Regional Geology Reviews

Siegfried Siegesmund
Miguel Angelo Stipp Basei
Pedro Oyhantçabal
Sebastian Oriolo *Editors*

Geology of Southwest Gondwana

Springer

Regional Geology Reviews

The Geology of—series seeks to systematically present the geology of each country, region and continent on Earth. Each book aims to provide the reader with the state-of-the-art understanding of a regions geology with subsequent updated editions appearing every 5 to 10 years and accompanied by an online “must read” reference list, which will be updated each year. The books should form the basis of understanding that students, researchers and professional geologists require when beginning investigations in a particular area and are encouraged to include as much information as possible such as: Maps and Cross-sections, Past and current models, Geophysical investigations, Geochemical Datasets, Economic Geology, Geotourism (Geoparks etc.), Geo-environmental/ecological concerns, etc.

More information about this series at http://www.springer.com/series/8643

Siegfried Siegesmund
Miguel Angelo Stipp Basei
Pedro Oyhantçabal · Sebastian Oriolo
Editors

Geology of Southwest Gondwana

Springer

Editors
Siegfried Siegesmund
GZG—Structural Geology and Geodynamics University of Göttingen
Göttingen
Germany

Miguel Angelo Stipp Basei
Geosciences Institute
University of São Paulo
São Paulo
Brazil

Pedro Oyhantçabal
Departamento de Geodinámica Interna
Universidad de la República
Montevideo
Uruguay

Sebastian Oriolo
GZG—Structural Geology and Geodynamics University of Göttingen
Göttingen
Germany

and

Instituto de Geociencias Básicas, Aplicadas y Ambientales de Buenos Aires (IGEBA)
CONICET-Universidad de Buenos Aires
Buenos Aires
Argentina

ISSN 2364-6438 ISSN 2364-6446 (electronic)
Regional Geology Reviews
ISBN 978-3-319-68919-7 ISBN 978-3-319-68920-3 (eBook)
https://doi.org/10.1007/978-3-319-68920-3

Library of Congress Control Number: 2017955254

"The cover photo shows the low-grade and folded sediments of the Ediacaran Rocha Formation (Dom Felicano Belt) at the Atlantic coast of Uruguay. These metasediments, based on the detrital zircon ages pattern and geological similarities are considered the counterpart of the Oranjemund Group (Gariep Belt) cropping out in the western borders of Namibia and South Africa. They were split up in the Mesozoic during the south Atlantic Ocean opening". Photo by Mathias Hueck

Printed on acid-free paper

This Springer imprint is published by the registered company Springer International Publishing AG part of Springer Nature
The registered company address is: Gewerbestrasse 11, 6330 Cham, Switzerland

Preface

Why This Book?

Our understanding of the Earth during the Precambrian has changed dramatically during the last decades. Discussions concerning the onset of plate tectonics, the supercontinent cycle and crustal growth processes have also diversified, with deep implications for Precambrian geodynamics. For this reason, this volume presents an updated synthesis of the state of the art of the Precambrian geology of Southwest Gondwana, including the main controversies and discussions concerning the tectonic and geodynamic evolution of this region during the Precambrian. Major tectonometamorphic, magmatic and sedimentary processes and paleogeographic implications during the late Neoproterozoic are evaluated in detail, as this period represents a key step in the Earth's evolution linked to the assembly of Gondwana.

Gondwana, in Retrospect

After publication of the first world atlas, *Theatrum Orbis Terrarum* (Ortelius 1570), the geographer Abraham Ortelius was the first to recognize the match of the South American and African Atlantic margins (Ortelius 1596). Later, these geometrical similarities constituted one of the main pieces of evidence to support plate tectonics (e.g., Wegener 1915; Bullard et al. 1965). However, geological similarities between both continents were first reported in the nineteenth century.

The term 'Gondwana', coined in the geological literature to refer to a plant-bearing series in India and afterwards extended to the Gondwana system (Feistmantel 1876; Medlicott and Blanford 1879), had previously been used in ethnographic works (Craig Robertson pers. comm.). Remarkably, the Austrian geologist Eduard Suess (1831–1914) was the first to establish regional correlations by the end of the nineteenth century, indicating the existence of a 'larger continent' (Suess 1885). This definition, probably the oldest precursor of the supercontinent concept, was stated by Suess as 'Versucht man ähnliche Vergleichungen auf die vereinigte Masse von Asien, Afrika und Europa anzuwenden, so zeigt sich sofort, dass hier verschiedenartige Gebiete zu einem grossen Continente aneinander geschweisst sind […] Wir nennen es Gondwána-Land nach der gemeinsamen alten Gondwána-Flora', and which can be roughly translated to 'if comparisons are made between Asia, Africa and Europe, it is clear that different areas in these regions were juxtaposed as part of a large continent […] We name it Gondwána-Land, after the shared Gondwana flora.'

Already in his first edition of *Die Entstehung der Kontinente und Ozeane*, Alfred Wegener considered South America, Africa, India and Australia as the main parts of Gondwana (Wegener 1915). Key contributions concerning South America and Africa correlations were first presented by Hans Keidel (1914, 1916) and Alexander du Toit (1927, 1928) and constituted one of the main lines of evidence considered by Alfred Wegener to support continental drift theory (Wegener 1929). Keidel described Upper Paleozoic glacial deposits in the Sierras

Australes de Buenos Aires in Argentina and correlated them with comparable deposits in the Cape Fold Belt (Keidel 1914, 1916, 1938). Motivated by Keidel's contributions, du Toit visited South America and provided further correlations across the South Atlantic (du Toit 1927, 1928, 1937).

First attempts to correlate the Precambrian rocks of South America and Africa were also established during the first half of the twentieth century. Based on the work of Brouwer (1921), Wegener (1929) recognized similarities in the 'old granites' of Brazil and southern Africa. On the other hand, du Toit (1927) stated:

> Prominent are the various belts of pre-Devonian strata in the lengthy stretch between the Río de la Plata and Pernambuco, of which some are probably of Ordovician age, while others may be older. They, however, have a general lithological resemblance to the folded Nama succession on the eastern side of the Atlantic, between Cape Town and Lüderitz, and also possess a strike that is more or less parallel to the coast. This likeness is highlighted by the fact that in certain localities the granite by which these belts are flanked are intrusive, just as in the Nama beds between Cape Town and Namaqualand.

These rocks were characterized by 'a general north-northeasterly trend', and du Toit (1927) attributed them both African and South American margins to the 'Brazilian system' defined by Alcide d'Orbigny in Brazil (Beaumont 1844), arguably corresponding to the oldest correlation of Brasiliano–Pan-African belts (Fig. 1).

After these first correlations, similarities in the Precambrian record of South America and Africa were tightened up significantly. Porada (1979) was one of the first to correlate the Damara and Gariep belts of southern Africa with the Ribeira Belt of South America, and to interpret their evolution in terms of continent collision. These correlations were strongly strengthened by the massive explosion in the application of first geochronological methods

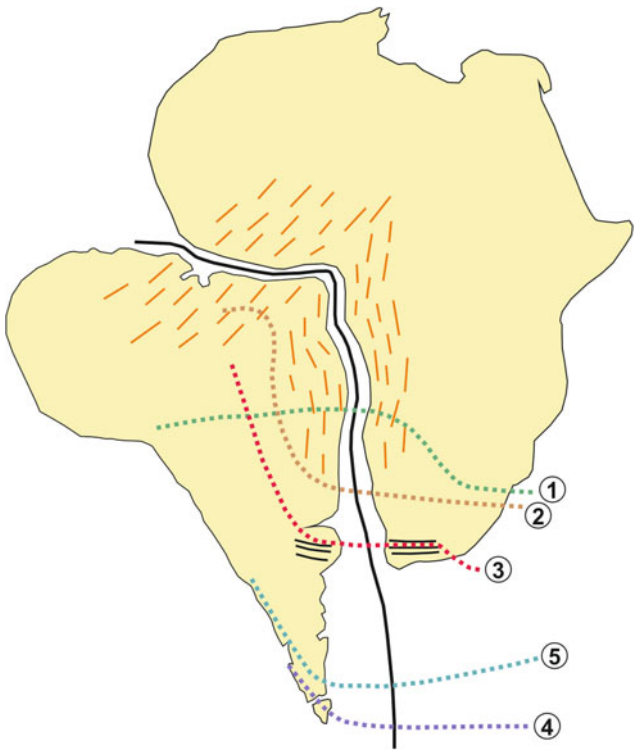

Fig. 1 Schematic reconstruction presented by Wegener (1915), including similarities between the Sierras Australes de Buenos Aires and the Cape Fold Belt (black lines). Handwritten notes made by Alfred Wegener on a copy of Wegener's (1915) work are schematically included in colour (after Wegener 2005): structural trends of basement rocks along both margins of the South Atlantic (orange lines) and northern boundary of marine deposits (1: Lower Cambrian, 2: Lower Devonian, 3: Upper Carboniferous, 4: Upper Triassic, 5: Upper Jurassic)

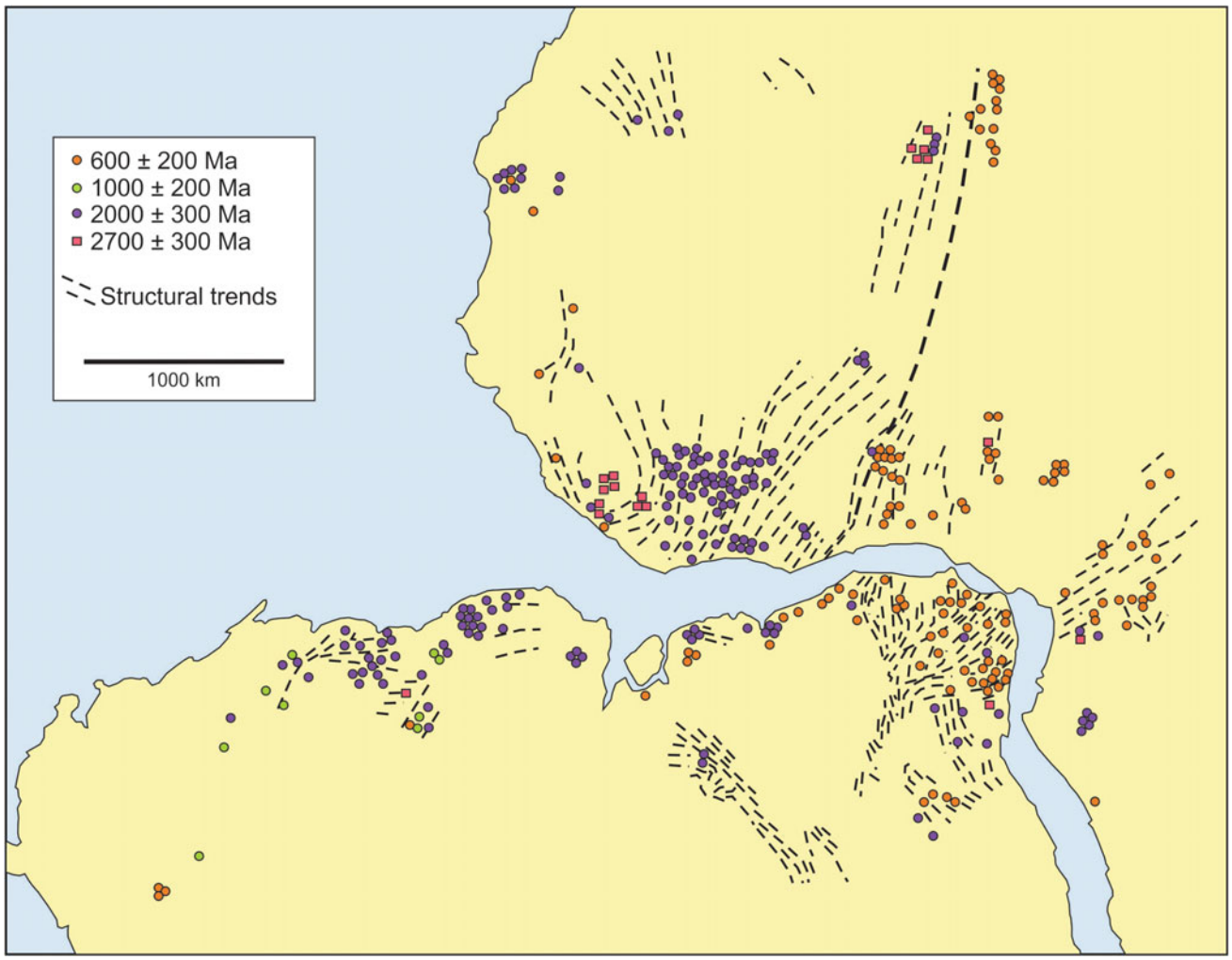

Fig. 2 Geochronological database presented by Hurley et al. (1967) showing similarities in the Precambrian record of South America and Africa (reconstruction after Bullard et al. 1965). Bold dashed line indicates the boundary between domains showing Paleoproterozoic and Neoproterozoic ages

(Torquato and Cordani 1981 and references therein). Correlations of Precambrian rocks of northeastern South America and western Africa, including similarities in structural and metamorphic characteristics, were presented by Pflug (1963), Almeida and Black (1968), and Allard and Hurst (1969). Along with this geological evidence, Hurley et al. (1967) provided a large database of K–Ar and Rb–Sr data, emphasizing similarities in the Paleoproterozoic and Neoproterozoic geological record (Fig. 2). Once again, these correlations constituted a central proof during renewed discussions about the validity of continental drift theory (Hurley 1968).

Likewise, several contributions focused particularly on the southwestern Gondwanan correlations across the Atlantic. Similarities in terms of collisional events and oceanic realms recorded in Brasiliano–Pan-African belts were presented by Almeida et al. (1973), Porada (1979, 1989), Torquato and Cordani (1981), and Hartnady et al. (1985). Based on paleomagnetic data, McWilliams (1981) provided the first apparent polar wander path for Western Gondwana (Fig. 3). The first geochronological data of the Precambrian basement of southern Brazil, Uruguay and Argentina were reported by Hart (1966), Halpern et al. (1970), Halpern and Linares (1970), and Umpierre and Halpern (1971), discussing their possible connection with African counterparts.

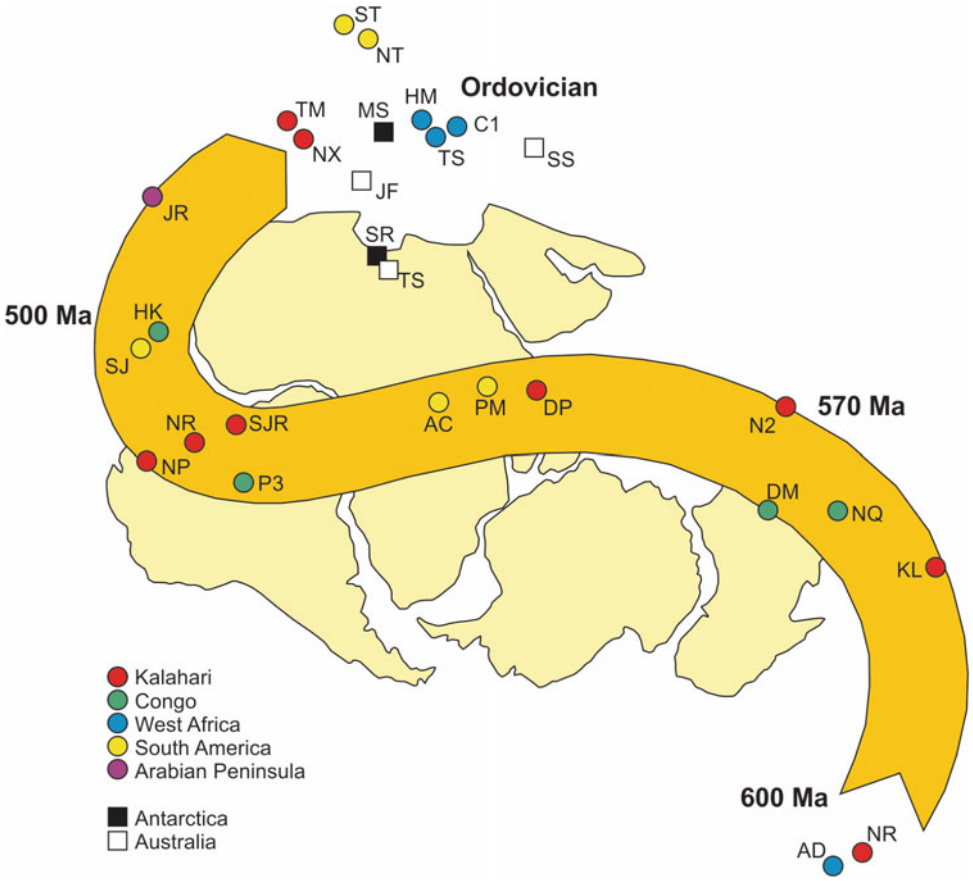

Fig. 3 First apparent polar wander path of Western Gondwana for the late Ediacaran-Ordovician after McWilliams (1981). Equal area projection, reconstruction after Smith and Hallam (1970) with fixed Africa. AD—Adma diorite; NR—Ntonya ring structure; KL—Klipheuvel Formation; NQ—Nosib Group; DM—lower Mulden Group; N2—upper Nama Group; DP—Doornpoort Formation; PM—Purmamarca sediments; AC—Abra de Cajas; P3—Plateau series; SJR—Sijarira Group; NR—Ntonya ring structure; NP—Nama Group—overprint-; SJ—Salta-Jujuy redbeds; HK—Hook intrusives; JR—Jordan redbeds; TM—Table Mountain series; NX—Blaubeker Formation; ST—S. Tilcara; NT—N. Tilcara; HM—Hasi-Mesaud sediments; TS—Tassili sediments; C1—Groupe de la Falaise d'Atar; MS—Mirnyy charnockites; JF—Jinduckin Formation; SR—Sor Rondane intrusives; TS—Tumblagooda sandstone; SS—Stairway sandstone. See McWilliams (1981) for further references

During the last two decades, however, Southwest Gondwana connections were significantly tightened up, particularly as a result of large-scale geological mapping programmes and the massive application of analytical techniques such as SHRIMP and LA-ICP-MS zircon geochronology (e.g. Siegesmund et al. 2011). The aim of this volume is thus to present an up-to-date overview of the Precambrian geology of Southwest Gondwana, emphasizing the role of the main Archean to Paleoproterozoic crustal blocks and the late Neoproterozoic orogenic belts related to the Brasiliano–Pan-African orogeny.

Content

This volume contains 24 chapters written by 54 authors. In Part I, regional overviews based on paleomagnetic and geophysical data are presented, together with a synthesis of the Adamastor Ocean evolution. The evolution of the main crustal blocks—the Río de la Plata, Congo and Kalahari cratons—is summarized in the chapters of Part II. Smaller continental fragments such

as the Nico Pérez Terrane, the Luis Alves and Curitiba microplates, and the Angolan Shield are also presented here, whereas the southwestern Brasiliano–Pan-African orogenic belts are described in the chapters in Part III. In Part IV a series of special chapters address key topics regarding the evolution of Southwest Gondwana: ore deposits, BIFs, Brasiliano–Pan-African shear zones, Neoproterozoic glaciations, Late Neoproterozoic-Early Paleozoic sedimentary basins, Ediacaran fauna and the impact crater record.

Rapalini presents an overview of available paleomagnetic data for Western Gondwana blocks and compares them with paleomagnetic constraints of Laurentia and Eastern Gondwana, discussing implications for the Ediacaran-Cambrian paleogeography. Data indicate that, by the early Ediacaran, the Amazonian and West Africa Cratons were probably still attached to Laurentia. On the other hand, the Río de la Plata and Congo-São Francisco cratons were already amalgamated by *c*. 575 Ma, whereas the Arabian-Nubian Shield was probably attached prior to *c*. 570 Ma. Paleomagnetic data from Australia constrain the apparent polar wander path for Eastern Gondwana, pointing to a late Ediacaran-Cambrian assembly with Western Gondwana. Interestingly, the author also outlines the absence of reliable paleomagnetic constraints for the Kalahari Craton.

Corner and Durrheim provide an integrated geophysical and geological framework for the lithospheric structure of southern Africa. A large database comprising geological, borehole, aeromagnetic, gravimetric, magnetotelluric, seismic reflection and refraction, and teleseismic data is carefully evaluated in order to provide insights not only into the Precambrian geology of areas covered by Phanerozoic sequences but also into major terrane boundaries, crustal lineaments and the lower crust-upper mantle structure. As a result, correlations between the main tectonostratigraphic domains and structures of the region are presented, together with implications for the thermal state of the main cratonic domains.

Basei et al. revise the Neoproterozoic history of opening and closure of the Adamastor Ocean between African and South American domains. The authors emphasize in particular the role of magmatic arc petrotectonic assemblages and associated major crustal-scale shear zones. Tonian-Cryogenian crustal extension gave rise to the opening of the Adamastor, succeeded by subduction starting at *c*. 640 Ma. Subduction led to magmatic arc development and, finally, to continental collision of South American and African cratons at *c*. 600 Ma, thus triggering crustal thickening in the Brasiliano–Pan-African belts.

Oyhantçabal et al. review geological, geochronological, isotopic and geophysical data of the Río de la Plata Craton of Argentina and Uruguay. Neoarchean to Paleoproterozoic crustal growth is indicated by Sm-Nd and Lu-Hf data. Widespread granitic-gneissic domains record accretional tectonics at *c*. 2.2–2.1 Ga and were intruded by late- to post-orogenic undeformed granitoids, gabbros and dolerites with a calcalkaline signature at *c*. 2.07 Ma. Subsequent exhumation, cooling and cratonization occurred at *c*. 2050–1800 Ma, succeeded by tholeiitic dyke intrusions at *c*. 1.8 and 1.6 Ga in Uruguay and Argentina, respectively. Despite being involved in the Brasiliano orogeny, the Río de la Plata Craton does not show significant reworking, revealing the presence of a thick and strong lithospheric mantle when it was amalgamated with the rest of Gondwana.

Thiéblemont et al. present an up-to-date geological overview of Precambrian domains in Western Central Africa, including the Congo Craton and adjacent blocks. Archean to Neoproterozoic lithostratigraphical domains are described in detail, along with novel geological maps and a summary of geochronological and Sm-Nd data. As a corollary, the Precambrian tectonic evolution of Western Central Africa is revised, emphasizing the role of crustal growth vs. crustal recycling processes.

Oriolo and Becker summarize the main tectonostratigraphic units of the Kalahari Craton. Geological, geochronological and isotopic data are presented, including a large compilation of U-Pb and Lu-Hf zircon data. The data show episodic crustal growth and accretion of minor crustal blocks during the Archean, also implying reworking of Hadean crustal remnants. The subsequent addition of juvenile Paleoproterozoic crust took place along the western margin of the proto-Kalahari margin, whereas Mesoproterozoic subduction zones were present all

around the Archean-Paleoproterozoic proto-Kalahari Craton. The latter gave rise to the accretion of several microcontinents and island arcs along the southern margin during the Namaqua-Natal orogeny. Afterwards, Cryogenian intraplate magmatism was succeeded by the incorporation of the Kalahari Craton into Gondwana during the protracted Pan-African orogeny.

Oyhantçabal et al. integrate geological, geochronological, isotopic and geochemical data of the Nico Pérez Terrane in Brazil and Uruguay in order to constrain its regional extension and Precambrian tectonic evolution. Archean crustal growth was succeeded by major Paleoproterozoic crustal reworking related to multistage magmatism and high-grade metamorphism. The Mesoproterozoic record is restricted to intraplate magmatism and related sedimentary sequences, whereas significant Neoproterozoic crustal reworking during the Brasiliano–Pan-African orogeny is attested by cooling ages, shear zones and granitic intrusions. In addition, the authors emphasize the African origin of the Nico Pérez Terrane, linked to the Congo Craton, and present novel correlations between the southern Brazilian and Uruguayan sectors.

Passarelli et al. revise geological, geochronological, isotopic and geochemical data of the Luis Alves and Curitiba terranes of southern Brazil, establishing the main characteristics of these two Paleoproterozoic crustal blocks. The Luis Alves Craton is composed of a TTG suite, mafic-ultramafic intrusions and scarce paragneisses, whereas the Curitiba terrane comprises migmatites and amphibole-gneissic rocks. On the other hand, Sm-Nd data indicate dominantly Neoarchean to Paleoproterozoic crustal growth for the Luis Alves Craton, and older Meso- to Neoarchean crustal growth for the Curitiba terrane. Both blocks were amalgamated during the Ediacaran along the Pien Suture Zone, triggering significant deformation and migmatization in the Curitiba terrane.

Jelsma et al. summarize new and available geological, geochronological and geochemical data of the Angolan Shield. Three main crustal domains are recognized: the Central Shield Zone in the east, and the Central Eburnean Zone and Lubango Zone in the west. Magmatism recorded in these domains is attributed to continental arcs developed along the active western and southern margins of the Congo Craton, with peak magmatic events at *c*. 2.0–1.96 Ga (Eburnean Event), 1.88–1.83 Ga (Kamanjab-Bangweulu Event) and 1.80–1.77 Ga (Epupa Event).

Phillip et al. evaluate the tectonic evolution of the São Gabriel Terrane in southern Brazil, linked to the evolution of the Charrua Ocean. A large database of geological and isotopic data are presented. Based on these data, the authors provide a three-stage tectonic evolution for the São Gabriel Terrane, which can be divided into the Passinho (*c*. 0.89–0.85 Ga), São Gabriel (*c*. 0.77–0.68 Ga) and Dom Feliciano (*c*. 0.65–0.54 Ma) orogenic events.

Hueck et al. compile geological, geochronological and structural data of the Dom Feliciano Belt in Brazil and Uruguay, discussing models and controversies related to the tectonic evolution of this major transpressional belt. The first phase is recorded in the São Gabriel Terrane, associated with juvenile magmatism and accretional tectonics at *c*. 870–680 Ma. Subsequent high-grade metamorphism, shear zone nucleation and deformation of metavolcanosedimentary units were related to a collision at *c*. 650–600 Ma, succeeded by strike-slip deformation and voluminous post-collisional magmatism at *c*. 600–550 Ma. The final stage corresponds to the development of foreland basins, probably associated with transtension occurring up to the Early Paleozoic.

Goscombe et al. provide a detailed tectonic evolution of the Kaoko-Damara Belt system, evaluating geological, structural, metamorphic and geochronological constraints. The collision of the Río de la Plata and Congo cratons resulted in obduction of the Coastal Terrane over the latter at *c*. 590 Ma and it was succeeded by collision of the Kalahari with the Congo Craton along the Damara Belt at *c*. 555–550 Ma, giving rise to northwest–southeast shortening between *c*. 550 and 530 Ma and consequent transpression with the development of strike-slip shear zones. At *c*. 530–525 Ma, shear zones of the Kaoko Belt underwent transtension, whereas peak metamorphism and deformation associated with north-northwest-south-

southeast crustal shortening is recorded in the Damara Belt, succeeded by northeast-southwest shortening by *c*. 512–508 Ma. A switch to east–west shortening and north–south extension is evident in the Damara Belt at *c*. 508 Ma, probably resulting from far-field effects of tectonic processes along the southern margin of Southwest Gondwana. This north–south extension triggers both decompression melts at *c*. 508–504 Ma and gravitational collapse and extension of the thermally weakened Damara Orogen core at *c*. 505–500 Ma.

Frimmel reviews the tectonostratigraphy of the Gariep Belt and provides an integrated evolution of Neoproterozoic tectonic processes, including interesting insights into contemporaneous sedimentary and paleoclimatic processes. The author indicates the existence of Tonian alkaline magmatism related to crustal thinning and associated late Tonian continental sedimentation that record a progressive transition to shallow marine conditions. At *c*. 750 Ma, the first glaciations of the Gariep Belt are recorded. After a hiatus of *c*. 100 Myr, oceanic magmatism is recorded by the Marmora Terrane, which is interpreted as a late Cryogenian-Ediacaran back-arc basin. Closure of the Marmora Basin took place at *c*. 550–545 Ma, contemporaneously with climatic recovery after the Numees glaciation. Transpressive deformation led to exhumation and erosion, providing detritus for the Nama basin, and was succeeded by post-orogenic Cambrian alkaline magmatism.

Kisters and Belcher present an overview of the stratigraphy, structure, magmatism and tectonic evolution of the Saldania Belt, interpreted as a forearc crustal section that evolved between the late Ediacaran and the Cambrian along the Kalahari Craton margin. The structurally lower Swartland Complex resulted from tectonic underplating during southeast-directed subduction below the Kalahari Craton and is unconformably overlain by low-grade metasediments and minor metavolcanic rocks of the Malmesbury Group that represent the late Neoproterozoic to Cambrian forearc basin fill. Regional deformation of the forearc is characterized by partitioned sinistral transpression related to oblique convergence and was probably associated with slab break-off, thus accounting for voluminous, syn- to late-tectonic magmatism of the Cape Granite Suite.

Schmitt et al. evaluate Cambrian Brasiliano–Pan-African tectonic events in the context of the assembly of Southwest Gondwana, based on the geological database of the new geological map of Gondwana. Not only collisional events but also extensional processes leading to the development of oceanic and back-arc basins are evaluated. Based on this synthesis, the authors establish correlations between Ediacaran-Cambrian orogens of Eastern and Western Gondwana, highlighting potential causal relationships between them.

López de Luchi et al. compile isotopic and geochemical data of the Eastern Sierras Pampeanas and provide a revised tectonic evolution for this key area of the proto-Pacific margin of Gondwana. The authors characterize the metamorphism, magmatism, deformation and tectonic implications of three main events: the Ediacaran to Early Cambrian (580–530 Ma) Pampean, the Late Cambrian-Ordovician (500–460 Ma) Famatinian and the Devonian-Carboniferous (400–350 Ma) Achalian orogenies, which resulted from the complex alternation of subduction-related and collisional processes.

Smith summarizes the main geological, stratigraphic and geochemical characteristics of iron formations of southern Africa. Additionally, he presents an overview of depositional models and the economic significance of these iron formations.

Rosière et al. provide a summary of iron formations of the South American Platform, separating them based on their age and location. Based on the main geological, stratigraphic, mineralogical and geochemical characteristics, implications for the genesis and ore deposit significance are evaluated.

Poiré et al. revise the Neoproterozoic glacial record of South America. They provide stratigraphic, isotopic and geobiological insights into the genesis of these deposits, exposed in Brazil, Paraguay, Bolivia, Uruguay and Argentina. As a corollary, sedimentary successions are divided into “Snowball Earth” and “Phantom Glacial” deposits in order to separate glaciogenic from non-glaciogenic deposits that were, however, influenced by global glaciation processes. Neoproterozoic major climatic and sea level fluctuations are also discussed.

Gaucher reviews the Ediacaran to Early Cambrian fossil record of Southwest Gondwana. Details of the characteristics and occurrence of acritarchs, soft-bodied biota, skeletonized metazoans and protists, and trace fossils are described, discussing the biostratigraphic and paleographic implications.

Zimmermann presents an up-to-date synthesis of provenance data of major Neoproterozoic to Lower Paleozoic sedimentary basins in southern South America and Africa, including key lithostratigraphic features as well as age and provenance constraints. The author provides a thorough discussion of the limitations of the available data and its implications for regional geodynamic and tectonic models. Based on the missing links of the current database, future lines of research are also presented.

Oriolo et al. review geometrical, structural, kinematic, microstructural and geochronological data of crustal-scale shear zones of the Brasiliano–Pan-African belts and discuss the role of these shear zones in the construction of Western Gondwana. Likewise, insights into Phanerozoic shear zone reactivation are also presented, particularly during the Cretaceous opening of the South Atlantic Ocean.

Borg and Gauert describe ore deposits of southern Africa, including some world-class deposits such as the Central African Copperbelt, and evaluate their age, genetic processes and tectonic setting. They emphasize the enormous potential of this region in terms of base (Cu, Pb, Zn, Co, Ni), precious (Au, Ag) and strategic metals (U, W, Sn, Li, Ta, REE). VHMS and SHMS deposits are related to extensional settings, mostly Mesoproterozoic in age, though sediment-hosted stratabound Cu-Ag deposits are also recorded in other volcanosedimentary basins. On the other hand, mantle-derived mafic melts allowed the formation of ore deposits of Cu, Co and Ni, whereas highly fractionated intrusions related to collisional orogens host a range of highly incompatible elements. As a result, the authors emphasize the role of the complex tectonic and geodynamic evolution of Southwest Gondwana, identifying alternating episodes of crustal shortening and extension as one of the main triggers of the wide diversity and availability of ore deposits.

Reimold et al. provide an overview of impact craters of Gondwanan regions. Though the African and South American record is emphasized, Eastern Gondwana craters occurring in Australia and India are also mentioned. A detailed list of impact crater location, size and age, among others, are provided. Finally, the authors emphasize the potential of the region in terms of possibly hidden impact craters, which might be discovered by future studies.

References

Allard GO, Hurst VJ (1969) Brazil-Gabon geologic link supports continental drift. Science 163:528–532

Almeida FFM et al (1973) The Precambrian evolution of the South American cratonic margin, South of Amazonas River. In: Nairn ACM et al (eds) The Ocean Basins and Margins. Plenum, New York, pp 411–446

Beaumont ME (1844) Report on M. Alcide D'Orbigny's memoir, entitled General considerations on the geology of South America. The Edinburgh New Philos J 37:111–131.

Bullard E. et al (1965) The fit of the continents around the Atlantic. Philos T Roy Soc A 258:41–51.

du Toit AL (1927) A Geological Comparison of South America with South Africa. Carnegie Institution of Washington, Washington, 158 p

du Toit AL (1928) Some reflections upon a geological comparison of South Africa with South America. Proc Geol Soc South Africa 19–38.

du Toit AL (1937) Our Wandering Continents. Oliver and Boyd, Edinburgh, 366 p

Feistmantel O (1876) Notes on the age of some fossils of India. Rec Geol Surv India 9:28–42

Halpern M, Linares E (1970) Edad rubidio-estroncio de las rocas graníticas del basamento cristalino del área de Olavarría, Provincia de Buenos Aires, República Argentina. Rev Asoc Geol Argentina 25:303–306

Halpern M et al (1970) Radiometric ages of crystalline rocks from southern South America, as related to Gondwana and Andean geologic provinces. Solid Earth Problems Conference, Buenos Aires

Hart SR (1966) Radiometric ages in Uruguay and Argentina and their implications concerning continental drift. Geological Society of America Annual Meeting, San Francisco

Hartnady C et al (1985) Proterozoic crustal evolution in southwestern Africa. Episodes 8:236–244
Hurley P (1968) The confirmation of continental drift. Sci Am 218:52–64
Hurley PM et al (1964) Test of continental drift by comparison of radiometric ages. Science 157:495–500
Keidel H (1914) Über das Alter, die Verbreitung und die gegenseitigen Beziehungen der verschiedenen tektonischen Strukturen in den argentinischen Gebirgen. International Geological Congress, Toronto
Keidel J (1916) La geología de las sierras de la provincia de Buenos Aires y sus relaciones con las montañas de Sud África y los Andes. *Anales del Ministerio de Agricultura de la Nación*, Sección Geología, Mineralogía y Minería 11:1–78
Keidel H (1938) Über die "Gondwaniden" Argentiniens. Geologische Rundschau 30:148–240
McWilliams MO (1981) Palaeomagnetism and Precambrian tectonic evolution of Gondwana. In: Kröner A (ed) Precambrian Plate Tectonics. Elsevier, Amsterdam, pp 649–687
Medlicott HB, Blanford WT (1879) A Manual of the Geology of India and Burma. Records of the Geological Survey of India, Calcutta
Ortelius A (1570) Theatrum Orbis Terrarum. Gilles Coppens de Diest
Ortelius A (1596) Thesaurus Geographicus
Pflug R (1963) Präkambrische Strukturen in Afrika und Südamerika. Neues Jb Geol P M 7:355–358
Porada H (1979) The Damara-Ribeira orogen of the Pan-African/Brasiliano Cycle in Namibia (South West Africa) and Brazil as interpreted in terms of continental collision. Tectonophysics 57:237–265
Porada H (1989) Pan-African rifting and orogenesis in southern to equatorial Africa and eastern Brazil. Precambrian Res 44:103–106
Siegesmund S, Basei MAS, Oyhantcabal P (2011) Multi-accretional tectonics at the Rio de la Plata Craton margins. Int J Earth Sci 100(2–3):197–694
Smith AG, Hallam A (1970) The fit of the southern continents. Nature 225:139–144
Suess E (1885) Das Antlitz der Erde. Temsky, Vienna
Torquato JR, Cordani UG (1981) Brazil-Africa geological links. Earth-Sci Rev 17:155–176
Umpierre M, Halpern M (1971) Edades Sr–Rb del Sur de la República Oriental del Uruguay. Rev Asoc Geol Argentina 26:133–155
Wegener A (1915) Die Entstehung der Kontinente und Ozeane. Friedrich Vieweg & Sohn, Braunschweig
Wegener A (1929) Die Entstehung der Kontinente und Ozeane, 4th edn. Friedrich Vieweg & Sohn, Braunschweig
Wegener A (2005) Die Entstehung der Kontinente und Ozeane, reprint of 1st edn with handwritten comments by Alfred Wegener and reprint of 4th edn. Gebrüder Borntraeger Verlargsbuchhandlung, Berlin-Stuttgart

Acknowledgements

The authors are greatly indebted to Carlos Cingolani, Víctor Ramos and Mathias Hueck for facilitating Keidel and du Toit's contributions. Craig Robertson is acknowledged for his valuable comments about the origin of the term 'Gondwana'.

The editors gratefully acknowledge the following colleagues for their reviews: Monica Lopez de Lucci, Guido Meinhold, Hartwig Frimmel, Stephen McCourt, Bert De Waele, Carlos Alberto Rosiere, Gerard Germs, Sebastian Oriolo, Pedro Oyhantcabal, Chris Gauert, Mathias Hueck, Thomas Becker, Miguel Basei, Klaus Wemmer, Alex Kisters, Christie Rowe, Carlos Cingolani, Johan de Beer, Siegfried Siegesmund, Wolfram Geissler, Wolf Uwe Reimold, Malte Drobe and Ben Goscombe

Contents

About the Editors

Siegfried Siegesmund is Professor of Geology at the Geoscience Center, Department of Structural Geology and Geodynamics, University of Goettingen, Germany. He began his geological studies at Freiberg University of Mining and Technology. He completed his Ph.D. thesis in 1989 at the University of Kiel, followed by his habilitation in 1995 at the University of Goettingen. He has been a visiting research fellow at the University of Hawaii, University of Harare, University of Laramie, University of Basel, INGEIS Buenos Aires, Universidad de la República (Uruguay), University of São Paulo, University of Granada, University of Oviedo, University of Villa Real, University of Padua, University of San Luis Potosi and others. He has been a member of various international scientific collaborations, including research projects in Antarctica, and was awarded a Heisenberg professorship. His research utilizes an interdisciplinary approach by combining structural geological surveys, geophysical explorations of structures at depth, kinematic studies of shear zones, emplacement of granites, microtectonics, geochronology, neotectonics, geochemistry and provenance studies (i.e. the geodynamic evolutionary development of mountain building processes in general). More recently his geological interests have included aspects of applied geology and geomaterial research (e.g., natural stones in architecture, exploration of dimensional stone deposits and ore deposits) plus geothermal exploration, the deposition of radioactive waste, and petrophysics. He has published more than 25 special issues and monographs, and more than 350 scientific articles and geological maps.

Miguel Angelo Stipp Basei holds a doctorate from 1985 from the Geosciences Institute at the University of São Paulo, where he is currently a full professor. He is a member of the Brazilian Academy of Sciences and a researcher for the National Research Council (CNPq). He was a visiting research fellow for the Open University, UK, from 1988 to 1989 with a specialization in isotope geochemistry, and he developed a postdoctoral program in U-Pb zircon geochronology at the University of Kansas, USA, in 1989. He has a specialization in U-Pb studies in zircon through the systematic SHRIMP technique obtained during several stages at the Australian National University, Canberra in 2000–2006. Since 2009 he has been coordinator of the LA MC ICPMS laboratory of the Geochronological Research Center of the University of São Paulo. He has a scientific interest in topics related to geochronology, geotectonics and structural geology, with a main focus on the tectonic evolution of the Precambrian terrains of the southeastern part of South America and its African counterparts, a topic on which he has already published numerous articles in international journals.

Pedro Oyhantçabal is Professor of Geology at the Universidad de la República of Uruguay and researcher for the Pedeciba and ANII (National Research Council of Uruguay). He obtained his degree in 1982 and his Ph.D. at the University of Göttingen, Germany. He has published more than 30 articles in peer-reviewed journals and has acted as co-editor of a special issue of *International Journal of Earth Sciences*. His interests are in geochemistry and the isotope

geology of magmas, geochronology, structural geology, and tectonics. His work currently focuses on the evolution of the Neoproterozoic belts of Uruguay, Southern Brazil, and southwestern Africa.

Sebastian Oriolo is a researcher at the National Scientific and Technical Research Council (CONICET) and the University of Buenos Aires (UBA), Argentina. He obtained his degree in geology in 2012 at the University of Buenos Aires and his Ph.D. in 2016 at the University of Göttingen, Germany. His main interests are structural geology, tectonics, geochronology and petrology, particularly focused on the Precambrian to Paleozoic evolution of Western Gondwana.

Part I

Paleomagnetism, Geophysics and Adamastor

The Assembly of Western Gondwana: Reconstruction Based on Paleomagnetic Data

1

Augusto E. Rapalini

Abstract

In the last two decades some consensus has been reached with regard to the assembly of Gondwana being a long and complex process. Reliable paleomagnetic data are essential to determine the paleogeographic and kinematic evolution of each Gondwana-forming block during its assembly as well as to place chronological constraints on such a process. A review of paleomagnetic data from Western Gondwana blocks indicates that the available Ediacaran to Cambrian database is still scarce and uneven for different cratons, despite clear improvement in the quantity and quality of paleomagnetic information in recent decades. The main constraints placed by the available information are as follows:

- The Río de la Plata and Congo–Sao Francisco cratons were likely already attached by mid-Ediacaran times (*c*. 575 Ma) and not part of Rodinia.
- The Arabian-Nubian Shield was part of proto-Gondwana by 550 Ma and probably even earlier.
- Paleomagnetic constraints are virtually absent for the Kalahari craton.
- Amazonia and West Africa were probably still part of Rodinia and attached to eastern Laurentia by the Early Ediacaran (*c*. 615 Ma), suggesting that a large Ediacaran Clymene Ocean existed between Amazonia and the Congo–Sao Francisco–Río de la Plata block.
- The age of Amazonia amalgamation is poorly constrained by paleomagnetic data as $\geq$ 525 Ma.
- The accretion of Eastern Gondwana blocks probably occurred in the latest Ediacaran-Cambrian times as suggested by the apparent polar wander path of Australia.

Keywords

Western Gondwana • Paleomagnetism • Ediacaran Cambrian • South America

1.1 Introduction

The assembly of Gondwana in Ediacaran-Cambrian times (e.g., Meert and Lieberman 2008) was a long and complex process that may have lasted well over 50 million years and involved several different 'orogenies'. Since this process was coetaneous with the major biotic changes occurring during the Earth's history (i.e., the Cambrian radiation; for detailed references, see Meert and Lieberman 2008), as well as large climatic and environmental changes (Hoffman 1999; Evans 2000; Xiao 2004; Canfield et al. 2007; Meert 2007 and references therein), unravelling the role that these dramatic paleogeographic configuration changes, produced by the assembly of such a continent, had in these events is of paramount importance.

Detailed kinematic and paleogeographic reconstruction of Gondwana assembly is a huge task that must involve several independent disciplines (i.e., geochronology, structural geology, biogeography, biostratigraphy, sedimentology and basin analysis, petrology, geophysics, tectonics etc.). Paleomagnetism is an essential tool for these purposes since it is the only known methodology that provides quantitative determination of paleolatitude and orientation of any continental block at different times (e.g., Butler 1992; Van der Voo 1993). Paleomagnetism is not without caveats and ambiguities, and it only provides a broad paleogeographic picture of distribution of continents along the Earth's history because its precision will be at its best in a few hundred kilometers. However, it is irreplaceable in producing first-order paleogeographic sketches as well as independently testing many opposing tectonic models. It is also a powerful tool to test whether actualistic climatic and geodynamic processes are valid in Precambrian and Early

A. E. Rapalini (✉)
Departamento de Ciencias Geológicas, Facultad de Ciencias Exactas y Naturales, Consejo Nacional de Investigaciones Científicas y Técnicas (CONICET), Instituto de Geociencias Básicas, Aplicadas y Ambientales de Buenos Aires (IGEBA), Universidad de Buenos Aires, Buenos Aires, Argentina
e-mail: rapalini@gl.fcen.uba.ar

S. Siegesmund et al. (eds.), *Geology of Southwest Gondwana*, Regional Geology Reviews,
https://doi.org/10.1007/978-3-319-68920-3_1

Paleozoic times (e.g., Kirschvink 1992; Williams 2008; Mitchell et al. 2010).

Many different paleogeographic models for the assembly of Gondwana, based on paleomagnetic data, have been published (e.g., Meert 2003; Collins and Pisarevsky 2005; Meert and Lieberman 2008; Li et al. 2013). Original proposals of a single episode of continental collision (McWilliams 1981) between East Gondwana (East Antarctica, Australia, India and Madagascar) and West Gondwana (South American and African cratons) along the Eastern African orogen have been replaced by models that prescribe a protracted process of collision of several independent crustal blocks (e.g., Powell and Pisarevsky 2002). Although some common ground has been reached among most models, like the complex nature of the amalgamation process that involved more than a dozen different crustal blocks with independent kinematic history, major controversies and uncertainties remain (compare, e.g., Murphy et al. 2013; Johansson 2014). On the basis of these shortcomings are the scarce reliable paleomagnetic data available, despite important progress achieved in the last two decades (e.g., Meert et al. 2001; Sánchez Bettucci and Rapalini 2002; Trindade et al. 2006; Rapalini 2006; Moloto-A-Kenguemba et al. 2009; Gregory et al. 2009; Schmidt et al. 2009; Mitchell et al. 2010; Rapalini et al. 2013, 2015; Schmidt 2014).

In this chapter a brief review of the available paleomagnetic constraints on the Gondwana assembly process, with a main focus on Western Gondwana, is presented.

1.2 Main Cratons and Paleomagnetic Database

Figure 1.1 presents a sketch of the main crustal blocks that constitute Western Gondwana. This is composed of five major Archean to Paleoproterozoic cratons—that is, Amazonia, West Africa, Congo–Sao Francisco, Kalahari and Río de la Plata, and many, generally smaller, crustal blocks with Archean to Mesoproterozoic basements but extensively reworked during the Pan-African and Brasiliano orogenies that led to the final assembly of Gondwana. The blocks represented in Fig. 1.1 are not exhaustive because several minor ones have been omitted for clarity of the sketch [e.g., Punta del Este/Cuchilla Dionisio terrane in eastern Uruguay (Bossi and Gaucher 2004) or the Sao Gabriel block in southern Brazil (Saalmann et al. 2006)], as well as long Neoproterozoic thrust and fold belts (e.g., Dom Feliciano, Araguaia, Paraguay, Brasilia, Namara and Gariep) that most probably developed along the margins of some of the larger crustal blocks (e.g., Prave 1996; Brito Neves et al. 2000; Gray et al. 2008; Santos et al. 2008; Oyhantçabal et al. 2009; Pimentel et al. 2011; McGee et al. 2012).

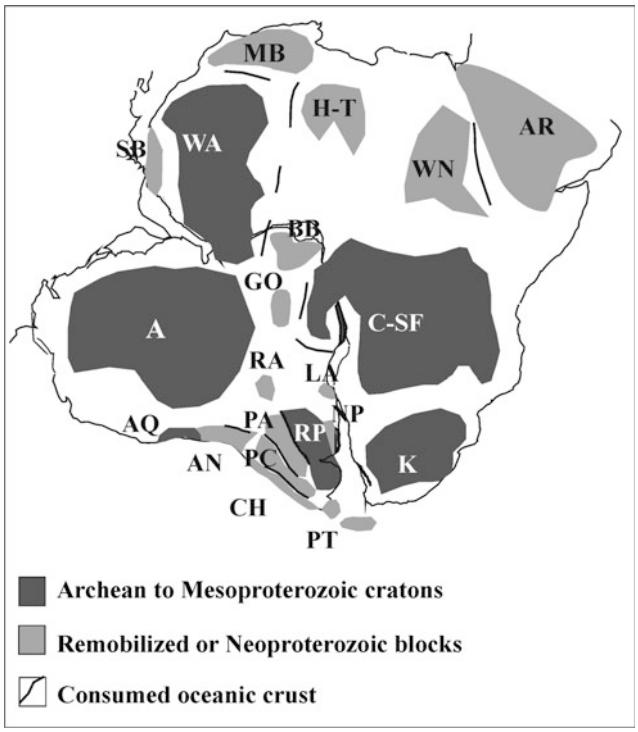

Fig. 1.1 Sketch of main crustal blocks of Western Gondwana in the Neoproterozoic. *A* Amazonia; *AN* Antofalla; *AQ* Arequipa; *AR* Central Arabia; *BB* Borborema, *CH* Chilenia; *C-SF* Congo–Sao Francisco; *GO* Goias; *H-T* Hoggar-Tibesti; *K* Kalahari; *LA* Luis Alves; *MB* Moroccan block; *NP* Nico Perez, *PA* Pampia; *PC* Cuyania; *PT* Patagonian/Malvinas block; *RA* Rio Apa; *RP* Rio de la Plata; *SB* Senegalese block; *WA* West Africa; *WN* West Nile. Modified from Sánchez-Bettucci and Rapalini (2002)

Unravelling the kinematic and paleogeographic evolution of the major cratons in Neoproterozoic-Early Paleozoic times to constrain how the amalgamation of West Gondwana occurred is a major endeavour, let alone if the smaller crustal fragments are considered.

Table 1.1 presents a selection of moderately to highly reliable available paleomagnetic poles for West Gondwana forming pieces for the Ediacaran-Cambrian. Their implications in the models of the continent assembly are discussed below.

1.2.1 The Río de la Plata Craton and Luis Alves Block

Table 1.1 and Fig. 1.2a show that several paleomagnetic poles are available for the Río de la Plata craton for the interval *c*. 600–500 Ma. Although some of them should be considered virtual geomagnetic poles (VGPs) because the small number of samples involved in their computation do not guarantee full average of paleosecular variation (McElhinny and McFadden 2000), and the age of most is loosely bracketed by stratigraphic

Table 1.1 Selected Ediacaran to Cambrian paleomagnetic poles for the Western Gondwana main crustal blocks

Geologic unit	PP	Lat (°)	Long (°)	A95 (dp/dm)	Age (Ma)	Method	References
Río de la Plata craton							
Cerro Victoria F. (remag)	CVc	29	13	11/16	500?	APWP	Rapalini and Sanchez Bettucci (2008)
Sierra de Animas (remag)	SA1	23	9	20/27	520	K/Ar	Sánchez Bettucci and Rapalini (2002)
Cerro Negro F.	SBc	18	354	10/13	520?	Strat. and APWP	Rapalini et al. (2013)
Polanco F. (remag)	P	15	359	14/17	520?	APWP	Rapalini and Sanchez Bettucci (2008)
Olavarría F.	SBd	4	323	6/9	535?	APWP	Rapalini et al. (2013)
Los Barrientos	LB	−47	313	11/14	570?	APWP	Rapalini (2006)
Sierra de Animas	SAn	−41	318	15	579	U–Pb and Ar/Ar	Rapalini et al. (2015)
Cerro Largo F.	SBe	−67	257	8/14	580?	APWP	Rapalini et al. (2013)
Villa Mónica F.	SBf	−76	159	6/11	590?	APWP	Rapalini et al. (2013)
Playa Hermosa F.	PH	−66	130	12	590	U–Pb and Strat	Rapalini et al. (2015)
Luis Alves Block							
Campo Alegre F	CA	−80	68	10	595	U–Pb	D'Agrella-Filho and Pacca (1988)
Congo–Sao Francisco (plus Borborema province)							
Piquete Formation	PF	24	22	10	500	K–Ar	D'Agrella Filho et al. (1986)
Juiz de Fora Complex	JF	10	357	10	510	K–Ar, APWP	D'Agrella Filho et al. (2004)
Bambuí + Salitre C (remag)	B + S	32	337	3	525	Pb–Pb, APWP	Trindade et al. (2004)
Itabiana Dykes	ID	29	330	8	525	Ar/Ar	Trindade et al. (2006)
Sinyai Dolerite	SD	−40	321	5	547	Ar/Ar	Meert and Van der Voo (1996)
Nola dykes	ND	−62	305	5/11	571	Ar/Ar	Moloto-A-Kenguemba et al. (2008)
Arabian-Nubian shield							
Mirbat Sandstones	MS	−25	317	4/7	550	Strat	Kempf et al. (2000)
Nabati Complex	NC	−56	132	18	575	K–Ar	Saradeth et al. (1989)
Bir Saf-Saf dykes	BS	−71	101	11	586	K–Ar	Saradeth et al. (1989)
Dokhan volcanics	DV	−42	47	5	592	U–Pb	Davies et al. (1980), Breitkreutz et al. (2010)
West Africa							
Sidi-Said volcanics	SS	−9	53	6	510	Strat.	Khattach et al. (1995)
Adma Diorite	AD	32	345	16	613	U–Pb	Morel (1981)
Tin Dioulaf	TD	36	246	7	630	Strat	Boudzoumou et al. (2011)
Amazonia							
Araras Group B (remag)	AB	36	338	10	525	APWP	Trindade et al. (2003)
Planalto da Serra	PS	37	315	11	615	Ar–Ar	Garcia et al. (2013)
Kalahari							
Equeefa dykes and Mzumbe gneiss (remag)	ED	25	17	11	530	Fission-tracks	Gose et al. (2004)

Age method: argument used to compute more likely age for the paleomagnetic pole

considerations, a single track can easily be seen for Río de la Plata. In a Gondwana reconstruction (Reeves et al. 2004; Trindade et al. 2006) to southern Africa, the apparent polar wander path (APWP) describes a long track from a position close to the present-day south pole at *c*. 590–600 Ma into northern Africa for the Late Early to Middle Cambrian (520–510 Ma). The Sierra de las Animas Complex new pole (Rapalini et al. 2015) can be considered a key pole for the craton since it was obtained from a sufficient number of sites on volcanic and hypabyssal rocks, shows both magnetic polarities, passes a tilt test and the rocks are accurately dated by U–Pb SHRIMP in zircons (578 Ma; Rapalini et al. 2015) and Ar–Ar in biotite (579 Ma; Oyhantçabal et al. 2009). The age of the sedimentary Playa Hermosa Formation, in turn, is bracketed between the youngest detrital zircon found in the lowermost, glacially influenced, levels (594 Ma; Rapalini et al. 2015) and the *c*. 580 Ma volcanic dykes that intrude into its upper section (Sánchez-Bettucci et al. 2010). Pecoits et al. (2016) have recently published detrital zircon ages from the upper levels of the Playa Hermosa Formation suggesting a *c*. 575 Ma for their deposition. Since the paleomagnetic data comes from the lowermost levels, *c*. 590 Ma for the Playa Hermosa paleomagnetic pole is likely. The long APWP for Río de la Plata (Fig. 1.2) corresponds largely to a counter-clockwise rotation of the craton during West Gondwana assembly, a timespan in which it was at middle to low southern latitudes. Low paleolatitudes for the Gaskiers glaciation recorded in the lower section of the Playa Hermosa Formation and the Colombo diamictite (Poiré and Spalletti 2005; Arrouy et al. 2015) are supported by the Playa Hermosa and SBf mean VGPs (Fig. 1.2a). Since the Late Early Cambrian (*c*. 510–520 Ma), all paleomagnetic poles from Río de la Plata fall over northern Africa.

The only available paleomagnetic pole for the Luis Alves Block in southeastern Brazil is that from the Campo Alegre lavas (D'Agrella-Filho and Pacca 1988). The age of these rocks has been determined as 595 ± 16 Ma (U–Pb TIMS in zircons; Cordani et al. 1999). The consistency of Campo Alegre lavas with Playa Hermosa and SBf suggest little or no relative displacement between the Luis Alves block and the Río de la Plata craton since the Early to Middle Ediacaran. This is consistent with most tectonic models of the region (see Campos Neto 2000; Rapela et al. 2007). However, Font et al. (2011) have suggested that the Campo Alegre lavas might have been remagnetized during the Cretaceous and therefore the Campo Alegre lavas might not be a reliable pole for constructing an Ediacaran APWP.

1.2.2 The Congo–Sao Francisco Craton

The Ediacaran-Cambrian paleogeographic evolution of the Congo–Sao Francisco craton is constrained by three high-quality paleomagnetic poles—that is Nola dykes (571 ± 6 Ma; Moloto-A-Kenguemba et al. 2009), Sinyai dolerite (547 ± 4 Ma; Meert and Van der Voo 1996) and Itabiana dykes (525 ± 5 Ma; Trindade et al. 2006), allowing the position of the craton to be determined at intervals of around 25 Ma from the Early Late Ediacaran to the Early Cambrian. All other poles are Cambrian and fall on northern Africa (Fig. 1.3). However, the Itabiana dykes are exposed in the Borborema province and not exactly on the Sao Francisco craton, and the Sinyai dolerite corresponds to the Mozambique Belt, which is adjacent to the Congo craton. Nevertheless, the consistency of the poles' distribution along a path similar to that of Río de la Plata, in both position and age, strongly supports the idea that by the Late Ediacaran (*c*. 575 Ma) both major cratons were already assembled, or nearly so. Taking into account the scarce database, the slight difference in the positions of the respective reference poles, Sierra de las Animas Complex new pole (579 Ma) and Nola dykes (571 Ma), does not allow us to firmly establish any relative movement between the Rio de la Plata and Congo–Sao Francisco cratons after 580 Ma, considering that both APWPs are nearly identical.

1.2.3 The Kalahari Craton

This craton is virtually devoid of any reliable paleomagnetic pole for the Ediacaran-Cambrian. A single pole has been selected for this in Table 1.1. It belongs to a remagnetization dated by fission tracks (Gose et al. 2004) on the Equeefa dykes and the Mzumbe gneiss. This pole is assigned an age of *c*. 530 Ma. Its position in northern Africa (Fig. 1.4), consistent with somewhat younger poles (520–500 Ma) from the Río de la Plata and Congo–Sao Francisco cratons (as well as other Gondwana blocks as shown below) can be interpreted in terms of a slightly younger age of remagnetization than that proposed by the authors. Otherwise, a northward (present-day coordinates) and clockwise rotation of Kalahari during final Gondwana assembly in the Cambrian could be speculated. Much geological evidence has been proposed in favour of a late accretion of Kalahari to the already assembled Rio de la Plata–Congo–Sao Francisco blocks (Prave 1996; Gray et al. 2006; Oyhantçabal et al. 2011; Oriolo et al. 2016).

1.2.4 Amazonia-West Africa

These two cratons have apparently behaved as a single crustal block since the Middle Paleoproterozoic until the opening of the South Atlantic in the Cretaceous (see Nomade et al. 2003 and references therein). Paleomagnetic data for the Ediacaran-Cambrian is scarce. The Araras

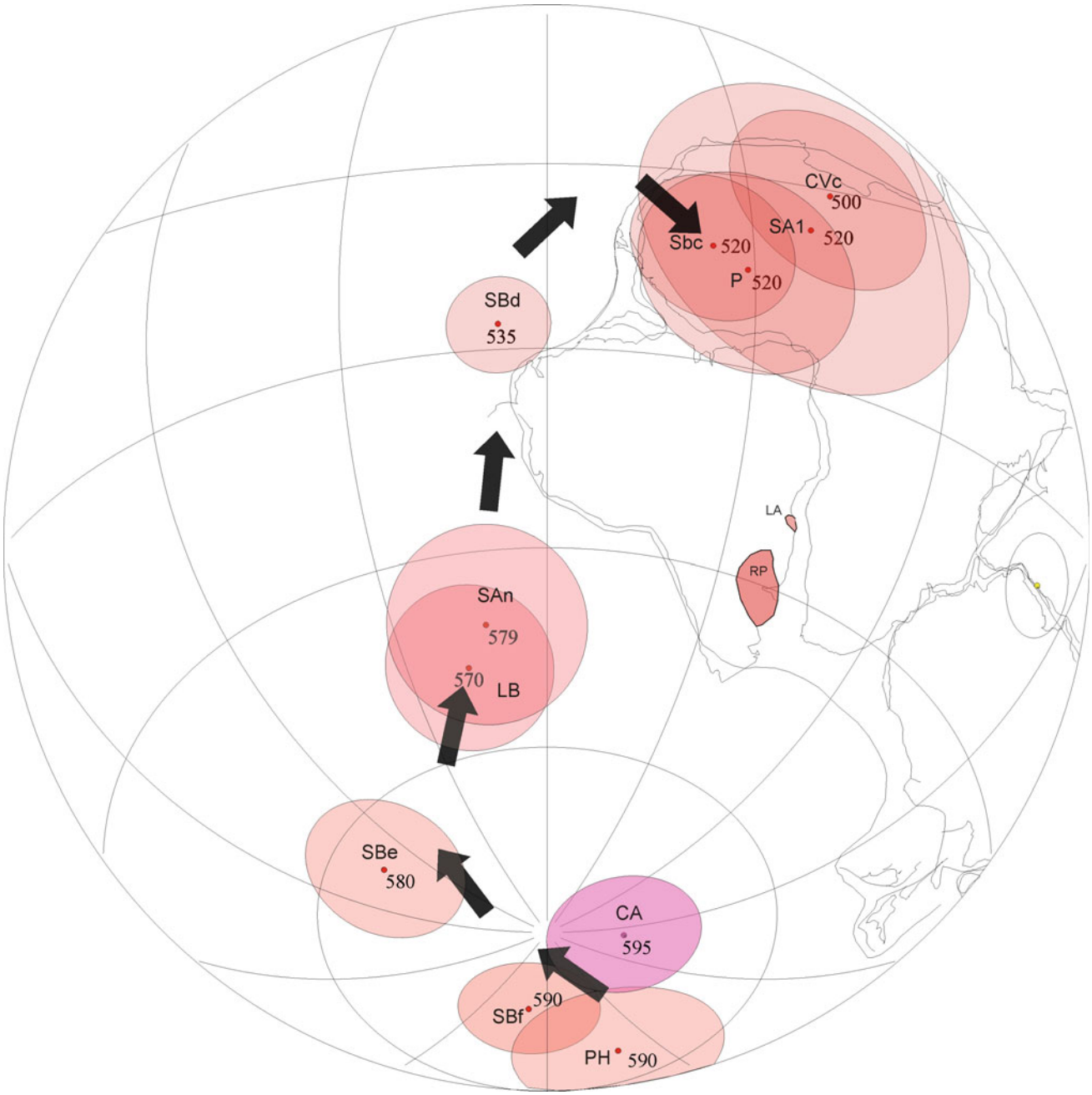

Fig. 1.2 Ediacaran to Cambrian paleomagnetic poles for the Río de la Plata cratón (red) and Luis Alves block (magenta) in a Gondwana reconstruction (after Trindade et al. 2006) in South Africa coordinates. Numbers indicate the more likely age of the pole and the arrows show the APWP inferred from the poles' distribution. Details of poles in Table 1.1

Group B component (Trindade et al. 2003), originally thought to correspond to a primary magnetization and therefore showing the paleogeographic position of Amazonia at *c*. 600 Ma, was demonstrated to be a later (Cambrian?) remagnetization (see Font et al. 2012). However, a new preliminary pole has been obtained from the Planalto da Serra lavas (Garcia et al. 2013; Trindade et al., in preparation), dated by Ar–Ar techniques at 615 Ma and suggesting a slow APWP for Amazonia along the Ediacaran. In turn, the Adma Diorite pole (Morel 1981) with a putative age of 613 Ma falls on top of the remagnetized Araras B pole, suggesting that either it is remagnetized too or the Amazonia-West Africa block was virtually 'static' for 100 Ma since the Early Ediacaran until the Early Cambrian. Other poles from the West Africa block are the Tin Dioulaf sedimentary rocks pole (Boudzoumou et al. 2011), whose age is only determined by stratigraphic relations and suggests an Early Ediacaran time for deposition (*c*. 630 Ma).

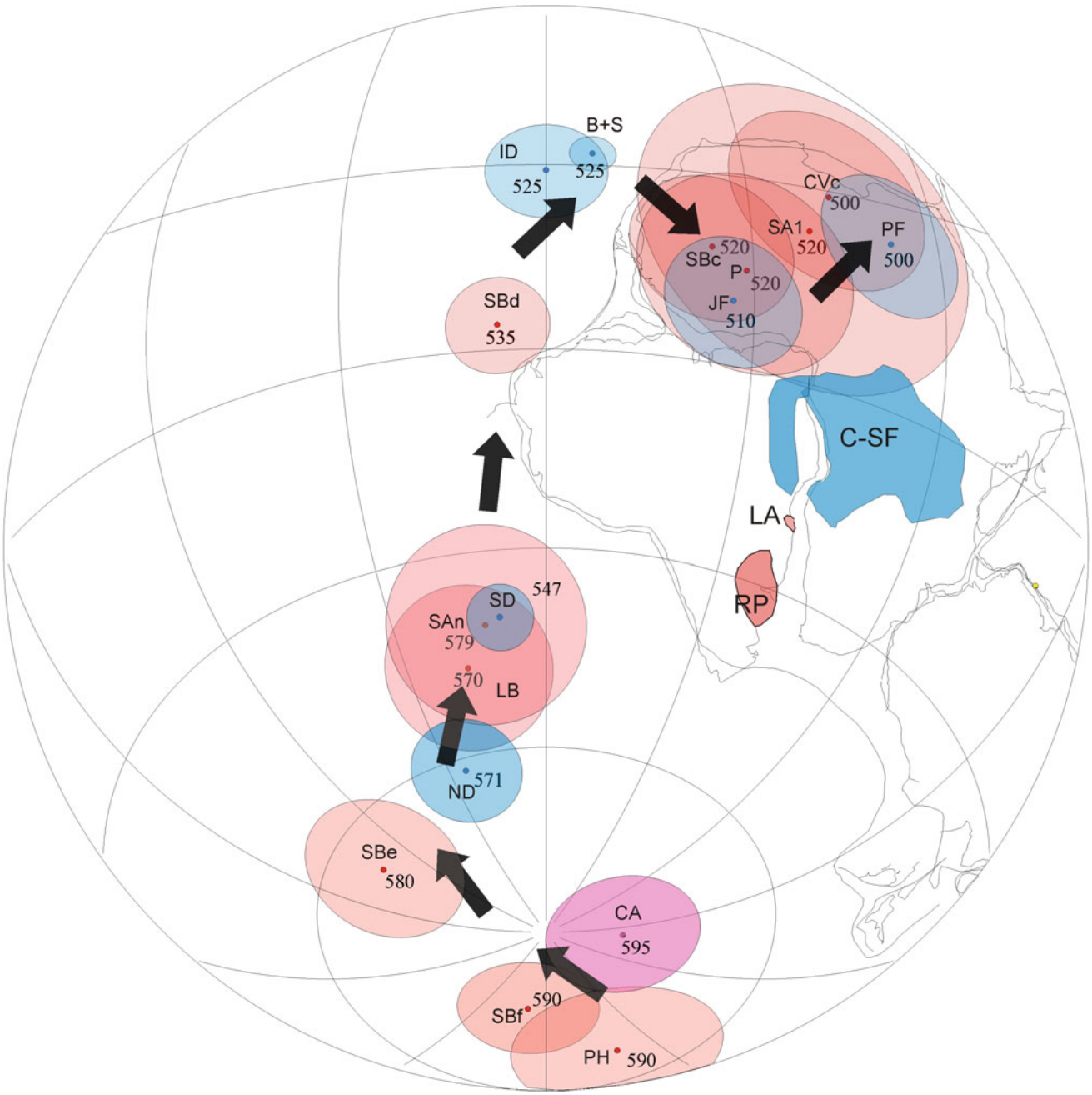

Fig. 1.3 As Fig. 1.2 plus the Ediacaran-Cambrian poles from the Congo–Sao Francisco craton (blue). Details in Table 1.1

This pole falls far away from the Adma Diorite and Planalto da Serra lavas poles suggesting either a very fast displacement between 630 and 615 Ma or a Late Paleozoic remagnetization, when the reference poles for Gondwana fall over Antarctica (e.g., McElhinny and McFadden 2000). Note that in Fig. 1.5, if an opposite polarity is chosen for the Tin Dioulaf sedimentary rocks pole, a fast but nearly rectilinear path can be defined between Tin Dioulaf sedimentary rocks, Planalto da Serra and Adma diorite poles. As discussed below, Planalto da Serra and Adma diorite poles are consistent with Amazonia (plus Western Africa) still attached to eastern Laurentia during final stages of Rodinia break-up about 615 Ma. If this is valid, a significantly different path is defined for Amazonia-West Africa with respect to Rio de la Plata–Congo–Sao Francisco in the Ediacaran. By around 525 Ma, poles from all blocks are consistent, suggesting a minimum age for final assembly of Amazonia-West Africa to form Gondwana. A lack of poles with ages between 600 and 530 Ma for this block precludes a better constrain on that age. The age of final assembly of

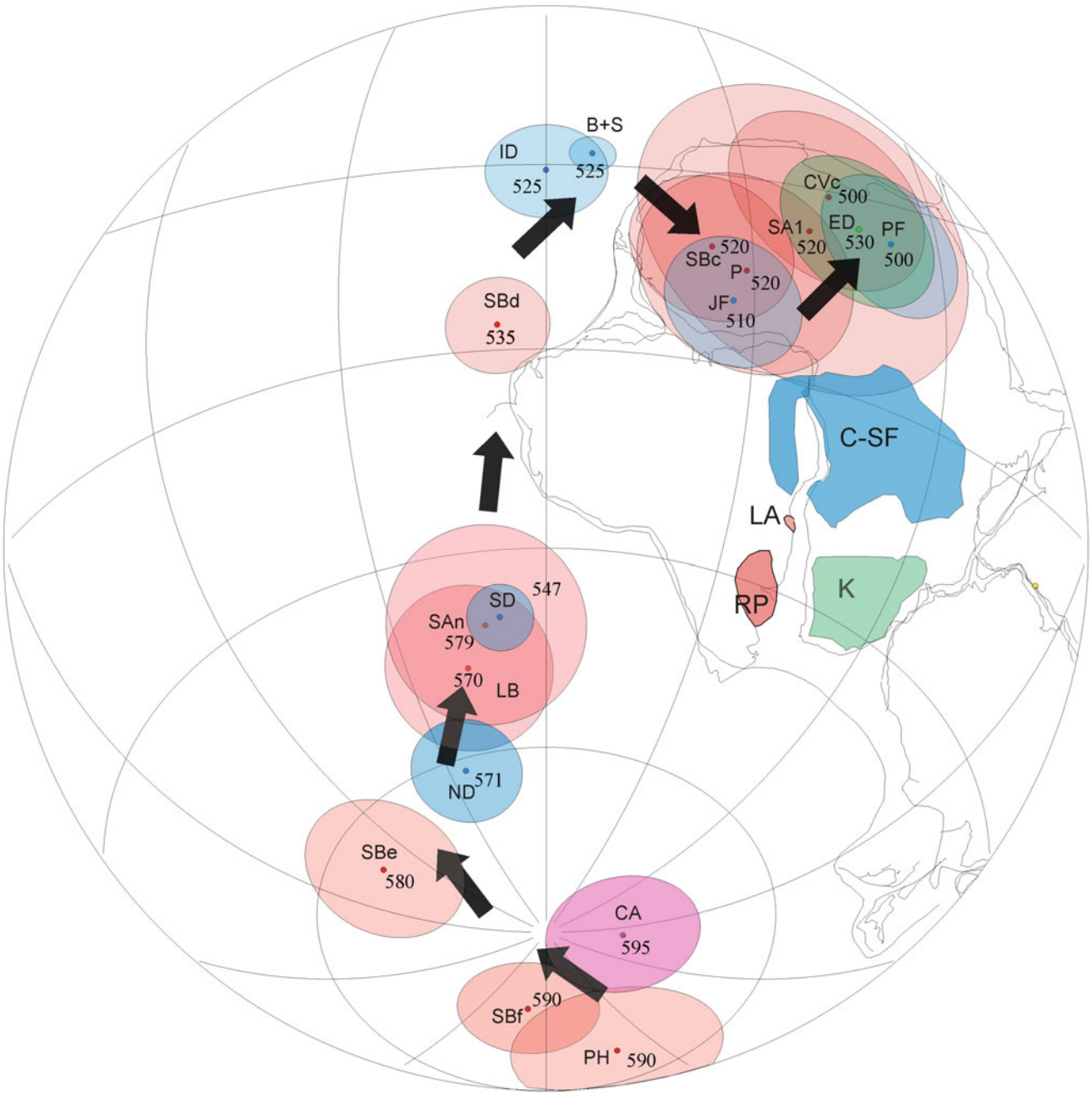

Fig. 1.4 As Fig. 1.3 plus the only pole selected for the Kalahari cratón (ED) in green. Details in Table 1.1

Amazonia (plus West Africa) has been a matter of hot debate (see Cordani et al. 2013; Tohver and Trindade 2014) and it is discussed below.

The pole from the Sidi Said Middle Cambrian volcanics (Khattach et al. 1995), assigned to the West Africa craton, is notoriously anomalous, possibly reflecting remagnetization at a later time (Late Paleozoic?), although a positive contact test is interpreted by the authors, or a displacement of the Moroccan Coastal Meseta from Gondwana since the Middle Cambrian, for which no significant geological evidence is available (Khattach et al. 1995; Tahiri et al. 2005). However, Remmal et al. (2009) have questioned the contemporaneity of the lavas and the dykes, the latter interpreted to be Early Silurian and associated with a regional thermal anomaly that reset K–Ar datings in the area. This suggests that the positive contact test may not apply to the Cambrian lavas and that the Sidi Said pole is significantly younger.

1.2.5 The Arabian-Nubian Shield

This block differs from previously mentioned cratons in that it lacks large areas of Archean or Paleoproterozoic stable crust and it is mainly a very large composite block formed by the accretion of terranes of different origins, mainly in Neoproterozoic times (e.g., Stern 1994; Abdelsalam and Stern 1996; Yibas et al. 2002; Johnson and Woldehaimanot 2003). Four paleomagnetic poles of different quality represent this block and describe a very fast APWP. The 592 Ma Dokhan volcanics pole (Davies et al. 1980, Fig. 6), if not remagnetized in the Late Paleozoic, suggests a fast wander by the Middle Ediacaran, as indicated by the positions of the slightly younger Bir Saf Saf dykes (586 Ma) and the Nabati Complex (575 Ma). The latter two are consistent with *c*. 590 Ma poles from the Río de la Plata craton and may

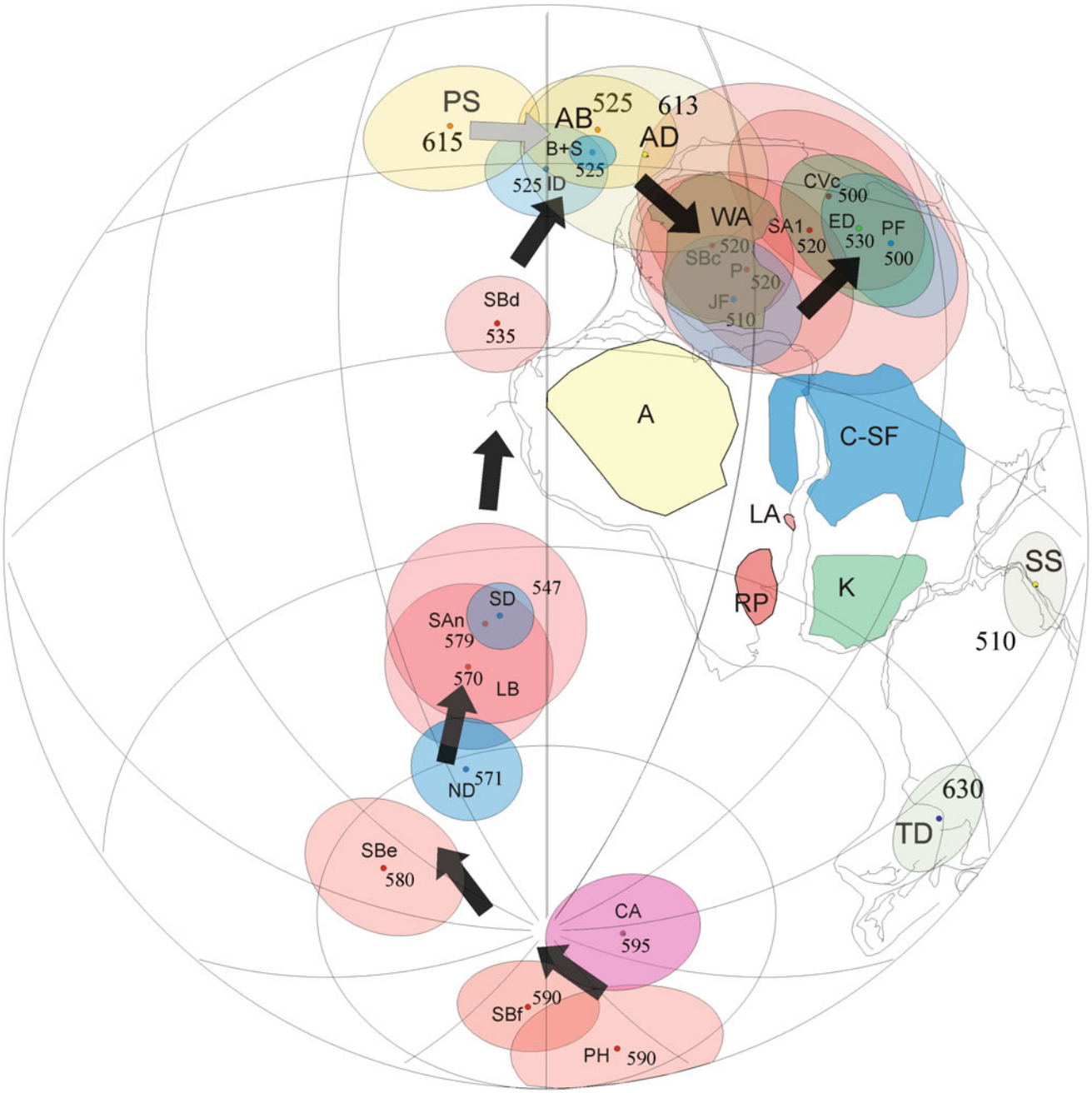

Fig. 1.5 As Fig. 1.4 plus selected poles for Amazonia (yellow) and West Africa (light brown). Larger numbers on these poles are for easier identification. Grey arrow shows hypothetical APWP for Amazonia in the Ediacaran. Details in Table 1.1. See text for discussion

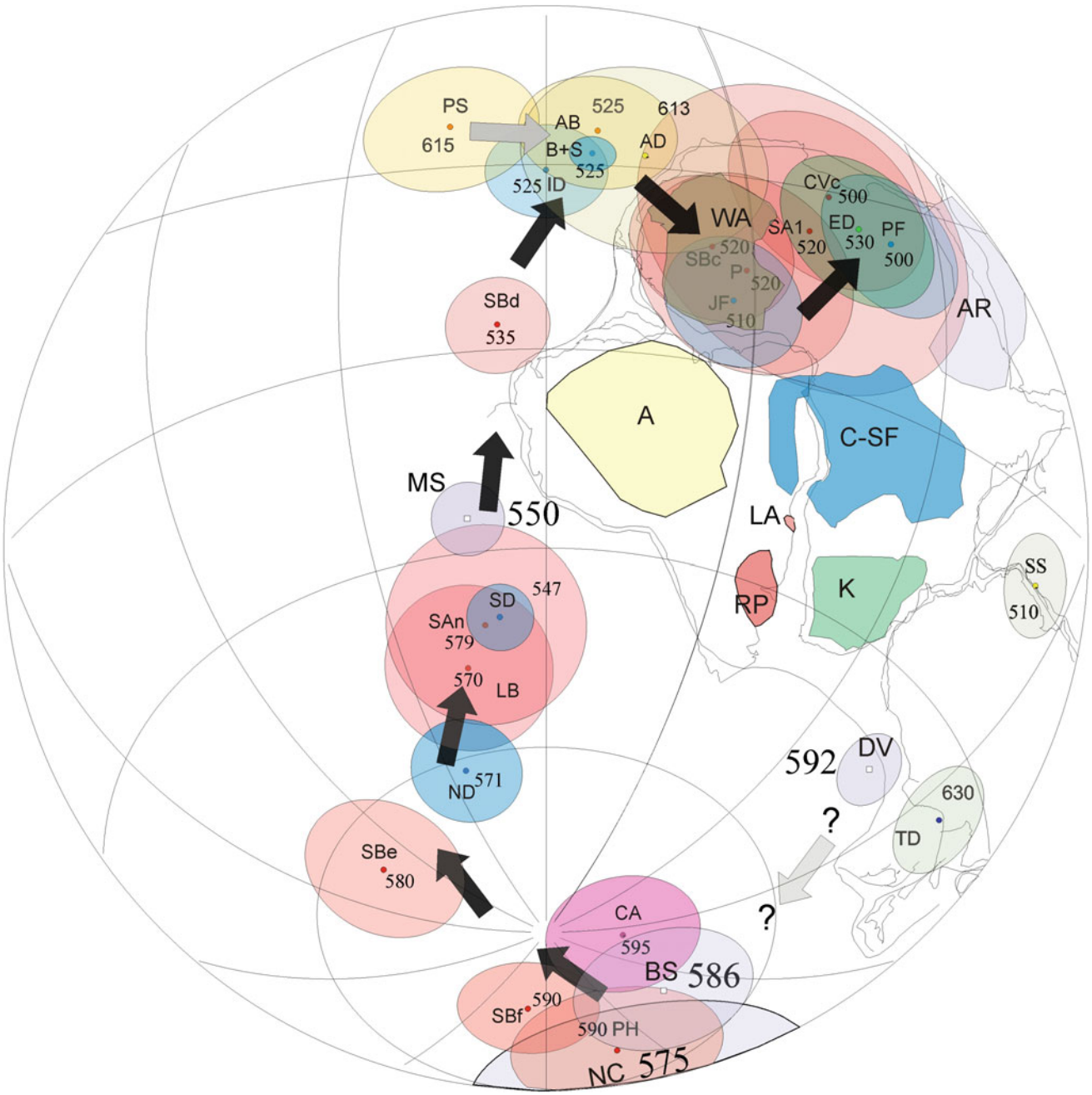

Fig. 1.6 As Fig. 1.5 plus selected poles from the Arabian-Nubian shield (light violet). Larger numbers on these poles are for easier identification. Details in Table 1.1

suggest that the Arabian-Nubian shield was already assembled into Gondwana or close to it by that time. In any case, the perfectly consistent 550 Ma pole from the Mirbat sandstone (Kempf et al. 2000) with coeval poles from the Río de la Plata and Congo–Sao Francisco strongly suggests that it was part of Gondwana at least by the Late Ediacaran (Fig. 1.6).

1.2.6 East Gondwana

The East Gondwana blocks (Australia, Antarctica, India, Madagascar, South China) also had a complex kinematic history before assembly into Gondwana (e.g., Collins and Pisarevsky 2005) and will not be analysed in detail here. However, it is interesting to illustrate some of the data as in

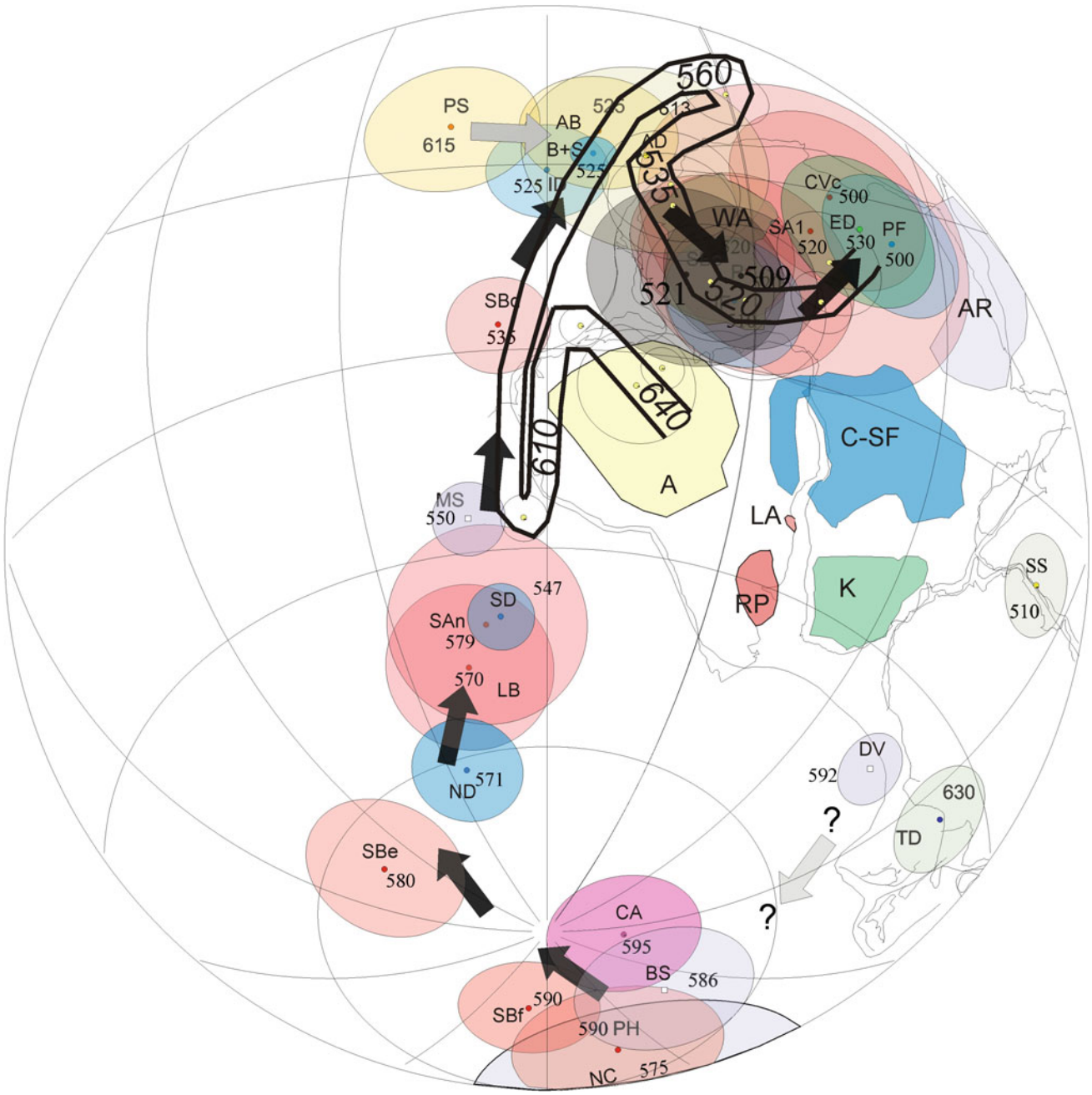

Fig. 1.7 As Fig. 1.6 plus the Ediacaran-Cambrian APWP for Australia (thick black lines) as computed by Schmidt (2014). Numbers along the path indicate likely ages. Two Cambrian paleomagnetic poles for Madagascar have also been included (Meert et al. 2001, 2003) and are identified with large numbers and grey circles. See text for discussion

Fig. 1.7. Here, the Ediacaran-Cambrian APWP for Australia, as recently computed by Schmidt (2014), is represented by the respective ages. As already discussed by this author, Australia apparently experienced a complex and long APWP. Although this overlaps in some sections with poles from Western Gondwana blocks, the ages for Australia are systematically much older. A confluence of its APWP and the Western Gondwana poles does not seem to occur until the Early Cambrian (*c.* 520 Ma). The assembly of other Eastern Gondwana blocks is illustrated by the high-quality paleomagnetic poles from the Carion granite (509 Ma; Meert et al. 2001) and the Virgation Zone (521 Ma; Meert et al. 2003) shown in Fig. 1.7 with large numbers. Their location, consistent with coeval poles from different Western Gondwana blocks, further confirms that by Late Early Cambrian most of Gondwana had been assembled.

1.3 Discussion

The briefly exposed paleomagnetic database available for the Ediacaran-Cambrian of the Western Gondwana main crustal blocks illustrates advances achieved with respect to the chronology, kinematics and paleogeography of the Western Gondwana assembly. However, it also exposes the scarcity and problems of such data. Even for the best cases (Congo–Sao Francisco, Río de la Plata), paleomagnetic poles are not enough for a precise description of the paleogeographic evolution of each craton and only broad pictures can be depicted with any certainty. Available paleomagnetic data shows that by the Early Late Ediacaran (*c*. 575 Ma) the Congo–Sao Francisco and Rio de la Plata cratons were already assembled, or nearly so. The Arabian-Nubian Shield was also part of 'proto-Gondwana' by Late Ediacaran (*c*. 550 Ma) and may already have been assembled to Congo–Sao Francisco and Río de la Plata by 575 Ma or even earlier. Approaching and accretion of Kalahari is basically unconstrained by paleomagnetic data, although geological evidence suggests that it post-dated the Río de la Plata–Congo–Sao Francisco collision (Prave 1996; Gray et al. 2006; Oyhantçabal et al. 2011; Oriolo et al. 2016). The major Western Gondwana crustal block, the composite Amazonia-West Africa continent, is poorly constrained by paleomagnetic data. The available poles suggest that this was already part of Gondwana in Early Cambrian times (*c*. 525 Ma). Older poles such as the Adma diorite (Table 1.1) may represent an Early Cambrian remagnetization and not the Early Ediacaran paleomagnetic field. However, recently obtained paleomagnetic data from well-dated lavas from the Planalto da Serra Complex in Amazonia (*c*. 615 Ma; Garcia et al. 2013) tend to confirm a pole position for this block similar to that suggested by the Adma diorite and far away from slightly younger poles from the Río de la Plata craton and the Arabian-Nubian Shield. This suggests that Amazonia-West Africa was more likely located far from the Río de la Plata–Congo–Sao Francisco-Arabian-Nubian blocks in the Early Ediacaran.

Most paleogeographic reconstructions of Rodinia (e.g., Hoffman 1991; Weil et al. 1998; Meert 2001; Pisarevsky et al. 2003; Li et al. 2008) place Amazonia as the conjugate margin of eastern Laurentia. Characteristic rift magmatism has been widely studied and dated in eastern Laurentia (see Cawood et al. 2001; McCausland et al. 2011) as occurring between *c*. 575 and 550 Ma, strongly indicating that the final Rodinia break-up took place along that margin in Middle Ediacaran times. Figure 1.8 shows that the traditional reconstruction of Amazonia attached to eastern Laurentia in the Early Ediacaran is consistent with the available paleomagnetic poles. These are the already discussed Adma Diorite and Planalto da Serra poles (Fig. 1.8) and the Long Range dykes pole for Laurentia (*c*. 615 Ma; Murthy et al. 1992; Fig. 1.8). Considering this, and although the paleomagnetic data is still scarce, the simplest interpretation is that Amazonia (plus West Africa) remained attached to eastern Laurentia until mid-Ediacaran times. It is to be recognized, however, that Chew et al. (2008, 2011) suggested an alternative interpretation, in which Amazonia separated from Laurentia in older times (*c*. 770–690 Ma), mainly based on the lack of exposed mid-Ediacaran rift-related magmatic rocks on the Amazonian side and an interpreted buried Ediacaran magmatic arc on Amazonia.

The mid-Ediacaran (590–570 Ma) paleogeography of Laurentia has been a matter of controversy for a long time (see McCausland et al. 2011 and references therein). This controversy derives from the existing Ediacaran paleomagnetic database that suggest high latitudes for Laurentia for the interval 590–570 Ma, while low paleolatitudes are suggested for 610 Ma and from 565 Ma and later times. The fast polar wander implied by these results for Laurentia has led to an alternative ('non-actualistic') hypothesis or direct dismissal of the data suggesting high paleolatitudes (e.g., Pisarevsky et al. 2001). Since the controversy is not yet resolved, despite recent advances made by Bono and Tarduno (2015), two options (the 'high' and the 'low' latitude options) remain when choosing the paleolatitudinal position of Laurentia in mid-Ediacaran times.

A more recent controversy concerns the age of accretion of the Amazon craton to Gondwana and whether a large Ediacaran ocean (the 'Clymene' Ocean) existed between Amazonia on one side and the Congo–Sao Francisco and Río de la Plata blocks on the other (for radically different positions on this subject, see Trindade et al. 2006; Cordani et al. 2013; Tohver and Trindade 2014). The controversy involves numerous geological arguments that will not be described here. The reader is referred to the above-cited papers and the references therein for a full comprehension of the issue. I shall simply mention that in the 'Clymene' hypothesis, the accretion of Amazonia must have occurred in the latest Ediacaran or even Early Cambrian times, while in the opposite view the collision of Amazonia occurred well before 600 Ma, when the 'Goias Ocean' was closed (Cordani et al. 2013). It is interesting to test whether the available paleomagnetic data from the Western Gondwana cratons can be useful in independently testing these models. Figure 1.9 shows paleogeographic sketches of Laurentia, Baltica, Amazonia, West Africa, Rio de la Plata, Congo–Sao Francisco and the Arabian-Nubian blocks by mid-Ediacaran times (*c*. 575 Ma), consistent with the available paleomagnetic data. Both options for Laurentia are presented. Figure 1.9a corresponds to the 'low-latitude' option. Laurentia has been positioned according to the Sept-Iles 'A' pole (Tanczyk et al. 1987), which has been confirmed by Bono and Tarduno (2015) as being derived from a primary

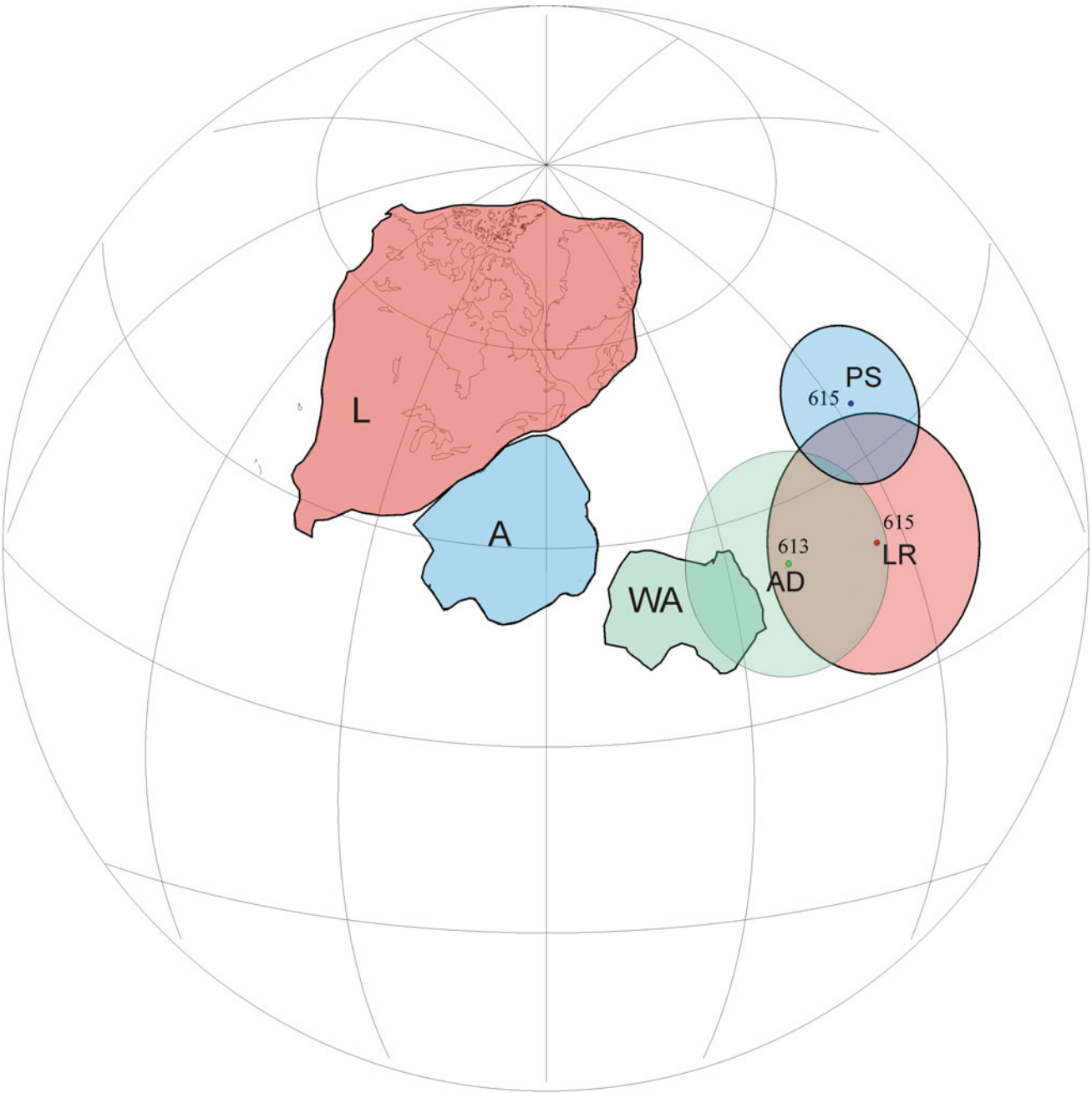

Fig. 1.8 Paleogeographic reconstruction of Laurentia, Amazonia and West Africa for the early Ediacaran (*c*. 615 Ma) consistent with coeval paleomagnetic poles for these cratons [Adma Diorite pole (Morel 1981); Planalto da Serra pole (Garcia et al. 2013); Long Range dykes pole (Murthy et al. 1992)]. See text for discussion

magnetization. Rio de la Plata, Congo–Sao Francisco and Arabia–Nubia are positioned according to the new Sierra de las Animas Complex pole (Table 1.1). Meanwhile, Amazonia (plus West Africa) has been positioned attached to Laurentia as in the paleogeographic reconstruction of Fig. 1.8 for the Early Ediacaran, since no mid-Ediacaran poles are available for those blocks. Nevertheless, if the configuration presented in Fig. 1.8 is valid, Amazonia began its breaking apart from Laurentia by *c*. 570 Ma (Cawood et al. 2001), and therefore the paleogeographic reconstruction shown in Fig. 1.9a is almost unavoidable. From this it is evident that the available paleomagnetic data indicate that the Río de la Plata craton was not part of Rodinia by those times and that a large ocean ('Clymene') must have existed between Río de la Plata–Congo–Sao Francisco and Amazonia in the mid-Ediacaran. Figure 1.9b shows the

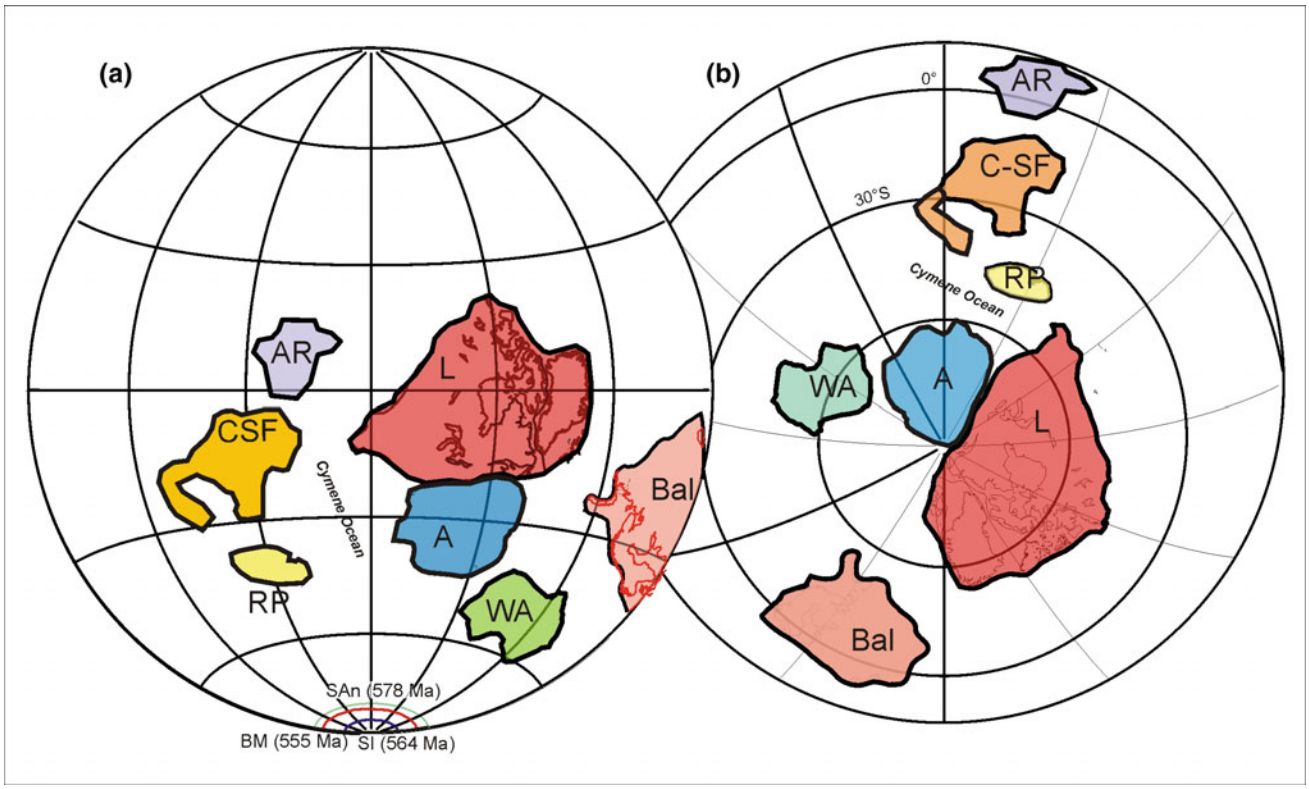

Fig. 1.9 **a** paleomagnetically controlled paleogeographic reconstruction of Laurentia, Baltica, Amazonia, West Africa, Río de la Plata, Congo–Sao Franciso and Arabian-Nubian shield for mid-Ediacaran times (*c*. 570 Ma). Laurentia has been placed according to the Sept-Iles A pole (SI; 564 Ma; Tanczyk et al. 1987) following the 'low latitude' option. Baltica is positioned according to the 555 Ma mean Baltica pole (BM; Meert 2007). The Río de la Plata, Congo–Sao Francisco and Arabian-Nubian shield are positioned according to the new Sierra de las Animas Complex pole (Table 1.1). Amazonia and West Africa are not controlled paleomagnetically and are kept attached to Laurentia, as in Fig. 1.8. **b** As in **a** with Laurentia positioned following the 'high latitude' option according to the Callander Complex pole (577 Ma; Symons and Chiasson 1991). Again, Amazonia and West Africa are kept attached to Laurentia

alternative 'high latitude' option for Laurentia. In this case, Laurentia was positioned according to the Callander Complex pole (Symons and Chiasson 1991) of *c*. 575 Ma. Amazonia plus West Africa remain attached to its eastern margin as in Fig. 1.8, while the same reconstruction is adopted for the Río de la Plata, Congo–Sao Francisco and Central Arabia blocks. In this option, again, a significant separation between these blocks and Amazonia is observed, supporting the existence of the Clymene Ocean in the mid-Ediacaran.

The existence of a large Ediacaran Clymene Ocean is therefore the simplest explanation that arises from the available paleomagnetic database, the traditional reconstructions of Amazonia as the conjugate margin of eastern Laurentia during the Rodinia break-up and the well-dated mid-Ediacaran age of rift along this margin. The lack of paleomagnetic data from Amazonia and West Africa between 600 and 540 Ma does not permit us to confirm the paleogeographic scenarios of Fig. 1.9 nor the exact time of accretion of Amazonia to form Gondwana. Further paleomagnetic support for a Cambrian accretion of Amazonia, albeit indirect, has been reported by the study of the Paraguay arcuate fold belt in south-central Brazil by Tohver et al (2010). These authors present paleomagnetic data that indicates an oroclinal bending of nearly 90° of this belt, located along the suture of Amazonia with the Sao Francisco and Río de la Plata cratons, in Cambrian times (<*c*. 528 Ma). The unlikely scenario of a truly intracontinental orocline of such curvature and dimensions strongly argues for a direct relation of this megastructural feature with the collision of Amazonia with the other blocks in Cambrian times. Alternative models, such as that presented by Chew et al. (2008, 2011) for a much older separation of Amazonia from Laurentia (>650 Ma), may not need a Clymene Ocean in Ediacaran times. However, this model lacked any independent paleomagnetic support until now and would imply that the consistency in Early Ediacaran poles between Amazonia, West Africa and Laurentia (Fig. 1.8) is casual.

This contribution has been limited to an analysis of the available paleomagnetic database from the Western Gondwana main crustal blocks and their paleogeographic

implications. No mention has been made of the paleomagnetic constraints placed on the tectonic and kinematic evolution of 'outboard' terranes of south-western Gondwana, such as Pampia, Arequipa-Antofalla, Cuyania and Chilenia. This has been reviewed by Rapalini et al. (2017) and the reader is referred to that work for a detailed analysis. In any case, an allochthonous origin for the Cuyania terrane of western Argentina, which broke away from southeastern Laurentia in the Early Cambrian to collide against Gondwana in Middle to Late Ordovician times, is supported by paleomagnetic data (see also Rapalini 2012). For the other terranes the paleomagnetic data is absent (Chilenia), too scarce (Arequipa-Antofalla) or ambiguous (Pampia).

Finally, the tectonic relations of the (composite?) terrane of Patagonia with Gondwana have also been widely debated. A para-autochthonous origin of this terrane with a Permo-Triassic collision against the southern Gondwana margin seems to be supported by very recent paleomagnetic data (Luppo et al. 2017).

1.4 Conclusions

A slow but systematic improvement in the Ediacaran-Cambrian paleomagnetic database of most major crustal blocks forming Gondwana has been produced in the last two decades. This allows some paleographic constraints to be established with greater certainty regarding the complex process of Gondwana assembly.

In particular, for Western Gondwana, some key paleomagnetic poles and broad APWPs are available from some of the cratons, which permits the following, but preliminary, conclusions:

- The Río de la Plata and Congo–Sao Francisco cratons were already assembled, or nearly so, by mid-Ediacaran times (575 Ma)
- The Arabian-Nubian Shield was already forming 'proto'-Western Gondwana by *c*. 550 Ma, and probably prior to 570 Ma
- None of these blocks was part of Rodinia by those times
- The Kalahari is virtually unconstrained by paleomagnetic data, with most geological evidence suggesting that it accreted relatively late in the Gondwana assembly process
- Amazonia and West Africa were probably still attached to Laurentia by the Early Ediacaran and a large Clymene Ocean likely existed in Ediacaran times between Amazonia and Congo–Sao Francisco–Río de la Plata
- The Eastern Gondwana blocks probably merged with their western counterparts by the latest Ediacaran or Early Cambrian as mainly suggested by the APWP defined for Australia.
- Accretion of other, minor, terranes to the southwest margin of Gondwana in the Paleozoic is only well supported by paleomagnetic data in the case of the Cuyania terrane, while for others the paleomagnetic evidence is absent, scarce or ambiguous.
- The kinematics of minor blocks trapped between the major players during Western Gondwana assembly is yet to be determined by paleomagnetism.

Acknowledgements I wish to thank S. Segesmund for the invitation to present this review. Deep gratitude goes to Leda Sánchez Bettucci (Universidad de la República, Uruguay), Daniel Poiré (Universidad Nacional de La Plata, Argentina), Ricardo Trindade (Universidade de Sao Paulo, Brazil) and Eric Tohver (University of Western Australia) for long and productive cooperation in the study of Neoproterozoic successions of the Río de la Plata craton. Many thanks also go to many graduate and postgraduate students at Laboratorio de Paleomagnetismo Daniel A. Valencio (IGEBA, Universidad de Buenos Aires) and especially to Dr Carlos A. Vásquez of that institution. GMAP software was used to perform paleogeographic reconstructions and to plot paleomagnetic poles. A grant by Universidad de Buenos Aires (UBACyT-20020130100465BA) provided financial support. This is a contribution to IGCP 648.

References

Abdelsalam MG, Stern RJ (1996) Sutures and shear zones in the Arabian-Nubian Shield. J Afr Earth Sci 23(3):289–310

Arrouy MJ et al (2015) Sedimentología y estratigrafía del Grupo La Providencia (nom. nov.): cubierta superior neoproterozoica, Sistema de Tandilia, Argentina. Lat Am J Sedimentol Basin Anal 22(2):171–189

Bono RK, Tarduno JA (2015) A stable Ediacaran Earth recorded by single silicate crystals of the ca. 565 Ma Sept-Îles intrusion. Geology 43(2):131–134

Bossi J, Gaucher C (2004) The Cuchilla Dionisio Terrane, Uruguay: an allochthonous block accreted in the Cambrian to SW-Gondwana. Gondwana Res 7(3):661–674

Boudzoumou F et al (2011) Neoproterozoic paleomagnetic poles in the Taoudeni basin (West Africa). CR Geosci 343(4):284–294

Brito Neves BB et al (2000) Tectonic history of the Borborema Province, NW Brazil. In: Cordani UG et al (ed) Tectonic Evolution of South America: Rio de Janeiro, pp 151–182

Butler RF (1992) Paleomagnetism: magnetic domains to geologic terranes. Blackwell Scientific Publications, Boston

Campos Neto MC (2000) Orogenic systems from Southwestern Gondwana: an approach to Brasiliano-Pan African Cycle and orogenic collage in South Eastern Brasil. In: Cordani UG et al (eds) Tectonic evolution of South America, 31st international geological congress, Río de Janeiro, Brazil, pp 335–365

Canfield DE et al (2007) Late-Neoproterozoic deep-ocean oxygenation and the rise of animal life. Science 315(5808):92–95

Cawood PA et al (2001) Opening Iapetus: constraints from the Laurentian margin in Newfoundland. Geol Soc Am Bull 113(4):443–453

Chew DM et al (2008) Detrital zircon fingerprint of the Proto-Andes: evidence for a neoproterozoic active margin? Precambrian Res 167(1):186–200
Chew DM et al (2011) Tectonic evolution of western Amazonia from the assembly of Rodinia to its break-up. Int Geol Rev 53(11–12):1280–1296
Collins AS, Pisarevsky SA (2005) Amalgamating eastern Gondwana: the evolution of the circum-Indian Orogens. Earth Sci Rev 71(3):229–270
Cordani UG et al (1999) Idades U-Pb (SHRIMP) de rochas vulcânicas das bacias de Campo Alegre, Itajai e Castro (SC e PR). Resumos An Acad Bras Cienc 71:835
Cordani UG et al (2013) Was there an Ediacaran Clymene ocean in central South America? Am J Sci 313(6):517–539
D'Agrella-Filho MS, Pacca IG, Sato K (1986) Paleomagnetism of metamorphic rocks from the Piquete region—Ribeira Valley, Southeastern Brazil. Rev Bras Geof 4:79–84
D'Agrella-Filho MSF, Pacca IG (1988) Paleomagnetism of the Itajai, Castro and Bon Jardim Groups from southern Brazil. Geophys J 93:365–376
D'Agrella-Filho MS, Raposo MIB, Egydio-Silva M (2004) Paleomagnetic study of the Juiz de Fora Complex, SE Brazil: implications for Gondwana. Gondwana Res 7(1):103–113
Davies J et al (1980) The paleomagnetism of certain late Precambrian and early Paleozoic rocks from the Red Sea Hills, eastern desert. Egypt J Geophys Res Solid Earth 85(B7):3699–3710
Evans DA (2000) Stratigraphic, geochronological, and paleomagnetic constraints upon the Neoproterozoic climatic paradox. Am J Sci 300 (5):347–433
Font E et al (2011) Paleomagnetism and rock magnetism of the Neoproterozoic Itajaí Basin of the Rio de la Plata craton (Brazil): Cambrian to cretaceous widespread remagnetizations of South America. Gondwana Res 20(4):782–797
Font E et al (2012) Episodic remagnetizations related to tectonic events and their consequences for the South America Polar Wander Path. Geol Soc Lond Spec Publ 371(1):55–87
Garcia MSR et al (2013) Paleomagnetismo do Complexo Alcalino Planalto Da Serra (Mato Grosso): Implicações para a formação do Gondwana. Latin Lett 3(Special Issue OB19):1–8
Gose WA et al (2004) Age of magnetization of Mesoproterozoic rocks from the Natal sector of the Namaqua-Natal belt, South Africa. J Afr Earth Sci 40(3):137–145
Gray DR et al (2006) 40 Ar/39 Ar thermochronology of the Pan-African Damara Orogen, Namibia, with implications for tectonothermal and geodynamic evolution. Precambrian Res 150(1):49–72
Gray DR et al (2008) A Damara orogen perspective on the assembly of southwestern Gondwana. Geol Soc Lond Spec Publ 294(1): 257–278
Gregory LC et al (2009) Paleomagnetism and geochronology of the Malani Igneous Suite, Northwest India: implications for the configuration of Rodinia and the assembly of Gondwana. Precambrian Res 170(1):13–26
Hoffman PF (1991) Did the breakout of Laurentia turn Gondwanaland inside-out? Science 252:1409–1412
Hoffman PF (1999) The break-up of Rodinia, birth of Gondwana, true polar wander and the snowball Earth. J Afr Earth Sci 28(1):17–33
Johansson Å (2014) From Rodinia to Gondwana with the 'SAMBA'-model—a distant view from Baltica towards Amazonia and beyond. Precambrian Res 244:226–235
Johnson PR, Woldehaimanot B (2003) Development of the Arabian-Nubian Shield: perspectives on accretion and deformation in the northern East African Orogen and the assembly of Gondwana. Geol Soc Lond Spec Publ 206(1):289–325
Khattach D et al (1995) A Cambrian pole for the Moroccan coastal meseta. Geophys J Int 120(1):132–144
Kempf O et al (2000) Paleomagnetic directions in late Precambrian glaciomarine sediments of the Mirbat Sandstone Formation, Oman. Earth Planet Sci Lett 175:181–190
Kirschvink JL (1992) Late Proterozoic low-latitude global glaciation: the snowball Earth. The proterozoic biosphere: a multidisciplinary Study. Cambridge University Press, New York, pp 51–52
Li ZX et al (2008) Assembly, configuration, and break-up history of Rodinia: a synthesis. Precambrian Res 160(1):179–210
Li ZX et al (2013) Neoproterozoic glaciations in a revised global palaeogeography from the breakup of Rodinia to the assembly of Gondwanaland. Sediment Geol 294:219–232
Luppo T et al (2017) Permo-Triassic collision of Patagonia? Paleomagnetic evidence. Latinmag Lett 7 (Special Issue, PM04):1–5
McCausland PJ et al (2011) Ediacaran paleogeography of Laurentia: Paleomagnetism and 40 Ar–39 Ar geochronology of the 583 Ma Baie des Moutons syenite, Quebec. Precambrian Res 187(1):58–78
McElhinny MW, McFadden PL (2000) Paleomagnetism, continents and oceans. Int Geophys Ser 73:386
McGee B et al (2012) G'day Gondwana—the final accretion of a supercontinent: U-Pb ages from the post-orogenic São Vicente Granite, northern Paraguay Belt, Brazil. Gondwana Res 21(2):316–322
McWilliams MO (1981) Palaeomagnetism and Precambrian tectonic evolution of Gondwana. Dev Precambrian Geol 4:649–687
Meert JG (2001) Growing Gondwana and rethinking Rodinia: a paleomagnetic perspective. Gondwana Res 4(3):279–288
Meert JG (2003) A synopsis of events related to the assembly of eastern Gondwana. Tectonophysics 362(1):1–40
Meert JG (2007) Testing the Neoproterozoic glacial models. Gondwana Res 11(4):573–574
Meert JG, Lieberman BS (2008) The Neoproterozoic assembly of Gondwana and its relationship to the Ediacaran-Cambrian radiation. Gondwana Res 14(1):5–21
Meert JG, Van Der Voo R (1996) Paleomagnetic and 40Ar/39Ar Study of the Sinyai Dolerite, Kenya: implications for Gondwana Assembly. J Geol 104(2):131–142
Meert JG et al (2001) Paleomagnetism, geochronology and tectonic implications of the Cambrian-age Carion granite, Central Madagascar. Tectonophysics 340(1):1–21
Meert JG et al (2003) The stratoid granites of central Madagascar: paleomagnetism and further age constraints on Neoproterozoic deformation. Precambrian Res 120(1):101–129
Mitchell RN et al (2010) Rapid early Cambrian rotation of Gondwana. Geology 38(8):755–758
Moloto-A-Kenguemba GR et al (2009) A late Neoproterozoic paleomagnetic pole for the Congo craton: tectonic setting, paleomagnetism and geochronology of the Nola dike swarm (Central African Republic). Precambrian Res 164:214–226
Morel P (1981) Palaeomagnetism of a Pan-African diorite: a late Precambrian pole for western Africa. Geophys J R Astron Soc 65:493–495
Murphy J et al (2013) Potential geodynamic relationships between the development of peripheral orogens along the northern margin of Gondwana and the amalgamation of West Gondwana. Mineral Petrol 107:635–650
Murthy G et al (1992) Paleomagnetism of Eocambrian long range dykes and double mer formation from Labrador, Canada. Can J Earth Sci 29:1224–2123
Nomade S et al (2003) The Guiana and the West African shield Palaeoproterozoic grouping: New palaeomagnetic data for French Guiana and the Ivory Coast. Geophys J Int 154(3):677–694
Oriolo S et al (2016) Timing of deformation in the Sarandí del Yí Shear Zone, Uruguay: Implications for the amalgamation of western

Gondwana during the Neoproterozoic Brasiliano-Pan-African Orogeny. Tectonics 35(3):754–771
Oyhantçabal P et al (2009) Geochronological constraints on the evolution of the southern Dom Feliciano Belt (Uruguay). J Geol Soc 166(6):1075–1084
Oyhantçabal P et al (2011) The Río de la Plata Craton: a review of units, boundaries, ages and isotopic signature. Int J Earth Sci 100(2–3):201–220
Pecoits E et al (2016) U Pb detrital zircon ages from some Neoproterozoic successions of Uruguay: provenance, stratigraphy and tectonic evolution. J S Am Earth Sci 71:108–130
Pimentel MM et al (2011) The tectonic evolution of the Brasilia Belt, central Brazil, based on SHRIMP and LA-ICPMS U-Pb sedimentar provenance data. J S Am Earth Sci 31(4):345–357
Pisarevsky SA et al (2001) Reply to comment by J.G. Meert and R. Van der Voo on 'New palaeomagnetic result from Vendian red sediments in Cisbaikalia and the problem of the relationship of Siberia and Laurentia in the Vendian'. Geophys J Int 146(3): 871–873
Pisarevsky SA et al (2003) Models of Rodinia assembly and fragmentation. Geol Soc Lond Spec Publ 206(1):35–55
Poiré DG, Spalletti LA (2005) La cubierta sedimentaria precámbrica/paleozoica inferior del Sistema de Tandilia. In: De Barrio RE et al (eds) Geología y Recursos Minerales de la provincia de Buenos Aires. Relatorio del XVI Congreso Geológico Argentino, pp 51–68
Powell CM, Pisarevsky SA (2002) Late neoproterozoic assembly of east Gondwana. Geology 30(1):3–6
Prave AR (1996) Tale of three cratons: tectonostratigraphic anatomy of the Damara orogen in northwestern Namibia and the assembly of Gondwana. Geology 24(12):1115–1118
Rapalini AE (2006) New late Proterozoic paleomagnetic pole for the Rio de la Plata craton: implications for Gondwana. Precambrian Res 147(3):223–233
Rapalini AE (2012) Paleomagnetic evidence for the origin of the Argentine Precordillera, fifteen years later: what is new, what has changed, what is still valid? Latin Lett 2:1–20
Rapalini AE et al (2013) The La Tinta pole revisited: paleomagnetism of the Neoproterozoic Sierras Bayas Group (Argentina) and its implications for Gondwana and Rodinia. Precambrian Res 224: 51–70
Rapalini AE et al (2015) The late Neoproterozoic Sierra de las Ánimas magmatic complex and playa Hermosa formation, southern Uruguay, revisited: paleogeographic implications of new paleomagnetic and precise geochronologic data. Precambrian Res 259:143–155
Rapalini AE et al (2017) Paleogeographic and kinematic constraints in the tectonic evolution of the Pre-Andean basement blocks. In: Folguera A et al (eds) The making of the Chilean-Argentinean Andes. Elsevier, Amsterdam
Rapela CW et al (2007) The Río de la Plata craton and the assembly of SW Gondwana. Earth Sci Rev 83(1):49–82
Reeves CV et al (2004) Tight reassembly of Gondwana exposes phanerozoic shears in Africa as global tectonic players. Gondwana Res 7(1):7–19
Remmal T et al (2009) Evidence of syn tectonic tephrites with nepheline in the Sidi Said Maachou Cambrian basin (coastal Meseta, Morocco); geo dynamic implications. Estudios Geologicos (Madrid) 65(2):147–156
Saalmann K et al (2006) Tectonic evolution of the Neoproterozoic Sao Gabriel block, southern Brazil: constraints on Brasiliano orogenic evolution of the Río de la Plata cratonic margin. J S Am Earth Sci 21(3):204–227
Sánchez-Bettucci L, Rapalini AE (2002) Paleomagnetism of the Sierra de Las Animas Complex, southern Uruguay: Its implications in the assembly of western Gondwana. Precambrian Res 118(3):243–265
Sánchez-Bettucci L et al (2010) Neoproterozoic tectonic synthesis of Uruguay. Int Geol Rev 52(1):51–78
Santos TJS et al (2008) Comparisons between the northwestern Borborema Province, NE Brazil, and the southwestern Pharusian Dahomey Belt, SW Central Africa). In: Pankhurst RJ et al (eds) West Gondwana: Pre-Cenozoic correlations across the Atlantic region. Geological Society of London Special Publications vol 294, pp 49–67
Schmidt PW (2014) A review of Precambrian palaeomagnetism of Australia: palaeogeography, supercontinents, glaciations and true polar wander. Gondwana Res 25(3):1164–1185
Schmidt PW et al (2009) Palaeomagnetism and magnetic anisotropy of late Neoproterozoic strata, South Australia: implications for the palaeolatitude of late Cryogenian glaciation, cap carbonate and the Ediacaran system. Precambrian Res 174(1):35–52
Stern RJ (1994) Arc assembly and continental collision in the Neoproterozoic East African Orogen: implications for the consolidation of Gondwanaland. Annu Rev Earth Planet Sci 22(1):319–351
Symons DTA, Chiasson AD (1991) Paleomagnetism of the Callander Complex and the Cambrian apparent polar wander path for North America. Can J Earth Sci 28(3):355–363
Tahiri A et al (2005) A comparison of the neoproterozoic/lower palaeozoic lithostratigraphy of morocco and southwestern Iberia. Geodynamic interpretations. Geogaceta 38:203–206
Tanczyk EI et al (1987) A paleomagnetic study of the layered mafic intrusion at Sept-Iles, Quebec. Can J Earth Sci 24(7):1431–1438
Tohver E, Trindade RI (2014) Comment on 'Was there an Ediacaran Clymene Ocean in central South America?' By UG Cordani and others. Am J Sci 314(3):805–813
Tohver E et al (2010) Closing the Clymene ocean and bending a Brasiliano belt: evidence for the Cambrian formation of Gondwana, southeast Amazon craton. Geology 38(3):267–270
Trindade RIF et al (2003) Low-latitude and multiple geomagnetic reversals in the Neoproterozoic Puga cap carbonate, Amazon craton. Terra Nova 15(6):441–446
Trindade RIF et al (2006) Paleomagnetism of Early Cambrian Itabaiana mafic dikes (NE Brazil) and the final assembly of Gondwana. Earth Planet Sci Lett 244(1):361–377
Van der Voo R (1993) Paleomagnetism of the Atlantic, Tethys and Iapetus oceans. Cambridge University Press, Cambridge
Weil AB et al (1998) The Proterozoic supercontinent Rodinia: paleomagnetically derived reconstructions for 1100 to 800 Ma. Earth Planet Sci Lett 154(1):13–24
Williams GE (2008) Proterozoic (pre-Ediacaran) glaciation and the high obliquity, low-latitude ice, strong seasonality (HOLIST) hypothesis: Principles and tests. Earth Sci Rev 87(3):61–93
Xiao S (2004) Neoproterozoic glaciations and the fossil record. In: Jenkins GS et al (eds) The extreme proterozoic: geology, geochemistry, and climate, pp 199–214
Yibas B et al (2002) The tectonostratigraphy, granitoid geochronology and geological evolution of the Precambrian of southern Ethiopia. J Afr Earth Sc 34(1):57–84

2 An Integrated Geophysical and Geological Interpretation of the Southern African Lithosphere

Branko Corner and Raymond J. Durrheim

Abstract

Southern Africa, here taken as the region that comprises the Kalahari and southern Congo Cratons, and the important orogenic belts that surrounded or separated them during the assembly of Gondwana, was situated in the heart of the supercontinent. As such, the region is an ideal site to study the lithospheric structure, composition and evolution of the supercontinent. A plethora of data sets, both geological and geophysical, are available in the public domain, including outcrop mapping, drilling results, aeromagnetic, gravity and magnetotelluric surveys, allowing mapping of extensive regions under cover. Deeper penetrating seismic reflection, refraction and teleseismic data, and also magnetotelluric data, have allowed the lithospheric interpretation to be extended to the middle and lower crust, and to the upper mantle. Interpretation has included, *inter alia*, mapping, or refinement of existing mapping, of the craton boundaries and associated terranes; major faults, structural lineaments and ring structures; specific features which have a geophysical expression, such as the Witwatersrand Basin, the Xade Complex and the tectonostratigraphic zones of the Damara-Ghanzi-Chobe Orogenic Belt; the Namaqua-Natal Belt and extensions thereof as the Maud Belt in Antarctica, as well as associated features such as the Beattie Magnetic Anomaly and Southern Cape Conductivity Belt; and the Namibian volcanic passive margin. Interpretations of the large-scale seismic, electrical resistivity, geomagnetic induction and magnetotelluric data by many workers have revealed conductive zones, terrane boundaries and continental-scale shear zones concealed by younger strata, and yielded important insights into the deep structure and evolution of the subcontinent. The topography of the Moho and the Lithosphere–Asthenosphere Boundary has also been mapped, showing that the Archaean Kaapvaal, Zimbabwe and Congo Cratons have deep roots that are relatively cold. As far as possible, the interpreted features honour the geological and geophysical data sets within the resolution of the data. Integration of these results in the unified interpretation map presented here brings new insights into both the disposition of selected geological features under cover, and the evolution of the Precambrian geology of southern Africa, extending into Antarctica within a Gondwana framework.

Keywords

Southern Africa • Geophysical studies • Integrated interpretation • Continental crust • Lithosphere Craton • Gondwana • Aeromagnetic • Gravity Magnetotelluric • Seismic • Kaapvaal • Zimbabwe Congo • Maud Belt • Namaqua-Natal Belt Damara-Ghanzi-Chobe Belt • Beattie Magnetic Anomaly Southern Cape Conductive Belt

2.1 Introduction and Chapter Layout

Southern Africa is an ideal site to study the structure, composition and evolution of the Gondwana supercontinent. Geophysical methods, integrated with the results of geological field mapping and exploratory drilling, play an increasingly important role in mapping rocks and structures, concealed by younger cover, from the near surface to the upper mantle. The Archaean-to-Palaeoproterozoic Kaapvaal, Zimbabwe and Congo Cratons are surrounded by Proterozoic metamorphic belts, platforms and basins, preserving more than 3600 million years of the Earth's history (Hunter et al. 2006). These terranes are penetrated by kimberlite intrusions, which provide samples of the lower crust and

B. Corner (✉)
Manica Minerals Ltd., Swakopmund, Namibia
e-mail: branko@iafrica.com.na

R. J. Durrheim
School of Geosciences, University of the Witwatersrand, Johannesburg, South Africa
e-mail: Raymond.Durrheim@wits.ac.za

S. Siegesmund et al. (eds.), *Geology of Southwest Gondwana*, Regional Geology Reviews,
https://doi.org/10.1007/978-3-319-68920-3_2

upper mantle (Skinner and Truswell 2006). Hart et al. (1981, 1990a, b) propose that the 2023 Ma Vredefort meteorite impact near the centre of the Kaapvaal Craton turned the crust 'on edge', providing a window into the deeper crystalline basement. Geophysical studies of the structure of the continental crust and upper mantle have also been driven by the search for hydrocarbons, diamonds, base metals, and precious metals. While the resolution and accuracy of geophysical images and models has improved as technology and knowledge have advanced, early studies still remain relevant because they provide important constraints on lithospheric models, especially in areas where surveys have not been repeated. De Beer (2015a, b, c) provides a comprehensive review of the history of geophysics in South Africa. We briefly also review the historic investigations that were conducted 20 or more years ago. More recent work is discussed in greater detail, as well as new aspects of interpretation of magnetic and gravity data sets. The scope of coverage is enormous, thus the mapping is selective, focusing on geophysically evident features and selected geological units that may not have a geophysical expression but which are relevant to the interpretation.

The early regional aeromagnetic and gravity data sets covering southern Africa have proved invaluable in mapping regional structure. More recently, higher-resolution data sets have become available in Namibia and Botswana, as well as magnetotelluric (MT), seismic reflection and teleseismic array studies. The interpretation presented here follows the norm of working from known, mapped geology, as published by the various geological surveys and geoscience councils, to mapping extensions thereof under cover using the geophysical data sets presented here, either by us or as referenced. Emphasis is placed on the mapping of large-scale structures, including major faults, lineaments and ring structures, and extensions of specific lithologies and tectonostratigraphic zones, many of which were not recognized in past studies of these geoscience data sets. Much of what is presented here is, in the first instance, observational, identifying and mapping many new features and thus creating a basis for further research on their nature, genesis and geological evolution. Although potential field data has formed the basis of the presented interpretation, and includes consideration of the MT and seismic results, we recognize that complete integration of the data sets has not been fully achieved. The prime reason for this is that the various geophysical studies had different key questions, and depths of investigation that did not always overlap, ranging from the near surface to the mantle. In addition, aspects of the chapter address potentially different readership interests, particularly in Sects. 2.2 and 2.3. Figure 2.1 shows the extent of the interpretation area within southern Africa.

The coverage of the chapter, bearing the above comments in mind, is based on the type of geophysical data used—that is,

Fig. 2.1 Location of the interpretation area. The red outline delineates the Proto-Kalahari Craton (Jacobs et al. 2008). See Sect. 2.2.10.3 for a discussion of the Gondwana reconstruction used. *DCB* Damara-Chobe Belt; *KVC* Kaapvaal Craton; *LT* Limpopo Terrane; *NNB* Namaqua-Natal Belt; *ZC* Zimbabwe Craton; *CC* Congo Craton; *GC* Grunehogna Craton

commencing with potential field data integrated with known geology, progressing to published magnetotelluric and seismic data and interpretations, as summarized briefly below:

- Interpretative mapping of specific Archaean and Proterozoic geological features and their boundaries, in areas covered by Phanerozoic or younger sediments, largely using magnetic and gravity data sets integrated with published outcrop geology—that is:
  - Kaapvaal, Zimbabwe, Kalahari and southern Congo Cratons, their boundaries and intracratonic belts or zones (e.g., Limpopo Terrane (LP) and Magondi Belt);
  - aspects of crustal magnetization;
  - the Witwatersrand Basin and its extensions;
  - the Xade Complex in Botswana;
  - the Meso-Proterozoic Sinclair-Rehoboth Groups, and Grootfontein Metamorphic Complex;
  - tectonostratigraphic zones of the Damara-Ghanzi-Chobe Belt, and the Gariep Belt;
  - the Rehoboth Terrane, and deep Neo- and Late Meso-Proterozoic basins in Namibia, Botswana and Angola;
  - the Karas Impact Structure;
  - the offshore Namibian passive volcanic margin;
  - the Namaqua-Natal Belt, the Khoisan Province, the Beattie Magnetic Anomaly and the Southern Cape Conductivity Belt;
  - extensions of the Namaqua-Natal Belt within Gondwana—the Maud Belt, Antarctica;

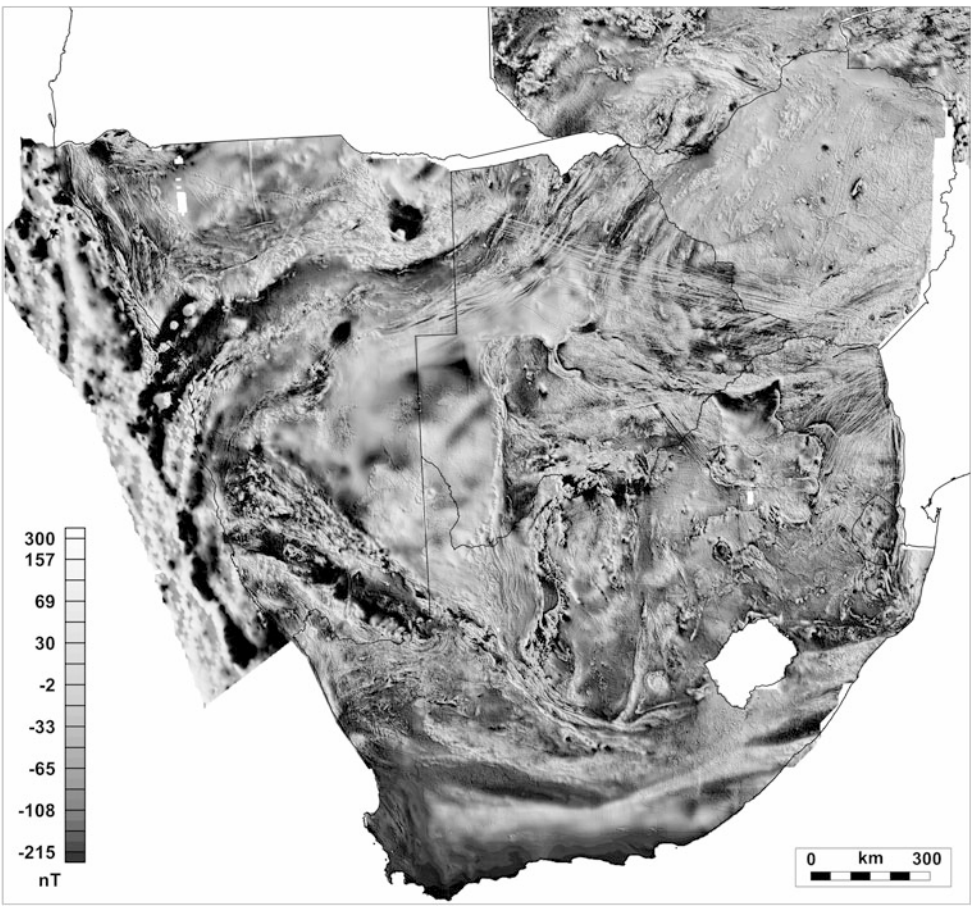

Fig. 2.2 Reduced-to-the Pole regional aeromagnetic image of southern Africa, including offshore aeromagnetic data over the continental shelf of Namibia. A grey-scale image is shown here, in preference to colour, because it best shows the magnetic relief of some of the features. (With acknowledgement to Fugro/CGG airborne Surveys, the Council for Geoscience of SA (formerly Geological Survey), the Geological Surveys of Namibia, Botswana, Swaziland, Mozambique, Zambia and Zimbabwe, and NAMCOR Pty Ltd. No data is available in the public sector for Angola, Lesotho or portions of Mozambique.)

  - major, geophysically evident faults and structural lineaments.
- Electrical resistivity, magnetotelluric, and regional seismic investigations which complement the above interpretation and extend it to the deeper crust and upper mantle:
  - reflection seismic data sets which have been used to search for reservoirs containing oil and gas on land and at sea, and also to map and explore for extensions of the Witwatersrand Basin and Bushveld Complex;
  - electrical and seismic characteristics which have been used to determine the thickness of the crust and lithosphere and to map the boundaries between cratons and mobile belts;
  - several important regional zones of anomalous conductivity and magnetization have been discovered, as noted also above—that is, the Southern Cape Conductivity Belt, Damara-Chobe Conductivity Belt and the Beattie Magnetic Anomaly. Considerable research has been conducted to map, and determine the cause of, these anomalous zones.

2.2 Potential Field Data Sets: An Integrated Interpretation

2.2.1 Magnetic and Gravity Data

The regional aeromagnetic data sets covering southern Africa, mostly acquired pre-1990, have proved invaluable in mapping stratigraphic units, specific lithologies and regional structure under the cover sequences. These data, shown as a reduced-to-the-pole (RTP, of the total magnetic intensity) image in Fig. 2.2, were acquired at flight-line spacings varying from mostly 1–4 km, under contract to the various geological surveys and geoscience councils of the countries covered by the map. The more recent medium-resolution Botswana aeromagnetic data (200–250 m line spacing, degraded to a 500 m grid interval) was merged into this grid. The image also includes an offshore aeromagnetic survey, flown under contract to the National Petroleum Corporation of Namibia (Pty) Ltd (NAMCOR) over the continental shelf area at a line spacing of 25 km. Some of the interpreted

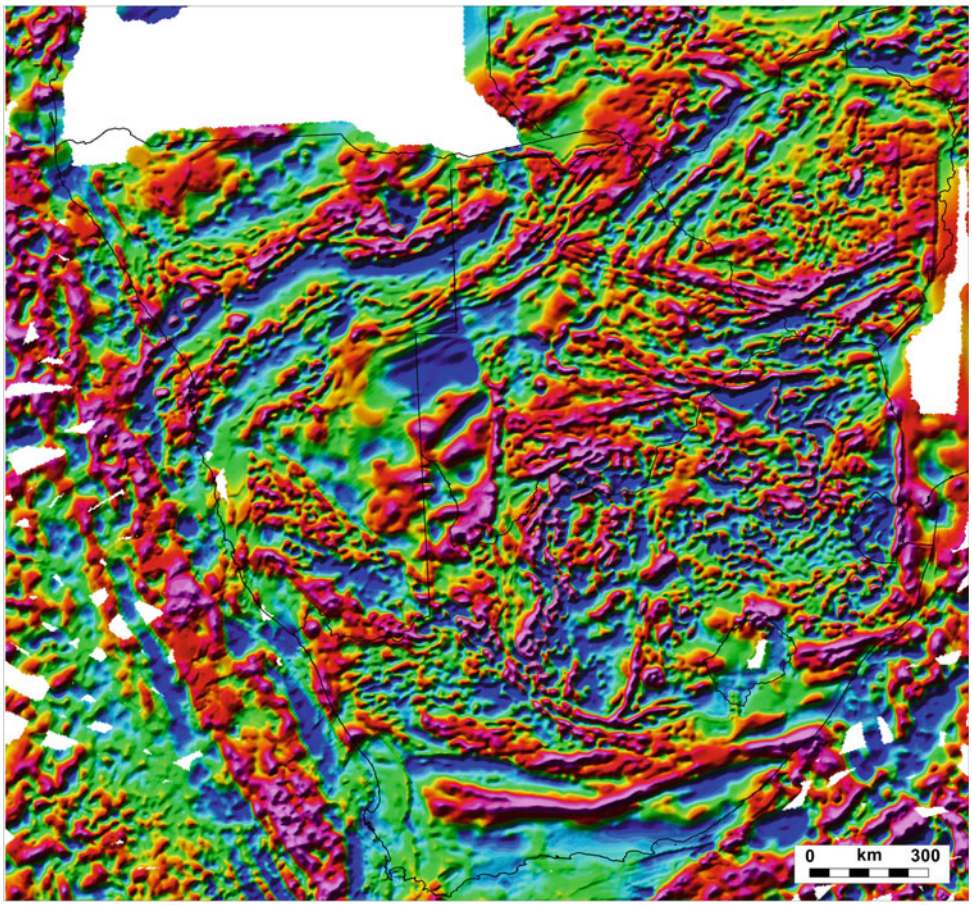

Fig. 2.3 Total Magnetic Intensity Worldwide Earth Magnetic Anomaly image, derived from satellite, airborne and ship-track magnetic data (Maus et al. 2009)

geological features are derived from the higher-resolution data sets in Botswana and Namibia. Also used in the interpretation was the Worldwide Earth Magnetic Anomaly data set, compiled from merged satellite, airborne and marine magnetic data (EMAG2; Maus et al. 2009). Given the relatively low 2 arc-min grid spacing, the higher-frequency (shallower) anomalies are degraded but the grid preferentially enhances some of the regional structures (Fig. 2.3). The offshore areas of this data set, compiled from satellite and marine magnetic data sets, provide a wealth of structural and seafloor spreading information.

The Bouguer Anomaly image shown in Fig. 2.4, to which a regional-residual separation filter has been applied, was derived from mostly ground-based national gravity data sets of Botswana, Namibia, Zambia, Mozambique, Swaziland and Lesotho, as well as from an older-generation South African data set of the Geological Survey (now the Council for Geoscience). Also shown in Fig. 2.4 is the satellite-derived NAMCOR offshore Free-Air anomaly data set covering the continental shelf of Namibia. Further gravity data sets used for interpretation were extracted from the World Gravity Map and related products, compiled by the Bureau Gravimetrique International (Balmino et al. 2012; Bonvalot et al. 2012) from satellite, airborne and ground data. Four data products were available in XYZ format at a 2 arc-min grid spacing—that is, the Bouguer Anomaly data shown in Fig. 2.5, and the Isostatic Anomaly, surface Free-Air Anomaly data and the ETOP-1 Topographic data, which are not shown here owing to space constraints. These data sets were gridded at a 3500 m interval. Although the resolution is reduced with the Bureau Gravimetrique International gravity data sets, the regional structure is relatively clear, as with the aeromagnetic data. Of particular value is the gravity data over Angola, where more detailed private sector ground and airborne data sets are not available.

2.2.2 Interpretation Methodology

The interpretation maps in Figs. 2.6 and 2.7 show geological units, stratigraphy and tectonostratigraphic zones that have been derived from either (1) published outcrop mapping, as indicated in the caption to the interpretation map (Fig. 2.6) or (2) from geophysical interpretation by the authors and their co-authors, or other authors as referenced in each case. Interpretation was aided in part by numerous magnetotelluric (MT) surveys discussed in Sect. 2.3. A number of filters were applied to the above potential field data sets prior to

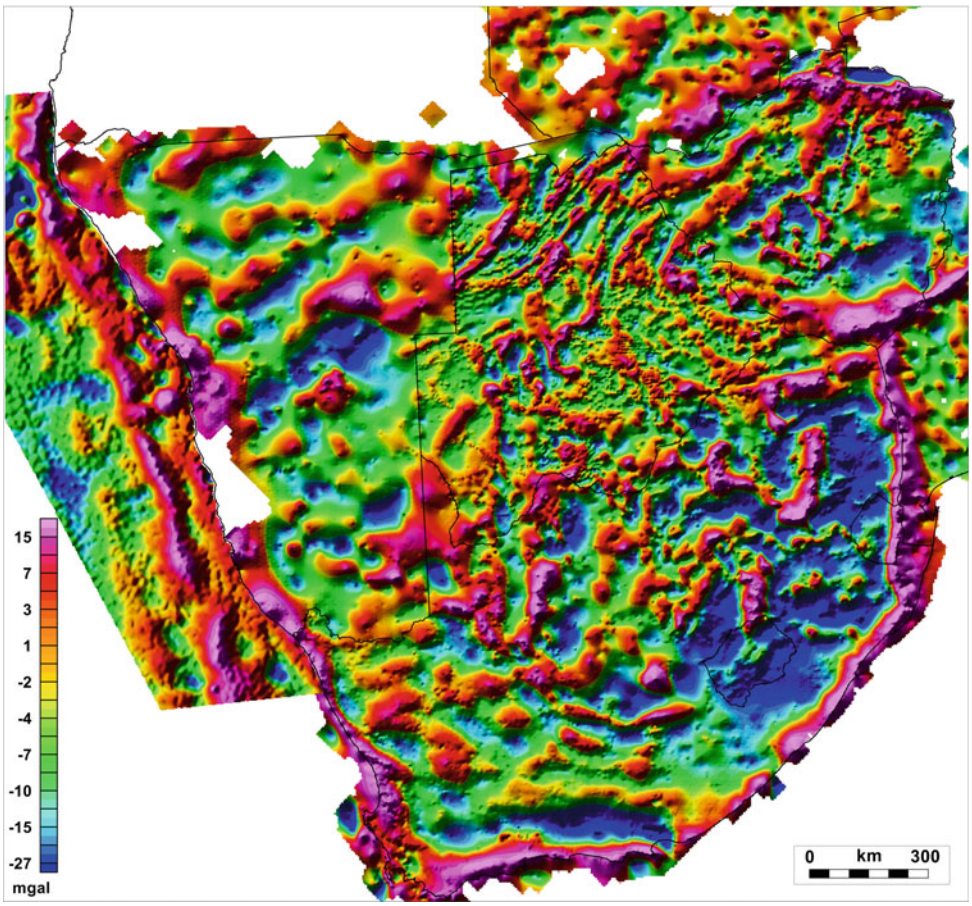

Fig. 2.4 Residual-filtered Bouguer Gravity image and Free Air data offshore Namibia. The onshore data was derived from ground surveys and the offshore Free Air data from satellite measurements (Acknowledgements as in Fig. 2.2)

interpretation so as to enhance structure, lithological fabric and contact locations. In the case of the magnetic data, Reduction-to-the-Pole (RTP) of the Total Magnetic Intensity (TMI) was applied for specific local-scale interpretations. Filters applied to the RTP data set included the First Vertical Derivative, Gaussian residual filters, Analytical Signal, and Total Horizontal Derivative. In the case of the gravity data sets, a Gaussian regional-residual separation filter was applied to each of the three Bureau Gravimetrique International gravity grids in order to reduce high-frequency noise, evident in the data, before further filtering to enhance lithological anomalies. The interpretation methodology followed the norm of working from the known, mapped geology and structure to a projection thereof under areas of cover using the above geophysical data sets. The derivative and residual filters provided the resolution required to map both local- and regional-scale structures. However, owing to the scale of presentation, many of the smaller, local structures have been excluded from the interpretation maps presented here. All features shown in the maps honour both the mapped geology and the geophysical data sets as best possible within the resolution of the data sets.

The interpretation maps (Figs. 2.6 and 2.7) show numerous geophysically evident faults and lineaments, many of which have been previously identified and discussed (e.g., Corner 2008). The term 'lineament' is used here, in the definition of Richards (2000), to denote a large-scale fault zone, or structural corridor, having a much broader swathe of manifestation up to 50 km in width, either continuous or disrupted. Geophysically, lineaments reflect approximately linear structures or zones with anomalous physical properties that range in depth from surface to 5 km or more, depending on the size of the source bodies and their physical property contrast. The lineaments, shown as lines on the interpretation maps, thus reflect the locus of a much broader structural corridor.

A number of ring features have also been identified (Corner 2000, 2008), which are considered to be the manifestation of ring fractures or faults, or alteration aureoles. Their origins may be varied and possibly include:

- ring fractures or faults associated with magmatism and associated intrusions;
- alteration aureoles associated with intrusions;
- alteration aureoles associated with exhalative vents;
- meteorite impact;
- craton-scale ring structures resulting from plate rotation or changes in lithospheric thickness.

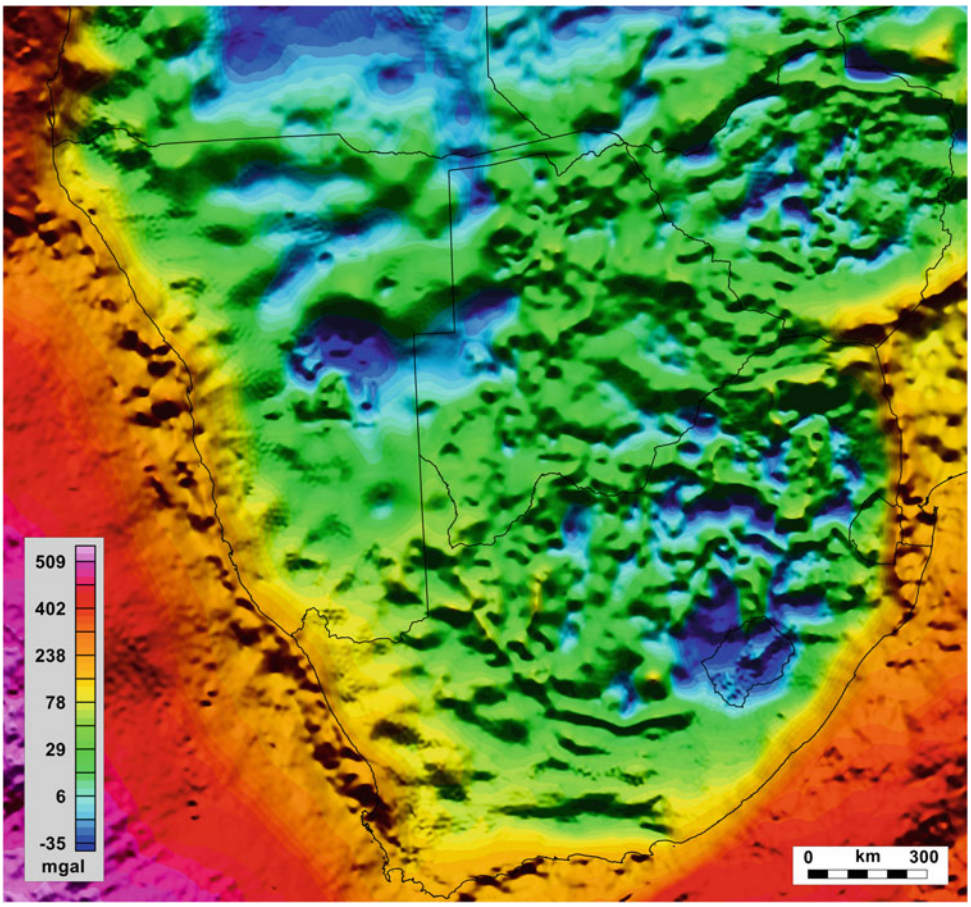

Fig. 2.5 Bouguer Gravity image of southern Africa derived from the World Gravity Map (Balmino et al. 2012; Bonvalot et al. 2012)

Fig. 2.6 **a** Integrated interpretation of southern Africa. Legend and text key are in Fig. 2.6, **b** Legend to Fig. 2.6a. Note that the stratigraphic units marked with an asterisk denote mapping published by the geological surveys, and geoscience councils or institutes, of the countries covered by the map. The following abbreviations are used *ASZ(WA)* Amanzimtoti Shear Zone (Williston Anomaly); *Au-L* Autseib Lineament; BA, Bloemfontein Arch; *Bb* Brandberg Complex; *BDSL* Botswana dyke swarm, main limits; *Be-L* Bethlehem Lineament; *BGH* Bethlehem Gravity High; *BIC* Bushveld Igneous Complex; *BK-L* Barberton-Kimberley Lineament; *BMA* Beattie Magnetic Anomaly; *CC* Congo Craton; *Cc* Cape Cross Complex; *CFB* Cape Fold Belt; *Co-L* Colesberg Lineament; *Cs* Cape Seal Complex; *d* deep features; *D* Daneib intrusion; *EF* Elliot fault; *EI* Epupa Inlier; *Er* Erongo Complex; *Et* Etosha pan; *Ga-L* Gam Lineament; *GD* Great Dyke; *GI* Grootfontein Inlier; *GMB* Grootfontein Mafic Body; *GSP* Gordonia Subprovince; *Gu* Gunib Intrusions; *HZ* Hinge Zone of seaward dipping seismic reflectors; *Ka* Soekor borehole; *Kal-L* Kalahari Lineament; *KB-L* Kuboos-Bremen Lineament; *KVC* Kaapvaal Craton; *KVC-OB* Kaapvaal Craton Okwa Block; *Kc* Soekor borehole; *Kf* Koegelfontein Complex; *KG-L* Khorixas-Gaseneirob Lineament; *KH* Karas Horst; *Kh-L* Kheis Lineament; *KIC* Kunene Igneous Complex; *KIS* Karas Impact Structure; *KI* Kamanjab Inlier; *KP* Khoisan Province; *Ku-L* Kudu Lineament; *LB* Lebombo Belt; *LMSZ* Lilani-Matigulu Shear Zone; *LSZ* Lovat Shear Zone; *LT* Limpopo Terrane; *M*2,4 Offshore magnetic anomalies; *M* Messum Complex; *MAB* Matchless Amphibolite Belt; *Mf* Molopo Farms Complex; *MGB* Magondi-Gweta Belt; *MGB-L* Magondi-Gweta Belt limit; *MIS* Morokweng Impact Structure; *MkF* Makgadikgadi Fault; *MSZ* Mwembeshi Shear Zone; *MT* Melville Thrust; *N* Naukluft Nappe Structure; *NamqP* Namaqua Province; *NatP* Natal Province; *Naq-L* Namaqua Lineament; *NcB* Ncojane Basin; *NNF* Namaqua-Natal Front; *NoB* Nosob Basin; *Ok-L* Okahandja Lineament; *Om-L* Omaruru Lineament; *OR* Omatako remanent anomalies; *Op-L* Opuwo Lineament; *OtM* Otjiwarongo Massif; *Ov* Okavango delta; *P* Pilanesberg Complex; *Pa* Paresis Complex; *PB* Passarge Basin; *Pof-L* Pofadder Lineament; *PaSZ* Palala Shear Zone; *PuSZ* Purros Shear Zone; *PV* Phoenix Volcano; *QI* Quangwadum Inlier; *Qu* Soekor borehole; *RGFZ* Rio Grande Fracture Zone; *RT* Rehoboth Terrane; *SMA* Steinhausen Magnetic Anomaly; *SRZ* Sinclair-Rehoboth Zone; *ST* Sesfontein Thrust; *St-L* Strydenburg Lineament; *TA* Tugela Allochthon; *TC* Trompsburg Complex; *TI* Tsumkwe Inlier; *TK-L* Trans-Kalahari Lineament; *T-G-C-B* Tsumis-Ghanzi-Chobe-Belt; *TM-L* Thabazimbi-Murchison Lineament; *Ts-L* Tsodilo Lineament; *Tsh* Tshane Complex; *Tst* Tsetseng Complex; *TTF* Tugela Thrust Front; *VIS* Vredefort Impact Structure; *Wb* Walvis Bay Complex; *We* Soekor borehole; *We-L* Welwitschia Lineament; *WFZ* Walvis Fracture Zone; *WR* Walvis Ridge; *WT* Waterberg Thrust; *XC* Xade Complex (SL, NL South, North Lobes); *ZFZ* Zoetfontein Fault Zone; *ZC* Zimbabwe Craton ▶

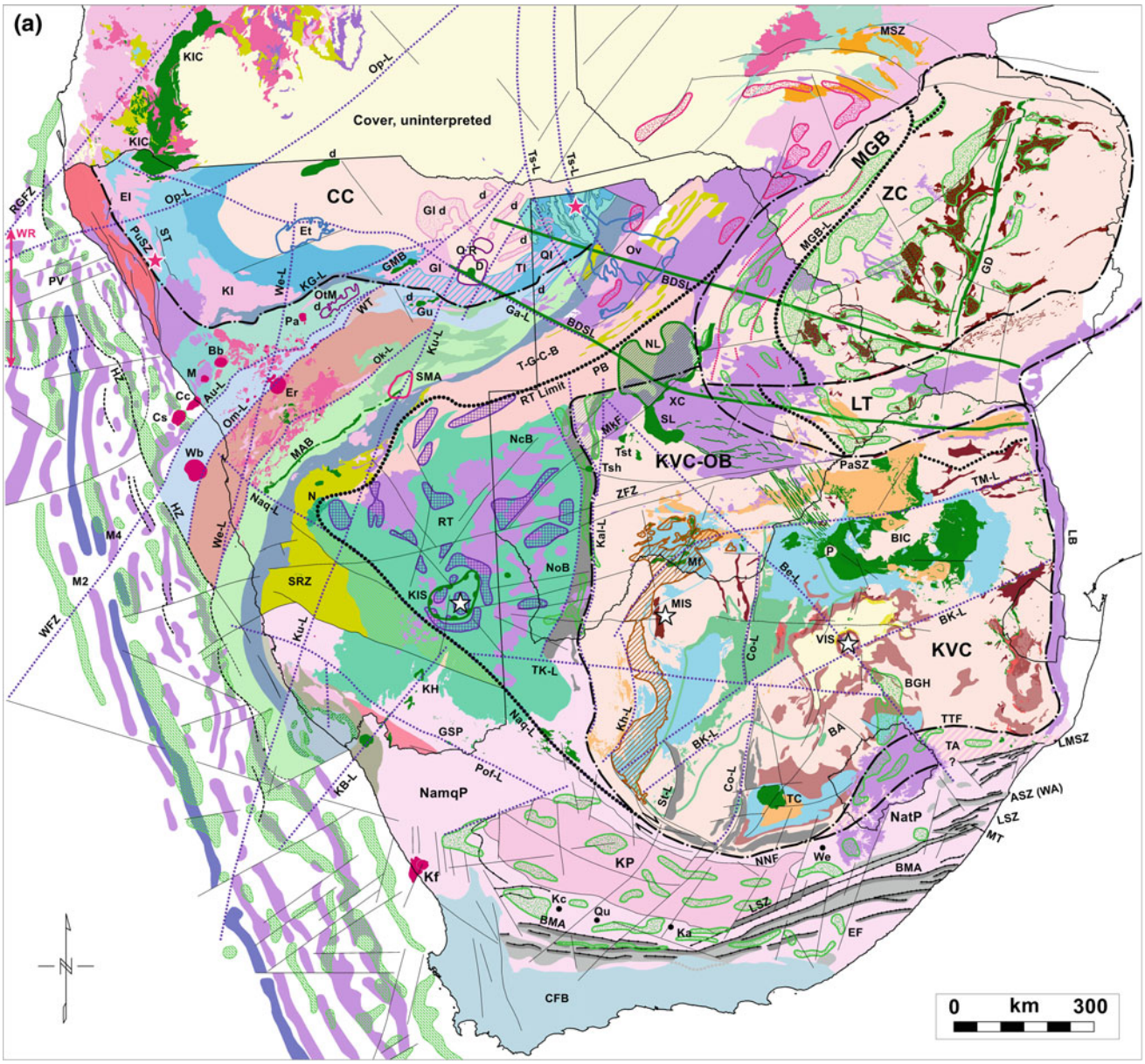

Examples of ring features are provided and discussed by Corner (2008) and Corner et al. (1997). For their arcuate geometry to be preserved, which may cut across older structural fabric, the ring features would have to be post- or late-tectonic in the first instance. It is also considered possible, as with many major faults, that the above foci or causative sources may have been reactivated through geological time owing to crustal weakness. In this sense, a ring feature may be evidence of an older reactivated focal source. A craton-scale source (last item in list above) is best exemplified by the Kaapvaal Ring Structure (KVRS; Fig. 2.7), which may have resulted from rheological or structural variations in the deep crust or upper mantle. It is evident in the south as the arcuate Namaqua-Natal Front, separating the Kaapvaal Craton and the Namaqua-Natal Belt, whereas its northern arcuate sector is evidenced through fault-trace analysis of the aeromagnetic data. Figure 2.16 shows an overlay of the KVRS on the 200 km P-wave velocity model depth slice. It clearly encompasses the high-velocity root of the Kaapvaal Craton and is interpreted here to arise from relative movement between this root and the surrounding lower velocity zones, perhaps initiated during plate movement along the zones of competency contrast.

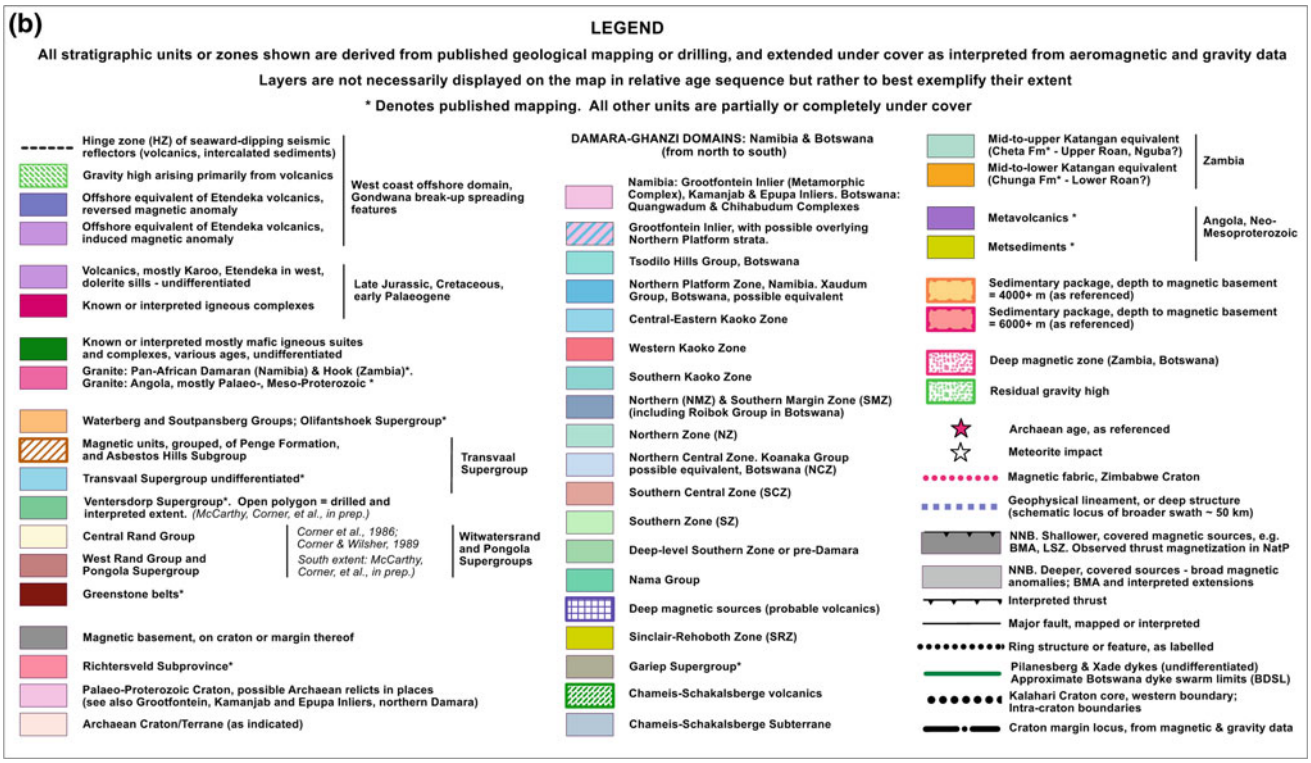

Fig. 2.6 (continued)

Examples of ring structures that are interpreted to arise from meteorite impact events are, firstly, due to the Morokweng Impact event (MIS; Fig. 2.6; MRS; Fig. 2.7; e.g. Corner 1994a; Andreoli et al. 1995; Corner et al. 1997) and, secondly, due to the interpreted Karas Impact event (KIS; Fig. 2.6; KRS; Fig. 2.7; Corner 2008; Section 2.2.7.2)

2.2.3 Archaean and Palaeoproterozoic Cratons

2.2.3.1 Introduction to the Interpretation of the Archaean and Proterozoic Geology

The various Archaean and Proterozoic stratigraphic units shown in the interpretation map (Fig. 2.6a, Legend 2.6b) are derived, first, from mapped geology as published by the relevant geological surveys, geoscience councils and institutes of the countries covered, and, second, from the interpretation of magnetic and gravity data sets, constrained by the outcrop data and limited published borehole data in the areas of cover. Cover sequences that have not been shown in this interpretation are defined here as being Phanerozoic in age, ranging approximately from the Cambrian to recent, with one exception—that is, the magnetic basalt flows and dolerite sills of Karoo age, including the Etendeka basalts. The distribution of these rocks is shown so as to indicate those areas where interpretation of the underlying suboutcrop geology is compromised as a result of the presence of these highly magnetized strata in the cover sequence.

Much geophysical research has been conducted in the southern African region. Aspects that are highlighted and referenced in this review include (1) interpretation of gravity and magnetic data, particularly of Precambrian features which have a clear expression in this data; (2) geomagnetic induction, Magnetotelluric (MT) and deep electrical resistivity studies; (3) deep seismic reflection surveys, conducted both by industry in its quest to locate extensions to the Witwatersrand Basin and by the South African National Geophysics Programme; (4) deep seismic refraction surveys; and (5) teleseismic studies of the cratons, underlying mantle, and adjacent polymetamorphic terranes. Many geological publications on the Precambrian geology of southern Africa show variable boundaries or delineations of the cratons and surrounding terranes in the areas of cover, as well as of key regional structures. Often, the detail which geophysical data can and does give has been ignored or at best loosely interpreted. We have sought to be rigorous in the mapping of these features, carefully honouring the detail of geological, magnetic and gravity data sets on both regional and local scales. The latter interpretations are not shown here owing to the scale of this presentation, but have been used to constrain the regional mapping shown here, as referenced where appropriate. The lines indicating craton and terrane

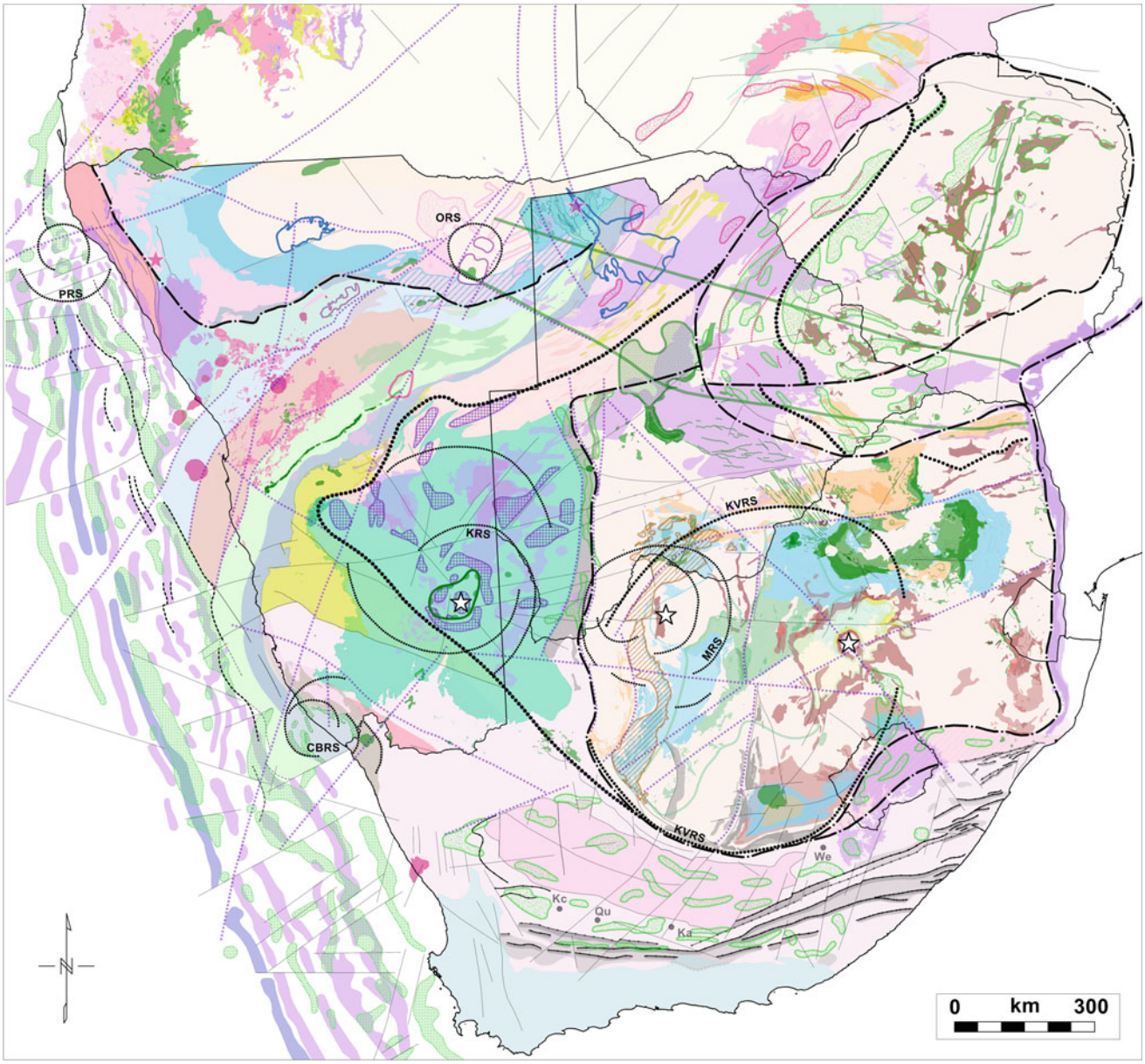

Fig. 2.7 Regional ring or arcuate structures are superimposed on the interpretation map of Fig. 2.6. *CBRS* Chameis Bay ring structure; *KRS* Karas ring structure; *KVRS* Kaapvaal ring structure; *MRS* Morokweng ring structure; *ORS* Omatako ring structure; *PRS* Phoenix ring structure

boundaries should be considered to represent broader complex swathes of varying structural style and dip, drawn at their shallowest manifestation.

2.2.3.2 Kaapvaal Craton

The Kaapvaal and Zimbabwe cratons were formed and have grown through accretion, thus comprising crustal blocks of different ages with different structural styles, from the Archaean to the Proterozoic. The boundaries thereof are mostly clearly revealed by the gravity and magnetic data. The assumption is made here that major structures or structural zones, as evidenced in the geophysical data, with geological control where available, constitute the craton boundaries. This applies similarly to the surrounding polymetamorphic terranes. De Beer and Meyer (1984) were the first to geophysically map a portion of the Kaapvaal Craton boundary covered by Phanerozoic rocks, delineating the arcuate southern craton margin by modelling a number of gravity profiles across it, where it is juxtaposed against the Namaqua-Natal Belt.

The Kalahari Lineament (Kal-L; Fig. 2.6; Kalahari Line, Reeves 1978), interpreted as the western Meso-, Palaeo-Proterozoic boundary of the Kaapvaal craton, is one of the most dramatic features in the aeromagnetic image of southern Africa (Figs. 2.2 and 2.6), separating relatively

shallow basement to the east (with mostly less than 1 km of cover) from extremely deep magnetic basement beneath the Rehoboth Terrane (RT) to the west, where cover thicknesses have been determined to vary from 6 to 10 km (Reeves 1978; Corner 2008). The magnetic signature of the Kal-L changes towards the south, where it bounds the Kheis Province (comprising the Olifantshoek Supergroup rocks) in the west, but the craton boundary is nevertheless clear as mapped in Fig. 2.6. Moen (1999) places the western limit of the Olifantshoek Supergroup at the Dabeep fault, which lies roughly centrally between the craton boundary and the Kheis Lineament (Kh-L) in Fig. 2.6. No justification for a major structural boundary is seen in the geophysical data in this central area. Recent gravity data (Botswana Geoscience Institute) indicates that a gravity high is associated with the Kal-L, although not ubiquitously. This suggests that the Kal-L magnetic signature results in part from mafic intrusions, probably mostly of late Mesoproterozoic Umkondo age (*c*. 1.1 Ga; Meixner and Peart 1984; Hanson et al. 2006; Cornell et al. 2011), and in part from magnetization interpreted to arise from hydrothermally altered granite-gneiss, associated with this major suture, where no clear gravity high is evident (Corner 2008). Localized high magnetic anomalies evident within the anomalous gravity zone are most likely associated with smaller-scale mafic intrusions, such as the Tshane Complex.

A number of features hallmark the Kal-L as a major crustal structure, including the enormous change in depths to basement, as described above, and apparent separation of Precambrian stratigraphy and terranes of differing structural styles, from its east to its west. It has been inferred to be a zone of major collision (Meixner and Peart 1984) or a zone of major transpression (Cornell et al. 2011). Its age has been inferred to be post-Waterberg (Olifantshoek Supergroup equivalent)—that is, post-Eburnean (Reeves 1978). Early interpretations of the Kal-L (e.g., Reeves 1978) identify a separate crustal terrane, the Okwa basement, north of the Makgadikgadi Fault, where it cuts the Kal-L. Many authors interpret the Zoetfontein fault to be the northern boundary of the Kaapvaal craton, constituting the southern boundary of the larger Okwa terrane north thereof (e.g., De Wit and Tinker 2004), a view most likely based on the original interpretation by Reeves (1978), who separated the basement north of the Zoetfontein fault from cratonic basement to the south. Corner (1998) does not support the interpretation of the larger Okwa terrane (i.e., north of the Zoetfontein fault, Kaapvaal Craton Okwa Block; Fig. 2.6) as a crustal entity separate from the Kaapvaal Craton, since it is bounded in the west by the uninterrupted Kal-L. That the Zoetfontein fault is a major early fault, with post-Karoo faulting as its youngest manifestation, is beyond question. However, as with the Makgadikgadi fault, there is no disruption of the Kal-L by the Zoetfontein fault. The continuity of the Kal-L thus suggests that the crustal blocks accreted north and south of the Zoetfontein fault are at least of Meso-, Palaeo-Proterozoic age, if not earlier. Nevertheless, interpretation of the aeromagnetic data confirms a clear change in basement fabric north and south of the Zoetfontein fault, the two most dramatic examples being the truncation of the north-northwest-trending Pilanesberg dykes against it, with minor continuation north thereof beneath Karoo basalt, and the east-west disposition of the interpreted feeder dykes to the Xade Complex to its north (Figs. 2.2 and 2.6; Corner et al. 2012). A change in crustal level within the Kaapvaal Craton is thus inferred across the Zoetfontein fault zone. The Okwa terrane, as described above, is referred to as the Okwa Block here, and interpreted to be part of the Kaapvaal Craton. Other authors also recognize the possibility that the Okwa Block is one of a mosaic of blocks making up the Kaapvaal Craton (e.g., Eglington and Armstrong 2004). Further subdivisions internal to the Kaapvaal Craton have been published. For example, Schmitz et al. (2004) recognize separate entities west (Witwatersrand Block) and east (Kimberley Block) of the Colesberg Lineament.

Reeves (1978) identified two sub-basins west of the Kal-L, overlying the Rehoboth Terrane—that is, the Ncojane Basin north of the Makgadikgadi fault, and the Nosob Basin to the south. The distinction between these two sub-basins is not recognized here, other than a probable change in deformation northwards as the Tsumis-Ghanzi-Chobe Belt is approached (T-G-C-B; Fig. 2.6). The northern margin of the Kaapvaal Craton, adjoining the Kal-L, is clearly evidenced by a similar dramatic change in depth to basement beneath the Passarge Basin (PB; Fig. 2.6), which is underlain by the T-G-C-B. Further east, the Palala shear zone (PaSZ; Fig. 2.6) is seen to trend north-westwards towards the PB, in both the gravity and magnetic data sets, constituting the boundary between the Kaapvaal Craton and the Limpopo Terrane (LT; Fig. 2.6). The eastern craton margin is well delineated by the Lebombo Belt (LB; Fig. 2.6), both geophysically and geologically.

The southeastern boundary of the Kaapvaal Craton, extending through Lesotho to the Tugela Thrust Front (TTF; Fig. 2.6), is a broad complex tectonic zone of inherited Archaean and Mesoproterozoic crust separating the craton from the Natal Province. This zone has been termed the Tugela Allochthon (TA; Fig. 2.6), based on geophysical and isotopic studies by Barkhuizen and Matthews (1990), De Wit and Tinker (2004), Eglington and Armstrong (2004); Schmitz and Bowring (2004). Although no magnetic data is available for Lesotho, the full gravity coverage has been merged into the residual Bouguer Gravity image of Fig. 2.4. Two gravity highs are evident in Lesotho, roughly parallel to the craton margin. At first sight these might be taken to be part of the Kaapvaal Craton, roughly on-strike with, although detached from, the gravity high (and coincident magnetic high) flanking the southern Witwatersrand Basin in the south. Alternatively, these highs might be interpreted to be relicts of the (unknown)

source of the Bethlehem Gravity High (BGH; Fig. 2.6). However, the latter is of much higher amplitude and lacks any magnetic expression. Schmitz and Bowring (2004) have shown, from geochronological and isotopic data on lower crustal xenoliths from the Lesotho kimberlites located just northeast of the two Lesotho gravity highs, that granulitization of the lower crust was a relatively young phenomenon, *c*. 1.0–1.1 Ga, which affected pre-existing Archaean to Mesoproterozoic crust. The gravity highs are thus assumed to be within the allochthonous zone (e.g., of De Wit and Tinker 2004), as are the smaller-scale gravity highs further east (excluding the known mafic intrusive sources). The Tugela Thrust Front clearly demarcates the northern boundary of the TA in the northern sector of the Natal Province. A possible continuation of the Kaapvaal Craton into Dronning Maud Land, Antarctica, where the Grunehogna Craton has been identified, is discussed in Sect. 2.2.10.3.

2.2.3.3 Zimbabwe Craton, Limpopo Terrane, Magondi Belt and the Kalahari Craton

The disposition of the Zimbabwe Craton (ZC; Fig. 2.6), and associated Magondi-Gweta Belt (MGB; Fig. 2.6) and Limpopo Terrane (LT; Fig. 2.6), has been revisited here in as much detail as the mapped geology and geophysical data sets allow. The boundary between the ZC and LT is relatively well defined from geological mapping in southern Zimbabwe, northern South Africa and eastern Botswana, and from a clear change in magnetic fabric across the boundary. Working westwards, this magnetic fabric loses clarity under the cover of Karoo basalts, although it is still evident in places. The MGB has a semilinear magnetic fabric that is not dissimilar to that of the LT. A faulted contact is suggested between the two belts in Fig. 2.6, but this may be a local feature, and the possibility thus exists that the LT and MGB constitute a continuous deformation zone encompassing the ZC in the south and west. Mapping of the eastern boundary of the ZC is limited by the both the paucity and the coarseness of the geophysical data.

The Mwembeshi Shear Zone in southern Zambia (MSZ; Fig. 2.6), a major roughly east–west dislocation zone, has been extended using the aeromagnetic data, as shown in Fig. 2.6 (see also Fig. 2.2)—that is, in the east it is seen to curve southeastwards toward the ZC boundary. Two other regional structures, with a similar roughly east–west trend, are mapped to its south. Fault mapping, derived from both the geological mapping and the geophysical interpretation, shows a continuation of these regional structures eastward into Zimbabwe. One of these (in northern Zimbabwe) is a major post-Karoo fault, at its youngest manifestation, preserving a deep Karoo basin to the north—that is, the Lower Zambezi Zone of the Cabora Bassa Basin. These regional fault zones appear to curve into the ZC boundary, suggesting possible later transpressional movement along the boundary. Of interest is that the northeast-trending magnetic fabric of the Magondi-Gweta Belt in Zimbabwe is seen to change direction dramatically, truncating against the above east–west-striking fault zone, and trending westwards into Zambia south of the Mwembeshi Shear Zone, initially following the east–west trend of this zone. Deep-seated magnetic sources are also shown within the basement in Zambia (Fig. 2.6), which mimic the interpreted westward trend of the Magondi-Gweta Belt. We find no evidence in the geophysical data for any continuity between the LT and the so-called Okwa Block, as inferred by a number of workers.

Jacobs et al. (2008) discuss the evolution of the Kalahari Craton, describing it as 'having been spawned from a small Archaean core which grew by prolonged crustal accretion in the Palaeoproterozoic … to form the Proto-Kalahari Craton by 1750 Ma'. They include the Grunehogna Craton in Dronning Maud Land, Antarctica, in their definition of this Archaean core (as discussed in Sect. 2.2.10.3). From *c*. 1400 Ma, all margins of the Proto-Kalahari Craton recorded intense tectonic activity, and by *c*. 1050 Ma the Proto-Kalahari nucleus was almost completely rimmed by voluminous Mesoproterozoic crust, becoming a larger entity, the Kalahari Craton (Jacobs et al. 2008). The outline of the Proto-Kalahari Craton, as defined by Jacobs et al. (2008) above, is shown in Fig. 2.1.

2.2.3.4 Congo Craton in Namibia and Botswana

McCourt et al. (2013) describe the Angolan Shield, *c*. 2.0 Ga, as being a Palaeoproterozoic basement terrane dominated by granitoids, together with a limited amount of Neo-Archaean crust, which extends from south of Lubango in Angola into Namibia, and eastward under cover into Zambia. This defines the southwest section of the Congo Craton. The craton was intruded by the *c*. 1385 Ma Kunene Complex, the areal extent of which indicates an extensive period of Mesoproterozoic crustal extension (McCourt et al. 2013). Delineation of the southern boundary of the Congo Craton in northern Namibia, and its continuation into Botswana and Zambia, has been the subject of much speculation in view of, firstly, the extensive Karoo and Kalahari cover in the central and eastern areas of northern Namibia and, secondly, the complex structural evolution that hallmarks the Kaoko Zone in the northwest (see Sect. 2.2.6.3). One is left with geophysical signatures (magnetic and magnetotelluric), and in places a lack thereof, which have often been variably interpreted, to map the craton boundary.

A significant crustal-scale magnetic anomaly, characterized by deep-seated high-amplitude anomalies arising from the crust beneath the Namibian Northern Platform and a southern dominant magnetic low, strikes northeastwards across northern Namibia, as is readily evident in Fig. 2.2. Eberle et al. (1995) modelled a number of magnetic profiles across key structural features in Namibia, of which three traversed this regional magnetic anomaly. Their modelling,

based on dipping prism-shaped bodies with induced (normal) magnetization, consistently suggested the presence of a regional-scale antiformal structure situated beneath the southern portion of the carbonate platform. This may indicate the southern abutment of the Congo Craton (CC). We thus interpret this regional magnetic anomaly and associated structure to delineate the boundary of the Congo Craton, as shown in Fig. 2.6, which is a refinement of an earlier interpretation which placed the boundary further north (Corner 2008). The magnetotelluric work of Khoza et al. (2013a, b), and seismic tomography studies of Raveloson et al. (2015), provide support for the boundary mapped here. The Khorixas-Gaseneirob Lineament (KG-L; Miller 2008a; Fig. 2.6) is thus considered to constitute the near-surface manifestation of the southern boundary of the Congo Craton. The continuity of the southern east–west-trending portion of the craton boundary has been disrupted by a number of major structural lineaments, as mapped in Fig. 2.6, including the Welwitschia (We-L) and Kudu (Ku-L) Lineaments in particular. This relatively well-defined regional magnetic signature of the southern Congo Craton boundary disappears northwestwards, where the craton boundary is inferred to continue along the north-northwest-trending Purros Shear Zone (PuSZ; Fig. 2.6). Similarly, in the east, the Congo Craton boundary, as evidenced in the magnetic data, appears to terminate abruptly in northwestern Botswana against what is newly interpreted here as the north-trending Tsodilo Lineament (Ts-L; see also Sect. 2.2.6.3).

The Mesoproterozoic Grootfontein Inlier (GI; also known as the Grootfontein Metamorphic Complex; Miller 2008b) is located in north-northeastern Namibia and extends eastward into Botswana, where it is inferred to continue as the Quangwadum Inlier (QI; Fig. 2.6) and to include the Chihabudum Complex. A singular combination of geophysically evident regional-scale features occurs within the Inlier—that is, an annular zone of high magnetization encompasses a low-magnetic central zone, referred to as the Omatako remanent anomalies (OR; Fig. 2.6; Corner 2000), which suggest deep, probably remanent, sources. These, and the encompassing annular high-magnetic zone, are collectively referred to as the Omatako Ring Structure (ORS; Fig. 2.7). The ORS occurs at the intersection of a number of major lineaments, including the Omaruru and Kudu Lineaments, and lies within the swathe of the west-northwest-trending Botswana dyke swarm that crosses the subcontinent (BDSL; Fig. 2.6). A number of deep, roughly linear magnetic anomalies radiate to the east, north and west of the OR/ORS, forming part of a much larger regional structural feature. The Grootfontein Inlier is mostly characterized by strongly magnetic gneisses. The radial anomalies are thus interpreted to arise from radial faults within the Complex, with a focus on the ORS. The area is covered by Kalahari and Karoo sediments, as well as by Karoo basalts, thus the origin of the ORS and associated features is unknown. Possible causes include a major volcanic eruptive centre, or even a meteorite impact site.

McCourt and Jelsma (this volume) discuss the Angolan Craton and, of relevance here, age aspects of the Congo Craton in Namibia. They describe the continental crust forming the Grootfontein Inlier as comprising plutonic rocks of dominantly alkaline/calc-alkaline composition. The protolith of granitic gneisses from the related Tsumkwe and Quangwadum Inliers (TI, QI; Fig. 2.6) have been dated at 2022 ± 15 Ma (Hoal et al. 2000) and at 2051 ± 1 Ma (Singletary et al. 2003), which are compatible with inherited zircon grains at 2052 ± 44 Ma and 1987 ± 4 Ma in granite and felsic lava in the Kamanjab Inlier (KI; Fig. 2.6). They take this as evidence of correlation between the older crust, interpreted to be present at a depth below the KI, and the granite gneisses exposed in the Grootfontein, and related Quangwadum and Tsumkwe, Inliers. Archaean ages within the Palaeoproterozoic basement inliers of northern Namibia and Botswana have been reported in the Epupa Inlier (e.g., 2585.4 ± 1.2 Ma and 2645 ± 6 Ma; Seth et al. 1998; EI; Fig. 2.6) and in the Tsodilo Hills area associated with the QI (2548 ± 65 Ma, Gaisford 2010). The Archaean localities are shown as red stars in Fig. 2.6.

2.2.3.5 Crustal Magnetization

Interpretation of the aeromagnetic and gravity data covering the Witwatersrand Basin (Figs. 2.6), and its potential extensions to the south and west of the main basin, led to some fundamental new insights into the underlying craton (Corner et al. 1986a, b; Corner et al. 1990). As part of these studies, long-wavelength magnetic anomalies within the craton, relating to deep sources, were interpreted through forward modelling. The Vredefort Impact Structure (VIS; Fig. 2.6) has an annular highly magnetic zone in its gneissic basement core which, accepting the crust-on-edge model for the structure, would thus lie some 8 km beneath the West Rand Group of the Witwatersrand Basin. This zone was interpreted, using a typical P-wave velocity for the basement, to correspond with seismic reflectors in the granite-gneissic basement evident in a reflection seismic line traversing the basin west of VIS (Durrheim et al. 1991). These reflectors are parallel, or subparallel to the base of the basin. Projection of this intermediate-crustal magnetic, reflective zone, through forward modelling of the magnetic data, to its suboutcrop beneath the Karoo Sequence to the southwest of the Witwatersrand Basin, suggested that the deep, high-amplitude semilinear magnetic anomalies trending northward from Colesberg (Co-L; Fig. 2.6) were due to this same level of magnetized basement. Drilling by a mining company (Goldfields SA, pers. comm.) confirmed this interpretation. Corner et al. (1986c) named this anomalous belt the Colesberg Trend, here termed Lineament

(Co-L; Fig. 2.6). This is inferred to be the locus of an early orogenic belt west of the Witwatersrand Basin, along which a major section of the upper crust has been eroded, possibly being the main source of the sediments that filled the western portion of the basin.

The confirmation of this interpretation led Corner (1998) to propose a model that attributed many of the high-amplitude, regional long-wavelength magnetic anomalies to arise from intermediate-crustal magnetization, particularly to the west of the Witwatersrand Basin, including the Colesberg Lineament (Figs. 2.2 and 2.6). Comparisons were made with other cratonic areas, particularly with studies of the structure of Russian cratons based on numerous deep crustal seismic refraction profiles (Pavlenkova 1987). These studies led Pavlenkova to propose a generalized three-layer craton model, distinguished on the basis of geological structure, seismic boundaries and P-wave velocities. Corner (1998) compared the above magnetization model with both the Pavlenkova three-layer craton model and the deep electrical resistivity results for southern Africa (Van Zijl 1978; De Beer and Meyer 1984; De Beer and Stettler 1988). Corner (1998) noted that the three-layer craton model could fully explain the extremely low resistivities observed in the deeper crust, which would thus occur below the upper, brittle, resistive crust, in an underlying hydrofractured, aseismic, probably fluid-filled middle crust (in the three seismic-layer model) where horizontal displacement stresses predominate. It is in this electrically conductive intermediate-crustal zone that Corner proposed the development of magnetization, through the growth of magnetite from iron in the protolith at elevated temperatures (below the Curie temperature for magnetite), in the presence of fluid.

Invoking the presence of an intermediate-crustal zone of magnetization, not necessarily ubiquitous throughout the craton but certainly prevalent in many areas particularly along major structures that may have allowed fluid movement, readily allows the interpretation, through forward modelling of both magnetic and gravity data sets, to explain many of the deeper features, such as the long-wavelength anomalies west of the Witwatersrand Basin near Wolmaransstad and Vryburg, the Colesberg Lineament (Co-L; Fig. 2.6), the Strydenburg Lineament to the west of the Colesberg Lineament (St-L; Fig. 2.6) and possibly portions of the Kal-L in Botswana (Corner 1998).

2.2.4 The Witwatersrand Basin

The main Witwatersrand (Wits) Basin is situated roughly centrally on the Kaapvaal Craton (Fig. 2.6). Economic exploitation since the discovery of gold in 1886 has seen the development of more than 150 mines, some of which have yielded uranium as a by-product. In terms of value of metal recovered, the basin's mineralization must rank as one of the most valuable mineral deposits ever found. However, more than 90% of the basin is covered by younger sequences, ranging from Neo-Archaean, through the Palaeoproterozoic, to Phanerozoic. Geophysics played a critical role, at an early stage, in the discovery of new mines, in particular through the application of magnetic and gravity techniques. More recently, reflection seismic techniques have also been very successfully applied, both to locate new extensions and to map, in 3D, structures on a mine scale (e.g., Pretorius et al. 1989). This technology was further applied to mapping and evaluation of the Bushveld Igneous Complex in the search for platinum (e.g., Pretorius et al. 2010).

In terms of mapping the basin under cover, Borchers (1964) produced the first geological map based on outcrop, mining and drilling data. A more recent map, based mostly on additional geological data acquired since that time, partially constrained by geophysical data, was published by Pretorius (1986). Using this map and associated data as a base to work from, Corner and Wilsher (1989) conducted a rigorous reinterpretation of the basin, using both the aeromagnetic and ground gravity data to further upgrade the mapping. Corner et al. (1986a, b) also published the first ever digitally printed colour images, in the public sector, of the aeromagnetic and gravity data covering the basin. The mapping of Corner and Wilsher (1989) is replicated in Fig. 2.6. Although older than the overlying Ventersdorp and Transvaal Supergroups, the main Wits Basin and outliers are placed on top of these in Fig. 2.6 so as to provide the reader with a view of their actual extent and disposition. Corner et al. (1986c) extended their interpretation southwards, covering the southern portion of the Kaapvaal Craton. They identified the possible presence of outliers of Witwatersrand rocks southeast of the main basin in the Bethlehem area, and south of Bloemfontein, confirming what many geologists had proposed in the past. High gold prices at the time resulted in extensive exploration activities commencing in these areas.

The ensuing quest, by major and junior mining companies, for extensions of the Wits Basin in the Bethlehem area and south of Bloemfontein, using aeromagnetic, gravity and extensive seismic reflection surveys, resulted in many successful boreholes being drilled which intersected Witwatersrand Supergroup rocks, and Waterberg-equivalent rocks, in previously untested areas. Unfortunately, most of the intersections were in the barren West Rand Group and, in time, these activities were terminated. One such exploration programme was conducted by AfriOre (Pty) Ltd, which built on the data available from other companies that had withdrawn from the area. The first author (Corner) was a member of a team that interpreted these data as well as a more recent aeromagnetic survey flown by AfriOre (McCarthy et al. in preparation). Drilling intersected both Witwatersrand and Transvaal Supergroup rocks east and southeast of the Trompsburg Complex. Integrated interpretation, in a team

approach, of all data resulted in the delineation of major Wits and Transvaal sub-basins underlying the Trompsburg Complex south of Bloemfontein, extending eastwards to Lesotho and to the Bethlehem area north of Lesotho (Fig. 2.6; McCarthy et al. in preparation). Both the Wits and the Transvaal sub-basins are separated from the main Wits Basin by the Bloemfontein Arch (BA; Fig. 2.6). This is a major contribution, built on all past exploration programmes, to the mapping of Archaean and Palaeoproterozoic rocks beneath an extensive cover of Karoo Supergroup rocks, in excess of 1000 m in thickness, in the southern portion of the Kaapvaal Craton.

2.2.5 Xade Complex

The Xade Complex (XC), situated in central Botswana, is a large singularly anomalous feature in the aeromagnetic and gravity images of southern Africa (Figs. 2.2, 2.4 and 2.6), occurring under a complete cover of sediments of the Kalahari Group and Karoo Supergroup, including Karoo volcanics in places, with a combined thickness that varies from 220 to 1000 m, probably extending to greater depths in the north beneath the Passarge Basin (PB). As such, it has drawn much attention both academically and from a minerals exploration point of view. It was first identified during the regional aeromagnetic survey of the country in 1975–1977 (Reeves 1978; Meixner et al. 1984; Figs. 2.2 and 2.4). The Xade Complex was originally interpreted to comprise a high-amplitude kidney-shaped zoned magnetic anomaly with two semilinear anomalies extending to the northwest and northeast in a Y-shaped form (e.g., Meixner et al. 1984). It is also evidenced by a coincident Bouguer gravity anomaly. Historical work was limited, with only three cored-boreholes having been drilled. Two of these were drilled as part of the Kalahari Drilling Project in the early 1980s, following interpretation of the aeromagnetic data (Meixner et al. 1984). One borehole intersected gabbroic rocks at 815 m, and the other a weathered basalt at 419 m, passing into dolerite. A third borehole was drilled by the Anglo American Corporation (Ambot 1998), which held exploration licences over the complex in the late 1990s. Amygdaloidal lava was intersected at 621 m, passing into dolerite, and shales assigned to the Waterberg Group. An U-Pb zircon age of 1109.0 ± 1.3 Ma, which is coeval with the Umkondo Igneous episode, has been published for the gabbroic unit intersected in the first borehole (Hanson et al. 2004).

A junior exploration company, Manica Minerals Ltd, held prospecting licences over the Xade Complex from 2005. Its exploration activities, conducted in joint venture partnerships with two other companies, included use of both the medium-resolution aeromagnetic data, acquired under contract to the Botswana Geoscience Institute at a 250 m line spacing, and the Institute's ground Bouguer gravity data. An additional higher-resolution aeromagnetic survey was conducted over a portion of the complex. Detailed ground gravity surveys and time domain electromagnetic soundings were conducted on selected profiles traversing the complex. Forward modelling of the magnetic and gravity profiles helped constrain the zoning and structure of the complex. Three boreholes were subsequently drilled (Corner et al. 2012). A parallel interpretation was conducted using the Institute's data, but without the benefit of the further exploration data, by Pouliquen and Key (2007).

The interpretation of the work of Corner et al. (2012) showed for the first time that the Xade Complex comprises two lobes: a Southern Lobe (XC-SL; Fig. 2.6), which is the historically identified kidney-shaped zoned magnetic anomaly, as well as a hitherto unrecognized large Northern Lobe (XC-NL; Figs. 2.2 and 2.6). The NL is mostly deeply buried in the north and northwest beneath the Neo-Proterozoic PB, as evidenced by deep magnetic and gravity anomalous sources, but its southern and eastern margins partially suboutcrop beneath Karoo sediments, forming the Y-shaped anomalies north of the SL. An apparent transgressive contact between the two lobes is indicated by the aeromagnetic data, suggesting that the NL may be slightly younger. Inversion depths to the complex range from 220 to 1000 m beneath the Kalahari and Karoo sediments, and greatly in excess of this beneath the PB. Forward modelling, of both magnetic and gravity data along a number of sections traversing the both lobes, indicates that they are lopolithic features with a depth extent of approximately 4 km. This is supported by the interpretation of Pouliquen and Key (2007) for the SL, as well as from dips derived from the drill cores. The total of four boreholes drilled into the SL shows that it comprises a volcanic sequence with subordinate gabbro (Corner et al. 2012). The basalts are partly highly magnetic, giving rise to the zoned high-amplitude anomalies of the larger kidney-shaped anomaly, and partly magnetically subdued owing to less magnetic basalts that appear to underlie the rocks of the main SL anomaly. The three boreholes drilled into the NL margins, as published to date, indicate that it comprises a texturally heterogeneous and magmatically differentiated sequence of gabbroic rocks, with minor dioritic and monzonitic rocks, as well as basalt (Corner et al. 2012).

The interpretation of Corner et al. (2012) has also identified a dyke system associated with the NL, which may represent either feeder or exit magmatic conduits. The interpretation further shows that the Xade Complex is located in a craton margin setting—that is, the SL lies on the northern margin of the Kaapvaal Craton, whereas the eastern suboutcrop of the NL extends along the margins of the Kaapvaal and Zimbabwe cratons (Fig. 2.6). The combined extent of both lobes of the Xade Complex is approximately a third the size of the Bushveld Complex, making it the largest Late-Mesoproterozoic magmatic complex in southern Africa, with a potential for nickel-copper mineralization.

2.2.6 Tectonostratigraphic Zones of the Damara-Chobe Orogenic Belt

2.2.6.1 Regional Aspects of the Interpretation

The tectonostratigraphic zones of the Namibian Damara Belt and its Mesoproterozoic basement, extending eastward into Botswana as the Damara-Chobe Orogenic Belt, were mapped under Kalahari cover to the eastern border with Botswana by Corner (2000, 2008), based on published mapping and stratigraphy, known bounding regional structures, and the overall internal magnetic signature of the zones. The aeromagnetic data used at that time was the national regional data set compiled from surveys flown at line spacings varying between 1 and 4 km. The interpretation has since been refined and updated, as shown in Fig. 2.6, being more accurate in local detail, based on the higher-resolution aeromagnetic data (200 m flight line spacing) and mapped geology at a 1:250 000 scale (all data from the Geological Survey of Namibia). Ongoing extension of this work into Botswana was facilitated by the publication of the 1998 edition of the National geological map of Botswana, in both digital and hard copy form; the work of Key and Ayers (2000), Singletary et al. (2003) and Rankin (2015); and the availability of the medium-resolution National aeromagnetic data of Botswana. These products have been reviewed, revised in places, and integrated with the Namibian interpretation shown in Fig. 2.6. Brief lithological, stratigraphic and structural summary descriptions of each tectonostratigraphic zone shown in the interpretation map of Fig. 2.6 follow below. For the Damara Belt in Namibia, these are based on detailed descriptions by Corner (2008) and Miller (2008a). Furthermore, an aeromagnetic survey covering the continental shelf of Namibia, flown under contract to NAMCOR (Fig. 2.2), although relatively coarse, has facilitated mapping of the extension of some of the tectonostratigraphic zones offshore, up to the seismically interpreted hinge zone (Sect. 2.2.9). It should be noted that the systematics of stratigraphic classification generally do not take cognizance of geophysical responses. Stratigraphic boundaries may thus differ from geophysically apparent boundaries. The Damara Sequence does, however, show a strong correlation in that the lower units, which include diamictites, psammitic rocks and volcanics of the Nosib and lower Swakop Groups, are often strongly magnetic, while the overlying pelitic and carbonate sequences of the Swakop Group tend to be relatively subdued magnetically.

2.2.6.2 Mesoproterozoic Sinclair-Rehoboth Zone

The Mesoproterozoic Sinclair-Rehoboth Zone (SRZ; Fig. 2.6) comprises the southern Damara Basement and is dominated by volcano-sedimentary cycles of the Rehoboth Group and the Sinclair Supergroup, as well as by granitic and mafic rock suites. The overall magnetic signature of this terrane is visibly different from that of the Gordonia Subprovince to the south, being dominated by relatively high-amplitude, curvilinear magnetic anomalies arising from the volcanic sequences. Some of the granites, granodiorites and orthogneisses are also magnetic. In contrast, the Gordonia Subprovince displays highly variable magnetic responses owing to a range of rock types, which include ortho- and para-gneisses, granites, granodiorites, ultramafics, charnockites, metasediments and metavolcanics of the Namaqua Metamorphic Complex, the Orange River Group and the Vioolsdrif Intrusive Suite. Both the Gordonia Subprovince (the northern extension of the Namaqua Province; GSP; Fig. 2.6) and Sinclair Supergroup are characterized by numerous remanent magnetic anomalies, which are distinctly different from the induced anomalies arising from the Sinclair basalts. These result from gabbroic, ultramafic and charnockite bodies, although their individual signatures are indistinguishable. Their magnetization is of uncertain age but is expected to be post-Sinclair, possibly being set at the time of emplacement during the *c*. 1000 Ma Namaqua metamorphic event.

2.2.6.3 Pan-African Tectonostratigraphic Zones

Gariep Group

The current geophysical interpretation has not as yet been extended to include the Gariep Belt, thus what is shown in Fig. 2.6 is based entirely on published mapping (e.g., Frimmel 2008). However, the offshore geophysical data sets, although of low resolution, have facilitated mapping of the offshore extensions of the Port Nolloth Zone, and the Marmora Terrane with its associated Schakalsberge volcanics (Fig. 2.6).

Tsumis Group of Namibia and the Ghanzi Group of Botswana

The Tsumis Group comprises sediments of the Doornpoort, Eskadron and Klein Aub Formations, which post-date the period of large-scale Sinclair-Rehoboth Mesoproterozoic igneous activity. The group has been considered as either encompassing both the lower Nosib Group and the Klein Aub Formation (e.g., Schalk 1988), or as occurring within the Sinclair Supergroup (e.g., Miller 2008c). However, Hoffman (1989a) and Becker et al. (2005), based on field observations and new geochronological evidence, place the Tsumis Group in unconformable contact with, and thus younger than, the Sinclair Supergroup. Although overlaid para- to dis-conformably by the Damaran Nosib Group, the Tsumis Group is considered to constitute the lowermost part of the Damara Sequence (Hoffmann 1989a). The latter interpretation, although equivocal, is favoured in this review and is shown as such in Fig. 2.6.

Intra-Tsumis stratigraphic units display clear magnetic signatures, which allow mapping of these units under cover, eastward in Namibia and into Botswana. The main stratigraphic units, with the Namibia nomenclature given first, followed by the Botswana nomenclature and general magnetic signature, are: Doornpoort Formation = Ngwako Pan Formation (low, quiet magnetic response); Klein Aub Formation = D'Kar Formation (strongly magnetic fabric); Nosib Group = Mamuno Formation (intermediate to low magnetic fabric). These units, mapped with outcrop control where available, are grouped together in Fig. 2.6 as the T-G-C-B (Fig. 2.6). This belt is also commonly referred to as the Kalahari Copperbelt in view of its numerous copper-silver occurrences (e.g., Maiden and Borg 2011). The T-G-C-B thus constitutes the southern flank of the Damara-Chobe Orogenic Belt.

Southern Margin Zone of Namibia and Its Extension into Botswana

Miller (1983) describes the Southern Margin Zone (SMZ) as comprising 'two subzones, a southern, less intensely deformed subzone containing mainly thrust slices of pre-Damaran rocks, and a northern subzone consisting of complex thrust sheets containing both Damaran and pre-Damaran rocks'. Stratigraphic units present in the SMZ thus include pre-Damara basement, gneissic basement, the Nosib Group and the lithologically variable passive margin succession of the Hakos Group (Miller 2008a). The northern subzone of the SMZ contains relatively little-deformed cover sequences of the early Damaran Nosib Group along the northeastern margin (Hoffman 1983). The SMZ is bounded in the south by the Frontal Thrust and in the north by the Gomab River Line (Corner 2008; Miller 2008a). High-amplitude magnetic fabric is associated with the Chuos diamictites within the SMZ. Magnetic fabric, characterized by lower levels of magnetization, is associated with the Nosib Group. This is particularly evident in the higher-resolution data.

The extension of the SMZ under cover eastwards to the Botswana border, as interpreted by Corner (2008) working from the western and central and delineation thereof by Miller (1983, 2008a), shows that it continues into Botswana as what has been mapped as the Roibok Formation by Key and Ayres (2000). The interpretation of Rankin (2015) does not appear to support continuity of the SMZ throughout the southern Damaran boundary, but does support the continuation of a portion thereof in eastern Namibia, associated with high-amplitude magnetic anomalies. His interpretation favours mapping the extension of the Botswana Roibok Formation into Namibia, where it also inter-fingers with these high amplitude magnetic anomalies. This package is considered here to be an integral part of the SMZ, extending into Botswana as mapped in Fig. 2.6, recognizing that the Roibok Formation may only be part of a much more complex SMZ extension in Botswana.

Southern Zone or Khomas Zone

The Southern Zone (SZ), bounded by the SMZ in the south and the Okahandja Lineament in the north, comprises a thick, deformed succession of Kuiseb schists arising from both active and passive margins of the Khomas Sea, which are placed into separate formations—that is, the Khomas and Hureb Formations (Miller 2008a). The SZ is also often referred to as the Khomas Zone or Khomas trough. This succession mostly shows a low-order relatively quiet magnetic fabric in the higher-resolution data, but it is significantly more magnetic in the lower stratigraphic sequence, particularly north and northeast of Windhoek, and also due to the magnetic quartzites associated with the Matchless Amphibolite Belt.

The eastward extension of the SZ into Botswana, based on the magnetically quiet signature, follows on north of the SMZ (Roibok Formation) in Botswana, where it is seen to pinch out (Fig. 2.6). The offshore extension of the SMZ and SZ, southwards toward the Gariep Belt, has been interpreted as a package, from both the offshore aeromagnetic and Free Air gravity data sets. The location of the boundary between these two zones may not be exact as a result of the poor data quality, but the trend of the package is clear, also abutting against the hinge zone (Fig. 2.6).

Deep-Level Southern Zone

The magnetic signature of the Southern Zone (SZ) and southern Central Zone (SCZ, described below) changes dramatically in the Steinhausen area and northeast thereof (note the Steinhausen anomaly, SMA, for location in Fig. 2.6). Here, the Kuiseb Formation schists display high-amplitude magnetic anomalies within the SZ. Magnetic rock types in the area also include epidosite and gabbro, uncommon for the Kuiseb schist sequence elsewhere. To the north, a belt of very high-amplitude magnetic anomalies striking roughly east–west and cutting across the SZ and SCZ fabric correlate with Fe–Mn reefs, and both magnetic and glassy quartzites. Hoffman (1989b) and K Kasch (pers. comm. 2006) have questioned the inclusion of these strata in the Damara Supergroup and have suggested that they form part of the pre-Damara basement. They are thus tentatively mapped in Fig. 2.6 as the Deep-level Southern Zone (Corner 2008), characterized by intense thrusting and deep stratigraphic levels (Kasch 1986). The Deep-level Southern Zone is largely centred between the Okahandja and Kudu Lineaments (Ok-L and Ku-L; Fig. 2.6), continuing east of the latter with a significant change in strike, suggesting a possible fault throw controlled by the latter lineament.

Southern and Northern Central Zones

The Central Zone is subdivided into northern and southern parts—that is, the Northern Central Zone (NCZ) and the Southern Central Zone (SCZ), as shown in Fig. 2.6—both of which are characterized by dome structures with an overall northeast elongation (Miller 2008a). Voluminous syn- to post-tectonic granite plutons occur in both. The SCZ is a regional horst, bounded by the Okahandja and Omaruru Lineaments (Ok-L and Om-L; Fig. 2.6), and characterized by high-amplitude magnetic anomalies arising from the exposure of deeper-level sequences, primarily of the Nosib Group, lower Swakop Group (Chuos Formation diamictites) and the Meso- to Palaeo-Proterozoic basement. These units are exposed in dome and anticlinal structures with a pronounced northeasterly trend. The relatively magnetically quiet lower Swakop Group carbonates and schists are preserved in the intervening synclines. Some of the granite phases are magnetic, particularly if derived in part from the basement and Nosib Group. In the western portion of the SCZ, where metamorphic grades are higher, the Etusis and Khan Formations of the Nosib Group, as well as the granitic derivatives therefrom (and also from basement), are strongly magnetic with high-amplitude anomalies that have retained the Damaran remanence (Corner 1983). This magnetic signature of the Khan Formation constitutes an important geophysical marker horizon for the uraniferous granites (e.g., at the Rössing and Husab mines), which mostly occur immediately above it in the Rössing Formation.

Much higher stratigraphic levels are exposed in the NCZ which largely comprises rocks of the Swakop Group. It is bounded by the Omaruru and Autseib Lineaments (Om-L and Au-L; Fig. 2.6). Regional-scale downthrow, or rapid deepening, to the north of the Omaruru Lineament, as also modelled magnetically by Corner (1983), has preserved this thick succession of higher stratigraphic-level Karibib Formation carbonates and Kuiseb Formation schists, deformed in numerous basin and dome structures. The dome structures are generally not cored by granitic basement but rather by Karibib Formation marbles and Usakos Subgroup schists, calcsilicates and marbles. The Swakop Group rocks are relatively magnetically inert, giving an overall quiet magnetic signature to the NCZ. Some low-order fabric is nevertheless seen in the higher-resolution data. Extensive syn- and post-tectonic granite emplacement has taken place, although less so in the areas where the highest levels of the Kuiseb Formation are exposed (Miller 2008a).

The offshore continuation of the SCZ and NCZ, westward up to the hinge zone where they are dramatically truncated, is clearly visible in the aeromagnetic image of Fig. 2.2. Eastwards, the northeast trend of the Damaran Belt is of particular interest as it changes dramatically east of the Kudu Lineament (Ku-L; Fig. 2.6) in the following respects:

- The SCZ terminates against the Ku-L, whereas the NCZ changes strike east of the Om-L trending east-southeastwards up to the Ku-L, thereafter regaining a northeasterly trend, pinching out in Botswana (as does the SZ). An alternative interpretation could be considered, given the relatively quiet, thus ambiguous, magnetic signature of both the SZ and the NCZ—that is, that the NCZ also terminates against the Ku-L. Thus what is shown in Fig. 2.6 as NCZ (blue) east of the Ku-L may in fact constitute part of the SZ.
- Recent interpretations of an area, focused on mineral exploration, which straddles the Ku-L in the vicinity of the Steinhausen Magnetic Anomaly (SMA; Fig. 2.6) reveal a significant change in the Damaran stratigraphy eastwards as the Ku-L is crossed—that is, with a much deeper level of erosion to the west thereof, exposing basement domes such as the Ekuja dome and deeper-level southern zone stratigraphy (e.g., Corner 2008; Naudé 2012; K. Hartmann, pers. comm.). Thus, not surprisingly, the Matchless Amphibolite Belt (MAB; Fig. 2.6) terminates against the Ku-L, and is not expected to continue on-strike further to the east.
- The width of the Damara-Chobe Mobile Belt taken from the SMZ to NMZ is approximately 350 km, west of the Ku-L. The NMZ, NZ, NCZ and SCZ appear to truncate against, or are in disconformable contact with, the Grootfontein Inlier (GI; Fig. 2.6). East of the Ku-L, this width decreases dramatically to less than 150 km, striking roughly parallel to the contact with the GI, pinching out altogether as it progresses further northeastwards into Botswana towards the Tsodilo Lineament. Similarly, the Okahandja Lineament (Ok-L) appears to terminate against the Ku-L and cannot be definitively followed east thereof in the aeromagnetic data.

Northern Zone

The Northern Zone (NZ; Fig. 2.6), comprising rocks of both the Nosib and Swakop Groups, has been thrust northwards onto Otavi, Mulden and pre-Damara rocks along the Khorixas-Gaseneirob Thrust (KG-L; Fig. 2.6; Miller 2008a). The Autseib Lineament (Au-L; Fig. 2.6), in part including the Autseib Thrust, forms the southern boundary of the highly and complexly deformed NZ, which shows an overall strongly magnetic signature owing largely to the highly magnetic diamictites of the Chuos and Ghaub Formations and the mafic volcanics of the Askevold Formation. The NZ, together with the northern part of the NCZ, formed the floor of the Outjo Sea during spreading (Miller 2008a).

Northern Margin Zone

The NMZ, constituting in-part the Khorixas-Gaseneirob Lineament (the inferred Congo Craton boundary), is a narrow transition zone which Miller (2008a) describes as the northern platform foreslope region where the rather uniform

facies of the Otavi Group to the north become more variable and include deep-water-facies carbonates of the Otavi Group. Mulden Group rocks are preserved in tight synclines within this zone, which, although generally magnetically quiet, display high-amplitude remanent magnetic anomalies. Corner (2008) ascribes these to secondary magnetization arising from the development of pyrrhotite in the phyllites through the passage of fluids along the lineament.

Northern Otavi Platform, and the Tsodilo Lineament

Damaran rocks are only exposed along the southern and western edges of the Northern Platform (NP) but continue northwards and eastwards below Karoo and Kalahari cover. The limits of the NP in Namibia, as shown in Fig. 2.6, are determined by the distribution of the shallow-water facies of the Otavi Group, extending westwards to the Sesfontein thrust (ST; Fig. 2.6; Miller 2008a). Predominant east–west-trending anticlinal structures are seen in the magnetic data in the southern sector of the NP. These separate expansive magnetically quiet areas that comprise higher stratigraphic levels, including Mulden Formation strata, in the synclines. The antiforms have an anomalous magnetic signature largely due to the exposure, or shallow suboutcrop, of the diamictites and possibly volcanics associated with the lower Damara strata. The tight folding of the antiforms close to the NMZ becomes progressively more open to the north.

Geophysical mapping of the eastward extension of the NP under cover in Namibia, and into Botswana, is complicated by the largely highly magnetic basement rocks of the Grootfontein Inlier. Outcrops of the NP do nevertheless occur at the Aha Hills close to the Botswana border, which allows continuity to be inferred. The intervening area is hatched in Fig. 2.6 to indicate the ambiguity of continuity owing to the low-magnetic signature of the overlying NP carbonates. On strike to the northeast of the Aha hills, in Botswana, is the Xaudum Group, which correlates with the Aha Hills Formation (e.g., Rankin 2015), and hence with the NP in Namibia. Extension of the NP into Botswana is indicated as such in Fig. 2.6. The Tsodilo Hills Group (Figs. 2.6a, b), however, is of uncertain correlation. Miller (1983), Breitkopf (1988) and Bűhn et al. (1992) correlate it with the Chuos Formation in Namibia in view of the abundant iron formations and ferruginous quartzites. Rankin (2015), based on further interpretation using potential field data, concluded that the Tsodilo Hills Group cannot be confidently correlated with a single tectonostratigraphic zone of the Damaran Belt, and that it may even be a correlative of units in Angola or Zambia. What appears to be singularly unique in the area is the dramatic change in structural style displayed by the Tsodilo Hills Group, from the expected northeast trend of the Damara-Ghanzi-Chobe Mobile Belt to tight folding and faulting striking north-northwest (e.g., Rankin 2015). The Tsodilo Hills Group is thus specifically separately colour coded in Fig. 2.6.

The question may thus be asked as to the reason for this dramatic change in structural style. In the current interpretation, we single out the regional Bouguer Gravity low in the Botswana Geosciences Institute data, with which the Tsodilo Hills Group is associated (Fig. 2.4; see also Rankin 2015), as providing the clue. We have the further benefit of the WGM Bouguer Gravity data (Fig. 2.5), which shows that the gravity low trends further north-northwestwards and northwards into Angola. The gravity low thus appears to hallmark a major, roughly north–south lineament which we have termed the Tsodilo Lineament (Ts-L; Fig. 2.6). That it constitutes a major regional structural zone is not only evidenced by the structural style displayed by the Tsodilo Hills Group and environs, but also provides an explanation as to why the regional east-northeast-trending magnetic low in northern Namibia, correlated with the southern Congo Craton margin, abruptly terminates in northwestern Botswana at the Tsodilo Hills gravity low. Viewed in a regional context, it is possible that the Ts-L was the northward continuation of the Kalahari Lineament (Kal-L) in pre-Pan-African times, as they are virtually on strike with each other, given some local north-northwest deformation in the Tsodilo Hills area. The continuity between the two may thus have been interrupted by the Damaran Orogeny (see also Sect. 2.2.8).

Kaoko Belt

The Kaoko Belt is subdivided into four subzones (Goscombe et al. 2003, 2005; Miller 2008a): the Southern, Eastern, Central and Western Kaoko Zones:

- The pelitic sequences of the Southern Kaoko Zone (SKZ), which are tightly folded in north–south-striking chevron folds, display a low-amplitude magnetic fabric, giving an overall quiet appearance to this zone which nevertheless has enabled better definition of this subzone's boundaries. In contrast, the strong, roughly north-northwest magnetic fabric of the Western, Central and Eastern Kaoko Zones results from complex deformation and variable grades of metamorphism (Goscombe et al. 2003).
- The Eastern Kaoko Zone (EKZ) comprises upright folds of subgreenschist-facies shelf carbonates (Goscombe et al. 2003). These rocks are relatively non-magnetic, but where lower stratigraphic levels are exposed or are in shallow suboutcrop, a strong magnetic fabric is seen. Miller (2008a) points out that the stratigraphy of the EKZ is almost identical to that of the Northern Platform (NP), but that the two regions are structurally distinct. This is also observed in the magnetic data, which shows a distinct magnetic, and hence tectonic, eastern boundary between the EKZ and the NP. The Sesfontein Thrust (ST) marks the western boundary of the EKZ.

- The Central Kaoko Zone (CKZ) comprises east-vergent nappes of Swakop Group passive margin rocks (Goscombe et al. 2003; Miller 2008a). Within the CKZ, the Damara stratigraphic units, the Okapuka Formation and the Palaeoproterozoic crystalline basement of the Epupa Inlier show variable magnetic responses, in some places subdued and in other places with a slight magnetic fabric. Higher-amplitude anomalies arise from the lower Swakop Group diamictites and amphibolites, and from amphibolitic and gabbroic units within the pre-Damara basement. The CKZ has no clear eastern boundary with the EKZ as evidenced in the magnetic data. Based on geological premises, the boundary is thus set, as above, at the Sesfontein Thrust (ST; Fig. 2.6; Miller 2008a). The western boundary of the CKZ is the Purros Shear Zone (PuSZ; Fig. 2.6), which comprises a series of closely spaced, steeply westward-dipping ultramylonites (Miller 2008a).
- The Western Kaoko Zone (WKZ) is predominantly a deep basin facies sequence of high metamorphic grade, intruded by numerous granites, which has experienced intense wrench-style deformation along steep, crustal-scale shear zones (Goscombe et al. 2003). Much of the magnetic fabric results from the mylonitic shear zones. The Purros Shear Zone constitutes the eastern boundary of the WKZ, which is further subdivided into a Coastal Terrane and an Orogen Core. The latter comprises a number of internal subdomains, which are separated by the Three Palms Mylonite Zone (Goscombe et al. 2005; Miller 2008a).

2.2.7 Rehoboth Terrane

2.2.7.1 Sedimentary Sequences

The Rehoboth Terrane (RT) has a unique expression in the aeromagnetic image of southern Africa (Figs. 2.2 and 2.6). It is hallmarked by long-wavelength anomalies that reflect deep magnetic basement sources, an overlying thick package of magnetically-inert sedimentary rocks including pre-Nama, Nama, Karoo and Kalahari sequences, and some shallow, high-frequency magnetic anomalies arising from Karoo basalts and sills. The interpreted deep-source magnetic and gravity anomalies which underlie the above sedimentary package (Corner 2008), are shown in Fig. 2.6.

The RT, which forms the western Palaeoproterozoic core of the Kalahari Craton (Jacobs et al. 2008; Fig. 2.1), is bounded in the east by the Kal-L. The change in depth to magnetic basement on either side of the Kal-L is dramatic, from ~500 m east thereof to 8–10 km west thereof (Corner 2008). Isopach contour levels, derived by Corner (2008) from a depth-to-basement analysis, of >4000 m (i.e., pre-Karoo sediments) and >6000 m, are shown in Fig. 2.8. This analysis is in agreement with the earlier, more regional, or localized, interpretation of Reeves (1978) and of an interpretation by Petro-Canada (a hydrocarbon exploration group which conducted seismic surveys in western Botswana and an aeromagnetic interpretation; Botswana Geoscience Institute archives, Wright and Hall 1990). In the southwest, the RT is bounded by the northwestward extension of the Namaqua Lineament (Naq-L; Fig. 2.6; an extension of the Namaqua-Natal Front), which also shows a dramatic increase in depth to basement across it into the RT, in excess of 4000 m to the northeast (Fig. 2.8). A considerable package of sediments, up to 10 km in total thickness, is thus preserved within the RT. Karoo and Nama strata, or Kalahari cover, are evident at surface. However, the deepest section of Nama rocks yet drilled was in the Masethleng Pan borehole in western Botswana, passing through the base of the Nama at 3844 m. Underlying red beds were intersected in both this and the Tses borehole in Namibia. Known red beds, outcropping to the northwest and west of the Nama Group, belong to the Doornpoort and Aubures Formations, respectively, which have been variably correlated with either the Tsumis or Sinclair Groups (Becker et al. 2005; Miller 2008a). The implication is thus that a red bed sequence of Mesoproterozoic age, and possibly older strata, may form a remarkably thick succession of up to approximately 6 km beneath the Nama Group.

2.2.7.2 Interpreted Basement Geology, the Karas Impact Structure

The only southern area proximal to the RT where basement is exposed is in the 130 km-wide north-northeast-trending Karas Horst (KH; Fig. 2.6), with which a dyke swarm is also associated. The Karas Horst forms a beautiful mountain land in southern Namibia, indicating relatively recent reactivation along the north-northeast bounding faults. A focus of attention arising from the deep magnetic and gravity sources mentioned in Sect. 2.2.7.1 is a roughly circular set of magnetic anomalies in the southern portion of the RT proximal to the Namaqua Lineament, approximately on strike with the Karas Horst (Fig. 2.6; Corner 2008). Concentric gravity highs collar the magnetic anomalies in the south and east but centrally the circular magnetic anomalies and their core correlate with a strong gravity low. This group of magnetic and gravity anomalies is also the centre of focus of a number of possible far-field ring features which were mapped by Corner (2008) from a number of the filtered magnetic data sets (Karas Ring Structure (KRS); Fig. 2.7). Despite the coarseness of gravity data, this combination of features, together with numerous apparently associated radial faults, has been interpreted to arise from a major meteorite impact named the Karas Impact Structure (KIS; Fig. 2.6; Corner 2008). The depth solutions, discussed above, of ~6 km in this area suggest a pre-Aubures (Sinclair Group) age.

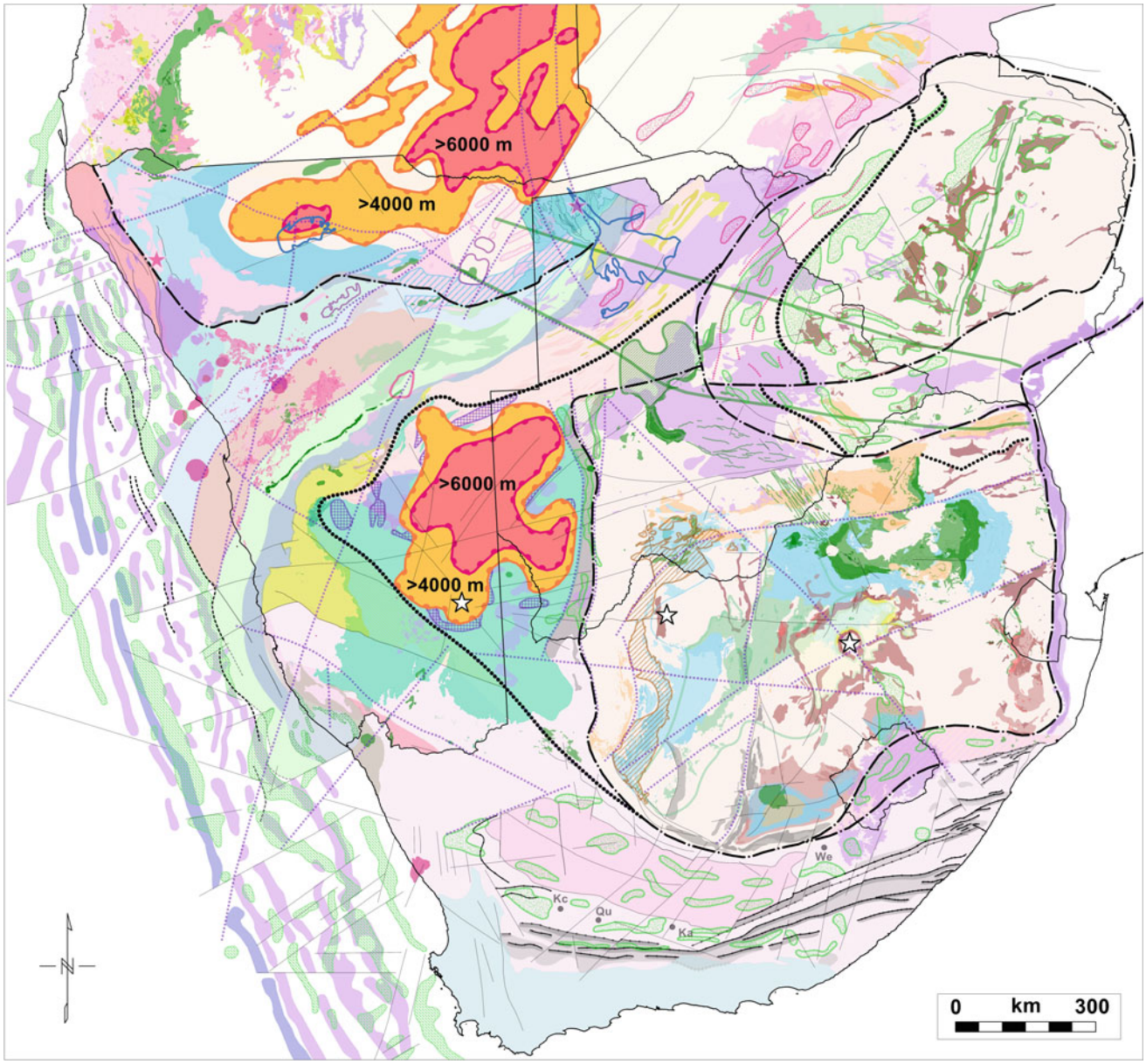

Fig. 2.8 Deep sedimentary basins in Namibia and Angola are superimposed on the interpretation map of Fig. 2.6. The basins are considered to comprise Meso- to Neo-Proterozoic sequences but are overlaid here on younger sequences to illustrate their extent. Depth-to-basement ranges of greater than 4000 and 6000 m are shown

Furthermore, the deep magnetic anomalies appear to be largely terminated against the Namaqua Lineament, possibly also suggesting a Mesoproterozoic or earlier age.

2.2.8 Deep Neo- and Meso-Proterozoic Basins in Namibia and Angola

The extent, and interpreted thickness of up to 10 km, of the magnetically inert sedimentary succession which overlies the basement of the Rehoboth Terrane is described in Sect. 2.2.7.1 (Fig. 2.8). Note that the depth-to-basement contours, which commence at 4000 m and extend to greater than 6000 m, largely reflect the thickness of a pre-Nama Mesoproterozoic succession. Similar sedimentary successions have been interpreted in northern Namibia and southern Angola from, firstly, a preliminary interpretation of Angolan airborne gravity and magnetic data (Sonangol & NAMCOR AAPG presentation 2009) and, secondly, a hydrocarbon exploration interpretation of the Owambo Basin in northern Namibia by Hoak et al. (2014). The 4000 m and 6000 m isopach contours are approximately

merged in Fig. 2.8 to show the full extent of a combined northern sedimentary succession. The former (Angolan) interpretation stopped at the eastern border with Zambia. An eastward thinning of the succession was nevertheless evident, thus the extent of the basin in Zambia, as shown in Fig. 2.8, is schematic. Structural controls of the basin are clearly evidenced from structures mapped in Namibia and extended into Angola using the World Bouguer Gravity data shown in Fig. 2.5. The basin is largely constrained by the Opuwo and Kudu Lineaments (Op-L and Ku-L; Fig. 2.6) in the northwest and southeast, respectively. The latter lineament has a more complex, broader swathe as indicated in Figs. 2.6 and 2.7. Whether these lineaments were active during sedimentation, or subsequently controlled the interpreted distribution of the sedimentary succession through faulting, is unknown.

Viewed in a regional context, there is a remarkable similarity in the extent, thickness of sedimentary pile, and location of the two basins with respect to the Kalahari (Ka-L) and Tsodilo (Ts-L) Lineaments which bound them in the east (Fig. 2.8). As noted in Sect. 2.2.6.3, it is possible that the Ts-L was the northward continuation of the Kal-L in pre-Pan-African times, and that the continuity between the two was interrupted by the Pan-African Damaran Orogeny.

2.2.9 West Coast Offshore Domain and the Namibian Passive Volcanic Margin

Corner and Swart (1997) and Corner et al. (2002) interpreted the Namibian offshore airborne and ship-track magnetic data, satellite Free Air gravity data, as well as numerous seismic lines that traverse the continental shelf. The offshore magnetic and gravity data sets are merged with the onshore data in Figs. 2.2 and 2.4. Significant contributions to the interpretation of the offshore domain have been made by Clemson et al. (1997) and Bauer et al. (2000). Corner and Swart (1997) used more recent reflection seismic surveys covering the Hinge Zone (HZ; Fig. 2.6) to update the mapping by Clemson et al. (1997) of the onset of the basalt-related seaward-dipping reflectors (SDR). Two boundaries were mapped—that is, the HZ itself, and the feather edge of the SDRs to the east of the Hinge Zone (Fig. 2.6). The continental crust occurring offshore east of the Hinge Zone was found not to have undergone any observable extension during the break-up of Gondwana. The extent of this block to the south of the Khorixas-Gaseneirob Lineament is clearly evident in the offshore aeromagnetic data. East of the HZ, the offshore extension of the Damara Orogen was clearly evidenced by the magnetic data for the first time, allowing the offshore extensions of the NCZ, SCZ, SZ and SMZ to be mapped (Fig. 2.6). A further significant result is that the mapped Mesozoic gravity and magnetic anomalies have been clearly offset along the offshore continuations of a number of Pan-African lineaments—for example, the Autseib (Au-L), Omaruru (Om-L) and Welwitschia (We-L) Lineaments (Corner et al. 2002, Fig. 2.6). The abrupt termination of Damaran rocks at the Au-L offshore is particularly dramatic. This observation suggests that these Late Proterozoic to Early Palaeozoic structures not only determined the architecture of the extended crust but were likely reactivated during the Late Mesozoic, having directions favourable for the initiation of transform faults. An important implication arising from this interpretation is that these structures may have provided potential pathways for the larger drainage systems and hence the focus of major offshore sedimentation, controlling the evolution of the offshore basins.

The M-type apparent spreading-related magnetic anomalies of previous workers (e.g., Rabinowitz and LeBrecque 1979; Gladczenko 1994) are readily evident in the recent offshore data—for example, M2 and M4 in Fig. 2.6. These are now more definitively delineated, and are seen to converge towards the northern Namibian and Angolan coastlines, in contrast to their previous placement much further out to sea. This has major implications for relative rates of extension from the southern to northern offshore areas, and for the relative ages of the offshore sedimentary sequences. The interpretation of Corner et al. (2002) fundamentally clarifies, through forward modelling of the magnetic and gravity data, the origin of the classical M-type anomalies. These high-low pairs are shown to arise from shallow westerly dipping wedges of lava (SDRs) at their suboutcrop feather edge, as opposed to the classical steep-dyke seafloor-spreading model. Such dykes are not expected to occur *senso stricto* on the continental shelf or within the extended continental crust, thus negating the 'M' nomenclature.

At least four coast-parallel gravity highs are seen in the offshore data, the highest amplitude being closest to shore (shallowest). These are also structurally disrupted along offshore extensions of the major onshore Pan-African lineaments, similarly signifying either later reactivation of these lineaments or the control by these early lineaments of the architecture of the extended crust. Corner et al. (2002) showed, through modelling, that the eastern, and most prominent, gravity high is caused primarily by the onset of a major package of SDRs that define the HZ. The amplitude of this gravity high increases as the lava sequence starts to thicken, but disappears completely further seaward as the overlying low-density sedimentary pile progressively neutralizes the effect of the deeper lava-related gravity high. The gravity response to the resultant centres of mass may thus be offset from the associated magnetic anomalies, which delineate the shallower feather edge of the basalts. The interpretation does not take cognizance of the

long-wavelength component, which is likely to be associated with deep magmatic underplating, but does explain the anomalies very well in the first order. This interpretation is in contrast with that of Watts and Fairhead (1999), who applied a process-orientated approach to modelling 'edge effect' anomalies such as the HZ gravity high. The processes which they considered included rifting, sedimentation and magmatic underplating. By quantifying these, they were able to model the 'edge effect' gravity anomalies. However, they did not consider the effect of the basaltic seaward-dipping reflectors and associated magnetic anomalies.

A number of probable offshore Cretaceous igneous complexes were interpreted, the largest being the Walvis Bay Complex (Wb; Fig. 2.6), situated close to the Om-L, and hallmarked by significant gravity and magnetic anomalies (Corner and Swart 1997; Corner et al. 2002). The inland Cretaceous Erongo Complex (Er) also occurs along the Om-L. The offshore Cape Seal Complex (Cs) and the offshore extension of the Cape Cross Complex (Cc) were also newly identified. The offshore magnetic and gravity data adjacent to South Africa have not been rigorously interpreted, but the significant anomalies and possible faults have been mapped from the EMAG2 and World Gravity Map data, as shown in Figs. 2.6 and 2.7. Noteworthy is the presence of the only Cretaceous igneous complex associated with the South African west coast region—that is, the Koegelfontein Complex (Kf; Fig. 2.6; Whitehead et al. 2016).

2.2.10 Namaqua-Natal Belt and Its Extension as the Maud Belt in Antarctica

2.2.10.1 Namaqua-Natal Belt

The Namaqua-Natal Belt (Namaqua-Natal Metamorphic Belt (NNB)) is an arcuate orogenic belt roughly 1400 km in length which bounds the Kalahari Craton to the south (Figs. 2.2, 2.6 and 2.7). It comprises igneous and metamorphic rocks formed or metamorphosed during the Proterozoic, with four periods of activity being evident at ~1.8–2.00 Ga, ~1.2 Ga, ~1.15 Ga and ~1.06 Ga, (Cornell et al. 2006; Eglington 2006)—that is, essentially two phases of activity of Palaeo- and Meso-Proterozoic age. The extensive outcrops in the west and east constitute the Namaqua and Natal Provinces, respectively (NamqP and NatP; Fig. 2.6), the former extending into Namibia as the Gordonia Subprovince (GSP; Fig. 2.6). The region between the outcrop areas is covered by Phanerozoic Karoo sediments, which hide the boundary between the NNB and the younger Palaeozoic rocks of the Cape Supergroup. The boundary is expected to be complex in view of the late Permian to early Triassic Cape Orogeny. It is thus only possible to map the southern boundary of the NNB using geophysical techniques.

The NNB comprises a number of tectonostratigraphic terranes (i.e., areas of common lithostratigraphy and structural fabric bounded by shear zones), which were assembled during the Namaqua Orogeny (Cornell et al. 2006). However, the structural fabric of the Namaqua and Natal Province differs considerably (e.g., Cornell et al. 2006), as is also evidenced in the magnetic images of Figs. 2.2 and 2.3. The Natal Province may be subdivided into three distinct, structurally complex, discontinuity-bound terranes: the northern Tugela, central Mzumbe and southern Margate Terranes. These are bounded by major shears and thrusts: the Tugela (thrust) Front, Lilani-Matigulu Shear Zone, the Lovat Shear Zone and the Melville Thrust (Thomas 1989; Jacobs et al. 1993; Jacobs and Thomas 2004; Cornell et al. 2006). Thrust tectonics are extensively preserved within the Tugela Terrane, where rocks were obducted northwards onto the Kaapvaal Craton during the Namaqua Orogeny, whereas the Mzumbe and Margate Terranes are dominated by major wrench faults (Matthews 1972; Jacobs and Thomas 2004). The thrust and shear zones are clearly evidenced by high-amplitude, linear magnetic anomalies, as seen in Figs. 2.2, 2.6 and 2.7 (Corner 1989; Corner et al. 1991; Hunter et al. 1991; Thomas et al. 1992). This structural fabric, as seen in the aeromagnetic data, is in contrast to that of the approximately coeval Namaqua Province, which has an irregular, unstructured or curvilinear fabric. The magnetically anomalous zone correlating with the mapped portion of the Lovat Shear Zone (LSZ; Fig. 2.6) in the Natal Province can be followed west-southwestwards in the aeromagnetic data, and has been mapped as such in Figs. 2.6 and 2.7.

The continuity of the NNB from the Namaqua to the Natal Provinces has commonly been accepted since the early recognition thereof by Nicolaysen and Burger (1965). More recently, Eglington and Armstrong (2003) conducted geochronological and isotope studies on cores from four deep boreholes drilled by SOEKOR (Ka, Kc, Qu and We; Fig. 2.6), comparing these with known signatures from the Namaqua and Natal Provinces. In particular, this study showed that the four boreholes reflect a Palaeoproterozoic crustal history similar to that of the Namaqua Province, and that reworked crust of this age is not evident in the Natal Province nor in the Cape Meredith Complex of the Falkland Islands. They thus concluded that there must be a significant terrane boundary between the exposures of the Natal Province and the easternmost borehole studied (We; Fig. 2.6; Eglington and Armstrong 2003). They further concluded that this clear evidence for isotopically distinct terranes during the Mesoproterozoic needs to be taken into account in reconstructions of the NNB, and its easterly extensions within Gondwana.

In the present study, a variety of regional-residual separation and upward continuation filters were used to enhance the sub-Karoo magnetic anomalies, including the Beattie

Magnetic Anomaly (Sect. 2.2.10.2), to assess the relationship between the Namaqua and Natal Provinces (Figs. 2.2 and 2.6). It is clear that the central area within the NNB has a distinctly different structural fabric to either the Namaqua or Natal Provinces. This central area, here named the Khoisan Province (KP; Fig. 2.6), is hallmarked by a disrupted but nevertheless roughly continuous belt of magnetic anomalies, of longer wavelength in the south as a result of the thicker Karoo cover. The KP shows apparent closure, through possible folding or thrusting in the west, where it adjoins the Namaqua Province; whereas in the southeast it appears to be discordantly truncated against the westward extension of the Lovat Shear Zone. The distribution of residual gravity anomalies in Figs. 2.4 and 2.6 also suggests apparent closure in the west, despite the coarseness of the data. In the east, the KP appears to terminate against a north-northeast-striking fault just west of the SOEKOR borehole We (Fig. 2.6). A further major north-northeast-striking fault occurs east of borehole We, which appears to bound the Natal Province in the west. This fault is here named the Elliot fault (EF; Fig. 2.6; after the nearby town of Elliot). In part, the northern sector of the Elliot fault coincides with the escarpment, and it could be argued that it is simply the manifestation of a dramatic increase in terrain clearance during the airborne survey east of the fault. However, the fault is also associated with a long-wavelength anomaly at its northern end, and is interpreted to continue southwards away from the escarpment. The intermediate area between these two faults is hallmarked by a zone of high-frequency anomalies arising from Karoo-age sills. The isotopic results of borehole We discussed above (Eglington and Armstrong 2003) suggests a correlation of this area with the Namaqua Province. No clear deeper sources, from either the KP or the Natal Province, were evident in this intermediate area in any of the filter products applied to the magnetic data. None of the four SOEKOR boreholes was sited within the KP, and its origin thus remains unknown. Given the location of the KP, and its offset with respect to the Kaapvaal Craton, it could be speculated that it may contain relicts of the southern portion of a proto-Kaapvaal Craton, and associated Archaean basins, assimilated during the Namaqua Orogeny. In the first instance, it is thus proposed here that, firstly, the Khoisan Province constitutes a subterrane of the Namaqua Province and, secondly, the Elliot fault is the western boundary of the Natal Province.

2.2.10.2 Beattie Magnetic Anomaly and the Southern Cape Conductivity Belt

Two remarkable, broadly spatially coincident, continental-scale geophysical anomalies are evident within the NNB: the Beattie Magnetic Anomaly (BMA; Beattie 1909) and the Southern Cape Conductivity Belt (SCCB; Gough et al. 1973; De Beer and Gough 1980; De Beer et al. 1982a; De Beer and Meyer 1984). The BMA extends for more than 950 km, has an apparent suboutcrop width in the order of 50 km, and correlates spatially with the northern margin of the broader SCCB, which extends from the western to the eastern coastal margins for more than 1100 km (Figs. 2.6 and 2.12). Their origin is enigmatic, with some earlier authors suggesting a common source owing to their apparent correlation in approximate location and scale, while more recent studies indicate separate sources, but with a common evolutionary origin. The SCCB is discussed in more detail in Sect. 2.3.2, but reference is made to it here where relevant. Many geophysical studies have been directed at mapping and understanding the SCCB and the BMA, including interpretations of aeromagnetic data, gravity data, magnetotelluric data, reflection seismic data and wide-angle seismic refraction studies (e.g., Gough et al. 1973; De Beer and Gough 1980; De Beer et al. 1982a; De Beer and Meyer 1984; De Beer and Stettler 1988; Corner 1989; Pitts et al. 1992; Thomas et al. 1992; Lindeque et al. 2007, 2011; Weckmann et al. 2007a, 2007b; Stankiewicz et al. 2008; Quesnel et al. 2009; Scheiber-Enslin et al. 2014).

The BMA is not a single magnetic anomaly but rather comprises a series of subparallel anomalies that may be separated with spectral filtering into residual anomalies reflecting the shallower (in a relative sense, but nevertheless deep) suboutcrop of magnetic sources beneath Phanerozoic Karoo strata, and deeper sources within the crystalline crust, which together give the appearance of a broad magnetically anomalous belt. There is no gravity anomaly associated with the BMA. Scheiber-Enslin et al. (2014) have mapped the extent of the residual magnetic anomalies, extending into the Natal Province. In parallel studies, Corner (e.g., 2015) conducted more rigorous mapping of the residual anomalous sources, an interpretation which is further refined and presented in Figs. 2.6 and 2.10. Forward models of magnetic profiles over the BMA, conducted by a number of researchers (e.g., Maher and Pitts 1989; Du Plessis and Thomas 1991; De Beer and Stettler, unpublished) show similar results—that is, the BMA is readily modelled with prism-shaped sources dipping at a shallow angle to the south. These models are indicative of a possible northward-directed thrust zone, as discussed further below. An early model for the origin of the BMA was that of a dipping slab of oceanic crust, representing a Pan-African suture zone, with serpentinization being invoked to explain the absence of an associated gravity high (De Beer et al. 1982a; De Beer and Meyer 1984).

Other forward models, conducted more recently, do not necessarily agree with southward dips of the BMA but are based on more simplistic source geometry models such as horizontal prisms and spheres (Quesnel et al. 2009) or a very coarse polygonal body interpreted to mimic a deeper-level resistive crust (Weckmann et al. 2008). On the strength of

the model of Maher and Pitts (1989), Corner et al. (1991) proposed that the linear magnetic anomalies in the Natal Province associated with the known major craton-directed thrust zones may share a common origin with the BMA. Palaeomagnetic studies in northern Natal (Corner and Maccelari unpublished) confirmed the presence of highly magnetic mylonites associated with the Lilani-Matigulu Thrust Zone (LMSZ; Fig. 2.6). Thomas et al. (1992) further confirmed this, also indicating that the thrusts and shears of the Natal Province are associated with linear magnetic anomalies, giving a magnetically 'striped appearance' to the province, and named the anomaly near Amanzimtoti the Williston anomaly (ASZ/WA; Figs. 2.6 and 2.10). They also supported the possibility that these may be associated with the BMA, which is present south of the Williston anomaly. Based on this model, Corner and Groenewald (1991), Corner et al. (1991) and Hunter et al. (1991) proposed that the regional-scale, high-amplitude magnetic anomalies in Dronning Maud Land (DML), Antarctica, were the extension of the BMA within a Gondwana framework. Fieldwork in DML, including palaeomagnetic sampling (Corner, unpublished), showed strong similarities with northern Natal: highly magnetic mylonites associated with craton-directed thrusts were observed in the Kirwanveggen, where the DML anomaly was observed in outcrop (see also Sect. 2.2.10.3). Large euhedral magnetite grains were also observed to be pervasive in the gneisses adjacent to the thrusts. The similarity of signature between the magnetized thrust zones of the Natal Province and the BMA was confirmed in a comprehensive study by Scheiber-Enslin et al. (2014). The finding that high-amplitude magnetization is pervasively associated with thrust zones and associated gneisses in both the Natal Province and DML, as well as the observation of the similar strike and linear magnetic signature of units within the BMA and in DML, is the best evidence we have to date on the origin of the BMA. A reflection seismic section crossing the BMA (Figs. 2.11 and 2.13, discussed in Sect. 2.3.3) shows a bean-shaped zone of strong reflections at the sub-Karoo location of the BMA. No diagnostic dips or depth extent could, however, be determined.

2.2.10.3 Extensions of the Namaqua-Natal Belt Within Gondwana: The Maud Belt, Antarctica

Early regional-scale aeromagnetic surveys were carried out in Antarctica over Dronning Maud Land (DML) and the Weddell Sea by the Polar Marine Geological Research Expedition (PMGRE, VNIIOkeangeologia, USSR) during the 1970s and 1980s, at a flight-line spacing of 20 km, with a higher-resolution 5 km flight-line spacing survey being flown over the Kirwanveggen region (Golynsky et al. 2000a). Regional aeromagnetic data sets had also been acquired by the German Federal Institute for Geosciences and Natural Resources (BGR) and Alfred Wegener Institute (AWI). A collaborative interpretation of these combined data sets showed that the major magnetic anomalies in DML were likely to be the continuation of counterparts in southern Africa and the Falkland Plateau (Corner 1989; Fűtterer 1989). In addition, the geophysical components of the South African National Antarctic Research Programme (SANARP) included limited, but nevertheless diagnostic, regional surface gravity profiles traversing the Grunehogna and Maud Provinces, limited helicopter-borne magnetic surveys, and palaeomagnetic studies (Hodgkinson 1989; Hunter et al. 1991; Corner 1994b; Jones et al. 2003). More recently, higher-resolution surveys, with a mostly 10 km flight-line spacing, were undertaken in specific areas by the British Antarctic Survey (BAS) in the Jutulstraumen region of DML, by the BGR and AWI (Johnson et al. 1992; Riedel et al. 2013). The area of early aeromagnetic coverage in DML was partly reflown, and extended, as part of the AWI VISA project during the period 2001–2005, at flight-line spacings of 10 km (mostly) and 20 km (Riedel et al. 2013).

A zone of regional-scale linear or semi-linear en-echelon magnetic lineaments (*c*. 40 km wide and extending over 700 km), revealed by the early and subsequent aeromagnetic surveys, was termed the H.U. Sverdrupfjella-Kirwanveggen Anomaly (SKA; Golynsky and Aleshkova 2000; Golynsky et al. 2000a). Golynsky et al. (2000a, 2000b) did not conduct a detailed analysis of the anomalies owing to the regional scale of their interpretation, but they attributed the anomalies to high-grade meta-igneous gneisses of 1000–1200 Ma (Grenvillian/Kibaran age), thrust or shear zones, and other larger crustal structures and zones of weakness. The associated magnetic anomalies were seen to be interrupted by changes in strike and inferred faulting. Later deformation and magmatism associated with the Ross orogeny (Pan-African) is described as being considerably less intense, with contrastingly weaker manifestation in the magnetic data (Moyes et al. 1993; Golynsky et al. 2000b). Importantly, Golynsky et al. (2000b) also recognized the additional complexity of interpretation, in that many magnetic anomalies could arise from Mesozoic magmatism associated with the break-up of Gondwana. The recent interpretation of Riedel et al. (2013) is more rigourous, given the larger area of coverage, the acquisition of data at a closer flight-line spacing (other than over the Kirwanveggen), the development and use of new data-filtering techniques, and the benefit of more fieldwork having been conducted in the interim.

The digital PMGRE aeromagnetic data set covering a portion of DML was passed on to SANARP by PMGRE in 1989 as part of a collaborative research programme, and interpreted by Corner (1989), Corner and Groenewald

(1991), Corner et al. (1991), Hunter et al. (1991) and Corner (1994b). The aeromagnetic data is shown in Fig. 2.9 and the interpretation is presented in Fig. 2.10, juxtaposed with southern Africa within a Gondwana framework. That early interpretation does not differ substantively from the more recent interpretation of Riedel et al. (2013), but it benefits in detail locally from the higher-resolution 5 km PMGRE flight-line coverage over the Kirwanveggen, where outcrop occurs and ice cover is relatively thin in places. By comparison, the interpretation of Riedel et al. (2013) benefits from the much larger area of coverage of the VISA Project in areas outside the higher-resolution PMGRE survey.

The continuation of the Namaqua-Natal Belt of southern Africa into DML, as the Maud Belt (MB; Fig. 2.10) within Gondwana, thus comprising the larger Namaqua-Natal-Maud Belt (NNMB), has been established geologically for some time (e.g., Groenewald et al. 1991; Hunter et al. 1991; Jacobs et al. 1993; Riedel et al. 2013). The interpretation of Corner (1989) above was based, firstly, on the similarity of the Beattie and SKA anomalies, in terms of scale and signature; and secondly, on the fact that the former is clearly truncated by the Agulhas Fracture Zone, implying possible eastward extension in Gondwana. The Gondwana reconstruction (Martin and Hartnady 1986), initially used by Corner (1989), aligned the SKA with the extension of the

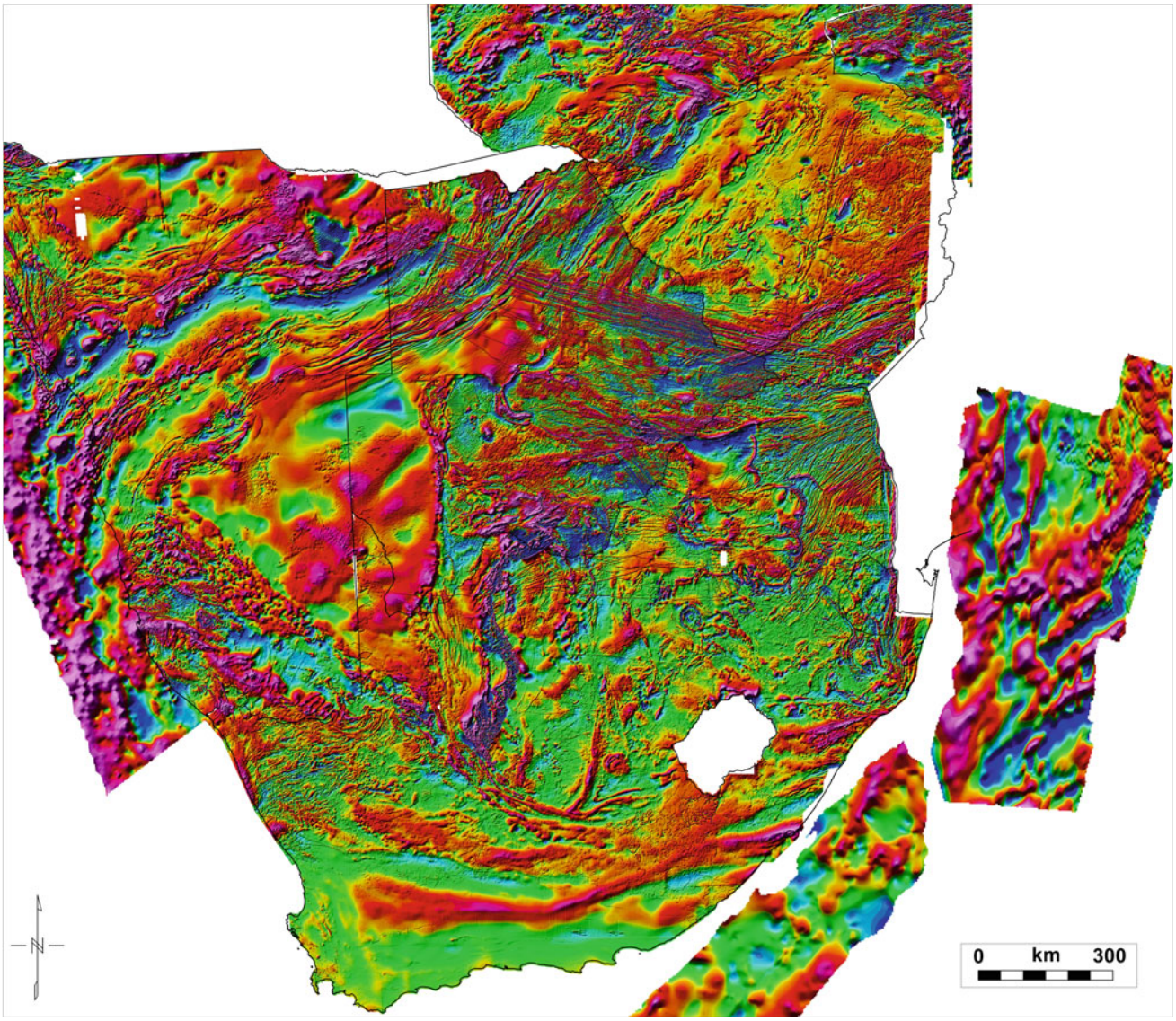

Fig. 2.9 Total magnetic intensity image of southern Africa, the Falkland Plateau (ship-track data) and Dronning Maud Land in Antarctica. The closer Gondwana reconstructions, after Martin and Hartnady (1986) and Grantham et al. (1988), have been relaxed here so as to accommodate the interpreted Mesozoic basalt anomalies (Fig. 2.10). The fit is thus indicative, rather than rigorous, for the purposes of this discussion

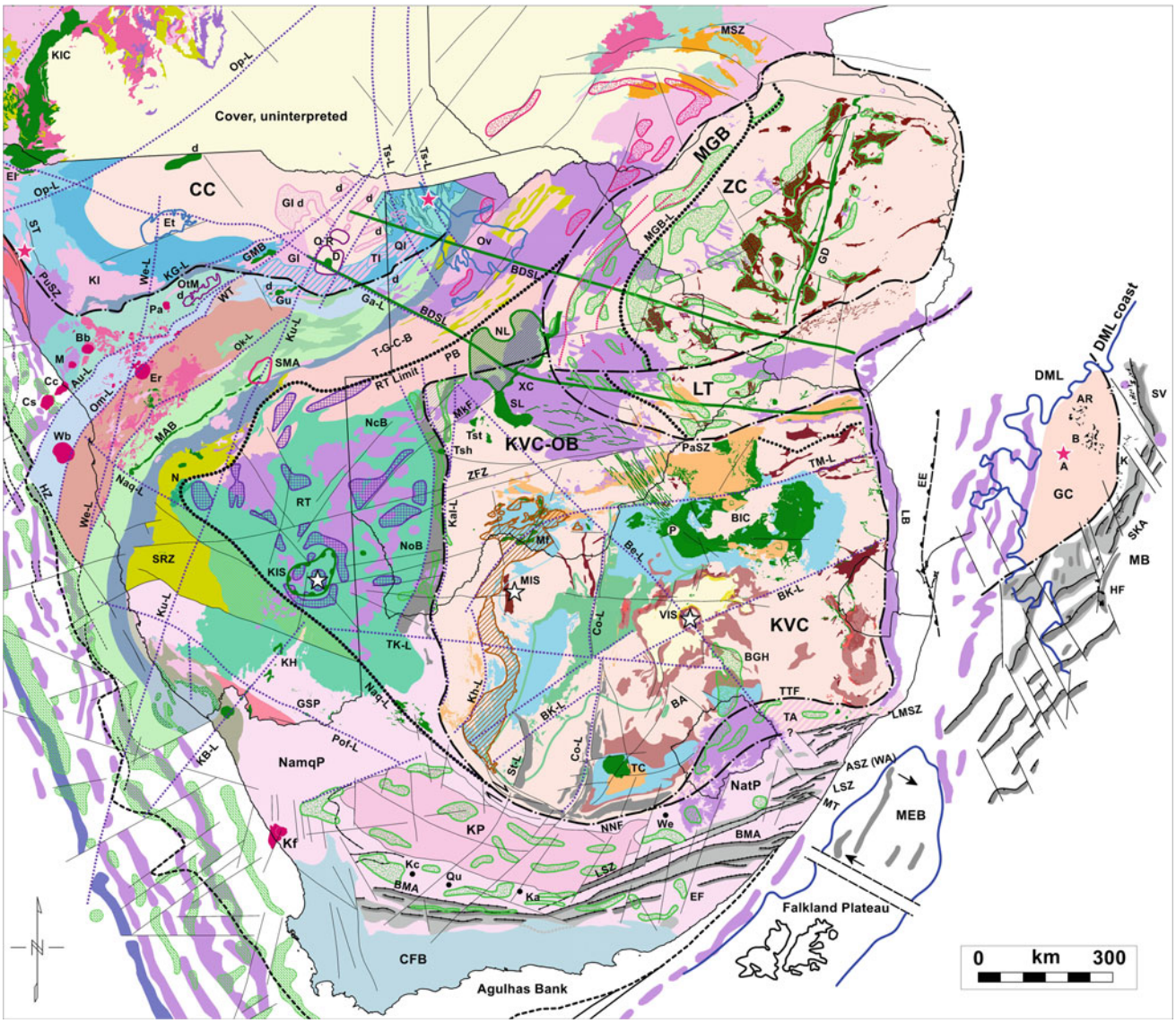

Fig. 2.10 Interpreted extension of the Namaqua-Natal Belt and Kaapvaal Craton in Dronning Maud Land, Antarctica, based on the correlation of the BMA (Beattie Magnetic Anomaly) and SKA (HU Sverdrupfjella-Kirwanveggen Anomaly) magnetic anomalies. As with Fig. 2.9, the closer Gondwana reconstructions, after Martin and Hartnady (1986) and Grantham et al. (1988), have been relaxed here so as to accommodate the interpreted Mesozoic basalt anomalies. *A* Annandagstoppane; *AR* Ahlmanryggen; *B* Borgmassivet; *DML* Dronning Maud Land; *EE* Explora Escarpment; *GC* Grunehogna Craton; *HF* Heimefrontfjella; *K* Kirwanveggen; *MB* Maud Belt; *MEB* Maurice Ewing Bank microplate; *SKA* Sverdrupfjella-Kirwanveggen Anomaly; *SV* H.U. Sverdrupfjella. All other text abbreviations are given in Fig. 2.6

Beattie into DML. The intervening gap, known as the Natal Embayment (Jacobs and Thomas 2004), was occupied by the Maurice Ewing Bank (MEB) microplate of the Falkland Plateau, over which marine magnetic data revealed a linear magnetic anomaly which, if the MEB microplate is rotated slightly as suggested in Figs. 2.9 and 2.10, would also constitute a possible continuation of the Beattie anomaly, and a link between the BMA and SKA (Figs. 2.9 and 2.10). In the interpretation of Corner (in Hunter et al. 1991), refined here, magnetic units and faulting within the larger SKA zone were mapped using higher-resolution residual-filtered aeromagnetic data. One aspect that complicated this interpretation was the presence of numerous magnetic anomalies owing to the Mesozoic basalts associated with the break-up of Gondwana, progressively dominating westwards from the SKA towards the Explora Escarpment (EE; Fig. 2.10). However, these appeared to have a strike direction different from that of the SKA anomalous units, and were thus subjectively separated, as shown in Fig. 2.10. This interpretation may be equivocal in the zone where both of these anomalous sources are present. The closer fit of DML to southern

Africa of Grantham et al. (1988) has been relaxed in Fig. 2.10 so as to accommodate the interpreted Mesozoic basalt anomalies. It is thus an indicative, rather than rigorous, fit for the purposes of this discussion. The continuation of the Namaqua-Natal Belt and BMA into DML in Antarctica has been further supported by the more recent work of Golynsky and Jacobs (2001); Jacobs and Thomas (2004) and Riedel et al. (2013).

The postulated preservation of an Archaean cratonic microplate in DML (the Grunehogna Craton), Antarctica, is supported by Archaean ages of *c*. 3000 Ma (Halpern 1970), and 3067 Ma (Marschall et al. 2010), determined on isolated exposures of basement at the Juletoppane and Annandagstoppane nunataks, respectively (red star; Fig. 2.10; see also Barton et al. 1987; Hunter et al. 1991). Corner (1994b), in interpreting the DML aeromagnetic data and ground gravity profiles, outlined the extent in DML of this microplate (Figs. 2.1 and 2.10) and juxtaposed it with the eastern margin of the Kaapvaal craton within a Gondwana reconstruction, suggesting the possibility that the cratonic microplate constituted the eastward extension of an early Kaapvaal craton. However, the location of the Kaapvaal Craton within Rodinia, and subsequently Gondwana, has been the topic of much controversy. An early view was that the DML Archaean microplate (Grunehogna Craton) is not related to the Kaapvaal-Zimbabwe Province (Barton et al. 1987; Barton and Moyes 1990). Dalziel (1991, 2000) and Moores (1991) hypothesized that Laurentia and East Antarctica were juxtaposed in an early Neoproterozoic supercontinent. This was named the SWEAT hypothesis (Southwest United States—East Antarctica). Moyes et al. (1993) examined the hypothesis by comparing coeval magmatism, regional isotopic resetting and structural deformation styles, and they concluded that this data neither supports nor contradicts the SWEAT hypothesis. Storey et al. (1994) compared geochronological, isotopic and aeromagnetic data between Coats Land and DML, confirming rocks of Grenvillian age in both, and concluded that this data supports the SWEAT hypothesis. On the other hand, Golynsky et al. (2000b) investigated the tectonic development of Coats Land and western DML using aeromagnetic data and correlative outcrop data, and concluded that Coats Land was never part of the Kaapvaal-Zimbabwe craton. Overall support for or against the SWEAT hypothesis is thus equivocal. It has also been suggested that Western Australia was a collision partner for the Kalahari Craton. This hypothesis was investigated by Ksienzyk and Jacobs (2015), who could not find support from a geochronological point of view. In summary, much recent work supports the extension of the Kaapvaal-Zimbabwe Cratons into DML, and the existence of a continuous Grenvillian/Kibaran belt bounding this proto-Archaean craton to the south and east.

2.3 Electrical Resistivity, Magnetotelluric and Regional Seismic Investigations

2.3.1 Introduction

Over the past half-century, a series of passive and active seismic experiments, and resistivity, geomagnetic induction and magnetotelluric (MT) surveys, have been conducted in southern Africa. Most of the early work was stimulated by curiosity, with the objective of learning more about the structure and evolution of the African continent. Much of the later work was done with commercial intent, with the aim of discovering new gold, platinum, diamond and hydrocarbon resources. In particular, reflection seismology surveys, while much more expensive to carry out than gravity and magnetic surveys, are able to produce far better images of the subsurface. The locations of MT and broadband seismic stations, Schlumberger resistivity soundings, seismic refraction, seismic reflection and MT profiles are superimposed on the geological interpretation map in Fig. 2.11.

In Sect. 2.2, magnetic and gravity data was used to map features of the southern African crust (e.g., Fig. 2.6). These regional surveys were mostly conducted by geological surveys, geoscience councils and other government agencies with the aim of stimulating exploration for metals and minerals. Exploration and mining companies use these surveys to identify target areas, secure prospecting licences, conduct higher-resolution geophysical and geochemical surveys, and, depending on the outcome, drill boreholes. In this section we use the electrical resistivity, MT and seismic data and their interpretations to validate and extend the interpretation of the potential field data. We recognize that the data sets have not been fully integrated. The prime reason for this is that the various geophysical studies addressed different key questions. Consequently, the survey footprints and depths of investigation (ranging from the near surface to the mantle) do not always overlap. Nevertheless, we believe that there is merit in providing the reader with a brief but comprehensive review of all the major geophysical surveys that have been conducted in southern Africa.

2.3.2 Electrical Resistivity and Magnetotelluric Studies

2.3.2.1 Deep Electrical Resistivity and Geomagnetic Induction Soundings

Between 1967 and 1986 the Council for Scientific and Industrial Research in South Africa (CSIR) conducted 11 ultradeep electrical resistivity soundings using the Schlumberger array with electrode spacings of up to 1200 km,

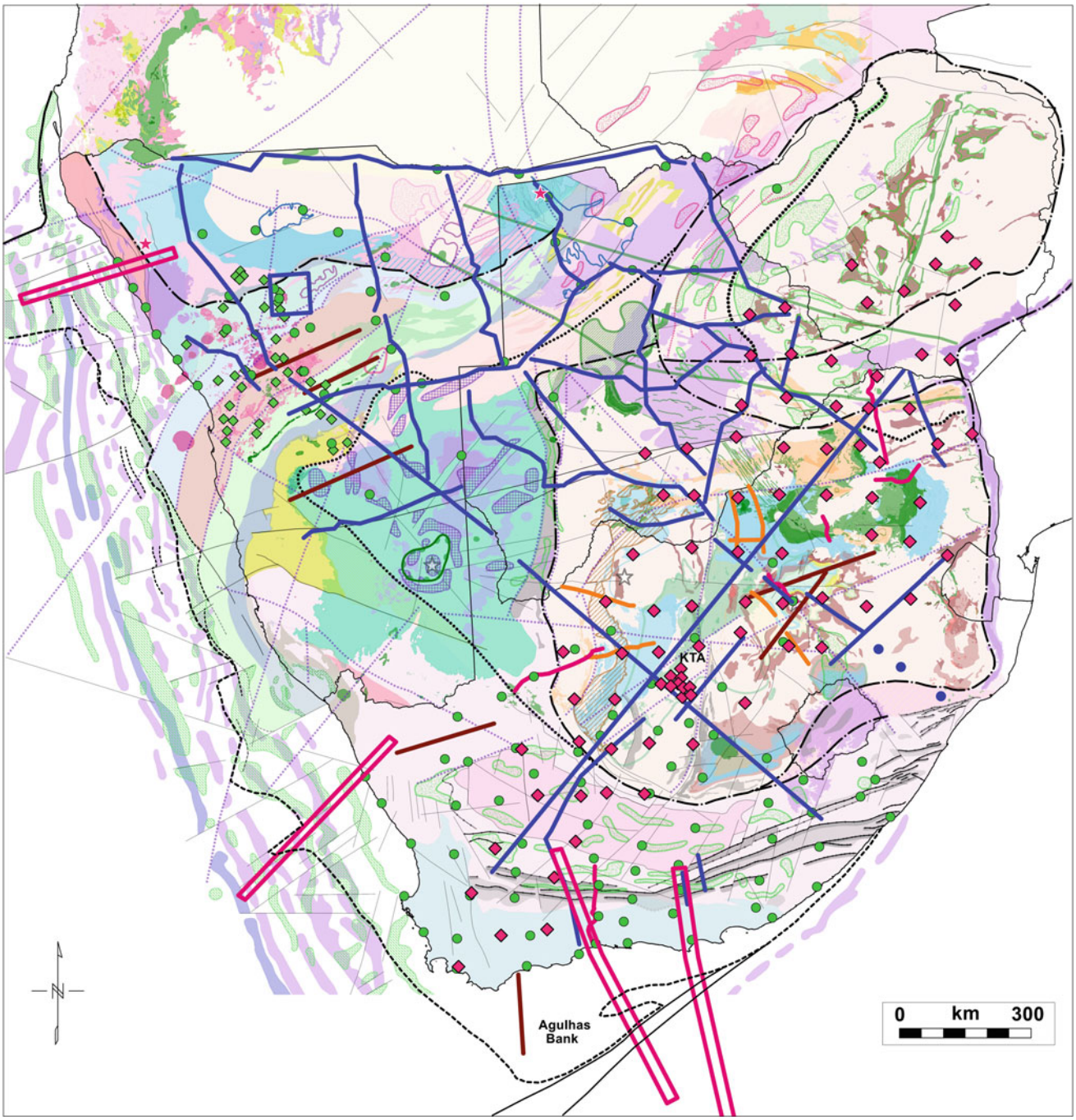

Fig. 2.11 Southern African seismic and magnetotelluric surveys. Blue, recent Magnetotelluric (MT) traverses conducted by the SAMTEX and Inkaba ye Africa programmes; green circles, MT soundings; green diamonds, vertical electrical soundings; red diamonds, SASE Broadband seismometer stations; red lines, national reflection seismic profiles; orange lines, AAC reflection seismic profiles; brown lines, refraction seismic profiles; red boxes, geotransects. *KTA* Kimberley Telemetered Array. The interpretation backdrop is from Fig. 2.6

probing the crust and upper mantle in the Kaapvaal, Zimbabwe and Congo cratons, the Bushveld Complex, and the Limpopo, Namaqua-Natal, Gariep and Damara Belts (De Beer 2015b; Fig. 2.11). In general, ignoring the surficial weathered layer, a five-layer electrical structure was found in both cratons and mobile belts:

- A high-resistivity layer ($\rho > 30{,}000\ \Omega m$) extending to about 10 km was found in 'massive terrains'—that is, in the granitic, Archaean cratonic nuclei.
- A moderate-resistivity zone ($2000\ \Omega m < \rho < 20{,}000$ m), indicating the presence of water-filled fractures associated with deformed metamorphic rocks in mobile belts, was observed at a depth range of 0–30 km and in the middle crust in Archaean cratons.
- A highly conductive zone ($\rho < 100\ \Omega m$), observed in the depth range 25–30 km, was speculated to consist of serpentinized ultramafic mantle rock.
- The uppermost mantle was found to be highly resistive ($\rho > 20{,}000\ \Omega m$).
- Thereafter the resistivity was found to decrease gradually as mantle temperatures increase with depth.

The CSIR supplemented the resistivity surveys with a series of geomagnetic induction campaigns (e.g., De Beer 2015c). Some 26 three-component magnetometers were deployed in 1971 in a triangular array over central South Africa, which straddled the boundary between the Kaapvaal Craton and the Namaqua-Natal Belt (Gough et al. 1973; Fig. 2.11). No significant resistivity difference was found between these domains, but a significant induction anomaly was evident under the southern edge of the array. In 1977 an array of 52 magnetometers was used to map this electrical conductivity anomaly, named the Southern Cape Conductive Belt (SCCB; Fig. 2.12). This coincides in part with the Beattie Magnetic Anomaly (De Beer and Gough 1980; see also Sect. 2.2.10.2 for further discussion).

A magnetometer array was deployed in northeastern Namibia, northern Botswana and northeastern Zimbabwe in 1971/1972 (De Beer et al. 1976; Fig. 2.11). A zone of low resistivity was discovered that runs from the Zambezi Valley to south of the Okavango Delta, and into the Damara Orogenic Belt (Fig. 2.12). Further surveys were conducted in the Damara Belt in 1977 (De Beer et al. 1982b), which tracked the Damara conductor to the Atlantic coast. The geomagnetic surveys were complemented by more than 40 Schlumberger soundings with maximum electrode spacings of 40 km, which showed that the northeast-striking conductor has steep sides, is 3–10 km deep and at least 20 km thick, and has a resistivity of less than $20\ \Omega m$ (Van Zijl and De Beer 1983; Fig. 2.12).

Magnetotelluric (MT) surveys conducted in northern Zimbabwe (Losecke et al. 1988, cited by Weckman 2012) detected highly conductive layers in the Lower Zambezi Valley situated in the Zambezi Mobile Belt (lying between the Congo and Kalahari cratons), which were tentatively linked with the conductive structures of the Damara Belt. In the late 1990s a series of MT surveys were carried out in shallow Karoo-age basins in the Zambezi Valley (Whaler and Zengeni 1993; Bailey et al. 2000a, b). The underlying cratonic rocks had quite high resistivities, which Bailey et al. (2000a, b) interpreted to indicate that cratons were not affected by the basin-forming processes in the adjacent mobile belts.

2.3.2.2 SAMTEX and Inkaba Ye Africa Magnetotelluric Experiments

Between 2003 and 2008 the Southern African Magnetotelluric Experiment (SAMTEX) deployed more than 740 stations at a nominal spacing of 20 km on lines, with a total length of some 15,000 km, straddling the major tectonic provinces (Evans et al. 2011; Fig. 2.11). SAMTEX was led by Dr A Jones of the Dublin Institute for Advanced Studies and involved many African and international scientists and institutions. MT arrays were also deployed under the auspices of the Inkaba ye Africa programme (Weckmann 2012). The principal findings of these investigations are reviewed below.

Kaapvaal Craton and Rehoboth Terrane (see also Sect. 2.2.7***):*** The MT observations were integrated with various geophysical and petrological observables (viz. elevation, surface heat flow, xenoliths) to derive an electrical conductivity model (Fullea et al. 2011). The depth of the present-day thermal lithosphere–asthenosphere boundary (LAB) was estimated to be at depths of 230–260 km and 150 km for the western block of the Kaapvaal Craton and Rehoboth Terrane, respectively. (It is important to note that the thermal LAB may differ from the chemical and mechanical LABs.)

Kaapvaal Craton—Limpopo Terrane—Zimbabwe Craton (see also Sect. 2.2.3.3***):*** Three profiles were used to investigate the electrical structure of this region (Khoza et al. 2013b; Fig. 2.11). The 30 km-wide Sunnyside-Palala-Tshipise shear zone (PaSZ; Fig. 2.6) was found to be a subvertical conductive feature that was interpreted to be the collisional suture between the Kaapvaal and Zimbabwe cratons.

Congo Craton—Damara Belt (see also Sects. 2.2.3.4 ***and*** 2.2.6.3***):*** The boundary between the Congo Craton and the Damara Belt is largely concealed by younger sediments. Four semiparallel MT profiles were used to investigate the electrical structure (Khoza et al. 2013a; Fig. 2.11). The Damara Belt lithosphere was found to be considerably thinner and more conductive than the Congo Craton lithosphere. Resistive features in the upper crust are interpreted as igneous intrusions emplaced during the Pan-African orogenic event, while highly conductive zones within the Central Zone of the Damara Belt are believed to be related to graphite- and possible sulphide-bearing stratigraphic units. The boundary between the Congo Craton and Damara Belt was shifted southwards, compared to prior models. A local

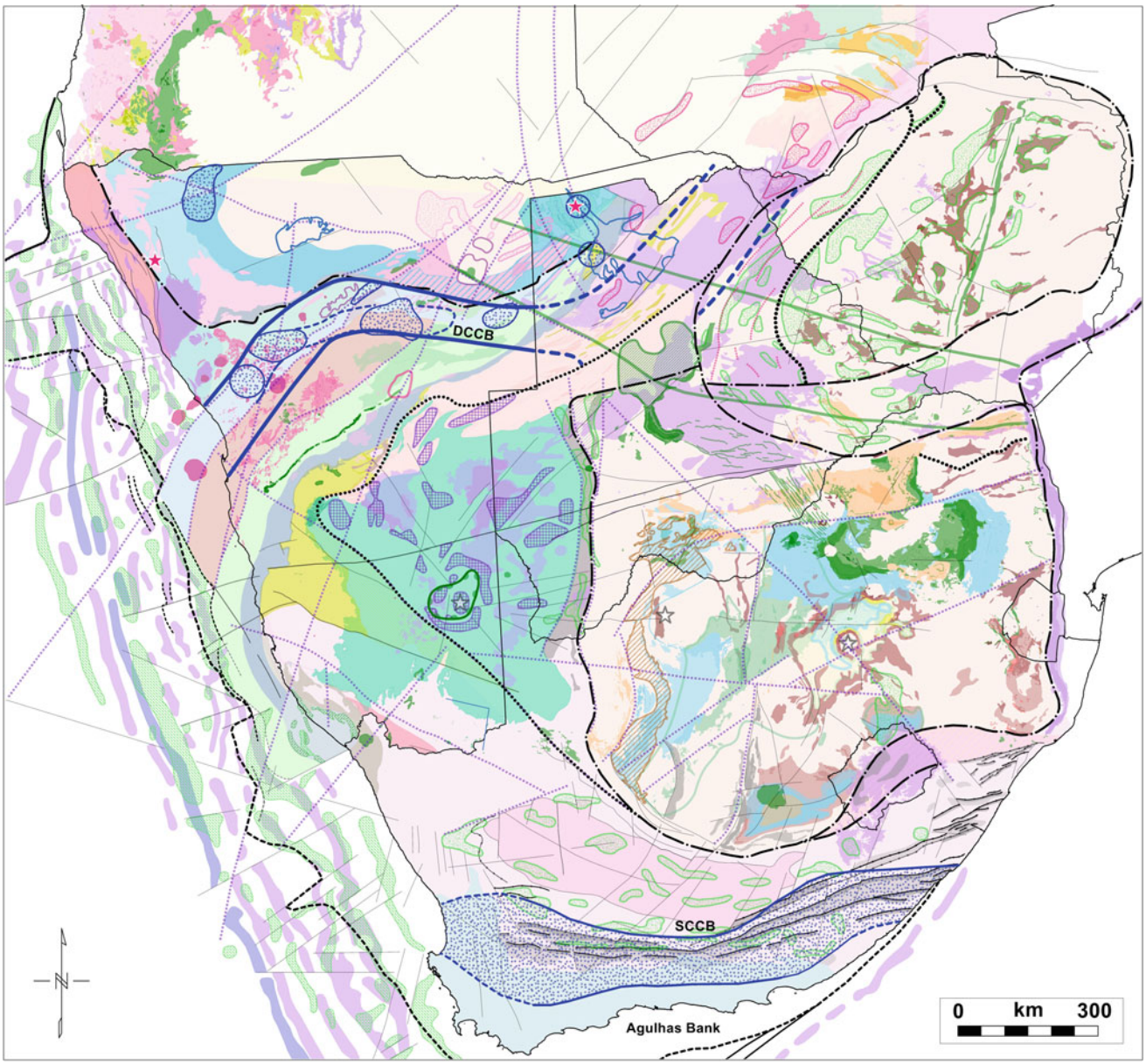

Fig. 2.12 Regional-scale conductivity anomalies overlaid on the interpretation backdrop of Fig. 2.6. The blue-speckled polygons are the conductivity anomalies mapped from the Magnetotelluric surveys described in Sects. 2.2.10.2 and 2.3.2 (*SCCB* Southern Cape Conductivity Belt; *DCCB* Damara-Chobe Conductivity Belt). The local anomalies shown are mapped from individual traverse data, with inferred extensions shown as dashed lines. The bold solid-blue lines show the DCCB of van Zijl et al. (1983) and the dashed lines show the inferred extensions into Botswana

study across the Waterberg Thrust/Omaruru Lineament (WT/Om-L; Fig. 2.6) found a 10 km-wide and at least 14 km-deep zone of anisotropic conductivity in the shallow crust parallel to the WT/Om-L (Ritter et al. 2003; Weckmann et al. 2003) and was interpreted to be the exhumed deep roots of ancient active shear zones.

Zimbabwe Craton—Magondi Belt—Ghanzi-Chobe Belt (see also Sect. 2.2.3.3): Kalahari sands cover most of northeastern Botswana and little was known about lithospheric structure and thickness prior to the study by Miensopust et al. (2011). A 600 km-long profile (Fig. 2.11) was interpreted. The Zimbabwe Craton is characterized by thick (~220 km) resistive lithosphere; the Tsumis-Ghanzi-Chobe Belt (TGCB; Fig. 2.6) by a somewhat thinner (~180 km) resistive lithosphere; while two lower- to mid-crustal conductors were found in the intervening Magondi Belt (MB; Fig. 2.6). The terrane boundary between the Magondi and Ghanzi-Chobe Belts was

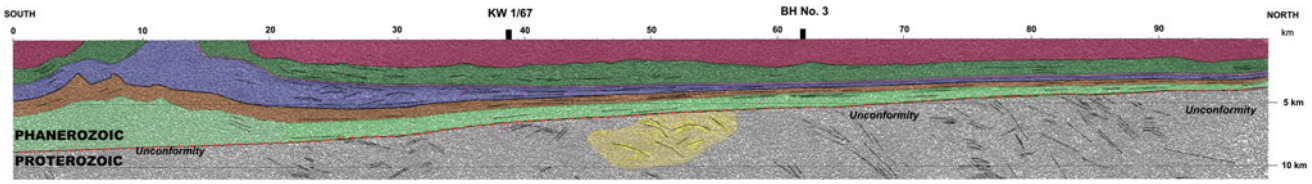

Fig. 2.13 Interpreted image of the upper 10 km of the 105 km-long southern Karoo reflection seismic profile. The source of the BMA is interpreted to lie within the yellow zone in the centre of the profile (*Source* Loots 2013)

interpreted to be further north than previously inferred from regional potential field data.

Kaapvaal Craton—Namaqua Natal Belt (see also Sect. 2.2.10.1): Karoo Supergroup strata conceal the contact between the Kaapvaal Craton and the Namaqua Natal Belt, but a large contrast in resistivity (>5000 Ωm and ~30 Ωm, respectively) makes it possible to map the contact (Weckmann 2012).

Southern Cape Conductivity Belt (see also Sect. 2.2.10.2): The source of the SCCB, discovered by De Beer et al. (1982a; Fig. 2.12), was studied in detail at specific locations by Weckmann et al. (2007a, b; Fig. 2.10). The Namaqua-Natal and Cape Fold Belts were found to have a generally high 'background' conductivity (~30 Ωm). Several distinct zones of high conductivity were identified, one 5–10 km below the surface trace of the Beattie Magnetic Anomaly, and the other linked to an extensive 50–70 m-thick pyritic-carbonaceous shale formation in the Karoo Basin (the White Hill Formation). Weckmann (2012) suggests that the SCCB, largely mapped using a sparse magnetometer array, may be the integrated result of the generally conductive NNB and the conductivity anomalies within it, or overlying it.

Cape Fold Belt: MT imaging of the structure of the CFB (Fig. 2.6) showed deep and resistive roots that are incompatible with a major crustal detachment zone and thick-skinned tectonics (Weckmann et al. 2012).

Lithospheric Mantle: Large variations in maximum resistivity at depths of 200–250 kmarine seismic refraction surveysm were found to relate directly to the age and provenance of upper crustal structure (Evans et al. 2011)—for example, beneath the central parts of the Kaapvaal craton the resistive mantle extends to depths as great as 230 km, while the mantle beneath the Bushveld Complex was found to be highly conductive at 60 km depth.

One of the main objectives of the extensive MT work was to investigate the use thereof to identify regions that are prospective for diamondiferous kimberlites. Images of electrical resistivity and electrical resistivity anisotropy at depths of 100 km and 200 km show that resistive regions correlated with the Kaapvaal, Zimbabwe and Congo (Angola) cratons, and more conductive regions correlated with the neighbouring mobile belts and the Rehoboth Terrane (Jones et al. 2009; Muller et al. 2009). Known diamondiferous kimberlites are inferred to lie mainly within the resistive or isotropic regions, and on their boundaries with conductive or anisotropic regions. Comparison with seismic body and surface wave tomographic images (see also Sect. 2.3.3.5 and Fig. 2.16) show that high-velocity regions are resistive and low-velocity regions are conductive.

2.3.3 Seismic Surveys

2.3.3.1 Refraction Seismic Surveys Using Mining-Induced Tremors

Seismic investigations of the Kaapvaal Craton, using recordings of earth tremors induced by deep gold mining, began in the 1940s (Willmore et al. 1952; Gane et al. 1956; Hales and Sacks 1959; Green 1980). Seismometers were deployed on profiles radiating from the Witwatersrand gold fields. The longest profile extended as far as Lusaka (Green 1980). The crust–mantle boundary (known as the Mohorovičić discontinuity or simply the Moho) was found to be at a depth of 33–36 km beneath the Kaapvaal Craton, with unusually high subcrustal P- and S-wave velocities of about 8.2 and 4.8 km/s, respectively. Long-period surface wave studies were conducted as part of the international Upper Mantle Project, in which a five-station long-period seismograph array was deployed on the Kaapvaal Craton (Bloch et al. 1969). Analysis of the dispersion of the surface waves produced by earthquakes in Malawi and Zambia confirmed that the shear wave velocities in the upper mantle beneath the Kaapvaal Craton were unusually high. The approach was used again in the 1980s with more modern technology (Durrheim and Green 1992). Seismographs were deployed at *c*. 10 km intervals on profiles linking the Klerksdorp, East Rand and Free State gold fields (Fig. 2.11); seismograms were recorded on magnetic tape and digitized; and ray-tracing and the reflectivity method were used to interpret the travel times and amplitudes. A P- and S-wave velocity model of the crust, upper mantle and crust–mantle transition zone was derived and integrated with xenolith and geochemical data to produce a model of evolution of the central Kaapvaal Craton (Durrheim and Mooney 1994). They postulated that there was a fundamental change in lithosphere-forming processes at the end of the Archaean. Hotter Archaean mantle temperatures led to the eruption of

komatiitic lavas and the formation of a lithosphere that was ultradepleted in FeO, intrinsically buoyant and sufficiently cool for diamonds to form. As the Earth cooled, the mantle temperature passed through a critical point and komatiitic volcanism ceased. The fertile Proterozoic mantle lithosphere had an FeO content similar to the asthenosphere and was prone to partial melting during heating events. Thickening of the Proterozoic crust occurred by the extrusion of basalt and underplating, the latter forming a high-velocity layer at the base of the crust.

2.3.3.2 Marine and Onshore Refraction Seismic Surveys Using Artificial Sources

Early marine seismic refraction surveys were conducted over the Agulhas-Bank, -Basin and -Plateau, and the Transkei Basin (Green and Hales 1966; Spence 1970; Chetty and Green 1977; Hales and Nation 1972; Barrett 1977; Tucholke et al. 1981; Fig. 2.11). The Agulhas Bank crust was found to be 33 km thick, with a high-velocity lower-crustal layer (7.2 km/s). The 2.5 km-deep Agulhas Plateau, to the south, was interpreted to be continental in origin, which was confirmed by dredging, while the crust beneath the 5 km-deep Agulhas Basin was interpreted to be oceanic in origin.

Three refraction profiles parallel to the axis of the Damara Orogen in Namibia were surveyed in 1975 (Baier et al. 1983; Green 1983; Fig. 2.11). The Moho was found to be at a depth of 36 km beneath the Pan-African Damara Orogen, deepening to 50 km along the southern margin of the orogeny, and to 60 km beneath the Proterozoic Kalahari Craton. A 290 km-long refraction seismic profile over the Proterozoic Namaqua Province (see also Sect. 2.2.10.1) was shot in 1983 (Green and Durrheim 1990; Fig. 2.11). The Namaqualand crust was found to be 42 km thick, with a lower crust P-wave velocity of 6.6–6.9 km/s, indicating the presence of rocks of intermediate composition.

2.3.3.3 Reflection Seismic Surveys for Hydrocarbons

From 1965 to 1979, about 11,000 line kilometres of seismic reflection data were acquired on land by the Southern Oil Exploration Corporation Ltd (SOEKOR) over the Karoo, Algoa, Gamtoos and Zululand basins in South Africa, and 138 boreholes were drilled (Wood 2015). The seismic surveys were complemented by aeromagnetic, gravity and deep resistivity investigations. It was concluded that the quality of sandstone reservoirs was poor, potential structural traps were small and high-quality source rocks were absent. Surveys of the continental shelf also commenced in the 1960s. The first discoveries of gas in southern South African waters were made in 1970 about 60 km offshore Plettenberg Bay and 90 km offshore Mossel Bay. Black oil was discovered in the Bredasdorp basin in 1986. Surveys for oil were also conducted in the Nosob Basin in Botswana (Wright and Hall 1990; NoB; Fig. 2.6), the Owambo Basin in northern Namibia (Hoak et al. 2014) and the coastal plain and continental shelf of Mozambique (Brownfield 2016).

2.3.3.4 Deep Continental Reflection Seismic Surveys

In the 1980s it was realized that the reflection seismic method, routinely used to search for hydrocarbons, could effectively probe the entire continental crust. Many countries established deep reflection seismic programmes, such as COCORP (US), Lithoprobe (Canada), DEKORP (Germany), ECORS (France) and BIRPS (UK). The South African National Geophysical Programme (NGP) was launched in 1985 and six deep reflection seismic profiles were surveyed, targeting some of the region's most interesting and important geological features. Other deep seismic reflection profiles were surveyed during mineral and hydrocarbon exploration programmes and the Inkaba ye Africa programme.

Agulhas Bank: The first deep reflection profile in southern Africa, shot in 1985 on the Agulhas Bank by SOEKOR, straddled the Cape Seal Arch (Durrheim 1987). The folded Cape and Kaaimans sediments gave rise to occasional strong reflections, and strong reflections at 9–10 s two-way time (TWT) were interpreted to arise from the Moho.

Central Kaapvaal Craton (see also Sects. **2.2.3.2** and **2.2.4** ***):*** Beginning in 1982, reflection seismics was used to explore for extensions of the gold-bearing Archaean Witwatersrand Basin and the platinum-bearing Bushveld Complex. Tens of thousands of line kilometres were surveyed (Pretorius et al. 2003; Campbell 2011). In 1988 the NGP surveyed a 112 km-long 16 s TWT profile from the Ventersdorp dome, across the Potchefstroom syncline, to the Vredefort Dome (Fig. 2.11). Using this data, Durrheim et al. (1991) mapped the present-day structure of the Witwatersrand Basin and the crystalline basement between the Ventersdorp dome and Potchefstroom, and found that it is characterized by several zones of strong, subhorizontal reflections (see also Sect. 2.2.3.5). Other geophysical data sets used to constrain interpretations of the reflection seismic profile included gravity and magnetics, and refraction seismics (Green and Chetty 1990; Durrheim and Green 1992). Between 1983 and 1994 the Gold Division of Anglo American Corporation of South Africa (now Anglogold Ashanti Ltd) acquired more than 16,000 kilometres of reflection data across the Kaapvaal Craton. As the main objective of these surveys was to explore for deeply buried gold-bearing Witwatersrand sediments, most of the sections were 5 or 6 s TWT. However, several 16 s TWT profiles were acquired, of which eight were made available for research and publication (Tinker 2001; Tinker et al. 2002; de Wit and Tinker 2004; Fig. 2.11). Seven of these profiles

were projected onto a common section that strikes northeast–southwest across the central part of the Kaapvaal Craton, stretching from the Vredefort Dome to Vryburg and straddling the Colesberg Lineament (see also Sect. 2.2.3.5). The seismic data suggests a tectonically stacked series of crustal slivers that were thrust over the Kaapvaal Craton during the Neoarchaean. The eighth profile crosses the boundary between the Kaapvaal Craton and the Namaqua-Natal Belt (NNB) in the Eastern Cape, and indicates that the NNB is thrust over the Kaapvaal Craton (location not shown in Fig. 2.11, see also Sect. 2.2.3.2).

Bushveld Complex: The NGP acquired two profiles over the Bushveld Complex (Fig. 2.11). In 1986 a 50 km-long profile was surveyed along a line starting west of Pretoria and running northwards across the Bushveld Complex (Odgers et al. 1993). In 1989 a 117 km-long profile was surveyed across the eastern lobe of the Bushveld Complex. Odgers and du Plessis (1993) interpreted the seismic profiles and concluded that the data supported a model of a sheet-like structure for the Rustenburg Layered Suite. They interpreted the Malope Dome to be a diapir of Nebo Granite Suite rocks that rose through the denser Rustenburg Layered Suite.

Limpopo Terrane (see also Sect. 2.2.3.3): In 1987 the NGP acquired a 200 km-long profile from Pont Drift (on the Limpopo River), traversing the Central and Southern Marginal Zones of the Limpopo Terrane (LT; Fig 2.6), and ending on the Kaapvaal Craton near Polokwane (Fig. 2.11). De Beer and Stettler (1992) found that the reflection seismic data provided excellent information about shallow structure, but lacked detail on the lower crustal and the crust–mantle boundary structures. Combining the seismic reflection data and results from geoelectrical studies, De Beer and Stettler (1992) concluded that the high-grade metamorphic rocks of the Southern Marginal Zone were thrust southward over the low-grade cratonic rocks. The reflection data were reprocessed and reinterpreted by Barker (1992), and subsequently integrated with gravity observations and refraction profiles surveyed from Johannesburg to Musina (Gane et al. 1956), Polokwane to Lusaka (Green 1980) and across the Limpopo Belt (Stuart and Zengeni 1987). It was found that the crust ranges in thickness from about 30 km in the centre of the LT to 40 km in the Zimbabwe Craton (Durrheim et al. 1992).

Kaapvaal Craton—Namaqua Natal Belt (see also Sects. 2.2.3.2 and 2.2.10.1): In 1991 a 226 km-long profile was surveyed under the auspices of the NGP between Sishen and Keimoes in the Northern Cape Province, straddling the western Kaapvaal Craton boundary (Fig. 2.11). Following the seismic survey, eleven magnetotelluric sounding stations were located at 20 km intervals along the same profile. Stettler et al. (1998, 1999) integrated the seismic, magnetotelluric, magnetic and gravity data along this traverse. In their interpretation, the reflective package west of Sishen is located on the western margin of the Kaapvaal Craton, coinciding with conductive, dense and partially magnetized material, which may be indicative of an ophiolitic sequence that was thrust onto the Craton margin to form an accretionary wedge between the Kheis Terrane and the Kaapvaal Craton.

Southern Karoo—Cape Fold Belt (see also Sect. 2.2.10): Loots (2013) reprocessed and interpreted the 105 km-long Karoo seismic reflection profile that was acquired under the auspices of the NGP in 1992 (Figs. 2.11 and 2.13). The upper crust consists of Karoo and Cape Supergroup rocks that dip slightly to the south. The middle crust is interpreted to consist of granitic gneisses belonging to the Bushmanland Terrane, part of the Namaqua-Natal Belt (NNB). The middle crust also hosts the source of the Beattie Magnetic Anomaly, which is characterized by a bean-shaped cluster of strong reflections, ~10 km wide, with a thickness of ~8 km and an apparent greatest depth at ~8 km. The Moho is encountered at ~37 km at one section of the profile, but no clear Moho reflections are seen elsewhere.

2.3.3.5 Southern African Seismic Experiment

The Kaapvaal Project, initiated in 1996, consisted of a range of geological, geophysical, geochemical and petrological investigations (Carlson et al. 1996). A key component was the Southern African Seismic Experiment (SASE), which comprised two broadband seismograph arrays: the regional Kaapvaal Seismic Array (KSA) of 82 stations along an 1800 km × 600 km transect that stretched from the Cape to Zimbabwe (James and Fouch 2002, Fig. 2.11); and the dense Kimberley Telemetered Array (KTA; Fig. 2.11), a six-month deployment of 32 stations in a 65 × 50 km area covering a region with several kimberlite intrusions. We review the main findings of a range of seismological investigations that were conducted by members of the Kaapvaal Seismic Group, and, following the release of the data into the public domain, by the international seismological community (Fig. 2.14).

African Superswell and Superplume Anomaly: Southern Africa is characterized by a high (~1.5 km) inland plateau, the 'African Superswell' (Nyblade and Robinson 1994). Geomorphological and geochronological studies indicate that the rise occurred between 5 and 30 Ma (McCarthy and Rubidge 2005). One of the largest shear wave anomalies in the lower mantle, the 'African Superplume' or simply the 'African Anomaly', is found beneath southern Africa. It is a 7000 km-long, 1000 km-wide and 1500 km-high structure, striking roughly northwest and characterized by a 3% drop in the shear-wave velocity Vs (Ni and Helmberger 2003; Wang and Wen 2007). An investigation of the phenomena that caused the Superswell (e.g., buoyancy caused by heating and/or convection forces) and the Superplume

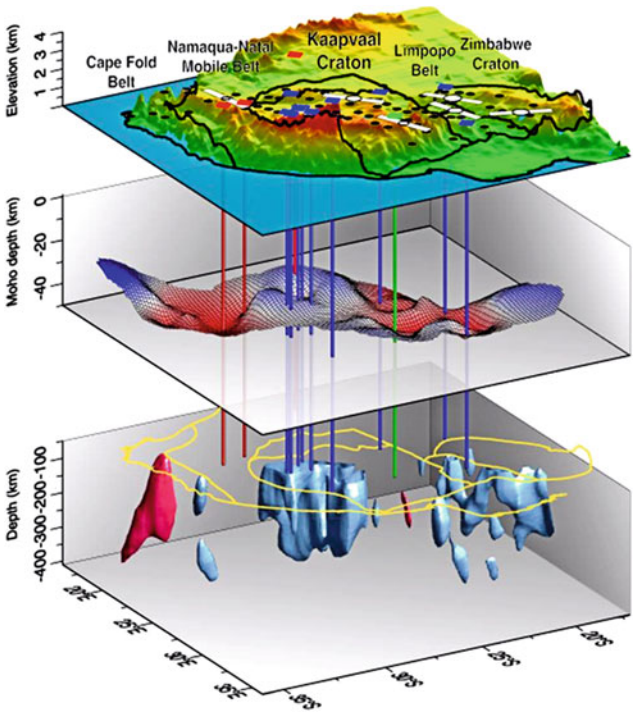

Fig. 2.14 Schematic of the South African Seismic Experiment (SASE), showing the topography of southern Africa, the main geological provinces (black outlines of the cratons), the disposition of seismograph stations (blue dots), the topography of the Moho shaded to show the seismic velocity of the uppermost mantle (blue is fast, red is slow), and seismic velocity anomalies in the upper mantle. This image was featured on the front cover of the 1 July 2001 issue of *Geophysical Research Letters*

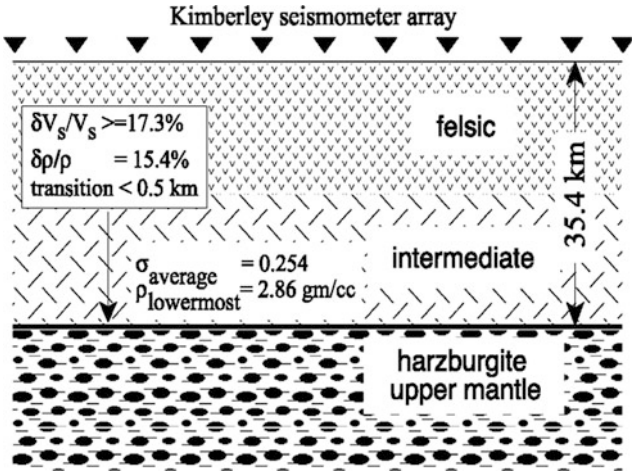

Fig. 2.15 Model of the crust and uppermost mantle beneath the Kimberley Telemetered Array (Niu and James 2002; James et al. 2003)

(e.g., thermal and/or chemical variations in the lower mantle), and the connection (if any) between the two features, were important drivers of SASE.

Crust: Receiver functions, which rely on the conversion of P-wave to S-wave energy at the Moho, have been used by several workers to map the structure and thickness of the crust (Harvey et al. 2001; Midzi and Ottemőller 2001; Nguuri et al. 2001; Stankiewicz et al. 2002; Kgaswane et al. 2009, 2012). It was found that the crust beneath undisturbed parts of the Archaean Kaapvaal and Zimbabwe Cratons is relatively thin (35–40 km), unlayered and characterized by a strong velocity contrast across a relatively sharp Moho. This contrasts with the crust beneath post-Archaean terranes or Archaean regions affected by large-scale Proterozoic events (e.g., Bushveld Complex), where the crust is relatively thick and the Moho is complex. The KTA enabled more detailed investigations to be performed in the Kimberley area. It was found (Fig. 2.15) that the crust is 35 km thick with an average Poisson's ratio of 0.25; the lower crust has a density of 2.86 g/cc, Vp of 6.75 km/s and Vs of 3.9 km/s, indicating a felsic to intermediate composition; the Moho transition is less than 0.5 km, with a 15% density contrast across it; and the uppermost mantle has Vp of 8.2 km/s and Vs of 4.79 km/s (Niu and James 2002; Stankiewicz et al. 2002; James et al. 2003).

Upper Mantle: Tomographic inversion of 3D body wave delay times (P, PKP, S, SKS) and surface wave phase and group velocities showed that high-velocity mantle roots extend to depths of at least 250 km and locally to 300 km beneath the Kalahari craton (comprising the Kaapvaal and Zimbabwe Cratons, and the Limpopo and Rehoboth Terranes, as shown in Fig. 2.1; Ritsema and Van Heijst 2000; James et al. 2001; James and Fouch 2002; Fouch et al. 2004). An example of a seismic-tomography P-wave-anomaly depth slice at 150 km is shown in Fig. 2.16 (after James and Fouch 2002). The mantle beneath the Bushveld Complex has relatively low velocities. Evidence for a seismic low-velocity zone (LVZ) in the upper mantle was eagerly sought in order to test the hypotheses regarding the cause of the Superswell. A LVZ is regarded as evidence of the presence of warm and/or low-density material. However, the body wave tomography did not provide evidence for a LVZ. Several surface wave studies were carried out using a variety of methods. Chevrot and Zhao (2007) confirmed that high-velocity cratonic roots are confined to the Archaean cratons, and that the roots extend to at least 250 km. Larson et al. (2006) found that Vs decreases slightly with depth from 4.7 km/s in the uppermost mantle to 4.60 km/s at 200 km. No evidence was found of Vs < 4.55 km/s shallower than 250 km. Larson et al. (2006) concluded that the present-day mantle velocity structure is similar to that at the time of kimberlite eruption at 70–90 Ma. Li and Burke (2006) imaged a fast, lithospheric lid beneath most parts of southern Africa, ranging in thickness from *c*. 80 km beneath the Namaqua-Natal Belt to 180 ± 20 km beneath the Kaapvaal Craton. Relatively low

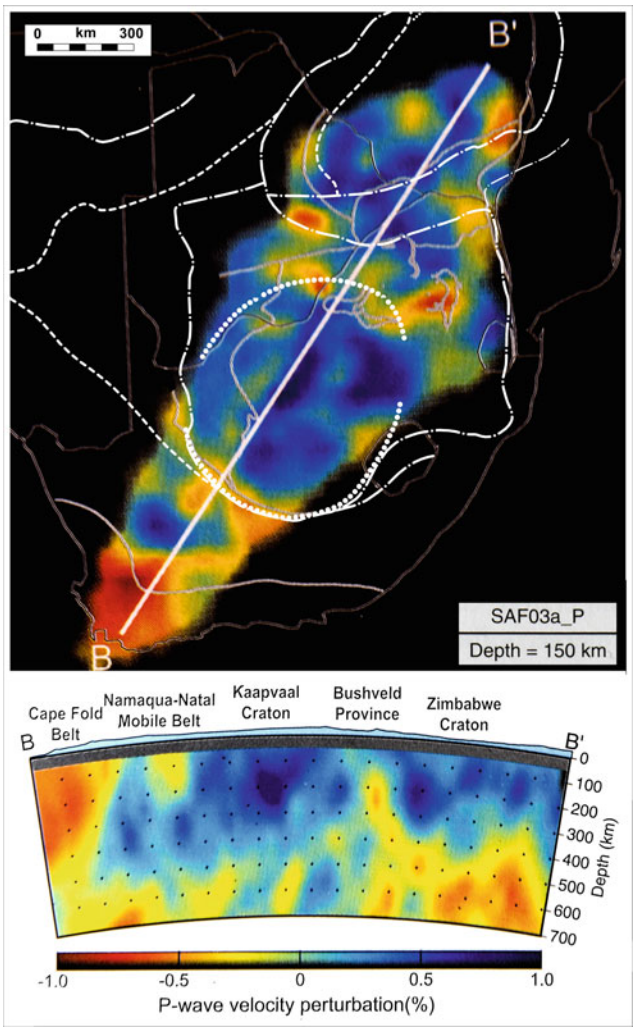

Fig. 2.16 Seismic tomography P-wave anomaly depth slice at 150 km (from James and Fouch 2002), with overlay of the Kaapvaal Ring Structure (KVRS; Fig. 2.7), the Zoetfontein fault (ZFZ; Fig. 2.6) and the interpreted craton boundaries. Cold colours indicate that the wave velocities are faster than the reference model, and warm colours indicate that they are slower

velocities were observed under the Cape Fold Belt and in the shallow upper mantle beneath the tectonic border regions. The basement to the Bushveld Complex was found to be relatively slower than its surroundings above 100 km. A LVZ was observed at depths of 160–260 km across southern Africa with an average velocity of 4.5 km/s. This layer, although not absolutely slow, is 4% slower than the fast lithosphere above it. Li and Burke (2006) suggested that the LVZ is largely caused by high temperature associated with sublithospheric mantle convection, which could contribute to the high elevation of southern Africa, rather than compositional and petrologic effects.

2.3.4 Agulhas Bank—Cape Fold Belt—Namaqualand Geotransects

The Cape Fold Belt-Agulhas Bank Geotransect (Central Geotransect, Fig. 2.11), compiled by Hälbich (1993), integrated much of the prior work in the region. The 600 km north-northwest-south-southeast-trending transect stretches from the central Karoo, across the Cape Fold Belt to the edge of the continental shelf, traversing several unusual features, such as the Southern Cape Conductivity Belt, the Beattie Magnetic Anomaly, a belt of Jurassic Karoo dolerites and the Agulhas Fracture Zone. Geophysical data sets used to compile the transect included seismic reflection profiles acquired by Soekor to image the offshore Cretaceous basins, including a deep (12 s two-way time) profile (Durrheim 1987); a combined refraction seismic and gravity profile along 21°50′E (Hales and Nation 1972); a refraction seismic profile in Namaqualand (Green and Durrheim 1990); and Bouguer gravity, magnetic and magnetotelluric data. The main conclusion drawn from the study was that old sutures, manifested by linear magnetic and conductive belts, probably played an important role in the subsequent geotectonic evolution of the continental crust.

A similar transect, east of the above, was compiled more than 20 years later under the auspices of the German-South African multidisciplinary earth science project Inkaba ye Africa. The 800 km Agulhas-Karoo Geoscience Transect runs north-northwestwards from the Agulhas Plateau across the Agulhas Passage, Agulhas-Falkland Transform Fault and Agulhas Bank to the coastline, then across the Cape Fold Belt, Beattie Magnetic Anomaly, the Karoo Basin, the Great Escarpment, and onto the Namaqua Natal Belt. The 457 km offshore profile, from the Agulhas Passage to the Agulhas Bank, was shot in 2005 (Parsiegla et al. 2007). It was extended landward using 48 seismic stations spaced over 240 km (Stankiewicz et al. 2007). The offshore profile shows a 52 km-wide transition from oceanic to continental crust, with crustal thickness increasing from 7 to 30 km. The upper and lower crust has P-wave velocities of 5.6–6.6 km/s and 6.4–7.1 km/s, respectively. The onshore profile enabled a P-wave velocity model to be derived to a depth of 25 km. A 100 km-long reflection seismic line was shot along the same line, beginning at Prince Albert and terminating near Fraserburg (Lindeque 2008; Lindeque et al. 2007), clearly imaging the Karoo and Cape Supergroup supracrustal strata. The unconformity at the base of these strata deepens from ~5 km in the north to ~10 km in the south. The mid-crustal layer is ~20 km thick, and the source of the Beattie Magnetic Anomaly is associated with reflectors 7–15 km deep. Reflections, that were interpreted to represent the Moho, range in depth from ~43 km in the north

to ~35 km in the centre, thickening to ~45 km beneath the tectonic front of the Cape Fold Belt.

2.4 Summary and Conclusions

The scope of this chapter is vast, presenting an integrated geophysical-geological interpretation of the major Archaean and Proterozoic domains concealed beneath Phanerozoic and younger cover in southern Africa. The interpretation is focused on specific regional-scale features that have been the subject of numerous investigations over the last five decades and current work by the authors. Where no geophysical interpretation has been conducted or sourced, the published geological mapping is shown for the sake of completeness. As far as possible, the interpreted features honour all geological and geophysical data sets within the resolution of the data. Integration of these results in the unified interpretation map presented here brings new insights into the disposition and evolution of the Precambrian geology of southern Africa, extending into Antarctica within a Gondwana framework. Improvement of this work will, no doubt, be further facilitated by in-house mining and exploration data when this becomes available. Interpretation highlights are summarized below:

- The craton boundaries have been mapped, or existing interpretations refined. Although indicated as 'line' boundaries, they reflect the locus of what is likely to be a much more complex structural swathe. What has often been referred to as the Okwa basement, excluding correlations with the Magondi-Gweta Belt by some workers, is considered to be an integral part of the Kaapvaal Craton, here termed the Okwa Block. The Magondi-Gweta Belt is suggested by the potential field data to be a separate entity, and is mapped extending westwards into Zambia. A possible link between this and the Limpopo Belt is suggested but is difficult to define owing to the cover of Karoo basalts. The high P-wave velocity anomaly associated with the Magondi-Gweta Belt, at a depth of 150 km, appears to continue southwards into the mapped western portion of the Limpopo Belt. The Congo Craton is interpreted to have a definable but complex southern boundary. Mapping the extent thereof into Angola is, however, hampered by extensive cover and lack of published detailed aeromagnetic and gravity data.
- Major structural lineaments have been mapped. As with the craton boundaries, the traces should be considered to be the locus of broader structural swathes or corridors. Many of the lineaments have been mapped previously and documented. However, the present study identifies a previously unrecognized lineament, here termed the Tsodilo Lineament, which extends from northwest Botswana into Angola, trending north-northwest to north. It is suggested that it may have been an early, northern extension of the Kalahari Lineament prior to the development of the Damaran Orogenic Belt. Many faults have been mapped from the potential field data, but only a select few are shown owing to the scale of presentation. It should be borne in mind that the data sets reflect sources at a range of depths. The fault traces should thus be considered as structural trends that include, but are not exclusive to, faults mapped at surface.
- A number of ring features have been mapped which may be associated with a variety of sources, such as intrusions, basalt vents and meteorites. Examples of the latter include the Morokweng and proposed Karas meteorite impact sites. The preservation of the arcuate geometry of ring structures, cutting across older structural fabric, suggests that they would have to be post- or late-tectonic features, or foci of older causative sources which have been reactivated through geological time as a result of associated crustal weakness. In this sense, a ring feature may be evidence of an older focal source. Further possible sources may result from rheological or structural variations in the deep crust or upper mantle. In particular, the Kaapvaal Ring Structure (KVRS) is thought to be such a feature, encompassing the high-velocity root of the Kaapvaal Craton. It is suggested that movement along a probable competency contrast between low and high mantle velocity zones may have resulted in the near-surface manifestation of the KVRS. A number of significant kimberlites, or clusters thereof, are associated with the KVRS.
- Mapping of the extent and structure of the Witwatersrand Basin, in previous studies by a number of workers, has been manifestly improved and documented here, not only with regard to the main basin but also through the identification and mapping of a southern extension of the main basin close to the southern boundary of the Kaapvaal Craton. Southern extensions of the Transvaal Supergoup have also been mapped.
- The Xade Complex in Botswana, a layered sequence of mafic intrusive and extrusive rocks forming part of the more extensive Umkondo magmatic province, has been found to comprise Northern and Southern Lobes. The Northern Lobe was not previously recognized as a separate entity, since it extends under a thick succession of sediments in the Passarge Basin, where it continues with diminished gravity and magnetic signatures. The Xade-related magmatic event is interpreted to have extended locally westwards to include the Tsetseng and Tshane intrusions, as well as along the northern portions of the Kalahari Lineament.
- On the Zimbabwe Craton, the residual gravity highs, despite the coarse data, show strong correlation with the

greenstone belts as a result of their volcanic and banded iron sequences.

- The tectonostratigraphic zones of the Damara-Chobe Belt have been refined, and built on, from previous interpretations by a number of workers, both westwards to offshore Namibia and northeastwards into Botswana. Major features of the belt are, firstly, the apparent disconformable truncation of these zones against the interpreted Congo Craton boundary and the disruption of continuity across this boundary into the Northern Platform; secondly, the dramatic change in the apparent width of the belt, as well as stratigraphic level, as the Kudu Lineament is crossed eastwards; and, thirdly, the rapid pinching out of the belt, as bounded by the Southern Margin Zone in the south, eastwards into Botswana. The northeastward extension of the belt in northern Botswana, and into Zambia, where it is almost entirely covered, has been the subject of much research and debate. The identification in northwestern Botswana of the Tsodilo Lineament, a structural corridor transverse to the strike of the belt, serves to explain the north-northwest structural disposition of the Tsodilo Hills Group seen in the aeromagnetic data, as well as the apparent abrupt termination of the eastern Congo Craton boundary. This structural corridor is thought to have played a significant role in controlling the extent and continuity of the Damaran-Katangan strata into southern Zambia south of the Mwembeshi Shear Zone.
- An aspect of interest within the Rehoboth Terrane is the identification of a potential meteorite impact site termed the Karas Impact Structure. The structure is possibly of Mesoproterozoic age, but the interpretation suggests that it was the focus of continued crustal weakening and reactivation until recent times.
- Published interpretations of depth to magnetic basement west of the Kalahari and Tsodilo Lineaments suggest the preservation of two extensive, thick sedimentary successions in excess of 6000 m, probably of Neoproterozoic age or older. Of interest is, firstly, their common occurrence west of these respective Lineaments; secondly, the possible control of a number of regional structures, which appear to constrain the basins, on the development of the basins or of their subsequent structural disruption; and, thirdly, that they straddle the Damara-Ghanzi-Chobe Belt to the north and south, suggesting that they may have formed a continuous basin in pre-Pan-African times.
- Improved definition of the Beattie Magnetic Anomaly (BMA), separating it into individual magnetic zones, suggests that the significant strike change from roughly east–west in the west to east–northeast in the east may have resulted from a change in transpressive direction affecting the eastern sector, possibly in Pan-African times. In addition, the parallelism of strike in the east with known highly magnetic thrust zones that crop out in Natal suggests that the origin of the BMA is thrust related. Furthermore, continuation of the belt of BMA-type anomalies into Dronning Maud Land (DML) in Antarctica, within the more extensive Namaqua-Natal-Maud Belt (NNMB) in a Gondwana framework, has provided additional field evidence for similar thrust-related magnetization seen to be associated with these anomalies in DML. The sense of thrusting at all observed field sites is craton directed, which is supported by the magnetic modelling of dips of the anomalous units in areas of cover.
- The interpretation identifies an area, under Phanerozoic cover, between the Namaqua and Natal Provinces of the Namaqua-Natal Belt, which has magnetic and gravity signatures distinctly different from either of these provinces. This is here termed the Khoisan Province which, based on a single deep borehole east thereof (SOEKOR borehole WE), is interpreted to be affiliated to the Namaqua Province, rather than to the Natal Province.
- The Southern Cape Conductivity Belt (SCCB), one of the largest deep crustal conductivity anomalies on Earth, remains enigmatic in its origin. Although the BMA lies within its swathe, paralleling its northern boundary, the SCCB is interpreted to lie deeper than the BMA. The majority of workers believe that the two anomalous belts do not have a common source but may be the result of a common evolutionary process. It has also been proposed that the SCCB, mapped largely from sparse magnetotelluric stations, results from an integrated effect of the elevated conductivity of the Namaqua-Natal basement, of higher conductivity zones therin, and of the high conductivities observed in overlying Phanerozoic strata.
- Interpretation of the aeromagnetic and satellite gravity data offshore Namibia has provided significant insights into the evolution of this passive volcanic margin. Firstly, the tectonostratigraphic zones of the Damara Orogen are clearly evidenced and mapped up to the offshore hinge zone where seaward-dipping reflectors (SDR), associated with basalt flows, first appear. Secondly, the mapped offshore Mesozoic gravity and magnetic anomalies are seen to be clearly offset along the offshore continuations of a number of Pan-African or older lineaments, suggesting that these structures not only determined the architecture of the extended crust but also were reactivated during the late Mesozoic, having directions that favoured the initiation of transform faults offshore. Thirdly, the M-type apparent spreading-related magnetic anomalies have been better delineated, and are seen to converge towards the northern Namibian and Angolan coastlines, in contrast to their previous placement much further out to sea. This has significant implications for the relative rates of extension from the southern to northern offshore areas, and hence for the relative ages of the

offshore sedimentary sequences. Forward modelling of the magnetic data has clarified the origin of the apparent M-type anomalies. These are shown to arise from the feather-edge suboutcrop of lava flows with a very shallow westerly dip, rather than to the classical vertical dyke-like seafloor spreading model.

- Several large-scale seismic, electrical resistivity, geomagnetic induction and magnetotelluric investigations have been conducted over the past five decades. They have yielded important insights into the deep structure and evolution of the subcontinent, and provided constraints on magnetic and gravity interpretations. The resultant published data sets have made it possible to extend our view of shallow crustal features to greater depths, and into the upper mantle. Conductive zones were recognized, and sedimentary basins, igneous intrusions, terrane boundaries and continental-scale shear zones concealed by younger strata were mapped. The topography of the Moho and the Lithosphere-Asthenosphere Boundary was mapped, showing that the Archaean Kaapvaal, Zimbabwe and Congo Cratons have deep roots that are relatively cold.

References

Ambot (Anglo American Botswana) (1998) Kalahari gold project, Final relinquishment report, CR 5/2/20

Andreoli MAG, Ashwal LD, Hart RJ, Smith CB, Webb SJ, Tredoux M, Gabrielli F, Cox RM, Hambleton-Jones BB (1995) The impact origin of the morokweng ring structure, southern Kalahari, South Africa. Centennial Geocongress, extended abstracts, Congr Geol Soc S Afr, Johannesburg, 541-544

Baier B, Berckhemer H, Gajewski D, Green RWE, Grimsel C, Prodehl C, Vees R (1983) Deep seismic sounding in the area of the Damara Orogen, Namibia, South West Africa. In: Martin H, Eder FW (eds) Intracontinental Fold Belts. Springer Verlag, Berlin, pp 885–900

Bailey D, Whaler K, Zengeni T (2000a) Comparison of geoelectric and seismic reflection models of the Zambezi Valley basins, northern Zimbabwe. Geophys J Int 142:898–914

Bailey D, Whaler KA, Zengeni T, Jones PC, Gwavava O (2000b) A magnetotelluric model of the Mana Pools basin, Northern Zimbabwe. J Geophys Res 105(5):11185–11202

Balmino G, Vales N et al (2012) Spherical harmonic modelling to ultra-high degree of Bouguer and Isostatic anomalies. J Geod 86 (7):499–520. https://doi.org/10.1007/s00190-011-0533-4

Barker W (1992) Geophysical studies of the Limpopo Belt. Unpublished MSc thesis. University of the Witwatersrand, Johannesburg

Barkhuizen JG, Matthews PE (1990) Gravity modelling of the Natal thrust front: a mid-proterozoic crustal suture in southeastern Africa. In: Geocongress'90, extended abstracts: Cape Town, Geol Soc S Afr, 32–35

Barrett DM (1977) The Agulhas Plateau off southern Africa: a geophysical study. Geol Soc Am Bull 88:749–763

Barton JM (Jr), Moyes AB (1990) Cooling patterns in western Dronning Maud Land, Antarctica and southeastern Africa, and their implication to Gondwana. Zbl Geol Paläeont, I(1/2):33–43

Barton JM Jr, Klemd R, Allsopp HL, Auret SM, Copperthwaite Y (1987) The geology and geochronology of the Annandagstopane granite, western Dronning Maud Land. Contrib Mineral Petrol 97:488–496

Bauer K, Neben S, Schrekenberger B, Emmerman R, Hinz K, Jokat W, Schultz A, Trumbull R, Weber K (2000) Deep structure of the Namibia continental margin as derived from integrated geophysical studies. J Geophys Res 105:25829–25853

Beattie J (1909) Report on the magnetic survey of South Africa. Cambridge University Press, New York

Becker T, Garoeb H, Ledru P, Milesi J-P (2005) The Mesoproterozoic event within the Rehoboth basement inlier of Namibia: review and new aspects of stratigraphy, geochemistry, structure and plate tectonic setting. S Afr J Geol 108:465–492

Bloch S, Hales AL, Landisman M (1969) Velocities in the crust and upper mantle of southern Africa from multi-mode surface wave dispersion. Bull Seism Soc Am 59:1599–1629

Bonvalot S, Balmino G et al (2012) World Gravity Map. Bureau Gravimetrique International (BGI), map, CGMW-BGI-CNES-IRD (ed), Paris

Borchers R (1964) Exploration of the Witwatersrand and its extensions. In: Haughton SH (ed) The geology of some ore deposits in Southern Africa, 1:1–24

Breitkopf JH (1988) Iron formations related to mafic volcanism and ensialic rifting in the Southern Margin Zone of the Damara orogen, Namibia. Precamb Res 38:111–130

Brownfield ME (2016) Assessment of undiscovered oil and gas resources of the Mozambique Coastal Province, East Africa. In: Brownfield ME (ed) Geologic assessment of undiscovered hydrocarbon resources of Sub-Saharan Africa. US Geol Surv Digital Data Series 69-GG(10): pp13

Bűhn B, Stannistreet IG, Okrusch M (1992) Late Proterozoic outer shelf manganese and iron deposits at Otjosondu (Namibia) related to the Damaran ocean opening. Econ Geol, SEG 87(5):1393–1411

Campbell G (2011) Exploration geophysics of the Bushveld Complex in South Africa. Leading Edge 30:622–637

Carlson RW, Grove TL, De Wit MJ, Gurney JJ (1996) Program to study crust and mantle of the Archaean craton in southern Africa. Eos 77(29):273–277

Chetty P, Green RWE (1977) Seismic refraction observations in the Transkei Basin and adjacent areas. Mar Geophys Res 3:197–208

Chevrot S, Zhao L (2007) Multiscale finite-frequency Rayleigh wave tomography of the Kaapvaal Craton. Geophys J Int 169:201–215

Clemson J, Cartwright J, Booth J (1997) Structural segmentation and the influence of basement structure on the Namibian passive margin. J Geol Soc London 154:477–482

Cornell DH, Thomas RJ, Moen HFG, Reid DL, Moore JM, Gibson RL (2006) The Namaqua-Natal Province. In: Johnson MR, Anhaeusser CR, Thomas RJ (eds) The Geology of South Africa, 325–373

Cornell DH, Van Schijndel V, Ingolfsson O, Schersten A, Karlsson L, Wojtyla J, Karlsson K (2011) Evidence from Dwyka tillite cobbles of Archaean basement beneath the Kalahari sands of southern Africa. Lithos 125:482–502

Corner B (1983) An interpretation of the aeromagnetic data covering the western portion of the Damara Orogen in South West Africa/Namibia. In: Miller R McG (ed) Evolution of the Damara Orogen of South West Africa/Namibia, National Geodynamics Programme, Spec Publ Geol Soc S Afr 11:339–354

Corner B (1989) The Beattie anomaly and its significance for crustal evolution within the Gondwana framework. S Afr Geophys Ass, First technical meeting, Extended abstracts, 15–17

Corner B (1994a) Crustal framework of the Kaapvaal Province from geophysical data. In: Proterozoic Crustal and Metallogenic Evolution, Conf Abstr, Windhoek

Corner B (1994b) Geological evolution of western Dronning Maud Land within a Gondwana Framework: Geophysics Subprogramme. Final Rep SA Committee for Antarctic Research (SACAR), p 21
Corner B (1998) A geophysical perspective of the Kaapvaal Province. S Afr Geophys Rev 2:19–28
Corner B (2000) Crustal framework of Namibia derived from magnetic and gravity data. Communs Geol Surv Namibia, Henno Martin Special 12:13–19
Corner B (2008) The crustal framework of Namibia derived from an integrated interpretation of geophysical and geological data. In: The Geology of Namibia, Miller R McG (ed) Ministry of Mines and Energy, Namibia. 1(2):1–9
Corner B (2015) Gravity and magnetic studies of the Kaapvaal Craton. In: De Beer JH (ed) The History of Geophysics in Southern Africa, ISBN 978-1-920689-80-3, Sun Media, 139–146
Corner B, Groenewald PB (1991) Gondwana reunited. Leader page, In: S Afr J Ant Res 21(2):172
Corner B, Swart R (1997) Structural insights gained from a comparison of offshore Namibia satellite data with onshore magnetic and gravity data. Poster presentation, In: Proc 5th Technical Meeting, S Afr Geophys Ass, Swakopmund
Corner B, Wilsher WA (1989) Structure of the Witwatersrand Basin derived from interpretation of aeromagnetic and gravity data. In: Garland GD (ed) Proceedings of Exploration 87, Ontario Geological Survey, Special Volume 3:532–546
Corner B, Wilsher WA, Du Plessis JG, Durrheim RJ, Nicolaysen LO, Du Plessis A (1986a) Bouguer gravity map of the Witwatersrand basin. Published by the Dept Geophys, Witwatersrand University
Corner B, Niccol SL, Wilsher WA, Durrheim RJ (1986b) Aeromagnetic map of the Witwatersrand basin—total field intensity upward continued by 500m. Published by Dept Geophys, Witwatersrand University
Corner B, Durrheim RJ, Nicolaysen LO (1986c) The structural framework of the Witwatersrand Basin as revealed by gravity and aeromagnetic data. In: Proc Geocongress86, Extended Abstracts, Geol Soc S Afr, 27–30
Corner B, Durrheim RJ, Nicolaysen LO (1990) Relationships between the Vredefort structure and the Witwatersrand basin within the tectonic framework of the Kaapvaal craton as interpreted from regional gravity and aeromagnetic data. Tectonophysics 171 (1-4):49–61
Corner B, Maccelari JCD, Niccol S (1991) Major magnetic anomalies in western Dronning Maud Land: their origin and possible correlates in southern Africa. In Abstracts: Sixth Int Ant Earth Sci Symp, Tokyo, National Institute of Polar research, 113
Corner B, Reimold WU, Brandt D, Koeberl C (1997) Morokweng impact structure, Northwest Province, South Africa: geophysical imaging and shock petrographic studies. Earth Sci Planet Lett 146:351–364
Corner B, Cartwright J, Swart R (2002) Volcanic passive margin of Namibia: a potential fields perspective. Geol Soc Am Spec Paper 362:203–220
Corner B, Verran DR, Hildebrand PR (2012) Geophysical interpretation of the nature and extent of the Xade Complex, Botswana. S Afr J Geol, 115(4), JM Moore Special Volume: 485–498
Dalziel IWD (1991) Pacific margins of Laurentia and East Antarctica-Australia as a conjugate rift pair: evidence and implications for an Eocambrian supercontinent. Geology 19:598–601
Dalziel IWD, Mosher S, Gahagan LM (2000) Laurentia-Kalahari collision and the assembly of Rodinia. J Geology 108:499–513
De Beer JH (ed) (2015a) The History of Geophysics in Southern Africa. Sun Media, Stellenbosch
De Beer JH (2015b) Ultra-deep electrical soundings to investigate the southern African crust and upper mantle. In: De Beer JH (ed) The History of Geophysics in Southern Africa. Sun Media, Stellenbosch, pp 217–230
De Beer JH (2015c) Geomagnetic induction studies in southern Africa. In: De Beer JH (ed) The History of Geophysics in Southern Africa. Sun Media, Stellenbosch, pp 231–236
De Beer JH, Gough DI (1980) Conductive structures in southernmost Africa: a magnetometer array study. Geophys J Int 63(2):479–95
De Beer JH, Meyer R (1984) Geophysical characteristics of the Namaqua-Natal Belt and its boundaries, South Africa. J Geodyn 1:473–494
De Beer JH, Stettler EH (1988) Geophysical characteristics of the southern African continental crust. Special Issue, J Petrology, pp 163–184
De Beer JH, Stettler EH (1992) The deep structure of the Limpopo Belt from geophysical studies. Precamb Res 55:173–186
De Beer JH, Van Zijl JS, Huyssen RM, Hugo PL, Joubert SJ, Meyer R (1976) A magnetometer array study in South West Africa, Botswana and Rhodesia. Geophys J Int 45(1):1–7
De Beer JH, Van Zijl JSV, Gough DI (1982a) The Southern Cape conductive belt (South Africa): its composition, origin and tectonic significance. Tectonophysics 83:205–225
De Beer JH, Huyssen RM, Joubert SJ, Van Zijl JS (1982b) Magnetometer array studies and deep Schlumberger soundings in the Damara orogenic belt South West Africa. Geophys J Int 70(1):11–29
De Wit MJ, Tinker J (2004) Crustal sutures across the central Kaapvaal Craton from deep seismic reflection data. S Afr J Geol 107 (1/2):185–206
Durrheim RJ (1987) Seismic reflection and refraction studies of the deep structure of the Agulhas Bank. Geophys J Roy Astr Soc 89:395–398
Durrheim RJ, Green RWE (1992) A seismic refraction investigation of the Archaean Kaapvaal Craton, South Africa, using mine tremors as the energy source. Geophys J Int 108:812–832
Durrheim RJ, Mooney WD (1994) Evolution and the Precambrian lithosphere: seismological and geochemical constraints. J Geophys Res 99(B8):15359–15374
Durrheim RJ, Nicolaysen LO, Corner B (1991) A deep seismic reflection profile across the Archaean-Proterozoic Witwatersrand basin, South Africa. In: Meissner R, Brown L, Dürbaum H-J, Franke W, Fuchs K, Seifert F (eds) Continental lithosphere: deep seismic reflections. Am Geophys Union, Geodynamics Series 22:213–224
Durrheim RJ, Barker WH, Green RWE (1992) Seismic studies in the Limpopo. Precam Res 55:187–200
Du Plessis AJ, Thomas RJ (1991) Discussion on the Beattie set of magnetic anomalies. In: Proc 2nd Technical Meeting, Extended Abstracts, S Afr Geophys Ass, Pretoria, 57–59
Eberle D, Andritzky G, Wackerle R (1995) The new magnetic data set of Namibia: its contributions to the understanding of crustal evolution and regional distribution of mineralisation. Communs Geol Surv Namibia 10:141–150
Eglington BM (2006) Evolution of the Namaqua-Natal Belt, southern Africa—a geochronological and isotope geochemical review. J Afr Earth Sci 46:93–11
Eglington BM, Armstrong RA (2003) Geochronological and isotopic constraints on the Mesoproterozoic Namaqua-Natal Belt: evidence from deep borehole intersections in South Africa. Precam Res 125:179–189
Eglington BM, Armstrong RA (2004) The Kaapvaal Craton and adjacent orogens, southern Africa: a geochronological database and overview of the geological development of the craton. S Afr Jour Geol 107(1/2):13–32
Evans R, Jones A, Garcia X, Muller M, Hamilton M, Evans SFS, Spratt J, Webb S, Jelsma H, Hutchins D (2011) Electrical

lithosphere beneath the Kaapvaal Craton, southern Africa. J Geophys Res 116:B04105
Fouch M, James DE, VanDecar JC, Van der Lee S (2004) Mantle seismic structure beneath the Kaapvaal and Zimbabwe Cratons. S Afr J Geol 107:33–44
Frimmel HE (2008) Neoproterozoic Gariep Orogen. In: Miller R McG (ed) The Geology of Namibia, Ministry of Mines and Energy, Namibia. 2(14):1–39
Fullea J, Muller MR, Jones AG (2011) Electrical conductivity of continental lithospheric mantle from integrated geophysical and petrological modeling: application to the Kaapvaal Craton and Rehoboth Terrane, southern Africa. J Geophys Res 116:B10202
Fűtterer D (1989) Crustal transects from the Weddell Sea to Dronning Maud Land. Poster presentation, IGC, Washington DC
Gaisford J (2010) Geochronology, petrography and tectonic implications of lithologies and base metal mineralization encountered in NW Ngamiland, Botswana. University of Cape Town, BSc Honours Dissertation, p 55
Gane PG, Atkins AR, Sellschop JPF, Seligman P (1956) Crustal structure in the Transvaal. Bull Seism Soc Am 46:293–316
Gladczenko TP (1994) Crustal structure and composition of selected transient large igneous provinces. Cand Scient Thesis (unpubl), Applied Geophysics, Univ Oslo, p 220
Golynsky AV, Aleshkova D (2000) Regional magnetic anomalies of the Weddell Sea region and their geological significance. Polarforsch 67(3):101–117
Golynsky AV, Jacobs J (2001) Grenville-age versus Pan-African magnetic anomaly imprints in western Dronning Maud Land, East Antarctica. J Geol 109:136–142
Golynsky AV, Masolov VN, Jokat W (2000a) Magnetic anomaly map of the Weddell Sea region: a new compilation of the Russian data. Polarforschung 67(3):125–132
Golynsky AV, Grikurov GE, Kamenev EN (2000b) Geological significance of regional magnetic anomalies in Coats Land and western Dronning Maud Land. Polarforsch 67(3):91–99
Goscombe B, Hand M, Gray D (2003) Structure of the Kaoko Belt, Namibia: progressive evolution of a classic transpressional orogen. J Struct Geol 25:1049–1081
Goscombe B, Gray D, Hand M (2005) Extrusional tectonics in the core of a transpressional orogen; the Kaoko Belt. Namibia. J Petrol 46 (6):1203–1241
Gough DI, De Beer JH, Van Zijl JSV (1973) A magnetometer array study in southern Africa. Geophys J Int 34(4):421–433
Grantham GH, Groenewald PB, Hunter DR (1988) Geology of the northern HU Sverdrupfjella, western Dronning Maud Land, and implications for Gondwana reconstructions. S Afr J Ant Res. 18:2–10
Green RWE (1980) A data acquisition and processing system, with application to seismological problems in southern Africa. Unpublished Ph.D. thesis. University of the Witwatersrand, Johannesburg
Green RWE (1983) Seismic refraction observations in the Damara Orogen and flanking craton, and their bearing on deep-seated processes in the Orogen. In: Miller R McG (ed) Evolution of the Damara Orogen of South West Africa/Namibia. National Geodynamics Programme. Geol Soc S Afr, Spec Publ 11:355–367
Green RWE, Chetty P (1990) Seismic studies in the basement of the Vredefort structure. Tectonophysics 171:105–113
Green RWE, Durrheim RJ (1990) A seismic refraction investigation of the Namaqualand Metamorphic Complex, South Africa. J Geophys Res 95(B12):19927–19932
Green RWE, Hales AL (1966) Seismic refraction measurements in the south-western Indian Ocean. J Geophys Res 71:1637–1647
Groenewald PB, Grantham GH, Watkeys MK (1991) Geological evidence for a Proterozoic to Mesozoic link between south-eastern Africa and Dronning Maud Land, Antarctica. In: Findlay RH, Banks HR, Veevers JJ, Unrug R (eds) Gondwana 8: Assembly, Evolution and Dispersal. Balkema AA, Rotterdam
Hälbich IW (1993) The Cape Fold Belt-Agulhas platform transect across the Gondwana suture in Southern Africa. Global Geoscience Transect 9. International Lithosphere Program, Publication No 202. American Geophys Union and the Inter-Union Commission on the Lithosphere
Hales AL, Nation JB (1972) A crustal structure profile on the Agulhas Bank. Bull Seism Soc Am 62:1029–1051
Hales AL, Sacks IS (1959) Evidence for an intermediate layer from crustal structure studies in the eastern Transvaal. Geophys J 2 (1):15–33
Halpern M (1970) Rb-Sr date of possibly 3 billion years for a granitic rock from Antarctica. Sci, 169:977–978, Washington
Hanson RE, Crowley JL, Bowring SA, Ramezani J, Gose WA, Dalziel IWD, Pancake JA, Seidel EK, Blenkinsop TG, Mukwakwami J (2004) Coeval large scale magmatism in the Kalahari and Laurentian Cratons during Rodinia assembly. Science 304:1126–1129
Hanson RE, Harmer RE, Blenkinsop TG, Bullen DS, Dalziel IWD, Gose WA, Hall RP, Kampanzu AB, Key RM, Mukwakwami J, Munyanyiwa H, Pancake JA, Seidel EK, Ward SE (2006) Mesoproterozoic intraplate magmatism in the Kalahari Craton: a review. J Afr Earth Sci 46:141–167
Hart RJ, Nicolaysen LO, Gale NH (1981) Radioelement concentrations in the deep profile through Precambrian basement of the Vredefort structure. J Geophys Res 86(B11):10639–10652
Hart RJ, Andreoli MA, Tredoux M, De Wit MJ (1990a) Geochemistry across an exposed section of Archaean crust at Vredefort, South Africa: with implications for mid-crustal discontinuities. Chem Geol 82:21–50
Hart RJ, Andreoli MA, Smith CB, Otter ML, Durrheim R (1990b) Ultramafic rocks in the centre of the Vredefort structure (South Africa): possible exposure of the upper mantle? Chem Geol 83(3–4):233–248
Harvey JD, De Wit MJ, Stankiewicz J, Doucoure CM (2001) Structural variations of the crust in the south-western Cape deduced from seismic receiver functions. S Afr J Geol 104:231–242
Hoak TE, Klawitter AL, Dommer CF, Scaturro PV (2014) Integrated exploration of the Owambo Basin, onshore Namibia: hydrocarbon exploration and implications for a modern frontier basin. Search and Discovery article 10609, adopted from poster presentation at AAPG Convention, Houston, Texas
Hoal KO, Hoal BG, Griffin WL, Armstrong RA (2000) Characterisation of the age and nature of the lithosphere in the Tsumkwe region of Namibia. Comms geol Surv Namibia 12:21–28
Hodgkinson G (1989) Palaeomagnetic studies in western Dronning Maud Land, Antarctica. University of the Witwatersrand, MSc dissertation: p155
Hoffman KH (1983) Lithostratigraphy and facies of the Swakop Group of the southern Damara Belt, SWA/Namibia. Spec Publ Geol Soc S Afr 11:43–63
Hoffman KH (1989a) New aspects of lithostratigraphic subdivision and correlation of late Proterozoic to early Cambrian rocks of the southern Damara Belt, and their correlation with the central and northern Damara Belt and the Gariep Belt. Comms Geol Survey Namibia 5:59–67
Hoffman KH (1989b) Aspects of relative age, stratigraphic correlation and origin of metaquartzites and associated Fe-Mn deposits of the Otjosondu mine in the eastern Okahandja district. Geol Survey Namibia, Internal Report
Hunter DR, Corner B, Krynauw JR, Le Roex A, Grantham GH, Groenewald PB, Moyes AB, Bergh HW, Harris C (1991) A recent history of South African earth science research in Antarctica and adjacent regions. S Afr J Ant Res 21(2):173–183

Hunter DR, Johnson MR, Anhaeusser CR, Thomas RJ (2006) Introduction. In: Johnson MR, Anhaeusser CR and Thomas RJ (eds) The Geology of South Africa, 1–7

Jacobs J, Thomas RJ (1994) Oblique collision at about 1.1 Ga along the southern margin of the Kaapvaal continent, southeast Africa. Geol Rundsch 82:322–333

Jacobs J, Thomas RJ (2004) Himalayan-type indenter-escape tectonics model for the southern part of the late Neoproterozoic-early Palaeozoic East African-Antarctic Orogen. Geol 32(8):721–724

Jacobs J, Thomas RJ, Weber K (1993) Accretion and indentation tectonics at the southern edge of the Kaapvaal Craton during the Kibaran (Grenville) orogeny. Geol 21:203–206

Jacobs J, Pisarevsky S, Thomas RJ, Becker T (2008) The Kalahari Craton during the assembly and dispersal of Rodinia. Precam Res 160:142–158

James DE, Fouch MJ, VanDecar JC, Van der Lee S, the Kaapvaal Seismic Group (2001) Tectospheric structure beneath southern Africa. Geophys Res Lett 28(13):2485–2488

James DE, Fouch MJ (2002) Formation and evolution of Archaean cratons: insights from southern Africa. Spec Publ Geol Soc London 199:1–26

James DE, Niu F, Rokosky J (2003) Crustal structure of the Kaapvaal Craton and its significance for early crustal evolution. Lithos 71:413–429

Johnson AC, Aleshkova AD, Barker PF, Golynsky AV, Masolov VN, Smith AM (1992) A preliminary aeromagnetic anomaly compilation map for the Weddell Province of Antarctica. In: Yoshida Y, Kaminuma K, Shiraishi K (eds) Recent progress in Antarctic Earth Science. Terra Pub, Tokyo, pp 545–553

Jones DL, Bates MP, Li ZX, Corner B, Hodgkinson G (2003) Palaeomagnetic results from the ca. 1100 Ma Borgmassivet intrusions in the Ahlmanryggen region of Dronning Maud Land, Antarctica, and tectonic implications. Tectonophysics 375:247–260

Jones AG, Evans RL, Muller MR, Hamilton MP, Miensopust MP, Garcia X, Cole P, Ngwisanyi T, Hutchins D, Fourie CJ, Jelsma H (2009) Area selection for diamonds using magnetotellurics: examples from southern Africa. Lithos 112:83–92

Kasch KW (1986) Tectonic subdivision, lithostratigraphy and structural geology of the Upper Black Nossob River area. Communs Geol Surv SWA/Namibia 2:117–129

Key RM, Ayres N (2000) The 1998 edition of the National geological map of Botswana, 1:1 000 000 scale. J Afr Earth Sci 30(3):427–451

Kgaswane EM, Nyblade AA, Julià J, Dirks PHGM, Durrheim RJ, Pasyanos ME (2009) Shear velocity structure of the crust in southern Africa: evidence for compositional heterogeneity within Archaean and Proterozoic terrains. J Geophys Res 114:B12304

Kgaswane EM, Nyblade AA, Durrheim RJ, Julià J, Dirks PHGM, Webb SJ (2012) Shear wave velocity structure of the Bushveld Complex, South Africa. Tectonophysics 554–557:83–104

Khoza TD, Jones AG, Muller MR, Evans RL, Miensopust MP, Webb SJ (2013a) Lithospheric structure of an Archaean craton and adjacent mobile belt revealed from 2-D and 3-D inversion of magnetotelluric data: example from southern Congo Craton in northern Namibia. J Geophys Res 118(8):4378–4397

Khoza D, Jones AG, Muller MR, Evans RL, Webb SJ, Miensopust M (2013b) Tectonic model of the Limpopo belt: constraints from magnetotelluric data. Precam Res 226:143–156

Ksienzyk AK, Jacobs J (2015) Western Australia-Kalahari (WAlahari) connection in Rodinia: not supported by U/Pb detrital zircon from the Maud Belt (East Antarctica) and the Northampton Complex (Western Australia). Precam Res 259:207–221

Larson AM, Snoke JA, James DE (2006) S-wave velocity structure, mantle xenoliths and the upper mantle beneath the Kaapvaal Craton. Geophys J Int 167:171–186

Li A, Burke K (2006) Upper mantle structure of southern Africa from Rayleigh wave tomography. J Geophys Res 111:B10303

Lindeque AS (2008) Deep crustal profile across the southern Karoo Basin, South Africa. Unpublished MSc thesis. University of Cape Town, Cape Town

Lindeque AS, Ryberg T, Stankiewicz J, Weber M, De Wit MJ (2007) Deep crustal seismic reflection experiment across the southern Karoo Basin, South Africa. S Afr J Geol 110:419–438

Lindeque AS, De Wit MJ, Ryberg T, Weber M, Chevalier L (2011) Deep crustal profile across the southern Karoo Basin and Beattie Magnetic Anomaly, South Africa: an integrated interpretation with tectonic implications. S Afr J Geol 114:265–292

Loots L (2013) Investigation of the crust in the southern Karoo using the seismic reflection technique. Unpublished MSc thesis. University of the Witwatersrand, Johannesburg

Losecke W, Knödel K, Müller W (1988) Magnetotelluric survey in the northern Zambezi valley of Zimbabwe. Tech. Rep. 84.2171.1, Bundesanstalt für Geowissenschaften und Rohstoffe, Hannover, Germany

Maher MJ, Pitts BE (1989) Interpretation of a potential field profile over the Cape Fold Belt. S Afr Geophys Ass., Proc 1st Tech Meeting, Ext Abstr: 135–140

Maiden KJ, Borg G (2011) The Kalahari Copperbelt in central Namibia: controls on copper mineralization. SEG Newslett 87:14–19

Marschall HR, Hawkesworth CJ, Storey CD, Dhuime B, Leat PT, Meyer H-P, Tamm-Buckle S (2010) The Annandagstoppane granite, East Antarctica: evidence for Archaean intracrustal recycling in the Kaapvaal-Grunehogna Craton from Zircon O and Hf isotopes. J Petrol 51(11):2277–2301

Martin PK, Hartnady C (1986) Plate tectonic development of the south-west Indian ocean: a revised reconstruction of East Antarctica and Africa. J Geoph Res 91(B5):4767–4786

Matthews PE (1972) Possible Precambrian obduction and plate tectonics in southeastern Africa. Nat 240:37–39

Maus S, Barckhausen U, Berkenbosch H, Bournas N, Brozena J, Childers V, Dostaler F Fairhead JD, Finn C, Von Frese RRB, Gaina C, Golynsky S (2009) EMAG2: a 2-arc min resolution Earth Magnetic Anomaly Grid compiled from satellite, airborne, and marine magnetic measurements. Geochem Geophys Geosys, Technical Brief 10(8):1–12

McCourt S, Jelsma H (This volume) The Angola Craton

McCarthy T, Rubidge B (2005) The Story of Earth and Life: a Southern Africa perspective on a 4.6 Billion-year Journey. Struik, Cape Town

McCourt S, Armstrong RA, Jelsma H, Mapeo RBM (2013) New U-Pb ages from the Lubango region, southwest Angola: insights into the Proterozoic evolution of Angolan Shield, southern Congo Craton, Africa. J Geol Soc London 170:353–363

McCarthy TS, Corner B, Lombard H, Beukes NJ, Armstrong RA, Cawthorn RG (in Prep.) The Pre-Karoo geology of the southern portion of the Kaapvaal Craton

Meixner HM, Peart RJ (1984) The Kalahari drilling project: a report on the geophysical and geological results of the follow-up drilling to the aeromagnetic survey of Botswana. Botswana Geol Surv Bull 27:224

Miller R McG (1983) The Pan-African Damara Orogen of South West Africa/Namibia. Spec Publ Geol Soc S Afr 11:431–515

Miller R McG (2008a) Neoproterozoic and early Palaeozoic rocks of the Damara Orogen, In: Miller R McG (ed) The Geology of Namibia, Ministry of Mines and Energy, Namibia. 2(13):1–410

Miller R McG (2008b) Palaeoproterozoic metamorphic complexes, In: Miller R McG (ed) The Geology of Namibia, Ministry of Mines and Energy, Namibia. 1(4):9–11

Miller R McG (2008c) The Sinclair Supergroup. In: Miller R McG (ed) The Geology of Namibia, Ministry of Mines and Energy, Namibia. 1(8):1–104

Midzi V, Ottemőller L (2001) Receiver function structure beneath three southern African seismic broadband stations. Tectonophysics 339:443–454

Miensopust MP, Jones AG, Muller MR, Garcia X, Evans RL (2011) Lithospheric structures and Precambrian terrane boundaries in northeastern Botswana revealed through magnetotelluric profiling as part of the Southern African Magnetotelluric Experiment. J Geophys Res 116(B2)

Moen HFG (1999) The Kheis tectonic province, southern Africa: A lithostratigraphic perspective. S Afr J Geol 102:27–42

Moores EM (1991) Southwest US-East Antarctic (SWEAT) connection: a hypothesis. Geology 19:425–428

Moyes AB, Barton JM, Groenewald PB (1993) Late Proterozoic to early Palaeozoic tectonism in Dronning Maud Land, Antarctica: supercontinental fragmentation and amalgamation. J Geol Soc London 150(5):833–842

Muller MR, Jones AG, Evans RL, Grütter HS, Hatton C, Garcia X, Hamilton MP, Miensopust MP, Cole P, Ngwisanyi T, Hutchins D (2009) Lithospheric structure, evolution and diamond prospectivity of the Rehoboth Terrane and western Kaapvaal Craton, southern Africa: constraints from broadband magnetotellurics. Lithos 112:93–105

Naudé C (2012) Target selection from airborne magnetic and radiometric data in the Steinhausen area, Namibia. MSc Thesis, Geology Dept, Rhodes University, p 138

Nguuri TK, Gore J, James DE, Webb SJ, Wright C, Zengeni TG, Gwavava O, Snoke JA, the Kaapvaal Seismic Group (2001) Crustal structure beneath southern Africa and its implications for the formation and evolution of the Kaapvaal and Zimbabwe Cratons. Geophys Res Lett 28(13):2501–2504

Ni S, Helmberger DV (2003) Seismological constraints on the South African superplume; could be the oldest distinct structure on earth. Earth Planet Sci Lett 206:119–131

Nicolaysen LO, Burger AJ (1965) Note on an extensive zone of 1000 million-year old metamorphic and igneous rocks in southern Africa. Sci Terres 10:497–518

Niu F, James DE (2002) Fine structure of the lowermost crust beneath the Kaapvaal Craton and its implications for crustal formation and evolution. Earth Planet Sci Lett 200:121–130

Nyblade AA, Robinson SW (1994) The African Superswell. Geophys Res Lett 21(9):765–768

Odgers ATR, Du Plessis A (1993) Interpretation of a regional reflection seismic survey in the north-eastern Bushveld Complex. Proceedings of the third technical meeting, S Afr Geophys Ass, Cape Town. Expanded Abstracts. 125–129

Odgers ATR, Hinds RC, Von Gruenewaldt G (1993) Interpretation of a seismic reflection survey across the southern Bushveld Complex. S Afr J Geol 96:205–212

Parsiegla N, Gohl K, Uenzelmann-Neben G (2007) Deep crustal structure of the sheared South African continental margin: first results of the Agulhas-Karoo Geoscience Transect. S Afr J Geol 110:393–406

Pavlenkova NI (1987) Properties of the middle and lower crust in platform areas. Annales Geophysicae 5B:651–656

Pitts BE, Maher MJ, De Beer JH, Gough DI (1992) Interpretation of the magnetic, gravity and magnetotelluric data across the Cape Fold Belt and Karoo basin. In: De Wit MJ, Ransome IDG (eds) Inversion tectonics of the Cape Fold Belt. Karoo and Cretaceous basins of southern Africa, Balkema, Rotterdam, Netherlands, pp 27–32

Pouliquen G and Key R (2007) 3D Geometry of the Xade Complex inferred from gravity and magnetic data. In: Milkeriet B (ed) Proceedings of Exploration 07, 5th Decennial International Conference on minerals exploration, Toronto, 1043–1047

Pretorius DA (1986) The Witwatersrand Basin - surface and subsurface geology and structure. 1:500 000 map enclosure, In: Anhaeusser CR and Maske S (eds) Mineral Deposits of South Africa, J Geol Soc S Afr, p 2376

Pretorius CC, Jamieson AA, Irons C (1989) Seismic exploration in the Witwatersrand Basin, Republic of South Africa. In: Garland GD (ed) Proceedings of Exploration 87, Ontario Geological Survey, Spec 3:241–253

Pretorius CC, Muller MR, Larroque M, Wilkens C (2003) A review of 16 years of hardrock seismics on the Kaapvaal Craton. In: Eaton DW, Milkeriet B, Salisbury MH (eds) Hardrock seismic exploration. Society of Exploration Geophysicists, Geophysical Developments Series, 10:247–268

Pretorius CC, Gibson MAS, Snyman Q (2010) Development of high-resolution 3D vertical seismic profiles. In: Proceedings 4th Int Platinum Conf, S Afr Inst Mining & Metallurgy, 47–56

Quesnel Y, Weckmann U, Ritter O, Stankiewicz J, Lesur V, Mandea M, Langlais B, Sotin C, Galdeano A (2009) Simple models for the Beattie Magnetic Anomaly in South Africa. Tectonophysics 478:111–118

Rabinowitz PD, LaBrecque J (1979) The Mesozoic south Atlantic Ocean and evolution of its continental margins. J Geoph Res 84 (B11):5973–6002

Rankin W (2015) Cross border correlation of the Damara Belt in Namibia and equivalent lithologies in northwestern Botswana from potential field and magnetotelluric interpretations. MSc dissertation, Univ. Witwatersrand, Johannesburg, p 542

Raveloson A, Nyblade A, Fishwick S, Mangongolo A, Master S (2015) The upper mantle seismic velocity structure of south-central Africa and the seismic architecture of Precambrian lithosphere beneath the Congo Basin. In: Geology and Resource Potential of the Congo Basin Springer Verlag, Berlin, pp. 3–18

Reeves CV (1978) Interpretation of the reconnaissance aeromagnetic survey of Botswana, Final Report, Terra Surveys Ltd. Geol Surv Dept Botswana, pp199 (and Appendices)

Richards JR (2000) Lineaments revisited. SEG Newsletter, 42, July 2000

Riedel S, Jacobs J, Jokat W (2013) Interpretation of new regional aeromagnetic data over Dronning Maud Land (East Antarctica). Tectonophysics 585:161–171

Ritsema J, Van Heijst H (2000) New seismic model of the upper mantle beneath Africa. Geology 28:63–66

Ritter O, Weckmann U, Vietor T, Haak V (2003) A magnetotelluric study of the Damara belt in Namibia 1. Regional scale conductivity anomalies. Phys Earth Planet Inter 138:71–90

Schalk KEL (1988) Pre-Damaran basement rocks in the Rehoboth and southern Windhoek districts (areas 2217D, 2316, 2317A-C) a regional description. Unpublished report of the Geol Surv Namibia, IR0074 of Namibia, (1/2): p185

Scheiber-Enslin S, Ebbing J, Webb SJ (2014) An integrated study of the Beattie Magnetic Anomaly, South Africa. Tectonophysics 636:228–243

Schmitz MD, Bowring SA (2004) Lower crustal granulite formation during Mesoproterozoic Namaqua-Natal collisional orogenesis, southern Africa. S Afr J Geol 107:261–284

Schmitz MD, Bowring SA, De Wit MJ, Gartz V (2004) Subduction and terrane collision stabilized the western Kaapvaal Craton tectosphere 2.9 billion years ago. Earth Planet Sci Lett 222:363–376

Seth B, Kröner A, Mezger K, Nemchin AA, Pidgoen RT, Okrusch M (1998) Archaean to Neoproterozoic magmatic events in the Kaoko Belt of NW Namibia and their geodynamic significance. Precambr Res 92:341–363

Singletary SJ, Hanson RE, Martin MW, Crowley JL, Bowring SA, Key RM, Ramokate LV, Direng BB, Krol MA (2003) Geochronology of basement rocks in the Kalahari desert of Botswana, and implications for regional Proterozoic tectonics. Precamb Res 121:47–71

Skinner EM, Truswell JF (2006) Kimberlites. In: Johnson MR, Anhaeusser CR and Thomas RJ (eds) The Geology of South Africa, 651–59

Sonangol (Gas Natural) and Namcor (2009) Snowball earth and the search for Neoproterozoic petroleum systems in Angola and Namibia. Joint presentation, AAPG, Rio de Janeiro

Spence D (1970) A seismic refraction study of sedimentary structure on the Agulhas Bank south of Cape Infanta. Unpublished MSc thesis. University of the Witwatersrand, Johannesburg

Stankiewicz J, Chevrot S, Van Der Hilst RD, De Wit MJ (2002) Crustal thickness, discontinuity depth, and upper mantle structure beneath southern Africa: constraints from body wave conversions. Phys Earth Planet Inter 130:235–251

Stankiewicz J, Ryberg T, Schulze A, Lindeque A, Weber MH, De Wit MJ (2007) Initial results from wide-angle seismic refraction lines in the southern Cape. S Afr J Geol 110(2/3):407–418

Stankiewicz J, Ryberg T, Parsiegla N, Gohl K, Trumbull R, Weber M (2008) Crustal structure of the southern margin of the African plate: results from geophysical experiments. J Geophys Res 113:B10313

Stettler EH, Prinsloo J, Hauger ME (1998) A geophysical transect between Avondale on the Kheis tectonic province and Keimoes on the Namaqua Metamorphic Province, South Africa. S Afr Geophys Rev 2:83–93

Stettler EH, Prinsloo J, Hauger ME, du Toit MC (1999) A crustal geophysical model for the Kheis tectonic province, South Africa, based on magnetotelluric, reflection seismic, gravity and magnetic data sets. S Afr Geophys Rev 3:54–68

Storey BC, Pankhurst R, Johnson A (1994) The Grenville Province within Antarctica: a test of the SWEAT hypothesis. J Geol Soc London 151(1):1–4

Stuart GW, Zengeni TG (1987) Seismic crustal structure of the Limpopo mobile belt. Tectonophysics 144:323–335

Thomas RJ (1989) A tale of two terranes. S Afr J Geol 92:306–321

Thomas RJ, Du Plessis AJ, Fitch F, Marshall CGA, Miller JA, Von Brunn V, Watkeys MK (1992) Geological studies in southern Natal and Transkei: implications for the Cape Orogen. In: De Wit MJ, Ransome IGD (eds) Inversion tectonics of the Cape Fold Belt, Karoo and Cretaceous basins of southern Africa. Balkema, Rotterdam, pp 229–236

Tinker JH (2001) Stratigraphic and structural interpretation of seismic reflection data across selected sections of the Kaapvaal Craton. Unpublished MSc thesis. University of Cape Town, Cape Town

Tinker J, De Wit MJ, Grotzinger J (2002) Seismic stratigraphic constraints on Neoarchean-Palaeoproterozoic evolution of the western margin of the Kaapvaal Craton. S Afr J Geol 105:107–134

Tucholke BE, Houtz RE, Barrett DM (1981) Continental crust beneath the Agulhas Plateau, Southwest Indian Ocean. J Geophys Res 86:3791–3806

Van Zijl JSV (1978) The relationship between the deep electrical resistivity structure and tectonic provinces in Southern Africa. Trans Geol Soc S Afr 81:129–142

Van Zijl JS, De Beer JH (1983) Electrical structure of the Damara orogen and its tectonic significance. Spec Publ Geol Soc S Afr 11:369–379

Wang Y, Wen L (2007) Geometry and P and S velocity structure of the 'African Anomaly'. J Geophys Res 112:B05313

Watts AB, Fairhead JD (1999) A process-oriented approach to modelling the gravity signature of continental margins. Leading Edge 18(2):258–263

Weckmann U (2012) Making and breaking of a continent: following the scent of geodynamic imprints on the African continent using electromagnetics. Surv Geophys 33(1):107–134

Weckmann U, Ritter O, Haak V (2003) A magnetotelluric study of the Damara Belt in Namibia 2. MT phases over 90° reveal the internal structure of the Waterberg Fault/Omaruru Lineament. Phys Earth Planet Inter 138:91–112

Weckmann U, Jung A, Branch T, Ritter O (2007a) Comparison of electrical conductivity structures and 2D magnetic model along two profiles crossing the Beattie Magnetic Anomaly, South Africa. S Afr J Geol 110:449–464

Weckmann U, Ritter O, Jung A, Branch T, De Wit M (2007b) Magnetotelluric measurements across the Beattie Magnetic Anomaly and the Southern Cape conductive belt South Africa. J Geophys Res 112:B05416

Weckmann U, Ritter O, Becken M, Pek J, De Wit M (2008) Electrical conductivity images of South African continental collision zones. Eos Trans AGU, 89(53), Fall meeting supplement, Abstract GP41A–0779

Weckmann U, Ritter O, Chen X, Tietze K, De Wit M (2012) Magnetotelluric image linked to surface geology across the Cape fold belt. South Africa. Terra Nova. 24(3):207–212

Whaler K, Zengeni T (1993) An audiofrequency magnetotelluric traverse across the Mana Pools basin, northern Zimbabwe. Geophys J Int 114:673–686

Whitehead BA, Harris C, Sloan A, Olianti C (2016) Origin of low δ18O values in the Cretaceous Koegelfontein Complex: evidence for pre-existing ^{18}O-depletion in the country rock. In: 35th Int Geol Congress Abstracts, Poster Presentation, Cape Town

Willmore PL, Hales AL, Gane PG (1952) A seismic investigation of crustal structure in the western Transvaal. Bull Seism Soc Am 42(1):53–80

Wood M (2015) Soft rock exploration seismics: the search for oil and gas. In: De Beer JH (ed) The History of Geophysics in Southern Africa. Sun Media, Stellenbosch, pp 473–484

Wright JA, Hall J (1990) Deep seismic profiling in the Nosop Basin, Botswana: cratons, mobile belts and sedimentary basins. Tectonophysics 173(1–4):333–343

The Tectonic History of the Southern Adamastor Ocean Based on a Correlation of the Kaoko and Dom Feliciano Belts

3

Miguel Angelo Stipp Basei, Hartwig Ernest Frimmel, Mario da Costa Campos Neto, Carlos Eduardo Ganade de Araujo, Neivaldo Araujo de Castro, and Claudia Regina Passarelli

Abstract

Closure of the southern Adamastor Ocean led to the development of the Neoproterozoic-Early Cambrian orogens on both margins of the present South Atlantic Ocean, which preserve a rich record of West Gondwana assembly and large-scale crustal evolution. Here we describe the distinct stages and tectonic regimes related to the evolution of the southern Adamastor Ocean as reconstructed from the geological record in southeastern Brazil, Uruguay and southwestern Africa. The welding of the Rio de la Plata/Paranapanema and African cratons was the result of a long history that generated the Dom Feliciano Belt in southeastern Brasil and Uruguay and its African counterparts, the Kaoko, Gariep and Saldania belts. Recent ideas and previous hypotheses are discussed and integrated into a tectonic model for the evolution of the southern Adamastor Ocean, largely based on comparison of the Neoproterozoic Kaoko and Dom Feliciano belts. The history of the southern Adamastor Ocean spans between 900 and 590 Ma, from the earliest records of magmatism related to Rodinia break-up (980–780 Ma), through the climax of the extensional phase that led to the opening of a vast ocean (780–640 Ma). Tectonic inversion led to subduction towards the east (in today's coordinates), which generated an extensive magmatic arc on the western margin of the Congo and Kalahari cratons (640–600 Ma) and eventually the collision between the Congo and Rio de La Plata Cratons (600–590 Ma) juxtaposing the magmatic arc and the western South American schist belts. At around 530 Ma, still under the influence of plate convergence, a positive flower structure was generated causing the extrusion of the Granite Belt, the eroded remnant of the magmatic arc, and reactivation of the doubly verging thrusts that affected the supracrustal units of the Kaoko and Dom Feliciano belts. Only at that time did deformation reach the Itajaí and Nama foreland basins.

Keywords

Kaoko and Dom Feliciano belts • Adamastor Ocean Sierra Ballena-Major Gercino suture zone • South African–South America connection

3.1 Introduction

Since the formation of the first larger masses of continental crust and preservation thereof, several cycles of continental dispersion and subsequent convergence of continental fragments have taken place. By the end of the Precambrian, four large supercontinental masses had formed (Hoffman 1991): Laurentia (North America), Gondwana (southern continents), Baltica and Siberia. In addition, several smaller peri-Gondwana blocks existed.

Comparative studies of the Western Gondwana segments in South America and Africa started with Almeida (1965), Hurley et al. (1967) and Porada (1979), and were followed by many more. In South America, recent geologic syntheses, such as those by Kröner and Cordani (2003), Cordani et al. (2010) and Brito Neves and Fuck (2013), divided the Precambrian rocks into two major geotectonic domains, roughly bounded by the Transbrasiliano Lineament: the Amazonas or pre-Brasiliano domain (of Laurentian affinity) and the Brasiliano domain (of Gondwana affinity). The latter

M. A. S. Basei (✉) · M. da C. Campos Neto · C. R. Passarelli
Geosciences Institute, University of São Paulo, São Paulo, Brazil
e-mail: baseimas@usp.br

H. E. Frimmel
Institute of Geography and Geology, University of Würzburg, Würzburg, Germany

H. E. Frimmel
Department of Geological Sciences, University of Cape Town, Rondebosch, South Africa

C. E. G. de Araujo
Geological Survey of Brazil, Rio de Janeiro, Brazil

N. A. de Castro
Geosciences Institute, Federal University of Santa Catarina, Florianópolis, Brazil

S. Siegesmund et al. (eds.), *Geology of Southwest Gondwana*, Regional Geology Reviews,
https://doi.org/10.1007/978-3-319-68920-3_3

comprises a Neoproterozoic framework of orogens adjacent to cratonic entities, such as the Rio de la Plata, Paranapanema and São Francisco cratons (Alkmim and Teixeira 2017; Assumpção et al. 2017; Barbosa and Barbosa 2017; Teixeira et al. 2017).

The geological records of convergent oceanic plate regimes and a succession of collisions between continental blocks along a continuous belt define the Western Gondwana Orogenic System (Ganade Araujo et al. 2012, 2016). This orogenic system reflects the diachronous closure of a large ocean—the Ocean (Caby 2003; Cordani et al. 2013; D'Agrela-Filho and Cordani 2017)—along a suture that is represented by today's Transbrasiliano Lineament, a product of a long-term geological history of *c.* 250 million years. As the example of the Mozambique Orogen in Eastern Africa-Antarctica (Squire et al. 2006), the Western Gondwana Orogenic System, as a result of its deep continental deformation, most likely formed a huge mountain chain by the end of the Neoproterozoic, comparable with today's Alpine-Himalayan system of orogenic belts (Ganade Araujo et al. 2014).

The paleogeographic starting point for the Neoproterozoic tectonic history, including the opening and closure of the Farusian-Goiás Ocean, remains a matter of debate but is generally assumed to start with the existence of a supercontinent—that is, Rodinia. Various configurations have been proposed for Rodinia, such as Urung (1997), and more recently Fuck et al. (2008) and Li et al. (2008). Alternative paleogeographic reconstructions of the Rodinia supercontinent, with continental masses of Laurentian and Gondwana affinities, such as the Rio de la Plata Craton, have been suggested on geological (Cordani et al. 2003a, b; Kröner and Cordani 2003; Johnson et al. 2005; Teixeira et al. 2013; Fuck et al. 2017) and geophysical grounds (Pisarevsky et al. 2003; Tohver et al. 2006; D'Agrela-Filho and Cordani 2017). An alternative model involves a large ocean between Rodinia and proto-Gondwana (Tohver et al. 2006), next to the Amazonian-Rio Apa Block and between Pampia (Ramos et al. 2010) and Rio de la Plata—named Clymene Ocean, as proposed by Tohver et al. (2010). The corresponding rock record is suggested to be in the Paraguai-Araguaia belts and the Pampean magmatic arc.

A map of Western Gondwana (Fig. 3.1) shows the orogenic systems related to the diachronous closure of the Farusian-Goiás and Adamastor oceans, and the continental blocks and cratons involved in plate convergence in the Neoproterozoic. While oceanic plate convergence in the South American sector marked the Farusian-Goiás domain in the Tonian to early Cryogenian periods (Cordani et al. 2013), divergent plate regimes segmented the Congo-São Francisco (Tack et al. 2001; Pedrosa-Soares et al. 2008; Babinski et al. 2012; Affaton et al. 2016) and Kalahari-Rio de la Plata continental blocks (Basei et al. 2005, 2008a, 2011a; Frimmel et al. 2011, 2013), resulting in the opening of the Adamastor Ocean. In this context, the Luís Alves and Curitiba continental blocks would represent microcontinents with an active margin by the end of the Neoproterozoic (Basei et al. 1992, 1998, 2000, 2009).

Beyond the Mesoproterozoic units of the Irumide Belt (Johnson et al. 2005, 2007; De Waele et al. 2009; Fernandez-Alonso et al. 2012; Hauzenberger et al. 2014), between the Congo and Kalahari cratons, the Damara Belt reflects the evolution from continental rifting to spreading and formation of a narrow oceanic basin in the Ediacaran (Miller et al. 2009; Frimmel et al. 2011; Lehmann et al. 2015; Nascimento et al. 2016). This suggests an aulacogen opening of lithospheric proportions, synchronous with the closure of the Adamastor Ocean.

The Ediacaran formation of magmatic arcs in active continental margins (Campos Neto and Figueiredo 1995; Basei et al. 2000, 2008a; Prazeres Filho et al. 2003; Leite et al. 2007; Frimmel et al. 2013; Hueck et al. 2016; Philipp et al. 2016a, b; Tedeschi et al. 2016; Heilbron et al. 2017) marked the end of ocean opening. Except for the hot roots of the Araçuaí Orogen (Valeriano et al. 2016), plate tectonic processes were fast and culminated in end-Ediacaran collisions (Basei et al. 2008a, 2010; Faleiros et al. 2011; Santos et al. 2015), which were followed by lithospheric extensional regimes, with subalkaline volcanism and continental basins (Teixeira et al. 2004b), and with elongated orogen-parallel provinces of A-type alkaline plutonism (Vlach and Galda 2007; Janasi et al. 2009; Pimentel 2016).

The term 'Adamastor Ocean' was originally coined by Hartnady et al. (1985) based on the areal distribution of mafic oceanic crustal rock assemablages in southwestern Africa, notably the Matchless amphibolite zone in the southern Damara Belt and the metavolcanic rocks of ophiolitic affinity in the Gariep Belt. These oceanic crustal rock suites continue south(west)ward from the Kalahari Craton towards southern South America and the Transantarctic Province. Oceanic opening towards the north up to the São Francisco-Congo gulf, ancestor of the Araçuaí-West Congo Orogen (Pedrosa Soares et al. 2001; Degler et al. 2017), seems to have been linked with the peripheral collision of the São Francisco Craton against the Paranapanema Block and Amazonian Craton. The Ediacaran magmatic arcs mark the end of ocean opening and record an extensive system of accretionary orogens that led to the Ediacaran-Cambrian assembly of western Gondwana.

The term 'Adamastor Ocean' is here considered in a broader sense than originally proposed by Hartnady et al. (1985), who regarded it as a kind of proto-South Atlantic ocean. In the current view, illustrated in Fig. 3.1, this Neoproterozoic ocean would include several branches, such as those that eventually led to the Ribeira and Araçuaí belts. In their midst several continental fragments with different shapes and sizes existed—namely the Nico Peres,

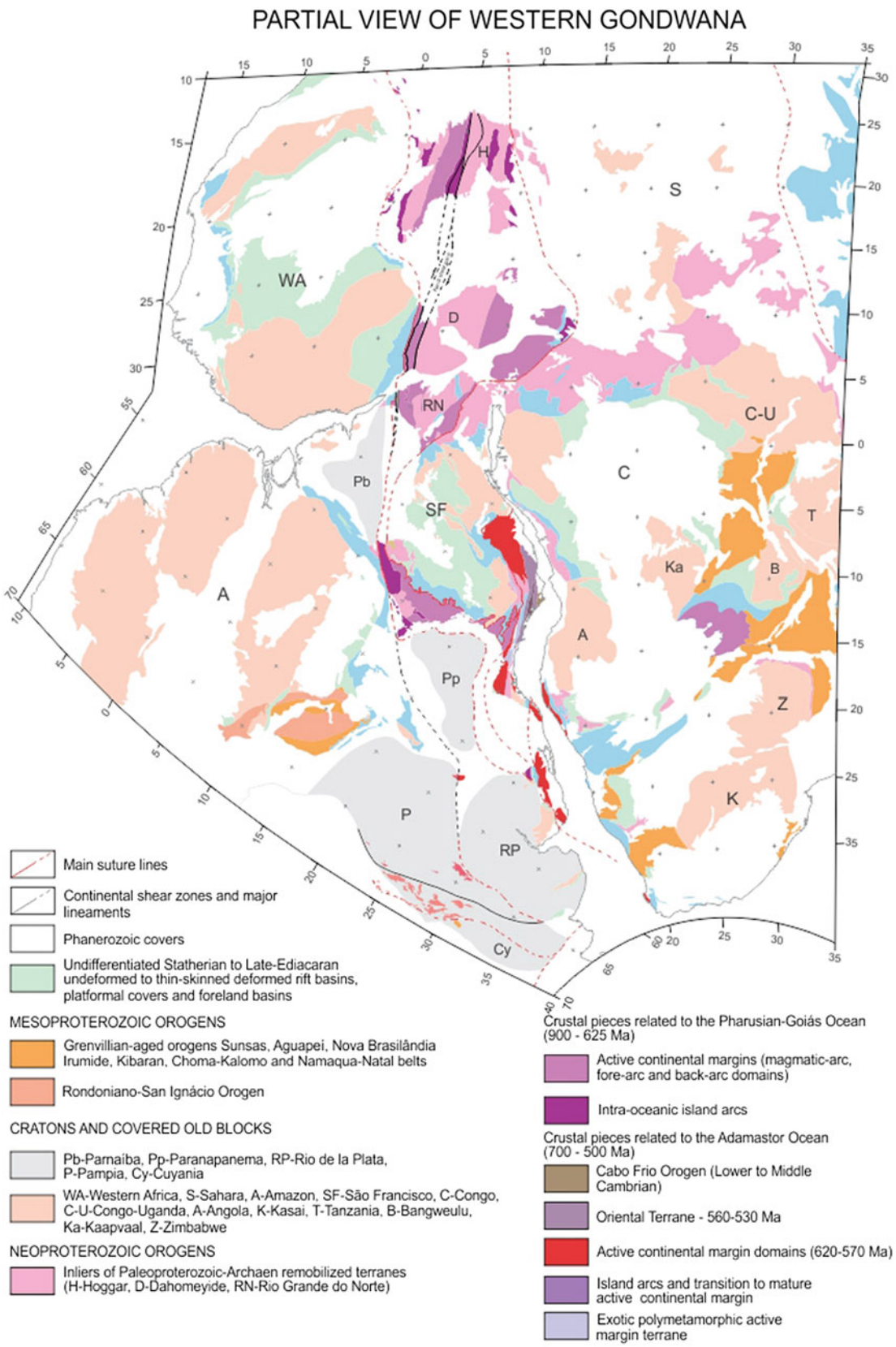

Fig. 3.1 Western Gondwana reconstruction (modified from de Wit et al. 1988). *RP* Rio de la Plata Craton; *P* Pampia Block; *A* Amazonian Craton; *SF* São Francisco Craton; *Pp* Paranapanema Block; *WA* West Africa Craton; *Pb* Parnaíba Block; *C* Congo Craton; *C–U* Congo-Uganda Craton; *A* Angola Craton; *KA* Kazai Block; *B* Bangweulu Block; *T* Tanzania Craton; *Z* Zimbabwe Craton; *K* Kalahari Craton; *Cy* Cuyania Terrane; *H* Hoggar Inlier; *D* Dahomei Inlier; *RN* Rio Grande do Norte Inlier

Encantadas, Luis Alves, and Curitica blocks—and in Africa possibly the Angola cratonic block. All these segments were diachronously amalgamated around 600 Ma during the closure of the Adamastor Ocean.

3.2 Pan-African/Brasiliano Belts Along the Southern South Atlantic Margins

Remnants of former southwestern Gondwana exist on both sides of the present South Atlantic Ocean with Neoproterozoic fold belts along the coasts and old cratons towards the interior. This symmetry is defined by a central granitic belt bounded on both sides by fold-and-thrust belts with opposite tectonic vergence: towards the west in the Dom Feliciano Belt and to the east in the Kaoko and Gariep belts (Trompette 1997; Goscombe and Gray 2007; Basei et al. 2008a). Supracrustal rocks predominate on the African side, where only small magmatic segments may correspond to the magmatic arc associated with the tectonic evolution of the Neoproterozoic belts. The domain on the African side that most closely resembles a magmatic arc occurs in the westernmost Kaoko Belt in the form of the Skeleton Coast granitoids. This African segment most likely corresponds to the 1200 km-long Granite Belt in the Dom Feliciano Belt in southeastern South America. As the main goal of this chapter is to characterize the geological history of the Southern Adamastor Ocean, we shall focus on a comparison between the Kaoko and Dom Feliciano belts.

3.2.1 Dom Feliciano Belt

The Dom Feliciano Belt (DFB) represents the geotectonic unit of greatest continuity of the southern portion of the Mantiqueira Province (Almeida et al. 1981) (Fig. 3.2). It defines an extensive north-northeast-trending polyphase belt of some 1200 km length, which occupies the whole southeastern portion of Brazil and Uruguay (Fragoso Cesar, 1980; Basei et al. 2000, 2008a, 2010; Oyhantçabal et al. 2009b; Philipp et al. 2016a, b). From its northern limit in Santa Catarina to its termination in Uruguay, it unifies three crustal segments with distinct lithological and tectonic characteristics. These are, from southeast to northwest, the Granitoid Belt (deformed calc-alkaline to alkaline granitoid rocks), a metamorphic (greenschist to amphibolite facies) volcano sedimentary belt, and a former foreland basin filled with anchimetamorphic sedimentary and volcanic rocks. In spite of younger sedimentary cover in many places, the continuity of these three segments is indicated by similarities in rock types, structural characteristics and gravimetric signatures (Schukowsky et al. 1991; Halinann and Mantovani 1993). The present constitution of the DFB was reached only in the Ediacaran Period when its different components were juxtaposed.

Northeast-southwest contacts between the different domains and the tectonic vergence pointing to the foreland westwards are conspicuous features of the entire DFB. This late geometry reflects different pulses of an overall continuous tectonic process between 640 and 530 Ma (Basei et al. 2008a).

The Dom Feliciano schist belt, referred to in the following as the Schist Belt, constitutes the Brusque (Santa Catarina), Porongos (Rio Grande do Sul) and Lavalleja (Uruguay) supracrustal sucessions, which represent the passive margin deposit on the western side of the Adamastor Ocean. Continuity of these supracrustal belts, besides geophysical evidence, is suggested by several similarities, including the predominance of lower-pressure metamorphism, the same geotectonic position of all sequences and also granitic magmatism intrusive into these supracrustal rocks. These units are polydeformed sequences, with three folding phases associated with a northwestward mass transport, which evolved to late lateral transpression. In structural terms the main foliation in the majority of the metamorphic rocks is a syn-peak metamorphic S_2 foliation. The regional metamorphism is of greenschist facies, locally reaching the lower amphibolite facies (Silva et al. 1980; Sanchez-Bettucci et al. 2001, 2004; Philipp et al. 2004; Basei et al. 2011b).

Along the Schist Belt, syn- to late-collisional, *c*. 600 Ma granitoids were emplaced into the supracrustal rocks and developed contact metamorphic aureoles that post-date the main foliation of the regional metamorphic rocks. They are more frequent in the Brusque Belt and decrease in abundance towards the south, with hardly any expression in the rocks of the Lavalleja Group in Uruguay (Plate 3.1).

Despite numerous new U–Pb detrital zircon age data, the precise age of sedimentation along the entire belt remains poorly constrained. The basement of all sedimentary units is Paleoproterozoic (Basei et al. 2008a, 2013). Late Neoproterozoic granite emplacement at around 600 Ma sets a minimum limit for the age of sedimentation. Volcanic rocks interspersed in the sedimentary sequences indicate ages along the belt that vary between 780 and 640 Ma.

3.2.2 Kaoko Belt

In southwestern Africa, the Pan-African Orogeny led to a system of three coast-parallel belts—namely, the Kaoko, Gariep and (western) Saldania belts—and an intracontinental belt, the Damara Belt (Fig. 3.3). This system evolved through successive phases of rifting and continental break-up, drifting, subduction and continental collision. In this chapter the emphasis is placed on the Kaoko Belt.

A range of basement rocks are exposed in the Kaoko Belt, most prominently in the Kamanjab Inlier and the Epupa Complex, containing Archean orthogneiss of *c*. 2600 Ma

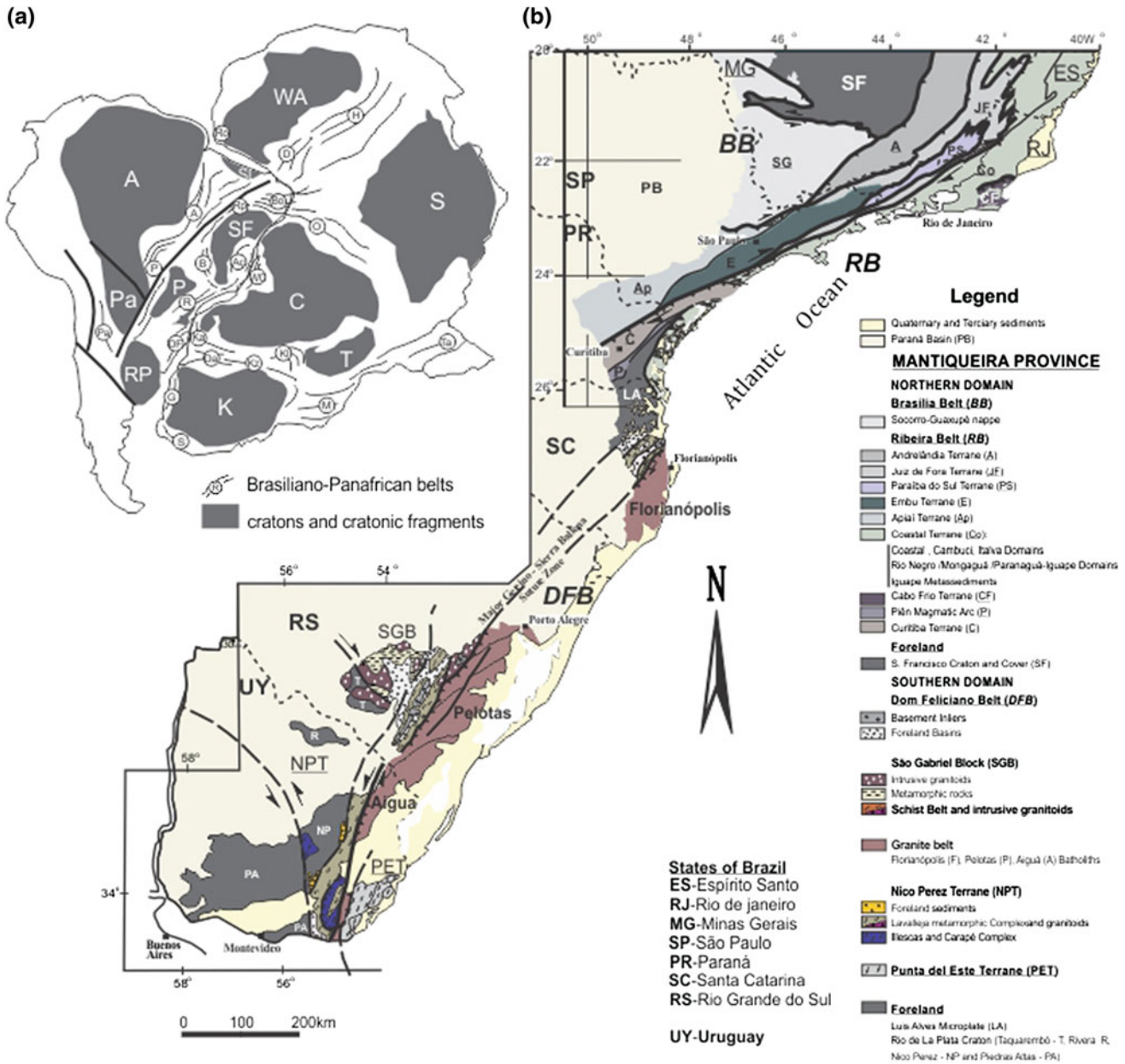

Fig. 3.2 Main geological features of Southern Mantiqueira Province focusing on the Dom Feliciano Belt (Brazil–Uruguay) **a** Reconstruction of West Gondwana after Heilbron and Machado (2003) and Heilbron et al. (2017); de Wit et al. (1988) and Cordani et al. (2013), showing cratonic blocks and Brasiliano–Panafrican belts. Cratons shown in grey: *A* Amazonia; *C* Congo; *K* Kalahari; *LA* Luis Alves; *P* Paranapanema; *SF* São Francisco; *WA* West Africa. Brasiliano–Panafrican belts (ringed): *Bo* Borborema; *Rp* Rio Preto; *A* Araguaia; *Aç* Araçuaí; *P* Paraguai; *B* Brasília; *R* Ribeira; *DF* Dom Feliciano; *Pa* Pampean; *H* Hoggar; *D* Dahomey; *Ro* Rockelides; *O* Oubangides; *Ta* Tanzania; *WC* West Congo; *Ka* Kaoko; *Da* Damara; *K/Z* Katangan/Zambezi; *Kl* Katanga-Lufilian Arc; *M* Mozambique; *G* Gariep; *S* Saldania. Location of the Mantiqueira Province is shown. **b** General outline of the Mantiqueira Province (Brazil–Uruguay). Simplified from Basei et al. (2008a), Passarelli et al. (2011, unpublished)

(Seth et al. 1998). Mesoproterozoic rocks occur in several places, predominantly quartzite and amphibolite with subordinate felsic rocks, with ages grouping in the 1350–1500 Ma interval (Seth et al. 1998; Kröner et al. 2004; Goscombe et al. 2005).

The Kaoko Belt has been subdivided into several zones. The Eastern Kaoko Zone consists of Neoproterozoic platform sediments on the western margin of Congo Craton. The metamorphic grade is only very low. A marine ingression prior to 750 Ma is evident from a carbonate, deep-water rhythmic argillite and shallow-water stromatolite succession (Ombombo Subgroup), which lies on siliciclastic deposits of the Nosib Group and is covered by the Chuos Formation diamictite (Hoffman et al. 1998).

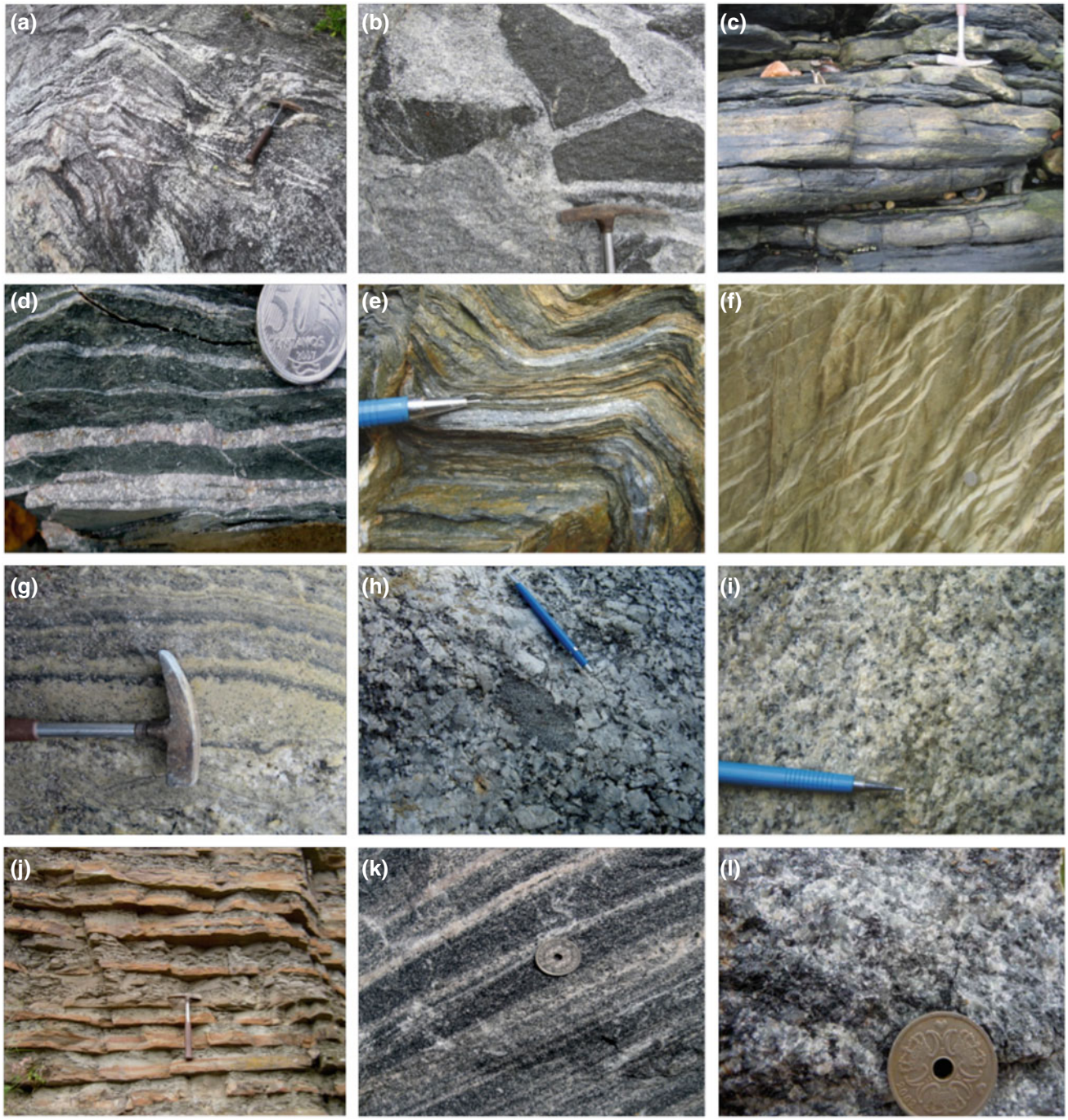

Plate 3.1 Field photographs from the Dom Feliciano Belt. Granite Belt: **a** banded gneisses of Aguas Mornas Complex; **b** São Pedro de Alcantara biotite-monzogranite with mafic enclaves; Schist Belt: **c** 640 Ma amphibolite interlayered with metasedimentary units; **d** thinly bedded limestone; **e** late-stage folds in biotite-quartzschist; **f** two sets of crenulation folds deforming quartz-sericiteschist; Granitoids intrusive into the Schist Belt: **g** São João Batista banded tourmaline-muscovite leucogranite; **h** coarse-grained Valsungana biotite granite with microgranular enclaves; **i** homogeneous Nova Trento two mica granite; Foreland Basin: **j** banded turbidite of Itajaí Basin; Luis Alves Craton (Foreland): **k** orthopyroxene banded gneiss; **l** typical massif charno-enderbitic gneiss

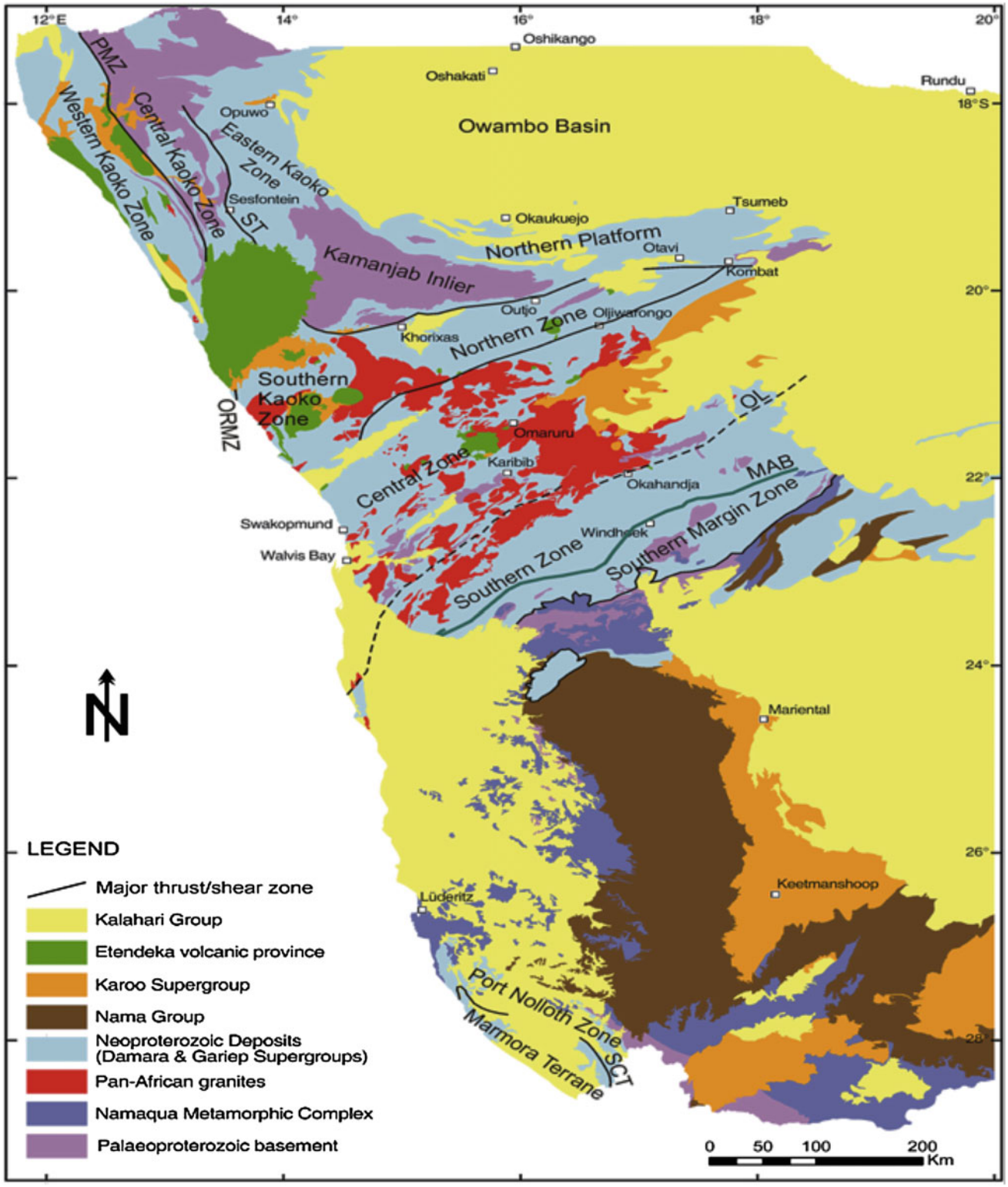

Fig. 3.3 Main tectonostratigraphic units of southwestern Africa. Lineaments: *ORMZ* Ogden mylonitic zone; *PMZ* Purros mylonitic zone; *ST* Sesfontein thrust; *SCT* Schakalsberge thrust. After Frimmel et al. (2011)

The Central Kaoko Zone is bounded to the east by a shallow late Pan-African thrust zone (Sesfontein Thrust) (Goscombe et al. 2003), and to the west by the mylonitic Purros Shear Zone (Fig. 3.3). It is composed of an Archean to Paleoproterozoic gneissic-granitic basement, with Paleo- to Mesoproterozoic granitoid bodies, and covered by Neoproterozoic metapelitic to metapsammitic supracrustal rocks (Seth et al. 1998; Kröner et al. 2004). Konopásek et al. (2008) reported U–Pb zircon ages (SIMS) between 840 and 805 Ma for felsic rocks of bimodal metavolcanic suites and interpreted them as dating continental rift-related volcanism. The metamorphic grade increases from east to west, passing from lower greenschist to upper amphibolite facies, and reflecting a Barrovian-type P/T gradient.

Both basement and sedimentary cover display an intense sinistral transpressional superposed fabric and folds associated with series of thrusts and nappes transported eastwards (Goscombe et al. 2003; Will et al. 2004). The sequences observed in the Ugab zone correspond to turbidites (Gray et al. 2006) containing two thin cap carbonate units possibly associated with Sturtian glaciation at 720–700 Ma (oldest) and the youngest with the Ghaub Formation diamictite of supposedly Marinoan age of 635 Ma (Hoffman et al. 1998; Hoffmann et al. 2004).

The Western Zone of the Kaoko Belt, also referred to as Coastal Terrane (Fig. 3.3), records two high-grade (upper amphibolite to granulite facies) low-P/high-T metamorphic episodes around 645 and 550 Ma (Franz et al. 1999) associated with Neoproterozoic granitoids. Type-I calc-alkaline granitoids of 650–630 Ma age are also present (Seth et al. 1998; Konopásek et al. 2016). All rocks in this domain were affected by sinistral shearing, isoclinal folding (Goscombe et al. 2003) and high-grade metamorphism (Seth et al. 1998; Franz et al. 1999; Konopásek et al. 2008). The Three Palms Mylonite Zone defines the eastern limit of the Coastal Terrane. It represents, analogous to the Major Gercino-Sierra Ballena Shear Zone on the western flank of the Granite Belt in the DFB, a low-angle shear zone that in the course of progressing crustal shortening was gradually transformed into high-angle faults with a predominantly directional component.

The abundance of calc-alkaline intrusive rocks, which form a large batholith (the Skeleton Coast Batholith), is generally explained as representing a former magmatic arc in the Coastal Terrane. These rocks range in composition from mafic, intermediate to felsic (Seth et al. 1998; Franz et al. 1999; Masberg et al. 2005), and were emplaced into metamorphosed supracrustals rocks (Goscombe and Gray 2007). The absence of a tectonic boundary between the metasedimentary cover and the rocks of the Skeleton Coast Batholith suggests an intimate relation between deposition of the metasedimentary rocks and the evolution of the magmatic arc. Interestingly, similar sedimentary cover as in the Coastal Terrane and with the same detrital zircon populations also occurs as roof pendants of the granitoids in the DFB (Basei et al. 2008a). Part of the detrital zircon age patterns of the metasedimentary units in the Coastal Terrane cannot be reconciled with any source in the Central Zone of the belt but match very well the age pattern of the magmatic arc rocks (Goscombe and Gray 2007, 2008; Konapásek et al. 2014; Basei et al. unpublished data). It is therefore concluded that the Coastal Terrane as a whole (magmatic arc and its sedimentary cover) would be a para-autochthonous unit and not an exotic terrane without genetic links with the rest of Kaoko Belt.

In a similar way to that observed in the DFB, where a set of S-type granitoids occurs adjacent to the Major Gercino-Sierra Ballena Suture Zone, marking the contact between the Schist Belt and the magmatic arc, a significant volume of S-type granitoids also marks the eastern contact of the magmatic arc of the Coastal Terrane in the vicinity of the Three Palms Mylonite Zone (Goscombe and Gray 2007; Konapásek et al. 2008, 2014) (Plate 3.2).

3.3 Depositional Age and Provenance Constraints from Detrital Zircon Ages from the Dom Feliciano and Kaoko Belts

U–Pb ages (SHRIMP and LAICPMS) on detrital zircon have been used as the main tool to define the provenance and maximum age of deposition of the metasedimentary rocks that constitute the schist belts. When this type of information is combined with ages of volcanic rocks interlayered in sedimentary sequences as well as ages of metamorphic and magmatic events, it becomes possible to reconstruct the geological evolution of a given belt with a high degree of confidence.

Zircon age dating on mylonitic quartzite that occurs in the northern portion of the Brusque Group (Hartmann et al. 2003) yielded largely Paleoproterozoic values in the range 2180–2090 Ma and a single crystal with 2220 Ma. Basei et al. (2008a) analysed two samples of metasedimentary rocks, a volcanosedimentary micaschist and a garnet-biotite schist. The zircon grains therein revealed age peaks in the ranges 2250–1700, 1500–1300 and 1300–1100 Ma, and two grains with anomalously young ages of 540 and 570 Ma. A metaconglomerate at the top of the metavolcanosedimentary unit in Morro do Carneiro gave detrital zircon ages mainly between 2100 and 1850 Ma with some older, Archean grains (2600–3000 Ma). In this sample the main age peak is around 2000 Ma and the youngest concordant age is 1250 Ma. Another sample, from a quartzitic bed in the micaschist, yielded a similar age distribution, with populations of 1500–1300 and 2200–1800, and some Archean values between 2600 and 3100 Ma. The main peak is at 2200 Ma (Yamamoto and Basei 2009).

Plate 3.2 Field photographs from the Kaoko Belt. Basement rocks: **a** deformed granitoid of Kamanjab Inlier; **b** sheared pink megacrystic granite at Marien Fluss, Kunene River; Eastern Domain (carbonate platform); **c** thinly bedded limestone of the Tsumeb formation; **d** limestone of the Hüttenberg formation; Central Domain; **e** general view of medium-grade Kaoko mica schist just above the Sesfontein thrust; **f** folded diamictite of Chuos formation; Orogen core; **g** deformed coarse-grained biotite granite, near Purros shear zone; **h** Porphyroclastic augen gneiss of three palm Mylonite zone; Costal Terrane; **i** banded high-grade migmatite with metasedimentary paleosome; **j** feldspathic garnet-mica schist of supracrustal units near Terrace Bay; **k** deformed tonalite with elongated mafic enclaves; **l** deformed biotite monzogranite with elongated mafic bands

Considering the detrital zircon age patterns of the Brusque Group, the predominance of Paleoproterozoic values is evident, as well as a moderate Archean contribution. In terms of provenance, the origin of these zircon grains can be essentially South American, with the Archean to Paleoproterozoic domains constituting the Luis Alves, Paranapanema and Rio de la Plata cratons, as well as the Camboriú Complex, representing the likely source areas. On the other hand, the origin of the few Mesoproterozoic ages found in these rocks, with values between 1200 and 1300 Ma, is more problematic as there are no known rocks of this age exposed in southern and southeastern Brazil. A probable African origin for these Mesoproterozoic zircons has been suggested by Basei et al. (2005, 2008a). The two young grains obtained, with ages of 540 and 570 Ma, confirm the Neoproterozoic depositional age of the Brusque Group. However, the values are much younger than one might expect and may reflect loss of radiogenic Pb.

Late Cryogenian deposition of most of the Brusque Group is confirmed by age data of around 637 and 640 Ma obtained on intercalated felsic and mafic metavolcanic rocks (Silva et al. 2002; Basei et al. 2011b). In addition, U–Pb zircon ages from four calsilicatic samples with a probable tuffecous contribution indicate several detrital zircon populations, with age peaks in the ranges 2350–2040, 2000–1880 and 1270–780 Ma, whereas the age of volcanism is around 640 Ma (Brentan 2011).

Recent U–Pb detrital zircon studies on the Porongos Group revealed the existence of two sedimentary sucessions with different ages and tectonic contexts. An older sedimentary sequence is Tonian to Cryogenian, as evidenced by 810 and 770 Ma felsic and mafic metavolcanic rocks (Porcher et al. 1999; Chemale 2000; Gruber et al. 2011; Saalmann et al. 2011; Arena et al. 2017; Pertille et al. 2017). In the enclosing sedimentary rocks, a younger population of detrital zircon with ages between 800 and 1300 Ma is distinguished from an older group with ages mainly between 2000 and 2200 Ma and a few Archean values (Gruber et al. 2011; Höfig et al. accepted). The younger depositional sequence is Ediacaran, with 610 Ma metatuff layers (Höfig et al. accepted) intercalated in the psamopelitic sedimentary rocks, and deformed 600 Ma alkaline leucosyenogranite (Zvirtes et al. 2015) crosscutting the metasedimentary rocks. The detrital zircon age pattern of the Ediacaran succession is marked by 580 and 610 Ma major peaks, with subordinate populations between 2200 and 2000 Ma and some Archean values between 2900 and 2700 Ma (Pertille et al. 2015b, 2017; Höfig et al. accepted).

The possibility of Paleo- to Mesoproterozoic metasedimentary units having formed part of the basement of the Porongos Basin is suggested by the existence of quartzite beds that contain detrital zircon populations of quite different provenance. These rocks occur on the western edge of the Santana Dome, the best exposure of the Paleoproterozoic basement of the Porongos Group occurs. Detrital zircon in this quartzite yielded ages in the 3200–1990 Ma range with a main peak around 2100 Ma (Hartmann et al. 2004; Gruber et al. 2011; Pertille et al. 2015a). A few grains yielded an age of *c*. 1750 Ma (Gruber et al. 2011) but no Meso- or Neoproterozoic data has been obtained.

The absence of Neoproterozoic detrital zircon grains is a critical feature that continues into the mica schists of the eastern and southern flanks of the Santana Dome. There, however, Mesoproterozoic detrital zircon ages from 1010 to 1060 Ma are abundant. In addition, the sedimentary succession contains intercalations of acidic and intermediate volcanic rocks that have been dated around 770 Ma (Porcher et al. 1999; Gruber et al. 2011; Saalmann et al. 2011; Pertille et al. 2017), thus suggesting a correlation with the oldest Tonian succession of the Porongos Group.

The oldest Tonian-Cryogenian metasedimentary succession of the Porongos Group corresponds to remnants of a marginal basin fill (including the rift units) that were laid down on the margin of the Rio de la Plata and Paranapanema cratons at the western end of the Adamastor Ocean. The Ediacaran upper units of the Porongos Group are related to the synorogenic deposits of the collisional phase of the DFB. The Meso-Paleoproterozoic quartzites may correspond, similar to those observed in the Kaoko Belt, to an old platform cover.

From the Lavalleja Group, which represents the continuation of the Schist Belt in Uruguay, only few data is available. SHRIMP U-Pb detrital zircon ages for two samples were presented by Basei et al. (2008a). The first corresponds to a quartz-sericite schist of the Fuente del Puma Formation (Sanchez-Bettucci et al. 2001, 2004) collected from a well-exposed outcrop on Road 60. A range of zircon ages was obtained with Archean (2600–3400 Ma), Paleoproterozoic (1780–2400 Ma) and Neoproterozoic ages (600–1000 Ma). The age pattern observed in a sample from the Zanja del Tigre Formation (Sanchez-Bettucci et al. 2001, 2004) is quite different from the previous sample. This rock corresponds to a rhythmic metapsammitic rock collected on Road 12. In this sample, some Archean grains were found (some older than 3000 Ma), with the majority being Paleoproterozoic (1800–2300 Ma). No Meso- or Neoproterozoic zircon grains were found in this sample. Here the older zircon populations are of particular interest because no corresponding Archean units are known so far in Uruguay.

On the African side, the number of provenance studies on (meta)sedimenatary units of the Kaoko Belt remains limited. Nevertheless, the control on the timing of sediment deposition is reasonably good thanks to age data for interlayered volcanic rocks. An additional control is provided by the age of metamorphism and granitoids that cut these metasedimentary units.

Two of the three lithostructural segments that make up the Kaoko Belt were studied by Konapásek et al. (2014), who presented a set of detrital zircon U–Pb ages. For the Central Domain, three samples yielded a large variation of ages, with main peaks at 650–750, 1250–1400 and 1850–2000 Ma. Only a few grains gave Archean ages of 2600–2700 Ma. The Orogen Core, located between the Purros and Three Palms Mylonite shear zones, contains detrital zircon grains with the main age groups around 650, 1000, 1450 and 1800 Ma. Neoproterozoic ages in this segment are more abundant than in the Central Domain. The well-documented increase in the grade of metamorphism towards the Orogen Core is well reflected by an abundance of U–Pb zircon overgrowth ages between 570 and 620 Ma. In the Coastal Terrane, the vast majority of detrital zircon grains in the metasedimentary rocks is Neoproterozoic in age, with a main peak around 650 Ma. Minor age peaks are at 950–1050, 1250–1050, 1850 and 2150 Ma. High-grade metamorphism in the Coastal Terrane is recorded in orthogranulitic gneisses and reflected by metamorphic zircon overgrowths with ages of 630–650 Ma.

For the metasedimentary units that occur south of the Kamanjab basement inlier, a set of U–Pb results in detrital zircon were presented for the Otavi-Swakop groups ranging from Nabis Formation to the Mulden Group molasse (Nascimento et al. 2017). The age pattern observed by Nascimento et al. shows an unimodal distribution around 1750 Ma for the Nabis Formation whereas in the Chuos Formation of the Nosib Group, additional populations with ages of *c*. 1250 Ma and to a lesser extent 740 Ma exist. The latter is in good agreement with the intercalated volcanic rocks that provided ages between 745 and 760 Ma (Hoffman et al. 1996; DeKock et al. 2000; Halverson et al. 2002; Nascimento et al. 2016) for spatially associated diamictite, which has been related to the Sturtian glaciation. In the Ghaub/Black River Formation, detrital zircon ages of around 1970 Ma predominate with a few grains having older ages of 1000–2600 Ma. In addition, younger values of 660–680 Ma are in agreement with a Marinoan age generally postulated for these units based on a precise U–Pb zircon age of 635 Ma obtained on an intercalated tuff layer in a supposedly correlatable unit further south in the Damara Belt (Hoffman et al. 2004). In contrast to the above, the molasse sediments of the Mulden Group contain detrital zircon grains that are predominantly Neoproterozoic (650–710 Ma), with a second population around 1030 Ma and minor contributions from Paleoproterozoic (~1860 Ma) and Archean (2600 Ma) sources.

For the intracontinental branch of the Damara Belt, Foster et al. (2015) could distinguish sediment sources in the Congo Craton and in the Kalahari Craton. The former is characterized by age peaks of 1150–1000 and 800–600 Ma, whereas the latter is characterized by ages between 1300 and 1150 Ma. This difference led them to conclude that both cratons were widely separated from each other at the end of the Mesoproterozoic and became juxtaposed only in Ediacaran times. Such a strict separation of Congo and Kalahari provenance is, however, problematic because elsewhere the Kalahari Craton contains voluminous units with ages that correspond to those allegedly typical of the Congo Craton—for example, in the Bushmanland Subprovince of the Namaqua-Natal Belt (Robb et al. 1999) and in the Richtersveld Igneous Complex (Frimmel et al. 2001).

Foster et al. (2015) also suggested a maximum depositional age for the Mulden Group in the Northern Foreland of ~590 Ma, which is supported by the youngest concordant detrital zircon ages of *c*. 620 Ma obtained from the Hartmann Subgroup (Goscombe et al. 2005).

The main sediment sources in both the DFB and the Kaoko Belts are evidently their basement and adjacent cratons (Goscombe et al. 2005; Basei et al. 2008a; Konapásek et al. 2014; Foster et al. 2015; Pertille et al. 2015a, 2017; Höfig et al. accepted; Nascimento et al. 2017). In most sedimentary sequences of these two belts, zircon populations with Paleoproterozoic ages predominate. Mesoproterozoic ages are abundant on the African side but are very minor on the South American side of the DFB, with only few such grains in the Brusque Group and increasing in number towards the south. However, in both belts, Cryogenian and Ediacaran zircon populations predominate in the younger syn- to late-orogenic units. This is due to the extrusion of the magmatic arc, represented by the Granite Belt, which became a high ground and thus constituted the main sediment source for the younger units in both belts. Similarly, the Coastal Terrane metasedimentary units are unequivocally related to magmatic arc evolution and probably had the Granite Belt as their main sediment source area. Metasedimentary remnants that occur as large roof-pendants in the middle of the Granite Belt probably have an African provenance of Meso- to Neoproterozoic age, which seems to be a fingerprint of Neoproterozoic supracrustal rocks of (southern) African affinity.

3.4 Tectonic Model

In the last 15 years, advances in the correlation of tectonothermal events, and Neoproterozoic sedimentation history on both sides of the Southern Atlantic Ocean have helped to fill gaps in the tectonopaleogeographic interpretation of the Neoproterozoic fold belts in southwestern Africa and southeastern South America.

A new tectonic model is proposed here, which hinges essentially on five findings: (1) The westernmost domain of the Kaoko Belt (Coastal Terrane) can be correlated with the Florianópolis-Pelotas-Aiguá magmatic arc in the DFB;

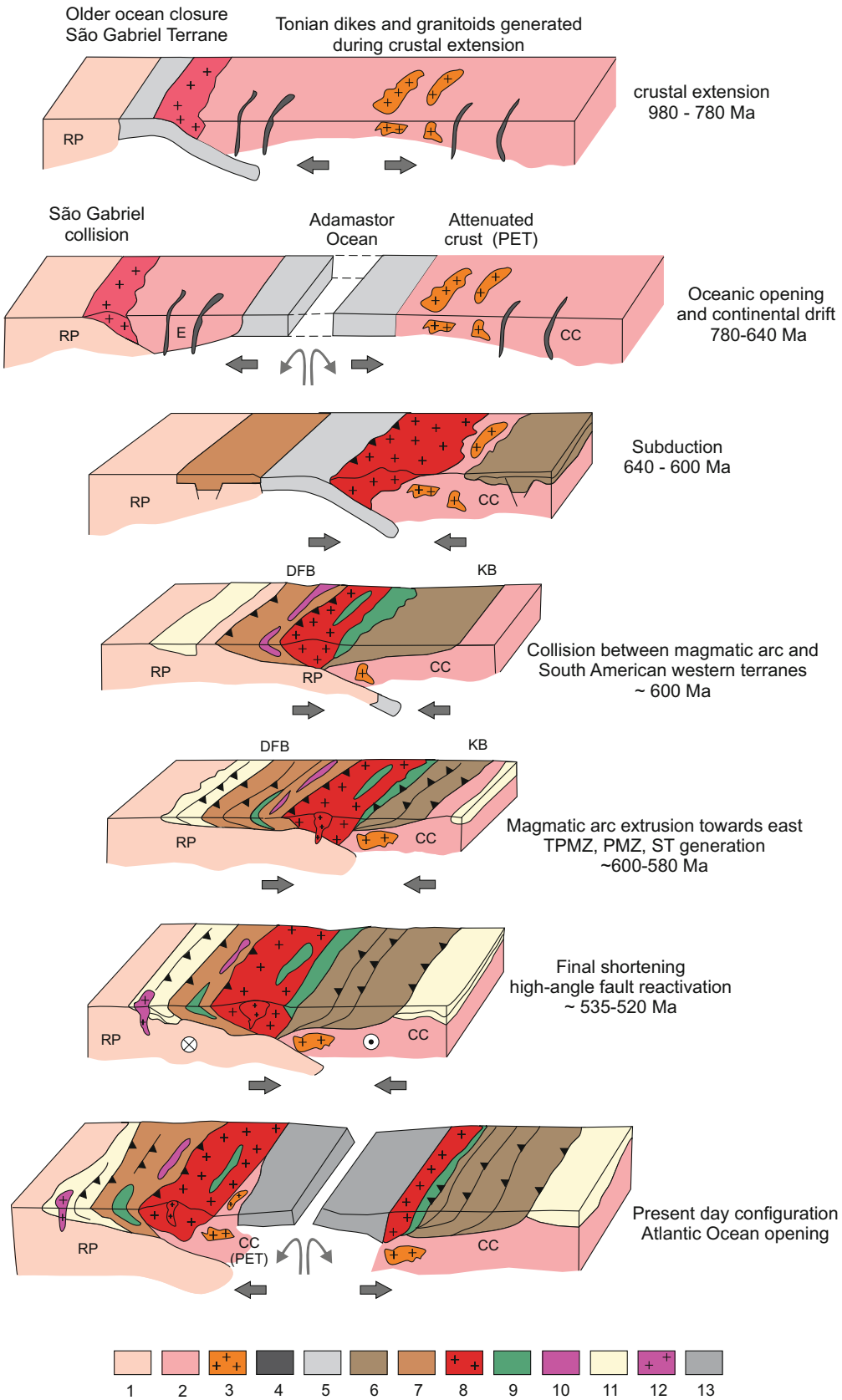

Fig. 3.4 Principle tectonic stages in the evolution of the Adamastor Ocean from Rodinia's fragmentation around 850 Ma to Adamastor closure *c*. 600 Ma: 1—Rio de la Plata Craton; 2—Congo Craton (and Nico Perez, Encantadas, Luis Alves crustal fragments); 3—Tonian granitoids generated during crustal extension; 4—Tonian mafic dykes; 5—Tonian oceanic crust; 6—Kaoko schist belt; 7—Dom Feliciano schist belt; 8—Granite Belt (magmatic arc granitoids); 9—arc related Ediacaran sediments; 10—syncollisional granitoids; 11—Foreland basin deposits; 12—late-stage 529 Ma Subida syenogranite; 13—South Atlantic oceanic crust

(2) the late-Ediacaran detrital zircon population in the supracrustal sequences of the western portion of the Kaoko, Gariep and Saldania belts and in the Rocha Group were probably derived from the above magmatic arc; (3) the Dom Feliciano Schist Belt represents the passive margin deposits that accumulated on the eastern margin of the South American cratons and on the plate that eventually became subducted; (4) the late Ediacarian synorogenic units in the Porongos Group register a second stage of sedimentary deposition in DFB owing to the magmatic arc collision against the DFB passive margin deposits around 600 Ma; and (5) the estimated time for the existence of the Adamastor Ocean would be 180 myr from first oceanic crust formation at *c*. 780 Ma to its closure around 600 Ma.

In addition to the above points, but equally important for the proposed tectonic model, is the finding that the upper units and mafic rocks of the Marmora Terrain in the Gariep Belt in southwestern Africa bear many similarities to those of the Rocha Group and Paso del Dragón Formation mafic-ultramafic rocks in northeastern Uruguay and are likely to represent the same original basin (Will et al. 2014).

Eastward subduction of Adamastor oceanic crust explains the positions of the 640–600 Ma Florianópolis-Pelotas-Aiguá granitoid belt (magmatic arc) and the passive margin reflected by the Brusque-Porongos-Lavalleja groups located between that arc and the Rio de la Plata/Paranapanema cratonic margins, as well as the back-arc domains of the Kaoko-Gariep-western Saldania belts (Basei et al. 2005, 2008a; Frimmel et al. 2011, 2013). The Major Gercino-Cordilheira-Sierra Ballena lineament represents the Neoproterozoic suture that separates the terranes with African and South American affinities. Around 535 Ma, crustal shortening in the region came to a close when folding and thrusting reached the foreland basins of the Kaoko-Gariep-western Saldania belts and the Dom Feliciano Belt. Thus the history of the Adamastor Ocean as suggested here reflects a complete Wilson Cycle.

3.5 Principle Tectonic Stages in the Evolution of the Adamastor Ocean

Figure 3.4 shows a diagram displaying the main steps related to the evolution of the Adamastor Ocean as well as the final shortening phase when the major faults zones began to present a predominant directional displacent and more vertical planes. The final step represents the present situation, with the rupture plane that generated the Atlantic Ocean developed predominantly along the eastern portion of the former Granite Belt—that is, along the corresponding back-arc basin (Marmora Basin).

3.5.1 Crustal Extension (980–780 Ma)

Although the Adamastor Ocean is considered to be one of the main products of Rodinia fragmentation, there is no direct evidence of its existence as there are no unequivocal remnants of corresponding oceanic crust recorded. All evidence is indirect and mainly in the form of significant marine deposits in the Neoproterozoic sedimentary successions on both the African and South American sides.

Age data on rift-related siliciclastic and bimodal volcanic rocks preserved in the Neoproterozoic schist belts from both Rio de la Plata/Paranapanema and Congo/Kalahari cratonic margins suggest a protracted continental rifting phase between 900 and 780 Ma (Frimmel et al. 1996; Hoffman et al. 1996; Basei et al. 2000; Pedrosa Soares and Alkmin 2011). However, considering the size of the area related to the Adamastor Ocean, it is likely that rifting was diachronous, with the period of 980–780 Ma covering different stages of crustal thinning that occurred simultaneously at different places.

On the African side, the granitoids of the Richtersveld Suite in the Gariep Belt with magmatic pulses at 835, 800 and 770 Ma are a good example of the magmatism associated with the taphrogenic phase (Frimmel et al. 2001). Ages between 880 and 820 Ma obtained on the Lufilian Belt, the eastern continuation of the Damara Belt, have also been attributed to continental rifting (Johnson et al. 2007; Frimmel et al. 2011). In the Kaoko Belt, a similar range of U–Pb ages (840–805 Ma) obtained on metavolcanic rocks of a bimodal suite in the Central Domain have been interpreted as dating continental rift magmatism (Konopásek et al. 2008). Further zircon age data of 770–710 Ma from amphibolite at the eastern side of the Three Palms Mylonite Zone (Konapásek et al. 2014) indicate that rift-related magmatism there continued into the Cryogenian Period.

For the northern Mantiqueira Province in the eastern part of South America, Pedrosa-Soares and Alkmin (2011) suggested several episodes of fissural magmatism in the Araçuaí Belt, which preceded the opening of the Adamastor Ocean. The oldest of these events would correspond to emplacement of 1000 Ma mafic dykes in the southern portion of Bahia State (Renné et al. 1990). A second event between 960 and 875 Ma is marked by the association of basic dykes and A-type granitoids (Machado et al. 1989; Silva et al. 2008; Queiroga et al. 2012; Castro 2014; Souza 2016). Alkaline magmatism between 730 and 700 Ma (Rosa et al. 2007, 2015) is the youngest event of this phase. In the central and southern portion of the Ribeira Belt, this taphrogenic phase can be associated with the emplacement of dykes and mafic bodies with ages between 900 and 800 Ma (Heibron and Machado 2003; Siga et al. 2009; Campanha et al. 2016).

A good example of Tonian magmatism associated with continental rifting in the south-southeastern part of Brazil is the mylonitic Parapente syenogranite, which pre-dates the deposition of the sediments of the Brusque Group at the northern end of the DFB. This syenogranite has a composition akin to A-type granite and yielded a U–Pb zircon age of 845 Ma (Basei et al. 2008b). Also in the same area, a 930 Ma deformed gabbro occurs (Basei et al. 2011b), which, together with the above syenogranite, evidences magmatism related to crustal thinning prior to volcanism and sedimentation in the Brusque Belt.

Large serpentinite bodies in the Pien region might represent remnants of the oceanic crust exhumed during the closure of the Adamastor Ocean branch that would have existed between the Luis Alves Craton and the Curitiba Block. Gabbro and norite occurring among these serpentinite bodies, with U–Pb zircon ages around 630 Ma (Harara 2001), suggest that the generation of this oceanic crust occurred in the Ediacaran. Arc-related calc-alkaline granitoids ranging in age between 614–610 Ma mark the onset of subduction (Harara et al. 2004).

On the other hand, in Rio Grande do Sul, remnants of oceanic crust of Tonian age were identified in two distinct sites associated with ophiolitic complexes. One of them is the mafic-ultramafic complex of the São Gabriel terrain and yielded ages of 900–850 Ma. The closure of that ocean would have occurred around 750 Ma with the generation of island arc granitoids (Gubert et al. 2016; Arena et al. 2016). The second site where oceanic crust was also identified is in the Capané Antiform area, where 750 Ma deformed mafic-ultramafic rocks were found interstratified in the Tonian metasedimentary successions of the Porongos Group of the DFB (Arena et al. 2017).

Crustal thinning in the course of continental rifting should have invariably led to an increase in the regional geothermal gradient resulting from a rise of the asthenospheric mantle. Partial melting of the lower crust, thus generating granitic melts and migmatites, and low P/T metamorphism, can be expected for this stage. On the African side, little evidence is recorded for this metamorphic overprint, except for the noted increase in metamorphic grade towards the west within the Kaoko Belt.

On the South American side, evidence for such Tonian metamorphism is recorded by rocks in the Punta del Este Terrane (PET) of eastern Uruguay (Preciozzi et al. 1999; Basei et al. 2011a; Masquelin et al. 2012). The Jaguarão Terrane in southeastern Rio Grande do Sul (Brazil) has been suggested to represent a continuation of the PET because of similarities in lithology and geochronology (Cruz et al. 2017).

The PET is the continuation into South America of the Gariep Belt and its Namaqua metamorphic basement in Namibia and South Africa. Correlation of the PET with the Namaqua Metamorphic Belt was initially proposed by Preciozzi et al. (1999) and confirmed by subsequent studies on the supracrustal rocks on both sides of the South Atlantic Ocean (Basei et al. 2000, 2005, 2011a; Frimmel et al. 2011, 2013; Masquelin et al.2012). The PET consists of a high-grade metamorphic gneissic to migmatitic basement, the Cerro Olivo Complex, and its low-grade supracrustal cover, the Rocha Group. This terrain, along with the Granite Belt, thus represents a remnant of the Kalahari Plate under which the Adamastor oceanic crust was subducted.

The Cerro Olivo Complex comprises orthogneisses, constituting the Cerro Bori unit, and paragneisses of the Chefalote unit (Masquelin 2000). The Chefalote migmatites and mafic granulites contain four distinct metamorphic assemblages, recording M2 peak-metamorphic conditions of 7–10 kbar and 830–950 °C on a clockwise P–T path (Gross et al. 2009). The tectonic evolution of this segment is characterized by Mesoproterozoic Namaqualand Metamorphic Complex-type rocks having been overprinted by several Neoproterozoic tectonometamorphic events (Masquelin 2000; Oyhantçabal et al. 2009a; Basei et al. 2011a; Lenz et al. 2011; Masquelin et al. 2012).

Tonian 850–760 Ma granitoids in the PET have been interpreted as products of either subduction (Lenz et al. 2011; Masquelin et al. 2012) or continental rifting (Oyhantçabal et al. 2009a). We prefer the latter interpretation because of the omnipresence of Namaqua-age zircon xenocrysts and inherited nuclei in dated zircon grains (Basei et al. 2011a; Lenz et al. 2011). It is proposed, therefore, that crustal thinning prior to the opening of the Adamastor Ocean led to decompression-induced anatexis of Namaqua-type basement and associated low P/T metamorphism along the western margin of the Kalahari continental plate. Remnants of this modified crust with Tonian granitoids can also be found within the Granite Belt, notably in the Pelotas and Florianópolis batholiths, where several 780–800 Ma tonalitic, dioritic and orthogneissic xenoliths have been observed (Silva et al. 1999; Frantz and Botelho 2000; Koester et al. 2008; Basei unpublished data).

Inversion from extension to compression occurred only in Ediacaran times, as evident from deformation and granulite-facies metamorphism in the PET (Gross et al. 2009; Masquelin et al. 2012). An age of 614 Ma for this stage of high-grade metamorphism is indicated by U–Pb data obtained on metamorphic zircon overgrowths around Tonain magmatic zircon cores (Oyhantçabal et al. 2009a). Metamorphic monazite ages from Chefalote Formation paragneisses corroborate syncompressional metamorphism and migmatite formation between 645 and 632 Ma (Basei et al. 2011a).

3.5.2 Drifting Phase (780–640 Ma)

Crustal thinning and continental rifting eventually led to continental break-up and first formation of oceanic crust at around 780 Ma. First evidence of subduction and thus onset of closure of the Adamastor Ocean at 640 Ma leaves at least 140 myr for the opening of this ocean. This would be enough time to generate an ocean as wide as the modern South Atlantic and to accumulate a thick pile of sediments (largely siliciclastic) on its margins.

Recent studies have revealed three major depositional episodes associated with the tectonic history of the Adamastor Ocean—that is, continental rifting, followed by marine deposits of sag basins (predominantly siliciclastic units), both associated with the main extension phases and sediment supply mainly from the adjacent cratons. During closure of the Adamastor Ocean, Ediacaran synorogenic deposits related to subduction (back-arc) and collisional phases are distinguished by their sediment derivation mainly from the Ediacaran magmatic arc (Basei et al. 2008a; Frimmel et al. 2013; Pertille et al. 2015b, 2017; Höfig et al. in revision).

The above scenario was built by compiling information from the different Neoprotezoic belts that occur on both sides of the South Atlantic (Ribeira, Dom Feliciano, Kaoko, Gariep and Saldania belts). However, it is not straightforward to assemble this puzzle because of intense deformation with tectonic imbrication, which makes it difficult to recognize and characterize the tectonic context that controlled the deposition of the various units. For most units the identification of their real tectonic setting remains precarious.

In many cases, the provenance and age of detrital zircon grains have been valuable tools in the characterization of the depositional tectonic context. Several authors have suggested the existence of two main periods for the filling of the Neoproterozoic Kaoko/Gariep paleobasins using changes in the sedimentary successions that suggest a depositional hiatus separating the rift basins from the subsequent thick marine siliciclastic deposits.

Most of the Neoproterozoic sedimentary successions on the African side are either rift graben fills or represent Ediacaran back-arc basins (Goscombe et al. 2003, 2005; Frimmel et al. 2011, 2013). In contrast, sedimentation in the DFB schist belts (Brusque, Porongos and Lavalleja) reflects a passive margin setting on the western side of the Adamastor Ocean. The influence of the magmatic arc on the sedimentary units of the DFB became significant only after the collision between the arc and the terranes located to the west, when the Ediacaran late synorogenic units were deposited. These units are well identified in the Porongos Group (Pertille et al. 2015a, b, 2017; Höfig et al. in revision).

3.5.3 Subduction and Magmatic Arc Formation (640–600 Ma)

The best geological record of the former existence of the Adamastor Ocean are the Granite Belt (Florianópolis-Pelotas and Aiguá magmatic arc) in South America and its equivalent, the Coastal Terrane, in northwestern Namibia (Basei et al. 2000; Goscombe et al. 2005; Goscombe and Gray 2007). Eastward subduction of the Adamastor oceanic crust must have begun prior to 640 Ma, which is the oldest age of granitoids in the magmatic arc that developed above the subduction zone.

The *c*. 1200 km long Granite Belt is composed of the Florianópolis, Pelotas and Aiguá batholiths. Remains of the metasedimentary cover occur in the three segments, with its best exposure in Santa Catarina, represented by paragneiss (with minor calcareous intercalations) and by the low-grade metasedimentary rocks of the Queçaba Formation. In the latter, the abundance of detrital zircon with ages of 900–1200 Ma suggests that the Namaqualand Metamorphic Complex of southwestern Africa as a likely sediment source (Basei et al. 2008a).

In Santa Catarina the Florianópolis Batholith exhibits three main lithological associations (Aguas Mornas, São Pedro de Alcantara and Pedras Grandes) that bear strong resemblance, both lithological and geochronological, to the rock associations defined by Philipp and Machado (2005) and Philipp et al. (2016a, b) for the Pelotas Batholith in Rio Grande do Sul. In Uruguay, the Aiguá Batholith has the same age range but presents greater uniformity, and its internal units have not been mapped in any greater detail yet.

In Santa Catarina, the oldest unit, Aguas Mornas, is composed of deformed meso- to leucocratic grayish granitoids, with composition ranging from quartz-monzonite, granodiorite to granite. Gabbro and diorite stocks and plutons are common. The intermediate suite, São Pedro de Alcantara, is the most voluminous, consisting predominantly of equi- to inequigranular grayish leucocratic granitoids. Among the porphyritic types, hornblende-biotite granodiorite to monzogranitic granitoids predominate. Enclaves of amphibolite, diorite and quartz-diorite are common. The youngest association, Pedras Grandes, is composed predominantly of pink leucocratic syeno- to monzogranitic granitoids. These rocks are equigranular to slightly porphyritic, medium-grained and texturally isotropic, and they are associated with felsic volcanic and volcaniclastic rocks and microgranite dykes.

The first two groups represent the least differentiated magmatites ($SiO_2 < 60$wt%), whereas the younger syenogranite and felsic volcanic rocks contain >73wt% SiO_2. A strong negative correlation between P_2O_5 and TiO_2 in granitoids of the Florianópolis Batholith suggests that

fractional crystallization involving apatite was important (Basei et al. 2015). Negative correlation of SiO_2 with Sr and Ba (except for the Águas Mornas Complex) and positive correlation with Rb indicates that the fractional crystallization process involved a considerable volume of feldspar. Calc-alkaline and subalkaline compositions predominate. Some of the two older units are metaluminous whereas the younger ones are transitional between meta- and peraluminous (Basei et al. 2015).

Fractionation between light and heavy rare-earth elements is observed in all the granitoid suites, with the Pedras Grandes Suite showing the smallest fractionation and most intense negative Eu anomaly. Virtually all the analysed samples plot in the field defined as post-collisional granite, indicating strong contamination of the magmas in the arc by continental crustal material.

All available U–Pb zircon ages (LAICPMS and SHRIMP) for the entire magmatic arc cover a range from 640 to 590 Ma (Silva et al. 2005; Florisbal et al. 2012a, b; Basei et al.2015). The younger values were obtained from the late Pedras Altas syenogranite and the oldest from augen gneiss of the Águas Mornas association. Whole rock Sm–Nd model ages are between 1200 and 1600 Ma (Basei et al. 2008a). High initial $^{87}Sr/^{86}Sr$ (>0.708) and moderate negative epsilon Nd values are further strong support of continental crust contribution in the generation of the magmatic arc.

Thus the Florianópolis, together with its corresponding Pelotas and Aiguá batholiths, corresponds to the roots of a Neoproterozoic magmatic arc, with strong crustal signature. Basei et al. (2000, 2008a) suggested that, based on the Nd model ages, and detrital zircon age pattern of its sedimentary cover, this arc would have an isotopic affinity with the terrains on the African side and that its genesis was related to the consumption of an oceanic crust subducted towards the east under the Kalahari and Congo cratons.

The generation of the magmatic arc on the edge of the African cratons, in a setting similar to the modern Andean Orogen, implies that the greatest extension of the Adamastor Ocean was to the west of the arc. The incorporation of the magmatic arc into the Dom Feliciano Belt took place only in the Ediacaran, after closure of the Adamastor Ocean and continent–continent collision in the course of Western Gondwana assembly. Its current position in South America is the result of the opening of the Atlantic Ocean along the eastern edge of the arc, following the contact with the back-arc deposits that correspond to the westernmost deposits of the Kaoko, Gariep and Saldania belts in southwestern Africa (Basei et al. 2008a; Frimmel et al. 2011, 2013).

Considering that this magmatic arc was active for at least 40 myr, it can be concluded that the Adamastor Ocean had reached at least 2000 km in width, assuming an average subduction rate of 5 cm/year. This value was obtained only for the ocean that existed between the Kaoko and the DFB, not including the branches between the Luis Alves and Curitiba Terranes and the Ribeira Belt, which would imply a much larger ocean. However, the total width of the ocean could have been much greater, possibly as much as 6000 km, if one takes the entire timespan of some 100 myr for the opening of the ocean into account (and using the same rate of subduction). This is close to the value suggested by Meert (2003) based on paleomagnetic data from African and South American cratons.

The Coastal Terrane has been recognized as the African counterpart of the magmatic arc consisting of calc-alkaline mafic, intermediate and felsic granitoids of 660–620 Ma age and metasedimentary rocks whose sediment load was derived from the magmatic arc (Seth et al. 1998; Kröner et al. 2004; Goscombe et al. 2005; Goscombe and Gray 2007; Foster et al. 2015; Konapásek et al. 2016). There the arc-rocks are calc-alkaline granitoids, such as monzodiorite, granodiorite and monzogranite with minor amount of diorite, quartz diorite and gabbro. All of them were affected by high-grade metamorphism (Seth et al. 1998; Franz et al. 1999; Masberg et al. 2005).

The Coastal Terrane is considered an exotic domain when compared with the Kaoko Belt turbiditic units deposited on the Congo Craton margin (Goscombe et al. 2003, 2005; Goscombe and Gray 2007, 2008; Frimmel et al. 2011; Konapásek et al. 2014). Differences in sedimentary provenance, magmatism and metamorphism in relation to the other segments of the Kaoko Belt are observed. Despite these differences the isotopic signature of its magmatic rocks and the detrital zircon provenance of its metasedimentary rocks are good indicators of the African roots of this segment, whose origin is also linked to the attenuated margin of the Congo Craton. The tectonic contacts and thrusts along which the Coastal Terrane were emplaced onto the other Kaoko Belt domains resulted from crustal shortening of the Kaoko and Dom Feliciano belts that followed the collision between the African and South American cratons.

3.5.4 Continental Collision (~600 Ma)

The Adamastor Ocean was much larger to the western side of the magmatic arc developed along the border of southwestern African cratons. Final closure of this ocean culminated in the collision of the magmatic arc with the South American continental segments. This collision occurred in the Ediacaran and left behind the Major Gercino-Cordillera-Sierra Ballena Suture Zone along which the sedimentary succession from the western margin of the Adamastor Ocean was juxtaposed to magmatic arc granitoids.

The suture zone, which stretches over a strike length of some 1200 km, is marked by up to a few kilometres-thick mylonite zones that display dextral displacement in Santa Catarina (Passarelli et al. 2011) and sinistral displacements in Rio Grande do Sul and Uruguay (Oyhantçabal et al. 2009b, 2011; Philipp et al. 2016a, b). The opposite displacements that took place at the same time along the shear zone are interpreted to reflect local partitioning of the collision vectors related to the different shapes of the continental masses involved in the collision.

This collision, although diachronic along its length, would have occurred around 600 Ma as suggested by U–Pb zircon age data from mylonitic arc granites, as well as by K–Ar cooling ages of synkinematic micas (Basei et al. 2011b; Passarelli et al. 2011). Compared with the age of arc magmatism (640–590 Ma), continental collision and suturing took place close to the end of arc magmatism, but about 10 myr after this magmatic episode had reached its peak (~610 Ma). In the Schist Belt, contact metamorphism overprinted, however, main syncollisional S2 fabric evident in the supracrustal rocks.

In Santa Catarina, the geochronological and geochemical-isotopic information of the intrusive bodies in the Schist Belt, all of them with a remarkable crustal signature (São João Batista, Valsungana and Nova Trento suites), suggest that these granitoids were generated around 590 Ma as a result of the thickening of the crust and heat introduced into the area by the 600 Ma collision of the magmatic arc with the Schist Belt (Basei et al. 2011b; Hueck et al. 2016, unpublished data). The 10 myr difference between the collision and the emplacement of the granitoids in the middle of the supracrustal rocks underlying the arc may result from the time required for the generation of granitic melts and their rise to shallower crustal levels.

In Rio Grande do Sul, the Cordillera Suite is the best example of collision-related magmatism. It consists of deformed, peraluminous granites that are now in many places mylonitic (Koester et al. 2001a, b; Philipp et al. 2013), intrusives in the metasedimentary rocks of the Porongos Group that outcrop parallel to the suture zone that follows the tectonic contact between the Pelotas Batholith (magmatic arc) and the Schist Belt. U–Pb zircon ages of these granitoids are around 600 Ma (Koester et al. 2001c).

Correlation of magmatic arc granitoid emplacement and its collision with the Schist Belt was first suggested by Passarelli et al. (1993) through the identification of a gradational change of the magmatic fabrics to subsolid shear deformation associated with the development of the Major Gercino Suture Zone in Santa Catarina. In the Rio Grande do Sul, a similar relationship has been observed between the granitoids of the Pelotas Batolith and the Cordillera shear zone (Philipp et al. 2016a, b).

Considering the above scenario, the magmatic-arc granitoids related to the Florianópolis, Pelotas and Aiguá batholiths are pre- to syncollisional. On the other hand, the younger granitoids that correspond to the syenogranites of the Pedras Grandes and Dom Feliciano Suites, with ages around 590 Ma, must be post-collisional, generated by decompression melting of continental crust as a result of orogenic collapse.

The filling of the Kaoko and Dom Feliciano depositional basins continued to about 590–580 Ma in the course of synorogenic basin development associated with the collision of the magmatic arc with the schist belts. This process was also concomitant with the installation of the foreland basins in both belts (Prave 1996; Hoffmann et al. 1998, 2004; Foster et al. 2015; Pertille et al. 2015a,b, 2017; Höfig et al. in revision).

The stress field that prevailed during the closure of the Adamastor Ocean and subsequent continental collision remained active and was responsible for the transpressive system that reactivated the main pre-existing lineaments with predominantly sinistral movements in the African domains and dextral displacement in the South American counterpart. This accentuated the extrusion of the arc, its double vergence, and caused its displacement towards the south (Goscombe et al. 2005) (Fig. 3.5).

3.6 Final Remarks and Conclusions

The comparative analysis of the Dom Feliciano and Kaoko belts made it possible to establish a protracted Wilson Cycle for the birth and demise of the Adamastor Ocean, but not in the position originally suggested by Hartnady et al. (1985), passing through lithospheric thinning, passive margin development, subduction, magmatic arc generation, collision and crustal thickening.

Originally, the Adamastor Ocean was perceived as a kind of proto-South Atlantic, and the modern South Atlantic has been thought to have opened along the Pan-African suture along which the Rio de la Plata Craton and the amalgamated Congo and Kalahari cratons became welded together. Although this notion is still being upheld by many workers (e.g. Buiter and Torsvik 2014), evidence reviewed in this chapter rather supports a more recently proposed model of the modern South Atlantic having opened up not along a suture zone but along a former back-arc basin (Frimmel et al. 2011; Will and Frimmel 2018). Subduction, which had led to the development of a large Andean-type magmatic arc,

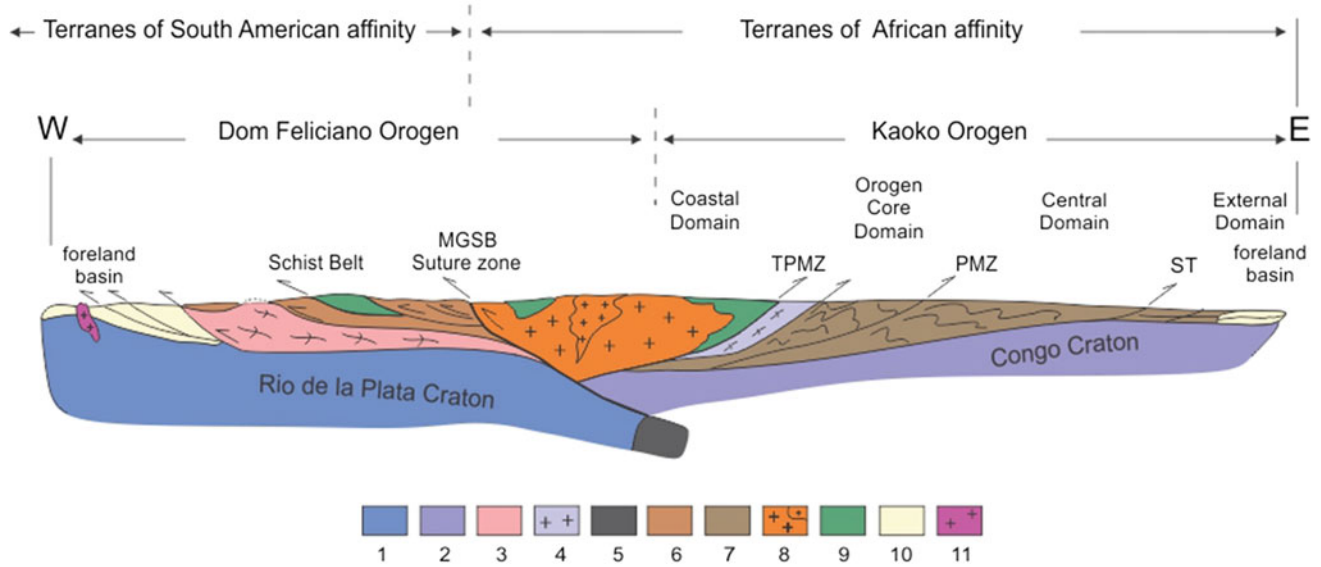

Fig. 3.5 Idealized cross-section juxtaposing Dom Felicano and Kaoko Belts: 1—Rio de la Plata Craton; 2—Congo Craton; 3—Encantadas, Luis Alves, Nico Perez crustal fragments; 4—tectonic exposures of basement belts inlier probably related to attenuated upper plate; 5—Adamastor oceanic crust remnant; 6—Dom Feliciano schist belt; 7—Kaoko schist belt; 8—Granite Belt (magmatic arc granitoids); 9—arc-related Ediacaran sediments; 10—Foreland basin deposits; 11—late stage 529 Ma Subida syenogranite

was not to the west but towards the east, implying the existence of a wide ocean, the redefined Adamastor Ocean, to the west of this magmatic arc. Integration of available data on the sedimentation history, magmatism and tectonometamorphic evolution of the various Neoproterozoic units of both sides of the modern South Atlantic, specifically the Dom Feliciano and Kaoko belts, revealed the following stages of a Wilson Cycle:

(1) Thinning and rifting of the Rodinia supercontinent, during the Tonian, with the climax of mafic dyke swarm emplacement, probably feeding a rift-related flood basalt province, around 850 Ma. This was followed by decompression- and mantle heat transfer-induced anataxis of the lower crust, the resulting emplacement of granitoids and formation of migmatites between 800 and 770 Ma. Evidence of this is best preserved in the PET in Uruguay. Transition from rifting to drifting occurred around 780 Ma. At the same time, further rift grabens opened to the east, along today's African west coast, but failed (see Chap. 13).
(2) Opening of the Adamastor Ocean lasted for at least 100 myr, and by 640 Ma subduction must have been well under way as evident from the oldest granitoids in the corresponding magmatic arc. Over this extended period of time, passive margin deposits accumulated on the margins of the Kalahari/Congo and Paranapanema/Rio de la Plata cratons.
(3) Peak of arc magmatism in the western edge of the Kalahari Craton was reached around 610–600 Ma. At the same time, a back-arc basin, the Marmora Basin, opened up east of the arc, probably reactivating pre-existing rift structures along the modern African west coast (see Chap. 13).
(4) Collision of the African cratons and the terranes of the South American portion began around 600 Ma shortly after the last manifestations of the magmatic arc, resulting in thickening of the continental crust along the Pan-African orogenic belts.

The importance of the magmatic arc in the structuring of the Kaoko and Dom Feliciano belts is striking, both because it represents the main product of the subduction process and because it formed, after collision, an important sediment source for the synorogenic deposits in both belts. The major tectonic boundaries are now present as important lineaments —that is, the Major Gercino-Cordilheira-Sierra Ballena Suture Zone in the DFB and the Three Palms Mylonite Zone in the Kaoko Belt. These doubly vergent shear zones were originally of low angle, being generated during the collision of Rio de La Plata and Congo cratons, progressing later to high-angle faults with directional movement owing to the crustal shortening process that followed the collision.

References

Affaton P et al (2016) The Pan-African West Congo belt in the Republic of Congo (Congo Brazzaville): stratigraphy of the Myombe and West Congo supergroups studied by detrital zircon geochronology. Precambr Res 272:185–202

Alkmim FF, Teixeira W (2017) The Paleoproterozoic Mineiro Belt and the Quadrilátero Ferrífero. In: Heilbron M et al (eds) São Francisco Craton, tectonic genealogy of a miniature continent. Springer, Eastern Brazil, pp 71–94

Almeida FFM (1965) Precambrian geology of North Eastern Brazil and Western Africa and the theory of Continental Drift. In: symposium on the granites of West Africa, Ivory Coast, Nigeria and Cameron. Proceedings, Paris: UNESCO, p 151–162

Almeida FFM et al (1981) Brazilian structural provinces: an introduction. Earth Sci Rev 17:1–29

Arena KR et al (2016) Evolution of Neoproterozoic ophiolites from the southern Brasiliano Orogen revealed by zircon U–Pb–Hf isotopes and geochemistry. Precambr Res 285:299–314

Arena KR et al (2017) U-Pb–Hf isotopes and trace elements of metasomatic zircon delimit the evolution of neoproterozoic Capané ophiolite in the southern Brasiliano Orogen. Int Geol Rev. https://doi.org/10.1080/00206814.2017.1355269

Assumpção M et al (2017) Lithospheric features of the São Francisco Craton. In: Heilbron M et al (eds) São Francisco Craton, tectonic genealogy of a miniature continent. Springer, Eastern Brazil, pp 15–25

Babinski M et al (2012) Neoproterozoic glacial deposits from the Araçuaí Orogen, Brazil: age, provenance and correlations with the São Francisco craton and West Congo belt. Gondwana Res 21:451–465

Barbosa JSF, Barbosa RG (2017) The Paleoproterozoic Eastern Bahia Orogenic domain. In: Heilbron M et al (eds) São Francisco craton, tectonic genealogy of a miniature continent. Springer, Eastern Brazil, pp 57–69

Basei MAS et al (1992) Evolução Tectonica dos Terrenos entre os Cinturões Ribeira e Dom Feliciano (PR e SC). Rev Bras Geoc 2:216–221

Basei MAS et al (1998) The Santa Catarina granulite complex of Southern Brazil, a review. Gondwana Res 1:383–391

Basei MAS et al (2000) The Dom Feliciano belt of Brazil and Uruguay and its foreland domain. In: Cordani U (ed) Tectonic evolution of South America, 31st International Geological Congress, Rio de Janeiro, Brazil, pp 311–334

Basei MAS et al (2005) A connection between the Neoproterozoic Dom Feliciano (Brazil/Uruguay) and Gariep (Namibia/South Africa) orogenic belts—evidence from a reconnaissance provenance study. Precambrian Res 139:195–221

Basei MAS et al (2008a) West Gondwana amalgamation based on detrital zircon ages from Neoproterozoic Ribeira and Dom Feliciano belts of South America and comparison with coeval sequences from SW Africa. Geol Soc Lond Spec Publ 294:239–256

Basei MAS et al (2008b) A-type rift-related granite and the lower Cryogenian age for the beginning of the Brusque Belt basin. In: Proceedings of South American symposium on isotope geology, vol 6, San Carlos de Bariloche, Argentina (CD-ROM)

Basei MAS et al (2009) The evolution and tectonic setting of the Luis Alves Microplate of Southeastern Brazil: an exotic terrane during the assembly of Western Gondwana. In: Gaucher C et al (eds) Special issue: Neoproterozoic-Cambrian tectonics, global change and evolution: a focus on Southwestern Gondwana Dev Precambriam Geol 16:273–291

Basei MAS et al (2010) Contribution of SHRIMP U–Pb zircon geochronology to unravelling the evolution of Brazilian Neoproterozoic fold belts. Precambrian Res 183:112–144

Basei MAS et al (2011a) The basement of the Punta del Este Terrane (Uruguay): an African Mesoproterozoic fragment at the eastern border of the South American Río de La Plata craton. Int J Earth Sci 100:289–304

Basei MAS et al (2011b) Tectonic evolution of the Brusque Group, Dom Feliciano Belt, Santa Catarina, Southern Brazil. J South Am Earth Sci 32:324–350

Basei MAS et al (2013) Polycyclic evolution of Camboriú Complex migmatites, Santa Catarina, Southern Brazil: integrated Hf isotopic and U–Pb age zircon evidence of episodic reworking of a Mesoarchean juvenile crust. Braz J Geol 43:427–443

Basei MAS et al (2015) Florianópolis Batholith—the roots of an Ediacaran Magmatic Arc generated during Gondwana Amalgamation, Dom Feliciano Belt, Santa Catarina State, South Brazil 2016 8th Hutton Symposium on Granites and Related Rocks. Florianópolis, Brazil, Abstracts, p 180

Brentan F (2011) Unidades turmaliníferas do Grupo Brusque, Rio do Oliveira, Tijucas, SC. 41 p, (graduation monograph). Instituto de Geociências, Universidade de São Paulo—USP, Brazil

Brito Neves BB, Fuck RA (2013) Neoproterozoic evolution of the basement of the South-American platform. J S Am Earth Sci 47:72–89

Buiter SJH, Torsvik TH (2014) A review of wilson cycle plate margins: a role for mantle plumes in continental break-up along sutures? Gondwana Res 26:627–653

Caby R (2003) Terrane assembly and geodynamic evolution of central-western Hoggar: a synthesis. J Afr Earth Sc 37:133–159

Campanha GAC et al (2016) The Mesoproterozoic to early Neoproterozoic passive margin Lajeado Group and Apiaí Gabbro, Southeastern Brazil. Geosci Front 7:683–694

Campos Neto MC, Figueiredo MCH et al (1995) The Rio Doce Orogeny, Southeastern Brazil. J S Am Earth Sci 8:13–162

Castro MP (2014) Caracterização Geológica da Formação Capelinha como uma unidade basal do Grupo Macaúbas em sua área tipo, Minas Gerais. Unpublished MSc thesis, Universidade Federal de Ouro Preto, 146 pp

Chemale F (2000) Evolução geológica do Escudo Sul-Riograndense. In: Holz M, De Ros LF (eds) Geologia Do Rio Grande Do Sul. Universidade Federal do Rio Grande do Sul, Porto Alegre, pp 13–52

Cordani UG et al (2003a) From Rodinia to Gondwana: a review of the available evidence from South America. Gondwana Res 6:275–283

Cordani UG et al (2003b) Tearing up Rodinia: The Neoproterozoic palaeogeography of South American cratonic fragments. Terra Nova 15:350–359

Cordani UG et al (2010) On the origin and tectonic significance of the intra-plate events of Grenvillian-type age in South America: a discussion. J South Am Earth Sci 29:143–159

Cordani UG et al (2013) The significance of the Transbrasiliano-Kandi tectonic corridor for the amalgamation of West Gondwana. Braz J Geol 43:583–597

Cruz RF et al (2017) O Terreno Jaguarão: Caracterização de Novo Domínio Geológico no Sudeste do Rio Grande do Sul. In: X international symposium on tectonics, 4 pp (CD-ROM)

D'Agrela-Filho MS, Cordani UG (2017) The paleomagnetic record of the São Francisco-Congo Craton. In: Heilbron M et al (eds) São Francisco Craton, Tectonic genealogy of a miniature continent. Springer, Eastern Brazil, pp 305–320

Degler R et al (2017) Contrasting provenance and timing of metamorphism from paragneisses of the Araçuaí-Ribeiraorogenic system, Brazil: hints for Western Gondwana assembly. Gondwana Res 51:30–50

DeKock GS et al (2000) U–Pb and Pb–Pb ages of the Naauwpoort rhyolite, Kawakeup leptite and Okongava diorite: implications for

the onset of rifting and of orogenesis in the Damara belt, Namibia. Commun Geol Surv Namibia 12:81–88
De Waele B et al (2009) The geochronological framework of the Irumide Belt: a prolonged crustal history along the margin of the Bangweulu Craton. Am J Sci 309:132–187
De Wit M et al (1988) Geological map of sectors of Gondwana: reconstructed to their disposition ~150 Ma. scale 1:10.000.000: Lambert equal area projection-centred at 20°S, 40°E. American Association of Petroleum Geologists, Tulsa, USA
Faleiros FM et al (2011) Ediacaran high-pressure collision metamorphism and tectonics of the southern Ribeira Belt (SE Brazil): evidence for terrane accretion and dispersion during Gondwana assembly. Precambr Res 189:263–291
Fernandez-Alonso M et al (2012) The Mesoproterozoic Karagwe-Ankole Belt (formely the NE Kibara belt): the result of prolonged extensional intracratonic basin development punctuated by two short-lived far-field compressional events. Precambr Res 216–219:63–86
Florisbal LM et al (2012a) Space–time relation of post-collisional granitic magmatism in Santa Catarina, Southern Brazil: U–Pb LA–MC–ICP–MS zircon geochronology of coeval mafic–felsic magmatism related to the Major Gercino Shear Zone. Precambr Res 216–219:132–151
Florisbal LM et al (2012b) Petrogenesis of syntectonic granites emplaced at the transition from thrusting totranscurrent tectonics in post-collisional setting: whole-rock and Sr–Nd–Pb isotope geochemistry in the Neoproterozoic Quatro Ilhas and Mariscal Granites, Southern Brazil. Lithos 153:53–71
Foster DA et al (2015) U–Pb age and Lu–Hf isotopic data of detrital zircons from Neoproterozoic Damara Sequence: implications for pre-Gondwana proximity of Congo and Kalahari. Gondwana Res 28:179–190
Fragoso Cesar ARS (1980) O Cráton do Rio de La Plata e o Cinturão Dom Feliciano no Escudo Uruguaio-Sul Riograndense, Camboriu, SC. In: An. XXXI Congresso Brasileiro de Geologia, pp 2879–2892
Frantz JC, Botelho NF (2000) Neoproterozoic granitic magmatism and evolution of the Eastern Dom Feliciano Belt in Southernmost Brazil: a tectonic model. Gondwana Res 3:7–19
Franz L et al (1999) Diachronous Pan-African granulite-facies metamorphism (650 Ma and 550 Ma) in the Kaoko Belt, NW Namibia. Eur J Mineral 11:167–180
Frimmel HE et al (2011) Neoproterozoic geodynamic evolution of SW-Gondwana: a southern African perspective. Int J Earth Sci 100:323–354
Frimmel HE et al (2013) A new lithostratigraphic subdivision and geodynamic model for the Pan-African western Saldania Belt, South Africa. Precambr Res 231:218–235
Frimmel HE et al (1996) New Pb–Pb single zircon age constraints on the timing of Neoproterozoic glaciation and continental break-up in Namibia. J Geol 104:459–469
Frimmel HE et al (2001) The Richtersveld Igneous Complex, South Africa: U–Pb zircon and geochemical evidence for the beginning of Neoproterozoic continental breakup. J Geol 109:493–508
Fuck RA et al (2008) Rodinia descendentes in South America. Precambr Res 160:108–126
Fuck RA et al (2017) The Northern Brasília Belt. In: Heilbron M et al (eds) São Francisco Craton, tectonic genealogy of a miniature continent. Springer, Eastern Brazil, pp 205–220
Ganade Araujo CE et al (2012) U–Pb detrital zircon provenance of metasedimentary rocks from the Ceará Central and Médio Coreaú domains, Borborema province, NE-Brazil: tectonic implications for a long-lived Neoproterozoic active continental margin. Precambr Res 206–207:36–51
Ganade Araujo CE et al (2014) Ediacaran 2500-km-long synchronous deep continental subduction in the West Gondwana Orogen. Nat Commun 5:5198
Ganade Araujo CE et al (2016) Rightening-up NE Brazil and NW Africa connections: New U–Pb/Lu–Hf zircon data of a complete plate tectonic cycle in the Dahomey Belt of the West Gondwana Orogen in Togo and Benin. Precambr Res 276:24–42
Goscombe BD, Gray D (2007) The Coastal Terrane of the Kaoko Belt, Namibia: outboard arc terrane and tectonic significance. Precambr Res 155:139–158
Goscombe BD, Gray D (2008) Structure and strain variation at mid-crustal levels in a transpressional orogen: a review of Kaoko Belt structure and the character of West Gondwana amalgamation. Gondwana Res Focus Paper 13:45–85
Goscombe BD et al (2003) Structure of the Kaoko Belt, Namibia: progressive evolution of a classic transpressional orogen. J Struct Geol 25:1049–1081
Goscombe BD et al (2005) Event geochronology of the Pan-African Kaoko Belt, Namibia. Precambr Res 140:1–41
Gray DR et al (2006) 40Ar/39Ar thermochronology of the Pan-African Damara Orogen, Namibia, with implications for tectonothermal and geodynamic evolution. Precambr Res 150:49–72
Gross AOMS et al (2009) Petrology and thermobarometry of mafic granulites and migmatites from the Chafalote Metamorphic Suite: new insights into the Neoproterozoic P-T evolution of the Uruguayan-Sul-Rio-Grandense shield. Precambr Res 170(157):174
Gruber L et al (2011) Proveniência de metassedimentos das sequências Arroio Areião, Cerro Cambará e Quartzo Milonitos no Complexo Metamórfico Porongos, Santana da Boa Vista. RS Pesqui Em Geociências 38:205–223
Gubert ML et al (2016) The Bossoroca Complex, São Gabriel Terrane, Dom Feliciano Belt, southermost Brazil: U–Pb geochronology and tectonic implications for the Neoproterozoic São Gabriel Arc. J S Am Earth Sci 70:1–17
Halinann SE, Mantovani SMM (1993) Structural framework of the Southern Brazilian shield: the perspective from gravity models. In: III International Geoph. Congress, vol 2. Anais. SBGF, RJ, pp 1078–1083
Halverson GP et al (2002) A major perturbation of the carbon cycle before the Ghaub glaciation (Neoproterozoic) in Namibia: prelude to snowball earth? Gechem Geophys Geosyst 3:1–24
Harara OMM (2001) Mapeamento e investigação petrológica e geocronológica dos litotipos da região do Alto Rio Negro (PR-SC): um exemplo de sucessivas e distintas atividades magmáticas durante o Neoproterozóico. Unpublished PhD thesis, Institute of Geosciences—University of São Paulo, 206 p
Harara OMM et al (2004) Neoproterozoic supra subduction zone (SSZ) ophiolitic rocks from Piên (PR), southern Brazil. Quarenta anos de geocronologia no Brasil. In: Boletim de Resumos N. 89
Hartmann LA et al (2003) Prolonged Paleoproterozoic magmatic participation in the Neoproterozoic Dom Feliciano Belt, Santa Catarina, Brazil, based on zircon U–Pb SHRIMP geochronology. J S Am Earth Sci 16:477–492
Hartmann LA et al (2004) Paleoproterozoic magmatic provenance of detrital zircons, porongos complex quartzites, Southern Brazilian shield. Int Geol Rev 46:127–157
Hartnady CJH et al (1985) Proterozoic crustal evolution in southwestern Africa. Episodes 8:236–244
Hauzenberger CA et al (2014) Termination of the Southern Irumide Belt, Tanzania: Zircon U/Pb geochronology. Precambrian Res 255:144–162
Heilbron M, Machado N (2003) Timing of terrane accretion in the Neoproterozoic-Eopaleozoic Ribeira orogen (SE Brasil). Precambr Res 125:87–112

Heilbron M et al (2017) The Ribeira Belt. In: Heilbron M et al (eds) São Francisco Craton, genealogy of a miniature continent Tectonic. Springer, Eastern Brazil, pp 277–302

Hoffman PF (1991) Did the breakout of Laurentia turn Gondwanaland inside out? Science 252:1409–1412

Hoffman PF et al (1996) Precise U–Pb zircon ages for early Damaran magmatism in the Summas Mountains and Welwitschia Inlier, northern Damara belt, Namibia. Commun Geol Surv Namibia 11:47–52

Hoffman PF et al (1998) A Neoproterozoic snowball earth. Science 281:1342–1346

Hoffmann KH et al (2004) U–Pb zircon date from the Neoproterozoic Ghaub Formation, Namibia: constraints on Marinoan glaciation. Geology 32:817–820

Höfig DF et al (accepted) Polyphasic evolution of the Porongos metamorphic complex, Dom Feliciano Belt, southernmost Brazil: implications for the assembly of southwestern Gondwana. Precambrian Res

Hueck M et al (2016) Origin and evolution of the granitic intrusions in the Brusque Group of the Dom Feliciano Belt, south Brazil: petrostructural analysis and wholerock/isotope geochemistry. J S Am Earth Sci 69:131–151

Hueck M et al (unpublished data) Tracking the sources and the emplacement of the Neoproterozoic granitic intrusions in the Brusque Group, Dom Feliciano Belt, South Brazil: LA-ICP-MS and SHRIMP U–Pb zircon geochronology coupled to Hf isotopic analysis

Hurley PM et al (1967) Test of continental drift by comparison of radiometric ages. A pre-drift reconstruction shows matching geologic age provinces in West Africa and Northern Brazil. Science 157:495–500

Janasi VA et al (2009) Associated A-type subalkaline and high-K calc-alkaline granites in the Itu Granite Province, Southeastern Brazil: petrological and tectonic significance. Canadian Mineral 47:1505–1526

Johnson SP et al (2005) A review of the Mesoproterozoic to early Palaeozoic magmatic and tectonothermal history of south-central Africa: implications for Rodinia and Gondwana. J Geol Soc Lond 162:433–450

Johnson SP et al (2007) Geochronology of the Zambezi supracrustal sequence, southern Zambia: A record of Neoproterozoic divergent processes along the southern margin of the Congo Craton. J Geol 115:355–374

Koester E et al (2001a) Geologia e Geoquímica de Granitóides sintectônicos à Zona de Cisalhamento Transcorrente Dorsal do Canguçu, Encruzilhada do Sul, RS. Revista Brasileira de Geociências 31(2):141–154

Koester E et al (2001b) Petrologia dos Granitóides sintectônicos à Zona de Cisalhamento Transcorrente Dorsal do Canguçu, Encruzilhada do Sul, RS. Revista Brasileira de Geociências 31(2):131–140

Koester E et al (2001c) SHRIMP U–Pb age for the emplacement of the Santana granite and Reactivation of the Porto Alegre Suture, southern Brazil. J S Am Earth Sci 14:91–99

Koester E et al (2008) U–Pb ages of Granitoids from Eastern Sul-Riograndense shield. In: VI South American symposium on isotope geology, San Carlos de Bariloche—Argentina, 8 pp

Konopásek J et al (2008) Neoproterozoic igneous complex emplaced along major tectonic boundary in the Kaoko Belt (NW Namibia)—ion probe and laser ablation ICP-MS dating of magmatic and metamorphic zircons. J Geol Soc Lond 165:153–165

Konopásek J et al (2014) Timing and sources of pre-collisional Neoproterozoic sedimentation along the SW margin of the Congo Craton (Kaoko Belt, NW Namibia). Gondwana Res 26:386–401

Konopásek J et al (2016) Linking the basement geology along the Africa-South America coasts in the South Atlantic. Precambrian Res 280:221–230

Kröner A, Cordani UG (2003) African and South American cratons were not part of the Rodinia supercontinent: evidence from field relationships and geochronology. Tectonophysics 375:325–352

Kröner S et al (2004) U–Pb and Pb–Pb zircon ages for metamorphic rocks in the Kaoko Belt of Northwestern Namibia: a Paleo- to Mesoproterozoic basement reworked during the Pan-African orogeny. S Afr J Geol 107:455–476

Lehmann J et al (2015) Structural and geochronological constraints on the Pan-African tectonic evolution of the northern Damara Belt, Namibia. Tectonics 35:103–135

Leite RJ et al (2007) The late-to postorogenic transition in the Neoproterozoic Agudos Grandes Batholith (Apiaí Domain, SE Brazil): constraints from geology, mineralogy, and U–Pb geochronology. J S Am Earth Sci 23:193–212

Lenz C et al (2011) U–Pb SHRIMP ages for the Cerro Bori Orthogneisses, Dom Feliciano Belt in Uruguay: Evidences of a 800 Ma magmatic and 650 Ma metamorphic event. Precambrian Res 185:149–163

Li ZX et al (2008) Assembly, configuration, and break-up history of Rodinia: a synthesis. Precambr Res 160:179–210

Machado N et al (1989) Resultados preliminares da geocronologia U–Pb na Serra do Espinhaço Meridional. In: V Simpósio de Geologia de Minas Gerais. Belo Horizonte, SBG, Anais, pp 171–174.

Masberg P et al (2005) Major and trace element and isotopic (Sr, Nd, O) constraints for Pan-African crustally contaminated grey granite gneisses from the southern Kaoko belt, Namibia. Lithos 84:25–50

Masquelin HC (2000) A Evolução Estrutural e Metamórfica do Terreno Punta del Este, Sudeste Uruguaio. Unpublished PhD thesis, University of Rio Grande do Sul, Brazil, 350 pp

Masquelin HC et al (2012) The Cerro Olivo complex: a pre-collisional neoproterozoic magmatic arc in Eastern Uruguay. Int Geol Rev. 54:1161–1183

Meert JG (2003) A synopsis of events related to the assembly of eastern Gondwana. Tectonophysics 362:1–40

Miller RM et al (2009) Geodynamic synthesis of the Damara Orogen sensu lato. Neoproterozoic to early Palaeozoic evolution of the Southwestern Africa (In: Gaucher C et al (eds) Neoproterozoic-Cambrian Tectonics, global change and evolution: focus on southwestern Gondwana). Dev Precambrian Geol 16:231–235

Nascimento DB et al (2016) Stratigraphy of the Neoproterozoic Damara sequence in northwest Namibia: slope to basin sub-marine mass transport deposits and olistolith fields. Precambr Res 278:108–125

Nascimento DB et al (2017) Depositional ages and provenance of the Neoproterozoic Damara Supergroup (northwest Namibia): Implications on the Angola-Congo and Kalahari cratons connection. Gondwana Res 52:153–171

Oyhantçabal P et al (2009a) The Sierra Ballena Shear Zone in the southernmost Dom Feliciano Belt (Uruguay): evolution, kinematics, and deformation conditions. Int J Earth Sci (Geol Rundsch) 99 (6):1227–1246

Oyhantçabal P et al (2009b) Geochronological constraints on the evolution of the southern Dom Feliciano Belt (Uruguay). J Geol Soc Lond 166:1–11, 1075–1084

Oyhantçabal P et al (2011) The transpressional connection between Dom Feliciano and Kaoko Belts at 580–550 Ma. Int J Earth Sci (Geol Rundsch) 100:379–390

Passarelli CR et al (1993) Caracterização geométrica e cinemática da Zona de Cisalhamento Major Gercino e sua importância na compartimentação dos terrenos Pré-Cambrianos de Santa Catarina. Revista Brasileira de Geociências 23:234–241

Passarelli CR et al (2011) Deformation and geochronology of syntectonic granitoids emplaced in the Major Gercino Shear Zone, southeastern South America. Gondwana Res 17:688–703

Pedrosa Soares AC, Alkmin FF (2011) How many rifting events preceded the development of the Araçuaí-west Congo Orogen? Geonomos 19:244–251

Pedrosa Soares AC et al (2001) The Araçuaí West Congo orogeny in Brazil: an overview of a confined orogeny formed during Gondwanaland assembly. Precambr Res 110:30–323

Pedrosa Soares AC et al (2008) Similarities and differences between the Brazilian and African counterparts of the Neoproterozoic Araçuaí-West Congo Orogen. In: Pankhurst JR et al (eds) West Gondwana: Pre-Cenozoic Correlations across the South Atlantic region. Geol Soc Lond Spec Publ 294:153–172

Pertille J et al (2015a) Zircon U–Pb age constraints on the Paleoproterozoic sedimentary basement of the Ediacaran Porongos Group, Sul-Riograndense Shield, southern Brazil. J South Am Earth Sci 63:334–345

Pertille J et al (2015b) Origin of the Ediacaran Porongos Group, Dom Feliciano Belt, southern Brazilian Shield, with emphasis on whole rock and detrital zircon geochemistry and U–Pb, Lu–Hf isotopes. J South Am Earth Sci 64:69–93

Pertille J et al (2017) Reconstructing the Cryogenian-Ediacaran evolution of the Porongos fold and thrust belt, Southern Brasiliano Orogen, based on Zircon U–Pb–Hf–O isotopes. Int Geol Rev 6814:1–29

Philipp RP, Machado R (2005) The late Neoproterozoic granitoid magmatism of the Pelotas Batholith, southern Brazil. J S Am Earth Sci 19:461–478

Philipp RP et al (2004) Caracterização litológica e evolução metamórfica da porção leste do ComplexoMetamórficoBrusque, Santa Catarina. Rev Bras Geocienc 34:21–34

Philipp RP et al (2013) Peraluminous leucogranites of the Cordilheira suite: a record of Neoproterozoic collision and the generation of the Pelotas Batholith, Dom Feliciano Belt, Southern Brazil. J South Am Earth Sci 43:8–24

Philipp RP et al (2016a) Tectonic evolution of the Dom Feliciano Belt in Southern Brazil: geological relationships and U–Pb geochronology. Braz J Geol 46(Suppl 1):83–104

Philipp RP et al (2016b) SHRIMP U–Pb age and high temperature conditions of the collisional metamorphism in the Várzea do Capivarita complex: implications for the origin of Pelotas Batholith, Dom Feliciano Belt, southern Brazil. J S Am Earth Sci 66:196–207

Pimentel MM (2016) The tectonic evolution of the Neoproterozoic Brasília Belt, central Brazil: a geochronological and isotopic approach. Braz J Geology 46:67–82

Pisarevsky SA et al (2003) Models of Rodinia assembly and fragmentation. Geol Soc Lond Sp Publ 206:35–55

Porada H (1979) The Damara-Ribeira Orogen of the Pan-African-Brasiliano cycle in Namibia (Southwest Africa) and Brazil as interpreted in terms of continental collision. Tectonophysics 57:237–265

Porcher CC et al (1999) Idade SHRIMP em zircão: vulcanismo ácido do Complexo Metamórfico Porongos. I Simpósio de Vulcanismo e Ambientes Associados. Brazilian Geological Society, Gramado, Brazil, p 110

Prave AR (1996) Tale of three cratons: tectonostratigraphic anatomy of the Damara Orogen in northwestern Namibia and the assembly of Gondwana. Geology 24:1115–1118

Prazeres Filho HJ et al (2003) Litoquímica, geocronologia U–Pb e geologia isotópica (Sr–Nd–Pb) das rochas graníticas dos batólitos Cunhaporanga e Três Córregos na porção sul do Cinturão Ribeira, Estado do Paraná. Geologia USP, Série Científica 3: 51–70

Preciozzi F et al (1999) The Namaqua/Grenville terrane of eastern Uruguay. In: Proceedings of the II South American symposium on isotope geology. Actas, Cordoba (Argentina), pp 338–340

Queiroga GN et al (2012) Geologia e Recursos Minerais da Folha Nova Venécia SE 24-Y-B-IV, Espirito Santo, 1:1000.000. Belo Horizonte, CPRM, p 76

Ramos VA et al (2010) Pampia: a large cratonic block missing in the Rodinia supercontinent. J Geodyn 50:243–255

Renné PR et al (1990) 40Ar/39Ar dating of 1.0–1.1 Ga magnetizations from the São Francisco and Kalahari Cratons: tectonic implications for Pan-African and Brasiliano mobile belts. Earth Planet Sci Lett 101(2–4):349–366

Robb LJ et al (1999) The history of granulite-facies metamorphism and crustal growth from singlezircon U–Pb geochronology: Namaqualand, South Africa. J Petrol 40:1747–1770

Rosa MLS et al (2007) Neoproterozoic anaorogenic magmatism in the southern Bahia Alkaline Province of NE Brazil: U–Pb and Pb–Pb ages of the blue sodalite syenites. Lithos 97:88–97

Rosa MLS et al (2015) Idade Pb–Pb do stock Nefelina Sienito Serra da Gruta, Província alcalina do sul do Estado da Bahia. Sci Plena 11 (3):1–5

Saalmann K et al (2011) Multiple accretion at the eastern margin of the Río de la Plata craton: the prolonged Brasiliano orogeny in southernmost Brazil. Int J Earth Sci Geol Rundsch 100:355–378

Sanchez-Bettucci L et al (2001) Tectonic setting of the late Proterozoic Lavalleja Group (Dom Feliciano Belt), Uruguay. Gondwana Res 4:395–407

Sanchez-Bettucci L et al (2004) Mineralizations of the Lavalleja Group (Uruguay), a probable Neoproterozoic Volcano-Sedimentary Sequence. Gondwana Res 7(3):745–751

Santos TMB et al (2015) Diachronic collision, slab-break-off and long-term high thermal flux in the Brasiliano-Pan African orogeny: implications for the geodynamic evolution of the Mantiqueira Province. Precambr Res 260:1–22

Schukowsky W et al (1991) Estruturação dos terrenos Pré-Cambrianos da região sul do Brasil e oeste do Uruguai: um estudo por modelamento gravimétrico. Rev Bras de Geofísica 9(2):275–287

Seth B et al (1998) Archaean to Neoproterozoic magmatic events in the Kaoko belt of NW Namibia and their geodynamic significance. Precambr Res 92:341–363

Siga Jr O et al (2009) Magmatic records of lower Neoproterozoic and upper Neoproterozoic in Itaiacoca Belt (Parana–Brazil): zircon ages and Lithostratigraphy studies. Gondwana Res, pp 197–208

Silva LC et al (1980) História metamórfica do Grupo Brusque em SC e Análise comparativa entre as regiões do Russo e da Catinga. In: Anais XXXI Congr. Bras. Geol. Balneario Camboriu, Santa Catarina, vol 5, pp 2982–2995

Silva LC et al (1999) SHRIMP U/Pb zircon dating of Neoproterozoic Granitic Magmatism and collision in the Pelotas Batholith, Southernmost Brazil. Int Geol Rev 41(6):531–551

Silva LC et al (2002) Dataçoes U–Pb SHRIMP do vulcanismo felsico na Bacia Brusque, Orogeno Pelotas, SC. SBG, Congresso Brasileiro de Geologia, 41, Anais, João Pessoa, p. 510

Silva LC et al (2005) SHRIMP U–Pb zircon geochronology of Neoproterozoic crustal granitoids (Southern Brazil): a case for discrimination of emplacement and inherited ages. Lithos 82:503–525

Silva LC et al (2008) Tonian rift-related, A-type continental plutonism in the Araçuaí orogen, eastern Brazil: new evidence for the breakup stage of the São Francisco-Congo Paleocontinent. Gondwana Res 13:527–537

Souza MES (2016) Caracterização Estrutural e Geocronológica dos Xistos Verdes e Metagabros do Grupo Macaúbas na Faixa Terra Branca-Planalto de Minas, Minas Gerais. Federal University of Ouro Petro. Unpublished master's thesis 215 pp

Squire RJ et al (2006) Did the Transgondwanan supermountain trigger the explosive radiation of animals on Earth? Earth Planet Sci Lett 250:116–133

Tack L et al (2001) Early Neoproterozoic magmatism (1000–910 Ma) of the Zadinian and Mayumbian Groups (Bas-Congo): onset of Rodinia rifitng and the western edge of the Congo craton. Precambr Res 110:277–306

Tedeschi M et al (2016) The Ediacaran Rio Doce Magmatic Arc revisited (Araçuaí-Ribeira orogenic system, SE Brazil). J S Am Earth Sci 68:167–186

Teixeira AL et al (2004) Bacias do estágio de transição da plataforma sul-americana. In: Mantesso-Neto V, Bartorelli A, Carneiro CDR, Brito-Neves BB (eds) Geologia do Continente Sul-Americano—Evolução da obra de Fernando Flávio Marques de Almeida, capítulo 29. BECA, São Paulo, pp 487–536

Teixeira W et al (2013) U–Pb (ID-TIMS) Baddeleyite ages and paleomagnetism of 1.79 and 1.59 Ga tholeiitic dyke swarms, and position of the Rio de la Plata Craton within the Columbia supercontinent. Lithos 174:157–174

Teixeira W et al (2017) The nature and evolution of the Archean Crust of the São Francisco craton. In: Heilbron M et al (eds) São Francisco Craton, Eastern Brazil: tectonic genealogy of a miniature continent. Regional geology review series. Springer, Berlin, pp 29–56 (CH 3)

Tohver E et al (2006) Paleomagnetic record of Africa and South America for the 1200–500 Ma interval, and evaluation of Rodinia and Gondwana assemblies. Precambr Res 147(3–4):193–222

Tohver E et al (2010) Closing the Clymene ocean and bending a Brasiliano belt: evidence for the Cambrian formation of Gondwana, southeast Amazon craton. Geology 38:267–270

Trompette R (1997) Neoproterozoic ($\sim$600 Ma) aggregation of western Gondwana: a tentative scenario. Precambr Res 82:101–112

Unrug R (1997) Rodinia to Gondwana: the geodynamic map of Gondwana supercontinent assembly. GSA Today 7(1):1–6

Valeriano CM et al (2016) Cambro-Ordovician post-collisional granites of the Ribeira Belt, SE-Brazil: a case of terminal magmatism of a hot orogen. J S Am Earth Sci 68:569–581

Vlach SRF, Gualda GAR (2007) Allanite and chevkinite in A-type granites and syenites of the Graciosa Province, southern Brazil. Lithos 97:98–121

Will TM, Frimmel HE (2018) Where does a continent prefer to break up? Lessons from the South Atlantic margins. Gondwana Res 53:9–19

Will TM et al (2004) Barrovian and Buchan type metamorphism in the Pan-African Kaoko belt, Namibia: Implications for its geotectonic position within the framework of Western Gondwana. S Afr J Geol 107:431–454

Will TM et al (2014) Geochemical and isotopic composition of Pan-African metabasalts from southwestern Gondwana: evidence of Cretaceous South Atlantic opening along a Neoproterozoic back-arc. Lithos 202–203:363–381

Yamamoto MT, Basei MAS (2009) Geoquímica isotópica e idade U-Pb em zircão do magmatismo básico do Grupo Brusque no Estado de Santa Catarina, SC. Simpósio 45 anos de Geocronologia no Brasil, Boletim de Resumos Expandidos. São Paulo, Brasil, pp 328–330

Zvirtes G et al (2015) Evidências de rifteamento e metamorfismo orogênico nos estágios finais de evolução do Cinturão Dom Feliciano na Antiforme Capané, Cachoeira do Sul, RS. In: 9th South-Brazilian geological symposium. Brazilian Geological Society, pp 141

Part II
Old Continental Landmasses

4 The Río de la Plata Craton of Argentina and Uruguay

Pedro Oyhantçabal, Carlos A. Cingolani, Klaus Wemmer, and Siegfried Siegesmund

Abstract

The geology and the tectonic evolution of the Río de la Plata Craton is reviewed, taking into account geochronological, isotopic and geophysical data. The craton consists of voluminous granite-gneissic terrains (2.2–2.1 Ga) that represent magmatism during the accretional stage of the orogeny. Coeval volcano-sedimentary basins are preserved as relics of supracrustal rocks, deformed and metamorphosed during a collisional event that occurred at ca. 2.1 Ga. Sm–Nd and Hf model ages between 2.7 and 2.2 Ga, and positive to slightly negative $\varepsilon Nd_{(t)}$ values indicate a Neoarchean to Paleoproterozoic juvenile crust which underwent a short period of crustal recycling. Undeformed granitoids, gabbros and dolerite swarms with calc-alkaline signature intruded at ca. 2.07 Ga correspond to the late- to post-tectonic stages of the orogeny. Exhumation, cooling and cratonization occurred during the Orosirian (2050–1800 Ma) and later anorogenic extension is recorded in tholeiitic dyke swarms intruded at ca. 1.8 Ga in Uruguay and at ca. 1.6 Ga in the Buenos Aires province of Argentina. There is no evidence of Meso- or Neoproterozoic orogenic reworking and only one shallow granite intrusion in Uruguay and low-temperature hydrothermal alteration in the Neoproterozoic cover of the Tandilia System can be ascribed to far-field effects of the Brasiliano orogeny.

Keywords

Río de la Plata Craton • Piedra Alta Terrane
Tandilia system • Geodynamics

4.1 Introduction

Almeida et al. (1973) defined the Río de la Plata Craton to include the 'ancient cratonic areas' of the southernmost South American Platform, 'already consolidated in the upper Precambrian'. The main outcrop regions of the craton are the Piedra Alta Terrane in central and southwestern Uruguay (Oyhantçabal et al. 2011) and the Tandilia System in Argentina (Cingolani 2011), but most of its assumed regional extension is covered by Phanerozoic sediments (Fig. 4.1). The westernmost area of the craton reaches the eastern border of the Pampean ranges near the city of Córdoba, as demonstrated by U–Pb SHRIMP data in zircon from drill cores (Rapela et al. 2007) and magnetotelluric investigations that allow the tracing of the unexposed boundary (Peri et al. 2013; Favetto et al. 2015). To the south, Tohver et al. (2008, 2012) report a Paleoproterozoic age for the Agua Blanca Granite, suggesting that the Río de la Plata Craton may be extended to the Ventania System, approximately 200 km south of the Tandilia outcrops. This interpretation is based on two zircon grains from an unfoliated two-mica-granite, assuming they are not inherited from the source. To the east, the Sarandí del Yí Shear Zone separates the craton from the Nico Pérez Terrane, an allochthonous block with African isotopic signature, amalgamated to the Río de la Plata Craton during the Ediacaran (Rapela et al. 2011; Oriolo et al. 2016a). The northern extension of the craton is also a matter of debate. The Paleoproterozoic basement of the Río Tebicuary area (Paraguay) could represent the northernmost outcrop of the Río de la Plata Craton

P. Oyhantçabal (✉)
Departamento de Geodinámica Interna, Facultad de Ciencias, Universidad de La República, Iguá 4225, C.P. 11400 Montevideo, Uruguay
e-mail: oyhantca@fcien.edu.uy

C. A. Cingolani
Centro de Investigaciones Geológicas (UNLP-CONICET) and División Geología del Museo de La Plata, Diag. 113 N. 275, La Plata, Argentina
e-mail: carloscingolani@yahoo.com

K. Wemmer · S. Siegesmund
Geoscience Centre, Georg-August University Göttingen, Goldschmidtstr 3, 37077 Göttingen, Germany
e-mail: kwemmer@gwdg.de

S. Siegesmund
e-mail: ssieges@gwdg.de

S. Siegesmund et al. (eds.), *Geology of Southwest Gondwana*, Regional Geology Reviews,
https://doi.org/10.1007/978-3-319-68920-3_4

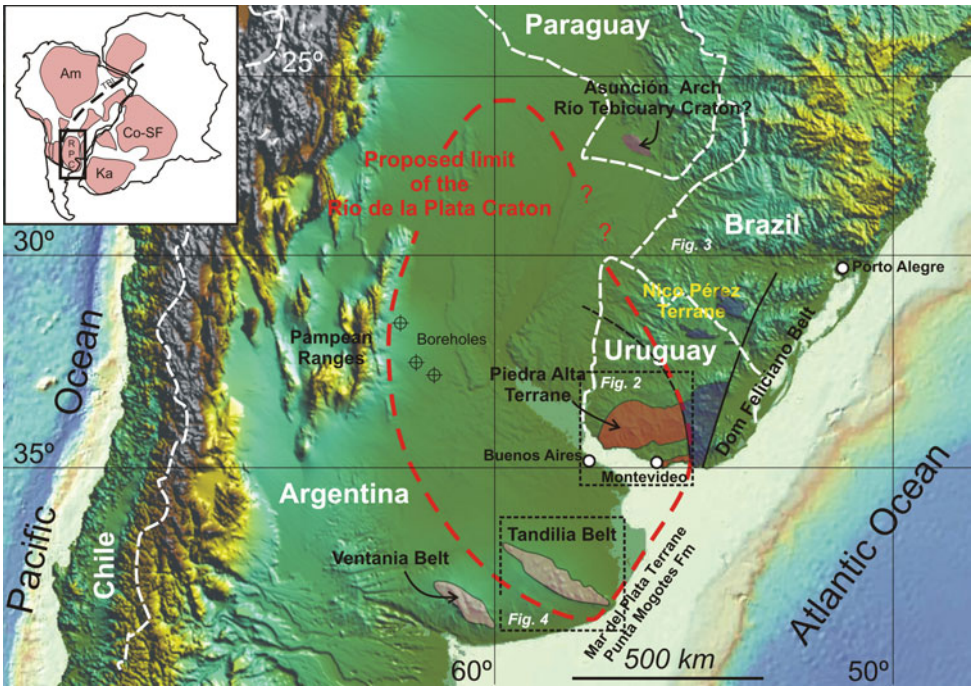

Fig. 4.1 The main outcrop areas of the Río de la Plata Craton and its boundaries. Interpretation based on Cingolani (2011), Oyhantçabal et al. (2011), Rapela et al. (2011), Peri et al. (2013), Favetto et al. (2015), Tohver et al. (2008, 2012) and Dragone et al. (2017)

(Rapela et al. 2007), though Dragone et al. (2017) based on geophysical arguments claim this should be considered a different craton.

The Río de la Plata Craton is a key piece in the reconstructions of western Gondwana, but its paleogeographic position during the Precambrian is far from being resolved (Rapalini et al. 2015). The collisions with Congo and Kalahari cratons on its eastern margin are related to the evolution of the Dom Feliciano, Kaoko and Gariep Belts, while the collision against the Pampia Terrane on its western margin resulted in the Eastern Sierras Pampeanas. This chapter reviews the recent additions to the knowledge of the craton and discusses its tectonic evolution.

4.2 Geological Overview

4.2.1 The Río de la Plata Craton in Uruguay (Piedra Alta Terrane)

The Piedra Alta Terrane of southwestern Uruguay is the region where the craton is best exposed and the only one where its boundary is not hidden by Phanerozoic sediments. The Sarandí del Yí Shear Zone is the tectonic boundary of the craton with the Archean-Paleoproterozoic Nico Pérez Terrane (Hartmann et al. 2001). The latter was formerly thought to be part of the Río de la Plata Craton (Oyhantçabal et al. 2011) (Fig. 4.2).

The Piedra Alta Terrane is composed of vast granitic gneiss areas separated by supracrustal metamorphic belts. Two main belts have been recognized: the Arroyo Grande Belt (Bossi and Ferrando 2001) which crops out in the northern part of the terrane; and the San José Belt (Bossi et al. 1993b; Oyhantçabal et al. 2003, 2007, 2011) located in southernmost Uruguay (Fig. 4.2).

4.2.1.1 Arroyo Grande Belt

This belt is a low metamorphic grade supracrustal block bounded by faults, about 15 km in width and 50 km in length. It strikes east–west and is located at the northern edge of the exposed area of the Piedra Alta Terrane (Ferrando and Fernández 1971; Fernández and Preciozzi 1974; Bossi et al. 1993b; Preciozzi 1993). The belt contains the Arroyo Grande Formation, a greenschist facies folded volcanosedimentary assemblage, with the base of the succession in the north and cut across by the Paso de Lugo fault in the south. Siliciclastic rocks predominate, including metarenites, quartzites, metarkoses, metapelites and metaconglomerates. Primary structures are frequently preserved. The metavolcanic rocks are restricted to the southern zone and include metabasalts and meta-andesites, with the paragenesis chlorite + epidote + albite + amphibole + quartz + opaque minerals ± calcite, and metadacites. Observed mineral assemblages indicate greenschist facies metamorphism (Fernández and Preciozzi 1974).

A felsic metavolcanic rock of this formation was dated at 2113 ± 8 Ma, while the age of intrusive post-orogenic granites range between 2108 ± 23 Ma and 2076 ± 18 Ma (U–Pb in zircon, Ferrando, pers. comm., cited by Bossi and Piñeyro 2014; see Table 4.1). LA-ICPMS U–Pb detrital zircon data in metasediments from the Arroyo Grande Formation show a rather simple age pattern with only one

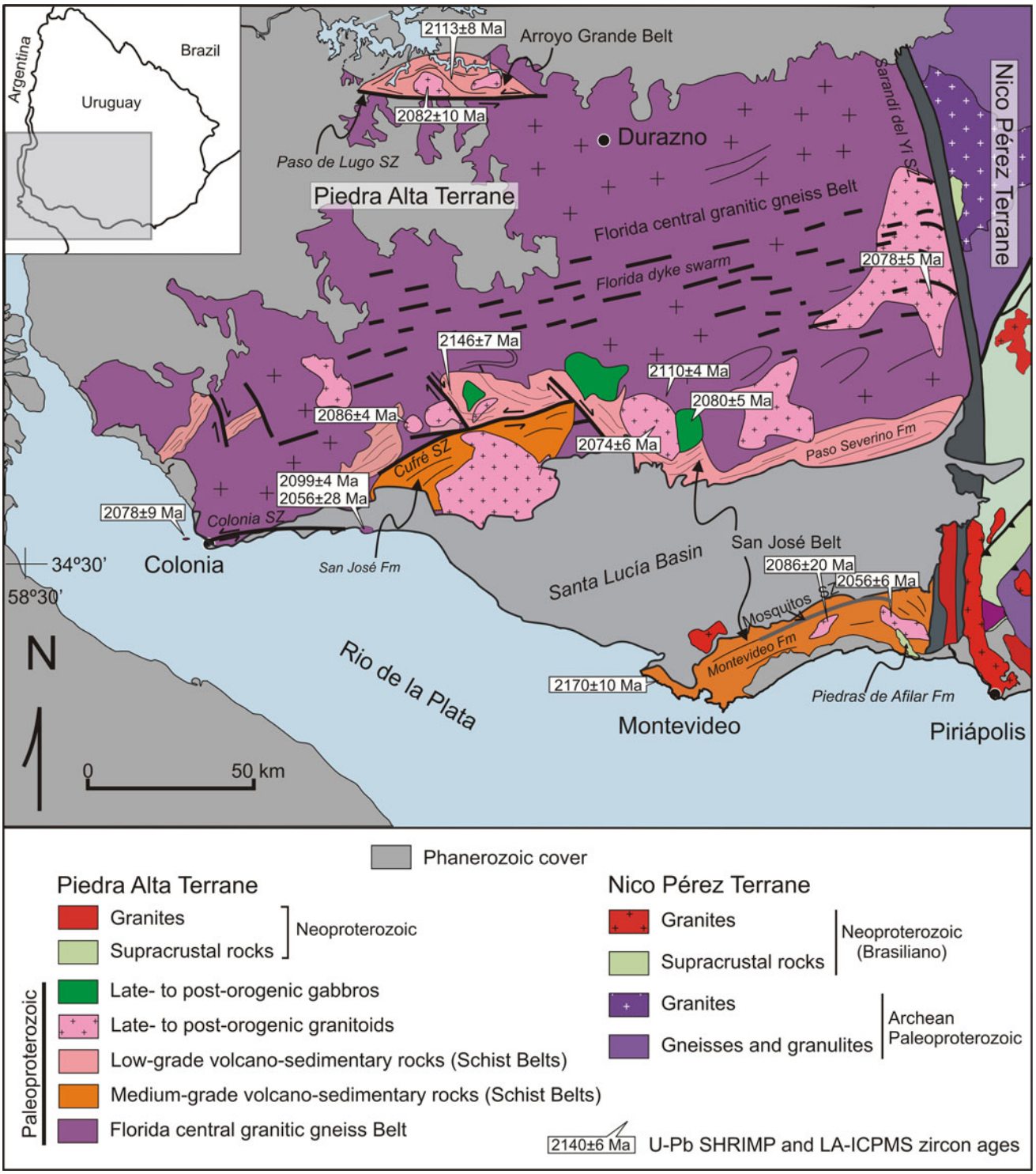

Fig. 4.2 Geological map of the Piedra Alta Terrane (Uruguay). Based on Preciozzi et al. (1985), Bossi and Ferrando (2001), Oyhantçabal et al. (2007, 2011)

Table 4.1 Selection of published zircon and titanite U-Pb SHRIMP, U-Pb LA-ICPMS and U-Pb multigrain geochronology data from the Río de la Plata Craton in the Tandilia Belt (Argentina) and the Piedra Alta Terrane (Uruguay)

Boreholes in westernmost domain			Tandilia Belt				Piedra Alta Terrane			
Lithology	Age (Ma)	References	Area/unit	Lithology	Age (Ma)	References	Area/unit	Lithology	Age (Ma)	References
			Tandil	Tonalite	2228 ± 6	1				
			Balcarce	Gneiss	2194 ± 5	1	San José	Amphibolic gneiss	2202 ± 8	5
			Buenos Aires	Gneiss	2186 ± 10	7	Montevideo	Orthogneiss	2165 ± 38	2
			Tandil	Tonalitic gneiss	2183 ± 4	1	Montevideo	Porphyritic granite	2158 +24/-23	5
			Tandil	Tonalite	2166 ± 7	1	Paso Severino	Metadacite	2146 ± 7	2
			Buenos Aires	Gneiss	2164 ± 5	7	Piedra Alta	Granodiorite	2110 ± 4	6
			Balcarce	Gneiss	2163 ± 8	1	Boca del Rosario	Migmatites/ melanosome	2099 ± 4	6
Amphibolite	2189 ± 14	4	Azul	Granitoid	2162 ± 5	1		Migmatites/ leucoosome	2056 ± 28	6
			Balcarce	Gneiss	2126 ± 11	1	Pajas Blancas	Orhogneiss	2170 ± 10	6
			Azul	Mylonitized granitoid	2113 ± 12	1				
Diorite	2162 ± 6	4	Buenos Aires	Gneiss	*2120 ± 11 (Zrn)*	7				
			Buenos Aires	Gneiss	*2120 ± 11 (Ttn)*	7				
			Buenos Aires	Gneiss	*2069 ± 13 (Ttn)*	7				
							Post-orogenic granitoids and gabbros	Empalme Olmos granite	2086 ± 20	6
								Rospide gabbro	2086 ± 7	5
			Tandil	Tonalite	2073 ± 6	1			2076 ± 6	5
			Post-orogenic granitoids and gabbros	Granitoid	2051 ± 3	1		Granitic mylonite (protolith age)	2078 ± 9	8
								Isla Mala granite	2074 ± 6	3
Granite	2088 ± 6	4							2065 ± 9	3
									2131 ± 13	6
								Soca granite	2056 ± 6	2
									2079 ± 8	6
								Cufré granite	2086 ± 4	6

References: (1) Cingolani et al. (2002), (2) Santos et al. (2003), (3) Hartmann et al. (2000), (4) Rapela et al. (2007), (5) Peel and Preciozzi (2006), (6) Basei et al. (2016), (7) Chernicoff et al. (2015), (8) Ribot et al. (2005)

Italics and gray background: metamorphic event. *Ttn* Titanite, *Zrn* Zircon

maximum at around 2.1 Ga (Basei et al. 2016). Thus a Rhyacian age of ca. 2.1 Ga is indicated for this formation, based on U–Pb data constraints.

4.2.1.2 San José Belt

The San José Belt is a low- to medium-grade metamorphic supracrustal sequence exposed in the central and southern area of the Piedra Alta Terrane. It is composed of two formations running nearly east–west separated by the Cufré Shear Zone (Fig. 4.2).

The Paso Severino Formation occurs to the north of the shear zone and is a greenschist facies folded volcano-sedimentary succession including predominant metapelites, and rarely dolomitic marbles and banded iron formations; while orthoderived rocks include metabasalts and meta-andesites, metadacites and metatuffs. U–Pb SHRIMP ages in zircon from a metadacite of the Paso Severino Formation yielded an age of 2146 ± 7 Ma (Santos et al. 2003; see Table 4.1). This is similar to the crystallization age of the felsic volcanic protoliths in the Arroyo Grande Belt. Positive values of $\delta^{13}C$ seem to confirm that the dolomitic limestones of Paso Severino formation were deposited during the global Lomagundi isotope excursion and are consistent with the age indicated for this succession by the interbedded felsic volcanic rocks (Maheshwari et al. 2010).

The Montevideo Formation crops out south of the Cufré Shear Zone and includes rocks formed under amphibolite-facies metamorphic conditions. It comprises ortho- and para-amphibolites, paragneisses and micaschists. The paragneisses and garnet and staurolite-bearing micaschists of the San José Formation of Preciozzi et al. (1985) are considered here part of the Montevideo Formation. The orthoamphibolites show geochemical signature similar to mid-oceanic ridge basalts (N-MORB) and partially preserved pillow structures (Oyhantçabal et al. 2003; Pascale and Oyhantçabal 2016).

The Montevideo Belt is divided into northeast and northwest-trending sectors owing to the influence of conjugate north-northwest dextral and east-northeast sinistral shear zones and its easternmost extreme is rotated clockwise as a result of the influence of the Sarandí del Yí Shear Zone. At least two deformation events are recognized in the belt

(Campal 1990; Preciozzi 1993; Oyhantçabal et al. 2007). The last event is associated with syntectonic granites and the abovementioned conjugate shear system.

4.2.1.3 Florida Central Granitic Gneiss Belt

Gneisses and granites make up the bulk of the central area located between Arroyo Grande and San José belts. Decametre- to kilometre-sized blocks of supracrustal rocks are common within the granites and gneisses. They include micaschists, paragneisses and amphibolites. Orthogneisses with similar features are also observed invading the supracrustals of the Montevideo Formation in southernmost Uruguay. These have slightly peraluminous medium-K calc-alkaline compositions (Pascale and Oyhantçabal 2016) and have been dated at 2170 ± 10 Ma (LA-ICPMS in zircon; Basei et al. 2016). A similar age was obtained in the mesosome of migmatites in southwestern Uruguay (2170 ± 24 Ma; LA-ICPMS in zircon; Basei et al. 2016). Ages and field observations indicate that most of these orthogneisses correspond to intrusions coeval with volcanosedimentary basins and that do not represent a basement related to a previous orogeny.

4.2.1.4 Paleoproterozoic Late- to Post-orogenic Granitoids and Gabbros

Several late- and post-orogenic plutons intrude the Piedra Alta Terrane. Available major element data summarized in Fig. 4.3 indicates that most of the intrusions are calc-alkaline with medium- to high-K content, although some alkaline plutons have also been recognized.

In the San José Belt, SHRIMP U–Pb ages of 2065 ± 9 and 2074 ± 6 Ma were obtained for the Isla Mala pluton (Hartmann et al. 2000) and 2086 ± 4 Ma for the Cufré Granite (LA-ICPMS U–Pb age in zircon, Basei et al. 2016). In the Arroyo Grande Belt, the Marincho Complex yielded a concordia age of 2081 ± 1 Ma (Basei et al. 2016). These similar ages point to a single magmatic event in both areas.

Post-orogenic gabbros are also frequently associated in both supracrustal belts (e.g., Mahoma, Rospide and Carreta Quemada gabbros). U–Pb SHRIMP ages for zircons from the Rospide Gabbro yielded 2076 ± 6 and 2086 ± 7 Ma (Hartmann et al. 2008a). The similar ages of gabbros and granites and the signature of the gabbros in the FeOt/MgO versus SiO_2 plot of Miyashiro (1974) point to coeval calc-alkaline magmatism (Fig. 4.3).

Several post-tectonic granites intrude the central granitic gneiss belt. The Cerro Colorado Granite yielded a concordia age of 2078 ± 5 Ma and two inherited concordant zircon grains show ages around 2.2 Ga (LA-ICPMS U–Pb in zircon; Oriolo et al. 2016a). This age is similar to the Rb-Sr whole-rock age of 2071 ± 70 Ma reported for this granite by Cingolani et al. (1990). The Piedra Alta granodiorite yielded a 2110 ± 4 Ma age (LA-ICPMS U–Pb in zircon, Basei et al. 2016). Additionally, Rb-Sr whole-rock data gave similar ages (2015 ± 40 Ma, Piedra Alta granodiorite; 2030 ± 75 Ma, Carmelo granodiorite; 1970 ± 55 Ma, Conchillas granitic gneiss; Umpierre and Halpern 1971). These age constraints and the field relationships (Oyhantçabal et al. 2007) indicate that these intrusions correspond to the same magmatic event responsible for the post-orogenic plutons that intruded into the Arroyo Grande and San José belts.

The Soca granite has compositions similar to that of the rapakivi granites from southern Finland, including high contents of LIL and HFS elements and high FeO*/[FeO* + MgO] ratios (Oyhantçabal et al. 1998), but Nb, Y and Ce contents show it belongs to the A2-type post-collisional granites of Eby (1992). Zircon U–Pb age constraints include a SHRIMP age of 2056 ± 6 Ma (Santos et al. 2003) and a LA-ICPMS age of 2079 ± 8 Ma (Basei et al. 2016). These ages are similar to those obtained for calc-alkaline granites (e.g., Isla Mala, Cufré and Marincho plutons) and confirm that the Soca granite should not be considered an example of anorogenic rapakivi association, but an A2-type rapakivi granite formed after continent collision (Eby 1992; Larin 2009).

In summary, this late- to post-orogenic association of granite and gabbro magmatism occurred at 2080–2050 Ma and includes medium to high K_2O calc-alkaline mafic to felsic and felsic alkaline rapakivi intrusions.

4.2.1.5 Mylonites and Shear Zones

Sinistral shear zones trending 090°–060° and dextral shear zones trending ca. 340° build up a system of conjugate strike-slip faults that controls the architecture of the Piedra Alta Terrane. Sinistral shear zones prevail and some of the best-known examples include the Colonia (Bossi et al. 2005; Ribot et al. 2005; Gianotti et al. 2010) and the Mosquitos shear zones.

The Colonia Shear Zone (Fig. 4.2) comprises two parallel branches striking ca. 090º and cropping out ca. 4 km apart in Colonia City and its surroundings. Subvertical foliations with subhorizontal stretching lineations and kinematic indicators point to a strike-slip wrench component, but frequent sinistral and dextral indicators are found, suggesting pure shear dominated deformation. Microstrucures in quartz and feldspar indicate deformation conditions of *c*. 450–550º C. The deformation age is bracketed by a K–Ar cooling age of 1796 ± 16 Ma in muscovite (Gianotti et al. 2010) and a U–Pb LA-ICPMS age in magmatic zircon of 2078 ± 9 Ma considered as the age of the protolith (Ribot et al. 2005; Ribot et al. 2013).

Similar time constraints were obtained for the Mosquitos Shear Zone (Fig. 4.2). K–Ar data in muscovite yielded cooling ages that range between 1909 ± 23 Ma and 2049 ± 25 Ma (Oyhantçabal et al. 2006).

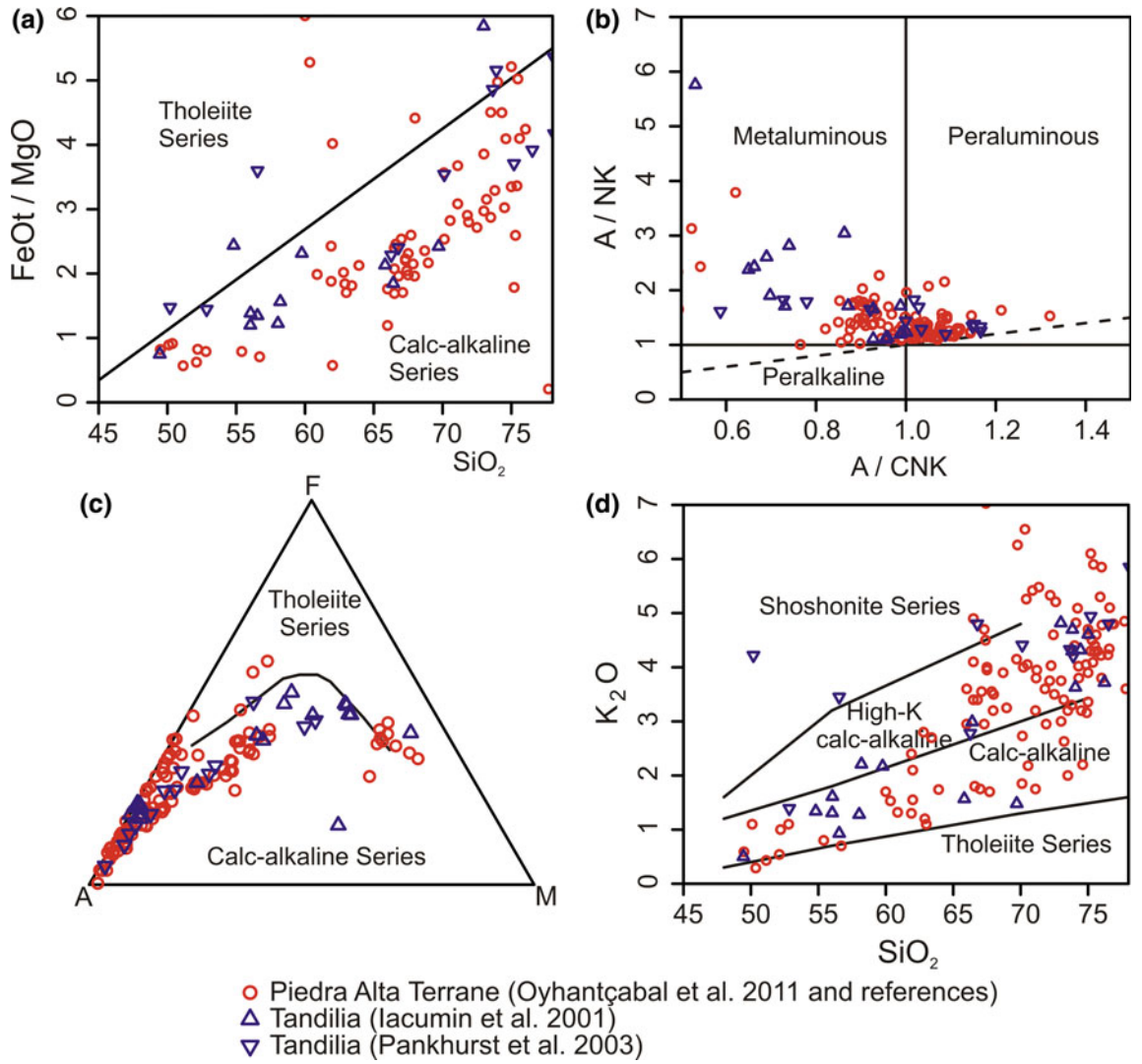

Fig. 4.3 Geochemistry of the Paleoproterozoic late- to post-orogenic magmatism in the Río de la Plata Craton. SiO_2 versus FeOt/MgO (Miyashiro 1974) **a**, A/NK versus A/CNK diagram (Shand 1943) **b**, AFM diagram (Irvine and Baragar 1971) **c**, SiO_2 versus K_2O plot (Peccerillo and Taylor 1976) **d**. Data for the granitoids and gabbros of the Piedra Alta Terrane (Oyhantçabal et al. 2011 and references therein). Tandilia granites (Pankhurst et al. 2003). Tandilia calc-alkaline Dyke Swarm (Iacumin et al. 2001)

4.2.1.6 Florida Dyke Swarm

The Florida Dolerite Dyke Swarm (also known as Uruguayan Dike Swarm; Teixeira et al. 1999) is more than 100 km in width, trends ca. 060º and extends for more than 250 km from westernmost Uruguay to the Sarandí del Yí Shear Zone in the east. When the dykes approach the shear zone, they are rotated clockwise, being a sense indicator of the first shear event (Oriolo et al. 2015 and references therein).

Individual dykes are subvertical, with a thickness attaining 50 m and a length up to 20 km. Whole-rock geochemistry and petrographic features allow the distinction of high and low TiO_2 tholeiitic dykes of andesitic-basalt and andesite composition, respectively (Bossi et al. 1993a). The swarm displays positive εSr and negative εNd values typical of an EM1-type mantle source (Mazzucchelli et al. 1995). A U–Pb age on baddeleyite of 1790 ± 5 Ma is the best estimate of the crystallization age of the high Ti dykes, considered younger than the low Ti dykes (Halls et al. 2001).

4.2.1.7 Neoproterozoic Record, Sedimentary Successions and Granites

A Neoproterozoic cover is usually lacking in the Piedra Alta Terrane. An exception is a small outcrop area corresponding to the Piedras de Afilar Formation (see Fig. 4.2). The formation comprises low-grade arenites, shales and limestones intruded by dolerite sills (Coronel et al. 1982; Pecoits et al. 2008; Pamoukaghlian 2012). It lies in sedimentary contact above the Coronilla and Soca granites. The detrital zircon pattern shows dominantly Paleo- and Mesoproterozoic

sources with the youngest peak at ca. 1009 Ma, which constrains the upper stratigraphic age limit of this unit (Gaucher et al. 2008). The Archean, Paleo- and Mesoproterozoic zircons observed in these sediments suggest that the Nico Pérez Terrrane was most probably the main source. A Neoproterozoic age is also consistent with $\delta^{13}C$ values (+5 to +6‰ V-PDB) reported by Pamoukaghlian et al. (2006) and the lack of Ediacaran zircons could indicate that the age is >650 Ma (see discussion in Pecoits et al. 2016).

The sequence strikes north-northwest, with the monoclinal structure dipping towards the southeast, and is intruded by diabase sills showing greenschist facies mineral assemblage (Coronel et al. 1982).

The La Paz Granite is a small intrusion located some kilometres north of the city of Montevideo. It is the only Neoproterozoic granite recognized in the Río de la Plata Craton in Uruguay. Two petrographic facies are recognized in this pluton: porphyritic granite with K-feldspar megacrysts and equigranular granite. The presence of miarolitic cavities and hypersolvus textures in alkali feldspar is indicative of shallow emplacement. The mineralogy is K-feldspar, quartz albite, biotite and amphibole, with epidote, apatite and zircon as accessory minerals. Whole-rock geochemistry data presented by Oyhantçabal et al. (1990) and Abre et al. (2014) show the typical signature of the post-collisional A2-type granites of Eby (1992): metaluminous, high $Na_2O + K_2O$ content, Eu negative anomaly and low Nb/Y ratio. The La Paz Granite was dated by U–Pb LA-ICPMS in zircon at 587 ± 8 Ma (Cingolani et al. 2012), roughly similar to a previous Rb–Sr whole-rock isochron age of 547 ± 15 Ma (Umpierre and Halpern 1971).

4.2.2 The Río de la Plata Craton in Argentina: The Tandilia System

4.2.2.1 Paleoproterozoic Basement: The Buenos Aires Complex

The Buenos Aires Complex (Marchese and Di Paola 1975) is a basement association including large areas of granitic gneisses and small occurrences of amphibolites, high-grade schists and marbles. Mylonite belts up to several kilometres wide crosscut this basement. Additionally, post-orogenic granite intrusions are frequent.

Metamorphic rocks different from the otherwise dominant granitic gneiss are conspicuous in the Balcarce area. These include granulite facies gneisses with orthopyroxene and hornblende, schists, olivine marbles (Punta Tota, Balcarce area), pyroxene-rich ultramafic rocks (Cinco Cerros and Punta Tota, Balcarce area) and migmatites (Fig. 4.4). Metamorphic conditions were estimated at 750–800 °C and 5–6 kb, followed by near isobaric cooling to about 500–450 °C and 5.5–6.5 kb (Delpino et al. 2001; Delpino and Dristas 2008; Massonne et al. 2012). The studied reactions indicate a metamorphic evolution along a counterclockwise P–T path.

In contrast, granitic gneisses dominate in the Tandil area, and only scarce outcrops of amphibolites, granulites and charno-enderbites have been found (Dalla Salda et al. 1988, 2005; Hartmann et al. 2002).

Orthogneisses

The orthogneisses occur in the Balcarce and Tandil areas, show a distinct foliation and the composition ranges from tonalitic to granodioritic and granitic. The mineral association comprises quartz + K-feldspar + plagioclase + biotite ± amphibole ± garnet ± epidote ± pyroxene ± muscovite ± sillimanite (Dalla Salda et al. 2006). Major and trace element data indicate that the basement orthoderived rocks are of calc-alkaline composition (Dalla Salda et al. 1988, 2006). On the other side, Rapela et al. (2007) present a complete set of geochemical and isotopic data, but from rocks obtained in boreholes located more than 800 km to the northwest of the Tandilia System in the western edge of the Río de la Plata Craton, and they indicate that these rocks are associated with intraoceanic subduction systems or primitive continental arc settings. U–Pb SHRIMP ages in zircon for the orthogneisses of the Buenos Aires Complex range from 2228 ± 6 Ma to 2113 ± 12 Ma (Cingolani et al. 2002; Hartmann et al. 2002). Despite their geochemical features being different, the ages from boreholes near Córdoba (Rapela et al. 2007) are similar to those that have been determined for the Buenos Aires Complex, pointing to events that occurred in a quite narrow timespan.

High-Grade Supracrustal Rocks

Two marble bodies were identified within the basement of the Tandilia System. One is in the Punta Tota area, near Balcarce city, described by Delpino and Dristas (2008 and references therein) where thin beds of dolomitic marble are intercalated in amphibolites and constitute the upper part of a layered basement sequence, which starts at the base with garnet migmatites showing a great abundance of pegmatitic segregates. Another marble crops out at the San Miguel quarry, near the town of Barker, and was revisited by Lajoinie et al. (2013, 2014). It occurs associated with prevalent garnet-biotite gneiss and both rocks are intruded by Paleoproterozoic granites. The marbles are whitish and coarse-grained; the calcite + diopside + quartz mineral association indicates upper amphibolite metamorphic facies conditions. The intrusion of thin granitic bodies composed of quartz + plagioclase + K-feldspar generated a wollastonite + vesuvianite + grossular mineral association in the contact aureole. Isotopic $\delta^{13}C$ and $\delta^{18}O$ data in calcite grains

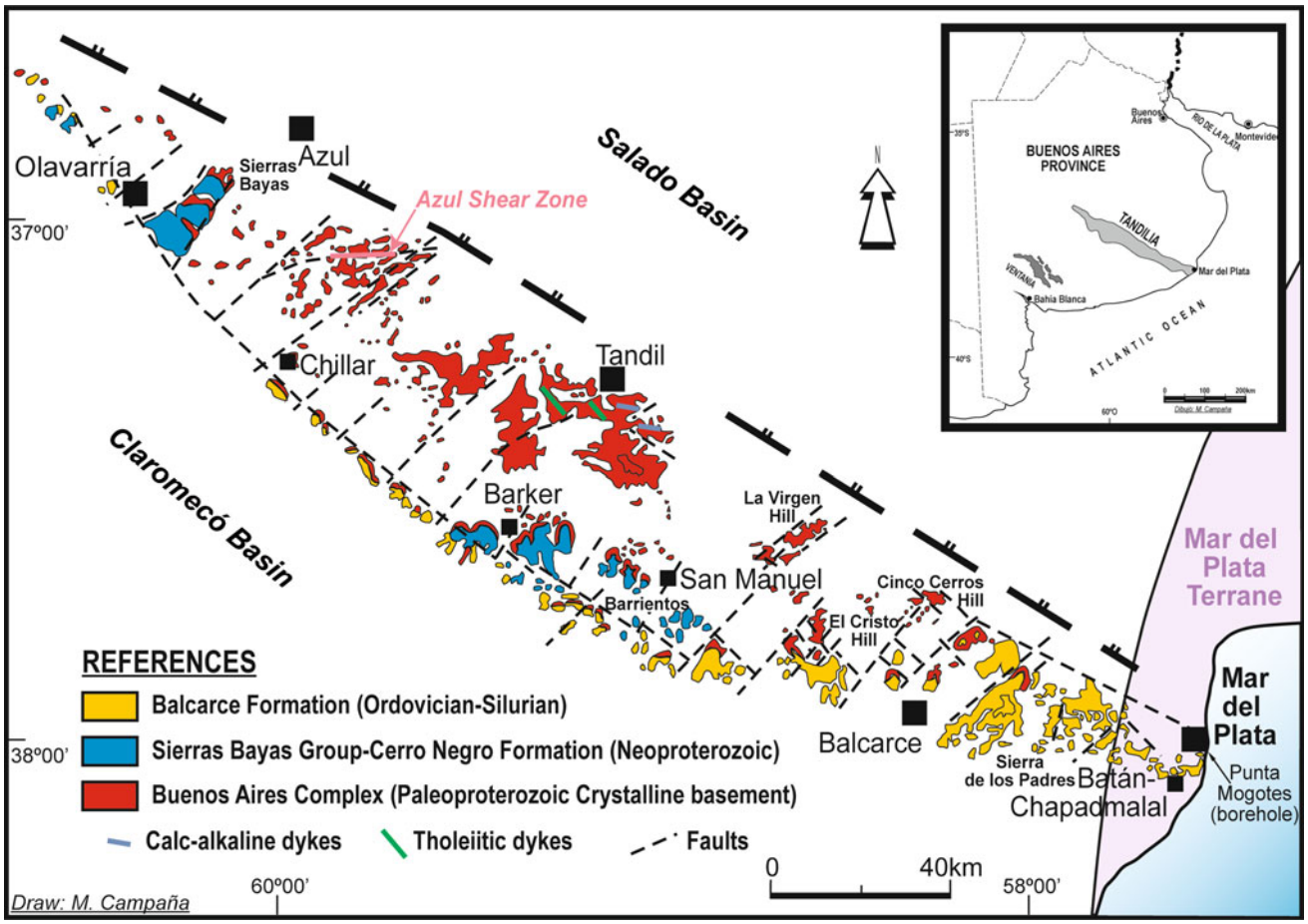

Fig. 4.4 Geological map of the Tandilia System showing the main outcrops of the Paleoproterozoic basement (Buenos Aires Complex) and the Neoproterozoic to lower Paleozoic sedimentary cover. Note the location of the Mar del Plata Terrane and the Punta Mogotes borehole. Based on Cingolani (2011) and references therein

revealed important positive anomalies. Values of $\delta^{18}O$ obtained from two diopside populations, proximal and distal to the contact marble-granite, together with the $\delta^{18}O$ values in calcite, allow the determination of temperatures of 716 °C for the metamorphic and 451 °C for the metasomatic processes. The concordance of the geological and isotopic characteristics of the marble from the San Miguel area (Lajoinie et al. 2014) with the worldwide record of Paleoproterozoic carbonates, together with the estimated age of the protolith, identify it as a marine carbonate deposited during the 'Lomagundi-Jatuli event'. This event is also recorded in Uruguay in the San José Belt (Maheshwari et al. 2010), in South Africa (Schröder et al. 2008) and in other Paleoproterozoic areas worldwide.

Mylonites and Shear Zones

Shear zones are widespread along the Tandilia System and the associated mylonites are derived mainly from granitic protoliths. In the Azul region, a mylonite belt is developed with east–west strike for about 40 km long and 3 km wide (Fig. 4.4) (Gonzalez Bonorino et al. 1956; Frisicale 1999). Deformation microstructures observed in quartz and feldspars allow an estimation of upper greenschist to amphibolite facies conditions for the deformation (Frisicale et al. 2001, 2005). Analysis of structures and microstructures in this shear zone indicate the deformation regime as pure shear dominated with an important component of flattening and minor wrenching (Frisicale et al. 2001). Other shear belts were recognized south of the Tandil city and in the Alta de Vela Range (Dalla Salda 1981).

Post-collisional Granites

The abovementioned metamorphic rocks have been intruded by several granite plutons. These are typically grey granitoids, except in the northernmost part of the complex where the granitoid rocks are reddish, as observed in the Sierra Chica and other quarries near Olavarría city. In the central region of the complex (Tandil area) a wide belt consisting of tonalite, granodiorite and granite occurs. These rocks show magmatic arc affinity, possibly representing syn- to

post-tectonic phases of the Paleoproterozoic evolution. The Alta de Vela and Montecristo leucogranites of the Tandil area (Fig. 4.4) are heterogeneous with high radiogenic, typically post-collisional signature (Dalla Salda et al. 2006). The undeformed tonalite in the Chacofi quarry (Balcarce area) was dated at 2073 ± 7 Ma and shows clear intrusive relationships with the country rock (mafic garnet orthogneiss) dated at 2194 ± 6 Ma (Hartmann et al. 2002), thus being a clear indication of the timing of the post-orogenic magmatism.

A garnet-bearing leucogranite and two country rocks from the El Cristo—San Verán hills (Balcarce area) were studied recently by Martínez et al. (2017) using mineral chemistry to decipher the P–T evolution. The leucogranite records an isothermal decompression from 5.3 to 3.8 kbar at 665 °C. The garnet-biotite migmatite was exhumed from 5.5 kbar at 630 °C to 4.3 kbar at 615 °C. Several analyses of monazite grains of the country rocks yielded three groups of U-Th–Pb ages, which these authors relate to a collisional event (ca. 2.13–2.14 Ga.), a post-collisional thermal overprint (ca. 2.01 Ga) and slow cooling of the orogen (1.80–1.90 Ga). Inherited ages of 2.28 and 2.25 Ga could refer to an early accretionary stage of the orogen. These results are consistent with mentioned SHRIMP ages older than 2.1 Ga for the orthogneisses and younger than 2.1 Ga for the post-collisional granites.

The Case of Punta Mogotes Formation on the Eastern Side of the Tandilia System

The Punta Mogotes Formation was defined in a borehole near the city of Mar del Plata and includes more than 80 m of mainly slightly deformed metapelites beneath a ca. 400 m-thick quartz-arenite cover (Borrello 1962). The metamorphism in the metapelites was dated by K–Ar in illite fine fraction at around 600 Ma (Cingolani and Bonhomme 1982). These metapelites are the only rocks that could be correlated with the Brasiliano cycle (Ramos 1988) of eastern Uruguay. After Rapela et al. (2011) the Punta Mogotes Formation at the bottom of the borehole contains a 740–840 Ma detrital zircon age peak (obtained in two samples) that is assigned to a widespread Neoproterozoic rifting event. The Punta Mogotes Formation could be correlated with other units that crop out in the Dom Feliciano Belt of Uruguay. These authors suggested, based on isotopic data, the existence of a new terrane, the 'Mar del Plata Terrane', about 20 km west of the homonymous city, that would have drifted away from the southwestern corner of the Angola block at ca. 780 Ma. Negative $\varepsilon Hf_{(t)}$ and $\delta^{18}O > 6.5\%$ values suggest derivation by melting of old crust during a protracted extensional episode.

4.2.2.2 Neoproterozoic—Lower Paleozoic Sedimentary Cover

Sedimentary processes in the Tandilia System began at ca. 800 Ma with an unconsolidated arkosic saprolite that records a paleoweathering basement surface (Zalba et al. 1993; Dristas et al. 2003). In the currently accepted stratigraphic scheme (see Poiré and Spalletti 2005; Gómez Peral et al. 2007; Poiré and Gaucher 2009; Cingolani 2011 and references therein) the Sierras Bayas Group (ca. 185 m thick) is a Neoproterozoic siliciclastic-carbonate sedimentary sequence. It is overlain by the siliciclastic Cerro Negro Formation (ca. 150–400 m thick) containing the first reliable record of Ediacaran soft-bodied organisms in South America (Arrouy et al. 2016) and the final Lower Paleozoic sedimentary strata, the 100–400 m thick Balcarce Formation. Rapela et al. (2007) reported from this unit new U–Pb detrital zircon age patterns showing detrital zircons as young as 475–480 Ma (Early Ordovician), suggesting a Late Ordovician to Lower Silurian sedimentation age. After detailed provenance studies including mineralogy and geochemistry by Zimmermann and Spalletti (2009), the Balcarce Formation comprises mainly detrital material derived from the basement of the Río de la Plata Craton and Upper Neoproterozoic to Lower Paleozoic igneous rocks. High concentrations of tourmaline and Ti-rich heavy minerals, including zircon and nearly euhedral chromite, are common. The source of chromite may be associated with convergent tectonics causing the obduction of oceanic crust during pre-Upper Ordovician times. Trace element geochemistry of recycled pyroclastic material, associated with the quartz-arenites, also suggests volcanic arc sources.

Diamictite levels were recognized at the Sierra del Volcán (Balcarce area) in between the crystalline basement and the Balcarce Formation. The diamictite is 4 m thick and bears polyhedral dropstones, often in a vertical position, affecting both ripple bedding and lamination structures. Zimmermann and Spalletti (2009) suggested a possible Hirnantian age for this glacial event, as this member of the Balcarce Formation can be correlated with an important glacial event in southern South America and South Africa. Some subalkaline dolerite sills intruded in kaolinitic shales assigned to the Balcarce Formation in the Los Barrientos area (Rapela et al. 1974) yielded whole-rock K–Ar ages of 450 and 490 Ma and represent the youngest event recorded.

4.2.2.3 Diagenesis and Hydrothermal Activity

In the Tandilia System, evidence for hydrothermal activity (clay deposits, quartz crystals, alunite and iron-rich levels) was recognized several times (Dristas and Frisicale 1988; Dristas et al. 2003). These deposits were interpreted to occur

along faults, fractures and breccias through which the hydrothermal fluids percolated. The consequent mixing of hydrothermal fluids with meteoric water gave rise to more oxidizing conditions and to the formation of alunite veins. The iron-rich deposits of the Barker region were studied by Dristas and Martínez (2007) and Martínez et al. (2010). These authors concluded that the deposits were formed at an unconformity by associated large-scale hydrothermal activity under low temperature conditions. Angeletti et al. (2014) obtained a Neoproterozoic U–Pb SHRIMP age of 652 ± 37 Ma in zircon rims and overgrowths interpreted as recording the hydrothermal event. Martínez and Dristas (2006, 2008) demonstrated that the lower part of the Neoproterozoic sequence, along the contact with the basement, was intensively altered by hydrothermal activity (Cuchilla de las Águilas and Cerrito La Cruz). On the other hand, Gómez Peral et al. (2007) divided the diagenetic processes that affected the dolostones from the lower part of the sedimentary cover (Villa Mónica and Loma Negra formations) into several stages. More recently, Martínez et al. (2010, 2013) presented K–Ar ages in clay minerals that confirm the Late-Neoproterozoic age of the hydrothermal fluid activity in the Tandilia Belt.

As recently established by Dristas et al. (2017) in the Barker area, the megabreccias, limestone breccias and phosphate-bearing breccias hosted in black limestone and along the contact with the Cerro Negro Formation are the result of extensive hydrothermal alteration of the original micritic limestone and other fine-grained clastic sediments. Quartz and calcite cements from hydraulic breccias in the limestone contain low-salinity aqueous fluid inclusions. Corresponding homogenization temperatures display 200–220 °C and 110–140 °C in hydrothermal quartz, and 130–150 °C in late calcite cement. Carbon and oxygen stable isotope analyses of carbonates from the Loma Negra Formation support the major role of hydrothermal activity dated ca. 590–620 Ma.

4.3 Geophysics

The isostatic residual Bouguer anomaly map of the Río de la Plata Craton is shown in Fig. 4.5. Gravity signature confirms most structural features of the Precambrian Basement of Argentina and Uruguay. The Piedra Alta Terrane shows east–west oriented gravity highs matching the San José and Arroyo Grande supracrustal Belts. The Sarandí del Yí Shear Zone coincides with a low gravity lineament, which prolongation can be traced with northwest trend to Argentina. In eastern Uruguay, the gravity signature is characterized by ca. north–south trend, in concordance with the structure of the southern Dom Feliciano Belt and a roughly east–west gravity high related to the Mesozoic Laguna Merín Basin (Fig. 4.5).

A similar east–west pattern is observed in the Buenos Aires province in residual gravity (Miranda et al. 2015) and magnetic maps (Chernicoff et al. 2014). Again, these geophysical features match the structural trend in the basement. In the Tandil area, a magnetic low has been interpreted as a suture zone, the El Cortijo Suture Zone, by Chernicoff et al. (2014). Another possible suture zone, the Salado Suture Zone, was put forward by Pángaro and Ramos (2012) based on Bouguer gravity anomalies. Nevertheless, the similarity of isotope data in all areas of the Río de la Plata Craton indicates that, in case these sutures were confirmed, the involved terranes would be only para-autochthonous.

4.4 U–Pb Geochronology

Selected U–Pb ages, most of them SHRIMP ages in zircon, from the basement of the Río de la Plata Craton are presented in Table 4.1. The magmatic crystallization ages obtained are always Paleoproterozoic (Rhyacian), in the range 2234–2065 Ma, but some inherited ages from the cores of a few zircon crystals indicate older events: 2368 Ma (Siderian) to 2185 Ma (Early Rhyacian) and only one Neoarchean age of ca. 2657 Ma in a tonalite from the Tandil region. The data suggests that crustal growth started in the Río de la Plata during the Neoarchean, while most of the magmatism is juvenile and occurred during the Rhyacian, in agreement with Hf-Sr-Nd isotope data (see Sect. 4.5). The lack of recrystallization or new zircon growth during the Meso- and Neoproterozoic suggests that the Río de la Plata Craton was preserved from younger events such as those of the Greenville or Brasiliano orogenies.

The U–Pb ages obtained point to two main magmatic events at 2.25–2.12 Ga and 2.1–2.06 Ga. These have been interpreted as two different orogenies—Encantadas and Camboriú, respectively (Hartmann et al. 2002; Santos et al. 2003)—but most probably represent the accretionary and post-collisional phases of the same orogeny (Oyhantçabal et al. 2011; Martínez et al. 2017). In the latter model, ages in the range 2.22–2.1 Ga are considered crystallization ages of the protoliths, generated during the pre- to syncollisional stage, while 2.0–2.1 Ga ages, in agreement with field observations, correspond to the late- to post-orogenic igneous activity. A similar tectonic evolution scheme considering subduction, collision and post-collision stages is envisaged by Chernicoff et al. (2016).

4.5 Nd and Hf Isotope Data

Sm–Nd model ages show similar values in the Piedra Alta Terrane and the Tandilia System (average 2.43 Ga) and indicate that the main crustal growth episode happened at the

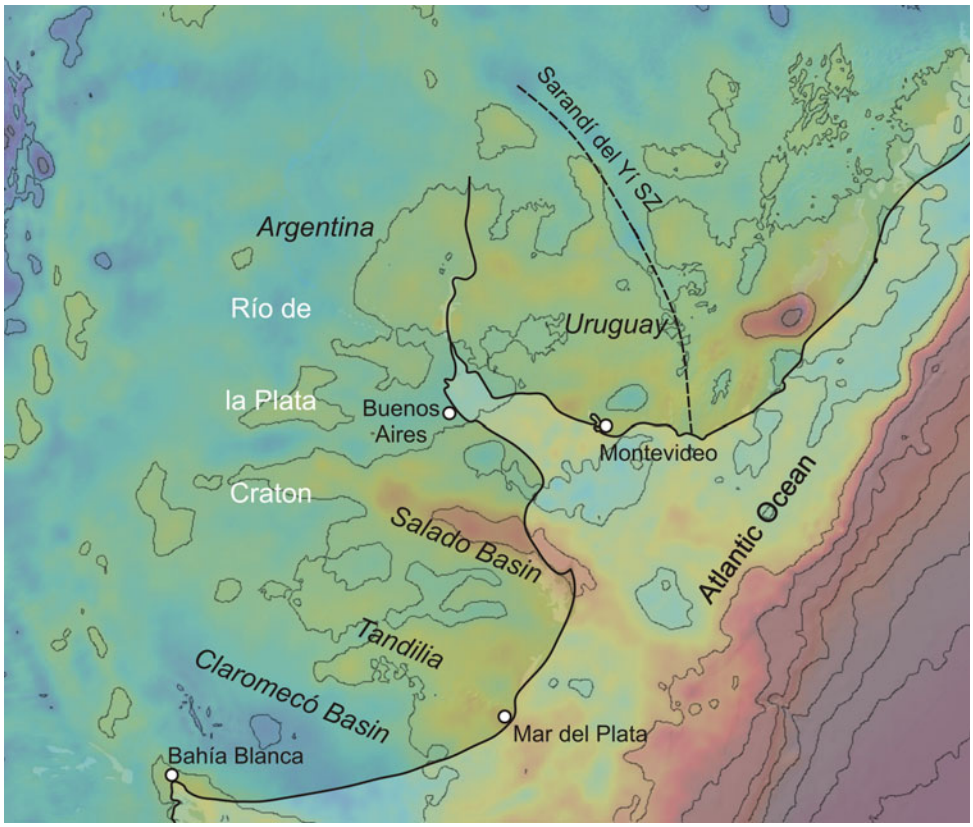

Fig. 4.5 Bouguer gravity anomaly map of the Río de la Plata Craton. WGM2012 Bouguer anomalies were obtained with GeoMapApp (Ryan et al. 2009; http://www.geomapapp.org)

Neoarchean–Paleoproterozoic boundary (Fig. 4.6). The Rhyacian U–Pb crystallization ages and the highly evolved signature of gneissic and granitic rocks, derived mostly indirectly from mantle sources, point to a short period of crustal recycling between the Neoarchean and the Rhyacian. The slightly negative $\varepsilon Nd_{(t)}$ values (−0.7 to −3.30) in Tandilia are another proof of a crustal source for most of the granitoids in the Río de la Plata Craton (Hartmann et al. 2002; Pankhurst et al. 2003). Still scarce zircon Hafnium isotope data is consistent with the observed neodymium results (Cingolani et al. 2010; Oriolo et al. 2016a); $\varepsilon Hf_{(t)}$ values are positive to slightly negative and Hf model ages are slightly older than U–Pb ages.

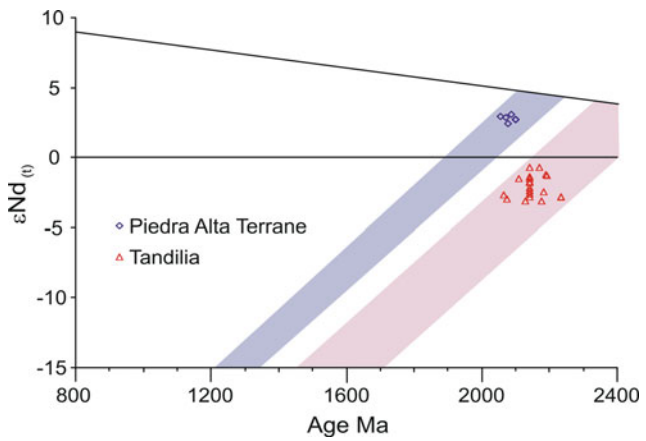

Fig. 4.6 $\varepsilon Nd_{(t)}$ versus age plot showing Nd isotopic data from granitoid and orthogneisses from the Piedra Alta Terrane (data from Peel and Preciozzi 2006; Basei et al. 2016) and from the Tandilia Belt (data from Hartmann et al. 2002; Pankhurst et al. 2003)

The similarity in crustal residence times, together with the abovementioned similarity in U–Pb geochronology, indicates that Piedra Alta and Tandilia terranes are most probably not allochthonous as considered by Bossi and Cingolani (2009), but rather should represent the accretion of para-autochthonous terranes.

4.6 Constraints on Metamorphic Events, Exhumation and Cooling

As mentioned above, the age of the main metamorphic event in the Río de la Plata Craton is constrained between the age of the metamorphic protoliths (2.2–2.1 Ga) and the age of the undeformed (post-collisional) granites dated at ca. 2.07 Ga. Chernicoff et al. (2015, 2016) reported the first direct dating of the metamorphism at 2120 ± 11 Ma (metamorphic titanite) and interpreted it as corresponding to the collisional stage. Additionally, shear zones in Tandilia and in southern Uruguay evolved under a comparable deformation regime and temperature conditions, and show

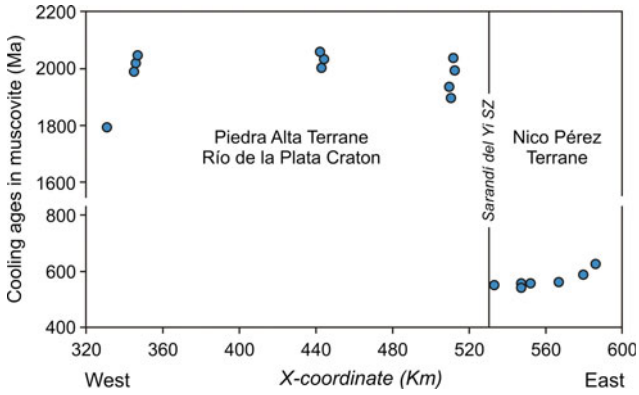

Fig. 4.7 Time-space diagram of muscovite K–Ar cooling ages across the Piedra Alta Terrane (Río de la Plata Craton), the Nico Pérez Terrane and the Dom Feliciano Belt (east–west profile). *X* coordinates in kilometres. Origin of coordinates 55º48′W

similar time constraints (Frisicale et al. 2001; Ribot et al. 2005; Gianotti et al. 2010).

K–Ar cooling ages along a transect across the major tectonic units of the Precambrian Uruguayan Shield (Piedra Alta Terrane, Nico Pérez Terrane and Dom Feliciano Belt) were presented by Oyhantçabal et al. (2011). The transect (Fig. 4.7) shows Paleoproterozoic cooling ages for the Piedra Alta Terrane in sharp contrast with the Neoproterozoic cooling ages from the Nico Pérez Terrane and the Dom Feliciano Belt. Likewise, in the Tandilia System the K–Ar and Ar–Ar cooling ages are Paleoproterozoic (Teixeira et al. 2002). The results demonstrate that the Río de la Plata Craton was not thermally overprinted during the Meso- or Neoproterozoic in contrast to the Nico Pérez and Mar del Plata terranes and the Dom Feliciano Belt, which show widespread Neoproterozoic reworking (Cingolani and Bonhomme 1982; Cingolani 2011; Oyhantçabal et al. 2011; Rapela et al. 2011).

4.7 Proterozoic Mafic Dyke Swarms

Available petrological and geochronological data for the Precambrian dyke swarms of the Río de la Plata Craton is presented in Table 4.2. A calc-alkaline dyke swarm intruded in Tandilia is near-coeval with the post-orogenic granitic plutonism (Teixeira et al. 2002). In Uruguay, a dyke swarm of similar age has not been recognized yet but numerous calc-alkaline gabbros could be the equivalent of this mafic post-orogenic magmatism.

Despite some geochemical similarities, the Florida dyke swarm of Uruguay (1.79 Ga, Halls et al. 2001) and the dykes of Tandilia (1.59 Ga) are not coeval (Teixeira et al. 2013). Nevertheless, both swarms reflect anorogenic extension after the Paleoproterozoic orogeny in the Río de la Plata Craton.

4.8 Tectonic Evolution

The tectonostratigraphic chart in Fig. 4.8 shows the main events on the different domains of the Río de la Plata Craton. Neoarchean to Early Paleoproterozoic crustal growth is documented by Nd and Hf model ages ranging between 2.6 and 2.1 Ga, while epsilon-$(Nd)_{(t)}$ and -$(Hf)_{(t)}$ positive to slightly negative values suggest a short period of crustal reworking. In an overview of the Tandilia System, Cingolani (2011) showed that the evolution could be represented by a first stage (ca. 2.2 Ga) during which Neoarchean juvenile separated continental blocks (Buenos Aires, El Cortijo and Tandilia blocks) converge. Calc-alkaline orthogneisses dated at ca. 2.2–2.1 Ga are widespread in all areas of the Río de la Plata Craton and should be the result of subduction-related magmatism. A similar model, but implying two subductions, was presented by Chernicoff et al. (2014), who suggested that extension of Neoarchean crust during Siderian times (2500–2300 Ma) caused the separation of the Balcarce, Tandilia and Buenos Aires terranes, and the development of narrow oceans. An island arc represented by the El Cortijo Formation was developed at this time. Evidence for relics of oceanic crust and suture zones is elusive in Precambrian terranes, and other possible suture zones have been suggested in the craton in Uruguay (e.g., the Ojosmin Complex or the Colonia Shear Zone; Bossi and Piñeyro 2004). Whether this magmatism reflects subduction resulting from reamalgamation between para-autochthonous terranes or not is a topic for future research. In any case, if the proposed suture zones were confirmed, the isotopic similarity of involved terranes indicates that they were para-autochthonous.

During the Late Rhyacian (ca. 2.1 Ga), continent–continent collision occurred, as suggested by thick mylonite belts, and suspected relics of ocean floor rocks. The collision caused thrusting and transcurrent tectonics favouring the anatexis of the crustal rocks. The age of the main metamorphism has been dated at ca. 2.1 Ga in metamorphic titanites from the basement in Buenos Aires city (Chernicoff et al. 2016). This age is bracketed by the protolith age of the orthogneisses (2.2–2.1 Ga) and the age of the post-orogenic granites and gabbros (ca. 2.07 Ga), and it is similar to the age of the shear zones, thus further confirming the timing of the collision. Late- to post-collision granitoids and gabbros (ca. 2.1–2.0 Ga) represent post-orogenic crustal extension.

K–Ar cooling ages indicate Paleoproterozoic cratonization (Hart 1966; Cingolani 2011; Oyhantçabal et al. 2011), consistent with subsequent crustal extension and emplacement of anorogenic tholeiitic dyke swarms (at ca. 1.8 Ga in Uruguay and ca. 1.6 Ga in Argentina). These dykes do not show any metamorphic overprint or deformation, except at

Table 4.2 Summary of available petrological and geochronological data of the Precambrian dyke swarms of the Río de la Plata Craton

	Calc-alkaline swarm of Tandilia	Tholeiitic swarm of Tandilia	Tholeiitic swarm of Florida
Age	2020 ± 24 Ma (Ar–Ar in biotite of the country rock)[a] (Teixeira et al. 2002)	1589 ± 3 Ma (U–Pb in baddeleyite) (Teixeira et al. 2013)	1790 ± 5 Ma (Halls et al. 2001) SHRIMP U–Pb in baddeleyite
Isotopic signature	Positive ε_{Sr} and negative ε_{Nd} (Teixeira et al. 2002)	Slightly positive ε_{Sr} and ε_{Nd} (Iacumin et al. 2001)	Positive ε_{Sr} and negative ε_{Nd} (Mazzucchelli et al. 1995)
Mantle source	IE enriched mantle source	IE depleted mantle source (Iacumin et al. 2001)	EM1 type, dominated by ε_{Nd} variation (Mazzucchelli et al. 1995)
Tectonic setting	Post-collisional extension	Anorogenic extension	Anorogenic extension

[a]U–Pb SHRIMP ages for zircons from the Rospide Gabbro yielded 2053 ± 14 Ma (Hartmann et al. 2008). This age is more or less similar to the Isla Mala Granite 2065 ± 9 Ma (Hartmann et al. 2000)

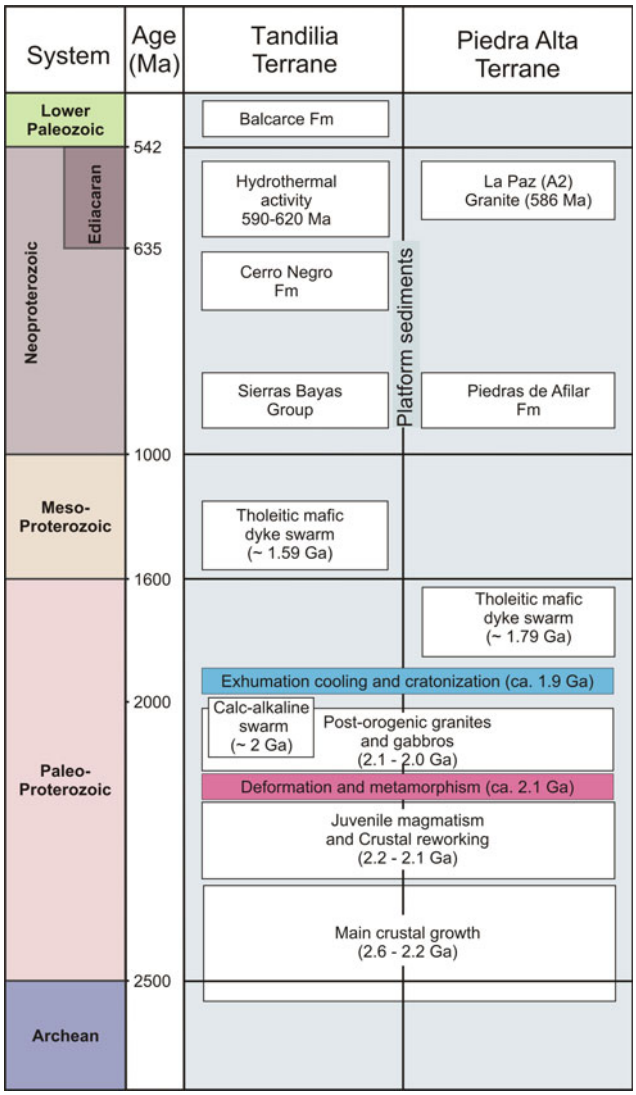

Fig. 4.8 Tectonostratigraphic chart of the Rio de la Plata Craton in Argentina and Uruguay

the edge of the craton in Uruguay, because of the influence of the Sarandí del Yí Shear Zone (Oriolo et al. 2015).

Afterwards, the basement suffered a long period of cooling, uplift, weathering and peneplanization, and the geological record begins again during the Neoproterozoic with deposits on a stable platform (the Villa Mónica Formation of the Sierras Bayas Group in Argentina and the Piedras de Afilar Formation in Uruguay).

Rapela et al. (2011) indicate, based on U–Pb, Hf and O isotope data in zircons, that the Río de la Plata Craton abuts against a distinct terrane to the east during the Ediacaran: the 'Mar del Plata Terrane'. As they point out, the Río de la Plata Craton is bounded by transcurrent faults and no Neoproterozoic belts were developed. The assembly of this part of Southwest Gondwana was accomplished before the deposition of the Ordovician (to Silurian?) siliciclastic platform sediments of the Ba1carce Formation in the Tandilia System. A comparable situation is observed in Uruguay, where the Nico Pérez Terrane was accreted to the eastern Río de la Plata Craton along the Sarandí del Yí Shear Zone (Oriolo et al. 2016a, b; Chap. 7) without the formation of a Neoproterozoic belt.

4.9 Conclusions

A review of the geology of the Río de la Plata Craton, including geochronological, isotopic data and geophysics, reveal the following main conclusions:

- Nd and Hf isotopic data for the Río de la Plata Craton is characterized by Nd and Hf model ages between 2.7 and 2.1 Ga, and positive to slightly negative epsilon values, thus indicating a single event of crustal growth and a short period of crustal recycling. Eo- Paleo- or Mesoarchean crust-forming events are absent in the craton.

- Granitic gneisses dated at 2.2–2.1 Ga predominate in the craton and are evidence of a large magmatic event, probably subduction related. The supracrustal successions (e.g., San José and Arroyo Grande belts of Uruguay) are roughly coeval with this magmatism as indicated by detrital zircon data and the age of interbedded lavas, and they may represent intra-arc basins.
- Crystallization ages of 2.2–2.1 Ga for the metamorphic protoliths and 2.1–2.05 Ga for the granitoids represent pre- and post-collisional magmatism of a Rhyacian orogeny.
- The uniformity of isotopic signature indicates that if suspected Paleoproterozoic suture zones are confirmed inside the craton, they should represent the accretion of para-autochthonous terranes.
- Cratonization occurred in Paleoproterozoic times (Statherian) and a lack of Meso- or Neoproterozoic overprinting is a distinctive feature, pointing out that this craton had a thick and strong lithosphere when it was amalgamated with Gondwana in the Neoproterozoic.

Acknowledgements Field and laboratory work by C. Cingolani was funded by CONICET and UNLP grants. P. Oyhantçabal gratefully acknowledges grants provided by the DAAD, the German Science Foundation and Comisión Sectorial de Investigación Científica (CSIC) of the Universidad de la República.

References

Abre P et al (2014) El Terreno Tandilia en Uruguay y Argentina. In: Bossi J, Gaucher C (eds) Geología del Uruguay, Tomo 1: Predevónico. Universidad de la República, Montevideo, pp 89–119

Almeida FFM et al (1973) The Precambrian evolution of the South American cratonic margin, South of Amazonas River. In: Nairn ACM et al (eds) The ocean basins and margins. Plenum, New York, pp 411–446

Angeletti M et al (2014) Nuevas edades radiométricas U–Pb SHRIMP en Tandilia, Cerro Siempre Amigos, Sierras de Azul, Buenos Aires, Argentina. XIX Congreso Geológico Argentino, abstract T81

Arrouy MJ et al (2016) Ediacaran discs from South America: probable soft bodied macrofossils unlock the paleo-geography of the Clymene ocean. Scientific Reports 6:30590. https://doi.org/10.1038/srep30590

Basei MAS et al (2016) LAICPMS U–Pb zircon ages from basement and metamorphic cover of Piedra Alta Terrane, Rio de la Plata Craton, Uruguay. Actas VIII Congreso Uruguayo de Geología, Montevideo

Borrello AV (1962) Formación Punta Mogotes (Eopaleozoico—Provincia de Buenos Aires). Notas Comisión de Investigación Científica Provincia de Buenos Aires 1(1):1–9

Bossi J, Cingolani C (2009) Extension and general evolution of the Río de la Plata Craton. In: Gaucher C et al (eds) Neoproterozoic-Cambrian tectonics, global change and evolution: a focus on southwestern Gondwana. Develop Precambrian Geol 16: 73–85

Bossi J, Ferrando L (2001) Carta geológica del Uruguay. Geoeditores. CD-ROM, Montevideo

Bossi J, Piñeyro D (2004) Complejo Ojosmin: fragment of ophiolite Transamazonian. Actas IV Congreso Uruguayo de Geologia—II Reunion de Geologia Ambiental y ordenamiento Territorial del Mercosur, Montevideo

Bossi J, Piñeyro D (2014) Terreno Piedra Alta. In: Bossi J, Gaucher C (eds) Geología del Uruguay. Tomo 1: Predevónico. Universidad de la República, Montevideo, pp 45–86

Bossi J et al (1993a) Early Proterozoic dike swarms from western Uruguay: geochemistry, Sr-Nd isotopes and petrogenesis. Chem Geol 106:263–277

Bossi J et al (1993b) Predevoniano del Uruguay. Parte 1: Terreno Piedra Alta. DINAMIGE, Montevideo, pp 1–50

Bossi J et al (2005) El límite sur del terreno Piedra Alta (Uruguay). Importancia de la faja milonítica sinistral de Colonia. Actas del XVI Congreso Geológico Argentino (La Plata) vol I, pp 173–179

Campal N (1990) Aportes al conocimiento de la estratigrafía durante el Precámbrico medio del Uruguay (con énfasis en los departamentos de Florida y San José). In: 1º Congreso Uruguayo de Geología. Resúmenes Ampliados vol 1. Montevideo, Uruguay, pp 65–69

Chernicoff CJ et al (2014) The Rhyacian El Cortijo suture zone: aeromagnetic signature and insights for the geodynamic evolution of the southwestern Río de la Plata craton, Argentina. Geosci Front 5:43–52

Chernicoff CJ et al (2015) Primeras edades UPb SHRIMP del Cratón Río de la Plata en el subsuelo del área metropolitana de Buenos Aires. Rev Asoc Geol Argent 72(4):575–577

Chernicoff CJ et al (2016) Zircon and Titanite U–Pb SHRIMP dating of unexposed basement units of the Buenos Aires region, southeastern Río de La Plata Craton, Argentina. Int Geol Rev 58:643–652

Cingolani CA (2011) The Tandilia system of Argentina as southern extension of the Río de la Plata craton: an overview. Int J Earth Sci 100:221–242

Cingolani CA, Bonhomme MG (1982) Geochronology of La Tinta Upper Proterozoic sedimentary rocks, Argentina. Precambrian Res 18(1–2):119–132

Cingolani CA et al (1990) Nuevos datos geológicos y geocronológicos del macizo granítico de Cerro Colorado, Florida, Uruguay. In: Resúmenes Ampliados del Primer Congreso Uruguayo de Geología, vol 1, pp 101–105

Cingolani CA et al (2002) U–Pb SHRIMP dating of zircons from the Buenos Aires complex of the Tandilia Belt. In: Río de la Plata Craton, Argentina. XV Congreso Geológico Argentino. Actas vol 1, pp 149–154

Cingolani CA et al (2010) New insights of the Paleoproterozoic basement of Tandilia belt. In: Río de la Plata Craton, Argentina: first Hf isotope studies on zircon crystals. GeoSur Mar del Plata, Argentina, pp 21–24

Cingolani CA et al (2012) U–Pb (LA-ICP-MS) zircon age of the La Paz Granite (Pando Belt, Uruguay): an upper Neoproterozoic magmatic event in the Río de la Plata Craton. In: VIII Simposio Sudamericano de Geología Isotópica, Medellin, Colombia, 5–7 July 2012

Coronel N et al (1982) Consideraciones estructurales de la Formación Piedras de Afilar. Departamento de Canelones. Uruguay. In: Actas V Congreso Latinoamericano de Geología. Buenos Aires, Argentina

Dalla Salda LH (1981) Tandilia, un ejemplo de tectónica de transcurrencia en basamento. Rev Asoc Geol Argent 36(2):204–207

Dalla Salda LH et al (1988) The Río de la Plata cratonic region of southwest-ern Gondwana. Episodes 11(4):263–269

Dalla Salda LH et al (2005) El basamento de las Sierras de Tandilia. In: de Barrio RE et al (eds) Geología y recursos minerales de la provincia de Buenos Aires. Relatorio del 16 Congreso Geológico Argentino, La Plata, pp 31–50

Dalla Salda LH et al (2006) Tandilia. In: Temas de Geología Argentina 1. Serie Correlación Geológica, vol 21, pp 17–46. San Miguel de Tucumán

Delpino SH, Dristas J (2008) Dolomitic marbles and associated calc-silicates, Tandilia belt, Argentina: geothermobarometry, metamorphic evolution, and P-T path. J South Am Earth Sci 25:501–525

Delpino SH et al (2001) Sucesión de eventos deformacionales en base a las correlaciones entre mesoestructuras, Punta Tota, basamento Paleoproterozoico de Tandilia, Argentina. Rev Asoc Geol Argent, Serie D: Publicación Especial

Dragone GN et al (2017) Western Paraná suture/shear zone and the limits of Río Apa, Río Tebicuary and Río de la Plata cratons from gravity data. Precambrian Res 291:162–177

Dristas JA, Frisicale MC (1988) Rocas piroclásticas en el sector suroeste de las Sierras Septentrionales de la provincia de Buenos Aires. Rev Asoc Argentina de Mineralogía, Petrología y Sedimentología, Buenos Aires 18(1–4):33–46

Dristas JA, Martínez JC (2007) Hydrothermal low temperature Late Proterozoic unconformity-related hydrothermal iron deposits, in the northern Barker area (Tandilia Ranges, Argentina). Neues Jahrb Geol Paläont 246(3):267–281

Dristas JA et al (2003) High-REE APS minerals associated with advanced argillic alteration in the Cerrito de la Cruz deposit, Barker, Buenos Aires province, Argentina. Göttinger Arb Geol Paläont Sb (Festschrift Behr) 5:pp. 1–6

Dristas JA et al (2017) Hydrothermal karst and associated breccias in Neoproterozoic limestone from the Barker-Villa Cacique area (Tandilia belt), Argentina. J South Am Earth Sci 76:182–197

Eby GN (1992) Chemical subdivision of the A-type granitoids: petrogenetic and tectonic implications. Geology 20:641–644

Favetto A et al (2015) A new limit for the NW Río de la Plata Craton border at about 24°S (Argentina) detected by Magnetotellurics. Geologica Acta 13(3):243–254

Fernández AN, Preciozzi F (1974) La formación Arroyo. Grande y los granitoides asociados. In: Annales. XXVIII Congreso Brasilero de Geologia, pp 212–226

Ferrando L, Fernández A (1971) Esquema tectónico-cronoestatigráfico del predevoniano en Uruguay. XXV Congreso Brasilero de Geología, vol 1. San Pablo, Paulo, pp 199–210

Frisicale MC (1999) Megacizalla en Boca de la Sierra, Tandilia. Actas 14 Congreso Geológico Argentino. Salta, vol 1, 168–171

Frisicale MC et al (2001) Cinemática de las milonitas del basamento proterozoico en Boca de la Sierra, Sierras de Azul, Buenos Aires. Rev Asoc Geol Argent 56(3):319–330

Frisicale MC et al (2005) Microstructural analysis and P-T conditions of the Azul megashear zone, Tandilia, Buenos Aires province, Argentina. J South Am Earth Sci 19(4):433–444

Gaucher C et al (2008) Detrital zircon ages of neoproterozoic sedimentary successions in Uruguay and Argentina: insights into the geological evolution of the Río de la Plata Craton. Precambrian Res 167:150–170

Gianotti V et al (2010) Caracterización Geológico-Estructural Y Estudio Microtectónico de las Zonas de Cizalla de Colonia. VI Congreso Uruguayo de Geología. Minas, CD-ROM

Gómez Peral LE et al (2007) Chemo-stratigraphy and diagenetic constraints on neoproterozoic carbonate successions from the Sierras Bayas group, Tandilia system, Argentina. Chem Geol 237:109–128

Gonzalez Bonorino F et al (1956) Estudio geológico de las Sierras de Olavarría y Azul (Provincia de Buenos Aires). LEMIT, Serie 2(63): 5–22. La Plata

Halls HC et al (2001) Magnetic studies and U–Pb geochronology of the Uruguayan dike swarm, Río de la Plata Craton, Uruguay: paleomagnetic and economic implications. J South Am Earth Sci 14: 349–361

Hart SR (1966) Radiometric ages in Uruguay and Argentina and their implications concerning continental drift. In: Geological Society of America. Annual Meeting, vol 86. San Francisco, EEUU

Hartmann LA et al (2000) Zircon U–Pb SHRIMP dating of Paleoproterozoic Isla Mala granitic magmatism in the Río de la Plata Craton, Uruguay. J South Am Earth Sci 13:105–113

Hartmann LA et al (2001) Archean crust in the Río de la Plata Craton, Uruguay—SHRIMP U–Pb zircon reconnoissance geochronology. J South Am Earth Sci 14:557–570

Hartmann LA et al (2002) Two Paleoproterozoic Orogenies in the evolution of the Tandilia belt, Buenos Aires, as evidenced by zircon U–Pb SHRIMP geochronology. Int Geol Rev 44:528–543. https://doi.org/10.2747/0020-6814.44.6.528

Hartmann LA et al (2008) Geocronología SHRIMP U–Pb en circones del Gabro Rospide del Cinturón Paleoproterozoico San José, Terreno Piedra Alta, Uruguay: una prueba geocronológica de magmas coetáneos. Rev Soc Uru Geol 15:40–53

Iacumin M et al (2001) Early Proterozoic calc-alkaline and middle Proterozoic tholeiitic dykes swarms from central-eastern Argentina: petrology, geochemistry, Sr–Nd isotopes and tectonic implications. J Petrology 42:2109–2143

Irvine TN, Baragar WRA (1971) A Guide to the Chemical Classification of the Common Volcanic Rocks. Canadian J Earth Sci 8:523–548

Lajoinie MF et al (2013) Zonación mineral vinculada a procesos geoquímicos en el skarn San Miguel, Sierras Septentrionales de la provincia de Buenos Aires. Rev Asoc Geol Argent 70:402–412

Lajoinie MF et al (2014) First records of the 'Lomagundi-Jatuli carbon isotope Event' in Paleoproterozoic marble of the basement of the Sierras Septentrionales in the Buenos Aires Province, Río de la Plata craton. Rev Asoc Geol Argent 71(4):585–597

Larin AM (2009) Rapakivi granites in the geological history of the earth. Part 1, magmatic associations with rapakivi granites: age, geochemistry, and tectonic setting. Stratigr Geol Correl 17:235–258

Maheshwari A et al (2010) Global nature of the Paleoproterozoic Lomagundi carbon isotope excursion: a review of occurrences in Brazil, India, and Uruguay. Precambrian Res 182:274–299

Marchese HG, Di Paola EC (1975) Reinterpretación estratigráfica de la Perforación Punta Mogotes N° 1, Provincia de Buenos Aires. Rev Asoc Geol Argent 30:17–44

Martínez JC, Dristas JA (2006) Perfiles de alteración en la discordancia entre el Complejo Buenos Aires y la Formación La Tinta, área de Barker, Tandilia. Avances en mineralogía, meta-logenia y petrología. Congreso de Mineralogía y Metalogenia. Actas, pp 409–412

Martínez JC, Dristas JA (2008) Mineralogía y petrología del nivel dolomítico de las Sierras de la Siempre Verde y Cuchilla de las Águilas, Sierras de Tandilia, provincia de Buenos Aires. 17° Congreso Geológico Argentino. Jujuy, Argentina

Martínez JC et al (2010) A hydrothermal clay mineral assemblage at the Late-Proterozoic unconformity Buenos Aires Complex—La Tinta Formation: Barker area, Tandilia Ranges (Argentina). Clay Miner 45:209–224

Martínez JC et al (2013) Late-Neoproterozoic hydrothermal fluid activity in the Tandilia belt, Argentina. Rev Asoc Geol Argent 70:410–426

Martínez JC et al (2017) Trans-Amazonian U-Th-Pb monazite ages and P-T-d exhumation paths of garnet-bearing leucogranite and migmatitic country rock of the southeastern Tandilia belt, Río de la Plata craton in Argentina. Lithos 274:328–348

Massonne HJ et al (2012) Metamorphic evolution of the Río de la Plata Craton in the Cinco Cerros area, Buenos Aires Province, Argentina. J South Am Earth Sci 38:57–70

Mazzucchelli M et al (1995) Petrology of the Proterozoic mafic dyke swarms of Uruguay and constraints on their mantle source composition. Precambrian Res 74:177–194

Miranda SA et al (2015) Fractalness of land gravity data and residual isostatic anomalies map of Argentina, Chile and western Uruguay. Geofís Int 54(4):315–322
Miyashiro A (1974) Volcanic rock series in island arcs and active continental margins. Am J Sci 274:321–355
Oriolo S et al (2015) Structural evolution of the Sarandí del Yí Shear Zone, Uruguay: kinematics, deformation conditions and tectonic significance. Int J Earth Sci 104(7):1759–1777
Oriolo S et al (2016a) The Nico Pérez Terrane (Uruguay): from Archean crustal growth and connections with the Congo Craton to late Neoproterozoic accretion to the Río de la Plata Craton. Precambrian Res 280:147–160
Oriolo S et al (2016b) Timing of deformation in the Sarandí del Yí Shear Zone, Uruguay: implications for the amalgamation of Western Gondwana during the Neoproterozoic Brasiliano–Pan-African Orogeny. Tectonics 35(3):754–771
Oyhantçabal P et al (1990) Contribución al conocimiento petrográfico, geoquímico y estructural del granito de La Paz. Resúmenes ampliados del Primer Congreso Uruguayo de Geología. Montevideo
Oyhantçabal P et al (1998) The Soca intrusion: a rapakivi granite of Uruguay. J South Am Earth Sci 11(2):169–178
Oyhantçabal P et al (2003) Proterozoico del suroeste del Uruguay: nueva propuesta estratigráfica para la Formación Montevideo y el magmatismo asociado. Rev Soc Urug Geol Pub Esp 1:38–48
Oyhantçabal P et al (2006) K–Ar geochronology of the Mosquitos Shear Zone (Piedra Alta Terrane-Río de la Plata craton-Uruguay). In: V South American symposium on isotope geology, short papers, Punta del Este, p 149
Oyhantçabal P et al (2007) Caracterización geológica de las rocas paleoproterozoicas de la región Centro-Sur del Uruguay (Terreno Piedra Alta—Cratón del Río de la Plata). In: Actas V Congreso Uruguayo de Geología. CD-ROM
Oyhantçabal P et al (2011) The Río de la Plata Craton: a review of units, boundaries, ages and isotopic signatures. Int J Earth Sci 100:201–220
Pamoukaghlian K (2012) Sedimentología y estratigrafía de la formación Piedras de Afilar, Terreno Tandilia, Uruguay. Doctoral dissertation, Facultad de Ciencias Naturales y Museo
Pamoukaghlian K et al (2006) First C and O isotopic data for the Piedras de Afilar Formation (Tandilia Terrane, Uruguay): their bearing on its correlation and age. In: Proceedings of the V South American symposium on isotope geology, short papers, Punta del Este, pp 277–283
Pángaro F, Ramos VA (2012) Paleozoic crustal blocks of onshore and offshore central Argentina: new pieces of the southwestern Gondwana collage and their role in the accretion of Patagonia and the evolution of Mesozoic south Atlantic sedimentary basins. Mar Petrol Geol 37(1):162–183. https://doi.org/10.1016/j.tecto.2013.02.008
Pankhurst RJ et al (2003) Antiquity and evolution of the Río de la Plata craton in Tandilia, southern Buenos Aires province, Argentina. J South Am Earth Sci 16:5–13
Pascale A, Oyhantçabal P (2016) Geoquímica de las anfibolitas de Formación Montevideo y los ortoneises asociados. Actas VIII Congreso Uruguayo de Geología, Montevideo, 2016
Peccerillo R, Taylor SR (1976) Geochemistry of Eocene calc-alkaline volcanic rocks from the Kastamonu area, Northern Turkey. Contrib Miner Petrol 58:63–81
Pecoits E et al (2008) Ediacaran in Uruguay: palaeoclimatic and palaeobiological implications. Sedimentology 55:689–719
Peri VG, Pomposiello MC, Favetto A, Barcelona H, Rossello E (2013) Magnetotelluric evidence of the tectonic boundary between the Río de La Plata Craton and the Pampean Terrane (Chaco-Pampean Plain, Argentina): the extension of the Transbrasilian Lineament. Tectonophysics 608:685–699
Pecoits E et al (2016) U–Pb detrital zircon ages from some Neoproterozoic successions of Uruguay: provenance, stratigraphy and tectonic evolution. J South Am Earth Sci 71:108–130
Peel E, Preciozzi F (2006) Geochronologic Synthesis of the Piedra Alta Terrane, Uruguay. In: V South American Symposium on Isotope Geology, Punta del Este, Uruguay, pp. 234–237
Poiré DG, Gaucher C (2009) Lithostratigraphy. Neoproterozoic Cambrian evolution of the Río de la Plata Palaeocontinent. In: Gaucher C et al (eds) Neoproterozoic-Cambrian tectonics, global change and evolution: a focus on southwestern Gondwana. Developments in precambrian geology, vol 16, no 4.2, pp 87–101. https://doi.org/10.1016/S0166-2635(09)01605-3
Poiré DG, Spalletti LA (2005) La cubierta sedimentaria Precámbrica-Paleozoica inferior del Sis-tema de Tandilia. In: de Barrio RE, Etcheverry RO, Caballé MF, Llambías E (eds) Geología y Recursos Minerales de la Provincia de Buenos Aires. 16° Congreso Geológico Argentino, La Plata, Relatorio, vol 4, pp 51–68
Preciozzi F (1993) Petrography and geochemistry of five granitic plutons from south-central Uruguay. Contribution to knowledge of the Piedra Alta Terrane. Unpublished Ph.D. thesis, Université du Québec, 143 pp
Preciozzi F et al (1985) Carta Geológica del Uruguay a escala 1:500.000, Dirección Nacional de Minería y Geología, Montevideo, 92 pp
Ramos VA (1988) Late Proterozoic-Early Paleozoic of South America: a collisional history. Episodes 11:168–174
Rapalini AE et al (2015) Paleomagnetic study on mid-Paleoproterozoic rocks from the Rio de la Plata craton: implications for Atlantica. Gondwana Res 27(4):1534–1549
Rapela C et al (1974) Un filón básico ordovícico en la Formación La Tinta, Sierra de los Barrientos Provincia de Buenos Aires. Rev Asoc Geol Argent XXIX 3:319–331
Rapela CW et al (2007) The Río de la Plata craton and the assembly of SW Gondwana. Earth Sci Rev 83:49–82
Rapela CW et al (2011) The Río de la Plata craton and the adjoining Pan-African/Brasilian terranes: their origins and incorporation into south-west Gondwana. Gondwana Res 20:673–690
Ribot AM et al (2005) Caracterización petrográfica y cinemática de la faja milonítica Colonia-Arroyo Pavón en el sur del terreno Piedra Alta, Uruguay: zona de cizalla principal en basamento Precámbrico? Actas del XVI Congreso Geológico Argentino, La Plata. I: 457–464
Ribot AM et al (2013) Milonitas graníticas de la Isla San Gabriel, Uruguay: cinemática de la deformación y Geocronología U–Pb. VII Congreso Uruguayo de Geología, I Simposio de Mineria y Desarrollo del Cono Sur. pp 147–153
Ryan WBF et al (2009) Global multi-resolution topography synthesis. Geochem Geophys Geosyst 10:Q03014. https://doi.org/10.1029/2008GC002332
Santos JOS et al (2003) Duration of the Trans-Amazonian cycle and its correlation within South America based on U–Pb SHRIMP geochronology of the La Plata Craton, Uruguay. Int Geol Rev 45:27–48
Schröder S et al (2008) Rise in seawater sulphate concentration associated with the Paleoproterozoic positive carbon isotope excursion: evidence from sulphate evaporites in the ~2.2–2.1Gyr shallow marine Lucknow formation, South Africa. Terra Nova 20:108–117
Shand HS (1943) Eruptive Rocks. John Wiley and Sons. 444 pp
Teixeira W et al (1999) ^{40}Ar–^{39}Ar and Rb–Sr geochronology of the Uruguayan dike swarm, Río de la Plata Craton and implications for Proterozoic intraplate activity in western Gondwana. Precambrian Res 93:153–180
Teixeira W et al (2002) Calc-alkaline and tholeiitic dyke swarms of Tandilia, Río de la Plata craton, Argentina: U–Pb, Sm-Nd, Rb-Sr

and ^{40}Ar–^{39}Ar data provide new clues for intraplate rifting shortly after Trans-Amazonian orogeny. Precambrian Res 119:329–353

Teixeira W et al (2013) U–Pb (ID-TIMS) baddeleyite ages and paleomagnetism of 1.79 and 1.59 Ga tholeiitic dyke swarms, and position of the Río de la Plata Craton within the Columbia supercontinent. Lithos 174:157–174

Tohver E et al (2008) New SHRIMP U–Pb and $^{40}Ar/^{39}Ar$ constraints on the crustal stabilization of southern South America, from the margin of the Río de Plata (Sierra de Ventana) craton to northern Patagonia. American Geophysical Union, Fall Meeting 2008, abstract #T23C-2052

Tohver E et al (2012) Closure of the Clymene ocean and formation of west Gondwana in the Cambrian: evidence from the Sierras Australes of the southernmost Rio de la Plata craton, Argentina. Gondwana Res 21:394–405

Umpierre M, Halpern M (1971) Edades Sr-Rb del Sur de la República Oriental del Uruguay. Rev Asoc Geol Argent 26:133–151

Zalba PE et al (1993) Precambrian and lower Paleozoic records and paleosurfaces of the Tandilia System, Buenos Aires Province, Argentina. In: Schmitt JM, Gall Q (eds) Mineralogical and geochemical records of paleoweathering. Memoire des Sciences de la Terre, vol 18, pp 93–113

Zimmermann U, Spalletti LA (2009) Provenance of the lower Paleozoic Balcarce formation (Tandilia system, Buenos Aires province, Argentina): implications for paleogeographic reconstructions of SW Gondwana. Sediment Geol 219:7–23

5 A Geological and Isotopic Framework of Precambrian Terrains in Western Central Africa: An Introduction

Denis Thiéblemont, Yannick Callec, Max Fernandez-Alonso, and Frédéric Chène

Abstract

This chapter presents an up-to-date geological map of Western Central Africa, the region of equatorial Africa extending from the East-African rift to the Atlantic Ocean. Some 18 geological domains of Precambrian age are distinguished in this region, covering all the geological periods from the Paleoarchean to the Neoproterozoic. An overview of the lithostratigraphy of each domain is presented, based on the most recent geochronological data. A compilation of Sm–Nd isotopic data enables these domains to be discriminated by their isotopic signatures and integrated into a crustal growth model.

Keywords

Western Central Africa • Geological Map
Archean • Proterozoic • Geochronology • Nd-isotopes
Crustal growth

5.1 Introduction

Since the pioneer works of Cahen et al. (1984), followed at the end of the 1980s by the first edition of the Geological Map of Africa at 1:5,000,000 scale (Choubert and Faure-Muret 1985–1990), the degree of knowledge of the geology of Africa has greatly increased, especially owing to the more and more intensive use of precise geochronological methods. Integration of these works into a geological map covering the whole of Africa was achieved in 2004, with the presentation, of the second edition of the Geological and Major Mineral Deposits Map of Africa at 1:10,000,000 scale (Milesi et al. 2004) in the frame of the 21 Congress on African Geology.

Starting from the same cartographical framework, the Tectonic Map of Africa was published in 2010 (Milesi et al. 2010). This expressed, in a finished cartographical form on a continental scale, the project of Cahen et al. (1984) to draw a temporal scenario of the geological evolution of Africa.

As far as Western Central Africa is concerned (i.e., the region comprised between latitudes 10°N and 10°S, west of the East-African rift), two recent syntheses have been published, thus making useless any attempt to re-expose in a concise way the geology of this region: the Geological and Mineral Deposits map at 1:4,000,000 scale presented by Milesi et al. (2006) and the SIG-based synthesis of the basement of the Congo Basin exposed by De Wit and Linol (2015). Nevertheless, important geological mapping projects have been conducted since 2004 (Delor et al. 2007; Fernandez-Alonso et al. 2015a, b; Callec and Fullgraf 2015; Thiéblemont 2009; Thiéblemont et al. 2009; Pinna et al. 2008; Fernandez-Alonso 2007), which have resulted in significant improvements in the cartographical framework and geological understanding of large regions of Central Africa, including its basement region of Archean to Paleoproterozoic age. This region is sometimes referred to as the Congo Craton. However, the extension of what can be called the Congo Craton—that is, the extent to which individual 'blocks' of Archean rocks may be correlated to others across Central Africa and even South America—is still a matter of debate (e.g., Fernandez-Alonso et al. 2011; De Wit and Linol 2015). Thus we avoid using the term Congo Craton and do not enter this debate, which is beyond the scope of this chapter.

The recent large-scale mapping projects conducted in Central Africa and other regions of this continent have motivated the preparation of the third edition of the Geological Map of Africa at 1:10,000,000 by a team of European and African geologists under the supervision of the Commission for the Geological Map of the World and Geological Society of Africa. This map was first presented at the 35th

D. Thiéblemont (✉) · Y. Callec · F. Chène
BRGM, DGR, B.P. 6009 45060 Orléans Cedex, France
e-mail: d.thieblemont@brgm.fr

M. Fernandez-Alonso
Department of Geology, Royal Museum for Central Africa, Steenweg op Leuven 13, 3080 Tervuren, Belgium

S. Siegesmund et al. (eds.), *Geology of Southwest Gondwana*, Regional Geology Reviews,
https://doi.org/10.1007/978-3-319-68920-3_5

International Geological Congress held in Capetown in 2016 (Thiéblemont et al. 2016a), and a slightly revised version was printed afterwards in France with the financial support of the Total company (Thiéblemont et al. 2016b).

In this chapter devoted to the geology of the Precambrian terrains of Western Central Africa, we present first an improved version of this map, with some details on the lithostratigraphical organization of Precambrian terrains. Then we combine the geological and Nd-isotopic information to show how the addition of new domains with time produced a continental block with a highly variable isotopic signature.

5.2 Cartographical and Geochronological Background

5.2.1 Geological Maps

Starting from the Geological and Major Mineral Deposits Map published in 2004 (Milesi et al. 2004), improvements were made using the following maps of national scale (1:2,500,000–1:500,000):

- Angola: 1:2,000,000 scale (Delor et al. 2007);
- Democratic Republic of Congo (referred to as DRC in the following): 1:2,500,000 scale (Fernandez-Alonso et al. 2015a, b);
- Western Congo: 1:500,000 scale (Callec and Fullgraf 2015);
- Gabon: 1:1,000,000 scale (Thiéblemont 2009; Thiéblemont et al. 2009);
- Tanzania: 1:2,000,000 scale (Pinna et al. 2008);
- Rwanda-Burundi (i.e., Karagwe-Ankole Belt; Fernandez-Alonso 2007).

Because the lithostratigraphic scheme of the 2004 map was extensively revised, some older maps were also reconsidered in detail:

- Central African Republic (referred to as CAR in the following): 1:1,500,000 scale (Rolin 1995);
- South-West Cameroon: 1:500,000 scale (Maurizot 1986).

5.2.2 Geochronological Information

To draw the most up-to-date map from the available information, much attention was paid to the geochronological information. Precise examination of the geochronological data allows us to assess the point where the lithostratigraphic attribution of a given cartographical unit is founded, and to which extent it can be changed in order to harmonize the geological contours across national boundaries when contradictions exist between countries.

Indeed, the quantity and quality of the geochronological information available varies greatly from one country to another. Extensive geochronological investigations are planned in the frame of recent national mapping surveys, which give a solid ground for lithostratigraphical charts on the country scale. In other cases, such extensive data is not available. New data is provided through local studies, and such information may imply significant modifications. Therefore the lithostratigraphical scheme adopted in the original map of a given country has to be revised.

A typical example is provided by the west-Congo Belt, a Panafrican belt running along the Atlantic coast, from 9°S in Angola to 2°S in Gabon (Fig. 5.1). Recent mapping projects combined with substantial geochronological investigations (Callec and Fullgraf 2015; Fernandez-Alonso et al. 2015a, b) have significantly increased the knowledge of the Paleoproterozoic basement of the belt (known as the Kimezian Supergroup; Tack et al. 2001), motivating important changes in its cartography. Comparable works are still lacking in western Angola, where the Paleoproterozoic basement (PPpm in Fig. 5.1) appears considerably more developed than in the DRC. Thus the synthetic map of Western Central Africa (Fig. 5.1) features a sudden change in the organization of the W-Congo belt at the Angola–DRC boundary (Fig. 5.1). It is in fact probable that this change is only apparent as a consequence of the overestimation of the extent of the Kimezian basement in previous cartographical surveys.

In some regions, similar terrains mapped on each of the sides of two adjacent countries may be attributed to different geological periods. In such cases, we base the interpretation on the works providing the geochronological data of the better quality and/or better regional lithostratigraphical consistency.

An example is given by the central-northern part of the studied region, where the supposedly Mesoproterozoic Linki Bembe Supergroup of DRC (Lepersonne 1974) passes to the Paleoproterozoic Bangui series of CAR (Poidevin and Pin 1986; Rolin 1995). We prefer to retain this latter interpretation because it is the most consistent from a regional perspective. In fact, precise geochronological information exists in the western part of the considered region (CAR, Cameroon, Gabon), which shows that no Mesoproterozoic terrains exist which could represent the westward extension of the Linki Bembe Supergroup in this region of Africa. It is rather improbable that this unit could be circumscribed to DRC, so attribution to the Paleoproterozoic is the best hypothesis in a regional perspective.

Such modifications have been made in all regions where they appeared necessary. The sources of the data used are

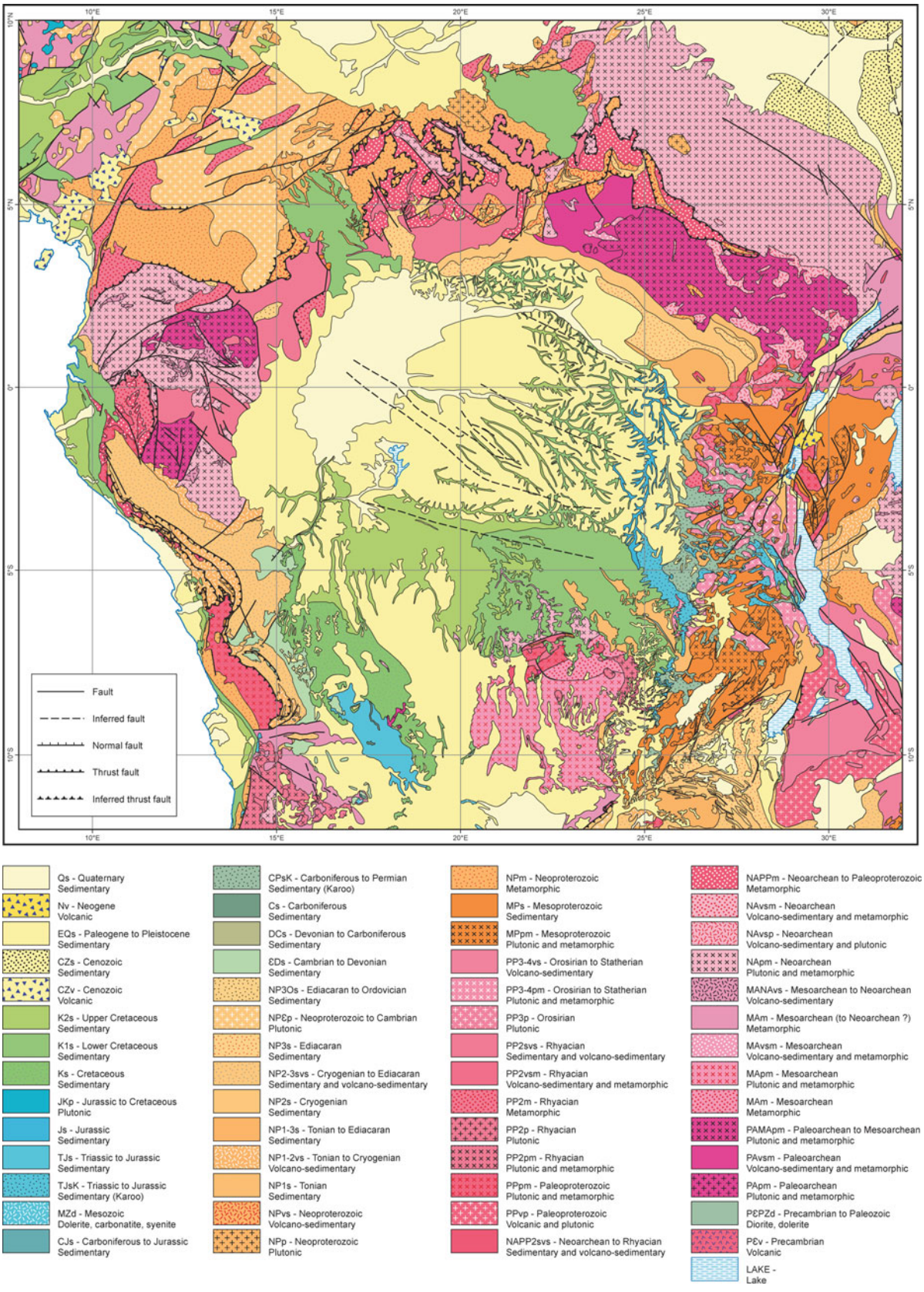

Fig. 5.1 Geological map of Western Central Africa extracted and modified from the third edition of the Geological Map of Africa at 1:10 M scale (Thiéblemont et al. 2016b)

Table 5.1 Summary of the references of the geochronological data used to improve the geological map and their corresponding domains (Fig. 5.1)

References	Geological domain
Abdelsalam et al. (2016)	Ruwenzori-Toro belt (Uganda)
Armstrong et al. (1999)	Lufilian belt, Irumide belt
Armstrong et al. (2005)	Lufilian belt
Boniface et al. (2012)	Ubendian belt
Brewer et al. (1979)	Bangweulu block
Buchwaldt et al. (2008)	Kibaran belt
Cahen et al. (1975)	Mbuji Mayi domain
Cahen et al. (1984)	All domains
Cahen and Ledent (1979)	Kibaran belt
De Carvalho et al. (2000)	Angola block
Censier (1990)	West Central African belt (CAR)
De Waele et al. (2006)	Irumide belt/Bangweulu block
De Waele and Fitzsimons (2007)	Irumide belt/Bangweulu block
De Wit (2004) in De Wit and Linol (2015)	Ntem-Chaillu block
Debruyne et al. (2015)	Kibaran belt (Burundi)
Delhal et al. (1986)	Kasai block
Delhal and Liégeois (1982)	Kasai block
Djama et al. (1992)	West Congo belt (Congo)
	West Central African belt (Congo)
Feybesse et al. (1998)	West Central African belt (Gabon)
Ganwa et al. (2016)	Oubanguides belt (Cameroon)
Ganwa et al. (2008a, b)	Oubanguides belt (Cameroon)
Gérards and Ledent (1976)	Kibaran belt (Rwanda)
Hanson et al. (1993)	Lufilian belt
Kabengele et al. (1990)	Irumide belt/Bangweulu block
Kampunzu et al. (1998)	Lufilian belt
Kampunzu and Cailteux (1999)	Lufilian belt
Key et al. (2001)	Lufilian belt (+basement)
Kokonyangi et al. (2001)	Kibaran belt
Kokonyangi et al. (2004)	Kibaran belt
Kokonyangi et al. (2005)	Kibaran belt
Kokonyangi et al. (2006)	Kibaran belt
Lavreau et al. (1980)	NE Congo block (CAR)
Lavreau et al. (1991)	NE Congo block (CAR)
Leggo (1974)	North Uganda block
Lenoir et al. (1994)	Ubendian belt (Tanzania)
Lerouge et al. (2006)	West Central African belt (Cameroon)
Link et al. (2010)	Ruwenzori-Toro belt (Uganda)
Maier et al. (2015)	Ntem-Chaillu block
Mänttäri et al. (unpublished) in De Wit and Linol (2015)	North Uganda block
Master et al. (2005)	Lufilian belt
Mayer et al. (2004)	Lufilian belt
McCourt et al. (2013)	Angola block
Moloto-A-Kenguemba et al. (2008)	West Central African belt (CAR)

(continued)

Table 5.1 (continued)

References	Geological domain
Mosoh Bambi et al. (2013)	Oubanguides belt (Cameroon)
Pasteels (1971)	Kasai block
Pin and Poidevin (1987)	Oubanguides belt (CAR)
Pinna (unpublished)	Ruwenzori-Toro belt (Uganda)
Poidevin (1985)	Oubanguides belt (CAR)
Poidevin and Pin (1986)	West Central African belt (CAR)
Rainaud et al. (2003)	Lufilian belt (+basement)
Rainaud et al. (2005b)	Lufilian belt (+basement)
Rainaud et al. (2005a)	Lufilian belt
Rolin (1995)	Oubanguides belt (CAR)
	West Central African belt (CAR)
	NE Congo block (CAR)
Shang et al. (2004a, b)	Ntem-Chaillu block (Cameroon)
Shang et al. (2010)	Ntem-Chaillu block (Cameroon)
Tack et al. (1994)	Kibaran belt (Burundi)
Tack et al. (2001)	West Congo belt
Tack et al. (2010)	Kibaran belt (Rwanda, Burundi)
Thiéblemont et al. (2009)	Ntem-Chaillu block (Gabon)
	West Central African belt (Gabon)
	Cent. Afric. Paleoprot. basins (Gabon)
Theunissen et al. (1992)	Ubendian belt (Tanzania)
Toteu et al. (1987, 2001, 2006b)	Oubanguides belt (Cameroon)
Toteu et al. (1994)	West Central African belt (CAR)
	Ntem-Chaillu block (Cameroon)
Turlin et al. (2016)	Lufilian belt (Zambia)
Walraven and Rumvegeri (1993)	Kasai block

listed in Table 5.1. For each set of data we indicate the regions covered by the geochronological information.

5.3 Precambrian Geological Domains Over Western Central Africa

5.3.1 General Framework

Present-day geological knowledge about Western Central Africa enables its Precambrian basement to be subdivided into a certain number of geological domains, including blocks, orogenic belts and sedimentary basins (Fig. 5.1). The term 'block' is used here to refer to regions made of crystalline rocks which are supposed to have been part of the deep regions of ancient orogenic belts, now highly eroded and split. Such blocks are sometimes designated as cratons, but this term is also used for combinations of blocks supposed to have been parts of the same crustal domain at the end of Archean times (De Wit and Linol 2015). Likewise, despite its wide use, the term 'Congo Craton' is not clearly defined (Fernandez-Alonso et al. 2011). For many authors it designates the basement region of Central Africa thought to have been stabilized before the Neoproterozoic and aggregated with northern (Nigeria) and southern (Kalahari) continental masses owing to the Panafrican orogenesis (e.g., Castaing et al. 1994; Kampunzu and Cailteux 1999; Trompette 2000). However, no agreement appears to exist concerning the exact limits of this craton. Therefore we avoid the term 'Congo Craton' and prefer to give a factual description of the lithostratigraphical organization of the different domains included in the studied area (i.e., Central Africa west of the East-African rift and north of 10°S).

In this area, three main blocks of Archean age may be distinguished (Fig. 5.2): the Ntem-Chaillu block to the west, the NE-Congo block to the northeast and the Kasai block to the south.

Beside the Archean blocks, different Proterozoic orogenic belts of continental extension are distinguished (Fig. 5.2). Two orogenic belts are of Paleoproterozoic age. One, in its

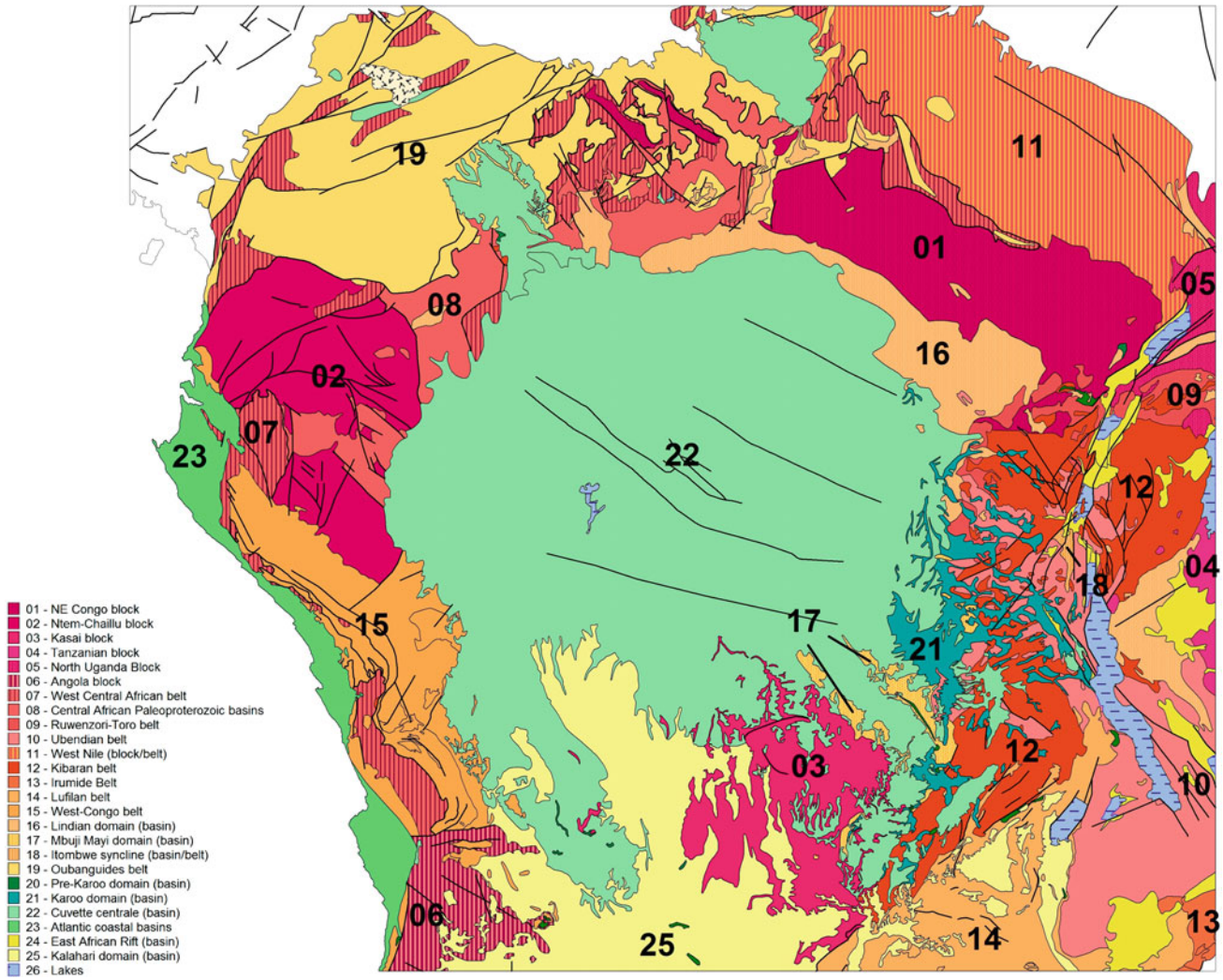

Fig. 5.2 Simplified geological map of Western Central Africa showing the different geological domains in this region. All these domains are numbered according to the legend. Some of them do not appear in the text because they are either younger than Precambrian or outside the considered region (e.g., the Tanzanian, North Angola and West-Nile blocks)

western and northern regions, may be traced from Angola to northern Cameroon (Fig. 5.2), and is classically designated as the Paleoproterozoic (Eburnean) belt of Western Central Africa (WCAB; Toteu et al. 1994; Feybesse et al. 1998). The other, in the eastern part of the studied region, covers a suite of individual belts straddling the southern and western margins of the Tanzania block: (1) the Usagaran belt (not considered in the present study); (2) the Ubendian belt, which occupies the northeast side of Lake Tanganyika in Tanzania, and extends toward the northwest in the DRC territory where it constitutes the poorly documented Ruzizi belt (Fig. 5.2); and (3) the Ruwenzori-Toro belt, which extends from Uganda to DRC in a broadly East–West direction (Fig. 5.2).

Also in the eastern part of the considered region, the Kibaran belt is the unique belt of Mesoproterozoic age in Central Africa west of the East-African Rfit. It shows a marked north-northeast structural trend, running along the eastern DRC border and covering most of Rwanda and Burundi.

Three Neoproterozoic belts are distinguished, all of which are part of the continental-scale Panafrican orogen. Two are situated at the edges of the cratonic domain aggregating the preceding blocks and belts (the so-called 'Congo Craton'): the Oubanguides belt, which separates Central Africa from a province of reworked basement covering Nigeria ('Nigerian province' of Castaing et al. 1994); and the Lufilian belt, which extends toward the southwest into the Damara belt and separates Central Africa from the cratonic domain of Southern Africa ('Kalahari craton' of Kampunzu and Cailteux 1999). In addition, a Neoproterozoic belt exists in the west: the W-Congo belt, generally considered to be an intracratonic belt resulting from the closure of a continental rift (Tack et al. 2001).

Basin domains of Western Central Africa are represented by an ensemble of sedimentary units resting unconformably over crystalline basement. These intracratonic basins are either of Paleoproterozoic or Neoproterozoic age, but none is of Mesoproterozoic age. More generally, the occurrences of Mesoproterozoic rocks outside the Kibaran belt are very limited in Western Central Africa, the most significant being a string of Mesoproterozoic ('Kibaran') granites evidenced in the southwestern part of CAR (Censier 1991) and considered as reflecting a post-Kibaran and pre-Panafrican extensional event (Vicat et al. 2001).

The Paleoproterozoic basins form a discontinuous suite of sedimentary groups extending from Gabon in the southwest to CAR in the northeast and including (Figs. 5.1 and 5.2): (1) the Francevillian basins (E-Gabon, *c*. 12–14°E to 2–0°S); (2) the Sembé-Ouesso basins (N-Congo, SE-Cameroon, *c*. 14–16°E to 0–4°S); (3) the Bangui and related basins (CAR, *c*. 19–22°E to 5–7°N); and (4) the Linki Bembé basin (DRC, *c*. 19–21°E to 4–5°S). These basins may be grouped into a single system classically considered as representing the foreland domain of the West Central African belt (e.g., Weber et al. 2016).

Three main basins of Neoproterozoic age are known which rest indifferently on Archean, Paleoproterozoic or Mesoproterozoic basement rocks. These intracratonic basins attest to the occurrence of extensional events outside the Panafrican belts. They include the Mbuji-Mayi basin in the south; the Itwombe syncline in the east; and the Lindian domain in the north (Fig. 5.2).

5.3.2 Archean Domains

The Archean domains in the studied zone include two main lithological units which are the typical constituents of many Archean terrains worldwide:

- a granito-gneissic association which mixes a variety of plutonic and metamorphic rocks including the so-called 'TTG-suite' (Tonalite-Trondhjemite-Granodiorite suite), but many other types of rocks such as potassic (pink) granites, charnockites or diorites;
- a supracrustal member, referred to as greenstone belt, which generally occurs as narrow and elongated units including metasedimentary rocks (schists, paragneisses, metaconglomerates), banded-iron formations (BIF) and basic to ultrabasic metavolcanites (metabasalts, amphibolites, chlorite-schists).

Depending on the quality of the geological and geochronological information available for a given region, more or less details may be brought on this general scheme. Major questions are as follows: What is the chronology of emplacement of the greenstone belts relative to that of the surrounding granitic rocks? How many events of magmatism, metamorphism and tectonism affected the granito-gneissic domains? And what is the precise timing of these events?

5.3.2.1 The NE-Congo Block

Among the three Archean blocks, NE-Congo is probably the less well known. The available geological and geochronological information (Lavreau 1982; Cahen et al. 1984) suggests the existence of a very ancient (*c*. 3.4 Ga) basement core (Bomu Complex) in its western part, overlain by a first generation of greenstone belts of Mesoarchean age (Fig. 5.1). To the east lies a vast and poorly known domain including a granitic and gneissic member and different greenstone belts, more abundant in its eastern than its western part (Fig. 5.1). Scarce and imprecise geochronological data (mainly by the Rb–Sr method on whole rock) suggests a Mesoarchean age for this whole basement, with a probable intrusion of granitoids within supracrustal units (Lavreau 1982; Cahen et al. 1984).

To the north of the NE-Congo block, extending over some 1000 km from CAR to Uganda, the huge West-Nile complex is even less well documented. Its age is generally considered as Neoarchean (Fig. 5.1) based on scarce geochronological data obtained in Uganda (Lavreau 1982).

5.3.2.2 The Ntem-Chaillu Block

On the western side of the studied region, the Ntem-Chaillu block is probably the best known owing to a recent mapping programme in Gabon (Thiéblemont 2009) and different field and geochronological works performed in Cameroon (see Table 5.1 for references). This information enables a precise scenario to be proposed for the geological evolution of this block (Thiéblemont et al. 2009).

Geological mapping at a 1:200,000 scale performed in Gabon allowed the granite-gneissic ensembles to be divided into two cartographical ensembles (Thiéblemont et al. 2009):

- A granitic basement including grey granitoids (mainly tonalite and granodiorite) intruded by pink granites (mainly monzogranite) ranging in size from metric injections to large and diffuse massifs. Over wide areas, this basement passes into granulitic domains characterized by a range of rock types (granulitic gneisses, charnockites, enderbites etc.) with a common high-temperature paragenesis, such as orthopyroxene, clinopyroxene and antipertithic feldspar.
- A migmatitic and granitic unit which includes a huge domain of migmatitic gneisses cut by well-delimited massifs of leucocratic granites.

Field studies enable a cartographical distinction to be drawn between the two main types of association (Fig. 5.1). The grey to pink granitic basement occurs as two domains, respectively, in the southern and northern parts of the Ntem-Chaillu block (Fig. 5.1). The migmatitic and granitic areas occur all around the two preceding domains covering about two-thirds of the surface of the Ntem-Chaillu block.

The geological mapping showed that the greenstone belts were located indifferently in the granitoid or migmatitic domains (Fig. 5.1), but that they were more intensively metamorphosed in the latter. In fact, the metamorphism in the greenstone belts (up to the high-grade amphibolite facies) and the surrounding migmatitic domains are of the same grade, which testifies to an emplacement of the greenstone belts before the migmatitic event.

Finally, a fourth cartographical unit was mapped in the western part of the Ntem-Chaillu block but not figured on the 1:10,000,000 scale because of its limited extension. It consists of a swarm of more or less linear hectometer- to kilometer-large intrusions of mafic and ultramafic rocks including orthopyroxenite cumulates, and less abundant olivine orthopyroxenites, norites and scarce harzburgites and dunites, crosscutting the granitic-gneissic basement.

Compilation of all the available geochronological data (Caen-Vachette et al. 1988 and other references in Thiéblemont et al. 2009) and more than 20 new high-precision datings (Thiéblemont 2009) indicated the following intervals for the emplacement of the different members of the granitic-gneissic basement and the cross-cutting mafic-ultramafic intrusions:

- *c*. 3.4–3.5 Ga (?) for the oldest phase of crustal accretion deduced from U–Pb ages obtained on granitic pebbles included in Paleoproterozoic conglomerates around the Archean domain and Nd-model ages in high-grade basic rocks (Mayaga-Mikolo 1996);
- *c*. 3.1–2.82 Ga for the emplacement of the grey granites;
- *c*. 2.88–2.81 Ga for the emplacement of the pink granites;
- 2.77 Ga for the mafic-ultramafic intrusions (Maier et al. 2015).

Dating of the BIF, granulitic and migmatitic events was not straightforward:

- Detrital zircons recovered from two quartzites and a conglomerate from the greenstone belt unit displayed U–Pb ages of 2868 ± 9 Ma, 2915 ± 12 Ma, 2918 ± 7 Ma, the youngest age of 2868 Ma therefore being considered as the maximum (oldest possible) age for sediment deposition.
- The U–Pb zircon ages obtained on the granulitic rocks ranged from *c*. 3020–2830 Ma (i.e., in the same range as those obtained on the granitoids from the non granulitic basement). However, a biotite pegmatite cutting a granulitic gneiss was dated to 2819 ± 22 Ma (U–Pb zircon), an age considered as the upper limit (youngest possible age) for the granulitic event.
- The age of the migmatitic event was determined by a leucocratic injection (leucosome) hosted in a banded gneiss. An U–Pb age of 2746 ± 7 Ma was obtained, clearly distinct from that deduced for the granulitic event, therefore indicating the occurrence of two distinct metamorphic events.
- Finally, a dyke of leucocratic granite cutting across the migmatites was dated to 2706 ± 7 Ma, an age consistent with others (*c*. 2.75–2.68 Ma) obtained from isolated massifs of post-orogenic leucocratic granites well represented in northern Gabon (Caen-Vachette et al. 1988; Mayaga-Mikolo 1996) and southern Cameroon (Shang et al. 2010).

The above results allow the proposal of the following scenario for the succession of magmatic, sedimentary and metamorphic events within the Ntem-Chaillu block (Thiéblemont et al. 2009, 2011a):

- *c*. 3.5 Ga (?) early stage of continental crust formation;
- *c*. 3.1–2.82 Ga emplacement of the grey granites (TTG type);
- *c*. 2.84–2.82 Ga granulitic event (first metamorphic event);
- *c*. 2.88–2.81 Ga emplacement of the pink granites;
- *c*. <2.87 Ga (2.8 Ga?) and >2.75 Ga deposition of the greenstone belts and intrusion of the mafic-ultramafic dykes;
- 2.75 Ga major tectonometamorphic event (second metamorphic event) involving recrystallization at high temperatures (migmatite formation), and deformation of the granitic-gneissic basement and the overlying greenstone belts;
- *c*. 2.7–2.6 Ga, intrusion of the post-orogenic potassic granites.

5.3.2.3 The Kasai Block

Though less well known, the Kasai block has been studied sufficiently to enable a comparison with the Ntem-Chaillu block. The geological map at a 1:10,000,000 scale features this block as the aggregation of granito-gneissic domains of different ages and metamorphic grades, with superposition of a volcanosedimentary group of Paleoproterozoic age (Fig. 5.1). The available geochronological data (Cahen et al.

1984; Delhal et al. 1986; Walraven and Rumvegeri 1993; Batumike et al. 2009) (Table 5.1) enables the following succession to be drawn (Deblond 2004):

- *c*. 3.4 Ga: Oldest age obtained on the gneissic basement represented by a restricted cartographical unit in the centre of the block (*c*. 22°E–7.5°S (Haute Luanyi Complex, unit indexed PApm in Fig. 5.1).
- *c*. 3.1–2.8 Ga: This range covers the ages obtained from the vast domain located in the southern part of the block (Sandoa granitic-gneissic Complex, unit indexed MApm in Fig. 5.1), showing an ensemble of granitoids and gneisses, sometimes with granulitic parageneses. The oldest ages (*c*. 3.1–2.86 Ga) were obtained on magmatic rocks (tonalites and granites), whereas a high-T metamorphic event (migmatites, granulites) is thought to have occurred around 2.8 Ga.
- *c*. 2.8 Ga: Age of the high-T metamorphic event recorded in a granulitic unit, often with charnockitic rocks (charnockites, charno-enderbites, enderbites), located in the central part of the block (Musefu Complex, indexed NAvsm in Fig. 5.1).
- *c*. 2.7–2.6 Ga: This range covers the ages obtained for migmatites (*c*. 2.7 Ga) and subsequent granitic intrusions (*c*. 2.6 Ga) within the gneissic and granitic domain covering the northern part of the block (Dibaya Complex, indexed MApm in Fig. 5.1).
- *c*. 2.4 Ga: Age of the high-temperature metamorphism within a gabbro-noritic unit located in the northwest part of the block (Lueta Complex, indexed PPpm in Fig. 5.1).
- *c*. 2.1–2 Ga: Deposition of a low-grade volcano-sedimentary unit located in the northwest part of the block (Lusanza Supergroup, indexed PP2svs in Fig. 5.1).
- *c*. 2 Ga: Emplacement of post-tectonic granites in the central and eastern parts of the block (indexed PP2p in Fig. 5.1).

As far as the Archean is considered, strong similarities may be noted between the Ntem-Chaillu and Kasai blocks:

- geological history starting in the Paleoarchean (*c*. 3.5–3.4 Ga);
- major accretion event between 3.1 and 2.8 Ga; Sandoa Complex in Kasai, granito-gneissic basement in the Ntem-Chaillu block;
- granulitic event around 2.8 Ga; Musefu granulitic Complex in Kasai and granulitic event (first metamorphic event) in the Ntem-Chaillu block;
- 2.7–2.6 Ga migmatization followed by granite intrusion; Dibaya Complex in Kasai and basement remobilization (second metamorphic event) and post-tectonic granite emplacement within the Ntem-Chaillu block.

5.3.3 Paleoproterozoic Domains

5.3.3.1 Paleoproterozoic Belts Around the Tanzania Craton

The Usagaran belt, which straddles the southeast edge of the Archean Tanzania Craton (Tanzania Block in Fig. 5.2), is not considered in the present study. Towards the south, this northeast-trending belt ends at the northern part of the Nyasa Lake, where it is orthogonally relayed by the Ubendian belt. The latter is well dated in Tanzania (Priem et al. 1979; Theunissen et al. 1992; Lenoir et al. 1994; Pinna et al. 2008; Boniface et al. 2012), where most of the ages obtained on magmatic rocks scatter between *c*. 2.05 and 1.75 Ga, indicating an Orosirian to Statherian age (Pinna et al. 2008; Fig. 5.1). It displays a pronounced northwest-oriented structural trend attributed to the predominance of strike-slip shear zones, at least in the final stages of structuration of the belt. Indeed, Neoproterozoic U–Pb zircon ages (*c*. 800–700 Ma) obtained from rocks associated with the shear zones suggest that this structuration could be related to the Panafrican orogenesis (Theunissen et al. 1992). Towards the northeast in DRC, the Ubendian belt passes into the poorly known Ruzizi belt. The Paleoproterozoic age of this belt is mainly supported by the fact that it displays a metamorphism of higher grade than that of the surrounding Mesoproterozoic rocks of the Kibaran belt, and that it relays the well-dated Ubendian terrains towards the northwest (Deblond 2004). Nevertheless, the distinction between Paleoproterozoic (Ruzizian) and Mesoproterozoic (Kibaran) terrains in eastern DRC is still very imprecise owing to the lack of recent mapping surveys (Fernandez-Alonso 2015b).

To the southwest the Ubendian belt is in contact with the Bangweulu block (Andersen and Unrug 1984), a triangular cartographical domain (Fig. 5.1) showing a plutonic suite covered by thick volcanosedimentary and sedimentary series. Abundant geochronological data (Cahen et al. 1984; De Waele et al. 2006; De Waele and Fitzsimons 2007) shows that most of the growth of the block occurred during Orosirian to Statherian times—that is, synchronously with that of the adjacent Ubendian belt (Lenoir et al. 1994). An Archean basement is postulated by De Waele et al. (2008) to exist below the Bangweulu block.

The occurrence of high-grade metamorphic rocks within the Ubendian-Usugarian belt has been taken as possibly indicative of an origin of the belt by a process of convergence (subduction/collision) involving the Tanzania craton to the north and another cratonic block to the south (Ring et al. 1997). Paleoproterozoic eclogites with MORB-type geochemical signature recovered at different places along the belt are considered as another piece of evidence for the formation of the Ubendian belt by modern-type mechanisms including oceanic subduction (Boniface et al. 2012).

On the northwest side of Lake Victoria, the Ruwenzori-Toro belt marks the boundary between two Archean domains: the SW-Uganda basement complex in the north (Cahen et al. 1984) and the Tanzania Craton in the south (Fig. 5.2). It includes metamorphic rocks dated between 2.21 and 2.15 Ga crosscut by 2–1.8 Ga-old granites (Abdelsalam et al. 2016). Recent structural and geochronological data (Link et al. 2010) indicates that the northern limit of the Ruwenzori-Toro belt consists of a west-southwest–east-northeast trending fold and thrust system involving slices of either Paleoproterozoic- or Archean-age thrusts to the north onto the Archean terrains.

The structural trend of the Ruwenzori-Toro belt, as well as its Rhyacian to Orosirian age, makes it different from the Ubendian belt, being, however, comparable to the Paleoproterozoic belt of Western Central Africa (see Sect. 5.3.3.2).

5.3.3.2 The Paleoproterozoic Belt and Foreland Basin of Western Central Africa

The Paleoproterozoic terrains of Western Central Africa, which form a discontinuous suite of cartographical ensembles running from the southwest edge to the central-northern part of Central Africa (Fig. 5.1), include an Eburnean orogenic belt (the Western Central African Belt) and a foreland domain (Feybesse et al. 1998; Vicat et al. 2001) (Figs. 5.1 and 5.2). The orogenic belt appears as a succession of metamorphic and plutonic rocks of Neoarchean to Rhyacian and Rhyacian age extending form W-Angola to CAR (Fig. 5.1). In Angola, DRC, Congo and Gabon the southern segment of the belt constitutes the basement of the Neoproterozoic W-Congo belt. It is known as the Kimezian Supergroup in Angola and DRC (Tack et al. 2001), and Mayombe basement in Congo and Gabon (Djama et al. 1992; Thiéblemont et al. 2009; Callec and Fullgraf 2015). Further north, in SW-Cameroon, the WCAB is represented by a high-grade metasedimentary and metaplutonic unit known as the Nyong Group (Toteu et al. 1994; Lerouge et al. 2006), which extends towards the north and northeast as a suite of cartographic ensembles intercalated within the Neoproterozoic Oubanguides belt owing to strike-slip shear zones of Panafrican age (Ngako et al. 2008). Further east, in CAR, the Eburnean terrains are represented by a series of epi- to mesozonal metasedimentary units (schists to micaschists) and less extensive metabasaltic rocks, superimposed on a Neoarchean basement and crosscut by *c*. 2 Ga-old granites and migmatites (Rolin 1995) (Fig. 5.1). As in Cameroon, the Paleoproterozoic terrains of RCA are located at the northern limit of the so-called 'Congo Craton' and are therefore strongly involved in the Panafrican Oubanguides belt. In CAR, the Paleoproterozoic (and Archean) terrains occur as tectonic windows underlying a huge system of southward-thrusted panafrican nappes made of Neoproterozoic rocks (Rolin 1995; Fig. 5.1).

The original WCA belt and its foreland basin are best preserved in central Gabon (Fig. 5.1). The deformed segment, known as the Ogooué orogenic domain (Feybesse et al. 1998), is constituted of a mesozonal metasedimentary and metavolcanic series thrust to the east over the Archean Ntem-Chaillu basement (Fig. 5.1). The foreland segment of this orogenic system lies in the eastern part of Gabon, as an ensemble of undeformed basins forming the Francevillian Group. A gradual transition is observed from the orogenic to the foreland domain, with the existence of an intermediate zone where the deformation attenuates (Thiéblemont 2009).

The whole architecture of the Gabonese Eburnean belt was recently reviewed by Thiéblemont et al. (2009) in the frame of the realization of the third edition of the geological map of Gabon (Thiéblemont 2009). About 45 high-quality geochronological datings were compiled (see Weber et al. 2016, table), enabling significant improvements in the model initially proposed by Feybesse et al. (1998). At least three major phases are distinguished, at *c*. 2.5 Ga, *c*. 2.15 Ga and *c*. 2 Ga. The first one corresponds to a high-grade metamorphic event recorded in the western and central part of the belt and affecting the Archean basement. This event is attributed by Weber et al. (2016) to the initial extensional event precursor to the opening of the Ogooué basin. This basin existed for *c*. 300 Ma, from about 2.45 to 2.15 Ga. Around 2.12 Ga it was affected by a major phase of deformation and metamorphism under relatively high-P conditions (Feybesse et al. 1998). Basins did not close after this major event, and sedimentation started again around *c*. 2.1 Ga. The final closure of the Eburnean domain occurred around 2 Ga with the eastward thrusting of the Ogooué domain, and intense plutonism and exhumation in a western block now surrounded by the Cretaceous series for the coastal basin (Fig. 5.1).

In the foreland domain, opening of the Francevillian basins could have occurred as early as 2.45 Ga, with a deposit of about 1 km of quartzitic sandstones and conglomerates (FA unit; Weber et al. 2016). Further rift-related pelitic to quartzo-pelitic sedimentation (FB unit) and associated alkaline volcanism could have occurred between 2.12 and 2.04 Ga. After a break marked by a jasper and stromatolite-rich horizon (FC unit), sedimentation and volcanism could have restarted with deposition of a volcanosedimentary series (FD unit) including a felsic calcalkaline member (Thiéblemont et al. 2014). Renewed coarse-grained detrital sedimentation (FE unit) at the top of the basin (i.e., $\sim$2 Ga) could have resulted from the erosion of the newly formed reliefs in the adjacent orogenic domain.

5.3.4 Mesoproterozoic Domain: The Kibara Belt

The north-northeast-trending Kibara belt extends over a distance of *c*. 1500 km from the Katanga province, in southern DRC, to SW-Uganda, crossing the entire DRC territory and covering most of Burundi and Rwanda (Fig. 5.2). In Burundi it lies on an Archean or Paleoproterozoic basement (Villeneuve and Chorowicz 2004) and, in its southern part, it is unconformably covered by Neoproterozoic rocks of the Mbuji-Mayi and Lufilian terrains (Cahen et al. 1984; Fig. 5.1).

The sedimentary terrains of the Kibara belt (Kibara Supergroup) are divided into four groups with a total thickness of at least 10,000 m, and maybe up to 20,000 m (Cahen et al. 1984). In the Kibara-type region of SE-DRC (Kokonyangi et al. 2006) a hiatus is observed within the lithostratigraphical succession, at the top of the basal group. This is marked by an erosional unconformity, deposition of a conglomerate and slight decrease in the degree of metamorphism. Deformation in the lower group was accompanied by the emplacement of felsic volcanism (Cahen et al. 1984). Metabasic rocks (amphibolites, greenstones) are also reported in some places in the basal section of the lower group. However, basaltic volcanism is rather rare in the Kibara Supergoup, and no mafic complex is reported which could be interpreted as the remnant of an old oceanic crust (i.e., ophiolite; Tack et al. 2010).

Towards the north, in Kivu and Burundi, the lithostratigraphical organization of the Mesoproterozoic succession (here referred to as the Burundian Supergroup) is closely comparable to that observed in SE-DRC. In particular, an unconformity is documented at the top of a basal group (Villeneuve and Chorowicz 2004), this latter displaying characteristics very similar to those of the lower group of the Kibara region (Cahen et al. 1984). This organization of the Kibaran into two units separated by an unconformity is confirmed by the presence of zircons inherited from the lower unit, within the upper one (Villeneuve and Chorowicz 2004; Kokonyangi et al. 2006). Such occurrences clearly indicate that the lower unit was likely to be eroded, and therefore partly erected, before deposition of the remaining Kibara succession.

The age of the Kibara succession is mainly constrained by the ages obtained from the granites crosscutting it (Cahen et al. 1984). These ages indicate a total time interval of about 450 MA, between *c*. 1.4 and 0.95 Ga. Four groups of intrusions were classically defined: the first two leucocratic, often deformed, and considered as synorogenic, and the younger two more or less leucocratic and post-orogenic (Cahen et al. 1984). Recent work based on precise geochronological data points to the existence of a major episode of bimodal magmatism around *c*. 1.4–1.35 Ga (Tack et al. 2010), followed by two periods of granitic intrusions, one around 1.2 Ga and the other at the Mesoproterozoic-Neoproterozoic boundary (*c*. 1–0.95 Ga). Post-tectonic tin-bearing granites were emplaced during this last phase.

Prominent structures in the Kibara belt include north-northeast- to northeast-trending westward verging folds and thrusts which were developed under moderate pressure, moderate temperature metamorphic conditions (Cahen et al. 1984; Kokonyangi et al. 2006). They were probably related to a second tectonic phase which followed a first one characterized by a northward thrusting of Kibaran terrains over a pre-existing basement (Theunissen and Klerkx 1980; Rumvegeri 1991). The age of the first phase is estimated at *c*. 1380 Ma constrained by the ages obtained on syntectonic granites, whereas the second phase could have taken place around 1080 Ma (Kokonyangi et al. 2006) and clearly occurred before the emplacement of the tin-bearing granites (*c*. 1000–950 Ma).

Geodynamic models for the formation of the Kibara belt is still a matter of debate with two main conceptions being proposed:

- A subduction/collision model (Rumvegeri 1991; Kokonyangi et al. 2006; Debruyne et al. 2015), involving the eastward subduction of an oceanic slab during the first phase, with an almost total consumption of the oceanic rocks.
- An intracontinental deformation model, initially considered by Cahen et al. (1984) and more recently by Tack et al. (2010). According to these authors the 'Kibaran event' around 1375 Ma could have been a phase of intense bimodal magmatism associated with an extensional process in an intracratonic setting. Later, closure of the system could have resulted from limited compression induced by movements of a distant plate.

5.3.5 Neoproterozoic Domains

Six Neoproterozoic domains are distinguished in the studied region (Fig. 5.2). Three are orogenic belts (Oubanguides belt, W-Congo belt, Lufilian Belt), whereas the others correspond to intracratonic basins (Mbuji-Mayi domain, Itwombe syncline, Lindian domain).

5.3.5.1 The Oubanguides Belt

On the northwest side of the studied region, the Oubanguides belt (also 'Oubanguides') covers large regions of Cameroon and CAR (Figs. 5.1 and 5.2), and it runs to the northeast of DRC, where scarce available ages obtained in

the W-Nile block attest for important structuration during the Neoproterozoic (Cahen et al. 1984).

The Oubanguides is a major Panafrican collisional belt (Poidevin 1985) interpreted as the result of the collision between two cratonic blocks—namely, the East-Saharan craton in the north and the so-called Congo Craton in the south (Ngako et al. 2008). This collision has resulted in continental-scale thrusts with a north–south emplacement of crustal nappes (Poidevin 1985; Fig. 5.1). These thrusts and nappes are clearly shown on the geological maps of CAR (Rolin 1995) and South-Cameroon (Maurizot 1986); they brought Neoproterozoic metamorphic terrains onto Archean to Paleoproterozoic basements (Fig. 5.1).

Intense granitization (Fig. 5.1) covering a large interval of time is another striking aspect of the Oubanguides. The geological map of Cameroun at a 1:1,000,000 scale compiled at the end of the 70th (Anonymous 1979) distinguished between different generations of intrusion:

- early calcalkaline and frequently orthogneissified granitoids;
- anatectic granites;
- syntectonic monzonitic granites;
- post-tectonic alkaline granites and microgranites;
- last-stage syenitic and gabbroic intrusions.

Around these granites, large high-grade metamorphic domains were also distinguished, often in migmatitic conditions, and with common granulitic parageneses.

These high-grade metamorphic rocks were classically considered to be the members of a 'basal (or basement) complex' of supposed Archean age, but U–Pb and Sm–Nd data on granulites from CAR clearly demonstrated that the high-grade metamorphic event was related to the Neoproterozoic (Panafrican) continental collision (Pin and Poidevin 1987). Likewise, Toteu et al. (1987) obtained a U–Pb zircon age of 630 Ma (emplacement age) in plutonic rocks ascribed to the basement complex in Cameroon. Nevertheless, the work of Pin and Poidevin (1987) and Toteu et al. (1987), as well as further investigations (Toteu et al. 1994; Feybesse et al. 1998; Lerouge et al. 2006), attest to an important reworking of old terrains within the Panafrican belt, and some gneisses of the 'basal complex' are in fact remnants of the Paleoproterozoic Western Central African belt. Indeed, the map of Oubanguides in Cameroon distinguishes a suite of elongated slices of Paleoproterozoic rocks adjacent to metasedimentary or plutonic terrains of Neoproterozoic age (Fig. 5.1).

Recent studies (Tchakounté et al. 2007; Ganwa et al. 2008a, b) have also documented the presence of detrital zircons of Archean to Mesoproterozoic age within the Neoproterozoic metasedimentary formations, and Paleoproterozoic and Mesoproterozoic magmatic inheritance was documented in Panafrican granites from SW-Cameroon, indicating that such granites were partly derived from the melting of old crustal basements (Mosoh Bambi et al. 2013).

Finally, Nd model ages obtained from a range of Panafrican granitoids, metasediments and gneisses are mostly Paleo- and Mesoproterozoic (Toteu et al. 1994, 2001, 2006b; Tchakounté et al. 2007; Djouka-Fonkwe et al. 2008; Ganwa et al. 2008b), suggesting that most of the crustal accretion within the Oubanguides occurred after the Archean and with only limited inputs from Archean materials.

The geological map of Africa at 1:1,000,000 conforms to the present state of knowledge, including the geochronological results summarized before, in distinguishing four major lithostratigraphic ensembles within the Oubanguides (Fig. 5.1):

- the Paleoproterozoic domains which were initially parts of the Eburnean belt of Western Central Africa;
- the Neoproterozoic metamorphic units (*c*. 1000–700 Ma);
- the pre- to syntectonic orthogneisses (*c*. 660–600 Ma);
- the syn- to poast-tectonic granites (*c*. 600–500 Ma).

Note that no Mesoproterozoic domain is distinguished around the Oubanguides which could explain the occurrence 1.6 Ga-old detrital zircons within some Neoproterozoic metasediments. According to Tchakounté et al. (2007), such zircons could have derived from a continental domain located to the north, a region which is still poorly known.

5.3.5.2 The W-Congo Belt

The W-Congo belt is a rather narrow domain (100–200 km wide) with a length of about 1000 km, running along the Atlantic coast and forming the eastern 'wall' of the Cretaceous to recent coastal basins of Gabon, Congo, DRC and Angola. In fact, despite being older than 500 Ma, the W-Congo belt still stands as a marked relief which north-northeast-orientation conforms to the original structural trend of the belt. This high domain, designated as the Mayombe massif, is generally less than 100 km and is followed to the east by a low and flat domain, known as the Niari-Nyanga basin in Gabon and Congo, where it is limited to the northeast by basement rocks of the Ntem-Chaillu block (Fig. 5.1). This morphological distinction also reflects a geological division between an internal domain (Mayombe) and an external foreland basin (Niari-Nyanga basin), the former being composed of highly deformed crystalline and metamorphic rocks, and the latter of a slightly deformed sedimentary series. Just north of 5°S the external limit of the basin suddenly suffers a 180° inflection, becoming southwest (Fig. 5.1). This change results from a huge network of

strike-slip faults perpendicular to the main direction of the belt. This enables the distinction of a new basin, the Comba basin, whose sedimentary sequence is similar to that observed elsewhere in the foreland domain (Alvarez and Maurin 1991).

At the northern limit of the W-Congo belt, in the Gabonese territory, the Neoproterozoic rocks of the external domain are surrounded by the Paleoproterozoic basement and rest unconformably on it (Fig. 5.1). Cartographical mapping in this region shows that this termination in fact corresponds to the limit of the initial sedimentary basin, the northwest-prograding sedimentary series overlapping here the Eburnean basement (Thiéblemont 2009).

Three major lithostratigraphical ensembles are recognized within the W-Congo belt:

- A mainly Paleoproterozoic basement (Fig. 5.1), well represented in the internal domain of the belt (Mayombe massif). In this chapter, this ensemble is attributed to the Western Central Africa Belt because it passes to the north to Eburnean terrains related to this belt forming the basement of the sediments of the external Nyanga basin.
- A metamorphic and strongly deformed ensemble, restricted to the internal domain, which includes the oldest units (the 'deepest' ones) of the Neoproterozoic succession, including a huge acid and basic magmatic complex in the central part of the belt (Congo and DRC territories).
- A more or less folded but non(or slightly)-metamorphic ensemble which correspond to the late sedimentary series of the foreland domain.

The Neoproterozoic rocks of the W-Congo belt are collectively grouped into a W-Congo Supergroup (Tack et al. 2001), for which no homogeneous lithostratigraphic scheme is yet available. This is especially true for the terrains of the internal domain, which display important differences along the belt and are generally less developed in Gabon, probably because they are here located at the northwest termination of the belt.

In Congo and DRC the lower part of the W-Congo Supergroup starts with a basal felsic member dated around *c*. 1 Ga (Mesoproterozoic-Neoproterozoic boundary), represented by different granitic massifs: Noqui granite (999 ± 7 Ma; Tack et al. 2001), Mfoubou granite (1050 ± 25 Ma; Djama et al. 1992) and Mont-Kanda granite (930 ± 8 Ma; Callec and Fullgraf 2015). This basal member is overlain by a series of clastic sediments passing to a thick (*c*. 1600–2400 m) basaltic unit. This huge volcanic formation was emplaced at *c*. 920 Ma in DRC (Tack et al. 2001) and is precisely dated at 915 ± 8 Ma in Congo (Callec and Fullgraf 2015). An ophiolitic nature was attributed to this complex (Vellutini et al. 1983), which conflicts with the within-plate and continental rift-affinity well documented by Tack et al. (2001) in DRC. This lower acid and basic unit is unknown in Gabon (Thiéblemont 2009).

In DRC the basal magmatic unit is overlain by a thick (*c*. 3000–4000 m) ensemble of volcanoclastic, volcanosedimentary and felsic metavolcanic rocks. U–Pb zircon ages obtained in rhyolites from the lower (920 ± 3 Ma) and upper (912 ± 3 Ma) parts of the succession indicate emplacement in an interval of *c*. 920–910 Ma (Tack et al. 2001). Slightly younger ages were obtained in Gabon for a gabbro (904 ± 6 Ma) and an alkaline granite (876 ± 4 Ma; Thiéblemont 2009; Thiéblemont et al. 2009), which correlate with ages of 912 ± 7 Ma and 898 ± 28 Ma obtained in a huge volcanosedimentary and volcanic unit forming a significant part of the series of the Mayombe massif in Congo (Callec and Fullgraf 2015).

The upper section of the W-Congo Supergroup, referred to as the Cataractes Group in DRC (Fernandez-Alonso et al. 2015a, b), includes the following units (Tack et al. 2001):

- A thick metabasaltic unit (1650 m).
- A lower glaciogenic unit ('Lower Diamictite') with an estimated thickness of 400 m and postulated Sturtian age (*c*. 740 Ma).
- A *c*. 1000 m-thick volcanosedimentary unit ('Haut Shiloango'). A probably correlative tuffaceous rock sampled in Gabon was imprecisely dated at 713 ± 49 Ma (Thiéblemont et al. 2009), being consistent with the supposed Cryogenian age of the W-Congolian glaciogenic formations. The value of the $^{87}Sr/^{86}Sr$ ratio (=0.7068) obtained in carbonates from this unit led Poidevin (2007) to give these rocks a post-Sturtian age.
- A second glaciogenic unit ('Upper Diamictite'), with an estimated thickness of 150 m and supposed Marinoan age (*c*. 650 Ma).
- A carbonate ensemble (Schisto-calcaire Subgroup) (*c*. 1100 m) with a $^{87}Sr/^{86}Sr$ ratio (=0.7075) indicating a post-Marinoan age (Poidevin 2007).
- A detrital clay to sandy (±conglomeratic) ensemble (Mpioka Subgroup) (*c*. 1000 m).

The interval extending from the Upper Diamictite to the Mpioka Subgroup constitutes the typical section present in the foreland domain, showing strong similarities in Gabon, Congo and DRC. On the eastern side of this external basin, the rocks overlay the crystalline basement of the Ntem-Chaillu block, and the upper Diamictite has a typical fluviatile to shoreline facies (Thiéblemont et al. 2009) (Fig. 5.1). The age of this sedimentary contact becomes younger from southeast to northwest, thus suggesting that

the external basin opened in the same sense (Thiéblemont et al. 2009). Likewise, the thickness of the upper units (Schisto-calcaire and Mpioka Subgroup) is no more than a fifth of the width at this northwest end (Gabon, Thiéblemont et al. 2009) compared with the central part of the basin (DRC).

Structurally the W-Congo belt is a typical fold-and-thrust belt with a marked verging towards the northeast (Boudzoumou and Trompette 1988; Tack et al. 2001; Callec and Fullgraf 2015). The intensity of metamorphism and deformation increases from the external to the internal domain, where mesozonal conditions (biotite-garnet paragenesis) are reached (Thiéblemont et al. 2009; Callec and Fullgraf 2015). This metamorphism is considered by Tack et al. (2001) to have ended before *c*. 566 Ma based on Ar–Ar ages obtained from greenschist facies rocks sampled in DRC (Frimmel et al. 2006.). On the other hand, illite K–Ar ages obtained from argilites of the Mpioka unit in Congo reveal mainly late Neoproterozoic ages, and detritic zircons in coarse detrital rocks are as young as 565 ± 37 Ma, this age being considered to be the maximum deposition age (Callec and Fullgraf 2015). This indicates deposition of the Mpioka unit in the course of the Mayombe surrection, in a context of foreland molassic basin (Tack et al. 2001; Callec and Fullgraf 2015).

From a geodynamic point of view, the 'ophiolitic' hypothesis of Vellutini et al. (1983), which interpreted the W-Congo as a subduction-collision belt, is no longer supported. A model most consistent with the recent data considers the W-Congo domain as a former intracontinental rift developed at the western edge of the Congo craton and which was affected only to a limited extent in the collisional processes involved in the Panafrican orogeny (Tack et al. 2001).

5.3.5.3 The Lufilian Belt

The Lufilian belt is located in the southern part of the studied region, overlapping DRC and Zambian. It includes the Copperbelt province, one of the major mining regions of Central Africa. To the south, the Lufilian belt appears as an arcuate domain (Lufilian arc), which extends for about 500 km from the Irumide belt in the east to the Kibara Belt and Kasai block in the west. To the north of this domain the Lufilian belt is represented by a triangular domain, the Kundelungu foreland, limited by the Bangweulu block on its eastern side and by the Kabara belt on its western side.

The Lufilian belt exposes a volcanosedimentary series of Neoproterozoic age known as the Katanga Supergroup. Its thickness is estimated as 5–10 km (e.g., Fernandez-Alonso et al. 2015b). These rocks are strongly deformed in the southern part of the belt, whose arcuate shape reflects the inflection of the structural trend from a northwest direction in the east to a northeast direction in the west. In the southern part of the arc, mainly in the Zambian territory, the sedimentary sequences are punctuated by a succession of domes of metamorphic and plutonic rocks in a direction more or less consistent with the general structural trend of the arc. Abundant U–Pb SHRIMP zircon ages obtained by Rainaud et al. (2005a, b) indicate a constant Paleoproterozoic age (*c*. 2.05–1.85 Ga) for these basement rocks, clearly distinct from the Neoproterozoic age of the overlying Katanga Supergroup. The widespread 'arc-signature' of these rocks led Rainaud et al. (2005a, b) to interpret the whole Lufilian basement as part of a regionally extensive Paleoproterozoic magmatic arc stretching from northern Namibia to northern Zambia and the DRC, which collided with the Archaean Tanzanian craton during the *c*. 2.0–1.9 Ga Ubendian orogeny.

Thanks to an IPGC working group, a unified lithostratigraphic chart is now available for the Katanga Supergroup. Three groups are distinguished from the bottom to the top: the Roan, Nguba and Kundelungu groups (Fernandez-Alonso et al. 2015a, b and references therein). The Roan Group hosts the main Cu stratiform mineralizations of the Copperbelt (Kampunzu and Cailteux 1999). It displays a succession of alternating siliciclastic, carbonatic (mainly dolomitic) and pyroclastic rocks. Hematitic facies and cherts are restricted to the uppermost part of the sequence. The Nguba Group displays a basal glaciogenic unit known as the 'Grand Conglomérat', covered by a cap carbonate hosting the main Zn–Pb–(Cu) mineralizations of DRC. These units are parts of a lower subgroup mixing carbonatic and siliciclastic rocks, and passing upwards to an upper subgroup dominated by siliciclastic rocks. The upper Kundelungu Group exposes a basal glaciogenic and cap-carbonate succession covered by a siliciclastic (argilite, siltstone, sandstone) unit passing upwards to a coarse-grained ensemble mixing conglomerates, arkoses and sandstones, these latter showing in places a red sandstone facies.

Three structural zones are distinguished by Unrug (1989) within the Lufilian belt: (1) an outer zone, which corresponds to the Kundelungu plateau of triangular shape forming the northern part of the belt; (2) an internal zone, the most southern, which covers Paleoproterozoic basement inliers; and (3) an intermediate zone, located between the two preceding zones.

The intermediate zone exposes the most complete succession, referred to as the Katanga Supergroup, and likely to have been deposited above a pre-Katangan (Paleoproterozoic) basement (Porada and Berhorst 2000; De Waele et al. 2008). Metamorphism in this zone is of low grade (greenschist facies or lesser) and deformation consists of north-verging folds and thrusts.

A higher grade of metamorphism is recorded in the internal zone (upper greenschist to amphibolite facies), and several nappes juxtapose Neoproterozoic metasediments and

basement-related migmatitic gneisses (Eglinger et al. 2016). The domes of Paleoproterozoic basement rocks present in this internal zone are low-amplitude structures but display a large cartographical extension.

The external zone is often considered to be a foreland basin with a large predominance of the upper part of the Katanga Supergroup (Kundelungu Group), which is supposed to be contemporaneous with deformation of the internal and intermediate domains.

On the scale of the African continent, the Lufilian arc is considered to be part of a huge Panafrican belt covering the Damara belt in its western part and is supposed to have resulted from the collision between the Kalahari craton to the south and the Congo craton to the north (Kampunzu and Cailteux 1999; Batumike et al. 2009).

The nature of the basins at the beginning of the orogenic cycle is still a matter of debate, but there is no indication that an oceanic domain could have existed within the Katanga belt. According to Unrug (1989), initial rifting could have proceeded in three directions, two corresponding to the northeast and northwest arms of the Lufilian arc and the third to the Kudelungu foreland, considered to be an aulacogen.

The main period of deformation was supposed by Cahen et al. (1984) to have occurred between 656 and 503 Ma, but further geochronological data has led to significantly enlarge this interval. According to Kampunzu and Cailteux (1999), following the rifting and deposition of the Katanga Supergroup in the internal and intermediate zones (*c*. 1000–800 Ma), the building of the Lufilian arc could have resulted from three major phases covering a period of more 300 Ma: (1) a D1 phase (*c*. 800–710 Ma), which resulted in north-verging folds and thrusts, followed by south-directed back thrusts of local extension; (2) a D2 phase (*c*. 690–540 Ma), which resulted in strike-slip structures and clockwise rotation of the Lufilian arc, giving the belt its present convex shape; and (3) a D3 phase of Paleozoic age (i.e., <540 Ma) marked by transverse structures and deposition of the upper part of the Kundelungu Group in a foreland position.

More recent work (John et al. 2004; Eglinger et al. 2016) casts a rather different light on the tectonic evolution of the Lufilian arc. These new perspectives result mainly from the geothermobarometric estimations and geochronological data obtained from metasedimentary formations straddling the contact between the Katanga series and axial basement domes. A high-pressure, high-temperature event ($P \sim 13$ kb for $T \sim 750$ °C) of Cambrian age (*c*. 530 Ma) was determined for kyanite-talc micaschists, indicating a tectonic burial of the internal part of the belt at depths of 40–50 km. Such results suggested the possible occurrence of continental collision at a rather late stage in the evolution of the Lufilian belt.

5.3.5.4 Intracratonic Domains: Lindian, Itwombe and Mbuji-Mayi

These three intracratonic domains (Figs. 5.1 and 5.2) are mainly represented in DRC. The Lindian domain is located at the northern border of the Bassin central and separates it from the Archean to Paleoproterozoic basement. An extension of the Lindian domain occurs in CAR beyond the southern limits of the Panafrican nappes (Fig. 5.1). The Itwombe synclinorium, oriented north–south, forms a narrow zone with a length of 160 km at the northwest border of Lake Tanganyika. The Mbuji-Mayi domain, localized in the southeast part of DRC, is mainly composed of two rather long northwest-directed strips of sedimentary rocks, one being in contact with the Kasai block and the other with the Kibara belt. To the north, the Mbuji-Mayi succession is covered by the Mesozoic sedimentary sequences of the Congo Basin (Cuvette centrale).

The Lindian domain (or Lindian Supergroup) has been mapped at a 1:500,000 scale by Verbeek (1970), work which served as a reference for the compilations of the DRC at a 1:2,000,000 scale (Lepersonne 1974) and a 1:2,500,000 scale (Fernandez-Alonso et al. 2015a, b).

Three groups separated by discontinuities are distinguished within the Lindian Supergroup, totalling a thickness of *c*. 2500 m. The lower (Ituri) group lies unconformably on the pre-Neoproterozoic basement. It shows a 200 m-thick succession of siliciclastic to carbonated sediments of marine origin. A low Sr-isotopic ratio (0.7066) in the carbonate rocks led Poidevin (2007) to consider them as pre-Sturtian.

The intermediate (Lokoma) group starts with a lenticular glaciogenic unit (tillite), followed by a siliciclastic (sandstone, conglomerate, arkose, shale) ensemble alternating with carbonates (limestones, dolostones) in its lower part. The total thickness is estimated at 500–900 m. From Sr-isotope stratigraphy and lithostratigraphic considerations, Poidevin (2007) considered the glaciogenic unit as a witness of the Sturtian ice age. The overlying sedimentary sequence shows important lateral and vertical facies variations, with alternating periods of continental or marine sedimentation. Carbonates, which occur as lenticular bodies intercalated with shales, in the lower part of the series, display considerable variation in thickness, from some decimeters to more than 100 m.

The upper (Aruwimi) group includes a lower sliciclastic unit of continental origin with conglomeratic horizons attesting for the sedimentary reworking of the lower part of the Lindian Supergroup. Above lies a thick (*c*. 400 m) ensemble of carbonated shales supposed to have accumulated in a context of alluvial plain (Deblond 2004). Within this ensemble, dark limestone horizons might record a lagoon environment. Indeed, very high Sr-isotopic (0.71222–0.71325) measured in these rocks led Poidevin (2007) to preclude a marine origin.

Above the shales of the Aruwimi Group stands a very thick (up to 1200 m) sliciclastic unit (Banalia formation) with a typical 'red beds' facies. This ensemble, considered to be Paleozoic (Kadima et al. 2011), is interpreted by Poidevin (2007) as a late-Panafrican molasse.

The Itwombe domain is interpreted as a basin graben filled with mainly detrital sediments: shales, quartzites and conglomerates, subordinate glaciogenic deposits and scarce carbonates, resting unconformably on Ruzizian (Paleoproterozoic) and Kibaran (Mesoproterozoic) basements (Fig. 5.1; Villeneuve 1973; Deblond 2004). The term 'syncline' is used for this domain because the Itwombe rocks are affected by folding associated with a low-grade metamorphism (occurrence of sericite and locally biotite).

The sedimentary sequence is divided into two groups, each of them reaching 1000–2000 m in thickness (Villeneuve 1973). The lower group includes a basal conglomerate, passing upwards to a succession of alternating sansdstones, conglomerates and shales. The upper group includes a basal diamictite (tillite) covered by siltstones and black shales. The existence of a tectonic contact separating the two groups has been postulated by Walemba (2001).

The Itwombe graben is coincident with first-order tectonic structures existing in the Paleo- and Mesoproterozoic basement. Reactivation of these structures under extensional conditions promoted graben formation and sediment deposition. Later, a compressional event induced north-trending and west-verging isoclinal folds (Villeneuve 1977) and recrystallization under epizonal conditions.

In SE-DRC the Mbuji-Mayi Supergroup is considered to be an equivalent of the Roan Group, the lower unit of the Katanga Supergroupse. Three units are distinguished from bottom to top: B0, B1 and B2.

The B0 Group presents an estimated thickness of 1000–2000 m and is composed of arkoses, quartzites, red shales and conglomerates. It is not represented in Kasaï, being only present at the southern end of the Katanga Supergroup, along the Kibara belt. It might be older than the Roan Group.

The B1 Group presents an estimated thickness of *c*. 1000 m and comprises units of varied lithologies: calc-schists to conglomerates with boulders of basement in the lower part, white quartzites and shales in the intermediate section, and shales and calc-schists in the upper part.

The B2 Group presents an estimated thickness of 800–1000 m and is composed of carbonates, including limestones (sometimes silicified, oolitic or stromatolitic) and dolomites.

Together with sedimentary rocks, the Mbuji-Mayi Supergroup exposes basaltic pillow lavas, whose relationship with the sedimentary sequence is not fully understood. Ages obtained from different flows give a consistent result at 950 ± 20 Ma (Cahen 1982), suggesting a single volcanic event. Abundant dolerites cutting across the sedimentary sequence are considered to be dykes feeding the eruptive unit (Fernandez-Alonso et al. 2015a, b).

5.4 Geological and Isotopic Differentiation of Western Central Africa

The construction of the Precambrian basement of western Central Africa spent around 3 Ga (from *c*. 3.5 to 0.5 Ga) and covered all the geological periods from the Paleoarchean to the Precambrian–Cambrian boundary. The simplified sketch map in Fig. 5.3 summarizes this history by showing which regions were stabilized at a given period, leaving a blank in the central part of the craton, whose basement is hidden under the Mesozoic to recent sedimentary series of the Bassin central of DRC.

According to De Wit and Linol (2015), this basement might be composed of three different Archean cratons: (1) the SouthWest Congo Craton, including the Ntem-Chaillu, Cuango (Archean terrains in North Angola) and Kasai blocks; (2) the almost entirely hidden Central Congo Craton; and (3) the NorthWest Congo Craton, covering the NW-Congo block. Between these cratons, two broadly north-northwest-directed Neoproterozoic belts attest to the amalgamation of the whole continental region during the Panafrican orogeny.

One of these belts would run from the Mbuji-Mayi (or Bushimay) domain (southeast) to the Sembé-Ouesso basin (northwest). Such a hypothesis is in fact not consistent with the arguments put forward by different authors (Vicat and Vellutini 1987; Vicat et al. 2001; Poidevin and Pin 1986) and adopted in the present study (Fig. 5.1) that the Sembé-Ouesso formations correlate with those of the well-dated Paleoproterozoic Franceville Supergroup. Moreover, as summarized above, the Mbuji-Mayi domain is not an orogenic belt but an undeformed sedimentary sequence resting unconformably on the Kasai block in the southwest and the Ubendian belt in the northeast (Fig. 5.2).

The other Panafrican belt would be more or less coincident with the Lindian domain, making this intracratonic basin (see Sect. 5.3.5.4) a suture zone of continental scale. Again, the hypothesis of De Wit and Linol (2015) is not easily supported by geological evidence.

A strongly different view is proposed by De Waele et al. (2008) and Fernandez-Alonso et al. (2011), who consider that the whole of Central Africa was stabilized at *c*. 1 Ga, forming a single 'proto-Congo Craton' extending from the Saõ Francisco craton in the west to the Tanzania craton in the east.

As far as the process of crustal growth is concerned, a useful tool for distinguishing between reworked and juvenile continental crust in a given orogen is provided by the Nd-isotopes (e.g., Abouchami et al. 1990; Boher et al. 1992).

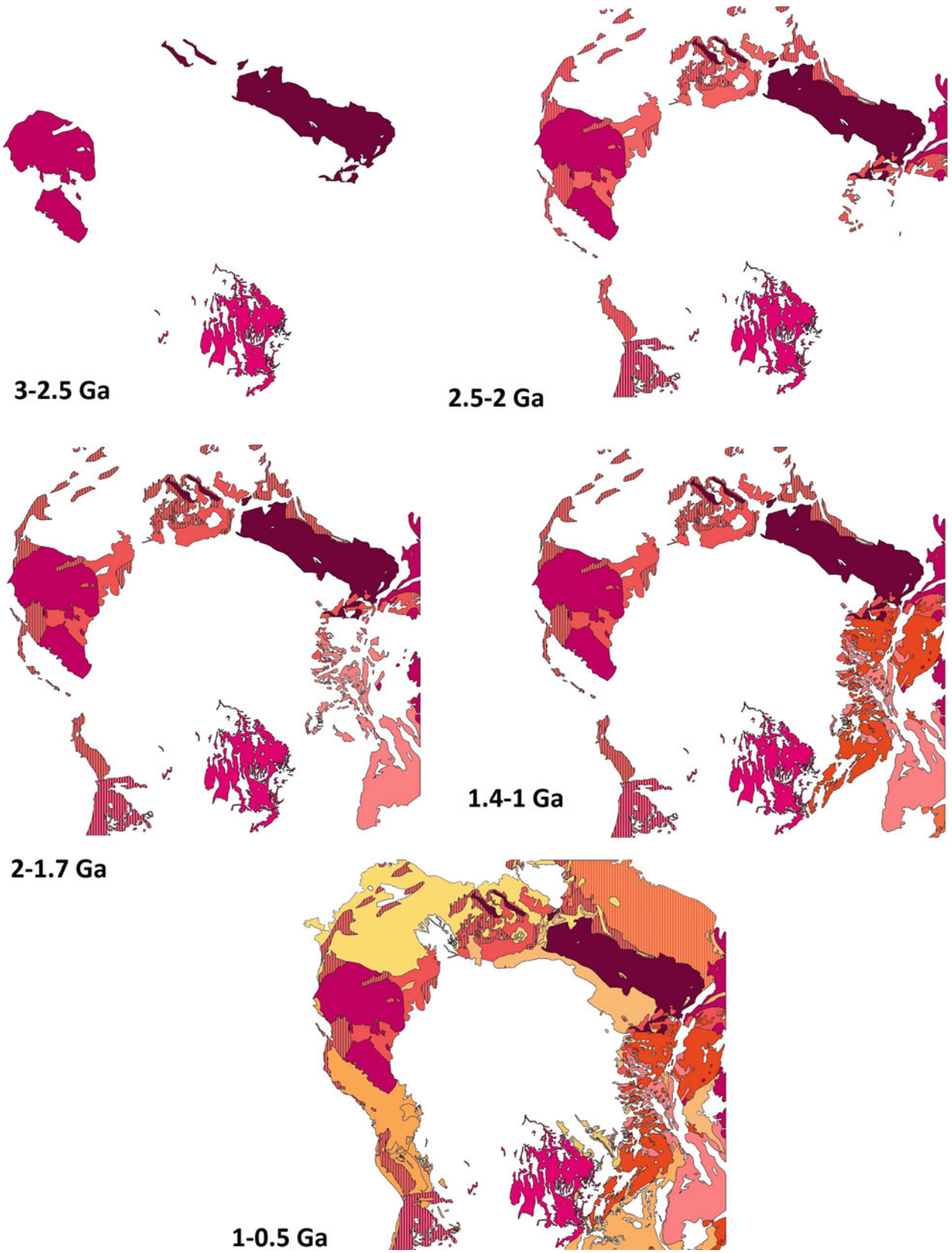

Fig. 5.3 Sketch map summarizing the geological construction of Western Central Africa during the Precambrian

Table 5.2 Summary of the references of the Nd-isotopic data used to draw the isotopic framework of Western Central Africa (Figs. 5.4 and 5.5) and their corresponding domains (Fig. 5.1)

References	Domains
Affaton et al. (2016)	West Congo belt (Congo)
Bros (1993)	Central African Paleoproterozoic basins (Gabon)
Buchwaldt et al. (2008)	Kibaran belt (Uganda)
Debruyne et al. (2015)	Kibaran belt (Burundi)
Delhal et al. (1986)	Kasaï block
Djama et al. (1992)	West Congo belt (Congo)
	West Central African belt (Congo)
Djouka-Fonkwe et al. (2008)	Oubanguides belt (Cameroon)
Frimmel et al. (2006)	West Congo belt (Congo)
Ganwa et al. (2008a, b)	West Central African belt (Cameroon)
Mayaga-Mikolo (1996)	West Central African belt (Gabon)
	Ntem-Chaillu block (Gabon)
Pin and Poidevin (1987)	Oubanguides belt (CAR)
Poidevin and Pin (1986)	West Central African belt (CAR)
Pouclet et al. (2007)	Ntem-Chaillu block (Cameroon)
Shang et al. (2004a, b)	Ntem-Chaillu block (Cameroon)
Shang et al. (2010)	Ntem-Chaillu block (Cameroon)
Thiéblemont et al. (2009)	Central African Paleoproterozoic basins (Gabon)
	Ntem-Chaillu block (Gabon)
Tack et al. (1994)	Kibaran belt (Burundi)
Tack et al. (2001)	W-Congo belt
Tchakounté et al. (2007)	West Central African belt (Cameroon)
Tchameni et al. (2000)	Ntem-Chaillu block (Cameroon)
Tchameni et al. (2001)	West Central African belt (Cameroon)
Toteu et al. (1994)	Oubanguides belt (Cameroon)
	West Central African belt (Cameroon)
	Ntem-Chaillu block (Cameroon)
Toteu et al. (2001)	Oubanguides belt (Cameroon)
	West Central African belt (Cameroon)
Toteu et al. (2006b)	Oubanguides belt (Cameroon)
	West Central African belt (Cameroon)
Vicat and Pouclet (2000)	West Congo belt (Congo)
	West Central African belt (Congo)

To test this tool for the Central African rocks, we have compiled a great number of Nd-isotopic analyses from the literature, covering most of the regions covered by the present study. The references and geological domains involved are listed in Table 5.2. Some 25 studies were used to provide an incomplete but useful database of the Nd-isotopic signatures of Western Central Africa. Indeed, because of missing data, some domains are not considered in the present study—namely, the NW-Congo block and the Ubendian and Ruwemzori-Toro belts. In fact, the best-documented domains are those on the western side of Central Africa: Ntem-Chaillu block, Western Central African Eburnean belt and foreland basins, W-Congo belt and Oubanguides belt. Thus the following section must be considered only a preliminary scenario of crustal growth in Central Africa, at least for the western side of the region.

The analyses undertaken are reported in a $(Sm/Nd)_N$ versus εNd_T diagram (Figs. 5.4 and 5.5). $(Sm/Nd)_N$ is the value of the Sm/Nd ratio of a given sample normalized to chondrite, and εNd_T is a chondrite normalized expression of the $^{143}Nd/^{144}Nd$ ratio at a given time '*T*'.

The first diagram (Fig. 5.4) was drawn for a value of *T* equal to 0. This illustrates the present-day variability of the bulk Nd-isotopic signature of the studied region and the variability in each specific domain. Only sedimentary and felsic igneous (e.g., granite, gneisse, rhyolite) rocks were

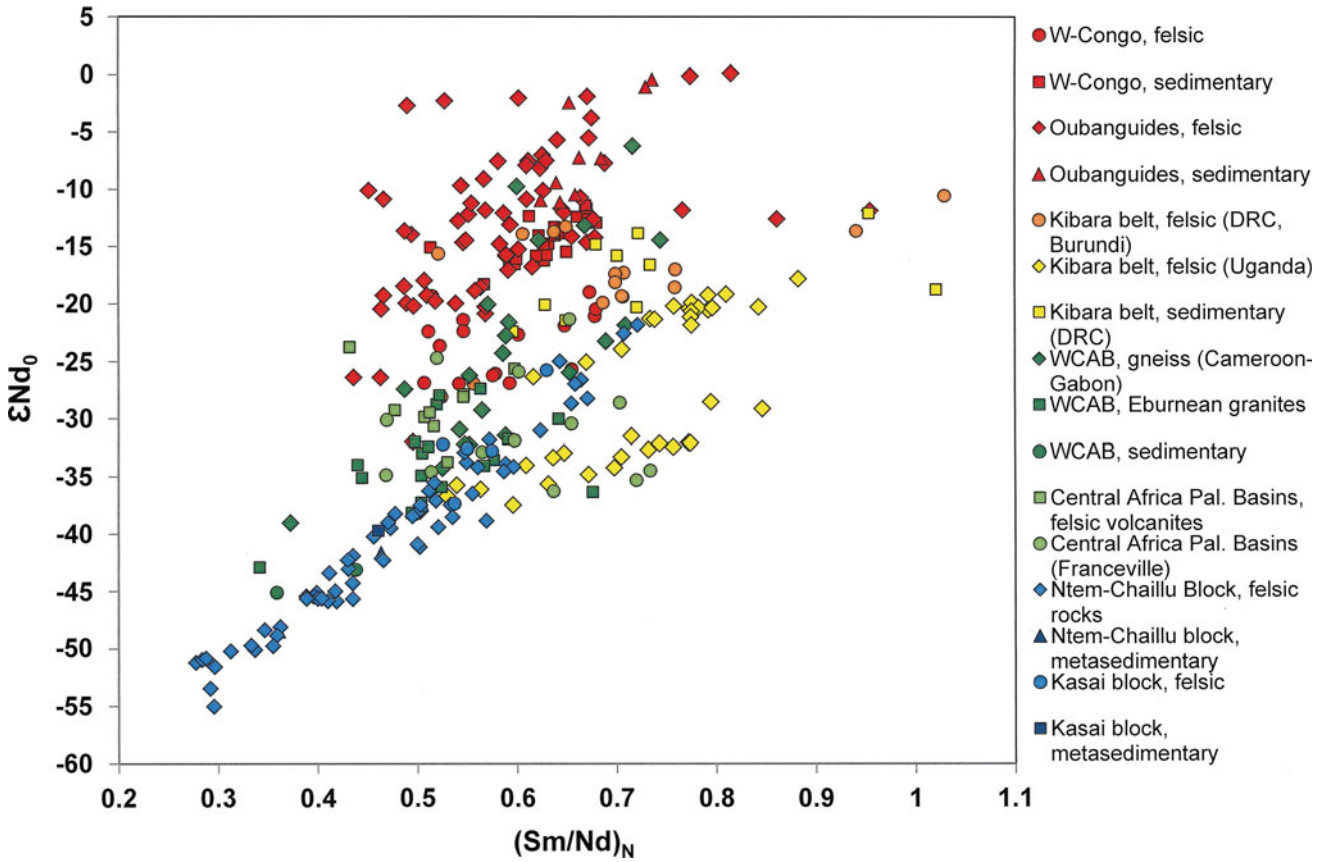

Fig. 5.4 $(Sm/Nd)_N$ versus εNd_0 diagram showing the bulk present-day variability in the LREE fractionation and Nd-isotopic signature of Precambrian terrains over Western Central Africa

reported because they confer on a domain its largely prevailing Nd-isotopic signature: (1) they are far more abundant than the basic or ultrabasic rocks; and (2) they display higher concentrations of Nd than the basic rocks.

The diagram illustrates a considerable isotopic variability, with εNd_0 ranging from *c.* −55 in Archean rocks to *c.* 0 in Neoproterozoic ones. At the bottom of Fig. 5.4 the Archean rocks (Ntem-Chaillu and Kasai bloks) define a broad linear correlation which reflects the predominance of a time-induced decrease of $^{143}Nd/^{144}Nd$ over initial differences in this isotopic ratio and elemental Sm:Nd ratio. As far as the isotopic ratio is concerned, the value of εNd_0 shows a general increase as the age of the rocks decreases, especially for the samples from the western side of the studied region (Gabon, Congo, W-DRC, Cameroon). The rather low εNd_0 (*c.* −38 to −15) determined in Kibaran (i.e., Mesoproterozoic) granites from Uganda (Buchwaldt et al. 2008) departs from the general trend, but the isotopic context of these rocks is today too incompletely documented to enable any explanation for this. Thus these samples will not be considered further in the following section.

A suite of $(Sm/Nd)_N$ versus εNd_T diagrams is presented (Fig. 5.5a–f) to illustrate the evolution of the Nd-isotopic signature during the succession of geological periods starting from 2.8 Ga and ending around 0.6 Ga. All rocks were taken into account: sedimentary, felsic and mafic-ultramafic.

At 2.8 Ga (Fig. 5.5a) the only existing rocks in the Netm-Chaillu and Kasai blocks are the Paleo- and Mesoarchean rocks of the granitic–gneissic association—that is, the granitoids, charnockites and associated basic rocks (norites), as well as those of the greenstone belts, paragneisses and basic rocks. In the great majority of the felsic samples, $\varepsilon Nd_{2.8\ Ga}$ ranges from −4 to 2.5. No correlation is observed between $(Sm/Nd)_N$ and $\varepsilon Nd_{2.8\ Ga}$, indicating that the variability of the $^{143}Nd/^{144}Nd$ mainly reflects isotopic differences in the source of the rocks (including all the components involved in these sources). The basic rocks generally display higher $(Sm/Nd)_N$ (*c.* 0.8–1.1 against *c.* 0.3–0.7) ratios. This reflects their depletion or slight enrichment in light rare-earth elements (LREE) relative to chondrite. The two basic rocks from greenstone belts have $\varepsilon Nd_{2.8\ Ga}$ values close to that calculated for the depleted mantle at this time, indicating a contribution from a juvenile source. However, $\varepsilon Nd_{2.8\ Ga}$ values in the basic rocks of the charnockitic suite are mostly negative, suggesting a significant contamination of their source by an old crustal component.

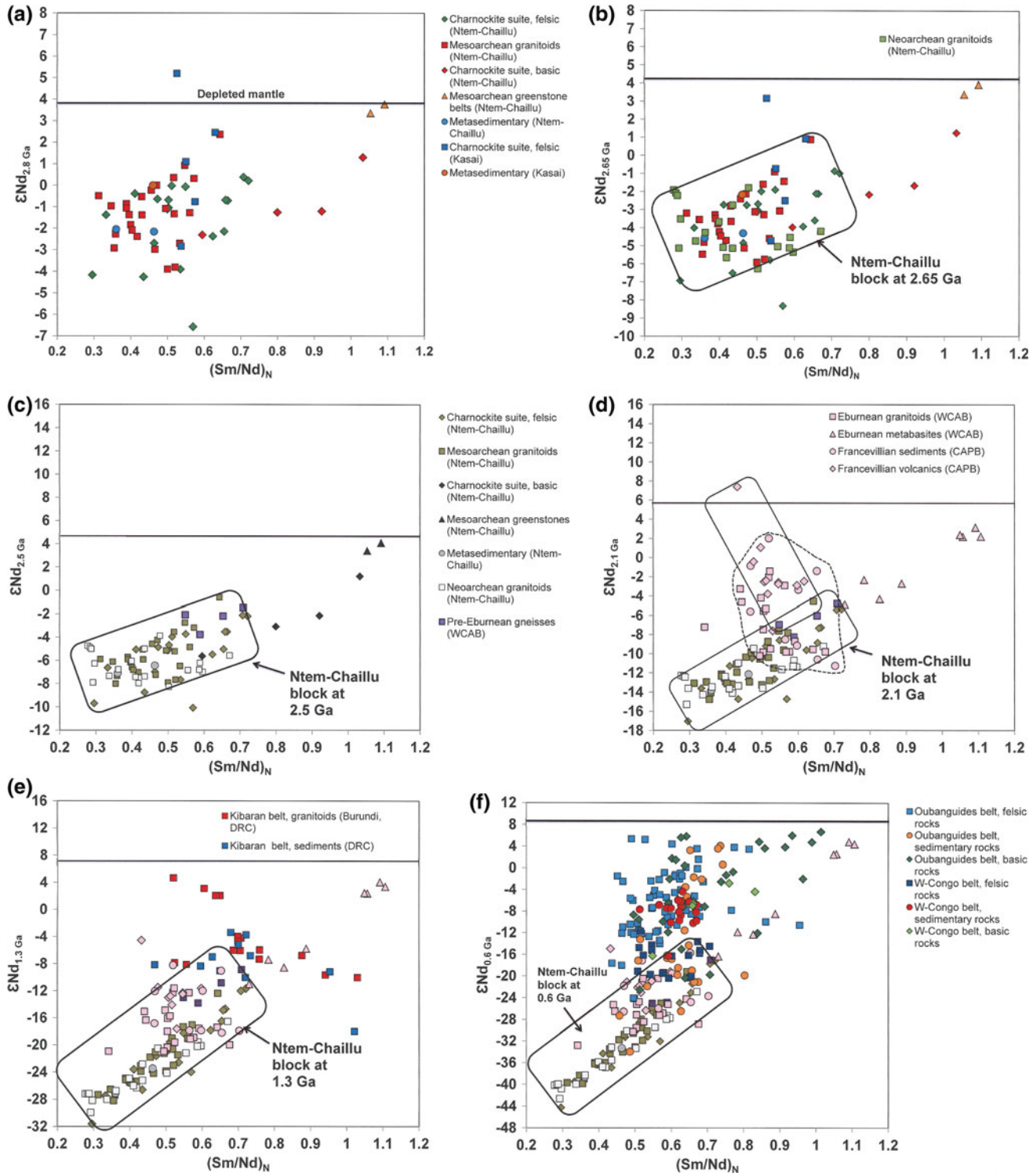

Fig. 5.5 Suite of $(Sm/Nd)_N$ versus εNd_T diagrams showing the variability of the Nd-isotopic signature of Western Central Africa through time as a result of radioactive decay (Sm–Nd system) and the addition of new geological domains

From the εNd values calculated at 2.65 Ga for the Mesoarchean felsic and metasedimentary rocks, a field was drawn which shows the bulk isotopic and Sm/Nd variability of the Ntem-Chaillu block at this time. The influence of basic rocks was considered to be insignificant because of their low abundance and rather low Nd contents relative to felsic rocks (Fig. 5.5b). The $\varepsilon Nd_{2.65\ Ga}$ ranges from *c.* −8 to 1 and a broad correlation is becoming apparent.

The subsequent Neoarchean granites are almost entirely included in the field of Mesoarchean rocks, suggesting that they were derived from a remobilization of the Mesoarchean basement, with no detectable juvenile input.

At 2.5 Ga (i.e., Pre-Eburnean period), εNd in the Ntem-Chaillu block ranges from *c*. −10 to 0 and the correlation noted above is better defined (Fig. 5.5c). In the diagram the pre-Eburnean gneisses are circumscribed in the field defined for the Ntem-Chaillu basement, suggesting that they were derived mainly from the remobilization of this basement.

At 2.1 Ga (Eburnean period) the elongated shape of the field of the Archean block became well-marked and the εNd value in this old basement ranges from −17 to −4 (Fig. 5.5d). Four groups of Paleoproterozoic rocks were distinguished: two from the Western Central Africa belt (Eburnean basic rocks and Eburnean granitoids), and two from its foreland basin (Francevillian volcanics and Francevillian sediments). These groups plot in fields more or less different from each other, and from the field of the Ntem-Chaillu block.

The Eburnean basic rocks plot in a totally distinct field, showing the highest $(Sm/Nd)_N$ and $\varepsilon Nd_{2.1\ Ga}$ in the range −6 to 3. Similarly, most of the Francevillian volcanic rocks plot outside the Archean field. Their εNd values (*c*. −8 to 7) are in fact comparable to those of the Eburnean metabasites, but their $(Sm/Nd)_N$ ratios (*c*. 0.45–0.65) are lower. These rocks show no depletion for LREE, displaying alkaline to calcalkaline geochemical signatures (Thiéblemont et al. 2014). The volcanic episodes in the Eburnean belt and its foreland basin attest to a juvenile input within the Archean block. However, the cartographic extent (and maybe bulk volume) of this volcanism is rather limited (Thiéblemont et al. 2009).

The Eburnean granitoids and Francevillian sediments display comparable ranges of $(Sm/Nd)_N$ (*c*. 0.45–0.7) and $\varepsilon Nd_{2.1\ Ga}$ (*c*. −12 to 2). They partly overlap the field of the Ntem-Chaillu block and extend towards higher $\varepsilon Nd_{2.1\ Ga}$ values. Slightly positive $\varepsilon Nd_{2.1\ Ga}$ values in the Francevillian sediments could reflect some contribution of juvenile material, as recorded by volcanic rocks. Among the Eburnean granitoids, those with the highest $\varepsilon Nd_{2.1\ Ga}$ are typically located in regions distant from the Ntem-Chaillu block, such as western Congo (Djama et al. 1992; Vicat and Pouclet 2000) and CAR (Poidevin and Pin 1986), suggesting the addition of juvenile crust along the margins of the Archean core. On the other hand, the granitoids emplaced within (Tchameni et al. 2001) or close to the Archean block (Mayaga-Mikolo 1996) are isotopically similar to Archean rocks.

The $(Sm/Nd)_N$ versus εNd_T diagram for $T = 1.3$ Ga (Fig. 5.5e) takes into account sediments and granites from the southwest (DRC, Debruyne et al. 2015) and northeast (Burundi; Tack et al. 1994) segments of the Kibara belt. All these rocks display Nd-isotopic signatures more or less distinct and always more juvenile ($\varepsilon Nd_{1.3\ Ga}$ = *c*. −10–4) than those of the Ntem-Chaillu block. At first sight, this appears consistent with a significant input of juvenile material to the Central African crust during the Kibaran event (Tack et al. 1994; Debruyne et al. 2015). However, owing to a lack of data, the isotopic signature of the neighbouring Ubendian (Ruzizi) belt (Figs. 5.1 and 5.2) could not be shown in the diagram, so the possible reworking of this domain during the Kibaran event could not be evaluated.

The $(Sm/Nd)_N$ versus εNd_T diagrams for $T = 0.6$ Ga (Fig. 5.5f) include all the data available for Neoproterozoic rocks of the W-Congo and Oubanguides belts. Three groups were distinguished in each belt: basic igneous rocks, felsic igneous rocks and sedimentary rocks. Actually, these three groups include rocks of strongly contrasted ages (*c*. 1 Ga to <600 Ma), but much of the available data (e.g., Toteu et al. 2001) does not enable the placement of significant age distinctions within each group. Thus a unique age of 0.6 Ga was used for the calculation of εNd_T, and comparison between the Nd-isotopic signature of the Ntem-Chaillu block and those of the two Panafrican belts around it.

Because of the higher $\varepsilon Nd_{0.6\ Ga}$, most of these rocks plot outside the field of the Ntem-Chaillu block as defined by both Archean and Paleoproterozoic rocks. This testifies to a significant input of juvenile material during the Panafrican event.

In the W-Congo belt, most of the felsic magmatic rocks (granitoids and rhyolites) display rather low $\varepsilon Nd_{0.6\ Ga}$ (i.e., <−10), making them similar to Paleoproterozoic granitoids (Fig. 5.5f). This suggests the contribution of an old lithospheric component in their genesis, either crustal (Djama et al. 1992) or subcrustal (lithospheric mantle; Tack et al. 2001). The sedimentary rocks in the W-Congo belt display moderately low εNd (i.e., −9 to 4). U–Pb geochronological data obtained from detrital zircons in these sediments in Congo and DRC indicates a proportion of 53% of Paleoproterozoic and Archean zircons, and 34% of Mesoproterozoic and Neoproterozoic (i.e., $T = 1.2$–0.5 Ga) zircons (Frimmel et al. 2006; Affaton et al. 2016). Comparable results were obtained in Gabon where 50% of the zircon extracted from volcanoclastic sediments from the Mayombe massif have Mesoproterozoic–Neoproterozoic ages (1.2–0.7 Ga), and the remaining 50% Archean–Paleoproterozoic ages (3.05–1.85 Ga) (Thiéblemont et al. 2011b). These results are constitent with the participation of both juvenile (Mesoproterozoic(?)-Neoproterozoic mafic magmas) and old (Archean-Paleoproterozoic basement) materials in the genesis of these sediments.

Except for some metasedimentary rocks, most of the Neoproterozoic rocks of the Oubanguides belt plot outside the field of the Ntem-Chaillu craton. However, the location

of metasedimentary rocks within this field is consistent with the occurrence of Archean and Paleoproterozoic zircons in metasedimentary rocks located close to the margin with the Ntem-Chaillu block (Toteu et al. 2006b). The important proportion of rocks with $\varepsilon Nd_{0.6\ Ga} > 0$ in the Oubanguides belt (Fig. 5.5f) indicates a significant input of long-time depleted material consistent with a major event of continent accretion during the Panafrican at the northern edge of the Ntem-Chaillu block (Trompette 2000).

5.5 Conclusion

This introductory chapter to the geology of the western part of Central Africa is based on an up-to-date geological map of Africa at 1:10,000,000 scale (Thiéblemont et al. 2016b). Its main objective is to show how different domains may be traced and dated within this region, and how the aggregation of these domains at different times and by different processes has given Central Africa a considerable isotopic variability. However, a lot of work has still to be done to build a precise sequence of events in a given domain and to allow correlations between domains. In our opinion, regional mapping sustained by important programmes of geochronological investigation is the key to such an objective.

Acknowledgements Many thanks to Sebastián Oriolo for his constructive review and Siegfried Siegesmund for his efforts in the editing of this book.

References

Abdelsalam MG, Katumwehe AB, Atekwana EA, Le Pera AK, Achang M (2016) The Paleoproterozoic Singo granite in south-central Uganda revealed as a nested igneous ring complex using geophysical data. J Afr Earth Sci 116:198–212

Abouchami W, Boher M, Michard A, Albarede F (1990) A major 2.1 Ga event of mafic magmatism in West Africa; an early stage of crustal accretion. J Geophys Res B Solid Earth Planets 95 (B11):17605–17617

Affaton P, Kalsbeek F, Boudzoumou F, Trompette R, Thrane K, Frei R (2016) The Pan-African West Congo belt in the Republic of Congo (Congo Brazzaville): stratigraphy of the Mayombe and West Congo Supergroups studied by detrital zircon geochronology. Precambrian Res 272:185–202

Alvarez P, Maurin J-C (1991) Evolution sédimentaire et tectonique du bassin protérozoïque supérieur de Comba (Congo): stratigraphie séquentielle du Supergroupe Ouest-Congolien et modèle d'amortissement sur décrochements dans le contexte de la tectogénèse panafricaine. Precambrian Res 50:137–171

Andersen LS, Unrug R (1984) Geodynamic evolution of the Bangweulu Block, Northern Zambia. Precambrian Res 25:187–212

Anonymous (1979) Carte géologique de la République Unie du Cameroun. Ministère des Mines et de l'Energie

Armstrong RA, Robb LJ, Master S, Kruger FJ, Mumba PACC (1999) New U–Pb age constraints on the Katangan Sequence, Central African Copperbelt. J Afr Earth Sci, Sp Abstr Issue, GSA11: Earth Resources for Africa 28:6–7

Armstrong RA, Master S, Robb LJ (2005) Geochronology of the Nchanga Granite, and constraints on the maximum age of the Katanga Supergroup, Zambian Copperbelt. J Afr Earth Sci 42:32–40

Batumike JM, Griffin WL, O'Reilly SY, Belousova EA, Pawlitschek M (2009) Crustal evolution in the central Congo-Kasai Craton, Luebo, D.R. Congo: insights from zircon U–Pb ages, Hf-isotope and trace-element data. Precambrian Res 170:107–115

Boher M, Abouchami W, Michard A, Albarede F, Arndt NT (1992) Crustal growthin West Africa at 2.1 Ga. J Geophys Res B Solid Earth Planets 97:345–369

Boniface N, Schenk V, Appel P (2012) Paleoproterozoic eclogites of MORB-type chemistry and three Proterozoic orogenic cycles in the Ubendian Belt (Tanzania): evidence from monazite and zircon geochronology, and geochemistry. Precambrian Res 192–195:16–33

Boudzoumou F, Trompette R (1988) La chaîne panafricaine ouest-congolienne au Congo (Afrique Equatoriale): un socle polycyclique charrié sur un domaine subautochtone formé par l'aulacogène du Mayombe et le bassin de l'Ouest-Congo. Bull Soc Géol France 6:889–896

Brewer MS, Haslam HW, Darbyshire, DPE, Davis AE (1979) Rb–Sr age determinations in the Bangweulu block, Luapula Province, Zambia. Inst Geol Sci Rep 79(5)

Bros R (1993) Géochimie isotopique (Sm–Nd, Rb–Sr, K–Ar) des argiles du Bassin protérozoïque de Franceville et des réacteurs d'Oklo (Gabon). Thesis, University Louis Pasteur, Strasbourg

Buchwaldt R, Toulkeridis T, Todt W, Ucakuwun EK (2008) Crustal age domains in the Kibaran belt of SW-Uganda: combined zircon geochronology and Sm–Nd isotopic investigation. J Afr Earth Sci 51:4–20

Caen-Vachette M, Vialette Y, Bassot J-P, Vidal P (1988) Apport de la géochronologie isotopique à la connaissance de la géologie gabonaise. Chroniques de la recherche minie`re 491:35–54

Cahen L (1982) Geochronological correlation of the late Precambrian sequences on and around the stable zones of Equatorial Africa. Precambrian Res 18:73–86

Cahen L, Ledent D (1979) Précisions sur l'âge, la pétrogenèse et la position stratigraphique des 'granites à étain' de l'est de l'Afrique Centrale. Bull Soc Géol Belg 88:33–49

Cahen L, Ledent D, Snelling NJ (1975) Données géochronologiques dans le Katangien inférieur du Kasai oriental et du Shaba nord-oriental (République du Zaïre). Musée Royal de l'Afrique Centrale, Tervuren, Belgique, Département Géologie et Minéralogie, Rapport Annuel (1974):59–69

Cahen L, Snelling NJ, Delhal J, Vail J-P (1984) The geochronology and evolution of Africa. Clarendon, Oxford, p 512

Callec Y, Fullgraf T (eds) (2015) Carte géologique à 1/500,000, 1ère édn. Programme National de Cartographie Géologique de la République du Congo, Ministère des Mines et de la Géologie, Direction Générale des Mines et de la Géologie

Castaing C, Feybesse J-L, Thiéblemont D, Triboulet C, Chèvremont P (1994) Palaeogeographical reconstructions of the Pan-African/Brasiliano orogen: closure of an oceanic domain or intracontinental convergence between major blocks? Precambrian Res 69:327–344

Censier C (1990) Characteristics of Mesozoic fluvio-lacustrine formations of the western Central African Republic (Carnot Sandstones) by means of mineralogical and exoscopic analyses of detrital material. J Afr Earth Sci 10(1–2):385–398

Censier C (1991) Dynamique sédimentaire d'un système fluviatile diamantifère mésozoïque: la Formation de Carnot (République Centrafricaine). Thesis Bourgogne University, Mém. BRGM 205, p 600

Choubert G, Faure-Muret A (eds) (1985–1990) International Geological Map of Africa, Scale 1/5,000,000, 3rd edn. CGMW/UNESCO 1990

Deblond A (2004) Updated Geological Framework of Central Africa. GEONET, Scientific case study no 7. Africa Museum, Tervuren

Debruyne D, Hulsbosch N, Van Wilderode J, Balcaen L, Vanhaecke F, Muchez P (2015) Regional geodynamic context for the Mesoproterozoic Kibara Belt (KIB) and the Karagwe-Ankole Belt: evidence from geochemistry and isotopes in the KIB. Precambrian Res 264:82–97

De Carvalho H, Tassinari C, Alves PH, Guimarães F, Simões MC (2000) Geochronological review of the Precambrian in western Angola: links with Brazil. J Afr Earth Sci 31(2):383–402

Delhal J, Liégeois J-P (1982) Le socle granito-gneissique du Shaba occidental (Zaïre)—Pétrographie et géochronologie. Ann Soc Géol Belg 105:295–301

Delhal J, Deutsch S, Denoiseux B (1986) A Sm–Nd isotopic study of heterogeneous granulites from the Archean Kasai-Lomami gabbro-norite and charnockite complex (Zaïre, Africa). Chem Geol 57:235–245

Delor C, Théveniaut H, Cage M, Pato D (2007) Carta geológica da Repùblica de Angola a escala 1:2,000,000. Ministerio da Geologia e Minas—Instituto geológico de Angola

De Waele B, Fitzsimons ICW (2007) The nature and timing of Palaeoproterozoic sedimentation at the southeastern margin of the Congo Craton; zircon U–Pb geochronology of plutonic, volcanic and clastic units in northern Zambia. Precambrian Res 159:95–116

De Waele B, Liégeois J-P, Nemchin AA, Tembo F (2006) Isotopic and geochemical evidence of proterozoic episodic crustal reworking within the irumide belt of south-central Africa, the southern metacratonic boundary of an Archaean Bangweulu Craton. Precambrian Res 148:225–256

De Waele B, Johnson SP, Pisarevsky SA (2008) Palaeoproterozoic to Neoproterozoic growth and evolution of the eastern Congo Craton: its role in the Rodinia puzzle. Precambrian Res 160:127–141

De Wit MJ, Linol B (2015) Precambrian basement of the Congo Basin and its flanking terrains. In: de Wit MJ et al (eds) Geology and resource potential of the Congo Basin regional geology reviews. Springer, Berlin, Heidelberg, pp 19–37

Djama LM, Leterrier J-L, Michard A (1992) Pb, Sr and Nd isotope study of the basement of the Mayumbian belt (Guena gneisses and Mfoubou granite, Congo): implications for crustal evolution in Central Africa. J Afr Earth Sci 14(2):227–237

Djouka-Fonkwe ML, Schulz B, Schüssler U, Tchouankoue J-P, Nzolang C (2008) Geochemistry of the Bafoussam Pan-African I- and S-type granitoids in western Cameroon. J Afr Earth Sci 50:148–167

Eglinger A, Vanderhaeghe O, André-Mayer AS, Goncalves P, Zeh A, Durand C, Deloule E (2016) Tectono-metamorphic evolution of the internal zone of the Pan-African Lufilian orogenic belt (Zambia): implications for crustal reworking and syn-orogenic uranium mineralizations. Lithos 240–243:167–188

Fernandez-Alonso M (2007) Geological map of the Mesoproterozoic Northeastern Kibaran Belt. Royal Museum for Central Africa, Tervuren (Belgium): catalogue of map and digital data

Fernandez-Alonso M (ed) et al. (2015a) Carte géologique de la république démocratique du Congo au 1/2,500,000. République Démocratique du Congo, Ministère des Mines

Fernandez-Alonso M (ed) et al (2015b) Carte géologique de la république démocratique du Congo au 1/2,500,000. Notice explicative République Démocratique du Congo Ministère des Mines, p 100

Fernandez-Alonso M, Tack L, Tahon A, De Waele B (2011) The Proterozoic history of the proto-Congo Craton of Central Africa. Paper presented at the 23th colloquium on Africa geology, Johannesburg, 10–15 Jan 2011

Feybesse J-L, Johan V, Triboulet C, Guerrot C, Mayaga-Mikolo F, Bouchot V, Eko N'dong J (1998) The West Central African belt: a model of 2.5–2.0 Ga accretion and two-phase orogenic evolution. Precambrian Res 87:161–216

Frimmel HE, Tack L, Basei MS, Nutman AP, Boven A (2006) Provenance and chemostratigraphy of the Neoproterozoic West Congolian Group in the Democratic Republic of Congo. J Afr Earth Sci 46:221–239

Ganwa AA, Frisch W, Siebel W, Ekodeck GE, Shang KC, Ngako V (2008a) Archean inheritances in the pyroxene-amphibole-bearing gneiss of the Méiganga area (Central North Cameroon): geochemical and $^{207}Pb/^{206}Pb$ age imprints. C R Geosci 340:211–222

Ganwa AA, Frisch W, Siebel W, Shang KC, Mvondo Ondoa J, Satir M, Tchakounte Numbem J (2008b) Zircon $^{207}Pb/^{206}Pb$ evaporation ages of Panafrican metasedimentary rocks in the Kombe´-II area (Bafia Group, Cameroon): constraints on protolith age and provenance. J Afr Earth Sci 51:77–88

Ganwa AA, Klötzli US, Hauzenberger C (2016) Evidence for Archean inheritance in the pre-Panafrican crust of Central Cameroon: insight from zircon internal structure and LA-MC-ICP-MS U/Pb ages. J Afr Earth Sci 120:12–22

Gérards J, Ledent D (1976) Les réhomogénéisations isotopiques d'gtge lufilien clans les granites du Rwanda. Musée Royal de l'Afrique Centrale, Tervuren, Belgique, Département Géologie et Minéralogie, Rapport Annuel (1975):91–103

Hanson RE, Wardlaw MS, Wilson TJ, Mwale G (1993) U–Pb zircon ages from the Hook granite massif and Mwembeshi dislocation: constraints on Pan-African deformation, plutonism, and transcurrent shearing in central Zambia. Precambrian Res 63:189–209

John T, Schenk V, Mezger K, Tembo F (2004) Timing and PT evolution of whiteschist etamorphism in the Lufilian Arc-Zambezi Belt rogen (Zambia): implications for the Assembly of Gondwana. J Geol 112:71–90

Kabengele M, Tshimanga K, Lubala RT, Kapenda D, Walraven E (1990) Geochronology of the calcalcaline granitoids of the Marungu plateau (eastern Zaire—central Africa). In: Rocci G, Deschamps M (eds) Recent data in African Earth sciences. International Center for Training and Exchanges in the Geosciences Occasional Publication 22:51–55

Kadima E, Delvaux D, Sebagenzi SN, Tack L, Kabeyaz SM (2011) Structure and geological history of the Congo Basin: an integrated interpretation of gravity, magnetic and reflection seismic data. Basin Res 23:499–527

Kampunzu AB, Cailteux J (1999) Tectonic Evolution of the Lufilian Arc (Central Africa Copper Belt) During Neoproterozoic Pan African orogenesis. Gondwana Res 2(3):401–421

Kampunzu AB, Wendorff M, Kruger EJ, Intiomale MM (1998) Pb isotopic ages of sediment-hosted Pb–Zn mineralisation in the Neoproterozoic Copperbelt of Zambia and Democratic Republic of Congo (ex-Zaire): reevaluation and implications. Chron Min Rech Min 530:55–61

Key RM, Liyungu AK, Njamu FM, Somwe V, Banda J, Mosley PN, Armstrong RA (2001) The western arm of the Lufilian Arc in NW Zambia and its potential for copper mineralization. J Afr Earth Sci 33:503–528

Kokonyangi J, Armstrong R, Kampunzu AB, Yoshida M (2001) SHRIMP U–Pb Zircon Geochronology of Granitoids in the Kibaran Type-Area, Mitwaba-Central Katanga (Congo). Gondwana Res 4 (4):661–663

Kokonyangi J, Armstrong R, Kampunzu AB, Yoshida M, Okudaira T (2004) U–Pb zircon geochronology and petrology of granitoids

from Mitwaba (Katanga, Congo): implications for the evolution of the Mesoproterozoic Kibaran belt. Precambrian Res 132:79–106

Kokonyangi J, Kampunzu AB, Poujol M, Okudaira T, Yoshida M, Shabeer KP (2005) Petrology and geochronology of Mesoproterozoic mafic–intermediate plutonic rocks from Mitwaba (D.R. Congo): implications for the evolution of the Kibaran belt in central Africa. Geol Mag 142(1):109–130

Kokonyangi JW, Kampunzu AB, Armstrong R, Yoshida M, Okudaira T, Arima M, Ngulube DA (2006) The Mesoproterozoic Kibaride belt (Katanga, SE D.R. Congo). J Afr Earth Sci 46:1–35

Lavreau J (1982) Etude geologique du Haut-Zaïre. Genèse et evolution d'un segment lithospherique archéen. Ann Mus Roy Afr Centr, Sc Geol 88:118

Lavreau J, Ledent D, Poidevin J-L (1980) Age archéen de la ceinture de granites et roches vertes des Bandas (R.C.A.). C R Acad Sci Paris 291(D):151–153

Lavreau J, Poidevin J-L, with the collaboration of Ledent D, Liégeois J-P, Weiss D (1991) Contribution to the geochronology of the basement of the Central African Republic. J Afr Earth Sci 11(1–2):69–82

Leggo PJ (1974) A geochronological study of the basement complex of Uganda. J Geol Soc London 130:263–277

Lenoir J-L, Liégeois J-P, Theunissen K, Klerkx J (1994) The Palaeoproterozoic Ubendian shear belt in Tanzania: geochronology and structure. J Afr Earth Sci 19(3):169–184

Lepersonne J (1974) Carte géologique du Zaïre au 1/2,000,000 et notice explicative. République du Zaïre, Département des mines, Direction de Ia Géologie, Kinshasa, p 67

Lerouge C, Cocherie A, Toteu SF, Penaye J, Milesi J-P, Tchameni R, Nsifa EN, Fanning CM, Deloule E (2006) Shrimp U–Pb zircon age evidence for Paleoproterozoic sedimentation and 2.05 Ga syntectonic plutonism in the Nyong Group, South-Western Cameroon: consequences for the Eburnean-Transamazonian belt of NE Brazil and Central Africa. J Afr Earth Sci 44:413–427

Link K, Koehn D, Barth MG, Tiberindwa JV, Barifaijo E, Aanyu K, Foley SF (2010) Continuous cratonic crust between the Congo and Tanzania blocks in western Uganda. Int J Earth Sci (Geol Rundsch) 99:1559–1573

Maier WD, Rasmussen B, Fletcher IR, Godel B, Barnes SJ, Fisher LA, Yang SH, Huhma H, Lahaye Y (2015) Petrogenesis of the ~2.77 Ga Monts de Cristal Complex, Gabon: evidence for Direct Precipitation of Pt-arsenides from Basaltic Magma. J Petrol 56 (7):1285–1308

Master S, Rainaud C, Armstrong RA, Phillips D, Robb LJ (2005) Provenance ages of the Neoproterozoic Katanga Supergroup (Central African Copperbelt), with implications for basin evolution. J Afr Earth Sci 42:41–60

Maurizot P (1986) Carte géologique du sud-ouest Cameroun. Direction des Mines et de la Géologie, Ministère des Mines, de l'eau et de l'Energie, République du Cameroun

Mayaga-Mikolo F (1996) Chronologie des évènements sédimentaires, magmatiques et tectono-métamorphiques du Précambrien d'Afrique Centrale Occidentale (Gabon): tectogenèse Ogooué et héritage archéen. Thesis, Blaise Pascal University, Clermont-Ferrand, p 185

Mayer A, Hofmann AW, Sinigoi S, Morais E (2004) Mesoproterozoic Sm–Nd and U–Pb ages for the Kunene Anorthosite Complex of SW Angola. Precambrian Res 133:187–206

McCourt S, Armstrong RA, Jelsma H, Mapeo RBM (2013) New U–Pb SHRIMP ages from the Lubango region, SW Angola: insights into the Palaeoproterozoic evolution of the Angolan Shield, southern Congo Craton, Africa. J Geol Soc London 170:353–363

Milesi J-P, Feybesse J-L, Pinna P, Deschamps Y, Kampunzu HAB, Muhonogo S, Lescuyer J-L, Toteu SF (2004) Géologie et principaux gisements de l'Afrique, échelle 1/1,000,000. 20th Congress on African Geology, Orléans, BRGM Ed

Milesi J-P, Toteu SF, Deschamps Y, Feybesse J-L, Lerouge C, Cocherie A, Penaye J, Tchameni R, Moloto-A-Kenguemba G, Kampunzu HAB, Nicol N, Duguey E, Leistel J-M, Saint-Martin M, Ralay F, Heinry C, Bouchot V, Doumnang Mbaigane JC, Kanda Kula V, Chene F, Monthel J, Boutin P, Cailteux J (2006) An overview of the geology and major ore deposits of Central Africa: explanatory note for the 1:4,000,000 map "Geology and major ore deposits of Central Africa". J Afr Earth Sci 44:571–595

Milesi J-P, Frizon de Lamotte D, De Kock G, Toteu S (2010) Tectonic Map of Africa at 1:10 M scale. CGMW ed

Moloto-A-Kenguemba GR, Trindade RIF, Monié P, Nédélec A, Siqueira R (2008) A late Neoproterozoic paleomagnetic pole for the Congo craton: tectonic setting, paleomagnetism and geochronology of the Nola dike swarm (Central African Republic). Precambrian Res 164:214–226

Mosoh Bambi CK, Frimmel HE, Zeh A, Suh CE (2013) Age and origin of Pan-African granites and associated U–Mo minelralization at Ekomédion, southwestern Cameroon. J Afr Earth Sci 88:15–37

Ngako V, Affaton P, Njonfang E (2008) Pan-African tectonics in northwestern Cameroon: implication for the history of western Gondwana. Gondwana Res 14:509–522

Pasteels P (1971) Age du granite de la Lunge (près de Kamina, Katanga). Musée Royal de l'Afrique Centrale, Département Géologie et Minéralogie,Tervuren, Belgique, Rapport Annuel (1970):41

Pin C, Poidevin J-L (1987) U–Pb zircon evidence for a Pan-African granulite facies metamorphism in the Central African Republic. A new interpretation of the high-grade series of the northern border of the Congo Craton. Precambrian Res 36:303–312

Pinna P, Muhongo S, Mcharo BA, Le Goff E, Deschamps Y, Ralay F, Milesi J-P (2008) Geology and mineral map of Tanzania, scale 1:2,000,000. BRGM–Geologicla Survey of Tanzania

Poidevin J-L (1985) Le Protérozoïque supérieur de la République Centrafricaine. Stratigraphie et structure. Annates du Musée royal de!'Afrique centrale, Tervuren–Belgique, in-8, Sciences géologiques 91:75

Poidevin J-L (2007) Stratigraphie isotopique du strontium et datation des formations carbonatées et glaciogéniques néoprotérozoiques du Nord et de l'Ouest du craton du Congo. C R Geosci 339:259–273

Poidevin J-L, Pin C (1986) 2 Ga U–Pb zircon dating of Mbi granodiorite (Central African Republic) and its bearing on the chronology of the Proterozoic of Central Africa. J Afr Earth Sci 5(6):581–587

Porada H, Berhorst V (2000) Towards a new understanding of the Neoproterozoic–early Palæozoic Lufilian and northern Zambezi belts in Zambia and the Democratic Republic of Congo. J Afr Earth Sci 30:727–771

Pouclet A, Tchaméni R, Mezger K, Vidal M, Nsifa E, Shang C, Penaye J (2007) Archaean crustal accretion at the northern border of the Congo Craton (South Cameroon). The charnockite-TTG link. Bull Soc Géol Fr 178(5):331–342

Priem HNA, Boelrijk NAIM, Hebeda EH, Verdumene EATh, Verschure RH (1979) Isotopic age determination on granitic and gneissic rocks from the Ubendian-Usagaran system in southern Tanzania. Precambrian Res 9:227–239

Rainaud C, Master S, Armstrong RA, Robb LJ (2003) A cryptic Mesoarchean terrane in the basement to the central African Copperbelt. J Geol Soc London 160:11–14

Rainaud C, Master S, Armstrong RA, Phillips D, Robb LJ (2005a) Monazite U–Pb dating and 40Ar–39Ar thermochronology of metamorphic events in the Central African Copperbelt during the Pan-African Lufilian Orogeny. J Afr Earth Sci 42:183–199

Rainaud C, Master S, Armstrong RA, Robb LJ (2005b) Geochronology and nature of the Palaeoproterozoic basement in the Central African Copperbelt (Zambia and the Democratic Republic of Congo), with regional implications. J Afr Earth Sci 42:1–31

Ring U, Kröner A, Toukeridis T (1997) Palaeproterozoic granulite-facies metamorphism and granitoid intrusions in the Ubendian-Usagaran Orogen of northern Malawi. Precambrian Res 85:27–51

Rolin P (1995) Carte tectonique de la République centrafricaine, au 1:1,500,000. BRGM ed

Rumvegeri BT (1991) Tectonic significance of Kibaran structures in Central and Eastern Africa. J Afr Earth Sci 13(2):267–276

Shang CK, Satir M, Siebel W, Nsifa EN, Taubald H, Liégeois J-P, Tchoua FM (2004a) TTG magmatism in the Congo craton; a view from major and trace element geochemistry, Rb–Sr and Sm–Nd systematics: case of the Sangmelima region, Ntem complex, southern Cameroon. J Afr Earth Sci 40:61–79

Shang CK, Siebel W, Satir M, Chen F, Mvondo JO (2004b) Zircon Pb–Pb and U–Pb systematics of TTG rocks in the Congo Craton: constraints on crust formation, magmatism, and Pan-African lead loss. Bull Geosci 79(4):205–219

Shang CK, Liégeois J-P, Satir M, Frisch W, Nsifa EN (2010) Late Archaean high-K granite geochronology of the northern metacratonic margin of the Archaean Congo craton, Southern Cameroon: evidence for Pb-loss due to non-metamorphic causes. Gondwana Res 18:337–355

Tack L, Liégeois J-P, Deblond A, Duchesne J-C (1994) Kibaran A-type granitoids and mafic rocks generated by two mantle sources in a late orogenic setting (Burundi). Precambrian Res 68:323–356

Tack L, Wingate MTD, Liégeois J-P, Fernandez-Alonso M, Deblond A (2001) Early Neoproterozoic magmatism (1000–910 Ma) of the Zadinian and Mayumbian Groups (Bas-Congo): onset of Rodinia rifting at the western edge of the Congo craton. Precambrian Res 110:277–306

Tack L, Wingate MTD, De Waele B, Meert J, Belousova E, Griffin B, Tahona A, Fernandez-Alonso M (2010) The 1375 Ma "Kibaran event" in Central Africa: prominent emplacement of bimodal magmatism under extensional regime. Precambrian Res 180:63–84

Tchakounté JN, Toteu SF, Van Schmus WR, Penaye J, Deloule E, Ondoua JM, Houketchang MB, Ganwa AA, White WM (2007) Evidence of ca 1.6-Ga detrital zircon in the Bafia Group (Cameroon): implication for the chronostratigraphy of the Pan-African Belt north of the Congo craton. C R Geosci 339:132–142

Tchameni R, Mezger K, Nsifa NE, Pouclet A (2000) Neoarchaean crustal evolution in the Congo Craton: evidence from K rich granitoids of the Ntem Complex, southern Cameroon. J Afr Earth Sci 30(1):133–147

Tchameni R, Mezger K, Nsifa NE, Pouclet A (2001) Crustal origin of Early Proterozoic syenites in the Congo Craton (Ntem Complex), South Cameroon. Lithos 53:27–42

Theunissen K, Klerkx J (1980) Considérations préliminaires sur l'évolution tectonique du "Burundien" au Burundi. Rapp Ann Mus R Afr Centr Tervüren Dépt Géol Min 1979:207–213

Theunissen K, Lenoi, J-L, Liegeois J-P, Delvaux D, Mruma A (1992) Empreinte pan-africaine majeure dans Ia cha·ine ubendienne de Tanzanie sud-occidentale. Geochronologie U–Pb sur zircon et contexte structural. C R Acad Sci Paris 314(II):1355–1362

Thiéblemont D (2009) Carte géologique et des Ressources minérales de la République gabonaise à 1/1,000,000, 3ième édn. DGMG Editions, Ministère des Mines, du Pétrole, des Hydrocarbures. Libreville

Thiéblemont D, Castaing C, Billa M, Bouton P, Préat A (2009) Notice explicative de la Carte géologique et des Ressources minérales de la République gabonaise à 1/1,000,000. DGMG Editions, Ministère des Mines, du Pétrole, des Hydrocarbures, Libreville, p 384

Thiéblemont D, Agenbacht A, Boulingui B, Bouton P, Ekogha H, Goujou J-C, Kassadou AB, Moussavou M, Prian J-P, Theunissen K, Cocherie A, Guerrot C (2011a) Synchronous BIF, HT metamorphism and granitic plutonism at ca. 2.8 Ga in Gabon. Paper presented at the 23th Colloquium on Africa Geology, Johannesburg, 10–15 Jan 2011, Abstract Book

Thiéblemont D, Prian JP, Goujou JC, Boulingui B, Ekogha H, Kassadou AB, Simo NS, Walemba A, Préat A, Theunissen K, Cocherie A, Guerrot C (2011b) Timing and characteristics of Neoproterozoic magmatism in SW-Gabon. Paper presented at the 23th Colloquium on Africa Geology, Johannesburg, 10–15 Jan 2011, Abstract Book and Poster

Thiéblemont D, Bouton P, Préat A, Goujou J-C, Tegyey M, Weber F, Ebang-Obiang M, Joron J-L, Treuil M (2014) Transition from alkaline to calc-alkaline volcanism during evolution of the Paleoproterozoic Francevillian basin of eastern Gabon (Western Central Africa). J Afr Earth Sci 99:215–227

Thiéblemont D, Liégeois J-P, Fernandez-Alonso M, Ouabadi A, Le Gall B, Maury R, Jalludin M, Vidal M, Ouattara-Gbélé C, Tchaméni R, Michard A, Nehlig P, Rossi P, Chêne F (2016a) An updated geological map of Africa at 1/10,000,000 scale, by Thiéblemont D. and partners of the new Africa 10 M map project. 35th IGC, Capetown

Thiéblemont D (ed), Liégeois J-P, Fernandez-Alonso M, Ouabadi A, Le Gall B, Maury R, Jalludin M, Vidal M, Ouattara-Gbélé C, Tchaméni R (2016b) Geological map of Africa at 1:10 M scale, CGMW-BRGM, 2016

Toteu SF, Michard A, Bertrand J-M, Rocci G (1987) U/Pb dating of Precambrian rocks from northern Cameroon, orogenic evolution and chronology of the Pan-African belt of Central Africa. Precambrian Res 37:71–87

Toteu SF, Van Schmus WR, Penaye J, Nyobé JB (1994) U–Pb and Sm–Nd evidence for Eburnian and Pan-African high-grade metamorphism in cratonic rocks of southern Cameroon. Precambrian Res 67:321–347

Toteu SF, Van Schmus WR, Penaye J, Michard A (2001) New U–Pb and Sm–Nd data from north-central Cameroon and its bearing on the pre-PanAfrican history of central Africa. Precambrian Res 108(1–2):45–73

Toteu SF, Fouateu RY, Penaye J, Tchakounte J, Mouangue ACS, Van Schmus WR, Deloule E, Stendal H (2006a) U–Pb dating of plutonic rocks involved in the nappe tectonic in southern Cameroon: consequence for the Pan-African orogenic evolution of the central African fold belt. J Afr Earth Sci 44(4–5):479–493

Toteu SF, Penaye J, Deloule E, Van Schmus WR, Tchameni R (2006b) Diachronous evolution of volcano-sedimentary basins north of the Congo craton: insights from U–Pb ion microprobe dating of zircons from the Poli, Lom and Yaoundé Groups (Cameroon). J Afr Earth Sci 44(4–5):428–442

Trompette R (2000) Gondwana evolution; its assembly at around 600 Ma. C R Acad Sci Paris Earth Planet Sci 330:305–315

Turlin F, Eglinger A, Vanderhaeghe O, André-Mayer AS, Poujol M, Mercadier J, Bartlett R (2016) Synmetamorphic Cu remobilization during the Pan-African orogeny: microstructural, petrological and geochronological data on the kyanite-micaschists hosting the Cu(–U) Lumwana deposit in the Western Zambian Copperbelt of the Lufilian belt. Ore Geol Rev 75:52–75

Unrug R (1989) Landsat-based structural map of the Lufilian fold belt and the Kundelungu aulacogen, Shaba (Zaïre)—Zambia and Angola, and the regional position of Cu, Co, U, Au, Zn, and Pb mineralization. In: Boyle et al. (eds) Sediment-hosted stratiform copper deposits, Geological Association of Canada, Special paper, 36:519–524

Vellutini P, Rocci G, Vicat J-P, Gioan P (1983) Mise en évidence de complexes ophiolitiques dans la chaîne du Mayombe (Gabon-Angola) et nouvelle interprétation géotectonique. Precambrian Res 22:1–21

Verbeek T (1970) Géologie et lithologie du Lindien (Précambrien supérieur du Nord de la République démocratique du Congo). Ann Mus Roy Afr Centr in-8°, Sc Géol 70:309

Vicat J-P, Pouclet A (2000) Palaeo- and Neoproterozoic granitoids and rhyolites from the West Congolian Belt (Gabon, Congo, Cabinda, north Angola): chemical composition and geotectonic implication. J Afr Earth Sci 31:597–617

Vicat J-P, Vellutini P (1987) Sur la nature et la signification des dolérites du bassin précambrien de Sembé-Ouesso (République du Congo). Precambrian Res 37:57–69

Vicat J-P, Moloto-A-Kenguemba G, Pouclet A (2001) Les granitoïdes de la couverture protérozoïque de la bordure nord du craton du Congo (Sud-Est du Cameroun et Sud-Ouest de la République centrafricaine), témoins d'une activité magmatique post-kibarienne à pré-panafricaine. C R Acad Sci Paris 332:235–242

Villeneuve M (1973) Essai de synthèse des études sur les formations burundiennes du synclinal de l'Itombwe (Région du Kivu, République du Zaïre). Conséquences sur la structure de ce synclinal.—I.R.S.A.C. Département de Géologie, Publication spéciale, vol 5, p 4

Villeneuve M (1977) Précambrien du Sud du lac Kivu (région du Kivu, Zaïre). Etude stratigraphique, pétrographique et tectonique. Thèse 3^{e} Cycle, Faculté des Sciences St-Jérôme, Université d'Aix-Marseille, p 195

Villeneuve M, Chorowicz J (2004) Les sillons plissés du Burundien supérieur dans la chaîne Kibarienne d'Afrique centrale. C R Geosci 336(9):807–814

Walemba KMA (2001) Geology, geochemistry, and tectono-metallogenic evolution of Neoproterozoic gold deposits in the Kadubu area, Kivu, Democratic Republic of Congo. Ph.D. thesis (unpublished), University of the Witwatersrand, Johannesburg, South Africa, 491 pp. + Appendix 16 pp

Walraven F, Rumvegeri BT (1993) Implications of whole-rock Pb–Pb and zircon evaporation dates for the early metamorphic history of the Kasai Craton, southern Zaire. J Afr Earth Sci 16(4):395–404

Weber F, Gauthier-Lafaye F, Whitechurch H, Ulrich M, El Albani A (2016) The 2-Ga Eburnean Orogeny in Gabon and the opening of the Francevillian intracratonic basins: a review. CR Geosci 348:572–586

The Kalahari Craton, Southern Africa: From Archean Crustal Evolution to Gondwana Amalgamation

6

Sebastián Oriolo and Thomas Becker

Abstract

The Kalahari Craton comprises all Archean to Mesoproterozoic rocks of southern Africa, which are surrounded by Pan-African orogenic belts that resulted from the amalgamation of Gondwana. Progressive crustal growth and accretion of minor crustal blocks is recorded during the Archean and also involved reworking of Hadean crustal remnants, suggesting modern plate tectonics was already operating in the late Neoarchean. The first widespread Paleoproterozoic tectonomagmatic event is recorded by intracontinental magmatism of the Bushveld Complex and the Okwa Terrane, and coeval magmatism in the Limpopo Belt, which separates the Archean Kaapvaal and Zimbabwe cratons. Afterwards, Paleoproterozoic transpression took place along the Limpopo Belt and was contemporaneous with the Magondi Orogeny. Subsequent addition of juvenile Paleoproterozoic crust took place along the western margin of the proto-Kalahari Craton, as recorded by the Rehoboth Basement Inlier. During the Mesoproterozoic, subduction zones were present all around the Archean-Paleoproterozoic proto-Kalahari Craton. The accretion of several microcontinents and island arcs along the southern margin gave rise to the Namaqua-Natal Orogeny. Tonian to Cryogenian intraplate magmatism was finally succeeded by the incorporation of the Kalahari Craton into Gondwana during the protracted Late Neoproterozoic-Early Paleozoic Pan-African Orogeny.

Keywords

Pan-African • Precambrian tectonics • Crustal growth
Crustal recycling • Geochronology

6.1 Introduction

The aim of this chapter is to present an overview of the geology of the Kalahari Craton, including the main tectonostratigraphic units, crustal growth events and tectonic framework. This review focuses on the Archean-Mesoproterozoic history, which culminates with the incorporation of the craton into Gondwana during the Late Neoproterozoic-Early Paleozoic.

The term 'Kalahari Craton' was introduced by Clifford (1970). This definition was later refined by Hartnady et al. (1985) to include Archean to Mesoproterozoic rocks of southern Africa that are surrounded by Pan-African orogenic belts, though the term 'Kgalagadi (Kalahari) Province' was also indicated by Hartnady et al. (1985) to nucleate Paleoproterozoic domains (e.g., Rehoboth, Okwa, Magondi). In contrast, other authors only considered the Archean-Paleoproterozoic domains under this term, thus regarding the Mesoproterozoic belts not as part of the craton (e.g., Dalziel et al. 2000; Powell et al. 2001). Based on contrasting geophysical and petrological characteristics between Archean and post-Archean terranes, de Wit et al. (2008) alternatively proposed the 'Kalahari Shield' to nucleate all Archean to Mesoproterozoic domains and the 'craton' restricted to Archean areas. In this work, the definition of Hartnady et al. (1985) is followed. Therefore the term 'Kalahari Craton' refers to Archean to Mesoproterozoic domains that behaved as a stable coherent block during the Neoproterozoic Pan-African Orogeny, thus fitting the classical craton definition (Neuendorf et al. 2005). More specifically, the term 'proto-Kalahari Craton' (e.g., Jacobs

S. Oriolo
Geoscience Centre, Georg-August-Universität Göttingen, Goldschmidtstraße 3, 37077 Göttingen, Germany

S. Oriolo (✉)
CONICET-UBA. Instituto de Geociencias Básicas, Aplicadas y Ambientales de Buenos Aires, Intendente Güiraldes 2160, C1428EHA Buenos Aires, Argentina
e-mail: seba.oriolo@gmail.com; soriolo@gl.fcen.uba.ar

T. Becker
Bureau de Recherches Géologiques et Minières (BRGM), 3 avenue Claude-Guillemin, BP 36009, 45060 Orléans Cedex 2, France

S. Siegesmund et al. (eds.), *Geology of Southwest Gondwana*, Regional Geology Reviews,
https://doi.org/10.1007/978-3-319-68920-3_6

et al. 2008) is used for all Kalahari nuclei that behaved as a single block prior to the Neoproterozoic.

The Archean domains of the Kalahari Craton crop out in Zimbabwe, eastern Botswana, Swaziland and central-northeastern South Africa (Fig. 6.1). Further to the west, the enigmatic Rehoboth Subprovince is geophysically distinct and is separated from the Kaapvaal Craton by the Kheis and Magondi belts and the Okwa Terrane, despite being hidden beneath Phanerozoic sediments (Fig. 6.1; Clifford 1970; Becker et al. 2006). Paleoproterozoic domains are surrounded by Mesoproterozoic provinces, which are mainly the southern Namaqua-Natal Belt and the northern Sinclair-Ghanzi-Chobe Belt. The Kalahari Craton is bounded by several Neoproterozoic-early Paleozoic Pan-African orogenic belts that resulted from the incorporation of the craton into Gondwana. The Mozambique Belt bounds the Kalahari Craton to the east, whereas the Damara and Zambezi belts are located to the north and separate the Kalahari and Congo cratons. Likewise, the Gariep and Saldania belts crop out to the west and south of the Kalahari Craton, respectively.

6.2 Archean Rocks of the Proto-Kalahari Craton

6.2.1 Introduction

Archean rocks were recognized in the Kaapvaal and Zimbabwe cratons, and the central high-grade Limpopo Belt (Fig. 6.1; Hartnady et al. 1985). Both cratons are characterized by low-grade metavolcanic and metasedimentary rocks, gneisses and granitoids, which represent the typical Archean greenstone belt-TTG (tonalite-trondhjemite-granodiorite) association.

6.2.2 The Kaapvaal Craton

The Kaapvaal Craton extends across northeastern South Africa, northwestern Lesotho, Swaziland and southeastern Botswana (Fig. 6.1). The margins of the craton are overthrust by orogenic belts of different ages. The northern margin is overthrust by rocks of the Limpopo Belt (e.g., Kramers et al. 2006), the western margin by the

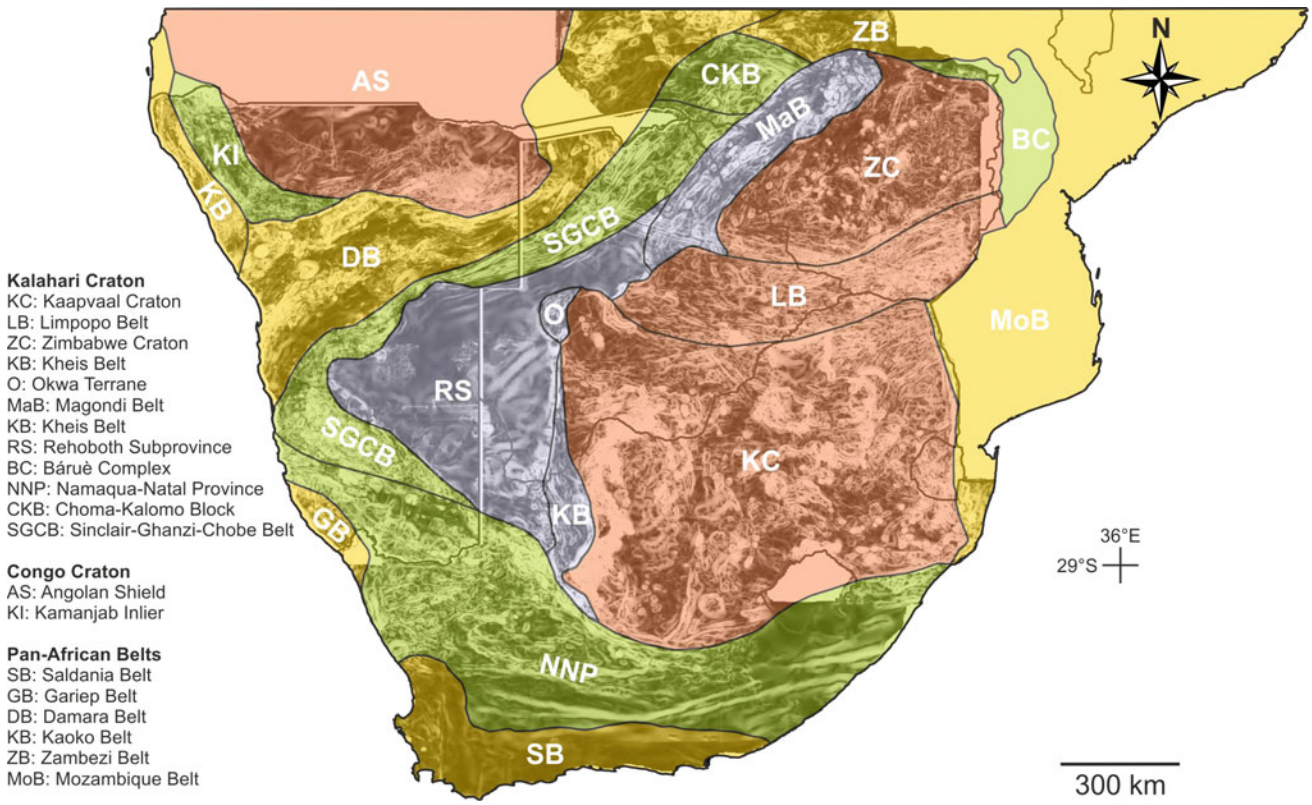

Fig. 6.1 Main Precambrian tectonostratigraphic domains of southern Africa (modified after Hanson 2003 and McCourt et al. 2013). Map of magnetic anomaly (first horizontal derivative) after Becker et al. (2006)

Paleoproterozoic Kheis Belt (Hanson 2003), the southern margin by the Mesoproterozoic Namaqua-Natal Metamorphic Province (de Wit and Tinker 2004) and the eastern margin by the Neoproterozoic Mozambique Belt, albeit overprinted by sinistral shearing (Grantham 2001).

The Kaapvaal Craton is mostly made up of greenstone belts, TTGs and granitoids (Lowe and Byerly 1999, 2007; Brandl et al. 2006; Robb et al. 2006; Kröner 2007; Moyen et al. 2007; Poujol 2007). The main exposures of these rocks are located to the east of the craton in the area from Pietersburg to Barberton and south into Swaziland, and in the west around Gaborone, Amalia, Kimberley and Marydale (e.g., Brandl et al. 2006; Robb et al. 2006). Archean granitoid-TTG-greenstone associations are accompanied by Archean and Paleoproterozoic sedimentary basins and igneous complexes (e.g., Witwatersrand Basin, Bushveld Complex; Robb and Meyer 1995; Eales and Cawthorn 1996; Cawthorn and Walraven 1998; Anhaeusser 2006; Cawthorn et al. 2006; Eriksson et al. 2006; Gold 2006; McCarthy 2006; van der Westhuizen et al. 2006; Verwoerd and du Toit 2006; Manzi et al. 2013).

The Barberton Greenstone Belt comprises the best-preserved association of Archean volcanic and sedimentary rocks of the Kaapvaal Craton (Lowe and Byerly 1999; Brandl et al. 2006 and references therein). Despite being originally referred to as the Swaziland Supergroup assuming an undisturbed supracrustal pile (Anhaeusser 1975), more recent contributions indicate that the Barberton Greenstone Belt constitutes a lithotectonic complex owing to its structural complexity (Brandl et al. 2006 and references therein). The complex presents an age of *c*. 3.54–3.23 Ga and consists of the basal Onverwacht Group, which is dominated by basalts and komatiites; the central Fig Tree Group comprising greywackes, shales, cherts and felsic volcanic rocks; and the upper Moodies Group, characterized by sandstones with minor intercalations of conglomerates and shales (Lowe and Byerly 1999, 2007; Brandl et al. 2006 and references therein).

The oldest intrusions of the Kaapvaal Craton comprise the Eoarchean Ancient Gneiss Complex, which presents the typical Archean TTG association (Hunter 1970; Compston and Kröner 1988; Kröner 2007; Zeh et al. 2011). However, intrusions yielding Paleo- to Neoarchean ages are widespread and include not only TTG suites but also sanukitoids, two-mica granites, monzogranites and syenites, among others (e.g., Robb et al. 2006; Laurent et al. 2011, 2014)

6.2.3 The Zimbabwe Craton

The Zimbabwe Craton is located in Zimbabwe and northeastern Botswana. It is overthrust by the Zambezi Belt in the north, the Báruè Complex in the east and the Limpopo Belt in the south (Hargrove et al. 2003; Kramers et al. 2006; Koistinen et al. 2008). Its western margin is unconformably overlain by rocks of the Magondi Supergroup (Master et al. 2010).

Greenstone belts are distinguished into few Paleoarchean slivers within the Tokwe Terrane (Dodson et al. 1988; Kusky 1998) and late Mesoarchean and Neoarchean rocks, which are ubiquitously recorded (Wilson 1979; Wilson et al. 1995; Kusky 1998).

On the other hand, intrusions present ages between *c*. 3.5 and 2.6 Ga and comprise mostly TTGs and granites (Kusky 1998; Jelsma and Dirks 2000). The oldest intrusions present Paleoarchean ages and crop out within the Tokwe terrane (Kusky 1998; Horstwood et al. 1999; Jelsma and Dirks 2002 and references therein). Late Neoarchean granitoids and TTGs are contemporaneous with the intrusion of the mafic Great Dyke at *c*. 2.58 Ga (Mukasa et al. 1998; Oberthür et al. 2002).

6.2.4 Archean Tectonics and Crustal Growth

The temporal and spatial relationships between Archean greenstone belts and TTG-granitoid intrusions and their tectonic implications have been the matter of a longstanding debate (e.g., Shackleton 1995; Kusky 1998; Dziggel et al. 2002; Jelsma and Dirks 2002; Moyen et al. 2006, 2007; Kröner 2007; Stevens and Moyen 2007; Schoene et al. 2008; Lana et al. 2009; Arndt 2013; Laurent et al. 2014). Mafic and ultramafic rocks of greenstone belts are typically interpreted to result from partial melting of mantle rocks in extensional settings (e.g., Parman et al. 1997; Jelsma and Dirks 2002; Brandl et al. 2006; Lowe and Byerly 2007). On the other hand, TTG suites often represent the oldest components of continental crust, and are typically modelled as forming by partial melting of mafic rocks (Dziggel et al. 2002; Moyen et al. 2006, 2007; Lowe and Byerly 2007; Arndt 2013; Laurent et al. 2014). However, the latter can result not only from subduction-like settings but also from progressive maturation related to mantle upwelling or lower crust delamination (Moyen and Martin 2012; Arndt 2013; Laurent et al. 2014 and references therein). A possible mechanism to explain mobility and accretion of these early crust nuclei in

non-subduction settings was proposed by Bédard et al. (2013), who considered small protocratons that would 'actively' drift as a result of mantle convection, thus contrasting with stable modern cratons that are only deformed along marginal orogenic belts. If present, Archean subduction was most likely related to spatially limited and short-lived subduction zones rather than to long-lived and stable subduction zones, as in modern settings (Moyen and van Hunen 2012). Instead of an abrupt change, the transition from Archean to modern plate tectonics probably constituted a maturation process that took place between the late Archean and the Paleoproterozoic (*c*. 2 Ga), which might result from a thickness decrease of the oceanic crust and/or increasing volume/strength of the continental crust (Moyen and Martin 2012; Moyen and van Hunen 2012; Laurent et al. 2014). This maturation process fundamentally implied stabilization of cratons and subduction along their margins after the cessation of protocraton amalgamation (Moyen and van Hunen 2012).

Archean crustal growth of the proto-Kalahari craton is documented by U–Pb and Lu-Hf zircon data from magmatic and metasedimentary rocks (Fig. 6.2). Even though intrusions older than 3.6 Ga are scarce (Compston and Kröner 1988; Kröner and Tegtmeyer 1994; Kröner et al. 1996; Zeh et al. 2011), Lu-Hf zircon data from granitoids and the detrital zircon record of greenstone belts indicate the existence of juvenile Eoarchean and Hadean crust (Fig. 6.2; Dodson et al. 1988; Zeh et al. 2007, 2008, 2011, 2013a, 2014). Subsequent widespread late Paleo- and Mesoarchean magmatic events are characterized by both addition of juvenile crust and crustal reworking, as recorded by suprachondritic and subchondritic ε_{Hf} values, respectively (Zeh et al. 2007, 2008, 2009, 2010, 2011, 2013b; Zeh and Gerdes 2012; Laurent and Zeh 2015). On the other hand, Neoarchean magmatism was dominated by crustal recycling processes, as recorded by negative ε_{Hf} values (Fig. 6.2). Two main trends can be recognized (Fig. 6.2), implying recycling of Meso- to Eoarchean crust, though subordinated Neproterozoic juvenile crust is recorded as well (Zeh et al. 2007, 2009, 2011).

On the other hand, amalgamation of minor crustal blocks took place in the Kaapvaal and Zimbabwe cratons up to the Neoarchean, giving rise to the development of a relatively thick and stable continental crust in both cratons (Kusky 1998; Jelsma and Dirk 2000, 2002; Moyen et al. 2006, 2007; Stevens and Moyen 2007; Lana et al. 2009; Zeh et al. 2009, 2011; Laurent et al. 2014). Subsequent post-collisional igneous bodies dominated by sanukitoids, peraluminous and K-rich granites and high-K granites intruded the Kaapvaal Craton (Laurent et al. 2014). In a similar way, late Neoarchean post-collisional magmatism is recorded in the Zimbabwe Craton by the Chilimanzi and Razi intrusions, contemporaneously with intraplate mafic magmatism of the Great Dyke intrusion (Frei et al. 1999; Jelsma and Dirks 2002; Oberthür et al. 2002). Thermal relaxation, crustal anatexis and extension are typical processes of post-collisional phases, which would account for the post-collisional magmatism recorded in both cratons (Laurent et al. 2014 and references therein). The great abundance of Neoarchean magmatic zircons with negative ε_{Hf} up to *c*. −20 indicates the dominance of crustal reworking during this time, thus further supporting a collisional to post-collisional setting, for which crustal reworking processes are more likely to occur (Collins et al. 2011). Hence, Archean nuclei of the Kalahari Craton were blocks of tectonically thickened crust already at *c*. 2.6–2.5 Ga (Jelsma and Dirks 2002; Oberthür et al. 2002; Laurent et al. 2014), supporting proposals that modern-style plate tectonic processes were operating at *c*. 2.5 Ga (e.g., Moyen and van Hunen 2012; Laurent et al. 2014).

6.2.5 The Limpopo Belt

The east-northeast-trending Limpopo Belt occurs in northeastern South Africa, southern Zimbabwe and eastern Botswana. It is separated from the Zimbabwe and Kaapvaal cratons by the North Limpopo Thrust Zone and the Hout River Shear Zone, respectively.

The Limpopo Belt is mostly composed of high-grade gneisses and granitoids (MacGregor 1953; Kramers et al. 2006 and references therein), and consists of the Southern and Northern Marginal Zones and the Central Zone, which are separated from each other by major shear zones (Mason 1973; Coward et al. 1976; van Biljon and Legg 1983; Coward and Daly 1984; van Reenen et al. 1987; McCourt and Vearncombe 1992; Roering et al. 1992). Granulite facies paragneisses, charnockites and granitoid gneisses dominate in the Southern Marginal Zone; whereas high-grade metasedimentary rocks, leucocratic orthogneisses and mafic rocks constitute the Central Zone. The Northern Marginal Zone is characterized by granulite facies orthogneisses (Kramers et al. 2006 and references therein).

Three distinct magmatic events are recorded at *c*. 3.3–3.1 Ga, 2.75–2.50 Ga and 2.06–1.90 Ga, and two high-grade metamorphic and deformation events are associated with the younger magmatic episodes (Kramers et al. 2006, 2014; Zeh et al. 2007 and references therein). Paleo- to Mesoarchean magmatic rocks and Sm–Nd and Lu–Hf model ages indicate crustal reworking of the basement of the Kaapvaal and Zimbabwe cratons in the Southern and Northern Marginal Zones, respectively (Zeh et al. 2007; Nicoli et al. 2015). In the case of the Neoarchean tectonomagmatic event, some authors considered continental collision of the Kaapvaal and Zimbabwe cratons along the Limpopo Belt (Watkeys et al. 1983; Burke et al. 1985; Van Reenen et al. 1987; Ranganai et al. 2002; Kramers et al.

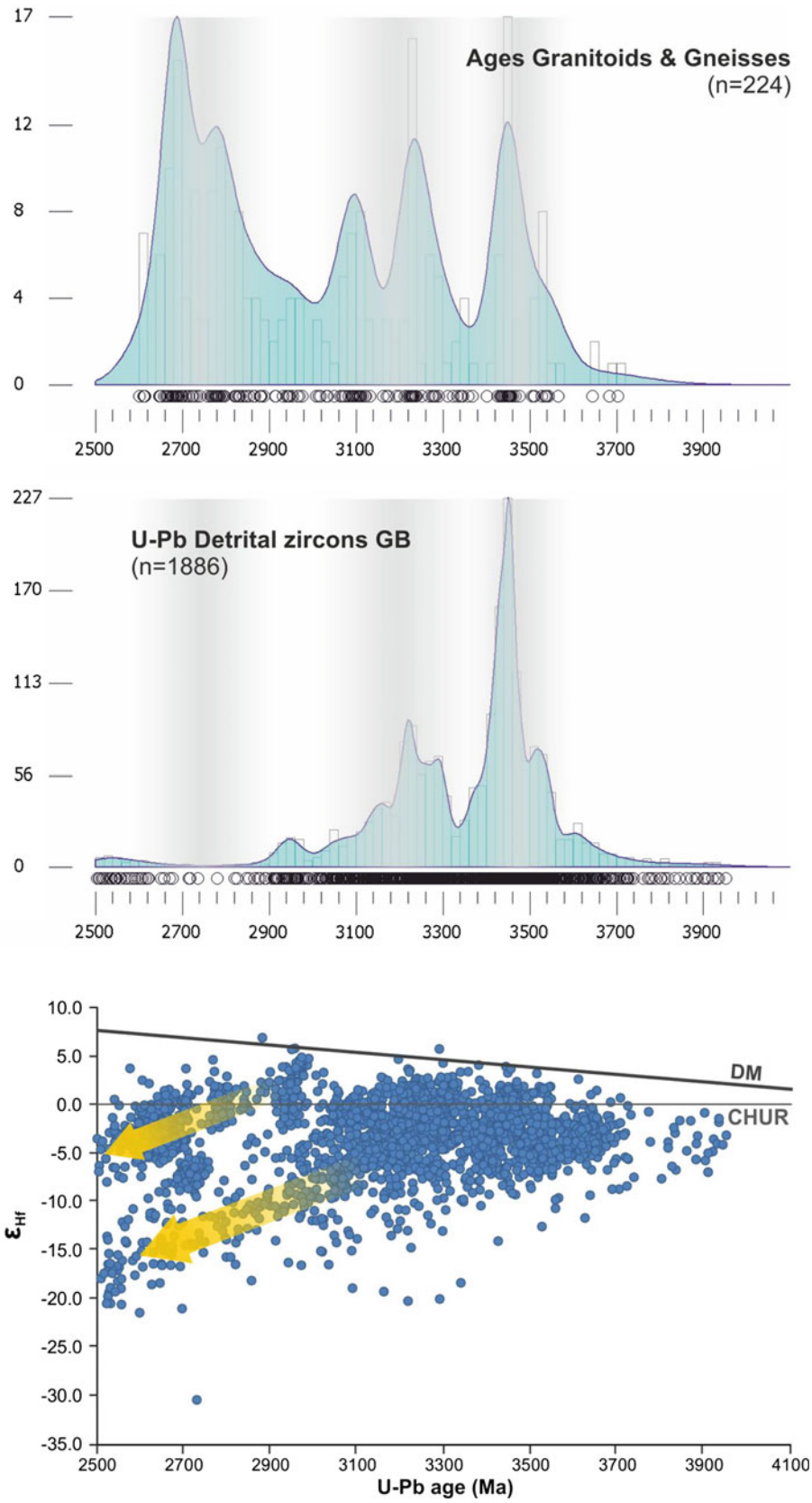

Fig. 6.2 Kernel density estimation plots (KDE) and histograms of available U–Pb and Pb–Pb (age vs. cumulative frequency) zircon ages from Archean intrusions and greenstone belts (GB) plotted using DensityPlotter (Vermeesch 2012) and ε_{Hf} versus U–Pb ages of both magmatic and detrital zircons (n = 2632). Lu–Hf data were recalculated considering a constant decay λ $^{176}Lu = 1.867 \times 10^{-11}$ year^{-1} (Söderlund et al. 2004) and CHUR values of $^{176}Hf/^{177}Hf = 0.282772$ and $^{176}Lu/^{177}Hf = 0.0332$ (Blichert-Toft and Albarède 1997). Data from Anhaeusser and Burguer (1982), Tegtmeyer and Kröner (1987), Compston and Kröner (1988), Dodson et al. (1988), Matthews et al. (1989), Walraven (1989), York et al. (1989), Armstrong et al. (1990), Kamo et al. (1990), Kröner et al. (1991, 1992, 1996, 2000), Taylor et al. (1991), Barton et al. (1992), Kamo (1992), Layer et al. (1992), Robb et al. (1992, 1993), de Wit et al. (1993), Grobler and Walraven (1993), Maphalala and Kröner (1993), Moore et al. (1993), Reimold et al. (1993), Kamo and Davis (1994), Kröner and Tegtmeyer (1994), Jelsma et al. (1996), Poujol et al. (1996, 2002), Thomas et al. (1997), Anhaeusser and Walraven (1999), Horstwood et al. (1999), Poujol and Robb (1999), Amelin et al. (2000), Henderson et al. (2000), Moser et al. (2001), Poujol (2001), Poujol and Anhaeusser (2001), Bagai et al. (2002), Dziggel et al. (2002), Fletcher (2003), Anhaeusser and Poujol (2004), Zeh et al. (2007, 2008, 2009, 2010, 2011, 2013a, b, 2014), Grosch et al. (2011), Sánchez-Garrido et al. (2011), Zeh and Gerdes (2012), Heubeck et al. (2013) and Laurent and Zeh (2015)

2011; Khoza et al. 2013; Rajesh et al. 2014; Nicoli et al. 2015), whereas others interpreted it as the result of the accretion of minor crustal blocks in the Limpopo Belt (Rollinson 1993; Zeh et al. 2007, 2009; Laurent et al. 2014; Laurent and Zeh 2015). The Paleoproterozoic event was characterized by transpression along large-scale shear zones and was attributed to either amalgamation of the Kaapval and Zimbabwe cratons (Kamber et al. 1995; Holzer et al. 1998, 1999; Schaller et al. 1999; Zeh et al. 2004, 2005a, b, 2007) or intracontinental deformation triggered by thermal weakening resulting from magmatic underplating (Kramers et al. 2011).

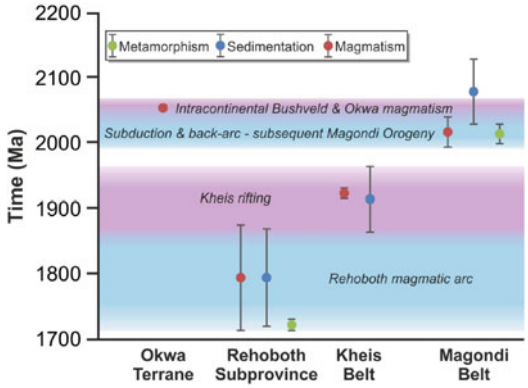

Fig. 6.3 Timing and duration of the main tectonic processes during the Paleoproterozoic (see text for further explanation and references)

6.3 Paleoproterozoic Blocks and Belts

6.3.1 Introduction

The Archean core of the Kalahari Craton is bounded by the Kheis and Magondi belts and the Okwa Terrane to the west and northwest (Fig. 6.1; Hartnady et al. 1985; Hanson 2003; McCourt et al. 2013). The Rehoboth Subprovince is located further to the west and is mostly hidden under a thick pile of Paleozoic to Cenozoic sedimentary rocks. However, Paleoproterozoic rocks of the Rehoboth Group and pre-Rehoboth high-grade metamorphic complexes are exposed at its northern and western margins in Namibia (Becker and Schalk 2008a).

6.3.2 The Okwa Terrane

The Okwa Terrane comprises a small isolated basement inlier, which crops out in the Kalahari Desert in Botswana. It is aligned with the Kheis and Magondi belts to the south and north, respectively, and bounded to the southeast by the Kaapvaal Craton, although this contact is covered beneath Cenozoic sands of the Kalahari Group. To the northwest it is unconformably overlain by rocks of the Ghanzi-Chobe Belt (Ramokate et al. 2000).

This basement inlier is mostly made up of metarhyolites, foliated and unfoliated monzogranites and microgranitoids (Ramokate et al. 2000; Mapeo et al. 2006 and references therein). U–Pb ID-TIMS zircon ages of 2.06–2.05 Ga constrain the age of the felsic magmatism (Fig. 6.3; Ramokate et al. 2000; Mapeo et al. 2006). K–Ar and Rb–Sr data, in turn, show ages of *c*. 2.0–1.8 and 1.2–1.0 Ga (Key and Rundle 1981), the latter probably being the result of isotopic resetting during the evolution of the Mesoproterozoic Namaqua-Natal Belt.

6.3.3 The Rehoboth Subprovince

The Rehoboth Subprovince lies in eastern Namibia, the adjacent part of southwest Botswana and western South Africa (Fig. 6.1; Hartnady et al. 1985). Despite being mostly covered by Paleozoic to Cenozoic sedimentary rocks, the Rehoboth Subprovince is clearly recognizable through geophysical data (Fig. 6.1; Becker et al. 2006; Corner 2008; Muller et al. 2009) and is well exposed in the Rehoboth Basement Inlier along its western and northwestern margins.

The Pre-Rehoboth Group units include orthogneisses, migmatites and amphibolites of the Kangas Metamorphic Complex, which yield U–Pb zircon ages of *c*. 1.83–1.78 Ga (Burger and Walraven 1978; Becker et al. 1996; Nagel et al. 1996; Becker and Brandenburg 2000; Becker and Schalk 2008a; van Schijndel et al. 2014). Orthogneisses of the Kangas Metamorphic Complex show Lu-Hf model ages of 2.26–2.24 Ga with ε_{Hf} and $\delta^{18}O$ values of 2.7–3.2 and 4.30–5.27‰, respectively (van Schijndel et al. 2014).

The Rehoboth Group comprises the Marienhof, Ellim and Gaub Valley formations and is made up of metaquartzites, metaconglomerates, metapelites, schists, marbles and voluminous felsic and mafic metavolcanic rocks (Becker and Brandenburg 2000; Becker et al. 2000; Becker and Schalk 2008a). U–Pb zircon ages of metavolcanic rocks constrain the deposition age of the Rehoboth Group between 1.79 and 1.75 Ga (Becker et al. 1996; Nagel et al. 1996; van Schijndel et al. 2014). Zircons from these rocks have Lu-Hf model ages of *c*. 2.35–2.15 Ga, ε_{Hf} =+0.5 to + 4.1 and $\delta^{18}O$ = 4.31–9.35‰ (van Schijndel et al.2014), whereas mafic metavolcanic rocks of the Elim Formation present Sm–Nd T_{DM} model ages of 1.98–1.95 Ga and ε_{Nd} values

from +1.92 to +2.26 (Becker et al. 2004). Based on a U–Pb LA-ICP-MS zircon age of a unit interpreted as a tuffaceous marl, van Schijndel et al. (2014) considered the Elim Formation to be older than the Rehoboth Group. Detrital zircons of the Marienhof Formation scatter mainly between 2.1 and 1.75 Ga, although a few Rhyacian and late Archean grains are present as well, suggesting mixing of a local source and an older source situated possibly further south (van Schijndel et al. 2014). Subsequent Paleoproterozoic metamorphism of the volcanoclastic successions of the Rehoboth Group reached peak amphibolite facies conditions (Becker and Schalk 2008a).

The Weener Igneous Complex and the Piksteel Intrusive Suite represent the main calc-alkaline suites of the Rehoboth Basement Inlier and are intrusive into both the Rehoboth Group and its basement (Becker et al. 1996). They comprise tonalitic, dioritic and granodioritic intrusions yielding U–Pb zircon ages between *c*. 1.78 and 1.72 Ga (Fig. 6.3; Ziegler and Stoessel 1991, 1993; Becker et al. 1996; Becker and Schalk 2008a; van Schijndel et al. 2014). Despite being almost contemporaneous according to geochronological data, field relationships indicate that the Piksteel Intrusive Suite intruded the Weener Igneous Complex (Becker et al. 1996). These intrusions yield Sm–Nd T_{DM} model ages of *c*. 2.30–1.78 Ga with ε_{Nd} between −0.18 and 5.49 (Ziegler and Stoessel 1991; Becker et al. 2000, 2004). Comparable Lu-Hf T_{DM} model ages of 2.19–2.17 Ga and ε_{Hf} values of 3.0–3.1 were reported for zircons of these units, which also yield $\delta^{18}O$ values of 5.95–7.55 (van Schijndel et al. 2014).

The mafic and ultramafic Alberta and Doornboom Mafic Complexes intrude the Elim Formation and the Rehoboth Group (Becker and Brandenburg 2000; Becker and Schalk 2008a). In the case of the Alberta Mafic Complex, Sm–Nd data show T_{DM} values of 2.25–1.58 Ga with associated ε_{Nd} between 0.21 and 4.52 (Becker et al. 2004).

Geochemical, isotopic and geochronological data indicate that the Rehoboth Group evolved within a Statherian magmatic arc setting, probably located at the proto-Kalahari Craton margin (Becker et al. 1996, 2000, 2004; Becker and Schalk 2008a; van Schijndel et al. 2014). A final tectonometamorphic event was recorded at *c*. 1.72 Ma, reaching amphibolite conditions (Becker and Schalk 2008a), though the characteristics and tectonic significance of this event remain uncertain. Afterwards, the Rehoboth Subprovince was overlain by Mesoproterozoic volcanoclastic successions and intruded by associated voluminous granites and granodiorites (Sect. 6.4.4.3).

6.3.4 The Kheis Belt

The north-trending Kheis Belt is exposed to the west of the Kaapvaal Craton in South Africa and Botswana (Fig. 6.1). It comprises an east-verging thin-skinned fold-and-thrust belt, which overthrusts the western margin of the Kaapvaal Craton along the Blackridge Thrust (Visser 1944; Hanson 2003; van Niekerk 2006). The Kalahari Lineament defines the boundary between the Kheis Belt and the Rehoboth Subprovince and, though covered by younger sediments, it is well defined by geophysical data (Hutchins and Reeves 1980; Jacobs et al. 2008). To the southwest, the Dabep Thrust forms the boundary between the Kheis Belt and the Mesoproterozoic Namaqua-Natal Province (Moen 1999, 2006; Cornell et al. 2006).

The Kheis Belt is made up by rocks of the Olifantshoek Supergroup, which represents a low-grade metamorphic succession of quartzites, sandstones, conglomerates, greywackes, tuffs and andesitic lavas (Moen 1999, 2006). Geochronological data constrain the age of the synsedimentary magmatism at 1.92–1.93 Ga (Fig. 6.3; Cornell et al. 1998; da Silva 2011), whereas the age distribution of detrital zircons shows a main peak at *c*. 2.2–1.9 Ga with few zircons of Archean age (van Niekerk 2006; da Silva 2011). Sedimentation of the Olifantshoek Supergroup took place along the western margin of the Kaapvaal Craton in a fluvial to shallow marine platform setting, with magmatism probably related to an Orosirian rifting event (Fig. 6.3; Hanson 2003; Moen 2006).

The metamorphic grade of the Kheis Belt increases westward but does not surpass low-grade conditions (Hanson 2003; Moen 2006). Associated deformation was related to east-verging folding and thrusting, with strain increasing to the west (Hanson 2003; Moen 2006). Ar/Ar muscovite data show ages of *c*. 1.1 Ga (van niekerk 2006), thus supporting a Mesoproterozoic age for deformation and metamorphism of the Kheis Belt related to the Namaqua-Natal Belt (Moen 1999), although previous contributions considered a Paleoproterozoic age (e.g., Cornell et al. 1998).

6.3.5 The Magondi Belt

The Magondi Belt extends between northwestern Zimbabwe and northeastern Botswana (Fig. 6.1). It unconformably overlays rocks of the Zimbabwe Craton to the east, whereas its western margin is covered by younger sediments (Carney et al. 1994; Master et al. 2010).

The Magondi Belt comprises the Magondi Supergroup and rocks of the Dete-Kamativi Inlier (Treloar 1988; Master 1991a, b; Master et al. 2010). The Magondi Supergroup can be subdivided into the Deweras, Lomagundi and Piriwiri groups, which are dominated by siliciclastic sediments with subordinated dolomites, mafic to felsic volcanites and volcaniclastic rocks (Master et al. 2010 and references therein). In turn, the Dete-Makativi Inlier consists of garnet- and sillimanite-bearing paragneisses, metavolcanites, micaschists, metaquartzites, orthogneisses and granites

(Master et al. 2010 and references therein). Despite being unclear, the intrusion of granites in the Dete-Makativi Inlier might be coeval with sedimentation of the upper sequences of the Magondi Supergroup (Master et al. 2010).

Deformation of the Magondi Supergroup is related to a southeast-verging thin-skinned fold-and-thrust belt (Treloar 1988). On the other hand, the metamorphic grade of the Magondi Supergroup varies from greenschist facies in the southeast to granulite facies in the northwest, whereas metasedimentary rocks of the Dete-Kamativi Inlier show amphibolite to granulite facies metamorphism and represent higher-grade counterparts of the Magondi Supergroup (Treloar 1988; Munyanyiwa et al. 1995; Master et al. 2010). U–Pb SHRIMP detrital zircon data provide a maximum sedimentation age of 2.13–2.12 Ga in a back-arc setting, whereas the metamorphism was dated at 2.03–2.00 Ga during closure and deformation of the basin (Fig. 6.3; Treloar and Kramers 1989; Master 1991a, b; Mapeo et al. 2001; Master et al. 2010), coinciding with the 2.0 Ga age of the late synkinematic Hurungwe granite (McCourt et al. 2001). Although the age of granitoids associated with the belt is Paleoproterozoic (Fig. 6.3; Priem et al. 1972; McCourt et al. 2001; Majaule et al. 2001; Mapeo et al. 2001), zircon xenocrysts as well as Archean Sm–Nd model ages indicate that the Magondi Belt possibly comprised reworked Archean crust of the Zimbabwe Craton (Majaule et al. 2001).

6.3.6 Tectonic Implications

Although several contributions attempted to correlate different Paleoproterozoic tectonostratigraphic units (e.g., Hanson 2003; Master et al. 2010), tectonic models to explain the complete Paleoproterozoic evolution of the proto-Kalahari Craton are scarce (Master 1993). The oldest record corresponds to magmatism in the Okwa Terrane at *c*. 2.05 Ga, which was correlated with intraplate magmatism of the Bushveld Complex in the Kaapvaal Craton (Figs. 6.3 and 6.4a; Mapeo et al. 2006). Coeval sedimentation is recorded in the Magondi Belt and is probably related to crustal extension in a back-arc setting (Fig. 6.4a), which was associated with subduction beneath the proto-Kalahari Craton (Master et al. 2010). This is supported by Archean zircon xenocrysts as well as Archean Sm–Nd model ages recorded in granitoids of the Magondi Belt (Majaule et al. 2001), indicating reworking of Archean crust. Hence intraplate magmatism and crustal extension took place in the proto-Kalahari Craton at 2.05 Ga, probably with coeval subduction along its western margin.

The timing of the Magondi Orogeny matches the timing of the Paleoproterozoic metamorphic and deformation event of the Limpopo Belt, indicating a common evolution of both areas (Figs. 6.3 and 6.4b; Master et al. 2010). Furthermore, approximately northwest-directed shortening giving rise to southeast-verging folding and thrusting of the Magondi Belt (Treloar 1988) would satisfactorily explain dextral transpression of Limpopo Belt (Holzer et al. 1999), with deformation of the latter probably being triggered by thermal weakening (Kramers et al. 2011). Although a collision of an unknown terrane at the northwestern margin of the Archean nucleus was tentatively proposed to account for this tectonic event (Master et al. 2010), the tectonic setting of the Magondi Orogeny remains unclear.

Despite being classically correlated (e.g., Hanson 2003; Master et al. 2010), sedimentation and magmatism in the Kheis Belt are younger than in the Magondi Belt (Figs. 6.3 and 6.4c; Cornell et al. 1998). Hence, rifting-related magmatism and sedimentation along the western margin of the proto-Kalahari Craton post-dates the Magondi Orogeny (Fig. 6.3). Although a Paleoproterozoic event cannot be discarded, geochronological data point to a Mesoproterozoic tectonic event as the trigger of deformation and metamorphism of the Olifantshoek Supergroup in the Kheis Belt (Moen 1999; van Niekerk 2006).

On the other hand, the Rehoboth Subprovince arises as a more singular tectonostratigraphic unit, not only because it records arc-related magmatism and sedimentation after *c*. 1.9 Ga but also because it preserves evidence of Paleoproterozoic juvenile crust (Fig. 6.3). Pre-Rehoboth units seem to represent oceanic and island arc sequences that were accreted to the continental margin (Fig. 6.4d; van Schijndel et al. 2014), although other contributions indicated a back-arc setting for rocks of the Elim Formation (e.g., Becker and Brandenburg 2000; Becker and Schalk 2008a). Isotopic, geochemical and geochronological data indicate that subsequent deposition of the Rehoboth Group and intrusion of associated magmatic rocks were related to a convergent margin at *c*. 1.77–1.72 Ga (Fig. 6.4e; Becker and Brandenburg 2000; Becker and Schalk 2008a; van Schijndel et al. 2014), comprising either an island arc (Becker et al. 2004) or a volcanic arc related to a thickened continental margin due to the previous accretionary complexes (Becker and Schalk 2008a; van Schijndel et al. 2014). Associated back-arc sedimentation and magmatism are recorded as well (Becker and Brandenburg 2000; Becker et al. 2000; Becker and Schalk 2008a; van Schijndel et al. 2014). The presence of Archean Lu-Hf model ages and ε_{Hf} subchondritic values in zircons of the Gaub Valley Formation may indicate the presence of an older crustal component in the Rehoboth Inlier (van Schijndel et al. 2014). Assuming that this area occupied a marginal position close to the proto-Kalahari margin, the Lu-Hf isotopy could alternatively be explained by the presence of an enriched mantle source, which was clearly documented in the Bushveld Complex (Zirakparvar et al. 2014). Hence the Kangas Metamorphic Complex and the Rehoboth Group record the progressive

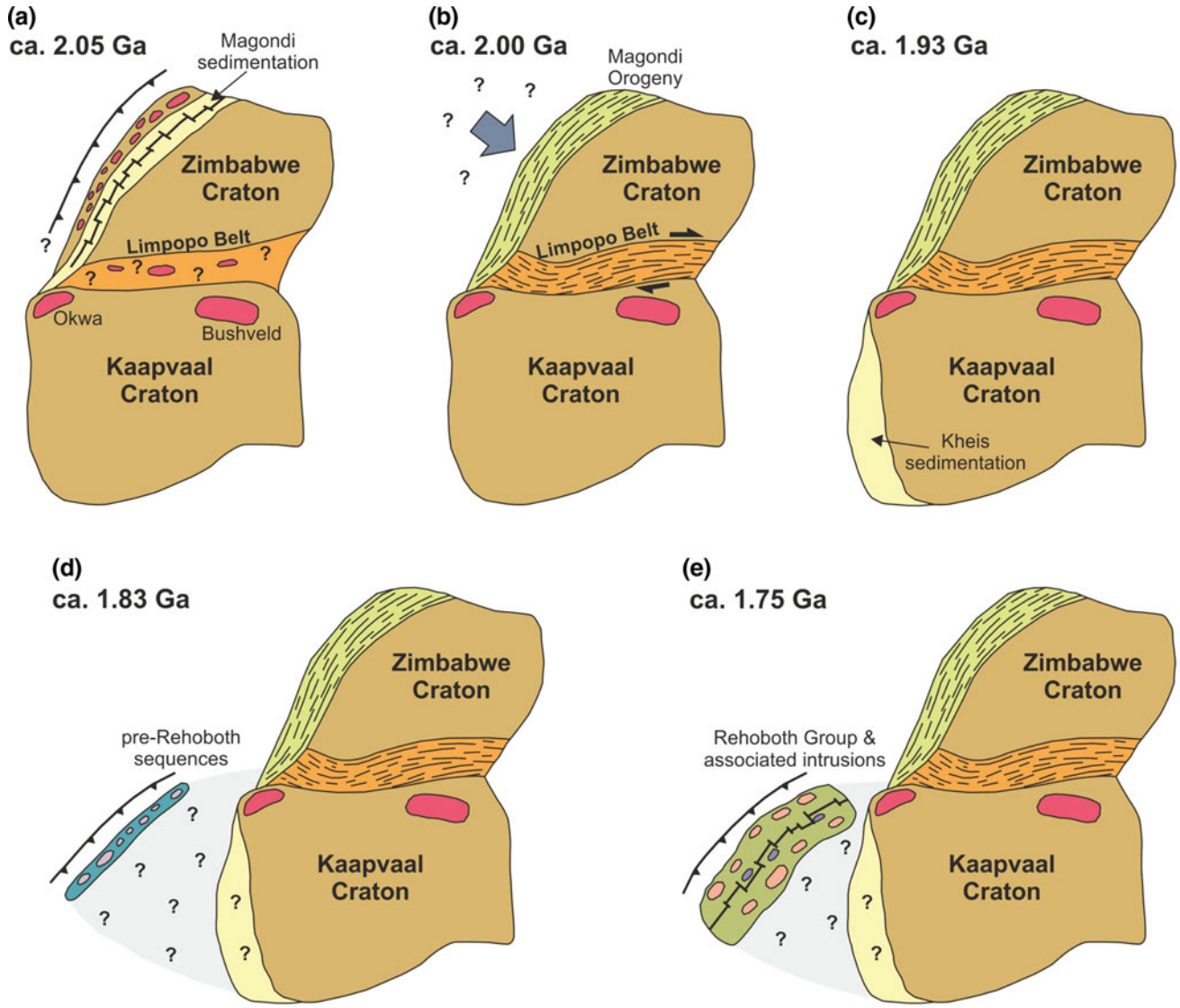

Fig. 6.4 Schematic Paleoproterozoic tectonic evolution modified after Becker et al. (2000, 2004), Becker and Schalk (2008a), Master et al. (2010) and van Schijndel et al. (2014). See text for further discussion. **a** Subduction and back-arc extension with associated magmatism and sedimentation in the Magondi Belt. The Limpopo Belt, Okwa Terrane and Bushveld Complex record coeval magmatism. Question marks in the Limpopo Belt indicate uncertainties regarding the accretion of the Kaapvaal and Zimbabwe cratons during or prior to the Paleoproterozoic (Sect. 6.2.5). **b** Magondi Orogeny and transpressional event in the Limpopo Belt. **c** Sedimentation along the southwestern proto-Kalahari Craton margin after the Magondi Orogeny. **d** Early subduction recorded by pre-Rehoboth sequences. **e** Subduction with associated arc magmatism (pink) and back-arc mafic intrusions (violet)

evolution of an active margin from an arc to a back-arc setting, implying also accretionary tectonics.

6.4 Mesoproterozoic Terranes

6.4.1 Introduction

Major tectonometamorphic events affected the margins of the proto-Kalahari Craton that was consolidated at the end of Paleoproterozoic times. These orogenic events gave rise to the development of four tectonostratigraphic units—the Báruè Complex, the Choma-Kalomo Block, the Sinclair-Ghanzi-Chobe Belt and the Namaqua-Natal Province (Fig. 6.1)—whereas they also reworked several Archean and Paleoproterozoic domains.

6.4.2 The Báruè Complex

The Báruè Complex lies at the northeastern Kalahari Craton in central-western Mozambique (Fig. 6.1). It is in contact

with Archean gneisses and Paleoproterozoic metasediments of the Zimbabwe Craton along a major sinistral strike-slip shear zone to the west, whereas it is bounded by faults to the east and south that separate it from Phanerozoic sediments (Koistinen et al. 2008).

The Báruè Complex includes mainly granitoids, medium- to high-grade felsic orthogneisses and migmatites, with minor intercalations of marbles, quartzites and mafic rocks (Koistinen et al. 2008). Zircons from igneous and metaigneous units yield crystallization U–Pb SHRIMP and TIMS ages of *c*. 1.20–1.04 Ga (Fig. 6.5), whereas Sm–Nd whole-rock isochron ages of *c*. 1.0–1.15 Ga were obtained for the mafic rocks (Manhica et al. 2001; Mänttäri 2008). Although sedimentation of these rocks might be related to a passive margin setting at the proto-Kalahari margin during the Mesoproterozoic, they show Neoproterozoic reworking related to deformation and metamorphism of the Mozambique Belt (Manhica et al. 2001; Koistinen et al. 2008; Mänttäri 2008).

6.4.3 The Choma-Kalomo Block

The Choma-Kalomo Block is located in southern Zambia and comprises a small basement inlier at the northern edge of the Kalahari Craton (Fig. 6.1). Despite being covered by Neoproterozoic and younger sedimentary sequences, subsurface data suggest correlations to the southwest with the Sinclair-Ghanzi-Chobe Belt (Hanson 2003; Singletary et al. 2003)

The Choma-Kalomo Block is made up of granitoids, orthogneisses and migmatites as well as amphibolite facies paragneisses, schists and metabasic rocks (Fig. 6.1; Hanson et al. 1988; Hanson 2003; Bulambo et al. 2006). Few U–Pb TIMS and SHRIMP zircon ages record two distinct magmatic events at *c*. 1.37–1.34 Ga and 1.20–1.15 Ga (Fig. 6.5; Hanson et al. 1988; Bulambo et al. 2006).

The structure of the Choma-Kalomo Block is characterized by distinct northeast-trending tight to isoclinal folds, which overprint a previous north- to northwest-striking structural grain (Hanson et al. 1988 and references therein). Both sets of structures are crosscut by pegmatites with Rb–Sr and K–Ar muscovite ages of *c*. 1.10–1.06 Ga, thus constraining the end of metamorphism and deformation (Hanson et al. 1988). Hence the tectonometamorphic event of the Choma-Kalomo Block probably took place at *c*. 1.20–1.15 Ga (Hanson et al. 1988; Singletary et al. 2003; Bulambo et al. 2006).

6.4.4 The Sinclair-Ghanzi-Chobe Belt

6.4.4.1 Introduction

The Sinclair-Ghanzi-Chobe Belt extends from southern Namibia to northern Botswana (Fig. 6.1) but is mainly exposed in its southwestern portion. In eastern Namibia and Botswana, it comprises a series of isolated basement inliers within sands of the Kalahari Group (e.g., Modie 1996). The southwesternmost part of the belt is represented by the Sinclair-Helmeringshausen-Awasib Terrane, which is separated by the west-northwest-trending Hauchab-Excelsior-Lord Hill Shear Zone from the Namaqua Belt to the southwest and can be correlated to the north and the northeast with Mesoproterozoic rocks of the Rehoboth Basement Inlier and the Ghanzi-Chobe Belt, respectively (Fig. 6.1; e.g., Hoal 1985, 1990; Modie 1996; Becker et al. 2006). Mesoproterozoic metamorphic complexes of similar character are exposed as basement inliers in the Damara Belt and are thus analysed here.

6.4.4.2 The Sinclair-Helmeringshausen-Awasib Terrane

The oldest Mesoproterozoic rocks of the Sinclair-Helmeringshausen-Awasib Terrane are represented by the medium-grade Kairab-Kumbis Metamorphic Complex (Watters 1974; Hoal 1985; Becker et al. 2006). This comprises paragneisses, amphibolites, serpentinites, schists and mafic to felsic metaigneous rocks, intruded by orthogneisses yielding protolith crystallization ages of *c*. 1.38–1.37 Ga (Fig. 6.5; Watters 1974; Hoal 1985, 1990; Hoal and Heaman 1995; Becker et al. 2006).

The Kairab-Kumbis Metamorphic Complex is unconformably overlain by the Sinclair Group, which comprises lavas, volcaniclastic rocks, conglomerates, sandstones, quartzites, and pelites showing subgreenschist to greenschist facies metamorphism (Watters 1976; Becker et al. 2006; Becker and Schalk 2008b and references therein). The maximum age of the Sinclair Group is constrained by *c*. 1.38–1.37 Ga-old gneisses of the underlying Kairab-Kumbis Metamorphic Complex (Hoal and Heaman 1995; Becker et al. 2006). U–Pb multigrain and single-grain zircon data show ages between *c*. 1.29 and 1.08 Ga for magmatism during sedimentation of the Sinclair Group (Fig. 6.5). This is supported by U–Pb LA-ICP-MS detrital zircon data, which provide a maximum deposition age of 1.11 Ga for the Aubures Formation, the uppermost unit of the Sinclair Group (Kasbohm et al. 2015). Additionally, these data indicate a main source with ages of *c*. 1.4–1.1 Ga and a minor Paleoproterozoic and Archean contribution (Kasbohm et al. 2015).

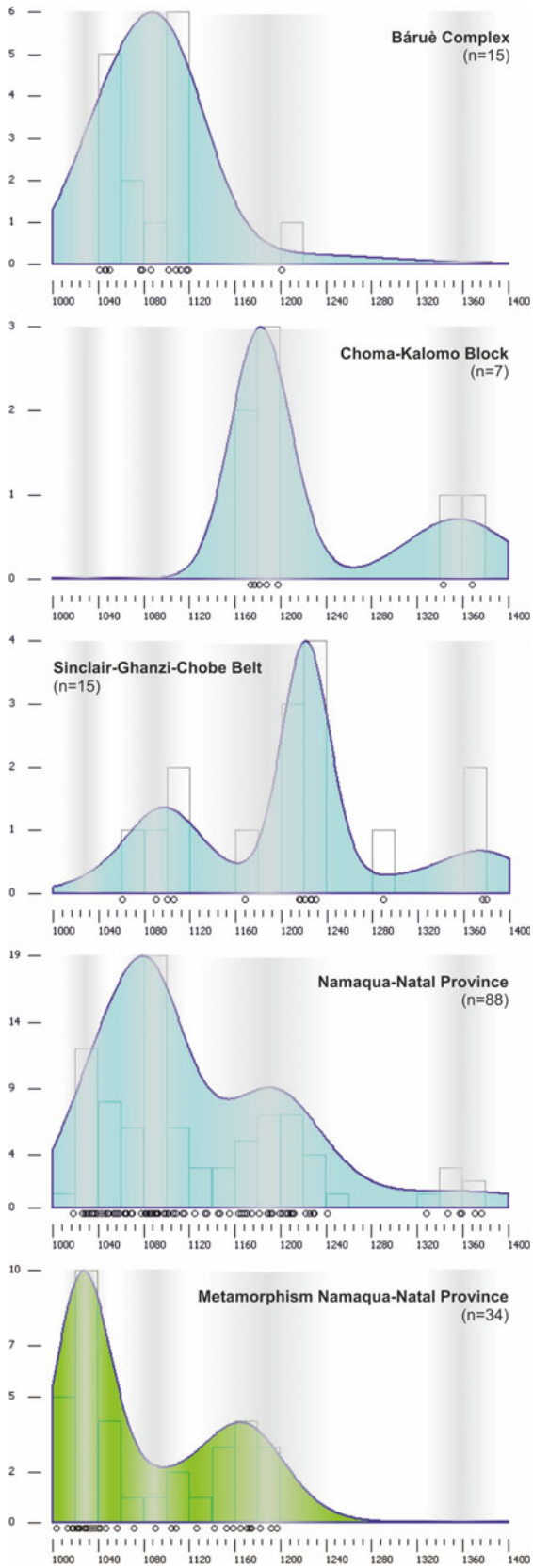

Fig. 6.5 Kernel density estimation plots (KDE) and histograms of available geochronological zircon data (age vs. cumulative frequency) for Mesoproterozoic intrusions and metamorphism plotted using DensityPlotter (Vermeesch 2012). Data from Hanson et al. (1988), Thomas and Eglington (1990), Thomas et al. (1993, 2003), Hoal and Heaman (1995), Schwartz et al. (1996), Robb et al. (1999), Johnston et al. (2001), Manhica et al. (2001), Mendonidis et al. (2002, 2009, 2015), Eglington and Armstrong (2003), Eglington et al. (2003, 2010), Clifford et al. (2004), Schneider et al. (2004), Becker et al. (2006), Bulambo et al. (2006), Cornell and Thomas (2006), Bailie et al. (2007), Cornell and Pettersson (2007), Pettersson et al. (2007), Mänttäri (2008), Mendonidis and Armstrong (2009), Cornell et al. (2012, 2015), Mapani et al. (2014), van Schijndel et al. (2014), Bachmann et al. (2015), Bial et al. (2015a, b), Colliston et al. (2015) and Spencer et al. (2015)

6.4.4.3 Mesoproterozoic Rocks of the Rehoboth Basement Inlier

Paleoproterozoic rocks of the Rehoboth Basement Inlier are overlain by Mesoproterozoic metavolcanosedimentary units and intruded by coeval granitoids. Volcanosedimentary units comprise three main sequences (SACS 1980; Schneider et al. 2004; Becker et al. 2005).

The basal Billstein Formation comprises mainly metapelitic rocks with minor metaconglomerates and metaquartzites, and intercalated metabasalts (Schneider et al. 2004; Becker et al. 2005). The deposition age of the Billstein Formation is poorly constrained, as a maximum age of *c*. 1.7 Ga is indicated by detrital zircon data and a minimum age of *c*. 1.21 Ga is provided by porphyritic intrusions (Ziegler and Stoessel 1993; van Schijndel et al. 2011, 2014).

The overlying Nauzerus Group represents the northern equivalent of the Sinclair Group and comprises volcaniclastic sequences with associated felsic magmatism (Schneider et al. 2004; Becker et al. 2005, 2006 and references therein). Volcanic rocks yield U–Pb zircon ages of *c*. 1.23–1.09 Ga (Schneider et al. 2004; Becker et al. 2006 and references therein). Detrital zircon data show a main peak at *c*. 1.32–1.10 Ga and a minor Paleoproterozoic contribution (van Schijndel et al. 2011a). The Nauzerus Group is intruded by calc-alkaline granites of the Gamsberg Granitic Suite, which yield U–Pb zircon multigrain ages between *c*. 1.22–1.01 Ga (Becker et al. 2006; Becker and Schalk 2008b and references therein) and are further supported by U–Pb SIMS zircon data (van Schijndel et al. 2014). A Lu-Hf model age of 2.06 Ga was obtained for a granite of this suite (van Schijndel et al. 2014).

The uppermost sequence is represented by the Skumok and Opdam formations, starting with a basal clastic association of quartzites, conglomerates and slates that are conformably overlain by basaltic flows, flow breccias and scarce pillow basalts (Schneider et al. 2004; Becker et al. 2005, 2006; Becker and Schalk 2008a, b). Although poorly constrained, the age of these units is regarded to be *c*. 1.1–1.0 Ga (Schneider et al. 2004; Becker et al. 2005).

6.4.4.4 The Ghanzi-Chobe Belt

The northeast-trending Ghanzi-Chobe Belt comprises greenschist facies metavolcanosedimentary sequences, which overlay Paleoproterozoic rocks of the Okwa Terrane and were strongly deformed during the evolution of the Damara Belt (Borg 1988; Modie 1996; Schwartz et al. 1996; Ramokate et al. 2000). The basal Kgwebe Formation is made up of metasandstones, metaconglomerates, metabasalts, metarhyolites and metavolcaniclastic rocks (Modie 1996; Kampunzu et al. 1998). A U–Pb zircon age of 1.11 Ga was obtained for a metarhyolite of this unit (Schwartz et al. 1996), thus allowing for correlation with the upper part of the Nauzerus Group in Namibia.

6.4.4.5 Mesoproterozoic Basement Inliers of the Damara Belt

The Hohewarte Metamorphic Complex comprises a basement inlier exposed in nappes of the Southern Damara Belt and is correlated with rocks of the northwestern margin of the Kalahari Craton (Miller 2008). It is made up of felsic orthogneisses, paragneisses, schists and amphibolites (Miller 2008). The felsic magmatism is constrained at *c*. 1.29–1.06 Ga by U–Pb LA-ICP-MS zircon data from the orthogneisses, although Paleoproterozoic crust is documented as well (Mapani et al. 2014). These data together with Lu-Hf zircon data showing the dominance of late Paleoproterozoic model ages for these gneisses support the correlation of the Hohewarte Metamorphic Complex with the Rehoboth Basement Inlier (Mapani et al. 2014).

6.4.5 The Namaqua-Natal Metamorphic Province

6.4.5.1 Introduction

The southern proto-Kalahari Craton is bounded by the Mesoproterozoic Namaqua-Natal Province (Fig. 6.1; Stockwell et al. 1970; SACS 1980), which is exposed in two main areas: the Namaqua sector, which extends from the northern Cape Province of South Africa northwestwards into Namibia, and the Natal sector, located in southeastern South Africa. Rocks of the Namaqua sector overthrust the Kheis Belt along the Dabep Thrust to the east, whereas they are in turn overthrust by rocks of the Gariep Belt to the west (Frimmel and Frank 1998; Cornell et al. 2006). In the Natal sector, Mesoproterozoic rocks are in tectonic contact with the Kaapvaal Craton along the Natal Thrust Belt (Matthews 1981), while the southern boundary, although obscured by Phanerozoic rocks, is correlated with a zone of geophysical anomalies referred to as the Southern Cape Conductive Belt (De Beer and Meyer 1984).

6.4.5.2 The Namaqua Belt

The Namaqua Belt comprises a complex array of Paleo- and Mesoproterozoic subprovinces and terranes—the Richtersveld Subprovince, the Bushmanland Terrane/Subprovince, the Kakamas Terrane, the Areachap Terrane and the Kaaien Terrane—which are separated by major shear zones (SACS 1980; Thomas et al. 1994). Alternatively, the Gordonia

Subprovince was proposed to include rocks from both the Kakamas and Areachap terranes (Eglington 2006; Miller 2008).

The Richtersveld Subprovince is located in the western part of the belt and comprises metavolcanosedimentary sequences of the Orange River Group, which are intruded by the Vioolsdrif Suite (Miller 2008). Metavolcanic rocks of the Orange River Group have an age of *c*. 2.0 Ga based on Rb–Sr, Pb–Pb and Sm–Nd whole-rock isochron data (Reid et al. 1987; Reid 1997 and references therein). The Vioolsdrif Suite is made up of gabbros, granodiorites, tonalites and granites yielding Rb–Sr, Pb–Pb and Sm–Nd whole-rock isochron ages of 2.00–1.73 Ga (Reid 1997 and references therein). Paleoproterozoic magmatism recorded in the Richtersveld Subprovince is characterized by Sm–Nd T_{DM} ages of *c*. 2.3–2.1 Ga (Reid 1997; Pettersson et al. 2009).

Paleoproterozoic supracrustal sequences and granitoids are also present within the Bushmanland Terrane, although Mesoproterozoic metavolcanosedimentary sequences and igneous bodies were identified as well (e.g., Robb et al. 1999; Cornell et al. 2006; Cornell and Pettersson 2007). The Bushmanland and Okiep groups comprise the main metavolcanosedimentary units. U–Pb detrital zircon data provide a maximum sedimentation age of *c*. 1.64 Ga for the Bushmanland Group, whereas a minimum age of *c*. 1.2 Ga is constrained by zircon metamorphic overgrowths (Bailie et al. 2007). The Okiep Group might have a Mesoproterozoic age because it unconformably overlays Mesoproterozoic intrusions of the Little Namaqualand Suite, although in some places an intrusive relationship is observed (Bailie et al. 2007). The timing of magmatism and metamorphism in the orthogneisses of the Little Namaqualand Suite is constrained by U–Pb zircon core and rim ages of *c*. 1.22–1.10 and 1.08–1.03 Ga, respectively (Robb et al. 1999; Cornell and Pettersson 2007; Colliston et al. 2015). Similar ages were reported for basic to intermediate intrusions of the Koperberg Suite, whereas zircons from granitoids of the Spektakel Suite yield U–Pb SHRIMP ages of *c*. 1.06–1.05 Ga (Robb et al. 1999). Sm–Nd and Lu–Hf T_{DM} data in the Bushmanland Terrane are scattered. Paleoproterozoic model ages between *c*. 2.2–1.8 Ga and scarce Neoarchean ages are present in the north, whereas *c*. 1.42–1.54 Ga model ages dominate in the south, indicating the composite nature of the Bushmanland Terrane (Clifford et al. 1995; Yuhara et al. 2001; Bailie et al. 2007; Pettersson et al. 2009; Colliston et al. 2015).

The Kakamas Terrane comprises several high-grade supracrustal sequences such as the Korannaland and Arribees groups and the Koelmanskop and Vyfbeker metamorphic suites, which include mostly metaquarzites, metapelites, metacalc-silicate rocks, marbles, and garnet- and biotite-bearing gneisses and migmatites (Cornell et al. 2006 and references therein). U–Pb detrital zircon data reveal two main age populations of *c*. 2.00–1.60 and 1.3–1.05 Ga for the Korannaland Group and constrain the metamorphic overprint of the Vyfbeker Metamorphic Suite at 1.20–1.18 Ga (Fransson 2008). Intrusions comprise mostly orthogneisses, granitoids and subordinated mafic rocks (Stowe 1983; Kruger et al. 2000; Cornell et al. 2006; Miller 2008). U–Pb zircon ages show multistage magmatism at *c*. 1.35–1.30, 1.22–1.18 and 1.10–1.08 Ga, the latter two being coeval with metamorphic events dated by zircon overgrowth and monazite geochronological data (Bailie et al. 2011; Cornell et al. 2012; Bial et al. 2015a, b; Colliston et al. 2015). Although Mesoproterozoic Sm–Nd model ages are widespread within the Kakamas Terrane (Kruger et al. 2000; Pettersson et al. 2009), Lu–Hf and Sm–Nd model ages between *c*. 2.2 and 1.8 Ga are present as well (Pettersson et al. 2009; Cornell et al. 2012; Colliston et al. 2015).

The Areachap Terrane comprises the Areachap Group and the Keimoes Suite. The Areachap Group is made up of amphibolites, intermediate metavolcanic rocks, paragneisses and migmatites, and records synsedimentary magmatism at *c*. 1.28–1.24 Ga (Cornell et al. 1990; Pettersson et al. 2007). The Areachap Group is intruded by the Keimoes Suite, which is also present in the Kakamas Terrane and yields U–Pb zircon ages of *c*. 1.10–1.08 Ga (Bailie et al. 2011; Cornell et al. 2012). The Areachap Terrane shows similar Lu–Hf and Sm–Nd model ages to those recorded in the Kakamas Terrane, although Mesoproterozoic model ages are restricted to 1.50–1.33 Ga and Paleoproterozoic T_{DM} values extend up to 2.41 Ga (Pettersson et al. 2009; Bailie et al. 2011; Cornell et al. 2012).

The Kaaien Terrane consists of metaquartzites and quartz-micaschists of the Brulpan and Vaalkoppies groups and metavolcanosedimentary sequences of the Wilgenhoutsdrif Group, although mafic to felsic intrusions are present as well (Cornell et al. 2006; Pettersson et al. 2007 and references therein). All these units are unconformably overlain by the Koras Group, which records synsedimentary volcanism at *c*. 1.18–1.16 and 1.10–1.19 Ga (Pettersson et al. 2007; Bailie et al. 2011). The Kaaien Terrane shows dominance of Sm–Nd model ages between 1.98 and 1.57 Ga (Pettersson et al. 2009).

Eglington and Armstrong (2003) reported Paleo- and Mesoproterozoic Sm–Nd T_{DM} in Mesoproterozoic intrusions that were sampled from boreholes located between the Namaqua and Natal Belts. Hence the Namaqua sector might extend further east, buried below younger units at the southern Kalahari Craton margin (Eglington and Armstrong 2003).

The main metamorphic and deformation events of the Namaqua Belt are contemporaneously recorded with magmatism. Peak metamorphic low-pressure amphibolite to granulite conditions were determined for rocks from the Bushmanland, Kakamas and Areachap terranes (Clifford

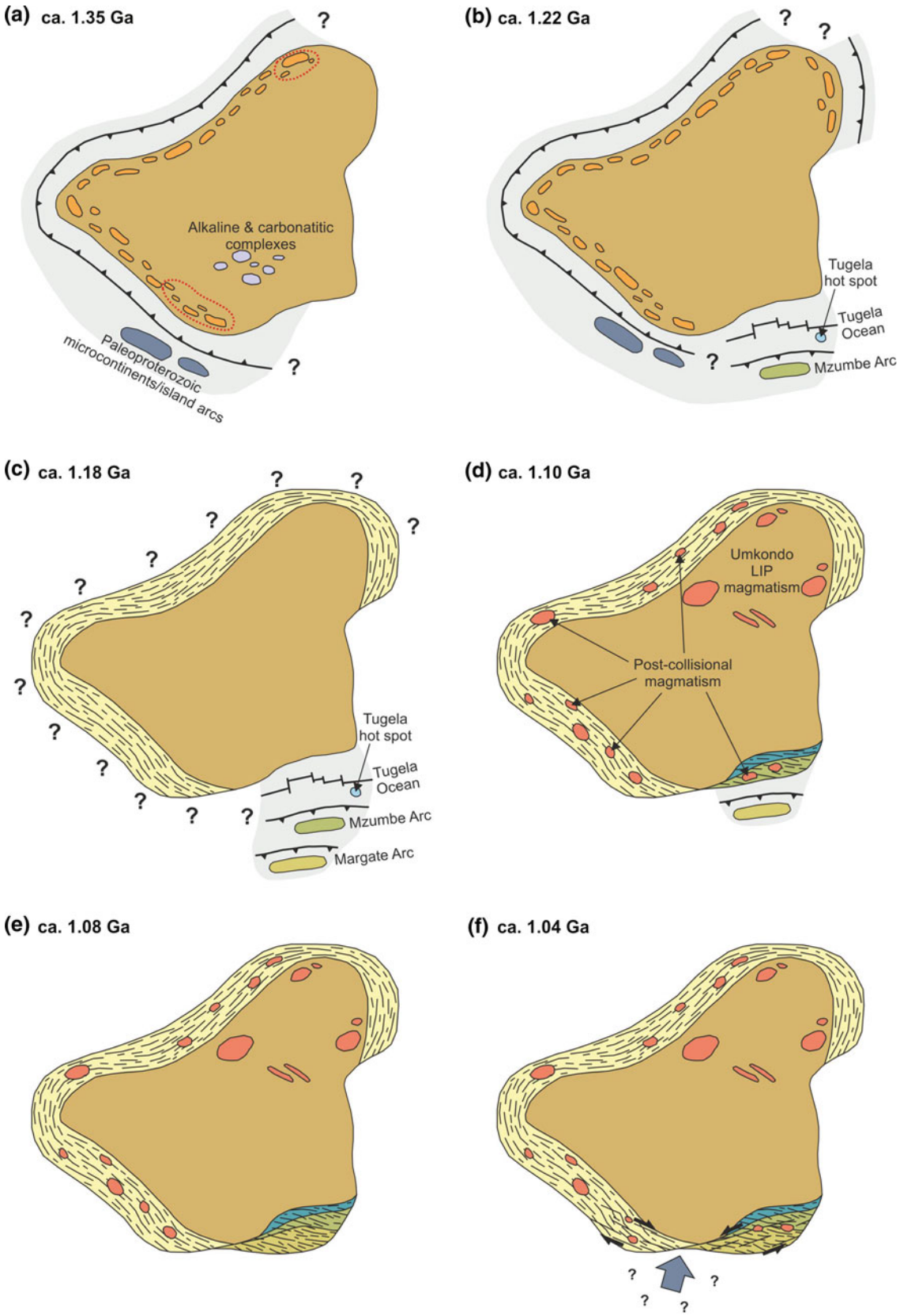
(a) ca. 1.35 Ga
Alkaline & carbonatitic complexes
Paleoproterozoic microcontinents/island arcs
(b) ca. 1.22 Ga
Tugela hot spot
Tugela Ocean
Mzumbe Arc
(c) ca. 1.18 Ga
Tugela hot spot
Tugela Ocean
Mzumbe Arc
Margate Arc
(d) ca. 1.10 Ga
Umkondo LIP magmatism
Post-collisional magmatism
(e) ca. 1.08 Ga
(f) ca. 1.04 Ga

◀ **Fig. 6.6** Schematic Mesoproterozoic tectonic evolution modified after Watters (1976), Hoal (1990), Jacobs and Thomas (1994), Kampunzu et al. (1998), Becker et al. (2005, 2006), McCourt et al. (2006), Jacobs et al. (2008), Miller (2008), Spencer et al. (2015). See text for further discussion. **a** Subduction along the proto-Kalahari margin. Red dashed lines indicate areas where it is unclear whether magmatism was arc- or extension-related (northeastern area: Choma-Kalomo Block, southwestern area: Namaqua Belt). Coeval alkaline and carbonatitic complexes are recorded at *c*. 1.4–1.35 Ga in the southern proto-Kalahari margin (Hanson et al. 2006). **b** Further subduction along the proto-Kalahari margin, which is also recorded along the northeastern margin in the Báruè Complex. **c** Widespread deformation and metamorphism during the collisional phase of the Namaqua Orogeny. Further subduction is only recorded in the Natal Belt. **d** Post-collisional magmatism coeval with the Umkondo LIP magmatism. In the Natal Belt, post-collisional magmatism postdates the obduction of the Tugela ophiolite and the accretion of the Mzumbe Terrane. **e** Accretion of the Margate Terrane in the Natal Belt. **f** Strike-slip deformation along the Namaqua-Natal Belt

et al. 1975, 1981; Stowe 1983; Waters 1986, 1989; Cornell et al. 1992; Raith and Harley 1998; Robb et al. 1999; Bachmann et al. 2015; Bial et al. 2015a). In contrast, the westernmost Richtersveld Subprovince shows greenschist to amphibolite facies metamorphism, whereas greenschist conditions dominate the easternmost Kaaien Terrane (Cornell et al. 2006 and references therein).

6.4.5.3 The Natal Belt

The Natal Belt is subdivided into the northern Tugela, central Mzumbe and southern Margate terranes, which are separated by east- to east-northeast-striking shear zones (Hartnady et al. 1985; Thomas 1989; Thomas et al. 1994; Cornell et al. 2006; Eglington 2006).

The Tugela Terrane comprises metasedimentary rocks, metabasalts and metamorphosed mafic/ultramafic intrusions, which are interpreted as an ophiolitic complex, and orthogneisses (Matthews 1972; Thomas 1989; Cornell et al. 2006; McCourt et al. 2006). U–Pb detrital zircon data constrain the maximum deposition age of the metasediments at *c*. 1.18 Ga and indicate a Mesoproterozoic source with ages up to *c*. 1.3 Ga (Johnston et al. 2001; McCourt et al. 2006). Orthogneisses, in turn, show U–Pb zircon ages between *c*. 1.21 and 1.16 Ga recording magmatism prior to collision, whereas late syn- to post-collisional magmatism is recorded at *c*. 1.15–1.14 Ga (Johnston et al. 2001; McCourt et al. 2006). Amphibolite facies metamorphism and deformation related to the obduction of the ophiolitic sequence is, in turn, constrained at 1.14–1.13 Ga by Ar/Ar amphibole data (Jacobs et al. 1997).

The Mzumbe Terrane is constituted by amphibolite-facies paragneisses of the Mapumulo Group, which is intruded by voluminous granitoids and locally by mafic and ultramafic rocks of the Equeefa Suite (Thomas 1989; Thomas and Eglington 1990; Cornell et al. 1996, 2006; McCourt et al. 2006). Thin volcanic intercalations yield U–Pb SHRIMP ages of *c*. 1.24–1.23 Ga, thus constraining the sedimentation age of the Mapumulo Group (Thomas et al. 1999). An orthogneiss of the Mzumbe Suite intruding the paragneisses presents a slighty younger U–Pb zircon age of *c*. 1.22–1.20 Ga (Thomas and Eglington 1990). Nevertheless, metavolcanosedimentary units yielding U–Pb SHRIMP zircon ages of *c*. 1.16 Ga were also reported for the Mapumulo Group (Cornell et al. 1996), which might indicate the presence of younger sedimentary units in the Mzumbe Terrane. Pre- to syncollisional intrusions with U–Pb zircon ages between *c*. 1.18 and 1.08 Ga were emplaced prior to and during the assembly of the Mzumbe and Margate terranes (Eglington et al. 2010; Spencer et al. 2015). Post-collisional magmatism at *c*. 1.05–1.03 Ga is recorded by the Oribi Gorge Suite, which intruded both the Mzumbe and Margate terranes (Thomas et al. 1993; Eglington et al. 2003; Cornell et al. 2006; Mendonidis et al. 2015; Spencer et al. 2015).

The Margate Terrane is made up of paragneisses, orthogneisses and mafic granulites, which are intruded by granitoids (Thomas 1989; Thomas and Eglington 1990; Cornell et al. 1996, 2006; McCourt et al. 2006). Supracrustal rocks are grouped under the Mzimkulu Group (Thomas 1989). Widespread plutonic activity since *c*. 1.18 Ga is recorded by the Banana Beach Gneiss; the Munster, Turtle Bay and Margate suites, and the Glenmore and Sikombe granites (Mendonidis et al. 2002, 2015; Thomas et al. 2003; Spencer et al. 2015). As in the Mzumbe Terrane, the Oribi Gorge Suite indicates the last stage of post-collisional magmatism.

Lu–Hf zircon and Sm–Nd whole-rock data indicate the dominance of Mesoproterozoic T_{DM} model ages and suprachondritic ε_{Hf} and ε_{Nd} values for the three terranes, indicating that the Natal Belt essentially comprises Mesoproterozoic juvenile crust (Eglington et al. 1989; Thomas and Eglington 1990; Eglington 2006; Spencer et al. 2015).

Metamorphism in the Natal Sector progressively increases from northeast to southwest (Thomas 1989; Cornell et al. 2006; McCourt et al. 2006). The Tugela Terrane attained peak greenschist to amphibolite facies metamorphic conditions, whereas conditions are restricted to amphibolite facies in the Mzumbe Terrane. Further south, the Margate Terrane records granulite facies metamorphism. Metamorphic facies distribution is parallel to the main structural grain that is characterized by northeast-verging folds and thrusts, which were subsequently overprinted by subvertical east-northeast-striking shear zones (Jacobs and Thomas 1994; Jacobs et al. 1997; Spencer et al. 2015).

6.4.5.4 Mesoproterozoic Tectonic Evolution

Most tectonic models assessing the Mesoproterozoic evolution of the Kalahari Craton are based on the Namaqua-Natal Province and the Sinclair-Ghanzi-Chobe Belt, whereas correlations with the Báruè Complex and the Choma-Kalomo Block are scarce (e.g., Jacobs et al. 2008). Nevertheless, some similarities can be found in their geological records. Geochronological data record a distinct magmatic event at *c*. 1.38–1.34 Ga in the Kairab-Kumbis Metamorphic Complex of the Sinclair-Ghanzi-Chobe Belt, Choma-Kalomo Block and the Namaqua-Natal Belt (Fig. 6.5; Hanson et al. 1988; Hoal 1990; Hoal and Heaman 1995; Becker et al. 2006; Bulambo et al. 2006; Pettersson et al. 2007; Bial et al. 2015a; Cornell et al. 2015). In the Namaqua-Natal Belt, this event was regarded as extensional (Bial et al. 2015a; Cornell et al. 2015), resulting either from rifting (Cornell et al. 2015) or back-arc extension (Bial et al. 2015a). The existence of coeval alkaline and carbonatite magmatism in the southern Kalahari Craton would further indicate intraplate magmatism (Fig. 6.6a; Hanson et al. 2006). In contrast, an active margin was indicated for the northwestern Kalahari Craton margin since *c*. 1.4 Ga, implying subduction towards the southeast and island arc accretion (Fig. 6.6a; e.g., Hoal 1990; Becker et al. 2006; Jacobs et al. 2008; Miller 2012). In the Choma-Kalomo Block, an extensional rifting event was indicated by Bulambo et al. (2006), whereas Hanson et al. (1988) suggested an active margin (Fig. 6.6a), which fits correlations with the Sinclair-Ghanzi-Chobe Belt (e.g., Hanson 2003; Singletary et al. 2003).

Intrusive magmatism and volcanism are recorded after 1.24 Ga in the Namaqua-Natal Province, showing a peak at *c*. 1.18–1.22 Ga (Figs. 6.5 and 6.6b; Robb et al. 1999; Thomas and Eglington 1990; Johnston et al. 2001; Eglington and Armstrong 2003; Thomas et al. 2003; Bial et al. 2015a, b; Colliston et al. 2015; Cornell et al. 2015; Mendonidis et al. 2015; Spencer et al. 2015). Likewise, coeval magmatism is recorded in the Báruè Complex and the Chola-Kalomo Block (Figs. 6.5 and 6.6b; Hanson et al. 1988; Bulambo et al. 2006; Mänttäri 2008). This event was interpreted as the result of arc magmatism, which was present from *c*. 1.4 Ga in the Sinclair-Ghanzi-Chobe Belt (Watters 1976; Hoal 1990; Becker et al. 2006).

The subsequent collision gave rise to metamorphism and deformation at *c*. 1.20–1.18 Ga in the Namaqua Sector (Figs. 6.5 and 6.6c; Manhica et al. 2001; Clifford et al. 2004; Miller 2008; Colliston et al. 2015; Cornell et al. 2015). Nevertheless, Bial et al. (2015a, b) argued for an extensional event in a back-arc setting for the magmatism and ultra-high-temperature metamorphism of the Namaqua Belt up to *c*. 1.1 Ga. In the Natal Sector, the first collisional event seems to be slightly younger, resulting from closure and obduction of oceanic crust of the Tugela Terrane and the accretion of the Mzumbe Terrane to the Kalahari Craton margin at 1.16–1.14 Ga (Fig. 6.6d; Jacobs et al. 1997; Cornell et al. 2006; Eglington et al. 2010; Spencer et al. 2015). In contrast, McCourt et al. (2006) indicated accretion of the Tugela Terrane to the Kaapvaal Craton margin prior to 1.16 Ga. In the case of the Sinclair-Ghanzi-Chobe Belt, the collisional phase can be placed at *c*. 1.20–1.11 Ga (Kampunzu et al. 1998; Becker et al. 2006).

Post-collisional magmatism is recorded after *c*. 1.18, 1.14 and 1.11 Ga in the Namaqua, Natal and Sinclair-Ghanzi-Chobe Belts, respectively (Figs. 6.5 and 6.6d; Kampunzu et al. 1998; Becker et al. 2005, 2006; Bailie et al. 2012; Spencer et al. 2015). Bailie et al. (2012) suggested a transtensional setting for the 1.17 and 1.1 Ga magmatism in the Namaqua Sector, which may explain the scarce metamorphic ages between 1.14 and 1.06 Ga (Fig. 6.5), although folding and thrusting were reported between *c*. 1.17 Ga and 1.08 for the same area (Colliston et al. 2015). Likewise, extension and associated post-collisional magmatism resulting from slab break-off and consequent astenospheric upwelling was indicated for the Sinclair-Ghanzi-Chobe Belt at *c*. 1.1 Ga (Kampunzu et al. 1998; Becker et al. 2006). Mantle upwelling is also indicated by voluminous mafic magmatism that produced the Umkondo LIP within the proto-Kalahari Craton at this time (Fig. 6.6d; Hanson et al. 2004, 2006). Hence, magmatism and extension/transtension related to mantle upwelling is well documented at 1.1 Ga, although it is unclear whether these processes took place in a post-collisional or intraplate setting (Kampunzu et al. 1998; Becker et al. 2006; Hanson et al. 2006; Jacobs et al. 2008; Cornell et al. 2015). The Natal Belt is the only area that shows a different evolution because it records the accretion of the Margate Terrane to the Mzumbe/Kalahari system at 1.10–1.08 Ga (Mendonidis et al. 2009; Spencer et al. 2015). According to McCourt et al. (2006), accretion of the Mzumbe Terrane to the proto-Kalahari Craton margin took place during this event and not during obduction of the Tugela Terrane oceanic rocks. In any case, Mesoproterozoic collisional and accretional tectonics at the proto-Kalahari margin was completed at *c*. 1.08–1.07 Ga (Fig. 6.6e; Cornell and Thomas 2006; McCourt et al. 2006; Miller 2012; Colliston and Schoch 2013).

The last period of significant deformation and associated magmatism and metamorphism started at *c*. 1.05 Ga, which is reflected by a peak of both magmatic and metamorphic ages at *c*. 1.04–1.02 Ga (Fig. 6.5; Thomas et al. 1993; Jacobs and Thomas 1994; Jacobs et al. 1997; Robb et al. 1999; Eglington et al. 2003; Clifford et al. 2004; Cornell and Thomas 2006; Eglington 2006; Bailie et al. 2007; Colliston and Schoch, 2013; Colliston et al. 2015; Mendonidis et al. 2015; Spencer et al. 2015). This event resulted from crustal thickening, low-pressure granulite metamorphism and strike-slip deformation along crustal-scale ductile shear

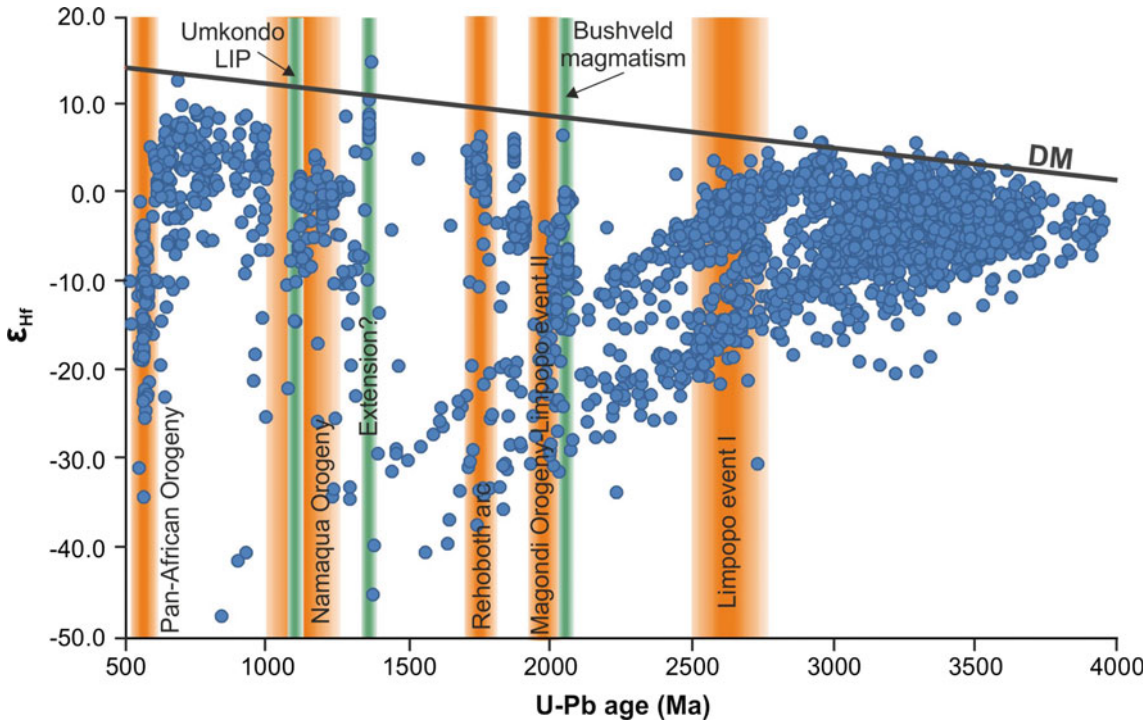

Fig. 6.7 Synthesis of ε_{Hf} versus U–Pb zircon data of the Kalahari Craton (n = 3515; Zeh et al. 2007, 2008, 2009, 2010, 2011, 2013a, b, 2014; Zeh and Gerdes 2012; Frimmel et al. 2013; Foster et al. 2014; Hofmann et al. 2014; van Schijndel et al. 2014; Zirakparvar et al. 2014; Colliston et al. 2015; Cornell et al. 2015; Milani et al. 2015). Data were recalculated considering a constant decay λ $^{176}Lu = 1.867 \times 10^{-11}$ year^{-1} (Söderlund et al. 2004) and CHUR values of $^{176}Hf/^{177}Hf$ = 0.282772 and $^{176}Lu/^{177}Hf$ = 0.0332 (Blichert-Toft and Albarède 1997). Main tectonic events are indicated (see text for further explanation)

zones, which are well documented in the Namaqua-Natal Belt (Fig. 6.6f; Jacobs and Thomas 1994; Jacobs et al. 1997; Robb et al. 1999; Eglington et al. 2003; Eglington, 2006; Colliston and Schoch 2013; Colliston et al. 2015; Mendonidis et al. 2015; Spencer et al. 2015).

6.5 Neoproterozoic: From Rodinia Break-up to Gondwana Amalgamation

The Neoproterozoic geological history of the Kalahari Craton is mostly recorded in the Pan-African belts that define the boundaries of the craton. As these belts are analysed in detail by other authors in this volume (Chaps. 12–14), they are outside the scope of this chapter. Nevertheless, some major points regarding the Neoproterozoic evolution of the Kalahari Craton are outlined.

Tonian and Cryogenian rocks located mostly at the craton margins have traditionally been interpreted as the result of extensional events (Jacobs et al. 2008 and references therein). In the Gariep Belt, the Richtersveld Suite records anorogenic intrusions at *c*. 840–770 Ma (Frimmel et al. 2001; Miller 2008), whereas metavolcanosedimentary sequences of comparable age are recorded in the lower portions of the Gariep Supergroup (e.g., Frimmel et al. 2002). In the Damara Belt, rifting is recorded by several Cryogenian metavolcanosedimentary rocks (Foster et al. 2014 and references therein), whereas evidences of late Tonian-Cryogenian magmatism and sedimentation were documented in the Zambezi Belt (e.g., Vinyu et al. 1999; Hargrove et al. 2003).

Assessing the timing of the Pan-African Orogeny is a difficult task owing to its diachronism, as it implied the interaction of the Kalahari Craton with several continental blocks, such as the Congo and Río de la Plata cratons. Nevertheless, the oldest events related to the Pan-African evolution of the Kalahari Craton were constrained at *c*. 590 Ma and are associated with the onset of the Congo-Kalahari convergence (Lehmann et al. 2015; Oriolo et al. 2016, 2017). The youngest Pan-African events, in turn, were recorded at *c*. 480 Ma, indicating that during the assembly of Gondwana, the margins of the Kalahari Craton experienced crustal reworking over a period of more than 100 myr (Gray et al. 2008; Bingen et al. 2009; Lehmann et al. 2015).

6.6 Final Considerations

U–Pb and Lu–Hf zircon data indicate the existence of Hadean and Early Archean crust-forming events up to *c*. 3.4 Ga, with a major peak at *c*. 3.6–3.4 Ga (Fig. 6.2). These events were probably related to the formation of minor crustal blocks, which collided between *c*. 3.3–3.2 Ga to form larger blocks that comprised the nuclei of the Kaapvaal and Zimbabwe cratons (Jelsma and Dirks 2002; Moyen et al. 2006, 2007; Lowe and Byerly 2007; Stevens and Moyen 2007; Lana et al. 2009; Zeh et al. 2009, 2011). A second peak of magmatism is recorded between *c*. 3.3 and 3.0 Ga by both magmatic and detrital zircon data, whereas there are very few ages between 3.0 and 2.8 Ga (Fig. 6.2), indicating a period of relative stability. Though some evolutionary crustal trends can be inferred considering $^{176}Lu/^{177}Hf$ values between 0.015 and 0.001, Lu–Hf data most probably reflect both crustal recycling and juvenile crust addition during the Paleo- and Mesoarchean (Zeh et al. 2007, 2008, 2009, 2010, 2011, 2013b; Zeh and Gerdes 2012; Laurent and Zeh 2015). Subsequent Neoarchean magmatism was related to the first episode recognized in rocks of the Limpopo Belt (Figs. 6.2 and 6.7; Zeh and Gerdes 2012; Zeh et al. 2007, 2008, 2009, 2010, 2011, 2013b; Laurent and Zeh 2015). Subchondritic ε_{Hf} values obtained for Neoarchean zircons point to crustal recycling of Mesoarchean and Paleo- to Eoarchean crust considering $^{176}Lu/^{177}Hf = 0.0113$ (Fig. 6.2; e.g., Zeh and Gerdes 2012; Zeh et al. 2013a). Hence Neoarchean tectonic events implied dominantly crustal reworking processes with little addition of juvenile material, suggesting that the proto-Kalahari Craton attained relative stability prior to *c*. 2.85 Ga (Laurent et al. 2014).

Paleoproterozoic zircon U–Pb ages between *c*. 2.5 and 2.1 Ga are mostly related to intrusions located between the Limpopo Belt and the northern Kaapvaal Craton (Zeh et al. 2007, 2009, 2013b). These zircons yield negative ε_{Hf} values and follow the same evolutionary trends as Neoarchean zircons, indicating the existence of local magmatism emplacement that took place between the two main events recorded in the Limpopo Belt and reworked older crust (Fig. 6.7).

A distinct event is recorded by zircon U–Pb data at *c*. 2.06–1.9 Ga, which is coeval with the timing of the second Limpopo Belt event and the Magondi Orogeny (Fig. 6.7). Zircons from intrusions in the Limpopo Belt yield negative ε_{Hf} values and Neo- to Paleoarchean Lu–Hf model ages, whereas zircon xenocrysts as well as Archean Sm–Nd model ages were reported for intrusions from the Magondi Belt, pointing to significant crustal reworking for both areas (Zeh et al. 2007, 2009). However, Paleoproterozoic magmatism recorded in the Limpopo Belt is coeval with intrusions of the Bushveld Complex at *c*. 2.05 Ga (Zeh et al. 2015), which present a Lu-Hf and O isotopic fingerprint of the parental magmas that indicate crustal contamination, more likely owing to subducted Archean oceanic rocks (Harris et al. 2005; Zirakparvar et al. 2014). Hence, juvenile mantle-derived magmas might also intrude during the Paleoproterozoic evolution of the Limpopo and Magondi belts, given that their isotopic signature is most likely the result of both reworked Archean crust and a metasomatized mantle source. The subsequent Rehoboth magmatism implied a significant addition of Paleoproterozoic mantle-derived material as evidenced by dominant positive ε_{Hf} values (Fig. 6.7; Becker et al. 1996, 2000, 2004; Becker and Brandenburg 2000; Becker and Schalk 2008a; van Schijndel et al. 2014), despite probably being restricted to the proto-Kalahari Craton margin.

The Mesoproterozoic tectonic events represent a key stage in the evolution of the Kalahari Craton, as they probably record the participation of this block during Rodinia amalgamation, although its position in Rodinia is still under debate (e.g., Powell et al. 2001; Jacobs et al. 2008; Li et al. 2008; Colliston and Schoch 2013; Oriolo et al. 2017). Zircons yielding ages of *c*. 1.36 Ga are characterized by positive ε_{Hf} between 6 and 11 (Fig. 6.7; Cornell et al. 2015), thus indicating local juvenile input. In contrast, Mesoprotezoic magmatism at *c*. 1.2–1.0 Ga records participation of both juvenile and older crust material, as shown by Sm–Nd and Lu–Hf data (Fig. 6.7; Eglington 2006; Frimmel et al. 2013; Hofmann et al. 2014; Cornell et al. 2015; Foster et al. 2014). The contribution of Archean material is almost absent and may thus indicate that the polarity of Mesoproterozoic subduction during the amalgamation of the various island arcs should be away from the margin of the proto-Kalahari Craton, which fits tectonic models proposed for the Natal Sector (Jacobs and Thomas 1994; Johnston et al. 2001; Cornell et al. 2006; McCourt et al. 2006; Mendonidis et al. 2015). In the Namaqua and Sinclair-Ghanzi-Chobe belts, subduction towards the craton was indicated (e.g., Hoal 1990; Becker et al. 2006; Bailie et al. 2012; Cornell et al. 2015), although dual polarity was proposed for subduction stages during the accretion of some terranes (Colliston et al. 2014). The lack of Archean contributions in these areas may thus be explained by subduction under relative juvenile Paleoproterozoic blocks that were previously accreted to the proto-Kalahari Craton.

Neoproterozoic tectonic processes are well recorded all around the Kalahari Craton. Zircons yielding Tonian to Cryogenian crystallization ages are mostly characterized by suprachondritic ε_{Hf} values resulting from juvenile input, probably during intraplate magmatism (Frimmel et al. 2013; Foster et al. 2014). In contrast, Ediacaran magmatism mostly reworked Archean to Mesoproterozoic crust, as revealed by subchondritic ε_{Hf} values (Fig. 6.7; Villaros et al. 2012;

Frimmel et al. 2013; Foster et al. 2014; Milani et al. 2015; Oriolo et al. 2017). Hence all units of the Kalahari Craton behaved as a coherent block that shared a common history from the Neoproterozoic.

Acknowledgements The authors are greatly indebted to Stephen McCourt for his observations and comments, which greatly improved the manuscript. Filiz Afşar is acknowledged for his assistance with GIS.

References

Amelin Y, Lee D-C, Halliday AN (2000) Early-middle Archaean crustal evolution deduced from Lu-Hf and U-Pb isotopic studies of single zircon grains. Geochim Cosmochim Acta 64:4205–4225

Anhaeusser CR (1975) The geological evolution of the primitive Earth: evidence from the Barberton Mountain Land. Economic Geology Research Unit, University of the Witwatersrand, Johannesburg, information circular 98, p 22

Anhaeusser CR (2006) Ultramafic and mafic intrusions of the Kaapvaal Craton. In: Johnson MR, Anhaeusser CR, Thomas RJ (eds) The geology of South Africa. Geological Society of South Africa and Council for Geoscience, Johannesburg and Pretoria, pp 95–134

Anhaeusser CR, Burguer AJ (1982) An interpretation of U-Pb zircon ages for Achaean tonalitic gneisses from the Johannesburg-Pretoria granite dome. Trans Geol Soc S Afr 852:111–116

Anhaeusser CR, Walraven F (1999) Episodic granitoid emplacement in the western Kaapvaal Craton: evidence from the Archaean Kraaipan granite-greenstone terrane, South Africa. J Afr Earth Sci 28:289–309

Anhaeusser CR, Poujol M (2004) Petrological, geochemical and U-Pb isotopic studies of Archaean granitoid rocks of the Makoppa Dome, northwest Limpopo Province, South Africa. S Afr J Geol 107:521–544

Armstrong RA, Compston W, de Wit MJ, Williams IS (1990) The stratigraphy of the 3.5–3.2 Ga Barberton greenstone belt revisited: a single zircon ion microprobe study. Earth Planet Sci Lett 101:90–106

Arndt NT (2013) Formation and evolution of the continental crust. Geochem Perspect 2:405–533

Bachmann K, Schulz B, Bailie R, Gutzmer J (2015) Monazite geochronology and geothermobarometry in polymetamorphic host rocks of volcanic-hosted massive sulphide mineralizations in the Mesoproterozoic Areachap Terrane, South Africa. J Afr Earth Sci 11:258–272

Bagai Z, Armstrong R, Kampunzu AB (2002) U-Pb single zircon geochronology of granitoids in the Vumba granite-greenstone terrain (NE Botswana): Implications for the evolution of the Archaean Zimbabwe craton. Precambrian Res 118:149–168

Bailie R, Armstrong R, Reid D (2007) The Bushmanland Group supracrustal succession, Aggeneys, Bushmanland, South Africa: Provenance, age of deposition and metamorphism. S Afr J Geol 110:59–86

Bailie R et al. (2011) Age of ferroan A-type post-tectonic granitoids of the southern part of the Keimoes Suite, Northern Cape Province, South Africa. J Afr Earth Sci 60:153–174

Bailie R et al. (2012) Bimodal volcanism at the western margin of the Kaapvaal Craton in the aftermath of collisional events during the Namaqua-Natal Orogeny: The Koras Group, South Africa. Precambrian Res 200–203:163–183

Barton JM Jr, Doig R, Smith CB, Bohlender F, van Reenen DD (1992) Isotopic and REE characteristics of the intrusive charnoenderbite and enderbite geographically associated with the Matok Pluton, Limpopo Belt, southern Africa. Precambrian Res 55:451–467

Becker T, Brandenburg A (2000) The evolution of the Alberta Complex, Naub Diorite and Elim Formation within the Rehoboth basement linlier, Namibia: geochemical constraints. Communs Geol Surv Namibia 12:31–42

Becker T, Schalk KEL (2008a) Rehoboth Group. In: Miller RMcG (ed) The geology of Namibia. Geological Survey of Namibia, Windhoek, pp 5-29–5-61

Becker T, Schalk KEL (2008b) The Sinclair Supergroup of the Rehoboth Volcanic Arc from the Sossusvlei-Gamsberg area to the Gobabis Region. In: Miller RMcG (ed) The geology of Namibia. Geological Survey of Namibia, Windhoek, pp 8-68–8-104

Becker T, Hansen BT, Weber K, Wiegand B (1996) U-Pb and Rb-Sr isotopic data for the Mooirivier Complex, Weener Igneous Suite and Gaub Valley Formation (Rehoboth Sequence) in the Nauchas area and their significance for Paleoproterozoic crustal evolution in Namibia. Communs Geol Surv Namibia 11:33–48

Becker T, Diedrichs B, Hansen BT, Weber K (2000) Weener Igneous Complex: geochemistry and implications for the evolution of the Palaeoproterozoic Rehoboth basement inlier; Namibia. Communs Geol Surv Namibia 12:43–55

Becker T, Wiegand B, Hansen BT, Weber K (2004) Sm/-Nd, Rb/-Sr and U/-Pb data from the Rehoboth Basement Inlier, Namibia: Evidence of a Paleoproterozoic magmatic arc. Communs Geol Surv Namibia 13:75–84

Becker T, Ledru P, Garoeb H, Milesi JP (2005) The Mesoproterozoic event within the Rehoboth Basement Inlier of Namibia—review and new aspects of metamorphism, structure and stratigraphical subdivision. S Afr J Geol 108:317–344

Becker T, Schreiber U, Kampunzu AB, Armstrong R (2006) Mesoproterozoic rocks of Namibia and their plate tectonic setting. J Afr Earth Sci 46:112–140

Bédard JH, Harris LB, Thurston PC (2013) The hunting of the snArc. Precambrian Res 229:20–48

Bial J, Büttner SH, Schenk V, Appel P (2015a) The long-term high-temperature history of the central Namaqua Metamorphic Complex: evidence for a Mesoproterozoic continental back-arc in southern Africa. Precambrian Res 268:243–278

Bial J, Büttner SH, Frei D (2015b) Formation and emplacement of two contrasting late-Mesoproterozoic magma types in the central Namaqua Metamorphic Complex (South Africa, Namibia): evidence from geochemistry and geochronology. Lithos 224–225:272–294

Bingen B, Jacobs J, Viola G, Henderson IHC, Skår Ø, Boyd R, Thomas RJ, Solli A, Key RM, Daudi EXF (2009) Geochronology of the Precambrian crust in the Mozambique belt in NE Mozambieque, and implications for Gondwana assembly. Precambrian Res 170:231–255

Blichert-Toft J, Albarède F (1997) The Lu-Hf geochemistry of chondrites and the evolution of the mantle-crust system. Earth Planet Sci Lett 148:243–258

Borg G (1988) The Koras-Sinclair-Ghanzi Rift in southern Africa. volcanism, sedimentation, age relationships and geophysical signature of a late middle Proterozoic rift system. Precambrian Res 38:75–90

Brandl G, Cloete M, Anhaeusser CR (2006) Archaean greenstone belts. In: Johnson MR, Anhaeusser CR, Thomas RJ (eds) The geology of South Africa. Geological Society of South Africa and Council for Geoscience, Johannesburg and Pretoria, pp 9–56

Bulambo M, De Waele B, Kokonyangi J, Johnson SP, Kampunzu AB, Tembo F (2006) SHRIMP U-Pb geochronology and geochemistry

of the Choma-Kalomo Block granitoids (Zambia): geological implications. 21° Colloquium on African Geology, Orléans
Burger AJ, Walraven F (1978) Summary of age determinations carried out during the period April 1975 to March 1976. Ann Geol Surv S Afr 11:323–329
Burke K, Kidd WSF, Kusky T (1985) Is the Ventersdorp Rift System of Southern Africa related to a continental collision between the Kaapvaal and Zimbabwe Cratons at 2.64 Ga ago? Tectonophysics 1–2:1–24
Carney JN, Aldiss DT, Lock NP (1994) The geology of Botswana. Geological Survey Department, Lobatse
Cawthorn RG, Eales HV, Walraven F, Uken R, Watkeys MK (2006) The Bushveld Complex. In: Johnson MR, Anhaeusser CR, Thomas RJ (eds) The geology of South Africa. Geological Society of South Africa and Council for Geoscience, Johannesburg and Pretoria, pp 261–281
Cawthorn RG, Walraven F (1998) Emplacement and crystallization time for the Bushveld Complex. J Petrol 39:1669–1687
Clifford TN (1970) The structural framework of Africa. In: Clifford TN, Gass IG (eds) African magmatism and tectonics. Oliver and Boyd, Edinburgh, pp 1–26
Clifford TN, Gronow J, Rex DC, Burguer AJ (1975) Geochronological and petrogenetic studies of high-grade metamorphic rocks and intrusives in Namaqualand, South Africa. J Petrol 16:154–188
Clifford TN, Stumpfl EF, Burguer AJ, McCarthy TS, Rex DC (1981) Mineral-chemical and isotope studies of Namaqualand granulites, South Africa: a Grenville analogue. Contrib Mineral Petrol 77:225–250
Clifford TN, Barton ES, Retief EA, Rex DC, Fanning CM (1995) A crustal progenitor for the intrusive anorthosite-charnockite kindred of the cupriferous Koperberg Suite, O'okiep District, Namaqualand, South Africa; new isotope data for the country rocks and intrusives. J Petrol 36:231–258
Clifford TN, Barton ES, Stern RA, Duchesne J-C (2004) U-Pb zircon calender ofr Namaquan (Grenville) crustal events in the granulite-facies terrane of the O'okiep Copper district of South Africa. J Petrol 45:669–691
Collins WJ, Belousova E, Kemp AIS, Murphy JB (2011) Two contrasting Phanerozoic orogenic systems revealed by hafnium isotope data. Nat Geosci. https://doi.org/10.1038/NGEO1127
Colliston WP, Schoch AE (2013) Wrench-shearing during the Namaqua Orogenesis-Mesoproterozoic late stage deformation effects during Rodinia assembly. Precambrian Res 233:44–58
Colliston WP, Schoch AE, Cole J (2014) The Grenvillian Namaqua-Natal fold belt adjacent to the Kaapvaal Craton: 1. Distribution of Mesoproterozoic collisional terranes deduced from results of regional surveys and selected profiles in the western and southern parts of the fold belt. J Afr Earth Sci 100:7–19
Colliston WP, Cornell WP, Schoch AE (2015) Geochronological constraints on the Hartbees River Thrust and Augrabies Nappe: new insights into the assembly of the Mesoproterozoic Namaqua-Natal Province of Southern Africa. Precambrian Res 265:150–165
Compston W, Kröner A (1988) Multiple zircon growth within early Archean tonalitic gneiss from the Ancient Gneiss Complex, Swaziland. Earth Planet Sci Lett 87:13–28
Cornell DH, Thomas RJ (2006) Age and tectonic significance of the Banana Beach Gneiss, KwaZulu-Natal South Coast, South Africa. S Afr J Geol 109:335–340
Cornell DH, Pettersson Å (2007) Ion probe dating of the Achab gneiss, a young basement to the Central Bushmanland Ore District? J Afr Earth Sci 47:112–116
Cornell DH, Kroener A, Humphreys H, Griffin G (1990) Age of origin of the polymetamorphosed Copperton Formation, Namaqua-Natal Province, determined by single grain zircon Pb-Pb dating. S Afr J Geol 93:709–716
Cornell DH, Humphreys H, Theart HFJ, Scheepers DJ (1992) A collision-related pressure-temperature-time path for Prieska Copper Mine, Namaqua-Natal tectonic province, South Africa. Precambrian Res 59:43–71
Cornell DH, Thomas RJ, Bowring SA, Armstrong RA, Grantham GH (1996) Protolith interpretation in metamorphic terranes: a back-arc environment with Besshi-type base metal potential for the Quha Formation, Natal Province, South Africa. Precambrian Res 77:243–271
Cornell DH, Armstrong RA, Walraven F (1998) Geochronology of the Proterozoic Hartley Basalt formation, South Africa: constraints on the Kheis tectogenesis and the Kaapvaal Craton´s earliest Wilson Cycle. J Afr Earth Sci 26:5–27
Cornell DH, Thomas RJ, Gibson R, Moen HFG, Moore JM, Reid DL (2006) Namaqua-Natal Province. In: Johnson MR, Anhaeusser CR, Thomas RJ (eds) The geology of South Africa. Geological Society of South Africa and Council for Geoscience, Johannesburg and Pretoria, pp 325–379
Cornell DH, Pettersson Å, Simonsen SL (2012) Zircon U-Pb emplacement and Nd-Hf crustal residence ages of the Straussburg granite and Friersdale charnockite in the Namaqua-Natal Province, South Africa. S Afr J Geol 115:465–484
Cornell DH, van Schijndel V, Simonsen SL, Frei D (2015) Geochronology of Mesoproterozoic hybrid intrusions in the Konkiep Terrane, Namibia, from passive to active continental margin in the Namaqua-Natal Wilson Cycle. Precambrian Res 265:166–188
Corner B (2008) The crustal framework of Namibia derived from an integrated interpretation of geophysical and geological data. In: Miller RMG (ed) The geology of Namibia. Geological Survey of Namibia, Windhoek, p p2-1–2-19
Coward MP, Daly MC (1984) Crustal lineaments and shear zones in Africa: their relationship to plate movements. Precambrian Res 24:27–45
Coward MP, James PR, Wright L (1976) Northern margin of the Limpopo mobile belt, southern Africa. Geol Soc Am Bull 87:601–611
da Silva R (2011) Distribution and geochronology of unconformity-bound sequences in Paleoproterozoic Elim-Olifantshoek red beds: implications for timing of formation of Sishen-type iron ore and heavy carbonate carbon isotope excursion. M.Sc. thesis, University of Johannesburg
Dalziel IWD, Mosher S, Gahagan LM (2000) Laurentia-Kalahari collision and the assembly of Rodinia. J Geol 108:499–513
De Beer JH, Meyer R (1984) Geophysical characeristics of the Namaqua-Natal Belt and its boundaries, South Africa. J Geodyn 1:473–494
de Wit MJ, Armstrong RA, Kamo SL, Erlank AJ (1993) Gold-bearing sediments in the Pietersburg greenstone belt: age equivalents of the Witwatersrand Supergroup sediments, Sotuh Africa. Econ Geol 88:1242–1252
de Wit MJ, Tinker J (2004) Crustal structures across the central Kaapvaal craton from deep-seismic reflection data. S Afr J Geol 107:185–206
de Wit MJ, Brito Neves BB, Trouw RAJ, Pankhurst RJ (2008) Pre-Cenozoic correlations across the South Atlantic region: "the ties that bind". In: Pankhurst RJ, Trouw RAJ, Brito Neves BB, de Wit MJ (eds) West Gondwana: pre-Cenozoic correlations across the South Atlantic Region. Special Publications, vol 294. Geological Society of London, London, pp 1–8
Dodson MH, Compston W, Williams IS, Wilson JF (1988) A search for ancient detrital zircons in Zimbabwean sediments. J Geol Soc London 145:977–983
Dziggel A, Stevens G, Poujol M, Anhaeusser CR, Armstrong RA (2002) Metamorphism of the granite-greenstone terrane south of the

Barberton greenstone belt, South Africa: an insight into the tectono-thermal evolution of the "lower" portions of the Onverwacht Group. Precambrian Res 114:221–247

Eales HV, Cawthorn RG (1996) The Bushveld Complex. In: Cawthorn RG (ed) Layered intrusions. Elsevier, Amsterdam, pp 181–229

Eglington BM (2006) Evolution of the Namaqua-Natal Belt, southern Africa-A geochronological and isotope geochemical review. J Afr Earth Sci 46:93–111

Eglington BM, Armstrong RA (2003) Geochronological and isotopic constraints on the Mesoproterozoic Namaqua-Natal Belt: evidence from deep borehole intersections in South Africa. Precambrian Res 125:179–189

Eglington BM, Harmer RE, Kerr A (1989) Isotope and geochemical constraints on Proterozoic crustal evolution in south-eastern Africa. Precambrian Res 45:159–174

Eglington BM, Thomas RJ, Armstrong RA, Walraven F (2003) Zircon geochronology of the Oribi Gorge Suite, KwaZulu-Natal, South Africa: constraints on the timing of trans-current shearing in the Namaqua-Natal Belt. Precambrian Res 123:29–46

Eglington BM, Thomas RJ, Armstrong RA (2010) U-Pb SHRIMP zircon dating of Mesoproterozoic magmatic rocks from the Scottburgh area, central Mzumbe Terrane, KwaZulu-Natal, South Africa. S Afr J Geol 113:229–235

Eriksson PG, Altermann W, Hartzer FJ (2006) The Traansval Supergroup and ist precursors. In: Johnson MR, Anhaeusser CR, Thomas RJ (eds) The geology of South Africa. Geological Society of South Africa and Council for Geoscience, Johannesburg and Pretoria, pp 237–260

Fletcher JA (2003) The geology, geochemistry and fluid inclusion characteristics of the Wyldsdale gold-bearing pluton, northwest Swaziland. Ph.D. thesis, University of Witwatersrand

Foster DA, Goscombe BD, Newstead B, Mapani B, Mueller PA, Gregory LC, Muvangua E (2014) U-Pb age and Lu-Hf isotopic data of detrital zircons from the Neoproterozoic Damara Sequence: Implications for Congo and Kalahari before Gondwana. Gondwana Res 28:179–190

Fransson, M (2008) U-Pb zircon dating of metasedimentary rocks in the Areachap, Kakamas and Bushmanland terranes in Namaqua Province, South Africa. MSc thesis, Göteborgs Universitet

Frei R, Schoenberg R, Blenkinsop TG (1999) Geochronology of the late Archaean Razi and Chilimanzi suites of granites in Zimbabwe; implications for the late Archaean tectonics of the Limpopo Belt and Zimbabwe Craton. S Afr J Geol 102:55–63

Frimmel HE, Frank W (1998) Neoproterozoic tectono-thermal evolution of the Gariep Belt and its basement, Namibia and South Africa. Precambrian Res 90:1–28

Frimmel HE, Zartman RE, Späth A (2001) Dating Neoproterozoic continental break-up in the Richtersveld Igneous Complex, South Africa. J Geol 109:493–508

Frimmel HE, Fölling PG, Eriksson P (2002) Neoproterozoic tectonic and climatic evolution recorded in the Gariep Belt, Namibia and South Africa. Basin Res 14:55–67

Frimmel HE, Basei MAS, Correa VX, Mbangula N (2013) A new lithostratigraphic subdivision and geodynamic model for the Pan-African western Saldania Belt, South Africa. Precambrian Res 231:218–235

Frimmel et al. (2018) The Gariep belt. In: S. Siegesmund et al. (eds) Geology of southwest gondwana, Regional geology reviews, Springer, Heidelberg, pp 354–383

Gold DJC (2006) The Pongola Supergroup. In: Johnson MR, Anhaeusser CR, Thomas RJ (eds) The geology of South Africa. Geological Society of South Africa and Council for Geoscience, Johannesburg and Pretoria, pp 135–147

Goscombe et al. (2018) The Evolution of the Damara Orogenic System: A Record of West Gondwana Assembly and Crustal Response. In: S. Siegesmund et al. (eds) Geology of southwest gondwana, Regional geology reviews, Springer, Heidelberg, pp 303–346

Gray DR, Foster DA, Meert JG, Goscombe BD, Armstrong R, Trouw RAJ, Passchier CW (2008) A Damaran orogeny perspective on the assembly of southwestern Gondwana. In: Pankhurst RJ, Trouw RAJ, Brito Neves BB, de Wit MJ (eds) West Gondwana: pre-Cenozoic correlations across the South Atlantic Region. Special Publications, vol 294. Geological Society of London, London, pp 257–278

Grantham GH (2001) Cryptic Pan-African transpression along the eastern margin of the Kalahari craton and beyond—a possible suture between East and West Gondwana. Gondwana Res 4:623–624

Grobler DF, Walraven F (1993) Geochronology of Gaborone Granite Complex extensions in the area north of Mafikeng, South Africa. Chem Geol 105:319–337

Grosch EC, Kosler J, McLoughlin N, Drost K, Slama J, Pedersen RB (2011) Paleoarchean detrital zircon ages from the earliest tectonic basin in the Barberton Greenstone Belt, Kaapvaal craton, South Africa. Precambrian Res 191:85–99

Hanson RE (2003) Proterozoic geochronology and tectonic evolution of southern Africa. In: Yoshida M, Windley BF, Dasgupta S (eds) Proterozoic East Gondwana: Supercontinent assembly and breakup. Special Publications, vol 206. Geological Society of London, London, pp 427–463

Hanson RE, Wilson TJ, Brueckner HK, Onstott TC, Wardlaw MS, Johns CC, Hardcastle KC (1988) Reconnaissance geochronology, tectonothermal evolution, and regional significance of the middle Proterozoic Choma-Kalomo Block, southern Zambia. Precambrian Res 42:39–61

Hanson RE, Crowley JL, Bowring SA, Ramezani J, Gose WA, Dalziel IWD, Pancake JA, Seidel EK, Blenkinsop TG, Mukwakwami J (2004) Coeval large-scale magmatism in the Kalahari and Laurentian cratons during Rodinia assembly. Science 304:1126–1129

Hanson RE, Harmer RE, Blenkinsop TG, Bullen DS, Dalziel IWD, Gose WA, Hall RP, Kampunzu AB, Key RM, Mukwakwami J, Munyanyiwa H, Pancake JA, Seidel EK, Ward SE (2006) Mesoproterozoic intraplate magmatism in the Kalahari Craton: a review. J Afr Earth Sci 46:141–167

Hargrove US, Hanson RE, Martin MW, Blenkinsop TG, Bowring SA, Walker N, Munyanyiwa H (2003) Tectonic evolution of the Zambezi orogenic belt: geochronological, structural, and petrological constraints form northern Zimbabwe. Precambrian Res 123:159–186

Harris C, Pronost JJM, Ashwal LD, Cawthorn RG (2005) Oxygen and hydrogen isotope stratigraphy of the Rustenburg Layered Suite, Bushveld Complex: constraints on crustal contamination. J Petrol 46:579–601

Hartnady C, Joubert P, Stowe C (1985) Proterozoic crustal evolution in southwestern Africa. Episodes 8:236–244

Henderson DR, Long LE, Barton JM (2000) Isotopic ages and chemical and isotopic composition of the Archaean Turfloop Batholith, Pietersburg granite-greenstone terrane, Kaapvaal Craton, South Africa. S Afr J Geol 103:38–46

Heubeck C, Engelhardt J, Byerly GR, Zeh A, Sell B, Luber T, Lowe DR (2013) Timing of deposition and deformation of the Moodies Group (Barberton Greenstone Belt, South Africa): Very-high-resolution of Archaean surface processes. Precambrian Res 231:236–262

Hoal BG (1985) Preliminary report on the geology of the south-eastern part of Diamond area n° 2, South West Africa/Namibia. Communs Geol Surv South West Africa/Namibia 1:9–22

Hoal BG (1990) The geology and geochemistry of the Proterozoic Awasib Mountain Terrain, Southern Namibia. Memoirs of the Geological Survey of Namibia, Windhoek, vol 11, 163 p

Hoal BG, Heaman LM (1995) The Sinclair Sequence: U-Pb age constraints from the Awasib Mountain area. Communs Geol Surv Namibia 10:83–92

Hofmann M, Linnemann U, Hoffmann K-H, Gerdes A, Eckelmann K, Gärtner A (2014) The Namuskluft and Dreigratberg sections in southern Namibia (Kalahari Craton, Gariep Belt): a geological history of Neoproterozoic rifting and recycling of cratonic crust during the dispersal of Rodinia until the amalgamation of Gondwana. Int J Earth Sci 103:1187–1202

Holzer L, Frei R, Barton JR Jr, Kramers JD (1998) Unraveling the record of successive high grade events in the Central Zone of the Limpopo Belt using Pb single phase dating of metamorphic minerals. Precambrian Res 87:87–115

Holzer L, Barton JR, Paya BK, Kramers JD (1999) Tectonothermal history of the western part of the Limpopo Belt: tectonic models and new perspectives. J Afr Earth Sci 28:383–402

Horstwood MSA, Nesbitt RW, Noble SR, Wilson JF (1999) U-Pb zircon evidence for an extensive early Archean craton in Zimbabwe: a reassessment of the timing of craton formation, stabilization, and growth. Geology 27:707–710

Hunter DR (1970) The ancient Gneiss Complex in Swaziland. Trans Geol Soc S Afr 73:107–150

Hutchins DG, Reeves CV (1980) Regional geophysical exploration of the Kalahari in Botswana. Tectonophysics 69:201–220

Jacobs J, Thomas RJ (1994) Oblique collision at about 1.1 Ga along the southern margin of the Kaapvaal continent, south-east Africa. Geol Rundsch 83:322–333

Jacobs J, Falter M, Thomas RJ, Kunz J, Jeßberger EK (1997) $^{40}Ar/^{39}Ar$ thermochronological constraints on the structural evolution of the Mesoproterozoic Natal Metamorphic Province, SE Africa. Precambrian Res 86:71–92

Jacobs J, Pisarevsky S, Thomas RJ, Becker T (2008) The Kalahari Craton during the assembly and dispersal of Rodinia. Precambrian Res 160:142–158

Jelsma HA, Dirks PHGM (2000) Tectonic evolution of a greenstone sequence in northern Zimbabwe: sequential early stacking and pluton diapirism. Tectonics 19:135–152

Jelsma HA, Dirks PHGM (2002) Neoarchaean tectonic evolution of the Zimbabwe Craton. In: Fowler CMR, Ebinger CJ, Hawkesworth CJ (eds) The early Earth: physical, chemical and biological development. Special Publications, vol 199. Geological Society of London, London, pp 183–211

Jelsma H, Vinyu M, Valbracht P, Davies G, Wijbrans J, Verdurmen E (1996) Constraints on Archean crustal evolution of the Zimbabwe craton: A U-Pb zircon. Sm-Nd and Pb-Pb whole rock isotope study: Contrib Mineral Petrol 124:55–70

Johnston ST, Armstrong R, Heaman L, McCourt S, Mitchell A, Bisnath A, Arima M (2001) Preliminary U-Pb geochronology of the Tugela terrane, Natal belt, eastern South Africa. Mem Natl Inst Polar Res Spec Issue 55:40–58

Kamber BS, Blenkinsop TG, Villa IM, Dahl PS (1995) Proterozoic transpressive deformation in the Northern Marginal Zone, Limpopo Belt, Zimbabwe. J Geol 103:493–508

Kamo SL (1992) Archean crustal evolution in the Barberton Mountain Land, South Africa: U-Pb and Nd isotopic constraints. MSc thesis, McMaster University

Kamo SL, Davis DW (1994) Reassessment of Archaean crustal development in the Barberton Mountain Land, South Africa, based on U-Pb dating. Tectonics 13:167–192

Kamo SL, Davis DW, de Wit MJ (1990) U-Pb geochronology of Archean plutonism in the Barberton region, South Africa: 800 Ma of crustal evolution. 7° International Congress on Geochemistry, Canberra

Kampunzu AB, Akanyang P, Mapeo RBM, Modie BN, Wendorff M (1998) Geochemistry and tectonic significance of the Mesoproterozoic Kgwebe metavolcanic rocks in northwest Botswana: implications for the evolution of the Kibaran Namaqua-Natal Belt. Geol Mag 135:669–683

Kasbohm J, Evans DAD, Panzik JE, Hofmann M, Linnemann U (2015) Palaeomagnetic and geochronological data from Late Mesoproterozoic redbed sedimentary rocks of the western margin of Kalahari Craton. In: Li ZX, Evans DAD, Murphy JB (eds) Supercontinent cycles through Earth history. Special Publications, vol 242. Geological Society of London, London. doi:https://doi.org/10.1144/SP424.4

Key RM, Rundle CC (1981) The regional significance of new isotopic ages from Precambrian windows through the Kalahari Beds in north-western Gondwana. Trans Geol Soc S Afr 84:51–66

Khoza D, Jones AG, Muller MR, Evans RL, Webb SJ, Miensopust M, the SAMTEX team (2013) Tectonic Model of the Limpopo Belt: Constraints from magnetotelluric data. Precambrian Res 226:143–156

Kisters A, Belcher R The stratigraphy and structure of the western saldania belt, south africa and geodynamic implications. In: S. Siegesmund et al. (eds) Geology of southwest gondwana, Regional geology reviews, Springer, Heidelberg, pp 387–408

Koistinen T, Lehtonen MI, Fernando S, Matola R (2008) Contribution to the structure at the eastern margin of the Archaean Zimbabwe Craton, Mozambique. In: Pekkala Y, Lehto T, Mäkitie H (eds) GTK Consortium Geological Surveys in Mozambique 2202-2007. Geological Survey of Finland Special Papers, vol 48, pp 141–144

Kramers JD, McCourt S, van Reenen DD (2006) The Limpopo Belt. In: Johnson MR, Anhaeusser CR, Thomas RJ (eds) The geology of South Africa. Geological Society of South Africa and Council for Geoscience, Johannesburg and Pretoria, pp 209–236

Kramers JD, McCourt S, Roering C, Smit CA, van Reenen DD (2011) Tectonics models proposed for the Limpopo Complex: mutual compatibilities and constraints. Geol Soc Am Mem 207:311–324

Kramers JD, Henzen M, Steidle L (2014) Greenstone belts at the northernmost edge of the Kaapvaal Craton: timing of tectonic events and a possible crustal fluid source. Precambrian Res 253:96–113

Kröner A (2007) The Ancient Gneiss Complex of Swaziland and Environs: Record of early Archean crustal evolution in southern Africa. In: van Kranendonk MJ, Smithies H, Bennett VC (eds) Earth´s oldest rocks. Developments in Precambrian Geology, vol 15. Elsevier, Amsterdam, pp 465–480

Kröner A, Tegtmeyer A (1994) Gneiss-greenstone relationships in the Ancient Gneiss Complex of southwestern Swaziland, southern Africa, and implications for early crustal evolution. Precambrian Res 67:109–139

Kröner A, Byerly GR, Lowe DR (1991) Chronology of early Archean granite-greenstone evolution in the Barberton Mountain Land, South Africa, based on precise dating by single grain zircon evaporation. Earth Planet Sci Lett 103:41–54

Kröner A, Hegner E, Byerly GR, Lowe DR (1992) Possible terrane identification in the early Archean Barberton greenstone belt, South Africa, using single zircon geochronology. Trans Amer Geophys Union 73:616

Kröner A, Hegner E, Went JI, Byerly GR (1996) The oldest part of the Barberton granitoid-greenstone terrain, South Africa: evidence for crust formation at 3.5 nd 3.7 Ga. Precambrian Res 78:105–124

Kröner A, Jaeckel P, Brandl G (2000) Single zircon ages for felsic to intermediate rocks from the Pietersburg and Giyani greenstone belts and bordering granitoid orthogneisses, northern Kaapvaal Craton, South Africa. J Afr Earth Sci 30:773–793

Kruger FJ, Geringer GJ, Havenga AT (2000) The geology, petrology, geochronology and source region character of the layered gabbronoritic Oranjekom Complex in the Kibaran Namaqua Mobile Belt, South Africa. J Afr Earth Sci 30:675–687

Kusky TM (1998) Tectonic setting and terrane accretion of the Archean Zimbabwe craton. Geology 26:163–166

Lana C, Kisters A, Stevens G (2009) Exhumation of Mesoarchean TTG gneisses from the middle crust: Insights from the Steyndorp core complex, Barberton granitoid-greenstone terrain, South Africa. Geol Soc Am Bull 122:183–197

Laurent O, Zeh A (2015) A linear Hf isotope-array despite different granitoid sources and complex Archean geodynamics: example from the Pietersburg block (South Africa). Earth Planet Sci Lett 430:326–338

Laurent O, Martin H, Doucelance R, Moyen J-F, Paquette JL (2011) Geochemistry and petrogenesis of high-K "sanukitoids" from the Bulai pluton, Central Limpopo Belt, South Africa: implications for geodynamic changes at the Archaean-Proterozoic boundary. Lithos 123:73–91

Laurent O, Martin H, Moyen JF, Doucelance R (2014) The diversity and evolution of late-Archean granitoids: evidence for the onset of "modern-style" plate tectonics between 3.0 and 2.5 Ga. Lithos 205:208–235

Layer PW, Kröner A, York D (1992) Pre-3000 Ma thermal history of the Archean Kaap Valley pluton, South Africa. Geology 20:717–720

Lehmann J, Saalmann K, Naydenov KV, Milani L, Belyanin GA, Zwingmann H, Charlesworth G, Kinnaird JA (2015) Structural and geochronological constraints on the Pan-African tectonic evolution of the northern Damara Belt, Namibia. Tectonics 35:103–135

Li ZX, Bogdanova SV, Collins AS, Davidson A, De Waele B, Ernst RE, Fitzimons ICW, Fuck RA, Gladkochub DP, Jacobs J, Karlstrom KE, Lu S, Natapov LM, Pease V, Pisarevsky SA, Thrane K, Vernikovsky V (2008) Assembly, configuration, and break-up history of Rodinia: a synthesis. Precambrian Res 160:179–210

Lowe DR, Byerly GR (1999) Geologic evolution of the Barberton Greenstone Belt, South Africa. Geological Society of America Special Paper 329, Colorado

Lowe DR, Byerly GR (2007) An overview of the geology of the Barberton Greenstone Belt and vicinity: Implications for early crust development. In: van Kranendonk MJ, Smithies H, Bennett VC (eds) Earth´s oldest rocks. Developments in Precambrian Geology, vol 15. Elsevier, Amsterdam, pp 481–526

MacGregor AM (1953) Precambrian formations of tropical Africa. 19° International Geological Congress, Algeria

Majaule T, Hanson RE, Key RM, Bowring SA (2001) The Magondi Belt in northeast Botswana: regional relations and new geochronological data from the Sua Pan area. J Afr Earth Sci 32:257–267

Manhica ADST, Grantham GH, Armstrong RA, Guise PG, Kruger FJ (2001) Polyphase deformation and metamorphism at the Kalahari Craton-Mozambique Belt boundary. In: Miller JA, Holdsworth RE, Buick IS, Hand M (eds) Continental reactivation and reworking. Special Publications, vol 184. Geological Society of London, London, pp 303–322

Mänttäri I (2008) Mesoarchaean to lower Jurassic U-Pb and Sm-Nd ages from NW Mozambique In: Pekkala Y, Lehto T, Mäkitie H (eds) GTK Consortium Geological Surveys in Mozambique 2202-2007. Geological Survey of Finland Special Papers, vol 48, pp 81–119

Manzi MSD, Hein KAA, King N, Durrheim RJ (2013) Neoarchaean tectonic history of the Witwatersrand Basin and Ventersdorp Supergroup: new constraints from high-resolution 3D seismic reflection data. Tectonophysics 590:94–105

Mapani B, Cornell D, van Schijndel V (2014) Geochronology and tectonic evolution of the Hohewarte Complex, central Namibia: new insights in Paleoproterozoic to Early Neoproterozoic crustal accretion processes. J Afr Earth Sci 99:228–244

Mapeo RBM, Armstrong RA, Kampunzu AB (2001) SHRIMP U-Pb zircon geochronology of gneisses from the Gweta borehole, northeast Botswana: implications for the Palaeoproterozoic Magondi Belt in southern Africa. Geol Mag 138:299–308

Mapeo RBM, Ramokate LV, Corfu F, Davis DW, Kampunzu AB (2006) The Okwa basement complex, western Botswana: U-Pb zircon geochronology and implications for Eburnean processes in southern Africa. J Afr Earth Sci 46:253–262

Maphalala RM, Kröner A (1993) Pb-Pb single zircon ages for the younger Archaean granitoids of Swaziland, southern Africa. 16° Colloquium African Geology, Mbabane

Mason R (1973) The Limpopo mobile belt-southern Africa. Philos T R Soc A 273:463–485

Master S (1991a) Stratigraphy, tectonic setting, and mineralization of the early Proterozoic Magondi Supergroup, Zimbabwe: a review. Economic Geology Research Unit, University of the Witwatersrand, Johannesburg, information circular 238, p 75

Master S (1991b) The origin and controls on the distribution of copper and precious metal mineralization at the Mangula and Norah mines, Mhangura, Zimbabwe. PhD thesis, University of the Witwatersrand

Master S (1993) Early Proterozoic assembly of "Ubendia" (Equatorial and Southern Africa and adjacent parts of South America): tectonic and metallogenic implications. In: Dia A (eds) Symposium on the Early Proterozoic: geochemical and structural constraints, Metallogeny. CIFEG Occ. Publ., 23, Dakar, pp 103–107

Master S, Bekker A, Hofmann A (2010) A review of the stratigraphy and geological setting of the Palaeoproterozoic Magondi Supergroup, Zimbabwe—type locality for the Logamundi carbon isotope excursion. Precambrian Res 182:254–273

Matthews PE (1972) Possible Precambrian obduction and plate tectonics in southeastern Africa. Nature 240:37–39

Matthews PE (1981) Eastern or Natal sector of the Namaqua-Natal mobile belt in southern Africa. In: Hunter DR (ed) Precambrian of the southern hemisphere. Elsevier, Amsterdam, pp 705–715

Matthews PE, Charlesworth EG, Eglington BM, Harmer RE (1989) A minimum 3.29 Ga age for the Nondweni greenstone complex in the south-eastern Kaapvaal Craton. S Afr J Geol 92:272–278

McCarthy TS (2006) The Witwatersrand Supergroup. In: Johnson MR, Anhaeusser CR, Thomas RJ (eds) The geology of South Africa. Geological Society of South Africa and Council for Geoscience, Johannesburg and Pretoria, pp 155–186

McCourt S, Vearncombe JR (1992) Shear zones of the Limpopo Belt and adjacent granitoid-greenstone terranes: implications for late Archaean collision tectonics in southern Africa. Precambrian Res 55:553–570

McCourt S, Hilliard P, Armstrong RA, Munyanyiwa H (2001) SHRIMP U-Pb zircon geochronology of the Hurungwe granite northwest Zimbabwe: age constraints on the timing of the Magondi orogeny and implications for the correlation between the Kheis and Magondi Belts. S Afr J Geol 104:39–46

McCourt S, Armstrong RA, Grantham GH, Thomas RJ (2006) Geology and evolution of the Natal belt, South Africa. J Afr Earth Sci 46:71–92

McCourt S, Armstrong RA, Jelsma H, Mapeo RBM (2013) New U-Pb SHRIMP ages from the Lubango region, SW Angola: insights into the Palaeoproterozoic evolution of the Angolan Shield, southern Congo Craton, Africa. J Geol Soc London 170:353–363

Mendonidis P, Armstrong RA (2009) A new U-Pb zircon age for the Portobello granite from the southern part of the Natal Metamorphic Complex. S Afr J Geol 112:197–208

Mendonidis P, Armstrong RA, Eglington BM, Grantham GH, Thomas RJ (2002) Metamorphic history and U-Pb zircon (SHRIMP) geochronology of the Glenmore Granite: implications

for the tectonic evolution of the Natal Metamorphic Province. S Afr J Geol 105:325–336
Mendonidis P, Armstrong RA, Grantham GH (2009) U-Pb SHRIMP ages and tectonic setting of the Munster Suite of the Margate Terrane of the Natal Metamorphic Belt. Gondwana Res 15:28–37
Mendonidis P, Thomas RJ, Grantham GH, Armstrong RA (2015) Geochronology of emplacement and charnockite formation of the Margate Granite Suite, Natal Metamorphic Province, South Africa: Implications for Natal-Maud belt connections. Precambrian Res 265:189–202
Milani L, Kinnaird JA, Lehmann J, Naydenov KV, Saalmann K, Frei D, Gerdes A (2015) Role of crustal contribution in the early stage of the Damara Orogen, Namibia: new constraints from combined U-Pb and Lu-Hf isotopes from the Goas Magmatic Complex. Gondwana Res 28:961–986
Miller RMG (2008) The geology of Namibia. Geological Survey of Namibia, Windhoek
Miller RMG (2012) Review of Mesoproterozoic magmatism, sedimentation and terrane amalgamation in southwestern Africa. S Afr J Geol 115:417–448
Modie BNJ (1996) Depositional environments of the Meso- to Neoproterozoic Ghanzi-Chobe belt, northwest Gondwana. J Afr Earth Sci 22:255–268
Moen HFG (1999) The Kheis tectonic subprovince, Southern Africa; a lithostratigraphic perspective. S Afr J Geol 102:27–42
Moen HFG (2006) The Olifantshoek Supergroup. In: Johnson MR, Anhaeusser CR, Thomas RJ (eds) The geology of South Africa. Geological Society of South Africa and Council for Geoscience, Johannesburg and Pretoria, pp 319–324
Moore M, Davis DW, Robb LJ, Jackson MC, Grobler DF (1993) Archean rapakivi granite-anorthosite-rhyolite complex in the Witwatersrand Basin hinterland, southern Africa. Geology 21:1031–1034
Moser D, Flowers RM, Hart RJ (2001) Birth of the Kaapvaal tectosphere 3.08 billion years ago. Science 291:465–468
Moyen J-F, Martin H (2012) Forty years of TTG research. Lithos 148:312–336
Moyen J-F, van Hunen J (2012) Short-term episodicity of Archaean plate tectonics. Geology 40:451–454
Moyen J-F, Stevens G, Kisters A (2006) Record of mid-Archaean subduction from metamorphism in the Barberton terrain, South Africa. Nature 442:559–562
Moyen J-F, Stevens G, Kisters A, Belchier RW (2007) TTG plutons of the Barberton granitoid-greenstone terrain, South Africa. In: van Kranendonk MJ, Smithies H, Bennett VC (eds) Earth´s oldest rocks. Developments in Precambrian Geology, vol 15. Elsevier, Amsterdam, pp 606–667
Mukasa SB, Wilson AH, Carlson RW (1998) A multielement geochronologic study of the Great Dyke, Zimbabwe: significance of the robust and reset ages. Earth Planet Sci Lett 164:353–369
Muller MR, Jones AG, Evans RL, Grütter HS, Hatton C, Garcia X, Hamilton MP, Miensopust MP, Cole P, Ngwisanyi T, Hutchins D, Fourie CJ, Jelsma HA, Evans SF, Aranavis T, Pettit W, Webb SJ, Wasborg J, the SAMTEX Team (2009) Lithospheric structure, evolution and diamond prospectivity of the Rehoboth Terrane and western Kaapvaal Craton, southern Africa: Constraints from broadband magnetotellurics. Lithos 112:93–105
Munyanyiwa H, Kröner A, Jaeckel P (1995) U-Pb and Pb-Pb single zircon ages for charno-enderbites from the Magondi mobile belt, northwest Zimbabwe. S Afr J Geol 98:52–57
Nagel R, Warkus F, Becker T, Hansen BT (1996) U/Pb-Zirkondatierungen der Gaub Valley Formation am Südrand des Damara Orogens-Namibia und ihre Bedeutung für die Entwicklung des Rehoboth Basement Inlier. Zt Geol Wiss 24:611–618
Neuendorf KEK, Mehl JP Jr, Jackson JA (2005) Glossary of geology, 5th edn. American Geological Institute, Virginia
Nicoli G, Stevens G, Moyen J-F, Frei D (2015) Rapid evolution from sediment to anatectic granulite in an Archean continental collision zone: the example of the Bandelierkop Formation metapelites, South Marginal Zone, Limpopo Belt, South Africa. J Metamorph Geol 33:177–202
Oberthür T, Davis DW, Blenkinsop TG, Höhndorf A (2002) Precise U-Pb mineral ages, Rb-Sr and Sm-Nd systematics for the Great Dyke, Zimbabwe – constraints on late Archean events in the Zimbabwe craton and Limpopo belt. Precambrian Res 113:293–305
Oriolo S, Oyhantçabal P, Wemmer K, Basei MAS, Benowitz J, Pfänder J, Hannich F, Siegesmund S (2016) Timing of deformation in the Sarandí del Yí Shear Zone, Uruguay: Implications for the amalgamation of western Gondwana during the Neoproterozoic Brasiliano-Pan-African Orogeny. Tectonics 35:754–771
Oriolo S, Oyhantçabal P, Wemmer K, Siegesmund S (2017) Contemporaneous assembly of Western Gondwana and final Rodinia break-up: implications for the supercontinent cycle. Geosci Front 8:1431–1445. https://doi.org/10.1016/j.gsf.2017.01.009
Parman SW, Dann JC, Grove TL, de Wit MJ (1997) Emplacement conditions of komatiite magmas from the 3.49 Ga Komati Formation, Barberton Greenstone Belt, South Africa. Earth Planet Sci Lett 150:303–323
Pettersson Å, Cornell DH, Moen HFG, Reddy S, Evans D (2007) Ion-probe dating of 1.2 Ga collision and crustal architecture in the Namaqua-Natal Province of southern Africa. Precambrian Res 158:79–92
Pettersson Å, Cornell DH, Yuhara M, Hirahara Y (2009) Sm-Nd data for granitoids across the Namaqua sector of the Namaqua-Natal Province, South Africa. In: Reddy SM, Mazumder R, Evans DAD, Collins AS (eds) Palaeoproterozoic supercontinents and global evolution. Special Publications, vol 323. Geological Society of London, London, pp 219–230
Poujol M (2001) U-Pb isotopic evidence for episodic granitoid emplacement in the Murchinson greenstone belt, South Africa. J Afr Earth Sci 33:155–163
Poujol M (2007) An overview of the Pre-Mesoarchean Rocks of the Kaapvaal Craton, South Africa. In: van Kranendonk MJ, Smithies H, Bennett VC (eds) Earth´s oldest rocks. Developments in Precambrian Geology, vol 15. Elsevier, Amsterdam, pp 453–464
Poujol M, Anhaeusser CR (2001) The Johannesburg Dome, South Africa: new single zircon U-Pb isotopic evidence for early Archaean granite-greenstone development within the central Kaapvaal Craton. Precambrian Res 108:139–157
Poujol M, Robb LJ (1999) New U-Pb zircon ages on gneisses and pegmatite from south of the Murchinson greenstone belt, South Africa. S Afr J Geol 102:93–97
Poujol M, Robb LJ, Respaut JP, Anhaeusser CR (1996) 3.07-2.97 Ga greenstone belt formation in the northeastern Kaapvaal Craton: implications for the origin of the Witwatersrand Basin. Econ Geol 91:1455–1461
Poujol M, Anhaeusser CR, Armstrong RA (2002) Episodic granitoid emplacement in the Archaean Amalia-Kraaipan terrane, South Africa: confirmation from single zircon U-Pb geochronology. J Afr Earth Sci 35:147–161
Powell CMA, Jones DL, Pisarevsky S, Wingate MTD (2001) Palaeomagnetic constraints on the position of the Kalahari Craton in Rodinia. Precambrian Res 110:33–46
Priem HNA, Boelrijk NAIM, Hebeda EH, Verdurmen EAT, Verschure RH (1972) Isotopic dating in the Kamativi Tin Belt, Southern Rhodesia. Geol Mijnbouw 50:619–624
Raith JG, Harley SL (1998) Low-P/high-T metamorphism in the Okiep Copper District, western Namaqualand, South Africa. J Metamorph Geol 16:281–305
Rajesh HM, Santosh M, Wan Y, Liu D, Liu SJ, Belyanin GA (2014) Ultrahigh temperature granulites and magnesian charnockites:

evidence for Neoarchean accretion along the northern margin of the Kaapvaal Craton. Precambrian Res 246:150–159

Ramokate LV, Mapeo RBM, Corfu F, Kampunzu AB (2000) Proterozoic geology and regional correlation of the Ghanzi-Makunda area, western Gondwana. J Afr Earth Sci 30:453–466

Ranganai RT, Kampunzu AB, Atekwana EA, Paya BK, King JG, Koosimile DI, Stettler EH (2002) Gravity evidence for a larger Limpopo Belt in southern Africa and geodynamic implications. Geophys J Int 149:F9–F14

Reid DL (1997) Sm-Nd age and REE geochemistry of Proterozoic arc-related igneous rocks in the Richtersveld Subprovince, Namaqua Mobile Belt, Southern Africa. J Afr Earth Sci 26:621–633

Reid DL, Welke HJ, Erlank AJ, Moyes A (1987) The Orange River Group: a major Proterozoic calcalkaline volcanic belt in the Western Namaqua Province, southern Africa. In: Pharaoh TC, Beckinsale RD, Rickard D (eds) Geochemistry and mineralization of Proterozoic volcanic suites. Special Publications, vol 33. Geological Society of London, London, pp 327–346

Reimold WU, Meyer FM, Walraven F, Matthews PE (1993) Geochemistry and chronology of pre- and post-Pongola granitoids from northeastern Natal. 16° Colloquium African Geology, Mbabane

Robb DL, Armstrong RA, Waters DJ (1999) The history of granulite-facies metamorphism and crustal growth form single zircon U-Pb geochronology: Namaqualand, South Africa. J Petrol 40:1747–1770

Robb LJ, Meyer FM (1995) The Witwatersrand Basin, South Africa: geological framework and mineralization processes. Ore Geol Rev 10:67–94

Robb LJ, Davis DW, Kamo SL, Meyer FM (1992) Ages of altered granites adjoining the Witwatersrand Basin and implications for the origin of gold and uranium. Nature 357:677–680

Robb LJ, Meyer FM, Kröner A, Trumbull RB, Reimold WU, De Bruiyn H, Walraven F, Toulkeridis T (1993) Late-stage granite plutons in the Barberton region and Swaziland: an update. 16° Colloquium African Geology, Mbabane

Robb LJ, Brandl G, Anhaeusser CR, Poujol M (2006) Archaean granitoid intrusions. In: Johnson MR, Anhaeusser CR, Thomas RJ (eds) The geology of South Africa. Geological Society of South Africa and Council for Geoscience, Johannesburg and Pretoria, pp 57–94

Roering C, van Reenen DD, de Wit MJ, Smit CA, de Beer JH, van Schalkwyk JF (1992) Structural, geological and metamorphic significance of the Kaapvaal Craton-Limpopo Belt contact. Precambrian Res 55:69–80

Rollinson HR (1993) A terrane interpretation of the Archaean Limpopo Belt. Geol Mag 130:755–765

SACS, South African Committee for Stratigraphy (1980) Stratigraphy of South Africa. Handbook of the Geological Survey of South Africa, vol 8. Geological Survey of South Africa

Sánchez-Garrido CJMG, Stevens G, Armstrong RA, Moyen J-F, Martin H, Doucelance R (2011) Diversity in Earth's early felsic crust: Paleoarchean peraluminous granites of the Barberton Greenstone Belt. Geology 39:963–966

Schaller M, Steiner O, Studer I, Holzer L, Herwegh M, Kramers JD (1999) Exhumation of Limpopo Central Zone granulites and dextral continental-scale transcurrent movement at 2.0 Ga along the Palala Shear Zone, Northern Province, South Africa. Precambrian Res 96:263–288

Schneider T, Becker T, Borg G, Hilken U, Hansen BT, Weber K (2004) New U-Pb zircon ages of the Nückopf Formation and their significance for the Mesoproterozoic event in Namibia. Communs Geol Surv Namibia 13:63–74

Schoene B, de Wit MJ, Bowring SA (2008) Mesoarchean assembly and stabilization of the eastern Kaapvaal craton: a structural-thermochronological perspective. Tectonics 27:TC5010

Schwartz MO, Kwok YY, Davis DW, Akanyang P (1996) Geology, geochronology and regional corelation of the Ghanzi Ridge, Botswana. S Afr J Geol 99:245–250

Shackleton RM (1995) Tectonic evolution of greenstone belts. In: Coward MP, Ries AC (eds) Early Precambrian Processes.Special Publications, vol 95. Geological Society of London, London, p 53–65

Singletary SJ, Hanson RE, Martin MW, Crowley JL, Bowring SA, Key RM, Ramokate LV, Direng BB, Krol MA (2003) Geochronology of basement rocks in the Kalahari Desert, Botswana, and implications for regional Proterozoic tectonics. Precambrian Res 121:47–71

Söderlund U, Patchett PJ, Vervoort JD, Isachsen CE (2004) The ^{176}Lu decay constant determined by Lu-Hf and U-Pb isotope systematics of Precambrian mafic intrusions. Earth Planet Sci Lett 219:311–324

Spencer CJ, Thomas RJ, Roberts NMW, Cawood PA, Millar I, Tapster S (2015) Crustal growth during island arc accretion and transcurrent deformation, Natal Metamorphic Province, South Africa: New isotopic constraints. Precambrian Res 265:203–217

Stevens G, Moyen J-F (2007) Metamorphism in the Barberton Granite Greenstone Terrain: a record of Paleoarchean accretion. In: van Kranendonk MJ, Smithies H, Bennett VC (eds) Earth´s oldest rocks. Developments in Precambrian Geology, vol 15. Elsevier, Amsterdam, pp 606–698

Stockwell CH, McGlynn JC, Emslie RF, Sanford BV, Norris AW, Donaldson JA, Fahrig WF, Curie KL (1970) Geology of the Canadian Shield. In: Douglas RJW (ed) Geology and economic minerals of Canada. Economic Geology Report, vol 1. Geological Survey of Canada, Ottawa, pp 43–150

Stowe CW (1983) The Upington geotraverse and its implications for craton margin tectonics. In: Botha BJV (ed) Namaqualand metamorphic complex. Geological Society of South Africa Special Publications, Johannesburg, vol 10, pp 147–171

Taylor PN, Kramers JF, Moorbath S, Wilson JF, Orpen JL, Martin A (1991) Pb/Pb, Sm-Nd, and Rb-Sr geochronology in the Archean craton of Zimbabwe. Chem Geol 87:175–196

Tegtmeyer AR, Kröner A (1987) U-Pb zircon ages bearing on the nature of early Archean greenstone belt evolution, Barberton Mountain Land, southern Africa. Precambrian Res 36:1–20

Thomas RJ (1989) A tale of two tectonic terranes. S Afr J Geol 92:306–321

Thomas RJ, Eglington BM (1990) A Rb-Sr, Sm-Nd and U-Pb zircon isotopic study of the Mzumbe Suite, the oldest intrusive granitoid in southern Natal, South Africa. S Afr J Geol 93:761–765

Thomas RJ, Eglington BM, Bowring SA (1993) Dating the cessation of Kibaran magmatism in Natal, South Africa. J S Afr Earth Sci 16:247–252

Thomas RJ, Agenbacht ALD, Cornell DH, Moore JM (1994) The Kibaran of southern Africa: tectonic evolution and metallogeny. Ore Geol Rev 9:131–160

Thomas RJ, Gold DJC, Verbeek JA, Walraven F (1997) Geology of the Archaean Nzimane Inlier, Zululand. S Afr J Geol 100:123–136

Thomas RJ, Cornell DH, Armstrong RA (1999) Provenance age and metamorphic history of the Quha Formation, Natal Metamorphic Province: a U-Th-Pb zircon SHRIMP study. S Afr J Geol 102:83–88

Thomas RJ, Armstrong RA, Eglington BM (2003) Geochronology of the Sicombe granite, Transkei, Natal Metamorphic Province, South Africa. S Afr J Geol 106:403–408

Treloar PJ (1988) The geological evolution of the Magondi Mobile Belt, Zimbabwe. Precambrian Res 38:55–73

Treloar PJ, Kramers JD (1989) Metamorphism and geochronology of granulites and magmatic granulites from the Magondi Mobile Belt, Zimbabwe. Precambrian Res 38:55–73

van Biljon WJ, Legg JH (eds) (1983) The Limpopo Belt. Geological Society of South Africa Special Publications, Johannesburg

van der Westhuizen WA, de Bruiyn H, Meintjes PG (2006) The Ventersdorp Supergroup. In: Johnson MR, Anhaeusser CR, Thomas RJ (eds) The geology of South Africa. Geological Society of South Africa and Council for Geoscience, Johannesburg and Pretoria, pp 187–208

van Niekerk HS (2006) The origin of the Kheis Terrane and its relationship with the Archean Kaapvaal Craton and the Grenvillian Namaqua Province in southern Africa. PhD thesis, University of Johannesburg

van Reenen DD, Barton JM Jr, Roering C, Smith CA, van Schalkwyk JF (1987) Deep crystal response to continental collision: the Limpopo belt of southern Africa. Geology 15:11–14

van Schijndel V, Cornell DH, Hoffmann K-H, Frei D (2011) Three episodes of crustal development in the Rehoboth Province, Namibia. In: van Hinsbergen DJJ, Buiter SJH, Torsvik TH, Gaina C, Webb SJ (eds) The formation and evolution of Africa: A synopsis of 3.8 Ga of Earth history. Special Publications, vol 357. Geological Society of London, London, pp 27–47

van Schijndel, V. et al. (2014) Crustal evolution of the Rehoboth Province from Archaean to Mesoproterozoic times: Insights from theRehoboth Basement Inlier. Precambrian Res 240:22–36

Vermeesch P (2012) On the visualisation of detrital age distributions. Chem Geol 312:190–194

Verwoerd WJ, du Toit MC (2006) The Phalaborwa and Schiel complexes. In: Johnson MR, Anhaeusser CR, Thomas RJ (eds) The geology of South Africa. Geological Society of South Africa and Council for Geoscience, Johannesburg and Pretoria, pp 291–299

Villaros A, Buick IS, Stevens G (2012) Isotopic variations in S-type granites: an inheritance from a heterogeneous source? Contrib Mineral Petrol 163:243–257

Vinyu ML, Hanson RE, Martin MW, Bowring SA, Jelsma HA, Krol MA, Dirks PHGM (1999) U-Pb and $^{40}Ar/^{39}Ar$ geochronological constraints on the tectonic evolution of the easternmost part of the Zambezi orogenic belt, northeast Zimbabwe. Precambrian Res 98:67–82

Visser DJL (1944) Stratigraphic features and tectonics of portions of Bechuanaland and Griqualand West. Trans Geol Soc S Afr 47:197–254

Walraven F (1989) The geology of the Pilgrim´s Rest area. Explanation Sheet 2430 (1:250000). Geological Survey of South Africa, Johannesburg

Waters DJ (1986) Metamorphic zonation and thermal history of politic gneisses from western Namaqualand, S Africa. Trans Geol Soc S Afr 89:97–102

Waters DJ (1989) Metamorphic evidence for the heating and cooling path of Namaqualand granulites. In: Daly JS, Cliff RA, Yardley BWD (eds) Evolution of metamorphic belts. Special Publications, vol 43. Geological Society of London, London, pp 357–363

Watkeys MK, Light MPR, Broderick TJ (1983) A retrospective view of the Limpopo belt, Zimbabwe. In: van Biljon WJ, Legg JH (eds) The Limpopo Belt. Special Publications, vol 8. Geological Society of South Africa, Johannesburg, pp 65–80

Watters BR (1974) Stratigraphy, igneous petrology and evolution of the Sinclair Group in southern SWA. Bulletin of the Precambrian Research Unit, University of Cape Town, Cape Town

Watters BR (1976) Possible late Precambrian subduction zone in South West Africa. Nature 259:471–473

Wilson JF (1979) A preliminary reappraisal of the Rhodesian basement complex. Geological Society of South Africa Special Publications, Johannesburg

Wilson JF, Nesbitt RW, Fanning CM (1995) Zircon geochronology of Archean felsic sequences in the Zimbabwe craton: a revision of greenstone stratigraphy and a model for crustal growth. In: Coward MP, Ries AC (eds) Early Precambrian processes. Special Publications, vol 95. Geological Society London, London, pp 109–126

York D, Layer PW, López Martínez M, Kröner A (1989) Thermal histories from the Barberton greenstone belt, southern Africa. 28° International Geological Congress, Washington

Yuhara M, Kagami H, Tsuchiya N (2001) Rb-Sr and Sm-Nd systematics of granitic and metamorphic rocks in the Namaqualand Complex, South Africa: Implications for evolution of marginal part of Kaapvaal Craton. Special Issue, vol 55. Memoir of the National Institute of Polar Research, Tokyo, pp 127–144

Zeh A, Gerdes A (2012) U-Pb and Hf isotope record of detrital zircons from gold-bearing sediments of the Pietersburg Greenstone Belt (South Africa)—is there a common provenance with the Witwatersrand Basin? Precambrian Res 204–205:46–56

Zeh A, Klemd R, Buhlmann S, Barton JM (2004) Pro- and retrograde P-T evolution of granulites of the Beit Bridge Complex (Limpopo Belt, South Africa): constraints from quantitative phase diagrams and geotectonic implications. J Metamorph Geol 22:79–95

Zeh A, Klemd R, Barton JM Jr (2005a) Petrological evolution in the roof of the high-grade metamorphic Central Zone of the Limpopo Belt, South Africa. Geol Mag 142:229–240

Zeh A, Holland TJB, Klemd R (2005b) Phase relationships in grunerite-garnet-bearing amphibolites in the system CFMASH, with applications to metamorphic rocks from the Central Zone of the Limpopo Belt, South Africa. J Metamorph Geol 23:1–17

Zeh A, Gerdes A, Klemd R, Barton JM Jr (2007) Archaean to Proterozoic crustal evolution in the Central Zone of the Limpopo Belt (South Africa-Botswana): Constraints from combined U-Pb and Lu-Hf isotope analyses of zircon. J Petrol 48:1605–1639

Zeh A, Gerdes A, Klemd R, Barton JM Jr (2008) U-Pb and Lu-Hf isotope record of detrital zircon grains from the Limpopo Belt-Evidence for crustal recycling at the Hadean to early-Archean transition. Geochim Cosmochim Acta 72:5304–5329

Zeh A, Gerdes A, Barton JM Jr (2009) Archean Accretion and crustal evolution of the Kalahari Craton—the Zircon age and Hf isotope record of granitic rocks from Barberton/Swaziland to the Francistown Arc. J Petrol 50:933–966

Zeh A, Gerdes A, Barton JM Jr, Klemd R (2010) U-Th-Pb and Lu-Hf systematics of zircon from TTG's, leucosomes, anorthosites and quartzites of the Limpopo Belt (South Africa): constraints for the formation, recycling, and metamorphism of Paleoarchean crust. Precambrian Res 179:50–68

Zeh A, Gerdes A, Millonig L (2011) Hafnium isotope record of the Ancient GneissComplex, Swaziland, southern Africa: evidence for Archaean crust-mantle formation and crust reworking between 3.66 and 2.73 Ga. J Geol Soc London 168:953–963

Zeh A, Gerdes A, Heubeck C (2013a) U-Pb and Hf isotope data of detrital zircons from the Barberton Greenstone Belt: constraints on provenance and Archaean crustal evolution. J Geol Soc London 170:215–223

Zeh A, Jaguin J, Poujol M, Boulvais P, Block S, Paquette J-L (2013b) Juvenile crust formation in the northeastern Kaapvaal Craton at 2.97 Ga-Implications for Archean terrane accretion, and the source of the Pietersburg gold. Precambrian Res 233:20–43

Zeh A, Stern R, Gerdes A (2014) The oldest zircons of Africa-Their U-Pb-Hf-O isotope and trace element systematics, and implications for Hadean to Archean crust-mantle evolution. Precambrian Res 241:203–230

Zeh A, Ovtcharova M, Wilson AH, Schaltegger U (2015) The Bushveld Complex was emplaced and cooled in less than one

million year-results of zirconology, and geotectonic implications. Earth Planet Sci Lett 418:103–114

Ziegler URF, Stoessel GFU (1991) New constraints on the age of the Weener Intrusive Suite, the Gamsberg Granite and the crustal evolution of the Rehoboth Basement Inlier, Namibia. Communs Geol Surv Namibia 7:81–85

Ziegler URF, Stoessel GFU (1993) Age determinations in the Rehoboth Basement Inlier, Namibia. Memoirs of the Geological Survey of Namibia, Windhoek

Zirakparvar NA, Mathez ED, Scoates JS, Wall CJ (2014) Zircon Hf isotope evidence for an enriched mantle source for the Bushveld Igneous Complex. Contrib Mineral Petrol 168:1050

The Nico Pérez Terrane of Uruguay and Southeastern Brazil

7

Pedro Oyhantçabal, Sebastián Oriolo, Ruy Paulo Philipp, Klaus Wemmer, and Siegfried Siegesmund

Abstract

The Nico Pérez Terrane of Uruguay and southeastern Brazil is characterized by an important component of Archean crustal growth and extensive post-Archean crustal reworking recorded in Paleoproterozoic zircon magmatic crystallization ages in widely distributed granitic orthogneisses. Supracrustal blocks of an older Neoarchean to Siderian sedimentary cover including BIFs, quartzites and marbles are preserved only as minor relics. Additionally, an intraplate Mesoproterozoic record includes anorthosite complexes, metagabbros, amphibolites, felsic volcanic rocks and sediments assumed to correspond to a stable platform cover. Rocks with similar isotopic features occur also as basement inliers and roof pendants in the batholiths of the Dom Feliciano Belt. Two different subterranes are recognized in the Nico Pérez Terrane, separated by the north-northeast-trending Caçapava–Sierra de Sosa Shear Zone. The granulite-facies Valentines Rivera and Santa Maria Chico granulitic complexes crop out in the western side of the shear zone and were less reworked during the Neoproterozoic, while the Pavas Block of Uruguay and several basement inliers in the Tijucas Terrane and Pelotas Batholith of Brazil were strongly reworked. Cooling ages, extensive shear zones and granite intrusions document this reworking that was probably facilitated by a thin lithosphere. The Nico Pérez Terrane represents a fragment of the Congo Craton separated during the Neoproterozoic.

Keywords

Exotic crustal blocks • Gondwana
Brasiliano/Pan-African • Archean crustal growth
Crustal reworking

7.1 Introduction

The Neoproterozoic Brasiliano/Pan-African orogenic cycle in southwestern Gondwana was the consequence of convergence and collision between three main continental fragments: the Río de la Plata, Congo and Kalahari cratons (Fig. 7.1). Several minor crustal blocks were also incorporated during these collisional events, mostly being preserved as basement inliers within Neoproterozoic mobile belts (e.g., Oriolo et al. 2017). However, Neoproterozoic paleogeographic reconstructions focused on major cratons and paid little attention to these subordinated blocks (e.g., Alkmim et al. 2001; Tohver et al. 2006; Li et al. 2008; Saalmann et al. 2011; Rapalini et al. 2015), which in the eastern margin of South America in Uruguay and southern Brazil are mostly represented by the Nico Pérez Terrane and the Luís Alves and Curitiba microplates (Bossi and Campal 1992; Basei et al. 2009; Philipp et al. 2016a; 2018; Oriolo et al. 2016a) (Fig. 7.2).

Despite being traditionally considered as part of the Río de la Plata Craton (e.g., Mallmann et al. 2007; Bossi and Cingolani 2009), recent contributions have indicated the allochthony of the Nico Pérez Terrane and its African derivation (Oyhantçabal et al. 2011a; Rapela et al. 2011; Oriolo et al. 2016a; Philipp et al. 2016a). The Taquarembó

P. Oyhantçabal (✉)
Departamento de Geodinámica Interna, Facultad de Ciencias, Universidad de la República, Iguá 4225, 11400 Montevideo, Uruguay
e-mail: oyhantca@fcien.edu.uy

S. Oriolo
CONICET-Universidad de Buenos Aires. Instituto de Geociencias Básicas, Aplicadas y Ambientales de Buenos Aires (IGEBA), Intendente Güiraldes 2160, C1428EHA Buenos Aires, Argentina

R. P. Philipp
Instituto de Geociências, Universidade Federal do Rio Grande do Sul (UFRGS), Porto Alegre, RS, Brazil
e-mail: ruy.philipp@ufrgs.br

K. Wemmer · S. Siegesmund
Geoscience Centre, Georg-August-Universität Göttingen, Goldschmidtstraße 3, 37077 Göttingen, Germany
e-mail: kwemmer@gwdg.de

S. Siegesmund
e-mail: ssieges@gwdg.de

S. Siegesmund et al. (eds.), *Geology of Southwest Gondwana*, Regional Geology Reviews,
https://doi.org/10.1007/978-3-319-68920-3_7

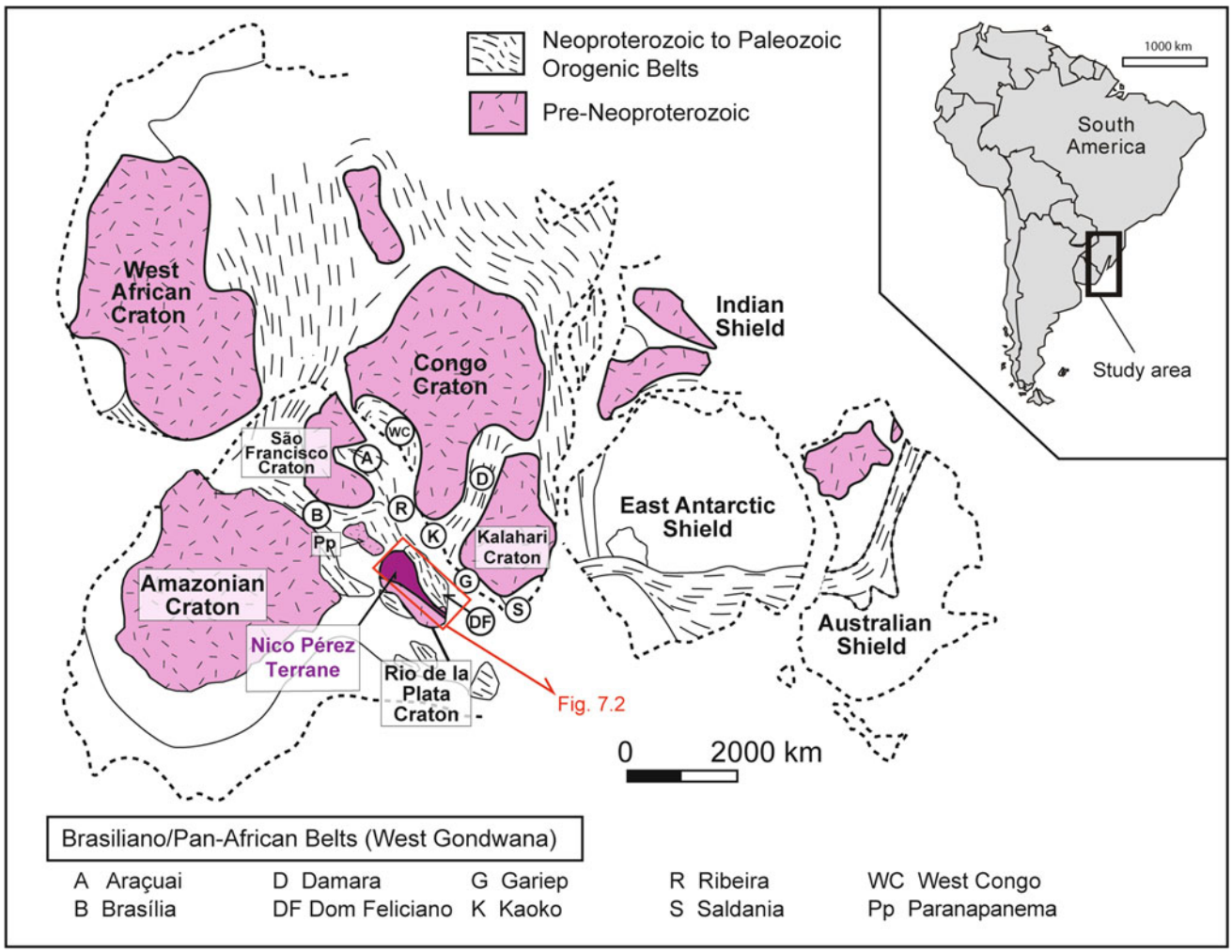

Fig. 7.1 Schematic reconstruction of south-western Gondwana showing the main Archean to Paleoproterozoic cratons and the Neoproterozoic orogenic belts. (Modified from Rapela et al. 2011 and Philipp et al. 2017a, b.)

Block and several basement inliers in the Dom Feliciano Belt in southernmost Brazil show similarities with the Nico Pérez Terrane in Uruguay, thus suggesting a more regional extension of the latter (Oyhantçabal et al. 2011a). A possible extension of the Nico Pérez Terrane even further to the north, including the suspected Paranapanema Craton (Mantovani and de Brito Neves 2005) and Luís Alves Microplate (Basei et al. 2009), is still unclear owing to the sedimentary cover of the Paraná Basin.

This contribution aims to present an updated review of the geology and tectonic evolution of the Nico Pérez Terrane in Uruguay and Rio Grande do Sul state in Brazil, also comparing it with adjacent basement blocks in order to determine the regional extension and tectonic evolution of this crustal terrane.

7.2 Geology of the Nico Pérez Terrane (Uruguay)

7.2.1 Introduction

The Nico Pérez Terrane is mostly exposed in central Uruguay and further north in the Isla Cristalina de Rivera (Fig. 7.3). The Sarandí del Yí Shear Zone constitutes the western margin of the Nico Pérez Terrane (Bossi and Campal 1992; Oriolo et al. 2015, 2016b), separating it from the Río de la Plata Craton. To the east, basement inliers of this terrane have been recognized within the Dom Feliciano Belt up to the Sierra Ballena Shear Zone (Bossi and Campal 1992; Oyhantçabal 2005; Oyhantçabal et al. 2009a, 2011b). Though the Nico Pérez Terrane was

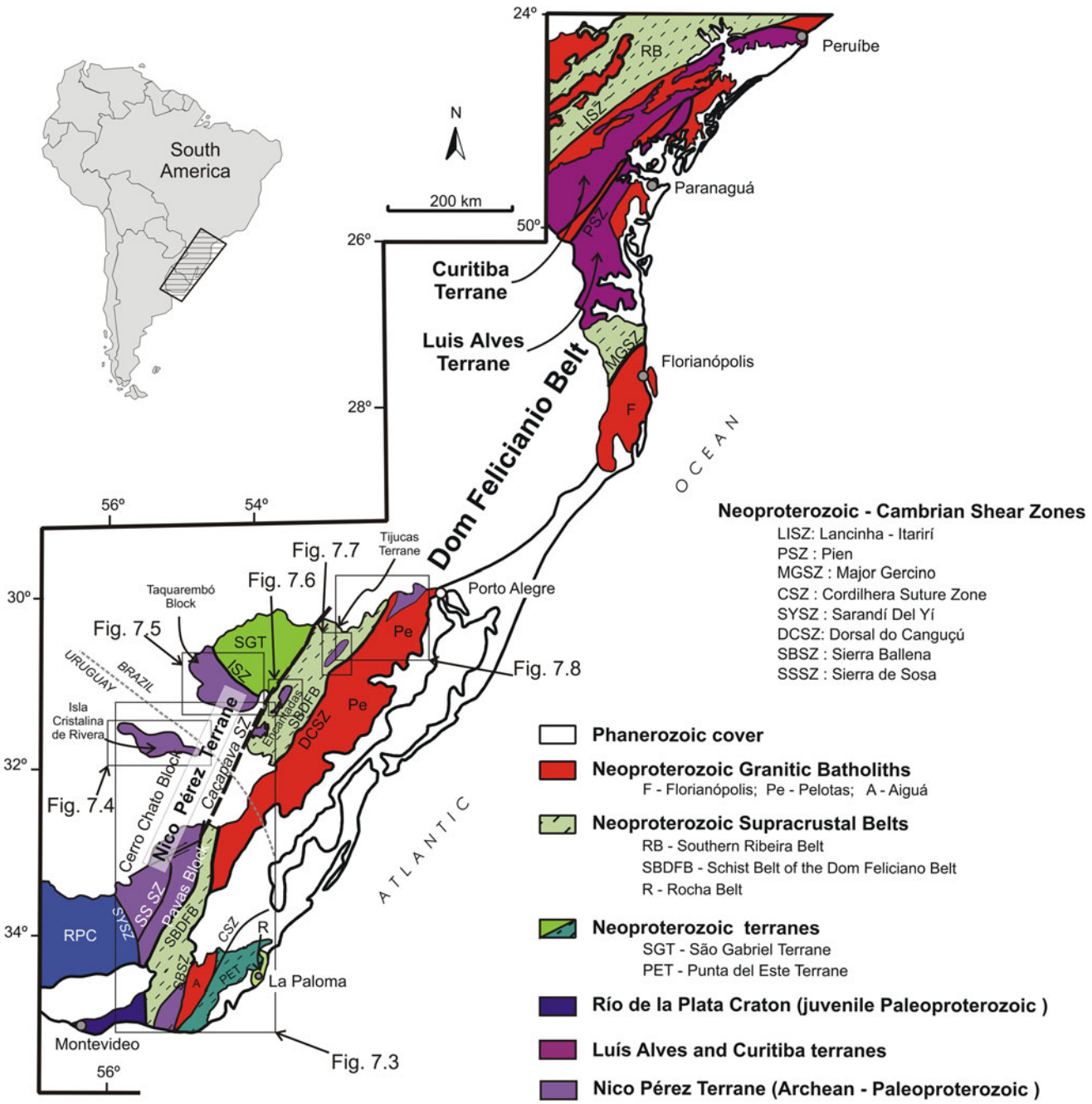

Fig. 7.2 Main tectonic units of the Precambrian of southern Brazil and Uruguay. (Modified from Basei et al. 2010.) The location of detailed geological maps (Figs. 7.3, 7.4, 7.5, 7.6, 7.7 and 7.8) of areas with Archean-Paleoproterozoic and Mesoproterozoic outcrops is indicated

originally defined as a Paleoproterozoic block with Neoproterozoic magmatism and deformation (Bossi and Campal 1992), recent contributions have demonstrated a much more complex evolution extending up to the early Archean (Hartmann et al. 2001; Mallmann et al. 2007; Oyhantçabal et al. 2011a; Oriolo et al. 2016a).

The Nico Pérez Terrane in Uruguay can be divided into two major blocks: Pavas and Cerro Chato, separated by the Sierra de Sosa Shear Zone (Fig. 7.3). Both blocks expose different crustal levels of Paleoproterozoic or older rocks. While the Pavas Block is characterized by amphibolite-facies metamorphism, the Cerro Chato Block displays granulite-facies metamorphism. In both blocks, granitic gneisses, mafic rocks and volcanosedimentary supracrustal sequences occur in the basement. The post-Paleoproterozoic cover in the Cerro Chato Block comprises only scarce Late Neoproterozoic metasediments, whereas in the Pavas Block both pre-Neoproterozoic and

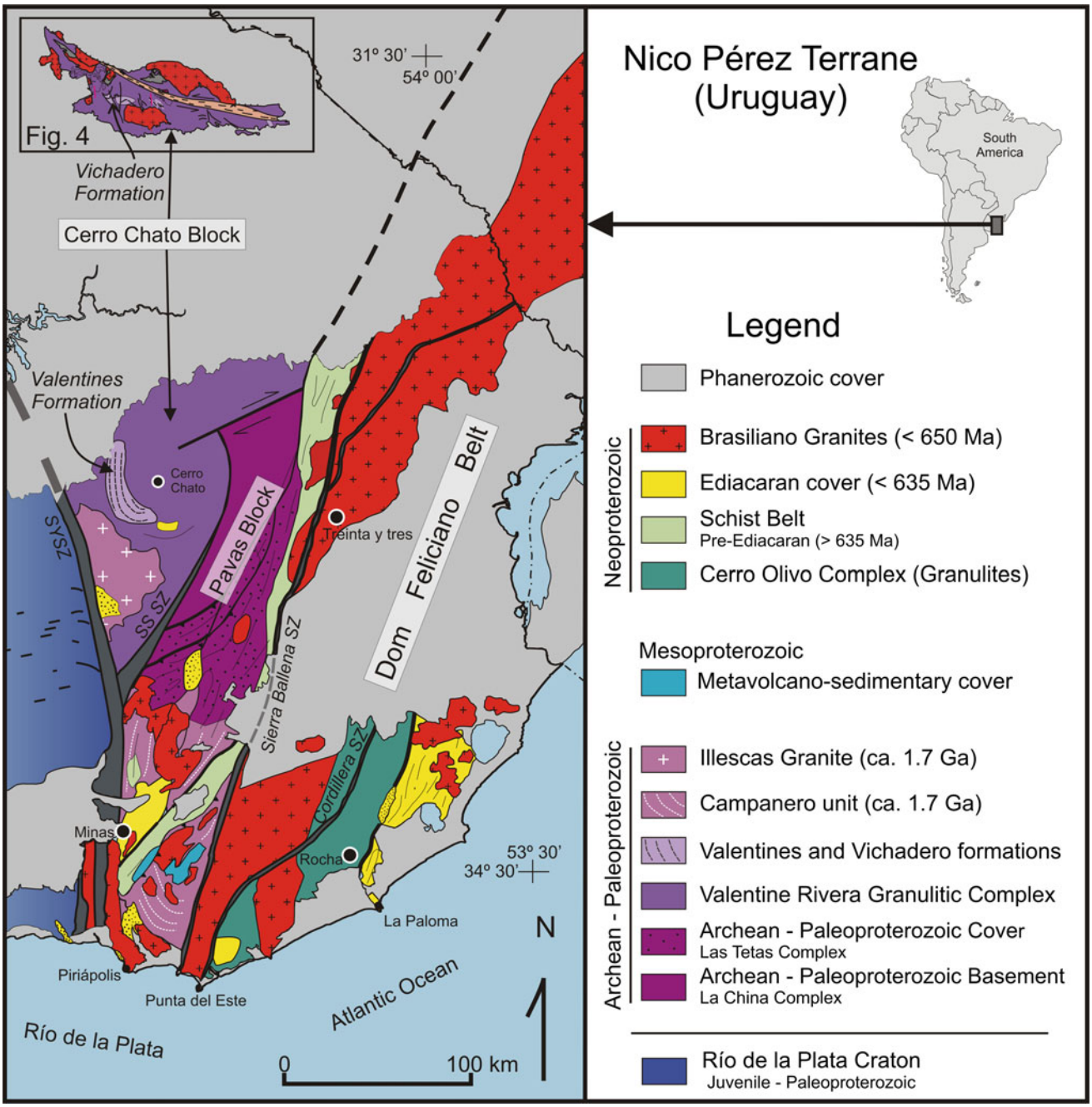

Fig. 7.3 Geological map of the Nico Pérez Terrane and adjacent blocks. (Modified from Oyhantçabal et al. 2011a, b, Spoturno et al. in press and Masquelín et al. 2017.)

Neoproterozoic metasediments are widespread. A summary of available geochronological data from this terrane in Uruguay is presented in Table 7.1.

7.2.2 The Cerro Chato Block

This crustal block is bounded by the Sarandí del Yí and the Sierra de Sosa shear zones to the west and east, respectively (Oriolo et al. 2015, 2016b, c), and it comprises high-grade felsic and mafic orthogneisses with scattered relics of a supracrustal succession and an unmetamorphosed Late Paleoproterozoic granite intrusion.

7.2.2.1 The Valentines—Rivera Granulitic Complex

The Valentines-Rivera Granulitic Complex is one of the most important lithostratigraphic units of the Cerro Chato Block. It

Table 7.1 Summary of available geochronological data of the Nico Pérez Terrane in Uruguay

Domain	Unit	Lithology	Age (Ma)	Method	References
Nico Pérez Terrane Central and southern	La China Complex	Metatonalite	3404 ± 8 (inherited)	U–Pb SHRIMP zircon	Hartmann et al. (2001)
	La China Complex	Metatonalite	2721 ± 7 (metamorphic)	U–Pb SHRIMP zircon	Hartmann et al. (2001)
	La China Complex	Migmatite	3096 ± 45 (magmatic)	U–Pb LA-ICP-MS zircon	Gaucher et al. (2011)
	Valentines–Rivera Granulitic Cx	Granulite	2163 ± 22 (magmatic)	U–Pb SHRIMP zircon	Santos et al. (2003)
	Valentines–Rivera Granulitic Cx	Felsic granulite	2106 ± 21	U–Pb LA-ICP-MS zircon	Oriolo et al. (2016a, b, c)
	Valentines–Rivera Granulitic Cx	Granulite	2058 ± 3 (metamorphic)	U–Pb SHRIMP zircon	Santos et al. (2003)
	Campanero Unit	Mylonitic granite	1754 ± 7	U–Pb SHRIMP zircon	Mallmann et al. (2007)
	Campanero Unit	Amphibolite	564.0 ± 4.1	Ar–Ar hornblende	Oyhantçabal et al. (2009a)
	Illescas Granite	Rapakivi granite	1760 ± 32	Rb–Sr WR	Bossi and Campal (1992)
	Parque UTE Group	Metagabbro	1492 ± 4	U–Pb ID-TIMS zircon	Oyhantçabal et al. (2005)
	Parque UTE Group	Metarhyolite	1429 ± 21	U–Pb ID-TIMS zircon	Oyhantçabal et al. (2005)
	Mina Verdún Group	Metatuff	1433 ± 6	U–Pb LA-ICP-MS zircon	Gaucher et al. (2011)
	Neoproterozoic granitoids	Puntas del Santa Lucía monzogranite	633 ± 8	U–Pb SHRIMP zircon	Hartmann et al. (2002)
	Neoproterozoic granitoids	Puntas de Mataojo granodiorite	627 ± 33	U–Pb SHRIMP zircon	Oyhantçabal et al. (2009a)
	Neoproterozoic granitoids	Lavaderos granite	610 ± 3	U–Pb LA-ICP-MS zircon	Gaucher et al. (2014a)
	Neoproterozoic granitoids	Zapicán granodiorite	610 ± 2	U–Pb LA-ICP-MS zircon	Oriolo et al. (2016a, b, c)
	Neoproterozoic granitoids	Mangacha granite	583 ± 7	U–Pb SIMS zircon	Gaucher et al. (2008)
Isla Cristalina de Rivera	Valentines–Rivera Granulitic Cx	Mesocratic gneiss	2147 ± 8.7 (magmatic)	U–Pb SHRIMP zircon	Oyhantçabal et al. (2012)
	Valentines–Rivera Granulitic Cx	Metatrondhjemite	2140 ± 6 (magmatic)	U–Pb SHRIMP zircon	Santos et al. (2003)
	Valentines–Rivera Granulitic Cx	Metatrondhjemite	2077 ± 6 (metamorphic)	U–Pb SHRIMP zircon	Santos et al. (2003)

(continued)

Table 7.1 (continued)

Domain	Unit	Lithology	Age (Ma)	Method	References
	Valentines–Rivera Granulitic Cx	Leucocratic gneiss	2172 ± 8 (magmatic)	U–Pb SHRIMP zircon	Oyhantçabal et al. (2012)
	Valentines–Rivera Granulitic Cx	Mesocratic gneiss	2114 ± 3 (magmatic)	U–Pb SHRIMP zircon	Oyhantçabal et al. (2012)
	Valentines–Rivera Granulitic Cx	Mesocratic gneiss	2094 ± 17 (metamorphic)	Pb–Pb stepwise leaching titanite	Oyhantçabal et al. (2012)
	Valentines–Rivera Granulitic Cx	Leucocratic gneiss	2093 ± 36 (magmatic/metamorphic?)	U–Pb SHRIMP zircon	Oyhantçabal et al. (2012)
	Valentines–Rivera Granulitic Cx	Mafic granulite	2095 ± 15	U–Pb LA-ICP-MS zircon	Oriolo et al. (2016a, b, c)
	Valentines–Rivera Granulitic Cx	Tonalitic gneiss	2087 ± 7	U–Pb LA-ICP-MS zircon	Oriolo et al. (2016a, b, c)
	Valentines–Rivera Granulitic Cx	Leucocratic gneiss	2069 ± 16	U–Pb LA-ICP-MS zircon	Oriolo et al. (2016a, b, c)
	Valentines–Rivera Granulitic Cx	Mesocratic gneiss	1982 ± 5	Th–U–Pb CHIME-EPMA monazite	Oyhantçabal et al. (2012)
	Valentines–Rivera Granulitic	Leucocratic gneiss	1975 ± 5	Th–U–Pb CHIME-EPMA monazite	Oyhantçabal et al. (2012)
	Rivera Shear Zone	Mylonite	606 ± 10	Th–U–Pb CHIME-EPMA monazite	Oyhantçabal et al. (2012)
	Rivera Shear Zone	Mylonite	606 ± 10	K–Ar muscovite	Oyhantçabal et al. (2012)
	Neoproterozoic granitoids	Amarillo Granite	596 ± 2	U–Pb LA-ICP-MS zircon	Oriolo et al. (2016a, b, c)
	Neoproterozoic granitoids	Sobresaliente granite	585 ± 2.5	U–Pb SHRIMP zircon	Oyhantçabal et al. (2012)
	Neoproterozoic granitoids	Las Flores granite	586 ± 2.7	U–Pb SHRIMP zircon	Oyhantçabal et al. (2012)

was originally defined as the Valentines Formation for the central region of Uruguay and was subsequently recognized further north in the Isla Cristalina de Rivera (Bossi and Umpierre 1969; Preciozzi et al. 1985; Ellis 1998; Oyhantçabal et al. 2011a). Felsic and subordinated mafic to intermediate granulitic orthogneisses are the main lithologies.

The felsic granulites present a mineral assemblage of mesoperthitic alkali feldspar, plagioclase and quartz with biotite, clinopyroxene and garnet as the main accessories. The texture is granoblastic to gneissic. Triple junctions, cusps and grain-boundary migration microstructures evidence fluid-assisted diffusional and dislocation creep of feldspars and pyroxene under high-T conditions. These high-T deformation features are partially overprinted by low-T deformation.

The mafic granulites, in turn, contain clinopyroxene, orthopyroxene, plagioclase and garnet, and show granoblastic texture with triple junctions at *c*. 120°. Retrograde metamorphic minerals are frequently present.

The available geochemical data (Oyhantçabal et al. 2012) indicate that granulitic orthogneisses have compositions ranging from gabbro to granite with calc-alkaline affinity and exhibit marked negative Nb, Ta and Ti anomalies. These features are compatible with a genesis of the protoliths in a continental magmatic arc setting.

U–Pb ages in zircon for this complex demonstrate multistage magmatism at 2.18–2.10 Ga, followed by high-grade metamorphism at 2.10–2.02 Ga (Santos et al. 2003; Oyhantçabal et al. 2012; Oriolo et al. 2016a). On the other hand, *c*. 1.8 Ga monazite ages (Th–U–Pb monazite; CHIME-EPMA method) reported by Oyhantçabal et al. (2012) record amphibolite-facies retrograde metamorphism and probably correspond to a different event from the one recorded by zircons. The slightly discordant U–Pb age in zircon obtained by Oriolo et al. (2016a) for a mafic granulite seems to confirm that felsic and mafic rocks are coeval. Archean zircon inheritance was reported for the Valentines and Isla Cristalina de Rivera areas (Santos et al. 2003; Oyhantçabal et al. 2012; Oriolo et al. 2016a).

7.2.2.2 Archean to Paleoproterozoic Supracrustal Rocks (Valentines and Vichadero Formations)

A high-grade platform metavolcanosedimentary sequence rich in BIFs crops out in two main areas in the Cerro Chato Block. The Vichadero Formation (Preciozzi et al. 1985; Ellis 1998; Oyhantçabal et al. 2011a, 2012) occurs in northern Uruguay in the Isla Cristalina de Rivera (Fig. 7.4), while the Valentines Formation (Bossi and Umpierre 1969) is located in the centre of the Nico Pérez Terrane.

The Vichadero Formation (Ellis 1998) comprises BIFs, metaquartzites, forsterite marbles, mafic volcanic rocks and pyroxene granofelses. All lithologies were affected by high-grade metamorphism and occur as isolated and scattered kilometre-scale bodies hosted in the granulitic orthogneisses.

The Valentines Formation comprises lithologies similar to those of the Vichadero Formation including BIFs, leucocratic to mesocratic gneisses, pyroxene granofelses and rare forsterite marbles. The gneisses contain mesoperthitic alkali feldspar, plagioclase, pyroxene, amphibole and biotite, and they are finely interbedded with the BIF bands, thus suggesting a volcanic protolith. Retrograde metamorphism is recorded by secondary chlorite and epidote.

Both formations share the same lithological association and mineral parageneses. They are therefore considered to be part of the same platform succession of Neoarchean to Siderian age, the BIF deposits probably being of the Lake Superior type (Ellis 1998; Chap. 18).

7.2.2.3 The Late Paleoproterozoic Illescas Granite

The Illescas intrusion is a rapakivi-type granite (Campal and Schipilov 1995), which presents a high-K subalkaline signature based on scarce geochemical data (Gaucher and

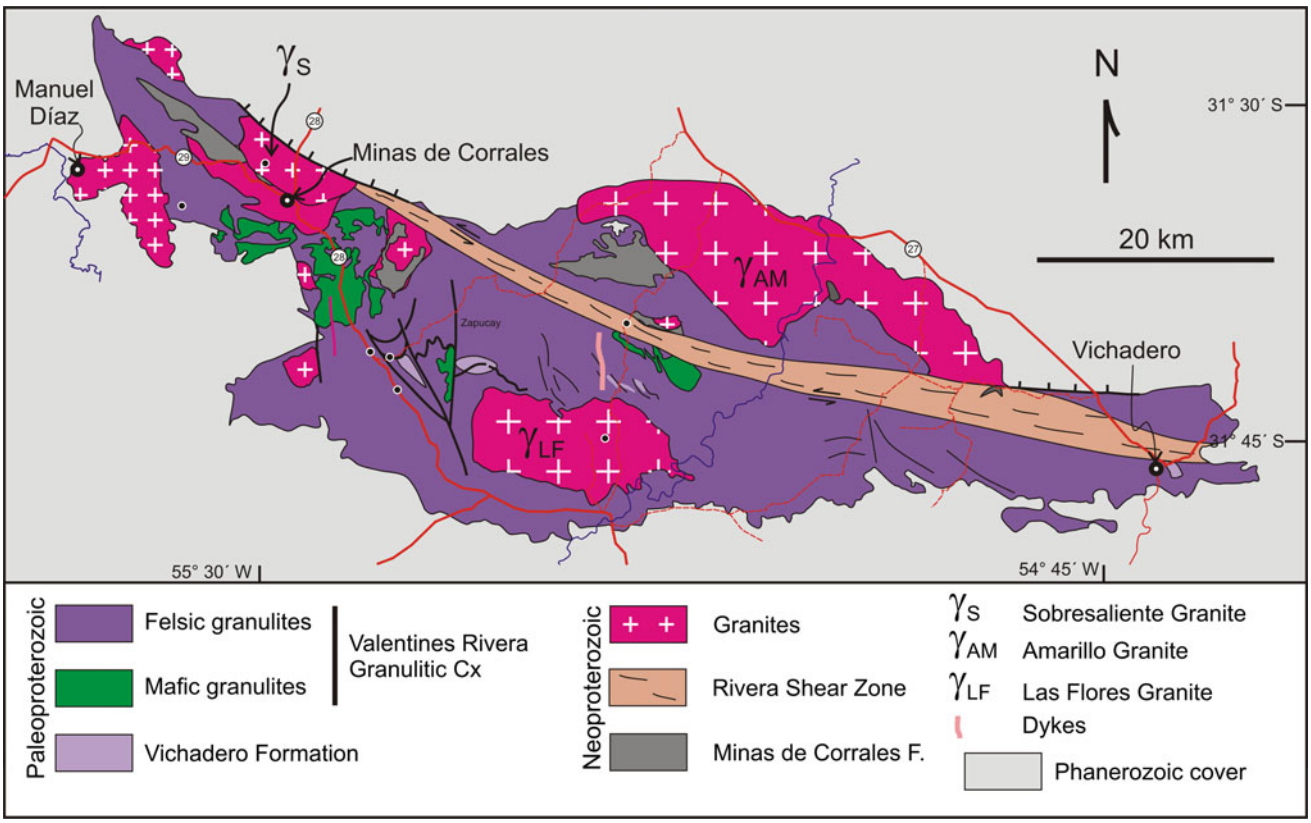

Fig. 7.4 Geological map of the Isla Cristalina de Rivera in northern Uruguay. (Modified from Oyhantçabal et al. 2012.)

Blanco 2014). Subalkaline affinity and low Ga/Al ratios suggest that this intrusion belongs to the A2-type post-collisional granites of Eby (1992). Therefore an anorogenic (within-plate) setting for this granite can be ruled out and the correlation with the coeval calc-alkaline Campanero Unit is possible. The age of this intrusion is constrained at 1760 ± 32 Ma by Rb-Sr whole-rock data (Bossi and Campal 1992) and a comparable $^{207}Pb/^{206}Pb$ zircon age of *c*. 1.75 Ga (Campal and Schipilov 1995). Although ductile to brittle deformation is observed in the margins of the pluton, most of the intrusion preserves magmatic textures and mineralogy, and thus represents an important constraint for the tectonothermal evolution of the Cerro Chato Block.

7.2.3 The Pavas Block

The Pavas Block comprises the La China Complex and the Las Tetas sedimentary platform cover (Preciozzi et al. 1979, 1985; Hartmann et al. 2001). The contact between both units is tectonic, including low-angle thrusts as well as high-angle transcurrent shear zones. Hartmann et al. (2001) indicated that both complexes are separated by a thrust, which imbricates orthogneisses of the La China Complex over metasediments of the Las Tetas Complex. On the other hand, Oriolo et al. (2016c) recognized the María Albina Shear Zone as the main boundary separating the La China Complex to the west from the Las Tetas Complex to the east, although minor tectonic slices of metasediments and orthogneisses were also identified to the west and east, respectively.

7.2.3.1 The Gneissic-Migmatitic Basement (La China Complex)

The La China Complex is made up of orthogneisses, migmatites, amphibolites, actinolitites, talc-bearing schists and serpentinites (Preciozzi et al. 1979, 1985; Oyhantçabal and Vaz 1990; Hartmann et al. 2001). A metatonalite of this complex yields an age of 3404 ± 8 Ma (U–Pb SHRIMP) in zircon cores interpreted as the age of the magmatism, while slightly younger ages could represent partial resetting as a result of upper amphibolite-facies metamorphism documented in low Th/U zircon rims dated at 3.1 Ga (Hartmann et al. 2001). On the other hand, Gaucher et al. (2011) obtained a U–Pb LA-ICP-MS zircon age of 3096 ± 45 Ma in a migmatite cropping out in the surroundings of the metatonalite. This age seems to reflect partial melting during the upper amphibolite-facies event.

Although the La China Complex has only been recognized locally in the central Nico Pérez Terrane, the existence of Archean Sm–Nd and Lu–Hf model ages and zircon inheritance in Paleo- and Neoproterozoic magmatic units indicates the ubiquitous presence of Archean crust in the Nico Pérez Terrane (Santos et al. 2003; Mallmann et al. 2007; Oyhantçabal et al. 2011a; Oriolo et al. 2016a). Despite the lack of geochemical data for these rocks, a tonalite–trondhjemite–granodiorite (TTG) association affinity is assumed for the orthogneisses of this complex.

7.2.3.2 The Sedimentary Platform Cover (Las Tetas Complex)

The Las Tetas Complex comprises fuchsite-bearing quartzites, metaconglomerates, micaschists, marbles and BIFs (Oyhantçabal and Vaz 1990; Hartmann et al. 2001; Gaucher et al. 2014a, b, c).

The rocks of this complex show variable deformation, frequently very strong, and they are thrust stacked and crosscut by transcurrent shear zones. Mineral parageneses indicate variable metamorphic grade ranging from sillimanite-bearing quartzites in the north (Oyhantçabal and Vaz 1990) to staurolite-garnet micaschists in the south (Hartmann et al. 2001), and even anchimetamorphic rocks according to Gaucher et al. (2014a, b, c).

The depositional environment for this lithological association was a siliciclastic-carbonate platform in a stable shelf (Hartmann et al. 2001). According to Gaucher et al. (2014a, b, c), a shallowing up trend is observed in the facies association.

The maximum deposition age is constrained by the youngest detrital zircon yielding a concordant $^{207}Pb/^{206}Pb$ age of 2717 ± 24 Ma (U–Pb SHRIMP, Hartmann et al. 2001), which is further supported by similar detrital zircon ages of *c*. 2.8–2.7 Ga (Hartmann et al. 2001). The minimum age is poorly constrained by an Ar/Ar phlogopite age of 621.4 ± 1.0 Ma (Oriolo et al. 2016c). A Neoarchean or Siderian deposition age is the most plausible, taking into account the fact that Rhyacian protolith ages are widespread in the basement of the Nico Pérez Terrane, but detrital zircons of this age are not observed in this complex. On the other hand, Ar/Ar and K–Ar data between *c*. 630 and 580 Ma obtained in metasediments dates an Ediacaran metamorphic overprint and deformation event in the Las Tetas Complex (Oriolo et al. 2016c).

7.2.4 Basement Inliers of the Nico Pérez Terrane in the Dom Feliciano Belt

Several basement inliers occur within the schist belt of the Neoproterozoic Dom Feliciano Belt in Uruguay. They comprise gneissic basement as well as pre-Neoproterozoic supracrustal successions.

7.2.4.1 Late Paleoproterozoic Orthogneisses (Campanero Unit)

The Campanero Unit is one of the largest basement inliers and is located between the schist belt and the Sierra Ballena Shear Zone (Fig. 7.3). It comprises felsic orthogneisses, with scattered slivers of supracrustal rocks including amphibolites, micaschists, BIFs and migmatites (Sánchez-Bettucci 1998; Sánchez-Bettucci et al. 2003; Oyhantçabal 2005) that are interpreted as relicts of the Las Tetas Complex. Geochemical data indicate that felsic orthogneisses mostly display a high-K calc-alkaline, slightly peraluminous signature (Oyhantçabal 2005). A U–Pb conventional zircon age of 1735 ± 32 Ma was obtained from orthogneisses (Sánchez-Bettucci et al. 2004), later confirmed by an U–Pb SHRIMP zircon age of 1754 ± 7 Ma (Mallmann et al. 2007), and interpreted as the age of the gneiss protolith. High-T foliation and development of striped gneisses are typical microstructural features in these rocks. On the other hand, an Ar/Ar hornblende age of 564.0 ± 4.1 Ma reported for an amphibolite provides a minimum age for the high-T foliation and indicates cooling during the Ediacaran period (Oyhantçabal et al. 2009b).

7.2.4.2 Mesoproterozoic Metavolcanosedimentary Cover

Though scarce, two Mesoproterozoic low- to medium-grade metavolcanosedimentary sequences—the Parque UTE and Mina Verdún groups—were recognized in the schist belt of the southern Dom Feliciano Belt (Fig. 7.3). In the case of the Parque UTE Group, neither base nor top are exposed (Chiglino et al. 2008, 2010). On the other hand, the base of the Mina Verdún Group is not exposed, whereas the top is separated by a tectonic contact from the Verdún quartzites and is discordantly overlain by the Ediacaran Las Ventanas Formation (Poiré et al. 2003, 2005).

From base to top, the Parque UTE Group comprises mostly mafic and felsic metavolcanic rocks with intercalations of metapelites, dolomitic marbles, marble-metamarl-metapelite alternations and metatuffs (Chiglino et al. 2008, 2010). In the case of the Mina Verdún Group, metarhyolites are exposed at the base and overlain by metapelites, scarce metamarls and marbles, the latter corresponding mostly to limestones and minor dolostones only recognizable at the top (Poiré et al. 2003, 2005; Poiré and Gaucher 2009).

For the Parque UTE Group, Oyhantçabal et al. (2005) reported U–Pb ID-TIMS zircon ages of 1492 ± 4 Ma from a metagabbro at the base of the unit and of 1429 ± 21 Ma from a metavolcanoclastic rock at the top, whereas Gaucher et al. (2014a) reported a U–Pb SIMS zircon age of 1461.8 ± 3.9 Ma from a metatuff probably corresponding to the base. The age of the Mina Verdún Group is constrained by a U–Pb LA-ICP-MS zircon age of 1433 ± 6 Ma obtained from a basal metarhyolite (Gaucher et al. 2011).

Available geochronological data for the felsic volcanic rocks point to a similar time period. This fact, the very close geographic proximity and the lithological similarities demonstrate that both units most probably belong to one Mesoproterozoic stable platform cover above the Nico Pérez Terrane, subsequently incorporated into the Dom Feliciano Belt. Geochemical data for the metagabbros also support an anorogenic setting.

7.3 The Nico Pérez Terrane in Southernmost Brazil

7.3.1 Introduction

Several medium- to high-grade metamorphic complexes showing similarities with the Nico Pérez Terrane basement are recognizable in southern Brazil (Tables 7.2 and 7.3). These include the Santa Maria Chico Granulitic Complex in the Taquarembó Terrane, the Encantadas and Vigia complexes in the Tijucas Terrane and the Arroio dos Ratos Complex within the Neoproterozoic Pelotas Batholith (e.g., Hartmann et al. 2000; Leite et al. 2000; Santos et al. 2003; Philipp et al. 2008, 2016a; Oyhantçabal et al. 2011a; Camozzato et al. 2013a, b).

7.3.2 The Santa Maria Chico Granulitic Complex (Taquarembó Block)

The Santa Maria Chico Granulitic Complex constitutes the basement of the Taquarembó Terrane. To the northeast it is bounded by units of the São Gabriel Terrane and is partially covered by Ediacaran sedimentary and volcanic rocks of the Camaquã Basin and Carboniferous to Permian sedimentary rocks of the Paraná Basin. Neoproterozoic granite intrusions (*c*. 630–570 Ma) are also frequent in this complex (Fig. 7.5).

The Santa Maria Chico Granulitic Complex comprises three main rock associations: (1) mafic to ultramafic granulites with associated metapyroxenites and meta-anorthosites; (2) sillimanite-garnet-biotite paragneisses, marbles, calc-silicate rocks, quartzo-feldspathic gneisses and BIFs; and (3) tonalitic to throndjemitic TTG orthogneisses (Hartmann 1998; Philipp et al. 2016a, 2017a) (Fig. 7.6). U–Pb SHRIMP and LA-MC-ICPMS detrital zircon ages between 2167 ± 15 and 2331 ± 31 Ma constrain the interval of the sedimentary deposition in the paragneisses (Table 7.2; Laux et al. 2012). In turn, U–Pb ages indicate two episodes of magmatism for the protoliths of the TTG gneisses. The older one have ages of 2380–2280 Ma (Girelli et al. 2016a, b) and the younger ones ages of 2240–2130 Ma (Girelli et al. 2016a, b; Philipp et al. 2017b).

Table 7.2 Summary of available geochronological data in the Taquarembó Block of the Nico Pérez Terrane in Brazil

Unit	Locality	Lithology	Age (Ma)	Method	References
The Santa Maria Chico Granulitic Complex	Dom Pedrito	Mafic granulite	2550 ± 150	Pb–Pb TIMS (isochron)	Soliani (1986)
		Sillimanite gneiss	2119 ± 17 (metamorphic)	Sm–Nd	Hartmann (1987)
		Mafic granulite	1877 ± 66 (metamorphic)	Sm–Nd	Hartmann (1987)
		Mafic granulite	2100 (metamorphic)	Sm–Nd	Hartmann (1987)
		Garnet granulite	2509 ± 13	U–Pb SHRIMP in zircon	Hartmann et al. (2008)
			2022 ± 18 (metamorphic)		Hartmann et al. (2008)
		Metabasalt	2301 ± 17	U–Pb SHRIMP in zircon	Hartmann et al. (2008)
			900 (metamorphic)		Hartmann et al. (2008)
		Throndjemite	2553 ± 9	U–Pb SHRIMP in zircon	Hartmann et al. (2008)
		Alm-Ab granulite	2489 ± 6	U–Pb SHRIMP in zircon	Hartmann et al. (2008)
			2006 ± 3 (metamorphic)		Hartmann et al. (2008)
		Metagrawacke	2200 ± 32	U–Pb SHRIMP in zircon	Hartmann et al. (2008)
		Granodioritic gneiss	2366 ± 8	U–Pb SHRIMP in zircon	Hartmann et al. (2008)
			2035 ± 9 (metamorphic)		Hartmann et al. (2008)
		Mafic granulite	2413 ± 13	U–Pb LA-ICPMS in zircon	Laux et al. (2010)
		Metasedimentary granulite	2617 ± 15	U–Pb LA-ICPMS in zircon	Laux et al. (2012)
			2072 ± 44 (metamorphic)		Laux et al. (2012)
			2462 ± 26	U–Pb LA-ICPMS in zircon	Laux et al. (2012)
			2331 ± 31	U–Pb LA-ICPMS in zircon	Laux et al. (2012)
		Metasedimentary granulite	2550–2390 (Detrital zrn)	U–Pb LA-ICPMS in zircon	Girelli et al. (2016a, b)
			2050 (metamorphic)		Girelli et al. (2016a, b)
		Granodioritic gneiss	2380–2280 (Detrital zrn)	U–Pb LA-ICPMS in zircon	Girelli et al. (2016a, b)
			2130–2240 (Detrital zrn)	U–Pb LA-ICPMS in zircon	Girelli et al. (2016a, b)
		Metagabbro	2173 ± 20	U–Pb LA-ICPMS in zircon	Girelli et al. (2016a, b)
		Metapyroxenite	2186 ± 17	U–Pb LA-ICPMS in zircon	Girelli et al. (2016a, b)
		Meta-anorthosite	2244 ± 17	U–Pb LA-ICPMS in zircon	Girelli et al. (2016a, b)
		Meta-leucogabbro	2349 ± 6	U–Pb LA-ICPMS in zircon	Girelli et al. (2016a, b)
		Metased. Granulite	2500–2150 (Detrital zrn)	U–Pb LA-ICPMS in zircon	Girelli et al. (2016a, b)
	Bagé	Dioritic gneiss	2178 ± 6	U–Pb LA-ICPMS in zircon	Philipp et al. (2017a, b)
			1761 ± 10 (metamorphic)		Philipp et al. (2017a, b)
		Dioritic gneiss	2163 ± 9	U–Pb LA-ICPMS in zircon	Philipp et al. (2017a, b)
		Mafic granulite	2124 ± 8	U–Pb LA-ICPMS in zircon	Philipp et al. (2017a, b)
			2078 ± 6 (metamorphic)		Philipp et al. (2017a, b)
		Metatonalite	1766 ± 14	U–Pb LA-ICPMS in zircon	Philipp et al. (2017a, b)

Table 7.3 Summary of available geochronological data of Paleo- and Mesoproterozoic rocks related to the Nico Pérez Terrane cropping out as basement inliers and roof pendants in the Tijucas Block and the Pelotas Batholith of Brazil

Unit	Locality	Lithology	Age (Ma)	Method	References
Encantadas Complex	Santana de Boa Vista	Tonalitic gneiss	2272 ± 235	Rb/Sr WR	Cordani et al. (1974)
			553 ± 10 (metamorphic)	K–Ar WR	Cordani et al. (1974)
		Tonalitic gneiss	2164 ± 91	Rb/Sr WR	Soliani (1986)
			1077 ± 41 (metamorphic)	K–Ar WR	Soliani (1986)
		Tonalitic gneiss	2083 ± 41	Rb/Sr WR	Porcher (1992)
			1883 ± 56	Rb/Sr WR	Porcher (1992)
		Tonalitic gneiss	2263 ± 18	U–Pb SHRIMP in zircon	Hartmann et al. (2000)
			2045 ± 10 (metamorphic)		Hartmann et al. (2000)
		Pegmatite	2263 ± 6	U–Pb SHRIMP in zircon	Hartmann et al. (2000)
			2021 ± 11 (metamorphic)		Hartmann et al. (2000)
		Granodiorite	2078 ± 13	U–Pb SHRIMP in zircon	Hartmann et al. (2000)
			631 ± 6 (metamorphic)		Hartmann et al. (2000)
		Metahornblendite	2257 ± 12	U–Pb SHRIMP in zircon	Hartmann et al. (2003)
			1989 ± 21 (metamorphic)		Hartmann et al. (2003)
			702 ± 21 (metamorphic)	U–Pb SHRIMP in zircon	Hartmann et al.(2003)
		Tonalitic gneiss	2234 ± 28	U–Pb LA-ICPMS in zircon	Saalmann et al. (2011)
	Vila Torrinhas	Tonalitic gneiss	2112 ± 22	U–Pb LA-ICPMS in zircon	Camozzato et al. (2013a, b)
	Pinheiro Machado	Augen gneiss	2153 ± 20	U–Pb LA-ICPMS in zircon	Camozzato et al. (2013a, b)
			643 ± 3 (metamorphic)		Camozzato et al. (2013a, b)
	Santana de Boa Vista	Tonalitic gneiss	2340 ± 19	U–Pb LA-ICPMS in zircon	Lusa et al. (2017)
			875 ± 160 (metamorphic)		Lusa et al. (2017)
		Metamonzogranite	2211 ± 17	U–Pb LA-ICPMS in zircon	Lusa et al. (2017)
		Metasienogranite	2210 ± 16	U–Pb LA-ICPMS in zircon	Lusa et al. (2017)
	Hulha Negra	Granodiritic gneiss	2404 ± 23	U–Pb LA-ICPMS in zircon	Camozzato et al. (2017)
			679 ± 49 (metamorphic)		Camozzato et al. (2017)
		Granitic gneiss	2231 ± 19	U–Pb LA-ICPMS in zircon	Camozzato et al. (2017)

(continued)

Table 7.3 (continued)

Unit	Locality	Lithology	Age (Ma)	Method	References
		Granitic gneiss	2187 ± 71	U–Pb LA-ICPMS in zircon	Camozzato et al. (2017)
		Granitic gneiss	2157 ± 13	U–Pb LA-ICPMS in zircon	Camozzato et al. (2017)
			626 ± 15 (metamorphic)		Camozzato et al. (2017)
		Metagranite	565 ± 2 (metamorphic)	U–Pb LA-ICPMS in zircon	Camozzato et al. (2017)
Arroio dos Ratos Complex	Butiá	Tonalitic gneiss	2078 ± 13	U–Pb TIMS in zircon	Tommasi (1991)
		Granodioritic gneiss	2067 ± 17	U–Pb SHRIMP in zircon	Leite et al. (2000)
		Trondhjemite	780	U–Pb SHRIMP in zircon	Leite et al. (2000)
		Granodiorite	580	U–Pb SHRIMP in zircon	Leite et al. (2000)
	Arroio dos Ratos	Metatonalite	2148 ± 33	U–Pb LA-ICPMS in zircon	Gregory et al. (2015)
		Metatonalite	2150 ± 28	U–Pb LA-ICPMS in zircon	Gregory et al. (2015)
		Metatonalite	2136 ± 27	U–Pb LA-ICPMS in zircon	Gregory et al. (2015)
		Metatonalite	2099 ± 10	U–Pb LA-ICPMS in zircon	Gregory et al. (2015)
		Granodioritic gneiss	2081 ± 7	U–Pb LA-ICPMS in zircon	Gregory et al. (2015)
		Granodioritic gneiss	2077 ± 13	U–Pb LA-ICPMS in zircon	Gregory et al. (2015)
			635 ± 6 (metamorphic)		Gregory et al. (2015)
Vigia Complex		Granitic gneiss	2056 ± 38	U–Pb LA-ICPMS in zircon	Camozzato et al. (2017)
		Dioritic gneiss	2008 ± 52	U–Pb LA-ICPMS in zircon	Camozzato et al. (2017)
Seival Metagranite	Hulha Negra	Granodiorite	1785 ± 42	U–Pb LA-ICPMS in zircon	Camozzato et al. (2013a, b)
		Monzogranite	1768 ± 24	U–Pb LA-ICPMS in zircon	Camozzato et al. (2013a, b)
		Granodiorite	1764 ± 29	U–Pb LA-ICPMS in zircon	Camozzato et al. (2013a, b)
		Monzogranite	1763 ± 28	U–Pb LA-ICPMS in zircon	Camozzato et al. (2013a, b)
Capivarita Meta-anorthosite		Meta-anorthosite	1573 ± 21	U–Pb LA-ICPMS in zircon	Chemale et al. (2011)
			606 ± 6 (metamorphic)		Chemale et al. (2011)
		Metagabbro	1530 ± 33	ttn	Chemale et al. (2011)
			652 ± 9 (metamorphic)		Chemale et al. (2011)
			597 ± 6 (metamorphic)	U–Pb LA-ICPMS in zircon	Chemale et al. (2011)

(continued)

Table 7.3 (continued)

Unit	Locality	Lithology	Age (Ma)	Method	References
Tupi Silveira Amphibolite		Gt-Diop-Hb gneiss	1567 ± 21	U–Pb LA-ICPMS in zircon	Camozzato et al. (2013a, b)
			643 ± 3 (metamorphic)		Camozzato et al. (2013a, b)

The mafic to ultramafic association presents two groups of U–Pb zircon ages. The older ages range from 2413 ± 13 Ma for a mafic granulite to 2349 ± 6 Ma for a metaleucogabbro (Laux et al. 2012; Girelli et al. 2016a, b). The younger group of ages includes 2244 ± 17 Ma (meta-anorthosite), 2186 ± 17 Ma (metapyroxenite), 2173 ± 20 Ma (metagabbro) and 2124 ± 8 Ma (mafic granulite) (Girelli et al. 2016a, b; Philipp et al. 2017b).

The main orogenic metamorphic event is indicated by U–Pb SHRIMP and LA-MC-ICPMS concordia zircon ages of 2078 ± 6, 2031 ± 40, 2022 ± 18, 2035 ± 9 and 2006 ± 3 Ma (Hartmann et al. 1999, 2008; Philipp et al. 2017b). Unmetamorphosed granites intruding the gneisses yielded U–Pb LA-MC-ICPMS zircon ages of 1840 ± 13 and 1766 ± 14 Ma (Table 7.2; Girelli et al. 2016a, b; Philipp et al. 2017b). These ages are similar to that of the unmetamorphosed Illescas Granite of Uruguay demonstrating the similar Paleoproterozoic evolution of Valentines (UY) and Taquarembó (BR) areas.

7.3.3 Pre-neoproterozoic Basement Inliers in the Tijucas Terrane

The Encantadas and Vigia complexes constitute two northeast–southwest elongated structural domes that occur as basement inliers in the central and southwestern portions of the Tijucas Terrane (Figs. 7.2, 7.6 and 7.7). The orthogneisses of these complexes occur tectonically interleaved with metavolcanosedimentary rocks of the Neoproterozoic Porongos Complex (Jost 1981; Saalmann et al. 2011; Camozzato et al. 2013a, b, 2017).

7.3.3.1 The Encantadas Complex

The Encantadas Complex represents the deepest portion of the Santana da Boa Vista Dome (Fig. 7.6) and comprises gneisses of tonalitic to trondhjemitic and minor dioritic composition with associated metahornblendites (Philipp et al. 2008). The orthogneisses are intruded by porphyritic and equigranular metagranites. These metagranites show the same deformation phases founded in the tonalitic to trondhjemitic gneisses, indicating a common structural and metamorphic history. The magmatic protoliths of the Encantadas Complex show the features of a typical high-Al TTG association, like high-K calc-alkaline signature, high LREE/Nb ratios, and trace element patterns that are consistent with an active continental margin setting. The metagranites present high-K calc-alkaline composition, metaluminous to slightly peraluminous affinity, enrichment in LRRE and LIL elements, with strong negative anomalies of Nb, Ta, Ti and P.

Several U–Pb SHRIMP and LA-MC-ICPMS zircon ages of *c*. 2263–2234 Ma constrain the timing of intrusive magmatism to the Rhyacian period (Table 7.3; Hartmann et al. 2000, 2003; Saalmann et al. 2011). However, new U–Pb ages indicate that the complex is composed by two magmatic associations. The older belongs to the Siderian period with U–Pb LA-MC-ICPMS zircon ages of 2404 ± 23 Ma (granodioritic gneiss) and U–Pb SHRIMP zircon ages of 2352 ± 26 Ma (tonalitic gneiss) (Table 7.3; Camozzato et al. 2017; Lusa et al. 2017). The younger association is Rhyacian and comprises tonalitic to dioritic gneisses and equigranular metagranites intruding the orthogneisses and yielded LA-MC-ICPMS U–Pb zircon ages of 2211 ± 17 and 2210 ± 16 Ma (Lusa et al. 2017).

Upper amphibolite-facies metamorphism is dated by U–Pb SHRIMP Orosirian zircon ages of 2045 ± 10 and 2021 ± 11 Ma (Hartmann et al. 2000). A younger metamorphic overprint yielded U–Pb LA-MC-ICPMS zircon ages of 679 ± 49, 643 ± 3.2, 631 ± 6 and 626 ± 15 Ma (Camozzato et al. 2013a, b, 2017), indicating reworking during the Brasiliano orogeny.

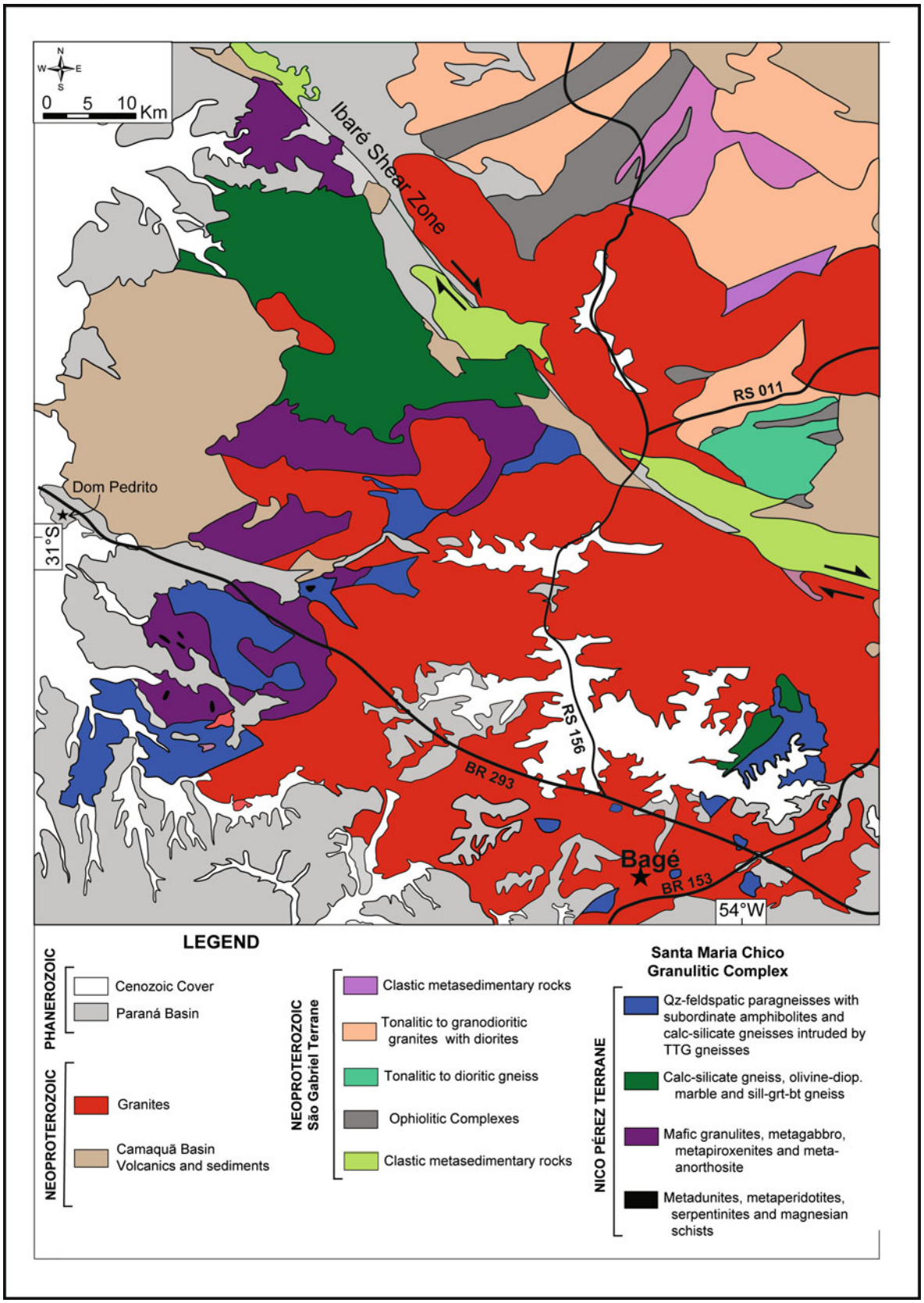

Fig. 7.5 Geological map of the Santa Maria Chico granulitic Complex, Taquarembó Terrane. (Modified from Philipp et al. 2016a, 2017a, b.)

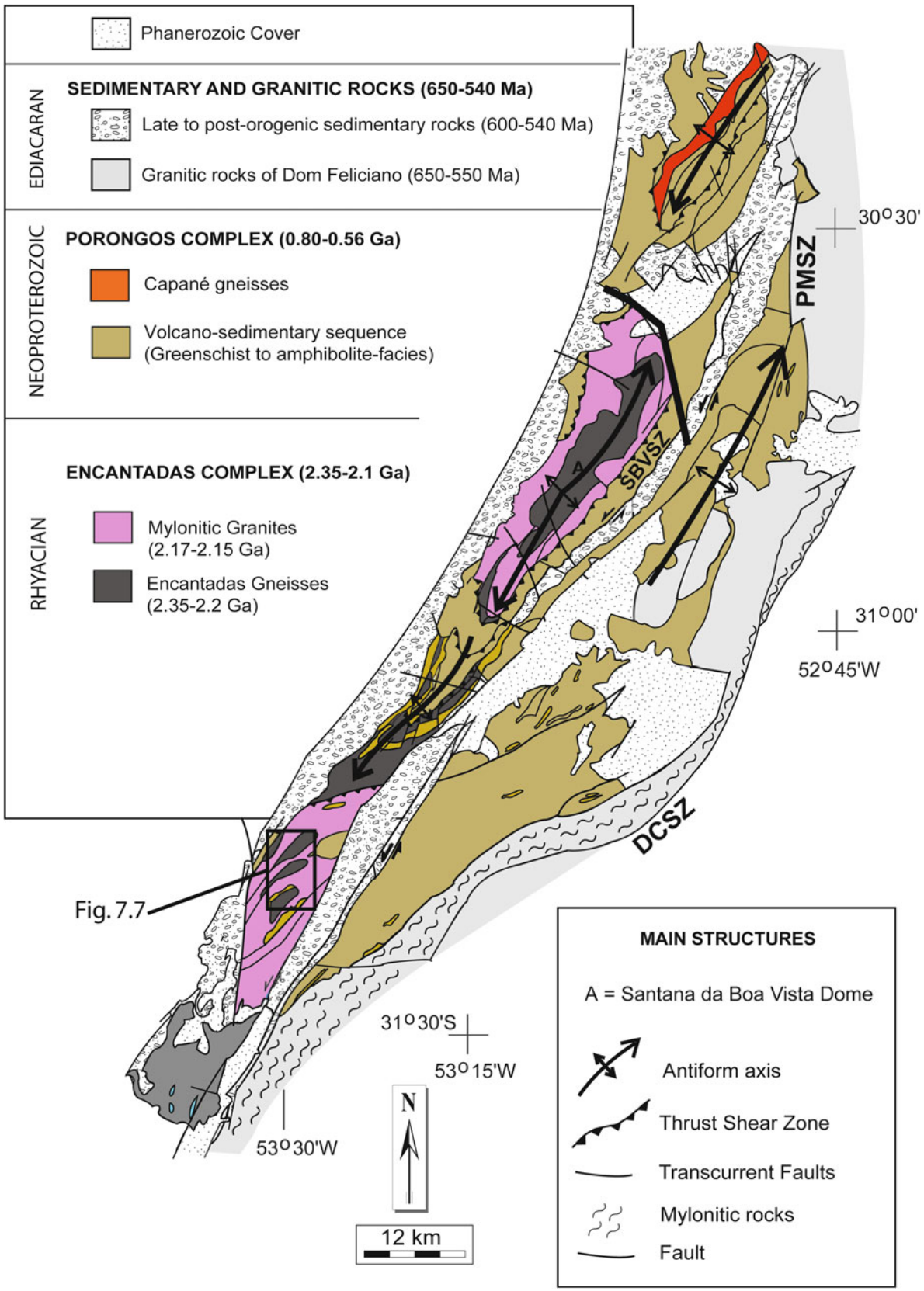

Fig. 7.6 Geological map of the Encantadas Complex in the Santana da Boa Vista region. (Modified from Philipp et al. 2016b, 2017a, b.) *DCSZ* Dorsal do Canguçu Shear Zone; *SBSZ* Santana da Boa Vista Shear Zone; *PMSZ* Passo do Marinheiro Shear Zone

7.3.3.2 The Vigia Complex

The Vigia Complex occurs in the southwestern portion of the Tijucas Terrane as a 25 km long and 10 km wide elongated body oriented north-northeast and surrounded by sedimentary rocks of the Camaquã Basin (Figs. 7.2 and 7.7). The Vigia Complex represents a north-northeast–south-southwest-trending dome, plunging towards both directions of strike. The core of the structure is occupied by tonalitic, trondhjemitic and granodioritic gneisses of the Vigia Complex, with the occasional occurrence of amphibolites and metahornblendites. In the eastern portion of the dome, the contact between the orthogneisses of the Vigia Complex and

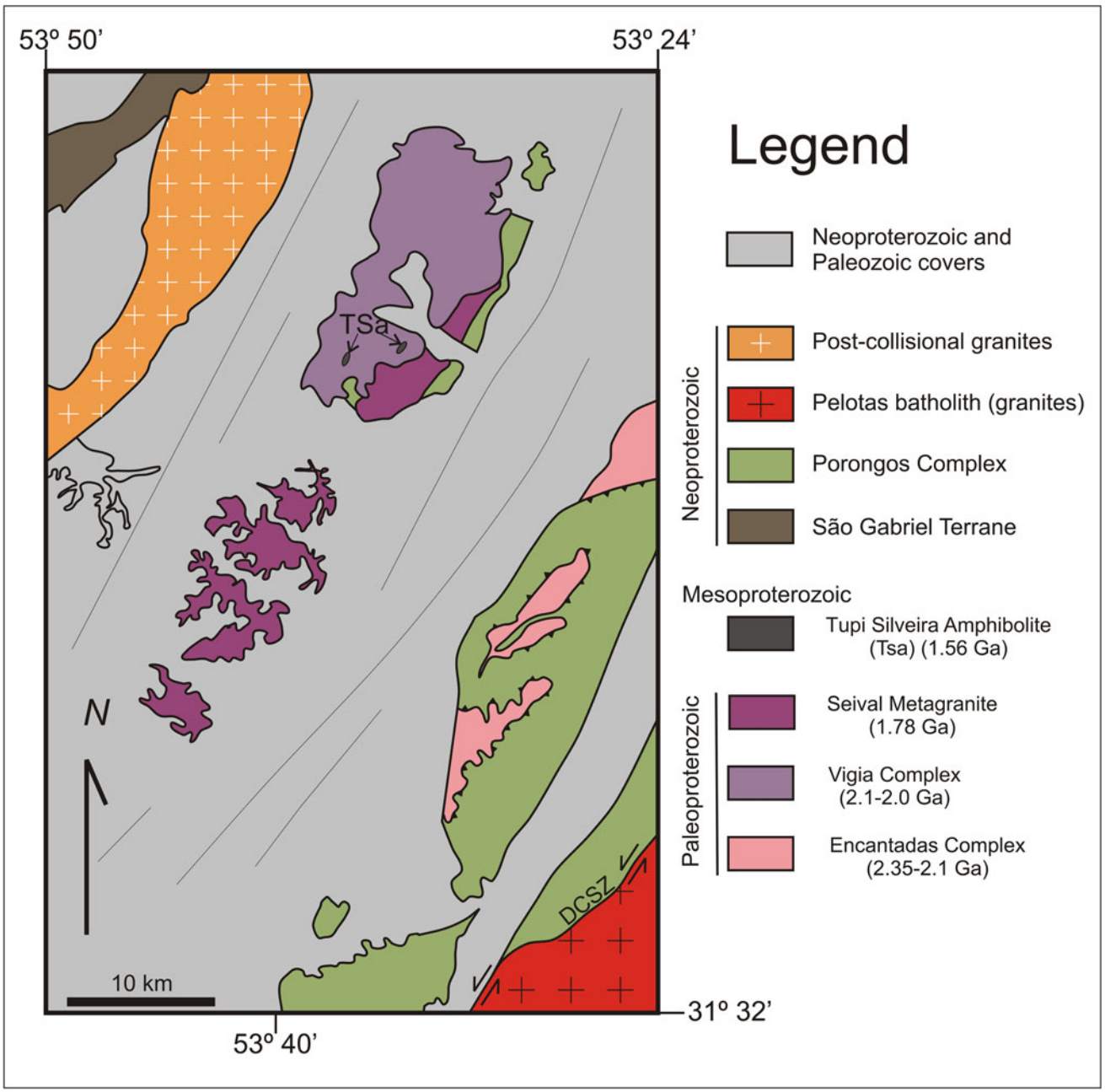

Fig. 7.7 Geological map of Vigia Dome, southern portion of Tijucas Block. (Modified from Camozzato et al. 2013a, b.) *DCSZ* Dorsal do Canguçu Shear Zone

the metasedimentary and metaultramafic rocks of the Porongos Complex is defined by a low- to medium-angle ductile shear zone. U–Pb zircon data (LA-MC-ICPMS) of a syenogranitic gneiss and a quartz dioritic gneiss yielded crystallization ages of 2056 ± 38 Ma and 2008 ± 52 Ma, respectively (Camozzato et al. 2013a, b, 2017).

7.3.3.3 Seival Metagranite

The Seival Metagranite is a north-northeast–south-southwest-trending elongated body extending continuously up to the vicinity of the Seival Farm, site of its type locality. The metagranite is located in the southeastern portion of the Vigia Dome and intrudes into the orthogneisses of the Vigia Complex (Fig. 7.7). The Seival Metagranite consists of granodiorites and monzogranites of pinkish colour, and subordinate bodies of leucogranite. The composition of this metagranite plots in the volcanic arc and post-collisional fields of the Rb versus Y + Nb diagram (Camozzato et al. 2017). The fabric is near isotropic. However, on the southeastern edge of the body a mylonitic foliation is defined by the preferred orientation of K-feldspar porphyroclasts, stretched quartz grains and biotite laths.

U–Pb LA-MC-ICPMS in zircon yielded concordant ages of 1785 ± 42, 1768 ± 24, 1764 ± 29 and 1763 ± 28 Ma (Camozzato et al. 2013a, b, 2017) interpreted as the time of intrusion during the Statherian period (Table 7.3).

7.3.3.4 Tupi Silveira Amphibolite

The Tupi Silveira Amphibolite occurs in the southern portion of the Vigia dome, being constituted by two small bodies up to some tens of metres long (Fig. 7.7) (Camozzato et al. 2013a, b, 2017). The bodies are intrusive into the orthogneisses of the Vigia Complex.

The amphibolite displays a millimetre banding, defined by the intercalation of layers composed mainly of granoblastic plagioclase and layers rich in hornblende with nematoblastic texture. The metamorphic assemblage plagioclase + hornblende + garnet + diopside is indicative of regional metamorphism under conditions compatible with upper-amphibolite to granulite-facies and medium pressure.

A U–Pb zircon age (LA-MC-ICPMS) of 1567 ± 21 Ma was obtained by Camozzato et al. (2013a, b) interpreted to be the age of magma emplacement (Table 7.3). The time of the metamorphism is recorded by a U–Pb zircon age of 643 ± 3 Ma.

7.3.4 Pre-Neoproterozoic Basement Inliers, Roof Pendants and Septas in the Pelotas Batholith

7.3.4.1 The Arroio Dos Ratos Complex

The Arroio dos Ratos Complex was originally defined by Fernandes et al. (1990, 1992) as a sequence of orogenic intrusions of granodioritic to trondhjemitic composition including three generations named G_1, G_2 and G_3. The complex is mostly exposed as roof pendants, septas and in situ wall rock fragments in Neoproterozoic intrusions in the Pelotas Batholith of the Dom Feliciano Belt (Fig. 7.8; Fernandes et al. 1990; Philipp and Campos 2004; Gregory et al. 2011; Martil et al. 2011). It is made up of tonalitic to granodioritic gneisses intruded by metatonalites, metadiorites and metagranodiorites (Philipp and Campos 2004; Gregory et al. 2011, 2015).

Geochemical data indicate that orthogneisses and metagranitoids mostly correspond to medium- to high-K calc-alkaline, metaluminous to slightly peraluminous intrusions (Philipp and Campos 2004; Martil et al. 2011; Gregory et al. 2015). The behaviour of major and trace elements and the pattern of moderate fractionation of the REE, with enrichment of LREE in relation to the HREE, indicate a mature continental arc setting for the magmatism of this association.

U–Pb SHRIMP and LA-MC-ICPMS zircon data (Table 7.3; Leite et al. 2000; Gregory et al. 2015) for this complex show Rhyacian-Orosirian magmatic ages for the protoliths. The first U–Pb TIMS zircon age yielded 2078 ± 13 Ma (Tommasi 1991). Afterwards, Leite et al. (2000) obtained a U–Pb SHRIMP in zircon age of 2067 ± 17 Ma. More recently, Gregory et al. (2015) dated this complex using LA-MC-ICPMS and obtained a concordia magmatic U–Pb zircon age of 2148 ± 33 Ma from a metatonalite of the G_1 association; ages of 2150 ± 28 and 2136 ± 27 Ma for metatonalites of the G_2 association; and ages of 2099 ± 10, 2081 ± 07 and 2077 ± 13 Ma for metatonalites to metagranodiorites of G_3 association. Scarce inherited zircons dated at *c*. 2.7 Ga are reported in the G_1 association (Gregory et al. 2015). Orosirian upper amphibolite to granulite-facies metamorphism (Lima et al. 1998) is dated by U–Pb SHRIMP at around 2.0 Ga (Leite et al. 2000).

The Neoproterozoic record includes granites that intrude into the complex, dated by Leite et al. (2000) at *c*. 780 Ma and U–Pb zircon metamorphic ages of 631 ± 13 Ma and

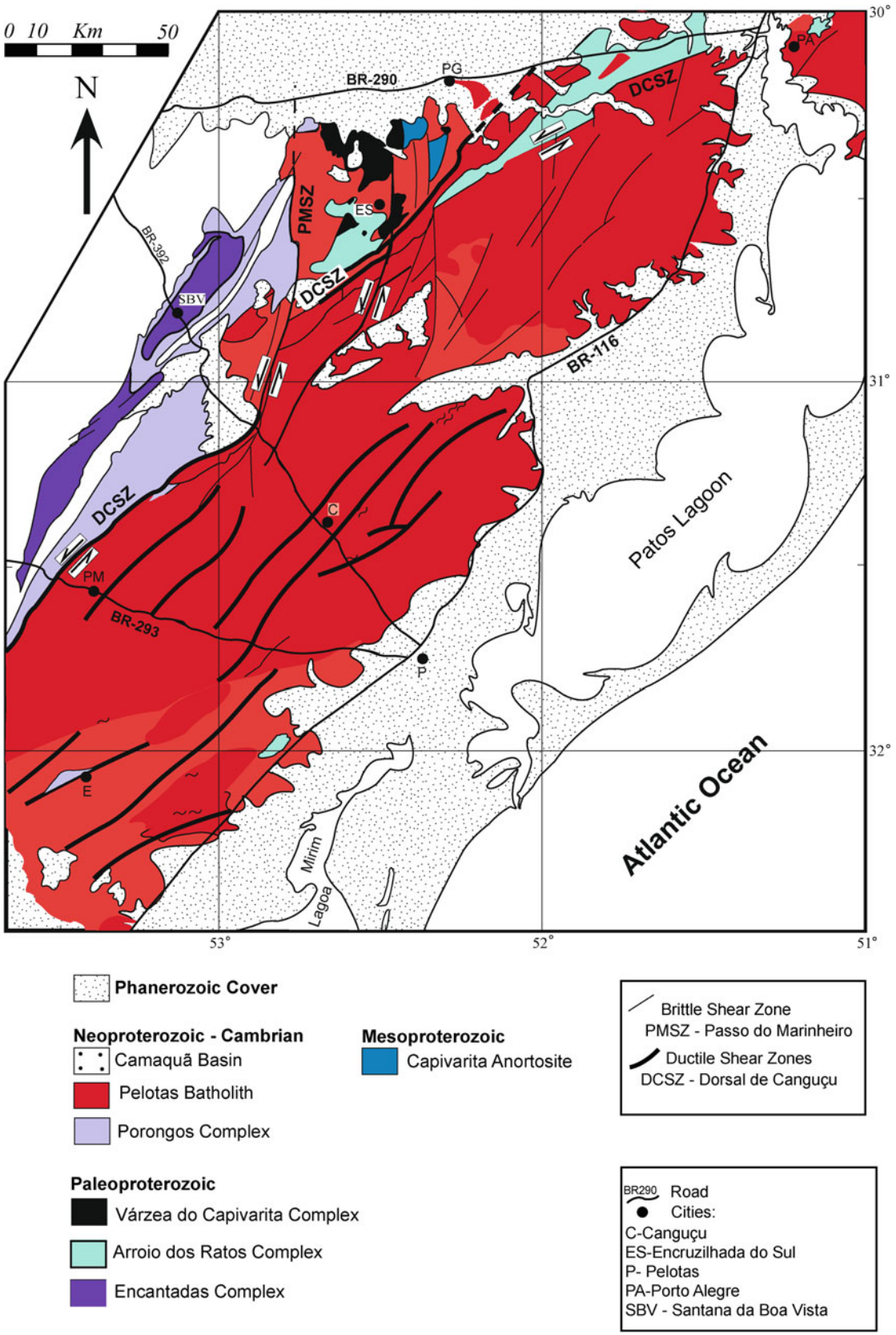

Fig. 7.8 Simplified map of the Neoproterozoic Pelotas Batholith showing the Paleoproterozoic Várzea do Capivarita, Arroio dos Ratos and Encantadas complexes and the Mesoproterozoic Capivarita Meta-anorthosite. (Modified from Philipp et al. 2016a.)

635 ± 6 Ma in the tonalitic and granodioritic gneisses (Leite et al. 2000; Gregory et al. 2015).

7.3.4.2 The Capivarita Meta-anorthosite

The Capivarita Meta-anorthosite crops out in two main bodies, oriented east–west and north–south, in the north-eastern portion of the Rio Grande do Sul state. It mainly occurs as roof pendants in the Neoproterozoic Encruzilhada do Sul Suite granites of the Pelotas Batholith that are part of the Dom Feliciano Belt (Fernandes et al. 1990; Philipp et al. 2010) (Fig. 7.8).

The Capivarita Meta-anorthosite is bounded to the southeast by the Dorsal do Canguçu Shear Zone and to the west by the Passo do Marinheiro Shear Zone (Fig. 7.8), and it is covered to the north by the Phanerozoic sediments of the Paraná Basin (Philipp et al. 2010). The Capivarita Meta-anorthosite and the Paleoproterozoic basement rocks of this area are metamorphosed under medium-amphibolite to granulite-facies conditions. The Paleoproterozoic basement is represented by Al-rich, calc-silicate rocks and quartz-feldspar paragneisses of the Várzea Capivarita Complex, and by the Paleoproterozoic orthogneisses of the Arrroio dos Ratos Complex (Fernandes et al. 1990; Gregory et al. 2011; Martil et al. 2011; Philipp et al. 2013, 2016a, b).

Anorthosite is the dominant lithotype, but there are subordinate occurrences of metagabbros (amphibolites) and thin layers of Fe–Ti oxide-rich rocks. The Capivarita Meta-anorthosite is homogeneous, light grey, equigranular and medium- to coarse-grained, with a mafic content ranging from 2 to 5%. A discontinuous millimetre-thick layering is defined by the distribution of hornblende plus some titanite and Fe–Ti oxides (ilmenite and magnetite), grossular and rare diopside (Philipp et al. 2010; Chemale et al. 2011). Metagabbro layers and dykes are up to 5 m thick, tabular and concordant. The primary igneous layering is frequently preserved. The fabric of the hornblende is parallel to the regional tectonic grain and is connected with the main regional deformational phase observed in the Neoproterozoic Várzea Capivarita Complex (Philipp et al. 2013).

U–Pb LA-MC-ICPMS zircon and titanite data constrain the timing of the magmatism at 1573 ± 21 and 1530 ± 33 Ma, respectively, thus indicating a Calymmian age (Chemale et al. 2011). The metamorphic age is defined in the rims of zircon crystals and in metamorphic titanite, yielding ages of 652 ± 9 Ma for the collisional metamorphism and 606 ± 6 and 597 ± 6 Ma for the thermal metamorphism related to emplacement of Encruzilhada do Sul Granite (Chemale et al. 2011).

7.4 Discussion

7.4.1 Origin and Extension of the Nico Pérez Terrane

The Nico Pérez Terrane has been regarded as the eastern part of the Río de la Plata Craton (Bossi and Campal 1992; Mallmann et al. 2007; Chiglino et al. 2010; Frimmel et al. 2011; Gaucher et al. 2011; Chernicoff et al. 2015), although some recent contributions argued for an allochthonous origin of the Nico Pérez Terrane (Oyhantçabal et al. 2011a; Rapela et al. 2011; Oriolo et al. 2016a). Interestingly, Almeida et al. (1973) stated the following in their definition of the Río de la Plata Craton:

> In Uruguay and Argentina, the Río de la Plata craton occurs, exhibiting Trans-Amazonian structures, which surely extend over the nearby continental shelf. The predominant trends are nearly east-west in disagreement with the NNE-NE trends of the Ribeira belt. This latter belt extends down to the Uruguay coastal region, close to the border of the cratonic area, indicating that the Río de la Plata craton also, in late Precambrian times, probably did not extend much further to the east.

After the redefinition of units by Fragoso Cesar (1980), the Neoproterozoic mobile belt that extends along eastern Rio Grande do Sul and Uruguay is considered to be the Dom Feliciano Belt and not the prolongation of the Ribeira Belt. The Dom Feliciano Belt clearly overprints the basement of the Nico Pérez Terrane (e.g., Oyhantçabal et al. 2011a, 2012; Oriolo et al. 2016a, c). Hence the assumption that the Nico Pérez Terrane was part of the Río de la Plata Craton can be ruled out, even if considering the original definition of the latter and an allochthonous origin related to the Congo Craton is well supported by recent geological, structural and isotopic data (Oyhantçabal et al. 2011a; Rapela et al. 2011; Oriolo et al. 2016a).

On the other hand, Oyhantçabal et al. (2011a, 2012) correlated the Valentines-Rivera Granulitic Complex of the Nico Pérez Terrane with the Santa María Chico Complex of the Taquarembó Terrane. The correlation is well established based on lithological association, age and isotopic constraints, metamorphic grade and geographic proximity. Leite et al. (2000), Saalmann et al. (2011) and Philipp et al. (2016a) in turn indicated that the Arroio dos Ratos and Encantadas complexes were part of the same block. Correlations are mostly based on Rhyacian-Orosirian multistage magmatism, the medium- to high-grade metamorphism recorded in all these complexes and the Neoproterozoic reworking (Tables 7.1, 7.2 and 7.3).

All pre-Neoproterozoic basement complexes of Uruguay located east of the Sarandí del Yí Shear Zone as well as those of Rio Grande do Sul state in southeastern Brazil represent reworked Archean crust. This fact was recognized using Sm–Nd data by Cordani and Sato (1999) in a revision of the South American Platform. Archean zircon inheritance was reported for gneisses of the Valentines-Rivera Granulitic Complex (Santos et al. 2003; Oriolo et al. 2016a), which are also dominated by Archean Sm–Nd and Lu–Hf model ages (Oyhantçabal et al. 2011a; Oriolo et al. 2016a). Archean zircons and Sm–Nd model ages were also obtained in the Santa Maria Chico Granulitic Complex (Mantovani et al. 1987; Hartmann 1998; Hartmann et al. 1999), whereas Saalmann et al. (2011) and Gregory et al. (2015) reported Neoarchean zircon inheritance in the Encantadas and Arroio dos Ratos complexes, respectively. Camozzato et al. (2017) present Lu–Hf data of the orthogneisses of Encantadas Complex, indicating $\varepsilon_{Hf(t)}$ between −7 and −15, with T_{DM} ages between 3.2 and 3.6 Ga for the dioritic gneisses, and $\varepsilon_{Hf(t)}$ in the range −1.30 to −10 with T_{DM} between 2.7 and 3.1 Ga for the syenogranitic gneiss.

The detrital zircon age patterns of the metavolcanosedimentary complexes in Rio Grande do Sul also record the ages observed in the Nico Pérez basement. LA-MC-ICPMS U–Pb ages in detrital zircons of the Porongos Complex (Dom Feliciano Belt) and in the Passo Feio Complex (São Gabriel Terrane) show a dominant Paleoproterozoic component and a subsidiary Archaean component up to 3.6 Ga (Hartmann et al. 2004; Gruber et al. 2011; Lopes et al. 2015; Pertille et al. 2015a, b), with subordinate occurrence of Proterozoic ages between 1.8 and 1.2 and between 1.0 and 0.6 Ga. This data confirm the presence of very old sources in the southern region of Brazil (Philipp et al. 2016a). A similar scenario is observed in Uruguay, as a compilation of detrital zircon age data from the metasedimentary cover shows these sediments were mainly derived from Paleoproterozoic sources, with subordinate contribution of Archean (up to 3.7 Ga), Meso- and Neoproterozoic sources (Gaucher et al. 2008; Blanco et al. 2009; Pecoits et al. 2016).

Reworking of Paleoproterozoic gneisses as a result of Neoproterozoic magmatism and metamorphism is also recorded in all units. Negative ε_{Nd} and ε_{Hf} values and T_{DM} ages between 3 and 2 Ga for most of the granitic plutons in the Nico Pérez Terrane and in the Dom Feliciano Belt suggest a protracted recycling process of Paleoproterozoic to Late Archaean sources (e.g., Silva et al. 1999, 2000; Hartmann et al. 2000; Oyhantçabal et al. 2012; Basei et al. 2013; Camozzato et al. 2013a, b, 2017; Gregory et al. 2015; Oriolo et al. 2016a; Philipp et al. 2016a; Lara et al. 2016).

Further similarities are revealed by geochemical data. A medium-K calc-alkaline signature suggesting emplacement in a continental arc tectonic setting is a common feature of the roughly coeval Paleoproterozoic magmatism of the Valentines-Rivera (Ellis 1998; Oyhantçabal et al. 2012), Santa Maria Chico (Laux et al. 2012; Girelli et al. 2016a), Encantadas (Philipp et al. 2008), Arroio dos Ratos (Philipp and Campos 2004; Gregory et al. 2011, 2015) and Vigia complexes (Camozzato et al. 2017). Though poorly constrained, available data for high-grade metamorphism show similar conditions and timing in the Valentines-Rivera, Santa Maria Chico, Encantadas and Arroio dos Ratos complexes (Hartmann 1998; Lima et al. 1998; Massonne et al. 2001; Philipp et al. 2008, 2013, 2016a; Martil et al. 2011; Oyhantçabal et al. 2012; Basei et al. 2013).

Furthermore, the geochemistry of the early Mesoproterozoic magmatism shows characteristics that match a within-plate tectonic setting. The Capivarita Meta-anorthosite (1.57 Ga) and Tupi Silveira Amphibolite (1.55 Ga) in Rio Grande do Sul and bimodal magmatism including felsic volcanic rocks (*c*. 1.45 Ga) and metagabbros (*c*. 1.5 Ga) in the southern Dom Feliciano Belt in Uruguay support an extensional environment in an intraplate tectonic setting.

A tectonostratigraphic chart summarizing the observed Archean, Paleo- and Mesoproterozoic events and the proposed correlation between different areas is presented in Fig. 7.9. Despite the above-indicated common features of all outcrop areas considered here as belonging to the Nico Pérez Terrane, two contrasting subterranes are clearly defined when taking into account the degree of Neoproterozoic reworking. The Caçapava Shear Zone (Hartmann et al. 2016 and references therein) or Caçapava do Sul Lineament (Philipp et al. 2016a) of Rio Grande do Sul is, in its southern segment, the boundary between the Tijucas Terrane and the Taquarembó Terrane of the Nico Pérez Terrane, while its northern prolongation separates the São Gabriel Terrane from the Tijucas Terrane (Chemale 2000). An equivalent structure in Uruguay is the Sierra de Sosa Shear Zone, separating the Cerro Chato and the Pavas blocks of the Nico Pérez Terrane. Although the Phanerozoic cover hinders a final conclusion, it seems quite likely that the Sierra de Sosa Shear Zone represents the prolongation of the Caçapava do Sul Shear Zone. The Cerro Chato (UY)—Taquarembó (BR) subterrane is characterized by granulite-facies metamorphism and, even though Brasiliano granite intrusions and volcanosedimentary associations are common, the crustal architecture is not strongly overprinted by the north-northeast Brasiliano structural grain. The Pavas (UY)—Tijucas (BR) subterrane, on the other hand, displays a strong structural reworking, and basement inliers in the Dom Feliciano belt are normally parallel to the orogen structural grain. The basement shows mostly amphibolite-facies metamorphism and the pre-Ediacaran cover is widely extended. This different behaviour of both subterranes during the

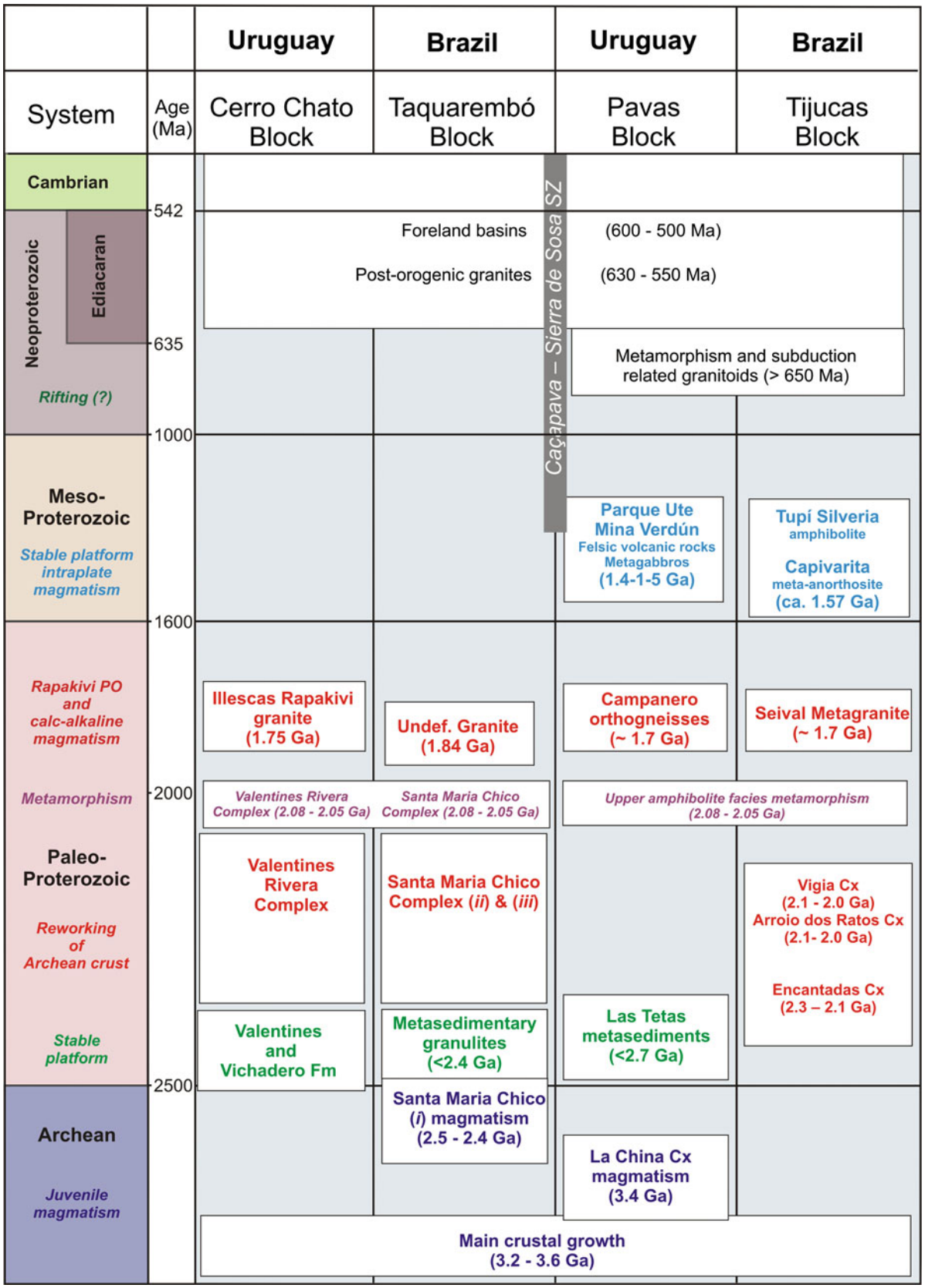

Fig. 7.9 Tectonostratigraphic chart of the Nico Pérez Terrane in Uruguay and southern Brazil. *Rapakivi PO* Post-orogenic rapakivi granites

evolution of the Dom Feliciano Belt could be related to different degrees of crustal attenuation before the Brasiliano collision and the distance to the orogenic core.

7.4.2 Tectonic Evolution

The Nico Pérez Terrane is dominated by Paleoproterozoic rocks. However, available geochronological and isotopic data reveals that in the Nico Pérez the main crustal growth occurred in the Archean and was subsequently reworked during the Paleo-, Meso- and Neoproterozoic (e.g., Oyhantçabal et al. 2011a; Girelli et al. 2016a; Oriolo et al. 2016a; Philipp et al. 2017b) (Fig. 7.9). Based on Hf isotopic data, Girelli et al. (2016a, 2016b), Oriolo et al. (2016a), Camozzato et al. (2017) and Philipp et al. (2017b) indicated Archean episodic crustal growth with Paleo- and Mesoarchean peaks of crust generation.

The Archean crust of the Nico Pérez Terrane underwent mostly crustal reworking during a major Rhyacian-Orosirian tectonometamorphic event (Tables 7.1, 7.2 and 7.3). The Valentines-Rivera Granulitic Complex records magmatism at *c*. 2.2–2.1 Ga succeeded by high-grade metamorphism and associated crustal anatexis at *c*. 2.1–2.0 Ga (Oyhantçabal et al. 2012; Santos et al. 2003; Oriolo et al. 2016a). Magmatism and metamorphism indicated for the Santa Maria Chico Granulitic Complex is coeval with that of the Valentines-Rivera Granulitic Complex (Hartmann et al. 1999, 2008; Laux et al. 2012; Girelli et al. 2016a, b; Philipp et al. 2017b), although Hartmann et al. (2008) and Camozzato et al. (2017) present U–Pb zircon data from the Siderian period. Even though this age seems to be older than those of the Valentines-Rivera Granulitic Complex, Siderian xenocrysts were also recognized in orthogneisses of the latter (Oriolo et al. 2016a). Rhyacian magmatism was reported for the Encantadas and Arroio dos Ratos complexes as well (Hartmann et al. 2000, 2003; Leite et al. 2000; Saalmann et al. 2011; Camozzato et al. 2013a, b; Gregory et al. 2015; Lusa et al. 2017), which in the latter is accompanied by Late Rhyacian to Early Orosirian metamorphism and magmatism, also recorded in the Vigia Complex (Hartmann et al. 2000, 2003; Camozzato et al. 2013a, b, 2017). Based on the existence of high-grade metamorphism and an arc geochemical fingerprint of orthogneisses, most tectonic models have favoured a magmatic arc setting for this major Paleoproterozoic event (e.g., Philipp et al. 2008, 2016a; Oyhantçabal et al. 2012; Gregory et al. 2015; Lusa et al. 2017), culminating in a collisional episode (Hartmann et al. 2000, 2003).

Subsequent Statherian magmatism is recorded during the intrusion of the Rapakivi-type Illescas granite and the protolith of the orthogneisses of the Campanero Unit (Bossi and Campal 1992; Campal and Schipilov 1995; Sánchez-Bettucci et al. 2004; Mallmann et al. 2007). Archean model ages of the latter also indicate the dominance of crustal reworking processes (Mallmann et al. 2007), whereas geochemical data point to a possible magmatic arc setting (Oyhantçabal 2005). Recently, Camozzato et al. (2013a, b) also presented Statherian U–Pb data for the magmatism of the Seival Metagranite in the Tijucas Terrane.

On the other hand, the Mesoproterozoic record of the Nico Pérez Terrane seems to be restricted to few passive margin metavolcanosedimentary units and mafic complexes with ages between *c*. 1.6 and 1.4 Ga (Table 7.1). The Capivarita Meta-anorthosite, which occurs as roof pendants in the Neoproterozoic granites of the Dom Feliciano Belt in southern Brazil, was correlated with the contemporaneous Mesoproterozoic units of Uruguay (Table 7.2; Chemale et al. 2011). Likewise, the age of the Tupi Silveira Amphibolite in the Tijucas Terrane is similar to that of the Capivarita Meta-anorthosite and an intraplate setting was suggested for this magmatism in southern Brazil (Camozzato et al. 2013a, b). In Uruguay, some authors suggested a major tectonometamorphic event related to the assembly of Rodinia for this magmatism (Campal and Schipilov 1999; Bossi and Cingolani 2009; Gaucher et al. 2011), whereas Oriolo et al. (2016a) argued for a more likely intraplate event. The latter hypothesis would also fit the tectonic setting inferred for this Calymmian event in southern Brazil, which implied local addition of relatively juvenile continental crust with some degree of crustal contamination (Chemale et al. 2011; Basei et al. 2013; Camozzato et al. 2013a, b, 2017).

Though elusive, the presence of a Cryogenian tectonomagmatic event seems to be well documented. U–Pb SHRIMP ages of 781 ± 5 and 777 ± 4 Ma were obtained for orthogneisses occurring as xenoliths within the Pelotas Batholith (Silva et al. 1999; Koester et al. 2016), whereas similar ages were reported in a metarhyolite and metadacites of the Porongos Complex. U–Pb SHRIMP and LA-MC-ICPMS zircon Cryogenian ages for metavolcanic rocks of the Porongos Complex were also presented by Chemale Jr. et al. (1997), Porcher et al. (1999), Saalmann et al. (2011) and Pertille et al. (2015b).

Metamorphic overprint at 875 ± 160, 702 ± 21 and 679 ± 49 Ma was indicated by U–Pb SHRIMP and LA-MC-ICPMS zircon data in rocks of the Encantadas Complex (Hartmann et al. 2003; Camozzato et al. 2017; Lusa et al. 2017). In Uruguay, no Cryogenian ages have

been identified so far in the Nico Pérez Terrane basement. Nevertheless, Oriolo et al. (2016a) indicated that the Cerro Olivo Complex, which is located to the east of the Sierra Ballena Shear Zone and records Cryogenian magmatism (Hartmann et al. 2002; Oyhantçabal et al. 2009b; Basei et al. 2011; Lenz et al. 2011), might be linked to the evolution of the Nico Pérez Terrane.

Cryogenian magmatism has traditionally been assumed to be the result of an extensional event, mostly based on the coeval timing of Rodinia break-up (e.g., Oyhantçabal et al. 2009b; Basei et al. 2011; Rapela et al. 2011; Oriolo et al. 2016a, b, c). In contrast, Lenz et al. (2011, 2013), Koester et al. (2016) and Philipp et al. (2016a) indicated a magmatic arc setting resulting from the arc-like geochemical signature. Within this framework, the western margin of the Nico Pérez Terrane was probably the upper plate during subduction to the east in the Tonian and Cryogenian (Philipp et al. 2016a; Oriolo et al. 2017). Extensional tectonics and the disconnection of the Nico Pérez Terrane from the Congo Craton most probably took place during the Early Neoproterozoic (Cryogenian) and resulted in crustal attenuation (Goscombe and Gray 2007, 2008; Konopásek et al. 2014; Oriolo et al. 2016a,b, c).

During the Late Neoproterozoic, involvement of the Nico Pérez Terrane in convergent tectonics associated with the Pan-African/Brasiliano orogeny and the evolution of the Dom Feliciano Belt gave rise to widespread crustal reworking, probably facilitated by previous crustal attenuation (Oriolo et al. 2016a, 2017). High-K to shoshonitic calc-alkaline to alkaline magmatism is recorded at *c*. 630–580 Ma (Table 7.1; Hartmann et al. 2002; Philipp et al. 2002, 2003, 2005, 2007; Oyhantçabal et al. 2007, Oyhantçabal et al. 2009b, 2012; Gaucher et al. 2008, 2014b; Oriolo et al. 2016a; Lara et al. 2016). Contemporaneous metamorphism, extensive deformation along shear zones and cooling were also reported for basement units (Philipp et al. 2003, 2016b; Oyhantçabal et al. 2009b, 2011a, 2012; Oriolo et al. 2016a, c). In a similar way, Ediacaran overprint resulting from metamorphism and magmatism of the Dom Feliciano Belt is well documented in basement metamorphic complexes (e.g., Hartmann et al. 2000; Leite et al. 2000; Chemale et al. 2011; Basei et al. 2013; Camozzato et al. 2013a, b; Philipp et al. 2013, 2016b; Gregory et al. 2015). This major Late Neoproterozoic tectonometamorphic event resulted from the collision of the Río de la Plata and Congo cratons at *c*. 650–620 Ma, which also implied the accretion of the Nico Pérez Terrane to the Río de la Plata Craton margin along the Sarandí del Yí Shear Zone (Oriolo et al. 2015, 2016a, b, c; Philipp et al. 2016a, b).

As mentioned above, derivation of the Nico Pérez Terrane from the Congo Craton seems to be well supported based on the predominance of Archean model ages, widespread Paleoproterozoic crustal reworking at 2.2–2.0 and 1.8–1.7 Ga, and anorogenic magmatism at 1.5–1.4 Ga. Luft et al. (2011) reported 1.8–1.7 Ga ages for the gneisses of the Mudorib Complex in Namibia, and the 1.5–1.4 Ga event is also clearly present in the Congo Craton (e.g., Kibaran belt; Tack et al. 2010; or the Kunene Complex), further supporting the African signature of Nico Pérez.

7.5 Conclusions

- The Nico Pérez Terrane of southernmost Brazil and Uruguay includes pre-Neoproterozoic basement evidencing an important component of Archean crustal growth. These basement rocks occur not only as basement blocks but also as basement inliers and roof pendants in the batholiths of the Dom Feliciano Belt. Though Sm–Nd and Lu–Hf Archean model ages predominate, zircon data indicate dominant Paleoproterozoic magmatic ages for the protoliths of the gneisses, which resulted from extensive Paleoproterozoic reworking associated with crustal anatexis. This terrane also contains relics of a Neoarchean to Siderian sedimentary cover including BIFs, quartzites and marbles.
- Intraplate Mesoproterozoic magmatism is recorded in Uruguay and southernmost Brazil and includes meta-anorthosite complexes, metagabbros, amphibolites and felsic volcanic rocks. The latter are interbedded with sediments assumed to correspond to a Mesoproterozoic platform cover.
- Two different subterranes are recognized separated by the north-northeast-trending Caçapava—Sierra de Sosa Shear Zone. The western subterrane includes the granulite-facies Valentines Rivera (UY) and Santa Maria Chico (BR) complexes and is less reworked by the Brasiliano Orogeny. The eastern subterrane was strongly reworked during the Brasiliano and comprises the Pavas Block of Uruguay and several basement inliers in the Dom Feliciano Belt of Uruguay and Brazil.
- Neoproterozoic reworking recorded in cooling ages, extensive shear zones and granite intrusions evidence that, despite its Archean origin, the Nico Perez terrane was not endowed with a thick lithosphere during the Neoproterozoic, leading to its metacratonization during the Brasiliano.
- A derivation of the Nico Pérez Terrane from the Congo Craton seems most likely owing to the similar tectonic evolution. Separation probably occurred during the Neoproterozoic and resulted in crustal attenuation that favoured subsequent metacratonization.

Acknowledgements S. Oriolo thanks DAAD for a long-term Ph.D. scholarship (A/12/75051). R.P. Philipp express thanks for the research grant and resources for research projects from the Brazilian National Council for Scientific and Technological Development (CNPq). P. Oyhantçabal gratefully acknowledges grants provided by the DAAD, the German Science Foundation and Comisión Sectorial de Investigación Científica (CSIC) of the Universidad de la República.

References

Alkmim FF, Marshak S, Fonseca MA (2001) Assembling West Gondwana in the Neoproterozoic: clues from the São Francisco craton region, Brazil. Geology 29:319–322

Almeida FFM, Amaral G, Cordani UG, Kawashita K (1973) The Precambrian evolution of the South American cratonic margin, South of Amazonas River. In: Nairn ACM, Kanes WH, Stehli FG (eds) The Ocean basins and margins. Plenum, New York, pp 411–446

Basei MAS, Nutman A, Siga Jr O, Passarelli CR, Drukas CO (2009) The evolution and tectonic setting of the Luís Alves Microplate of southeastern Brazil: An exotic terrane during the assembly of Western Gondwana. In: Gaucher C, Sial AN, Halverson GP, Frimmel HE (eds) Neoproterozoic-Cambrian tectonics, global change and evolution: a focus on southwestern Gondwana. Dev Precambrian Geol 16:273–291

Basei MAS, Neves BBB, Siga O Jr, Babinski M, Pimentel MM, Tassinari CCG, de Hollanda MHBM, Nutman AP, Cordani UG (2010) Contribution of SHRIMP U–Pb zircon geochronology to unravelling the evolution of Brazilian Neoproterozoic fold belts. Precambrian Res 183(1):112–144

Basei MAS, Peel E, Sánchez Bettucci L, Preciozzi F, Nutman AP (2011) The basement of the Punta del Este Terrane (Uruguay): an African Mesoproterozoic fragment at the eastern border of the South American Río de la Plata craton. Int J Earth Sci 100:289–304

Basei MAS, Campos Neto MC, Pacheco Lopes A, Nutman AP, Liu D (2013) Polycyclic evolution of Camboriú Complex migmatites, Santa Catarina, Southern Brazil: integrated Hf isotopic and U–Pb age zircon evidence of episodic reworking of a Mesoarchean juvenile crust. Braz J Geol 43:427–443

Blanco G, Rajesh HM, Gaucher C, Germs GJB, Chemale F (2009) Provenance of the Arroyo del Soldado group (Ediacaran to Cambrian, Uruguay): implications for the paleogeographic evolution of southwestern Gondwana. Precambr Res 171:57–73

Bossi J, Campal N (1992) Magmatismo y tectónica transcurrente durante el Paleozoico inferior del Uruguay. In: Gutiérrez J, Saavedra J, Rábano I (eds) Paleozoico Inferior de Ibero-América. Universidad de Extremadura, Alicante, pp 343–356

Bossi J, Cingolani C (2009) Extension and general evolution of the Río de la Plata Craton. In: Gaucher C, Sial AN, Halverson GP, Frimmel HE (eds): Neoproterozoic-Cambrian tectonics, global change and evolution: a focus on southwestern Gondwana. Dev Precambrian Geol 16:73–85

Bossi J, Umpierre M (1969) La petrología del yacimiento de hierro de Valentines. Cuartas Jornadas Geológicas Argentinas, Mendoza, 1969, Actas pp 127–147

Camozzato E, Philipp R P, Chemale F Jr (2013a) Idades Estaterianas no Domo da Vigia: complexos Vigia e Porongos, Metagranito Seival e Anfibolito Tupi Silveira, Bagé, RS In: VIII Symposium International on Tectonics, XIV Simpósio Nacional de Estudos Tectônicos. *Boletim de Resumo Expandidos*, Chapada dos Guimarães, Cuiabá, SBG-MT, v.1, p 15–19

Camozzato E, Philipp RP, Chemale F Jr (2013b) Evolução Tectônica e Geocronologia U–Pb em zircão da terminação sul do Terreno Tijucas (RS, Brasil). In: VII Congreso Uruguayo de Geología, Montevideo, Resúmenes Extendidos, pp 7–11

Camozzato E, Philipp RP, Chemale F Jr (2017). Siderian-Ryacian and Staterian magmatism of the Encantadas and Vigia complexes and Seival Metagranite at the Vigia Dome, southern portion of the Tijucas Terrane, Dom Feliciano Belt, RS, Brazil. J South Am Earth Sci (Manuscript submitted for publication)

Campal N, Schipilov A (1995) The Illescas bluish quartz rapakivi granite (Uruguay-South America): some geological features. In: Symposium rapakivi granites and related rocks, Belem

Campal N, Schipilov A (1999) The eastern edge of the Rio de la Plata Craton: a history of tangential collisions. Basement Tectonics 13:33–48

Chemale F Jr (2000) Evolução Geológica do Escudo Sul-Rio-Grandense. In: Holz M, De Ros LF (eds.) Geologia do Rio Grande do Sul. Editora UFRGS, Porto Alegre, pp 13–52

Chemale F Jr, Babinski M, Van Schmus WR, Wildner W, Lima EF (1997) U-Pb and Sm-Nd isotopic studies of Neoproterozoic to early Paleozoic belts in southern Brazil. In: South American symposium on isotope geology, Sa˜o Paulo. Boletim de Resumos Expandidos Sa˜o Paulo, SGB, 71

Chemale F Jr, Philipp RP, Dussin IA, Formoso MLL, Kawashita K, Berttotti AL (2011) Lu-Hf and U–Pb age determination of Capivarita Anorthosite in the Dom Feliciano Belt, Brazil. Precambrian Res 186:117–126

Chernicoff CJ, Zappettini EO, Santos JOS, Pesce A, McNaughton NJ (2015) Zircon and titanite U–Pb SHRIMP dating of unexposed basement units of the Buenos Aires region, southeastern Río de la Plata Craton, Argentina. Int Geol Rev 58:643–652

Chiglino L, Gaucher C, Sial AN, Bossi J, Ferreira VP (2008) Chemostratigraphy of Mesoproterozoic carbonates in the Nico Pérez Terrane (Río de la Plata Craton). In: 33 International Geological Congress, Oslo

Chiglino L, Gaucher C, Sial AN, Bossi J, Ferreira VP, Pimentel MM (2010) Chemostratigraphy of Mesoproterozoic and Neoproterozoic carbonates of the Nico Pérez Terrane, Río de la Plata Craton, Uruguay. Precambrian Res 182:313–336

Cordani UG, Sato K (1999) Crustal evolution of the South American Platform, based on Nd isotopic systematics on granitoid rocks. Epis Newsmag Int Union Geol Sci 22(3):167–173

Cordani UG, Halpern M, Berenholc M (1974) Idades radiométricas de rochas do Escudo Sul-Riograndense e sua significação tectônica. Actas XXVIII Congresso Brasileiro de Geologia, 1974. Porto Alegre Bol 1:696–697

Cordani UG, Cubas N, Sato K, Nutman AP, Gonzales ME, Presser JLB (2001) Geochronological constraints for the evolution of the metamorphic complex near the Tebicuary River, Southern Precambrian Region of Paraguay. In: 3 South American Symposium on Isotope Geology, Pucón

Eby GN (1992) Chemical subdivision of the A-typegranitoids: petrogenetic and tectonic implications. Geology 20:641–644

Ellis J (1998) The Precambrian supracrustal rocks of the Isla Cristalina de Rivera in northern Uruguay and their ore deposits, vol 90. Heidelberger Geowissenschaftliche Abhandlungen, Heidelberg, pp 1–196

Fernandes LA, Tommasi A, Porcher CC (1990) Esboço estrutural de parte do Batólito Pelotas, região de Quitéria—Capivarita. Acta Geológica Leopoldensia 30:117–138

Fernandes LAD, Tommasi A, Porcher CC (1992) Deformation patterns in the southern Brazilian branch of the Dom Feliciano Belt: a reappraisal. J S Am Earth Sci 5:77–96

Fragoso Cesar ARS (1980) O Craton do Rio de La Plata e o Cinturáo Dom Feliciano no Escudo Uruguaio-Sul Riograndense. In: *Congresso Brasileiro de Geologia*, vol 31. SBG Anais, Camboriú, pp 2879–2891

Frimmel HE, Basei MAS, Gaucher C (2011) Neoproterozoic geodynamic evolution of SW-Gondwana: a southern African perspective. Int J Earth Sci (Geol Rundsch) 100:323–354

Gaucher C, Blanco G (2014) Batolito de Illescas. In: Bossi J, Gaucher C (eds) Geología del Uruguay, Predevónico. Universidad de la República, Montevideo, pp 209–214

Gaucher C, Finney SC, Poiré DG, Valencia VA, Grove M, Blanco G, Pamoukaghlián K, Gómez Peral L (2008) Detrital zircon age of Neoproterozoic sedimentary successions of Uruguay and Argentina: insights into the geological evolution of the Río de la Plata Craton. Precambrian Res 167:150–170

Gaucher C, Frei R, Chemale F Jr, Frei D, Bossi J, Martínez G, Chiglino L, Cernuschi F (2011) Mesoproterozoic evolution of the Río de la Plata Craton in Uruguay: at the heart of Rodinia? Int J Earth Sci 100:273–288

Gaucher C, Bossi J, Martínez G, Chiglino L, Frei R, Sial AN (2014a) Grupo Parque UTE. In: Bossi J, Gaucher C (eds) Geología del Uruguay, Predevónico. Universidad de la República, Montevideo, pp 215–232

Gaucher C, Sial AN, Frei R, Ferreira V, Frei D, Bossi J, Cabrera J (2014b) Magmatismo anorogénico ediacárico. In: Bossi J, Gaucher C (eds) Geología del Uruguay, Predevónico. Universidad de la República, Montevideo, pp 283–298

Gaucher C, Frei R, Sial AN, Castiglione E, Ferreira V (2014c) Grupo Cebollatí. In: Bossi J, Gaucher C (eds) Geología del Uruguay, Predevónico. Universidad de la República, Montevideo, pp 283–298

Girelli T, Chemale Jr F, Lavina ELC, Lana CC, Laux JH (2016a) Novos dados de geocronologia U–Pb e Lu-Hf para o Complexo Granulítico Santa Maria Chico, RS. In: Congresso Brasileiro de Geologia, 48, Porto Alegre, Sociedade Brasileira de Geologia, Boletim de Resumos

Girelli T, Chemale Jr F, Lavina ELC, Laux JH, Bongiolo E, Lana C (2016b) Proterozoic evolution of Santa Maria Chico Granulitic Complex and adjacent areas. In: Congresso Brasileiro de Geologia, 48, Porto Alegre, Sociedade Brasileira de Geologia, Boletim de Resumos

Goscombe B, Gray DR (2007) The coastal terrane of thekaoko belt, Namibia: outboard arc-terrane and tectonic significance. Precambr Res 155:139–158

Goscombe B, Gray DR (2008) Structure and strain variation at mid-crustal levels in a transpressional orogen: a review of Kaoko Belt structure and the character of West Gondwana amalgamation and dispersal. Gondwana Res 13:45–85

Gregory TR, Bitencourt MF, Nardi LVS (2011) Caracterização estrutural e petrológica de metatonalitos e metadioritos do Complexo Arroio dos Ratos na sua seção-tipo, região de Quitéria, RS. Pesqui em Geociênc 38:85–108

Gregory TR, Bitencourt MF, Nardi LVS, Florisbal LM, Chemale F Jr (2015) Geochronological data from TTG-type rock associations of the Arroio dos Ratos Complex and implications for crustal evolution of southernmost Brazil in Paleoproterozoic times. J S Am Earth Sci 57:49–60

Gruber L, Porcher CC, Lenz C, Fernandes LAD (2011) Proveniência dos metassedimentos das seqüências Arroio Areião, Cerro Cambará e Quartzo Milonitos no Complexo Metamórfico Porongos, Santana da Boa Vista, RS. Pesquisas em Geociências 38(3):205–223

Hartmann LA (1987) Isócrona Sm–Nd de 2,1 Ga em minerais de duas amostras do Complexo Granulítico Santa Maria Chico, RS. Congresso Brasileiro de Geoquímica 1, SBGq, Porto Alegre, Anais 1:105–111

Hartmann LA (1998) Deepest exposed crust of Brazil—Geochemistry of Paleoproterozoic depleted Santa María Chico granulites. Gondwana Res 1:331–341

Hartmann LA, Leite JAD, McNaughton NJ, Santos JOS (1999) Deepest exposed crust of Brazil—SHRIMP establishes three events. Geology 27:947–950

Hartmann LA, Leite JAD, da Silva LC, Remus MVD, McNaughton NJ, Groves DI, Ir Fletcher, Santos JOS, Vasconcellos MAZ (2000) Advances in SHRIMP geochronology and their impact on understanding the tectonic and metallogenic evolution of southern Brazil. Aust J Earth Sci 47:829–844

Hartmann LA, Campal N, Santos JOS, McNaughton NJ, Bossi J, Schipilov A, Lafon JM (2001) Archean crust in the Río de la Plata Craton, Uruguay. J S Am Earth Sci 14:557–570

Hartmann LA, Santos JOS, Bossi J, Campal N, Schipilov A, McNaughton NJ (2002) Zircon and titanite U–Pb SHRIMP geochronology of Neoproterozoic felsic magmatism on the eastern border of the Río de la Plata Craton, Uruguay. J S Am Earth Sci 15:229–236

Hartmann LA, Santos JOS, Leite JAD, Porcher CC, McNaughton NJ (2003) Metamorphic evolution and U–Pb zircon SHRIMP geochronology of the Belizário ultramafic amphibolite, Encantadas Complex, southernmost Brazil. An Acad Bras Cienc 75:393–403

Hartmann LA, Philipp RP, Liu D, Wan Y, Wang Y, Santos JOS, Vasconcellos MAZ (2004) Paleoproterozoic Magmatic Provenance of Detrital Zircons, Porongos Complex Quartzites, Southern Brazilian Shield. Int Geol Rev 46:127–157

Hartmann LA, Liu D, Wang Y, Massonne HJ, Santos JOS (2008) Protolith age of Santa María Chico granulites dated on zircons from an associated amphibolite-facies granodiorite in southernmost Brazil. An Acad Bras Cienc 80:543–551

Hartmann LA, Lopes WR, Savian JF (2016) Integrated evaluation of the geology, aerogammaspectrometry and aeromagnetometry of the Sul-Riograndense Shield, southernmost Brazil. An Acad Bras Ciênc 88(1):75–92. https://dx.doi.org/10.1590/0001-3765201520140495

Jost H (1981) Geology and Metallogeny of the Santana da Boa Vista region, South Brazil. University of Athens, Georgia, PhD thesis, pp 1–208

Konopásek J, Košler J, Sláma J, Janoušek V (2014) Timing and sources of pre-collisional Neoproterozoic sedimentation along the SW margin of the Congo Craton (Kaoko Belt, NW Namibia). Gondwana Res 26:386–401

Koester E, Porcher CC, Pimentel MM, Fernandes LAD, Vignol-Lelarge ML, Oliveira LD, Ramos RC (2016) Further evidence of 777 Ma subduction-related continental arc magmatism in Eastern Dom Feliciano Belt, southern Brazil: The Chácara das Pedras Orthogneiss. J S Am Earth Sci 68:155–166

Lara P, Oyhantçabal P, Dadd K (2016) Post-collisional, late Neoproterozoic, high-Ba-Sr granitic magmatism from the Dom Feliciano Belt and its cratonic foreland, Uruguay: petrography, geochemistry, geochronology and tectonic implications. Lithos 277:178–198

Laux JH, Bongiolo EM, Chemale F Jr, Gross AOMS, Santos TC dos (2010) Reavaliação da idade do complexo granulítico Santa Maria Chico, RS. Resumos, Congresso Brasileiro de Geologia, 45, 2010, Belém

Laux JH, Bongiolo EM, Klein C, Iglesias CMF (2012) Programa de Geologia do Brasil-PGB. Folha Lagoa da Meia Lua, SH.21-Z-B-VI. Estado do Rio Grande do Sul. Carta Geológica. Porto Alegre, CPRM, 1 mapa colorido, Escala 1:100.000

Leite JAD, Hartmann LA, Fernandes LAD, McNaughton NJ, Soliani E Jr, Koester E, Santos JOS, Vasconcellos MAZ (2000) Zircon U–Pb SHRIMP dating of gneissic basement of the Dom Feliciano Belt, southernmost Brazil. J S Am Earth Sci 13:739–750

Lenz C, Fernandes LAD, McNaughton NJ, Porcher CC, Masquelin H (2011) U–Pb SHRIMP ages for the Cerro Bori Orthogneisses, Dom Feliciano Belt in Uruguay: evidences of a ~800 Ma magmatic and a ~650 Ma metamorphic event. Precambrian Res 185:149–163

Lenz C, Porcher CC, Fernandes LAD, Masquelin H, Koester E, Conceição RV (2013) Geochemistry of the Neoproterozoic (800-767 Ma) Cerro Bori orthogneisses, Dom Feliciano Belt in Uruguay: tectonic evolution of an ancient continental arc. Miner Petrol 107:785–806

Li ZX, Bogdanova SV, Collins AS, Davidson A, De Waele B, Ernst RE, Fitzsimons ICW, Fuck RA, Gladkochub DP, Jacobs J, Karlstrom KE, Lu S, Natapov LM, Pease V, Pisarevsky SA, Thrane K, Vernikovsky V (2008) Assembly, configuration, and break-up history of Rodinia: a synthesis. Precambrian Res 160:179–210

Lima EF, Porcher CA, Wildner W (1998) Granulitos da Região da Várzea do Capivarita - Bloco Encruzilhada do Sul, RS. Pesquisas em Geociências 25(1):27–33

Lopes CG, Pimentel MM, Philipp RP, Gruber L, Armstrong R, Junges S (2015) Provenance of the Passo Feio complex, Dom Feliciano Belt: Implications for the age ofsupracrustal rocks of the São Gabriel Arc, southern Brazil. J South Amer Earth Sci 58:9–17

Luft JL Jr, Chemale F Jr, Armstrong R (2011) Evidence of 1.8- to 1.7-Ga collisional arc in the Kaoko Belt, NW Namibia. Int J Earth Sci 100:305–321

Lusa M, Philipp RP, Chemale Jr F, Nardi LVS, Archanjo C (2017) The Paleoproterozoic (Siderian-Rhyacian) continental-arc magmatism of the Encantadas Complex, Santana da Boa Vista, southernmost Brazil and his significance for evolution of the Rio de la Plata Craton. J South Am Earth Sci (Manuscript submitted for publication)

Mallmann G, Chemale F Jr, Ávila JN, Kawashita K, Armstrong RA (2007) Isotope geochemistry and geochronology of the Nico Pérez Terrane, Rio de la Plata Craton, Uruguay. Gondwana Res 12:489–508

Mantovani MSM, de Brito Neves BB (2005) The Paranapanema Lithospheric Block: Its Importance for Proterozoic (Rodinia, Gondwana) Supercontinent Theories. Gondwana Res 8:303–315

Mantovani MSM, Hawkesworth CJ, Basei MAS (1987) Nd and Pb isotope studies bearing on the crustal evolution of southeastern Brazil. Rev Bras Geociências 17:263–268

Martil MMD, Bitencourt MF, Nardi LVS (2011) Caracterização estrutural e petrológica do magmatismo pré-colisional do Escudo Sul-rio- grandense: os ortognaisses do Complexo Metamórfico Várzea do Capivarita. Pesquisas em Geociências 38(2):181–201

Masquelin H, Lara HS, Sánchez-Bettucci L, Demarco PN, Pascual S, Muzio R, Peel E, Scaglia F (2017) Lithologies, structure and basement-cover relationships in the schist belt of the Dom Feliciano Belt in Uruguay. Brazilian J Geol 47(1):21–42

Massonne HJ, Tikovsky T, Hartmann LA (2001) Petrology of the 2.0 Ga old Santa Maria Chico granulites in southern Rio Grande do Sul, Brazil, and implications for crustal thickening in Paleoproterozoic times. In: 11 Congreso Latinoamericano de Geologia, Montevideo

Oriolo S, Oyhantçabal P, Heidelbach F, Wemmer K, Siegesmund S (2015) Structural evolution of the Sarandí del Yí Shear Zone, Uruguay: kinematics, deformation conditions and tectonic significance. Int J Earth Sci 104:1759–1777

Oriolo S, Oyhantçabal P, Basei MAS, Wemmer K, Siegesmund S (2016a) The Nico Pérez Terrane (Uruguay): from Archean crustal growth and connections with the Congo Craton to late Neoproterozoic accretion to the Río de la Plata Craton. Precambrian Res 280:147–160

Oriolo S, Oyhantçabal P, Wemmer K, Basei MAS, Benowitz J, Pfänder J, Hannich F, Siegesmund S (2016b) Timing of deformation in the Sarandí del Yí Shear Zone, Uruguay: implications for the amalgamation of Western Gondwana during the Neoproterozoic Brasiliano–Pan-African Orogeny. Tectonics 35:754–771

Oriolo S, Oyhantçabal P, Wemmer K, Heidelbach F, Pfänder J, Basei MAS, Hueck M, Hannich F, Sperner B, Siegesmund S (2016c) Shear zone evolution and timing of deformation in the Neoproterozoic transpressional Dom Feliciano belt, Uruguay. J Struct Geol 92:59–78

Oriolo S, Oyhantçabal P, Wemmer K, Siegesmund S (2017) Contemporaneous assembly of Western Gondwana and final Rodinia break-up: implications for the supercontinent cycle. Geosci Front. https://doi.org/10.1016/j.gsf.2017.01.009

Oyhantçabal P (2005) The Sierra Ballena shear zone: kinematics, timing and its significance for the geotectonic evolution of southeast Uruguay. PhD Thesis, Georg-August-Universität Göttingen

Oyhantçabal P, Vaz N (1990) Una asociación de cuarcitas y rocas máficas y ultramáficas en los alrededores de Isla Patrulla, Treinta y Tres, Uruguay. In: 1 Congreso Uruguayo de Geología, Montevideo

Oyhantçabal P, Sánchez Bettucci L, Pecoits E, Aubet N, Peel E, Preciozzi F, Basei MAS (2005) Nueva propuesta estratigráfica para las supracorticales del Cinturón Dom Feliciano (Proterozoico Uruguay). In: 12 Congreso Latinoamericano de Geología, Quito

Oyhantçabal P, Siegesmund S, Wemmer K, Frei R, Layer P (2007) Post-collisional transition from calc-alkaline to alkaline magmatism during transcurrent deformation in the southernmost Dom Feliciano Belt (Braziliano–Pan-African, Uruguay). Lithos 98:141–159

Oyhantçabal P, Siegesmund S, Wemmer K, Layer P (2009a) The Sierra Ballena Shear Zone in the southernmost Dom Feliciano Belt (Uruguay): evolution, kinematics, and deformation conditions. Int J Earth Sci. https://doi.org/10.1007/s00531-009-0453-1

Oyhantçabal P, Siegesmund S, Wemmer K, Presnyakov S, Layer P (2009b) Geochronological constraints on the evolution of the southern Dom Feliciano Belt (Uruguay). J Geol Soc London 166:1075–1084

Oyhantçabal P, Siegesmund S, Wemmer K (2011a) The Río de la Plata Craton: a review of units, boundaries, ages and isotopic signature. Int J Earth Sci 100:201–220

Oyhantçabal P, Siegesmund S, Wemmer K, Passchier CW (2011b) The transpressional connection between Dom Feliciano and Kaoko Belts at 580-550 Ma. Int J Earth Sci 100:379–390

Oyhantçabal P, Wegner-Eimer M, Wemmer K, Schulz B, Frei R, Siegesmund S (2012) Paleo- and Neoproterozoic magmatic and tectonometamorphic evolution of the Isla Cristalina de Rivera (Nico Pérez Terrane, Uruguay). Int J Earth Sci 101:1745–1762

Pecoits E, Aubet NR, Heaman LM Philippot P, Rosière C, Veroslavsky G, Konhauser KO (2016) UPb detrital zircon ages from some Neoproterozoic successions of Uruguay: Provenance, stratigraphy and tectonic evolution. J South Amer Earth Sci 71:108–130

Pertille J, Hartmann LA, Philipp RP (2015a) Zircon U–Pb age constraints on the Paleoproterozoic sedimentary basement of the Ediacaran Porongos Group, Sul-Riograndense Shield, southern Brazil. J South Am Earth Sci 63:334–345

Pertille J, Hartmann LA, Philipp RP, Petry TS, Lana CC (2015b) Origin of the Ediacaran Porongos Group, Dom Feliciano Belt, southern Brazilian Shield, with emphasis on whole rock and detrital zircon geochemistry and U–Pb, Lu-Hf isotopes. J South Am Earth Sci 64:69–93

Philipp RP, Campos RS (2004) Geologia, Petrografia e Litogeoquímica dos Gnaisses Porto Alegre, RS, Brasil: Implicações Geotectônicas. Revista Pesquisas em Geociências 31(2):79–94

Philipp RP, Machado R (2005) The Neoproterozoic to Cambrian granitic magmatism of Pelotas Batholith, Southern Brazil. J South Am Earth Sci 19:461–478

Philipp RP, Wild F, Duarte LC, Arend S, Rivera CB, Samberg E, Morales LF, Malmann G (2001) Caracterização litológica, estrutural e condições metamórficas do Complexo Camboriú, Itapema. In: SC. VIII Simpósio Nacional de Estudos Tectônicos, II International Symposium on Tectonics of Brazilian Geological Society, Boletim de Resumos Expandidos, Sociedade Brasileira de Geologia, Recife, vol 1. pp 103–105

Philipp RP, Machado R, Nardi LVS, Lafon JM (2002) O magmatismo granítico Neoproterozóico do Batólito Pelotas no sul do Brasil: novos dados e revisão de geocronologia regional. Revista Brasileira de Geociências 32(2):277–290

Philipp RP, Machado R, Chemale F Jr (2003) Reavaliação e novos dados geocronológicos sobre o Batólito Pelotas: implicações petrogenéticas e idade das zonas de cisalhamento. Boletim do Instituto de Geociências da USP, São Paulo 3:71–84

Philipp RP, Machado R, Chemale Jr F (2007) A Geração dos granitóides Neoproterozóicos do Batólito Pelotas: evidências dos isótopos de Sr e Nd e implicações para o crescimento continental da porção sul do Brasil. In: 50 anos de Geologia. Instituto de Geociências. Contribuições, Ianuzzi R, Frantz JC (eds.) Porto Alegre, Editora Comunicação e Identidade, CIGO, IG-UFRGS 1:59–77

Philipp RP, Lusa M, Nardi LVS (2008) Geochemistry and petrology of dioritic, tonalitic and trondhjemitic gneisses from Encantadas Complex, Santana da Boa Vista, southernmost Brazil, a Paleoproterozoic continental-arc magmatism. An Acad Bras Ciênc 80:1–14

Philipp RP, Massone HJ, Campos RS (2013) Peraluminous leucogranites of Cordilheira Suite,record of Neoproterozoic collision and generation of Pelotas Batholith, Dom Feliciano Belt, southern Brazil. J S Am Earth Sci 43:8–24

Philipp RP, Massonne HJ, Theye T, Campos RS (2009) U-Th-Pb EPMA geochronology of polygenetic monazites of the metapelite migmatitic gneisses of Camboriú Complex, SC, Southern Brazil: evidences for the collisional and post-collisional events in Dom Feliciano Belt. Simpósio 45 anos de geocronologia no Brasil, São Paulo. Boletim de Resumos Expandidos, EDUSP 1:289–291

Philipp RP, Formoso MLL, Dossin I, Chemale F Jr, Campos RS (2010) Estruturas primárias e tectônicas do Anortosito Capivarita, Pântano Grande, RS: significado e implicações para o entendimento da evolução petrológica. Revista Brasileira de Geociências 40(1):99–110

Philipp RP, Pimentel MM, Chemale F Jr (2016a) Tectonic evolution of the Dom Feliciano belt in Southern Brazil based on geological relationships and U–Pb geochronology. Brazilian J Geol 46(1):83–104

Philipp RP, Bom FM, Pimentel MM, Junges SL, Zvirtes G (2016b) SHRIMP U–Pb age and high temperature conditions of the collisional metamorphism in the Várzea do Capivarita Complex: implications for the origin of Pelotas Batholith, Dom Feliciano Belt, southern Brazil. J South Am Earth Sci 66:196–207

Philipp RP, Girelli TG, Lopes RC, Sander A (2017a) Geologia do Complexo Granulítico Santa Maria Chico, Dom Pedrito, RS: significado tectônico e implicações sobre a evolução do Cráton Rio de La Plata. Boletim do Instituto de Geociências USP, (Manuscript submitted for publication).

Philipp RP, Quintela O, Bruckmann MP, Lana CC (2017b) U–Pb and Lu-Hf zircon geochronology and geochemistry of the qzo-feldspatic (meta-arenites) gneisses and metagranites of the Santa Maria Chico Granulitic Complex, Dom Pedrito (RS, Brazil) and his tectonic significance and implications on the evolution of the Rio de la Plata Craton. J South Am Earth Sci, (Manuscript submitted for publication).

Philipp RP, Pimentel MM, Basei MAS (2018) The Tectonic Evolution of the São Gabriel Terrane, Dom Feliciano Belt, Southern Brazil: The Closure of the Charrua Ocean. In: S. Siegesmund et al. (eds) Geology of southwest gondwana, Regional geology reviews, Springer, Heidelberg, pp 243–265

Poiré D, Gaucher C (2009) Lithostratigraphy. Neoproterozoic-Cambrian evolution of the Río de la Plata Palaeocontinent. In: Gaucher, C, Sial, AN, Halverson, GP, Frimmel, HE (eds) Neoproterozoic-Cambrian tectonics, globalchange and evolution: a focus on southwestern Gondwana. Developments in Precambrian Geology, 16, Elsevier, pp 87–101

Poiré DG, González PD, Canalicchio JM, García Repetto F (2003) Litoestratigrafía y estromatolitos de la sucesión sedimentaria Precámbrica de la cantera Mina Verdún, Minas, Uruguay. Rev Soc Uruguaya Geol 108–123

Poiré DG, González PD, Canalicchio JM, García Repetto F, Canessa ND (2005) Estratigrafía del Grupo Mina Verdún, Proterozoico de Minas, Uruguay. Lat Am J Sedimentol Basin Anal 12:125–143

Porcher CC (1992) Caracterização das condições de fluxo em uma zona de cisalhamento tangencial na região de Santana da Boa Vista (RS). Unpublished MSc Thesis, Universidade Federal do Rio Grande do Sul, p 192

Porcher CC, McNaughton NJ, Leite JAD, Hartmann LA, Fernandes LAD (1999) Idade U–Pb SHRIMP em zircão do vulcanismo ácido do Complexo Metamórfico Porongos. In: 1 Simpósio sobre vulcanismo e ambientes associados, Gramado. Boletim de Resumos. São Paulo: Sociedade Brasileira de Geologia

Preciozzi F, Spoturno J, Heinzen W (1979) Carta geo-estructural del Uruguay, escala 1:2.000.000. Instituto Geológico Ing. Terra Arocena, Montevideo

Preciozzi F, Spoturno J, Heinzen W, Rossi P (1985) Carta Geológica del Uruguay a escala 1:500.000. Dirección Nacional de Minería y Geología, Montevideo

Rapalini AE, Tohver E, Sánchez-Bettucci L, Lossada AC, Barcelona H, Pérez C (2015) The late Neoproterozoic Sierra de las Ánimas Magmatic Complex and Playa Hermosa Formation, southern Uruguay, revisited: paleogeographic implications of new paleomagnetic and precise geochronologic data. Precambrian Res 259:143–155

Rapela CW, Fanning CM, Casquet C, Pankhurst RJ, Spalletti L, Poiré D, Baldo EG (2011) The Río de la Plata craton and the adjoining Pan-African/brasiliano terranes: Their origins and incorporation into south-west Gondwana. Gondwana Res 20:673–690

Saalmann K, Gerdes A, Lahaye Y, Hartmann LA, Remus MVD, Läufer A (2011) Multiple accretion at the eastern margin of the Rio de la Plata craton: the prolonged Brasiliano orogeny in southernmost Brazil. Int J Earth Sci 100:355–378

Sánchez-Bettucci L (1998) Evolución Tectónica del Cinturón Dom Feliciano en la región Minas-Piriápolis, República Oriental del Uruguay. PhD Thesis, Universidad de Buenos Aires

Sánchez-Bettucci L, Oyhantçabal P, Page S, Ramos VA (2003) Petrography and geochemistry of the Carapé Granitic Complex (southeastern Uruguay). Gondwana Res 6:89–105

Sánchez-Bettucci L, Oyhantçabal P, Loureiro J, Ramos VA, Preciozzi F, Basei MAS (2004) Mineralizations of the Lavalleja group (Uruguay), a probable neoproterozoic volcano-sedimentary sequence. Gondwana Res 6:89–105

Santos JOS, Hartmann LA, Bossi J, Campal N, Schipilov A, Piñeyro D, McNaughton NJ (2003) Duration of the Trans-Amazonian Cycle and its correlation within South America based on U–Pb SHRIMP geochronology of the La Plata Craton, Uruguay. Int Geol Rev 45:27–48

Silva LC, Hartmann LA, McNaughton NJ, Fletcher IR (1999) SHRIMP U–Pb zircon dating of Neoproterozoic granitic magmatism and collision in the Pelotas batholith, southernmost Brazil. Int Geol Rev 41:531–551

Silva LC, Hartmann LA, McNaughton NJ, Fletcher IR (2000) Zircon U/Pb SHRIMP dating of a Neoproterozoic overprint in Paleoproterozoic granitic-gneissic terranes, southern Brazil. Am Min 85:649–668

Soliani Jr E (1986) Os dados geocronológicos do escudo Sul-rio-grandense e suas implicações de ordem geotectônica. Ph. D. thesis. Instituto de Geociências. Universidade de São Paulo, p 425. http://www.teses.usp.br/teses/disponiveis/44/44131/tde-15072015-153916/publico/Soliani_Junior_Doutorado.pdf. https://doi.org/10.11606/T.44.1986.tde-15072015-153916

Spoturno J, Oyhantçabal P.,Faraone M (2017) Mapa geológico del Departamento de Lavalleja, a escala 1:100000. Facultad de Ciencias —DINAMIGE (*in press*)

Tack L, Wingate MTD, De Waele B, Meert J, Belousova E, Griffin B, Tahon A, Fernandez-Alonso M. (2010) The 1375 Ma "Kibaran event" in Central Africa: Prominent emplacement of bimodal magmatism under extensional regime. Precambr Res 180:63–84

Tohver E, D'Agrella Filho MS, Trindade RIF (2006) Paleomagnetic record of Africa and South America for the 1200-500 Ma interval, and evaluation of Rodinia and Gondwana assemblies. Precambrian Res 147:193–222

Tommasi A (1991) Evolução cinemática do Cinturão Dom Feliciano durante o Ciclo Brasiliano, Unpublished MsSc Thesis. Instituto de Geociências, UFRGS, Porto Alegre, p 207

8 The Luis Alves and Curitiba Terranes: Continental Fragments in the Adamastor Ocean

Claudia Regina Passarelli, Miguel Angelo Stipp Basei, Oswaldo Siga Jr., and Ossama Mohamed Milah Harara

Abstract

The Luis Alves and Curitiba terranes represent pre-existent continental fragments of unknown origin involved in the Adamastor closure during the Western Gondwana assembly. These basement domains separate the low- to medium-grade Ribeira and Dom Feliciano belts that were generated as a result of the convergence of São Francisco, Paranapanema, Rio de la Plata, Congo and Kalahari Cratons. The Paleoproterozoic Luis Alves Craton is composed of a TTG suite, mafic-ultramafic bodies and a few paragneiss remnants representing a crustal block that had already been cold since the Paleoproterozoic. The Curitiba terrane comprises Paleoproterozoic migmatites and amphibole-gneissic rocks that underwent intense deformation and migmatization during the Neoproterozoic. The Pien magmatic arc was generated around 610 Ma as a result of the oceanic crust consumption that existed between the Luis Alves and Curitiba terranes. The culmination of the compressional process was the collision of these blocks in a few million years. The juxtaposition of the Luis Alves and Curitiba domains was already finished around 590 Ma when post-tectonic granitoids were emplaced. The northeast-trending Pien-Suture Zone is the limit between these crustal segments.

Keywords

Luis Alves and Curitiba terranes • Brasiliano-Pan African orogeny • Granulitic complex • Gneiss-migmatitic rocks

8.1 Introduction

The closure of the Adamastor Ocean during the Brasiliano-Pan African orogeny involved the interaction between the São Francisco, Paranapanema, Congo and Kalahari cratons and several terranes (Fig. 8.1a). The resulting Mantiqueira Province (MP), which exhibits mainly northeast structural trends, includes the Araçuaí, Ribeira and Dom Feliciano fold belts (Fig. 8.1b). The largest geotectonic unit of the MP (Fig. 8.1) is the Ribeira Belt (RB), which occupies the southeastern part of this large domain (Almeida et al. 1981; Heilbron et al. 2004; Silva et al. 2005). The RB consists of several tectonic domains limited either by thrust or transpressive shear zones juxtaposed at Ediacaran time (Fig. 8.1b). The Northern and Central Ribeira belt comprise the Occidental, Paraíba do Sul-Embú, Oriental (Serra do Mar Microplate) and Cabo Frio terranes (Rio de Janeiro and southern Espírito Santo states (Heilbron et al. 2004; Tupinambá et al. 2012). Socorro, Apiaí, Embú and Curitiba terranes in São Paulo and Paraná states compose the Southern Ribeira belt (Campos Neto 2000; Basei et al. 2009b; Siga Jr et al. 2011a, b).

The understanding of the juxtaposition history of these different domains, many of them displaying only deep structural levels, is hard to recognize by the presence of significant crustal-scale shear zones, whose resulting displacements are poorly known. Supracrustal terranes to the north, Embu and Apiaí, are separated by the Cubatão–Itariri Shear System (CISS) from the granite-gneissic migmatitic terranes that occur to the south (Mongaguá Domain and Curitiba Terrane-Registro Domain) (Fig. 8.1b).

The central portion of the Mantiqueira Province in the south-southeastern region of Brazil incorporates four tectonic domains, juxtaposed between 600 and 570 Ma as part of the western Gondwana assembly processes (Fig. 8.1b). Two of the four major domains are constituted of gneissic-migmatitic rocks represented by the Neo-Archean Luís Alves and Paleoproterozoic Curitiba Microplates, which separate the Neoproterozoic Ribeira belt to the northwest and

C. R. Passarelli (✉) · M. A. S. Basei · O. Siga Jr.
Instituto de Geociências—Universidade de São Paulo, São Paulo, Brazil
e-mail: cr.passarelli@usp.brcr_passarelli@hotmail.com

O. M. M. Harara
Instituto de Geociências—Universidade Federal do Paraná, Curitiba, Brazil

S. Siegesmund et al. (eds.), *Geology of Southwest Gondwana*, Regional Geology Reviews,
https://doi.org/10.1007/978-3-319-68920-3_8

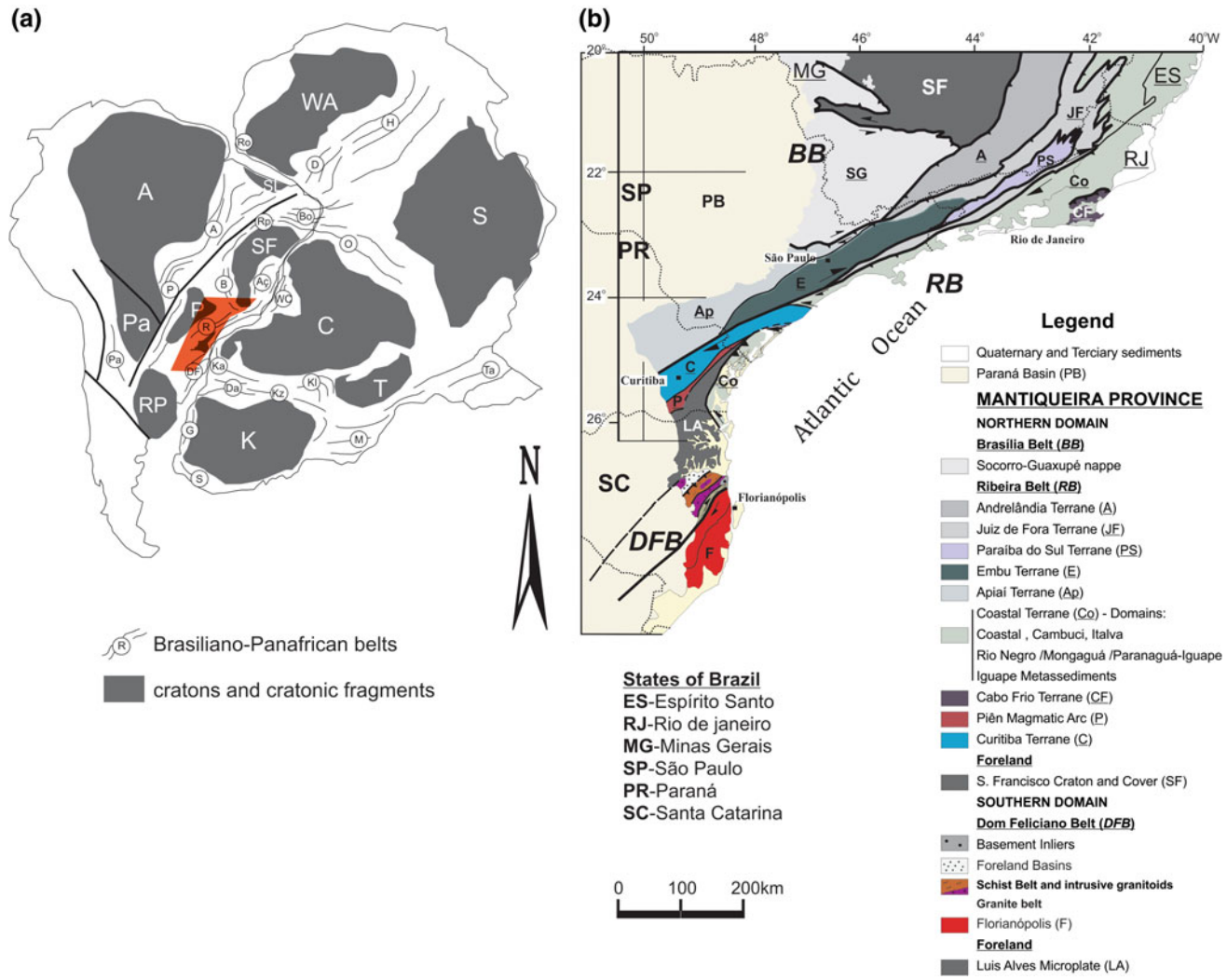

Fig. 8.1 **a** Reconstruction of West Gondwana after Abdelsalam et al. (2002), Mantovani and Brito Neves (2005), Heilbron et al. (2008), Vaughan and Pankhurst (2008), Rapela et al. (2011) and Cordani et al. (2013), showing cratonic and Brasiliano–Panafrican components. Cratons shown in grey: *A* Amazonia; *C* Congo; *K* Kalahari; *LA* Luis Alves, *P* Paranapanema, *SF* São Francisco; *WA* West Africa. Brasiliano–Panafrican belts (ringed): *Bo* Borborema; *Rp* Rio Preto; *A* Araguaia; *Aç* Araçuaí; *P* Paraguai; *B* Brasília; *R* Ribeira; *DF* Dom Feliciano; *Pa* Pampean; *H* Hoggar; *D* Dahomey; *Ro* Rockelides; *O* Oubangides; *Ta* Tanzania; *WC* West Congo; *Ka* Kaoko; *Da* Damara; *K/Z* Katangan/Zambezi; *Kl* Katanga-Lufilian Arc; *M* Mozambique; *G* Gariep; *S* Saldania. Location of the Mantiqueira Province is shown. **b** General outline of part of the Mantiqueira Province. Simplified from Campos Neto and Figueiredo (1995), Basei et al. (1999, 2000), Heilbron et al. (2004), Tupinambá et al. (2007), Passarelli et al. (2011)

the Dom Feliciano belt to the southeast. The Ediacaran Piên Domain composed of granitoids and an ultramafic sequence occurs between Luis Alves and Curitiba Terranes (Basei et al. 2000, 2008). The other segment occurs in the coastal region, being represented by the Ediacaran Costeiro Granitic Belt (Siga Jr et al. 1993; Cury 2009), and constituted by a variety of granitoids and supracrustal remnants.

The main purpose of this contribution is to summarize and evaluate the geological evolution of the Luis Alves and Curitiba Terranes. Several important open questions resulting from this evaluation will be discussed here.

8.2 Geological Setting

The tectonic structure of the southern Ribeira Belt (São Paulo and Paraná states) comprises several tectonostratigraphic terranes defined as Apiaí, Embú, Curitiba and Luis Alves Cratons (Campos Neto 2000).

The Apiaí and Embu terranes, part of the Ribeira Belt (RB), are composed of Mesoproterozoic to Neoproterozoic metasedimentary successions deposited on the eastern margin of the Paranapanema paleocontinent. In the Neoproterozoic the RB, as an active margin, was intensely affected by calcalkaline magmatism represented by granitic batholiths that constitute the roots of the Três Córregos, Cunhaporanga and Agudos Grandes magmatic arcs. The main metamorphism and deformation superimposed also occurred at this time (Basei et al. 1992; Siga Jr et al. 2009).

The Embu terrane is composed of several units of different ages with partially migmatized mica schists, paragneisses and quartzite (Hasui 1975; Cordani et al. 2002). Several Neoproterozoic orthogneisses with predominantly high-K calcalkaline and peraluminous signatures intrude these units (Janasi et al. 2003; Alves et al. 2016). The Rio Capivari Complex is recorded in the northern portion of this terrane and comprises the stretched Paleoproterozoic basement inliers composed mainly of metatexitic orthogneisses and amphibolitic rocks, consistently reworked by the Brasiliano Orogeny (Babinski et al. 2001; Meira et al. 2015; Maurer et al. 2015). Isotopic evidence suggests that the Rio Capivari Complex was not the basement of the metasedimentary sequence of the Embu Complex (Benetti Silva 2017). Passarelli et al. (2018) suggest that the orthogneisses and amphibolitic rocks of the Rio Capivari Complex and Curitiba Terrane may have constituted a single microplate before 600 Ma.

The Lancinha-Cubatão-Itariri Shear Zone (LCISZ) is interpreted as a suture between the Curitiba Terrane to southeast and Ribeira Belt (Embu/Apiaí terranes) to the northwest (Basei et al. 1998b, 2008; Passarelli et al. 2011). In turn, the Itariri Shear Zone separates the Curitiba Terrane (Registro and Itatins Complexes) from the Coastal Terrane (Fig. 8.1b).

Fiori (1990) and Fassbinder et al. (1994) described related structures to the Lancinha shear zone using simple shear and Riedel models, and recognized ductile-brittle transpressive character and an average dextral displacement of 100–140 km.

From seismic anisotropy data, Assumpção et al. (2001) suggest that the high-angle foliation and subhorizontal lineation of the system spreads on all crust reaching the upper mantle, consequently characterizing a lithospheric scale for this shear zone.

However, the absence of the geophysical signature corresponding to this shear zone would be explained by the progression of the strike-slip (Faleiros 2008) and the consequent modification of its geophysical answer (Castro et al. 2014; Castro and Ferreira 2015). Thus the LCISZ would be the record of a Neoproterozoic collision (suture), modified by the progression of shear, setting the boundary between the Curitiba and Apiaí as a mainly dextral shear zone.

Granulite-migmatitic rocks that constitute the basement of the Curitiba microplate were grouped into the Atuba Complex (Siga Jr et al. 1995) defined in the Paraná state. Neoproterozoic metasedimentary rocks covering the northern part of the Atuba Complex composed of dolomitic marble, quartzite and subordinated phyllite characterized the Turvo-Cajati, Setuva and Capiru Sequences (Basei et al. 2008; Faleiros et al. 2011). In the southeast of São Paulo state, the Registro Domain was correlated to the Atuba Complex (Passarelli et al. 2004, 2007) and is represented mainly by granite-gneissic-migmatitic and paragneissic rocks. Nevertheless, despite its lithological and geochronological similarities, important distinguishing characteristics occur in Registro Domain as Calymmian extensional and Tonian metamorphic events.

Within the basement gneisses, nuclei of high metamorphic-grade rocks of predominantly charno-enderbitic composition are preferentially distributed in the northern portion of these terranes. The best exposition occurs in the Peruíbe region (Itatins Massif), southeastern São Paulo State and the Paulo Leminski Quarry, in Curitiba City, Paraná state.

The Curitiba and Luis Alves terranes are separated by the northeast-trending Piên shear zone (Siga Jr et al. 1995). Two important units occur in the area (Harara 2001): the Piên--Mandirituba granite belt characterized by arc-related granitoids and the Piên mafic-ultramafic suite, interpreted as an incomplete ophiolite suite. These units are evidence of a suture zone and a record of a northwestward subduction (Basei et al. 2000).

The Luis Alves Terrane consists of medium to high-grade metamorphic granulitic gneisses (Basei et al. 1992, 1998a, b). Subordinate migmatites, granites and basic and ultramafic rocks occur, besides calc-silicate gneisses, kinzigites, iron formations and quartzites (Cury 2009). The Archean to Paleoproterozoic basement rocks are orthogneisses characterized by alternating quartz-feldspatic and mafic bands affected by granulite facies metamorphism. The gneisses predominantly have TTG geochemical affinity, with some mafic components and metasedimentary contributions (Basei et al. 1998a).

The Dom Feliciano Belt in the Santa Catarina State is characterized by three tectonic domains described from east-southeast to north-northwest (Basei et al. 2000, 2005, 2008): (1) Eastern Granitoid Belt, which comprises the calcalkaline Florianópolis Batholith and represents the roots of a Neoproterozoic magmatic arc; (2) Supracrustal Schist

Belt, composed of the Brusque Group, a low-grade metavolcanosedimentary sequence with northwestward tectonic transports, intruded by several late- to post-tectonic granitoids; and (3) Foreland basin, represented by a thick pack of sedimentary (mostly turbidites) rocks filling the Itajaí Basin, less affected by deformation and metamorphism than the adjacent Schist Belt.

8.3 Luis Alves Terrane

Three main distinct units compose the Luis Alves terrane: an Archaean to Palaeoproterozoic migmatitic granitic-gneissic basement (Hartmann et al. 1979, 2000; Basei et al. 1998a), a Neoproterozoic cover composed of volcanosedimentary basins and A-type alkaline-peralkaline granitoids (Fig. 8.2).

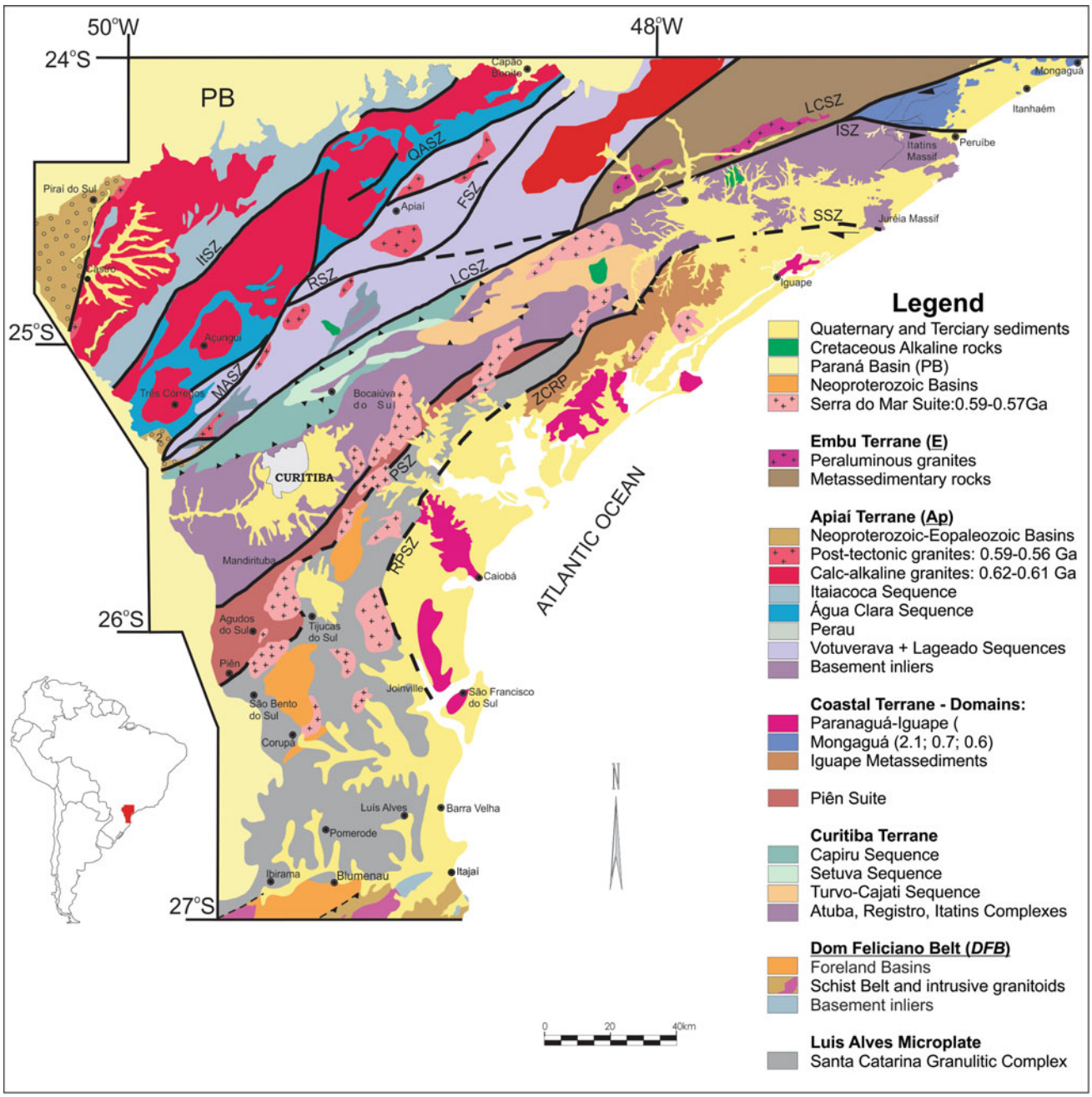

Fig. 8.2 Tectonic and geological sketch of the south-southeast Brazilian Precambrian terranes. Tectonic subdivision of the South-central portion of the Ribeira Belt. (Modified from Basei 2000; Basei et al. 1992, 2000; Campos Neto and Figueiredo 1995.)

Fig. 8.3 Granulite gneiss migmatitic rocks from Santa Catarina Granulitic Complex (LAT): **a** ultramafic granulite gneiss; **b** banded and folded tonalitic amphibole gneiss with pink veined axial plan pegmatoids; **c** banded gneiss with highly plastic ductile deformation; **d** charnockites strongly retrogressed; **e** banded gneiss with transposition foliation; and **f** detail of massif charnockite

8.3.1 Basement Rocks–Santa Catarina Granulitic Complex

The typical basement rocks included in the Santa Catarina Granulitic Complex (Hartmann et al. 1979) are Archean to Paleoproterozoic hypersthene orthogneisses, migmatites and granitic rocks (Fig. 8.3).

The southern portion of the Santa Catarina Granulitic Complex is composed mainly of biotite-amphibole gneisses and migmatites with biotite-bearing mesosome and pink granitic leucosome, together with porphyritic biotite granites and pink mylonitic leucogranites. Charnockitic-enderbitic rocks occur rarely. The central domain is characterized by charnockitic-enderbitic gneisses with predominantly tonalitic-granodioritic compositions. A conspicuous characteristic of this domain is the presence of basic and ultrabasic rocks (pyroxenites, metagabbros, amphibolites and magnesian schists), which in some places (e.g., Barra Velha-SC state) constitute the predominant rock type (Basei et al. 2009b).

The north-northwestern portion as in other segments of the complex is characterized by the majority of Palaeoproterozoic orthogneisses. Among the several rock types are greenish-grey, mafic amphibole-biotite gneisses with orthopyroxene relicts, mafic granulites with associated charnockitic-enderbitic portions, and subordinate lenses of amphibolitic schists, serpentinites, garnet-rich amphibolites, amphibolitic gneisses and felsic granulites (Basei et al. 2009b).

The orthogneisses are greenish-grey, usually leuco- to mesocratic and fine- to medium-grained affected by granulite facies metamorphism followed by an amphibolite facies retrograde metamorphic event (Fig. 8.3d), and then by the development of greenschist facies mineral assemblages along shear zones (Basei et al. 1998a). These gneisses predominantly have TTG geochemical affinity, with some mafic components and metasedimentary contributions (Basei et al. 1998a). Structures trend predominantly northwest-southeast.

8.3.2 Neoproterozoic Units

The Neoproterozoic units of the Luis Alves Terrane exhibit evident contrasts with the gneissic rocks of the Santa Catarina Granulitic Complex concerning metamorphism and deformation. These units either lie discordantly on top of or are clearly intrusive into the gneisses. The cover units are represented by the volcanosedimentary Campo Alegre, Corupá and Guaratubinha basins. Anorogenic alkaline-peralkaline granitoids are intrusive into the gneiss rocks (Basei et al. 1998b, 2009b).

8.3.2.1 Extensional Late Collision Basins

The lower sedimentary sequence of Campo Alegre basin was divided into two facies, one conglomeratic and the other arenaceous (Fig. 8.4a). The lower volcanic sequence is composed of basalts and andesites with rare dacites and more differentiated rhyodacites and quartz-trachytes. The intermediate sedimentary sequence consists mainly of pyroclastic (Fig. 8.4b, c) and fine-grained epiclastic sediments. The upper sedimentary sequence has a transitional contact with the underlying pyroclastic rocks. There is a predominance of fine-grained tuffs intercalated with less abundant fine-grained epiclastic rocks at the base (Fig. 8.4d).

The sedimentary filling of the Corupá Basin is similar to that of the Campo Alegre basin, but several authors have noted that the rocks of this graben are more intensely deformed than those of the Campo Alegre basin. Except for the lower volcanic sequence, all units of the Campo Alegre basin are present in the Corupá basin. In the graben, the intermediate sedimentary sequence has a small pyroclastic component, whereas such rocks are common in the upper sedimentary sequence.

The sediments of Guaratubinha basin and associated intermediate to acid volcanic rocks are in angular unconformity with underlying migmatites and granites. Arkoses are predominant, siltstones and claystones form intercalations, and conglomerates are present in isolated occurrences. The rudaceous rocks seem to occupy the base of the sequence, and are ortho-conglomerates with clasts of a range of dimensions, derived from a variety of source rocks including acid volcanics, in an arkosic matrix with quartz, alkaline and plagioclase feldspars, opaque and other minerals. The conglomerates have poorly defined stratification.

8.3.2.2 Foreland Basin

In contrast to the extensional Campo Alegre Basin, the Itajaí Basin evolved under an overall convergent regime. It consists of a thick package of sedimentary rock, with significant turbiditic contribution, besides important felsic volcanic activity, common throughout its evolution, culminating with the emplacement of the Cambrian Subida Granite (Fig. 8.5a).

Its sediments are interpreted to have been deposited in the Dom Feliciano foreland basin, the southern border of which underwent thrusting and folding, resulting from late deformations that affected the Brusque Group (Dom Feliciano Belt). Most studies of the Itajaí Basin (Salamuni et al. 1961; Silva and Dias 1981; Appi and Cruz 1990; Rostirolla 1991; Basei et al. 2011) recognize the existence of two main units, from bottom to top: a predominantly psammitic unit with intercalations of conglomerates (Fig. 8.5b) and acid tuffs,

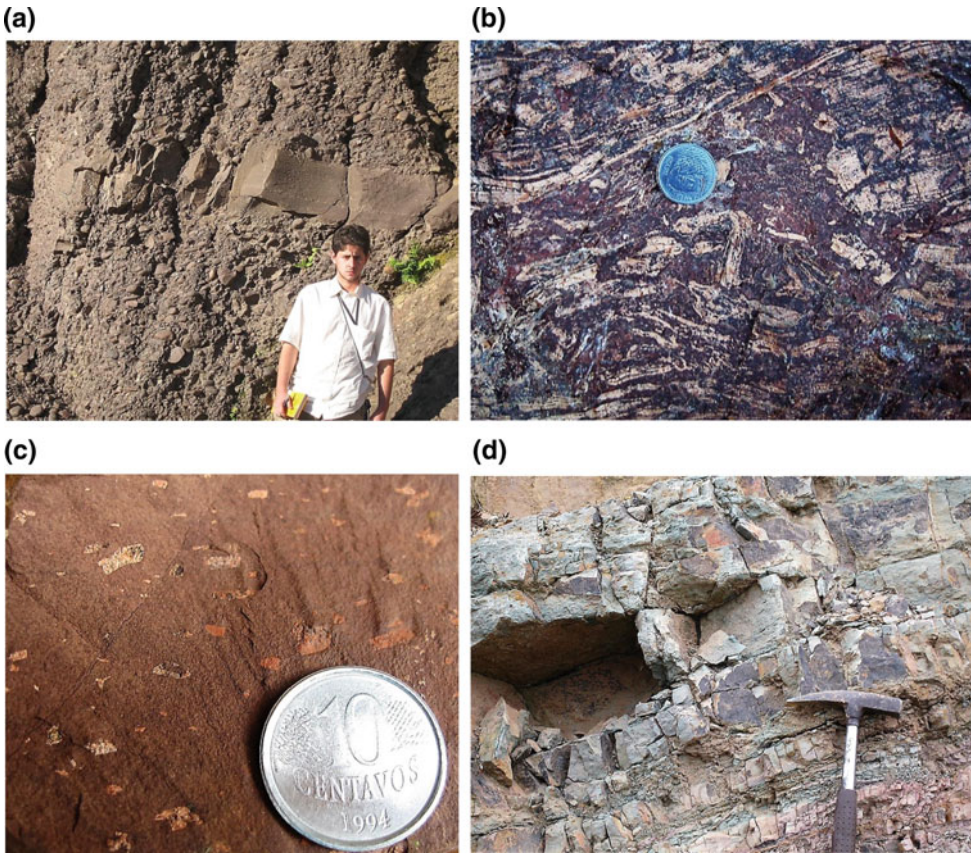

Fig. 8.4 Campo Alegre volcanosedimentary basin: **a** sandstone layer intercalated in thick conglomerate of the basal unit; **b** common aspect of the ignimbrite flows with many gas tubes frequently observed in the surroundings of São Bento do Sul- Santa Catarina State; **c** welded tuffs of the intermediate volcanic unit with feldspar antecrystals; and **d** outcrop with predominance of volcanic ash falls layer from the intra-caldera upper unit

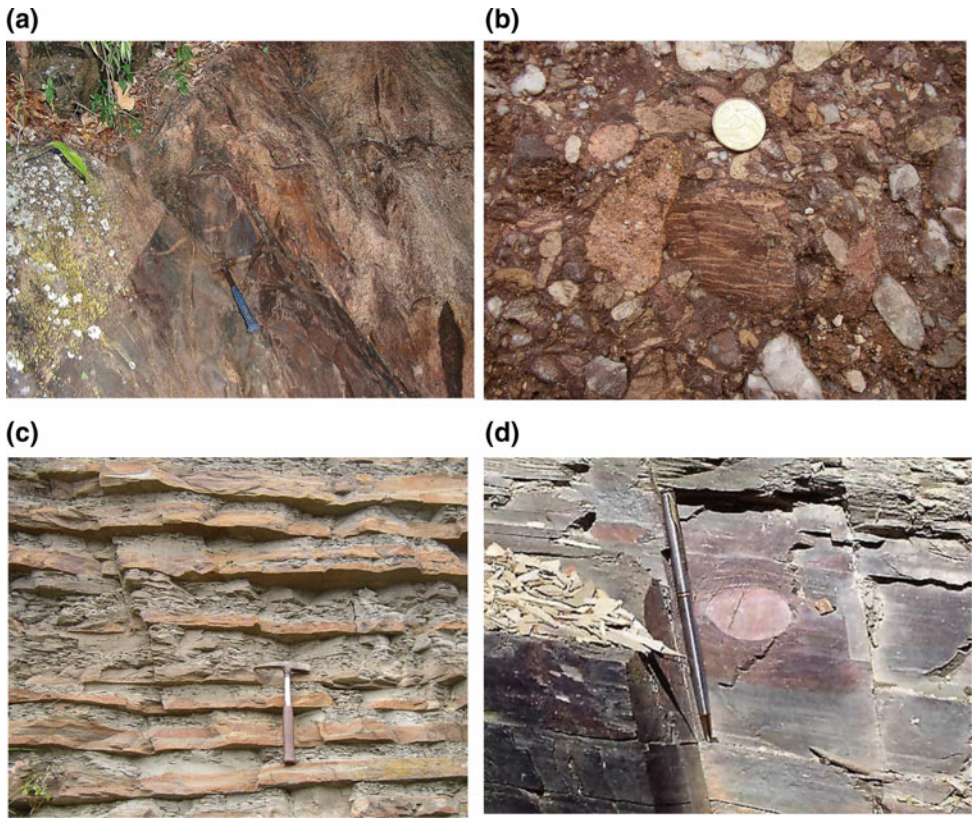

Fig. 8.5 **a** Xenoliths of laminated siltstones in the Subida Granite confirming its intrusive character; **b** normal appearance of the polymictic conglomerates of the basal unit; **c** rithymites with alternation of fine siltstones and sandstones of the turbiditic sequence; and **d** rare pebble (drop-stone) observed in upper siltic unit

and a finer and more distal pelitic-psammitic one with abundant rhythmites (Fig. 8.5c). The continental lower sequence, Baú Formation, grades laterally and towards the top to the upper marine sequences: the Ribeirão Carvalho, Ribeirão Neisse and Ribeirão do Bode Formations (Basei et al. 2011). Predominantly acid volcanic and subvolcanic rocks are more abundant than the pyroclasts, and are intercalated within the sediments of the top of the sequence (Fig. 8.5d).

8.4 Curitiba Terrane

The Curitiba Terrane, located between the Luis Alves and the Paranapanema cratonic fragments (Fig. 8.1), is constituted by distinct units: the Atuba Complex (AC), Registro Complex (RC), Itatins Complex (IC) and the metasedimentary assemblages. South of the Lancinha Shear Zone, the Atuba Complex defined in Paraná state exemplifies the Curitiba Terrane basement (Basei et al. 2009a). This complex is covered by low-grade Meso-Neoproterozoic metavolcanosedimentary sequences (Capiru, Setuva and Turvo-Cajati) and has been intruded by anorogenic alkaline-peralkaline granitoids of the Serra do Mar Suite/Graciosa Province (Siga Jr et al. 1999; Kaul and Cordani 2000; Gualda and Vlach 2007; Basei et al. 2009b). The Registro Complex, defined in São Paulo state, has already been correlated to the Atuba Complex by Passarelli et al. (2007). In this work, we correlate the Itatins Complex with the other two complexes.

The contact between the Curitiba and Luís Alves terranes is marked by the Piên Suture Zone (Fig. 8.2) characterized by deformed arc-related calcalkaline granitoids where basic and ultrabasic rocks are present. The roots of this Neoproterozoic magmatic arc lying between these Terranes are thought to be an Ediacaran active margin, where oceanic crust was consumed (Basei et al. 1992, 2009b; Machiavelli et al. 1993; Harara 2001).

8.4.1 Basement Units–Atuba, Registro and Itatins Complexes

The Atuba Complex (AC) is composed of Rhyacian banded biotite-amphibole gneisses, amphibolites and a variety of granitoids, which underwent medium- to high-grade metamorphism associated with extensive remigmatization (Siga Jr et al. 1995; Sato et al. 2003).

The mesosome is represented by leuco to mesocratic gray biotite-amphibole-gneisses; medium-grained, with granodioritic, monzodioritic to quartz-dioritic composition. The first migmatization phase of leucosomes is foliated and folded, occurring as millimetre to centimetre white tonalitic to granodioritic bands parallel to the main foliation (Fig. 8.6a, d). Pinkish segregations of granitic to alkali-feldsphatic granite composition occur concordant

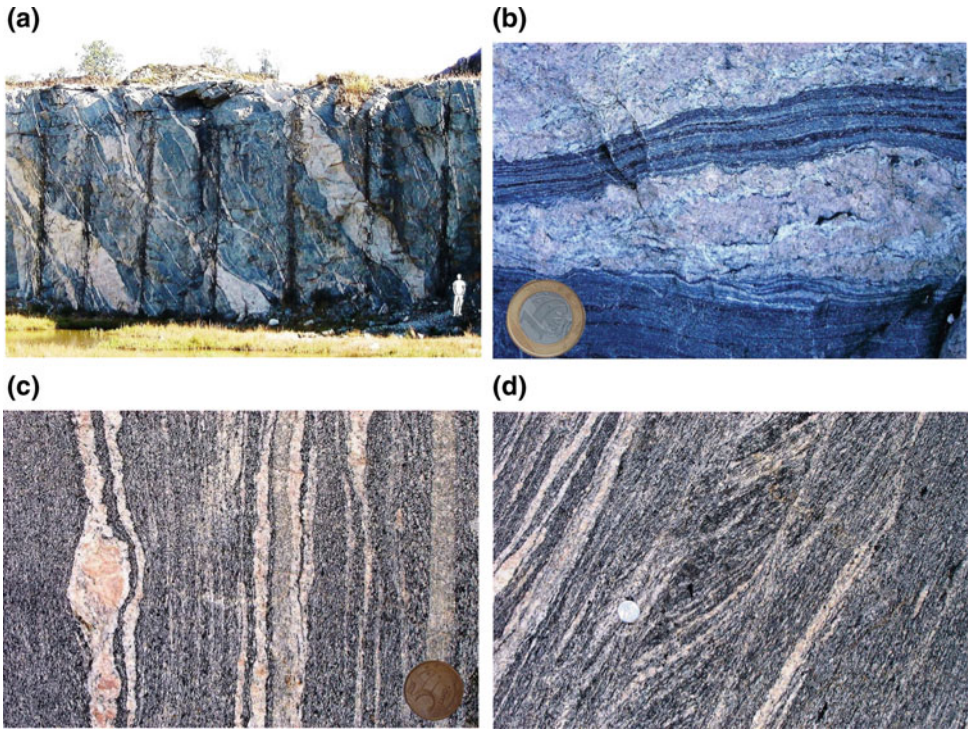

Fig. 8.6 Gneiss-migmatitic rocks from Atuba Complex: **a** Atuba Quarry large outcrop north of Curitiba city showing remigmatization (pinkish leucosome); **b** detail of banded migmatite with Paleoproterozoic anphibole-biotite gneiss and Neoproterozoic leucossomatic pink granitoid; **c** banded gneiss with pink granite injections; and **d** banded gneiss with clear evidence of transposition of previous foliation

with the regional gneissic banding, indicating a migmatitic structure with Neoproterozoic ages. A previous foliation can be recognized in banded gneiss (Fig. 8.6d) evidenced by intense transposition. The leucosomes of the second migmatitic phase are slightly foliated to frankly isotropic (Fig. 8.6a–c).

Among the migmatitic gneisses is the usual occurrence of magnesian schists, mangerites, jotunites, foliated norites and mafic-ultramafic rocks. The AC rocks show a north-northeast-trending steeply dipping mylonitic foliation parallel to the gneissic foliation and a shallowly south-southwest plunging stretching lineation (Siga Jr et al. 1995; Faleiros et al. 2011).

The Registro Complex (RC) was characterized south of the Cubatão and Itariri shear zones (Passarelli 2001; Passarelli et al. 2004). The RC is represented mainly by Paleoproterozoic biotite-amphibole gneisses, migmatites and a variety of granitoids (Fig. 8.7). Calymmian gabbro-dioritic dykes intrude Rhyacian amphibole-biotite granodiorites (Fig. 8.7a) and both are extremaly deformed and migmatized (Fig. 8.7b). The Neoproterozoic regional metamorphism and deformation result in a succession of diverse migmatitic rocks, metatexites and diatexites with several complex structures with different proportions of neosomes. Notably agmatic (Fig. 8.7c), phlebitic (Fig. 8.7d), surreitic (Fig. 8.7e), schlieren (Fig. 8.7f), and schollen (Fig. 8.7g) structures and folded-layer structured (Fig. 8.7h) migmatites are observed. A record of gneissic foliation trending northwest is observed, although northeast and east–west mylonitic foliation, parallel to the Itariri and Cubatão shear zones trend with moderately to steeply north-northwest dipping, predominates.

The Itatins Complex (IC) (Silva et al. 1978; Dantas et al. 1987; Picanço et al. 1998) was described south of the Itariri shear zone. This massif is composed of kinzigites, kinzigitic gneiss and amphibolites (Cachoeira Sequence), enderbites and charnoenderbites (Itatins Suite), in association with melanocratic granitoids and migmatitic rocks (Fig. 8.8).

8.4.2 Metasedimentary Units

The Neoproterozoic metasedimentary assemblages interpreted as a shallow continental shelf (Faleiros et al. 2011) are represented by the Turvo-Cajati Complex, Setuva and Capiru Formations (Siga Jr et al. 2012) and are in tectonic contact with the gneiss-migmatitic Atuba Complex.

The Setuva (SF) and Capiru (CF) Formations correspond to a greenschist to amphibolite facies metasedimentary cover. According to Bigarella and Salamuni (1956), SF would be covered by the CF in angular unconformity. There is no consensus in relation to stratigraphic position of the SF, but some studies propose that SF could represent a related CF tectonofacies (Fiori 1994; Yamato 1999).

Phyllites and slates with laminations and primary bedding preserved compose the CF. Usually these structures are folded, where a associated slaty cleavage is identified. Elongated quartzites, as well as metacherts and calcitic or dolomitic marbles, occur (Fig. 8.9a, b). The SF includes sequences of mica-schists, aluminous-schists, paragneisses, quartzites and quartz-schists characterized by a low to medium metamorphic grade (Campanha and Sadowski 1999). This formation corresponds to a shallow shelf sequence (Campanha and Sadowski 1999; Siga Jr et al. 2012; Faleiros et al. 2016).

The Turvo-Cajati Complex (TCC) is represented by a sequence of mica-schists, quartz-mica-schists, calcium schists, dolomitic marbles, quartzites, calc-silicate rocks, paragneisses, aluminous/calc-silicate migmatites and para-amphibolites (Vasconcelos et al. 1999; Faleiros 2008). Low to high metamorphic-grade units are distinguished in the TCC (Faleiros et al. 2011).

The Juréia Massif, southeastern São Paulo State, is constituted of mylonitic paragneisses (garnet-muscovite-biotite gneisses) with Tonian high amphibolite facies (Fig. 8.9c, d). This unit was already correlated to the Cachoeira Sequence (Passarelli et al. 2007) described in the Itatins Massif (Picanço et al. 1998). The rocks of the Cachoeira Sequence are considered to be supracrustal remains of volcanosedimentary sequences, preserved from the intense Neoproterozoic migmatization and anatexis (Dantas et al. 1987). In the area, calci-silicatic rocks, dolomitic marbles, schists, quartzites and metabasic rocks were also mapped, as well as gneisses and kinzigitic gneisses (Dantas et al. 1987; Picanço et al. 1998). The rocks of both Juréia Massif and Cachoeira Sequence may be associated with the Turvo-Cajati Complex. However, further geological-isotopic investigation is necessary.

8.4.3 Piên Suite

High K calcalkaline I-type deformed granite suites compose the Piên Granite Belt (PGB) which was formed in Ediacaran times (Harara 2001). The PGB is interpreted as a northwest subduction-related magmatic arc (Fig. 8.10a).

Two mafic-ultramafic bodies, tectonically emplaced between the Santa Catarina Complex (Luis Alves terrane) and the Piên Granite Belt and as a klippe, compose the Piên Mafic-Ultramafic Suite (PMUS) (Fig. 8.10b–d), 11 km long and N40-50E-trending (Harara et al. 2004). This suite

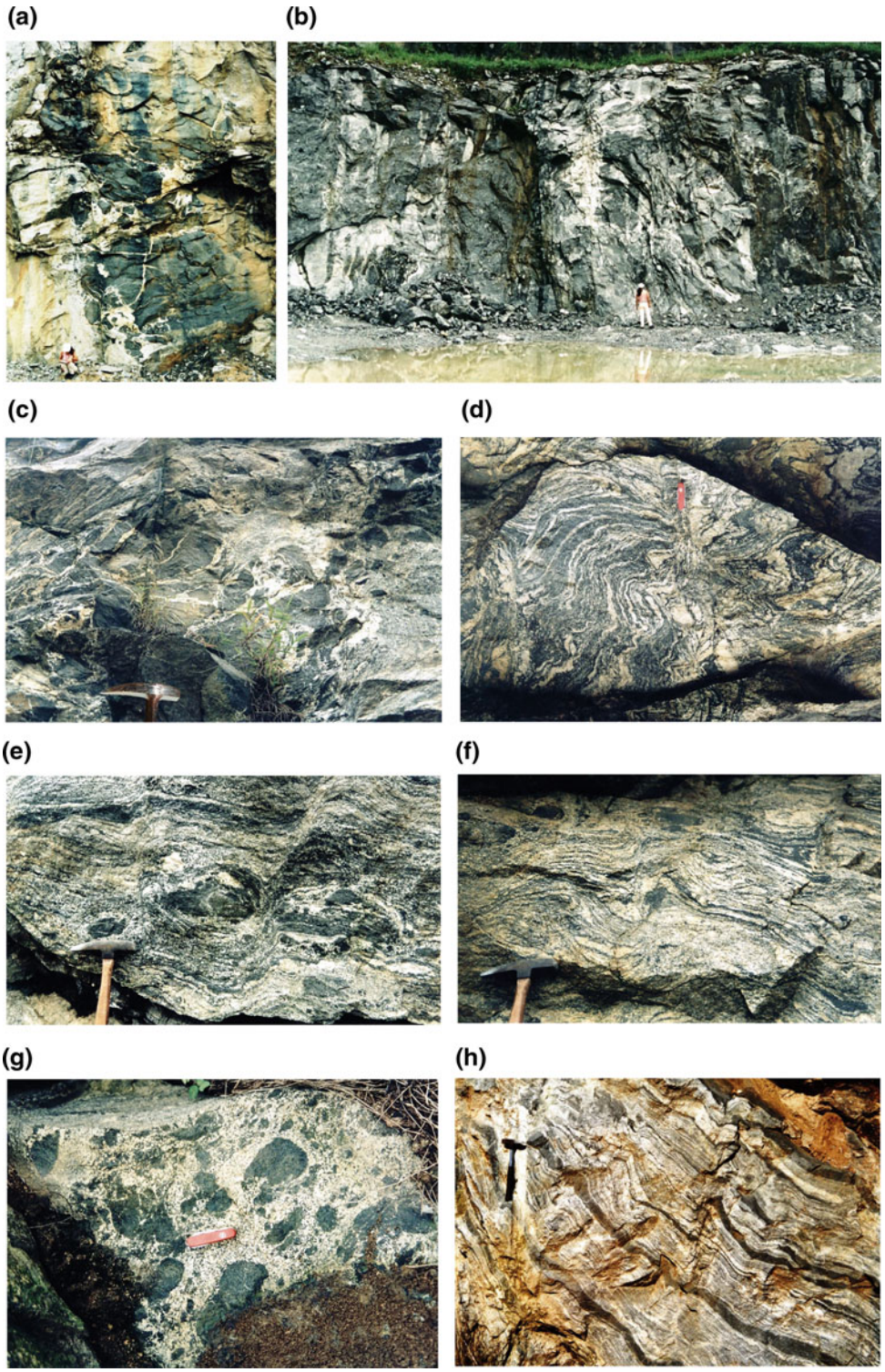

Fig. 8.7 Gneiss migmatitic rocks from Registro Complex: **a** gabbro-dioritic dyke intrusive into amphibole-biotite granodiorites; **b** Granodiorite and gabbro rocks intensely deformed and migmatized; **c** breccia-structured metatexite (agmatite) with sharp-edged gneiss blocks surrounded br leucosome dykes; **d** veined structure (phlebite) migmatite with neosome folded veins; **e** surreitic structure where leucosome tends to locate in the spaces between boudins of more competent layer; **f** schlieren structure of a diatexite with flame-like melanosome and coarse-grained leucosome; **g** schollen-structured migmatite with roundish paleosome blocks enveloped by neosome; and **h** folded banded gneiss paleosome and leucosome

composed by deformed and serpentinized peridotites (Fig. 8.10c), pyroxenites, gabbros and magnesian schists is interpreted as Neoproterozoic oceanic crust remnant, obducted in a fore-arc setting during the collision between the arc and the continental margin (Luis Alves Terrane).

Based on the ophiolite typology determined by chemical compositions of their mafic and ultramafic rocks and on its tectonic position, the PMUS is considered to be an incomplete Supra Subduction Zone ophiolite with mainly the mantle section (Harara et al. 2004).

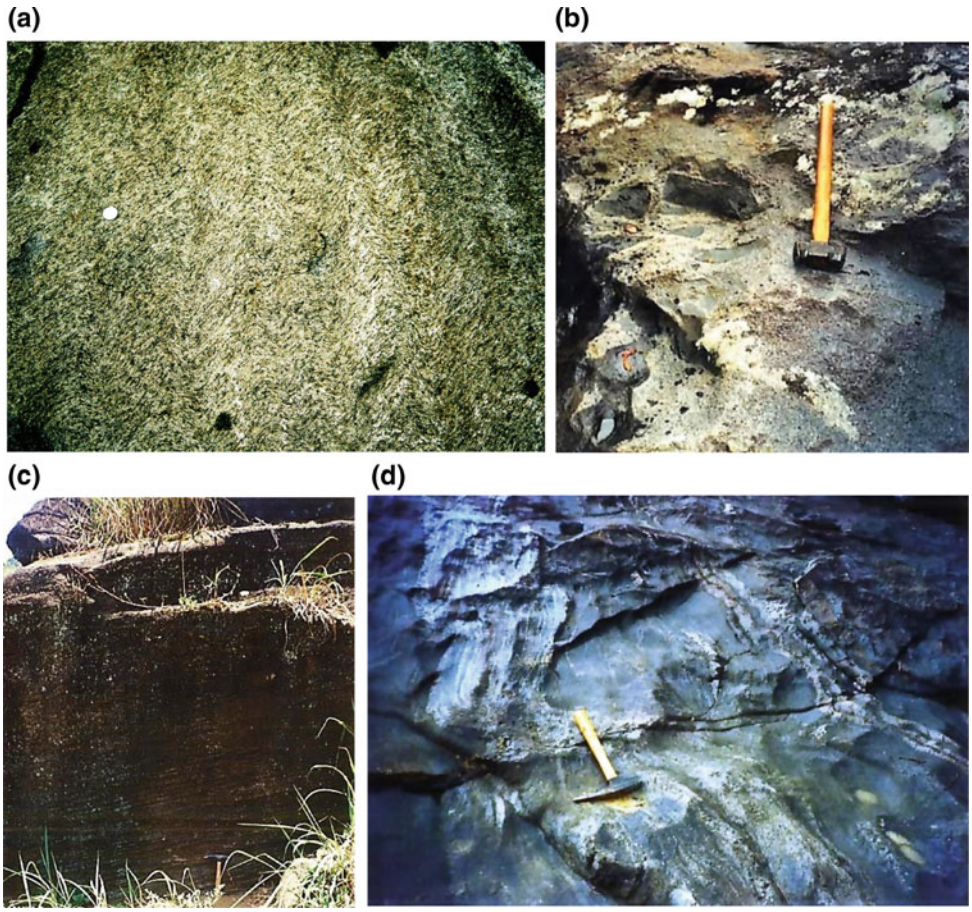

Fig. 8.8 Charnocktic rocks from Itatins Complex: **a** crenulation cleavage; **b** schollen structures with enclaves of basic granulite; **c** centimetric compositional band pattern; and **d** quartz-feldsphatic leucosomatic thick portions. (Photos b, c and d from Azevedo Sobrinho 1995)

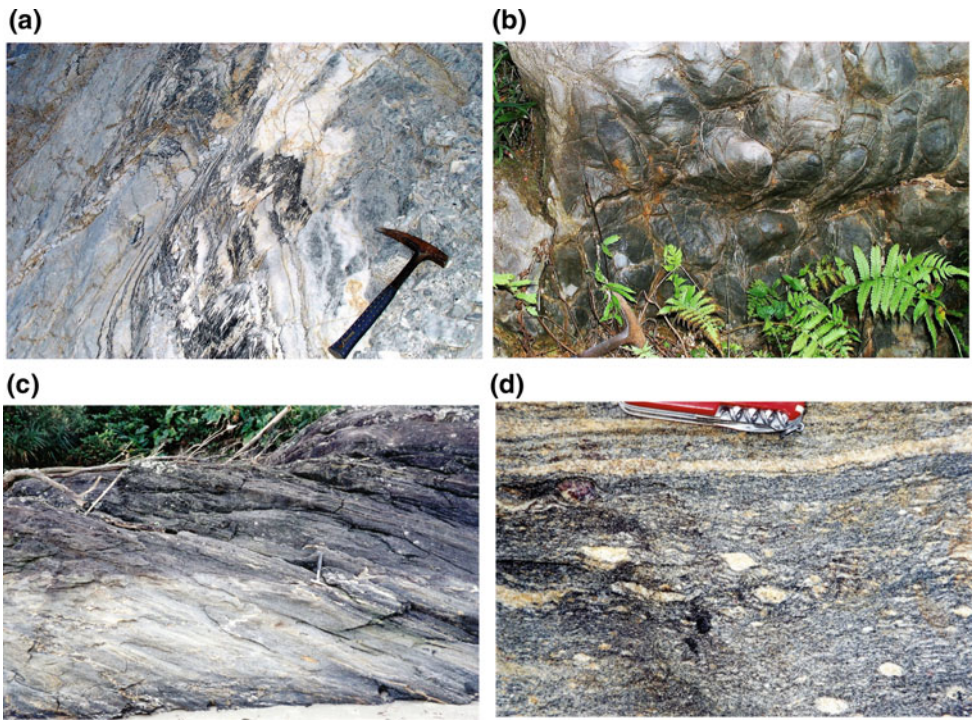

Fig. 8.9 Metasedimentary units of Curitiba Terrane. Capiru Formation: **a** laminated limestone; **b** stromatolites on dolomites; Juréia Massif (Cachoeira Sequence/Turvo-Cajati Complex); **c** low-angle mylonitic foliation on garnet-biotite paragneiss with quartzous-feldspathic beds parallel or cutting the main foliation; and **d** mylonitic foliation in paragneiss defined by quartz-feldsphatic bands, orientation and stretching of centimetre-sized feldspar and garnet porphyroclasts

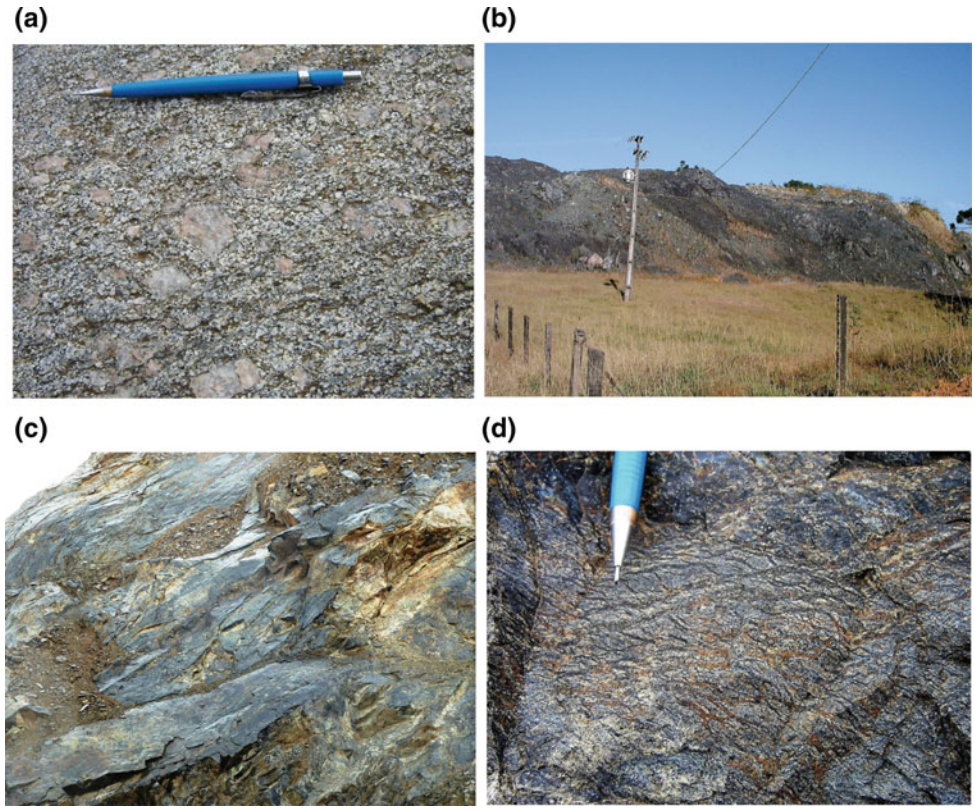

Fig. 8.10 Piên Suite: **a** deformed quartz granodiorites; **b** ophiolitic sequence; **c** serpentinites (picture covers *c*. 30 m^2); and **d** anastomosed foliated ultramafic rock

8.5 Anorogenic Alkaline-Peralkaline Granitoids

The Serra do Mar Suite/Graciosa Province was initially proposed by Kaul (1984) and is composed of isotropic, A-type anorogenic granitoid bodies aligned in a north-northeast trend, parallel to the modern coastline. The plutons are intrusive in the gneissic-migmatitic basement rocks of the Luis Alves and Curitiba Microplate and the Coastal Terrane (Fig. 8.2). Lithologies are monzonites, monzogranites, syenogranites and alkali-feldspar granites usually containing biotite and amphibole, and locally arfvedsonite and riebeckite (Fig. 8.11).

The suite can be grouped in two A-type granite associations (Pitcher 1995): an alkaline, which includes a peralkaline with associated metaluminous varieties (Fig. 8.11a–c), and an aluminous, with associated peraluminous (Fig. 8.11c) and metaluminous diversities (Basei et al. 2009b).

8.6 Available Geochronological and Isotopic Data

Luis Alves Terrane–Santa Catarina Granulitic Complex

The U–Pb, Rb–Sr, Sm–Nd and K–Ar available geochronological data for the SCGC indicate an Archean to Paleoproterozoic geological history, involving tectonic stabilization at the end of the Paleoproterozoic. Table 8.1 presents the main geochronological and isotopic data available for the SCGC.

U–Pb ages around 2350 Ma attributed to a high-grade metamorphic event were obtained in all domains of the complex and were preceded by a second high-grade metamorphism in granulitic paragneisses at around 2180 Ma (Basei et al. 1998a, 1999, 2009b). Therefore an apparent episode for erosion and deposition of sedimentary rocks between the two high-grade metamorphic events must be considered (Basei et al. 2009b). In spite of this, Hartmann et al. (2000) recognized two granulite-facies events dated by U/Pb zircon SHRIMP at about 2.68 and 2.17 Ga, whereas the amphibolite facies event probably occurred close to the 2.17 Ga granulitic metamorphism (Hartmann et al. 2000). The age of around 2480 Ma (U/Pb zircon SHRIMP, Hartmann et al. 2000) may correspond to a metamorphic event, although additional work is required. Archaean U–Pb values close to 2720 Ma were obtained from U–Pb zircon cores dated by the SHRIMP method (Hartmann et al. 2000), and similar Archaean values between 2720 and 2580 Ma were observed in Rb–Sr and Sm–Nd whole-rock isochrons (Basei et al. 1998a). Even though Archaean rocks have not yet been recognized, magmatic protoliths of the Santa Catarina granulite complex were formed at this time (Hartmann et al. 2000; Basei et al. 2009a).

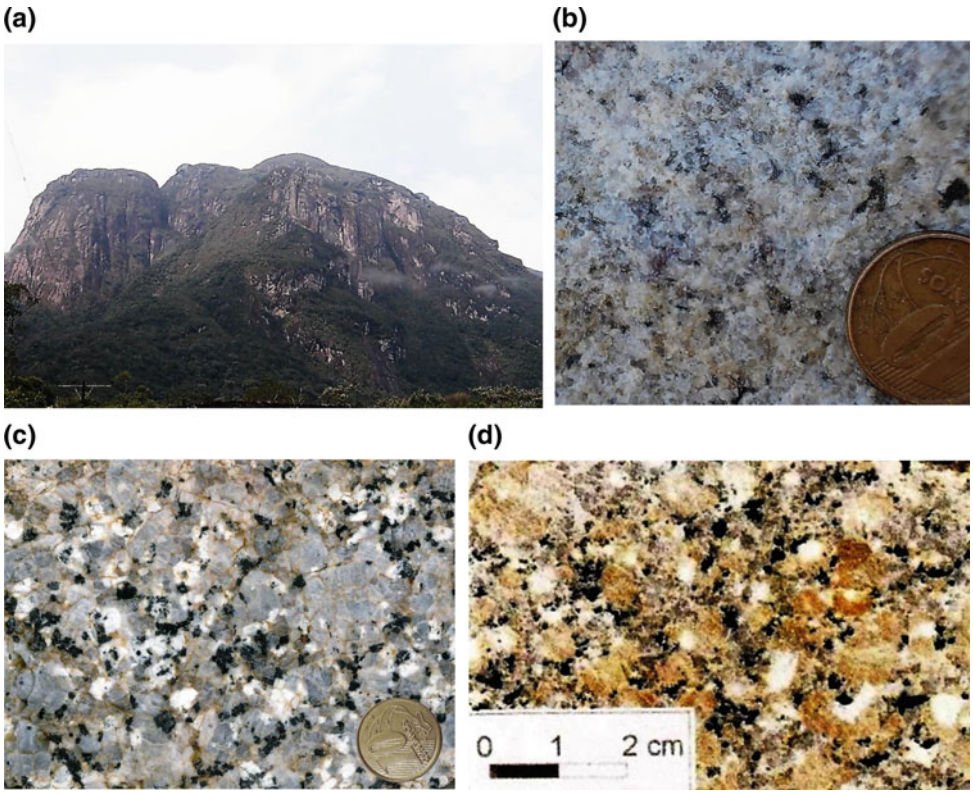

Fig. 8.11 Serra do Mar Suite/Graciosa Province: **a** Marumbi granite mountain range (Paraná State); **b** biotite sienogranite Guaraú (São Paulo State); **c** amphibole-biotite monzogranite Palermo (Paraná State); and **d** biotite-monzogranite with garnet and tourmaline Serra do Paratiú/Cordeiro (São Paulo State)

Sm–Nd model ages fall into two groups: 2800–2700 and 2400–2300 Ma. The former reflects the initial mantle-crust differentiation, while the latter may be due to either the injection of crustally derived magmas or the closure of systems at the end of the granulite facies metamorphism. εNd (2.4 Ga) ranges from 4.9 to −7.2 (Basei et al. 1998a).

At 1800 Ma the Santa Catarina Granulitic Complex had already cooled below the 450 °C isotherm, as indicated by the K–Ar ages in biotite (Siga Jr et al. 1995; Basei et al. 1998a), and mainly remained as a stable block during the Brasiliano orogenic cycle, establishing the Luís Alves craton (Kaul and Teixeira 1982). Table 8.2 summarizes the proposed tectonic evolution for the Luis Alves terrane.

8.7 Curitiba Terrane–Basement Rocks

The evolution of the Atuba Complex (AC) starts in the Meso-Neoarchean, around 3.0–2.7 Ga (Sato et al. 2003) recorded in oscillatory zoned inner parts of zircon crystals (U–Pb zircon SHRIMP ages).

Sm–Nd T_{DM} ages suggest that the AC rocks differentiated from the mantle and were incorporated into the continental crust between 3.1 and 2.7 Ga (Siga Jr et al. 1995; Sato et al. 2003).

Two metamorphic events are recognized on the AC associated with widespread migmatization. Rhyacian ages between 2200 and 2100 Ma (TIMS U–Pb zircon, Rb–Sr WR, Siga Jr et al. 1993, 1995; EV-TIMS and SHRIMP U–Pb ages; Sato et al. 2003) are associated with the main granulite to high-amphibolite facies metamorphism (Siga Jr et al. 1995; Faleiros 2008). This metamorphic event is observed in mesosomes of granulitic gneisses and biotite-amphibole gneiss with tonalitic-trondhjemitic leucosomes. Paleoproterozoic ages were also obtained in Rb-Sr isochrons diagrams, with initial $^{87}Sr/^{86}Sr$ values of between 0.703 and 0.710 (Siga Jr et al. 1995), suggesting both the presence of mantle-derived material and/or lower crust as a reworking of upper crustal rocks.

A second migmatization phase associated with amphibolite facies metamorphism occurred in Ediacaran times. The mobilized granite to granodiorite leucosome is white and pinkish, fine to medium grained, even pegmatitic in places, foliated or not. U–Pb SHRIMP ages obtained in zircon rims at 560–600 Ma, the mineral Rb–Sr isochron age of 570 Ma (Sato et al. 2003) and Rb–Sr isochrons between 585–600 Ma (Siga Jr et al. 1995) all register this activity. Although imprecise, the minimum age of AC remigmatization was obtained by 588 ± 1 Ma biotite $^{40}Ar/^{39}Ar$ age (Siga Jr et al. 2007).

The initial ratios ($^{87}Sr/^{86}Sr$) of these leucosome are in the range 0.716–0.713 (Siga Jr et al. 1995), implying an origin from crustal reservoirs.

In the Itatins Complex, charno-enderbite rocks provide a U–Pb SHRIMP age of 2173 ± 18 Ma (Picanço et al. 1998) interpreted as the crystallization age of metamorphic zircons

Table 8.1 Available isotopic data for the Luis Alves Terrane

Method/material	Localization	Lithotype	Age/petrogenetic parameter	References
U–Pb zr (SHRIMP)	Near Luis Alves-SC	Felsic granulite	2.68; 2.17 Ga granulite-facies events	Hartmann et al. (2000)
U–Pb zr (SHRIMP)	Near Luis Alves-SC	Felsic granulite	≅2.17 Ga amphibolite-facies event	Hartmann et al. (2000)
U–Pb zr (SHRIMP)	Central domain	Quartzose paragneisses	2182 ± 9 Ma	Sato et al. (2008)
U–Pb zr (SHRIMP)	Southern portion	Hbl-bio-granodiorite	2202 ± 25 Ma	Basei et al. (2009a)
U–Pb zr (ID-TIMS)	Luis Alves-SC	Granulitic gneiss	2400 Ma	Basei (1985)
U–Pb zr (ID-TIMS)	Luis Alves-SC	Migmatites	2890 Ma	Basei (1985)
U–Pb zr (ID-TIMS)	Dona Francisca-SC	Granulitic gneiss	2200 ± 2 Ma	Siga Jr (1995)
U–Pb zr (ID-TIMS) (pink)	Dona Francisca-SC	Granulitic gneiss	2247 ± 18 Ma	Siga Jr (1995)
U–Pb zr (ID-TIMS) (brown)	Dona Francisca-SC	Granulitic gneiss	2360 ± 100 Ma	Siga Jr (1995)
U–Pb zr (ID-TIMS)	Central domain	Charnockite-Enderbite	2372 ± 48 Ma	Basei et al. (1998a)
U–Pb zr (ID-TIMS)	southern portion	Mylonitic Leucogranite	2112 ± 21 Ma	Basei et al. (1998a)
U–Pb zr (ID-TIMS) (spherical)	Luis Alves-SC	Charnockite-Enderbite	2338 ± 37 Ma	Basei et al. (1999, 2000)
U–Pb zr (ID-TIMS) (prismatic)	Luis Alves-SC	Charnockite-Enderbite	2204 ± 30 Ma	Basei et al. (1999, 2000)
U–Pb zr (ID-TIMS)	Ibirama-SC	Leucogranite	2112 ± 21 Ma	Basei et al. (1999, 2000)
U–Pb mz (ID-TIMS)	SW-Pomerode-SC	Garnet-quartzite	2283 ± 3 Ma	Basei et al. (2000)
U–Pb zr (ID-TIMS)	Near Piên-PR	Mafic charnockite	2200 ± 7 Ma	Harara (2001)
U–Pb zr (ID-TIMS)	Near Piên-PR	Mafic charnockite	2068 ± 15 Ma	Harara (2001)
U–Pb zr (ID-TIMS)	Near Piên-PR	Felsic granulitic gneisses	2125–2060 Ma	Harara (2001)
U–Pb zr (ID-TIMS)	Central domain	Qz-feldspathic-Hygneiss	2200 ± 4.4 Ma	Basei et al. (2009b)
U–Pb zr (ID-TIMS)	Central domain	Charnockite-Enderbite	2338 ± 37 and 2204 ± 30	Basei et al. (2009b)
U–Pb zr (ID-TIMS)	Central domain	Quartzose paragneisses	2179 ± 9 Ma	Basei et al. (2009b)
U–Pb zr (ID-TIMS)	Southern portion	Hyp-garnet gneiss	2322 ± 32 Ma	Basei et al. (2009b)
U–Pb zr (SHRIMP)	Southern portion	Hyp-garnet gneiss	2311 ± 25 Ma	Basei et al. (2009b)
U–Pb mz (ID-TIMS)	Southern portion	Hyp-garnet gneiss	2288 ± 26 Ma	Basei et al. (2009b)
U–Pb zr (ID-TIMS)	Barra Velha region	Granulite	2192 ± 14 Ma (basic + felsic rocks)	Basei et al. (2009b)
Rb–Sr WR	Luis Alves-SC	Granulitic gneisses	2663 ± 72 Ma/0.70397	Hartmann et al. (1979)
Rb–Sr WR	Pomerode-SC	Granulitic gneisses	2478 ± 37 Ma/0.70129	Siga Jr (1995)
Rb–Sr WR	Luis Alves-SC	Migmatite-Leucosome	2581 ± 277 Ma/0.70418	Basei (1985)
Rb–Sr WR	Luis Alves-SC	Migmatite-Mesosome	1900 ± 200 Ma/0.70460	Basei (1985)
Rb–Sr WR	Dona Francisca-SC	Granulitic gneisses	2700 ± 90 Ma/0.70409	Siga Jr (1995)

(continued)

Table 8.1 (continued)

Method/material	Localization	Lithotype	Age/petrogenetic parameter	References
Rb–Sr WR	Dona Francisca-SC	Granulitic gneisses	1900 ± 70 Ma/0.70451	Siga Jr (1995)
Rb–Sr WR	Blumenau-SC	Granulitic gneisses	2169 ± 177 Ma/0.70150	Basei (1985)
Rb–Sr WR	Luis Alves-SC	Granulitic gneisses	1970 ± 36 Ma/0.70245	Siga Jr (1995)
Rb–Sr WR	Jaraguá do Sul-SC	Granulitic gneisses	2184 ± 48 Ma/0.70257	Siga Jr (1995)
Rb–Sr WR	Piên-PR	Granulitic gneisses	2067 ± 199 Ma/0.70244	Girardi et al. (1974)
Rb–Sr WR	S. Bento do Sul-SC	Granulitic gneisses	2107 ± 69 Ma/0.70284	Machiavelli (1991)
Rb–Sr WR	Serra Negra-PR	Granulitic gneisses	2200 ± 69 Ma/0.70850	Siga Jr (1995)
Sm–Nd isochron	Near Piên-PR	Mafic granulitic gneisses	1704 and 1831 Ma (cooling age)	Harara (2001)
Sm–Nd isochron	Barra Velha-SC	Granulite	2258 ± 67 Ma	Hartmann et al. (1999)
Sm–Nd TDM WR	Near Piên-PR	Granulitic gneisses	2.75–2.56 Ga	Harara (2001)
Sm–Nd TDM WR	Near Piên-PR	Felsic granulitic gneisses	2.5 Ga	Harara (2001)
Sm–Nd TDM WR	Near Piên-PR	Mafic charnockites	3.4 Ga	Harara (2001)
Sm–Nd TDM WR	Near Piên-PR	Granulites; Metanorite	3.1–3.0; 2.8–2.7; 2.3–2.2 Ga	Siga Jr (1995)
Pb–Pb WR	Luis Alves-SC	Felsic-mafic granulites	2100 ± 500 Ma/μ1 = 8.9	Basei (1985)
K–Ar hbl, bio, pla, hyp	All areas	Granulite	2100–1700 Ma	Girardi et al. (1974), Hartmann et al. (1979), Basei (1985), Machiavelli (1991), Siga Jr (1995), Harara (2001)
K–Ar hbl, bio	Near shear zones	Gneiss, amphibolites	1700–600 Ma	Siga Jr (1995)

Qz, quartz; bio, biotite; pla, plagioclase; hyp, hypersthene; hbl, hornblende; zr, zircon; mz, monazite; WR, whole rock; ID-TIMS, isotope dilution thermal ionization mass spectrometry; SHRIMP, sensitive high-resolution ion microprobe

Table 8.2 Summary of the evolution of the Luis Alves Terrane

Event	Characteristics and methods	Age (Ga)
Itajaí Basin		
Sedimentation, volcanism	Sedimentary rocks with subordinate felsic volcanics	0.58–0.56
Serra do Mar Suite		
Magmatism	A-type granites	0.59–0.58
Campo Alegre, Corupá and Guaratubinha basins		
Volcanism, sedimentation	Felsic volcanics with subordinate sedimentary rocks	0.60–0.59
Santa Catarina Granulite Complex		
Local regeneration/reactivation	Near contact with adjacent terranes,internal faults (K–Ar mineral)	0.66–0.62
Tectonic stabilization	Regional cooling (K–Ar mineral)	1.80–1.70
Retrograde metamorphism	U–Pb mineral -upper crust	2.00–1.90
Amphibolite-facies regional metamorphism	Pb–Pb, Rb–Sr WR isochrons, U–Pb mineral, Sm–Nd mineral isochrons-middle crust	2.10–2.00
GranuIite-facies event	Felsic granulite-U/Pb zircon SHRIMP-middle crust	2.17
Magmatism	Deformed granitoids U–Pb (SHRIMP)	2.25–2.15
GranuIite-facies regional metamorphism	Development of orthopyroxene in many rocks (U–Pb zircon, Sm–Nd mineral isochrone)	2.35
Mantle/crust differentiation	Addition of mantle-derived material to the crust (Sm–Nd T_{DM})	2.40–2.30
Amphibolite-facies event?	Felsic granulite-U/Pb zircon SHRIMP	2.48
Magmatism	Intrusion of igneous rocks (Rb–Sr WR isochrons)	2.60
GranuIite-facies event	Felsic granulite-U/Pb zircon SHRIMP-middle crust	2.68
Magmatism	TTG igneous activityU–Pb (SHRIMP), Rb–Sr WR isochrons	2.70
Mantle/crust differentiation	Addition of mantle-derived material to the crust (Sm–Nd T_{DM})	3.40?;2.80–2.70

under granulite facies. In the neossome of migmatites an imprecise age of *c*. 720 Ma (Rb–Sr isochron) is interpreted as a high-amphibolite grade metamorphism with associated migmatization of this complex. Imprecise ages around 600 Ma (Sm–Nd isochrons WR and minerals) are also associated with high-amphibolite grade metamorphism (Picanço et al. 1998).

During the Mesoproterozoic there was little activity in the Curitiba terrane. However, in the Registro Complex (RC) an extensional Calimian event was recorded by U–Pb SHRIMP zircon age of *c*. 1430 Ma in dismembered alkali gabbro-dioritic dykes intrusive in 2100 Ma Rhyacian granodioritic rocks (Passarelli et al. 2012).

In the Ribeira Belt this extensional event is well marked on the Apiaí terrane by basic magmatism in the Água Clara, Perau and Votuverava successions (Siga Jr et al. 2011a, b, c). Up to now the Caliminian event was not identified on the corresponding Atuba Complex in the Paraná state.

8.8 Metasedimentary Units

The Atuba complex provides the infrastructure of the Capiru/Setuva Formations and Turbo-Cajati Complex metasediments. However, the correlations between the metasediments and the assertion that these sequences were deposited on the AC are obstructed particularly by the thrust contacts.

Capiru Formation is probably an allochthonous unit in relation to the AC, with its basal segments severely intertwined in thrust systems to the east (Fiori 1992; Yamato 1999). This may have led to the SF deformation generating a

tectonofacies of the CF (Yamato 1999; Fiori et al. 2003; Faleiros 2008). The majority of TCC and CF geological contacts are given by high-angle reverse shear zones with top-to-southwest transport so the CF units are thrust over the TCC. Back thrust also occurs with an east-northeast direction of transport of CF on the TCC (Faleiros 2008).

Remarkably, since the 2000s, the use of U–Pb ages of detrital zircons to constrain the maximum depositional ages and to elucidate the possible provenance area of these sequences has expanded.

8.8.1 Turvo Cajati Zircon and Monazite Ages

Most of the detrital zircon from TCC has nuclei or rims with 690–640, 790–730 Ma ages, while other ages fall in the 880–800, 1180–1050, 1250–1240, ~1340, 1540–1520, 1790–1730 and 2200–2000 Ma intervals, with a few Archaean grain contributions (2700–2600 and 3100 Ma) (Siga Jr et al. 2012, 2014). The results show that the Neoproterozoic terranes were important sources, and the age of sedimentation of the Turvo-Cajati Complex cannot be older than 640 Ma. Some of the εHf(t) values are positive for Neoproterozoic ages, suggesting that 'primitive' sources are involved.

LA-ICP-MS U–Pb zircon geochronology in kyanite migmatite from the high-grade TCC (Faleiros et al. 2016) provided six main populations of ages, grouped in the intervals of 575–600 Ma, 630–750 Ma, 1000–1200 Ma, *c*.1450 Ma, 1700–1800 Ma and 2000–2200 Ma, which corroborate previous studies (Siga Jr et al. 2012, 2014). The age of 584 ± 4 Ma is inferred as the peak metamorphic age for the sample. This interpretation is corroborated by previous in situ chemical dating of monazite that yields an average age of 589 ± 12 Ma for a sillimanite migmatite sample from the High-TCC followed by a greenschist facies metamorphic overprint at 579 ± 8 Ma, associated with late transcurrent shear zones (Faleiros et al. 2011). The youngest age group (630–650 Ma) is considered to be the maximum depositional age for the high-TCC.

8.8.2 Capiru Detrital Zircons

SHRIMP U–Pb ages of detrital zircons from the CF quartzites provide unimodal distribution around 2.2 Ga (Basei et al. 2008).

New LA-ICP-MS U–Pb ages of detrital zircons from Siga Jr et al. (2012) provide the same absence of Neoproterozoic zircons, but the presence of Mesoproterozoic grains (1.4–1.0 Ga) for the CF. The youngest ages obtained show that the upper age limit of deposition must be close to 1.0 Ga. The older grains include mainly 2.2–2.1 Ga Paleoproterozoic sources, with a 2.9–2.6 Ga Archaean contribution. Some of the Mesoproterozoic grains have negative ƐHf(t) values, which suggest that they have crustal origins. The main component of the Capiru Formation is dolomitic marble with stromatolites, quartzite and phyllite. The youngest age group between 1.0 and 0.9 Ga is considered to be the maximum depositional age for the CF and 630–580 Ma the minimum age (metamorphic event that affects the unit; Faleiros 2008).

8.8.3 Cachoeira Sequence–Juréia Massif Monazite Ages

The Juréia Massif is composed of amphibolite facies mylonitic paragneisses and was exposed to more than one episode of metamorphism and deformation.

The metamorphic Tonian event (750–740 Ma) that reached the high amphibolite facies in garnet-biotite gneiss from Juréia Massif, in the southeastern area of the Registro Complex, was recorded by monazite ID-TIMS U–Pb ages (Passarelli et al. 2007).

This event was corroborated by in situ chemical dating of monazite that provided two distinct populations of ages of 754 ± 9 and 594 ± 8 Ma (unpublished data), indicating two amphibolite metamorphic events in this unit. The Tonian and Ediacaran amphibolite metamorphic events are also recorded in rocks from the Itatins Complex (2200–580 Ma).

Table 8.3 presents the main geochronological and isotopic data available for the Curitiba terrane and Table 8.4 summarizes the proposed tectonic evolution for this terrane.

8.9 Piên Suite

The high K calcalkaline I-type granites that compose the Piên-Mandirituba Granite Belt provided U–Pb TIMS zircon ages between 620 and 615 Ma (quartz-monzodiorites-granodiorites) and 595 Ma (proto-mylonitic quartz-monzodiorites), interpreted as the crystallization ages of these rocks (Harara 2001).

The U–Pb (SHRIMP) data obtained on prismatic magmatic zircons of the gabbros form the Piên Mafic-Ultramafic Suite yielded a concordant crystallization age around 631 ± 17 Ma. The rare rounded zircon ages of the gabbros and the Sm–Nd (whole-rock) isochronic ages of the peridotites and pyroxenites suggest Paleoproterozoic infracrustal contaminations of this suite.

As a consequence of oceanic crust consumption and the continental collision between the Luis Alves terrane and Piên Suite, the granites was deformed and the mafic-ultramafic rocks obducted between 605 and 595 Ma.

Table 8.3 Available isotopic data for the Curitiba Terrane

Method/material	Localization	Lithotype	Age/petrogenetic parameter	Reference
Atuba Complex				
U–Pb zr (SHRIMP)/ EV-TIMS	Near Curitiba-PR	Banded granitic gneisses	3.10–2.90; 2.80–2.60; 2.20–2.00; 0.61–0.59 Ga	Sato et al. (2003)
U–Pb zr (SHRIMP)	Near Curitiba-PR	Banded granitic gneisses	600 Ma	Kaulfuss (2001)
U–Pb zr (ID-TIMS)	Near Curitiba-PR	Granulitic gneiss	2095 ± 5 Ma	Siga Jr et al. (1995)
U–Pb zr (ID-TIMS)	Mandirituba-PR	Amphibole-gneiss	2138 ± 6 Ma	Siga Jr et al. (1995)
U–Pb zr (ID-TIMS)	Near Curitiba-PR	Banded granitic gneisses	560–570 Ma (lower intercept)	Kaulfuss (2001)
U–Pb zr (ID-TIMS	Near Curitiba-PR	Banded granitic gneisses	*c*. 570 Ma (lower intercept)	Siga Jr et al. (2007)
U–Pb zr (ID-TIMS)	Serra do Azeite-SP	Banded granitic gneisses	2148 ± 37 Ma (upper intercept)	Vasconcelos et al. (1999)
Rb–Sr WR	Serra do Azeite-SP	Banded gneisses	1.9–2.0 Ga	Campagnoli (1996)
Rb–Sr WR	Near Curitiba	Banded gneisses	*c*. 595 Ma	Siga Jr et al. (1995)
Rb–Sr minerals	Near Curitiba	Banded gneisses	577–617 Ma	Siga Jr et al. (1995)
Rb–Sr WR	North of Curitiba	Granulitic gneiss	1826 ± 96 Ma/0.71051	Siga Jr et al. (1995)
Rb–Sr WR	NE of Curitiba	Granulitic gneiss	2116 ± 95 Ma/0.70160	Siga Jr et al. (1995)
Rb–Sr WR	NE of Curitiba	Biotite-amphibole-gneiss migmatitic	2220 ± 26 Ma/0.70660	Siga Jr. et al. (1995)
Rb–Sr WR	Atuba Quarry	Biotite-amphibole-gneiss migmatitic	598 ± 48 Ma/0.71650	Siga Jr et al. (1995)
Rb–Sr mineral	Atuba Quarry	Biotite-amphibole-gneiss migmatitic	617 ± 14 Ma	Siga Jr et al. (1995)
Rb–Sr WR	Mandirituba-PR	Amphibole migmatitic gneiss	2010 ± 60 Ma/0.70327	Siga Jr et al. (1995)
Rb–Sr WR	Quitandinha-PR	Biotite-amphibole-gneiss migmatitic	1868 ± 89 Ma/0.70584 (tonalite)	Siga Jr et al. (1995)
Rb–Sr WR	Quitandinha-PR	Biotite-amphibole-gneiss migmatitic	595 ± 41 Ma/0.71308 (granite)	Siga Jr et al. (1995)
Rb–Sr mineral	Quitandinha-PR	Biotite-amphibole-gneiss migmatitic	577 ± 17 Ma (gra)	Siga Jr. et al. (1995)
Sm–Nd isochron	Near Curitiba-PR	Banded gneisses	595 ± 30 Ma	Siga Jr et al. (1995)
Sm–Nd TDM WR	Near Curitiba-PR	Migmatite	2.73 Ga	Sato (1998)
Sm–Nd TDM WR	Near Curitiba-PR	Amphibolite	1.16 Ga	Sato (1998)
Sm–Nd TDM WR	Near Curitiba-PR	Diorite	1.22 Ga	Siga Jr (1995)
Sm–Nd TDM WR	North of Curitiba	Granulitic gneiss	2.82 Ga	Siga Jr et al. (1995)
Sm–Nd TDM WR	Atuba Quarry	Migmatite	2.65 Ga	Siga Jr (1995)
Sm–Nd TDM WR	Atuba Quarry	Biotite-amphibole migmatitic gneiss	2.76 Ga	Siga Jr et al. (1995)
Sm–Nd TDM WR	Quitandinha-PR	Migmatite (mesosome)	2.83 Ga	Siga Jr (1995)
Sm–Nd TDM WR	Mandirituba-PR	Migmatite	2.77 Ga	Siga Jr (1995)
Sm–Nd TDM WR	Mandirituba-PR	Amphibole migmatitic gneiss	2.43 Ga	Siga Jr et al. (1995)
Sm–Nd TDM WR	Mandirituba-PR	Biotite-gneiss migmatitic	2.28 Ga	Siga Jr et al. (1995)
Sm–Nd TDM WR	Quitandinha-PR	Biotite-amphibole-gneiss migmatitic	2.81 Ga	Siga Jr et al. (1995)
Sm–Nd TDM WR	Near Curitiba-PR	Migmatites (leuco + mesossome)	2.9–2.6 Ga	Sato et al. (2003)
Sm–Nd isochron	Mandirituba-PR	Amphibole migmatitic gneiss	585 ± 30 Ma	Siga Jr et al. (1995)

(continued)

Table 8.3 (continued)

Method/material	Localization	Lithotype	Age/petrogenetic parameter	Reference
K–Ar hbl	Serra do Azeite-SP	Orthogneiss	565 ± 39 Ma	Campagnoli (1996)
K–Ar bio	Serra do Azeite-SP	Orthogneiss	527 ± 26 Ma	Campagnoli (1996)
K–Ar bio,/bio/pla	Atuba Complex - PR	Gneiss migmatitic	600 ± 20 Ma	Siga Jr et al. (1995)
Ar-Arbio	Núcelo Setuva-PR	Orthogneiss	588 ± 1 Ma	Siga Jr et al. (2007)
Ar–Ar hbl	Serra do Azeite-SP	Orthogneiss	594 ± 1 Ma	Machado et al. (2007)
Ar–Ar hbl	Serra do Azeite-SP	Pegmatitic vein	577 ± 3 Ma	Machado et al. (2007)
Itatins Complex				
U–Pb zr (SHRIMP)	Itatins Massif-SP	Granulites	2173 ± 18 Ma	Picanço et al. (1998)
Rb–Sr WR	Itatins Massif-SP	Migmatite	722 ± 30/07147	Picanço (1994)
Rb–Sr WR	Itatins Massif-SP	Kinzigitic gneiss	601 ± 32/0.7069	Picanço (1994)
Sm–Nd isochron	Itatins Massif-SP	Granulites	607 ± 136 Ma	Picanço (1994)
Sm–Nd TDM WR	Itatins Massif-SP	Granulites	2.52 Ga	Picanço (1994)
K–Ar hbl	Itatins Massif-SP	Granulites	656 Ma	Picanço (1994)
K–Ar bio	Itatins Massif-SP	Granulites	590–580 Ma	Picanço (1994)
Registro Complex				
U–Pb zr (SHRIMP)	Oliveira Barros-SP	Deformed granodiorite	2100 Ma	Passarelli et al. (2012)
U–Pb zr (SHRIMP)	Oliveira Barros-SP	Gabbro dyke	1430 Ma	Passarelli et al. (2012)
U–Pb zr (ID-TIMS)	Oliveira Barros-SP	Biotite gneiss	2151 ± 62 Ma	Passarelli (2001)
U–Pb zr (ID-TIMS)	South of Miracatu-SP	Biotite gneiss	2197 ± 41 Ma (upper intercept)	Passarelli (2001)
U–Pb zr (ID-TIMS)	South of Miracatu-SP	Biotite gneiss	580 ± 24 Ma (lower intercept)	Passarelli (2001)
Sm–Nd TDM WR	South of Miracatu-SP	Biotite gneiss	2.7–2.9 Ga; 2.4 Ga	Passarelli (2001)
K–Ar bio	South of Miracatu-SP	Biotite gneiss	504 ± 9 Ma	Passarelli (2001)
Cachoeira Sequence				
U–Pb mz (ID-TIMS)	Jureia Massif	Garnet-biotite paragneiss	752 ± 4 Ma; 741 ± 7 Ma	Passarelli et al. (2007)
Rb–Sr WR	Itatins Massif-SP	Kinzigitic gneiss	1469 ± 48/0.7145	Picanço (1994)
Rb–Sr WR	Itatins Massif-SP	Kinzigitic gneiss	601 ± 32 Ma	Picanço (1994)
Sm–Nd isochron	Itatins Massif-SP	Kinzigitic gneiss	582 ± 22 Ma	Picanço (1994)
Turvo Cajati				
LA-ICP-MS U–Pb zr	Serra do Azeite-SP	Kyanite migmatite	0.575–0.6, 0.63–0.75, 1.0–1.2, *c*. 1.45, 1.7–1.8; 2.0–2.2 Ga	Faleiros et al. (2016)
LA-ICP-MS U–Pb zr	Serra do Azeite-SP	Low-grade siliciclastic units	0.8–0.6; 1.4–1.0, 1.8–1.7, 2.2–2.0 Ga	Siga Jr et al. (2012)
Chemical dating mz	Serra do Azeite-SP	Paragneisses	590–575 Ma (metamorphic peak)	Faleiros (2008)

(continued)

Table 8.3 (continued)

Method/material	Localization	Lithotype	Age/petrogenetic parameter	Reference
Chemical dating mz	Serra do Azeite-SP	Sillimanite migmatite	589 ± 12 Ma	Faleiros et al. (2011)
K–Ar flogopite	Serra do Azeite-SP	Paragneisses	587 ± 21 Ma	Campagnoli (1996)
Capiru				
SHRIMP U–Pb ages	North of Curitiba city-PR	Quartzites	2.2 Ga	Basei et al. (2008)
LA-ICP-MS U–Pb zr	North of Curitiba city-PR	Low-grade siliciclastic units	2.9–2.6; 2.2–2.1; 1.4–1.0 Ga	Siga Jr et al. (2012)

Qz quartz; *bio* biotite; *pla* plagioclase; *hyp* hypersthene; *hbl* hornblende; *zr* zircon; *mz* monazite; *WR* whole-rock; *ID/EV-TIMS* Isotope Dilution/Evaporation Thermal ionization mass spectrometry; *SHRIMP* Sensitive high-resolution ion microprobe; *LA-ICP-MS* Laser Ablation Inductively Coupled Mass Spectrometry

The Piên Mafic-Ultramafic Suite is interpreted as a Neoproterozoic oceanic crust remnant, obducted in a fore-arc setting during the collision between the arc and the continental margin (Basei et al. 1992; Machiavelli et al. 1993; Harara 2001).

8.10 Sedimentation Environments and Viable Source-Areas

Petrographic criteria and field relations allowed the correlation between the Capiru and Turvo-Cajati Formations (Faleiros 2008), particularly from the clear similarities in their sedimentary protoliths as pelites interbedded with dolomitic limestones, calc-silicatic rocks and arenites, and additionally the lack of volcanic and subvolcanic rocks. The author interprets that both TCC and CF are Neoproterozoic shallow continental-shelf metasedimentary assemblages. Additionally, the Setuva Formation may represent a tectonofacies Capiru Formation (Yamato 1999; Fiori et al. 2003; Faleiros 2008).

The protholiths sediments of CF indicates a marine sequence of shallow water platform and coastal (Campanha et al. 1987; Campanha and Sadowski 1999). Based on morphological features of the stromatolites and the observed sedimentary structures (Guimarães et al. 2002), the authors suggest distinct shelf environments for this sequence: supratidal and an environment varying from intertidal to infratidal.

The tectonic contact between these units and the isotopic-geochronological data indicate alternative interpretations of the sedimentary environment for TCC rocks. Some positive ƐHf(t) values for 0.8–0.6 and 1.4–1.0 Ga detrital zircons from TCC suggest that primitive Neoproterozoic and Mesoproterozoic sources are involved. An unstable active continental margin with the development of Neoproterozoic magmatic arcs would be an appropriate tectonic situation for the deposition of this pelitic-psammitic sequence, south of the Lancinha suture zone (Siga Jr et al. 2012, 2014).

In contrast, in the Capiru Formation, no Ediacaran zircon grains or overgrowths were found and the youngest ages obtained show that the upper age limit of deposition must be close to 1.0 Ga. The older grains include mainly 2.2–2.1 Ga Paleoproterozoic sources, with a 2.9–2.6 Ga Archaean contribution. Some of the Mesoproterozoic grains (1.4–1.0 Ga) have negative ƐHf(t) values, which suggest that they have crustal origins (Siga Jr et al. 2012). As the main component of the Capiru Formation is dolomitic marble with stromatolites, quartzite and phyllite, a platform sequence deposited in a pre-Gondwana configuration would be an appropriate tectonic situation for the deposition of this sequence, as suggested by many authors.

The absence of Neoproterozoic detrital zircons in the CF, the low green-schist metamorphic grade and Neoproterozoic migmatization of the basement rocks (Atuba Complex) implies that the thrusting of the CF on the basement rocks (AC) occurred after the Brasilian migmatization. On the other hand, the Setuva Formation, as a tectonofacies of the CF in contact with AC (Fiori et al. 2003) with higher grade metamorphic rocks, may indicate that the AC was still hot during these thrust tectonics (Faleiros 2008).

Although detrital zircons of the Capiru and Turvo-Cajati metasedimentary sequences between 2.0 and 2.2 Ga are found in zircons from Atuba Complex and basement rocks of Luis Alves terrane, the other age signatures are characteristically absent from the known zircon U–Pb age patterns found for southeastern Brazil. On the pre-Gondwana African side, rocks with ages in the range 1.4–1.0 Ga are found mainly in belts in SW Africa, discussed below as a viable source area for the Capiru and Turvo-Cajati sequences.

Table 8.4 Summary of the evolution of the Curitiba Terrane

Event	Characteristics and methods	Age (Ga)
Magmatism	A-type granites—Serra do Mar/Graciosa Suite: U–Pb zr	0.59–0.58
Regional cooling	Turvo-Cajati Formation: K–Ar; Ar–Ar	0.575–0.565
Regional cooling	Gneiss-migmatitic basement rocks: K–Ar	0.6–0.58
Peak of metamorphism	Turvo-Cajati Formation: Chemical dating mz; LA-ICP-MS zr	0.59–0.575
High-amphibolite-facies regional metamorphism	Migmatites, gneiss: U–Pb zr (TIMS-lower intercepts; SHRIMP, LA-ICP-MS) Atuba, Registro, Itatins	0.62–0.60
Amphibolite-facies event	Jureia Paragneiss Massif: U/Pb mz; migmatites Itatins Complex: Rb-Sr WR	0.75–0.74
Sedimentation	Turvo-Cajati Formation:U–Pb zr LA-ICP-MS	<0.8–0.6
Sedimentation	Capiru Formation: U–Pb zr LA-ICP-MS	<1.4–1.0
Extensional Event	Gabbros dykes Registro Complex: U/Pb zircon SHRIMP	1.43
Granulite to Amphibolite facies event	Granulites Itatins Complex: U/Pb zircon SHRIMP gneiss-migmatites Atuba + Registro: U–Pb zr and Rb–Sr (WR)	2.2–2.0
Mantle/crust differentiation	Addition of mantle-derived material to the crust (Sm–Nd T_{DM})	2.9–2.6

On the Southern Angola craton in SW Africa, rocks with ages in the range 1.4–1.0 Ga are found, but isotopic information about the source of these rocks is scarce. The Angola Craton can be subdivided into several tectonic zones (Carvalho et al. 2000; Heilbron et al. 2008): (1) Central Shield; (2) Central Eburnian zone; (3) Lubango–Cassinga zone; (4) Gabbro–Anorthosite complexes of SW Angola; and (5) Coastal Poliorogenic zone.

The coastal poliorogenic belt (CPB) is mainly composed of granitoids, gneiss, migmatites and metasedimentary sequences. The Mesoproterozoic rocks (Kibaran orogeny) in the region are represented by the Chela Supergroup, a volcanosedimentary sequence deposited in an epicratonic basin that extends to south of the Lubango region in the southwest of Angola (Pereira et al. 2011). After the deposition of the Chela Group, a period of crustal accretion is marked by the emplacement of leucocratic peraluminous granites and an extensional Mesoproterozoic (1.4–1.1 Ga) bimodal magmatism, followed by deposition of the Damara Supergroup and development of the Brasilian/Pan-African belt (Pereira et al. 2011).

Mafic magmatism yielded ages around 1380 Ma (U–Pb SHRIMP; McCourt et al. 2004). Several occurrences of the 'Red Granites' (Carvalho et al. 1987) and associated rocks are known in southwestern Angola, many of them intruding the Gabbro–Anorthosite complex (Central Eburnian zone). The A-type red granites, syenites, porphyries and volcanics provided Rb–Sr WR isochrone ages between 1410 and 1300 Ma, with initial $^{87}Sr/^{86}Sr$ ratios between 0.706 and 0.705 (Carvalho et al. 1987). In NW Namibia, intrusions of alkaline rocks dated at *c*. 1215 Ma (U–Pb zircon ages; Littmann et al. 2000) reflected the youngest known pre-Pan-African magmatic activity in that region (Seth et al. 2003).

In northern Namibia, red granitic rocks associated with anorthosites yielded a U–Pb zircon age of *c*. 1380 Ma (Drüppel et al. 2000). Sills and dykes of dolerites and gabbros (intruded into the red granites), and noritic-dolerite gabbros forming extensive intrusions, were included in the 1.2–1.1 Ga age range (Carvalho et al. 1979).

Additionally, gneissic rocks of the CPB from northwest Namibia have yielded concordant U–Pb (zircon) ages of 1470–1408 Ma, but petrogenetic information about these rocks is not available (Carvalho et al. 2000). The Lufico orthogneisses (outcropping from Northwestern Angola to the Congo) yielded concordant U–Pb zircon ages of *c*. 1030 Ma (Cahen et al. 1978).

The Kunene Complex (KC) in SW Angola which is intrusive at the southern margin of the Congo Craton yielded a concordant U–Pb zircon age of *c*. 1370 ± 2.5 Ma and Sm–Nd mineral isochrons between 1470 and 1320 Ma (Mayer et al. 2004).

Mesoproterozoic granitoids with zircon ages of 1176–1534 Ma intrude Palaeoproterozoic gneisses of the Epupa Metamorphic Complex in northwestern Kaokoland, Namibia. The Okapuka Formation, a supracrustal assemblage with felsic volcanic rocks similar to some rocks of the Chela Group, overlies the Epupa gneisses. Some A-type granites and Okapuka basin formation in northwestern Kaokoland were related to crustal extension as also documented by emplacement of the 1385 ± 8 Ma Kunene Gabbro-Anorthosite Complex (Kröner and Rojas-Agramonte 2017). The supposition that the Mesoproterozoic magmatism probably extended along the southwestern margin of the Congo craton (Kröner and Rojas-Agramonte 2017) is supported by these Mesoproterozoic granitoids, together with abundant Mesoproterozoic

detrital zircons in Kaoko Belt metasediments (Konopásek et al. 2014).

8.11 Tectonic Interpretations

The lithotypes of the Curitiba Terrane exhibit geological, geochronological and distinct structural characteristics from those of the Luis Alves Terrane. Although Paleoproterozoic records (2150–1800 Ma) are preserved in that domain, the main migmatization/granitization period occurred during the Brasiliano cycle (620–550 Ma). The main northeast structural fabric differs from the frankly northwest pattern observed in the Luis Alves Terrane. The contact between these domains is mostly marked by Neoproterozoic calcalkaline Piên granitoids (615–595 Ma).

Basei et al. (1992, 2008, 2009a) admit processes of subductions and collisions in the Neoproterozoic-Cambrian, leading the juxtaposition of Curitiba Terrane and Paranapanema Craton, under the Ribeira Belt, considering this terrane a microplate (Curitiba Microplate). Subsequently, the collision between the Luis Alves and Curitiba Microplates, with the closure of the pre-existing ocean, would be due to the northeast movement of these terranes. Tectonically, the model seems perfectly plausible owing to the presence of calcalkali granites in the Ribeira Belt (Três Córregos, Cunhaporanga and Agudos Grandes batholiths) and in the Piên Suite, added to the remains of obducted oceanic crust (Piên mafic-ultramafic suite). This model is widely accepted by most of the geoscientific community (e.g., Janasi et al. 2001; Silva et al. 2005; Fuck et al. 2008; Heilbron et al. 2008; Brito Neves et al. 2014). Figure 8.12 shows a schematic northwest–southeast section from the southern Ribeira Belt covering the Apiaí and Embu terranes, and the Curitiba microplate and the Luis Alves craton.

Nevertheless, the absence of related metasediments in the evolution of the Brasilian Ocean (Adamastor) requires additional research, once the metamorphism of the arc-related granitic rocks and of the ultramafic rocks (potential remains of a seafloor) is greenschist facies. Likewise, further studies should be carried out on the mafic-ultramafic rocks, to better elucidate its tectonic meaning.

An alternative model was proposed by Siga Jr et al. (1993) based mainly on the similarities of the Sm–Nd TDM ages of the Luis Alves and Curitiba terranes and the absence of metasedimentary rocks of the Adamastor Ocean. The

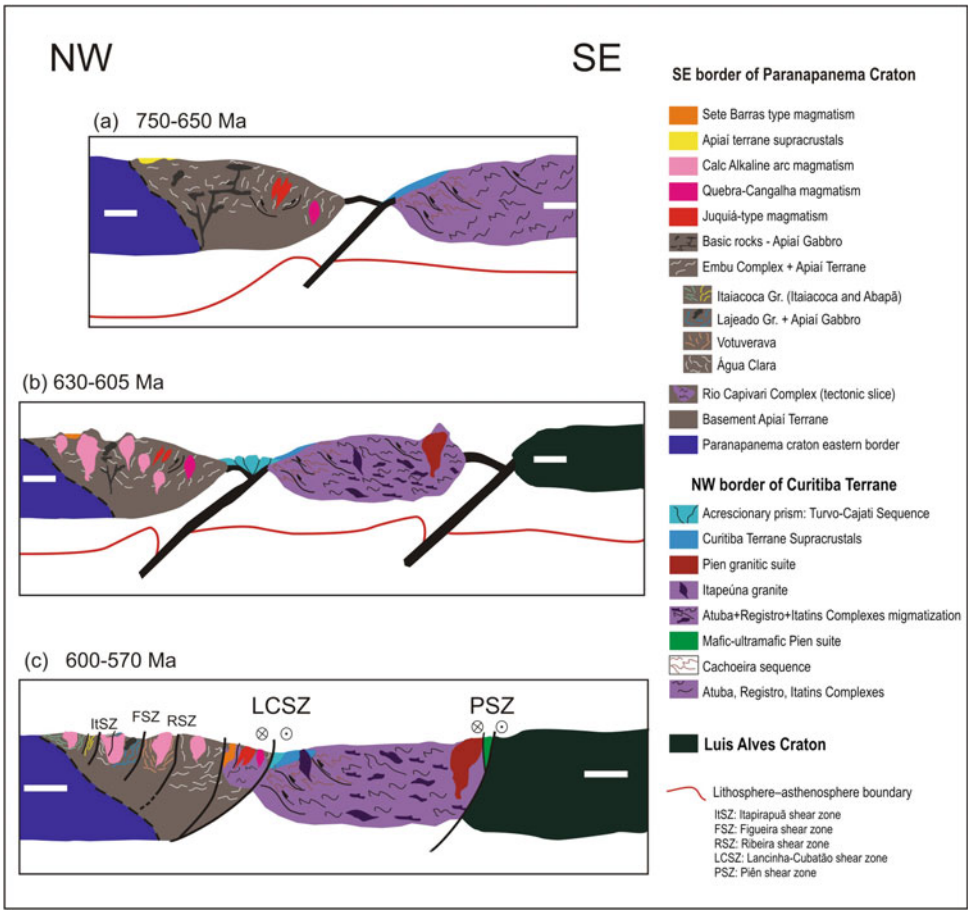

Fig. 8.12 Schematic northwest–southeast sections from the southern Ribeira Belt, Curitiba Microplate and Luis Alves craton. Simplified tectonic model showing the main geological units that were juxtaposed during collisions associated with Gondwana formation. (Modified from Passarelli et al. 2018.)

authors suggest the derivation of the Curitiba Terrane gneisses from Luis Alves terrane rocks by the $^{87}Sr/^{86}Sr$ evolution ratios through geological time. Additionally, the presence of 1800 Ma (K–Ar ages) granulitic rocks side by side with Neoproterozoic rocks of the Curitiba terrane could indicate that the latter does not represent a Microplate but the northeast reworked margin of the Luis Alves terrane, involved in the Neoproterozoic tectonics, a reflection of its collision against the Paranapanema Craton.

Several models for structural development of shear zones (sutures) for the juxtaposition of the distinct terranes of the Ribeira Belt should be taken into consideration (Fiori 1990; Campanha 2002; Faleiros 2008; Carreiro-Araújo 2012).

The models suggest the northwest direction of maximum horizontal compressive stress σ1 that first produced northeast thrusts with a southeast direction of tectonic transport. With the progress of compression, these northeast faults evolved to transcurrent/transpressive fault systems predominantly in a dextral sense, and secondary sinistral shear zones were generated, characterizing the tectonic escape to accommodate the continuing compression (Passarelli et al. 2011). The process, from the initial collision phase until the lateral escape phase predominantly marked by dextral and subordinate sinistral transpressional shear zones, lasted for *c*. 60 Ma, between *c*. 625 and 595 Ma in its central-southern portion.

In this context, the juxtaposition of the Curitiba and Apiaí terranes would have occurred by lateral dispersion along the Lancinha-Cubatão shear zone with considerable slip, but still undefined. Therefore it must be considered that the Curitiba Terrane could have collided originally with the Apiaí Terrane in an unknown position, different from the present.

Therefore the paleogeographic reconstruction of the southeastern portion of the Ribeira Belt must consider a model of collage of suspect or exotic terranes whose boundaries are fault systems (earlier suture zones) that have undergone large but usually unknown amounts of lateral movement progressively. A model of opening and closing of oceans at least in part of the Ribeira belt would not be justified.

The Palermo and Rio Negro Granites (Harara 2001) of Serra do Mar Suite intrusive in the Santa Catarina Granulitic Complex and in the Piên Granite Belt provide U–Pb zircon ages of 593 Ma, and therefore constrain the minimum age of the juxtaposition of the Luis Alves and Curitiba terranes.

8.12 Conclusions

The Luís Alves Microplate is an exotic continental fragment in relation to the other geotectonic units of southeastern Brazil. The migmatitic-gneissic at granulite facies or retrogressed under amphibolite facies conditions formed from a TTG association that since 1.8–1.7 Ga has been cold and stable. Two high-grade metamorphic events at *c*. 2.3 Ga and 2.1 Ga are characterized.

South of the Lancinha Shear Zone, the Curitiba Microplate is composed of basement rocks of the Atuba Complex covered by low-grade Neoproterozoic metavolcanosedimentary sequences (Capiru, Setuva and Turvo-Cajati). Banded migmatitic gneisses of Paleoproterozoic age (2.2–2.1 Ga) predominate in the Atuba Complex, strongly affected by a second Neoproterozoic migmatization phase. The contact between the southern portion of the Curitiba Microplate and the Luís Alves Microplate is marked by the heterogeneously deformed *c*. 615 ± 5 Ma calcalkaline granitoids that constitute the Rio Piên Batholith. Basic and ultrabasic rocks (630 Ma) are also present, and are possible remains of obducted oceanic floor.

In the period *c*. 750–650 Ma, orthogneisses and amphibolitic rocks of the Rio Capivari Complex and Curitiba Terrane (Atuba, Registro and Itatins Complexes) may constitute a single microplate. At this time, subduction zone was active with calcalkaline and S-type magmatism being generated at *c*. 680–660 Ma in the Embu terrane (Fig. 8.12a). Metamorphism at 750 and 705 Ma affected Tonian granites and the metasedimentary sequence of the Embu Complex. At 750 Ma, amphibolite to granulite facies metamorphism affected the Cachoeira Sequence–Registro Complex and intrusive granitic magmatism in the Atuba Complex. Capiru and Turvo Cajati sedimentary sequences in the Curitiba terrane with sedimentation ages between 0.8 and 0.6 Ga, probably with maximum depositional age of 650 Ma occurred.

A *c*. 630–605 Ma synorogenic calcalkaline magmatism in the Ribeira Belt (Embu and Apiaí terranes) took place during the juxtaposition of the Curitiba microplate and the Ribeira belt (Santa Catarina Granite −630 Ma; Agudos Grandes −610 Ma; Três Córregos, Cunhaporanga Batholits −620 to 590 Ma; Fig. 8.12b). During the closure of the Adamastor ocean also occurred the collision between the Curitiba microplate and the Luis Alves craton with calcalkaline granites of Piên magmatic arc generation. The Turvo-Cajati Sequence may represent an accretionary prism at this time. Metamorphism and partial melting at Rio Capivari, Atuba, Registro and Itatins Complexes took place at 620–590 Ma.

The closure of the Adamastor Ocean with the orogenic collage between Paranapanema craton, Curitiba Terrane and Luis Alves craton must have occurred in the 600–570 Ma interval (Fig. 8.12c).

The Lancinha-Cubatão Shear Zone (LCSZ) separates the supracrustal terranes of the eastern border of the Paranapanema craton (northwest) from the Curitiba Terrane (southeast). The oblique component of the arrangements of the colliding tectonic blocks defined the transpressional character of this suture zone. The initial collision phase

evolved into a dextral transpressional shear zone. Nevertheless, the Curitiba Microplate may have collided initially with the Paranapanema craton in an unidentified position, different from that of the present day.

The final stages of the collisions generated several peraluminous granites in the Embu terrane in around 590 Ma (e.g., Sete Barras granite) that preceded the extensional tectonics responsible for emplacing the alkaline-peralkaline granitoids of the Serra do Mar Suite/Graciosa Province and Itu Province of the Apiaí Terrane with ages in the range 590–580 Ma. The juxtaposition of the Curitiba and Luis Alves Microplates evolved with the subduction of Neoproterozoic oceanic crusts towards the northwest. No ocean remnants between Curitiba and Ribeira belt are recorded. The Rio Capivari Complex may be added to the ET at this time.

References

Abdelsalam MG, Lieegeois JP, Stern RJ (2002) The Saharan Metacraton. J Afr Earth Sci 34(3):119–136

Almeida FFM, Hasui Y, Brito Neves BB, Fuck RA (1981) Brazilian structural provinces, an introduction. Earth Sci Rev 17:1–29

Alves A, Janasi VA, Campos Neto MC (2016) Sources of granite magmatism in the Embu Terrane (Ribeira Belt, Brazil): Neoproterozoic crust recycling constrained by elemental and isotope (Sr-Nd-Pb) geochemistry. J S Am Earth Sci 68:205–223

Appi CJ, Cruz CES (1990) Estratigrafia de Sequências na Bacia do Itajaí, SC. In: XXXVI Congresso Brasileiro de Geologia, Natal, pp 93–106

Assumpção M, Heintz M, Vauchez A, Egydio Silva M, Barbosa JR, Benevides T (2001) Upper mantle anisotropy in SE and Central Brazilfrom SKS. Congresso Brasileiro de Geofísica, Salvador. Anais Salvador, SBGf, pp 1–4

Azevedo Sobrinho JM (1995) Petrologia dos chranockitos da região de Itariri (SP). MSc Dissertation, Institute of Geosciences—University of São Paulo, p 112

Babinski M, Tassinari CGC, Nutman AP, Sat K, Martin PR, Iye SS (2001) U/Pb shrimp zircon ages of migmatites from the basement of the Embu Complex Ribeira Fold Belt Brazil: indications for $\sim$1.4–1.3 Ga Pb–Pb and Rb-Sr "isochron" ages of no geological meaning. In: III South America Symposium on Isotope Geology, Pucón, pp 91–93 (Book of abstracts)

Basei MAS (1985) O Cinturão Dom Feliciano em Santa Catarina. PhD thesis, Institute of Geosciences—University of São Paulo, p 191

Basei MAS, Siga Jr O, Machiavelli A, Mancini F (1992) Evolução tectônica dos terrenos entre os Cinturões Ribeira e Dom Feliciano (PR - SC). Braz J Geol Former Rev Brasil Geociênc 22(2):216–221

Basei MAS, McReath I, Siga Jr O (1998a) The Santa Catarina Granulite Complex of Southern Brazil, a review. Gondwana Res 1:383–391

Basei MAS, Citroni SB, Siga Jr O (1998b) Stratigraphy and age of Fini-Proterozoic Basins of Paraná and Santa Catarina States, Southern Brazil. Bol IG USP, Série Científica 29:195–216

Basei MAS, Siga Jr O, Reis Neto JM, Passarelli CR, Prazeres HJ, Kaulfuss G, Sato K, Lima OS (1999) Paleoproterozoic granulitic belts of the Brazilian southern region (PR-SC) In: II South American Symposium on Isotope Geology, Cordoba, Argentina, Short Papers, vol 1, pp 291–294

Basei MAS (2000) Geologia e modelagem geotectônica dos terrenos Pré-Cambrianos das regiões sul-oriental brasileira e uruguaia: possíveis correlações com províncias similares do sudoeste africano. Full Professors Thesis, Institute of Geosciences—University of São Paulo, p 124

Basei MAS, Siga Jr O, Masquelin OM, Reis Neto JM, Preciozzi P (2000) The Dom Feliciano Belt of Brazil and Uruguay and its foreland domain, the Rio de la Plata craton. In: Cordani UG, Milani EJ, Thomaz Filho A, Campos DA (eds) Tectonic Evolution of South America, 31st International Geological Congress, Rio de Janeiro, pp 311–334

Basei MAS, Frimmel HE, Nutman AP, Preciozzi F, Jacob J (2005) The connection between the Neoproterozoic Dom Feliciano (Brazil/Uruguay) and Gariep (Namibia/South Africa) orogenic belts. Precambr Res 139:195–221

Basei MAS, Frimmel HE, Nutman AP, Preciozzi F (2008) West Gondwana amalgamation based on detrital ages from Neoproterozoic Ribeira and Dom Feliciano belts of South America and comparison with coeval sequences from SW Africa. In: Pankhurst, R.J., Trouw, R.A.J., Brito Neves, B.B., De Wit, M.J. (eds.) West Gondwana Pre-Cenozoic correlations across the South America. Geological Society of London, Special Publication 294, pp 239–256

Basei MAS, Siga Jr O, Passarelli CR, Drukas CO; Sato K, Sproesser WM (2009a) The role of the Curitiba and Luis Alves Microplates during the west Gondwana assembly. Boletim de Resumos Expandidos Simpósio 45 Anos de Geocronologia no Brasil, pp 26–31

Basei MAS, Nutman A, Siga Jr O, Passarelli CR, Drukas CO (2009b) The evolution and tectonic setting of the Luis Alves Microplate of Southeastern Brazil: an exotic terrane during the assembly of Western Gondwana. In: Gaucher C, Sial AN, Halverson GP, Frimmel HE (eds) Neoproterozoic-Cambrian tectonics, global change and evolution: a focus on southwestern Gondwana. Developments in Precambrian Geology vol 16, pp 273–291

Basei MAS, Drukas CO, Nutman A, Wemmer K, Dunyi L, Santos PR, Passarelli CR, Campos Neto MC, Siga Jr O, Osako L (2011) The Itajaí foreland basin: a tectono-sedimentary record of the Ediacaran period, Southern Brazil. Int J Earth Sci Geol Rundsch 100:543–569

Benetti Silva BY (2017) Evolução tectônica da porção central do terreno Embu ao norte da Zona de Cisalhamento Taxaquara-Guararema. MSc Dissertation, Institute of Geosciences—University of São Paulo, p 121

Bigarella JJ, Salamuni R (1956) Estudos preliminares na Série Açungui: algumas estruturas singenéticas nos dolomitos da Formação Capiru. Bol Arq Biol Tecn 1:11–197

Brito Neves Bb, Fuck RA, Pimentel MM (2014) The Brasiliano collage in South America: a review. Braz J Geol 44(3):493–518

Cahen L, Ledent D, Tack L (1978) Données sur la geochronologie du Mayumbien (Bas-Zaire). Bull Soc Géol Belg 87:101–112

Campagnoli F (1996) Consideracões sobre a geologia da Sequência Turvo–Cajati, na região do Alto Rio Jacupiranguinha, SP. MSc Dissertation, Institute of Geosciences—University of São Paulo, p 96

Campanha GAC (2002) O papel do sistema de zonas de cisalhamento transcorrentes na configuração da porção meridional da Faixa Ribeira. Full Professors Thesis, Institute of Geosciences—University of São Paulo, p 104

Campanha GAC, Bistrichi CA, Almeida MA (1987) Considerações sobre a organização litoestratigráfica e evolução tectônica da Faixa de Dobramentos Apiaí. Simpósiosul-brasileiro de Geologia, 3, Curitiba, vol 2. Atas, Curitiba, SBG, pp 725–742

Campanha GAC, Sadowski GR (1999) Tectonics of the southern portion of the Ribeira Belt (Apiaí Domain). Precambr Res 98:31–51

Campos Neto MC (2000) Orogenic systems from Southwestern Gondwana, an approach to Brasiliano-Pan African cycle and

orogenic collage in Southeastern Brazil. In: Cordani UG, Milani EJ, Thomaz Filho A, Campos DA (eds) Tectonic Evolution of South America, 31st International Geological Congress, Rio de Janeiro, pp 335–365

Campos Neto MC, Figueiredo MCH (1995) The Rio Doce Orogeny, southeastern Brazil. J S Am Earth Sci 8:143–162

Carvalho H, Crasto J, Silva ZC, Vialette Y (1987) The Kibaran cycle in Angola: a discussion. In: Bowden P, Kinnaird J (eds) African Geology Reviews. Geological Journal 22 (1): 85–102

Carvalho H, Tassinari CG, Alves F, Guimarães D, Simões MC (2000) Geochronological Review of the Precambrian in western Angola: links with Brazil. J Afr Earth Sci 31:383–402

Carvalho H, Fernandez A, Vialette Y (1979) Chronologie absolute du Précambrien du Sud-Ouest de l'Angola. Comptes Rendus Académie Sci Paris 288:1647–1650

Carreiro-Araújo SA (2012) Métodos potenciais aplicados ao estudo do arcabouço crustal da porção meridional da Faixa Ribeira, margem continental da Bacia de Santos. MSc Dissertation, Institute of Geosciences University of Brasília 295, p 137

Castro LG, Ferreira FJF, Cury LF, Soares PC, Lopes AP, Oliveira MJ (2014) Qualitative and semiquantitative interpretation of aeromagnetic data over the Lancinha Shear Zone, Southern Ribeira Belt, in Paraná State, Southern Brazil. Geologia USP, Série Científica 14 (4):3–18

Castro LG, Ferreira FJF (2015) Geophysical-structural framework of southern Ribeira Belt. Braz J Geol 45(4):499–516

Cordani UG, Coutinho JMV, Nutman AP (2002) Geochronological constraints on the evolution of the Embu Complex, Sao Paulo, Brazil. J S Am Earth Sci 14(8):903–910

Cordani UG, Pimentel MM, Ganade de Araújo CE, Basei MAS, Fuck RA, Girardi VAV (2013) Was there an Ediacaran Clymene Ocean in central South America? Am J Sci 313:517–539

Cury LF (2009) Geologia do Terreno Paranaguá. PhD Thesis, Institute of Geosciences—University of São Paulo, p 188

Dantas ASL, Gimenez Filho A, Teixeira AL, NagataN, Fernandes LA, Albuquerque Filho JL, Frasca MHBO (1987) Evolução geológica e estrutural da faixa costeira nas regiões de Juquiá e Miracatu, Sul do Estado de São Paulo. In: Simpósio Regional de Geologia 6, Rio Claro, SP, Brasil, SBG, vol 1, pp 173–189

Drüppel K, Littmann S, Okrusch M (2000) Geo- und isotope chemische Untersuchungen der Anorthosite des KuneneIntrusiv Komplexes (KIC) in NW Namibia. Berichte der Deutschen Mineralogischen Gesellschaft, Beih. Z. Eur J Min 12(1):37

Faleiros FM (2008) Evolução de terrenos tectono-metamórficos da Serrania do Ribeira e Planalto Alto Turvo (SP, PR). PhD thesis, Institute of Geosciences—University of São Paulo, p 318

Faleiros FM, Campanha GAC, Martins L, Vlach SRF, Vasconcelos PM (2011) Ediacaran high-pressure collision metamorphism and tectonics of the southern Ribeira Belt (SE Brazil): evidence for terrane accretion and dispersion during Gondwana assembly. Precambr Res 189:263–291

Faleiros FM, Campanha GAC, Pavan M, Almeida VV, Rodrigues SWO, Araújo BP (2016) Short-lived polyphase deformation during crustal thickening and exhumation of a collisional orogen (Ribeira Belt, Brazil). J Struct Geol 93:106–130

Fassbinder E, Sadowski GR, Fiori AP (1994) Modelo de Riedel aplicado ao Lineamento da Lancinha, no Estado do Paraná. Bole Parana Geociên 42:173–184

Fiori AP (1990) Tectônica e Estratigrafia do Grupo Açunguia norte de Curitiba. Full Professors Thesis, Institute of Geosciences—University of São Paulo, p 261

Fiori AP (1992) Tectônica e Estratigrafia do Grupo Açungui. Boletim do Instituto de Geociências—USP. São Paulo 23:55–74

Fiori AP (1994) Evolução geológica da Bacia do Açungui. Bole Parana Geociên 42:7–27

Fiori AP, Fassbinder E, Salamuni E (2003) Evolução geológica do Grupo Açungui. SBG, Boletim de Resumos, VIII Simpósio de Geologia do Sudeste, São Pedro, SP, p 16p

Fuck RA, Brito Neves BB, Schobbenhaus C (2008) Rodinia descendants in South America. Precambr Res 160:108–126

Girardi VAV, Cordani UC, Candido A, Melfi AJ, Kawashita K (1974) Geocronologia do Complexo Básico-Ultrabásico de Piên, PR. Anais XXVIII Congresso Brasileiro de Geologia 6:245–252

Gualda GAR, Vlach SRF (2007) The Serra da Graciosa A-type Granites and Syenites, southern Brazil. Part 1: Regional setting and geological characterization. An Acad Bras Ciênc 79(3):405–430

Guimarães SB, Reis Neto JM, Siqueira RBL (2002) Caracterização dos estromatólitos da Formação Capiru (Proterozóico) nas regiões Morro Azul e Morro Grande—leste do Paraná. Bole Parana Geociên 51:77–88

Harara OMM (2001) Mapeamento e investigaçãopetrológica e geocronológica dos litotipos da regiãodo Alto Rio Negro (PR-SC): um exemplo de sucessivas e distintas atividades magmáticas durante o Neoproterozóico. PhD thesis, Institute of Geosciences —University of São Paulo, p 206

Harara OMM, Basei MAS, Siga Jr O, Campos Neto MC (2004) Neoproterozoic supra subduction zone (SSZ) ophiolitic rocks from Piên (PR), southern Brazil. Quarenta anos de geocronologia no Brasil. Boletim de Resumos, 89

Hartmann LA, Silva LC, Orlandi Filho V (1979) O Complexo Granulítico de Santa Catarina. Descrição e implicações genéticas. Acta Geol Leopoldensia 3(6):93–112

Hartmann LA, Basei MAS, Simas MW (1999) Geochemistry of the Lower Proterozoic granulite-facies Grant syenite gneiss, Barra Velha, Santa Catarina State, southern Brazil. Pesquisas 25:3–9

Hartmann LA, Santos JOS, McNaughton NJ, Vasconcellos MAZ, Silva LC (2000) SHRIMP dates recurrent granulite facies metamorphism in the Santa Catarina granulites, southern Brazil. Anais Academia Brasileira de Ciências 72:559–572

Hasui Y (1975) Evolução Polifásica do Pré-Cambriano a Oeste de São Paulo. Boletim Instituto de Geociências-USP 6:95–108

Heilbron M, Pedrosa-Soares AC, Campos Neto MC, Silva LC, Trouw RAJ, Janasi VC (2004) A Província Mantiqueira. In: Mantesso-Neto V, Bartorelli A, Carneiro CDR, Brito Neves BB (eds) O Desvendar de um Continente: a moderna geologia da América do Sul e o Legado da Obra de Fernando Flávio Marques de Almeida. Ed. Beca, São Paulo, pp 203–234

Heilbron M, Valeriano CM, Tassinari CCG, Almeida J, Tupinambá M, Siga Jr O, Trouw R (2008) Correlation of Neoproterozoic terranes between the Ribeira Belt, SE Brazil and its African counterpart: comparative tectonic evolution and open questions. In: Pankhurst RJ, Trouw RAJ, Brito Neves BB and De Wit MJ (eds) West Gondwana: Pre-Cenozoic Correlations across the South Atlantic Region, vol 294. Geological Society London Special Publications, pp 211–237

Janasi VA, Leite RJ, Van Schmus WR (2001) U-Pb chronostratigraphy of the granitic magmatism in the Agudos Grandes Batholith (west of São Paulo, Brazil): implications for the evolution of the Ribeira Belt. J S Am Earth Sci 14(4):363–376

Janasi VA, Alves A, Vlach SRF (2003) Granitos peraluminosos da porção central da Faixa Ribeira, Estado de São Paulo: sucessivos eventos de reciclagem da crosta continental no Neoproterozóico. Geologia USP 3:13–24

Kaul PFT (1984) Significado dos granitos anorogênicos da Suíte Intrusiva Serra do Mar na evolução da crosta do sul-sudeste do Brasil, no âmbito das folhas SG-22, Curitiba e SG-23, Iguape. In: Congresso Brasileiro de Geologia 33, vol 6. Rio de Janeiro, RJ, Brasil, SBG, pp 2815–2825

Kaul PFT, Cordani UG (2000) Geochemistry of the Serra do Mar (southern Brazil) granitoids magmatism and tectonic implications. Braz J Geol 30:115–119

Kaul PFT, Teixeira W (1982) Archean and early Proterozoic complexes of Santa Catarina, Paraná and São Paulo states, south-southeastern Brazil: an outline of their geological evolution. Rev Bras Geociên 12:172–182

Kaulfuss GA (2001) Geocronologia dos núcleos de embasamento Setuva, Betara e Tigre, Norte de Curitiba, Paraná. MSc Dissertation, Institute of Geosciences—University of São Paulo, p 115

Konopásek J, Košler J, Sláma J, Janoušek V (2014) Timing and sources of pre-collisional Neoproterozoic sedimentation along the SW margin of the Congo Craton (Kaoko Belt, NWNamibia). Gondwana Res 26:386–401

Kröner A, Rojas-Agramonte Y (2017) Mesoproterozoic (Grenville-age) granitoids and supracrustal rocks in Kaokoland, northwestern Namibia. Precambr Res. https://doi.org/10.1016/j.precamres.2017.07.008

Littmann S, Romer RL, Okrusch M (2000) Nephelinsyenite der Epembe-Swartbooisdrif-Alkali-Provinz (ESAP)/NW Namibia. Beih Z Eur J Min 12:1

Machado R, Dehler NM, Vasconcelos P (2007) $^{40}Ar/^{39}Ar$ ages (600-570 Ma) of the Serra do Azeite transtensional shear zone: evidence for syncontractional extension in the Cajati area, southern Ribeira belt. An Acad Bras Ciênc 79(4):713–723

Machiavelli A (1991) Os Granitóides Deformados da Região de Pien (PR): Um provável Arco Magtnático do Proterozóico Superior. MSc Dissertation, Institute of Geosciences—University of São Paulo, p 89

Machiavelli A, Basei MAS, Siga Jr O (1993) Suíte Granítica Rio Piên: um arco magmático do Proterozóico Superior na Microplaca Curitiba. Geochim Brasiliensis 7(2):113–129

Mantovani MSM, Brito Neves BB (2005) The Paranapanema lithospheric block: its importance for Proterozoic (Rodinia, Gondwana) supercontinent theories. Gondwana Res 8:303–315

Maurer VC, Alves A, Campos Neto MC (2015) Characterization of the Rio Capivari Complex, basement of the Embu Terrane: Geochemical and Geochronological constraints. In: 8th Hutton Symposium on Granites and Related Rocks. Book of abstracts, PT, p 164

Mccourt S, Armstrong RA, Kampunzu AB, Mapeo RBM, Morais E (2004) New U-Pb SHRIMP ages for zircons from the Lubango region, SW Angola: insights into the proterozoic evolution of South-Western Africa. In: Geoscience Africa 2004. Geological Society of South Africa, pp 438–439

Meira VT, García-Casco A, Juliani C, Almeida RP, Schorscher JHD (2015) The role of intracontinental deformation in supercontinent assembly: insights from the Ribeira Belt, Southeastern Brazil (Neoproterozoic West Gondwana). Terra Nova 27:206–217

Mayer A, Hofmann AW, Sinigoi S, Morais E (2004) Mesoproterozoic Sm–Nd and U-Pb ages for the Kunene Anorthosite Complex of SW Angola. Precambr Res 133:187–206

Passarelli CR (2001) Caracterização estrutural e geocronológica dos domínios tectônicos da porção sul-oriental do Estado de São Paulo. PhD thesis, Institute of Geosciences—University of São Paulo, p 254

Passarelli CR, Basei MAS, Campos Neto MC, Siga Jr O, Prazeres Filho HJ (2004) Geocronologia e geologia isotópica dos terrenos Pré-cambrianos da porção sul-oriental do Estado de São Paulo. Geologia USP Série Científica 4:55–74

Passarelli CR, Basei MAS, Prazeres Filho HJ, Siga Jr O, Szabó GAJ, Marco-Neto J (2007) Structural and geochronological constraints on the evolution of the Juréia Massif, Registro Domain, State of São Paulo, Brazil. An Acad Bras Ciênc 79:441–455

Passarelli CR, Basei MAS, Wemmer K, Siga Jr O, Oyhantçabal P (2011) Major shear zones of southern Brazil and Uruguay: escape tectonics in the eastern border of Rio de la Plata and Paranapanema cratons during the Western Gondwana amalgamation. Int J Earth Sci Geol Rundsch 100:391–414

Passarelli CR, Basei MAS, Prazeres Filho HJ, Siga Jr O (2012) First evidence of Calimian basic magmatism in Registro Terrane—Ribeira Belt—State of São Paulo. Book of Abstracts, VIII South American Symposium on Isotope Geology, Medellin, Colombia, p 53

Passarelli CR, Mcreath I, Basei MAS, Siga Jr O (2018) Juquiá and Sete Barras granites and their implications for the tectonic evolution of the Embu Terrane, SE Brazil: tracing the history from the extension to the final collision. J S Am Earth Sci (Submitted, September 2017)

Pereira E, Tassinari CCG, Rodrigues JF, Van-Dúnem MV (2011) New data on the deposition age of the volcano-sedimentary Chela Group and its Eburnean basement: implications to post-Eburnean crustal evolution of the SW of Angola. Comunicações Geológicas 98:29–40

Picanço JL (1994) Aplicação das sistemáticas Sm/Nd e Rb/Sr no Maciço de Itatins (SP). MSc Dissertation, Institute of Geosciences—University of São Paulo, p 140

Picanço J, Tassinari CCG, Cordani UG, Nutman AP (1998) Idades U-Pb (SHRIMP), Sm-Nd e Rb-Srem rochas do Maciço de Itatins (SP): Evidências de Evolução Policíclica. Anais da Academia Brasileira de Ciências 70(1):139–150

Pitcher WS (1995) Origin and nature of granite. Blackie Academic and Professional, New York, p 321

Rapela CW, Fanning M, Casquet C, Pankhurst RJ, Spalletti L, Poiré D, Baldo EG (2011) The Rio de la Plata craton and the adjoining Pan-African/brasiliano terranes: their origins and incorporation into south-west Gondwana. Gondwana Res 20(4):673–690

Rostirolla SP (1991) Tectônica e sedimentação da Bacia de Itajaí–SC. Universidade Federal de Ouro Preto, Ouro Preto. MSc Dissertation, Institute of Geosciences—University of São Paulo, p 132

Salamuni R, Bigarella JJ, Takeda FK (1961) Considerações sobre a estratigrafia e tectônica da Série Itajaí. Bol Parana de Geogr Curitiba 4–5:188–201

Sato K (1998) Evolução Crustal da Plataforma Sul Americana, com base na geoquimica isotópica Sm-Nd. PhD thesis, Institute of Geosciences—University of São Paulo, p 300

Sato K, Siga Jr O, Nutman AP, Basei MAS, McReath I, Kaulfuss G (2003) The Atuba Complex, southern South American platform: archean components and paleoproterozoic to Neoproterozoic tectono thermal events. Gondwana Res 6(2):51–263

Sato K, Williams I, Hyder J, Yaxley G, Cordani UG, Tassinari CCG, Basei MAS, Siga Jr O (2008) Multicollector SHRIMP IIe of Brazil—first results. In: Barilloche SC (ed) VI South American Symposium on Isotope Geology

Seth B, Armstrong RA, Brandt S, Villa IM, Kramers JD (2003) Mesoproterozoic U-Pb and Pb–Pb ages of granulites in NWNamibia: reconstructing a complete orogenic cycle. Precambr Res 126:147–168

Siga Jr O (1995) Domínios tectônicos da região sudeste do Paraná e Nordeste de Santa Catarina. Geocronologia e Evolução Crustal. PhD thesis, Institute of Geosciences—University of São Paulo, p 290

Siga Jr O, Basei MAS, Machiavelli A (1993) Evolução geotectônica da porção NE de Santa Catarina e SE do Paraná, com base em interpretações geocronológicas. Rev Bras Geociên 23(3):215–223

Siga Jr O, Basei MAS, Reis Neto JM, Machiavelli A, Harara OM (1995) O Complexo Atuba: um cinturão Paleoproterozóico intensamente retrabalhado no Neoproterozóico. Boletim IG-USP Serie Científica 26:69–98

Siga Jr O, Basei MAS, Sato K, Citroni SB, Reis Neto JM, Weber W, Lima PS, Sproesser WM (1999) Post-orogenic magmatism and sedimentation in Neoproterozoic extensional regimes in the

Brazilian southern region. South American Symposium on Isotope Geology 2. Cordoba, Argentine, pp 367–370

Siga Jr O, Basei MAS, Passarelli CR, Harara OMM, Sato K, Cury LF, Prazeres Filho HJ (2007) Geocronologia das rochas gnáissico-migmatíticas e sienograníticas do Núcleo Setuva (PR): implicações tectônicas. Rev Bras Geociên 37:114–128

Siga Jr O, Basei MAS, Passarelli CR, Sato K, Cury LF, McReath I (2009) Lower and Upper Neoproterozoic magmatic records in Itaiacoca Belt (Paraná-Brazil): Zircon ages and lithostratigraphy studies. Gondwana Res 15:197–208

Siga Jr O, Basei MAS, Nutman AP, Sato K, Mcreath I, Passarelli CR, Liu D (2011a) Extensional and colisional magmatic records in the Apiaí Terrane, south-southeastern Brazil: integration of geochronological U-PB Zircon ages. Geologia USP 11:149–175

Siga Jr O, Cury LF, Mcreath I, Ribeiro LMAL, Sato K, Basei MAS, Passarelli CR (2011b) Geology and geochronology of the Betara Region in South-Southeastern Brazil: evidence for possible Statherian (1.80–1.75 Ga) and Calymmian (1.50–1.45 Ga) extension events. Gondwana Res 19:260–274

Siga Jr O, Basei MAS, Passarelli CR, Sato K, Nutman A, Mcreath I, Prazeres Filho HJ (2011c) Calymmian (1.50–1.45) magmatic records in Votuverava and Perau Sequences, south-southeastern Brazil: Zircon ages and Nd-Sr isotopic geochemistry. J S Am Earth Sci 32:301–308

Siga Jr O, Campanha GAC, Faleiros FM, Basei MAS, Sato K, Dantas E, McReath I (2012) Detrital Zircon U-Pb and Hafnio Geochronology from the Capiru and Turvo-Cajati Formations (S-SE Brazil): Tectonic Implications. In: VIII South American Symposium on Isotope Geology—SSAGI, 2012, Colombia. Summaries. Colombia

Siga Jr O, Faleiros FM, Campanha GAC, Basei MAS, Sato K, Passarelli CR (2014) Neoproterozoic records in metasedimentary sequenceof Turvo-Cajati Complex (S-SE Brazil): U-Pb detrital zircon geochronology. In: 9th South American Symposium on Isotope Geology, São Paulo, vol 219. Book of Abstracts

Silva ATSF, Chiodi Filho C, Chiodi DK, Algarte JP (1978) Geologia Integrada das Folhas Cananéia e Iguape. In: Congresso Brasileiro de Geologia 30, Recife, PE, Brasil, SBG 1: 208–221

Silva LC, Dias AA (1981) Projeto Timbó—Barra Velha, Brasil. Porto Alegre, p 282 (Convênio DNPM/CPRM—relatório inédito)

Silva LC, McNaughton NJ, Armstrong R, Hartmann LA, Fletcher IR (2005) The Neoproterozoic Mantiqueira Province and its African connections: a zircon-based U-Pb geochronologic subdivision for the Brasiliano/Pan-African systems of orogens. Precambr Res 136:203–240

Tupinambá M, Heilbron M, Duarte BP, Nogueira JR, Valladares C, Almeida J, Silva LGE, Medeiros SR, Almeida CG, Miranda A, Ragatky CD, Mendes J, Ludka I (2007) Geologia da Faixa Ribeira Setentrional: Estado da Arte e Conexões com a Faixa Araçuaí. Geonomos 15:67–79

Tupinambá M, Heilbron M, Valeriano CM, Porto R Jr, Dios FB, Machado N, Silva LGE, Almeida JCH (2012) Juvenile contribution of the Neoproterozoic Rio Negro Magmatic Arc (Ribeira Belt, Brazil): implications for Western Gondwana amalgamation. Gondwana Res 21:422–438

Vasconcelos CS, Yamato AA, Dehler NM, Lopes Jr. I (1999) Projeto Jacupiranga – Rio Guaraú, Estado de São Paulo. São Paulo, Convênio CPRM/ Secretaria de Energia do Governo do Estado de São Paulo (inédito)

Vaughan APM, Pankhurst RJ (2008) Tectonic overview of the West Gondwana margin. Gondwana Res 13:150–162

Yamato AA (1999) Mapeamento geológico de parte da Folha Bocaiúva do Sul (SG.22-X-D-I-2), escala 1:50.000. MSc Dissertation, Institute of Geosciences - University of São Paulo, p 108

The Geology and Evolution of the Angolan Shield, Congo Craton

9

Hielke A. Jelsma, Steve McCourt, Samantha H. Perritt, and Richard A. Armstrong

Abstract

New U–Pb zircon SHRIMP ages are presented and used together with published age and geochemical data and geological observations to review the Palaeoproterozoic evolution of the Angolan Shield of Central Africa. The shield comprises at least three main crustal tectonic domains: the Central Shield Zone in the east and the Central Eburnean Zone and Lubango Zone in the west. The latter extends south into Namibia as the Epupa Metamorphic Complex and further south is exposed in the Kamanjab and Grootfontein inliers. The magmatic events associated with these tectonic domains have been attributed to the formation of a system of arcs that developed along the active western and southern continental margins of the Congo Craton, with peak magmatic events at 2.0–1.96 Ga (Eburnean Event), 1.88–1.83 Ga (Kamanjab-Bangweulu Event) and 1.80–1.77 Ga (Epupa Event). Along the western continental margin, precise age data confirms the presence of Eburnean granitoids from the Huambo-Andulo region in Angola south to the Kamanjab-Grootfontein region in NW Namibia, a distance of over 1000 km. Geochronology and isotope geochemistry indicates that Neoarchaean crust was involved in the formation of these granitoids. Field relations indicate that this ~2.0 Ga granitic crust was metamorphosed and deformed during orogeny at 1967 Ma. Along the southern continental margin within the Kamanjab Inlier a second magmatic event is documented at *c*. 1.84 Ga, with inherited grains suggesting the involvement of older crust with a similar age to that exposed in SW Angola and in the nearby Grootfontein-Tsumkwe Inlier. This event may be related to magmatism within the basement to the Lufilian Arc and Bangweulu Block. In the Epupa Metamorphic Complex a third magmatic event is documented at *c*. 1.77 Ga. It is likely that additional events will be recognized with further high precision geochronology, as is observed for instance along the Andean continental margin which has been periodically active at least since the early Paleozoic.

Keyword

Angolan Shield • SHRIMP • Geochronology Tectonics

9.1 Introduction

The Congo Craton of Central Africa (Fig. 9.1) comprises Precambrian continental crust that preserves evidence for crustal growth from the Mesoarchaean through to the Mesoproterozoic. At current levels of erosion, a large part of the Congo (alt. Central African) Craton is buried below Neoproterozoic and Phanerozoic cover rocks but Archaean and Palaeoproterozoic basement has been recognized in four shield areas around the edges of the block. One of these basement terranes is the Angolan Shield (Fig. 9.1), which lies at the southwest margin of the Congo Craton and is exposed in Angola, Namibia and Botswana between 9 and 20°S and west of longitude 22°E.

In this paper we use new and published age and geochemical data, field observations and information gleaned from historic geological maps as well as geophysical and remote sensing data to outline our understanding of the geology and evolution of the Angolan Shield. Within

H. A. Jelsma (✉)
Anglo American Group Discovery and Geosciences, Johannesburg, South Africa
e-mail: hielke.jelsma@angloamerican.com

S. McCourt
Geological Sciences, School of Agricultural, Earth and Environmental Sciences, University of KwaZulu-Natal, Durban, South Africa

S. H. Perritt
De Beers Exploration, Johannesburg, South Africa

R. A. Armstrong
Research School of Earth Sciences, Australian National University, Canberra, ACT, Australia

S. Siegesmund et al. (eds.), *Geology of Southwest Gondwana*, Regional Geology Reviews,
https://doi.org/10.1007/978-3-319-68920-3_9

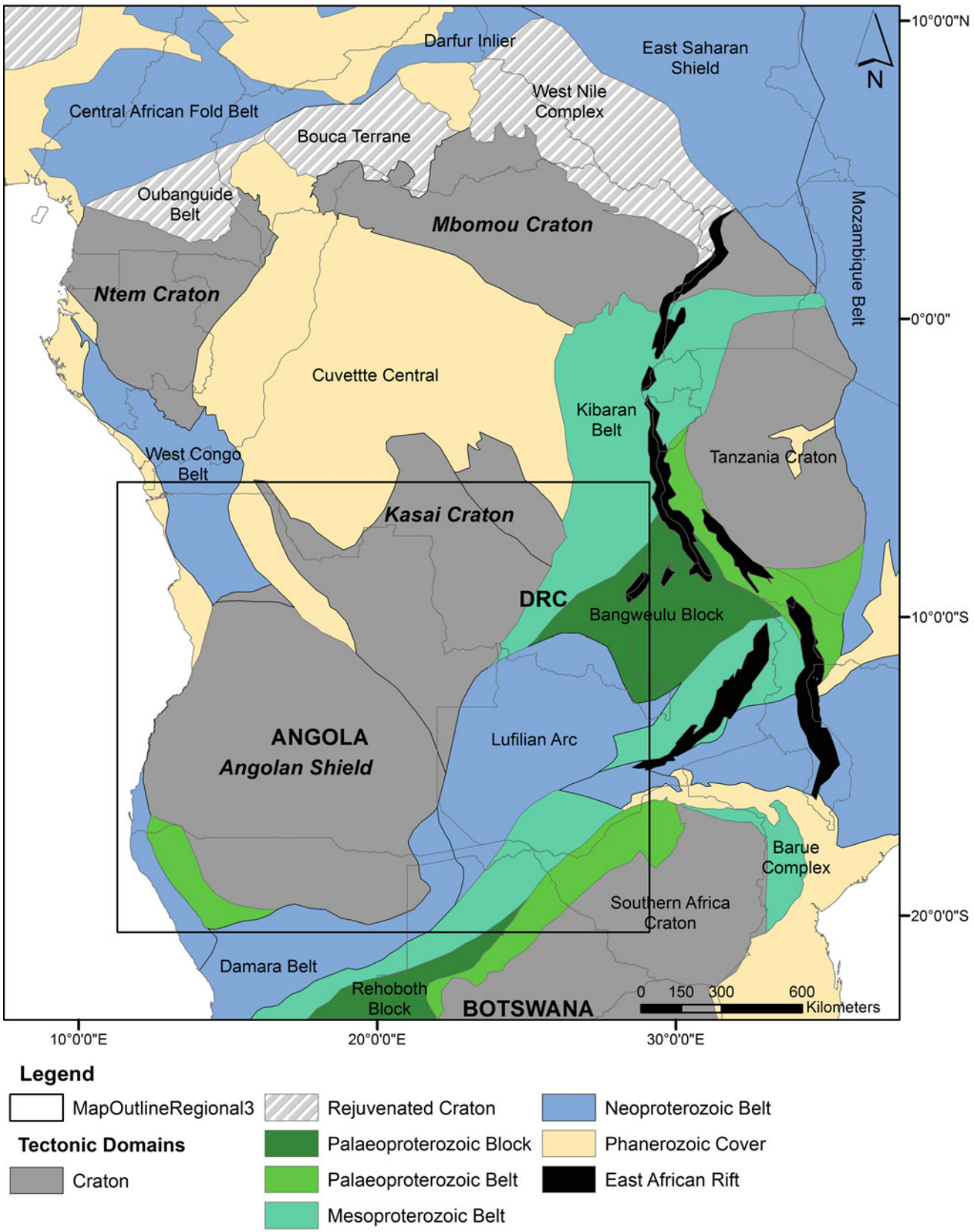

Fig. 9.1 Precambrian tectonic framework of south-central Africa showing the Congo Craton and exposed shield areas: Kasai Craton (south) and Angolan Shield (southwest), Ntem (Chaillu-Gabon) Craton (northwest) and Mbomou (NE DRC) Craton (northeast), which were once joined with the Saõ Francisco Craton

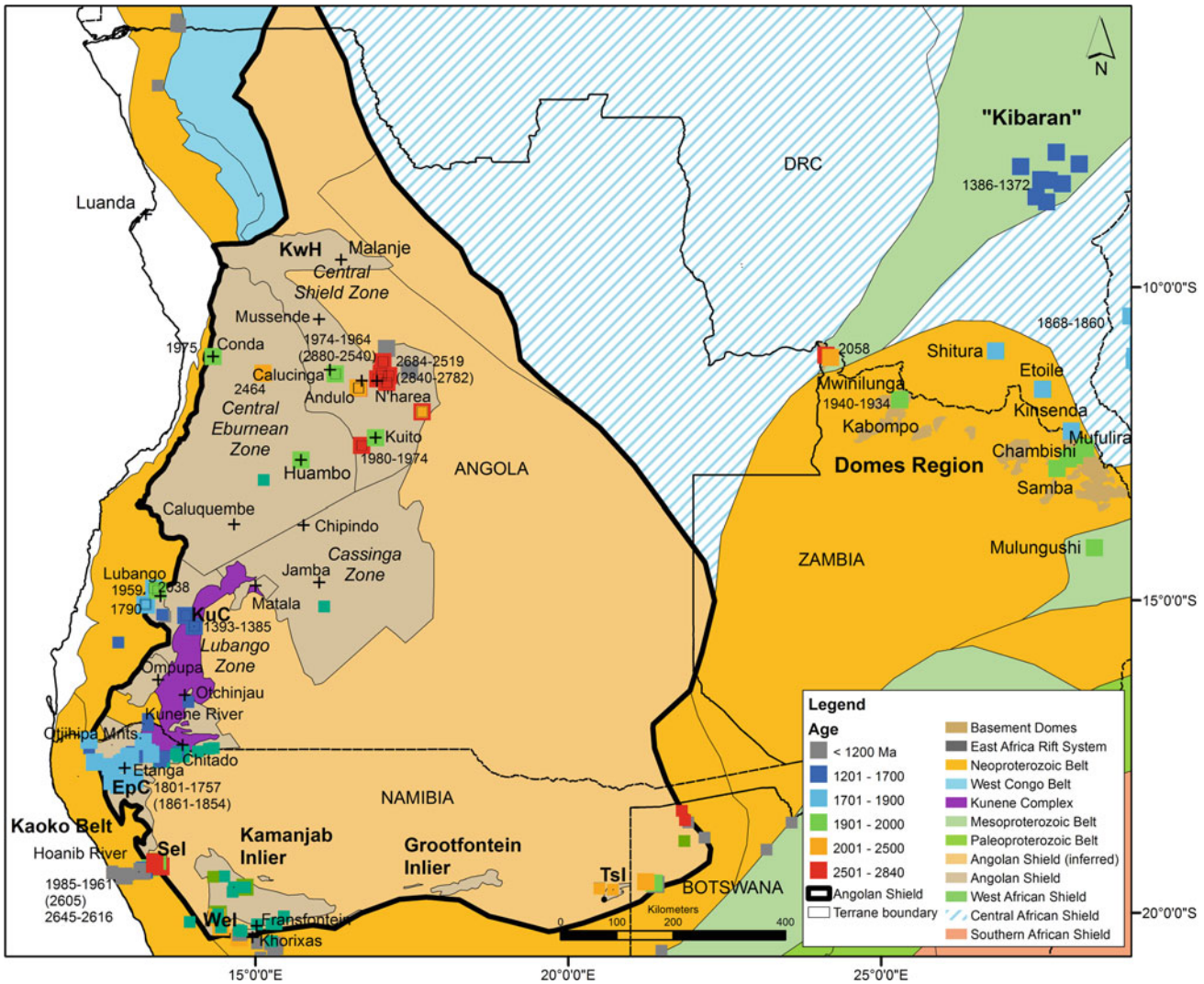

Fig. 9.2 Geographic information system (GIS)-based map showing the Precambrian tectonic framework of the Angolan Shield, modified after de Carvalho and Alves (1993) with the location of the main crustal tectonic domains as well as basement inliers in northern Namibia, Botswana and Zambia, and several towns for reference. Geochronological data shown is recently published U–Pb zircon ages and age ranges for granitoids and associated volcanic rocks along the southern margin of the Congo Craton as cited in the text; ages in brackets are from zircon grains interpreted as xenocrysts. *EMC* Epupa Complex; *KuC* Kunene Complex; *KwH* Kwanza Horst; *SeI* Sesfontein Inlier; *TsI* Tsumkwe Inlier; *WeI* Welwitschia Inlier

Angola, we identify three main crustal tectonic domains: the Central Shield Zone in the east and the Central Eburnean Zone and Lubango Zone in the west. The latter extends south into Namibia as the Epupa Metamorphic Complex and further south is exposed in the Kamanjab and Grootfontein inliers (Fig. 9.2).

9.2 Analytical Techniques

SHRIMP II U–Pb zircon analyses were conducted at the Research School of Earth Sciences, Australian National University on samples from key stratigraphic units to assess the extent of Archaean basement and to provide age constraints on the nature and timing of magmatic, tectonic and sedimentation events. Analytical procedures follow, for example, Stern (1997) with data reduction via SQUID and ISOPLOT (Ludwig 1998, 2003). The standard mount for SHRIMP analysis is a 25 mm round disk that is held in a mount holder. Samples are polished and characterized through various types of imaging (visual, electron). Samples are coated with a conductive material (typically gold, carbon) to avoid sample charging. Finally experimental routines were followed to convert the measured ion abundances into actual concentrations and isotopic ratios.

9.3 Regional Geology of the Angolan Shield

9.3.1 SW Angola

Previous accounts of the regional geology of Angola included de Carvalho et al. (1987, 2000) and de Carvalho and Alves (1993). McCourt et al. (2013) published the first precise U–Pb zircon age data for granitoids from the Lubango Zone while conference abstracts by Delor et al. (2006) and Jelsma et al. (2011) include U–Pb zircon ages for granitoids and associated volcanic rocks in the Central Eburnean Zone and the Central Shield Zone. This age data, although limited, suggests that the Central Shield Zone is characterized by Archaean age granitoid gneisses with Palaeoproterozoic granites dominant in the Central Eburnean and Lubango zones (see details below).

9.3.1.1 Archaean Crust

Archaean basement rocks are common constituent rocks of the Central Shield Zone and have been documented from the Kwanza Horst (alt. Block) with ages between 2590 and 2520 Ma (de Carvalho et al. 2000; Delor et al. 2006) and from the Andulo Region of Bié Province. The latter include intermediate to felsic gneisses and granitoids and associated metavolcanic and metasedimentary rocks. De Carvalho et al. (2000) documented an Rb–Sr whole rock isochron age of 2520 ± 36 Ma for granitoid gneisses from the Andulo region. This age was confirmed by Jelsma et al. (2011, 2013) through U–Pb zircon ages on biotite gneisses between 2682 and 2519 Ma. Delor et al. (2006) did not identify any rocks of Archaean age in their study of the Central Eburnean Zone, but did report inherited zircons from Palaeoproterozoic granitoids and rhyolites with ages between 2.71 and 2.51 Ga.

Here we report previously unpublished data on the basement rocks from the Andulo area (Central Shield Zone).

CVZ609 Sample CVZ609 (coordinates 16.956°E, 11.466°S) is a megacrystic biotite gneiss that contains feldspar megacrysts (3–5 cm in size) and shows a well-developed fabric in outcrop, hand specimen and thin section (Fig. 9.3a). The rock contains biotite (5%) and garnet (1%), with accessory opaque minerals, secondary chlorite, zircon, apatite, epidote and rutile. Twenty-one spots on 19 zircons were analysed (Fig. 9.4a; Appendix 9.1). Discordance varies between 0 and 57%. Six concordant zircons (discordance of 0%) give a mean $^{207}Pb/^{206}Pb$ age of 2533 ± 11 Ma (MSWD = 0.76, probability 0.58). The Concordia age of 2533 ± 11 Ma (Fig. 9.4a) is interpreted as the crystallization age of the protolith.

CVZ612 Sample CVZ612 (coordinates 17.100°E, 11.525°S) is a reddish biotite granite showing decimetre-scale banding (Fig. 9.3b). The rock is medium-grained, equigranular and massive (in hand section) and contains biotite (2%), secondary chlorite (5%), opaque minerals (2%) and accessory zircon (abundant), apatite and euhedral epidote. The red colouration is a product of extensive alteration and replacement of feldspars and micas by clay minerals. Twenty-three spots were analysed on 20 zircons (Fig. 9.4b; Appendix 9.1). Discordance varies between −2 and 70%. Five (near) concordant zircons (discordance of −3 to 2%) give a mean $^{207}Pb/^{206}Pb$ age of 2519.4 ± 5 Ma (weighted by data point errors only), with MSWD = 0.13, probability 0.97. Two zircons give older $^{207}Pb/^{206}Pb$ ages of 2782 ± 6 Ma (2% discordant) and 2670 ± 11 Ma (1% discordant). The mean and (near)-concordant $^{207}Pb/^{206}Pb$ age of 2519.4 ± 5 Ma (Fig. 9.4b) is interpreted as the crystallization age of the intrusion. The two older zircons with $^{207}Pb/^{206}Pb$ ages of 2782 ± 6 Ma and 2670 ± 11 Ma have been interpreted as inherited zircons.

CVZ614 Sample CVZ614 (coordinates 17.131°E, 11.414°S) is a grey biotite gneiss with 2–3 cm sized feldspar megacrysts (Fig. 9.3c). The rock is coarse-grained, inequigranular and gneissic and contains biotite (6%), metamorphic garnet (5%) and accessory sericite, secondary chlorite, opaque minerals, apatite and tourmaline. Twenty-three spots on 20 zircons were analysed (Fig. 9.4c; Appendix 9.1). Discordance varies between −2 and 55%. Seven concordant zircons (discordance of −2 to 1%) give a Concordia age of 2521.8 ± 5 Ma. A model 2 solution regression on all 23 zircons (± 95% conf.) gives an upper intercept of 2518 ± 12 Ma and a lower intercept of 603 ± 42 Ma, with MSWD = 19, probability 0. The Concordia age of 2521.8 ± 5 Ma (Fig. 9.4c) is interpreted as the crystallization age of the protolith.

CVZ862 Sample CVZ862 (coordinates 17.014°E, 11.379°S) is a medium- to coarse-grained equigranular and massive granodiorite and contains biotite (3%), secondary chlorite, epidote (both euhedral crystals and as saussurite) and accessory opaque minerals, zircon, apatite and titanite (Fig. 9.4d; Appendix 9.1). Twenty spots on 20 zircons were analysed showing varying discordance. Eight concordant and near-concordant zircons (−2 to 1% discordance) give an age of 2681.6 ± 4.6 Ma (Fig. 9.4d), which is the preferred magmatic age.

In the eastern part of the Central Shield Zone Archaean gneisses and granites are well preserved. In the western part, field relationships of Archaean gneisses are typically as enclaves within the Palaeoproterozoic Regional Granite (de Carvalho and Alves 1993; Jelsma et al. 2011). In the southern part of the Central Shield Zone, Korpershoek (1984) described a sequence of schist, greywacke, pillow lava, chert, felsic volcanic rocks and pelite resting unconformably on gneissic basement and intruded by granite. De Carvalho and Ayles (1993) named this sequence the Jamba Group and interpreted it as the remnant of an Archaean

Fig. 9.3 Plate showing some of the petrographic characteristics of Archean rocks from the Central Shield Zone of west-central Angola. **a** CVZ609 megacrystic biotite gneiss. **b** CVZ612 biotite granite. **c** CVZ614 biotite gneiss. **d** CVZ862 granodiorite

greenstone belt, although no age data was reported. Schists, quartzites, cherts and amphibolites have also been mapped in the N'harea area, enveloped by Archaean granite-gneiss domes.

9.3.1.2 Palaeoproterozoic Crust

Infracrustal and supracrustal rocks related to Palaeoproterozoic tectonics are widespread in southwest Angola (Cahen et al. 1984; de Carvalho and Alves 1993). The infracrustal rocks, referred to as the Regional Granite, are the dominant component and occur in each of the tectonic zones originally recognized by de Carvalho et al. (2000) and redefined here. The ages published by Cahen et al. (1984) and de Carvalho et al. (2000) are exclusively Rb–Sr whole rock isochron dates and thus of uncertain significance. More recently, however, a number of studies have reported U–Pb ages on zircon. Delor et al. (2006) working in the Central Eburnean Zone provide constraints of 1980 ± 9 and 1987 ± 16 Ma on granite from the Huambo area; 1975 ± 23 Ma on granodiorite from the Conda area further north (Fig. 9.2); and 1964 ± 9 and 1978 ± 11 Ma on rhyolite and rhyodacite from the overlying supracrustal package. The indistinguishable ages of the intrusive granitoids and the overlying felsic lavas prompted Delor et al. (2006) to suggest the magmatism was linked to an extensional regime rather than orogeny. Jelsma et al. (2011, 2013) report U–Pb SHRIMP ages of between 1974 ± 5 and 1966 ± 3 Ma for granite and granodiorite from the Central Shield Zone, while McCourt et al. (2013) report SHRIMP ages of 2038 ± 28 and 1954 ± 6 Ma for granite from the Lubango Zone. In contrast to Delor et al. (2006), Jelsma et al. (2011) and McCourt et al. (2013) relate the granitoid magmatism to an active continental margin along the southern margin (present coordinates) of the developing Congo Craton.

New unpublished age constraints on Palaeoproterozoic granitoids from the Central Shield Zone are summarized here.

CVZ605/CVZ606 Samples CVZ605 and CVZ606 are exposed in a road-cutting at coordinates 16.275°E and

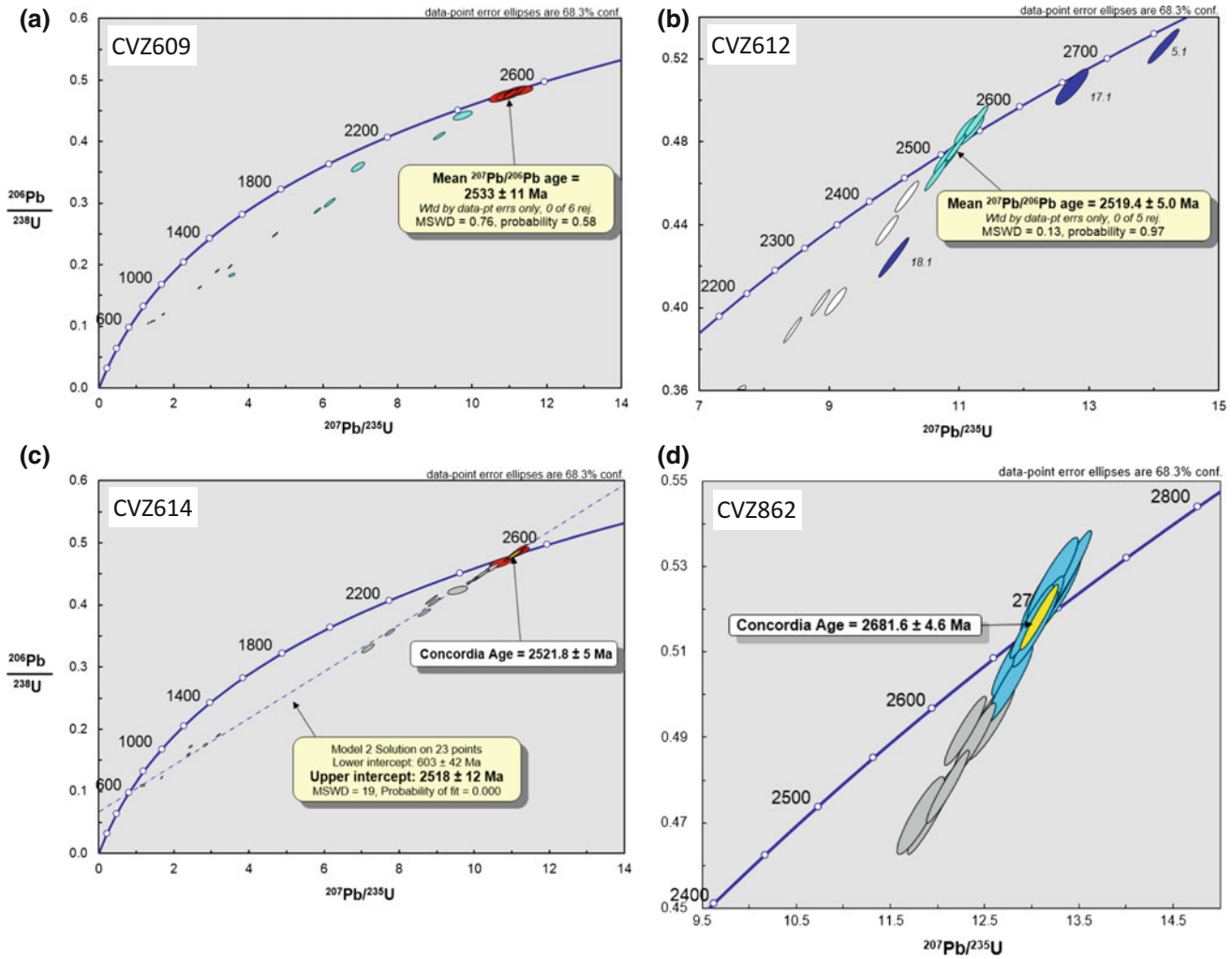

Fig. 9.4 Concordia plots showing zircon isotopic ratios and derived ages for Archean rocks from the Central Shield Zone of west-central Angola

11.389°S (Figs. 9.5a, b). Sample CVZ605 (Fig. 9.5a) is a granodioritic augen gneiss, with plagioclase megacrysts and anastomosing biotite fabric, and is intruded by a granodiorite with xenoliths of augen gneiss (CVZ606, Fig. 9.5b). The augen gneiss (CVZ605) is coarse grained and inequigranular and contains biotite (4%), secondary chlorite, opaque minerals and abundant rutile, and accessory apatite and zircon. Sample CVZ606 is a medium-grained, massive granodiorite showing intrusive field relationships and containing xenoliths of augen gneiss. The granodiorite (CVZ606) is medium grained and shows a weakly defined gneissic fabric. It contains biotite (6%), opaque minerals (2%, euhedral to anhedral) and accessory zircon and apatite. Seventeen (near)-concordant zircons (discordance between −2 and 7%) give a mean $^{207}Pb/^{206}Pb$ age of 1965.6 ± 3.1 Ma (MSWD = 0.30, probability 0.997) for sample CVZ605 (Fig. 9.6a; Appendix 9.1). A model 1 solution regression on all 22 zircons (± 95% conf.) gives an upper intercept of 1973.5 ± 4.3 Ma and a lower intercept of 358 ± 48 Ma, with MSWD = 0.91, probability 0.57. The mean and (near)-concordant $^{207}Pb/^{206}Pb$ age of 1965.6 ± 3.1 Ma is interpreted as the crystallization age of the protolith (Fig. 9.6a). Twenty spots on 20 zircons were analysed from sample CVZ606 (Fig. 9.6b; Appendix 9.1). Discordance varies between −3 and 38%. Fourteen spots (discordance between −3 and 2%) give a Concordia age of 1967.5 ± 4.5 Ma (Fig. 9.6b) and a mean $^{207}Pb/^{206}Pb$ age of 1967.3 ± 4.5 Ma (MSWD = 0.62, probability 0.84). The Concordia age of 1967.5 ± 4.5 Ma is interpreted as the crystallization age of the granodiorite. The two ages are within error of each other and interpreted to constrain the timing of deformation in the area at ~1965 Ma.

CVZ856 Sample CVZ856 (coordinates 16.699°E, 12.532°S) is composed of two phases: (1) gneissic biotite granite with weakly defined fabric and biotite clots; and (2) leucocratic granite, intrusive in the former (Fig. 9.5c). The gneissic biotite granite is medium-grained and contains biotite (7%, with deformation bending), euhedral epidote

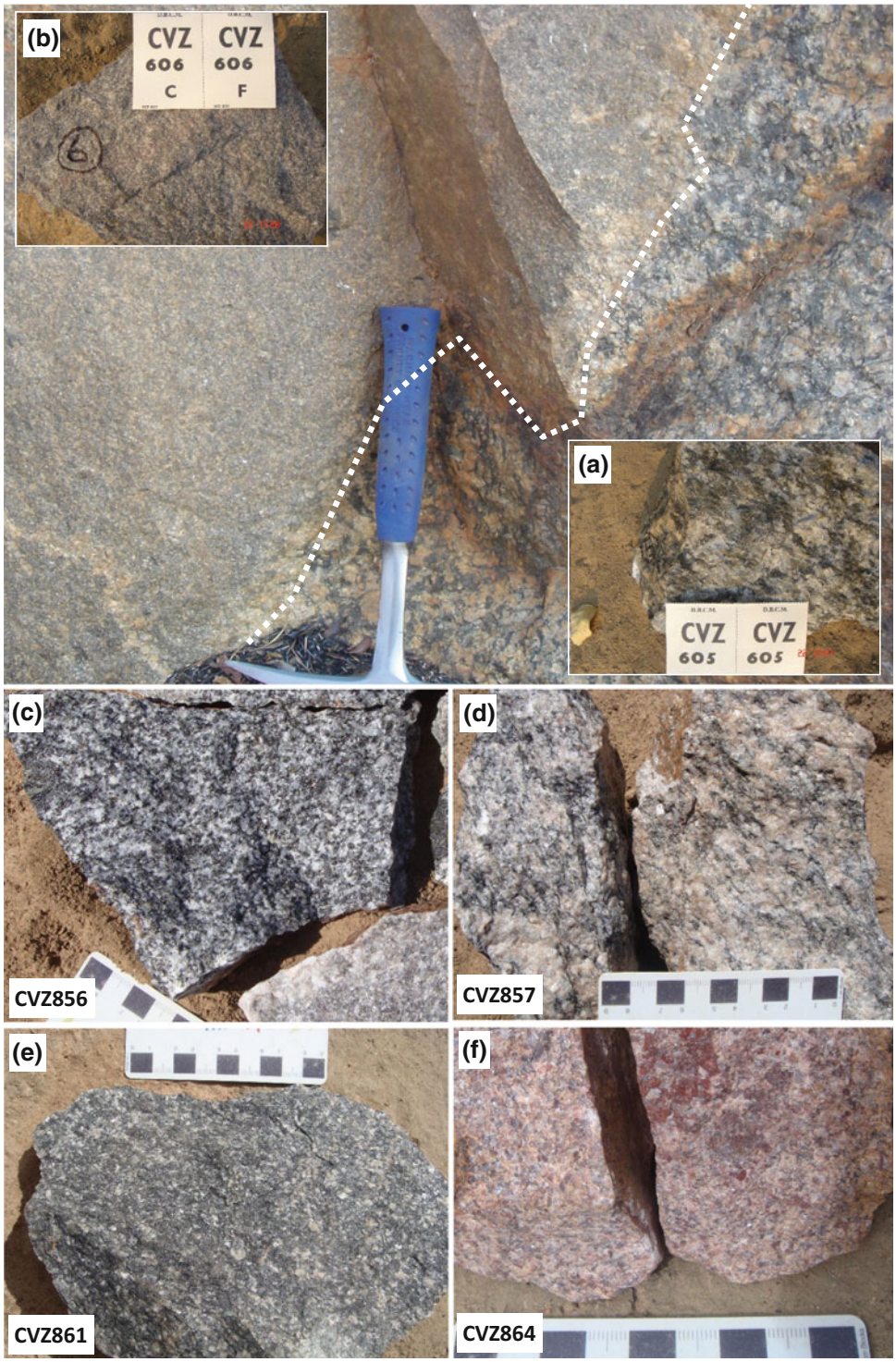

Fig. 9.5 Plate showing some of the petrographic characteristics of Palaeoproterozoic rocks from the Central Eburnean Zone and Central Shield Zone of west-central Angola. **a** CVZ605 granodioritic augen gneiss. **b** CVZ606 granodiorite. **c** CVZ856 biotite granite. **d** CVZ857 megacrystic biotite gneiss. **e** CVZ861 quartz diorite. **f** CVZ864 leucogranite

(2%), opaque minerals and accessory zircon, apatite and titanite. Twenty-two spots on 20 zircons were analysed (Fig. 9.6c; Appendix 9.1). Discordance varies between −2 and 35%. Ten (near) concordant zircons (discordance of −2 to 1%) give a Concordia age of 1973.5 ± 4.9 Ma (Fig. 9.6c). One concordant zircon gives a $^{207}Pb/^{206}Pb$ age of 2599 ± 7 Ma. The Concordia age of 1973.5 ± 4.9 Ma is interpreted as the crystallization age of the biotite granite. The older zircon with a $^{207}Pb/^{206}Pb$ age of 2599 ± 7 Ma is interpreted as an inherited zircon.

CVZ857 Sample CVZ857 (coordinates 16.652°E, 11.614°S is a megacrystic biotite gneiss (Fig. 9.5d). The rock is medium to coarse grained and contains 40–50% feldspar porphyroclasts, anastomosing biotite films and

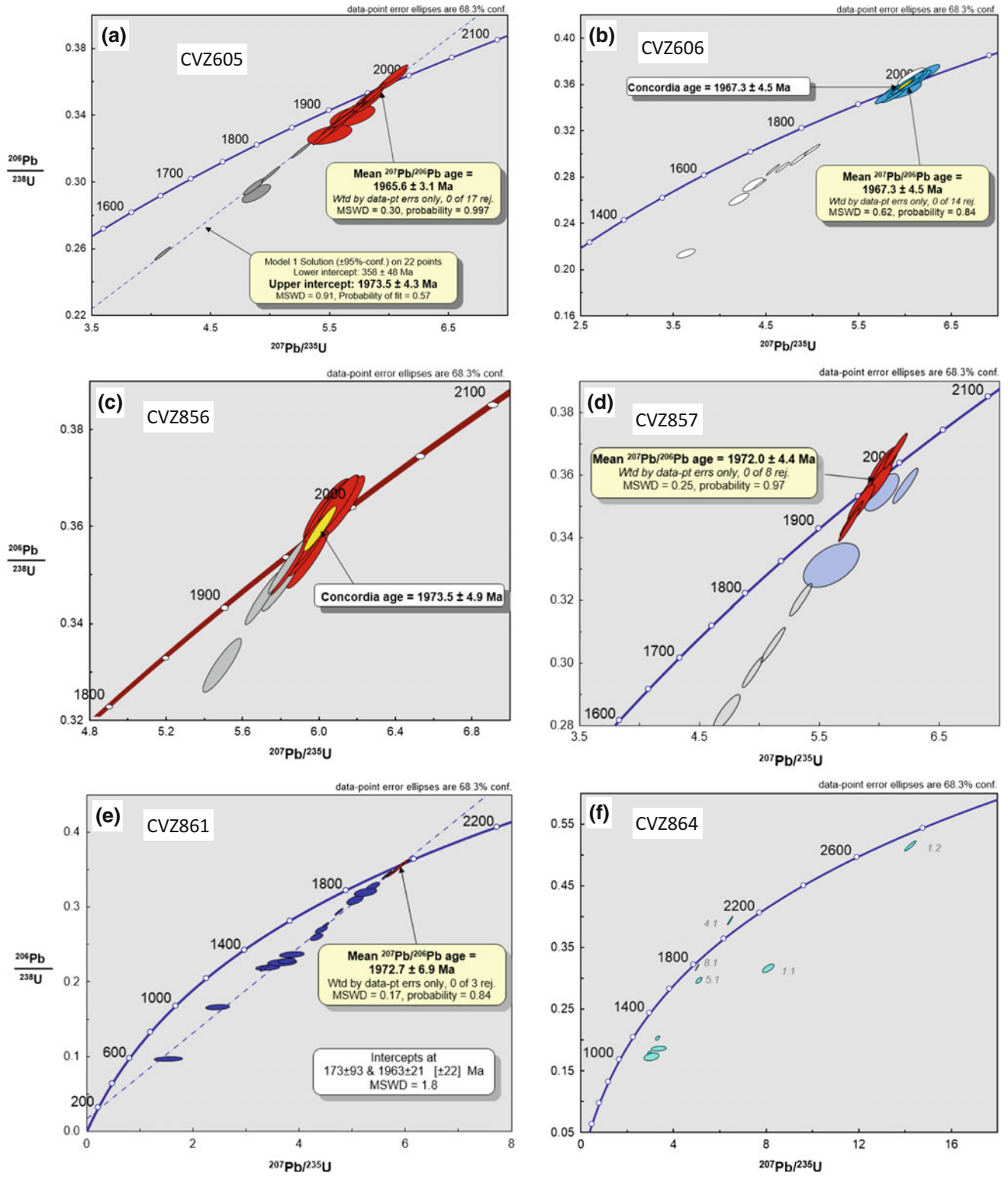

Fig. 9.6 Concordia plots showing zircon isotopic ratios and derived ages for Palaeoproterozoic rocks from the Central Eburnean Zone and Central Shield Zone of west-central Angola

quartz ribbon grains, and can be classified as mylonite. It contains biotite (3%), muscovite (1%) and accessory opaque minerals, zircon and apatite. Twenty-two spots on 20 zircons were analysed (Fig. 9.6d; Appendix 9.1). Excluding analysis 20.1 discordance varies between –2 and 27%. Eight (near) concordant zircons (discordance of −2 to 3%) give a mean

$^{207}Pb/^{206}Pb$ age of 1972 ± 4.4 Ma (Fig. 9.6d); interpreted as the crystallization age of the protolith. Four older zircons with ages between 2540 and 2880 Ma are interpreted as inherited zircons. Within this subgroup, three (near) concordant zircons yield ages of 2539 ± 14 Ma (1% discordant), 2617 ± 24 Ma (−1% discordant) and 2832 ± 12 Ma (−3% discordant).

CVZ861 Sample CVZ861 (coordinates 17.01349°E, 11.41979°S) is a massive quartz diorite showing a high content of hornblende and plagioclase and 1 cm sized tabular hornblende crystals (Fig. 9.5e). In thin section the rock is medium to coarse grained, inequigranular and massive, and contains quartz (15–20%), hornblende (20%), biotite (6%), epidote (6%, both as euhedral crystals and secondary saussurite), and accessory opaque minerals, zircon, apatite and titanite. There is significant scatter superimposed on some highly discordant data, making establishment of a precise age difficult. Three (near)-concordant zircons give a mean $^{207}Pb/^{206}Pb$ age of 1972.7 ± 6.9 Ma (Fig. 9.6e; Appendix 9.1), which is interpreted as the magmatic age. Two older (near) concordant and high Th/U zircon cores yielded $^{207}Pb/^{206}Pb$ ages of 2515 ± 14 Ma (−1% discordant) and 2816 ± 8 Ma (−3% discordant), and have been interpreted as inherited zircons.

CVZ864 Sample CVZ864 (coordinates 17.038°E, 11.192°S) is a medium-grained, massive and equigranular leucogranite, with very low contents of mafic minerals (Fig. 9.5f). The rock is altered and shows abundant iron oxides. The rock contains muscovite (2%) and accessory opaque minerals, epidote, zircon and apatite. Nine spots on eight zircons were analysed. The sample yielded only a very small number of zircons and a heterogeneous population with significant Pb loss in most grains. The zircons are generally of very poor quality, being dark, opaque and highly altered. One grain (#1) has well-developed oscillatory zoning preserved, and is quite different to the remainder of the population. The analyses show that the dark grains have extreme U contents (and high Th) of up to 1.2%. This not only means that the zircon structure has been inevitably badly damaged (metamict) but also severely compromises any U–Pb calibration. The effect of this compromised calibration is to artificially shift the data points up on the Concordia plot, giving high apparent U/Pb 'ages'. The data is discordant, as expected, with the relatively well-preserved grain #1 giving the least discordant results in line with the moderate U contents in both the centre (#1.2) and the margin (#1.1) analyses (Fig. 9.6f; Appendix 9.1). The central area gives a minimum $^{207}Pb/^{206}Pb$ age of 2826 ± 7 Ma (1 sigma). The rim is highly discordant (34%) but is probably not much different in age. The remaining data is scattered and discordant, indicating a complex history of Pb loss and possibly inheritance. The grains with extreme U concentrations have compromised U/Pb ages but give an indication of Palaeoproterozoic $^{207}Pb/^{206}Pb$ ages of about 1933 Ma, although these are minimum ages.

This new U–Pb zircon data identifies Palaeoproterozoic granitoids occurring as intrusive phases within the Archaean gneisses and becoming the predominant basement rock west of Andulo town. In Central Angola these intrusions were emplaced over a very short time span between 1972 and 1965 Ma. Inherited zircon grains with ages between 2832 and 2515 Ma indicate reworking of Archaean basement. Crosscutting gneisses and intrusive rock types yield ages that are within error at ~1967 Ma, thereby constraining the age of regional deformation related to Palaeoproterozoic (Eburnean) orogeny.

Amongst the supracrustal rocks, to the east and northeast of Lubango (Fig. 9.2), de Carvalho and Alves (1993) document three packages of supracrustal material, which they refer to as the Bale, Chivanda (locally Cuandja) and Oendolongo Groups. The Bale Group occurs within the southern part of the Central Shield Zone and lies unconformably on the rocks of the Jamba Group. De Carvalho and Alves (1993) describe the Bale Group as a clastic succession comprising quartzite with interbedded conglomerates at the base, overlain by finely laminated shale and, at the top, a siltstone-sandstone facies. They interpreted it as younger than and unconformable on the Chivanda Group, but older than the Oendolongo Group. There are, however, no direct age constraints on the rocks of the Bale Group.

The Chivanda Group is a deformed meta-volcano-sedimentary sequence comprising quartzite with conglomeratic layers, sandstone, greywacke and occasional limestone overlain by mafic volcanic rocks, including pillow lava, followed by conglomerate and felsic volcanics. The top of the succession is black manganiferous schist. In the Chipindo region further south, felsic schists, interpreted as tuffs, from the base of the locally named Cuandja Group have yielded imprecise Rb–Sr ages, indicating a Palaeoproterozoic age (De Carvalho and Alves 1993). These supracrustal rocks are intruded by the Regional Granite (see below), which thus provides a minimum age for the group.

The Oendelongo Group is a package of metasedimentary rocks outcropping over a large area in the Caluquembe region to the north of Lubango (Fig. 9.2) and thus within the Central Eburnean Zone. De Carhalvo and Alves (1993) note that, like the Bale Group, the rocks of the Oendelongo Group are unconformable on the Chivanda Group and interpret them as a molasse sequence related to uplift following deformation and metamorphism of the latter. They further note that whereas rocks of the Bale Group are intruded by granite, those of the Oendelongo Group are younger than the basement granitoids.

Delor et al. (2006) report sandstone and conglomerate with interbedded felsic volcanics as forming significant topography in the central and eastern part of the Central

Eburnean Zone. Although they do not attempt to correlate these rocks with the subdivisions of de Carhalvo and Alves (1993), they note the supracrustal rocks are deformed, with both open and tight folding reported, and that they are unconformable on the regionally dominant granitoid gneisses and undeformed granite.

The Chela Group is a supracrustal sequence best exposed on the Humpata Plateau near Lubango that was previously interpreted as being both Mesoproterozoic (de Carvalho and Alves 1993) and Neoproterozoic (Kröner and Correia 1980) in age. McCourt et al. (2013) analysed zircon grains from three units within the Chela Group. An ignimbrite from the Humpata Formation was dated at 1798.4 ± 10.6 Ma and interpreted as a direct constraint on the Palaeoproterozoic age of this unit, while detrital grains from two samples of quartz-arenite provided a maximum age of 1782 ± 6 Ma of deposition for the overlying Bruco Formation.

In the extreme south of Angola along the border with Namibia are isolated occurrences of what de Carhalvo and Alves (1993) refer to as the Tchipa-Iona Formation. In the type area, this formation comprises quartzites, arkoses, cherts and rare marbles, and is locally folded. There are felsic-volcanic rocks (porphyries, rhyolites and tuffs) associated with the metasedimentary units. Although there are no direct age constraints on the rocks of the Tchipa-Iona Formation, the intrusive Mesoproterozoic Red Granite provides a minimum age constraint. De Carvalho and Alves (1993) regard the Tchipa-Iona Formation as Palaeoproterozoic in age and suggest it may be equivalent to the Khoabendus Group of NW Namibia (see below) (Table 9.1).

9.3.1.3 Mesoproterozoic Crust

The Red Granite (De Carvalho and Alves 1993) occurs in the Lubango Zone and is best exposed in the area around Matala and the Ompupa-Otchinjau-Chitado region to the southeast (see McCourt et al. 2013, Fig. 2). The granite occurs as elongate northeast–southwest trending bodies intrusive into the anorthosite of the Kunene Complex and the supracrustal rocks of the Tchipa-Iona Formation. The reddish colour is due to disseminated iron oxide. The texture is usually porphyritic and the matrix is coarse to medium grained. Mafic minerals are typically rare but both hornblende and biotite have been described (De Carvalho and Alves 1993). In addition to granite, monzonite, syenite, charnockite, mangerite and rhyolitic porphyry have also been documented (De Carvalho and Alves 1993). Published ages for the occurrences in Angola are based on the Rb–Sr system and are best constrained by 1302 ± 20 Ma from the Chitado Red Granite (de Carvalho and Alves 1993). In NW Namibia, however, Seth et al. (2005) obtained a precise SHRIMP U–Pb age of 1374±5 Ma on zircon from Red Granite intruding granitoid gneiss of the Epupa Metamorphic Complex (see later).

The Kunene Complex dominates the geology of southwest Angola and the neighbouring part of Namibia. The Complex intruded along the southern margin of the Congo Craton and in outcrop and suboutcrop defines a north-northeast trending elongate shape that in Angola covers an area of *c*. 15,000 km^2 (Ashwal and Twist 1994). Country rocks exposed along the western margin of the Complex comprise a variety of metamorphic and igneous rocks that include the Regional Granite (De Carvalho and Alves 1990). The dominant rock type of the Complex is massive anorthosite followed by leucotroctolite, troctolite, gabbro, leucogabbro and subordinate norite (de Carhalvo and Aves 1993 and references therein). Ultramafic rocks appear to be absent (Ashwal and Twist 1994). Mayer et al. (2004) note the presence of dolerite at the northwestern margin of the Complex and based on mutually intrusive relationships suggest the dolerite is co-genetic with the anorthosite. Mayer et al. (2004) further note that in proximity to the Red Granite the Kunene Complex is characterized by massive Fe–Ti ore bodies, and they propose a genetic link between anorthosite, Fe–Ti ore bodies and at least some of the Red Granite.

The age of the Kunene Complex is well constrained. Mayer et al. (2004) document a near concordant upper intercept age of 1371 ± 2.5 Ma for a mangerite dyke cutting anorthosite in the northern part of the Complex. This age is supported by a U–Pb single zircon age of 1385 ± 25 Ma on anorthosite from the Kunene Complex in Namibia (Druppel et al. 2007) and 1385 ± 7.6 Ma on samples from the Dongue area in Angola (McCourt et al. 2013). In addition to the U–Pb zircon ages, Mayer et al. (2004) reported a Sm–Nd mineral age of 1319 ± 13 Ma, which they interpreted as dating the end of magmatism. The Kunene Complex is one of the largest massif-type anorthosite bodies in the world (Ashwal and Twist 1994), and its intrusion signifies a period of significant crustal extension along the southwest margin of the Congo Craton at *c*. 1385 Ma, possibly related to the prominent ~1375 Ma tectono-magmatic 'Kibaran Event' (Fig. 9.2), which comprises intraplate emplacement of abundant coeval bimodal magmatism under an extensional regime (Tack et al. 2008).

9.3.2 NW Namibia

Within Namibia, rocks interpreted as representing the southwestern margin of the Congo Craton are exposed in the Epupa Metamorphic Complex, the Kamanjab Inlier and the Grootfontein Inlier, and along the Hoanib River near Sesfontein (Fig. 9.2).

Kröner et al. (2010) define the Epupa Metamorphic Complex (EMC) as the gneiss terrane extending from Hoanib River valley near Sesfontein in NW Namibia

Table 9.1 Precambrian lithostratigraphic units of southwest Angola and northern Namibia

Lithostratigraphic unit	Principal rock types	Age (Ma)	Comment
Neoproterozoic			
Damara Supergroup	Quartzites, conglomerates, marble, amphibolites, schists	No published ages	Interpreted as an extension of the Nosib Group in northern Namibia
Mesoproterozoic			
Leba-Tchamalindi Formation	Stromatolitic dolomites, chert and anhydrite	No published ages	Unconformable on Chela Group (de Carvalho et al. 1987)
Red Granite	Granites, granodiorites, syenites, rhyolitic porphyries	1374 ± 5 Ma (Seth et al. 2005); 1302 ± 20 Ma Chitado granite; 1411 ± 24 Ma Otechinjau granite; 1407 ± 26 Ma Ompupa granite; 1350 ± 65 Ma Matala granite (de Carvalho and Alves 1993, Rb–Sr ages)	Intrusive into the anorthosite of the Kunene Complex and the supracrustal rocks of the Tchipia-Iona and Cahama-Otechinjau formations (de Carvalho et al. 1987)
Kunene Complex	Massive anorthosite, leucotroctolite, leucogabbro, mangerite, syenodiorite	1385 ± 25 Ma anorthosite; 1371 ± 3 Ma mangerite dyke (Mayer et al. 2004, U–Pb zircon)	Ages from McCourt et al. (2013), Mayer et al. (2004) and Drüppel et al. (2007), U–Pb zircon
Palaeoproterozoic			
Epupa Metamorphic Complex	Orue Unit metapelites, metagreywackes and amphibolites	No published ages	Inherited cores of 1997–1731 Ma providing maximum age constraint (Seth et al. 2003)
	Epembe Unit metapelites		Inherited cores of 1810–1660 Ma providing maximum age constraint (Seth et al. 2003)
	Epupa granitic gneisses, migmatites and anatectic granites	1808 ± 12 Ma biotite gneiss (Seth et al. U–Pb zircon); 1789 ± 2 Ma and 1758 ± 3 Ma gneiss; 1757 ± 4 Ma Otjitanda granite (Kröner et al. 2010, U–Pb zircon)	Protoliths to the gneiss samples and age of crystallization. Inheritance documented at 186 ± 7 and 1854 ± 8 Ma (Kröner et al. 2010)
Chela Group	Conglomerates, quartzites, sandstones, felsic volcanic rocks, argillites	1798 ± 11 Ma Humpata Formation ignimbrite (McCourt et al. 2013, U–Pb zircon)	Maximum age of deposition of overlying 1782 ± 6 Ma Bruco Formation quartz-arenite (McCourt et al. 2013). Intruded by 1407 ± 6 Ma Ompupa granite, 1119 ± 27 Ma (Rb–Sr) norite sills and dykes
Kamanjab Inlier	Fransfontein granite suite granodiorites and granites	1841 ± 14 Ma Franken granodiorite, 1836 ± 17 Ma Kamdescha granite, 1834 ± 14 Ma Kaross granite (Kleinhanns et al. 2013, U–Pb zircon)	Metamorphic overprint documented at ~ 1.77 Ga (1756 Ma zircon rim, 1778 ± 49 Ma Concordia age; 2.7–2.3 Ga Nd model ages (Kleinhanns et al. 2013)
	Huab Metamorphic Complex. Lower metasedimentary (Welwitschia Inlier to N of Khorixas) and upper metavolcanic sequence (WNW of Fransfontein)	1830 ± 17 Ma granodiorite gneiss, 1801 ± 27 Ma red orthogneiss, 1826 ± 30 Ma meta-rhyolite (Kleinhanns et al. 2013, U–Pb zircon)	Inheritance documented at 2052 Ma and xenoliths in red orthogneiss dated at 1967 and 1941 Ma (Kleinhanns et al. 2013)
	Khoabendus Group metavolcanic and metasedimentary units	1862 ± 6 Ma quartz porphyry near top of unit (Steven and Armstrong 2002, U–Pb zircon)	Correlated with the Tchipa-Iona Formation
	Tchipa-Iona formation quartzites, arkoses, chert, rare marble; felsic volcanic rocks (porphyries, rhyolites, tuffs)	No published ages	Correlated with the *c.* 1860 Ma Khoabendus Group (de Carvalho and Alves 1993). Intruded by Red Granite
Oendolongo Group	Coarse siliciclastic succession (interpreted molasse)	No published ages	Unconformable on Chivanda Group (de Carvalho and Alves 1993)

(continued)

Table 9.1 (continued)

Lithostratigraphic unit	Principal rock types	Age (Ma)	Comment
Bale Group	Clastic succession with quartzite and conglomerate at base, overlain by finely laminated shale, and a siltstone-sandstone sequence	No published ages	Unconformable on Chivanda Group and intruded by granite (de Carvalho and Alves 1993)
Lufubu Metamorphic Complex (Zambia and DRC)	Bangweulu (intermediate to felsic volcanic and volcaniclastic rocks) and coeval granitoids	1874 ± 8 Ma Kinsenda trachyandesite (Rainaud et al. 2005), 1884 ± 10 Ma Kabompo granite, 1874 ± 9 Ma Solwezi granite (John 2001)	
	Lufubu Schists (intermediate to felsic volcanic and volcaniclastic rocks) and coeval granitoids	1994 ± 7 Ma Mufulira pink granite, 1984 ± 5 Ma Chambishi granite, 1980 ± 7 Ma Chambishi meta-trachyandesite, 1976 ± 5 Ma Mulungushi Bridge augen gneiss, and 1968 ± 9 Ma Mufulira schist, 1964 ± 12 Ma Samba felsic metavolcanic schist (Rainaud et al. 2005), 1940 ± 3 Ma and 1934 ± 6 Ma Kabompo Dome granites (Key and Armstrong 2000, Key et al. 2001), 194 ± 6 and 1927 ± 10 Ma Luwalizi granite (De Waele et al. 2006); earlier magmatism indicated by 2049 ± 6 Ma Mkushi biotite gneiss (Rainaud et al. 2005; basement to southern Irumide Belt) and 2058 ± 7 Ma Mwinilunga granite (Key et al. 2001)	Basement rocks in Domes Region of Copperbelt. Protoliths to the schist samples and age of crystallization. Inheritance documented at 2174 ± 13, 2160 ± 25 and 2052 ± 6 Ma (Rainaud et al. 2005). Basement to the Muva Supergroup and Roan Group of Copperbelt
Regional granite (Angola and Namibia)	Felsic volcanic and volcaniclastic rocks	1964 ± 9 Ma rhyolite, 1978 ± 11 Ma rhyodacite (Delor et al. 2006, U–Pb zircon)	Coeval with regional granite; association with Bale Group uncertain
	Undifferentiated granitoids (Namibia and Botswana)	1971 ± 7 and 1961 ± 4 Ma Hoanib River granitoids (Seth et al. 1998, U–Pb zircon); 1979 ± 92 Ma pink granite from NW Botswana (Gaisford 2010, U–Pb zircon)	
	Tonalites, granodiorites and granites and their gneissic equivalents	2038 ± 28 Ma Lubango granite, 1954 ± 6 Ma (McCourt et al. 2013, U–Pb zircon); 1987 ± 16, 1980 ± 9 Ma Huambo granitoids; 1975 ± 23 Ma Conda granitoids (Delor et al. 2006, U–Pb zircon); 1966 ± 3 Ma granodioritic augen gneiss, 1967 ± 5 Ma granodiorite west of Andulo; 1974 ± 5 Ma gneissic biotite granite south of Kuito; 1972 ± 4 Ma south of Andulo, 1973 ± 7 Ma quartz diorite north of N'harea (this study, U–Pb zircon)	Regionally dominant granitoid, intrusive into Archaean gneiss-migmatite complex; basement to Chela Group rocks. Palaeoproterozoic protoliths with xenocrysts of 2873–2515 Ma (**this study**)
Chivanda Group (locally Cuandja)	Deformed volcano-sedimentary sequance comprising quartzite and conglomerate, sandstone, greywacke and limestone overlain by mafic volcanics, conglomerates, felsic volcanic rocks, and black manganiferous schist	2149 ± 83 Ma felsic schist, 1915 ± 58 Ma black schist at Chipinda (de Carvalho and Alves 1993, Rb–Sr ages)	Metamorphosed supracrustal sequences; intruded by the regional granite

(continued)

Table 9.1 (continued)

Lithostratigraphic unit	Principal rock types	Age (Ma)	Comment
Grootfontein Metamorphic Complex, Tsumkwe and Quangwadum Inliers	Foliated gneisses, amphibolites and metasedimentary rocks, gabbros and granites	2022 ± 15 Ma granitic gneiss (Hoal et al. 2000, U–Pb zircon); 2052 ± 1 Ma augne gneiss (Singletary et al. 2003); 1939 ± 64 Ma porphyritic biotite granite (Sanz 2005, U–Pb zircon)	
Archaean			
Jamba Group	Schists, quartzites, greywackes, pelites, pillow lavas, amphibolites, felsic volcanic rocks, chert, marble	No published ages	Unconformable on gneissic basement, intruded by Regional Granite (Korpershoek 1984; **this study**—field observations from N'herea-Catacala)
Basement complex	Orthogneiss and amphibolite (Namibia and Botswana)	2645–2585 Ma Hoanib River orthogneisses (Seth et al. 1998, U–Pb zircon); 2548 ± 65 Ma migmatitic gneiss (Gaisford 2010, U–Pb zircon) and 2641 ± 82 Ma (Witbooi 2011, U–Pb zircon) for granitic gneisses from NW Botswana	~2.7 Ga Nd model ages (Seth et al. 1998)
	Tonalitic to granitic gneisses, migmatites, quartz diorites and granites (Angola)	2522 ± 108 Ma Cariango granitoids (de Carvalho et al. 2000, Rb–Sr); 2533 ± 11 Ma megacrystic biotite gneiss; 2519 ± 5 Ma biotite granite; 2522 ± 5 Ma biotite gneiss, 268 ± 5 Ma quartz diorite near N'harea east of Andulo (this study; U–Pb age)	Neoarchaean protoliths with xenocrysts of 2782 Ma-2670 Ma (**this study**)

northwards into southwest Angola. The geology of the EMC comprises granitoid gneisses (the Epupa gneisses) that are variably migmatized and minor amounts of supracrustal gneisses. The latter are subdivided into the amphibolite facies Orue Unit (Seth et al. 2005) and the granulite facies Epembe Unit (Brandt et al. 2003, 2007; Seth et al. 2003), but contacts between these supracrustal gneisses and the Epupa gneisses are not exposed (Kröner et al. 2010). Regionally, the Epupa gneisses are overlain along a nonconformity by the rocks of the Neoproterozoic Damara Supergroup and are intruded by anorthosite of the *c*. 1385 Ma Kunene Complex, which provides a minimum age constraint on the formation of the EMC. Kröner et al. (2010) note that in the western part of the Otjihipa Mountains the Epupa gneisses are folded together with the Okapuka Formation. The latter is a sequence of quartzite, quartzite-sericite schist and mafic schist intruded by gabbroic sills and dykes, but there are no direct age constraints on any of these rocks.

The U–Pb zircon study reported by Kröner et al. (2010) involved granitoid rocks from the northern part of the EMC between Etanga and the Kunene River. Samples included granitic gneiss, migmatite and undeformed anatectic granite. Protoliths to the gneiss samples were emplaced between 1789 ± 2 and 1758 ± 3 Ma; migmatization occurred at 1762 ± 4 Ma and intrusion of the anatectic Otjitanda Granite at 1757 ± 4 Ma. These latter two ages are within analytical error, suggesting that the peak of metamorphism and anatectic granite formation in the Epupa Complex were coeval at around 1760 Ma. Kröner et al. (2010) also reported whole rock Nd isotope data for several samples. These data are very similar to $\varepsilon_{Nd(t)}$ values between −1.9 and +0.6 corresponding to mean crustal residence ages between 2.26 and 2.0 Ga, suggesting the protolith formed from a source that separated from the mantle at that time (Kröner et al. 2010). The only deviation from these values was the Otjitanda Granite, with initial $\varepsilon_{Nd(t)}$ value of +3.2 suggesting a major component of juvenile crustal for the protolith (Kröner et al. 2010). In addition to the ages around 1770 Ma, Kröner et al. (2010) reported a single sample with an age of 1861 ± 7 Ma and a single xenocryst at 1854 ± 8 Ma as evidence for older crust below the Epupa Metamorphic Complex, but there was no evidence for an Archaean component in the source area. Major and trace element geochemistry on the dated samples from the EMC indicate a calcalkaline crustal protolith for the granitoids which Kröner et al. (2010) interpret as a batholith within a Palaeoproterozoic magmatic arc.

The gneisses of the Epembe and Orue units are exposed in two east to west trending bands along the southern margin of the Kunene Complex in NW Namibia. The gneisses of the upper amphibolite facies Orue Unit are immediately adjacent to the Kunene Complex, with the granulite facies Epembe Unit further south. Seth et al. (2005) note that the contacts of both units are either not exposed or defined by faults. The granulites of the Epembe Unit comprise felsic and mafic orthogneisses and metasedimentary paragneisses (Brandt et al. 2003) and are the product of an ultra-high temperature event (960 °C at 9.5 kbar) with prograde zircon growth dated between 1520 and 1510 Ma and peak metamorphic conditions at 1490–1447 Ma (Seth et al. 2003). U–Pb analyses of core regions in zircon grains from a metapelite sample range between 1810 and 1660 Ma, indicating derivation from a Palaeoproterozoic source terrane and deposition post-1660 Ma (Seth et al. 2003). The upper amphibolite facies rocks of the Orue Unit comprise metasedimentary gneisses derived from pelite and greywacke and garnet amphibolite derived from mafic intrusions or lava. Geochronological studies by Seth et al. (2005) show growth of zircon rims at around 1357 Ma and of metamorphic zircon between 1340 and 1320 Ma. Analyses of inherited zircon cores produced ages of between 1731 ± 17 and 1997 ± 12 Ma, indicating that the metasedimentary rocks of the Orue Unit, like those of the Epembe Unit, were derived from the erosion of Paleoproterozoic crust. Despite this link, it should be noted that in the original metamorphic study, Brandt et al. (2003) could find no evidence that the upper amphibolite facies gneisses of the Orue Unit were derived by retrogression of the granulite facies Epembe Unit. Seth et al. (2005) also dated zircon grains from a grey biotite gneiss that from field relationships did not intrude the metasedimentary gneisses of the Orue Unit. The data from these grains plots in a tight cluster defining a Concordia age of 1808 ± 12 Ma. Seth et al. (2005) interpreted this as the age of the igneous protolith to the gneiss, and by extension the age of the basement to the Orue Unit.

The Kamanjab Inlier lies south of the Epupa Metamorphic Complex and comprises rocks of Palaeoproterozoic age subdivided into a northern domain characterized by low-grade supracrustal rocks of the Khoabendus Group (KG) and the southern high-grade Huab Metamorphic Complex (HMC). These contrasting metamorphic terranes are separated by the Fransfontein Granite Suite (FFG) with a number of granitoids from the latter occurring as batholiths in the Khoabendus Group. Reconnaissance mapping by the Geological Survey of Namibia (Becker 2004, 2005, 2006) suggests the HMC comprises a lower metasedimentary sequence and an upper metavolcanoclastic sequence. The lower sequence is well exposed in the Welwitschia Inlier to the north of Khorixas and the upper sequence to the west-northwest of Fransfontein (for more information, Kleinhanns et al. 2013, Fig. 2). The upper and lower sequences of the HMC are intruded by large numbers of mafic sills and dykes, now represented by amphibolite, and by voluminous amounts of granitic material occurring as both mega-sills (Kleinhanns et al. 2013) and plutons. Two main varieties of granitic material are recognized: coarse-grained K-feldspar megacrystic quartz-feldpar-biotite gneiss and equigranular red orthogneiss (Kleinhanns et al. 2013). Interestingly (cf. Epupa Complex) Kleinhanns et al. (2013) note that the granitoid gneisses are overprinted by incipient migmatization such that some of the mega-sills may represent anatectic granite. The Khoabendus Group (KG) is poorly documented (see review in Miller 2008), but again a twofold subdivision can be recognized with a lower part dominated by metavolcanic rocks but including intercalated metasedimentary units and an upper unit comprising metasedimentary rocks and subordinate metavolcanics. Precise age data on the Khoabendus Group is limited to a SHRIMP U–Pb zircon age of 1862 ± 6 Ma on a quartz-porphyry from near the top of the unit (Steven and Armstrong 2002). Recent geochemical studies on rhyolite from the Khoabendus Group (Muvangua 2006) suggest an active continental margin as the tectonic setting for the volcanism.

Documented studies on the granitoids of the Fransfontein Granite Suite are limited to the published work of Clifford et al. (1969), a student thesis by Muvangua (2006) and the detailed study of Kleinhanns et al. (2013). The latter group document the results of a comprehensive petrographic and geochemical study on both granitoids from the FFG and orthogneisses from the Huab Metamorphic Complex (HMC). The geochemical data is supported by Rb–Sr and Sm–Nd isotope systematics and U–Pb age data on zircon, and the following description is based on that study.

Kleinhanns et al. (2013) studied five samples of (meta-) granitoid from the FFG, including the previously described red Kaross granite, porphyritic Kamdescha granite and the Franken granodiorite. Samples from the HMC included granodioritic gneiss, red orthogneiss and metarhyolite. Major element signatures indicate that the FFG granitoids range in composition from monzogranite to alkali-feldspar granite; trace element data have a strong subduction signature. As a result, Kleinhanns et al. (2013) interpreted the FFG samples as I-type magnesian Cordilleran granitoids formed in an active continental margin setting. The granodioritic gneiss from the HMC has a similar geochemical signature to the FFG granitoids and, based on both whole-rock major and trace element data, can be interpreted as the high grade equivalent of the FFG suite (Kleinhanns et al. 2013). The red orthogneisses crystallized from highly differentiated melts and show a strong affinity to A-type granitoids with high concentrations of SiO_2 together with very low values of MgO. The geochemistry of the HMC

metarhyolite is intermediate between that of the FFG granitoids/HMC granodiorite and the HMC red orthogneiss, but were linked to the former by Kleinhanns et al. (2013) based on calcalkaline character and the subduction zone signature of their trace element budget.

U–Pb age data for granitoids from the Kamanjab Inlier was obtained by LA-ICP-MS and for the FFG samples give Concordia ages between 1841 ± 14 Ma (Franken granodiorite) and 1834 ± 14 Ma (Kaross granite) interpreted as the emplacement age of the relevant intrusions (Kleinhanns et al. 2013). The data from the 1836 ± 17 Ma Kamdescha granite includes younger ages of *c*. 1756 Ma on a zircon rim and a Concordia age of 1778 ± 49 Ma on a group of four grains interpreted as an overprint leading to Pb loss at around 1770 Ma. The majority of zircon grains from the HMC granodioritic gneiss gave a Concordia age of 1830 ± 17 Ma, with one grain yielding a concordant age of 2052 ± 44 Ma. The age of 1830 ± 17 Ma is within error of the emplacement ages of the FFG intrusions and is therefore interpreted as the age of the igneous protolith to the gneiss. The older age of 2052 ± 44 Ma is interpreted as a xenocryst by Kleinhanns et al. (2013) and linked to the existence of older crust below the Kamanjab Inlier. Support for this older crust comes from xenocrysts obtained from a sample of HMC red orthogneiss, which gave ages of 1967 Ma and 1941 Ma. The emplacement age of the protolith to this red gneiss was 1801 ± 27 Ma. Finally zircon grains from the HMC meta-rhyolite gave a Concordia age of 1826 ± 30 Ma, indicating emplacement of volcanic and plutonic rocks was coeval. Kleinhanns et al. (2013) note the occurrence of core and rim structures in several zircon grains, but where analysis was possible no age difference was identified. Kleinhanns et al. (2013) also report data from Sm–Nd isotope analyses on the samples collected, which yielded T_{DM} (Nd) ages of between 2.7 and 2.3 Ga for samples from the FFG and between 2.0 and 2.2 Ga for the samples from the HMC. The latter data is compatible with an age of around 2124 Ma for a xenocryst found in the Neoproterozoic Oas Syenite intruding the southern part of the Kamanjab Inlier (Tegtmeyer and Kröner 1985).

The rocks of the Grootfontein Inlier comprise the Grootfontein Metamorphic Complex (GMC), Grootfontein gabbro and Grootfontein granite (Miller 2008). Exposure is poor and data scarce, but a recent study by Laukamp (2006) indicates that the GMC comprises plutonic rocks of dominantly alkaline/calcalkaline composition that are interpreted to have formed in an active continental marginal arc. The rocks of the Tsumkwe Inlier along the border with Botswana are regarded as an extension of the GMC (Hoal et al. 2000), and a granitic gneiss from this region has been dated at 2022 ± 15 Ma. This is interpreted as the age of the igneous protolith to the gneiss.

Basement gneisses to the Damara Supergroup in the southern part of the Kaoko Belt are well exposed in the Hoanib River west of Sesfontein. Regionally the gneisses lie west of the Kamanjab Inlier and at the southern tip of the gneissic terrane defined as the Epupa Metamorphic Complex by Kröner et al. (2010). Age data published by Seth et al. (1998) shows that the eastern part of the Hoanib River section is characterized by Neoarchaean orthogneisses intruded by Palaeoproterozoic granitoids. The Neoarchaean gneisses have protolith emplacement ages between 2645 Ma and 2585 Ma (Seth et al. 1998) with Nd crustal resident ages of ~2.7 Ga, suggesting the protolith was derived from the partial melting of even older Archaean crust. The emplacement ages of the Palaeoproterozoic granitoids are constrained by U–Pb SHRIMP ages of 1971 ± 7 and 1961 ± 4 Ma, with Nd isotope data indicating a crustal residence age of 2.6 Ga. This, together with xenocrysts dated at 2605 ± 11 Ma, strongly suggests the protoliths of the Palaeoproterozoic granitoids were derived from Neoarchaean crust similar in age to the orthogneisses further east (Seth et al.

9.4 Discussion and Conclusion

The geology of the Angolan Shield is dominated by granitoid rocks of both igneous and metamorphic character. Recent studies using modern techniques have shown that although these granitoids preserve a history of crustal formation stretching back to the Neoarchaean, the major crust forming events occurred in the Palaeoproterozoic with significant magmatism and related orogeny in the interval 1987–1965 Ma and again at 1830–1760 Ma (Fig. 9.7).

The oldest rocks occur in the Central Shield of Angola around the town of Andulo and on the Kwanza Horst. These granitoid gneisses and granites have ages between 2681.6 ± 4.6 and 2519.4 ± 5 Ma with inheritance back to 2782 Ma. The only other occurrence of Archaean rocks in the Angolan Shield is in the eastern part of the Hoanib Valley west of Sesfontein in NW Nambia, where Seth et al. (1998) documented ages of 2645 ± 6, 2616 ± 5 and 2585 ± 0.4 Ma for zircon grains from orthogneisses exposed as basement in the western Kaoko Belt. In both Angola and Namibia, the Archaean granitoids are intruded by Palaeoproterozoic granite and granodiorite (now gneisses) that in Angola characterize the Central Eburnean Zone. In the CEZ. the granitoids and coeval felsic volcanics rocks are linked to magmatism dated between 1987 ± 16 and 1964 ± 9 Ma (Delor et al. 2006) and between 1973 ± 6.9 and 1966 ± 3.1 Ma (this study). Inherited grains dated at 2539 ± 14, 2617 ± 24 and 2832 ± 12 Ma indicate the reworking of older, predominantly Neoarchean, crust in the

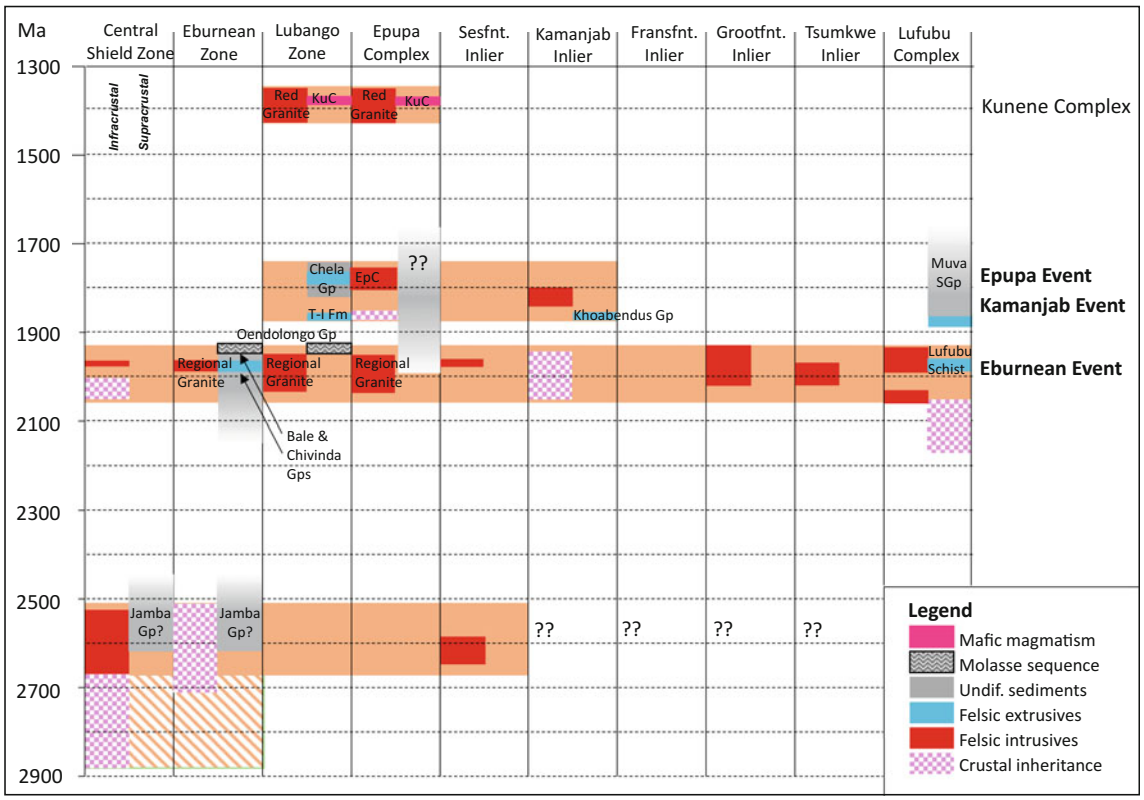

Fig. 9.7 Time line for the Angolan Shield, showing continental growth between 2.82 and 2.62 Ga, with craton stabilization at 2.52 Ga marked by the emplacement of granites. Between 2.0 and 1.96 Ga the craton margin was reworked during the Eburnean event, with the emplacement of ubiquitous granites and volcanics. Subsequent magmatic events may be attributed to the continued development of arcs along the southern continental margin of the Congo Craton in the Palaeoproterozoic at 1.86–1.83 Ga (Kamanjab Event) and 1.80–1.77 Ga (Epupa Event). *KuC* Kunene Complex, *EMC* Epupa Complex, *T–I Fm* Tchipa-Iona Formation

formation of these magmas. Crosscutting gneisses and intrusive rock types that yield ages within error at ~1967 Ma (samples CVZ605 and CVZ606 above) constrain the age of regional deformation and metamorphism related to Palaeoproterozoic orogeny. The Lubango Zone lies south of the CEZ and extends into Namibia, where it has been mapped and sampled as the Epupa Metamorphic Complex. Precise age data on the Palaeoproterozoic crust of the Lubango Zone is limited to U–Pb SHRIMP ages of 2038 ± 28 and 1954 ± 6 Ma on slightly deformed granite acting as basement for the Chela Group and an age of 1798.4 ± 10.6 Ma on ignimbrite from the Humpata Formation within that group (McCourt et al. 2013). This direct data is supported by xenocrysts from the ignimbrite dated between 1920 and 1995 Ma and detrital zircon grains ranging between 1752 and 2043 Ma from the clastic Bruno Formation towards the top of the Chela Group. In addition, the regionally developed granitoid gneisses referred to as the Regional Granite by all previous workers are identical to those of the CEZ, and the Rb–Sr whole rock isochron dates on these rocks published by de Carvalho et al. (2000) are compatible with the new U–Pb data cited here. We interpret this data to indicate that the *c*. 1970 Ma Palaeoproterozoic crust recognised in the CEZ extends south to the border with Namibia. In addition however, there is evidence of younger felsic magmatism between 1860 and 1752 Ma.

The Epupa Metamorphic Complex (EMC) comprises granitic gneiss, migmatite and undeformed anatectic granite. Based on the data published by Kröner et al. (2010) the protoliths to these granitoids were emplaced between 1789 ± 2 and 1758 ± 3 Ma and peak metamorphism, deformation and anatexis, as indicated by migmatization and the formation of the Otjitanda Granite, was at ~ 1760 Ma. Kröner et al. (2010) reported a single sample with an age of 1861 ± 7 Ma and a single xenocryst at 1854 ± 8 Ma as evidence for older crust below the Epupa Metamorphic Complex, but there is no indication of the extent of this crust. Major and trace element geochemistry on the dated samples dated by Kröner et al. (2010) indicates the protolith to the granitoids was calcalkaline crust linked to a Palaeoproterozoic magmatic arc, and Nd isotope data suggests the EMC granitoids were derived from a source that separated from the mantle between 2.26 and 2.0 Ga. Thus, although the Epupa Event is over 200 million years younger than the

magmatism responsible for the granitoids in the Lubango and Central Eburnean Zones to the north, there is some indication that the protoliths to the Epupa granitoids may have been part of the *c*. 2.0 Ga Regional Granite. In support of this link, Seth et al. (1998) dated Palaeoproterozoic granite in the Hoanib Valley, which lies at the southern tip of the EMC, at 1971 ± 7 and 1961 ± 4 Ma.

Crustal formation in the Kamanjab Inlier in NW Namibia is informed by geochemical, isotope and age data on the Fransfontein Granite Suite (FFG) and the Huab Metamorphic Complex (Kleinhanns et al. 2013). This data supports an interpretation that the rocks of the FFG and HMC are I-type magnesian Cordilleran granitoids formed in an active continental margin between 1841 ± 14 and 1830 ± 17 Ma. Inheritance at 2052 ± 44; 1967 ± 39 and 1941 ± 48 Ma indicates the involvement of older crust in the formation of these magmas. Evidence of new zircon growth and Pb-loss at ~1770 Ma provides a link with the Epupa Event further north. The granites of the FFG intrude into the supracrustal rocks of the Khoabendus Group, which is compatible with the older age of 1862 ± 6 Ma for rhyolite within that supracrustal package (Steven and Armstrong 2002). An older age of 1987 ± 4 Ma cited in Seth et al. (1998) is indistinguishable from the age of xenocrysts yielded by red orthogneiss from the HMC and is taken as further evidence for older crust beneath the Kamanjab Inlier. Finally, Nd isotope data from Kleinhanns et al. (2013) indicates T_{DM} ages between 2.7 and 2.3 Ga for samples from the FFG and between 2.2 and 2.0 Ga for the samples from the HMC, with the source material for the latter characterized by relatively high amounts of juvenile material.

The continental crust forming the Grootfontein Inlier comprises plutonic rocks of dominantly alkaline/calcalkaline composition that are interpreted to have formed in an active continental marginal arc (Laukamp 2006). The protolith of granitic gneisses from the related Tsumkwe and Quangwadum Inliers have been dated at 2022 ± 15 Ma (Hoal et al. 2000) and at 2051 ± 1 Ma, which is compatible with inherited zircon grains at 2052 ± 44 and 1987 ± 4 Ma in granite and felsic lava in the Kamanjab Inlier. This is taken as evidence that the older crust involved in the formation of the FFG and HMC granitoids and interpreted to be present at depth below the Kamanjab Inlier is exposed in the Grootfontein-Tsumkwe-Quangwadum inliers, and was presumably part of the active continental margin identified by Kleinhanns et al. (2013).

Farther to the northeast, in the Lufilian Arc and Central African Copperbelt in Angola, Zambia and DRC, basement rocks underlying the Katanga Supergroup include Neoarchaean granites and gneisses of the Kasai Craton and schists, granites and gneisses of the Lufubu Metamorphic Complex (LMC). The latter was identified as Paleoproterozoic basement by Rainaud et al. (2005) and is exposed in the Domes Region (Fig. 9.2) and the external fold and thrust belt of the Copperbelt. It continues eastwards as the granitoids and felsic volcanic rocks of the Bangweulu Block (Rainaud et al. 2005; De Waele et al. 2009), which forms the foreland to, and basement of, the Mesoproterozoic Irumide Belt (De Waele et al. 2006, 2009).

The LMC comprises the Lufubu Schists and intrusive granitoids and gneisses. The Lufubu Schists include mica schists, quartzites and biotite paragneisses, with conglomerates, greywackes, arkoses and metamorphosed calcareous rocks, and have been intruded by granites. In the Copperbelt region, the Lufubu schists and the intrusive granites are unconformably overlain by quartzites and metapelites of the Muva Supergroup that were deposited between *c*. 1850 and 1650 Ma (de Waele et al. 2006).

Petrography and geochemistry have shown that the precursors of the Lufubu Schists were mainly volcanic in origin and of calcalkaline character, and are predominantly andesites, rhyodacites, trachyandesites and alkali basalts (Rainaud et al. 2005). SHRIMP zircon geochronology suggests that volcanism was coeval with the emplacement of granitoids and took place during at least three events.

A widespread and common event represented by both extrusive and intrusive phases has been constrained between 1994 ± 7 and 1964 ± 12 Ma (Rainaud et al. 2005). This event is reflected by the Mufulira porphyritic andesites, Chambishi trachyandesite quartz porphyry, Samba felsic volcanic schists, and the Mufulira and Chambishi granites and Mulungushi gneisses. Younger ages of 1940 ± 3 and 1934 ± 6 Ma are documented by feldspar-phyric granites from the Kabompo Dome (Key and Armstrong 2000; Key et al. 2001) and of 1942 ± 6 and 1927 ± 10 Ma by the Luwalizi granite of the Irumide belt (De Waele et al. 2006), and are probably compatible with those from the LMC, albeit slightly younger.

Inheritance suggests the involvement of older crust with zircon ages of 2174 ± 13 and 2052 ± 6 Ma (at Mufulira) and 2160 ± 25 Ma (at Samba). The 2050 Ma age is very similar to the emplacement age of the precursor to the Mkushi biotite gneisses dated at 2049 ± 6 Ma (Rainaud et al. 2005) and the emplacement age of 2058 ± 7 Ma for a pink granite in the Mwinilunga area of northwest Zambia (Key et al. 2001).

Younger ages of ~1.88 Ga are provided by a trachyandesite porphyry at Kinsenda (1874 ± 8 Ma, Rainaud et al. 2005) and a rhyolite in the Chinsali area (1880 ± 12, de Waele and Mapani 2002; 1868 ± 7 Ma, de Waele et al. 2006, 2009). The Chinsali rhyolite gives a depositional age for the Manshya River Group of the Muva Supergroup and is thought to represent the early, volcanic equivalents of the 1.88–1.83 Ga granitoids of the Bangweulu Block, which de

Waele et al. (2006, 2009) interpreted as having formed in a continental arc related to the Palaeoproterozoic Ubendian belt.

Rainaud et al. (2005) interpreted the Lufubu Metamorphic Complex lithologies as having formed in a subduction-related Palaeoproterozoic magmatic arc terrane, a terrane they regarded as a continuation of the Kamanjab Inlier of Namibia and, by extension of the present study, the Angolan Shield, and which they referred to as the Kamanjab-Bangweulu terrane.

In summary, therefore, although the geochemical and isotope data is limited to the crust exposed in NW Namibia, precise age data confirms the presence of granitoids formed at $\sim$2.0 $\pm$ 0.04 Ga from the Huambo-Andulo region in Angola south to Kamanjab-Grootfontein region in NW Namibia, a distance of over 1000 km. Inherited grains from samples collected in Central Angola, indicate that Neoarchaean crust was involved in the formation of these *c*. 2.0 Ga granitoids, an interpretation supported by Nd crustal residence ages of 2.7–2.6 Ga in the Sesfontein area of NW Namibia (Seth et al. 1998). Field relations in Angola indicate that this $\sim$2.0 Ga granitic crust was metamorphosed and deformed during orogeny at $\sim$1967 Ma. Jelsma et al. (2011) and McCourt et al. (2013) linked the formation of this *c*. $\sim$2.0 Ga crust to an active continental margin associated with the developing Congo Craton. The continental crust forming the Kamanjab Inlier is the product of I-type magmatism in a continental margin arc that was active between 1841 and 1830 Ma, with inherited grains suggesting the involvement of older crust with a similar age to that exposed in Central and SW Angola (Delor et al. 2006; Jelsma et al. 2011; McCourt et al. 2013) and in the nearby Grootfontein-Tsumke Inlier. Protoliths to the granitoids of the Epupa Metamorphic Complex were emplaced into the crust between 1789 $\pm$ 2 and 1758 $\pm$ 3 Ma, with peak metamorphism and deformation to produce gneisses occurring before the formation of the Otjitanda Granite at 1757 $\pm$ 4 Ma. Although the crust into which these granitoid magmas were intruded is not exposed, and the cause of the orogenic event is not obvious from the available data, Kröner et al. (2010) suggest the protoliths were derived from a granitoid batholith formed in an active marginal arc and that the source separated from the mantle between 2.26 and 2.0 Ga.

The three events defined probably formed part of a system of magmatic arcs that developed along the western and southern continental margins of the Congo Craton in the Palaeoproterozoic, with peak magmatic events described $\sim$100 million years apart at 2.0–1.93 Ga (Eburnean Event), 1.88–1.83 Ga (Kamanjab-Bangweulu Event) and 1.80–1.77 Ga (Epupa Event). It is likely that additional events will be recognized with further high precision geochronology, as is observed for instance along the Andean continental margin (e.g., Oncken et al. 2006), which has been periodically active at least since the early Palaeozoic. Active continental margins are principal sites for growth of continental crust, but also of recycling and destruction of continental crust, which is observed in the Angolan Shield by the diversity of supracrustal rock types (mafic to felsic volcanics, arenaceous, argillaceous and calcareous successions including possible molasse sequences).

Acknowledgements The authors gratefully acknowledge Charles Skinner of De Beers Exploration for his support of research on the geology of Angola and Gleuber Alves, Heraldo Ferreira and Josinaldo Souza for support during the field surveys. Bert de Waele is thanked for reviewing the manuscript and Siegfried Siegesmund for editorial handling.

Appendix 9.1

SHRIMP zircon U–Th–Pb isotopic compositions and age data

Grain.spot	% $^{206}Pb_c$	ppm U	ppm Th	$^{232}Th/^{238}U$	ppm $^{206}Pb^*$	$^{206}Pb/^{238}U$ age[a]		$^{207}Pb/^{206}Pb$ age[a]		% discordant
CVZ605										
1.1	0.12	128	95	0.77	37.6	1894	±19	1961	±12	3
2.1	0.00	440	187	0.44	132	1934	±17	1972	±7.1	2
3.1	0.04	226	149	0.68	70.7	2002	±19	1961.6	±7.4	−2
4.1	0.00	110	101	0.95	34.1	1987	±20	1970	±10	−1
5.1	0.00	847	358	0.44	245	1874	±17	1964.7	±4.3	5
6.1	1.29	123	91	0.76	35.2	1829	±18	1976	±35	7
7.1	0.03	559	277	0.51	165	1902	±17	1964.1	±4.7	3
8.1	0.01	921	366	0.41	241	1712	±15	1942.9	±3.8	12
9.1	0.05	125	72	0.59	35.7	1851	±18	1965.6	±9.9	6
10.1	0.20	131	142	1.12	39.3	1931	±19	1965	±12	2
11.1	0.04	291	117	0.41	88.5	1951	±18	1962.4	±6.7	1
12.1	0.00	1041	450	0.45	285	1783	±16	1949.4	±3.6	9
13.1	0.03	213	139	0.67	63.8	1923	±18	1977.6	±7.9	3
14.1	0.03	954	454	0.49	210	1472	±13	1889	±5.3	22
15.1	–	483	173	0.37	136	1825	±17	1966.7	±6.3	7
16.1	0.00	1077	422	0.40	274	1674	±15	1937.4	±8.5	14
17.1	0.00	644	331	0.53	186	1866	±17	1962	±6.1	5
19.1	0.01	989	300	0.31	291	1897	±17	1965	±4.4	3
19.2	1.38	115	77	0.69	34	1883	±20	1979	±32	5
18.1	0.02	666	279	0.43	199	1926	±17	1966.3	±5.3	2
20.1	0.00	120	60	0.51	30.3	1655	±18	1968	±19	16
21.1	0.02	799	382	0.49	241	1941	±17	1965.5	±4.7	1
CVZ606										
1.1	0.18	125	113	0.93	39.8	2029	±22	1985	±15	−2
1.2	0.01	535	204	0.39	164	1964	±18	1968.3	±5.9	0
2.1	0.00	321	132	0.43	97.7	1956	±18	1966.5	±7.4	1
3.1	0.20	78	55	0.73	18.3	1556	±19	1888	±19	18
4.1	0.00	76	58	0.78	24	2013	±23	1954	±15	−3
5.1	0.02	207	124	0.62	64.1	1983	±20	1974	±13	0
6.1	0.00	76	65	0.89	22.9	1940	±23	1973	±15	2
7.1	0.02	1192	520	0.45	280	1559	±14	1912.8	±4.3	18
8.1	0.00	71	60	0.87	15.9	1492	±19	1908	±19	22
9.1	0.02	488	274	0.58	151	1986	±18	1960.2	±6.2	−1
10.1	0.09	181	123	0.70	54.3	1931	±19	1958	±11	1
11.1	2.00	228	198	0.90	42.6	1247	±13	2004	±25	38
12.1	0.02	586	293	0.52	181	1982	±18	1969.1	±5.4	−1
13.1	0.03	1666	295	0.18	410	1622	±15	1889.5	±3.8	14
14.1	0.02	747	251	0.35	185	1631	±15	1919.6	±5.9	15
15.1	0.01	273	167	0.63	85.4	2004	±19	1970.1	±7.8	−2

(continued)

Grain.spot	% $^{206}Pb_c$	ppm U	ppm Th	$^{232}Th/^{238}U$	ppm $^{206}Pb^*$	$^{206}Pb/^{238}U$ age[a]		$^{207}Pb/^{206}Pb$ age[a]		% discordant
16.1	0.03	514	208	0.42	131	1673	±21	1939.5	±6.3	14
17.1	0.00	96	63	0.67	30.2	2006	±22	1985	±13	−1
17.2	0.01	674	275	0.42	176	1708	±16	1944.1	±5.1	12
18.1	0.00	49	38	0.81	15	1959	±25	1983	±29	1
19.1	0.02	133	125	0.97	41.6	2006	±21	1974	±11	−2
20.1	0.01	437	279	0.66	135	1984	±18	1962.4	±6.3	−1
CVZ856										
1.1	0.00	135	100	0.76	42.3	2002	±20	1974	±8.9	−1
2.1	0.17	338	73	0.22	104	1966	±18	1970	±6.9	0
3.1	0.00	102	70	0.71	31.8	1997	±21	1970	±10	−1
4.1	0.24	923	164	0.18	217	1553	±14	1882.6	±5.6	18
5.1	0.11	189	173	0.94	53.9	1842	±18	1959.9	±9.7	6
5.2	0.09	775	185	0.25	234	1940	±17	1958.7	±4.5	1
6.1	0.10	341	183	0.55	103	1939	±18	1962.7	±6.6	1
7.1	0.00	107	77	0.74	33.5	1997	±21	1965	±12	−2
8.1	0.02	189	131	0.72	57.3	1948	±19	1985.1	±8.3	2
9.1	0.02	135	120	0.92	57.5	2602	±25	2598.8	±6.6	0
9.2	0.50	303	75	0.26	61.9	1370	±13	2110	±21	35
10.1	0.08	217	197	0.94	65	1924	±18	1969.7	±7.7	2
11.1	1.65	716	135	0.20	175	1589	±15	1920	±19	17
12.1	–	284	328	1.20	86.5	1959	±18	1974.6	±6.5	1
13.1	0.92	326	114	0.36	80.9	1624	±15	1938	±14	16
14.1	0.32	431	201	0.48	113	1705	±16	1945.4	±8.4	12
15.1	0.00	116	78	0.70	36.1	1991	±20	1969	±10	−1
16.1	0.00	133	85	0.66	41.6	2001	±20	1985.6	±9.3	−1
17.1	0.00	128	93	0.75	40.1	2001	±20	1975.8	±9.4	−1
18.1	1.06	880	81	0.10	152	1169	±11	1766	±14	34
19.1	0.15	318	150	0.49	72.6	1519	±15	1965.7	±8.1	23
20.1	0.14	462	247	0.55	137	1909	±17	1955.4	±6.1	2
CVZ857										
1.1	0.13	117	45	0.40	36.4	1995	±20	1966	±12	−1
2.1	0.16	130	54	0.43	31.9	1613	±19	1966	±14	18
3.1	0.06	375	155	0.43	98.7	1721	±18	1975.2	±6.3	13
4.1	0.01	386	31	0.08	118	1966	±18	2051.1	±7.4	4
5.1	0.06	163	89	0.56	50.7	1994	±19	1971.3	±9.1	−1
6.1	0.03	996	32	0.03	295	1907	±17	1974.5	±4.5	3
7.1	0.03	670	49	0.08	199	1917	±17	1969.4	±4.1	3
8.1	0.22	374	47	0.13	103	1792	±17	1971.8	±7.5	9
9.1	0.14	345	301	0.90	88.1	1677	±16	1967.7	±7.2	15
10.1	0.39	301	77	0.26	86.1	1844	±23	1997	±42	8
11.1	0.01	416	94	0.23	132	2019	±18	1972.3	±5.3	−2
12.1	0.13	147	54	0.38	45.2	1971	±19	1980.1	±9.4	0
13.1	0.02	109	128	1.21	53.5	2909	±29	2832	±6	−3
14.1	1.44	813	40	0.05	172	1398	±16	1925	±17	27

(continued)

Grain.spot	% $^{206}Pb_c$	ppm U	ppm Th	$^{232}Th/^{238}U$	ppm $^{206}Pb^*$	$^{206}Pb/^{238}U$ age[a]		$^{207}Pb/^{206}Pb$ age[a]		% discordant
14.2	0.77	203	100	0.51	89.1	2649	±28	2617	±12	−1
15.1	0.85	740	146	0.20	156	1408	±15	1934	±13	27
16.1	0.13	150	74	0.51	45.2	1940	±19	1970.3	±9.8	2
17.1	0.39	217	78	0.37	66.4	1962	±19	1971	±10	0
19.1	0.02	168	40	0.24	68.6	2509	±23	2539.3	±7.1	1
20.1	5.11	1352	31	0.02	97.8	495.2	±5.5	1674	±74	70
20.2	1.49	179	77	0.44	55.3	1956	±19	2004	±20	2
21.1	0.06	80	29	0.37	35.5	2686	±26	2873.4	±8.9	7
CVZ861										
1.1	0.00	447	173	0.40	132	1899	±17	1955.3	± 4.8	3
1.2	1.15	366	85	0.24	104	1829	±17	1947	±19	6
3.1	1.95	689	236	0.35	187	1738	±18	1938	±30	10
2.1	14.89	2590	284	0.11	254	598	±11	1883	±200	68
5.1	1.21	573	193	0.35	159	1787	±17	1947	±43	8
6.1	1.83	354	93	0.27	80.6	1490	±15	1972	±27	24
7.1	6.79	852	239	0.29	172	1276	±14	1852	±75	31
8.1	0.03	327	145	0.46	101	1976	±18	1974.7	± 5.9	0
9.1	9.37	1023	419	0.42	161	991	±13	1770	±110	44
10.1	0.90	786	310	0.41	149	1273	±13	1821	±18	30
11.1	6.48	535	131	0.25	111	1313	±14	1934	±85	32
12.1	0.28	328	110	0.35	77.7	1565	±16	1931.4	± 9	19
13.1	1.95	566	234	0.43	134	1540	±14	1943	±22	21
14.1	0.13	427	148	0.36	127	1912	±17	1970	± 5.9	3
15.1	4.98	584	154	0.27	120	1324	±13	1959	±50	32
16.1	0.01	121	83	0.71	50.4	2550	±24	2514.7	± 7	−1
17.1	0.01	414	883	2.20	202	2897	±29	2815.8	± 4.4	−3
17.2	0.25	671	250	0.38	170	1660	±15	1922.2	± 6.1	14
18.1	0.07	449	198	0.46	136	1949	±18	1973.6	± 6.7	1
19.1	4.27	465	119	0.26	98.8	1370	±14	1939	±68	29
CVZ864										
1.1	3.52	296	512	1.79	83.6	1774	±22	2697	±25	34
1.2	0.42	272	140	0.53	121	2678	±23	2826.1	± 6.7	5
2.1	2.37	574	400	0.72	91	1068	±10	1933	±25	45
3.1	8.11	434	1108	2.64	70.3	1031	±22	2060	±120	50
4.1	0.62	8249	2132	0.27	2810	2142	±21	1933	± 5.8	−11
5.1	1.69	282	506	1.85	73.5	1680	±16	2017	±20	17
6.1	2.62	10,738	2553	0.25	1930	1197	±11	1916	±27	38
7.1	10.67	585	1844	3.26	105	1103	±13	2099	±110	47
8.1	0.11	12,099	2488	0.21	3310	1782	±16	1866.8	± 2.8	5

Errors are 1-sigma; Pb_c and Pb^* indicate the common and radiogenic portions, respectively
Error in Standard calibration was 0.24% (not included in above errors but required when comparing data from different mounts)
[a]Common Pb corrected using measured ^{204}Pb

References

Ashwal LD, Twist D (1994) The Kunene Complex Angola/Namibia: a composite massif-type anorthosite complex. Geol Mag 131:579–591

Becker T (2004) Sheets 2014AB Suiderkruis, 2014AD Bethanis, and 2014BA Welcom. Geological maps of Namibia, geological series scale 1:50,000. Ministry of Mines and Energy, Geological Survey of Namibia, Windhoek, Namibia

Becker T (2005) Sheets 2014BB Rockeys, 2014BC Petrified Forest, and 2014BD Khorixas. Geological maps of Namibia, geological series scale 1:50,000. Ministry of Mines and Energy, Geological Survey of Namibia, Windhoek, Namibia

Becker T (2006) Sheets 1914CB Atlanta, 1914DA Bruno, and 1914DB Kamanjab. Geological maps of Namibia, geological series scale 1:50,000. Ministry of Mines and Energy, Geological Survey of Namibia, Windhoek, Namibia

Brandt S, Klemd R, Okrusch M (2003) Ultrahigh-temperature metamorphism and multistage evolution of garnet–orthopyroxene granulites from the Proterozoic Epupa complex, NW Namibia. J Petrol 44:1121–1144

Brandt S, Will TM, Klemd R (2007) Magmatic loading in the Proterozoic Epupa complex, NW Namibia, as evidenced by ultrahigh-temperature sapphirine-bearing orthopyroxene-sillimanite-quartz granulites. Precambr Res 153:143–178

Cahen L, Snelling NL, Delhal J, Vaill JR (1984) The geochronology and evolution of Africa. Clarendon Press, Oxford

Clifford TN, Rooke JM, Allsopp HL (1969) Petrochemistry and age of the Franzfontein granitic rocks of northern SW Africa. Geochim Cosmochim Acta 33:973–986

Delor C, Iafin JM et al (2006) Unravelling Precambrian crustal growth of central west Angola: Neoarchaean to Siderian inheritance, main Orosirian accretion and discovery of the 'Angolan' Pan African Belt. Abstract Volume, 21st Colloquium of African Geology. Geological Mining Association of Mozambique, Maputo, pp 40–41

De Carvalho H, Alves P (1990) Gabbro–anorthosite complex of SW Angola/NW Namibia. Communicações Instituto de Investigação Cientifica Tropical série de ciencias da terre 2:1–66

De Carvalho H, Alves P (1993) The Precambrian of SW Angola and NW Namibia. Communicações Instituto de Investigação Cientifica Tropical série de ciencias da terre 4:1–38

De Carvalho H, Crasto J, Silva ZC, Vialette Y (1987) The Kibaran cycle in Angola: a discussion. Geol J 22:85–102

De Carvalho H, Tassinari C, Alves P, Guimarães F, Simões MC (2000) Geochronogical review of the Precambrian in western Angola: Links with Brazil. J Afr Earth Sc 31:383–402

De Waele B, Mapani B (2002) Geology and correlation of the central Irumide Belt. J Afr Earth Sc 35:385–397

De Waele B, Wingate MTD, Fitzsimons ICW, Mapani BSE (2003) Untying the Kibaran knot: a reassessment of Mesoproterozoic correlations in southern Africa based on SHRIMP U–Pb data from the Irumide belt. Geology 31:509–512

De Waele B, Kampunzu AB, Mapani BSE, Tembo F (2006) The Mesoproterozoic Irumide belt of Zambia. J Afr Earth Sc 46:36–70

De Waele B, Fitzsimons ICW, Wingate MTD, Tembo F, Mapani B, Belousova EA (2009) The geochronological framework of the Irumide Belt: a prolonged crustal history along the margin of the Bangweulu Craton. American Journal of Science 309:132–187

Drüppel K, Littmann S, Romer RL, Okrusch M (2007) Petrology and isotope geochemistry of the Mesoproterozoic anorthosite and related rocks of the Kunene Intrusive Complex, NW Namibia. Precambrian Res 156:1–31

Gaisford J (2010) Geochronology, petrography and tectonic implications of lithologies and base metal mineralisation encountered in NW Ngamiland, Botswana, B.Sc Honours Thesis, University of Cape Town

Hoal KO, Hoal BG, Griffin WI, Armstrong RA (2000) Characterization of the age and nature of the lithosphere in the Tsumkwe region Namibia. Comm Geol Surv Namibia 12:21–28

Jelsma H, Perritt SH, Armstrong RA, Ferreira HF (2011) SHRIMP U–Pb zircon geochronology of basement rocks of the Angolan Shield, western Angola. In: Proceedings of the 23rd CAG, Johannesburg. Council for Geoscience, Pretoria, p 203

Jelsma H, Krishnan U, Perritt S, Preston R, Winter F, Lemotlo L, van der Linde G, Armstrong R, Phillips D, Joy S, Costa J, Facatino M, Posser A, Kumar M, Wallace C, Chinn I, Henning A (2013) Kimberlites from central Angola: a case study of exploration findings. In: Pearson G, Grütter HS, Harris JW, Kjarsgaard BA, O'Brien H, Chalapathi Rao NV, Sparks S (eds) Proceedings of 10th International Kimberlite Conference, Vol 1. Special Issue of the Journal of the Geological Society of India, Springer, India, pp 173–190

John T (2001) Subduction and Continental Collision in the Lufilian Arc–Zambezi Belt Orogen: a petrological, geochemical, and geochronological study of Eclogites and Whiteschists (Zambia). Ph.D. Thesis, Kiel

Key RM, Armstrong RA (2000) Geology and geochronology of pre-Katangan igneous and meta-igneous rocks north of the Lufilian Arc in northwest Zambia. J Afr Earth Sc 31:36–37

Key RM, Liyungu AK, Njamu FM, Somwe V, Banda J, Mosley PN, Armstrong RA (2001) The Western arm of the Lufilian Arc in NW Zambia and its potential for copper mineralization. J Afr Earth Sc 33:503–528

Kleinhanns IC, Fullgraf T, Wilsky F, Nolte N, Fliegel D, Klemd R, Hansen BT (2013) U–Pb zircon ages and (isotope) geochemical signatures of the Kamanjab Inlier (NW Namibia): constraints on Palaeoproterozoic crustal evolution along the southern Congo craton. Geol Soc London SP 389:165–195

Korpershoek HR (1984) The geology of the Cassinga district (Angola) and its potential as compared to that of the Serra dos Carajás (Brazil). In: 33° Congresso Braisileiro Geologia, Rio de Janeiro, Brasil

Kröner A, Correia H (1980) Continuation of the Pan African Damara belt into Angola: a proposed correlation of the Chela Group in southern Angola with the Nosib Group in northern Namibia. Geol Soc S Afr Trans 83:5–16

Kröner A, Rojas-Agramonte Y, Hegner E, Hoffman KH, Wingate MTD (2010) SHRIMP zircon dating and Nd isotopic systematics of Palaeoproterozoic migmatitic orthogneisses in the Epupa Metamorphic Complex of northwestern Namibia. Precambr Res 183:50–69

Laukamp C (2006) Structural and fluid system evolution in the Otavi Mountainland (Namibia) and its significance for the genesis of sulphide and nonsulphide mineralisation. Ph.D. Thesis, Universität Heidelberg

Ludwig KR (1998) On the treatment of concordant uranium-lead ages. Geochim Cosmochim Acta 62:665–676

Ludwig KR (2003) User's manual for Isoplot 3.0, a geochronological toolkit for Microsoft Excel. SP 4, Berkeley Geochronology Center, Berkeley, California, pp 1–70

Mayer A, Hofmann AW, Sinigoi S, Morais E (2004) Mesoproterozoic Sm–Nd and U–Pb ages for the Kunene Anorthosite Complex of SW Angola. Precambr Res 133:187–206

McCourt S, Armstrong RA, Jelsma H, Mapeo RBM (2013) New U − Pb SHRIMP ages from the Lubango region, SW Angola: insights into the Palaeoproterozoic evolution of the Angolan Shield, southern Congo Craton, Africa. J Geol Soc 170:353–363

Miller RM (2008) The Geology of Namibia. Ministry of Mines and Energy, Geological Survey, Windhoek, Namibia, p 1

Muvangua E (2006) Petrology and geochemistry of the Khoabendus Group and the Fransfontein Suite in the Kamanjab Area, northwestern Namibia. B.Sc Thesis, University of Stellenbosch

Oncken O, Chong G, Franz G, Giese P, Götze HJ, Ramos VA, Strecker MR, Wigger P (eds) (2006) The Andes: Active Subduction Orogeny. Springer, Berlin, p 574

Rainaud C, Master S, Armstrong RA, Robb LJ (2005) Geochronology and nature of the Palaeoproterozoic basement in the Central African Copperbelt (Zambia and the Democratic Republic of Congo), with regional implications. J Afr Earth Sc 42:1–31

Sanz ALG (2005) Pre- and post-Katangan granitoids of the Greater Lufilian Arc—geology, geochemistry, geochronology and metallogenic significance. Ph.D. Thesis, University of the Witwatersrand

Seth B, Kröner A, Mezger K, Nemchin AA, Pidgeon RT, Okrusch M (1998) Archaean to Neoproterozoic magmatic events in the Kaoko belt of NW Namibia and their geodynamic significance. Precambr Res 92:341–363

Seth B, Armstrong RA, Brandt S, Villa IM, Kramers JD (2003) Mesoproterozoic U–Pb and Pb–Pb ages of granulites in NW Namibia: reconstructing a complete orogenic cycle. Precambr Res 126:147–168

Seth B, Armstrong RA, Büttner B, Villa IM (2005) Time constraints for Mesoproterozoic upper amphibolite facies metamorphism in NW Namibia: A multi-isotope approach. Earth Planet Sci Lett 230: 355–378

Singletary SJ, Hanson RE, Martin MW, Crowley JL, Bowring SA, Key RM, Krol MA (2003) Geochronology of basement rocks in the Kalahari Desert, Botswana, and implications for regional Proterozoic tectonics. Precambr Res 121:47–71

Stern RA (1997) The GSC Sensitive High Resolution Ion Microprobe (SHRIMP): analytical techniques of zircon U–Th–Pb age determinations and performance evaluation. Radiogenic, age and isotope studies: report 10, GSC. Curr Res 1997f:1–31

Steven N, Armstrong RA (2002) The potential for clastic-hosted zinc deposits in the upper Khoabendus Group near Kamanjab, N.W. Namibia. In: Extended Abstracts, 11th IAGOD symposium and Geocongress, Windhoek. Geological Survey of Namibia/Geological Society of South Africa (CD-ROM)

Tack L, Wingate MTD, De Waele B, Meert J, Belousova E, Griffin B, Tahon A, Fernandez-Alonso M (2008) The 1375 Ma "Kibaran Event" in Central Africa: prominent emplacement of bimodal magmatism under extensional regime. Precambr Res 180:63–84

Tegtmeyer A, Kröner A (1985) U–Pb zircon age for granitoid gneisses in northern Namibia and their significance for Proterozoic crustal evolution of southwestern Africa. Precambr Res 28:311–326

Witbooi EH (2011) Petrology, petrography, geochemistry and geochronology of base-metal mineralisation in the Lufilian Arc extension in the Tsodilo Hills Area, NW Botswana, B.Sc Honours Thesis, Nelson Mandela Metropolitan University, Port Elizabeth

Part III

Neoproterozoic Fold Belts related to Western Gondwana Formation

The Tectonic Evolution of the São Gabriel Terrane, Dom Feliciano Belt, Southern Brazil: The Closure of the Charrua Ocean

10

Ruy Paulo Philipp, Marcio Martins Pimentel, and Miguel Angelo Stipp Basei

Abstract

The Dom Feliciano Belt (DFB) is an important Neoproterozoic to Cambrian orogenic complex, extending from eastern Uruguay to southern Brazil. It comprises a collage of oceanic domains and continental fragments developed between 0.9 and 0.54 Ga between the Rio de La Plata Craton (RLPC), Nico Perez Terrane (NPT) and Kalahari Craton. In southern Brazil, the DFB comprises two metamorphic-granitic terranes, a batholith and a foreland basin that cover all units. The São Gabriel Terrane (SGT) consists of two Neoproterozoic (Tonian and Cryogenian) juvenile arcs and a late-collisional basin, interleaving with relicts of ophiolitic complexes. A review of the geologic and geochronological data of the SGT is presented. Sm–Nd T_{DM} model ages between 1.2 and 0.8 Ga and positive $\varepsilon Nd(t)$ values between +1 and +5 characterize the SGT units. Plate tectonic evolution started with the opening of the Charrua Ocean to the east of the RLPC and west of NPT, between 0.93 and 0.90 Ga. An intraoceanic island arc (Passinho Arc), between 0.89 and 0.86 Ga, and a continental margin arc (São Gabriel Arc), between 0.77 and 0.72 Ga, was generated by eastward and westward subduction and was subsequently accreted to the western margin of the NPT, between 0.71 and 0.70 Ga. The post-collisional stage is marked by the emplacement of late orogenic granites (0.70–0.68 Ga). The late orogenic Pontas do Salso basin presents zircon provenance between 0.86 and 0.68 Ga and represents the collapse of the SGT.

Keywords

West Gondwana • Dom Feliciano Belt • São Gabriel Terrane • Charrua Ocean • Brasiliano orogeny Neoproterozoic • Gondwana assembly

10.1 Introduction

There are two large geological domains in South America, the Amazonian (also referred to as pre-Brasiliano, or northwest domain) and the "Brasiliano" (or central-east domain), according to Brito Neves and Fuck (2013, 2014) (Fig. 10.1). Over the last five decades the phrase "Brasiliano cycle" has been used to refer to the orogenic cycle of the Neoproterozoic geology of Brazil, comprising the period from 800 to 500 Ma (Cordani et al. 1973, 2003; Almeida 1971; Almeida et al. 1973; Silva et al. 2005).

The Mantiqueira Province is one of the main Neoproterozoic orogenies formed during the assembly of West Gondwana. This orogenic system is a northeast to southwest mobile belt running parallel to the southern and eastern coast of Brazil and extending for over 3000 km from Bahia to Uruguay. It comprises the Dom Feliciano (southern Brazil and Uruguay), Ribeira (Paraná, São Paulo, Minas Gerais and Rio de Janeiro states) and Araçuaí belts (Espírito Santo, eastern Minas Gerais and southern Bahia states) (e.g., Heilbron and Machado 2003; Silva et al. 2005). Its African counterpart includes the Saldania-Gariep, Damara, Kaoko and West Congo belts (Fig. 10.1). Several models have been developed to explain the tectonic evolution of this orogen and its role in the assembly of West Gondwana (e.g.,

R. P. Philipp (✉)
Geosciences Institute, Federal University of Rio Grande do Sul (UFRGS), Av. Bento Gonçalves, 9500, Porto Alegre, RS CEP: 91501-970, Brazil
e-mail: ruy.philipp@ufrgs.br

M. M. Pimentel
Geosciences Institute, Federal Unversity of Brasília (UnB), Campus Universitário Darcy Ribeiro ICC—Ala Central, Brasilia, DF CEP: 70.910-900, Brazil
e-mail: pimentel@unb.br

M. A. S. Basei
Geosciences Institute, Geochronological Research Center (CEPEGEO), São Paulo University (USP), R. do Lago, 562—Vila Universitaria, São Paulo, SP CEP: 05508-080, Brazil
e-mail: baseimas@usp.br

S. Siegesmund et al. (eds.), *Geology of Southwest Gondwana*, Regional Geology Reviews,
https://doi.org/10.1007/978-3-319-68920-3_10

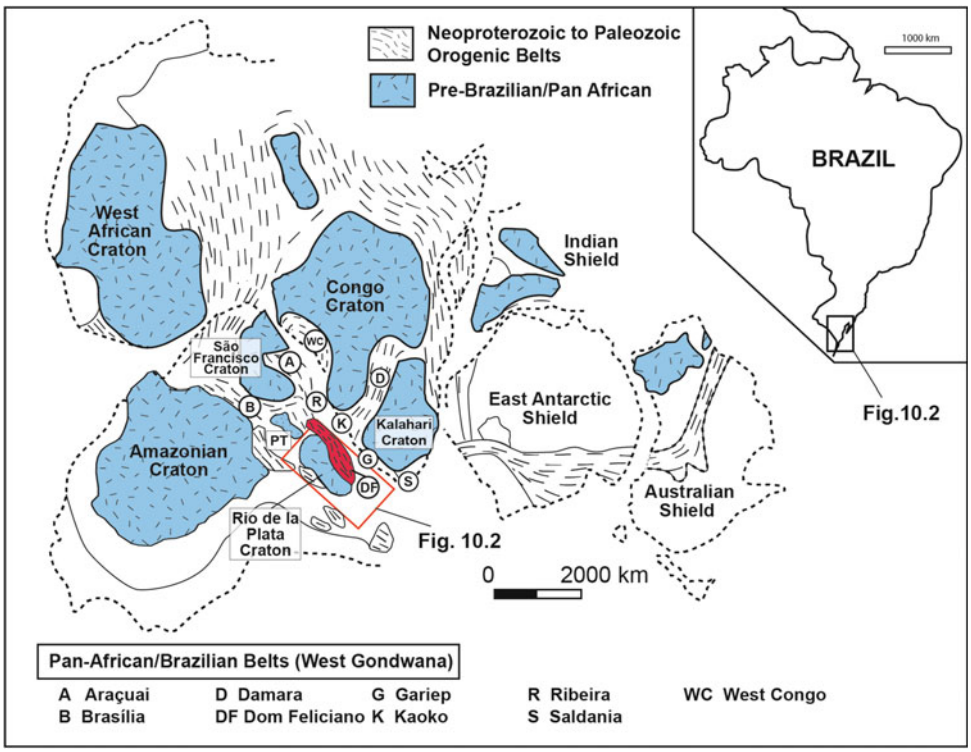

Fig. 10.1 Southern portion of the Gondwana continent showing the location of the main cratonic areas and of the DFB (in red) and related belts in Africa. *PT* Paranaguá Terrane. Modified from Oyhantçabal et al. (2011), Rapela et al. (2011) and Philipp et al. (2016a)

Chemale 2000; Cordani et al. 2003; Hartmann et al. 2007; Basei et al. 2008; Saalmann et al. 2010; Philipp et al. 2016a).

A review of recent geological and U–Pb geochronological data from the basement of the South American platform shows that the Brasiliano orogenic collage occurred in four distinct tectonic phases: (1) Upper Tonian-Early Cryogenian (*c*. 890–720 Ma), (2) Late Cryogenian-Early Ediacaran (*c*. 660–610 Ma), (3) Early-Middle Ediacaran (*c*. 590–560 Ma); and (4) Late Cambrian (520–500 Ma) (Almeida et al. 1973; Cordani et al. 2003; Silva et al. 2005; Brito Neves and Fuck 2013, 2014; Brito Neves et al. 2014). The first three phases are well represented in most Neoproterozoic structural provinces in West Gondwana. The interval between approximately 800 and 500 Ma is, in part, comparable to that reported for the amalgamation of various continental fragments in East (Arabian-Nubian, Mozambique, Kuunga) and North Gondwana (Cadomian). However, there are important differences in the tectonic process and in the age intervals of the events as a function of the magnitude of the Gondwana agglutination and the diversity of paleogeographic scenarios. West Gondwana shows an interesting peculiarity: lithologically and tectonically diversified Tonian terranes that underlie Brasiliano orogenic buildups (Brito Neves et al. 2014). These terranes were strongly reworked during younger orogenic phases. The Tonian terranes (1000–900 Ma) and their relationship with Rodinia or with the Gondwana fusion processes remain undefined (Brito Neves et al. 2014).

The history of the evolution of orogenic belts rarely preserves all its constructive episodes. The São Gabriel Terrane (SGT) presents one of the best exhibitions of the initial evolution period of the so-called Brasiliano Event or Orogenic Cycle, with all elements related to the construction and closure of Neoproterozoic oceans. The Dom Feliciano Belt (DFB) was formed during a long-lived evolution of about 450 My, starting with the opening of the Charrua Ocean in the southwestern portion of Gondwana, at 930–900 Ma, between the Rio de La Plata Craton (RLPC) and the Nico Perez Terrane (NPT) (Philipp et al. 2016a). The closure of this ocean generated two juvenile magmatic arcs between 890 and 860 Ma and 770 and 720 Ma. The collision of the arc systems against the NPT (Taquarembó Terrane in Brazil) was recorded by a metamorphism event between 720 and 700 Ma. This was followed by the opening and closure of the Adamastor Ocean and the collision between the Rio de la Plata and Kalahari cratons at the end of the Neoproterozoic, set between 650 and 620 Ma. The collapse of the belt is represented by the foreland or late-collisional basins with a maximum depositional age of 540 Ma. Four distinct events may be recognized by the development of four arc systems, (1) Passinho, (2) São Gabriel, (3) Porongos and (4) Dom Feliciano, defining two main orogenies (Chemale 2000;

Hartmann et al. 2007; Saalmann et al. 2010; Philipp et al. 2016a).

This work is based on a review of K–Ar, Rb–Sr and U–Pb zircon geochronology, available for the lithostratigraphic units of the SGT. To assess the sources of magmas we used Rb–Sr, Sm–Nd and ^{18}O data. The interpretation of geochronological and isotopic data was then combined with a review of field geological data produced by regional geological mapping projects and a Ph.D. thesis. The magmatic crystallization ages are more abundant and were predominantly obtained by the K–Ar (cooling), Rb–Sr, U–Pb SHRIMP and LA-MC-ICPMS methods. Metamorphic ages were obtained by zircon and titanite dating by U–Pb LA-MC-ICPMS, by the combination of whole-rock and mineral Rb–Sr and Sm–Nd data and by the monazite composition by EMPA. The U–Pb zircon data also include provenance studies of metavolcanosedimentary complexes, including *c*. 450 analyzed zircon grains, some of which were not yet published data. The data used in the present review are shown in Tables 10.1 and 10.2.

Table 10.1 Summary of the published geochronological data of the lithostratigraphic units of the São Gabriel Terrane

Unit/location	Rock type	Crystalization age	Metamorp.	Sr^{87}/Sr^{86}	Method	Reference
Mata Grande gabbro (São Sepé)	Gabbro	2.182 ± 10 Ma 1.826 ± 55 Ma 1.867 ± 56 Ma 960 Ma			K–Ar K–Ar Nd T_{DM}	Issler et al. (1973) Teixeira (1982) Babinski et al. (1996)
Pontas do Salso Complex (Palma)	Metassediments	805 ± 38 Ma 745 ± Ma 755 ± Ma			Rb–Sr LA-ICPMS (z)	Soliani (1986) Laux et al. (2012)
Lagoa da Meia Lua Suite (Vila Nova do Sul)	Granite Microdiorite Pegmatite Granodiorite Sanga do Jobim Gr. Tonalito Buriti Santa Zélia Gr. Trondhjemite Tonalito Sanga do Jobim Gr. Cerca de Pedra Gr.	647 Ma 654 Ma 620 Ma 601 Ma 614 Ma 666 ± 20 Ma 658 ± 126 Ma 643 ± 28 Ma 661 ± 29 Ma 665 ± 25 Ma 703 ± 7 Ma 704 ± 3 Ma 694 ± 5 Ma 690 ± 2 Ma 680 ± 2 Ma 682 ± 1 Ma		0.704 0.704 0.704	Rb-Sr (WR) Rb-Sr (WR) Rb-Sr (WR) Rb–Sr K–Ar U-Pb SHRIMP (z)	Cordani et al. (1973) Soliani (1986) Silva and Soliani (1987) Remus (1991) Hartmann et al. (2011)
Palma Complex (Palma)	Metabasalt Metabasalt	559 ± 17 Ma 805 ± 38 Ma			K–Ar K–Ar	Teixeira (1982) Soliani (1986)
Cambaí Complex (Vila Nova do Sul)	Tonalitic gn. Amphibolite Amphibolite Tonalitic gn. Amphibolite Tonalitic gn. Tonalitic gn. Tonalitic gn. Diorite Tonalite Trondhjemite Amphibolite Diorite Diorite Diorite Tonalitic gn. Santa Siria Diorite	690 ± 18 Ma 744 ± 19 Ma 725 ± 26 Ma 700 ± 21 Ma 755 ± 23 Ma 738 ± 22 Ma 694 ± 23 Ma 682 ± 29 Ma 714 ± 49 Ma 759 ± 326 Ma 703 ± 41 Ma 879 ± 14 Ma 750 ± 16 Ma 736 ± 10 Ma 733 ± 13 Ma 704 ± 13 Ma 860 Ma 718 ± 2 Ma 735 ± 7 Ma 745 ± 2 Ma	850 730 720 730 Ma	0.704 0.705 0.704	K–Ar K–Ar Rb–Sr Rb-Sr SHRIMP (z) TIMS (z) LA-ICPMS (z) SHRIMP (z) LA-ICPMS (z)	Cordani et al. (1973) Teixeira (1982) Soliani (1986) Silva and Soliani (1987) Leite et al. (1998) Babinski et al. (1996) Bongiolo et al. (2010) Hartmann et al. (2011) Lusa et al. (2018)

(continued)

Table 10.1 (continued)

Unit/location	Rock type	Crystalization age	Metamorp.	Sr^{87}/Sr^{86}	Method	Reference
Bossoroca Complex (São Sepé)	Metavolcanic Metadacite Metadacite Meta-agglomerate Metacrystal Tuff	681 ± 44 Ma 753 ± 2 Ma 756 ± 14 Ma 767 ± 3 Ma 765 ± 10 Ma	698 ± 16 Ma		K–Ar TIMS (z) SHRIMP (z) LA-ICPMS (z)	Soliani (1986) Machado et al. (1990) Remus et al. (1999) Gubert et al. (2016)
Cambaizinho Complex (Vila Nova do Sul)	Gt-bt-plag-qz gn. Gt-bt-plag-qz gn.		807 ± 31 Ma 682 ± 1 Ma		Sm-Nd Gt-Whole Rock SHRIMP (z)	Philipp et al. (2008a) Hartmann et al. (2011)
Imbicuí Complex (Lavras do Sul)	Dioritic gn. Dioritic gn. Dioritic gn. (Amphibolite) Metadiorite Passinho Tonalitic gn.	2.149 ± 13 Ma (h) 2.087 ± 10 Ma (h) 2.100 ± 15 Ma (h) 2.761 ± 17 Ma (h) 1.866 ± 11 Ma (h) 879 ± 14 Ma 875 ± 5 Ma	741 ± 2 Ma 746 ± 2 Ma 750 ± 3 Ma 790 ± 7 Ma 786 ± 6 Ma		SHRIMP (z) SHRIMP (z) LA-ICPMS (z)	Hartmann et al. (2009) Leite et al. (1998) Philipp et al. (2014)
Cerro Mantiqueiras Ophiolite (Lavras do Sul)	Amphibolite Metabasal Cloritite	911 ± 276 Ma 773 ± 10 Ma 923 ± 3 Ma	787 ± 13 Ma		K–Ar SHRIMP (z) SHRIMP (z)	Teixeira (1982) Leite et al. (1998) Arena et al. (2016)
Ibaré Ophiolite (Ibaré)	Plagiogranite	892 ± 3 Ma			SHRIMP (z)	Arena et al. (2016)
Pedras Pretas Complex (São Sepé)	Mafic to ultramafic rocks	1004 ± 55 Ma 839 ± 29 Ma 891 ± 79 Ma 681 ± 44 Ma			K–Ar K–Ar	Sartori (1978) Soliani Jr. (1986)

The compilation includes a historical review, with pioneer K–Ar and Rb–Sr studies (Cordani et al. 1973; Teixeira 1982; Silva Filho 1984; Soliani 1986), and the use of Pb–Pb and U–Pb ID-TIMS systematics (Machado et al. 1990; Babinski et al. 1996, 1997). More recently, the use of the SHRIMP (Leite et al. 1998, 2000; Remus et al. 1999, 2000; Hartmann et al. 1999, 2000, 2011; Lena et al. 2014; Lopes et al. 2015) and LA-MC-ICPMS (Philipp et al. 2014; Gubert et al. 2016; Vedana and Philipp 2016; Vedana et al. 2017; Lusa et al. 2018) techniques has produced abundant new isotopic data, allowing significant progress in the understanding of tectonic processes in southern Brazil.

10.2 Geotectonic Context

The southern Brazilian Shield is an association of Precambrian rocks exposed in the Rio Grande do Sul state (RS), and comprises Paleo- and Neoproterozoic tectono-stratigraphic units. The geology of this area consists of fragments of Paleoproterozoic metamorphic and granitic rocks gathered in the NPT (Oyhantçabal et al. 2011; Rapela et al. 2011; Philipp et al. 2016a), surrounded by Neoproterozoic associations of the DFB (Fig. 10.2).

The DFB is the southern segment of the Mantiqueira Province and represents a crustal segment, partially strongly deformed and migmatized between *c*. 650 and 620 Ma (e.g., Fernandes et al. 1992; Chemale et al. 1995; Bitencourt and Nardi 2000; Philipp and Machado 2005; Hartmann et al. 2007; Saalmann et al. 2010; Philipp et al. 2013, 2016b. Remnants of older continental crust are represented by septa exposed in Santa Catarina (Hartmann et al. 2000; Basei et al. 2008), Rio Grande do Sul (Philipp et al. 2008a; Hartmann et al. 2008, 2011) and Uruguay (Hartmann et al. 2002; Oyhantçabal et al. 2011).

The DFB is divided from west to east into the following domains: (1) SGT, (2) Tijucas Terrane, (3) Florianópolis-Pelotas-Aigua batholiths and (4) Punta Del Este Terrane (Fig. 10.2). In southern Brazil, the belt comprises rock units developed during four major orogenic events: the Passinho (890–860 Ma), Porongos (800–750 Ma), São Gabriel (770–680 Ma) and Dom Feliciano (650–540 Ma) (e.g., Hartmann et al. 2000; Saalmann et al. 2010; Philipp et al. 2016a).

The relationships between the units of the SGT and DFB are shown in Figs. 10.3 and 10.4, including time relationships between lithostratigraphic and geotectonic units and time, U–Pb and Pb–Pb geochronology (crystallization,

Table 10.2 Isotopic data from the lithostratigraphic units of the SGT

Sample	Lithology	Age	$^{87}Sr/^{86}Sr$	Sm	Nd	$^{143}Nd/^{144}Nd$	$^{147}Sm/^{144}Nd$	$E_{Nd}(0)$	$E_{Nd}(t)$	T_{DM}
PVN-1117	Gran-Bt gn. (Cz)	800	–	11.31	54.78	0.512,346	0.12490	−5.70	1.69	1.28
PVR-6060	Musc-bt gn. (Cz)	800	–	4.93	24.26	0.512269	0.12290	−7.20	0.39	1.59
BR-131/1	Musc-bt gn. (Cz)	800	0.7022	3.3	12.6	0.512670	0.158207	0.62	4.59	1.03
BR126/10	Amphibolitic gn. (Cz)	800	0.7028	2.8	12.1	0.512631	0.140402	−0.13	5.64	0.86
BR-126/6	Psammitic schist (Cz)	800	0.7014	1.1	6.4	0.512208	0.102918	−8.4	1.20	1.15
BR-146/1	Amphibolitic gn. (Cz)	800	0.7033	4.6	18.8	0.512534	0.148829	−2.03	2.90	1.19
BR-147/1	Gran-bt gn. (Cz)	800	0.703	3.3	18.7	0.512269	0.107061	−7.02	2.03	1.11
BR-167/1	Chlo-ep. schist (PSC)	750	0.7154	0.22	0.74	0.511232	0.183068	−2.08	−0.68	2.57
BR-31/2	Phylitte (BC)	750	0.7016	3.2	12.6	0.512739	0.152501	1.98	6.23	0.77
BR-32/2	Phylitte (BC)	750	0.7039	4.5	20	0.512578	0.134953	−1.17	4.77	0.90
BR-137/1	Chlo. schist (BC)	800	0.7036	2.3	10	0.512478	0.141620	−3.11	2.53	1.19
RS-19	Metarhyodacite (BC)	750	–	3.94	12.94	0.512978	0.18434	6.6	7.8	0.96
BR-126/8	Tonalitic gn. (CC)	720	–	1.5	8.8	0.512414	0.105941	−4.34	3.98	0.89
BR-148/1	Tonalitic gn. (CC)	720	0.7035	3.8	15.9	0.512713	0.142760	1.46	6.43	0.73
GRF-45	Tonalitic gn. (CC)	720	–	3.01	11.86	0.512624	0.15340	−0.27	3.71	1.68
GRF-01a	Tonalitic gn. (CC)	720	–	5.61	25.32	0.512444	0.13390	−3.78	1.99	1.27
GRF-03c	Dioritic gn. (CC)	720	–	7.31	36.69	0.512210	0.12050	−8.35	−1.34	1.04
GRF-21e	Metadiorite (CC)	705	–	5.83	27.27	0.512464	0.12930	−3.39	2.68	1.04
GRF-01e	Metatonalite (CC)	705	–	5.24	25.56	0.512487	0.12390	−2.95	3.61	1.31
GRF-22e	Metatonalite (CC)	705	–	5.13	28.61	0.512436	0.10830	−3.94	4.03	0.88
RS-20E	Dioritic gn. (CC)	700	–	4.03	19.23	0.512460	0.12653	−3.5	2.8	1.03
RS-20F	Metatonalite (CC)	700	–	5.90	35.36	0.512415	0.10089	−4.4	4.3	0.86
RS-20G	Pegmatite (CC)	700	–	1.28	5.51	0.512603	0.14059	−0.7	4.4	0.93
RS-20H	Metadiorite (CC)	700	–	6.39	33.27	0.512498	0.11615	−2.7	4.5	0.86
GRF-35a	Granodiorite (LMLS)	695	–	3.91	24.80	0.512165	0.09520	−9.23	−0.22	1.13
GRF-21d	Monzogranite (LMLS)	695	–	5.25	31.26	0.512359	0.10150	−5.44	3.01	0.93
GRF-26 g	Diorite (LMLS)	695	–	7.62	36.27	0.511936	0.12700	–13.69	−7.52	1.93
RS-24	Sanga do Jobim G.	700	–	4.16	19.31	0.512600	0.13026	−0.7	5.2	0.82
BR123/2b	Santa Zélia G. (LMLS)	660	0.708	3.6	17.3	0.512252	0.12714	−7.53	−1.66	1.38
BR123/2b	Santa Zélia G. (LMLS)	660	0.7068	3.6	17	0.512264	0.12916	−7.29	−1.59	1.39
BR-114/1	Phylitte (PSC)	750	0.7034	2.9	9.9	0.512834	0.17623	3.82	5.79	0.87
BR-138/1	Amphib.gn. (ultram.)	800	0.7035	3.9	14.5	0.512740	0.16438	2.00	5.31	0.94
BR-138/3	Amphibolite (ultram.)	800	0.7048	3.9	18.5	0.512563	0.12719	−1.47	5.66	0.85

Complexes Cz Cambaizinho, *BC* Bossoroca, *CC* Cambaí and *PSC* Pontas do Salso, *LMLS* Lagoa da Meia Lua Suite. Samples PVN, PVR and GRF from Philipp et al. (2008b), samples BR from Saalmann et al. (2005a, b, c) and samples RS from Babinski et al. (1996)

metamorphic ages and detrital zircon provenance in metasediments), geochemistry and main orogenic cycles. The geochronological data indicate four main Neoproterozoic orogenic events: (1) Passinho: initial crustal accretion phase with intraoceanic arc magmatism, *c*. 890–860 Ma, (2) Porongos Arc: continental arc magmatism and crustal accretion, 800–750 Ma, (3) São Gabriel Arc: continental arc magmatism and accretion, 770–680 Ma, and (4) Dom Feliciano: a main magmatic and sedimentary phase, with intense crustal anatexis promoted by the injection of mantle magmas, *c*. 650–550 Ma. In all units of the DFB a younger regional metamorphic event (570–540 Ma) associated with transcurrents shear zones is recognized. A summary of the main events and tectonic processes in the DFB and NPT in the southern portion of Brazil is presented in Fig. 10.3.

The fragments of the NPT (sensu Oyhantçabal et al. 2011; Rapela et al. 2011; Oriolo et al. 2016) in RS were designated as Encantadas Microplate (Chemale 2000), Block

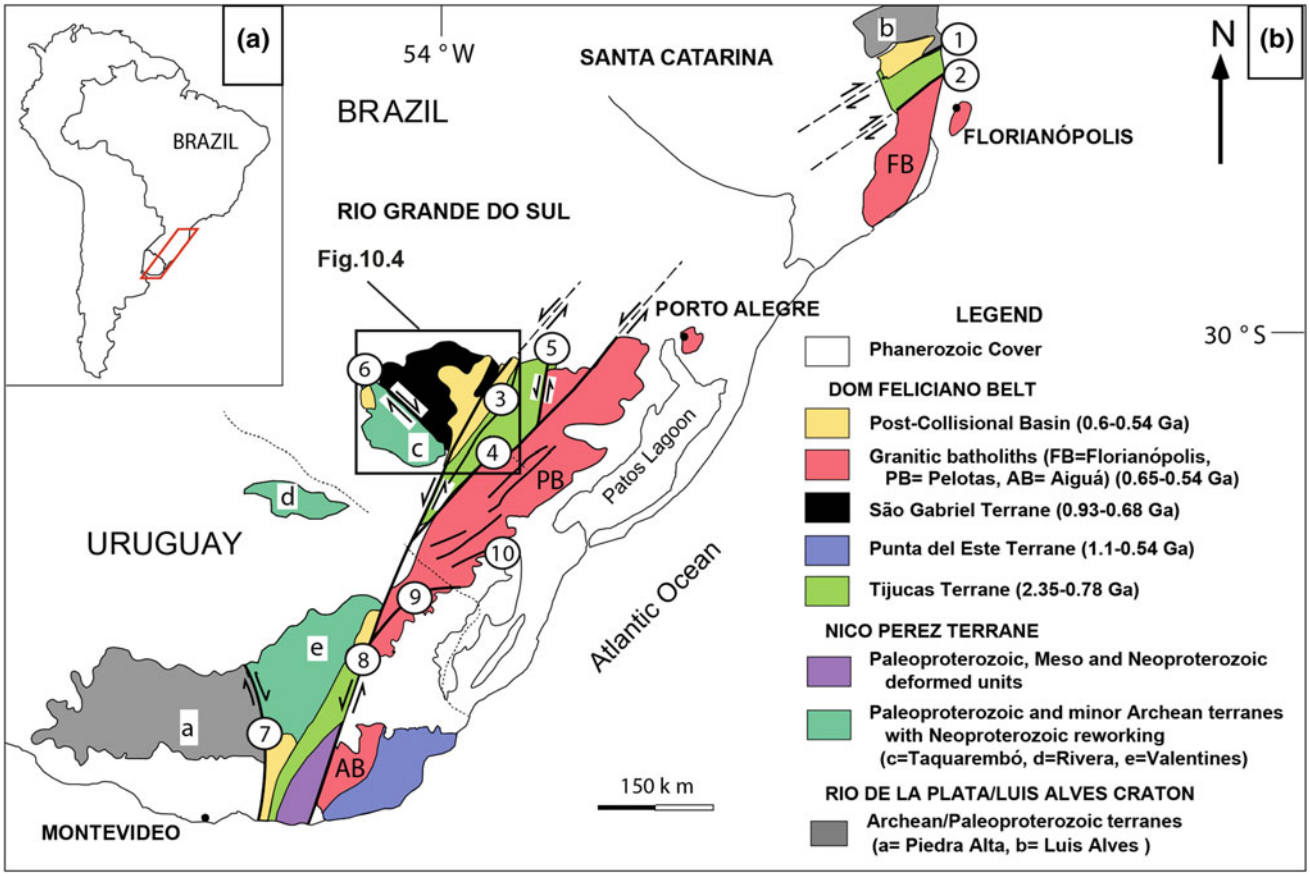

Fig. 10.2 Geotectonic units of the southern Brazilian and Uruguayan shields (modified after Oyhantçabal et al. 2011; Philipp et al. 2016a). Shear Zones: *1* Itajai-Perimbó, *2* Major Gercino, *3* Caçapava do Sul, *4* Dorsal de Canguçu, *5* Passo do Marinheiro, *6* Ibaré, *7* Sarandí del Yí, *8* Sierra Ballena, *9* Cerro Amaro, *10* Arroio Grande

(Saalmann et al. 2005a, b, c, 2006) or Microcontinent (Hartmann et al. 2007). These fragments, several hundred meters to a few kilometers wide, occur as "basement inliers" in the Taquarembó and Tijucas terranes and in the Pelotas Batholith of the DFB. They are represented by Paleoproterozoic gneisses and metagranites. These rocks comprise associations formed in three main events: (1) the Santa Maria Chico (Siderian, 2.4–2.3 Ga), (2) the Encantadas (Rhyacian, 2.2–2.0 Ga) and (3) the Seival (Statherian, 1.8–1.7 Ga) (Chemale 2000; Hartmann et al. 2007; Philipp et al. 2016a). After that, the continental crust in southern Brazil experienced a period of tectonic quiescence, marked by the emplacement of basic-ultrabasic complexes of Callymian age (1.57–1.55 Ga), represented by the Capivarita Anorthosite (Chemale et al. 2011) and Tupi Silveira Amphibolite (Camozzato et al. 2012, 2013).

The Taquarembó Terrane (TT) is located in the southwestern portion of the shield and represents the largest exposed fragment of the NPT in Brazil (Fig. 10.2). The TT comprises the Paleoproterozoic Santa Maria Chico Granulitic Complex, which is intruded by Staterian and Neoproterozoic granites and covered by the volcano-sedimentary sequence of the Ediacaran Camaquã Basin.

The Tijucas Terrane (TjT) is elongated in the N30–40°E direction, extending for 170 km, 15–30 km wide (Fig. 10.2). It is in tectonic contact with the SGT to the west along the Caçapava do Sul Shear Zone. The eastern boundary, with the Pelotas Batholith, is marked by the ductile strike-slip Dorsal do Canguçu Shear Zone (e.g., Fernandes et al. 1992; Philipp et al. 2003). The northeastern contact of the TjT with the Pelotas Batholith is affected by the Passo do Marinheiro Shear Zone. The TjT consists of: (1) basement inliers made of Paleoproterozoic orthogneisses of the Encantadas and Vigia complexes, (2) Statherian Seival Metagranite, (3) Calymminian Tupi Silveira Amphibolite and (4) Neoproterozoic metavolcanic and metasedimentary rocks of the Porongos Complex.

The Pelotas Batholith is composed of a set of Neoproterozoic (Ediacaran) and Paleozoic (Cambrian-Ordovician) granitic suites, generated during and after the climax of the Dom Feliciano orogeny, between 650 and 550 Ma. The

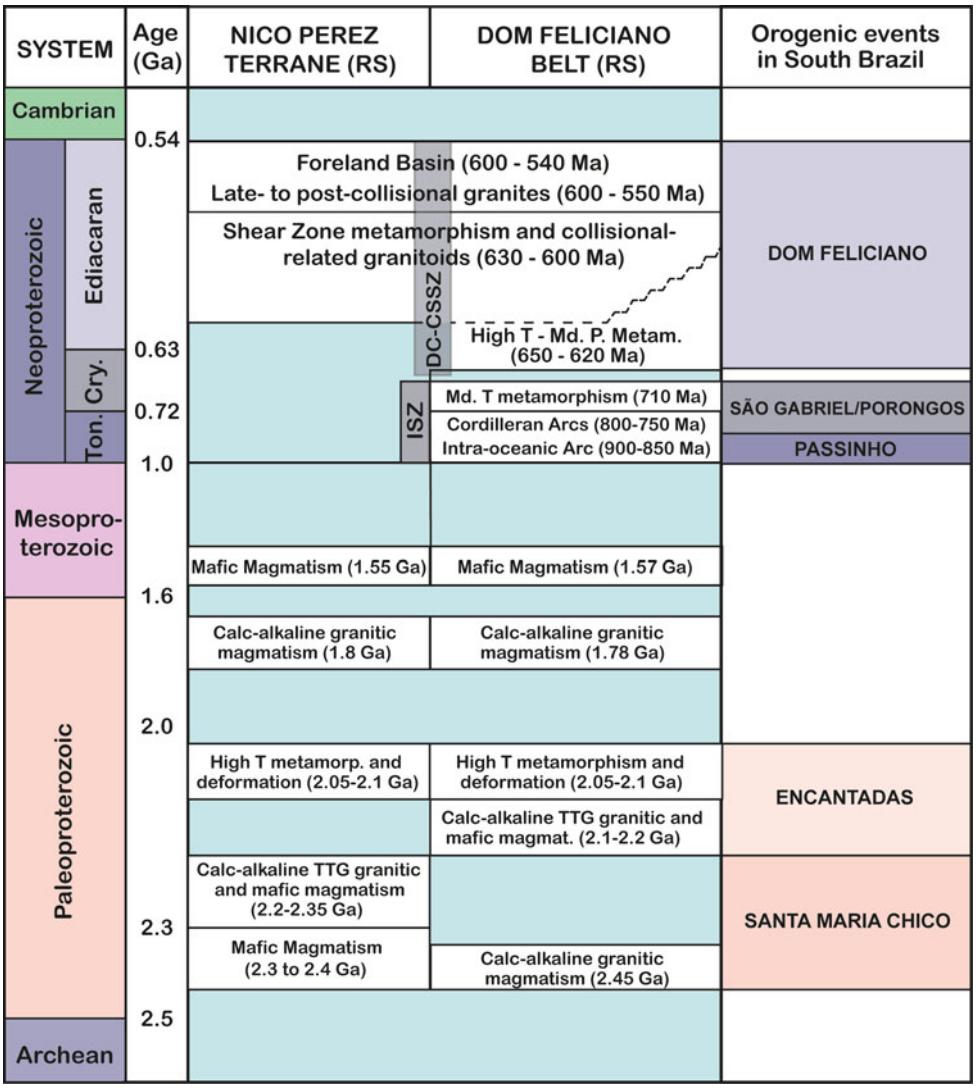

Fig. 10.3 Main events and tectonic processes in the DFB and NPT. Shear zones: *ISZ* Ibaré Shear Zone; *DCSZ* Dorsal de Canguçu Shear Zone, *CSSZ* Caçapava do Sul Shear Zone

granitic suites are elongated in the N50–70°E direction, and their generation and emplacement were controlled by high-angle ductile transcurrent shear zones. The batholith is a multi-intrusive 400 × 120 km plutonic complex including granite, gabbro and diorite, as well as rhyolitic to basaltic volcanic rocks (Fig. 10.2) (Philipp and Machado 2005). The granitoids represent an early generation of high-K calcal-kaline suites with metaluminous to peraluminous affinity, followed by alkaline magmatism and, finally, less voluminous peralkaline intrusions (Philipp and Machado 2005; Oliveira et al. CR004). Shear zones in the batholith are defined by mylonitic belts with subvertical foliation, accompanied by subhorizontal stretching lineation, and were active during the development of the batholith, controlling the intrusion of the granitic suites (Fernandes et al. 1992; Koester et al. 2001; Philipp et al. 2003). Syn- to late collisional episodes (650–620 Ma) of compressional ductile movements were followed by an extensional post-collisional period (600–550 Ma) (Philipp et al. 2016a).

10.2.1 Geotectonic Units of the São Gabriel Terrane

The São Gabriel Terrane (SGT) occurs in the western portion of the DFB and has an elongated shape in the N20–30°E direction, underlying an area of approximately 110 km × 60 km (Fig. 10.2). This region is covered in the west and north by the Phanerozoic units of the Paraná Basin, and is limited to the south by the N70°W–S70°E trending Ibaré

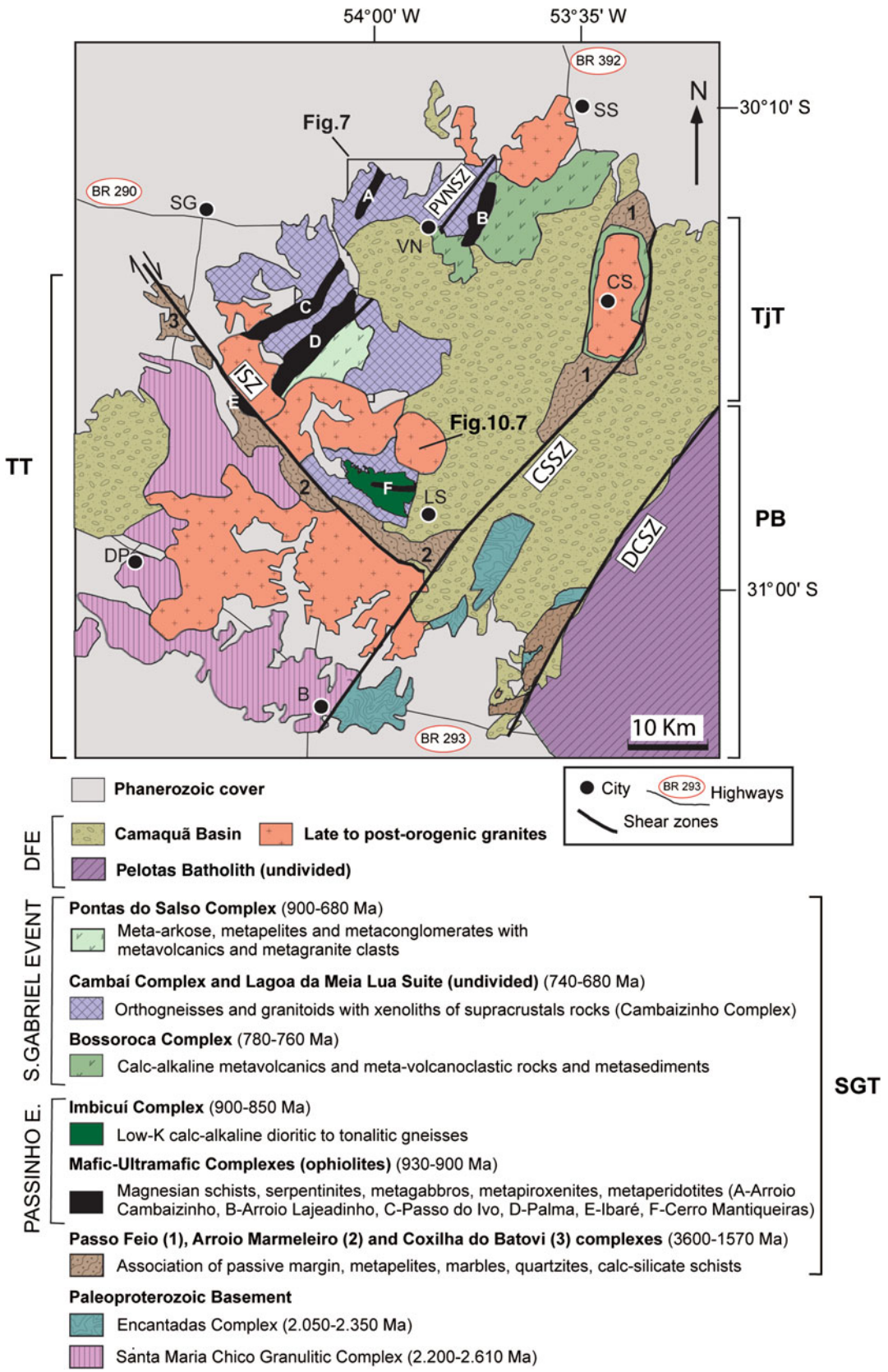

Fig. 10.4 Geological map of the SGT. Modified from Philipp et al. (2016a). Shear Zones: *ISZ* Ibaré, *PVNSZ* Palma-Vila Nova, *CSSZ* Caçapava do Sul and *DCSZ* Dorsal do Canguçu. Cities: *VN* Vila Nova do Sul, *SG* São Gabriel, *LS* Lavras do Sul, *DP* Dom Pedrito and *B* Bagé

Shear Zone (ISZ) and to the east by the Caçapava do Sul Shear Zone (CSSZ). Geophysical modeling of the CSSZ shows that this structure is deep seated and may be interpreted as the suture zone between the São Gabriel and Tijucas terranes (Chemale 2000 and references therein).

The SGT consists of remnants of ophiolitic complexes and two Neoproterozoic magmatic arcs; the older one is an intraoceanic arc (Passinho) and the younger one represents an active continental margin arc (São Gabriel) (Fig. 10.4). They are covered by the sedimentary and volcanic sequences of the Neoproterozoic (Ediacaran) Camaquã Association, and cut by related granitic rocks associated with the Dom Feliciano orogeny. The units of the SGT are strongly controlled by N30–40°E trending shear zones, which are rotated to the N70°W direction by the ISZ in the southern border of the terrane. This tectonic structure is recognized by magnetic anomalies as well as the elliptical shape of the Neoproterozoic intrusive plutonic bodies.

The different rock units of the SGT may be grouped into four main associations: (1) metasedimentary complexes, (2) the Palma Accretionary Prism, (3) arc-related rocks and (4) volcanosedimentary rocks of the Camaquã Basin and plutonic rocks associated (Fig. 10.4). The Palma Accretionary Prism is made of tectonic slabs of ophiolitic complexes, comprising magnesian schist, serpentinite and amphibolite, with subordinate metaperidotite, metagabbro, metapyroxenite and meta-anortosite. The arc-related rocks are the Cambaizinho Complex paragneisses, Passinho Complex orthogneisses (890–860 Ma) and São Gabriel rocks, represented by the metavolcanosedimentary Bossoroca Complex (780–760 Ma), orthogneisses and metagranitoids of Cambaí Complex (CC) (740–700 Ma) and granitoids of the Lagoa da Meia Lua Suite (LMLS) (700–680 Ma). The Pontas do Salso Complex is a late orogenic basin, older than 680 Ma and characterizing the collapse of the SGT (Vedana and Philipp 2016; Vedana et al. 2017). These associations are in tectonic contact with passive margin metasedimentary rocks represented by the Passo Feio and Marmeleiro complexes. The Camaquã volcanosedimentary association and granites associated was formed between 610 and 540 Ma and is represented by a foreland basin and granites related to the late to post-orogenic stages of the Dom Feliciano orogeny (Chemale et al. 1995).

A summary of the main tectonic events, lithostratigraphic units and orogenesis of the rocks associations of the SGT can be seen in Fig. 10.5. The detailed description of the SGT units can be found in the studies by Leite et al. (1998), Remus et al. (1999), Garavaglia et al. (2002), Saalmann et al. (2005b, c, 2006), Hartmann et al. (2011), Lena et al. (2014), Arena et al. (2016), Gubert et al. (2016), Vedana and Philipp (2016), Vedana et al. (2017) and Lusa et al. (2018).

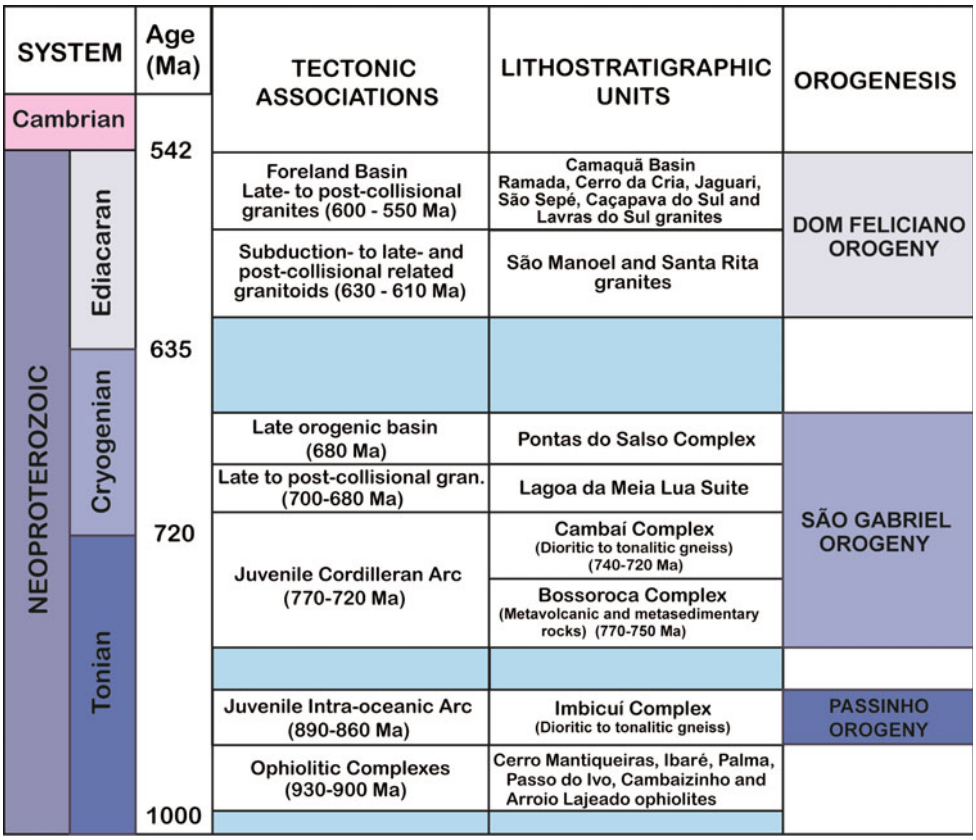

Fig. 10.5 Tectonostratigraphic chart of the SGT and the orogenesis of the DFB in south Brazil

10.2.2 Geology and Geochronological Data

The first geochronological data obtained by the K–Ar and Rb–Sr methods for the SGT units in the 1970s and 1980s indicated the existence of magma-generating processes developed in the Tonian and Cryogenic periods between 1000 and 680 Ma (Table 10.1) (Cordani et al. 1973; Teixeira 1982; Soliani 1986; Silva Filho and Soliani 1987). Subsequently, U–Pb zircon dating by TIMS confirmed these observations with the research of Machado et al. (1990), Babinski et al. (1996, 1997) and Leite et al. (1998). More recently, the U–Pb method zircon dating by SHRIMP and LA-MC-ICPMS represents an important contribution to the understanding of the SGT geochronology (Philipp et al. 2014; Lena et al. 2014; Lopes et al. 2015; Hartmann et al. 2011; Gubert et al. 2016).

10.2.2.1 Metasedimentary Complexes

The Cambaizinho, Passo Feio, Marmeleiro and Cerro do Batovi complexes together with the ophiolitic rocks are the oldest units of the SGT (Fig. 10.4). The metasediments of the Pontas do Salso Complex represent a late orogenic basin and mark the collapse and the final evolution of the SGT.

The Cambaizinho Complex (CbzC) comprises quartz-feldspatic paragneiss with interspersed calc-silicate rocks, marbles and impure quartzite (Lena et al. 2014). The rocks of this complex occur as kilometer-long elongated strips as well as metric-decametric xenoliths and roof pendants in the orthogneisses and metagranitoids of the CC and in the granites of the LMLS (Hartmann et al. 2011). Metamorphic paragenesis indicates metamorphism in mid- to upper amphibolite facies conditions. Sm–Nd isotope data presented by Saalmann et al. (2006) and Philipp et al. (2008b) indicate that the original sediments of the CbzC derived from the erosion of juvenile rocks of the Passinho and São Gabriel arcs. Lena et al. (2014) presented the results of combined U–Pb SHRIMP and LA-MC-ICPMS ages of detrital zircon grains from the metasedimentary rocks of the Cambaizinho Complex. The igneous U–Pb ages range from 840 to 700 Ma, peaking around 750 and 700 Ma, suggesting that the tectonic setting of the original sediments was part of a fore-arc or back-arc basin (Table 10.1). The $\delta^{18}O$ values of the detrital zircon ranged from 3.2 to 9.6‰ and are grouped into three distinct groups of sediment sources (Lena et al. 2014). They indicate a progressive evolution of the SGT from an intraoceanic arc to a continental active margin.

The Passo Feio Complex (PFC) is exposed in the eastern part of the SGT and was defined originally as a sequence of metapelite, marble, calc-silicate schist, quartzite, amphibolite, metavolcanic/metavolcanoclastic rocks and magnesium schist (Fig. 10.4). The metavolcanic rocks are related to the Bossoroca Complex and the amphibolites and ultramafic schists belong to ophiolitic complexes (Gubert et al. 2016). The U–Pb SHRIMP zircon provenance work was carried out by Remus et al. (2000) in one sample of metasediment from the northwestern part of the PFC, and shows zircon grains ranging in age from Archean to Neoproterozoic, suggesting that the PFC was originated from the erosion of complex continental sources. Based on U–Pb detrital zircon data of the PFC metasedimentary rocks, Lopes et al. (2015) also recognized zircon ages ranging from 0.8 to 3.6 Ga with Neoproterozoic, Mesoproterozoic, Paleoproterozoic and Archean distribution patterns.

The Marmeleiro and Cerro do Batovi complexes represent the continuity of the PFC metasediments to the south. Both units are composed of thick meta-arkose packages, interbedded with metapelites, marbles and low- to medium-grade calcsilicate schists. These complexes, however, were affected at the end of Neoproterozoic (Ediacaran) by the ISZ, responsible for bending and redirecting metamorphic foliations to the N40–50°W direction. They show regional schistosity with mineral stretching lineation with low plunge angle (<8°). The structure of the complex is related to transcurrent tectonics and suggests that the ISZ represents a lateral ramp, originated during the SGT thrusting over the Paleoproterozoic units of the Tijucas and Taquarembó terranes (Philipp et al. 2016a).

The metasedimentary rocks of the Pontas do Salso Complex are exposed in the southeastern portion of the SGT (Fig. 10.4). Meta-arkoses are dominant, with subordinate lenses of conglomeratic metasandstone and phyllites (Fig. 10.6). The metaconglomerates and metasandstones are immature with clasts of metavolcanic rocks with andesitic to dacitic composition, orthogneisses and granitic rocks. Petrographic and geochemical data indicate that the sources of the metasedimentary rocks were metavolcanic and metagranitic rocks of the Passinho and São Gabriel arcs (Vedana and Philipp 2016; Vedana et al. 2017). LA-MC-ICPMS detrital zircon provenance data for a meta-arkose and muscovite phyllite indicated that the sources of the complex have ages between 900 and 680 Ma (Vedana et al. 2017) (Table 10.1). The youngest ages suggest that the complex represents a late orogenic basin associated with the collapse of the SGT.

10.2.2.2 Palma Accretionary Prism

The mafic-ultramafic complexes from this unit comprise amphibolite and metaultramafic rocks including serpentinized harzburgite, metapyroxenite, metagabbro, serpentinite and Mg-rich schist with tholeiitic signature (Leite et al. 1998; Remus et al. 1999; Chemale 2000). Six major ophiolite complexes occur as northeast to southwest elongated

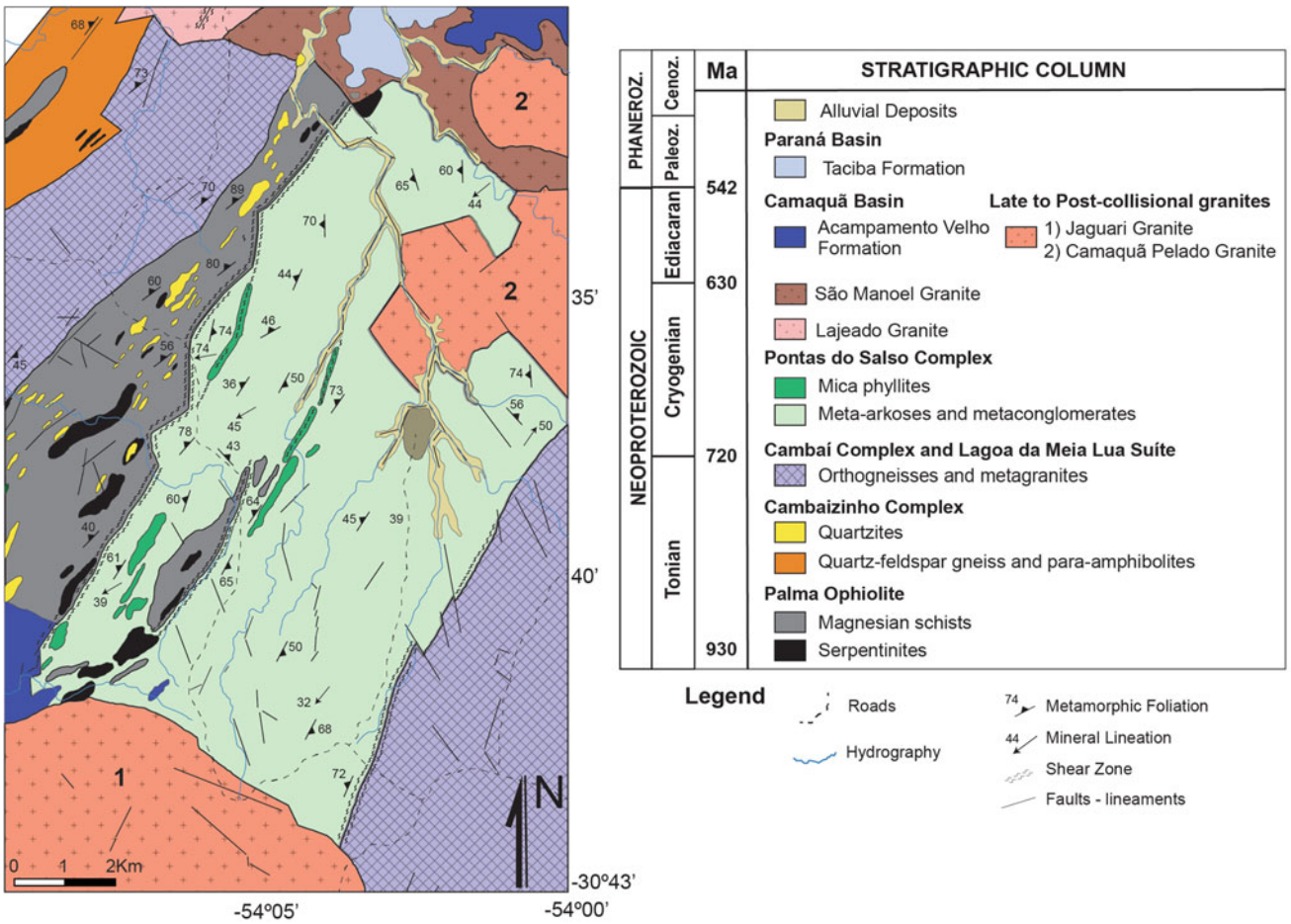

Fig. 10.6 Geological map of the Palma region (from Vedana and Philipp 2016; Vedana et al. 2017)

bodies parallel to regional structures: Cambaizinho, Arroio Lajeadinho, Passo do Ivo, Palma, Ibaré and Cerro Mantiqueira (Fig. 10.4).

The metaultramafic rocks show M_1 assemblage comprising antophilite + forsterite + enstatite, defining conditions of high grade and low pressure (Hartmann and Chemale 2003). Younger metamorphic events were accompanied by the formation of ductile shear zones, which characterize the later regional deformation and mark the M_2 greenschist facies metamorphism. The authors interpreted the amphibolite metamorphism (M_1) and the late greenschist facies event (M_2) as related to the São Gabriel and Dom Feliciano events respectively. Relicts of olivine and spinels have a chemical composition typical of ophiolitic rocks (Hartmann and Chemale 2003). U–Pb SHRIMP zircon ages for metasomatic albitites (plagiogranites) and cloritites formed during low-temperature serpentinization of ultramafic rocks of the Cerro Mantiqueira and Ibaré ophiolites are 923 ± 3 and 892 ± 3 Ma respectively, which are interpreted by Arena et al. (2016) as the emplacement age (Table 10.1). Metamorphic rims dated at 787 ± 13 Ma were found in the Cerro Mantiqueira Ophiolite.

10.2.2.3 Arc-Related Rocks

Passinho Arc

The rocks of the Passinho Arc are exposed in the southern portion of the SGT in a small area located south and north of the Cerro da Mantiqueira Ophiolite (Fig. 10.4). The arc rocks occur as an east to west elongated belt and are represented by orthogneisses of the Imbicuí Complex. This unit includes tonalitic to trondhjemitic gneisses in the central portion, involved by dioritic gneisses with subordinate lenses of metahornblendites (Lusa et al. 2018) (Fig. 10.7). The gneisses present tholeiitic to low-K calc-alkaline chemical composition and have U–Pb crystallization ages between *c*. 890 and 860 Ma (Table 10.1). Dioritic gneisses exposed to the south of the Cerro Mantiqueiras complex have SHRIMP U–Pb ages of 879 ± 14 Ma (Leite et al. 1998) and LA-MC-ICPMS ages of 875 ± 5 Ma (Philipp et al. 2014),

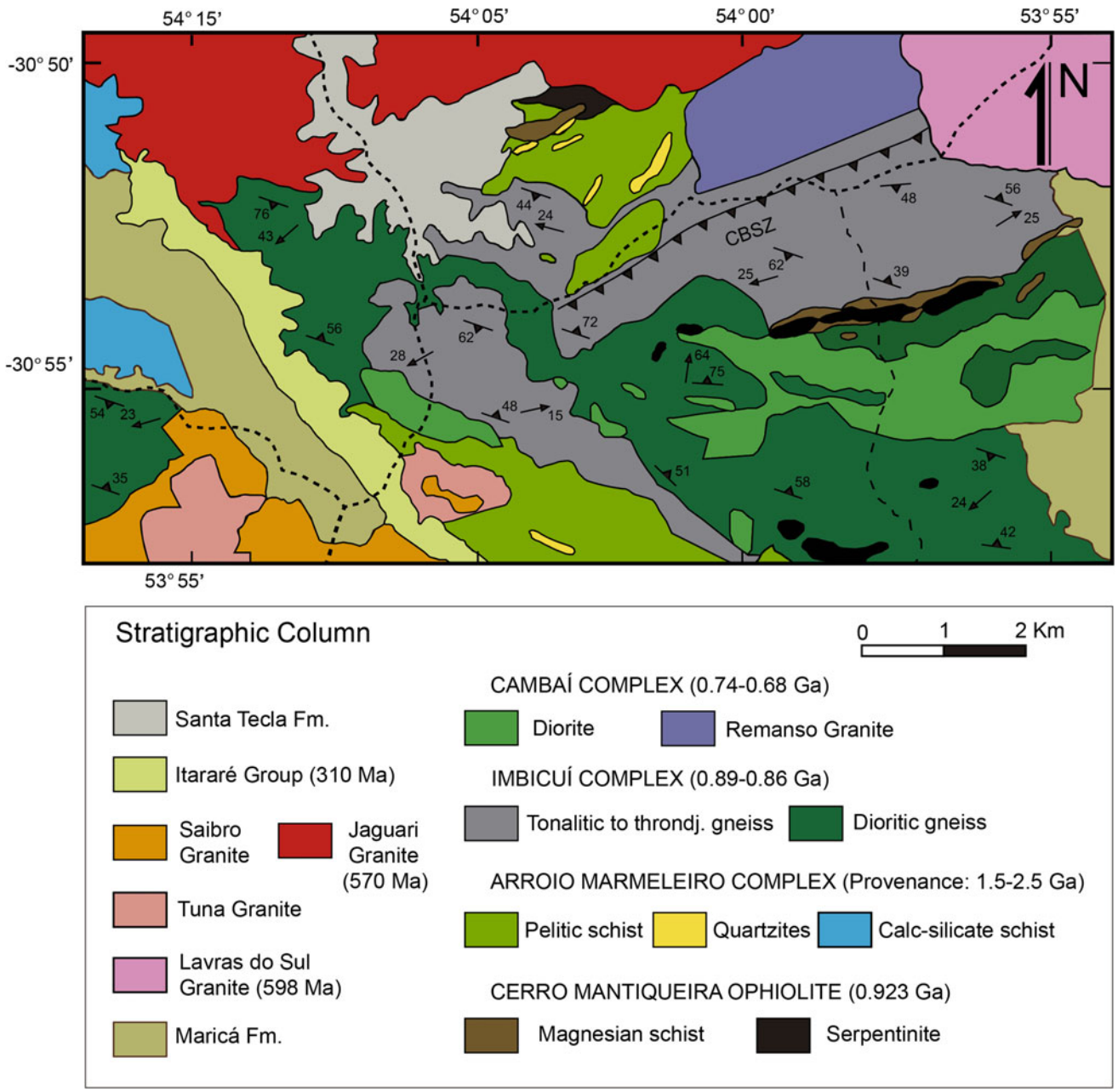

Fig. 10.7 Geological map of the Imbicui Complex, Cerro Mantiqueira region, southwestern portion of Lavras do Sul region (from Lusa et al. 2018)

890 ± 9 and 885 ± 3 Ma (Lusa et al. 2018). They are intruded by diorites and tonalites related to the CC with U–Pb ages between 740 and 710 Ma (Leite et al. 1998; Lusa et al. 2018).

The regional metamorphism of the Imbicuí Complex is marked by the assemblage Ca plagioclase + hornblende + biotite and Ca plagioclase + hornblende + diopside, indicative of the mid- to upper amphibolite facies and low-pressure conditions. A retrograde metamorphic event associated with shear zone development is marked by a greenschist to lower amphibolite paragenesis formed of albite + actinolite/hornblende + chlorite + epidote + white mica.

São Gabriel Arc

The São Gabriel Arc is exposed in a large area extending from São Gabriel, Vila Nova do Sul and São Sepé cities, in

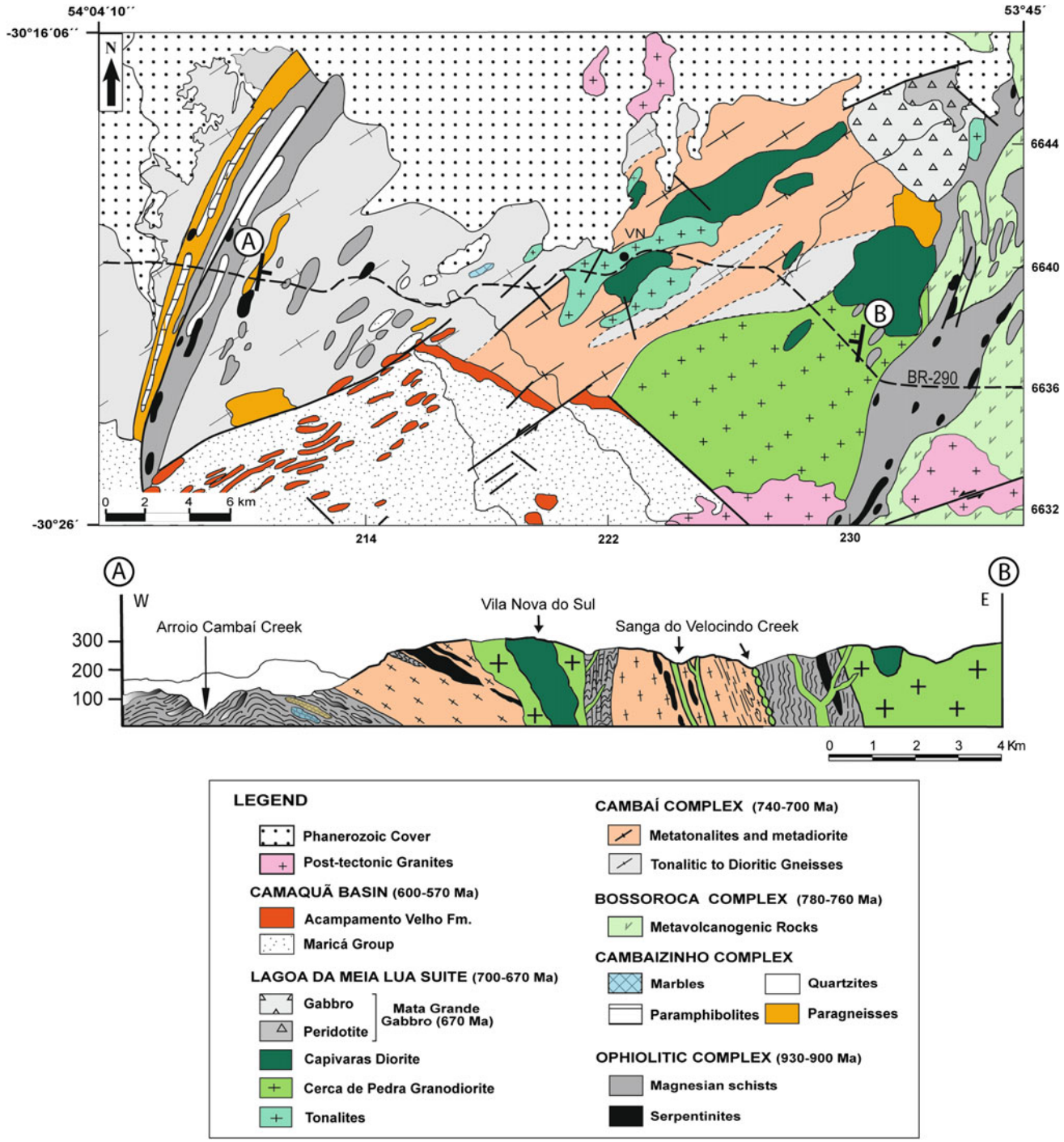

Fig. 10.8 Geological map and section of the Vila Nova region (modified from Hartmann et al. 2011)

the west, to Lavras do Sul, in the south (Fig. 10.4). The São Gabriel Arc consists of metavolcano-sedimentary rocks of the Bossoroca Complex, orthogneiss and metagranitoids of the CC, cut by late- to post-collisional granites and diorites of the LMLS (Garavaglia et al. 2002; Saalmann et al. 2005c; Hartmann et al. 2011; Gubert et al. 2016) and mafic to ultramafic rocks of Mata Grande Complex (Simões et al. 2014) (Figs. 10.4 and 10.8). The metamorphic rocks are interlayered with the ophiolitic complexes and the metasedimentary rocks of the Cambaizinho (Lena et al. 2014) and Passo Feio (Lopes et al. 2015) complexes. These associations are covered by the metasedimentary rocks of the Pontas do Salso Complex (Vedana and Philipp 2016; Vedana et al. 2017).

Metavolcanic Rocks

The Bossoroca Complex consists of Neoproterozoic metavolcano-sedimentary rocks including acid to intermediate metatuffs, meta-lapilli tuffs and lava flows (metadacites, meta-andesites and metabasalts), which are associated with metapelitic, carbonaceous and chemical sediments (Saalmann et al. 2005c; Gubert et al. 2016). Metavolcanoclastic rocks, pillowed metabasalts, amphibole schists and amphibolites exposed in the western part of the PFC may be correlated with the metavolcanic rocks of the Bossoroca Complex, according to the existing petrographic and geochemical data. The metavolcanic rocks have low- to medium-K calc-alkaline affinity. Machado et al. (1990) reported the U-Pb TIMS age of *c*. 753 Ma for a metadacite, which is identical to the U–Pb SHRIMP age of 756 ± 14 Ma reported by Remus et al. (1999) (Table 10.1). New LA-MC-ICPMS data for metacrystal tuff and meta-agglomerate of dacitic composition showed ages of 767 ± 3 and 765 ± 10 Ma (Gubert et al. 2016). Remus et al. (1999) and Hartmann et al. (2011) obtained ages of *c*. 700 Ma for the metamorphic event that affected this sequence.

Metagranitic Rocks

The CC is composed of two magmatic associations: (1) tonalitic, trondhjemitic and dioritic gneiss and (2) intrusive metatonalites, metagranodiorites and metadiorites (Fig. 10.8). The paragneisses of the Cambaizinho Complex are either interlayered with, or occur as xenoliths in, the CC rocks. The magmatism of the CC is composed of mid- to high-K calc-alkaline rocks with metaluminous composition. The orthogneisses presents a complex deformational history. The metamorphic segregation banding is affected by three regional folding stages. The metagranitic rocks are intrusive in the orthogneisses and are deformed by oblique ductile shear zones. Both units are cut by undeformed intrusions of the LMLS (Garavaglia et al. 2002; Hartmann et al. 2011). The CC orthogneisses yielded U–Pb SHRIMP and LA-MC-ICPMS zircon ages of *c*. 740 and 720 Ma, interpreted by Leite et al. (1998), Hartmann et al. (2011) and Vedana et al. (2017) as the age of igneous crystallization. U–Pb SHRIMP zircon ages of slightly deformed tonalites and diorites of the CC are between *c*. 710 and 690 Ma (Babinski et al. 1996; Hartmann et al. 2011), and those reported for tonalites and diorites in the Lavras do Sul region range between 740 and 720 Ma (Leite et al. 1998; Lusa et al. 2018).

The LMLS is made of tonalite-granodiorite to diorite forming N20–30°E elongated bodies, concordant with the main ductile shear zones of the SGT. This suite includes the youngest magmatic rocks of the São Gabriel orogen and is intrusive into the Cambaizinho and Cambaí complexes (Fig. 10.8). The LMLS represents a late orogenic intrusive event, including the Capivara Diorite, the Sanga do Jobim Granodiorite, the Cerca de Pedra Granodiorite and the Buriti Tonalite (Garavaglia et al. 2002; Hartmann et al. 2011 and references therein). The U–Pb SHRIMP zircon ages indicate that the granitoid emplacement occurred between 700 and 680 Ma, including ages of 703 ± 7 Ma for the Buriti Tonalite, 704 ± 3 Ma for the Santa Zélia Granite, 690 ± 2 Ma for the BR-290 Tonalite, 694 ± 5 Ma for the BR-290 Trondhjemite, 682 ± 2 Ma for the Cerca de Pedra Granodiorite and 680 ± 2 Ma for the Sanga do Jobim Granodiorite (Hartmann et al. 2011) (Table 10.1).

The Mata Grande and the Pedras Pretas complexes are the two main mafic plutonic bodies of the LMLS. The Mata Grande is a layered intrusion composed by gabbro-peridotite and other cumulate rock units dated by LA-MC-ICPMS U-Pb zircon method at 668 ± 3 Ma (Table 10.1).

10.3 Isotopic Geochemistry (Rb–Sr and Sm–Nd Data)

The few available isotopic data for the SGT rocks include those produced by Soliani (1986), Silva Filho and Soliani (1987), Remus (1991), Babinski et al. (1996), Saalmann et al. (2005b, 2006) and Philipp et al. (2008). Data from the initial $^{87}Sr/^{86}Sr$ ratio of the SGT units show characteristic compositions of rocks generated from mantle sources, with most of the available data showing values between 0.701 and 0.703 (Tables 10.1 and 10.2). The initial $^{87}Sr/^{86}Sr$ ratio data obtained for the metasediments of the Cambaizinho and Bossoroca complexes range from 0.7014 to 0.7039. The orthogneisses and metagranites of the CC had ratio values between 0.701 and 0.705, and the granites of the LMLS showed higher values between 0.704 and 0.708.

Most Sm–Nd data show positive epsilon Nd(t) values and T_{DM} model age values between 0.77 and 1.2 Ga (Fig. 10.9). The ages of the protolith selected for calculation of ENd (*t*) for each lithostratigraphical unit are based on geological relationships, such as intrusive contacts and xenoliths, and in U–Pb zircon age determinations of the same samples available in the literature. The metasedimentary rocks of Cambaizinho and Bossoroca complexes are older than the Cambaí gneisses, and the granites of the LMLS are the youngest rocks.

The Nd T_{DM} model ages of metavolcanic and metasedimentary rocks show Neoproterozoic ages. All the lithostratigraphic units of SGT show positive initial ENd(*t*) values (Table 10.2). Only a few samples of tonalitic gneisses of the CC and some granites and diorites of the LMLS exhibit negative initial ENd(*t*) values and older Nd T_{DM} model ages between 1.38 and 1.93 Ga, suggesting limited crustal

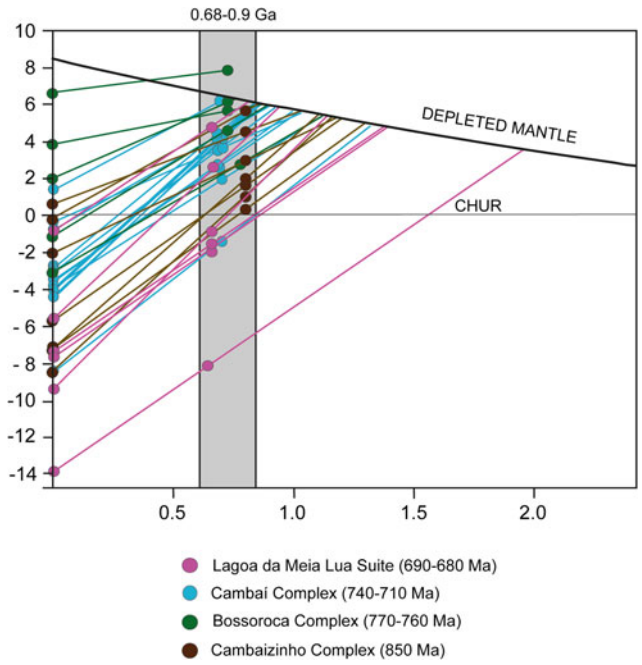

Fig. 10.9 Sm–Nd X Time diagram for the units of the SGT

contamination. A chlorite-epidote schist of the PFC shows higher Nd T_{DM} model ages of 2.57 Ga (Table 10.2).

The paragneisses of the Cambaizinho Complex show higher Nd T_{DM} model ages and lower ENd(t) values than the metarhyodacite of Bossoroca Complex. Nd T_{DM} model ages range between 0.86 and 1.28 Ga, with one sample at 1.59 Ga. The ENd(t) values range between 0.39 and 5.64; however, most of them are between 2.03 and 2.9 (Table 10.2).

The metasedimentary rocks of the Bossoroca Complex show positive ENd(t) values, between 2.53 and 6.23, and T_{DM} model age values between 0.77 and 1.19 Ga. The metavolcanic rocks show an ENd(t) value of 7.8 and T_{DM} model age value of 0.96.

The tonalitic to dioritic gneisses and the metagranitoids of the CC also exhibit positive ENd(t) values, between 1.99 and 6.43, and T_{DM} model ages values between 0.86 and 1.04 Ga. One sample of dioritic gneiss shows a negative ENd(t) value of −1.34 and three samples show T_{DM} model ages values between 1.27 and 1.68 Ga.

The granites of the LMLS yield the highest T_{DM} model ages, with values between 0.82 and 1.93 Ga, and negative ENd(t) values, between −7.52 and −0.22, with two samples showing positive ENd(t) values of +3.01 and +5.2 (Table 10.2). The negative values and the old T_{DM} ages suggest a crustal contamination in the granites of this suite.

10.4 Evolution of the São Gabriel Terrane

The metamorphic evolution of the SGT took place during three main collisional events. The first collision occurred between the Passinho arc and the RLPC. The second collision involved the RLPC and the NPT at *c*. 720–710 Ma along the western portion of the belt, associated with the closure of the Charrua Ocean. Subduction-related low- to medium-K calc-alkaline plutonic and volcano-sedimentary associations were formed in this process, represented by the Passinho and São Gabriel arcs (Saalmann et al. 2005b, c, 2006, 2010; Hartmann et al. 2007; Philipp et al. 2016a). The third and most intense collisional event is believed to have been an oblique collision between the RLPC/NPT and the Kalahari Craton between 650 and 620 Ma (Chemale et al. 2011; Camozzato et al. 2013; Gregory et al. 2015; Philipp et al. 2016a, b). This event also caused the strong deformation of the arc-related rocks, passive margin sedimentary rocks and of units of the sialic basement. The process led to the anatexis of the high grade metamorphic units of para and orthogneisses complexes in the DFB (Philipp et al. 2013, 2016b).

The units that compose the SGT are structured as elongated bodies, in the N20–30°E general direction, juxtaposing orthogneisses and arc-related metagranitoids of low- to medium-K calc-alkaline composition (Imbicuí and Cambaí complexes), ultramafic and mafic rocks (ophiolitic complexes), arc metavolcanosedimentary (Bossoroca Complex) and metasedimentary rocks (Cambaizinho Complex) and chemical and mature clastic metasediments of passive margin (Passo Feio, Marmeleiro and Cerro do Batovi) (Fig. 10.4). The definition of an order of structural events based on geometric elements such as foliations and folding stages has limitations and generalizations that have not been considered in previous analyses (Chemale 2000; Saalmann et al. 2005a, 2006, 2010; Hartmann et al. 2007; Laux et al. 2012). The combined analysis shows particularities associated with different ages of the metamorphic foliations, indicating that the SGT structure was generated in several stages, associated mainly with the Passinho (890–860 Ma) and São Gabriel (770–680 Ma) orogenies. However, this evolution involved three separate orogenic metamorphic events at the age intervals 800–780 Ma (M_1—pre-collisional), 710–720 Ma (M_2—syn-collisional), and 700–680 Ma (M_3—late- to post-collisional) (Fig. 10.5). The two initial stages are associated with the subduction and closure of the Charrua Ocean, with the SGT thrusting over the NPT. The SGT rocks were also partially affected by the younger Dom Feliciano orogeny, associated with the closure

of the Adamastor Ocean and the collision between the Rio de La Plata and Kalahari cratons, between 650 and 620 Ma. The post-collisional period of this orogeny also shows significant transcurrent shear zone movements between 600 and 540 Ma, responsible for the uplift of the basement and by the deposition of sedimentary and volcanic rocks of a foreland basin (Camaquã Basin) and the emplacement of late- to post-collisional (M_4) granites (Philipp et al. 2016a).

The SGT structure was developed from three major deformation phases or evolutionary stages herein called: (1) thrust-, (2) oblique- and (3) transcurrent phases. The first deformational events were related to the beginning of the closure of the Charrua Ocean, with the development of M_1 orogeny metamorphism associated with oceanic crust subduction (thrust phase). The structuring of this phase is associated with the final process of ocean closure, with the collision of arc systems against the Paleoproterozoic gneissic rocks of the Rio de La Plata and NPT (Taquarembó Terrane in RS) located to the west and east. This oblique phase has low-angle shear zones with front and oblique movements as main structures, responsible in part for the current contact relationships between the SGT units. The late movement of the transcurrent shear zones is responsible for the rise and emplacement control of the LMLS and deposition of metasediments of the Pontas do Salso Complex.

The first major deformational phase (thrust phase) generated the low-angle metamorphic foliations (S_1 and S_2) and low-angle ductile thrust shear zones. These structures are recorded in the rocks of the Imbicuí, Cambaizinho, Bossoroca and in the metasedimentary complexes. The metamorphic foliations show N20–40° general orientation, with low to medium northwest dipping. The mineral stretching lineation has low northwest plunge. Primary sedimentary structures are still partially preserved in the metasediments of the Passo Feio, Marmeleiro, Cerro do Batovi and Cambaizinho complexes, and in the metavolcano-sedimentary rocks of the Bossoroca Complex. The compositional and grain size layering and schistosity/banding of these rocks were generated owing to the transposition of S_0 during the formation of S_1 foliation.

The Passo Feio, Marmeleiro and Cerro do Batovi complexes represent associations of sediments found in a passive margin environment. Based on their geographical location, next to the Paleoproterozoic orthogneisses further east, these metasediments represent the passive margin of the NPT, greatly deformed by the late transcurrent phase associated with the Dom Feliciano orogeny. These complexes were deformed and metamorphosed by different metamorphism events. The main S_1 foliation of the Marmeleiro and Cerro do Batovi metasediments varies between slaty cleavage and schistosity, deformed and transposed by S_2 foliation, represented by well-developed crenulation, mainly near the low-angle shear zones (thrust shear zones). The metamorphic foliations show N30–40°W direction, dipping southwest and northeast, with low-angle mineral stretching lineation with N30–40°W direction and transcurrent kinematics. The PFC features a very similar structure; however, the mineral stretching lineations show low plunge angle and N20–40°E direction, with transcurrent kinematics. An S_3 foliation is also observed, varying from fracture cleavage to crenulation, with a subvertical northeast direction, associated with a stage of inclined normal folds (F_3), with open to smooth shapes and axis with a northeast to southwest direction. There is no information about the metamorphism age of the Marmeleiro and Cerro do Batovi complexes. The metamorphic ages of the PFC rocks, between 580 and 570 Ma, obtained in U–Pb zircon (SHRIMP and LA-MC-ICPMS), and monazite (EPMA) dating (unpublished data), indicate that this metamorphism is late and occurred in the transcurrent stage after the collisional peak of the Dom Feliciano orogeny (Philipp et al. 2016a) (Table 10.1).

Geochronological evidence indicates that the metamorphism recorded in the Cambaizinho Complex metasediments is aged between 800 and 780 Ma (Philipp et al. 2008; Hartmann et al. 2011) (Table 10.1). The Sm–Nd isotopic composition of this complex shows a mantle and juvenile signature, indicating that these rocks represent an older arc basin (Saalmann et al. 2005b; Philipp et al. 2008) (Table 10.2). These metasediments occur as metric to decametric xenoliths in orthogneisses and metagranitoids of the CC, with U–Pb ages between 740 and 720 Ma (Table 10.1). Thus, this older back-arc basin could be associated with the formation of the Imbicuí Complex orthogneisses, which feature crystallization U–Pb zircon ages between 890 and 860 Ma. These metasediments show S_1 metamorphic segregation banding, which is deformed and transposed by S_2 foliation, especially near the low-angle shear zones (ductile thrust shear zones). This crenulation is associated with a phase of isoclinal folds (F_2), with and without root (sheath folds). The banding shows N10–30°E direction, with main northwest dipping and mineral stretching lineation with low angle plunge in the N30–50°W direction. The previous foliations are affected by a phase of inclined normal folds (F_3), with open to smooth shapes and axes with northeast to southwest direction. The S_3 foliation is defined by fracture cleavage and/or crenulation with northeast subvertical direction.

The metavolcanic and metasedimentary rocks of the Bossoroca Complex show S_1 schistosity with N20–30°E arrangement and northwest dipping. This schistosity is affected in a much restricted manner by isoclinal F_2 folds,

with and without root, whose axial surface is defined by S_2 crenulation. These rocks show weak mineral lineation with low northwest plunge. The few metamorphic ages obtained by U–Pb SHRIMP in zircon crystal edges indicate ages of around 700 Ma (Remus et al. 1999) (Table 10.1).

There is development of right-lateral transpression along northeast to southwest oriented oblique and high angle strike-slip shear zones, associated with the oblique deformational phase. The granites of the LMLS, the Santa Zélia Granite, Sanga do Jobim and Buriti tonalites and Capivaras Diorite, among others, show late collisional mylonitic foliation parallel to pluton borders. This dextral strike-slip combination with oblique thrusting is responsible for the tectonic superimposing of different lithostratigraphic units. The general structuring is characterized by a southeast-vergent transpressional thrust stack (Saalmann et al. 2005a).

The gneisses of the Imbicuí Complex represent a relict of the lower portion of Middle Tonian intraoceanic arc, while the gneisses of the CC and metavolcano-sedimentary rocks of the Bossoroca Complex represent relicts of the lower and upper portion of a younger continental margin arc of Upper Tonian age (Chemale 2000; Saalmann et al. 2005a; Hartmann et al. 2007; Gubert et al. 2016; Philipp et al. 2016a). The tectonic juxtaposition of slices of oceanic crust (Cerro Mantiqueiras, Ibaré, Palma, Passo do Ivo, Cambaizinho e Arroio Lajeadinho ophiolitic complexes), metavolcano-sedimentary sequence (Bossoroca Complex), arc-related orthogneisses and metagranitoids (Imbicuí and Cambaí complexes) and metasedimentary rocks (Passo Feio and Marmeleiro complexes) due to southeast-directed ductile transpressive thrusting and stacking correspond to an accretionary wedge setting (Chemale 2000; Saalmann et al. 2005a; Hartmann et al. 2007).

The last deformation phase (transcurrent) took place under retrograde conditions and is characterized by northeast to southwest oriented brittle to ruptile-ductile strike-slip shear zones. These structures reactivated the pre-existing oblique to high-angle transcurrent shear zones of the oblique phase.

10.4.1 Closure of the Charrua Ocean

The construction of the Neoproterozoic SGT starts with the closure of the Charrua Ocean during the Passinho and São Gabriel orogenies and later with the collision between the arc systems and the western margin of the NPT (Fig. 10.10).

During the last two decades, arc-related Neoproterozoic plutonic complexes and volcanosedimentary sequences have been recognized in Goiás (Pimentel and Fuck 1992; Junges et al. 2002; Laux et al. 2005) and Rio Grande do Sul states (Fragoso Cesar et al. 1990; Machado et al. 1990; Babinski et al. 1996; Saalmann et al. 2005b, 2006; Hartmann et al. 2011; Lena et al. 2014; Gubert et al. 2016; Lusa et al. 2018). These are important subduction-related juvenile crustal accretions, which took place during the Tonian (Leite et al. 1998; Hartmann et al. 2007; Saalmann et al. 2010; Philipp et al. 2014, 2016a; Arena et al. 2016). These associations suggest that the duration of the Brasiliano orogeny and ocean plate subduction was substantially longer than what has been suggested in previous models. They demonstrate the existence of small ocean basins separating continental microplates, which were later amalgamated.

The new geochronological and isotopic data indicate that in the south of Brazil the subduction processes occurred between 890 and 850 Ma and 770 and 700 Ma, marking the initial stages of the Neoproterozoic orogenic events in the region (e.g., Machado et al. 1990; Babinski et al. 1996; Leite et al. 1998; Saalmann et al. 2005b, c, 2006; Hartmann et al. 2007, 2011; Philipp et al. 2014, 2016a; Arena et al. 2016; Gubert et al. 2016; Vedana and Philipp 2016; Vedana et al. 2017; Lusa et al. 2018). The rock units that represent this period of oceanic lithosphere consumption are exposed only in the SGT. Figure 10.11 presents a proposed evolutionary model based on the stratigraphic, structural, isotopic and geochronological data. Opening of the oceanic basin between the RLPC and NPT started at least 0.93–0.90 Ga ago (Saalmann et al. 2005b; Arena et al. 2016). Subduction of oceanic lithosphere started about 890 to 860 Ma, leading to the development of the Passinho Arc, an intraoceanic island arc above an east-dipping subduction zone (e.g., Philipp et al. 2016a; Lusa et al. 2018). Westward subduction beneath the Passinho Arc resulted in the establishment of the São Gabriel Arc, with active continental margin magmatism with main activity between 780 and 720 Ma (Hartmann et al. 2011 and references therein).

Dextral oblique collision of the arc systems and accretion to the west passive margin of the NPT occurred between *c*. 710 and 700 Ma (Remus et al. 1999; Saalmann et al. 2010; Hartmann et al. 2011). These processes resulted in eastward thrusting of the SGT units. The collapse of the orogen is defined by the emplacement of the post-collisional granites and diorites of the LMLS and the formation of a late-orogenic basin represented by the metasediments of the Pontas do Salso Complex, with a maximum age of ca. 680 Ma (Vedana and Philipp 2016; Vedana et al. 2017).

10.4.2 Tonian Associations of Brazil

Other associations of rocks generated in the Tonian-Cryogenian interval are found in the Mantiqueira

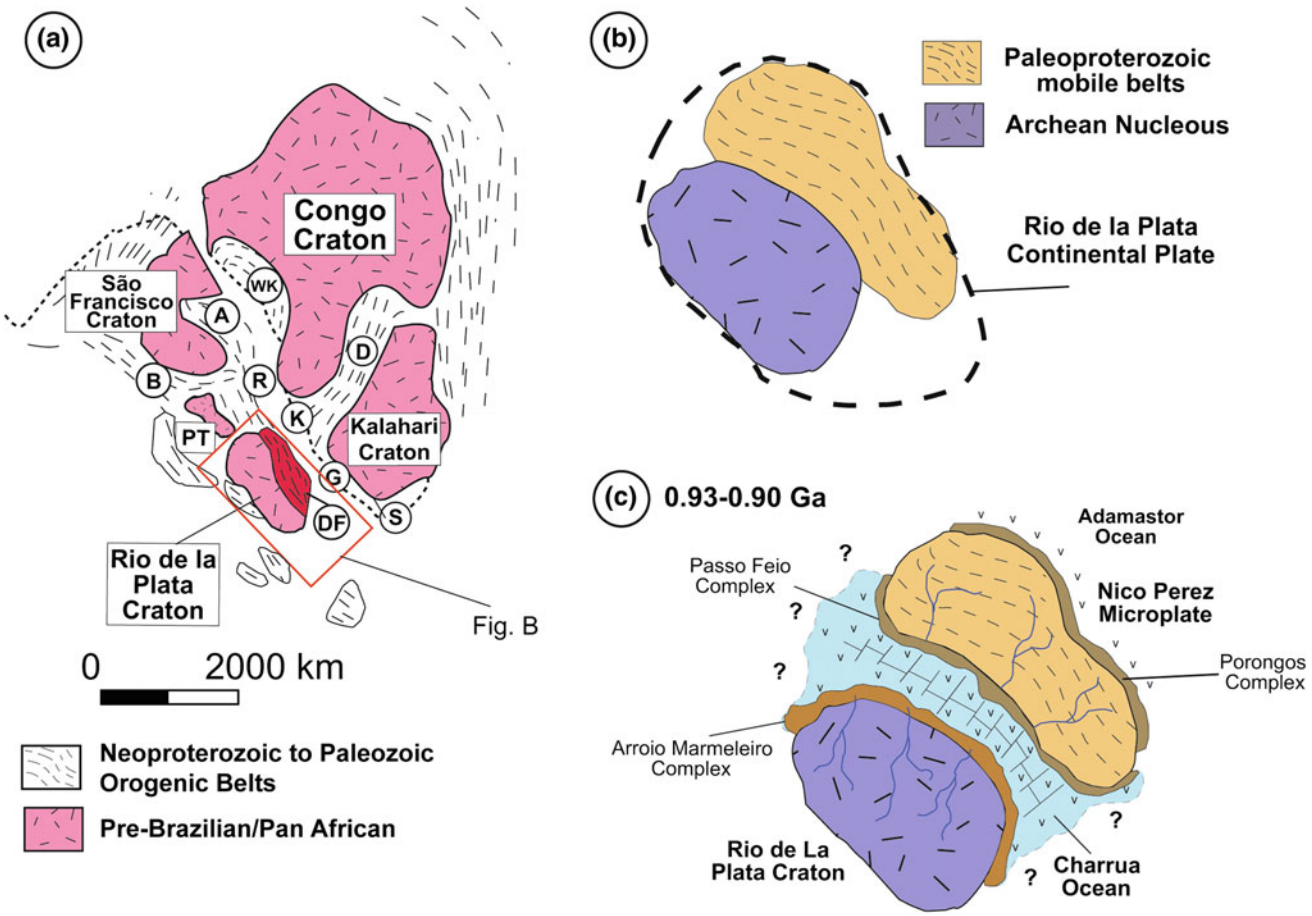

Fig. 10.10 **a** Southern portion of Gondwana showing the main cratonic areas and the location of the DFB (in red) and related belts of Africa, **b** detail of the composition of the Rio de La Plata continental plate, highlighting the archean core, **c** opening of the Charrua Ocean between the RLPC (old core) and the NPT (Paleoproterozoic mobile belt). From Philipp et al. (2016a)

(Cordani et al. 2002; Heilbron et al. 2004; Siga et al. 2009, 2011; Alves et al. 2013) and Borborema (Accioly et al. 2010) and Tocantins (Pimentel et al. 1997; Pimentel et al. 2004, 2011; Laux et al. 2004, 2005; Mantovani and Brito Neves 2009; Della Giustina et al. 2011) provinces in Brazil, and also in Uruguay (Lenz et al. 2011). These occurrences are represented by metamorphic complexes including ophiolites and magmatic arcs, constituted by orthogneisses, metagranitoids and metavolcanosedimentary associations with juvenile geochemistry and isotopic signatures. Figure 10.12 shows a geological synthesis of the main Tonian associations occurring in Brazil.

These rock associations are aligned and record the processes of formation of continental rifts and opening of small oceans probably generated at the end of the consolidation of the Rodinia supercontinent. The Tonian terranes in West Gondwana extend along strike for several thousands of kilometers (Fig. 10.13). The presence of Tonian terranes in Rodinia and Western Gondwana has actually been neglected, persisting as a challenging unresolved definition. Tonian processes and orogenies were absent and have not been considered in the Rodinia concept (Brito Neves and Fuck 2014). This supercontinent was formed *c*. 900 Ma ago, and it is still an open question whether the Tonian processes precede (or follow) Rodinia amalgamation, which has important implications on the configuration of this supercontinent (Li et al. 2008). It appears that, in general, awareness of this problem is absent in the international scientific community, as highlighted by Brito Neves and Fuck (2014).

During the same period in the center of Brazil, the most important geotectonic unit of the Brasília Belt, the Goiás magmatic arc, is generated. It comprises a large area along the western part of the orogen and consists mainly of: (1) calc-alkaline metaplutonic suite made of tonalites-granodiorites recording two main periods of intrusion (860–800 and 660–610 Ma), (2) metavolcano-sedimentary

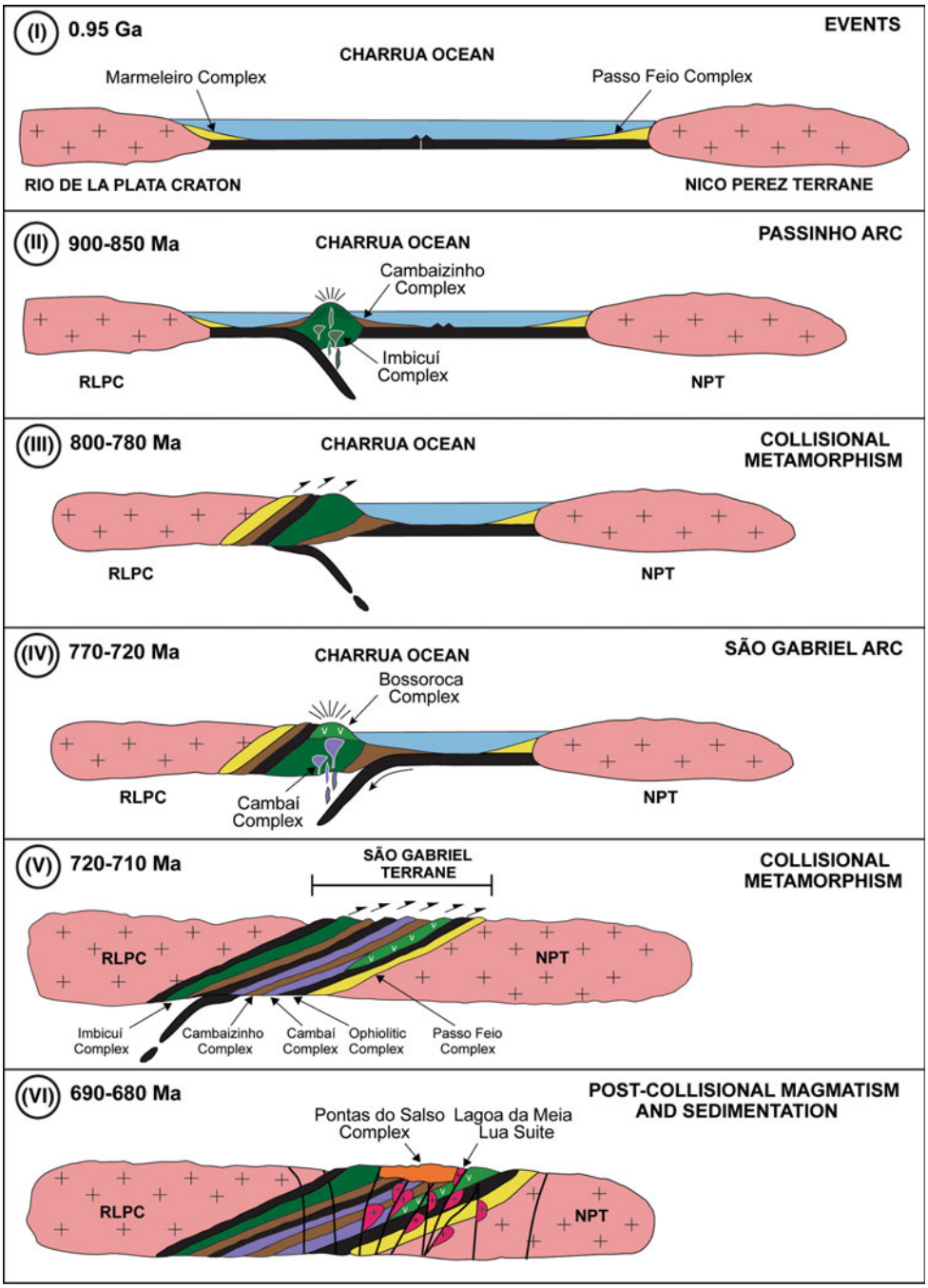

Fig. 10.11 Plate tectonic model for the Brasiliano orogenic cycle in the SGT and southern Brazil

sequences of calcalkaline nature, ranging in age from *c*. 900 to 620 Ma, (3) post-tectonic granite intrusions forming large bimodal complexes, emplaced between *c*. 600 and 500 Ma (Pimentel et al. 2011). Most of these rocks present a juvenile character with a strong mantle input, as indicated by the positive epsilon Nd(T) values and T_{DM} model ages mostly between 0.9 and 1.2 Ga (Pimentel and Fuck 1992). The metasediments of Ibiá and Araxá Groups represent the period of sedimentation in the fore-arc basin setting of this arc. The arc of Goiás and the SGT present several similarities and represent the two most complete Tonian associations in Brazil.

Provinces	Borborema	Tocantins		Mantiqueira				
				Brasil				Uruguay
Units	1-Alto Paejú Terrane	2-Goiás Magmatic Arc	3-Ceres-Rialma Metam. Belt	4-Italva Klippe Terrane	5-Embu Terrane	6-Itaiacoca Group	7-Passinho and São Gabriel arcs	8-Cerro Bori orthogneisses
Rock Types	Volcanic-sedimentary association and felsic, mafic associations with ultramafic rocks.	Primitive tholeiitic to calc-alkaline volcanics and tonalites to granodiorites	Metasedimentary and metavolcanic rocks	Tonalite and granodiorite, gneiss,marble, amphibolite	Tonalite and granodiorite gneiss and granite intrusions	Metavolcano-sedimentary sequence, quartzite, pelite, marble	**Calc-alkaline TTG gneiss, metavolcano-sedimentary sequence, tonalite to diorite intrusions, ophiolite complex**	Tonalite and granodiorite gneisses, mafic and felsic granulites and amphibolite
Ages	1050 - 930 Ma	930 - 810 Ma	1270-800 Ma	848 ±11 Ma	810 - 500 Ma	950 - 630 Ma	**890 - 680 Ma**	800 - 770 Ma
Setting	Island arc, Juvenile geochemical and isotopic signatures	Island and continental arc, Positive εNd(T)	Rift environment	Extensional magmatism, back arc-type environment	Magmatic arc affiliation	Continental passive margin deposits	**Island and continental arcs Positive εNd(T) NdTDM: 0.8-1.2 Ga**	Magmatic arc affiliation
References	Accioly *et al.* (2010), Santos *et al.* (2010), Van Schmus *et al.* (2011).	Pimentel & Fuck (1992), Pimentel et al. (1997, 2000)	Brito Neves & Fuck (2013), Pimentel *et al.* (2004), Della Giustina *et al.* (2011)	Peixoto & Heilbron (2010), Heilbron & Machado (2003)	Heilbron *et al.* (2004), Cordani *et al.* (2002), Alves *et al.*(2013)	Siga Jr. *et al.* (2009, 2011), Mantovani & Brito Neves (2009)	**Machado *et al.* (1990), Leite *et al.* (1998), Saalmann *et al.*(2005) Hartmann *et al.*(2011) Philipp *et al.* (2014), Lena *et al.* (2014)**	Lenz *et al.* 2011, Silva *et al.* 2005.

Fig. 10.12 Tectonostratigraphic chart of the Tonian associations in the Mantiqueira, Borborema and Tocantins provinces in Brazil

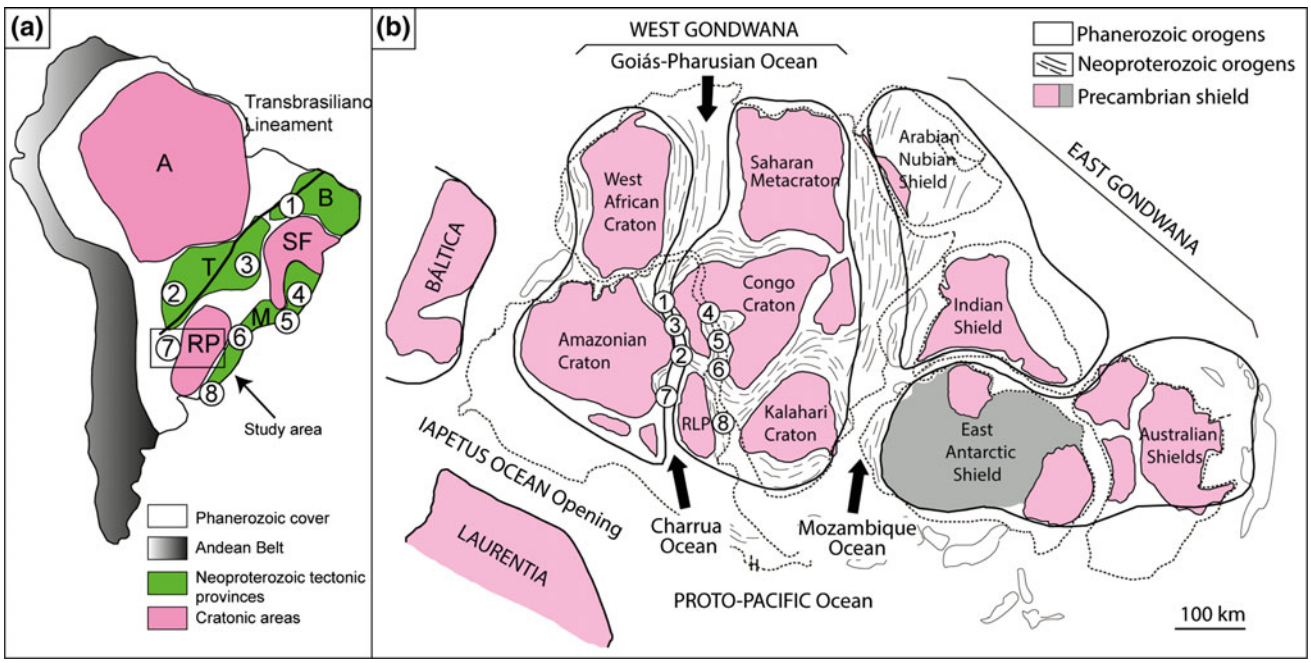

Fig. 10.13 Disposition of the Tonian associations in the Mantiqueira (M), Borborema (B) and Tocantins (T) provinces in Brazil and relationships with the main cratonic areas of Brazil. Cratons: *RP* Rio de La Plata, *SF* São Francisco, *A* Amazonian. Tonian associations: *1* Alto Paejú Terrane, *2* Goiás Magmatic Arc, *3* Ceres-Rialma Metamorphic Belt, *4* Italva Klippe Terrane, *5* Embu Terrane, *6* Itaiacoca Group, *7* SGT, *8* Cerro Bori orthogneisses

10.5 Conclusions

The rock associations of the Tonian and Cryogenian periods represent the beginning of the evolution of the Brasiliano cycle orogenesis and the closing of small oceans generated probably from the fragmentation of the Rodinian continent about 0.93 Ga ago.

Rocks of the SGT show positive initial epsilon Nd values and low initial $^{86}Sr/^{87}Sr$ ratios, indicating juvenile nature of the original magmas. The recent isotope data indicate that the evolution of the SGT took place between 0.89 and 0.68 Ga with the development of three orogenic events known as the Passinho (0.89–0.85 Ga), São Gabriel (0.77–0.68 Ga) and Dom Feliciano (650–540 Ma).

The evolution of the SGT is preserved in igneous zircon grains indicating ages of 0.93 to 0.90 Ga for the opening of the Charrua Ocean and 0.89 to 0.68 Ga for the closure and generation of the intraoceanic Passinho Arc (0.89–0.86 Ga) and the São Gabriel Arc (0.77–0.68 Ga). The collision of the arc systems against the NPT occurred around 0.7–0.71 Ga, and the collapse of the SGT is marked by the deposition of the Pontas do Salso Complex at 0.68 Ga.

The emplacement of granitoids and diorites of the LMLS represents the post-collisional magmatism associated with high-angle transcurrent shear zones. The stratiform gabbros and peridotites of the Mata Grande Complex characterize the younger magmatism associated with this period. The high occurrence of dioritic bodies in the LMLS, associated with mafic-ultramafic rocks, may suggest the existence of slab-break-off processes associated with the detachment of the oceanic plate during the final process of the SGT collision with the Paleoproterozoic units of the NPT.

All units of the SGT were mapped on a regional scale and the inclusion of this database with the current set of geochronological and isotopic data has provided significant advances in the understanding of its units and the correlation of the processes with other orogenic belts of Brazil and Africa.

Acknowledgements We would like to acknowledge the Brazilian National Council for Scientific and Technological Development (CNPq) for the research grants, the Geoscience Institute of Rio Grande do Sul Federal University (UFRGS) for field work support and laboratories, and the Geochronology Research Center of São Paulo University (USP), for the access to LA-MC-ICP-MS laboratories. We are grateful to reviewers for the helpful comments and suggestions and to the editors for comments and editorial handling of the manuscript.

References

Almeida FFM (1971) Geochronological division of the Precambrian of South America. Rev Bras Geociências 1:13–21

Almeida FFM et al (1973) The precambrian evolution of the South America cratonic margin south of the Amazon River. In: Nairn AEM, Stehli FG (eds) The Ocean Basins and Margins. Plenum Publishing, New York, pp 411–446

Alves A et al (2013) U–Pb geochronology of the granite magmatism in the Embu terrane: implication for the evolution of Central Ribeira Belt, SE Brazil. Precambr Res v(230):1–12

Arena KR et al (2016) Evolution of neoproterozoic ophiolites from the southern Brasiliano Orogen revealed by zircon U-Pb-Hf isotopes and geochemistry. Precambr Res 285:299–314

Babinski M et al (1996) Juvenile accretion at 750–700 Ma in southern Brazil. Geology 24:439–442

Babinski M et al (1997) U–Pb and Sm–Nd geochronology of the Neoproterozoic granitic-gneissic Dom Feliciano Belt, southern Brazil. J South Am Earth Sci 3–4:263–274

Basei MAS et al (2008) West Gondwana amalgamation based on detrital zircon ages from Neoproterozoic Ribeira and Dom Feliciano belts of South America and comparison with coeval sequences from SW Africa. In: Pankhurst RJ et al. (eds) West Gondwana, Pre-Cenozoic Correlations across the South Atlantic Region. Geological Society London *Special* Publications 294:239–256

Bitencourt MF, Nardi LVS (2000) Tectonic setting and sources of magmatism related to the Southern Brazilian Shear Belt. Rev Bras Geociências 30:186–189

Brito Neves BB, Fuck RA (2013) Neoproterozoic evolution of the South-American platform. J S Am Earth Sci 47:72–89

Brito Neves BB, Fuck RA (2014) The basement of South American platform: half Gondwana + half Laurentia. Precambr Res 244:75–86

Brito Neves BB et al (2014) The Brasiliano collage in South America: a review. Braz J Geol 44(3):493–518

Camozzato E et al (2012). Mapa Geológico da Folha Hulha Negra (SH.22.Y-C-1), escala 1:100.000. In: Programa Levantamentos Geológicos, CPRM, Rio de Janeiro, vol 1, 128 p

Camozzato E et al (2013) Evolução Tectônica e Geocronologia U–Pb em zircão da terminação sul do Terreno Tijucas (RS, Brasil). In: VII Congreso Uruguayo de Geología, Montevideo, Resúmenes Extendidos, p 7

Chemale F Jr (2000) Evolução Geológica do Escudo Sul-Rio-Grandense. In: Holz M, De Ros LF (eds) Geologia do Rio Grande do Sul. Porto Alegre, Editora UFRGS, pp 13–52

Chemale F Jr, Philipp et al. (2011) Lu–Hf and U–Pb age determination of the Capivarita Anorthosite, Dom Feliciano belt, Brazil. Precambr Res 186:117–126

Chemale F Jr et al (1995) Stratigraphy and tectonism of precambrian to early paleozoic units in Southern Brazil and uruguay—excursion guidebook. Acta Geologica Leopoldensia 43:4–115

Cordani UG et al (1973) The Precambrian evolution of South America. Geol Rundsch 62:309–317

Cordani UG et al (2002) Geochronological constraints on the evolution of the Embu Complex, S. Paulo, Brazil. J South Am Earth Sci v (14):903–910

Cordani UG et al (2003) From Rodínia to Gondwana: a review of the available evidence from South America. Gondwana Res 6:275–283

Della Giustina MES et al. (2011) U–Pb, Hf-trace element systematics and geochronology of zircon from a granulite-facies metamorphosed mafic-ultramafic layered complex in central Brazil. Precambr Res v(189):176–192

Fernandes LA et al (1992) Deformation patterns in the southern Brazilian branch of the Dom Feliciano Belt, a reappraisal. J S Am Earth Sci 5(1):77–96

Fragoso-Cesar ARS (1990) Tectônica de placas no Bloco São Gabriel (RS) em base dos dados geológicos, geocronológicos e geoquímicos. Workshop Geoquímica Isotópica, Geocronologia e litogeoquímica das regiões sul e sudeste do Brasil, Boletim de Resumos, SBGq, São Paulo, pp 8–16

Garavaglia L et al (2002) Cumulatic diorites related to Post-collisional, Brasiliano/Pan-African mafic magmatism in the Vila Nova Belt, Southern Brazil. Gondwana Res 5:519–534

Gregory TR et al (2015) Geochronological data from TTG-type rock associations of the Arroio dos Ratos Complex and implications for crustal evolution of southernmost Brazil in Paleoproterozoic times. J S Am Earth Sci 57:49–60

Gubert M, Philipp RP, Basei MAS (2016) Geochronology of the Bossoroca Complex, São Gabriel Terrane, Dom Feliciano Belt, southernmost Brazil: tectonic implications for a Neoproterozoic São Gabriel Arc. J S Am Earth Sci 70:1–17

Hartmann LA (2008) Protolith age of santa maria chico granulites dated on zircons from an associated amphibolite-facies granodiorite in southernmost Brazil. *A*nais da Academia Brasileira de Ciências 80:543–551

Hartmann LA, Chemale F Jr (2003) Mid amphibolite facies metamorphism of harzburgites in the Neoproterozoic Cerro Mantiqueiras Ophiolite, southernmost Brazil. Anais da Acad Bras Ciências 75 (1):109–128

Hartmann LA et al (1999) Deepest exposed crust of Brazil–SHRIMP establishes three events. Geology 27:947–950

Hartmann LA et al (2000) Advances in SHRIMP geochronology and their impact on understanding the tectonic and metallogenic evolution of southern Brazil. Aust J Earth Sci 47:829–843

Hartmann LA et al (2002) Two paleoproterozoic orogenies in the evolution of the tandilia belt, buenos aires, as evidenced by Zircon U–Pb SHRIMP geochronology. Int Geol Rev 44:528–543

Hartmann LA, Chemale F Jr, Philipp RP (2007) Evolução Geotectônica do Rio Grande do Sul no Pré-Cambriano. In: Frantz JC, Ianuzzi R (Eds) 50 anos de Geologia no Rio Grande do Sul, Porto Alegre: UFRGS-PETROBRÁS, p 97–123

Hartmann LA et al (2011) Time frame of 753–680 Ma juvenile accretion during the São Gabriel orogeny, southern Brazil. Gondwana Res 19:84–99

Heilbron M, Machado N (2003) Timing of terrane accretion in the Neoproterozoic-Eopaleozoic Ribeira orogen (SE, Brazil). Precambr Res 125(1–2):87–112

Heilbron M et al (2004) Província Mantiqueira. In: Mantesso-Neto V et al (eds) Geologia do Continente Sul-Americano: Evolução da Obra de Fernando Flávio Marques de Almeida. São Paulo, Beca, pp 203–234

Junges SL et al (2002) Nd isotopic study of the Neoproterozoic Mara Rosa Arc, central Brazil: implications for the evolution of the Brasília Belt. Precambr Res 117:101–118

Koester E, Soliani E Jr, Leite JAD, Hartmann LA, Fernandes LAD, Santos JOS, Oliveira LD (2001) SHRIMP U-Pb age for the emplacement of Santana granite and reactivation of the Porto Alegre Suture, southern Brazil. J S Am Earth Sci 14:91–99

Laux JH, Pimentel MM, Dantas EL, Armstrong R, Armele A, Nilson AA (2004) Mafic magmatism associated with the Goiás Magnatic Arc in the Anicuns region, Goiás central Brazil: Sm–Nd isotopes and new ID-TIMS and SHRIMP U–Pb data. J S Am Earth Sci 16(7):599–614

Laux JH et al (2005) Two neoproterozoic crustal accretion events in the Brasília belt, central Brazil. J S Am Earth Sci 18:183–198

Laux JH, Bongiolo EM, Klein C, Iglesias CM, de F (2012) Programa de Geologia do Brasil-PGB. *Folha Lagoa da Meia Lua, SH.21-Z-B-VI*. Estado do Rio Grande do Sul. Carta Geológica. Porto Alegre, CPRM, 1mapa colorido, Escala 1:100.000

Leite JAD et al (1998) SHRIMP U/Pb zircon geochronology of Neoproterozoic juvenile and crustal-reworked terranes in southernmost Brazil. Int Geol Rev 40:688–705

Leite JAD et al (2000) Zircon U–Pb SHRIMP dating of gneissic basement of the Dom Feliciano Belt, southernmost Brazil. J S Am Earth Sci 13:739–750

Lena LOF et al (2014) The evolution of the Neoproterozoic São Gabriel juvenile terrane, southern Brazil based on high spatial resolution U-Pb ages and ^{18}O data from detrital zircons. Precambr Res 247:126–138

Lenz C et al (2011) U–Pb SHRIMP ages for Cerro Bori orthogneisses, Dom Feliciano belt in Uruguay: evidence of a ~800 Ma magmatic and 650 Ma metamorphic event. Precambr Res 185:149–163

Li ZX et al (2008) Assembly, configuration and break-up history of Rodinia: a synthesis. Precambr Res 160:169–210

Lopes CG et al (2015) Provenance of the passo feio complex, São Gabriel Terrane, Dom Feliciano Belt, southern Brazil, implications for the tectonic setting of deposition, age of the São Gabriel Arc and origin of Paleoarchean detrital zircons (3.3–3.63 Ga). J S Am Earth Sci 58:9–17

Lusa M et al. (2018) The Neoproterozoic São Gabriel orogeny, Dom Feliciano Belt, southernmost Brazil: The intra-oceanic Passinho arc and the active continental margin of the São Gabriel-Vila Nova Arc, Lavras do Sul, southernmost Brazil. J S Am Earth Sci

Machado N et al (1990) A late proterozoic U–Pb age for the Bossoroca Belt, Rio Grande do Sul, Brazil. J S Am Earth Sci 3:87–90

Mantovani MSM, Brito Neves BB (2009) The Paranapanema lithospheric block: its nature and role in the accretion of Gondwana. In: Gaucher C et al. (eds) Neoproterozoic-cambrian tectonics global changes and evolution: a focus on southwestern Gondwana, Development in Precambrian Geology 16, Elsevier, Amsterdam, pp 257–272

Oliveira DS, Sommer CA, Philipp RP, Lima EF, Basei MAS (2015) Post-collisional subvolcanic rhyolites associated to the neoproterozoic pelotas batholith, Southern Brazil. J S Am Earth Sci 63:84–100

Oriolo S et al (2016) Timing of deformation in the Sarandí del Yí Shear Zone, Uruguay: implications for the amalgamation of western Gondwana during the Neoproterozoic Brasiliano-Pan-African Orogeny. AGU Tectonics 1–18. doi:https://doi.org/10.1002/2015TC004052

Oyhantçabal P et al (2011) The Rio de la Plata Craton, a review of units, boundaries, ages and isotopic signature. Int J Earth Sci 100:201–220

Philipp RP, Machado R (2005) The Neoproterozoic to Cambrian granitic magmatism of Pelotas Batholith, Southern Brazil. J S Am Earth Sci 19:461–478

Philipp RP et al (2003) Reavaliação e novos dados geocronológicos sobre o Batólito Pelotas: implicações petrogenéticas e idade das zonas de cisalhamento. Bol Inst Geociênciasda USP, São Paulo 3:71–84

Philipp RP et al (2008a) Geochemistry and petrology of dioritic, tonalitic and trondhjemitic gneisses from Encantadas Complex, Santana da Boa Vista, southernmost Brazil, a Paleoproterozoic continental-arc magmatism. An Acad Bras Ciênc 80:1–14

Philipp RP, Bitencourt MF, Junges SL (2008b) Isótopos de Nd dos Complexos Neoproterozóicos Cambaí e Cambaizinho, Terreno Vila Nova: implicações para a evolução do Cinturão Dom Feliciano no RS. Congresso Brasileiro de Geologia, vol 46. SBG, Anais, Curitiba, p 21

Philipp RP et al (2013) Peraluminous leucogranites of Cordilheira Suite, record of Neoproterozoic collision and generation of Pelotas Batholith, Dom Feliciano Belt, southern Brazil. J S Am Earth Sci 43:8–24

Philipp RP et al. (2014) Oldest age of magmatism in the Passinho arc in the southwestern portion of Gondwana, Rio Grande do Sul, Brazil. In: 9 South American symposium on isotope Geology, Abstracts. São Paulo, p 186

Philipp RP et al (2016a) Tectonic evolution of the Dom Feliciano belt in Southern Brazil: geological relationships and U–Pb geochronology. Braz J Geol 46(1):83–104

Philipp RP et al (2016b) SHRIMP U–Pb age and high temperature conditions of the collisional metamorphism in the Várzea do Capivarita Complex: implications for the origin of Pelotas Batholith, Dom Feliciano Belt, southern Brazil. J S Am Earth Sci 66:196–207

Pimentel MM, Fuck RA (1992) Neoproterozoic crustal accretion in central Brazil. Geology 20:375–379

Pimentel MM et al (1997) The mara rosa arc in the tocantins province: further evidence for neoproterozoic crustal accretion in central Brazil. Precambr Res 81:299–310

Pimentel MM et al (2004) O Embasamento da Faixa Brasília e o Arco Magmático de Goiás. In: Mantesso-Neto V et al (eds) Geologia do Continente Sul-Americano: Evolução da Obra de Fernando Flávio Marques de Almeida. São Paulo, Beca, pp 355–368

Pimentel MM et al (2011) The tectonic evolution of the Neoproterozoic Brasília Belt, central Brazil, based on SHRIMP and LA-ICPMS UePb sedimentary provenance data: A review. J S Am Earth Sci 31:345–357

Rapela CW et al (2011) The Rio de la Plata craton and the adjoining Pan-African/brasiliano terranes: their origins and incorporation into south-west Gondwana. Gond Res 20:673–690

Remus MVD (1991) Geologia e Geoquímica do Complexo Cambaizinho, São Gabriel –RS. Instituto de Geociências, Universidade Federal do Rio Grande do Sul, UFRGS, Brasil. Master Degree thesis

Remus MVD et al (1999) Gold in the Neoproterozoic juvenile Bossoroca volcanic arc of southernmost Brazil, isotopic constraints on timing and sources. J S Am Earth Sci 12:349–366

Remus MVD et al (2000) The link between hydrothermal epigenetic copper mineralization and the Caçapava Granite of Brasiliano Cycle in southern Brazil. J S Am Earth Sci 13:191–216

Saalmann K et al (2005a) Tectonic evolution of two contrasting schist belts in southernmost Brazil, a plate tectonic model for the Brasiliano Orogeny. Int Geol Rev 47:1234–1259

Saalmann K et al (2005b) Sm–Nd isotope geochemistry of metamorphic volcano-sedimentary successions in the São Gabriel belt, southernmost Brazil: evidence for the existence of juvenile Neoproterozoic oceanic crust to the east of the La Plata Craton. Precambr Res 136:159–175

Saalmann K et al (2005c) Geochemistry and crustal evolution of volcano-sedimentary successions and orthogneisses in the São Gabriel belt, southernmost Brazil—relics of Neoproterozoic magmatic arcs. Gondwana Res 8:143–162

Saalmann K et al (2006) Tectonic evolution of the Neoproterozoic juvenile São Gabriel belt, southern Brazil—constraints on Brasiliano orogenic evolution of the La Plata Cratonic margin. J S Am Earth Sci 21:204–227

Saalmann K et al (2010) Multiple accretion at the eastern margin of the Rio de La Plata craton, the prolonged Brasiliano orogeny in southernmost Brazil. Int J Earth Sci 100:355–378

Siga O Jr et al (2009) Lower and upper Neoproterozoic magmatic records in Itaiacoca Belt (Paraná-Brasil): Zircon ages and lithostratigraphic studies. Gondwana Res 15:197–208

Siga O Jr et al (2011) Extensional and collisional magmatic records on the Apiaí Terrane, South-Southeastern Brazil: integration of geochronological U–Pb zircon ages. Revista do Instituto de Geociências—USP Série Científica 11:149–175

Silva Filho BC (1984) Geology of the poliphase deformed Precambrian Terrane of the Vila Nova Region, State of Rio Grande do Sul, Southern Brazil. Part I. Petrogenesis Acta Geológica Leopoldensia 17:35–152

Silva Filho BC, Soliani E Jr (1987) Origem e evolução dos Gnaisses Cambaí: exemplo de estudo integrado de análise estrutural, petroquímica e geocronologia. Atas, II, Simpósio Sul- Brasileiro de Geologia, vol 1, p 127–146

Silva LC et al (2005) The Neoproterozoic Mantiqueira Province and its African connections, a zircon-based U–Pb geochronologic subdivision of the Brasiliano/Pan-African systems of orogens. Precambr Res 136:203–240

Simões MS et al (2014) Geologia do complexo Máfico-ultramáfico Mata Grande, São Sepé, RS. Pesquisas em Geociências 41(2):105–120

Soliani E Jr (1986) Os dados geocronológicos do Escudo Sul-rio-grandense e suas implicações de ordem geotectônica. Ph.D. thesis, Instituto de Geociências, Universidade São Paulo, 425 p

Teixeira W (1982) Folhas SH.22 – Porto Alegre, SI.22 – Lagoa Mirim e SH.21 – Uruguaiana. Interpretação dos Dados Radiométricos e Evolução Geocronológica. Projeto RADAM BRASIL, Florianópolis (Relatório Interno, Inédito)

Vedana LA, Philipp RP (2016) Análise petrográfica e proveniência dos metassedimentos do Complexo Pontas do Salso, Terreno São Gabriel, Cinturão Dom Feliciano. RS Pesquisas em Geociências 43 (3):229–248

Vedana LA et al (2017) Petrology of the Pontas do Salso Complex, São Gabriel Terrane, Dom Feliciano Belt, southernmost Brazil: tectonic implications for a Neoproterozoic São Gabriel orogeny. Int J Geol. http://dx.doi.org/10.1080/00206814.2017.1328709

The Dom Feliciano Belt in Southern Brazil and Uruguay

11

Mathias Hueck, Pedro Oyhantçabal, Ruy Paulo Philipp, Miguel Angelo Stipp Basei, and Siegfried Siegesmund

Abstract

The Dom Feliciano Belt is an orogenic association that extends from southern Brazil to Uruguay parallel to the Atlantic coastline for over 1100 km. It was assembled in the Neoproterozoic, during the Brasiliano orogenic cycle, and is the result of interaction between the Río de la Plata, Congo and Kalahari cratons, together with several microplates, juxtaposed along major shear zones. Along its extension, the Dom Feliciano Belt is exposed in three sectors: in the Brazilian states of Santa Catarina and Rio Grande do Sul, and in Uruguay. The blocks that acted as direct forelands to the belt in South America are smaller fragments to the main cratons: Luís Alves and Nico Pérez. Three main lithotectonic domains are recognized in the belt, from east to west: a granitic batholith, a metasedimentary sequence and an association of foreland basins. Basement inliers are common, and evidence intense reworking and magmatism during the Neoproterozoic. Cryogenian to Ediacaran granitogenesis is widespread and voluminous, and usually displays an evolutionary tendency from medium- to high-K calc-alkaline, finishing with alkaline magmatism. The early evolution of the Dom Feliciano Belt is recorded in the São Gabriel Terrane, in which convergent tectonics is associated with intense juvenile magmatism, ophiolite complexes and accretion between 870 and 680 Ma. This is followed by two more deformational phases, identified in all three sectors. A convergent phase is associated with the deformation of the metavolcano-sedimentary complexes, shear zone nucleation and granitic magmatism associated with high-grade collisional metamorphism. This stage is constrained between *c*. 650–620 Ma in Santa Catarina and Rio Grande do Sul, and between *c*. 630–600 Ma in Uruguay. The last stage marks a transition to strike-slip deformation, with common shear zone reactivation associated with refolding in the metamorphic associations and widespread post-collisional granitic and volcanic magmatism. This phase is predominant from 610 to 550 Ma. The opening of the foreland basins was initiated during this period, probably associated with transtension along the main structures. Late-stage deformation and magmatism is common until 550–540 Ma. Abundant geochronological data have been added to the Dom Feliciano Belt in the last decades, leading to more precise time constraints for most of the geologic processes in the orogen. Details of its tectonic model, however, are still matters of debate, in terms of both the setting of its main units and its position into the assembly of southwestern Gondwana.

Keywords

Dom Feliciano Belt • Neoproterozoic • Brasiliano Pan-African • Gondwana

M. Hueck (✉) · S. Siegesmund
Geoscience Centre, Georg–August–Universität Göttingen, Göttingen, Germany
e-mail: mathiashueck@gmail.com

P. Oyhantçabal
Departamento de Geología, Facultad de Ciencias, Universidad de la República, Montevideo, Uruguay

R. P. Philipp
Instituto de Geociências, Universidade Federal do Rio Grande do Sul, Porto Alegre, RS, Brazil

M. A. S. Basei
Instituto de Geociências, Universidade de São Paulo, São Paulo, Brazil

11.1 Introduction

The Mantiqueira Province is the biggest mobile belt association in Brazil, extending for over 3000 km with a northeast to southwest direction parallel to its southern and eastern coast and into Uruguay (Almeida et al. 1973). It was formed in the Neoproterozoic during the Brasiliano-Pan African orogenic cycle, and was one of the most significant orogenic systems during the assembly of Southwestern Gondwana (Fig. 11.1). It is divided into three orogenic belts which are,

S. Siegesmund et al. (eds.), *Geology of Southwest Gondwana*, Regional Geology Reviews,
https://doi.org/10.1007/978-3-319-68920-3_11

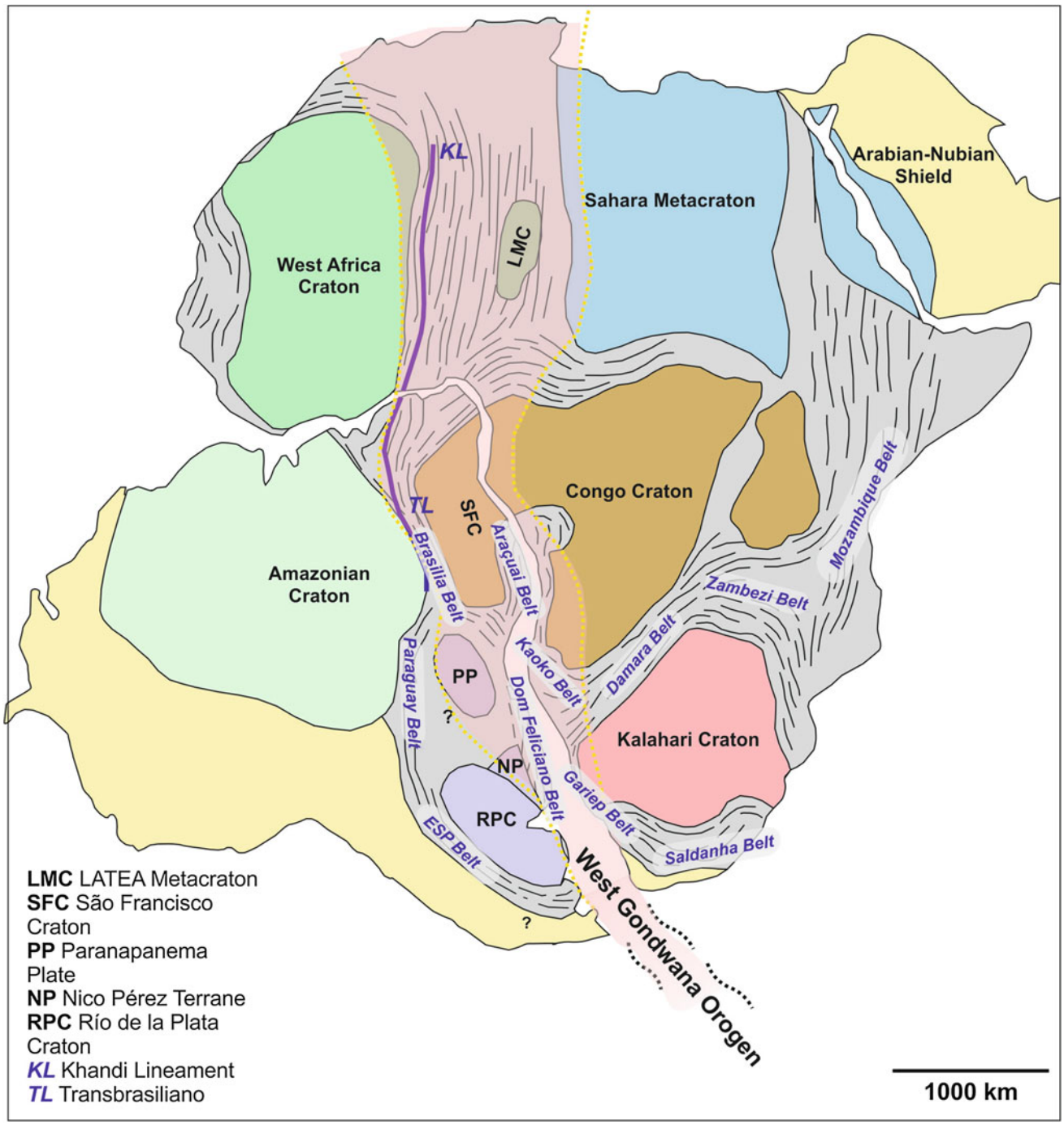

Fig. 11.1 Position of the Dom Feliciano Belt in relation to the surrounding cratons and other orogenic belts in Gondwana. ESP Belt—Eastern Sierras Pampeanas Belt. Modified from Oriolo et al. (2017)

from north to south: Araçuaí, Ribeira and Dom Feliciano (e.g.: Heilbron and Machado 2003; Silva et al. 2005a). At the African side of the Atlantic, its counterparts are the Saldania-Gariep, Damara, Kaoko and West Congo belts (Porada 1989; Basei et al. 2008, Oyhantçabal et al. 2011b).

In the southernmost portion of the Mantiqueira Province, the Dom Feliciano Belt extends for more than 1100 km, striking northeast to southwest to northnortheast to south-southwest, roughly following the coastline and with a maximum width of *c*. 200 km (Fig. 11.2). It is limited to the north by the cratonic Luís Alves Terrane, to the east by the shore of the South Atlantic Ocean and associated marine sediments, and to the south by the Río de la Plata estuary between Uruguay and Argentina. To the west, it is

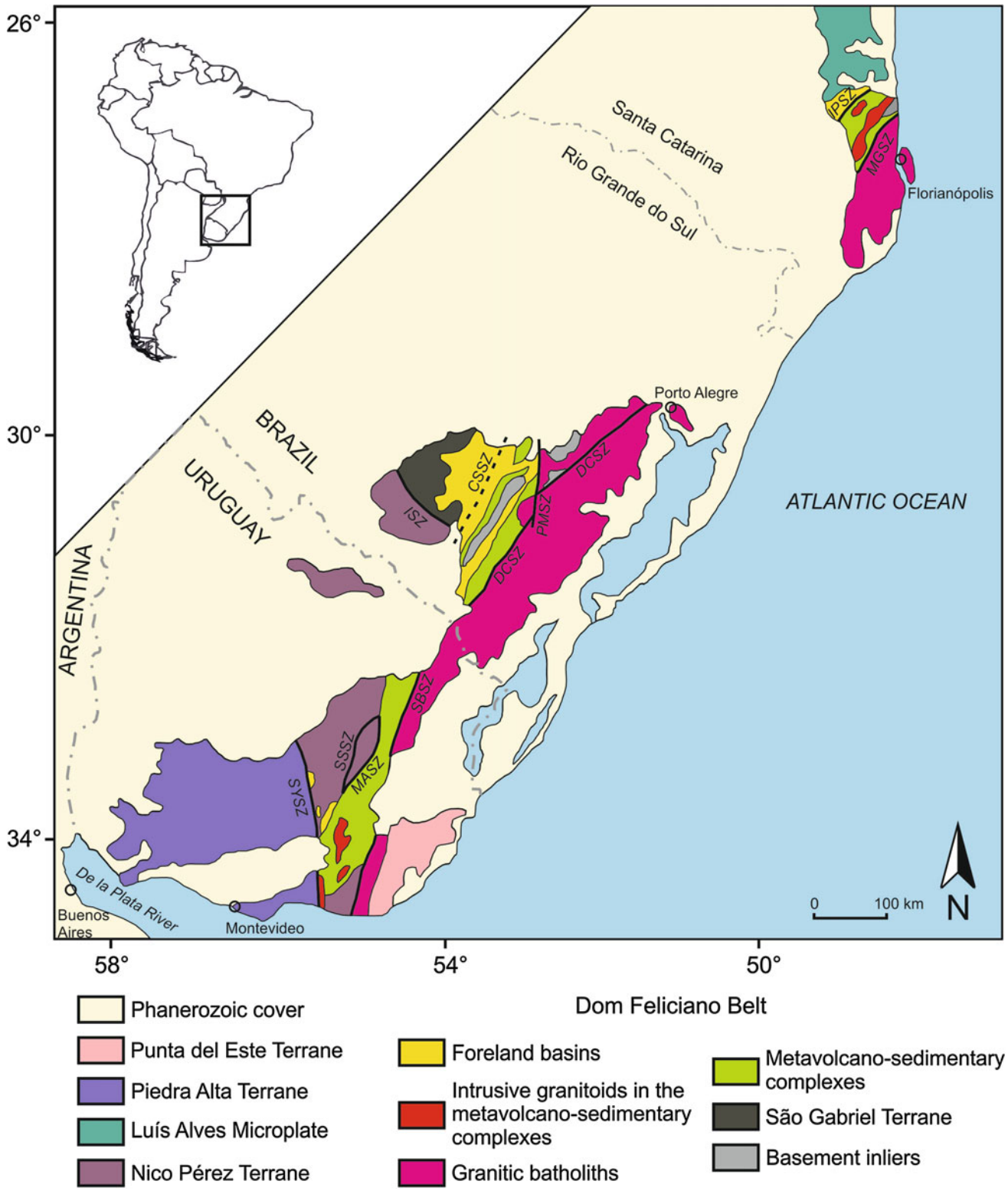

Fig. 11.2 Tectonic map of the Dom Feliciano Belt (Modified from Basei et al. 2000; Hueck et al. 2016). IPSZ - Itajaí-Perimbó Shear Zone; MGSZ - Major Gercino Shear Zone; DCSZ - Dorsal do Canguçu Shear Zone; PMSZ - Passo do Marinheiro Shear Zone; CSSZ - Caçapava do Sul Shear Zone; ISZ - Ibaré Shear Zone; SBSZ - Sierra Ballena Shear Zone; MASZ - Maria Albina Shear Zone; SSSZ - Sierra de Sosa Shear Zone; SYSZ - Sarandí del Yí Shear Zone

commonly covered by the Paleo- to Mesozoic sedimentary succession of the Paraná Basin, but locally it is in contact with foreland basement blocks such as the Nico Pérez Terrane. The belt is exposed in three structural windows, also known as shields, in different areas, from north to south, in the Brazilian states of Santa Catarina and Rio Grande do Sul, and in Uruguay. Each sector has its own particularities and has been the focus of recurrent research.

This chapter aims to revise the extensive bibliography accumulated in the last decades around the Dom Feliciano Belt. Each sector is described individually, with a synthesis of the main local units. When detail studies are present, the latest findings in terms of structural geology, geochemistry, isotopic geochemistry and geochronology are reviewed. This is followed by a discussion of the current tectonic models and interpretations of the origins and evolution of the belt, and its significance in the assembly of Gondwana.

11.2 Santa Catarina Sector

The northernmost occurrence of the Dom Feliciano Belt is exposed in the Brazilian state of Santa Catarina. It constitutes a *c*. 60 km wide corridor along the South Atlantic coastline, south of the city of Penha, covered to the west and to the south by Phanerozoic sediments of the Paraná Basin. The orogenic belt is limited, to the north, by the Luís Alves Microplate, a cratonic block that acted as a foreland during the Neoproterozoic orogenic event in this sector.

In Santa Catarina, the architecture of the Dom Feliciano Belt is especially clear, and since its original recognition (Basei 1985) it has been extended to the remaining portions of the belt (Basei et al. 2000). It is divided into three domains (Figs. 11.3 and 11.4): southeastern (internal), central and northwestern (external). Each domain has a characteristic lithological association and is separated from the bordering terrane by major shear zones.

The southeastern domain is an association of voluminous granitic intrusions, called the Florianópolis Batholith. It consists of several granitic suites with local occurrences of crystalline basement. The central domain is characterized by a metavolcano-sedimentary fold-and-thrust belt, the Brusque Group. Its crystalline basement, the Camboriú Complex, is exposed in the northeastern extremity of the domain. Both units are intruded by numerous granitic intrusions. Finally, the northwestern domain corresponds to the foreland Itajaí Basin, deposited on top of the Luís Alves Microplate.

Each unit will be detailed in the following sections, followed by a short discussion on the deformation history of the Dom Feliciano Belt in the Santa Catarina sector. The individual shear zones that mark the boundaries between the domains are described and discussed in an individual chapter (Oriolo et al. 2018).

11.2.1 The Cratonic Foreland

The cratonic foreland to the Dom Feliciano Belt in Santa Catarina is the Paleoproterozoic Luís Alves Microplate (Fig. 11.5a) (Basei et al. 2000, 2009; Hartmann et al. 2000a, 2003a). It comprises most of the northern segment of the Precambrian exposition in Santa Catarina, occurring north of the city of Penha. Its southern limits are covered by the Itajaí Foreland Basin, while the northern border is tectonic, along which it is juxtaposed to the Curitiba Microplate. Both terranes are described in detail by Passarelli et al. (2018).

11.2.1.1 Basement Inliers

The main exposure of pre-Brasiliano inliers in the central domain of the Dom Feliciano Belt in Santa Catarina is the Camboriú Complex (Basei et al. 2000). This association crops out in the northeastern extremity of the domain, along the South Atlantic coast, and is interpreted to represent the crystalline basement of the Brusque Group, although the contact relationship between both units seems to suggest a tectonic juxtaposition (Philipp et al. 2004).

The region comprises two main units. The first one consists of gneisses and stromatic migmatites, commonly identified as the Camboriú Complex proper (e.g., Hartmann et al. 2003a; Philipp et al. 2004; Peternell et al. 2010; Florisbal et al. 2012a), or alternatively the Morro do Boi Migmatites (Basei et al. 2013a) (Fig. 11.5b). Migmatitic rocks predominate in the unit, characterized by the presence of more than one generation of leucosome and associated with amphibolite. The unit has a NE-SW orientation and has been folded into a major antiform with numerous subordinate parasite folds. The second unit is a large monzogranitic to granodioritic intrusion characterized by abundant mafic enclaves and xenoliths from the migmatites, referred to as Itapema Granite (Hartmann et al. 2003a; Bitencourt and Nardi 2004; Philipp et al. 2004; Peternell et al. 2010) or, alternatively, Ponta do Cabeço Granite (Basei 2000; Basei et al. 2013a). It is a sheet-like body, intruded in the base of the migmatites and exposed in the center of the regional fold, and corresponds to schollen-rich diatexite originated from the main migmatization event in the Camboriú Complex. Later generations of granitic magmatism unrelated to the main migmatization event also intrude the unit and are either associated with narrow shear zones, such as the Corre-Mar Granite (Martini et al. 2015), or are part of the large granitic intrusions that also affect the Brusque Group (Florisbal et al. 2012a; Hueck et al. 2016).

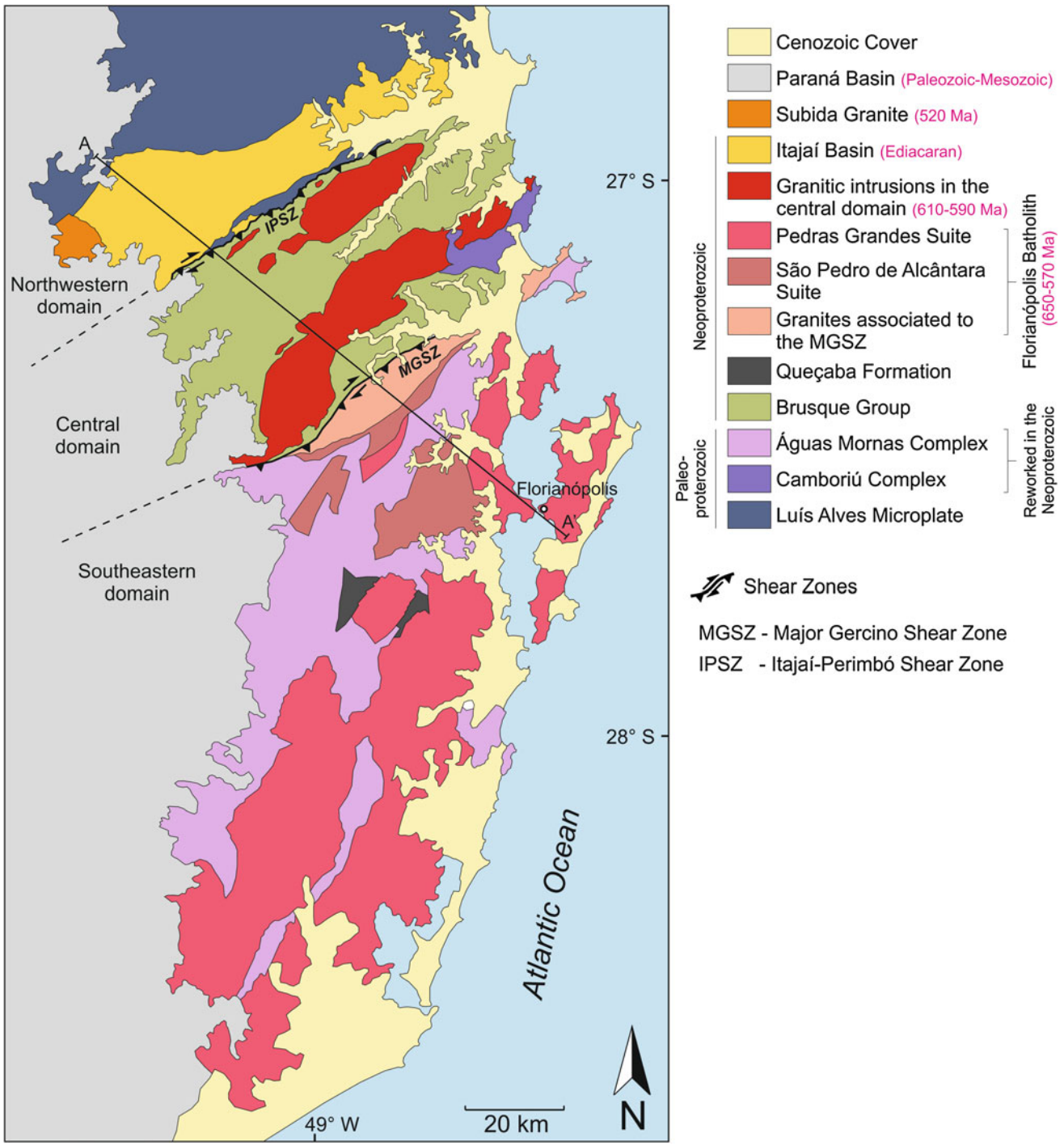

Fig. 11.3 Simplified geological map of the Santa Catarina sector of the Dom Feliciano Belt. Profile A-A′ is presented in Fig. 11.2. Modified from Basei et al. (2000, 2006), Silva et al. (2005b), and Wildner et al. (2014)

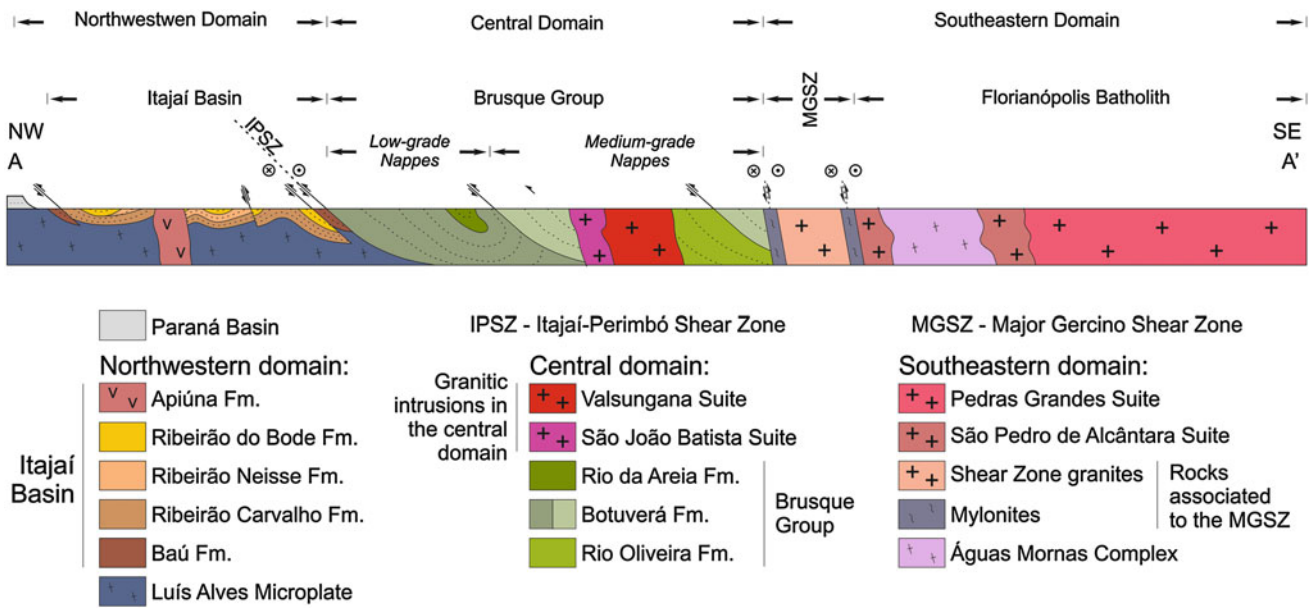

Fig. 11.4 Schematic geologic profile of the Dom Feliciano Belt in the Santa Catarina sector. Details of the stratigraphy of the Brusque Group and Itajaí Basin presented in this figure were omitted from Fig. 11.1 in order to comply with the scale of the map. Modified from Basei et al. (2006, 2011a, b)

U-Pb zircon dating in most lithologies of the Camboriú Complex yield predominantly Paleoproterozoic ages between 2.0 and 2.2 Ga (Silva et al. 2000, 2005b; Hartmann et al. 2003a; Basei et al. 2013a). Abundant Archean signatures have also been recognized, both in Nd and Hf T_{DM} model ages of the Sm-Nd and Lu-Hf isotopic systems and in widespread inherited zircon nuclei (Basei et al. 2013a). This is interpreted as the main extraction age for juvenile material. A third group of ages corresponds to the Neoproterozoic (640–610 Ma), including analyses performed in the neosome of the migmatites, in the Itapema Granite and on rims of inherited zircon crystals (Hartmann et al. 2003a; Silva et al. 2000, 2005b; Basei et al. 2013a; Martini et al. 2015). The significance of the geochronological data have been subject to alternative interpretations. Silva et al. (2000), Bitencourt and Nardi (2004) and Hartmann et al. (2003a) interpret the Paleoproterozoic ages to correspond to the event responsible for the migmatization of the Camboriú Complex and formation of the Itapema Granite, and attribute the Neoproterozoic ages to metamorphic overgrowth during the Brasiliano orogenic cycle. On the other hand, Silva et al. (2005b) acknowledges further melt generation during the Neoproterozoic, interpreted as the crystallization age of anatectic granodiorites. Finally, Basei et al. (2000, 2013a) consider the Paleoproterozoic ages to represent the crystallization age of the protoliths of the Camboriú Complex, and attribute the generation of the migmatites and of the Itapema Granite to the Neoproterozoic.

In the southeastern domain of the Dom Feliciano Belt, basement inliers within the Florianópolis Batholith are grouped into the Águas Mornas Complex. They occur predominantly in the northern portion of the domain, and are intruded by the diverse Neoproterozoic granites that constitute the batholith. Silva et al. (2000, 2002b, 2005b) recognize two main lithological associations. The first comprises restitic orthogneisses of tonalitic composition associated with amphibolites (G1), while the second includes foliated monzogranites of anatectic origin (G2), intrusive in the former. This second generation was dated by SHRIMP and yielded an age of *c*. 2.20 Ga, predominantly in magmatic zircon cores (Silva et al. 2005b). Two other zircon crystallization events were recognized by the same authors, the earliest one responsible for cores with metamorphic appearance dated at *c*. 1.75 Ga, while the latest one is responsible for the generation of new magmatic zircons and overgrowth rims around the earlier phases, dated at 592 ± 5 Ma. This last phase is interpreted as an intense reworking of the unit during the formation of the Dom Feliciano Belt, responsible for widespread melting and migmatization of the unit, similar to that proposed in the Camboriú Complex (Basei et al. 2000, 2013a; Silva et al. 2005b). An alternative designation for the basement rocks intruded by granites of the Florianópolis Batholith in its northeastern extremity is the Porto Belo Complex (Florisbal et al. 2012b, c). In this region, Neoproterozoic melts hosted in the gneisses have yielded a U-Pb zircon age of

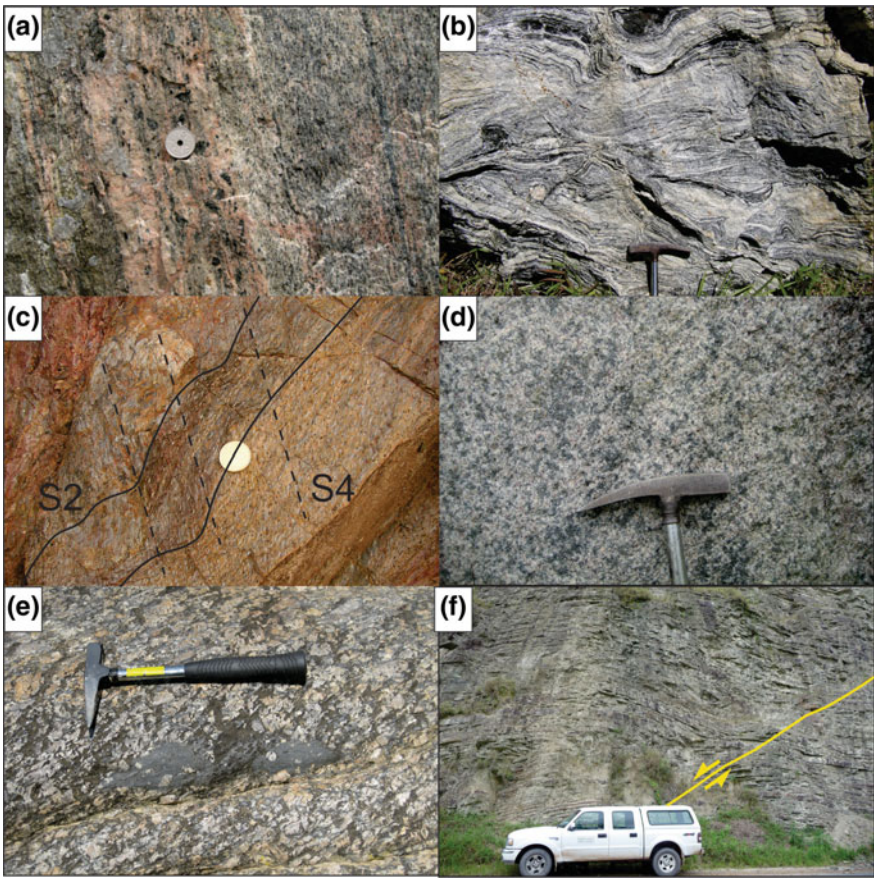

Fig. 11.5 Some field aspects of rocks from the Santa Catarina sector of the Dom Feliciano Belt. **a** Granulitic rocks overprinted by retrograde metamorphism, Luís Alves Complex; **b** Folded migmatites of the Morro do Boi unit, Camboriú Complex; **c** Metapelitic rocks from the Botuverá Formation, Brusque Group. Note that the compositional layering (S_2) is transposed by a pervasive crenulation foliation (S_4); **d** Late isotropic leucogranite of the Pedras Grandes Suite. **e** Mafic enclave in porphyritic Southern Valsungana Batholith, part of the granitic intrusions in the Brusque Group. Note cm-sized K-feldspar megacrysts within a coarse, biotite-rich matrix; **f** Turbidites of the Ribeirão Carvalho Formation, Itajaí Basin. Note the normal fault in the lower right corner of the picture

649 ± 10 Ma (Chemale et al. 2012), related to the early phases of migmatization and anatexis.

Alternatively, Basei et al. (2000, 2006) consider the Águas Mornas Complex to be the oldest intrusive Suite of the Florianópolis Batholith. In this interpretation, the magmatic rocks in it would predominantly be the product of Neoproterozoic melting, while the gneissic rocks would represent xenoliths or restites of the original Paleoproterozoic basement.

11.2.2 The Metavolcano-sedimentary Complex

The Brusque Group is the main geological unit of the central domain of the Dom Feliciano Belt in Santa Catarina. It corresponds to a volcano-sedimentary association that went through more than one phase of deformation and metamorphism (Basei 1985; Silva 1991; Caldasso et al. 1995a, b; Basei et al. 2000, 2008, 2011a; Philipp et al. 2004). The unit forms a *c*. 40 km-wide corridor with a northeast to southwest orientation, segmented by the intrusion of voluminous granitic plutons, in particular those of the Valsungana Suite. Both of its extremities are marked by tectonic contacts. The northwestern limit is the Itajaí-Perimbó Shear Zone, along which the Brusque Group is thrust over the foreland Itajaí Basin. From the other side, the dextral transcurrent Major Gercino Shear Zone separates the central domain from the Florianópolis Batholith to the southeast (Bitencourt and Kruhl 2000; Passarelli et al. 2010, 2011a, b; Oriolo et al. 2018). The only exposure of the crystalline basement of the metasupracrustal succession is the Camboriú Complex, on the northeastern portion of the central domain. An alternative designation commonly used in the literature is Brusque Metamorphic Complex (e.g., Silva 1991; Philipp et al. 2004).

Based on detailed mapping of the Brusque Group, Basei et al. (2006, 2011a) propose a stratigraphic division of the sequence into three formations: Rio Oliveira, Botuverá and Rio da Areia. This division takes as reference the main

metamorphic foliation of the sequence which transposes the original sedimentary bedding. Nonetheless, primary structures such as grain size variations between layers can be recognized locally (Philipp et al. 2004). It should be noted that some works on the Brusque Group opt to separate the sequence only in terms of lithology, instead of individual formations (e.g., Philipp et al. 2004; de Campos et al. 2012a, b), which may lead to the encompassing of rocks from different formations within a same unit.

The basal unit of the Brusque Group is the Rio Oliveira Formation. Its area of occurrence is limited to the eastern extent of central domain, south of the main Valsungana intrusion, where it is wedged between the pluton and an overthrusting nappe of metasediments (Silva 1991). It is divided into four units, from the oldest to the youngest: metavolcanic and calc-silicatic, volcanic-exhalative, metapelitic and metapsammitic units. The metavolcanic rocks include amphibolite and local metaultramafites (tremolite schists), while the main lithology in the volcano-exhalative unit is tourmalinite. Whole-rock geochemistry and isotopic geochemistry indicate that both the basic and ultramafic volcanic rocks have similar signatures and were probably generated in the same setting, and both contributed to the volcanoclastic components of the sedimentary associated metasediments (de Campos and Philipp 2007; de Campos et al. 2012a). Detailed geochemical characterization of the tourmalinites indicates more than one source for the hydrothermal fluids responsible for their generation (Garda et al. 2013). The metapelites are mostly mica-schists with quartz, garnet and andalusite, and the metapsammites include quartzites and paraconglomerates. Subordinate occurrences of acid metavolcanic rocks, mostly metarhyodacites, have also been identified in this formation (Silva 1991; Silva et al. 2002a).

In an intermediate position, the Botuverá Formation is the largest unit of the Brusque Group, and occupies most of the central domain both to the south and to the north of the large Valsungana intrusions. Three lithologic associations are recognized: metapelites (Fig. 11.5c), metarhythmites and metapsammites (Basei et al. 2011a). The metamorphic conditions to which these rocks were submitted vary from low to medium grade, leading to different associations of rocks. The lower metamorphic assemblage is predominant in the northern portion of the metamorphic complex, and consists of a gradation from sericitic schists to phyllites and metarhythmites to quartzites and mica quartzites. The medium-grade rocks transition from biotite schists with garnet and muscovite to an intercalation of mica schists with quartz schist and quartzite.

Finally, the uppermost unit of the association is the Rio da Areia Formation, which constitutes the metavolcano-sedimentary sequence of the northern portion of the Brusque Group. Four units are recognized: metapelitic-carbonatic, metacarbonatic, quartzitic and metavolcanic (Basei et al. 2011a). The first one is the largest, and corresponds to an association of metamarls, calc-schist and metalimestones. Large occurrences of metacarbonatic rocks, mostly comprising limestones and dolomites, are dismembered from this unit in map scale. In a similar position, the most significant incidences of quartzite can be singled out as an individual unit, in which massive quartzites are locally intercalated to micaceous and feldspatic layers. The topmost unit of the Rio da Areia Formation encompasses its metavolcanic rocks, mostly an association of basalts, tuffs and ultramafites metamorphosed into chlorite schists and tremolite schists.

From early studies onwards, the metamorphism of the Brusque Group has been characterized by high-temperature and low-pressure conditions (e.g., Basei 1985; Silva 1991; Caldasso et al. 1995a, b). The most recent detailed research on the metamorphic evolution of the unit (Philipp et al. 2004; Basei et al. 2011a) agree in a number of aspects but diverge in others. The consensus is that the structural and metamorphic evolution of the Brusque Group was polyphasic and can be characterized by two main stages. The first is associated with the development of the main foliation, which is a S_2 that transposes both the original sedimentary surface (S_0) and an early foliation (S_1). The second is related to the intrusion of voluminous granitic intrusions in the Brusque Group, of which the Valsungana Suite is the main example.

According to Philipp et al. (2004), the first stage corresponds to two metamorphic phases (M_1 and M_2), and is characterized with metamorphic conditions of low-pressure greenschist to lower amphibolite facies, also indicated by geothermometry of the metabasic rocks (de Campos and Philipp 2007; de Campos et al. 2012a). Progressive burial and heating of the sequence would then eventually lead to conditions capable of promoting partial melting of the metasedimentary sequence, associated with outcrop-scale granitic bodies interpreted as syn-D_2 (Philipp and Campos 2010). Philipp et al. (2004) also interpret the distribution of the metamorphic zones to be irregular and disrupted, and point to it as an evidence of tectonic reworking of the metamorphic framework preceding the intrusion of the granitic magmatism. Following partial exhumation of the sequence, the late metamorphic event (M_3) is triggered by the intrusion of the granitic plutons (Phillipp et al. 2004). During this phase, the contact metamorphism aureoles reached a width of up to 4 km and had temperature conditions varying from the albite-epidote hornfels facies to the pyroxene-hornfels facies.

In the model proposed by Basei et al. (2011a), the transition from S_1 to S_2 foliation was gradual and corresponds to the regional metamorphic event. Two paragenetic assemblages indicating greenschist-facies conditions record this event, which was followed by a slight retrogression due to D_2 thrusting (Fig. 11.4), associated with exhumation.

A second prograde sequence, with the development of four more typical parageneses, is coeval to the intrusion of the granites, which is described as syn- to late kinematic in relation to S_2. It was accompanied by reburial of the sequence, promoted by the emplacement of the biggest Valsungana Batholiths, and affects predominantly the southern portion of the Brusque Group. This event started from initial conditions close to 570 °C and 2.5 kbar and reached 760–850 °C and 4–5 kbar.

Both models described above agree that the time interval between the development of the main S_2 foliation and the intrusion of the granites in the Brusque Group must have been relatively short. They also have in common the observation that the S_2 is further affected by two more deformational events, although with different characteristics. Basei et al. (2011a) describe D_3 as a regional inverse folding event verging to the northnorthwest with development of plane-axial schistosity, while D_4 corresponds to smaller asymmetric folds associated with a persistent crenulation cleavage (Fig. 11.5c). On the other hand, Philipp et al. (2004) interpret D_3 to be a transcurrent event accompanied by normal folding, followed by a D_4 characterized by kink banding and open chevron folds. These late phases of deformation, in particular D_3, are likely coeval to the intrusion of the granitic magmatism.

The age of the sedimentation of the Brusque Group is also still unclear. Zircon SHRIMP dating of metabasic rocks from the Rio do Oliveira Formation yield an age of 936 ± 40 Ma (Basei et al. 2011a), interpreted by these authors as representative of mafic intrusions associated with the initial taphrogenesis of the Brusque Basin. Nd signatures from other samples of the same unit evidence a mantellic source contaminated with crustal material, yielding model ages between 1028 and 1762 Ma, suggestive of a Neoproterozoic extraction (de Campos et al. 2012a). Another constraint for the rift phase of the Brusque is the emplacement of the A-type Morro do Parapente Granite, also dated by SHRIMP at *c*. 840 Ma (Basei et al. 2008). Detrital zircon crystals are mostly limited to ages of 2.0–2.2 Ga (Hartmann et al. 2003a; Basei et al. 2011a), indicating fairly consistent sources for the sedimentary input. Nonetheless, some crystals from the Botuverá Formation reported by Basei et al. (2008) have younger Paleoproterozoic (1.7–2.0) and Mesoproterozoic (1.1–1.5 Ga) ages. An upper limit for the deposition of the Brusque Group is that of syn-sedimentary acid metavolcanic rocks, dated to around 640 Ma by SHRIMP (Silva et al. 2002a; Basei et al. 2011a). Diabase and lamprophyre dikes in the volcano-sedimentary sequence of the Rio da Areia Formation represent early magmatic intrusion after the development of the main foliation, and were dated by LA-ICP-MS in zircon at 618 ± 9 Ma (de Campos et al. 2012b). Thus the best estimate for the age of the regional metamorphism (syn-S_2) of the Brusque Group is given by the interval between the *c*. 640 Ma syn-depositional acid volcanism and the intrusion of the *c*. 620 basic rocks. The intrusion of the massive granitic magmatism is constrained to 610–590 Ma (Silva et al. 2002b, 2003, 2005b; Vlach et al. 2009; Basei et al. 2011a; Florisbal et al. 2012c; Hueck et al., in preparation).

Silva (1991) postulate a tectonic setting in which the metavolcano-sedimentary sequence of the Rio do Oliveira Formation would correspond to a mature rift system with generation of oceanic crust in a deep environment, later evolving to a marine setting corresponding to the main metasedimentary package (Botuverá Formation). Basei et al. (2011a) follow a similar interpretation, noting that although the metamorphic conditions of the Brusque Group most closely resemble those of a back-arc environment, this setting is incompatible with their model, which positions the Brusque basin to the west of a continental arc association. On the other hand, Philipp et al. (2004) propose a marine sedimentation in a continental rift system, without generation of oceanic crust, evolving to a passive margin. In this context, the volcanic association corresponds to an intraplate magmatic event, with tholeiitic to alkaline signatures indicating crustal contamination (de Campos and Philipp 2007; de Campos et al. 2012a).

11.2.3 Neoproterozoic Granitic Magmatism

11.2.3.1 Florianópolis Batholith

More than half of the exposition of the Dom Feliciano Belt in Santa Catarina corresponds to its southeastern domain, the Florianópolis Batholith. It comprises a large association of granitic intrusions grouped into different suites. While its eastern, southern and western limits are masked either by the coastline of the South Atlantic Ocean or by the sedimentary cover of the Phanerozoic Paraná Basin, its northern boundary is tectonic and sharply defined by the Major Gercino Shear Zone, separating it from the central domain (Bitencourt and Nardi 1993; Bitencourt and Kruhl 2000; Passarelli et al. 2010, 2011a, b; Oriolo et al. 2018)

The lithostratigraphic division of the various granites into intrusive suites has some variations in the literature devoted to the subject. Many divisions apply geochemical criteria, separating earlier calc-alkaline granites from later alkaline ones (Bitencourt and Nardi 2000; Silva et al. 2002b, 2005b). In addition, granites from the northern part of the batholith, associated with the Major Gercino Shear Zone, are commonly addressed separately from the rest of the batholith, owing to their close relationship to the development of this structure (Basei et al. 2000, 2006; Bitencourt and Kruhl 2000; Passarelli et al. 2010, 2011a; Florisbal et al. 2012b). Nonetheless, the isotopic signature of these rocks is compatible to that of the remaining Florianópolis Batholith,

instead of the bordering units of the central domain (Basei et al. 2000; Hueck et al. 2016). The granites associated with the shear zone are exposed in two distinct areas. The oldest are found in the coastal region, and correspond to early melts hosted in the crystalline basement of the region (Porto Belo Complex), dated at 649 ± 10 Ma (Chemale et al. 2012). The interior portion is enveloped by two mylonitic bands and comprises two calc-alkaline intrusions, Fernandes and Rolador, dated by U-Pb TIMS at 614 ± 2 and 609 ± 16 Ma respectively (Passarelli et al. 2010, 2011a). Comparable signatures and ages were obtained in the coastal sector of the shear zone, where the Mariscal and Quatro Ilhas granites yield U-Pb zircon ages between 625 and 610 Ma (Bitencourt and Kruhl 2000; Chemale et al. 2012; Florisbal et al. 2012b, 2012c). This early magmatism is followed in the same region by the Estaleiro Granite, an intrusion with shoshonitic affinity strongly correlated with the mylonitic deformation, dated at 602 ± 4 Ma (Bitencourt and Kruhl 2000; Chemale et al. 2012). The same authors identify a last granitic intrusion in the coastal portion, associated with the late alkaline magmatism of the batholith, the Zimbros Suite, with ages between 589 and 586 Ma.

In the stratigraphy proposed by Basei et al. (2000, 2006) for the main portion of the Florianópolis Batholith it is divided into three units, the oldest of which is the Águas Mornas Complex. Different from the traditional interpretation of this unit as the exposure of the Paleoproterozoic basement within the Batholith (e.g., Silva et al. 2000, 2002b, 2005b), these authors consider it to be an essentially Neoproterozoic unit, in which extensive reworking during the formation of the Dom Feliciano Belt was responsible for widespread magmatism. The original protoliths are commonly preserved as xenoliths and restites. In this conception, this unit includes rocks alternatively associated with the Paulo Lopes Suite (e.g., Zanini et al. 1997; Silva et al. 2002b, 2005b; Bitencourt et al. 2008; Florisbal et al. 2009). Predominant in the southern part of the batholith, such as in the Garopaba region, this association is characterized by the common presence of coeval basic rocks (Bitencourt et al. 2008) and is the result of the interaction of mantle-derived mafic magmas with abundant crustal contaminants (Florisbal et al. 2009). The best geochronological constraint for this suite is the SHRIMP age of 626 ± 8 Ma, obtained in the Paulo Lopes Granite (Silva et al. 2003).

In an intermediate stratigraphic position, the São Pedro de Alcântara Suite includes diverse granodiorites to monzogranites. Most rocks are gray to pink with medium-grained equi- to inequigranular textures, though porphyritic varieties may also occur. They usually show slight deformation. This unit has mostly calc-alkaline signatures and corresponds to most varieties with these signatures otherwise grouped into the Maruim Suite (e.g., Zanini et al. 1997; Silva et al. 2002b, 2005b). The geochronological record of this unit consists of SHRIMP ages ranging from *c*. 610 Ma in the Forquilha Granite (Silva et al. 2002b), to 579 ± 8 Ma in the Alto da Varginha Granite (Silva et al. 2002b).

Finally, the late alkaline magmatism is grouped into the Pedras Grandes Suite by Basei et al. (2000, 2006), and corresponds to the final stage of granitic magmatism in the Florianópolis Batholith. In this sense, it includes associated volcanic and subvolcanic rocks alternatively identified as the Cambirela Suite (e.g., Zanini et al. 1997; Bitencourt et al. 2008). The suite comprises a number of different rocks, but the predominant lithology corresponds to isotropic gray to pink or red leucocratic granites with medium to coarse granulation (Fig. 11.5d), such as the Serra do Tabuleiro and Ilha granites. Most volcanic rocks associated with this suite occur as rhyolitic flows and tuffs, besides numerous dikes intruding into older suites (Zanini et al. 1997; Bitencourt et al. 2008). SHRIMP dating of the Tabuleiro Granite has produced an age of 597 ± 9 Ma (Silva et al. 2003, 2005b).

Metasedimentary rocks occur sporadically overlying the Florianópolis Batholith, grouped into the Queçaba Formation (Basei 1985; Zanini et al. 1997). They correspond to quartzites associated with mica schists, quartz schist and phyllites, tectonically juxtaposed with the granites.

11.2.3.2 Granite Intrusions in the Central Domain

Both the Brusque Group and its exposed basement, the Camboriú Complex, were intruded by numerous granitic plutons during the Brasiliano orogenic cycle. Centimeter- to meter-thick bodies of peraluminous granites concordant with the metasupracrustal sequence were interpreted by Philipp and Campos (2010) as related to the main deformational event of the Brusque Group in a collisional context, and represent an early phase of granitic magmatism. Much more voluminous intrusions affect the domain after the main deformational phase in the metamorphic association and are associated with the sequence's thermal climax (Philipp et al. 2004; Basei et al. 2011a). A total of *c*. 40 individual intrusions from this event are recognized, including two large batholiths many tens of kilometers long. The intrusions are grouped into three different suites: São João Batista, Valsungana, and Nova Trento (Basei et al. 2000, 2011a; Hueck et al. 2016). An early division of the intrusions into Valsugana and Guarbiruba suites, after Trainini et al. (1978), is still followed in some publications (e.g. Silva et al. 2005b; Hartmann et al. 2003a).

According to the division proposed by Basei et al. (2000, 2006) and Hueck et al. (2016), the São João Batista Suite is the oldest of the three suites, and includes fine- to medium-grained leucocratic isotropic granitoids. The suite has characteristic peraluminous mineralogy, with widespread igneous muscovite and accessory minerals such as

garnet and tourmaline. The suite with the largest intrusions, by far, is the Valsungana Suite. It includes the two batholiths that occupy much of the central domain of the Dom Feliciano Belt in Santa Catarina. The most striking characteristic of the suite is its porphyritic texture, with K-feldspar megacrysts up to several centimeters long, within a medium- to coarse-grained matrix (Fig. 11.5e). Most rocks are leucocratic to mesocratic gray granites, with some varieties having pink K-feldspars. The main mafic mineral is biotite. Lastly, the Nova Trento Suite comprises numerous plutons, usually intruding in or around the main Valsungana batholiths. Rocks from this suite are mostly fine to medium grained, and have colors between gray and pink. Biotite is the most common mafic mineral, and common accessories include muscovite and, in the northernmost intrusions, hornblende.

With the exception of the rocks from the São João Batista Suite, most intrusions have magmatic foliations along their borders that are parallel to the orientation of their host rocks. Deformation in magmatic to submagmatic conditions that eventually evolve to solid-state deformation during magma cooling is indicated in microstructures (Peternell et al. 2010; Florisbal et al. 2012a; Hueck et al. 2016). This has been interpreted as evidence for a transcurrence-controlled emplacement (Peternell et al. 2010; Florisbal et al. 2012a), but might alternatively reflect magma-initiated strain localization (Hueck et al. 2016, in preparation).

All suites share a slightly peraluminous signature and have high-K calc-alkaline affinity (Castro et al. 1999; Florisbal et al. 2012a; Hueck et al. 2016). There is a geochemical distinction of some of the northernmost intrusions from the Valsungana and Nova Trento suites that suggest they underwent more oxidizing conditions (Castro et al. 1999; Hueck et al. 2016). A strong crustal signature is suggested for the granitic intrusions in the central domain by their isotopic signature (Florisbal et al. 2012a; Hueck et al. 2016). Nd and Hf T_{DM} model ages largely indicate Paleoproterozoic ages, with some early Mesoproterozoic and Archean influence as well. Mantellic input was limited to the Valsungana Suite, as suggested by the presence of mafic enclaves (Fig. 11.5e) and slightly less negative εNd values (Florisbal et al. 2012a).

Field relationships such as intrusive contacts and the presence of xenoliths are used to recognize the relative stratigraphy between the three suites (Basei et al. 2000, 2006, 2011a; Hueck et al. 2016). Nonetheless, most recent U-Pb dating of the granites obtained widely overlapping age intervals for all three suites of around 610–590 Ma (Silva et al. 2002b, 2003, 2005b; Vlach et al. 2009; Basei et al. 2011a; Florisbal et al. 2012c; Hueck et al., in preparation), suggesting a long-lasting magmatic event on which magmas of all three suites crystallized coevally (Hueck et al., in preparation). Although multiple sources were likely responsible for the generation of the granitic magmas (Florisbal et al. 2012a), both the isotopic record and zircon inheritance link them to the partial melt of rocks from the central domain of the Dom Feliciano Belt; that is, the Brusque Group and its crystalline basement, such as the exposed Camboriú Complex (Hueck et al. 2016, in preparation). The peraluminous São João Batista Suite probably had a bigger influence of paraderived source rocks, while the Valsungana and Nova Trento Suite might have had some degree of magmatic interaction (Hueck et al. 2016).

11.2.4 The Foreland Basin

The northwestern domain of the Dom Feliciano Belt in Santa Catarina is the Itajaí Basin. It is deposited on top of the Luís Alves Microplate and has an elongated shape, constituting a corridor up to 25 km wide, oriented east-northeast to west-southwest. The basin is asymmetric, with increasing thickness from north to south, where it reaches a sedimentary package as thick as 5000 m (Rostirolla et al. 1999; Guadagnin et al. 2010; Basei et al. 2011b; Costa and Nascimento 2015). Its northern contact is characterized by normal depositional contact, with the basal units of the Basin lying on top of the granulites from the Luís Alves Microplate. The southern limit, on the other hand, is tectonic in origin, and is characterized by the thrusting of the metavolcano-sedimentary rocks of the Brusque Group over the basin along the Itajaí-Perimbó Shear Zone (Basei 1985; Silva 1991; Rostirolla et al. 1992, 1999; Guadagnin et al. 2010; Oriolo et al. 2018).

The stratigraphy of the Itajaí Basin has been affected by thrust tectonics, causing local folding and numerous repetitions (Basei et al. 2011b). As a consequence, the total thickness of the sedimentary stack does not correspond to its stratigraphic thickness. The package has traditionally been designated as Itajaí Group (e.g., Silva and Dias 1981; Basei 1985) and most recent studies in the area identify three to four sedimentary units intruded by felsic volcanic rocks (Rostirolla et al. 1999; Guadagnin et al. 2010; Basei et al. 2011b; Costa and Nascimento 2015). The stratigraphy described below follows that of Basei et al. (2011b).

The basal unit corresponds to the Baú Formation, and comprises mainly polymitic conglomerates overlain by red massive sandstones. It has a thickness between 1 and 1.4 km and represents a system of continental fan deltas. Subordinate levels of volcanic tuff occur associated with the sandstones, and some layers of conglomerate are rich in felsic volcanogenic clasts. Further above is the Ribeirão Carvalho Formation, which consists of a 650–1000 m thick package of rhythmites, corresponding to a turbiditic system (Fig. 11.5f). This association transitions gradationally into the Ribeirão Neisse Formation, which mostly includes

immature arkosic sandstones. This unit has a thickness of *c*. 1000 m. Finally, the upper sedimentary unit is the Ribeirão do Bode Formation, a 1500 m-thick alternation of silty-argillitic and silty-sandy layers, occasionally associated with massive green siltites and polymitic conglomerates. After its deposition, the Itajaí Group was affected by the intrusion of rhyolites, grouped into the Apiúna Formation. They affect the two uppermost units of the sedimentary package, occurring as dikes and domes. Finally, the eastern portion of the basin was intruded by the Subida Granite in the early Cambrian.

Alternative lithostratigraphic divisions of the Itajaí Basin do not divide it into formations, but rather into depositional tracts (Costa and Nascimento 2015) or into facies associations ordered from A to D (Rostirolla et al. 1999; Guadagnin et al. 2010). In the case of the latter, while facies association A and B agree well to the Baú and Ribeirão Carvalho Formations described above, facies association C is described as dominated by shales and rhythmites, which would most likely correspond to the Rio do Bode Formation. This alternative column also interprets an additional unit (facies association D) characterized by the return of a prograding continental sequence mainly composed of sandstones associated with conglomerates. Basei et al. (2011b) interpret the same rocks as a tectonic recurrence of the basal Baú Formation (Fig. 11.4) and point to the similar isotopic signatures and detrital zircon pattern of both continental associations.

After deposition, the Itajaí Basin went through two phases of deformation (Basei 1985; Rostirolla et al. 1992, 1999; Schroeder 2006; Basei et al. 2011b). None of them led to transposition of the original depositional surfaces, which preserve its primary structures. The first event (D_1) is associated with the thrust tectonics responsible for juxtaposing the Brusque Group with the Itajaí Basin. It is recorded in regional open folds with an east to west to northeast to southwest orientation, coupled to the development of an oblique cleavage (Basei et al. 2011b). Furthermore, this phase also developed thrusting parallel to bedding and oblique strike-slip faults (Fig. 11.4) (Rostirolla et al. 1999). The second phase is usually associated with extensional tectonics (Fig. 11.5f), and is responsible for refolding the previous structural framework, this time with a north to south orientation, along with reactivation of previous faults (Rostirolla et al. 1999; Basei et al. 2011b). In contrast with the sedimentary succession, the rhyolites of the Apiúna Formation are affected only by the D_2 deformational phase, as indicated by its magnetic fabrics, and were therefore intruded after the D_1 event (Raposo et al. 2014).

The main source areas for the sediments of the Itajaí Basin are the rocks from the other domains of the Dom Feliciano Belt and the Luís Alves Microplate, as evidenced by isotopic signatures, detrital zircons and paleocurrent indicators (Guadagnin et al. 2010; Basei et al. 2011b; Costa and Nascimento 2015). There is, however a distinction between the provenance of the basal Baú Formation and the remaining superior sequences, reflected in contrasting whole-rock geochemical and isotopic signatures. Furthermore, the detrital record of the zircons from the lower sequence reveals a more pronounced Paleoproterozoic and Archean inheritance. Based on this evidence, Basei et al. (2011b) propose that the continental deposits from the Baú formation are mostly associated with basement rocks such as the Luís Alves Microplate and the Camboriú Complex, while in the superior sequence the Dom Feliciano Belt and its Neoproterozoic magmatism were the main source areas.

Geochronological constraints to the deposition of the Itajaí Basin derive from U-Pb zircon analyses of its detrital content, volcanic intrusions and volcanogenic components. Guadagnin et al. (2010) attribute the age of the youngest detrital zircons found in the basin, at *c*. 563 Ma, as a maximum age for the sedimentation of the basin. On the other hand, Basei et al. (2011b) interpret the volcanoclastic components of the basal Baú Formation as reworked syn-depositional volcanism, and consider its age of *c*. 595 Ma to be the lower limit for the Itajaí Basin. The intrusion of rhyolitic dikes and domes in the upper sequences of the sedimentary package establishes a minimum age to its deposition. These are dated at *c*. 550 and 560 Ma, by Guadagnin et al. (2010) and Basei et al. (2011b) respectively. This upper limit is in disagreement with Cambrian ages previously proposed for the basin, based on its limited fossil content (Paim et al. 1997). The late Subida Granite was dated by U-Pb in zircon at 520 Ma (Basei et al. 2011b).

11.2.5 Deformation History of the Dom Feliciano Belt in Santa Catarina

As this chapter aims to describe the evolution of the Dom Feliciano Belt, the previous geological history recorded in the cratonic foreland and basement inliers will not be discussed in detail here. It should be noted, however, that all basement units are characterized by widespread Paleoproterozoic magmatism and deformation (Fig. 11.5b), particularly in the period from the Rhyacian to the Orosirian (Basei et al. 2000, 2009, 2013a; Hartmann et al. 2000a, 2003a; Silva et al. 2000, 2002b, 2005b).

The first stages of deformation associated with the Neoproterozoic evolution of the Dom Feliciano Belt in Santa Catarina are characterized by a compressional regime with an important thrust component (650–620 Ma). This is most evident in the central domain, in which the transposition foliation (S_2) of the Brusque Group was developed during regional metamorphism (Philipp et al. 2004; Basei et al. 2011a). In addition, basement inliers both in the central and

in the southern domains (Camboriú and Águas Mornas complexes, respectively) were intensively reworked in this phase, generating flat-lying structures such as the gently-dipping antiform of the Camboriú Complex migmatites (Basei et al. 2000, 2013a; Bitencourt and Kruhl 2000; Philipp et al. 2004; Peternell et al. 2010; Chemale et al. 2012; Florisbal et al. 2012a, b). Geochronological constraints of this oldest event are given by the earliest Neoproterozoic melts recorded in the Camboriú and Porto Belo complexes, dated at 650–640 Ma (Chemale et al. 2012; Basei et al. 2013a). In the Brusque Group, the maximum age for the beginning of the thrust-related deformation (Fig. 11.4) is given by the syn-sedimentary metamorphosed acid volcanic rocks dated at 640 Ma (Silva et al. 2002a; Basei et al. 2011a). Conversely, this event should have ended by 620 Ma, as indicated by the intrusion of basic dikes (de Campos et al. 2012b) and by the first intrusions of transcurrent-associated granitic intrusions in the Florianópolis Batholith, along the Major Gercino Shear Zone (Passarelli et al. 2010, 2011a; Chemale et al. 2012; Florisbal et al. 2012c).

Following this initial stage, the deformation pattern transitioned to a transpressive setting (625–585 Ma). The earliest granites in the Florianópolis Batholith are associated with this period and intruded along the most significant structure of the region, the Major Gercino Shear Zone (Bitencourt and Kruhl 2000; Passarelli et al. 2010, 2011a, b; Florisbal et al. 2012b). Early stages of transcurrence in this structure indicate a transition from a convergent setting and span from 625 to 610 Ma (Passarelli et al. 2010; Chemale et al. 2012; Florisbal et al. 2012c), also recorded in limited shear zones in the Camboriú Complex basement inlier (Martini et al. 2015). Magmatism along the shear zone continued until *c*. 585 Ma (Bitencourt and Kruhl 2000; Chemale et al. 2012). The compressive component of this event is better recognized in the Brusque Group, in which the D_3 deformation phase led to the development of regional inverse folds (Basei et al. 2011a) locally evolving to transcurrent shear zones (Philipp et al. 2004). This stage of deformation in the metasupracrustal sequence is coeval with its second metamorphic phase, caused by the emplacement of large granitic intrusions between 610 and 590 Ma (Philipp et al. 2004; Basei et al. 2011a; Hueck et al. 2016, in preparation). The latter authors point out that this magmatic input led to strain localization along the intrusions. Concurrently, the latest granitic intrusions in the Florianópolis Batholith that are not associated with the Major Gercino Shear Zone are isotropic (Zanini et al. 1997; Basei et al. 2000, 2006; Bitencourt et al. 2008), indicating that the transcurrent deformation had relatively little impact outside high-strain zones. Considering a lower limit of 595 Ma for the sedimentation of the Itajaí Basin (Basei et al. 2011b), the effect of strike-slip faulting in its initial installation as advocated by Guadagnin et al. (2010) might be related to a transtensional component at the end of this stage.

Late stages of deformation are best evidenced in the thrusting that led to the placement of the Brusque Group on top of the Itajaí Basin (585–550 Ma). It corresponds to the D_1 event in the basin (Rostirolla et al. 1992, 1999; Schroeder 2006; Basei et al. 2011b) and is responsible for open folding associated with an oblique cleavage and recurrent thrusting, causing stratigraphic repetitions (Fig. 11.4). This event is constrained between the deposition of the sedimentary package of the basin and the intrusion of rhyolitic domes which were not affected by this phase (Raposo et al. 2014), dated between 560 and 550 Ma (Basei et al. 2011b; Guadagnin et al. 2010). It might correspond to the development of the D_4 deformation in the Brusque Group, characterized by abundant small folds and persistent cleavage (Fig. 11.5c) (Basei et al. 2011a). It is also synchronous to late-stage deformations along the Major Gercino Shear Zone and numerous K-Ar cooling ages from both muscovite and biotite in its associated granitic intrusions (Passarelli et al. 2010; Basei et al. 2011a).

Finally, the last significant deformation recorded in the Dom Feliciano Belt in Santa Catarina is an extensional event (550–520 Ma), responsible for the D_2 deformation recorded in the Itajaí Basin (Rostirolla et al. 1999; Basei et al. 2011b). This stage is associated with the refolding of the depositional package and the reactivation of previous faults.

11.3 Rio Grande do Sul Sector

The Dom Feliciano Belt in Rio Grande do Sul is part of the Precambrian Sul-rio-grandense Shield, an association of terranes juxtaposed in the Brasiliano orogenic cycle and composed of various geotectonic units with distinct characteristics. This wide area is bounded to the north and to the west by the Paleozoic sequences of the Paraná Basin, resting in sedimentary contact over the shield rocks, while to the east it is covered by the Cenozoic coastal sediments close to the South Atlantic shore. In its southern extremity it crops out across the national border into the Uruguayan sector of the Dom Feliciano Belt.

The Sul-rio-grandense Shield is traditionally divided into four geotectonic units, namely the Taquarembó, São Gabriel and Tijucas terranes, together with the Pelotas Batholith (Figs. 11.6 and 11.7). They are overlain by the Ediacaran to Cambrian Camaquã Basin (Chemale 2000; Philipp et al. 2016a). Each domain is separated from its neighbor by large shear zones, although not all are exposed. The Taquarembó Terrane is part of the Nico Pérez Terrane and constitutes the main foreland basement associated with the Dom Feliciano Belt in the region. On the other hand, the São Gabriel Terrane is a particularity of the Dom Feliciano Belt in Rio Grande do Sul, and corresponds to a juvenile Neoproterozoic

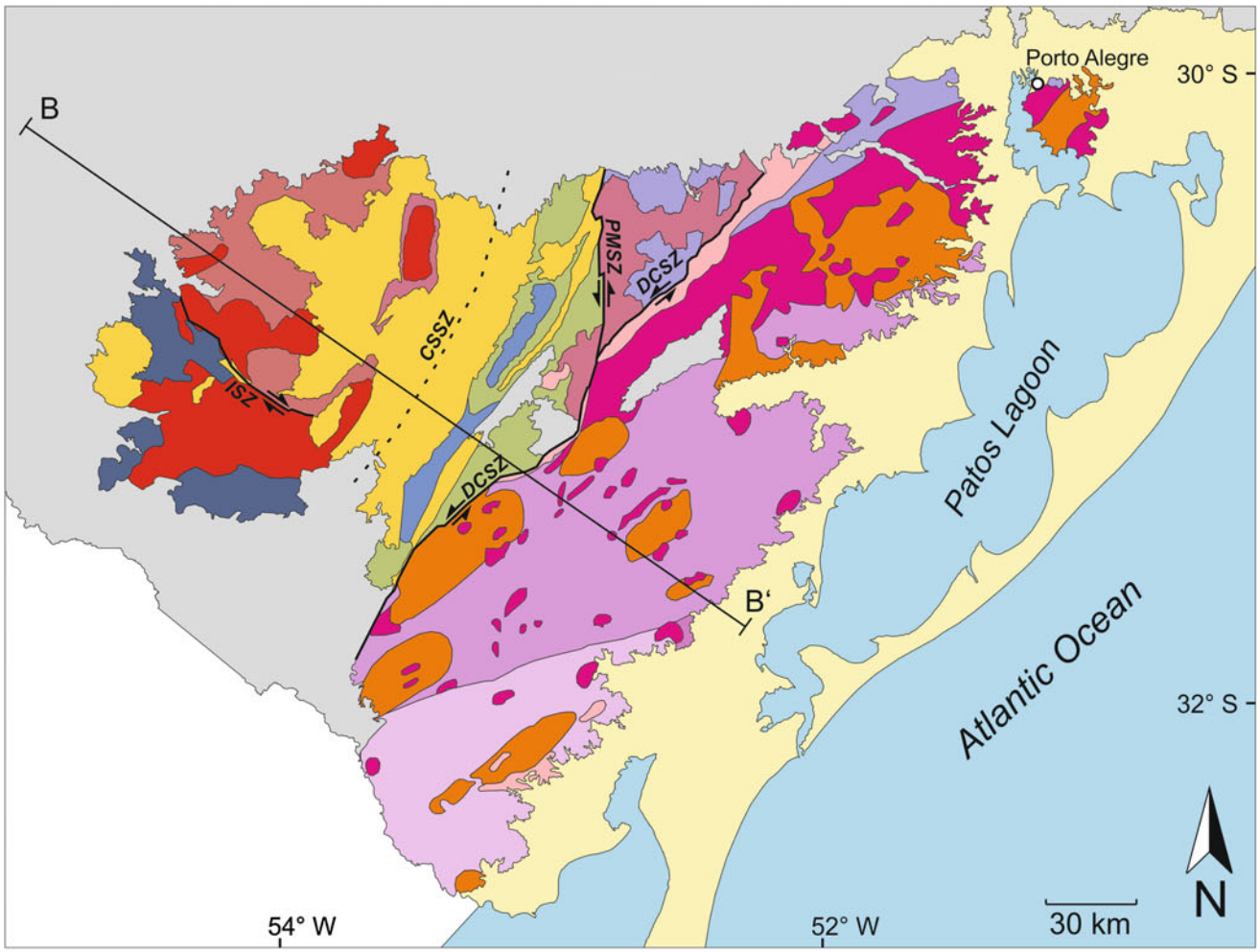

Cenozoic cover
Paraná Basin (Paleozoic-Mesozoic)
Camaquã Foreland Basin (Ediacaran)
Brasiliano granites (non-Pelotas Batholith) (630-550 Ma)
Dom Feliciano Suite
Encruzilhada do Sul and Piquiri suites
Viamão Suite
Erval Suite
Pinheiro Machado Suite
Quitéria and Cordilheira suites
Porongos Complex
São Gabriel Terrane (870-670 Ma)
Basement inliers in the Pelotas Batholith
Basement inliers in the Tijucas Terrane
Basement inliers in the Taquarembó Terrane

Neoproterozoic
Pelotas Batholith (650-550 Ma)
Paleo- to Mesoproterozoic

Shear Zones:

PMSZ - Passo do Marinheiro Shear Zone
DCSZ - Dorsal do Canguçu Shear Zone
ISZ - Ibaré Shear Zone
CSSZ - Caçapava do Sul Shear Zone

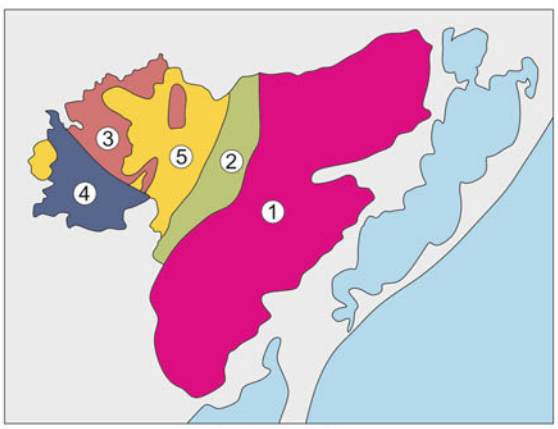

Tectonic units:

① Pelotas Batholith
② Tijucas Terrane
③ São Gabriel Terrane
④ Taquarembó Terrane
⑤ Camaquã Basin

◀ **Fig. 11.6** Simplified geological map of the Rio Grande do Sul sector of the Dom Feliciano Belt. Profile B-B′ is presented in Fig. 11.7. Modified from Wildner et al. (2006), Saalmann et al. (2011) and Philipp et al. (2016a)

terrane accreted to it during the earliest stages of the Brasiliano orogenic cycle. It contains the remnants of two magmatic arcs, besides ophiolitic sequences and metasedimentary passive margin deposits associated with its evolution.

The remaining domains roughly correspond to those recognized in the threefold division of the belt (Basei et al. 2000). The eastern domain comprises the Pelotas Batholith, part of the large granitic association that is one of the main characteristics of the orogenic belt. It is the largest unit in the Precambrian shield, corresponding to almost half of its area. The Tijucas Terrane represents the central domain of the Dom Feliciano Belt in Rio Grande do Sul, and is composed of a metavolcano-sedimentary complex associated with basement inliers, represented by Paleoproteozoic gneiss complexes. Finally, the western domain corresponds to the foreland Camaquã Basin, a thick sedimentary package with subordinate volcanic rocks deposited predominantly during the Ediacaran.

The following sections will describe the main lithostratigraphic units of each terrane, summarizing the state of the art in terms of geological knowledge. A short discussion of the shield's deformational history is also presented. A detailed description of the São Gabriel Terrane and a discussion of its significance in the Dom Feliciano Belt is presented in an individual chapter (Philipp et al. 2018), as is the Taquarembó Terrane, along with the rest of the Nico Pérez Terrane (Oyhantçabal et al. 2018). In addition, another chapter describes and discusses the main shear zones of the shield (Oriolo et al. 2018).

11.3.1 The Cratonic Foreland

11.3.1.1 Basement Inliers

Crystalline rocks of varied age are locally exposed in close connection with the new units generated during the Brasiliano orogenic cycle, representing the basement of the Dom Feliciano Belt in Rio Grande do Sul.

The basement inliers of the Tijucas Terrane are exposed in the core of large-scale antiforms known as the Santana da Boa Vista and Vigia domes. These basement rocks are composed by Paleoproterozoic TTG gneisses, the Encantadas and Vigia complexes, associated with the Statherian Seival Metagranite and the Calymmian Tupi Silveira Amphibolite (Jost 1981; Saalmann et al. 2006; Camozzato et al. 2013; Philipp et al. 2016a). The contact between these units and the metavolcano-sedimentary Porongos Complex is defined by low-angle ductile shear zones marked by mylonites, which obliterate the original stratigraphic relationships.

The Encantadas Complex is a Paleoproterozoic unit composed of tonalitic to trondhjemitic and dioritic gneisses (Fig. 11.8a) with minor amphibolite. The gneisses are metaluminous to slightly peraluminous, with medium-K calc-alkaline composition, representing a typical high-Al TTG association (Philipp et al. 2008; Lusa et al. submitted). This metamorphic complex is intruded by mylonitic monzo- and syenogranitic gneisses (Philipp et al. 2010; Lusa et al. submitted), and was metamorphosed under upper amphibolite facies conditions (Hartmann et al. 2003b; Philipp et al. 2008). The tonalitic gneisses have mostly Siderian crystallization zircon ages between 2.35 and 2.1 Ga, the intrusive

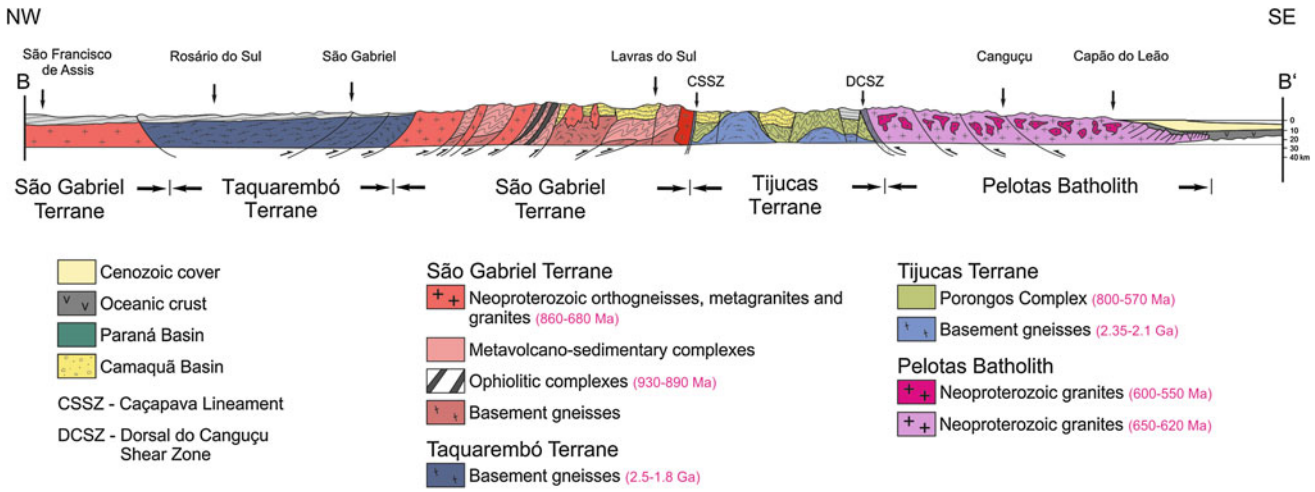

Fig. 11.7 Schematic geologic profile of the Dom Feliciano Belt in the Rio Grande do Sul sector

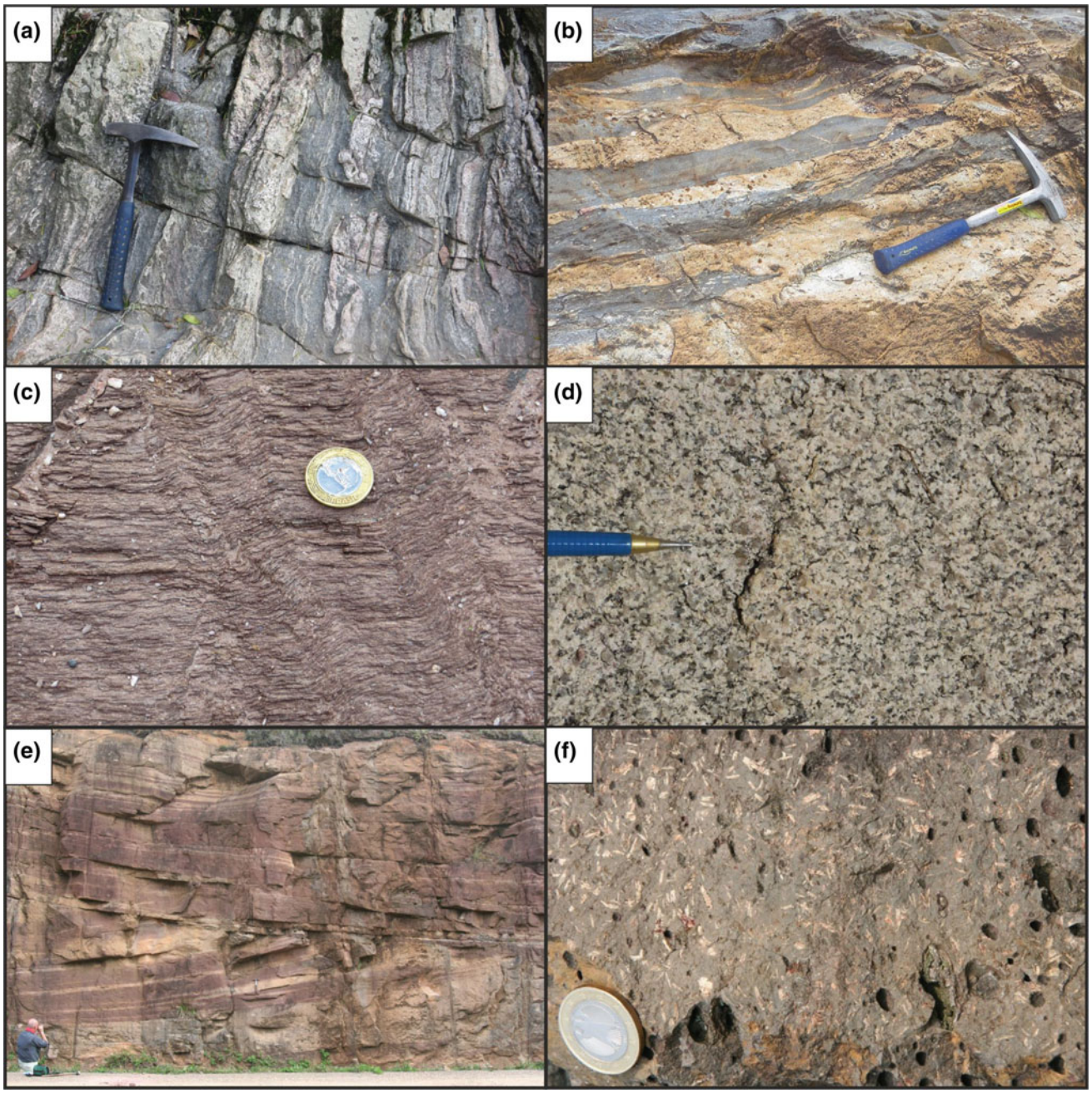

Fig. 11.8 Some field aspects of rocks from the Rio Grande do Sul sector of the Dom Feliciano Belt. **a** Banded gneiss of the Encantadas Complex; **b** Migmatitic paragneiss of the Várzea do Capivarita Complex; **c** Finely laminated phyllite of the Porongos Complex. Note the presence of kink bands representing late-stage deformation; **d** Fine- to medium-grained granite of the peraluminous Cordilheira Suite; **e** Arenites with metric cross-beddings ofthe Pedra Pintada Formation, Guaritas Group, Camaquã Basin; **f** Andesite of the Hilário Formation, Bom Jardim Group, Camaquã Basin

mylonitic gneisses present Rhyacian zircon ages varying from 2.17 to 2.15 Ga, and the metamorphism was dated in the Orosirian (2.06–2.02 Ga) (Hartmann et al. 2003b; Saalmann et al. 2011; Camozzato et al. 2013, submitted; Lusa et al., submitted).

The Vigia Complex is a Paleoproterozoic (Orosirian) unit composed of dioritic, tonalitic and trondhjemitic gneisses with subordinate amphibolite exposed at the southern portion of the Tijucas Terrane (Camozzato et al. 2013). Geochemical data indicate that these rocks are metaluminous to slightly peraluminous, with medium- to high-K calc-alkaline nature, similar to that of the Encantadas Complex (Camozzato et al. 2013, submitted). The age of this complex is constrained by LA-MC-ICPMS U-Pb crystallization ages in zircons at *c*. 2.05–2.0 Ga (Camozzato et al. 2013, submitted).

This metamorphic complex is intruded by the Seival Metagranite and by the Tupi Silveira Amphibolite. The former is a 40 × 10 km pluton elongated in the N30°E direction in the southeastern portion of the Vigia Dome. The monzogranitic to granodioritic rocks of the intrusion have a high-K calc-alkaline composition, with metaluminous to slightly peraluminous nature and trace elements characteristics similar to those of evolved arc-related associations (Camozzato et al. 2013). U-Pb LA-MC-ICPMS ages between 1.78 and 1.76 Ga place it as the only known Statherian granitic magmatism in southern Brazil (Camozzato et al. 2013, submitted; Philipp et al. 2016a). The Tupi Silveira Amphibolite crops out in the southern portion of the Vigia Dome, comprising two bodies about 1–2 km in length, elongated in the N10°E and N30°E directions. The amphibolites present a regular and continuous banding of millimetric thickness and polygonal granoblastic texture defined by plagioclase, hornblende, garnet and rare diopside. U-Pb zircon age of one sample revealed a crystallization age of 1,567 ± 21 Ma (Camozzato et al. 2013, submitted). It represents a Calymmian anorogenic magmatic event characterized by basic and ultrabasic layered complexes (Philipp et al. 2016a), to which the Capivarita Meta-anorthosite in the Pelotas Batholith might be associated (Chemale et al. 2011). After crystallization, both units were affected by collisional metamorphism under granulite facies, between c. 650 and 630 Ma (Philipp et al. 2016a, b).

Basement inliers in the Pelotas Batholith are represented by medium- to high- grade metamorphic rocks, captured as xenoliths and "roof pendants" during the ascent and emplacement of the granitic suites. Their dimensions vary from up to several kilometers across in large areas in the northern portion of the domain to enclaves of centimetric to decametric dimensions in the central and southern areas. Petrographic, geochemical and structural data for these xenoliths show that they are comparable to the adjacent metamorphic units of the Nico Pérez Terrane in RS and correlate with the basement occurring in Uruguay. The main exposures are within granites of the Encruzilhada do Sul Suite, and are xenoliths of paragneisses of the Várzea do Capivarita Complex and orthogneisses of the Arroio dos Ratos Complex (Fernandes et al. 1992).

The Arroio dos Ratos Complex is an association of orthoderived rocks, including tonalitic to granodioritic gneisses which underwent metamorphism under upper amphibolite to granulite facies conditions (Leite et al. 1998; Lima et al. 1998; Tickyj et al. 2004; Philipp and Campos 2004; Gross et al. 2006; Gregory et al. 2011, 2015; Martil et al. 2011). Three rock associations were identified in the field (Gregory et al. 2015), which are interpreted to represent successive magmatic pulses that mark the evolution of a Paleoproterozoic continental magmatic arc. Tectonic contacts separate this unit from the paraderived Várzea do Capivarita Complex. This latter complex mostly comprises pelitic migmatite (Fig. 11.8b), with subordinate calc-silicate gneiss, marble and rare quartzite (Philipp et al. 2016b). Structurally, the main S_2 foliation is a crenulation cleavage, responsible for transposing a previous S_1 banding. A later regional deformational event generated normal open F_3 folds. Both units record collisional metamorphism under upper amphibolite to granulite facies conditions (Fernandes et al. 1992; Lima et al. 1998; Gross et al. 2006; Philipp et al. 2010, 2013; Chemale et al. 2011). Based on pseudosection modeling for the paragenesis garnet-cordierite-sillimanite-biotite of the Várzea do Capivarita Complex, this metamorphism occurred at 720–820 °C and pressure of 8–9 kbar (Philipp et al. 2013).

The Capivarita Meta-anorthosite represents an intrusive association into the high-grade metamorphic rocks. The main lithology is a homogeneous light gray anorthosite, but subordinate varieties include garnet anorthosites, metagabbros and amphibolites (Philipp et al. 2010; Chemale et al. 2011). Structurally, the main foliation corresponds to that of the Várzea do Capivarita and Arroio dos Ratos complexes, and is defined by irregular and discontinuous millimeter-thick banding. This magmatism may represent an episode of continental accretion in an extensional setting during fragmentation of a supercontinent in the Early Mesoproterozoic, and is coeval with the intrusion of the Tupi Silveira Amphibolite in the Tijucas Terrane (Chemale et al. 2011; Philipp et al. 2016a).

The orthogneisses of the Arroio dos Ratos Complex have magmatic ages spreading around *c*. 2.2–2.0 Ga and juvenile signatures (Leite et al. 2000; Silva et al. 2005a; Gregory et al. 2015). The intrusion of the Capivarita Meta-anorthosite is constrained by magmatic zircon crystals dated at 1,573 ± 21 Ma (Chemale et al. 2011), with Lu–Hf model ages distributed into two clusters: from 1.81 to 2.03 Ga (εHf from +2.2 to +6.4) and from 2.55 to 2.62 Ga (εHf from −4.59 to −5.64). Neoproterozoic metamorphic overprint is recorded in all basement units between 650 and 600 Ma. Metamorphic zircon grains of gneisses from the Várzea do Capivarita Complex were dated at 620 ± 4 Ma, associated with the intrusion of a peraluminous leucogranite at 612 ± 5 Ma (Philipp et al. 2016b). Similarly, metamorphic zircon growth was dated at 631 ± 13 Ma (Silva et al. 2005a) in the Arroio dos Ratos Complex, while the Capivarita Meta-anorthosite yield metamorphic zircons dated at 606 ± 6 Ma and titanite grains with ages of 651 ± 9 and 601 ± 5 Ma (Chemale et al. 2011).

Gneissic rocks in the region of Porto Alegre have commonly been correlated with the Arroio dos Ratos Complex (Philipp and Campos 2004). Recently, however, Koester

et al. (2016) presented a Tonian U-Pb SHRIMP zircon age of 789 ± 13 Ma for the Chácara das Pedras orthogneiss, suggesting a new arc generation, similar to other signatures identified recently in the Dom Feliciano Belt (Lenz et al. 2011, 2013; Masquelin et al. 2012; Martil et al. 2017). Xenoliths of tonalitic gneiss inside the dated unit present a LA-MC-ICPMS U-Pb zircon age of 1,993 ± 25 Ma, probably related to inheritance of Arroio dos Ratos-type gneisses (Philipp et al., submitted).

11.3.2 The Metavolcano-sedimentary Complexes

The metavolcano-sedimentary complexes in Rio Grande do Sul are part of the Tijucas Terrane, which constitutes the central domain of the Dom Feliciano Belt in the region. It is elongated in the N30°–40°E direction, extending for 170 km with a width of between 15 and 30 km, in tectonic contact with the neighboring units by means of important shear zones (Chemale 2000; Philipp et al. 2016a; Oriolo et al. 2018). To the west, it is limited from the São Gabriel Terrane by the Caçapava do Sul Shear Zone, covered by the Camaquã Basin. The eastern boundary, with the Pelotas Batholith, is marked by the ductile strike-slip Dorsal do Canguçu Shear Zone. The northeastern contact of the Tijucas Terrane with the Pelotas Batholith is further affected by the brittle north to south Passo do Marinheiro Shear Zone.

The supracrustal rocks of this domain are grouped into the Porongos Complex. This comprises two distinct depositional sequences, as evidenced by petrographic, geochemical and U-Pb zircon data both in detrital crystals of metasediments and magmatic ones in metavolcanic rocks (Saalmann et al. 2006; Pertille et al. 2015a, b; Philipp et al. 2016a). The central-southern sequence is exposed in the Santana da Boa Vista, Pinheiro Machado and Hulha Negra areas and consists of a pile of quartzite, pelitic schists (Fig. 11.8c) and marble lenses, interlayered with Late Tonian metarhyolites, metadacites and meta-andesites, with subordinate ultramafic rocks (magnesian schists and serpentinites). This unit has traditionally been the most studied of the two. The schists have variable degrees of weathering, maturity and a mix of Paleoproterozoic to Neoproterozoic sources (Hartmann et al. 2004; Basei et al. 2008; Gruber et al. 2011; Pertille et al. 2015b). The lower and the dominant part of the complex were derived from the erosion of Archean, Paleo- and Mesoproterozoic sources with ages between 2.9 and 2.0 Ga, and between 1.6 and 1.0 Ga (Hartmann et al. 2004; Gruber et al. 2011; Pertille et al. 2015a, b). The first LA-MC-ICPMS U-Pb analyses in zircons of the metavolcanic rocks from Santana da Boa Vista area presented an age of 770 ± 14 Ma for a meta-andesite and 789 ± 74 Ma for a metarhyolite, with Nd T_{DM} model ages of *c*. 3.2 Ga, and later SHRIMP U-Pb zircon ages of 783 ± 6 Ma were obtained in a metarhyolite (Chemale Jr. 2000; Hartmann et al. 2000b). Recently, new SHRIMP U-Pb zircon analyses of metadacites and meta-andesites of the Santana da Boa Vista and of metarhyolites of the Piratini region yielded ages between 795 and 810 Ma (unpublished data).

On the other hand, the northern sequence, exposed in the Capané (Cachoeira do Sul) area, is younger and consists of metapelites and quartzites intercalated with Ediacaran fine-grained crystal metatuffs and metadacites intruded by alkaline granite (Marques et al. 1998a; Gollmann et al. 2008; Saalmann et al. 2011; Zvirtes et al. 2017). The metamorphism ranges from greenschist to amphibolite facies with medium pressure conditions (Jost 1981; Marques et al. 1998b). Detrital zircon ages of the Capané area range from Mesoproterozoic (pelitic schists) to Neoproterozoic ages (chlorite schist), and the whole rock geochemical parameters show mantellic affinity (Pertille et al. 2015a). However, the major Ediacaran population of zircon grains indicates exclusively reworked sources with strong similarity with the syn- to post- collisional granites of the Pelotas Batholith or with the Neoproterozoic calc-alkaline to alkaline granitic suites of the Taquarembó Terrane (Pertille et al. 2015a; Philipp et al. 2016a; Camozzato et al. submitted). Despite the mantellic affinity of the chlorite schists, the dated samples have minimum U-Pb ages of around 580 Ma. It is suggested that this part of the Porongos Complex represents a foreland basin that was deformed and metamorphosed (Pertille et al. 2015a).

11.3.3 Neoproterozoic Granite Magmatism

The Pelotas Batholith is the foremost expression of the extensive post-collisional granitic magmatism in the Dom Feliciano Belt, occupying most of the Sul-rio-grandense Shield. The Tijucas Terrane exhibits less abundant granitic intrusions, possibly associated with the main batholith. In addition, numerous granites with ages corresponding to the Dom Feliciano Belt intrude the São Gabriel and Taquarembó terranes, evidencing some degree of reworking of these domains. Their evolution, however, is more closely related to the magmatism of the Camaquã Foreland Basin, and will be discussed in the corresponding section.

11.3.3.1 Pelotas Batholith

The Pelotas Batholith is composed of a set of Upper Cryogenian to Ediacaran granite suites, generated during and after the orogenic climax of the Dom Feliciano Belt, between 650 and 550 Ma. It comprises a multi-intrusive 400 × 120 km plutonic complex including granite, diorite and gabbro, as well as rhyolitic to basaltic (Philipp and Machado 2005).

The granitic suites are elongated in the N50°–70°E direction, and their generation and emplacement were controlled by high angle ductile transcurrent shear zones (Fig. 11.7) (Fernandes et al. 1992; Philipp et al. 1993, 2002, 2003; Koester et al. 2001a, b). These structures were active during the batholith's development and are defined by mylonitic belts with subvertical foliation, accompanied by subhorizontal stretching lineation (Philipp et al. 2003). The structural evolution of the intrusive rocks suggests episodes of compressional ductile movements, followed by an extensional period with ample transcurrence. Large crustal xenoliths and roof pendants represent the basement inliers in the northern portion of the batholith, while xenoliths of schist, quartzite and marble of the Porongos Complex occur in the Herval and Pedro Osório regions.

The granitoids can be divided into an early generation of high-K calc-alkaline suites with metaluminous to peraluminous affinity, followed by alkaline magmatism and, finally, less voluminous peralkaline intrusions (Philipp and Machado 2005; Philipp et al. 2016a). High $^{87}Sr/^{86}Sr$ initial ratios and negative εNd values, with Nd T_{DM} model ages in the interval between 1.1 to 2.1 Ga, indicate anatexis of the Paleoproterozoic continental crust, associated with coeval mafic magmatism, as evidenced by mingling processes with dioritic rocks (Koester et al. 2001a, b; Philipp et al. 2003, 2007, 2013, 2016a).

The lithostratigraphic sequence of the batholith begins with the Quitéria Granite, followed by the Cordilheira Suite, Pinheiro Machado Complex, and the Viamão, Erval, Piquiri, Encruzilhada do Sul, Dom Feliciano and Itapuã suites (Koester et al. 2001a, b; Philipp et al. 2002, 2003, 2013).

The Quitéria Metagranite is the oldest granite in the batholith, with a U-Pb SHRIMP zircon age of 658 ± 4 Ma (Frantz et al. 2003). In the Quitéria region, the peraluminous granites of the Cordilheira Suite (Fig. 11.8d) have U-Pb SHRIMP zircon ages between *c*. 634 and 625 Ma (Cordilheira and Francisquinho granites) and 605 ± 8 Ma (Figueiras granite) (Frantz et al. 2003). In addition, new LA-MC-ICPMS U-Pb zircon ages of peraluminous leucogranite related to the Cordilheira Suite intrusive in migmatitic pelitic gneiss of the Várzea do Capivarita Complex indicate crystallization at 620 ± 6 Ma (Philipp et al. 2016b). Both suites are closely associated with the development of the Dorsal do Canguçu Shear Zone, and represent the early stages of formation of the Pelotas Batholith (Philipp et al. 2013, 2016a).

Following this early magmatism, the orogenic peak of the Dom Feliciano Belt was controlled by compression and new shear episodes, associated with the generation of acid to basic magmas, suggesting important anatexis. This event culminated in the generation of the granites of the Pinheiro Machado Complex and Viamão Suite. These suites present U-Pb and Pb-Pb TIMS zircon ages between 630 and 620 Ma, with the exception of the Arroio Moinho Granite, from the Viamão Suite, dated at 595 ± 1 Ma (Babinski et al. 1997; Philipp et al. 2002, 2003; Silva et al. 1997). More recent LA-MC-ICPMS U-Pb analyses yielded ages of 630 ± 6 Ma for the Viamão Granite and 627 ± 16 Ma for the Barão do Triunfo Granite (Philipp et al., submitted).

Late- to post-collisional reactivation of the shear zones between *c*. 610 and 550 Ma resulted in the emplacement of the alkaline and peralkaline Piquiri and Encruzilhada do Sul suites, and high-K calc-alkaline to alkaline granites of the Dom Feliciano Suite (Philipp et al. 2003, 2016a). Zircon crystals from syenites of the Piquiri Suite were dated by Pb-Pb evaporation TIMS method, with ages of 611 ± 3 and 612 ± 3 Ma (Philipp et al. 2002), while granites of the Encruzilhada do Sul Suite have the U-Pb TIMS zircon age of 595 ± 4 Ma (Babinski et al. 1997). New U-Pb LA-MC-ICPMS zircon analyses yielded an age of 595 ± 8 Ma for the porphyritic facies of the same granite (Philipp et al., submitted). The northern portion of the Pelotas Batholith is dominated by the voluminous post-collisional leucogranites of the Dom Feliciano Suite, emplaced at the end of the Neoproterozoic. The Ponta Grossa Granite has a U-Pb TIMS zircon age of 600 ± 9 Ma, and a pegmatoid leucogranite associated with this suite intruding basement gneisses in the Porto Alegre region yielded a crystallization age of 585 ± 6 Ma (Philipp et al., submitted).

Finally, the subvolcanic component traditionally associated with this suite is separated into the Itapuã Suite (Oliveira et al. 2001). It comprises granites, syenogranites, quartz syenites and subordinate syenites, as well as a dike swarms of comenditic rhyolite to basalt with alkaline to peralkaline affinity (Oliveira et al. 2015). A U-Pb SHRIMP zircon age of 600 ± 3 Ma was reported for the Santana Granite (Koester et al. 2001c), while new U-Pb LA-MC-ICPMS zircon data indicate ages of around 550 Ma for the felsic dikes, determining the youngest magmatism of the Pelotas Batholith (Oliveira et al. 2015; Zanon et al. submitted).

11.3.3.2 Granitic Intrusions in the Tijucas Terrane

Two groups of granite intrusions are recognized in the Tijucas Terrane. The first is represented by deformed bodies emplaced along the regional foliation of the Porongos Complex; these have a peraluminous composition, with muscovite, garnet and tourmaline. Compositional and textural characteristics suggest that they can be correlated with the Cordilheira Suite of the Pelotas Batholith (Camozzato et al. 2012). The second group of intrusions is associated with high-angle shear zones in the Capané and Candiotinha regions. They have alkaline compositions and comprise leucogranites with biotite and/or sodic pyroxene. The Capané Granite was investigated by conventional U-Pb zircon by Chemale (2000) yielding an age of 543 ± 6 Ma. More recently, new U-Pb LA-MC-ICPMS

zircon ages indicate crystallization at 589 ± 25 Ma for the Candiotinha Metagranite and 601 ± 7 Ma for the Capané Metagranite (Camozzato et al. 2013, submitted; Zvirtes et al. 2017). It is interpreted that these granites represent distinct orogenic settings: granites of the first group are coeval with collisional metamorphism, and the younger are late orogenic and associated with transcurrence along the high-angle shear zones internal to the Tijucas Terrane (Camozzato et al. 2013; Zvirtes et al. 2017).

11.3.4 The Foreland Basin

The plutonic-volcano-sedimentary Camaquã Association represents the late- to post-collisional stage of the Dom Feliciano Belt (Paim et al. 2000; Chemale 2000; Philipp et al. 2016a). The main unit of this association is the Camaquã Basin, formed by four different sedimentary and three volcano-sedimentary units. They are grouped into four depositional successions, separated from each other by angular or erosional unconformities of regional character. The basin was filled and deformed during the late stages of the Brasiliano orogenic cycle, between 620 and 540 Ma (Paim et al. 2000; Chemale 2000; Almeida et al. 2012; Janikian et al. 2012; Bicca et al. 2013; Oliveira et al. 2014).

The basin was initiated with the deposition of the Maricá Group in a marine environment. It is interpreted to correspond to a retro-arc foreland basin due to the collision of the Rio de la Plata Craton and the Encantadas microcontinent (Borba et al. 2006, 2008). This was followed by a transition between marine and lacustrine conditions during the deposition of the Bom Jardim and Santa Bárbara Groups. The former was associated with transpressive tectonics (Paim et al. 2000), while the latter marks the transition to the upper section of the Camaquã Basin, a transtensional rift basin developed when amalgamation of the shield was already completed (Bicca et al. 2013; Oliveira et al. 2014). In this context, the last sedimentary sequence, the Guaritas Group, was deposited in fluvial and lacustrine environments with aeolian facies (Fig. 11.8e).

In the last three sequences, activity of the main shear zones and extensional faults reached the mantle and lower crust levels to generate the volcanic rocks that characterize the upper Camaquã Basin. Large shoshonite to high-K calc-alkaline magmatism is represented by elongated volcanic bodies parallel to the main transcurrent fault systems. The volcanic evolution of the basin started with the eruption of volcanic rocks with tholeiitic, high-K calc-alkaline to shoshonitic compositions (Fig. 11.8f, Hilário Formation, Bom Jardim Group). Afterwards, the volcanism changed to magmas with bimodal tholeiitic to sodic alkaline signatures, as represented by the Acampamento Velho Formation, part of the Santa Barbara Group (Matté et al. 2016). Finally, alkaline basaltic volcanic rocks finish the succession (Rodeio Velho Formation, Guaritas Group) (Wildner et al. 2002; Sommer et al. 2005; Janikian et al. 2012).

Two main granitoid suites intruding into the São Gabriel and Taquarembó terranes are linked to this magmatism, first a shoshonitic to high-K calc-alkaline association followed by alkaline granites. The emplacement of the shoshonitic granitoids, such as the Lavras do Sul intrusion, is correlated with the deposition of the Bom Jardim Group. On the other hand, the sedimentary and volcanic rocks of the Santa Barbara Group are contemporaneous with the emplacement of the Acampamento Velho Formation rhyolites and high-K calc-alkaline granitoids such as the Caçapava do Sul Granite and of alkaline granitoids such as the Jaguari, Ramada, Cerro da Cria and São Sepé granites. The high-K calc-alkaline plutons have SHRIMP and LA-MC-ICPMS U-Pb ages between 598 and 570 Ma, whereas the alkaline plutons crystallized between 570 and 560 Ma (Philipp et al. 2016a).

11.3.5 Deformation History of the Dom Feliciano Belt in Rio Grande do Sul

The impact of the Dom Feliciano orogeny in the Sul-rio-grandense Shield cannot be overstated, as it was responsible for reworking most of the preceding units of the area and producing a voluminous granitogenesis that affects most of the shield. However, most domains record the evolution of previous orogenic events, representing a complex array of superposed deformational phases lasting from the Paleoproterozoic to the Early Cryogenian. As a consequence, it is sometimes difficult to separate the effect of the Dom Feliciano orogeny from earlier orogenic processes.

The initial construction of the Dom Feliciano Belt in Rio Grande do Sul is recorded in the São Gabriel Terrane, and begins with the formation of the Passinho and São Gabriel arcs during the closure of the Charrua Ocean between 890 and 680 Ma. This was followed by the collision between the arc systems and the western margin of the Nico Pérez Terrane, deforming the sedimentary rocks deposited at its western passive margin. This stage of the orogeny is discussed in detail by Philipp et al. (2018).

The main orogenic phase in the Dom Feliciano Belt comprises the Late Cryogenian and the Ediacaran periods, and can be best evaluated by analyzing the units that were generated during this period, in particular the granitic intrusions. The early evolution of the Pelotas Batholith magmatism corresponds roughly to the period from 650 to 620 Ma (Babinski et al. 1997; Silva et al. 1997; Frantz et al. 2003; Philipp et al. 2002, 2003, 2016a, b, submitted). The structural pattern observed in the granites of this period is dependent on the position relative to the different strain partition domains. Intrusions located closest to the main

shear zones, and in particular those associated with the Dorsal do Canguçu Shear Zone, have syn-deformational characteristics and indicate a transcurrent displacement, as evidenced by detail studies on both the Quitéria and Cordilheira suites, besides smaller intrusions in the same context (Fernandes et al. 1993; Philipp et al. 1993, 2016a; Tommasi et al. 1994; Fernandes and Koester 1999; Philipp and Machado 2005; Fontana et al. 2012; Knijnik et al. 2012). On the other hand, the period between 630 and 620 Ma marks the intrusion of the large Pinheiro Machado Complex and of the Erval and Viamão suites. In particular in the Pinheiro Machado Complex, most structural characteristics indicate a transpressional (oblique) deformation, with vergence to the northwest (Fernandes et al. 1992, 1993; Philipp et al. 1993; Philipp and Machado 2005).

This pattern indicates an important degree of strain partitioning in a transpressive context in the early evolution of the Dom Feliciano Belt in Rio Grande do Sul (650–620 Ma), with coeval intrusions developing different structural features according to the strain intensity under which they were emplaced (Fig. 11.7). This process is commonly interpreted to have evolved during the peak of the oblique collision that formed the Dom Feliciano Belt, which, in the case of the granitogenesis, was responsible for promoting anatexis in the continental crust and assisting the emplacement of the Pelotas Batholith (Chemale et al. 2011; Philipp et al. 2013, 2016a, b; Gregory et al. 2015).

Late-stage magmatism in Rio Grande do Sul encompasses intrusions and associated volcanism between 610 and 550 Ma (Babinski et al. 1997; Philipp et al. 2002, 2003, 2016a, submitted; Oliveira et al. 2015; Zanon et al. 2017). Intrusions related to this stage are not restricted to the Pelotas Batholith, but also occur in the Tijucas Terrane, and are coeval to the volcanic components of the Camaquã Basin and the post-collisional granitic intrusions in both the São Gabriel and Taquarembó Terranes (Philipp et al. 2016a). Reactivation of the main shear zones probably played an important role in this late-stage magmatism (Philipp et al. 2003, 2016a), as is exemplified by the Capané and Candiotinha mylonitic granitoids, intruded along shear zones in the Tijucas Terrane and dated at 600–590 Ma (Camozzato et al. 2013; Philipp et al. 2016a; Zvirtes et al. 2017). However, outside the areas directly influenced by the shear zones, rocks associated with this event are mostly isotropic.

The other major lithostratigraphic unit affected by the Dom Feliciano orogeny in Rio Grande do Sul is the metasupracrustal Porongos Complex. Some detailed structural studies of this unit propose a multistage evolution, in which the earliest deformational phases, recorded in successive isoclinal folding, would correspond to the late stages of the orogenic assembly of the São Gabriel Terrane and a tectonic interaction between this domain and the Tijucas Terrane (Saalmann et al. 2005, 2006, 2007, 2011). The same authors, however, note that the same sequence was also affected by the Dom Feliciano Belt, and recognize a phase of thrusting and stacking of the metavolcano-sedimentary sequence, followed by the development of sinistral strike-slip shear zones. As described above, this two-fold pattern is in agreement with the deformational history recorded in the Pelotas Batholith. Later deformations are also recognized (Fig. 11.8c).

11.4 Uruguay Sector

The southernmost outcrops of the Dom Feliciano Belt are exposed in eastern Uruguay over more than 300 km. The belt probably continues in the continental shelf up to the Mar del Plata Terrane, in Argentina, where it has been identified below the Paleozoic cover in the Punta Mogotes drill hole (Rapela et al. 2011). The belt is in tectonic contact to the west with the Archean–Paleoproterozoic Nico Pérez Terrane (Oyhantçabal et al. 2018) representing its cratonic foreland, while to the east the outcrops continue up to the Atlantic Ocean coastline.

The belt can be divided into two main domains, western and eastern (Figs. 11.9 and 11.10), bounded by the Sierra Ballena Shear Zone (Oriolo et al. 2016a). The Western Domain comprises the metavolcano-sedimentary association, basement inliers from the Nico Pérez Terrane and widespread Ediacaran granite intrusions. The Eastern Domain (also known as Punta del Este Terrane, Basei et al. 2011c) includes the Aiguá Batholith, the Cerro Olivo Complex and the Rocha and Sierra de Aguirre formations. The latter three units constitute a peculiarity of the Dom Feliciano Belt in Uruguay, as they are the only wide exposures of rocks to the east of the granite batholith. Widespread transcurrent shear zones are a common feature of both domains, as well as relics of foreland basin deposits. In contrast to the other sections of the Dom Feliciano Belt, however, these deposits do not constitute a single continuous domain. In this way, the Uruguayan sector differs from the traditional threefold division of the belt (Basei et al. 2000).

A general description of the main units of the belt in Uruguay is given in the next sections. Controversial aspects about stratigraphic details will be avoided when possible and focus placed on main tectonic units and their meaning for the evolution of the belt.

11.4.1 The Cratonic Foreland

In the Uruguayan sector of the Dom Feliciano Belt, the terrane that acted as cratonic foreland for the generation of the belt is known as Nico Pérez Terrane. It is exposed to the

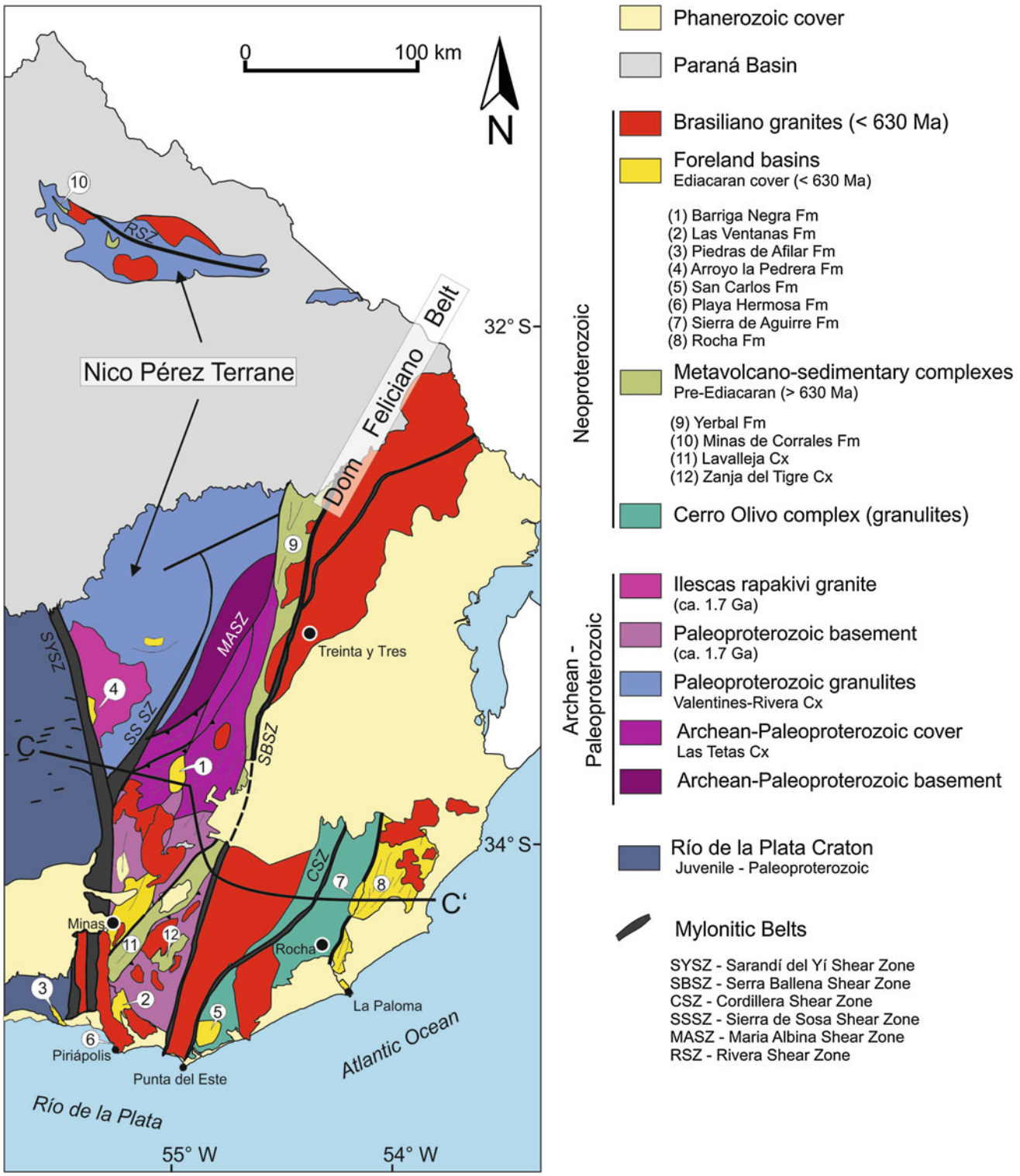

Fig. 11.9 Simplified geological map of the Uruguay sector of the Dom Feliciano Belt. Profile C-C′ is presented in Fig. 11.10. Shear Zones: SYSZ: Sarandí del Yí Shear Zone; SSSZ – Sierra de Sosa Shear Zone; MASZ: Maria Albina Shear Zone; RSZ: Rivera Shear Zone

west of the Dom Feliciano Belt in Uruguay and its western limit is the Sarandí del Yí Shear Zone, which separates it from the juvenile Paleoproterozoic Río de la Plata Craton. The Nico Pérez Terrane includes relics of Archean orthogneisses and of Archean to Paleoproterozoic supracrustal rocks, widespread areas of Paleoproterozoic orthogneisses

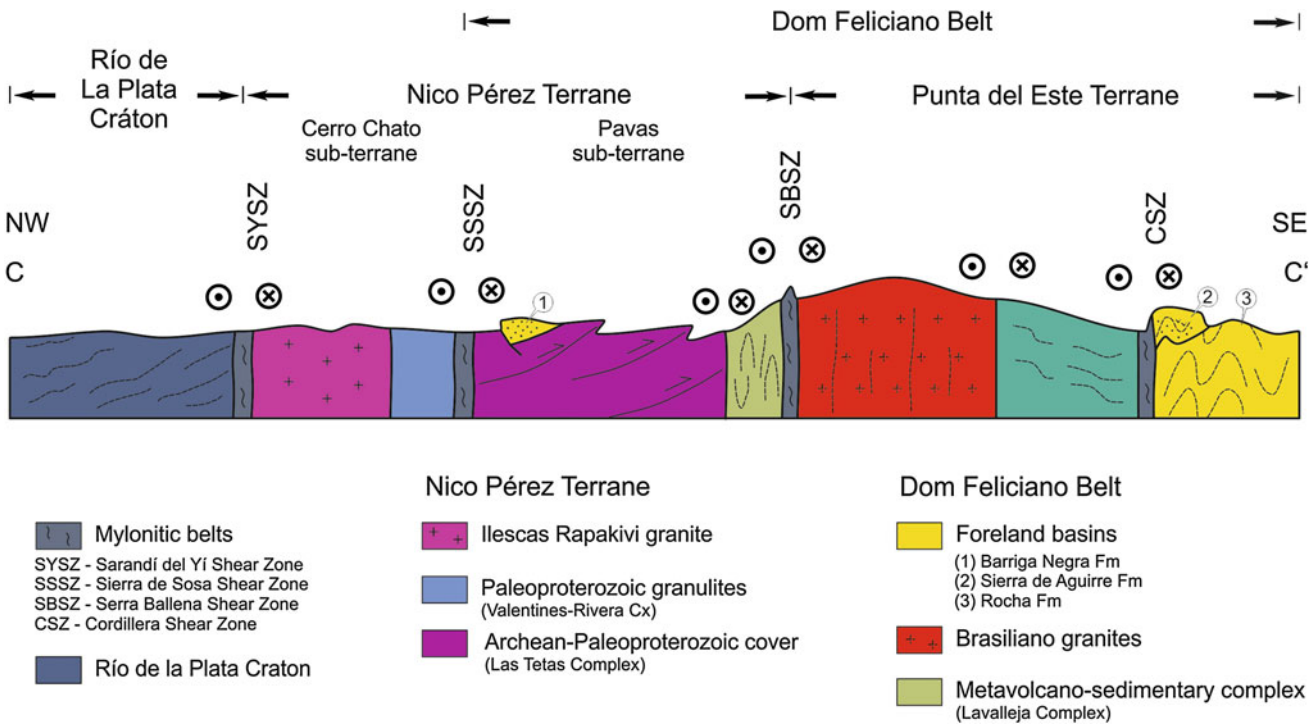

Fig. 11.10 Schematic geologic profile of the Dom Feliciano Belt in the Uruguay Sector

and a Mesoproterozoic metavolcano-sedimentary cover, and has experienced widespread reworking during the Brasiliano orogeny. This terrane is discussed in detail in an individual chapter (Oyhantçabal et al. 2018).

Another large exposure of basement rocks associated in the area is the Cerro Olivo Complex, an association of ortho- and paraderived rocks metamorphosed at high-grade conditions. They are part of the Punta del Este Terrane, which is discussed below.

The main basement inlier that can be considered a constituent part of the Dom Feliciano Belt proper in Uruguay is the Campanero Unit. It constitutes an association of orthogneisses, calc-silicatic gneisses, amphibolites, mica schists, BIFs and migmatites (Oyhantçabal 2005), and occurs in the southeastern portion of the western domain of the belt in Uruguay, south of the main expositions of the Lavalleja Complex.

11.4.2 The basement of the Punta del Este Terrane

A peculiarity of the Uruguayan sector of the Dom Feliciano Belt is the occurrence of basement rocks on the eastern side of the Aiguá Batholith, associated with a second metasedimentary association located further to the east of these rocks. The basement, known as Cerro Olivo Complex (Masquelin et al. 2012), contains high-grade metamorphic rocks comprising ortho- and paraderived granulites and migmatites (Fig. 11.11d). The orthoderived rocks yield protolith ages between c. 800 and 770 Ma, and zircon xenocrysts showing ages between c. 1.0 and 1.3 Ga. On the other hand, metamorphic overgrowths in the magmatic zircons provided ages at c. 650 Ma allowing to constrain the age of the granulite-facies metamorphism (Oyhantçabal et al. 2009; Basei et al. 2011c; Lenz et al. 2011; Masquelin et al. 2012). Similar ages in high-grade metamorphic rocks were identified in the Rio Grande do Sul sector of the Dom Feliciano Belt, in rocks associated with the basement inliers of the Pelotas Batholith (Gross et al. 2006; Koester et al. 2016; Philipp et al. 2016b; Martil et al. 2017). A continental magmatic-arc setting was suggested for the orthoderived rocks in both areas, based on their geochemistry (Lenz et al. 2011, 2013; Masquelin et al. 2012; Koester et al. 2016; Martil et al. 2017). The Cerro Olivo Complex is intruded by minor granite intrusions and is in tectonic contact with late Ediacaran folded metasediments.

11.4.3 The Metavolcano-sedimentary Complexes

The metavolcano-sedimentary complexes in Uruguay are considered to include different Mesoproterozoic to Cryogenian volcano-sedimentary successions affected by Brasiliano deformation and metamorphism, grouped by Masquelin et al. (2017) in the Lavalleja Complex. This association is up

Fig. 11.11 Some field aspects of rocks from the Uruguay sector of the Dom Feliciano Belt. **a** Compositional layering of metasediments and metabasic rocks of the Lavalleja Complex; **b** Stretched mafic enclaves in the syn-tectonic Maldonado Granite, of the Aiguá Batholith. Note the strong foliation in the rock; **c** Conglomerate of the San Carlos Formation; **d** Folded orthogneiss of the Cerro Olivo Complex; **e** Folded metasediments of the Rocha Formation; **f** Double enclave in the post-tectonic Santa Teresa Granite

to 40 km wide, and crops out in Uruguay with a north-northeast strike for more than 250 km. To the east the metavolcano-sedimentary complexes are mostly bounded by the Sierra Ballena Shear Zone, except in its southernmost part where it is in tectonic contact with the Paleoproterozoic orthogneisses of the basement inlier of the Campanero Unit.

The oldest succession of the belt is the Mesoproterozoic Zanja del Tigre Formation (Sánchez-Bettucci and Ramos 1999; Basei et al. 2008), which corresponds partially to the Parque UTE and Mina Verdún groups of Chiglino et al. (2008, 2010). This formation comprises metapelites, dolomitic marbles, metamarls, metatuffs, metagabbros and mafic and felsic metavolcanic rocks (Poiré et al. 2003, 2005; Chiglino et al. 2008, 2010; Poiré and Gaucher 2009). Interbedded volcanoclastic rocks (Fig. 11.11a) dated at 1429 ± 21 Ma (U-Pb ID-TIMS

zircon, Oyhantçabal et al. 2005) and 1461.8 ± 3.9 Ma (U-Pb SIMS in zircon; Gaucher et al. 2014a) constrain the age of these successions. Additionally, metagabbros intruding the succession yielded an age of 1492 ± 4 Ma (U-Pb ID-TIMS zircon, Oyhantçabal et al. 2005). These successions are interpreted as a Mesoproterozoic cover above the Nico Pérez Terrane, in the context of a stable platform (Oyhantçabal et al. 2018).

The age of the pre-Ediacaran Neoproterozoic successions is not well constrained. One of the best exposed areas, located northwest of the Treinta y Tres city, comprises metapelites (Yerbal Formation; Gaucher 2000) and limestones (wrongly included in the Polanco Formation by Gaucher et al. (2000); the latter is presently considered of Paleoproterozoic age, see Cabrera et al. 2014). U-Pb detrital zircon data and the ages of intrusive granites constrain the deposition between *c*. 1000 and 650 Ma (Pecoits et al. 2016). The tectonic setting for these metavolcano-sedimentary successions was probably a passive continental margin (Pecoits et al. 2016). Nevertheless, basic volcanic rocks interbedded with sediments are common in the southern part of the belt, and their geochemistry suggests the possibility of a back-arc setting (Sánchez-Bettucci and Ramos 1999) that later evolved to a passive margin.

11.4.4 Neoproterozoic Granite Magmatism

Similarly to the other section of the Dom Feliciano Belt, the orogen is characterized in Uruguay by voluminous and widespread magmatism, intruding in all domains associated with the fold belt. The biggest intrusive association is the Aiguá Batholith, the Uruguayan continuation of the granitic intrusions that also constitute the Florianópolis and Pelotas batholiths. Granitic magmatism is also common in the western domain of the belt, intruding into both the metavolcano-sedimentary complexes and its associated basement. Additional granitic intrusions also occur to the east of the Aiguá Batholith, intruding other units of the Punta del Este Terrane.

11.4.4.1 Aiguá Batholith

The central domain of the Dom Feliciano Belt in Uruguay corresponds to a large granitic area extending in a north-easterly direction from the surroundings of Punta del Este to the border with Brazil. The batholith comprises several plutons with different ages and geochemistry.

In the southern part of the Dom Feliciano Belt in Uruguay several plutons are recognized in the Aiguá batholith: Maldonado, Aiguá, Florencia, Valdivia, Puntas del Arroyo de Rocha and Cerrillos (Masquelin 1990; Spoturno et al. 2012). Most of these plutons correspond to equigranular to porphyritic biotite granites, with titanite as common accessory. A protomylonitic foliation parallel to the strike of the main shear zones of the area is frequently observed. The Florencia pluton is a very elongated and strongly deformed body (*c*. 5 × 50 km) oriented N30°E. The main lithology is a leucocratic alkali feldspar granite with biotite as the main accessory. Whole-rock geochemistry of the Aiguá pluton (Gómez Rifas 1995) indicates a highly fractioned high-K calc-alkaline signature. The Maldonado Granite (Masquelin 1990) is a strongly deformed and elongated pluton emplaced parallel to the Sierra Ballena Shear Zone (Fig. 11.11b). The most extended facies are porphyritic biotite monzogranite, granodiorite and leucogranite. The geochemical signature of the Maldonado Granite shows transitional features between highly fractionated calc-alkaline and alkaline (Oyhantçabal et al. 2007). U-Pb geochronological data in zircon for the Aiguá Batholith range from 616 to 564 Ma (Basei et al. 2000; Oyhantçabal et al. 2007; Gaucher et al. 2014; Lara et al. 2016).

Basei et al. (2000) suggest an important crustal component in the genesis of the granites of this batholith based on Sm-Nd data that yield very negative εNd between −9.8 and −12.6 and Nd T_{DM} model ages between 2.1 and 1.4 Ga. For the northern sector of the batholith, Peel et al. (2015) report U-Pb zircon ages (LA-ICP-MS) for high- K calc-alkaline granites that range from *c*. 625 Ma, interpreted as the time of initial magma generation, to *c*. 600 Ma, interpreted as the emplacement age. Nd isotopes in the same samples yielded εNd values from −4.2 to −6.4 and $^{87}Sr/^{86}Sr$ initial ratios between 0.708 and 0.718.

11.4.4.2 Granite Intrusions in the Western Domain

Numerous granite bodies are emplaced into the metavolcano-sedimentary association and in its cratonic foreland (the Nico Pérez Terrane). The ages of these intrusions range from 634 ± 7 Ma (Sierra de los Caracoles Granite, U-Pb LA-ICPMS in zircon, Lara et al. 2017) to 583 ± 7 Ma (Mangacha Granite, U-Pb SIMS in zircon, Gaucher et al. 2008). Most of these intrusions show high-K calc-alkaline, metaluminous to slightly peraluminous compositions and several of them can be classified as high Ba and Sr granites (Lara et al. 2016, 2017; Fort et al. 2016; Gallardo et al. 2016). An important crustal component and recycling of Paleoproterozoic to Late Archean sources for the genesis is indicated by intermediate $^{87}Sr/^{86}Sr$ initial ratios (0.7077–0.7090), very low initial Nd values (−15.8 to −19.3), old Nd T_{DM} model ages (2.2–2.8 Ga) and zircon inheritance ages (Lara et al. 2017). Shoshonitic granites have also been identified (Cortez Blanco pluton, Lara et al. 2016), as well as metaluminous to peralkaline intrusions associated with volcanic rocks of the Sierra de las Ánimas Complex, dated at 575–590 Ma (Oyhantçabal et al. 2007; Rapalini et al. 2015).

Most authors suggest a post-collisional environment for this high-K calc-alkaline to alkaline granitic magmatism (Oyhantçabal et al. 2007; Lara et al. 2017; Fort et al. 2016; Gallardo et al. 2016).

11.4.4.3 Granite Intrusions East of the Aiguá Batholith

The main granitic intrusions in the Punta del Este Terrane are the Santa Teresa Granite Complex (543 ± 7 Ma, U-Pb in zircon, LA ICPMS, Basei et al. 2013b) and the José Ignacio Granite (590 ± 25 Ma; 87Sr/86Sr initial ratio 0.708, Umpierre and Halpern 1971). For the Santa Teresa Complex (Fig. 11.11f), Muzio and Arthur (1999) defined a peraluminous suite, with muscovite, biotite, tourmaline, ilmenite and monazite, and a medium- to high-K calc-alkaline suite with biotite, titanite, allanite, magnetite and microgranular enclaves.

11.4.5 The Foreland Basins

The Uruguayan sector of the Dom Feliciano Belt distinguishes itself for not having a single, wide sedimentary foreland basin, such as the Itajaí and Camaquã successions in Santa Catarina and Rio Grande do Sul. Instead, the Ediacaran cover occurs as relicts covering different units throughout the Uruguayan Shield, leading to difficulties in chronostratigraphically correlating these units. This section describes the main occurrences and applies the latest nomenclature.

11.4.5.1 Playa Hermosa Formation

The Playa Hermosa Formation (Masquelin and Sánchez-Bettucci 1993) is a volcano-sedimentary unit that crops out close to the city of Piriápolis, in the southernmost Dom Feliciano Belt in Uruguay. Pazos et al. (2003) recognized two facies: a proximal association including breccias, conglomerates, sandstones and minor mudstones and a distal association with diamictites, rhythmites, sandstones and mudstones. These sedimentary facies show also evidences of glacial influence, such as dropstones and coarse-grained rhythmite intervals, representing rain-out processes from icebergs and deposition in a tectonically active basin (Pazos et al. 2003, 2011). Fambrini et al. (2003) recognized hummocky cross-stratification and consider the sedimentation to have occurred in shallow waters, probably in a shallow marine environment, but a lake environment is not ruled out.

Detrital zircons from the Playa Hermosa Formation show a main peak at 2.0 and 2.2 Ga and a secondary peak at around 600 Ma, without Archean ages (Rapalini et al. 2015; Pecoits et al. 2016). The main peak could indicate contribution of the basement of the Río de la Plata Craton (e.g., Oyhantçabal et al. 2011a), which is further supported by southwest-trending paleocurrent directions (Pazos et al. 2011).

The youngest U-Pb detrital zircon age from sediments of the Playa Hermosa Formation constrain maximum depositional age of deposition to 594 ± 16 Ma (Rapalini et al. 2015) or 563 ± 13 Ma (n = 6, Pecoits et al. 2016), while the age of the felsic dikes cutting the formation is c. 580 Ma (Rapalini et al. 2015). Evidence of interaction between magma and wet sediments, such as peperites (Sánchez-Bettucci et al. 2009), suggests that dike emplacement occurred a short time after deposition and therefore a sedimentation at c. 580 Ma is assumed. The formation can be correlated with the Maricá Formation of the Camaquã Basin from southern Brazil. Considering these age constraints, these sediments can be associated with the Gaskiers glaciation (Rapalini et al. 2015).

11.4.5.2 Barriga Negra Formation

The Barriga Negra Formation was defined by Midot (1984), Gaucher (2000), Blanco et al. (2009), Fambrini et al. (2005) and Nuñez et al. (2016) for sediments occurring in the central portion of the western domain.

According to Nuñez et al. (2016), the formation is a c. 3000 m thick volcano-sedimentary succession comprising (from bottom to top) felsic volcanic and volcanoclastic rocks, orthoconglomerates, calcareous breccia, clast-supported conglomerates, sandstones and pelites. All authors agree these deposits represent alluvial fan/braided rivers and fan-delta successions.

Detrital zircon age patterns (Blanco et al. 2009; Pecoits et al. 2016) reflect a major contribution from the basement of the Nico Pérez Terrane (main peaks at c. 0.58, 1.75, 2.1–2.2 and 2.6–3.4 Ga), and constrain the maximum age of deposition to c. 580 Ma (youngest peak age). Fambrini et al. (2005) considers this succession correlate with the Santa Bárbara Group of the Camaquã Basin in southern Brazil.

11.4.5.3 Las Ventanas Formation

The Las Ventanas Formation (Midot 1984) is a volcano-sedimentary succession comprising, from bottom to top, conglomerates, sandstones and pelites, and is exposed in the southern portion of the western domain. The association records the evolution from an alluvial fan-dominated environment to shallow marine conditions (Blanco and Gaucher 2005).

Based on the microfossil content, Blanco and Gaucher (2005) suggested an Ediacaran age, later corroborated by a 573 ± 11 Ma age in a felsic volcanoclastic rock of this unit ($^{207}Pb/^{206}Pb$ SHRIMP in zircon, Oyhantçabal et al. 2009). Detrital zircon age patterns of the Las Ventanas Formation show three main peaks at 2.7, 2.1 and 0.59 Ga (Pecoits et al. 2016), evidencing sources in the basement of the Nico Pérez Terrane. The youngest peak age is 548 ± 19 Ma, which

overlaps within error with the age obtained for the volcanoclastic rocks.

11.4.5.4 San Carlos Formation

The San Carlos Formation (Masquelin 1990) is a volcano-sedimentary sequence comprising conglomerates (Fig. 11.11c), sandstones, pelites and felsic volcanics in the southern portion of the eastern domain (Pecoits et al. 2008; Gaucher et al. 2010). Locally, a steep and strong foliation parallel to the Sierra Ballena Shear Zone is observed, especially in the westernmost outcrop area (Oyhantçabal et al. 2010). In this area, metamorphism reached at least lower greenschist facies conditions.

Detrital zircon age patterns show mainly Neoproterozoic peaks (0.55, 0.65 and 0.76 Ga) and minor Meso- and Paleoproterozoic contribution (Pecoits et al. 2008; Gaucher et al. 2010). The *c*. 0.76 and 0.65 Ga ages could represent a local source in the Cerro Olivo Complex, corresponding respectively to the igneous protolith and the high-grade metamorphism ages recorded in this basement, while older ages may correlate to inherited zircon grains recorded in the granulites of this complex (Oyhantçabal et al. 2009; Lenz et al. 2011; Masquelin et al. 2012). A maximum depositional age for the unit is constrained by a youngest zircon cluster at *c*. 552 Ma (Pecoits et al. 2016).

11.4.5.5 Sierra de Aguirre Formation

The Sierra de Aguirre Formation (Masquelin and Tabó 1988) is a volcano-sedimentary succession including felsic pyroclastic rocks, interbedded with lavas of basaltic to rhyolitic composition and siliciclastic sediments (Campal and Schipilov 2005; Fantin 2003). It is located in the central portion of the eastern domain. The succession is folded, a slaty cleavage is frequently observed, and the unit is in tectonic contact with the metasediments of the Rocha formation.

Chondrite-normalized trace-element patterns of the volcanic rocks show moderate enrichment in LILE with negative Nb anomalies and moderate enrichment in LREE with negative Eu anomalies. The age of Sierra de Aguirre is constrained by a 571 ± 8 Ma age (U-Pb—SHRIMP in zircon) in a dacitic pyroclastic rock (Hartmann et al. 2002). Campal and Schipilov (2005) have suggested a late extensional tectonic setting related to the Brasiliano orogenic cycle.

11.4.5.6 Rocha Formation

The Rocha Formation occurs as a north to northeast-striking folded belt with a width of c. 30 km east of the Cerro Olivo Complex (Sánchez-Bettucci and Burgueño 1993; Basei et al. 2011c). Blanco et al. (2014) describe the unit as a turbiditic sequence composed by sandstones, wackestones and mudstones affected by metamorphism in greenschist facies conditions (Fig. 11.11e). The maximum deposition age of the formation is constrained by the youngest detrital zircons (629 ± 17, 668 ± 20, 670 ± 18 Ma, Basei et al. 2005) and the minimum by the age of the intrusion of the Santa Teresa Granite in the transition of the Ediacaran to the Cambrian (Basei et al. 2013b). Basei et al. (2005) consider the Rocha Formation as the stratigraphic equivalent of the Oranjemund Group (Frimmel et al. 2002) split by the opening of the Atlantic Ocean.

11.4.6 Deformation History of the Dom Feliciano Belt in Uruguay

As observed in the other sectors of the Dom Feliciano Belt, most authors acknowledge two main deformation events associated with characteristic structures in the Uruguayan sector of the orogen (Oyhantçabal et al. 2009; Oriolo et al. 2016a, b; Masquelin et al. 2017). The older structures include southwest-verging northeast to southwest trending thrusts (Campal and Schipilov 1999; Oyhantçabal et al. 2009). These occur as recumbent folds with subhorizontal mylonitic foliation and a flat-lying stripped foliation, recognized in the Archean orthogneisses of the La China Complex (Masquelin et al. 2017), in the Paleoproterozoic orthogneisses of the Campanero Unit (Oyhantçabal et al. 2009) and in the quartzites and metaconglomerates of the Las Tetas Complex (Fig. 11.10). This event does not affect the late Ediacaran foreland basins, and available geochronological data from several isotopic systems allow a rough constraint on the period of 630–600 Ma (Oriolo et al. 2016a, b). This event can be correlated with the collision between the Río de la Plata and Congo cratons, leading to the reworking of the Nico Pérez cratonic foreland and the closure of the Lavalleja Complex basin.

The final architecture of the belt is controlled by younger structures including northwest-verging thrusts and north-northeast striking sinistral transcurrent shear zones, with subhorizontal stretching lineation parallel to the fold axis of the metasediments in the low-strain domains (Oyhantçabal et al. 2009; Oriolo et al. 2016a). This event affects the late Ediacaran foreland basin sequences (Figs. 11.10 and 11.11e), is well constrained by different isotopic systems in multiple minerals between 600 and 550 Ma, and is probably related to the convergence of the Kalahari Craton and the Río de la Plata-Congo cratons (Oyhantçabal et al. 2009, 2011b; Oriolo et al. 2016a).

11.5 Discussion and Final Remarks

11.5.1 Deformation Patterns in the Dom Feliciano Belt

It is evident that the main structural pattern of the Dom Feliciano Belt is the result of the transition from an early convergent setting to a later transcurrent one. This observation is not new (e.g., Fernandes et al. 1992) and has been abundantly documented, as described in the sections dedicated to each sector of the orogen. The first is responsible for the main folding phase in the metavolcano-sedimentary complexes, the nucleation of the main shear zones and the intrusion of the first granitic suites in the batholiths. The second stage is characterized by a transition to strike-slip deformation, a process that led to the reactivation of the previous shear zones associated with widespread granitic magmatism and a refolding of the metavolcano-sedimentary rocks. Some transtensional or even truly extensional episodes probably occurred during this protracted transpressional phase and were responsible of the opening of the foreland basins.

The geochronological constraints for each of these stages are well supported by extensive dating using various isotopic methods, including on granites that intruded during each phase. The initial convergent phase has been well recorded in both Santa Catarina and Rio Grande do Sul by the ages of the earliest granites associated with the belt dated at *c*. 650 Ma, and continues up to *c*. 620 Ma (Babinski et al. 1997; Silva et al. 1997; Frantz et al. 2003; Philipp et al. 2002, 2003, 2016a, b, submitted; Chemale et al. 2012; Basei et al. 2013a). In Uruguay, this stage was recorded a little later, mostly in the interval between 630 and 600 Ma (Oriolo et al. 2016a, b).

The second deformation stage is dominant from 610 Ma onwards in both Santa Catarina and Rio Grande do Sul, while in Uruguay it is recorded starting at 600 Ma (Babinski et al. 1997; Philipp et al. 2002, 2003, 2016a, submitted; Passarelli et al. 2010; Basei et al. 2011a; Oyhantçabal et al. 2011b; Chemale et al. 2012; Florisbal et al. 2012c). In Rio Grande do Sul and Uruguay this phase is commonly extended to the latest deformations and intrusions identified in the belt, up to *c*. 550 Ma, which in the latter is immediately followed by cooling to low-temperature ranges (Hueck et al. 2017). In Santa Catarina, two later phases were identified from 585 Ma onwards both in the Brusque Group and in the foreland basins (Rostirolla et al. 1992, 1999; Basei et al. 2011b; Raposo et al. 2014). The first one is compressional (585–550 Ma) and the second one is extensional (550–520 Ma).

11.5.2 Tectonic Evolution of the Dom Feliciano Belt

The popularization of modern geochronological tools in the last decades has led to the addition of abundant new data to the Dom Feliciano Belt, as reviewed in the items above. Consequently, most of the geologic processes in the orogeny have been well constrained recently, enhancing the understanding of the timing of the orogeny. Nonetheless, there is still an ongoing debate on the significance of these processes and on the tectonic evolution of the belt.

The interpretation of the tectonic significance of the Dom Feliciano Belt necessarily has to consider its entire extension. However, the discontinuous exposure of the belt, the administrative borders cut by it and the sheer size of the orogen have caused most tectonic models to focus on individual sectors. Consequently, particularities of each area may be overrepresented or underrepresented in models focusing more strongly on one of the regions, complicating the integration of the different hypotheses. This section aims to present the different evolutionary models proposed in the recent decades, highlighting their eventual similarities and differences.

The discussion will focus exclusively on the processes that led to the formation of the main domains that constitute the orogen (granite batholiths, metavolcano-sedimentary complexes, foreland basins and basement inliers). The early evolution of the cratonic blocks that acted as foreland to the collision that formed the Dom Feliciano Belt, such as the Luís Alves and Nico Pérez terranes, is the focus of individual chapters of this book (Passarelli et al. 2018; Oyhantçabal et al. 2018), as well as that of the exotic São Gabriel Terrane (Philipp et al. 2018).

From the early works on the Dom Feliciano Belt, its evolution has been tentatively interpreted in terms of tectonic processes. In the original definition of the belt, Fragoso-Cesar (1980, 1991) proposed for it a continental margin setting, in which the granitic batholiths and metavolcano-sedimentary associations would constitute a collisional continental magmatic arc and a back-arc association, respectively. This would represent the effect of the closure of the Adamastor Ocean, with subduction from east to west under the belt. This model has been very influential since its original proposition, in particular in its interpretation of the granitic belt as a collisional continental magmatic arc, still an integral part of many current models (e.g., Basei et al. 2000, 2005, 2008; Silva et al. 2005b; Passarelli et al. 2010, 2011a, b; Frimmel et al. 2011; Saalmann et al. 2011).

A more recent interpretation proposes that the granitic arc association formed on the eastern (African) side of the

system, over an east-dipping subduction zone during the closure of the Adamastor Ocean (Basei et al. 2000, 2005, 2008, 2011a; Passarelli et al. 2011a; Frimmel et al. 2011). In the later variations of this model, an initial compressional regime of the belt would have developed during the pre-collisional stage of the collision, forming the early granitic suites of the granite batholiths and the nappe development in the metavolcano-sedimentary complexes. The actual collision was oblique and caused the transition to a transpressive setting with abundant strike-slip deformation around *c*. 615 Ma, during which the remaining intrusions would have formed. A consequence of this model is the presence of an old suture zone between the granitic batholiths and the metasupracrustal associations, represented by the Major Gercino-Dorsal do Canguçu-Sierra Ballena-Lineament (Passarelli et al. 2011a). This model is in part based on contrasting isotopic signatures observed in both sides of this lineament, especially in the Santa Catarina sector (e.g., Basei et al. 2005, 2008, 2011a; Hueck et al. 2016).

An alternative conception of the Dom Feliciano Belt interprets the vast majority of the Neoproterozoic granitogenesis to correspond to post-collisional magmatism (e.g., Fernandes et al. 1992; Bitencourt and Nardi 1993, 2000; Bitencourt and Kruhl 2000; Oyhantçabal et al. 2007, 2009; Peternell et al. 2010; Florisbal et al. 2012a, b, c; Philipp et al. 2016a; Lara et al. 2017). In this model, the convergent phase of the Dom Feliciano belt represents the syn- to late-collisional stage of the orogeny, and is set from the early generations of the major batholiths, dated between 650 and 620 Ma in Brazil and 630–600 Ma in Uruguay (Frantz et al. 2003; Oyhantçabal et al. 2009; Chemale et al. 2012; Florisbal et al. 2012c; Oriolo et al. 2016a, b). This transition from a collisional to a within-plate setting led to the melting of the crustal rocks associated with the development of a system of deep shear zones, which contributed with variable contribution of mantellic material. The later transition of the deformation to a transcurrent setting promoted the development of shear zones and further granitic magmatism with more evolved continental signatures.

The models briefly exposed above have consequences in the tectonic setting of the metavolcano-sedimentary complexes. An east-dipping subduction with generation of a continental arc to the east of the metavolcano-sedimentary complex implicates in a deposition of this sequence at the passive margin of the western continent (Luís Alves or Nico Pérez), later juxtaposed along the old suture zone. This is in accordance with the setting proposed for this unit by Basei et al. (2008, 2011a). In the case of the Brusque Group, in Santa Catarina, it would agree with the suggestion that the volcanic components of the sequence correspond to the generation of oceanic crust (Basei et al. 2011a). On the other hand, alternative settings suggested for these units include back-arc basins and continental rifting without generation of oceanic crust (Philipp et al. 2004; Sánchez-Bettucci et al. 2010; de Campos et al. 2012a), both of which can be accommodated into a model proposing subduction from east to west.

The integration of the foreland basins into the tectonic models of the Dom Feliciano Belt is mostly based on correlations between the deformation observed in the basins with that of the remaining portions of the belt. Most authors consider the initial formation of the basins to represent the consequence of strike-slip tectonics within a transtensional-transpressive system (Paim et al. 2000; Borba et al. 2006, 2008; Basei et al. 2011b; Guadagnin et al. 2011; Pecoits et al. 2016), which are tentatively correlated with the second (transcurrent) deformation phase of the belt. Even later stages are responsible for folding and faulting of these sediments, an event that can be correlated with structures recognized in the metasupracrustal rocks (Rostirolla et al. 1999; Basei et al. 2011b; Masquelin et al. 2017). On the other hand, an alternative interpretation includes the same basins as part of a continental rift system developed in southern Brazil starting from 600 Ma, associated not with transpression, but with simple extensional tectonics (Almeida et al. 2010, 2012). In this interpretation, the strike-slip deformation recognized in this basin would represent later reactivation of the extensional structures, and not basin-forming processes. The implication of this model is that the Dom Feliciano Belt would have to be completely assembled and on the verge of collapse by 600 Ma.

A controversial aspect in the literature on the Dom Feliciano Belt that should be noted is the possible presence of an early arc association in the Tonian, between 800 and 770 Ma. The orthogneisses of the Cerro Olivo Complex, in the Punta del Este Terrain in Uruguay, are considered to be its main expression, but similar ages were recently recognized in zircon cores of strongly reworked basement inliers of the Pelotas Batholith in Rio Grande do Sul, associated with similar geochemical signatures (Lenz et al. 2011, 2013; Masquelin et al. 2012; Koester et al. 2016; Philipp et al. 2016a; Martil et al. 2017). One implication of this model proposed by some authors (Fernandes et al. 1995a, b; Fernandes and Koester 1999; Koester et al. 2001c) is an intraplate setting for the generation of the Pelotas Batholith, associated with the development of shear zones including the Dorsal do Canguçu Shear Zone, which would be generated by the reactivation of the old Tonian suture zone, the so-called Porto Alegre Suture.

Last, but decidedly not least, there is much debate regarding what continental blocks were involved in the assembly of the Dom Feliciano Belt. This discussion can be divided into two parts: the South American and the African sides of the collision. The South American part of the debate is straightforward, as there is some continuity between the

rocks of the belt and their foreland associations. Initially, those domains were associated with the Río de la Plata and Paranapanema Cratons. Over the years, smaller continental blocks have consistently been recognized and separated from the major structural provinces, so that now the domains that are interpreted as forelands to the Dom Feliciano Belt in South America are considered microplates accreted to the main cratonic cores: Luís Alves in Santa Catarina and Nico Pérez in Rio Grande do Sul and Uruguay (Basei et al. 2000, 2008; Oyhantçabal et al. 2011a, 2012; Saalmann et al. 2011; Oriolo et al. 2016c; Philipp et al. 2016a).

Based on isotopic data, Philipp et al. (2016a) suggest that many of the basement fragments identified in different domains of the Rio Grande do Sul sector might all correspond to pieces of a single paleocontinent, associated with the Nico Pérez Terrane (Philipp et al. 2016a). Furthermore Oriolo et al. (2016c) suggest that this terrane has similarities with the Congo Craton in Western Africa. Taken together, these evidences might indicate a setting in which many fragments of a same paleocontinent were separated in a rifting event, only to be later reworked and juxtaposed during the formation of the Dom Feliciano Belt. Some other models propose that parts of the main domains in the belt acted as individual microplates during the collision, such as the so-called Arachania Terrane (Frimmel et al. 2011), corresponding approximately to the Aiguá Batholith.

From the African side, many authors propose that the Kalahari Craton acted as foreland for the collision that generated the Dom Feliciano Belt (e.g., Basei et al. 2000, 2005, 2008, 2011c; Frimmel et al. 2011; Saalmann et al. 2011; Philipp et al. 2016a), a model endorsed by correlations proposed between the Dom Feliciano Belt and the Gariep Belt in Namibia (e.g., Basei et al. 2008). On the other hand, similarities between the crystalline basement of the Punta del Este Terrane in Uruguay and orthogneisses of the Coastal Terrane in the Kaoko Belt have led some authors to propose a link between this African belt and the Dom Feliciano Belt (e.g., Oyhantçabal et al. 2011b). Additionally, Konopásek et al. (2016) propose that the *c*. 620 and 580 Ma granitic suites of the coastal terrane of the Kako Belt represent the continuation of the Florianópolis Batholith on the African side. As a consequence, part of the evolution of the Dom Feliciano Belt would be related to a collision involving the Congo Craton while the last orogenic events are associated with a collision against the Kalahari Craton and the late Ediacaran closure of the Rocha-Gariep basin (Oyhantçabal et al. 2011b).

Oriolo et al. (2016a, 2017) propose a multistage process for the formation of the belt including all three cratonic blocks. In this model, the paleocontinents involved in the collision that formed the belt in Uruguay are the Congo Craton (from the east) and the Nico Pérez Terrane, accreted to the eastern Río de la Plata margin (from the west). This event would be responsible for the generation of the first (convergent) deformation stage of the orogeny. Afterwards, the onset of the convergence between the Congo Craton and Kalahari cratons around 600 Ma (Lehmann et al. 2016) would have triggered the transition to the transcurrent stage of deformation in the belt.

References

Almeida FFM, Amaral G, Cordani UG, Kawashita K (1973) The precambrian evolution of the South American cratonic margin, South of Amazonas River. In: Nairn ACM, Kanes WH, Stehli FG (eds) The Ocean basins and margins. Plenum, New York, pp 411–446

Almeida RP, Janikian L, Fragoso-Cesar AR, Fambrini GL (2010) The Ediacaran to Cambrian rift system of Southeastern South America: tectonic implications. J Geol 118:145–161

Almeida RP, Santos MGM, Fragoso-Cesar AR, Janikian L, Fambrini GL (2012) Recurring extensional and strike-slip tectonics after the Neoproterozoic collisional events in the Southern Mantiqueira Province. Ann Braz Acad Sci 84(2):347–376

Babinski M, Chemale F, Hartmann LA, Van Schmus WR, Silva LC (1997) U-Pb and Sm-Nd geochronology of the Neoproterozoic granitic-gneissic Dom Feliciano belt, Southern Brazil. J S Am Earth Sci 10(3–4):263–274

Basei MAS (1985) O Cinturão Dom Feliciano em Santa Catarina. Ph. D. thesis, Universidade de São Paulo, São Paulo

Basei MAS (2000) Geologia e Modelagem Geotectônica dos Terrenos Pré-Cambrianos das Regiões Sul-Oriental Brasileira e Uruguaia: Possíveis Correlações com Províncias Similares do Sudoeste Africano. IGc-USP, 124 pp

Basei MAS, Siga O Jr, Masquelin H, Harara OM, Reis Neto JM, Preciozzi F (2000) The Dom Feliciano Belt of Brazil and Uruguay and its Foreland Domain the Rio de la Plata Craton: framework, tectonic evolution and correlation with similar provinces of Southwestern Africa. In: Cordani UG, Milani EJ, Thomaz Filho A, Campos DA (eds) Tectonic evolution of South America, IGC 31, Rio de Janeiro, pp 311–334

Basei MAS, Frimmel HE, Nutman AP, Preciozzi F, Jacob J (2005) The connection between the Neoproterozoic Dom Feliciano (Brazil/Uruguay) and Gariep (Namibia/South Africa) orogenic belts. Precambr Res 139:139–221

Basei MAS, Campos Neto MC, Castro NA, Santos PR, Siga O Jr, Passarelli CR (2006) Mapa Geológico 1:100,000 das Folhas Brusque e Vidal Ramos, SC, Convênio USP-CPRM. In: XLII Congresso Brasileiro de Geologia, Aracaju, SE

Basei MAS, Frimmel HE, Nutman AP, Preciozzi F (2008) West Gondwana amalgamation based on detrital zircon ages from Neoproterozoic Ribeira and Dom Feliciano belts of South America and comparison with coeval sequences from SW Africa. In: Pankhurst RJ, Trouw RAJ, de Brito Neves BB, de Wit MJ (eds) West Gondwana: Pre-Cenozoic Correlations Across the South Atlantic Region, London. Geological Society London, Special Publication 294, pp 239–256

Basei MAS, Nutman A, Siga O Jr, Passarelli CR, Drukas CO (2009) The evolution and tectonic setting of the Luis Alves Microplate of Southeastern Brazil: an exotic terrane during the assembly of Western Gondwana. In: Gaucher C, Sial AN, Halverson GP, Frimmel HE (eds) Neoproterozoic-Cambrian tectonics, global change and evolution: a focus on southwestern Gondwana. Dev Precambr Geol 16:273–291

Basei MAS, Campos Neto MC, Castro NA, Nutman AP, Wemmer K, Yamamoto MT, Hueck M, Osako L, Siga O, Passarelli CR (2011a)

Tectonic evolution of the Brusque group, Dom Feliciano belt, Santa Catarina, Southern Brazil. J S Am Earth Sci 32(4):324–350

Basei MAS, Drukas CO, Nutman A, Wemmer PK, Dunyi L, Santos PR, Passarelli CR, Campos-Neto MC, Siga O Jr, Osako L (2011b) The Itajaí foreland basin: a tectono-sedimentary record of the Ediacaran period, Southern Brazil. Int J Earth Sci 100:543–569

Basei MAS, Peel E, Sánchez-Bettucci L, Preciozzi F, Nutman AP (2011c) The basement of the Punta del Este Terrane (Uruguay): an African Mesoproterozoic fragment at the eastern border of the South American Río de la Plata craton. Int J Earth Sci 100:289–304

Basei MAS, Campos Neto MC, Lopes AP, Nutman AP, Liu D, Sato K (2013a) Polycyclic evolution of Camboriú Complex migmatites, Santa Catarina, Southern Brazil: integrated Hf isotopic and U-Pb age zircon evidence of episodic reworking of a Mesoarchean juvenile crust. Braz J Geol 43:427–443 (São Paulo)

Basei MAS, Sánchez-Bettucci L, Peel E, Muzio R (2013b) Geocronología U-Pb LA-ICP-MS en circones del Complejo Granítico Santa Teresa, Terreno Punta del Este. VII Congreso Uruguayo de Geología, Montevideo, Proceedings, pp 30–31

Bicca MM, Chemale F Jr, Jelinek AR, Oliveira CHE, Guadagnin F, Armstrong R (2013) Tectonic evolution and provenance of the Santa Bárbara Group, Camaquã Mines region, Rio Grande do Sul, Brazil. J S Am Earth Sci 48:173–192

Bitencourt MF, Kruhl JH (2000) Crustal-scale shearing, magmatism and the development of deformation structures: an example from Santa Catarina (Southern Brazil). Zeitschrift für Angewandte Geologie SH1/2000, pp 229–236

Bitencourt MF, Nardi LSV (1993) Late- to pos-collisional Brasiliano Magmatism in the Southernmost Brazil. An Acad Bras Ciênc 65:3–16

Bitencourt MF, Nardi LVS (2000) Tectonic setting and sources of magmatism related to the Southern Brazilian shear Belt. Rev Brasil Geociênc 30:186–189

Bitencourt MF, Nardi LVS (2004) The role of xenoliths and flow segregation in the genesis and evolution of the Paleoproterozoic Itapema Granite, a crustally derived magma of shoshonitic affinity from southern Brazil. Lithos 73(1):1–19

Bitencourt MF, Bongiolo E, Philipp RP, Morales LF, Ruber RR, Melo CL, Luft JL Jr (2008) Estratigrafia do Batólito Florianópolis, Cinturão Dom Feliciano, na Região de Garopaba-Paulo Lopes, SC. Pesquisas em Geociênc 35:109–136

Blanco G, Gaucher C (2005) Estratigrafia, paleontologia y edad de la Formacion Las Ventanas (Neoproterozoico, Uruguay). Lat Am J Sedimentol Basin Anal 12(2):109–124

Blanco G, Rajesh HM, Gaucher C, Germs GJB, Chemale F Jr (2009) Provenance of the Arroyo del Soldado Group (Ediacaran to Cambrian, Uruguay): implications for the paleogeographic evolution of southwestern Gondwana. Precambr Res 171:57–73

Blanco G, Abre P, Cabrera J, Gaucher C (2014) Formación Rocha. In: Bossi J, Gaucher C (eds) Geología del Uruguay – Tomo 1: Predevónico. DIRAC, Montevideo, pp 401–408

Borba AW, Mizusaki AMP, Silva DRA, Noronha FL, Casagrande J (2006) Provenance of the Neoproterozoic Maricá Formation (Sul-rio-grandense Shield, Southern Brazil): petrographic and Sm-Nd isotopic constrains. Gondwana Res 9:464–474

Borba AW, Mizusaki AMP, Santos JOS, Mc Naughton NJ, Onoe AT, Hartmann LA (2008) U-Pb zircon and 40Ar–39Ar K-feldspar dating of syn-sedimentary volcanism of the Neoproterozoic Maricá Formation: constraining the age of foreland basin inception and inversion in the Camaquã Basin of southern Brazil. Basin Res 20:359–375

Cabrera J, Gaucher C, Frei R, Sial AN, Ferreira VP (2014) Formación Manguera Azul. In: Bossi J, Gaucher C (eds) Geología del Uruguay – Tomo 1: Predevónico. DIRAC, Montevideo, pp 191–208

Caldasso ALS, Krebs ASJ, Silva MAS, Camozzato E, Ramgrab GE (1995a) Programa de Levantamentos Geológicos Básicos 1: 100,000; Folha Brusque (SG-22-Z-D-II-1), SC. CPRM, Brasília.

Caldasso ALS, Krebs ASJ, Silva MAS, Camozzato E, Ramgrab GE (1995b) Programa de Levantamentos Geológicos Básicos 1: 100,000; Folha Botuveá (SG-22-Z-D-I-2), SC. CPRM, Brasília.

Camozzato E, Lopes RC, Philipp RP (2012) Mapa Geológico da Folha Hulha Negra (SH.22.Y-C-1), escala 1:100.000. Rio de Janeiro, Programa Levantamentos Geológicos, CPRM. vol 1, 128 p

Camozzato E, Philipp RP, Chemale F Jr (2013) Evolução Tectônica e Geocronologia U-Pb em zircão da terminação sul do Terreno Tijucas (RS, Brasil). In: VII Congreso Uruguayo de Geología, Montevideo, Resúmenes Extendidos, 7

Camozzato E, Philipp RP, Chemale Jr F. Tectonic evolution of the southern portion of the Tijucas Terrane, Dom Feliciano Belt, Brazil: the reworked border of Rio de La Plata Craton. Journal of South American Earth Sciences (submitted)

Campal N, Schipilov A (1999) The eastern edge of the Rio de la Plata Craton: a history of tangential collisions. Basement Tectonics 13:33–48

Campal N, Schipilov A (2005) La Formación Cerros de Aguirre: evidencias de magmatismo Vendiano en el Uruguay. Lat Am J Sedimentol Basin Anal 12:161–174

Castro NA, Basei MAS, Crósta AP (1999) The W(Sn-Mo) specialized Catinga and other intrusive granitoids in the Brusque group, Neoproterozoic of the state or Santa Catarina, southern Brazil. RBG 29(1):17–26

Chemale F Jr (2000) Evolução Geológica do Escudo Sul-Rio-Grandense. In: Holz M, De Ros LF (eds) Geologia do Rio Grande do Sul. Editora UFRGS, Porto Alegre, pp 13–52

Chemale F Jr, Philipp RP, Dussin I, Formoso MLL, Kawashita K, Berttotti AL (2011) Lu-Hf and U-Pb age determination of the Capivarita Anorthosite, Dom Feliciano belt, Brazil. Precambriam Res 186:117–126

Chemale F Jr, Mallmann G, Bitencourt MF, Kawashita K (2012) Time constraints on magmatism along the Major Gercino Shear Zone, southern Brazil: implications for West Gondwana reconstruction. Gondwana Res 22(1):184–199

Chiglino L, Gaucher C, Sial AN, Bossi J, Ferreira VP (2008) Chemostratigraphy of Mesoproterozoic carbonates in the Nico Pérez Terrane (Río de la Plata Craton). In: 33° International Geological Congress, Oslo, Abstracts

Chiglino L, Gaucher C, Sial AN, Bossi J, Ferreira VP, Pimentel MM (2010) Chemostratigraphy of Mesoproterozoic and Neoproterozoic carbonates of the Nico Pérez Terrane, Río de la Plata Craton, Uruguay. Precambr Res 182:313–336

Costa MS, Nascimento MS (2015) Tratos deposicionais e arquitetura estratigráfica de sucessões sedimentares da Bacia do Itajaí (Neoproterozoico), nordeste de Santa Catarina, Brasil. Geologia USP, série científica 15(2):111–134

de Campos RS, Philipp RP (2007) Petrografia e geoquímica das rochas metavulcânicas máficas e ultramáficas do Complexo Metamórfico Brusque, região da Serra da Miséria, Itapema, SC. Rev Brasil Geociênc 37(4):705–726

de Campos RS, Philipp RP, Massonne HJ, Chemale F Jr, Theye T (2012a) Petrology and isotope geology of mafic to ultramafic metavolcanic rocks of the Brusque Metamorphic Complex, southern Brazil. Int Geol Rev 54(6):686–713

de Campos RS, Philipp RP, Massonne HJ, Chemale F Jr (2012b) Early post-collisional Brasiliano magmatism in Botuverá region, Santa Catarina, southern Brazil: evidence from petrology, geochemistry, isotope geology and geochronology of the diabase and lamprophyre dikes. J S Am Earth Sci 37:266–278

Fambrini GL, Fragoso-Cesar ARS, Almeida RP, Riccomini C (2005) A Formaçao Barriga Negra (Ediacarano do Uruguai): caracterizaçao estratigráfica e correlaçao com unidades do estado do Rio Grande do Sul, Brasil. Rev Brasil Geociênc 35:515–524

Fantin M (2003) Geología de la Sierra de Aguirre, Departamento de Rocha, Uruguay. Graduation dissertation, Universidad de Buenos Aires, 92 pp

Fernandes LAA, Koester E (1999) The Neoproterozoic Dorsal de Canguqii strike-slip shear zone: its nature and role in the tectonic evolution of southern Brazil. J Afr Earth Sc 29(1):3–24

Fernandes LAD, Tommasi A, Percher CC (1992) Deformation Patterns in the southern Brazilian branch of the Dom Feliciano Belt: a reappraisal. J S Am Earth Sci 5:77–96

Fernandes LAD, Tommasi A, Vauchez A, Percher CC, Menegat R, Koester E (1993) Zona de cisalhamento transcorrente Dorsal de Canguçu: Caracterizacão e importancia na compartimentação tectônica do Cinturão Dom Feliciano. Rev Brasil Geocienc 23:1–10

Fernandes LAD, Menegat R, Costa AFU, Koester E, Porcher CC, Tommasi A, Kramer G, Ramgrab GE, Camazzoto E (1995a) Evolução Tectônica do Cinturão Dom Feliciano no Escudo Sul-riograndense: Parte I- Uma Contribuição a partir do registro geológico. Rev Brasil Geociênc 25:351–374

Fernandes LAD, Menegat R, Costa AFU, Koester E, Porcher CC, Tommasi A, Kramer G, Ramgrab GE, Camazzoto E (1995b) Evolução Tectônica do Cinturão Dom Feliciano no Escudo Sul-riograndense: Parte II- Uma Contribuição a partir do registro geofísico. Rev Brasil Geocienc 25:375–384

Florisbal LM, Bitencourt MF, Nardi LVS, Conceição RV (2009) Early postcollisional granitic and coeval mafic magmatism of medium- to high-K tholeiitic affinity within the Neoproterozoic Southern Brazilian Shear Belt. Precambr Res 175:135–148

Florisbal LM, Janasi VA, Bitencourt MF, Nardi LVS, Heaman LM (2012a) Contrasted crustal sources as defined by whole-rock and Sr–Nd–Pb isotope geochemistry of Neoproterozoic early post-collisional granitic magmatism within the Southern Brazilian Shear Belt, Camboriú, Brazil. J S Am Earth Sci 39:24–43

Florisbal LMF, Bitencourt MF, Janasi VA, Nardi LVS, Heaman LM (2012b) Petrogenesis of syntectonic granites emplaced at the transition from thrusting to transcurrent tectonics in post-collisional setting: whole-rock and Sr-Nd-Pb isotope geochemistry in the Neoproterozoic Quatro Ilhas and Mariscal granites, southern Brazil. Lithos 153:53–71

Florisbal LMF, Janasi VA, Bitencourt MF, Heaman LM (2012c) Space-time relation of post-collisional granitic magmatism in Santa Catarina, southern Brazil: U-Pb LAMC-ICP-MS zircon geochronology of coeval mafic-felsic magmatism related to the Major Gercino Shear Zone. Precambr Res 216–219:132–151

Fontana E, Nardi LVS, Bitencourt MF, Knijnik DB (2012) Caracterização geoquímica e petrogenética dos Granitoides Arroio Divisa, região de Quitéria, Rio Grande do Sul. Geologia USP, Série cientifica 12(3):3–56

Fort S, Peel E, Gallardo P (2016) Caracterización geoquímica de los Granitos Guazunambí, Policlínica y Yerbal. In: VIII Congreso uruguayo de Geología, Montevideo, Actas

Fragoso-Cesar ARS (1980) O Cráton do Rio de La Plata e o Cinturão Dom Feliciano no Escudo Uruguaio-Sul e Riograndense. In: An. XXXI Congresso Brasileiro de Geologia, Camboriú, Santa Catarina, Brazil. Anais, pp 2879–2892

Fragoso-Cesar ARS (1991) Tectônica de Placas no Ciclo Brasiliano: As orogenias dos cinturões Dom Feliciano e Ribeira no Rio Grande do Sul. Ph.D. thesis, Federal University of Rio Grande do Sul, Brazil

Frantz JC, McNaughton NJ, Marques JC, Hartmann LA, Botelho NF, Caravaca G (2003) SHRIMP U-Pb zircon ages of granitoids from southernmost Brazil: constrains on the temporal evolution of the Dorsal de Canguçu transcurrent Shear Zone and Eastern Dom Feliciano Belt. In: IV South American symposium on isotope geology, Salvador, Short Papers, pp 174–177

Frimmel HE, Fölling PG, Eriksson P (2002) Neoproterozoic tectonic and climatic evolution recorded in the Gariep Belt, Namibia and South Africa. Basin Res 14:55–67

Frimmel HE, Basei MAS, Gaucher C (2011) Neoproterozoic geodynamic evolution of SW–Gondwana: a southern African perspective. Int J Earth Sci 100:323–354

Gallardo P, Peel E, Fort S (2016) Geoquímica del Complejo Granítico Polanco (Ediacárico-Cámbrico). In: VIII Congreso uruguayo de Geología, Montevideo, Actas

Garda GM, Brentan F, Basei MAS (2013) Turmalinitos do Grupo Brusque na região entre São João Batista e Tijucas, Santa Catarina, Brasil. Geologia USP - Série Científica 13(1):73–94

Gaucher C (2000) Sedimentology, palaeontology, and stratigraphy of the Arroyo del Soldado Group (Vendian to Cambrian, Uruguay). Beringeria 26:1–120

Gaucher C, Finney SC, Poiré DG, Valencia VA, Grove M, Blanco G, Pamoukaghlián K, Gómez Peral L (2008) Detrital zircon age of Neoproterozoic sedimentary successions of Uruguay and Argentina: Insights into the geological evolution of the Río de la Plata Craton. Precambr Res 167:150–170

Gaucher C, Frei R, Frei D (2010) Detrital zircon U–Pb ages of the San Carlos Formation (latest Neoproterozoic, Uruguay) and the allochthonous nature of Arachania. In: VII South American symposium on isotope geology, Brasília, Extended Abstract, pp 556–559

Gaucher C, Frei R, Frei D, Blanco G (2014) Edad, proveniencia y paleogeografia de la Formacion San Carlos. In: Bossi J, Gaucher C (eds) Geologia del Uruguay - Tomo 1: Predevonico. UdelaR, Montevideo

Gollmann K, Marques JC, Frantz JC, Chemale F Jr (2008) Geoquímica e isótopos de Nd de rochas metavulcânicas da Antiforme Capané, Complexo Metamórfico Porongos, RS. Rev Pesquisas em Geociênc 35(2):83–95

Gómez Rifas C (1995) A Zona de Cisalhamento Sinistral "Sierra Ballena" no Uruguai. Ph.D. thesis, Universidade de São Paulo, 243 pp

Gregory TR, Bitencourt MAFS, Nardi LVS (2011) Caracterização estrutural e petrológica de metatonalitos e metadioritos do Complexo Arroio dos Ratos na sua seção-tipo, região de Quitéria, RS. Pesquisas em Geociênc 38(2):85–108

Gregory TR, Bitencourt MAFS, Nardi LVS, Florisbal LM, Chemale F Jr (2015) Geochronological data from TTG-type rock associations of the Arroio dos Ratos Complex and implications for crustal evolution of southernmost Brazil in Paleoproterozoic times. J S Am Earth Sci 57:49–60

Gross AOMS, Porcher CC, Fernandes LAD, Koester E (2006) Neoproterozoic low-pressure/high-temperature colisional metamorphic evolution in the Varzea do Capivarita Metamorphic Suite, SE Brazil: Thermobarometric and Sm/Nd evidence. Precambr Res 147:41–64

Gruber L, Porcher CC, Lens C, Fernandes LAD (2011) Proveniência dos metassedimentos das seqüências Arroio Areião, Cerro Cambará e Quartzo Milonitos no Complexo Metamórfico Porongos, Santana da Boa Vista, RS. Pesquisas em Geociênc 38(3):205–223

Guadagnin F, Chemale F Jr, Dussin IA, Jelinek AR, Santos MN, Borba ML, Justino D, Bertotti AL, Alessandretti L (2010) Depositional age and provenance of the Itajaí Basin, Santa Catarina State, Brazil: implications for SW Gondwana correlation. Precambr Res 180:156–182

Hartmann LA, Leite JAD, Silva LC, Remus MVD, McNaughton NJ, Groves DI, Fletcher IR, Santos JOS, Vasconcellos MAZ (2000a) Advances in SHRIMP geochronology and their impact on understanding the tectonic and metallogenic evolution of southern Brazil. Aust J Earth Sci 47:829–844

Hartmann LA, Porcher CC, Remus MVD (2000b) Evolução das rochas metamórficas do Rio Grande do Sul. In: Holz M, De Ros LF (eds.) Geologia do Rio Grande do Sul. Editora UFRGS, Porto Alegre, 13–52

Hartmann LA, Santos JOS, Bossi J, Campal N, Schipilov A, McNaughton NJ (2002) Zircon and titanite U-Pb SHRIMP geochronology of Neoproterozoic felsic magmatism on the eastern border of the Río de la Plata Craton, Uruguay. J S Am Earth Sci 15:229–236

Hartmann LA, Bitencourt MF, Santos JOS, McNaughton NJ, Rivera CB, Betiollo L (2003a) Prolonged Paleoproterozoic magmatic participation in the Neoproterozoic Dom Feliciano belt, Santa Catarina, Brazil, based on zircon U-Pb SHRIMP geochronology. J S Am Earth Sci 16:477–492

Hartmann LA, Santos JOS, Leite JAD, Porcher CC, McNaughton I, Neal J (2003b) Metamorphic evolution and U-Pb zircon SHRIMP geochronology of the Belizário ultramafic amphibolite, Encantadas Complex, southernmost Brazil. Anais Acad Brasil Ciências 75 (3):393–403

Hartmann LA, Philipp RP, Liu D, Wan Y, Wang Y, Santos JOS, Vasconcellos MAZ (2004) Paleoproterozoic provenance of detrital zircon, Porongos Complex quartzites, southern Brazilian Shield. Int Geol Rev 46:127–157

Heilbron M, Machado N (2003) Timing of terrane accretion in the Neoproterozoic-Eopaleozoic Ribeira orogen (SE, Brazil). Precambr Res 125(1–2):87–112

Hueck M, Basei MAS, de Castro NA (2016) Origin and evolution of the granitic intrusions in the Brusque Group of the Dom Feliciano Belt, south Brazil: Petrostructural analysis and whole-rock/isotope geochemistry. J S Am Earth Sci 69:131–151

Hueck M, Oriolo S, Dunkl I, Wemmer K, Oyhantçabal P, Schanofski M, Basei MAS, Siegesmund S (2017) Phanerozoic low-temperature evolution of the uruguayan shield along the South American passive margin. J Geol Society 174(4):609–626

Janikian L, Almeida RP, Fragoso-Cesar ARS, Martins VTS, Dantas EL, Tohver E, Mc Reath I, D'Agrella Filho MS (2012) Ages (U-Pb SHRIMP and LA-ICP-MS) and stratigraphic evolution of the Neoproterozoic volcano-sedimentary successions from extensional Camaquã Basin, Southern Brazil. Gondwana Res 21:466–482

Jost H (1981) Geology and metallogeny of the santana da boa vista region, South Brazil. PhD thesis, University of Athens, Georgia, 208p

Knijnik D, Bitencourt MF, Nardi LVS, Pinto VM, Fontana E (2012) Caracterização geoquímica e estrutural do Granodiorito Cruzeiro do Sul: magmatismo shoshonítico pós-colisional neoproterozoico em zona de transcorrência, região de Quitéria, RS. Geologia USP, Série científica 12(1):1–38

Koester E, Roisenberg A, Fernandes LAD, Soliani E Jr, Nardi LVS, Kraemer G (2001a) Petrologia dos granitóides sintectônicos à Zona de Cisalhamento Transcorrente Dorsal de Canguçu, Encruzilhada do Sul, RS. Rev Brasil Geociênc 31(2):131–140

Koester E, Fernandes LAD, Solani Jt ES, Nardi LVS, Kraemer G, Roisenberg A (2001b) Geologia e geoquímica de granitóides sintectônicos à Zona de Cisalhamento Transcorrente Dorsal do Canguçu, Encruzilhada do Sul, RS. Rev Brasil Geociênc 31(2):141–154

Koester E, Soliani E Jr, Leite JAD, Hartmann LA, Fernandes LAD, McNaughton NJ, Santos JOS, Oliveira LD (2001c) SHRIMP U-Pb age for the emplacement of the Santana Granite and reactivation of the Porto Alegre Suture, southern Brazil. J S Am Earth Sci 14:91–99

Koester E, Porcher CC, Pimentel MM, Fernandes LAD, Vignol-Lelarge ML, Oliveira LD, Ramos RC (2016) Further evidence of 777 Ma subduction-related continental arc magmatism in Eastern Dom Feliciano Belt, southern Brazil: the Chácara das Pedras Orthogneiss. J S Am Earth Sci 68:155–166

Konopásek J, Sláma J, Košler J (2016) Linking the basement geology along the Africa-South America coasts in the South Atlantic. Precambr Res 280:221–230

Lara P, Oyhantçabal P, Dadd K (2016) Post-collisional, Late Neoproterozoic, High-Ba-Sr Granitic Magmatism from the Dom Feliciano Belt and its Cratonic Foreland, Uruguay. In: VIII Congreso uruguayo de Geología, Montevideo, Actas

Lara P, Oyhantçabal P, Dadd K (2017) Post-collisional, Late Neoproterozoic, high-Ba-Sr granitic magmatism from the Dom Feliciano Belt and its cratonic foreland, Uruguay: Petrography, geochemistry, geochronology, and tectonic implications. Lithos 277:178–198

Lehmann J, Saalmann K, Naydenov KV, Milani L, Belyanin GA, Zwingmann H, Charlesworth G, Kinnaird JA (2016) Structural and geochronological constraints on the Pan-African tectonic evolution of the northern Damara belt, Namibia. Tectonics 35:103–135

Leite JAD, Hartmann LA, McNaughton NJ, Chemale F Jr (1998) SHRIMP U/Pb zircon geochronology of Neoproterozoic juvenile and crustal-reworked terranes in southernmost Brazil. Int Geol Rev 40:688–705

Leite JAD, Hartmann LA, Fernandes LAD, McNaughton NJ, Soliani E Jr, Koester E, Santos JOS, Vasconcellos MAZ (2000) Zircon U-Pb SHRIMP dating of gneissic basement of the Dom Feliciano Belt, southernmost Brazil. J S Am Earth Sci 13:739–750

Lenz C, Fernandes LAD, McNaughton NJ, Porcher CC, Masquelin H (2011) U-Pb SHRIMP ages for the Cerro Bori Orthogneisses, Dom Feliciano Belt in Uruguay: Evidences of a ~800 Ma magmatic and a ~650 Ma metamorphic event. Precambr Res 185:149–163

Lenz C, Porcher CC, Fernandes LAD, Masquelin H, Koester E, Conceição RV (2013) Geochemistry of the Neoproterozoic (800–767 Ma) Cerro Bori orthogneisses, Dom Feliciano Belt in Uruguay: tectonic evolution of an ancient continental arc. Mineral Petrol 107 (5):785–806

Lima EFL, Porcher CA, Wildner W (1998) Granulitos da região da Várzea do Capivarita – Bloco Encruzilhada do Sul, RS. Pesquisas em Geociênc 25(1):27–33

Lusa M, Philipp RP, Chemale F Jr, Archanjo C, Nardi LVS. The Paleoproterozoic (Siderian to Rhyacian) continental-arc magmatism of the Encantadas Complex, southernmost Brazil and his significance for evolution of the Rio de la Plata Craton. J S Am Earth Sci (submitted)

Marques JC, Jost H, Roisenberg A, Frantz JC (1998a) Eventos ígneos da Suíte Metamórfica Porongos na área da Antiforme Capané, Cachoeira do Sul – RS. Rev Brasil Geociênc 28:419–430

Marques JC, Jost H, Roisenberg A, Frantz JC (1998b) Rochas metassedimentares, geologia estrutural e metamorfismo da Suíte Metamórfica Porongos na área da Antiforme Capané, Cachoeira do Sul – RS. Rev Brasil Geociênc 28:467–472

Martil MMD, Bitencourt MF, Nardi LVS (2011) Caracterização estrutural e petrológica do magmatismo pré-colisional do Escudo Sul-rio- grandense: os ortognaisses do Complexo Metamórfico Várzea do Capivarita. Pesquisas em Geociênc 38(2):181–201

Martil MMD, Bitencourt MF, Nardi LVS, Koester E, Pimentel MM (2017) Pre-collisional, Neoproterozoic (ca. 790 Ma) continental arc magmatism in southern Mantiqueira Province, Brazil: geochemical and isotopic constraints from the Várzea do Capivarita Complex. Lithos 274–275:39–52

Martini A, Bitencourt MF, Nardi LVS, Florisbal LM (2015) An integrated approach to the late stages of Neoproterozoicpost-collisional magmatism from Southern Brazil: Structural geology, geochemistry and geochronology of the Corre-mar Granite. Precambr Res 261:25–39

Masquelin H (1990) Análisis estructural de las zonas de cizalla en las migmatitas de Punta del Este – Uruguay. Acta Geol Leopoldensia 30:139–158

Masquelin H, Sánchez-Bettucci L (1993) Propuesta de evolución tectono-sedimentaria para la fosa tardi-Brasliana en la región de Piriápolis, Uruguay. Rev Brasil Geocienc 23:313–322

Masquelin H, Tabó F (1988) Memoria Explicativa de la Carta Geológica del Uruguay, Hoja Chafalote, Escala 1:100.000. Dinamige-Fac. de Agron.-Fac. de H. y, Ciencias, p 20

Masquelin H, Fernandes LAD, Lenz C, Porcher CC, McNaughton NJ (2012) The Cerro Olivo complex: a pre-collisional neoproterozoic magmatic arc in eastern Uruguay. Int Geol Rev 54:1161–1183

Masquelin H, Lara HS, Betucci LS, Demarco PN, Pascual S, Muzio R, Peel E, Scaglia F (2017) Lithologies, structure and basement-cover relationships in the schist belt of the Dom Feliciano Belt in Uruguay. Braz J Geol 47(2):21–42

Matté V, Sommer CA, Lima EF, Philipp RP, Basei MAS (2016) Post-collisional Ediacaran volcanism in oriental Ramada Plateau, southern Brazil. J S Am Earth Sci 71:201–222

Midot D (1984) Etude Geologique et diagnostic Metallogenique pour l'exploration du Secteur de Minas (Uruguay).Ph.D. thesis, Universite Pierre et Marie Curie, Paris, 175 pp

Muzio R, Artur AC (1999) Petrological features of the Santa Teresa Granitic Complex Southeastern Uruguay. J S Am Earth Sci 12 (5):501–510

Nuñez P, Masquelin E, Sánchez-Bettucci L (2016) Estructura, estratigrafía, deformación y metamorfismo de la Formación Barriga Negra. In: VIII Congreso uruguayo de Geología, Montevideo, Actas

Oliveira LD, Koester E, Soliani E Jr (2001) Geoquímica das rochas graníticas pós-transcorrentes da região de Porto Alegre e Viamão, RS. Geochim Brasiliensis 15(2):65–92

Oliveira CHE, Chemale F Jr, Jelinek AR, Bicca MM, Phillip RP (2014) U-Pb and Lu-Hf Isotopes applied to the evolution of the late to post-orogenic transtensional basins of the Dom Feliciano Belt, Brazil. Precambr Res 246:240–255

Oliveira DS, Sommer CA, Philipp RP, Lima EF, Basei MAS (2015) Post-collisional subvolcanic rhyolites associated to the Neoproterozoic Batholith Pelotas, Southern Brazil. J S Am Earth Sci 63:84–100

Oriolo S, Oyhantçabal P, Wemmer K, Heidelbach F, Pfänder J, Basei MAS, Hueck M, Hannich F, Sperner B, Siegesmund S (2016a) Shear zone evolution and timing of deformation in the Neoproterozoic transpressional Dom Feliciano Belt, Uruguay. J Struct Geol 92:59–78

Oriolo S, Oyhantçabal P, Wemmer K, Basei MAS, Benowitz J, Pfänder J, Hannich F, Siegesmund S (2016b). Timing of deformation in the Sarandí del Yí Shear Zone, Uruguay: implications for the amalgamation of western Gondwana during the Neoproterozoic Brasiliano-Pan-African Orogeny. Tectonics 35. doi:https://doi.org/10.1002/2015TC004052

Oriolo S, Oyhantçabal P, Basei MAS, Wemmer K, Siegesmund S (2016c) The Nico Pérez Terrane (Uruguay): from Archean crustal growth and connections with the Congo Craton to late Neoproterozoic accretion to the Río de la Plata Craton. Precambr Res 280:147–160

Oriolo S, Oyhantçabal P, Wemmer K, Siegesmund S (2017) Contemporaneous assembly of Western Gondwana and final Rodinia break-up: implications for the supercontinent cycle. Geosci Front 8: 1431-1445

Oriolo S, Hueck M, Oyhantçabal P, Goscombe B, Wemmer K, Siegesmund S (2018) Shear Zones in Brasiliano-Pan-African Belts and Their Role in the Amalgamation and Break-Up of Southwest Gondwana. In: S. Siegesmund et al. (eds) Geology of southwest gondwana, Regional geology reviews, Springer, Heidelberg, pp 593–613

Oyhantçabal P (2005) The Sierra Ballena shear zone: kinematics, timing and its significance for the geotectonic evolution of southeast Uruguay. Ph.D. thesis, Georg–August–Universität Göttingen

Oyhantçabal P, Sánchez-Bettucci L, Pecoits E, Aubet N, Preciozzi F, Basei MAS (2005) Nueva propuesta estratigráfica para las supracorticales del Cinturón Dom Feliciano (Proterozoico, Uruguay). In: XII Congreso Latinoamericano de Geología, Quito, Abstracts

Oyhantçabal P, Siegesmund S, Wemmer K, Robert F, Lyer P (2007) Post-collisional transition from calc-alkaline to alkaline magmatism during transcurrent deformation in the southernmost Dom Feliciano Belt (Braziliano–Pan-African, Uruguay). Lithos 98:141–159

Oyhantçabal P, Siegesmund S, Wemmer K, Presnyakov S, Layer P (2009) Geochronological constraints on the evolution of the southern Dom Feliciano Belt (Uruguay). J Geol Soc London 166:1075–1084

Oyhantçabal P, Siegesmund S, Wemmer K, Layer P (2010) The Sierra Ballena Shear Zone in the southernmost Dom Feliciano Belt (Uruguay): evolution, kinematics, and deformation conditions. Int J Earth Sci. https://doi.org/10.1007/s00531-009-0453-1

Oyhantçabal P, Siegesmund S, Wemmer K (2011a) The Río de la Plata Craton: a review of units, boundaries, ages and isotopic signature. Int J Earth Sci 100:201–220

Oyhantçabal P, Siegesmund S, Wemmer K, Passchier CW (2011b) The transpressional connection between Dom Feliciano and Kaoko Belts at 580–550 Ma. Int J Earth Sci 100:379–390

Oyhantçabal P, Wegner-Eimer M, Wemmer K, Schulz B, Frei R, Siegesmund S (2012) Paleo- and Neoproterozoic magmatic and tectonometamorphic evolution of the Isla Cristalina de Rivera (Nico Pérez Terrane, Uruguay). Int J Earth Sci 101:1745–1762

Oyhantçabal P, Oriolo S, Philipp RP, Wemmer K, Siegesmund S (2018) The Nico Pérez Terrane of Uruguay and Southeastern Brazil. In: S. Siegesmund et al. (eds) Geology of southwest gondwana, Regional geology reviews, Springer, Heidelberg, pp 161–187

Paim PSG, Leipnitz II, Rosa ANZ, Rosa AAS (1997) Preliminary report on the occurrence of Chancelloria sp. In the Itajaí Basin, southern Brazil. Rev Brasil Geociênc 27(3):303–308

Paim PSG, Chemale F Jr, Lopes C (2000) A Bacia do Camaquã. In: Holz M, de Ros LF (eds) Geologia do Rio Grande do Sul. CIGO/UFRGS, Porto Alegre, pp 231–274

Passarelli CR, Basei MAS, Siga O Jr, Mc Reath I, Campos Neto MC (2010) Deformation and geochronology of syntectonic granitoids emplaced in the major Gercino Shear zone, southeastern South America. Gondwana Res 17:688–703

Passarelli CR, McReath I, Basei MAS, Siga O Jr, Campos Neto MC (2011a) Heterogeneity in syntectonic granitoids emplaced in a major shear zone, southern Brazil. J S Am Earth Sci 32:369–378

Passarelli CR, Basei MAS, Wemmer K, Siga O Jr, Oyhantçabal P (2011b) Major shear zones of southern Brazil and Uruguay: escape tectonics in the eastern border of Rio de La Plata and Paranapanema cratons during the Western Gondwana amalgamation. Int J Earth Sci (Geol. Rundsch) 100:391–414

Passarelli C.R, Basei MAS, Siga Jr. O, Harara MM (2018) The Luis Alves and Curitiba Terranes: Continental Fragments in the Adamastor Ocean. In: S. Siegesmund et al. (eds) Geology of southwest gondwana, Regional geology reviews, Springer, Heidelberg, pp 189–215

Pazos PJ, Sánchez-Bettucci L, Tofalo OR (2003) The record of the Varanger glaciation at the Río de la Plata craton, Vendian-Cambrian of Uruguay. Gondwana Res 6(1):65–77

Pazos P, Rapalini A, Sánchez-Bettucci L, Tófalo R (2011) The Playa Hermosa Formation, Playa Verde Basin, Uruguay. Geol Soc London Mem 36:547–553

Pecoits E, Gingras M, Aubet N, Konhauser K (2008) Ediacaran in Uruguay: palaeoclimatic and palaebiological implications. Sedimentology 55:689–719

Pecoits E, Aubet NR, Heaman LM, Philippot P, Rosière CA, Veroslavsky G, Konhauser KO (2016) U-Pb detrital zircon ages from some Neoproterozoic successions of Uruguay: Provenance, stratigraphy and tectonic evolution. J S Am Earth Sci 71:108–130

Pertille J, Hartmann LA, Philipp RP, Petry TS, Lana CC (2015a) Origin of the Ediacaran Porongos Group, Dom Feliciano Belt, southern

Brazilian Shield, with emphasis on whole rock and detrital zircon geochemistry and U-Pb, Lu-Hf isotopes. J S Am Earth Sci 64:69–93

Pertille J, Hartmann LA, Philipp RP (2015b) Zircon U-Pb age constraints on the Paleoproterozoic sedimentary basement of the Ediacaran Porongos Group, Sul-Riograndense Shielf, southern Brazil. J S Am Earth Sci 63:334–345

Peel E, Muzio R, Basei MAS (2015) U-Pb zircon ages and Sr-Nd isotopic composition of neoproterozoic magmatism, Dionisio-Sierra de los Ríos block, NE Uruguay. Goldschmidt Abstracts 2015:2442

Peternell M, Bitencourt MF, Kruhl JH, Stäb C (2010) Macro and microstructures as indicators of the development of syntectonic granitoids and host rocks in the Camboriú region, Santa Catarina, Brazil. J S Am Earth Sci 29:738–750

Philipp RP, Campos RS (2004) Geologia, Petrografia e Litogeoquímica dos Gnaisses Porto Alegre, RS, Brasil: Implicações Geotectônicas. Rev Pesquisas em Geociênc 31(2):79–94

Philipp RP, Campos RS (2010) Granitos peraluminosos intrusivos no Complexo Metamórfico Brusque: registro do magmatismo relacionado a colisão neoproterozóica no Terreno Tijucas, Itapema (SC). Rev Brasil Geociênc 40(3):303–320

Philipp RP, Machado R (2005) The Neoproterozoic to Cambrian granitic magmatism of the Pelotas Batholith, southern Brazil. J S Am Earth Sci 19:461–478

Philipp RP, Mesquita MJM, Gomes MEB, Almeida DPM (1993) Reconhecimento estrutural e geoquímico dos granitóides brasilianos da região de Pelotas-RS. Pesquisas em Geociênc 20(1):3–13

Philipp RP, Machado R, Nardi LVS, Lafon JM (2002) O magmatismo granítico Neoproterozóico do Batólito Pelotas no sul do Brasil: novos dados e revisão de geocronologia regional. Rev Brasil Geociênc 32(2):277–290

Philipp RP, Machado R, Chemale F Jr (2003) Reavaliação e novos dados geocronológicos (Ar/Ar, Rb/Sr e Sm/Nd) do Batólito Pelotas no Rio Grande do Sul: implicações petrogenéticas e idade de reativação das zonas de cisalhamento. Geol USP, Série Científica 3:71–84

Philipp RP, Mallmann G, Bitencourt MF, Souza ER, Souza MMA, Liz JD, Wild F, Arendt S, Oliveira A, Duarte L, Rivera CB, Prado M (2004) Caracterização litológica e evolução metamórfica da porção leste do Complexo Metamórfico Brusque, Santa Catarina. Rev Brasil Geociênc 34:21–34

Philipp RP, Machado R, Chemale F Jr (2007) A Geração dos granitóides Neoproterozóicos do Batólito Pelotas: evidências dos isótopos de Sr e Nd e implicações para o crescimento continental da porção sul do Brasil. In: Ianuzzi R, Frantz JC (eds) 50 anos de Geologia, Instituto de Geociências, Contribuições, Comunicação e Identidade-CIGO, Porto Alegre, vol 1, pp 59–77

Philipp RP, Lusa M, Nardi LVS (2008) Geochemistry and petrology of dioritic, tonalitic and trondhjemitic gneisses from Encantadas Complex, Santana da Boa Vista, southernmost Brazil: a Paleoproterozoic continental-arc magmatism. An Acad Bras Ciênc 80:1–14

Philipp RP, Dussin I, Formoso MLL, Chemale F Jr, Campos RS (2010) Estruturas primárias e tectônicas do Anortosito Capivarita, Pântano Grande (RS): significado e implicações na sua evolução petrogenética. Rev Brasil Geociênc 40(1):99–110

Philipp RP, Massonne HJ, de Campos RS (2013) Peraluminous leucogranites of the Cordilheira Suite: a record of Neoproterozoic collision and the generation of the Pelotas Batholith, Dom Feliciano Belt, Southern Brazil. J S Am Earth Sci 43:8–24

Philipp RP, Pimentel MM, Chemale F Jr (2016a) Tectonic evolution of the Dom Feliciano Belt in Southern Brazil: Geological relationships and U-Pb geochronology. Braz J Geol 46(1):83–104

Philipp RP, Bom FM, Pimentel MM, Junges SL, Zvirtes G (2016b) SHRIMP U-Pb age and high temperature conditions of the collisional metamorphism in the Varzea do Capivarita Complex: implications for the origin of Pelotas Batholith, Dom Feliciano Belt, southern Brazil. J S Am Earth Sci 66:196–207

Philipp RP, Pimentel MM, Basei MAS (2018) The Tectonic Evolution of the São Gabriel Terrane, Dom Feliciano Belt, Southern Brazil: The Closure of the Charrua Ocean. In: S. Siegesmund et al. (eds) Geology of southwest gondwana, Regional geology reviews, Springer, Heidelberg, pp 243–265

Philipp RP, Jelinek AR, Chemale F Jr. Post-collisional neoproterozoic magmatism of the Pelotas Batholith, Dom Feliciano Belt, RS, southernmost Brazil. Int Geol Rev (submitted)

Poiré D, Gaucher C (2009) Lithostratigraphy. Neoproterozoic-Cambrian evolution of the Río de la Plata Paleocontinent. Dev Precambr Geol 16:87–101

Poiré DG, González PD, Canalicchio JM, García Repetto F (2003) Litoestratigrafía y estromatolitos de la sucesión sedimentaria Precámbrica de la cantera Mina Verdún, Minas, Uruguay. Rev Soc Uruguaya Geol 1:108–123 (Publicación Especial)

Poiré DG, González PD, Canalicchio JM, García Repetto F (2005) Estratigrafía del Grupo Mina Verdún, Proterozoico de Minas, Uruguay. Lat Am J Sedimentol Basin Anal 12(2):125–143

Porada H (1989) Pan-African rifting and orogenesis in southern to equatorial Africa and eastern Brazil. Precambr Res 44:103–136

Rapalini AE, Tohver E, Sánchez-Bettucci L, Lossada AC, Barcelona H, Pérez C (2015) The late Neoproterozoic Sierra de las Ánimas Magmatic Complex and Playa Hermosa Formation, southern Uruguay, revisited: Paleogeographic implications of new paleomagnetic and precise geochronologic data. Precambr Res 259:143–155

Rapela CW, Fanning CM, Casquet C, Pankhurst RJ, Spalletti L, Poiré D, Baldo EG (2011) The Río de la Plata craton and the adjoining Pan-African/brasiliano terranes: their origins and incorporation into south-west Gondwana. Gondwana Res 20:673–690

Raposo MI, Drukas CO, Basei MAS (2014) Deformation in rocks from Itajaí basin, Southern Brazil, revealed by magnetic fabrics. Tectonophysics 629:290–302

Rostirolla SP, Alckmin FF, Soares PC (1992) O Grupo Itajaí, Estado de Santa Catarina, Brasil, exemplo de sedimentação em uma bacia flexural de antepaís. Bol Geociênc Petrobrás 6(3/4):109–122

Rostirolla SP, Ahrendt A, Soares PC, Carmingnani L (1999) Basin analysis and mineral endowment of the Proterozoic Itajaí Basin, south-east Brazil. Basin Res 11:127–142

Saalmann K, Hartmann LA, Remus MVD (2005) Tectonic evolution of two contrasting schist belts in southernmost Brazil, a plate tectonic model for the Brasiliano Orogeny. Int Geol Rev 47:1234–1259

Saalmann K, Remus MVD, Hartmann LA (2006) Structural evolution and tectonic setting of the Porongos belt, southern Brazil. Geol Mag 143:59–88

Saalmann K, Hartmann LA, Remus MVD (2007) The assembly of West Gondwana—The view from the Rio de la Plata craton. In: Linnemann U, Nance RD, Kraft P, Zulauf G (eds) The evolution of the Rheic Ocean: from Avalonian-Cadomian active margin to Alleghenian-Variscan collision. Geological Society of America Special Paper 423, pp 1–26

Saalmann K, Gerdes A, Lahaye Y, Hartmann LA, Remus MVD, Läufer A (2011) Multiple accretion at the eastern margin of the Rio de la Plata craton: the prolonged Brasiliano orogeny in southernmost Brazil. Int J Earth Sci 100:355–378

Sánchez-Bettucci LS, Burgueño AM (1993) Análisis Sedimentológico y Faciológico de la Formación Rocha (ex-Grupo Rocha). Rev Brasil Geocienc 23(3):323–329

Sánchez-Bettucci L, Ramos VA (1999) Aspectos geológicos de las rocas metavolcánicas y metasedimentarias del Grupo Lavalleja, sudeste de Uruguay. Rev Brasil Geociênc 29(4):557–570

Sánchez-Bettucci L, Koukharsky M, Pazos PJ, Stareczek S (2009) Neoproterozoic subaqueous extrusive–intrusive rocks in the Playa Hermosa formation in Uruguay: regional and stratigraphic significance. Gondwana Res 16(1):134–144

Sánchez-Bettucci L, Peel E, Masquelin H (2010) Neoproterozoic tectonic synthesis of Uruguay. Int Geol Rev 52(1):51–78

Schroeder GS (2006) Análise tectônica da Bacia do Itajaí. Mastership dissertation. Universidade Federal do Rio Grande do Sul, Porto Alegre

Silva LC (1991) O cinturão metavulcanossedimentar Brusque e a evoluç ão policíclica das faixas dobradas proterozóicas no sul do Brasil: uma revisão. Rev Brasil Geociênc 21:60–73

Silva LC, Dias AA (1981) Projeto Timbó-Barra Velha. DNPM/CPRM Internal Report, Porto Alegre, Brazil

Silva LC, Hartmann LA, McNaughton NJ, Fletcher IR (1997) SHRIMP U/Pb zircon dating of Neoproterozoic granitic magmatism and collision in the Pelotas batholith, southernmost Brazil. Int Geol Rev 41:531–551

Silva LC, Hartmann LA, McNaughton NJ, Fletcher I (2000) Zircon U-Pb SHRIMP dating of a Neoproterozoic overprint in Paleoproterozoic granitic-gneissic terranes, southern Brazil. Am Miner 85:649–667

Silva LC, McNaughton NJ, Santos JOS (2002a) Datações U-Pb SHRIMP do vulcanismo félsico na Bacia Brusque, Orógeno Pelotas, SC. In: Congresso Brasileiro de Geologia 41, João Pessoa, Brasil. Anais, 510

Silva LC, Armstrong R, Pimentel MM, Scandolara J, Ramgrab G, Wildner W, Angelim LAA, Vasconcelos AM, Rizzoto G, Quadros MLES, Sander A, Rosa ALZ (2002b) Reavaliação da evolução geológica em terrenos pré-cambrianos brasileiros com base em novos dados U-Pb SHRIMP, Parte III: Províncias Borborema, Mantiqueira Meridional e Rio Negro-Juruena. Rev Brasil Geociênc 32(4):529–544

Silva LC, McNaughton NJ, Hartmann LA, Fletcher IR (2003) Contrasting zircon growth patterns in Neoproterozoic granites of Southern Brazil revealed by SHRIMP U-Pb analyses and SEM imaging: consequences for the discrimination of emplacement and inheritance ages. In: IV South American Symposium on Isotope Geology, Salvador, Bahia, Brazil. Short Papers, pp 687–690

Silva LC, McNaughton NJ, Armstrong R, Hartman LA, Fletcher IR (2005a) The neoproterozoic Mantiqueira Province and its African connections: a zircon-based U-Pb geochronologic subdivision for the Brasiliano/Pan-African systems of orogens. Precambr Res 136:203–240

Silva LC, McNaughton NJ, Fletcher IR (2005b) Reassesment on complex zircon populations from Neoproterozoic granites in Brazil, through SEM imaging and SHRIMP analysis: consequences for discrimination of emplacement and inherited ages. Lithos 82(3–4): 503–525

Sommer CA, Lima EF, Nardi LVS, Figueiredo AMG, Pierosan R (2005) Potassic and low- and high-Ti mildly alkaline volcanism in the Neoproterozoic Ramada Plateau, southernmost Brazil. J S Am Earth Sci 18(3):237–254

Spoturno JJ, Oyhantçabal P, Loureiro J (2012) Mapa geológico del Departamento de Maldonado escala 1:100.000. Facultad de Ciencias (UdelaR)–Dirección Nacional de Minería y Geología (MIEM), Montevideo

Tickyj H, Hartmann LA, Vasconcellos MAZ, Philipp RP, Remus MVD (2004) Electron-microprobe dating of monazite substantiates ages of major geological events in the southern Brazilian Shield. J S Am Earth Sci 16(8):699–713

Tommasi A, Vauchez A, Fernandes LAD, Porcher CC (1994) Orogen-parallel strike-slip faulting and synkinematic magmatism in the Dom Feliciano Belt, Southern Brazil. Tectonics 13:421–437

Trainini DR, Dias AA, Krebs ASJ, Souza EC, Capeletti I, Toniolo JA, Silva LC, Silva MAS (1978) Projeto Vidal Ramos e Biguaçu. 1:250.000. DNPM/CPRM, Porto Alegre

Umpierre M, Halpern M (1971) Edades. Sr-Rb del Sur de la República Oriental del Uruguay. Rev Asoc Geológica Argent 26:133–155

Vlach SRF, Basei MAS, Castro NA (2009) Idade U-Th-Pb de monazita por microssonda eletrônica do Granito Nova Trento, Grupo Brusque, SC. In: Simpósio 45 anos de Geocronologia no Brasil, São Paulo, Brasil. Annals, pp 325–327

Wildner W, Lima EF, Nardi LVS, Sommer CA (2002) Volcanic cycles and setting in the neoproterozoic III to ordovician Camaquã Basin succession in Southern Brazil: characteristics of post-collisional magmatism. J Volcanol Geoth Res 118:261–283

Wildner W, Ramgrab GE, Lopes RC, Iglesias CMF (2006) Mapa geologico do Estado do Rio Grande do Sul, Escala 1:750.000. CPRM—Companhia de Pesquisa de Recursos Minerais, Porto Alegre

Wildner W, Camozzato E, Toniolo JA, Binotto RB, Iglesias CMF, Laux JH (2014) Mapa geológico do estado de Santa Catarina, Escala 1:500,000. CPRM—Companhia de Pesquisa de Recursos Minerais, Porto Alegre

Zanini LFP, Branco PDM, Camozzato E, Ramgrab GE (1997) Programa levantamentos geológicos básicos do Brasil. Florianópolis-Lagoa: folha SG. 22-ZDV-folha SG. 22-ZD-VI. 1:100.000. CPRM Porto Alegre

Zanon C, Machado R, Philipp RP, Cordani UG, Chemale Jr. F. Extensional magmatism after the emplacement of the Pelotas Batholith, Dom Feliciano Belt, southern Brazil: geochronological and mineral chemistry evidence. Brazilian J Geol (submitted)

Zvirtes G, Philipp RP, Camozzato E, Guadagnin F (2017) Análise estrutural do Metagranito Capané, Antiforme Capané, Complexo Porongos, Cachoeira do Sul, RS. Pesquisas em Geociênc 44(1):5–23

The Evolution of the Damara Orogenic System: A Record of West Gondwana Assembly and Crustal Response

12

Ben Goscombe, David A. Foster, David Gray, and Ben Wade

Abstract

The Damara Orogenic System is a well-exposed orogenic junction that preserves a rich record of West Gondwana assembly and crustal processes in classic examples of transpression (Kaoko Belt) and bivergent collisional orogenesis (Damara Belt). Both belts show typical orogenic cycles in common with orogenic belts universally: from rifted passive margin sequences, subduction at continental margin arcs with back-arc basins, collision, crustal overthickening, outwedging of orogenic margins, detachment of subducted lithosphere, upper-plate lithospheric thinning and eventual collapse. There is no controversy here, and, like all orogens, kinematic and metamorphic response is dynamic and strongly zonal, the patterns of which are strong evidence for crustal architectures and tectonic history. Large relational data sets are required to characterize these patterns of orogenic response, to test robustness, accuracy and internal consistency, and to build crustal and tectonic models. For this summary of the Damara Orogenic System, two large-scale internally consistent relational data sets have been integrated: (1) age-calibrated deformation histories have been correlated across the whole system on the basis of stress fields and absolute age constraints in common; and (2) deformation structures have been correlated with mineral growth and patterns of metamorphic response characterized by *P–T* evolutions, metamorphic maps and field gradients, quantified using a large data set of *PT* determinations. Collision of the Rio De La Plata Craton at ~590 Ma resulted in west over east obduction of the Coastal Terrane arc over the Congo Craton passive margin. The Kaoko Belt subsequently evolved through ~45° clockwise rotation of the stress field, showing progressive transpressional orogenesis, steepening and strain partitioning, resulting in a strike-slip shear system between ~550 and 530 Ma. Collision in the Damara Belt at ~555–550 Ma involved subduction of the Kalahari Craton margin, with a highly attenuated Congo Craton passive margin in an upper-plate setting. The Kaoko and Damara orogenic fronts were both operating between 550 and 530 Ma, and with the same northwest-southeast shortening direction. At ~530–525 Ma a stress switch to north-northwest-south-southeast shortening resulted in transtensional reactivation of the Kaoko Belt shear zones, rapid exhumation and cooling, terminating orogenesis in this belt. At this time, main phase orogenesis, burial and metamorphism peaked in the Damara Belt, and subsequent contraction in this belt dominated the stress field, which evolved through a roughly 70° clockwise rotation to northeast-southwest shortening by ~512–508 Ma. Barrovian metamorphism in the southern orogenic margin was diachronous, 530–522 Ma in the north to 517–514 Ma in the south, and accompanied ongoing contraction. Deep burial to 9.5–11.5 kb followed by rapid isostatic readjustment gave successive foreland propagating exhumation events at <522 and <517 Ma, by southward transport of crustal wedges along basal thrusts. Outwedging was accommodated by top down to the north transport of hanging walls at higher structural levels, indicated by major metamorphic discontinuities and extensional structures, resulting in extensional telescoping of the southern margin. In contrast, medium-*P*/high-*T* granulite facies metamorphic conditions persisted in the orogen core from 540 to 505 Ma, following low $\Delta P/\Delta$

B. Goscombe (✉)
Integrated Terrane Analysis Research (ITAR),
18 Cambridge Rd, Aldgate, SA 5154, Australia
e-mail: ben.goscombe@gmail.com
URL: http://www.terraneanalysis.com.au

D. A. Foster
Department of Geological Sciences, University of Florida,
Gainesville, FL 32611, USA

D. Gray
School of Earth Sciences, University of Tasmania,
Hobart, TAS, Australia

B. Wade
Adelaide Microscopy, University of Adelaide, Adelaide,
SA 5005, Australia

S. Siegesmund et al. (eds.), *Geology of Southwest Gondwana*, Regional Geology Reviews,
https://doi.org/10.1007/978-3-319-68920-3_12

T clockwise *P*–*T* paths indicating moderate burial and stable high-heat flow conditions, best explained by the detachment of subducted lithospheric during collision. A rapid stress switch to east–west directed shortening along the orogen at ~508 Ma generated crossfolding in the orogen core and northern margin. This stress field is inconsistent with any plausible trajectory between the Rio De La Plata, Congo and Kalahari Cratons and is interpreted as a far-field effect from the orogenic margin of Gondwana at that time: arc collisions in the Ross Orogen. This established a north–south extension direction exploited by 508–504 Ma decompression melts in many parts of the system, and at ~505–500 Ma triggered gravitational collapse and extension of the thermally weakened orogen core, resulting in a broad bivergent core complex, rapid exhumation and cooling from 700 to 400 °C between 500 and 470 Ma.

Keywords
Damara Belt • Kaoko Belt • Collisional Tectonics
Transpressional Tectonics • Structural Geology
Metamorphic Geology

12.1 Introduction

West Gondwana was assembled during three orogenic periods: the Mozambiquean/Brasiliano Phase (660–620 Ma), the Kaokoan/Ribeiran/Dronning Phase (590–535 Ma) and the Damaran/Kuungan Phase (555–505 Ma). The Damara Orogenic System is a triple junction orogen central to West Gondwana that tracks relative movements of the Rio De La Plata, Congo and Kalahari Cratons during the latter two orogenic cycles (Fig. 12.1). All three constituent belts are well exposed and experienced entirely different tectonic settings and tectonometamorphic responses. Consequently, the tectonic evolution of this region is crucial to understanding the assembly of Gondwana and the crustal response during different orogenic episodes. The north-trending Gariep Belt involved sinistral obduction of oceanic thrust sheets onto the Kalahari Craton (Frimmel and Frank 1998) and is summarized in Chap. 3. The north-northwest-trending Kaoko Belt involved sinistral transpressive obduction of the Coastal Terrane magmatic arc onto the Congo Craton margin, and subsequent sinistral transpressional orogenesis (Goscombe and Gray 2007, 2008). The east-northeast-trending Damara Belt involved closure of the Khomas ocean basin and high-angle collision of the Congo and Kalahari Cratons (Coward 1981; Miller 1983; Porada et al. 1983). The Kaoko and Damara Belts were contiguous, overlap in age and are simply components of the one Damara Orogenic System. Both belts are classic examples of transpressional and collisional orogens, and crucially they are well exposed and preserve boundary conditions and tectonic context intact. Furthermore, both contain Neoproterozoic stratigraphy devoid of earlier orogenic cycles and later reworking, giving an undisturbed record of crustal response during a protracted period of supercontinent assembly (Fig. 12.2). This chapter attempts to summarize the tectonic evolution of the Kaoko and Damara Belts on the basis of comprehensive deformation, metamorphism, magmatic and provenance-stratigraphic data layers that are now available. The approach taken was to integrate time-calibrated, internally consistent deformation frameworks (Goscombe et al. 2017b), with comprehensive metamorphic patterns and histories covering both belts (Goscombe et al. 2003b, 2004, 2005a, 2017a) as the basis for expanding on the tectonic history of the Damara Orogenic System established by Gray et al. (2006, 2008). As a result, the chapter summarizes our recent work and uses it to propose an internally consistent model for the Damara Orogenic System. Given limitations of space, it does not attempt a comprehensive summary of the geology or research history of the Damara System, which are readily available elsewhere (e.g., Kasch 1983b; Miller et al. 1983; Porada 1983; Miller and Grote 1988; Gray et al. 2006, 2008).

An integrated approach is crucial to reconstructing the dynamic architectures and evolution of orogenic systems (Goscombe et al. 2006, 2007, 2017a). Structural data sets on their own are insufficient to track particle paths in different parts of orogenic systems. Significant pressure and thermal gradient discontinuities in peak metamorphic patterns are indicative of superimposed deformational imprints and crustal-scale structures that would otherwise go unrecognized. Consequently, metamorphic patterns and metamorphic field gradients in particular, in combination with structural profiles, have been used to delineate dynamic evolving crustal architectures during orogenesis (e.g., Inger and Harris 1992; Vannay and Hodges 1996; Harrison et al. 1997; Goscombe et al. 2005a, 2006). Furthermore, small isolated data sets are insufficient to establish unambiguous constraints on the tectonic evolution of orogenic systems; large relational data sets are required. Large data sets permit testing of the robustness of individual results, pooled averages increase accuracy, and facilitate spatial and temporal patterns of tectonometamorphic responses on the orogenic scale. This simple and relational approach based on large data sets covering all parts of the orogenic system offers geological context that is otherwise unobtainable. Without large relational data sets, small sample sets in isolation (e.g., Cross et al. 2015) are insufficient to define variation across an orogenic system, and they remain unable to contribute well-constrained models for the tectonic evolution at the scale of an orogenic system.

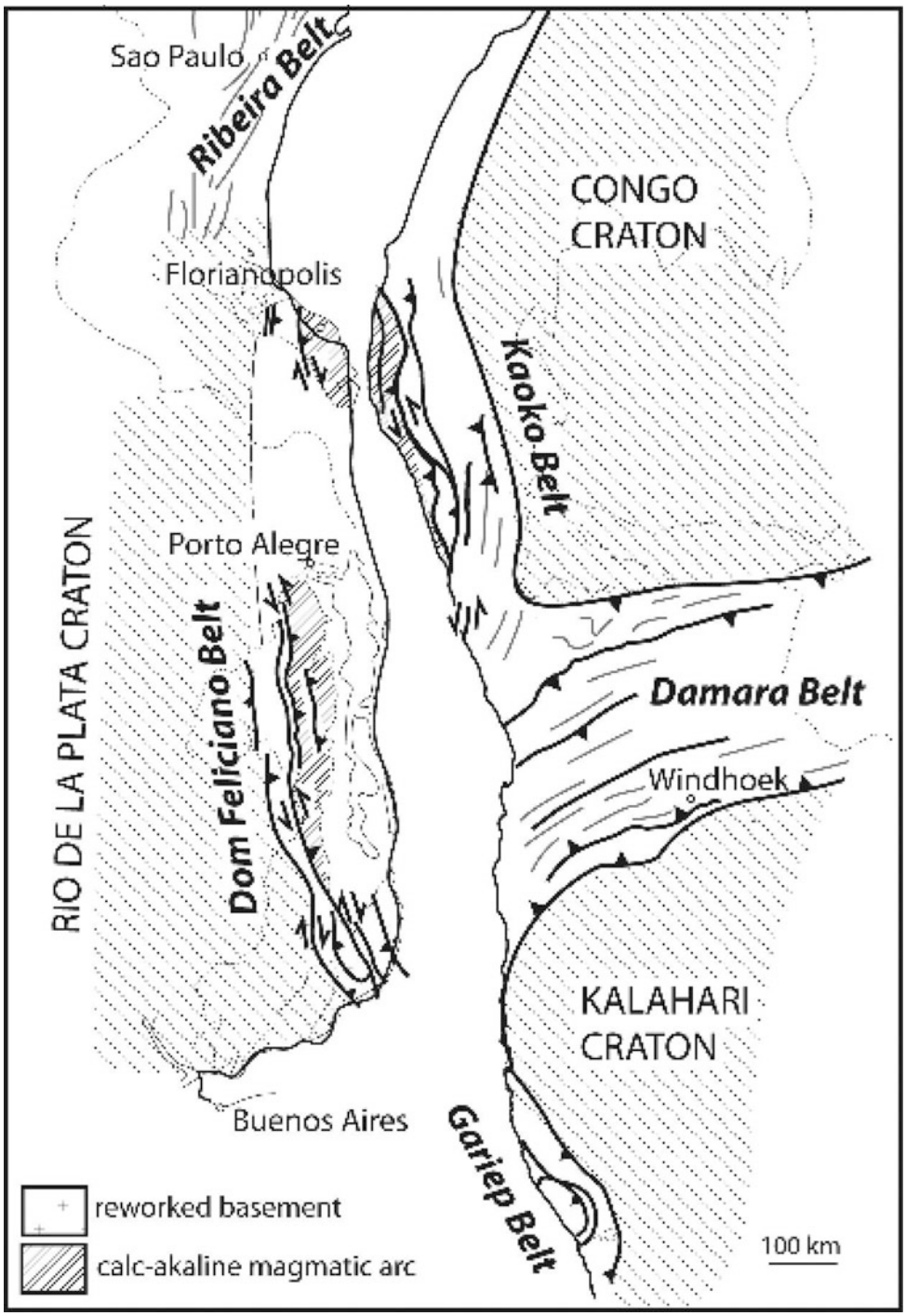

Fig. 12.1 Simplified map of West Gondwana with the Damara and Kaoko Belts located for context (from Gray et al. 2008)

12.2 Large-Scale Architecture of the Damara Orogenic System

12.2.1 Kaoko Belt

The Kaoko Belt is a classic transpressional orogen, formed during oblique collision between the Congo and Rio De La Plata Cratons (Coward 1983; Porada 1989; Trompette and Carozzi 1994; Trompette 1997; Prave 1996). Orogenesis evolved from east-directed obduction of the Coastal Terrane at ~590 Ma, main phase transpressional orogenesis and synkinematic granitoids at 580–560 Ma, progressive partitioning of wrench and shortening deformation, and finally strain localization in strike-slip shear zones after ~550 Ma (Seth et al. 1998; Goscombe et al. 2003a, 2005a, b;

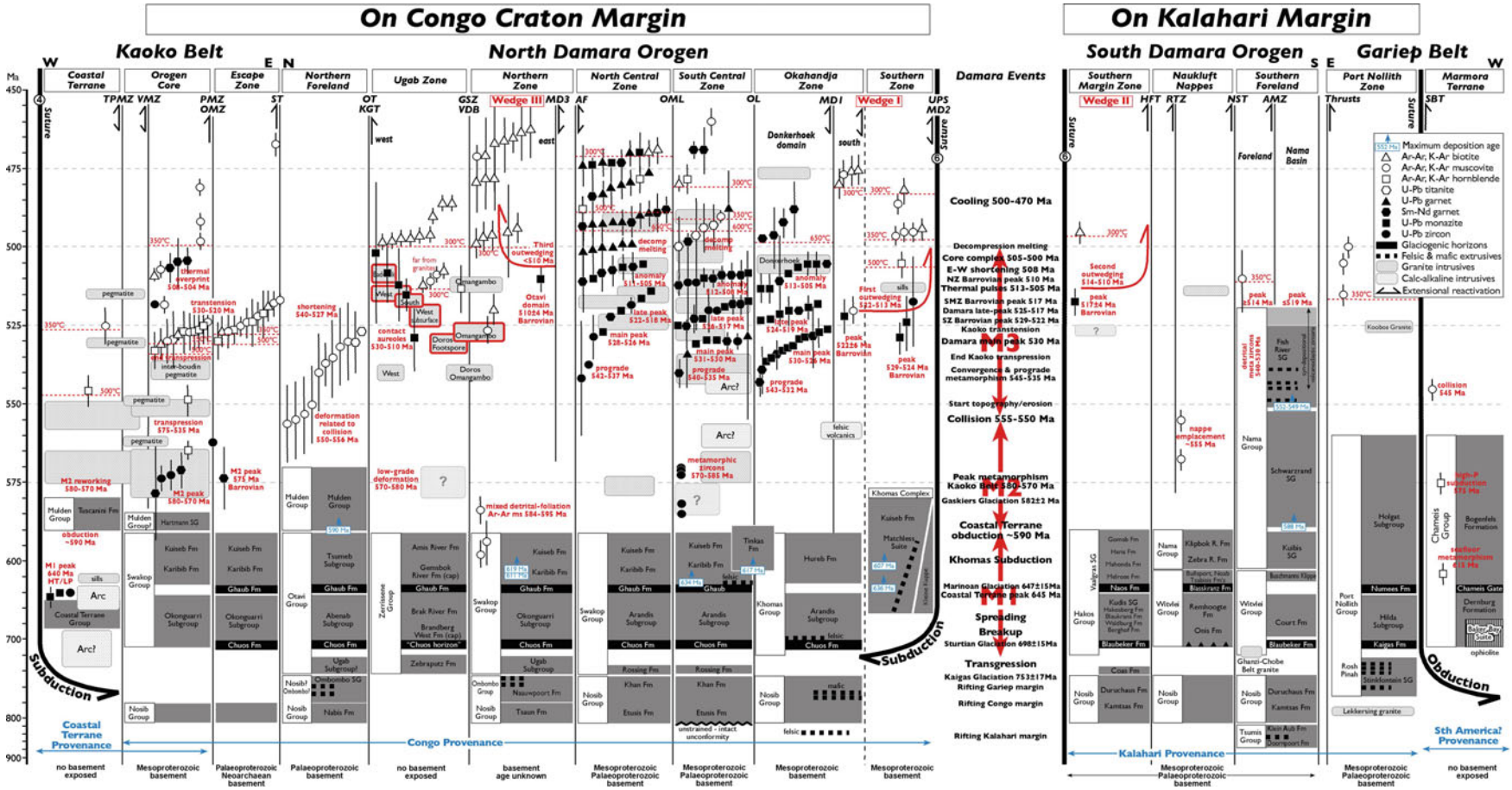

Fig. 12.2 Time-space diagram outlining the stratigraphy and chronology in different zones of the Damara Belt (modified after Goscombe et al. 2017a, b). Stratigraphy modified after Hoffmann (1989), with the latest corrections from Halverson et al. (2002) and Hoffmann et al. (2004), and recent geochronology of felsic extrusives (e.g., Hoffman et al. 1996). Older published stratigraphy for the internal parts of the Kaoko Belt (i.e., Guj 1970; Henry and Osborne 1992; Prave 1996; Stanistreet and Charlesworth 2001) are inconsistent with recently mapped geology, such as the recognition of two diamictites, and has been modified (Goscombe et al. 2005b; Goscombe and Gray 2007, 2008). Otherwise in other provices no changes have been made and the most recent and accepted stratigraphy is presented (Swart 1992; Hoffmann 1994, 1997, 1989; Hoffman et al. 1996, 1998; Becker et al. 1998, 2004; Hoffmann and Schreiber 1998; DeKock et al. 2000; Halverson et al. 2002; Hoffmann et al. 2004; Nascimento et al. 2016). All detrital, magmatic, metamorphic and cooling age determinations are sourced from the literature and listed in the appendicies in Goscombe et al. (2017a, b). The detrital zircon data used to constrain maximum deposition ages (blue) have been sourced from Newstead (2010) and Foster et al. (2015). Only robust U–Pb monazite, zircon, garnet and titanite metamorphic ages, Sm–Nd garnet metamorphic ages and Ar–Ar hornblende, muscovite and biotite cooling ages have been compiled. The age range for different episodes of granitoid crystallization is indicated by grey cross-hatching

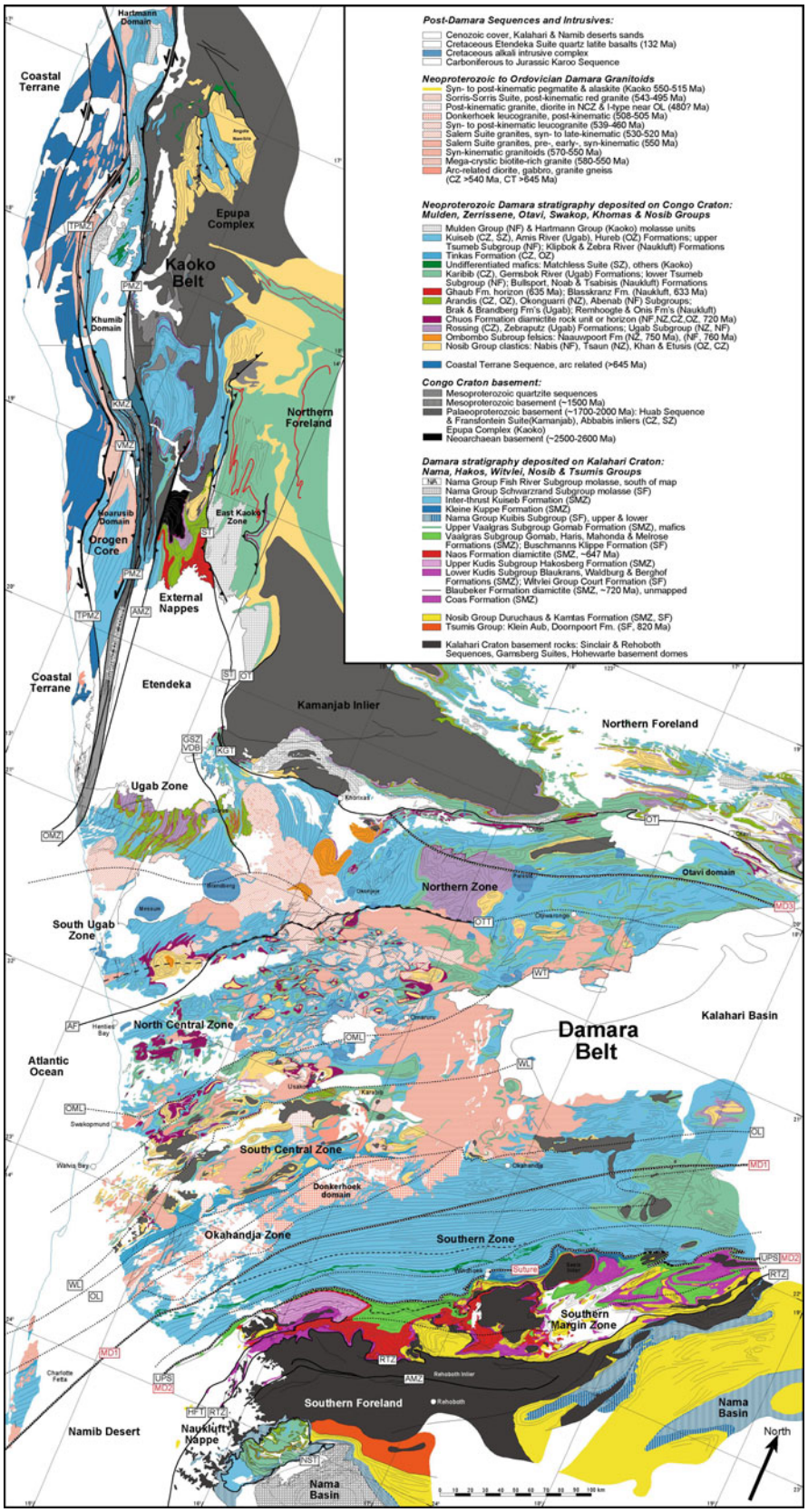
Post-Damara Sequences and Intrusives:
Cenozoic cover, Kalahari & Namib deserts sands
Cretaceous Etendeka Suite quartz latite basalts (132 Ma)
Cretaceous alkali intrusive complex
Carboniferous to Jurassic Karoo Sequence
Neoproterozoic to Ordovician Damara Granitoids
Syn- to post-kinematic pegmatite & alaskite (Kaoko 550-515 Ma)
Sorris-Sorris Suite, post-kinematic red granite (543-495 Ma)
Post-kinematic granite, diorite in NCZ & I-type near OL (480? Ma)
Donkerhoek leucogranite, post-kinematic (508-505 Ma)
Syn- to post-kinematic leucogranite (539-460 Ma)
Salem Suite granites, syn- to late-kinematic (530-520 Ma)
Salem Suite granites, pre-, early-, syn-kinematic (550 Ma)
Syn-kinematic granitoids (570-550 Ma)
Mega-crystic biotite-rich granite (580-550 Ma)
Arc-related diorite, gabbro, granite gneiss
(CZ >540 Ma, CT >645 Ma)
Neoproterozoic Damara stratigraphy deposited on Congo Craton:
Mulden, Zerrissene, Otavi, Swakop, Khomas & Nosib Groups
Mulden Group (NF) & Hartmann Group (Kaoko) molasse units
Kuiseb (CZ, SZ), Amis River (Ugab), Hureb (OZ) Formations; upper Tsumeb Subgroup (NF); Klipbok & Zebra River (Naukluft) Formations
Tinkas Formation (CZ, OZ)
Undifferentiated mafics: Matchless Suite (SZ), others (Kaoko)
Karibib (CZ), Gemsbok River (Ugab) Formations; lower Tsumeb Subgroup (NF); Bullsport, Noab & Tsabisis (Naukluft) Formations
Ghaub Fm. horizon (635 Ma); Blaskranz Fm. (Naukluft, 633 Ma)
Arandis (CZ, OZ), Okonguarri (NZ), Abenab (NF) Subgroups; Brak & Brandberg Fm's (Ugab); Rembhoogte & Onis Fm's (Naukluft)
Chuos Formation diamictite rock unit or horizon (NF,NZ,CZ,OZ, 720 Ma)
Rossing (CZ), Zebraputz (Ugab) Formations; Ugab Subgroup (NZ, NF)
Ombombo Subroup felsics: Naauwpoort Fm (NZ, 750 Ma), (NF, 760 Ma)
Nosib Group clastics: Nabis (NF), Tsaun (NZ), Khan & Etusis (OZ, CZ)
Coastal Terrane Sequence, arc related (>645 Ma)
Congo Craton basement:
Mesoproterozoic quartzite sequences
Mesoproterozoic basement (~1500 Ma)
Palaeoproterozoic basement (~1700-2000 Ma): Huab Sequence & Fransfontein Suite(Kamanjab), Abbabis inliers (CZ, SZ)
Epupa Complex (Kaoko)
Neoarchaean basement (~2500-2600 Ma)
Damara stratigraphy deposited on Kalahari Craton:
Nama, Hakos, Witvlei, Nosib & Tsumis Groups
Nama Group Fish River Subgroup molasse, south of map
Nama Group Schwarzrand Subgroup molasse (SF)
Inter-thrust Kuiseb Formation (SMZ)
Kleine Kuppe Formation (SMZ)
Nama Group Kuibis Subgroup (SF), upper & lower
Upper Vaalgras Subgroup Gomab Formation (SMZ), mafics
Vaalgras Subgroup Gomab, Haris, Mahonda & Melrose Formations (SMZ); Buschmanns Klippe Formation (SF)
Naos Formation diamictite (SMZ, ~647 Ma)
Upper Kudis Subgroup Hakosberg Formation (SMZ)
Lower Kudis Subgroup Blaukrans, Waldburg & Berghof Formations (SMZ); Witvlei Group Court Formation (SF)
Blaubeker Formation diamictite (SMZ, ~720 Ma), unmapped
Coas Formation (SMZ)
Nosib Group Duruchaus & Kamtas Formation (SMZ, SF)
Tsumis Group: Klein Aub, Doornpoort Fm. (SF, 820 Ma)
Kalahari Craton basement rocks: Sinclair & Rehoboth Sequences, Garnsberg Suites, Hohewarte basement domes
Hartmann Domain
Coastal Terrane
Epupa Complex
Kaoko Belt
Khumib Domain
Northern Foreland
Koarusib Domain
Orogen Core
East Kaoko Zone
External Nappes
Coastal Terrane
Etendeka
Kamanjab Inlier
Northern Foreland
Ugab Zone
Otavi domain
Northern Zone
South Ugab Zone
Kalahari Basin
Damara Belt
North Central Zone
Atlantic Ocean
South Central Zone
Donkerhoek domain
Okahandja Zone
Southern Zone
Southern Margin Zone
Southern Foreland
Rehoboth
Nama Basin
Namib Desert
Naukluft Nappe
Nama Basin
North

◀ **Fig. 12.3** Simplified geological map of the Damara Orogenic System. The Kaoko Belt component is reproduced from Goscombe et al. (2005a) and based on our mapping and published maps (Guj 1970; Goscombe 1998, 1999a, b, c; Schreiber 2002; Goscombe et al. 2003a, b). The crustal-scale shear zone abbreviations are *TPMZ* Three Palms Mylonite Zone; *PMZ* Puros Mylonite Zone; *HMZ* Hartmann Mylonite Zone; *VMZ* Village Mylonite Zone; *KMZ* Khumib Mylonite Zone; *AMZ* Ahub Mylonite Zone; *ST* Sesfontein Thrust. The Damara Belt part of the map is modified after the 1:500,000 geological map of Namibia (Miller and Grote 1988) and reproduced from Goscombe et al. (2017a). Tectonometamorphic zones are as currently accepted in the literature except for the South Ugab Zone, North Central Zone and Okahandja Zone, which have been modified in response to new metamorphic understanding (Goscombe et al. 2017a). Most zones are demarcated by crustal-scale shear zones, thrust or faults, which are indicated by abbreviations UPS, Uis-Pass Suture, crustal thrusts reactivated by extension, corresponding to the suture between stratigraphy deposited on either the Kalahari or Congo cratons, and containing dismembered serpentinites (Barnes 1983; Kasch 1983b; Kukla and Stanistreet 1991); *OT* Outjo thrust; *AF* Autseib fault; *KGT* Khorixas-Gaseneirob thrust; *OL* Okahandja lineament; *HFT* Hakos Frontal thrust; *ASZ* Areb shear zone; *ASZ* Areb shear zone; *RTZ* Rehoboth thrust zone; *WT* Waterberg thrust; *OTT* Otjorongo thrust; *OML* Omaruru lineament; *WL* Welwitchia lineament; *GSZ/VDB* Goantagab shear zone or Vrede–Doros–Brandberg line; *MD* metamorphic discontinuities inferred from metamorphic field gradients (Goscombe et al. 2017a)

Konopásek et al. 2005). Kaoko Belt orogenesis was terminated at ~530–525 Ma by Damaran north-northwest-south-southsoutheast shortening, resulting in the transtensional reactivation of shear zones, pegmatites, rapid exhumation and cooling (Goscombe et al. 2005b; Foster et al. 2009). Ongoing north–south shortening buckled the belt and coincides with north–south trending pegmatites of ~515 Ma age (Goscombe et al. 2005b). Final overprint was a stress switch to east–west shortening, resulting in north–south extension, pegmatites and thermal pulse at ~508–505 Ma.

The Kaoko Belt has steep bivergent flower and half-flower geometry controlled by arcuate crustal-scale shear zones (Dürr and Dingeldey 1996; Goscombe et al. 2003a, 2005a). Shear zones are predominantly steeply west-dipping and listric at depth (Guj 1970; Dingeldey et al. 1994; Goscombe et al. 2003a; Konopásek et al. 2005). The architecture and evolution of the belt were controlled by two long-lived crustal-scale shear zones that started as shallow west-dipping decollements (Fig. 12.3). At the highest structural levels, Three Palms Mylonite Zone was a sinistral-normal shear zone that transported Coastal Terrane southward and down with respect to the core of the belt. Purros Mylonite Zone is a sinistral-reverse shear zone that accommodated south-southeast-directed transport of the orogen core. Flower geometry resulted from the progressive rotation of shear zones into steeper orientations owing to shortening against thick Congo Craton lithosphere in the foreland, while continuing to localize transcurrent shear (Goscombe et al. 2003a; Konopásek et al. 2005). Kinematic partitioning, deformation style and metamorphic response are all controlled by these crustal-scale shear zones, and they divide the belt into distinct tectonometamorphic zones (e.g., Figs. 12.3, 12.7 and 12.11; Goscombe et al. 2005a).

The **Eastern Foreland** has subgreenschist facies Damara Sequence platform carbonates unconformably overlying unreworked Paleoproterozoic Congo Craton. Deformation involved east–west directed coaxial shortening of carbonates into large-scale upright, open to close cylindrical folds, box folds, ramp anticlines and steep discontinuous thrusts (Guj 1970; Coward 1983; Hoffman et al. 1994, 1998). Overlying phyllonitic Mulden Group molasse developed progressively shallower dipping folds and crenulations, ending with a discontinuous network of west-dipping thrusts, such as the Sesfontein Thrust (Guj 1970).

The **External Nappe Zone** is a strongly deformed slope to deep-sea facies Damara Sequence, with inverted greenschist to upper-amphibolite facies Barrovian series metamorphism (Dingeldey 1997; Goscombe et al. 2003b, 2005a; Will et al. 2004). Deformation was by large-scale east-directed folds and nappes with reworked Archaean-Paleoproterozoic basement cores. The structures are tighter and steeper in the west where they root into the Purros Mylonite Zone (Guj 1970; Dingeldey et al. 1994; Dürr and Dingeldey 1996; Stanistreet and Charlesworth 2001; Goscombe et al. 2003a).

The **Orogen Core** is mostly high-grade, deep-sea Damara Sequence intruded by synkinematic S-type granitoids of 580–562 and 559–549 Ma age, and dissected into lenticular panels by crustal-scale shear zones (Seth et al. 1998; Franz et al. 1999; Kröner et al. 2004; Goscombe et al. 2005b; Konopásek et al. 2005). Hartmann domain in the north is almost devoid of exposed basement, metamorphosed to upper-amphibolite grade, and syn- to post-kinematic pegmatite sills are common. Khumib domain is shallow crustal level, lower amphibolite facies turbidites with upright chevron folding similar to the Ugab Zone (Goscombe et al. 2005a). Hoarusib domain in the south consists of high-grade migmatitic metagreywacke gneiss, with isoclinal infolds of Mesoproterozoic basement and synkinematic granitoids (Seth et al. 1998; Kröner et al. 2004; Goscombe et al. 2005b).

The **Coastal Terrane** has provenance distinct from the rest of the Kaoko Belt and consists of juvenile meta-arkose Neoproterozoic sequences <650 Ma and intruded by 661–655 and 638–620 Ma arc-related, I-type intrusives (Seth et al. 1998; Kröner et al. 2004; Goscombe et al. 2005b; Goscombe and Gray 2007). These were metamorphosed to high-*T*/low-*P* conditions typical of arc settings between 650 and 640 Ma (Franz et al. 1999). Different lithostratigraphy, provenance, magmatism and thermal regime indicate that the Coastal Terrane was a continental margin arc at the leading edge of attenuated passive margin with back arc basin containing deep-sea turbidite and slope sequences (Fig. 12.4; Goscombe and Gray 2007, 2008). The

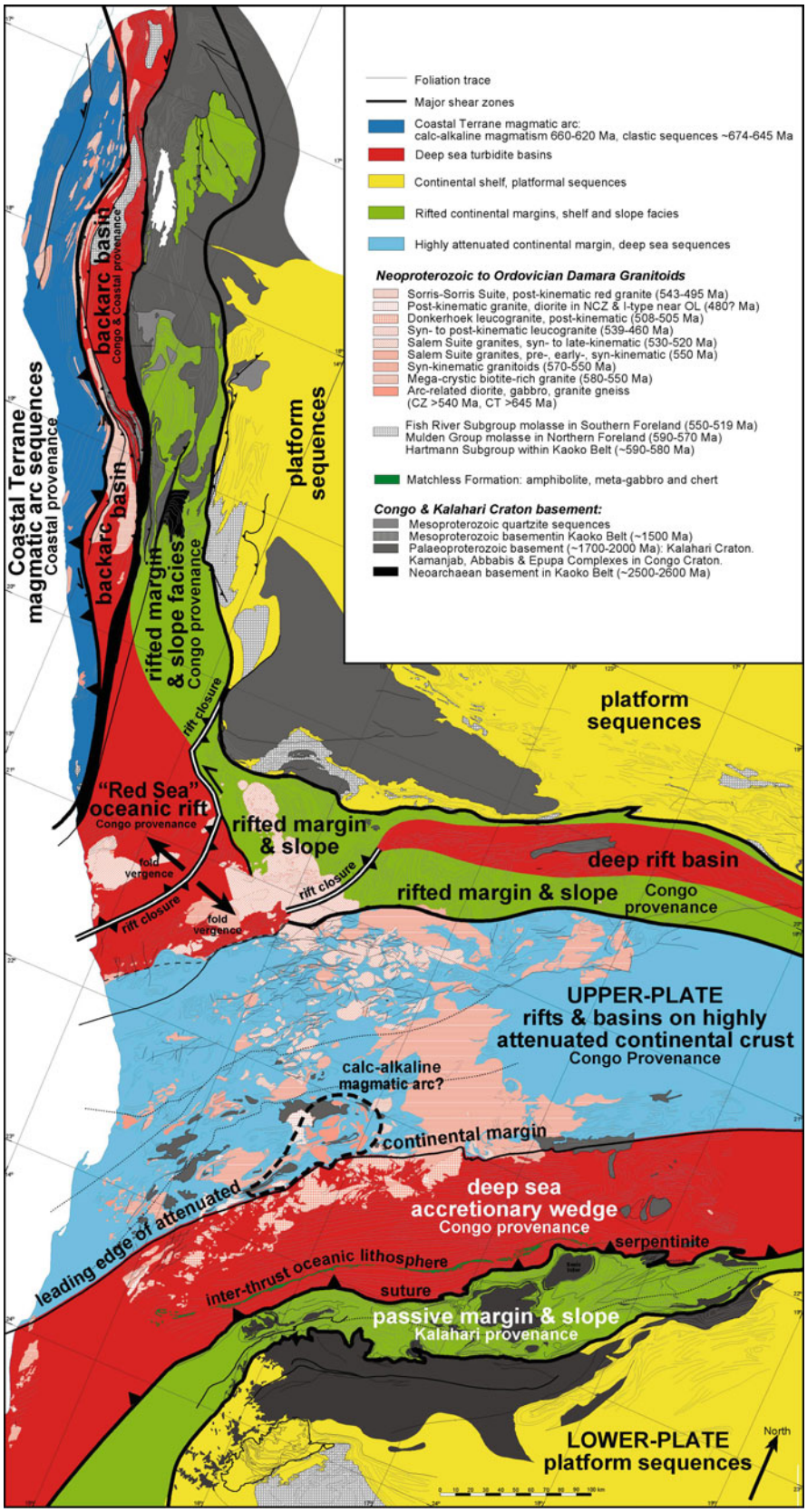

Fig. 12.4 Interpretive pre-orogenic depositional basin environments for the Damara Orogenic system

subduction outboard of the Coastal Terrane was terminated by the collision of the Rio De La Plata Craton, resulting in obduction along the Three Palms Mylonite Zone and reworking at shallow crustal levels during transpression.

12.2.2 Damara Belt

The Damara Belt involved closure of the Khomas ocean and high-angle collision of the Congo and Kalahari Cratons producing an asymmetric, bivergent orogen (Coward 1981, 1983; Miller et al. 1983; Porada et al. 1983; Gray et al. 2008). Decollements dip away from both cratons, and the Kalahari Craton is underthrust below attenuated Congo Craton in the upper-plate setting (Gray et al. 2008). Orogenesis evolved through consumption of oceanic crust, imbrication of an accretionary wedge, early calcalkaline magmatism, collision at ~555 Ma, crustal shortening and burial, culminating in peak metamorphism between ~530 and 510 Ma, extensional telescoping of orogenic margins between ~520 and 510 Ma, and collapse and cooling of the orogen core between ~505 and 470 Ma (Goscombe et al. 2017a, b). The belt shows pronounced zonation reflected by deformation and thermal regimes (e.g., Figs. 12.3, 12.7 and 12.11).

The **Northern Margin** shows dramatic along-orogen variation in deformation and metamorphic response (Goscombe et al. 2004) and it overlaps with the Kaoko Belt. Ugab Zone at the Kaoko-Damara junction is a 1.7 km thick sequence of deep-sea turbidites with no basement exposed (Swart 1992). Kaokoan transpression results in bivergent flower-structure geometry with map-scale chevrons verging both east and west (Coward 1983; Porada et al. 1983; Maloof 2000; Passchier et al. 2002). High shortening strains were accommodated by basal decollements dipping towards the central Ugab (Gray et al. 2006), and probably rooting into a sinistral transcurrent structure at depth (Goscombe et al. 2017b). Overprinting Damaran events are low-strain and produced complex fold and fabric interference (Coward 1981, 1983; Freyer and Halbich 1994; Maloof 2000; Passchier et al. 2002, 2007; Goscombe et al. 2004). Structures formed at low-grade metamorphic grades, punctuated by diachronous contact metamorphism during five episodes of granite and syenogranite plutonism at ~540, 534–526, 520, 516 and 513–508 Ma (Seth et al. 2000; Van de Flierdt et al. 2003; Lobo-Guerrero Sanz 2005; Schmitt et al. 2012; Lehmann et al. 2015; Goscombe et al. 2017b). The Northern Zone abuts thick crustal lithosphere of the Congo Craton, resulting in a steep fold-thrust belt with complex fold interference and penetrative foliations (Coward 1983; Miller et al. 1983; Gray et al. 2008; Lehmann et al. 2015). North of the steep bounding thrusts, the foreland has Paleoproterozoic basement overlain by a carbonate platform with low-amplitude folding (Hedberg 1979), and low-grade phyllites preserving early Damaran K–Ar deformation ages of 556–550 and 540–530 Ma (Clauer and Kröner 1979). The West Northern Zone has greenschist facies sequences and deformation history similar to the Ugab Zone (Porada et al. 1983; Goscombe et al. 2004; Lehmann et al. 2015). The East Northern Zone has a thick turbidite sequence deposited in a rift (Fig. 12.4; Porada 1979, 1983; Porada and Wittig 1983), which was deeply buried to Barrovian metamorphic conditions at 510 Ma and exhumed soon after (Goscombe et al. 2017a).

The **Orogen Core** consists of the high-grade Central Zone and northern Okahandja Zone, with relatively thin Damara strata deposited on attenuated Congo Craton passive margin. Deformation in the Central Zone was moderate strain northwest-southeast to northeast-southwest shortening with large-scale upright to inclined folds and later crossfolds producing dome and basin interference (Fig. 12.3; Jacob et al. 1983; Kisters et al. 2004; Longridge et al. 2011, 2014). The Central Zone developed only moderate foliation and lineation intensity and bulk strains, with grain refinement, mylonite and high-strain detachments being absent, and the basal unconformity preserved intact (Goscombe et al. 2017b). The metamorphic response was long-lived medium-P granulite facies conditions between 540–505 Ma (e.g., Jung et al. 1998a, 2000b; Masberg 2000; Goscombe et al. 2017a), and large volumes of S-type synkinematic granite of 546–515 Ma age originating from mid- to lower-crustal melting (e.g., McDermott et al. 2000; Jung et al. 2001; DeKock and Armstrong 2014). The Southern Central Zone contains 568–556 Ma I-type granitoids with some magmatic arc affinities (e.g., McDermott et al. 1996; Jacob et al. 2000; Jung et al. 2001). The Okahandja Zone is a steep, tightly folded synform of upper Damara stratigraphy sharing metamorphic events in common with the Central Zone, though at lower to upper amphibolite conditions, and overprinted by a post-kinematic Donkerhoek batholith of ~508–504 Ma age (Kukla et al. 1991; DeKock and Armstrong 2014). This zone is the leading edge of attenuated Congo Craton, transitional between the high-grade orogen core and Barrovian southern orogenic margin. Having stratigraphy, provenance and basement in common indicates that the Kaoko Belt and central and northern Damara Belt were contiguous; though expressions of Kaokoan orogenesis are restricted to rare pre-kinematic granites and metamorphic zircons of 580–570 Ma age (Allsopp et al. 1983; Armstrong et al. 1987; Bergemann et al. 2014; Milani et al. 2014; Foster et al. 2015).

The **Southern Orogenic Margin** is a highly strained fold-thrust belt with half-flower geometry that experienced south-directed transport, deep burial and inverted Barrovian metamorphic response almost void of granitic melt generation or emplacement (Fig. 12.3). At the highest structural levels the south Okahandja Zone is a steep wedge of deeply

buried Damara Sequence, juxtaposed with high-grade orogen core. The Southern Zone is a thick, homoclinal, intensely transposed accretionary wedge of deep-sea turbidites with Congo Craton provenance (Kukla and Stanistreet 1991; Gray et al. 2008; Foster and Goscombe 2013; Foster et al. 2015), devoid of basement and containing interthrust oceanic lithosphere of the Matchless Belt (Killick 2000). The lower-plate Southern Margin Zone consists of sequences deposited on the Kalahari Craton margin (Fig. 12.4) and it is highly strained in a fold-thrust belt with basement-cored nappes transported onto the Southern Foreland (Porada and Wittig 1983). The Uis-Pass Suture between these two zones is the site of closure of the Khomas Ocean basin and contains sheared Alpine serpentinite accreted during collision (Barnes 1983; Kasch 1983b; Killick 2000). This structure marks the boundary between sequences with Kalahari or Congo Craton provenance (Foster and Goscombe 2013; Foster et al. 2015), and, along with paleomagnetic poles (Meert et al. 1995; Meert and Torsvik 2003), a homoclinal accretionary wedge and gross structural asymmetry of the orogen, indicates ocean basin closure (Gray et al. 2008). The Uis-Pass Suture is a crustal-scale shear zone with a two-stage history: main phase north over south reverse shear and retrograde extensional reactivation during exhumation of the southern margin (Goscombe et al. 2017a). Collisional strain was partitioned into the southern orogenic margin, where main foliation intensity and bulk strain were highest, burial was deepest and significantly greater topography was developed. Deep burial produced inverted Barrovian series metamorphism and crustal overthickening, which led to rapid exhumation of crustal wedges resulting in extensional telescoping of the southern margin while still under contraction. Foreland-directed thrusting accommodated by broad, ductile to brittle extensional zones at higher structural levels produced pronounced metamorphic discontinuities (Goscombe et al. 2017a).

12.3 Stratigraphy and Provenance of Rock Units

Though overlapping in age and with clear age correlatives such as glaciogenic horizons, sequences on the Congo and Kalahari passive margins differ substantially in their provenance. Detrital zircon studies and whole rock εNd values have shown that the two sequences were isolated from each other, separated by a wide ocean basin, and sourced from their adjacent craton only (Newstead 2010; Foster et al. 2015). Consequently, stratigraphy of the Damara Belt is subdivided on the basis of provenance, as separate basinal sequences sharing no connection (Figs. 12.2 and 12.4). Detrital zircon data is also used to constrain maximum deposition ages, and in conjunction with overprinting magmatic and metamorphic age data, further constrains the well-established stratigraphic relationships in the literature, as listed in Fig. 12.2.

12.3.1 Coastal Terrane Sequences

The Coastal Terrane magmatic arc is an intimate mix of ~50% calcalkaline mafic, intermediate and felsic metaintrusives (Seth et al. 1998; Franz et al. 1999; Masberg et al. 2005) and metamorphosed supracrustals of the Coastal Terrane Group or Sequence (Goscombe and Gray 2007). The Coastal Terrane Group is dominated by a layered package of coarse clastic metafeldspathic psammite, meta-arkose, metagreywacke and minor metapsammopelite, devoid of metapelite, carbonate and quartzite. These metasedimentary rocks are of Cryogenian age, bracketed by maximum deposition ages of 674 Ma and minimum metamorphic ages of 645–640 Ma (Franz et al. 1999). These coarse juvenile clastics are interpreted to be volcanogenic and overlap in age with magmatism in the arc at 661–656 Ma (Seth et al. 1998; Kröner et al. 2004; Goscombe et al. 2005b). The εNd ratios indicate different provenance sources to those of the Damara Supergroup (Goscombe et al. 2005b; Goscombe and Gray 2007). Metasedimentary rocks in the Coastal Terrane have εNd ratios ranging from −6.1 to −4.1 and from −1.8 to 1.1, for model ages of 650 Ma, indicating mostly Neoproterozoic sources. In contrast, the Damara Supergroup samples from the remainder of the Kaoko Belt show a huge range of εNd ratios from −14.6 to −1.1 (Goscombe et al. 2005b), indicating Archaean, Mesoproterozoic and Neoproterozoic sources, consistent with basement within the belt and hinterland. The Coastal Terrane Group has a major detrital zircon peak at 820 Ma and others at 674 Ma and between 720 and 800 Ma, with none older than 820 Ma, indicating a juvenile provenance dominated by a probable magmatic event at 820 Ma.

Evidence for juvenile sources absent of a Mesoproterozoic to Archaean component, and deposition between 674–645 Ma overlapping with magmatism, indicates sedimentation during formation of the crust consistent with a magmatic arc setting (Goscombe and Gray 2007). These juvenile arkosic sediments are outboard of deep-sea turbiditic sediments of the Damara Supergroup deposited in the central Kaoko Belt to the east. Consequently, the Coastal Terrane Group must be sourced from the west, from within the Coastal Terrane. Different lithostratigraphy and provenance, and the absence of subduction parageneses in the Kaoko Belt, indicate that the Coastal Terrane magmatic arc was outboard of a deep back-arc basin floored by attenuated Mesoproterozoic-Neoarchaean basement, with east dipping subduction on the western margin of the arc (Goscombe and Gray 2008). Igneous, metamorphic and deposition histories

all support that the suggestion that Coastal Terrane evolved independently of the Kaoko Belt, prior to obduction at ~590–580 Ma (Goscombe et al. 2003b, 2005a, b; Goscombe and Gray 2007).

12.3.2 Sequences Deposited on the Congo Craton

12.3.2.1 Kaoko Belt

Damara Sequences in the Kaoko Belt are platform, slope and deep marine facies deposited on the western Congo Craton passive margin between ~800 and 580 Ma (Miller et al. 1983; Hoffman et al. 1994, 1998; Prave 1996). Basal sequences are rift-related siliciclastics of the Nosib Group, and possible rift-related mafic volcanics of ~840–805 Ma age at the leading edge in the footwall of Three Palms Mylonite Zone (Konopásek et al. 2005). The detrital zircon maximum deposition age for Nosib Group quartzite is ~811 Ma (Foster et al. 2015). Detrital peaks indicate the probable provenance from Stenian and Paleoproterozoic basement in the Congo Craton (Foster et al. 2015). The Ombombo Subgroup in the platform contains felsic volcanics of 759–756 Ma and 764 Ma age (Halverson et al. 2002). Overlying Otavi Group platform carbonates in the eastern Foreland are dominated by thick cap carbonates with three associated glaciogenic deposits. The oldest glacial horizon is correlated with the Kaigas glaciation and dated between 750–735 Ma (Halverson et al. 2002). The Swakop Group slope and basin facies consisting of turbidites, metagreywacke and subordinate mafic schists, calcsilicate, carbonate and quartzite, were deposited in the External Nappe Zone and Orogen Core of the Kaoko Belt (Guj 1970; Prave 1996; Hoffman et al. 1998; Stanistreet and Charlesworth 2001). Two diamictite units with associated iron formation are identified within the External Nappe Zone and correlated with Chuos Formation of ~720–700 Ma Sturtian glaciation and Ghaub Formation of ~635 Ma Marinoan glaciation (Goscombe 1998, 1999a, b, c; Hoffman et al. 1998; Goscombe et al. 2003a; Hoffmann et al. 2004). Khumib domain in the Orogen Core consists of low-grade turbidites correlated with Kuiseb Formation, and with detrital zircon maximum deposition ages of 622 and 643 Ma (Foster et al. 2015). Detrital zircon peaks from Kuiseb Formation samples in the Kaoko Belt have probable provenance from Stenian and Paleoproterozoic basement in the Congo Craton.

12.3.2.2 Ugab Zone

The Cryogenian to Ediacaran sequences in the Ugab Zone, the Zerrissene Group, are a 1.7 km thick package of turbidites deposited in a deep-sea basin (Swart 1992), possibly floored by oceanic crust (Fig. 12.4; Gray et al. 2006). The Zerrissene Group is correlated with Otavi Group platform carbonates of the Northern Foreland and Swakop Group slope and basin facies in the Kaoko and Damara Belts (Fig. 12.2; Swart 1992). Otavi Group carbonates occur east of the Goantagab Shear Zone in the eastern Ugab Zone (Miller et al. 1983; Swart 1992; Passchier et al. 2002). The Zerrissene Group contains two thin cap carbonate units correlated with glaciogenic horizons. The ldest carbonate is the Brandberg West Formation correlated with Sturtian age glaciation at ~720–700 Ma. It has no reported glaciogenic or mass flow deposits associated with it. The youngest cap carbonate is Gemsbok River Formation correlated with Karibib Formation in the Swakop Group. This overlies the Ghaub Formation mass flow diamictite horizon, correlated with Marinoan age glaciation at ~635 Ma (Hoffman et al. 1998; Hoffmann et al. 2004). The remaining Zerrissene Group is a monotonous sequence of pelagic turbidites contain metapelite, metapsammite and subordinate calcsilicate and chert bands. The Basal Zerrissene Group is Zebraputz Formation turbidites correlated with Ugab Subgroup of the Swakop Group. The Middle Zeissene Group is Brak River Formation turbidites correlated with Okonguarri or Arandis Subgroup in the Swakop Group. Top of the Zerrissene Group are Amis River Formation turbidites, correlated with the Kuiseb Formation in the Swakop Group. Rift facies felsic volcanics of the Nosib Group are not represented within the Ugab Zone, thusconstraining the deposition age for the Zerrissene Group to <740 Ma. The detrital zircon maximum deposition age for Brak River Formation is ~650 Ma, and detrital peaks indicate probable provenance from the Coastal Terrane, Nosib Group rhyolites and Stenian basement in the Congo Craton (Foster et al. 2015).

12.3.2.3 Damara Belt

The Cryogenian to Ediacaran Damara Supergroup was deposited on the attenuated Congo Craton passive margin between approximately 837 and 580 Ma (Fig. 12.2; Miller et al. 1983; Hoffman et al. 1994, 1998; Prave 1996; Hoffmann et al. 2004; Foster et al. 2015). These sequences range from passive margin carbonates of the Otavi facies that rimmed the oceanbasin, to deeper-water turbidites of the Swakop facies within the ocean basin (Hoffman et al. 1996; Hoffman et al. 1994, 2004; Halverson et al. 2002). Basal sequences are rift-related quartzite, conglomerate and arenite siliciclastics of the Nosib Group. The detrital zircon maximum deposition ages from Etusis and Khan Formations of the Nosib Group in the Central Zone are ~861 Ma (Foster et al. 2015), and they are further constrained by carbonatite extrusives in the Okahandja Zone at ~837 Ma (Buhn et al. 2001). The Upper Nosib Group contains quartz-syenite, alkaline ignimbrite and alkali-rhyolite volcanics of the Naauwpoort Formation of 748–746 and 757–752 Ma age in the Northern Zone (Hoffman et al. 1994; Hoffman et al.

1996; DeKock et al. 2000; Nascimento et al. 2016) and 750 Ma in the Central Zone (DeKock et al. 2000). Detrital zircon peaks in the Nosib Group indicate probable provenance from Stenian and Paleoproterozoic basement in the Congo Craton (Foster et al. 2015).

The overlying Swakop Group in the Damara Belt comprises slope and basin sequences dominated by turbiditic greywacke, with pelitic schists, psammites; rare mafic schists and turbiditic carbonate formations associated with diamictites (Hoffman et al. 1994, 1998). Diamictite horizons are mass flow deposits of remobilized glaciogenic material deposited on the platform and are associated with iron formation (Hoffmann et al. 1994; Nascimento et al. 2016). The oldest glaciogenic horizon is the Chuos Formation correlated with the Sturtian glaciation at ~720–700 Ma, and the youngest is the Ghaub Formation correlated with the Marinoan glaciation of 635 ± 1 Ma age, and with overlying Karibib Formation cap carbonates (Hoffman et al. 1994, 1998; Hoffmann et al. 2004). Top of the Swakop Group is the widespread Kuiseb Formation, consisting of turbiditic greywacke, with pelite schist and thin calcsilicate bands. The detrital zircon maximum deposition ages from the Karibib Formation are 634 and 651 Ma, and from the Kuiseb Formation are 607–611 and 619 Ma (Foster et al. 2015). The minimum deposition age for the Swakop Group is constrained by the oldest granite and metamorphic age determinations of ~580–570 Ma (Allsopp et al. 1983; Armstrong et al. 1987; Bergemann et al. 2014; Milani et al. 2014; Foster et al. 2015). The detrital zircon peaks in the Karibib and Kuiseb Formations indicate probable provenance from Coastal Terrane, Nosib Group felsic volcanics and Stenian, Tonian and Paleoproterozoic basement in the Congo Craton (Foster et al. 2015).

The Okahandja and Southern Zones contain the deep basin Khomas Group with basal Chuos Formation diamictite and ~714–705 Ma felsic volcanics (DeKock et al. 2000; DeKock and Armstrong 2014). The Khomas Group is otherwise dominated by Kuiseb Formation turbidites representing submarine fans shed off the Congo Craton into the Khomas Ocean basin (Fig. 12.4; Martin and Porada 1977; Hoffmann 1989; Kukla et al. 1991; Kukla and Stanistreet 1991; Gray et al. 2007; Foster et al. 2015; Foster and Goscombe 2013). The Tinkas Formation at the top of the sequence is a thick unit of massive metapsammopelite in the Okahandja Zone. The maximum deposition ages from Tinkas Formation are ~617 and ~645 Ma, and from the Kuiseb Formation are 636–638 Ma (Foster et al. 2015). The detrital zircon peaks in the Tinkas and Kuiseb Formations indicate provenance from Coastal Terrane, Nosib Group felsic volcanics and Stenian and Paleoproterozoic Congo Craton basement (Foster et al. 2015). The Matchless Suite within the Khomas Group comprises highly sheared tholeiitic gabbro, pillow basalt, amphibolite, serpentinite and metachert (Schmidt and Wedepohl 1983), interpreted as interthrust relict oceanic lithosphere (Barnes 1983; Killick 2000). The Matchless Belt is a 200–300 m wide and >350 km long belt containing discontinuous slivers of the Matchless Suite within a ~100 km wide accretionary wedge of sediment shed off the Congo Craton (Kukla and Stanistreet 1991; Gray et al. 2008).

The Damara Belt is contiguous, below the Kalahari Basin, with the Lufilian Arc and Zambezi Belt to the east. Upper Tonian to lower Cryogenian rift phase sequences of the Muva Supergroup in the Lufilian-Zambezi Belt record a ~940–735 Ma history, significantly longer than the Nosib Group in the Damara Belt. The basal units are quartzites of the Fombwe Group with maximum deposition ages of 962–957 Ma, overlain by the Kafue Group containing felsic volcanics of 880–879, 876 and 867 Ma (Johnson et al. 2007; Goscombe et al. in press b). The Nosib Group is correlated with rift-related quartzites of the Mpanshya Group in the upper Muva Supergroup. Rhyolite and mafic volcanics in the Mpanshya Group have 765–760, 747 and 735 Ma ages, overlapping with felsic volcanics in Naauwpoort Formation (Key et al. 2001; Johnson et al. 2005; Master et al. 2005). The overlying Katanga Supergroup in the Lufilian-Zambezi Belt spans ~750–580 Ma in common with the Swakop Group in the Damara Belt (e.g., Key et al. 2001). The Broken Hill Group in the middle Katanga Supergroup contains thick carbonate units interpreted as cap-carbonates, Matero-Chunga and Lusaka Formations, associated with the Sturtian and Marinoan glaciations, respectively. Maximum deposition ages of 705 and 729 Ma from the base of the Broken Hill Group confirm the Sturtian correlation (Goscombe et al. in press b).

12.3.3 Sequences Deposited on the Kalahari Craton

Whole-rock εNd values in metapelites and detrital zircons indicate that stratigraphic sequences either side of the Uis-Pass Suture have different provenance and were widely separated by an ocean basin (Fig. 12.2; Foster et al. 2015). The Damara Supergroup to the north has εNd values ranging from −3.0 to −5.0 and Congo provenance, and those in the Southern Margin Zone have εNd values of −8.0 and Kalahari provenance (Foster et al. 2015). Cryogenian to Ediacaran sequences in the Southern Margin Zone and Southern Foreland are shelf and slope facies deposited on the Kalahari Craton margin between approximately 840 and 550 Ma (Hoffmann 1989, 1994, 1997; Becker et al. 1998, 2004; Hoffmann and Schreiber 1998; Foster et al. 2015). The basal units are represented by rift-related quartzite, conglomerate and arenite siliciclastics confusingly called the Nosib Group and older Tsumis Group containing felsic volcanics of

820 Ma age (Kampunzu et al. 2000). Younger rift stage felsic volcanics of 729–742 Ma and 780 Ma age are preserved in the foreland of the Gariep Belt (Frimmel et al. 1996). The overlying Hakos Group in the Southern Margin Zone comprises slope facies dominated by greywacke, pelitic schist, psammite and minor mafic schist, and is correlated with the Witvlei Group in the Southern Foreland (Hoffman et al. 1998). The Hakos Group has two glaciogenic horizons: the Blaubeker Formation correlated with the Sturtian glaciation at ~720–700 Ma and the Naos Formation correlated with the Marinoan glaciation of ~635 Ma (Hoffmann et al. 2004). The Witvlei Group in the Southern Foreland is dominated by phyllite, siltstones and psammites, with basal Blaubeker Formation diamictite (Becker et al. 1998, 2004). The Witvlei Group is overlain by siliciclastics of the Nama Group deposited in the essentially unmetamorphosed Nama Basin on the Southern Foreland. The Kuibis and overlying Schwarzrand Subgroups are the uppermost units of the Damara platformal sequences. Deposition of the Schwarzrand Subgroup is constrained between 549–588 Ma on the basis of maximum deposition ages from detrital zircons and overlying felsic volcanics in the Fish River Subgroup (Foster et al. 2015), consistent with the fossil assemblages (Gresse and Scheepers 1993; Grotzinger et al. 1995). The detrital zircon peaks in the Kuibis and Schwarzrand Subgroups indicate probable provenance from the Sinclair Complex granites, Alberta Complex, Magondi Belt and Archaean of the Kalahari Craton (Foster et al. 2015). The Naukluft Nappe complex contains out-of-sequence thrust sheets that can be correlated with Southern Foreland stratigraphy, including Blasskranz Formation diamictite of 633 Ma age and correlated with the Naos Formation in the Southern Margin Zone (Fig. 12.2). The minimum deposition age for the Naukluft Nappe sequences is constrained by the oldest metamorphic age of 555 Ma (Gray et al. 2006).

12.3.4 Foreland Molasse Sequences

The Nama Basin in the Southern Foreland culminated in the Fish River Subgroup siliciclastic molasse, shed off the evolving Damara Belt between 552 and 519 Ma (Gresse and Scheepers 1993; Grotzinger et al. 1995; Foster et al. 2015). The Fish River Subgroup contains felsic volcanics of 539, 543–545 and 549 Ma age, and detrital zircon maximum deposition ages of 549, 550 and 552 Ma (Foster et al. 2015). The minimum deposition age is estimated from the youngest detrital metamorphic zircons and reworked volcanoclastic zircons of ~519 Ma age (Foster et al. 2015). These bracketing age constraints are confirmed by fossil assemblages (Gresse and Scheepers 1993; Grotzinger et al. 1995). The detrital zircons are predominantly 560–540 Ma, with metamorphic zircons ranging from 540 to 530 Ma, coinciding with prograde orogenesis, crustal thickening and maximum topography development in the Damara Belt. Other detrital zircon peaks at 615–645, 840 and 1060–1090 Ma indicate minor contribution from the Coastal Terrane and Sinclair Complex granites.

The Mulden Group siliciclastic molasse in the Northern Foreland (Guj 1970; Miller and Grote 1988) was deposited during obduction of the Coastal Terrane and the start of pervasive deformation in the Kaoko Belt from ~590 to 580 Ma (Hoffmann et al. 2004; Goscombe et al. 2005b; Gray et al. 2006). The Mulden Group in the eastern Kaoko Belt and the equivalent Hartmann Subgroup within the core of the belt were folded by shortening across the belt late in transpressional orogenesis, indicating the cessation of deposition and incorporation within the belt soon after peak orogenesis at ~580–570 Ma. The detrital zircon maximum deposition age from the Hartmann Subgroup is ~621 Ma (Goscombe et al. 2005b). Deposition of material shed off the Kaoko Belt may have persisted longer further east in the Northern Foreland and Northern Zone. The maximum deposition age from the Mulden Group metapsammite preserved in a Damaran Phase infold in the Northern Foreland is ~590 Ma (Foster et al. 2015). The oldest Damaran deformation fabrics recorded in the Northern Foreland ranges from ~556 to 550 Ma (Clauer and Kroner 1979), constraining the deposition of material shed off the Kaoko Belt between ~590 and 556 Ma. The detrital zircon peaks from the Mulden Group samples indicate probable provenance from the Coastal Terrane, Paleoproterozoic and Neoarchaean basement within the Kaoko Belt and Stenian and Paleoproterozoic basement in the Congo Craton (Goscombe et al. 2005b; Foster et al. 2015).

Molasse sequences associated with the Lufilian-Zambezi Belt show similarities with the Damara Belt. The Kundelunga Group at the highest stratigraphic level in the Lufilian Arc contains molasse and conglomerates with detrital zircon maximum deposition ages ranging from 565 to 560 Ma (Goscombe et al. in press b), consistent with main phase orogenesis in the Zambezi Belt and Lufilian Arc between ~550 and 525 Ma (e.g., Goscombe et al. 1998; John et al. 2004). Molasse shed to the south of the Zambezi Belt is preserved in Sijarira Group quartzites deposited onto the Zimbabwe Craton. The maximum deposition ages from the basal Sijarira Group are 570 Ma, and 527–515 Ma from the top of the sequence (Goscombe et al. in press b). Consequently, molasse shed from the Lufilian-Zambezi Belt post-date the Mulden Group molasse shed off the Kaoko Belt, and overlap in age with the Fish River Subgroup molasse shed off the Damara Belt. The detrital zircon peaks from the Lufilian-Zambezi molasse indicate probable provenance from sequences and basement within the Lufilian-Zambezi Belt, Bangweulu Block, Ubendian Belt,

Irumide Belt and South Irumide Province, all within the Congo Craton. Source regions are restricted to the north, implying that the Lufilian-Zambezi Belt shares a south vergent asymmetric architecture in common with the Damara Belt, with the Congo Craton in an upper-plate setting and the Kalahari Craton in the foreland.

12.3.5 Basement Units

A range of Neoarchaean to Neoproterozoic Congo Craton basement is exposed across the Northern Foreland such as the Kamanjab Inlier and Eupupa Complex, within antiformal infolds and nappes in the Kaoko Belt, and antiformal domes in the Northern, Central and Southern Zones of the Damara Belt (Fig. 12.2). The Kamanjab Inlier consists of a 1987 ± 4 Ma age Korbendus Sequence and a 1811 ± 35 Ma age Huab Sequence (Tegtmeyer and Kroner 1985), intruded by 1838, 1662 and 1580–1547 Ma granite suites (Burger et al. 1976). Antiformal nappes in the External Nappe Zone of the Kaoko Belt contain Archaean orthogneiss of 2645–2585 Ma age (Seth et al. 1998), correlated with 2606 Ma orthogneiss incorporated into the Ogden Mylonite Zone (Goscombe et al. 2017b). Most Kaoko Belt nappes are cored by the Paleoproterozoic Epupa Metamorphic Complex consisting of paragneiss, quartzite, mafic gneiss and granitic orthogneisses of 1985–1933, 1861 and 1776–1752 Ma age, and metamorphosed between 1697 and 1768 Ma (Tegtmeyer and Kroner 1985; Seth et al. 1998). The Supracrustal Epupa Group in the northern Epupa Complex has a maximum deposition age of ~1600 Ma and was metamorphosed at 1520–1592 Ma, indicating a rapid deposition-burial-metamorphism cycle. The Kunene Anorthosite Complex was emplaced into the northern Epupa Complex at ~1374 Ma. Paleoproterozoic ages are almost absent from the Orogen Core of the Kaoko Belt (Goscombe et al. 2005b). Mesoproterozoic basement containing quartzite, amphibolite and felsic orthogneiss of 1489–1513 Ma age occurs in both the External Nappe Zone and the Orogen Core of the Kaoko Belt (Seth et al. 1998; Kröner et al. 2004; Goscombe et al. 2005b). The Abbabis Complex basement infolds and inherited zircons from the Central Zone of the Damara Belt indicate at least four episodes of granitoids: 2090–2038, 2000–1945, 1115–1102 and 1063–1028 Ma, metmorphism at 1000 ± 12 Ma (Armstrong et al. 1987; DeKock et al. 2000; Steven et al. 2000; Singletary et al. 2002; Foster et al. 2015), and mafic intrusives of ~1081 Ma age in the Southern Zone (Steven et al. 2000). Parts of the Central Zone basement unconformity are preserved as an intact Fe–Al-rich meta-paleosoil profile up to 10 m thick (Fig. 12.10h; Goscombe et al. 2017b).

Paleoproterozoic to Neoproterozoic Kalahari Craton basement such as Rehoboth and Sinclair Complexes are exposed across the Southern Foreland and within large antiformal domes and nappes in the Southern Margin Zone. The Paleoproterozoic Rehoboth Complex has sequences and granites ranging from ~1747 to 1782 Ma and these were intruded by the Alberta mafic-granite complex of ~1376 Ma age (Becker and Hersfeld 1995). The Stenian age Sinclair Complex is part of the larger Sinclair-Ghanzi-Chobe Belt that stretches along the southern margin of the Damara Belt into Botswana. Sinclair Sequences and granites range from ~1078 to 1217 Ma, with mafic intrusives and volcanics of ~1104–1108 Ma age, and post-tectonic Gamsberg granites of ~1040 Ma age (Pfurr et al. 1991; Hoal and Heaman 1995; Kampunzu et al. 2000; Singletary et al. 2003).

12.4 Granite Magmatism

12.4.1 Coastal Terrane

The earliest intrusives in the Coastal Terrane are metamorphosed I-type intermediate granitoids such as monzodiorite, granodiorite and monzogranite with minor mafics, such as diorite, quartz diorite, quartz gabbro and mela-gabbro (Seth et al. 1998; Franz et al. 1999; Masberg et al. 2005). This calcalkaline suite has arc affinities with sources interpreted to be biotite- and/or hornblende-bearing, muscovite-free intermediate rocks such as diorite, granodiorite or greywacke, consistent with an arc setting (Masberg et al. 2005). All granitoids are metamorphosed and annealed at high metamorphic grades to polygonal granoblastic textures. Granitoid age determinations fall into three groups: inaccurate ages spanning 694–730 Ma, orthogneiss of 661–656 Ma age and granite sills of 638–620 Ma age (Seth et al. 1998; Kröner et al. 2004; Goscombe et al. 2005b). The younger granitoid episodes bracket 640.5 ± 1.0–645 ± 4 Ma high-grade metamorphism in the Coastal Terrane (Franz et al. 1999). These arc intrusives overlap in age with deposition of the Damara Sequence to the east, indicating an outboard setting for the Coastal Terrane. Granitoids of ~650–630 Ma age also occur in the footwall of the Three Palms Mylonite Zone (Konopásek et al. 2005), indicating that the Coastal Terrane was attached to the leading edge of the attenuated Congo Craton passive margin, outboard of a deep turbiditic back-arc basin containing Damara Sequences (Goscombe and Gray 2008).

12.4.2 Kaoko Belt

The Kaoko Belt was intruded by a suite of S-type granites emplaced at all stages of the transpressional orogenic cycle, contributing ~20% of the western part of the belt (Fig. 12.3). S-type granites are concentrated around the

Three Palms Mylonite Zone, intruding both the Coastal Terrane and the Orogen Core, but they are absent from the External Nappe Zone. Consequently, the Coastal Terrane was obducted prior to emplacement of the S-type granite suite (Goscombe and Gray 2007). In contrast to earlier I-type intrusives in the Coastal Terrane, these preserve magmatic textures though have been later sheared, grain-refined and foliated during transpressional orogenesis (Goscombe et al. 2005b). The S-type suite is dominated by large lenticular plutons of synkinematic biotite-rich megacrystic granite, medium-grained biotite granite and syenogranite of 580–562 Ma age (Seth et al. 1998; Franz et al. 1999; Goscombe et al. 2005b). Late-kinematic granite plutons and veins of 558–549 Ma age crosscut the main phase of regional foliation and are sheared by crustal-scale shear zones (Seth et al. 1998; Franz et al. 1999; Kröner et al. 2004; Goscombe et al. 2005b). The youngest episode of felsic magma associated with transpression is interboudin pegmatite infill of 539 ± 6 Ma age (Kröner et al. 2004). Three episodes of post-kinematic pegmatite sills and dykes are recognized that crosscut the major shear zones and both the Coastal Terrane and the Orogen Core. These include north-northwest-southeast trending pegmatites of 531–530 Ma age and northeast-southwest trending pegmatite dykes of 515 Ma age, dated from the southern Coastal Terrane (Goscombe et al. 2005b). Pegmatite dyke swarms of 508 Ma age trends east–west to east-southeast-west-northwest crosscut the Three Palms Mylonite Zone and are associated with a local thermal anomaly of 507–505 Ma age (Goscombe et al. 2005b).

12.4.3 Damara Belt

Granitic rocks are a major component of the Damara Belt, composing 25% of outcrop and concentrated in the Central Zone (Fig. 12.3; Miller et al. 1983). Granite plutons are an important component of the Ugab and Northern Zones, large post-kinematic Donkerhoek leucogranite batholith is the only significant granitoid in the Okahandja Zone, and the Southern Zone has only a single swarm of m-scale 513 ± 17 Ma granite sills (Goscombe et al. 2017b). Granitoids are predominantly S-type, and clear mantle signatures such as positive εNd and low δ18O are limited, even in the less common mafic I-type granitoids, indicating that crustal recycling dominated petrogenesis (McDermott and Hawkesworth 1990; Jung et al. 2000a). There is little evidence for typical subduction-generated magmatic arc models, with margin-parallel linear batholiths and margin-normal geochemical gradients being absent (Kasch 1983a), while felsic S-type granites dominate and mafic granitoids with mantle isotopic signatures rare (Jung et al. 2001). However, greater volumes of mafic magmas may have pooled below the zone of felsic crustal melting, resulting in magma hybridization within the crust. The combination of high heat flow from the thinned lithosphere (Goscombe et al. 2017a), high radiogenic heat production (Haack et al. 1983; Ballard et al. 1987) and the high fertility of Damara metasediments resulted in massive middle and lower-crustal melting (Haack et al. 1982; McDermott and Hawkesworth 1990; Jung et al. 2001). Granites predominate, making up 96%, granodiorite and tonalite only 2% and diorite and gabbro the remaining 2%. There are five broad periods of granitoid emplacement, largely overlapping with metamorphic peaks (Fig. 12.2), as follows:

1. Granites of Kaokoan age (580–570 Ma) and pre-dating collision in the Damara Belt contribute a minor component in the Central Zone (Allsopp et al. 1983; Armstrong et al. 1987; Bergemann et al. 2014; Milani et al. 2014). A small number of discordant metamorphic zircon age determinations from the Central Zone have similar ages of 585–570 Ma (Armstrong et al. 1987; Foster et al. 2015).
2. Pre- to synkinematic I-type intermediate metaluminous granitoids with hornblende and clinopyroxene are rare, and include partly calcalkaline quartz diorites and granodiorites with some magmatic arc affinities (Haack et al. 1982; Miller et al. 1983; Hawkesworth et al. 1986; McDermott et al. 1996; Jung et al. 2001, 2015). These are consistently among the oldest granitoids (>540 Ma), including 568–545 Ma Goas-Palmental in the South Central Zone (DeKock et al. 2000; Jacob et al. 2000; Jung et al. 2001, 2015; Milani et al. 2014). Other I-type complexes include Okongava dioritic complex in the Central Zone and Bandombaai Complex in cores of composite plutons in the Ugab Zone. Isotopic signatures vary significantly—$^{87}Sr/^{86}Sr$ range 0.704–0.713, εNd range 0.0 to −20.0 and δ18O range 7–13‰—indicating multiple magma sources (Hawkesworth et al. 1981; Haack et al. 1982; Miller et al. 1983; McDermott et al. 1996; Jung et al. 2001; van de Flierdt et al. 2003). Isotope and chemical signatures indicate multiple magma sources ranging from primitive lithospheric mantle-derived melts lacking assimilation to those indicating assimilation with remelting of metabasalt and granulite basement in the lower crust (Hawkesworth et al. 1981; Jung et al. 2001, 2015).
3. Syn- to late-kinematic peraluminous S-type granites of 546–515 Ma age (DeKock and Armstrong 2014) predominate in all regions. The Ugab Zone is intruded by at least five distinct episodes of S-type granite and syenogranite plutons of ~530, ~526, ~520, ~516 and ~512 Ma age (Seth et al. 2000; van de Flierdt et al. 2003; Lobo-Guerrero Sanz 2005; Schmitt et al. 2012; Lehmann et al. 2015; Goscombe et al. 2017b). S-type

granites include Salem-type porphyritic, biotite-rich granites and minor alaskite formed from disequilibrium dehydration melting of muscovite metapelites (McDermott et al. 1996; Basson and Greenway 2004). S-type granites show an exceptionally wide range in isotope composition: $^{87}Sr/^{86}Sr$ ranging from 0.708 to 0.740, εNd ranging from −2.0 to −19.0, and high δ18O values of 11–15‰ (Haack et al. 1982; McDermott et al. 1996; Jung et al. 2001). These signatures indicate crustal sources dominated by Damara metasediments and minor pre-Damara basement, generated by dehydration melting at mid-crustal levels >6 kb (Haack et al. 1982; McDermott and Hawkesworth 1990; Jung et al. 2000a, 2001).

4. Minor peraluminous A-type granites have slightly later ages, ranging from synkinematic 525 Ma to post-kinematic 486 Ma (Jung et al. 1998a, 2000a; McDermott et al. 2000). These are rich in high field strength elements and have within-plate signatures. Isotope signatures are less evolved, such as $^{87}Sr/^{86}Sr$ ranging 0.7034–0.709, εNd ranging 0.0 to −6.0 and as low as −16.0 in Sorris-Sorris A-type granites. These hot magmas of >800 °C involved remelting of lower crust at 8–10 kb, from metatonalite sources with mixed mantle and crustal isotopic signatures.
5. There is a variety of post-kinematic granitoids ranging from 515 to 464 Ma (DeKock et al. 2000; Jacob et al. 2000; Jung and Mezger 2003a; Longridge et al. 2014; Paul et al. 2014; Goscombe et al. 2017b). These include rare I-type granites in the south Central Zone and Sorris-Sorris Suite red granite in the Northern and Central Zones, and Donkerhoek leucogranite batholith of 508 ± 3–504 ± 4 Ma age in the Okahandja Zone (Kukla et al. 1991; DeKock and Armstrong 2014).

12.5 Deformation History

The Damara Orogenic System preserves evidence for three orogenic cycles (Fig. 12.2):

1. The **Coastal Phase or M1 metamorphic cycle** (660–620 Ma) involved subduction outboard of the Coastal Terrane, producing calcalkaline magmatism and low-*P*/high-*T* metamorphism within this magmatic arc (Franz et al. 1999; Kröner et al. 2004; Masberg et al. 2005; Goscombe et al. 2005b; Goscombe and Gray 2007).
2. The **Kaokoan Phase or M2 metamorphic cycle** (590–535 Ma) involved obduction of the Coastal Terrane onto the west Congo Craton margin, producing main phase transpressional orogenesis of the Kaoko Belt and Ugab Zone (Passchier et al. 2002; Goscombe et al. 2003a, b, 2004, a, b; Konopásek et al. 2005; Goscombe and Gray 2007, 2008).
3. The **Damaran Phase or M3 metamorphic cycle** (555–505 Ma) involved collision of the Kalahari Craton with the south Congo Craton, producing high-angle shortening in the Damara Belt (e.g., Hoffer 1978; Coward 1981; Miller et al. 1983; Porada et al. 1983; Gray et al. 2008).

Deformation structures, magmatic rocks and metamorphic parageneses preserve a detailed record of orogenesis from collision, main phase orogenesis, metamorphic response and exhumation and cooling. Detailed age-calibrated deformation histories from different parts of the Damara Orogenic System have been correlated on the basis of the stress fields, transport and age constraints they have in common (Table 12.1; Goscombe et al. 2017b). The principle compressive stress rotated clockwise through ~180° in total during evolution of the Kaoko Belt starting 590 Ma, and ~135° during evolution of the Damara Belt starting 555 Ma. Progressive rotation was punctuated by rapid stress switches at ~530–525, ~508 and ~505–500 Ma. A full description of the deformation history and structures developed in different tectonometamorphic zones is available in the work of Goscombe et al. (in press, 2017b) and represented diagrammatically in Figs. 12.5, 12.7 and 12.14. The main stages are summarized here.

12.5.1 Kaokoan Phase: 590–550 Ma

12.5.1.1 Obduction: ~590–580 Ma

The Kaoko Belt and Ugab Zone were contiguous from the inception of orogenesis and both preserve early flat-lying bedding-parallel *L*–*S* mylonitic fabrics, with pronounced mineral aggregate lineation in unfolded original orientations trending east–west (Figs. 12.6a and 12.7). Early boudins trains formed prior to main phase chevron folding in the Ugab Zone and are correlated with this event. These fabrics are partitioned into the footwall of the Thee Palms Mylonite Zone in the Kaoko Belt, and preserved in chert and carbonate bands throughout the Ugab Zone to the west of the Goantagab Shear Zone (Vrede–Doros–Brandberg line). These structures are interpreted to have formed at the earliest stages of orogenesis during collision and east-vergent obduction of the Coastal Terrane onto the Congo Craton margin (Goscombe et al. 2003a; Konopásek et al. 2005).

12.5.1.2 Progressive Transpression: 580–550 Ma

Main phase *S*–*L* foliations defining peak metamorphic parageneses in the Kaoko Belt formed under east-southeast- to southeast-directed transport at 580–570 Ma. Progressive sinistral transport under this stress field was partitioned into fold and nappe shortening across the belt, and oblique

Table 12.1 Simplified time-space table of deformation, magmatic and metamorphic correlations across the four distinct tectonometamorphic provinces of the Damara Orogenic System

σ1*	AGE	KAOKO BELT		NORTHERN MARGIN		OROGEN CORE		SOUTHERN MARGINS	
	Coastal Terrane Only:								
	660-655		Calc-alkaline arc granitoids						
	650-640		M1-peak metamorphism						
	640-620		Granite sills						
	~600-585			<598-584	Ar-Ar ms, defm/detrital [NZ]			Subduction / Accretion in Southern Zone	
to 090°	~590	Obduction of Coastal Terrane						D1sz	Bedding foliation, qtz-veins [SZ]
to 090°	~590-580	D1kz	Flat-lying early foliation	D1nz	E-W stretching lineation [UZ]				
to 120°	~580-570	D2kz	Main L-S fabric	D2nz	Chevron folds, main foliation		Metamorphic zircon		Schwarzrand SG deposition
	580-570		M2-peak metamorphism		M2-peak main foliation		End of deposition on Congo		End deposition on Kalahari
	580-560		Syn-kinematic granite		Granite		Pre-kinematic granite	D1sz	Bedding foliation, qtz-veins [SMZ]
to 120°	~570-550	D3kz	Progressive transpression	D3nz	NE-SW sinistral folds		I-type granitoids		
to ~140°	555	Collision Congo-Kalahari Cratons		556-550	K-Ar defm [Nth Foreland]			555	Nappe Ar-Ar ms [Naukluft]
	560-550		Late-kinematic granite			D1cz	Prograde, melt, gneissic fabric	D2sz	Axial planar main foliation
to 140°	~550-540	late-D3kz	Strike-slip sinistral shear zones				S-type syn-kinematic granite		Fish River SG deposition
to 140°	545-535		Final late-kinematic melt		West, Doros, Omangambo		M3a-prograde metamorphism		Detrital metamorphic zircons
	540-535				K-Ar phyllite age [Foreland]		Anatectic Red granites		
	535-530				K-Ar phyllite age [Foreland]	late-D1cz	Intrafolial isoclines	D3sz	Main folds, nappes
to 160°	530	D4kz	End ductile shearzones	early-D4nz	NNW-SSE shortening folds	D2cz	Peak metamorphic events, melt		
	530		Post-kinematic pegmatite	M3#1	Doros, Footspore Granites		M3b-peak#1 [main peak SCZ]		
	530				Mineralization [Foreland]		Syn-peak leucogranite sill [SCZ]		
	528-526				Omangambo Granite		Aplite-granite sills [NCZ]		
to 160°?	~530-525	D5kz	Transtension reactivation				M3b-peak#1 [NCZ, OZ]		
	530-525		Rapid cooling exhumation			D3cz	N over S folds, foliation, melt	D4-5sz	Peak mineral growth [SZ-OZ]
to 160°	525-522			mid-D4nz	NNW-SSE shortening		M3b-peak#2 [SCZ]	1st cycle	M3-peak [SZ]
	522-518			M3#2	South Ugab Granite		M3b-peak#2 [main peak NCZ]		M3-peak [Sth OZ]
	520-513		Regional cooling Ar-Ar		Cooling Ar-Ar [west NZ]		A-type syn-kinematic granite	D6-8sz	Initiate exhumation [SZ-OZ]
	521-520						Syn-kinematic grey granite	1st cycle	
	~518-516					D4cz	NNW over SSE tight folds		
	520-517						M3b-peak#3 [SCZ]		
	517						Late-kinematic pegmatite [NCZ]		
to 180°	~518-516	D6kz	N-S shortening folds	late-D4nz	N-S shortening	D5cz	Tight folds, S over N, foliation	D4-5sz	Peak mineral growth [SMZ-SF]
	516-513					early-D6cz	Magmatism, oblate shortening	2nd cycle	M3-peak [Nama]
	516-515		Post-kinematic N-S pegmatite	M3#3	West Ugab Granite		Alkali-feldspar pegmatite [NCZ]		M3-peak [SMZ]
	516-514						M3b-peak#3 [NCZ]		M3-peak [SF]
	516-513						Post-peak S-type granite	D6-8sz	Initiate exhumation [SMZ]
	513-508					late-D6cz	Thermal anomaly, extension		
	515-505						M3c-late thermal pulse [CZ]	2nd cycle	Post-kinematic granite [SF]
	513-511			M3#4	Omangambo, Baddocks Bay		Late-kinematic granite [CZ]		Post-kinematic granite [SZ]
	511-508						Extensional granite veins [SCZ]		
to 225°	<512			D5nz	NE-SW shortening, warps				
to 225°	<512			D6nz	NE-SW shortening, kinks			D9sz	NE-SW shortening, kinks
	~510				Distal cooling Ar-Ar ms				350°C cooling Ar-Ar ms, [SF]
	Otavi Domain Only:								
	510			D4-5	M3-peak metamorphism				
	<510			D6-8	Initiate exhumation [Otavi]				
to 270°	~512-508			D7nz	E over W shortening folds	D7cz	E over W upright folds, domes		
to 270°	~512-508			D8nz	Brittle E-W thrusting				
to 270°	508-505		Post-kinematic ESE pegmatite		Strathmore Granite		Donkerhoek granite		
vertical σ1	505	D7kz	N-S extension			D8cz	Flattening folds, N-S extension		500°C cooling Ar-Ar hbl
	507-505		M3c-late thermal pulse						
	502						Decompression melting		
vertical σ1	500					D9cz	Core complex, N-S extension		
	500-470		Late-cooling Ar-Ar ms,bt		Cooling Ar-Ar ms,bt		Cooling 700 to 500 °C		350°C cooling Ar-Ar ms
	490-460						Cooling 500 to 300 °C		300°C cooling Ar-Ar bt

Age determinations from intrusives, metamorphic parageneses and cooling ages have been used to constrain the probable age range for deformation events (Goscombe et al. 2017a). *, approximate trend of principle compressive stress (σ1), with arrow indicating transport direction of the upper plate; based primarily on the Kaoko Belt and west Ugab Zone. Deformation events are labelled by province: Dkz, Coastal Terrane and Kaoko Belt north of the Etendeka Plateau; Dnz, Ugab Zone and west Northern Zone; Dcz, South Ugab Zone, Central Zone and north and central Okahandja Zone; Dsz, south Okahandja, Southern and Southern Margin Zones, Southern Foreland

sinistral slip in crustal-scale shear zones (Fig. 12.8). Main phase transpressive deformation was more distributed in the shallow crustal Ugab Zone, forming pervasive map-scale chevron folding with axial planar schistosity (Figs. 12.6b, d and 12.7). Overprinting second generation folds and boudinage showing sinistral-reverse vergence, occurred in both regions and formed under shortening directions closer to northwest-southeast, indicating ~45° stress field rotation from collision through main phase transpression events (Figs. 12.5 and 12.6e). Both fold generations are overprinted by 530 Ma granites in the Ugab Zone (Seth et al. 2000; Goscombe et al. 2004; Passchier et al. 2007), restricting progressive sinistral transpression to between 570 and 530 Ma. The main phase events in the Kaoko Belt are coeval with synkinematic granites ranging in age from 580 to 550 Ma. Within the Damara Belt there are cryptic indications of Kaokoan events in the more distal Central Zone, such as rare pre-kinematic granite and metamorphic age determinations ranging from 580 to 570 Ma (Fig. 12.7; Allsopp et al. 1983; Armstrong et al. 1987; Bergemann et al. 2014; Milani et al. 2014; Foster et al. 2015). Kaokoan fold generations have not been documented in the Central Zone

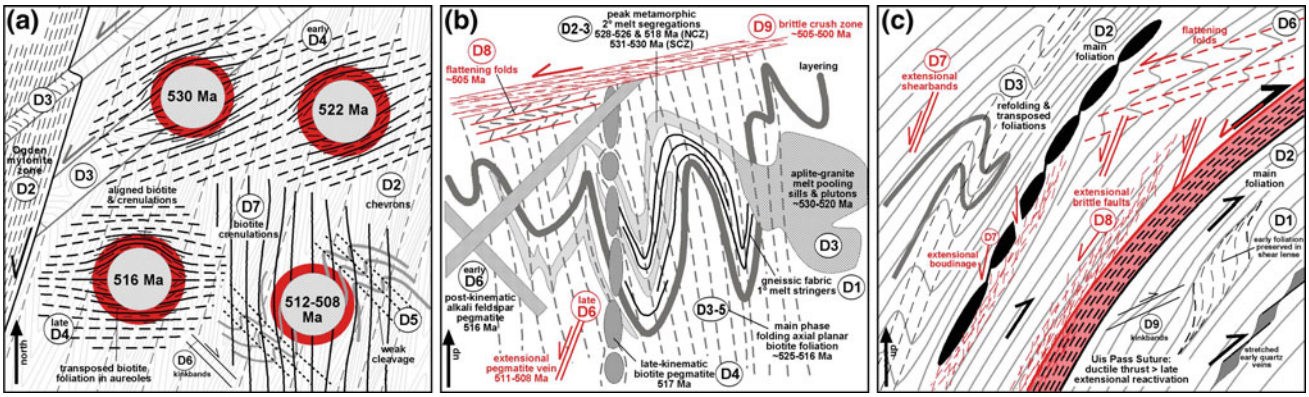

Fig. 12.5 Diagramatic summary of key overprinting relationships, timing and deformational styles in the key regions of the Ugab Zone, Central Zone and southern margin (from Goscombe et al. 2017b). The relationships between deformation fabrics such as main phase foliations and fold axial planes (black and grey lines) and granite-pegmatite intrusions (cross-hatch and patterns) are represented diagrammatically. Contact aureoles in the Ugab Zone are indicated by red margins. The red structures and symbols in the Central Zone and southern margin indicate vertical flattening extensional structures

either because strain was low and structures did not develop, or because developed structures are obscured by subsequent high-grade metamorphism, magmatism and deformation.

12.5.2 Damaran Phase: 555–508 Ma

12.5.2.1 Subduction and Collision: 555–550 Ma

Subduction of the Kalahari lithosphere below an already attenuated Congo Craton passive margin occurred prior to 555 Ma, without producing large-scale magmatic arcs, linear batholiths or significant volumes of mafic granitoids with mantle signatures (Kasch 1983b; Jung et al. 2000a). The leading edge of the upper plate does, however, contain pre-kinematic I-type intermediate metaluminous granitoids, including calcalkaline quartz diorites and granodiorites with some magmatic arc affinities (Fig. 12.4; Haack et al. 1982; Miller et al. 1983; Hawkesworth et al. 1986; McDermott et al. 1996; Jung et al. 2001). These include the Goas-Palmental and other complexes of 568–556 Ma age in the South Central Zone, sourced from remelting of the lower crust (DeKock et al. 2000; Jacob et al. 2000; Jung et al. 2001, 2015; Milani et al. 2014). In the absence of blueschist-eclogite subduction parageneses and unambiguous magmatic arc suites, little evidence of the subduction stage is preserved in the rock record. Nevertheless, first-order constraints such as sediment provenance indicating cratons separated by an ocean basin (Foster et al. 2015), interthrust oceanic lithosphere (Barnes 1983; Killick 2000), homoclinal accretionary wedge and gross structural asymmetry of the orogen (Gray et al. 2008; Foster et al. 2015) are evidence for subduction at this margin (Fig. 12.8). Fine-grained, bedding-parallel schistosity preserved in shear lenses and widespread quartz veining in the Southern Zone probably formed in an accretionary wedge setting, prior to being transposed during collision and subsequent orogenesis (Figs. 12.5, 12.9a). Distal expressions of pre-collisional shortening that have been correlated with subduction are (1) early north–south stretching lineations in the west Northern Zone (Goscombe et al. 2004; Passchier et al. 2016); (2) 598–584 Ma Ar–Ar ages in the west Northern Zone (Lehmann et al. 2015), however, are maximum ages because the samples retain some detrital mica; and (3) uncommon 585–570 Ma granites and metamorphic zircons in the Central Zone (Allsopp et al. 1983; Armstrong et al. 1987; Bergemann et al. 2014; Milani et al. 2014; Foster et al. 2015). Ocean closure and collision are dated at ~555 Ma by Ar–Ar muscovite from phyllonite in the basal thrust of the Naukluft Nappe Complex (Gray et al. 2008). Early thin skin transport of the nappes onto the foreland removed them from resetting by later main phase events in the internal parts of the orogen. This age is confirmed by deposition of the Fish River Subgroup molasse in the Nama Basin starting from ~552 Ma (Grotzinger et al. 1995; Foster et al. 2015), and 556–550 Ma K–Ar deformation ages from phyllites in the Northern Platform (Clauer and Kroner 1979).

12.5.2.2 Prograde Northwest-Southeast Shortening: 550–530 Ma

Transpressional strain in the Kaoko Belt was progressively partitioned into oblique- to strike-slip shear zones, while shortening structures such as folds and nappes ceased to operate and were eventually overprinted by the shear zones (Figs. 12.6c and 12.7). This progression reflects rotation to northwest-southeast principle compressive stress, at lower angles to the grain of the belt producing a lower shortening component. Once established, these large-scale shear zones continued to operate and reactivate until ~525 Ma.

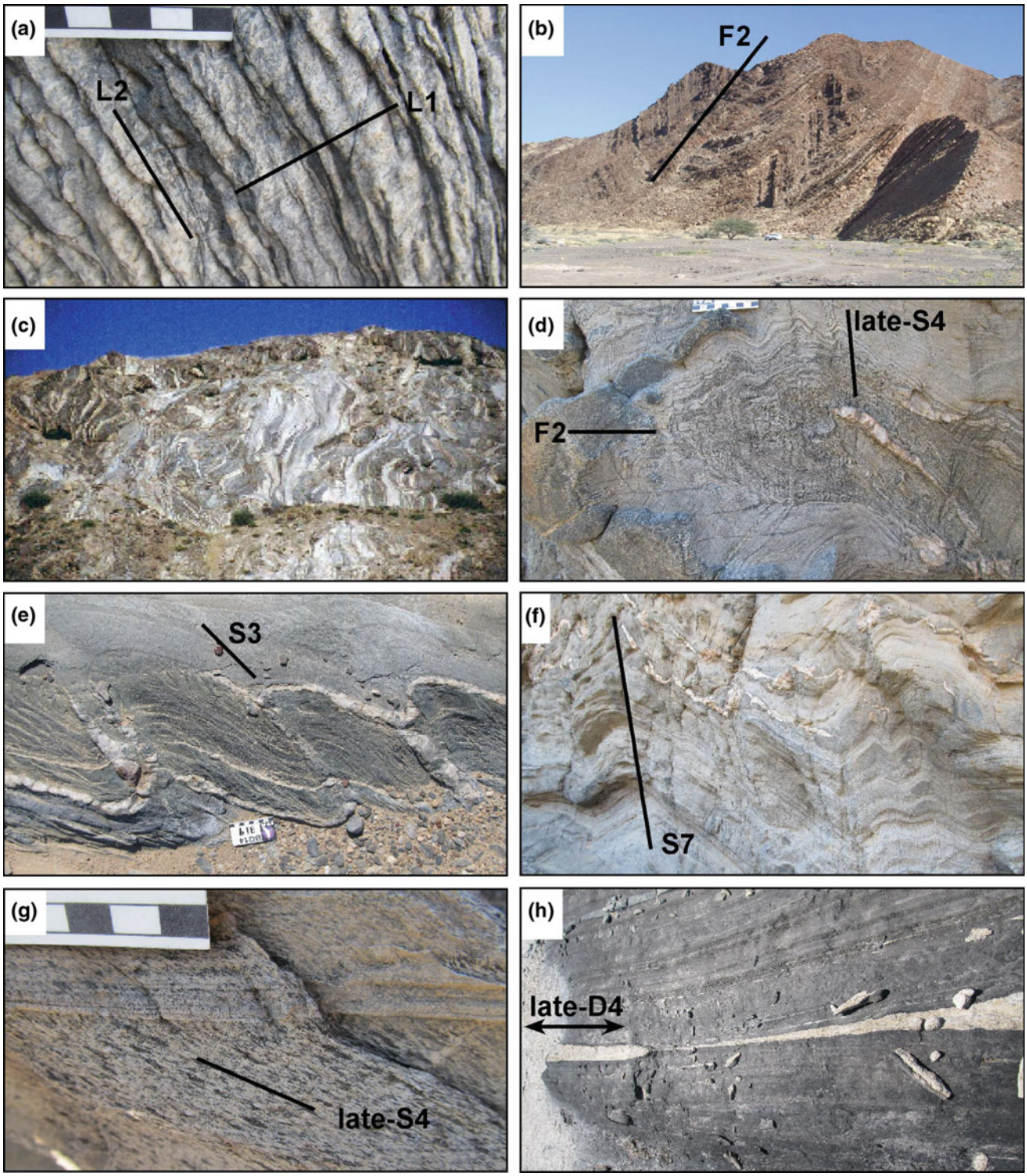

Fig. 12.6 Representative deformation structures from the Kaoko Belt and Ugab Zone. **a** Earliest phase D1nz quartz aggregate stretching lineation in thin metachert bed, overprinted by D2nz Kaokoan main phase intersection mullions. **b** Inclined Kaokoan Phase D2nz tight map-scale chevron folds. **c** Large-scale foliation boudinage of high-grade metaorthogneisses and strain partitioning into shear zones and lenticular lenses during transpressional orogenesis, typical of the west Kaoko Belt. **d** Kaokoan Phase D2nz fold transected by late-D4nz crenulations with biotite growth. **e** Kaokoan Phase D2nz boudins train sinistral sheared by D3nz producing weak foliation parallel to the rotated interboudin plane. **f** Asymmetric D7nz folds with weak axial planar crenulation with biotite growth. **g** Damaran Phase late-D4nz biotite foliation. **h** Strongly transposed D2nz and late-D4nz, and extreme stretch of aplite dyke in West Ugab granite contact aureole

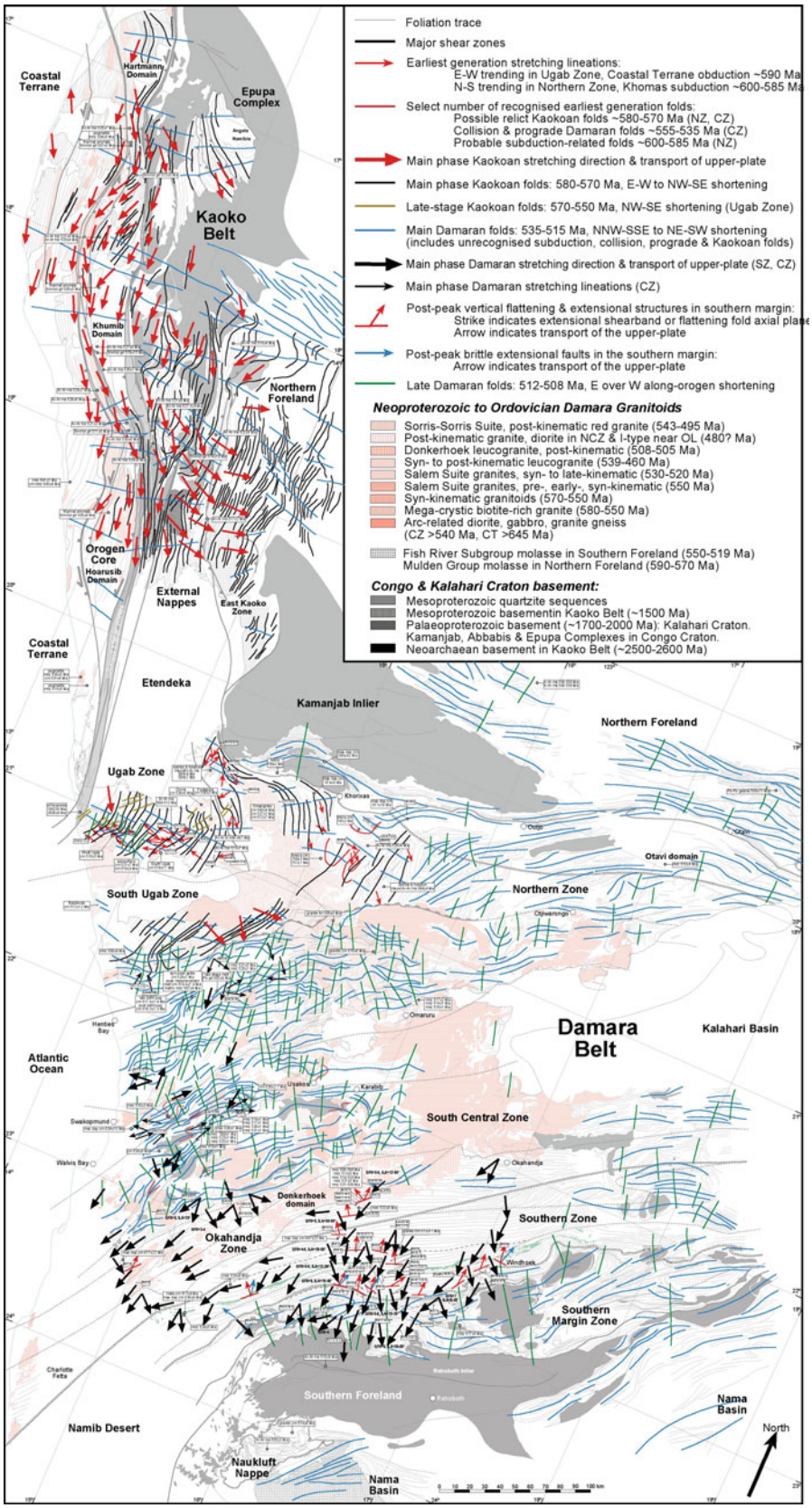

Fig. 12.7 Distribution of Kaokoan Phase and Damaran Phase deformation effects throughout the Damara Orogenic System, based on a synthesis of different generation deformation structures. The deformation structure symbology is outlined in the legend. The deformation structures for the Damara Belt are sourced from Goscombe et al. (2017b), and those of the Kaoko Belt are sourced from Goscombe et al. (2003) and Goscombe and Gray (2008). In general, main phase kaokoan folds (black), late-Kaokoan folds (gold), main phase Damaran folds (blue) and late-stage along orogen shortening (green). Main phase Kaokoan transport is indicated by thick red arrows and main phase Damaran transport by thick black arrows. Relict early-formed structures formed in different settings in the Ugab, Central and Northern Zones are indicated by thin red lines and arrows. Late-stage extensional and vertical flattening structures in the southern margin are indicated by red (ductile) and blue symbols (brittle). Robust peak metamorphic U–Pb age determinations are annotated (Goscombe et al. 2017a, b). A select number of U–Pb magmatic age determinations and maximum deposition ages crucial to constraining the deformation and metamorphic history are also indicated (Goscombe et al. 2017a, b). Semiquantitative strain ratio determinations, typical interlimb angles and qualitative foliation intensity domains (Goscombe and Gray 2008) are indicated

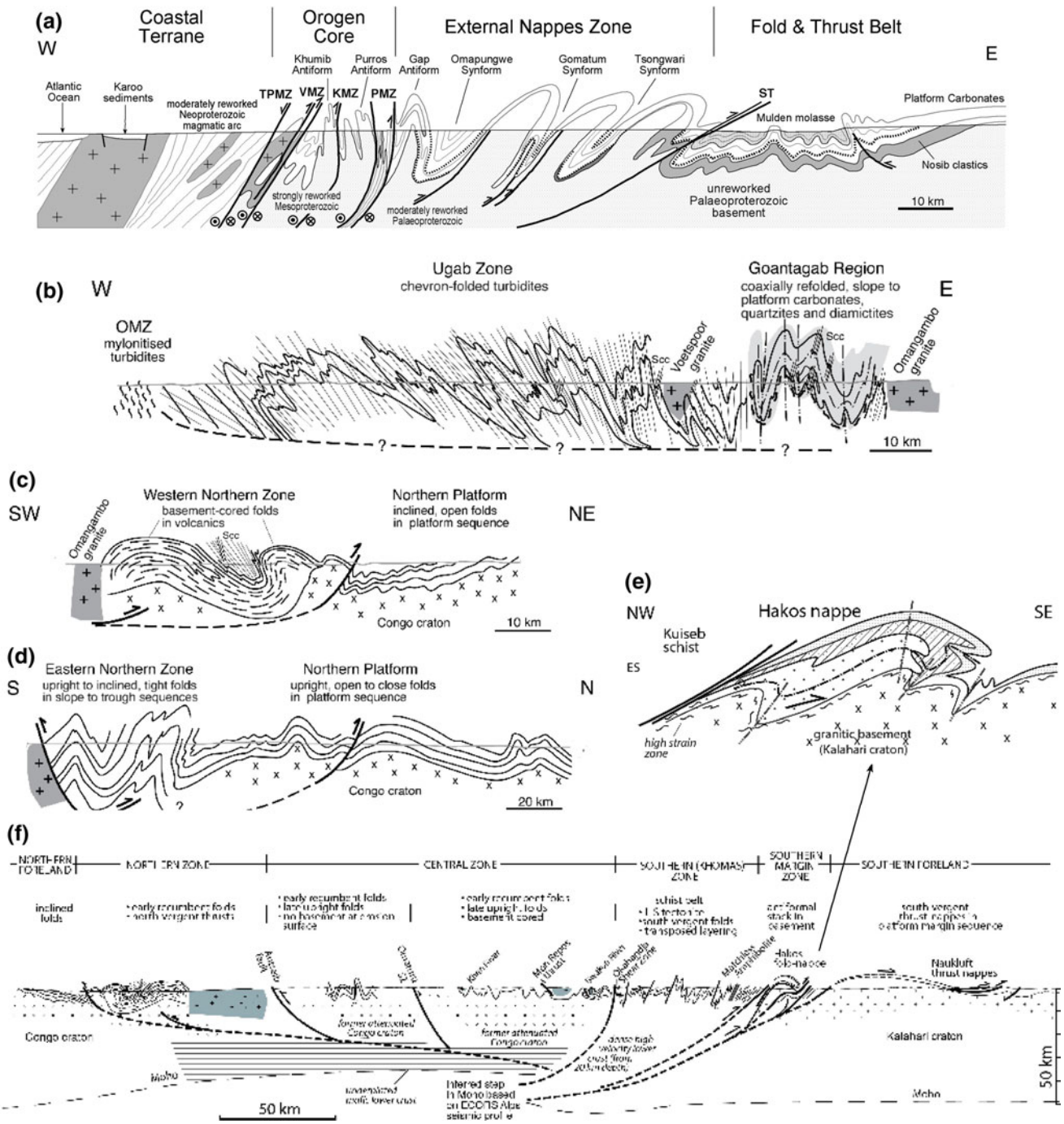

Fig. 12.8 Simplified structural profiles across the (**a**) Kaoko (from Goscombe et al. 2003a) (**b**) Ugab Zone (**c**) west Northern Zone (from Goscombe et al. 2004) (**d**) east Northern Zone (from Goscombe et al. 2004) (**e**) Hakos Nappe in the Southern Margin Zone and (**f**) Damara Belt (from Gray et al. 2007, 2008)

Transition to predominantly transcurrent slip occurred at ~550 Ma, constrained by late-kinematic granites and pegmatites of 559–549 Ma age that are cut by the crust-scale shear zones. Ongoing sinistral transcurrent slip continued to at least 539 Ma and the formation of interboudin melt infill, and it was terminated before 531–530 Ma crosscutting pegmatite dykes.

This 550–530 Ma period coincides with collision and prograde orogenesis in the Damara Belt, indicating a Damaran imprint imposed on the Kaoko Belt stress field

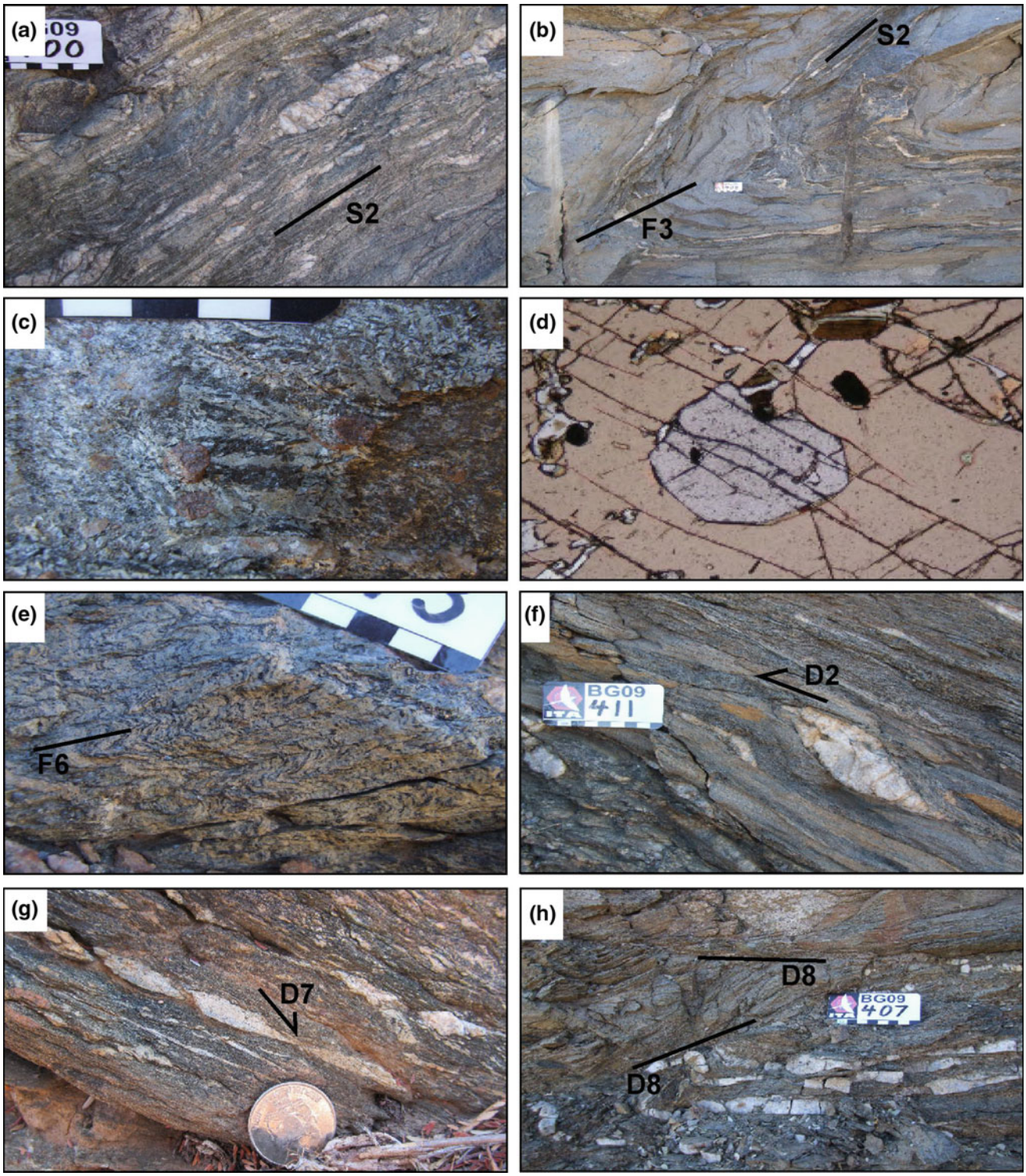

Fig. 12.9 Representative deformation structures from the southern orogenic margin, including the Southern and Southern Margin Zones. **a** Strong D2sz foliation intensity with extreme stretch of early layer-parallel quartz veins. **b** Main phase D3sz folding of psammite-pelite bedding and main phase D2sz foliation. **c** Peak metamorphic random biotite laths and idioblastic garnet overgrowing main foliation. **d** Prograde garnet idioblast overgrown and included within post-kinematic peak metamorphic staurolite porphyroblasts. Image in plain polarized light and field of view of 4.2 mm. **e** Shallow dipping D6sz flattening folds with spaced axial planar crenulation cleavage. **f** North over south main phase D2sz shear sense indicated by shearbands propogating off sigma clasts. **g** Top down to the north D7sz extensional shearbands in Matchless amphibolite. **h** D8sz brittle extensional fault zone

(Fig. 12.7). Contraction between the Congo and Kalahari Cratons started from 555 to 550 Ma (Clauer and Kroner 1979; Grotzinger et al. 1995; Gray et al. 2008; Foster et al. 2015). The prograde burial stage of orogenesis in the Damara Belt formed significant topography shedding detrital metamorphic zircons of 540–530 Ma age into molasse (Foster et al. 2015), and earliest metamorphic age determinations and widespread S-type granitoids of 546–534 Ma age within the orogen core (e.g., Jung et al. 2000b; Jung and Mezger 2003a). Prograde structures in the orogen core are pervasive gneissic layering, the earliest generation of thin stromatic melt segregations, and northwest-vergent inclined folds responsible for prograde crustal thickening (Kisters et al. 2004; Longridge et al. 2011, 2014). Prograde structures in the southern orogenic margin are early fine-grained bedding-parallel foliations. These are largely obliterated by main phase penetrative schistosity with down-dip stretching lineations (Fig. 12.9a, f), formed in associated with thrusts and southeast- to south-vergent tight to isoclinal inclined folds and nappes (Figs. 12.9b and 12.8). Progressive deformation in the Southern Zone was partitioned into strongly transposed and recycled foliations (Fig. 12.9a, f), resulting in folding of the main foliation being less common than expected for the high strains (Fig. 12.9b). At this time, the Kaoko and Damara Belts shared similar northwest-southeast shortening directions, and Naukluft Nappe transport was to the southeast (e.g., Gray et al. 2008; Longridge et al. 2011, 2014). Both Kaoko and Damara orogenic fronts were operating at the same time and all three cratons were convergent during the 550–530 Ma period: Rio De La Plata Craton southeast-directed over the west margin of the Congo Craton, while the southern margin was southeast-directed over the Kalahari Craton margin.

12.5.2.3 Peak Metamorphic North-Northwest-South-Southeast Shortening: 530–525 Ma

The rotation of principle compressive stress to acute angles with the orogenic grain of the Kaoko Belt led to sinistral-normal reactivation of crustal-scale shear zones in the west (Fig. 12.7). A shortening direction of north-northwest-south-southeast is estimated for transtensional reactivation of the Three Palms Mylonite Zone, resulting in south-southwest-directed downward transport of the Coastal Terrane and rapid exhumation of the orogen core. This ~25° rotation of the stress field led to a marked change in Kaoko Belt tectonics, terminating waning transpressional orogenesis and resulting in rapid exhumation and cooling of the belt. Timing of this switch is accurately constrained by post-kinematic pegmatites of 531–530 Ma age (Goscombe et al. 2005b) and thermochronology, indicating rapid cooling through 600–300 °C at 533–525 Ma (Foster et al. 2009). From this time, contraction across the Kaoko Belt ceased and all subsequent deformation was associated with the contractional stress fields in the Damara Belt. The earliest Damaran overprint in the Ugab Zone was also under north-northwest-south-southeast shortening at this time, forming fabrics in the contact aureoles of 530 Ma granites correlated with east-northeast-trending folds and crenulations (Fig. 12.5; Goscombe et al. 2004; Passchier et al. 2007).

Peak granulite metamorphism, dominant partial melting generation (Fig. 12.10a, c), early leucogranite sills and main phase folding around roughly east–west axes (Fig. 12.10g) all occurred between 530 and 518 Ma in the Central and Okahandja Zones (Jung et al. 2000a, b; Jung and Mezger 2001, 2003a; Armstrong et al. 1987; Kukla et al. 1991; Goscombe et al. 2017b). The minimum age for the metamorphic peak is constrained by post-kinematic granites and pegmatite of 516–515 Ma age that crosscut matrix parageneses and melt segregations (e.g., Jung et al. 2001; Jung and Mezger 2003a; Longridge et al. 2014; Paul et al. 2014; Goscombe et al. 2017b). Peak metamorphic parageneses experienced ongoing flattening strains that stretched garnet and cordierite porphyroblasts, developed the main phase biotite foliation and moderate boudinage (Figs. 12.5 and 12.10c, g). Main phase foliation in the Central Zone formed at only moderate strains with strain ratios <10, and high-strain grain refinement foliations such as mylonite did not form (Goscombe et al. 2017b). Peak Barrovian metamorphism in the southern orogenic margin was attained under relatively low-strain conditions immediately after main phase folding and foliation development, producing idioblastic garnet, staurolite and biotite porphyroblasts that overprint the main schistosity (Fig. 12.9c). Peak metamorphic conditions were attained at the same time in most parts of the Damara Belt: 530–518 Ma in the orogen core, 529–522 Ma in the Okahandja and Southern Zones, and 517 Ma in the Southern Margin Zone (Goscombe et al. 2017a). The thermal peak in the Ugab Zone also persisted from 530 to 516 Ma, with widespread contact metamorphism and regional growth of biotite in east-northeast-west-southwest and later east–west crenulations (Figs. 12.5 and 12.6d). This widespread thermal peak marks the culmination of main phase orogenesis, shortening, crustal thickening and burial in the Damara Belt, and all subsequent thermal and deformation events were superimposed during the waning stages of orogenesis.

12.5.2.4 Progressive North-Northwest-South-Southeast Shortening: 525–517 Ma

North-northwest-sout-southeast directed shortening persisted in both the Ugab and Central Zones until at least 517 Ma (Goscombe et al. 2017b). East-northeast-trending fabrics formed regionally in the Ugab Zone and are coeval with

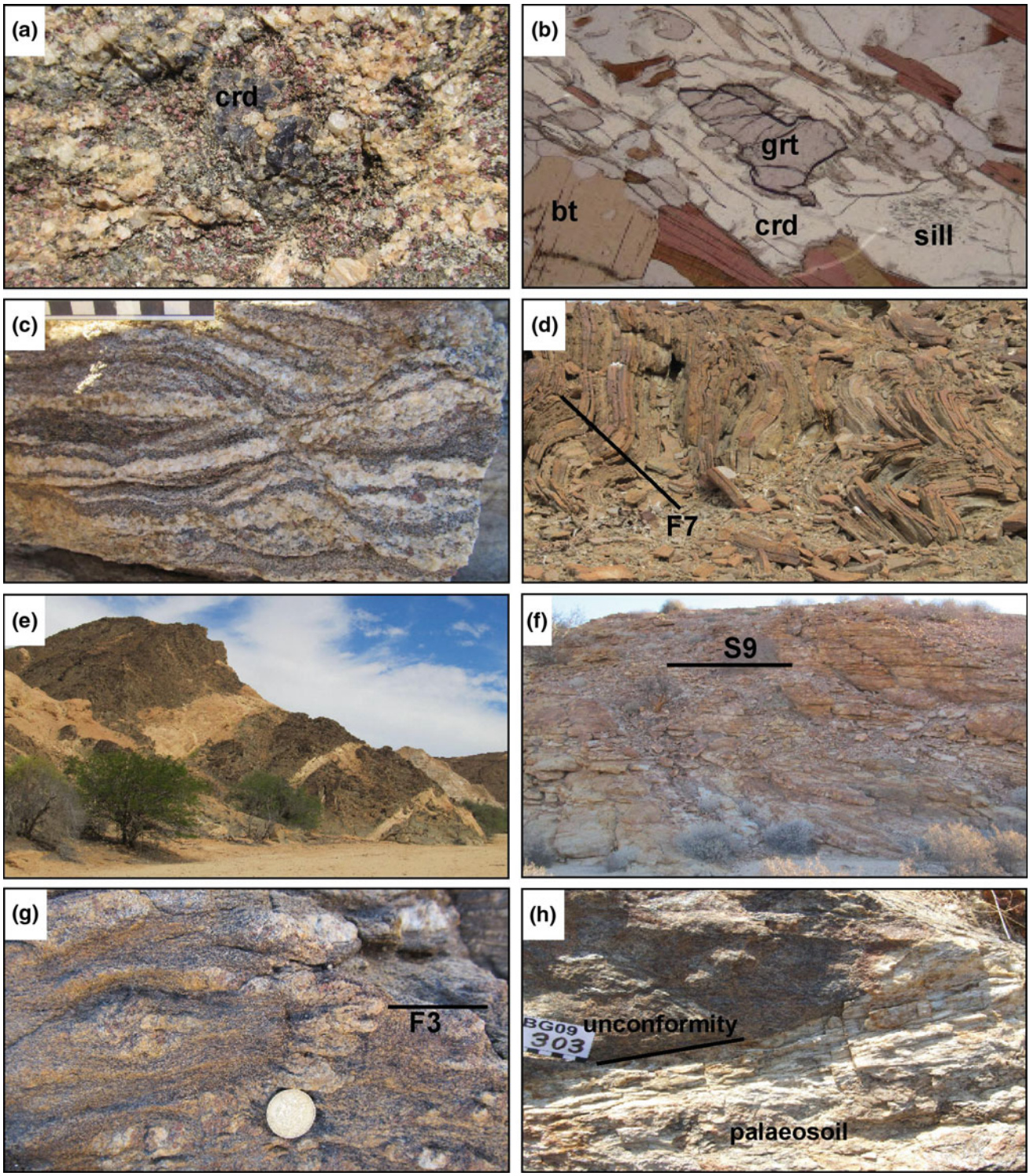

Fig. 12.10 Representative deformation structures from the Central Zone. **a** Coarse D3cz partial melt pool with paratectic cordierite in metapelite granulite. **b** High-grade metapelite gneiss with relict garnet and sillimanite resorbed and occluded by cordierite growth during decompression through the peak of metamorphism. Image in plain polarized light and field of view of 4.2 mm. **c** Typical D2cz stromatic partial melt segregations in metapelite granulite. **d** Asymmetric D7cz folds with east over west vergence. **e** Early-D6cz biotite-alkali feldspar dykes in the Omaruru river valley. **f** D9cz brittle crush zone within pegmatite and coarse granite in the Khan River region. **g** D2cz partial melt segregation folded by D3cz with axial planar biotite foliation. **h** Quartz-sillimanite aluminous metapaleosoil developed in the top 20 cm of basement at the unstrained unconformity immediately below the Etusis Formation Damara Sequence

fabrics developed in the contact aureoles of ~520 Ma granite (Fig. 12.5). Peak metamorphic parageneses and structures in the Central Zone were overprinted by second generation folding that produced large-scale south-southeast-vergent inclined folds that form long axes of basement domes. These are approximately coeval with 518–515 Ma granite magmatism and overprint peak metamorphic parageneses. At this time there was little deformation in the Kaoko Belt, except for east–west trending warps, indicating that almost all Congo-Kalahari convergence was accommodated within the Damara Belt.

In contrast, the deeply buried southern orogenic margin was exhumed at this time by foreland propagating upthrusting events that resulted in extensional telescoping of the margin (Fig. 12.8). Outwedging events occurred while under contraction, along basal thrusts, and accommodated by broad zones at the top of the crustal wedge showing top down to the north extensional structures and metamorphic discontinuity to lower pressures in the hanging wall (Fig. 12.5; Goscombe et al. 2017a). Exhumation of the south Okahandja-Southern Zone crustal wedge was initiated at ~522–513 Ma, resulting in further burial of the Southern Margin Zone, which attained peak metamorphism and maximum depths of burial at 517 ± 4 Ma, followed by outwedging soon after (Goscombe et al. 2017a). Extensional structures are developed in close association with metamorphic discontinuities in the southern margin; in the south Okahandja Zone, central Southern Zone near the Matchless Belt and vicinity of the Uis-Pass Suture, and the association is otherwise absent elsewhere in the Damara Belt. Extensional structures indicating vertical flattening, overprint main phase foliations and progressed from ductile to brittle, tracking exhumation through the crust. First formed are mesoscopic asymmetric folds and crenulations with shallow north-dipping axial surfaces, and top down to the north-northwest vergence in the Okahandja Zone and top down to the north-northeast in the southern zones (Fig. 12.9e). Axial planar crenulations and biotite growth are overprinted by post-kinematic secondary garnet overgrowths, indicating that the thermal peak of metamorphism accompanied early vertical flattening. Flattening folds are overprinted by top down to the north extensional shearbands (Fig. 12.9g) and shear zones at all scales, including reactivation of the Uis-Pass Suture, producing chlorite-muscovite retrogressive schist zones (Figs. 12.5 and 12.7). Brittle top down to the north extensional faults are last formed, and range from centimetre-scale fault planes, breccia zones, pseudotachylite and gouge zones, to laterally continuous 1–3 m wide fault zones (Fig. 12.9h).

12.5.2.5 North-South Shortening: ~518–515 Ma

A widespread switch to north–south shortening at ~518–515 Ma was experienced in both the Kaoko Belt and most parts of the Damara Belt (Fig. 12.7). North–south shortening produced late-stage kinkbands and large-scale east–west warping of the orogenic grain and shear zones of the Kaoko Belt, and north-northeast-south-southwest trending pegmatite dykes of 515 Ma age in the south Coastal Terrane (Goscombe and Gray 2007, 2008). Folding post-dates transtensional reactivation of these shear zones, constraining east–west warps to younger than 525 Ma. Further south in the Ugab Zone, widespread east–west trending biotite foliations (Fig. 12.6d, g), crenulations and folds are coeval with transposed fabrics and parageneses developed in the contact aureole of 516 ± 3 Ma West Ugab granite (Figs. 12.5 and 12.6h; Goscombe et al. 2017b). East–west foliations and folds are cut by younger granites of ~513–511 Ma age, narrowing north–south shortening to ~518–513 Ma. The youngest contraction contributing to the grain of the Damara Belt is east–west trending folds ranging from north-vergent asymmetric folds in the Central Zone to upright chevron folding in the Okahandja Zone. These folds are correlated with the waning stages of synkinematic S-type granite magmatism of 516–513 Ma age, and pre-date the post-kinematic Donkerhoek granite of 508–505 Ma age. South-directed upthrusting and outwedging of the Southern Margin Zone occurred at this time, with isothermal decompression indicating rapid exhumation immediately after peak metamorphism at 517 Ma (Goscombe et al. 2017a). Outwedging was accommodated by extensional reactivation of the Uis-Pass Suture, and indicated by a major metamorphic discontinuity. The initiation of exhumation of this footwall crustal wedge is constrained to between 517 and 513 Ma by post-kinematic granites of 514–513 Ma age that probably formed by decompression melting. This second stage of outwedging in the southern orogenic margin thus coincides with the switch to north–south directed shortening in the waning stages of contraction and initiation of insipient extensional events in the Central Zone starting from ~516 Ma, as discussed below (Table 12.1).

12.5.2.6 Northeast-Southwest Shortening: 512–508 Ma

Final phase of contraction across the Damara Belt is constrained by low-strain, low-grade relationships in the Ugab Zone (Figs. 12.5 and 12.7). Map-scale upright open folds with west-northwest-east-southeast to north-northwest-south-southeast trends are tightened against pre-existing 516 Ma and 513–511 Ma granite bodies (Fig. 12.5). Kinkbands formed by northeast-southwest shortening are developed in low-grade domains distal from granites and are correlated with this deformation period. Both kinks and open folds are devoid of axial planar foliations and mineral growth, and are interpreted to have formed at sub-biotite grades <450 °C. Ar–Ar muscovite closure and regional cooling through 400 °C far from granites was at 512–508 Ma, indicating northeast-southwest shortening at

~512–508 Ma, consistent with the granite age constraints. These structures bracket the end of contraction across the Damara Belt and indicate progressive clockwise rotation of the stress field through 70°, and possibly as much as 90°, from collision at 555 Ma to ~512–508 Ma. No deformation feature of this age is identified in the Kaoko Belt. Barrovian metamorphism in the east Northern Zone occurred at 510 ± 3 Ma, with peak conditions terminated by isothermal decompression, indicating rapid exhumation at <510 Ma (Goscombe et al. 2017a). Stress directions during this significant exhumation event are unknown, though there is an overlap in age with northeast-southwest shortening further west in the Ugab Zone.

12.5.3 Transitional Events in the Orogen Core: 516–508 Ma

Coinciding with waning contraction across the Damara Belt, the Okahandja and Central Zones experienced a complex transitional phase between 516 and 508 Ma. Conjugate post-kinematic alkali feldspar pegmatite dykes in the North Central Zone indicate east-northeast-west-southwest directed oblate shortening as early as 516 Ma (Figs. 12.5 and 12.10e; Goscombe et al. 2017b). These were followed by a widespread thermal anomaly between ~515 and 505 Ma, indicated by metamorphic age determinations throughout the Central Zone (Briqueu et al. 1980; Jung et al. 2000b; Jung and Mezger 2003b; Longridge et al. 2011; Goscombe et al. 2017b). This anomaly was associated with late-kinematic granites between 512 and 507 Ma (Allsopp et al. 1983; Jung et al. 2001; DeKock and Armstrong 2014) and granite veins intruded into extensional shear zones between 511 and 508 Ma (Longridge et al. 2011, 2014). Regional stress fields in the Central Zone at this time are not confidently known, though a secondary thermal peak accompanying extensional magmatic features and only minor deformation is indicative of a conductive thermal anomaly, either without stress or accompanying incipient extension localized to the Central Zone.

12.5.4 Along Orogen Shortening: 508–505 Ma

Waning contraction across the Damara Belt at 512–508 Ma was followed by a rapid stress switch of 45° to east–west directed shortening along the length of the belt at 508–505 Ma (Figs. 12.5 and 12.7). The youngest deformation recognized in the west Ugab Zone is west-vergent asymmetric folds with steep north–south trending crenulation cleavages with axial planar biotite growth (Figs. 12.5 and 12.6f). These post-date both 516 Ma and 513–511 Ma granites, as well as northwest-southeast trending open folds that formed at sub-biotite grade. Consequently, renewed biotite growth in these north–south crenulations indicate an increase in west Ugab Zone temperatures to >450 °C following earlier cooling to sub-biotite conditions. The Central Ugab Zone cooled below 400 °C at 512–508 Ma, indicating that the west Ugab Zone thermal anomaly post-dates regional cooling preserved in cooler parts of the Ugab Zone. A late-stage secondary thermal anomaly accompanying east–west shortening is also recognized in the Kaoko Belt. Pegmatite dyke swarms of 508 Ma age have trends ranging east–west to east-southeast-west-northwest, consistent with an imposed east–west shortening direction. These swarms are associated with a local thermal anomaly of 507–505 Ma age that resets Sm–Nd isotopics (Goscombe et al. 2005b).

Late-stage, upright to inclined west-vergent crossfolds in the Central Zone (Fig. 12.10d) produced dome and basin fold interference, with orientation and vergence in common with the west Ugab Zone (Fig. 12.7). Dome and basin folding in the Central Zone post-dates 511–508 Ma granite veins and has been constrained to ~508 Ma by Longridge et al. (2011, 2014). Widespread evidence for east–west directed shortening at ~508 Ma is significant because it indicates an essentially instantaneous rearrangement of the stress field by ~45°. Such a rapid stress switch implies an internal cause is unlikely and along-orogen shortening is inconsistent with any plausible trajectory between the Rio De La Plata, Congo and Kalahari Cratons. Consequently, far-field effects at the margin of Gondwana are the probable cause, such as arc collision and obduction in the Ross-Tasman Orogen (e.g., Foster et al. 2005). Furthermore, along-orogen shortening also implies the termination of contraction in the Damara Belt, and that the Congo and Kalahari Cratons were welded together.

12.5.5 Vertical Flattening and Orogen Collapse: 505–500 Ma

Along-orogen shortening of the Damara Belt between 508 and 505 Ma was followed by a switch at ~505 Ma from horizontal to vertical principle compressive stress, while still under north–south extension. This stress switch was restricted to the Central Zone where vertical flattening and north–south extension led to rapid vertical exhumation as a broad bivergent core complex (Fig. 12.11; Goscombe et al. 2017a). Vertical flattening evolved from ductile subhorizontal flattening folds to shallow north-dipping brittle breccia zones with top down to the north transport (Figs. 12.5 and 12.10f; Goscombe et al. 2017b). The initiation of significant Central Zone decompression is dated by the oldest decompression melts in the footwall of 502 ± 9 Ma age (Jung and Mezger 2003a), and the

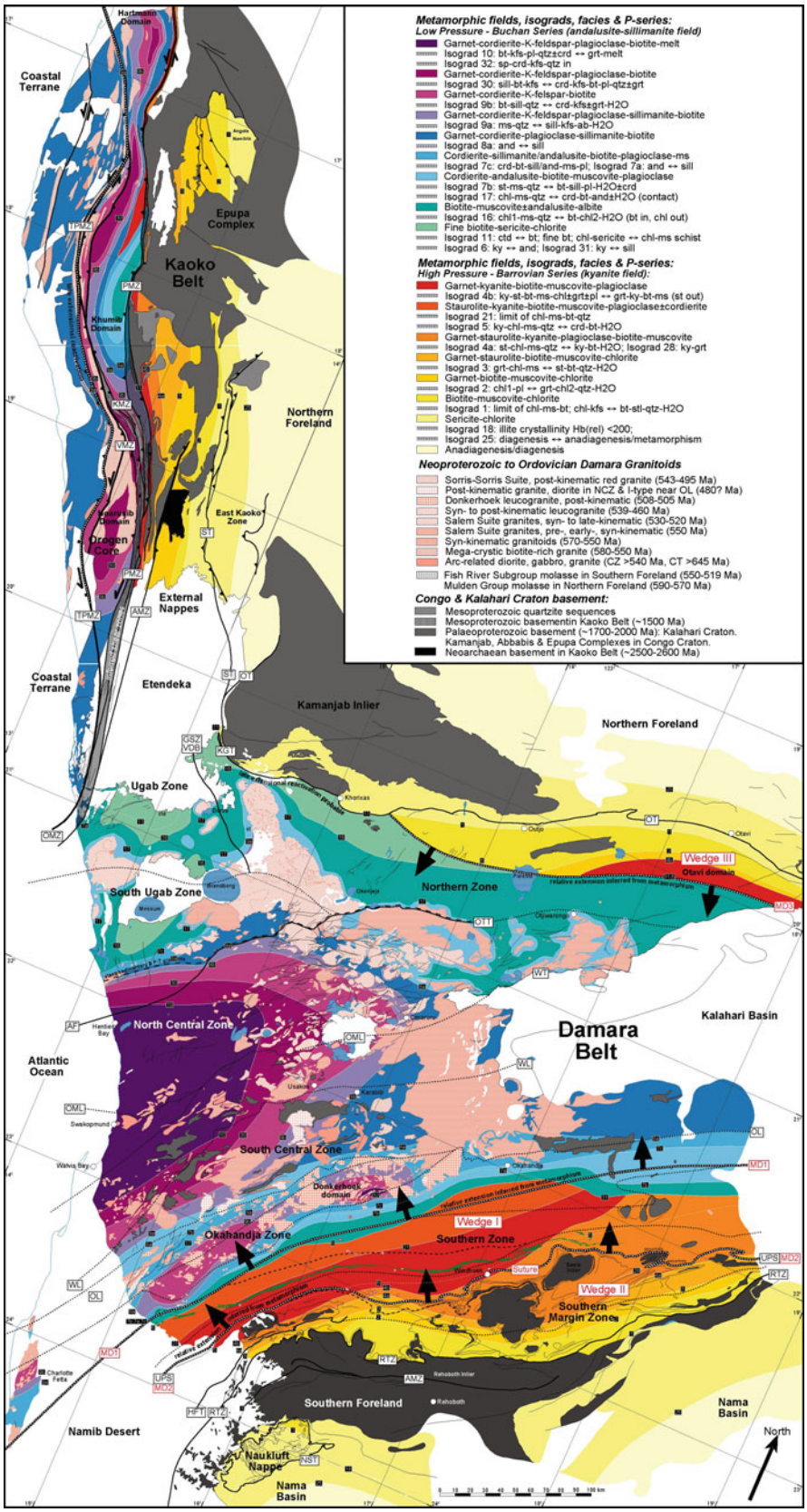

Fig. 12.11 Simplified metamorphic map of the Damara Orogenic System. The Kaoko Belt component is sourced from Goscombe et al. (2005) and represents M2 peak metamorphic parageneses developed during transpressional orogenesis. The Damara Belt component is sourced from Goscombe et al. (2017a). Metamorphic fields and isograds have been compiled from a large number of published sources (e.g., Hoffer 1977, 1978, 1983; Hoernes and Hoffer 1979, 1985; Sawyer 1981; Nitsch 1982; Hartmann et al. 1983; Kasch 1983a; Kukla 1992a, b; Goscombe et al. 2004), and new metamorphic mapping, petrology and quantitative *PT* (Goscombe et al. 2017a). MD, metamorphic discontinuities inferred from metamorphic field gradients (Goscombe et al. 2017a)

maximum age limited by youngest late-kinematic granites and granulite facies parageneses ranging from 512 to 507 Ma (Jung et al. 1998b, 2000a, b; Longridge et al. 2011, 2014; Goscombe et al. 2017a). Immediately pre-dating exhumation, leucogranite and pegmatites in the Central Zone are associated with north–south extension directions between 516 and 508 Ma (Allsopp et al. 1983; Jung et al. 2001; Longridge et al. 2011, 2014; Goscombe et al. 2017b). Elsewhere decompression melting, post-kinematic leucogranite and pegmatite dykes, also associated with north–south extension, occurred at 508–504 Ma in the South Ugab Zone, Kaoko Belt and Okahandja Zone (Kukla et al. 1991; Goscombe et al. 2005b; DeKock and Armstrong 2014).

Rapid exhumation and cooling of the Central Zone from high-grade conditions followed the 505 Ma stress switch. Thermochronometers spanning monazite closure at ~700 °C to biotite closure at ~300 °C give cooling or recrystallization ages ranging from 500 to 470 Ma and define a cooling rate of ~11 °C/Ma (Hawkesworth et al. 1983; Jacob et al. 2000; Jung et al. 2000a, b; Singletary et al. 2002; Jung and Mezger 2003a; Goscombe et al. in press a). Elsewhere, slower cooling through 400–300 °C occurred between 499 and 481 Ma in all other parts of the Kaoko and Damara Belts. A stress switch to north–south extension at 508 Ma, followed by vertical flattening and collapse of the hot orogen core at 505 Ma, are most plausibly causally connected. A sudden switch to east–west directed shortening at 508 Ma is interpreted as a far-field effect imposed on the then intracontinental Damara Orogenic System. This imposed stress field established a north–south extension direction exploited by decompression melts, and it is interpreted to have triggered gravitational collapse of the thermally weakened hot orogen core at 505 Ma, producing the Central Zone core complex.

12.6 Metamorphic History

12.6.1 Kaoko Belt

12.6.1.1 Coastal Terrane

The oldest metamorphic parageneses in the Damara Orogenic System is 645 ± 4 Ma metamorphic monazite (Franz et al. 1999), restricted to the Coastal Terrane. Peak metamorphism was at low-*P*/high-*T* granulite to upper amphibolite conditions averaging 689 ± 43 °C and 4.9 ± 1.3 kb, with thermal regimes of 40.2 ± 11 °C/km (Goscombe et al. 2005a; Goscombe and Gray 2007). Matrix assemblages have coarse polygonal granoblastic textures, partial melt and clinopyroxene are common, and orthopyroxene and muscovite are absent. Metamorphic evolution followed tight, low $\Delta P/\Delta T$ clockwise *P–T* paths with no evidence for high pressures, and followed by near isobaric cooling. High thermal regimes, low pressures and shallow *P–T* paths indicate a high heat flow setting with little crustal thickening, consistent with a magmatic arc. The Coastal Terrane is dominated by I-type calcalkaline granitoids of 661–655 Ma and post-kinematic granitoids of 638–620 Ma, straddling peak metamorphism (Seth et al. 1998; Kröner et al. 2004; Goscombe and Gray 2007).

Magmatic arc parageneses were variably reworked and downgraded at shallow crustal levels during obduction along the Three Palms Mylonite Zone and subsequent transpressional orogenesis. In contrast, the remainder of the Kaoko Belt experienced prograde metamorphism and crystallization of matrix parageneses during transpression (Goscombe et al. 2005a). Reworking parageneses are defined by ductile recrystallization of earlier minerals to subgrains in mortar textures, pressure shadows, aggregate ribbons and as new mineral growth in foliation seams. Reworking foliations in metapsammopelites contain quartz, oligoclase, biotite, muscovite and ilmenite, and they are devoid of new K-feldspar, garnet and aluminosilicates growth. Whereas mafics contain quartz, plagioclase, biotite, epidote and titanate and are devoid of hornblende, garnet and pyroxene. *PT* calculations from reworking foliations and re-equilibrated outer rims of relict garnet porphyroclasts average 557 ± 50 °C and 4.5 ± 1.2 kb, with T/depth ratios of ~37 °C/km (Goscombe et al. 2005a). The low pressures are consistent with the high structural level during transpressional orogenesis.

12.6.1.2 Transpressional Metamorphic Pattern

The Kaoko Belt developed a paired metamorphic pattern during transpressional orogenesis, with contrasting thermal regimes on either side of the Purros Mylonite Zone, reflecting the marked kinematic partitioning of the belt (Fig. 12.11). The Damara Sequences within the Kaoko Belt experienced a single metamorphic cycle, with peak metamorphic parageneses defined by the main foliation matrix assemblage developed during transpressional orogenesis. The atrix assemblages have been dated directly using Sm–Nd garnet and U–Pb zircon (Goscombe et al. 2003b, 2005b), giving similar ages in all parts of the belts, indicating that the paired metamorphic pattern developed at the same time. Peak metamorphism occurred at 574.3 ± 9.7 Ma in the External Nappes, at 571.2 ± 6.1 to 572.4 ± 5.1 Ma in the high-grade parts of the Orogen Core and at 579 ± 15 to 573.8 ± 4.0 Ma in the low-grade Khumib domain in the Orogen Core (Goscombe et al. 2003b, 2005b). Peak metamorphism overlaps in age with the oldest synkinematic granites ranging from 580 to 562 Ma (Seth et al. 1998).

The Eastern Kaoko Belt developed inverted Barrovian series zonation: subgreenschist facies in the foreland, greenschist in the East Kaoko Belt and External Nappe Zone

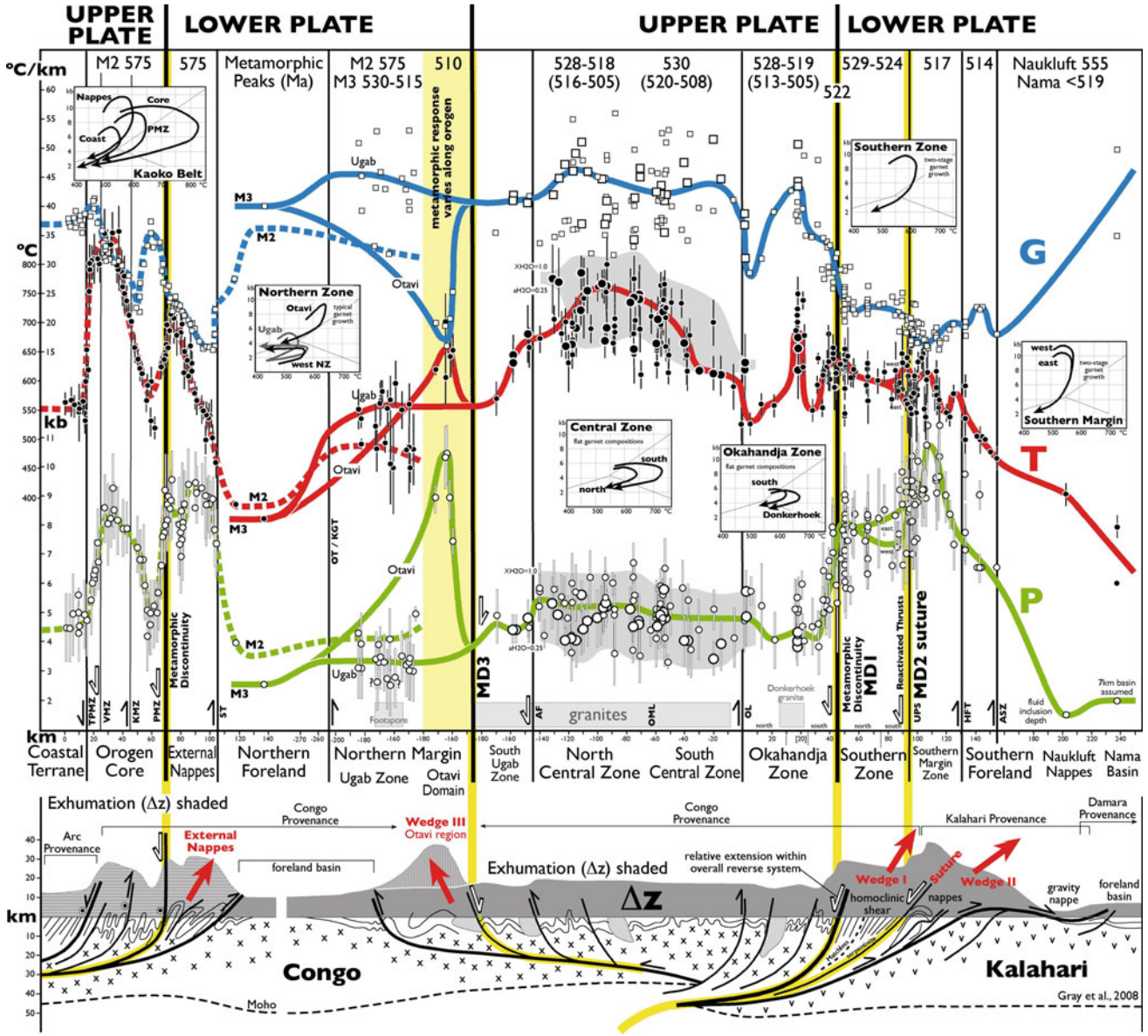

Fig. 12.12 Composite metamorphic field gradients describing metamorphic response to orogenesis in the Damara and Kaoko Belts, modified after Goscombe et al. (2017a). The field gradients are plotted against distance (km) north and south of the Okahandja Lineament and organized around distinct tectonometamorphic zones and bounding shear zones, with the abbreviations listed in Fig. 12.3. All *PT* calculations were made using THERMOCALC v3.21 (Powell and Holland 1988) with the same thermodynamic data set and so are directly comparable. Shading indicates upper and lower limits calculated from high-grade garnet-cordierite gneisses, on the basis of fluid and H_2O activity assumptions, bounding the region of permissible conditions. The upper limit assumes the presence of a hydrous fluid phase and the lower limit encompasses fluid-absent conditions and a H_2O value of 0.25. Best estimate *PT* results from garnet-cordierite gneisses (plotted as larger symbols) are calculated independent of fluid considerations by using fluid-free reactions and assuming a $H_2O = 0.25$ in cordierite. Metamorphic field gradients define major metamorphic discontinuities (MD) that demand extensional reactivation of the main foliation at boundaries between Southern and Southern Margin Zones at the Uis-Pass Suture (MD2), Okahandja and Southern Zones (MD1), and Central Zone and Otavi domain in the east Northern Zone (MD3). This relative extensional transport accommodated outwedging of the Southern Zone (Crustal Wedge I), Southern Margin Zone (Crustal Wedge II) and Otavi domain (Crustal Wedge III), terminating peak-*P* Barrovian conditions and accompanying decompression through the peak-*T* of metamorphism. Simplified crustal architecture at the bottom of the figure is modified after Gray et al. (2007). The summary of metamorphic age determinations is sourced from the compressive age data listing of Goscombe et al. (2017b)

ranges across biotite-, garnet-, staurolite-, kyanite-in isograds to sillimanite-kyanite upper amphibolite facies adjacent to the Purros Mylonite Zone. The Purros Mylonite Zone is coincident with the muscovite- and kyanite-out isograds and incoming of K-feldspar, sillimanite and partial melt. The metamorphic grade typically increases substantially across this shear zone. In contrast, the Orogen Core experienced Buchan series thermal regimes, varying substantially in grade from lower amphibolite in the Khumib domain, upper amphibolite in the Hartmann domain and granulite facies in the Hoarusib domain. The Hoarusib domain contains metapelite granulite with garnet-cordierite-sillimanite-K-feldspar assemblages and two pyroxene mafics. Metapelite zonation in the Khumib domain ranges from biotite-muscovite-garnet in the east to K-feldspar-sillimanite-melt in the west. There is a sharp decrease in the metamorphic grade across the Three Palms Mylonite Zone into the Coastal Terrane.

The peak metamorphic conditions vary substantially between different parts of the belt (Goscombe et al. 2003b, 2005a). Peak metamorphism was <450 °C in the East Kaoko Zone, and the External Nappe Zone ranges from 534 °C in the east to 689 °C in the west, at constant pressures of 8.5–8.6 kb, indicating an increase in thermal regime from 18 °C/km to 23 °C/km towards the core of the belt (Fig. 12.12). The Orogen Core is characterized by thermal regimes ranging from 28 to 34 °C/km and peak conditions averaging 769 °C/8.0 kb, 843 °C/8.1 kb, 811 °C/6.2 kb and 785 °C/6.7 kb in different high-grade panels. In contrast, the turbiditic Khumib domain at higher structural levels has peak conditions averaging 597 °C/5.2 kb and similar thermal regimes of 33 °C/km. The metamorphic grade varies smoothly across the Khumib Domain, from 573 °C/5.4 kb in the east to 704 °C/4.2 kb in the west. All regions experienced clockwise *P–T* paths (Fig. 12.13). The External Nappe Zone following steep trajectories, open clockwise loops with isothermal decompression followed by decompressive cooling, reflecting advection dominated metamorphism, whereas the Orogen Core panels experienced low $\Delta P/\Delta T$ clockwise paths with near isobaric cooling through 650 °C at 4.0–4.8 kb (Fig. 12.13). Elevated thermal regimes and shallow *P–T* paths in the Orogen Core indicate minor crustal thickening and subdued topographic development, giving long residence times with conduction outcompeting advection, typical of transcurrent orogenic systems (Thompson et al. 1997; Goscombe et al. 2005a).

The complex peak metamorphic pattern of the Orogen Core developed during transpressional orogenesis, resulting in discontinuous metamorphic variation between the different panels. Main phase stretching lineations and kinematic indicators define low-angle material transport trajectories with either an upward or downward component during transpression. Pressure variation and kinematics are consistent with each other: high-*P* panels such as the Hoarusib and Hartmann domains experienced upward-directed transport, and low-*P* panels such as the Khumib domain and Coastal Terrane experienced downwards shear trajectories. These low-angle transport trajectories resulted in the juxtaposition of different crustal levels during main phase transpression (Goscombe et al. 2005a). Peak pressures of ~4.0–6.0 kb in shear zones indicate that most of the exhumation of the Kaoko Belt occurred following clockwise *P–T* paths during the transpressional metamorphic cycle, before the shear zones developed; both by longitudinal extrusion in the Orogen Core and foreland-vergent transport in the External Nappe Zone (Fig. 12.14). From ~550 Ma, shear zones predominated and were responsible for further exhumation during transcurrent shear late in the orogenic cycle. Eventually the peak metamorphic pattern of the Orogen Core was modified further by transtensional reactivation of western shear zones at ~530–525 Ma (Foster et al. 2009).

12.6.1.3 Shear Zone Metamorphism and Exhumation

Late in the transpressional metamorphic cycle, after regional main phase fabrics and folding, strain was progressively partitioned into shear zones from ~550 Ma, producing new grain-refinement parageneses (Goscombe et al. 2003b). Peak metamorphic conditions in these shear zones are at slightly lower temperatures and pressures than in adjacent panels, consistent with clockwise *P–T* paths and decompression through main phase transpressional orogenesis (see above). Ductile shear zone parageneses also record decompressive cooling from peak to post-peak conditions, indicating a component of exhumation in these zones between ~550 and 530 Ma. Western shear zones such as the Village, Khumib and Three Palms Mylonite Zones were later reactivated by sinistral-normal slip producing retrogressive to brittle parageneses. Transtensional reactivation transported the hanging wall western domains down and to the sout-southwest, allowing rapid exhumation and cooling of the Kaoko Belt at ~530–525 Ma (Foster et al. 2009).

Peak metamorphic conditions in the Purros Mylonite Zone range from 620 to 650 °C/6.3–8.8 kb in the north, 720 °C/9.0 kb in the centre and 680 °C/4.5 kb in the south (Foster et al. 2009). Post-peak outer-rim parageneses record decompression to 5.3–5.6 kb in the north, 4.4 kb in the centre and 4.1 kb in the south. Having magnetic lineaments and mylonitized Neoarchaean and Paleoproterozoic basement in common links the Purros and Ogden Mylonite Zones, extending ~620 km length from Angola to the Ugab Zone (Seth et al. 1998; Corner 2000, 2004; Passchier et al. 2002; Goscombe et al 2003a, 2004, 2017b). The Ogden Mylonite Zone formed at shallower crustal levels of 479 °C and 4.7 kb. In contrast to all other shear zones, the Purros and Ogden Mylonite Zones are almost devoid of late-stage brittle reactivation and do not record sinistral-normal

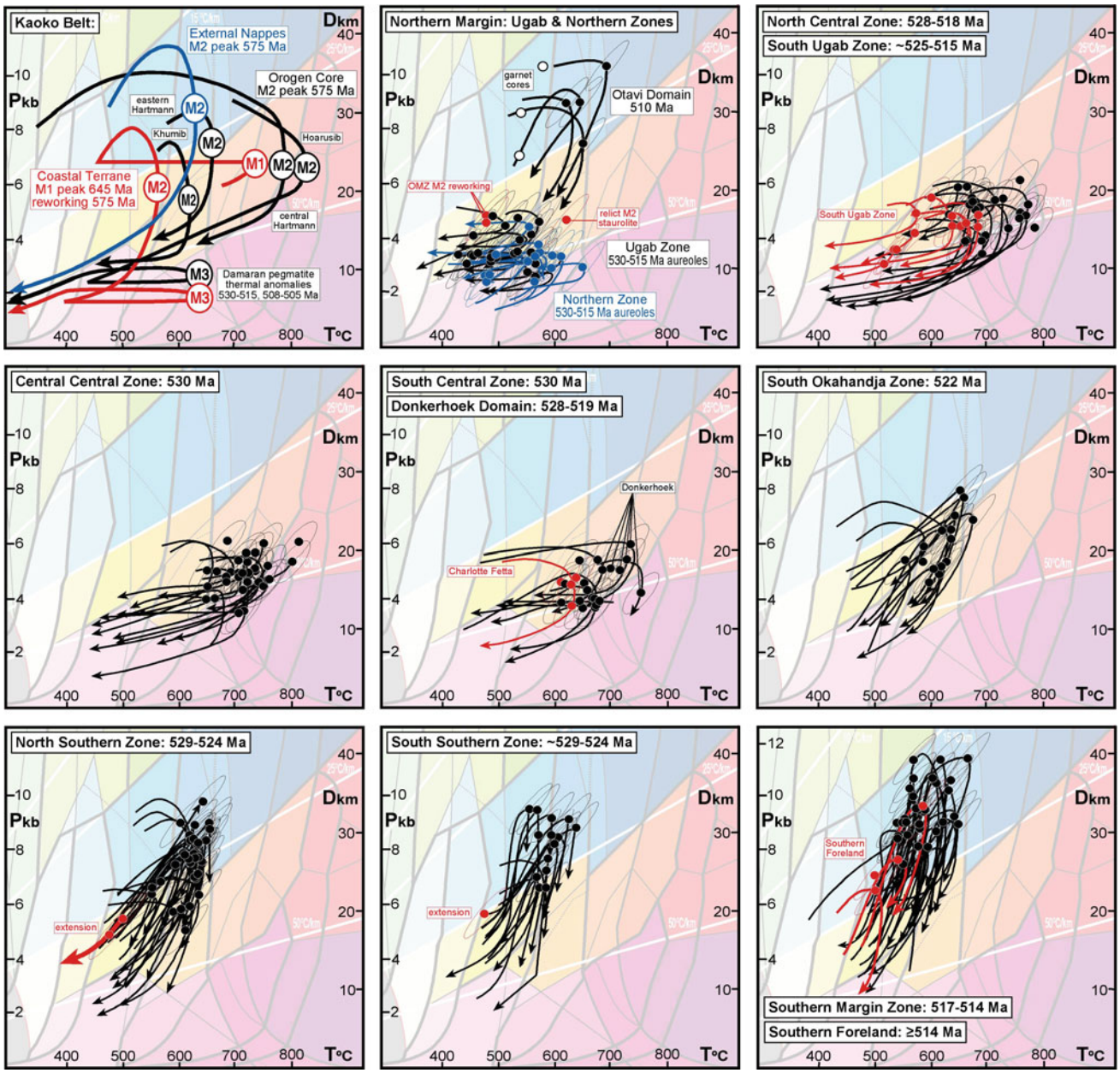

Fig. 12.13 Summary of *P–T* evolutions in all tectonometamorphic zones of the Kaoko and Damara Belts. Black dots are peak metamorphic *PT* determinations with error ellipses based on the average error for the sample population. The semiquantitative *P–T* paths interpreted for different samples are defined by prograde, peak and post-peak *PT* determinations, in conjunction with petrology evaluated in published *PT* pseudosections. The Kaoko Belt data was sourced from Goscombe et al. (2003b, 2005a) and that for the Damara Belt was sourced from Goscombe et al. (2004, 2017a)

kinematics. Peak metamorphic conditions in the Khumib Mylonite Zone are 704 °C/4.2 kb and in the Village Mylonite Zone are 709 °C/4.8 kb, both recording high thermal regimes of 42–48 °C/km. High-grade ductile parageneses, including stretched garnets, are progressively overprinted by mid-amphibolite facies mylonites at >500–590 °C, semiductile deformation at 400–480 °C, and brittle gouge and breccia indicating reactivation into the brittle field (Konopasek et al. 2005; Foster et al. 2009). At the highest structural level, the Three Palms Mylonite Zone obducted the Coastal Terrane and partitioned much of the subsequent transpressional strain, leaving the hanging wall only moderately reworked. The Three Palms Mylonite Zone is a broad ductile mylonite zone that reworked and down-graded older parageneses, at conditions ranging from 543 to 556 °C/4.3–4.8 kb and thermal regimes of 35 °C/km, shared in common with reworking fabrics in the overriding Coastal Terrane. Ductile shear fabrics were pervasively overprinted during

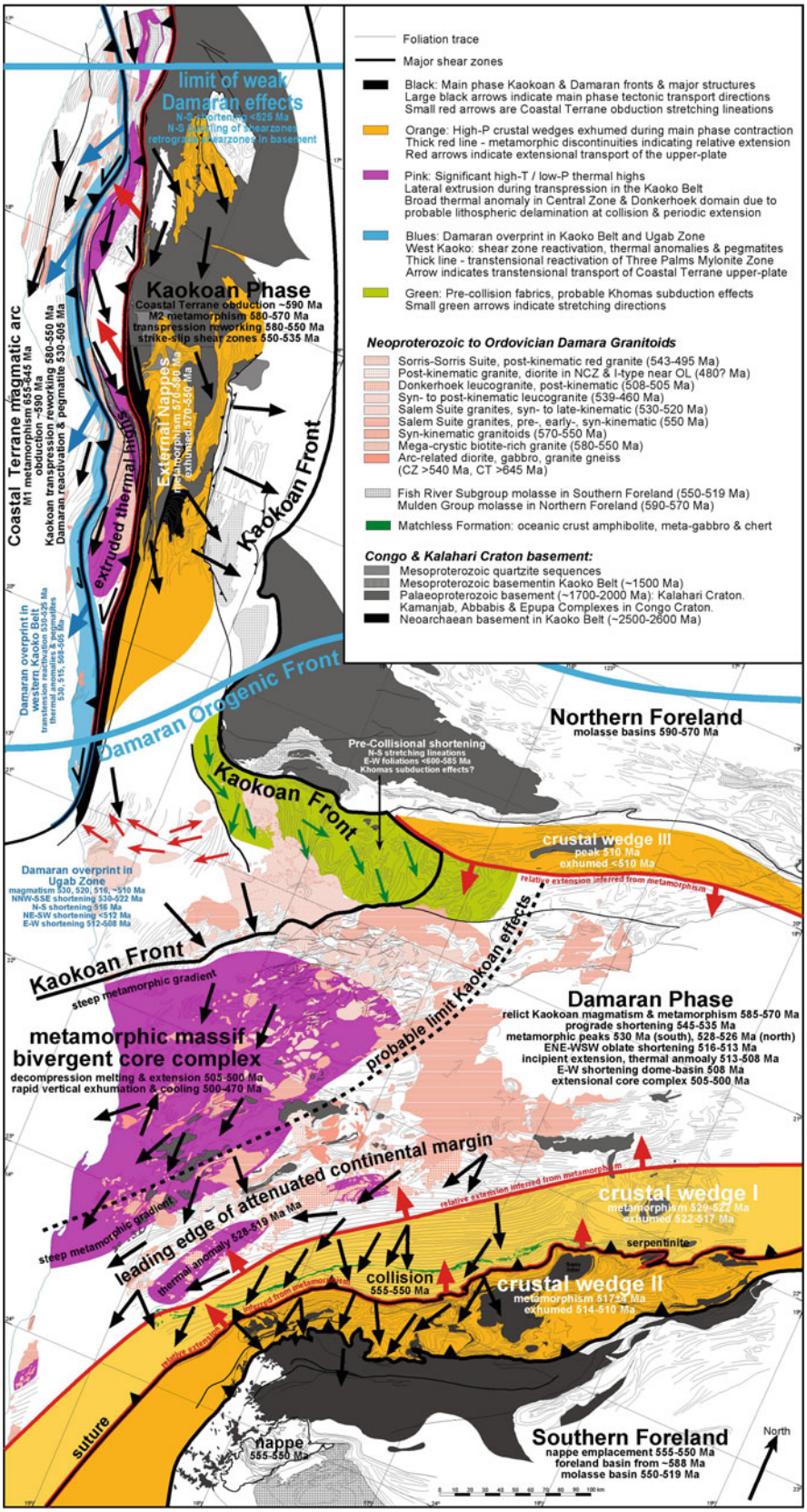

Fig. 12.14 Chronospatial interpretation of the orogenic history of the Damara Orogenic System based on the distribution of Kaokoan Phase and Damaran Phase deformation effects (Fig. 12.7; Goscombe et al. 2017b)

later transtensional reactivation of this zone, producing semiductile shearbands at 420–500 °C, brittle-ductile deformation at 300–450 °C and finally brittle faults, pseudotachylite and fracturing.

12.6.2 Damara Belt

12.6.2.1 Barrovian Orogenic Margins

Both the eastern part of the northern margin (Otavi domain) and southern orogenic margin experienced inverted Barrovian series metamorphism at lower to upper amphibolite facies, high pressures between 8.0 and 11.0 kb and low T/depth ratios between 17 and 25 °C/km (Fig. 12.11; Hoffer 1977, 1978; Sawyer 1981; Kasch 1987; Kukla 1992a, b; Goscombe et al. 2004, 2017a). Typical metapelite assemblages are biotite-muscovite-quartz-plagioclase matrix foliation with syn- to post-kinematic garnet, staurolite, biotite and rare kyanite porphyroblasts. Internally, all parts of these orogenic margins experienced steep, tight clockwise *P–T* paths showing deep burial culminating in peak metamorphic conditions at maximum pressures, and terminated by near isothermal decompression (Fig. 12.13; Behr et al. 1983; Kasch 1987, 1993; Puhan 1995; Cross et al. 2015; Goscombe et al. 2017a). Decompression through the peak is indicated in metapelites by early kyanite overprinted by sillimanite, garnet occluded by staurolite porphyroblasts (Fig. 12.9d) and garnet overprinted by plagioclase moats and sillimanite (e.g., Kasch 1987). The southern margin consists of two crustal wedges corresponding to the Southern Margin Zone in the footwall and the south Okahandja-Southern Zone at higher structural levels. Both were metamorphosed at deep crustal levels between 28 and 39 km and peak metamorphism was in relatively cool thermal regimes, with low *T*/depth ratios of 17 °C/km in the Southern Margin Zone and 25 °C/km in the Southern Zone. Moderately sharp metamorphic discontinuities define the upper boundaries of these crustal wedges (Fig. 12.12). The top of the Southern Margin Zone is defined by a metamorphic discontinuity coinciding with the Uis-Pass Suture, an extensionally reactivated crustal-scale thrust. There is a steep systematic increase in P from the Southern Foreland to the top of this crustal wedge, with a concomitant decrease in *T*/depth ratio. The Uis-Pass discontinuity is marked by a steep drop in P from 11.0 to 8.0 kb, and a change in thermal regime from 17 to 25 °C/km (Fig. 12.12). At higher structural levels there is no systematic variation in *P* and *T* across the south Okahandja-Southern Zone, and the T/depth ratio remains a constant 25 °C/km across this crustal wedge. The top of this crustal wedge has a broader metamorphic discontinuity in the southern Okahandja Zone, encompassing the transition from Barrovian to Buchan conditions in the north. This discontinuity is marked by a large drop in *P* from 9.0 to 5.5 kb and a change in thermal regime from 25 to 35 °C/km, to conditions typical of the internal parts of the orogen.

Large pressure drops across the two metamorphic discontinuities indicate extensional telescoping of the southern margin during the peak of metamorphism (Fig. 12.12). Extensional telescoping was accommodated by opposing, but coeval, shear kinematics at the top and bottom of the crustal wedges. Crustal wedges were exhumed by upthrusting along basal thrusts in the south, and accommodated by relative extensional shear at the top, juxtaposing low-*P* rocks against high-*P* rocks immediately below the discontinuity (Figs. 12.12 and 12.14). Southward propagation of outwedging events is indicated by the two-stage history of the Uis-Pass Suture: initially reverse during overthrusting of the Southern Zone and later extensional reactivation during outwedging of the Southern Margin Zone. Diachronous peak metamorphism ranging from 530 to 522 Ma in the south Okahandja-Southern Zone to 517 Ma in the Southern Margin Zone confirms foreland propagation of the outwedging event (Goscombe et al. 2017a). Deep burial followed by rapid exhumation of crustal wedges is expressed internally by *P–T* paths following near isothermal burial, hairpin clockwise loops and isothermal decompression (Fig. 12.13). Metamorphic zonation of the southern margin and steep clockwise *P–T* paths terminated by isothermal decompression are consistent with deep burial, metamorphism at low *T*/depth conditions and rapid exhumation in response to gravitational instability in overthickened crust (England and Thompson 1984; Jamieson et al. 1996).

The northern margin of the Damara Belt shows dramatic along-orogen variation in metamorphic response during Congo-Kalahari convergence (Goscombe et al. 2004), from diachronous and heterogeneous development of low-*P* contact metamorphic parageneses in the west, to high-*P* Barrovian metamorphism in the east. This is primarily the result of a large variation in thickness of basinal sequences from 1.7 km in the west (Swart 1992) to deep rift sequences in the east (Martin and Porada 1977; Porada 1979, 1983; Miller et al. 1983). Damaran deformation events involved biotite growth and temperatures >450 °C across most of the Ugab and Northern Zones. The highest grade parageneses in contact aureoles average 560 °C and 3.6 kb, and experienced tight anticlockwise *P–T* paths followed by isobaric cooling, with each pluton representing a different aged thermal anomaly (Goscombe et al. 2004, 2017a). In contrast, the Otavi domain in the east has similar metamorphic architecture to the southern orogenic margin. This sector experienced Barrovian peak metamorphic conditions of 637 °C, 9.2–10.4 kb and 20 °C/km (Goscombe et al. 2017a). This deeply buried crustal wedge is bound by steep metamorphic field gradients; to low-*P* greenschist facies conditions in the Northern Foreland, and at higher structural

levels across a metamorphic discontinuity to Buchan conditions in the Central Zone (Fig. 12.11). This pattern indicates overthrusting onto the Northern Foreland, accommodated by extension near the margin with the orogen core. Peak metamorphism and exhumation of the Otavi crustal wedge occurred after events in the southern margin. Peak metamorphism is constrained by the main foliation monazite of 510 ± 4 Ma age (Goscombe et al. 2017a), and exhumation was initiated soon after and was followed by cooling through 400 °C at 490 ± 11 Ma (Ahrendt et al. 1983).

12.6.2.2 High-Grade Orogen Core

All parts of the upper plate experienced Buchan series metamorphism at low to medium pressures between 4.0 and 6.0 kb and high T/depth ratios between 32 and 50 °C/km, and were associated with large volumes of in situ partial melt and crustal granitic melt (Fig. 12.3). The metamorphic grade varies from a lower amphibolite facies trough along the north Okahandja Zone margin, increasing to an elongate upper amphibolite facies anomaly along the central Okahandja Zone (Hoffer 1977; Hoernes and Hoffer 1979; Sawyer 1981; Haack et al. 1983; Kasch 1987; DeKock 1992; Kukla 1992a, b; Bühn et al. 1994; Jung et al. 1998b), whereas the Central Zone is a distinctive broad elliptical region of medium-P granulite facies rocks formed at 700–780 °C and 4.3–6.0 kb, with thermal regimes of 38–47 °C/km, and concentric zonation to lower-grade margins (e.g., Hoffer 1977; Goscombe et al. 2017a). Typical metapelite assemblages are garnet-cordierite-plagioclase-K-feldspar-biotite-quartz, with partial melt and cordierite coronas being common. Metamorphic field gradients show a broad asymmetric thermal high and a more subdued pressure maximum centred on the North Central Zone (Fig. 12.12). Metamorphic evolutions are uniform throughout, with tight, low $\Delta P/\Delta T$ clockwise *P–T* paths that experienced minor burial and low maximum pressures, extreme heating and near isobaric cooling after the peak of metamorphism (Fig. 12.13). Decompression through the peak of metamorphism is indicated by prograde garnet-sillimanite parageneses and highly resorbed relict garnet being occluded by peak metamorphic cordierite (Fig. 12.10b), and thin plagioclase coronas on garnet (Goscombe et al. 2017a). High thermal regimes with low $\Delta P/\Delta T$ *P–T* paths and isobaric cooling are indicative of metamorphism in stable settings with long residence times, where conduction outcompetes advection (Thompson et al. 1997).

Metamorphism occurred over a protracted period of time from 540 to 505 Ma. U–Pb metamorphic age determinations indicate three metamorphic events: 542–534, 530–516 and 515–505 Ma (Armstrong et al. 1987; Jung et al. 2000a, b; Jung and Mezger 2003a; Longridge et al. 2014; Goscombe et al. 2017a). Detrital metamorphic zircons from molasse in the Fish River Subgroup overlap with the oldest event, indicating main phase convergent orogenesis, topography development and prograde metamorphism at this time. Peak metamorphism, crystallization of matrix parageneses and predominant partial melting events were between 530 and 518 Ma throughout the Central Zone (Jung and Mezger 2003a; Longridge et al. 2011, 2014; Paul et al. 2014). However, the main peak metamorphic event that crystallized matrix parageneses and predominant melt segregations occurred at ~530 Ma in the South Central Zone, and in the North Central Zone was at ~528–526 Ma and persisted to 518 Ma (Goscombe et al. 2017b; Table 12.1). The 515–505 Ma age determinations are a late-stage thermal pulse that post-dates main phase events and coincides with post-kinematic granite, pegmatite and secondary partial melting (Briqueu et al. 1980; Allsopp et al. 1983; Jung et al. 2000b, 2001; Jung and Mezger 2003b; Longridge et al. 2011; DeKock and Armstrong 2014; Goscombe et al. 2017a). High-grade parageneses in the central Okahandja Zone formed at 534–519 Ma (Kukla et al. 1991; Jung and Mezger 2001) and at conditions of 650–720 °C, 4.0–5.5 kb and 40–50 °C/km (Goscombe et al. 2017a). The timing and thermal regime are shared in common with the Central Zone, indicating that the central Okahandja Zone represents the leading edge of attenuated passive margin and southern limit of high heat flow resulting from upper-plate lithospheric thinning.

Long residence times at high-grade conditions imply minor crustal thickening without major topographic development and relatively quiescent tectonic setting without rapid isostacy induced exhumation like the orogenic margins. The Central Zone is characterized by large volumes of granite, migmatite and in situ partial melt (30–60% of the current erosion surface), most of which was derived from melting of the Damara Sequence (McDermott et al. 1996), implying that these are a consequence of the high thermal gradient, not the cause. Similarly, there is no evidence for voluminous mafic magmatism, suggesting that the high thermal gradient was most probably a combination of thinned lithosphere (Ritter et al. 2003), and internal heat production from granites and metasediments highly enriched by radiogenic elements and with anomalous heat production values ranging from 4 to 24 μWm^{-3} (Haack et al. 1983; Ballard et al. 1987). It is proposed that prolonged high heat flow in the Central Zone is primarily the result of the thinned lithospheric architecture of the upper plate, established as (1) attenuated passive margin prior to collision and (2) further thinning processes subsequent to collision (Goscombe et al. 2017a). At collision it is probable that the subducted Khomas Ocean lithosphere was decoupled from the Kalahari lithosphere, sinking into the asthenosphere, driving countercirculation and further thinning of the upper plate in a setting akin to a continental 'back-arc' (e.g., Scharf et al.

2013). These initial conditions generating high-heat flow, and after a conductive delay of ~25 Ma from collision at ~555–550 Ma, resulted in high-grade metamorphism, significant partial melting and large volumes of S-type granite in the upper crust at ~530–520 Ma (e.g., Houseman et al. 1981; Houseman and Molnar 1997; Ducea 2011). Later extensional events may have contributed further lithospheric thinning, prolonging high heat flow conditions, and resulting in the secondary thermal anomaly at ~515–505 Ma. For example, extensional shear zones with granite veins of 511–508 Ma age have been documented in the Central Zone. It is also probable that extensional telescoping, outwedging and collapse of the southern orogenic margin at <522 Ma and <517 Ma may have resulted in a component of extensional stress in the Central Zone.

In contrast to lateral exhumation by outwedging in the Barrovian orogenic margins, the high-grade core of the orogen was exhumed vertically as an extensional core complex during late-stage collapse of the belt (Fig. 12.14). Metamorphic map patterns and field gradients across the Central Zone show upwards deflection of isobars, indicating that the hot orogen core was exhumed vertically as a broad core complex after the peak of metamorphism (Figs. 12.11 and 12.12). The granulite core of the Central Zone constitutes a ~140 km wide footwall dome showing weak uplift asymmetry, with pressures averaging ~4.8 kb in the south and ~5.5 kb in the north (Fig. 12.12). The margins show steep *PT*-gradients into low-grade hanging wall troughs with lower pressures averaging ~3.6 kb in the Ugab Zone and ~3.5–4.0 kb in the Okahandja Zone. This metamorphic pattern indicates the back tilting of isograds during vertical exhumation of the orogen core. The northern parts of the Central Zone experienced 3.5–7.7 km of uplift relative to the low-grade hanging wall, and 2.8–4.6 km of relative uplift in the south. The geometry, scale, mid-crustal exposure and high-grade nature of the Central Zone are consistent with a massif bivergent core complex type (Gessner et al. 2007; Wu and Laviers 2016). These are characterized by rapid uplift and cooling, 100–150 km widths, high-grade footwalls, bivergent marginal extensional detachments and a weak lower crust (Gessner et al. 2007; Wu and Laviers 2016). Marginal extensional detachments for the Central Zone would coincide with the Autseib Fault system in the north and the Okahandja Lineament in the south. Vertical exhumation of the Central Zone as a core complex is a natural consequence of the already thinned lithosphere and high heat flow in the Central Zone. This pre-existing condition of thin, hot lithosphere is conducive to extension and collapse of the orogen core, with thicker cooler lithosphere to both the north and south acting as steep lithospheric fronts that bound the central core complex. The imposed far-field stress switch from contraction across the Damara Belt, to shortening along the orogen at ~508 Ma, established a north–south extension direction exploited by melts and possibly triggered gravitational collapse of the thermally weakened orogen core soon after at ~505 Ma, followed by rapid cooling between 500 and 470 Ma.

12.7 Discussion and Conclusions

12.7.1 Plate-Tectonic Context of Damara System and West Gondwana Amalgamation

Being exceptionalla y well exposed, and consequently investigated intensively, there is now sufficient body of knowledge to put the Damara Orogenic System in a plate tectonic context. There has been a history of models proposed with special case scenarios and exceptional processes or settings to explain aspects of Damaran geology, such as lateral escape (Coward 1983; Oliver 1994; Kisters et al. 2004), high-strain basal detachments (Oliver 1994), ridge subduction (Meneghini et al. 2014; Cross et al. 2015) and intracontinental orogenesis (Kroner 1977; Miller et al. 1983). However, the Damara Orogenic System is typical to the point of being an archetypal example of transpressional orogenesis in the case of the Kaoko Belt and collisional orogenesis in the case of the Damara Belt. Both show typical orogenic cycles in common with orogenic belts universally: from rifted passive margin sequences, subduction with continental margin arcs and back arc basins, collision with detachment of subducted lithosphere, crustal overthickening, metamorphism and outwedging of orogenic margins, lithospheric thinning in the upper plate leading to protracted high heat flow and eventual collapse. There are no controversies here: both belts experienced orogenic cycles, histories, crustal processes and architectures in common with orogens globally. Possibly the only exceptional aspect of the Damara Orogenic System is its continuous exposure, and this rich geological record has allowed the construction of large relational data sets covering the entire system and facilitating the testing of hypotheses. This chapter is not intended as a comprehensive description of the Damara Orogenic System, and has specifically focused on the structural and metamorphic evolution (e.g., Goscombe et al. 2017a, b). Detailed data sets and summaries of other aspects, such as geological mapping, sedimentology, stratigraphy, magmatism and geophysics, are widely available elsewhere (e.g., Kasch 1983b; Miller et al. 1983, 2008; Porada 1983; Miller and Grote 1988). Building on our previous attempts to put the Damara Orogenic System into a broader plate tectonic context (Gray et al. 2006, 2008; Goscombe and Gray 2007, 2008; Goscombe et al. 2017a, b), an attempt is made here to develop an internally consistent model for crustal evolution and tectonic history, using the structural, metamorphic and

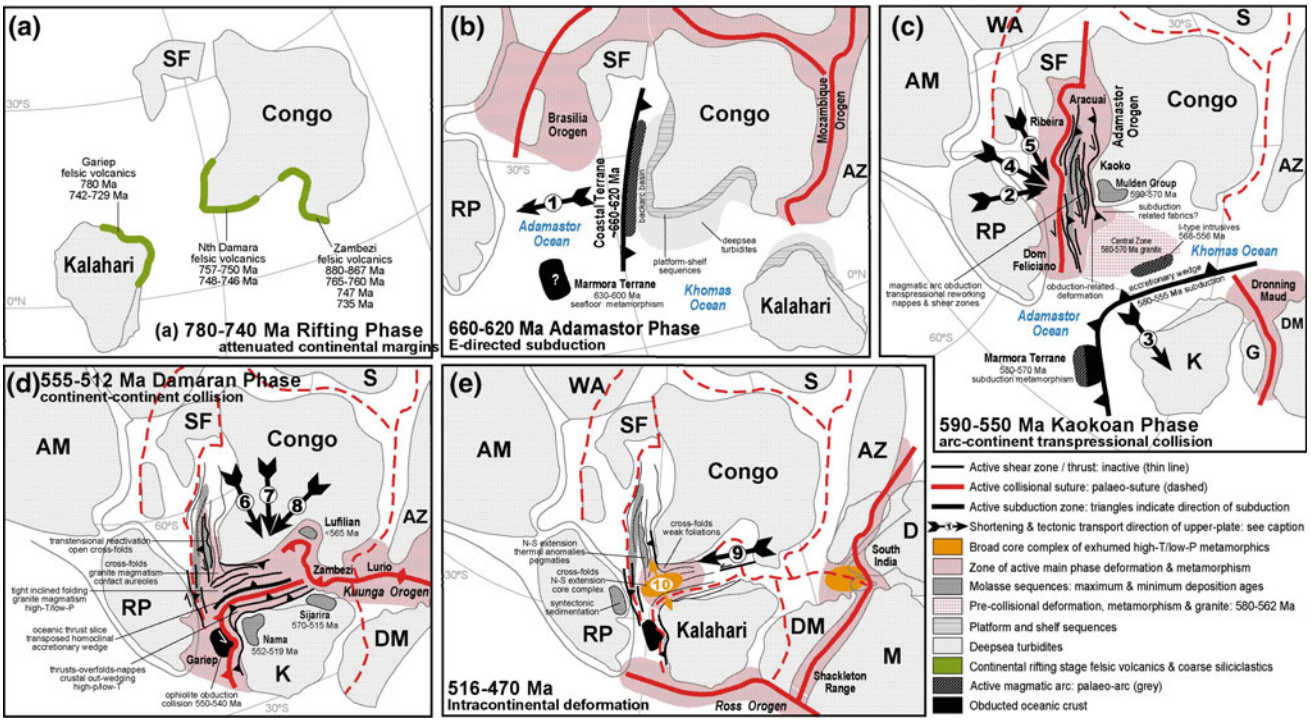

Fig. 12.15 Time sequence reconstruction of continents at key periods in the evolution of the Damara Orogenic System, modified after Gray et al. (2008). All figures are arranged relative to the affixed Congo Craton in the current orientation with respect to north. **a** Rifting of continental margins stage at ~780–740 Ma. **b** Coastal Terrane magmatic arc stage ~660–620 Ma. **c** Kaoko Belt transpressional collision stage ~590–550 Ma. **d** Damara Belt continent–continent collision stage ~555–512 Ma. **e** Reactivation, exhumation and cooling stage in an intracontinental setting ~516–470 Ma. Deformation episodes during evolution of the Damara Orogenic System are numbered along with the interpreted tectonic transport direction of the upper plate: (1) east-directed subduction and formation of the Coastal Terrane continental margin magmatic arc from ~660 to 620 Ma; (2) east-directed obduction of the Coastal Terrane at ~590 Ma; (3) north-directed subduction in the Khomas Ocean from ~600 to 555 Ma; (4) main phase transpressional orogenesis in the Kaoko Belt ~580–550 Ma; (5) progressive strike-slip shear in the Kaoko Belt from ~550 to 535 Ma; (6) Congo-Kalahari collision at the Uis-Pass Suture, north-northwest-south-southeast contraction and main phase orogenesis at ~555–520 Ma; (7) north–south contraction across the Damara Belt and outwedging of the Southern Margin between ~518 and 516 Ma; (8) northeast-southwest shortening and outwedging of the Southern Margin Zone between ~516 and 512 Ma; (9) east–west shortening, crossfolding and reactivation of the Damara Belt between ~510 and 508 Ma; and (10) north–south extension, vertical shortening and core complex in the high-grade core of the Damara Belt from ~505 to 500 Ma

chronological data sets we have been involved with (Figs. 12.2, 12.7, 12.12 and 12.14).

12.7.1.1 Rifted Cratonic Margins: ~880–700 Ma

Continental break-up, rifting of cratonic margins and formation of passive margins were well under way by ~750 Ma on both Kalahari and Congo cratonic margins (Fig. 12.15; Frimmel et al. 1996; Hoffman et al. 1996). Age determinations from rift = related siliciclastics and mafic-felsic volcanics preserved in the Congo Craton margin vary substantially, indicating a protracted rifting phase. The Lufilian-Zambezi Belt in the east preserves the oldest rift phase sequences with maximum deposition ages of 962–957 Ma in basal sequences (Goscombe et al. in press b), and mafic-felsic volcanism at 880–876, 867, 765–760 and 747–735 Ma (Key et al. 2001; Johnson et al. 2005, 2007; Master et al. 2005; Goscombe et al. in press b). Metamorphosed felsic extrusives in allochthonous terranes on the southern margin of the Zambezi Belt have a range of ages: 870–869, 858–849, 808–804, 797–794, 764 and 750–737 Ma (Dirks et al. 1998, 1999; Hanson et al. 1998; Vinyu et al. 1999). Only the later episodes in the Lufilian-Zambezi Belt overlap in age with volcanics preserved in the northern Damara Belt. The maximum deposition ages from the Nosib Group siliclastics range from 861 to 811 Ma (Foster et al. 2015), and possible rift-related mafic volcanics in the Kaoko Belt are ~840–805 Ma (Konopásek et al. 2005). Meanwhile, felsic volcanics of the Naauwpoort Formation at the top of the Nosib Group range from 759 to 756 Ma and 764 Ma in the Kaoko Belt (Halverson et al. 2002), 748–746 and 757–752 Ma age in the Northern Zone (Hoffmann 1994; Hoffman et al. 1996; DeKock et al. 2000; Nascimento et al. 2016), 750 Ma in the Central Zone (DeKock et al. 2000), and ~714–705 Ma in the Okahandja and Southern Zones

(DeKock et al. 2000; DeKock and Armstrong 2014). In contrast, rift-related siliciclastic Tsumis and Nosib Group deposited on the Kalahari margin contain felsic volcanic episodes at 820, 780 and 742–729 Ma, and do not overlap with eruptive events on the Congo margin and cannot be correlated (Frimmel et al. 1996; Kampunzu et al. 2000; Gray et al. 2008).

The width of the Khomas basin between the Congo and Kalahari Cratons has been disputed (e.g., Kroner 1977; Porada 1989). The Khomas basin has been interpreted as either (1) an intracontinental rift basin between the Congo and Kalahari Cratons with sedimentation on attenuated continental lithosphere (Kroner 1977; Martin and Porada 1977; Porada 1979, 1983, 1989; Hawkesworth et al. 1983; Hanson et al. 1994; Hanson 2003) or (2) a small ocean basin with minor spreading at ~700 Ma, formed after intracontinental rifting of contiguous Congo and Kalahari Cratons (e.g., Barnes and Sawyer 1980; Kasch 1983b; Miller et al. 1983; DeKock 1992). In both models, intracontinental rifting of once contiguous Congo and Kalahari Cratons was inferred on the basis of rift-related felsic volcanism thought to be the same age, and now known to differ (Gray et al. 2008). εNd values in metapelites and detrital zircon populations from metapsammites show distinctly different provenance for the sequences deposited on Congo and Kalahari margins. Sequences north of the Uis-Pass suture have εNd values ranging from −3.0 to −5.0, and detrital zircons with Congo provenance and those in the Southern Margin Zone have εNd values of −8.0 and zircons with Kalahari provenance (Foster et al. 2015). These sequences show no connection, and the Congo and Kalahari Cratons cannot have been contiguous or separated by an intracontinental rift but must have been separated by a wide ocean basin. Paleomagnetic data suggests that the positions of the Congo, Kalahari and Rio de la Plata Cratons were quite disparate at ~750 Ma during the rifting phase (Meert 2003). Gray et al. (2008) argued for 38° separation in latitude between the Congo and Rio De La Plata cratons. Meanwhile, the less well-constrained Kalahari Craton is inferred to have been separate on the basis of Grenvillian age paleomagnetic poles (Meert and Torsvik 2003; Pesonen et al. 2003) and a 755 Ma pole for the Congo Craton (Meert et al. 1995). Crucially, an intracontinental orogenic model for the Damara Belt lacks a plausible mechanism to drive contraction in the absence of a subducting slab pull, and requires far-field collision on the margin of Gondwana as early as 555 Ma to drive Congo-Kalahari contraction. Similarly, a complete absence of basement geology shared in common between the respective margins precludes an intracontinental rift model.

12.7.1.2 Khomas Ocean: ~700–580 Ma

Sedimentation into the Adamastor and Khomas Ocean basins continued until ~580 Ma, when passive margin sedimentation was terminated by collision in the Kaoko Belt (Miller et al. 1983; Hoffman et al. 1994, 1998; Prave 1996; Hoffmann et al. 2004; Foster et al. 2015). Deposition in the northern Khomas ocean basin occurred on highly attenuated Congo Craton crust, exposed in basement antiforms in the Kaoko Belt and Central-Okahandja Zones of the Damara Belt. South of the continental leading edge, the Southern Zone is a thick monotonous sequence of deep-sea turbidites. This sequence contains MORB-type Matchless Suite with sheared tholeiitic gabbro, pillow basalt, serpentinite and meta-chert-Cu/Zn mineralization association, interpreted as interthrust relict oceanic lithosphere (Barnes 1983; Schmidt and Wedepohl 1983; Killick 2000). The Southern Zone is devoid of continental basement and interpreted as turbidite fans shed into an ocean basin (Martin and Porada 1977; Barnes and Sawyer 1980; Kasch 1983b; Miller et al. 1983; Hoffmann 1989; Kukla et al. 1991; Kukla and Stanistreet 1991; DeKock 1992; Gray et al. 2006, 2007, 2008; Foster et al. 2015). It is a homoclinal, intensely transposed wedge of deep marine turbidites with Congo Craton provenance, entirely consistent with formation as an accretionary prism (Kukla and Stanistreet 1991; Gray et al. 2006, 2008; Foster et al. 2015). The Uis-Pass Suture between the Southern and Southern Margin Zones is a crustal-scale shear zone containing sheared Alpine serpentinites accreted during continent-continent collision (Barnes 1983; Kasch 1983b), and it marks the suture between the Kalahari and Congo sequences (Foster et al. 2015). Subduction at this suture did not, however, produce voluminous Andean-type magmatic arc with margin-parallel linear batholiths and margin-normal geochemical gradients (Barnes and Sawyer 1980; Kasch 1983b; Miller et al. 1983; DeKock 1992). Pre-collision, I-type intermediate granitoids of 568–556 Ma age in the South Central Zone have some magmatic arc affinities consistent with subduction of the Khomas Ocean lithosphere (Haack et al. 1982; McDermott et al. 1996; Jung et al. 2001). These complexes are small, mantle isotopic signatures are rare (Jung et al. 2001), and they had multiple magma sources, indicating assimilation of lower crust (Hawkesworth et al. 1981; Haack et al. 1982; McDermott et al. 1996; Jung et al. 2001).

High-*P*/low-*T* blueschist-eclogite subduction parageneses associated with the subduction of oceanic lithosphere at the Uis-Pass Suture have not been preserved in the rock record. Similarly, early low-*P*/high-*T* parageneses, with thermal regimes of at least 40–50 °C/km, associated with subduction of the spreading ridge, have not been preserved in the rock record. Recently, Cross et al. (2015) reported putative ridge subduction parageneses in the Southern Zone, yet current evidence for high-*P*/moderate-*T* parageneses with clockwise *P*–*T* paths is entirely incompatible with ridge subduction and typical of the Barrovian conditions during later collisional orogenesis, as extensively reported in the literature (Hoffer

1978; Sawyer 1981; Behr et al. 1983; Kasch 1987, 1993; Kukla 1992a, b; Puhan 1995; Goscombe et al. 2017a). Subduction parageneses are rarely preserved because (1) they need to be accreted into the hanging wall; and (2) they formed prior to collision and simply recrystallized and were obliterated by both ongoing shear in the accretionary wedge, and later high-strain penetrative deformation and burial during collisional orogenesis (Yardley 1982; Mortimer 2000). It is therefore no surprise that all parageneses reported from the Southern Zone are Barrovian series with thermal regimes in the range 17–25 °C/km, and steep clockwise *P–T* paths with isothermal decompression, typical of collisional orogenesis (England and Thompson 1984; Jamieson et al. 1996, 2002; Thompson et al. 1997; Huerta et al. 1998, 1999; Beaumont et al. 2001; Goscombe et al. 2006). Nevertheless, ocean basin closure is indicated by separate sediment provenance (Foster et al. 2015), interthrust oceanic lithosphere in both the suture and Matchless Belt at higher structural levels (Barnes 1983; Killick 2000), homoclinal accretionary wedge and gross structural asymmetry of the orogen (Gray et al. 2008). Northward subduction of Khomas Ocean lithosphere beneath attenuated Congo Craton is indicated by the homoclinal north-dipping southern margin with ubiquitous top to the south tectonic transports, and calcalkaline I-type complexes in the upper-plate Central Zone (Barnes and Sawyer 1980; Kasch 1983b; Maloof 2000; Gray et al. 2008). Furthermore, the Lufilian-Zambezi Belt contains ~575 Ma, MORB-type eclogite and whiteschist buried to 90 km depth, and clearly formed during subduction, inferring a closed ocean basin (John et al. 2003, 2004; Goscombe et al. in press b).

12.7.1.3 Adamastor Ocean: ~660–590 Ma

The geological record of the Adamastor ocean is preserved within the Damara Orogenic System in two widely separated obducted oceanic terranes: the Coastal Terrane of the Kaoko Belt and the Marmora Terrane of the Gariep Belt (Fig. 12.15). Ocean closure occurred earlier in the north, with obduction of the Coastal Terrane onto the Congo Craton margin at ~590–580 Ma (Goscombe et al. 2005b; Goscombe and Gray 2007) and Marmora Terrane obduction onto the Kalahari Craton margin at ~550 Ma (Frimmel 1995; Frimmel and Frank 1998).

The Coastal Terrane is a magmatic arc consisting of calcalkaline mafic, intermediate and felsic metaintrusives of 661–655 and 638–620 Ma age (Seth et al. 1998; Kröner et al. 2004; Goscombe et al. 2005b; Masberg et al. 2005; Goscombe and Gray 2007), and coarse juvenile meta-arenites with maximum deposition ages of 674 Ma (Goscombe and Gray 2007; Foster et al. 2015). Metasediments have detrital zircon populations <820 Ma and εNd ratios indicating Neoproterozoic sources, consistent with being juvenile sediments shed off the arc (Goscombe et al. 2005b; Goscombe and Gray 2007). Metamorphism aged at 650–640 Ma accompanied magmatism and was at low-*P*/high-*T* conditions of 40 °C/km consistent with magmatic arc thermal regimes (Franz et al. 1999; Goscombe et al. 2005a). Lithostratigraphy, provenance, magmatism and metamorphism differ from the remainder of the Kaoko Belt, indicating that the Coastal Terrane evolved independently of the Kaoko Belt prior to obduction at ~590–580 Ma (Goscombe et al. 2003b, 2005a, b; Goscombe and Gray 2007). In contrast, sequences in the remainder of the Kaoko Belt consist of deep basin turbidite and slope facies with Congo Craton provenance, deposited on attenuated passive margin floored by Mesoproterozoic to Neoarchaean basement (Goscombe and Gray 2007, 2008).

Two scenarios have been proposed: west-directed subduction and destruction of an ocean basin at the Three Palms Mylonite Zone (Porada 1979; Machado et al. 1996; Masberg et al. 2005), and outboard east-directed subduction with the Orogen Core occupying a back-arc position (Basei et al. 2000, 2005; Goscombe and Gray 2007, 2008). The geological evidence supports the latter, and interprets the originally shallow west-dipping Three Palms Mylonite Zone as accommodating obduction of the Coastal Terrane, resulting from collision of Rio De La Plata Craton in the west. There is no evidence that the Orogen Core of the Kaoko Belt was floored by oceanic crust, ophiolite is absent and basement infolds of Congo Craton crust occur across the zone (Konopásek et al. 2005). High-*P*/low-*T* subduction parageneses are also absent, and the Three Palms Mylonite Zone and adjacent rocks were buried no deeper than ~6 kb (Goscombe et al. 2005a; Goscombe and Gray 2007). Consequently, the Coastal Terrane is interpreted as a continental margin arc attached to the leading edge of attenuated passive margin with Damaran sequences deposited in a back arc floored by continental crust (Fig. 12.16; Goscombe et al. 2005a, b; Goscombe and Gray 2007, 2008).

The West Gondwana Orogen contains magmatic arc terranes of 680–580 Ma age strung along the core of this 2800 km-long composite orogenic system (Fig. 12.1; Trompette and Carozzi 1994; Trompette 1997; Basei et al. 2000; Heilbron and Machado 2003; Saalmann et al. 2005). The Coastal Terrane magmatism was contiguous with calcalkaline magmatism in the Oriental Terrane of the Ribeira Belt (Heilbron et al. 2004). Arc magmatism propagated southwards, ranging from 620 to 580 Ma along the Granite Belt in the Dom Feliciano Belt (Basei et al. 2000). Calcalkaline magmatism was long-lived in the east Dom Feliciano Belt, with episodes at 800, ~670, 630–617 and 600–585 Ma (Frantz and Botelho 2000). Further north, arc magmatism was at 680–670 Ma and metamorphism at 655–645 Ma in the Brasiliano Belt on the west side of the Sao Francisco Craton (Heilbron and Machado 2003; Heilbron et al. 2004), and 630–585 Ma within the Aracuai Belt on the

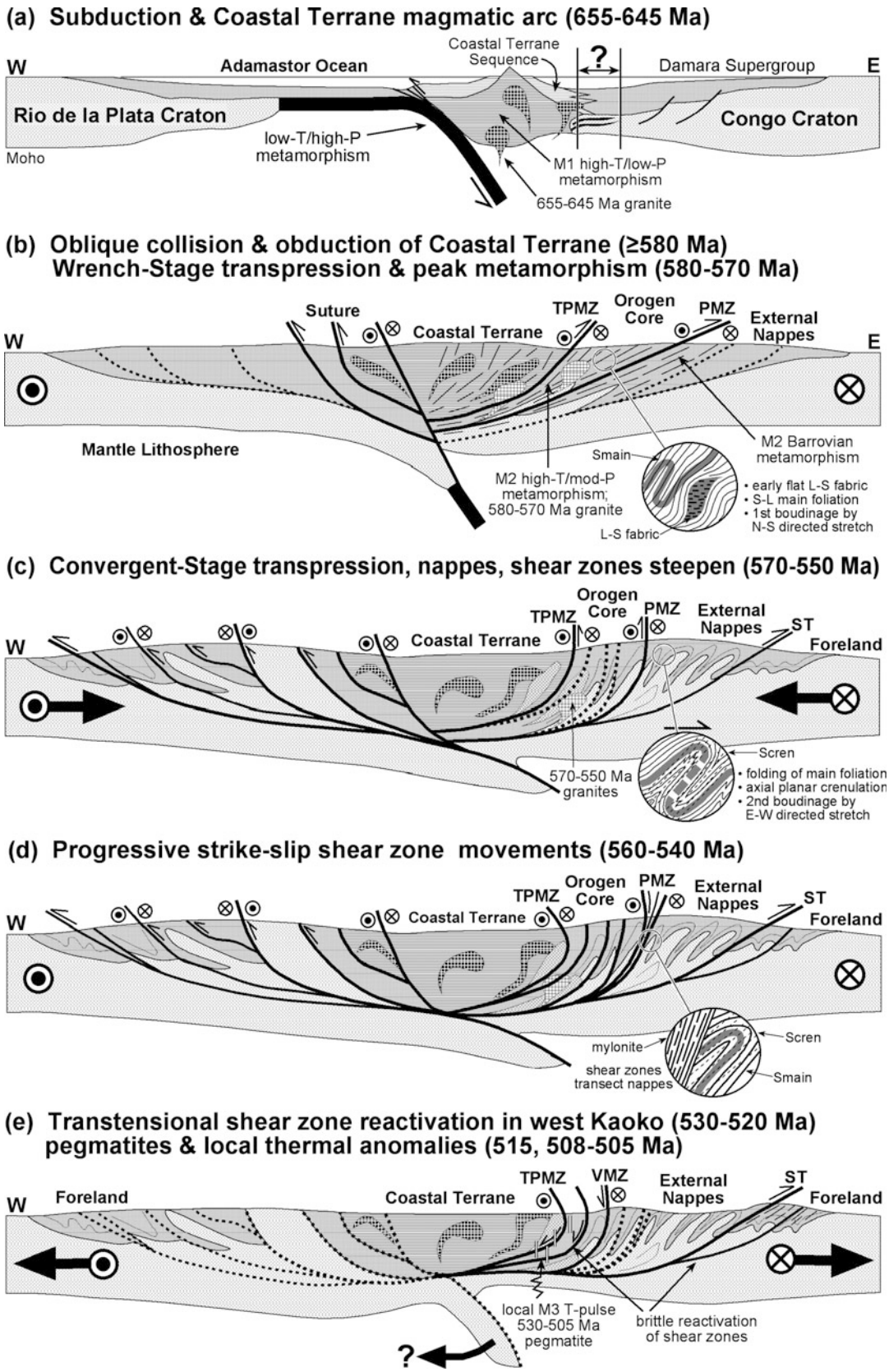

Fig. 12.16 Diagrammatic summary of the time-sequence evolution of crustal architecture in the Kaoko Belt, illustrating the relationship between deformation and metamorphic processes and probable tectonic settings, modified after Goscombe and Gray (2008)

east side of the Sao Francisco Craton (Alkmin et al. 2005). In common with interpretation of the Kaoko Belt, there is no evidence for west-dipping subduction below the Rio De La Plata Craton (Basei et al. 2000). The Aracaui Orogen in the north has ophiolite inboard of the magmatic arc, indicating east-directed subduction (Pedrosa-Soares et al. 1998, 2001). East-directed subduction has also been proposed for the Dom Feliciano Belt (Basei et al. 2000). West-directed obduction of the Granite Belt in the Dom Feliciano Belt was the result of attempted subduction of Rio De La Plata Craton upon ocean closure (Gray et al. 2008). The result was a doubly vergent architecture for the Kaoko-Dom Feliciano Orogen, with the Coastal Terrane-Granite Belt magmatic arc in the core, obducted onto both cratonic margins during collision.

Further south, magmatic arcs are absent, but the oceanic lithosphere of the south Adamastor Ocean is preserved in the Marmorma Terrane that was obducted onto the Kalahari Craton margin in the Gariep Belt (Frimmel 1995; Frimmel and Frank 1998). The ensimatic, subduction-related origin of the Marmora Terrane is indicated by the assemblage of a deep-sea turbidite, metavolcanic and Chameis Complex mélange containing mafic and ultramafic blocks with near blueschist facies parageneses formed at 6 kb and low temperatures (Frimmel and Hartnady 1992; Frimmel 2000). Seafloor metamorphism parageneses are also identified, and with Ar–Ar hornblende ages of 630 Ma age, indicating that seafloor spreading was still occurring at this time (Frimmel 1995; Frimmel and Frank 1998). The detrital zircon populations are similar in both the Rocha Group of the Dom Feliciano Belt and the Oranjemund-Stinkfontein Groups of the Gariep Belt, indicating that they shared the same oceanic basin (Basei et al. 2005). Consequently, the Gariep Belt was closed by west-directed subduction beneath the Rio De La Plata Craton (Frimmel et al. 1996). Collision by southeast-directed oblique obduction of the Marmora Terrane over the imbricated passive margin in the Gariep Belt occurred at 550–540 Ma (Frimmel 1995; Frimmel and Frank 1998). Tectonic transport and the age of collision is identical to 555–550 Ma closure of the Khomas Ocean at the Uis-Pass Suture in the Damara Belt. This establishes a continuous, arcuate northwest-directed subduction system that closed the southern Adamastor and Khomas Oceans at the same time, and the resultant Gariep-Damara Belt constitutes the westernmost sector of the greater Kuunga Orogen.

12.7.1.4 Closure of Northern Adamastor Ocean: ~590 Ma

Closure of the north Adamastor Ocean was by oblique collision and transpressional orogenesis at much the same time in the Dom Feliciano and Ribeira Belts flanking the Rio de la Plata Craton and the Kaoko Belt flanking the Congo Craton (Frantz and Botelho 2000; Heilbron and Machado 2003; Heilbron et al. 2004; Goscombe et al. 2005b). Subduction-related closure may have propagated southwards in concert with the younging direction of magmatic arcs (Stanistreet et al. 1991; Gresse and Germs 1993; Germs 1995; Frimmel and Frank 1998; Maloof 2000; Gray et al. 2008). The earliest collision occurred in the north within the Brasiliano Orogen at ~640 Ma, with east-directed nappe emplacement over the Sao Francisco Craton between 640 and 630 Ma (Valeriano et al. 2004, 2008). Collisional events further east and south started approximately 50 Ma later. The youngest calcalkaline magmatism in the Aracuai Belt was at 585 Ma, indicating ocean closure after this time. Obduction of the Coastal Terrane onto the Congo margin was initially east-directed along a shallow west-dipping Three Palms Mylonite Zone, and progressed to east-southeast- and southeast-directed transport as sinistral transpression progressed (Goscombe et al. 2003a; Goscombe and Gray 2008). Obduction is constrained between the 620 Ma end of magmatism and the 580–570 Ma main phase transpressional fabrics, parageneses and synkinematic granites (Seth et al. 1998; Goscombe et al. 2005b). Collision is interpreted to have been immediately prior to transpression and estimated at ~590 Ma (Goscombe and Gray 2007). The Mulden Group molasse is infolded and deformed during transpressional orogenesis in the Kaoko Belt, indicating deposition ages prior to 580–570 Ma (Gray et al. 2008). The maximum deposition ages of ~621 and ~590 Ma and detrital zircon peaks are consistent with the earliest formed topography being obducted Coastal Terrane at ~590 Ma (Goscombe et al. 2005b; Foster et al. 2015). Similarly, oblique collision of the Rio Negro arc in the Ribeira Orogen has been estimated at ~595–590 Ma and dextral transpressional orogenesis with steep transcurrent shear zones progressed throughout 590–560 Ma (Machado et al. 1996; Heilbron and Machado 2003; Heilbron et al. 2004). Collision in the Dom Felicianao Belt is estimated by the youngest arc magmatism at ~580 Ma (Basei et al. 2000), and experienced both sinistral and dextral transcurrent shear in major shear zones (Basei et al. 2000; Frantz and Botelho 2000; Saalmann et al. 2005).

Though complex, different sectors of the West Gondwana Orogen between the Rio De La Plata-Sao Francisco and Congo Cratons share similar architecture and histories, and together can be considered to be a large-scale transpressive orogenic system. Collisions at 595–585 Ma were initiated by the obduction of magmatic arcs, main phase transpressional orogenesis, magmatism and metamorphism between 585 and 560 Ma, and they were progressively partitioned into long-lived, steep crustal-scale transcurrent shear zones active to ~530 Ma (Pedrosa-Soares et al. 1998, 2001; Brueckner et al. 2000; Heilbron et al. 2004; Schmitt et al. 2004; Basei et al. 2005; da Silva et al. 2005; Goscombe et al. 2005b; Goscombe and Gray 2008). The crustal architecture of the

reconstructed West Gondwana Orogen has symmetrical bivergent form, dominated by crustal-scale shear zones of opposing listric inclination, dipping east in South America and west in Africa (Fig. 12.16; Basei et al. 2005; Trompette and Carozzi 1994; Trompette 1997; Goscombe and Gray 2007). Opposing shear zone kinematics across the orogen, sinistral in the east and predominantly dextral in the west (Brueckner et al. 2000; Basei et al. 2005), indicate local convergence and southwards transport of the central magmatic arc, rather than plate-scale trajectories (Gray et al. 2008). All belts show strong kinematic and metamorphic partitioning typical of transpressional orogens (e.g., Thompson et al. 1997). Internal parts are steep, wrench-dominated, thermally softened, intruded by granites and contain reworked magmatic arcs, whereas margins are foreland-vergent Barrovian fold-nappe-thrust belts with reworked basement (Trompette and Carozzi 1994; Dürr and Dingeldey 1996; Trompette 1997; Pedrosa-Soares et al. 1998, 2001; Brueckner et al. 2000; Heilbron et al. 2004; Basei et al. 2005; Goscombe et al. 2005a; Goscombe and Gray 2008).

12.7.1.5 Closure of Southern Adamastor and Khomas Oceans: ~555–550 Ma

Closure of both the South Adamastor Ocean at the Gariep Belt, and the Khomas Ocean at the Damara Belt, occurred at 555–550 Ma by northwest-directed collision of the Kalahari Craton with the already amalgamated Congo-Rio De La Plata Cratons (Fig. 12.15; Frimmel 1995; Frimmel and Frank 1998; Gray et al. 2006, 2008; Goscombe et al. 2017b). Ocean closure at the Uis-Pass Suture in the Damara Belt is recorded by southeast-directed transport of the Naukluft Nappe Complex onto the foreland, and dated at ~555 Ma by Ar–Ar muscovite from phyllonite in the basal thrust (Gray et al. 2006). Collision at this time is confirmed by the maximum deposition age of ~552 Ma for the Fish River Subgroup molasse in the Nama Basin (Grotzinger et al. 1995; Foster et al. 2015), and 556–550 Ma K–Ar deformation ages from phyllites in the Northern Platform (Clauer and Kroner 1979). Collision in the Gariep Belt was by southeast-directed oblique obduction of the Marmora Terrane onto the Kalahari passive margin at 550–540 Ma (Frimmel 1995; Frimmel and Frank 1998; Frimmel 2000), with erosion into the Nama Basin commencing at 540 Ma (Gresse and Germs 1993; Gresse 1994; Frimmel 2000).

Tectonic transport and collision at the same time in both belts establish that a single arcuate northwest-directed subduction system closed the southern Adamastor and Khomas Oceans at the same time, and the resultant Gariep-Damara Belt constitutes the westernmost sector of the greater Kuunga Orogen (Fig. 12.15; Meert 2003). Earlier collision and amalgamation of the Congo and Rio De La Plata Cratons is well established by main phase orogenesis, metamorphism and magmatism in the Kaoko Belt between 580 and 550 Ma (Seth et al. 1998; Franz et al. 1999; Kröner et al. 2004; Goscombe et al. 2005b). The northwest-directed collision of the Kalahari Craton against the already amalgamated Congo-Rio De La Plata Cratons is confirmed by overprinting relationships. The earliest Damaran overprint in the Kaoko Belt and the Ugab Zone involved northwest-southeast shortening, shared in common with the earliest northwest-vergent folding in the Central Zone and southeast-vergent folds, nappes and thrusts in the southern margin of the Damara Belt (Longridge et al. 2011, 2014). From 555 Ma onwards both the Kaoko and Damara Belts shared the same deformation history of progressive clockwise rotation of the stress field from northwest-southeast to east–west shortening at ~510 Ma (Goscombe et al. 2017b). Paleomagnetic poles indicate all components of West Gondwana had amalgamated by 550 Ma and shared a single apparent polar wander path (Rapalini 2006; Tohver et al. 2006), confirming that collision in the Damara and Gariep Belts had occurred by this time.

12.7.1.6 Collisional Orogenesis in the Damara Belt: ~550–510 Ma

Closure of the Khomas Ocean was complete by 555–550 Ma. The culmination of orogenesis and peak metamorphism was between 530 and 520 Ma in the Damara and Lufilian-Zambezi Belts, 530–510 Ma in the Ribeira Belt and similar ages along the length of the Kuunga Orogen (Goscombe et al. 1998; John et al. 2003, 2004; Meert 2003; Boger and Miller 2004; Schmitt et al. 2004; Gray et al. 2008). Collisional orogenesis in the Kuunga Orogen was responsible for stitching north and south Gondwana in the final phase of Gondwana's assembly. Subsequent events in the Damara Orogenic System therefore occurred in an intraplate setting driven by orogenesis on the margins of Gondwana. Subduction under the margins of Gondwana began at ~560 Ma off Antarctica and was established by ~530 Ma in Australia and South America, producing major accretionary orogens. Major arc collisions and magmatism in the Ross-Delamerian Orogen took place by 520–510 Ma, followed by extension along the margins of Gondwana and within older mobile belts (e.g., Goodge et al. 1993; Goodge 1997; Meert 2003; Boger and Miller 2004; Foster et al. 2005; Foden et al. 2006), significantly effecting late-stage evolution of the Damara Orogenic System.

The direction of convergence, and deformation and metamorphic response, evolved considerably through the Damaran orogenic cycle (Fig. 12.17). The collision and prograde crustal thickening stage in the Damara Belt, between 555 and 530 Ma, accompanied northwest-directed transport of the Kalahari Craton into the Congo-Rio De La Plata Cratons (Fig. 12.15). Both the Kaoko and Damara Belts shared similar northwest-southeast shortening

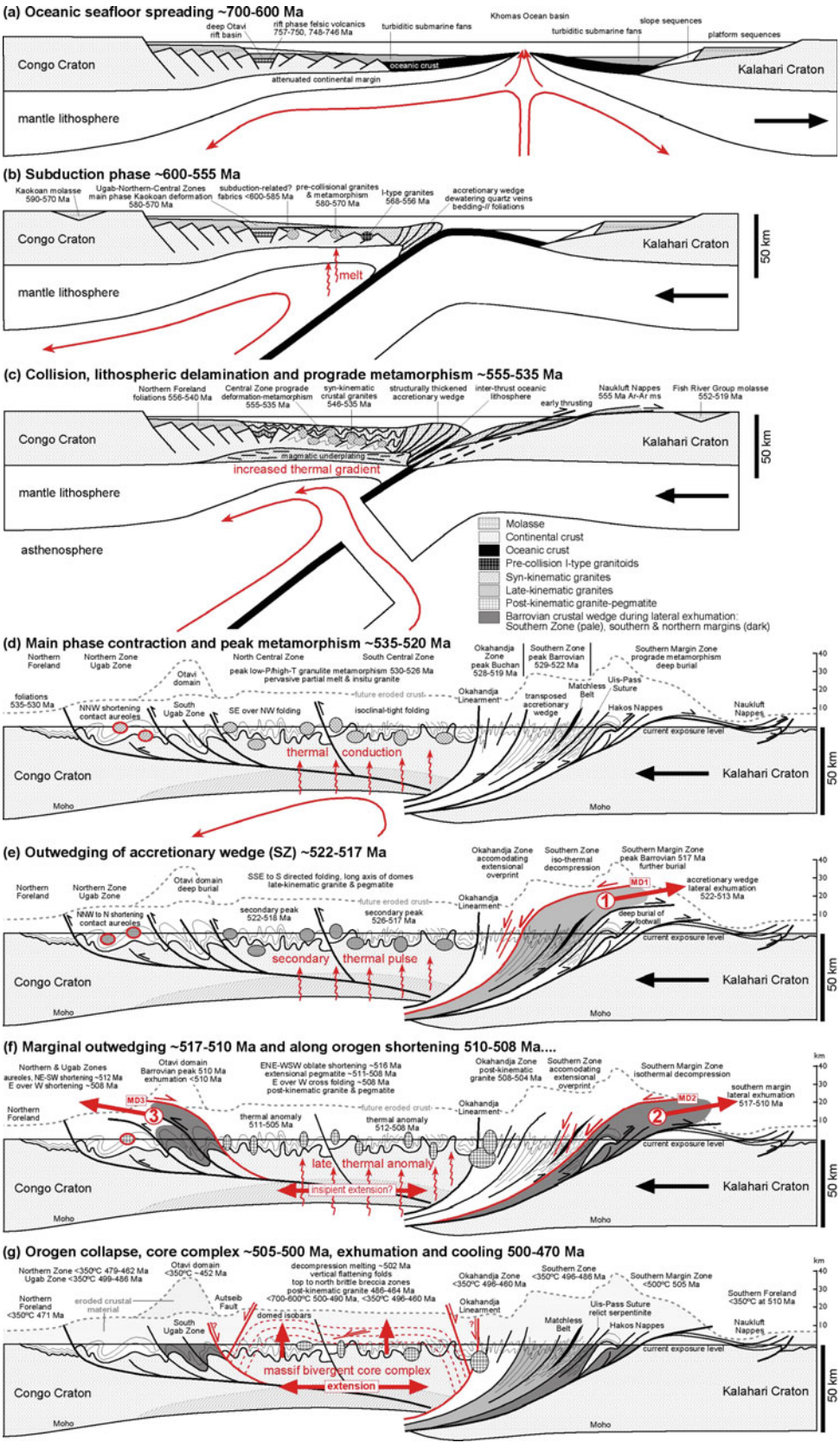

Fig. 12.17 Diagrammatic summary of the time-sequence evolution of crustal architecture in the Damara Belt, illustrating the relationship between deformation and metamorphic processes and probable tectonic settings, modified after Gray et al. (2007, 2008) and Goscombe et al. (2017a). See text for arguments and discussion of the tectonic models adopted. Extensional telescoping events and thermal features are indicated by red symbols

directions and both orogenic fronts were operating at this time: waning transpression in Kaoko Belt and high-angle collisional orogenesis in the Damara Belt (Gray et al. 2008). All three cratons were convergent: upper-plate Rio De La Plata Craton transported southeast over the west margin of the Congo Craton, while upper-plate Congo Craton in the southern margin was transported southeast over the Kalahari Craton margin. The earliest fold generations in the Damara Belt were northwest-vergent in the Central Zone (Kisters et al. 2004; Longridge et al. 2011, 2014) and southeast-vergent penetrative foliations, folds, thrusts and nappes in the southern orogenic margin, including the earliest Naukluft and Gariep nappes transported onto the foreland. Crustal thickening and burial in the orogen core led to prograde metamorphic parageneses, the earliest migmatization and widespread S-type granitoids of 546–534 Ma age (e.g., Jung et al. 2000b; Jung and Mezger 2003a). Significant topography was established, shedding molasse into the Nama Basin, dominated by material from the internal parts of the belt, with prograde magmatic and metamorphic zircons of 540–530 Ma age well represented (Gresse and Germs 1993; Gresse 1994; Foster et al. 2015).

A stress switch at 530–520 Ma in response to changes in the Kalahari Craton trajectory to north-northwest-directed transpor, resulted in higher angle convergence in the Damara Belt, which from this time partitioned almost all contractional strain (Fig. 12.17; Goscombe et al. 2017b). The culmination of the main phase of orogenesis, crustal thickening, partial melting and peak metamorphism in the Damara Belt coincides with this period (Armstrong et al. 1987; Kukla et al. 1991; Jung et al. 2000a, b; Jung and Mezger 2001, 2003a; Jung et al. 2001; Longridge et al. 2014; Paul et al. 2014). Metamorphism in the orogen core was characterized by granulite facies conditions, high thermal regimes of 32–50 °C/km, and low $\Delta P/\Delta T$ clockwise P–T paths showing only moderate burial and peak metamorphic conditions at only 4–6 kb (Goscombe et al. 2017a). High-grade conditions were long-lived, from ~540 to 505 Ma, and resulted in large volumes of partial melting and granite pooling in the mid-crust. Prolonged high heat flow in the orogen core is the result of anomalously high radiogenic heat production, from granites and metasediments enriched in radiogenic elements (Haack et al. 1983; Ballard et al. 1987), and thinned lithospheric architecture of the upper plate (Ritter et al. 2003). Thin upper-plate lithosphere was established by a combination of highly attenuated passive margin prior to collision, and probable further thinning by asthenospheric countercirculation in response to the decoupling and sinking of subducted Khomas Ocean lithosphere after collision (Fig. 12.17; e.g., Scharf et al. 2013). These initial conditions at ~550 Ma generated high heat flow, resulting in peak metamorphism after a conductive delay of ~25 Ma (e.g., Housman et al. 1981; Houseman and Molnar 1997; Ducea 2011). Peak Barrovian metamorphism in the southern orogenic margin was attained at the same time, under relatively low-strain conditions immediately after main phase folding, penetrative foliations and burial (Goscombe et al. 2017a). The Damaran thermal peak was widespread and coincides with shortening, metamorphism and granite plutonism in the Ugab and Northern Zones. Rearrangement of the stress field must have been accommodated by transcurrent sinistral slip outboard of the western margin of the Kalahari Craton, and led to a major rearrangement of the Kaoko Belt. Transpression was terminated in the Kaoko Belt, and the western shear zones were reactivated by sinistral-normal slip, resulting in rapid exhumation and cooling (Foster et al. 2009).

Ongoing north-northwest-south-southeast shortening persisted till at least 517 Ma, resulting in large-scale south-southeast-vergent folds that form the long axes of basement domes in the Central Zone, coeval with 525–515 Ma granite magmatism that overprints peak metamorphic parageneses. In contrast, the deeply buried (~28–39 km) southern orogenic margin was exhumed at this time by sequential, foreland propagating upthrusting events that resulted in extensional telescoping of the margin (Fig. 12.17). These outwedging events occurred while under contraction, along basal thrusts, while the top of the crustal wedges partitioned top down to the north extension, resulting in metamorphic discontinuities and lower pressures in the hanging wall (Goscombe et al. 2017a). Rapid exhumation by outwedging was in response to gravitational instability in overthickened crust (England and Thompson 1984; Jamieson et al. 1996). Peak metamorphism was diachronous across the southern margin, ranging from 530 to 522 Ma in the south Okahandja-Southern Zone to 517 Ma in the Southern Margin Zone, confirming foreland propagation of outwedging (Goscombe et al. 2017a). Exhumation of the south Okahandja-Southern Zone crustal wedge was initiated at ~522–513 Ma, resulting in further burial of the Southern Margin Zone, which attained peak metamorphism and maximum depths of burial at 517 ± 4 Ma, followed by outwedging soon after (Goscombe et al. 2017a). The Uis-Pass Suture between these two crustal wedges is a significant metamorphic discontinuity and records a two-stage history of early main phase thrusting followed by retrogressive extension. Extensional structures progressed from ductile to brittle, tracking rapid exhumation through the crust (Goscombe et al. 2017b). Metamorphic histories also record rapid exhumation, with P–T paths within crustal wedges following steep, tight clockwise paths followed by isothermal decompression (Goscombe et al. 2017a).

The waning stages of contraction in the Damara Belt saw ongoing rotation of the stress field to north–south shortening at ~517–515 Ma and northeast-southwest shortening at ~510 Ma, resulting in total ~90° clockwise rotation of the stress field during the Damaran orogenic cycle (Goscombe

et al. 2017b). Low-strain north–south shortening in the Kaoko Belt produced kinkbands, large-scale east–west warping of crustal-scale shear zones and 515 Ma pegmatites (Goscombe and Gray 2007, 2008). East–west trending biotite foliations and north-vergent folds in the Ugab Zone are coeval with 516 ± 3 Ma granite and pre-date ~513–511 Ma granites. North-vergent and upright east–west trending folds in the Central and Okahandja Zones overlap with the waning stages of synkinematic granite magmatism of 516–513 Ma age, and pre-date post-kinematic Donkerhoek granite of 508–505 Ma age. South-directed outwedging of the Southern Margin Zone also occurred at this time, immediately after the 517 Ma peak of metamorphism, and accompanying 514–513 Ma granites formed by decompression melting (Goscombe et al. 2017a). Extension directions in the top of crustal wedges, track rotation of the regional stress field, were top down to the N-northwest during exhumation of the south Okahandja-Southern Zone at ~522 Ma and top down to the north-northeast during exhumation of the Southern Margin Zone at ~517 Ma.

The final phase of contraction in the Damara Belt is constrained by low-strain, sub-biotite grade northeast-southwest shortening in the Ugab Zone, after 513–511 Ma granite plutons. Barrovian metamorphism in the east Northern Zone occurred at this time, with high-*P* (9.2–10.4 kb) peak metamorphic conditions attained at 510 ± 3 Ma, followed by rapid isothermal decompression (Goscombe et al. 2017a). The Okahandja and Central Zones also experienced a secondary thermal peak at this time, between ~515 and 505 Ma (Briqueu et al. 1980; Jung et al. 2000b; Jung and Mezger 2003b; Longridge et al. 2011; Goscombe et al. 2017b). This secondary thermal anomaly prolonged high-grade conditions in the orogen core, and may be the result of northwest-southeast extension direction associated with late-kinematic pegmatite and granite veins between 512 and 507 Ma (Allsopp et al. 1983; Jung et al. 2001; Longridge et al. 2011, 2014; DeKock and Armstrong 2014). It is also probable that extensional telescoping, outwedging and collapse of the southern orogenic margin at <522 Ma and <517 Ma may have contributed a component of extensional stress in the orogen core.

12.7.1.7 Along Orogen Shortening: ~508–505 Ma

Waning contraction in the Damara Belt at 512–508 Ma was followed by a rapid stress switch of 45° to low-strain, east–west directed shortening along the length of the belt between 508 and 505 Ma (Fig. 12.15). Late-stage upright to inclined west-vergent folds produced north–south trending crenulation cleavages with axial planar biotite in the Ugab Zone, and dome and basin fold interference in the Central Zone. North–south biotite foliations in the Ugab Zone post-date 513–511 Ma granites and sub-biotite grade folds that formed after regional cooling below 400 °C at 512–508 Ma, indicating a late-stage thermal anomaly and east–west shortening after ~508 Ma (Goscombe et al. 2017b). A late-stage secondary thermal anomaly accompanying east–west shortening is also recognized in the Kaoko Belt. East–west trending pegmatite dyke swarms of 508 Ma age are associated with a 507–505 Ma local thermal anomaly that reset Sm–Nd isotopics (Goscombe et al. 2005b). Central Zone cross-folding post-dates 511–508 Ma granite veins and extensional shear zones, and was interpreted at ~508 Ma (Longridge et al. 2011, 2014). East–west shortening at this time is not associated with main phase, high strain orogenesis, as would be implied by lateral escape models for the inclined dome and basin fold interference geometries in the Central Zone (e.g., Coward 1983; Oliver 1994; Kisters et al. 2004). Lateral escape models are dependent on high shear strains and a basal detachment, neither of which exists: high-strain grain-refinement fabrics (i.e., mylonite) are absent from any structural level in the Central Zone, and the basal unconformity is an unsheared, intact metapaleosoil profile (Fig. 12.10h; Goscombe et al. 2017b). Crucially, lateral escape models fail because there was no free margin at the time when crossfolds were forming; all three cratons were amalgamated and the Damara Belt was in an intraplate setting. Widespread evidence for east–west directed shortening at ~508 Ma indicates an essentially instantaneous and significant rearrangement of the stress field, inconsistent with any plausible trajectory between the Rio De La Plata, Congo and Kalahari Cratons. Consequently, far-field effects at the margin of Gondwana are the probable cause, and overlap in age with arc collisions in the Ross Orogen (Meert 2003; Boger and Miller 2004; Foster et al. 2005).

12.7.1.8 Orogen Collapse and Cooling: ~505–470 Ma

Along-orogen shortening in the Damara Belt between 508 and 505 Ma was followed by a switch at ~505 Ma from horizontal to vertical principle compressive stress, while still under north–south extension (Fig. 12.17). This stress switch was largely restricted to the Central Zone where vertical flattening and north–south extension led to rapid vertical exhumation as a core complex. Metamorphic field gradients document 3.5–7.7 km uplift relative to the northern margin and 2.8–4.6 km relative to the south (Goscombe et al. 2017a). Vertical flattening evolved from subhorizontal folding in the ductile field, to top down to the north shallow-dipping brittle breccia zones (Goscombe et al. 2017b). The initiation of decompression is bracketed by the youngest late-kinematic granites and granulite facies parageneses ranging from 512 to 507 Ma (Jung et al. 1998b, 2000a, b; Longridge et al. 2011, 2014; Goscombe et al. 2017a), and the oldest decompression melts of ~502 Ma age (Jung and Mezger 2003a). Rapid exhumation and

cooling were under way by 500 Ma, and Central Zone cooling from 700 to 300 °C between 500–470 Ma (Hawkesworth et al. 1983; Jacob et al. 2000; Jung et al. 2000a, b; Singletary et al. 2002; Jung and Mezger 2003a; Goscombe et al. in press a). Elsewhere, decompression melting, post-kinematic leucogranite and pegmatite dykes associated with north–south extension occurred immediately before this at 508–504 Ma in the Ugab Zone, Kaoko Belt and Okahandja Zone (Kukla et al. 1991; Goscombe et al. 2005b; DeKock and Armstrong 2014). Stress propagation from the margin of Gondwana at ~508 Ma established north–south extension exploited by decompression melts, and it is interpreted as having triggered gravitational collapse and extension of the thermally weakened hot orogen core between 505 and 500 Ma, producing a broad bivergent metamorphic core complex in the Central Zone.

Acknowledgements This research was a largely self-funded ITAR project that was generously supported by Prof. David Gray (ARC grant A00103456 and DP0210178) and Prof. David Foster (NSF grants EAR0738874 and EAR0440188), making the large-scale structure and metamorphic programme possible. The Namibian Geological Survey contributed to fieldwork while BG was on the staff. Dr. Ben Wade and Angus Netting (Adelaide Microscopy) helped with garnet maps and mineral analyses. Prof. David Foster, Dr. Richard Armstrong and Dr. Ben Wade contributed geochronology. Peter Weber, Jeanette Steiner, Ben Thompson, Mimi Dunaiski and Mr. Blum assisted with vehicles and logistics in Namibia. Avdale Namibia Pty Ltd and John Wilton (Teal Exploration and Mining) kindly supplied drill core. We acknowledge discussions with Richard Blewett, Karol Czarnota, Martin Hand, Charlie Hoffmann, Paul Hoffman, Cees Passchier, Rudolph Trouw, Galen Halverson and Roy Miller on a range of geology during this project. Mike and Rida Jacob, Mr. Gift, Dorette Knobel, Mark and Norma Jeanne, Miranda and Angus Campbell, Margaret and Roddy MacAskill, Mrs Gunn, Ronnie MacPhee and Alex Urquhart are thanked for their kind hospitality at bonnie camps, farms and crofts during analysis and write-up.

References

Ahrendt H, Behr HJ, Clauer N, Porada H, Weber K (1983) K/Ar age determinations of the northern Damara Branch and their implications for the structural and metamorphic evolution of the Damara Orogen, Namibia. In: Miller RMcG (ed) Evolution of the Damara Orogen of South West Africa/Namibia, vol 11. Geological Society South Africa Special Publication, pp 299–306

Alkmin FF, Marshak S, Pedrosa-Soares AC, Cruz S, Peres GG, Whittington A (2005) Nutcracker *Tectonics* during the Neoproterozoic assembly of west Gondwana: the development of the confined Aracuai-West Congo Orogen (Brazil/Africa). In: Supercontinents and Earth evolution symposium, abstracts 2005, p 98

Allsopp HL, Barton ES, Kröner A, Welke HJ, Burger, AJ (1983) Emplacement versus inherited isotopic age patterns: a Rb–Sr and U–Pb study of Salem-type granites in the central Damara Belt. In: Miller RMcG (ed) Evolution of the Damara Orogen, vol 11. Special Publication of the Geological Society of South Africa, pp 281–287

Armstrong et al (1987) In: Unpublished Australian National University Report

Ballard S, Pollack HN, Skinner NJ (1987) Terrestrial heat flow in Botswana and Namibia. J Geophys Res 92:6291–6300

Barnes SJ (1983) Pan-African serpentinites in central south West Africa/Namibia and the chemical classification of serpentinites. Spec Publ Geol Soc South Africa 11:147–155

Barnes SJ, Sawyer EW (1980) An alternative model for the Damara Mobile Belt: ocean crust subduction and continental convergence. Precambr Res 13:297–336

Basei MAS, Siga O, Masquelin H, Harara OM, Reis Neto JM Preciozzi F (2000) The Dom Feliciano Belt of Brazil and Uruguay and its foreland domain. In: Cordani U (ed), Tectonic evolution of South America, 31st International Geological Congress, Rio de Janiero, Brazil pp 311–334

Basei MAS, Frimmel HE, Nutman AP, Preciozzi F, Jacob J (2005) A connection between the Neoproterozoic Dom Feliciano (Brazil/Uruguay) and Gariep (Namibia/South Africa) orogenic belts—evidence from a reconnaissance provenance study. Precambr Res 139:195–221

Basson IJ, Greenway G (2004) The Rossing uranium deposit: a product of late-kinematic localization of uraniferous granites in the Central Zone of the Damara Orogen, Namibia. J Afr Earth Sc 38:413–435

Beaumont C, Jamieson RA, Nguyen MH, Lee B (2001) Himalayan tectonics explained by extrusion of a low-viscosity crustal channel coupled to focused surface denudation. Nature 414:738–742

Becker T, Hersfeld B (1995) Die Geologie, Geochemie under alterstellung des Weener Igneous Komplex und der Gaub Valley Formation am Südrand des Damara Orogens, Namibia und ihre bedeutung für die Genese der Frühproterozoischen Rehoboth Sequenz, pp 5–19

Becker T, Hoffmann KH, Schreiber UM (1998) Provisional draft of Rehoboth 250 K Geological map sheet. In: Namibian Geological Survey

Becker T, Hoffmann KH, Schreiber UM (2004) Rehoboth 1:250,000 geological map sheet. In: Namibian Geological Survey

Behr HJ, Horn EE, Porada H (1983) Fluid inclusions and genetic aspects of the Damara Orogen. Intracontinental Damara Orogen, Springer, Berlin, pp 617–635

Bergemann C, Jung S, Berndt J, Stracke A, Hauff F (2014) Generation of magnesian, high-K alkali-calcic granites and granodiorites from amphibolitic continental crust in the Damara orogen, Namibia. Lithos 198–199:217–233

Boger SD, Miller JMcL (2004) Terminal suturing of Gondwana and the onset of the Ross-Delamerian Orogeny: the cause and effect of an Early Cambrian reconfiguration of plate motions. Earth Planet Sci Lett 219:35–48

Briqueu L, Lancelot JP, Valois JP, Walgenwitz F (1980) Géochronologie UPB et genése d'un type de minéralization uranifere: les alaskites de Goanikontes (Namibie) et leur encaissant. Bull Cent Rech Explor Prod Elf-Aquitane 4:759–811

Brueckner HK, Cunningham D, Alkmin FF, Marshak S (2000) Tectonic implications of Precambrian Sm-Nd dates from the southern São Francisco craton and adjacent Araçuaí and Ribeira belts, Brazil. Precambr Res 99:255–269

Buhn B, Dorr W, Brauns CM (2001) Petrology and age of the Otjisazu carbonite complex, Namibia: implications for the pre- and synorogenic Damaran evolution. J Afr Earth Sc 32:1–17

Bühn B, Häussinger H, Kramm U, Kukla C, Kukla PA, Stanistreet IG (1994) Tectonometamorphic Patterns Developed during Pan-African continental collision in the Damara Inland Belt. Namibia Chem Erde 54:329–354

Burger AJ, Clifford TN, Miller R McG (1976) Zircon U–Pb ages of the Franzfontein Granitic Suite, Northern South West Africa. Precambr Res 3:415–431

Clauer N, Kroner A (1979) Strontium and argon isotopic homogenization of pelitic sediments during low-grade regional metamorphism:

the Pan-African Upper Damara Sequence of northern Namibia. Earth Planetary Science Letters 43:117–131
Corner B (2000) Crustal framework of Namibia derived from magnetic and gravity data. Communications of the Geological Survey of Namibia 12:13–19
Corner B (2004) Total magnetic intensity data of southern Africa, 1:3,000,000 map. Branko Corner Consulting
Coward MP (1981) The junction between Pan African Mobile belts in Namibia: its structural history. Tectonophysics 76:59–73
Coward MP (1983) The tectonic history of the Damara belt. In: Miller RMcG (ed), Evolution of the Damara Orogen, vol 11. Special Publication of the Geological Society of South Africa, pp 409–421
Cross CB, Diener JFA, Fagereng A (2015) Metamorphic imprint of accretion and ridge subduction in the Pan-African Damara Belt, Namibia. J Metamorph Geol 33:633–648
DeKock GS (1992) Forearc basin evolution in the Pan-African Damara Belt, central Namibia: the Hureb Formation of the Khomas Zone. Precambr Res 57:169–194
DeKock GS, Armstrong R (2014) SHRIMP dating on magmatic rocks from the Karabib-Otjimbingwe region, Namibia. In: Roy Miller symposium, Namibia, 2014
DeKock GS, Eglington B, Armstrong RA, Harmer RE, Walraven F (2000) U–Pb and Pb–Pb ages of the Naauwpoort rhyolite, Kawakeup leptite and Okongava Diorite: implications for the onset of rifting and of orogenesis in the Damara belt, Namibia. Commun Geol Surv Namibia 12:81–88
Dingeldey P (1997) *Tectono-metamorphic evolution of the Pan-African Kaoko Belt, NW-Namibia*. Ph.D. Thesis. Julius-Maximilians-Universitat Wurzburg, p 246
Dingeldey DP, Dürr SB, Charlesworth EG, Franz L, Okrusch M, Stanistreet IG (1994) A geotraverse through the northern coastal branch of the Damaran Orogen west of Sesfontein, Namibia. J African Earth Sci 19:315–329
Dirks PHGM, Jelsma HA, Vinyu ML, Munyanyiwa H (1998) The structural history of the Zambezi belt in N E Zimbabwe: evidence for crustal extension during the early Pan African. S Afr J Geol 101:1–16
Dirks PHGM, Kroner A, Jelsma HA, Sithole TA, Vinyu ML (1999) Pb-Pb zircon dates from the Makuti gneisses: evidence for a crustal-scale Pan African shear zone in the Zambezi Belt, NW Zimbabwe. J Afr Earth Sc 28:427–442
Ducea MN (2011) Fingerprinting orogenic delamination. Geology 39:191–192
Dürr SB, Dingeldey DP (1996) The Kaoko belt (Namibia): part of a late Neoproterozoic continental-scale strike-slip system. Geology 24:503–506
England PC, Thompson AB (1984) Pressure-temperature-time paths of regional metamorphism 1. Heat transfer during the evolution of regions of thickened continental crust. J Petrol 25:894–928
Foden J, Marlina AE, Dougherty-Page J, Burtt A (2006) The timing and duration of the Delamarian Orogeny: correlation with the Ross Orogen and implications for Gondwana Assembly. J Geol 114: 189–210
Foster DA, Goscombe BD (2013) Continental growth and recycling in convergent Orogens with large turbidite fans on oceanic crust. Geosciences 3:354–388. https://doi.org/10.3390/geosciences3030354
Foster DA, Goscombe BD Gray DR (2009) Rapid exhumation of deep crust in an obliquely convergent orogen: the Kaoko Belt of the Damara Orogen. Tectonics 28:TC4002
Foster DA, Gray DR, Spaggiari CV (2005) Timing of subduction and exhumation along the Cambrian East Gondwana margin, and the formation of Paleozoic backarc basins. Geol Soc Am Bull 117: 105–116
Foster DA, Goscombe BD, Newstead B, Mapani B, Mueller PA, Gregory LC, Muvangua E (2015) U–Pb age and Lu–Hf isotopic data of detrital zircons from Neoproterozoic Damara Sequence: Implications for pre-Gondwana proximity of Congo and Kalahari. Gondwana Res 28:179–190
Frantz JC, Botelho NF (2000) Neoproterozoic granitic magmatism and evolution of the eastern Dom Feliciano Belt in southernmost Brazil: a tectonic mosel. Gondwana Res 3:7–19
Franz L, Romer RL, Dingeldey DP (1999) Diachronous Pan-African granulite-facies metamorphism (650 and 550 Ma) in the Kaoko belt, NW Namibia. Eur J Mineral 11:167–180
Freyer EE, Halbich IW (1994) Deformation history of the lower Ugab Belt. In: Niall M, McManus C (eds) Proterozoic crustal and metallogenic evolution. In: Abstracts of geological society and geological survey of Namibia, vol 18, Windhoek
Frimmel HE (1995) Metamorphic evolution of the Gariep Belt. South African Tydskr Geology 98:176–190
Frimmel HE (2000) The Pan-African Gariep Belt in southwestern Namibia and western South Africa. In: Miller RMcG (ed), Henno Martin Commemorative volume, vol 12. Communications of the Geological Survey of Namibia, pp 197–209
Frimmel HE, Frank W (1998) Neoproterozoic tectono-thermal evolution of the Gariep Belt and its basement, Namibia and South Africa. Precambr Res 90:1–28
Frimmel HE, Hartnady CJH (1992) Blue amphiboles and their significance for the metamorphic history of the Pan-African Gariep belt, Namibia. J Metamorph Geol 10:651–669
Frimmel HE, Klotzli US, Siegfried PR (1996) New Pb–Pb single zircon age constraints on the timing of neoproterozoic glaciation and continental break-up in Namibia. J Geol 104:459–469
Frimmel HE (2017) The Gariep Belt. In: S. Siegesmund et al. (eds) Geology of southwest gondwana, Regional geology reviews, Springer, Heidelberg, pp 353–386
Germs GJB (1995) The Neoproterozoic of southwestern Africa, with emphasis on platform stratigraphy and paleontology. Precambr Res 73:137–151
Gessner K, Wijns C, Moresi L (2007) Significance of strain localization in the lower crust for structural evolution and thermal history of metamorphic core complexes. Tectonics 26(2),https://doi.org/10.1029/2004TC001768
Goodge JW (1997) Latest Neoproterozoic basin inversion of the Beardmore Group, central Transantarctic Mountains, Antarctica. Tectonics 16:682–701. https://doi.org/10.1029/97TC01417
Goodge JW, Hansen VL, Walker N (1993) Neoproterozoic-Cambrian basement-involved orogenesis within the Antarctic margin of Gondwana. Geology 21:37–40
Goscombe BD (1998) Geological map of the Sesfontein 1:250 000 sheet. *Geological Survey of Namibia*
Goscombe BD (1999a) Geological map of Tomakas 1:50 000 sheet. In: Geological survey of Namibia
Goscombe BD (1999b) Geological map of Omapungwe 1:50 000 sheet. In: Geological survey of Namibia
Goscombe BD (1999c) Geological map of Orumpembe 1:50 000 sheet. In: Geological survey of Namibia
Goscombe BD, Gray D (2007) The Coastal Terrane of the Kaoko Belt, Namibia: outboard arc-terrane and tectonic significance. Precambr Res 155:139–158
Goscombe BD, Gray D (2008) Structure and strain variation at mid-crustal levels in a transpressional orogen: a review of Kaoko Belt structure and the character of West Gondwana amalgamation. Gondwana Research Focus Paper 13:45–85
Goscombe BD, Armstrong R, Barton JM (1998) Tectonometamorphic evolution of the Chewore Inliers: partial re-equilibration of high-grade basement during the Pan-African Orogeny. J Petrol 39:1347–1384

Goscombe BD, Hand M, Gray D (2003a) Structure of the Kaoko Belt, Namibia: progressive evolution of a classic transpressional orogen. J Str Geol 25:1049–1081

Goscombe BD, Hand M, Gray D, Mawby J (2003b) The metamorphic architecture of a transpressional orogen: the Kaoko Belt, Namibia. J Petrol 44:679–711

Goscombe BD, Gray D, Hand M (2004) Variation in metamorphic style along the northern margin of the Damara Orogen, Namibia. J Petrol 45:1261–1295

Goscombe BD, Gray D, Hand M (2005a) Extrusional tectonics in the core of a transpressional orogen, the Kaoko Belt, Namibia. J Petrol 46:1203–1241

Goscombe B, Gray DR, Armstrong RA, Foster DA, Vogl J (2005b) Event geochronology of the Pan-African Kaoko Belt, Namibia. Precambr Res 140:e1–41

Goscombe B, Gray D, Hand M (2006) Crustal architecture of the Himalayan Metamorphic Front in eastern Nepal. Gondwana Res 10:232–255

Goscombe B, Blewett RS, Czarnota K, Maas R, Groenewald BA (2007) Broad thermo-barometric evolution of the Eastern Goldfields Superterrane. In: Bierlein FP, Knox-Robinson CM (eds). In: Proceedings of Geoconferences (WA) Inc. Kalgoorlie'07 conference. Geoscience Australia Record 2007/14, pp 33–38

Goscombe B, Gray D, Foster D, Wade B (in press a) Metamorphic evolution of Gondwana 2. The Damara Orogenic System: amalgamation of central Gondwana and evolution of orogen architecture. Geoscience Australia Record (in press)

Goscombe B, Gray D, Foster D (in press b) Metamorphic evolution of Gondwana 3. The Pan-African Orogenic system: thermo-mechanical response to orogenesis during Gondwana assembly. Geoscience Australia Record (in press)

Goscombe B, Foster D, Gray D, Wade B (2017a) Metamorphic response and crustal architecture in a classic collisional orogen: Damara Belt, Namibia. Gondwana Res. Focus Pap 52:80–124

Goscombe B, Foster DA, Gray D, Wade B, Marsellos A, Titus J (2017b) Deformation correlations, stress field switches and evolution of an orogenic intersection: the Pan-African Kaoko-Damara orogenic junction, Namibia. Geosci Front 8:1187–1232

Gray DR, Foster DA, Goscombe B, Passchier CW, Trouw RAJ (2006) 40Ar/39Ar thermochronology of the Pan-African Damara Orogen, Namibia, with implications for tectonothermal and geodynamic evolution. Precambr Res 150:49–72

Gray DR, Foster DA, Maas R, Spaggiari CV, Gregory RT, Goscombe B, Hoffmann KH (2007) Continental growth and recycling by accretion of deformed turbidite fans and remnant ocean basins: examples from Neoproterozoic and Phanerozoic orogens. In Hatcher RD Jr, Carlson MP, McBride JH, Martínez Catalán JR (eds), 4-D Framework of continental crust: geological society of America Memoir, vol 200, 63–92, https://doi.org/10.1130/2007.1200(05)

Gray DR, Foster DA, Meert JG, Goscombe BD, Armstrong R, Trouw RAJ, Passchier CW (2008) A Damara Orogen perspective on the assembly of southwestern Gondwana. Geol Soc Lond Spec Publ 294:257–278

Gresse PG (1994) Strain partitioning in the southern Gariep Arc as reflected by sheath folds and stretching directions. South Africa J Geol 97:52–61

Gresse PG, Germs GJB (1993) The Nama foreland basin: sedimentation, major unconformity and bounded sequences and multisided active margin advance. Precambr Res 63:247–272

Gresse PG, Scheepers R (1993) Neoproterozoic to Cambrian (Namibian) rocks of South Africa: a geochronological and geotectonic review. J Afr Earth Sc 16:375–393

Grotzinger JP, Bowring SA, Saylor BZ, Kaufman AJ (1995) Biostratigraphic and Geochronologic contraints on early animal evolution. Science 270:598

Guj P (1970) *The Damara Mobile Belt in the south-western Kaokoveld, South West Africa*. Ph.D. Thesis, University of Cape Town, p 168

Haack U, Hoefs J, Gohn E (1982) Constraints on the origin of Damaran granites by Rb/Sr and d18O data. Contrib Miner Petrol 79:279–289

Haack U, Hoefs J, Gohn E (1983) Genesis of Damaran granites in the light of Rb/Sr and d18O data. In: Martin H, Eder FW (eds) Intracontinental fold belts. Springer, Berlin, pp 848–872

Halverson GP, Hoffman PF, Schrag DP (2002) A major perturbation of the carbon cycle before the Ghaub glaciation (Neoproterozoic) in Namibia: Prelude to snowball earth? Gechem Geophys Geosyst 3:24

Hanson RE (2003) Proterozoic geochronology and tectonic evolution of southern Africa. Geol Soc Lond, Spec Publ 206:427–463

Hanson RE, Wilson TJ, Munyanyiwa H (1994) Geological evolution of the Neoproterozoic Zambezi Orogenic Belt in Zambia. J African Earth Sci 18:135–150

Hanson RE, Martin MW, Bowring SA, Munyanyiwa H (1998) U–Pb zircon age for the Umkondo dolerites, eastern Zimbabwe: 1.1 Ma large igneous province in southern Africa-east Antarctica and possible Rodinia correlations. Geology 26:1143–1146

Harrison TM, Ryerson FJ, LeFort P, Yin A, Lovera OM, Catlos EJ (1997) A late Miocene-Pliocene origin for the Central Himalayan inverted metamorphism. Earth and Planet Sci Lett 146:E1–E7

Hartmann O, Hoffer E, Haack U (1983) Regional metamorphism in the Damara Orogen: interaction of crustal motion and heat transfer. Spec Publ Geol Soc South Africa 11:233–241

Hawkesworth CJ, Kramers JD, Miller RMG (1981) Old model Nd ages in Namibian Pan-African rocks. Nature 289:278–282. https://doi.org/10.1038/289278a0

Hawkesworth CJ, Gledhill AR, Roddick JC, Miller RMcG, Kroner A (1983) RbSr and KAr studies bearing on models for the thermal evolution of the Damara belt, Namibia. In: Miller RMcG (ed) Evolution of the Damara Orogen, vol 11. Special Publication of the Geological Society of South Africa, pp 323–338

Hawkesworth CJ, Menzies MA, van Calsteren P (1986) Geochemical and tectonic evolution of the Damara Belt, Namibia. Collis Tecton, Geol Soc Spec Publ 19:305–319

Hedberg RM (1979) Stratigraphy of the Ovamboland Basin, South West Africa, vol 24. Bulletin of the Precambrian Research Unit, University of Cape Town, p 325

Heilbron M, Machado N (2003) Timing of terrane accretion in the Neoproterozoic-Eopaleozoic Ribeira orogen (SE Brasil). Precambr Res 125:87–112

Heilbron M, Pedrosa-Soares A, Neto M, da Silva L, Trouw R, Janasi V (2004) Brasiliano Orogens in Southeast and South Brazil. In: Weinberg R, Trouw R, Fuck R, Hackspacher P (eds), The 750–550 Ma Brasiliano Event of South America, J Virtual Explor Electron Ed 17; Paper 4, ISSN 1441-8142

Henry G, Osborne MA (1992) Tsongoari Project Exploration report for the period April 1992–January 1993. Randgold Tsongoari expl. Pty. Ltd. pp 1–43

Hoal BG, Heaman LM (1995) The sinclair sequence: U–Pb age constraints from the Awasib Mountain area. Commun Geol Surv Namibia 10:83–92

Hoernes S, Hoffer E (1979) Equilibrium relations of prograde metamorphic mineral assemblages. A stable isotope study of rocks of the Damara Orogen from Namibia. Contrib Miner Petrol 68:377–389

Hoernes S, Hoffer E (1985) Stable isotope evidence for fluid-present and fluid-absent metamorphism in metapelites from the Damara Orogen, Namibia. Contrib Miner Petrol 90:322–330

Hoffer E (1977) *Petrologische Untersuchungen zur regional metamorphose Al-reicher metapelite im sudlichen Damara Orogen (Sudwest Africa)*. PhD. Thesis Gottingen University

Hoffer E (1978) On the "late" formation of paragonite and its breakdown in pelitic rocks of the Southern Damara Orogen (Namibia). Contrib Miner Petrol 67:209–219

Hoffer E (1983) Compositional variations of minerals in metapelites involved in low- to medium grade isograd reactions in the southern Damara Orogen, Namibia, South West Africa. In: Martin H, Eder FW (eds), Intracontinental fold belts, Springer, Berlin

Hoffman PF, Swart R, Eckhardt EF, Guowei H (1994) Damara orogen of northwest Namibia. Geol excursion guide Geol Surv Namibia pp 55

Hoffman PF, Hawkins DP, Isachsen CE, Bowring SA (1996) Precise U–Pb zircon ages for early Damaran magmatism in the Summas Mountains and Welwitschia Inlier, northern Damara belt, Namibia. Commun Geol Surv Namibia 11:47–52

Hoffman PF, Kaufman AJ, Halverson GP, Schrag DP (1998) A Neoproterozoic snowball earth. Science 281:1342–1346

Hoffmann KH (1989) New aspects of lithostratigraphic subdivision and correlation of late Proterozoic to early Cambrian rocks of the southern Damara Belt, and their correlation with central and northern Damara Belt and the Gariep Belt. Commun Geol Surv Namibia 5:59–67

Hoffmann KH (1994) New constraints on the timing of continental breakup and collision in the Damara Belt. In: Niall M, McManus C (eds) Proterozoic crustal and metallogenic evolution. Abstracts of geological society and geological survey of Namibia conference, Windhoek, p 30

Hoffmann KH (1997) *Stratigraphy of the Damara Orogen*. Unpublished figure, Namibian Geological Survey

Hoffmann KH, Schreiber UM (1998) Windhoek 250 K Geological map sheet. Namibian Geological Survey

Hoffmann KH, Condon DJ, Bowring SA, Crowley JL (2004) U–Pb zircon date from the Neoproterozoic Ghaub Formation, Namibia: constraints on Marinoan glaciation. Geology 32:817–820

Houseman GA, Molnar P (1997) Gravitational (Rayleigh-Taylor) instability of a layer with non-linear viscosity and convective thinning of continental lithosphere. Geophys J Int 128:125–150

Houseman GA, McKenzie DP, Molnar P (1981) Convective instability of a thickened boundary-layer and its relevance for the thermal evolution of continental convergent belts. J Geophys Res 86: 6115–6132

Huerta AD, Royden LH, Hodges KV (1998) The thermal structure of collisional orogens as a reponse to accretion, erosion, and radiogenic heating. J Geophys Res 103:15287–15302

Huerta AD, Royden LH, Hodges KV (1999) The effects of accretion, erosion and radiogenic heat on the metamorphic evolution of collisional orogens. J Metamorph Geol 17:349–366

Inger S, Harris NBW (1992) Tectonothermal evolution of the High Himalayan Crystalline Sequence, Langtang Valley, northern Nepal. J Metamorph Geol 10:439–452

Jacob RE, Snowdon PA, Bunting FJL (1983) Geology and structural development of the Tumas basement dome and its cover rocks. In Miller RG (ed) Evolution of the Damara orogen of southwest Africa/Namibia, vol 11. Geological Society of South Africa Special Publication, pp 157–172

Jacob RE, Moore JM, Armstrong RA (2000) Zircon and titanite age determinations from igneous rocks in the Karibib District, Namibia: implications for Navachab vein-style gold mineralization. Commun Geol Surv Namibia 12:157–166

Jamieson RA, Beaumont C, Hamilton J, Fullsack P (1996) Tectonic assembly of inverted metamorphic sequences. Geology 24:839–842

Jamieson RA, Beaumont C, Nguyen MH, Lee B (2002) Interaction of metamorphism, deformation and exhumation in large convergent orogens. J Metamorph Geol 20:1–16

John T, Schenk V, Haase K, Scherer E, Tembo F (2003) Evidence for a Neoproterozoic ocean in south-central Africa from mid-oceanic-ridge-type geochemical signatures and pressure-temperature estimates of Zambian eclogites. Geology 31:243–246

John T, Schenk V, Mezger K, Tembo F (2004) Timing and *PT* evolution of whiteschist metamorphismin the Lufilian Arc-Zambezi Belt Orogen (Zambia): implications for the assembly of Gondwana. J Geol 112:71–90

Johnson SP, Rivers T, De Waele B (2005) A Review of the Mesoproterozoic to early Palaeozoic magmatic and tectonothermal history of south-central Africa: implications for Rodinia and Gondwana. J Geol Soc London 162:433–450

Johnson SP, De Waele B, Evans D, Banda W, Tembo F, Milton JA, Tani K (2007) Geochronology of the Zambezi Supracrustal Sequence, southern Zambia: a record of Neoproterozoic divergent processes along the southern margin of the Congo Craton. J Geol 115:355–374

Jung S, Mezger K (2001) Geochronology in migmatites—a Sm–Nd, U–Pb and Rb–Sr study from the Proterozoic Damara belt (Namibia: implications for polyphase development of migmatites in high-grade terranes. J Metamorph Geol 19:77–97

Jung S, Mezger K (2003a) U–Pb garnet chronometry in high-grade rocks; case studies from the central Damara Orogen (Namibia) and implications for the interpretation of Sm–Nd garnet ages and the role of high U–Th inclusions. Contribu Mineral Petrol 146:382–396

Jung S, Mezger K (2003b) Petrology of basement-dominated terranes: I. regional metamorphic T–t path from U–Pb monazite and Sm–Nd garnet geochronology (central Damara orogen, Namibia). Chem Geol 198:223–247

Jung S, Mezger K, Hoernes S (1998a) Petrology and geochemistry of syn- to post-collisional metaluminous A-type granites—a major and trace element and Nd-Sr-Pb-O-isotope study from the Proterozoic Damara Belt, Namibia. Lithos 45:147–175

Jung S, Mezger K, Masberg E, Hoffer E, Hoernes S (1998b) Petrology of an intrusion-related high-grade migmatite: implications for partial melting of metasedimentary rocks and leucosome-forming processes. J Metamorph Geol 16:425–445

Jung S, Hoernes S, Mezger K (2000a) Geochronology and petrogenesis of Pan-African, syn-tectonic, S-type and post-tectonic A-type granite (Namibia): products of melting of crustal sources, fractional crystallization and wall rock entrainment. Lithos 50:259–287

Jung S, Hoernes S, Mezger K (2000b) Geochronology and petrology of migmatites from the Proterozoic Damara Belt—importance of episodic fluid-present disequilibrium melting and consequences for granite petrology. Lithos 51:153–179

Jung S, Mezger K, Hoernes S (2001) Trace element and isotopic (Sr, Nd, Pd, O) arguments for a mid-crustal origin of Pan-African garnet-bearing S-type granites from the Damara Orogen (Namibia). Precambr Res 110:325–355

Jung S, Kroner A, Hauff F, Masberg P (2015) Petrogenesis of Synorogenic diorite-granodiorite-granite complexes in the Damara Belt, Namibia: Constraints from U–Pb zircon ages and Sr–Nd–Pb isotopes. J Afr Earth Sc 101:253–265

Kampunzu AB, Armstrong RA, Modis MP, Mapeo RBM (2000) Ion microprobe U–Pb ages on detrital zircon grains from the Ghanzi Group: implications for the identification of a Kibaran-age crust in northwest Botswana. J Afr Earth Sc 30:579–587

Kasch KW (1983a) Regional *P–T* variations in the Damara Orogen with particular reference to early high-pressure metamorphism along the southern margin. In: Miller RMcG (ed) Evolution of the Damara Orogen of South West Africa/Namibia, vol 11. Special Publication of Geological Society South Africa, pp 243–253

Kasch KW (1983b) Continental collision, suture propogation and thermal relaxation: a plate tectonic model for the Damara Orogen in

central Namibia. In: Miller RMcG (ed), Evolution of the Damara Orogen of South West Africa/Namibia, vol 11. Special Publication of Geological Society South Africa, pp 423–429
Kasch KW (1987) Metamorphism of pelites in the upper Black Nossob River area of the Damara Orogen. Commun Geol Soc Namibia 3:63–81
Kasch KW (1993) Metamorphic petrology of the eastern Damara Orogen in Namibia. In: 16th Colloquim of African Geology, Mbabne, Swaziland, abstracts, pp 177–178
Key RM, Liyungu AK, Njamu FM, Somwe V, Banda J, Mosley PN, Armstrong RA (2001) The western arm of the Lufilian Arc in NW Zambia and its potential for copper mineralization. Afr Earth Sci 33:503–528
Killick AM (2000) The matchless Belt and associated sulphide mineral deposits, Damara Orogen, Namibia. Commun Geol Surv Namibia 12:73–80
Lehmann J, Saalmann K, Naydenov KV, Milani L, Belyanin GA, Zwingmann H, Charlesworth G, Kinnaird, JA (2015) Structural and geochronological constraints on the Pan-African tectonic evolution of the northern Damara Belt, Namibia. Tectonics. https://doi.org/10.1002.2015TC003899
Kisters AFM, Jordaan LS, Neumaier K (2004) Thrust-related dome structures in the Karibib district and the origin of orthogonal fabric domains in the south central zone of the Pan-African Damara Belt, Namibia. Precambr Res 133:283–303
Konopásek J, Kröner S, Kitt SL, Passchier CW, Kröner A (2005) Oblique collision and evolution of large-scale transcurrent shear zones in the Kaoko belt, NW Namibia. Precambr Res 136:139–157
Kroner A (1977) Precambrian mobile belts of southern and eastern Africa—ancient sutures or sites of ensialic mobility? A case for crustal evolution towards plate tectonics. Tectonophysics 40: 101–135
Kröner S, Konopásek J, Kröner A, Passchier CW, Poller U, Wingate MTD, Hofmann KH (2004) U–Pb and Pb–Pb zircon ages for metamorphic rocks in the Kaoko Belt of Northwestern Namibia: A Palaeo- to Mesoproterozoic basement reworked during the Pan-African orogeny. S Afr J Geol 107:455–476
Kukla C (1992a) Strontium isotope heterogeeities in amphibolite facies, banded metasediments—a case study from the late Proterozoic Kuiseb Formation of the southern Damara Orogen, central Namibia. PhD. Thesis Julius-Maximilians-Universitat, Wurzburg
Kukla PA (1992b) Tectonics and sedimentation of a late Proterozoic Damaran Convergent continental margin, Khomas Hochland, central Namibia. Geol Surv Namibia Mem 12:95
Kukla PA, Stanistreet IG (1991) Record of the Damaran Khomas Hochland accretionary prism in central Namibia: Refutation of an "ensialic" origin of a Late Proterozoic orogenic belt. Geology 19:473–476
Kukla C, Kramm U, Kukla PA, Okrusch M (1991) U–Pb monazite data relating to metamorphism and granite intrusion in the northwestern Khomas Trough, Damara Orogen, central Namibia. Commun Geol Surv Namibia 7:49–54
Lobo-Guerrero Sanz A (2005) *Pre- and post-Katangan granitoids of the Greater Lufilian Arc: geology, geochemistry, geochronology and metallogenic significance*. PhD thesis, University of Witswatersrand
Longridge L, Gibson RL, Kinnaird JA, Armstrong RA (2011) Constraining the timing of deformation in the southwestern Central Zone of the Damara Belt, Namibia. Geol Soc Lond Spec Publ 357:107–135
Longridge L, Kinnaird JA, Gibson RL, Armstrong RA (2014) Amphibolites of the Central Zone: new SHRIMP U–Pb ages and implications for the evolution of the Damara Orogen, Namibia. S Afr J Geol 117:67–86
Machado N, Valladres C, Heilbron M, Valeriano C (1996) U–Pb geochronology of the central Ribeira belt (Brazil) and implications for the Brazilian Orogeny. Precambr Res 79:347–361
Maloof AC (2000) Superposed folding at the junction of the inland and coastal belts, Damara Orogen, NW Namibia. Commun Geol Surv Namibia 12:89–98
Martin H, Porada H (1977) The intracratonic branch of the Damara Orogen in South West Africa. II. Discussion of Relationships with the Pan-African mobile belt system. Precambr Res 5:339–357
Masberg P (2000) Garnet growth in medium-pressure granulite facies metapelites from the central Damara Orogen: igneous versus metamorphic history. Commun Geol Soc Namibia 12:115–124
Masberg P, Mihm D, Jung S (2005) Major and trace element and isotopic (Sr, Nd, O) constraints for Pan-African crustally contaminated grey granite gneisses from the southern Kaoko belt, Namibia. Lithos 84:25–50
Master S, Rainaud C, Armstrong RA, Phillips D, Robb LJ (2005) Provenance ages of the Neoproterozoic Katanga Supergroup (Central African Copperbelt), with implications for basin evolution. J Afr Earth Sc 42:41–60
McDermott F, Hawkesworth CJ (1990) Intracrustal recycling and upper-crustal evolution: A case study from the Pan-African Damara mobile belt, central Namibia. Chem Geol 83:263–280
McDermott F, Harris NBW, Hawkesworth CJ (1996) Geochmical constraints on crustal anatexis: a case study from the Pan-African Damara granitoids of Namibia. Contrib Miner Petrol 123:406–423
McDermott F, Harris NBW, Hawkesworth CJ (2000) Geochemical constraints on the petrogenesis of Pan-African A-type granites in the Damara Belt, Namibia. Commun Geol Surv Namibia 12:139–148
Meert JG (2003) A synopsis of events related to the assembly of eastern Gondwana. Tectonophysics 362:1–40
Meert JG, Torsvik TH (2003) A synopsis of events related to the assembly of eastern Gondwana. Tectonophysics 375:261–288
Meert JG, Van Der Voo R, Ayub S (1995) Palaeomagnetic investigation of the Neoproterozoic Gagwe lavas and Mbozi Complex, Tanzania and the assembly of Gondwana. Precambr Res 75: 225–244
Meneghini F, Kisters A, Buick I, Fagereng A (2014) Fingerprints of late Neoproterozoic ridge subduction in the Pan-African Damara belt, Namibia. Geology 42:903–906
Milani L, Kinnaird JA, Lehmann J, Naydenv KV, Saalmann K, Frei D, Gerdes A (2014) Role of crustal onribution in the early stage of the Damara Orogen, Namibia: new constraints from combined U–Pb and Lu–Hf isotopes from the Goas Magmatic Complex. Gondwana Res
Miller R McG Freyer EE Halbich IW (1983) A turbidite succession equivalent to the entire Swakop Group. In: Miller RMcG (ed), Evolution of the Damara Orogen, vol 11. Special Publication of the Geological Society of South Africa, pp 65–71
Miller RMcG (1983) The Pan-African Damara Orogen of Namibia. In: Miller RMcG (ed), Evolution of the Damara Orogen of South West Africa/Namibia, vol 11. Special Publication, Geological Society South Africa, pp 431–515
Miller RMcG (2008) The geology of Namibia. Geol Soc Namibia
Miller RMcG, Grote W (1988) Geological map of the Damara Orogen. In: Namibia (scale 1:500,000. Geological Survey of Namibia, Windhoek, 2 sheets
Mortimer N (2000) Metamorphic discontinuities in orogenic belts: example of garnet–biotite–albite zone in the Otago Schist, New Zealand. Inter J Earth Sci 89:295–306
Nascimento DB, Ribeiro A, Trouw RAJ, Schmitt RS, Passchier CW (2016) Stratigraphy of the Neoproterozoic Damara Sequence in northwest Namibia: slope to basin sub-marine mass-transport deposits and olistolith fields. Precambr Res 278:108–125

Newstead B (2010) Provenance of the Damara Sequence, Damara Orogen, Namibia. University of Florida Masters Thesis

Nitsch KH (1982) Petrologische utersuchungen an metapeliten des zentralen Damara Orogens, Namibia. Diploma of student of Prof. Nitsch at Gottingen University

Oliver GJH (1994) Mid-crustal detachment and domes in the central zone of the Damaran Orogen, Namibia. J Afr Earth Sc 19:331–344

Passchier CW, Trouw RAJ, Ribeiro A, Paciullo FVP (2002) Tectonic evolution of the southern Kaoko Belt, Namibia. J Afr Earth Sc 35:61–75

Passchier CW, Trouw R, Goscombe B, Gray D, Kroner A (2007) Intrusion mechanisms in a turbidite sequence: the Voetspoor and Doros plutons in NW Namibia. J Struct Geol 29:481–496

Passchier CW, Trouw R, Schmitt RS (2016) How to make a transverse triple junction—new evidence for the assemblage of Gondwana along the Kaoko-Damara belts, Namibia. Geology 44:843–846

Paul A, Jung S, Romer RL, Stracke A, Hauff F (2014) Petrogenesis of synorogenic high-temperature leucogranites (Damara orogen, Namibia): constraints from U–Pb monazite ages and Nd, Sr and Pb isotopes. Gondwana Res 25:1614–1626

Pedrosa-Soares AC, Vidal P, Leonardos OH, Brito-Neves BB (1998) Neoproterozoic oceanic remnants in eastern Brazil: further evidence and refutation of an exclusively ensialic origin for the Araçuaí-West Congo craton. Geology 26:519–522

Pedrosa-Soares AC, Noce AC, Widemann CM, Pinto CP (2001) The Araçuaí-West Congo Orogen in Brazil: an overview of a confined orogen formed during Gondwanaland assembly. Precambr Res 110:307–323

Pesonen LJ, Elming S-A et al (2003) Palaeomagnetic configuration of continents during the Proterozoic. Tectonophysics 375:289–324

Pfurr N, Ahrendt H, Hansen BT, Weber K (1991) U–Pb and Rb–Sr isotopic study of granitic gneisses and associated metavolcanic rocks from the Rostock massifs, southern margin oif the Damara Orogen: implications for litho stratigraphy of this crustal segment. Commun Geol Surv Namibia 7:35–48

Porada H (1979) The Damara-Ribeira Orogen of the Pan-African-Brasiliano cycle in Namibia (Southwest Africa) and Brazil as interpreted in terms of continental collision. Tectonophysics 57:237–265

Porada H (1983) Geodynamic model for the geosynclinal development of the Damara Orogen, Namibia, South West Africa. In: Martin H, Eder FW (eds) Intracontinental fold belts. Springer, Berlin, pp 502–538

Porada H (1989) Pan-African Rifting and Orogenesis in Southern to Equatorial Africa and Eastern Brazil. Precambr Res 44:103–136

Porada H, Wittig R (1983) Turbidites and their significance for the geosynclinal evolution of the Damara Orogen, South West Africa/Namibia. In: Miller RMcG (ed), Evolution of the Damara Orogen, vol 11. Special Publication of the Geological Society of South Africa, pp 21–36

Porada H, Ahrendt H, Behr HJ, Weber K (1983) The join of the coastal and intracontinental branches of the Damara Orogen, Namibia, South West Africa. Springer, Berlin, pp 901–912

Powell R, Holland TJB (1988) An internally consistent dataset with uncertainties and correlations: 3. Applications to geobarometry, worked examples and a computer program. J Metamorph Geol 6:173–204

Prave AR (1996) Tale of three cratons: Tectonostratigraphic anatomy of the Damara Orogen in northwestern Namibia and the assembly of Gondwana. Geology 24:1115–1118

Puhan D (1995) Metamorphic evolution of the assemblage tremolite + talc + calcite + dolomite + quartz within a sample of siliceous dolomite from the southern Damara Orogen (Namibia). Contribu Minera Petrol 120:180–185

Rapalini AE (2006) New late Proterozoic palaeomagnetic pole for the Rio de la Plata Craton: implications for Gondwana. Precambr Res 147:223–233

Ritter O, Weckmann U, Vietor T, Haak V (2003) A magnetotelluric study of the Damara Belt in Namibia 1. Regional scale conductivity anomalies. Phys Earth Planet Inter 138:71–90

Saalmann K, Hartmann LA, Remus MVD, Koester E, Conceiao RV (2005) Sm-Nd isotope geochemistry of metamorphic volcano-sedimenatry successions in the Sao Gabriel Block, southernmost Brazil: evidence for the existence of juvenile Neoproterozoic crust to the east of the Rio de la Plata Craton. Precambr Res 136:159–175

Sawyer EW (1981) Damaran structural and metamorphic geology of an area south-east of Walvis Bay, South West Africa/Namibia. Geol Surv South West Africa, Mem 7:94

Scharf A, Handy MR, Zieman MA, Schmid SM (2013) Peak-temperature patterns of polyphase metamorphism resulting from accretion, subduction and collision (eastern Tauern Window, European Alps)—a study with Raman microspectroscopy on carbonaceous material (RSCM). J Metamorph Geol 31:863–880

Schmidt A, Wedepohl KH (1983) Chemical composition and genetic relations of the Matchless amphibolite (Damara orogenic belt). In Miller RG (ed), Evolution of the Damara orogen of southwest Africa/Namibia, vol 11. Geological Society of South Africa Special Publication, pp 139–145

Schmitt RS, Trouw RAJ, Van Schmus WR, Pimentel MM (2004) Late amalgamation in the central part of West Gondwana: new geochronological data and the characterisation of a Cambrian collisional orogeny in the Ribeira Belt (SE Brazil). Precambr Res 133:29–61

Schmitt RS, Trouw RAJ, Passchier CW, Medeiros SR, Armstrong R (2012) 530 Ma syntectonic syenites and granites in NW Namibia—their relation with sollision along the junction of the Damara and Kaoko belts. Gondwana Res 21:362–377

Schreiber UM (2002) Geological map of the Swartbooisdrif 1:250 000 sheet. Geological Survey of Namibia

Seth B, Kroner A, Mezger K, Nemchin AA, Pidgeon RT, Okrusch M (1998) Archaean to Neoproterozoic magmatic events in the Kaoko belt of NW Namibia and their geodynamic significance. Precambr Res 92:341–363

Seth B, Okrusch M, Wilde M, Hoffmann KH (2000) The Voetspoor Intrusion, Southern Kaoko Zone, Namibia: mineralogical, geochemical and isotopic constraints for the origin of a syenitic magma. Commun Geol Surv Namibia 12:125–137

Singletary et al (2002) In: Hanson, 2003. Geological Society of London, Special Publications 206, 427–463

Singletary SJ, Hanson RE, Martin MW, Crowley JL, Bowring SA, Key RM, Ramokate LV, Direng BB, Krol MA (2003) Geochronology of basement rocks in the Kalahari desert, Botswana, and implications for regional Proterozoic tectonics. Precambr Res 121:47–71

Stanistreet IG, Charlesworth EG (2001) Damaran basement-cored fold nappes incorporating pre-collisional basins, Kaoko Belt, Namibia, and controls on Mesozoic supercontinent breakup. S Afr J Geol 104:1–12

Stanistreet IG, Kukla PA, Henry G (1991) Sedimentary basinal responses to a Late precambrian Wilson Cycle: the Damara Orogen and Nama Foreland, Namibia. J African Earth Sci 13(1):141–156

Steven N, Armstrong R, Smalley T, Moore J (2000) First geological description of a Late Proterozoic (Kibaran) metabasaltic andesite-hosted chalcocite deposit at Omitiomire, Namibia. In: Cluer JK, Price JG, Struhsacker EM, Hardyman RF, Morris CL (eds), Geology and ore deposits 2000: The Great Basin and beyond: Symposium Proceedings, Reno, Nevada, vol 2. Geological Society of Nevada, pp 711–734

Swart R (1992) The sedimentology of the Zerrissene turbidite system, Damara Orogen, Namibia. Mem Geol Surv Namibia 13:54

Tegtmeyer A, Kroner A (1985) U–Pb zircon ages for granitoids gneisses in northern Namibia and their significance for Proterozoic crustal evolution of southwestern Africa. Precambr Res 28:311–326

Thompson AB, Schulmann K, Jezek J (1997) Thermal evolution and exhumation in obliquely convergent (transpressive) orogens. Tectonophysics 280:171–184

Tohver E, D'Agrella-Filho MSD, Trindade RIF (2006) Palaeomagnetic record of Africa and South America for the 1200–500 Ma interval, and evaluation of Rodinia and Gondwana assemblies. Precambr Res 147:193–222

Trompette R (1997) Neoproterozoic (~600 Ma) aggregation of westernGondwana: a tentative scenario. Precambr Res 82:101–112

Trompette R, Carozzi AV (1994) Geology of Western Gondwana 2000–500 Ma. In: Pan-African-Brasiliano Aggregation of South America and Africa. A.A. Balkema, Rotterdam, Brookfield, p 350

Valeriano CM, Machado N, Simonetti A, Valladres CS, Seer HJ, Simoes LA (2004) U–Pb geochronology of the southern Brasilia belt (SE-Brazil): sedimentary provenance, Neoproterozoic orogeny and assembly of West Gondwana. Precambr Res 130:27–55

Valeriano CM, Pimentel MM, Heilbron M, Almeida JCH, Trouw RAJ (2008) Tectonic evolution of the Brasilia Belt, Central Brazil, and early assembly of Gondwana. In: Pankhurst RJ, Trouw RAJ, Britoneves BB, De Witt MJ (eds) West Gondwana: Pre-Cenozoic correlations across the South Atlantic Region, vol 294. Geological Society, London, Special Publications, pp 197–210

van de Flierdt T, Hoernes S, Jung S, Masberg P, Hoffer E, Schaltegger U, Friedrichsen H (2003) Lower crustal melting and the role of open-system processes in the genesis of syn-orogenic quartz diotite-granite-leucogranite associations: constraints from Sr–Nd–O isotopes from the Bandombaai Complex, Namibia. Lithos 67:205–226

Vannay JC, Hodges KV (1996) Tectonometamorphic evolution of the Himalayan metamorphic core between the Annapurna and Dhaulagiri, central Nepal. J Metamorph Geol 14:635–656

Vinyu ML, Hanson RE, Martin MW, Bowring SA, Jelsma HA, Krol MA, Dirks PHGM (1999) U–Pb and 40Ar/39Ar geochronological constraints on the tectonic evolution of the easternmost part of the Zambezi orogenic belt, northeast Zimbabwe. Precambr Res 98:67–82

Will TM, Okrusch M, Gruner BB (2004) Barrovian and Buchan type metamorphism in the Pan-African Kaoko belt, Namibia: implications for its geotectonic position within the framework of Western Gondwana. S Afr J Geol 107:431–454

Wu G, Lavier LL (2016) The effects of lower crustal strength and pre-existing midcrustal shear zones on the formation of continental core complexes and low-angle normal faults. Tectonics. https://doi.org/10.1002/2016TC004245

Yardley BWD (1982) The early metamorphic history of the Haast Schists and related rocks of New Zealand. Contrib Miner Petrol 81:317–327

The Gariep Belt

13

Hartwig Ernest Frimmel

Abstract

The Neoproterozoic to Early Cambrian Gariep Belt in southwestern Namibia and westernmost South Africa, together with the Damara and Kaoko belts further north and the Saldania Belt to the south, forms an important part of the larger network of Pan-African/Brasiliano orogenic belts in SW-Gondwana. It is subdivided into two major tectonostratigraphic units: the external, continental, para-autochthonous Port Nolloth Zone in the east and the largely oceanic, internal Marmora Terrane in the west. Owing to its generally low metamorphic grade, the rocks exposed in the Gariep Belt provide an excellent record of Neoproterozoic Earth history from continental break-up, multiple glaciations, opening of a narrow oceanic basin, to continental collision in the course of Gondwana assembly. Crustal thinning of the pre-existing, Late Mesoproterozoic supercontinent Rodinia prior to continental rifting led to repeated alkaline, predominantly acid, magmatism at shallow crustal levels, starting at 837 ± 2 Ma, widespread emplacement of a doleritic dyke swarm, which most likely served as feeders to a flood basalt province, and eventually bimodal, predominantly felsic, volcanic rocks along the principal growth fault at around 750 Ma. The continental, $\leq 771 \pm 6$ Ma rift deposits reflect alluvial plain and delta environments that evolved into a shallow sea. The prevailing glacial conditions at around 750 Ma are indicated by an older diamictite (Kaigas Formation), which is overlain by first regionally persistent carbonate deposits in the succession. Following a major hiatus of at least 100 million years, a new major sequence sets in, first with predominantly coarse-grained, largely immature siliciclastic sedimentary rocks, including dolomitic megabreccias above a major unconformity, and shallow marine stromatolitic reef mounds. These units grade into a second, regionally extensive sheet of glaciogenic diamictite with minor intercalated banded iron formation. At that stage the westernmost graben became reactivated into a probably narrow basin floored by oceanic crust (now partly preserved in the Marmora Terrane with equivalents in the Cuchilla Dionisio Terrane in Uruguay) and locally with oceanic islands that developed into guyots. The timing of oceanic magmatism is estimated at 610 Ma. So far, no evidence of the global *c*. 635 Ma Marinoan glaciation has been detected in the Gariep Belt and it is speculated that the area was land at that time. The formation of oceanic crust in the Marmora Terrane is explained by the reactivation of a previous rift-graben as back-arc basin behind the large 640–590 Ma Cuchilla Dionisio-Pelotas magmatic arc in the Dom Feliciano Belt in southeastern Brazil and Uruguay. Climatic recovery after the Numees glaciation coincided with the closure of the Marmora back-arc basin and was followed by flyschoid foredeep deposits on top and in front of the advancing thrust sheets of the Marmora Terrane prior to continental collision between 550 and 545 Ma. Contractional deformation was largely transpressive, directed towards the southeast, with a strong sinistral wrench component along its eastern margin, and led to a fold-thrust belt with a steep orogenic front against a basement ramp in the east and southeast. Eventual exhumation and erosion fed detritus into the Nama foreland basin. Post-orogenic alkaline magmatism affected the southern part of the belt and the adjoining basement at 507 ± 6 Ma.

Keywords

Gariep Supergroup • Neoproterozoic • Marmora Basin Glaciations

H. E. Frimmel (✉)
Department of Geodynamics and Geomaterials Research, Institute of Geography and Geology, University of Würzburg, Am Hubland, 97074 Würzburg, Germany
e-mail: hartwig.frimmel@uni-wuerzburg.de

H. E. Frimmel
Department of Geological Sciences, University of Cape Town, Rondebosch, 7701, South Africa

S. Siegesmund et al. (eds.), *Geology of Southwest Gondwana*, Regional Geology Reviews,
https://doi.org/10.1007/978-3-319-68920-3_13

13.1 Introduction

The Gariep orogenic belt is the dominant geological feature of southwestern Namibia, where it forms most of the basement rocks that are either exposed or covered by sand of the Namib Desert between Lüderitz and the Orange River. The belt extends from the coast inland for some 80 km as far as Rosh Pinah (Fig. 13.1a) and crosses the Orange River, after which it received its name ('Gariep' = 'great river' in the local Nama language), into South Africa, where it is well exposed in the western Richtersveld region. Following an arcuate north-northwest trend, it stretches southwards along the coast to Kleinzee (Fig. 13.1a).

The Gariep Belt is part of the extensive network of Pan-African-Brasiliano, Neoproterozoic to Cambrian orogens in West-Gondwana (Fig. 13.2). Its stratigraphy and tectonic evolution are thus comparable with those of the Damara Belt in central, and the Kaoko Belt in northwestern, Namibia (see Chap. 20). In South Africa the Gariep Belt re-emerges towards the south in an erosional window at 31° S along the South African west coast (Vredendal Outlier), and then continues into the Saldania Belt, which is exposed in a number of inliers within the Permo-Triassic Cape Fold Belt along the south coast of South Africa (Fig. 13.1c).

Different geodynamic models have been proposed for the formation of the various Pan-African belts in southwestern Africa. Traditionally, the coast-parallel branches of the network of Pan-African orogenic belts, including the Gariep Belt, have been viewed as the African portion of the suture between Neoproterozoic South America and Africa south of the Sào Francisco-Congo cratonic bridge. This commonly held view is based on a geodynamic model that involves the existence of a large Neoproterozoic ocean, the Adamastor Ocean, between the Rio de la Plata and the Kalahari cratons, and its subsequent closure having led to continent–continent collision peaking in the Gariepian orogeny. Accordingly, the

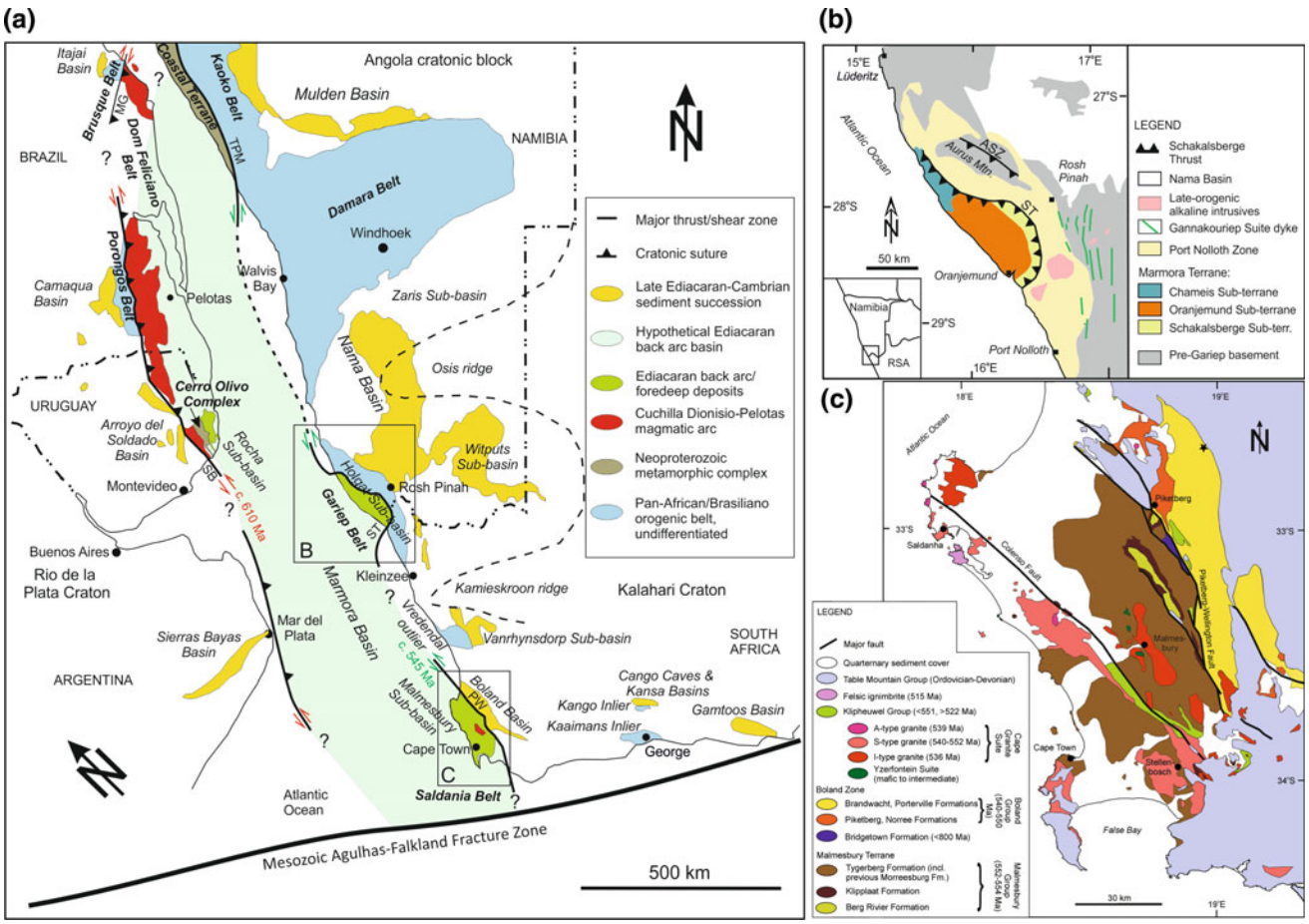

Fig. 13.1 **a** Position of the Gariep Belt within the framework of Pan-African orogenic belts and corresponding Ediacaran to Early Cambrian late- to post-orogenic basins in southwestern Africa and southeastern South America. Also indicated is the position of the inferred Ediacaran Marmora back-arc basin (modified from Frimmel et al. 2011). *MG* Major Gercino Shear Zone; *PW* Piketberg-Wellington Fault; *SB* Sierra Ballena Shear Zone; *ST* Schakalsberge Thrust; *TPM* Three Palms Mylonite Shear Zone. **b** Main tectonostratigraphic units of the Gariep Belt (modified from Frimmel and Hartnady 1992). Also shown are the principal Neoproterozoic shear zones: *ASC* Aurus Shear Zone; *ST* Schakalsberge Thrus. **c** Tectonostratigraphic map for the western Saldania Belt (modified from Frimmel et al. 2013)

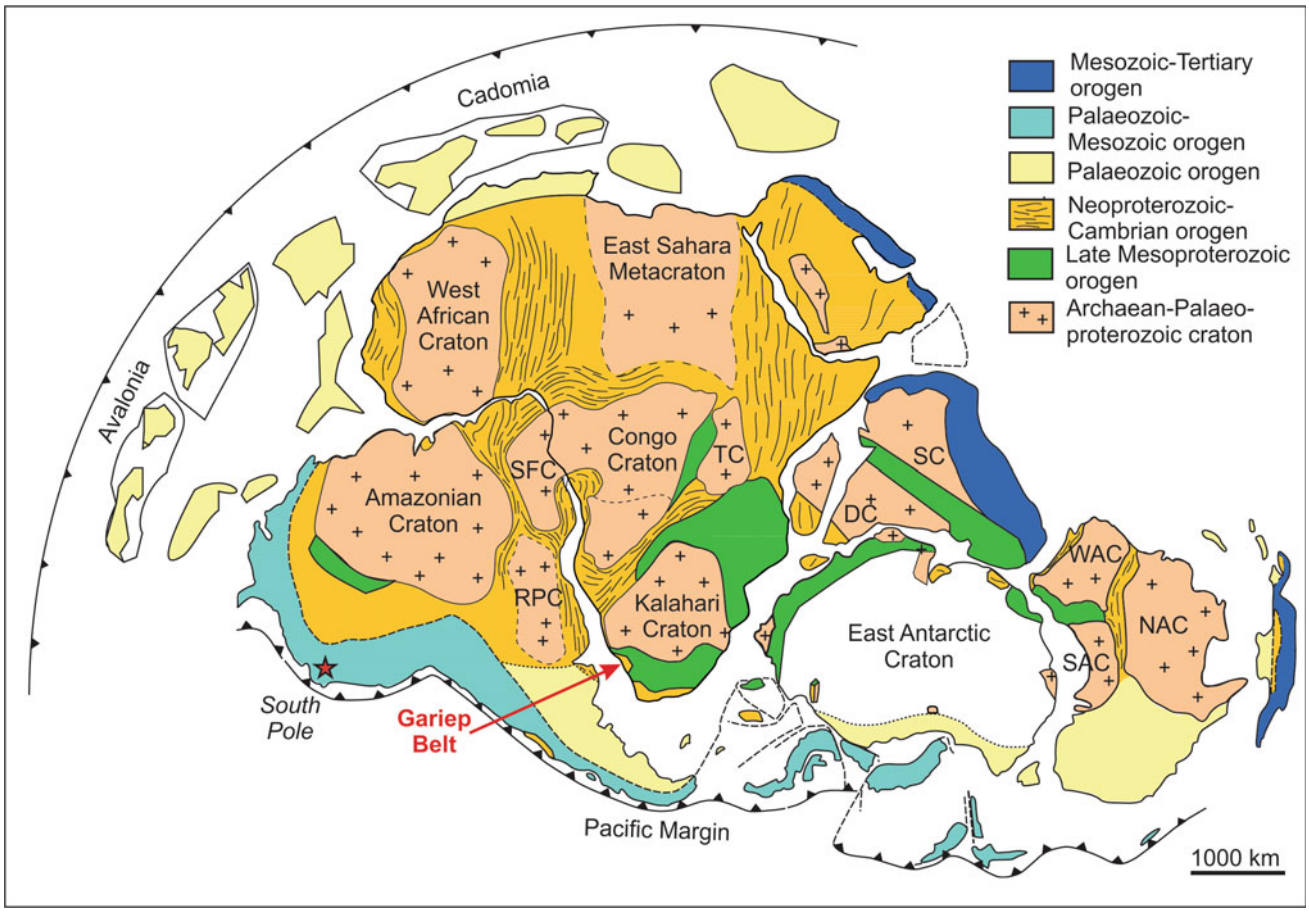

Fig. 13.2 Tectonic map of Gondwana in Ediacaran times (*c*. 570 Ma) and position of the Gariep Belt within SW Gondwana. *DC* Dharwar Craton; *NAC* North Australian Craton; *RPC* Rio de la Plata Craton; *SAC* South Australian Craton; *SC* Singhbhum Craton; *SF* Sao Francisco Craton; *TC* Tanzania Craton; *WAC* West Australian Craton (modified from Gray et al. 2008)

Gariep Belt should record an entire Wilson Cycle and should contain the deformed portion of a Neoproterozoic passive continental margin. The corresponding active continental margin would be located in the Dom Feliciano Belt in Uruguay and southern Brazil. Owing to the absence of proper high-pressure metamorphic zones in these belts, ambiguity remains as to the direction of subduction or even as to the existence of a former subduction zone between the Gariep and Dom Feliciano belts at all. Most previous studies favoured westward (in today's coordinates) subduction of Adamastor oceanic crust underneath the Rio de la Plata Craton (Porada 1989; Germs 1995; Frimmel et al. 1996a; Frimmel and Frank 1998), a notion that has been reinforced by Diener et al. (2017).

An alternative model, based on zircon provenance and sediment isotope geochemical data, has been suggested in which the main suture between Neoproterozoic southern Africa and South America is not located along the modern South Atlantic coastlines but inland of Uruguay and Brazil (Basei et al. 2005). According to that model, which involves southeast-directed subduction underneath Arachania—a continental fragment that split off from the Kalahari Craton during Rodinia break-up (Gaucher et al. 2009)—the metasedimentary rock record of the Gariep Belt would reflect the fill of initially a failed rift basin that later on became reactivated as back-arc basin behind the magmatic arc in the Dom Feliciano Belt in response to eastward subduction (Basei et al. 2005, 2008; Goscombe and Gray 2007; Frimmel et al. 2011, 2013; Konopásek et al. 2014).

In contrast to the Damara Belt in central Namibia (see Chap. 20), the Gariep Belt has received only limited attention for most of the twentieth century owing to difficulty in accessing the former Diamond Area No. 1. Early mapping was carried out by Rogers (1916) and Kaiser (1926), then later by De Villiers and Söhnge (1959), Martin (1965), McMillan (1968) and Kröner (1974), resulting in very different and conflicting interpretations of the stratigraphy. Davies and Coward (1982) provided a first interpretation of the belt's structural evolution. Subsequently, Von Veh (1993) remapped an important part of the South African

portion of the Gariep Belt and thus laid the foundation for the current stratigraphic subdivision and tectonic interpretation. The structural work was followed up in the Rosh Pinah area by Hälbich and Alchin (1995). Metamorphism (Frimmel 1995), geochemistry and the tectonic setting of the various igneous bodies (Frimmel et al. 1996a, 2001; Will et al. 2014), timing of the tectonic events and the thermal evolution were studied (Reid et al. 1991; Grotzinger et al. 1995; Frimmel et al. 1996b; Frimmel and Frank 1998), as well as the evolution of fluids across the external part of the belt (Frimmel and Board 2000). This was augmented by provenance studies on the siliciclastic successions of the Gariep Belt by Basei et al. (2005) and Hofmann et al. (2014). More recently the age and tectonothermal evolution of pre-Gariep basement within the belt have been investigated by Thomas et al. (2016) and Diener et al. (2017).

The Neoproterozoic sedimentary rock succession exposed in the Gariep Belt contains at least two glaciogenic diamictite units with corresponding overlying cap carbonates, which reflect the dramatic climatic changes for which the Cryogenian and Ediacaran periods have become famous. The stratigraphic correlation of these units with similar units in adjacent Pan-African orogenic belts has been contentious for decades, and conflicting correlations with well-dated successions elsewhere in the world can be found in the literature (e.g., Macdonald et al. 2010). The stratigraphic subdivision of the South African sector of the Gariep Belt, as currently accepted by the South African Committee for Stratigraphy (SACS), has been adopted also for the Namibian part (Frimmel 2000b) and is largely based on field observations by Von Veh (1993) and me, and on chemostratigraphic (Fölling and Frimmel 2002) as well as geochronological studies (Fölling et al. 2000). Not included in the stratigraphic scheme of SACS are the volcanosedimentary successions of the Rosh Pinah Formation (Alchin et al. 2005) and the Chameis Group (Frimmel 2000c), both of which are restricted to Namibia. The stratigraphic scheme suggested by Macdonald et al. (2010) deviates significantly from that of SACS. The latter authors questioned the glaciogenic nature of the older diamictite unit in the Kaigas Formation and instead introduced in addition to the glaciogenic Numees Formation a further glaciogenic unit, named 'Namaskluft diamictite'. This stratigraphic nomenclature has not been formally accepted by SACS and is based on the correlation of a vertical profile through a specific locality at the eastern part of the basin, at farm Namuskluft 88, Namibia, with other diamictite exposures elsewhere in the belt whose stratigraphic position was probably misinterpreted. It is also not in accordance with available geochronological data from the Gariep Belt and is therefore not adopted here.

The Gariep Belt has considerable economic significance. The variably metamorphosed and deformed rocks of this belt form the basement of one of the world's largest diamond placer deposits along the Atlantic coast and the Orange River. There the style and orientation of structures as well as the lithology of the basement rocks have influenced strongly the development of diamond trap sites and thus they form important tools in modern exploration (Jacob et al. 2006). Furthermore, the Gariep Belt hosts a major base metal ore province (the Rosh Pinah Province), with currently two active mines: the Zn–Pb mine at Rosh Pinah and the Zn mine at Skorpion. The largely restricted access to most of the area that forms the Gariep Belt in the past has hindered exploration and thus the belt is comparatively underexplored for further ore deposits. In addition, spectacular scenery and outcrops of the Gariep Belt in a transfrontier national park have the potential to form the basis for geotourism, which could add further economic value to the region.

13.2 Stratigraphy and Basin Architecture

Intense folding, top-to-southeast thrusting and wrench faulting during the Gariepian orogeny obliterated all direct evidence of the original extent, depth and structure of the depositional basin(s). Only the eastern margin is well defined in the form of inverted structures along which the Neoproterozoic rocks were thrust against their basement. Two main tectonostratigraphic zones are distinguished: the continental Port Nolloth Zone in the east and the largely oceanic Marmora Terrane in the west (Fig. 13.1b). These units are separated by a major thrust fault, the Schakalsberge Thrust. Although internally intensely deformed, the Port Nolloth Zone has retained a para-autochthonous relationship with its basement. This is evident from a number of basement slivers within the zone and from sedimentological and geochemical evidence that points to early sediment derivation from the basement in the immediate vicinity. In contrast, the Marmora Terrane is entirely thrust-bound and lacks a basement. The lower part of its stratigraphy is devoid of significant continental siliciclastic deposits and it is therefore considered allochthonous. The shape of the Port Nolloth Zone most likely reflects the outline of the eastern margin, along which the Rosh Pinah rift graben developed.

The rock record of the Gariep Belt is testimony to a series of tectonic stages that range from crustal thinning in preparation for Rodinia break-up, subsequent continental rifting and opening of an oceanic basin to basin closure and continent–continent collision during the amalgamation of West Gondwana at the end of the Neoproterozoic Era. Each of these stages left behind a distinct succession of sedimentary, volcanic and plutonic units with individual lithological, geochronological and geochemical characteristics. Based on the deformational and metamorphic history, the

areal distribution of individual stratigraphic units, and on limited geochronological data, the belt's rock record can be divided broadly into pre-, syn- and post-orogenic deposits. The pre- and synorogenic, predominantly sedimentary and subordinate volcanic to volcaniclastic units, make up the bulk of the belt and form the Gariep Supergroup (Fig. 13.3). The late- to post-orogenic deposits were laid down in the corresponding Nama foreland basin and constitute the Nama Group. As evident from Fig. 13.1a, the Nama foreland basin evolved in response not only to the emergence of the Gariep Belt but also to that of the Damara Belt further north and the Gariep's continuation to the south, the Saldania Belt in South Africa. Magmatic activity is recorded in the Gariep Belt both from the pre-rift to rift stage and from the post-orogenic stage. Evidence of synorogenic magmatism is notably absent.

The lithostratigraphic subdivision of the volcanosedimentary units in the Gariep Belt, especially within the Port Nolloth Zone, had been defined before a sequence stratigraphic understanding of the succession was achieved based on chemostratigraphic, sequence stratigraphic and geochronological data. This was at times when the whole succession was interpreted in terms of a classic full Wilson Cycle (Von Veh 1993). Thus sediment successions that had been deposited in two completely different types of basin at very different times were combined into single lithostratigraphic units. As can be seen in Fig. 13.3, the Port Nolloth Group contains deposits that represent three different sequences, laid down in a continental rift graben, a back-arc and a foredeep setting, respectively. Notwithstanding this major discrepancy between litho- and sequence stratigraphic subdivision, the lithostratigraphic terms as defined by SACS will be retained in the following summary of the stratigraphic make-up of the Gariep Supergroup, which comprises the Port Nolloth Group in the para-autochthonous Port Nolloth Zone, and the Chameis and Oranjemund groups as well as the Grootderm Formation in the allochthonous Marmora Terrane (Fig. 13.3). The only deviation from the formal stratigraphic scheme is the abolition of the term 'Hilda Subgroup' because it encompasses a number of formations that were formed in two entirely different settings with a first-order sequence stratigraphic boundary within this subgroup (Frimmel 2008a), as will be discussed further.

13.2.1 Port Nolloth Group

The Port Nolloth Group unifies all the Neoproterozoic sedimentary, and subordinately volcanic, units that are older than the Pan-African orogenic deformation in the region and that make up the Port Nolloth Zone. The latter stretches from south of Lüderitz in southwestern Namibia via Rosh Pinah to the coastal region around Port Nolloth in South Africa (Fig. 13.1b). Sediment deposition started with a siliciclastic

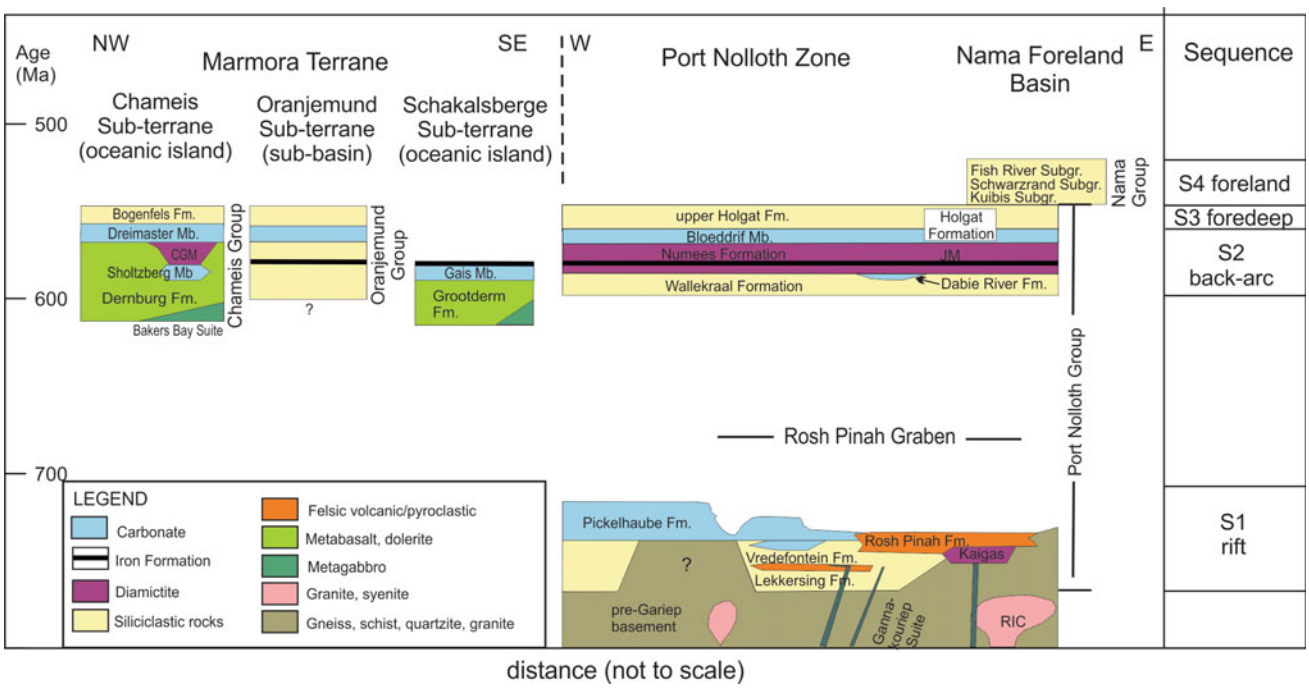

Fig. 13.3 Lithostratigraphic subdivision of the Gariep Supergroup, tentative correlation between units of the Marmora Terrane and the Port Nolloth Zone, and sequence stratigraphic interpretation. *CGM* Chameis Gate Member; *JM* Jakkalsberge Member; *RIC* Richtersveld Igneous Complex; *Fm* Formation; *Mb* Member; *Subgr.* Subgroup

continental rift graben sequence, accompanied by bimodal, predominantly felsic volcanism, the Stinkfontein Subgroup. Sedimentation took place along the western flank of an actively rising fault scarp, with alluvial fans, alluvial plains and fan deltas as dominant depositional environments. Volcanism was centred on or near this growth fault. Progressive subsidence led to pronounced facies changes with deeper water deposits further to the west. The local development of a proximal glaciogenic diamictite, the Kaigas Formation, was followed by the accumulation of carbonate sediments and abundant tempestite (Pickelhaube Formation) that contain intercalated near-shore volcanic and volcanoclastic deposits (Rosh Pinah Formation) and, after a major hiatus, breccias, conglomerates and other clastic deposits of highly variable energy regime (Wallekraal Formation) with locally developed reef-facies carbonates (Dabie River Formation). A second glacial period is represented by a massive diamictite unit, the Numees Formation. This is capped by the Holgat Formation, consisting of cap carbonates that are overlain by turbiditic, siliciclastic metasedimentary rocks.

13.2.1.1 Stinkfontein Subgroup

The Stinkfontein Subgroup, which is subdivided into the Lekkersing and Vredefontein formations, is best developed in South Africa along the southern and southeastern front of the Gariep Belt. In a few places, best seen in the Richtersveld in South Africa, the entire subgroup is crosscut by dolerite dykes of the *c*. 750 Ma Gannakouriep Suite.

South of the Orange River, the Lekkersing Formation, which reaches as much as 500 m in thickness, is made up mainly of medium-bedded quartz sandstone with sharp, flat bedding planes defined by partings. Erosional channels are common and continuous to discontinuous. Thin, flat laminated beds alternate with planar cross-beds and massive beds. Paleocurrent measurements indicate source areas to the east or southeast. Occasional reversals in the cross-bedding inclinations result from the presence of antidune structures. The sandstone is sparsely intercalated, in particular at the bottom of the formation, with conglomerate, which consists of subrounded to well-rounded pebbles of pre-Gariep basement provenance. Feldspathic sandstone becomes widespread in the upper parts of the formation where it undergoes a conformable and continuous transition into the overlying Vredefontein Formation.

The Vredefontein Formation reaches as much as 300 m in thickness. Internal sedimentary structures, accentuated by heavy mineral concentrations along laminations, are well preserved in the dominantly medium-bedded feldspathic sandstone. Cross-bedding of low-angle wedge, tabular planar or trough type alternates with parallel laminated bedding. Small-scale asymmetrical ripple marks with linguoid and cuspate crests occur. Paleocurrent directions are from the east or southeast. Soft sediment deformation takes the form of recumbent folds with a down-current direction of overturn near the top of cross-sets, oversteepened cross-laminae, convoluted laminae, disrupted and ripped-up clasts, and 'flame' structures (Von Veh 1993).

In the upper part of the Vredefontein Formation, a locally thick package of volcanic rocks is intercalated (Middlemost 1966). Their composition ranges from basic to acid (SiO_2 = 47–70 wt%), whereby intermediate varieties dominate. These rocks are only known from the Richtersveld in South Africa, where they are far more widespread than suggested by previous mapping (Macey, personal communication). Sandy to gritty breccia, composed of angular to subrounded vein quartz, granitoid, microgranite, gneiss, orthoquartzite, calcareous grit and felsic volcanic pebbles in a massive or indistinctly cross-bedded feldspathic grit matrix, occurs towards the top of the Vredefontein Formation.

The distribution of the Stinkfontein Subgroup in Namibia (Fig. 13.4) remains enigmatic because of the presence of similar siliciclastic successions also higher up in the stratigraphy, lateral facies changes that make long-distance correlation with the type sections in South Africa problematic, and because of the typically tectonic nature of its upper and lower contacts. Occurrences of the subgroup are confined to the northeastern basin margin. A good example of a primary lower contact with pre-Gariep basement is exposed on the farm Trekpoort 96 (Fig. 13.5) where the Neoproterozoic sediment succession starts with basal conglomerate a few metres thick, followed by coarse-grained, thickly bedded and locally laminated arkose. Although the section is strongly deformed with a near-vertical secondary northwest-trending crenulation cleavage, primary sedimentary structures, such as metre-scale trough cross-bedding, are still recognizable. The upper contact is not exposed but after a hiatus in outcrop of some 150 m a succession follows that corresponds lithologically to the Rosh Pinah Formation, which rests above the Stinkfontein Subgroup elsewhere in the region. Although the extent of deformation prohibits quantification of stratigraphic thickness, it is estimated to be *c*. 800 m. Such a maximum thickness compares well with that of the type section in the Richtersveld. Lithologically, the Stinkfontein Subgroup in Namibia is similar to the Vredefontein Formation in the Richtersveld. The relatively clean quartz sandstone, typical of the Lekkersing Formation, is only poorly developed in the northern parts of the Port Nolloth Zone.

The overall higher feldspar content in the siliciclastic rift deposits in the north might reflect an overall more proximal position of the depositional environments relative to the area further south in South Africa. This finds support from the observation that along the northwest-southeast trending branch of the basin to the north of the Aurus Mountains, the entire Stinkfontein Formation is missing and rocks of the

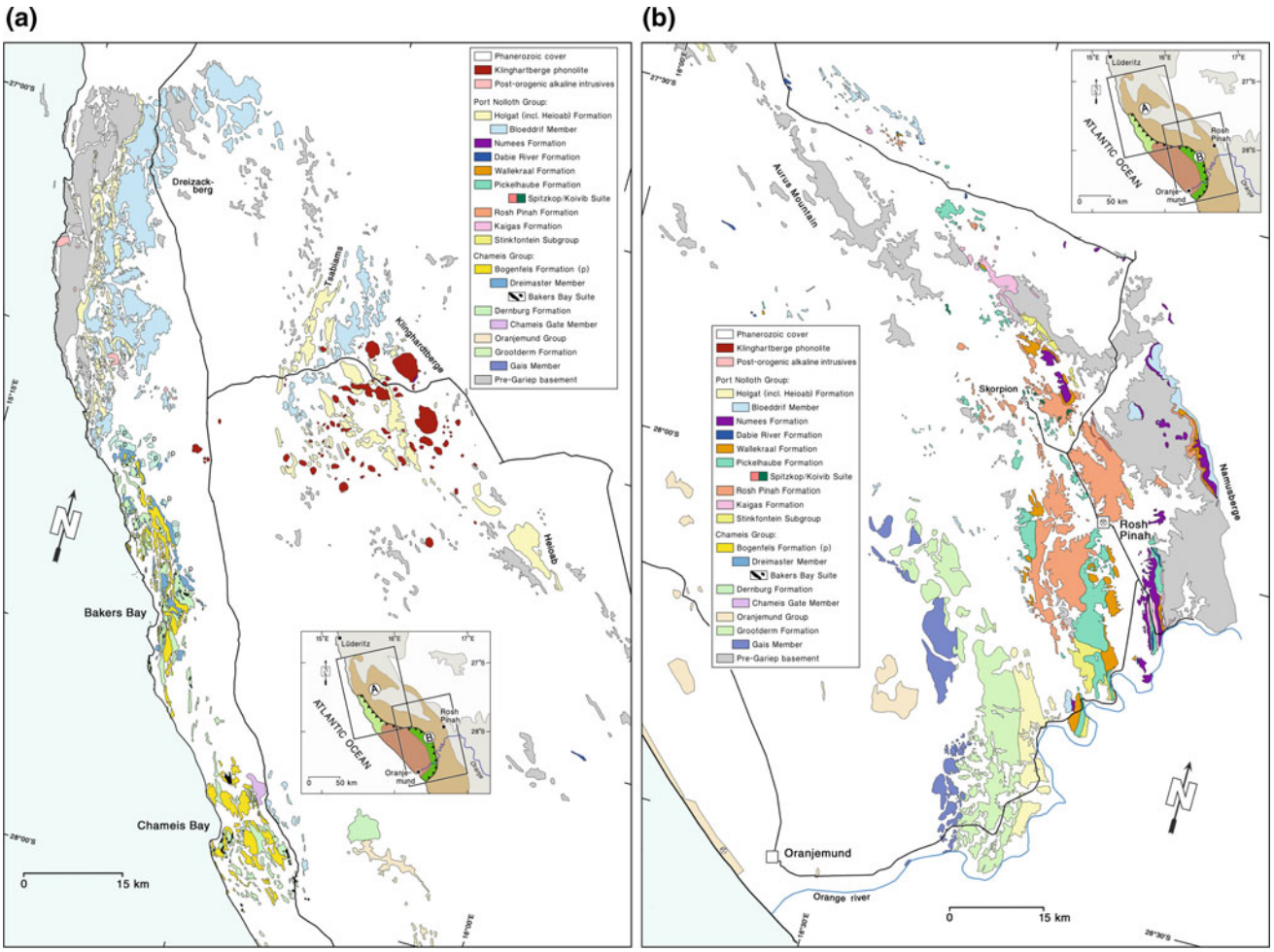

Fig. 13.4 Lithostratigraphic map of the Gariep Supergroup (Gariep Belt) in Namibia: **a** northwestern part, **b** southeastern part. *p* phyllonite within undifferentiated Bogenfels Formation, from Frimmel (2008a). For an explanation of the overview map (insert), see Fig. 13.3

next younger stratigraphic units, the Kaigas Formation, where present, rest directly on the basement.

13.2.1.2 Kaigas Formation

The Kaigas Formation is only locally developed along the eastern and northeastern margin of the former rift basin. At its type locality in the southern Richtersveld (South Africa), it reaches a thickness of 115 m. There it rests conformably on feldspathic sandstone of the Vredefontein Formation. Elsewhere its lower contact is unconformable. It comprises laterally discontinuous, medium- to thick-bedded diamictite and subordinate massive, locally cross-bedded or graded feldspathic sandstone, silt- and minor mudstone. Ripple cross-laminations, indicating paleocurrent directions from the east, mudstone rip-up clasts, load and flute casts, and sinuous ripple marks are locally present. The formation is characterized by its marked variations in thickness along strike, with individual occurrences, more than 100 m in thickness, pinching out over only several hundred metres.

The sedimentary features of the diamictite (Frimmel 2008a), such as sharp upper and lower bedding contacts, lack of internal structures, except for crudely graded bedding, correlation between clast size and bedding thickness, rapid decrease in clast size towards the basin centre, and the limited geographical distribution, suggest rapid deposition as debris flows. Transport by turbidity currents in a subaqueous fan environment is indicated by common upwards fining beds in the intercalated arkose and greywacke. The presence of westward-directed gravity flow deposits stepping back onto the basement foreland suggests a phase of marine transgression along an active fault scarp. This is also indicated by local dolomite clasts in the diamictite, which implies the presence of shallow-water carbonate deposits already prior to Kaigas sedimentation. It should be emphasized, however, that in contrast to a younger diamictite in the Port Nolloth Group, the clast lithology of the Kaigas Formation diamictite is, in general, dominated by basement-derived rock types, such as granite, gneisses, amphibolite, schists, and by

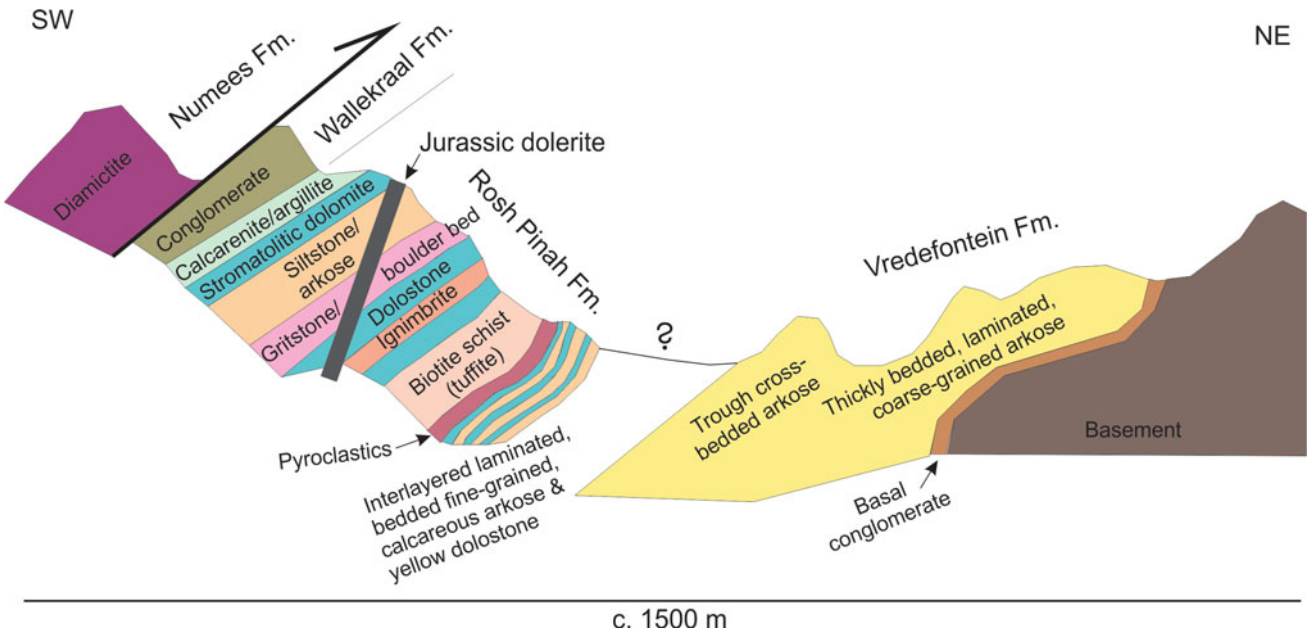

Fig. 13.5 Schematic southwest–northeast profile across the lower portion of the Port Nolloth Group above the pre-Gariep basement on the farm Trekpoort 96 (position of northeast end of section: 16.629°E, 27.740°S)

reworked sandstone from the underlying Stinkfontein Subgroup, whereas carbonate clasts are, in general, very rare and localized.

A component of melt-out glacial debris in the diamictite, such as dropstones, bimodal clast distribution, sandwiched and faceted clasts and outsized erratic blocks in shaly beds, suggest a glaciomarine or fluvioglacial origin of parts of the Kaigas Formation. Uplifted horsts along the margin of the basin may have been the sites of mountain glaciers which contributed some glacial material.

In Namibia, the formation reaches its maximum thickness in an area southeast of the Aurus Mountains at 16.527°E, 27.679°S (Fig. 13.4), where it rests directly on basement. From there it pinches out rapidly towards the southeast, but re-emerges in several small occurrences along the basement edge to the north and southeast of Rosh Pinah. On the farm Spitzkop 111, the Kaigas Formation diamictite grades laterally into a coarse-grained, proximal pyroclastic deposit (at 16.706°E, 27.827°S) that is assigned to the Rosh Pinah Formation (Frimmel 2008a), indicating an overlap in time between Kaigas sedimentation and Rosh Pinah volcanism. Elsewhere, background sedimentation towards the top of the Kaigas Formation gradually changed from siliciclastic to calcareous. An example of that can be found east of the Aurus Mountains at 16.486°E, 27.651°S, where the matrix of the diamictite and intercalated arenite becomes progressively dolomitic towards the top of the formation.

13.2.1.3 Pickelhaube Formation

Relatively undeformed successions through the Pickelhaube Formation with primary lower and upper contacts can be studied southeast of Rosh Pinah on the farm Namuskluft 88 and on the eastern flank of Dreigratberg near the Orange River (Fig. 13.6). At the former locality, the Pickelhaube Formation rests with an erosional unconformity on basement, whereas at the latter it rests conformably on Kaigas Formation diamictite. The Pickelhaube Formation starts with laminated, variably dolomitized, medium to dark grey limestone, followed by a varied sequence of predominantly mudstone and marl with minor feldspathic sandstone. Intercalated are a number of limestone and dolostone beds with the latter becoming thicker towards the middle of the formation. A further succession of intercalated shale and siltstone follows, which, in turn, is paraconformably overlain by massive dolostone of the Dabie River Formation. The Pickelhaube Formation reaches a maximum thickness of about 280 m at the Dreigratberg.

The feldspathic sandstone in this formation contains scour structures, load casts, rip-up shale clasts, sand dykes, ripple cross-laminations and small-scale channels indicating a paleocurrent direction from the southeast. The absence of conglomerate, scarcity of cross-bedding, presence of thin bedding, and the increasing carbonate content of the Pickelhaube Formation arenites indicate quieter, submerged conditions compared with the underlying Stinkfontein Subgroup and Kaigas Formation, as can be expected in the distal parts of

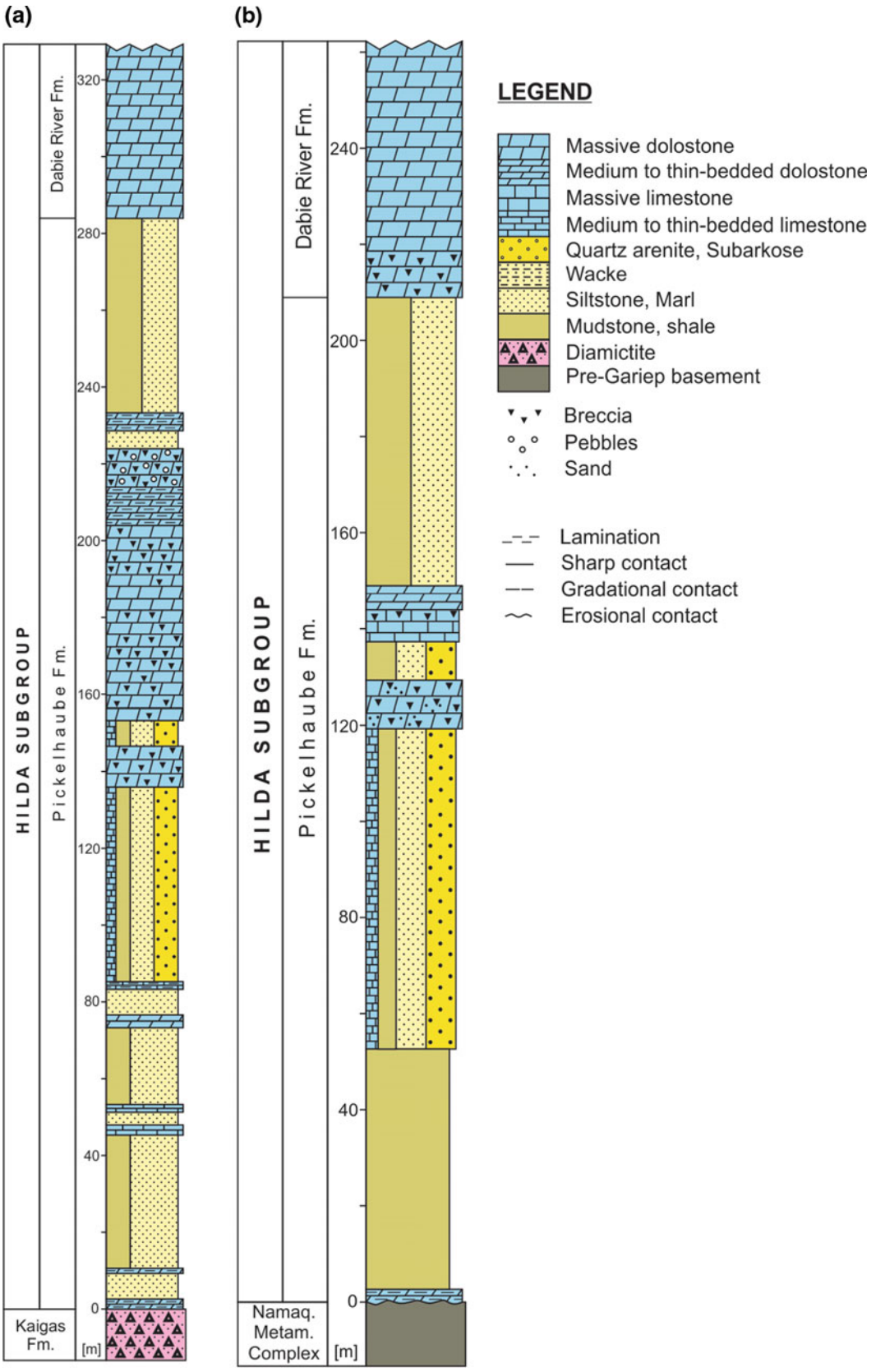

Fig. 13.6 Profiles through the Pickelhaube Formation **a** on the eastern flank of the Dreigratberg at 16.875°E, 28.105°S and **b** on farm Namuskluft at 16.845°E, 27.985°S (from Fölling and Frimmel 2002)

a fan complex. Some of the clastic beds may represent turbidites and minor debris flow deposits. The original limestone deposits are largely dolomitized in the more proximal positions but retained their synsedimentary mineralogy further away from the basin margin. Laminated allodapic limestone (calcarenite) is a ubiquitous feature of this formation. Where the formation on-laps directly onto basement, basement-derived clasts are embedded in such allodapic limestone of the lower Pickelhaube Formation (Frimmel 2008a). The carbonate beds in the middle of the formation show extensive synsedimentary brecciation that is reminiscent of tempestite. This is in contrast to slump breccias and carbonate debris flow deposits, some of which contain extrabasinal clasts. The latter are common in the thicker carbonate beds.

13.2.1.4 Rosh Pinah Formation

The economically significant Rosh Pinah Formation (Kapok Formation of Martin 1965) is distinguished from the more or less contemporaneous Pickelhaube Formation by the presence of felsic volcanic and volcaniclastic rocks. Clastic and volcanic facies are distinguished. The greatest accumulation of felsic volcanic rocks some 15–20 km north of Rosh Pinah (on farm Spitzkop 111) is considered to represent the main volcanic centre. The Rosh Pinah Formation displays repetitive sedimentary cycles that reflect rapid deposition with intervening quiescent periods related to reactivation on basin bounding faults with subsequent thermal and mechanical subsidence (Alchin et al. 2005). While deposition of the volcanosedimentary successions was sustained in the more active, proximal parts of the basin, distal background sedimentation ranged from planar laminated allodapic limestone to mudstone, followed by platform carbonates (Pickelhaube Formation). In proximal positions, tilting of the rift shoulders led to partial erosion of the Rosh Pinah Formation and thus to intraformational breccias and olistostromes.

The felsic volcanic outcrops at and near the inferred volcanic centre on the farms Spitskop 111 and Trekpoort 96 range in composition from rhyodacite to rhyolite (Frimmel et al. 1996b). They comprise massive to flow banded quartz-alkali-feldspar rhyolite to rhyodacite with locally spherulitic textures, autoclastic or hyaloclastic breccias, locally reworked (lapilli tuff breccias), and a variety of volcaniclastic units that reflect deposition in a different energy regime and, thus, at a greater distance from the eruptive centre. They range from proximal agglomerate and lapillistone to distal coarse- and fine-grained tuffs. In particular, the finer-grained varieties were affected by metamorphic recrystallization that resulted in biotite-chlorite-sericite schist with variable amounts of clinozoisite and calcite. Remnants of volcanic glass shards, though recrystallized, can still be discerned in many cases. Inversely graded lapillistone/tuff units are present and indicate water-lain pumice ash flow deposits. A special variety is crystal tuff rich in alkali-feldspar (5–15 vol.%). A bimodal character of the Rosh Pinah volcanism is indicated by the local presence of metabasalt and metagabbro, and the lack of igneous rocks of intermediate composition (see Sect. 13.4 below). Sedimentary rocks directly associated with the volcanic facies comprise intercalated ripple-marked quartzite and dolomite, which are, in places, highly ferruginous owing to fumarolic activity.

No continuous-type section through the entire Rosh Pinah Formation exists but a composite section has been described in greater detail by Alchin et al. (2005) and is depicted in Fig. 13.7, which shows a series of upward-fining depositional cycles. An unequivocally primary lower contact of the formation is exposed northeast of Rosh Pinah at 16.786°E, 27.923°S, where it conformably overlies a massive to thickly bedded, laterally discontinuous diamictite on the western limb of a southeast-trending anticline. By analogy with stratigraphically well-constrained comparable successions south of the Orange River where a similar diamictite unit is overlain by Pickelhaube Formation carbonates, this diamictite is assigned to the Kaigas Formation (Frimmel 2008a).

The Rosh Pinah Zn–Pb–Cu sulfide ore zone is bound to a strongly silicified carbonaceous mudstone with bedding-parallel laminations of pyrite, galena and sphalerite. It includes overlying dark grey arkose with mudstone intercalations and partly mineralized, dolomitized limestone lenses. A siliciclastic succession follows that shows upward-fining, graded bedding with coarse-grained, locally pebbly, sandstone at the base and fine-grained mudstone forming the top of individual cycles. The bottom contacts are typically sharp but the upper contacts are erosive with rip-up mudstone fragments. The influx of minor carbonate material during high-energy flows is indicated by the calcareous nature of the basal layers.

Pebbly to gritty, massive sandstone follows and contains unsorted, matrix-supported clasts of rounded to subrounded, mature quartz and angular carbonate clasts ranging from pebble to boulder size. This is overlain by an 8 m-thick carbonate unit representing the first unmineralized carbonates in the Rosh Pinah Formation. It is extensively broken at the base and grades down-slope into a zone that contains large carbonate clasts embedded in a gritty to pebbly sandstone matrix. An overlying cyclic sandstone-mudstone succession comprises individual units that grade upwards from pebbly to gritty to fine-grained sandstone, siltstone and mudstone, and, in places, to several decimetres-thick carbonate beds (Fig. 13.7). Overall, the carbonate content increases up section, whereby several of the original limestone beds experienced diagenetic dolomitization and ferruginization, possibly contemporaneous with sulfide mineralization lower down in the succession.

The upper part of the Rosh Pinah Formation in the vicinity of the Rosh Pinah mine comprises a

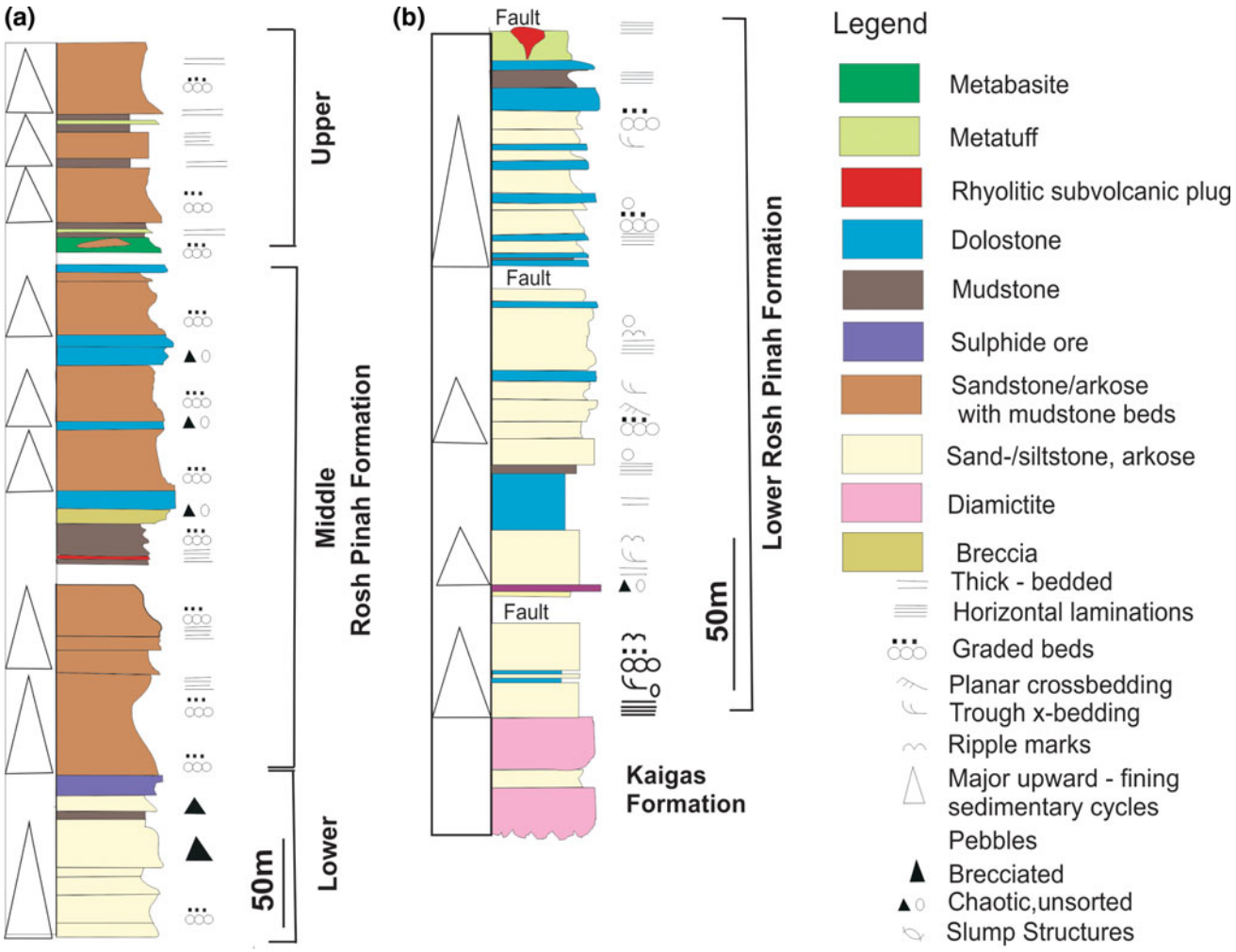

Fig. 13.7 Composite lithostratigraphic profiles through the Rosh Pinah Formation: **a** combination of three profiles through the Rosh Pinah Mine; **b** profile from about 5.5 km northeast of Rosh Pinah (modified from Alchin et al. 2005)

mudstone-sandstone lithofacies (Fig. 13.7) that is paraconformably overlain by coarse-grained siliciclastic rocks of the Wallekraal Formation at the top of Rosh Pinah Mountain. Intercalated with the siliciclastic succession is a horizontally discontinuous tuff or tuffite with, in places, a large proportion of angular, euhedral former sanidine grains set in a fine to very fine-grained quartz sericite matrix (crystal tuff). In some places the K-feldspar grains appear slightly rounded and occur together with well-rounded, evidently detrital quartz particles, as well as subrounded perthitic alkali feldspar grains of granitic provenance. The proportions of pyroclastic sanidine and detrital alkali feldspar and quartz are highly variable and document various degrees of sedimentary reworking of the crystal tuff (Frimmel et al. 1996b).

As a result of tectonic disruptions, the true stratigraphic thickness of the Rosh Pinah Formation cannot be deduced but in the Rosh Pinah area it is greater than 850 m as indicated by surface exposure and underground drilling (Alchin et al. 2005). The stratigraphic top of the formation is preserved at only a few localities, where conglomerates of the Wallekraal Formation rest on the Rosh Pinah Formation. Elsewhere, diamictite occurs incised into the Rosh Pinah Formation (e.g., at 27.930°S, 16.787°E). This diamictite contains a variety of dropstones of mainly basement-derived granite and gneisses and, to a lesser extent, carbonate and sandstone as well as felsic volcanic clasts which were derived from older units of the Port Nolloth Group. It is assigned to the Numees Formation.

13.2.1.5 Wallekraal Formation

A regional unconformity within the Port Nolloth Group represents a first-order sequence boundary and is overlain by the clastic succession of the Wallekraal Formation, named after its type locality in the western Richtersveld in South Africa (Von Veh 1993; Fig. 13.8). Although the highly tectonized nature of the Port Nolloth Zone makes it difficult

to map out this unconformity, evidence of it can be found in almost all parts of the Port Nolloth Zone whereby the clastic rocks of the Wallekraal Formation cut down to various levels of the older stratigraphy, and, in places, even to the pre-Gariep basement.

The Wallekraal Formation is dominated by coarse-grained siliciclastic sedimentary rocks consisting of mature, well-sorted, quartz-pebble conglomerate, gritstone and arkose that grade into mudstone in locally upward-fining cycles. Lateral and vertical facies changes reflect vastly different energy regimes, with boulder beds with individual, well-rounded basement-derived boulders reaching almost a metre in diameter occurring in some places and laminated mudstone displaying ripple marks in others (Frimmel 2008a). Locally, decimetre-thick, cream-coloured dolomite beds are intercalated with the arenite fraction. Isolated dolomite blocks and clasts (olistostromes) are conspicuous features. Where both are present, quartz pebbles are typically well rounded and well sorted whereas dolomite clasts are angular and very poorly sorted. A prime example of a huge olistostrome can be seen north of the Aurus Mountains at 16.335°E, 27.502°S, where a rotated block of more than 20 m in diameter of laminated limestone rests with unconformable contacts in a carbonate breccia that displays crudely defined, upward-fining graded bedding (Frimmel 2008a). The breccia grades into a limestone and, thus, a glaciogenic origin of this chaotic deposit is unlikely. More likely is that it resulted from a seismic event near the former basin margin.

The formation attains a thickness of as much as 180 m but it is laterally discontinuous and, in places, not developed at all. Overall, the lithology and sedimentary features are consistent with deposition in a submarine fan environment dominated by high-energy gravity-flow processes. The lateral discontinuity of the conglomerate and arenite units indicates deposition in channels in the upper fan or in suprafan lobes in the mid-fan region. Low-energy turbidity current deposition on channel levees or abandoned lobes is inferred for the fine-grained beds from parallel, even laminations and normal grading. The good rounding of pebbles, the isolated dolomite blocks and the dominance of gravity flow mechanisms indicate resedimentation from a shallow-water platform or shelf environment, probably represented by the Pickelhaube Formation.

13.2.1.6 Dabie River Formation

The Dabie River Formation, named after its type locality in the western Richtersveld, South Africa (Von Veh 1993), attains a thickness of as much as 160 m. It occurs in several small outcrops around the Aurus Mountains (Fig. 13.4) and in the western Richtersveld (Fig. 13.8). The formation is lithologically distinguished from the other carbonate-bearing successions of the subgroup by the presence of stromatolites displaying *Conophyton*-like forms, several centimetres to decimetres in height. Pisolites, oolites and oncolites are also present. The formation is almost exclusively calcareous, with original limestone being variably dolomitized. Macdonald et al. (2010) described giant wave ripples and sheet crack cement in dolomite of what they coined the 'Dreigratberg member'. In the stratigraphic scheme preferred in this chapter, that dolomite would be part of the Dabie River Formation. The carbonate rocks are typically massive, light to medium grey and, in places, intensely brecciated. Some of the carbonate breccias are interpreted as debris flow deposits while others are ascribed to gravitational slumping. Cyclical emergence and submergence is indicated by desiccation cracks (Von Veh 1993) and by the interbedding of limestone and dolostone.

A shallow-water, rimmed shelf environment, such as a barrier bar or shelf lagoon, passing seaward (westward) into a shelf margin, comprising reef build-ups and oolitic to pisolitic shoals, is envisaged as depositional environment. Reef rocks formed, or are preserved, particularly in those areas that escaped the pre-Wallekraal erosion. Consequently, the Dabie River Formation carbonates rest in many places paraconformably above dolostone of the Pickelhaube Formation and not necessarily on top of the clastic Wallekraal Formation rocks. Possibly the best example of this reef facies in outcrop is located as a tectonic sliver at 16.876°E, 28.085°S northeast of Dreigratberg near the Orange River. Good examples of stromatolitic dolostone of this formation can be found to the west of the Roter Kamm meteorite impact site in a sand dune field at 16.202°E, 28.802°S. Note that the observed giant wave ripples are not necessarily evidence of extreme wind conditions as originally inferred by Allen and Hoffman (2005) but are more likely a function of coarse grain size (Lamb et al. 2012), which is well reflected by the coarse-grained allodapic limestone of the formation.

13.2.1.7 Numees Formation

The Numees Formation, with its well-preserved varved pelites containing exotic dropstones, has long been regarded as glaciogenic (Rogers 1916; Martin 1965). Although the type section for this formation is located in the western Richtersveld, the diamictite at the Numees Prospect in that area, from which the formation obtained its name, does not belong to this formation but is part of the Kaigas Formation (Von Veh 1993). This reflects a considerable level of confusion surrounding the stratigraphic position of the diamictite and the existence of two diamictite units at different stratigraphic levels. For example, Hälbich and Alchin (1995) argued for the existence of only a single diamictite unit in the Gariep Belt. Detailed mapping in the western Richtersveld by Von Veh (1993) and in southwestern Namibia by me, combined with chemo- and chronostratigraphic data (Fölling et al. 2000; Fölling and Frimmel 2002), clearly

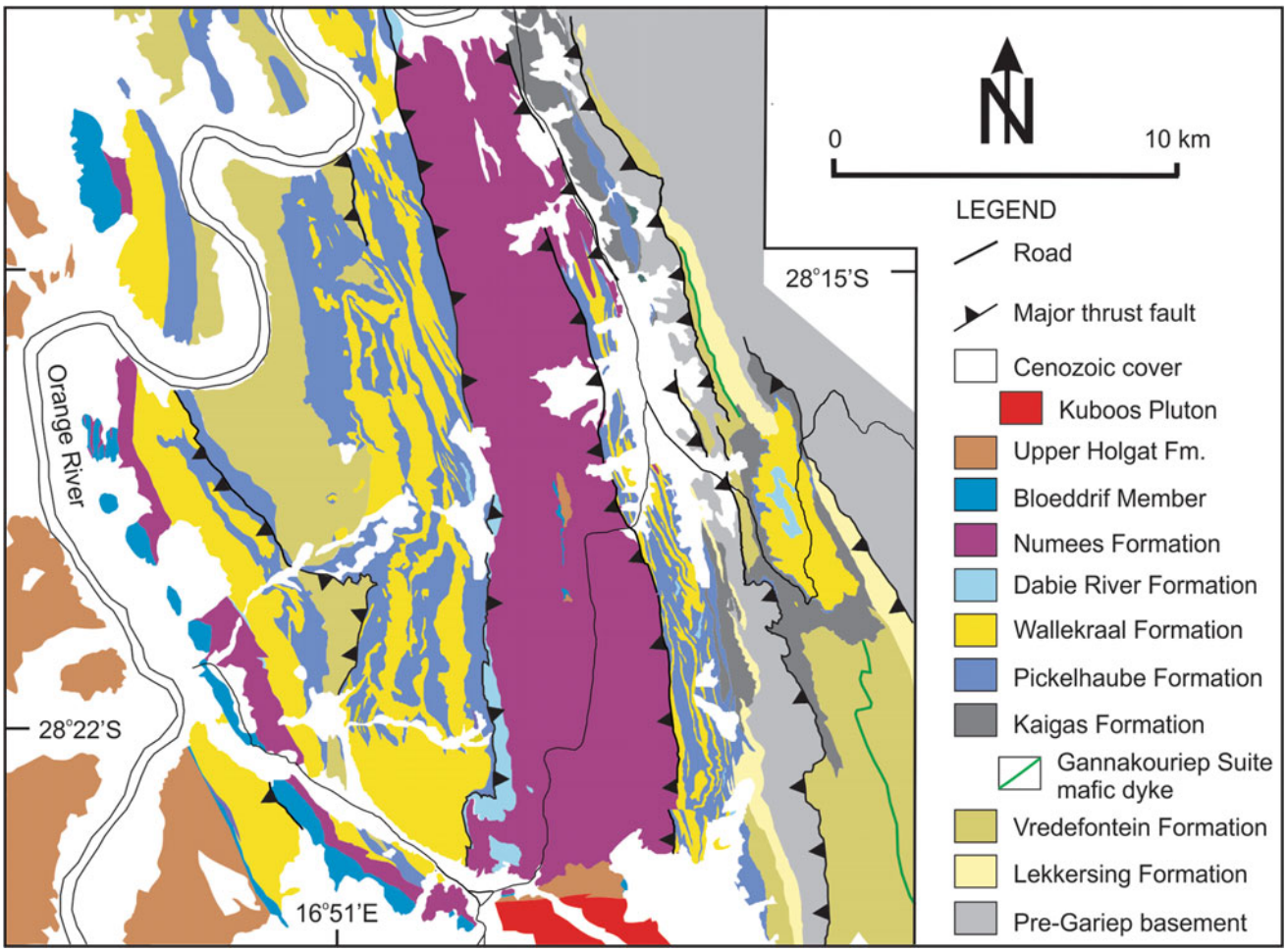

Fig. 13.8 Geological map of western Richtersveld area (based on a map by von Veh 1993 and remapping by me)

indicate, however, the presence of at least two different glaciogenic diamictite units in the Port Nolloth Zone, with the Numees Formation representing the younger of the two. Further confusion as to the stratigraphic position of the various glaciogenic diamictite units in the Port Nolloth Zone was added by Macdonald et al. (2010), who questioned the glaciogenic nature of the Kaigas Formation, assigned several outcrops of the Kaigas Formation to the Numees Formation and introduced a further glaciogenic unit, named 'Namaskluft diamictite', within the overlying Holgat Formation. This necessitated the positioning of the Wallekraal Formation above the Numees Formation, a notion that is not supported by field evidence elsewhere in the belt and based on the confusion between Kaigas and Numees Formation diamictite units. Figure 13.8 illustrates the regional distribution of the two diamicite units in the critical area of the western Richtersveld, South Africa.

Though in most places tectonic, the lower contact is locally conformable (Kröner 1974). In places where the Dabie River Formation carbonates are not developed, the siliciclastic Wallekraal Formation grades into the Numees Formation. A prime example of such a contact can be examined in the southeastern corner of farm Trekpoort 96 at 16.655°E, 27.799°S. The total thickness of the Numees Formation is estimated to be as much as 500 m but it decreases towards the east, where the formation on-laps directly onto pre-Gariep basement. The lithology of the clasts, which reach several cubic metres in size, comprises basement-derived pegmatite, leucogranite, granitic gneiss, quartzite and schist, as well as intrabasinal dolomite and minor limestone from the immediately underlying Dabie River Formation, and reworked diamictite (Frimmel 2008a). The latter is particularly abundant in the lower parts of the formation but becomes rare in the upper parts where basement-derived clasts dominate. Clast and matrix grain sizes decrease upwards. Intercalated minor ferrugineous, feldspathic sandstone is coarse-grained and medium bedded, and like the matrix of the diamictite of dark grey to blue-green colour that turns to dark brown on weathered surfaces. In addition, thin-bedded, varve-like siltstone beds

occur, with intercalated coarser-grained, graded sandstone beds. Some of these beds contain dropstones with soft-sediment deformation around their bottom contact.

A highly ferruginous unit, consisting of thinly laminated chlorite schist, iron formation and diamictite, is distinguished as the Jakkalsberg Member near the base of the formation. This is best developed in the southern portion of the belt in South Africa but is missing in the northeastern parts of the belt. Deposition adjacent to a glaciated continental margin by processes of settling from suspension and ice rafting is indicated by the extensive lateral distribution of the diamictite, its textural homogeneity and largely unbedded nature, and by the presence of outsized extrabasinal lonestones.

13.2.1.8 Holgat Formation

The youngest unit of the Port Nolloth Group is the Holgat Formation, which consists of a predominantly siliciclastic succession that comprises variably metamorphosed parasequences of upward-fining arkose and greywacke with interbedded mudstone and intraformational conglomerate. The formation is best developed in the western Richtersveld in South Africa (Fig. 13.8). The apparent thickness of the formation is about 7 km but, as a result of tectonic thickening, the true thickness is considerably less and estimated to be not more than several hundred metres.

The arenitic beds, typically a few decimetres in thickness, display graded bedding from which a turbiditic origin with a relatively proximal source may be inferred. The true thickness of the formation is difficult to constrain because of intense folding and duplication by thrusting. It appears, however, that stratigraphic on-lap led to a decrease in thickness from several hundred metres in the west to less than 100 m in the east.

Of particular interest is the formation's basal unit, a generally coarsely recrystallized, variably dolomitized, H_2S-rich, finely laminated limestone that is distinguished as the Bloeddrif Member (Figs. 13.3, 13.4 and 13.8). In the central part of the Port Nolloth Zone, the Bloeddrif Member attains a thickness of about 100 m but it thins towards the east. The significance of this formation lies in its conformable contact with the underlying glaciogenic deposits (Frimmel 2008a). It thus represents, at least in its lowermost beds, the cap carbonates to the Numees glaciation. In less deformed regions near the basin margin, such as some 17 km to the northeast of Rosh Pinah and on farm Nord Witputs 22, internal, vertical tube-like structures with a micritic sediment and cement infill form a conspicuous feature of the Bloeddrif Member limestone (Frimmel 2008a). Similar structures have been described from many other Neoproterozoic postglacial carbonates (Cloud 1974). Some workers have interpreted them as microbial in origin (Hegenberger 1993; Hoffman et al. 1998), whereas others have explained them by gas escape following the destabilization of gas hydrate during the warming of terrestrial permafrost (Kennedy 2001). Some microbial activity in the Bloeddrif Member is clearly indicated by the local presence of stromatolites. The limestone is notably rich in strontium (a few thousand parts per million). This has been interpreted as reflecting original aragonite in the form of deep-sea aragonite fan deposits (Hoffman et al. 1998), but a very shallow, restricted basin setting with elevated evaporation rates could have also caused this geochemical anomaly. The latter explanation is preferred because more distal, relatively pure limestone deposits that are characteristically devoid of continental detritus can be distinguished from proximal stratigraphic equivalents that experienced more intense, early diagenetic dolomitization and have intercalations of thin arenite beds (Frimmel and Fölling 2004). A particularly good example of a very shallow, proximal facies of this member occurs to the north of the Aurus Mountains at 16.216°E, 27.453°S, where a thinly laminated dark grey to cream-coloured limestone with numerous erosion surfaces and mud cracks grades upwards into a chaotic dolomitic breccia that is unconformably overlain by white, dolomitic arenite that is cross-bedded in places and became disrupted and filled with sand dykes (Frimmel 2008a).

In most places the laminated limestone is overlain by a massive, dark grey dolomite that is followed by a thickly bedded, distinctly pink dolomite. A good example of this sequence is exposed in the northernmost outcrop of the Bloeddrif Member at 15.667°E, 27.070°S, north of the Klinghardtberge (Fig. 13.4) where the Bloeddrif Member carbonates rest non-conformably above pre-Gariep basement gneisses (Frimmel 2008a).

13.2.2 Marmora Terrane, Chameis and Oranjemund Groups

The allochthonous Marmora Terrane is subdivided into three subterranes (or thrust sheets), from southeast to northwest and from tectonically lowest to highest position, the Schakalsberge, Oranjemund, and Chameis subterranes (Fig. 13.1b). Each of them has its own distinct stratigraphy, with the middle unit being essentially sedimentary and predominantly siliciclastic (Oranjemund Group), whereas the Schakalsberge and the Chameis subterranes consist to a large extent of mafic volcanic rocks that are overlain by carbonates and in the Chameis Subterrane by minor siliciclastic rocks (Chameis Group, Figs. 13.3 and 13.4).

13.2.2.1 Schakalsberge Subterrane

The Schakalsberge Subterrane consists of a thick pile of metabasalt with a local capping of stromatolitic and oolitic dolomite (Gais Member), all of which is lithostratigraphically

unified as the Grootderm Formation. Based on the geochemical character of the mafic, predominantly volcanic and to a lesser extent intrusive rocks, and the conspicuous lack of continental detrital input in the overlying carbonate rocks, the formation has been interpreted as representing former guyots with the Gais Member representing reef growth on top of an oceanic volcanic island (Frimmel et al. 1996a). Except for a ferruginous chert band that is not more than 1 m in thickness, no younger deposits above the reef carbonate of the Gais Member are present.

13.2.2.2 Oranjemund Subterrane

The rock record of this subterrane has been unified as the Oranjemund Group (Basei et al. 2005). It lacks the large number of mafic volcanic and intrusive rocks that are typical of the other two subterranes. Instead it is rich in chlorite schist that can be explained by erosion of adjacent oceanic seamounts. This mafic schist is overlain in places by a thin chert and minor carbonate, followed by a thick succession of decimetre- to metre-thick arenitic beds with upward-fining graded bedding of turbiditic character. As the rocks of the Oranjemund Group are largely covered by sand of the Namib Desert, the regional extent and distribution of the various subunits are only poorly known and thus a formal subdivision into formations remains outstanding.

13.2.2.3 Chameis Subterrane

The Chameis Subterrane is made up of the Dernburg and Bogenfels formations. The volcanic stratigraphy of the Dernburg Formation is similar to that of the Grootderm Formation and is locally overlain by stromatolitic and oolitic dolomite of the Sholtzberg Member, which has been correlated with the Gais Member (Fig. 13.3). In many places gabbro, and to a lesser extent serpentinized ultramafic rocks, occur within the metavolcanic rocks and constitute the Bakers Bay Suite.

The Sholtzberg Member dolomite is overlain by highly magnesian metapelite and dolomite beds, rich in albite, tourmaline and magnesioriebeckite. These have been identified as former marine evaporite deposits, which are believed to have formed within an atoll during a period of eustatic sea-level fall (Frimmel and Jiang 2001). Elsewhere, ophicarbonates, hornblendite, epidosite and magnesioriebeckite-bearing albitite are spatially associated with the predominant mafic rocks of the Dernburg Formation and have been ascribed to intense sodium metasomatism related to metamorphism of the former evaporite beds (Frimmel and Jiang 2001). Also associated with the mafic rocks is a locally developed diamictite (Chameis Gate Member) with exotic dropstones embedded in thinly laminated, predominantly mafic, metatuff beds (Frimmel 2000c, 2008a). Although no primary contact is exposed, field relationships suggest a stratigraphic position of the Chameis Gate Member, for which a glaciogenic origin is inferred, in the uppermost part of the Dernburg Formation. If this is correct, the eustatic sea-level fall that triggered the evaporation of seawater in an atoll on top of an oceanic island could be explained by global cooling in preparation for a glacial event that led to sea ice cover in the Gariep Basin.

13.2.2.4 Bogenfels Formation

Only those parts of Martin's (1965) original Bogenfels Formation that occur within the Marmora Terrane have been retained in a redefined Bogenfels Formation (Frimmel 2000c). Those parts located within the Port Nolloth Zone are ascribed to the Port Nolloth Group (Fig. 13.4). Diamictite associated with Martin's Bogenfels Formation is tentatively correlated with the Numees Formation.

Where exposed, the youngest formation of the Chameis Subterrane, the Bogenfels Formation, rests above the metabasic rocks of the Dernburg Formation. It begins with the carbonate-dominated Dreimaster Member (Frimmel 2000c), consisting of a 10 m-thick, thinly laminated, medium-grey limestone that is variably dolomitized and rich in H_2S—analogous to the lower Bloeddrif Member. The upper unit of the Dreimaster Member is made up of a few tens of metres of thickly bedded, micritic, light creamy white to medium grey dolomite, local ferruginous black chert and dolomite breccia in which the underlying rock types appear reworked. The Dreimaster Member is overlain by a varied succession of quartzite, meta-arkose, phyllite, chlorite schist and calcareous metapelite. The thickness of this siliciclastic succession is not constrained because of intense deformation but is estimated to be a few hundred metres—similar to the upper Holgat Formation. Turbiditic graded bedding is common in medium- to thick-bedded arenitic units that grade into argillaceous rocks towards the top of each cycle. Overall, a strong lithological similarity between the Bogenfels Formation, the upper Oranjemund Group and the Holgat Formation is noted.

13.3 Sediment Provenance

Analysis of paleocurrent directions and facies changes from high-energy, proximal deposits to lower-energy, distal deposits, clast lithology in conglomerate and diamicite beds (Frimmel 2008a), and sediment geochemical data together with detrital zircon age data (Basei et al. 2005; Hofmann et al. 2014), make it possible to draw inferences about the likely sources of the clastic sediments in the Gariepian strata. This data supports a broad division into older continental rift-related deposits, derived from the nearby pre-Gariep basement, and younger deposits that obtained their detritus largely from an Ediacaran volcanic arc to the west.

Detritus in the clastic rocks of the Stinkfontein Subgroup, the Kaigas and Pickelhaube formations of the proximal domains in the Port Nolloth Zone was delivered from the east—that is, from the Kalahari Craton. In the Stinkfontein Subgroup, detrital zircon ages of 1.1–1.3 Ga dominate, with a smaller proportion of ages between 1.7 and 1.9 Ga, whereas Paleoproterozoic ages between 1.8 and 2.0 Ga dominate in the Kaigas Formation diamictite [labelled 'Lower Diamictite by Hofmann et al. (2014)]. The ages conform to those known for the Mesoproterozoic Namaqua-Natal Belt and the Paleoproterozoic Richtersveld Terrane, both of which constitute the pre-Gariep basement in the Kalahari Craton. Notably no zircon grains younger than 1.0 Ga could be detected in the older Gariepian clastic rocks. Siliciclastic sediment geochemistry points to derivation from a continental magmatic arc (Hofmann et al. 2014)—a signature that is easily explained by the nature of the basement rocks: the Richtersveld Terrane represents an extensive Eburnean magmatic arc (Macey et al. 2017).

Siliciclastic rocks higher up in the Port Nolloth Group, including the Numees Formation diamictite [labelled 'Upper Diamictite' by Hofmann et al. (2014)], show identical detrital zircon age spectra, though with a dominance of Mesoproterozoic age data. Interestingly, no Neoproterozoic zircon grains have been observed in these younger strata, thus precluding zircon geochronology as a means of distinguishing between the various diamictite units (Hofmann et al. 2014).

The situation is different in the more distal parts of the belt, in the Marmora Terrane. There the upper Oranjemund Group rocks contain detrital zircon populations with a dominance of ages between 610 and 690 Ma, with a minor population at 800 Ma, in addition to late Mesoproterozoic (1.0–1.3 Ga) and Paleoproterozoic (1.7–1.9 Ga) age groups (Basei et al. 2005). The younger Neoproterozoic ages are unequivocal testimony to derivation from the Cuchilla Dionisio-Pelotas Arc in the Dom Feliciano Belt in the west, as there is no other potential magmatic source of the right age known (see below). This is supported by the chemistry of the siliciclastic units, although a mafic component in the upper Oranjemund Group rocks can be ascribed to erosion of the mafic rocks equivalent to those present in the adjacent Chameis and Schakalsberge subterranes (Basei et al. 2005). The *c*. 800 Ma age can be explained by zircon derived from the Richtersveld Suite.

A feature common to all detrital zircon age spectra from the Gariep Belt, irrespective of stratigraphic or tectonic position, is a total lack of Archaean ages. Clearly, no Archaean basement rocks had been exposed in the hinterland throughout the Neoproterozoic, neither on the African side nor on today's South American side of the belt.

13.4 Magmatic Evolution

13.4.1 Pre-rift Magmatism

The first major tectonothermal event that affected the pre-Gariep basement in preparation for Rodinia break-up and the opening of the Gariepian depositional basins was the emplacement of a range of predominantly felsic intrusive bodies along a northeasterly trend from the Richtersveld in South Africa to southern Namibia (Frimmel et al. 2001; Fig. 13.9). These are clearly post-tectonic with respect to the Namaqua tectonic events that shaped the Namaqua-Natal Belt between 1.2 and 1.0 Ga (Ritter 1980). In the past, these rocks were referred to as the Richtersveld Igneous Complex (Middlemost 1963; Ritter 1980) but they are better described as a suite (Frimmel 2008a).

In the extreme south of Namibia, the rocks of the Richtersveld Suite occur intrusive into low-grade metamorphosed and tectonized granitoids and metavolcanic rocks of the 1910–1865 Ma magmatic arc that constitutes the Richtersveld Subprovince (Macey et al. 2017). Further to the south in South Africa, the plutons, dykes and subvolcanic rocks of the Richtersveld Suite were emplaced into country rocks of the Bushmanland Terrane, which consists of high-grade gneisses and felsic intrusions, with the peak of metamorphism at 1.03–1.06 Ga (Robb et al. 1999).

Four major intrusive stages are distinguished within the Richtersveld Suite (Ritter 1980), from oldest to youngest: (1) an older leucogranite; (2) bostonite dykes (Fig. 13.10a); (3) subvolcanic quartz syenite; and (4) a younger subvolcanic leucogranite and its extrusive equivalent. Geochemically, these felsic rocks bear all the hallmarks of anorogenic magmatism, with trace element distributions conforming to those expected in a continental within-plate setting (Frimmel et al. 2001).

Uranium–Pb zircon age data indicates a prolonged phase of magmatism with individual pulses dated at 837 ± 2, 801 ± 8 and 771 ± 6 Ma (Frimmel et al. 2001). The youngest of these ages is of particular significance as it was obtained on granite that underlies the oldest sedimentary rocks of the Gariep Supergroup, thus providing a maximum age for the onset of Gariepian sedimentation. Hanson et al. (2011) reported older U–Pb zircon ages of 890–880 Ma for granite and syenite in the Richtersveld Suite. This would extend the timespan of magmatism to more than 100 myr or the older age data are an artefact due to older inherited core components in the dated zircon grains.

Undeformed, fine-grained, post-tectonic granite bodies (Uruchab Granite) in the pre-Gariep basement near the Aurus Mountains and along the margin of the Gariep Belt, respectively northwest and north of Rosh Pinah, appear

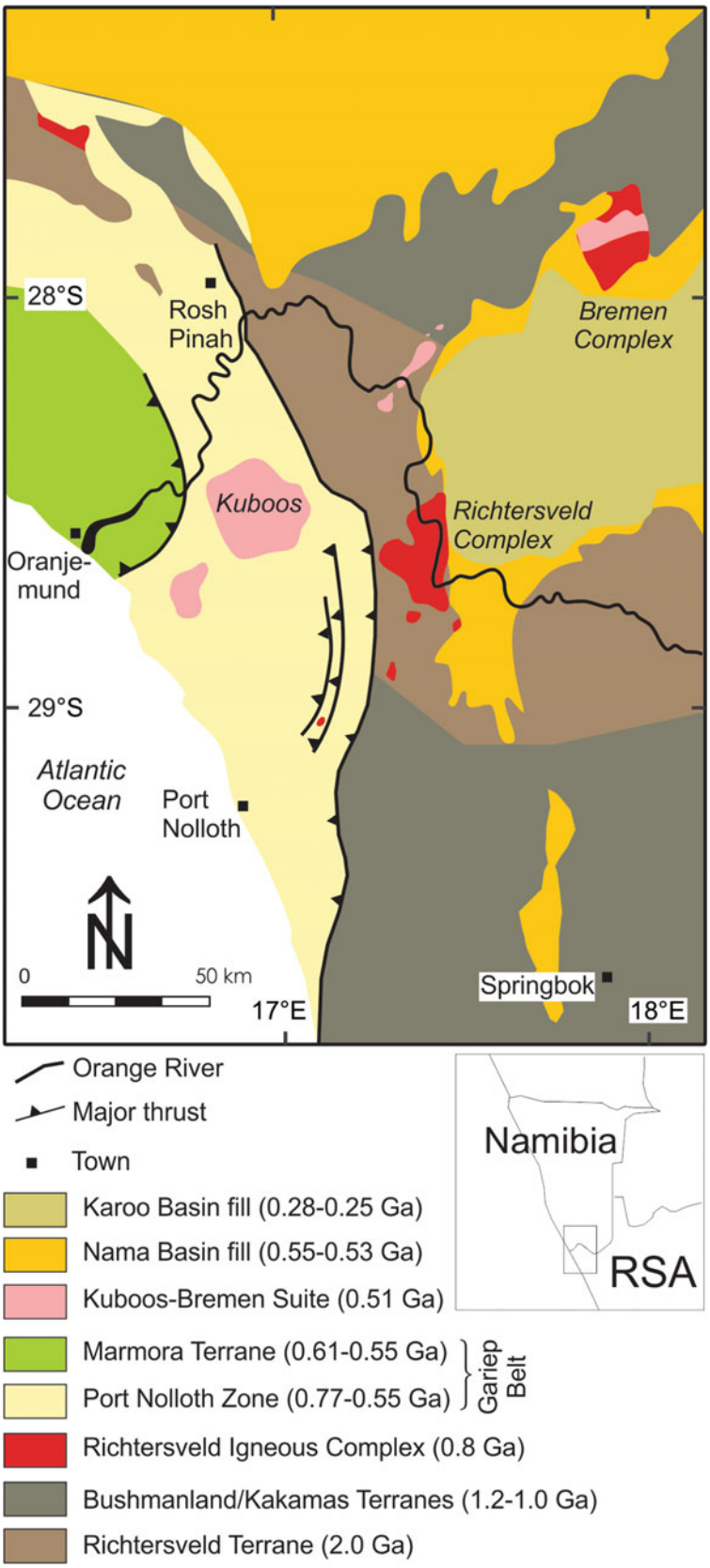

Fig. 13.9 Distribution of the 833–771 Ma Richtersveld Suite (Richtersveld Igneous Complex) and the *c*. 507 Ma Kuboos-Bremen Suite (along Kuboos-Bremen Line) within the main tectonic units of southernmost Namibia and adjoining South Africa (modified from Frimmel 2008a)

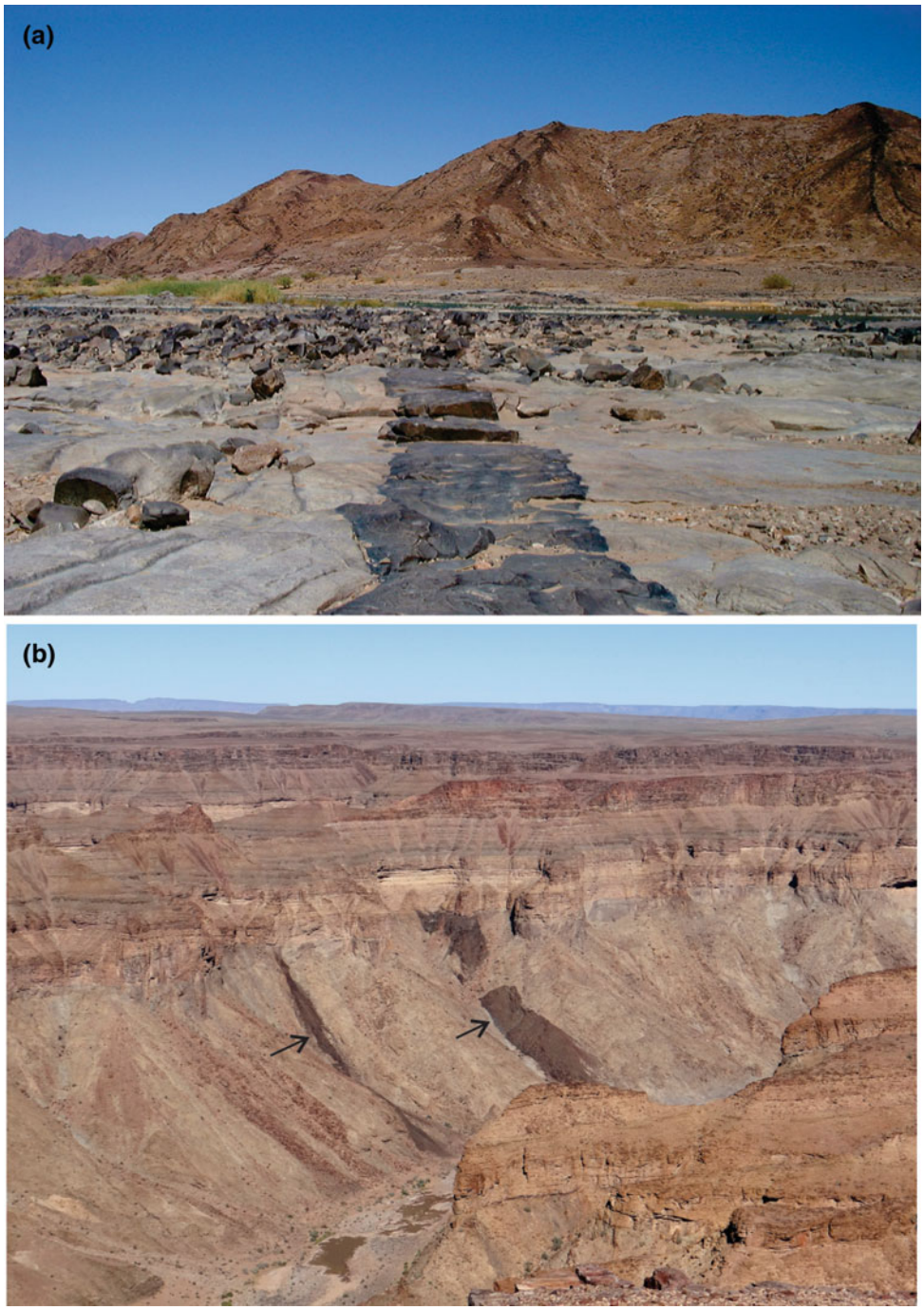

Fig. 13.10 **a** Bostonite dyke cutting across 837 Ma alkali granite, both of the Richtersveld Suite, at Sjamboksloof, Orange river pavement on farm Aussenkjer 147. **b** *c*. 750 Ma Gannakouriep Suite mafic dykes (arrows) crosscutting pre-Gariep basement, unconformably overlain by Lower Cambrian siliciclastic rocks of the Fish River Subgroup, Nama Group, Fish River Canyon

similar to the Richtersveld Suite granite both petrologically and in terms of relative timing of emplacement, but these granite bodies still await precise dating. Thomas et al. (2016) have reported a U–Pb zircon age of ~840 Ma for a felsic gneiss in the Aurus Mountains and interpreted this as the crystallization age of a volcanic protolith related to the Richtersveld Suite. The rocks there display a penetrative schistosity and are crosscut by pegmatite, thus indicating a tectonothermal overprint after 840 Ma (Diener et al. 2017).

13.4.2 Syn-rift Magmatism

The first magmatism after the onset of continental rift sedimentation is evident from a regionally extensive mafic dyke swarm, the Gannakouriep Suite. Most of the exposed dykes cut across pre-Gariep basement (Fig. 13.10b) but a few were emplaced also into the siliciclastic Stinkfontein Subgroup. Locally they are terminated by the Kaigas Formation diamictite, thus providing a relative age constraint. Available

radiometric age limits are a Rb–Sr whole-rock age of 717 ± 11 Ma (Reid et al. 1991) and a U–Pb baddeleyite age of 793 ± 2 (Rioux et al. 2010). The former is most likely younger than its true age owing to partial resetting during Pan-African metamorphism, whereas the latter age seems too old, considering the field relationship of some of the dykes crosscutting sedimentary strata that should be younger than 771 ± 6 Ma. Paleomagnetic data revealed a very tight clustering of calculated paleomagnetic poles for the Richtersveld Suite (including the older Bremen Complex; Fig. 13.9) and the Gannakouriep Suite (Bartholomew 2008), from which only a limited timespan between the two magmatic events can be inferred. The Gannakouriep Suite must be older than the *c*. 750 Ma Rosh Pinah volcanism (see below). Consequently, it should have been emplaced sometime between *c*. 770 and 750 Ma, a precise determination of which remains to be achieved.

The dyke swarm extends for more than 300 km from southern Namibia into westernmost South Africa. The width of individual dykes typically exceeds 5 m and their length can be as much as 100 km (Hunter and Reid 1987). The maximum width of the entire dyke swarm is about 150 km and integration of individual dykes' thickness amounts to about 10 km. The variably metamorphosed dykes are largely tholeiitic and their trace element distribution as well as ε_{Nd} and ε_{Sr} values conform to a within-plate setting (Ransome 1992; Frimmel et al. 1996a). Thus the suite's geochemistry, relative age and the spatial distribution of the dykes all indicate a genetic relationship between the stress field that induced continental break-up, early rift basin evolution and dyke emplacement, whereby the original rift axis most likely conforms to the northeasterly trend. A swing in the dyke trend towards northwest closer to the Gariep Belt, where the dykes also experienced metamorphic recrystallization, is then explained by reorientation in the compressional to transpressional stress field during the Gariepian orogeny.

Several felsic intrusive bodies—that is, fine-grained granite, quartz porphyry and feldspar porphyry, all of which constitute the Spitzkop Suite (Alchin et al. 2005)—occur in close proximity to the most proximal volcanic and volcaniclastic facies within the Rosh Pinah Formation. The microgranite contains abundant xenoliths of felsic volcanic material, several centimetres to decimetres in size, that appear identical to that of the surrounding Rosh Pinah Formation volcanic and pyroclastic rocks, thus pointing to a genetic relationship. At one locality, 2 km southeast of the Spitskop farmhouse, apophyses of glimmerite that emanate from this granite into adjacent felsic volcanic rock indicate an intrusive relationship (Frimmel 2008a).

Further to the west, in the Koivib Mountains, mafic intrusive rocks of the Koivib Suite (Alchin et al. 2005) are exposed in the form of irregularly shaped, crosscutting or concordant, relatively coarse-grained amphibolite bodies. No direct contact with a felsic intrusive body is known and therefore it remains unclear whether the mafic intrusions pre- or post-date the felsic ones. They are, however, clearly pre-orogenic. Because of the overall spatial association with the Rosh Pinah Formation and the proximity to the Spitzkop Suite, they are assumed to reflect the same magmatic episode. Comparable amphibolite with a subalkaline olivine-tholeiitic composition and geochemical and isotopic characteristics of within-plate basalt has been intersected in drill core on the farm Trekpoort further north (Frimmel et al. 1996b).

The volcanism evident in the Rosh Pinah Formation was bimodal, with eruptions of predominantly rhyolitic to rhyodacitic and subordinately basaltic chemistry (Frimmel et al. 1996b). In the Richtersveld, south of the Orange River, highly alkaline volcanic rocks occur with mainly tephriphonolitic to trachyandesitic but also tephritic and dacitic compositions. Their geochemistry is clearly different (Frimmel and Macey, unpublished data) and they occur at a slightly lower stratigraphic position within the Vredefontein Formation. Their genetic relationship to the Rosh Pinah volcanic units as described above remains to be established. The best available age constraints are Pb–Pb and U–Pb single zircon age data of respectively 741 ± 6 Ma obtained on a felsic volcanic bed from the Rosh Pinah Formation (Frimmel et al. 1996b) and 752 ± 6 Ma for a similar unit near the Skorpion mine (Borg et al. 2003).

The massive felsic volcanic units consist of alkalifeldspar phenocrysts embedded in a very fine-grained matrix of quartz and biotite. Pyrite, pyrrhotite, sphalerite and marcasite have been identified as accessory sulfides, whereas, in some flow units, magnetite occurs instead. Zircon is a common accessory phase. Locally, the volcanic rocks appear highly vesicular, with the vesicles being filled with calcite, quartz, chlorite and/or secondary iron oxides or sulfides. In places, the matrix shows banding that resembles original flow or quench textures. Pillow structures are locally well preserved in former basaltic lava flows. This, together with the presence of hyaloclastic breccias, attests to a subaqueous setting of at least some of the volcanism (Borg and Kottke-Levin 2007). In spite of a metamorphic overprint, the extent of recrystallization within the volcanic rocks is very limited. However, alteration is evident in spherulitic varieties, in which the spherules were preferentially silicified. The trace element distribution of the volcanic rocks, both felsic and mafic, is consistent with a typical continental within-plate setting, analogous to the Gannakouriep Suite (Frimmel et al. 1996b). However, the Rosh Pinah Formation metabasalt shows distinct differences to the Gannakouriep Suite dolerite by having higher age-corrected ε_{Nd} values (3.1–4.8) and lower Zr/Y ratios, both of which are transitional between within-plate and mid-ocean ridge basalt (Frimmel et al. 1996a).

13.4.3 Back-Arc Magmatism

The thick pile of predominantly mafic intrusive and extrusive rocks in the Marmora Terrane has been interpreted as post-rift but pre-orogenic in relative age. This is for the following reasons: (1) they lack any basement or continental sedimentary footwall; (2) they are associated with open marine, distal sediments in their hangingwall (Frimmel and Jiang 2001); (3) their geochemistry corresponds to oceanic within-plate and mid-ocean ridge basalts (Frimmel et al. 1996a; Will et al. 2014); (4) initial, though imprecise, geochronological evidence points to an age of emplacement at around 600–650 Ma (Frimmel and Fölling 2004)—that is, considerably younger than the rifting stage; and (5) they are metamorphosed, deformed and must be older than *c*. 575 Ma —the time of first syntectonic metamorphic hornblende formation (Frimmel and Frank 1998).

The mafic rocks of the Grootderm Formation in the Schakalsberge Subterrane are predominantly metabasaltic former lava flows with only very minor intrusive equivalents and a capping of thin dolomite that has been explained as former atoll deposit on top of a guyot (Frimmel and Jiang 2001). The most abundant basalt type is a fine-grained aphyric rock rich in vesicles and altered plagioclase, followed by plagioclase-phyric basalt. Metabasalt with ferromagnesian phenocrysts (now completely altered to actinolite and/or chlorite) and such with microphenocrysts of titanomagnetite are also abundant. Pillow structures are preserved in places, hyaloclastites are abundant, and agglomerates as well as tuff beds are also present. Intraformational, presumably penecontemporaneous, metadolerite dykes contain primary hornblende, titanomagnetite and apatite phenocrysts. Rare metagabbro and serpentinized picrite (cumulate) bodies are found in the lower parts of the formation.

In the Chameis Subterrane occur a number of tectonically dismembered slices of mafic rocks, predominantly metagabbro (Bakers Bay Suite), consisting originally of clinopyroxene, plagioclase and ilmenite. At the bottom of such bodies are, in several places, serpentinized ultramafic cumulates and serpentinized porphyric picrite (Frimmel et al. 1996a), whereas on top of the metagabbro bodies follow metabasalt and thinly laminated mafic tuff beds (Dernburg Formation). The mafic to ultramafic bodies cause magnetic highs and thus feature as prominent anomalies on aeromagnetic maps (Wackerle 2003). From the spatial distribution of these anomalies it can be inferred that the proportion between mafic/ultramafic rocks and sedimentary cover is greater than indicated on the surface. Moreover, the mafic/ultramafic rocks of the Chameis Subterrane seem to extend offshore for at least a further 60 km to the south.

In contrast to the Rosh Pinah Formation basites, which are subalkaline, those in the Marmora Terrane are alkalibasaltic and tholeiitic. Geochemically, two groups are distinguished among the mafic rocks of the Marmora Terrane (Frimmel et al. 1996a). One group is strongly enriched in light rare-earth elements, has a high Zr/Y (>6) and age-corrected ε_{Nd} of 0, whereas the other has flat to slightly light rare-earth element-depleted chondrite-normalized rare-earth patterns, and distinctly lower Zr/Y (2–3) and higher ε_{Nd} values (4–6). Most of the mafic rocks have trace element characteristics that correspond to those of oceanic within-plate basalt, whereas a few have compositions similar to those of mid-ocean ridge basalt (Frimmel et al. 1996a; Will et al. 2014). All these geochemical features, together with the lithological make-up of the Marmora Terrane and the available age constraints, point to deposition in a back-arc basin relative to the Cuchilla Dionisio-Pelotas Arc in the Dom Feliciano Belt, for which the term 'Marmora Basin' has been proposed (Frimmel et al. 2011).

13.4.4 Post-orogenic Magmatism

No evidence exists for any synorogenic magmatism in the entire Gariep Belt. Post-kinematic with respect to the main phase of orogenic deformation are a series of alkaline intrusive bodies that are located along a northeast-trending line over at least 270 km, the Kuboos-Bremen Line (Söhnge and de Villiers 1948; Fig. 13.9). These cut across the penetrative foliation and main structures of the deformed Neoproterozoic metasedimentary successions and include, from southwest to northeast, the Swartbank Pluton (largely covered), the Kuboos Pluton, the Tatasberg Pluton (all in South Africa), the Grootpenseiland ring complex at the Orange River, the Marinkas Kwela complex and associated carbonatite, the Kanabeam ring complex, the Mount Ai-Ais breccia pipe, the younger Bremen complex, the Haruchas stock and the Garub pipe in southern Namibia. Alkali-granite and alkali-syenite dominate the plutons in South Africa (southwestern part), whereas syenite, nepheline syenite, monzodiorite, phonolite and locally also carbonatite are more important in the Namibian examples further northeast. The best available geochronological datum for any of these bodies is a U–Pb zircon age of 507 ± 6 Ma for the Kuboos Pluton (Frimmel 2000a). The available age data is insufficient to assess a possible age progression along the Kuboos–Bremen line. Detailed petrographic and geochemical studies carried out on the Grootpenseiland-Marinkas Kwela (Smithies and Marsh 1996) and the Kanabeam complexes revealed that the parental melt composition may approximate that of gabbroic (basanitic) xenoliths within a phonolite breccia pipe at the Kanabeam ring complex (Reid 1991).

Comparable post-orogenic, largely syenitic bodies occur near the northwestern margin of the belt near the Atlantic

coast north of Bogenfels (Fig. 13.4). There, several stocks of alkali granite and syenite were emplaced either into pre-Gariep basement or younger strata of the Port Nolloth Group. They cut across the penetrative, synorogenic foliation of the host rocks and show little deformation themselves.

13.5 Chemo-, Chrono- and Biostratigraphic Correlation

As indicated above, controversy exists with regard to the number of glaciogenic diamictite units in the Gariep Belt, as well as to their correlation with global glacial events in the Neoproterozoic. Chemostratigraphy, specifically strontium, carbon and oxygen isotopic trends in calcareous successions, and biostratigraphic methods have been particularly helpful in establishing a stratigraphic scheme for the Gariep Supergroup. Isotopic variations (only taking near-primary signals into account) along profiles through carbonate-bearing sections above diamictite beds in various localities, summarized in Fig. 13.11, reveal distinct trends for the carbonate beds above the Kaigas and those above the Numees formations in the Port Nolloth Zone (Fölling and Frimmel 2002) and their equivalents in the Marmora Terrane (Frimmel 2000c). Additional data provided by Macdonald et al. (2010) conform to these trends, provided the analysed units are assigned to the correct stratigraphic position.

The carbonates immediately above the Kaigas Formation diamictite start with $\delta^{13}C$ as low as −4.6‰ (relative to V-PDB standard) and remain at negative values throughout the lower Pickelhaube Formation. This negative $\delta^{13}C$ excursion is, in itself, evidence of the glacial conditions that must have prevailed during Kaigas diamictite deposition. The upper Pickelhaube and lower Dabie River formations are marked by a positive $\delta^{13}C$ excursion, with ratios as high as 8.7‰. In the upper Dabie River Formation, this trend towards higher $\delta^{13}C$ reverses and a rapid drop in $\delta^{13}C$ is observed towards the contact with the overlying Numees Formation diamictite. The same trend is also observed immediately below the 'Namaskluft Diamictite' of Macdonald et al. (2010), which provides a further argument for that diamictite in fact representing the Numees Formation. The cap carbonates above the Numees Formation diamictite again have very low, negative $\delta^{13}C$ values (–4.6‰) but recover over some 30 m to values around 0‰ only to remain at that level for the remainder of the section (Fig. 13.11a). This trend applies to the distal portions of the Bloeddrif Member where it occurs as clean limestone (Fölling and Frimmel 2002). The same stratigraphic unit closer to the basin margin, that is in a proximal position where it appears largely dolomitized and with interbedded sandstone (Fig. 13.11b), shows a $\delta^{13}C$ trend from −3.3 to 4.1‰ (Frimmel and Fölling 2004). This highlights the fact that positive $\delta^{13}C$ excursions are not necessarily a global seawater signal that can be used for interbasinal correlation but can be a function of a depositional environment, specifically of higher evaporation rates (Frimmel 2009; Schmid 2017). Similarly, the $^{87}Sr/^{86}Sr$ ratios in the Gariepian carbonate rocks seem to be influenced by sedimentary facies with more proximal deposits having higher primary $^{87}Sr/^{86}Sr$ ratios (*c*. 0.7082–0.7085) than distal ones, as in the oceanic realm of the Marmora Basin (0.7075–0.7080). The lowest primary $^{87}Sr/^{86}Sr$ ratios have been observed in the upper Pickelhaube Formation carbonates (0.7071) and these seems to be independent of proximity to the paleocoastline. This is confirmed by the data of Macdonald et al. (2010) provided that their analyses are assigned to the correct stratigraphic position. The $\delta^{13}C$ values reported for the Wallekraal Formation (Fölling and Frimmel 2002; Macdonald et al. 2010) must be viewed with caution. They tend to be low (*c*. −2 to −4‰) but are unlikely to reflect contemporaneous seawater composition because the analysed rocks are largely allodapic.

Although more susceptible to post-depositional alteration, the $\delta^{18}O$ values obtained appear to be close to primary in many samples. They fluctuate between −11 and −3‰ (relative to V-PDB standard) with lower values in cap carbonates (Fölling and Frimmel 2002; Frimmel and Fölling 2004). Furthermore, no significant difference in $\delta^{18}O$ trends between calcite and dolomite samples could be noted, which suggests that dolomite precipitated either directly from seawater or replaced calcite during early diagenesis.

The available chemostratigraphic data from the Marmora Terrane (Frimmel 2000c; Frimmel and Fölling 2004), though still limited, confirm the lithostratigraphic correlation proposed above. The dolomite of the Gais Member in the Schakalsberge Subterrane is enriched in ^{13}C similar to the carbonates of the Dabie River Formation. By analogy, the diamictite in the uppermost Dernburg Formation in the Marmora Terrane is correlated with the Numees Formation. The carbonates of the Dreimaster Member in the Bogenfels Formation display a negative $\delta^{13}C$ excursion similar to the carbonates above the Numees Formation (Fig. 13.11d).

Low-grade metamorphosed sedimentary rocks of Neoproterozoic age also occur south of the Gariep Belt sensu stricto, where they rest unconformably on basement rocks of the Namaqua-Natal Belt along the Atlantic coast between latitudes 30° and 32°S, most concentrated in the Vredendal Outlier (Fig. 13.1a). They were thrust northeastwards onto subgreenschist-facies siliciclastic rocks to the east of Vanrhynsdorp (Gresse 1992). Although these two units have been described lithostratigraphically as separate entities—that is the Gifberg and Vanrhynsdorp groups—they are very similar to the metasedimentary successions of the Gariep and Saldania belts and to the syn- to post-orogenic foreland basin deposits of the Nama Group, respectively. Whereas the

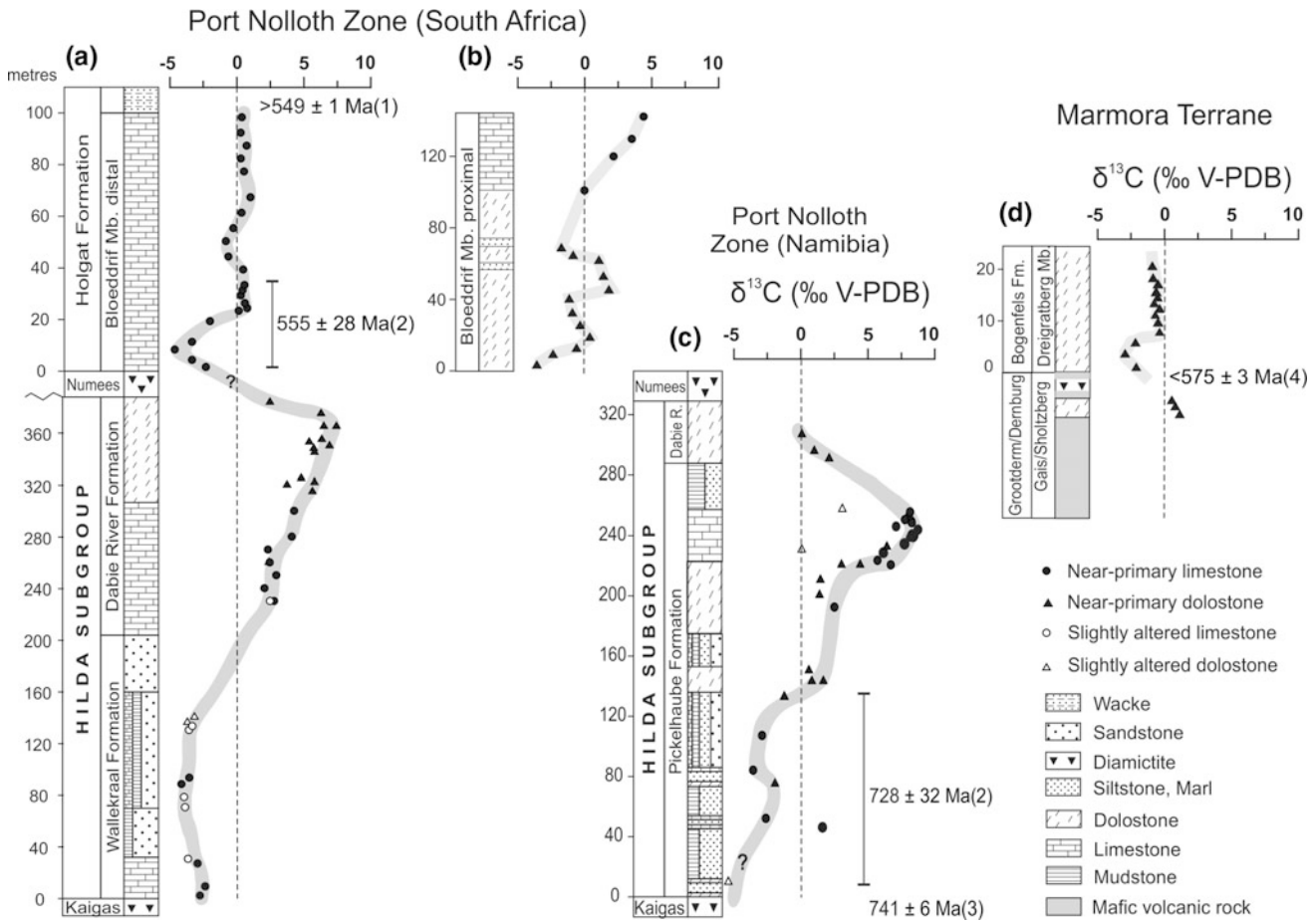

Fig. 13.11 Composite sections showing the variation in $\delta^{13}C$ of marine carbonates in the Gariep Supergroup: **a** western Richtersveld (South Africa) north of the Kuboos Pluton with Bloeddrif Member in a relatively distal position (from Fölling and Frimmel 2002); **b** section through the most proximal facies of the Bloeddrif Member south of the Kuboos Pluton (Frimmel and Fölling 2004); **c** Dreigratberg section (Fölling and Frimmel 2002), and **d** carbonates in the Marmora Terrane (Frimmel 2000c). Age constraints from (1) Grotzinger et al. (1995), (2) Fölling et al. (2000), (3) Frimmel et al. (1996b) and (4) Frimmel and Frank (1998)

Vanrhynsdorp Group represents the fill of a distinct sub-basin (Vanrhynsdorp Basin) within the larger Nama Basin (Germs et al. 2009), the Gifberg Group can be directly correlated with the Port Nolloth Group based on both litho- and chemostratigraphy (Frimmel 2008b). There again a lower and upper diamicite unit can be distinguished. The lower one of the Karoetjes Kop Formation is equivalent to the Kaigas Formation, and the overlying carbonates of the Widow Formation can be correlated with parts of the Pickelhaube Formation but represent a more evaporitic, proximal facies (Frimmel 2008b). The following Aties Formation is more siliciclastic and reflects the starvation of the basin under partly euxinic conditions. The overlying Bloupoort Formation contains stromatolitic carbonates that can be correlated with the Dabie River Formation and a massive diamictite with minor iron formation that bears all the hallmarks of the Numees Formation. It is overlain by a thinly laminated pink dolomite that can be correlated with the Bloeddrif Member (Frimmel 2008b). Thus the entire Gifberg Group can be regarded as equivalent to the Port Nolloth Group.

Chemostratigraphy helped in resolving the local stratigraphy but has been inconclusive regarding the regional and global correlation of key units of the Gariep Supergroup, specifically the glaciogenic Kaigas and Numees Formations. Although these two formations have been correlated with the global Sturtian and Marinoan glaciations, respectively, in the past (Frimmel et al. 2002), this notion can no longer be upheld in the light of improved geochronological constraints for these two glacial episodes elsewhere in the world. The Sturtian glaciation is estimated to have lasted from 717 to 660 Ma and the Marinoan from 650 to 632 Ma (Rooney et al. 2015). Neither of the two glaciogenic formations in the Port Nolloth Zone fit into these age brackets.

The Kaigas Formation is more or less contemporaneous with the Rosh Pinah Formation, the age of which is

constrained at around 750 Ma by Pb–Pb and U–Pb zircon age data of respectively 741 ± 6 Ma and 752 ± 6 Ma (Frimmel et al. 1996b; Borg et al. 2003). Furthermore, a Pb–Pb carbonate age of 728 ± 32 Ma obtained on the cap carbonate immediately above the Kaigas Formation (Fölling et al. 2000), though subject to a relatively large uncertainty, is older than the onset of the Sturtian glaciation. Consequently, the Kaigas Formation must be older than the Sturtian glaciation and reflects either an older pre-Sturtian global glacial event or a regional glaciation. It follows that the carbonate deposits of the Pickelhaube Formation must be pre-Sturtian as well.

More problematic is the correlation of the Numees Formation because of a lack of direct radiometric age control. A minimum age is given by a Pb–Pb carbonate age of 555 ± 28 Ma for the overlying cap carbonates, the Bloeddrif Member of the Holgat Formation (Fölling et al. 2000), and the age of regional, syncollisional metamorphism—that is, 545 ± 2 Ma (Frimmel and Frank 1998). The Pb–Pb carbonate age is considered to be robust because it could be repeated for a stratigraphically identical unit far away from the Port Nolloth Zone—that is, in the Saldania Belt (Fölling et al. 2000). For the overlying clastic and in places turbiditic flysch sediments of the upper Holgat and Bogenfels formations, a maximum sedimentation age is provided by the youngest concordant detrital zircon age data. From the Kaoko Belt in the north through the Gariep Belt to the Saldania Belt in the south, the maximum age is <630 Ma, in most areas <600 Ma, and in the Saldania Belt the timing of flysch sedimentation could be constrained to the very narrow interval of 554–552 Ma (Basei et al. 2005; Frimmel et al. 2013; Basei, unpublished data). In the absence of a significant hiatus between the Numees and Holgat formations, evident both in the field and from the $\delta^{13}C$ profiles, it follows that the former cannot be a correlative of the Marinoan glaciation but must be younger. In the light of currently available age data, a correlation with the global, very short-lived 581–579 Ma Gaskiers glaciation (Pu et al. 2016) seems most plausible.

Further attempts at correlation can be based on biostratigraphy of organic-walled microfossils (Gaucher et al. 2005). Poorly preserved, highly carbonized acritarchs are present in units beneath the Numees Formation, including *Bavlinella faveolata* in the Pickelhaube Formation. This acritarch assemblage is in stark contrast to that in the post-Numees Bloeddrif Member, which is similar to many upper Ediacaran assemblages described from SW-Gondwana and elsewhere. The assemblage is of low diversity and consists of *Soldadophycus*, *Myxococcoides*, *Coniunctiophycus and Leiosphaeridia*, with a dominance of *Soldadophycus bossii*, and the absence of acanthomorphs and large sphaeromorphs. Associated with this acritarch assemblage is the agglutinated foraminifer *Titanotheca* sp. This palynormorph assemblage is analogous to that found in the lower Kombuis Member of the Cango Caves Group in the Saldania Belt (South Africa), for which an identical Pb–Pb carbonate age of 553 ± 30 Ma and chemostratigraphic signals had been obtained previously (Fölling et al. 2000; Fölling and Frimmel 2002). The micropaleontological and isotopic peculiarities of the Bloeddrif and Kombuis members are also shared by the Buschmannsklippe Formation in the Witvlei Group of central Namibia and the uppermost Polanco-lowermost Cerro Espuelitas Formation in the Arroyo del Soldado Group in Uruguay (Gaucher et al. 2005).

Three informal acritarch biozones have been recognized between the Marinoan glacial deposits and the base of the Cambrian (Knoll 2000; Grey et al. 2003). The Marinoan deposits and strata immediately above are characterized by a simple leiosphere palynoflora, followed by a middle Ediacaran complex acanthomorph palynoflora, described from Australia, Siberia and China. In the uppermost Ediacaran, plankton diversity decreased dramatically, leading again to a depauperate assemblage dominated by small sphaeromorphs (Kotlin-Rovno assemblage of Vidal and Moczydlowska-Vidal 1997). Based on the above chemo-, chrono- and biostratigraphic data, correlation of the Holgat Formation palynomorph assemblage with the younger of the two Ediacaran low-diversity palynofloras has been suggested. This provides further support for the Numees Formation corresponding to the 581–579 Ma Gaskiers glacial event.

The interpretation of the Kaigas Formation reflecting a *c*. 750 Ma, either global or regional, pre-Sturtian glacial event and the Numees Formation the global Gaskiers glacial event has some major implications for the depositional history of the Gariep Belt. It implies a pre-Sturtian age for the post-Kaigas carbonate deposits of the Pickelhaube Formation and the absence of any tillite deposits related to the globally so significant Sturtian and Marinoan glaciations. This, in turn, implies that the area of today's Gariep Belt was land for most, if not all, of the Cryogenian Period and explains the position of the by far most important sequence boundary in the entire Port Nolloth Group—that is, the regional unconformity below the Wallekraal Formation. Moreover, it explains the lack of a thick passive continental margin development in the belt. Thus erosion of some of the older rift-graben fill prior to the Sturtian glaciation is proposed, with subsequent peneplanation, followed by the incision of glacial valleys during the Marinoan glaciation only to be filled by the Wallekraal sediments. Renewed subsidence in the Ediacaran Period would then have been related to the opening of the Marmora back-arc basin to the west. Finally, a hiatus of less than 5 million years is indicated for the erosive surface at the base of the Nama Group,

on the basis of available U–Pb age data of 549 ± 1 Ma for the lower Nama Group (Grotzinger et al. 1995) and the age suggested for the Holgat Formation.

Several tectonostratigraphic packages of the Damara and Kaoko belts contain two distinct glaciogenic units, similar to the Port Nolloth Zone in the Gariep Belt. These include the Northern Platform of the Damara Orogen, stretching from the Eastern Zone of the Kaoko Belt to the Otavi Mountainland northeast of the Damara Belt (e.g., Hoffman et al. 1998), the central and southern units of the Damara Belt (Hoffmann et al. 2004), including the Naukluft nappe complex, and the belt's southern foreland (Prave et al. 2011). This dichotomy can be extended to other Neoproterozoic successions of southern Africa, such as in the West Congo Belt (Frimmel et al. 2006; Cailteux et al. 2015) and the Lufilian Arc (e.g., Master and Wendorff 2011). In the past it was therefore tempting to correlate all of these respectively older and younger diamictite units across southern Africa as representing two distinct glacial episodes, which in turn have been correlated with the global Sturtian and Marinoan events (e.g., Halverson et al. 2005; Macdonald et al. 2010; Miller 2013). Much of this correlation is, for the lack of precise geochronological data for many of the glaciogenic units, based on indirect evidence, largely chemostratigraphy. It has been shown, however, that primary chemostratigraphic signals can reflect certain depositional environments rather than changes in global seawater composition (e.g., Jiang et al. 2007; Frimmel 2010; Schmid 2017) and are not as reliable for stratigraphic correlation as previously thought.

The above interpretation of the age of the two glaciogenic units in the Gariep Belt shows that a broad-brush correlation with other glaciogenic units on the subcontinent is not straightforward and is potentially misleading. The Kaigas Formation is seemingly older than the Chuos Formation in the Otavi Group, which has been used as one of the classic units on which the 'snowball Earth' hypothesis was built (Hoffman et al. 1998). The Chuos Formation diamictite contains clasts of an older volcanic unit, the precisely dated 746 ± 2 Ma Naauwpoort Formation, which is stratigraphically 720 m below the diamictite. Thus the diamictite must be 'substantially younger than 746 Ma' (Hoffman 2011), most likely Sturtian. The younger diamictite in the Otavi Group, the Ghaub Formation, was initially also considered to be Sturtian (Hoffman et al. 1998) but later described as the archetype of Marinoan glaciation (Hoffman and Schrag 2002), a notion that subsequently found support from a precise age of 635.5 ± 1 Ma obtained for a diamictite in the Central Zone of the Damara Belt (Hoffmann et al. 2004). While the correlation of this dated unit with the Ghaub Formation in the Northern Platform remains speculative, the above age provides unequivocal evidence of syn-Marinoan glacial deposits in the central Damara Belt, which were laid down at a time when the area of today's Gariep Belt was most likely land. A late Ediacaran (syn-Gaskiers) age for the Numees Formation, as suggested here, implies that glaciogenic and post-glacial deposits of the same age should also be present in other tectonostratigraphic units of southern Africa where sedimentation was still ongoing prior to the final assembly of Gondwana. Maybe the age of some of the younger diamictite units and corresponding cap carbonate successions in the wider region will be reassigned to that late Ediacaran time in the future.

13.6 Deformation and Metamorphism

The original sediment fill, now present in a fold-thrust belt, experienced a series of deformation events, some of which took place under metamorphic pressure-temperature conditions. From the distribution of sedimentary facies, aeromagnetic data and structural studies, pre-, syn- and post-orogenic stages of deformation are distinguished (Davies and Coward 1982; Von Veh 1993; Gresse 1994). Synorogenic deformation typically utilized pre-existing structures that had been formed during basin development (Hälbich and Alchin 1995; Frimmel 2000b).

13.6.1 Syndepositional Deformation

The presence of debris flow and turbidity fan deposits as well as large slump masses, particularly within the Kaigas and Rosh Pinah formations, indicates widespread syndepositional deformation related to continental rifting (Frimmel 2008a). Large but only locally developed dolomitic olistostromes near the (north-)eastern basin margin are explained by seismic activity along active, basin-bounding growth faults. These normal faults were subsequently reactivated during the opening of the Marmora Basin and later on inverted during the Gariepian orogeny, but the position of some of the major syn-rift faults is still recognizable. A major growth fault must have existed along today's eastern to northeastern margin of the belt, separating basement rocks to the east and northeast from the rift graben fill to the west and southwest. This fault is now present as an inverted northwest-southeast trending thrust fault system (e.g., Rosh Pinah Fault). Further to the southwest, thrust faults with basement slivers in their hangingwall represent inverted normal faults on the other side of a rift graben, the Rosh Pinah Graben. The orientation of the major syn-rift faults was subparallel to the north–south trending Gannakouriep dyke swarm, which demarcates the principal direction of extension during the rifting phase as east–west.

13.6.2 Synorogenic Deformation and Metamorphism

The Gariep Belt is made up of an arcuate arrangement of stacked thrust sheets, with the upper tectonic unit, the Marmora Terrane, being allochthonous. A first penetrative schistosity (s1) developed during a first phase of contractional deformation (D1). It is almost horizontal and subparallel to bedding (s0) in the western Port Nolloth Zone but steepens towards the eastern margin of the belt. Open to isoclinal F1 folds, thrusts, stretching lineations and sheath folds related to D1 all follow the arcuate shape of the belt (Gresse 1994). In the northern and northeastern part of the Port Nolloth Zone, F1 folds are northeast-vergent (Davies and Coward 1982), whereas in the eastern and southeastern parts, they are southeast-vergent (Von Veh 1993; Hälbich and Alchin 1995).

Tight, southwest- to west-verging, non-cylindrical F2 folds and associated axial-planar crenulation cleavage (s2) as well as a north-northwest-plunging mineral lineation (L2) in the respectively northeastern and eastern marginal domains of the Port Nolloth Zone are products of the second major phase of deformation (D2). They have been interpreted as both back-folds, associated with back-thrusts (Hälbich and Alchin 1995) and as shear folds related to plane sinistral wrenching (Von Veh 1993). In the inner parts of the Port Nolloth Zone, the F2 folds verge towards the foreland (Gresse 1994).

In the Marmora Terrane, the penetrative foliation s1 dips to the west and is axial-planar relative to tight to isoclinal, east-vergent F1 folds. Locally, s1 was refoliated around open to tight, northeast-trending F2 kinkbands. The contact with the underlying Port Nolloth Zone is a major thrust fault with top-to-southeast transport (Schakalsberge Thrust) and progressively higher intensity of folding towards the actual fault surface. At the northern boundary of the Marmora Terrane, F1 folds within the Chameis Subterrane are truncated by the Schakalsberge Thrust, attesting to its syn-D2 timing. The contact between the Oranjemund and the Schakalsberge subterranes is a west- to northwest-dipping fault plane along which the former was thrust on top of the latter. The contact between the Chameis and Oranjemund subterranes is a zone of intense F2 folding with top-to-southeast transport and subsequent back-folding that resulted in locally steeply southeast-dipping crenulation.

The main contractional structures in the Gariep Belt have been ascribed to two stages (Frimmel 2000b). First is eastward transport of the Marmora back-arc basin fill, internal stacking of this basin fill and eventually obduction onto the continental Port Nolloth Zone. The irregular geometry of the continental margin led to partitioning of the strain into different strike-slip and orthogonal components with northeast-, east- and southeast-directed transport along the northeastern, eastern and southeastern basin margin, respectively. Second is sinistral transpression with overall top-to-southeast transport as result of the overall oblique, southeast-directed convergence at an angle to the continental margin, leading to southeast-verging folds and thrusts along the southern frontal ramps within the outer Port Nolloth Zone (Gresse 1994).

Small-scale, north-northwest-trending F3 open gravity folds have been recorded mainly in the Port Nolloth Zone. Probably contemporaneous east–west striking normal faults, north–south striking reverse faults, veins and fractures, and a set of Riedel shears and conjugates that strike east-southeast and northeast, respectively, resulted from late-orogenic sinistral D3 transtension (Von Veh 1993). At this stage the alkaline igneous bodies along the Kuboos-Bremen Line were emplaced. Finally, a further phase of compressional deformation (D4) affected the region after the deposition of the Nama Group molasse sediments. It caused northeast-verging open to tight folds and related faults, which become the dominant structures in the southern extension of the Gariep Belt along the South African west coast and in the Nama Group rocks to the east and southeast of the Gariep Belt (Gresse 1994).

The two principal tectonostratigraphic units of the belt, the Marmora Terrane and the Port Nolloth Zone, differ not only with regard to stratigraphy and deformation but also in their metamorphic history. In the Port Nolloth Zone, only one stage of regional metamorphism is discerned, the peak of which was attained after D2 but prior to D3 and is ascribed to crustal thickening following the loading of the Marmora Terrane on top of the Port Nolloth Zone. Temperature-pressure conditions transitional between the greenschist and amphibolite facies of *c*. 520 °C and 3.0–3.5 kbar were attained (Frimmel 1995). The onset of exhumation during the transtensional D3 phase is evidenced by lower homogenization temperatures of aqueous fluid inclusions in related quartz veins, when compared with those of syn-D2 quartz veins (Frimmel and Board 2000). Yet when the alkaline igneous bodies of the Kuboos-Bremen Line were emplaced, the crust beneath the Gariep Belt was presumably still considerably thicker than under the foreland to the east; the rising melts crystallized at a depth of about 7 km, calculated from contact metamorphic phase relationships, within the Gariep Belt (Frimmel 1995), whereas in the foreland they reached the surface to form volcanoes (e.g., Grootpenseiland, Kanabeam).

Synorogenic deformation was accompanied by the movement of crustal fluids, particularly through siliciclastic sedimentary successions where they left behind deformed, s2-parallel, pinch-and-swell quartz veins. The fluids involved had a uniform composition across the belt. They were low-salinity aqueous fluids with densities that are in

good agreement with the regional metamorphic grade (Frimmel and Board 2000). An exception is local brines that can be explained by interaction with locally developed paleoevaporites, which are a prominent feature in the open marine sediment cover of the Dernburg Formation in the Chameis Subterrane (Frimmel and Jiang 2001). Stable isotope studies (Frimmel and Board 2000) revealed that the fluids were of mixed meteoric and metamorphic origin and that their composition was largely controlled by local infiltrated host rock composition. Late to post-orogenic fluids, preserved as inclusions in syn-D_3 and younger tabular quartz veins, are meteoric and of equally low-salinity aqueous composition. These studies further confirm the notion that the entire sediment succession was not a thick package with progressive metamorphic dehydration in its deeper parts but a fairly thin, more or less autochthonous cover above a relatively dry basement.

The metamorphic evolution of the Marmora Terrane is more complex. There the mafic and ultramafic rocks of the Dernburg Formation and Bakers Bay Suite experienced a polyphase metamorphic overprint that is not recorded by the sedimentary cover of the Bogenfels and the stratigraphically equivalent upper Oranjemund Group. The mafic rocks, particularly metagabbro, contain up to three metamorphic amphibole generations that not only reflect different metamorphic conditions of formation (Frimmel and Hartnady 1992) but also yielded distinctly different Ar–Ar age spectra (Frimmel and Frank 1998). The first amphibole generation crystallized at temperatures between 500 and 700 °C at a pressure of less than 2 kbar and has been explained by ocean-floor metamorphism, for which imprecise Ar–Ar data suggest an age of approximately 610 Ma. The second amphibole generation records elevated pressures between 4 and 6 kbar at lower amphibolite-facies temperatures, most likely due to tectonic stacking of these oceanic rocks, for which an age of 574 ± 9 Ma is indicated by Ar–Ar data. Finally, the third amphibole generation formed under lower greenschist-facies conditions and gave Ar–Ar ages consistently around 545 Ma, in accordance with the age of regional metamorphism determined for the Port Nolloth Zone (Frimmel and Frank 1998).

Peak metamorphic conditions reached in the upper, sedimentary portions of the Marmora Terrane did not exceed the lower greenschist facies (300–400 °C). This difference in the metamorphic history between the upper and lower stratigraphic parts of this terrane would imply a hiatus between them. As most stratigraphic contacts are tectonic, it has so far not been possible to verify such a hiatus by a field observation of an erosional, angular unconformity. However, for other reasons, relating to similarities in the stratigraphy of the younger units across the entire Gariep Belt and marked differences in the older parts of the Chameis and Port Nolloth groups, it has been suggested that a first tectonic pulse, leading to the accretion of oceanic crust, had already taken place prior to the deposition of the Bogenfels and Holgat formations sediments (Frimmel and Fölling 2004).

Recently, relatively high pressure-metamorphism has been documented for schists in the Aurus Mountains (Diener et al. 2017). Although these rocks form part of the pre-Gariep basement, the relatively high-pressure event, attaining P-T conditions of around 10 kbar and 500 °C, has been interpreted by Diener et al., based on structural and textural grounds, as post-dating the approximately 840 Ma Richtersveld Suite and as being related to northwest-southeast striking ductile shear zones, the largest of which is the Aurus Shear Zone (Fig. 13.3). This recent finding is similar to observations made in the pre-Gariep basement in the Vredendal Outlier by Waters et al. (1983). There the high-grade metamorphic rocks of the Mesoproterozoic Namaqua Metamorphic Complex experienced a kyanite-grade retrograde overprint with increasing intensity towards the coast in the west. That event, resulting in garnet-staurolite-kyanite mica schist, was associated with sinistral rotation and shearing of basement structures, which can be ascribed to the Gariepian orogeny based on field relations (Waters et al. 1983) and Ar–Ar age data (Frimmel and Frank 1998), though the latter only give cooling ages. The mineral paragenesis corresponds to metamorphic conditions of *c*. 630 °C and 6–7 kbar. Thus evidently the pre-Gariep basement rocks experienced a relatively high-pressure event that is not recorded by the Gariepian cover rocks. Either the basement rocks were exhumed prior to juxtaposition with the rocks of the Port Nolloth Group, as suggested by Diener et al. (2017), or the relatively high-pressure metamorphic event took place prior to the deposition of the Gariep Supergroup rocks. The latter possibility seems more likely, both because of primary contacts between basement and cover rocks at several localities and because of mounting evidence of a significant tectonothermal event in the Uruguayan sector at the time of continental rifting in the Gariep Belt (Oyhantçabal et al. 2009; Basei et al. 2011; Lenz et al. 2011; Will, unpublished data).

13.6.3 Post-orogenic Deformation

After the orogenic episode that amalgamated South America with southern Africa along the Kaoko-Gariep-Saldania-Dom Feliciano system of orgenic belts, the area formed part of southwestern Gondwana until the opening of the modern South Atlantic in the Cretaceous. This was accompanied by the emplacement of a series of north–south trending mafic dykes and subsequently the development of predominantly normal step faults with the western blocks down-faulted relative to the eastern ones.

13.7 An Integrated Geodynamic Model

The available data and observations from the Gariep Belt, when integrated with data from the corresponding Dom Feliciano Belt in Uruguay and southern Brazil, and with comparable information from the adjacent coast-parallel Pan-African belts in southern Africa, make it possible to formulate a model for the geodynamic evolution of the Gariep Belt.

13.7.1 The Rifting Stage (770–740 Ma)

The history of the Gariep Belt begins with continental rifting between *c*. 770 and 740 Ma, following a period of anorogenic, alkaline magmatism. The latter resulted from crustal thinning that led to decompression-related, mantle-derived melts rising, differentiating and finally crystallizing at shallow depths between 830 and 770 Ma, possibly even earlier (Richtersveld Suite). The pre-Gariep basement constitutes part of the late Mesoproterozoic Namaqua-Natal Belt along the margin of the Kalahari Craton that, in turn, is commonly regarded as a marginal fragment of Rodinia (Meert and Torsvik 2003), although some workers consider it to be a 'non-Rodinian block' (Oriolo et al., in press). U–Pb zircon ages between 800 and 750 Ma obtained from high-grade gneisses in basement inliers of the Dom Feliciano Belt in Uruguay (Cerro Olivo Complex) have been interpreted as dating a magmatic pulse that could be correlated with the Richtersveld Suite in southwestern Africa (Oyhantçabal et al. 2009; Basei et al. 2011; Lenz et al. 2011). If this correlation is correct, the basement of the Dom Feliciano Belt would form a part of the Kalahari Craton that was split off during this rifting stage (Fig. 13.12), as suggested, for example, in the Arachania model of Gaucher et al. (2009).

More locally in the Gariep Belt, the spatial distribution of the Stinkfontein Subgroup rift deposits suggests that the centre of the rift basin was in the south (in South Africa) and orientated more or less in a southwest–northeast direction, thus following the initial trend of the Gannakouriep Suite dyke swarm prior to its sinistral rotation during the Gariepian orogeny. Several basement highs, remnants of which now exist at the bottom of tectonic slivers, separated a number of subparallel sub-basins. One of the more prominent of these sub-basins is the Rosh Pinah Graben, which is now separated from the wider Gariep rift basin further to the west by a large, tectonically emplaced basement block in the Aurus Mountains, the so-called Sperrgebiet Domain of Thomas et al. (2016). Continental rift sedimentation was accompanied at an earlier stage by highly alkaline, later by bimodal, predominantly acidic magmatism at around 750 Ma.

Although this rifting phase appears to have been more or less synchronous across southern Africa—that is, around the Kalahari Craton—comparison of geochronological and paleomagnetic data from South America and Africa reveals not only that many continental fragments there were not part of Rodinia but also a diachronous progression of continental break-up (Cordani et al. 2003). In the West Congo Belt, continental rifting commenced as early as 1000 Ma (Tack et al. 2001), at a time for which juvenile granitoid magmatism is documented in the Brasilia Belt (Pimentel et al. 2000). Thus continental break-up in the Gariep region took place at a time when elsewhere—that is, to the northwest (in today's coordinates)—inversion of early Neoproterozoic basins had already led to their closure and to continental collision. It may therefore be speculated that rifting in the Gariep Basin was a far-field consequence of subduction along the perimeter of an emerging continent that consisted of the Congo-Sao Francisco, Borborema-Trans Sahara, Luis Alves, and Rio de la Plata cratonic blocks (Fig. 13.12). Maybe the relatively high-pressure event recorded in the pre-Gariep basement rocks is related to this subduction. Alternatively, continental rifting might have been related to a rising thermal anomaly in the underlying mantle.

The Gariep rift failed. First marine ingression towards the end of Stinkfontein Subgroup sedimentation was interrupted by the Kaigas glaciation at around 750 Ma. Whether this drop in sea level was eustatic, related to a global Kaigas glacial event, or a regional phenomenon caused by the rise of the area owing to contemporaneous volcanism, remains unclear. In any event, this sea level drop cut off the Rosh Pinah sub-basin from the rest of the rift basin, limited seawater circulation and led to a stratified water column with anoxic bottom waters. This enabled massive synsedimentary sulfide mineralization to take place from the discharge of hydrothermal, metal-bearing brines that ascended along basin-bounding growth faults (Frimmel and Jonasson 2003; Fig. 13.13).

Although the Pickelhaube Formation documents renewed transgression in the wake of either post-glacial eustatic sea level rise or post-volcanic subsidence, further sedimentation remained limited to shallow water depths. The final stages of rift sedimentation were marked by elevated evaporation rates as indicated by an increase in $\delta^{13}C_{Carb}$. The total thickness of the Pickelhaube Formation (except for the volcanically controlled Rosh Pinah area) is not more than 280 m. Applying the same carbonate accumulation rate of 52 m/myr as calculated for the platform carbonates in the northern Damara Belt (Hoffman et al. 1998) yields a timespan for sedimentation of only 5.4 million years, which is far less than the uncertainty for the age of the Pickelhaube Formation carbonates (728 ± 32 Ma). This points to a major hiatus, which is evident in the field in the form of the unconformity below the Wallekraal Formation—a first-order

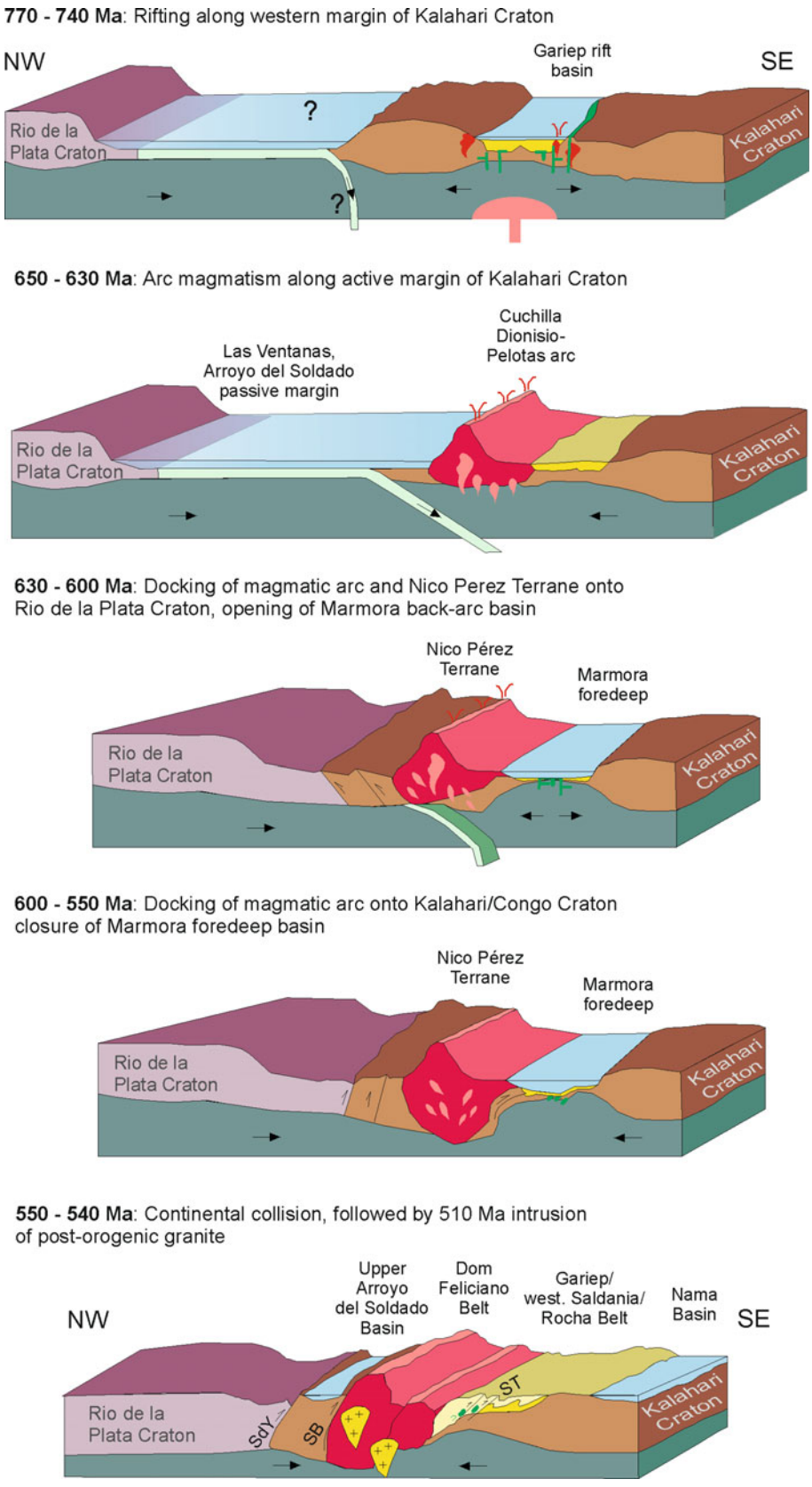

Fig. 13.12 Schematic cross-section illustrating a proposed geodynamic evolution of the Gariep Belt in the framework of Rio del la Plata–Kalahari collision in Ediacaran/Early Cambrian times. *SB* Sierra Ballena Shear Zone; *SdY* Sarandí del Yí Shear Zone; *ST* Schakalsberge Thrust

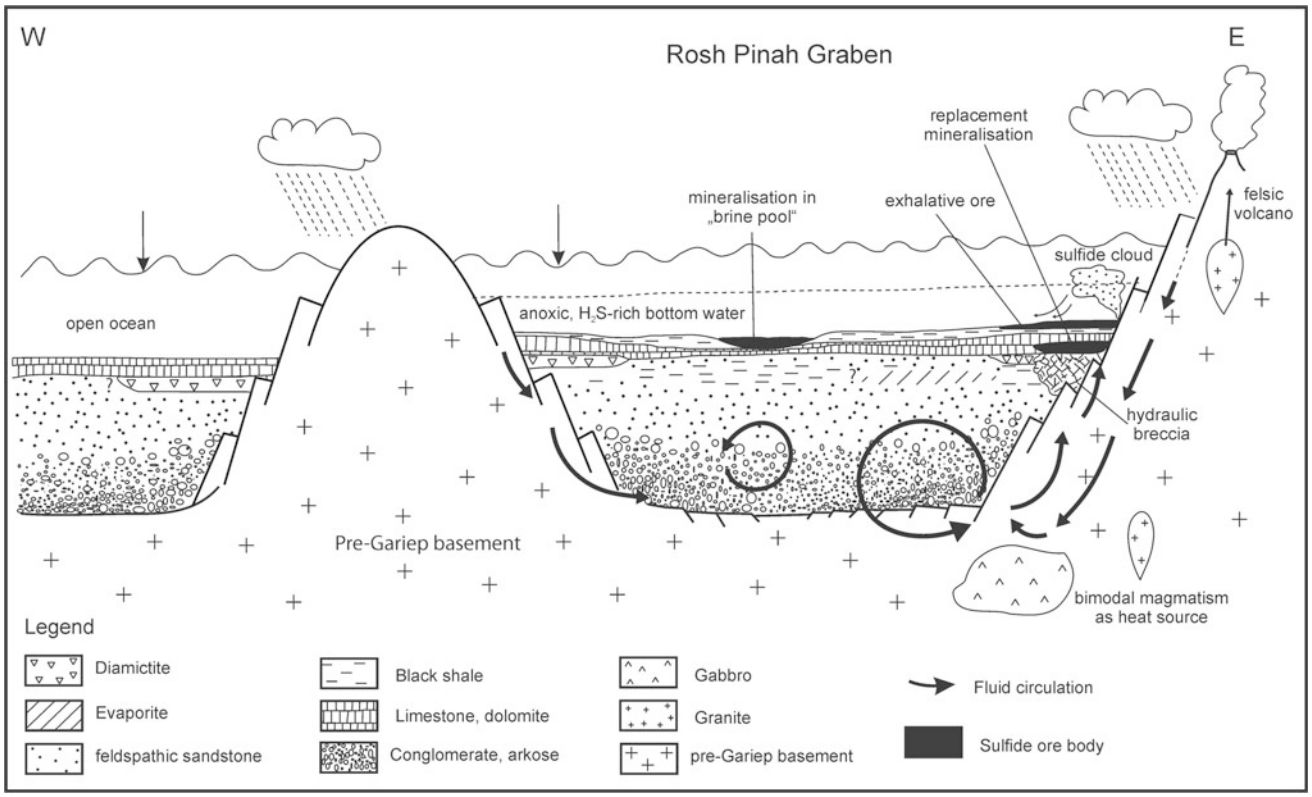

Fig. 13.13 Schematic profile through the Rosh Pinah Graben at the time of base metal mineralization, which is assumed to have been triggered by eustatic sea level drop that cut off the Rosh Pinah Graben from the open ocean, thus causing anoxic bottom waters. Magmatic heat-driven fluid flow in the rift sediments (and uppermost basement) leached metals and subsequently precipitated them as sulfides at or near the seafloor from hydrothermal discharge along basin-bounding growth faults (modified from Lohmeyer 2013)

sequence boundary (Frimmel 2008a). It is therefore suggested that the end of rift sedimentation was reached when extension of the failing rift basin came to a close and the entire region was uplifted and/or when the severe global Sturtian glaciation drew down the sea level below the bottom of the rift basin. In any event, by the time of the Sturtian glaciation, the area was land and subjected to erosion and peneplanation.

13.7.2 Post-rift Sedimentation (*c.* 640–580 Ma)

After a hiatus of some 100 million years, covering in time the entire Sturtian glaciation, renewed subsidence in the depo basin of the Port Nolloth Zone took place in response to probably eastward subduction that gave rise to a volcanic arc in the Dom Feliciano Belt—that is, the 640–590 Ma Cuchilla Dionisio-Pelotas arc. The timing of the onset of renewed sedimentation in the Port Nolloth Zone is poorly constrained but probably coincides with the waning stage of the Marinoan glaciation at around 635 Ma, when meltwaters flowing down deeply incised valleys that had been carved out by Marinoan glaciers led to high-energy sedimentation that is evident in the Wallekraal Formation. This was eventually followed by deposition of very shallow marine, in places reef, carbonates (Dabie River Formation) prior to tillite deposition (Numees Formation), most probably in the course of the 581–579 Ma Gaskiers glaciation.

Crustal extension in the Gariep area during the formation of the extensive Cuchilla Dionisio-Pelotas volcanic arc further west caused not only renewed sedimentation in the Port Nolloth Zone but also, closer to the arc, the formation of oceanic rocks in a back-arc basin (Fig. 13.12). These constitute the lower parts of the stratigraphy in the Marmora Terrane. Analogous oceanic mafic rocks with similar geochemical characteristics also occur in the Cuchilla Dionisio Terrane in Uruguay in the form of the La Tuna amphibolite and have been interpreted as remnants of the same back-arc basin (Will et al. 2014). The timing of back-arc basin opening is only poorly constrained but has been estimated by Will et al., based on detrital zircon ages, Ar–Ar data on the earliest amphibole generation and Nd model ages between *c.* 650 and 600 Ma.

At the same time, high-grade metamorphism affected basement inliers in the Dom Feliciano Belt, the Cerro Olivio Complex and the 'exotic' Coastal Terrane of the Kaoko Belt

which have been correlated with each other (Oyhantçabal et al. 2009; Lenz et al. 2011; Konopásek et al. 2016). This relatively low-pressure, high-temperature event has been explained as related to arc magmatism.

A minimum age for sedimentation in the Marmora back-arc basin is given by the Ar–Ar age of *c*. 575 Ma for relatively high-pressure amphibole in the Bakers Bay Suite (Frimmel and Frank 1998). At that stage the mafic rocks on the floor of the back-arc basin had already been stacked onto each other as the basin closed in preparation for subsequent continental collision.

13.7.3 The Orogenic Phase (580–540 Ma)

Whereas the lower stratigraphy of the Port Nolloth Zone is completely different from that of the Marmora Terrane, the upper parts in both, specifically the Holgat and Bogenfels formations and the Upper Oranjemund Group, are remarkably similar. They consist to a large extent of upwards-fining parasequences of sand-, silt- and mudstone beds of, in places, turbiditic character and can be interpreted as flysch sediments laid down in a foredeep during basin closure. The onset of basin closure must have been prior to 575 Ma when the stratigraphically lower mafic units had already been tectonically thickened to as much as *c*. 15 km, as indicated by the relatively high-pressure syntectonic hornblende generation therein (Frimmel and Hartnady 1992). This might explain why the younger flysch deposits are not present everywhere on top of the mafic rocks in the Marmora Terrane. The recently discovered relatively high-pressure metamorphic event in the Sperrgebiet Domain (Diener et al. 2017), the pre-Gariep basement inlier of the Aurus Mountains, might be related to this metamorphic episode but no reliable age data is available thus far and an alternative explanation is currently favoured (see above).

The interpretation of the Marmora Basin as a back-arc basin implies that the Gariepian orogeny was merely the eastward progression of contractional deformation in consequence of the collision between the Rio de la Plata Craton and the Cuchilla Dionisio-Pelotas Arc in the Dom Feliciano Belt (Fig. 13.12). Arc magmatism ceased at around 590 Ma, and shortly thereafter the inversion of basin tectonics in the Marmora Basin can be expected. This coincided with the global 581 to 579 Ma Gaskiers glacial event, which led to basin-wide deposition of glaciogenic deposits (Numees Formation in the Port Nolloth Zone and Chameis Gate Member in the Marmora Terrane) in the already closing basin. Ongoing sedimentation on top and in front of eastwards-advancing thrust sheets was uniform across the entire basin, which is evident from the uniform character of synorogenic deposits that make up the upper part of the Gariepian stratigraphy (Holgat and Bogenfels formations, Upper Oranjemund Group) across terrane boundaries. Only in the Schakalsberge Subterrane are these synorogenic deposits missing as it had been already thrust over at that stage. Post-glacial eustatic sea level rise, in combination with subsidence of the craton margin (emerging foreland basin) as the magmatic and sedimentary rock pile in the main Gariep Basin was becoming progressively thicker, led to drowning of the continental margin and sedimentation of synorogenic deposits of the Holgat Formation (and its equivalent, the Upper Oranjemund Group, in the Marmora Terrane) not only in the Marmora Basin but also further to the east in the autochthonous region on the basement.

The final closure of the Marmora Basin is marked by a regional angular unconformity at the interface between the Port Nolloth and Nama groups. This must have taken place prior to 549 Ma, which is the oldest available age for the foreland deposits of the Nama. The peak of regional metamorphism was reached within a few million years at around 545 Ma, at which time the first detritus from the young orogen was already shed off into the Nama Basin (Grotzinger et al. 1995).

The synorogenic deposits of the Gariep Belt can be correlated with lithologically and geochronologically equivalent units in eastern Uruguay, where the flysch deposits of the Rocha Group appear identical to those of the Upper Oranjemund Group (Basei et al. 2005), but also further south in the western Saldania Belt, where the Tygerberg Formation in the allochthonous Malmesbury Terrane reflect rapid sedimentation of a thick pile of turbiditic strata in a quickly shallowing basin between 554 and 552 Ma (Frimmel et al. 2013). Most likely a similarly short timespan also applies to the deposition of the flysch sediments in the Gariep Belt.

A comparable depositional evolution is also indicated for the Kaoko Belt further north. There the cratonic cover in the Central Kaoko Zone received its detritus from the ‘exotic’ Coastal Terrane, which has been interpreted as the continuation of the 650–630 Ma migmatized Punta del Este Terrane and Florianópolis Batholith in the Dom Feliciano Belt (Konopásek et al. 2014, 2016). The timing of docking of the Coastal Terrane onto the cratonic margin on the African side at *c*. 580 Ma (Konopásek et al. 2014) overlaps with the above timing of closure of the Marmora Basin. The short timespan available for sedimentation of the upper siliciclastic succession in the Central Kaoko Zone prior to collision of the Coastal Terrane effectively excludes the existence of a wide ocean between the Punta del Este Terrane/Coastal Terrane and the margin of the Kalahari/Congo cratons. It thus confirms the existence of only a narrow basin along the western margin of the Kalahari Craton that stretched from today’s position of the Kaoko Belt all the way via the Gariep Belt southwards to the western Saldania Belt. The long axis of that basin—the Marmora Basin—was parallel to the Cuchilla Dionisio-Pelotas Arc and the basin fill conforms to

an early evolution as back-arc basin that developed into a foredeep during Pan-African orogeny in the lead-up to Gondwana amalgamation (Fig. 13.12). Consequently, the main suture between the Rio de la Plata Craton and the Kalahari Craton was probably not located along a paleo-South Atlantic (Adamastor Ocean) but to the west of the Punta del Este Terrane.

Previously, the Sierra Ballena- Major Gercino (or Alferez-Cordillera-Punta del Este) Lineament within Brazil and Uruguay (to the west of the Cerro Olivo Complex) has been considered a potential candidate for such a suture (Basei et al. 2005, 2008; Frimmel et al. 2011), but more recent work by Oriolo et al. (2016a) attests to the Nico Pérez Terrane in Uruguay an 'African', that is Kalahari cratonic, affinity, which implies that the Sarandí del Yí Shear Zone, along which the Nico Pérez Terrane docked onto the Rio de la Plata Craton at 630–625 Ma (Oriolo et al. 2016b), is the more likely candidate for this suture (Fig. 13.12). Oriolo et al. regard the Nico Pérez Terrane as a splinter of the Congo Craton, but both the spatial distribution (taking into account strike-slip movement along major shear zones) and the age of recorded tectonothermal events are more akin to that recorded in the western Kalahari Craton (Macey et al. 2017). It is therefore suggested that the various crustal blocks with 'African affinity' in South America—that is, the Cerro Olivo Complex and Nico Pérez Terrane as well as the Coastal Terrane of the Kaoko Belt—all represent small blocks (microplates) of the Kalahari Craton, which split off during 800–750 Ma rifting along the margin of that craton. The later juxtaposition in the course of Pan-African Orogeny of the Coastal Terrane next to the Congo cratonic margin (Angola Block) between 580 and 550 Ma rather than the Kalahari Craton only became possible because of the convergence between the Congo and Kalahari cratons at that time, giving rise to the Damara Belt.

A Kalahari rather than Congo cratonic provenance of the said microplates would imply a major dextral shear component along the eastern boundary of the Coastal Terrane, which is in apparent conflict with the observed sinistral movement there. It should be noted, however, that the well-documented sinistral deformation only refers to the latest stages of the orogeny and to the stress field during rapid exhumation between 535 and 525 Ma (Foster et al. 2009). It pervasively overprinted earlier fabrics and consequently a dextral movement during the actual continental collision phase cannot be excluded.

Acknowledgements This chapter summarizes some 25 years of research on the Gariep Belt, which was only possible thanks to logistical and sometimes financial support from several mining companies, especially Kumba Resources and Namdeb, as well as several research grants from the South African National Research Foundation and more recently the German Research Foundation (DFG; grant No. FR 2183/8). Special thanks go to the guest editors, S. Siegesmund and M. A. S. Basei, for the invitation to contribute this chapter, and to the latter also for his repeated company during field work in Namibia and South Africa. A very careful examination of the manuscript by an anonymous reviewer is much appreciated. I thank the Royal Belgian Institute of Natural Sciences for providing office space during my sabbatical, during which the manuscript was drafted.

References

Alchin DJ et al (2005) Stratigraphic setting of the metalliferous Rosh Pinah Formation and the Spitzkop and Koivib Suites in the Pan-African Gariep Belt, southwestern Namibia. S Afr J Geol 108:19–34

Allen PA, Hoffman PF (2005) Extreme winds and waves in the aftermath of a Neoproterozoic glaciation. Nature 433:123–127

Bartholomew LT (2008) Paleomagnetism of Neoproterozoic intraplate igneous rocks in the southwest Kalahari Craton, Namibia and South Africa. Unpublished MSc thesis, College of Science and Engineering, Texas Christian University, Austin

Basei MAS et al (2005) A connection between the Neoproterozoic Dom Feliciano (Brazil/Uruguay) and Gariep (Namibia/South Africa) orogenic belts—evidence from a reconnaissance provenance study. Precambrian Res 139:195–221

Basei MAS et al (2008) West Gondwana amalgamation based on detrital zircon ages from Neoproterozoic Ribeira and Dom Feliciano belts of South America and comparison with coeval sequences from SW Africa. In: Pankhurst RJ et al (eds) West Gondwana: pre-cenozoic correlations across the South Atlantic Region. Geological Society of London, Special Publication, London, pp 239–256

Basei MAS et al (2011) The basement of Punta del Este Terrane: Grenvillian rocks reworked during Brasiliano/Pan-African orogenesis. Int J Earth Sci 100:289–304

Borg G, Kottke-Levin J (2007) Recognition of high-T rhyolite melts in the Rosh Pinah—Skorpion Zn-Pb district, Southern Namibia. In: Andrew CJ et al (eds) Digging deeper: Proceedings of the 9th Biennial SGA Meeting, Dublin, Ireland, pp 1049–1052

Borg G et al (2003) Geology of the Skorpion zinc deposit, southern Namibia. Econ Geol 98:749–771

Cailteux JLH et al (2015) The Neoproterozoic West Congo 'Schisto-Calcaire' sedimentary succession from the Bas-Congo region (Democratic Republic of the Congo) in the frame of regional tentative correlations. Geol Belgica 18:126–146

Cloud PE (1974) Giant stromatolites and associated vertical tubes from the Upper Proterozoic Noonday Dolomite, Death Valley region, eastern California. Geol Soc Am Bull 85:1869–1882

Cordani UG et al (2003) Tearing up Rodinia: the Neoproterozoic palaeogeography of South American cratonic fragments. Terra Nova 15:350–359

Davies C, Coward MP (1982) The structural evolution of the Gariep Arc in southern Namibia. Precambrian Res 17:173–198

De Villiers J, Söhnge PG (1959) The geology of the Richtersveld. Mem Geol Surv S Afr 48:1–295

Diener JFA et al (2017) Pan-African accretionary metamorphism in the Sperrgebiet Domain, Gariep Belt, SW Namibia. Precambrian Res 292:152–162

Fölling PG, Frimmel HE (2002) Chemostratigraphic correlation of carbonate successions in the Gariep and Saldania Belts, Namibia and South Africa. Basin Res 14:69–88

Fölling PG et al (2000) A novel approach to double-spike Pb-Pb dating of carbonate rocks: examples from Neoproterozoic sequences in southern Africa. Chem Geol 171:97–122

Foster DA et al (2009) Rapid exhumation of deep crust in an obliquely convergent orogen: the Kaoko Belt of the Damara Orogen. Tectonics 28:TC4002. doi:https://doi.org/10.1029/2008TC002317
Frimmel HE (1995) Metamorphic evolution of the Gariep Belt. S Afr J Geol 98:176–190
Frimmel HE (2000a) New U-Pb zircon ages for the Kuboos pluton in the Pan-African Gariep belt, South Africa: Cambrian mantle plume or far field collision effect? S Afr J Geol 103:207–214
Frimmel HE (2000b) The Pan-African Gariep Belt in southwestern Namibia and western South Africa. Commun Geol Surv Namib 12:197–209
Frimmel HE (2000c) The stratigraphy of the Chameis Sub-terrane in the Gariep Belt in southwestern Namibia. Commun Geol Surv Namib 12:179–186
Frimmel HE (2008a) The Gariep Belt. In: Miller RM (ed) The geology of Namibia. Geological Survey of Namibia, pp 14.11–14.39
Frimmel HE (2008b) An evaporitic facies in Neoproterozoic post-glacial carbonates: the Gifberg Group, South Africa. Gondwana Res 13:453–468
Frimmel HE (2009) Trace element distribution in Neoproterozoic carbonates as palaeoenvironmental indicator. Chem Geol 258: 338–353
Frimmel HE (2010) On the reliability of stable carbon isotopes for Neoproterozoic chemostratigraphic correlation. Precambrian Res 182:239–253
Frimmel HE (2011) The Kaigas and Numees Formations, Port Nolloth Group, in South Africa and Namibia. In: Arnaud E et al (eds) The Geological Record of Neoproterozoic glaciations. Geological Society, London. Memoirs 36:223–231
Frimmel HE, Board WS (2000) Fluid evolution in and around the Rosh Pinah massive sulphide deposit in the external Pan-African Gariep Belt, Namibia. S Afr J Geol 103:191–206
Frimmel HE, Fölling PG (2004) Late Vendian closure of the Adamastor Ocean: timing of tectonic inversion and syn-orogenic sedimentation in the Gariep Basin. Gondwana Res 7:685–699
Frimmel HE, Frank W (1998) Neoproterozoic tectono-thermal evolution of the Gariep Belt and its basement, Namibia/South Africa. Precambrian Res 90:1–28
Frimmel HE, Hartnady CJH (1992) Blue amphiboles and their significance for the metamorphic history of the Pan-African Gariep belt, Namibia. J Metamorph Geol 10:651–669
Frimmel HE, Jiang S-Y (2001) Marine evaporites from an oceanic island in the Neoproterozoic Adamastor ocean. Precambrian Res 105:57–71
Frimmel HE, Jonasson I (2003) The controls on Neoproterozoic base metal sulphide mineralization. In: Eliopoulos DG et al (eds) Mineral exploration and sustainable development. Proceedings of the 7th Biennial SGA Meeting, 24–28 Aug 2003, Athens. Millpress, Rotterdam, pp 661–664
Frimmel HE et al (1996a) Geochemistry and tectonic setting of magmatic units in the Pan-African Gariep Belt, Namibia. Chem Geol 130:101–121
Frimmel HE et al (1996b) New Pb-Pb single zircon age constraints on the timing of Neoproterozoic glaciation and continental break-up in Namibia. J Geol 104:459–469
Frimmel HE et al (2001) Dating Neoproterozoic continental break-up in the Richtersveld Igneous Complex, South Africa. J Geol 109: 493–508
Frimmel HE et al (2002) Neoproterozoic tectonic and climatic evolution recorded in the Gariep Belt, Namibia and South Africa. Basin Res 14:55–67
Frimmel HE et al (2006) Provenance and chemostratigraphy of the Neoproterozoic West Congolian Group in the Democratic Republic of Congo. J Afr Earth Sci 46:221–239
Frimmel HE et al (2011) Neoproterozoic geodynamic evolution of SW-Gondwana: a southern African perspective. Int J Earth Sci 100:323–354
Frimmel HE et al (2013) A new lithostratigraphic subdivision and geodynamic model for the Pan-African western Saldania Belt, South Africa. Precambrian Res 231:218–235
Gaucher C et al (2005) Organic-walled microfossils and biostratigraphy of the upper Port Nolloth Group (Namibia): implications for the latest Neoproterozoic glaciations. Geol Mag 142:539–559
Gaucher C et al (2009) The Neoproterozoic and Cambrian: a time of upheavals, extremes and innovations. In: Gaucher C et al (eds) Neoproterozoic-Cambrian tectonics, global change and evolution: a focus on Southwestern Gondwana. Elsevier, Amsterdam, pp 3–11
Germs GJB (1995) The Neoproterozoic of southwestern Africa, with emphasis on platform stratigraphy and paleontology. Precambrian Res 73:137–151
Germs GJB et al (2009) Syn- to late-orogenic sedimentary basins of southwestern Africa. Neoproterozoic to early Palaeozoic evolution of Southwestern Gondwana. In: Gaucher C et al (eds) Neoproterozoic tectonics, global change and evolution: a focus on Southwestern Gondwana. Elsevier, Amsterdam, pp 183–203
Goscombe B, Gray DR (2007) The coastal terrane of the Kaoko Belt, Namibia: outboard arc-terrane and tectonic significance. Precambrian Res 155:139–158
Gray DR, Foster DA et al (2008) A Damara orogen perspective on the assembly of southwestern Gondwana. In: Pankhurst RJ et al (eds) West Gondwana: pre-Cenozoic correlations across the South Atlantic Region. Geological Society of London, Special Publications, London, 294:279–296
Gresse PG (1992) The tectono-sedimentary history of the Vanrhynsdorp Group. Mem Geol Surv S Afr 79:1–163
Gresse PG (1994) Strain partitioning in the southern Gariep Arc as reflected by sheath folds and stretching lineations. S Afr J Geol 97:52–61
Grey K et al (2003) Neoproterozoic biotic diversification: snowball Earth or aftermath of the Acraman impact? Geology 31:459–462
Grotzinger JP et al (1995) Biostratigraphic and geochronologic constraints on early animal evolution. Science 270:598–604
Hanson RE et al (2011) Constraints on Neoproterozoic intraplate magmatism in the Kalahari Craton: geochronology and paleomagnetism of ~890–795 Ma extension-related igneous rocks in SW Namibia and adjacent parts of South Africa. Geological Society of America Annual Meeting, 9–12 Oct 2011, Minneapolis, Paper No. 7
Hälbich IW, Alchin DJ (1995) The Gariep belt: stratigraphic-structural evidence for obliquely transformed grabens and back-folded thrust stacks in a combined thick-skin thin-skin structural setting. J Afr Earth Sci 21:9–33
Halverson GP et al (2005) Towards a Neoproterozoic composite carbon isotope record. Geol Soc Am Bull 117:1181–1207
Hegenberger W (1993) Stratigraphy and sedimentology of the Late Precambrian Witvlei and Nama Groups, east of Windhoek. Mem Geol Surv Namib 17:1–82
Hoffmann K-H et al (2004) A U-Pb zircon date from the Neoproterozoic Ghaub formation, Namibia: constraints on Marinoan glaciation. Geology 32:817–820
Hofmann M et al (2014) The Namuskluft and Dreigratberg sections in southern Namibia (Kalahari Craton, Gariep Belt): a geological history of Neoproterozoic rifting and recycling of cratonic crust during the dispersal of Rodinia until the amalgamation of Gondwana. Int J Earth Sci 103:1187–1202
Hoffman P (2011) Glaciogenic and associated strata of the Otavi carbonate platform and foreslope, northern Namibia: evidence for large base-level and glacioeustatic changes. In: Arnaud E et al (eds)

The Geological Record of Neoproterozoic Glaciations. Geological Society of London. Memoirs, vol 36, pp 195–209
Hoffman PF, Schrag DP (2002) The snowball Earth hypothesis: testing the limits of global change. Terra Nova 14:129–155
Hoffman PF et al (1998) Comings and goings of global glaciations on a Neoproterozoic tropical platform in Namibia. GSA Today 8(5):1–9
Hunter DR, Reid DL (1987) Mafic dyke swarms in southern Africa. In: Halls HC, Fahrig WF (eds) Mafic dyke swarms. Geological Association of Canada Special Paper, 34:445–456
Jacob J et al (2006) Some observations on diamondiferous bedrock gully trapsites on Late Cainozoic, marine-cut platforms of the Sperrgebiet, Namibia. Ore Geol Rev 28:493–506
Jiang G et al (2007) Carbon isotope variability across the Ediacaran Yangtze platform in South China: implications for a large surface-to-deep ocean $\delta^{13}C$ gradient. Earth Planet Sci Lett 361:303–320
Kaiser E (1926) Die Diamanten Wüste. Dietrich Reimer, Berlin, 321 pp
Kennedy MJ (2001) Are Proterozoic cap carbonates and isotopic excursions a record of gas hydrate destabilization following Earth's coldest intervals? Geology 29:443–446
Knoll AH (2000) Learning to tell Neoproterozoic time. Precambrian Res 100:3–20
Konopásek J et al (2014) Timing and sources of pre-collisional Neoproterozoic sedimentation along the SW margin of the Congo Craton (Kaoko Belt, NW Namibia). Gondwana Res 26:386–401
Konopásek J et al (2016) Linking the basement geology along the Africa-South America coasts in the South Atlantic. Precambrian Res 280:221–230
Kröner A (1974) The Gariep Group, part I: late Precambrian formations in the western Richtersveld, northern Cape Province. Precambrian Research Unit, University of Cape Town. Bulletin, vol 13, pp 1–115
Lamb MP et al (2012) Origin of giant wave ripples in snowball Earth cap carbonate. Geology 40:827–830
Lenz C et al (2011) U-Pb SHRIMP ages for the Cerro Bori orthogneisses, Dom Feliciano Belt in Uruguay: evidences of a ~800 Ma magmatic and ~650 Ma metamorphic event. Precambrian Res 185:149–163
Lohmeyer M (2013) Methodische Entwicklung GIS-basierter geogener Rohstoffpotentialkarten am Beispiel des südwestlichen Namibia. Unpublished MSc thesis, Institute of Geography and Geology, University of Würzburg, 109 p
Macdonald FA et al (2010) Stratigraphy of the Port Nolloth Group of Namibia and South Africa and implications for the age of Neoproterozoic iron formations. Am J Sci 310:862–888
Macey PH et al (2017) Origin and evolution of the ~1.9 Ga Richtersveld magmatic Arc, SW Africa. Precambrian Res 292:417–451
McMillan MD (1968) The geology of the Witputs-Sendelingsdrif area. Precambrian Research Unit, University of Cape Town. Bulletin, vol 4, pp 1–177
Martin H (1965) The Precambrian geology of South West Africa and Namaqualand. Precambrian Research Unit, University of Cape Town. Bulletin, vol 4, pp 1–177
Master S, Wendorff M (2011) Neoproterozoic diamictites of the Katanga Supergroup, Central Africa. In: Arnaud E et al (eds) The Geological Record of Neoproterozoic Glaciations, Geological Society London. Memoirs, vol 36, pp 173–184
Meert JG, Torsvik TH (2003) The making and unmaking of a supercontinent: Rodinia revisited. Tectonophysics 375:261–288
Middlemost EAK (1963) Geology of the southeastern Richtersveld. PhD thesis, University of Cape Town, Cape Town
Middlemost EAK (1966) The genesis of the Stinkfontein Formation. Trans Geol Soc S Afr 69:87–98
Miller RM (2013) Comparative stratigraphic and geochronological evolution of the northern Damara Supergroup in Namibia and the Katanga Supergroup in the Lufilian Arc of Central Africa. Geosci Can 40:118–140
Oriolo S et al (2016a) The Nico Pérez Terrane (Uruguay): from Archean crustal growth and connections with the Congo Craton to late Neoproterozoic accretion to the Río de la Plata Craton. Precambrian Res 280:147–160
Oriolo S et al (2016b) Timing of deformation in the Sarandí del Yí Shear Zone, Uruguay: implications for the amalgamation of the Western Gondwana during the Neoproterozoic Brasiliano–Pan-African Orogeny. Tectonics 35. http://dx.doi.org/10.1002/2015TC004052
Oriolo S et al (in press) Contemporaneous assembly of Western Gondwana and final Rodinia break-up: Implications for the supercontinent cycle. Geosci Front. doi:http://dx.doi.org/10.1016/j.gsf.2017.01.009
Oyhantçabal P et al (2009) Geochronological constraints on the evolution of the southern Dom Feliciano Belt (Uruguay). J Geol Soc Lond 166:1075–1084
Pimentel MM et al (2000) The basement of the Brasilia Fold Belt and the Goiás Magmatic Arc. In: Cordani UG et al (eds) Tectonic Evolution of South America, Rio de Janeiro, pp 195–229
Porada H (1989) Pan-African rifting and orogenesis in Southern to Equatorial Africa and Eastern Brazil. Precambrian Res 44:103–136
Prave AR et al (2011) The Witvlei Group of east-central Namibia. In: Arnaud E et al (eds) The Geological Record of Neoproterozoic Glaciations. Geological Society of London. Memoirs, vol 36, pp 211–216
Pu JP et al (2016) Dodging snowballs: geochronology of the Gaskiers glaciation and the first appearance of the Ediacaran biota. Geology 44:955–958
Ransome IGD (1992) The geochemistry, kinematics and geodynamics of the Gannakouriep dyke swarm. MSc thesis, University of Cape Town, Cape Town, 182 pp
Reid DL (1991) Alkaline rocks in the Kuboos-Bremen igneous province, southern Namibia: the Kanabeam multiple ring complex. Commun Geol Surv Namib 7:3–13
Reid DL et al (1991) Time of emplacement and metamorphism of Late Precambrian mafic dykes associated with the Pan-African Gariep orogeny, Southern Africa: implications for the age of the Nama Group. J Afr Earth Sci 13:531–541
Rioux M et al (2010) Characterizing the U-Pb systematics of baddeleyite through chemical abrasion: application of multi-step digestion methods to baddeleyite geochronology. Contrib Miner Petrol 160:777–801
Ritter U (1980) The Precambrian evolution of the eastern Richtersveld. Precambrian Research Unit, University of Cape Town. Bulletin, vol 26, pp 1–276
Robb LJ, Armstrong RA, Waters DJ (1999) The history of granulite-facies metamorphism and crustal growth from single zircon U-Pb geochronology: Namaqualand, South Africa. J Petrol 40:1747–1770
Rogers AW (1916) The geology of part of Namaqualand. Trans Geol Soc S Afr 18(1915):72–101
Rooney AD et al (2015) A Cryogenian chronology: two long-lasting synchronous Neoproterozoic glaciations. Geology 43:459–462
Schmid S (2017) Neoproterozoic evaporites and their role in carbon isotope chemostratigraphy (Amadeus Basin, Australia). Precambrian Res 290:16–31
Smithies RH, Marsh JS (1996) Alkaline rocks in the Kuboos-Bremen Igneous Province, southern Namibia: the Grootpenseiland and Marinkas Kwela Complexes. Commun Geol Surv Namib 11:13–20
Söhnge PG, de Villiers J (1948) The Kuboos Pluton and its associated line of intrusives. Trans Geol Soc S Afr 51:1–31
Tack L et al (2001) Early Neoproterozoic magmatism (1000–910 Ma) of the Zadinian and Mayumbian Groups (Bas-Congo): onset of

Rodinia rifting at the western edge of the Congo craton. Precambrian Res 110:277–306

Thomas RJ et al (2016) The Sperrgebiet Domain, Aurus Mountains, SW Namibia: A ~ 2020–850 Ma window within the Pan-African Gariep Orogen. Precambrian Res 286:35–58

Vidal G, Moczydlowska-Vidal M (1997) Biodiversity, speciation, and extinction trends of Proterozoic and Cambrian phytoplankton. Paleobiology 23:230–246

Von Veh MW (1993) The stratigraphy and structural evolution of the Late Proterozoic Gariep Belt in the Sendelingsdrif-Annisfontein area, northwestern Cape Province. Precambrian Research Unit, University of Cape Town. Bulletin, vol 38, pp 1–174

Wackerle R (2003) High resolution airborne geophysical survey program: TMI colour image. Geological Survey of Namibia, Windhoek

Waters DJ et al (1983) A suggested reinterpretation of Namaqua basement and cover rocks south and west of Bitterfontein. Trans Geol Soc S Afr 86:293–299

Will T et al (2014) Geochemical and isotope evidence for initiation of Cretaceous South Atlantic opening along a former Neoproterozoic back-arc basin: implications for the location of the main Pan-African suture in southwest Gondwana. Lithos 202–203: 363–381

14 The Stratigraphy and Structure of the Western Saldania Belt, South Africa and Geodynamic Implications

Alexander Kisters and Richard Belcher

Abstract

The western Saldania belt in South Africa exposes a section through a fore-arc region that records deformation, sedimentation and plutonism in the late Neoproterozoic and Cambrian (>560 to <510 Ma) along the obliquely convergent continental margin of the Kalahari Craton. The belt comprises two main and structurally overlying units. Imbricated and pervasively transposed marine metasediments and relics of oceanic crust constitute the structurally lower Swartland complex. Kinematics and strains indicate formation of the accretionary complex during tectonic underplating and top-to-the west and northwest thrusting related to the southeast-directed subduction of the Adamastor ocean below the Kalahari Craton. The Swartland complex is unconformably overlain by low-grade metamorphic metasediments and minor metavolcanic rocks of the Malmesbury group that represent the late-Neoproterozoic to Cambrian fore-arc basin fill. Sedimentary facies suggest the presence of a volcanic arc in the east, succeeded in the west by metaturbidites of the inner fore-arc basin and deeper-water metapelitic successions in the northwest interpreted to form slope-apron deposits overlying the toe of the prim and facing the ocean basin. The regional deformation of the fore arc is characterized by partitioned sinistral transpression related to oblique convergence. The absence of collisional structures and very limited exhumation of the rocks suggest a soft collisional event, probably as a result of slab break-off. This break-off may also account for the voluminous, syn- to late-tectonic plutonism of the Cape Granite Suite in the fore-arc region, peaking around 540–530 Ma and accompanying the waning stages of regional tectonism.

Keywords

Saldania belt • Accretionary complex • Fore-arc basin
Partitioned transpression • Granite plutonism

14.1 Introduction

The Saldania belt is an arcuate fold belt along the southern tip of Africa (Fig. 14.1) and part of the larger system of Pan-African belts that led to the assembly of southwest Gondwana in the late Neoproterozoic and early Palaeozoic (e.g., Hartnady et al. 1985; Gaucher et al. 2009). In southern Africa, the chronology and geological evolution of these events are well documented from the better exposed coastal Kaoko, Gariep and Vanrhynsdorp belts (e.g., Von Veh 1983, 1993; Gresse 1994; Frimmel and Frank 1998; Goscombe et al. 2003; Basei et al. 2005; Konopasek et al. 2005; Goscombe and Gray 2008; Miller 2008). Lithological sequences, metamorphic P–T paths and sinistral transpressive tectonics record the oblique and diachronous closure of oceanic basins culminating in the collision of South American cratons and intervening arc terranes with the Kalahari and Congo Cratons in Africa (Fig. 14.1). A similarly well-constrained depositional and kinematic framework has not been established for the southernmost Saldania belt. Poor outcrop conditions, the apparent monotony of supracrustal sequences and uniformly low grades of metamorphism have resulted in a number of contrasting views about the tectonostratigraphic make-up and overall geodynamic setting of the belt (Hartnady et al. 1974; Von Veh 1983; Rozendaal et al. 1999; Belcher and Kisters 2003; Gresse et al. 2006; Frimmel 2009; Frimmel et al. 2011, 2013; Buggisch et al. 2010; Rowe et al. 2010). This has prevented regional correlations with similarly old belts to the north so that the Saldania belt has only featured sporadically and commonly controversially

A. Kisters (✉) · R. Belcher
Department of Earth Sciences, University of Stellenbosch, Stellenbosch, South Africa
e-mail: akisters@sun.ac.za

Present Address:
R. Belcher
RWB Exploration Ltd, Mottram House, 43 Greek Street, Stockport, SK3 8AX, UK

S. Siegesmund et al. (eds.), *Geology of Southwest Gondwana*, Regional Geology Reviews,
https://doi.org/10.1007/978-3-319-68920-3_14

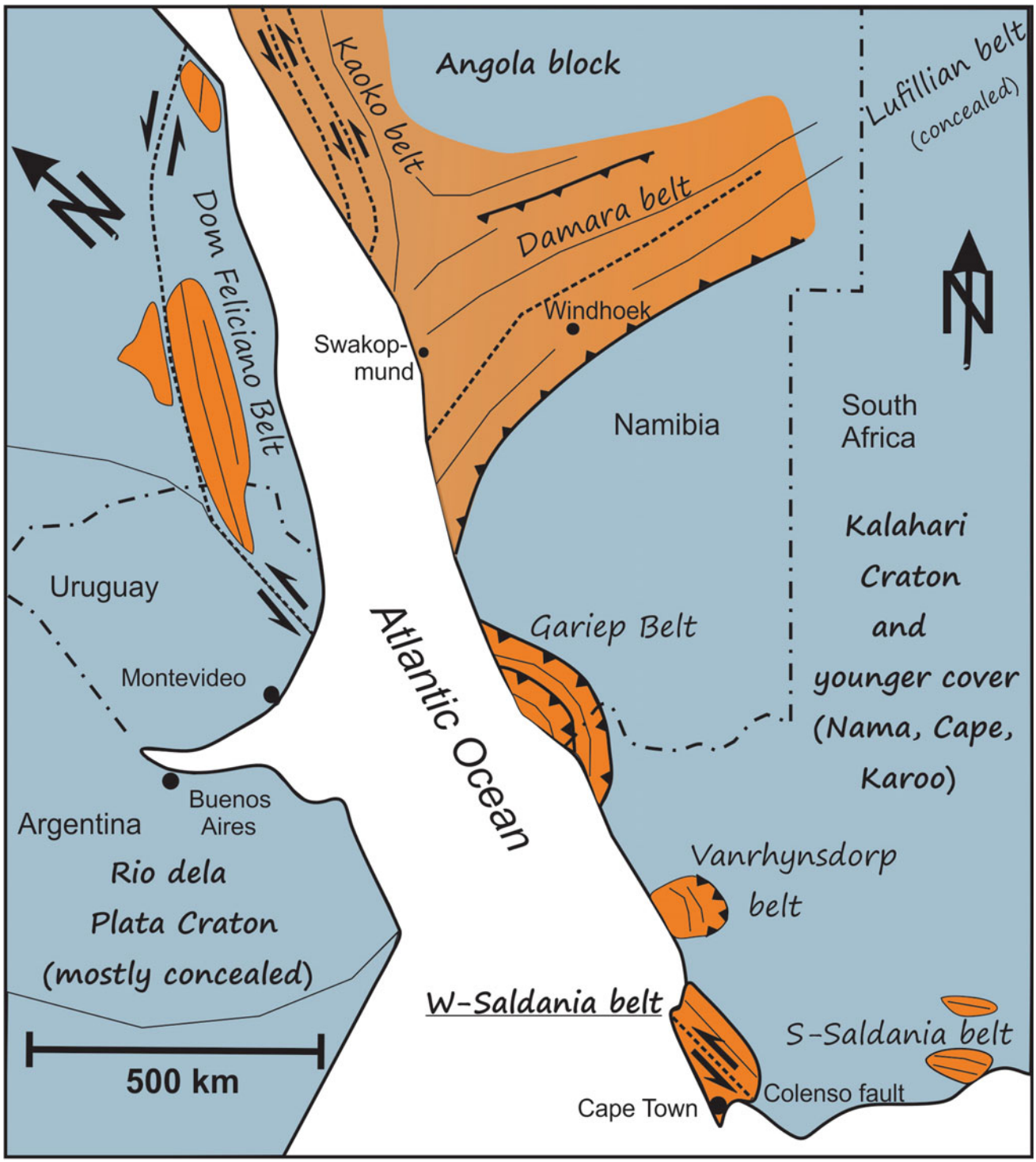

Fig. 14.1 Location of Neoproterozoic and Cambrian orogenic belts (orange) in the broader context of SW Gondwana in southern Africa and eastern South America (simplified after Rapela et al. 2011; Frimmel et al. 2013; Oriolo et al. 2016). Major strike-slip and thrust fault zones are shown and thin, solid lines indicate generalized structural formlines and trends

discussed in paleogeographic reconstructions of southwest Gondwana (e.g., Gaucher et al. 2009; Miller et al. 2009; Frimmel et al. 2011; Rapela et al. 2011).

The Saldania belt (sensu lato) is made up of an east–west trending southern branch and a northerly trending western branch (Fig. 14.1) (Gresse et al. 2006). This contribution focuses on the western branch of the Saldania belt stretching from Cape Town in the south to north of the coastal town of Saldanha from which the belt derives its name (Fig. 14.2). This part documents sedimentation, plutonism and deformation in what probably represented the eastern realm of the Adamastor ocean or related oceanic basins along the western margin of the Kalahari Craton in pre-Gondwana times. Our understanding of the geology of the western Saldania belt has been fundamentally influenced by the benchmark paper by Hartnady et al. (1974), which proposed the belt to be underlain by three allochthonous or para-autochthonous domains or terranes separated by prominent and supposedly terrane bounding strike-slip fault zones (Fig. 14.2). This view also forms the basis for currently accepted lithostratigraphic subdivisions that discuss the stratigraphy of the belt in terms of distinct, fault-bounded tectonostratigraphic packages (e.g., South African Committee for Stratigraphy (SACS) 1980; Gresse et al. 2006; Table 14.1). Despite this, the term 'Malmesbury Group' has been retained for the supracrustal succession across purported terrane boundaries and the belt in its entirety. This is obviously not without problems and also acknowledges lithological and structural similarities of rocks in large parts of the belt. Moreover, the uniformly low grades of metamorphism, contiguity of structures without any major breaks and similar age of rocks are not indicative of the presence of distinct terranes. As a result, not only the extent and delineation of terranes (Frimmel 2009; Frimmel et al. 2011, 2013; Buggisch et al. 2010) but also the presence of distinct tectonostratigraphic domains (Belcher 2003; Belcher and Kisters 2003) have been questioned. This highlights our only rudimentary understanding of the structural geology and lithostratigraphic relationships and, as a result, the rather diverse interpretations of original depositional environments and geodynamic setting of the belt.

The primary purpose of this chapter is to review the structural and lithological inventory of the belt with a view to integrating some of the conflicting interpretations and unresolved controversies that surround the geology of the belt. For this we intend to highlight similarities and/or differences of lithological packages and regional strains, particularly across purported terrane boundaries, and against a background of more recent geochronological, petrographic and structural data (e.g., Villaros et al. 2009; Rowe et al. 2010; Farina et al. 2012; Frimmel et al. 2013), and our own work. It is not our aim to provide a new stratigraphic subdivision but rather to suggest a geological framework that acknowledges lithological affinities and reconciles distinct structural domains within the belt. We hope this will allow for a better integration of the western Saldania belt into the broader framework of Pan-African belts in southwest Gondwana.

14.2 The Main Geological Characteristics of the Western Saldania Belt

The western Saldania belt is a low-grade metamorphic fold belt underlain by supracrustal rocks collectively referred to as the Malmesbury Group. Aerially extensive syn-, late- and post-tectonic granites of the 550–510 Ma Cape Granite Suite (CGS) are intrusive into the Malmesbury Group (Fig. 14.2). The group comprises a late Neoproterozoic, predominantly clastic marine sedimentary succession. Mafic to felsic metavolcanic rocks are volumetrically minor and are either intrusive or structurally interleaved with the metasediments (Hartnady et al. 1974; Theron et al. 1992; Slabber 1995; Gresse et al. 2006). Following Hartnady et al. (1974), the Saldania belt has been subdivided into three tectonostratigraphic domains or terranes: a southwestern Tygerberg, a central Swartland and a northeastern Boland terrane (Fig. 14.2). The former two are separated by the prominent Colenso fault zone, whereas the Swartland is interpreted to be separated from the Boland terrane by the Piketberg-Wellington fault (Fig. 14.2). Detrital zircon ages (Armstrong et al. 1998; Frimmel et al. 2013) and zircon crystallization ages from intercalated tuffs (Kisters et al. 2015) indicate a depositional age of *c*. 560–555 Ma for at least the upper parts of the Malmesbury Group. The base of the group is not exposed anywhere and the thickness and upper age of the sequence as well as the nature of the basement remain elusive.

The second and characteristic component of the belt are voluminous S- and minor I- and A-type granites of the CGS. The granites crosscut regional folds and fabrics, and are largely devoid of magmatic or solid-state fabrics. This has commonly been suggested to indicate a late- to post-tectonic emplacement of the CGS (e.g., Scheepers 1995; Scheepers and Schoch 2006). In contrast, granites that have intruded into or along prominent fault zones are invariably deformed and gneissic. The most prominent example of this synmagmatic deformation is the large Darling batholith that has intruded the central Colenso fault zone over a strike length of more than 40 km (Fig. 14.2). The deformation of the granites illustrates not only the syntectonic timing of at least parts of the CGS but also the pronounced regional-scale partitioning of strain in the belt (Kisters et al. 2002). U-Pb zircon ages indicate emplacement of the granites between *c*. 550 and 510 Ma with a peak of plutonic activity between *c*. 540 and 530 Ma (Schoch 1975; Scheepers 1995; Da Silva

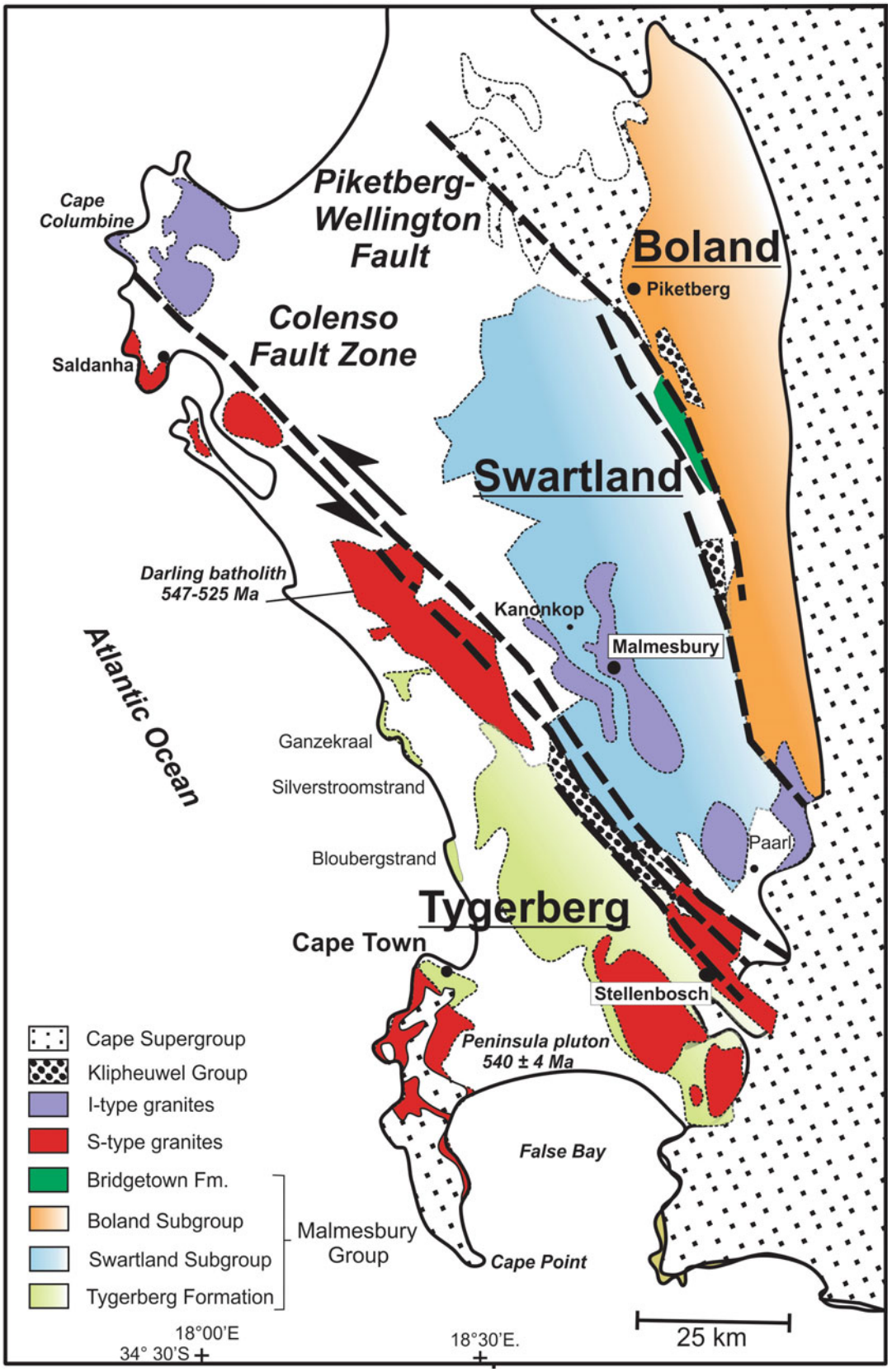
Cape Columbine
Piketberg-Wellington Fault
Boland
Piketberg
Colenso Fault Zone
Saldanha
Swartland
Darling batholith 547-525 Ma
Kanonkop
Malmesbury
Atlantic Ocean
Ganzekraal
Silverstroomstrand
Bloubergstrand
Paarl
Tygerberg
Cape Town
Stellenbosch
Peninsula pluton 540 ± 4 Ma
False Bay
Cape Point
Cape Supergroup
Klipheuwel Group
I-type granites
S-type granites
Bridgetown Fm.
Boland Subgroup
Swartland Subgroup
Tygerberg Formation
Malmesbury Group
18°00'E
34° 30'S
18°30'E.
25 km

◀ **Fig. 14.2** Schematic geological map of the western Saldania belt showing the currently accepted subdivision of the belt into three tectonostratigraphic domains or terranes (Tygerberg, Swartland and Boland), separated by strike-slip faults and intruded by plutons of the Cape Granite Suite (modified after Rozendaal et al. 1999; Gresse et al. 2006). Note that the extent of and contacts between geological formations are largely inferred given the very poor outcrop conditions. Blank areas on the map correspond to regions with less than 1% outcrop. Locations mentioned in the text are shown

et al. 2000; Scheepers and Schoch 2006; Villaros et al. 2009; Chemale et al. 2011; Farina et al. 2012). These intrusion ages also emphasize the only short timespan between the deposition, deformation and metamorphism of the Malmesbury Group and the onset of CGS plutonism. On a regional scale, earlier S-type granites are confined to the southwest of the Colenso Fault and the Tygerberg domain. I-type granites are only found east of the Colenso Fault and mainly in the Swartland domain (Fig. 14.2). The distribution of geochemically distinct granite suites on either side of the Colenso fault probably indicates the transcrustal extent of the fault zone, but has also been used to reiterate the terrane model for the belt (Rozendaal et al. 1999; Kisters et al. 2002; Frimmel et al. 2013).

The third but volumetrically minor lithological component of the belt are rocks of the Klipheuwel Group. The mainly clastic sedimentary rocks are somewhat transitional between the Pan-African basement of the Malmesbury Group and CGS, and the Paleozoic Cape Supergoup. Rocks of the Klipheuwel Group unconformably overlie folded strata of the Malmesbury Group and plutons of the CGS but are located below the regional unconformity with the overlying Cape Supergroup. For the most part, Klipheuwel Group rocks are confined to isolated, fault-bounded basins (Fig. 14.2). The rocks show steep dips, but it is not clear whether these strains are late-Pan-African or Permo-Triassic in age and part of the later Gondwanide evolution that has affected the southwest parts of the Gondwana supercontinent.

Structurally, the western Saldania belt is, for the most part, developed as a fold belt comprising northerly- to northwesterly-trending, gently doubly plunging, open to isoclinal and more or less upright to southwest-verging folds (F2) (Rabie 1948; Theron et al. 1992; Gresse et al. 2006; Rowe et al. 2010). Regional-scale thrusts have not been mapped, although this may be a function of the subdued topography and very limited outcrop. Domains of more complex low-angle fabrics (D1 fabric domains) and intensely disrupted stratigraphy are preserved in structural windows in the central parts of the belt, in the Swartland domain (Figs. 14.2 and 14.3) (Rabie 1948; Newton 1966; Hartnady et al. 1974; Belcher 2003; Belcher and Kisters 2003). Owing to the very poor outcrop conditions, the significance of these high-strain domains, their extent and also their contact relationship with the structurally overlying, relatively simple fold belt have not been resolved. The most prominent structural features of the belt are the northwesterly-trending subvertical Colenso and the less prominent Piketberg-Wellington fault zones (Rabie 1948, 1974; Schoch 1975; Theron et al. 1992; Kisters et al. 2002). Sinistral strike-slip kinematics are widely documented from the Colenso fault (Kisters et al. 2002) and an oblique slip, east-side up component is suggested by the deeper structural levels exposed on the eastern side of the fault (e.g., Hartnady et al. 1974; Rozendaal et al. 1999; Gresse et al. 2006). The location of the Piketberg-Wellington is largely inferred over much of its strike extent (Rabie 1974; Theron et al. 1992; Slabber 1995). Demonstrable displacement along the fault strands can only be shown to have affected the Paleozoic Cape Supergroup with a downthrow to the east (e.g., Belcher 2003).

Recent research has mainly focused on the delineation of actual tectonostratigraphic domains or terranes, and the original terrane model for the belt has undergone several permutations. Frimmel (2009) and Frimmel et al. (2011) suggest only the southwestern Tygerberg to represent a truly allochthonous terrane, separated from the autochthonous Swartland and Boland terranes by the Colenso fault zone. Buggisch et al. (2010) place the terrane boundary to the northeast and along the Piketberg-Wellington fault. The study by Buggisch et al. (2010) postulates the amalgamation of the Tygerberg and Swartland terranes against the Boland terrane during westward subduction and closure of an ocean basin. Supposed relics of this ocean basin are preserved as the metamafic Bridgetown Formation (Fig. 14.2; Table 14.1) between the Boland and Swartland terranes. In this scenario, the Swartland and Tygerberg terranes are suggested to have been part of South American cratons, whereas the Boland terrane represented the passive margin of the Kalahari Craton. Frimmel et al. (2013) report results of a detrital zircon study sampling different formations throughout large parts of the belt. The results indicate deposition of the rocks in the late Neoproterozoic, up to *c*. 560 Ma. However, zircon age spectra in the Boland domain show a far more prominent population of Mesoproterozoic zircons compared with the Tygerberg and Swartland domains that are dominated by Ediacaran-age zircons. Based on this, Frimmel et al. (2013) suggest a largely contemporaneous sedimentation of the rocks in the latest Neoproterozoic, but in two distinct basins and the two southwestern domains to represent part of a contiguous block, termed the Malmesbury terrane. In this scenario, the Piketberg-Wellingon fault is advocated as the main terrane boundary, separating the Malmesbury terrane in the southwest from an autochthonous Boland domain in the northeast. The results of the detrital zircon study also underline the similar late-Neoproterozoic timing of sedimentation in the Saldania belt and parts of the Gariep belt to the north (Fölling et al. 2002). Given the back-arc setting inferred for

Table 14.1 Synopsis of recent stratigraphic subdivisions suggested for the western Saldania belt following Gresse et al. (2006) and Frimmel et al. (2013)

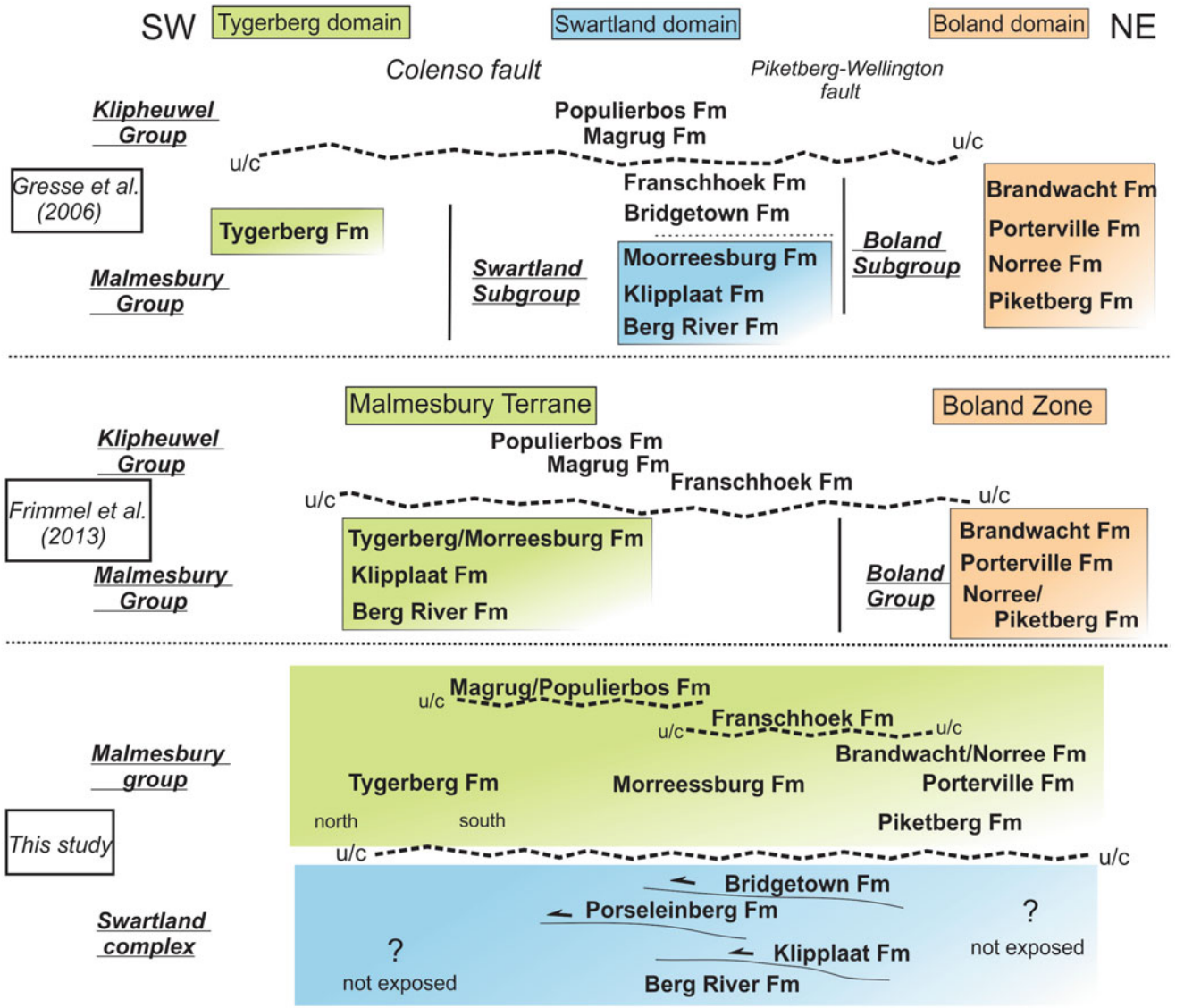

Formation names are those approved by SACS (1980). The subdivision suggested in this study is based on these formations but emphasizes the contiguity and similarities and/or differences of former lithological subdivisions and formations across purported terrane boundaries. The main difference from formerly accepted lithostratigraphic subdivisions is the recognition of a major tectonostratigraphic break between the two structurally overlying but similarly old packages of the Swartland complex and Malmesbury group fore-arc deposits

Note that formation names are taken from the officially approved lithostratigraphic subdivision of the Saldania belt (SACS 1980) but have not yet been approved in the form suggested here

the upper Gariep Supergoup (e.g., Basei et al. 2005), Frimmel et al. (2013) suggest a similar depositional setting for the Malmesbury Group having formed in the same back-arc realm to the east of the Dionisio Cuchilla-Pelotas magmatic arc (Fig. 14.1), now situated in the Dom Feliciano Belt of northeastern Brazil and Uruguay. In contrast to this, regional studies have long maintained similarities and rather gradual contacts of rocks of the Malmesbury Group and the contiguity of structures and similar metamorphic grades across the main fault zones (Rabie 1948; Von Veh 1983; Rozendaal et al. 1999; Belcher 2003; Belcher and Kisters 2003; Rowe et al. 2010). These studies rather advocate the autochthonous nature of the Saldania belt and its development along the western margin of the Kalahari Craton. The Colenso Fault is recognized as a regional-scale fault zone and significant structural break, but not as a terrane bounding fault.

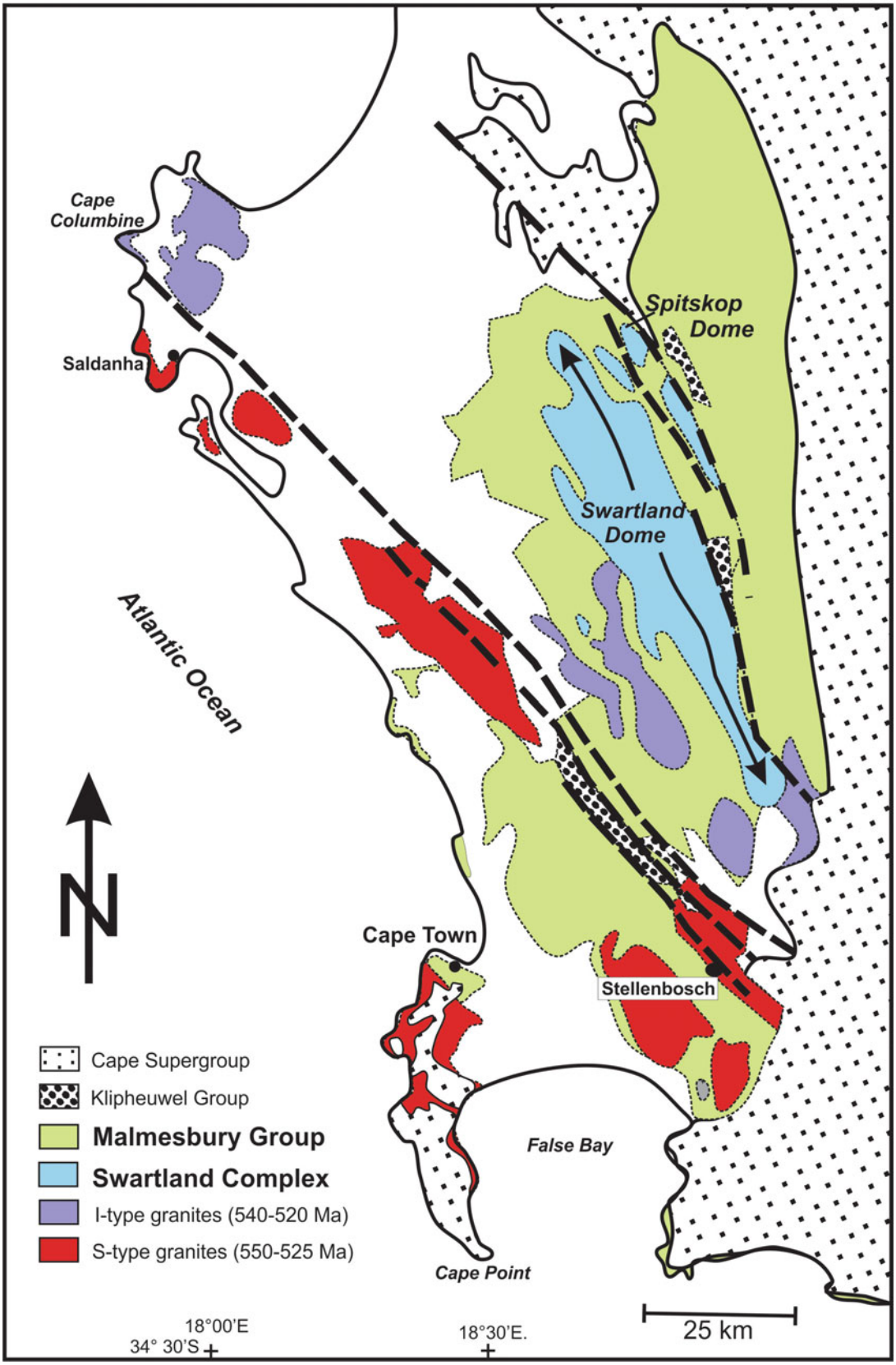

Fig. 14.3 Geological map of the western Saldania belt, as in Fig. 14.2 but highlighting the distribution of structural and lithological packages extending across purported terrane boundaries, emphasizing the presence of two structurally overlying packages, a lower Swartland complex and an upper Malmesbury group. Note that these terms are not officially approved by SACS. Details of this subdivision, and lithological and structural affinities within these two overlying domains, are discussed in the text

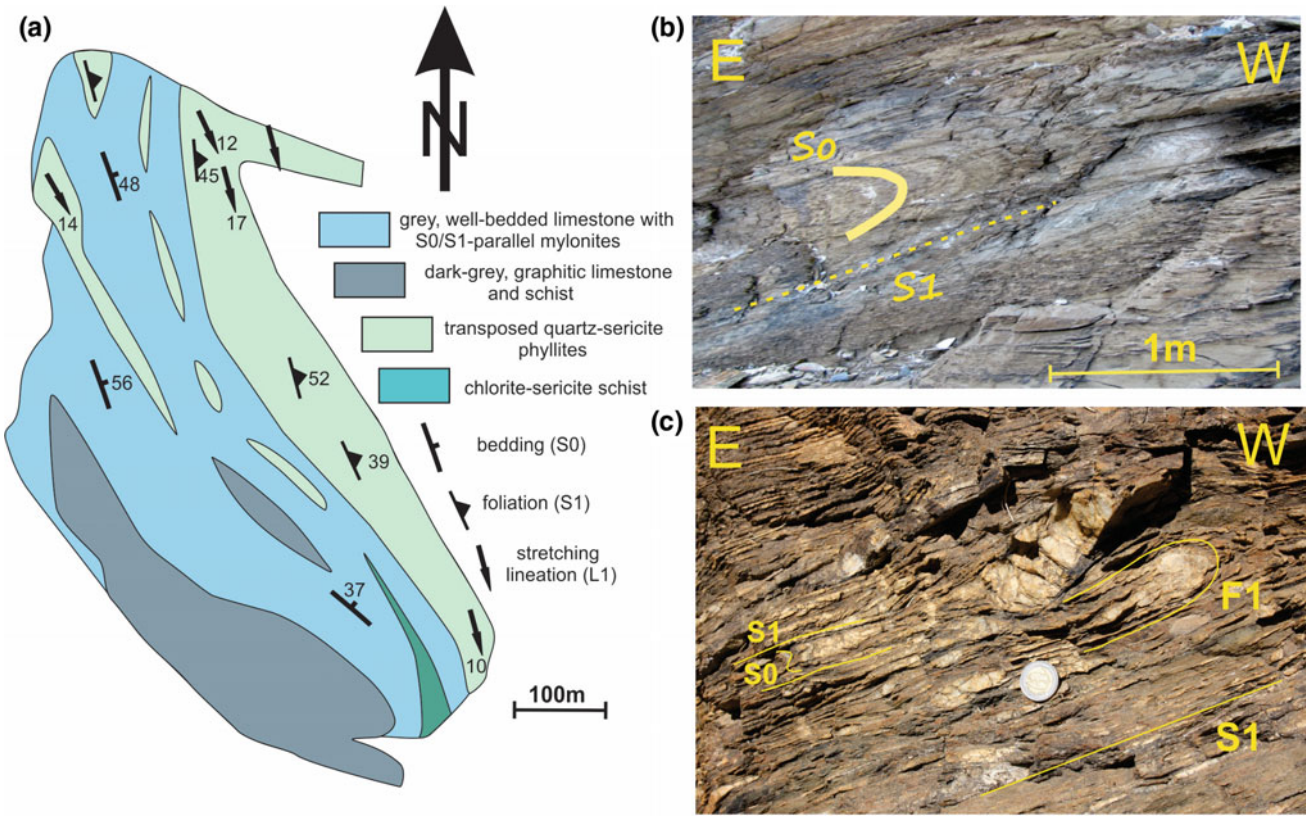

Fig. 14.4 **a** The lithological heterogeneity and complexity of rocks of the Swartland complex are best observed in quarry operations, illustrated here by the simplified geological map of the De Hoek quarry, outside Piketberg. Contacts between units are almost exclusively structural in nature, transposed into parallelism with the pervasive S1 foliation. The quarry is located on the steep northeast-dipping limb of a later (F2), large-scale fold, the Spitskop Dome (Fig. 14.3), which accounts for the steep dips of bedding (S0) and the foliation (S1). **b** Oblique cross-sectional view (to the southeast) of a metre-scale, isoclinal fold (F1) that refolds bedding (S0), enveloped by the pervasive S1 axial planar foliation (De Hoek Quarry, Piketberg). F1 folds are observed on a centimetre to metre scale and indicate the near-pervasive transposition of original bedding features in rocks of the Swartland complex into the subhorizontal S1 foliation. **c** Oblique cross-sectional view of a quartz-rich phyllite illustrating the progressive transposition of fabric elements into the composite S1 foliation in rocks of the Swartland complex (here taken from a roadcut at Bothmaskloof Pass, outside Riebeck Kasteel). Tightly folded bedding laminations (S0, left-hand side) and centimetre-scale, isoclinally folded (F1), rootless quartz veins (annotated by fine yellow line) are transposed into the pervasive S1 foliation. The dismembered, asymmetric quartz vein at the centre suggests deformation during top-to-the west shearing. Coin for scale is 2.5 cm in diameter

This brief synopsis highlights some of the discrepancies in our understanding of the overall structural evolution, but also stratigraphic framework, of the belt. The present review focuses on the structural inventory and lithological similarities or differences of sequences across purported terrane boundaries. Previous regional works have hinted at the presence of two overlying domains in the belt with distinct lithological and structural inventories and strain histories (Rabie 1948; Newton 1966; Hartnady et al. 1974; Belcher 2003; Belcher and Kisters 2003). These domains extend across the large strike-slip faults in the belt (Fig. 14.3), a view supported by the recent detrital zircon study by Frimmel et al. (2013). The upper and structurally seemingly more simple domain covers most of the Saldania belt and encompasses the former Tygerberg terrane, parts of the central Swartland and large parts of the eastern Boland terrane (Fig. 14.3). The lower domain is structurally more complex and lithologically hetereogeneous, and while strains are clearly regional, neither the significance nor the structural relationship between the two domains are fully understood.

14.3 Lithostratigraphic and Structural Relationships in the Western Saldania Belt

14.3.1 Lithological Inventory of the Lower Domain: The Swartland Complex

Rocks of the lower domain are mainly exposed in the cores of the regional-scale antiforms (F2 folds) of the Swartland

and Spitskop domes (Fig. 14.3) that provide windows into the lower structural levels of the belt (e.g., Rabie 1948, 1974; Newton 1966; Hartnady et al. 1974; Belcher 2003). Lower domain rocks broadly correspond to the Swartland Subgroup of previous subdivisions (SACS 1980; Gresse et al. 2006), including the Berg River and Klipplaat formations (Table 14.1). The two formations form supposedly more or less coherent stratigraphic packages distinguished by varying abundances of metapsammites versus metapelites. However, regional mapping cannot confirm the presence of laterally continuous lithological packages or marker units, and there seems little or no correlation of sequences between outcrops (Belcher 2003; Belcher and Kisters 2003). We also include the lower parts of the Morreesburg Formation, previously known as the Porseleinberg Formation (Hartnady et al. 1974), and metamafic rocks of the Bridgetown Formation into the lower domain. Importantly and in contrast to accepted subdivisions (e.g., SACS 1980), we consider the largest parts of the regionally widespread Morreesburg Formation not to be part of this lower domain or the Swartland Subgroup, rather forming part of the upper domain (see below). Given the degree of structural dismemberment, a subdivision of lower domain rocks into formations is a rather moot point and the rocks rather form part of a tectonostratigraphic complex, henceforth referred to as the Swartland complex (Fig. 14.3; Table 14.1).

Lithologically, the Swartland complex comprises a heterogeneous assemblage of quartz-sericite and chlorite-muscovite schists and phyllites, chlorite- and talc-carbonate schists, quartzites and muscovite quartzites, highly sheared chert horizons, graphitic schists and limestones, and grey, massive to well-bedded limestones (Fig. 14.4a) (Rabie 1948, 1974; Hartnady et al. 1974; SACS 1980; Theron et al. 1992; Belcher 2003; Belcher and Kisters 2003; Gresse et al. 2006). The main distinguishing characteristic of the Swartland complex in outcrop is the presence of a pervasively developed bedding-parallel phyllitic foliation (S1; see below) (Fig. 14.4b, c). Primary bedding is preserved in more competent units such as limestones or quartzites, but is largely obliterated by the pervasive S1 foliation and bedding transposition in metapelitic schists and phyllites (Fig. 14.4b). A further characteristic is the abundance of foliation (S1) parallel and mostly transposed quartz and quartz-carbonate veins (Fig. 14.4c). Quartz veins may constitute up to 20 vol.% of individual outcrops and testify to the pervasive fluid flow during formation of the bedding-parallel foliation and bedding transposition.

Despite the pervasive fabrics, the predominantly metapelitic sequence and interlayered metapsammite units preserve characteristics of an originally marine, probably metaturbiditic succession (Theron et al. 1992; Belcher 2003). A marine origin can also be inferred for the structurally interleaved graphitic schists and limestones. Chlorite and talc-carbonate schists are interpreted as altered mafic metavolcanic rocks (Rozendaal et al. 1994; Slabber 1995; Gresse et al. 2006). These chlorite schists are volumetrically minor but common throughout the Swartland complex. In quarries and in borehole sections the metamafic rocks form up to several metres thick, typically isolated lens-like bodies enveloped by the S1 foliation (Rozendaal et al. 1994; Belcher 2003). Scattered outcrops of chlorite-actinolite-epidote-carbonate schists and minor ultramafic talc-carbonate schist define a northwest-trending, *c*. 15 by 3 km sliver in the eastern parts of the Swartland domain (Rabie 1948, 1974; Hartnady et al. 1974; Theron et al. 1992; Slabber 1995). This largest, more or less coherent metamafic unit forms the Bridgetown Formation (Hartnady et al. 1974; SACS 1980) situated along the southern down plunge extent of the upright to southwest-verging F2 Spitskop dome (Fig. 14.2). The highly altered mafic metavolcanic rocks are intercalated with cherts and dolomite units along the western margins of the Bridgetown Formation against quartz-sericite phyllites (Theron et al. 1992; Belcher 2003). Geochemical signatures indicate that the Bridgetown Formation rocks represent original tholeiitic metabasalts (Slabber 1995; Rozendaal et al. 1999).

14.3.2 Lithological Inventory of the Upper Domain: The Malmesbury Group

Rocks outside D1 fabric domains and in large parts of the Saldania belt show significantly lower fabric intensities. The mainly metasedimentary and minor metavolcanic rocks lack the bedding-parallel foliation (S1), and primary bedding and even intricate depositional features are well preserved so that sedimentary environments are better constrained (Fig. 14.5a, b) (e.g., Von Veh 1983; Theron et al. 1992; Rowe et al. 2010; Frimmel et al. 2013). Wherever recorded, way-up criteria indicate the normal younging of the rocks (Fig. 14.5b). In the following, we highlight lithological similarities and the distribution of different facies across much of the belt that point to reasonable regional correlations between units, also across purported terrane boundaries. Following the current terminology, we henceforth refer to these rocks as the Malmesbury group. Importantly, and in contrast to currently accepted lithostratigraphic classifications, the structurally lower rocks of the Swartland complex are not included in the Malmesbury group described here (Table 14.1).

In current subdivisions (SACS 1988; Gresse et al. 2006), the westernmost parts of the Saldania belt are only underlain by one stratigraphic unit, the Tygerberg Formation. In coastal exposures and large quarries around Cape Town, this formation is developed as a greywacke-dominated succession with intercalated shales and siltstones (Hartnady et al. 1974;

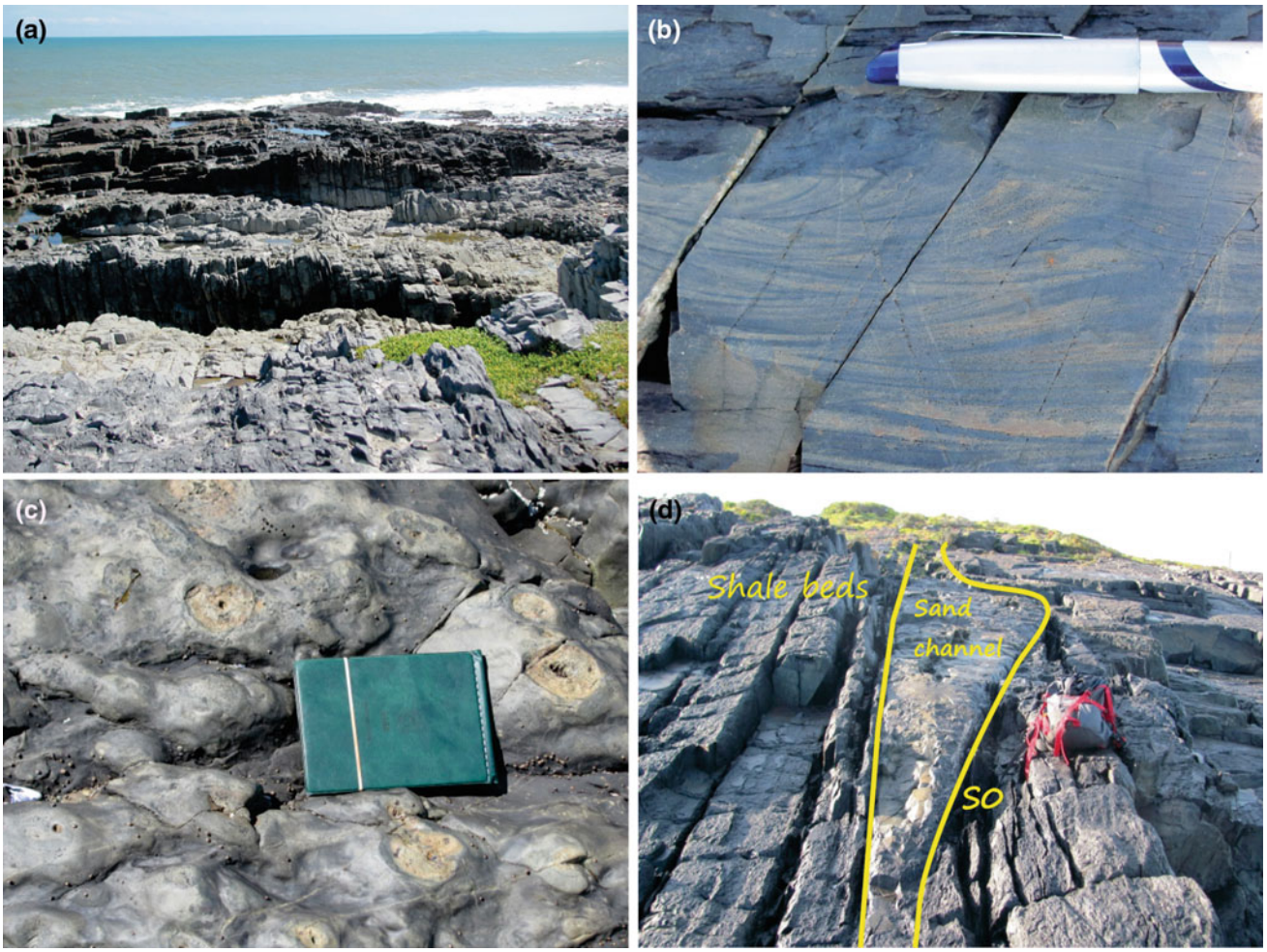

Fig. 14.5 **a** Rocks of the Malmesbury Group show well-preserved bedding, here developed as alternating shale and greywacke units exposed on the vertical limb of a F2 fold, looking northwest in rocks of the Tygerberg Formation along the Atlantic seaboard at Ganzekraal. **b** Intricate sedimentary features, here cross-bedding in the Tygerberg Formation, are well preserved throughout the Malmesbury Group. Despite the tight folding in many places, Malmesbury Group rocks show only very limited internal strain, which is in marked contrast to rocks of the underlying Swartland complex (Fig. 14.4b, c). **c** Synsedimentary deformation features are very common, particularly in the Tygerberg Formation (e.g., Von Veh 1983). The features shown here are interpreted as sand boils or sand volcanoes, forming ovoid sand protrusions through shale formed during the liquefaction of unconsolidated sands during seismic events. Tygerberg Formation, Silverstroomstrand (Fig. 14.2). **d** Oblique view of a greywacke channel fill erosive into thick black shale units that dominate the northern facies of the Tygerberg Formation, looking southeast, Ganzekraal

Von Veh 1983; Rowe et al. 2010; Frimmel et al. 2013). The predominance of massive greywacke units, presence of angular feldspar fragments and poor sorting of the rocks together with the occurrence of conglomerates and thin limestone units have commonly been inferred to indicate relatively proximal and shallow-marine conditions of deposition (Theron 1984; Theron et al. 1992). Soft-sediment deformation features are common and have been suggested to indicate a rapid deposition of the sediments, but also as records of seismic activity in the unconsolidated sediments (Fig. 14.5c) (e.g., Von Veh 1983). Detrital zircons from the southern parts of the Tygerberg Formation point to a late-Neoproterozoic timing of sedimentation and the youngest concordant zircons yield ages of *c*. 565–560 Ma (Armstrong et al. 1998; Frimmel et al. 2013). These ages correspond well with U-Pb ages of an intercalated felsic tuff from the metavolcanic Bloubergstrand Member in the Tygerberg Formation, north of Cape Town, indicating an age of volcanism of *c*. 554.5 ± 5 Ma (Kisters et al. 2015). The amygdaloidal textures of the intermediate lavas and eutaxitic textures of the tuff units are consistent with the shallow marine or, locally, even subaerial conditions of volcanism of the Bloubergstrand Member and deposition of the Tygerberg Formation in this part of the belt (Von Veh 1983). Coastal exposures of the Tygerberg Formation in the north, north of Silverstroomstrand, are dominated by massive to laminated

black shale. Intercalations of greywacke are subordinate and metapsammites mostly form 10–50 m wide erosive, often laterally and vertically stacked channel fills encased by thick units of black shales (Fig. 14.5d). The rocks resemble slope channel fills acting as sand bypasses and delivering sediment into deeper-water environments. This deeper marine northern facies has not been distinguished in the undifferentiated Tygerberg Formation. However, lateral stratigraphic correlations and age relationships between these different facies have to remain tentative given the only sporadic outcrop.

East of the Colenso Fault, large parts of the Swartland domain are underlain by rocks of the Moorreessburg Formation. The interlayered greywacke and shale units resemble those of the Tygerberg Formation and regional studies maintain the similarity between the two formations across the Colenso Fault (e.g., Von Veh 1983; Belcher and Kisters 2003). The lithological similarities are corroborated by near identical detrital zircon populations that point to the deposition of the rocks in the late Neoproterozoic and up to *c*. 560 Ma (Frimmel et al. 2013). The Franschhoek Formation in the central parts of the western Saldania belt is distinct from the laterally more extensive Tygerberg and Moorreessburg Formation in a number of ways. The sequence is dominated by quartzites, feldspathic greywackes and conglomerates, with only minor intercalated shales, but also tuffs and amygdaloidal lavas and intrusive quartz-porphyry dykes (De Villiers et al. 1964; Theron et al. 1992; Gresse et al. 2006). Clasts in conglomerates are made up of original quartz vein material, chert, and quartzite, but also granite and phyllite. In contrast to the laterally extensive Tygerberg and Morressburg formations, rocks of the Franschoek Formation form northwest-trending, elongate depositories that also occur on either side of the Colenso Fault on regional maps (Fig. 14.6) (Theron et al. 1992). The rocks have clearly been affected by the regionally upright, northwest-trending F2 fold and, as a result, show steep dips and, in places, a well-developed foliation and northwest-trending stretching lineation. Taken in conjunction, lithological and structural characteristics of the Franschhoek Formation indicate an origin of the rocks during the localized uplift, erosion and reworking of underlying rocks of the Swartland complex and Morreessburg Formation and during CGS plutonism pointing to a later, probably syntectonic (D2 shortening, see below), timing of deposition. This also agrees with the unconformable contacts of the Franschhoek formation against underlying phyllitic units, but also parts of the CGS (Theron et al. 1992).

Rocks in the eastern parts of the western Saldania belt are grouped under the Boland Subgroup that comprises the Piketberg, Porterville, Norree and Brandwacht formations. Contacts are not exposed and most studies suggest the lateral interfingering of, or gradual contacts between, formations, and also correlations with rocks of the Franschhoek Formation to the west (Hartnady et al. 1974; Theron et al. 1992). In general, the Boland Subgroup comprises coarser-grained and less well-sorted clastic rocks compared with the western Tygerberg or Morreessburg Formations. The sequence comprises sandstone and feldspathic sandstone interlayered with silt and shale, greywacke, gritty sandstone, conglomerate units and impure limestones. Most studies suggest a near-shore marine to deltaic and fluival and non-marine depositional environment for the mainly coarse-clastic rocks (Gresse and Theron 1992; Rozendaal et al. 1999). Conglomerates of the Piketberg and Porterville formations contain pebbles of vein quartz, phyllite and greywacke, suggesting a very proximal source for the sediments probably derived from the reworking of underlying rocks, similar to the Franschhoek Formation. Frimmel et al. (2013) document detrital zircon age spectra from the Porterville Formation that are similar to rocks from the western parts of the Saldania belt and possibly point to a slightly younger age of sedimentation of at least parts of the Boland Subgroup compared with the western Tygerberg and Morreessburg formations. Differences in the age spectra relate to the much more prominent input of late-Mesoproterozoic and early Neoproterozoic zircons. This likely reflects the proximity of the Namaqua-age (1200–950 Ma) metamorphic hinterland to the immediate east (e.g., Rozendaal et al. 1999). Parts of the Piketberg Formation in particular are strongly foliated and lineated, and fabric development resembles those found in rocks of the Swartland complex. The Brandwacht Formation in the far eastern parts of the western Saldania belt is unique in that it contains prominent metavolcanic units of broadly andesitic composition intercalated with conglomerates, greywackes and metapelites. Contacts of the Brandwacht Formation against older rocks are interpreted as either a basal conglomerate or a tectonic melange, possibly along a thrust plane (Hartnady 1969).

14.3.3 Klipheuwel Group

Clastic rocks of the Klipheuwel Group are preserved in a number of rhomb-shaped, narrow (<2–3 km), elongate (>10 km), northwesterly-trending basins (SACS 1980) that are spatially closely associated with the Colenso and, to a lesser extent, Piketberg-Wellington fault zones (Figs. 14.2 and 14.6). Correlations between individual basins are limited, suggesting that individual depositories were not interconnected. The rocks commonly show a coarse-clastic basis with conglomerates and poorly sorted sandstones, arkoses and intercalated shales that unconformably overlie shales and/or phyllites of the Swartland complex and/or Malmesbury group, but also granitic rocks of the CGS. Pebbles in conglomerates and gritty sandstones include vein quartz, shale and phyllite, clearly derived from the underlying

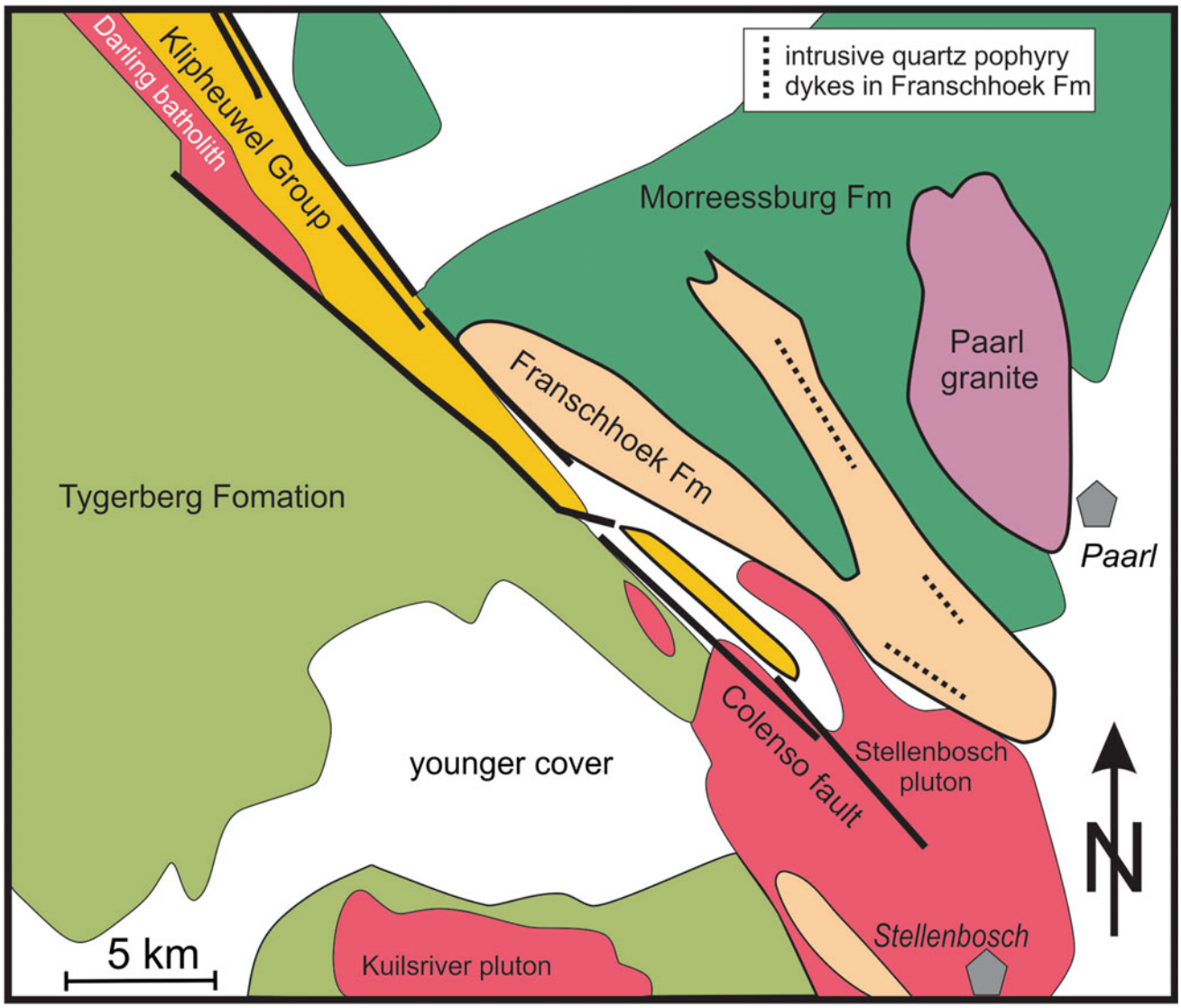

Fig. 14.6 Simplified geological map, modified after Theron et al. (1992), showing the relationships of the laterally more extensive Tygerberg and Morreessburg formations against the Franschhoek Formation and Klipheuwel Group. The latter are mainly confined to northeast-trending and, in the case of the Klipheuwel Group, fault-bounded basins. Granitic dykes are intrusive into the Franschhoek Formation but not into the Klipheuwel Group. Note also the seemingly unconformable contacts of the Franschhoek Formation against plutons of the CGS

metasediments, but also boulders of the CGS. The Klipheuwel Group is said to attain a maximum thickness of up to 2000 m (Gresse et al. 2006), and towards its upper parts the basin fills are commonly finer grained and dominated by shale and intercalated sandstones. This has led to the subdivision of the group into a lower Magrug and an upper Populierbos formation (Theron et al. 1992). Rocks of the Klipheuwel Group show mainly steep dips and northwesterly strikes. In places, a steeply dipping northwesterly-trending foliation is developed in shale units. Frimmel et al. (2013) suggested a maximum age of deposition of *c*. 550 Ma based on detrital zircon ages from the Magrug Formation in the lower parts of the Klipheuwel Group. Unconformable contacts between rocks of the Klipheuwel Group and the Darling batholith in the type locality of the Klipheuwel quarry provide a tighter age constraint of <535 Ma for sedimentation. An upper age of *c*. 480–500 Ma is provided by the age of the unconformably overlying Cape Supergroup that is considered to be lower Ordovician in age (Thamm and Johnson 2006).

Tankard et al. (2009) suggest that the Klipheuwel Group represents a rift-related precursor to the Cape Supergoup, but most other studies interpret the group as late-stage molasse-type basins more closely related to the Pan-African evolution of the Saldania belt (e.g., Gresse et al. 2006). Numerous workers emphasize similarities with rocks of the

Franschhoek Formation (Belcher and Kisters 2003; Frimmel et al. 2013). Lower fabric intensities, the lack of intrusive granite dykes, generally better preservation and the typically fault-bounded nature of the rocks may indicate a slightly later deposition of the Klipheuwel Group compared with that of the Franschhoek Formation.

14.3.4 Granites of the Cape Granite Suite

Granites of the CGS hardly ever feature in regional reconstructions and tectonic models for the Saldania belt when they are a volumetrically important component and a clear distinguishing feature compared with adjoining Pan-African belts in southern Africa. A detailed discussion of the CGS is beyond the scope of this chapter, so the reader is referred to, *inter alia*, Scheepers (1995), Scheepers and Schoch (2006), Stevens et al. (2007), Villaros et al. (2009, 2011), Chemale et al. (2011) and Farina et al. (2012) for more comprehensive accounts on the origin of the granites. However, any geodynamic considerations have to take the emplacement, petrogenesis and timing of the CGS into account that illustrate widespread partial melting of mid- and lower crustal levels underlying the belt. Aspects pertaining to the geodynamic setting of the granites are briefly presented below.

Most studies focus on the petrogenetic evolution of the peraluminous S-type granites (e.g., Stevens et al. 2007; Villaros et al. 2009, 2011; Harris and Vogeli 2010; Farina et al. 2012, to name but a few). S-type granites form five major and composite plutons that are confined to the west of the Colenso Fault (Fig. 14.2). Available age data points to an emplacement of the plutons between *c*. 550 and 535 Ma and as late as *c*. 525 Ma for the latest phases in the central Darling batholith (Da Silva et al. 2000; Villaros et al. 2009). Subvolcanic textures and miarolitic cavities in some of the *c*. 540 Ma S-type granites (e.g., Rozendaal and Bruwer 1995) point to fairly shallow emplacement levels of the plutons. This may also account for the presence of granitic pebbles in rocks of the Franschhoek and Piketberg formations and the Klipheuwel Group, and it also suggests only limited uplift and erosion of the rocks after their emplacement.

Most petrological studies discuss a lithologically heterogeneous but broadly aluminous metasedimentary mid- and lower crustal source for the S-type granites and partial melting of the rocks through fluid-absent reactions (e.g., Stevens et al. 2007; Villaros et al. 2009; Farina et al. 2012). As such, the granites provide windows into the deeper parts underlying the Saldania belt. Harris and Vogeli (2010) document oxygen isotope compositions of garnet in the *c*. 540 Ma S-type Pensinsula Pluton around Cape Town that are consistent with the partial melting of a metapelitic source with an oxygen isotope composition similar to that of the Malmesbury Group exposed on surface. Also from the Peninsula Pluton, Villaros et al. (2011) document ages as young as 570 Ma from cores of inherited zircons in the granites, showing magmatic overgrowths with ages of between 555 and 525 Ma. In another study, Villaros et al. (2009) document high-grade metamorphic assemblages from metapelitic xenoliths in the central Darling batholith that are compositionally similar to rocks of the Swartland complex. Mineral assemblages in xenoliths record P–T conditions of *c*. 10 kbar and T at *c*. 800 °C. On a similar point, although outside the CGS, Kisters et al. (2015) recorded xenocrystic zircon populations in 555 Ma old tuffs intercalated with the Tygerberg Formation that are near identical to detrital zircon populations from the Malmesbury Group and Swartland Complex (Frimmel et al. 2013). While being circumstantial, these results consistently point to Pan-African age, Malmesbury-type rocks in the anatectic source region of the magmas. This would indicate an at least structural thickness of Pan-African rocks of in excess of 25 km, about ten times the thickness of the similarly aged sequences in the Gariep belt to the north.

There are only a few studies of I-type granites of the CGS (for a comprehensive summary, see Scheepers and Schoch 2006). The I-type granites form elongate, northwest-trending plutons east of the Colenso Fault, largely intruding rocks of the central Swartland domain. Existing ages suggest that the 540–520 Ma I-type granites are slightly younger than S-types. However, the ever-improving geochronological database shows a considerable overlap of ages between S- and I-type granites and the two granite types are essentially coeval.

14.4 Structural Geology

14.4.1 D1 Structures and Fabrics of the Swartland Complex

The structural complexity and lithological heterogeneity of the Swartland complex is probably best appreciated in quarry operations that provide excellent 3D windows into the mélange-like sequence (e.g., Fig. 14.3a) (Belcher 2003; Belcher and Kisters 2003). The pervasive bedding-parallel phyllitic foliation (S1) is axial planar to and envelopes centimetre- to metre-scale isoclinal, intrafolial folds (F1) that testify to the widespread transposition of original bedding and the high-strain nature of the S1 foliation (Fig. 14.3b). Quartz and quartz-carbonate veins are abundant throughout the lower domain rocks where they appear almost invariably transposed into the S1 foliation, having undergone boudinage or pinch-and-swell within the foliation, particularly in phyllitic units (Fig. 14.3c). A northwesterly-trending, gently doubly plunging mineral and mineral stretching lineation

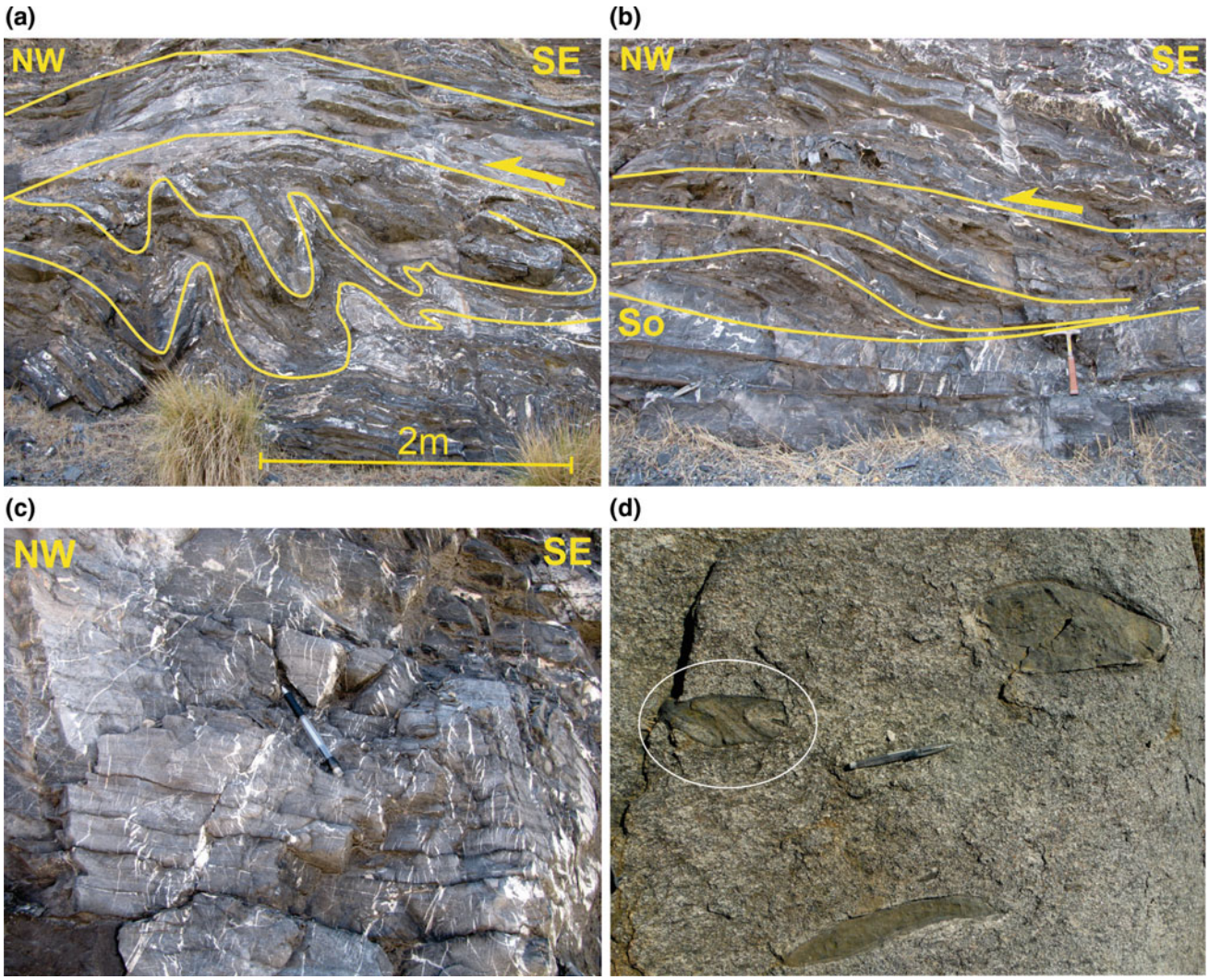

Fig. 14.7 **a** Vertical section of a mylonitic shear zone (top) and associated footwall deformation documenting top-to-the-northwest low-angle shearing in graphitic limestone of the De Hoek Quarry. Yellow lines annotate folded bedding and the shear zone boundaries. While strain is more distributed in phyllitic units (e.g., Fig. 14.3b, c), discrete calc-mylonites are developed in limestone units. **b** Metre-scale duplex structure in limestone suggesting top-to-the northwest and west low-angle thrusting at De Hoek quarry, Piketberg. **c** Cross-sectional view of conjugate calcite veins developed in low-strain domains within dark, graphitic limestones at limestone quarry, Riebeck West. The orientation of the conjugate sets together with the orientation of subvertical extensional veins points to the vertical shortening of the sequence during deformation and fluid flow. **d** Metasedimentary xenoliths within a finer-grained and low-strain phase of the Darling batholith, west of the Colenso fault (Fig. 14.2). Xenoliths preserving isoclinally folded bedding are common in the granites (here encircled xenolith on the left). These folds resemble F1 intrafolial folds developed in the Swartland complex and may indicate the wider extent of the lower, transposed domain at depth and across the Colenso fault

(L1) contained in S1 is prominent throughout the Swartland complex. L1 parallel rodding textures are particularly common in chert units (Belcher 2003). In phyllites, F1 intrafolial folds show shallow northwesterly and/or southeasterly plunges parallel to the L1 stretching lineations indicative of the rotation of fold hinges into the regional stretch during bedding transposition.

Contacts between thicker lithological packages are commonly sheared, which also accounts for the discontinuous extent of units (Hartnady et al. 1974; Belcher 2003; Gresse et al. 2006) (see below). Competent limestone units commonly preserve bedding, and S1 fabric intensities are lower than in the pervasively transposed phyllites and schists. Instead, strain is localized along discrete, bedding-parallel calc-mylonites (Fig. 14.7a). Shear sense indicators such as S–C′ fabrics and rotated quartz-calcite aggregates are common and consistently point to a top-to-the-northwest sense of shear, parallel to the L1 lineation. Similarly, metre-scale duplex structures point to the imbrication of the rocks during top-to-the-northwest thrusting (Fig. 14.7b). Fault-propagation folds associated with thrusts

show northeasterly trends at high angles to the thrust kinematics. Contrary to the pervasively transposed quartz veins in phyllitic units, carbonate and quartz-carbonate veins in limestones form a pervasive network of intersecting bedding-normal extensional veins and high-angle conjugate, and less abundant bedding-parallel veins (Fig. 14.7c). As such, D1 fabric development documents a distinctly mixed continuous-discontinuous deformation. Bedding transposition and the pervasive S1 foliation in schists and phyllites record, for the most part, continuous fabric development during distributed creep and ductile flow. The extensive high-angle vein networks and hydraulic breccias in more competent units record discontinuous brittle deformation, probably in the presence of temporarily supralithostatic fluid pressures. In general, foliation (S1) development, associated folding and boudinage of units, and the orientation of extensional and conjugate shear veins record the vertical shortening of lower domain rocks (Fig. 14.7c). Bedding-parallel thrusts, thrust-related folds and stretching lineations document a concomitant component of simple shear associated with a northwest stretch (Fig. 14.7a, b). Kinematic indicators consistently point to top-to-the-northwest and west thrusting along the low-angle thrusts. This strain pattern of vertical shortening and associated top-to-the-west and northwest non-coaxial shearing characterizes the Swartland complex throughout the central parts of the belt (Belcher 2003).

Rocks of the Swartland complex are not limited to the cores of the regional-scale Swartland and Spitskop domes, and several smaller windows expose transposed phyllitic units and, indeed, higher-grade metamorphic rocks. For example, Belcher (2003) describes isoclinally folded biotite gneisses from the farm Kanonkop north of Malmesbury (Fig. 14.2). These isolated outcrops highlight the much wider extent of the rocks in the western Saldania belt. This distinction has not been made on regional maps (e.g., Theron et al. 1992) but is clearly evident where low-angle foliations (dips < 40–50°) are indicated, pointing to the presence of D1 fabric domains. The distribution of these outcrops also suggests shallow dips along which rocks of the overlying Malmesbury Group rest on the Swartland complex, either along an unconformity (Belcher and Kisters 2003) or along a major low-angle fault (Rabie 1948). In this context, the abundance of high-grade metasedimentary xenoliths containing intrafolial folds and transposed bedding (e.g., Schoch 1975) typical of D1 fabric domains in the Darling batholith, west of the Colenso fault is conspicuous (Fig. 14.7d). Although circumstantial, the large number of these xenoliths may point to the extent of the Swartland complex at depth and across the Colenso fault.

14.4.2 D2 Regional Folding and Associated Strains

The D1 fabrics and strains described above are confined to rocks of the Swartland complex. The most obvious and regionally widespread structures that have affected the western Saldania belt are northerly- to northwesterly-trending folds and associated fabrics, collectively summarized under the D2 deformation event. Where rocks of the Swartland complex are exposed, F2 folds clearly refold earlier D1 fabrics, resulting in the steepening and crenulation of earlier low-angle fabrics (Hartnady et al. 1974; Belcher 2003; Belcher and Kisters 2003). Most mappable F2 folds are second- or third-order folds with wavelengths between *c*. 150 and 500 m (Fig. 14.8a). First-order F2 folds have wavelengths exceeding 3–5 km. The Swartland dome is probably the largest fold in the central parts of the Saldania belt with a width of *c*. 10 km. F2 folds are typically doubly plunging towards the northwest and southeast. The folds are more or less upright or steep southwesterly verging, but domains with northeast-verging folds also exist. Fold interlimb angles are highly variable and range from very gentle (>140°) to tight and isoclinal, even between adjacent folds. An upright, broadly axial planar cleavage (S2) is prominent in shaly units but is only very weak or absent in psammitic rocks (Fig. 14.8b). During their detailed analysis of F2 fold structures in the Tygerberg Formation on Robben Island, Rowe et al. (2010) showed the S2 foliation to be a transecting cleavage with a consistent clockwise rotation of S2 with respect to the axial planes for F2 folds. This finding can be extrapolated to F2 folds throughout much of the Saldania Belt and the S2 foliation commonly describes a clockwise rotation by 5–15° with respect to the axial surfaces of F2 folds (e.g., McGibbon 2012). Rowe et al. (2010) interpreted the transecting cleavage to indicate F2 folding during sinistral transpression. Quartz veins are common but are mainly restricted to more competent greywacke units. Along coastal exposures, quartz veins and vein sets show remarkably consistent orientations, also with respect to the orientation of F2 folds. Veins are high-angle extensional veins normal to the northwesterly-trending F2 folds or conjugate vein sets, both pointing to a component of subhorizontal, hinge-parallel north(west)-south(east) stretch during F2 folding (Fig. 14.8 c). The intersection between bedding (S0) and the upright S2 foliation results in a variably developed, northerly- to northeasterly-trending intersection lineation (L2). Stretching lineations comparable to those in rocks of the lower domain are conspicuous by their absence.


(a)
SW
NE
(b)
SW
S2
NE
So
(c)
SW
NE
shale
50 cm
greywacke
(d)
SE
NW
(e)
SE
NW
(f)
SE
NW
C'
S

◀ **Fig. 14.8** **a** Gentle, near-horizontal, upright F2 synform in black shales of the Tygerberg Formation, north of Ganzekraal, looking northwest, parallel to the trend of the fold. **b** Bedding (S0)–cleavage (S2) relationship in shale units on the southwest limb of an F2 antiform at Ganzekraal, looking northwest. **c** Oblique view of a central greywacke horizon interlayered with dark shales on the subvertical limb of a tight F2 fold at Ganzekraal. Systematic, high-angle quartz vein sets (annotated by yellow lines) are largely confined to the competent greywacke beds. Conjugate and extensional quartz veins indicate a layer-parallel stretch and, as such, hinge-parallel extension during F2 folding. **d** Magmatic fabric defined by the preferred orientation of k-feldspar megacrysts in the porphyritic phase of the Darling granite. Magmatic fabrics trend northwest-southeast, parallel to the Colenso fault, and are preserved in low-strain domains in the Darling batholith. **e** Gneissic textures in the Darling batholith result from the pervasive dynamic recrystallization of minerals and the overprint of originally magmatic textures. Here, augen textures are defined by ovoid, marginally recrystallized k-feldspar megacrysts and an anastomosing foliation defined by quartz ribbons and the preferred orientation of biotite. Plan view of the subvertical, northwest-southeast-trending foliation, parallel to the Colenso fault. **f** Plan view of mylonitic and protomylonitic textures in original granites of the Darling batholith define northwest-trending, up to 250 m wide mylonite belts overprinted on original magmatic and later solid-state gneissic fabrics. Shear sense indicators are common, here expressed by S–C′ fabrics, the majority of which indicate a sinistral sense of shear

14.4.3 D2 Strike-Slip Faults

The Colenso and Piketberg-Wellington fault zones are the largest structural features of the belt (Hartnady et al. 1974; Theron et al. 1992; Belcher 2003; Frimmel et al. 2011, 2013). The Colenso Fault is far more prominent and better exposed, and it can be traced for some 180 km along its northwesterly strike (Fig. 14.2). Deformation along the Colenso fault is distributed and the fault is developed as an up to 8 km wide anastomosing fault zone (Kisters et al. 2002). The best and most extensive exposures of the fault zone are in granites of the CGS, particularly the large, central Darling batholith. The batholith is bounded along its northeastern margin by mylonites and cataclasites related to the Colenso Fault. Intrusive and fabric relationships document the synmagmatic deformation of successively emplaced granite phases. Northwesterly-trending, steeply dipping magmatic foliations in the granites are commonly overprinted by high-temperature solid-state fabrics (Fig. 14.8d–f). This results in regionally widespread although variably pervasive gneissic textures (Schoch 1956; Theron et al. 1992; Kisters et al. 2002). Northwest-trending, subvertical mylonite and protomylonite zones show gradational contacts with magmatic and weak solid-state fabrics developed in large parts of the pluton. Brittle-ductile, anastomosing cataclasite and ultracataclasite zones indicate that deformation has continued under lower-grade conditions and accompanying the cooling of the granites. Magmatic and solid-state lineations are defined by the stretching of magmatic enclaves or xenoliths, the preferred alignment of k-felspar megacrysts or stretched quartz-feldspar aggregates in mylonites (Schoch 1975; Kisters et al. 2002). Lineations show mainly shallow northwest and/or southeast plunges consistent with the mainly strike-slip kinematics. The vast majority of magmatic and solid-state shear sense indicators point to sinistral kinematics (Fig. 14.8f), but there are also domains of seemingly conflicting dextral and sinistral kinematics. Available U-Pb ziron ages from granites of the Darling batholith point to deformation along the fault zones between at least 545 and 525 Ma (Da Silva et al. 2000; Villaros et al. 2009). The *c*. 510 Ma undeformed Klipberg granite (Scheepers 1995) crosscuts earlier magmatic and solid-state fabrics in the Darling batholith and indicates the cessation of deformation by that time. Northwest of the Darling batholith, fault rocks related to the Colenso Fault zones are developed in the Cape Columbine granite and Vredenburg adamellite. Faulting is evidenced by 2–3 km wide networks of anastomosing, northwesterly-trending mylonites, ultracataclasites and cataclasite zones (Schoch 1956). Shear sense indicators in these younger, 540–520 Ma granites mainly point to dextral kinematics, suggesting a late-stage reversal of shear along the Colenso fault (Kisters et al. 2002).

The Piketberg-Wellington fault is only poorly exposed and its actual trace and location are controversial (Rabie 1948, 1974; Slabber 1995; Belcher 2003). Rabie (1974) postulated the presence of the fault to account for the juxtaposition of sheared and transposed rocks of the Swartland complex in the west against only weakly deformed rocks of the Boland domain in the east. Notably, this area corresponds to the eastern limb of the first-order F2 Swartland dome and smaller Spitskop dome that are cored by the Swartland complex. Around Piketberg, faulting is evidenced by several northwest-trending, anastomosing fault strands and associated quartz veining. Where faulting can be identified with certainty, rocks of the Cape Supergroup have been displaced, forming downfaulted outliers surrounded by Pan-African basement. This suggests a significant component of post-Cape Supergroup displacement along the fault, with a mainly normal sense of movement and downthrow to the east. Along its southern extent, the trace of the Piketberg Wellington Fault can only be inferred (e.g., Theron et al. 1992). Despite this, Frimmel et al. (2013) suggest that the fault represents the major terrane boundary in the western Saldania Belt, but it should be emphasized that neither the location, nor the extent or actual timing and kinematics of the fault zone have been established with any certainty.

14.5 Discussion

The recognition of two structurally overlying tectonostratigraphic domains in the western Saldania belt is not new (e.g., Rabie 1948, 1974; Newton 1966; Hartnady et al. 1974; Belcher 2003; Gresse et al. 2006), but the significance of these contrasting domains for the overall evolution of the belt has never been discussed or fully appreciated. The detrital zircon study by Frimmel et al. (2013) demonstrates the, within error, identical late-Neoproterozoic age of rocks of the Malmesbury group and structurally underlying Swartland complex. Hence the notion expressed by Belcher and Kisters (2003) of an older D1 domain overlain by a younger, less deformed metasedimentary sequence cannot be upheld. This implies that the Swartland complex and the Malmesbury group represent two different structural levels, and we suggest that the contrasting lithological inventories, kinematics and strains illustrate a section through a fore-arc region situated along the western margin of the Kalahari Craton as has similarly been suggested by Von Veh (1983), Belcher (2003) and Rowe et al. (2010). The Swartland complex exposes the upper parts of an accretionary prism whereas rocks of the overlying Malmesbury group represent the relics of a reasonably coherent, although deformed, fore-arc basin on top of the accretionary prism. These aspects are detailed below.

14.5.1 Swartland Complex

The Swartland complex represents a highly sheared and transposed tectonostratigraphic sequence that records the offscraping and imbrication of marine sediments and slivers of oceanic crust (e.g., Hartnady et al. 1974; Belcher 2003). Strains record the vertical shortening of the sequence combined with a component of subhorizontal shear and top-to-the-west and northwest-thrusting along low-angle mylonites and phyllite zones. The combined vertical coaxial shortening strain and non-coaxial subhorizontal slip are diagnostic for accretionary systems formed by the underthrusting and basal accretion of rocks to the base of the accretionary complex, resulting in the thickening of the wedge during tectonic underplating of marine strata and oceanic crust (e.g., Fisher and Byrne 1987; Raimbourg et al. 2009; Malavieille 2010). The pervasive quartz and quartz-carbonate veins and vein networks document the progressive dehydration of underthrusted sediments during burial and basal accretion. Competent limestone units preserve the original geometries of these vein networks. The brittle vein networks and associated hydraulic breccias testify to episodically supralithostatic fluid pressures and associated seismic slip events during underplating of the rocks. In the regional context of southwest Gondwana, the top-to-the-west and northwest kinematics agree with an imbrication of the rocks during east- or southeast-directed convergence and subduction of oceanic crust below the Kalahari Craton. This corresponds to the kinematics recorded from coastal belts to the north (e.g., Hartnady et al. 1985; Von Veh 1993; Gresse 1995; Goscombe et al. 2003; Konopasek et al. 2005). The age spectra of detrital zircons in rocks of the Swartland complex provide further evidence of the setting of the rocks along an active continental margin. The ages of detrital zircons (Frimmel et al. 2013) suggest that deformation, burial and metamorphism of rocks in the Swartland complex followed shortly, within <5–10 Ma, the deposition of the rocks, typical of convergent plate margins (e.g., Cawood et al. 2012).

14.5.2 Malmesbury Group

Lithological assemblages and strains in the overlying Malmesbury group mark a sharp break against the underlying mélange-like rocks of the Swartland complex, although the actual contacts between the two are not exposed. Despite the only patchy outcrop and later folding of Malmesbury group rocks, the areal distribution of facies associations allows for the reconstruction of a depositional model for the Malmesbury group across purported terrane boundaries. The coarse-clastic sedimentary and intercalated volcanic rocks of the Boland Subgroup in the east define a northerly- to northwesterly-trending belt of non-marine to near-shore and shallow-marine sediments proximal to a volcanic arc located to the east. The proximal facies shows a pronounced influence and sediment input from the Kalahari Craton as an eastern hinterland (Tankard et al. 1982; Gresse and Theron 1992, 2006), which is underpinned by the prominence of Meso- to Neoproterozoic zircons in the rocks (Frimmel et al. 2013). To the west, the mainly proximal facies of the Boland Subgroup is replaced by the greywacke-dominated turbidite deposits of the Tygerberg and Morreesburg formations. The metaturbidites are laterally the most extensive units, showing mainly tabular geometries and a lack of channels at their base consistent with a depositional environment in the more central parts of the fore-arc basin. This agrees with the views of Von Veh (1983), who suggests deposition of the southern Tygerberg Formation along a progradational submarine fan along a continental slope. He also evokes the proximal facies of the southern Tygerberg Formation to be derived from rocks to the immediate east. The abundant soft-sediment deformation features agree with the deposition of the rocks along an

active continental margin (see also Von Veh 1983) and represent either the near-surface expression of seismic events as they are recorded by hydrothermal breccias and vein networks preserved in the Swartland complex or very high sedimentation rates and gravitational instabilities as expected in this environment.

A deeper-water environment is indicated for the shale-dominated and stacked channel fills of the northern Tygerberg Formation north of Silverstroomstrand (Fig. 14.3). Hartnady et al. (1974) and Tankard et al. (1982) envisage a hemipelagic, trench-like sedimentary environment for this northern facies of the Tygerberg Formation. The shallow marine and, in places, subaerial depositional conditions in parts of the southern Tygerberg Formation may correspond to the location of a trench-slope break. This outer arc high separates the inner fore arc basin in the east (southern Tygerberg and Morreessburg formations) from the slope apron deposits to the west and northwest (northern Tygerberg Formation). In general, the regional distribution of facies indicates the transverse sediment input from the arc side via river systems and deltas in the east into and across the deepening fore-arc basin towards the west, as is common for fore-arc basins (e.g., Heller and Ryberg 1983; Santra et al. 2013). Contacts between formations and facies are gradational and across purported terrane boundaries.

The reworking of underlying rocks, including phyllites and granites of the CGS in rocks of the Franschhoek and Piketberg formations, is indicative of the deposition of these formations during or very shortly after plutonism and metamorphism at depth. Folded, unconformable contacts of the Franschhoek Formation against underlying phyllites suggest the syntectonic formation of the coarse-clastic rocks, possibly related to episodes of intrabasinal uplift during regional shortening (D2) along either growth folds or steepened breakthrough thrusts (e.g., Noda 2016). The different basins may have formed at different times but they correspond to similar processes that signify the progressive shortening (D2), localized uplift, erosion and deposition within the larger Malmesbury fore-arc basin between at least 550 Ma to probably 520 Ma. The synsedimentary deformation will also have an effect on the basin topography and, hence, the geometry of sediment supply paths and resulting flow and transport directions recorded in the sediments (e.g., Buggisch et al. 2010; Rowe et al. 2010). Lower strain intensities, better preservation and the strictly fault-bounded nature of basins of the Klipheuwel Group point to a slightly later sedimentation compared with, for example, that of the Franschhoek Formation, probably related to the late-stage uplift history.

14.5.3 Deformation of the Fore Arc (D2)

The western Saldania belt shows a very characteristic domainal structural pattern in which regions of upright to southwest-verging folds (F2), up to several tens of kilometres wide, are bounded by the several kilometre-wide vertical sinistral strike-slip corridor of the Colenso fault zone as the central structure. This pattern of orogen-parallel transcurrent shear zones bordering or enveloping folded domains is characteristic of obliquely convergent margins and points to the partitioning of the overall transpressional deformation into a contractional and a transcurrent component (Fig. 14.10a, b) (e.g., Robin and Cruden 1994; Tikoff and Teyssier 1994; Fossen and Tikoff 1998; Tikoff and Peterson 1998). Folded (F2) domains record the largely coaxial shortening component whereas strike-slip faults, such as the Colenso Fault, accommodate the transcurrent component of the strain. The subparallel orientation of F2 folds and the northwest-trending Colenso fault corridor also suggest that parts of the strike-slip component during oblique convergence were accommodated by the strike-slip shear zones, rather than being distributed across the belt (Fig. 14.10a, b). This pronounced strain partitioning may be related to the very oblique subduction and convergence angles of <20° (Rowe et al. 2010) and/or point to the decoupling of the shortening and strike-slip components in the belt as a result of weak fault rheologies, particularly of the main Colenso fault. Notably, the Colenso fault zone is, for most of its strike extent, developed in granites of the CGS. While this may be an artefact of the outcrop conditions, the progressive fabric development from magmatic via high-temperature to low-temperature solid-state fabrics underlines the spatial and temporal relationships between granite emplacement and strain localization (Fig. 14.8d–f). The granitic magmas are rheologically weaker than the surrounding wall rocks and magma emplacement will most likely result in the weakening of the fault zones. This in turn promotes strain localization and partitioning of the strike-slip component into the faults. Given that repeated granite sheeting in the Darling batholith is recorded between *c*. 545 and 525 Ma, magma emplacement may have, at least intermittently, contributed to the decoupling and strain partitioning in the belt over a period of over 20 Ma. Despite this, the fold hinge-parallel stretch (Fig. 14.8c) and the widely recorded transecting S2 cleavage (e.g., Rowe et al. 2010) in F2 fold domains is evidence for more distributed D2 strains. Given that magmatic sheeting is most likely episodic, one could argue that these more distributed strains have developed during episodes of fault lock-up and fault zone strengthening related to intervals when the faults were not intruded by granitic sheets.

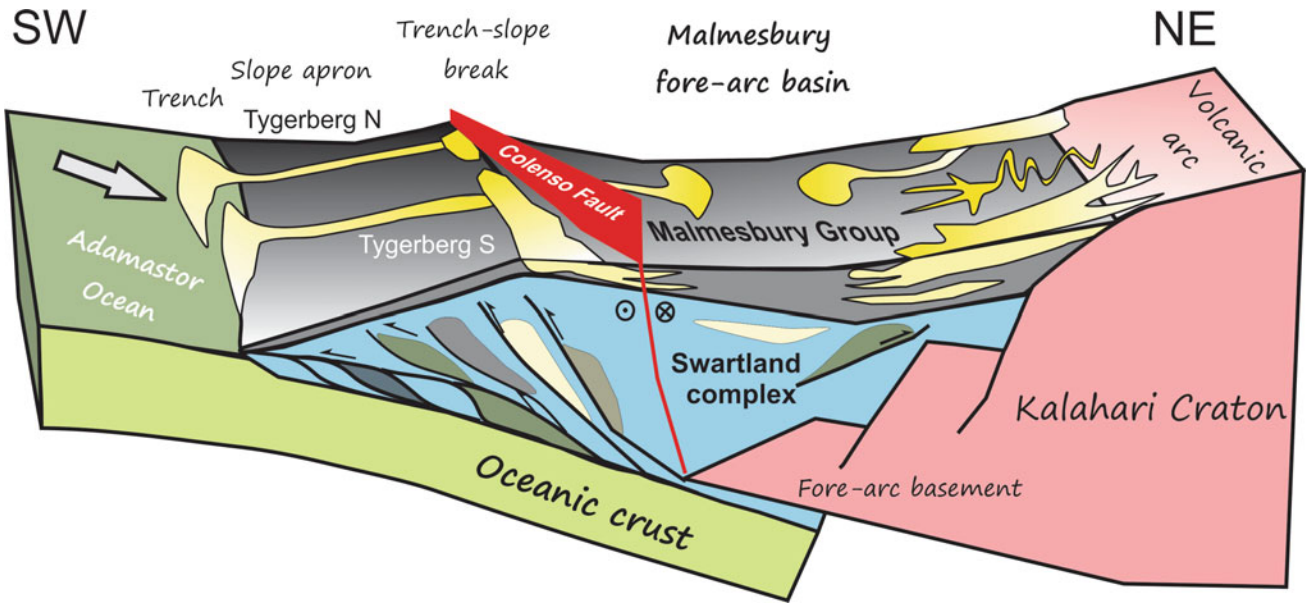

Fig. 14.9 Schematic sketch illustrating the different lithological and structural elements of the Malmesbury fore arc as discussed in this chapter, made up of an underlying accretionary complex, the Swartland complex, and sediments of the overlying fore-arc basin, represented by the Malmesbury group. Later deformation by F2 folds and plutons of the CGS are not shown for clarity. Tectonic underplating during subduction in the deeper parts of the prism and deposition of fore-arc sediments at higher structural levels are contemporaneous and can be recorded between >560 Ma and at least 520 Ma. See text for further detailed discussion

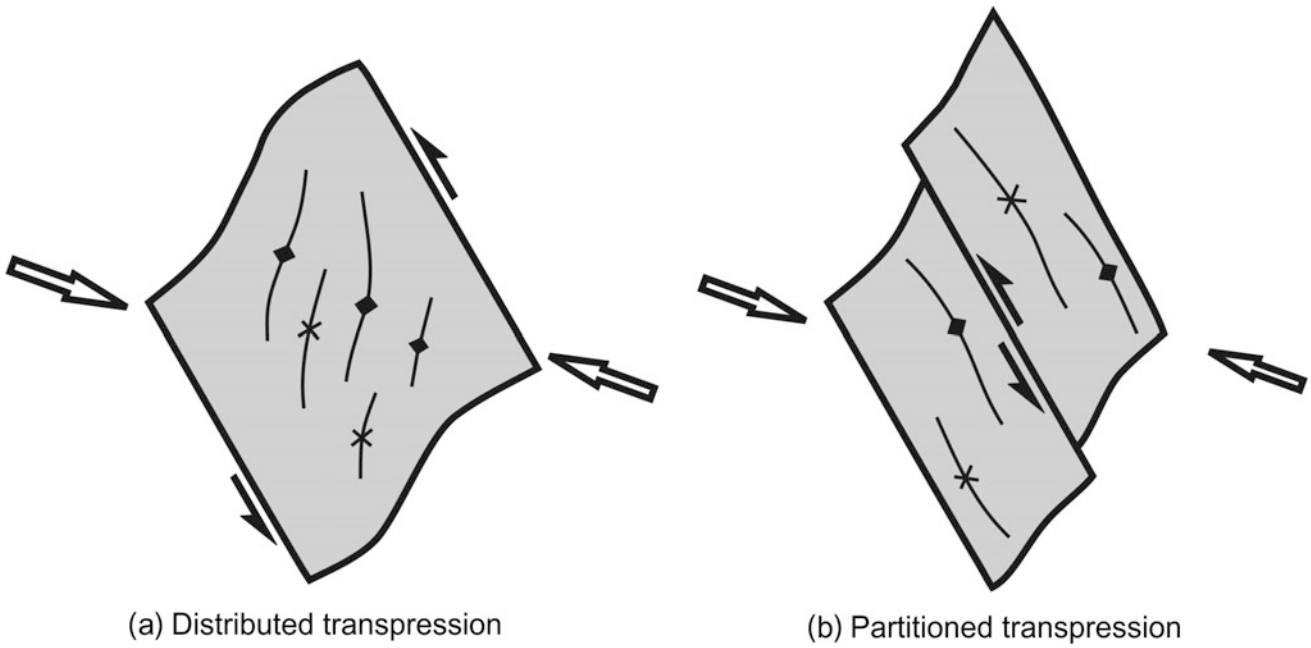

Fig. 14.10 Schematic sketch illustrating the effects of **a** homogeneous distribution of strain and **b** strike-slip partitioned strain in transpressional zones on the orientation of fold hinges (after Fossen and Tikoff 1998). In (**a**), folds form at high angles to the shortening direction and fold hinges rotate into parallelism with the regional stretch during progressive deformation. In (**b**), the strike-slip component is partitioned into discrete transcurrent shear zones whereas the contractional component is accommodated by domains of largely coaxial shortening (folding) and fold hinges are subparallel to transcurrent shear zones. This latter case seems to be realized in the Saldania belt and either indicates the very weak rheology of the Colenso fault as the main transcurrent shear zone and/or a low angle (<20°) of plate convergence

On a regional scale, the D2 strike slip faults will not have contributed significantly to the shortening of the belt, but the open to tight and isoclinal F2 folds suggest a shortening of the fore arc by at least 30–50%, although the highly variable fold interlimb angles and lack of outcrop render these estimates tentative at best. Rocks of the Franschhoek and Piketberg formations testify to the synsedimentary deformation of the fore arc. This is consistent with the timing of strike-slip shearing recorded from the Colenso fault between at least 545 Ma and probably 520 Ma (Kisters et al. 2002). Given that the oldest *c*. 550 Ma granites of the CGS crosscut F2 folds (e.g., Theron 1984; Theron et al. 1992), D2 strains related to convergence and subduction can be recorded over at least 30 Ma from >550 to *c*. 520 Ma.

Sinistral transpressive kinematics are similarly documented from coastal belts to the north over a distance of >2000 km. There is general consensus that these strains document the oblique closure of the Adamastor ocean or related basins, and the eventual collision of terranes (Von Veh 1993; Gresse 1994, 1995; Goscombe et al. 2003; Konopasek et al. 2005; Goscombe and Gray 2008). Despite the similar regional kinematics, the structural style of upright folds and vertical strike slip faults in the western Saldania belt is distinct from, for example, the Vanrhynsdorp and Gariep belts to the immediate north. These northern belts are developed as east- to southwest-verging fold-and-thrust belts, with only little evidence of major vertical transcurrent faults. Importantly, these belts lack syn- to late kinematic granites such as those of the CGS in the Saldania belt. This may underscore the close relationship between synkinematic granite intrusions and the effects of at least temporary rheological weakening and resulting strain partitioning in the belts that gives rise to markedly different structural patterns in adjacent belts. The intrusion of the granites in turn likely reflects different basement structures underlying the belts.

14.5.4 The Deeper Structure of the Western Saldania Belt

Neither the base nor the top of the Pan-African rocks are exposed, so thickness estimates must remain tentative. However, metamorphic, geochemical and geochronological data from the CGS (Villaros et al. 2009, 2011; Harris and Vogeli 2010) and tuffs in the Tygerberg Formation (Kisters et al. 2015) point to the partial melting of metapelite-dominated, Pan-African age rocks at depths of >20–25 km. If correct, these thickness estimates are an order of magnitude greater compared to the thicknesses considered for similarly old rocks of the Gariep Supergroup to the north (e.g., Frimmel and Frank 1998; Gresse et al. 2006). A structural thickness of >20 km agrees with the thickness for accretionary prisms but is unlikely to be realized in a back-arc setting, as has been suggested in regional correlations of rocks of the Saldania with those of the Gariep belt (Frimmel et al. 2011, 2013). More precisely, the substantial thicknesses would point to the inner parts of the prism that has been structurally thickened through the underplating of sediments and oceanic crust. This in turn would correspond to the position of the unconformably overlying fore-arc basin sediments of the Malmesbury group above the inner parts of the wedge. In this scenario, the toe of the accretionary prism would be located to the far west, and the eastern and top parts of the frontal wedge would correspond to the deeper-water facies of the northern Tygerberg Formation forming the slope apron facing the ocean basin to the west (Rowe et al. 2010).

The plutons of the CGS may provide additional clues about the deeper structure of the western Saldania belt. Compositional variations in granites or granite suites are thought to mainly reflect source heterogeneities (e.g., Clemens et al. 2009, 2010). S-type granites are derived from the partial melting of aluminous clastic sediments, whereas I-type granites indicate former arc material or orthogneissic basement rocks in the source (e.g., Chappell and White 1974; Wall et al. 1987; Clemens 2003). The Colenso fault forms a sharp divide between S- and I-type granites in the western Saldania belt (Scheepers 1995; Scheepers and Schoch 2006; Stevens et al. 2007; Villaros et al. 2009), suggesting that the fault separates two compositionally different source regions at depth. This may imply the location of the Colenso fault at depth along the leading edge of the fore-arc basement (Fig. 14.9). Partial melting west of the fault has only affected the metasediments of the thickened accretionary wedge yielding the voluminous S-type granites. I-type granites east of the fault, in contrast, indicate a more heterogenous source made up of metasediments and older basement gneisses.

This raises the question as to the heat source for partial melting. Fore-arc regions are commonly considered to be the coldest part of convergent margins refrigerated by the subducting oceanic slab. The syn- to late-stage timing and fore-arc position of the CGS has previously been explained in terms of a slab break-off (e.g., Belcher 2003). Late tectonic fore-arc magmatism related to slab break-off is invoked for a number of convergent orogens, such as the Acadian of Maine (Schoonmaker et al. 2005) or, more recently, the Pan-African Damara belt in Namibia (Meneghini et al. 2014; Clemens et al. 2017). The slab break-off may also explain the lack of a hard collision in the western Saldania belt (e.g., Rozendaal et al. 1999). Unlike adjoining coastal belts to the north, rocks of the Saldania belt have not experienced high-grade metamorphism and lack evidence of a post-collisional uplift prior to the onset of Cape Supergoup sedimentation at *c*. 480–500 Ma. This would agree with a slab break-off in which slab delamination has resulted in a

soft collision between the southern tip of the Kalahari Craton and the Rio de la Plata Craton.

14.6 Conclusions

This review is an attempt to present a different view of the geology of the western Saldania belt that is less based on the premise of allochthonous or parautochthonous domains and rather highlights correlations of lithological packages, facies and structures across purported terrane boundaries. The picture that emerges then is that of a deformed but reasonably well-preserved section through a fore arc that formed in the latest Neoproterozoic and into the Cambrian (>560 to <510 Ma) along the western margin of the Kalahari Craton. The structurally lower parts of the belt, the Swartland complex, record the imbrication of marine sediments and oceanic crust. Tectonic underplating and thrust imbrication have resulted in a complex tectonostratigraphic sequence with a thickness of likely >20–25 km. This section corresponds to the inner part of an accretionary prism that formed during southeast-directed oblique subduction of the Adamastor ocean below the Kalahari Craton. The accretionary prism is overlain by low-grade metamorphic metasediments and minor metavolcanic rocks with markedly lower fabric intensities, the Malmesbury group. Rocks of this group represent the late-Neoproterozoic to Cambrian fore-arc basin fill (Belcher 2003; Rowe et al. 2010). Contacts between formations are gradational and across purported terrane boundaries. Sedimentary facies suggest the presence of a volcanic arc in the east, succeeded in the west by shallow-marine turbidites of the inner fore-arc basin. Metapelitic successions and sandy channel fills in the far west and northwest indicate deeper-water deposits overlying the toe of the prim and facing the ocean basin. Late-stage, unconformably overlying coarse-clastic sediments in large parts of the belt represent syntectonic (D2) deposits that record the reworking of underlying sequences during shortening of the fore arc. Overall, the Malmesbury fore arc has been shortened by at least 30–50%, but strain (D2) is heterogeneous and partitioned into domains of coaxial northeast-southwest shortening and sinistral strike-slip shear. Coaxial shortening is documented by ubiquitous northerly- to northwesterly-trending, upright to southwest-verging folds (F2). The non-coaxial component of the strain is partitioned into regional-scale northwest-trending strike-slip fault zones, in particular the main Colenso Fault Zone. The sinistral transpressive strains agree with the oblique closure of the Adamastor ocean during the late Neoperoterozoic and probably until 520 Ma. The lack of burial metamorphism and subsequent exhumation that has also preserved original depositional environments and shallow intrusive features suggests that the deformation in the western Saldania records a soft collisional event, probably as a result of slab break-off. This break-off may also account for the voluminous, syn- to late-tectonic (550–510 Ma) granite plutonism of the CGS in the fore-arc region.

Acknowledgements Much of this work is based on the work of many Stellenbosch geology students over a period of more than 15 years. We thank these students for their enthusiasm, sharing their results and contributing to our knowledge of Western Cape geology. We also thank the geologists of the Council for Geoscience in the Bellville office for their continued support and discussions, and for providing unpublished maps and reports. AK gratefully acknowledges many enlightening discussions with Gary Stevens and John Clemens of Stellenbosch University on anything granite related. We thank Christie Rowe for a critical, highly detailed and very constructive review of an earlier version of the manuscript, and Siggi Siegesmund for additional comments, editorial guidance and patience.

References

Armstrong R, de Wit MJ, Reid D, York D, Zartman R (1998) Cape Town's table mountain reveals rapid Pan-African uplift of its basement rocks. J Afr Earth Sci 27(1A):10

Basei MAS, Frimmel HE, Nutman AP, Preciozzi F, Jacob J (2005) A connection between the Neoproterozoic Dom Feliciano (Brazil/Uruguay) and Gariep (Namibia/South Africa) orogenic belts—evidence from a reconnaissance provenance study. Precambr Res 139:195–221

Belcher RW (2003) Tectonostratigraphic evolution of the Swartland region and aspects of orogenic lode-gold mineralisation in the Pan-African Saldania Belt, Western Cape, South Africa. Ph.D thesis (unpubl.), University of Stellenbosch, 244 p

Belcher RW, Kisters AFM (2003) Lithostratigraphic correlations in the western branch of the Pan-African Saldania Belt, South Africa: the Malmesbury Group revisited. S Afr J Geol 106:327–342

Buggisch W, Kleinschmidt G, Krumm S (2010) Sedimentology, geochemistry and tectonic setting of the Neoproterozoic Malmesbury Group (Tygerberg Terrane) and its relation to neighbouring terranes, Saldania Fold Belt, South Africa. Neues Jahrbuch fur Geologie und Palaontologie 257:85–114

Cawood PA, Hawkesworth CJ, Dhuime B (2012) Detrital zircon record and tectonic setting. Geology 40(10):875–878

Chappell BW, White AJR (1974) Two contrasting granite types. Pac Geol 8:173–174

Chemale F, Scheepers R, Gresse PG, Schmus WRV (2011) Geochronology and sources of late Neoproterozoic to Cambrian granites of the Saldania Belt. Int J Earth Sci 100:431–444

Clemens JD (2003) S-type granitic magmas—petrogenetic issues, models and evidence. Earth-Sci Rev 61:1–18

Clemens JD, Belcher RW, Kisters AFM (2010) The Heerenveen batholith, Barberton Mountain Land, South Africa: Mesoarchaean felsic magmas formed by melting of an ancient subduction complex. J Petrol. https://doi.org/10.1093/petrology/egq014

Clemens JD, Helps PA, Stevens G (2009) Chemical structure in granitic magmas—a signal from the source? Proc R Soc Edinb 100:1–14

Clemens JD, Buick IS, Kisters AFM (2017) The Donkerhuk batholith, Namibia: a giant S-type granite emplaced in the mid crust, in a fore-arc setting. J Geol Soc London 174:157–169

Da Silva LC, Gresse PG, Scheepers R, McNaughton NJ, Hartmann LA, Fletcher I (2000) U-Pb and Sm-Nd age constraints on the timing and sources of the Pan-African Cape Granite Suite, South Africa. J Afr Earth Sci 30:795–815

De Villiers J, Jansen H, Mulder MP (1964) The geology of the area between Worcester and Hermanus. Explanations sheets 3319C Worcester and 3419A Caledon and parts of the sheets 3318D Stellenbosch and 3418B Somerset West. Geological Survey of South Africa, South Africa, p 69

Farina F, Stevens G, Villaros A (2012) Multi-batch incremental assembly of a dynamic magma chamber: the case of the Peninsula Pluton granite (Cape Granite Suite, South Africa). Mineral Petrol. https://doi.org/10.1007/s00710-012-0224-8

Fisher D, Byrne T (1987) Structural evolution of underthrusted sediments, Kodiak Islands, Alaska. Tectonics 6:775–793

Fölling PG, Zartmann RE, Frimmel HE (2002) A novel approach to double-spike Pb-Pb dating of carbonate rocks: examples from Neoproterozoic sequences in southern Africa. Chem Geol 171:97–122

Fossen H, Tikoff B (1998) Extended models of transpression and transtension, and applications to tectonic settings. In: Holdsworth RE, Strachan RA, Dewey JF (eds) Continental transpressional and transtensional tectonics, vol 135. Geological Society of London Special Publication, pp 15–33

Frimmel HE (2009) Configuration of Pan-African orogenic belts in southwestern Africa. In: Gaucher C, Sial AN, Halverson GP, Frimmel HE (eds) Neoproterozoic-Cambrian tectonics, global change and evolution: a focus on southwestern Gondwana, vol 16. Developments in Precambrian geology, Elsevier, pp 145–151

Frimmel HE, Frank W (1998) Neoproterozoic tectono-thermal evolution of the Gariep Belt and its basement, Namibia and South Africa. Precambr Res 90:1–28

Frimmel HE, Basei MAS, Gaucher C (2011) Neoproterozoic geodynamic evolution of SW Gondwana: a southern African perspective. Int J Earth Sci 100:323–354

Frimmel HE, Basei MAS, Correa VX, Mbangula N (2013) A new lithostratigraphic subdivision and geodynamic model for the western Pan-African Saldania Belt, South Africa. Precambr Res 231:218–235

Gaucher C, Frimmel HE, Germs GJB (2009) Tectonic events and paleogeographic evolution of southwestern Gondwana in the Neoproterozoic and Cambrian. In: Gaucher C, Sial AN, Halverson GP, Frimmel HE (eds) Neoproterozoic-Cambrian tectonics, global change and evolution: a focus on southwestern Gondwana, vol 16. Developments in Precambrian Geology, Elsevier, pp 295–316

Goscombe BD, Gray DR (2008) Structure and strain variation at mid-crustal levels in a transpressional orogen: a review of the Kaoko Belt structure and the character of West Gondwana amalgamation and dispersal. Gondwana Res 13:45–85

Goscombe BD, Hand M, Gray D (2003) Structure of the Kaoko Belt, Namibia: progressive evolution of a classic transpressional orogen. J Struct Geol 25:1049–1081

Gresse PG (1994) Strain partitioning in the southern Gariep arc as reflected by sheath folds and stretching lineations. S Afr J Geol 97:52–61

Gresse PG (1995) Transpression and transection in the late Pan-African Vanrhynsdorp foreland thrust-fold belt, South Africa. J Afr Earth Sci 21:91–105

Gresse PG, Theron JN (1992) The geology of the Worcester area. Explanation sheet 3319 Worcester (1:250.000), Geological Survey of South Africa, 79 p

Gresse PG, Von Veh MW, Frimmel HE (2006) Namibian (neoproterozoic) to early Cambrian successions. In: Johnson MR, Anhaeusser CR, Thomas RJ (eds) The geology of South Africa. Geological Society of South Africa, Johannesburg/Council for Geoscience, Pretoria, pp 395–420

Hartnady CJH (1969) Structural analysis of some pre-Cape formations in the Western Province, vol 6. Bulletin Precambrian Research Unit, University of Cape Town

Hartnady CJH, Newton AR, Theron JN (1974) The stratigraphy and structure of the Malmesbury Group in the southwestern Cape, vol 15. Bulletin Precambrian Research Unit, University Cape Town, pp 193–213

Hartnady CJ, Joubert P, Stowe CW (1985) Proterozoic crustal evolution of southwestern Africa. Episodes 8:236–244

Harris CJ, Vogeli J (2010) Oxygen isotope composition of garnet in the Peninsula granite, Cape Granite Suite, South Africa: constraints on melting and emplacement mechanisms. South African J Geol 401–412

Heller PL, Ryberg PT (1983) Sedimentary record of subduction to fore-arc transition in the rotated Eocene basin of western Oregon. Geology 11(7):380–383

Kisters AFM, Belcher RW, Armstrong RA, Scheepers R, Rozendaal A, Jordaan LS (2002) Timing and kinematics of the Colenso Fault; the Early-Paleozoic shift from collisional to extensional tectonic in the Pan-African Saldania Belt, South Africa. S Afr J Geol 105:257–270

Kisters AFM, Agenbach C, Frei D (2015) Age and tectonic significance of the volcanic Bloubergstrand member in the Pan-African Saldania Belt, South Africa. S Afr J Geol 118:213–224

Konopasek J, Kröner S, Kitt SL, Passchier CW, Kröner A (2005) Oblique collision and evolution of large-scale transcurrent shear zones in the Kaoko belt, SW Namibia. Precambr Res 136:139–157

Malavieille J (2010) Impact of erosion, sedimentation and structural heritage on the structure and kinematics of orogenic wedges: analog models and case studies. GSA Today 20:4–10

McGibbon D (2012) Structural inventory and style of the Tygerberg formation along coastal outcrops near Grotto Bay, West Coast, South Africa: Implications for the tectonic evolution of the Pan-African Saldania Belt. BSc Honours thesis (unpubl.), University of Stellenbosch, 67 p

Meneghini F, Kisters AFM, Buick IS, Fagereng A (2014) Fingerprints of Late-Neoproterozoic ridge subduction in the Pan-African Damara Belt, Namibia. Geology 42:903–906

Miller RM (2008) Neoproterozoic and early Palaeozoic rocks of the Damara Orogen. In: Miller RM (ed) The geology of Namibia, vol 2. Geological Survey of Namibia, Windhoek

Miller RM, Frimmel HE, Will TM (2009) Geodynamic synthesis of the Damara Orogen sensu lato. Neoproterozoic to early Palaeozoic evolution of Southwestern Africa. In: Gaucher C, Sial AN, Halverson GP, Frimmel HE (eds) Neoproterozoic-Cambrian tectonics, global change and evolution: a focus on Southwestern Gondwana, vol 16. Developments in Precambrian Geology, Elsevier, Amsterdam, pp 231–235

Newton AR (1966) Preliminary report on work on Malmesbury Rocks. In: 4th annual report, Precambrian Res. Unit, University of Cape Town, pp 16–17

Noda, A. (2016) Fore arc basins: Types, geometries and relationships to subduction zone dynamics. Geological Society of America Bulletin. https://doi.org/10.1130/B31345.1

Oriolo S, Oyhantcabal P, Basei MAS, Wemmer K, Siegesmund S (2016) The Nico Perez Terrane (Uruguay): from Archaean crustal growth and connections with the Congo Craton to Late neoproterozoic accretion to the Rio de la Plata Craton. Precambr Res 280:147–160

Rabie LP (1948) Geological Map of the Morreesburg-Wellington area. University of Stellenbosch

Rabie IP (1974) Geological map of the Morreessburg-Wellington area. Annals of the University of Stellenbosch, vol 49 (A5)

Raimbourg H, Tadahiro S, Yamaguchi A, Yamaguchi H, Gaku K (2009) Horizontal shortening versus vertical loading in accretionary prisms. Geochem Geophys Geosyst (G3) 10(4):1–17

Rapela CW, Fanning MC, Casquet C, Pankhurst RJ, Spalletti C, Poire D, Baldo EG (2011) The Ria de la Plata Craton and adjoining Pan-African/Brasiliano terranes: their origin and incorporation into SW Gondwana. Gondwana Res 20:673–690

Robin P-YF, Cruden AR (1994) Strain and vorticity patterns in ideally ductile transpression zones. J Struct Geol 15:1–20

Rowe CD, Backeberg NR, Van Rensberug T, McLennan SA, Faber C, Curtis C, Viglietti PA (2010) Structural geology of Robben Island: implications for the tectonic environment of Saldanian deformation. S Afr J Geol 113:57–72

Rozendaal A, Bruwer L (1995) Tourmaline nodules: indicators of hydrothermal alteration and Sn-Zn-(W) mineralization in the Cape Granite Suite, South Africa. J Afr Earth Sci 21:141–155

Rozendaal A, Gresse PG, Scheepers R De, Beer CH (1994) Structural setting of the Riviera W-Mo deposit, Western Cape, South Africa. S Afr J Geol 97:184–195

Rozendaal A, Gresse PG, Scheepers R, Le Roux JP (1999) Neoproterozoic to early Cambrian crustal evolution of the Pan-African Saldania belt, South Africa. Precambr Res 97:303–323

Santra M, Steel RJ, Olariu C, Sweet ML (2013) Stages of sedimentary prism development on a convergent margin—Eocene Tyee forearc basin, Coast Range, Oregon, USA. Global Planet Change 103:207–231

Scheepers R (1995) Geology and petrogenesis of the Late-Precambrian S-, I-, and A-type granitoids in the Saldania belt, Western Cape Province, South Africa. J Afr Earth Sci 21:35–58

Scheepers R, Schoch AE (2006) The Cape granite suite. In: Johnson MR, Anhaeusser CR, Thomas RJ (eds) The geology of South Africa. Geological Society of South Africa, Johannesburg/Council for Geoscience, Pretoria, pp 421–432

Schoch AE (1956) The cataclasites of Northwest Bay. Ann Univ Stellenbosch 37A(10):659–808

Schoch AE (1975) The Darling granite batholith. Ann Univ Stellenbosch 1(A1):1–104

Schoonmaker A, Kidd WSF, Bradley DC (2005) Foreland-forearc collisional granitoid and mafic magmatism caused by lower lithospheric slab breakoff: the Acadian of Maine, and other orogens. Geology 33:961–964

Slabber N (1995) The geology and geochemistry of the Bridgetown Formation of the Malmesbury group, Western Cape province. M.Sc. Thesis (unpubl), University of Stellenbosch, 99 p

South African Committee for stratigraphy (SACS) (1980) Stratigraphy of South Africa. Part 1 (Comp. L. E. Kent). Lithostratigraphy of the Republic of South Africa, SW Africa/Namibia, and the Republics of Bophuthatswana, Transkei and Venda. Handbook Geol Surv S A 8

Stevens G, Villaros A, Moyen J-F (2007) Selective peritectic garnet entrainment as the origin of geochemical diversity in S-type granites. Geology 35:9–12

Tankard AJ, Jackson MPA, Eriksson KA, Hobday DK, Hunter DR, Minter WEL (1982) Crustal evolution of Southern Africa: 3.5 billion years of earth history. Springer, New York, p 523

Tankard A, Welsink H, Aukes P, Newton R, Stettler E (2009) Tectonic evolution of the Cape and Karoo basins of South Africa. Mar Pet Geol 26:1379–1412

Thamm AG and Johnson MR (2006) The Cape Supergroup. In: Johnson MR, Anhaeusser CR, Thomas RJ (eds) The geology of SouthAfrica. Geological Society of South Africa, Johannesburg/Council for Geoscience, Pretoria, pp 443–460

Theron, J.N. (1984) The geology of Cape Town and environs, explanation of sheets 3318CD and DC and 3418 AB, AD and BA. Geological Survey of South Africa, 77 p

Theron JN, Gresse PG, Siegfried HP, Rogers J (1992) The geology of the Cape Town area. Explanation Sheet 3318. Department of Mineral and Energy Affairs, Geological Survey, Pretoria, 140 p

Tikoff B, Teyssier C (1994) Strain modelling of displacement field partitioning in transpressional orogens. J Struct Geol 10:1575–1588

Tikoff B, Peterson K (1998) Physical experiments of transpressional folding. J Struct Geol 20:661–672

Villaros A, Stevens G, Buick IS (2009) Tracking S-type granite from source to emplacement: clues from garnet in the Cape granite suite. Lithos 112:217–235

Villaros A, Buick IS, Stevens G (2011) Isotopic variations in S-type granites: an inheritance from a heterogeneous source? Contributions to Mineralogy and Petrology. https://doi.org/10.1007/s00410-011-0073-9

Von Veh MW (1983) Aspects of Sedimentation, structure and tectonic evolution in the Tygerberg Terrane, southwestern Cape Province, vol 32. Bulletin of the Precambrian Research Unit, University of Cape Town, 84 p

Von Veh MW (1993) The stratigraphy and structural evolution of the Lste Proterozoic Gariep Belt in the Sendelingsdrif-Annisfontein area, northwestern Cape Province, vol 38. Bulletion Precambrian Research Unit University of Cape Town, 174 p

Wall VJ, Clemens JD, Clarke DB (1987) Models for granitoid evolution and source composition. J Geol 95:731–750

Suturing Gondwana in the Cambrian: The Orogenic Events of the Final Amalgamation

15

Renata da Silva Schmitt, Rafael de Araújo Fragoso, and Alan Stephen Collins

Abstract

Gondwana was consolidated in the late Cambrian after 180 myr of tectonic convergence among Neoproterozoic paleocontinents and smaller fragments. We present a compilation of 55 orogens that record its final amalgamation. Collisional events are registered by the metamorphic peak assemblages and contractional deformational structures. Two main periods of orogenic activity are recognized. The first at *c*. 670–575 Ma includes few orogens (*c*. 15) but over larger areas. During this stage, the Saharan, West African, São Francisco-Congo and Paranapanema paleocontinents, along with the Arabian Nubian shield that consisted of juvenile Tonian terranes and some East African Orogen microcontinents, were accreted to form the proto-Gondwana core. The second stage, at 575–480 Ma, incorporated more orogens, *c*. 40, that sutured the Amazonia, Rio de La Plata, Kalahari, Dhawar, East Antarctica and Australian paleocontinents. The collisional orogen pattern throughout both western and eastern Gondwana is similar, indicating that although Gondwana was built up by the convergence of distinct paleocontinents, their approximation might be orchestrated by global geodynamics. In SW Gondwana, the opening of *c*. 610–570 Ma basins, some with oceanic crust, coincided with the suturing of the proto-Gondwana core. They were rapidly formed but even more quickly inverted during the second and last 575–480 Ma collisional stage, represented by the major east–west Kuunga and north–south South Atlantic belts. We propose that the 570–500 Ma collision of the Damara-Lufilian-Zambesi belt was coeval with the Cuchilla Dionisio-Saldania-Gariep-Dom Feliciano-Kaoko-Ribeira-Cabo Frio orogens. This South Atlantic orogenic system consists of the main SW Gondwana suture, reactivated 350 myr later to form the South Atlantic Ocean. The suture is preserved by old orogenic high-pressure and oceanic-derived rocks on the actual conjugate continental margins.

Keywords

Gondwana • Ediacaran-Cambrian tectonics
Sutures • South Atlantic orogenic system

15.1 Introduction

Gondwana amalgamation was the product of a diachronic convergence of Neoproterozoic continents that culminated in the Early Paleozoic (Kennedy 1964; Boger and Miller 2004; Collins and Pisarevsky 2005; Li et al. 2008; Meert and Lieberman 2008; Merdith et al. 2017a). The convergent margins were a mix of long-lived margins inherited from the Mesoproterozoic, and new convergent margins that succeeded the break-up of the Tonian supercontinent Rodinia. The Neoproterozoic can be summarized as a combinaton of a transition from Rodinia to Gondwana (Hoffman 1991) along with the closure of a vast pre-Rodinian accretionary orogen by the collision of Neoproterozoic India with an East African-Antarctic-West Australian margin (Merdith et al. 2017a). A number of models for this rifting and reconfiguration have been proposed (Dalziel 1991, 1997; Hoffman 1991; Moores 1991; Karlstrom et al. 1999; Burrett and Berry 2000; Wingate et al. 2002; Li et al. 2008, Merdith et al. 2017a). These have recently been kinematically tested by comparing their plate tectonic motion implications (Merdith et al. 2017b).

It has long been proposed that two major tectonic periods were responsible for Gondwana construction (Clifford 1967; Stern 1994; Meert 2003; Collins and Pisarevsky 2005; Cawood and Buchan 2007; Merdith et al. 2017a). The older

R. da S. Schmitt (✉) · R. de A. Fragoso
Departamento de Geologia, Universidade Federal do Rio de Janeiro, Rio de Janeiro, 21949-900, Brazil
e-mail: schmitt@geologia.ufrj.br

A. S. Collins
Department of Earth Sciences, Centre for Tectonics, Resources and Exploration (TRaX), The University of Adelaide, Adelaide, SA 5005, Australia

S. Siegesmund et al. (eds.), *Geology of Southwest Gondwana*, Regional Geology Reviews,
https://doi.org/10.1007/978-3-319-68920-3_15

Table 15.1 Data compilation of Gondwana post-670 Ma orogens with references

Name	Continent	Meta. Deform. (Id) (Ma)	Meta. Deform. (Id) (Ma)	References
Ribeira Belt—Paralba/Embu/Apiaf Terranes	South America	670–640	600–570	Heilbron et al. (2008) and references therein, Duffles et al. (2016)
Ribeira Belt—Oriental Terrane/Costeiro Domain	South America	580–500	–	Heilbron et al. (2008) and references therein
Ribeira Belt—Cabo Frio Tectonic Domain	South America	540–490	–	Schmitt et al. (2004, 2008), Fernandes et al. (2015), Bongiolo et al. (2016)
Araçuaí Belt—West	South America	590–560	–	de Campos et al. (2016), Richter et al. (2016), Degler et al. (2017)
Araçuaí Belt—East	South America	585–535	–	Gradim et al. (2014), de Campos et al. (2016), Richter et al. (2016), Degler et al. (2017)
Cuchilla Dionisio Terrane	South America	570–520	–	Bossi and Gaucher (2004), Will and Frimmel (2018)
Nico Perez Terrane	South America	630–580	–	Oriolo et al. (2016)
Dom Feliciano Belt	South America	650–610	–	Philipp et al. (2016) and references therein
Brasilia Belt (North and South)	South America	650–610	–	Trouw et al. (2013) and references therein, Ganade de Araujo et al. (2014a, b) and references therein
Gurupi Belt	South America	580–520	–	Klein et al. (2012) and references therein
Araguaia Belt	South America	560–530	–	Moura et al. (2008), Paixão et al. (2008), Tohver et al. (2012)
Paraguay Belt	South America	540–500	–	Godoy et al. (2010), Bandeira et al. (2012), Hasui et al. (2012) and references therein, McGee et al. (2012), Piacentini et al. (2013)
Borborema Province—North	South America	610–570	–	Ganade de Araujo et al. (2014a, b) and references therein
Borborema Province—Central	South America	610–570	–	Van Schmus et al. (2008), Ganade de Araujo et al. (2014b) and references therein
Rio Preto Belt	South America	590–540	–	Caxito et al. (2016)
Mar del Plata Terrane—Punta Mogotes	South America	550–520	–	Rapela et al. (2011)
Borborema Province—South (Sergipano)	South America	590–540	–	Oliveira et al. (2010), Ganade de Araujo et al. (2014b) and references therein
Caapucu High	South America	580–530	–	Ramos et al. (2010) and references therein
Pampean Orogen	South America	530–510	–	Lira et al. (1997), Rapela et al. (1998, 2002), Schwartz et al. (2008), Martino et al. (2009), Escayola et al. (2011)
Ad Dawadimi and Ar Rayn Terranes	Africa	620–607	–	Johnson et al. (2011), Cox et al. (2012)
Arabian Nubian Shield—North	Africa	650–605	–	Fritz et al. (2013) and references therein
Arabian Nubian Shield—South	Africa	650–610	–	Fritz et al. (2013) and references therein
Mozambique Belt	Africa	650–610	–	Fritz et al. (2013) and references therein
Mozambique Belt—Nampula Block	Africa	520–480	–	Fritz et al. (2013) and references therein
Bemarivo Belt—Madagascar	Africa	540–500	–	Tucker et al. (2014)
Vohibori/Androyen Domains—-Madagascar	Africa	630–600	580–550	Boger et al. (2015)
Antananarivo Block—Madagascar	Africa	580–520	–	Berger et al. (2006), Collins (2006), Grégoire et al. (2009), Goodenough et al. (2010), Giese et al. (2011)
Hoggar	Africa	625–590	–	Berger et al. (2014), Ganade de Araujo et al. (2014a, b) and references therein
Dahomey	Africa	610–570	–	Ganade de Araujo et al. (2016) and references therein
West Congo Belt	Africa	630–560	–	Tack et al. (2001), Frimmel et al. (2006)
Lufilian Belt	Africa	560–530	–	Frimmel et al. (2011) and references therein
Zambesi Belt	Africa	580–540	–	Fritz et al. (2013)

(continued)

Table 15.1 (continued)

Name	Continent	Meta. Deform. (Id) (Ma)	Meta. Deform. (Id) (Ma)	References
Angolan Belt	Africa	550–510	–	Monié et al. (2012)
Damara Belt	Africa	590–550	580–510	Frimmel et al. (2011) and references therein
Kaoko Belt—Central East	Africa	580–540	–	Frimmel et al. (2011) and references therein; Goscombe et al. (2017)
Kaoko Belt—Coastal Terrane	Africa	650–630	530–510	Frimmel et al. (2011) and references therein; Goscombe et al. (2017)
Gariep Belt	Africa	575–545	–	Frimmel et al. (2011) and references therein, Diener et al. (2017)
Anti–Atlas Belt	Africa	590–540	–	Garfunkel (2015)
Rokelides Belt	Africa	550–530	–	Villeneuve (2008)
Oubanguides Belt	Africa	615–570	–	Owona et al. (2011)
Saldania Belt	Africa	550–520	–	Frimmel et al. (2011) and references therein, Frimmel et al. (2013)
Galana Terrane	Africa	580–550	–	Fritz et al. (2013) and references therein
Western Granulites	Africa	560–530	–	Fritz et al. (2013) and references therein
Meghalaya Plateau	India	540–500	–	Kumar et al. (2016)
Southern Granulite terrane	India	590–510	–	Collins et al. (2014) and references therein, Richard et al. 2015
Eastern Ghats Mobile Belt	India	550–500	–	Crowe et al. (2001) and references therein, Collins and Pisarevsky (2005)
Dronning Maud Land—SRM and YBC[a]	Antarctica	640–600	–	Shiraishi et al. (2003, 2008), Jacobs et al. (2015)
Dronning Maud Land (West)	Antarctica	580–550	–	Pauly et al. (2016) and references therein
Prince Olaf Coast/Kemp Land—Lutzow–Holm Complex	Antarctica	560–520	–	Tsunogae et al. (2015)
Princess Elizabeth Land	Antarctica	530–490	–	Corvino et al. (2008) and references therein
Ross Orogeny—North Victoria Land	Antarctica	550–480	–	Paulsen et al. (2013) and references therein; Estrada et al. (2016) and references therein
Ross Orogeny—South Victoria Land	Antarctica	530–480	–	Paulsen et al. (2016) and references therein
Ross Orogeny—Pensacola Mountains	Antarctica	560–490	–	Schmidt and Ford (1969); Curtis et al. (2004) and references therein
Delamerian Orogen	Australia	530–480	–	Gibson et al. (2015) and references therein, Johnson et al. (2016) and references therein
Petermann Orogen	Australia	570–530	–	Major and Conor (1993), Wade et al. (2008), Haines et al. (2016) and references therein
Pinjarra Orogen	Australia	540–510	–	Collins et al. (2003)

EAO Eastern African Orogen; *EGCD* Eastern Granulite-Cabo Delgado
[a]*SRM* Sor Rondane Mountains, *YBC* Yamato-Belgica Complex

comprised Late Tonian and Cryogenian (pre-670 Ma) mostly accretionary orogens, preserved within the belts, normally reworked by younger orogenic events. The second and later period included Cryogenian through Cambrian (post-670 Ma) accretionary/collisional settings, responsible for suturing the newly formed supercontinent. These final Gondwana 'internal orogens' (e.g., Buzios, Damara, Saldania, Paraguay, Araguaia, Malagasy, Kuunga orogenies) overlapped in time with the initiation of convergent settings on the newly formed margins, certainly influencing the coeval Cambro-Ordovician 'external' orogens (e.g., Pampean, Ross, Delamerian, Bhimphedian; Rapela et al. 1998, 2011; Schmitt et al. 2004; Foden et al. 2006; Oriolo et al. 2017). Therefore, by the end of the Cambrian, Gondwana was laced by a series of internal Himalayan-style belts formed by continent–continent collision superimposed on earlier accretionary orogens and ringed by accretionary orogens that although may have been initiated during the final Gondwana formation were to last for the duration of the Phanerozoic. These are dominated by the accretion of oceanic materials along the Gondwana margins (Murphy and Nance 1991; Cawood 2005; Collins et al. 2011).

However, the nature of the 'internal orogens' is still a matter of debate. Some authors suggest that they are products of the closure of large oceans, culminating with the collision of faraway paleocontinents (e.g., Clymene Ocean, Tohver et al. 2012; Khomas Ocean, Foster et al. 2015; Adamastor Ocean, Heilbron et al. 2008; Mozambique Ocean, Stern 1994; Meert and Van Der Voo 1997; Collins and Windley 2002; Boger and Miller 2004). Another point of view suggests that these orogens were the product of intracontinental rifting and basin inversion in between blocks that were never far apart (e.g., Araguaia Belt, Cordani et al. 2013a; Damara belt, Nascimento et al. 2017; Ribeira Belt, Meira et al. 2015). These two end members produced distinctive collisional processes during the last convergent phase, providing either a Himalayan or an Alpine-type orogenic style. Differences include the occurrence of a pre-collisional arc in the former, and the development of a hyperextended margin with exhumation of subcontinental lithospheric mantle in the second type (Manatschal and Müntener 2009).

Here we present a review of the main orogenic belts that consolidated Gondwana, using the geological database of the new geological map of Gondwana (Schmitt et al. 2016a), focusing on the post-670 Ma orogenic pulses. The geological data confirms that the Cryogenian-Cambrian orogenic events are widespread in all belts that sew Gondwana together, in both eastern and western major fragments. In addition, we discuss these events in SW Gondwana, mostly preserved on the actual coastal regions of South America and Africa with an inland branch (Damara belt). This implies that the basement of the Atlantic continental margins comprises Ediacaran-Cambrian belts (Schmitt et al. 2016b). Our data also shows that during the last period of Gondwana formation, there was an extensional stage (*c*. 610–570 Ma) that pre-dated the final collisional events. The 'South Atlantic orogenic system' contains geological units of oceanic nature from this stage. The cause of closing these Ediacaran basins could have been the initiation of the marginal Gondwana convergent settings or the far-field effects of the Himalayan-scale collision caused by Neoproterozoic India colliding with both Australia and Africa at this time (Merdith et al. 2017a).

15.2 Gondwana Amalgamation

Although not including all of the Earth's major continental fragments (e.g., Laurentia, Baltica), Gondwana is commonly referred to as a supercontinent (Fig. 15.1). Its landmass represents around 64% of today's continental crust (Torsvik and Cocks 2013), composed of the continents of Africa, South America, India, Australia and Antarctica, including several smaller fragments now incorporated into Asia, Europe and North America. The supercontinent title is not only related to the amount of participating continental crust but also to its endurance, rarely registered in the evolution of the Earth's history. Gondwana lasted as a merged landmass *c*. 320 myr, from the Cambrian (*c*. 500 Ma) until the Jurassic (*c*. 180 Ma), comparing only to the lifetime of Archean cratons (Condie et al. 2015). Gondwana's lifetime expands to a value between 800 and 600 myr when taking into account the amalgamation and break-up processes. Supercontinental cycles are assumed to vary from 250 to 1000 myr, including both assembly and dispersal (Condie et al. 2015). Gondwana's break-up interval started at *c*. 183 Ma, with Madagascar splitting away from East Africa, and ended at *c*. 85 Ma, with Antarctica and Australia's separation (White et al. 2013; Reeves 2014), lasting *c*. 100 myr. Nevertheless, the amalgamation period was longer, from 670 to 480 Ma (*c*. 190 myr), considering all the orogenic belts that sutured the Neoproterozoic cratons (Fig. 15.2). However, if the Late Tonian-Cryogenian tectonic events (850–670 Ma) are included in this timeframe, then the amalgamation period lasted for more than 370 myr.

The earlier Tonian-Cryogenian events are dispersed within some belts. In terms of the volume of continental crust reworked or generated, these are minor in comparison with the equivalent Ediacaran–Cambrian regions. It is noteworthy that the Tonian-Cryogenian domains have a large percentage of juvenile material (Johnson et al. 2011; Oriolo et al. 2017), suggesting that much of the continental crust was generated at this time, in contrast to the Ediacaran-Cambrian, which involved more tectonothermal reworking of existing crust.

Here we consider the 670–480 Ma tectonic events to be directly responsible for Gondwana amalgamation. According to the compiled data, within this timeframe, two stages of convergent tectonics are identified, overlapping partially with a transitional extensional period (*c*. 610–570 Ma) (Figs. 15.2 and 15.3).

The birth of Gondwana is best represented by the map of Neoproterozoic cratons and Neoproterozoic-Cambrian belts (Trompette 1994; Collins 2006; Gray et al. 2008; Fig. 15.1). We present a new version of the Gondwana cratons-belts map, based on the new geological map of Gondwana (Schmitt et al. 2016a). Our compilation shows 55 post-670 Ma belts which register Gondwana's final amalgamation, suturing *c*. 16 cratonic blocks (Figs. 15.1 and 15.2).

Many authors suggest that the approximation and collision between the Neoproterozoic paleocontinents was orchestrated by the Rodinia supercontinent break-up (Hoffman 1991; Cawood and Buchan 2007). This common sense is based mostly on the similarities between the cratons' 'barcodes' (age pattern of crustal growth) and paleomagnetic data. However, some western Gondwana cratons (and possibly India; Merdith et al. 2017a) might not have been Rodinian participants (Cordani et al. 2003; Oriolo et al.

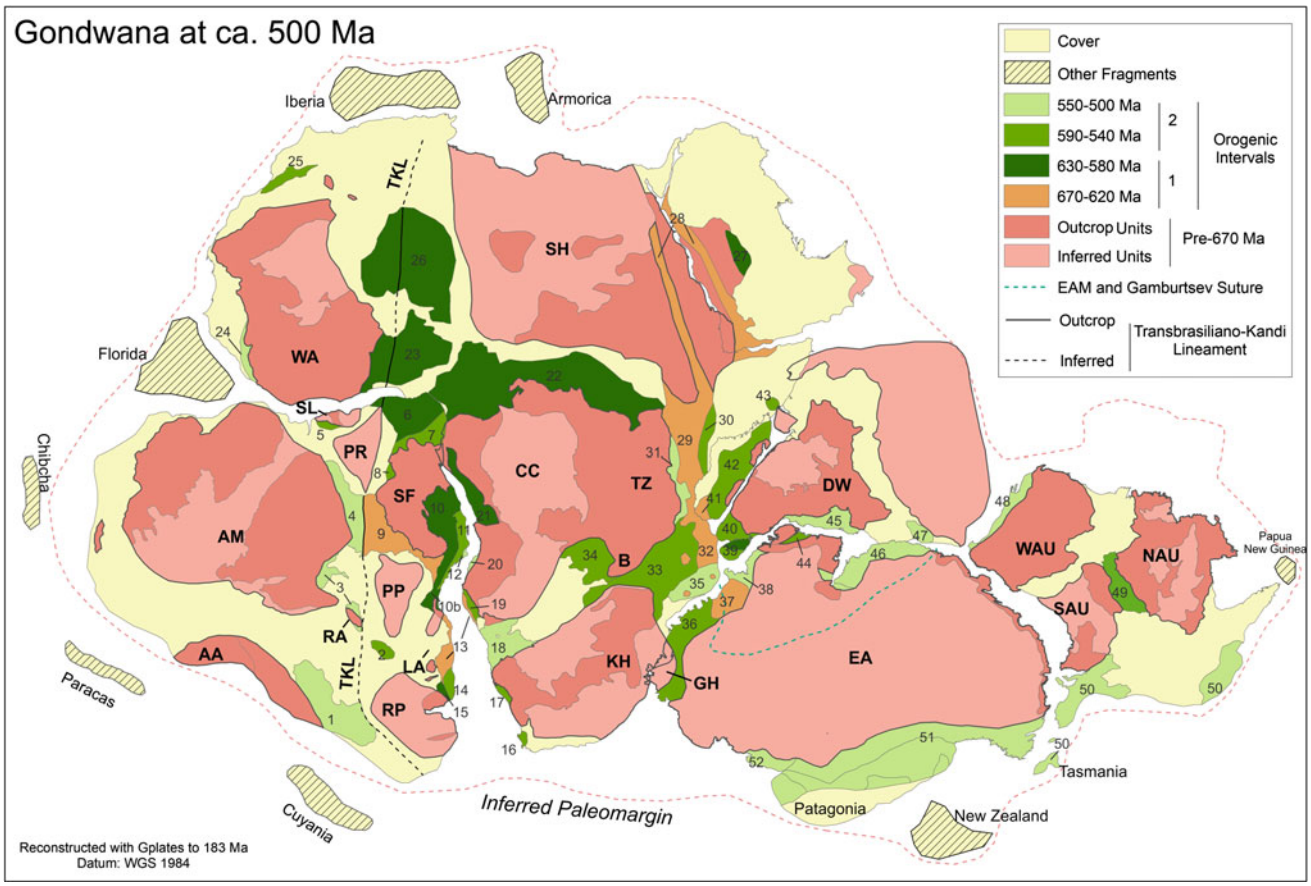

Fig. 15.1 Gondwana configuration at *c.* 500 Ma with cratons (pre-Gondwana continents) sutured by Gondwana mobile belts. This figure is mostly compiled from the new Gondwana geological map at 1:5 M scale (Schmitt et al. 2016a). It is also compiled from Collins (2003), Kröner and Cordani (2003), Heilbron et al. (2004), Jacobs et al. (1998, 2008), Schmitt et al. (2008), Ramos (2010), Frimmel et al. (2011), Offler et al. (2011), Fritz et al. (2013), Torsvik and Cocks (2013), Ramos and Naipauer (2014). Reconstruction by Richetti et al. (2016). The letters and numbers represent Gondwanan cratons and mobile belts, respectively. They are *AA* Arequipa/Antofalla; *AM* Amazonia; *RA* Río Apa; *SL* São Luís; PR, Parnaíba; SF, São Francisco; PP, Paranapanema; *LA* Luís Alves; *RP* Río de La Plata; KH, Kalahari; *B* Bangweulu Block; *TZ* Tanzania; *CC* Congo; *WA* West Africa; *SH* Sahara; *DW* Dharwar; *GH* Grunehogna; *EA* East Antarctica; *WAU* West Australia; *SAU* South Australia; *NAU* North Australia. 1—Pampeana; 2—Caapucú High; 3—Paraguai; 4—Araguaia; 5—Gurupi; 6—Borborema (North and Central); 7—Borborema (South); 8—Rio Preto; 9—Brasília; 10—Araçuaí (West), Ribeira (Paraíba/Embu); 10b—Apiaí; 11—Araçuaí (East), Ribeira (Oriental Terrane) and Costeiro Domain; 12—Cabo Frio Tectonic Domain; 13—Dom Feliciano, Kaoko (Coastal); 14—Cuchilla Dionísio; 15—Nico Pérez; 16—Saldania; 17—Gariep; 18—Damara; 19—Kaoko (Central-East); 20—Angolan Belt; 21—West Congo; 22—Oubanguides; 23—Dahomey; 24—Rockelides; 25—Anti-Atlas; 26—Hoggar; 27—Ad Dawadimi and Ar Rayn; 28—Arabian/Nubian Shield (North); 29—Arabian/Nubian Shield (South); 30—Galana (Azania); 31—Western Granulite; 32—Eastern Granulite; 33—Zambesi; 34—Lufilian; 35—Nampula Block; 36—Dronning Maud Land (West); 37—Dronning Maud Land (Sor Rondane Mountains and Yamato-Belgica Complex); 38—Prince Olaf Coast/Kemp Land, (Lützow-Holm Complex); 39—Sri Lanka; 40—Southern Granulites; 41—Madagascar (Vohibori); 42—Madagascar (Antananarivo, Androyen and Bemarivo); 43—Seychelles; 44—Reworked border of the Napier Complex; 45—Eastern Ghat; 46—Princess Elizabeth Land; 47—Meghalaya Plateau; 48—Pinjarra; 49—Petermann; 50—Delamerian; 51—Ross (Northern and Southern Victoria Land); 52—Ross (Pensacola Mountains). TKL stands for Transbrasiliano-Kandi Lineament

2017). Over recent decades it has become clear that the Neoproterozoic was an Era of several individual continents, inconsistent with the earlier ideas of only two single continents, named East and West Gondwana (cf. Shackleton 1996).There are large differences between the eastern and western orogens, but we will show that at the end of the amalgamation process (late Ediacaran-Cambrian), these orogens started to share a similar evolution.

15.2.1 Eastern Gondwana Orogens (Including the EAO)

Rocks deformed and metamorphosed in the East African Orogen (EAO; Stern 1994) extend, in a reconstructed Gondwana, from the eastern Mediterranean in the north (e.g., Candan et al. 2016), through Arabia (including NW India/Pakistan/Afghanistan), eastern Africa, Madagascar,

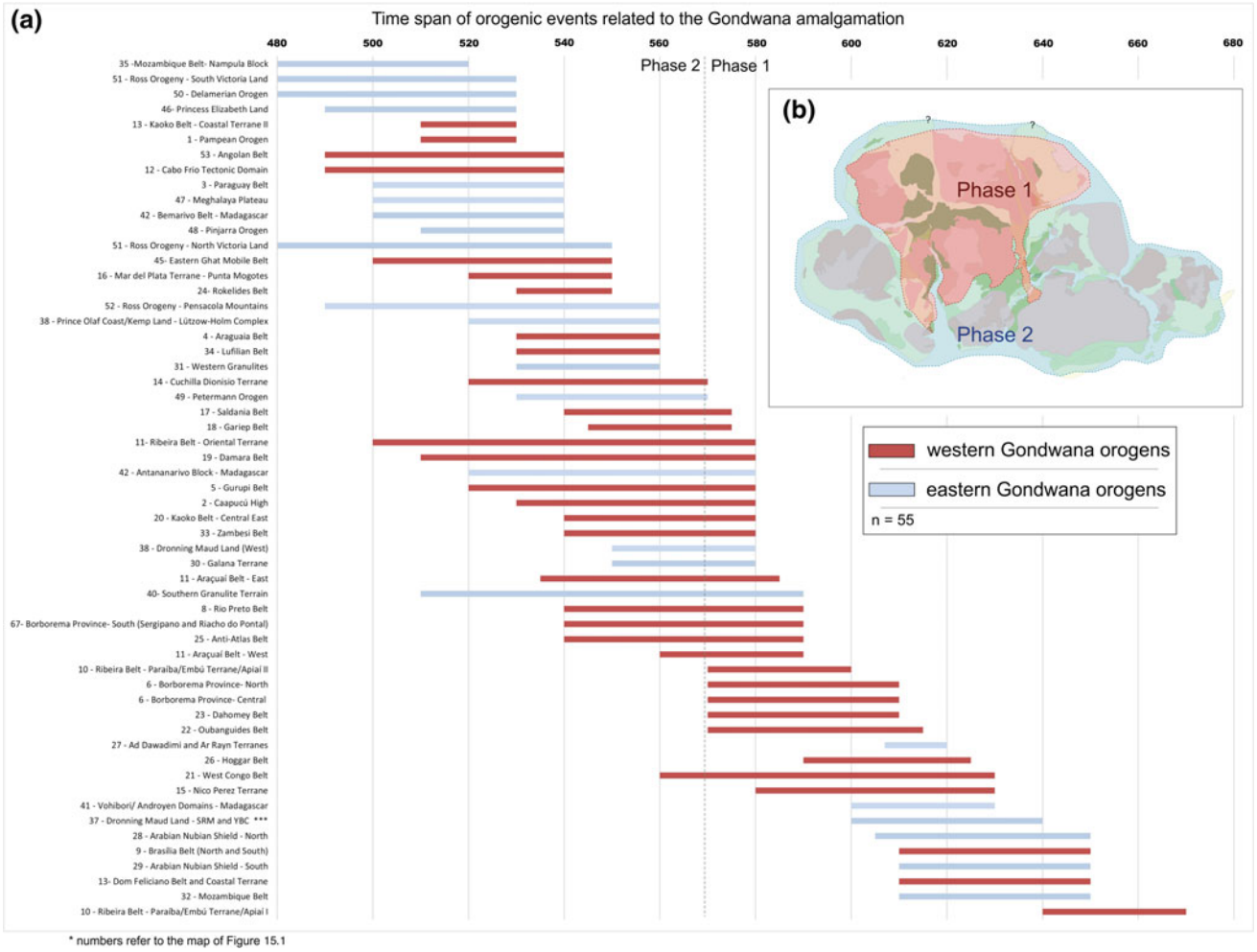

Fig. 15.2 **a** Time-space chart with all recorded eastern and western Gondwana orogens from the Ediacaran and Cambrian. The data was compiled from references listed in Table 15.1. **b** At the top right there is an insert of Gondwana with the areas corresponding to the two main amalgamation phases. Note that the proto-Gondwana core is centred on Africa

southern India and Sri Lanka to East Antarctica (Fig. 15.1). The orogen is likely to follow the subglacial East Antarctica Mountain Range (An et al. 2015) to the Gambutschev suture (Ferraccioli et al. 2011), where it meets the Kuunga Orogen (Meert et al. 1995; also known as the Pinjarra-Prydz-Denman Orogen; Fitzsimons 2003a, b; Fig. 15.1). Together these orogens delineate the western, southern and eastern margins of Neoproterozoic India.

The northern East African Orogen is part of the Arabian-Nubian Shield (Johnson et al. 2011) and is characterized by voluminous juvenile Neoproterozoic crust that formed as a series of volcanic arcs (Robinson et al. 2014, 2015a, b; Blades et al. 2015, 2017; Fig. 15.1). Less extensive continental terranes exist in the region, particularly in the Sinai (Be'eri-Shlevin et al. 2012; Eyal et al. 2014), in the Khida and Afif Terranes of Saudi Arabia (Stoeser et al. 2001; Whitehouse et al. 2001) and in Yemen (Windley et al. 1996, 2001; Whitehouse et al. 1998, 2001) with corollaries along the southern Gulf of Aden escarpment (Sassi et al. 1993; Whitehouse et al. 2001; Collins and Windley 2002). The eastern margin of the East African Orogen in Arabia is often left at the margin of the exposed Neoproterozoic in Saudi Arabia, but similar magnetic anomalies to the easternmost exposed Saudi terrane (the Ar-Rayn terrane; Doebrich et al. 2007; Cox et al. 2012) occur beneath the Ediacaran Rub Al-Khali Basin of Saudi Arabia (Johnson and Stewart 1995). Where Precambrian basement is exposed in the east of the Arabian Peninsula in Oman, it is again Neoproterozoic juvenile crust that formed in volcanic arc tectonic environments (Bowring et al. 2007; Whitehouse et al. 2016; Alessio et al. 2017). This led Cozzi et al. (2012) and Merdith et al. (2017a) to extend the East African Orogen to regions that now form the basement of southern Afghanistan, Pakistan and NW India.

The Mozambique Belt is the common name for the southern East African Orogen. Here, Tonian and pre-Tonian

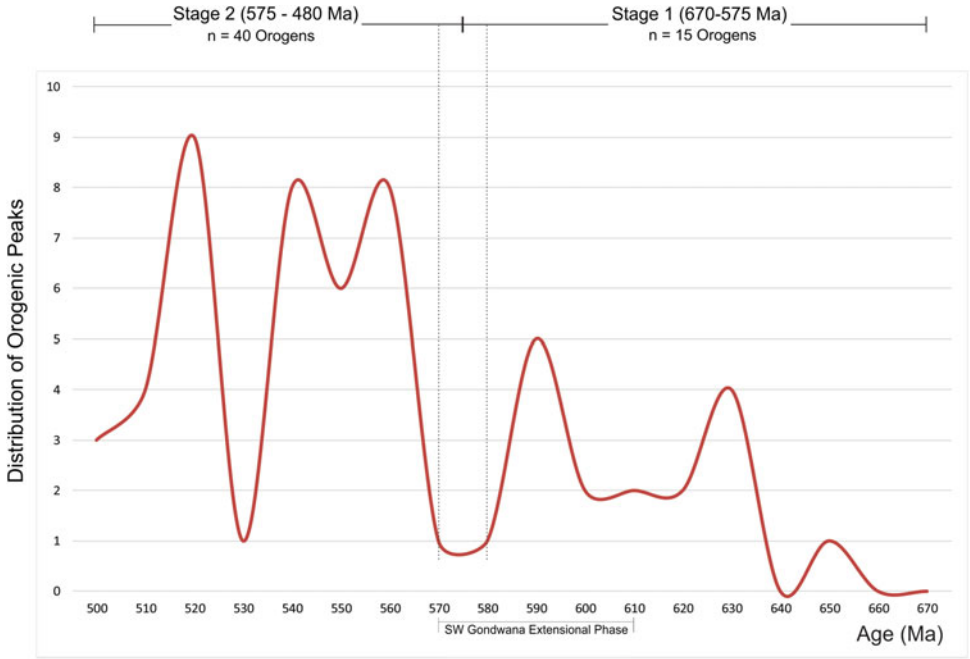

Fig. 15.3 Diagram with distribution of 670–480 Ma orogenic peaks in Gondwana. Based on Fig. 15.2

terranes came together in two main orogenic events (Fig. 15.1). Many of these Tonian and pre-Tonian terranes have a long history of pre-Cryogenian arc-related subduction-arc magmatism (Handke et al. 1999; Blades et al. 2015; Elburg et al. 2015; Jacobs et al. 1998, 2015; Archibald et al. 2016, 2017a, b). The earlier one occurred at *c*. 650–640 Ma as indicated by the time of peak metamorphism in Uganda, Kenya, Tanzania and northern Mozambique (Appel et al. 1998; Hauzenberger et al. 2004; 2007; Fritz et al. 2013; Tenczer et al. 2013). This orogenic event was interpreted as being the result of intra-arc extension (Appel et al. 1998), based on its counterclockwise P-T-t path, but on a regional scale it correlates with the amalgamation of the main Arabian-Nubian Shield along the Keraf Suture to the north, and it is focused along the suture of Azania (an extensive pre-Neoproterozoic terrane including central Madagascar, parts of Somalia, Ethiopia, Yemen and the Madurai Block of southern India) with the Congo-São Francisco continent. This is particularly apparent in Madagascar, where *c*. 650–640 Ma metamorphic ages were reported from the west of the country (Jöns and Schenk 2011), whereas in the eastern part, metamorphic ages of *c*. 570–540 Ma dominate (Tucker et al. 1999, 2014; Collins et al. 2003; Jöns and Schenk 2011; Fig. 15.1). This younger, eastern orogenesis correlates with the Ediacaran arc accretion recorded in the far east of the Saudi Arabian Shield that separates the exposed Saudi Shield from the basement of Oman (Fig. 15.1). These observations led Collins and Pisarevsky (2005) to propose that the western *c*. 650–640 Ma orogenesis was due to late Cryogenian collision of Azania with the Congo-São Francisco continent (the East African Orogeny sensu stricto; e.g., Stern 1994; Meert and Van der Voo 1997), while the younger *c*. 570–540 Ma orogenesis was the result of the final collision of Neoproterozoic India with the then amalgamated Azania/Congo-São Francisco continent, closing the Mozambique Ocean (and forming the Malagasy Orogeny; Collins and Pisarevsky 2005). Studies from southern India support this hypothesis because orogenesis in the Southern Granulite Belt is restricted to 570–520 Ma and forms a part of the Malagasy Orogeny (Collins et al. 2007a, b, 2014; Plavsa et al. 2012, 2014, 2015; Clark et al. 2015; Johnson et al. 2015; Taylor et al. 2015; Richard et al. 2015; Vijaya Kumar et al. 2017).

The Pinjarra-Prydz-Denman (Kuunga) orogeny led to the final major amalgamation of continental crust in eastern Gondwana, with the suturing of Australia-East Antarctica against India and Kalahari. The Pinjarra orogeny refers to the entire orogen, but here we separate the three to discretely treat varying tectonic events. The Pinjarra orogeny preserves the suture along the west coast of Australia (Fig. 15.1). Further south, in Antarctica, ice covers most exposures, but the suture crops out in the Denman glacier area, and, further south, in the Prince Charles Mountains-Prydz Bay area, where India and the Rayner province collided with the main crustal part of Antarctica (e.g., Boger 2011).

Exposure of the Pinjarra orogeny in Australia is limited to small inliers along the western coastline of the continent, such as the Leeuwin, Northampton and Mullingara Complexes (Fig. 15.1). The Leeuwin Complex in the southwest best preserves the orogeny (e.g., Collins and Fitzsimons 2001; Collins 2003). Here, pink granitic gneisses had their protoliths emplaced at *c*. 750 Ma and they exhibit upper

amphibolite-granulite metamorphism dated at *c*. 522 Ma (Collins 2003). This is broadly coeval with the end of tectonism, as *c*. 520 Ma dykes that intrude the Leeuwin Complex exhibit no deformation (e.g., Fitzsimons 2003a, b). The tectonic environment of emplacement was inferred to be a rift, related to Rodinia break-up (Collins 2003), since at the time it was postulated that Kalahari was attached to this margin of Australia (e.g., Powell and Pisarevsky 2002). Sinistral shearing is preserved in the Northampton Complex (Embleton and Schmidt 1985), and alkali granitoids in the Leeuwin Complex, originally inferred to be rift related, are now thought to have been emplaced in a sinistral transpressive environment (e.g., Harris 1994; Fitzsimons 2003a, b).

Further south, the Antarctica Denman Glacier area fits tightly against the Leeuwin Complex in a reconstructed Gondwana (Fig. 15.1). Here, U–Pb dating of zircon from syenite yielded an age of *c*. 516 Ma, and orthogneisses with a protolith age of *c*. 3 Ga record a metamorphic overprint age of between 550 and 520 Ma (e.g., Halpin et al. 2008). Some data shows substantial lead loss between 600 and 520 Ma (Black et al. 1992), indicating an Ediacaran history similar to that of rocks further north in Australia. The suture between India-Antarctica and Australia-Antarctica is typically traced south of this area, towards Prydz Bay and the Prince Charles Mountains (e.g., Boger et al. 2001).

The Prydz Bay area is further south and east in Antarctica and is also strongly affected by the Gondwana-forming orogeny between India-Antarctica and Australia-Antarctica. Owing to the similarity of protoliths, neodymium model ages and metamorphic events, the Prydz Bay area is inferred to be part of the Indo-Antarctica plate (e.g., Zhao et al. 1995; Kelsey et al. 2007; Wang et al. 2008; Liu et al. 2009; Boger 2011). Here, too, late Ediacaran-early Cambrian metamorphism up to granulite facies (Liu et al. 2003; Kelsey et al. 2007) is evident, with 540–500 Ma charnockite and granite plutons intruding gneisses (Liu et al. 2006, 2009; Mikhalsky and Sheraton 2011). Further inland from Prydz Bay, zircon from gneiss in the Grove Mountains suggests magmatic emplacement at *c*. 900 Ma, with a high-grade metamorphic overprint between 530 and 520 Ma (Zhao et al. 2000; Liu et al. 2003). Younger *c*. 500 Ma granitic dykes exhibit no metamorphism, suggesting that deformation had finished by this time (Zhao et al. 2000).

A broad region of Ediacaran-Cambrian deformation and metamorphism occurs within Australia. This stretches from the eastern Pilbara, where it is called the Patterson Orogen (Martin et al. 2017), and then passes through central Australia, where it is known as the Petermann Orogen. This intra-Australian orogen involves significant dextral transpressional deformation (Raimondo et al. 2009, 2010) and has been linked to a suggested Neoproterozoic 40° anticlockwise rotation between the North Australian Craton and the South Australian Craton interpreted from paleomagnetic data (Li and Evans 2011). Cryogenian sedimentary rocks of the Centralian Superbasin are found on both sides of the Petermann Orogen, supporting the hypothesis that the orogen is an intracontinental orogen and, although there is significant crustal shortening (Raimondo et al. 2010), it doesn't represent an oceanic suture (Close et al. 2003).

15.2.2 Western Gondwana Orogens (Pan-African–Brasiliano Events)

Amazonia, West Africa, São-Francisco-Congo, Kalahari and Rio de La Plata are the major outcropping paleocontinents of western Gondwana (Fig. 15.1). The Saharan block, considered to be a metacraton, is poorly exposed but also may have played an important role in the amalgamation process (Abdelsalam et al. 2002). These Neoproterozoic paleocontinents are partially covered by Phanerozoic deposits, also comprising Gondwana intracratonic basins. Two cratonic blocks are inferred below the Paraná (Paranapanema paleocontinent) and Parnaíba (Parnaíba block) basins in Brazil, based on geophysical and geological data from the basement (Mantovani and Brito Neves 2009; Daly et al. 2014; Fig. 15.1). Smaller blocks are São Luis (which links with the West Africa Craton), Luis Alves (which might link with Paranapanema) and Rio Apa (an inlier within the Cambrian Paraguay-Pampean orogens; respectively, Basei et al. 2008; Klein and Moura 2008; Dragone et al. 2017; Fig. 15.1).

One of the major crustal scale structures within western Gondwana, the Transbrasiliano-Kandi shear zone (Cordani et al. 2013b; Fuck et al. 2014), is considered by Ganade de Araujo et al. (2014a) to have developed in a *c*. 3000 km collisional orogen (the West Gondwana Orogen). According to Ganade de Araujo, this orogen, which includes at least the Brasilia, Borborema, Dahomey and Hogar belts, is comparable to the East African Orogen because it represents the closure of a large oceanic basin and evolved from a long-lasting subduction environment (Fig. 15.1). The West Gondwana Orogen was formed as a result of the convergence of two groups of blocks: Amazonia-West African cratons and Central African blocks (Saharan, São Francisco-Congo, Kalahari and Rio de La Plata). The consequent closure of the Goais-Pharusian Ocean is registered by high-pressure subduction-related rocks along the orogen and also some mafic oceanic units. These collisional events occurred between 630 and 580 Ma (Ganade de Araujo et al. 2014b).

At first glimpse it might seem logical to visualize the Gondwana amalgamating framework as three blocks and two major north–south running orogens. However, when one looks in detail, the framework is more complex, crosscut by roughly east–west-trending orogens. These interference

zones, or transverse orogenic triple junctions (Passchier et al. 2016; Goscombe et al. 2017), demonstrate that Gondwana amalgamated through the collision of multiple blocks. However, the various belts do not eliminate the possibility that there was a previous connection between larger blocks or linked smaller fragments.

The oldest western Gondwana orogens, grouped in the 670–575 Ma interval, include mostly the West Gondwana Orogen (Hoggar, Dahomey, Oubanguides, Borborema north and Brasilia belts; Ganade de Araujo et al. 2014a, 2016) and the Dom Feliciano belt (in southern South America; Philipp et al. 2016; Fig. 15.1). Some authors suggest that these connect in one superorogen (Oriolo et al. 2016, 2017). The Hoggar–Dahomey belts are products of convergence among the West African and Saharan cratons (Fig. 15.1). In the northern Borborema province (the South American counterpart), it is not clear which are the colliding blocks. To the east, the Borborema province is composed of Paleoproterozoic blocks reworked in the Brasiliano events, the São Francisco-Congo Craton representing one of these blocks. To the west, underneath the Paleo-Mesozoic Parnaiba basin, the mostly inferred Parnaíba cratonic block possibly represents the other colliding block (Daly et al. 2014; Fig. 15.1). Continuing to the south, the northern sector of the Brasilia belt represents the collision between the São Francisco Craton western margin with the Goiás block (Pimentel 2016; Fig. 15.1). Further south the Paranapanema Craton (mostly covered by the Paraná Paleo-Mesozoic basin) is the counterpart for the agglutination and generation of the southern Brasilia belt (Fig. 15.1). The Dom Feliciano belt is a product of the intereaction between Paranapanema, Rio de La Plata and Kalahari blocks, and seems to have an important period of magmatism c. 650–590 Ma, attributed to collision, as discussed in item 3.

A smaller group of *c*. 600–550 Ma western Gondwana orogenic belts are characterized, some on the fringes of the 670–590 belts. The Sergipano-Oubanguides collisional belt accomplished the suturing of the northern São Francisco Craton margin and the Saharan Metacraton at this time (Fig. 15.1). On the southern São Francisco margin, the Araçuai-West Congo Orogen, plus the Central and South Ribeira belts, have a more enigmatic evolution. It is agreed that there is a *c*. 600–550 Ma metamorphic peak event, but the cause is still controversial (Pedrosa-Soares et al. 2008; Degler et al. 2017; Bento dos Santos et al. 2010; Richter et al. 2016). Some propose that the metamorphism is related to arc emplacement in a subduction environment (Duffles et al. 2016), while others propose a collisional setting (Heilbron et al. 2004; Vinagre et al. 2014). An alternative model suggests an intracontinental setting and a major extension that produced the large granitic batholiths and hence the regional metamorphism (Meira et al. 2015).

The period 560–510 Ma comprises the largest Neoproterozoic-Cambrian peak of collisional metamorphism and tectonic activity (Fig. 15.3). In western Gondwana these belts are related to the approximation of two major blocks: the Kalahari in the south and the Amazonia in the north (Fig. 15.1). The Rockelides-Araguaia belts register the collision of the Amazonia Craton suturing western Gondwana. Tohver et al. (2012) and Trindade et al. (2006) attribute this collision to the closure of the Clymene Ocean, after a long-lasting subduction zone, with a hidden magmatic arc below the cover of the Parnaiba Basin (Fig. 15.1). Cordani et al. (2013a) advocate that this belt is the result of the closure of an intracontinental basin. Towards the south the Araguaia belt merges into the Paraguai belt that runs until the Rio Apa cratonic inlier (Fig. 15.1). The metamorphic ages here are younger, coeval with the Pampean belt and the Puncoviscana belt, possibly related to the collision of the Pampia and Arequipa-Antofalla blocks (Rapela et al. 2002; Ramos 2008; Ramos et al. 2010; Escayola et al. 2011; Fig. 15.1) or the final closure of the Clymene Ocean separating the Paranapanema from Rio Apa (and Amazonia; McGee et al. 2015a, b). These younger belts of *c*. 530–480 Ma represent the transition between the internal suturing Gondwana belts and the external marginal belts.

In the central part of western Gondwana there is also a generation of Cambrian belts (530–480 Ma) fringing the Ediacaran-Cambrian domains (560–510 Ma; Brito Neves et al. 2014). There are two major ramifications of orogenic systems: the Damara-Lufilian-Zambesi and the Ribeira-Kaoko-Dom Feliciano-Gariep-Cuchilla Dionisio (named here the South Atlantic orogenic system, detailed on item Sect. 15.3). The former has recently received extensive attention in the literature with metamorphic and geochronological data (Goscombe et al. 2017). The Damara Belt is a classical product of convergence between the Kalahari Craton and the southern Congo Craton, named the Angola block (some authors even suggest that this block had independent kinematics, not linked with Congo cratonic blocks; Heilbron et al. 2008; Fig. 15.1). Evidence suggests at least two hypotheses for the origin of the Damara Belt: (1) an intracontinental orogeny with a small ocean formed during an extensional period (Porada 1979; Nascimento et al. 2017); and (2) a large ocean separating both cratons (de Waele et al. 2003; Johnson et al. 2005; Schmitt et al. 2012). The conclusion is key to the understanding of eastern and western Gondwana amalgamation (see Sect. 15.4).

15.3 Ediacaran-Cambrian Orogens in SW Gondwana—the South Atlantic Orogenic System

SW Gondwana was constructed as a result of the interaction between the Kalahari, Rio de La Plata, Southern São--Francisco-Congo, Paranapanema and Luis Alves paleocontinents (Figs. 15.1 and 15.4). Our review focuses on the orogens that are *younging* towards today's South Atlantic continental margins, registering Ediacaran-Cambrian tectonic events (Fig. 15.4). Although controversial at some points (Will and Frimmel 2018; see Sect. 15.4), it is certain that the South Atlantic break-up followed the youngest sutures of Gondwana's amalgamation (Schmitt et al. 2016b). Therefore we propose the name South Atlantic Orogenic System for the following belts in conjunction: Gariep-Saldania-Cuchilla Dionisio-West-Kaoko-Dom Feliciano-South and Central Ribeira and Angola.

Even though separated today by more than 6000 km of ocean, these belts share some important features that hide the final amalgamation of Gondwana: (1) the tectonometamorphic evolution occurred between 670 and 480 Ma; (2) most of the belts present mafic-ultramafic lithostratigraphic units as tectonic slivers; (3) all belts show contraction structures and evidence for crustal thickening; and (4) all belts present extensional Cambrian structures and late Ediacaran-Cambrian basins.

Below we briefly describe the evolution of this orogenic system through the Ediacaran-Cambrian.

15.3.1 670–575 Ma Orogens

The Dom Feliciano is the only belt developed during this interval in SW Gondwana that corresponds to the Cryogenian to early Ediacaran period. It is mostly a granitic domain that extends from Uruguay (Aigua Batholith) to south Brazil (Pelotas-Florianópolis batholiths; Fig. 15.4; Bitencourt and Nardi 2000; Florisbal et al. 2012; Philipp et al. 2016). It is predominantly composed of calcalkaline magmatic rocks, with shoshonitic and alkaline terms (Lara et al. 2017). Xenoliths of Paleoproterozoic and Tonian gneisses are present. This igneous unit also intrudes Tonian metavolcanosedimentary sequences (Gruber et al. 2011). The emplacement is controlled by low-angle structures with west vergence that evolve to steep northeast–southwest shear zones segmenting the belt after *c*. 610 Ma (Martil et al. 2017).

The generation of the batholiths is considered to be related to a syn to post-collisional setting at *c*. 650–550 Ma (Oyhantçabal et al. 2011; Philipp et al. 2016). This collision between the Kalahari and Rio de La Plata cratons would be the consequence of the Adamastor ocean closure along a southeast dipping subduction zone (Basei et al. 2008). Its correspondent in Africa is interpreted by some to be the 660–620 Ma Coastal Terrane, which is considered to be an exotic domain in the Kaoko belt thrust over the Congo-Angola Craton margin at *c*. 590 Ma (Goscombe and Gray 2007; Figs. 15.1and 15.4). In agreement with the Brazilian counterpart it is also interpreted as a product of southeast subduction (Goscombe et al. 2017).

In Figs. 15.1 and 15.4, the Dom Feliciano belt is represented as a domain with peak metamorphism at *c*. 640–590 Ma, coeval with the Brasilia Belt. However, its surrounding terranes register the influence of a younger metamorphic tectonic event, well represented in the Cuchilla Dionisio, Eastern Kaoko, Damara, Gariep and Saldania belts (Figs. 15.1 and 15.4). The 585–485 Ma orogenic events that fringe the eastern sector of the Dom Feliciano belt are largely overlooked when authors interpret this domain as the product of the collision between the Kalahari and Rio de La Plata Craton (see Sect. 15.4).

Further north, the Ribeira belt contains a series of 640–590 Ma arc-related batholiths (Campanha et al. 2008; Faleiros et al. 2011; Tupinambá et al. 2012; Vinagre et al. 2014; Fig. 15.4). The southwestern segment is interpreted as having developed due to a northwest dipping subduction zone (Campanha et al. 2015), while to the northeast a southeast dipping subduction is proposed (Heilbron et al. 2004; Trouw et al. 2013). The work of Heilbron et al. (2004) and Trouw et al. (2013) considers a collisional phase, regarding the docking of the magmatic arc domain onto the São Francisco Craton, and the end of this subduction at *c*. 580–560 Ma. A similar period is attributed to the final stage of subduction in the southwestern sector (Apiaí Terrane) due to collision between the arc terrane and the Curitiba terrane (Campanha et al. 2008; Faleiros et al. 2016; Fig. 4).

15.3.2 575–480 Ma Orogens

The best representative of the Ediacaran-Cambrian orogens is the Damara belt (Fig. 15.4). The convergence between the Kalahari Craton and the southern Congo Craton (Angola Block) resulted in a collisional event starting at *c*. 550 Ma with late collisional plutons at *c*. 530–500 Ma (Schmitt et al. 2012). Lehmann et al. (2016) and Passchier et al. (2016) suggested that precollisional convergence started as early as *c*. 590 Ma, based on Ar–Ar data in biotite, with the metamorphic climax in the central part of the orogen at *c*. 530 Ma related to the final collision (Schmitt et al. 2012; Goscombe et al. 2017).

Today the Damara belt is an inland branch of the Gondwana-forming orogens (Miller 2008; Nascimento et al.

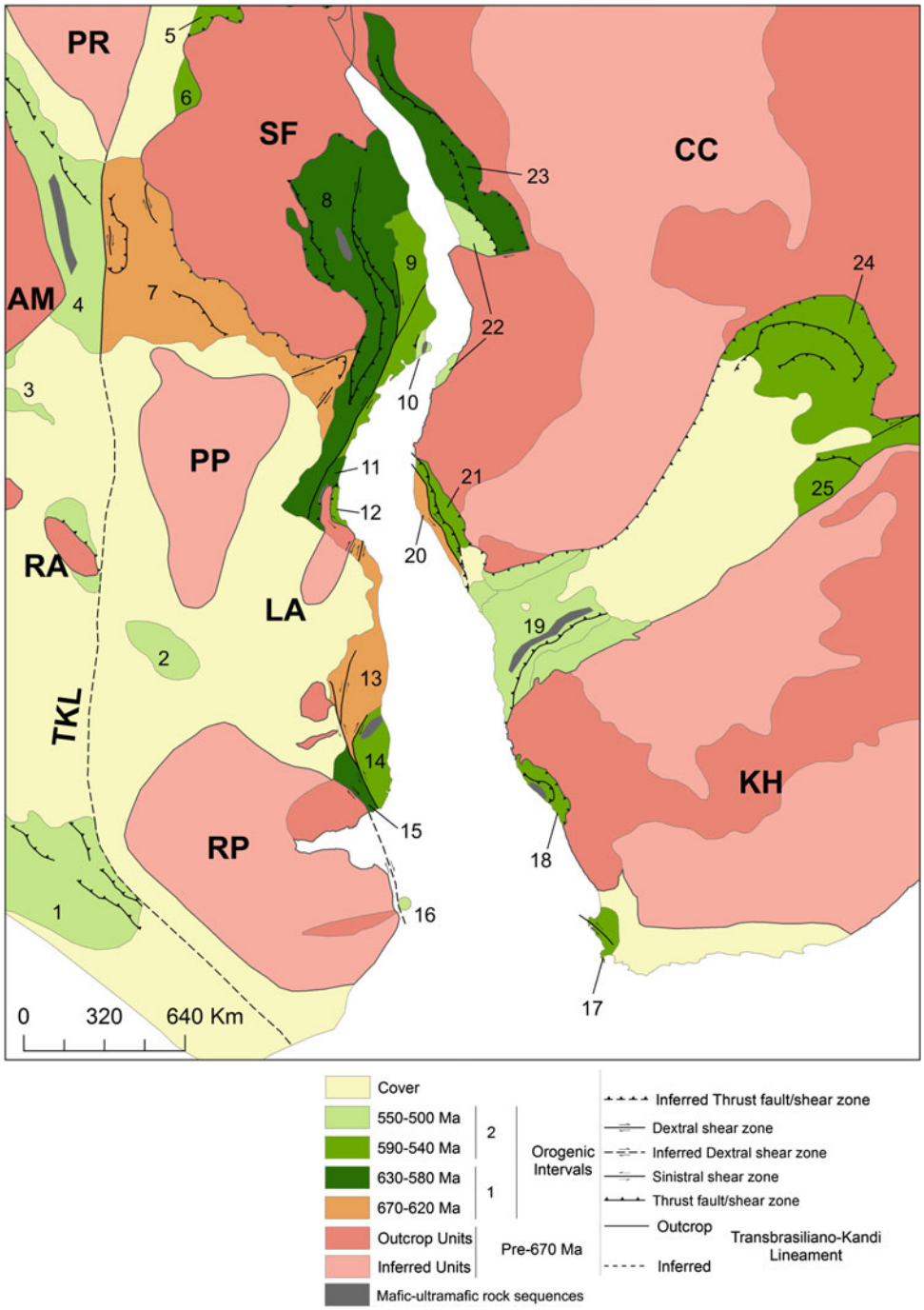

Fig. 15.4 SW Gondwana with cratons, and post-670 Ma orogens, major crustal-scale structures and oceanic-derived units. The letters and numbers on the map stand for the Gondwana cratons and mobile belts, respectively. They are *AM* Amazonia; *PR* Parnaíba; *SF* São Francisco; *PP* Paranapanema; *LA* Luís Alves; *RA* Río Apa; *RP* Río de La Plata; *KH* Kalahari; *CC* Congo. 1—Pampeana; 2—Caapucú High; 3—Paraguay; 4—Araguaia; 5—Borborema (South); 6—Rio Preto; 7—Brasília; 8a—Araçuaí (West), 8b—Ribeira (Paraíba/Embu) and 8c—Apiaí to East Araçuai and Occidental Terrane; 9—Ribeira (Oriental Terrane); 10—Cabo Frio Tectonic Domain; 11—Curitiba Terrane; 12—Paranaguá Terrane; 13—Dom Feliciano; 14—Cuchilla Dionísio; 15—Nico Pérez; 16—Mar del Plata Terrane; 17—Saldania; 18—Gariep; 19—Damara; 20—Kaoko (Coastal); 21—Kaoko (Central-East); 22—Angola; 23—West Congo; 24—Lufilian; 25—Zambesi. TKL stands for Transbrasiliano-Kandi Lineament

2016). The South Atlantic continental margins also show younger metamorphic/collisional ages, represented by the Gariep Belt, Saldania Belt, Cuchilla Dionisio Terrane, Kaoko Belt, Paranaguá Block, Oriental Terrane (Ribeira Belt), Cabo Frio Tectonic Domain (Buzios Orogen) and Angolan belt (Figs. 15.1 and 15.4).

These Ediacaran-Cambrian domains have several common features: (1) medium- to high-grade metamorphic rocks; (2) mafic-ultramafic lenses tectonically interleaved with supracrustals; (3) ductile compressional structures; and (4) late extensional structures with syntectonic Cambrian to Ordovician magmatic intrusions.

The Cabo Frio Tectonic Domain is the only one that shows high P-T metamorphism dated at *c*. 530 Ga, interpreted as being related to the collision between the Angolan Block and the southern São Francisco Craton (Fig. 15.4; Schmitt et al. 2016b). These metamorphic conditions were attained during the collisional-exhumation phase by

supracrustal sequences from a basin developed on transitional crust between the continent and the ocean (Schmitt et al. 2008; Fernandes et al. 2015; Capistrano et al. 2017).

The mafic-ultramafic rocks of the Forte de São Mateus unit are considered to be relics of an oceanic crust, dated at *c*. 610 Ma (Schmitt et al. 2008, 2016b). Other mafic-ultramafic occurrences are (Fig. 15.4) the Araçuai belt (Pedrosa-Soares et al. 1998), Pien Suite (in between the Luis Alves Craton and Curitiba Terrane; Cury 2009), Paso del Dragon Complex and Arroio Grande Complex (in the northern Cuchilla Dionisio Terrane; Bossi and Gaucher 2004; Ramos and Koester 2014), and Marmora Terrane (in the Gariep Belt; Frimmel and Frank 1998). The Damara Belt contains the Matchless Amphibolite, interleaved with accretionary prism sedimentary and volcanoclastic deposits (Kukla and Stanistreet 1991; Meneghini et al. 2014). These are interpreted as representing oceanic crust formed in a precollisional stage, and most of them are attributed to a back-arc basin setting (Will and Frimmel 2018). Some ultramafic occurrences are alternatively interpreted as exhumed subcontinental lithospheric mantle (e.g., Paso del Dragon Complex in Uruguay; Benedek et al. 2017). Regardless of the origin, this 610–570 Ma extensional phase is also well recorded in the older domains, such as the Dom Feliciano belt (Camaqua Basin), the Luis Alves Craton (Itajai Basin), the Paranapanema Block (Castro Basin) and the Oriental Terrane of the Ribeira Belt (Pico do Itapeva Basin; Riccomini et al. 1996; Almeida et al. 2012; de Oliveira et al. 2014), and even in eastern Gondwana sectors, as in Madagascar (Collins 2006).

The tectonic inversion of these basins started with convergence at *c*. 580 Ma and culminated with continental collision between 560 and 520 Ma (Fig. 15.3). The oceanic crust from the Buzios basin (in the Cabo Frio Tectonic Domain) is interpreted to be subducted towards the northwest-west, based on the high P-T conditions of the sequence (Schmitt et al. 2016b). A 570–540 Ma igneous domain in the Oriental Terrane of the Ribeira belt (to the northwest) is considered to be representative of a magmatic arc related to this Cambrian subduction (Martins et al. 2016). On the other hand, to the south, the Marmora terrane, obducted at *c*. 545 Ma onto the Kalahari Craton, is considered to be an oceanic unit of a back-arc basin developed in a post-collsional setting (Frimmel and Frank 1998; Will and Frimmel 2017).

Widespread ductile deformational phases are related to convergence and collision in all of these South Atlantic belts from 580 Ma until 530 Ma, coeval with high- to low-grade metamorphism, which varies according to the exposed crustal level and proximity to the suture zones. Low-angle structures predominate in the Cabo Frio Tectonic Domain, Angolan Belt, Apiaí and Curitiba terranes, Gariep belt and the external parts of the Damara and Kaoko belts.

High-angle structures related to steep shear zones are common in the Dom Feliciano Belt, Central Ribeira Belt and Western Kaoko Belt, mostly attributed to late collisional strain zones, developed during the final amalgamation of the cratons (Oyhantçabal et al. 2010; Konopásek et al. 2016; Oriolo et al. 2016; Passchier et al. 2016; Philipp et al. 2016). The age of this last kinematic activity of these mylonitic zones is constrained to the period 580–480 Ma. These transpressional and transtensional kinematics are probably the result of lateral adjustments of the multiple collisions. Some authors try to make transatlantic correlations between the shear zones (de Wit et al. 2008; Konopásek et al. 2016). Although they are subvertical structures, the connection is very speculative since the opening of the South Atlantic produced wide continental margins and probably a rifted microcontinent (Rio Grande Rise; Santos et al. 2014; Szatmari and Milani 2016). Approximately 300–500 km of continental crust is estimated on both conjugate margins submerged in this Atlantic sector (Schmitt et al. 2016b).

Magmatism at *c*. 580–550 Ma is related to these shear zone systems in the Dom Feliciano Belt, Cuchilla Dionisio and the Coastal Terrane of Kaoko Belt (e.g., Oyhantçabal et al. 2011; Konopásek et al. 2016). In the northern sector of the South Atlantic belt, a pre-eminent 540–440 Ma magmatic event intrudes into these high strain zones (Martins et al. 2016). During their reactivation in a transtentional phase, 510–440 Ma plutons intrude into this shear zone system (Bongiolo et al. 2016).

15.4 Discussion

The main contribution of this chapter is to present a compilation of all the collisional orogens/metamorphic belts that sutured Gondwana in the late Ediacaran Early Cambrian (Fig. 15.1). The timeframe attributed to orogenic activity in each of the 55 belts comprises the metamorphic peak and deformational structures representing the continental collision phase, which includes the extrusion of nappes and development of steep shear zones (Figs. 15.1 and 15.2). Two main periods of orogenic activity related directly to the amalgamation processes can be recognized (Fig. 15.3). The first period, starting *c*. 670 Ma, includes relatively few orogens (*c*. 15) but involves larger areas in Gondwana than subsequent orogenesis. These orogens are shown in orange and dark green in Fig. 15.1. This period amalgamated the Saharan, West African, São Francisco-Congo and Paranapanema paleocontinents, and also the juvenile Tonian terranes of the Arabian Nubbian shield and some

microcontinents of the East African Orogen. This *c*. 575 Ma proto-Gondwana was the core of the supercontinent, centred on Africa (Fig. 15.2b).

The second and last period of Gondwana amalgamation includes a vast number of orogens, *c*. 40 (Fig. 15.3). These, shown in light- and very light-green, were responsible for suturing the Amazonia, Rio de La Plata, Kalahari, Dhawar, East Antarctica and Australian paleocontinents (Fig. 15.1). The external (marginal) orogens overlapped in time with this second amalgamation stage. They are the Pampean, Ross and Delamerian belts (also plotted in Fig. 15.3).

15.4.1 Correlating Ediacaran-Cambrian Orogens Throughout Gondwana

The distribution of the collisional orogens throughout western and eastern Gondwana is similar (Fig. 15.2), with coeval and interleaving events in the period 670–480 Ma (Figs. 15.1 and 15.3). This pattern indicates that although Gondwana was constructed by the convergence of several paleocontinents and microcontinents (Neoproterozoic Cratons) with different geological evolutions, their approximation might be orchestrated by global geodynamics (Hoffman 1991; Condie et al. 2015; Merdith et al. 2017a). The two stages of Gondwana amalgamation interpreted here, 670–575 Ma and 575–480 Ma, represent periods with abundant collisions in all sectors of Gondwana (Fig. 15.2). The younger stage has many more orogens (*c*. 40 orogens) than the first stage (*c*. 15 orogens; Fig. 15.3).

The separation was arbitrarily drawn at *c*. 580–570 Ma (Fig. 15.3). These 10 myr of low orogenic activity match with the opening of extensional/transtensional basins (e.g., SW Gondwana; Riccomini et al. 1996; Almeida et al. 2012; de Oliveira et al. 2014). These Ediacaran rifting events, sometimes forming oceanic crust (e.g., Buzios, Cuchilla Dionisio, Gariep; Fig. 15.4), probably indicate a period when the convergence rate slowed down. These basins were rapidly formed and even more quickly inverted in the second and final stage of Gondwana amalgamation. One important global tectonic event that coincides with the beginning of this second stage is the opening of the Iapetus ocean (Nance et al. 2014).

The 575–480 Ma collisional orogens that sutured Gondwana are recognized in the east–west Kuunga and north–south South Atlantic belts (Fig. 15.1). The intersection zone between these composite belts is located in the central part of SW Gondwana, today in the South Atlantic (Fig. 15.4). In this zone, the final amalgamation was completed by the Kalahari and Rio de La Plata collision with the São Francisco-Congo Craton. This was coeval with the development of the marginal orogens of the Pampean-Ross-Delamarian events (Fig. 15.1).

15.4.2 Do the Internal Western Gondwana Ediacaran-Cambrian Orogens Represent Closure of Oceanic Realms?

The Ediacaran-Cambrian South Atlantic rogenic system is here considered to be the record of the final suturing of western Gondwana. These orogens share certain features that might indicate that there was mantle exhumation and/or generation of oceanic crust at *c*. 610–590 Ma (Fig. 15.4). The sediments deposited in these basins present a major Ediacaran provenance (Basei et al. 2005; Foster et al. 2015; Fernandes et al. 2016) mostly from volcanic and plutonic sources. These igneous domains are interpreted as continental magmatic arcs (Basei et al. 2008; Heilbron et al. 2008; Gaucher et al. 2009; Goscombe et al. 2017) ovelapping partially in age with syn- to post-collisional intrusions (Oyhantçabal et al. 2011; Florisbal et al. 2012) and extensional intraplate magmatism (Meira et al. 2015). Most authors agree that these basins were developed in a back-arc environment at the end of southeast-directed subduction (Basei et al. 2008; Heilbron et al. 2008; Gradim et al. 2014).

The map shows that the reality is more complex, exposing flaws in this model that should be reviewed (Fig. 15.4). The back-arc basin model apparently works well for the Marmora basin-Cuchilla Dionisio Terrane, but, northwards, in the Apiaí Terrane and the Cabo Frio Tectonic Domain, evidence suggests that the major metamorphic peak, probably related to continental collision, is much yonger, *c*. 570–520 Ma (Schmitt et al. 2004, 2008, 2016b; Cury 2009; Faleiros et al. 2011). High- to medium-pressure rock units, identified in both domains, are not compatible with a back-arc setting.

Transform limits are usually not considered in Neoproterozoic-Cambrian tectonic models. The opening of the Khomas sea (Damara belt), Adamastor Ocean (Dom Feliciano belt) and Buzios Ocean (Cabo Frio Tectonic Domain) is geometrically plausible including transform limits, which are intrinsic to oceanic crust formation. However, the closure of all these oceans/seas within a short period implicates a complex array that would need to be resolved with triple junction migration along subduction zones (e.g., Passchier et al. 2016).

In addition, the evolution of the Damara belt is well constrained to the period 570–500 Ma with a major metamorphic peak and magmatism around 540–530 Ma (Miller 2008; Goscombe et al. 2017). It shows that the Kalahari-southern Congo main frontal collision was coeval approximately with the Buzios orogen (Cabo Frio Tectonic Domain; Schmitt et al. 2004), the Apiai-Embu orogenic domains (Cury 2009; Faleiros et al. 2011), and the deformation and metamorphism in the Cuchilla Dionisio-Gariep-Saldania domains/belts

(Bossi and Gaucher 2004; Gaucher et al. 2009; Frimmel et al. 2013).

A major 620–600 Ma collision in the Dom Feliciano belt is not compatible with the evolution of the fringing post-585 Ma belts (Fig. 15.4). The reconstruction shown in the SW Gondwana cratons-belts maps suggests a connection between the Cuchilla Dionisio and the Damara-Kaoko orogenic junction (Fig. 15.4). This 570–500 Ma orogenic system strongly reworks the Coastal Terrane of the Kaoko Belt (Foster et al. 2015; Goscombe et al. 2017; Nascimento et al. 2017). On the South American side, the Florianopolis batholith does not offer published data relating to this younger orogenic activity, though the Paranagua Terrane (still with very limited geochronological data) has Cambrian syntectonic magmatism, and the Curitiba-Apiai terranes also show this younger metamorphism (Cury 2009).

We propose that the collision on the Damara belt developed coevally with the Cuchilla Dionisio-Saldania-Gariep-Dom Feliciano-Kaoko-Ribeira-Cabo Frio orogenic system between 570 and 500 Ma, including the Mar del Plata Terrane (Rapela et al. 2011; Fig. 15.4). This South Atlantic orogenic system contains the main SW Gondwana suture that was reactivated in the extensional setting 350 myr later. Indeed, most of the the South Atlantic opening follows the rule of suture inheritance, with old orogenic high-pressure and oceanic-derived rocks preserved on its actual continental margins (Beltrando et al. 2010, 2014). In disagreement with the interpretation of Will and Frimmel (2018), we consider that back-arc basins are not likely to favour continental break-up since they usually do not represent major lithospheric boundaries.

In addition, the recent discovery of offshore continental units, 1000 km off the Brazilian coast at the Rio Grande Rise (Santos et al. 2014), reinforces the idea that a large volume of Gondwana lithosphere is hidden in the continental margins and even as remnants encrusted on the Atlantic oceanic floor. Therefore the *c*. 630–600 Ma Dom Feliciano Belt in southern South America and its probable counterpart Coastal Terrane in Namibia might represent the external limits of a belt that only terminated its evolution in the Cambrian.

15.5 Conclusion

The compilation of 55 orogenic belts that sutured Gondwana in the period 670–480 Ma provides the following conclusions:

- Two main orogenic stages are recognized. The first, 670–575 Ma, includes few orogens (*c*. 15) but larger areas. During this stage, Saharan, West African, São Francisco-Congo and Paranapanema paleocontinents, Arabian Nubian shield juvenile Tonian terranes and some East African Orogen microcontinents were amalgamated, forming the proto-Gondwana core.
- The second stage, from 575 to 480 Ma, incorporates more orogens, *c*. 40, suturing the Amazonia, Rio de La Plata, Kalahari, Dhawar, East Antarctica and Australian paleocontinents.
- The collisional orogen pattern throughout Gondwana is similar, indicating that Gondwana was built up by the convergence of distinct paleocontinents. This comparable pattern regarding metamorphic and deformational peaks suggests that Gondwana amalgamation processes, although complex, were partially orchestrated by global geodynamic forces.
- In SW Gondwana the South Atlantic system of Ediacaran-Cambrian orogens is here considered to register the final suturing of western Gondwana.
- The belts share certain features, such as the opening of basins, coinciding with the interval between the two main orogenic stages. Mafic-ultramafic sequences might indicate that there was mantle exhumation and/or generation of oceanic crust at *c*. 610–570 Ma.
- These basins were rapidly formed and even more quickly inverted during the 575–480 collisional stage, represented by the major east–west Kuunga and north–south South Atlantic belts.
- We propose that the 570–500 Ma convergence and collision of the Damara belt was coeval with the Cuchilla Dionisio-Saldania-Gariep-Dom Feliciano-Kaoko-Ribeira-Cabo Frio orogenic system. This South Atlantic orogenic system holds the key to the SW Gondwana suture, reactivated 350 myr later, evidenced by old orogenic high-pressure and oceanic-derived rocks preserved in the present conjugate continental margins.

Acknowledgements The authors acknowledge the careful reviews from Sebástian Oriolo and Rudolph Trouw. Renata Silva Schmitt thanks the CNPq for research grant 309216/2015-0. Alan S. Collins is supported by Australian Research Council Future Fellowship FT120100340 and his contribution forms TRaX Record #392. This chapter is a product of the project 'Revisão do mapa geológico do Gondwana', a collaboration between PETROBRAS and UFRJ, and a contribution to IGCP-628 'The Gondwana Map and the tectonic evolution of Gondwana'.

References

Abdelsalam MG, Liégeois J-P, Stern RJ (2002) The Saharan Metacraton. J African Earth Sci 34:119–136

Alessio B, Blade M, Murray G, Thorpe B, Collins A, Kelsey D, Foden J, Payne J, Al-Khirbash S, Jourdan F (2017). Origin and tectonic evolution of the NE basement of Oman: a window into the Neoproterozoic accretionary growth of India? Geol Mag 1–25

Almeida RP, Santos MGM, Fragoso-Cesar ARS, Janikian L, Fambrini GL (2012) Recurring extensional and strike-slip tectonics after the Neoproterozoic collisional events in the southern Mantiqueira province. An Acad Bras Cienc 84:347–376

An M, Wiens DA, Zhao Y, Feng M, Nyblade AA, Kanao M, Li Y, Maggi A, Lévêque J-J (2015) S -velocity model and inferred Moho topography beneath the Antarctic Plate from Rayleigh waves. J Geophys Res Solid Earth 120:359–383

Appel P, Moller A, Schenk V (1998) High-pressure granulite facies metamorphism in the Pan-African belt of eastern Tanzania: P-T-t evidence against granulite formation by continent collision. J Metamorph Geol 16:491–509

Archibald DB, Collins AS, Foden JD, Payne JL, Holden P, Razakamanana T, De Waele B, Thomas RJ, Pitfield PEJ (2016) Genesis of the Tonian Imorona-Itsindro magmatic Suite in central Madagascar: insights from U-Pb, oxygen and hafnium isotopes in zircon. Precambrian Res 281:312–337

Archibald DB, Collins AS, Foden J, Payne J, Macey P, Razakamanana T, Holden P (2017a) Stenian–Tonian arc magmatism in west–central Madagascar: the genesis of the Dabolava Suite. J Geol Soc. https://doi.org/10.1144/jgs2017-028

Archibald DB, Collins AS, Foden JD, Razakamanana T (2017b) Tonian Arc magmatism in central Madagascar: the petrogenesis of the Imorona-Itsindro Suite. J Geol 125:271–297

Bandeira J, McGee B, Nogueira ACR, Collins AS, Trindade R (2012) Sedimentological and provenance response to Cambrian closure of the Clymene ocean: the upper Alto Paraguai Group, Paraguay belt, Brazil. Gondwana Res 21:323–340

Basei MAS, Frimmel HE, Nutman AP, Preciozzi F, Jacob J (2005) A connection between the Neoproterozoic Dom Feliciano (Brazil/Uruguay) and Garlep (Namibia/South Africa) orogenic belts—evidence from a reconnaissance provenance study. Prec Res 139:195–221

Basei MAS, Frimmel HE, Nutman AP, Preciozzi F (2008) West Gondwana amalgamation based on detrital zircon ages from Neoproterozoic Ribeira and Dom Feliciano belts of South America and comparison with coeval sequences from SW Africa. Geol Soc Lond (Spec Publ) 294:239–256

Be'eri-Shlevin Y, Eyal M, Eyal Y, Whitehouse MJ, Litvinovsky B (2012) The Sa'al volcano-sedimentary complex (Sinai, Egypt): a latest Mesoproterozoic volcanic arc in the northern Arabian Nubian Shield. Geology 40:403–406

Beltrando M, Compagnoni R, Lombardo B (2010) (Ultra-) High-pressure metamorphism and orogenesis: an Alpine perspective. Gondwana Res 18:147–166

Beltrando M, Manatschal G, Mohn G, Dal Piaz GV, Vitale Brovarone A, Masini E (2014) Recognizing remnants of magma-poor rifted margins in high-pressure orogenic belts: the Alpine case study. Earth-Science Rev 131:88–115

Benedek MR, Schmitt RS, Bossi J, Marmól S, Gaucher C (2017) Inversão Tectônica de uma Margem Continental Ediacarana - Geologia dos Xistos La Micaela, Terreno Cuchilla Dionísio, NE do Uruguai. In: Anais do X Simpósio Sul - Brasileiro de Geologia

Bento dos Santos TM, Munhá JM, Tassinari CCG, Fonseca PE, Dias Neto C (2010) Thermochronology of central Ribeira Fold Belt, SE Brazil: Petrological and geochronological evidence for long-term high temperature maintenance during Western Gondwana amalgamation. Precambrian Res 180:285–298

Berger A, Gnos E, Schreurs G, Fernandez A, Rakotondrazafy M (2006) Late Neoproterozoic, Ordovician and Carboniferous events recorded in monazites from southern-central Madagascar. Precambrian Res 144:278–296

Berger J, Ouzegane K, Bendaoud A, Liegeois J-P, Kienast J-R, Bruguier O, Caby R (2014) Continental subduction recorded by Neoproterozoic eclogite and garnet amphibolites from Western Hoggar (Tassendjanet terrane, Tuareg Shield, Algeria). Precambrian Res 247:139–158

Bitencourt MF, Nardi LVS (2000) Tectonic setting and sources of magmatism related to the Southern Brazilian Shear Belt. Revista Brasileira de Geociências 30(1):186–189

Black LP, Sheraton JW, Tingey RJ, McCulloch MT (1992) New U-Pb zircon ages from the Denman Glacier area, East Antarctica, and their significance for Gondwana reconstruction. Antarct Sci 4:447–460

Blades ML, Collins AS, Foden J, Payne JL, Xu X, Alemu T, Woldetinsae G, Clark C, Taylor RJM (2015) Age and hafnium isotopic evolution of the Didesa and Kemashi Domains, western Ethiopia. Precambrian Res 270:267–284. https://doi.org/10.1016/j.precamres.2015.09.018

Blades ML, Foden J, Collins AS, Alemu T, Woldetinsae G (in press) The origin of the ultramafic rocks of the Tulu Dimtu Belt, western Ethiopia—do they represent remnants of the Mozambique Ocean?' Geol Mag

Boger SD (2011) Antarctica—before and after Gondwana. Gondwana Res 19:335–371

Boger SD, Miller JM (2004) Terminal suturing of Gondwana and the onset of the Ross-Delamerian Orogeny: the cause and effect of an Early Cambrian reconfiguration of plate motions. Earth Planet Sci Lett 219:35–48

Boger SD, Wilson CJL, Fanning CM (2001) Early Paleozoic tectonism within the East Antarctic craton: the final suture between east and west Gondwana? Geology 29:463–466

Boger SD, Hirdes W, Ferreira CAM, Jenett T, Dallwig R, Fanning CM (2015) The 580–520 Ma Gondwana suture of Madagascar and its continuation into Antarctica and Africa. Gondwana Res 28:1048–1060

Bongiolo EM, Renac C, Piza P, d'Almeida T, Schmitt RS, Mexias AS (2016) Origin of pegmatites and fluids at Ponta Negra (RJ, Brazil) during late- to post-collisional stages of the Gondwana Assembly. Lithos 240–243:259–275

Bossi J, Gaucher C (2004) The Cuchilla Dionisio Terrane, Uruguay: an allochthonous block accreted in the Cambrian to SW-Gondwana. Gondwana Res 7:661–674

Bowring SA, Grotzinger JP, Condon DJ, Ramezani J, Newall MJ, Allen PA (2007) Geochronologic constraints on the chronostratigraphic framework of the Neoproterozoic Huqf Supergroup, Sultanate of Oman. Am J Sci 307:1097–1145

Brito Neves BB, Fuck RA, Pimentel MM (2014) The Brasiliano collage in South America: a review. Braz J Geol SciELO Brasil 44(3):493–518

Burrett C, Berry R (2000) Proterozoic Australia-Western United States (AUSWUS) fit between Laurentia and Australia. Geology 28:103–106

Campanha GAC, Basei MAS, Tassinari CCG, Nutman AP, Faleiros FM (2008) U-Pb SHRIMP and Sm-Nd analysis for Ribeira Belt mesoproterozoic and neoproterozoic terranes. In: VI South American symposium on isotope geology, p 4

Campanha GAC, Faleiros FM, Basei MAS, Tassinari CCG, Nutman AP, Vasconcelos PM (2015) Geochemistry and age of mafic rocks from the Votuverava Group, southern Ribeira Belt, Brazil: Evidence for 1490 Ma oceanic back-arc magmatism. Precambrian Res 266:530–550

Candan O, Akal C, Koralay OE, Okay AI, Oberhänsli R, Prelević D, Mertz-Kraus R (2016) Carboniferous granites on the northern margin of Gondwana, Anatolide-Tauride Block, Turkey—evidence for southward subduction of Paleotethys. Tectonophysics 683:349–366

Capistrano GG, Schmitt RS, Medeiros SR, Fernandes GLF (2017) Evidence of a Neoproterozoic active continental margin—geochemistry and isotope geology of high-grade paragneiss from the Ribeira Orogen, SE Brazil. J South Am Earth Sci 77:170–184

Cawood PA (2005) Terra Australis Orogen: Rodinia breakup and development of the Pacific and Iapetus margins of Gondwana during the Neoproterozoic and Paleozoic. Earth-Science Rev 69:249–279

Cawood PA, Buchan C (2007) Linking accretionary orogenesis with supercontinent assembly. Earth-Sci Rev 82:217–256

Caxito FA, Uhlein A, Dantas EL, Stevenson R, Salgado SS, Dussin IA, Sial AN (2016) A complete Wilson Cycle recorded within the Riacho do Pontal Orogen, NE Brazil: implications for the Neoproterozoic evolution of the Borborema Province at the heart of West Gondwana. Precambrian Res 282:97–120

Clark C, Healy D, Johnson T, Collins AS, Taylor RJ, Santosh M, Timms NE (2015) Hot orogens and supercontinent amalgamation: a Gondwanan example from southern India. Gondwana Res 28: 1310–1328

Clifford TN (1967) The Damaran episode in the Upper Proterozoic—Lower Paleozoic structural history of Southern Africa. In: Clifford TN (ed) The Damaran episode in the Upper Proterozoic—Lower Paleozoic structural history of Southern Africa. Geol Soc Am 1–78

Close D, Scrimgeour IR, Edgoose CJ (2003) Compilation of geochronological data from the northwestern Musgrave Block, Northern Territory, Technical Report 2003-006, Northest Territories Geological Survey, Darwin, Australia

Collins AS (2003) Structure and age of the northern Leeuwin Complex, Western Australia: Constraints from field mapping and U-Pb isotopic analysis. Aust J Earth Sci 50:585–599

Collins AS (2006) Madagascar and the amalgamation of Central Gondwana. Gondwana Res 9:3–16

Collins AS, Fitzsimons ICW (2001) Structural, isotopic and geochemical constraints on the evolution of the Leeuwin Complex, southwest Australia. In: Geological Society of Australia Abstracts. Geological Society of Australia, pp 16–19

Collins AS, Pisarevsky SA (2005) Amalgamating eastern Gondwana: the evolution of the Circum-Indian Orogens. Earth-Sci Rev 71: 229–270

Collins AS, Windley BF (2002) The tectonic evolution of central and northern Madagascar and its place in the Final Assembly of Gondwana. J Geol 110:325–339

Collins AS, Kröner A, Fitzsimons ICW, Razakamanana T (2003) Detrital Footprint of the Mozambique Ocean: U/Pb SHRIMP and Pb Evaporation Zircon geochronology of metasedimentary gneisses in Eastern Madagascar. Tectonophysics 375:77–99

Collins AS, Clark C, Sajeev K, Santosh M, Kelsey DE, Hand M (2007a) Passage through India: the Mozambique Ocean suture, high-pressure granulites and the Palghat-Cauvery shear zone system. Terra Nov 19:141–147

Collins AS, Santosh M, Braun I, Clark C (2007b) Age and sedimentary provenance of the Southern Granulites, South India: U-Th-Pb SHRIMP secondary ion mass spectrometry. Precambrian Res 155:125–138

Collins WJ, Belousova EA, Kemp AIS, Murphy JB (2011) Two contrasting Phanerozoic orogenic systems revealed by hafnium isotope data. Nat Geosci 4:333–337

Collins AS, Clark C, Plavsa D (2014) Peninsular India in Gondwana: the tectonothermal evolution of the Southern Granulite Terrain and its Gondwanan counterparts. Gondwana Res 25:190–203

Condie K, Pisarevsky SA, Korenaga J, Gardoll S (2015) Is the rate of supercontinent assembly changing with time? Precambrian Res 259:278–289

Cordani UG, D'Agrella-Filho MS, Brito-Neves BB, Trindade RIF (2003) Tearing up Rodinia: the Neoproterozoic palaeogeography of South American cratonic fragments. Terra Nov 15:350–359

Cordani UG, Pimentel MM, De Araújo CEG, Basei MAS, Fuck RA, Girardi VAV (2013a) Was there an Ediacaran Clymene ocean in central South America? Am J Sci 313:517–539

Cordani UG, Pimentel MM, de Araújo CEG, Fuck RA (2013b) The significance of the Transbrasiliano-Kandi tectonic corridor for the amalgamation of Western Gondwana. Brazilian J Geol 43:583–597

Corvino AF, Boger SD, Henjes-Kunst F, Wilson CJL, Fitzsimons ICW (2008) Superimposed tectonic events at 2450 Ma, 2100 Ma, 900 Ma and 500 Ma in the North Mawson Escarpment, Antarctic Prince Charles Mountains. Precambrian Res 167:281–302

Cox GM, Lewis CJ, Collins AS, Halverson GP, Jourdan F, Foden J, Nettle D, Kattan F (2012) Ediacaran terrane accretion within the Arabian-Nubian Shield. Gondwana Res 21:341–352

Cozzi A, Rea G, Craig J (2012) From global geology to hydrocarbon exploration: Ediacaran–Early Cambrian petroleum plays of India, Pakistan and Oman. Geol Soc Lond (Spec Pub) 366

Crowe WA, Cosca MA, Harris LB (2001) 40Ar/39Ar geochronolgy and Neoproterozoic tectonics along the northern margin of the Eastern Ghats Belt in north Orissa, India. Precambrian Res 108:237–266

Curtis ML, Millar IL, Storey BC, Fanning M (2004) Structural and geochronological constraints of early Ross orogenic deformation in the Pensacola Mountains, Antarctica. Geol Soc Am Bull 116:619–636

Cury LF (2009) Geologia do Terreno Paranaguá. Biblioteca Digital de Teses e Dissertações da Universidade de São Paulo

Daly MC, Andrade V, Barousse CA, Costa R, McDowell K, Piggott N, Poole AJ (2014) Brasiliano crustal structure and the tectonic setting of the Parnaíba basin of NE Brazil: Results of a deep seismic reflection profile. Tectonics 33:2102–2120

Dalziel IWD (1991) Pacific margins of Laurentia and East Antarctica-Australia as a conjugate rift pair: evidence and implications for an Eocambrian supercontinent. Geology 19:598–601

Dalziel IWD (1997) Overview: Neoproterozoic-Paleozoic geography and tectonics: review, hypothesis, environmental speculation. Geol Soc Am Bull 109:16–42

de Campos CP, de Medeiros SR, Mendes JC, Pedrosa-Soares AC, Dussin I, Ludka IP, Dantas EL (2016) Cambro-Ordovician magmatism in the Araçuaí Belt (SE Brazil): snapshots from a post-collisional event. J South Am Earth Sci 68:248–268. https://doi.org/10.1016/j.jsames.2015.11.016

de Oliveira CHE, Chemale F, Jelinek AR, Bicca MM, Philipp RP (2014) U-Pb and Lu–Hf isotopes applied to the evolution of the late to post-orogenic transtensional basins of the dom feliciano belt, Brazil. Precambrian Res 246:240–255

de Waele B, Wingate MTD, Fitzsimons ICW, Mapani BSE (2003) Untying the Kibaran knot: areassessment of Mesoproterozoic correlations in southern Africa based on SHRIMP U-Pb data from the Irumide belt. Geology 31:509–512

de Wit MJ, de Brito Neves BB, Trouw RAJ, Pankhurst RJ (2008) Pre-Cenozoic correlations across the South Atlantic region: (the ties that bind). Geol Soc Lond (Spec Publ) 294:1–8

Degler R, Pedrosa-Soares A, Dussin I, Queiroga G, Schulz B (2017) Contrasting provenance and timing of metamorphism from paragneisses of the Araçuaí-Ribeira orogenic system, Brazil: hints for Western Gondwana assembly. Gondwana Res 51:30–50

Diener JFA, Thomas RJ, Macey PH (2017) Pan-African accretionary metamorphism in the Sperrgebiet Domain, Gariep Belt, SW Namibia. Precambrian Res 292:152–162

Doebrich JL, Al-Jehani AM, Siddiqui AA, Hayes TS, Wooden JL, Johnson PR (2007) Geology and metallogeny of the Ar Rayn terrane, eastern Arabian shield: evolution of a Neoproterozoic continental-margin arc during assembly of Gondwana within the East African orogen. Precambrian Res 158:17–50

Dragone GN, Ussami N, Gimenez ME, Klinger FGL, Chaves CAM (2017) Western Paraná suture/shear zone and the limits of Rio Apa, Rio Tebicuary and Rio de la Plata cratons from gravity data. Precambrian Res 291:162–177

Duffles P, Trouw RAJ, Mendes JC, Gerdes A, Vinagre R (2016) U-Pb age of detrital zircon from the Embu sequence, Ribeira belt, Se Brazil. Precambrian Res 278:69–86

Elburg MA, Andersen T, Jacobs J, Läufer A, Ruppel A, Krohne N, Damaske D (2015) One hundred fifty million years of intrusive activity in the Sør Rondane Mountains (East Antarctica): implications for Gondwana Assembly. J Geol 124:1–26

Embleton BJJ, Schmidt PW (1985) Age and significance of magnetizations in dolerite dykes from the Northampton Block, Western Australia. Aust J Earth Sci 32:279–286

Escayola MP, van Staal CR, Davis WJ (2011) The age and tectonic setting of the Puncoviscana Formation in northwestern Argentina: an accretionary complex related to Early Cambrian closure of the Puncoviscana Ocean and accretion of the Arequipa-Antofalla block. J South Am Earth Sci 32:438–459

Estrada S, Läufer A, Eckelmann K, Hofmann M, Gärtner A, Linnemann U (2016) Continuous Neoproterozoic to Ordovician sedimentation at the East Gondwana margin—implications from detrital zircons of the Ross Orogen in northern Victoria Land, Antarctica. Gondwana Res 37:426–448

Eyal M, Be'eri-Shlevin Y, Eyal Y, Whitehouse MJ, Litvinovsky B (2014) Three successive Proterozoic island arcs in the Northern Arabian-Nubian Shield: evidence from SIMS U-Pb dating of zircon. Gondwana Res 25:338–357

Faleiros FM, Campanha GAC, Martins L, Vlach SRF, Vasconcelos PM (2011) Ediacaran high-pressure collision metamorphism and tectonics of the southern Ribeira Belt (SE Brazil): evidence for terrane accretion and dispersion during Gondwana assembly. Precambrian Res 189:263–291

Faleiros FM, Campanha GAC, Pavan M, Almeida VV, Rodrigues SWO, Araújo BP (2016) Short-lived polyphase deformation during crustal thickening and exhumation of a collisional orogen (Ribeira Belt, Brazil). J Struct Geol 93:106–130

Fernandes GLF, Schmitt RS, Bongiolo EM, Basei MAS, Mendes JC (2015) Unraveling the tectonic evolution of a Neoproterozoic-Cambrian active margin in the Ribeira Orogen (Se Brazil): U-Pb and Lu-Hf provenance data. Precambrian Res 266:337–360

Ferraccioli F, Finn CA, Jordan TA, Bell RE, Anderson LM, Damaske D (2011) East Antarctic rifting triggers uplift of the Gamburtsev Mountains. Nature 479:388–392

Fitzsimons ICW (2003a) Proterozoic basement provinces of southern and southwestern Australia, and their correlation with Antarctica. Geol Soc London (Spec Publ) 206:93–130

Fitzsimons ICW (2003) Proterozoic basement provinces of southern and southwestern Australia, and their correlation with Antarctica. Geol Soc Lond (Spec Publ) 206(1):93–130

Florisbal LM, Bitencourt MF, Janasi V, Nardi LVS, Heaman L (2012) Petrogenesis of syntectonic granites emplaced at the transition from thrusting to transcurrent tectonics in post-collisional settings. Lithos 153:53–71

Foden J, Elburg MA, Dougherty-Page J, Burtt A (2006) The timing and duration of the Delamerian Orogeny: correlation with the Ross Orogen and implications for Gondwana Assembly. J Geol 114:189–210

Foster DA, Goscombe BD, Newstead B, Mapani B, Mueller PA, Gregory LC, Muvangua E (2015) U-Pb age and Lu–Hf isotopic data of detrital zircons from the Neoproterozoic Damara Sequence: implications for Congo and Kalahari before Gondwana. Gondwana Res 28:179–190

Frimmel HE, Frank W (1998) Neoproterozoic tectono-thermal evolution of the Gariep Belt and its basement, Namibia and South Africa. Precambrian Res 90:1–28

Frimmel HE, Tack L, Basei MS, Nutman AP, Boven A (2006) Provenance and chemostratigraphy of the Neoproterozoic West Congolian Group in the Democratic Republic of Congo. J African Earth Sci 46:221–239

Frimmel HE, Basei MS, Gaucher C (2011) Neoproterozoic geodynamic evolution of SW-Gondwana: a southern African perspective. Int J Earth Sci 100:323–354

Frimmel HE, Basei MAS, Correa VX, Mbangula N (2013) A new lithostratigraphic subdivision and geodynamic model for the Pan-African western Saldania Belt, South Africa. Precambrian Res 231:218–235

Fritz H, Abdelsalam M, Ali KA, Bingen B, Collins AS, Fowler AR, Ghebreab W, Hauzenberger CA, Johnson PR, Kusky TM, Macey P, Muhongo S, Stern RJ, Viola G (2013) Orogen styles in the East African Orogen: a review of the Neoproterozoic to Cambrian tectonic evolution. J African Earth Sci 86:65–106

Fuck RA, Dantas EL, Pimentel MM, Botelho NF, Armstrong R, Laux JH, Junges SL, Soares JE, Praxedes IF (2014) Paleoproterozoic crust-formation and reworking events in the Tocantins Province, central Brazil: a contribution for Atlantica supercontinent reconstruction. Precambrian Res 244:53–74

Ganade de Araujo CE, Weinberg RF, Cordani UG (2014b) Extruding the Borborema Province (NE-Brazil): a two-stage Neoproterozoic collision process. Terra Nov 26:157–168

Ganade de Araujo CE, Cordani UG, Agbossoumounde Y, Caby R, Basei MAS, Weinberg RF, Sato K (2016) Tightening-up NE Brazil and NW Africa connections: new U-Pb/Lu–Hf zircon data of a complete plate tectonic cycle in the Dahomey belt of the West Gondwana Orogen in Togo and Benin. Precambrian Res 276:24–42

Ganade de Araújo CE, Rubatto D, Hermann J, Cordani UG, Caby R, Basei MAS (2014b) Ediacaran 2,500-km-long synchronous deep continental subduction in the West Gondwana Orogen. Nat Commun 5:5198

Garfunkel Z (2015) The relations between Gondwana and the adjacent peripheral Cadomian domain—constrains on the origin, history, and paleogeography of the peripheral domain. Gondwana Res 28:1257–1281

Gaucher C, Frimmel HE, Germs GJB (2009) Tectonic events and Palaeogeographic evolution of Southwestern Gondwana in the Neoproterozoic and Cambrian. Developments in Precambrian Geology 16:295–316

Gibson GM, Champion DC, Ireland TR (2015) Preservation of a fragmented late Neoproterozoic–earliest Cambrian hyper-extended continental-margin sequence in the Australian Delamerian Orogen. Geol Soc Lond (Spec Publ) 413:269–299

Giese J, Berger A, Schreurs G, Gnos E (2011) The timing of the tectono-metamorphic evolution at the Neoproterozoic-Phanerozoic boundary in central southern Madagascar. Precambrian Res 185:131–148

Godoy AM, Pinho FEC, Manzano JC, de Araújo LMB, da Silva JA, Figueiredo M (2010) Estudos isotópicos das rochas granitóides neoproterozóicas da Faixa de Dobramento Paraguai. Rev Bras Geociências 40:380–391

Goodenough KM, Thomas RJ, De Waele B, Key RM, Schofield DI, Bauer W, Tucker RD, Rafahatelo J-M, Rabarimanana M, Ralison AV, Randriamananjara T (2010) Post-collisional magmatism in the central East African Orogen: the Maevarano Suite of north Madagascar. Lithos 116:18–34

Goscombe B, Gray DR (2007) The Coastal Terrane of the Kaoko Belt, Namibia: outboard arc-terrane and tectonic significance. Precambrian Res 155:139–158

Goscombe B, Foster DA, Gray D, Wade B, Marsellos A, Titus J (2017) Deformation correlations, stress field switches and evolution of an orogenic intersection: the Pan-African Kaoko-Damara orogenic junction. Namibia, Geosci Front 8(6):1187–1232

Gradim C, Roncato J, Pedrosa-Soares AC, Cordani U, Dussin I, Alkmim FF, Queiroga G, Jacobsohn T, da Silva LC, Babinski M (2014) The hot back-arc zone of the Araçuaí orogen, Eastern Brazil: from sedimentation to granite generation. Brazilian J Geol 44:155–180

Gray DR, Foster DA, Meert JG, Goscombe BD, Armstrong R, Trouw RAJ, Passchier CW (2008) A Damara orogen perspective on the assembly of southwestern Gondwana. Geol Soc Lond (Spec Publ) 294:257–278

Grégoire V, Nédélec A, Monié P, Montel J-M, Ganne J, Ralison B (2009) Structural reworking and heat transfer related to the late-Panafrican Angavo shear zone of Madagascar. Tectonophysics 477:197–216

Gruber L, Porcher CC, Lenz C, Fernandes LAD (2011) Proveniência de metassedimentos das sequências Arroio Areião, Cerro Cambará e Quartzo Milonitos no Complexo Metamórfico Porongos, Santana da Boa Vista. Pesqui em Geociências 38:205–223

Haines PW, Kirkland CL, Wingate MTD, Allen H, Belousova EA, Gréau Y (2016) Tracking sediment dispersal during orogenesis: A zircon age and Hf isotope study from the western Amadeus Basin, Australia. Gondwana Res 37:324–347

Halpin JA, Crawford AJ, Direen NG, Coffin MF, Forbes CJ, Borissova I (2008) Naturaliste Plateau, offshore Western Australia: a submarine window into Gondwana assembly and breakup. Geology 36:807–810

Handke MJ, Tucker RD, Ashwal LD (1999) Neoproterozoic continental arc magmatism in west-central Madagascar. Geology 27:351–354

Harris LB (1994) Neoproterozoic sinistral displacement along the Darling Mobile Belt, Western Australia, during Gondwanaland assembly. J Geol Soc Lond 151:901–904

Hasui Y, Carneiro CDR, de Almeida FFM, Bartorelli A (2012) Geologia do Brasil. Beca, p 900

Heilbron M, Pedrosa-Soares AC, Campos Neto M da C, Silva LC da, Trouw RAJ, Janasi V de A (2004) Província Mantiqueira. Geol do Cont sul-americano evolução da obra Fernando Flávio Marques Almeida: 203–235

Heilbron M, Valeriano CM, Tassinari CCG, Almeida J, Tupinambá M, Siga O, Trouw R (2008) Correlation of Neoproterozoic terranes between the Ribeira Belt, SE Brazil and its African counterpart: comparative tectonic evolution and open questions. Geol Soc Lond (Spec Publ) 294:211–237

Hoffman PF (1991) Did the Breakout of Laurentia Turn Gondwanaland Inside-Out? Science 252:1409–1412

Jacobs J, Fanning CM, Henjes-Kunst F, Olesch M, Paech H (1998) Continuation of the Mozambique Belt into East Antarctica: Grenville-Age Metamorphism and Polyphase Pan-African High-Grade Events in Central Dronning Maud Land. J Geol 106:385–406

Jacobs J, Pisarevsky S, Thomas RJ, Becker T (2008) The Kalahari Craton during the assembly and dispersal of Rodinia. Precambrian Res 160:142–158

Jacobs J, Elburg M, Läufer A, Kleinhanns IC, Henjes-Kunst F, Estrada S, Ruppel AS, Damaske D, Montero P, Bea F (2015) Two distinct Late Mesoproterozoic/Early Neoproterozoic basement provinces in central/eastern Dronning Maud Land, East Antarctica: The missing link, 15o-21oE. Precambrian Res 265:249–272

Johnson PR, Stewart ICF (1995) Magnetically inferred basement structure in central Saudi Arabia. Tectonophysics 245:37–52

Johnson SP, Rivers T, De Waele B (2005) A review of the Mesoproterozoic to early Palaeozoic magmatic and tectonothermal history of south–central Africa: implications for Rodinia and Gondwana. J Geol Soc Lond 162:433–450

Johnson PR, Andresen A, Collins AS, Fowler AR, Fritz H, Ghebreab W, Kusky T, Stern RJ (2011) Late Cryogenian-Ediacaran history of the Arabian-Nubian Shield: a review of depositional, plutonic, structural, and tectonic events in the closing stages of the northern East African Orogen. J African Earth Sci 61:167–232

Johnson TE, Clark C, Taylor RJM, Santosh M, Collins AS (2015) Prograde and retrograde growth of monazite in migmatites: an example from the Nagercoil Block, southern India. Geosci Front 6:373–387

Johnson EL, Phillips G, Allen CM (2016) Ediacaran-Cambrian basin evolution in the Koonenberry Belt (eastern Australia): Implications for the geodynamics of the Delamerian Orogen. Gondwana Res 37:266–284

Jöns N, Schenk V (2011) The ultrahigh temperature granulites of southern Madagascar in a polymetamorphic context: implications for the amalgamation of the Gondwana supercontinent. Eur J Mineral 23:127–156

Karlstrom KE, Harlan SS, Williams ML, McLelland J, Geissman JW, Ahall K-I (1999) Refining Rodinia: Geologic evidence for the Australia–western US connection in the Proterozoic. GSA Today 9:1–7

Kelsey DE, Hand M, Clark C, Wilson CJL (2007) On the application of in situ monazite chemical geochronology to constraining P-T–t histories in high-temperature (> 850 °C) polymetamorphic granulites from Prydz Bay, East Antarctica. J Geol Soc London 164:667–683

Kennedy WQ (1964) The structural differentiation of Africa in the PanAfrican (±500 m. y.) tectonic episode. Univ Leeds Res Inst African Geol Annu Rep 8:48–49

Klein EL, Moura CAV (2008) São Luís Craton and Gurupi Belt (Brazil): possible links with the West African Craton and surrounding Pan-African belts. Geol Soc Lond (Spec Publ) 294:137–151

Klein EL, Rodrigues JB, Lopes ECS, Soledade GL (2012) Diversity of Rhyacian granitoids in the basement of the Neoproterozoic-Early Cambrian Gurupi Belt, northern Brazil: Geochemistry, U-Pb zircon geochronology, and Nd isotope constraints on the Paleoproterozoic magmatic and crustal evolution. Precambrian Res 220–221: 192–216

Konopásek J, Sláma J, Košlerc J (2016) Linking the basement geology along the Africa-South America coasts in the South Atlantic. Precambrian Res 280:221–230

Kröner A, Cordani U (2003) African, southern Indian and South American cratons were not part of the Rodinia supercontinent: evidence from field relationships and geochronology. Tectonophysics 375:325–352

Kukla PA, Stanistreet IG (1991) Record of the Damara Khomas Hochland accretionary prism in central Namibia: refutation of an ''ensialic'' origin of a Late Proterozoic orogenic belt. Geology 19:473–476

Lara P, Oyhantçabal P, Dadd K (2017) Post-collisional, Late Neoproterozoic, high-Ba-Sr granitic magmatism from the Dom Feliciano Belt and its cratonic foreland, Uruguay: petrography, geochemistry, geochronology, and tectonic implications. Lithos 277:178–198

Lehmann J, Saalmann K, Naydenov KV, Milani L, Belyanin GA, Zwingmann H, Charlesworth G, Kinnaird JA (2016) Structural and geochronological constraints on the Pan-African tectonic evolution of the northern Damara Belt, Namibia. Tectonics 35:103–135

Li ZX, Evans DA (2011) Late Neoproterozoic 40° intraplate rotation within Australia allows for a tighter-fitting and longer-lasting Rodinia. Geology 39(1):39–42

Li ZX, Bogdanova SV, Collins AS, Davidson A, De Waele B, Ernst RE, Fitzsimons ICW, Fuck RA, Gladkochub DP, Jacobs J,

Karlstrom KE, Lu S, Natapov LM, Pease V, Pisarevsky SA, Thrane K, Vernikovsky V (2008) Assembly, configuration, and break-up history of Rodinia: a synthesis. Precambrian Res 160: 179–210

Lira R, Millone HA, Kirschbaum AM, Moreno RS (1997) Calc-alkaline arc granitoid activity in the Sierra Norte-Ambargasta Ranges, central Argentina. J South Am Earth Sci 10:157–177

Liu X, Zhao Z, Zhao Y, Chen J, Liu X (2003) Pyroxene exsolution in mafic granulites from the Grove Mountains, East Antarctica: constraints on Pan-African metamorphic conditions. Eur J Mineral 15:55–65

Liu X, Jahn B, Zhao Y, Li M, Li H, Liu X (2006) Late Pan-African granitoids from the Grove Mountains, East Antarctica: age, origin and tectonic implications. Precambrian Res 145:131–154

Liu X, Zhao Y, Song B, Liu J, Cui J (2009) SHRIMP U-Pb zircon geochronology of high-grade rocks and charnockites from the eastern Amery Ice Shelf and southwestern Prydz Bay, East Antarctica: Constraints on Late Mesoproterozoic to Cambrian tectonothermal events related to supercontinent assembly. Gondwana Res 16:342–361

Major RB, Conor CHH (1993) Musgrave Block. In: Drexel JF, Preiss WV, Parker AJ (eds) The geology of South Australia, vol 1. The Precambrian, 54th edn. Mines and Energy South Australia, Bulletin, pp 157–167

Manatschal G, Müntener O (2009) A type sequence across an ancient magma-poor ocean–continent transition: the example of the western Alpine Tethys ophiolites. Tectonophysics 473:4–19

Mantovani MSM, Brito Neves BB (2009) The Paranapanema Lithospheric Block: its nature and role in the accretion of Gondwana. Dev Precambrian Geol 16:257–272

Martil MMD, de Fátima Bitencourt M, Nardi LVS, Koester E, Pimentel MM (2017) Pre-collisional, Tonian (ca. 790 Ma) continental arc magmatism in southern Mantiqueira Province, Brazil: geochemical and isotopic constraints from the Várzea do Capivarita Complex. Lithos 274–275:39–52

Martin EL, Collins WJ, Kirkland CL (2017) An Australian source for Pacific-Gondwanan zircons: implications for the assembly of northeastern Gondwana. Geology 45(8):699–702. https://doi.org/10.1130/G39152.1

Martino RD, Guereschi AB, Sfragulla JA (2009) Petrology, structure and tectonic significance of the Tuclame banded schists in the Sierras Pampeanas of Córdoba and its relationship with the metamorphic basement of northwestern Argentina. J South Am Earth Sci 27:280–298

Martins GG, Mendes JC, Schmitt RS, Armstrong R, Valeriano CM (2016) 550–490 Ma pre-to post-collisional shoshonitic rocks in the Ribeira Belt (SE Brazil) and their tectonic significance. Precambrian Res 286:352–369

McGee B, Collins AS, Trindade RIF (2012) G'day Gondwana - the final accretion of a supercontinent: U-Pb ages from the post-orogenic São Vicente Granite, northern Paraguay Belt, Brazil. Gondwana Res 21:316–322

McGee B, Collins AS, Trindade R, Jourdan F (2015a) Investigating mid-Ediacaran glaciation and final Gondwana amalgamation using coupled sedimentology and 40Ar/39Ar detrital muscovite provenance from the Paraguay Belt, Brazil. Sedimentology 62:130–154

McGee B, Collins AS, Trindade R (2015b) Age and Provenance of the Cryogenian to Cambrian passive margin to foreland basin sequence of the northern Paraguay Belt, Brazil. Geol Soc Am Bull 127:76–86

Meert JG (2003) A synopsis of events related to the assembly of eastern Gondwana. Tectonophysics 362:1–40

Meert JG, Lieberman BS (2008) The Neoproterozoic assembly of Gondwana and its relationship to the Ediacaran-Cambrian radiation. Gondwana Res 14:5–21

Meert JG, Van Der Voo R (1997) The assembly of Gondwana 800–550 Ma. J Geodyn 23:223–235

Meert JG, Van Der Voo R, Ayub S (1995) Paleomagnetic investigation of the Neoproterozoic Gagwe lavas and Mbozi complex, Tanzania and the assembly of Gondwana. Precambrian Res 74:225–244

Meira VT, García-Casco A, Juliani C, Almeida RP, Schorscher JHD (2015) The role of intracontinental deformation in supercontinent assembly: insights from the Ribeira Belt, Southeastern Brazil (Neoproterozoic West Gondwana). Terra Nov 27:206–217

Meneghini F, Kisters A, Buick I, Fagereng Å (2014) Fingerprints of late Neoproterozoic ridge subduction in the Pan-African Damara belt, Namibia. Geology 42:903–906

Merdith AS, Williams SE, Müller RD, Collins AS (2017a) Kinematic constraints on the Rodinia to Gondwana transition. Precambrian Res 299:132–150

Merdith AS, Collins AS, Williams SE, Pisarevsky S, Foden JD, Archibald DB, Blades ML, Alessio BL, Armistead S, Plavsa D, Clark C, Müller RD (2017b) A full-plate global reconstruction of the Neoproterozoic. Gondwana Res 50:84–134

Mikhalsky EV, Sheraton JW (2011) The Rayner tectonic Province of East Antarctica: compositional features and geodynamic setting. Geotectonics 45:496–512

Miller RM (2008). Neoproterozoic and early Palaeozoic rocks of the Damara Orogen. In: Miller RM (ed) The geology of Namibia. Geological Survey of Namibia, Windhoek, 13-1–13-410

Monié P, Bosch D, Bruguier O, Vauchez A, Rolland Y, Nsungani P, Buta Neto A (2012) The Late Neoproterozoic/Early Palaeozoic evolution of the West Congo Belt of NW Angola: geochronological (U-Pb and Ar-Ar) and petrostructural constraints. Terra Nov 24:238–247

Moores EM (1991) Southwest U.S.-East Antarctic (SWEAT) connection: a hypothesis. Geology 19:425–428

Moura CAV, Pinheiro BLS, Nogueira ACR, Gorayeb PSS, Galarza MA (2008) Sedimentary provenance and palaeoenvironment of the Baixo Araguaia Supergroup: constraints on the palaeogeographical evolution of the Araguaia Belt and assembly of West Gondwana. Geol Soc Lond (Spec Publ) 294:173–196

Murphy JB, Nance RD (1991) Supercontinent model for the contrasting character of Late Proterozoic orogenic belts. Geology 19:469–472

Nance RD, Murphy JB, Santosh M (2014) The supercontinent cycle: a retrospective essay. Gondwana Res 25:4–29

Nascimento DB, Ribeiro A, Trouw RAJ, Schmitt RS, Passchier CW (2016) Stratigraphy of the Neoproterozoic Damara Sequence in northwest Namibia: slope to basin sub-marine mass-transport deposits and olistolith fields. Precambrian Res 278:108–125

Nascimento DB, Schmitt RS, Ribeiro A, Trouw RAJ, Passchier CW, Basei MS (2017) Depositional ages and provenance of the Neoproterozoic Damara Supergroup (northwest Namibia): implications for the Angola-Congo and Kalahari cratons connection. Gondwana Res 52:153–171

Offler R, Phillips G, Fergusson CL, Green TJ (2011) Tectonic Implications of Early Paleozoic Metamorphism in the Anakie Inlier, Central Queensland, Australia. J Geol 119:467–485

Oliveira EP, Windley BF, Araújo MNC (2010) The Neoproterozoic Sergipano orogenic belt, NE Brazil:a complete plate tectonic cycle in western Gondwana. Precambrian Res 181:64–84

Oriolo S, Oyhantçabal P, Basei MAS, Wemmer K, Siegesmund S (2016) The Nico Pérez Terrane (Uruguay): from Archean crustal growth and connections with the Congo Craton to late Neoproterozoic accretion to the Río de la Plata Craton. Precambrian Res 280:147–160

Oriolo S, Oyhantçabal P, Wemmer K, Siegesmund S (2017) Contemporaneous assembly of Western Gondwana and final Rodinia break-up: Implications for the supercontinent cycle. Geosci Front

Owona S, Schulz B, Ratschbacher L, Mvondo Ondoa J, Ekodeck GE, Tchoua FM, Affaton P (2011) Pan-African metamorphic evolution in the southern Yaounde Group (Oubanguide Complex, Cameroon) as revealed by EMP-monazite dating and thermobarometry of garnet metapelites. J African Earth Sci 59:125–139

Oyhantçabal P, Siegesmund S, Wemmer K, Layer P (2010) The Sierra Ballena Shear Zone in the southernmost Dom Feliciano Belt (Uruguay): evolution, kinematics, and deformation conditions. Int J Earth Sci 99:1227–1246

Oyhantçabal P, Siegesmund S, Wemmer K, Passchier CW (2011) The transpressional connection between Dom Feliciano and Kaoko Belts at 580–550 Ma. Int J Earth Sci 100:379–390

Paixão MAP, Nilson AA, Dantas EL (2008) The Neoproterozoic Quatipuru ophiolite and the Araguaia fold belt, central-northern Brazil, compared with correlatives in NW Africa. Geol Soc Lond (Spec Publ) 294:297–318

Passchier C, Trouw R, Schmitt RS (2016) How to make a transverse triple junction—new evidence for the assemblage of Gondwana along the Kaoko-Damara belts, Namibia. Geology 44:843–846

Paulsen TS, Encarnación J, Grunow AM, Valencia VA, Pecha M, Layer PW, Rasoazanamparany C (2013) Age and significance of "outboard" high-grade metamorphics and intrusives of the Ross orogen, Antarctica. Gondwana Res 24:349–358

Paulsen TS, Deering C, Sliwinski J, Bachmann O, Guillong M (2016) Detrital zircon ages from the Ross Supergroup, north Victoria Land, Antarctica: implications for the tectonostratigraphic evolution of the Pacific-Gondwana margin. Gondwana Res 35:79–96

Pauly J, Marschall HR, Meyer H-P, Chatterjee N, Monteleone B (2016) Prolonged Ediacaran-Cambrian Metamorphic History and Short-lived High-pressure Granulite-facies Metamorphism in the H.U. Sverdrupfjella, Dronning Maud Land (East Antarctica): Evidence for Continental Collision during Gondwana Assembly. J Petrol 57:185–228

Pedrosa-Soares AC, Vidal P, Leonardos OH, de Brito Neves BB (1998) Neoproterozoic oceanic remnants in eastern Brazil: Further evidence and refutation of an exclusively ensialic evolution for the Araçuaí-West Congo orogen. Geology 26:519–522

Pedrosa-Soares AC, Alkmim FF, Tack L, Noce CM, Babinski M, Silva LC, Martins-Neto MA (2008) Similarities and differences between the Brazilian and African counterparts of the Neoproterozoic Araçuaí-West Congo orogen. Geol Soc London, Spec Publ 294:153–172

Philipp RP, Pimentel MM, Chemale F Jr (2016) Tectonic evolution of the Dom Feliciano Belt in Southern Brazil: geological relationships and U-Pb geochronology. Brazilian J Geol 46:83–104

Piacentini T, Vasconcelos PM, Farley KA (2013) 40Ar/39Ar constraints on the age and thermal history of the Urucum Neoproterozoic banded iron-formation, Brazil. Precambrian Res 228:48–62

Pimentel MM (2016) The tectonic evolution of the Neoproterozoic Brasília Belt, central Brazil: a geochronological and isotopic approach. Braz J Geol 46:67–82

Plavsa D, Collins AS, Foden JF, Kropinski L, Santosh M, Chetty TRK, Clark C (2012) Delineating crustal domains in Peninsular India: age and chemistry of orthopyroxene-bearing felsic gneisses in the Madurai Block. Precambrian Res 198–199:77–93

Plavsa D, Collins AS, Payne JL, Foden JD, Clark C, Santosh M (2014) Detrital zircons in basement metasedimentary protoliths unveil the origins of southern India. GSA Bull 126:791–811

Plavsa D, Collins AS, Foden JD, Clark C (2015) The evolution of a Gondwanan collisional orogen: a structural and geochronological appraisal from the Southern Granulite Terrane, South India. Tectonics 34:820–857

Porada H (1979) The damara-ribeira orogen of the Pan-Africanbrasiliano cycle in Namibia (Southwest Africa) and Brazil as interpreted in terms of continental collision. Tectonophysics 57:237–265

Powell CM, Pisarevsky SA (2002) Late Neoproterozoic assembly of East Gondwana. Geology 30:3–6

Raimondo T, Collins AS, Hand M, Walker-Hallam A, Smithies RH, Evins PM, Howard HM (2009) Ediacaran Intracontinental Channel Flow. Geology 37:291–294

Raimondo T, Collins AS, Hand M, Walker-Hallam A, Smithies RH, Evins PM, Howard HM (2010) The anatomy of a deep intracontinental Orogen. Tectonics. https://doi.org/10.1029/2009TC002504

Ramos VA (2008) The basement of the Central Andes: the Arequipa and related terranes. Annu Rev Earth Planet Sci 36:289–324

Ramos VA (2010) The Grenville-age basement of the Andes. J South Am Earth Sci 29:77–91. https://doi.org/10.1016/j.jsames.2009.09.004

Ramos RC, Koester E (2014) Geologia da associação metamáfica-ultramáfica da região de Arroio Grande, sudeste do Escudo Sul-Rio-Grandense. Pesqui em Geociências 41:25–38

Ramos VA, Naipauer M (2014) Patagonia: where does it come from? J Iber Geol 40:367–379

Ramos VA, Vujovich G, Martino R, Otamendi J (2010) Pampia: A large cratonic block missing in the Rodinia supercontinent. J Geodyn 50:243–255

Rapela CW, Pankhurst RJ, Casquet C, Baldo E, Saavedra J, Galindo C, Fanning CM (1998) The Pampean Orogeny of the southern proto-Andes: Cambrian continental collision in the Sierras de Córdoba. Geol Soc London, Spec Publ 142:181–217

Rapela CW, Baldo EG, Pankhurst RJ, Saavedra J (2002) Cordieritite and Leucogranite Formation during Emplacement of Highly Peraluminous Magma: the El Pilón Granite Complex (Sierras Pampeanas, Argentina). J Petrol 43:1003–1028

Rapela CW, Fanning CM, Casquet C, Pankhurst RJ, Spalletti L, Poiré D, Baldo EG (2011) The Rio de la Plata craton and the adjoining Pan-African/brasiliano terranes: their origins and incorporation into south-west Gondwana. Gondwana Res 20:673–690

Reeves C (2014) The position of Madagascar within Gondwana and its movements during Gondwana dispersal. J African Earth Sci 94:45–57

Riccomini C, Coimbra AM, Rocha-Campos AC (1996) Stratigraphy of the Pico de Itapeva basin (neoproterozoic-cambrian, southeastern Brazil). An Acad Bras Cienc 68:602

Richard J, Taylor M, Clark C, Johnson TE, Santosh M, Collins AS (2015) Unravelling the complexities in high-grade rocks using multiple techniques: the Achankovil Zone of southern India. Contrib to Mineral Petrol 169:1

Richetti PC, Schmitt RS, Reeves C (2016) Dividing South America into continental blocks and applying it to West Gondwana re-assemble. In: Abstracts 35th International Geological Congress, Cape Town

Richter F, Lana C, Stevens G, Buick I, Pedrosa-Soares AC, Alkmim FF, Cutts K (2016) Sedimentation, metamorphism and granite generation in a back-arc region: records from the Ediacaran Nova Venécia Complex (Araçuaí Orogen, Southeastern Brazil). Precambrian Res 272:78–100

Robinson FA, Foden JD, Collins AS, Payne JL (2014) Arabian Shield magmatic cycles and their relationship with Gondwana 2 assembly: Insights from zircon U-Pb and Hf isotopes. Earth Planet Sci Lett 408:207–225

Robinson FA, Foden JD, Collins AS (2015a) Geochemical and isotopic constraints on island arc, synorogenic, post-orogenic and anorogenic granitoids in the Arabian Shield, Saudi Arabia. Lithos 220–223:97–115

Robinson FA, Foden JD, Collins AS (2015b) Zircon geochemical and geochronological constraints on contaminated and enriched mantle sources beneath the Arabian Shield, Saudi Arabia. J Geol 123:463–489

Santos RV, Glasmacher UA, Geldmacher J (2014) Scientific drilling in the South Atlantic. In: IODP Workshop, Rio de Janeiro, Brazil, 2–5 April 2014. EOS, Transactions, American Geophysical Union 95, 249

Sassi FP, Visonà D, Ferrara G, Gatto GO, Ibrahim HA, Said AA, Tonarini S (1993) The crystalline basement of northern Somalia: lithostratigraphy and the sequence of events. In: Abbate E, Sagri M, Sassi FP (eds) Geology and mineral resources of Somalia and surrounding regions. Istituto Agronomico l'Otremare, Firenze, pp 3–40

Schmidt DL, Ford AB (1969) Geology of the Pensacola and Thiel mountains. Antarctic map folio series, Folio, p 12

Schmitt RS, Trouw RAJ, Van Schmus WR, Pimentel MM (2004) Late amalgamation in the central part of West Gondwana: new geochronological data and the characterization of a Cambrian collisional orogeny in the Ribeira Belt (SE Brazil). Precambrian Res 133:29–61

Schmitt RS, Trouw RAJ, Van Schmus WR, Passchier CW (2008) Cambrian orogeny in the Ribeira Belt (SE Brazil) and correlations within West Gondwana: ties that bind underwater. Geol Soc Lond (Spec Publ) 294:279–296

Schmitt RS, Trouw RAJ, Passchier CW, Medeiros SR, Armstrong R (2012) 530 Ma syntectonic syenites and granites in NW Namibia—their relation with collision along the junction of the Damara and Kaoko belts. Gondwana Res 21:362–377

Schmitt RS, Silva EA, Collins AS, Reeves C, Fragoso RA, Richetti PC, Fernandes GL de F, Benedek MR, Costa RL, Assis AP (2016a) Gondwana tectonic evolution recounted through the Gondwana map—IGCP-628. In: Abstracts 35th International Geological Congress, Cape Town

Schmitt RS, Trouw R, Van Schmus WR, Armstrong R, Stanton NSG (2016b) The tectonic significance of the Cabo Frio Tectonic Domain in the SE Brazilian margin: a Paleoproterozoic through Cretaceous saga of a reworked continental margin. Braz J Geol 46:37–66

Schwartz JJ, Gromet PL, Miró R (2008) Timing and Duration of the Calc-Alkaline Arc of the Pampean Orogeny: implications for the Late Neoproterozoic to Cambrian Evolution of Western Gondwana. J Geol 116:39–61

Shackleton RM (1996) The final collision zone between East and West Gondwana: where is it? J African Earth Sci 23:271–287

Shiraishi K, Hokada T, Fanning CM, Misawa K, Motoyoshi Y (2003) Timing of thermal events in eastern Dronning Maud Land, East Antarctica. Polar Geosci 16:76–99

Shiraishi K, Dunkley DJ, Hokada T, Fanning CM, Kagami H, Hamamoto T (2008) Geochronological constraints on the Late Proterozoic to Cambrian crustal evolution of eastern Dronning Maud Land, East Antarctica: a synthesis of SHRIMP U-Pb age and Nd model age data. Geol Soc Lond (Spec Publ) 308:21–67

Stern RJ (1994) Arc assembly and continental collision in the Neoproterozoic East African Orogen: implications for the consolidation of Gondwanaland. Annu Rev Earth Planet Sci 22:319–351

Stoeser DB, Whitehouse MJ, Stacey JS (2001) The Khida terrane—geology of Paleoproterozoic rocks in the Muhayil area, eastern Arabian Shield, Saudi Arabia. Gondwana Res 4:192–194

Szatmari P, Milani EJ (2016) Tectonic control of the oil-rich large igneous-carbonate-salt province of the South Atlantic rift. Mar Pet Geol 77:567–596

Tack L, Wingate MTD, Liégeois J-P, Fernandez-Alonso M, Deblond A (2001) Early Neoproterozoic magmatism (1000–910 Ma) of the Zadinian and Mayumbian Groups (Bas-Congo): onset of Rodinia rifting at the western edge of the Congo craton. Precambrian Res 110:277–306

Taylor RJM, Clark C, Johnson TE, Santosh M, Collins AS (2015) Unravelling the complexities in high-grade rocks using multiple techniques—the Achankovil Zone of southern India. Contrib Miner Petrol 165:51. https://doi.org/10.1007/s00410-015-1147-2

Tenczer V, Hauzenberger C, Fritz H, Hoinkes G, Muhongo S, Klötzli U (2013) Crustal age domains and metamorphic reworking of the deep crust in Northern-Central Tanzania: a U/Pb zircon and monazite age study. Mineral Petrol 107 (5):679–707

Tohver E, Cawood PA, Rossello EA, Jourdan F (2012) Closure of the Clymene Ocean and formation of West Gondwana in the Cambrian: evidence from the Sierras Australes of the southernmost Rio de la Plata craton, Argentina. Gondwana Res 21:394–405

Torsvik TH, Cocks LRM (2013) Gondwana from top to base in space and time. Gondwana Res 24:999–1030

Trindade RIF, D'Agrella-Filho MS, Epof I, Neves BBB (2006) Paleomagnetism of Early Cambrian Itabaiana mafic dikes (NE Brazil) and the final assembly of Gondwana. Earth Planet Sci Lett 244:361–377

Trompette R (1994) Geology of Western Gondwana (2000-500 Ma): Pan-African-Brasiliano aggregation of South America and Africa. Balkema 364

Trouw RAJ, Peternel R, Ribeiro A, Heilbron M, Vinagre R, Duffles P, Trouw CC, Fontainha M, Kussama HH (2013) A new interpretation for the interference zone between the southern Brasília belt and the central Ribeira belt, SE Brazil. J South Am Earth Sci 48:43–57

Tsunogae T, Yang Q-Y, Santosh M (2015) Early Neoproterozoic arc magmatism in the Lützow-Holm Complex, East Antarctica: Petrology, geochemistry, zircon U-Pb geochronology and Lu–Hf isotopes and tectonic implications. Precambrian Res 266:467–489. https://doi.org/10.1016/j.precamres.2015.05.040

Tucker RD, Ashwal LD, Handke MJ, Hamilton MA, Le Grange M, Rambeloson RA (1999) U-Pb geochronology and isotope geochemistry of the Archean and Proterozoic rocks of north-central Madagascar. J Geol 107:135–153

Tucker RD, Roig J-Y, Moine B, Delor C, Peters SG (2014) A geological synthesis of the Precambrian shield in Madagascar. J African Earth Sci 94:9–30

Tupinambá M, Heilbron M, Valeriano C, Júnior RP, de Dios FB, Machado N, Silva LGE, de Almeida JCH (2012) Juvenile contribution of the Neoproterozoic Rio Negro Magmatic Arc (Ribeira Belt, Brazil): Implications for Western Gondwana amalgamation. Gondwana Res 21:422–438

Van Schmus WR, Oliveira EP, Da Silva Filho AF, Toteu SF, Penaye J, Guimarães IP (2008) Proterozoic links between the Borborema Province, NE Brazil, and the Central African Fold Belt. Geol Soc London (Spec Publ) 294:69–99

Vijaya Kumar T, Bhaskar Rao YJ, Plavsa D, Collins AS, Tomson JK, Gopal BV, Babu E (2017) Zircon U-Pb ages and Hf isotopic systematics of charnockite gneisses from the Ediacaran-Cambrian high-grade metamorphic terranes, southern India: constraints on crust formation, recycling, and Gondwana correlations. Geol Soc Am Bull 129(5–6):625–648

Villeneuve M (2008) Review of the orogenic belts on the western side of the West African craton: the Bassarides, Rokelides and Mauritanides. Geol Soc Lond (Spec Publ) 297:169–201

Vinagre R, Trouw RAJ, Mendes JC, Duffles P, Peternel R, Matos G (2014) New Evidence of a Magmatic Arc in the Southern Brasília Belt, Brazil: the Serra da Água Limpa Batholith (Socorro-Guaxupé Nappe). J South Am Earth Sci 54:120–139

Wade BP, Kelsey DE, Hand M, Barovich KM (2008) The Musgrave Province: stitching north, west and south Australia. Precambrian Res 166:370–386

Wang Y, Liu D, Chung S-L, Tong L, Ren L (2008) SHRIMP zircon age constraints from the Larsemann Hills region, Prydz Bay, for a late Mesoproterozoic to early Neoproterozoic tectono-thermal event in East Antarctica. Am J Sci 308:573–617

White LT, Gibson GM, Lister GS (2013) A reassessment of paleogeographic reconstructions of eastern Gondwana: bringing geology back into the equation. Gondwana Res 24:984–998

Whitehouse MJ, Windley BF, Ba-Bttat MAO, Fanning CM, Rex DC (1998) Crustal evolution and terrane correlation in the eastern Arabian Shield, Yemen: geochronological constraints. J Geol Soc Lond 155:281–295

Whitehouse MJ, Windley BF, Stoeser DB, Al-Khirbash S, Ba-Bttat MAO, Haider A (2001) Precambrian basement character of Yemen and correlations with Saudi Arabia and Somalia. Precambrian Res 105:357–369

Whitehouse MJ, Pease V, Al-Khirbash S (2016) Neoproterozoic crustal growth at the margin of the East Gondwana continent–age and isotopic constraints from the easternmost inliers of Oman. Int Geol Rev 58:2046–2064

Will TM, Frimmel HE (2018) Where does a continent prefer to break up? Some lessons from the South Atlantic margins. Gondwana Res 53:9–19

Windley BF, Whitehouse MJ, Ba-Bttat MAO (1996) Early Precambrian gneiss terranes and Pan-African island arcs in Yemen: crustal accretion of the eastern Arabian Shield. Geology 24:131–134

Windley BF, Whitehouse MJ, Stoeser DB, Al-Khirbash S, Ba-Bttat MAO, Al-Ghotbah A (2001) The Precambrian terranes of Yemen and their correlation with those of Saudi Arabia and Somalia: implications for the accretion of Gondwana. Gondwana Res 4:206–207

Wingate MTD, Pisarevsky SA, Evans DAD (2002) Rodinia connections between Australia and Laurentia: no SWEAT, no AUSWUS? Terra Nov 14:121–128

Zhao Y, Song B, Zhang Z, Fu Y, Chen T, Wang Y, Ren L, Yao Y, Li J, Liu X (1995) Early Paleozoic (Pan African) thermal event of the Larsemann Hills and its neighbours, Prydz Bay, East Antarctica. Sci China B 38:74–84

Zhao Y, Liu XC, Fanning CM, Liu XH (2000) The Grove Mountains, a segment of a Pan-African orogenic belt in East Antarctica

16

Untangling the Neoproterozoic-Early Paleozoic Tectonic Evolution of the Eastern Sierras Pampeanas Hidden in the Isotopical Record

Mónica G. López de Luchi, Carmen I. Martínez Dopico, Klaus Wemmer, and Siegfried Siegesmund

Abstract

The Sierras Pampeanas of Central Argentina are an example of a continuous and fast overlap of episodes of high- to medium- and low-grade metamorphism, deformation, anatexis, magmatism and mineralization along the belts that bounded the margins of the South American cratons during the Neoproterozoic and early Paleozoic. A compilation and critical revision of the massive isotopic and geochemical data for the basement rocks of the Eastern Sierras Pampeanas is presented. The Eastern Sierras Pampeanas are defined by three main events: the Ediacaran to early Cambrian (580–530 Ma) Pampean, the late Cambrian–Ordovician (500–460 Ma) Famatinian and the Devonian-Carboniferous (400–350 Ma) Achalian orogenies. The mean average crustal residence age (Sm–Nd T_{DM}) varies between 1.8 and 1.7 Ga with $\varepsilon Nd_{(540)}$ (−6 to −8). Pampean and Famatinian granitoids exhibit a similar T_{DM} interval except for the Ordovician TTG suites of the Sierras de Córdoba (T_{DM} 1.3–1.0 Ga). Achalian magmatism exhibits more radiogenic $\varepsilon Nd_{(540)}$ values (0.5 to −4) and T_{DM} ages younger than 1.3 Ga. Two types of Pampean-related mafic rocks are recognized: one with a depleted mantle signature and another younger group with an enriched mantle signature, which is associated with the peak of metamorphism. Ordovician mafic-ultramafic rocks result from mixing/assimilation of depleted mantle and crustal magmas. Detrital zircon data for the metaclastic sequences indicates mainly Grenvillian and Brasiliano sources. The difference between the measured crystallization age for detrital zircon grains and the depositional age of the succession indicates that most of the Pampean basins are collisional, i.e. foreland basins except for Sierra Norte metaclastic host rocks that correspond to a convergent setting signature. The results for the post-Pampean Famatinian basins indicate mostly collisional convergent settings for the Ambato and La Cébila (type locality) metamorphic complexes and the Olta (northern sector) and Achavil formations. The Negro Peinado Formation is the only post-Pampean basin that corresponds to a collisional setting. Data from Green Quarry, Nogolí Metamorphic Complex, and Olta Formation in the central part of the Sierra de Chepes, Suri Formation and La Cébila Metamorphic Complex at Quebrada La Rioja yielded convergent margin settings. These exhibit the highest correlation among the post-Pampean basins showing a relatively large number of Middle Cambrian age detrital zircons apart from having Ordovician magmatic zircons in the detrital record. Sources were apparently more restricted than in the rest of the Famatinian post-Pampean basins. The two samples of post-Pampean basins that exhibit Río de la Plata age peaks (2.2–2.0 Ga; Paleoproterozoic) belong to the collisional convergent group. Therefore the exhumed Pampean rocks probably formed a drainage divide that blocked westward transport of the Río de la Plata-derived sediments. Intense erosion owing to an unstable tectonic scenario would have led to the progressive appearance of the Río de la Plata signature.

Keywords

Early Paleozoic orogenies • Eastern Sierras Pampeanas
Detrital zircon data • Sm–Nd systematic

M. G. López de Luchi (✉) · C. I. Martínez Dopico
Instituto de Geocronología y Geología Isotópica (INGEIS), CONICET-UBA, Intendente Güiraldes 2160, Ciudad Universitaria, C1428EGA Buenos Aires, Argentina
e-mail: deluchi@ingeis.uba.ar

C. I. Martínez Dopico
e-mail: carmenmd@ingeis.uba.ar

K. Wemmer · S. Siegesmund
Geoscience Centre of the University of Göttingen (GZG), Goldschmidtstr. 3, 37077 Göttingen, Germany
e-mail: kwemmer@gwdg.de

S. Siegesmund
e-mail: ssieges@gwdg.de

S. Siegesmund et al. (eds.), *Geology of Southwest Gondwana*, Regional Geology Reviews,
https://doi.org/10.1007/978-3-319-68920-3_16

16.1 Introduction

The Sierras Pampeanas of Central Argentina (26°–33°S) are a series of N-S striking blocks that originated during the latest Neoproterozoic–Early Paleozoic as a result of the evolution of the tectonically active western margin of Gondwana, after the breakdown of Rodinia. The final uplift of the Sierras Pampeanas was closely related to the inception of the Miocene to Recent 27°–33° 30′S flat-slab segment of the Nazca plate in the Southern Andes (Ramos et al. 2002; Bense et al. 2013a). Previous exhumation processes causing the main uplift were pinpointed in Devonian, Carboniferous, Permian and late Cretaceous times (Steenken et al. 2010; Löbens et al. 2011, 2013a, 2013b, 2016; Bense et al. 2013b, 2017). The Sierras Pampeanas developed at a key locality for understanding the orogenic events along the Pacific margin of SW Gondwana, between the Paleoproterozoic Río de la Plata Craton against which they probably have a continental fault contact (Booker et al. 2004; Rapela et al. 2007; Peri et al. 2015) to the east and the Grenvillian (e.g., Kay et al. 1996; *c*. 1200–1000 Ma), Cuyania-Precordillera Terrane to the west. An overview of the geology of the Río de la Plata Craton is presented by Oyhantçabal et al. (2010), Rapela et al. (2011) and in Chap. 4. The final configuration of Gondwana was achieved by the end of the mid-Ediacaran time at the latest stages of the Pan-African/Brasiliano cycle. The main cratons involved were Amazonia–Arequipa–Río Apa, Kalahari, Río de la Plata, Congo, East Antarctica etc. Several collisional orogenic belts resulted, notably the East Africa–Antarctica, Brasiliano–Panafrican, Pampean–Saldania, and the Ross–Delamerian orogens (Casquet et al. 2012). The Brasiliano orogenic collage took place in four distinct phases: (a) Late Tonian (*c*. 800–740 Ma); (b) Late Cryogenian-Early Ediacaran (*c*. 660–610 Ma); (c) Early-Middle Ediacaran (*c*. 590–560 Ma); and (d) Late Cambrian (520–500 Ma; de Brito Neves et al. 2014). For the latest discussion see Oriolo et al. (2017).

Caminos (1979) established a lithologically based separation of the Sierras Pampeanas into (1) the Eastern Sierras Pampeanas dominated by abundant granites, metasedimentary and metaigneous rocks; and (2) the Western Sierras Pampeanas characterized by abundant metabasic, ultrabasic and calcsilicate rocks. This original separation corresponds to different geological provinces. The Western Sierras Pampeanas (WSP) expose (1330–1030 Ma 'Grenville-age') Mesoproterozoic crystalline basement intruded by relatively scarce Ordovician granites of the Famatinian cycle (e.g., Pankhurst and Rapela 1998; Casquet et al. 2001, 2006, 2008; Sato et al. 2003; Vujovich et al. 2004; Rapela et al. 2010). The Eastern Sierras Pampeanas (ESP) constitute a polyphase deformed morphotectonic unit which is defined by three main events: the late Ediacaran to mid-Cambrian (560–510 Ma) Pampean, the late Cambrian–Ordovician (500–445 Ma) Famatinian, and the Devonian (400–360 Ma) Achalian orogenic cycles (Aceñolaza and Toselli 1981; Ramos et al. 1986; Aceñolaza et al. 1988; Sims et al. 1997, 1998; Rapela et al. 1998a, b, 2001, 2007; Stuart-Smith et al. 1999; Siegesmund et al. 2004, 2010; Steenken et al. 2004, 2006, 2011; López de Luchi et al. 2007; Drobe et al. 2009). These mountain-building processes are related to the accretion of different terranes integrated into the proto-Andean margin of Gondwana. Moreover, a distinct Carboniferous tectonic event in the Sierras Pampeanas, which post-dates the late Devonian collisional orogeny and pre-dates the Permian San Rafael orogenic phase, has been proposed by Dahlquist et al. (2015). This possible transtensional event played a major role during the development and evolution of the late Paleozoic Paganzo Basin as well as during the emplacement of alkaline magmatism in the retroarc (Alasino et al. 2012; Löbens et al. 2016).

The aim of this contribution is to present an overview of the main geological features of the Eastern Sierras Pampeanas, mainly focused on the area located between 28° and 38°S (Figs. 16.1 and 16.2). Furthermore, the investigation aims to set time constraints for the metamorphism and magmatism, to analyse petrogenetic events and track potential sources through the WR Sm–Nd isotopic system. A comprehensive statistical approach to detrital zircon ages of the metaclastic rocks and the WR Sm–Nd data provides a summary that may support a revised model for the Early Paleozoic tectonic evolution.

16.2 Geological Background of the Main Basement Units of the Eastern Sierras Pampeanas

The Eastern Sierras Pampeanas extend from southern Salta (26°S) to the San Luis and La Pampa provinces (38°S) (Fig. 16.2). The eastern sector of these basement units is mainly affected by the Pampean orogeny, which is characterized by late Neoproterozoic sedimentation and Ediacaran to Cambrian deformation, magmatism and medium- to high-grade metamorphism (e.g., Rapela et al. 2007; Siegesmund et al. 2010; Steenken et al. 2011). The western sector is dominated by the Famatinian orogeny, which is characterized by Late Cambrian to Early-Middle Ordovician marine and volcaniclastic successions and Early to Middle Ordovician I- and S-type intrusions, minor tonalite–trondhjemite–granodiorite suites in the foreland (e.g., Sims et al. 1998; Steenken et al. 2006). The Famatinian belt is characterized by low- to high-grade temperature, low- to intermediate-pressure metamorphism coeval with foliation development, folding and thrusting. The Achalian orogeny

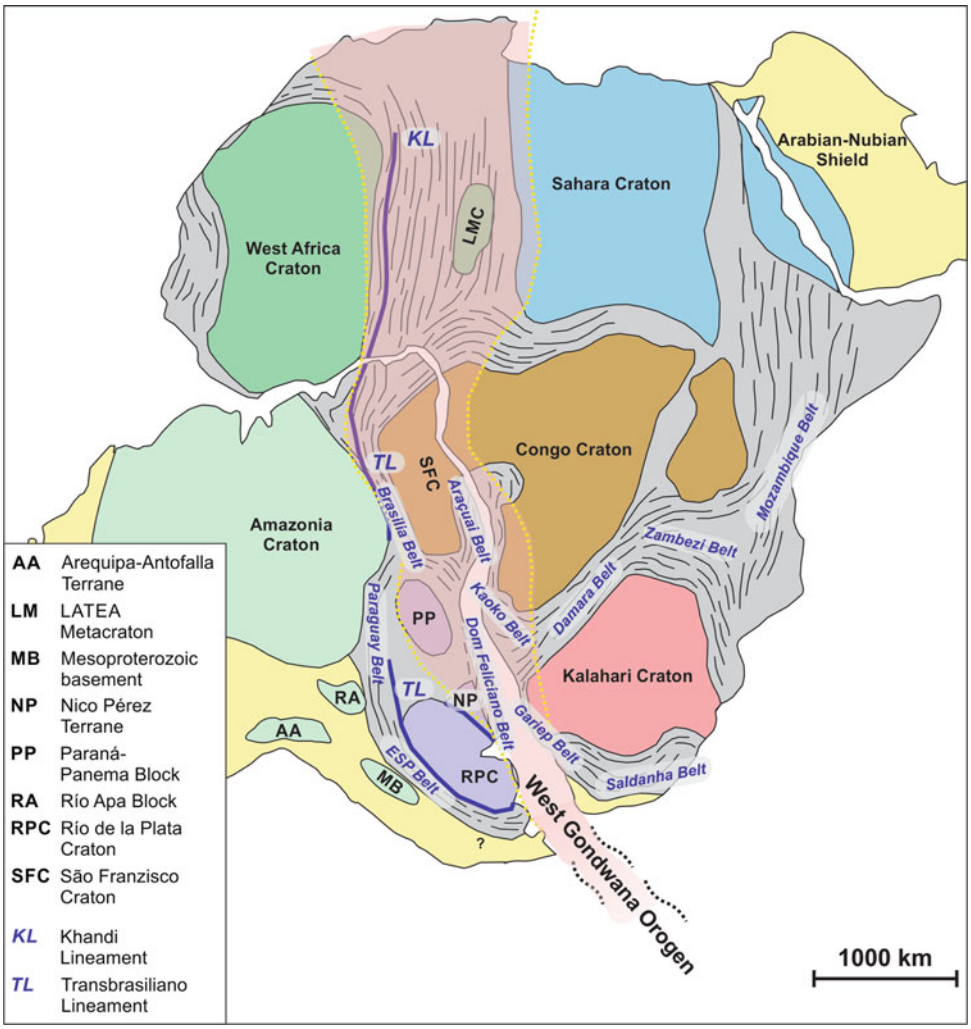

Fig. 16.1 Cratonic blocks and Neoproterozoic belts of southwestern Gondwana. ESP = Eastern Sierras Pampeanas

overprints this basement (Sims et al. 1998; Siegesmund et al. 2010). The 393 and 360 Ma mid- to late-Devonian magmatism is developed mainly in the Sierra de Córdoba and San Luis, whereas Lower Carboniferous magmatism is more conspicuous towards the north in the Sierra de Velasco (Fig. 16.2). Most of these Devonian batholiths display elongated shapes and are composed of plutons that have discordant contacts with the country rocks and produce wide thermal aureoles. Post-Pampean cooling of the basement domains in the Cambrian to Early Ordovician is related to imbrication and uplift along different shear zones, while Middle to Late Silurian K/Ar biotite ages register different stages of the exhumation (Steenken et al. 2010).

The Late Ediacaran to Early Paleozoic low- to high-grade metasedimentary successions of the Eastern Sierras Pampeanas were considered to be an extension of the very low- to low-grade turbiditic metaclastic rocks of the Puncoviscana Formation that developed along the Cordillera Oriental (e.g., Schwartz and Gromet 2004; Steenken et al. 2004; Zimmermann 2005; Drobe et al. 2009, 2011). These protoliths were deposited in the Late Ediacaran (Omarini et al. 1999) to Early Cambrian and were folded in the Early Cambrian (537–523 Ma; Escayola et al. 2011 and references therein).

The Sierras de Córdoba and the Sierra Norte as well as its continuation in the Sierras de Ambargasta and Sumampa are the easternmost group of the Sierras Pampeanas. These Sierras are made up of Neoproterozoic to Paleozoic plutonic-metamorphic basement intruded by Paleozoic intermediate and felsic plutonic rocks. They consist of a series of submeridian mountain chains limited by west-vergent reverse thrust faults on its western side and separated by intermontane Mesozoic and Cenozoic sediments, which are partially covered by a localized series of trachiandesitic volcanites and pyroclastic deposits of the upper Tertiary age.

The Sierra Norte, Sierras de Ambargasta and Sumampa constitute a major block mostly made up of the Ediacaran to early Cambrian arc-related I-type calcalkaline Sierra Norte-Ambargasta Batholith (SNAB) (Lira et al. 1997; Siegesmund et al. 2010). This batholith comprises

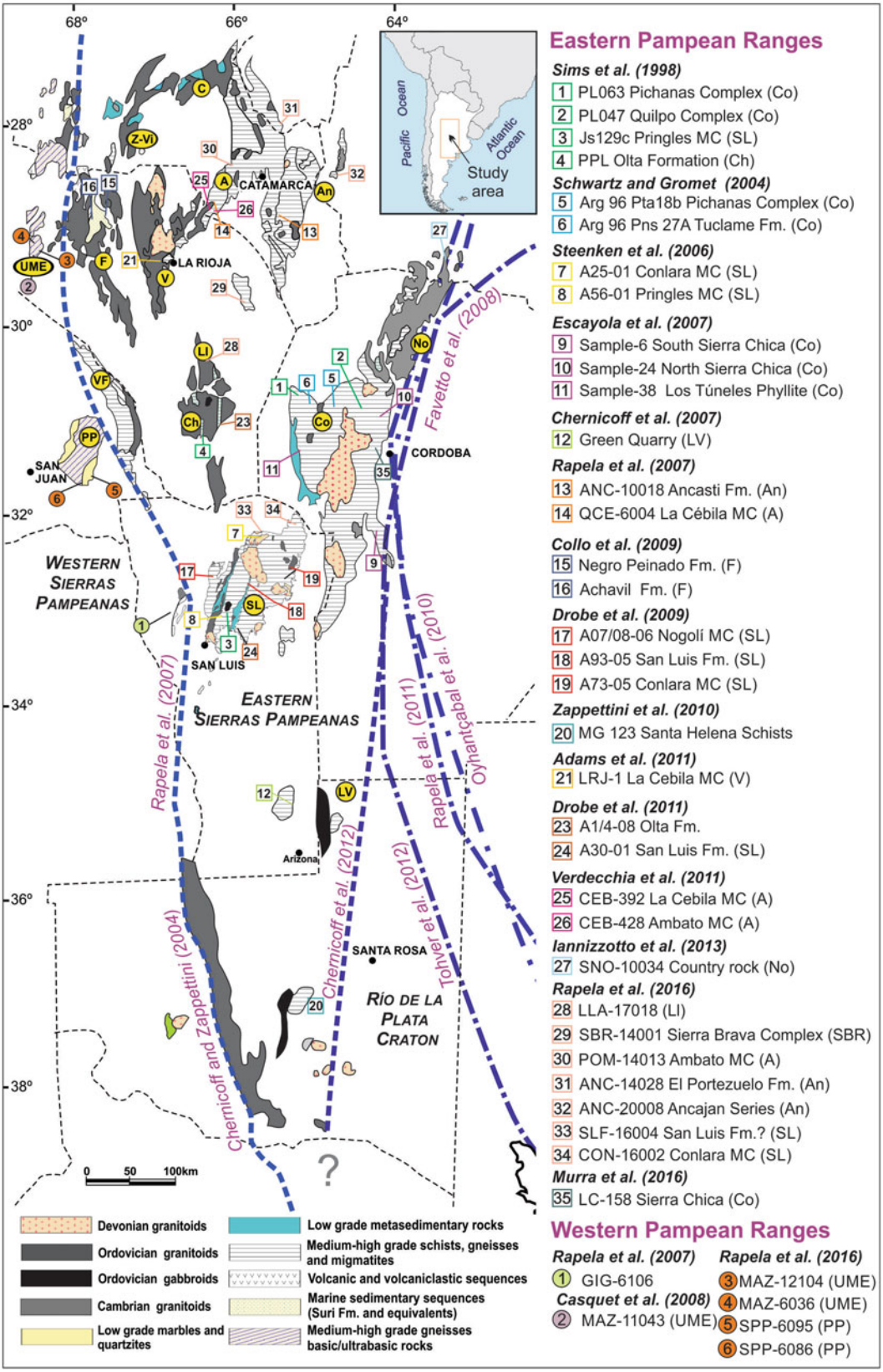

Fig. 16.2 Schematic map of the Early Paleozoic sequences of the Sierras Pampeanas between 24°–38° S with location of the published detrital zircon data. Limits of the Pampean and Famatinian orogens were taken from Chernicoff and Zappettini (2004) and Rapela et al. (2007). Limits of the Rio de la Plata craton were taken from Favetto et al. (2008), Oyhantçabal et al. (2010), Rapela et al. (2011), Chernicoff et al. (2012), and Tohver et al. (2012). Code for the names of the mountain chain A = Ambato; An = Ancasti; C = Capillitas; Co = Sierras de Córdoba; Ch = Chepes; F = Famatina; Fi = Fiambalá; LL = Llanos; No = Sierra Norte de Córdoba; PP = Pie de Palo; SL = Sierra de San Luis; LP = La Pampa hills; LV = Lonco Vaca; UME = Umango, Espinal, Maz; V = Velasco; VF = Valle Fértil; Z-Vi = Zapata-Vinquis

537 ± 4 Ma granitoid rocks affected by Pampean D_2 dextral shearing and mylonitization, and 530 ± 4 Ma granitoids emplaced after deformation had ceased (Iannizzotto et al. 2013). Late magmatic activity represented by a series of volcanic rocks associated with an extensional regime took place at 521 ± 2 Ma (Ramos et al. 2015; Oncan Rhyolite). The SNAB encloses large roof pendants of a locally contact overprinted late Neoproterozoic metamorphic complex (Siegesmund et al. 2010 and references therein). Ignimbritic rhyolites intercalated in conglomerates record synsedimentary igneous activity at 584 + 22/−14 Ma (conventional U–Pb zircon date in Llambías et al. 2003).

The Sierras de Córdoba constitute a unit of igneous and low- to high-grade metamorphic para- and orthogneisses, pure and impure marbles, amphibolites and ultramafic rocks, which underwent local partial melting processes that led to migmatitization (migmatite massifs are described in Gordillo 1979; Guereschi and Martino 2014). Several peraluminous and metaluminous granites and granodiorites of different ages intrude this basement (Rapela et al. 1998a, b; Sims et al. 1998; Escayola et al. 2007). The polymetamorphic complexes are organized in lithological and structural domains (Fig. 16.2): Sierra Chica, Sierra Grande and Sierra de Comechingones separated by ductile shear zones and mafic and ultramafic rocks (Siegesmund et al. 2010 and references therein). These domains are characterized by Ediacaran sedimentation and late Ediacaran to Cambrian deformation, magmatism and metamorphism with a more restricted Ordovician magmatic event (Rapela et al. 1998b; Siegesmund et al. 2010) and voluminous intrusions of Devonian granites (López de Luchi et al. 2007, 2017; Dahlquist et al. 2015). A NNW trending trending belt of granulite facies metamorphic rocks and related S-type granitoids (Fig. 16.2) can be split into the San Carlos Massif in the northwest and the Sierra de Comechingones in the southeast (Guereschi and Martino 2008, 2014 and references therein). Low-grade metamorphic rocks, the Los Túneles Phyllites are recognized in the western region of the Sierra Grande. Geochronological data supports the idea that the most important tectonothermal evolution of the crystalline rocks of Córdoba occurred in the lower Cambrian during the Pampean orogeny (*c*. 530–577 Ma; Rapela et al. 1998a, b; Sims et al. 1998; Siegesmund et al. 2010). In Table 16.1 a characterization of the metamorphic events is depicted. Peraluminous granitoids associated with migmatites were generated during a high-grade regional 525–519 Ma post M2 metamorphic event (Escayola et al. 2007; Siegesmund et al. 2010). Ordovician (480–490 Ma) granitoids are non-collisional, whereas the Devonian granitoids, e.g. Achala Batholith, Cerro Aspero pluton and Capilla del Monte pluton are alkali-calcic peraluminous granitoids.

Mafic and ultramafic rocks that were in part interpreted as ophiolites were separated into an eastern Sierra Chica belt and a western Sierra Grande belt (Mutti 1992; Escayola et al. 1996). The NNW-SSE trending eastern belt is composed of lherzolites with interlayered websterites and subordinate harzburgites, abundant pyroxenites and gabbros. Escayola et al. (1996) assigned the tectonic setting to an ensialic back-arc basin, whereas Ramos et al. (2000) interpreted the belt as ophiolite remnants of a back-arc zone. The ultramafic-mafic units of the western belt (Escayola et al. 2007), which extend for *c*. 300 km, are made up of harzburgites that were metasomatized by intrusive basaltic dykes. Escayola et al. (1996) interpreted the western belt as a suture zone and considered the ultramafic rocks as dismembered ophiolites with MORB affinities. Escayola et al. (2007) suggested a suprasubduction-zone ophiolitic complex formed during a back-arc stage. Sm–Nd dating of basalt and gabbro dykes, pyroxenites and impregnated peridotites of the western belt yielded an isochron age of 647 ± 77 Ma. The $\varepsilon Nd_{(647)}$ value of 5.2 is consistent with an oceanic or back-arc origin for the ophiolite sequence (Escayola et al. 2007).

The Sierra de Comechingones encompasses the Calamuchita, Monte Guazú and Achiras complexes (Otamendi et al. 2004). The Calamuchita Complex, north of the Cerro Aspero, is essentially composed of a metasedimentary sequence synkinematically intruded at the time of the metamorphic peak by an OIB-type affinity basic unit (Tibaldi et al. 2008). The Monte Guazú and Achiras complexes appear at the southern end of the mountain range and are in tectonic contact with the Las Lajas shear belt (Stuart-Smith and Skirrow 1997; Otamendi et al. 2000). The Monte Guazú Complex, interpreted by Fagiano et al. (2008) as the southern culmination of the Calamuchita complex, is characterized by an Ordovician (?) calcalkaline igneous rock suite (Gromet et al. 2001; Drobe et al. 2011) intercalated with gneisses, schists, amphibolites and marbles, derived from protoliths similar to the Calamuchita Complex (Otamendi et al. 2000; Fagiano et al. 2008). The Achiras Complex is a monotonous sequence comprising discontinuous belts of greywacke-derived amphibolite-facies gneisses and schists that are interlayered with peraluminous leucogranites. The complex is intruded by Devonian peraluminous granites, like the Achiras Granite (384 ± 6 Ma, U–Pb zircon; Stuart-Smith et al. 1999). Fagiano et al. (2008) proposed an Ordovician age for the metamorphism of the Achiras Complex.

Gabbros with OIB signatures located in the Sierra de Comechingones, which result from the subduction of a mid-ocean ridge beneath the paleo-Pacific Gondwana margin, are related to the high-grade metamorphic overprint (Tibaldi et al. 2008 and references therein). Intrusive relationships suggest that emplacement varied from preceding (e.g., Cerro San Lorenzo; Chincarini et al. 1998) to coincident with peak metamorphism of the metasedimentary rocks (e.g., Suya Taco mafic complex; Otamendi et al. 2005; Tibaldi et al. 2008). Gromet et al. (2005) reported an U–Pb

Table 16.1 Mineral paragenesis, P–T constraints and ages of the Pampean metamorphic events

Basement unit	Paragénesis	P–T	Metamorphic age (Ma)	References
North Sierra de Córdoba	Cdr+Sill migmatites Cdr+Sill+Grt gneiss Bt-Grt gneiss	M2 P = 5.5–6.5 kbar T = 700 ºC M1	543 ± 4* 531 ± 10* 561 ± 10* 581 ± 16*	Martino and Guereschi (2005) Siegesmund et al. (2010) Sims et al. (1998)
Sierra Chica de Córdoba	Cdr migmatite Grt+Cdr+Sill Metabasites	M2 P = 6 kbar T = 820 ºC	522 ± 8**	Rapela et al. (1998a)
Santa Rosa Massif *Sierra de Córdoba*	Grt+Cdr migmatite	M2 = ca. 7.5 kbar T = 850–900 ºC	536 ± 11* 511 ± 6**	Siegesmund et al. (2010) Otamendi et al. (2006)
Tala Cruz Stromatite Cañada del Sauce Diatexite *South Sierra de Córdoba*	Bt–Sil–Grt–Kfs migmatite Bt–Grt–Crd–Kfs diatexite	M1 P = 8.5–9 kbar T = 810–840 °C P = 5.5–6 kbar T = 725–780 °C	553 ± 3* 577 ± 11*	Guereschi and Martino (2008) Siegesmund et al. (2010)
Monte Guazu Complex *Sierra de Comechingones*	Kfs+Si l+Grt Gneiss	P = 7 kbar T = −∼750 ºC		Fagiano (2007)
Conlara Metamorphic Complex *Sierra de San Luis*	Bt±Grt±Ms schist-gneiss	M1 P = 5–6 kbar T = 550−600 ºC	564 ± 21***	Siegesmund et al. (2010)
Ancasti Formation *Sierra de Ancasti*	Ms+Bt+And+Crd Schist		524 ± 28****	Knüver (1983)
Santa Helena schist *La Pampa province*	Bt+Grt Schist Sill+Grt gneiss	T > 700 ºC	Pre 530 Ma	Zappetini et al. (2010) Chernicoff et al. (2008)

*Zircon ages; **Monazite ages; ***garnet(PbSL); ****Rb–Sr WR isochron

age of 520 ± 2 Ma for igneous monazites in a migmatitic granitic leucosome developed in the aureole of a mafic dyke in the Suya Taco mafic complex. This age might be considered to be a cooling age from granulite facies metamorphism since an age of 536 ± 11 Ma was calculated for the Santa Rosa Grt-Crd granulite, which is the restite of the melting event that is associated with the metamorphic peak (Siegesmund et al. 2010).

The Sierra de San Luis (Figs. 16.1 and 16.2) records an Ediacaran to Devonian metamorphic and magmatic evolution and comprises three NNE-SSW striking basement domains of amphibolite- to granulite-facies complexes: the Nogolí, Pringles and Conlara metamorphic complexes (Sims et al. 1997). The domains are generally (Fig. 16.2) separated by an assemblage of metaquartz arenites and phyllites, e.g., the San Luis Formation (Prozzi and Ramos 1988; Wemmer et al. 2011) and are intruded by Ordovician and Devonian granitoids (Sims et al. 1997, 1998; López de Luchi et al. 2007). The metamorphic events and mineral parageneses are summarized in Table 16.1.

The Conlara Metamorphic Complex (CMC) is the easternmost of these complexes. The western margin of the CMC is affected by the Devonian Río Guzmán shear zone, whereas its eastern margin towards the Sierra de Comechingones (Sims et al. 1997) is controlled by the Guacha Corral shear zone. The metamorphic series of the CMC comprises NNE trending metagreywackes, and scarce metapelites and metaigneous components, which encompass basic sills and granitic rocks. These belong to two distinct groups: an earlier one represented by tonalitic to granodioritic orthogneisses, locally migmatites, and scarce amphibolites, and a later granitic one, which comprises Late Cambrian to Early Ordovician monzogranite to tonalitic plutons (i.e., La Tapera, El Peñón, El Salado plutons) and a group of large granitic pegmatites.

Within the CMC, ultramafic rocks have not been reported yet. However, scarce amphibolites are distributed in a N-S belt through Sierra del Morro, San Felipe and Villa de Praga. Some tungsten deposits are genetically related to them (de Brodtkorb et al. 2005).

The Pringles Metamorphic Complex (PMC) consists of paragneisses, mica schists, migmatites and amphibolites. Discontinuous lenses of mafic (mainly norites) to ultramafic units occur along a narrow NNE-SSW central belt concordant with the NNE trending S2 foliation. Granulite facies metamorphism, which would result from the emplacement of (ultra-)mafic intrusions, occurred during the beginning of the Famatinian cycle (Fig. 16.3; Hauzenberger et al. 2001; Steenken et al. 2005, 2006; Delpino et al. 2007). Granulite facies assemblages grade into amphibolite and greenschist facies assemblages (Hauzenberger et al. 2001; Delpino et al. 2007). Mafic to ultramafic 506–480 Ma Mid-Cambrian to

earliest Ordovician complexes developed in the central part of the Sierra de San Luis (Sims et al. 1998; Hauzenberger et al. 2001; Steenken et al. 2008) and are represented by norites to gabbro-norites with minor ultramafic rocks. A back-arc or marginal basin setting was assigned to them. On both sides of the mafic to ultramafic bodies, a metamorphic gradient from granulite to greenschist facies is observed (Delpino et al. 2007), and therefore a contact metamorphic origin for the granulite facies paragenesis was suggested (Hauzenberger et al. 2001; Steenken et al. 2005, 2006).

The Nogolí Metamorphic Complex (NMC) is composed of paragneisses, mica schists, metaquartzites and migmatites, with minor amphibolite and small lenses of two mica- and garnet-leucogranites. González et al. (2009 and references therein) proposed that part of the amphibolites are metakomatiites and high-Fe tholeiite metabasalts, which are interlayered with marbles and banded iron formation. Prograde regional metamorphism accompanies deformational phases, from at least middle greenschist to high amphibolite facies conditions (Table 16.2).

The NNE trending low-grade phyllites and metaquartz-arenites of the San Luis Formation appear in two belts (Fig. 16.2). NNE trending large-scale tight folds with a moderate plunge is the main deformation style in the San Luis Formation, corresponding to the Famatinian event recorded in the PMC (Steenken et al. 2006, 2008). Isoclinally folded quartz layers within the phyllites (Fig. 16.2) suggest a preceding deformation phase. The transpressional Río Guzmán shear zone that accommodated the 'east-side-up' displacement of the CMC is developed along the eastern belt of this formation (Steenken et al. 2008).

López de Luchi et al. (2007) considered that the Late Cambrian– Early Ordovician granitoids (*c*. 500–470 Ma) of the Sierra de San Luis are synkinematic with compressive deformation related to the early stages of Famatinian convergence. The melting of crustal sources relates to a contemporaneous mafic magmatism as expressed in the mafic-ultramafic complexes of the Pringles Metamorphic Complex (Steenken et al. 2006, 2008 and references therein). Devonian magmatism is represented by voluminous alkali-calcic ellipsoidal granodiorite-monzogranite units, for example, Las Chacras-Potrerillos and Renca batholiths and La Totora, San José del Morro and El Hornito plutons associated with lamprophyres and monzonitic rocks, which suggest an enriched lithospheric mantle source (López de Luchi et al. 2017).

The Sierras de Chepes, Malanzán and Los Llanos (Fig. 16.2) are composed of Early Ordovician metaluminous, calcalkaline I-type granitoids and restricted peraluminous S-type monzogranites (Dahlquist and Galindo 2004). Small bodies of gabbro diorite or quartz diorite frequently mingled with the surrounding granodiorites. The most important granitoid unit is the 490 ± 5 Ma Chepes granodiorite (Pankhurst et al. 1998). The greenschist to amphibolite grade metasedimentary rocks are largely metapelites with intercalations of metarenites that occur as discontinuous

Table 16.2 Mineral paragenesis, P–T constraints and ages of the Ordovician metamorphic events

Basement unit	Paragenesis	P–T	Metamorphic age (Ma)	References
Pringles metamorphic complex	Grt–Sill Gneiss Pl–Kfs–Grt–Bt–Sil±Cd	P = 5.7–6.4 kbar T = 740– 790 °C	498 ± 10*	Steenken et al. (2006)
Nogolí metamorphic complex	Bt+Sill+Pl migmatite Bt–Pl–Grt gneiss	Not determined P = 5–8 kbar T = 660–791 °C	478 ± 4* 475–457*	Steenken et al. (2006)
Green quarry	Qz–Feld–Bt schist		Between 502–480	Chernicoff et al. (2007)
Olta Fm Sierra de Chepes	Low to medium grade schist	P = 3 kbar 400–700 °C	Pre 478 ± 9 (age anatetic Tuani granite)	Pankhurst et al. (2000)
La Cebila metamorphic complex Sierra de Velasco	Low to medium grade gneiss/migmatites	P = 5–7 kbar T = 600 °C	478 ± 4**	Larrovere et al. (2011)
El Portezuelo Igneous metamorphic complex	Bt+Pl±Grt metatexites Bt+Pl+Grt+Crd migmatites	P = 4.5–5.3 kbar T = 670–820 °C	477–470**	Larrovere et al. (2011)
Sierra Brava metamorphic complex	Bt+Pl+Grt gneiss/migmatite Bt+Pl schist Metabasite			Dahlquist et al. (2010)
Achavil Fm	Ill+Chl	P = 2.5–3 kbar T = 200–280	495–475 ± 15***	Collo et al. (2009)
Negro Peinado Fm	Ili+Chl±Bt	P = 4.5 kbar T = 290–400 °C	463 ± 14***	Collo et al. (2009)

*Zircon ages; **Monazite ages; ***garnet(PbSL); ****Rb–Sr WR isochron

roof pendants (Pankhurst et al. 1998). The first metamorphic imprint is represented by fine-grained inclusions of biotite, magnetite, quartz and muscovite preserved in cordierite porphyroblasts that would correspond to a second low-pressure metamorphism, which was considered to be coeval with the granitoid emplacement (Pankhurst et al. 1998) grades from phyllite to an anatectic zone (Pankhurst et al. 1998). Metamorphic events and mineral parageneses are summarized in Table 16.2.

The Sierra de Velasco (Fig. 16.2) is dominated by granitoids (Grosse et al. 2011). Low-grade metamorphic rocks (Table 16.2) consisting of phyllites and mica schists correlate with the lower Ordovician metasedimentary La Cébila Formation (Verdecchia et al. 2007; Larrovere et al. 2012). These separate the Sierra de Velasco from the Sierra de Ambato (Fig. 16.2) and are only present as small outcrops along the eastern flank. The granitoid units (Báez et al. 2005; Toselli et al. 2005) comprise older weakly to strongly foliated Ordovician metagranitoids and younger Lower Carboniferous undeformed granites. These plutons share some features with the Devonian granitoids: nearly circular shapes, general lack of pervasive solid-state deformation, discordant relationships with the host rocks, shallow emplacement in the upper crust, syeno- to monzogranitic compositions, high SiO_2 and K_2O content, porphyritic textures and an abundance of pegmatites and aplites. They were possibly generated during a regional crustal heating event (e.g., 96.Miller and Söllner 2005) that occurred during the Late Devonian–Early Carboniferous.

The Sierra de Ancasti (Fig. 16.2) comprises three metamorphic domains:

- The Sierra Brava Complex in the eastern flank is composed of paragneisses and migmatites (Aceñolaza and Toselli 1981), as well as marbles, schists and amphibolites.
- The central sector is mostly formed by folded NNE-SSW trending banded schist of the Ancasti Formation (Aceñolaza and Toselli 1981; Willner 1983), which records a low-pressure Pampean metamorphism that was overprinted by a syndeformational medium grade event (Knüver 1983; Willner 1983; Gaido 2003).
- In the western flank, metasediments of the Ancasti Formation prograde into gneiss and migmatites of the El Portezuelo Formation (Willner 1983). Ordovician granites and tourmaline- and beryl-bearing pegmatites are emplaced in the Sierra Brava Complex and the Ancasti Formation (Dahlquist et al. 2012).

The metamorphic events and mineral parageneses are summarized in Table 16.2.

The Sierra de Ambato (Fig. 16.2) is dominated by widespread metasedimentary rock sequences metamorphosed under different metamorphic grades, such as granulites, migmatites, gneisses, schists, phyllites, shales, and less abundant marbles, amphibolites, and calcsilicate rocks (Caminos 1979; Toselli et al. 1996). The Ambato metamorphic complex mainly consists of high-grade metasedimentary rocks (migmatites and gneisses) and discordant granitic and pegmatitic bodies (Caminos 1979). Larrovere et al. (2009) obtained an Early to Mid-Ordovician metamorphic age on monazites from a migmatite in the central northern part of the Sierra de Ambato. At the southern tip of the Sierra de Ambato, next to Sierra de Velasco, the Ambato Metamorphic Complex overlies the low-grade successions of the La Cébila Metamorphic Complex across a west-directed Cenozoic reverse fault (Larrovere et al. 2011, 2012). Granitoid rocks intruded the metamorphic basement of both Sierra de Ancasti and Ambato during two major events: the Lower–Middle Ordovician (Famatinian) and Late Devonian–Early Carboniferous (Achalian). The former and more important is characterized by the Capillitas Batholith, an Ordovician peraluminous S-type Famatinian granitoid (Toselli et al. 1996; Pankhurst et al. 2000; Rossi et al. 2005). On the other hand, the Devonian–Carboniferous magmatism in the area is restricted to discordant bodies.

The Famatina Ranges are characterized by widespread Cambro-Ordovician volcanosedimentary successions and Ordovician plutonism. These low-grade rocks accumulated adjacent to a subduction-related magmatic arc (Astini 2003) and are separated into three units: the Negro Peinado, Achavil and La Aguadita Formations (Astini et al. 2005; Collo and Astini 2008). The dominance of Cambrian detrital ages in the Negro Peinado Formation suggests derivation principally from the eastern Pampean Belt, whereas the dominance of late Neoproterozoic ages in the Achavil Formation suggests that input from the Pampean Belt was overwhelmed by older sources (Collo et al. 2009). Detrital zircon ages from the La Aguadita Formation, a synorogenic Ordovician clastic wedge developed along a retroarc foreland basin, indicate that it must be younger than 452 ± 6 Ma (Astini 2003; Astini et al. 2005). The Achavil Formation is unconformably covered by the Late Cambrian–Early Ordovician Volcancito Formation. Calcalkaline metaluminous epizonal granitoids are recognized in the central area of the Famatina Ranges (Dahlquist et al. 2008 and references therein). Contact metamorphism is observed in the Negro Peinado/La Aguadita Formations (Rossi et al. 2005).

The Neoproterozoic–Cambrian basement of south-central La Pampa province is represented by metapelites and metapsammites, and minor quartzites and marbles. These rocks formed in a platform environment on the Río de la

Plata Craton, called the Las Piedras Formation. On the Pampia Terrane, minor outcrops are grouped in the Santa Helena Schist and the Green Quarry Schist. The first one represents a metamorphic unit, whose protolith was deposited after *c*. 556 Ma and prior to *c*. 530 Ma in a foreland basin possibly equivalent to the late Puncoviscana basin (Zappetini et al. 2010). Cambrian metasedimentary rocks are grouped in the Green Quarry Schist, whose protolith was deposited after *c*. 515–500 Ma and prior to *c*. 465 Ma (Chernicoff et al. 2007) in a post-collisional basin (mostly sourced from the Pampean orogen), slightly post-dating Middle- to Late Cambrian sedimentation that occurred in more northern latitudes

The 528 Ma Carancho Igneous Complex (Chernicoff et al. 2012) comprises calcalkaline metadiorites and metagranites, as well as tholeiitic metapyroxenites, and is considered as representing remains of the suture between the Río de la Plata Craton and the Pampia Terrane. Both the Santa Helena Schist and the Green Quarry Schist are the host rocks of Ordovician metaigneous rocks.

16.3 Time Constraints on the Pampean Metamorphism

The maximum depositional age for the sedimentation of the protolith that later constituted the Pampean metamorphic basement is provided by the 560–555 Ma detrital zircon age peak of the Puncoviscana Formation (Adams et al. 2008; Escayola et al. 2011) and equivalent rocks from various sectors (Sierras de Córdoba, the Conlara Metamorphic Complex and the Sierra de Ancasti, Sierra Brava) of the Eastern Sierras Pampeanas and further south in La Pampa province (the Santa Helena Schist) (e.g., Schwartz and Gromet 2004; Steenken et al. 2004, 2006, Escayola et al. 2007; Rapela et al. 2007, 2016; Drobe et al. 2009, 2011; Siegesmund et al. 2010; Zappetini et al. 2010; Ramos et al. 2015).

In the Sierra de Córdoba, complex metamorphic textures and parageneses (Guereschi and Martino 2003, 2008, 2014) suggest the existence of at least two metamorphic regional events (here named M1 and M2). The zircon ages of older rims reported by Sims et al. (1998) indicate a stage of zircon growth between 580 and 560 Ma. In the Sierra de Comechingones the first metamorphic peak produced a high-grade paragenesis (M1) and the first anatexis generating the stromatic migmatites, named the Tala Cruz type (Martino et al. 1994; Guereschi and Martino 2002, 2003, 2008). These rocks yield a concordant SHRIMP U/Pb zircon age of 553.5 ± 3.2 Ma (2σ, *n* = 5; Siegesmund et al. 2010). This age corresponds closely to the *c*. 560 Ma peaks on the detrital zircon patterns of the metaclastic Pampean rocks. In this connection, rocks that were considered as resulting from anatexis of the abovementioned stomatites, the Cañada del Sauce diatexite (M4 after Guereschi and Martino 2008), yielded a population of an igneous zircon concordant cluster at 581 ± 15 Ma (2σ, *n* = 3) (Siegesmund et al. 2010). The calcalkaline signature of this rock led Guereschi and Baldo (1993) to consider it to be an indication of an arc-related magmatism.

The M2 event (810–840 °C and 8.5–9 kbar) was determined in the Sierra Grande, where the metamorphism pre-dating the formation of cordierite was dated by the Sil + Kfs Las Palmas Gneiss, which lacks cordierite and yielded a zircon age of 543.1 ± 3.6 Ma (Siegesmund et al. 2010). Together with datings on the cooling history recorded by a 534 ± 13 Ma K/Ar hornblende age (Steenken et al. 2010), a metamorphic history pre-dating the onset of a lower pressure event is reinforced. Cordierite formation and diatexites resulting from a second melting of the metatexites at 725–780 °C and 5.5–6 kbar occurred at *c*. 530 Ma or even slightly later (Rapela et al. 1998b). Martino (2003) and Otamendi et al. (2005) related the main migmatization event and cordierite formation to the decompressional history of the M2 metamorphic stage, which lasted approximately 10 Ma (Camacho and Ireland 1997; Lyons et al. 1997; Fantini et al. 1998; Gromet and Simpson 1999; Rapela et al. 1998a, b; Sims et al. 1998). However, Ramos et al. (2015) proposed that granulite formation, migmatites and peraluminous granites at *c*. 518 Ma are related to an important heat advection in the crust, which controlled anatexis and cordierite formation in localized areas. Acidic volcanic rocks and peraluminous granitic intrusions that are widespread within the northern portion of the San Carlos massif as well as in the Sierra Norte yielded ages between 530 and 520 Ma (Rapela et al. 1998a, b; Escayola et al. 2007; Siegesmund et al. 2010; Ramos et al. 2015). The early Cambrian M2 event in the Sierra de Comechingones is recorded by the 536 ± 11 Ma Santa Rosa Grt-Crd granulite (Siegesmund et al. 2010). Monazite grains from this granulite yield a mean $^{206}Pb/^{232}Th$ age of 507.4 ± 6.1 Ma, supporting PbSL dating of one titanite separate (A20-04), yielding 506 ± 26 Ma. Additional constraints on the younger limit of the metamorphism are provided by PbSL titanite ages obtained from calcsilicate intercalations in the San Carlos Massif, which yielded an age of 505.7 ± 7.3 Ma (Siegesmund et al. 2010). This new Pb/Pb titanite age supports the earlier U–Pb data on titanite at 509 ± 2 Ma (Fantini et al. 1998). This closely follows a U/Pb age of 515 ± 2 Ma for prograde metamorphic monazite in the Guamanes shear zone in the east of the massif (Gromet and Simpson 1999). K/Ar and Ar/Ar muscovite ages starting at 502 Ma were also

reported (Krol and Simpson 1999; Steenken et al. 2010). Most of these micas are large muscovite booklets from pegmatites and are considered to have a closure temperature significantly higher than 410 °C (Willigers et al. 2001), as pointed out by Steenken et al. (2008). These ages would mark the end of the last metamorphic episode in the ESP. The mid to low temperature ages that cluster around Mid-Cambrian times denote a short-lived cooling, and hence an accelerated exhumation of the Pampean orogen at around 505 Ma and a fast formation of the Famatinian arc (Ducea et al. 2017). This correlates with the first activation of the different compressional shear zones along the western margin of the basement complex, the Guacha Corral and Los Túneles shear zones (Steenken et al. 2010), and with the initiation of compression along the Gondwana margin (Steenken et al. 2006 and references therein) and, albeit more speculative, with the Irúyica deformation phase (Astini et al. 2008).

Therefore, portions of the basement of the Sierra de Córdoba might be older than the ubiquitous metamorphic equivalents of the Puncoviscana Formation. Geochemical results may indicate a calcalkaline granodioritic composition for the Cañada del Sauce diatexite (Guereschi and Baldo 1993), relating this intrusion to an active continental margin. The first metamorphic (M1) overprint took place at *c*. 560 Ma, whereas the more extended prograde event (M2) is constrained between 540 and 533 Ma.

Post-liminary fusion (migmatization), granulite formation (i.e., M3, M4 Steenken et al. 2011) and derived peraluminous magmatism are younger than 530 Ma and probably unrelated to the decompressional evolution of the main clockwise metamorphic overprint. Table 16.1 gives a summary of the Pampean metamorphism.

16.4 Time Constraints for the Famatinian Metamorphism

Famatinian metamorphism is mostly related to the closure of ensialic back-arc or inter-arc basins developed east of or inside the main Famatina magmatic arc (Balhburg 1991; Steenken et al. 2006; Dahlquist et al. 2008; Collo et al. 2009 and references therein).

Steenken et al. (2004) were the first to recognize at least two different sedimentary protoliths (P) in the Eastern Sierras Pampeanas: (P1) a *c*. 560 Ma source and (P2) a younger post-Pampean. Steenken et al. (2006) suggested resumption of subduction and sedimentation in the west of the Pampean terrane in the Late Cambrian and the subsequent amalgamation of the Cuyania and/or Precordillera Terrane during the Famatinian orogenic cycle (Ramos et al. 1986; Sims et al. 1998). Drobe et al. (2009) indicate that extensional tectonics after the Pampean metamorphism controlled the development of the back-arc basins in which the protoliths of the Nogolí and Pringles metamorphic complexes were deposited. Age constraints between 500 and 480 Ma for the (ultra)mafic rocks (Sims et al. 1998; Hauzenberger et al. 2001; Steenken et al. 2008) of the Pringles Metamorphic Complex argue for a thermal input and LP/HT metamorphism in a thinned crust. On both sides of the mafic to ultramafic bodies a metamorphic gradient from granulite to greenschist facies is observed (Delpino et al. 2007), and therefore a contact metamorphic origin for the granulite facies paragenesis was suggested (Hauzenberger et al. 2001; Steenken et al. 2005, 2006). Ducea et al. (2010) proposed that high-grade Famatinian metamorphism and migmatization were synchronous with 485–465 Ma magmatic emplacement. Inherited ages in some of the plutonic rocks as well as detrital zircons in the metasedimentary framework suggest that the Famatinian arc was emplaced into a thick miogeoclinal cover to the thinned margin of the proto-South American continent. Therefore it could be proposed that the Famatinian orogen consists of two stages of compression: one related to the onset of subduction at around 500 Ma and another stage related to docking of the Precordilleran terrane at 480 Ma (Ramos et al. 1998) and the cessation of the Famatinian magmatism.

Table 16.2 gives a summary of the P–T constraints and ages of the Famatinian metamorphism.

16.5 Magmatism in the Eastern Sierras Pampeanas

Rapela et al. (1990) separated granitoids of the Sierras Pampenas into G1, G2 and G3, which roughly correspond in time to the Pampean (Ediacaran to Cambrian), Famatinian (Ordivician) and Achalian (Devonian to Carboniferous) orogenies. Pampean magmatism is arc-related with minor post-collisional peraluminous intrusions and minor acid volcanic rocks. Famatinian magmatism is also arc-related. I-type granitoids occur in the west and grade into S-type towards the continent. Devonian magmatism would be either arc-related with a Devonian subduction along the western margin of the Precordillera Terrane or the result of post-Ordovician uplift.

16.5.1 Ediacaran to Cambrian Granitoids

Calcalkaline magmatic rocks of Ediacaran and Cambrian age form the batholith of Sierra Norte and extend discontinuously southwards along the Sierra Chica (Rapela et al. 1998b) and in Sierra de Guasayan (Dahlquist et al. 2016; Fig. 16.2). These rocks consist of calcalkaline metaluminous to weakly peraluminous granodiorites and monzogranites

that intruded a metasedimentary host. Aplites, porphyries and pegmatites intrude all the sequences (Rapela et al. 1991). Late-stage rhyodacites and miarolitic monzogranites are also present (Lira et al. 1997). Geochemistry suggests (Lira et al. 1997) subduction related magmatism and convergent margin tectonics along the western margin of Gondwana in the late Neoproterozoic. Geochronological studies from the Sierra Norte granitoids (Schwartz et al. 2008) indicate a period of emplacement bracketed between 550 and 530 Ma. Cambrian granitoids (the G1b suite of Rapela et al. 1998a, b) located in the Sierra Grande and Sierra de Comechingones are peraluminous anatectic melts of the metasedimentary country rocks (Rapela et al. 1998a, b). The ages of these groups of plutons is bracketed between 523 ± 2 Ma for El Pilón (Rapela et al. 1998a, b, 2001) and 529 ± 3.4 Ma for the Juan XXIII pluton (Escayola et al. 2007). The 521.1 ± 1.6 Ma Oncan rhyolite cuts the older granites of the Sierra Norte and is considered to be related to the Cambrian peraluminous granites (Iannizzotto et al. 2013; Ramos et al. 2015).

Cambrian magmatism is represented further south in the La Pampa province by the 528 Ma El Carancho Igneous Complex (Chernicoff et al. 2012), which comprises calcalkaline metadiorites and metagranites, as well as tholeiitic metapyroxenites, and is considered as representing remains of the suture between the Río de la Plata Craton and the Pampia Terrane. Alternatively, this complex might represent the mantle-derived rocks related to the slab break-off that post-dated the M2 Pampean metamorphic event.

16.5.2 Ordovician Magmatism

The Famatinian magmatic belt was short-lived (*c*. 20 Ma) and without a significant asthenospheric contribution (Pankhurst et al. 1998; Dahlquist et al. 2008 and references therein). Three distinct 484–463 Ma Famatinian granite types were identified (Pankhurst et al. 2000): a dominant I-type, a small-scale S-type and a tonalite-trondhjemite-granodiorite. I-type magmatism is represented by tonalites, granodiorites, minor monzogranites and gabbros that can be traced from the northwest in Catamarca and La Rioja down to the Sierras de Valle Fértil-La Huerta in the San Juan province and the Sierra de San Luis. The S-type granitoids are developed in Sierra de Velasco, Sierra de Chepes and in a sector of the Sierra de San Luis (Steenken et al. 2006, 2008; Grosse et al. 2011). The TTG group (i.e., El Hongo, Calmayo, La Fronda, Guiraldes, La Playa and Paso del Carmen tonalite to granodiorite plutons) is emplaced in the Sierra Grande except for the Calmayo group (500–480 Ma, U–Pb zircon; Rapela et al. 1998a, b), which intrudes the Sierra Chica Complex.

López de Luchi et al. (2007) considered that the Late Cambrian-Ordovician granitoids (*c*. 500–470 Ma) of the Sierra de San Luis (Fig. 16.2) are synkinematic with compressive deformation related to Famatinian convergence. They proposed a separation of these granitoids into an Ordovician tonalite suite (OTS; metaluminous to mildly peraluminous calcic tonalite-granodiorites) and an Ordovician granodiorite-granite suite (OGGS; peraluminous calcic to calcalkaline granodiorite-monzogranites).

Lower Ordovician metaluminous calcalkaline granitoids, which constitute the principal lithologies of the Sierras de Chepes, Malanzán and Los Llanos (Fig. 16.2), frequently exhibit mingling relationships with gabbro diorite or quartz diorite. The most important granitoid unit is the 490 ± 5 Ma (U/Pb zircon age) Chepes Granodiorite (Pankhurst et al. 1998).

Weakly to strongly foliated (481 ± 3 Ma, Pankhurst et al. 2000; 481 ± 2 Ma, Rapela et al. 2001) peraluminous metagranitoids are the dominant lithology of the Sierra de Velasco (Báez et al. 2005; Toselli et al. 2005). Subordinate varieties include strongly peraluminous porphyritic biotite-cordierite metamonzogranites and moderately peraluminous coarse- to medium-grained biotite metagranodiorites and metatonalites. In the southern part of the Sierra de Velasco, the main lithologies are metaluminous to weakly peraluminous biotite-hornblende metagranodiorites and metatonalites (Bellos 2005).

In the Sierra de Ancasti, Ordovician granitoid magmatism is represented by calcalkaline metaluminous plutons, minor garnet-bearing two-mica granite stocks (Reissinger 1983; Rapela et al. 2005) and tourmaline- and beryl-bearing pegmatites that are emplaced in the Sierra Brava Complex and in the Ancasti Formation (Dahlquist et al. 2010, 2012). The metaluminous Las Cañadas Complex was emplaced close to 468 Ma (Dahlquist et al. 2012).

Calcalkaline metaluminous epizonal granitoids are recognized in the central area of the Famatina Ranges (Dahlquist et al. 2008 and references therein). Rapela et al. (1999) calculated a U–Pb SHRIMP zircon age of 484 ± 5 Ma for the Cerro Ñuñorco biotite granite. Rubiolo et al. (2002) determined a U–Pb age of 485 ± 7 for the Narváez Granite. Dahlquist et al. (2008) calculated U–Pb zircon SHRIMP ages of 481 ± 4 Ma for a tonalite of the weakly peraluminous Cerro Toro Complex and of 463 ± 4 Ma for a monzogranite of the Ñuñorco Complex. Rhyolites interbedded with sediments of a volcanic sedimentary sequence yielded 477 ± 4 Ma.

Further south, in the southernmost tip of the Sierras Pampeanas, both the Santa Helena Schist and the Green Quarry Schist are found intruded by Ordovician metaigneous rocks: the 475.7 ± 2.3 Ma (U–Pb zircon SHRIMP age) Paso del Bote metaquartz-diorites and associated rocks

(Chernicoff et al. 2010) and the *c*. 450 Ma (U–Pb zircon SHRIMP age) back-arc-related Valle Daza metagabbros (Chernicoff et al. 2009). Both Famatinian rock assemblages define narrow, roughly N-S trending belts.

16.5.3 Devonian to Lower Carboniferous Magmatism

Paleozoic magmatism in the Sierras Pampeanas ended with the intrusion of a suite of Middle Devonian to Lower Carboniferous batholiths (López de Luchi 1996; Stuart-Smith et al. 1999; Pinotti et al. 2002; Siegesmund et al. 2004). They were considered to be either post-Famatinian or post-orogenic (Rapela et al. 1998a, b) or the Achalian granite group. In the Sierra de Córdoba, the Devonian Achala Batholith is a peraluminous, alkali-calcic granitoid with sharp and discordant contacts, which would represent variable proportions of a juvenile mantle component and crustal melts formed by dehydration melting of biotite-bearing gneisses (Rapela et al. 2008). The Cerro Aspero Batholith in Sierra de Comechingones is made up of biotite-granite and leucogranites (Pinotti et al. 2002). In the Sierra de San Luis, voluminous Devonian batholiths (Las Chacras-Potrerillos, Renca, La Totora and El Hornito) are made up of an I-type hybrid monzonite-granite suite with metaluminous alkali-calcic (393–385 Ma) monzonite-quartz monzonite-granodiorite ± monzogranite and peraluminous alkali-calcic monzogranites (Fig. 16.3a, b; López de Luchi et al. 2007, 2017). Undeformed granites of Lower Carboniferous age (Dahlquist et al. 2008) are located in the north (Báez et al. 2005) and central (Grosse et al. 2008) parts of the Sierra de Velasco. They have some features in common with the Devonian granitoids, in particular, nearly circular shapes, general lack of pervasive solid-state deformation, discordant relationships with the host, shallow emplacement, syeno- to monzogranitic compositions, porphyritic textures and an abundance of pegmatites and aplites. Miller and Söllner (2005) proposed that the Devonian to Early Carboniferous magmatism is related to post-orogenic regional crustal heating, whereas Grosse et al. (2008) proposed that the general age decrease in the Achalian magmatism from south to north could have been related to a progressive delamination of the crust coupled with upper mantle upwelling from south to north.

16.5.4 Neoproterozoic-Ordovician (Ultra-)Mafic Rocks

Mafic to ultramafic units of the Sierras de Córdoba which trend NNW to NE and dip between 50°–70° to the east were separated into an eastern and a western belt (Escayola et al. 1996). The NNW-SSE trending eastern belt is composed of lherzolite with interlayered websterite and subordinate harzburgite, abundant pyroxenite and gabbros. Escayola et al. (1996) assigned the tectonic setting to an ensialic back-arc basin, whereas Ramos et al. (2000) interpreted the belt as ophiolite remnants of a back-arc zone. The mafic to ultramafic units of the western belt, which extend along *c*. 300 km, are made up of harzburgites that were metasomatized by intrusive basaltic dykes (Escayola et al. 2007). Escayola et al. (1996) interpreted the western belt as a suture zone and considered the ultramafic rocks as dismembered ophiolites with MORB affinities, whereas Escayola et al. (2007) suggested a suprasubduction zone ophiolitic complex formed at a back-arc stage. Sm–Nd dating of basalt and gabbro dykes, pyroxenites and impregnated peridotites of the western belt yielded an isochron age of 647 ± 77 Ma. The $\varepsilon Nd_{(647)}$ value of 5.2 is consistent with an oceanic or back-arc origin for the ophiolite sequence (Escayola et al. 2007).

Gabbros with OIB signatures located in the Sierra de Comechingones, which result from the subduction of a mid-ocean ridge beneath the paleo-Pacific Gondwana margin, are related to the high-grade metamorphism of the Sierras de Córdoba (Tibaldi et al. 2008).

In the Cambrian Pampean Conlara Metamorphic Complex, ultramafic rocks have not been reported yet. Scarce amphibolites are distributed in a N-S belt through Sierra del Morro, San Felipe and Villa de Praga. Tholeiitic metapyroxenites of the 528 Ma Carancho Igneous Complex (Chernicoff et al. 2012) were interpreted as slivers of arc and back-arc rocks related to the inferred Late Early Cambrian suture between the Río de la Plata Craton and the Pampia Terrane.

Mafic to ultramafic Ordovician complexes are developed in the central part of the Sierra de San Luis, whereas gabbros are recognized as small plutons associated with the calcalkaline granitoids of the Sierra de Chepes, in the Famatina Complex in the Sierra de Famatina and in La Pampa province as scattered outcrops (Fig. 16.2). In the Pringles Metamorphic Complex, mafic to ultramafic bodies for which back-arc or marginal basin settings were proposed (Sims et al. 1998; Steenken et al. 2008, 2011) are represented by norites to gabbro-norites with minor ultramafic rocks. They have ages between 506 and 480 Ma. Amphibole-bearing gabbros associated with the calcalkaline complexes of the Sierra de Chepes, e.g. the Tama gabbro exhibit mingling relationships with the host granodiorite (Pankhurst et al. 1998).

Combined geological, geochronological, geochemical and geophysical studies have led to the identification of a large (*c*. 300 km long, *c*. 5 km wide) N-S trending belt of metagabbros in the province of La Pampa. This belt, though

only poorly exposed in the localities of Valle Daza and Sierra de Lonco Vaca, stands out in the geophysical data (aeromagnetics and gravity) (Chenicoff et al. 2010). The main rock type is metagabbro with relict magmatic nucleii where layering is preserved. A counterclockwise P–T evolution affected these rocks, while during the Middle Ordovician the protolith reached an initial granulite facies metamorphism (M1), evolving to amphibolite facies (M2).

16.6 Isotopic Constraints for the Neoproterozoic-Early Paleozoic Geodynamic Evolution of the Gondwana Margin

16.6.1 Sm–Nd Fingerprints for the Metamorphic Rocks

Steenken et al. (2011) suggested that the T_{DM1} = 1.8–1.7 Ga and $\varepsilon Nd_{(540)}$ = −6 to −8 can be considered as the mean average crustal composition of the Eastern Sierras Pampeanas (Fig. 16.3). Younger T_{DM1} ages and more radiogenic εNd values in metaclastic rocks could reflect the addition of juvenile material, a different source or a petrogenetic process. Although detrital zircon age patterns for the Pampean metaclastic rocks exhibit prominent Mesoproterozoic and Brasiliano peaks (Fig. 16.4), those for the post-Pampean metamorphic rocks independent of their metamorphic grade show Pampean and a less pronounced Grenvillian peak, suggesting a limited Grenvillian input. The average interval of crustal residence ages is similar. Since the Sm–Nd model ages (Fig. 16.3) are older than these peaks, the magmatic-metamorphic events sampled by the zircon cores/rims mainly represent recycled crustal sources.

Metamorphic rocks of the same grade from different parts of the Eastern Sierras Pampeanas show similar T_{DM1} ages (Fig. 16.3a), and crustal $f_{Sm/Nd}$ values but less radiogenic $\varepsilon Nd_{(540)}$ for those with older metamophic ages, which implies a higher degree of recycling between the Pampean and the Famatinian metaclastic rocks. Therefore increasing the amount of zircons from Grenville sources introduces a relatively more positive epsilon (Steenken et al. 2011). The La Cébila Metamorphic Complex at Quebrada La Rioja is not part of this trend, since T_{DM1} values vary between 1.3 and 1.5 Ga, and $\varepsilon Nd_{(t)}$ is less negative (Larrovere et al. 2011). Interestingly, the 526 Ma youngest age peak (Fig. 16.4) calculated for samples from this area is defined by only 20 zircons.

Increasing metamorphic grade in rocks with similar sources and detrital ages as in the Sierras de Córdoba is associated with a younging of the T_{DM} ages and less negative $\varepsilon Nd_{(540)}$ values. Pampean high-grade metaclastic rocks of the Sierra Grande de Córdoba and Sierra de Comechingones (Fig. 16.3) show consistently younger T_{DM} ages of 1.6–1.5 Ga and $\varepsilon Nd_{(540)}$ values between −4 and −3, whereas the $f_{Sm/Nd}$ value is above the average of −0.4 for the continental crust. Although SHRIMP zircon data for the granulite of the Sierra de Comechingones is scarce, the persistence of the Mesoproterozoic peaks (Fig. 16.4) in the Pampean units (Siegesmund et al. 2010) suggests that younging of the T_{DM1} ages results from a petrogenetic process. Otamendi et al. (2006) proposed that the granulites formed by a short-lived event of local thermal input, which enhanced the possibility that melting was rapid enough to trigger isotopic disequilibrium. The Ordovician high-grade rocks of the Pringles Metamorphic Complex exhibit T_{DM1} ages of 1.7–1.6 Ga (Fig. 16.3a) and a mean $\varepsilon Nd_{(540)}$ value of −5.5 (Fig. 16.3a). To summarize, increasing metamorphic grade in rocks with similar sources and ages as in the Sierras de Córdoba is associated with a younging of the T_{DM} ages and less negative $\varepsilon Nd_{(540)}$ values. In metaclastic rocks of different metamorphic age, the Grenville source introduces a relatively less negative epsilon. The change in source between the Pampean and the Famatinian metaclastic rocks is related to a higher degree of recycling as evidenced by the less radiogenic epsilon.

16.6.2 Sm–Nd Fingerprints for the Magmatic Rocks

16.6.2.1 Mafic-Ultramafic Complexes

Sm/Nd isotopes and Nd model ages of whole rock samples give the crustal residence age, this T_{DM} age corresponds to the actual mantle separation age of the crustal material (Patchett 1992). However, in the case of igneous rocks directly derived from the mantle, as can be expected for the (ultra-)mafic rocks, the T_{DM} model age could be close to the crystallization age if the rocks were stabilized over a period of up to 100 Ma (Patchett 1992) and thus provide the age of formation of the rock. Based on the analysis of the Sm–Nd results from various authors, Steenken et al. (2011) indicate two types of Pampean-related mafic rock in which no interaction with the continental crust in the sense of mixing or assimilation process is recognized. One group shows a depleted mantle-like signature and LREE depleted sources, which could indicate a stage of ocean crust formation, and the other, younger group has a signature of enrichment (cf. Siegesmund et al. 2010).

Rocks of the Eastern belt located in the Sierra Chica de Córdoba (Fig. 16.2) can be separated into two groups: (1) mafic to ultramafic rocks with a depleted mantle signature with $\varepsilon Nd_{(today)}$ values around 11, $\varepsilon Nd_{(540)}$ values of 6–8.5 and positive $f_{Sm/Nd}$; and (2) another more variable group located in the northern sector of the Sierras de Córdoba in which amphibolites are characterized by negative $\varepsilon Nd_{(today)}$ values,

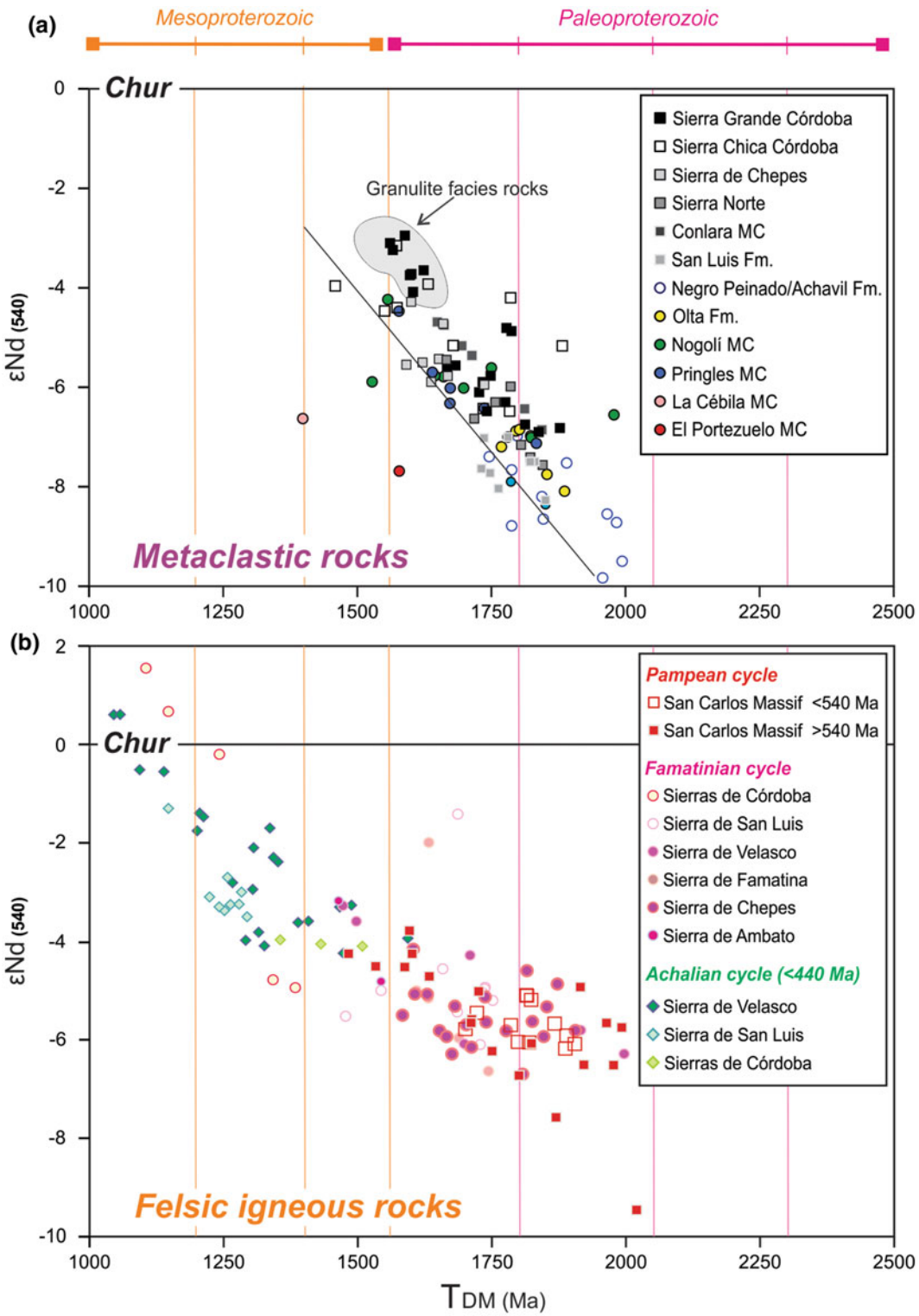

Fig. 16.3 **a** $\varepsilon Nd_{(t)}$ versus T_{DM} diagrams showing the Eastern Sierras Pampeanas clastic and felsic igneous rocks. Most of the metamorphic rocks are restricted to crustal values of fSm/Nd Pampean high grade rocks metaclastic rocks show more radiogenic compositions. Felsic igneous rocks exhibit more ample the data and the overlapping of the Ordovician and Pampean granitoids. Pampean rocks older than 540 Ma separate into two groups. The group with $\varepsilon Nd_{(t)} > -5$ corresponds to the rocks that show $T_{DM} < 1.6$ Ga. Rocks with less radiogenic $\varepsilon Nd_{(t)}$ correspond to older T_{DM} which suggest recycling nevertheless $\varepsilon Nd_{(t)}$ is more radiogenic in comparison with metaclastic rocks of similar T_{DM}. Devonian granitoids exhibit the more radiogenic signature. **b** $\varepsilon Nd_{(t)}$ versus fSm/Nd showing the Eastern Sierras Pampeanas mafic rocks in relation to the depleted mantle (DM) and the enriched reservoir represented by the oldest recorded crust i.e. T_{DM} between 1.7 and 1.8 Ga. Any mixture between these two reservoirs should lie along the mixing line (crust incorporation-thick line). Field limited for dashed line corresponds to the dominant values for the Eastern Sierras Pampeanas continental crust. See text for further explanation

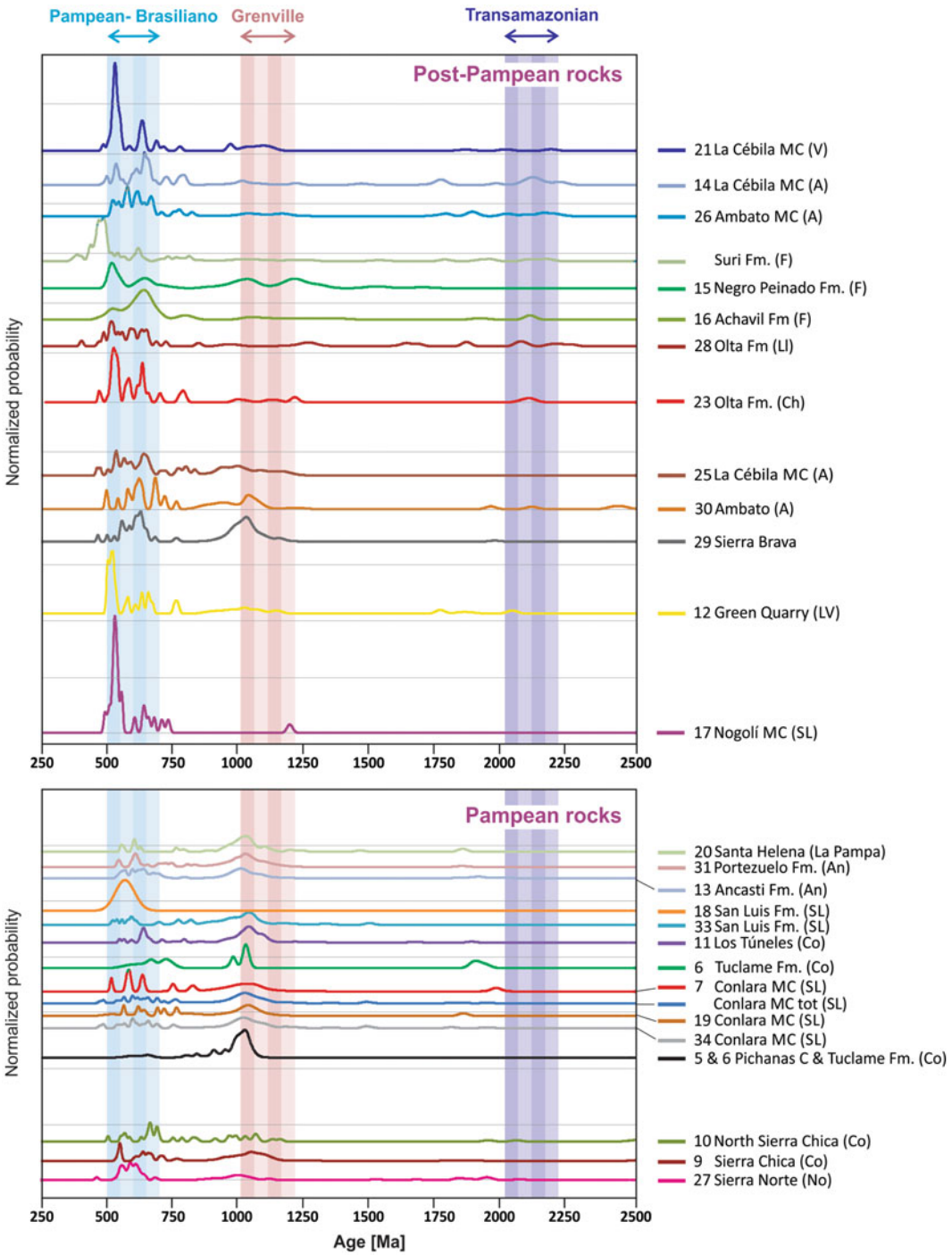

Fig. 16.4 Comparison of the detrital zircon provenance of the metaclastic rocks of the Pampean and post-Pampean basins using normalized zircon plots (Gehrels 2014). Data are display ordered from east (bottom side of the each figure) to west. Note that although the dominant peaks are of Brasiliano and Grenvillian ages, the relative proportion of each zircon population changes. See text for comments. Sample codes as in Fig. 16.2

positive $\varepsilon Nd_{(540)}$ values and negative $f_{Sm/Nd}$. T_{DM2} ages vary between 570 and 560 Ma. In the western belt in the Sierra de Comechingones, two groups can be recognized (Fig. 16.2). One includes serpentinites and metabasaltic dykes in which $\varepsilon Nd_{(today)}$ values can be higher or lower than the depleted mantle. The other group is made up of the gabbros related to the granulite facies metamporphism, such as Intihuasi, Suya Taco and Sol de Mayo in which the $\varepsilon Nd_{(today)}$ values are significantly lower than that of the contemporary depleted mantle. If the serpentinites and peridotites are discarded owing to the complex processes involved in their genesis, the remaining primitive rocks yield a T_{DM2} age range of 700–600 Ma. Therefore formation of oceanic crust in the Sierra Chica could have been active up to 560 Ma, whereas in the Sierra de Comechingones formation of oceanic crust was active up to 700–600 Ma (Steenken et al. 2011).

Ultramafic rocks of the Pringles Metamorphic Complex exhibit positive $\varepsilon Nd_{(480)}$ with T_{DM2} ages between 1100 and 800 Ma, whereas the norites with a negative $\varepsilon Nd_{(480)}$ plot on a mixing line (Fig. 16.3b) connecting the DM signature at 600–500 Ma with the average values for the metaclastic rocks of the complex. Amphibolites and komatiitic basalts of the Nogolí Metamorphic Complex, which show negative $\varepsilon Nd_{(480)}$ and $f_{Sm/Nd}$ values, and T_{DM2} ages between 1500 and 1300 Ma, suggest a process of mixing with a crustal component. A T_{DM2} age of 1100 Ma is calculated for the mafic rocks with positive $\varepsilon Nd_{(480)}$. The only available data for the gabbros of Sierra de Famatina and Sierra de Chepes exhibit negative $\varepsilon Nd_{(480)}$ and T_{DM2} ages between 1600 and 1500 Ma. The $\varepsilon Nd_{(480)}$ values for the Valle Daza gabbro are positive and show T_{DM2} ages of 800 Ma. Therefore the geodynamic scenario for the Ordovician mafic rocks could imply thicker continental crust than for the emplacement of the Pampean mafic rocks or, alternatively, a fast extensional process (extensional collapse) could prevent modification of the mafic melts in their ascent to the emplacement level.

The less evolved Devonian magmatic rock of the Las Chacras batholith indicates a T_{DM} age younger than any granitoid of the Sierra de San Luis (Fig. 16.3b) coupled with an εNd value of around zero.

16.6.2.2 Felsic Rocks

The overall high abundance of felsic intrusive rocks and the paucity of intermediate compositions suggest that crystal fractionation of mafic parental magmas was not an important process. Partial melting of crustal sources during basalt underplating or during crustal delamination is the dominant process at least during the Pampean and Famatinian cycles. Pre-540 Ma (Figs. 16.2 and 16.3), granitoids of the Sierra de Córdoba make up two clusters: one that would be entirely crustal, since they have T_{DM} ages older than 1.75 Ga and $\varepsilon Nd_{(540)}$ values of less than −5, and another cluster which corresponds to samples from Sierra Chica de Córdoba in which $\varepsilon Nd_{(540)}$ values are more radiogenic and T_{DM} ages are younger. In the first cluster, melting of a large amount of old sedimentary protoliths can be suggested, whereas in the second, since the host is less radiogenic and older, melting of a variably rejuvenated crust could be assumed. In this area, tonalites and granodiorites carry dioritic enclaves, suggesting a mixture of a mafic precursor with metasedimentary sources (Siegesmund et al. 2010; Iannizzotto et al. 2013).

In spite of the episode of mafic magma input to the crust as shown by the *c*. 540 Ma gabbros of the Sierra de Comechingones, no evidence of this juvenile input is seen in the post-540 Ma Pampean felsic rocks, which would represent partial melts derived from the older than 1.75 Ga basement (Fig. 16.3). Therefore it could be proposed that Cambrian OIB mafic magma should have just controlled the melting process through delamination or underplating.

Although juvenile input is suggested by the mafic rocks in the Pringles Metamorphic Complex or the gabbros of the Sierra de Chepes, widespread Famatinian magmatism with the exception of the minor TTG suites reworked the old lithospheric sources (Pankhurst et al. 1998). Mostly evolved granitoids dominate the rock spectrum in the Famatinian subduction stage. This fact suggests melting of mostly crustal sources as expected in regions of thick continental crust.

Sources for TTG suites of the Sierra de Córdoba are younger. Data from the Guiraldes and La Fronda throndhjemite together with a leucogranite from the northern sector of Sierra Chica de Córdoba cluster at a T_{DM} age of *c*. 1.3 Ga (see Fig. 16.3), which is accompanied by an $\varepsilon Nd_{(540)}$ value of −5 and a $f_{Sm/Nd}$ value of −0.55. One throndhjemite of the San Carlos Massif and the La Playa granodiorite shows the youngest T_{DM} age and a positive or slightly negative value of $\varepsilon Nd_{(470)}$, which suggests a juvenile input (Steenken et al. 2011).

16.7 Detrital Zircon Constraints on Protoliths of the Metaclastic Sequences

All 28 detrital zircon samples included in this study were compiled from the literature (see captions for references). Data was filtered by accepting values of less than 10% discordant for ages younger than 800 Ma. All the provenance and maximum depositional age analyses are based on published data that was obtained by different sampling strategies and numbers of points per sample. Differences in the method of age peak calculations, number of data, errors and strategy of measurement have a strong influence on the results, and thus interpretations must be careful and combine several analytical approaches.

To simplify the process of statistical provenance analysis, samples were separated into those belonging to Pampean

and post-Pampean basins following first the idea proposed by Steenken et al. (2004) in which the post-Pampean basins have detrital zircons younger than 530 Ma. Post-Pampean basins were further separated on the basis of a westwards rejuvenation of the protoliths of the Famatinian back-arc metamorphic complexes owing to the development of less stable basins associated with the emplacement to the west of the Ordovician orogenic front on the Gondwana margin (Larroverre et al. 2012).

Samples were analysed using normalized plots, the K–S test, the age pick 2010 test and by plotting the distribution of the difference between the measured crystallization ages (CA) of individual zircon grains present in the sediment and the depositional age (DA) of the (meta)sediment (Cawood et al. 2012)

Normalized probability plots are formed by calculating a normal distribution for each age from the data, summing the probability distribution of all accepted analyses and dividing the area under the curve by the number of analyses. Peak heights are a function of the number of grains at a particular age and the precision associated with that analysis. On normalized probability diagrams, significant age populations are only defined as clusters with three or more overlapping analyses (Gehrels et al. 2006).

The K–S test (Kolmogorov-Smirnov test) is a statistical approach that compares the maximum probability difference between two cumulative distribution function (CDF) representations of the age spectra. The test is a measure of the percentage of statistically indistinguishable spectra in a given grouping. Dependence on the CDF, which sums probabilities with increasing age, results in heightened sensitivity to the relative abundance of age peaks rather than their presence or absence. This characteristic caused samples with fewer grains or skewed peak abundances to be rejected (Laskowski et al. 2013).

The age pick test was performed to identify the statistically significant peaks in a set of detrital zircon ages. The youngest peak is considered to be a maximum depositional age.

Cumulative proportions were calculated using as the maximum depositional age the youngest calculated peak and as the minimum depositional age the fossil record or the age of the oldest intrusion.

On the normalized plots, samples are ordered from east to west based on the growth of successive Pampean and Famatinian belts towards the west from the margin of the Río de la Plata Craton. As previously mentioned, in various provenance studies the two main provenance populations are from Grenvillian and Brasiliano sources (e.g., Schwartz and Gromet 2004; Steenken et al. 2006; Escayola et al. 2007; Rapela et al. 2007; Drobe et al. 2009, 2011; Ramos et al. 2010).

Samples from the easternmost sector of the Eastern Sierras Pampeanas (Fig. 16.2) exhibit a predominance of Brasiliano sources while towards the west, Grenvillian sources exhibit a more prominent normalized plot peak, as for example point 6 in Fig. 16.4. This observation was first mentioned by Escayola et al. (2007), who considered a Grenvillian source towards the west. This feature of increasing the presence of Grenvillian sources in the detrital record is also observed in the rest of the Pampean basins, except for one sample from the San Luis Formation, A93-05 (Drobe et al. 2009), which has a small amount of data.

The available data for the retroarc post-Pampean Famatinian basins from San Luis, e.g. the Nogolí Metamorphic Complex and the fine-grained schist of the Green Quarry exhibit a well-defined Brasiliano-Pampeano peak and a less pronounced Grenvillian one. In the remaining three samples, data from the Sierra Brava Complex and one sample from the Ambato Complex are more similar to the Pampean basins, whereas the Ambato Formation sample has a predominance of Brasiliano-Pampeano peak. All these detrital patterns show peaks at *c*. 500 Ma or older than 480 Ma.

The Famatinian arc basins are characterized by the Brasiliano-Pampean peaks and the peaks between 520 and 480 Ma or younger in the case of the Suri Fm. Verdecchia et al. (2011) mentioned that the presence of a Paleoproterozoic age peak between 2.2 and 2.0 Ga, which is an indication of a Río de la Plata Craton source, indicates that sedimentation post-dates the juxtaposition with the craton which would have occurred after the main Pampean tectonothermal event (530–520 Ma). This peak is exhibited by the Olta, La Cébila and Achavil Formations (Fig. 16.4). Nevertheless, all these detrital records exhibit peaks in the normalized plots between 500 and 480 Ma, a feature that is preserved even if the Río de la Plata Craton imprint is absent from the rest of the post-Pampean basins.

An alternative explanation is that the exhumed Pampean rocks formed a drainage divide that blocked westward transport of the Río de la Plata-derived sediments. Intense erosion owing to an unstable tectonic scenario led to the progressive appearance of the Río de la Plata signature.

Application of the K–S test to the Pampean and post-Pampean basins indicates a high degree of correlation, which would suggest common/recycled sources. Detrital zircon data from Pampean basins exhibits the highest internal correlation. This may suggest a relatively stable availability of sources, whereas post-Pampean basins show, on average, lower values, which could be an indication of greater instability or barrier erosion (Figs. 16.4 and 16.5; Table 16.3)

Age peak analysis results can be seen in Table 16.4, together with the total number of zircons and the number of zircons that define the peak. Only samples with more than 25 zircon data were used. Based on the calculated peak ages, sample POM14013 from the Ambato Metamorphic-Igneous Complex and SBR14001 from the Sierra Brava

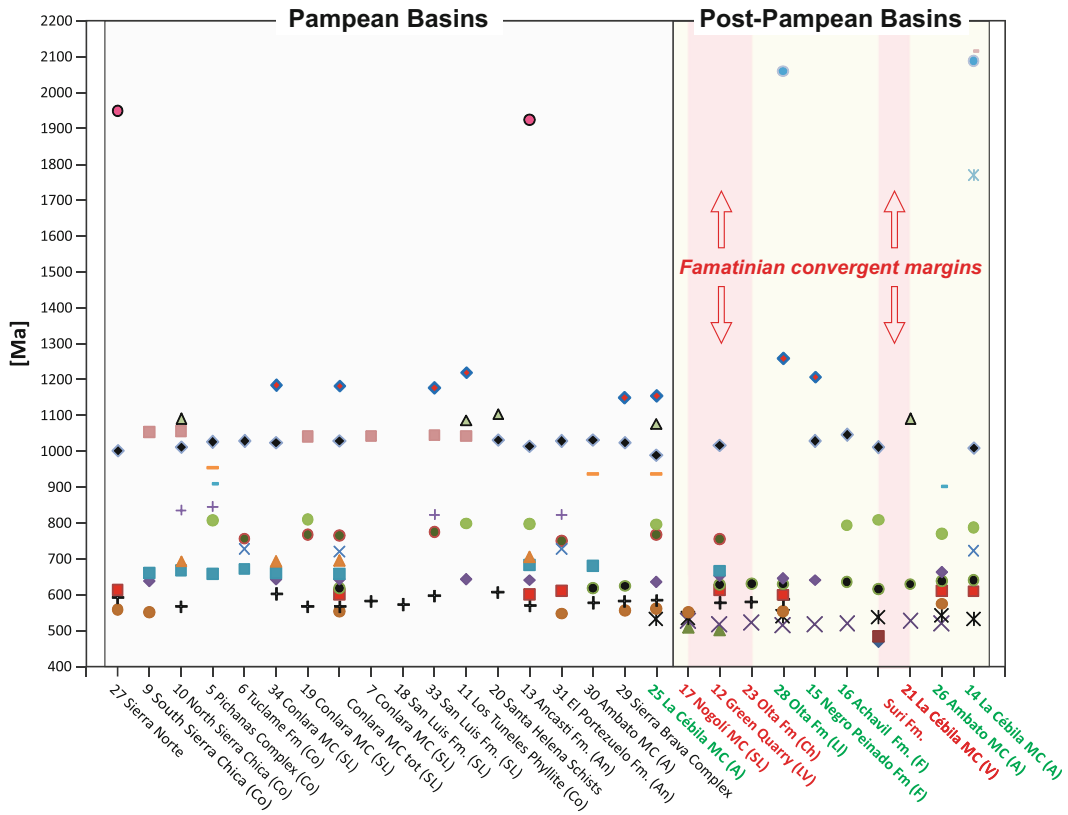

Fig. 16.5 Age picks of the detrital zircons of the metaclastic rocks derived from the Pampean and post Pampean basins. Dominant peaks are of Brasiliano and Grenvillian ages, Pampean ages appear in the post Pampean basins. Note that although several Post Pampean basins have a record of Ordovician sedimentation based not only on the youngest zircon data but also in the fossil record, the only Famatinian Ordovician peak corresponds to the Suri Formation (sample FAM 7082; Rapela et al. 2007). Sample codes as in Fig. 16.2

Metamorphic Complex are akin to the Pampean basins, since they lack younger peaks despite having younger detrital ages, as can be seen in the normalized plots (Fig. 16.4). All the samples exhibit Brasiliano peaks, which correspond to the mean peaks as defined by de Brito Neves et al. (2014; Early Cryogenian to Middle Ediacaran ages for the Pampean basins plus the Late Ediacaran–Middle Cambrian peak for the post-Pampean basins) and Grenvillian peaks. The Río de la Plata peaks are only present in one of the samples of the Olta Formation and in the sample of the La Cébila Metamorphic Complex. This corresponds to the one that Verdecchia et al. (2011) interpreted as an indication of its sedimentation post-dating the juxtaposition of the Río de la Plata Craton. Figure 16.5 is a graphical representation of the age peaks in which the importance of Late Cambrian to Early Ordovician peaks towards the west stand out.

Detrital zircon spectra reflect the tectonic setting of the basin in which they are deposited (Cawood et al. 2012). Convergent plate margins are characterized by a large proportion of zircon ages close to the depositional age of the sediment, whereas sediments in collisional, extensional and intracratonic settings contain greater proportions of older ages that reflect the history of the underlying basement. The difference between the measured crystallization ages (CA) of individual zircon grains present in the sediment and the depositional age (DA) of the sediment provides an indication of the type of margin. The youngest peak calculated from the Age Pick calculus routine (Table 16.4; Fig. 16.5) values was used as the CA, whereas the DA was obtained from the age of cover sequences, plutons intruding the units or the fossil record (Fig. 16.6).

The analysis of the cumulative distribution function (Table 16.4; Fig. 16.6) of highly concordant detrital zircon ages suggests, from east to west, that:

- 'Pampean' basins (sensu Steenken et al. 2011) are collisional, they are foreland basins except for Sierra Norte metaclastic host rocks that yield a convergent setting, and Sierra Brava and one of the samples from the Conlara Metamorphic Complex that would correspond to a collisional-convergent margin.
- Results from the post-Pampean Famatinian basins (Fig. 16.6b) indicate mostly collisional-convergent basins for the Ambato Metamorphic Complex, La

Table 16.3 K–S statistical correlation analysis of detrital zircon ages of the Pampean and Post Pampean metaclastic rocks

	Post-Pampean											Pampean											
Sample	Ch 23	Ch 28	F 16	F 15	A 26	A 25	A 14	GQ 12	V 21	SL 8	SL 17	Co 11	SL 33	Co 10	Co 9	No 27	SL 34+19	SBR. 29	An 13	An 31	SL 7	AIMC 30	SHS 20
23		0,052						0,442	0,985	0,250													
28	0,052		0,279	0,207	0,569	0,105	0,081	0,220								0,163			0,051			0,175	
16		0,279			0,428	0,069		0,131								0,070						0,053	
15		0,207			0,110	0,178		0,098				0,101	0,193	0,450	0,448	0,357	0,202		0,220	0,121	0,193	0,496	0,097
26		0,569	0,428	0,110		0,476	0,291								0,053	0,948		0,079	0,098			0,347	
25		0,105	0,069	0,178	0,476			0,088						0,064	0,141	0,805		0,417	0,215			0,879	
14		0,081			0,291									0,058	0,153	0,186			0,060			0,176	
12	0,442	0,220	0,131	0,098		0,088			0,782	0,083													
21	0,985							0,782		0,177	0,065												
8	0,250							0,083	0,177		0,313												
17									0,065	0,313													
11				0,101									0,909	0,418	0,926		0,922		0,245	0,800	0,909		0,998
33				0,193								0,909		0,484	0,761		0,894	0,057	0,160	0,987	1,000		0,843
10				0,450		0,064	0,058					0,418	0,484		0,508	0,089	0,366	0,301	0,393	0,389	0,484	0,140	0,508
9				0,448	0,053	0,141	0,153					0,926	0,761	0,508			1,000	0,271	0,893	0,983	0,761	0,360	0,509
27		0,163	0,070	0,357	0,948	0,805	0,186							0,089				0,237	0,108			0,555	
34+19				0,202								0,922	0,894	0,366	1,000			0,085	0,626	0,961	0,894	0,111	0,622
29					0,079	0,417							0,057	0,301	0,271	0,237	0,085		0,691	0,065	0,057	0,805	
13		0,051		0,220	0,098	0,215	0,060					0,245	0,160	0,393	0,893	0,108	0,626	0,691		0,310	0,160	0,575	0,077
31				0,121								0,800	0,987	0,389	0,983		0,961	0,065	0,310		0,987	0,087	0,764
7				0,193								0,909	1,000	0,484	0,761		0,894	0,057	0,160	0,987			0,843
30		0,175	0,053	0,496	0,347	0,879	0,176							0,140	0,360	0,555	0,111	0,805	0,575	0,087			
20				0,097								0,998	0,843	0,508	0,509		0,622		0,077	0,764	0,843		

P values > 0.05 indicate that two detrital zircon populations are statistically indistinguishable. Blue color indicate the highest degree of correlation from 0.8 to 1.0, yellow from 0.7 to 0.5

Note that the Pampean basins exhibit the highest degree of correlation. Samples with less than 25 zircon age data were excluded. Sample codes as in Fig. 16.2

Cébila Metamorphic Complex at the type locality, the sample from the northern sector of the Olta Formation (LLA-17018) and Achavil Formation in the Sierra de Famatina.

- Data from Green Quarry, Nogolí Metamorphic Complex, Olta Formation in the central part of the Sierra de Chepes, Suri Formation and La Cébila Metamorphic Complex at Quebrada La Rioja (LRJ1-1) yielded convergent margins. Negro Peinado Formation is the only post-Pampean basin sample that yielded a collisional setting. This could be an artefact of sampling, data acquisition routine or even misrepresentation. The two samples that exhibit Río de la Plata age peaks (2.2–2.0 Ga; Paleoproterozoic), LLA-17018 and CEB-428, belong to the collisional-convergent group. Samples that yielded convergent margin patterns in the cumulative distribution function plots exhibit the highest correlation among the post-Pampean basins (Table 16.3). They show a relatively large number of Middle Cambrian age zircons that define the corresponding peak, apart from having Ordovician magmatic zircons in the detrital record. It seems as if sources were more restricted than in the rest of the Famatinian to post-Pampean basins.

16.8 Orogenic Events of the Eastern Sierras Pampeanas

16.8.1 Pampean Orogeny

The western margin of South America and west Gondwana between 22° and 38°S (present coordinates) underwent an almost continuous convergent history extending from the Neoproterozoic–Early Cambrian to the Devonian through collisional/accretionary mechanisms, recycling processes and limited juvenile additions related to the Pampean, Famatinian and Achalian orogenies (Ramos 1988; Sims et al. 1998; Steenken et al. 2011). Final Gondwana amalgamation corresponds to the Cambrian closure of the Clymene Ocean that separated Amazonia from proto-Gondwana (Trindade et al. 2006). A large orogenic belt encompassing

Table 16.4 Main statistical peaks calculated with Age Pick 2010 (Gehrels 2014) for the Pampean and Post Pampean detrital zircon data. Colors of the columns correspond to the colors of the lines in Fig. 6.5

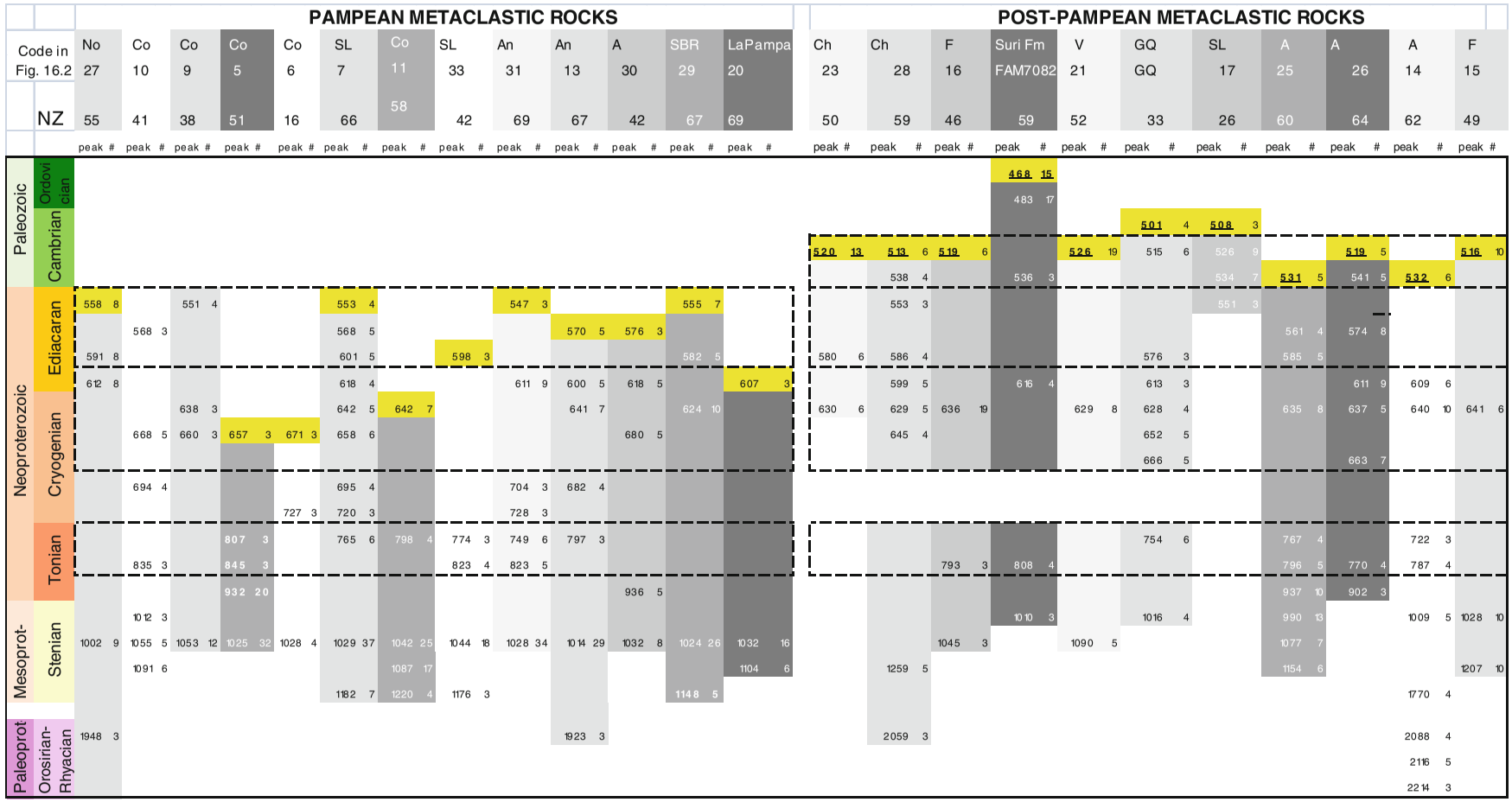

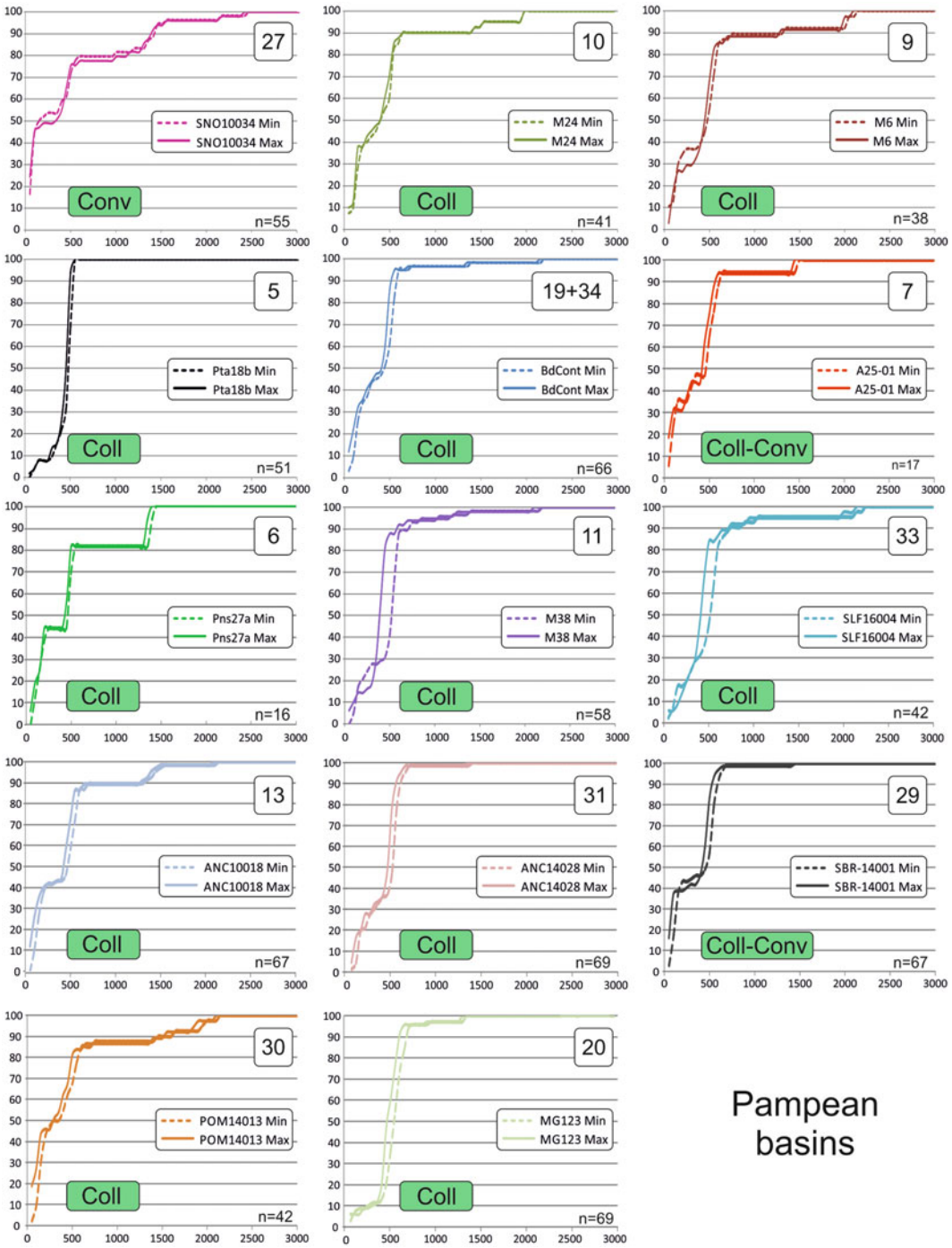

Fig. 16.6 Cumulative proportion curves (Cawood et al. 2012) for the **a** Pampean and **b** Post Pampean basins. Variation of the difference between the measured crystallization age for the youngest detrital zircon grain and the depositional age of the succession lead to the identification of the tectonic regime of the depositional system. *Coll* collisional setting, *Conv* convergent setting, *Coll-Conv* transitional between collisional and convergent. *N* number of zircon data. *Min* minimun depositional age, *Max* maximum depositional age

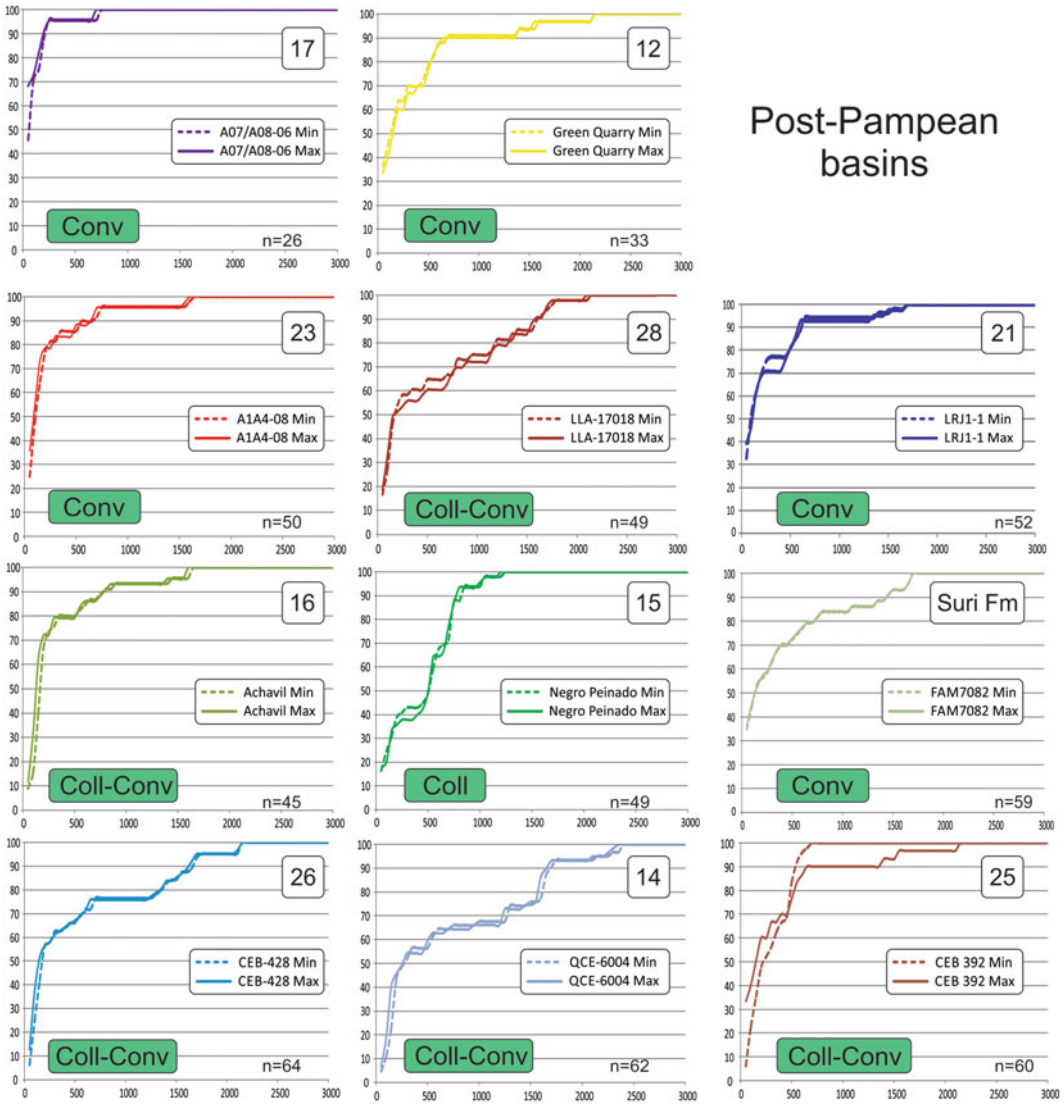

Fig. 16.6 (continued)

the Araguaia, Paraguay and Pampean Belts would record the closure of this ocean, which occurred between 530 and 520 Ma (Trindade et al. 2006).

Driving mechanisms for the Early Cambrian Pampean Orogeny involve competing scenarios of accretion of an allochthonous/para-autochthonous terrane or major block to the Río de la Plata Craton or subduction-related orogeny without any terrane addition (Piñán-Llamas and Simpson 2006; Schwartz et al. 2008) (Fig. 16.7a–d). These different hypotheses are based on deformational history, polymetamorphic evolution, detrital zircon patterns and/or magmatic signatures.

The terrane collision accretion models (Fig. 16.7a–c) involve the hypothesis that the substratum of the metamorphic basement of the Eastern Sierras Pampeanas is the Pampia Terrane (Ramos 1988), the Arequipa-Antofalla Terrane (Escayola et al. 2011) or that its basement is limited to the west by the MARA block (Rapela et al. 2016 and references therein). The Pampia Terrane was considered to be allochthonous and colliding with the Río de la Plata Craton in the Late Proterozoic (Ramos 1988; Kraemer et al. 1995), or para-autochthonous with an Early Cambrian collision with the Río de la Plata Craton (e.g., Rapela et al. 1998a, b). Ramos et al. (2010) proposed that it was originally attached to the Amazon craton since the Mesoproterozoic, jointly colliding with the Paranapanema block during the Neoproterozoic, and finally colliding with the Río de la Plata Craton during Early Cambrian. On the other hand, Chernicoff et al. (2012) considered that the Pampia Terrane derived from a Mesoproterozoic belt that detached from the Río de la Plata Craton to collide back at around 530 Ma. The collision of an island arc or a minor

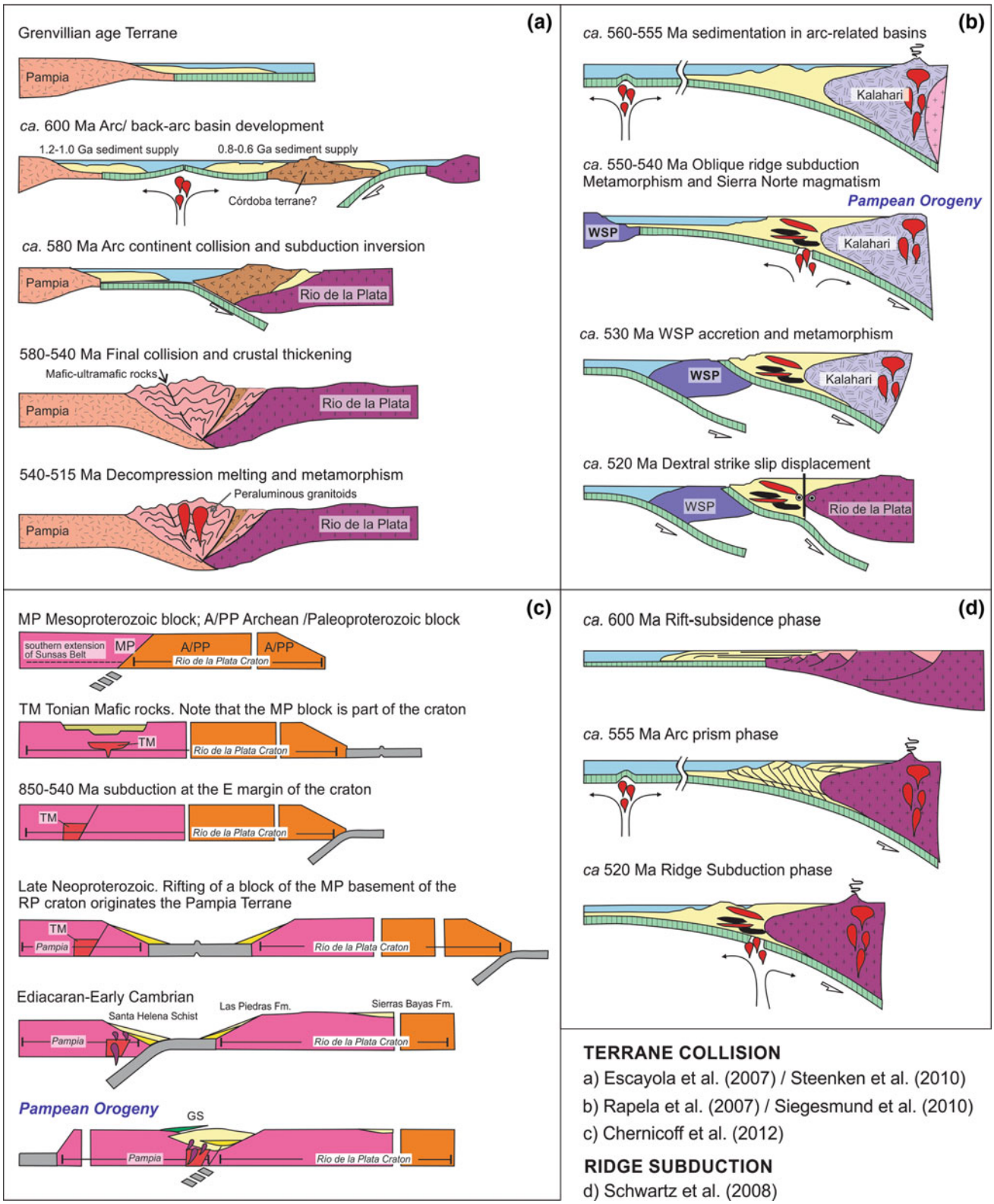

Fig. 16.7 Different models for the Pampean orogen. **a**, **b** and **c** are terrane accretion models whereas **d** correspond to the ridge subduction model. See text for comments

Mesoproterozoic block (Steenken et al. 2011) terrane against the Río de la Plata Craton would have preceded the collision of the Pampia Terrane (Ramos et al. 2015).

Rapela et al. (2007, 2016) proposed the collision of a ridge with the Kalahari Craton, and the subsequent displacement of the Pampean Belt along a transform fault was related to the collision/accretion with the MARA main terrane that includes the Western Sierras Pampeanas Terrane. This process ended with the juxtaposition with the Río de la Plata Craton.

Some variations on the terrane collisional model hypotheses correspond to Siegesmund et al. (2010) and Steenken et al. (2011), who combine the proximity to the Kalahari craton, the development of a magmatic arc at 580 Ma, with the collision of a Mesoproterozoic block. Chernicoff et al. (2012) proposed that the sedimentation and collisional episodes were developed on the Pampia Terrane facing the Río de la Plata Craton.

Ramos (1988) and later Kraemer et al. (1995) and Escayola et al. (2007) proposed that the evolution of the Eastern Sierras Pampeanas involved orthogonal subduction and terrane collision with the Río de la Plata Craton (Fig. 16.7a). An initial stage involved the Neoproterozoic accretion of the Córdoba Terrane, an island-arc terrane, against the Río de la Plata Craton following west-dipping (present coordinates) subduction (Escayola et al. 2007). Steenken et al. (2011) proposed a Mesoproterozoic terrane as responsible for this accretion that would have closed an ocean as indicated by ophiolite remnants of the Sierras de Córdoba. This early stage is supported by the M1-D1 metamorphic ages of 560 Ma and arc magmatism dated at 580 Ma at the south of the Sierras Córdoba (Sims et al. 1998; Siegesmund et al. 2010; Guereschi and Martino 2014 and references therein). The accretion of the Pampia Terrane (a Grenville age basement terrane or a Mesoproterozoic basement) is initiated by the subduction of a ridge to the already amalgamated Córdoba/Mesoproterozoic basement terrane in the Neoproterozoic-earliest Cambrian (Escayola et al. 2007; Ramos et al. 2010; Steenken et al. 2011). This collision controlled the M2 metamorphic event in the Sierras de Córdoba and produced the Pampean orogen with subsequent decompression melting and intrusion of peraluminous granitoids.

Based on a geochronological study of the Río de la Plata Craton, Rapela et al. (2007) proposed that these supracrustal sequences or protoliths of the metasedimentary rocks of the Eastern Sierras Pampeanas could initially have been deposited as large submarine fans at the southern tip of the Río de la Plata Craton and the Kalahari Craton, and fed by a magmatic arc located at the present African side. They concludes that the closing of the Clymene Ocean (Trindade et al. 2006), which might have separated the Río de la Plata Craton from the Grenvillian terranes such as Amazonia, Arequipa-Antofalla and Western Sierras Pampeanas, would have led to a right-lateral accretion between the MARA/Western Sierras Pampeanas Craton and the Pampean Belt at *c*. 540–520 Ma. After the collision, a continued right-lateral movement would have displaced the Pampean mobile belt to its present position alongside the Río de la Plata Craton through the dextral Trans-Brasiliano shear zone.

Schwartz et al. (2008) (Fig. 16.7d) proposed a long-lived early subduction between 555 and 525 Ma and a calcalkaline magmatic arc, which could partially provide the sediments to build a long accretionary prism. This process would have ended with the subduction of a seismic ridge beneath the accretionary prism developed in the Río de la Plata Craton, excluding a continental collision (Schwartz and Gromet 2004).

As noted previously by Escayola et al. (2007) and Ramos et al. (2015), the models, apart from those put forward by Rapela et al. (2007) and Drobe et al. (2011), have two statements in common: (1) the subduction of oceanic lithosphere was east dipping beneath the Río de la Plata Craton for the main metamorphic event; and (2) the supracrustal sequences of the Eastern Pampean Ranges represent passive/active margin deposits along the continental platform of that craton or facing the craton on the Pampia Terrane.

Detrital zircon ages for the Pampean basins show important Brasiliano and Grenvillian age peaks: Mesoproterozoic ages are typical of the (1250–950 Ma) Sunsás–Aguapeí province, located in southern Brazil (Teixeira et al. 2010). The lack of additional isotopic data, as for example Hf data, hampers our ability to determine whether the Grenvillian ages are derived from the Namaqualand Belt or the Sunsás-Aguapeí. The lack of a Río de la Plata signature in the Pampean basins could be derived from the existence of orogenic barriers, for instance, related to the Córdoba or island arc *c*. 580–560 Ma accretion that controlled the exhumation of Brasiliano rocks. After the final collision of the Pampia/Arequipa-Antofalla terrane at *c*. 530 Ma, cannibalization of the older granites together with recycling of the metasediments fed the post-Pampean foreland basins. Figure 16.7 illustrates the different models for the Pampean orogen.

16.8.2 Famatinian Orogeny

The Famatinian orogen consists of a continuous upper-plate continental arc, associated with some contribution from juvenile mantle material and ensialic basins (Dahlquist et al. 2008; Collo et al. 2009), which would stretch between southern Peru and northern Patagonia (Casquet et al. 2006; Chew et al. 2007; Martínez Dopico et al. 2011). The

Famatina Belt between 28° and 38°S has been interpreted as part of the accretionary margin built along Western Gondwana during the early Paleozoic after the Pampean Orogeny. The Famatinian arc started at *c*. 495 Ma when subduction was established along the outboard boundary of the Pampean Orogen. The final stages at *c*. 465 Ma (Ramos 1988; Thomas and Astini 2003) related to the collision of the Metamorphic Complex are akin to the Pampean basins allochthonous Laurentia-derived Precordillera/Cuyania Terrane during the Ordovician Ocloyic Orogeny (see Dahlquist et al. 2008 and references therein). An alternative para-autochthonous model proposed that the Cuyania Terrane (sedimentary sequence of the Precordillera of Argentina plus Grenville basement of the Western Sierras Pampeanas) migrated along a transform fault, from a position on the southern margin of West Gondwana (present coordinates) in the mid-Ordovician to its modern position outboard of the Famatina magmatic belt in Devonian time (Finney 2007 and references therein).

Dahlquist et al. (2008) proposed a model for the development of a relatively short-lived (481–463 Ma) Famatina Complex (Famatina magmatic arc and related ensialic basins) along the border of the Pampean basement, related to an ongoing subduction along the margin of the Western Sierras Pampeanas Terrane. Magmatism and closure of the ensialic basin was related to a compressive event. Steenken et al. (2006, 2008, 2011) proposed that the interval between the end of the Pampean orogen and the initiation of the Famatinian subduction encompasses the uplift and erosion of the Pampean-related rocks that fed Middle Cambrian foreland basins, which developed along the margin of the Pampean terrane and the initiation of a new subduction along the western margin of the Pampean Terrane. The first deformation and metamorphism in these basins were related to the onset of the Famatina subduction at around 500 Ma. Subsequently an extensional back-arc regime was established. The initiation of granulite facies metamorphism due to the transient anomaly associated with the 506–480 Ma mafic and ultramafic intrusions is contemporaneous or closely followed by the emplacement of crustal-derived granitoids, such as the northern stock of the 491 Ma Paso del Rey granite, parallel to the S1 foliation of the country rock and the 480–460 Ma OTS tonalite-granodiorite in the low-grade phyllites. The inferred post-D1 emplacement of those granitoids indicates that D1 and M1 pre-date the generally assumed mid-Ordovician accretion of the Precordillera/Cuyania Terrane. If Steenken et al. (2006) are right, the mafic to ultramafic rocks of the PMC emplaced in a back-arc basin at the lower levels of a continental crust had undergone D1 and amphibolite facies M1. Higher-grade metamorphism M2 and crustal melting closely followed this event. This magmatic arc would have developed in a crust that was already at amphibolite facies conditions owing to D1 that would be related to the Iruyic deformation. Collo et al. (2009) suggested a foreland tectonic context for the quartz-rich Mesón Group (NW Argentina), which unconformably covers the folded Puncoviscana Formation, and proposed that the initiation of the Famatinian orogenic cycle could correspond to the Iruyic unconformity in NW Argentina. Extensional basins post-dating the initiation of the Famatinan arc were developed along the entire margin of the Pampean Terrane (Collo et al. 2009). Ordovician volcanic rocks and volcaniclastic successions of the northern and central sector of the Famatina Complex (Dahlquist et al. 2008 and references therein) form an essentially bimodal association of basalt and subalkaline rhyolite interpreted as ensialic back-arc or inter-arc basins (e.g., Astini 2003 and references therein).

16.8.3 Achalian Orogeny

Achalian orogeny or the Achalian cycle (Sims et al. 1997) resulted from the collision of the allochthonous Chilenia terrane with Gondwana (Ramos et al. 1986; Ramos 1988; Sims et al. 1997, 1998; Quenardelle and Ramos 1999). This event roughly corresponds to the late to post-Famatinian events of the Famatinian cycle of Dalla Salda et al. (1998). The Achalian cycle is a period of heterogeneous deformation along crustal-scale fault lines that may have resulted from the resumption of the convergence on the western margin of Gondwana (Siegesmund et al. 2004). Achalian granitoids intruded the older basement and are especially widespread in the Sierra de San Luis and the Sierras de Córdoba (Sims et al. 1997; Siegesmund et al. 2004; López de Luchi et al. 2007; Rapela et al. 2007). The voluminous Achalian granite magmatism has raised much speculation regarding the underlying geodynamic causes (López de Luchi et al. 2007). It was first discussed as post-tectonic in relation to the Famatinian cycle (Llambías et al. 1998) or as resulting from slab break-off during the late stages of the subduction that ended with the collision of Chilenia (López de Luchi 1996; López de Luchi et al. 2007).

16.9 Concluding Remarks and Critical Topics for a Renewed Proposal for the Early Paleozoic Tectonic Evolution of the Eastern Sierras Pampeanas

A geodynamic model for the early Paleozoic orogenic evolution of the proto-Andean margin of Gondwana must combine the reliable geochronological evidence with petrological observations, structural features and physical parameters of the involved lithospheric segments (Fig. 16.8).

In evaluating alternatives for a tectonic model, critical data are as follows:

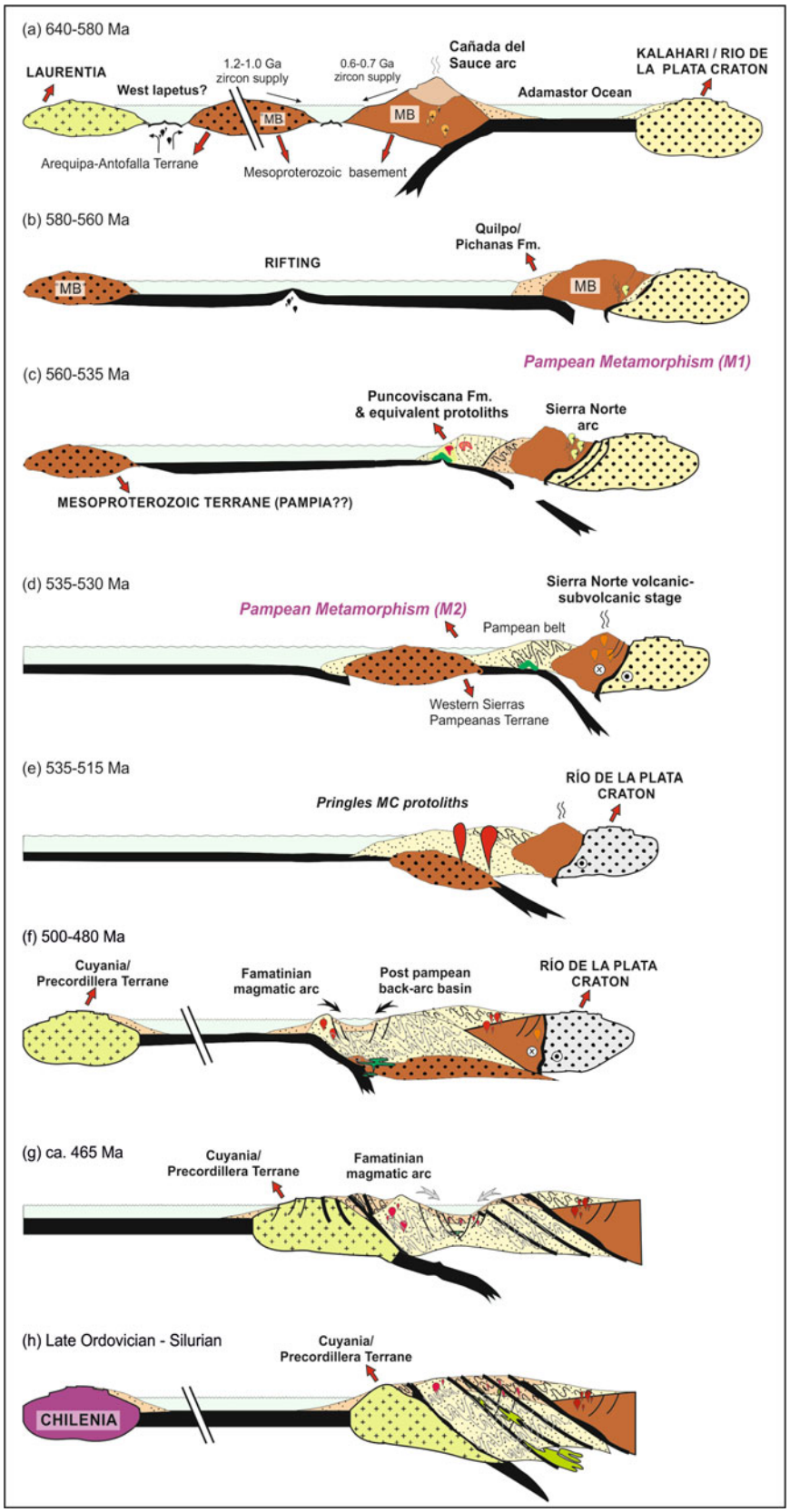
(a) 640-580 Ma
LAURENTIA
West Iapetus?
1.2-1.0 Ga zircon supply
0.6-0.7 Ga zircon supply
Cañada del Sauce arc
KALAHARI / RIO DE LA PLATA CRATON
Adamastor Ocean
MB
MB
Arequipa-Antofalla Terrane
Mesoproterozoic basement
(b) 580-560 Ma
RIFTING
Quilpo/ Pichanas Fm.
MB
MB
Pampean Metamorphism (M1)
(c) 560-535 Ma
Puncoviscana Fm. & equivalent protoliths
Sierra Norte arc
MESOPROTEROZOIC TERRANE (PAMPIA??)
(d) 535-530 Ma
Sierra Norte volcanic-subvolcanic stage
Pampean Metamorphism (M2)
Pampean belt
Western Sierras Pampeanas Terrane
(e) 535-515 Ma
RÍO DE LA PLATA CRATON
Pringles MC protoliths
(f) 500-480 Ma
Cuyania/ Precordillera Terrane
Famatinian magmatic arc
Post pampean back-arc basin
RÍO DE LA PLATA CRATON
(g) ca. 465 Ma
Cuyania/ Precordillera Terrane
Famatinian magmatic arc
(h) Late Ordovician - Silurian
Cuyania/ Precordillera Terrane
CHILENIA

Fig. 16.8 Schematic evolution of the Eastern Sierras Pampeanas between 30 and 32° SL from the Neoproterozoic to the Silurian. **a** Back-arc extension according to Escayola et al. (2007) and Steenken et al. (2011). Note that arc magmatism is developed in an inferred Mesoproterozoic (Arequipa derived?) block. Rapela et al. (2007) proposed that the location of this margin was close to the Kalahari craton. **b** Initial development of accretionary prism along an active margin that started after the closure of the Adamastor or Clymene ocean (Frimmel and Fölling 2004). Ages to constrain a *ca* 560 Ma metamorphic overprint are taken from Sims et al. (1998) and Siegesmund et al. (2010). **c** Late Neoproterozoic to Early Cambrian development of the Sierra Norte arc magmatism post dating M1 and concomitant deposition of accretionary prism and foreland basin sediments. **d** Metamorphism and deformation of the Puncoviscana Formation equivalents and cessation of arc magmatism is ascribed to the accretion of a slice of Mesoproterozoic basement that may correspond to the Pampia Terrane. **e** Post collisional collapse as indicated by Ramos et al. (2015). **f** Initiation of the subduction that migrated to the western border of the Pampean belt. Incipient development of extensional basins. Age constraints for the initiation of sedimentation are interpreted from the detrital data of the Post Pampean basins. **g** Accretion of the Precordillera Terrane. Age constraints for the Pringles Metamorphic Complex according to Steenken et al. (2006). Synorogenic deposition of Negro Peinado and Achavil formations according to Collo et al. (2009). **h** Post-Famatinian margin of Gondwana. **i** Convergence of Chilenia based on Ramos (1988)

- High-grade metamorphism either Pampean or Famatinian was ascribed to the thermal input by mafic intrusions. Most of the physical processes capable of raising temperatures in the upper mantle involve upwelling of hot asthenospheric material following attenuation or removal of the mantle lithosphere via convective thinning, delamination detachment via 'slab break-off', or extension either preceding or post-dating shortening (Bodorkos et al. 1999 and references therein). Attenuation of the mantle lithosphere is often accompanied by decompression melting and the emplacement of mantle-derived mafic magmas at the base of the crust as an underplate (Bodorkos et al. 1999 and references therein).
- In the Pampean orogen, high-grade granulite metamorphism post-dates a collisional stage and would result from the collapse of the subducting slab and delamination of the mantle lithosphere. This combination of processes resulted in the upwelling of hot asthenospheric material (the OIB signature of Tibaldi et al. 2008) beneath the crust of the Sierras de Córdoba, triggering plutonism and metamorphism in the middle crust. Uplift, which would be the isostatic response to asthenospheric upwelling and the initiation of the mantle-related temperature anomaly, would enhance melting of the middle crust and would control the *c*. 530–520 Ma crustal magmatism.
- In the Famatinian orogen the close temporal and spatial relationships between mid-crustal felsic plutonism, mafic magmatism and zones of high-grade metamorphism are controlled by active subduction. High-grade metamorphism in the Pringles Metamorphic Complex could result from a mantle-related transient thermal anomaly initiated at around 500 Ma as the primary heat source for high-T, relatively low-P metamorphism in an extensional setting. Subsequent compression during active convergence may explain the extensive crustal and mafic derived melts. At higher crustal levels, as exposed in the Sierra de Chepes, Ordovician metamorphism is driven by magma advection because it is typically localized and characterized by high lateral metamorphic field gradients in the vicinity of intrusions.
- Grenvillian detrital ages in Pampean metaclastic rocks are independent of the present location of the sampled rock. The average crustal residence time is *c*. 1.8 Ga, significantly older than the dominant detrital ages, a fact which implies recycled sources. These Grenvillian detrital ages could be ascribed to the approaching Mesoproterozoic terranes or, as proposed by Rapela et al. (2016 and references therein), either to the Mesoproterozoic rocks of the Natal–Namaqua Belt, southern Kalahari Craton or to the Brasiliano–Panafrican granites of southern Africa and SE Brazil and Uruguay (Schwartz and Gromet 2004; Rapela et al. 2007). Detrital zircons in the Rocha Group of SE Uruguay and the Oranjemund Group of the Gariep Belt of southwest Africa show similar bimodal patterns with a 1.0 Ga component (Basei et al. 2005), suggesting extensive offshore source rocks of these ages. In addition, Peri et al. (2013) showed that the tectonic limit between the Río de la Plata Craton and the basement of the Eastern Sierras Pampeanas dips to the east, which makes it difficult to explain a transcurrent regional displacement from the Kalahari to the Río de la Plata Craton.
- Concerning the lack of 'Río de la Plata' 2.2–2.0 Ga sources in Sierras Pampeanas, the model proposed initially by Ramos (1988) involving a 'Córdoba terrane' implies that its accretion could lead to exhumation of the associated metamorphic rocks, which would constitute the barrier for the detrital input of the Río de la Plata Craton, an idea put forward by Ramos et al. (2014).
- Ocean crust formation at 640 Ma at the present site of the Sierra de Comechingones is coherent with the existence of the Adamastor (or Clymene) ocean, which may have survived up to 560 Ma based on the data of the Sierra Chica mafic rocks with a respective DM signature. The closure of the Adamastor Ocean would be reflected in the older metamorphic age of 553 Ma recorded by the Tala Cruz metatexite (Siegesmund et al. 2010). Guereschi and

Martino (2008) calculated P–T constraints of 810–840 °C and 8.5–9 kbar for the metamorphism of the Tala Cruz stromatites.

- The *c*. 580 Ma metamorphic/igneous ages found in the easternmost extension of the Eastern Sierras Pampeanas determined by Siegesmund et al. (2010) for the Cañada del Sauce diatexite, and previously mentioned by Sims et al. (1998), would support the existence of a Mid-Ediacaran magmatic arc. Interestingly, the so-called Ancajan Series of Rapela et al. (2016 and references therein) could correspond to relicts of the host rocks of the 580 Ma magmatic rocks.
- The penetrative deformational phase at around 530 Ma is recognized in the Sierra Norte and in the Sierra Chica orthogneiss, and would correspond to the collision of the Pampia Terrane.
- The emplacement of OIB-type magmas at *c*. 535 Ma is closely associated in space with the generation of granulite facies rocks, where subsequent anatexis was associated with a decompressional path and massive anatectic crustal derived granitoids (younger than 530 Ma).
- Intrusive ages in the Sierra Norte between 555 and 535 Ma post-date the 560 Ma M 1 metamorphism and pre-date the M2 metamorphic peak and deformation history at *c*. 530 Ma (Rapela et al. 1998a) that represented the final closure of the Puncoviscan-like basins. Two stages during the magmatism in the Sierra Norte are further indicated by the intrusion of undeformed granite. Later exhumation is indicated by the *c*. 521 Ma rhyolites.
- The interval of Famatinian magmatism predates 460 Ma, which was considered to be the age of accretion of Cuyania. Therefore magmatism is related to subduction and no important collision-related Ordovician magmatism is present in the Eastern Sierras Pampeanas.
- The degree of interaction between the crust and the mafic magmas indicates a thicker crust and a protracted emplacement process in the Ordovician, which involves I-and S-type coeval magmatism.
- Detrital zircon spectra indicate a minor contribution of Grenvillian sources to the post-Pampean basins, which suggest either a barrier or the separation from these sources as a result of the relative displacement.
- Achalian Cycle magmatism is unrelated to Famatinian history and involves a transient heat anomaly that controlled extensive melting of an enriched mantle source, and probably a segment of a crust different from the Neoproterozoic to Ordovician continental crust of the Eastern Sierras Pampeanas.

Acknowledgements We gratefully acknowledge the support we have received from the German Science Foundation, which has funded our research projects in Argentina over the years (Grants Si 438/16, Si 438/17 and Si 438/24, Si 438/31), as well from the DAAD-ANTORCHAS programme. M. López de Luchi also thanks the DAAD for its support through grants A/03/39422 and A/ 07/10368. The authors thank Gabriel Giordanengo and F. Wilski for the final polishing of all figures. We are thankful to A. Steenken, R.D. Martino, C. Costa, M. Drobe, S. Löbens, F.A. Bense and numerous students from Göttingen for fruitful fieldwork and discussion.

References

Aceñolaza FG, Toselli AJ (1981) Geología del Noroeste Argentino. Publicación Especial de la Facultad de Ciencias Naturales, Universidad Nacional de Tucumán 1287: 1–212

Aceñolaza FG, Miller H, Toselli AJ (1988) The puncoviscana formation (late precambrian-early Cambrian). Sedimentology, tectonometamorphic history and age of the oldest rocks of NW Argentina. In: Bahlburg H, Breitkreuz C, Giese P (eds) The Southern Central Andes, vol 17. Lect Notes Earth Science. Springer, Heidelberg, pp 25–37

Adams CJ, Miller H, Toselli AJ, Griffin WL (2008) The Puncoviscana Formation of Northwest Argentina: U–Pb geochronology of detrital zircons and Rb–Sr metamorphic ages and their bearing on its stratigraphic age, sediment provenance and tectonic setting. Neues Jahrb Geol P-A 247:341–352

Alasino PH, Dahlquist JA, Pankhurst R, Galindo C, Casquet C, Rapela CW, Larrovere MA, Fanning CM (2012) Early Carboniferous sub-to mid-alkaline magmatism in the Eastern Sierras Pampeanas, NW Argentina: a record of crustal growth by the incorporation of mantle-derived material in an extensional setting. Gondwana Res 22:992–1008. https://doi.org/10.1016/j.gr.2011.12.011

Astini RA (2003) The Ordovician Proto-Andean basins. In: Benedetto JL (ed) Ordovician fossils of Argentina. Universidad Nacional de Córdoba, Secretaría de Ciencia y Tecnología, pp 1–74

Astini RA, Dávila F, Collo G, Martina F (2005) La Formación La Aguadita (Ordovícico medio-superior?): Su implicancia en la evolución temprana del Famatina. In: Dahlquist JA, Baldo EG, Alasino PH (eds) Geología de la Provincia de La Rioja (Precámbrico-Paleozoico inferior), vol 8. Rev Asoc Geol Arg, Serie D, Publicación Especial, pp 67–84

Astini RA, Dávila FM, Collo G (2008) Las discordancias Tilcárica e Irúyica en el noroeste argentino: una perspectiva regional. XVIII Congreso Geológico Argentino, Santiago, Chile, October 2008, Actas I, pp 3–4

Báez MA, Bellos LI, Grosse P, Sardi FG (2005) Caracterización petrológica de la Sierra de Velasco. In: Dahlquist J, Rapela C, Baldo E (eds) Geología de la provincia de La Rioja-Precámbrico-Paleozoico Inferior, vol 8. Asoc Geol Argent Spec Pub, Serie D, pp 123–130

Balhburg H (1991) The Ordovician back-arc to foreland successor basin in the Argentinian-Chilean Puna: tectonosedimentary trends and sea-level changes. In: MacDonald DIM (ed) Sedimentation, tectonics, and eustasy, vol 12. Spec Pub Inter Assoc Sedimentology, pp 465–484

Basei MAS, Frimmel HE, Nutmann AP, Preciozzi F, Jacob J (2005) The connection between the Neoproterozoic Dom Feliciano (Brazil/Uruguay) and Gariep (Namibia/South Africa) orogenic belts. Precambrian Res 139:139–221. https://doi.org/10.1016/j.precamres.2005.06.005

Bellos LI (2005) Geología y petrología del sector austral de la sierra de Velasco, al sur de los 29° 44′S, La Rioja, Argentina. In: Aceñolaza FG, Hünicken M, Toselli AJ, Aceñolaza GF (eds) Simposio Bodenbender: Trabajos completos. Serie de Correlación Geológica,

Nº19. INSUGEO (CONICET), San Miguel de Tucumán, pp 261–278

Bense F, Löbens S, Dunkl I, Wemmer K, Siegesmund S (2013a) Is the exhumation of the Sierras Pampeanas only related to Neogene flat-slab subduction? Implications from a multi-thermochronological approach. J S Am Earth Sci 48:123–144

Bense F, Wemmer K, Löbens S, Siegesmund S (2013b) Fault gouge analyses: K/Ar illite dating, clay mineralogy and tectonic significance—a case study from the Sierras Pampeanas, Argentina. Int J Earth Sci 103(1):189–218

Bense F, Costa C, Oriolo S, Löbens S, Dunkl I, Wemmer K, Siegesmund S (2017) Exhumation history and landscape evolution of the Sierra de San Luis (Sierras Pampeanas, Argentina)—new insights from low-temperature Thermochronological data. Andean Geol 44(3)

Booker JR, Favetto A, Pomposiello MC (2004) Low electrical resistivity associated with plunging of the Nazca flat slab beneath Argentina. Nature 429:399–403. https://doi.org/10.1038/nature02565

Bodorkos S, Oliver NHS, Cawood PA (1999) Thermal evolution of the central Halls Creek Orogen, northern Australia. Australian J Earth Sci 46:453–465

Brito Neves BB de, Fuck RA, Pimentel MM (2014) The Brasiliano collage in South America: a review. Braz J Geol 44(3):493–518

de Brodtkorb MK, Ostera H, Pezzutti N, Tassinari C (2005) Sm/Nd and K-Ar data from W-bearing amphibolites of Eastern Pampean Ranges, San Luis and Córdoba, Argentina. V South American Symp Isotope Geol, Punta del Este, 2006, Actas, pp 478–482

Camacho A, Ireland TR (1997) U/Pb Geochronology, final report. Geoscientific mapping of the Sierras Pampeanas Argentine–Australia Cooperative Project. Servicio Geológico Minero Argentino (unedited). Buenos Aires

Caminos R (1979) Sierras Pampeanas Noroccidentales. Salta, Tucumán, Catamarca, La Rioja y San Juan. II Simposio de Geol Reg Argentina 1:225–291

Casquet C, Baldo E, Pankhurst RJ, Rapela CW, Galindo C, Fanning CM, Saavedra J (2001) Involvement of the Argentine Precordillera Terrane in the Famatinian mobile belt: U–Pb SHRIMP and metamorphic evidence from the Sierra de Pie de Palo. Geology 29:703–706

Casquet C, Pankhurst RJ, Fanning CM, Baldo E, Galindo C, Rapela C, González-Casado JM, Dahlquist JA (2006) U–Pb SHRIMP zircon dating of Grenvillian metamorphism in Western Sierras Pampeanas (Argentina): correlation with the Arequipa Antofalla craton and constraints on the extent of the Precordillera Terrane. Gondwana Res 9:524–529

Casquet C, Pankhurst RJ, Rapela CW, Galindo C, Fanning CM, Chiaradia M, Baldo E, González-Casado JM, Dahlquist J (2008) The Mesoproterozoic Maz terrane in the Western Sierras Pampeanas, Argentina, equivalent to the Arequipa-Antofalla block of southern Peru? Implications for West Gondwana margin evolution. Gondwana Res 13:163–175. https://doi.org/10.1016/j.gr.2007.04.005

Casquet C, Rapela CW, Pankhurst RJ, Baldo EG, Galindo C, Fanning CM, Dahlquist JA, Saavedra J (2012) A history of Proterozoic Terranes in Southern South America: from Rodinia to Gondwana. Geosci Front 2:137–145

Cawood PA, Hawkesworth CJ, Dhuime B (2012) Detrital zircon record and tectonic setting. Geology 40(10):875–878. https://doi.org/10.1130/G32945.1

Chernicoff CJ, Zappettini EO (2004) Geophysical evidence for terrane boundaries in South Central Argentina. Gondwana Res 7(4):1105–1116

Chernicoff CJ, Santos JOS, Zappettini EO, McNaughton NJ (2007) Early Paleozoic schists in the Green Quarry (35° 0′S–65° 28′O), Southern San Luis: U–Pb SHRIMP ages and geodynamic implications. Rev Asoc Geol Arg 62:154–158

Chernicoff CJ, Santos JOS, Zappettini EO, McNaughton NJ (2008) U–Pb SHRIMP dating of the Famatinian (Lower Paleozoic) metamorphism in La Pampa province, Argentina. In: Digital Proceedings of the 5th South American symposium on isotope geology, San Carlos de Bariloche, Apr 2008

Chernicoff CJ, Zappettini EO, Villar LM, Chemale F, Hernández L (2009) The belt of metagabbros of La Pampa: lower paleozoic back-arc magmatism in south-central Argentina. J S Am Earth Sci 28:383–397

Chernicoff CJ, Zappettini EO, Santos JOS, Allchurch S, McNaughton NJ (2010) The southern segment of the Famatinian magmatic arc, La Pampa province, Argentina. Gondwana Res 17:662–675

Chernicoff CJ, Zappettini EO, Santos JOS, Godeas M, Belousova E, McNaughton NJ (2012) Identification and isotopic studies early Cambrian magmatism (El Carancho Igneous Complex) at the boundary between Pampia terrane and the Río de la Plata craton, La Pampa province, Argentina. Gondwana Res 21:378–393

Chew DM, Schaltegger U, Kosler J, Whitehouse MJ, Gutjahr M, Spikings RA, Miskovic A (2007) U–Pb geochronologic evidence for the evolution of the Gondwanan margin of the north–central Andes. GSA Bull 119:697–711

Chincarini AD, Martino RD, Guereschi AB (1998) Origen alóctono del gabro del cerro San Lorenzo, Sierra de Comechingones. Córdoba. Rev Asoc Geol Arg 53(4):435–444

Collo G, Astini RA (2008) La Formación Achavil: una nueva unidad de bajo grado metamórfico en la evolución cámbrica superior del Famatina. Rev Asoc Geol Arg 63(3):344–362

Collo G, Astini RA, Cawood PA, Buchan C, Pimentel M (2009) U–Pb detrital zircon ages and Sm–Nd isotopic features in low-grade metasedimentary rocks of the Famatina belt: implications for late neoproterozoic-early paleozoic evolution of the proto-Andean margin of Gondwana. J Geol Soc London 166:303–319

Dahlquist JA, Galindo C (2004) Geoquímica isotópica de los granitoides de La Sierra de Chepes: un modelo geotectónico y termal, implicancias para el orógeno famatiniano. Rev Asoc Geol Arg 59 (1):57–69

Dahlquist JA, Pankhurst RJ, Rapela CW, Galindo C, Alasino P, Fanning CM, Saavedra J, Baldo E (2008) New SHRIMP U–Pb data from the Famatina complex: constraining early-mid ordovician Famatinian magmatism in the Sierras Pampeanas, Argentina. Geol Acta 6(4):319–333

Dahlquist JA, Colombo F, Murra JA, Locati F, Alasino PH, Baldo EG, Verdecchia SO (2010) El Stock álcali-feldespático El Pilón (Sierra Brava, La Rioja): un ejemplo de magmatismo granítico turmalinífero. Rev Asoc Geol Arg 67(3):369–382

Dahlquist JA, Rapela CW, Pankhurst RJ, Fanning CM, Vervoort JD, Hart JDG, Baldo EG, Murra JA, Alasino PH, Colombo F (2012) Age and magmatic evolution of the Famatinian granitic rocks of Sierra de Ancasti, Sierras Pampeanas, NW Argentina. J S Am Earth Sci 34:10–25

Dahlquist JA, Pankhurst RJ, Rapela CW, Basei MAS, Fanning CM, Alasino PH,Saavedra J, Baldo EG, Murra JA, Neto MCC (2015). The Capilla del Monte pluton, Sierras de Córdoba, Argentina: the easternmost Early Carboniferous magmatism in the pre-Andean SW Gondwana margin. Int J Earth Sci. doi:https://doi.org/10.1007/s00531-015-1249-0

Dahlquist JA, Verdecchia SO, Baldo EG, Basei MAS, Alasino PH, Urán GA, Rapela CW, Neto MCC, Zandomeni PS (2016) Early Cambrian U–Pb zircon age and Hf-isotope data from the Guasayán pluton, Sierras Pampeanas, Argentina: implications for the northwestern boundary of the Pampean arc. Andean Geol 43:137–150

Dalla Salda LH, López de Luchi MG, Cingolani C, Varela R (1998) Laurentia–Gondwana collision: the origin of the Famatinian–Appalachians Orogenic Belt. In: Pankhurst RJ, Rapela CW (eds) The Proto-Andean Margin of Gondwana, Geological Society of London, London, vol 142, pp 219–234, Special Publications

Delpino SH, Bjerg EA, Ferracutti GR, Mogessie A (2007) Counter-clockwise tectonometamorphic evolution of the Pringles Metamorphic Complex, Sierras Pampeanas of San Luis (Argentina). J S Am Earth Sci 23:147–175

Drobe M, López de Luchi MG, Steenken A, Frei R, Naumann R, Wemmer K, Siegesmund S (2009) Provenance of the Late Proterozoic to Early Cambrian metaclastic sediments of the Sierra de San Luis (Eastern Sierras Pampeanas) and Cordillera oriental, Argentina. J S Am Earth Sci 28:239–262

Drobe M, López de Luchi MG, Steenken A, Wemmer K, Naumann R, Frei R, Siegesmund S (2011) Geodynamic evolution of the Eastern Sierras Pampeanas (central Argentina) based on geochemical, Sm–Nd, Pb–Pb and SHRIMP data. Int J Earth Sci 100:631–658

Ducea MN, Otamendi JE, Bergantz G, Stair K, Valencia V, Gehrels G (2010) Timing constraints on building an intermediate plutonic arc crustal section: U–Pb zircon geochronology of the Sierra Valle Fértil, Famatinian arc, Argentina. Tectonics 29:TC4002. doi:https://doi.org/10.1029/2009TC002615

Ducea MN, Bergantz GW, Crowley JL, Otamendi JE (2017) Ultrafast magmatic buildup and diversification to produce continental crust during subduction. Geology. https://doi.org/10.1130/G38726.1

Escayola MP, Ramé GA, Kraemer PE (1996) Caracterización y significado geotectónico de las fajas ultramáficas de las Sierras Pampeanas de Córdoba. XIII Congreso Geológico Argentino y III Congreso de Exploración de Hidrocarburos, Buenos Aires, October 1996. Actas 3:421–438

Escayola MP, Pimentel MM, Armstrong R (2007) A Neoproterozoic Back-Arc Basin: SHRIMP U–Pb and Sm–Nd isotopic evidence from the Eastern Pampean Ranges, Argentina. Geology 35(6):495–498. https://doi.org/10.1130/G23549A.1

Escayola MP, van Staal C, Davis W (2011) The age and tectonic setting of the Puncoviscana Formation in NW Argentina: an accretionary complex related to Early Cambrian closure of the Puncoviscana Ocean and accretion of the Arequipa-Antofalla block. J S Am Earth Sci 32:437–458

Fagiano M (2007) Geología y petrología del basamento cristalino de Las Albahacas, Sur de la Sierra de Comechingones,Córdoba. Unpublished doctoral thesis, Universidad Nacional de Río Cuarto, p 375

Fagiano M, Otamendi JE, Nullo F (2008) Los orógenos Pampeano y Famatiniano en la evolución de los complejos Monte Guazú y Achiras, Sierra de Comechingones, Córdoba. In: Proceedings of the 17th congress geology Argent, Jujuy, Oct 2008, Actas, pp 1008–1009

Fantini R, Gromet P, Simpson C, Northrup CJ (1998) Timing of high temperature metamorphism in the Sierras Pampeanas of Córdoba, Argentina: implications for Laurentia-Gondwana Interactions. X Congr Latinoam Geol and VI Congr Nacional Geología Econ, Buenos Aires, November 1998. Actas 2:388–392

Favetto A, Pomposiello C, López de Luchi MG, Booker J (2008) 2D Magnetotelluric interpretation of the crust electrical resistivity across the Pampean Terrane- Rio de la Plata Suture in Central Argentina. Tectonophysics 459(1–4):54–65

Finney SC (2007) The parautochthonous Gondwanan origin of the Cuyania (greater Precordillera) terrane of Argentina: a reevaluation of evidence used to support an allochthonous Laurentian origin. Geol Acta 5:127–158

Frimmel HE, Fölling P (2004) Late Vendian Closure of the Adamastor Ocean: timing of tectonic inversion and syn orogenic sedimentation in the Gariep Basin. Gondwana Res 7:685–699

Gaido MF (2003) Informe petrográfico de la hoja geológica Recreo 2966-IV, escala 1:250.000. Servicio Geológico Minero Argentino, Delegación Córdoba, 12 p

Gehrels GE (2014) Detrital zircon U Pb geochronology applied to tectonics. Annu Rev Earth Pl Sci 42:127–149

Gehrels GE, Valencia V, Pullen A (2006) Detrital zircon geochronology by Laser-Ablation Multicollector ICPMS at the Arizona LaserChron Center. In: Loszewski T, Huff W (eds) Geochronology: Emerging Opportunities, Paleontology Society Short Course Papers, vol 11, p 10

González PD, Sato AM, Llambías EJ, Petronilho LA (2009) Petrology and geochemistry of the banded iron formation in the Eastern Sierras Pampeanas of San Luis (Argentina): Implications for the evolution of the Nogolí Metamorphic Complex. J S Am Earth Sci 28(2):89–112

Gordillo CA (1979) Observaciones sobre la petrología de las rocas cordieríticas de la Sierra de Córdoba: Córdoba, Argentina. Boletín de la Academia Nacional de Ciencia 53:3–44

Gromet LP, Simpson C (1999) Age of the Paso del Carmen pluton and implications for the duration of the Pampean Orogeny, Sierras de Córdoba, Argentina. In: Proceeding of the 14th Congress Geology Argent, Salta, Actas, vol 1, pp 149–151

Gromet LP, Simpson C, Miro R, Whitmeyer SJ (2001) Apparent truncation and juxtaposition of Cambrian and Ordovician arc-accretionary complexes, Eastern Sierras Pampeanas, Argentina. Geological Society America Annual Meeting, Boston, vol 33, pp A–155

Gromet LP, Otamendi JE, Miró RC, Demichelis AH, Schwartz JJ, Tibaldi AM (2005) The Pampean orogeny: ridge subduction or continental collision? Gondwana 12 Conference. Academia Nacional de Ciencias, Mendoza, p 185

Grosse P, Söllner F, Báez MA, Toselli AJ, Rossi JN, de la Rosa D (2008) Lower Carboniferous post-orogenic granites in central-eastern Sierra de Velasco, Sierras Pampeanas, Argentina: U–Pb monazite geochronology, geochemistry and Sr–Nd isotopes. Inter J Earth Sci 98(5):1001–1025

Grosse P, Bellos L, de los Hoyos CR, Larrovere MA, Rossi JN, Roselli AJ (2011) Across-arc variation of the Famatinian magmatic arc (NW Argentina) exemplified by I, S and transitional I/S-type Early Ordovician granitoids of the Sierra de Velasco. J S Am Earth Sci 32(1):110–126

Guereschi AB, Baldo E (1993) Petrología y geoquímica de las rocas metamórficas del sector centro-oriental de la Sierra de Comechingones, Córdoba. In: Proceedings of the 7th Congress Geol Argent y II Congr Explor Hidrocarb, Mendoza, Actas 4:319–325

Guereschi A, Martino RD (2002) Geotermobarometría de migmatitas y gneises del sector centro-oriental de la Sierra de Comechingones, Córdoba. Rev Asoc Geol Argent 57(4):365–375

Guereschi A, Martino RD (2003) Trayectoria textural de las metamorfitas del sector centro-oriental de la Sierra de Comechingones, Córdoba. Rev Asoc Geol Argent 58(1):61–77

Guereschi A, Martino RD (2008) Field and textural evidence of two migmatization events in the Sierras de Córdoba, Argentina. Gondwana Res 13:176–188

Guereschi AB, Martino RD (2014) Las migmatitas de las Sierras de Córdoba. In: Martino, R, Guereschi, AB (eds) Geología y Recursos Naturales de la provincia de Córdoba, Asociación Geológica Argentina, XIX Congreso Geologico Argentino, Córdoba, Relatorio, vol 1, pp 67–94

Hauzenberger C, Mogessie A, Hoinkes G, Felfernig A, Bjerg E, Kostadinoff J, Delpino S, Dimieri L (2001) Metamorphic evolution of the Sierras de San Luis, Argentina: Granulite facies metamorphism related to mafic intrusions. Min Petrol 71(1–2):95–126

Iannizzotto N, Rapela CW, Baldo EG, Galindo C, Fanning CM, Pankhurst RJ (2013) The Sierra Norte-Ambargasta batholith: Late Ediacarian-Early Cambrian magmatism associated with Pampean transpressional tectonics. J S Am Earth Sci 42:127–143

Kay S, Orrell S, Abbruzzi JM (1996) Zircon and whole rock Nd–Pb isotopic evidence for a Grenville Age and a Laurentian origin for the basement of the Precordillera in Argentina. J Geol 104:637–648

Knüver M (1983) Dataciones radimétricas de rocas plutónicas y metamórficas. In: Aceñolaza FG, Miller H, Toselli J (eds) Geología de la sierra de Ancasti, Münstersche Forschungen zur Geologie und Pälaontologie. Münster, vol 59. Heft, pp 201–218

Kraemer PE, Escayola MP, Martino RD (1995) Hipótesis sobre la evolución tectónica neoproterozoica de las Sierras Pampeanas de Córdoba (30º 40′-32º 40′) Argentina. Rev Asoc Geol Argentina 50 (1–4):47–59

Krol MA, Simpson C (1999) Thermal history of the eastern Sierras Pampeanas accretionary prism rocks, constraints from $^{40}Ar/^{39}Ar$ mica data. GSA Abstr Prog 31(7):114–115

Larrovere MA, Rossi J, Toselli A, de los Hoyos CR, Basei MAS (2009) Nuevas edades U–Pb en monacitas y proveniencia cortical del Complejo Metamórfico-ígneo El Portezuelo, Sierras Pampeanas, Argentina. Boletin de Resumos Expandidos Simposio 45 Anos de Geocronologia no Brasil. Universidade de Sao Paulo. Resumen, p 42

Larrovere MA, de los Hoyo CR, Toselli AJ, Rossi JN, Basei MAS, Belmar ME (2011) High T/P evolution and metamorphic ages of the migmatitic basement of northern Sierras Pampeanas, Argentina: characterization of a mid-crustal segment of the Famatinian belt. J S Am Earth Sci 31(2–3):279–297

Larrovere MA, de los Hoyos CR, Grosse P (2012) Los complejos metamórficos del retroarco famatiniano (noroeste de Argentina): caracterización geoquímica e isotó-pica de sus protolitos e implicancias tectónicas, RevMex Geol 29(3):676–695

Laskowski AK, De Celles PG, Gehrels G (2013) Detrital zircon geochronology of Cordilleran retroarc foreland basin strata, western North America. Tectonics 32:1–22

Lira R, Millone HA, Kirschbaum AM, Moreno RS (1997) Calc-alkaline arc granitoid activity in the Sierra Norte Ambargasta ranges, Central Argentina. J S Am Earth Sci 10:157–177

Llambías EJ, Sato AM, Ortiz Suárez, A, Prozzi C (1998) The granitoids of the Sierra de San Luis. In: Pankhurst RJ, Rapela CW (eds.) The Proto-Andean margin of Gondwana, Geological Society of London, London, vol 142, pp 325–341, Special Publications

Llambías EJ, Gregori D, Basei MAS, Varela R, Prozzi C (2003) Ignimbritas riolíticas neoproterozoicas en la Sierra Norte de Córdoba: ¿evidencia de un arco magmático temprano en el ciclo Pampeano? Rev Asoc Geol Arg 58(4):572–582

Löbens S, Bense F, Wemmer K, Dunkl I, Costa CH, Layer P, Siegesmund S (2011) Exhumation and uplift of the Sierras Pampeanas: preliminary implications from K-Ar fault gauge dating and low-T thermochronology in the Sierra de Comechingones (Argentina). Int J Earth Sci 100:671–694. https://doi.org/10.1007/s00531-010-0608-0

Löbens S, Bense F, Dunkl I, Wemmer K, Kley J, Siegesmund S (2013a) Thermochronological constrains of the exhumation and uplift of the Sierra de Pie de Palo, NW Argentina constrained by methods. J S Am Earth Sci 48:209–219

Löbens S, Sobel ER, Bense F, Wemmer K, Dunkl I, Siegesmund S (2013b) Refined exhumation history of the northern Sierras Pampeanas, Argentina. Tectonics 32:453–472. https://doi.org/10.1002/tect.20038

Löbens S, Oriolo S, Benowitz J, Wemmer K, Layer P, Siegesmund S (2016) Late Paleozoic deformation and exhumation in the Sierras Pampeanas (Argentina): first $^{40}Ar/^{39}Ar$-feldspar dating constraints. Int. J. Earth Sci. doi:https://doi.org/10.1007/s00531-016-1403-3

Lopez de Luchi MG (1996) Enclaves en un Batolito Postectónico: petrología de los enclaves microgranulares del Batolito de Renca. Rev Asoc Geol Argentina 51(2):131–146

López de Luchi MG, Siegesmund S, Wemmer K, Steenken A, Naumann R (2007) Geochemical constraints on the petrogenesis of the Paleozoic granitoids of the Sierra de San Luis, Sierras Pampeanas, Argentina. J S Am Earth Sci 24:138–166. https://doi.org/10.1016/j.jsames.2007.05.001

López de Luchi MG, Siegesmund S, Wemmer K, Nolte N (2017) Petrogenesis of the postcollisional Middle Devonian monzonitic to granitic magmatism of the Sierra de San Luis, Argentina. Lithosdoi. doi:https://doi.org/10.1016/j.lithos.2017.05.018

Lyons P, Skirrow RG, Stuart-Smith PG (1997) Report on geology and metallogeny of the Sierras Septentrionales de Córdoba, Province of Córdoba: Geoscientific mapping of the Sierras Pampeanas: Canberra ACT Argentine–Australian Cooperative Project, Australian Geological Survey Organization, scale 1:250,000, sheet 1

Martínez Dopico CI, López de Luchi MG, Rapalini AE, Kleinhanns IC (2011) Distinguishing crustal segments in the North Patagonian Massif, Patagonia: an integrated perspective based on Nd systematics. J S Am Earth Sci 31(2–3):324–341

Martino RD (2003) Las fajas de deformación dúctil de las Sierras Pampeanas de Córdoba: una reseña general. Rev Asoc Geol Argent 58:549–571

Martino RD, Guereschi AB (2005) Estructuras primarias, secundarias y evolución estructural de las corneanas de La Clemira, Sierra de Ambargasta, Santiago del Estero. Rev Asoc Geol Argent 60 (2):327–335

Martino RD, Munn B, Kraemer P, Escayola M, Guereschi AB (1994) Thermobarometry at 32º 00′S in the Pampean Ranges of Córdoba, Argentina. GSA Abstracts with Programs, pp A–226. Seattle

Miller H, Söllner F (2005) The Famatinian complex (NW Argentina): back-docking of an island arc or terrane accretion? Early Palaeozoic geodynamics at the western Gondwana margin. In: Vaughan APM, Leat PT, Pankhurst RJ (eds) Terrane Processes at the Margins of Gondwana. Geological Society of London, London, vol 246, pp 241–256, Special Publications

Mutti D (1992) Las rocas ultrabásicas-básicas de la provincia de Córdoba: interpretaciones geoquímicas e implicancias geotectónicas. I Reunión de Mineralogía y Metalogénesis and I Jornada de Mineralogía, Petrografía y Metalogénesis de Rocas Ultrabásicas. Publicación del Instituto de Recursos Minerales, La Plata 2:411–432

Omarini RH, Sureda RJ, Toselli A, Rossi J (1999) Ciclo Pampeano. Magmatismo. In: González Bonorino G, Omarini RH, Viramonte J (eds) Geología del Noroeste Argentino. Salta, Relatorio XIV Congreso Geológico Argentino, pp 29–40

Oriolo S, Oyhantçabal P, Wemmer K, Siegesmund S (2017) Contemporaneousassembly of Western Gondwana and final Rodinia break-up: implications for the supercontinent cycle. Geosci Frontieres. https://doi.org/10.1016/j.gsf.2017.01.009

Otamendi JE, Fagiano MR, Nullo FE (2000) Geología y evolución metamórfica del Complejo Monte Guazú, sur de la sierra de Comechingones, provincia de Córdoba. Rev Asoc Geol Argent 55 (3):265–279

Otamendi JE, Castellarini PA, Fagiano MR, Demichelis AH, Tibaldi AM (2004) Cambrian to Devonian geologic evolution of the Sierra de Comechingones, Eastern Sierras Pampeanas, Argentina: evidence for the development and exhumation of continental crust on the Proto-Pacific Margin of Gondwana. Gondwana Res 7:1143–1155

Otamendi JE, Ribaldi AM, Demichelis AH, Rabbia OM (2005) Metamorphic evolution of the Rio Santa Rosa granulites, north Sierra de Comechingones, Argentina. J S Am Earth Sci 18:163–181. https://doi.org/10.1016/j.jsames.2004.10.006

Otamendi JE, Demichelis A, Tibaldi A, de la Rosa J (2006) Genesis of aluminous and intermediate granulites: a study case in the eastern Sierras Pampeanas, Argentina. Lithos 89:66–88

Oyhantçabal P, Siegesmund S, Wemmer K (2010) The Río de la Plata Craton: a review of units, boundaries, ages and isotopic signature. Int J Earth Sci 100(2–3):201–220. https://doi.org/10.1007/s00531-010-0616-0

Oyhantçabal P, Cingolani CA, Wemmer K, Siegesmund S (this volume) The Río de la Plata Craton of Argentina and Uruguay

Pankhurst RJ, Rapela CW (1998) The Proto Andean margin of Gondwana. Geological Society of London, London, p 383, Special Publications

Pankhurst RJ, Rapela CW, Saavedra J, Baldo E, Dahlquist J, Pascua I, Fanning CM (1998) The Famatinian magmatic arc in the central Sierras Pampeanas: an early to Mid-Ordovician continental arc on the Gondwana margin. In: Pankhurst RJ, Rapela CW (eds) The Proto-Andean Margin of Gondwana, Geological Society of London, London, vol 142, pp 343–367, Special Publications

Pankhurst RJ, Rapela CW, Fanning CM (2000) Age and origin of coeval TTG, I- and S-type granites in the Famatinian belt of NW Argentina. Trans Royal Soc Edinburgh Earth Sci 91(1/2):151–168

Patchett PJ (1992) Isotopic studies of proterozoic crustal growth and evolution. Develop Precambrian Geol 10(13):481–508

Peri VG, Pomposiello C, Favetto A, Barcelona H, Rossello EA (2013) Magnetotelluric evidence of the tectonic boundary between the Río de La Plata Craton and the Pampean terrane (Chaco-Pampean Plain, Argentina): the extension of the Transbrasiliano Lineament. Tectonophysics 608:685–699

Peri VG, Barcelona H, Pomposiello C, Favetto A (2015) Magnetotelluric characterization through the Ambargasta-Sumampa range: the connection between the northern and southern trace of the Río de La Plata Craton-Pampean Terrane tectonic boundary. J S Am Earth Sci 59:1–12. https://doi.org/10.1016/j.jsames.2015.01.003

Piñán-Llamas A, Simpson C (2006) Deformation of Gondwana margin turbidites during the Pampean orogeny, north-central Argentina. Geol Soc Am Bull 118:1270–1279

Pinotti LP, Coniglio JE, Esparza AM, D'Eramo FJ, Llambias EJ (2002) Nearly circular plutons emplaced at shallow crustal levels, Cerro Aspero batholith, Sierras Pampeanas de Córdoba, Argentina. J S Am Earth Sci 15:251–265

Prozzi CR, Ramos G (1988) La Formación San Luis. In: Primeras Jornadas de trabajo de Sierras Pampeanas, San Luis Abstracts, p 1

Quenardelle S, Ramos VA (1999) Ordovician western Sierras Pampeanas magmatic belt: record of Precordillera accretion in Argentina. In: Ramos VA, Keppie JD (eds) Laurentia Gondwana Connections before Pangea. Geol Soc Am Special Paper, vol 336, Boulder, Colorado, pp 63–86

Ramos VA (1988) Late Proterozoic-Early Paleozoic of S America: a collisional story. Episodes 11:168–174

Ramos VA, Jordan TE, Allmendinger RW, Mpodozis C, Kay SM, Cortés JM, Palma M (1986) Paleozoic Terranes of the Central Argentine Chilean Andes. Tectonics 5:855–880. https://doi.org/10.1029/TC005i006p00855

Ramos VA, Dallmeyer RD, Vujovich G (1998) Time constraints on the early paleozoic docking of the Precordillera, central Argentina. In: Pankhurst RJ, Rapela CW (eds) The Proto-Andean margin of Gondwana, Geological Society of London, London, vol 142, pp 143–158, Special Publications

Ramos VA, Escayola M, Mutti DI, Vujovich GI (2000) Proterozoic–early Paleozoic ophiolites of the Andean basement of southern S America. GSA Spec Pap 349:331–349

Ramos VA, Cristallini EO, Pérez DJ (2002) The Pampean flat-slab of the Central Andes. J S Am Earth Sci 15:59–78

Ramos VA, Vujovich G, Martino RD, Otamendi J (2010) Pampia: a large cratonic block missing in the Rodinia supercontinent. J Geodyn 50:243–255

Ramos VA, Chemale F Jr, Naipauer M, Pazos P (2014) A Provenance study of the paleozoic Ventania system (Argentina): Transient complex sources from western and eastern Gondwana. Gondwana Res 26:719–740

Ramos VA, Escayola M, Leal P, Pimentel MM, Santos JOS (2015) The late stages of the Pampean Orogeny, Cordoba (Argentina): evidence of postcollisional early Cambrian slab break-off magmatism. J S Am Earth Sci 64:351–364

Rapela CW, Toselli A, Heaman L, Saavedra J (1990) Granite plutonism of the Sierras Pampeanas: an inner cordilleran Paleozoic arc in the southern Andes. In: Kay SM, Rapela CW (eds) Plutonism from Antarctica to Alaska, vol 241. Geological Society America, pp 77–90, Special Paper

Rapela CW, Pankhurst RJ, Bonalumi AA (1991) Edad y geoquímica del Pórfido Granítico de Oncán, Sierra Norte de Córdoba, Sierras Pampeanas, Argentina. In: Proceedings of the 6th Congress geology Chil, Viña del Mar, Actas, vol 1, pp 19–22

Rapela CW, Pankhurst RJ, Casquet C, Baldo E, Saavedra J, Galindo C (1998a) Early evolution of the proto-Andean margin of South America. Geology 26:707–710

Rapela CW, Pankhurst RJ, Casquet C, Baldo EG, Saavedra J, Galindo C, Fanning CM (1998b) The Pampean Orogeny of the southern proto-Andes: Cambrian continental collision in the sierras de Córdoba. In: Pankhurst R, Rapela CW (eds) The Proto-Andean Margin of Gondwana, Geological Society of London, London, vol 142, pp 181–217, Special Publications

Rapela CW, Pankhurst RJ, Dahlquist J, Fanning CM (1999) U-Pb SHRIMP ages of Famatinian Granites: new constraints on the timing, origin and tectonic setting of I-and S-type magmas in an ensialic arc. II South American Symposium on Isot Geol Actas 264–267

Rapela CW, Pankhurst RJ, Casquet C, Baldo EG, Galindo C, Fanning CM, Saavedra J (2001) Ordovician metamorphism in the Sierras Pampeanas: new U–Pb SHRIMP ages in central-east Valle Fértil and the Velasco Batholith. III S Am Symp Isotope Geol 1:616–619

Rapela CW, Fanning CM, Baldo EG, Dahlquist J, Pankhurst RJ, Murra J (2005) Coeval S- and I-type granites in the Sierra de Ancasti, Eastern Sierras Pampeanas, Argentina. In: Pankhurst RJ, Veiga G (eds) Gondwana 12: Geol Biol Herit Gondwana, Abstract, p 307

Rapela CW, Pankhurst RJ, Casquet C, Fanning CM, Baldo EG, González-Casado JM, Galindo C, Dahlquist J (2007) The Río de la Plata craton and the assembly of SW Gondwana. Earth Sci Rev 83:49–82

Rapela CW, Baldo EG, Pankhurst RJ, Fanning CM (2008) The Devonian Achala Batholith of the Sierras Pampeanas: F-rich aluminous A-type granites. abstracts 6th South American Symposium on Isotope. Geology 1:104

Rapela CW, Pankhurst RJ, Casquet C, Baldo EG, Galindo C, Fanning CM, Dahlquist JA (2010) The Western Sierras Pampeanas: protracted Grenville-age history (1330–1030 Ma) of intra-oceanic arcs, subduction-accretion at continental edge and intraplate magmatism. J S Am Earth Sci 29:105–127

Rapela CW, Fanning CM, Casquet C, Pankhurst RJ, Spalletti L, Poiré D, Baldo EG (2011) The Rio de la Plata craton and the adjoining Pan-African/Brasiliano terranes: their origins and incorporation into south-west Gondwana. Gondwana Res 20:673–690

Rapela CW, Verdecchia SO, Casquet C, Pankhurst RJ, Baldo EG, Galindo C, Murra JA, Dahlquist JA, Fanning CM (2016)

Identifying Laurentian and SW Gondwana sources in the Neoproterozoic to Early Paleozoic metasedimentary rocks of the Sierras Pampeanas: Paleogeographic and tectonic implications. Gondwana Res 32:193–212

Reissinger M (1983) Geología de la Sierra de Ancasti. Evolución geoquímica de las rocas plutónicas. Munster Forsch Geol Palaont 59:101–112

Rossi JN, Toselli AJ, Báez MA (2005) Evolución termobárica del ortogneis peraluminoso del noroeste de la sierra de Velasco, La Rioja. Rev Asoc Geol Argent 60(2):278–289

Rubiolo D, Cisterna CE, Villeneuve M (2002) Edad U/Pb del granito de Las Angosturas en la sierra de Narváez (Sistema de Famatina, provincia de Catamarca). XV Congr Geol Argent Actas 1:359–362

Sato AM, González PD, Llambías EJ (2003) Evolution of the Famatinian orogen in the Sierra de San Luis: arc magmatism, deformation, and low to high-grade metamorphism. Rev Asoc Geol Argent 58:487–504

Schwartz JJ, Gromet PL (2004) Provenance of a late Proterozoic-early Cambrian basin, Sierras de Córdoba, Argentina. Precambrian Res 129:1–21

Schwartz JJ, Gromet LP, Miro R (2008) Timing and duration of the calc-alkaline arc of the Pampean orogeny: implications for the late Neoproterozoic to Cambrian Evolution of Western Gondwana. J Geol 116:39–61

Siegesmund S, Steenken A, López de Luchi MG, Wemmer K, Hoffmann A, Mosch S (2004) The Las Chacras-Potrerillos batholith (Pampean Ranges, Argentina): structural evidence, emplacement and timing of the intrusion. Int J Earth Sci 93:23–43

Siegesmund S, Steenken A, Martino RD, Wemmer K, López de Luchi MG, Frei R, Presnyakov S, Guereschi A (2010) Time constraints on the tectonic evolution of the Eastern Sierras Pampeanas (Central Argentina). Int J Earth Sci 99:1199–1226

Sims JP, Skirrow RG, Stuart-Smith PG, Lyons P (1997) Informe geológico y metalogenético de las Sierras de San Luis y Comechingones (provincias de San Luis y Córdoba), 1:250,000. Anales 28, IGRM, SEGEMAR, Buenos Aires, pp 1–148

Sims JP, Ireland TR, Camacho A, Lyons P, Pieters PE, Skirrow RG, Stuart-Smith PG, Miro R (1998) U–Pb, Th–Pb and Ar–Ar geochronology from the southern Sierras Pampeanas, Argentina: implications for the Palaeozoic tectonic evolution of the western Gondwana margin. In: Pankhurst R, Rapela CW (eds) The Proto-Andean Margin of Gondwana, Geological Society of London, London, vol 142, 259–281, Special Publications

Steenken A, López de Luchi MG, Siegesmund S, Wemmer K, Pawlig S (2004) Crustal provenance and cooling of basement complexes of the Sierra de San Luis: An insight into the tectonic history of the proto-Andean margin of Gondwana. Gondwana Res 7(4):1171–1195

Steenken A, López de Luchi MG, Siegesmund S, Wemmer K (2005) The thermal impact of the accommodation of mafic melts within the central basement complex of the Sierra de San Luis: constraints from numeric modeling. In: XVI Congress Geological Argent, La Plata. Actas vol 1, pp 889–896

Steenken A, Siegesmund S, López de Luchi MG, Frei R, Wemmer K (2006) Neoproterozoic to early Palaeozoic events in the Sierra de San Luis: implications for the Famatinian geodynamics in the Eastern Sierras Pampeanas (Argentina). J Geol Soc London 163:965–982

Steenken A, Siegesmund S, Wemmer K, López de Luchi MG (2008) Time constraints on the Famatinian and Achalian structural evolution of the basement of the Sierra de San Luis (Eastern Sierras Pampeanas, Argentina). J S Am Earth Sci 25(3):336–358

Steenken A, Wemmer K, Martino RD, López de Luchi MG, Guereschi AB, Siegesmund S (2010) Post-Pampean cooling and the exhumation of the Sierras Pampeanas in the West of Córdoba (Central Argentina). Neues Jahrb Geol P-A 256:235–255

Steenken A, López de Luchi MG, Martínez Dopico CI, Drobe M, Wemmer K, Siegesmund S (2011) The Neoproterozoic-early Paleozoic metamorphic and magmatic evolution of the Eastern Sierras Pampeanas: an overview. Int J Earth Sci 10:465–488

Stuart-Smith PG, Skirrow RG (1997) 1:100000 scale geologicaland metallogenic maps sheet 3366–24. Provinces of San Luis and C′ 0rdoba. Mapeo Geocientífico de las Sierras Pampeanas, Servicio Geológico Minera Argentino, pp 43, Buenos Aires

Stuart-Smith PG, Camacho A, Sims JP, Skirrow RG, Lyons P, Pieters PE, Black LP (1999) Uranium-lead dating of felsic magmatic cycles in the southern Sierras Pampeanas, Argentina: Implications for the tectonic development of the proto-Andean Gondwana margin. In: Ramos VA, Keppie JD (eds) Laurentia-Gondwana Conections before Pangea. Geol Soc America, Boulder, Colorado vol 336, pp 87–114, Special Paper

Teixeira W, Geraldes MC, Matos R, Ruiz AS, Saes G, Vargas-Mattos G (2010) A review of the tectonic evolution of the Sunsas belt SW Amazonian Craton. J South Am Earth Sci 29:47–60

Thomas W, Astini R (2003) Ordovician accretion of the Argentine Precordillera Terrane to Gondwana: a review. J S Am Earth Sci 16:67–79

Tibaldi AM, Otamendi JE, Gromet LP, Demichelis AH (2008) Suya Taco and Sol de mayo mafic complexes from Eastern Sierras Pampeanas, Argentina: evidence for the emplacement of primitive OIB-like magmas into deep crustal levels at a late stage of the Pampean orogeny. J S Am Earth Sci 26:172–187

Tohver E, Cawood PA, Rossello EA, Jourdan F (2012) Closure of the Clymene Ocean and formation of West Gondwana in the Cambrian: evidence from the Sierras Australes of the southernmost Rio de la Plata craton, Argentina. Gondwana Res 21:394–405

Toselli AJ, Sial AN, Saavedra J, Rossi de Toselli JN, Pinto Ferreira V (1996) Geochemistry and genesis of the S type, cordierite andalusite- bearing Capillitas Batholith, Argentina. Int Geol Rev 38(11):1040–1053

Toselli JA, Rossi JN, Miller H, Báez M, Grosse P, López JP, Bellos L (2005) Las rocas graníticas y metamórficas de la sierra de Velasco. In: Aceñolaza FG, Aceñolaza GF, Hünicken M. Toselli AJ (eds) Simposio Bodenbender, Instituto Superior de Correlación Geológica, Serie Correlación Geológica vol 19, pp 211–220

Trindade R, Dagrellafilho M, Epof I, Brito Neves BB de (2006) Paleomagnetism of early Cambrian Itabaiana mafic dikes (NE Brazil) and the final assembly of Gondwana. Earth Planet Sc Lett 244:361–377

Verdecchia SO, Baldo E, Benedetto L, Borghi R (2007) The first shelly faunas from metamorphic rocks of the Sierras Pampeanas (La Cébila Formation), Sierra de Ambato, Argentina): age and paleogeographic implications. Ameghiniana 44:493–498

Verdecchia SO, Casquet C, Baldo EG, Pankhurst RJ, Rapela CW, Fanning M, Galindo C (2011) Mid- to Late Cambrian docking of the Rio de la Plata craton to southwestern Gondwana: age constraints from U–Pb SHRIMP detrital zircon ages from Sierras de Ambato and Velasco (Sierras Pampeanas, Argentina). J Geol Soc London 168:1061–1071

Vujovich GI, van Staal CR, Davis W (2004) Age constraints on the tectonic evolution and provenance of the Pie de Palo complex, Cuyania Composite Terrane, and the Famatinian Orogeny in the Sierra de Pie de Palo, San Juan, Argentina. Gondwana Res 7:1041–1056

Wemmer K, Steenken A, Müller S, López de Luchi MG, Siegesmund S (2011) The tectonic significance of K/Ar Illite fine fraction from the San Luis Formation (Eastern Sierras Pampeanas, Argentina). Int J Earth Sci 100:659–669

Willigers BJA, Krogstad EJ, Wijbrans JR (2001) Comparison of thermochronometers in a slowly cooled granulite terrain: Nagssugtuqidian Orogen, West Greenland. J Petrol 42(9):1729–1749. https://doi.org/10.1093/petrology/42.9.1729

Willner A (1983) Evolución metamórfica. In: Aceñolaza FG, Miller H, Toselli A (eds) Geología de la Sierra de Ancasti. Münst Forsch Geol Paläont vol 59, pp 189–200

Zappetini EO, Chernicoff CJ, Santos JOS, McNaughton NJ (2010) Los es-quistos neoproterozoicos de Santa Helena, Provincia de La Pampa, Argentina: eda-des U-Pb SHRIMP, composición isotópica de hafnio e implicancias geodinámicas. Rev Asoc Geol Argent 66 (1–2):21–37

Zimmermann U (2005) Provenance studies of very low to low-grade metasedimentary rocks of the Puncoviscana complex, northwest Argentina. In: Vaughan APM, Leat PT, Pankhurst RJ (eds) Terrane processes at the margin of Gondwana, Geological Society of London, London, vol 246, pp 381–416, Special Publications

Part IV
Special Topics

The Iron Formations of Southern Africa

17

Albertus J. B. Smith

Abstract

Iron formations (IFs) are Fe-rich chemical sedimentary rocks that show a unique distribution through Precambrian time, with abundant deposition from approximately 3.8 Ga, reaching a volumetric peak at 2.5 Ga, disappearing at 1.8 Ga and returning at 0.8 to 0.6 Ga. They are important paleoenvironmental proxies, recording possible ancient marine water signatures. IFs also host the largest Fe ore deposits in the world. IFs can be classified based on three criteria: Texture; Mineralogy; and Stratigraphic setting. The geological record of Southern Africa contains examples of all IF types as based on all three classification criteria that also span most of the geological time periods that mark abundant IF deposition. Meso- to Neoarchean greenstone belt-hosted (Algoma-type) IFs occur within the majority of the Kaapvaal and Zimbabwe Cratons' greenstone belts. Some of the world's oldest Superior-type IFs, which occur within marine successions that mark stable shelf depositional settings, occur within the Mesoarchean Witwatersrand and Pongola Supergroups on the Kaapvaal Craton. The volumetric bulk of the IFs in Southern Africa occur in the Neoarchean to Paleoproterozoic Transvaal Supergroup on the Kaapvaal Craton, which contains multiple Superior-type IFs throughout its stratigraphy. Of these, the thickest and best developed IF is the approximately 2.5 Ga Asbesheuwels-Penge IF. Neoproterozoic, Rapitan-type IFs occur in the Gariep Belt of the Northern Cape Province of South Africa and southern Namibia as well as in the Damara and Otavi Belts of northern Namibia. These are associated with glacial diamictites and were deposited during the global Sturtian glaciation. The two major geochemical components in IFs are Fe_2O_3 and SiO_2, with the Superior-type IFs of southern Africa generally having higher Fe_2O_3 and lower SiO_2 contents than Algoma- and Rapitan-type IFs. Some IFs in the Pongola and Transvaal Supergroups are also enriched in MnO. The rare earth element contents of IFs generally indicate that they were precipitated from marine water, with Archean and Paleoproterozoic occurrences showing significant hydrothermal inputs. The stable C isotopes of Fe-rich carbonates in Superior-type IFs are depleted in ^{13}C which suggest that it was sourced from organic C, implying biological activity during IF deposition. The depositional models developed for the Superior-type IFs of Southern Africa take into account lateral mineralogical facies variations in IFs, with Fe-silicate facies more proximal, Fe-carbonate facies intermediate and Fe-oxide facies more distal to the paleo-coastline. The precipitation of Fe was thought to have occurred through the oxidation of dissolved, hydrothermally-derived Fe^{2+} to Fe^{3+} by Fe-oxidizing bacteria, with the preserved mineralogical facies being formed during diagenesis or metamorphism. Although free oxygen is not required for Fe oxidation by photoferrotrophic bacteria, studies on Mn contents, Mo isotopes and the sequence stratigraphy of Fe-enrichment suggest that free oxygen was present during IF deposition in some instances. The Rapitan-type IFs of Southern Africa, due to their association with the Sturtian glaciation, are thought to have been deposited as a by-product of the global-scale glacial activity. Almost complete glacial ice cover would have led to reduced water bodies building up dissolved Fe^{2+}, with melting of the ice sheets causing the oxidation and precipitation of Fe. Enrichment of IF to Fe ore took place by either top-down supergene (ore overlying oxidized IF) or bottom-up hydrothermal (ore underlying oxidized IF) processes that leached SiO_2 and oxidized all Fe-bearing minerals. The ore-forming fluids likely had high Eh and high pH. The largest and

A. J. B. Smith (✉)
DST-NRF Centre of Excellence for Integrated Mineral and Energy Resource Analysis, Department of Geology, University of Johannesburg, Auckland Park, 2006, South Africa
e-mail: bertuss@uj.ac.za

A. J. B. Smith
Paleoproterozoic Mineralization Research Group, Department of Geology, University of Johannesburg, Auckland Park, 2006, South Africa

S. Siegesmund et al. (eds.), *Geology of Southwest Gondwana*, Regional Geology Reviews,
https://doi.org/10.1007/978-3-319-68920-3_17

best known supergene Fe ore deposits of Southern Africa are the Asbesheuwels Subgroup-hosted deposits at Sishen, Khumani, Beeshoek and Kolomela in the Nothern Cape Province of South-Africa. The best known hydrothermal Fe ore deposit is the Penge IF-hosted deposit at Thabazimbi in the Limpopo Province of South Africa. Other smaller Fe ore deposits occur in the Transvaal Supergroup of South Africa and in the greenstone belts of the Zimbabwe Craton.

Keywords
Iron formation • Iron ore • Kaapvaal Craton
Zimbabwe Craton • Gariep Belt • Damara Belt
Otavi Belt

17.1 Introduction

Iron formations (IFs) are defined as chemical sedimentary rocks that have an anomalously high Fe content (traditionally placed at $\geq$15 wt% Fe) that commonly, but not necessarily, contain layers of chert (James 1954; Trendall 1983; Klein 2005). IFs show a unique distribution through Precambrian time, with the earliest-known examples deposited at approximately 3.8 Ga (Isua Greenstone Belt) and continuing to be deposited until a volumetric peak at approximately 2.5 Ga (e.g., Transvaal Supergroup and Hamersley Group), before IF deposition temporarily ceased at approximately 1.8 Ga (Klein 2005 and references therein). IFs made a temporary return to the geological record between 0.8 and 0.6 Ga (Klein 2005), being closely associated with Snowball Earth-related glacial diamictites (Klein and Beukes 1993a). IFs are not to be confused with Phanerozoic ironstones, with the latter commonly ooidal in texture and having a very different depositional setting and mineralogy to IFs (Gross 1980; Klein 2005).

IFs can host high-grade haematite ore deposits where post-depositional supergene and/or hydrothermal processes have leached silica from the primary IF (Beukes et al. 2003; Smith and Beukes 2016), leaving the residual rock strongly enriched in Fe (typically >60 wt% Fe; Hagemann et al. 2008). IF-hosted Fe ores have for many decades provided the bulk of Fe ores mined globally (Smith and Beukes 2016), and as such IFs have been the subject of many studies (Bekker et al. 2014). Except for their economic importance and debates surrounding the epigenetic enrichment processes of IF-hosted ores (e.g., Smith and Beukes 2016), IFs have also been at the heart of numerous other geological debates. These include, but are not limited to, the following (Smith 2015): the source, mode of transport and deposition of Fe in marine settings prior to, during and after the great oxidation event (GOE; e.g., Bekker et al. 2010; Smith et al. 2013); the use of IFs as a proxy for marine and surface environments during the Early Earth (e.g., Bau and Dulski 1996; Planavsky et al. 2014; Viehmann et al. 2015); and the nature of primitive marine life on the Early Earth and its role in the deposition of Fe (e.g., Konhauser et al. 2002; Kappler et al. 2005).

The geological record of southern Africa contains numerous IFs that cover the majority of geological time over which IFs were deposited (Fig. 17.1; Table 17.1). Numerous of these IFs have also been the subject of research that has led to great progress in the understanding of not only the IFs themselves but also the nature of ancient depositional environments and life on Earth. This contribution summarizes the temporal and stratigraphic occurrence of IFs in the geological record of southern Africa, as well as the significance of these units within the geological evolution of southern Africa and the Earth. A previous, detailed review of the IFs of southern Africa was conducted by Beukes (1973). This contribution aims to be briefer and more up to date.

17.2 The Classification of Iron Formations

IFs can be classified according to three criteria: texture, mineralogy and stratigraphic setting. More detail on the classification of IFs can be found in the work of Clout and Simonson (2005), Klein (2005), Beukes and Gutzmer (2008) and Bekker et al. (2010, 2014). All of the subtypes of IF defined below occur within the geological record of southern Africa.

17.2.1 Texture

The textural classification of IFs presented here is a summary of a detailed classification originally developed by Beukes (1983) and expanded on by Beukes and Gutzmer (2008). In broad terms, IFs can be defined into two textural subtypes: micritic iron formation (MIF) and granular iron formation (GIF).

MIFs are IFs deposited as chemical muds and include two subtypes: massive poorly bedded IFs (termed felutite) and banded IFs (BIF; also termed ferhythmite; Beukes and Gutzmer 2008). The term BIF has traditionally been used for all chemically precipitated IF (e.g., Klein 2005). However, this can lead to confusion because IFs do not necessarily contain laminations or banding. Therefore the more generic term IF is used throughout, unless reference is made to a textural subtype of IF.

GIFs are IFs that were generally deposited as endoclastic sands (Beukes and Gutzmer 2008). However, a granular texture in IFs does not necessarily point to endoclastic

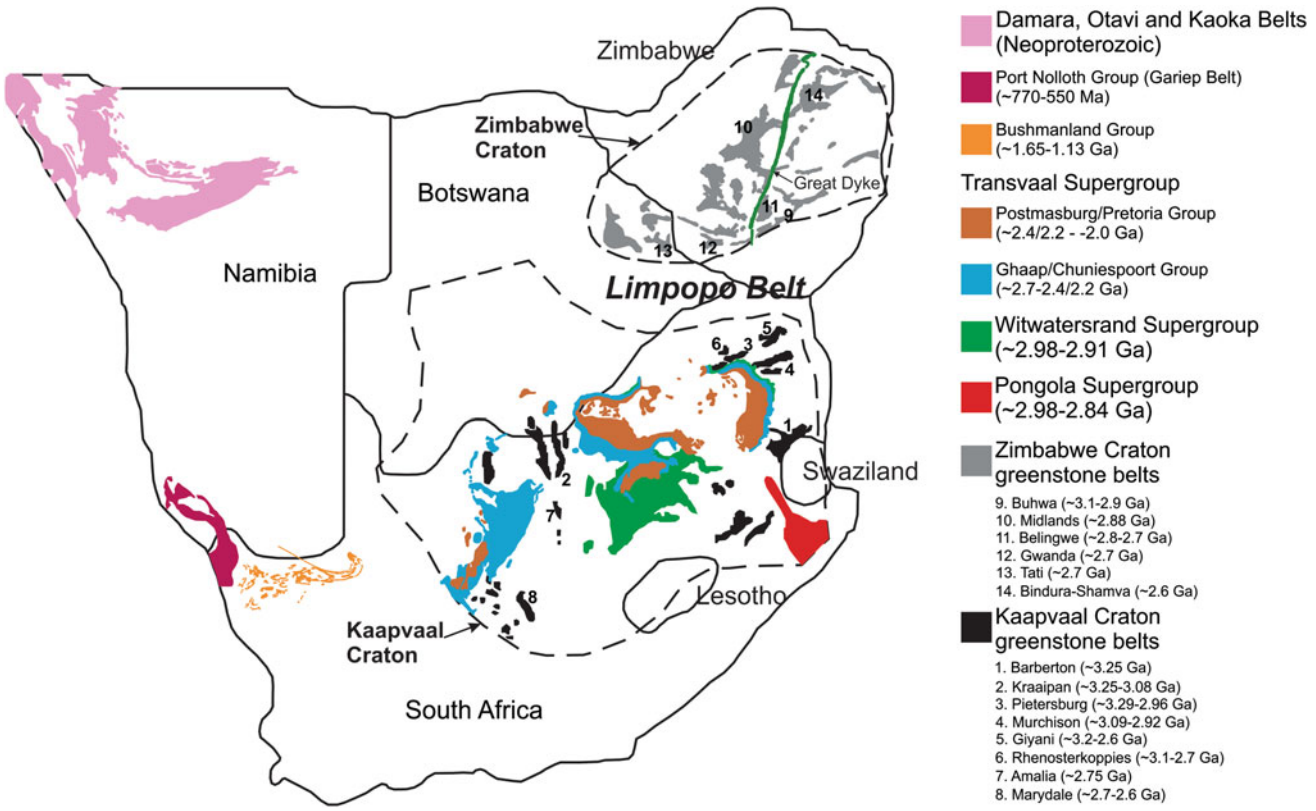

Fig. 17.1 Simplified map of southern Africa indicating the locations, geological outlines and approximate ages of the IF-hosting successions. Kaapvaal Craton greenstone belts, Pongola Supergroup and Witwatersrand Supergroup maps adapted from Poujol et al. (2003). Zimbabwe Craton greenstone belts map adapted from Kusky (1998), Oberthür and Weiser (2008) and Døssing et al. (2009). Transvaal Supergroup map adapted from Eriksson et al. (2006) and Smith and Beukes (2016). Bushmanland Group map adapted from McClung (2006). Gariep Belt and Port Nolloth Group map adapted from Basei et al. (2005). Damara, Otavi and Kaoka Belts map adapted from Miller (2013)

depositional processes, as some authors have implied a diagenetic origin for granules in some instances (e.g., Köhler et al. 2013). GIFs can be further classified into fearenite, which includes grainstone, packstone and wackestone; and ferudite, which includes flat-pebble and edgewise conglomerates (Beukes and Gutzmer 2008).

17.2.2 Mineralogy

IFs contain two major mineral component groups: quartz, usually in the form of chert; and Fe-rich minerals. IFs can be classified according to the Fe-bearing mineralogy into three groups (termed mineralogical facies): oxide, carbonate and silicate facies (Beukes and Gutzmer 2008; Bekker et al. 2010, 2014). Older publications include sulphide facies IFs (e.g., James 1954; Klein and Fink 1976). However, these are better classified as pyritic carbonaceous shales and are therefore excluded from newer classifications (Beukes and Gutzmer 2008; Bekker et al. 2010, 2014). Although individual mineralogical facies can occur over significant stratigraphic thicknesses and lateral extents in IFs, it is very common for mixed facies to occur (e.g., Klein and Fink 1976; Klein 2005; Smith et al. 2013).

Oxide facies IFs are characterized by Fe-rich minerals comprising magnetite and/or haematite. Carbonate facies IFs contain significant Fe-rich carbonates which include siderite, ankerite and ferrodolomite. Silicate facies IFs contain abundant Fe-rich silicates which include greenalite, minnesotaite, stilpnomelane, riebeckite and, where detrital contents are higher, Fe-rich chlorites. At higher metamorphic grades, other silicates such as amphiboles, pyroxenes and fayalite can also occur (Klein 2005). Multiple other minor and trace minerals also occur in IFs, such as calcite, apatite, monazite, xenotime, biotite, actinolite and ilmenite.

It is important to note that the mineralogical facies of IFs are used in conjunction with the textural classification presented earlier to properly define IFs in a petrographic sense. For example, an IF comprising alternating microbands that are respectively chert- and magnetite-rich would be petrographically defined as an oxide facies microbanded ferhythmite, whereas an IF with a massive texture comprising mixed chert, minnesotaite and stilpnomelane would be petrographically defined as a silicate facies felutite.

Table 17.1 A summary of the documented occurrences of IFs within the geological record of southern Africa

	Geological sequence		Location	Age	Mineralogy	Other comments/characteristics	References
Meso- to Neoarchean Kaapvaal Craton algoma-type	Barberton greenstone belt	Fig Tree Group, Ngwenya Formation Moodies Group	Eastern margin of Kaapvaal Craton Mpumalanga Province, South Africa; Swaziland	~3.25 Ga ~3.2 Ga	Oxide facies in outcrop. Mixed facies in drill core. Oxide facies	Two 50 m thick sequences of jaspillitic BIF. Occurs within ferruginous shales. Associated surrounding greenstone fragments also contain BIF. Interbedded with cm-scale sandstone at base and top.	Hofmann (2005) Brandl et al. (2006) Bontognali et al. (2013)
	Kraaipan greenstone belt	Kraaipan Group, Gold Ridge Formation	West-central Kaapvaal Craton Northwest Province, South Africa	~3.25–3.08 Ga	Mixed facies.	15–45 m thick. Hosted in metasediments interlayered with metavolcanics. Hosts lode gold mineralization.	Brandl et al. (2006) Hammond and Moore (2006)
	Pietersburg greenstone belt	Pietersburg Group, Mothiba and Ysterberg Formations	Northern Kaapvaal Craton Limpopo Province, South Africa	~3.29–2.96 Ga	NA	BIF intercalated with mafic metavolcanics.	Zeh and Gerdes (2012)
	Murchison greenstone belt	Leydsdorp Formation Weigel Formation MacKop Formation	Northeastern Kaapvaal Craton Limpopo Province, South Africa	~3.09–2.92 Ga	Mixed facies.	200 m thick IF interbedded with mafic lavas and clastic sediments.	Brandl et al. (2006) Block et al. (2013)
	Giyani greenstone belt	Giyani Group	Northern margin of Kaapvaal Craton Limpopo Province, South Africa	~3.2–2.6 Ga Poorly constrained	NA	BIF occurs within mafic to ultramafic metvolcanics. Hosts lode gold mineralization.	McCourt and Van Reenen (1993) Brandl et al. (2006)
	Rhenosterkoppies greenstone belt	Pietersburg Group, Zandrivierspoort Formation	Northern margin of Kaapvaal Craton Limpopo Province, South Africa	~3.1–2.7 Ga	Oxide and silicate facies.	Up to five distinct layers of BIF. Associated with quartzite and garnetiferous schist.	Miyano and Van Reenen (1987) Brandl et al. (2006)
	Amalia greenstone belt		West-central Kaapvaal Craton Northwest Province, South Africa	~2.75 Ga	Oxide facies.	BIF intercalated with mafic metavolcanics and pyroclastics. Hosts lode gold mineralization.	Vearncombe (1986) Jones and Anhaeusser (1993) Poujol et al. (2003) Brandl et al. (2006)
	Marydale greenstone belt	Marydale Group, Modderfontein Formation	Southwestern margin of Kaapvaal Craton Northern Cape Province, South Africa	~2.7–2.6 Ga	Oxide facies.	IF overlying carbonates and underlying amphibolites.	Brandl et al. (2006)
Meso- to Neoarchean Zimbabwe Craton algoma-type	Buhwa greenstone belt	Buhwa Group	Southern margin of Zimbabwe Craton	~3.1–2.9 Ga	Oxide facies	100s of m thick IF occurring within shale in shelf association. <50 m thick IF associated with mafic volcanics in basin association.	Fedo and Eriksson (1996)
	Midlands greenstone belt	Bulawayan Group correlative, Mafic Formation	Central Zimbabwe Craton	~2.88 Ga	Oxide facies	BIF caps cycles of basalt grading into sandstone, shale and BIF.	Hofmann et al. (2003)
	Belingwe greenstone belt	Ngezi Group, Manjeri and Chesire Formations	Southern Zimbabwe Craton	~2.8–2.7 Ga	NA	Fe-rich units of debated origin. Originally thought to be BIF. Recently interpreted as deformed and sheared shales.	Kusky and Kidd (1992) Hofmann et al. (2003)
	Gwanda greenstone belt	Buluwayan Group correlative, "Mafic unit"	Southern margin of Zimbabwe Craton	~2.7 Ga	Oxide and carbonate facies.	BIF intercalated with mafic to ultramafic metavolcanics. Hosts stratiform gold mineralization.	Saager et al. (1987)
	Tati greenstone belt	Lady Mary Formation Matsiloje Formation Penhalonga Formation	Southwestern margin of Zimbabwe Craton Southeastern Botswana	~2.7 Ga	Oxide facies	BIF with associated epiclastics as well as mafic to felsic volcanics. Hosts gold mineralization.	Beukes (1973) Døssing et al. (2009)
			Northern Zimbabwe Craton	~2.6 Ga	Oxide facies		Jelsma et al. (1993)

(continued)

Table 17.1 (continued)

	Geological sequence		Location	Age	Mineralogy	Other comments/characteristics	References
	Bindura-Shamva greenstone belt	Buluwayan Group, Arcturus Formation	80 km north of Harare			30–100 m thick BIF intercalated with mafic to ultramafic volcanics.	Hofmann et al. (2003)
Mesoarchean limpopo belt	Central Zone	Mount Dowe Group	Border between South Africa and Zimbabwe	~3.30–3.15 Ga	NA	Highly metamorphosed banded and massive magnetite quartzite.	Beukes (1973) Kramers et al. (2006)
Neoarchean to Kaapvaal Craton Superior-type	Pongola Supergroup Mozaan Group	Vlakhoek Member, Sinqeni Formation Mhlatuze Member, Ntombe Formation Scotts Hill Member, Ntombe Formation Nconga Formation	Southeastern margin of Kaapvaal Craton Kwazulu-Natal and Mpumalang Provinces, South Africa; Swaziland	~2.98–2.84 Ga	All facies. NA Oxide-silicate facies All facies.	~2–5 m thick. Ferhythmite and felutite. Anomalous Mn enrichment. Up to 80 m thick and microfolded. Ferhythmite. ~3–12 m thick. Also contains GIF interbedded with IF.	Beukes and Cairncross (1991) Smith (2007) Hicks and Hofmann (2012) Planavsky et al. (2014) Ossa Ossa et al. (2016) Smith et al. (2017)
	Witwatersrand Supergroup West Rand Group	Parktown Formation, Water Tower IF Parktown Formation, Contorted Bed IF Promise Formation Coronation Formation, Silverfield Member IF	Central Kaapvaal Craton Gauteng, Northwest and Free State Provinces, South Africa	~2.98–2.91 Ga	Oxide-carbonate facies Oxide-carbonate facies Oxide-carbonate facies Oxide-silicate facies	>10 m thick. Felutite. ~30 m thick. Ferhythmite. Microfolded in many outcrops. ~5 m thick. Ferhythmite. Overlies diamictite of glacial origin. ~5–10 m thick. Ferhythmite. Overlies diamictite of glacial origin.	Smith (2007) Smith et al. (2013)
Neoarchean to Paleoproterozoic Kaapvaal Craton Superior-type	Transvaal Supergroup	Schmidtsdrift Subgroup, Lokammona Formation Asbesheuwels Subgroup, Kuruman IF Asbesheuwels Subgroup, Griquatown IF Koegas Subgroup, Doradale IF Koegas Subgroup, Rooinekke IF Koegas Subgroup, Klipputs IF Koegas Subgroup, Nelani IF Makganyene Formation Hotazel Formation	Western to southwestern Kaapvaal Craton Griqualand West basin, Northern Cape Province, South Africa	~2.6 Ga ~2.52–2.43 Ga ~2.41 Ga ~2.4 or ~2.2 Ga	Carbonate facies All facies. Carbonate-silicate facies All facies. All facies. Oxide-silicate facies Carbonate-silicate facies All facies. All facies.	Felutite. 120–750 m thick. Ferhythmites and clastic textured IF. ~250 m thick. Felutite, grainstones and conglomerates. ~35 m thick. Ferhythmite, felutite and GIF. ~120 m thick. Felutite. ~20 m thick. Felutite. Stromatolitic carbonate bioherms at top. ~130 m thick. Felutite. ~3–5 m thick IF of limited extent interbedded with glacial diamictites. Four IF units interbedded with three Mn formation units.	Beukes (1983, 1984) Eriksson et al. (2006) Nel (2013) Beukes and Gutzmer (2008) Preliminary field work (UJ) Gutzmer and Beukes (1995, 1996) Tsikos and Moore (1997)
Mesoproterozoic Superior-type?	Bushmanland Group	Wortel Subgroup, Namies Formation Kouboom Subgroup, Gams Formation	Central Namaqua Province Northern border of Northern Cape Province, South Africa	~1.65–1.13 Ga	Oxide-silicate facies	0.3–0.5 m thick. 0.3–5 m thick.	Stalder and Rozendaal (2002, 2005) McClung (2006)
Neoproterozoic Rapitan-type	Damara Belt	Khomas Subgroup, Chuos Formation	Northwest Namibia	~717–660 Ma	Oxide facies	Ferhythmite interbedded with glacial diamictites likely related to Sturtian global glaciation.	Beukes et al. (2016) Lechte and Maxwell (2016) Lechte et al. (2016)
	Gariep Belt	Port Nolloth Group, Numees Formation	West coast of Northern Cape Province, South Africa and southern Namibia	~580 or 717 Ma	NA	IF occurring within glacial diamictite sequence likely related to either Sturtian or Marinoan global glaciation.	Fölling and Frimmel (2002) Frimmel et al. (2002) McDonald et al. (2010)

17.2.3 Stratigraphic Setting

The stratigraphic classification of IFs also shows a strong correlation with their occurrence in time. Although the original classification only contained the first two types (Gross 1980), today three stratigraphic IF types are defined: Algoma-type IFs; Superior-type IFs; and Rapitan-type IFs (Beukes and Gutzmer 2008). It is important to note that in successions affected by strong deformation and shearing, the differentiation between Algoma- and Superior-type IFs can be difficult (Bekker et al. 2014).

Algoma-type IFs are generally associated with volcanic rocks and greywacke, and they commonly occur within greenstone belts (Gross 1980; Beukes and Gutzmer 2008; Bekker et al. 2014). They have been interpreted to have mostly formed close to volcanic centres through fumarolic, effusive and exhalative hydrothermal processes (Gross 1980). Although Algoma-type IFs were mostly deposited in greenstone belts during the Archean, examples are found in numerous greenstone belt-like volcanosedimentary successions of younger age (e.g., Isley and Abbott 1999; Stalder and Rozendaal 2002; Huston and Logan 2004). Algoma-type IFs are generally thinner (10–100 m) and smaller in lateral extent (<10 km) than Superior-type IFs (Isley and Abbott 1999; Bekker et al. 2014), although much larger Algoma-type IFs are known (Beukes and Gutzmer 2008). The Algoma-type IFs are more abundant in number of individual occurrences than Superior-type IFs (Beukes and Gutzmer 2008).

Superior-type IFs are typically interbedded with carbonates, quartz arenites and black shales. They are considered to have been deposited in nearshore continental shelf environments (Gross 1980; Beukes and Gutzmer 2008; Bekker et al. 2014). Some are hundreds of metres thick and in general have better lateral continuity and are less deformed than the Algoma-type IFs, with larger examples covering areas greater than 10^5 km^2 (Isley and Abbott 1999; Beukes and Gutzmer 2008). The majority of Superior-type IFs were deposited in the Paleoproterozoic, although some Mesoarchean examples are known (e.g., Smith 2007; Smith et al. 2013).

Rapitan-type IFs are associated with glacial diamictites and most commonly formed during the Neoproterozoic Snowball Earth event (Beukes and Gutzmer 2008). However, smaller occurrences of glacially associated IFs are also found in Paleoproterozoic (Beukes 1983) and Mesoarchean (Smith 2007; Smith et al. 2013) successions. Rapitan-type IFs are commonly interbedded with shale and sandstone (Klein and Beukes 1993a).

17.3 Meso- to Neoarchean Algoma-Type Iron Formations of Southern Africa

Numerous Archean greenstone belts occur on the Kaapvaal Craton of South Africa, Swaziland and Botswana (Poujol et al. 2003) and the Zimbabwe Craton of Zimbabwe and Botswana (Dirks and Jelsma 1998; Kusky 1998). The majority of these contain Algoma-type IFs within their volcanosedimentary successions. Below is a chronological summary of selected occurrences across these two cratons with a special note on IF occurrences in the Limpopo Belt, which lies between these two cratons (Fig. 17.1; Table 17.1).

17.3.1 Algoma-Type Iron Formations in the Greenstone Belts of the Kaapvaal Craton

The oldest known IF of southern Africa occurs in the Ngwenya Formation of the approximately 3.25 Ga Fig Tree Group of the Barberton greenstone belt of southern Africa, located on the eastern margin of the Kaapvaal Craton (Fig. 17.1; Hofmann 2005). The IF occurs above a ferruginous shale as two approximately 50 m thick beds of jaspilitic BIF that are separated by fine-grained sandstone to siltstone. Although the BIF mostly comprises chert and haematite in surface outcrops (Fig. 17.2a), drill core intersections produced by the Barberton Drilling Project (Arndt et al. 2012) show a more complicated mineralogy, with carbonate and silicate facies IFs also present. Even though the Fig Tree Group is mostly a sedimentary succession, the IFs can still be considered to be Algoma-type. This is because the underlying Onverwacht Group contains significant ultramafic to mafic volcanics, and in some parts of the Barberton greenstone belt the top of the Fig Tree Group contains intercalated felsic volcanics (Hofmann 2005). The approximately 3.2 Ga Moodies Group, which overlies the Fig Tree Group in the Barberton greenstone belt, also contains an oxide facies BIF (Bontognali et al. 2013). The base and top of the BIF is interbedded with cm-scale fine-grained sandstones and a volcanic tuff is also present towards the base of the BIF. Numerous greenstone fragments to the south of the Barberton greenstone belt in Mpumalanga and Kwazulu-Natal provinces also contain IFs (Brandl et al. 2006).

The approximately 3.25–3.08 Ga (Poujol et al. 2003) Kraaipan greenstone belt, located on the west-central part of

the Kaapvaal Craton (Fig. 17.1), also contains a 15–45 m thick Algoma-type IF within a metasedimentary succession that interlayers mafic metavolcanics and volcaniclastics (Hammond and Moore 2006). This IF also hosts significant lode gold mineralization in some parts. The IF comprises all mineralogical facies, with abundant crosscutting quartz, carbonate and sulphide veins developed in areas marked by gold mineralization (Hammond and Moore 2006). The Pietersburg greenstone belt, located close to the northern margin of the Kaapvaal Craton (Fig. 17.1) and similar in age to the Kraaipan greenstone belt (Poujol et al. 2003), also contains IFs intercalated with basalts, mafic metatuffs, metagabbros and serpentinites within its basal Mothiba and Ysterberg Formations (Zeh and Gerdes 2012).

The approximately 3.09–2.92 Ga Murchison greenstone belt occurs to the east of the Pietersburg greenstone belt at the northeastern margin of the Kaapvaal Craton (Fig. 17.1) and contains up to 200 m thick IFs interbedded with mafic lavas and clastic sediments (Block et al. 2013; Brandl et al. 2006).

Two greenstone belts at the northernmost margin of the Kaapvaal Craton, directly to the south of the Southern Marginal Zone of the Limpopo belt, contain IFs. The Giyani greenstone belt, formerly known as the Sutherland greenstone belt, occurs northeast of the Pietersburg greenstone belt (Fig. 17.1). It has a poorly constrained age that appears to fall between 3.5 and 2.8 Ga and contains IFs within its mostly mafic to ultramafic metavolcanic succession (Brandl et al. 2006; McCourt and Van Reenen 1993). Both the mafic metavolcanics and IFs can host gold mineralization. The approximately 3.1–2.7 Ga Rhenosterkoppies greenstone belt, located less than 10 km to the north of the Pietersburg greenstone belt (Fig. 17.1), contains up to five distinct layers of IFs (Brandl et al. 2006; Miyano and Van Reenen 1987).

The approximately 2.75 Ga (Poujol et al. 2003) Amalia greenstone belt, located on the west-central part of the Kaapvaal Craton just south of the Kraaipan greenstone belt (Fig. 17.1), contains IFs intercalated with mafic metavolcanics (Jones and Anhaeusser 1993). Just as observed in parts of the Kraaipan greenstone belt, the IFs in the Amalia greenstone belt can host lode gold mineralization in quartz veins (Vearncombe 1986).

Located on the southwestern margin of the Kaapvaal Craton close to the town of Prieska (Fig. 17.1), the approximately 2.7–2.6 Ga Marydale greenstone belt contains IFs overlying carbonates in the Modderfontein Formation. The IFs are overlain by the Uitzigt Formation amphibolites (Brandl et al. 2006).

17.3.2 Algoma-Type Iron Formations in the Greenstone Belts of the Zimbabwe Craton

The Zimbabwe Craton (Fig. 17.1) has more than 20 Archean greenstone belt occurrences (Kusky 1998), the majority of which contain IFs. Important to note is that numerous of these IFs are known to host orogenic gold deposits (Fripp 1976). Table 17.1 provides a short summary of a selection of documented Algoma-type IF occurrences in these greenstone belts.

At the southernmost margin of the Zimbabwe Craton lies the approximately 3.0 Ga Buhwa greenstone belt (Fig. 17.1), which contains IFs in the shelf association of its cover succession (Fedo and Eriksson 1996). The IFs are estimated to be between 300 and more than 500 m thick and gradationally overlie and underlie shale units which, in turn, are overlain by mafic volcanics. The basinal association of the Buhwa greenstone belt also contain IFs that are less than 50 m thick and are associated with mafic volcanics and metachert (Fedo and Eriksson 1996).

In the centre of the Zimbabwe Craton, the approximately 2.88 Ga Mafic Formation of the Bulawayan Group of the Midlands greenstone belt (Fig. 17.1) contains multiple approximately 20 m-thick jaspillitic IFs at the top of asymmetric cycles that comprise basalt overlain by sandstone grading into shale and then IFs (Hofmann et al. 2003).

The approximately 2.8–2.7 Ga Ngezi Group of the Belingwe greenstone belt, situated on the southern margin of the Zimbabwe Craton (Fig. 17.1), contain Fe-rich units (termed 'ironstones' by Hofmann et al. 2003) at the top of the Manjeri Formation and base of the Chesire Formation (Kusky and Kidd 1992; Hofmann et al. 2003). Although these Fe-rich units have earlier been interpreted to be BIFs (Martin 1978; Wilson 1979), they have recently been reinterpreted to represent highly deformed and sheared shale (Hofmann et al. 2003).

The Gwanda greenstone belt, located at the southern margin of the Zimbabwe Craton in Zimbabwe close to the border with South Africa (Fig. 17.1), contains carbonate and oxide facies IFs intercalated at numerous stratigraphic levels with mafic to ultramafic metavolcanics in what is termed the 'Mafic unit' (Saager et al. 1987). This succession is thought to correlate with the Upper Greenstones of the Bulawayan Group and is likely approximately 2.7 Ga (Wilson et al. 1978; Foster and Wilson 1984; Saager et al. 1987). The IFs have been noted to host significant stratiform gold mineralization (Fripp 1976; Saager et al. 1987).

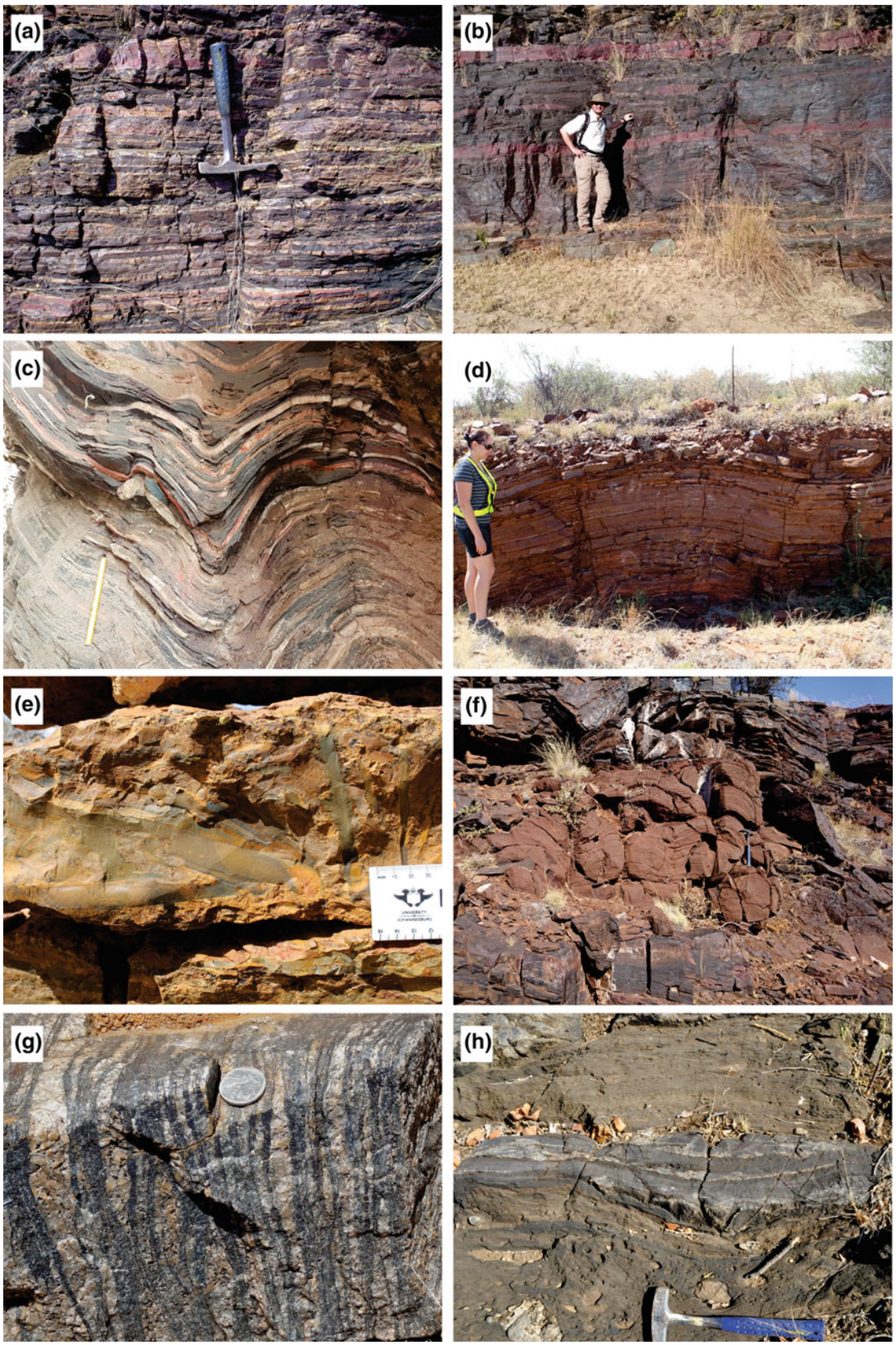
(a)
(b)
(c)
(d)
(e)
(f)
(g)
(h)

Fig. 17.2 Photographs of surface outcrops of IF occurrences in southern Africa. **a** The Ngwenya Formation ferhythmite of the approximately 3.25 Ga Fig Tree Group of the Barberton greenstone belt along the Komati River near the border between Mpumulanga Province in South Africa and Swaziland (photograph courtesy of Axel Hofmann). **b** The Vlakhoek Member felutite of the approximately 2.98–2.84 Ga Mozaan Group of the Pongola Supergroup in the White Umfolozi inlier in the Kwazulu-Natal Province of South Africa. **c** The Contorted Bed ferhythmite of the approximately 2.98–2.91 Ga West Rand Group of the Witwatersrand Supergroup in Johannesburg, South Africa. **d** The Groenwater Member ferhythmite of the Kuruman IF of the Transvaal Supergroup near Griquatown in the Northern Cape Province of South Africa. **e** Rip-up clasts in the reworked IF edgewise conglomerates of the Skietfontein Member of the Griquatown IF of the Transvaal Supergroup near Griquatown in the Northern Cape Province of South Africa. **f** Stromatolitic dolomite bioherms within the Rooinekke IF of the Koegas Subgroup of the Transvaal Supergroup near Griquatown in the Northern Cape Province of South Africa. **g** Micro- to mesobanded Mn–Fe-rich chemical metasedimentary rock from the Bushmandland Group, Gambserg, Northern Cape Province, South Africa (picture courtesy of Nic Beukes). **h** Ferhythmite interbedded with ferruginous diamictite in the Chuos Formation of the Damara Belt near Lowenfontein in northern Namibia (picture courtesy of Maxwell Lechte)

The approximately 2.7 Ga Tati greenstone belt, situated on the southwestern margin of the Zimbabwe Craton in Botswana (Fig. 17.1), contains IFs within its basal Lady Mary and middle Matsiloje and Penhalonga Formations (Beukes 1973; Døssing et al. 2009). The IFs are associated with epiclastic sedimentary rocks as well as mafic to felsic volcanic rocks. Their thickness varies from tens of metres to approximately 100 m at Mupane gold mine (Døssing et al. 2009).

The Bindura-Shamva greenstone belt (also known as the Harare-Shamva-Bindura or Harare-Bindura-Shamva greenstone belt; e.g., Huizenga and Touret 1993; Oberthür and Weiser 2008), situated in the northern Zimbabwe Craton (Fig. 17.1), contains 30–100 m-thick IFs within sedimentary horizons that are intercalated with the mafic to ultramafic volcanics of the approximately 2.6 Ga Arcturus Formation of the basal Bulawayan Group (Jelsma et al. 1993; Hofmann et al. 2003).

17.3.3 A Note on Iron-Rich Metasediments in the Limpopo Belt

The Limpopo Belt is a broad zone of gneisses that occurs between the Kaapvaal and Zimbabwe Cratons and extends from eastern Botswana through southern Zimbabwe and northern South Africa (Fig. 17.1; Kramers et al. 2006). The Mount Dowe Group of the Beit Bridge Complex, which occurs within the Central Zone of the Limpopo Belt, contains a metasedimentary succession that contains banded and massive magnetite quartzite. This banded magnetite quartzite has been interpreted to be metamorphosed BIF (Beukes 1973; Kramers et al. 2006). The Mount Dowe Group's age has been bracketed at approximately 3.30–3.15 Ga (Kramers et al. 2006). However, the Limpopo Belt has experienced major metamorphism and deformation at approximately 2.7–2.0 Ga (Kramers et al. 2006), which makes the interpretation of metasedimentary units, especially the origin of the massive magnetite quartzite, uncertain (Beukes 1973). The high levels of metamorphism and deformation also make a definite interpretation of the Fe-rich units' stratigraphic classification problematic, although the age and tectonic setting suggest that these were Algoma-type IFs.

17.4 Mesoarchean Superior-Type Iron Formations of Southern Africa

The Kaapvaal Craton of southern Africa is unique with regard to IF occurrences in that it contains the oldest known Superior-type IFs. These occur within the approximately 2.98–2.84 Ga (Hegner et al. 1994; Gutzmer et al. 1999) Mozaan Group of the Pongola Supergroup on the southeastern margin of the Kaapvaal Craton and the approximately 2.98–2.91 Ga (Armstrong et al. 1991; Kositcin and Krapež 2004) West Rand Group of the Witwatersrand Supergroup on the central Kaapvaal Craton (Fig. 17.1; Smith 2007; Smith et al. 2013). The Mozaan Group and West Rand Group are considered to be depositional correlatives (Beukes and Cairncross 1991; Smith 2007). This correlation is based, in part, on both succession containing Fe-rich units (IF or Fe-rich mudstone) at corresponding sequence stratigraphic points (Fig. 17.3a). All these IFs, with two exceptions, are interbedded with marine shelf mudstone and sandstone. In the West Rand Group the IFs of the Promise and Coronation Formations directly overlie diamictites (Fig. 17.3a; Smith 2007; Smith et al. 2013) which, along with their correlatives in the Mozaan Group, are interpreted to be of glacial origin (Von Brunn and Gold 1993; Beukes 1995; Young et al. 1998; McCarthy 2006). To illustrate the thickness and lateral extent of these IFs, one can consider the correlatable Contorted Bed and Scotts Hill Member IFs of the West Rand and Mozaan Groups, respectively (Fig. 17.3a). The thickness varies between approximately 30 m (Contorted Bed IF) and 80 m (Scotts Hill Member IF), and both IFs are known to be developed across the entirety of their currently preserved depositional basins. This suggests a currently preserved lateral extent of more than 600 km for the Contorted Bed-Scotts Hill Member IF from Ottosdal in Northwest Province to Pongola in Kwazulu-Natal Province of South Africa.

The Mozaan Group contains IFs within the following stratigraphic units, from the base upwards (Fig. 17.3a): the

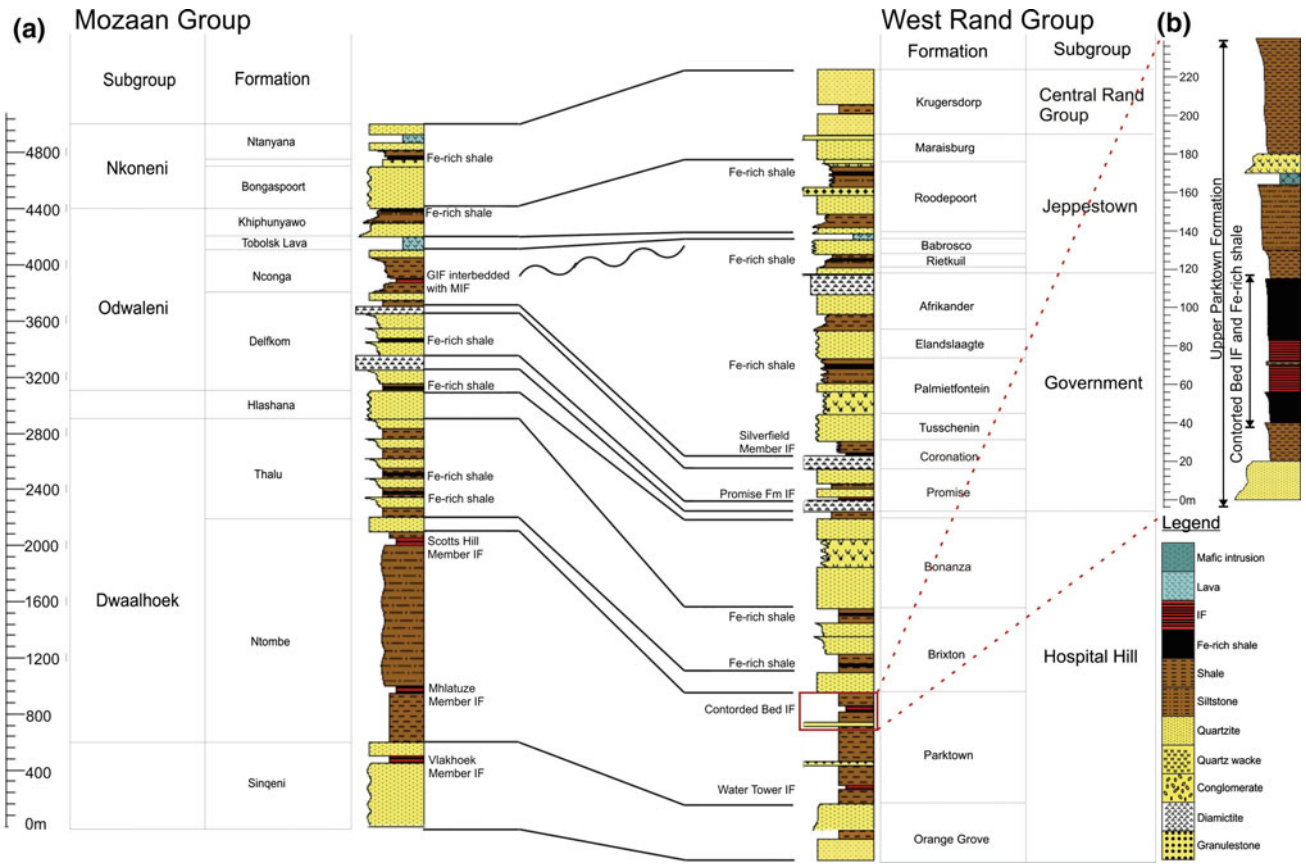

Fig. 17.3 **a** Lithostratigraphic correlation of the Mozaan Group of the Pongola Supergroup and the West Rand Group of the Witwatersrand Supergroup (adapted from Nhleko 2003; Smith 2007). **b** Detailed section of the Contorted Bed IF as intersected in exploration drill core drilled near Mazista, Northwest Province, South Africa (adapted from Smith 2007; Smith et al. 2013)

Ijzermijn IF within the Vlakhoek Member shale in the Sinqeni Formation; the Mhlatuze and Scotts Hill Member IFs within the Ntombe Formation; and an IF with associated GIF in the Nconga Formation (Table 17.1). The latter GIF within the Nconga Formation is unique in that it is the oldest known GIF in the global geological record and it contains microstromatolitic structures in the granule rims (Smith et al. 2017). Fe-rich mudstone units also occur in the Thalu (two units), Delfkom (two units), Khiphunyawo and Ntanyana Formations (Smith 2007).

The Vlakhoek Member of the Sinqeni Formation is unique in that it contains one of the oldest known Superior-type IFs in the world. The IF, also referred to as the Ijzermijn IF Bed, which is a combination of mixed carbonate-oxide-silicate facies felutite and ferhythmite, is approximately 2–5 m thick (Fig. 17.2b) and occurs within the approximately 11–80 m thick Vlakhoek Member shale. The shale is ferruginous, interpreted to mark a transgressive cycle and separates the Dipka Member quartzite below and the Kwaaiman Member quartzite above it (Beukes and Cairncross 1991; Smith 2007; Hicks and Hofmann 2012; Ossa Ossa et al. 2016). The Vlakhoek Member is also unique in that it has an anomalously high Mn content, occurring as Mn-rich carbonates, in the White Mfolozi area of the Kwazulu-Natal Province (Smith 2007; Planavsky et al. 2014; Ossa Ossa et al. 2016). With regard to the other IFs in the Mozaan Group, detailed descriptions of the Scotts Hill and Nconga Formation IFs can be found in the work of Smith (2007), whereas a proper detailed description of the Mhlatuze Member IF is lacking from the literature.

The West Rand Group contains IFs within the following stratigraphic units, from the base upwards (Fig. 17.3a): the Water Tower and Contorted Bed IFs in the Parktown Formation; an IF in the Promise Formation; and the Silverfield Member IF in the Coronation Formation (Table 17.1). Fe-rich mudstone units also occur in the Brixton, Palmietfontein, Rietkuil and Roodepoort Formations (Smith 2007; Smith et al. 2013). The IF in the Promise Formation is not as laterally consistent as the other three IFs, with only Fe-rich shale developed in certain sections of the Promise Formation.

Best known of the West Rand Group IFs is the Contorted Bed IF (formerly known as the Jan Smuts Bed), which is laterally continuous across the whole West Rand Group and has acted as an important marker bed in gold exploration

(McCarthy 2006; Smith et al. 2013). This IF is also well known for having outcrops of folded ferhythmite (hence the 'contorted' in its name) at the western border of Johannesburg's central business district (Fig. 17.2c). The Contorted Bed IF is an approximately 30 m-thick oxide-carbonate facies ferhythmite that occurs within an Fe-rich shale succession (Fig. 17.3b). Thinner shale interbeds can also occur within the IF. The whole Fe-rich shale-IF package is approximately 80 m thick and considered to be a transgressive to regressive marine cycle as it is underlain and overlain by quartzite. The IF therefore marks the point of maximum transgression (Smith 2007; Smith et al. 2013). With regard to the other IFs in the Mozaan Group, detailed descriptions of the Water Tower, Promise Formation and Silverfield Member IFs can be found in Smith (2007) and Smith et al. (2013).

17.5 Neoarchean-Paleoproterozoic Superior-Type Iron Formations of Southern Africa

By far the most volumetrically significant IFs in southern Africa (e.g., the Asbesheuwels-Penge IFs are ~350–1000 m-thick over a lateral extent of approximately 1000 km) occur in the Neoarchean to Paleoproterozoic (~2.7–2.2 Ga; Eriksson et al. 2006) Transvaal Supergroup in the Kaapvaal Craton of South Africa and Botswana (Figs. 17.1 and 17.4a). The Transvaal Supergroup is developed in three regions (Fig. 17.4a), sometimes referred to as sub-basins: the Transvaal (Mpumalanga, Limpopo, Northwest and Gauteng Provinces, South Africa), Griqualand West (Northern Cape Province, South Africa) and Kanye (southern Botswana) regions (Eriksson et al. 2006; Smith and Beukes 2016). IFs occur in all three regions and have been documented, from the base to the top, in: the Lokammona Formation of the Schmidtsdrift Subgroup of the Griqualand West region; the correlating Asbesheuwels Subgroup, Penge Formation and Masoke Formation of the Griqualand West, Transvaal and Kanye regions, respectively; the Koegas Subgroup of the Griqualand West region; near the base of the Pretoria Group in the Transvaal region; the Makganyene Formation of the Griqualand West region; and the Hotazel Formation of the Griqualand West region (Table 17.1; Beukes 1973, 1983, 1984; Tsikos et al. 2003; Eriksson et al. 2006; Nel 2013). All of these occurrences, with the exception of the Makganyene Formation, are known to host significant high-grade Fe ore (Smith and Beukes 2016). This contribution will focus on IF occurrences in the Griqualand West region specifically (Fig. 17.4b) as these are better developed and more abundant (Beukes 1983). The IF near the base of the Pretoria Group is poorly developed and of limited lateral extent (Beukes 1983). Descriptions of the Penge IF of the Transvaal region can be found in the work of Miyano et al. (1987) and Miyano and Beukes (1997). The Lokammona Formation within the lowermost Schmidtsdrift Subgroup in the Griqualand West region only contains two less than 1 m thick

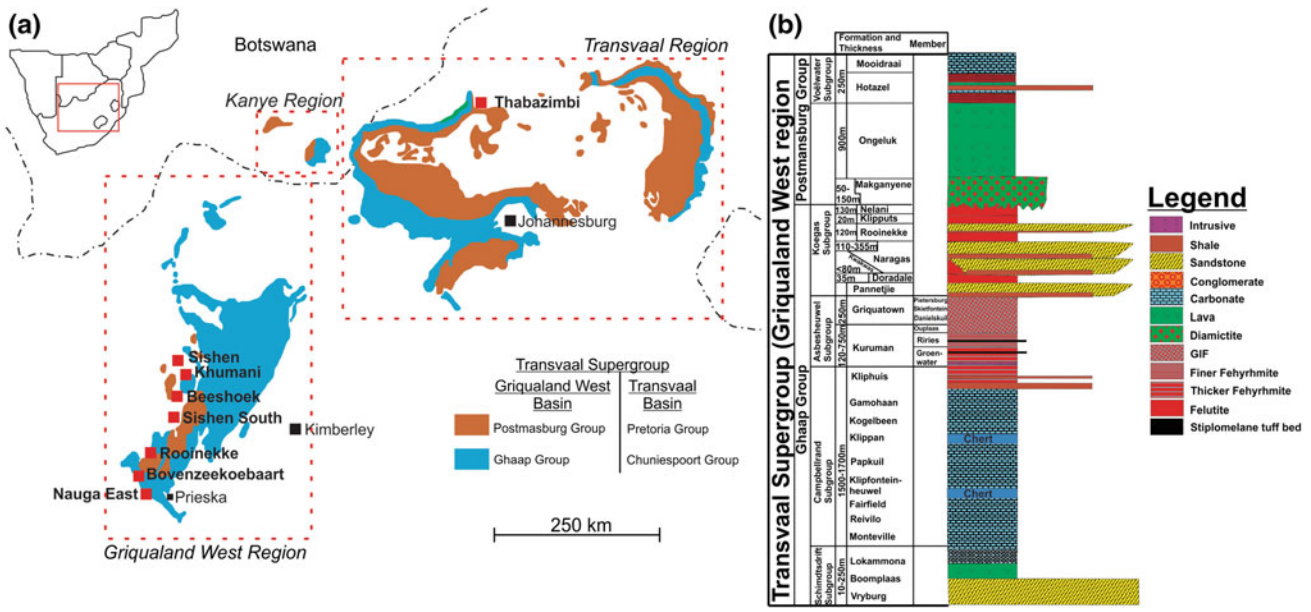

Fig. 17.4 **a** A general locality map indicating the position of the Transvaal, Griqualand West and Kanye regions of the Transvaal Supergroup in South Africa. Also indicated are the locations of the main IF-hosted Fe ore deposits of South Africa (adapted from Eriksson et al. 2006; Smith and Beukes 2016). **b** General stratigraphic column of the Transvaal Supergroup in the Griqualand West region (compiled from Van Schalkwyk and Beukes 1986; Eriksson et al. 2006; Schröder et al. 2011)

carbonate facies felutite beds which are of limited lateral extent (Beukes 1983).

The approximately 2.52–2.43 Ga (Trendall et al. 1990; Sumner and Bowring 1996) Asbesheuwels Subgroup of the Ghaap Group comprises the lower Kliphuis, middle Kuruman and upper Griquatown (also called Daniëlskuil) Formations (Fig. 17.4b; Beukes 1984; Eriksson et al. 2006). The Kliphuis Formation, originally included by Beukes (1983, 1984) in the Kuruman Formation as the basal Kliphuis Member, is transitional from the Campbellrand Subgroup carbonates and comprises carbonate shales, and carbonate and haematite cherts, and is only 8–13 m thick (Eriksson et al. 2006). The Kuruman Formation, which correlates not only with the Penge IF but potentially also with the Brockman IF in Australia (Beukes 1984), is the thickest IF in the stratigraphic record of southern Africa and has been found to be up to 750 m thick close to the town of Koegas, although it is generally around 120–250 m thick (Beukes 1983, 1984; Eriksson et al. 2006). The Kuruman IF comprises the following members from its base upwards (Fig. 17.4b; Beukes 1984): the Groenwater Member (chert-banded carbonate and oxide facies ferthythmite; Fig. 17.2d); the Riries Member (chert-poor silicate-carbonate facies ferthythmite); and the Ouplaas Member (carbonate facies clastic textured IF). Overlying the Kuruman IF, the Griquatown IF is on average 250 m thick and comprises the following members from its base upwards (Fig. 17.4b; Beukes 1983, 1984): the Daniëlskuil Member (carbonate-silicate lutite interbedded with grainstones); the Skietfontein Member (silicate facies disclutites/edgewise conglomerate; Fig. 17.2e); the Middelwater Member (silicate facies lutite); and the Pietersberg Member (silicate facies lutite). From an economic geology perspective, the IFs of the Asbesheuwels Subgroup are world renowned because they host the superlarge haematite ore deposits of the Maremane Dome of the Northern Cape Province of South Africa, which include the deposits at Sishen, Khumani, Beeshoek and Kolomela (Smith and Beukes 2016).

The Koegas Subgroup gradationally overlies the Griquatown IF and contains four IFs from its base upwards (Fig. 17.4b; Beukes 1983; Nel 2013): the approximately 35 m-thick Doradale IF (mixed facies ferhythmite and felutite with carbonate facies GIF); the approximately 120 m-thick Rooinekke IF (mixed facies felutite with carbonate facies GIF); the approximately 20 m-thick Klipputs IF (oxide-silicate facies felutite); and the approximately 130 m-thick Nelani IF (carbonate-silicate facies felutite), which is cut unconformably at the top by the Makganyene Formation diamictite. An interesting feature at the base of the Rooinekke IF and the top of the Klipputs IF are transgression surfaces that are marked by stromatolitic dolomite bioherms (Fig. 17.2f; Beukes 1983; Beukes and Gutzmer 2008). The Rooinekke IFs also contain two approximately 1 m-thick ferruginous Mn ore beds (Beukes et al. 2016). A poorly constrained U-Pb zircon age of approximately 2.41 Ga was determined from a tuff bed in the Rooinekke IF (Gutzmer et al. 1999; Beukes and Gutzmer 2008).

The Makganyene Formation mostly consists of diamictites interpreted to signify a Snowball Earth glacial event (Kirschvink et al. 2000) and it marks the base of the Postmasburg Group of the Transvaal Supergroup in the Griqualand West region (Fig. 17.4a, b). Although not yet described in detail in the literature, in some areas the base of the Makganyene Formation contains IFs interbedded with the diamicitite. The IFs occur as approximately 3–5 m-thick interbeds in the diamictite and show all the IF mineralogical facies.

Higher up in the Postmasburg Group, occurring conformably above the Ongeluk Formation lavas, the Hotazel Formation comprises four IF units interbedded with three Mn formations grading upwards into the carbonates of the Mooidraai Formation (Fig. 17.4b; Gutzmer and Beukes 1995, 1996). The total thickness of the Hotazel Formation is approximately 100 m, with the IF thicknesses being antithetic to those of the Mn formations (Tsikos and Moore 1997). The mineralogy of the IFs includes oxide, mixed and carbonate facies whereas the textures vary between ferhythmites, microgranular interbeds and irregularly banded and podded IFs (Tsikos and Moore 1997). The Mn beds of the Hotazel Formation are world renowned because they make up the Kalahari Manganese Field (KMF), the largest land-based deposit of Mn in the world (Beukes et al. 2016). The age of the Hotazel Formation is highly controversial and subject to contradictory age data with regard to the Ongeluk and Mooidraai Formations, which respectively underlie and overlie the Hotazel Formation conformably. The Ongeluk lavas have been correlated to the Hekpoort lavas in the Transvaal region, with both originally dated at approximately 2.2 Ga by Rb–Sr whole rock for the Hekpoort (Burger and Coertze 1973–74) and a Pb–Pb whole-rock model age for the Ongeluk (Cornell et al. 1996). However, Bau et al. (1999) dated the Mooidraai carbonates at approximately 2.4 Ga using a bulk rock Pb–Pb age, and Gumsley et al. (2017) dated a dolerite appearing to crosscut the Ongeluk lavas at approximately 2.43 Ga using U–Pb in baddelyites.

17.6 Mid-Proterozoic Iron-Rich Metasediments of Southern Africa

The Bushmanland Group, a less than 1500 m-thick sequence of deformed amphibolite facies metavolcanics and metasediments that occurs in the central Namaqualand

Province of the Northern Cape Province of South Africa (Fig. 17.1), is well known for hosting the Broken Hill-type base metal deposits of the Aggeneys Gamsberg district (Stalder and Rozendaal 2002, 2005). Within the Kouboom Subgroup towards the top of the Bushmanland Group, the Gams Formation contains chemical precipitates, of which an approximately 0.3–5 m-thick layer has been described either as manganiferous IFs (Stalder and Rozendaal 2002) or chemogenic stratabound Mn–Fe-rich metasedimentary rocks (McClung 2006). McClung also documents the presence of an approximately 0.3–0.5 m-thick stratabound Mn–Fe-rich metasedimentary unit in the Namies Schist Formation of the lower Wortel Subgroup. Both Fe–Mn-rich units occur within aluminous schist successions and show micro- to mesobands of alternating recrystallized quartz-garnet, quartz-Fe-oxides (Fig. 17.2g) and quartz-garnet-Fe-oxides. Generally referred to as IFs by mine geologists in the region, these Mn–Fe-rich strata have been used as an exploration tool in identifying prospective areas for base metal mineralization (McClung 2006).

Although generally referred to as IFs, the Mn–Fe-rich chemical metasedimentary units of the Bushmanland Group are difficult to definitely classify as true IFs. The high metamorphic grade and polydeformed nature of the stratigraphy make it difficult to properly classify the original depositional setting, although a shallow, locally restricted basin (Von Gehlen et al. 1983) or small third-order basins (McClung 2006) have been proposed. The major element geochemical composition is very similar to that of IFs. However, the Al_2O_3 content (~5 wt% average) is generally greater than for IFs (McClung 2006), suggesting, at least in part, that some of the lithologies were originally ferruginous shales. Another characteristic making it problematic to classify these units as true IFs is their depositional age. Deposition of the Wortel and Kouboom Subgroups has been bracketed between approximately 1650 and 1130 Ma in a detrital zircon provenance study by McClung (2006). This falls outside the generally accepted depositional age ranges of IFs, as discussed in the Introduction. If these highly deformed and metamorphosed units can be classified as true IFs, their occurrence within metasedimentary successions of aluminous schists would suggest that they are Superior-type IFs.

17.7 Neoproterozoic Rapitan-Type Iron Formations of Southern Africa

The geological record of southern Africa contains, within the Damara and Gariep Belts along its west coast (Fig. 17.1), true Rapitan-type IFs related to the Neoproterozoic Snowball Earth event (Kirschvink 1992; Hoffman et al. 1998).

The Neoproterozoic Damara and Otavi Belts that occur in northern Namibia (Fig. 17.1) contain the Chuos Formation

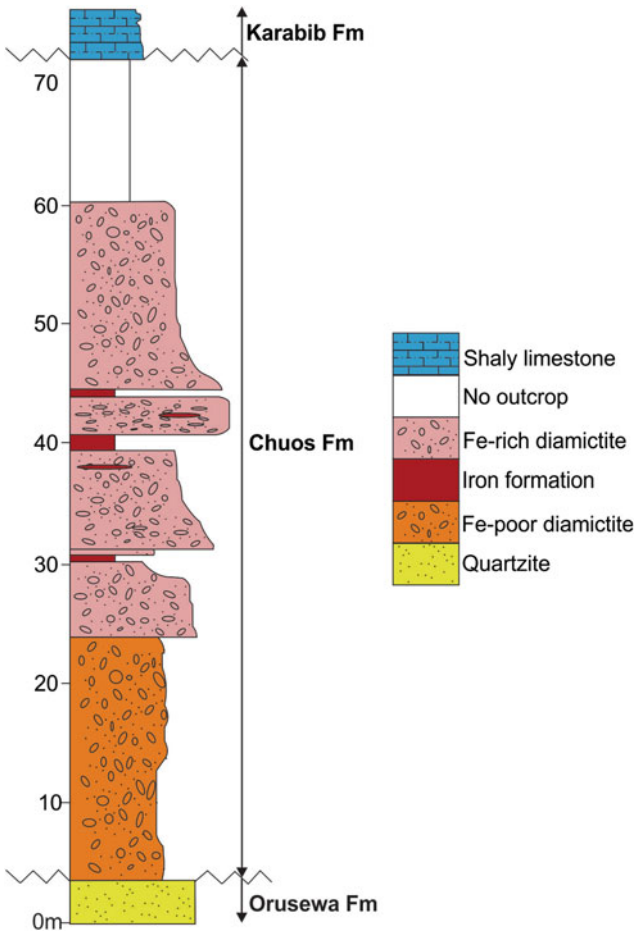

Fig. 17.5 A stratigraphic section of the Chuos Formation in the Damara Belt measured at Lowenfontein towards the southern margin of the Damara Belt (adapted from Lechte et al. 2017)

of the Swakop (NE Namibia) and Otavi (NW Namibia) Groups, which is a glacial diamictite deposited during the approximately 717–660 Ma global Sturtian glaciation (Gaucher et al. 2015; Beukes et al. 2016; Lechte and Wallace 2016). The Chuos Formation mostly comprises glacial diamictite and contains a ferruginous facies that contains ferruginous diamictite and an IF (Table 17.1; Figs. 17.2h and 17.5). The IF is finely laminated (i.e., ferhythmite) and composed of mostly magnetite and chert (Lechte and Wallace 2016), making it an oxide facies IF. The Chuos Formation is approximately 70 m thick in the Damara Belt (Fig. 17.5), although some sections towards the northern margin are almost 300 m thick. The thickness (<1–10 m) and number (1–6) of IF horizons interbedded with diamictite in the Chuos Formation varies across the Gariep Belt (Lechte et al., in review). At Otjosondu, a correlative section of the Chuos Formation has an approximately 30–40 m thick IF under- and overlain by a 4–6 m thick Mn formation. This chemical sedimentary succession, which is limited in its lateral extent when compared to the diamictite section of the

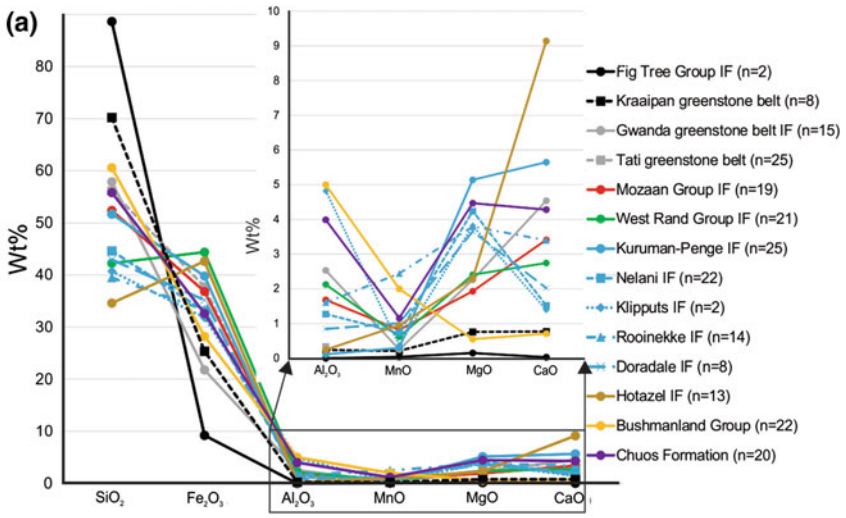
(a)
Wt%
SiO2
Fe2O3
Al2O3
MnO
MgO
CaO
Fig Tree Group IF (n=2)
Kraaipan greenstone belt (n=8)
Gwanda greenstone belt IF (n=15)
Tati greenstone belt (n=25)
Mozaan Group IF (n=19)
West Rand Group IF (n=21)
Kuruman-Penge IF (n=25)
Nelani IF (n=22)
Klipputs IF (n=2)
Rooinekke IF (n=14)
Doradale IF (n=8)
Hotazel IF (n=13)
Bushmanland Group (n=22)
Chuos Formation (n=20)

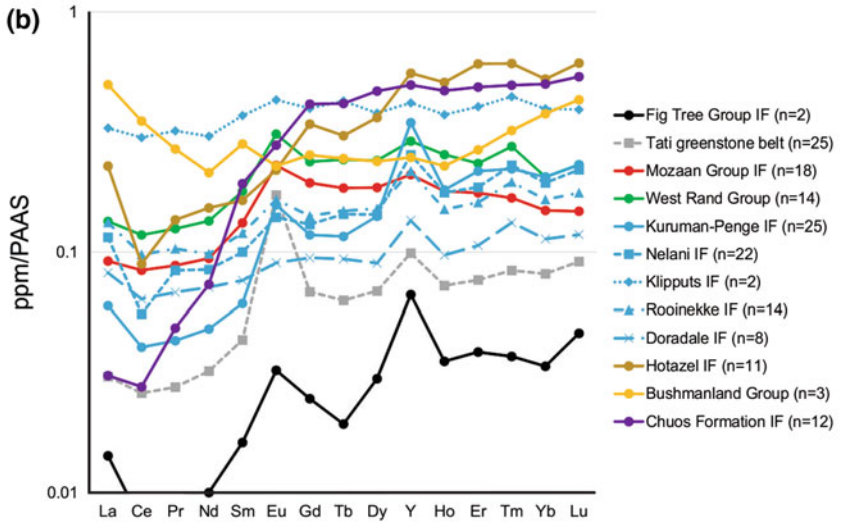
(b)
ppm/PAAS
La Ce Pr Nd Sm Eu Gd Tb Dy Y Ho Er Tm Yb Lu
Fig Tree Group IF (n=2)
Tati greenstone belt (n=25)
Mozaan Group IF (n=18)
West Rand Group (n=14)
Kuruman-Penge IF (n=25)
Nelani IF (n=22)
Klipputs IF (n=2)
Rooinekke IF (n=14)
Doradale IF (n=8)
Hotazel IF (n=11)
Bushmanland Group (n=3)
Chuos Formation IF (n=12)

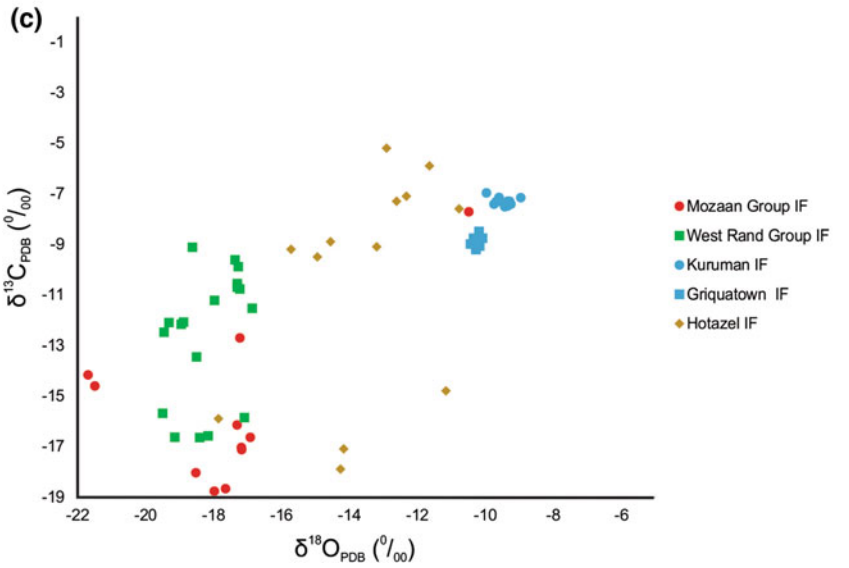
(c)
δ13CPDB (‰)
δ18OPDB (‰)
Mozaan Group IF
West Rand Group IF
Kuruman IF
Griquatown IF
Hotazel IF

Fig. 17.6 Selected geochemical data from the literature for the IFs of southern Africa. **a** Spider diagram plot of selected average major element contents from the Ngwenya IF of the Fig Tree Group of the Barberton greenstone belt (Hofmann 2005); the Kraaipan greenstone belt IF (Hammond and Moore 2006); the Gwanda greenstone belt IF (Saager et al. 1987); the Matsijole and Penhalonga IFs of the Tati greenstone belt (Døssing et al. (2009); the Mozaan Group IFs (Smith 2007); the West Rand Group IFs (Smith et al. 2013); the Kuruman-Penge IFs (Gutzmer et al. 2008); the Nelani, Klipputs, Rooinekke and Doradale IFs (Nel 2013); the Hotazel IF (Tsikos et al. 2003); the Bushmanland Group Mn–Fe-rich chemical metasedimentary rocks (McClung 2006); and the Chuos IF (Lechte and Wallace 2016). **b** Post-Archean Australian Shale (PAAS; Taylor and McLennan 1985) normalized average REY spider diagram plot from the Ngwenya IF of the Fig Tree Group of the Barberton greenstone belt (Hofmann 2005); the Matsijole and Penhalonga IFs of the Tati greenstone belt (Døssing et al. (2009); the Mozaan Group IFs (Smith 2007); the West Rand Group IFs (Smith et al. 2008, 2013); the Kuruman-Penge IFs (Gutzmer et al. 2008); the Nelani, Klipputs, Rooinekke and Doradale IFs (Nel 2013); the Hotazel IF (Blignaut 2017); the Bushmanland Group Mn–Fe-rich chemical metasedimentary rocks (McClung 2006); and the Chuos IF (Lechte and Wallace 2016). Oxygen (normalized to Peedee Belemnite; PDB) versus carbon (normalized to PDB) in carbonate stable isotope XY scatter plot from the Mozaan Group IFs (Smith 2007); the West Rand Group IFs (Smith et al. 2013); the Kuruman and Griquatown IFs (Kaufman 1996); and the Hotazel IF (Tsikos et al. 2003)

Chuos Formation, occurs between two quartzite units (Beukes et al. 2016).

The Port Nolloth Group of the approximately 770–550 Ma Gariep Belt that lies along the west coast of the Northern Cape Province of South Africa and southern Namibia contains the Jakkalsberg Member IF within the approximately 500 m-thick glaciogenic diamictite of the Numees Formation (Table 17.1; Fölling and Frimmel 2002). The deposition of the Numees Formation was originally linked to the approximately 580 Ma Marinoan global glaciation (Frimmel et al. 2002). However, a geological mapping, stratigraphic and sedimentological study of the Port Nolloth Group by MacDonald et al. (2010) concluded that the Numees Formation is older than previously thought and associated with the approximately 717 Ma Sturtian global glaciation.

17.8 Selected Geochemical Characteristics of the Iron Formations of Southern Africa

When assessing published data on the whole-rock geochemistry of IFs occurring in southern Africa, the major elements show a clear trend that the greenstone belt-hosted Algoma-type IFs on average have higher SiO_2 and lower Fe_2O_3 content than the Superior-type IFs (Fig. 17.6a). However, the effects of secondary alteration on the SiO_2 content in Algoma-type IFs should not be ignored because the primary IFs might have had a lower SiO_2 content. The Mn–Fe-rich chemical metasedimentary units of the Bushmanland Group show similar SiO_2 and Fe_2O_3 content to that of the Algoma-type IFs. With regard to Al_2O_3, which is generally considered to be of detrital origin and can act as an indicator of chemical precipitate purity, the majority of the IFs, with the exception of the Bushmanland Group Mn–Fe-rich chemical metasedimentary units and the Klipputs IF, have an average Al_2O_3 content of less than 3 wt%. The average MnO content is generally low (<1 wt%) with elevated content only observed in the Bushmanland Group and Rooinekke IFs. The average MgO and CaO content show a wide spread. However, the IFs of the Asbesheuwels Group of the Transvaal Supergroup (Kuruman-Penge, Nelani, Klipputs, Rooinekke and Doradale IFs) are all enriched in average MgO content. The Hotazel IF has an anomalously high average CaO content.

The rare earth-element and yttrium (REY) geochemistry of IFs has been extensively studied because it can reflect the chemistry of the water column from which the IFs were precipitated, so it can be used as a robust geochemical proxy of the paleoenvironment (e.g., Bau and Dulski 1996; Viehmann et al. 2015). When assessing the average REY content of the IFs of southern Africa normalized to Post-Archean Australian Shale (PAAS), some important trends and characteristics are observed (Fig. 17.6b). The majority of the IFs show heavy rare-earth element (HREE) over light rare-earth element (LREE) enrichment, which is typical of most Precambrian IFs (Klein and Beukes 1993b) and modern seawater (Bau and Dulski 1996). Only at elevated REY contents, which could be due to elevated detrital influxes during deposition, do the patterns become flatter and more shale-like (e.g., Klipputs IF and Bushmanland Group). Different positive or negative REE anomalies (anomaly calculations in Bau and Dulski 1996) are also assessed because these can be used as paleoenvironmental indicators. For example, a prominent feature in the Algoma-type and the older Superior-type IFs is the presence of a prominent positive Eu anomaly (Fig. 17.6b), which, along with the HREE over LREE enrichment, are observed for hydrothermal fluids mixed with ocean water (Dymek and Klein 1988; Klein and Beukes 1993b; Bekker et al. 2010). However, it appears that there is a temporal correlation with the positive Eu anomaly because it is absent in the younger IFs (Doradale IF and onwards). True Ce anomalies, which are indicative of Ce oxidation and imply complete oxidation and precipitation of all Fe in the original depositional system (Bau and Dulski 1996; Smith 2007), are only observed in the Hotazel Formation IFs. This implies that by the time the Hotazel Formation was being deposited, the system was completely oxic, as also supported by apparent Mn oxidation and deposition into the interbedded Mn formations. The positive Y anomalies, which are observed in all the IFs documented here except for the Klipputs IF, Bushmanland Group and

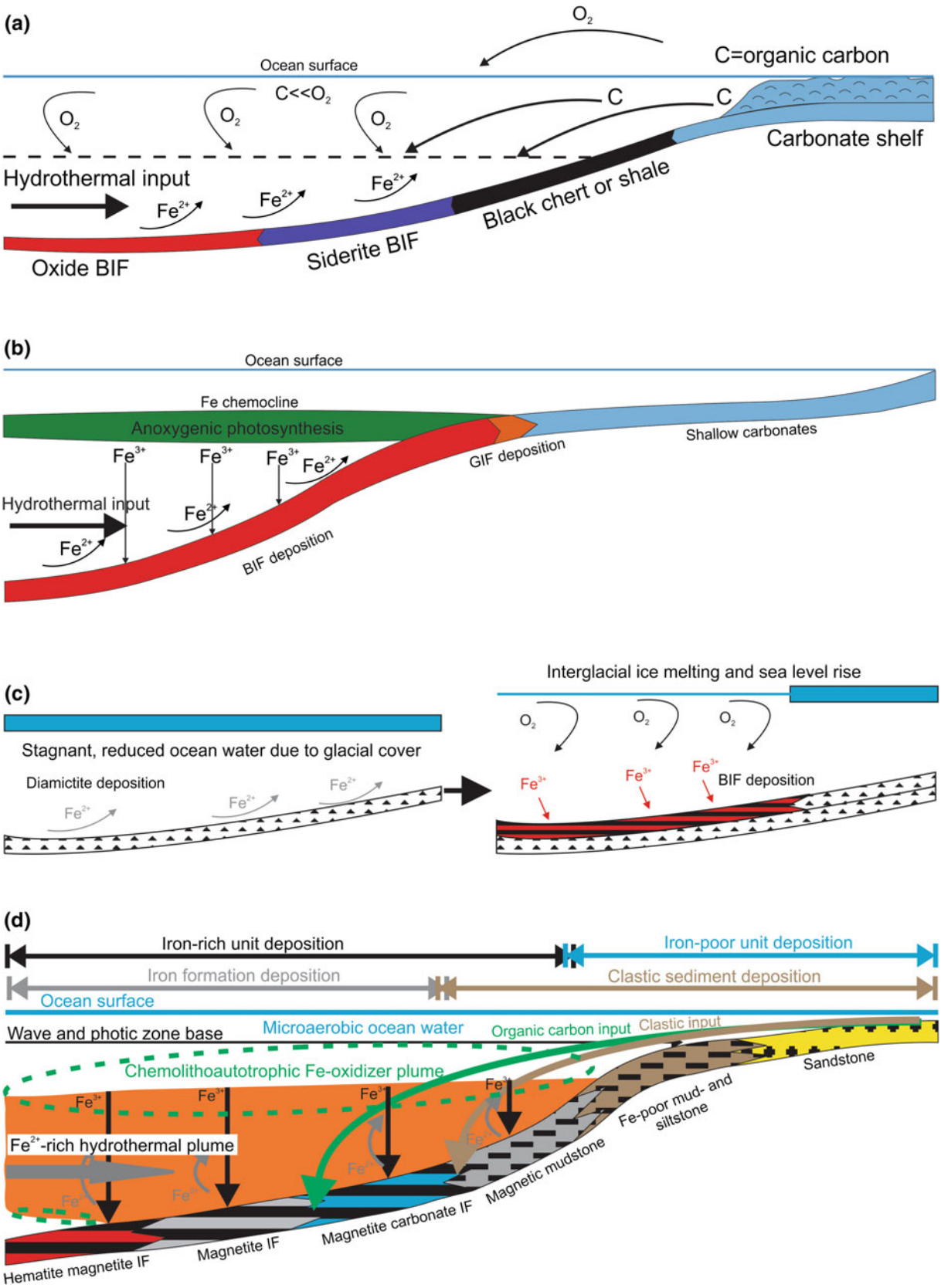
(a)
O2
C=organic carbon
Ocean surface
C<<O2
C
C
O2
O2
O2
Carbonate shelf
Hydrothermal input
Fe2+
Fe2+
Fe2+
Black chert or shale
Oxide BIF
Siderite BIF
(b)
Ocean surface
Fe chemocline
Anoxygenic photosynthesis
Fe3+
Fe3+
Fe3+
Fe2+
Shallow carbonates
GIF deposition
Hydrothermal input
Fe2+
Fe2+
BIF deposition
(c)
Interglacial ice melting and sea level rise
Stagnant, reduced ocean water due to glacial cover
O2
O2
O2
Diamictite deposition
Fe2+
Fe2+
Fe2+
Fe3+
Fe3+
Fe3+
BIF deposition
(d)
Iron-rich unit deposition
Iron-poor unit deposition
Iron formation deposition
Clastic sediment deposition
Ocean surface
Wave and photic zone base
Microaerobic ocean water
Organic carbon input
Clastic input
Chemolithoautotrophic Fe-oxidizer plume
Sandstone
Fe3+
Fe3+
Fe3+
Fe3+
Fe2+-rich hydrothermal plume
Fe-poor mud- and siltstone
Magnetic mudstone
Magnetite carbonate IF
Magnetite IF
Hematite magnetite IF

Fig. 17.7 Depositional models for IFs. **a** Abiological stratified ocean depositional model for IF through upwelling hydrothermal Fe^{2+} encountering a redox chemocline leading to oxidation and precipitation of Fe. Siderite deposition in shallower facies was attributed to increased p_{CO_2} as a result of degrading organic C closer to the carbonate shelf (adapted from Klein and Beukes 1989; Beukes and Gutzmer 2008). **b** Biologically mediated depositional model for IFs under completely anoxic conditions. Fe is sourced from hydrothermal Fe^{2+} upwelling and Fe deposition is mediated by Fe-oxidizing anoxygenic phototrophic bacteria (adapted from Bekker et al. 2010). **c** Depositional model for Neoproterozoic glacially associated Rapitan-type IFs where ice cover caused an anoxic, stagnant water column where dissolved Fe^{2+} could accumulate. Glacial retreat introduced O_2 into the ocean, leading to Fe oxidation and IF deposition into the diamictite (adapted from Beukes and Klein 1992, 1993a). **d** Depositional model for the Mesoarchean Superior-type IFs of the West Rand Group where no Fe was preserved above the wave base or the photic zone. Fe^{2+} was introduced by hydrothermal plumes and the oxidation of Fe took place below the photic zone through chemolithoautotrophic Fe-oxidizing bacteria in a low concentration of free O_2 (adapted from Smith et al. 2013)

Chuos Formation, are indicative of fairly rapid IF deposition (Bau and Dulski 1996).

In carbonate and mixed facies IFs, the stable C and O isotopes of the carbonate minerals can be measured. In the Superior-type IFs of southern Africa, all the Fe-bearing carbonates show prominently depleted $\delta^{13}C_{PDB}$ (~ -5 to $-19^0/_{00}$) and $\delta^{18}O_{PDB}$ (~ -9 to $-22^0/_{00}$) values (Fig. 17.6 c). The depleted $\delta^{13}C_{PDB}$ values suggest that the C in the carbonates was sourced from the oxidation of organic C in the sediment (Schidlowski 1987; Des Marais 2001), implying that biological activity played a role in IF deposition (e.g., Kaufman 1996; Beukes and Gutzmer 2008; Bekker et al. 2010). This also highlights a likely diagenetic origin of Fe-rich carbonates where the reduction of Fe^{3+} to Fe^{2+} in the sediment oxidized the organic C, thereby producing Fe-rich carbonates (Smith et al. 2013). The depleted $\delta^{18}O_{PDB}$ values could be the result of the ocean temperature during IF deposition or a metamorphic effect (Smith et al. 2013).

Other, less traditional geochemical characteristics have also been studied in the IFs of southern Africa. For example, studies on the Fe isotopes of the Asbesheuwels Subgroup IFs found that haematite and magnetite generally had zero to positive $\delta^{56}Fe$ values, and siderite generally had negative $\delta^{56}Fe$ values (Johnson et al. 2003, 2008). The positive $\delta^{56}Fe$ values were concluded to be caused by incomplete oxidation of the hydrothermal Fe^{2+} source during IF deposition, whereas the negative $\delta^{56}Fe$ values were concluded to be the result of dissimilatory Fe reduction during the diagenetic formation of carbonates. The Nd isotopes of the Vlakhoek Member IF (Alexander et al. 2008) and Contorted Bed and Water Tower IFs (Viehmann et al. 2015) have also been documented, with the studies reporting highly negative ε_{Nd} values, indicating that the Nd was derived from continental sources. However, the greater detrital influx in these IFs likely had a large effect on some of these values (Viehmann et al. 2015). Another study by Døssing et al. (2009) reported on the Pb isotopes of the IFs of the Tati greenstone belt. The Pb isotopes provided an approximate depositional age of 2.7 Ga, a metamorphic age of approximately 2 Ga, and also suggested a complex extraction prehistory of the Pb sources from an older Archean mantle reservoir. A study of the Mo isotopes of the Vlakhoek Member IF by Planavsky et al. (2014) is discussed in more detail in the next section.

17.9 Depositional Models and the Geological Significance of the Iron Formations of Southern Africa

IFs, being interpreted as the product of direct precipitation from seawater, may serve as proxies to provide information about the environment in which they were deposited. The increased geological occurrence of IFs during the Neoarchean to Paleoproterozoic, with cessation at approximately 1.8 Ga and a recurrence during the Neoproterozoic, has also been interpreted to be the result of changes in the paleoenvironments on Earth through time (see reviews by Bekker et al. 2010; Smith 2015). Detailed discussions on the depositional models of Mesoarchean to Paleoproterozoic IFs, which integrate stratigraphy, sedimentology, petrography, mineralogy and geochemistry, can be found in the work of Klein (2005), Beukes and Gutzmer (2008), Bekker et al. (2010) and Smith et al. (2013). This section will summarize published depositional models for the Superior- and Rapitan-type IFs. Some studies conducted on IFs in southern Africa and how they played a role in a better understanding of the Earth's marine paleoenvironments will also briefly be discussed.

With regard to Superior-type IFs, it is generally accepted that the source of Fe in these IFs was dissolved Fe^{2+} from hydrothermal influx into the marine basin, as implied by positive Eu anomalies (e.g., Dymek and Klein 1988; Bau and Dulski 1996; Beukes and Gutzmer 2008; Smith et al. 2013). It has also been recognized that there is a lateral depositional facies control on the mineralogical IF facies observed, with oxides more distal, carbonates intermediate and silicates more proximal to the coastline (Beukes and Gutzmer 2008; Smith et al. 2013). Another challenge in developing depositional models was that it was clear from mineralogical evidence, such as abundant magnetite with positive $\delta^{56}Fe$ values (e.g., Johnson et al. 2003, 2008) and the presence of primary haematite (e.g., Smith et al. 2013), that Fe oxidation was the major mechanism in Fe deposition. This creates a redox problem with regard to the large-scale transport of dissolved Fe^{2+} and then precipitation by oxidation (Smith 2015). Initially an abiological, chemically stratified ocean model was developed by Klein and Beukes

(1989) for IF deposition in the Campbellrand Subgroup carbonate to Asbesheuwels Subgroup IF transition (Fig. 17.7a). In this model, upwelling, Fe^{2+}-enriched bottom waters from hydrothermal input encountered oxygenated surface waters along a chemocline where the oxidation and precipitation of ferrihydrite took place. In areas more proximal to the coast, where there was greater organic matter production closer to the carbonate platform, siderite was precipitated as a result of increased p_{CO_2}, leading to the lateral mineralogical facies variations seen in IFs. However, due to the pre-GOE setting of many of these IFs, the presence of any free oxygen in IF depositional models was considered problematic. Photo-oxidation, now considered too inefficient to account for IFs, and later anoxygenic phototropic Fe-oxidizing bacteria (e.g., Konhauser et al. 2002; Kappler et al. 2005; Posth et al. 2008), became the preferred precipitation mechanism for IF deposition during pre-GOE times (Bekker et al. 2010). Later depositional models therefore envisioned a chemocline defined by anoxygenic photosynthesis (i.e., anoxygenic phototropic Fe-oxidizing bacteria) rather than shallow water oxygenic photosynthesis (Fig. 17.7b; Bekker et al. 2010). Lateral mineralogical facies variations could be explained by variable diagenetic processes, controlled by proximity to the coast, in the sediment (e.g., Beukes and Gutzmer 2008; Smith et al. 2013). However, there is still some debate around oxygen-free IF deposition on the pre-GOE Earth, which will be briefly highlighted at the end of this section.

With regard to the Neoproterozoic Rapitan-type Snowball Earth-related IFs, there are important differences from the older Algoma- and Superior-type IFs. First, mixed facies are generally absent and mostly oxide facies are present (Table 17.1). Also, positive Eu anomalies are lacking (Fig. 17.6b) and these IFs were deposited well after the GOE in what is considered to have been well-oxygenated surface environments. A major difference, however, is the geological setting, where the Rapitan-type IFs are interbedded with glacial diamictites rather than upwards fining stable shelf or volcaniclastic successions. A depositional model, taking into account the unique sedimentological setting of these IFs as well as their differences from older IFs, was developed by Klein and Beukes (1992, 1993a). In this model (Fig. 17.7c), depositional basins became stagnant and reducing as a result of complete ice cover during the Neoproterozoic Snowball Earth period. This caused a build-up of dissolved Fe^{2+} in the water column. During interglacial periods, the ice would melt and the glaciers would retreat, exposing the water mass to the oxygenated atmosphere, leading to Fe oxidation and IF deposition along with diamictites. Lechte and Wallace (2016) changed this depositional model based on their observations in the Neoproterozoic IFs of Namibia. No transitional facies between the diamictites and IFs were observed, and the fine interbedding of IF and diamictite did not support drastic environmental changes, such as glacial retreat. They proposed that these IFs were deposited below the ice shelf through an ice pump mechanism where cold, oxygenated glacial fluid mixed with ferruginous seawater.

An important topic with regard to the study of IFs relates to the pre-GOE Earth's surface environments. Detailed studies of the geochemistry of the early Earth rock record, with a focus on sulphur mass independent fractionation (SMIF) in particular, resulted in the conclusion that the Earth's surface environments were mostly anoxic before approximately 2.5– 2.3 Ga (e.g., Holland 2002; Guo et al. 2009; Hoffman 2013). As stated, Fe oxidation in the deposition of IFs has been mostly ascribed to anoxygenic phototropic Fe-oxidizing bacteria (e.g., Kappler et al. 2005; Posth et al. 2008). However, studies of the Mesoarchean Superior-type IFs of the Kaapvaal Craton have put these anoxic pre-GOE environments into question. Planavsky et al. (2014) reported Mo isotopic data for the Vlakhoek Member, including its IF, of the approximately 2.98–2.84 Ga Mozaan Group (Figs. 17.1 and 17.3a; Table 17.1). They concluded that the Mo isotopic signature indicates Mo interaction with Mn oxides, with the latter only being able to form under oxic conditions. This implies IF deposition in the presence of free oxygen during the Mesoarchean. The study by Planavsky et al. (2014) was also supported by a later one by Ossa Ossa et al. (2016), also conducted on the Vlakhoek Member, which found MnO concentrations of up to 15 wt% in the IF and shale. The latter group concluded that secondary hydrothermal Mn enrichment took place, but that original MnO content was likely as high as 8.5 wt%. They interpreted the high primary Mn content as being due to Mn deposition through oxidation by free oxygen in a shallow marine environment. Further support for these conclusions came from a study on the IFs of the laterally equivalent West Rand Group of the Witwatersrand Supergroup (Table 17.1) by Smith et al. (2013). In their depositional model (Fig. 17.7d) they concluded that the lateral facies of the sandstone to shale to IF sedimentary sequence shows a depletion of Fe in all lithologies deposited above wave base, whereas below wave base lithologies are Fe-rich. Further, they suggested that because the wave base and the base of the photic zone sit at similar depths, there is no sedimentological evidence that Fe was ever present within the photic zone, negating the role of anoxygenic phototropic Fe-oxidizing bacteria and implying

that chemolithoautotrophic Fe-oxidizing bacteria (Konhauser et al. 2002) in the presence of free oxygen must have played a role in the deposition of certain pre-GOE IFs.

17.10 The Economic Significance of the Iron Formations of Southern Africa

IF-hosted high-grade haematite ore deposits have provided the bulk of iron ore mined across the world in modern times (Smith and Beukes 2016). Most of southern Africa's IF-hosted ores occur in the Transvaal Supergroup, with these deposits producing 78 million tonnes of high-grade haematite ore during 2014 (United States Geological Survey 2015). High-grade ore deposits are developed in the following units of the Transvaal Supergroup (Fig. 17.4a): the Sishen, Khumani, Beeshoek, Sishen South, Bovenzeekoebaart and Nauga East deposits in the Asbesheuwels Subgroup; the Thabazimbi deposit in the Penge IF; the Rooinekke deposit in the Rooinekke IF of the Koegas Subgroup; and some deposits in the Hotazel Formation. Of these, the superlarge deposits of the Maremane Dome of the Northern Cape Province of South Africa—namely, Sishen, Khumani, Beeshoek and Sishen South—provide by far the bulk of the ore production (Smith and Beukes 2016).

For IF-hosted high-grade haematite ores to develop, an epigenetic residual Fe-enrichment process has to occur where silica is removed from IFs. Three genetic ore types are recognized in the Transvaal Supergroup (Beukes et al. 2003; Smith and Beukes 2016): supergene, hydrothermal and magmatically induced hydrothermal ores. Supergene deposits are typically characterized by the high-grade ore being developed below an erosional unconformity, grading downwards into oxidized IF (Fig. 17.8a). Downwards migrating meteoric water with a high pH and Eh in a lateritic weathering profile is interpreted to have removed silica from IFs (e.g., Van Schalkwyk and Beukes 1986; Carney and Mienie 2003; Van Deventer 2009). Supergene ore deposits in the Transvaal Supergroup include Sishen, Khumani, Beeshoek, Sishen South, Rooinekke and occurrences in the Hotazel Formation (Fig. 17.4a). All these deposits occur directly below the regional pre-Gamagara unconformity of the Northern Cape Province of South Africa, with reworked conglomeratic ore occurring above the unconformity in many instances (Fig. 17.8a; Smith and Beukes 2016).

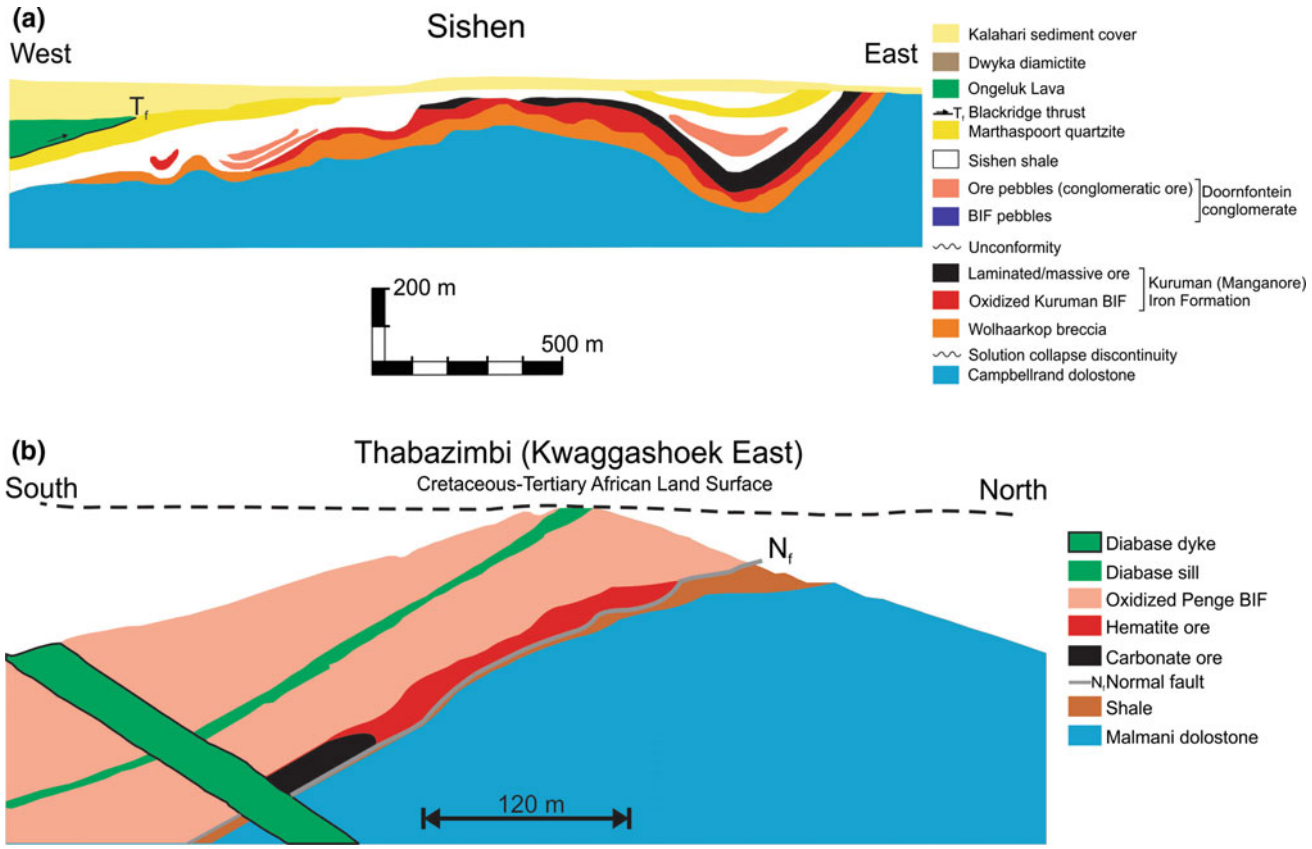

Fig. 17.8 Cross-sections through parts of the Sishen supergene (**a** adapted from Carney and Mienie 2003; Van Deventer 2009; Smith and Beukes 2016) and Thabazimbi hydrothermal (**b** adapted from Netshiozwi 2002; Smith and Beukes 2016) IF-hosted high-grade haematite ore deposits

Hydrothermal deposits are typically characterized by the high-grade ore occurring at the basal contact between the IF and underlying shale, grading upwards into the oxidized IF (Fig. 17.8b). Thrust fault systems typically intersect the deposits, and faulted contacts also occur between lithological units (e.g., Netshiozwi 2002; Harding 2004). Crosscutting dykes and sills within the overlying IFs are also common. Laterally and upwards migrating fluids with a high pH and Eh, related to either orogenesis or large intrusions, are interpreted to have removed silica and oxidized all remaining Fe-bearing minerals (e.g., Netshiozwi 2002; Beukes et al. 2003; Harding 2004). Hydrothermal ore deposits in the Transvaal Supergroup include Thabazimbi in the Limpopo Province and Bovenzeekoebaart in the Northern Cape Province of South Africa (Fig. 17.4a).

Magmatically induced hydrothermal deposits have the high-grade ore occurring exclusively above syenite-carbonatite intrusions, with the removal of silica and oxidation of Fe-bearing minerals by carbonatitic fluids. The only known example of such an ore deposit in the Transvaal Supergroup is the Nauga East deposit in the Northern Cape Province of South Africa (Fig. 17.4a).

A more detailed review of the IF-hosted high-grade haematite ore deposits of the Transvaal Supergroup and their characteristics was carried out by Smith and Beukes (2016). Fe ore deposits are also developed in: the greenstone belts of Zimbabwe, for example the Buhwa greenstone belt (Fedo and Eriksson 1995) and the Bulawayan Group IFs (Du Toit 2014); the Masoke IF of the Transvaal Supergroup in the Kanye region of Botswana (http://www.strata-africa.com/botswana-iron-ore.html); and poorly documented occurrences in the Chous Formation of Namibia, with Mn deposits in this unit enjoying more attention (e.g., Beukes et al. 2016).

Acknowledgements I wish to thank the Department of Geology at the University of Johannesburg, the Paleoproterozoic Mineralisation Research Group (PPM), Kumba Iron Ore and the Department of Science and Technology (DST) and the National Research Foundation (NRF) funded Centre of Excellence for Integrated Mineral and Energy Resource Analysis (CIMERA) for its funding and support. Thanks go to Nic Beukes and Jens Gutzmer for their guidance and mentorship, especially during my first research on iron formations; to Axel Hofmann and Maxwell Lechte for providing literature and photographs that helped in preparing this chapter; and to Conrad de Kock for assisting in the preparation of some of the figures.

References

Alexander BW, Bau M, Andersson P, Dulski P (2008) Continentally-derived solutes in shallow Archean seawater: Rare earth element and Nd isotope evidence in iron formation from the 2.9 Ga Pongola Supergroup, South Africa. Geochimica et Cosmochimica Acta 72:378–394

Armstrong RA, Compston W, Retief EA, William LS, Welke HJ (1991) Zircon ion microprobe studies bearing on the age and evolution of the Witwatersrand triad. Precambr Res 53:243–266

Arndt NT, Wilson A, Hofmann A, Mason P, Bau M, Byerly G, Chunnett G (2012) Peering into the cradle of life: scientific drilling in the Barberton Greenstone Belt. Sci Drilling 13:71

Basei MAS, Frimmel HE, Nutman AP, Preciozzi F, Jacob J (2005) A connection between the Neoproterozoic Dom Feliciano (Brazil/Uruguay) and Gariep (Namibia/South Africa) orogenic belts—evidence from a reconnaissance provenance study. Precambr Res 139:195–221

Bau M, Dulski P (1996) Distribution of yttrium and rare-earth elements in the Penge and Kuruman iron-formations, Transvaal Supergroup, South Africa. Precambr Res 79:37–55

Bau M, Romer RL, Lüders V, Beukes NJ (1999) Pb, O, and C isotopes in silicified Mooidraai dolomite (Transvaal Supergroup, South Africa): implications for the composition of Paleoproterozoic seawater and 'dating' the increase of oxygen in the Precambrian atmosphere. Earth and Planetary Science Letters 174:43–57

Bekker A, Slack JF, Planavsky N, Krapež B, Hofmann A, Konhauser KO, Rouxel OJ (2010) Iron formation: the sedimentary product of a complex interplay among mantle, tectonic, oceanic, and biospheric processes. Econ Geol 105:467–508

Bekker A, Planavsky NJ, Krapež B, Rasmussen B, Hofmann A, Slack JF, Rouxel OJ, Konhauser KO (2014) Iron formations: their origins and implications for ancient seawater chemistry. In: Holland H, Turekian K (eds) Treatise on geochemistry. Elsevier, Waltham, pp 561–625

Beukes NJ (1973) Prebambrian iron-formations of Southern Africa. Econ Geol 68:960–1004

Beukes NJ (1983) Palaeoenvironmental setting of iron-formations in the depositional basin of the Transvaal supergroup, South Africa. In: Trendall AF, Morris RC (eds) Iron-formation: facts and problems. Elserivier, Amsterdam, pp 131–209

Beukes NJ (1984) Sedimentology of the Kuruman and Griquatown iron-formation, Transvaal supergroup, Griqualand West, South Africa. Precambr Res 24:47–84

Beukes NJ (1995) Stratigraphy and basin analyses of the West Rand Group with special reference to prospective areas for placer gold deposits. Rand Afrikaans University Geology Department, Johannesburg, Unpublished Report, 117 p

Beukes NJ, Cairncross B (1991) A lithostratigraphic-sedimentological reference profile for the Late Archaean Mozaan Group, Pongola sequence: application to sequence stratigraphy and correlation with the Witwatersrand supergroup. S Afr J Geol 94:44–69

Beukes NJ, Gutzmer J (2008) Origin and paleoenvironmental significance of major iron formations at the Archean-Paleoproterozoic boundary. Rev Econ Geol 15:5–47

Beukes NJ, Gutzmer J, Mukhopadhyay J (2003) The geology and genesis of high-grade iron ore deposits. Appl Earth Sci (Trans. Inst Min Metall B) 112:B18–B25

Beukes NJ, Swindell EPW, Wabo H (2016) Manganese deposits of Africa. Episodes 39:285–317

Blignaut LC (2017) A petrographical and geochemical analysis of the upper and lower Maganese Ore Bodies from the Kalahari Manganese Deposit, Northern Cape, South Africa—Controls on Hydrothermal Metasomatism and Metal Upgrading. Unpublished Ph.D. thesis, University of Johannesburg, Johannesburg, 257 p

Block S, Moyen J-F, Zeh A, Poujol M, Jaguin J, Paquette J-L (2013) The Murchison Greenstone Belt, South Africa: accreted slivers with contrasting metamorphic conditions. Precambr Res 227:77–98

Bontognali TRR, Fischer WW, Föllmi KB (2013) Siliciclastic associated banded iron formation from the 3.2 Ga Moodies Group, Barberton Greenstone Belt, South Africa. Precambr Res 226:116–224

Brandl G, Cloete M, Anhaeusser CR (2006) Archaean greenstone belts. In: Johnson MR, Anhaeusser CR, Thomas RJ (eds) The geology of South Africa. Geological Society of South Africa, Johannesburg, Council for Geoscience, Pretoria, pp 9–56

Burger AJ, Coertze FJ (1973–74) Age determinations—April 1972–March 1974. Annal Geol Surv S Afr 10:135–141

Carney MD, Mienie PJ (2003) A geological comparison of the Sishen and Sishen South (Welgevonden) iron ore deposits, Northern Cape Province, South Africa. Appl Earth Sci (Trans. Inst Min Metall B) 112:B81–B88

Clout JMF, Simonson BM (2005) Precambrian iron formations and iron formation-hosted iron ore deposits. Economic Geology 100th Anniversary Volume, pp 643–679

Cornell DH, Schütte SS, Eglington BL (1996) The Ongeluk basaltic andesite formation in Griqualand West, South Africa: Submarine alteration in a 2222 Ma proterozoic sea. Precambr Res 79:101–124

Des Marais DJ (2001) Isotopic evolution of the biogeochemical carbon cycle during the Precambrian. Rev Min Geochem 43:555–578

Dirks PHGM, Jelsma HA (1998) Horizontal accretion and stabilization of the Archean Zimbabwe Craton. Geology 26:11–14

Døssing LN, Frei R, Stendal H, Mapeo RBM (2009) Characterization of enriched lithospheric mantle components in ~2.7 Ga banded iron formations: an example from the Tati Greenstone Belt, Northeastern Botswana. Precambr Res 172:334–356

Du Toit A (2014) Ripple Creek iron ore deposit. The Geological Society of Zimbabwe, http://www.geologicalsociety.org.zw/atlas/ripple-creek-iron-ore-deposit

Dymek RF, Klein C (1988) Chemistry, petrology and origin of banded iron-formation lithologies from the 3800 Ma Isua supracrustal belt, West Greenland. Precambr Res 39:247–302

Eriksson PG, Altermann W, Hartzer FJ (2006) The Transvaal supergroup and its precursors. In: Johnson, MR, Anhaeusser, CR, Thomas, RJ (eds.) The Geology of South Africa. Geological Society of South Africa, Johannesburg, Council for Geoscience, Pretoria, pp 237–260

Fedo CM, Eriksson KA (1995) Geologic setting and ideas concerning the origin of the iron-ore deposits at Buhwa, Zimbabwe. In: Blenkinsop TG, Tromp PL (eds) Sub-Saharan economic geology 1993. AA Balkema, Rotterdam, pp 43–53

Fedo CM, Eriksson KA (1996) Stratigraphic framework of the ~3.0 Ga Buhwa Greenstone Belt: a unique stable-shelf succession in the Zimbabwe Craton. Precambr Res 77:161–178

Fölling PG, Frimmel HE (2002) Chemostratigraphic correlation of carbonate carbonate successions in the Gariep and Saldania Belts, Namibia and South Africa. Basin Res 14:69–88

Foster RP, Wilson JF (1984) Geological setting of Archaean gold deposits in Zimbabwe. In: Foster RP (ed) Gold '82. AA Balkema Publishing, Rotterdam, pp 521–549

Frimmel HE, Fölling PG, Eriksson PG (2002) Neoproterozoic tectonic and climatic evolution recorded in the Gariep Belt, Namibia and South Africa. Basin Res 14:55–67

Fripp REP (1976) Stratabound gold deposits in Archean banded iron-formation, Rhodesia. Econ Geol 71:58–75

Gaucher C, Sial AN, Frei R (2015) Chemostratigraphy of neoproterozoic banded iron formation (BIF): types, age and origin. In: Ramkumar MU (ed) Chemostratigraphy. Elsevier, Amsterdam, pp 433–449

Gross GA (1980) A classification of iron formations based on depositional environments. Can Min 18:215–222

Gumsley AP, Chamberlain KR, Bleeker W, Söderland U, De Kock MO, Larsson ER, Bekker A (2017) Timing and tempo of the great oxidation event. PNAS 114:1811–1816

Guo Q, Strauss H, Kaufman AJ, Schröder S, Gutzmer J, Wing B, Baker MA, Bekker A, Jin Q, Kim S-T, Farquhar J (2009) Reconstructing earth's surface oxidation across the Archean-Proterozoic transition. Geology 37:399–402

Gutzmer J, Beukes NJ (1995) Fault-controlled metasomatic alteration of early proterozoic sedimentary manganese ores in the Kalahari Manganese field, South Africa. Econ Geol 90:823–844

Gutzmer J, Beukes NJ (1996) Mineral paragenesis of the Kalahari manganese field, South Africa. Ore Geol Rev 11:405–428

Gutzmer J, Beukes NJ, Pickard NJ, Barley ME (1999) SHRIMP age of a quartz porphyry sill in the Mozaan group: geochronological implication for the Pongola and the Witwatersrand Supergroups. S Afr J Geol 102(2):139–146

Gutzmer J, Chisonga BC, Beukes NJ, Mukhopadhyay J (2008) The geochemistry of banded iron formation-hosted high-grade hematite-martite iron ores. Rev Econ Geol 15:157–183

Hagemann S, Rosière C, Gutzmer J, Beukes NJ (2008) Introduction: banded iron formation-related high-grade iron ore. In: Hagemann S, Rosière C, Gutzmer J, Beukes NJ (eds) Reviews in economic geology, vol 15. Society of Economic Geologists, Littleton, pp 1–4

Hammond NG, Moore JM (2006) Archaean lode gold mineralisation in banded iron formation at the Kalahari Goldridge deposit, Kraaipan Greenstone Belt, South Africa. Miner Deposita 41:483–503

Harding CJ (2004) Origin of the Zeekoebaart and Nauga East high grade iron ore deposits, Northern Cape Province, South Africa. Unpublished M.Sc. dissertation, Rand Afrikaans University, Johannesburg, 128 p

Hegner E, Kröner A, Hunt P (1994) A precise U–Pb zircon age for the Archean Pongola Supergroup volcanics in Swaziland. J Afr Earth Sci 18(4):139–141

Hicks N, Hofmann A (2012) Stratigraphy and Provenance of the auriferousuraniferous, fluvial to shallow-Marine Sinqeni Formation, Mozaan Group, Northern KwaZulu-Natal, South Africa. S Afr J Geol 115:327–344

Hoffman PF, Kaufman AJ, Halverson GP, Schrag DP (1998) A neoproterozoic snowball earth. Science 281:1342–1346

Hoffman PF (2013) The great oxidation and a Siderian snowball earth: MIF-S based correlation of paleoproterozoic glacial epochs. Chem Geol 362:143–156

Hofmann A (2005) The geochemistry of sedimentary rocks from the Fig Tree Group, Barberton greenstone belt: Implications for tectonic, hydrothermal and surface processes during mid-Archaean times. Precambr Res 143:23–49

Hofmann A, Dirks PHGM, Jelsma HA, Natura N (2003) A tectonic origin for ironstone horizons in the Zimbabwe craton and their significance for greenstone belt geology. J Geol Soc London 160:83–97

Holland HD (2002) Volcanic gases, black smokers, and the Great Oxidation Event. Geochim Cosmochim Acta 66:3811–3826

Huizenga JM, Touret LR (1993) Fluid inclusions in shear zones: the case of the Umwindsi shear zone in the Harare-Shamva-Bindura greenstone belt, NE Zimbabwe. Eur J Min 11:1079–1090

Huston DL, Logan GA (2004) Barite, BIFs and bugs: evidence for the evolution of the Earth's early hydrosphere. Earth Planet Sci Lett 220:41–55

Isley AE, Abbott DH (1999) Plume-related volcanism and the deposition of banded iron formation. J Geophys Res 104:15461–15477

James HL (1954) Sedimentary facies of iron-formation. Econ Geol 49:235–293

Jelsma HA, Van der Beek PA, Vinyu ML (1993) Tectonic evolution of the Bindura-Shamva greenstone belt (northern Zimbabwe): progressive deformation around diapiric batholiths. J Struct Geol 15:163–176

Johnson CM, Beard BL, Beukes NJ, Klein C, O'Leary JM (2003) Ancient geochemical cycling in the Earth as inferred from Fe

isotope studies of banded iron formations from the Transvaal Craton. Contrib Miner Petrol 144:523–547
Johnson CM, Beard BL, Klein C, Beukes NJ, Roden EE (2008) Iron isotopes constrain biologic and abiologic processes in banded iron formation genesis. Geochim Cosmochim Acta 72:151–169
Jones IM, Anhaeusser CR (1993) Accretionary lapilli associated with Archaean banded iron formations of the Kraaipan Group, Amalia greenstone belt, South Africa. Precambr Res 61:117–136
Kappler A, Pasquero C, Konhauser KO, Newman DK (2005) Deposition of banded iron formations by anoxygenic phototrophic Fe(II)-oxidizing bacteria. Geology 33:865–868
Kaufman AJ (1996) Geochemical and mineralogical effects of contact metamorphism on banded iron-formation: an example from the Transvaal Basin, South Africa. Precambr Res 79:171–194
Kirschvink JL (1992) Late Proterozoic low-latitude global glaciation: the Snowball Earth. In: Schopf JW, Klein C (eds) The proterozoic biosphere: a multidisciplinary study. Cambridge University Press, New York, pp 51–52
Kirschvink JL, Gaidos EJ, Bertani LE, Beukes NJ, Gutzmer J, Maepa LN, Steinberger RE (2000) Paleoproterozoic snowball earth: extreme climatic and geochemical global change and its biological consequences. PNAS 97:1400–1405
Klein C (2005) Some Precambrian banded iron-formations (BIFs) from around the world: Their age, geologic setting, mineralogy, metamorphism, geochemistry, and origin. Am Miner 90:1473–1499
Klein C, Beukes NJ (1989) Geochemistry and sedimentology of a facies transition from limestone to iron-formation in the early proterozoic Transvaal Supergroup, South Africa. Econ Geol 84:1733–1774
Klein C, Beukes NJ (1992) Models for iron-formation deposition. In: Schopf JW, Klein C (eds) The proterozoic biosphere: a multidisciplinary study. Cambridge University Press, Cambridge, pp 147–151
Klein C, Beukes NJ (1993a) Sedimentology and geochemistry of the glaciogenic late Proterozoic Rapitan iron-formation in Canada. Econ Geol 88:542–565
Klein C, Beukes NJ (1993b) Proterozoic iron-formations. In: Condie K (ed) Proterozoic crustal evolution. Elsevier, Amsterdam, pp 383–418
Klein C, Fink RP (1976) Petrology of the Sokoman iron formation in the Howells River area, at the western edge of the Labrador Trough. Econ Geol 71:453–487
Konhauser KO, Hamade T, Raiswell R, Morris RC, Ferris FG, Southam G, Canfield DE (2002) Could bacteria have formed the Precambrian banded iron formations? Geology 30:1079–1082
Kositcin N, Krapež B (2004) SHRIMP U-Pb detrital zircon geochronology of the Late Archaean Witwatersrand Basin of South Africa: relation between zircon provenance age spectra and basin evolution. Precambr Res 129:141–168
Kramers JD, McCourt S, Van Reenen DD (2006) The Limpopo Belt. In: Johnson MR, Anhaeusser CR, Thomas RJ (eds) The geology of South Africa. Geological Society of South Africa, Johannesburg, Council for Geoscience, Pretoria, pp 209–236
Kusky TM (1998) Tectonic setting and terrane accretion of the Archean Zimbabwe craton. Geology 26:163–166
Kusky TM, Kidd WSF (1992) Remnants of an Archean oceanic plateau, Belingwe greenstone belt, Zimbabwe. Geology 20:43–46
Lechte M, Wallace M (2016) Sub–ice shelf ironstone deposition during the neoproterozoic Sturtian glaciation. Geology 44:891–894
Lechte MA, Wallace MW, Hoffmann K-H (2017) Glaciomarine ironstone deposition in a ~700 Ma glaciated margin: insights from the Chuos Formation, Namibia. Geological Society of London Special Publications, in review
MacDonald FA, Strauss JV, Rose CV, Dudás FŌ, Schrag DP (2010) Stratigraphy of the Port Nolloth Group of Namibia and South Africa and implications for the age of neoproterozoic iron formations. Am J Sci 310:862–888
Martin, A (1978) The geology of the Belingwe-Shabani schist belt. Rhodesia Geol Surv Bull 83, 213
McCarthy TS (2006) The Witwatersrand Supergroup. In: Johnson MR, Anhaeusser CR, Thomas RJ (eds) The geology of South Africa. Geological Society of South Africa, Johannesburg, Council for Geoscience, Pretoria, pp 155–186
McClung CR (2006) Basin analysis of the Mesoproterozoic Bushmanland Group of the Namaqua Metamorphic Province, South Africa. Unpublished Ph.D. Thesis, University of Johannesburg, Johannesburg, 307 p
McCourt S, Van Reenen DD (1993) Structural geology and tectonic setting of the Sutherland Greenstone Belt, Kaapvaal Craton, South Africa. Precambr Res 55:93–110
Miller RMCG (2013) Comparative stratigraphic and geochronological evolution of the northern Damara Supergroup in Namibia and the Katanga Supergroup in the Lufilian Arc of Central Africa. Geosci Canada 40:118–140
Miyano T, Van Reenen DD (1987) Metamorphic conditions of the Rhenosterkoppies iron formation in the Southern Marginal Zone of the Limpopo Belt, South Africa. Annual Report of the Institute of Geoscience vol 13, University of Tsukuba, pp 119–122
Miyano T, Beukes NJ (1997) Mineralogy and petrology of the contact Metamorphosed Amphibole Asbestos-bearing Penge iron formation, Eastern Transvaal, South Africa. J Petrol 38:651–676
Miyano T, Beukes NJ, Van Reenen DD (1987) Metamorphic evidence for the early post-Bushveld sills in the Penge iron formation, Transvaal Sequence, Eastern Transvaal. S Afr J Geol 90:37–43
Nel BP (2013) Petrogaphy and geochemistry of iron formations of the Paleoproterozoic Koegas Subgroup, Transvaal Supergroup, Griqualand West, South Africa. Unpublished M.Sc. thesis, University of Johannesburg, Johannesburg, 133 p
Netshiozwi ST (2002) Origin of high-grade hematite ores at Thabazimbi Mine, Limpopo Province, South Africa. Unpublished M.Sc. dissertation, Rand Afrikaans University, Johannesburg, 135 p
Nhleko N (2003) The Pongola Supergroup in Swaziland. Unpublished Ph.D. thesis, Rand Afrikaans University, Johannesburg, 300 p
Oberthür T, Weiser TW (2008) Gold-bismuth-telluride-sulphide assemblages at the Viceroy Mine, Harare-Bindura-Shamva greenstone belt, Zimbabwe. Min Mag 72:953–970
Ossa Ossa F, Hofmann A, Vidal O, Kramers JD, Belyanin G, Cavalazzi B (2016) Unusual manganese enrichment in the Mesoarchean Mozaan Group, Pongola Supergroup, South Africa. Precambr Res 281:414–433
Planavsky NJ, Asael D, Hofmann A, Reinhard CT, Lalonde SV, Knudsen A, Wang X, Ossa Ossa F, Pecoits E, Smith AJB, Beukes NJ, Bekker A, Johnson TM, Konhauser KO, Lyons TW, Rouxel OJ (2014) Evidence for oxygenic photosynthesis half a billion years before the great oxidation event. Nat Geosci 7:283–286
Posth NR, Hegler F, Konhauser KO, Kappler A (2008) Alternating Si and Fe deposition caused by temperature fluctuations in Precambrian oceans. Nat Geosci 1:703–708
Poujol M, Robb LJ, Anhaeusser CR, Gericke B (2003) A review of the geochronological constraints on the evolution of the Kaapvaal Craton, South Africa. Precambr Res 127:181–213
Saager A, Oberthür T, Tomschi H-P (1987) Geochemistry and mineralogy of banded iron-formation-hosted gold mineralization in the Gwanda Greenstone Belt, Zimbabwe. Econ Geol 82:2017–2032
Schidlowski M (1987) Application of stable carbon isotopes to early biochemical evolution on earth. Annu Rev Earth Planet Sci 15: 47–72
Schröder S, Bedorf D, Beukes NJ, Gutzmer J (2011) From BIF to red beds: sedimentology and sequence stratigraphy of the paleoproterozoic Koegas Subgroup (South Africa). Sed Geol 236:25–44

Smith AJB (2007) The paleo-environmental significance of the iron-formations and iron-rich mudstones of the Mesoarchean Witwatersrand-Mozaan Basin, South Africa. Unpublished M.Sc. thesis, University of Johannesburg, Johannesburg, 208 p

Smith AJB (2015) The life and times of banded iron formations. Geology 43:1111–1112

Smith AJB, Gutzmer J, Beukes NJ, Reinkie C, Bau M (2008) Rare earth elements (REE) in banded iron formations—link between geochemistry and mineralogy. In: Proceedings of the 9th international congress for applied mineralogy, Australian Institute for Mining and Metallurgy (AusIMM), Brisbane, Australia, 8–10 Sept 2008, pp 651–658

Smith AJB, Beukes NJ (2016) Palaeoproterozoic banded iron formation-hosted high-grade hematite iron ore deposits of the Transvaal Supergroup, South Africa. Episodes 39:269–284

Smith AJB, Beukes NJ, Gutzmer J (2013) The composition and depositional environments of Mesoarchean iron formations of the West Rand Group of the Witwatersrand Supergroup, South Africa. Econ Geol 108:111–134

Smith AJB, Beukes NJ, Gutzmer J, Czaja AD, Johnson CM, Nhleko N (2017) Oncoidal granular iron formation in the Mesoarchaean Pongola Supergroup, southern Africa: textural and geochemical evidence for biological activity during iron deposition. Geobiology 15:731–749

Stalder M, Rozendaal A (2002) Graftonite in phosphatic iron formations associated with the mid-Proterozoic Gamsberg Zn–Pb deposit, Namaqua Province, South Africa. Min Mag 66:915–927

Stalder M, Rozendaal A (2005) Distribution and geochemical characteristics of barite and barium-rich rocks associated with the Broken Hill-type Gamsberg Zn–Pb deposit, Namaqua Province, South Africa. S Afr J Geol 108:35–50

Sumner DY, Bowring SA (1996) U-Pb geochronologic constraints on deposition of the Campbellrand Subgroup, Transvaal Supergroup, South Africa. Precambr Res 79:25–35

Taylor RT, McLennan SM (1985) The continental crust: its composition and evolution. Blackwell Scientific, London, p 312

Trendall AF (1983) Introduction. In: Trendall AF, Morris RC (eds) Iron-formation: facts and problems. Elserivier, Amsterdam, pp 1–11

Trendall AF, Compston W, Williams IS, Armstrong RA, Arndt NT, McNaughton NJ, Nelson DR, Barley ME, Beukes NJ, De Laeter JR, Retief EA, Thorne AM (1990) Precise zircon U–Pb chronological comparison of the volcano-sedimentary sequences of the Kaapvaal and Pilbara Cratons between about 3.1 and 2.4 Ga. In: Abstracts of the 3rd IAS conference, Perth, pp 81–83

Tsikos H, Moore JM (1997) Petrographay and geochemistry of the paleoproterozoic Hotazel iron-formation, Kalahar manganese field, South Africa: implications for Precambrian manganese metallogenesis. Econ Geol 92:87–97

Tsikos H, Beukes NJ, Moore JM, Harris C (2003) Deposition, diagenesis, and secondary enrichment of metals in the paleoproterozoic Hotazel iron formation, Kalahari manganese field, South Africa. Econ Geol 98:1449–1462

United States Geological Survey (2015) Mineral commodity summaries 2015

Van Schalkwyk JF, Beukes NJ (1986) The Sishen iron ore deposit, Griqualand West. In: Anhaeusser CR, Maske S (eds) Mineral deposits of Southern Africa. Geological Society of South Africa, Johannesburg, pp 931–956

Van Deventer WF (2009) Textural and geochemical evidence for a supergene origin of the paleoproterozoic high-grade BIF-hosted iron ores of the Maremane Dome, Northern Cape Province, South Africa. Unpublished M.Sc. dissertation, University of Johannesburg, Johannesburg, 107 p

Von Gehlen K, Nielsen H, Chunnett I, Rozendaal A (1983) Sulphur isotopes in metamorphosed Precambrian Fe–Pb–Zn–Cu sulphides and baryte at Aggeneys and Gamsberg, South Africa. Mineral Mag 47:481–486

Vearncombe JR (1986) Structure of veins in a gold-pyrite deposit in banded iron formation, Amalia greenstone belt, South Africa. Geol Mag 123:601–609

Viehmann S, Bau M, Smith AJB, Beukes NJ, Dantas EL, Bühn B (2015) The reliability of ~2.9 Ga old Witwatersrand banded iron formations (South Africa) as archives for Mesoarchean seawater: Evidence from REE and Nd isotope systematics. J Afr Earth Sc 111:322–334

Von Brunn V, Gold DJC (1993) Diamictite in the Archaean Pongola sequence of southern Africa. J Afr Earth Sci (and the Middle East) 16:367–374

Wilson JF (1979) A preliminary reappraisal of the Rhodesian basement complex. Geol Soc S Afr Spec Publ 5:1–23

Wilson JF, Bickel MJ, Hawkesworth CJ, Martin A, Nisbet E, Orpen JL (1978) Granite-greenstone terranes of the Rhodesian Archaean craton. Nature 271:23–27

Young GM, Von Brunn V, Gold DJC, Minter WEL (1998) Earth's oldest reported glaciation: physical and chemical evidence from the Archean Mozaan Group (~2.9 Ga) of South Africa. J Geol 106:523–538

Zeh A, Gerdes A (2012) U–Pb and Hf isotope record of detrital zircons from gold-bearing sediments of the Pietersburg Greenstone Belt (South Africa)—is there a common provenance with the Witwatersrand Basin? Precambr Res 204–205:46

The Iron Formations of the South American Platform

18

Carlos Alberto Rosière, Adriana Heimann, Pedro Oyhantçabal, and João Orestes Schneider Santos

Abstract

The Precambrian of South America contains world-class iron formation (IF) occurrences of Archean, Paleo-, and Neoproterozoic age preserved in its different cratonic fragments and surrounding collisional belts developed during their amalgamation along a protracted Neoproterozoic to Early Paleozoic event known as the Brasiliano-Pan-African collage that formed the southwest part of the Gondwana supercontinent. In the domain of South America located west of the Transbrasiliano Lineament, most Archean IFs are spatially and genetically associated with volcanosedimentary sequences and crop out as discontinuous tectonic fragments of relatively small dimensions and seldom with economic concentrations of iron. An exception is the Carajás mineral Province in the Amazon Craton, where voluminous IFs from the Neoarchean Carajás Formation host giant high-grade iron ore deposits associated with the recurrent circulation of fluids of magmatic origin. Giant ore deposits of this metal are also present in the Paleoproterozoic Imataca granulite facies Complex in the Transamazon/Guianas Province of the Amazon Craton, but the information available about their primary geological setting, age, and mineralization processes is very limited. In the domain located east of the Transbrasiliano Lineament, on the other hand, the São Francisco Craton stands out with large Paleoproterozoic platform sequences containing banded IF (BIF) deposits, including some of the most important high-grade iron-ore deposits in the world. These are hosted by the Siderian Cauê Formation of the Minas Supergroup in the well-known Quadrilátero Ferrífero Mining District, and found also in the north–south-trending Orosirian-Statherian Serra da Serpentina IF, all IFs having been deposited along the eastern coast of an Archean protocraton. The Nico Pérez Terrane of southern Brazil and Uruguay, assumed to be a fragment of the São Francisco-Congo Craton, also preserves relics of BIF-bearing Paleoproterozoic platform successions. These BIFs contain significant but sub-economic iron ore resources as a result of a weak secondary iron enrichment and their relatively small size. The Paleoproterozoic Río de la Plata Craton lacks an Archean core and does not show any evident link with the other cratons of the South American Platform. In contrast with the other terranes, it hosts only small, scarce occurrences of BIFs associated with metavolcanosedimentary sequences. Neoproterozoic BIFs associated with Fe-rich clastic sediments are widespread in the Cryogenian sediments of the mobile schist belts, but economic deposits are few. The best-known examples of sequences hosting Neoproterozoic BIFs include the Jacadigo Group of Brazil and Bolivia, and the Yerbal Formation of Uruguay.

Keywords

Iron Formations • Gondwana • South America Cratons

C. A. Rosière (✉)
Departamento de Geologia, Universidade Federal de Minas Gerais, Belo Horizonte, MG 31270-901, Brazil
e-mail: crosiere@gmail.com

A. Heimann
Department of Geological Sciences, East Carolina University, Greenville, NC 27858, USA
e-mail: heimanna@ecu.edu

P. Oyhantçabal
Departamento de Geodinámica Interna, Universidad de la República, Iguá 4225, CP 11600 Montevideo, Uruguay
e-mail: ohyantca@fcien.edu.uy

J. O. S. Santos
Centre for Exploration Targeting, The University of Western Australia, 35 Stirling Highway, Crawley, Perth, WA 6009, Australia
e-mail: orestes.santos@bigpond.com

18.1 Introduction

Iron formation (IF) is a term introduced by James (1954) for chemical sedimentary rocks containing ≥ 15 wt% Fe and commonly characterized by alternating, Fe- and SiO_2-rich

S. Siegesmund et al. (eds.), *Geology of Southwest Gondwana*, Regional Geology Reviews,
https://doi.org/10.1007/978-3-319-68920-3_18

layers or laminations. IFs are the main source of iron ore for the steel industry and, in addition to their economic significance, they are of great scientific interest because they provide clues about the compositional evolution of the early Earth's oceans and atmosphere and the evolution of marine life. They occur in the early Precambrian geological record distributed over a wide timespan (3.8–0.6 Ga). Their relative abundance correlates with periods of large volumes of Fe input from the Earth's mantle into seawater and with the evolution of atmospheric O_2 content (e.g., Bekker et al. 2010). They may occur in greenstone belts, mainly as deformed, metamorphosed, and dismembered units intimately associated with volcanosedimentary sequences, as what is referred to as Algoma-type IFs (Goodwin 1962; Gross 1980, 1983). Interpretations about their depositional environment and the mechanism of Fe precipitation in Archean Algoma BIFs are contentious. Different authors propose local conditions with discontinuous hydrothermal Fe input during the deposition of greenstone belt sequences (Barley et al. 1998; Huston and Logan 2004) and precipitation as oxides (Hoashi et al. 2009; Sun et al. 2015), silicates, or "green rust" (Bekker et al. 2010; Zegeye et al. 2012, Rasmussen et al. 2016) aided by organic oxygenic/anoxygenic photosynthesis (Konhauser et al. 2002, in press; Gourcerol et al. 2016), inorganic precipitation by decreasing pH (Gourcerol et al. 2016), or local oxic conditions of brines owing to boiling from submarine volcanic emanations (Bekker et al. 2010).

However, the largest and thickest sequences of IFs in the world's geological record are the Lake Superior-type IFs (Gross 1980, 1983), which are most abundant in the early Paleoproterozoic and occur in platform environments along the border of cratonic areas. It is widely accepted that these sequences are associated with a global and rather rapid increase in atmospheric O_2 content referred to as the Great Oxidation Event (Holland 2006). The precipitation of iron compounds from seawater, as evidenced in the volume of IFs, reached a maximum at about 2.5 Ga and nearly ceased at ~1.8 Ga, purportedly as a result of the total consumption of extreme amounts of dissolved Fe accumulated from the Archean until the early Proterozoic. After a long hiatus, IFs reappear in the geologic record in the Neoproterozoic between ~1 and 0.6 Ga as what are known as Rapitan-type IFs (Klein and Beukes 1993). These IFs are related to a change in global environmental conditions and the recurrent prevalence of stagnated anoxic conditions in the oceans beneath a near-global ice cover during world glaciation events referred to as Snowball Earth, and the resulting accumulation of dissolved Fe in seawater (Kirschvink 1992; Hoffman et al. 1998).

Because of the association between specific periods of the Earth's history and IF deposition, large IF deposits occur in areas where old cratons are preserved, including those in Australia, Brazil, northern North America, southern Africa, and Greenland. South America is endowed with significant world-class IF occurrences, including Algoma-type (i.e., Carajás, Brazil), Lake Superior-type (Minas Supergroup, Brazil), and Rapitan-type IFs (Urucum, Brazil and Bolivia). In this chapter we review the main IF occurrences in South America, including their tectonic setting, and discuss the possible correlations within western Gondwana.

18.2 Iron Formations: Main Characteristics

Iron Formations are chemical sedimentary rocks rich in Fe and SiO_2, typically laminated to layered, and devoid of detrital components. Primary iron phases precipitated under oxic to suboxic conditions are usually linked to microbial activity from original hydrothermal-Fe-rich fertilized seawater first concentrated as ferrous Fe in deep anoxic environments (Konhauser et al. 2002). Recent studies using Fe isotopes, rare-earth element content, and Nd isotope compositions suggest that the source of Fe is a combination of marine hydrothermal fluids and biologically recycled (reduced), riverine continental Fe (Li et al. 2015). Although James (1954) established a minimum content of 15 wt% Fe for IFs, it typically ranges from ~20 to 40 wt%. The SiO_2 content varies from 40 to 60 wt%, the CaO and MgO content is always less than 10 wt%, and Al_2O_3 and alkalis are less than 2 wt%. Fe-rich minerals include iron oxides (hematite, magnetite), carbonates (siderite, ankerite), and silicates (greenalite), depending on metamorphic grade (Klein 2005). Silica occurs as microcrystalline quartz or individual quartz crystals. Although most of the current minerals in IFs are the product of post-depositional processes, including diagenesis, metamorphism, and hydrothermal alteration, minerals such as siderite and greenalite were originally considered of "primary" origin and several authors (e.g., James 1954) historically used them to define depositional facies. Ferric oxy-hydroxides were probably, in most cases, the primary phases that during diagenesis extensively underwent dehydration, recrystallization, and phase transformation, or reacted with other chemical components undergoing post-depositional inorganic or microbially mediated processes (bacterial Fe reduction, oxidation; Johnson et al. 2003, 2008; Konhauser et al. 2005; Heimann et al. 2010) to form oxides, silicates, and carbonates, depending on the pH-Eh conditions (Klein 2005). Local contamination by volcanogenic alkalis in some IFs is evidenced by the presence of silicates such as riebeckite and stilpnomelane.

The most striking primary features of IFs are bands defined by alternating layers of Fe-rich minerals and chert or quartz of varying scales that define banded IFs (BIFs). These bands are classified as macro-, meso-, and microbands according to their thickness and spatial distribution (Trendall and Blockley 1970). The bands reflect original

sedimentary beds, but chert is considered to be a product of syndiagenetic cementation by direct precipitation or flocculation in the sediment–water interface, or by diagenetic decomposition of primary silicates. Some IFs display detrital textures from erosion and redeposition of Fe-rich chemical muds (Krapez et al. 2003). They are characteristically composed of oxides or silicates, occur in the shallow environment of basins as discontinuous lenses with a thickness of a few meters (usually <2 m), and are named Granular Iron Formations.

Iron formations of the basin-hosted Lake Superior-type usually occur in upwards-deepening marine successions underlain by black, carbon-rich shales. They may be associated with shaly turbidites in deep-water sequences or with quartz sands and platform carbonates in shallow-water environments (Beukes 1983; Simonson 1984; Klein and Beukes 1989; Krapez et al. 2003). Algoma-type IFs are associated with volcanosedimentary sequences interlayered with shales, greywackes, chert, mafic and felsic volcanic rocks, and volcanogenic sedimentary rocks, are commonly deposited in pelagic hydrothermal environments, and are typically of Archean age. Continental rift-hosted IFs typical of Neoproterozoic age (Rapitan-type IFs) display much less conspicuous banding, contain dropstones and striated clasts, and are interlayered with banded jaspilite. These IFs are typically spatially associated with slates and glaciogenic ferruginous diamictite lenses and calcareous silty layers. Basaltic and volcaniclastic rocks in the sequence are associated with the break-up of Rodinia (Young et al. 1979; Cox et al. 2013).

18.3 Iron Formation-Hosted Iron-Ore Deposits

The largest high-grade iron ore deposits are hosted by Paleoproterozoic, Lake Superior-type BIF sequences, although economically important deposits may also occur associated with Archean Greenstone Belt successions (Figueiredo e Silva et al. 2008, 2013; Duuring and Hagemann 2013a, b). Iron enrichment may upgrade IFs from their primary 20–40 wt% up to 60–68 wt% Fe content under the effects of supergene, hypogene, or the superposition of both processes (Gruner 1930, 1937; Dorr 1965; Beukes et al. 2002). Some authors (e.g., Lascelles 2002) alternatively consider the possibility of loss of chert and residual Fe enrichment during compaction still in the diagenetic stage as preparation for supergene enrichment to form high-grade iron ore.

The enrichment process comprises mainly leaching of gangue minerals, although quartz is hardly soluble at low temperatures (i.e., <250 °C), specifically during weathering. The recently observed superposition of hydrothermal alteration stages in mineralized BIFs, where the substitution of quartz by highly soluble carbonate plays a major role, supporting new models to explain the genesis of giant iron ore deposits (Barley et al. 1999; Taylor et al. 2001). Hydrothermal metasomatic replacement (carbonatization of cherty BIF) is evident in most high-grade deposits worldwide, together with many other complementary processes such as iron remobilization (high temperature), metasomatic replacement and oxidation/reduction (high and low temperature), laterization and ferrolysis (low-temperature), and decarbonation (high- and low-temperature; for a thorough discussion, see Hagemann et al. 2016 and references therein).

Hypogene genetic models are based on structural, microchemical, fluid inclusion, and stable isotope studies. According to these models, hydrothermal fluids of variable origins such as basinal brines, magmatic fluids, or heated meteoric water are responsible for multistage processes controlled by large- and microscale structures. Supergene models explain high-grade iron ores by residual concentration in IF but not necessarily related to a laterization process. The superposition of supergene processes on hydrothermal alteration is considered to be of chief importance in the formation of extra-large world-class iron-ore deposits by the removal of residual gangue minerals via elutriation of quartz grains, solution of primary or hydrothermal carbonates and apatite, and concentration of hematite. Iron oxides, mainly magnetite, and silicates decompose to goethite and other related hydrated iron oxide minerals. Manganese-bearing carbonates alter to manganese oxy-hydroxides and aluminum silicates to clays.

18.4 Iron Formations of SW Gondwana

Well-preserved remnants of several IF-bearing basins are widely distributed in the South American Platform (Cordani et al. 2009), recording different periods of Fe sedimentation in the Earth's history in the Amazon, São Luis, São Francisco, Luiz Alves, Río de la Plata, and Nico Pérez cratons and terranes. These terranes collided and amalgamated during successive events, starting in the Lower Cryogenian (*c.* 800 Ma) and lasting until the Upper Cambrian (~500 Ma; Brito Neves et al. 2014), to form the Western Gondwana Supercontinent during the Brasiliano/Pan-African orogeny. In this mosaic of crustal fragments, the Nigeria-Borborema and the Nico Pérez provinces hold singular positions, being comprised of Archean-Early Paleoproterozoic crust strongly reworked during the Brasiliano orogenesis. In the following sections we review the lithological associations, mineralogical features, depositional environment, age constraints, and tectonic setting of the main IF deposits of Brazil and Uruguay.

18.4.1 The Amazon Craton

The Amazon Craton is one of the largest cratons in the world, spanning an area of about 6 million km^2. It is covered by Phanerozoic basins in the northeast (Parnaíba), center (Amazon), south (Xingu-Alto Tapajós), southwest (Parecis), and west (Solimões) sectors. It is surrounded by the Andes Orogenic Belt to the west, and by the Neoproterozoic Tocantins/Araguaia Neoproterozoic orogenic belts to the east and southeast (Fig. 18.1). The craton was first divided by Tassinari and Macambira (1999) into six major geochronological provinces based on Rb–Sr data, and more recently Santos (2003) and Santos et al. (2006), based on U–Pb data, reinterpreted these provinces and proposed the following subdivisions: Carajás (3.10–2.53 Ga), Transamazon (Guianas, 2.25–2.00 Ga), Tapajós-Parima (2.10–1.87 Ga), Central Amazon (1.88–1.70 Ga); Rio Negro (1.86–1.52 Ga), Rondônia-Juruena (1.76–1.47 Ga), and Sunsás (1.33–0.99 Ga, including the K'Mudku Shear Belt, 1.10–1.33 Ga) (Fig. 18.1).

18.4.1.1 Iron Formations in Greenstone Belts and Volcanosedimentary Sequences of the Amazon Craton

In the Carajás Province, several Algoma-type BIF-bearing greenstone belts such as the Rio Maria from the Carajás area, have been mapped and prospected. However, they have been generically considered by geologists of the DOCEGEO in 1988 as part of the Archean Andorinhas Supergroup (3.0–2.90 Ga). Other similar sequences have been named Serra do Inajá, Sapucaia, and Tucumã, but little information is available in the literature about these sequences.

The Transamazon Province comprises juvenile Paleoproterozoic crust and an area of reworked Archean terrane in the southwest of the State of Amapá that evolved during a protracted event over the period 2.26–2.10 Ga, ending with the closure of oceanic basins and arc-continent collision during Neorhyacian times (see Barreto et al. 2013 and references therein). This province is dominated by metavolcanosedimentary sequences, all purportedly of Rhyacian age, that contain BIF layers at the top and extend from Brazil

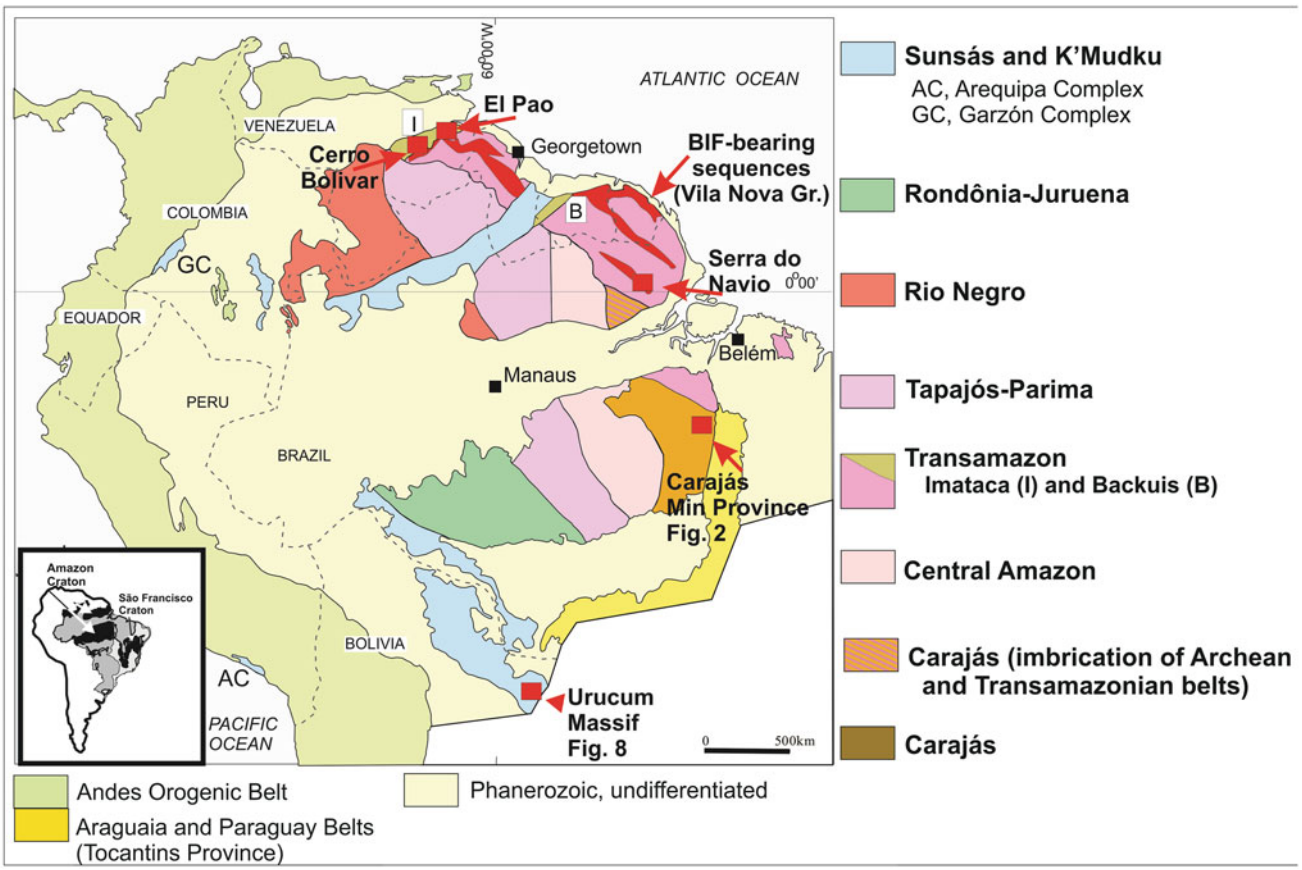

Fig. 18.1 Geochronological Provinces of the Amazon Craton showing the location of major BIF occurrences. Modified from Santos (2003) and Santos et al. (2000, 2006)

(Vila Nova Group) to Venezuela (Pastora Group) and Guyana (Barama-Mazaruni Supergroup). In Suriname and French Guyana, Paramaka volcanic rocks that belong to the Marowijne Group have been dated at 2112–2155 Ma (Delor et al. 2003) and correlated with the adjacent Pastora and Barama sequences.

In northern Brazil, in the Amapá Block of the Transamazon Province (Fig. 18.1), BIFs occur in the northwest-southeast-trending Vila Nova Group (~2.26 Ga; Barreto et al. 2009) on top of mafic and ultramafic metavolcanic rocks (schists). The Vila Nova Group includes several greenstone belts with BIFs, Mn-carbonates, pelitic schists, and quartzites that contain some high-grade iron and manganese ore deposits, such as in the Serra do Navio, Tartarugalzinho, Serra das Coambas, and Ipitinga areas. The sequence of the Serra do Navio area is characterized by biotite and graphitic schist and manganiferous carbonate rocks. The sedimentary succession is similar to many other black shale- and chert-hosted manganese carbonate deposits and interpreted by Chisonga et al. (2012) as deposited in an intra-arc basin. According to these authors, positive Ce anomalies and $\delta^{13}C_{VPDB}$ values of −4.3 to 9.4‰ indicate a

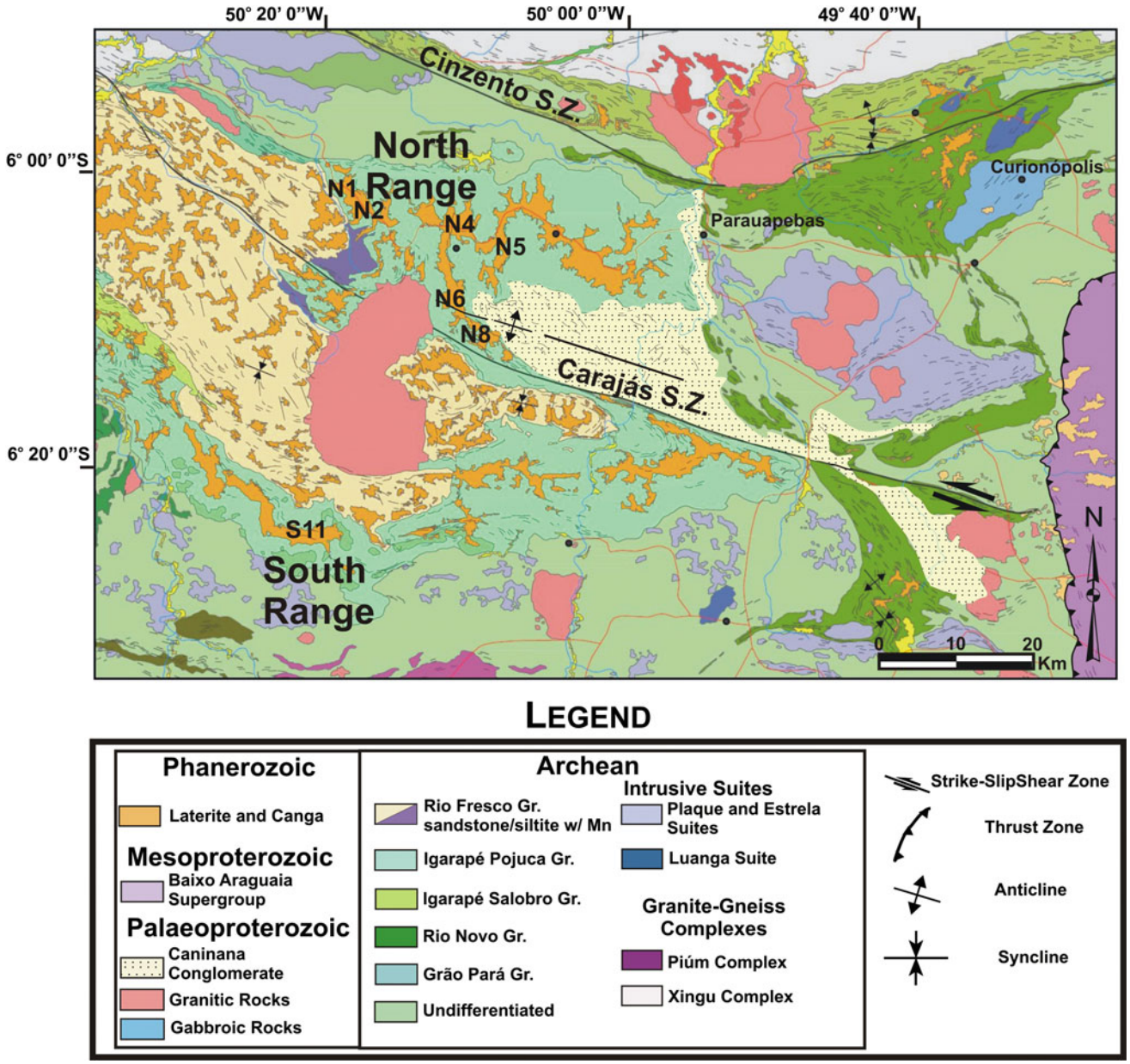

Fig. 18.2 Geological map of the Carajás Mineral Province showing the location of the main iron ore deposits in the northern and southern ranges (Serras Norte and Sul; N1, N2, N4, N5, N6 e N8 and S11). After Lobato et al. (2005). Modified with data from Seoane et al. (2004), Rosière et al. (2006), Costa (2007) and Pereira et al. (2009), based on Landsat images ETM7, RGB 321, 752, PC1-52

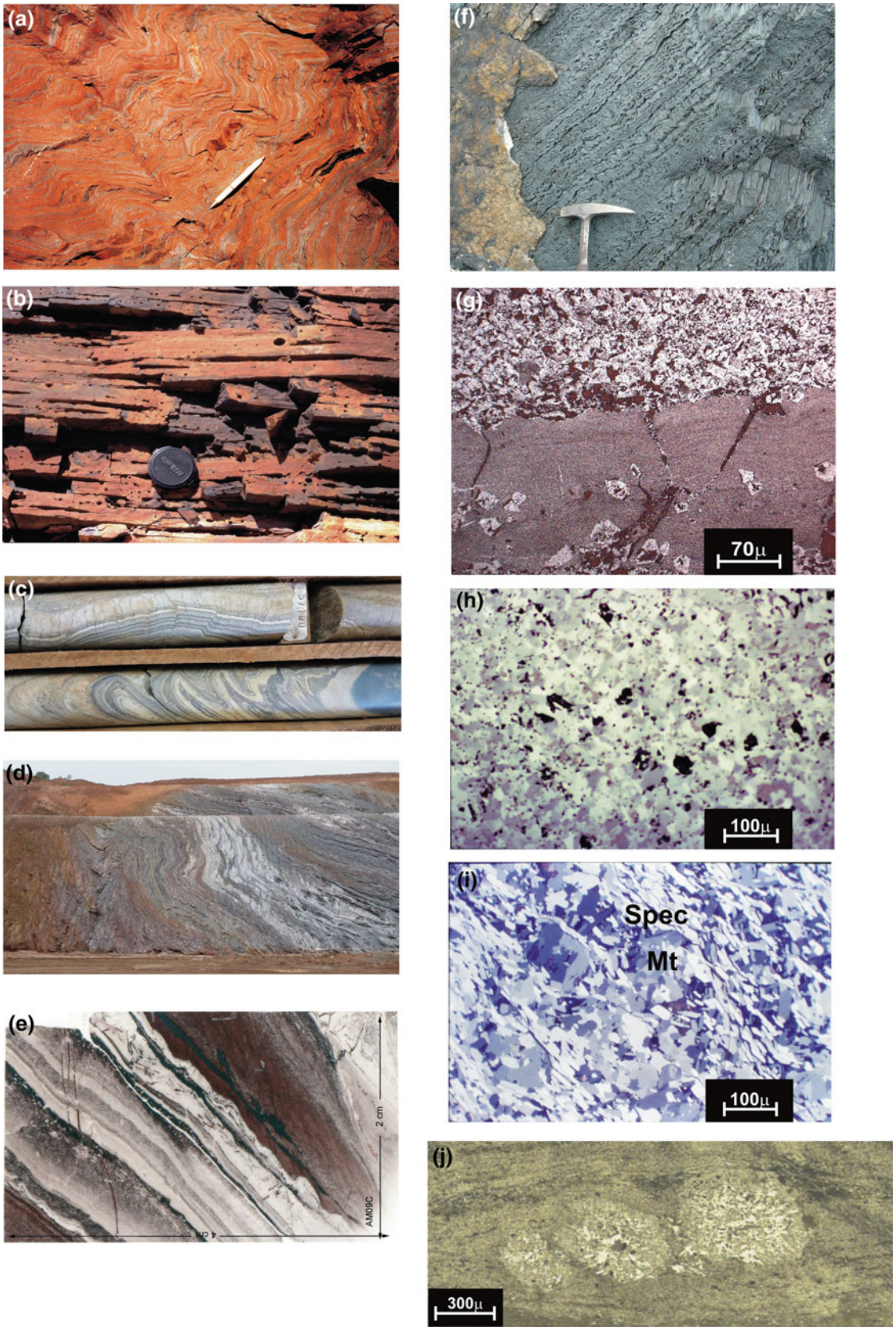
(a)
(b)
(c)
(d)
(e)
2 cm
AM09C
(f)
(g)
70µ
(h)
100µ
(i)
Spec
Mt
100µ
(j)
300µ

◀ **Fig. 18.3** Meso- and microscopic features of Brazilian IFs and high-grade iron ores. **a** Jaspilite from the Carajás Fm, mine N4E, Carajás Province, Amazon Craton. **b** Supergene enriched, weathered BIF from the Jacadigo Fm, Urucum District. Quartz has been thoroughly leached leaving a residual prime high-grade iron ore. **c** Ankerite-dolomite-quartz BIF from the Cauê Formation, Alegria mine, Quadrilátero Ferrífero District, São Francisco Craton. Slump folds are well developed in one of the cores, detached from the thick SiO_2 (quartz) layer. **d** Sheared and refolded (second-generation open folds) IF from the Serra do Sapo Mine, Serra do Sapo IF, Serra da Serpentina, São Francisco Craton. **e** Fine microbanding and compositional variation in quartz (white) and dolomite (red) layers of IF. Cauê Formation, Minas Supergroup, Aguas Claras Deposit (exhausted), São Francisco Craton. **f** Banded hypogene high-grade iron ore. The fine primary structure of the BIF can be recognized. Fazendão mine, Quadrilátero Ferrífero, São Francisco Craton. **g** Mineralized BIF from the Carajás Formation. Hydrothermal idiomorphic magnetite-martite crystals overgrow microcrystalline hematite layer and substitutes former quartz (?) band. Mine N5E. Carajás Province, Amazon Craton. **h** Granoblastic hematite fabric with magnetite relics. Hypogene high-grade ore, Tamanduá Mine, Quadrilátero Ferrífero District, São Francisco Craton. **i** Specularite (platy hematite-specularite) crystals anastomose around hematite-martite (Mt) aggregate, high-grade ore, Pico mine, Quadrilátero Ferrífero District, São Francisco Craton. **j** Spherulitic structure metasomatically substituted by hematite in hypogene high-grade ore hosted by jaspilite from the Carajás Formation, N5E mine, Carajás Provice, Amazon Craton

diagenetic origin under suboxic conditions for the Mn carbonate rocks at the expense of sedimentary Mn^{4+} oxyhydroxide precipitates. Manganese silicates such as rhodonite, tephroite, and spessartine formed by metamorphic reaction of carbonate and Al-clay minerals under upper greenschist facies conditions (1–2 kbars and 400–500 °C). Rhodochrosite and Mn-calcite are interpreted as secondary products formed by carbonation during retrograde metamorphism. These BIFs and carbonate rocks have undergone deep tropical weathering that resulted in the formation of large supergene iron and manganese oxide deposits.

18.4.1.2 Iron Formations in the Imataca Complex

The Imataca Complex is an east-northeast-trending 80 km-wide and 300 km-long granulite facies belt located to the south of the lower Orinoco River in Venezuela, NW Amazon Craton (Fig. 18.1). It contains orthogneisses, paragneisses (hornblende-pyroxene- and epidote-bearing varieties) metamorphosed to almandine-amphibolite facies, granulite facies gneiss, and intercalated BIFs (Goodwin 1991). The principal iron-bearing minerals are hematite and magnetite, with local amphibole or pyroxene. The oxide-bearing BIFs host giant iron deposits (Cerro Bolivar, El Pao) and others of more modest dimensions, such as San Isidro, Cerro Altamira, Cerro Redondo, La Estrella, Cerro Arimagua, Cerro Toribio, and Cerro Frontera. The belt was considered to include the oldest rocks of the Amazon Craton, dated at 3.7–3.4 Ga by Montgomery (1979) using whole-rock U–Pb data. Using zircon U–Pb SHRIMP data, Santos et al. (2005) demonstrated that the complex, instead of being pre-Transamazonian, is post-Transamazonian in age, and that a major metamorphic event at granulite facies conditions recrystallized zircons at 2018 ± 5 Ma. Some 95% of the detrital material in the Imataca Basin is derived from Transamazonian rocks (2123–2061 Ma) and only 5% originated from Neoarchean rocks (2677 and 2521 Ma).

18.4.1.3 The Neoarchean Carajás Iron Formation

The Neoarchean Carajás Iron Formation, together with volcanic rocks of the Parauapebas Formation, make up the voluminous volcanosedimentary sequence of the Grão Pará Group, Itacaiúnas Supergroup (*c*. 2.76 Ga; Machado et al. 1991) (Fig. 18.2), dominated by mafic metavolcanic rocks (2759 ± 2 Ma; Machado et al. 1991) associated with BIFs in the Carajás Province and possibly deposited in a back-arc environment on attenuated continental crust (Zucchetti 2007). The basement consists of the Pium (3002 ± 14 Ma; Pidgeon et al. 2000) and Xingu (2859 ± 2 Ma; Machado et al. 1991) complexes. The Itacaiúnas Supergroup (Wirth et al. 1986) is subdivided by several authors into the Igarapé Salobo, Igarapé Pojuca, Grão Pará, and Igarapé Bahia Groups. Another volcanosedimentary unit in the Carajás area is the Rio Novo Group (*c*. 2.9 Ga; Avelar et al. 1999; Villas and Santos 2001), consisting of meta-mafic to ultramafic with minor felsic volcanic rocks (schists) and BIF.

The iron mineralized Carajás Formation of the Grão Pará Group contains jaspilitic and cherty IFs (Fig. 18.3a) and minor dolomitic rocks under- and overlain by basalts (Parauapebas Formation) and covered by psamopelitic strata of the Aguas Claras Formation, all metamorphosed to greenschist facies conditions. Mineralization developed associated with a multistage history of hydrothermal alteration, possibly by magmatic fluids that affected jaspilites and volcanic rocks controlled by west-northwest- and west-southwest-trending folds of second order to the regional Carajás Fold (Rosière et al. 2006), and by the Carajás and Cinzento strike-slip systems (Pinheiro and Holdsworth 1997, 2000). The major Serra Norte N1, N4E, N4W, N5E, and N5S iron-ore deposits of the Carajás Province are distributed along and structurally controlled by the northern flank of the Carajás fold. High-grade iron ore (>65% Fe) is made up of hard and soft ore. The hard ores can be banded, massive, and/or brecciated, and they are characterized by hematite-martite and hematite types (Fig. 18.3g). The soft ores are very porous, discontinuous, tabular, friable, and banded. The basal contact of high-grade iron ore is defined by a hydrothermally altered basaltic rock mainly composed of chlorite and microplaty hematite (Figueiredo e Silva et al. 2008). At the southern limb of the Carajás Fold, several

important high-grade ore bodies also occur, and these are currently being explored.

The age of iron mineralization is uncertain. The presence of iron ore clasts in the Paleoproterozoic Caninana conglomerate, unconformable over the Grão Pará Group, indicates an age of >2.01 Ga for the hydrothermal mineralization (Pereira et al. 2009). Santos et al. (2010) determined the age of hydrothermal monazite inclusions in platy hematite (1613 ± 21 Ma; $^{208}Pb/^{232}Th$) and of anatase crystals from Fe-mineralized volcanic rocks (1717 ± 12 Ma; Pb–Pb). Hydrothermal minerals from various iron-oxide-copper-gold (IOCG) deposits in the Carajás Province yielded U–Pb and Re–Os ages of *c*. 2.71–2.68 Ga and 1.90–1.88 Ga, respectively (Moreto et al. 2015). These ages are coeval with the emplacement of Neoarchean and Paleoproterozoic granitoids, which indicate a recurrent circulation of hydrothermal fluids that were probably responsible for the formation of the giant high-grade iron deposits.

18.4.2 The São Francisco Craton

The São Francisco Craton (Almeida 1977) comprises several Archean fragments reworked and assembled together with Paleoproterozoic segments in a proto-craton during an orogenic cycle (*c*. 2.2–1.8 Ga) coined as Transamazonian by Almeida (1971). The São Francisco Craton is surrounded by the Neoproterozoic Araçuaí Belt in the east and southeast, the Rio Negro and Brasilia Belts in the northwest to southwest, and by the Riacho do Pontal and Sergipano Belts in the north (Fig. 18.4). In the northern half of the craton, several Archean blocks are exposed, unveiling a complex mosaic of terranes: the oldest Gavião Block (~3.4 Ga), the Jequié, the Serrinha, and the youngest Itabuna-Salvador-Curaçá Belt that amalgamated during the Rhyacian (Transamazonian) orogeny (2.14–1.94 Ga) (Barbosa and Sabaté 2002, 2004). These terranes are assembled together with Paleoproterozoic segments along the Jacobina–Contendas Mirante belts, also encasing Archean rocks of the Mairí inlier.

The southern half of the craton is widely covered by Neoproterozoic and Phanerozoic sedimentary rocks. Archean terranes are exposed mostly in a small area at its southern extremity and made up of TTG gneissic rocks, migmatites, granitoid plutons, mafic-ultramafic intrusions, and greenstone belts overlain by Proterozoic sedimentary successions. The Archean core is bordered in the southeast by the collisional Rhyacian (Transamazonian) Mineiro Belt (Teixeira et al. 1996). Further east, the Mineiro Belt is bounded by the Mantiqueira Complex, which comprises partially molten Archean terranes and Paleoproterozoic igneous bodies (2137 ± 19 to 2041 ± 7 Ma). The Mineiro Belt was generated and accreted into the Archean São Francisco protocraton during the Transamazonian orogeny, becoming the basement for the Proterozoic sediments (Noce et al. 2007) along the eastern border of the craton.

18.4.2.1 Iron Formations in Volcanosedimentary Sequences of the Northern São Francisco Craton

The Gavião Block contains several exposed Archean to Paleoproterozoic volcanosedimentary sequences, including Riacho de Santana, Boquira, Guajeru, Ibitira-Ubiraçaba, Umburanas, Contendas-Mirantes, and Urandi-Caetité-Licínio de Almeida, all enclosed in Archean TTG terranes (Silva and Cunha 1999). SHRIMP U/Pb and Pb/Pb dating on zircon indicates ages of 3.3 Ga (Umburanas) and 3.0 Ga (Contendas-Mirante) for mafic rocks, whereas felsic units yielded ages of 2.75 and 2.70 Ga. The Contendas-Mirante and Jacobina belts also contain a Paleoproterozoic sedimentary unit, as indicated by detrital zircon populations (see Marinho 1991; Cunha et al. 1996; Bastos-Leal et al. 1997; Bastos-Leal 1998). The Urandi-Caetité-Licínio de Almeida sequence (Fig. 18.4) is characterized by Mn-rich, calcitic and dolomitic marbles, quartzite, schist, and calcsilicate rocks associated with the Mosquito IF that hosts significant high-grade, iron-ore bodies as well some manganese deposits (Borges 2012; Borges et al. 2015). Other important BIF-bearing sequences are the Rio Itapicuru greenstone belt in the Serrinha Block and the Ibicui-Iguaí Metasedimentary Sequence (Fig. 18.4) in the southern Itabuna-Salvador-Curaçá Belt (Santos 2015).

18.4.2.2 Iron Formations in Volcanosedimentary Sequences of the Southern São Francisco Craton

The economically relevant Fortaleza de Minas/Morro do Ferro Greenstone Belt strikes northwest–southeast along the Neoproterozoic Campos Altos Lineament at the southeastern boundary of the Tocantins Province (Figs. 18.4 and 18.7) and comprises tectonic lenses of ultramafic and mafic metavolcanic rocks, iron formation, and pelitic schists intercalated with slices of gneissic rocks and mylonitic schists. A Rb/Sr isochron age of 2918 ± 105 Ma was obtained by Schrank and Silva (1993) from migmatites in thermal equilibrium with the rocks from the greenstone belt. In close proximity is located the Piumhi Greenstone Belt (Schrank 1982) (Figs. 18.4 and 18.7), which comprises a 3000 m-thick sequence of metavolcanic rocks in tectonic contact with schists of the Canastra Group and gneisses of the Campo Gerais granite-gneissic Complex. Dating by U/Pb of zircon grains from gabbroic rocks yielded ages of

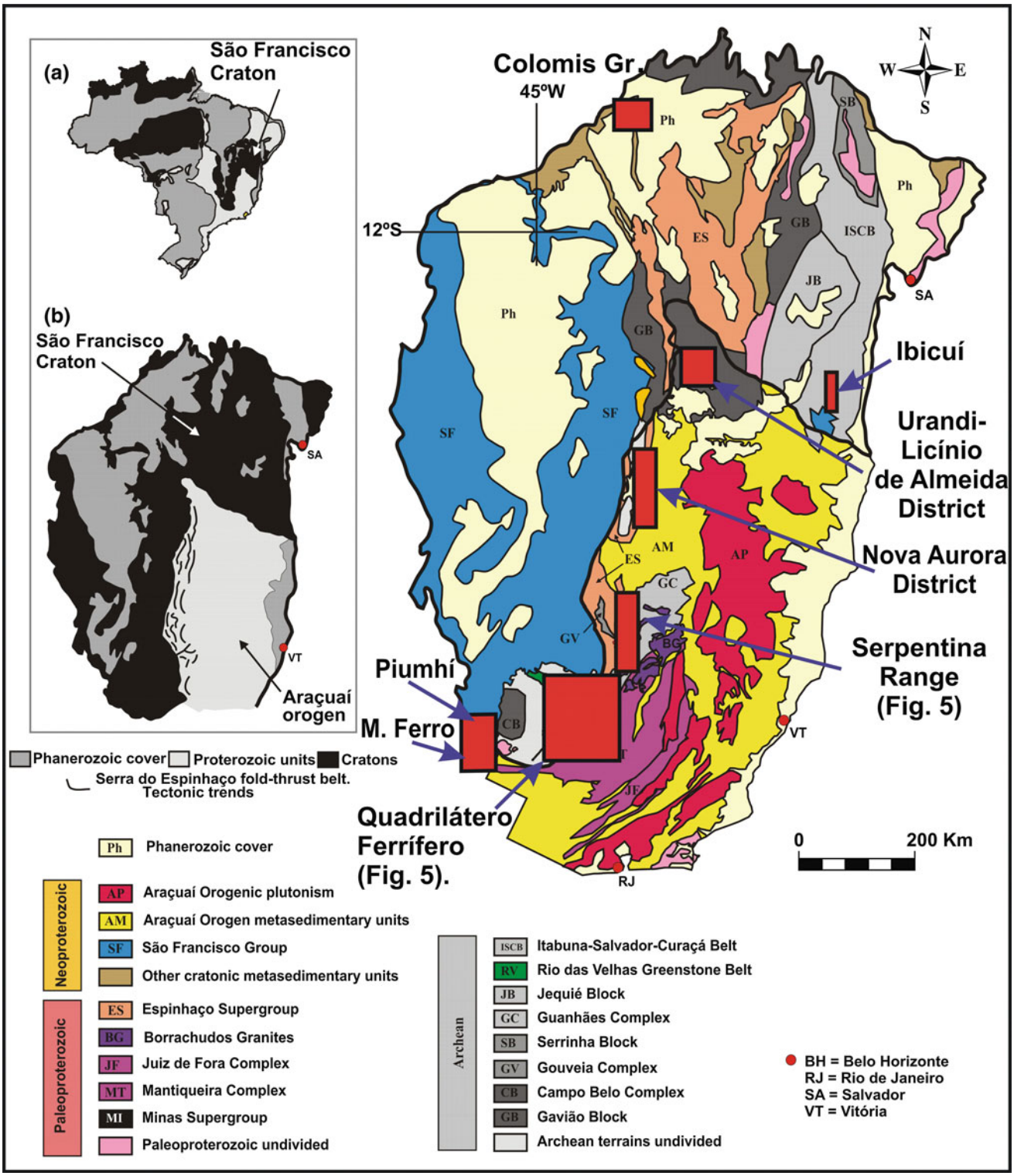

Fig. 18.4 Geologic map of the São Francisco Craton depicting the main lithotectonic units and showing the location of the principal occurrences of iron formations. **a** Location of the São Francisco Craton. **b** Sketch of the São Francisco Craton and Araçuaí Orogen. Modified after Almeida (1977), Teixeira et al. (1996), Silva et al. (2002), Souza et al. (2003), Barbosa and Sabaté (2004), Noce et al. (2007), Danderfer Filho et al. (2009), Pinto and Silva (2014) and Rolim et al. (2016)

3116 + 10/−7 Ma and $^{207}Pb/^{206}Pb$ zircon ages from a rio-dacitic intrusion ranged from 3.00 to 2.97 Ga (Machado and Schrank 1989). Other ill-defined and discontinuous upper amphibolite facies BIF-bearing volcanosedimentary sequences occur scattered enclosed in the gneissic terranes and host high-grade magnetite orebodies.

The Rio das Velhas Greenstone Belt (Fig. 18.5) is the economically most important volcanosedimentary sequence in the São Francisco Craton territory hosting large gold deposits. In map view the sequence displays a complex regional outcrop pattern, roughly following the quadrangular shape of the overlying Paleoproterozoic sequence of the

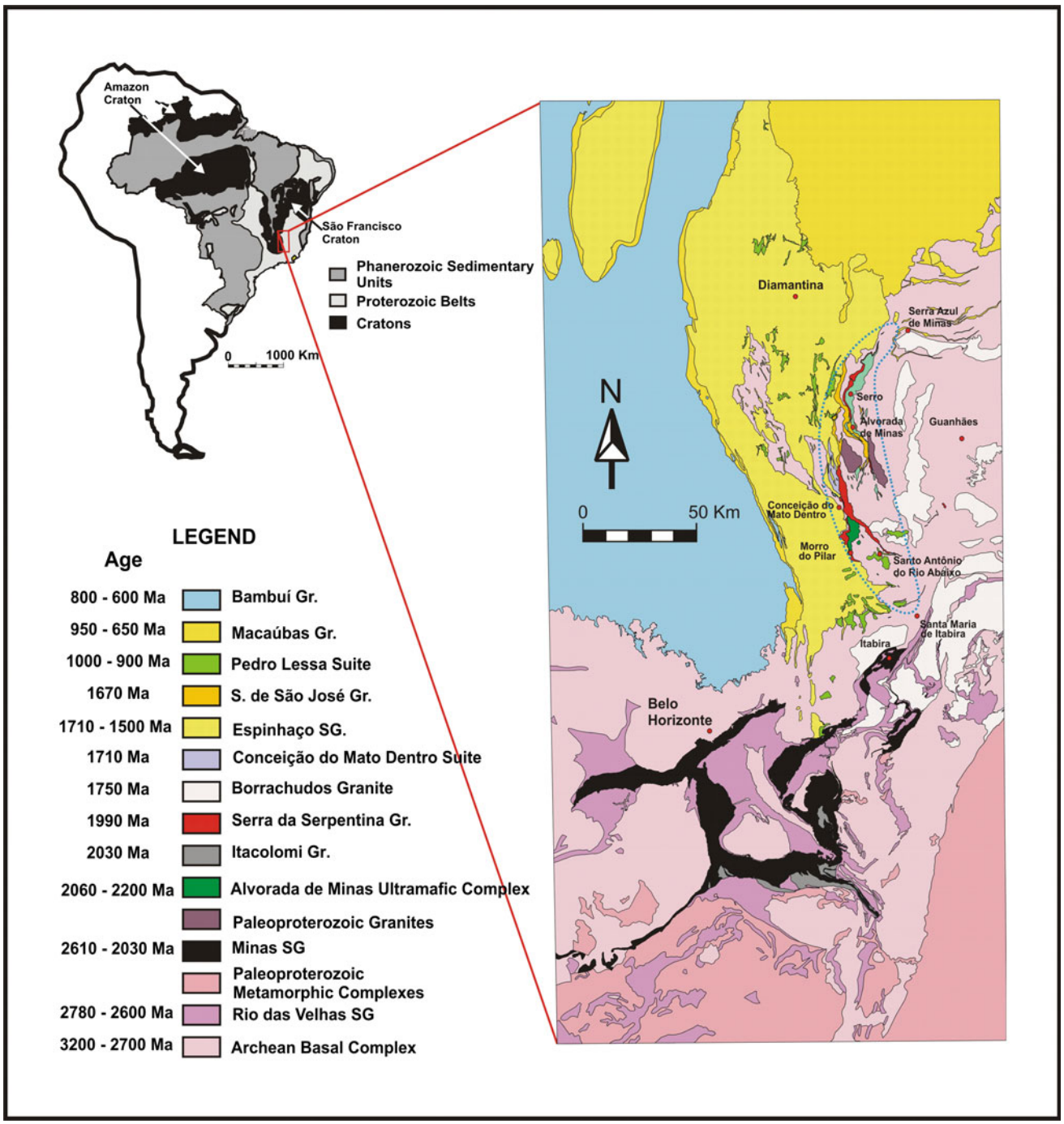

Fig. 18.5 Simplified geologic map of the Quadrilátero Ferrífero District and eastern border of the Southern Espinhaço Range. Modified from Pedrosa-Soares et al. (1994), Grossi-Sad et al. (1997), Knauer and Grossi-Sad (1997), CPRM (2004) and Rolim et al. (2016)

Minas Supergroup (see below) as a result of the superposition of fold directions developed during the Neoarchean Rio das Velhas Orogenic Event (Carneiro 1992; Machado et al. 1992), and the subsequent Paleoproterozoic Transamazonic and Neoproterozoic Brasiliano orogenies. The metamorphic grade varies from greenschist facies to amphibolite facies conditions.

Iron formations occur in the lower Nova Lima Group associated with mafic and ultramafic lavas, ferruginous chert, carbonaceous pelite, turbidites, rare felsic volcaniclastic rocks and intrusions of gabbro, anorthosite, and peridotite (Baltazar and Zuchetti 2007). The IF usually displays a secondary hydrothermal mineralogy comprising sulfides (pyrite, pyrrhotite, arsenopyrite), magnetite, siderite, and quartz (silicification) associated with gold mineralization (Lobato et al. 2001). The timespan for the felsic magmatic activity of the greenstone belt has been estimated by Noce et al. (2005) to range from 2792 ± 11 to 2751 ± 9 Ma (SHRIMP and ID-TIMS U–Pb zircon) and by Machado et al. (1992) from 2776 + 23/−10 to 2772 ± 6 Ma (TIMS U–Pb in zircon).

18.4.2.3 The Paleoproterozoic Minas Supergroup, Quadrilátero Ferrífero District, Southern São Francisco Craton

The lithologic record of the 3700 m-thick lower Minas Supergroup (Caraça, Itabira, and Piracicaba Groups; Dorr 1969) represents a sequence that grades from fluvio-deltaic to open-marine shelf, deposited in a long-living basin covered by the immature foreland marine deposits of the Sabará Group and now located at the southern margin of the São Francisco Craton (Almeida 1977). The basal Moeda Formation of the Caraça Group consists of a clastic sequence of U-Au pyrite-bearing quartzites, metasandstones, and metaconglomerates (Wallace 1965; Villaça 1981; Renger et al. 1994). The siliciclastic layer is covered by carbonaceous and sericitic phyllites of the Batatal Formation that may be locally hydrothermally altered to chlorite and carbonate (Hensler et al. 2017). U–Pb ages of detrital zircons from the Moeda quartzites (Machado et al. 1992, 1996; Hartmann et al. 2006) indicate a maximum depositional age of 2584 Ma for this unit. The Batatal Formation also comprises, in addition to metapelitic phyllites, subordinate volcaniclastic rocks interlayered with fine-grained quartzite (metachert) and carbonate rocks that grade into BIF (Suckau et al. 2005). The deposition of fine-grained sandstones (upper Moeda Formation) and shales (Batatal Formation) registers the first stages of a period of marked transgression-regression during the opening of the Minas basin that is followed by the conformable deposition of the Cauê Formation and the Gandarela dolomites that grade both laterally and vertically into each other and comprise the Itabira Group.

The Cauê Formation contains a single prominent BIF layer *c*. 250–300 m-thick that hosts all high-grade, iron-ore deposits of the district, interlayered with lenses of sericitic phyllite, dolomite phyllite, and pyroclastic rocks (Suckau et al. 2005). The metamorphosed BIFs of the Quadrilátero Ferrífero District are described by the term "itabirite", which is widely used in Brazil (Rosière et al. 2008) and other mining districts worldwide. The layered structure of the itabirites is usually inherited from the primary Fe-rich sediment (Fig. 18.3c, e), although it may be locally obliterated by transposition and metamorphic differentiation. Four major mineralogical/compositional types of metamorphosed IF were distinguished by Dorr and Barbosa (1963) and Dorr (1964, 1965, 1969): quartz itabirite, the most widespread type, grades upwards or laterally into dolomite- and amphibole itabirite (Fig. 18.3e). Amphibole is usually of the grunerite-cummingtonite series (Guild 1957; Gair 1962; Dorr and Barbosa 1963; Pomerene 1964; Wallace 1965; Reeves 1966; Simmons 1968; Maxwell 1972; Pires 1995).

The Gandarela Formation has a maximum thickness of 500 m, as estimated by Renger et al. (1994), and is dominated by carbonate rocks (calcitic and dolomitic marbles), some with well-preserved stromatolites, thin itabirite layers, and at least two intraformational conglomerate horizons (Lopes-Silva et al. 2007), all of which reflect sea level fluctuations in the carbonate platform by the end of the period of deposition of the Itabira Group. The depositional age of the Itabira Group was first constrained by Babinski et al. (1995), who dated stromatolitic carbonate rocks at 2419 ± 19 Ma (Pb–Pb isochron), and this is currently the most reliable data. Based on this upper limit, and considering the Pb–Pb ages on detrital zircons of the Moeda Formation, the authors suggested that the deposition of the BIF of the Cauê Formation took place between 2520 and 2420 Ma.

The overlying units of the Piracicaba Group represent the sedimentation of a basin subjected to tectonoeustatic oscillations that developed into a foreland basin during the Rhyacian Transamazonian orogeny with the deposition of flysch, volcaniclastic sediments, and BIFs of the Sabará Group. The units of the Minas Supergroup are covered by quartzites and conglomerates of the Itacolomi Group, whose maximum depositional age is constrained by the youngest detrital zircon age of 2059 ± 58 Ma obtained by Machado et al. (1996).

The tectonic structure of the Minas Supergroup in the Quadrilátero Ferrífero District was shaped primarily by the Transamazonian orogenic event initiated at *c*. 2.1 Ga (Alkmim and Marshak 1998) at the end of the Rhyacian Period, although the surrounding Archean domes have strongly influenced the morphological configuration of the sequence (Chemale et al. 1994). The Rhyacian event caused deformation and greenschist to lower amphibolite facies metamorphism of the sedimentary sequences encompassing two

main penecontemporaneous deformational phases: the first is defined by northeast-southwest-trending folds (Alkmim and Marshak 1998) superposed by approximately northwest-southeast-trending structures, yielding large- and mesoscale dome and basin interference patterns. The Brasiliano collage (Brito Neves et al. 2014) caused the tectonic reworking of the sequence and modification of the older structures with the development of major thrusts, subordinate tight to isoclinal folds, and ductile shear zones.

18.4.2.4 High-Grade Iron Ore

High-grade iron ores in the Quadrilátero Ferrífero District (typically >64 wt% Fe) occur as economically significant deposits widespread in the entire region. Iron ores are subdivided into "hard" and "soft", or "blue" and "brown" types. Blue ores (Fig. 18.3f) are composed mainly of hematite, whereas brown ores contain considerable amounts of goethite and other iron hydroxides. Hard ore may occur as partially concordant to discordant, massive, banded, or schistose bodies, usually has a gray-blue color, a dull to metallic luster, and is composed of hematite, martite, and kenomagnetite/maghemite. Both massive and banded ore types display a granoblastic fabric (Fig. 18.3h), but the schistose varieties comprise largely oriented platy hematite crystals identified as specularite (Rosière and Chemale 1991) (Fig. 18.3i). Soft or friable blue ores are usually associated with hard ores and do not differ significantly in their mineralogy but are commonly devoid of internal structures, and locally exhibit large cavities up to several meters in diameter.

The formation of massive iron ore in the itabirite is mainly driven by the widespread and intense leaching and removal of gangue minerals involving multiphase hypogene-supergene alteration and enrichment processes associated with carbonate alteration of the Cauê itabirite that also affected the adjacent layers of the Batatal and Cercadinho Formations (Sanglard et al. 2014; Hensler et al. 2015, 2017). Hypogene mineralization is structurally controlled (Rosière et al. 2013), usually in shear zones or concentrated in folded blind tips of faults (Sanglard et al. 2014).

Supergene alteration is generally accompanied by the depletion of most elements, except for MnO_2 and K_2O. Its overprint increases the efficiency of the BIF mineralization by solubilization of residual carbonates, elutriation of loosened quartz grains, and concentration of goethite near the present land surface. The replacement of iron oxides and silicates and filling of open spaces produce a hard lateritic duricrust (known as "canga") as the end product.

18.4.2.5 The Orosirian-Statherian BIF-Bearing Sequences of the Serpentina Range

The Serra da Serpentina Range comprises two distinct BIF-bearing metasedimentary sequences, the Serra da Serpentina Group and the Serra de São José Group, both of which border the eastern edge of the Statherian-Calymmian Espinhaço Supergroup (1731 ± 5 and 1582 ± 8 Ma; Danderfer Filho et al. 2009) (Figs. 18.4 and 18.5). The Upper Paleoproterozoic Serra do Sapo IF of the Serra da Serpentina Group and the Canjica IF of the Serra de São José Group were deposited at the boundary between the Orosirian and Statherian periods during the early opening stages of the Espinhaço Basin (Rolim et al. 2016). The Serra da Serpentina Group has an Orosirian maximum depositional age (youngest detrital zircon age 1990 ± 16 Ma; Rolim et al. 2016) and is probably contemporaneous with the Itacolomi Group of the Quadrilátero Ferrífero District. The sequence consists of fine clastic metasediments of the Meloso Formation at the base that grade upward to BIF and dolomite lenses of the Serra do Sapo Formation. Lenses of sericitic quartzites, ferruginous quartzites, hematite-sericite-quartz phyllites, and meter-thick banded iron-manganese rock are sparsely found within the BIF layer. The BIF displays typical meso- and microbanding, although primary features may be commonly transposed by the pervasive tectonic foliation (Fig. 18.3d). The true thickness varies from 80 to 350 m in its northern portion, thinning down to 15–35 m along the southernmost part of the ridge.

The younger Serra de São Jose Group is separated from the Serra da Serpentina by an erosional unconformity. This sequence was deposited in a tectonically active north–south continental rift basin in the early stages of the opening of the Espinhaço Basin. It comprises a complete cycle of transgressive sedimentary deposits that were subdivided, from base to top, into the Lapão, Itapanhoacanga, Jacém, and Canjica formations. The coarse, BIF-boulder orthoconglomerates and psammitic sediments of the Lapão Formation were deposited over the Serra do Sapo Formation and transgressive on the basement complex in the active Serra de São Jose rift system. The quartzite of the Itapanhoacanga Formation has a maximum depositional age of 1666 ± 32 Ma (Statherian). The Jacém Formation (Almeida-Abreu et al. 1989; Knauer 1990) is a monotonous white, fine- to medium-grained quartzite that turns progressively Fe richer and grades into the Canjica BIF. This BIF occurs discontinuously with thicknesses that vary from 20 to 40 m and display drastic lateral changes. The BIF has typical banding defined by alternating layers of white, fine-to-medium grained quartz and iron oxides with granoblastic and lamellar hematite (specularite) and accessory magnetite.

The supracrustal rocks have undergone two stages of deformation during the west-verging Brasiliano orogeny that affected the eastern margin of the São Francisco Craton. The orogenic event generated a regional-scale, north–south trending fold-thrust belt developed during two compressional phases, and partially involved the crystalline basement.

Rare, high-grade (>62 wt% Fe), lens-shaped iron-ore bodies that are parallel to the regional schistosity are occasionally encountered in the Serra do Sapo BIF layer. The ore bodies are strongly foliated, 100–300 m long, with a thickness varying from 5 to 30 m (Fig. 18.3d), and comprising mainly millimeter-long platy hematite (specularite). East of the Serpentina and Espinhaço Ranges, several irregular, lens-shaped, discontinuous, folded and sheared bodies of BIF-bearing metasedimentary sequences occur enclosed in gneissic rocks of the Guanhães Crystalline Complex (GC; Fig. 18.4; 2867 ± 10 Ma; Silva et al. 2002) and host medium-sized, high-grade, magnetite-rich ore bodies (e.g., Morro Escuro, Candonga, Piçarrão, Baratinha, and Cuité). Tectonic analyses supported by U–Pb SHRIMP dating of detrital zircons constrained a maximum Statherian age (1668 Ma) for the Morro Escuro supracrustal rocks (Silveira Braga et al. 2015). Preliminary geochronologic studies by Barrote (2015) and Barrote et al. (2017) obtained similar results for several small amphibolite facies bodies near Guanhães, indicating that they represent tectonic outliers correlated with the IF sequences of the Serra da Serpentina Range over a large area eastwards from the southern Espinhaço Range.

18.4.2.6 The Colomis Group

The Colomis Group (Fig. 18.4) is a folded metamorphic sequence exposed in the surroundings of the Sobradinho Dam in the northwestern border of the Craton. It comprises lower amphibolite facies metapsamitic and metapelitic rocks (schists and phyllites) associated with quartz-hematite-magnetite BIF and quartz-hematite/magnetite-amphibole BIFs interlayered with dolomites and hosting high-grade hematite and magnetite iron ore bodies. This sedimentary sequence covers hydrothermally altered and partially sheared schists, possibly of magmatic origin. The age of the Colomis Group is uncertain but it underlies horizontal quartzites of the Mesoproterozoic Chapada Diamantina Group and displays a sheared contact with basement granitic-gneissic rocks, suggesting that they are contemporaneous with the Statherian Serra da Serpentina Group in the eastern border of the Espinhaço Range.

18.4.2.7 Neoproterozoic Iron Formations in the Cover Sequences of the São Francisco Craton

The Nova Aurora Formation (Macaúbas Group)

The Neoproterozoic Macaúbas Group records the long-lasting evolutionary stages from the opening of a Tonian continental rift as the precursor basin system of the Aracuaí-West Congo orogen to the development of a glaciomarine environment in a continental sea basin (Noce et al. 1997; Pedrosa-Soares and Wiedemann-Leonardos 2000; Kuchenbecker et al. 2015, 2016). Noce et al. (1997) subdivided the Macaúbas Group into the Duas Barras, Domingas, Rio Peixe Bravo, Serra do Catuni, Nova Aurora, Chapada Acauã, Ribeirão da Folha, Salinas, and Capelinha formations.

The sequence of the Macaúbas Group begins with sandstones, pelitic rocks (Rio Peixe Bravo Formation), and conglomerate lenses (Duas Barras Formation) with maximum sedimentation age constrained by U–Pb SHRIMP dating of detrital zircons of 900 ± 21 Ma (Babinski et al. 2012). Glaciogenic metasedimentary rocks of the Serra do Catuni are older than 740 ± 22 Ma. The glaciomarine Nova Aurora Formation that covers the Rio Peixe Bravo Formation is a distal correlative of the Chapada Acauã Formation, comprising quartzite, schists, metadiamictites, iron diamictites, and fine clastic iron rocks (Riacho Poções Member) (Figs. 18.4 and 18.6). The lithotypes of the Riacho Poções Member reach a thickness of 600 m and are considered to be a Rapitan-type sequence, probably deposited in the Cryogenian. The Fe_2O_3 (total) content of the diamictite varies from 10 to 78 wt%, whereas SiO_2 varies from approximately 13–78 wt% and Al_2O_3 is invariably high (up to 12 wt%). The rare-earth element content is very variable but lacks considerable fractionation and is devoid of anomalies when normalized to NASC (Vilela et al. 2014 and references therein).

The Lagoa Formosa Formation (Bambuí Group)

The Bambuí Group comprises a carbonate siliciclastic cover on the São Francisco Craton deposited in a restricted marine basin at the Neoproterozoic/Paleozoic Boundary (~635–570 Ma) with local glacial sediments. The sediments of the Bambuí Group were deposited directly over the cratonic basement (orthogneisses, amphibolite, schists, quartzites) or cover older Tonian sediments of the Macaúbas Group. In the southwestern São Francisco Craton, the Bambuí Group comprises massive diamictites and is associated with sandstones, conglomerates, laminated siltstones, carbonates, and subordinate jaspilite interlayered with siltites of the Lagoa Formosa Formation. The sequence suggests a slope and base-of-slope system with subaqueous gravitational flows (submarine fans) in the foreland basin of the Brasilia Belt (Uhlein et al. 1998) with a maximum age of ~612 Ma and a minimum of ~567 Ma (Uhlein et al. 2011).

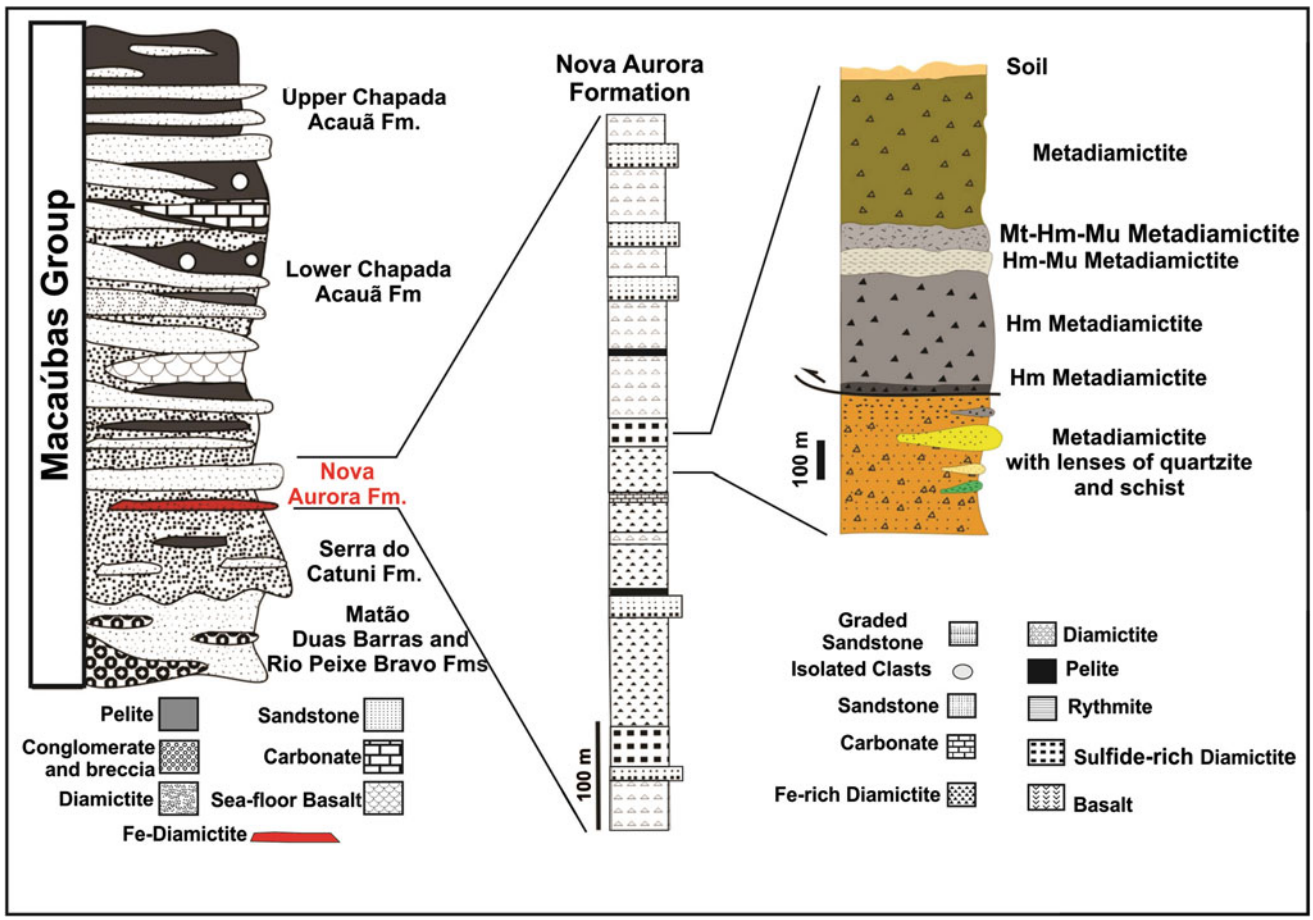

Fig. 18.6 Stratigraphy of the Macaúbas Group in the Nova Aurora District. Mt—magnetite, Hm—hematite, Mu—muscovite. Modified after Vilela et al. (2014)

18.4.3 The Tocantins Province: Archean Greenstone Belts, Paleoproterozoic Terranes and Neoproterozoic Belt of the Western Border of the São Francisco Craton

The Tocantins Province (Almeida et al. 1981) in central Brazil comprises the Neoproterozoic Araguaia and Paraguay belts that border the eastern and southeastern margins of the Amazon Craton, and the Brasilia Belt on the western edge of the São Francisco Craton (Fig. 18.7), all tectonically active during the Brasiliano collage. In the central part of the province and between both orogenic belts, several terranes of different ages occur which are reworked by the tectonothermal events associated with the Brasilia Belt: (1) Paleoproterozoic supracrustal belts comprising orthogneiss and volcanosedimentary sequences of the Almas-Dianópolis Terrane and the Anápolis-Itauçu high-grade metamorphic complex; (2) the Central Goias Massif, made up of the Crixás-Goiás Archean granite-greenstone terranes and the Paleo-Mesoproterozoic mafic-ultramafic layered complexes of Barro Alto, Niquelândia, Cana Brava, and related marine volcanosedimentary sequences; and (3) the Neoproterozoic Goias magmatic arc (Pimentel et al. 2000a, b, 2004; Pimentel 2016).

Granite-gneisses represent *c*. 80% of the Archean terranes, whereas the greenstone belts occur distributed in 6 km narrow strips over 60–100 km long separated by gneisses (Fig. 18.7). Three of them are located in the north (Crixás, Guarinos, and Pilar de Goiás) and two are located in the southern part (Faina and Serra de Santa Rita). The five belts display a lower stratigraphic sequence of metavolcanic rocks starting with metakomatiites followed by tholeiitic metabasalt. Felsic volcanic rocks have so far only been described in the Santa Rita Greenstone Belt. Iron formations are ubiquitous in all greenstone belts: in Pilar de Goiás, a continuous, on average 10 m-thick, silicate-bearing (garnet and amphiboles) BIF layer extends for several kilometers; in Faina and Guarinos, BIF is associated with metaconglomerate, quartzite, phyllite, and dolomite of uncertain age.

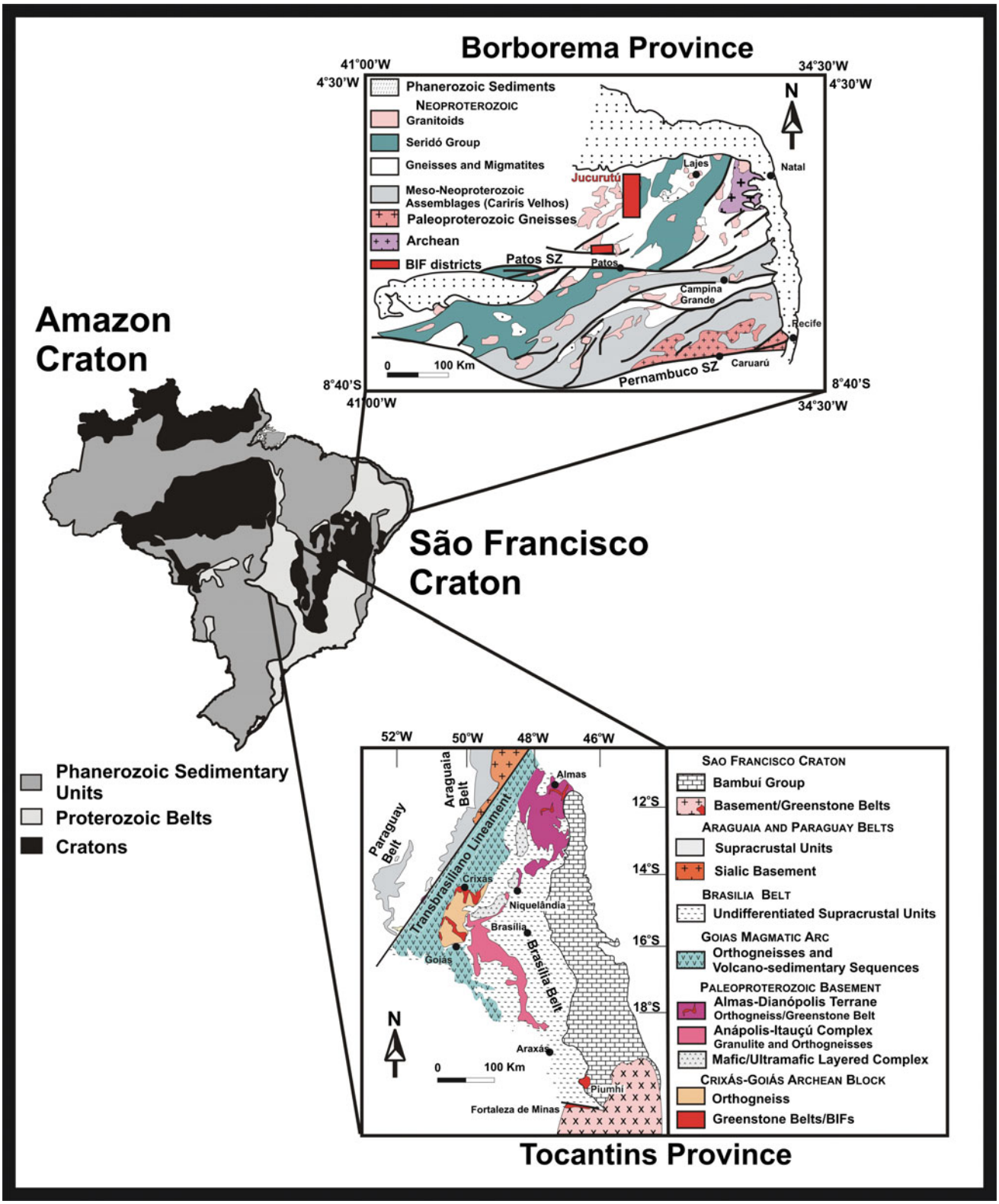

Fig. 18.7 Simplified geologic maps of the Tocantins and Borborema Provinces with the location of the main BIF-bearing sequences. Modified after Pimentel et al. (2000a) and Brito Neves et al. (2000), respectively

18.4.4 The Borborema Province

In the northeastern region of the South American Platform, the Borborema Province (Almeida et al. 1981; Almeida 1997) (Fig. 18.7) encompasses several terranes that have undergone a complex evolution over different orogenic events and were amalgamated during the Neoproterozoic Brasiliano Orogeny. Nevertheless, the definition, correlation, and integration of these events in the accretional history and reconstruction of Western Gondwana is still unsubstantial. In these terranes, the presence of several minor and ill-defined BIF-bearing sequences have stimulated mineral exploration with limited success. In the Brasiliano Seridó and Piancó-Alto Brígida Belts, in the northern part of the Province, occur several BIF layers, where the metamorphic Jucurutu (or Serra dos Quintos) Formation is regionally the economically most important BIF unit (Fig. 18.7). This formation is interpreted as being deposited at the boundary between the Upper Cryogenian to Lower Ediacaran (Sial et al. 2015), but further studies are necessary to better understand the stratigraphy and sedimentary environment as well as the tectonic setting. Regionally, the BIF strikes northeast–southwest, being strongly sheared at its southernmost extremity by the Patos Shear Zone. Several massive hematitic and magnetitic high-grade lenses (Fe > 65%) associated with low-grade ore (35–52% Fe) are present.

18.4.5 The Paraguay Belt

The Paraguay Belt (Figs. 18.7 and 18.8) is an orocline of Brasiliano age associated with the closure of the Clymene Ocean that marks the Neoproterozoic limit of the SE Amazon craton. The opening of the basin is associated with the break-up of the Rodinia supercontinent and the basin was filled with Cryogenian to Ediacaran deposits, including glaciogenic, continental to glaciomarine, and marine sediments that comprise the basal Puga Formation, and the Cuiabá, Jacadigo, Corumbá, Araras, and Alto Paraguay Groups.

18.4.5.1 Iron Formations of the Jacadigo Group

The Jacadigo Group comprises the Cryogenian Band'Alta/-Santa Cruz Rapitan-type IF interlayered with Mn-rich units, associated with purportedly glaciogenic (Marinoan?) sediments (sandstone and diamictite), and capped by Ediacaran stromatolitic carbonates of the Corumbá Group. These units crop out south of the Sunsas Province and west of the Paraguay-Araguaia fold Belt in the west-northwest-east-southeast-trending, 500 km-long Chiquitos-Tucavaca aulacogen (Litherland and Bloomfield 1981; Almeida and Hasui 1984) and in the northeast-southwest-trending, 10–20 km-long, Corumbá graben system (Jones 1985). The Band'Alta Formation hosts jaspilites, dolomitic-cherty BIFs, and IFs with nodular structure (Fig. 18.3b) along with massive hematite pelites and Fe-rich, fine-to-coarse grained clastic sedimentary rocks (Fig. 18.8).

The age of the Jacadigo Group is poorly constrained by its regional correlation with the Puga diamictite (Alvarenga and Trompette 1993), which is overlain by a Marinoan-type cap dolostone (Nogueira et al. 2003). The Jacadigo Group is also stratigraphically correlated with the Boqui Group in Bolivia (Graf et al. 1994), and sedimentation is considered to have occurred at *c*. 590 Ma by the fragmentation of the Amazon Craton (Pimentel et al. 1996; Trompette et al. 1998; Cordani et al. 2009).

18.4.6 The Nico Pérez Terrane of Southern Brazil and Uruguay

East of the Sarandí del Yí Shear Zone in Uruguay and in the Rio Grande do Sul State of Brazil, the Nico Pérez Terrane (NPT) crops out as basement blocks and several basement inliers within the Dom Feliciano Belt (Figs. 18.9 and 18.10; Chap. 7). Neodymium and Hf isotopic studies evidence an important component of Archean crustal growth in all areas of the NPT, whereas zircon U–Pb geochronology shows extensive Paleoproterozoic crustal reworking by anatexis (Oyhantçabal et al. 2012; Oriolo et al. 2016). Relics of a Neoarchean to Siderian sedimentary cover, including BIF, quartzite, and marble, are a frequent feature, particularly in the Valentines and Isla Cristalina de Rivera areas (Figs. 18.9 and 18.10). Additionally, anorthosite complexes, metagabbro, amphibolite, and felsic volcanic rocks record a Mesoproterozoic anorogenic event not observed in the Río de la Plata Craton (see Sect. 4.7). The Neoproterozoic reworking during the Brasiliano orogeny was extensive and the cratonization age remains uncertain in this terrane (Chap. 7). Two different subterranes, separated by the north-northeast-trending Caçapava–Sierra de Sosa Shear Zone, are recognized. The western subterrane (Cerro Chato Block) includes the granulite facies Valentines Rivera (Uruguay) complex and Santa Maria Chico (Brazil) complex, and it is less reworked by the Brasiliano orogeny than the eastern part. The eastern subterrane (Pavas Block) was strongly reworked during the Brasiliano and comprises the Pavas Block of Uruguay and several basement inliers in the Dom Feliciano Belt of Uruguay and Brazil (Chap. 7).

The endowment of mineral resources confirms the difference between the Río de la Plata Craton and the Nico Pérez Terrane. Iron resources from BIFs in the NPT in

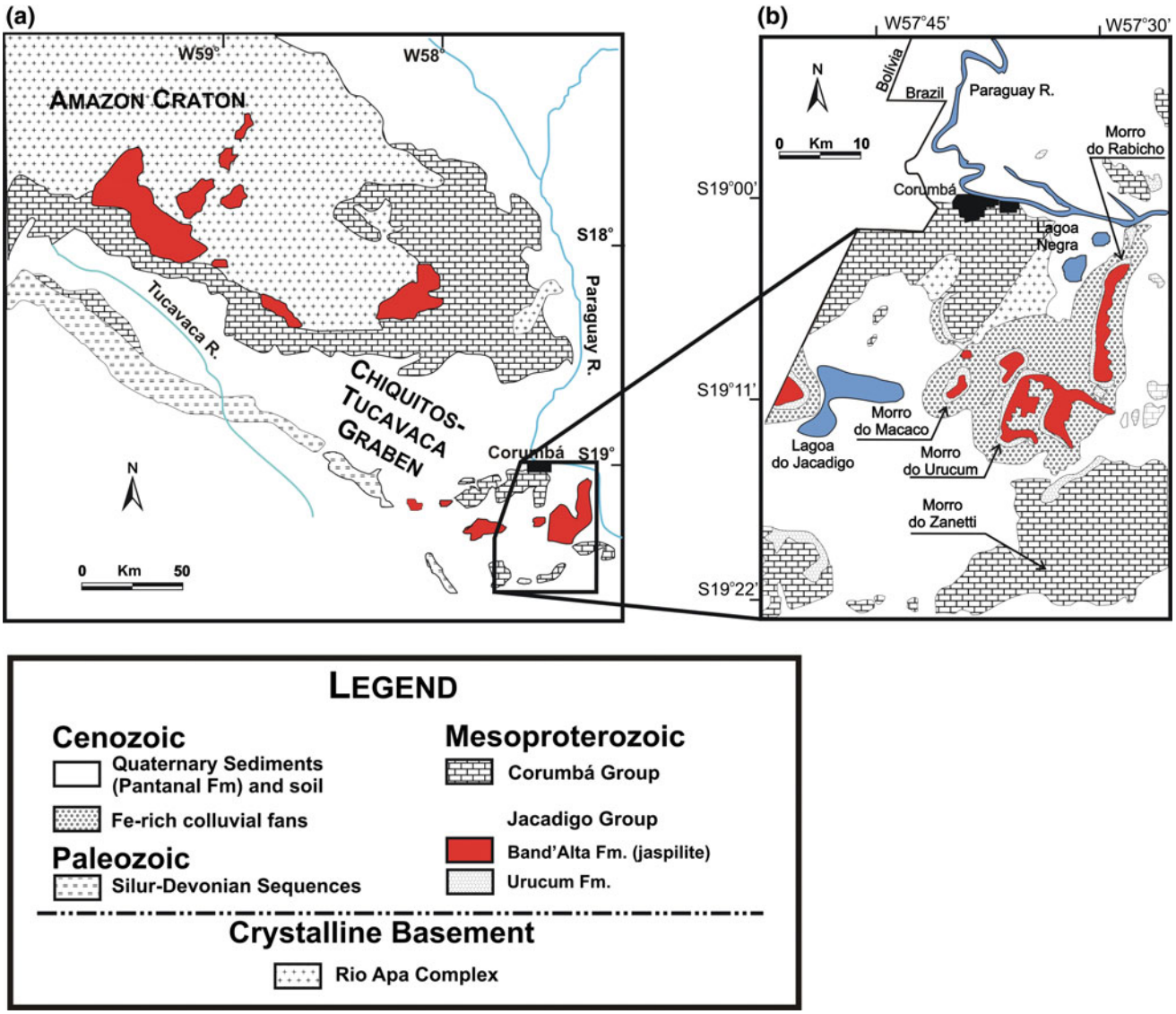

Fig. 18.8 Geologic map of the Urucum District, Mato Grosso do Sul. **a** Simplified regional geological map. **b** Inset from **a**, modified from Schobbenhaus and Oliva (1979), Urban et al. (1992), Trompette et al. (1998), and Geologic Map Embrapa Pantanal geological map, based on images TM-Landsat-5, WRS 227/73D, 1:100.000; TM-Landsat-5, and WRS 227/73D, on the topography sheets Corumbá (SE.21-Y-D-II, MI 2469) and Albuquerque (SE.21-Y-D-III, MI 2470) and on the geological map 1:1.000.000, Del'Arco et al. (1982)

central and northern Uruguay are significant, with more than 600 Mt with *c*. 28 wt% Fe. These BIFs are part of the Vichadero and Valentines formations, described below. These formations share the same lithological association and mineral parageneses and are therefore considered to be part of the same platform succession of Neoarchean to Siderian age, being the BIF deposits probably of the Lake Superior-type. In the northern NPT of Uruguay, shear zone-hosted gold vein deposits of Neoproterozoic age are well known and currently mined. In contrast, these mineral resources are scarce to absent in the Río de la Plata Craton.

18.4.6.1 Iron Formations in the Cerro Chato Block of the Nico Pérez Terrane

Iron Formation of the Vichadero Formation

Geologic Setting, Dates, and Associated Lithologies

The Vichadero Formation (Ellis 1998; Oyhantçabal et al. 2011, 2012), with a strike length of about 100 km, occurs in a Precambrian basement horst referred to as Isla Cristalina de Rivera that crops out within a Phanerozoic sedimentary basin of northern Uruguay. The formation is composed

mostly of metasedimentary and minor metavolcanic rocks, including BIF, manganese IF, quartzite, forsterite marble, calcsilicate granofels, clinopyroxene granofels, tremolite granofels, and mafic metavolcanic rocks (including two-pyroxene granulite). All lithologies were affected by high-grade metamorphism and deformation, and they occur as isolated and scattered, kilometer-scale bodies hosted by granulitic orthogneisses. Several varieties of BIF and manganese IF occur as the thickest member of the Vichadero Formation within the Isla Cristalina de Rivera. There they reach a maximum of ~100 m and form low hills in an undulating relief (Ellis 1998).

Zircon U–Pb ages are only available for granulitic gneisses enclosing the relics of supracrustal rocks (Vichadero Formation) that contain the IFs. Felsic and mafic orthogneisses have Rhyacian U–Pb zircon ages ranging from 2171 ± 6 to 2069 ± 16 Ma (Santos et al. 2003; Oyhantçabal et al. 2012; Oriolo et al. 2016). Older ages reflect the magmatic crystallization of the protolith, whereas the younger ones record the high-grade metamorphic event. Field relationships and similar metamorphism indicate that these ages constrain the minimum age of the IF-bearing supracrustal rocks. Because U–Pb ages are not available for the supracrustal rocks and it is not obvious if the protolith of the gneisses was a volcanic or plutonic rock, it is not possible to determine whether these supracrustal rocks are older or coeval with the dated gneisses.

Even though age dating is not available for the Vichadero Formation, field and petrographic relationships, the BIF and manganese formation association, and rare-earth element (REE) characteristics (see next section for details), suggest an early Paleoproterozoic depositional age, a main granulite facies metamorphic event at *c*. 2.1 Ga, and a well-defined amphibolite facies metamorphic event at *c*. 1.94 Ga (Oyhantçabal et al. 2012).

Petrography and Geochemistry

Ellis (1998) performed detailed studies of BIF and manganese formation of the Vichadero Formation in the Vichadero, Cerro Iman, Cerro Iman east, Papagayo deposit (many localities), Minas de Corrales, and Manuel Diaz localities. Based on mineralogical and fabric characteristics, he classified the different varieties of BIF and Mn formation into four end-member groups within a continuum. The main groups and their lithologies and mineralogy, described in more detail below, are (1) banded rocks composed of >90% quartz and iron oxide layers; (2) mostly banded rocks composed of quartz, iron-(manganese) oxides, and iron-(manganese) silicates; (3) garnet-bearing rocks composed of iron-(manganese) oxides and manganese-iron silicates, and variable amounts of quartz; and (4) massive Mn-rich rocks composed of manganese-iron silicates and iron-(manganese) oxides with subordinate to absent quartz. Groups 1 and 2 are mostly oxide dominated, groups 3 and 4 are oxide-silicate dominated, but group 4 is mostly silicate manganese IF. Hematite is a common secondary mineral partially replacing magnetite in lamellae or as patches.

Group 1 of IF is composed of monomineralic layers of quartz and magnetite (and hematite) up to several centimeters thick. Chemically, these rocks are mostly Fe and Si, with very low concentration of other elements. *Group 2* of IF is similar to Group 1 but is less abundant and contains iron-(manganese) silicates, including pyroxene, pyroxenoid, and amphibole. Groups 1 and 2 of IFs are mostly composed of SiO_2 and Fe_2O_3, with both oxides together being 90–99 wt%. However, Group 2 IFs have slightly higher Al, Mg, and Ca, which are hosted by the silicates. *Group 3* IFs are garnet-bearing to garnet-rich (almandine dominant, <77.2 mol%), composite Fe–Mn rocks. Garnet-rich rocks are coarse grained and tend to have less quartz and are banded, in contrast to rocks in Groups 1 and 2. Group 3 IFs have higher Mn (4.2–10.2 wt% MnO), Al (0.5–5.7 wt% Al_2O_3), Ca (0.3–9.5 wt% CaO), Mg (0.4–5.5 wt% MgO), Sc, Y, and REEs compared with those of Groups 1 and 2. *Group 4* IF is composed of massive, heterogeneous, composite iron-manganese rocks, with minor to absent quartz and with manganese silicates that include knebelite, pyroxferroite or pyroxmangite, braunite, manganoan augite or manganoan hedenbergite/diopside, and spessartine-rich garnet. They are characterized by a variable content of Al (0.2–14.4 wt% Al_2O_3), Mg (0.4–5.5 wt% MgO), and Ca (1.2–7.2 wt% CaO). Amphiboles of various compositions, including those of Fe–Mg–Mn groups (cummingtonite, dannemorite, tirodite) and Ca amphiboles (tremolite, actinolite), may be present in all groups of IF, but they are of retrograde origin in all but one occurrence and replace clinopyroxene and quartz. Apatite is a common accessory phase in all groups of IF. Limonite and manganomelane are prevalent supergene minerals.

Metamorphic conditions reached granulite facies, as evidenced by the occurrence of two-pyroxene granulite and spinel-bearing forsterite marble. In one of the localities (Cerro Papagayo), the association orthopyroxene + clinopyroxene + plagioclase in a mafic granulite indicates, using the petrogenetic grid of Pattison (2003), that peak metamorphic conditions reached granulite facies at around 800–1000 °C and 8–10 kbar (Oyhantçabal et al. 2012). An amphibolite to greenschist facies retrograde metamorphic event dated at *c*. 1.94 Ga (Oyhantçabal et al. 2012) is evident by the replacement of pyroxene by amphibole in BIF and manganese formation and other lithologies of the Vichadero Formation.

Rare-earth element patterns normalized to the North American Shale Composite (NASC) of the various IF and Mn formations from Vichadero (Ellis 1998) are characterized by relatively flat to smoothly dropping trends, mostly small negative Eu anomalies, and small negative to positive Ce anomalies (physical visual anomalies in the patterns). The rare-earth element content is low to moderate and less

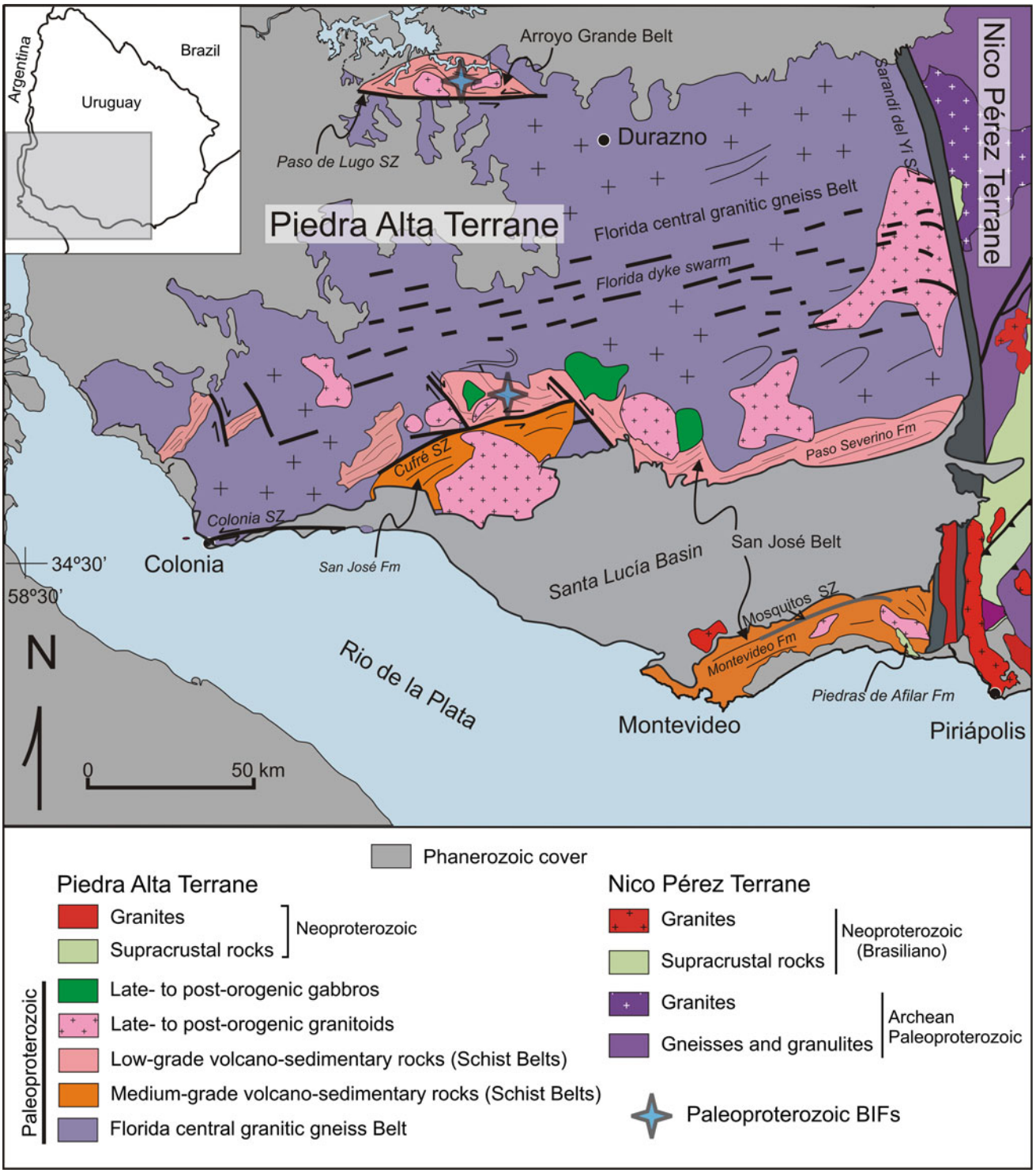

Fig. 18.9 Regional geologic map of western Uruguay depicting the Piedra Alta Terrane and part of the Nico Pérez Terrane. The area of the Piedra Alta Terrane shown comprises the Arroyo Grande Belt and the San José Belt. Modified from Preciozzi et al. (1985), Bossi and Ferrando (2001), Oyhantçabal et al. (2011)

than 10× NASC and <1× the Post Archean Australian Shale (PAAS) in samples with low detrital contents (Ellis 1998; Fig. 18.11a). Samples of IF and manganese formation that have a higher REE content correspond to those with garnet and/or apatite, and likely reflect contamination by carbonate and/or detrital input.

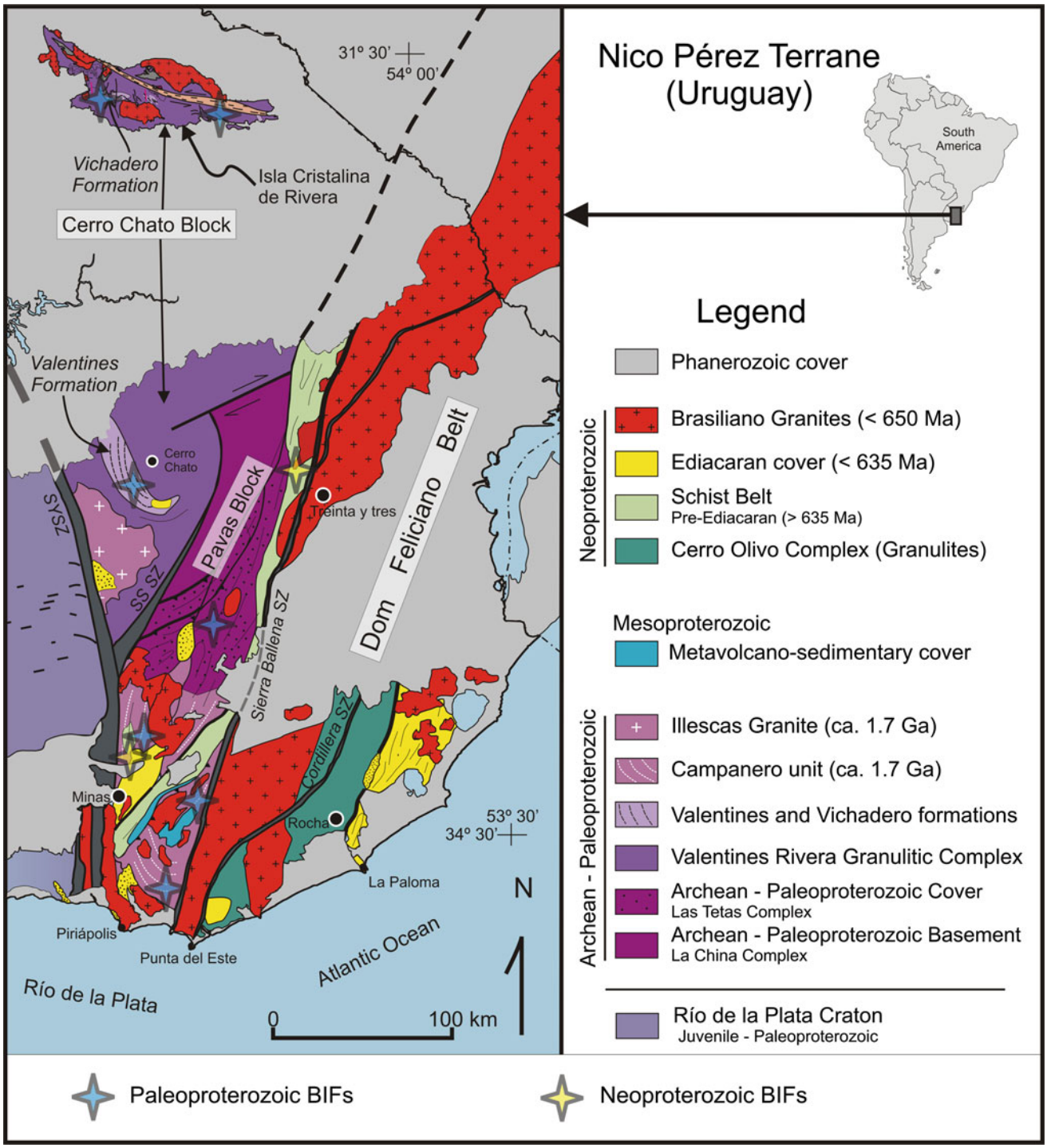

Fig. 18.10 Geologic map of the Nico Pérez Terrane and the contiguous Dom Feliciano Belt. Modified from Preciozzi et al. (1985), Bossi and Ferrando (2001) and Oyhantçabal et al. (2011)

Genesis of the IF

Because of the association with metasedimentary rocks, and minor meta-mafic rocks, the BIF and manganese formation were interpreted as chemical sediments formed as part of a sedimentary sequence (Ellis 1998). The protoliths of the BIF and manganese formation are considered to have been Fe- and Fe–Mn-rich, cherty, carbonate-bearing, mudstone sediment with a (bio)chemical precipitation origin and a minor detrital component. Submarine hydrothermal volcanogenic fluids provided most of the Fe, Mn, and Si, the Ca and Mg

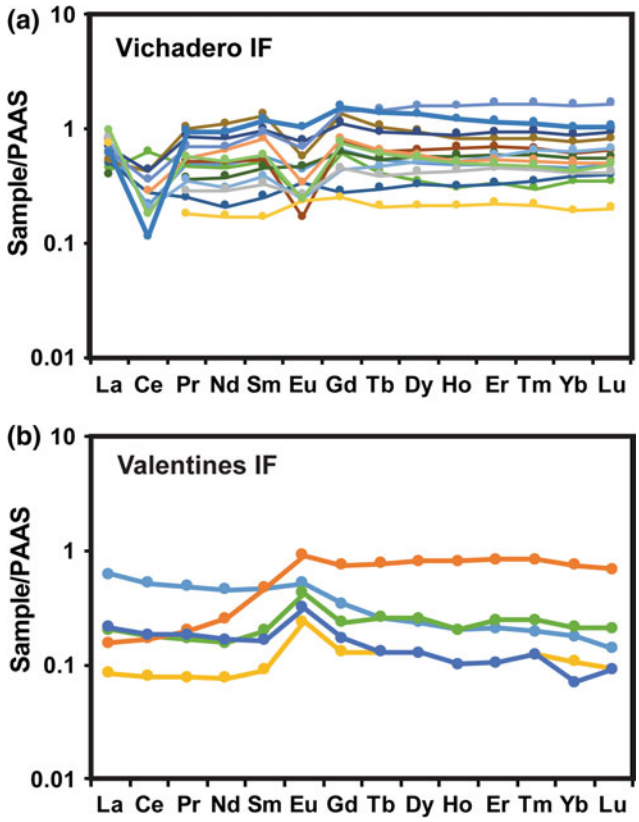

Fig. 18.11 Representative REE patterns of IF normalized to Post-Archean Australian Shale (McLennan 1989). **a** Valentines IF (Lancaster 2015 and A. Heimann, unpublished data), and **b** Vichadero IF (Ellis 1998)

were derived from seawater, and the Al and some Si reflect minor clastic contributions. Rare-earth element patterns of associated quartzite suggest that the silica formed as a chemical precipitate, and there is no evidence of detrital quartz in the BIF and manganese formation. Impure carbonate rocks are also considered to contain chemically precipitated chert: forsterite marble represents a siliceous dolomite protolith, whereas tremolite granofels and clinopyroxene granofels represent cherty carbonates with variable chert content. These associations were interpreted as reflecting deposition of the Vichadero Formation in a chert and carbonate shelf of a passive continental margin. The overall characteristics of REE patterns of BIF and manganese formation, in particular the lack of positive Eu anomalies, led Ellis (1998) to suggest formation in a Proterozoic marginal basin in a passive continental margin environment, and/or precipitation distal from the main source hydrothermal fluids. The mentioned characteristics and the absence of separate basins suggest that the BIF and manganese formation are similar to Lake Superior-type BIF. Higher Al content in Fe–Mn-rich formations of Groups 3 and 4 reflect a higher detrital (clay) component. This is also consistent with higher Mn content compared with that of IF of Groups 1 and 2, which indicates precipitation closer to shore and under more oxidizing conditions for the Mn-bearing formations of Groups 3 and 4.

The available information suggests that the BIF and manganese formation of the Vichadero Formation could be correlated with the IF of the Valentines Formation in the Nico Pérez Terrane of central Uruguay (see elaboration below).

Iron Formation of the Valentines Formation

Geological Setting, Ages and Associated Lithologies

The Valentines Formation (Bossi et al. 1965) is a high-metamorphic grade, folded sequence located in the central part of the Nico Pérez Terrane (Fig. 18.10) and composed of felsic granulite, mafic granulite, pyroxene granofels, augite-magnetite quartzite, clinopyroxene granofels (Bossi et al. 1965; Bossi and Umpierre 1968), amphibole-magnetite quartzite, and rare forsterite marble (Preciozzi et al. 1979, 1985; Bossi and Gaucher 2014). The granulites contain mesoperthitic alkali feldspar, plagioclase, pyroxene, amphibole, and biotite. Based on mineralogy, peak metamorphism of the Valentines Formation reached granulite facies (Bossi and Umpierre 1968). Characteristics of high-grade metamorphism include the presence of garnet, cordierite, and pyroxene, lobated grain edges evidencing grain boundary migration, mesoperthitic alkali feldspar, and triple junctions at 120 °C. Retrograde metamorphism is recorded by amphibole, secondary chlorite, epidote, and calcite (Bossi and Umpierre 1968; Lancaster 2015). The lithologies and the high-grade metamorphism are similar to those of the Vichadero Formation in Rivera.

Iron formation exposures of the Valentines Formation are part of the Nico Pérez terrane in central Uruguay (Fig. 18.12a). The IF, which is referred to as the Valentines Iron Formation, has been studied in some detail, including associated lithologies, petrography, mineral chemistry, and rock chemistry (Guillemain 1910a, b; Bossi 1963; Bossi and Umpierre 1968; Lancaster 2015). Exploration campaigns focused on this IF took place in the 1950s and 1960s and returned in the 2010s with detailed drilling and mapping, and a view on mining.

As is the case of the Vichadero IF, age dates are only available for the enclosing rocks and not for the IF itself. Dating by U–Pb SHRIMP in zircon of a felsic granulite in the Valentines Formation determined a 2.16 Ga magmatic crystallization age, a high-grade metamorphic overprint at 2053 Ma, and partially reset inherited Archean zircons (Santos et al. 2003). Similar magmatic crystallization ages at 2106 ± 21 Ma and Archean inheritance were reported for zircon from felsic orthogneiss (Oriolo et al. 2016).

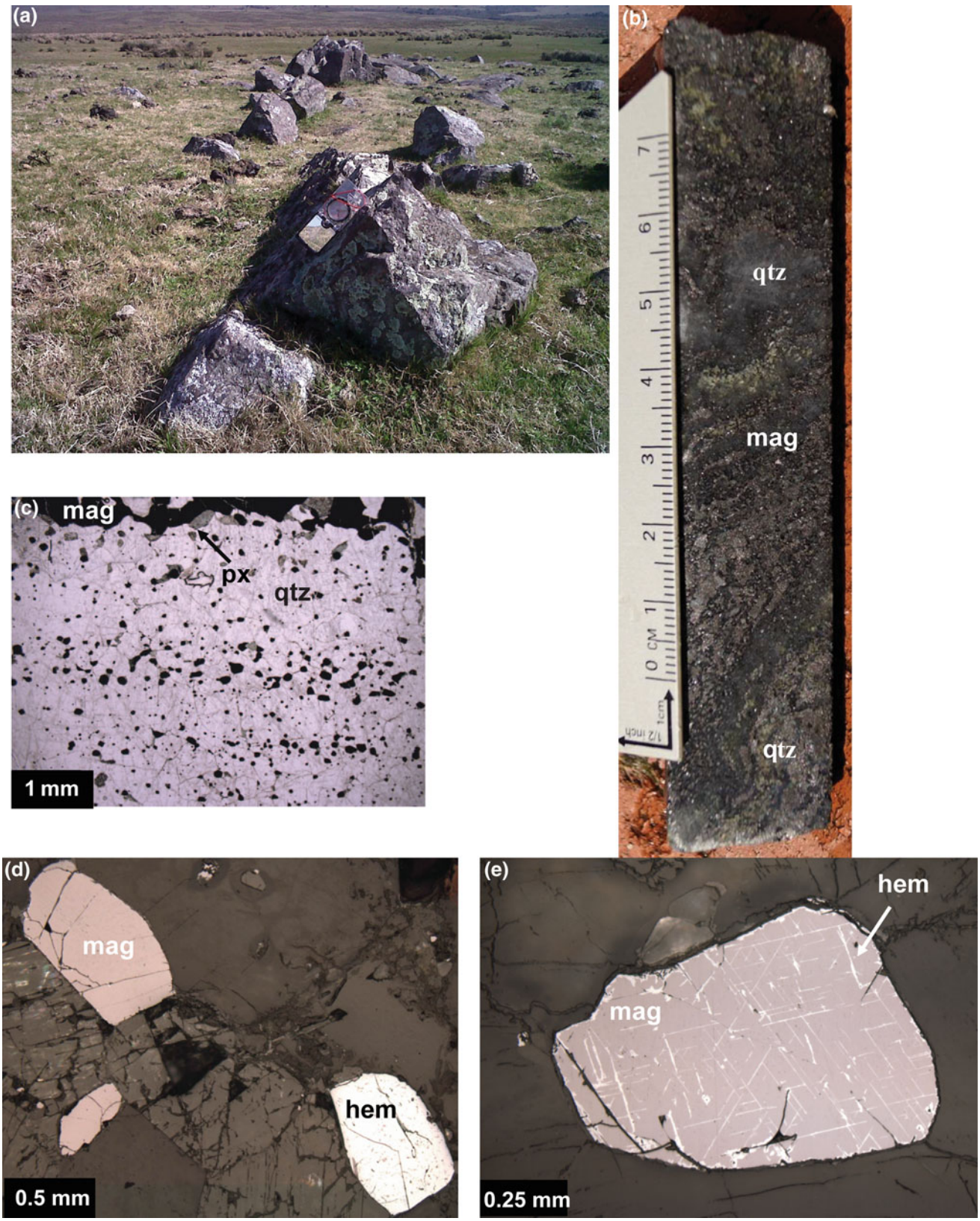

Fig. 18.12 Field (**a**) and hand sample photos (**b**) and photomicrographs (**c–e**) showing typical outcrops, appearance, petrography, and textures of the Valentines Iron Formation. **a** Field photo showing the typical outcrop of the Valentines IF. **b** Slab of core sample showing typical alternating layers of magnetite (mag) and quartz (qtz) of the Valentines IF. **c** Banded iron formation showing layers mostly composed of qz, mag, and greenish clinopyroxene (cpx). **d** Magnetite martitized, replaced by hematite (hem). **e** Individual crystals of magnetite with hematite

Additional metamorphic ages of 2011–2039 ± 10 Ma were also obtained for zircon from felsic granulite via in situ U–Pb LA-ICP-MS (Lancaster 2015).

Petrography and Geochemistry of the IF and Associated Lithologies

Bossi and Umpierre (1968) described the petrology and field relationships, and presented some rock and mineral chemical compositions of the rocks of the Valentines Formation, focusing on the Valentines Iron Formation. Lancaster (2015) performed a petrographic, mineral chemistry, and major- and trace-element chemical study of the IF and associated lithologies using drill core from the Las Palmas and Valentines areas (Fig. 18.12b). The Valentines Iron Formation is defined by an augite-magnetite quartzite (locally referred to as "Valentinesite") characterized by a granoblastic texture with crystals between 0.5 and 1 mm (Bossi 1963; Bossi et al. 1965; Bossi and Umpierre 1968; Lancaster 2015). This rock is composed of quartz (40 vol.%), magnetite (33%), and clinopyroxene (25%) as the main minerals, whereas hematite (1%), apatite (0.5%), titanite (0.2%), and pyrite (0.1%) are the accessory phases present (Fig. 18.12c–e; Bossi and Umpierre 1968; Lancaster 2015). Petrographic analysis shows a green clinopyroxene described in early studies as aegirine-augite (Bossi and Umpierre 1968). The rocks are banded, with laminations and bands ranging from 1 to 3 cm in thickness defined by mineralogical changes (Lancaster 2015; Fig. 18.12b, c). Close to the surface the rock grades into a quartz hematite assemblage (Bossi and Umpierre 1968). Hematite and ilmenite also occur in the BIF along with magnetite (Lancaster 2015) (Fig. 18.12d).

Magnetite is characterized by very low Mn (<0.5 wt% MnO) and Ti (<0.05 wt% TiO_2) content (Lancaster 2015). The dominant pyroxene present in the BIF shows pleochroism from light-yellow, yellow-green to slight pinkish yellow. The pyroxene is mainly diopside-hedenbergite solid solution (80%) with minor acmite-jadeite (10%) and enstatite (10%) components (Bossi and Umpierre 1968). The most common pyroxene present in the BIF contains large amounts of CaO (20.14–23.63 wt%) and roughly equal proportions of FeO and MgO (6.96–13.77 wt% FeO, 9.15–14.99 wt% MgO), putting it in the diopside field (Lancaster 2015). When plotted on a discrimination diagram using the wollastonite-enstatite-ferrosilite (Wo-En-Fs)-jadeite (Jd)-aegirine (Ae) end-members, this pyroxene does not contain enough Na to reach an aegirine-augite composition (Lancaster 2015). Pyroxene present in less banded IF samples that are rich in pyroxene contains similar amounts of CaO, larger amounts of FeO (up to 18.64 wt%), and less MgO (up to 9.38 wt%) than pyroxene in the BIF, belonging to the diopside-hedenbergite series, and most analyses classify it as hedenbergite.

Amphiboles are present in some of the rocks, and the species vary with depth. In shallow rocks, amphibole occurs as fibrous actinolite likely replacing pyroxene, whereas in deeper rocks it appears as small (<1 mm) individual hornblende crystals (Lancaster 2015). Hematite contains almost exclusively Fe and small amounts of MnO (up to 0.2 wt%) and TiO_2 (up to 0.6 wt%). Ilmenite contains less than 0.1 wt% MgO, and significant amounts of MnO (up to 16.26 wt%; Lancaster 2015).

The well-banded IF has Fe concentrations ranging from 40.83 to 52.25 wt% Fe_2O_{3T}, extremely low MnO, TiO_2, Na_2O, and K_2O content (<1 wt%), very low Al_2O_3 (<2.99 wt%), and low to moderate Mg (<4.26 wt% MgO) and Ca (4.11 wt% CaO) (Lancaster 2015). In terms of their Al, Fe, and Mn content, banded quartz-magnetite-pyroxene rocks have compositions that fall in the previously defined field of hydrothermal sediments close to the Fe end-member and along the Fe–Al join with minor Al content (Lancaster 2015). Minor elements indicative of a hydrogenous component occur in very small amounts, with (Ni + Co + Cu) ×10 close to 0 mol%. Similarly, Al/(Al + Fe + Mn) ratios are very low (<0.1) for banded quartz-magnetite-pyroxene rocks, indicating an extremely small to absent detrital component (Fig. 18.13). Iron/titanium ratios range from very high (>1000 Fe/Ti), and similar to those of active ridge sediments, to lower values (100–1000) similar to those of the Cauê Iron Formation and the Quadrilátero Ferrífero, Brazil, and the Isua Iron Formation, Greenland. Other magnetite-rich rocks with less well-defined fine-scale banding contain more Al and have larger Al/(Al + Fe + Mn) and lower Fe/Ti (< ~ 100) ratios that fall along the mixing line between the East Pacific Rise hydrothermal sediments and the continental crust, indicating a larger detrital component compared to the more banded variety of quartz-magnetite-pyroxene rock (Lancaster 2015).

Rare-earth element signatures of quartz-magnetite-pyroxene rocks normalized to PAAS are characterized by

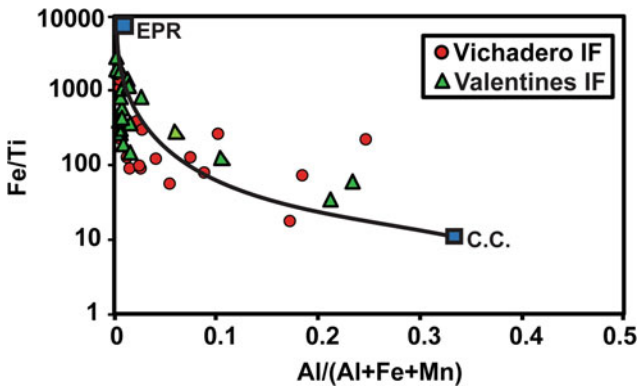

Fig. 18.13 Geochemical diagram of Al versus Al/(Al + Fe + Mn) comparing the Valentines and Vichadero iron formations. Curve represents mixing line between the average continental crust and East Pacific Rise (EPR) metalliferous sediments. Modified after Boström (1973) and Lancaster (2015)

relatively flat patterns and absent or small positive and negative (not shown) Eu anomalies (Lancaster 2015; Fig. 18.11b). In a $(Pr/Pr^*)_{SN}$ versus $(Ce/Ce^*)_{SN}$ plot (SN = PAAS normalized), most samples of banded rocks analyzed do not have a true Ce anomaly but a few have a very small positive La anomaly. Iron formations uncontaminated by detrital input, evidenced by low Sc, Hf, and Th (<2 ppm), lack or have a small negative Ce anomaly and are similar to those of Archean IFs (Lancaster 2015). These characteristics suggest that the protoliths of the Valentines Iron Formation were deposited in suboxic to anoxic waters influenced by high-temperature hydrothermal fluids.

The felsic granulite is composed of oligoclase ($An_{20–25}$) and quartz, and accessory biotite, hornblende, or augite. Clinopyroxene granofels is a dark, granoblastic rock with up to 5 vol.% magnetite that appears with two different mineralogies. One variety of clinopyroxene granofels is associated with quartz-magnetite-pyroxene rock and composed of green-pink pleochroic clinopyroxene, andesine ($An_{30–50}$), quartz, microcline, magnetite, hornblende, and titanite (Bossi and Umpierre 1968; Lancaster 2015). When andesine is absent, garnet may account for up to 50% of the rock. The other variety of clinopyroxene granofels is not associated with quartz-magnetite-pyroxene rock and is composed of diopside-hedenbergite, andesine, hornblende, and accessory magnetite (Bossi and Umpierre 1968).

Genesis of the IF

The chemical composition of the Valentines Iron Formation suggests that the original sediments were mostly iron oxides/oxy-hydroxides and chert formed from seawater influenced by hydrothermal fluids. The low concentration of Ti in magnetite suggests that it is of sedimentary origin and formed at low temperatures (Lancaster 2015). Rare-earth element signatures suggest that the precursor Fe and Si minerals of the IF were deposited in suboxic to anoxic waters. Overall, REE characteristics and age dating of spatially associated felsic granulites suggest a Paleoproterozoic to Archean time of deposition for the Valentines Iron Formation.

Comparison of the Valentines and Vichadero Iron Formations

Available U–Pb zircon age data and geological similarities, including associated lithologies and mineralogy of the IFs, suggest that the Valentines and Vichadero IFs could be part of the same coeval sedimentary sequence. Geochemically, the main difference is the greater Mn content (up to 10 wt% MnO; Ellis 1998) in some of the Vichadero manganese IF samples compared with the Valentines IF that has a much lower Mn content (<1 wt% MnO in bulk rocks; Lancaster 2015), even though ilmenite in the latter contains Mn. We note that, in general, greater Mn content in IFs tend to be typical of younger, upper Paleoproterozoic IFs, such as those from the ~2.22 Ga Hotazel Formation that reflects a somewhat oxygenated coeval deep ocean (e.g., Tsikos et al. 2003; Planavsky et al. 2010) at the time of deposition. Post-Archean Australian Shale-normalized REE patterns are similar in that both have relatively flat patterns. Some samples from the Vichadero IF that contain greater REE content than those of the Valentines IF correspond to rocks with greater detrital contributions, as evidenced by the Fe/Ti and Al/(Al + Fe + Mn) ratios (Figs. 18.11 and 18.13). The main difference is the presence of positive Eu anomalies in the Valentines IF and the lack of clear positive Eu anomalies and presence of negative Eu anomalies in the Vichadero IF (Fig. 18.11). This, along with the higher Mn content of the Vichadero IF, may indicate an older age for the Valentines IF and/or a higher temperature of or closer proximity to source hydrothermal fluids (e.g., Bekker et al. 2010; Planavsky et al. 2010) compared to the Vichadero IF and manganese formation.

18.4.6.2 Iron Formations in the Pavas Block of the Nico Pérez Terrane

Geological Setting, Dating and Associated Lithologies

In southeastern Uruguay, several scattered occurrences of IFs are found within the western block of the Nico Pérez Terrane (Bossi and Gaucher 2004). These occurrences are hematite-rich rocks associated with amphibolite facies metasedimentary rocks that occur near the localities of Zapicán, Villa Serrana (Piedra del Gigante mine), Puntas del Santa Lucía (Carreras mine), Arroyo del Sauce, and Cerro de las Cuentas (Piedra de Fierro outcrop), among others. Some of these occurrences constitute mines for the extraction of iron ore to be utilized in flour or "pasta" to obtain clinker for the Portland cement industry.

The best-preserved stratigraphic section of these IF-bearing successions is located south of Zapicán village along the upper course of the Cebollatí River. The succession, named Las Tetas Complex (Hartmann et al. 2001), comprises metaconglomerate, quartzite, paragneiss, micaschist, marble, and BIFs. The youngest detrital zircon dated in this unit yielded a $^{207}Pb/^{206}Pb$ age of 2717 ± 24 Ma, and the age of the main cluster is 2.8–2.7 Ga (U–Pb SHRIMP; Hartmann et al. 2001). The maximum age is therefore Neoarchean and the minimum age is not well constrained but assumed to be no younger than Paleoproterozoic owing to the absence of Paleo-, Meso-, or Neoproterozoic detrital zircons despite rocks of these ages being frequent in the neighboring basement. The age of these scattered IF occurrences is only constrained in the main outcrop area of the Las Tetas Complex in the surroundings of Zapicán village.

Except for the type locality of the Las Tetas Complex, most of the outcrops of this complex are scattered tectonic slivers, for which the exact stratigraphic position of these IF occurrences is uncertain and stratigraphic correlations are difficult to establish. Nevertheless, some geological features, such as the abundance of specularite, association with quartzite (frequently fuchsite-bearing), micaschist, and marble, and amphibolite-facies metamorphism allows a tentative correlation of all these occurrences.

Only the Piedra del Gigante (ANCAP) iron deposit, located near Villa Serrana, has been investigated in some detail (Oyhantçabal et al. 2007). From north to south in this locality, IF occurs in a sequence of quartz-muscovite schist; coarse-grained, altered meta-mafic rock with amphibole phenoblasts; muscovite schist; banded rocks with bands rich in quartz, iron minerals, carbonate, and amphibole; quartz-muscovite schist; and fine-grained meta-mafic volcanic rock (Oyhantçabal et al. 2007). The exact stratigraphic position needs to be determined with additional age dating, but, as mentioned above, based on local and regional geological similarities, this occurrence could correspond to one of the slivers of the Las Tetas Complex. Considering the available age constraints, it is not unexpected that these platform sequences composed of marble, quartzite, IF, and metamorphosed mafic volcanic rocks are Neoarchean or Siderian and possibly correlated with the occurrences of Valentines and the Isla Cristalina de Rivera.

Mineralogy and Genesis of the IF

The common feature of these IF occurrences is the existence of hematite as the dominant iron oxide and magnetite only being subordinated. The IF is strongly deformed and characterized by martitization of magnetite and formation of medium-to-coarse grained specularite-rich layers with local relics of partly martitized magnetite. Magnetite-rich layers alternate with banded rocks composed of hematite, carbonate, and amphibole. The magnetite-rich layers contain 70–80%, medium-grained (1–2 mm), euhedral magnetite crystals with partial martitization and interstitial, well-crystallized quartz (0.5–1 mm) (Oyhantçabal et al. 2007). In the banded levels, magnetite and martitized magnetite occur. Hematite forms twinned, elongated crystals (1 × 0.2 mm) of specularite. Partially martitized magnetite relics associated with specularite indicate that specular hematite formed by replacing magnetite. The associated carbonate is iron-bearing dolomite ($Mg_{0.7}Ca_{1.08}Mn_{0.05}Fe_{0.11}(CO_3)_2$). Amphibole occurs as pale-green, radiating crystals up to several centimeters long and corresponds to an Fe-bearing tremolite ($Na_{0.18}Ca_{1.68}Mn_{0.07}Mg_{4.16}Fe^{3+}{}_{0.2}Fe^{++}{}_{0.55}Al_{0.03}(Si_{7.86}Al_{0.13})O_{22}(OH)_2$; Oyhantçabal et al. 2007). These crystals have clearly crystallized/recrystallized during a late event after the main deformation event (Oyhantçabal et al. 2007). Cummingtonite has been reported as a frequent accessory phase (Bossi and Navarro 1998). The banding of the rocks is considered to be transposed during a deformation event associated with hydrothermalism and martitization of magnetite (Oyhantçabal et al. 2007).

It is not clear yet how the IF formed. Low iron content in the amphibole and the association with dolomite do not point to a regular BIF origin. However, the low Al, V, Mn, and Zn content in magnetite does not indicate an igneous origin. High oxygen fugacity conditions during martitization under medium-temperature metamorphic conditions (e.g., Popp et al. 1977; Evans and Ghiorso 1995) could have prevented the formation of Fe-rich amphiboles typical of IF (Oyhantçabal et al. 2007).

18.4.7 Río de la Plata Craton, Piedra Alta Terrane, Southwestern Uruguay

The Río de la Plata Craton, whose outcrop area in Uruguay is known as the Piedra Alta Terrane, consists of a central granitic gneiss region, two metamorphic belts (Arroyo Grande Belt and Montevideo Belt), and frequent, smaller (up to several kilometers long) relict paragneiss and amphibolite (Fig. 18.9; Oyhantçabal et al. 2011). The other main outcrop area of the craton is represented by the Tandil area in the Buenos Aires province of Argentina (Cingolani 2011). This craton is characterized by a Neoarchean to Palaeoproterozoic single event of crustal growth, and crystallization ages for the pre-metamorphic protoliths (U–Pb in zircon by LA-ICP-MS and SHRIMP) from the gneisses and the felsic volcanic rocks of the supracrustal belts at ~2.2–2.1 Ga. On the other hand, the post-orogenic granitoids have U–Pb zircon ages of 2.1–2.05 Ga, thus indicating that a juvenile crust was followed by a short period of crustal recycling and a relative short and simple orogenic event. Cratonization, as revealed from K–Ar and Ar–Ar cooling ages (in muscovite), occurred during Paleoproterozoic times (Statherian), and the lack of Meso- or Neoproterozoic overprinting is a distinctive feature. Dolerite dyke swarms intruded during intraplate extension at *c*. 1.7 Ga (Halls et al. 2001), but the Río de la Plata Craton remained unaffected by younger tectonothermal events after this occurrence (Basei et al. 2006; Oyhantçabal et al. 2011; Chap. 7).

Small occurrences of Paleoproterozoic age IFs exist in the Piedra Alta Terrane of southwestern Uruguay (Bossi and Navarro 1998). The deposits are of small dimensions and spatially associated with mafic metavolcanic rocks of the Paso Severino Formation within the Arroyo Grande Belt (Fig. 18.9; Spoturno et al. 2004). Because of the lack of

stable continental platform deposits, their restricted occurrence associated with mafic volcanic rocks, and their likely Paleoproterozoic age, they can be classified as Algoma-type IFs (Oyhantçabal et al. 2007).

18.4.8 The Dom Feliciano Belt

18.4.8.1 Geological Setting, Dating and Associated Lithologies

Occurrences of BIFs are found in southeastern Uruguay spatially associated with the Neoproterozoic supracrustal sequence of the Ediacaran age Arroyo del Soldado Group (Yerbal and Cerro Espuelitas formations; Gaucher and Schipilov 1994; Gaucher 2000; Gaucher et al. 2003; Pecoits 2010) within the Dom Feliciano Belt (Fig. 18.10). The metasedimentary rocks of Yerbal and Cerro Espuelitas formations are thought to have been deposited between ~1000 and 650 Ma based on detrital zircon ages and geological considerations (Pecoits et al. 2016).

The Cerro Espuelitas Formation is composed of intercalated metamorphosed dark shales and chemical sediments, including oxide-facies BIFs and chert (Gaucher 2000). Only one occurrence of these Neoproterozoic BIFs has been mineralogically and geochemically studied in some detail (Oyhantçabal et al. 2007; Pecoits 2010). In the locality of Cerro la Higuerita, the sequence of rocks is composed of, from bottom to top, metapelites, finely laminated Fe-rich metapelites, and IFs. The volcanic contribution in the metapelites is evidenced by the occurrence of quartz phenocrysts with a typical habit of felsic volcanic rocks (beta quartz), alkali feldspar phenocrysts, and shard fragments in a fine-grained matrix, suggesting the possibility of some volcanic contribution to the iron as well (Oyhantçabal et al. 2007).

The Yerbal Formation is a fining- and thinning-upward succession composed of interbedded mudstone and sandstone with minor contributions of carbonate, chert, and IFs (Pecoits 2010). The IFs consist of rhythmic alternations of chert and iron oxide-rich layers of roughly equal thickness (0.3–15 cm). Both layers are composed of quartz, hematite, and magnetite, and accessory monazite, corundum, maghemite, apatite, goedkenite, and kaolinite (Pecoits 2010). Magnetite is oxidized to hematite to various degrees.

Mineralogy, Geochemistry, and Age Constrains of the IF

In the Cerro Espuelitas IF, iron minerals account for less than 40%. The IF contains disseminated, partially martitized, euhedral magnetite crystals (~0.2 mm) and a matrix with fine (0.2 × 0.05 mm), disseminated hematite laths oriented parallel to the foliation/stratification, along with grunerite ($Na_{0,04}Ca_{0,17}Mn_{0,02}Mg_{1,36}Fe_{5,35}Al_{0,07}(Si_{7,97}Al_{0,03})O_{22}(OH)_2$) and greenish yellow to green chlorite (diabantite; $K_{0.84}Na_{0.85}Ca_{0.10}Mg_{6.22}Fe^{2+}{}_{2.21}Al_{1.93}Fe^{3+}{}_{0.17}Mn_{0.05}[Si_{6.97}Al_{1.03}O_{20}](OH)_{16}$). These characteristics are consistent with Rapitan-type IF for this Neoproterozoic IF.

Iron and manganese concentrations in the IF from the Cerro Espuelitas and Yerbal formations reach 40 wt% Fe_2O_3 and 110 ppm Mn, respectively (Pecoits 2010). The detrital contribution is small (<2.7 wt% Al_2O_3). Normalized REE + Y patterns of Neoproterozoic IFs of Uruguay are similar to that of seawater, with negative Ce and absent Eu anomalies, and were interpreted as indicative of a subaqueous, distal hydrothermal source and deposition in oxygenated shallow waters (Frei et al. 2009, 2013). Post-Archean Australian Shale-normalized REE patterns of IF from the Yerbal Formation are quite flat and homogeneous, and are characterized by slight enrichment in middle REEs (MREEs), positive La anomalies, and very small negative to absent Eu anomalies (Pecoits 2010). Positive Ce anomalies are seen in chert from the Cerro Espuelitas Formation. These and other geochemical observations indicate that oxygen levels in the water column were high enough to oxidize Ce during the deposition of the uppermost Yerbal Formation (Pecoits 2010).

Fossil content and geological evidence are consistent with a Neoproterozoic age for this BIF-bearing metasedimentary succession, but the former assumed Ediacaran age (Blanco et al. 2009) is challenged by recent sampling (three new samples) and dating by Pecoits et al. (2016), indicating that the youngest detrital zircon is 1036 Ma, even though most are much older (see discussion in Aubet et al. 2014; Pecoits et al. 2016).

Genesis of the IF

Petrography and associated lithologies indicate that the IF from the Yerbal Formation is of sedimentary origin. Associated banded siltstone is interpreted as reflecting deposition in a deep-water setting, and the IF of the uppermost Yerbal Formation is interpreted to reflect the maximum flooding surface (Pecoits 2010). Geochemical characteristics of REE patterns in IF of this formation, specifically the absence of positive Eu anomalies, suggest that high-temperature hydrothermal fluids did not contribute to the origin of the IFs (Pecoits 2010). In contrast, enrichment in MREEs is similar to that in low-temperature (<200 °C) hydrothermal fluids, and these fluids seem to have provided the components of the IF (Pecoits 2010). Positive Ce anomalies seen in chert of the Cerro Espuelitas Formation (post Gaskiers) were interpreted as reflecting anoxic conditions during deposition of the upper part of the formation. The absence of positive Ce anomalies and the presence of negative Ce anomalies in IF from the Yerbal Formation (pre-Gaskiers) were interpreted to reflect oxygenation conditions good enough to

oxidize Ce during precipitation of the uppermost part of the formation (Pecoits 2010). However, U/Th ratios suggest a source of the components of the IFs in shallow oxic water and deposition in reducing or suboxic bottom waters.

18.5 Depositional Record of IFs in Southwestern Gondwana

The earliest record of IFs in the studied areas of the South American Platform is represented by Algoma-type BIFs of greenstone belt successions and volcanosedimentary sequences from the Amazon Craton, Brazil. Iron formations in this craton include typically discontinuous Algoma-type BIFs, as well as continuous and thick deposits of the Carajás Formation (Itacaiunas Supergroup), which is spatially and temporally related to mafic rocks in the Carajás Province, the Archean core of the craton.

Archean, Algoma-type BIFs are also present in the São Francisco Craton. However, typical of this craton are large, Paleoproterozoic, Lake Superior-type BIFs with high-grade iron ore bodies originated via metamorphic fluids. This record of IFs is represented by the Archean-early Paleoproterozoic (2.5–2.4 Ga) Cauê IF (Minas Supergroup) of the east-southeast São Francisco Craton (Fig. 18.14), which formed in a platform setting spatially and temporally associated with carbonates. This IF is host to giant iron-ore deposits (>300 Mt reserves of high-grade ore) that comprise the Quadrilátero Ferrífero, one of the most important mining districts in the world.

The deposition of subsequent IFs during the early Paleoproterozoic took place in stable platforms of the Pavas ($\geq$ Paleoproterozoic to Archean Las Tetas Complex IFs, Uruguay) and Taquarembó (Brazil) blocks, and the Cerro Chato Block (early Paleoproterozoic or older Vichadero and Valentines IFs, Uruguay). The available information suggests that the BIF and manganese formation of the Vichadero Formation in the Isla Cristalina de Rivera could be correlated with the Lake-Superior-type IF of the Valentines Formation in the Nico Pérez Terrane of central Uruguay.

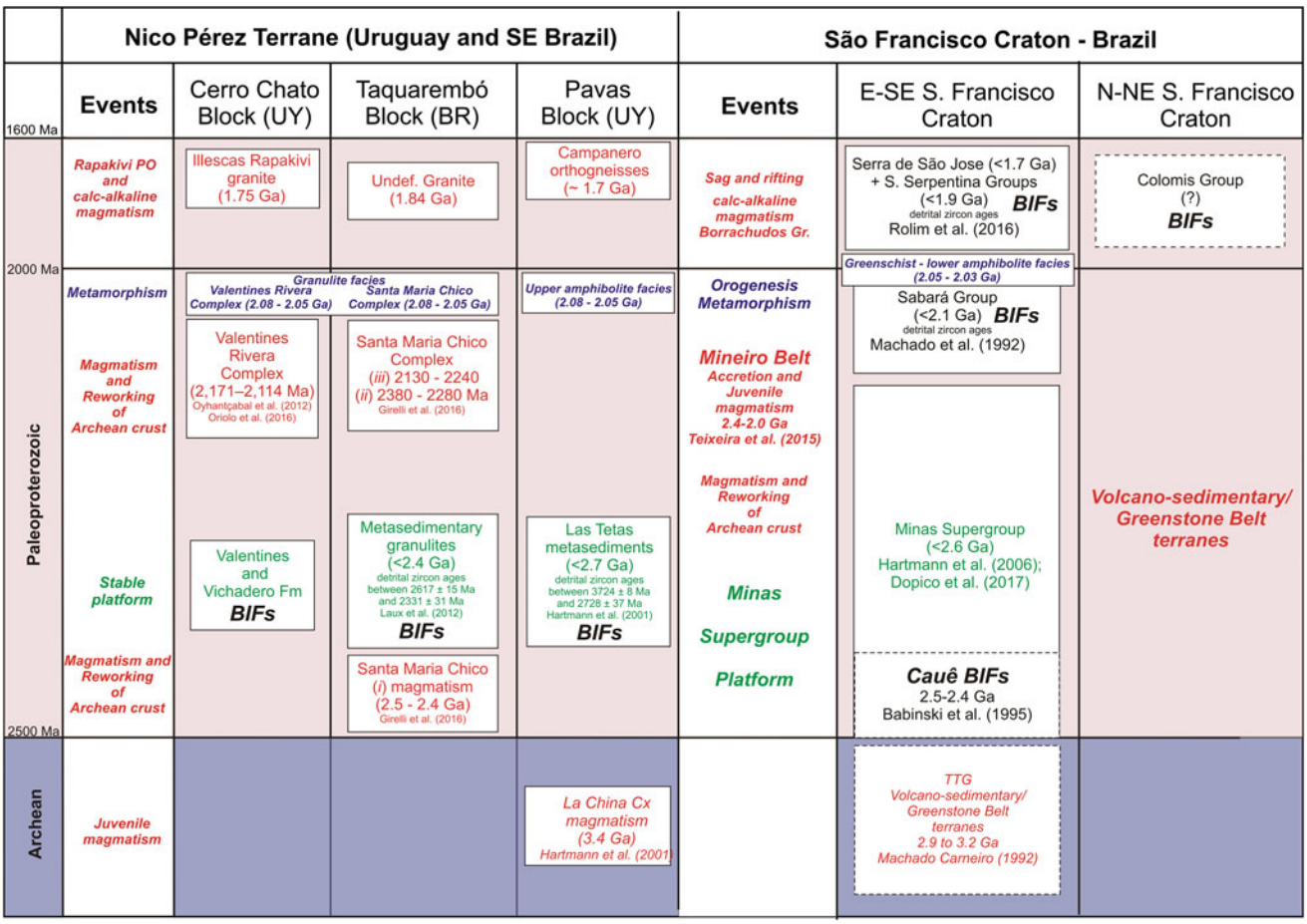

Fig. 18.14 Stratigraphic correlation chart showing the various units from the Nico Pérez Terrane of Uruguay and SE Brazil and the São Francisco Craton of Brazil indicating available age dating and the approximate or estimated stratigraphic position of IF occurrences. References shown are the same as in the text

Smaller occurrences of Paleoproterozoic age IFs occur in the Piedra Alta Terrane of the Río de la Plata Craton (SW Uruguay) spatially associated with mafic metavolcanic rocks of the Paso Severino Formation within the Arroyo Grande Belt, and interpreted to be of Algoma-type affiliation owing to their lithologic associations and likely age. The available data indicates that the Río de la Plata Craton represents a portion of the São Francisco Craton of Brazil.

Based on geology, structural details, age dating, and lithological associations, likely correlations among Archean and Paleoproterozoic units of the Nico Pérez Terrane in Uruguay and Brazil and the São Francisco Craton of Brazil can be made (Fig. 18.14). All data indicates that the Nico Pérez Terrane of Uruguay and southern Brazil represent a piece of the Congo Craton separated during the Neoproterozoic (see Chap. 7). Therefore the correlation with the São Francisco Craton is quite straightforward, despite the geological record of supracrustal sequences here being only relics.

The next early Paleoproterozoic occurrence of IFs takes place as small, discontinuous lenses between flysch and other schists in the east-southeast of the São Francisco Craton as part of the foreland sequence of the Sabará Group (<2.1 Ga). In the mid-Paleoproterozoic, IFs occur in the continuous north–south-trending Serra de Serpentina (<1.9 Ga) and the Serra de São Jose Groups (<1.7 Ga) during the opening of the Espinhaço Basin in the east-southeast of the craton (Fig. 18.14) and probably as part of the Colomis Group, in the north-northwest of the craton.

Neoproterozoic, Rapitan-type IFs and iron-bearing diamictites, including those from the Lagoa Formosa (612 to ~567 Ma) and Nova Aurora (Cryogenian) formations, were deposited as cover sequences of the São Francisco Craton associated with typical diamictite-associated glaciomarine sequences. Occurrences of Neoproterozoic IFs are also found in southeastern Uruguay spatially associated with Neoproterozoic supracrustal sequences (black shale, chert, carbonate, mudstone, and sandstone) of the Arroyo del Soldado Group in the Dom Feliciano Belt (Yerbal and Cerro Espuelitas formations; uncertain age of ~1000–650 Ma or >1306 Ma).

18.6 Concluding Remarks

Differences in IF occurrences among the Amazonian domain (Laurentian), located to the west of the Transbrasiliano Lineament, the Gondwana domain, to the east of the Transbrasiliano Lineament, and the Río de la Plata Craton are evident. The Amazonian domain hosts mainly Archean and Algoma-type IF deposits, the Gondwana domain is characterized by the dominance of Paleoproterozoic and Superior-type IF deposits, and the Río de la Plata Craton has almost an absence of IFs. The Río de la Plata Craton seems to be different in the context of the South American Platform. There is no Archean (Nd model ages reach a maximum 2.6 Ga), there is no Mesoproterozoic record, and it has no African (Gondwana) affinity. The open question is whether the Río de la Plata Craton has Laurentian affinity or not.

The iron mineralizing system of the Amazonian domain also strongly contrasts with the one found in the Gondwana domain. In the core of the Amazon Craton, the Carajás Province hosts a large number of mineral deposits that, in addition to high-grade iron ore bodies, include IOCG, Au–(Pt–PG), and Mn deposits. This ore system apparently resulted from a long-lived, protracted circulation of magmatic fluids that lasted from the Archean to the Paleoproterozoic and that was controlled by kilometer-scale, strike-slip faults. Probably long-lasting slow circulation of fluids was responsible for the preservation in high-grade ores of many primary/diagenetic textural features inherited from the iron formation (Fig. 18.3g, j).

In the Proterozoic areas of the Gondwana domain, a much different scenario comes into perspective when comparing it with the Amazonian province: in the eastern border of the São Francisco Craton, Lake Superior-type IFs were extensively mineralized by percolation of metamorphic fluids associated with the development of folds and thrusts, the first during the Rhyacian Transmazonian Orogeny and recurrently during the Brasiliano orogeny. In contrast with Carajás, here the iron ore acquired a metamorphic fabric (Fig. 18.3h, i) with the formation of platy crystals of hematite (specularite) in high strain domains that define an anastomosed to continuous schistosity and obliterate pre-ore characteristics.

Neoproterozoic BIF-bearing units are apparently not present in the Amazon Craton. In the Gondwana domain they do not display evidence of tectonic-associated hypogene mineralization, except possibly for the case of Jucurutu in the Borborema Province. Supergene processes responsible for Fe enrichment, on the other hand, were very effective in the Urucum District (Fig. 18.3b).

The presence of sedimentary/diagenetic or hydrothermal carbonate in the IFs played an important role in the formation of voluminous, high-grade iron ore deposits of all ages owing to its greater reactivity and solubility. This becomes obvious when comparing the number and size of deposits in the Quadrilátero Ferrífero and in the Serra da Serpentina, or when evaluating the effectiveness and depth of supergene

enrichment of the Jacadigo IF in the Urucum District compared with the regular tropical weathering profile observed in shallow deposits in the Quadrilátero Ferrífero.

Acknowledgements This chapter summarizes knowledge and information gathered from several research projects with the support of various funding agencies, including the Brazilian CNPq, FAPEMIG, FINEP, CAPES, ADIMB, and the DAAD and COFECUB, also with the help from many mining companies that generously gave access to inestimable information: MBR, SAMARCO, Ferrous Resources, Anglo American, CSN, Gerdau, Vallourec, Crusader, Centaurus, MMX, USIMINAS, GME4, BEMISA, VALE, BHP, Rio Tinto, and Tata Steel. We particularly thank Richard Lateulade and Minera Aratirí for providing samples, geological maps, and sample information for the Valentines IF of Uruguay. Access to cores and permission to send samples was granted by Derek Helm, Minera Aratirí, Uruguay. CAR extends his gratitude to his late supervisor and friend Prof. Dr. H. Quade from the TU Clausthal. CAR is recipient of a CNPq Grant 305115/2016-2. Useful comments and suggestions from reviewer C. Gauert are appreciated.

References

Alkmim FF, Marshak S (1998) Transamazonian orogeny in the southern Sao Francisco craton region, Minas Gerais, Brazil: evidence for Paleoproterozoic collision and collapse in the Quadrilátero Ferrífero. Precambr Res 90:29–58

Almeida FFM (1971) Geochronological division of the Precambrian of South America. Revista Brasileira de Geociências 1:13–21

Almeida FFM (1977) O Craton de Sao Francisco. Revista Brasileira de Geociências 7:349–364

Almeida FFM, Hasui Y (eds) (1984) O Pré-Cambriano do Brasil. São Paulo, Blücher Ltda., p 378 p

Almeida FFM et al (1981) Brazilian structural provinces: an introduction. Earth Sci Rev 17(1):1–29

Almeida-Abreu PA et al (1989) Estratigrafia, faciologia e tectônica do Supergrupo Espinhaço na região de Serro—Conceição do Mato Dentro, Minas Gerais, Brasil. Zbl Geol Paläontol 5:857–873

Alvarenga CJS, Trompette R (1993) Evolução tectônica Brasiliana da faixa Paraguai: a estruturação da região de Cuiabá. Revista Brasileira de Geociências 23:18–30

Aubet NR et al (2014) Ediacaran in Uruguay: facts and controversies. J S Am Earth Sci 55:43–57

Avelar VG et al (1999) O Magmatismo arqueano da região de Tucumã—Província Mineral de Carajás: novos resultados geocronológicos. Revista Brasileira de Geociências 29(4):453–460

Babinski M et al (1995) The Pb/Pb age of Minas Supergroup carbonate rocks, Quadrilatero Ferrifero, Brazil, and its implications to the correlation with BlFs from South Africa and Australia. Precambr Res 72:235–245

Babinski M et al (2012) Neoproterozoic glacial deposits from the Araçuaí orogen, Brazil: age, provenance and correlations with the São Francisco craton and West Congo belt. Gondwana Res 21 (2):451–465

Baltazar OF, Zucchetti M (2007) Lithofacies associations and structural evolution of the Archean Rio das Velhas Greenstone belt, Quadrilátero Ferrífero, Brazil: a review of the setting of gold deposits. Ore Geol Rev 32:471–499

Barbosa JSF, Sabaté P (2002) Geological features and the Paleoproterozoic collision of four Archean crustal segments of the São Francisco Craton, Bahia, Brazil. A synthesis. An Acad Bras Ciênc 74(2):343–359

Barbosa JSF, Sabaté P (2004) Archean and Palaeoproterozoic crust of the São Francisco Craton, Bahia, Brazil: geodynamic features. Precambr Res 133:1–27

Barley ME et al (1998) The 2.72–2.60 Ga bonanza: metallogenic and environmental consequences of the interaction between mantle plumes, lithospheric tectonics and global cyclicity. Precambr Res 91:65–90

Barley ME et al (1999) Hydrothermal origin for the 2 billion year old Mount Tom Price giant iron ore deposit, Hamersley province, Western Australia. Miner Deposita 34:784–789

Barreto CJS et al (2009) Magmatismo eo-riaciano (2.26 Ga) na porção norte do Bloco Amapá, região central do Amapa: nova evidência e implicações geodinâmicas. In SBG, Simpósio de Geologia da Amazônia, 11, Resumos, CD-ROM

Barreto CJS et al (2013) Paleoproterozoic granitoids from the northern limit of the Archean Amapá block (Brazil), Southeastern Guyana Shield: Pb–Pb evaporation in zircons and Sm–Nd geochronology. J S Am Earth Sci 45:97–116

Barrote VR (2015) A sequência portadora de formações ferríferas de Guanhães, Minas Gerais, Brasil. M.Sc. thesis, Universidade Federal de Minas Gerais, Belo Horizonte

Barrote VR et al (2017) As formações ferríferas bandadas proterozóicas de Guanhães, borda sudeste do Cráton São Francisco, Brasil: evidências de contaminação detrítica. Geologia USP, Série Científica 17(2):303–324

Basei MAS et al (2006) Provenance and depositional age of the Dom Feliciano Belt Supracrustal units, Brazil—Uruguay: correlations with SW Africa. V South American symposium on isotope geology Punta del Este Uruguay. Short papers, pp 45–48

Bastos-Leal LR (1998) Geocronologia U/Pb (Shrimp), $^{207}Pb/^{206}Pb$, Rb/Sr, Sm/Nd e K/Ar dos terrenos granito-greenstone do Bloco Gavião: Implicações para a evolução Arqueana e Paleoproterozóica do Cráton do São Francisco. Brasil. Ph.D. thesis, University of São Paulo, Brazil

Bastos-Leal LR et al (1997) Crustal evolution of Gavião block of the São Francisco Craton: a geochronological study with U–Pb, Pb–Pb, Sm–Nd, Rb–Sr and K–Ar. Extended Abstracts. South Am Symp Isot Geol 2:161–162

Bekker A et al (2010) Iron formation: the sedimentary product of a complex interplay among mantle, tectonic, oceanic, and biospheric processes. Econ Geol 105:467–508

Beukes NJ (1980) Lithofacies and stratigraphy of the Kuruman and Griquatown Iron-formations, northern Cape Province, South Africa. Trans Geol Soc S Afr 83:69–86

Beukes NJ (1983) Palaeoenvironmental setting of iron-formations in the depositional basin of the Transvaal Supergroup, South Africa. In: Trendall AF, Morris RC (eds) Iron-formation: facts and problems. Elsevier, Amsterdam, pp 131–209

Beukes NJ et al (2002) The geology and genesis of high-grade hematite iron ore deposits. Iron Ore 2002:23–29

Blanco G et al (2009) Provenance of the Arroyo del Soldado Group (Ediacaran to Cambrian, Uruguay): implications for the paleogeographic evolution of southwestern Gondwana. Precambr Res 171:57–73

Borges JO (2012) Geologia e evolução metalogenética do minério de manganês da mina Lagoa D'anta, subdistrito ferro-manganesífero de Caetité-Licínio de Almeida, Bahia. M.Sc. thesis, Universidade Federal da Bahia, 216 p

Borges JO et al (2015) Structural framework of rocks of the Lagoa D'anta mine area, iron-manganese Urandi-Caetité-Licínio de Almeida District, Bahia, Brasil. Braz J Geol 45(2):173–192

Bossi J (1963) El yacimiento de hierro del Arroyo Valentines, Florida, Uruguay; Parte I. La mena ferrífera. Boletim Sociedade Brasileira de Geología 12:109–133

Bossi J, Ferrando L (2001) Carta Geologica del Uruguay, Escala 1:500.000. Version 2.0 Digital. Facultad de Agronomía, Montevideo

Bossi J, Gaucher C (2004) The Cuchilla Dionisio Terrane, Uruguay: an allochthonous block accreted in the Cambrian to SW-Gondwana. Gondwana Res 7:661–674

Bossi J, Gaucher C (2014) Formación Valentines. In: Bossi J, Gaucher C (eds) Geología del Uruguay—Tomo 1: Predevónico. pp 171–189

Bossi J, Navarro R (1998) Las formaciones ferríferas de Uruguay: su significado económico y tectono-estratigráfico. Abstracts of the X Congreso Latinoamericano Geologia—VI Congreso Argentino Geologia Economica, Buenos Aires

Bossi J, Umpierre M (1968) La petrología de la formación ferrífera Valentines, Departamento de Florida, República Oriental del Uruguay. Unpublished report, Universidad de la República, Facultad de Química, Sector Geoquímica, Montevideo, 102 p

Bossi J et al (1965) Predevoniano en el Uruguay. Boletín Facultad de Agronomía Nº 78. Montevideo, Uruguay

Boström K (1973) The origin and fate of ferromanganoan active ridge sediments. Stockholm Contrib Geol 27:147–243

Brito Neves BB et al (2000) Tectonic history of the Borborema Province. In: Cordani UG et al (eds) Tectonic evolution of South America. 31st International Geological Congress, Rio de Janeiro, pp 151–182

Brito Neves BB et al (2014) The Brasiliano collage in South America: a review. Braz J Geol 44(3):493–518

Carneiro MA (1992) O Complexo metamórfico Bonfim Setentrional (Quadrilátero Ferrífero, MG): Litoestratigrafia e evolução geológica de um segmento de crosta continental do Arqueano. Ph.D. thesis, Instituto de Geociências, Universidade de São Paulo. São Paulo, Brasil, 233 p

Chemale F Jr et al (1994) The tectonic evolution of the Quadrilátero Ferrífero, Minas Gerais, Brazil. Precambr Res 65:25–54

Chisonga BC et al (2012) Nature and origin of the protolith succession to the Paleoproterozoic Serra do Navio manganese deposit, Amapá Province, Brazil. Ore Geol Rev 47:59–76

Cingolani CA (2011) The Tandilia system of Argentina as southern extension of the Río de la Plata craton: an overview. Int J Earth Sci 100:221–242

Cordani UG et al (2009) The position of the Amazonian Craton in supercontinents. Gondwana Res 15:396–407

Costa LP (2007) Caracterização das sequências metavulcanossedimentares da porção leste da Província Mineral Carajás, Pará. M.Sc. thesis, Universidade Federal de Minas Gerais, Belo Horizonte, Brasil, 113 p

Cox GM et al (2013) Neoproterozoic iron formation: an evaluation of its temporal, environmental and tectonic significance. Chem Geol 362:232–249

CPRM (Companhia de Pesquisa de Recursos Minerais) (2004) http://geosgb.cprm.gov.br/ (last accessed 24.8.2017)

Cunha JC et al (1996) Idade dos greenstone belts e dos terrenos TTG's associados da região de Brumado, centro oeste do Cráton do São Francisco (Bahia-Brasil). SBG, Congresso Brasileiro de Geologia 39, Anais, pp 67–70

Danderfer Filho A et al (2009) New geochronological constraints on the geological evolution of Espinhaço basin within the São Francisco Craton—Brazil. Precambr Res 170:116–128

Del'Arco JO et al (1982) Geologia. Projeto RADAMBRASIL Folha SE.21 Corumbá. Rio de Janeiro. Levantamento de Recursos Naturais 27:25–160

Delor C et al (2003) Transamazonian crustal growth and reworking as revealed by the 1:500,000-scale geological map of French Guiana, 2nd edn. Géologie de la France 2–4:5–57

Dorr JVN II (1964) Supergene iron ores of Minas Gerais, Brazil. Econ Geol 59:1203–1240

Dorr JVN II (1965) Nature and origin of the high-grade hematite ores of Minas Gerais, Brazil. Econ Geol 60:1–46

Dorr JVN II (1969) Physiographic, stratigraphic and structural development of the Quadrilatero Ferrifero, Minas Gerais. U.S. geological survey professional paper 641-A, 110 p

Dorr JVN II, Barbosa ALM (1963) Geology and ore deposits of the Itabira district Minas Gerais, Brazil. U.S. geological survey professional paper 341-C, 110 p

Duuring P, Hagemann S (2013a) Genesis of superimposed hypogene and supergene Fe ore bodies in BIF at the Madoonga deposit, Yilgarn Craton, Western Australia. Miner Deposita 48:371–395

Duuring P, Hagemann S (2013b) Leaching of silica bands and concentration of magnetite in Archean BIF by hypogene fluids: Beebyn Fe ore deposit, Yilgarn Craton, Western Australia. Miner Deposita 48:341–370

Ellis J (1998) The Precambrian supracrustal rocks of the "Isla Cristalina de Rivera" in northern Uruguay and their ore deposits: definition of a new lithostratigraphic unit ("Vichadero Formation") and a contribution to the genesis of banded iron-formation and manganese-formation. Ph.D. thesis, Ruprecht-Karls-Universitat, Heidelberg, 181 p

Embrapa Pantanal, Laboratório de Geoprocessamento, Mapa de Geologia, http://www.cpap.embrapa.br/agencia/001bdado1.htm (last accessed 25.8.2017)

Evans BW, Ghiorso MS (1995) Thermodynamics and petrology of cummingtonite. Am Miner 80:649–663

Figueiredo e Silva RC et al (2008) A hydrothermal origin for the jaspilite-hosted giant Sierra Norte deposits in the Carajas Mineral Province, Pará State, Brazil. Econ Geol 15:255–290

Figueiredo e Silva RC et al (2013) Hydrothermal fluid processes and evolution of the giant Serra Norte jaspilite-hosted iron ore deposits, Carajás Mineral Province, Brazil. Econ Geol 108:739–779

Frei R et al (2009) Fluctuations in Precambrian atmospheric oxygenation recorded by chromium isotopes. Nature 461(7261):250–253

Frei R et al (2013) Fluctuations in late Neoproterozoic atmospheric oxidation-Cr isotope chemostratigraphy and iron speciation of the late Ediacaran lower Arroyo del Soldado Group (Uruguay). Gondwana Res 23:797–811

Gair JE (1962) Geology and ore deposits of the Nova Lima and Rio Acima Quadrangles, Minas Gerais, Brazil. U.S. geological survey professional paper 341-A, 65 p

Gaucher C (2000) Sedimentology, palaeontology and stratigraphy of the Arroyo del Soldado Group (Vendian to Cambrian, Uruguay). Beringeria 26:1–120

Gaucher C, Schipilov A (1994) Formaciones de hierro bandeadas del Vendiano del Uruguay. Paleociencias del Uruguay (Serie Didáctica) 2:3–5 (Facultad de Ciencias, Montevideo, Uruguay)

Gaucher C et al (2003) Integrated correlation of the Vendian to Cambrian Arroyo del Soldado and Corumbá Groups (Uruguay and Brazil): palaeogeographic, palaeoclimatic and palaeobiologic implications. Precambr Res 120:241–278

Goodwin AM (1962) Structure, stratigraphy, and origin of iron formations, Michipicoten Area, Algoma District, Ontario, Canada. Geol Soc Am Bull 73(5):561–586

Goodwin AM (1991) (reprinted in 2016) Precambrian geology: the dynamic evolution of the continental crust. Academic Press, Harcourt Brace Jovanovich Publishers, Toronto

Gourcerol B et al (2016) Depositional setting of Algoma-type banded iron formation. Precambr Res 281:47–79

Graf J et al (1994) Rare earth element evidence of origin and depositional environment of Late Proterozoic ironstone beds and manganese-oxide deposits, SW Brazil and SE Bolivia. J S Am Earth Sci 7:115–133

Gross GA (1980) A classification of iron-formation based on depositional environments. Can Miner 18:215–222
Gross GA (1983) Tectonic systems and the deposition of iron-formation. Precambr Res 20:171–187
Grossi-Sad JH et al (1997) Geologia da Folha Conceição do Mato Dentro. In: Grossi-Sad JH et al (eds) Projeto Espinhaço CD-ROM (textos, mapas e anexos). COMIG—Companhia Mineradora de Minas Gerais, Belo Horizonte, pp 2533–2693
Gruner JW (1930) Hydrothermal oxidation and leaching experiments: their bearing on the origin of Lake Superior hematite-limonite ores: part II. Econ Geol 25:837–867
Gruner JW (1937) Hydrothermal leaching of iron ores of the Lake superior type—a modified theory. Econ Geol 32:121–130
Guild PW (1957) Geology and mineral resources of the Congonhas district, Minas Gerais, Brazil. US geological survey professional paper 290, 90 p
Guillemain C (1910a) Lagerstätten in der Republik Uruguay. Bergwirtschaftliche Mitteilung 1:189–192
Guillemain C (1910b) Der erste Versuch einer geologischen Karte von Uruguay. Dr. A. Petermanns Mitteilungen aus Justus Perthes' geographischer Anstalt 56, p 306
Hagemann SG, Angerer T, Duuring P, Rosière CA, Figueiredo e Silva RC, Lobato L, Hensler AS, Walde DHG (2016) BIF-hosted iron mineral system: a review. Ore Geology Reviews 76:317–359
Halls HC et al (2001) Magnetic studies and U–Pb geochronology of the Uruguayan dyke swarm, Río de la Plata craton, Uruguay: paleomagnetic and economic implications. J S Am Earth Sci 14:349–361
Hartmann LA et al (2001) Archean crust in the Rio de la Plata Craton, Uruguay—SHRIMP U–Pb zircon reconnaissance geochronology. J S Am Earth Sci 14:557–570
Hartmann LA et al (2006) Provenance and age delimitation of Quadrilátero Ferrífero sandstones based on zircon U–Pb isotopes. J S Am Earth Sci 20:273–285
Heimann A et al (2010) Fe, C, and O isotope compositions of banded iron formation carbonates demonstrate a major role for dissimilatory iron reduction in ~2.5 Ga marine environments. Earth Planet Sci Lett 294:8–18
Hensler A-S et al (2015) Hydrothermal and metamorphic fluid-rock interaction associated with hypogene hard iron ore mineralisation in the Quadrilátero Ferrífero, Brazil: implications from in-situ laser ablation ICP-MS iron oxide chemistry. Ore Geol Rev 69:325–351
Hensler A-S et al (2017) Iron oxide mineralization at the contact zone between phyllite and itabirite of the Pau Branco deposit, Quadrilátero Ferrífero, Brazil-Implications for fluid-rock interaction during iron ore formation. Econ Geol 112:941–982
Hoashi M et al (2009) Primary haematite formation in an oxygenated sea 3.46 billion years ago. Nat Geosci 2:301–306
Hoffman PF et al (1998) A neoproterozoic snowball earth. Science 281:1342–1346
Holland HD (2006) The oxygenation of the atmosphere and oceans. Philos Trans Roy Soc Biol Sci 361:903–915
Huston DL, Logan GA (2004) Barite, BIF and bugs: evidence for the evolution of the earth's early hydrosphere. Earth Planet Sci Lett 220:41–55
James HL (1954) Sedimentary facies iron formation. Econ Geol 49 (3):235–293
Johnson CM et al (2003) Ancient geochemical cycling in the Earth as inferred from Fe isotope studies of banded iron formations from the Transvaal craton. Contrib Miner Petrol 144:523–547
Johnson CM et al (2008) Iron isotopes constrain biologic and abiologic processes in banded iron formation genesis. Geochim Cosmochim Acta 72:151–169
Jones JP (1985) The southern border of the Guaporé Shield in western Brazil and Bolivia: an interpretation of its geologic evolution. Precambr Res 28(2):111–135
Kirschvink JL (1992) Late Proterozoic low-latitude global glaciation: the snowball earth. Section 2.3. In: Schopf JW et al (eds) The proterozoic biosphere: a multidisciplinary study. Cambridge University Press, Cambridge, pp 51–52
Klein C (2005) Some Precambrian banded iron-formations (BIFs) from around the world: their age, geologic setting, mineralogy, metamorphism, geochemistry, and origin. Am Miner 90:1473–1499
Klein C, Beukes NJ (1989) Geochemistry and sedimentology of a facies transition from limestone to iron-formation deposition in the Early Proterozoic Transvaal Supergroup, South Africa. Econ Geol 84:1733–1774
Klein C, Beukes NJ (1993) Sedimentology and geochemistry of the glaciogenic late Proterozoic Rapitan iron-formation in Canada. Econ Geol 88(3):542–565
Knauer LG (1990) Evolução geológica do Pré-cambriano da porção centro-oeste da Serra do Espinhaço Meridional e metalogênese associada. M.Sc. thesis. Universidade de Campinas, São Paulo, Brazil, 298 p
Knauer LG, Grossi-Sad JH (1997) Geologia da Folha Serro. In: Grossi-Sad JH et al (eds) Projeto Espinhaço em CD-ROM (textos, mapas e anexos). COMIG—Companhia Mineradora de Minas Gerais, Belo Horizonte, pp 2057–2316
Konhauser KO et al (2002) Could bacteria have fonned the Precambrian banded iron formations? Geology 30:1079–1082
Konhauser KO et al (2005) The potential significance of microbial Fe (III) reduction during deposition of precambrian banded iron formations. Geobiology 3:167–177
Konhauser KO et al (in press) Iron formations: a global record of neoarchean to palaeoproterozoic environmental history. Earth-Sci Rev. https://doi.org/10.1016/j.earscirev.2017.06.012
Krapez B et al (2003) Hydrothermal and resedimented origins of the precursor sediments to banded iron formation: sedimentological evidence from the early palaeoproterozoic brockman supersequence of Western Australia. Sedimentology 50:979–1011
Kuchenbecker M et al (2015) Detrital zircon age patterns and provenance assessment for pre-glacial to post-glacial successions of the Neoproterozoic Macaúbas Group, Araçuaí orogen, Brazil. Precambr Res 266:12–26
Kuchenbecker M et al (2016) Chemostratigraphy of the lower Bambuí Group, southwestern São Francisco Craton, Brazil: insights on Gondwana paleoenvironments. Braz J Geol 46:145–162
Lancaster H (2015) Mineralogy, geochemistry, and genesis of the valentines iron formation, Nico Pérez Terrane, eastern Uruguay, and significance for the redox conditions of early Earth's oceans. M.Sc. thesis, East Carolina University, 141 p
Lascelles D (2002) A new look at old rocks—an alternative model for the origin of in situ iron ore deposits derived from banded iron formation. Proc Iron Ore 2002:1–20
Li W et al (2015) Biologically-recycled continental iron: a major component in banded iron formations. Proc Nat Acad Sci 112:8193–8198
Litherland M, Bloomfield K (1981) The proterozoic history of eastern Bolivia. Precambr Res 15:157–179
Lobato LM et al (2001) Brazil's premier gold province: part II. Geology and genesis of gold deposits in the Archean Rio das Velhas greenstone belt, Quadrilátero Ferrífero. Miner Deposita 36:249–277
Lobato LM et al (2005) A mineralização hidrotermal de ferro da Província Mineral de Carajás—Controle estrutural e contexto na evolução metalogenética da provincia. In: Marini OJ et a. (eds) Caracterização de depósitos minerais em distritos mineiros da Amazônia: Departamento Nacional da Produção Mineral (DNPM)/Fundo Setorial Mineral (CT-Mineral/FINEP)/Agência para o Desenvolvimento Tecnológico da Indústria Mineral Brasileira (ADIMB), Brasília, Brazil, pp 25–92

Lopes-Silva L et al (2007) Lithological review of the Socorro Quarry, Gandarela Minerios Ltda., Minas Gerais, Brazil: Quarry logs, drilling logs and litho-geochemical model: Internal report, Limelette/Sao Jose da Lapa, 55 p

Machado N, Schrank A (1989) Geocronologia U/Pb no Maciço de Piumhi: Resultados Preliminares. Anais symposium Geologia de Minas Gerais, 5th, Belo Horizonte, pp 45–49

Machado N et al (1991) UPb geochronology of Archean magmatism and basement reactivation in the Carajás área, Amazon shield, Brazil. Precambr Res 49:329–354

Machado N et al (1992) U–Pb geochronology of the Archean magmatism and Proterozoic metamorphism in the Quadrilátero Ferrífero, southern Sao Francisco Craton, Brazil. Geol Soc Am Bull 104:1221–1227

Machado N et al (1996) Ages of detrital zircon from archean-paleoproterozoic sequences: implications for greenstone belt setting and evolution of a transamazonian foreland basin in Quadrilátero Ferrífero, southeast Brazil. Earth Planet Sci Lett 141:259–276

Marinho MM (1991) Le sequence Volcano-Sedimentaire de Contendas Mirante et la Bordure Ocidentale du Bloc de Jequié (Craton du São Francisco, Brésil): um example de transition Archean-Proterozoic. Unpublished Ph.D. thesis, University of Clermont-Ferrand, 257 p

Maxwell CH (1972) Geology and ore deposits of the Alegria district, Minas Gerais, Brazil. US geological survey professional paper 341-J, 72 p

McLennan S (1989) Rare earth elements in sedimentary rocks: influence of provenance and sedimentary processes. Rev Mineral Geochem 21:169–200

Montgomery CW (1979) Uranium-lead geochronology of the Archean Imataca Series, Venezuelan Guayana Shield. Contrib Miner Petrol 69(2):167–176

Moreto CPN et al (2015) Timing of multiple hydrothermal events in the iron oxide–copper–gold deposits of the Southern Copper Belt, Carajás Province, Brazil. Miner Deposita 50:517–546

Noce CM et al (1997) Nova subdivisão estratigráfica regional do Grupo Macaúbas na Faixa Araçuaí: O registro de uma bacia Neoproterozóica. Boletim do Núcleo Minas Gerais-Sociedade Brasileira de Geologia 14:29–31

Noce CM et al (2005) Age of felsic volcanism and the role of ancient continental crust in the evolution of the Neoarchean Rio das Velhas greenstone belt (Quadrilátero Ferrífero, Brazil): U–Pb zircon dating of volcaniclastic graywackes. Precambr Res 141:67–82

Noce CM et al (2007) Evolution of polycyclic basement complexes in the Araçuai Orogen, based on U–Pb SHRIMP data: Implications for Brazil-Africa links in Paleoproterozoic time. Precambr Res 159(1–2):60–78

Nogueira ACR et al (2003) Soft-sediment deformation at the Neoproterozoic Puga cap carbonate (southwestern Amazon Craton, Brazil): confirmation of rapid icehouse to greenhouse transition in snowball Earth. Geology 31:613–616

Oriolo S et al (2016) The Nico Pérez Terrane (Uruguay): From Archean crustal growth and connections with the Congo Craton to late Neoproterozoic accretion to the Río de la Plata Craton. Precambr Res 280:147–160

Oyhantçabal P et al (2007) Petrografía y química mineral de dos ocurrencias de formaciones de hierro bandeado (BIF) del sureste del Uruguay (Terreno Nico Pérez). Abstracts, Congreso Uruguayo de Geología, 19 p

Oyhantçabal P et al (2011) The Río de la Plata Craton: a review of units, boundaries, ages and isotopic signature. Int J Earth Sci 100:201–220

Oyhantçabal P et al (2012) Paleo- and Neoproterozoic magmatic and tectonometamorphic evolution of the Isla Cristalina de Rivera (Nico Pérez Terrane, Uruguay). Int J Earth Sci 101(7):1745–1762

Pattison DRM (2003) Petrogenetic significance of orthopyroxene-free garnet + clinopyroxene + plagioclase-bearing metabasites with respect to the amphibolite and granulite facies. J Metamorph Geol 21:21–34

Pecoits E (2010) Ediacaran iron formations and carbonates of Uruguay: palaeoceanographic, palaeoclimatic and palaeobiologic implications. Ph.D. thesis, University of Alberta, 237 p

Pecoits E et al (2016) U–Pb detrital zircon ages from some Neoproterozoic successions of Uruguay: provenance, stratigraphy and tectonic evolution. J S Am Earth Sci 71:108–130

Pedrosa-Soares AC, Wiedemann-Leonardos CM (2000) Evolution of the Araçuaí belt and its connection to the Ribeira belt, Eastern Brazil. In: Cordani U et al (eds) Tectonic evolution of South America. Sociedade Brasileira de Geologia, São Paulo, pp 265–285

Pedrosa-Soares AC et al (1994) Nota explicativa dos mapas geológico, metalogenético e de ocorrências minerais do Estado de Minas Gerais, Escala 1:1.000.000

Pereira RMP et al (2009) Unidade Caninana: Sequência clástica Paleoproterozóica revelada por datação U–Pb em zircões detríticos da Província Mineral Carajás. XI Simpósio de Geologia da Amazônia 2009, Manaus. Anais. SBG, CD-ROM, Brasília

Pidgeon R et al (2000) Th-U–Pb isotopic systems and internal structures from an enderbite from the Pium Complex, Carajás Province, Brazil: evidence for the ages of granulite facies metamorphism and the protolith of the enderbite. Chem Geol 166:159–171

Pimentel MM (2016) The tectonic evolution of the Neoproterozoic Brasília Belt, central Brazil: a geochronological and isotopic approach. Braz J Geol 46:67–82

Pimentel MM et al (1996) Dados Rb–Sr e Sm–Nd da região de Jussara-Goiás-Mossâmedes (GO), e o limite entre terrenos antigos do Maciço de Goiás e o Arco Magmático de Goiás. Revista Brasileira de Geociências 26:61–70

Pimentel MM et al (2000a) The basement of the Brasília fold belt and the goiás magmatic arc. In: Cordani UG et al (eds) Tectonic evolution of South America. 31st International Geological Congress, Rio de Janeiro, pp 195–229

Pimentel MM et al (2000b) The Neoproterozoic Goiás magmatic arc, central Brazil: a review and new Sm–Nd isotopic data. Revista Brasileira de Geociências 30(1):35–39

Pimentel MM et al (2004) O embasamento da faixa Brasília e o arco magmático de Goiás. In: Mantesso-Neto V et al (Org) Geologia do continente Sul-Americano. Evolução da obra de Fernando Flávio Marques de Almeida. 1 ed. São Paulo. Beca 2004:355–368

Pinheiro RVL, Holdsworth RE (1997) The structure of the Carajás N-4 ironstone deposit and associated rocks: relationship to Archean strike-slip tectonics and basement reactivation in the Amazon region, Brazil. J S Am Earth Sci 10:305–319

Pinheiro RVL, Holdsworth RE (2000) The anatomy of shallow-crustal transpressional structures: insights from the Archean Carajás fault zone, Amazon, Brazil. J Struct Geol 22:1105–1123

Pinto CP, Silva MA (2014) Mapa Geológico do Estado de Minas Gerais, 1:1.000.000. CPRM-CODEMIG, Belo Horizonte (CD-ROM)

Pires FRM (1995) Textural and mineralogical variations during metamorphism of the proterozoic itabira iron formation in the Quadrilatero Ferrifero, Minas Gerais, Brazil. Anais Academia Brasileira de Ciencias 67:77–105

Planavsky N et al (2010) Rare earth element and yttrium compositions of archean and paleoproterozoic Fe formations revisited: new perspectives on the significance and mechanisms of deposition. Geochim Cosmochim Acta 74:6387–6405

Pomerene IB (1964) Geology and mineral deposits of the Belo Horizonte, Ihirite and Maeacos quadrangles. U.S. geological survey professional paper 341-D, pp 1–84

Popp RK et al (1977) Stability of Fe-Mg amphiboles with respect to oxygen fugacity. Am Miner 62:1–12
Preciozzi F et al (1979) Carta geo-estructural del Uruguay, Escala 1:2.000.000. Instituto Geologico Ing. Terra Arocena, Montevideo, 62 p
Preciozzi F et al (1985) Carta Geológica del Uruguay a escala 1:500.000. Dirección Nacional de Minería y Geología, Montevideo, 92 p
Rasmussen B et al (2016) Dust to dust: Evidence for the formation of "primary" hematite dust in banded iron formations via oxidation of iron silicate nanoparticles. Precambr Res 284:49–63
Reeves RG (1966) Geology and mineral resources of the Monlevade and Rio Piracicaba Quadrangles, Minas Gerais, Brazil. U.S. geological survey professional paper 341-E, 58 p
Renger FE et al (1994) Evolução sedimentar do Supergrupo Minas: 500 Ma. de registro geológico no Quadrilátero Ferrífero, Minas Gerais, Brasil. Geonomos 2:1–11
Rolim VK et al (2016) The Orosirian-Statherian banded iron formation-bearing sequences of the southern border of the Espinhaço range, southeast Brazil. J S Am Earth Sci 65:43–66
Rosière CA, Chemale F Jr (1991) Textural and structural aspects of iron ores from iron quadrangle, Brazil. In: Pagel M, Leroy JL (Org) Source, transport and deposition of metals. Balkema, Amsterdam, pp 485–488
Rosière CA et al (2006) Structure and iron mineralisation in the Carajás Province. Proceedings iron ore 2005, Applied earth science. Trans Inst Min Metall B 115(4):126–136
Rosière CA et al (2008) The itabirites of the Quadrilátero Ferrífero and related high-grade iron ore deposits: an overview. Rev Econ Geol 15:223–254
Rosière CA et al (2013) Domainal fabrics of hematite in schistose, shear zone-hosted high-grade Fe ores: the product of the interplay between deformation and mineralization. J Struct Geol 55:150–166
Sanglard J et al (2014) A estrutura do segmento oeste da Serra do Curral, Quadrilátero Ferrífero, e o controle tectônico das acumulações compactas de alto teor em Fe. Geologia USP. Série Científica 13:81–95
Santos JOS (2003) Geotectônica dos Escudos das Guianas e Brasil-Central. In: Bizzi LA et al (eds) Geologia, tectônica e recursos minerais do Brasil. Companhia de Pesquisa e Recursos Minerais–CPRM, pp 169–226
Santos JS (2015) Geologia da sequência metassedimentar Ibicuí-Iguaí na Serra do Lontra com ênfase no controle estrutural dos depósitos de ferro hipogênico. M.Sc. thesis, Universidade Federal da Bahia, Salvador
Santos JOS et al (2000) A new understanding of the Amazon Craton Provinces based on integration of field mapping and U–Pb and Sm–Nd geochronology. Gondwana Res 3(4):453–488
Santos JOS et al (2003) Duration of the trans-amazonian cycle and its correlation within South America based on U–Pb SHRIMP geochronology of the La Plata Craton, Uruguay. Int Geol Rev 45:27–48
Santos JOS et al (2005) Metasedimentary rocks of the Imataca Complex, Venezuela: from Archean to Orosirian (Late-Transamazonian). In 12º Congreso Latinoamericano de Geologia, Anais, Quito, Equador
Santos JOS et al (2006) A compartimentação do Cráton Amazonas em províncias: Avanços ocorridos no período 2000–2006. SBG, Simpósio de Geologia da Amazônia, IX, CD-ROM, Belém
Santos JOS et al (2010) Two Statherian hydrothermal events in the Carajás Province: evidence from Pb–Pb SHRIMP and Pb–Th SHRIMP dating of hydrothermal anatase and monazite. VII SSAGI South American symposium on isotope geology. Anais, CD-ROM, Brasília
Schobbenhaus C, Oliva LA (1979) Carta geológica do Brasil ao milionéssimo: folha Corumbá (SE.21), DNPM, Brasília. Escala de 1:1.000.000
Schrank A (1982) Petrologie des komatiites et des rochesassociées de la ceintures verte du Massif Précambrien de Piumhi (Minas Gerais—Brazil). Thèse (3ème Cycle), Université de Paris-Sud, Orsay, 270
Schrank A, Silva MG (1993) (1993) Greenstone Belts do Cráton do São Francisco, Brasil. In: Misi A, Dominguez JML (eds) O Craton do São Francisco. SBG/SGM/CNPq, Salvador, pp 85–118
Seoane JCS et al (2004) Mapeamento litoestrutural 3-D do Grupo Grão Pará, Província Mineral de Carajás, PA. In: Simpósio Brasileiro Exploração Mineral, May 2004, CD ROM, ADIMB, Ouro Preto
Sial AN et al (2015) Algoma-type Neoproterozoic BIFs and related marbles in the Seridó Belt (NE Brazil): REE, C, O, Cr and Sr isotope evidence. J S Am Earth Sci 61:33–52
Silva LC et al (2002) Reavaliação da evolução geológica em terrenos pré-cambrianos brasileiros com base em novos dados U–Pb SHRIMP, parte II: orógeno Araçuaí, Cinturão Mineiro e Cráton São Francisco Meridional. Revista Brasileira de Geociências 32 (4):513–528
Silva MG, Cunha JC (1999) Greenstone belts and equivalent volcano-sedimentary sequences of the São Francisco Craton, Bahia, Brasil, Brasil—Geology and mineral potential. In: Silva MG, Misi A (eds) Base Metal deposits of Brazil. MME/CPRM/DNPM, Belo Horizonte, pp 92–99
Silveira Braga FC et al (2015) The Statherian itabirite-bearing sequence from the Morro Escuro Ridge, Santa Maria de Itabira, Minas Gerais, Brazil. J S Am Earth Sci 58:33–53
Simmons GC (1968) Geology and iron deposits of the western Serra do Curral, Minas Gerais, Brazil U.S. geological survey professional paper 341-G, 57 p
Simonson BM (1984) High-energy shelf deposit: early Proterozoic wishart formation, northeastern Canada. SEPM Spec Publ 34:251–268
Souza JD et al (2003) Mapa geológico do Estado da Bahia. CPRM
Spoturno J et al (2004) Mapa geológico y de recursos minerales del Departamento de San José. Escala 1/100.000 DINAMIGE-Facultad de Ciencias. CD-ROM
Suckau VE et al (2005) Transitional pyroclastic, volcanic-exhalative rocks to iron ores in the Caue Formation, Tamandua and Capitao do Mato Mines: An overview of metallogenetic and tectonic aspects. Simpósio do Craton de Sao Francisco, III, Companhia Bahiana de Pesquisa Mineral/Universidade Federal da Bahia/Sociedade Brasileira de Geologia, Anais, Salvador, pp 343–346
Sun S et al (2015) Primary hematite in neoarchean to paleoproterozoic oceans. Geol Soc Am Bull 127:850–861
Tassinari CCG, Macambira MJB (1999) Geochronological provinces of the Amazonian Craton. Episodes 22(3):174–182
Taylor D et al (2001) Genesis of high-grade hematite orebodies of the Hamersley Province, Western Australia. Econ Geol 96:837–873
Teixeira W et al (1996) Pb, Sr and Nd isotope constraints on the Archean evolution of gneissic-granitoid complexes in the southern São Francisco Craton, Brazil. Precambr Res 78:151–164
Trendall AF, Blockley JG (1970) The iron formations of the Precambrian Hamersley Group, Western Australia. Geol Surv West Austral Bull 119:366
Trompette R et al (1998) Geological evolution of the Neoproterozoic Corumba graben system (Brazil). Depositional context of the stratified Fe and Mn ores of the Jacadigo Group. J S Am Earth Sci 11:587–597
Tsikos H et al (2003) Deposition, diagenesis, and secondary enrichment of metals in the Paleoproterozoic Hotazel iron-formation, Kalahari manganese field, South Africa. Econ Geol 98:1449–1462
Uhlein A et al (1998) Proterozoic rifting and closure, SE border of the São Francisco Craton, Brazil. J S Am Earth Sci 11:191–203

Uhlein A et al (2011) A Formação Lagoa Formosa, Grupo Bambuí (MG): sistema deposicional de leque submarino em bacia de ante-país. Geonomos 19:163–172

Urban H et al (1992) Iron and manganese deposits of the Urucum District, Mato Grosso do Sul, Brazil. Econ Geol 87:1375–1392

Vilela FT et al (2014) Metalogênese da Faixa Araçuaí: o distrito ferrífero de Nova Aurora (Grupo Macaúbas, norte de Minas Gerais) no contexto dos recursos minerais do Orógeno Araçuaí. In: Silva MGS et al (Org) Metalogênese das Províncias tectônicas brasileiras, pp 415–530

Villaça JN (1981) Alguns aspectos sedimentares da Formação Moeda. Belo Horizonte, Bol. 2 SBG-MG:93–137

Villas RN, Santos MD (2001) The gold deposits of the Carajás mineral province: deposit types and metallogenesis. Miner Deposita 36(3–4):300–331

Wallace RM (1965) Geology and mineral resources of the Pico do Itabirito district, Minas Gerais, Brazil. U.S. geological survey professional paper 341 F, 68 p

Wirth KR et al (1986) U–Pb ages of zircons from the Grão-Pará Group and Serra dos Carajás Granite, Pará, Brazil. Revista Brasileira de Geociências 16:195–200

Young GM et al (1979) Middle and late Proterozoic evolution of the northern Canadian cordillera and shield. Geology 7:125–128

Zegeye A et al (2012) Green rust formation controls nutrient availability in a ferruginous water column. Geology 40:599–602

Zucchetti M (2007) Rochas máficas do Supergrupo Grão Pará e sua relação, com a mineralização de ferro dos depósitos N4 e N5, Carajás (PA). Ph.D. thesis, Belo Horizonte, Brazil, Universidade Federal de Minas Gerais, 125 p

The Glaciations in South America

19

Daniel G. Poiré, Lucía E. Gómez Peral, and María J. Arrouy

Abstract

Neoproterozoic successions in South America are recorded in many areas of Brazil, Paraguay, Bolivia, Uruguay and Argentina. Some of these units show glaciogenic formations like those represented in the Puga and Serra Azul formations in the Northern Paraguay Belt (Brazil) in agreement with their accumulation in a Snowball Earth context. However, in other cases, tillites or other glaciomarine deposits are absent, which may indicate a distant position (tropical) regarding the ice cap, as occurs in the Tandilia System (Argentina) related to a "Phantom glacial" context. In this contribution we show the comparison between direct and indirect evidence of glaciations in the Neoproterozoic successions of South America. The Puga and Serra Azul formations in the Paraguay Belt and Sierras Bayas Group in the Río de la Plata Craton have been chosen to describe the "Snowball Earth" and "Phantom glacial" models, respectively. By means of multiproxy analysis it is also possible to indicate changes in paleoclimate conditions in both cases. The presence of tillites is considered to be direct evidence of the extreme climatic conditions during deposition during a glaciation. Meanwhile, more subtle evidence such as regional unconformities related to drastic sea level changes, trends in $\delta^{13}C$, events of phosphogenesis, constitute, among others, the tools to indicate the influence of Neoproterozoic global glaciations during the deposition of the sedimentary units.

Keywords

Paleoclimatic proxies • Neoproterozoic • Tillite records Phantom glacial deposits

D. G. Poiré (✉) · L. E. Gómez Peral · M. J. Arrouy
Centro de Investigaciones Geológicas–CONICET–FCNyM (UNLP), Diag.113 N° 275, esq. 64, 1900, La Plata, Argentina
e-mail: dgpoire@yahoo.com.ar

19.1 Introduction

Neoproterozoic diamictite rocks such as tillites or glaciomarine deposits have been recorded as the product of regional glaciations around the world, in accordance with the Snowball Earth hypothesis (Hoffman et al. 1998). However, in some parts of the planet, contemporaneous non-glaciogenic sedimentary rocks have also been observed related to sedimentation in non-glacial environments but influenced by planetary glaciation, which was termed "Phantom glacial" (Cozzi et al. 2002; Poiré 2004) in a "slushball Earth" scenario. In the first model, the glacial mass covers the whole planet during glaciations, whereas in the slushball hypothesis the Earth was not completely frozen during periods of extreme glaciation (Hyde et al. 2000; Lewis et al. 2007; Micheel and Montenari 2008). Floating ice would have covered up to 60% of the ocean, but this left a lot of the ocean open, and littoral and low continental environments in the tropics without any ice cover. In this case, the total glacial mass was increasing while the sea level was falling, producing diamictites in the frozen areas around the world and falling sea-level deposits in tropical and equatorial regions. Phantom glacial deposits are those that are not glacial diamictites but show glacial sea level dropping sedimentation, such as deltas progradation, fluvial erosional unconformities and karstic surfaces on limestone shelves.

As synthesized by Sohl and Chandler (2007), of these two end-member climate conditions, the Snowball Earth glaciations have attracted most attention in recent years, in large part because of the discussion about the possible climatic influence on the evolution of macroscopic life. Previous iterations of the Snowball Earth hypothesis (Hoffman et al. 1998; Hoffman and Schrag 2002) have taken the geological evidence for widespread cold climates and extrapolated a vision of the world practically entombed in ice, with the oceans totally frozen. Proponents of the "hard" Snowball Earth have suggested that total or near-total sea-ice cover is

S. Siegesmund et al. (eds.), *Geology of Southwest Gondwana*, Regional Geology Reviews,
https://doi.org/10.1007/978-3-319-68920-3_19

necessary to explain both an interpreted rapid transition from the glacial to the non-glacial state, and unusual $\delta^{13}C$ signatures, as low as –5‰, in carbonate rocks ("cap carbonates") directly overlying the glacial deposits (Hoffman et al. 1998; Hoffman and Schrag 2002). Those in favor of a slightly less extreme scenario, the slushball Earth, point to sedimentary deposits (ice-rafted debris in deep marine settings) that can be used to argue in favor of more open ocean rather than less (e.g., McMechan 2000; Condon et al. 2002; Kellerhals and Matter 2003). Furthermore, some authors have suggested that icebergs have never reached equatorial positions, but the strong polar glaciations have led to falling sea levels with karstic surfaces in tropical and equatorial latitudes over carbonate platforms (Poiré 2004; Gómez Peral et al. 2014a, b, 2017).

The South American geological record shows both types of occurring given by successions with the presence of tillites ("Snowball Earth") and others without these diamictite deposits ("Phantom glacial"). The aim of this contribution is to make a comparison between evidence of the direct and indirect influence of glaciations in the Neoproterozoic successions of the Tandilia System and Northern Paraguay Belt (Fig. 19.1) as end-members of the climate conditions in South America. Thus the Puga Formation in Northern Paraguay Belt, Amazonia Craton in Brazil, and the Sierras Bayas Group in the Rio de la Plata Craton of Argentina have been chosen to describe both models. By means of multiproxy analysis it is also possible to indicate changes in paleoclimatic conditions in both cases.

The Paraguay Belt shows the occurrence of tillite deposits associated with glacial events and is in agreement with the Snowball Earth hypothesis.

In particular, the example of Phantom glacial is postulated on the basis of the development of regional karstic unconformities related to drastic sea level changes, trends in $\delta^{13}C$ and phosphogenesis events, which among others constitute indirect evidence that can be used to indicate the influence of Neoproterozoic global glaciations during the deposition of the sedimentary units of the Tandilia System.

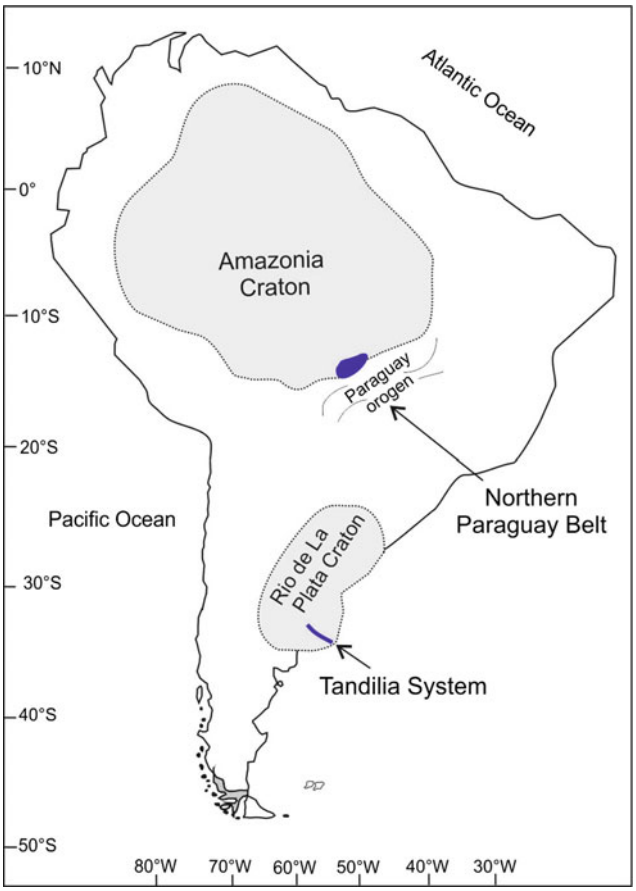

Fig. 19.1 General map of the Rio de la Plata craton and Amazonia craton of southern South America (modified from Rapela et al. 2016 and references therein)

19.2 Glacial Deposits in South America

19.2.1 Northern Paraguay Belt in the Amazonia Paleocontinent

The Paraguay Belt is an extended region located on the southeastern edge of the Amazon Craton (Fig. 19.1), also defined as Amazonia Paleocontinent by Alvarenga et al. (2009). In the Northern Paraguay Belt, two indubitable Neoproterozoic tillite units have been recognized (Fig. 19.2): the Marinoan-aged Puga Formation and the Gaskiers-aged Serra Azul Formation (Alvarenga and Trompette 1992; Alvarenga et al. 2004, 2007, 2009).

Marinoan glacial deposits have also been identified in the Southern Paraguay Belt with carbonate rocks overlying the glaciogenic deposits. The Santa Cruz (Fig. 19.3a) and Puga formations in the Corumbá area have been correlated with this glacial event (635 Ma) based on cap-dolomite lithofacies, paleomagnetic data, and associated $\delta^{13}C$ and $^{87}Sr/^{86}Sr$ isotope trends (Boggiani 1998; Trompette et al. 1998; Nogueira et al. 2003; Trindade et al. 2003; Alvarenga et al. 2004, 2009, 2011; Boggiani et al. 2004; Sial et al. 2016). However, tillites of the Puga Formation are better represented in the Northern Paraguay Belt (Figs. 19.2 and 19.3b). According to Alvarenga et al. (2011) and Sial et al. (2016), the Puga Formation was originally described from the Southern Paraguay Belt (Maciel 1959) but is not necessarily coeval with the homonymous unit in the Northern Paraguay Belt. Besides, the deposition of these Puga Formation terrigenous sediments in the south is probably associated with the development of a rift basin (Boggiani 1998; Gaucher et al. 2003).

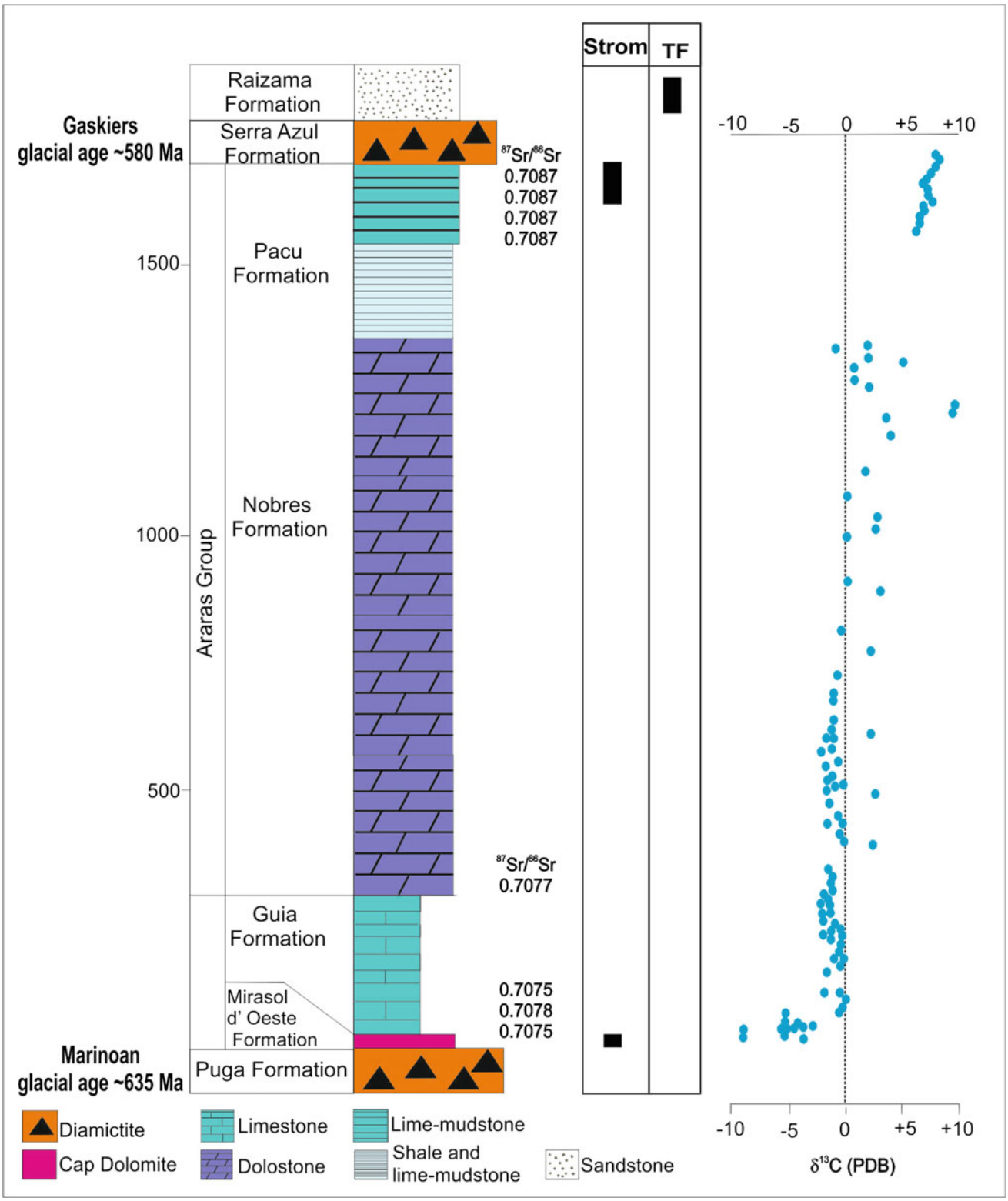

Fig. 19.2 Stratigraphic and bioestratigraphic section and variations in δ13C and 87Sr/86Sr for the Araras Group (modified from Sial et al. 2016)

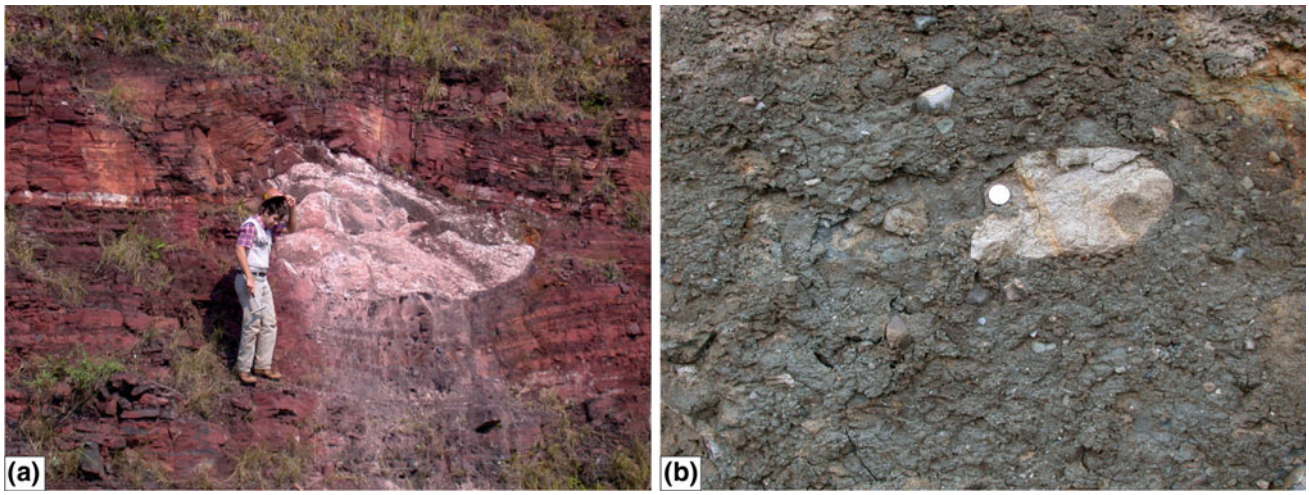

Fig. 19.3 Field photographs. **a** Granite megaclast dropstone in Santa Cruz Formation, Southern Paraguay Belt, Brazil. **b** Tillite of Puga Formation, Northern Paraguay Belt, Brazil

19.2.1.1 Lithostratigraphy

Lithostratigraphically, this region comprise a crystalline basement complex (gneisses, schists, granites, meta-quartzites) overlain by a Neoproterozoic sedimentary succession that from bottom to top is composed of the Puga Formation, Araras Group (Mirassol d´Oeste, Guia, Nobres and Pacu formations) and Serra Azul Formation, all covered by the Ediacaran/Cambrian Razaima Formation (Fig. 19.2).

The Puga Formation (Maciel 1959) is the oldest depositional unit (100 m thick) and comprises purple, reddish, brownish or dark-greenish gray, pebbly tillite with striated clasts of granite and sandstone (Fig. 19.3b), also accompanied by conglomerates, sandstones, and shales. It has been interpreted as a glacial-marine deposit (Maciel 1959; Alvarenga and Trompette 1992). Based on detrital zircon ages (Babinski et al. 2013), paleomagnetic data (Trindade et al. 2003) and chemostratigraphy of the overlying limestones (Nogueira et al. 2003), this unit is considered Cryogenian in age.

The basal unit of the Araras Group is the Mirassol d´ Oeste Formation (up to 30 m thick), which is composed of pinkish dolostones bearing stromatolites, tube-like structures, breccia, giant wave ripples, deformed microbialites dislocated by synsedimentary faults, red iron-oxide-rich mudstones in the top level (Nogueira et al. 2003; Alvarenga et al. 2004, 2008; Nogueira and Riccomini, 2006) and fan-like crystals interpreted as aragonite pseudomorphs (Alvarenga et al. 2008). The unit is interpreted as a moderately deep euphotic platform (Nogueira et al. 2003).

The middle one, the Guia Formation (up to 250 m thick), consists of dark-gray laminated limestones and shales, with slumps and other deformational sedimentary structures, interpreted as deposited in a deep platform environment (Nogueira et al. 2003).

The Nobres Formation (up to 1100 m thick) is composed mainly of light-gray grainstone, packstone dolostones, with some interlayered breccias. This unit was interpreted as a carbonate platform deposited under shallow-water sedimentation.

The uppermost unit of the Araras Group is the Pacu Formation (~300 m thick), described as carbonate mudstones and stromatolitic limestones (Souza et al. 2012), in a coarsening upward succession, which was interpreted as deposited by a marine transgression followed by a regression with the development of a carbonate shallow marine platform during the Ediacaran (Souza 2015).

Above the Araras Group through an erosional surface, the Serra Azul Formation (up to 270 m thick) is recorded, composed of a very thick basal diamictite unit (70 m) of massive reddish diamictite with an abundant clay-silty matrix. Well-rounded to highly angular clasts (from millimeters to centimeters in diameter) are dispersed throughout the matrix, some of them reaching up to 30 cm in diameter. The composition of the clasts is sandstones, quartz, quartzites, arkoses, carbonates, cherts, basalts, rhyolites, diabases and weathered granitic rocks. Some faceted, polished and striated clasts have also been preserved in the diamictite (Alvarenga et al. 2007, 2009). These tillites are overlain by a succession of reddish laminated siltstone (25 m thick), which is overlaid by a rhythmite unit (175 m thick) interbeded with episodic sandstones (Alvarenga et al. 2009).

The Razaima Formation (up to 700 m thick) covers the Neoproterozoic sedimentary cover of the Northern Paraguay Belt, which consists of a siliciclastic succession. The lower part of this unit consists of whitish parallel-laminated and small-scale hummocky cross-stratified sandstone and pebbly sandstone, interbedded with parallel-laminated mudstone that grades upwards into swaley cross-stratified sandstone,

forming a shallowing upward succession (Santos et al. 2017). The ichnogenera *Skolithos*, *Arenicolites* and *Diplocraterion* have been reported by Santos et al. (2017). According to these authors, (1) these trace fossils are therefore consistent with sedimentologic data which indicates a wave-dominated nearshore environment, and (2) the ichnofauna are suggesting an early Cambrian age or younger for the Raizama Formation in contrast to the previously held view of an Ediacaran age for this unit.

19.2.1.2 Glacial Deposits of Puga Formation

The Puga Formation tillites were correlated with the Marinoan glaciation related to Araras Group cap-carbonate lithofacies, paleomagnetic data, and associated $\delta^{13}C$ and $^{87}Sr/^{86}Sr$ isotope trends (Nogueira et al. 2003; Pinho et al. 2003; Trindade et al. 2003; Alvarenga et al. 2004). Over the diamictites of the Puga Formation, the cap dolostone of the Mirassol d'Oeste Formation is succeeded by transgressive, deep-platform deposits of dark-gray laminated lime-mudstone and shales of the Guia Formation, reaching up to 250 m thick in the middle shelf domain (Alvarenga et al. 2004, 2008, 2011; Nogueira et al. 2007; Riccomini et al. 2007).

Ca isotopic compositions of post-glacial carbonate successions in central Brazil (Mirassol d'Oeste-Cáceres and Tangará) have been reported by Silva-Tamayo et al. (2010a, b). These authors indicate that the Ca-isotope secular variation trend is similar to those of Marinoan post-glacial carbonate successions in Namibia, suggesting that the perturbation of the marine Ca cycle was, perhaps, global. Carbon isotope data for rocks of the Guia Formation revealed predominantly negative $\delta^{13}C$ values, from –3.5 to 0.1‰, and $\delta^{18}O$ values from –13.5‰ to –6.3‰ (Nogueira et al. 2003, 2007; Alvarenga et al. 2004, 2008; Figueiredo 2006). $^{87}Sr/^{86}Sr$ ratios for limestones with a higher Sr content (>750 ppm) and low Mn/Sr ratios (<0.2) range from 0.7076 to 0.7078 (Alvarenga et al. 2008, 2011).

19.2.1.3 Glacial Deposits of Serra Azul Formation

Dropstones and striated clasts provide evidence of a glacial setting for the Serra Azul diamictite (Fig. 19.2). This unit is composed of massive diamictite with an abundant clay-silty matrix (70 m thick), followed by a thick succession of laminated siltstone (200 m). This unit is not overlaid by a cap carbonate, as was reported for the Puga Formation. The Serra Azul Formation was described as discontinuous outcrops of diamictites and siltstones above post-Marinoan carbonates of the Araras Group (Fig. 19.2), and it represents a record of the Gaskiers glaciation (Alvarenga et al. 2007) with an age of *c*. 580 Ma (Knoll et al. 2004).

19.3 Phantom Glacial Deposits in South America

19.3.1 Tandilia System in the Río de La Plata Craton

The Neoproterozoic sedimentary cover of the Tandilia System in the Sierras Bayas- Olavarría area comprises a ~455 m-thick succession, which overlays a crystalline basement. The Sierras Bayas Group (Villa Mónica, Colombo, Cerro Largo, Olavarría and Loma Negra formations) and La Providencia Group (Avellaneda, Alicia and Cerro Negro formations) are compound this sedimentary cover (Fig. 19.4a), which are composed of different carbonate and siliciclastic units separated by regional unconformities (Poiré 1987; Iñiguez et al. 1989; Poiré and Spalletti 2005; Poiré and Gaucher 2007, 2009; Arrouy et al. 2015).

19.3.1.1 Lithostratigraphy

Crystalline Basement

The Buenos Aires Complex (Marchese and Di Paola 1975) is composed of granitoids, migmatites, mylonites, amphibolites and basic dykes (Cingolani and Dalla Salda 2000), yielding U-Pb SHRIMP ages of between 2234 and 2065 Ma (Cingolani et al. 2002; Hartmann et al. 2002a, b; Cingolani 2011) and Sm-Nd model ages averaging around 2620 ± 80 Ma (Pankhurst et al. 2003).

Sierras Bayas Group

In the Olavarría-Barker area (Fig. 19.4a) the overlying Neoproterozoic lithostratigraphic units are grouped into five depositional intervals (Fig. 19.4b) (Poiré et al. 2003; Poiré and Spalletti 2005; Poiré and Gaucher 2009). Detrital zircon U-Pb ages indicate a Paleoproterozoic to Mesoproterozoic source of clastic material in the Neoproterozoic succession (Rapela et al. 2007, 2011; Gaucher et al. 2008; Cingolani 2011). Gaucher et al. (2008) and Cingolani (2011) observe an obvious change in detrital provenance from the basal to the upper formations (see also Zimmerman et al. 2011, who provide geochemical evidence for a change in provenance).

The basal unit, the Villa Mónica Formation (52–70 m thick), exhibits two sedimentary facies associations: quartz-arenite and arkosic sandstone at the base, and dolostone including shallow marine stromatolites and shale-marls at the top (Poiré 1993; Gaucher and Poiré 2009a).

The erosional surface above the Villa Mónica Formation, the Piedra Amarilla Surface, is followed by breccias and diamictites of the Colombo Formation (Poiré and Gaucher

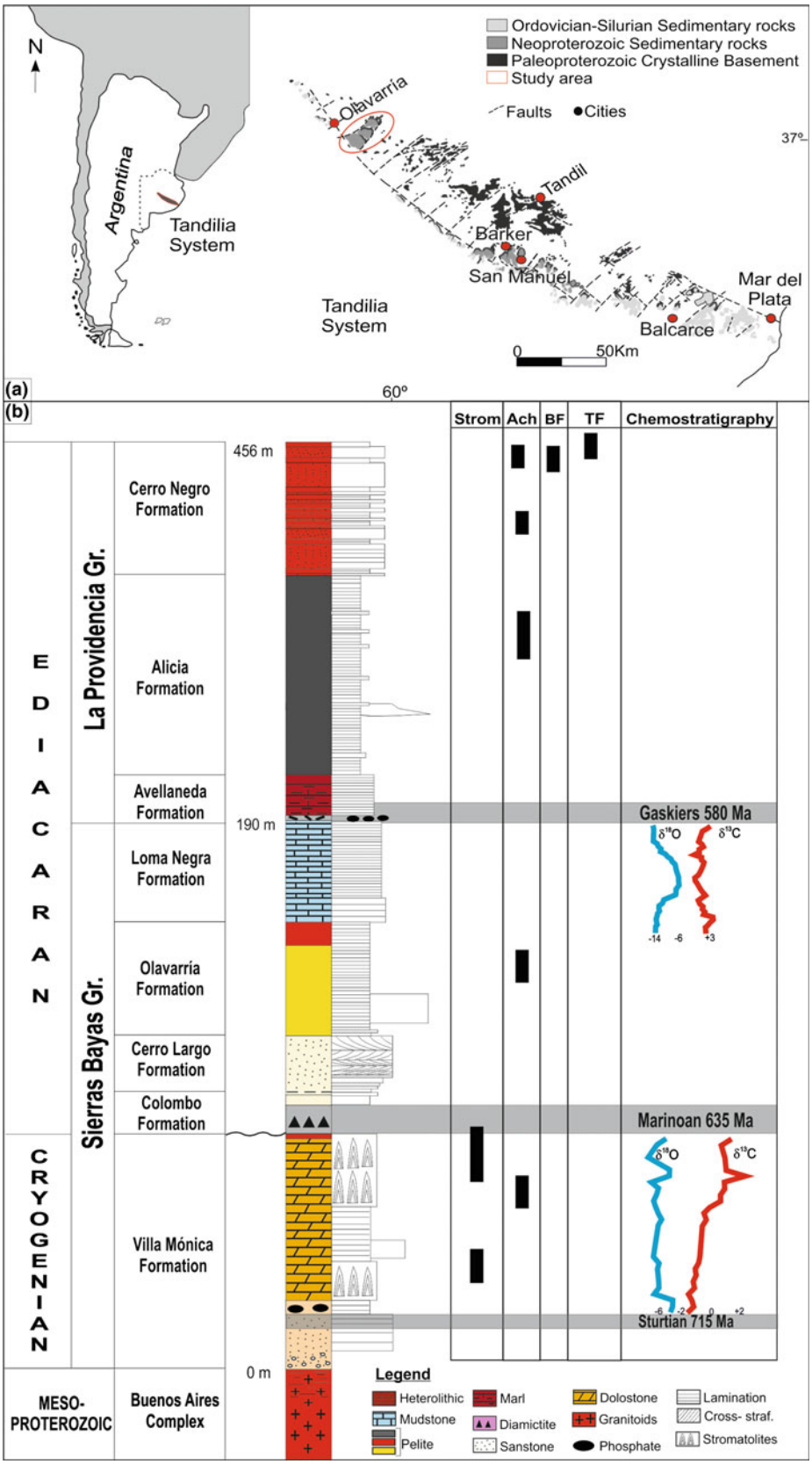

Fig. 19.4 **a** Location map of Argentina in South America and study area in the Tandilia System, Buenos Aires Province, Argentina (modified from Iñiguez 1989). **b** Schematic representation of the lithostratigraphic, biostratigraphic and quimiostratigraphic successions of Sierras Bayas and La Providencia Groups (Poiré and Gaucher 2009; Arrouy et al. 2015; Gómez Peral et al. 2017)

2009; Gómez-Peral et al. 2011). The diamictites (Gaucher and Poiré 2009b) contain blocks up to 3 m in diameter (i.e., sandstone, shale, dolostone and chert breccia), synsedimentary deformation structures, and a sandy-muddy matrix (Gómez-Peral et al. 2011). Rapalini et al. (2013) assigned a tentative age for the Piedra Amarilla Surface of 590 Ma on the basis of paleomagnetic data. Above the diamictite, finely laminated glauconitic shales and fine-grained sandstones appear in the basal part of the Cerro Largo Formation. The upper part of this unit consists of cross-bedded quartz sandstones with sigmoidal, herringbone and hummocky cross-stratification (Gómez-Peral et al. 2011). This succession represents a shallowing-upward succession, ranging from subtidal nearshore to tidal-flat deposits (Poiré 1987; Poiré and Gaucher 2009).

The overlying Olavarría Formation is approximately 35 m thick and includes a transitional basal contact represented by quartzite to mudstone heterolithic facies. Mudstone and heterolithic facies contain 8–20 cm concretionary iron-rich beds (Gómez-Peral et al. 2011).

The youngest depositional unit of the Sierras Bayas Group is the Loma Negra Formation (Figs. 19.2b), which is represented by 40 m exclusively composed of micritic limestones originating from suspension fall-out in open marine platform environment. The age of the Loma Negra Formation was debated. It was suggested first as ~540–550 Ma, based on the presence of *Cloudina* (Gaucher et al. 2005), but it could be older (~580–590 Ma) considering $\delta^{13}C$ and $^{87}Sr/^{86}Sr$ combined trends (Gómez Peral et al. 2007). Moreover, in the overlying Cerro Negro Formation, Arrouy et al. (2016) described typical morphs of *Aspidella* (related to the 560–550 Ma White Sea assemblage; Wagooner 2003).

La Providencia Group

The Sierras Bayas Group is overlain discordantly by La Providencia Group. The basal Avellaneda Formation is the filling of a channelized paleosurface (Barker surface, Fig. 19.4b) composed on common chert breccias (Barrio et al. 1991) with phosphate concretions first recognized by Leanza and Hugo (1987). The Avellaneda Formation (up to 25 m thick) is composed mostly of red to purple laminated and massive marls at the base, which grade vertically into red massive mudstones (Fig. 19.2b). This formation was interpreted as deposited under supratidal conditions in a tidal-flat depositional environment, probably in well-oxygenated conditions (Arrouy 2015; Arrouy et al. 2015).

The Alicia Formation (up to 150 m thick) conformably overlies the previous one and is composed of dark fissile mudstones and massive gray siltstones, as well as gray heterolithics with lenticular and wavy bedding (Fig. 19.2b). This facies succession was interpreted to represent low-energy subtidal settings, likely with suboxic to anoxic bottom conditions (Arrouy 2015; Arrouy et al. 2015).

The Cerro Negro Formation (~100 m) unconformably rests on the previous, and represents an abrupt change to red heterolithics with wavy and flaser bedding, together with cross-laminated and massive, fine- to medium-grained sandstones (Fig. 19.4b). Mudcracks, scour marks and flutes are common in this succession, which was interpreted to represent subtidal to intertidal settings, probably with well-oxygenated substrates. The top of this succession has been removed by erosion in both the subsurface and outcrops (Arrouy 2015; Arrouy et al. 2015).

19.3.1.2 Geobiology

The Neproterozoic sedimentary cover of the Tandilia System is very rich in signs of primitive life. These include stromatolites, Ediacaran Biota, trace fossils, microbial induced sedimentary structures (MISS) and acritarchs.

Stromatolites of the Villa Monica Formation of the Sierras Bayas Group include *Colonnella* fm., *Conophyton* fm., *Conophyton ressoti*, *Cryptozoon* fm., *Gongylina* fm., *Gymnosolen* fm., *Inzeria* fm., *Jacutophyton* fm., *Jurusania* cf. *nisvensis*, *Katavia* fm., *Kotuikania* fm., *Kussiella* fm., *Minjaria* fm., *Parmites* fm., *Parmites* cf. *concrescens* and *Stratifera* fm (Poiré 1987, 1989, 2002; Poiré and Spalletti 2005). Megascale studies show that the lower and upper parts of this dolostone unit are composed of 0.5–1.4 m-thick domal biostromes and 0.1–0.5 m-thick interbiostromal green shales. A few bioherms are present at the top of this unit. In contrast, in the middle part the stromatolites are completely absent. Domal biostromes are very conspicuous and they reflect the strong influence of paleocurrents in their morphogenesis. The direction of elongation was perpendicular to the shoreline. Two types of elongated bioconstruction are distinguished: symmetrical and asymmetrical. The latter suggests their acute end-points out to sea. The measured paleocurrents suggest a north–south local shoreline direction with open sea towards the east (Poiré 1987, 1989).

Very abundant and diverse discoidal structures in fine-grained micaceous sandstones, associated with abundant MISS, in the Cerro Negro Formation of the La Providencia Group, were assigned to the genera *Aspidella* sp. as the oldest record of Ediacaran macrobiota in South America (Arrouy et al. 2016). In this unit, *Skolithos* isp., *Helminthopsis* isp. and bilobate trace fossils are also reported (Poiré and Spalletti 2005; Arrouy et al. 2016).

In terms of microfossils, the Sierras Bayas Group contains acritarchs assigned to *Chuaria circularis*, *Leiosphaeridia minutissima, L. tenuissima* and *Synsphaeridium* sp. In addition, *Leiosphaeridiajacutica*, *L. tenuissima* and *Synsphaeridium* sp. from Sierras Bayas and La Providencia

groups were also recognized in the shales (Gaucher et al. 2005; Gaucher and Poiré 2009a).

19.3.1.3 Synglacial Sea Level Falls

Two major stratigraphic discontinuities are recorded in the Sierras Bayas Group, including the lower surface at the contact between the Villa Mónica and Cerro Largo formations, "Piedra Amarilla Surface" (Fig. 19.5a), and the upper surface on top of the Loma Negra Formation, "Barker Surface" (Fig. 19.5b). The latter may have been expressed worldwide and related to glacial eustacy insofar as it has been correlated with other Neoproterozoic omission surfaces in Uruguay, Brazil, South Africa and Namibia (Poiré et al. 2007; Praekelt et al. 2008; Germs and Gaucher 2012). Both of the Sierras Bayas unconformities are associated with the development of karst on carbonate lithologies filled with diamictite, chert and phosphate concretions, and intraformational breccia (Fig. 19.5). On the other hand, the transitional or planar contacts between the Cerro Largo and Olavarría formations, and the Olavarría and Loma Negra formations, reflect variations in paloenvironmental conditions, recognized primarily by pronounced lithological changes (Fig. 19.5b).

The Piedra Amarilla Surface was defined as a karstic surface (Gómez Peral et al. 2011), which is located at the contact between the Villa Mónica and Colombo formations (Fig. 19.5a) dividing the Sierras Bayas Group in two sections with very different depositional and diagenetic stories. Some iron-rich levels related to the basal Colombo Formation were placed by paleomagnetic studies in ~595 Ma (Rapallini et al. 2013). On the other hand, some iron concentrations were related to hydrothermal activity (Gómez Peral et al. 2012), as well as in the Barker area (Martínez et al. 2010) related to hydrothermal activity between 620 and 590 Ma based on K/Ar ages (Martínez et al. 2013).

Siliceous cementation and replacement were assumed for subaerial exposure when the pH dropped. This subaerial exposure is associated with an important sea-level fall whose relation to glaciation can be assumed, probably as a response to the Marinoan global event.

The Barker surface (Fig. 19.5b) is on top of the Sierras Bayas Group and has been correlated with other Neoproterozoic surfaces in SW Gondwana in Uruguay, Brazil, South Africa and Namibia, and related tentatively to the Gaskiers glaciation (Poiré et al. 2007; Gaucher and Poiré 2009b; Gaucher et al. 2009). This surface is associated with a drastic regional sea-level fall that exposed the Loma Negra shelf carbonates (Barrio et al. 1991; Gómez Peral 2008).

Telodiagenetic processes were defined in detail by Gómez Peral (2008), where besides the intense silicification also hematite constitutes a frequent type of cementation related to meteoric fluids during kastification. This is strong evidence of subaerial exposure.

19.3.1.4 Paleoclimate-Controlled Chemostratigraphy

Trends in $\delta^{13}C$ curves from the dolostones of Villa Mónica Formation showed consistent values from –2 to 2.6‰ (Gómez Peral et al. 2017) and $\delta^{18}O$ values vary from –2 to –6‰. Dolostones immediately above a subtle diamictite level show the lowest $\delta^{13}C$ value. $^{87}Sr/^{86}Sr$ values are ~0.7069. The clear positive trend of $\delta^{13}C$ was considered to suggest this unit as a cap dolostone (Fig. 19.4b; Gómez Peral et al. 2017). In addition, low Sr content in was associated with precipitation influenced by fresh water (Brand and Veizer 1981; Veizer 1983), Mn/Sr ratios <6 and Rb/Sr <0.002 (Gómez Peral et al. 2017).

The Loma Negra Formation, composed almost exclusively of micritic limestones, shows constant positive values of $\delta^{13}C$ ranging between 2.2 and 4.5‰ (Fig. 19.4b), $\delta^{18}O$ values varying from –8 to –14‰, and $^{87}Sr/^{86}Sr$ values from 0.7070 to 0.7082. The later uplift of the succession in relation to the implantation of the karstic surface on top of the sequence was related to a regional sea level fall, later linked to the Gaskiers glacial event (~580 Ma), but no negative $\delta^{13}C$ anomalies have been mentioned to date. The Sr content is ~400 ppm on average and Mn/Sr <1.4 (Gómez Peral et al. 2007) are in agreement with carbonate platforms developed in warmer conditions. In addition, the paleogeographic position of the Río de La Plata Craton suggested by Merdith et al. (2017) between 600 and 560 Ma coincides with a tropical latitude.

19.3.1.5 Post-glacial Events of Phosphogenesis

Two phosphogenic events were recorded in the Neoproterozoic successions of the Tandilia System. The older one occurring just below the cap-dolostone (Upper Villa Mónica Formation) was considered to be Cryogenian based on stromatolite assemblages, carbon isotope trends and strontium isotope abundances of <0.7071 (Gómez Peral et al. 2014a, b). This level (Fig. 19.6a) occurs in the contact between the lower and upper sections of the Villa Mónica Formation, where phosphate concretions are interbedded with iron-rich shales (Gómez Peral et al. 2014a, b).

The later event of phosphogenesis was over the karstic Barker surface and was Ediacaran in age (Gómez Peral et al. 2014a, b). This phosphate horizon is at the base of the Avellaneda Formation and is composed of phosphate and chert concretions in either a laminated shale or mudstone matrix (Fig. 19.6b; Gómez Peral et al. 2014a, b). This level was first recognized by Leanza and Hugo (1987), who interpreted it as the filling of a channelized paleosurface resulting from sea-level regression.

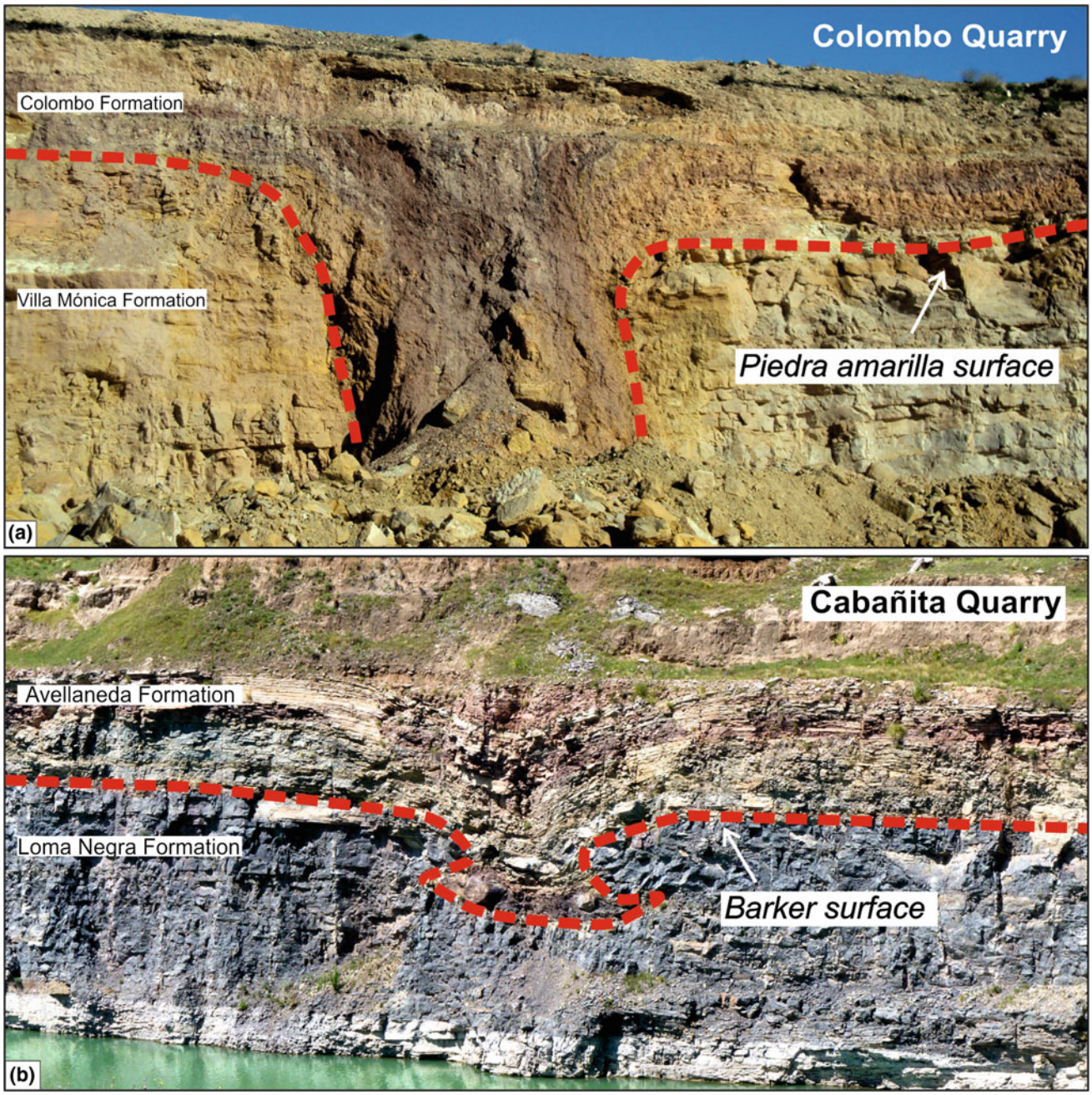

Fig. 19.5 Field photographs. **a** Piedra Amarilla karstic surface in the Colombo Quarry, Olavarría, Argentina. **b** Barker karstic surface in the Polcecal Quarry (Olavarría)

These two levels have been suggested as the result of events of generalized phosphogenesis related to relative sea-level fall and exposure in response to glacial eustacy. The reported oxic seawater conditions where phosphate was concentrated in the Neoproterozoic Tandilia System were markedly different for both levels. The Villa Mónica phosphates was related to stratified ocean under reducer conditions, while the Avellaneda level reveals well oxygenated conditions regarding Ce anomalies (Fig. 19.6; Gómez Peral et al. 2014a, b).

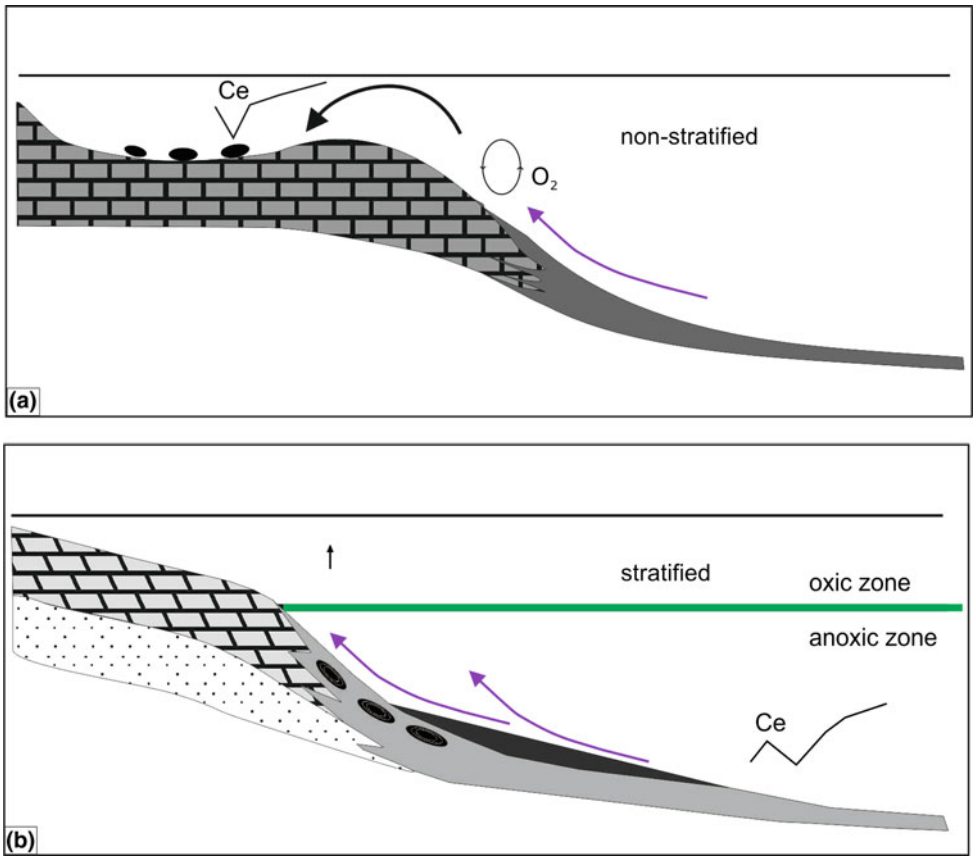

Fig. 19.6 Schematic representation of the two phosphogenesis events in the Tandilia System. **a** Paleoenvironment of the Villa Mónica phosphate level with a stratified basin (positive Ce anomaly). **b** Paleoenvironment scheme of the Avellaneda phosphate level (ex Cerro Negro Formation) with well-mixed ocean and normal circulation of oxygen (negative Ce anomaly) (modified from Gómez Peral et al. 2014a, b)

19.4 Other Examples of Tillites, Phantom Glacial Deposits and Indeterminate Diamictites in South America

Besides the above mentioned glacial deposits of the Puga and Serra Azul formations in the Northern Paraguay Belt, and the Santa Cruz Formation in the Southern Paraguay Belt, other Neoproterozoic tillites were referred to in South America (Fig. 19.7). In the Nico Perez Terrane, Uruguay, the diamictites of the Playa Hermosa Formation show the presence of glacial deposits as was suggested by Pazos et al. (2003). Meanwhile the contemporaneous Las Ventanas Formation in the same terrane seems to be associated with rift deposits below the Arroyo del Soldado Group (Blanco and Gaucher 2005, 2014) or above the Mina Verdún Group (Poiré et al. 2005; Poiré 2014) (Fig. 19.7).

Other regions of Brazil show different types of diamictite. For instance, the origin of the Puga Formation conglomerates in its type locality seems to be related to a tectonic event, as previously mentioned (Boggiani 1998; Gaucher et al. 2003) (Fig. 19.7). The Tamengo Formation of the Corumbá Group (Boggiani 1998; Gaucher et al. 2003; Boggiani et al. 2010) bearing *Cloudina* and *Corumbella* fossils associated with volcanic ash levels at the top, which yielded a U-Pb SHRIMP age of 543 ± 2 Ma (Babinski et al. 2008), is another good example of the Phantom glacial model. Over the Tamengo Formation limestones, the shales of the Guaicurus Formation have been correlated with the regional karstic "Barker surface" (Poiré et al. 2007; Poiré and Gaucher 2009b). The Itapucumí Group in Paraguay (Fig. 19.7) also reflects a Phantom glacial model because there are no tillites in the siliciclastic units below the limestones and the upper limestones are perfectly correlated with the Tamengo Formation (Warren 2011; Warren et al. 2011, 2012). The Tucavaca Group in Bolivia near Corumbá suggests the same environmental conditions during its sedimentation (Fig. 19.7).

The Bambuí and Una groups (São Francisco Supergroup) in Brazil are formed by carbonate and siliciclastic successions, with some diamictites overlaid by limestones. However, the glacial origin of these diamictites is still under discussion (Kaufman et al. 2009; Warren et al. 2014; Sial et al. 2016 and references therein).

In Argentina the Colombo Formation in the Río de la Plata Craton constitutes a dubious diamictite deposit considering its origin, but this needs further detailed analysis to understand the depositional processes during its sedimentation (Fig. 19.7). In the Sierras Pampeanas terrane, some limestones and marls are interpreted as Phantom glacial

Glacial (tillites)	Phantom glacial deposits	Undefined, dubious or tectonic diamictites
Santa Cruz Formation Southern Paraguay Belt	Villa Mónica Formation Rio de la Plata Craton	Puga Formation Southern Paraguay Belt
Puga Formation Northern Paraguay Belt	Loma Negra/Avellaneda Formations Río de la Plata Craton	Las Ventanas Formation Nico Pérez Terrane
Serra Azul Formation Northern Paraguay Belt	Sierra de Ancasti metacarbonates Sierras Pampeanas Terrane	Colombo Formation Río de la Plata Craton
Playa Hermosa Formation Nico Pérez Terrane	Difunta Correa marbles Sierras Pampeanas Terrane	Bambui Group San Francisco Craton
	Tamengo Formation Souther Paraguay Belt	Una Group San Francisco Craton
	Itapucumí Group Paraguay	
	Tucavaca Group Bolivia	

Fig. 19.7 Compilation of glacial, phantom glacial deposits and undefined, dubious or tectonic conglomerates in South America

deposits because there are no diamictites below the carbonate levels ("pseudo-cap carbonate"). The metacarbonates of La Calera Quarry in the Ancasti Range (Murra et al. 2011, 2016) is one example of Phantom glacial deposits, with $^{87}Sr/^{86}Sr$ ratios of 0.70831–0.70860 and 0.70747–0.70781, and values of C and O in three samples of $\delta^{13}C_{PDB} \sim 8.36$ to 9.05‰, $\delta^{18}O_{SMOW} \sim 19.37$ to 22.23‰ (Murra et al. 2011). According to Murra et al., these carbonates are post-Marinoan in age. A similar consideration was proposed by Galindo et al. (2004) for the Difunta Correa marbles in Córdoba Province in the same Sierras Pampeanas terrane (Fig. 19.7).

19.5 Discussion and Conclusions

In this chapter we focus on a comparison between Snowball Earth and Phantom glacial scenarios represented in different successions of South America. Regarding different evidence of glaciations in the Neoproterozoic successions, we choose the Puga and Serra Azul formations in the Paraguay Belt, Amazonia Craton, and the Sierras Bayas Group in the Río de la Plata Craton in order to compare the two models, also related to their different paleolatitudinal position.

The Snowball Earth hypothesis (Hoffman et al. 1998) proposes that Neoproterozoic tillite deposits are recorded as the product of regional glaciations around the world. However, in the Río de La Plata Craton, contemporaneous successions are related to sedimentation in non-glacial environments or Phantom glacial (Cozzi et al. 2002; Poiré 2004).

The Snowball Earth context is well represented by some units of undoubted glaciogenic origin such as the Puga and Serra Azul formations in Northern Paraguay Belt (Brazil) that were related to Marinoan (~635 Ma) and Gaskiers (~580 Ma) glacial events.

On the other hand, the Phantom glacial context is characterized by the successions of the Tandilia System (Argentina) related to a tropical paleogeographic position for this time interval and even older (Cryogenian), in which indirect evidence of those glaciations is also postulated.

Although no tillites were recorded in the Río de La Plata Craton (Argentina), synglacial sea level falls represented by two main karstic discordances over carbonate platforms, the Piedra Amarilla and Barker Surfaces, are considered to be a response of seawater cooling in a distant position with respect to the ice cover.

Conversely, cap-carbonates are defined as deposited over glacial diamictites (Mirasol d´Oeste Fm, Paraguay Belt, Brazil), but a "cap-dolostone" was also referred to (Upper Villa Mónica Formation) by the isotopic trends, Sr content, direct dolomicrite precipitation and tubestone stromatolitic

morphologies related to deglacial meltwater environmental conditions (Gómez Peral et al. 2017). A Cryogenian phosphogenic event reported in the Neoproterozoic successions of the Tandilia System, associated with a very discrete level of mudstones with dropstones (Fig. 19.6, Lower Villa Mónica Formation; Gómez Peral et al. 2014a, b) of age ~710 Ma, is postulated as another indirect piece of evidence of the influence of the Sturtian glaciation.

The Barker surface (Fig. 19.5b) on top of the carbonates of the Loma Negra Formation was correlated with others in SW-Gondwana in Uruguay, Brazil, South Africa and Namibia, and related tentatively to the Gaskiers glaciation (Poiré et al. 2007; Gaucher and Poiré 2009b). These micritic limestones show constant positive values of $\delta^{13}C$ ranging between 2.2 and 4.5‰ and $^{87}Sr/^{86}Sr$ from 0.7070 to 0.7082 (Gómez Peral et al. 2007). Later uplift drive in subaerial exposure and meteoric diagenesis in relation to the implantation of the karstic surface on top of the sequence that was also linked to the Gaskiers glacial event (~580 Ma). However, no negative $\delta^{13}C$ anomalies have been mentioned to date. The age of this karst in association with the Ediacaran phosphogenesis event (Fig. 19.6b; Gómez Peral et al. 2014a, b) is supported by the presence of *Aspidella* in the overlying succession (Arrouy et al. 2016).

The two phosphate levels were suggested as being the result of events of generalized phosphogenesis related to relative sea-level fall and exposure in response to glacial eustacy.

Finally, we consider that multiproxy analysis allows the identification of changes in paleoclimate conditions in both cases. In one case, the presence of tillites is considered irrefutable evidence of glaciation particularly when a cap-carbonate is involved, but in the other model the development of regional karstic unconformities related to drastic sea level falls and associated phosphogenesis and trends in $\delta^{13}C$ constitute indirect evidence of the influence of a Phantom glacial during their deposition, under a less extreme climate context.

References

Alvarenga CJS et al (2004) C-O-Sr isotopic stratigraphy of cap carbonates overlying Marinoan-age glacial diamictites in the Paraguay, Brazil. Precambrian Res 131:1–21

Alvarenga CJS et al (2007) Glacial diamictites of Serra Azul Formation (Ediacaran, Paraguay belt): Evidence of the Gaskiers glacial event in Brazil. J South Am Earth Sci 23:236–241

Alvarenga CJS et al (2009) The amazonian palaeocontinent. In: Gaucher C et al (eds) Neoproterozoic-Cambrian Tectonics, global change and evolution: a focus on Southwestern Gondwana. Developments in Precambrian Geology, vol 16. Elsevier, pp 15–28

de Alvarenga CJS, Trompette R (1992) Glacial influenced turbidite sedimentation in the uppermost Proterozoic and Lower Cambrian of the Paraguay belt (Mato Grosso, Brazil). Palaeogeogr Palaeoclimatol Palaeoecol 92:85–105

Alvarenga CJS, Boggiani PC, Babinski M, Dardenne MA, Figueiredo MF, Dantas EL, Uhlein A, Santos RV, Sial AN, Trompette R (2011) Glacially infuenced sedimentation of the Puga Formation, Cuiabá Group and Jacadigo Group, and associates carbonates of the Araras and Corumbá groups, Paraguay Belt, Brazil. In: Arnaud E, Halverson GP, Shields-Zhou G (eds) The Geologiacal Record of Neoproterozoic Glaciations, vol 36. Geological Society, London, Memoirs, pp 487–497

Alvarenga CJS, Dardenne MA, Santos RV, Brod ER, Gioia SMCL, Sial AN, Dantas EL, Ferreira VP (2008) Isotope stratigraphy of Neoproterozoic cap carbonates in the Araras Group, Brazil. Gondwana Res 13:469–479

Arrouy MJ (2015) Sedimentología y estratigrafía de los depósitos ediacareano-paleozoicos suprayacentes a las calizas del precámbrico del Sistema de Tandilia, provincia de Buenos Aires, Argentina. Tesis doctoral, Facultad de Ciencias Naturales y Museo, Universidad Nacional de La Plata, pp 285 (online SEDICI-UNLP)

Arrouy MJ et al (2015) Sedimentología y estratigrafía del grupo La Providencia (Nom. Nov.): Cubierta Neoproterozoica, Sistema de Tandilia, Argentina. Lat Am J Sedimentol Basin Anal 22(2):1–38

Arrouy MJ et al (2016) Ediacaran discs from South America: probable soft-bodied macrofossils unlock the paleogeography of the Clymene Ocean. Sci Rep 6(30590):1–10. https://doi.org/10.1038/srep30590

Babinski M et al (2013) Detrital zircon ages and geochronological constraints on the Neoproterozoic Pugadiamictites and associated BIFs in the southern Paraguay Belt, Brazil. Gondwana Res 23:988–997

Babinski M, Boggiani PC, Fanning CM, Fairchild TR, Simon CM, Sial AN (2008) On isotope geology U-Pb SHRIMP geochronology and isotope chemostratigraphy (C, O, Sr) of the Tamengo Formation, Southern Paraguay Belt, Brazil. In: Linares E, Caballeri NG, do Campo MD, Ducós EI, Panarello HO (eds) Proceedings of VI South American Symposium. CDROM, Buenos Aires

Barrio C et al (1991) El contacto entre la Formación Loma Negra (Grupo Sierras Bayas) y la Formación Cerro Negro, un ejemplo de paleokarst, Olavarría, provincia de Buenos Aires. Revista de la Asociación Geológica Argentina 46:69–76

Blanco G, Gaucher C (2005) Estratigrafa, paleontologia y edad de la Formacion Las Ventanas (Neoproterozoico, Uruguay). Latin American J Sedimentol Basin Anal 12(2):109–124

Blanco G, Gaucher C (2014) Formación Las Ventanas. In: Bossi J, Gaucher C (eds) Geología del Uruguay. Tomo 1. Predevónico. Polo, Montevideo, pp 299–312

Boggiani PC (1998) Analise estratigráfica da Bacia Corumba (Neoproterozoíco), Mato Grosso do Sul. Unpublished PhD thesis, University of Sao Paulo, Brazil, pp 181

Boggiani PC et al (2004) New level of diamictites in the Corumbá Group (Ediacaran), Paraguay belt, South America. Symposium on Neoproterozoic-Early Paleozoic Events in SW-Gondwana, 1, Extended Abstracts, IGCP Project 478, Second Meeting, Brazil, pp 10–12

Boggiani PC, Gaucher C, Sial AN, Babinski M, Simon CM, Riccomini C, Ferreira VP, Fairchild TR (2010) Chemostratigraphy of the Tamengo Formation (Corumbá Group, Brazil): a contribution to the calibration of the Ediacaran carbon isotope curve. Precambrian Res 182:382–401

Brand U, Veizer J (1981) Chemical diagenesis of multicomponent carbonate system: Stable isotopes. J Sediment Petrol 51:987–997

Cingolani CA, Dalla Salda L (2000) Buenos Aires cratonic region. In: Cordani U et al (eds) Tectonic evolution of South America. Proceedings 31st International Geological Congress, Río de Janeiro, pp 139–146

Cingolani CA et al (2002) U-Pb SHRIMP dating of zircons from the Buenos Aires complex of the Tandilia belt, Río de La Plata cratón, Argentina. 15 Congreso Geológico Argentino (El Calafate, Santa Cruz). Actas 1:149–154

Cingolani C (2011) The Tandilia System of Argentina as a southern extension of the Río de la Plata craton: An overview. Int J Earth Sci 100:221–242

Condon DJ et al (2002) Neoproterozoic glacial-rainout intervals: observations and implications. Geology 30:35–38

Cozzi A et al (2002) Last gasp of "snowball Earth"? 2 A "phantom" glacial from the Late Neoroterozoic Shuram Formation of Oman. 16 International Sedimentological Congress, Abstracts, pp 68–69

Figueiredo MF (2006) Quimioestratigrafia das rochas ediacaranas no extremo norte da Faixa Paraguai, Mato Grosso. Unpublished dissertação de Mestrado, Instituto de Geociências, Universidade de São Paulo, Brazil

Galindo C et al (2004) Sr, Cand O isotope geochemistry and stratigraphy of Precambrian and lower Paleozoic carbonate sequences from the Western Sierras Pampeanas of Argentina: Tectonic implications. Precambr Res 131:55–71

Gaucher C, Finney SC, Poiré DG, Valencia VA, Grove M, Blanco G, Pamoukaghlián K, Gómez Peral L (2008) Detrital zircon ages of Neoproterozoic sedimentary successions in Uruguay and Argentina: insights into the geological evolution of the Río de la Plata Craton. Precambrian Res 167:150–170

Gaucher C, Poiré DG (2009a) Biostratigraphy. Neoproterozoic-Cambrian evolution of the Río de la Plata Palaeocontinent. In: Gaucher C et al (eds) Neoproterozoic–Cambrian Tectonics, Global change and evolution: a focus on Southwestern Gondwana. Developments in Precambrian Geology, vol 16. Elsevier, pp 103–114

Gaucher C, Poiré DG (2009b) Palaeoclimatic events. Neoproterozoic-Cambrian evolution of the Río de la Plata Palaeocontinent. In: Gaucher C et al (eds) Neoproterozoic–Cambrian tectonics, Global change and evolution: a focus on Southwestern Gondwana. Developments in Precambrian Geology, vol 16. Elsevier, pp 123–130

Gaucher C et al (2003) Integrated correlation of Vendian to Cambrian Arroyo del Soldado and Corumbá Groups (Uruguay and Brazil): Palaeogeographic, palaeoclimatic and palaeobiologic implications. Precambr Res 120:241–278

Gaucher C et al (2005) Litoestratigrafía, bioestratigrafía y correlaciones de las sucesiones sedimentarias del Neoproterozoico-Cámbrico del Cratón del Río de La Plata (Uruguay y Argentina). Lat Am J Sedimentol Basin Anal 12(2):145–160

Gaucher C et al (2009) Chemostratigraphy. Neoproterozoic–Cambrian evolution of the Río de la Plata Palaeocontinent. In: Gaucher C et al. (eds) Neoproterozoic–Cambrian tectonics, global change and evolution: a focus on Southwestern Gondwana. Developments in Precambrian Geology, vol 16. Elsevier, pp 115–122

Germs GJB, Gaucher C (2012) Nature and extent of a late Ediacaran (ca. 547 Ma) glacigenic erosion surface in southern Africa. South African J Geol 115:91–102

Gómez-Peral LE (2008) Petrología y diagénesis de las unidades sedimentarias precámbricas de Olavarría, Provincia de Buenos Aires. Tesis doctoral, Facultad de Ciencias Naturales y Museo, Universidad Nacional de La Plata Tomo I: pp 327 y tomo II: pp 292 (online SEDICI-UNLP)

Gómez-Peral LE, Poiré DG, Strauss H, Zimmermann U (2007) Chemostratigraphy and diagenetic constraints on Neoproterozoic carbonate successions from the Sierras Bayas Group, Tandilia System, Argentina. Chem Geol 237, 127–146

Gómez-Peral LE et al (2011) Petrología y evolución diagenética de las facies silicoclásticas del Grupo Sierras Bayas, Sistema de Tandilia, Argentina. Lat Am J Sedimentol Basin Anal 18(1):3–41

Gómez-Peral LE et al (2012) Isotope stratigraphic evidence for a Neoproterozoic cap-carbonate in Sierras Bayas Group, Tandilia System, Argentina. VIII Simposio Sudamericano de Geología isotópica, 5 al 7 de julio de 2012, Medellín, Colombia, Actas CD

Gómez-Peral LE et al (2014a) Paleoenvironmental implications of two phosphogenic events in Neoproterozoic sedimentary successions of the Tandilia System, Argentina. Precambr Res 252: 88–106

Gómez-Peral LE et al (2014b) Origen y diagénesis del karst del Tope de la Formación Villa Mónica, Sistema de Tandilia, Argentina. Actas XIV Reunión Argentina de Sedimentología, Madryn, 1–5 Septiembre de 2014

Gómez-Peral LE et al (2017) Paleoclimatic and paleoenvironmental evolution of the Early Neoproterozoic basal dolomitic platform, Río de La Plata Craton, Argentina: Insights from the $\delta^{13}C$ chemostratigraphy. Sed Geol 353:139–157

Hartmann LA et al (2002a) Zircon and titanite U-Pb SHRIMP geochronology of Neoproterozoic felsic magmatism on the eastern border of the Rio de la Plata Craton, Uruguay. J South Am Earth Sci 15:229–236

Hartmann LA et al (2002b) Two Paleoproterozoic orogenies in the evolution of the Tandilia Belt, Buenos Aires, as evidenced by zircon U-Pb SHRIMP geochronology. Int Geol Rev 44:528–543

Hoffman PF, Schrag DP (2002) The snowball Earth hypothesis: Testing the limits of global change. Terra Nova 14:129–155

Hoffman PF et al (1998) A Neoproterozoic snowball Earth. Science 281:1342–1346

Hyde WT et al (2000) Neoproterozoic snowball Earth simulations with a coupled climate/ice-sheet model. Nature 405:425–429

Iñiguez AM et al (1989) Cuenca precámbrica-paleozoica inferior de Tandilia, Provincia de Buenos Aires. In: Chebli G, Spalletti LA (eds) Cuencas Sedimentarias Argentinas. Serie Correlación Geológica 6: 245–263

Kaufman AJ et al (2009) Neoproterozoic to Cambrian Palaeoclimatic events in Southwestern Gondwana. In Gaucher C et al (eds) Neoproterozoic-Cambrian tectonics, global change and evolution: a focus on Southwestern Gondwana. Developments in Precambrian Geology, vol 16. Elsevier, Amsterdam, pp 369–388

Kellerhals P, Matter A (2003) Facies analysis of a glaciomarine sequence, the Neoproterozoic Mirbat Sandstone Formation, Sultanate of Oman. Eclogae Geologicae Helvetiae 96:49270

Knoll AH et al (2004) A new period for the geologic time scale. Science 305:621–622

Knoll AH et al (2006) The Ediacaran period: a new addition to the geologic time scale. Lethaia 39:13–30

Leanza HA, y Hugo CA (1987) Descubrimiento de fosforitas sedimentarias en el Proterozoico superior de Tandilia, Buenos Aires, Argentina. Revista Asociación Geológica Argentina 42(3–4): 417–428

Lewis JP et al (2007) Snowball versus slushball Earth: dynamic versus nondynamic sea ice? J Geophys Res112(C11)

Maciel P (1959) Tilito Cambriano (?) no Estado de Mato Grosso. Boletim da Sociedade Brasileira de Geologia 81(1):31–39

McMechan ME (2000) Neoproterozoic glaciogenic slope deposits, Rocky Mountains, northeast British Columbia. Bull Can Pet Geol 48:2462261

Marchese HG, Di Paola E (1975) Miogeosinclinal Tandil. Revista de la Asociación Geológica Argentina 30(2):161–179

Martínez JC et al (2010) A hydrothermal clay mineral assemblage at the Late Proterozoic unconformity in the Buenos Aires Complex—La Tinta Formation, Barker area, Tandilia Ranges (Argentina). Clays Minerals 45:209–224

Martínez JC et al (2013) Late-Neoproterozoic hidrotermal fluid activity in the Tandilia Belt, Agentina. Revista de la Asociación Geológica Argentina 70(3):410–426

Merdith AS et al (2017) A full-plate global reconstruction of the Neoproterozoic. Gondwana Res. https://doi.org/10.1016/j.gr.2017.04

Micheels A, Montenari M (2008) A snowball Earth versus a slushball Earth: Results from Neoproterozoic climate modeling sensitivity experiments. Geosphere 4(2):401–410

Murra JA et al (2011) Sr, C and O isotope composition of marbles from the Sierra de Ancasti, Eastern Sierras Pampeanas, Argentina: age and constraints for the Neoproterozoic-Lower Paleozoic evolution of the proto-Gondwana margin. Geological Acta 9:79–92

Murra JA et al (2016) Isotope (Sr, C) and U-Pb SHRIMP zircon geochronology of marble-bearing sedimentary series in the Eastern Sierras Pampeanas, Argentina. Constraining the SW Gondwana margin in Ediacaran to early Cambrian times. Precambr Res 181:602–617

Nogueira ACR, Riccomini C (2006) O Grupo Araras (Neoproterozoico) na parte norte da Faixa Paraguai e sul do Craton Amazônico, Brazil. Revista Brasileira de Geociências 36(4):623–640

Nogueira ACR et al (2003) Soft-sediment deformation at the base of the Neoproterozoic Puga cap carbonate (Southwestern Amazon Craton, Brazil): confirmation of rapid icehouse to greenhouse transition in Snowball Earth. Geology 31:613–616

Nogueira ACR et al (2007) Carbon and strontium isotope fluctuations and paleoceanographic changes in the late Neoproterozoic Araras carbonate platform, Southern Amazon Craton, Brazil. Chem Geol 237:168–190

Pankhurst RJ et al (2003) Antiquity of the Río de la Plata craton in Tandilia, southern Buenos Aires province, Argentina. J S Am Earth Sci 16:5–13

Pazos PJ et al (2003) The Record of the Varanger Glaciation at Río de la Plata Craton. Vendian-Cambrian of Uruguay. Gondwana Research 6(1):65–78

Pinho FEC et al (2003) Contribution to the Neoproterozoic C and O isotopic record: Carbonate rocks from the Paraguay Belt, Mato Grosso, Brazil, vol 1. In: IV South American symposium on isotope geology, Salvador, Brasil, Short Papers, pp 386–389

Poiré DG (1987) Mineralogía y sedimentología de la Formación Sierras Bayas en el Núcleo Septentrional de las sierras homónimas, partido de Olavarría, provincia de Buenos Aires. Unpublished PhD thesis 494, Facultad de Ciencias Naturales y Museo, Universidad Nacional de La Plata pp 27

Poiré DG (2004) Sedimentary history of the Neoproterozoic of Olavarría, Tandilia System, Argentina: new evidence from their sedimentary sequences and unconformities: a "snowball Earth" or a "phantom" glacial? 1º Symposium on Neoproterozoic-Early Paleozoic Events in SW-Gondwana.Extended Abstract: 46–48, San Pablo, Brasil.

Poiré DG (1989) Stromatolites of the Sierras Bayas Group, Upper Proterozoic of Olavarría, Sierras Septentrionales, Argentina. Stromatolite Newsl 11:58–61

Poiré DG (1993) Estratigrafía del Precámbrico sedimentario de Olavaría, Sierras Bayas, Provincia de Buenos Aires, Argentina. XII Congreso Geológico Argentino y II Congreso de Exploración de Hidrocarburos Actas II:1–11

Poiré DG (2002) The Precambrian/lower Paleozoic sedimentary cover of Tandilia System, Argentina. In: Gaucher C, Poiré DG (eds) II International Colloquium Vendian-Cambrian of W. Gondwana, field trip guide. Facultad de Ciencias-UNESCO, Montevideo, pp 55–66

Poiré DG (2014) Grupo Mina Verdún, In Bossi, J., Gaucher, C. (eds) Geología del Uruguay. Tomo 1: Predevónico, Montevideo, Polo, pp 233–251

Poiré DG, Gaucher C (2007) Lithostratigraphy and correlations of two Neoproterozoic basins from the Río de la Plata Craton, SW-Gondwana. In: III Symposium on neoproterozoic-early palaeozoic events in Southwestern Gondwana, Programme and Short Papers, Stellenbosch, pp 23–27

Poiré DG, Gaucher C (2009) Lithostratigraphy. Neoproterozoic-Cambrian evolution of the Río de la Plata Palaeocontinent. In: Gaucher C et al (eds) Neoproterozoic–cambrian tectonics, global change and evolution: a focus on Southwestern Gondwana. Developments in Precambrian Geology, vol 16, pp 87–101

Poiré, D.G., Spalletti, L.A. (2005) La cubierta sedimentaria precámbrica/paleozoica inferior del Sistema de Tandilia. In De Barrio, R.E. et al. (eds) Geología y Recursos Minerales de la provincia de Buenos Aires. Relatorio del XVI Congreso Geológico Argentino, 51–68. La Plata

Poiré DG et al (2003) The Cambrian-Ordovician siliciclastic platform of the Balcarce Formation (Tandilia System, Argentina): Facies, trace fossils, palaeoenvironments and sequence stratigraphy. Geologica Acta 1:41260

Poiré DG et al (2005) Estratigrafía del Grupo Mina Verdún, Precámbrico de Minas, Uruguay. Lat Am J Sedimentol Basin Anal 12(2):125–143

Poiré DG et al (2007) La superficie 'Barker' y su importancia regional, Neoproterozoico del Cratón del Río de La Plata. VI Jornadas Geológicas y Geofísicas Bonaerenses. Actas 36. Mar del Plata, Argentina

Praekelt HE, Germs GJB, Kennedy JH (2008) A distinct unconformity in the Cango Caves Group of the Neoproterozoic to early Paleozoic Saldania Belt in South Africa: its regional significance. South African J Geol 111:357–368

Rapalini AE et al (2013) The La Tinta pole revisited: Paleomagnetism of the Neoproterozoic Sierras Bayas Group (Argentina) and its implications for Gondwana and Rodinia. Precambr Res 224:51–70

Rapela CW et al (2007) The Río de la Plata Craton and the assembly of SW Gondwana. Earth-Sci Rev 83:49–82

Rapela CW et al (2011) The Rio de la Plata craton and the adjoining Pan-African/brasiliano terranes: their origins and incorporation into south-west Gondwana. Gondwana Res 20:673–690

Rapela CW, Verdecchia SO, Casquet C, Pankhurst RJ, Baldo EG, Galindo C, Murra JA, Dahlquist JA, Fanning CM (2016) Identifying Laurentian and SW Gondwana sources in the Neoproterozoic to Early Paleozoic metasedimentary rocks of the Sierras Pampeanas: Paleogeographic and tectonic implications. Gondwana Res 32:193–212

Riccomini C et al (2007) Carbon and oxygen isotope geochemistry of Ediacaran outer platform carbonates, Paraguay Belt, central Brazil. An Acad Bras Ciênc 79(3):519–527

Santos HP et al (2017) Ichnologic evidence of a Cambrian age in the southern Amazon Craton: Implications for the onset of the Western Gondwana history. J S Am Earth Sci 76:482–488

Sial AN et al (2016) Correlations of some Neoproterozoic carbonate-dominated successions in South America based on high-resolution chemostratigraphy. Braz J Geology 46(3):439–488

Silva-Tamayo JC et al (2010a) Global Ca isotope variations in c. 0.7 Ga old post-glacial carbonate successions. In: Karhu J et al (eds) Precambrian Isotope Stratigraphy, vol 182. Special issue. Precambrian Research, pp 373–381

Silva-Tamayo JC et al (2010) Global Ca isotope variations in Post-Sturtian carbonate successions. Terra Nova 22:188–194

Sohl LE, Chandler MA (2007) Reconstructing Neoproterozoic palaeoclimates using a combined data/modelling approach. In: Williams M et al (eds) Deep-time perspectives on climate change: marrying the signal from computer models and biological proxies. The Micropalaeontological Society, Special Publications. The Geological Society, London, pp 61–80

Souza JO et al (2012) Projeto Planalto da Serra. Estado de Mato Grosso, Programa Geologia do Brasil, CPRM, Goiânia, p 105

Souza SCR (2015) Detalhamento Estratigráfico das Unidades superiores do Neoproterozóico da Faixa Paraguai. Unpublished MSc thesis, Instituto de Geociências, Universidade de Brasília, Brazil

Trindade RIF et al (2003) Low-latitude and multiple geomagnetic reversals in the Neoproterozoic Puga cap carbonate of Amazonia. Terra Nova 15:441–446

Trompette R et al (1998) Geological evolution of the Neoproterozoic Corumbágraben system (Brazil). Depositional context of the stratified Fe and Mn ores of the Jacadigo Group. J S Am Earth Sci 11:587–597

Veizer J (1983) Chemical Diagenesis of carbonates: theory and application of trace element technique. Stable Isotopes in Sedimentary Geology. S.E.P.M. Short Course 10(3–1): 3–100

Waggoner B (2003) The Ediacaran biotas in space and time. Integr Comp Biol 43:104–113

Warren LV (2011) Tectônica e sedimentação do Grupo Itapucumi (Neoproterozóico, Paraguai Setentrional. Unpublished doctoral thesis, Institute of Geosciences, University of São Paulo, São Paulo, pp 215

Warren LV et al (2011) Corumbella and in situ Cloudina in association with thrombolites in the Ediacaran Itapucumi Group, Paraguay. Terra Nova 23:382–389

Warren LV et al (2012) The dawn of animal skeletogenesis: ultrastructural analysis of the Ediacaran metazoan Corumbella werneri. Geology 40:691–694

Warren LV et al (2014) The puzzle assembled: Ediacaran guide fossil Cloudina reveals an old proto-Gondwana seaway. Geology 42:391–394

Zimmermann U et al (2011) Neoproterozoic to Lower Palaezoic successions of Tandilia system in Argentina: implication for the palaeotectonic framework of southwest Gondwana. Int J Earth Sci 100:489–510

The Ediacaran-Early Cambrian Fossil Record in Southwest Gondwana

20

Claudio Gaucher

Abstract

A review of the Ediacaran-Early Cambrian fossil record in SW Gondwana is presented. Organic-walled microfossils (acritarchs) reported from the region can be assigned for the most part to the Late Ediacaran Leiosphere Palynoflora (LELP), with only a few occurrences of lower Ediacaran acritarchs. So far, complex acanthomorphs (ECAP assemblage) are absent in fossil-bearing units of lower to mid-Ediacaran age, which may be the result of an adverse paleoclimate. The Ediacara soft-bodied biota is best recorded in the Nama Group, with occurrences recently reported in South America. Biostratigraphically, soft-bodied fossils are best assigned to the latest Ediacaran Nama Association. Ediacaran shelly fossils are widespread in SW Gondwana, including biostratigraphically relevant genera such as *Cloudina*, *Namacalathus*, *Corumbella* and *Titanotheca*. The only group with a record across the Ediacaran–Cambrian boundary are trace fossils. Whereas simple, mostly bedding-parallel burrows and biomat structures occur in Ediacaran "matgrounds," diverse vertical bioturbations characterize Early Cambrian "mixgrounds." Ediacaran fossils can be useful for biostratigraphy. The early and Mid-Ediacaran are best zoned using acritarchs, the Late Ediacaran with shelly fossils and the Ediacaran–Cambrian boundary can be determined using trace fossils. Biostratigraphy, in turn, enables the correlation of distant sedimentary successions, which may have paleogeographic implications. Ediacaran paleobiogeography, on the other hand, is hampered by the cosmopolitan nature of most taxa found in SW Gondwana.

Keywords

Acritarchs • Shelly fossils • Ediacara biota
Cambrian explosion • Biostratigraphy

C. Gaucher (✉)
Facultad de Ciencias, Instituto de Ciencias Geológicas, Universidad de La República, Iguá 4225, 11400 Montevideo, Uruguay
e-mail: gaucher@chasque.net

20.1 Introduction

SW-Gondwana includes several sedimentary successions of predominantly Late Ediacaran age (Figs. 20.1 and 20.2), which preserve a rich fossil record. Early studies of these fossils include in southern Africa the reports by Gürich (1930, 1933) of vendobionts (*Pteridinium*, *Rangea*), which were some of the first descriptions of Ediacaran soft-bodied fossils.

In South America, Beurlen and Sommer (1957) described the first skeletal fossils from Precambrian rocks, although they were assigned a Cambrian age. Later, Germs (1972a, b) erected the genus *Cloudina* and accepted a Neoproterozoic age for the fossils, representing the first Precambrian skeletal fossils to be described worldwide.

This chapter deals with the latest advances in Ediacaran paleontology and biostratigraphy in southwestern Gondwana. Four main fossil groups will be dealt with: acritarchs, the Ediacara soft-bodied biota, skeletonized metazoans and protists, and trace fossils. Ediacaran-Early Cambrian metaphytes (vendotaenids) also occur in SW Gondwana, but because of the paucity of their record the reader is directed to the few studies dealing with these fossils (Grant et al. 1991; Gaucher et al. 2003; Cohen et al. 2009).

20.2 Acritarchs

Ediacaran acritarchs (i.e., organic-walled microfossils of uncertain affinity) were first described in SW Gondwana from the Nama Group in Namibia (Germs 1972b; Germs et al. 1986) and from the Sierras Bayas Group in Argentina (Pothe de Baldis et al. 1983; Cingolani et al. 1991; Fig. 20.2).

Acritarchs were thereafter reported for other units in the region (Figs. 20.1 and 20.2), such as the Corumbá Group in SW Brazil (Zaine 1991; Gaucher et al. 2003), the Bambuí Group in central Brazil (Fairchild et al. 1996; Sánchez, 2010), the Arroyo del Soldado Group in Uruguay (Gaucher

S. Siegesmund et al. (eds.), *Geology of Southwest Gondwana*, Regional Geology Reviews,
https://doi.org/10.1007/978-3-319-68920-3_20

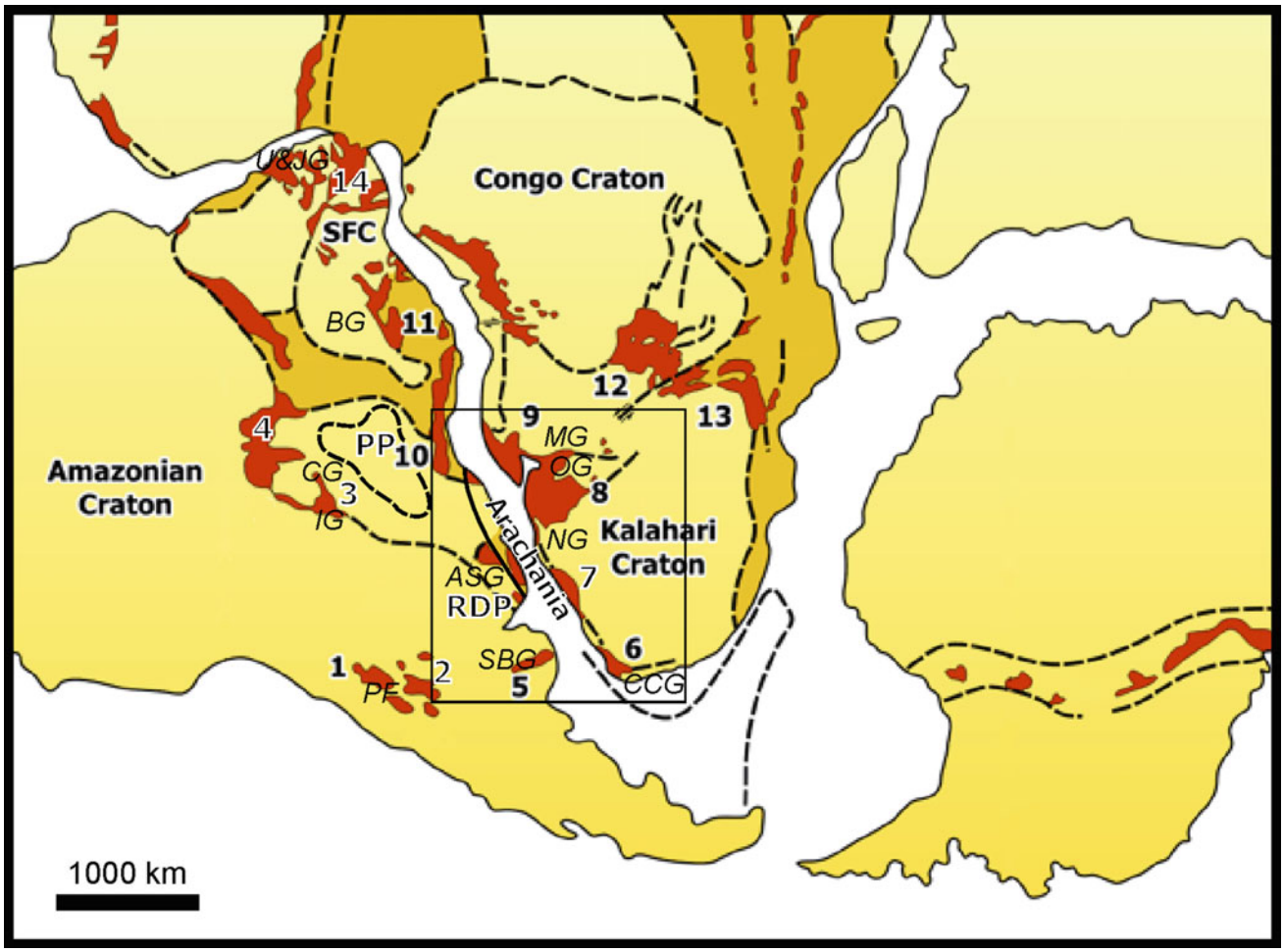

Fig. 20.1 Fossiliferous Ediacaran units indicated on a pre-drift reassembly of Gondwana, modified after Porada (1989). *PP* Paranapanema Craton; *RPC* Río de la Plata Craton; *SFC* São Francisco Craton. Red areas: Neoproterozoic to Early Paleozoic belts. (1) Western Sierras Pampeanas, (2) Eastern Sierras Pampeanas, (3) Southern Paraguay Belt, (4) Northern Paraguay Belt, (5) Tandilia System, (6) Saldania Belt, (7) Gariep Belt, (8) Damara Belt, (9) Kaoko Belt, (10) Ribeira Belt, (11) Aracuaí Belt, (12) Lufilian Belt, (13) Zambezi Belt. Ediacaran fossiliferous units are indicated in italics: *ASG* Arroyo del Soldado Group (and Las Ventanas Formation); *BG* Bambuí Group; *CCG* Cango Caves and Gamtoos groups; *CG* Corumbá Group; *IG* Itapucumí Group; *MG* Mulden Group; *NG* Nama Group; *OG* Otavi Group; *PF* Puncoviscana Formation; *SBG* Sierras Bayas and La Providencia groups; *U&JB* Ubajara and Jaibaras groups. Rectangle: see detail in Fig. 20.2

et al. 1996, 1998, 2003, 2004; Gaucher 2000, 2014; Gaucher and Poiré 2009), the Eleutério-Pico de Itapeva and Pouso Alegre basins (SE Brazil; Teixeira and Gaucher 2004), the Holgat Formation in Namibia (Gaucher et al. 2005b) and the Cango Caves and Gamtoos groups in the Saldania Belt, South Africa (Gaucher and Germs 2006).

More recently, acritarchs were described for the Las Ventanas Formation in Uruguay (Blanco and Gaucher 2005; Gaucher et al. 2008a), the Otavi and Mulden groups in Namibia (Germs et al. 2009), the Alicia Formation of the La Providencia Group in Argentina (Poiré et al. 2010; Arrouy et al. 2015) and the Frecheirinha Formation of the Ubajara Group, NE Brazil (Chiglino et al. 2015; Fig. 20.1).

Early Cambrian acritarchs have not been found in SW Gondwana because the sparse sedimentary record of that age is either continental or very shallow marine, such as the upper Nama Group (Germs 1995) and the upper Arroyo del Soldado Group (Sprechmann et al. 2004). Early Cambrian shales of the Puncoviscana Formation in NW Argentina were deposited in deeper settings, but so far no acritarchs have been found in these strata.

Biostratigraphically, almost all of the known occurrences belong to the "Kotlin-Rovno" assemblage of Vidal and Moczydłowska-Vidal (1997), synonymous with the Late Ediacaran Leiosphere Palynoflora (LELP) of Gaucher and Sprechmann (2009).

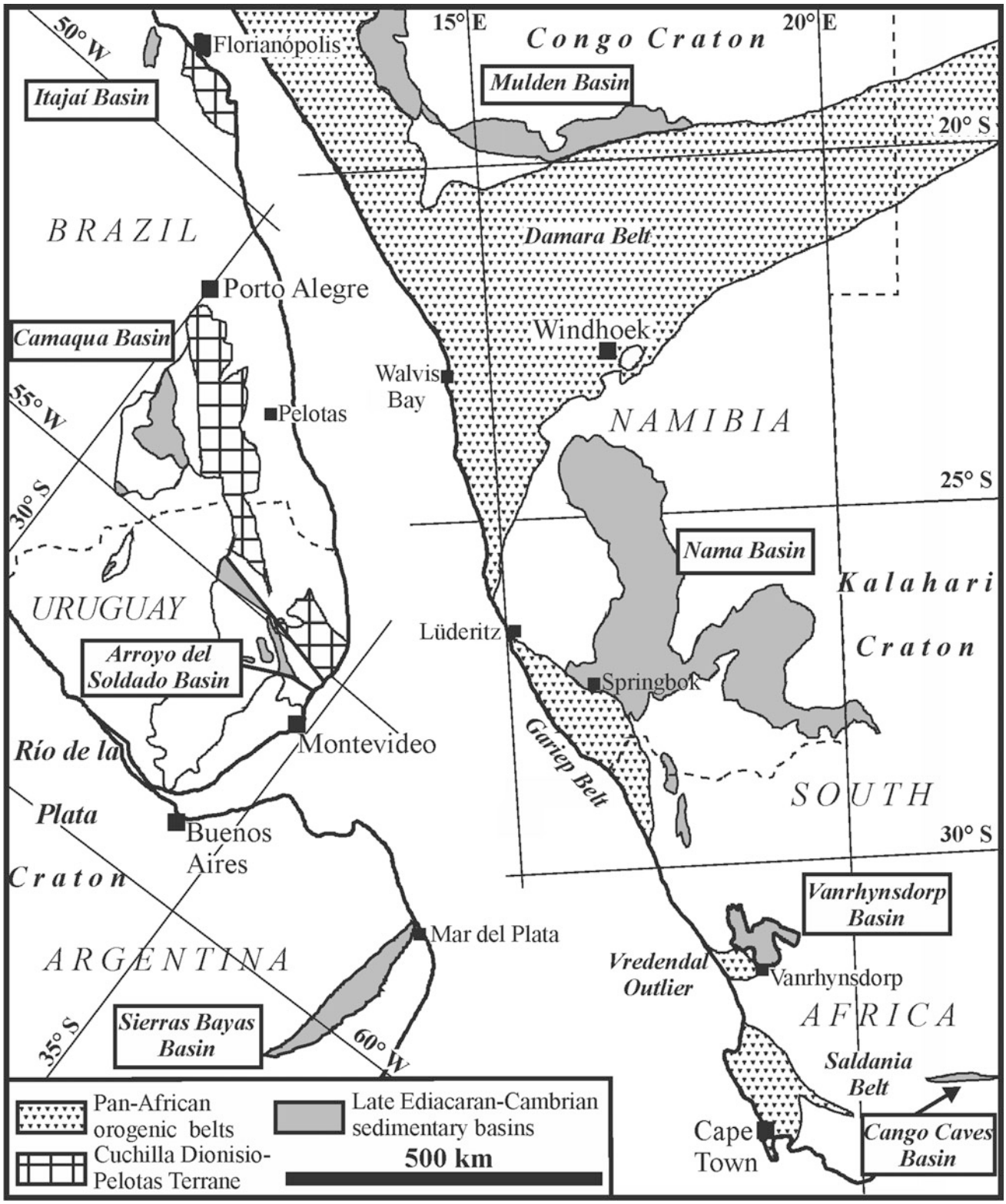

Fig. 20.2 Map showing the location of fossiliferous Ediacaran units dealt with in this work, modified after Gaucher et al. (2005b)

The low-diversity LELP assemblage is dominated by small (<150 μm) and predominantly thin-walled *Leiosphaeridia* (Fig. 20.3c), *Bavlinella faveolata* (Fig. 20.3d, e), colonial microfossils of the genus *Soldadophycus* (Fig. 20.3f), small (<20 μm) acanthomorphs of the genus *Asteridium* (=*Micrhystridium*) and large sphaeromorphs of the genus *Chuaria* (Germs et al. 1986; Steiner 1994).

The LELP represents a depauperate assemblage which characterizes the last 20 myr of the Neoproterozoic (*c*. 560–541 Ma), just before the Cambrian Explosion. It follows an extinction event that wiped out the diverse acritarchs of the Ediacaran Complex Acanthomorph Palynoflora (ECAP; Grey et al. 2003; Grey 2005). Between 75 and 90% of acritarch species became extinct during this event (Vidal and Moczydłowska-Vidal 1997; Knoll et al. 2006), which may have been caused by ocean eutrophication and the exclusion of eukaryotic plankton by massive cyanobacterial blooms (e.g., *Bavlinella faveolata* blooms; Gaucher and Sprechmann 2009).

Interestingly, no occurrences of morphologically complex acanthomorphs belonging to the ECAP have been found so far in SW Gondwana. The ECAP is recorded in Australia (Grey 2005), Baltica (Vorob'eva et al. 2009), in the upper Doushantuo Formation in China (McFadden et al. 2008; Liu et al. 2013; Fig. 20.4) and in Siberia (Moczydłowska 2005), and it probably represents a relatively short period, possibly between the Gaskiers Glaciation (580 Ma; Pu et al. 2016) and *c*. 560 Ma. This entire period is characterized by positive $\delta^{13}C$ values known in the Doushantuo Formation as EP2 excursion (Liu et al. 2013; Fig. 20.4).

Deposition of the rift succession of the Las Ventanas Formation in Uruguay is radiometrically constrained by the U–Pb SHRIMP method between 590 ± 2 Ma for basalts at its base (Mallmann et al. 2007) and 573 ± 11 Ma for volcanoclastics at its top (Oyhantçabal et al. 2009). Glaciogenic diamictites occur near the base of the unit and were assigned to the Gaskiers Glaciation (Gaucher et al. 2008a). Thus the Las Ventanas Formation encompasses the time period in

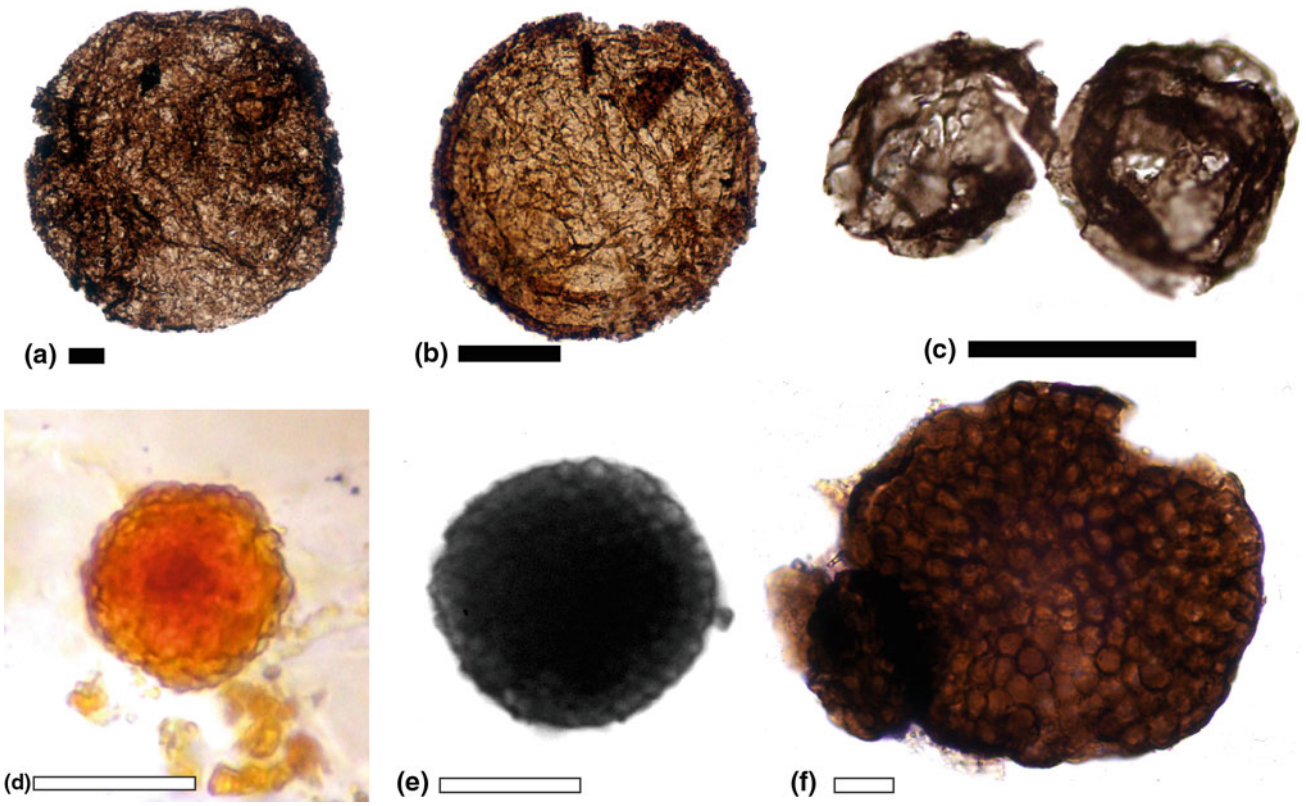

Fig. 20.3 Ediacaran acritarchs from SW Gondwana. **a** *Leiosphaeridia tenuissima*, large specimen from the Villa Mónica Formation, Sierras Bayas Group (Gaucher et al. 2005a). **b** *Leiosphaeridia tenuissima*, Las Ventanas Formation (Gaucher et al. 2008a). **c** *Leiosphaeridia minutissima*, two attached carbonized specimens from the Alicia Formation, La Providencia Group. **d** *Bavlinella faveolata*, thin section from the Yerbal Formation, Arroyo del Soldado Group (Gaucher 2000). **e** *Bavlinella faveolata*, Kombuis Member, Cango Caves Group (Gaucher and Germs 2006). **f** *Soldadophycus bossii*, a saucer-shaped colony attached to a smaller, sphaeroidal colony. Yerbal Formation (Arroyo del Soldado Group; Gaucher et al. 2004). White scale bars represent 10 μm and black scale bars 50 μm

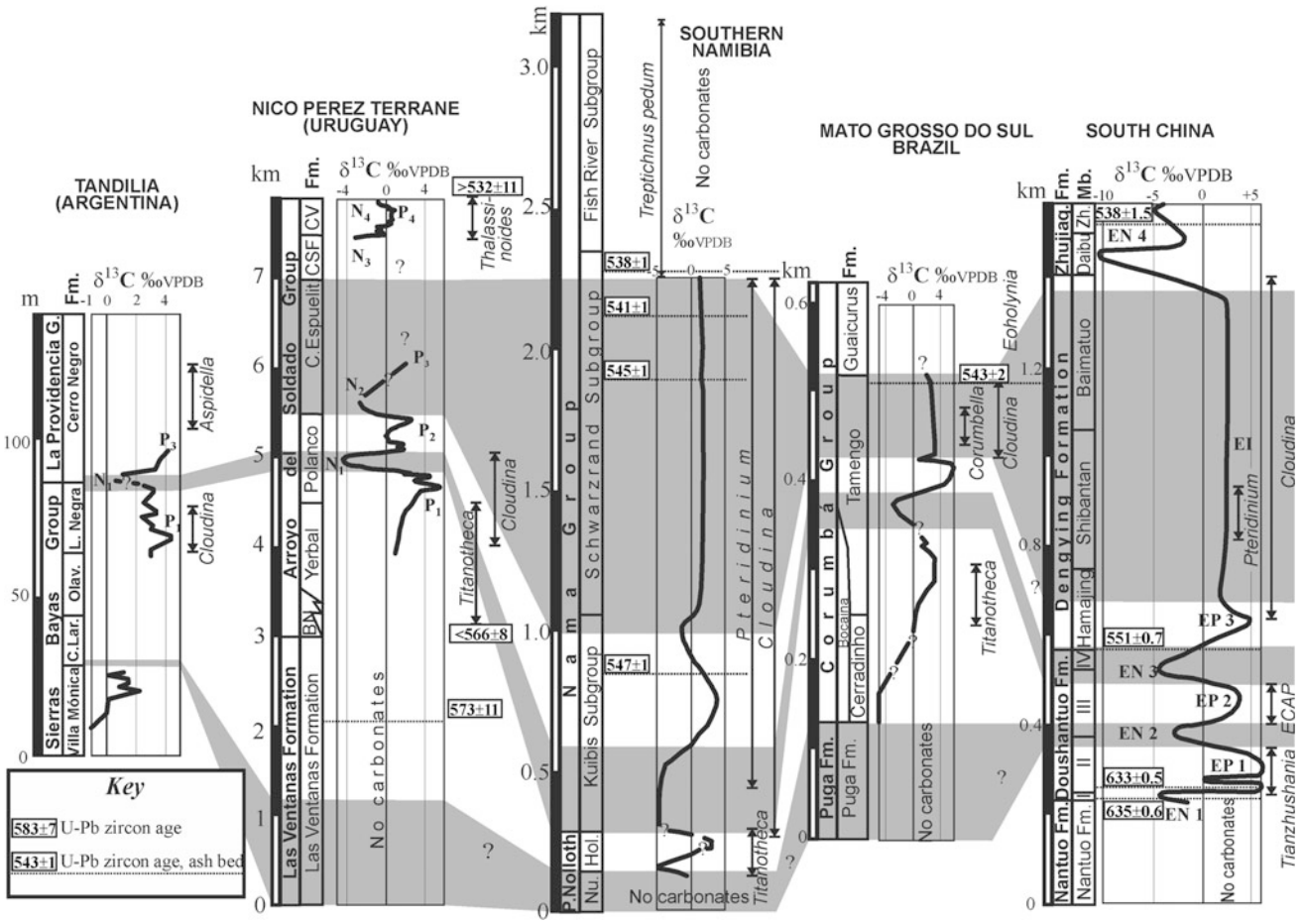

Fig. 20.4 Correlation chart between different Ediacaran-Cambrian successions in SW Gonwdana with South China as a reference, showing biostratigraphic, radiochronological and chemostratigraphic data (modified from Boggiani et al. 2010 and references therein). Recalculated U–Pb ages for the Nama Group (Smith et al. 2017 and references therein). Biostratigraphic data: see text. Tandilia: *C. Lar* Cerro Largo; *Olav.* Olavarría; *L. Negra* Loma Negra. Arroyo del Soldado Group: *BN* Barriga Negra; *CSF* Cerros San Francisco; *CV* Cerro Victoria. Namibia: *P. Nolloth:* Port Nolloth Group; *Nu.* Numees Formation; *Ho.* Holgat Formation. South China: *Zhuiaq.* Zhujiaqing Formation; *Zh.* Zhongyicun Member; *ECAP* Ediacaran Complex Acanthomorph Palynoflora

which the ECAP dominated. However, acritarchs reported from the upper third of the unit are mostly leiosphaerids (Blanco and Gaucher 2005; Gaucher et al. 2008a; Gaucher and Poiré 2009; Fig. 20.3b), albeit significantly larger (up to 400 µm) than those characteristic of Late Ediacaran assemblages (LELP). Why complex acanthomorphs are missing from the Las Ventanas Formation remains to be explained.

Large leiosphaerids were also described from shales of the Villa Mónica and Cerro Largo formations (lower Sierras Bayas Group, Argentina), including *Leiosphaeridia tenuissima* up to 450 µm in diameter (Gaucher et al. 2005a; Fig. 20.3a). A diamictite (Colombo Diamictite) occurs between both occurrences and has been interpreted as being correlative to the Las Ventanas Formation (Fig. 20.4), and thus Gaskiers in age (Rapalini et al. 2013; Gaucher 2014). It could be argued in this case that the relatively short-lived ECAP assemblage may coincide with the basal erosional unconformity of the Cerro Largo Formation.

20.3 Ediacara Soft-Bodied Biota

Soft-bodied macrofossils were first described from the Nama Group by Gürich (1930, 1933). Thereafter, a number of researchers expanded our knowledge of these remarkable fossils (e.g., Richter 1955; Pflug 1966, 1970, 1972; Germs 1973a, b, 1995). These studies and more recent work have shown that the Nama Group hosts one of the most remarkable Ediacara biota *Lagerstätten* worldwide. For a comprehensive bibliographical review of the Ediacara biota in Namibia, the reader is referred to McCall (2006).

The Nama Group hosts the youngest of the three assemblages (547–541 Ma; Grotzinger et al. 1995; Narbonne et al. 1995; Smith et al. 2017) so far recognized in the Ediacara biota: the Avalon, White Sea and Nama Associations (Waggoner 2003; Laflamme et al. 2013). The Nama Association occurs in both the Kuibis and Schwarzrand

subgroups, three-dimensionally preserved within sandstone beds (Fig. 20.5a), which for the most part represent tempestites (storm deposits). The best-known *Lagerstätten* are in the quartz-arenites of the Kliphoek Member, Dabis Formation (Kuibis Subgroup), such as the world-class Aar Farm occurrence.

The preservation is unusual for soft-bodied organisms, and it prompted Seilacher (1984) to propose the "quilted air mattress" model, which means that the organisms had a relatively compact shape but a large surface area. The high surface/volume ratio points to a metabolism dependent on interactions across the tegument, such as respiration, nutrient uptake and excretion (Seilacher 2007). Apart from a few examples of fossils belonging to known metazoan phylla (e.g., the mollusk *Kimberella* Fedonkin and Waggoner 1997 or the hexactinellid sponge *Palaeophragmodictya* Gehling and Rigby 1996), the Ediacara biota represents a failed experiment of evolution, or as Seilacher (2007) put it, "strange as life on another planet, but easier to reach." Seilacher (1992) proposed the (kingdom-level?) taxon Vendobionta, which currently continues to encompass all Ediacara soft-bodied fossils that cannot be assigned to known phyla.

In the Nama Group, two groups of vendobionts occur: those that grew by serial quilting (addition of "segments") and the more remarkable fractal vendobionts. Among the serial vendobionts, *Pteridinium* (Fig. 20.5a, b), *Ernietta*, *Namalia* and *Swartpuntia* occur in the Nama Group (e.g., Grazhdankin and Seilacher 2002). *Rangea*, on the other hand, grew by means of fractal quilting (Narbonne 2004; Grazhdankin and Seilacher 2005), unlike any other known organism outside the Vendobionta. Discoidal soft-bodied fossils assigned to *Aspidella* sp. have been described from the Schwarzrand Subgroup in the Zaris sub-basin (Darroch et al. 2016).

In South Africa (southern Cape Province), an Ediacara-type soft-bodied fossil occurs in the Groenefontein Formation of the Cango Caves Group (Praekelt et al. 2008) but it is still under study (G.J.B. Germs, pers. comm. 2017). *Beltanelloides* has been found in the Groenefontein and Huis Rivier formations of the Cango Caves Group, and microbial mats and enigmatic discoidal fossils (*Aspidella*?) throughout the unit (G.J.B. Germs, pers. comm.).

In South America the Ediacara soft-bodied biota was conspicuously absent until very recently. Aceñolaza and Aceñolaza (2007) described discoidal to bulbous fossils from the latest Ediacaran Puncoviscana Formation at Purmamarca (Jujuy Province) and assigned them to *Beltanelloides* sp. (Fig. 20.5c, d). Aceñolaza et al. (2009) and Aceñolaza (2012) reassigned the material to *Nemiana simplex*. The fossils are preserved as positive hyporelief, range in diameter between 0.9 and 2.5 cm and often show a circular structure (opening?) near their center (Fig. 20.5d). The discs resemble the type material from Ukraine and Russia (Leonov 2007). Interestingly, *Nemiana simplex* also occurs in the lower Nama Group, originally described as the species *Hagenetta aarensis* (Hahn and Pflug 1988) and later reinterpreted as *Nemiana simplex* (Grazhdankin and Seilacher 2005; Leonov 2007; Ivantsov et al. 2014). An Ediacaran age for the Puncoviscana fossils is consistent with U–Pb detrital zircon ages from the host sandstones (Adams et al. 2011).

Barroso et al. (2014) reported the occurrence of soft-bodied Ediacaran macrofossils in sandstones of the Jaibaras Group in NE Brazil (Ceará State; Fig. 20.1). Both discs and fronds were described, including *Cyclomedusa*, *Ediacaria*, *Medusinites* and *Charniodiscus*, most of them represented by a single specimen each. Barroso et al. (2014) also figured one specimen of *Kimberella*, which has been interpreted as a mollusk (Fedonkin and Waggoner 1997). Barroso et al. (2014) assign the fossils to the White Sea Association of Waggoner (2003), which is in accordance with a Late Edaicaran age for the Jaibaras Group, as indicated by acritarchs and Sr isotope ratios of the underlying carbonates (see Chiglino et al. 2015).

More recently, Arrouy et al. (2016) have reported the occurrence of discoid fossils with radial grooves and circular structures at their center in the Cerro Negro Formation (La Providencia Group), which they classify as *Aspidella* sp. (Fig. 20.5e, f). The diameter of the discs is typically between 1 and 2.5 cm, but some "giant" specimens exceed 15 cm. The fossils occur in the underside of fine-grained, tempestitic sandstone beds intercalated with reddish siltstones (Arrouy et al. 2016). Interestingly, the discs are associated with wrinkle structures (microbially induced sedimentary structures), a characteristic feature that has been compared to a "microbial death mask" (Gehling 1999). The age of the Cerro Negro Formation is considered latest Ediacaran on the basis of the occurrence of the LELP acritarch assemblage and also because of *Cloudina* preserved in underlying limestones of the Loma Negra Formation (Gaucher et al. 2005a; Fig. 20.4).

Other possible occurrences of Ediacaran soft-bodied macrofossils in South America are the Itajaí and Camaquã basins in southern Brazil (Fig. 20.2). In the Itajaí Basin, Zucatti-da-Rosa (2006) described *Cyclomedusa* and *Charniodiscus*, *Aspidella* sp. and *Parvancorina* sp. from the Itajaí Group (Fig. 20.2). The depositional age of the fossil-bearing beds has been constrained by U–Pb zircon ages between 563 ± 3 Ma and 549 ± 4 Ma (Guadagnin et al. 2010), which is in agreement with the known range of the Ediacara soft-bodied biota. However, the poor preservation of the fossils and lack of more detailed studies demand more work to confirm this occurrence (Netto 2012). The same can be said for *Aspidella* sp. described from the Camaquã Supergroup (Netto 2012; Fig. 20.2).

A different type of Ediacaran soft-bodied fossil are tubular (vermiform) fossils best known from the Dengying

Fig. 20.5 Ediacaran soft-bodied fossils. **a** *Pteridinium*, Kliphoek Member, Kuibis Subgroup (Nama Group) at Farm Plateau. **b** *Pteridinium carolinaense*, youngest occurrence of the genus in the Spitzkopf Member, upper Schwarzrand Subgroup at Farm Swartpunt (see Narbonne et al. 1997). **c**, **d** *Nemiana simplex* from the Puncoviscana Formation at Purmamarca. Note circular structure near the center in specimens in d, as well as the considerable relief. **e**, **f** *Aspidella* sp. from the Cerro Negro Formation (La Providencia Group) at El Polvorín Quarry, showing radial grooves and circular structures at the center. Scale in **b**, **e** and **f** is 8 cm

Formation in South China (Fig. 20.4), such as *Gaojiashania* (Cai et al. 2013), *Shaanxilithes* (Meyer et al. 2012) and *Wutubus* (Chen et al. 2014). Therefore these fossils form part of the latest Ediacaran Nama Assemblage, and probably represent multiple phyla and even multiple kingdoms. They inhabit an important transition from the latest Ediacaran to the early Cambrian (Schiffbauer et al. 2016). Tubular organisms co-existed with erniettomorphs for at least the last

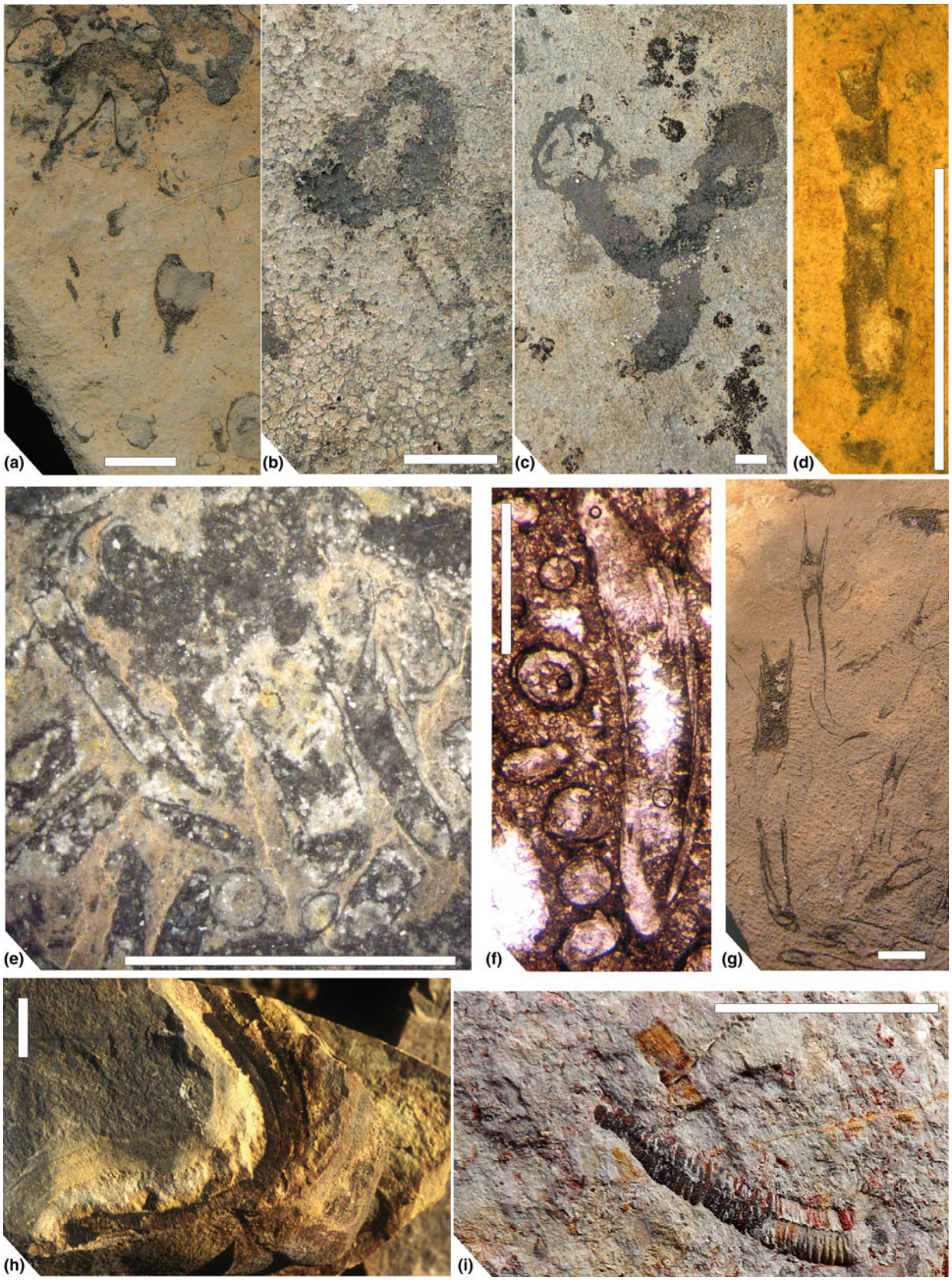

Fig. 20.6 Ediacaran fossils with a carbonate shell. **a** *Namacalathus hermanastes*, Omkyk Member, Nama Group at Farm Zwartmodder. **b** *Namacalathus hermanastes*, in thrombolitic carbonates of the Itapucumí Group, Paraguay. **c** *Namacalathus hermanastes*, Itapucumí Group, two attached specimens. **d** *Cloudina lucianoi*, Itapucumí Group. Note cone in cone structure. **e** *Cloudina lucianoi*, Tamengo Formation, Corumbá Group (polished slab). **f** *Cloudina riemkeae*, Kuibis Subgroup. Nama Group, both longitudinal and cross-sections (Germs et al. 2009). **g** *Cloudina hartmannae*, longitudinal sections, Nama Group. **h**, **i** *Corumbella werneri*, from marl of the Tamengo Formation, Corumbá Group. Note flexibility in **h** and considerable relief and longitudinal ridge in **i** Scale bars equal 1 cm, except for f (1 mm)

6 Ma of the Ediacaran period from about 547 Ma until 541 Ma (Smith et al. 2017). The disappearance of this cosmopolitan assemblage may represent the first Phanerozoic-style mass extinction (Smith et al. 2017).

Soft-bodied tubular fossils assigned to *Shaanxilithes* have been reported from the Schwarzrand Subgroup of the Nama Group (Darroch et al. 2016). *Gaojiashania*, in turn, has been reported from the *c*. 547 Ma Hoogland Member of the Kuibis Subgroup (Smith et al. 2017). The tubular fossil *Archaeichnium* occurs in the *c*. 545 Ma Nasep and Huns Members of the Schwarzrand Subgroup (GJB Germs, pers. comm.). The trace fossil *Buchholzbrunnichnus* (Germs 1973b) is now considered to represent a tubular fossil resembling *Gaojiashania* (GJB Germs, pers. comm.). In South America, *Corumbella* could be considered to be a tubular fossil but, as will be explained below, it has been related to either the cloudinids or the conularids.

20.4 Skeletonized Metazoans and Protists

Ediacaran skeletonized metazoans are probably the most promising group of fossils for late Neoproterozoic biostratigraphy. SW Gondwana has an unmatched diversity and abundance of these fossils, which was first recognized by the pioneering work of Germs (1972a), who created the genus *Cloudina* and postulated a Late Neoproterozoic age for the fossils. An earlier report by Beurlen and Sommer (1957) recognized the same fossils in the Corumbá Group in Brazil, but they were assigned to the Cambrian genus *Aulophycus*.

The Nama Group hosts abundant calcified fossils, which in some cases form real coquinas, the oldest in Earth history. *Cloudina* is represented by two species, which differ essentially in their size: the larger *C. hartmannae* (Fig. 20.6g) and the smaller *C. riemkeae* (Germs 1972a; Fig. 20.6f). *Cloudina* has since been reported from all continents, including Antarctica. Grant (1990) recognized the biostratigraphic importance of the genus as an index fossil, and Gaucher and Germs (2009) formally proposed the *Cloudina* Range Zone. The biological affinities of *Cloudina* are still debated but its most likely that its modern analogs are annelids, possibly serpulids (Germs 1972a; Hua et al. 2005).

Another common calcareous metazoan in the Nama Group is *Namacalathus hermanastes* (Grotzinger et al. 2000). The species occurs, along with *Cloudina*, associated with thrombolite reefs, and it accounts for more than 75% of specimens there (Grotzinger et al. 2000). *Namacalathus* is characterized by a hollow stem attached to a spheroidal cup with openings, whose distribution exhibits radial symmetry (Fig. 20.6a). This, along with its sessile mode of life, suggests phylogenetic affinities with anthozoan cnidarians.

The last skeletonized fossil to be found in the Nama Group is at the same time the largest and more heavily mineralized, reaching 1 m in size. *Namapoikia rietoogensis* has been reported from Driedoornvlakte reef carbonates (Kuibis Subgroup, Omkyk Member), associated with thrombolite and stromatolites (Wood et al. 2002). The colonies are made up of tubules of polygonal or labyrinthine cross-section, and the outer habit of the colony is domal, columnar or sheet-like. A cnidarian affinity related to tabulate corals is probable (Wood et al. 2002; Gaucher and Germs 2009), which would make *Namapoikia* the oldest corals in the Earth's history.

Also in southern Africa, *Titanotheca* has been reported by Gaucher et al. (2005b) from the upper Port Nolloth Group (Holgat Formation) of southern Namibia. As will be explained below, *Titanotheca* is characterized by an agglutinated skeleton and has been assigned to the Foraminiferida (Gaucher and Sprechmann 1999).

The greatest diversity of Ediacaran skeletal fossils of SW-Gondwana—unlike other fossil groups—is found on the South American side. The genus *Cloudina* occurs in bioclastic calcarenites of the Corumbá Group (Brazil). It is in fact another species, *Cloudina lucianoi* (Beurlen and Sommer; Zaine and Fairchild 1985), which has a size-frequency distribution intermediate between *C. hartmannae* and *C. riemkeae* (Gaucher et al. 2003; Fig. 20.6e). Along with *Cloudina*, the species *Corumbella werneri* (Hahn et al. 1982) occurs in marls of the Tamengo Formation (Corumbá Group; Fig. 20.6h, i). The fossils were long considered to be soft-bodied and possibly related to the Cnidaria. However, more recent work has shown that they were lightly mineralized with calcium carbonate (Warren et al. 2012; Pacheco et al. 2015). Whereas a group of researchers has postulated a conularian affinity for *Corumbella* (Babcock et al. 2005; Van Iten et al. 2014; Pacheco et al. 2015), another group currently favors a cloudinid affinity (Walde et al. 2015). Finally, *Titanotheca coimbrae* has also been described from phosphorites of the Bocaina Formation in the Corumbá Group, *c*. 150 m stratigraphically below the first *Cloudina* occurrences (Gaucher et al. 2003; Fig. 20.4).

So far the most abundant and well-preserved Ediacaran shelly fossils in South America have been described from the Itapucumí Group, which represents the southward extension of the Corumbá Group into Paraguay. *Cloudina lucianoi* was first reported by Boggiani and Gaucher (2004; Fig. 20.6d). An association of *Cloudina lucianoi* and *Corumbella werneri* occurs in thrombolitic facies, much like in the Nama Group (Warren et al. 2011). As in the latter unit, *Namacalathus hermanastes* also occurs in the thrombolitic facies (Warren et al. 2017; Fig. 20.6b, c), although it is relatively less abundant than in the Nama Group.

The most diverse shelly fossils in the whole of SW Gondwana possibly occur in the Arroyo del Soldado Group in Uruguay. An assemblage of skeletal fossils, the Yerbal biota, occurs in the homonymous Yerbal Formation

(Gaucher and Sprechmann 1999) and also in the overlying limestones of the Polanco Formation (Gaucher and Poiré 2009). It includes *Cloudina riemkeae*, which occurs in life position (perpendicular to bedding) in siltstones of the Yerbal Formation, or disarticulated in limestones of the Polanco Formation (Gaucher and Sprechmann 1999; Gaucher 2000, 2014; Gaucher and Poiré 2009). In both cases the shells are replaced by hematite or silica.

Apart from *Cloudina*, the Yerbal biota also includes abundant *Titanotheca coimbrae*, a foraminifer with a test made up of agglutinated rutile grains (Gaucher and Sprechmann 1999; Gaucher and Germs 2009; Fig. 20.7a–c), much like present-day *Bathysiphon* (Lowenstam and Weiner 1989). The fossils show reproduction by budding and often occur in groups, denoting a gregarious life mode (Gaucher and Poiré 2009). The advantage of a rutile exoskeleton could be related to its impervious nature against predators, which could penetrate *Cloudina* shells and were extant in the Late Ediacaran (e.g., Hua et al. 2003). The species *Waltheria marburgensis* is also abundant in siltstones of the upper Yerbal Formation, and possibly had a phosphatic shell (Gaucher and Sprechmann 1999). It is characterized by a multilayered, septate, rigid skeleton, which often shows branching and reaches 1 cm in length (Gaucher 2000, 2014; Gaucher and Poiré 2009; Fig. 20.7d, e). It occurs in life position or reworked as thin shell beds (Gaucher and Germs 2009).

Two other genera of skeletal fossils were described from the Yerbal Formation: *Soldadotubulus*, which resembles *Waltheria*, and the genus *Palaeodiscus* (Gaucher and Sprechmann 1999; Gaucher 2000). In both cases the fossils are preserved as steinkerns and nothing can be said about the original composition of the shell.

A sixth, still unnamed, species of shelly fossil occurs in the middle Yerbal Formation, some 1100 m stratigraphically below the first *Cloudina* occurrence (Gaucher and Poiré 2009). It occurs in large numbers, current-reworked on bedding planes, and reaches 3 cm in length. Its shape is conical to tubular and it exhibits deeply stacked cones but differs from *Cloudina* in that the cones share the same apex (Fig. 20.7f). It is solitary, branched and arranged in X- or star-shaped clusters. The fossils show Burgess Shale-type reservation of the shell walls, which are replaced by chamosite and sericite (Fig. 20.7f). Ongoing work is attempting to reconstruct the morphology by means of digital tomography (Gaucher et al. 2016).

Other occurrences of Ediacaran shelly fossils in sedimentary successions in SW Gondwana include the following: (1) *Cloudina* cf. *C. riemkeae* occurs in limestones of the Loma Negra Formation of the Sierras Bayas Group, Argentina (Gaucher et al. 2005a). (b) Warren et al. (2014) described *Cloudina* sp. and fragments assigned to *Corumbella* from the Sete Lagoas Formation, lower Bambuí Group (Brazil). (c) *Titanotheca coimbrae* has been reported from the late Neoproterozoic Pico de Itapeva and Cajamar basins in SE Brazil, and *Cloudina* cf. *C. riemkeae* from the correlative Eleutério basin (Teixeira and Gaucher 2004).

20.5 Trace Fossils

Trace fossils are the only fossils in SW Gondwana with a record across the Ediacaran–Cambrian boundary.

In the Nama Group, trace fossils occur throughout the succession. Ediacaran trace fossils of the Kuibis and lower Schwarzrand subgroups are sparse, small, mostly bedding-parallel and of low diversity (Germs 1972c; Crimes and Germs 1982; Aceñolaza et al. 2009; Germs et al. 2009; Fig. 20.8c). *Streptichnus narbonnei*, a complex trace fossil similar to *Treptichnus pedum* (=*Phycodes pedum*), has been described by Jensen and Runnegar (2005) from the uppermost Urusis Formation (middle Schwarzrand Group). In the Nomtsas Formation (uppermost Schwarzrand Subgroup) and in the Fish River subgroup, the species *Treptichnus pedum* occurs (Germs 1972c; Crimes and Germs 1982; Geyer 2005; Germs et al. 2009 and references therein; Fig. 20.4), which indicates an early Cambrian age (Brasier et al. 1994) in accordance with U–Pb ages of interbedded ash beds and detrital zircons (Grotzinger et al. 1995; Blanco et al. 2011). Vertical traces, such as *Skolithos*, appear in these units, although they were also described with doubts from the Ediacaran portion of the Nama Group (Germs et al. 2009). Other ichnogenera occurring in the upper Nama Group include *Trichophycus*, *Paleophycus*, *Gordia and Enigmatichnus* (Crimes and Germs 1982; Geyer 2005; Aceñolaza et al. 2009 and references therein; Germs et al. 2009).

In the correlative Vanrhynsdorp Group in South Africa, a similar pattern is observed. Simple, horizontal traces such as *Planolites*, *Helminthopsis* and *Helminthoidichnites* occur in the Kwanous and lower Knersvlakte subgroups (Fig. 20.8b), lower Vanrhynsdorp Group (Aceñolaza et al. 2009 and references therein). *Oldhamia geniculata* has been reported from the middle Knersvlakte Subgroup, marking the lowermost occurrence of Cambrian trace fossils in the Vanrhynsdorp Group (Gresse 1992; Aceñolaza et al. 2009). *Treptichnus pedum* occurs in subtidal to intertidal facies of the upper Knersvlakte and Brandkop subgroups (Buatois et al. 2012).

At the South American side, the Puncoviscana Formation in NW Argentina is the Ediacaran-Cambrian unit with the most diverse trace fossil record. Two assemblages were recognized—the *Oldhamia* and *Nereites* ichnoassociations—but the relative age of each association is difficult to determine owing to the complex, multiphase deformation that affected the unit (Aceñolaza and Toselli 2009). Both assemblages are Early Cambrian in age, as indicated by

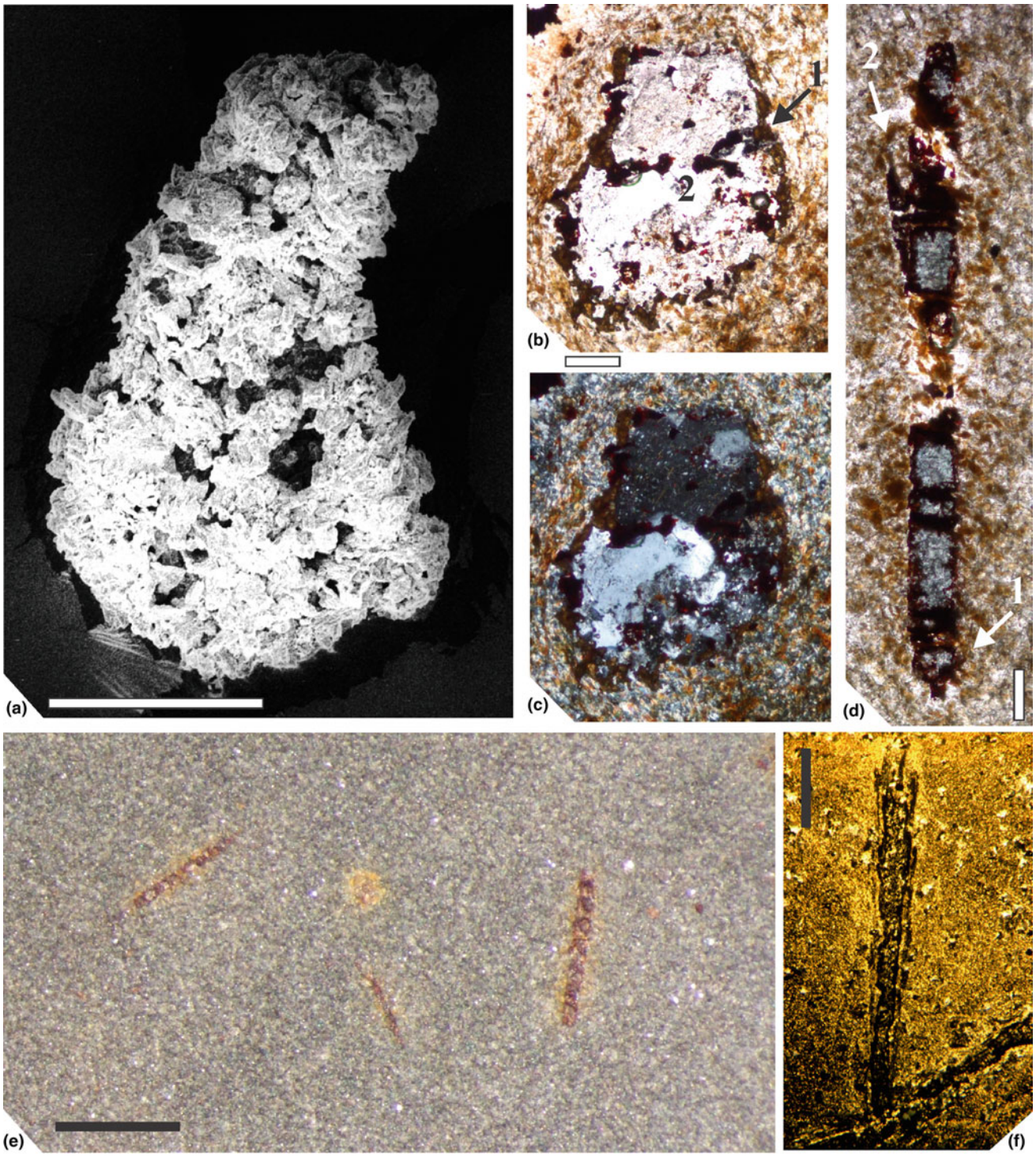

Fig. 20.7 Other Ediacaran shelly fossils from pelites of the Yerbal Formation, Arroyo del Soldado Group (Uruguay). **a** *Titanotheca coimbrae*, paratype, SEM image (Gaucher and Sprechmann 1999). **b** *Titanotheca coimbrae*, bilocular specimen in thin section, showing (1) septum and (2) pore between chambers (Gaucher and Sprechmann 1999). **c** Same as previous with cross nicols. **d** *Waltheria marburgensis*, thin section of holotype showing (1) initial sphaerical chamber and (2) small branch (Gaucher and Sprechmann 1999). **e** *Waltheria marburgensis* on bedding plane, showing two larger, septated, hematized specimens. **f** Thin section of branched, tubular fossils with deeply nested cones and walls replaced by chamosite (Gaucher 2014). White scale bars represent 0.1 mm and black scale bars 1 mm

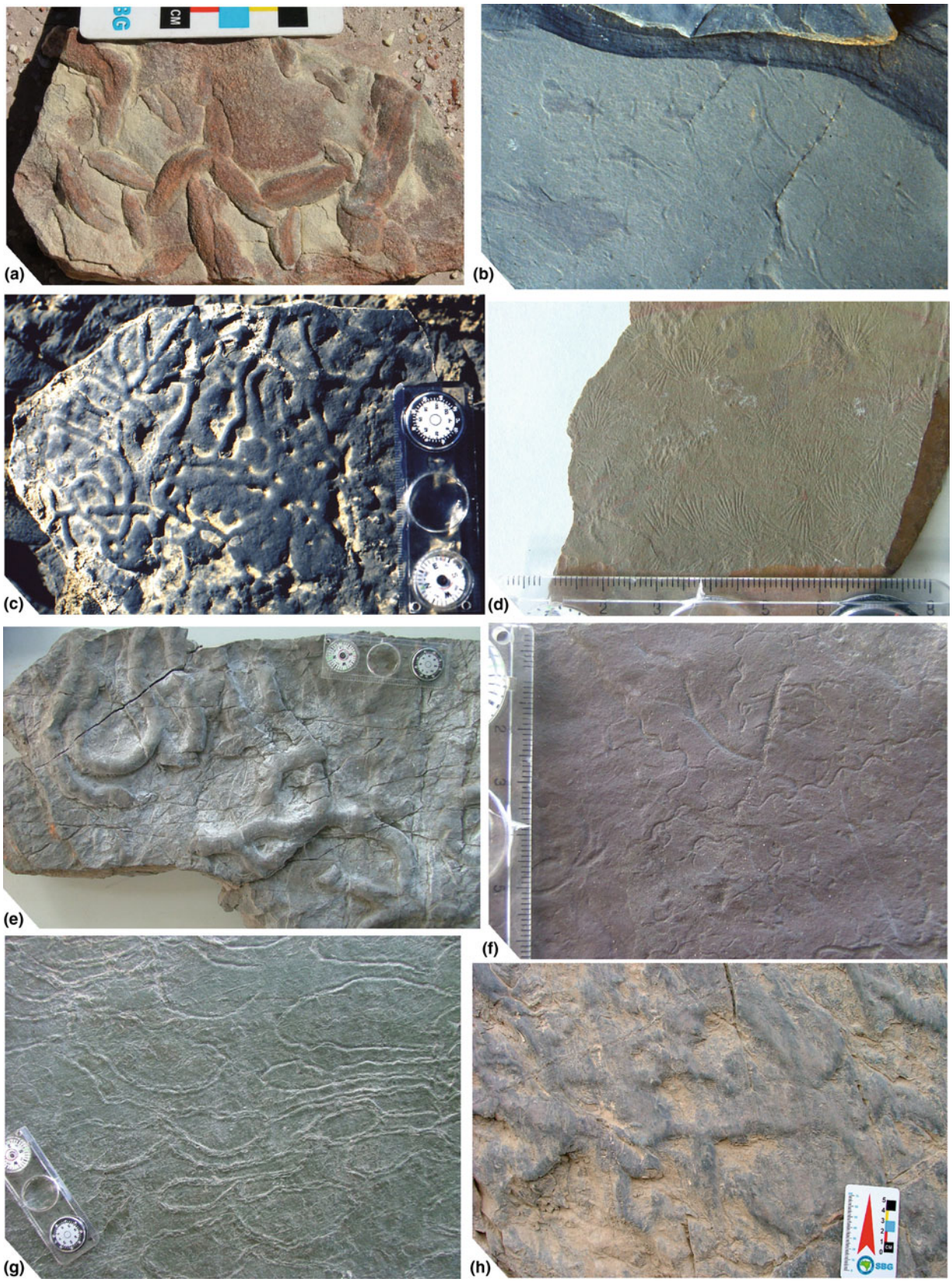

Fig. 20.8 Ediacaran and Early Cambrian trace fossils. **a** Biomat desiccation structures, Las Aguilas Formation, Sierras Bayas Group at Taglioretti Quarry. **b** *Planolites* isp. from the Besonderheid Formation, middle Vanrhynsdorp Group. **c** *Planolites* isp. in limestone of the Spitzkopf Member, upper Schwarzrand Subgroup at Swartpunt Farm. **d** *Oldhamia radiata*, Puncoviscana Formation (specimen from the collection of INSUGEO, Tucumán, Argentina). **e** *Helminthoraphe* isp., Puncoviscana Formation (INSUGEO collection). **f** Cochlichnus isp., Puncoviscana Formation (INSUGEO collection). **g** *Nereites saltensis* (holotype at INSUGEO collection), Puncoviscana Formation. **h** *Thalassinoides* isp. boxworks, Puncoviscana Formation near San Antonio de los Cobres. Except for a and h, the scale is 8 cm

detrital zircon age data (Adams et al. 2011). The *Oldhamia* assemblage comprises six *Oldhamia* ichnospecies (*O. alata*, *O. antiqua*, *O. curvata*, *O. flabellata*, *O. geniculata* and *O. radiata*; Fig. 20.8d), *Monomorphichnus lineatus*, *Monomorphichnus* isp., *Dimorphichnus*, *Cochlichnus anguineus* (Fig. 20.8f), *Nereites*, *Helmintoidichnites tenuis*, *Didymaulichnus lyelli* and *Thalassinoides* isp. (Fig. 20.8h; Aceñolaza and Aceñolaza 2005, 2007; Aceñolaza et al. 2009). The more diverse *Nereites* association includes *Nereites saltensis* (Fig. 20.8g), meandering burrows assigned to *Helminthopsis* spp. and *Helminthoraphe* sp. (Fig. 20.8e), *Treptichnus*, *Monomorphichnus*, *Cochlichnus*, *Didymaulichnus*, *Diplichnites*, *Glockerichnus*, *Dimorphichnus*, *Asaphoidichnus* and *Tasmanadia* (Aceñolaza and Aceñolaza 2005, 2007; Aceñolaza et al. 2009 and references therein).

The ichnoassociations of the Puncoviscana Formation occur as northeast-trending belts and have been used to divide the otherwise lithologically monotonous unit. Whereas the *Oldhamia* association occurs in the west in deeper facies, the *Nereites* association occurs in the east in shallower depositional environments. Thus it is not yet clear if the different assemblages respond to different ages or merely to facies/paleoenvironmental control (Aceñolaza and Aceñolaza 2005; Aceñolaza et al. 2009).

In stromatolitic carbonates of the uppermost Arroyo del Soldado Group (Cerro Victoria Formation, Fig. 20.4), large *Thalassinoides* boxworks were described by Sprechmann et al. (2004). *Gyrolithes* and *Palaeophycus* also occur, and all traces show concretionary growth by silica. *Thalassinoides* of the Cerro Victoria Formation is similar in its large size to the same ichnogenus from the Puncoviscana Formation, and also resembles large, carbonate-facies *Thalassinoides* from the late Cambrian La Flecha and La Silla formations (e.g., Sial et al. 2008; Gaucher and Poiré 2009).

The Sierras Bayas and La Providencia groups in Argentina, on the other hand, mainly preserve Ediacaran trace fossils. Apart from well-preserved biomat desiccation structures (Fig. 20.8a; Porada and Bouougri 2008), *Helminthopsis* has been reported from the Loma Negra Formation (Gaucher and Poiré 2009 and references therein). Bilobed burrows assigned to *Archaeonassa*, and *Arumberia* biomat strucures were reported by Arrouy et al. (2016) from the Cerro Negro Formation. A similar assemblage of *Archaeonassa* and Palaeophycus was reported by Warren et al. (2014) from the Sete Lagoas Formation of the Bambuí Group (Brazil).

Finally, Ediacaran trace fossils also occur in the Itajaí Group and Camaquã Supergroup in southern Brazil (Fig. 20.2). In the Itajaí Group, horizontal, meandering burrows were described by Zucatti-da-Rosa (2006) and assigned to *Helminthoidichnites* isp. The late Ediacaran (568–549 Ma; de Oliveira et al. 2014) Santa Bárbara Group, upper Camaquã Supergroup, on the other hand, hosts a more diverse trace fossil assemblage. Netto (2012) described *Arthraria antiquata*, *Bergaueria hemispherica*, *Cochlichnus*, *Palaeophycus*, *Planolites* and so far undetermined treptichnid burrows. Microbially induced sedimentary structures, such as *Arumberia* and *Kinneya*-type structures, are also quite common (Netto 2012).

20.6 Biostratigraphy and Paleogeography

20.6.1 Biostratigraphy

One interesting pattern observed in SW Gondwana is the abundance of Ediacaran, and especially Late Ediacaran, fossils. Apart from acritarchs of the Otavi Group (Germs et al. 2009), Early Ediacaran and Cryogenian fossils are almost absent in SW Gondwana.

In the Maieberg Formation (lower Otavi Group), the polygonomorph acritarch *Octoedryxium truncatum* occurs in marls of the Maieberg Formation, 170 m stratigraphically above the contact with glacial diamictites of the Ghaub Formation (Gaucher and Germs 2007; Germs et al. 2009), which has been dated at 635 ± 1 Ma by Hoffmann et al. (2004). The Maieberg Formation is comparable in age to the lower Doushantuo Formation in China, which yielded large and complex acanthomorphs of the *Tianzhushania spinosa* assemblage (Liu et al. 2013; Fig. 20.4). More work is required to establish whether this assemblage is also represented in the upper Otavi Group.

Complex acanthomorphic acritarchs of the ECAP assemblage are so far absent in SW Gondwana. This is quite puzzling because microfossil-bearing rocks of the same age (580–570 Ma) occur in the Las Ventanas Formation in Uruguay (Fig. 20.4) but these yielded only large leiosphaerids. Paleoenvironmental, including paleoclimatic, factors may have played a role. Whereas the environments represented in the Las Ventanas Formation are glacial to cold, as indicated by sedimentary structures and the Chemical Index of Alteration (Gaucher et al. 2008a; Blanco and Gaucher 2014), the classical localities of ECAP acritarchs (South China, Australia, Siberia) occur in successions deposited in tropical settings (Li et al. 2013).

Shelly fossils are the most promising group from a biostratigraphic point of view. Apart from the well-established, latest Ediacaran *Cloudina* Range Zone and associated taxa (*Namacalathus*, *Corumbella*; Fig. 20.4), other taxa may prove useful as index fossils. So far the first appearance of *Titanotheca coimbrae* always occurs well beneath the first appearance of *Cloudina* (Fig. 20.4; Gaucher and Germs 2009), and both species overlap at least in the Arroyo del Soldado Group for a few hundred meters of the section (Gaucher and Sprechmann 1999).

Biostratigraphically, the Ediacaran–Cambrian boundary has been established in SW Gondwana only with the use of trace fossils. The "agronomic revolution" that occurred at the boundary, owing to which the Precambrian matgrounds were irreversibly succeeded by Phanerozoic mixgrounds (Seilacher 1999), is well represented in several units in the region. Recently described vermiform fossils may prove useful in establishing the Ediacaran–Cambrian boundary as well (Schiffbauer et al. 2016).

In summary, it can be stated that—biostratigraphically—the Early and Mid-Ediacaran are best zonated using acritarchs, the Late Ediacaran with shelly fossils and the Ediacaran–Cambrian boundary can be identified using trace fossils.

20.6.2 Paleogeography

The question arises as to whether the fossil record can aid the complex paleogeographic reconstructions of the assembly of SW Gondwana.

Biostratigraphy can surely contribute to our understanding of regional paleogeography by enabling the correlation between different successions. As an example, the Sierras Bayas, Arroyo del Soldado, Itapucumí and Corumbá groups (Figs. 20.1 and 20.2) have many genera and species in common, such as *Cloudina* and a low-diversity acritarch palynoflora (LELP assemblage). Their lithostratigraphy is very similar (Fig. 20.4), with interbedded carbonates and siliciclastics, which reflect their deposition in a passive margin setting. Gaucher et al. (2003, 2005a, 2008b) proposed that all these units were deposited in the same platform, which opened to the east and southeast and which they named the Corumbá-Arroyo del Soldado-Sierras Bayas shelf (Gaucher et al. 2008b, 2009). Closure of the shelf took place in the basal Cambrian around 540–530 Ma (e.g., Gaucher et al. 2008b; McGee et al. 2015) at the end of the Brasiliano-Pan African Cycle.

A few studies have also suggested that Ediacaran fossils could be used for paleobiogeographic reconstructions in SW Gondwana, specifically in support of the existence of the Clymene Ocean (e.g., Warren et al. 2014; Arrouy et al. 2016). However, it seems premature to use the Ediacaran fossil record in SW Gondwana for paleobiogeographic reconstructions. Most of the taxa, such as *Cloudina*, are cosmopolitan and have a global distribution, which could be explained by these organisms having planktonic larvae. In other cases, such as acritarchs, the organisms themselves were planktonic. Thus their occurrence alone cannot be used to delimitate different biogeographical provinces. It should be asked why similar benthic assemblages, such as the *Cloudina-Namacalathus-Corumbella* skeletal assemblage, occur on both sides of the Clymene Ocean, in the Kalahari and São Francisco cratons in the west and in the Río Apa/Amazonia and Laurentian cratons in the east according to the proposed reconstructions (Warren et al. 2014; Arrouy et al. 2016). The discipline of Ediacaran paleobiogeography is clearly still in its infancy.

Acknowledgements This contribution is dedicated to the memory of the late Peter Sprechmann (1938–2017), a pioneer of Precambrian paleontology in South America, professor, colleague and long-time friend. An earlier draft of the chapter was significantly improved thanks to comments and data provided by Gerard Germs, to whom I am deeply indebted. Thanks go to the book editors, Siegfried Siegesmund, Miguel Basei and Pedro Oyhantçabal, for inviting me to write this contribution and for their patience. Support from the Polo de Desarrollo Universitario "Geología y Recursos Minerales" (CURE-Universidad de la República) is gratefully acknowledged.

References

Aceñolaza FG (2012) Biodiversity of the Ediacaran-early Cambrian transition in northwestern Argentina and related areas. Revue de Paléobiologie, 11:299–309

Aceñolaza G, Aceñolaza FG (2005) La Formación Puncoviscana y unidades estratigráficas vinculadas en el Neoproterozoico-Cámbrico temprano del Noroeste Argentino. Lat Am J Sediment Basin Anal 12(2):65–87

Aceñolaza G, Aceñolaza FG (2007) Insights in the Neoproterozoic–early Cambrian transition of NW Argentina: facies, environments and fossils in the proto-margin of western Gondwana. In: Vickers_Rich P, Komarower P (eds) The Rise and Fall of the Ediacaran Biota, vol 286. Geological Society of London Special Publication, The Geological Society, London, pp 1–13

Aceñolaza FG, Toselli A (2009) The Pampean Orogen: Ediacaran-lower Cambrian evolutionary history of Central and Northwest region of Argentina. In: Gaucher C, Sial AN, Halverson GP, Frimmel HE (eds) Neoproterozoic-Cambrian tectonics, global change and evolution: a focus on southwestern Gondwana. Developments in Precambrian Geology, vol 16. Elsevier, Amsterdam, pp 239–254

Aceñolaza GF, Germs GJB, Aceñolaza FG (2009) Trace fossils and the Agronomic Revolution at the Neoproterozoic-Cambrian transition in southwest Gondwana. In: Gaucher C, Sial AN, Halverson GP, Frimmel HE (eds) Neoproterozoic-Cambrian tectonics, global change and evolution: a focus on southwestern Gondwana. Developments in Precambrian Geology, vol 16. Elsevier, Amsterdam, pp 339–347

Adams CJ, Miller H, Aceñolaza FG, Toselli AJ, Griffin WL (2011) The Pacific Gondwana margin in the late Neoproterozoic–early Paleozoic: detrital zircon U–Pb ages from metasediments in northwest Argentina reveal their maximum age, provenance and tectonic setting. Gondwana Res 19:71–83

Arrouy MJ, Poiré DG, Gómez Peral LE, Canalicchio JM (2015) Sedimentología y estratigrafía del Grupo La Providencia (nom. nov.): cubierta superior neoproterozoica, Sistema de Tandilia, Argentina. Lat Am J Sediment Basin Anal 22(2):171–189

Arrouy MJ, Warren LV, Quaglio F, Poiré DG, Simões MG, Rosa MB, Gómez Peral LE (2016) Ediacaran discs from South America: probable soft-bodied macrofossils unlock the paleogeography of the Clymene Ocean. Sci Rep 6:30590

Babcock LE, Grunow AM, Sadowski GR, Leslie SA (2005) *Corumbella*, an Ediacaran-grade organism from the late Neoproterozoic of Brazil. Palaeogeogr Palaeoclimatol Palaeoecol 220:7–18

Barroso FRG, Viana MSS, Lima Filho MF, Agostinho SMO (2014) First Ediacaran Fauna occurrence in Northeastern Brazil (Jaibaras Basin,? Ediacaran-Cambrian): preliminary results and regional correlation. An Acad Bras Ciênc 86:1029–1042

Beurlen K, Sommer FW (1957) Observações estratigráficas e paleontológicas sôbre o calcário Corumbá. Boletim Divisão Geologia e Mineralogia/ DNPM 168:1–47

Blanco G, Gaucher C (2005) Estratigrafia, paleontologia y edad de la Formacion Las Ventanas (Neoproterozoico, Uruguay). Lat Am J Sediment Basin Anal 12(2):109–124

Blanco G, Gaucher C (2014) Formación Las Ventanas. In: Bossi J, Gaucher C (eds) Geología del Uruguay. Tomo 1: Predevónico. Polo, Montevideo, pp 299–312

Blanco G, Germs GJB, Rajesh HM, Chemale F Jr (2011) Provenance and palaeogeographic evolution of the Nama Group (Ediacaran-early Palaeozoic, Namibia): petrography, geochemistry and U–Pb zircon ages. Precambr Res 187:15–32

Boggiani PC, Gaucher C (2004) *Cloudina* from the Itapucumí Group (Vendian, Paraguay): age and correlations. In: 1st symposium Neoproterozoic-early Palaeozoic events in SW-Gondwana, extended abstracts, São Paulo, 2004

Boggiani PC, Gaucher C, Sial AN, Babinski M, Simon CM, Riccomini C, Ferreira VP, Fairchild TR (2010) Chemostratigraphy of the Tamengo formation (Corumbá Group, Brazil): a contribution to the calibration of the Ediacaran carbon-isotope curve. Precambr Res 182:382–401

Brasier M, Cowie J, Taylor M (1994) Decision on the Precambrian-Cambrian boundary stratotype. Episodes 17:3–8

Buatois LA, Almond J, Germs GJB (2012) Environmental tolerance and range offset of *Treptichnus pedum*: implications for the recognition of the Ediacaran-Cambrian boundary. Geology 41:519–522

Cai Y, Hua H, Zhang X (2013) Tube construction and life mode of the late Ediacaran tubular fossil *Gaojiashania cyclus* from the Gaojiashan Lagerstätte. Precambr Res 224:255–267

Chen Z, Zhou C, Xiao S, Wang W, Guan C, Hua H, Yuan X (2014) New Ediacara fossils preserved in marine limestone and their ecological implications. Sci Rep 4:4180

Chiglino L, Gaucher C, Sial AN, Ferreira VP (2015) Acritarchs of the Ediacaran Frecheirinha Formation, Ubajara Group, Northeastern Brazil. Anais da Academia Brasileira de Ciencias 87(2):635–649

Cingolani CA, Rauscher R, Bonhomme M (1991) Grupo La Tinta (Precámbrico y Paleozoico inferior) provincia de Buenos Aires, República Argentina. Nuevos datos geocronológicos y micropaleontológicos en las sedimentitas de Villa Cacique, partido de Juarez. Revista Técnica de YPFB 12(2):177–191

Cohen PA, Bradley A, Knoll AH, Grotzinger JP, Jensen S, Abelson J, Hand K, Love G, Metz J, McLoughlin N, Meister P, Shepard R, Tice M, Wilson JP (2009) Tubular compression fossils from the Ediacaran Nama Group, Namibia. J Paleontol 83(1):110–122

Crimes TP, Germs GJB (1982) Trace fossils from the Nama Group (Precambrian-Cambrian) of South West Africa/Namibia. J Paleontol 65:890–907

Darroch SAF, Boag TH, Racicot RA, Tweedt S, Mason SJ, Erwin DH, Laflamme M (2016) A mixed Ediacaran-metazoan assemblage from the Zaris Sub-basin, Namibia. Palaeogeogr Palaeoclimatol Palaeoecol 459:198–208

de Oliveira CHE, Chemale F Jr, Jelinek AR, Bicca MM, Philipp RP (2014) U–Pb and Lu–Hf isotopes applied to the evolution of the late to post-orogenic transtensional basins of the dom feliciano belt, Brazil. Precambr Res 246:240–255

Fairchild TR, Schopf JW, Shen-Miller J, Guimarães EM, Edwards MD, Lagstein A, Li X, Pabst M, Melo-Filho LS (1996) Recent discoveries of Proterozoic microfossils in south-central Brazil. Precambr Res 80:125–152

Fedonkin MA, Waggoner BM (1997) The late Precambrian fossil Kimberella is a mollusc-like bilaterian organism. Nature 388:868–871

Gaucher C (2000) Sedimentology, palaeontology and stratigraphy of the Arroyo del Soldado Group (Vendian to Cambrian, Uruguay). Beringeria 26:1–120

Gaucher C (2014) Grupo Arroyo del Soldado. In: Bossi J, Gaucher C (eds) Geología del Uruguay. Tomo 1: Predevónico. Polo, Montevideo, pp 313–339

Gaucher C, Germs GJB (2006) Recent advances in South African Neoproterozoic-early Palaeozoic biostratigraphy: correlation of the Cango Caves and Gamtoos Groups, and acritarchs of the Sardinia Bay Formation, Saldania Belt. S Afr J Geol 109:193–214

Gaucher C, Germs GJB (2007) First report of organic-walled microfossils from the Otavi and Mulden groups (Neoproterozoic, Namibia). In: III symposium on Neoproterozoic-early Palaeozoic events in SW-Gondwana, short papers, Stellenbosch, 2007

Gaucher C, Germs GJB (2009) Skeletonised Metazoans and Protists. Neoproterozoic-Cambrian biota. In: Gaucher C, Sial AN, Halverson GP, Frimmel HE (eds) Neoproterozoic-Cambrian tectonics, global change and evolution: a focus on southwestern Gondwana. Developments in Precambrian Geology, vol 16. Elsevier, Amsterdam, pp 327–338

Gaucher C, Poiré D (2009) Biostratigraphy. Neoproterozoic-Cambrian evolution of the Río de la Plata Palaeocontinent. In: Gaucher C, Sial AN, Halverson GP, Frimmel HE (eds) Neoproterozoic-Cambrian tectonics, global change and evolution: a focus on southwestern Gondwana. Developments in Precambrian Geology, vol 16. Elsevier, Amsterdam, pp 103–114

Gaucher C, Sprechmann P (2009) Neoproterozoic acritarch evolution. Neoproterozoic-Cambrian biota. In: Gaucher C, Sial AN, Halverson GP, Frimmel HE (eds.) Neoproterozoic-Cambrian tectonics, global change and evolution: a focus on southwestern Gondwana. Developments in Precambrian Geology, vol 16. Elsevier, Amsterdam, pp 319–326

Gaucher C, Sprechmann P, Schipilov A (1996) Upper and Middle Proterozoic fossiliferous sedimentary sequences of the Nico Pérez Terrane of Uruguay: Lithostratigraphic units, paleontology, depositional environments and correlations. Neues Jahrbuch für Geologie und Paläontologie, Abh. 199:339–367

Gaucher C, Sprechmann P, Montaña J (1998) New advances on the geology and paleontology of the Vendian to Cambrian Arroyo del Soldado Group of the Nico Pérez Terrane of Uruguay. Neues Jahrbuch für Geologie und Paläontologie, Monatshefte 1998 (2):106–118

Gaucher C, Sprechmann P (1999) Upper Vendian skeletal fauna of the Arroyo del Soldado Group, Uruguay. Beringeria 23:55–91

Gaucher C, Boggiani PC, Sprechmann P, Sial AN, Fairchild TR (2003) Integrated correlation of the Vendian to Cambrian Arroyo del Soldado and Corumbá Groups (Uruguay and Brazil): palaeogeographic, palaeoclimatic and palaeobiologic implications. Precambr Res 120:241–278

Gaucher C, Chiglino L, Pecoits E (2004) Southernmost exposures of the Arroyo del Soldado Group (Vendian to Cambrian, Uruguay): palaeogeographic implications for the amalgamation of W-Gondwana. Gondwana Res 7(3):701–714

Gaucher C, Poiré DG, Gómez Peral L, Chiglino L (2005a) Litoestratigrafía, bioestratigrafía y correlaciones de las sucesiones sedimentarias del Neoproterozoico-Cámbrico del Cratón del Rio de la Plata (Uruguay y Argentina). Lat Am J Sedimentol Basin Anal 12 (2):145–160

Gaucher C, Frimmel HE, Germs GJB (2005b) Organic-walled microfossils and biostratigraphy of the upper Port Nolloth Group (Namibia): implications for the latest Neoproterozoic glaciations. Geol Mag 142(5):539–559

Gaucher C, Blanco G, Chiglino L, Poiré DG, Germs GJB (2008a) Acritarchs of Las Ventanas Formation (Ediacaran, Uruguay): implications for the timing of coeval rifting and glacial events in western Gondwana. Gondwana Res 13:488–501

Gaucher C, Finney SC, Poiré DG, Valencia VA, Grove M, Blanco G, Pamoukaghlián K, Gómez Peral L (2008b) Detrital zircon ages of Neoproterozoic sedimentary successions in Uruguay and Argentina: insights into the geological evolution of the Río de la Plata Craton. Precambrian Res 167:150–170

Gaucher C, Bossi J, Blanco G (2009) Palaeogeography. Neoproterozoic-Cambrian evolution of the Río de la Plata Palaeocontinent. In: Gaucher C, Sial AN, Halverson GP, Frimmel HE (eds) Neoproterozoic-Cambrian tectonics, global change and evolution: a focus on southwestern Gondwana. Developments in Precambrian Geology, vol 16. Elsevier, Amsterdam, pp 131–141

Gaucher C, Chiglino L, Tambusso S (2016) Ediacaran tubular fossils with Burgess Shale-type preservation, Arroyo del Soldado Group, Uruguay. In: 35th international geological congress, Cape Town, 2016

Gehling JG (1999) Microbial mats in terminal Proterozoic siliciclastics: Ediacaran death masks. Palaios 14:40–57

Gehling JG, Rigby JK (1996) Long expected sponges from the Neoproterozoic Ediacara fauna of South Australia. J Palaeontol 70:185–195

Germs GJB (1972a) New shelly fossils from Nama Group, South West Africa. Am J Sci 272:752–761

Germs GJB (1972b) The stratigraphy and paleontology of the lower Nama Group, South West Africa. Precambrian Research Unit, University of Cape Town, Bulletin 12:1–250

Germs GJB (1972c) Trace fossils from the Nama Group, South West Africa. J Paleontol 46:864–870

Germs GJB (1973a) A reinterpretation of *Rangea schneiderhoehni* and the discovery of a related new fossil from the Nama Group. South West Africa Lethaia 6(1):1–9

Germs GJB (1973b) Possible sprigginid worm and a new trace fossil from the Nama Group, South West Africa. Geology 1:69–70

Germs GJB (1995) The Neoproterozoic of southwestern Africa, with emphasis on platform stratigraphy and paleontology. Precambr Res 73:137–151

Germs GJB, Knoll AH, Vidal G (1986) Latest Proterozoic microfossils from the Nama Group, Namibia (South West Africa). Precambr Res 32:45–62

Germs GJB, Miller RMcG, Frimmel HE, Gaucher C (2009) Syn- to late-orogenic sedimentary basins of southwestern Africa. Neoproterozoic to Early Palaeozoic evolution of southwestern Africa. In: Gaucher C, Sial AN, Halverson GP, Frimmel HE (eds) Neoproterozoic-Cambrian tectonics, global change and evolution: a focus on southwestern Gondwana. Developments in Precambrian Geology, vol 16. Elsevier, Amsterdam, pp 183–203

Geyer G (2005) The Fish River Subgroup in Namibia: stratigraphy, depositional environments and the Proterozoic-Cambrian boundary problem revisited. Geol Mag 142:465–498

Grant SWF (1990) Shell structure and distribution of *Cloudina*, a potential index fossil for the terminal Proterozoic. Am J Sci 290-A:261–294

Grant SWF, Knoll AH, Germs GJB (1991) Probable calcified metaphytes in the latest Proterozoic Nama Group, Namibia: Origin, diagenesis and implications. J Paleontol 65:1–18

Grazhdankin D, Seilacher A (2002) Underground Vendobionta from Namibia. Palaeontology 45(1):57–78

Grazhdankin D, Seilacher A (2005) A re-examination of the Nama-type Vendian organism *Rangea schneiderhoehni*. Geol Mag 142: 571–582

Gresse PG (1992) The tectono-sedimentary history of the Vanrhynsdorp Group. Mem Geol Surv South Africa 79:1–163

Grey K (2005) Ediacaran palynology of Australia. Mem Assoc Australasian Palaeontol 31:1–439

Grey K, Walter MR, Calver CR (2003) Neoproterozoic biotic diversification: Snowball Earth or aftermath of the Acraman impact? Geology 31:459–462

Grotzinger JP, Bowring SA, Saylor BZ, Kaufman AJ (1995) Biostratigraphic and geochronologic constraints on early animal evolution. Science 270:598–604

Grotzinger JP, Watters WA, Knoll AH (2000) Calcified metazoans in thrombolite-stromatolite reefs of the terminal Proterozoic Nama Group, Namibia. Paleobiology 26:334–359

Guadagnin F, Chemale F, Dussin IA, Jelinek AR, dos Santos MN, Borba ML, Justino D, Bertotti AL, Alessandretti L (2010) Depositional age and provenance of the Itajaí Basin, Santa Catarina State, Brazil: implications for SW Gondwana correlation. Precambr Res 180(3):156–182

Gürich G (1930) Die bislang ältesten Spuren von Organismen in Südafrika. XV international geological congress. Comptes Rendus 2:670–680

Gürich G (1933) Die Kuibis Fossilien der Nama-Formation von Südwestafrika. Paläontologische Zeitschrift 15:137–154

Hahn G, Pflug HD (1988) Zweischalige Organismen aus dem Jung-Präkambrium (Vendium) von Namibia (SW-Afrika). Geol Palaeontol 22:1–19

Hahn G, Hahn R, Leonardos OH, Pflug HD, Walde DHG (1982) Körperlich erhaltene Scyphozoen- Reste aus dem Jungpräkambrium Brasiliens. Geol Palaeontol 16:1–18

Hoffmann KH, Condon DJ, Bowring SA, Crowley JL (2004) A U–Pb zircon date from the Neoproterozoic Ghaub Formation, Namibia: constraints on Marinoan glaciation. Geology 32:817–820

Hua H, Pratt BR, Zhang L (2003) Borings in *Cloudina* shells: complex predator–prey dynamics in the terminal Neoproterozoic. Palaios 18:454–459

Hua H, Chen Z, Yuan X, Zhang L, Xiao S (2005) Skeletogenesis and asexual reproduction in the earliest biomineralizing animal *Cloudina*. Geology 33:277–280

Ivantsov AY, Gritsenko VP, Konstantinenko LI, Zakrevskaya MA (2014) Revision of the problematic Vendian macrofossil *Beltanelliformis* (=*Beltanelloides*, *Nemiana*). Paleontol J 48:1423–1448

Jensen S, Runnegar BN (2005) A complex trace fossil from the Spitskop Member (terminal Ediacaran-? Lower Cambrian) of southern Namibia. Geol Mag 142:561–569

Knoll AH, Javaux EJ, Hewitt D, Cohen P (2006) Eukaryotic organisms in Proterozoic oceans. Philos Trans R Soc, B 361:1023–1038

Laflamme M, Darroch SA, Tweedt SM, Peterson KJ, Erwin DH (2013) The end of the Ediacara biota: extinction, biotic replacement, or Cheshire Cat? Gondwana Res 23:558–573

Leonov MV (2007) Comparative taphonomy of Vendian genera *Beltanelloides* and *Nemiana:* taxonomy and lifestyle. In: Vickers_Rich P, Komarower P (eds.) The Rise and Fall of the Ediacaran Biota. Geological Society of London Special Publication, vol 286. The Geological Society, London, pp 259–267

Li Z-X, Evans DAD, Halverson GP (2013) Neoproterozoic glaciations in a revised global palaeogeography from the breakup of Rodinia to the assembly of Gondwanaland. Sed Geol 294:219–232

Liu P, Yin C, Chen S, Tang F, Gao L (2013) The biostratigraphic succession of acanthomorphic acritarchs of the Ediacaran Doushantuo Formation in the Yangtze Gorges area, South China and its biostratigraphic correlation with Australia. Precambr Res 225:29–43

Lowenstam HA, Weiner S (1989) On biomineralization. Oxford University Press, Oxford

Mallmann G, Chemale F Jr, Avila JN, Kawashita K, Armstrong RA (2007) Isotope geochemistry and geochronology of the Nico Pérez Terrane, Río de la Plata Craton, Uruguay. Gondwana Res 12: 489–508

McCall GJH (2006) The Vendian (Ediacaran) in the geological record: enigmas in geology's prelude to the Cambrian explosion. Earth Sci Rev 77(1):1–229

McFadden KA, Huang J, Chu X, Jiang G, Kaufman AJ, Zhou C, Yuan X, Xiao S (2008) Pulsed oxidation and biological evolution in the Ediacaran Doushantuo formation. Proc Natl Acad Sci 105:3197–3202

McGee B, Collins AS, Trindade RI, Jourdan F (2015) Investigating mid-Ediacaran glaciation and final Gondwana amalgamation using coupled sedimentology and 40Ar/39Ar detrital muscovite provenance from the Paraguay Belt. Brazil Sedimentol 62(1):130–154

Meyer M, Schiffbauer JD, Xiao S, Cai Y, Hua H (2012) Taphonomy of the upper Ediacaran enigmatic ribbonlike fossil *Shaanxilithes*. Palaios 27(5):354–372

Moczydłowska M (2005) Taxonomic review of some Ediacaran acritarchs from the Siberian Platform. Precambr Res 136(3):283–307

Narbonne GM (2004) Modular construction of early Ediacaran complex life forms. Science 305:1141–1144

Narbonne GM, Saylor BZ, Grotzinger JP (1997) The youngest Ediacaran fossils from southern Africa. J Paleontol 71(6):953–967

Netto RG (2012) Evidences of life in terminal Proterozoic deposits of southern Brazil: a synthesis. In: Netto RG, Carmona NB, Tognoli FMW (eds) Ichnology of Latin America—selected papers. Monografias da Sociedade Brasileira de Palentologia, vol. 2, Sociedade Brasileira de Paleontologia, Porto Alegre, pp 15–26

Oyhantçabal PB, Siegesmund S, Wemmer K, Presnyakov S, Layer P (2009) Geochronological constraints on the evolution of the southern Dom Feliciano Belt (Uruguay). J Geol Soc London 166:1075–1084

Pacheco MLF, Galante D, Rodrigues F, Leme JDM, Bidola P, Hagadorn W, Stockmar M, Herzen J, Rudnitzki ID, Pfeiffer F, Marques AC (2015) Insights into the skeletonization, lifestyle, and affinity of the unusual Ediacaran fossil *Corumbella*. PLoS One 10: e0114219

Pflug HD (1966) Neue Fossilreste aus den Nama-Schichten in Suedwest-Afrika. Paläontologische Zeitschrift 40:14–25

Pflug HD (1970) Zur fauna der Nama-Schichten in Suedwest-Afrika. Teil I, Pteridinia, Bau und systematische Zugehoerigkeit. Palaeontographica A134(4–6):226–261

Pflug HD (1972) Systematik der jung-praekambrischen Petalonamae Pflug 1970. Paläontologische Zeitschrift 46:56–67

Poiré DG, Arrouy MJ, Canalicchio JM, Gaucher C (2010) Formación Alicia: una nueva unidad de lutitas negras del Neoproterozoico del Sistema de Tandilia, Argentina. In: VI Congreso Uruguayo de Geología, Programa. Sociedad Uruguaya de Geología, Minas, 2010

Porada H (1989) Pan-African rifting and orogenesis in Southern to Equatorial Africa and Eastern Brazil. Precambr Res 44:103–136

Porada H, Bouougri E (2008) Neoproterozoic trace fossils vs. microbial mat structures: examples from the Tandilia Belt of Argentina. Gondwana Res 13:480–487

Pothe de Baldis ED, Baldis BA, Cuomo J (1983) Los fósiles precámbricos de la Formación Sierras Bayas (Olavarría) y su importancia intercontinental. Asociación Geológica Argentina Revista 38:73–83

Praekelt HE, Germs GJB, Kennedy JH (2008) A distinct unconformity in the Cango Caves Group of the Neoproterozoic to early Paleozoic Saldania Belt in South Africa: its regional significance. S Afr J Geol 111:357–368

Pu JP, Bowring SA, Ramezani J, Myrow P, Raub TD, Landing E, Mills A, Hodgin E, Macdonald FA (2016) Dodging snowballs: Geochronology of the Gaskiers glaciation and the first appearance of the Ediacaran biota. Geology 44(11):955–958

Rapalini AE, Trindade RI, Poiré DG (2013) The La Tinta pole revisited: Paleomagnetism of the Neoproterozoic Sierras Bayas Group (Argentina) and its implications for Gondwana and Rodinia. Precambr Res 224:51–70

Richter R (1955) Die ältesten Fossilien Süd-Afrikas. Senckenb Lethaea 36:243–289

Sánchez EAM (2010) Micropaleontologia aplicada na interpretação estratigráfica e paleoclimática da transição entre o Grupo Paranoa e o Supergrupo São Francisco (Neoproterozoico, Cabeceiras, GO). MSc Thesis, Universidade de São Paulo, São Paulo, pp 1–125

Schiffbauer JD, Huntley JW, Darroch SAF, Laflamme M, Cai Y (2016) The latest Ediacaran wormworld fauna setting the ecological stages for the Cambrian explosion. GSA Today 26:4–11

Seilacher A (1984) Late Precambrian and early Cambrian Metazoa: preservational or real extinctions? In: Holland HD, Trendall AF (eds) Patterns of change in Earth evolution. Springer, Heidelberg, pp 159–168

Seilacher A (1992) Vendobionta and Psammocorallia: lost constructions of Precambrian evolution. J Geol Soc London 149:607–613

Seilacher A (1999) Biomat-related lifestyles in the Precambrian. Palaios 14:86–93

Seilacher A (2007) The nature of vendobionts. In: Vickers_Rich P, Komarower P (eds.) The Rise and Fall of the Ediacaran Biota. Geological Society of London Special Publication, vol 286. The Geological Society, London, pp 387–397

Sial AN, Peralta S, Ferreira VP, Toselli AJ, Aceñolaza FG, Parada MA, Gaucher C, Alonso RN, Pimentel MM (2008) Upper Cambrian carbonate sequences of the Argentine Precordillera and the Steptoean C-isotope positive excursion (SPICE). Gondwana Res 13:437–452

Smith EF, Nelson LL, Tweedt SM, Workman JB (2017) A cosmopolitan late Ediacaran biotic assemblage: new fossils from Nevada and Namibia support a global biostratigraphic link. The R Soc Proc B 284:20170934

Sprechmann P, Gaucher C, Blanco G, Montaña J (2004) Stromatolitic and trace fossils community of the Cerro Victoria Formation, Arroyo del Soldado Group (lowermost Cambrian, Uruguay). Gondwana Res 7:753–766

Steiner M (1994) Die neoproterozoischen Megaalgen Südchinas. Berliner geowissenschaftliche Abhandlungen, Reihe E 15:1–146

Teixeira AL, Gaucher C (2004) Bacias do Estágio de Transição dos setores Meridional (parcial) e Central da Província Mantiqueira. In: Mantesso-Neto V, Bartorelli A, Carneiro CDR, Brito-Neves BB (eds) Geologia do Continente Sul-Americano: Evolução da Obra de Fernando Flávio Marques de Almeida. Editora Beca, São Paulo, pp 503–525

Van Iten H, Marques AC, Leme JDM, Pacheco ML, Simões MG (2014) Origin and early diversification of the phylum Cnidaria Verrill: major developments in the analysis of the taxon's Proterozoic-Cambrian history. Palaeontology 57:677–690

Vidal G, Moczydłowska-Vidal M (1997) Biodiversity, speciation, and extinction trends of Proterozoic and Cambrian phytoplankton. Paleobiology 23(2):230–246

Vorob'eva NG, Sergeev VN, Knoll AH (2009) Neoproterozoic microfossils from the margin of the East European Platform and the search for a biostratigraphic model of lower Ediacaran rocks. Precambrian Res 173:163–169

Waggoner B (2003) The Ediacaran biotas in space and time. Integr Comp Biol 43:104–113

Walde DH, do Carmo DA, Guimarães EM, Vieira LC, Erdtmann BD, Sanchez EA, Adorno RR, Tobias TC (2015) New aspects of Neoproterozoic-Cambrian transition in the Corumbá region (state of Mato Grosso do Sul, Brazil). Annales de Paléontologie 101(3):213–224

Warren LV, Fairchild TR, Gaucher C, Boggiani PC, Poiré DG, Anelli LE, Inchausti JCG (2011) *Corumbella* and in situ *Cloudina* in association with thrombolites in the Ediacaran Itapucumi Group, Paraguay. Terra Nova 23:382–389

Warren LV, Pacheco MLAF, Fairchild TR, Simões MG, Riccomini C, Boggiani PC, Cáceres AA (2012) The dawn of animal skeletogenesis: ultrastructural analysis of the Ediacaran metazoan *Corumbella werneri*. Geology 40(8):691–694

Warren LV, Quaglio F, Riccomini C, Simões MG, Poiré DG, Strikis NM, Anelli LE, Strikis PC (2014) The puzzle assembled: Ediacaran guide fossil *Cloudina* reveals an old proto-Gondwana seaway. Geology 42:391–394

Warren LV, Quaglio F, Simões MG, Gaucher C, Riccomini C, Poiré DG, Freitas BT, Boggiani PC, Sial AN (2017) *Cloudina-Corumbella-Namacalathus* association from the Itapucumi Group, Paraguay: increasing ecosystem complexity and tiering at the end of the Ediacaran. Precambr Res 298:79–87

Wood RA, Grotzinger JP, Dickson JAD (2002) Proterozoic modular biomineralized metazoan from the Nama Group, Namibia. Science 296:2383–2386

Zaine M (1991) Análise dos fósseis de parte da Faixa Paraguai (MS, MT) e seu contexto temporal e paleoambiental. PhD Thesis, Universidade de São Paulo

Zaine MF, Fairchild TR (1985) Comparison of *Aulophycus lucianoi* Beurlen & Sommer from Ladário (MS) and the genus *Cloudina* Germs, Ediacaran of Namibia. Anais Academia Brasileira de Ciências 57(1):130

Zucatti-da-Rosa AL (2006) Evidências de vida no Ediacarano inferior da bacia do Itajaí, SC. MSc Thesis, Universidade do Vale do Rio dos Sinos

The Provenance of Selected Neoproterozoic to Lower Paleozoic Basin Successions of Southwest Gondwana: A Review and Proposal for Further Research

21

Udo Zimmermann

Abstract

A review and evaluation of existing provenance information together with their implication has been made of selected Neoproterozoic to Paleozoic successions of southwest Gondwana. This overview led to the identification of major underexplored areas of research and with often even basic issues still unresolved. Firstly, the data of U–Pb ages of detrital zircons needs to be adapted to the up-to-date knowledge of this methodological approach, which relates to sampling techniques, amount of grains and presentation of the data. Secondly, high resolution heavy mineral studies are nearly absent but powerful, especially in the identification of terrane boundaries and source compositions from active continental margins. Thirdly, the character of the geodynamic processes at the southern margin would be of importance, to differentiate the detritus derived from there from those related to the processes in the center of SW Gondwana, where allegedly the Kalahari, Congo and South American cratonic masses collided/interacted. Currently, it seems to be possible to argue that during the Neoproterozoic in the south of the Kalahari craton an active margin existed—of unknown distance to the modern continental margin. The central part of SW Gondwana is complex with an apparent minimum of three subduction zones to unify the Angola-Congo, South America and the Kalahari cratons, if they had been separated by oceanic crust. It is most probable that the tectonic regime changed from extensional to compressive during the Neoproterozoic, but how large had been the proposed oceanic basins and how was the proposed subduction zones orientated (if they have existed) is unknown. Subsequently, the area from central Argentina to southern Brazil and from the southern Gariep Belt to eastern South Africa have been covered with mainly recycled clastic successions of Cambro-Ordovican to Carboniferous ages. The western margin of Gondwana may have been affected by an active margin since c. 600 Ma until the Permian (or even today) interrupted by times of quiescence during the Upper Cambrian and Upper Ordovician to Lower Carboniferous.

Keywords

Provenance • U-Pb isotopic ages on detrital zircons
Sampling techniques

21.1 Introduction

Paleotectonic reconstructions are of major interest and concern in many studies regarding regional geodynamics. Several approaches gain supporting information to model the ancient geographic situation as a base for numerous application, even for the field of economic geology. Hence, mainly magmatic and metamorphic successions had been used in the past to decipher those mosaics, added later by paleomagnetic and sedimentological data combined with lithostratigraphic data. However, in the wake of quantitative sediment-petrography and sediment-geochemistry (including isotope geochemistry), sediment successions moved into the focus of those objectives. These quantitative methods are nowadays often used to compare, correlate or differentiate sedimentary successions in different modern geographic areas to test if there had been a relationship in ancient times, and which type of connection did exist. However, as clastic sediments and sedimentary rocks form, resulted from very different geological processes compared to crystalline rocks, careful sampling and a thorough understanding of the sedimentary pile is paramount for a successful provenance study. The application of different methods is always recommended, though not always feasible, which is a common problem in this field of study.

Southwest Gondwana (Fig. 21.1) with its wide range of Neoproterozoic to Lower Paleozoic rock record is a seducing

U. Zimmermann (✉)
Department of Petroleum Engineering, University of Stavanger, 4036 Stavanger, Norway
e-mail: udo.zimmermann@uis.no

S. Siegesmund et al. (eds.), *Geology of Southwest Gondwana*, Regional Geology Reviews,
https://doi.org/10.1007/978-3-319-68920-3_21

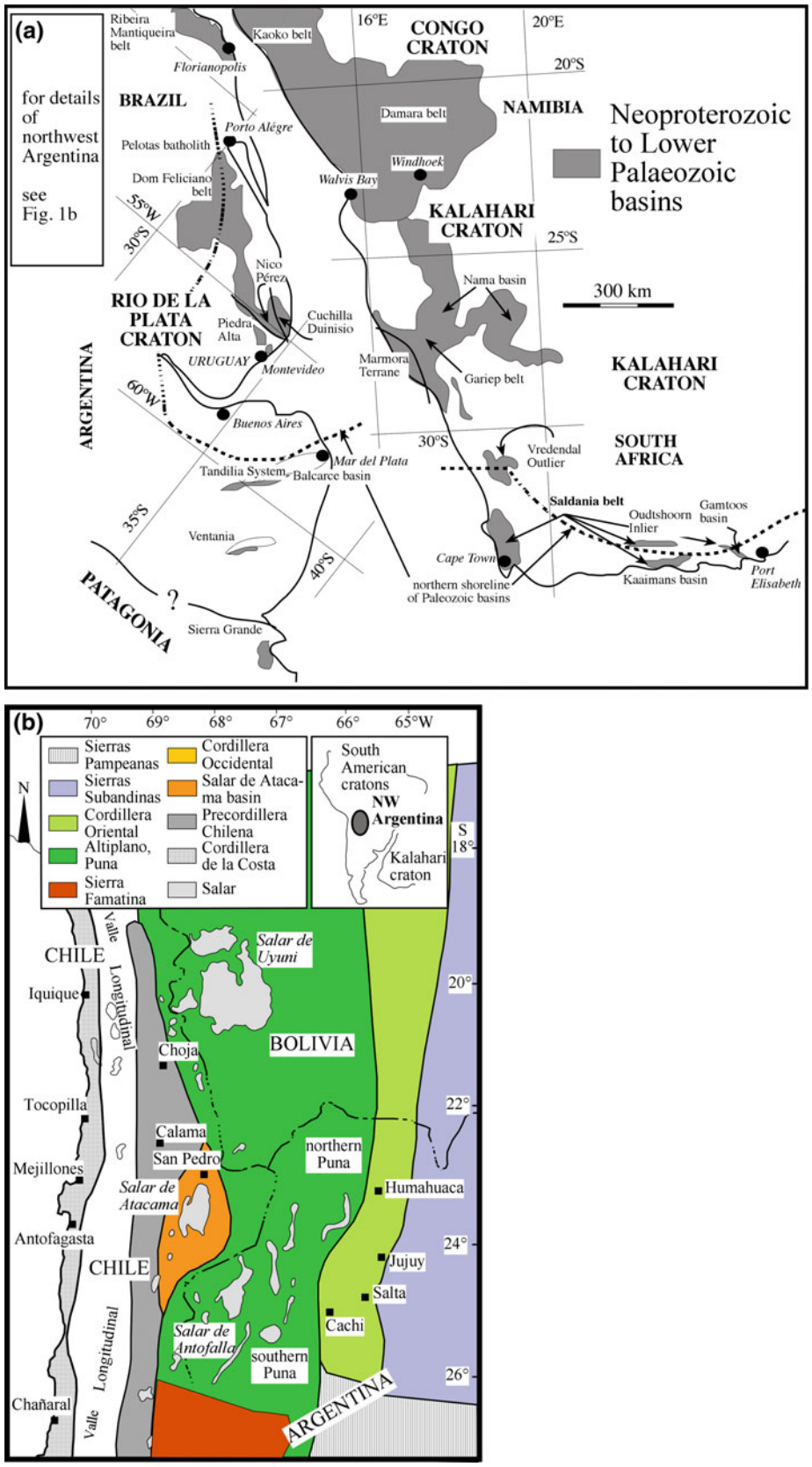

Fig. 21.1 Sketch map of SW Gondwana with basins discussed in this study. **a** Locations of basins of the Kalahari Craton (see detailed sketch map in Fig. 21.2) and Río de la Plata Craton. From Zimmermann et al. (2011b) with the northern shoreline of Paleozoic basins in eastern South America (after Uriz et al. 2016) and divisions of the Dom Feliciano and Gariep Belt (after Frimmel et al. 2010). **b** Sketch map of northwest Argentina (after Zimmermann et al. 2010)

field to test and apply the mentioned provenance methodology—and controversial as can be imagined. This is grounded in the obvious relation between western Africa and the eastern region of South America. Therefore, it represents a good, yet not perfect but sufficient, case study for comparison of successions at the eastern margin of southern South America and the successions fringing the southern part of South Africa (Fig. 21.1).

Southwest Gondwana can be described as the region from the Central Andes to the southern part of the Kalahari craton (Fig. 21.1). For the Neoproterozoic and Lower Paleozoic times the geological evolution of the southern South American continent contains already several controversial issues like the origin and the geographic location of Patagonia and the Precordillera (Fig. 21.1; compilation in Finney 2007; Pankhurst et al. 2014). These two areas are therefore here not discussed. The area mainly represented by the Angola-Congo Craton to the north and east as well to its west, towards the todays Brazilian areas is here also not covered, wherefore the major focus lies on the Central Andes (and here on the region covered by the Argentinean Puna, Cordillera Oriental and the Famatina Range, called from now on northwestern Argentina; Fig. 21.1b), the region of Uruguay and eastern Argentina (central SW Gondwana), the western (Gariep belt and Vredendal Outlier) and southern part of the Kalahari Craton (Saldania Belt) (Fig. 21.1). This is also related to specific issues of provenance studies in regard of an understanding what such an approach means.

All these areas had been involved in the formation and separation of Rodinia and placed in different models in different geographic areas (review in Evans 2013). However, controversial is still the exact paleogeographic position of the Río de la Plata craton as such that this block, as others like the Congo Craton have not been involved in the formation of Rodinia (Oriolo et al. 2017). However, the fact that South America and most parts of southern Africa have a common geological history as one larger block throughout most of the existence of Gondwana until the formation of Pangea implies a separation with a subsequent collision of these blocks after the formation of Rodinia, and to excel the complexity, in conjunction with the Angola-Congo craton. The mentioned possible amalgamation of these three major blocks, parts of South America, the Kalahari and the Angola-Congo craton is still enigmatic. The fact that the proposed separation had to produce oceanic crust, subsequently consumed via subduction complicates the interaction, and it is not entirely understood in this 'dance of three' (or even more). This process could not be resolved and explained by paleomagnetic data, lithostratigraphy and/or igneous and metamorphic petrogenesis, which called sediment provenance on the plan. The intensive sedimentological and structural study of sedimentary basins and their infill allowed to apply provenance studies and here discussed.

This contribution, therefore, will only review the status of knowledge of these areas, to point out well established knowledge and indicate where future work is necessary for a comprehensive model of geological processes, *all in terms and from the viewpoint of provenance studies solely*. Introduction into the lithostratigraphy, structure and geodynamic models as well as crystalline rocks are covered by other chapters in this book. The fact that the quality and the amount of provenance data varies significantly in between the different sedimentary successions, is challenging and affects the potential of interpretation. This contribution, therefore, will supply a pilot study of an evaluation of the class of provenance data based on the very modern approach in this field of geosciences. This is of importance as some contributions have been published earlier, when less was known about potential problems when using quantitative petrographical, geochemical and isotope geochemical data related to sedimentary rocks.

After an only very brief introduction in the different selected sedimentary deposits (as exhaustive literature does exist and this book here will add with several articles more information), the major trends of the existing provenance data will be addressed and evaluated. Again, the objective is not to introduce into the entire geology including the lithostratigraphic units, their genesis and significance discussing every single model or to present new models but to assist in the evaluation of the likelihood of existing models when discussing in specific selected cases only provenance related issues. This will give the way to asking kindly for focusing on what is known and fact, and what shall be added in the nearest future, again in the field of provenance studies.

21.2 Major Sedimentary Basins in Southwest Gondwana

Numerous publications have shown that sediment provenance studies are able to identify the paleotectonic evolution of a region and are able to pin-point a (paleo)tectonic setting for the studied areas based on the deduced principles by McLennan et al. (1990, 1993) and Taylor and McLennan (1985). This mostly geochemical approach combined with whole-rock Sm–Nd isotope geochemistry (after DePaolo 1981; DePaolo et al. 1991) was more recently substantially enhanced with the application of intensive isotope geochemistry of detrital grains like zircon (a large amount of literature here the compilation in Hanchar and Hoskin (2003) is only mentioned; Cawood et al. 2012) and recently rutile (Triebold et al. 2012) using U–Pb and Lu–Hf systematics on the same grain (Vervoort and Patchett 1996; Hanchar and Hoskin 2003; Vervoort and Kemp 2016).

21.2.1 Kalahari Craton

The monumental geological compilation by Tankard et al. (1982) comprises the knowledge of the southern African

geology and was recently up-dated with a focus on South African geology (Johnson et al. 2006) besides very detailed and brilliant studies on large sedimentary successions of the mentioned Neoproterozoic to Lower Paleozoic time frame (e.g. Germs 1995; Thamm and Johnson 2006) and descriptions on selected areas [(compiled in Tankard et al. (1982) and Johnson et al. (2006)]. Figure 21.2 shows the main Neoproterozoic basins on the western and southern margin of the Kalahari craton, which were mostly subsequently covered by the Cape Supergroup and its equivalents from the Cambrian on. These are as being relevant for this contribution the Gariep Belt and the Saldania Belt including the area around Port Elisabeth (Fig. 21.2). The Cape Supergroup and its equivalents (Thamm and Johnson 2006) represents a very thick craton-cover sequence and pinches out in the west towards the Gariep Belt and in the east towards Mozambique, but has its equivalents in eastern South America (Fourie et al. 2011; Uriz et al. 2011).

21.2.1.1 Gariep Belt

Generals

The Neoproterozoic basins in the west, to the south of the proposed suture to the Angola-Congo craton, are represented by the successions deposited in the Gariep Belt (compilation in Frimmel and Fölling 2004) and the northern margin successions of the Kalahari craton (the 'southern foreland' according to Frimmel et al. 2011) towards the so-called Khomas Sea, the oceanic area produced during the rifting of the Kalahari craton away from the Angola-Congo craton during the dismembering of Rodinia (compilations in Frimmel and Frank 1998; Gray et al. 2006). However, recently Foster et al. (2014) find that U–Pb combined with Lu–Hf isotopes on detrital zircons that the margin successions on both cratons allow in proposing a distance between these cratons during the break-up of Rodinia. The southwest

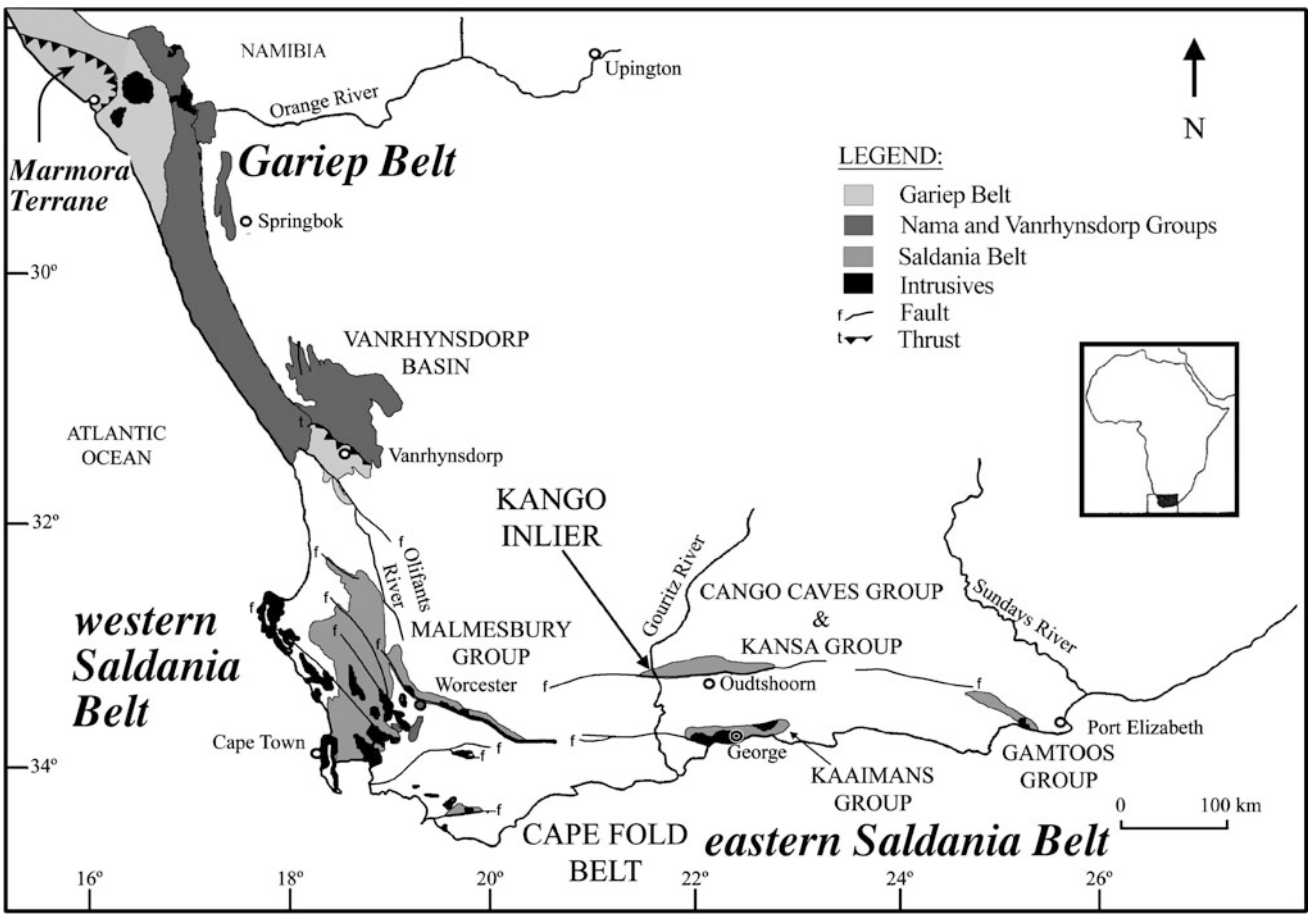

Fig. 21.2 **a** Sketch map of sedimentary basins of importance for the contribution here located on the Kalahari craton (from Zimmermann et al. 2011b)

'corner' of the Kalahari craton is represented by the successions of the Vredendal Outlier and the western Saldania belt (see below), while the eastern Saldania Belt is composed of three smaller basin units (compilation in Frimmel et al. 2013).

The successions in the Gariep Belt are divided in different areas or terranes (compilation in Frimmel 2011a) and interpreted to be deposited during the opening and closure of an oceanic basin (Adamastor Ocean or Brazilide Ocean), separating the Kalahari Craton from South America (Hartnady et al. 1985; Stanistreet et al. 1991; Frimmel et al. 1996a, b; Frimmel and Frank 1998), which supposedly constructed this orogenic belt when colliding again (c. 610–530 Ma; Basei et al. 2005, 2008; or 530–495 Ma; Gray et al. 2006) with South America. The extensional phase is supported by small-scale intrusive and extrusive rocks with ages between c. 850 and 740 Ma (Frimmel et al. 1996a, b, 2001). However, igneous rocks related to an active margin and volcano-sedimentary successions typical for active margins are absent or yet to be found or are already eroded. According to Basei et al. (2005, 2008) and Frimmel et al. (2010) they may have been located in the eastern part of South America (Uruguay, Cuchilla Dionisio or Punta del Este Terrane or Arachania), interpreted as a part of the western Kalahari craton during Neoproterozoic by the same authors and their peer-group, but disputed by other geologists (see Oyhantçabal et al. 2009).

The lithostratigraphy of the Gariep Belt records generally a very thin package of sediment with less than 2000 m (Frimmel and Fölling 2004) for a major rift-drift and collisional tectonic evolution stretching over 200–300 My (Frimmel et al. 1996a, b). The Gariep Belt sedimentation record is found on these three terranes with different lithostratigraphies (Frimmel 2011a) and interpreted as containing remnants of (back-arc) oceanic crust (Frimmel et al. 1996a, b; 2010). Sedimentary successions deposited after c. 740 Ma, the age of extensional magmatism, shall record the alkaline signature typical for rift tectonics, while those after the disputed timing of the collision or during the activity of the volcanic arc, need to record the active margin detritus including arc magmatism and possible oceanic detritus, either in the framework mineral composition (Dickinson and Suczek 1979), or in the geochemical signature (McLennan et al. 1990, 1993) or in their U–Pb ages of detrital zircons derived from the active margin (Cawood et al. 2012). The proposed arc had been separated by an oceanic basin (see compilation in Frimmel et al. 2010), which complicates the transport of detritus into the rifted margin basins of the Kalahari craton.

The thrusted terranes are covered by the Late Ediacaran to Cambrian Nama Group. The latter has been interpreted based on the lithostratigraphy as a foreland basin in an exceptional contribution by Germs (1995). While the rocks of the Gariep Belt suffered low grade metamorphism, the exact metamorphic grade of the Nama Group is unknown but its exceptional fossil record and the possible chemostratigraphic studies assume a lower metamorphic grade (e.g. Germs 1995; Grotzinger et al. 1995; Saylor et al. 1998).

Age constraints

Age constraints are partially absolute with U–Pb ages on felsic lava flows (Rosh Pinah Formation, a part of the Port Nolloth Group; Fig. 21.3) pointing to a depositional age at 750 Ma (SHRIMP method; Borg et al. 2003), supported by Pb–Pb ages on single zircon grains from the same unit dated at c. 742 Ma (Frimmel et al. 1996a). Chemostratigraphic tools have been applied to the carbonate units of the Port Nolloth Group and led to different age constraint interpretation related to an involvement of the 'snowball Earth hypothesis', which finally has been reviewed and reinterpreted by Frimmel (2010), concluding that chemostratigraphic data in the Gariep Belt are not free of doubt in terms of their possible primary nature and/or validity as reflector of the global trend. This issue has been discussed in detail in Zimmermann et al. (2011b), who proposed a more conservative interpretation until more data are available, which are not so far.

Paleontological data for the Pre-Nama successions are scarce and rely on non-global biostratigraphic data (pers. com. with K. Grey and M. Mocydlowska-Vidal in 2008; Pecoits et al. 2011) on acritarchs (Gaucher et al. 2005a, b). Again, more biostratigraphic data are necessary to avoid any misinterpretation or any doubts.

The Port Nolloth Group and the Gariep Belt successions are succeeded by rocks of the Nama Group, dated at its base at 549 ± 1 Ma (Grotzinger et al. 1995) and which host the world-famous Ediacara fauna which dates the rocks into the Late Ediacaran. The end of deposition for the Nama Group is assigned to be during the Lower Cambrian (Germs 1995; Geyer 2005), however based on trace fossils. Further south, equivalents of the Nama Group succession (Gresse and Germs 1993) are overlain by the Cape Supergroup, interpreted to be not younger than the Lower Ordovician (Thamm and Johnson 2006). The youngest detrital zircon found in the Fish River Group, the upper part of the Nama Group, is reported at 531 ± 9 Ma. However, the samples have been possibly unfortunately swapped (pers. com. G. Blanco, November 2008: pers. com. F. Chemale, January 2009) and a re-evaluation of the detrital zircon yield for the upper part of the Fish River Subgroup showed very different detrital zircon characteristics in terms of shape and size (Øxnevad 2017).

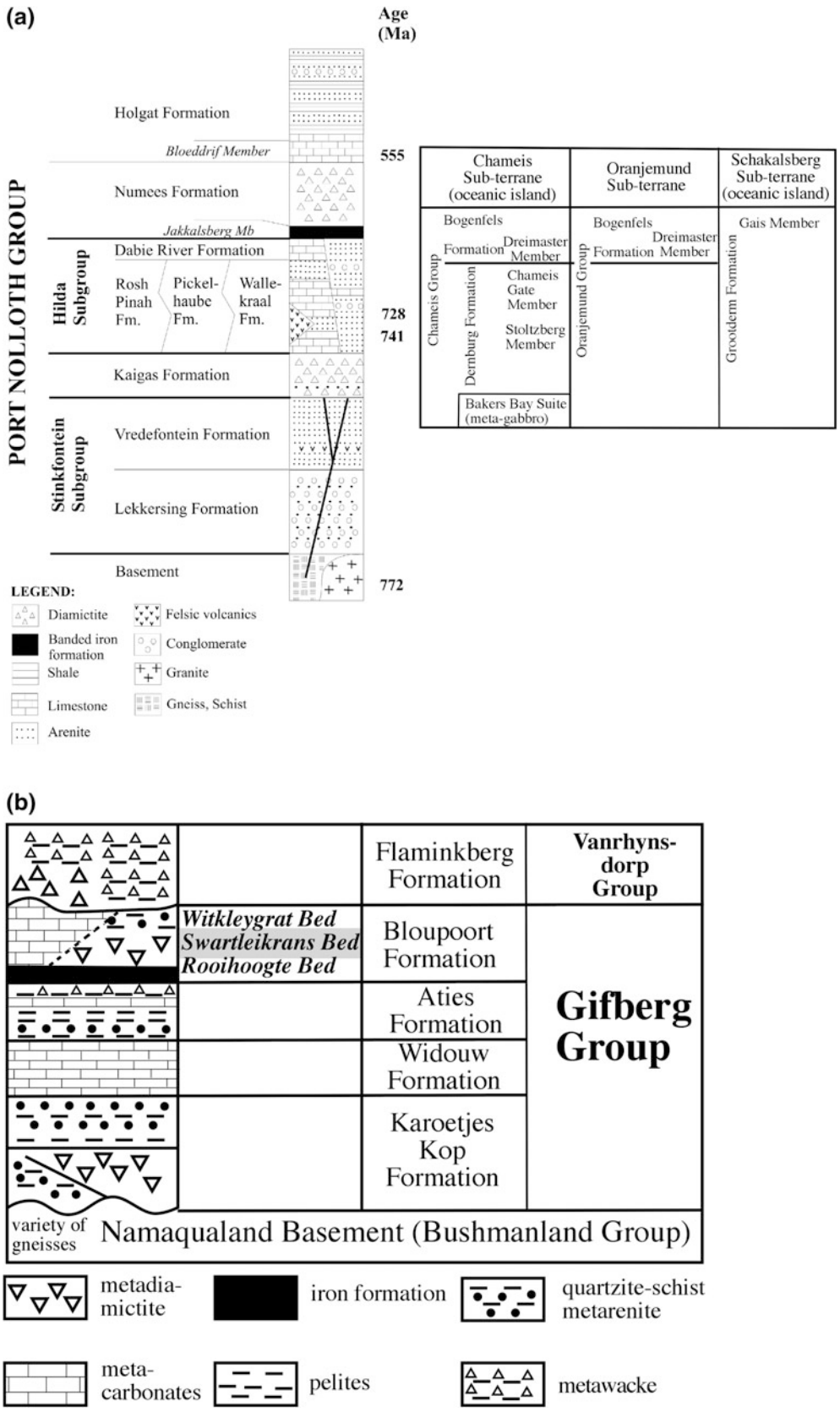

Fig. 21.3 Lithostratigraphy of the Gariep Belt and Vredendal Outlier (Part 1). **a** Port Nolloth Group (from Van Staden et al. 2006) and the lithologies of the Marmora Terrane (after Frimmel 2000a). **b** Stratigraphy of the Gifberg Group (from Van Staden et al. 2006). Detailed lithology descriptions can be found in this book and in Frimmel (2011) and Van Staden et al. (2006)

Exceptional lithostratigraphic characteristics

In the western area of the Kalahari craton, rock successions occur, including even type localities of the 'snowball Earth hypothesis' (Hoffman and Schrag 2002) containing diamictites and so-called cap carbonates. This interpretation and discussion is, as widely known, a highly sensitive topic and here is not the place to discuss this in detail. However, the hypothesis has re-initiated strongly the correlation efforts based on specific lithologies of the 'snowball Earth hypothesis' (like diamictites or glacial diamictites, so-called cap carbonates with pinkish colors and iron formations) are used for correlation, implying that the different exposed diamictites are (i) of glacial origin and (ii) related beyond doubt to the three/four assigned significant ice ages defined by Hoffman and Li (2009; Kaigas, Sturtian, Marinoan or Gaskier). Age determination using U–Pb ages of detrital zircons were unsuccessful (Zimmermann et al. 2011b; Hofmann et al. 2014; Naidoo et al. 2017), although several Neoproterozoic igneous events are well recorded in the detrital zircon record of younger, Late Ediacaran to Carboniferous rocks from the Kalahari craton (e.g. Blanco et al. 2009; Fourie et al. 2011; Naidoo et al. 2013). Hence, the diamictites remain undated, besides the Kaigas formation with an age around 745 Ma. Furthermore, so far there are very few detailed sedimentological study on the diamictites of the Gariep Belt (e.g. Zimmermann et al. 2011a, b). Earlier, Martin (1965)—often referenced—claimed to have identified numerous glacial diamictites, but the same author rectified his own studies in 1985 (Martin et al. 1985—nearly never referenced) practically completely to pin-point only one single deposit as of possible glacial nature (!). This coincides with the interpretations by Schermerhorn (1974). What is of utmost importance, is the fact that the deposits are not sufficiently studied in terms of clastic sedimentology and therefore shall not be used as correlation horizons of definite age, as earlier proposed by Zimmermann et al. (2011b), Naidoo et al. (2013), Van Staden et al. (2014) and Naidoo et al. (2017).

Puzzling (or not) is the observation that the Neoproterozoic rocks of the Gariep Belt do not host *significant* igneous rocks or epiclastic units related to the proposed syndepositional extensional event (rift) and formation of oceanic crust (drift) and active volcanic arc to the west (Basei et al. 2005, 2008; Frimmel et al. 2010). Aeolian deposits, derived from an active arc, may deposit proximal the active arc (or even in far distances), either to the west (in Uruguay and eastern Argentina) or east of the arc, depending on the paleoaeolian directions. This has been observed during the Ordovician in eastern Argentina or in the Precordillera of western Argentina and Laurentia (Huff et al. 1992, 1998; Zimmermann and Spalletti 2009), for example.

Provenance studies

Provenance studies in the light of modern isotope geochemical analyses (see below) (Vermeesch 2004; Andersen 2005), sampling techniques and awareness of facies (DeGraaf-Surplass et al. 2003; Zimmermann et al. 2015) are not available besides in small-scale local studies (Zimmermann et al. 2011b; Naidoo et al. 2017) and in Hofmann et al. (2014). Basei et al. (2005, 2008) presented very interesting pilot studies on samples from the different terranes of the Gariep Belt, but dated only few detrital zircons and did not determine for the younger grains their discordancies. Geochemical and isotope geochemical data are available from the Nama Group (Blanco et al. 2011) and for some successions of the Marmora Terrane and the Port Nolloth Group (Basei et al. 2005; Van Staden et al. 2006; Zimmermann et al. 2011b) and will be discussed below.

21.2.1.2 Vredendal Outlier

Generals

Rocks in the Vredendal Outlier to the north of the Saldania Belt (Fig. 21.2) are exposed as the Gifberg Group and the overlying Vanrhynsdorp Group, covered by rocks of the Paleozoic Cape Supergroup (De Beer et al. 2002). The Gifberg Group is interpreted to be an equivalent of the Port Nolloth Group of the Gariep Belt (e.g. Frimmel et al. 2010) and the Vanrhynsdorp Group rocks are equivalents to the upper Nama Group rocks (Gresse and Germs 1993; Fig. 21.4) based on lithostratigraphy and deformational history. The overlying rocks of the Cape Supergroup range from the Ordovician to the Carboniferous (De Beer et al. 2002).

As an equivalent of the Port Nolloth Group, the Gifberg Group should therefore represent a comparable geological evolution with a rift-drift and collisional event. Its thickness of not more than 1000 m and the fact to be devoid of igneous rocks (Bührmann 1981) is not typical for sedimentary successions accompanying such a geological history. It may be that a larger amount of those strata had been eroded during active syndepositional tectonics prior to the deposition of the overlying Vanrhynsdorp Group rocks. These have been, as the Nama Group rocks, deposited in a foreland basin (Gresse and Germs 1993) related to the proposed collision of the Kalahari craton with South America. The Cape Supergroup indicates the transition from extensional tectonics after the collisional event during the Cambro-Ordovician towards a large intracratonic basin, with characteristics of a passive margin in terms of the provenance indicators (Thamm and Johnson 2006; Fourie et al. 2011). Both, the Vanrhynsdorp Group and the Cape

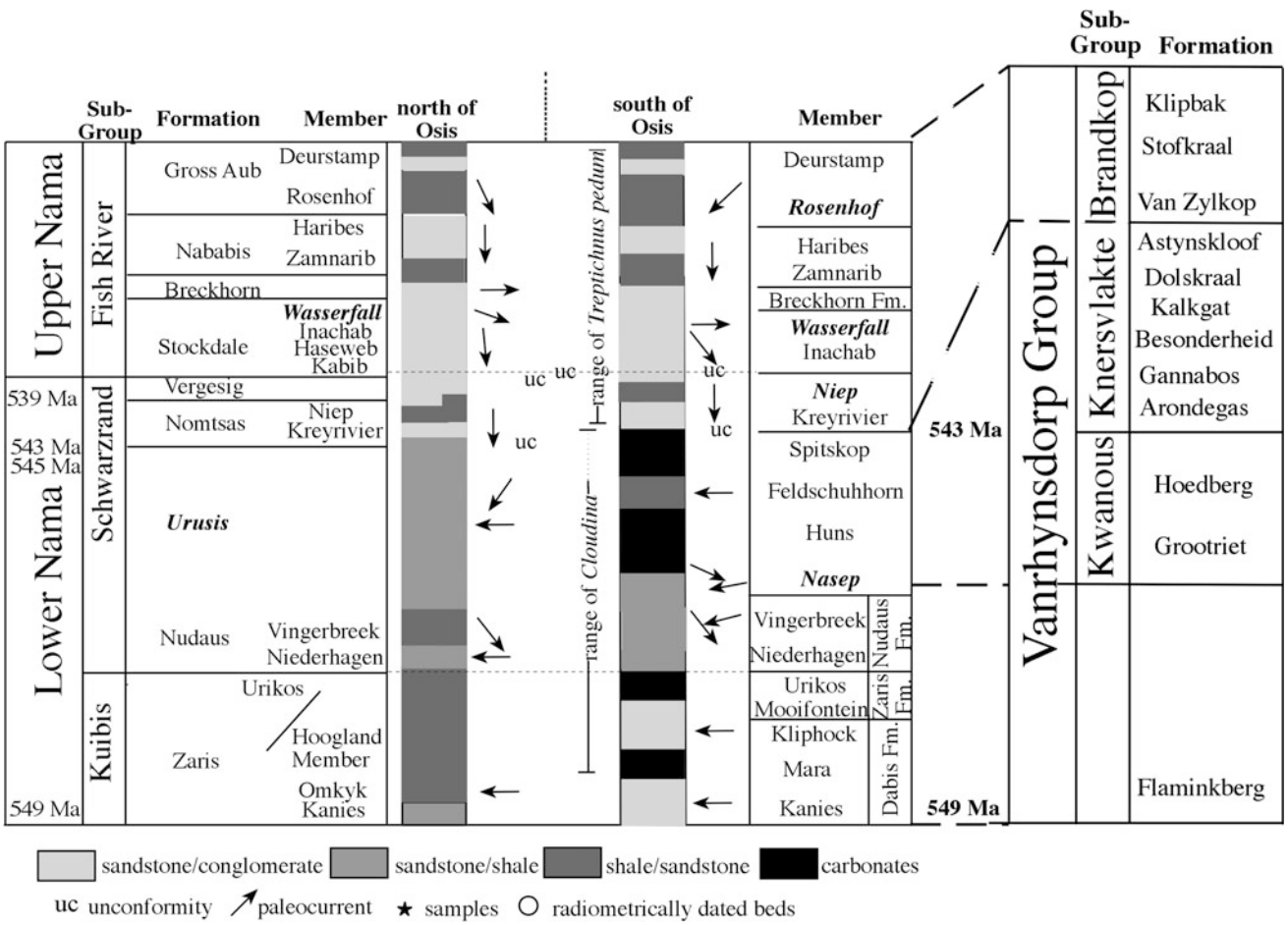

Fig. 21.4 Lithostratigraphy of the Nama and Vanrhynsdorp Group (Gariep Belt and Vredendal Outlier) (after Germs 1995; Frimmel et al. 2010). Detailed lithology descriptions can be found in Germs (1995) and Gresse et al. (2006 and references therein). The Vanrhynsdorp Group is covered by the Cape Supergroup successions

Supergroup should reveal detritus from the proposed active continental margin, if sediment dispersal systems had been favorable for such a reworking from the margin towards the east.

Age constraints

There are no age constraints for the Gifberg Group. Earlier, chemostratigraphic data had been used to determine an absolute age (given that this is a reliable method, which is controversial) but the reliability of the data in terms of a definite primary signature or a reflection of global seawater composition had been reviewed and an interpretation abandoned (Frimmel 2009, 2010). Paleontological constraints are absent and detrital zircon U–Pb ages gave a robust peak for grains of a Late Mesoproterozoic age but only two grains have been found of Neoproterozoic age (youngest 573 ± 8 Ma, 8% discordance) and an interpretation avoided (Naidoo et al. 2017) following recent lines of interpretations (e.g. Dickinson and Gehrels 2009). The Vanrhynsdorp Group rocks host trace fossils indicating a deposition straddling the Precambrian-Cambrian boundary (Buatois et al. 2013). The rocks of the overlying Cape Supergroup with samples from the Bokkeveld Group (Devonian) gave only few results from U–Pb age determination on detrital zircons but Neoproterozoic detritus could be observed.

Exceptional lithostratigraphic characteristics

The Gifberg Group, analog to the Port Nolloth Group, hosts two diamictites and two major carbonate units. However, the lower diamictite appears in the field rather as a paleovalley infill, hence a debris flow or gravity flow deposit, and shows no evidence of a glacial deposit (Van Staden et al. 2014). The upper diamictite, in turn, may point to a glacial environment based on few sedimentological and geochemical data and their interpretation (Van Staden et al. 2014; Naidoo et al. 2017), so also proposed by Bührmann (1981) based on interpreted 'dropstones'—however, the rocks are metamorphosed and strongly deformed. Hence, a glacial origin

beyond doubt is not possible to determine, *and* the depositional age is unknown.

The occurrence of *Treptichnus pedum,* which may mark the Precambrian-Cambrian boundary or strata close to this boundary, in the Vanrhynsdorp Group is spectacular and aided in defining the facies preference for this ichnofossil (Buatois et al. 2013).

Interesting is the absence of igneous rocks and even epiclastic deposits in the whole stratigraphy for the Neoproterozoic successions, although the proposed arc was not too far to the west exposed and active.

Provenance studies

Provenance studies are exercised based on petrographical and geochemical data (Van Staden et al. 2014) and U–Pb isotopic data from detrital zircons (Naidoo et al. 2017). The latter were so far unsuccessful in terms of determining a depositional age or a maximum sedimentation age—similar to all other attempts in diamictites of the region (Zimmermann et al. 2011a, b; Hofmann et al. 2014), which may would have been helpful for the geodynamic interpretation.

21.2.1.3 Western Saldania Belt

Generals

The rocks of the western part of the Saldania Belt (Fig. 21.2) have been deposited in three areas formerly defined as terranes, but reduced to two terranes based on provenance data (compilations in Frimmel et al. 2010, 2013). The rocks of the Malmesbury and Boland Group (sensu Frimmel et al. 2013) are overlain by the Klipheuwel Group of Cambrian age (Frimmel et al. 2013) and covered by the Cape Supergroup. The oldest successions, the Malmesbury and Boland Groups, have been interpreted to be deposited in a back-arc basin, but it is not proven that this basin has been floored by oceanic crust (Frimmel et al. 2013), while its northern prolongation contains such a crust-type (Frimmel et al. 2013). Subsequent rocks (Klipheuwel Group) have been deposited after the extinction of the arc and the closure of the different oceanic basins, and are interpreted to be related to the same retro-arc foreland basin as the Nama Group (Frimmel et al. 2013). Deposited in an extensional tectonic regime which is interpreted to point to a rift or pull-apart basin (Gresse et al. 2006 in Frimmel et al. 2013).

Age constraints

Frimmel et al. (2013) interpret a depositional age based on their interpretation of U–Pb ages for detrital zircons for the Malmesbury (557–552 Ma) and Boland (609–530 Ma) Groups ranging from the Ediacaran to Lower Cambrian. This will later be evaluated and more conservative interpreted.

Exceptional lithostratigraphic characteristics

The Neoproterozoic successions here, and this may be exceptional, are devoid of the 'snowball Earth hypothesis' successions, although the age interpretation by Frimmel et al. (2013) would allow such a deposition. However, it is obvious that these successions (diamictite/glacial deposit—cap carbonate and possible iron formation) do not *have* to be preserved, as many Neoproterozoic successions do not carry those (see Schermerhorn 1974; Eyles and Januszczak 2004). Rare—as in the Gariep Belt—are igneous or epiclastic rocks, although the successions are proposed to be deposited in a back-arc basin. However, as in the cases above, this may be related to preservation and/or to outcrop conditions.

Provenance studies

Very few studies have been carried out (Buggisch et al. 2010; Frimmel et al. 2013) in this area, the western Saldania Belt. Rocks of the Cape Supergroup have been subject of a provenance study using geochemical and isotope geochemical methods as well, but as in Frimmel et al. (2013), the major issue had been the high amount of discordant U–Pb ages in detrital zircons.

21.2.1.4 Eastern Saldania Belt (Southern Margin)

Generals

Precambrian rock successions at the southern margin (eastern branch of the Saldania Belt) of South Africa are exposed in the Kango Inlier around the town Oudtshoorn, as the Kaimaans Group close to the town George and as the Gamtoos Group north of Jeffrey's Bay close to Port Elisabeth (Fig. 21.2). They are associated with the Saldanian orogenic event (c. 600 Ma) and had been exposed during the Permian. These rocks were affected by low grade metamorphism, except locally where they have been intruded and metamorphosed to a higher degree during contact metamorphism caused by granites of the Cape Granite Suite (Gresse 1983; Frimmel and van Achterbergh 1995). In addition, these rocks are structurally complex and are folded and faulted—to the point that the stratigraphy is still unclear.

The rocks of the Kango Inlier are capped by the Kansa Group and the Schoemannspoort Formation, followed by the Cape Supergroup. The Kaimaans Group is associated with the Cape Granite Suite (although volcanic rocks are associated to this magmatic event), an igneous event during the

Cambrian which intruded in Neoproterozoic rocks and stretches from the Cape Town area to Port Elisabeth and covered by the Cape Supergroup. The Cape Granite Suite and the overlying clastic rocks of the Cape Supergroup have equivalents in eastern Argentina (Rozendaal et al. 1999; Rapela et al. 2003; Gregori et al. 2004; Uriz et al. 2011). This intrusion of felsic to intermediate plutonic and associated volcanic rocks took place before the deposition of the Table Mountain Group (Da Silva et al. 2000; Scheepers and Armstrong 2002; Chemale et al. 2010). However, granitic intrusions or volcanic rocks are not observed in the Cango Caves and Kansa Groups. The further east deposited Gamtoos Group, close to Port Elisabeth, is overlain by the Sardinia Bay Formation and, subsequently, the Cape Supergroup. All successions are affected by lower greenschist facies metamorphism and, in some areas, contact metamorphism is observed close to the intrusive bodies of the Cape Granite suite (Gresse 1983; Miller et al. 2016).

The rocks of the Cango Caves Group are interpreted to be deposited in a foreland basin (Van Staden et al. 2006; Naidoo et al. 2013) based on their sedimentological features, geochemical and isotope geochemical composition, although an active margin or general active margin deposits have not been found towards the south so far. It has been speculated that the area of the active margin may have been drifted away from the Kalahari craton, as Patagonia or an unknown exotic terrane (Fourie et al. 2011; Naidoo et al. 2013). A similar statement could be made for the Kansa Group (Van Staden et al. 2006). This active continental margin provenance signature changes strongly with the Schoemannspoort Formation (Fig. 21.5d) and the Cape Supergroup rocks, which are characterized by strongly recycled detritus and a different tectonic setting (intracratonic basin or passive margin) and/or a very different source, wherefrom mainly quartz-rich material resulted (Van Staden et al. 2006; Naidoo et al. 2013).

The rocks of the Kaimaans Group are comparable to those of the Cango Caves and Kansa Groups in terms of provenance data showing a typical retro-arc basin geochemical signature (Zimmermann et al. 2008a, b)—sedimentological interpretations are impossible because of the high metamorphic grade of the rocks. Their main isotope geochemical characteristics are the abundance of significant input of Neoproterozoic detritus (Naidoo et al. 2013; Naidoo 2016).

The Gamtoos Group rocks comprise mainly turbidites and quartz-arenites with a significant recycled component in its composition. Those clastic rocks are associated with carbonates but the exact stratigraphy is disputed (compiled in Gaucher and Germs 2006). Nevertheless, if compared to the rocks of the Oudtshoorn Inlier, the successions overlying the Gamtoos Group rocks are extremely enriched in quartz, hence their detritus is significantly recycled. U–Pb ages on detrital zircon are published but complex to interpret, as rarely groups of similar aged grains could be found and not enough grains were dated with the required concordance in their U–Pb isotope characteristics to exclude significant source components (Miller et al. 2016; Naidoo 2016). Both authors call for further studies.

Age constraints

All sedimentary successions are devoid of igneous rocks and some have been affected by intrusive bodies. U–Pb isotopic ages on detrital zircons from the metasedimentary rocks of the Cango Caves Group point to a sedimentation age older than the Cambrian Cape Granite Suite. The metasedimentary rocks, however, revealed no useful detrital zircon ages (see discussion later) for the purpose of excluding sources and to determine a definite maximum depositional age, as only very few grains had been concordant and the youngest grain at c. 571 ± 9 Ma was a single one, which shall not be used as an age constraint (Dickinson and Gehrels 2009; Naidoo et al. 2013). A small group of detrital zircon ages in the Huis Rivier Formation (Fig. 21.5d) scatter around 650 Ma. The rocks of the Kansa Group (Fig. 21.5d) are definitely younger, and point to a Late Cambrian depositional age (Barnett et al. 1997; Naidoo et al. 2013), so does the overlying Ordovician Peninsula Formation (Naidoo et al. 2013). The Neoproterozoic rocks show also few records of acritarchs, which are interpreted as being of Late Ediacaran age (Gaucher et al. 2005b), as similar acritarchs have been found in Uruguay together with *Cloudina* sp. (Gaucher et al. 2005b; Gaucher and Germs 2006), although the here described acritarchs are not global biostratigraphic markers (see above).

The rocks of the Kaimaans Group mark within their youngest detrital zircons a Late Ediacaran depositional ages (Naidoo 2016). This accounts for all successions but the Sandkraal Formation (Fig. 21.5b), which contains ages similar to the Cape Granite Suite—a characteristic which is still not understood (Naidoo 2016). The intruding granites have been dated with Lower Cambrian ages (Da Silva et al. 2000; Chemale et al. 2010) and post-date the Kaimaans Group rocks.

Detrital zircons of the Gamtoos Group have been dated and Naidoo (2016), could not determine younger ages than Mesoproterozoic ones, while Miller et al. (2016) interpret, based on their detrital zircon population, the age for the Kleinrivier Formation (Fig. 21.5c) into the Lower Cambrian (<529 Ma). This contradicts the paleontological findings by Gaucher and Germs (2006), who proposes a Late Ediacaran for the same formation based on the often used achritarch assemblage, which, however (as commented) is not biostratigraphical valid on a global scale. However, the age difference is not significant for the general geodynamic

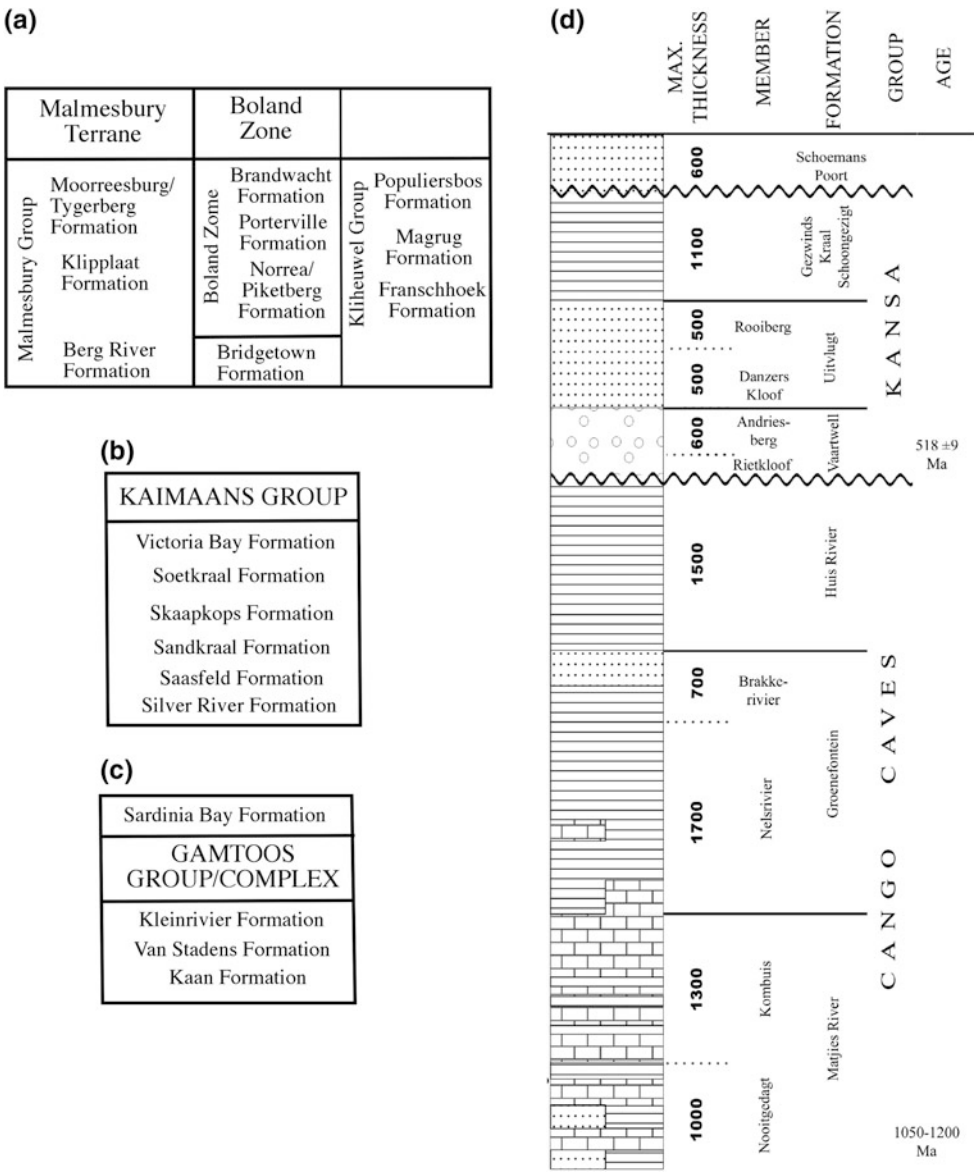

Fig. 21.5 Lithostratigraphy of the Western and Eastern Saldania Belt. **a** Stratigraphy of the western Saldania Belt (after Frimmel et al. 2010). **b** Stratigraphy of the Kaimaans Group (eastern Saldania Belt; after Frimmel and van Achterbergh 1995). **c** Stratigraphy of the Gamtoos Group/Complex and Sardinia Bay Formation (eastern Saldania Belt; after Miller et al. 2016). **d** Stratigraphy of the Cango Caves and Kansa Groups (eastern Saldania Belt; from Van Staden et al. 2006). The different units are covered by the Cape Supergroup successions

interpretation, but calls for a re-evaluation of both methods applied. Naidoo (2016) supports with her data the age determination of the Sardinia Bay Formation by Miller et al. (2016) of being Early Paleozoic. However, all authors (Naidoo, Miller et al.) here agree on the need to date more detrital zircons from these successions to gain sound results (see below).

Exceptional lithostratigraphic characteristics

As in the western Saldania Belt, the successions are devoid of definite glacial or diamictitic deposits or so-called cap carbonates in the terms of the 'snowball Earth hypothesis'. Two conglomeratic successions exist in the Oudtshoorn Inlier, but they are not resembling diamictitic or even glacial characteristics. Chemostratigraphy in carbonate rocks of the Cango Caves Group have been made to investigate isotope trends (Fölling and Frimmel 2002) but, similar to the above discussed deposits at the western margin of the Kalahari craton, it is not ensured that the values are of primary nature (Frimmel 2008, 2009, 2010).

Provenance studies

The rocks of the Cango Caves, Kaimaans and Gamtoos Groups (Fig. 21.5) have been subject of provenance studies and most of the data have been published (Van Staden et al. 2006; Naidoo et al. 2013; Miller et al. 2016) and some are unpublished (Naidoo 2008, 2016) and will here only be briefly discussed. This applies to the geochemical as to the isotope geochemical data. Recently, Miller et al. (2016) added interesting data for the Gamtoos Group and the

Sardinia Bay Formation. As in the western area, Fourie et al. (2011) studied the Cape Supergroup and supplied important age population of detrital zircons available in Ordovician to Carboniferous rocks.

21.2.2 South America

The here discussed successions have been accumulated in Uruguay and Argentina, at the eastern margin of the modern South America and in the northwestern part of Argentina, marking the Neoproterozoic to Lower Paleozoic western margin of SW Gondwana. In terms of provenance studies, the rocks of a small area in eastern Argentina (Tandilia System acc. Gómez Peral et al. 2007) and the Ventania region (Sierras de la Ventana; according to Uriz et al. 2011) and Sierra Grande region (according to Uriz et al. 2011; Fig. 21.1) are well studied as are the rocks of northwestern Argentina. The Uruguayan successions are in a way constrained that a number of controversial articles have been published and provokes strong discussion in terms of (i) the correct interpretation of the lithostratigraphy and basin evolution and (ii) an appropriate use of provenance methodologies, besides the validity of biostratigraphic data (Pecoits et al. 2011; Zimmermann 2011a, b; Aubet et al. 2014; Oriolo et al. 2016a, b, c; Gómez Peral et al. 2017). Lower to Upper Paleozoic rocks are exposed in the Ventania and Sierra Grande regions and will be discussed briefly to match with their most probable equivalents in South Africa, the Cape Supergroup (Fourie et al. 2011; Uriz et al. 2011).

21.2.2.1 Eastern South America: Uruguay and Eastern Argentina

Generals

The sedimentary successions of Neoproterozoic to Lower Paleozoic age of Uruguay (Fig. 21.5) are complex as they may have been deposited on different possible terranes, bounded by large scale shear zones, which are partly interpreted to be related either to the western Kalahari craton, to a volcanic arc (Dom Feliciano Belt) or the Río de la Plata Craton (Basei et al. 2008; Oyhantçabal et al. 2009; Frimmel et al. 2010, 2013; Fig. 21.2). In particular, following Oyhantçabal et al. (2011), the Río de la Plata Craton is limited to the east by the Sarandí del Yi Shear Zone, which separates it from the Nico Perez Terrane. The latter is clearly different from the Río de la Plata Craton and probably has a common origin with Congo-Angola Craton (Oriolo et al. 2016b).

Further east, the Punta del Este Terrane (or Cuchilla Dionisio Terrane (Gaucher et al. 2008), also named Arachania; Frimmel et al. 2010) as part of the Dom Feliciano Belt hosts a magmatic event around 770 Ma (Oyhantçabal et al. 2010), interpreted by Lenz et al. (2011) as being possibly related to a volcanic arc, comparable in age with the rift-related magmatic rocks in the Gariep Belt (Frimmel et al. 2010), followed by the evolution of a magmatic arc—absent in the Gariep Belt. Regional metamorphism during the Ediacaran is interpreted as the collisional event between the Dom Feliciano Belt and the Río de la Plata Craton, represented here by the Nico Perez and Piedra Alta Terranes according to Frimmel et al. (2013), while Oyhantçabal et al. (2010) exclude the Nico Pérez Terrane from the Río de la Plata craton and would argue with one arc region, the Dom Feliciano Belt. It is argued that the collision between the Piedra Alta (Río de la Plata) and the Nico Perez Terrane took place at ca. 630 Ma, giving rise to deformation and metamorphism in the Dom Feliciano Belt (see, e.g. Oriolo et al. 2016a) identifying the Nico Perez Terrane as a large basement inlier within the Dom Feliciano, being strongly reworked by the latter (Oriolo et al. 2016a).

However, the major subduction interpreted as subducting the Dom Feliciano Belt (Basei et al. 2008) or Cuchilla Dionisio-Pelotas arc (Frimmel et al. 2013) from the west implies a passive margin setting for Ediacaran rocks located on the Río de la Plata craton (e.g. Arroyo del Soldado Group). The Cuchilla Dionisio-Pelotas arc had been separated by oceanic back-arc crust during the Early Ediacaran from the Gariep Belt (Frimmel et al. 2013) to the east and by a mature ocean (Adamastor/Brazilide Ocean; Frimmel et al. 2010) to the west (Frimmel et al. 2010). The ocean between the eastern margin of the Río de la Plata and the arc was consumed during the Ediacaran to form the Dom Feliciano Belt (Frimmel et al. 2013). After the collision of the arc with the South American crustal blocks, the area in Uruguay, and to the south in Argentina evolved then to a peripheral foreland basin (Frimmel et al. 2010). This may be represented by the uppermost formation of the Arroyo del Soldado Group (Cerro San Francisco Formation) and Arroyo de Pedrera (Pecoits et al. 2008). However, this scenario would change when the subduction had been orientated from east to west below the Dom Feliciano Belt (e.g. Oyhantçabal et al. 2010) and when earlier biostratigraphic data (e.g. Gaucher 2000; Gaucher et al. 2005a, b) are discarded (Aubet et al. 2014; Gómez Peral et al. 2017), because then several formations would lack their age constraints, like parts of the Arroyo del Soldado Group, for example (see Aubet et al. 2014). The latter scenario would be supported by available structural, geochronological and geological data, as for instance, all pre-Neoproterozoic basement units are strongly reworked during the Neoproterozoic east of the Sarandí del Yi Shear Zone, while to the west, the Río de la Plata Craton remains almost unaffected (Sánchez Bettuci et al. 2010; Oyhantçabal et al. 2010; Oriolo et al. 2016a, b). Provenance data cannot confirm a retro-arc foreland basin scenario, using

petrographical, geochemical and isotope geochemical data, which would, if typical, imply possible volcano-sedimentary successions, higher relations between plagioclase to alkalifeldspar, large amounts of lithoclasts, a high amount of pseudomatrix, rather low Nb, Ta, TiO_2, and relatively low Th/Sc, La/Sc and Zr/Sc ratios (as proposed by McLennan et al. 1990, 1993; Jordan 1995 and many others). The rocks studied (Arroyo del Soldado Group, by Blanco et al. 2009) are characterized by rather strong reworked successions, with the exception of the Barriga Negra Formation. As commented by Zimmermann (2011a, b), the data do not allow for a definite constraint for a tectonic setting. Late Cambrian and Ordovician rocks are not reported so far from this region.

Correlation to successions in the Argentinean area of the Tandilia System (Figs. 21.2 and 21.6) are mainly based on chemostratigraphic and paleontological constraints (Gaucher et al. 2005a and discussion in Gómez Peral et al. 2017). The sedimentary rocks of the area of the Tandilia System (Fig. 21.6c), south of Buenos Aires in eastern Argentina (Fig. 21.1), comprises Neoproterozoic to Lower Paleozoic successions. The Neoproterozoic rocks are represented by the Sierras Bays Group and covered by the Late Ediacaran Cerro Negro Formation (Gómez Peral et al. 2017) followed unconformably by the Ordovician to Silurian Balcarce Formation (Van Staden et al. 2010). The latter has been subject of a detailed high resolution provenance study including detrital zircons and heavy mineral analyses and an Hirnantian age for the succession has been interpreted (Zimmermann and Spalletti 2009; Van Staden et al. 2010), based on meticulous sedimentological studies (Spalletti and del Valle 1984). In contrast, the ages of the Neoproterozoic rocks are unknown besides of one formation (Loma Negra), which supposedly comprises C*loudina* sp. (Gaucher et al. 2005a), which has been questioned by Gómez Peral et al. (2017). The Sierras Bayas Group was subject of a meticulous and extraordinary sedimentological study (Poiré 1987, 1993). The succession has been interpreted to represent a passive margin of the Rio de la Plata Craton (Poiré 1987, 1993; Zimmermann et al. 2011a). The overlying rocks of the Cerro Negro Formation are enigmatic, as they are composed of less recycled detritus and differ therefore significantly geochemically and mineralogically from the Sierras Bayas Group rocks (Zimmermann et al. 2011a). In turn, the Ordovician rocks of the Balcarce Formation resemble perfectly mineralogically age equivalent rocks of the Cape Supergroup: supermature quartz-arenites, in this case related to a glacial event, most possible the Hirnantian (Spalletti and del Valle 1984; Van Staden et al. 2010).

Further south, in the regions Ventania and Sierra Grande (Uriz et al. 2011; Fig. 21.1), Neoproterozoic to Paleozoic successions (Fig. 21.5) are exposed. Magmatism is typical for the Neoproterozoic time and metamorphic rocks are the most abundant ones (Uriz et al. 2011). Those rocks are overlain by rift-related Cambro-Ordovician rocks and subsequently magmatic rocks (region Sierra Grande) and clastic platform successions (region Ventania). The provenance data of this study (Uriz et al. 2011) can be compared and correlated with data from the Cape Supergroup successions (Fourie et al. 2011). This information has been merged and well interpreted within a provenance study on Silurian to Devonian rocks in Uruguay, as a whole basin unit from northern Uruguay to eastern South Africa and to northern Patagonia by Uriz et al. (2016) in an impressive study.

Age constraints

Some Neoproterozoic sedimentary successions in Uruguay are dated by absolute methods in terms of occurring magmatic rocks, like the Ediacaran Las Ventanas and San Carlos Formations (Oyhantçabal et al. 2009; Pecoits et al. 2011; Aubet et al. 2014), while others had been supposedly dated by fossils (e.g. *Cloudina* sp.; Yerbal Formation). With the exception of the Barriga Negra Formation, where numerous Ediacaran detrital zircons have been dated (Blanco et al. 2009), only very few single grains of Neoproterozoic ages were reported for the Yerbal and Cerro San Francisco Formations of the Arroyo del Soldado Group (Fig. 21.6a), respectively. However, the youngest detrital zircon ages in the Barriga Negra Formation are older than the biostratigraphic age of the so far underlying rocks of the Yerbal Formation (Blanco et al. 2009). This may be related to the very few number ($n = 34$) of concordant U–Pb ages in detrital zircon grains. However, this is only a possibility if the existence of *Cloudina* sp. in the upper Yerbal Formation is verified, which seems to be not the case. Aubet et al. (2014) reviewed earlier biostratigraphic data and added arguments for the need to abandon the biostratigraphic data by Gaucher (2000), and repeatedly published afterwards. Aubet et al. (2014) concluded that the Arroyo del Soldado Group is therefore much older (>580 Ma) and the Barriga Negra Formation should be excluded from this group and the latter formation is younger. Furthermore, other workers also considered the lack of validity of the Arroyo del Soldado Group as a formal unit, as it includes units that show no clear geological relationships (e.g. Pecoits et al. 2011; Masquelin et al. 2017). This new interpretation affects the correlation efforts with the Argentinean rocks of the Tandilia System and influences the determination of the geodynamic evolution (Oriolo et al. 2016a, b, c; Gómez Peral et al. 2017; Oriolo et al. 2017).

In the area of the Tandilia System, the situation is comparable concerning the detrital zircon record of Neoproterozoic rocks, as most of the formations do not show

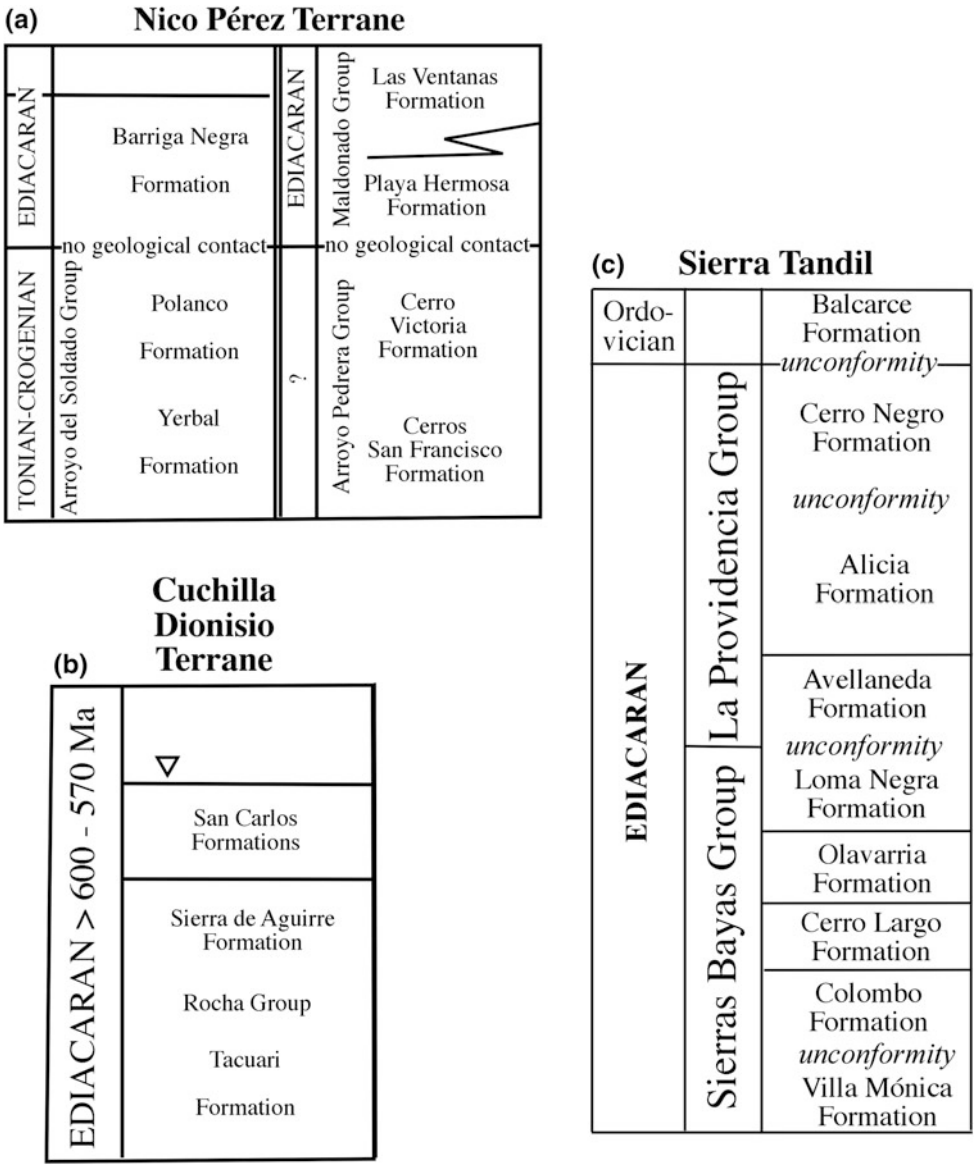

Fig. 21.6 Lithostratigraphy of Uruguay and the Sierra Tandil. **a** Revised stratigraphy after Aubet et al. (2014). Note that here as in **c** the reliability of *Cloudina* sp. is doubted as the Yerbal Formation, supposed to be hosting this hard-shell fossil is interpreted to be older than 575 Ma, not in the range of *Cloudina* sp.—stratigraphic Tables with other interpretations (e.g. Pecoits et al. 2008) are repeated in the literature and do not match anymore the data, hence here not shown (see Gaucher et al. 2008, f.e.). The Barriga Negra Formation is separated from the Arroyo del Soldado Group as proposed by Masquelin et al. (2017) and based on trends within provenance data. Note that this area contains four packages of sedimentary rocks, which are not clearly related to each other. **b** Stratigraphy for the Cuchilla Dionisio Terrane/Punta del Este Terrane (after Aubet et al. 2014). Note that relations between the formations and the Rocha Group are not clear. Depending on the geodynamic model the San Carlos Formation may be covering the Sierra Ballena Shear Zone and is an equivalent of the Las Ventanas Formation (Pecoits et al. 2008 suggest this but asks for further research). **c** Stratigraphy of the Tandilia System after Gómez Peral et al. (2017)

significant, if any, Neoproterozoic detrital zircon grains (Rapela et al. 2007; Gaucher et al. 2008; Cingolani 2011; unpublished data U.Z.). However, the overlying Ordovician Balcarce Formation (Fig. 21.6c), although supermature mineralogically (Zimmermann and Spalletti 2009), contains a well established provenance fingerprint of tectono-magmatic events to be expected for the Río de la Plata craton, including Neoproterozoic to Lower Cambrian aged detrital zircon grains (Rapela et al. 2007; Van Staden et al. 2010). It is not clear why this detrital record has not been deposited in the Ediacaran rocks of the Sierras Bayas Group and the Cerro Negro Formation. This would leave the age constraints for Neoproterozoic successions solely dependent on the reported occurrence of *Cloudina*

sp. (Gaucher et al. 2005b). Regarding the paleontological record, Pecoits et al. (2011) mentioned critically that some of the used fossil groups (acritarchs) are not biostratigraphic marker or of doubtful origin, similarly to earlier mentioned personal communications to the author (see above) for similar acritarchs. Moreover, the validity of *Cloudina* sp. in the Loma Negra Formation has been recently discarded (Gómez Peral et al. 2017). Hence, one major argument for correlation of both stratigraphic piles, the controversial Arroyo del Soldado Group and well defined Sierras Bayas Group, disappeared.

The Phanerozoic rocks investigated in areas to the south of the Tandilia System, the regions Ventania and Sierra Grande, show, similar to the Balcarce Formation, significant input of Neoproterozoic and Lower Paleozoic detritus (Uriz et al. 2011).

Exceptional lithostratigraphic characteristics

Equivalent to the successions of the Kalahari craton, efforts are made to identify lithotypes related to the 'snowball Earth hypothesis', as well to facilitate correlation and often diamictites have been interpreted as of glacial origin or glacial rocks of Neoproterozoic age (as in the case of the Balcarce Formation; Pazos and Rapalini 2011), which had been, however, dated as an Ordovician deposit (Van Staden et al. 2010). Nevertheless, until nowadays only very few successions are likely candidates like the diamictites deposited in the Playa Hermosa and Las Ventanas formations (Pecoits et al. 2008, 2011), which may be related to a major Neoproterozoic ice age according to the age constraints, which lie between 630 and 580 Ma (Pecoits et al. 2011). For the Playa Hermosa Formation Rapalini et al. (2015) claim to present a robust age around 590–580 Ma, which would point to possible relation-ship to the Gaskier event, but not necessarily. So-called cap carbonates, overlying glacial diamictites in the 'snowball Earth hypothesis' (Hoffman and Schrag 2002) are absent. It needs to be critically asked if the identification of glacial deposits is not rather triggered by the (seducing) hypothesis than actual hard data.

Both, the Barriga Negra Formation deposited in Uruguay (Fig. 21.6a) and the Cerro Negro Formation of the Tandilia System are different in terms of provenance and composition compared to their stratigraphically related rocks in their areas (Fig. 21.6; Gaucher 2000; Blanco et al. 2009; Zimmermann 2011b; Zimmermann et al. 2011a). Both do not point to a typical passive margin deposit, as they contain mostly unrecycled immature detritus (Blanco et al. 2009; Zimmermann 2011b; Zimmermann et al. 2011a). Hence, based on the critical re-interpretation of the stratigraphy by Aubet et al. (2014) and Masquelin et al. (2017) a correlation between those formations can be favored and is possible based on their provenance signatures. The age of the Barriga Negra Formation is younger than 566 Ma within error of the detrital zircon ages, while the Cerro Negro Formation contains microfossils of Late Ediacaran age (Arrouy et al. 2016). This implies the separation of the Barriga Negra Formation from the Arroyo del Soldado Group.

Provenance studies

Some provenance studies have been applied to the clastic rocks of the mentioned rocks in the region of which one focused on petrographical and geochemical data (Zimmermann et al. 2011a), others had U–Pb ages on detrital zircons as their main objective (e.g. Gaucher et al. 2008; Blanco et al. 2009; Uriz et al. 2010; Cingolani 2011), while others used several kinds of data set (petrographical, geochemical and isotope geochemical; Basei et al. 2008; Van Staden et al. 2010) or heavy mineral and geochemical data combined with sedimentology (Zimmermann and Spalletti 2009). Most of the Neoproterozoic successions contain very low input of Neoproterozoic detritus based on the U–Pb isotopic data of detrital zircons (Basei et al. 2008; Gaucher et al. 2008; Blanco et al. 2009; Cingolani 2011). In contrast, Phanerozoic successions in the same geographical regions contain significant Neoproterozoic detritus (Rapela et al. 2007; Van Staden et al. 2010; Uriz et al. 2011, 2016)—this is surprising. One possible explanation could be that the sampled successions represent only the local geology because they are small and very restricted basins. Another possibility may be the sampling itself, when not representative samples were taken and that may have influenced the detrital zircon record (e.g. DeGraaf-Surplass et al. 2003; Zimmermann et al. 2015). One exception is, however, the Barriga Negra Formation, which shows some Neoproterozoic detritus (10 grains from a total of 36 concordant U–Pb isotope ages in detrital zircons).

21.2.3 Western South America (Northwestern Argentina)

Generals

The Neoproterozoic to Lower Paleozoic successions in northwestern Argentina are well understood with one exception, the Ediacaran to Lower Cambrian Puncoviscana Complex (sensu Zimmermann 2005). The area in northwest Argentina and adjacent northern Chile is characterized by a metamorphic basement, which may be an equivalent of the less metamorphosed succession of the Puncoviscana Complex (Willner 1990; compilation in Zimmermann 2005;

Escayola et al. 2011) or partly older (Mon and Hongn 1991). The Puncoviscana Complex is followed by quartz-arenites (Mesón Group) and Ordovician successions, which demonstrate the beginning and the ending of a volcanic arc activity (e.g. Bahlburg 1990; Moya 1999; Zimmermann and Bahlburg 2003; compilation in Collo et al. 2009), the so-called Famatinian arc. The area in northwest Argentina contains no sutures between terranes during the Phanerozoic, and so far no positive evidence has been presented in regard of the existence of oceanic crust of Ediacaran age (see review in Zimmermann et al. 2014). The Puncoviscana Complex, nevertheless, contains mainly immature wackes with few carbonates and conglomerates associated with shales and can be interpreted as a retro-arc foreland or retro-arc basin deposit (Kraemer et al. 1995; Keppie and Bahlburg 1999; Zimmermann 2005; Escayola et al. 2011), although other authors interpret a passive margin (Ježek 1990; Do Campo and Guevara 2002) or as a rift and forearc deposit (Collo et al. 2009; Rapela et al. 2007). Hence, nearly every possible tectonic setting has been interpreted for the Puncoviscana Complex. Whatever the geodynamic situation had been during the Ediacaran, most probably the area was characterized by an active margin, and this detritus may be interpreted to be as well stored in the Late Cambrian quartz-arenites of the Mesón Group (Augustsson et al. 2011) and in the Lower Ordovician successions (Bock et al. 2000; Zimmermann and Bahlburg 2003; Augustsson et al. 2015; Naidoo 2016).

The subsequent Ordovician rock record in the Argentinean Puna and adjacent northern Chile is a textbook example for a successful provenance study, as the sedimentological, mineralogical, geochemical and isotope geochemical data were not only able to determine the major sources but also the syndepositional tectonic setting in successions as the rocks are associated with arc related volcanic and plutonic rocks, which also have been meticulously studied (Bahlburg 1990, 1998; Bock et al. 2000; Zimmermann and Bahlburg 2003; Kleine et al. 2004; Poma et al. 2004; Zimmermann et al. 2010). An arc signature could also be identified in the eastern margin deposits of the retro arc foreland basin in Lower Ordovician clastic rocks, as an ash layer of the San Bernardo Formation deposited close to the city of Salta in the Cordillera Oriental, derived from the active Famatinian arc by aeolian transport (Zimmermann 2011b). The sedimentary successions of the Famatina area are less intensively studied in terms of petrographical, geochemical and isotope geochemical provenance (e.g. Clemens 1993; Collo et al. 2009; see overview in Rapela et al. 2016).

Age constraints

The age constraint(s) of the Puncoviscana Complex is/are controversial as some detrital zircon ages point to different maximum depositional ages ranging from Ediacaran to nearly Middle Cambrian (compilation in Adams et al. 2010). Escayola et al. (2011) report syn-depositional volcanic rocks of Late Ediacaran ages (c. 535 Ma). If the rocks sampled and compiled in this complex are related to the same formation is still unresolved, therefore the expression 'complex' is preferred. The large exposure over hundreds of kilometer extension (compilation in Zimmermann 2005) hampers a thorough study, and different sampling strategies and dating methods applied to the rocks by different authors complicates the interpretation. However, most probably an active margin existed during the Lower Cambrian and possibly as well during the Ediacaran (630–570 Ma), as inferred by the massive occurrence of detrital zircons of that time frame in nearly all Lower Paleozoic successions (e.g. Collo et al. 2009; Augustsson et al. 2015; Naidoo 2016) and in some rock successions without paleontological record but possible maximum depositional ages in that range based on detrital zircons in southern Peru (Chew et al. 2007, 2008) and northwestern Argentina (Naidoo et al. 2016; Zimmermann et al., in prep.). It seems that the entire area of northwestern Argentina had been affected by a permanent change of an active margin and the absence of subduction activity (Bahlburg et al. 2009; Augustsson et al. 2016).

Exceptional lithostratigraphic characteristics

The situation that arc related clastic rocks are associated with arc related magmatic rocks in the Ordovician indicates this area as an ideal ancient example for provenance studies using petrographic, geochemical and isotope geochemical data to determine both, the tectonic setting of the source rocks and the tectonic setting of the depositional successions, as mentioned above (Bahlburg 1990, 1998; Zimmermann and Bahlburg 2003; Kleine et al. 2004; Poma et al. 2004; Zimmermann et al. 2010). Knowing this, the different clastic formations, which represents specific tectonic settings during the Ordovician in northwest Argentina, may be used for comparison with rock successions proposed to be deposited during the Ediacaran to Lower Cambrian in the same tectonic setting in the same area. For example, Zimmermann et al. (2010) could identify Lower Ordovician clastic rocks deposited on very thin crust in a most probable fore-arc position. Rapela et al. (2007) interpret a similar

tectonic setting for the Puncoviscana Formation, though the petrographic and mineralogical data do not match at all (Ježek 1990; Zimmermann 2005). The best match in terms of these two characteristics can be made between the Ordovician retro-arc (foreland) basin deposits and the Puncoviscana complex successions (Zimmermann and Bahlburg 2005). Escayola et al. (2011) also suggests an active margin and retro-arc basin positions for the Puncoviscana complex, as mentioned above. However, the abundance of volcano-sedimentary successions in the Lower Ordovician of northwest Argentina is by far larger (Bahlburg 1990; Clemens 1993; Moya 1999; Zimmermann and Bahlburg 2003) than similar rocks in the Puncoviscana Complex (Ježek 1990; Zimmermann 2005).

Also, deposits related to the 'snowball Earth hypothesis' have been proposed to be deposited in northwest Argentina (e.g. Toselli et al. 2005; López de Azarevich et al. 2010) with diamictites and overlying carbonates; and interpreted as part of the Puncoviscana Formation or equivalent. Unpublished U–Pb ages on detrital zircon show that the clastic rocks associated with the carbonates had been deposited during the Cambrian (unpublished data U.Z.). An Ordovician age is not possible as the rocks are overlying by Floian successions.

Provenance studies

Provenance studies in Neoproterozoic to Lower Paleozoic rocks in northwest Argentina are numerous (Clemens 1993; Bahlburg 1998; Bock et al. 2000; Do Campo and Guevara 2002; Zimmermann and Bahlburg 2003; Collo et al. 2009; Adams et al. 2010; Augustsson et al. 2011, 2015; Escayola et al. 2011; Aparicio González et al. 2014; Naidoo 2016; Naidoo et al. 2017) and helped significantly to resolve geodynamic issues. The major enigmatic aspect is still the paleotectonic setting of the Puncoviscana Complex. Have been all the rocks included in this complex deposited in the same tectonic setting or not? A second issue is the higher grade metamorphic basement and the central question if all these metamorphic units are equivalent of the Puncoviscana Complex or not (Willner 1990; Mon and Hongn 1991; Rapela et al. 2007; see compilation in Naidoo 2016; Rapela et al. 2016; Naidoo et al. 2017). As nearly all sampled clastic rocks from the Ediacaran to the Permian of very different facies (data in and compilation Augustsson et al. 2015, 2016), contain Late Mesoproterozoic detrital material, it seems very probable that rocks of this age may be part of the underlying basement and only rarely exposed (Augustsson et al. 2015; Rapela et al. 2016; Zimmermann et al., in review) and more may be identified in the future.

21.3 Provenance and Geodynamic Constraints

21.3.1 Important General Remarks for Minimum Requirements for Provenance Studies Today

Some short comments on the methodology are helpful, as the knowledge of the different quantifying method has been changed significantly over the years. Generally, it shall be remembered that unrecycled detritus of the Upper Continental Crust by definition shall have the same geochemical signature as a typical active continental margin (Taylor and McLennan 1985; McLennan et al. 1990, 1993). Furthermore, it is very important to recall that the whole-rock geochemistry and isotope geochemistry may be subject of reworking of (inherited from) older rocks and even are able to cross terrane boundaries (McLennan et al. 1990, 1993; McLennan 2001). It is also nowadays appropriate to use a sufficient number of detrital zircons for the sake of interpretation, when source areas shall be excluded with ideally not less than 60 and at best around 100 concordant grains (Vermeesch 2004; Andersen 2005) based on zircon selection described by Andersen (2005). The ideal article also states (in Figures, Tables or easy available methodology section) (i) the amount of dated grains, (ii) the number of concordant ages, (iii) the criteria of discordance and (iv) if 1- or 2-sigma age errors are reported combined with cathodoluminescence images and a brief description of the separated grains. As more frequently reports on the effect of sorting plays a paramount role in regard of the distribution pattern of detrital zircons (e.g. DeGraaf-Surplass et al. 2003; Adams et al. 2010; Zimmermann et al. 2015; Naidoo 2016), which in turn is dependent on facies, information about (i) the facies and (ii) the sampling technique are of utmost importance. It needs to be stated if several rocks or lithotypes have been sampled to cover the existing grain size variation of a formation in a specific outcrop, or one single sample has been taken (see in Puetz et al. 2017). If the latter is the case, then it shall be reported if this sample is representative for the formation—a sedimentological discussion would be 'helpful' (if not obligatory). It is helpful if the youngest group of detrital zircons dated is described when used to propose a maximum depositional age (Dickinson and Gehrels 2009). Other authors, however, use to determine the maximum depositional age of a sedimentary rock as well the age of one single grain—this may be possible but should be discussed. Some of these criteria have not been known earlier as of importance and are therefore difficult to evaluate—this is a very important issue when revising data and developing geodynamic models.

21.3.2 Gariep Belt

21.3.2.1 Provenance

This sedimentary package associated with volcanic and plutonic rocks has been divided in three major areas (Frimmel et al. 2010). It is interpreted as containing the geological history of a major rift with the formation of a back-arc basin, hence, floored by oceanic crust (Frimmel et al. 2010). This process has been succeeded by compression until a collisional event to close the short-lived oceanic basin, with the evolution of retro-arc and retro-arc foreland basins. The Ediacaran to Lower Cambrian Nama Group represents according to Frimmel et al. (2010) such a retro-arc foreland basin and at the same time would be a peripheral foreland basin in regard of the collision of the Kalhari craton with the Angola-Congo craton (Frimmel et al. 2010), which implies for the Nama basin being a 'double-foreland' comparable with areas in NE Italy during the alpine orogeny (e.g. Handy et al 2010).

To sustain a rift tectonic setting using sediment provenance is difficult (McLennan et al. 1990, 1993) and may be identifiable via significant alkaline geochemical input in the sedimentary detrital record (Winchester and Floyd 1977; Fralick 2003) and may be, in an ideal case, supported by thick sedimentary packages combined with rift-related magmatism. The rocks related to the evolution of the Gariep Belt are interpreted as such reflecting a rift-drift and collisional geodynamic evolution (e.g. Frimmel et al. 1996a, b, 2010), but the sedimentary rocks are quite thin for such a scenario (also pers. com. H. Frimmel in 2002). Nearly nothing is known geochemically about the sedimentary rocks of the Port Nolloth Group (Fig. 21.3) besides the two diamictites (Numees and Kaigas Formations), which show a strong geochemical alkaline fingerprint in its detrital composition but only for the deposits in South Africa, very different from rocks of the same successions deposited in Namibia (Van Staden et al. 2006). The associated Holgat Formation (Fig. 21.3), comparable with the mentioned diamictites, show a major unrecycled to recycled geochemical composition, which cannot be directly interpreted in terms of a tectonic setting of the depositional basin only in regard of the source(s).

Based on the sedimentological findings in the Gariep Belt (McMillan 1968; Kröner and Rankama 1972; Kröner 1974; Von Veh 1993; Van Staden et al. 2006; Zimmermann et al. 2011a, b), it is however possible to interpret rapid facies changes in interaction with tectonic movements to allow for a high sediment flux, which could explain the thin sedimentary package.

The enigmatic U–Pb ages of detrital zircons in all successions in terms of the extreme low abundance of Neoproterozoic aged detrital zircons, with the exception of the Kaigas Formation (Van Staden 2011), but the large dominance of Mesoproterozoic to Paleoproterozoic detritus, points to local sources and may allow to interpret localized smaller basins for the sedimentary successions than a large rift basin of regional significance (Van Staden et al. 2006; Zimmermann et al. 2011b). The geodynamic evolution of a large and long lasting rift event followed by the development of an active margin should have provided some igneous zircon and not nearly none. However, depending on the type of rifts, with large amounts of magmatic activity would allow for youngest detrital zircon ages close to the depositional age if even only as a small population (Cawood et al. 2012), while a rift infill with less abundant syn-depositional igneous rocks, would possibly record a larger time span between the youngest group of detrital zircons and the depositional age (Cawood et al. 2012). Interestingly, Neoproterozoic detrital zircons have been found in the overlying Nama Group and further south in the Cape Supergroup successions (Blanco et al. 2009; Fourie et al. 2011). Either these detrital zircons are not derived from the paleotectonic setting of the region or the regional magmatic rocks emplaced during the Neoproterozoic have been fertile enough to deliver detrital zircons but they never reached the Neoproterozoic basins older than the Late Ediacaran, but were then eroded into the Late Ediacaran and Paleozoic basins.

Few provenance data exist for the terranes hosting the proposed oceanic crust in the defined Marmora Terrane bounded by thrusts (Basei et al. 2005, 2008; Frimmel et al. 2010). The very few detrital zircon ages are not sufficient to exclude possible sources. The few Ediacaran and other Neoproterozoic U–Pb isotopic ages in detrital zircons are presented mostly without discordance and their errors (2-sigma) are in the range of 30–60 Ma (e.g. Basei et al. 2005). The geochemistry points to some input of mafic or intermediate detritus when studying the element concentrations of some provenance indicative trace elements, but are not significantly different from those of the Port Nolloth Group (Basei et al. 2005; Van Staden et al. 2006; Zimmermann et al. 2011b).

Conclusively, this geochemical fingerprint may nearly only be related to the major source components, which are Mesoproterozoic and Late Paleoproterozoic in age, based on detrital zircon data and significant mafic or even intermediate detritus has not been identified (although detrital zircons from such sources would be quite rare as those types of rocks are not the most fertile for zircon delivery).

The overlying Nama Group has been interpreted successfully as a foreland basin, 'even only' based on the outstanding sedimentological and stratigraphic work by Germs (compilation Germs 1995). Detrital zircon studies of the entire sedimentary pile reflect mainly the local geology only

and is nearly devoid of 'typical' Kaapvaal detritus, as frequently observed in basins fringing the Kalahari craton (Fourie et al. 2011; Frimmel et al. 2013; Naidoo et al. 2013; Miller et al. 2016; Naidoo et al. 2016). Interesting are the occurrence of Neoproterozoic grains, especially Ediacaran ones, interpreted to be related to the proposed arc to the west. The main area consisting Ediacaran magmatic rocks as representing that arc is the Dom Feliciano Belt, (i.e., intruding the Nico Perez and Punta del Este terranes). The rocks in question have been interpreted as arc-related earlier (Basei et al. 2005, 2008 and references therein) but as well as post-collisional in recent petrological works (e.g. Oyhantçabal et al. 2007; Florisbal et al. 2012; de Oliveira et al. 2015; Lara et al. 2017). However, other time equivalent candidates for the detrital material would be igneous rocks of the Cape Granite Suite towards the south; a very fertile source for detrital zircons. To differentiate these sources Lu–Hf isotope determination of the same detrital zircons are necessary ideally combined with O isotopes and trace element chemistry. Until then, all interpretations of the origin of these aged (Ediacaran to Lower Cambrian) detrital zircons are speculation.

21.3.2.2 Concluding Remarks

Regarding nearly all rock successions in this area petrographic and especially heavy mineral provenance data are lacking. The geochemical approach here is biased by the very dominant input from the lithologically quite heterogeneous Mesoproterozoic Namaqua Metamorphic Belt (Eglington 2006), hence from the local geology. Currently, it seems that most of the exposed pre-Nama rocks may represent small-scale basins, which would hamper correlation even more. As mentioned above, biostratigraphic and chemostratigraphic data are by far not conclusive and further efforts in dating of the carbonate succession and the so far unstudied clastic rocks are paramount before using provenance data for (i) geodynamic modelling and (ii) correlation, as proposed in Van Staden et al. (2006) and Zimmermann et al. (2011b). Combined with in depth high-resolution heavy mineral studies, the proposed Neoproterozoic active margin may be traceable in the detritus, if sedimentary transport pattern would allow this directed channeling of sediment (see for this discussion Zimmermann et al. 2008b).

21.3.3 Vredendal Outlier

21.3.3.1 Provenance

In the few here deposited rock succession (Fig. 21.3b) the provenance signatures are rather similar to those reported above (Van Staden et al. 2014; Naidoo et al. 2017) and would call for the same type of necessary further studies. The geochemical fingerprints reflect mainly the Namaqua Metamorphic Belt, which is also the major source in one studied immature sandstone unit (Swartleikrans Bed; Naidoo et al. 2017) and so far, nothing is known about the provenance of the successions of the Vanrhynsdorp Group (Fig. 21.4). A very fertile possible candidate to contain arc-related detritus may be the Aties Formation (Fig. 21.3b; see geochemistry by Van Staden et al. 2014) with U–Pb age determination on detrital zircons combined with high-resolution heavy mineral study. At this stage of knowledge, it is not possible to correlate the Gifberg Group rocks with other Neoproterozoic successions of the region, beside based on lithostratigraphic and structural grounds (although the exact stratigraphy is controversial; see discussion in Van Staden et al. 2014; Naidoo et al. 2017) as proposed by Frimmel et al. (2010). Isotope geochemical data shows that geochemical data rather relates to Mesoproterozoic detritus and not Neoproterozoic one (Van Staden et al. 2014; Naidoo et al. 2017) and chemostratigraphic data from this succession (Fig. 21.3b) is not useful for correlation (Frimmel 2008). However, based on sedimentological grounds the Vanrhynsdorp Group could be correlated with the Nama Group rocks (Gresse and Germs 1993; Fig. 21.4), which indicates a foreland basin setting for this part of the Neoproterozoic geology on the western margin of the Kalahari craton. Additionally, the rocks seem to be quite well dated using trace fossils within the Lower Cambrian close to the Precambrian-Cambrian boundary (Buatois et al. 2013), but provenance data are absent.

21.3.4 Western Saldania Belt

21.3.4.1 Provenance

Frimmel et al. (2013) reviewed and added to the few existing provenance data others and proposed a reinterpretation of the successions. The authors use their data to define this area as located during the Neoproterozoic in the southern prolongation of the oceanic crust floored back-arc basin, which opened during the Early Ediacaran. However, geochemical data cannot support this, because key values for TiO_2, Ta and Nb do not point to the influence of arc detritus. In contrast to the studied rocks in the Gariep belt and the Vredendal Outlier, the samples from the western Saldania Belt contain significant Neoproterozoic detritus (Frimmel et al. 2013). The youngest detrital zircon groups matching the criteria by Dickinson and Gehrels (2009) allow for the newly defined Malmesbury Terrane a possible maximum depositional age of 600–620 Ma. The overlying Boland Group rocks do not host a group of similar aged detrital zircons younger than c. 905 Ma and the youngest group (Klipheuwel) contains a larger group of detrital zircons around 619 Ma and two grains at c. 585 Ma. This all may be caused by the rather low amount of dated grains, mostly

<40. It may be necessary to add a larger statistic to verify the interpreted depositional ages.

21.3.4.2 Concluding Remarks

A significant change in provenance can be observed in these Neoproterozoic to possible Lower Paleozoic rocks, as significant Neoproterozoic material had been deposited in the sedimentary successions. Geochemical signatures do not point to an arc or retro-arc environment, as the key trace and minor elements are not depleted (Hofmann 1988) but enriched. Hence, the major intermediate to mafic component, which may be here present rather relates to extensional magmatism than subduction related magmas. However, the current provenance characteristics with the geochemical data cannot rule out an arc component, even of Ediacaran age, but it cannot be identified (only proposed). To resolve this issue, again high-resolution heavy mineral studies seems to be the only possibility nowadays.

21.3.5 Eastern Saldania Belt—Southern Margin

21.3.5.1 Provenance

Few studies are published besides the area around Oudtshoorn in regard of provenance (Van Staden et al. 2006; Naidoo et al. 2013). Similar to the western part of the Saldania Belt, is the fact that the rocks partly point to the influence of less fractionated detritus ('active continental margin' signature), with enrichment in Ti, Nb, Ta and other compatible elements combined with significant amounts of occurring Neoproterozoic detritus (Naidoo et al. 2013; Naidoo 2016). Hence, the Oudtshoorn Inlier (represented by the Cango Caves and Kansa Groups) and the Kaimaans basin (Kaimaans Group) are currently interpreted to be foreland basins, they also may be rift basins—this is not possible to differentiate (Naidoo et al. 2013; Naidoo 2016). However, no provenance signature points to a volcanic arc setting. Detrital zircon populations for most of the formations of the Kaimaans Group deposits fulfill the mentioned criteria above and point to possible maximum depositional ages around 560–580 Ma (Naidoo 2016). Critical is the situation for the Cango Cave Group with indeed a similar geochemical signature as the Kaimaans Group rocks (and the ones from the western part of the Saldania belt) but U–Pb ages are insufficient in number for interpretations and models. Unpublished data (UZ) on a new sample of the Huis Rivier Formation (Fig. 21.5d) points to a possible maximum depositional age of c. 580 Ma. This would, however, be in conflict with the proposed interpretation of biostratigraphic material in the Kombuis Member (Matjies River Formation; Fig. 21.5d), stratigraphically older than the Huis Rivier Formation (Fig. 21.5d), by Gaucher et al. (2005a, b) who assigned an age around 555 Ma to the Kombuis Member. This contradiction needs to be resolved.

It was speculated (Fourie et al. 2011; Naidoo et al. 2013) that a larger block may have been situated to the south of the Kalahari craton and rifted away from the latter (Rapela et al. 2003; Gregori et al. 2004) during the Lower Paleozoic. This would also explain as well the existence and evolution of the Cape Granite Suite (Rozendaal et al. 1999; Scheepers and Armstrong 2002) and subsequent opening of a large depositional area for the Cape Supergroup and its equivalents in South America (Fourie et al. 2011; Uriz et al. 2011, 2016).

The deposits further towards the East (Fig. 21.2), the Gamtoos Group and the Sardinia Bay Formation (Fig. 21.5 c), are compositional differently in terms of their mineralogy with a dominance of quartz-rich sediments. Naidoo (2016) could not date younger detrital zircons younger than c. 1000 Ma in the Kleinrivier Formation, in comparison to Miller et al. (2016) who presents few grains of Cambrian age for these rocks. However, it is not clear if the youngest dated Paleozoic detrital zircon grains are represented by a group or single grains as data are not given. The ages proposed by Miller et al. (2016) would also be in contrast, to the biostratigraphic data by Gaucher and Germs (2006). Then, the Cambrian successions of the Gamtoos basin could not be correlated with the other successions which are of Neoproterozoic ages. Miller et al. (2016) proposed to add in the nearest future more data to resolve this issue.

21.3.5.2 Conclusive Remarks

Conclusively, the Saldania Belt from west to east hosts more Neoproterozoic detritus than the rocks at the western margin of the Kalahari craton deposited prior to the Nama Group. If this material in the western area of the Saldania Belt can be related to the geodynamic scenario related to the Gariep belt is one possibility, it may also be shed by another tectonic event to the south of the craton (or even both). Perhaps overlapping with the last stages of the Brasiliano-Pan-African Orogeny with the beginning of the Terra Australis subduction (sensu lato), since c. 580 Ma, as both events overlap in time (e.g. Cawood 2005; Oriolo et al. 2017). None of the sampled successions at the southern margin of the Kalahari craton imply, based on provenance data, that the detritus is related to a subduction zone setting.

21.3.6 Uruguay and Eastern Argentina

21.3.6.1 Provenance

Few Neoproterozoic successions deposited in Uruguay are affected by the influence of Neoproterozoic detritus (e.g. Playa Hermosa Formation in Rapalini et al. 2015; Barriga Negra Formation in Blanco et al. 2009), but often the input

of Neoproterozoic detrital material is very scarce (Gaucher et al. 2008; Blanco et al. 2009). Besides, only few provenance studies exist providing geochemical data, of which one (Blanco et al. 2009) is, however, strongly controversial in terms of stratigraphy, structural data, age constraints and provenance interpretation (Sánchez Bettucci et al. 2010; Zimmermann 2011b). Furthermore, only few data exist on sedimentary successions of the most eastern part of Uruguay, interpreted by some authors to be the actual Ediacaran arc (Dom Feliciano Belt; Basei et al. 2005, 2008), which separated from the Kalahari craton as a single terrane (so-called Arachania) and collided again during the end of the Ediacaran until the Lower Cambrian (see Frimmel et al. 2010). This is not undebated (see Pecoits et al. 2008; Oyhantçabal et al. 2009; Aubet et al. 2014), as it is proposed that the two terranes Nico Perez and Cuchilla Dionisio, are exotic blocks to the Río de la Plata craton. However, in the model presented by Frimmel et al. (2010), the studied successions of the Nico Pérez and Piedra Alta Terranes are situated on the subducting plate during the proposed subduction event which closed the Brazilides Ocean, while the rocks of the Cuchillo dionisio Terrane and the Gariep Belt, prior to the deposition of the Nama Group, are part of the overriding block (Basei et al. 2008). According to the model of Oyhantçabal et al. (2011) and Oriolo et al. (2016a), the successions of the Nico Perez Terrane have not been part of the Río de la Plata Craton, but an exotic terrane possibly derived from the Congo Craton (Oriolo et al. 2016a). The paleotectonic setting for the Arroyo del Soldado Group rocks and associated formations remains unclear in this model. The subduction is interpreted to be from west to east (Oyhantçabal et al. 2011; Oriolo et al. 2016a, b, c) underneath the Kalahari craton in the south of the Brazilide Ocean. Consequently, the subduction should have propagated with the same orientation in the north of the same ocean, subducting from west to east. Several authors argue that the subduction was orientated from east to west, hence below South American blocks (Goscombe and Gray 2007; Frimmel et al. 2010; Konopásek et al. 2014). However, this is challenged by Trompette (1994), Oyhantçabal et al. (2009), Chemale et al. (2012) and Oriolo et al. (2016c) as well as supported by data from Hoffman et al. (2016). The major advantage of the model with a subduction to the east is the combination of different data pointing to a homogeneous geodynamic scenario. Detailed provenance studies are not existent and may prove this point, hence, shall be executed in the nearest future. This may also assist in defining 'terranes', which is characteristic for both models. Beyond doubt, the issues of the orientations of the different subduction zones, if they had been such, and the definition of terranes or crustal fragments of being exotic, are surely the two most challenging ones in the entire reconstruction of the area. Because, if the subduction worked underneath the Dom Feliciano Belt towards the east, then the latter lies on the overriding plate and the Ediacaran successions should indicate a different provenance compared to a model where they had been deposited on the subducting plate.

However, the Las Ventanas and San Carlos Formations, which seems to be deposited before 580 Ma (Pecoits et al. 2008, 2011; Oyhantçabal et al. 2009), are characterised by anorogenic magmatism dated in the timeframe 610–580 Ma and point to an extensional regime, containing even possible glacial deposits (Pazos and Rapalini 2011). The subsequently following Arroyo del Soldado Group (according to Gaucher 2000), including (Gaucher 2000) or excluding (Pecoits et al. 2011; Zimmermann 2011b) the uppermost formations (now included in the Arroyo Pedrera Group; after Pecoits et al. 2008; Aubet et al. 2014), is from a provenance point of view typical for a passive margin, but the same signature can be found in foreland basins elsewhere or at rifted margins (McLennan et al. 1990, 1993). However, the available data in the literature (e.g. Pecoits et al. 2008; compilation by Aubet et al. 2014) combined with the re-evaluation of the provenance data of the Arroyo del Soldado Group (Zimmermann 2011b) points to a small-scale basin, comparable to those in the Gariep and Saldania Belts and eastern Argentina. Those basins have rather less regional significance and reflect the provenance of the local geology, which is of less significance for geodynamic modeling.

Conclusively, it seems generally accepted that the Dom Feliciano Belt with its northern prolongation may represent a Neoproterozoic volcanic arc, but the orientation of the subduction, as mentioned, is debated as well as the boundaries and its relation to the Río de la Plata craton. However, it is indicated by some authors that this area represents rather a collisional setting, actually dominated by post-collisional processes (e.g. Oyhantçabal et al. 2007; Chemale et al. 2012; Florisbal et al. 2012; de Oliveira et al. 2015; Lara et al. 2017). Of interest and utmost important is therefore, the geology and the geodynamic role of the Cuchilla Dionisio Terrane. Is this area a sole terrane and a remnant of the Kalahari craton based on mainly Nd model age characteristics (Basei et al. 2008)? Or, is this area a part of the possible arc and the shear zone an intracontinental one (e.g. Oyhantçabal et al. 2009)? It should be possible to gain from the deposits here the necessary proof or deny of volcanic arc signatures in detailed petrogenesis studies with Nd–Sr–Pb isotope investigations and detailed provenance studies focusing on provenance indicating heavy minerals like chromites and rutiles, additional to systematic dating of detrital zircons with U–Pb.

However, the Barriga Formation (Fig. 21.6a) is still with its provenance character dubious as it contains less fractionated detritus and grains of Ediacaran age (Blanco et al. 2009). The formation is according to its geochemistry comparable to the Ediacaran Cerro Negro Formation of the

Tandilia System, but the latter contains in its detrital zircon record the same poor abundance of Neoproterozoic aged detritus (Cingolani 2011) as most of the so far studied Neoproterozoic successions (Gaucher et al. 2008; Blanco et al. 2009). Masquelin et al. (2017) proposed to exclude the Barriga Negra Formation from the Arroyo del Soldado Group and it seems it possibly would better fit in the geodynamic evolution of the region. Moreover, it seems that the biostratigraphic data of the Arroyo del Soldado Group are dubious (Aubet et al. 2014). The lack of Late Neoproterozoic detrital zircons may be caused by sampling techniques, as in such critical successions a wide range of grain sizes may be the best solution for sampling to avoid sorting effects (DeGraaf-Surplass et al. 2003; Naidoo 2016). Currently, the Arroyo del Soldado Group is interpreted to be not younger than 580 Ma (Aubet et al. 2014) and the Barriga Negra Formation is separated and represents an independent formation (Masquelin et al. 2017).

Comparing the Arroyo del Soldado Group (sensu Gaucher 2000) with successions in the Tandilia System, as proposed (Gaucher et al. 2005b), implies ideally thorough age constraints. One key element was the occurrence of *Cloudina* sp. in both stratigraphies (Arroyo del Soldado Group; Gaucher 2000; Sierras Bayas Group, Gaucher et al. 2005b). However, the validity of these findings is challenged in Aubet et al. (2014) and Gómez Peral et al. (2017). Acritarch biostratigraphy was as well, as mentioned above, has been criticised by Pecoits et al. (2011). This leaves the correlation to chemostratigraphic data. However, even those are interpreted of being not primary in for the rocks of the Arroyo del Soldado Group (Aubet et al. 2014), as for Neoproterozoic carbonates on the Kalahari craton (Frimmel 2008, 2009, 2010). If these critiques are correct then a correlation between the rocks of the Arroyo del Soldado Group (sensu lato) and the Sierras Bayas Group and the Cerro Negro Formation can at the moment be made only on lithological grounds.

The rocks of the Tandilia System are in terms of their sedimentology and chemostratigraphy and the understanding of the microfacies of the carbonates well understood (e.g. Poiré 1987, 1993; Gómez Peral et al. 2007, 2017). Unfortunately, age constraints are complicated for the rocks of the Sierras Bayas Group, as the proposed finding of *Cloudina* sp. in the Loma Negra Formation (Gaucher et al. 2005b) has been abandoned (Gómez Peral et al. 2017). None of the studied formations of the Sierras Bayas Group and the Cerro Negro Formation could reflect significant Neoproterozoic detritus or sufficient concordant detrital zircons to exclude certain source areas (Rapela et al. 2007; Gaucher et al. 2008; Cingolani 2011; see above). Chemostratigraphic values of the lowermost Villa Mónica Formation (Fig. 21.6c) are not indicative for a specific time frame during the Cryogenian (Gómez Peral et al. 2007, 2017). The overlying Cerro Largo Formation (Fig. 21.6c) has been studied (unpublished material by the author) in terms of Ar–Ar dating on glauconite, and a sample covering all grain sizes of the formation has been processed for U–Pb age dating of detrital zircons, with no younger age constraints as c. 800 Ma. Whole rock K–Ar and Rb–Sr isotope data by Cingolani and Bonhomme (1988) and Kawashita et al. (1999) resulted also in Cryogenian ages (793 ± 32 Ma; 725 ± 36 Ma) interpreted as diagenetic ages (Gómez Peral et al. 2007).

The Cerro Negro Formation from the Tandilia System (Fig. 21.6d) is different from the underlying successions as it contains less fractionated detritus and felsic detrital material derived from pre-Neoproterozoic rocks (Cingolani 2011). Biostratigraphic data assign a Late Ediacaran age to this formation (Arrouy et al. 2016), which allows a correlation with the Barriga Negra Formation.

Interesting is that younger formations, like the Lower Paleozoic Balcarce Formation (in the Tandilia System) or Siluro-Devonian rocks deposited in Uruguay (Uriz et al. 2016) or Paleozoic successions in the regions Ventania and Sierra Grande contain significant Neoproterozoic detritus (Uriz et al. 2010), while the rocks of the Sierras Bayas Group did not.

21.3.6.2 Conclusive Remarks

Although several provenance studies have been undertaken in the area of Uruguay and eastern Argentina, the only reliable and strong data are related to the regions of Ventania and Sierra Grande (Uriz et al. 2010), the Balcarce Formation (Tandilia System; Zimmermann and Spalletti 2009; Van Staden et al. 2010) and the Paleozoic successions of Uruguay (Uriz et al. 2016). However, in Neoproterozoic rocks either data are highly controversial and especially for the Arroyo del Soldado Group seems to need revision (Pecoits et al. 2011; Aubet et al. 2014; Masquelin et al. 2017) or Neoproterozoic age constraints are very weak or even absent, based on U–Pb isotopic ages on detrital zircons (Rapela et al. 2007; Gaucher et al. 2008; Blanco et al. 2009; Cingolani 2011). Finally, it is controversial what the geodynamic role of the Neoproterozoic magmatic rocks of the Dom Feliciano Belt is, either related to a volcanic arc (Basei et al. 2005, 2008; Frimmel et al. 2010) or to a collisional event with its ubiquitous deformation along shear zones during this period (e.g. Oyhantçabal et al. 2009; Oriolo et al. 2016a, c).

Provenance studies of several Neoproterozoic successions seems to reveal that the detritus is mostly related to Mesoproterozoic sources and may not therefore contribute to a solution of the geodynamic evolution during the Neoproterozoic (e.g. Rapela et al. 2007; Gaucher et al. 2008; Blanco et al. 2009; Zimmermann et al. 2011a). One reason may be that the studied successions tend to be deposited in small-scale basins reflecting rather local geology (e.g.

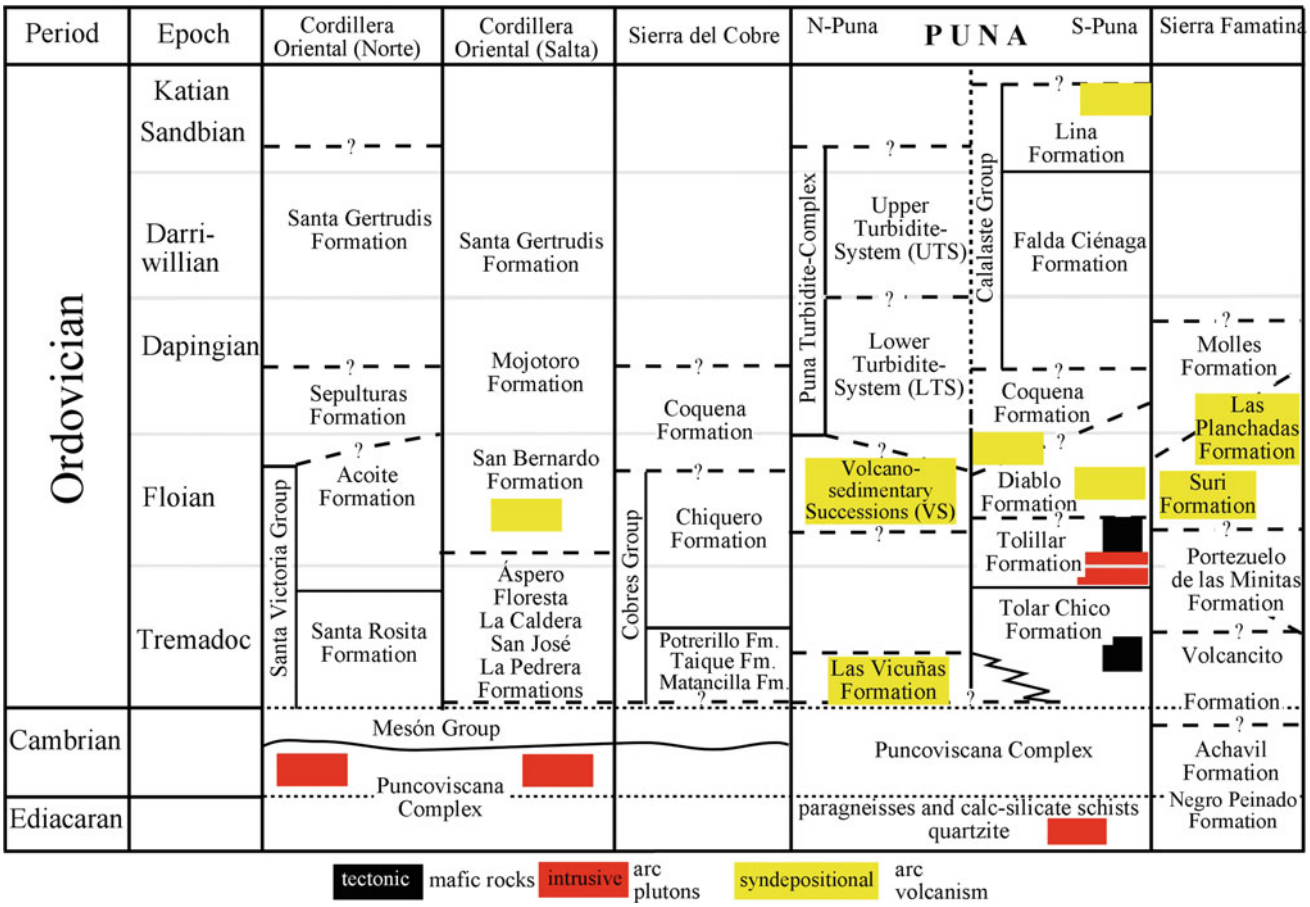

Fig. 21.7 Lithostratigraphy of northwest Argentina with focus on the active margin. Numerous successions deposited further away from the active margin in the Sierras Sub-Andinas, those are not mentioned as they received their detritus from the east, the central cratonic area and would not reveal significant data to those successions deposited at the margin. Note that the Puncoviscana Complex may be an equivalent of the gneisses, schists and quartzites (Willner 1990). (compiled from Zimmermann and Bahlburg 2003; Collo et al. 2009; Moya 1999; Zimmermann et al. 2014; Naidoo et al. 2017). To the west in northern Chile are equivalents of the Floian volcano-sedimentary successions of the Tolillar and Diablo Formation exposed, they are not named here separately here

Arroyo del Soldado basin). This may be quite comparable in regard of the provenance studies in the Gariep Belt, which reflect mainly local detritus. Some results in the Barriga Negra (Blanco et al. 2009), Cerro Negro (Zimmermann et al. 2011a) and Playa Hermosa Formation (Rapalini et al. 2015) show that Neoproterozoic detritus was reworked in Ediacaran formations Hence, it is proposed to focus in those formations on heavy mineral studies to possibly gain more provenance information about Neoproterozoic active margin sources.

Age constraints for well described sedimentary successions in the Tandilia System of eastern Argentina depended solely still on the finding of *Cloudina* sp. However, these findings and earlier achritarch occurrences are challenged (Pecoits et al. 2008; Gómez Peral et al. 2017). However, the base of the Sierras Bayas Group is most probably be Cryogenian (Gómez Peral et al. 2017) and the top Late Ediacaran (Cerro Negro Formation; Arrouy et al. 2016). If so, then the possible equivalent of the Cerro Negro Formation could be the Barriga Negra Formation, as the existence of *Cloudina* sp. in the Arroyo del Soldado Group has been abandoned.

21.3.7 Northwest Argentina

21.3.7.1 Provenance

In the defined area of the Puna, Cordillera Oriental and the Famatina region several successions have been studied and numerous provenance studies have been carried out (e.g. Bahlburg, 1990, 1998; Ježek 1990; Clemens 1993; Bock et al. 2000; Do Campo and Guevara 2002; Zimmermann et al. 2002, 2010; Zimmermann and Bahlburg 2003; Zimmermann 2005; Collo et al. 2009; Adams et al. 2010; Escayola et al. 2011; Hauser et al. 2011; Aparicio González et al. 2014; Augustsson et al. 2011, 2015, 2016; Naidoo

et al. 2016; and more references in Rapela et al. 2016) and could be combined with studies on magmatic rocks related to the geodynamic evolution of the Ordovician (Kleine et al. 2004; Poma et al. 2004; Zimmermann et al. 2014; Bahlburg and Berndt 2015).

At the western margin, fact seems to be that during the Late Neoproterozoic an active continental margin developed (e.g. Escayola et al. 2011), which was followed by a time of relative quiescence during the Upper Cambrian and deposition of quartz-arenites of Méson Group in an extensional regime, although the rocks contain significant amount of volcanic detritus (Augustsson et al. 2011, 2015). During the Uppermost Cambrian, another active margin developed ('Famatinian arc/cycle'; Pankhurst et al. 1998) until the Middle Ordovician, again succeeded by an extensional tectonic setting (Bahlburg 1990; Bahlburg and Berndt 2015) followed by a time of relative magmatic and tectonic silence until the Lower Carboniferous (Bahlburg et al. 2009; Augustsson et al. 2015, 2016). The location of the western margin of Gondwana seems to be clarified for the Ordovician (Zimmermann et al. 2010) as are the extensions of the arc-basins and adjacent succesions from north to south in northwest Argentina (Bahlburg 1990, 1998; Aceñolaza et al. 1996; Zimmermann and Bahlburg 2003; Collo et al. 2009; Zimmermann et al. 2010).

Enigmatic are two issues: firstly, the nature of the basement in the region and secondly the role of the exposed basement in the geodynamic models.

Late Mesoproterozoic detritus could be found in nearly every sampled sedimentary rock succession in the northwest Argentina (as defined above; e.g. Adams et al. 2010; Augustsson et al. 2015). Did this material derive from the same regional are or had it been introduced from non-regional areas? However, Nd-isotope data in metamorphic and sedimentary rocks in northwest Argentina point to the existence of Meso- and Paleoproterozoic basement (Pankhurst et al. 1998; Rapela et al. 1998; Bock et al. 2000; Lucassen et al. 2000; Zimmermann et al. 2002; Zimmermann and Bahlburg 2003) as well as possible Mesoproterozoic rock exposure in the Puna (Rapela et al. 2016) and to the south and north of the here discussed region (Rapela et al. 2010, 2016; Casquet et al. 2012).

The oldest rocks are low grade metamorphic succesions of the Puncoviscana Complex, intensively studied in terms of U–Pb ages on detrital zircons (Adams et al. 2010; Escayola et al. 2011; Aparicio González et al. 2014) combined with some thorough petrographic and geochemical studies (Ježek 1990; Do Campo and Guevara 2002; Zimmermann 2005). Associated with these low grade metamorphic rocks are higher grade metamorphic rocks, schists and gneisses, which are interpreted as equivalents (Willner 1990) of the Puncoviscana Complex or not (Mon and Hongn 1991). Only U–Pb ages on detrital zircons do exist as proper age constraints and identified a range of possible maximum depositional ages for the Puncoviscana Complex from 570 to 510 Ma, covering a wide range of time and explained as related to sorting effects (Adams et al. 2010). It might be that the Puncoviscana Complex contains several formations related to different tectonic settings. These are systematically older for the gneisses and schists (the assigned equivalents) with ages older than 540 Ma (Ancasti Formation in Rapela et al. 2007; Naidoo et al. 2016; Rapela et al. 2016).

It has been proposed that during the Neoproterozoic the western margin of South America rifted away from Laurentia possibly followed by either the initiation of a subduction zone (e.g. Chew et al. 2008) during the Ediacaran or/and a collision of a terrane with the Río de la Plata craton (Rapela et al. 1998). The unknown exact geodynamic evolution provoked a variety of interpretation for the paleotectonic setting of the Puncoviscana Complex deposited during the Ediacaran. However, as Zimmermann (2005) and Escayola et al. (2011) compile, a passive margin can be excluded and an interpretation of a deposition of the rocks close to a proposed subduction zone (Collo et al. 2009; Rapela et al. 2007) can be discarded as the rocks in Argentina and those in the Saldania Belt (for the model of Rapela et al. 2007) have not been deposited along a subduction zone. Hence, the most probable interpretation for the Puncoviscana Complex is either a retro-arc foreland basin deposit or a retro-arc basin infill (Kraemer et al. 1995; Keppie and Bahlburg 1999; Zimmermann 2005; Escayola et al. 2011) as the petrographical and geochemical do not point to a passive margin or forearc tectonic setting.

21.3.7.2 Concluding Remarks

The geodynamic evolution from the end of the Lower Cambrian to the Carboniferous is roughly well understood in northwest Argentina with phases of subduction-related magmatism and relative magmatic quiescence. However, the so-called 'basement' is less well understood. Detrital zircon age populations together with sedimentological, mineralogical, geochemical and isotope geochemical data point for low grade metasedimentary rocks (Puncoviscana Complex, sensu Zimmermann 2005) to a setting along an active margin, as a retro-arc or retro-arc foreland basin (Kraemer et al. 1995; Keppie and Bahlburg 1999; Escayola et al. 2011); or both when it is proposed that the complex is comprised of different units related to different tectonic settings and represent different ages. However, it seems less probable that the successions are older than c. 540–550 Ma based on provenance data (Adams et al. 2010; Escayola et al. 2011). Higher grade metamorphic rocks (schists and gneisses) may be of similar age or older, or both, this is still a matter of discussion (compilation in Naidoo et al. 2016). Hence, the age and the tectonic setting of these metamorphic successions need to be resolved in the future.

21.4 Conclusive Statements

The most important provenance results from the different regions here presented in a very short compilation related to southwest Gondwana showed that some possible important issues should be resolved to develop final geodynamic models for this interesting geological region.

Some short comments on the needs or usefulness of specific future research shall here be proposed:

- Resolving the orientation of the subduction below the Dom Feliciano Belt by provenacen studies
- Correlation (or not) of the possible small-scale Neoproterozoic basins on the Kalahari craton and in Uruguay with the one in the Tandilia System
- Clarify the Neoproterozoic lithostratigraphy of the Uruguayan 'terranes'
- Intensify the knowledge of the southern margin of Gondwana to allow a differentiation of detritus related to the geodynamic process in the 'centre' (the collisions of the Kalhari, Congo and Río de la Plata cratons) from those at the southern margin of southwest Gondwana
- Resolving the geodynamic processes between 600 and 540 Ma in northwest Argentina including a better understanding of the geodynamic role of the Puncoviscana Complex
- New biostratigraphic data of the Kalahari craton, Uruguay and the Tandilia System for the Neoproterozoic as the current data are controversial and contradictive in some areas with isotopic data
- Using high-resolution heavy mineral studies with a combination of quantifications and geochemical as well as isotope geochemical methods on selected successions which are candidates to contain active margin detrital material related to the Neoproterozoic subduction zones developed between the Kalahari, Congo and Río de la Plata cratons.

Acknowledgements First UZ likes to thank for the invitation for this review paper and is indebted for the patience of the editors until this contribution had been finished. This was and is extraordinary. Furthermore, S. Oriolo is thanked for several new ideas and important comments which enhanced the paper and comments by L. López de Luchi have been appreciated to augment the quality of the text.

References

Aceñolaza FG, Miller H, Toselli A (1996) Geología del Sistema de Famatina. Münchner Geologische Hefte, Reihe A Allgemeine Geologie, A 19:1–410

Adams CJ, Miller H, Aceñolaza FG, Toselli AJ, Griffin WL (2010) The Pacific Gondwana margin in the Late Neoproterozoic-Early Palaeozoic: detrital zircon U–Pb ages from metasediments in northwest Argentina reveal their maximum age, provenance and tectonic setting. Gondwana Res 19:71–83

Andersen T (2005) Detrital zircons as tracers of sedimentary provenance: limiting conditions from statistics and numerical simulation. Chem Geol 216:249–270

Aparicio González PA, Pimentel MM, Hauser N, Moya MC (2014) U–Pb LA-ICP-MS geochronology of detrital zircon grains from lowgrade metasedimentary rocks (Neoproterozoic e Cambrian) of the Mojotoro Range, northwest Argentina. J S Am Earth Sci 49:39–50

Arrouy MJ, Warren LV, Quaglio F, Poiré DG, Guimarães Simões M, Boselli MR, Gómez Peral LE (2016) Ediacaran discs from South America: probable soft-bodied macrofossils unlock the paleogeography of the Clymene Ocean. Sci Rep 6(30590):1–10. https://doi.org/10.1038/srep30590

Aubet NR, Pecoits E, Heaman LM, Veroslavsky G, Gingras MK, Konhauser KO (2014) Ediacaran in Uruguay: facts and controversies. J S Am Earth Sci 55:43–57

Augustsson C, Rüsing T, Adams CR, Chmiel H, Kocabayoğlu M, Büld M, Zimmermann U, Berndt J, Kooijman E (2011) Detrital quartz and zircon combined: the production of mature sand with short transportation paths along the Cambrian West Gondwana Margin, NW Argentina. J Sediment Res 81:284–298

Augustsson C, Rüsing T, Niemeyer H, Kooijman E, Berndt J, Bahlburg H, Zimmermann U (2015) 0.3 b. y. of drainage stability along the palaeozoic palaeo-Pacific Gondwana margin—a detrital zircon study. J Geol Soc Lond 172:186–200

Augustsson C, Willner AP, Rüsing T, Niemeyer H, Gerdes A, Adams CJ, Miller H (2016) The crustal evolution of South America from a zircon Hf-isotope perspective. Terra Nova 28:128–137

Bahlburg H (1990) The Ordovician basin in the Puna of NW Argentina and N Chile: geodynamic evolution from back-arc to foreland basin. Geotekton Forsch 75:1–107

Bahlburg H (1998) The geochemistry and provenance of Ordovician turbidites in the Argentine Puna. In: Pankhurst RJ, Rapela CW (eds) The Proto-Andean margin of Gondwana. Geological Society London, Special Publications, 142, pp 127–142

Bahlburg H, Berndt J (2015) Provenance from zircon U–Pb age distributions in crustally contaminated granitoids. Sed Geol. https://doi.org/10.1016/j.sedgeo.2015.08.006

Bahlburg H, Vervoort JD, Du Frane SA, Bock B, Augustsson C, Reimann RC (2009) Timing of crust formation and recycling in accretionary orogens: insights learned from the western margin of South America. Earth Sci Rev 97:227–253

Barnett W, Armstrong RA, de Wit MJ (1997) Stratigraphy of the upper Neoproterozoic Kango and lower palaeozoic table mountain groups of the cape fold belt revisited. S Afr J Geol 100:237–250

Basei MAS, Frimmel HE, Nutman AP, Preciozzi F, Jacob J (2005) A connection between the Neoproterozoic Dom Feliciano (Brazil/Uruguay) and Gariep (Namibia/South Africa) orogenic belts—evidence from a reconnaissance provenance study. Prec Res 139:195–221

Basei MAS, Frimmel HE, Nutman AP, Preciozzi F (2008) West Gondwana amalgamation based on detrital zircon ages from Neoproterozoic Ribeira and Dom Feliciano belts of South America and comparison with coeval sequences from SW Africa. Geol Soc Lond Spec Publ 294:239–254

Blanco G, Rajesh HM, Gaucher C, Germs GJB, Chemale F Jr (2009) Provenance of the Arroyo del Soldado Group (Ediacaran to Cambrian, Uruguay): implications for the palaeogeographic evolution of southwestern Gondwana. Prec Res 171:57–73

Blanco G, Germs GJB, Rajesh HM, Chemale F Jr, Dussin IA, Justino D (2011) Provenance and paleogeography of the Nama Group (Ediacaran to early Paleozoic, Namibia): petrography, geochemistry and U–Pb detrital zircon geochronology. Precambr Res 187:15–32

Bock B, Bahlburg H, Wörner G, Zimmermann U (2000) Tracing crustal evolution in the southern central Andes from the late precambrian to permian with geochemical and Nd and Pb isotope data. J Geol 108:515–535

Borg G, Kärner K, Buxton M, Armstrong R, Van der Merwe SW (2003) Geology of the skorpion zinc deposit, southern Namibia. Econ Geol 98:749–771

Buatois LA, Almond H, Germs GJB (2013) Environmental tolerance and range offset of *Treptichnus pedum*: implications for the recognition of the Ediacaran-Cambrian boundary. Geology 41:519–522

Buggisch W, Kleinschmidt G, Krumm S (2010) Sedimentology, geochemistry and tectonic setting of the Neoproterozoic Malmesbury Group (Tygerberg Terrane) and its relation to neighbouring terranes, Saldania Fold Belt, South Africa. Neues Jahrbuch für Geologie und Paläontologie 257:85–114

Bührmann HT (1981) The geology of the Lower Kobe Valley, Vanrhynsdorp District. Annals of the University of Stellenbosch, 3, Series A1, pp 67–144

Casquet C, Rapela CW, Pankhurst RJ, Baldo EG, Galindo C, Fanning CM, Dahlquist JA, Saavedra J (2012) A history of proterozoic terranes in southern South America: from Rodinia to Gondwana. Geosci Front 3:137–145

Cawood PA (2005) Terra Australis Orogen: Rodinia breakup and development of the Pacific and Iapetus margins of Gondwana during the Neoproterozoic and Palaeozoic. Earth Sci Rev 69:249–279

Cawood PA, Hawkesworth CJ, Dhuime B (2012) Detrital zircon record and tectonic setting. Geology 40(10):875–878

Chemale F, Mallmann G, de Fátima Bitencourt M, Kawashita K (2012) Time constraints on magmatism along the Major Gercino Shear Zone, Southern Brazil: implications for West Gondwana reconstruction. Gondwana Res 22(1):184–199

Chemale F Jr, Scheepers R, Gresse PG, Van Schmus WR (2010) Geochronology and sources of late Neoproterozoic to Cambrian granites of the Saldania Belt. Int J Earth Sci (Geol Rundsch). https://doi.org/10.1007/s00531-010-0579-1

Chew DM, Schaltegger U, Kosler J, Whitehouse MJ, Gutjahr M, Spikings RA, Miskovic A (2007) U–Pb geochronologic evidence for the evolution of the Gondwanan margin of the north-central Andes. Geol Soc Am Bull 119:697–711

Chew DM, Magna T, Kirkland CL, Miskovic A, Cardona A, Spikings R, Schaltegger U (2008) Detrital zircon fingerprint of the Proto-Andes: evidence for a Neoproterozoic active margin? Precam Res 167:186–200

Cingolani CA (2011) The Tandilia system of Argentina as a southern extension of the Río de la Plata craton: an overview. Int J Earth Sci (Geol Rundsch) 100:221–242

Cingolani C, Bonhomme MG (1988) Resultados geocronológicos en niveles pelíticos intercalados en las dolomías de Sierras Bayas (Grupo La Tinta), provincia de Buenos Aires. Segundas Jornadas Geológicas Bonaerenses. Buenos Aires, Argentina, pp 283–289

Clemens K (1993) Sedimentología, proveniencía y desarollo geotectónico del Sistema de Famatina en el Noroeste de Argentina durante el Paleozóico Inferior; XII Congreso Geológico Argentino y II Congreso de Exploración de Hidrocarburos, Actas, Tomo I, pp 310–320

Collo G, Astini RA, Cawood PA, Buchan C, Pimentel M (2009) U–Pb detrital zircon ages and Sm–Nd isotopic features in low-grade metasedimentary rocks of the Famatina belt: implications for late Neoproterozoic-Early Palaeozoic evolution of the proto-Andean margin of Gondwana. J Geol Soc 166:303–319

Da Silva LC, Gresse PG, Scheepers R, McNaughton NJ, Hartmann LA, Fletcher I (2000) U–Pb SHRIMP and Sm–Nd age constraints on the timing and sources of the Pan-African Cape Granite Suite, South Africa. J Afr Earth Sci 30:795–815

De Beer CH, Gresse PG, Theron JN, Almond JE (2002) The geology of the Calvinia area, explanation sheet 3118, scale: 1:250,000. Council for Geoscience, Pretoria, p 92

de Oliveira DS, Sommer CA, Philipp RP, Fernandes de Lima E, Basei MAS (2015) Post-collisional subvolcanic rhyolites associated with the Neoproterozoic Pelotas Batholith, southern Brazil. J S Am Earth Sci 63:84–100

DeGraaff-Surpless K, Mahoney JB, Wooden JL, McWilliams MO (2003) Lithofacies control in detrital zircon provenance studies: insights from the Cretaceous Methow basin, southern Canadian Cordillera. GSA Bull 115(8):899–915

DePaolo DJ (1981) Neodymium isotopes in the Colorado Front range and crust-mantle evolution in the Proterozoic. Nature 291:193–196

DePaolo DJ, Linn AM, Schubert G (1991) The continental crustal age distribution: methods of determining mantle separation ages from Sm–Nd isotopic data and application to the southwestern United States. J Geophys Res 96(B2):2071–2088

Dickinson WR, Gehrels GE (2009) Use of U–Pb ages of detrital zircons to infer maximum depositional ages of strata: a test against a Colorado Plateau Mesozoic database. Earth Planet Sci Lett 288 (2009):115–125

Dickinson WR, Suczek CA (1979) Plate tectonics and sandstone compositions. Am Assoc Petrol Geol Bull 63(12):2164–2182

Do Campo M, Ribeiro Guevara SR (2002) Geoquimica de las sequencias clásticas de la Formación Puncoviscana (Neoproterozoico, NO Argentina), proveniencia y marco tectónico. XV Congreso Geológico Argentino, El Calafate, CD Volume

Eglington BM (2006) Evolution of the Namaqua-Natal Belt, southern Africa—a geochronological and isotope geochemical review. J Earth Sci 46:93–111

Escayola MP, van Staal CR, Davis WJ (2011) The age and tectonic setting of the Puncoviscana formation in northwestern Argentina: an accretionary complex related to Early Cambrian closure of the Puncoviscana ocean and accretion of the Arequipa-Antofalla block. J S Am Earth Sci 32:438–459

Evans DAD (2013) The palaeomagnetically viable, long-lived and all-inclusive Rodinia supercontinent reconstruction. In: Murphy JB, Keppie JD, Hynes AJ (eds) Ancient orogens and modern analogues. Geological Society, London, Special Publications, 327, pp 371–404

Eyles N, Januszczak N (2004) "Zipper-rift": Neoproterozoic glaciations and the diachronous break up of Rodinia between 740 and 620 Ma. Earth Sci Rev 65:1–73

Finney SC (2007) The parautochthonous Gondwanan origin of the Cuyania (greater Precordillera) terrane of Argentina: a re-evaluation of evidence used to support an allochthonous Laurentian origin. Geologica Acta 5:127–158

Florisbal LM, Janasi VA, Bitencourt MF, Heaman LM (2012) Space-time relation of post-collisional granitic magmatism in Santa Catarina, southern Brazil: U–Pb LA-MC-ICP-MS zircon geochronology of coeval mafic-felsic magmatism related to the Major Gercinho Shear Zone. Precambr Res 216:132–151

Fölling PG, Frimmel HE (2002) Chemostratigraphic correlation of carbonate successions in the Gariep and Saldania Belts, Namibia and South Africa. Basin Res 14:69–88

Foster DA, Goscombe BD, Newstead B, Mapani B, Mueller PA, Gregory LC, Muvangua E (2014) U–Pb age and Lu–Hf isotopic data of detrital zircons from the Neoproterozoic Damara sequence: implications for Congo and Kalahari before Gondwana. Gondwana Res. https://doi.org/10.1016/j.gr.2014.04.011

Fourie PH, Zimmermann U, Beukes NJ, Naidoo T, Kobayashi K, Kosler J, Nakamura E, Tait J, Theron JN (2011) Provenance and reconnaissance study of detrital zircons of the Palaeozoic Cape

Supergroup in South Africa: revealing the interaction of the Kalahari and Río de la Plata Cratons. Int J Earth Sci 2–3:527–541
Fralick P (2003) Geochemistry of clastic sedimentary rocks: ratio techniques. In: Lentz DR (ed) Geochemistry of sediments and sedimentary rocks: evolutionary considerations to mineral-deposit-forming environments. Geological Association of Canada, GEOText, vol 4, pp 85–104
Frimmel HE (2000a) The stratigraphy of the Chameis Subterrane in the Gariep Belt in southwestern Namibia. Commun Geol Surv Namibia 12:179–186
Frimmel HE (2000b) The Pan-African Gariep Belt in Southwestern Namibia and Western South Africa. Commun Geol Surv Namibia 12:197–209
Frimmel HE (2008) An evaporitic facies in Neoproterozoic postglacial carbonates: the Gifberg Group, South Africa. Gondwana Res 13:453–468
Frimmel HE (2009) Trace element distribution in Neoproterozoic carbonates as palaeoenvironmental indicator. Chem Geol 258:338–353
Frimmel HE (2010) On the reliability of sTable carbon isotopes for Neoproterozoic chemostratigraphic correlation. Precambr Res 182:239–253
Frimmel HE (2011a) The Kaigas and Numees Formations, Port Nolloth Group, in South Africa and Namibia. In: Arnaud E, Halverson GP, Shields-Zhou G (eds) The geological record of Neoproterozoic glaciations. Geological Society, London, Memoirs, vol 36, pp 223–231
Frimmel HE (2011b) Chapter 18 The Karoetjes Kop and Bloupoort formations, Gifberg Group, South Africa. Geol Soc London, Mem 36(1):233–237
Frimmel HE, Fölling PG (2004) Late vendian closure of the Adamastor Ocean: timing of tectonic inversion and syn-orogenic sedimentation in the Gariep Basin. Gondwana Res 7:685–699
Frimmel HE, Frank W (1998) Neoproterozoic tectono-thermal evolution of the Gariep Belt and its basement, Namibia/South Africa. Precambr Res 90:1–28
Frimmel HE, van Achterbergh E (1995) Mineralogy petrology metamorphism of calc-silicate and associated rocks in the Pan-African Kaaimans Group, Saldania Belt, South Africa. Mineral Petrol 53:75–102
Frimmel HE, Basei MS, Gaucher C (2010) Neoproterozoic geodynamic evolution of SW-Gondwana: a southern African perspective. Int J Earth Sci (Geol Rundsch). https://doi.org/10.1007/s00531-010-0571-9
Frimmel HE, Hartnady CJH, Koller F (1996a) Geochemistry and tectonic setting of magmatic units in the Pan-African Gariep Belt, Namibia. Chem Geol 104:459–469
Frimmel HE, Klötzli U, Siegfried P (1996b) New Pb–Pb single zircon age constraints on the timing of the Neoproterozoic glaciation and continental break-up in Namibia. J Geol 104:459–469
Frimmel HE, Zartman RE, Spaeth A (2001) The Richtersveld igneous complex, South Africa; U–Pb zircon and geochemical evidence for the beginning of Neoproterozoic continental breakup. J Geol 109:493–508
Frimmel HE, Basei MS, Gaucher C (2011) Neoproterozoic geodynamic evolution of SW-Gondwana: a southern African perspective. Int J Earth Sci 100:323–354
Frimmel HE, Basei MAS, Correac VX, Mbangula N (2013) A new lithostratigraphic subdivision and geodynamic model for the Pan-African western Saldania Belt, South Africa. Precambr Res 231:218–235
Gaucher C (2000) Sedimentology, palaeoontology and stratigraphy of the Arroyo del Soldado Group (Vendian to Cambrian, Uruguay). Beringeria 26:1–120
Gaucher C, Germs GJB (2006) Recent advances in South African Neoproterozoic to early Palaeozoic biostratigraphy: correlation of the Cango Caves and Gamtoos Groups and acritarchs of the Sardinia Bay Formation, Saldania Belt. S Afr J Geol 109:193–214
Gaucher C, Poiré DG, Gómez Peral L, Chiglino L (2005a) Litoestratigrafía, bioestratigrafía y correlaciones de las sucesiones sedimentarias del Neoproterozoico-Cámbrico del Cratón del Río de La Plata (Uruguay y Argentina). Latin Am J Sedimentology Basin Anal 12:145–160
Gaucher C, Frimmel HE, Germs GJB (2005b) Organic-walled microfossils and biostratigraphy of the upper Port Nolloth Group (Namibia): implications for latest Neoproterozoic glaciations. Geol Mag 142:539–559
Gaucher C, Finney S, Poiré D, Valencia V, Grove M, Blanco G, Paoumukaghlian L, Peral L (2008) Detrital zircon ages of Neoproterozoic sedimentary successions in Uruguay and Argentina: insights into the geological evolution of the Río de la Plata Craton. Precam Res 167:150–170
Germs G (1995) The Neoproterozoic of southwestern Africa, with emphasis on platform stratigraphy and paleontology. Precambr Res 73(1–4):137–151
Geyer G (2005) The Fish River Subgroup in Namibia: stratigraphy, depositional environments and the Proterozoic-Cambrian boundary problem revisited. Geol Mag 142:465–498
Gómez Peral LE, Poiré DG, Strauss H, Zimmermann U (2007) Chemostratigraphy and diagenetic constraints on Neoproterozoic carbonate successions from the Sierras Bayas Group, Tandilia System, Argentina. Chem Geol 237:127–146
Gómez Peral L, Sial AM, Arrouy MJ, Richiano S, Ferreira VP, Kaufman AJ, Poiré DG (2017) Paleo-climatic and paleo-environmental evolution of the Neoproterozoic basal sedimentary cover on the Río de La Plata Craton, Argentina: Insights from the δ13C chemostratigraphy. Sed Geol 353(2017):139–157
Goscombe B, Gray DR (2007) The Coastal Terrane of the Kaoko Belt, Namibia: outboard arc-terrane and tectonic significance. Precambr Res 155(1–2):139–158
Gray RD, Foster DA, Goscombe B, Passchier C, Trouw AJ (2006) $^{40}Ar/^{39}Ar$ thermochronology of the Pan-African Damara Orogen, Namibia, with implications for tectonothermal and geodynamic evolution. Prec Res 150:49–72
Gregori DA, López VL, Grecco LE (2004) A late Proterozoic-early Paleozoic magmatic cycle in Sierra de la Ventana, Argentina. J S Am Earth Sci 19:155–171
Gresse PG (1983) Lithostratigraphy and structure of the Kaaimans Group. In: Hälbich IW (ed) Geodynamics of the Cape Fold Belt. Special Publications Geological Society of South Africa, 12, pp 7–19
Gresse PG, Germs GJB (1993) The Nama foreland basin: sedimentation, major unconformity bounded sequences and multisided active margin advance. Precambr Res 63:247–272
Gresse PG, von Veh MW, Frimmel HE (2006) Namibian (Neoproterozoic) to Early Cambrian sucessions. In: Johnson MR, Anhaeusser CR, Thomas RJ (eds) The geology of South Africa, Council of Geoscience, pp 395–420
Grotzinger JP, Bowring SA, Saylor BZ, Kaufman AJ (1995) Biostratigraphic and geochronologic constraints on early animal evolution. Science 270:598–604
Hanchar JM, Hoskin PWO (eds) (2003) Zircon. Reviews in mineralogy and geochemistry, vol 53, pp 1–499
Handy MR, Schmid G, Bousquet R, Kissling E, Bernoulli D (2010) Reconciling plate-tectonic reconstructions of Alpine Tethys with the geological–geophysical record of spreading and subduction in the Alps. Earth Sci Rev 102(2010):121–158
Hartnady C, Joubert P, Stowe C (1985) Proterozoic crustal evolution in southwestern Africa. Episodes 8:236–244

Hauser N, Matteini M, Omarini RH, Pimentel MM (2011) Combined U–Pb and Lu–Hf isotope data on turbidites of the Paleozoic basement of NW Argentina and petrology of associated igneous rocks: implications for the tectonic evolution of western Gondwana between 560 and 460 Ma. Gondwana Res 19:100–127

Hoffman PF, Li Z-H (2009) A palaeogeographic context for Neoproterozoic glaciation. Palaeogeogr Palaeoclimatol Palaeoecol 277 (2009):158–172

Hoffman PF, Schrag DP (2002) The snowball earth hypothesis. Terra Nova 14:129–155

Hoffman PF, Bellefroid EJ, Johnson BJ, Hodgskiss MSW, Schrag DP, Halverson GP (2016) Early extensional detachments in a contractional orogen: coherent, map-scale, submarine slides (mass transport complexes) on the outer slope of an Ediacaran collisional foredeep, eastern Kaoko belt, Namibia. Can J Earth Sci 53:1177–1189

Hofmann A (1988) Chemical differentiation of the Earth: the relationship between mantle, continental crust and oceanic crust. Earth Planet Sci Lett 90:297–314

Hofmann M, Linnemann U, Hoffmann K-H, Germs G, Gerdes A, Marko L, Eckelmann K, Gärtner A, Krause R (2014) The four Neoproterozoic glaciations of southern Namibia and their detrital zircon record: the fingerprints of four crustal growth events during two supercontinent cycles. Precambr Res 259:176–188

Huff WD, Bergstrøm SM, Kolata DR (1992) Gigantic Ordovician volcanic ash fall in North America and Europe: biological, tectonomagmatic, and event-stratigraphic significance. Geology 20:875–878

Huff WD, Bergström SM, Kolata DR, Cingolani CA, Astini RA (1998) Ordovician K-bentonites in the Argentine Precordillera: relations to Gondwana margin evolution. In: Pankhurst RJ, Rapela CW (eds) The Proto-andean margin of Gondwana. Geological Society, London, Special Publication, no. 142, pp 107–126

Ježek P (1990) Analisis sedimentológico de la Formación Puncoviscana entre Tucumán y Salta. In Aceñolaza FG, Miller H, Toselli AJ (eds) El Ciclo Pampeano en el Noroeste Argentino. Serie Correlación Geológico, Universidad Nacional de Tucumán, vol 12, pp 9–35

Johnson MR, Anhaeusser CR, Thomas RJ (eds) (2006) The geology of South Africa. Geological Society of South Africa and Council of Geoscience, Pretoria, pp 1–691

Jordan TE (1995) Retroarc foreland and related basins. In: Busby CJ, Ingersoll RV (eds) Tectonics of sedimentary basins. Blackwell Science, Oxford, pp 331–362

Kawashita K, Varela R, Cingolani C, Soliani E Jr, Linares E, Valencio SA, Ramos AV, Do Campo M (1999) Geochronology and chemostratigraphy of "La Tinta" Neoproterozoic sedimentary rocks, Buenos Aires Province, Argentina. II South American symposium on isotope geology, Brazil, pp 403–407

Keppie JD, Bahlburg H (1999) Puncoviscana formation of northwestern and central Argentina: passive margin or foreland basin deposits? In: Ramos VA, Keppie JD (eds) Laurentia-Gondwana connections before Pangaea. Geological Society of America Special Publication, 336, pp 139–144

Kleine T, Mezger K, Münker K, Zimmermann U, Bahlburg H (2004) Crustal evolution along the Early Ordovician ptoto-Andean margin of Gondwana: trace element and isotope evidence from the Complejo Igneo Pocitos (NW Argentina). J Geol 112:503–520

Konopásek J, Košler J, Sláma J, Janoušek V (2014) Timing and sources of pre-collisional Neoproterozoic sedimentation along the SW margin of the Congo Craton (Kaoko Belt, NW Namibia). Gondwana Res 26(1):386–401

Kraemer PE, Escayola MP, Martino RD (1995) Hipótesis sobre la evolución neoproterozoica de las Sierras Pampeanas de Córdoba (3084′–3284′S) Argentina. Revi Asoc Geol Arg 50(1–4):47–59

Kröner A (1974) The Gariep Group, Part I; Late Precambrian formations in the western Richtersveld, northern cape Province. Precam Res Unit Univ Cape Town Bull 13:1–87

Kröner A, Rankama K (1972) Late Precambrian glaciogenic sedimentary rocks in southern Africa: a compilation with definitions and correlations. Precambr Res Unit Univ Cape Town Bull 11:1–37

Lara P, Oyhantçabal P, Dadd K (2017) Post-collisional, Late Neoproterozoic, high-Ba-Sr granitic magmatism from the Dom Feliciano Belt and its cratonic foreland, Uruguay: petrography, geochemistry, geochronology, and tectonic implications. Lithos 277:178–198

Lenz C, Fernandes LAD, McNaughton NJ, Porcher CC, Koester E, Masquelin H (2011) Magmatic and metamorphic U–Pb SHRIMP ages in zircons for the Cerro Olivo Gneissic complex orthogneisses —Dom Feliciano Belt in Uruguay. Precambr Res 185:149–163

López de Azarevich VL, Omarini RH, Santos RV, Azarevich MB, Sureda RJ (2010) Nuevos aportes isotópicos para secuencias carbonáticas del Precámbrico superior (Formación Las Tienditas) del NO de Argentina: su implicancia en la evolución de la Cuenca Puncoviscana. Serie Correlación Geológica 26:1–15

Lucassen F, Becchio R, Wilke HG, Franz G, Thirwall MF, Viramonte J, Wemmer K (2000) Proterozoic-Palaeozoic development of the basement of Central Andes (18–26°)—a mobile belt of the South American craton. J S Am Earth Sci 13:697–715

Martin H (1965) The Precambrian geology of South Africa and Namibiaaqualand. Precam Res Unit Univ Cape Town 1–159

Martin H, Porada H, Walliser OH (1985) Mixtite deposits of the Damara sequence, Namibia: problem of interpretation. Palaeogeogr Palaeo-climatol Palaeoecol 51:159–196

Masquelin H, Lara HS, Sánchez Bettucci L, Núñez Demarco P, Pascual S, Muzio R, Peel E, Scaglia F (2017) Lithologies, structure and basement-cover relationships in the schist belt of the Dom Feliciano Belt in Uruguay. Braz J Geol 47:21–42

McLennan SM (2001) Relationships between the trace element composition of sedimentary rocks and upper continental crust. Geochem Geophys Geosyst 2:2000GC000109

McLennan SM, Taylor SR, McCulloch MT, Maynard JB (1990) Geochemical and Nd–Sr isotopic composition of deep-sea turbidites: crustal evolution and plate tectonic associations. Geochim Cosmochim Acta 54:2015–2050

McLennan SM, Hemming S, McDaniel DK, Hanson GN (1993) Geochemical approaches to sedimentation, provenance and tectonics. In: Johnsson MJ, Basu A (eds) Processes controlling the composition of clastic sediments, Geological Society of America, Special Publications 284, pp 21–40

McMillan MD (1968) The geology of the Witputs-Sendelingsdrif area. Precambr Res Unit Univ Cape Town Bull 4:1–177

Miller W, Armstrong R, De Wit MJ (2016) Geology and U/PB geochronology of the gamtoos complex and lower Paleozoic Table Mountain Group, Cape Fold Belt, Eastern Cape, South Africa. S Afr J Geol 119:147–170

Mon R, Hongn F (1991) The structure of the Precambrian and Lower Palaeozoic basement of the Central Andes between 22° and 32° Lat. Geol Rundsch 80:745–758

Moya MC (1999) El Ordovícico en los Andes del norte Argentino. In: González Bonorino G, Omarini R, Viramonte J (eds) Relatorio del XIV Congreso Geológico Argentino. Geología del Noroeste Argentino, pp 134–152

Naidoo T (2008) Provenance of the Neoproterozoic to Early Paleozoic Kango Inlier, Oudtshoorn, South Africa. University of Johannesburg, unpublished M.Sc. thesis, pp 1–261

Naidoo T (2016) The applicability of U–Pb and Lu–Hf isotopic signatures from detrital zircon in establishing tectonic setting, depositional environment and maximum depositional age constraints of clastic sedimentary successions. Unpublished Ph.D. thesis, University of Stavanger, pp 1–321

Naidoo T, Zimmermann U, Chemale F Jr (2013) The evolution of Gondwana: U–Pb, Sm–Nd, Pb–Pb and geochemical data from Neoproterozoic to Early Palaeozoic successions of the Kango Inlier (Saldania Belt, South Africa). Sed Geol 294:164–178

Naidoo T, Zimmermann U, Vervoort J (2016) Pre-Pampean metasedimentary rocks from the Argentinian Puna: evidence for the Ediacaran margin of Gondwana or the Arequipa-Antofalla-Western Pampeanas block. Precambr Res 280:139–146

Naidoo T, Zimmermann U, Vervoort J, Tait J (2017) The elusive snowball earth: U–Pb zircon ages from the upper diamictite of the Gifberg Group, South Africa. J Afr Earth Sci 129:307–317

Oriolo S, Oyhantçabal P, Wemmer K, Heidelbach F, Pfänder J, Basei MAS, Hueck M, Hannich F, Sperner B, Siegesmund S (2016a) Shear zone evolution and timing of deformation in the Neoproterozoic transpressional Dom Feliciano Belt, Uruguay. J Struct Geol 92:59–78

Oriolo S, Oyhantçabal P, Basei MAS, Wemmer K, Siegesmund S (2016b) The Nico Pérez Terrane (Uruguay): from Archean crustal growth and connections with the Congo Craton to late Neoproterozoic accretion to the Río de la Plata Craton. Precambr Res 280:147–160

Oriolo S, Oyhantçabal P, Wemmer K, Basei MAS, Benowitz J, Pfänder J, Hannich F, Siegesmund S (2016c) Timing of deformation in the Sarandí del Yí shear zone, Uruguay: implications for the amalgamation of western Gondwana during the Neoproterozoic Brasiliano-Pan-African Orogeny. Tectonics 35. doi:https://doi.org/10.1002/2015TC004052

Oriolo S, Oyhantçabal P, Wemmer K, Siegesmund S (2017) Contemporaneous assembly of Western Gondwana and final Rodinia break-up: implications for the supercontinent cycle. Geosci Front. https://doi.org/10.1016/j.gsf.2017.01.009

Oyhantçabal P, Siegesmund S, Wemmer K, Frei R, Layer P (2007) Post-collisional transition from calc-alkaline to alkaline magmatism during transcurrent deformation in the southernmost Dom Feliciano Belt (Braziliano–Pan-African, Uruguay). Lithos 277:178–198

Oyhantçabal P, Siegesmund S, Wemmer K, Presnyakov S, Layer P (2009) Geochronological constraints on the evolution of the southern Dom Feliciano Belt (Uruguay). J Geol Soc Lond 166:1075–1084

Oyhantçabal P, Siegesmund S, Wemmer K (2010) The Río de la Plata Craton: a review of units, boundaries, ages and isotopic signature. In: Siegesmund S, Basei M, Oyhantçabal P (eds) Multiaccretional Tectonics at the Rio de La Plata Margins. Int J Earth Sci. doi:https://doi.org/10.1007/s00531-010-0580-8

Oyhantçabal P, Siegesmund S, Wemmer K (2011) The Río de la Plata Craton: a review of units, boundaries, ages and isotopic signature. Int J Earth Sci 100:201–220

Øxnevad S (2017) High-resolution heavy mineral studies on "black sands" from the Nama Group (Fish River Subgroup) in Namibia – Part I. - Unpublished Master Thesis at the Department of Petroleum Engineering, University of Stavanger, pp 1–159 with appendices

Pankhurst RJ, Rapela CW, Saavedra J, Baldo E, Dahlquist J, Pascua I, Fanning CM (1998) The Famatinian magmatic arc in the central Sierras Pampeanas: an Early to Mid-Ordovician continental arc on the Gondwana margin. In: Pankhurst RJ, Rapela CW (eds) The Proto-Andean margin of Gondwana. Geological Society, London, Special Publications 142, pp 343–367

Pankhurst RJ, Rapela CW, Lopez De Luchi MG, Rapalini AE, Fanning CM, Galindo C (2014) The Gondwana connections of northern Patagonia. J Geol Soc Lond 171:313–328

Pazos PJ, Rapalini A (2011) Chapter 54: the controversial stratigraphy of the glacial deposits in the Tandilia System, Argentina. In: Arnaud E, Halverson GP, Shields-Zhou G (eds) The geological record of Neoproterozoic glaciations. Geological Society, London, Memoirs, 36, pp 565–569

Pecoits E, Gingras M, Aubet N, Konhauser K (2008) Ediacaran in Uruguay: palaeoclimatic and palaeobiological implications. Sedimentology 55:689–719

Pecoits E, Gingras MK, Konhauser KO (2011) Las Ventanas and San Carlos formations. Maldonado Group, Uruguay, Geological Society, London, Memoirs, 36, pp 555–564

Poiré DG (1987) Mineralogía y sedimentología de la Formación Sierras Bayas en el núcleo septentrional de las sierras homónimas, Partido de Olavarría, Provincia de Buenos Aires. Ph.D. thesis, Universidad Nacional de La Plata, Argentina, 545 pp

Poiré DG (1993) Estratigrafía del Precámbrico sedimentario de Olavaría, Sierras Bayas, Provincia de Buenos Aires, Argentina. XII Congreso Geológico Argentino y II Congreso de Exploración de Hidrocarburos Acta II:1–11

Poma S, Quenardelle S, Litvak V, Maisonnave EB, Koukharsky M (2004) The Sierra de Macon, Plutonic expression of the Ordovician magmatic arc, Salta Province Argentina. J S Am Earth Sci 16:587–597

Puetz S, Ganade C, Zimmermann U, Borchardt G (2017) Statistical analyses of global U–Pb database 2017. Geosci Front. https://doi.org/10.1016/j.gsf.2017.06.001

Rapalini AE, Tohver E, Sánchez Bettucci L, Lossada AC, Barcelona H, Pérez C (2015) The Late Neoproterozoic Sierra de Ánimas Magmatic complex and Playa Hermosa formation, southern Uruguay, revisited: paleogeographic implications of new paleomagnetic and precise geochronologic data. Precambr Res 259:143–155

Rapela CW, Pankhurst RJ, Casquet C, Baldo E, Saavedra J, Galindo C, Fanning CM (1998) The Pampean Orogeny of the southern proto-Andes: Cambrian continental collision in the Sierras de Cordoba. In: Pankhurst RJ, Rapela CW (eds) The Proto-Andean margin of Gondwana. Geological Society London, Special Publications 142, pp 181–217

Rapela CW, Pankhurst RJ, Fanning CM, Grecco LE (2003) Basement evolution of the Sierra de la Ventana Fold Belt: new evidence for Cambrian continental rifting along the southern margin of Gondwana. J Geol Soc Lond 160:613–628

Rapela CW, Pankhurst RJ, Casquet C, Fanning CM, Baldo EG, González-Casado JM, Galindo J, Dahlquist J (2007) The Río de la Plata craton and the assembly of SW Gondwana. Earth-Sci Rev 83:49–82

Rapela CW, Pankhurst RJ, Casquet C, Baldo EG, Galindo J, Fanning CM, Dahlquist JM (2010) The Western Sierras Pampeanas: protracted Grenville-age history (1330–1030 Ma) of intra-oceanic arcs, subduction–accretion at continental-edge and AMCG intraplate magmatism. J S Am Earth Sci 29:105–127

Rapela CW, Verdecchia SO, Casquet C, Pankhurst RJ, Baldo EG, Galindo C, Murra JA, Dahlquist JA, Fanning CM (2016) Identifying Laurentian and SW Gondwana sources in the Neoproterozoic to Early Paleozoic metasedimentary rocks of the Sierras Pampeanas: paleogeographic and tectonic implications. Gondwana Res 32:193–212

Rozendaal A, Gresse PG, Scheepers R, Le Roux JP (1999) Neoproterozoic to Early Cambrian crustal evolution of the Pan-African Saldania belt, South Africa. Precambr Res 97:303–323

Sánchez Bettucci L, Masquelin E, Peel E, Oyhantçabal P, Muzio R, Ledesma JJ, Preciozzi F (2010) Comment on "Provenance of the Arroyo del Soldado Group (Ediacaran to Cambrian, Uruguay): implications for the palaeogeographic evolution of southwestern Gondwana" by Blanco et al. [Precambr Res 171:57–73 (2009)]. Precambr Res 180:328–333

Saylor BZ, Kaufman AJ, Grotzinger JP, Urban F (1998) A composite reference section for terminal Proterozoic strata of southern Namibia. J Sed Res 68:1223–1235

Scheepers R, Armstrong R (2002) New U–Pb SHRIMP zircon ages of the Cape Granite Suite: implications for the magmatic evolution of the Saldania Belt. S Afr J Geol 105:241–256

Schermerhorn LJG (1974) Late Precambrian mixtites: glacial and/or nonglacial. Am J Sci 274:673–824

Spalletti LA, Del Valle A (1984) Las diamictitas del sector oriental de Tandilia: caracteres sedimentológicos y orígen. Rev de la Asoc Geol Arg 49:188–206

Stanistreet IG, Kukla PA, Henry G (1991) Sedimentary basinal responses to a Late Precambrian Wilson cycle: the Damara Orogen and Nama Foreland, Namibia. J Afr Earth Sci 13:141–156

Tankard AJ, Jackson MPA, Eriksson KA, Hobday DK, Hunter DR, Minter WEL (1982) Crustal evolution of southern Africa, 3.8 billion years of earth history. Springer, New York, pp 1–588

Taylor SR, McLennan SM (1985) The continental crust. Its composition and evolution; an examination of the geochemical record preserved in sedimentary rocks. Blackwell, Oxford

Thamm AG, Johnson MR (2006) The Cape supergroup. In: Johnson MR, Anhaeusser CR, Thomas RJ (eds) The geology of South Africa. Geological Society *of* South Africa and Council of Geoscience, Pretoria, pp 443–460

Toselli AJ, Aceñolaza FG, Sial AN, Rossi JN, Ferreira VP, Alonso R, Parada MA, Gaucher C (2005) Los carbonatos de la Formación Puncoviscana s.l.: Correlación quimioestratigráfica e interpretación geológica. X Congresso Brasileiro de Geoquímica e II Simpósio de Geoquímica dos Países do Mercosul Porto de Galinhas, Pernambuco, Brasil, 1–5 pp

Triebold S, von Eynatten H, Zack T (2012) A recipe for the use of rutile in sedimentary provenance analysis. Sed Geol 282:268–275

Trompette R (1994) Geology of Western Gondwana (2000–500 Ma). Pan-African-Brasiliano aggregation of South America and Africa. A.A. Balkema, Rotterdam, Brookfield, p 350

Uriz NJ, Cingolani CA, Chemale F Jr, Macambira MB, Armstrong R (2011) Isotopic studies on detrital zircons of Silurian-Devonian siliciclastic sequences from Argentinean North Patagonia and sierras de la Ventana regions: comparative provenance. Int J Earth Sci 100:571–589

Uriz NJ, Cingolani CA, Basei MAS, Blanco G, Abre P, Portillo NS, Siccardi A (2016) Provenance and paleogeography of the Devonian Durazno Group, southern Parana Basin in Uruguay. J S Am Earth Sci 66:248–267

Van Staden A (2011) Provenance analyses of Neoproterozoic/Early Palaeozoic glacial (?) deposits from southwestern Gondwana. Unpublished Ph.D. thesis, University of Johannesburg, pp 1–262 plus 6 appendices

Van Staden A, Naidoo T, Zimmermann U, Germs GJB (2006) Provenance analysis of selected clastic rocks in Neoproterozoic to lower Palaeozoic successions of southern Africa from the Gariep Belt and the Kango Inlier. S Afr J Geol 109:215–232

Van Staden A, Zimmermann U, Gutzmer J, Chemale F Jr, Germs GJB (2010) First regional correlation of Lower Paleozoic successions from Argentina and South Africa using glacial diamictite deposits and its consequences for the regional geology. J Geol Soc Lond 167:217–220

Vermeesch P (2004) How many grains are needed for a provenance study? Earth Planet Sci Lett 224:441–451

Vervoort JD, Kemp AIS (2016) Clarifying the zircon Hf isotope record of crust–mantle evolution. Chem Geol 425:65–75

Vervoort JD, Patchett PJ (1996) Behavior of hafnium and neodymium isotopes in the crust: constraints from Precambrian crustally derived granites. Geochim Cosmochim Acta 60(19):3717–3733

von Veh MW (1993) The stratigraphy and structural evolution of the Late Proterozoic Gariep Belt in the Sendelingsdrif-Annisfontein area, northwestern Cape Province. Precambr Res Unit Univ Cape Town Bull 38:1–174

Willner AP (1990) División tectonometamórfica del basamento del Noroeste Argentino. In: Aceñolaza FG, Miller H, Toselli AJ (eds) El Ciclo Pampeano en el Noroeste Argentino. Serie Correlación Geológico, Universidad Nacional de Tucumán, vol 12, pp 113–159

Winchester JA, Floyd PA (1977) Geochemical discrimination of different magma series and their differentiation products using immobile elements. Chem Geol 20:325–343

Zimmermann U (2005) Provenance studies of very low- to low-grade metasedimentary rocks of the Puncoviscana Formation in Northwest Argentina. In: Vaughan APM, Leat PT, Pankhurst RJ (eds) Terrane processes at the margins of Gondwana. Geological Society London, Special Publications, 246, pp 381–416

Zimmermann U (2011a) From fore-arc to foreland: a cross section of the Ordovician in the Central Andes. In: Gutíerrez-Marco JC, Rábano I, García-Bellido D (eds) Ordovician of the world. Cuadernos del Museo Minero, 14. Instituto Geológico y Minero de España, Madrid, pp 667–674

Zimmermann U (2011b) Comment on Blanco et al. (2009; Provenance of the Arroyo del Soldado Group (Ediacaran to Cambrian, Uruguay): implications for the palaeogeographic evolution of southwestern Gondwana)—a necessary remark to the use of provenance data. Precambr Res 186:233–236. https://doi.org/10.1016/j.precamres.2010.08.017

Zimmermann U, Bahlburg H (2003) Provenance analysis and tectonic setting of the Ordovician deposits in the southern Puna basin, NW Argentina. Sedimentology 50:1079–1104

Zimmermann U, Bahlburg H (2005) The crustal evolution of the Central Andes during the Neoproterozoic to the Silurian. Geochim Cosmochim Acta 69(10S):A877

Zimmermann U, Spalletti LA (2009) Provenance of the Lower Palaeozoic Balcarce formation (Tandilia System, Buenos Aires Province, Argentina): implications for palaeogeographic reconstructions of SW Gondwana. Sed Geol 219:7–23

Zimmermann U, Luna Tula G, Marchioli A, Narváez G, Olima H, Ramírez A (2002) Análisis petrográfico, geoquímico e isotópico geoquímicos de las arenitas de la Formación Falda Ciénaga (Ordovícico Medio) y sus implicaciones para le evolución de la cuenca ordovícica en la Puna (NO Argentina). Asociación Argentina de Sedimentología, vol 9, no 2, pp 165–188

Zimmermann U, Chemale F Jr, Dussin IA, Justino D, Germs GJB (2008a) Detrital zircon record of the Nama Group: implications for the Neoproterozoic to Lower Palaeozoic Palaeogeography of southern Africa; VI South American symposium of isotope geochemistry, Bariloche, Abstract volume, 7 p

Zimmermann U, Tait J, Miyazaki T, Naidoo T (2008b) Probable Neoproterozoic retro-arc basins on the southern Kalahari craton: the search for an active margin bordering southern Gondwana. 33th International Geological Congress, Oslo (Norway; 6.8.2009–14.8.2008), abstract volume

Zimmermann U, Niemeyer H, Meffre S (2010) Revealing the continental margin of Gondwana: the Ordovician arc of the Cordón de Lila (northern Chile). Int J Earth Sci 99(Suppl 1):S39–S56

Zimmermann U, Poiré DG, Gómez Peral L (2011a) Neoproterozoic to Lower Palaeozoic successions of the Tandilia System in Argentina:

implication for the palaeotectonic framework of southwest Gondwana. Int J Earth Sci 100:489–510

Zimmermann U, Tait J, Crowley QG, Pashley V, Straathof G (2011b) The Witputs diamictite in southern Namibia and associated rocks—constraints for a global glaciation? Int J Earth Sci 100:511–526. https://doi.org/10.1007/s00531-010-0621-3

Zimmermann U, Bahlburg H, Mezger K, Berndt J, Kay SM (2014) Origin and age of ultramafic rocks and gabbros in the southern Puna of Argentina: an alleged Ordovician suture revisited. Int J Earth Sci 103:1023–1036

Zimmermann U, Andersen T, Madland MV, Larsen IS (2015) The role of U–Pb ages of detrital zircons in sedimentology—an alarming case study for the impact of sampling for provenance interpretation. Sed Geol 320:38–60

Shear Zones in Brasiliano-Pan-African Belts and Their Role in the Amalgamation and Break-Up of Southwest Gondwana

22

Sebastián Oriolo, Mathias Hueck, Pedro Oyhantçabal, Ben Goscombe, Klaus Wemmer, and Siegfried Siegesmund

Abstract

Crustal-scale shear zones are ubiquitous in most Brasiliano–Pan-African belts of southwestern Gondwana and they resulted from the assembly of the Río de la Plata, Congo and Kalahari cratons. In the Dom Feliciano Belt, the Sierra Ballena-Dorsal do Canguçu-Major Gercino shear zone system and Sarandí del Yí Shear Zone are the most prominent structures, and they share a common history with shear zones of the Kaoko Belt, such as the Purros and Three Palms Mylonite Zones. The Purros Mylonite Zone, in turn, can be traced further south in the Damara Belt, where it is correlated with the Ogden Mylonite Zone. All these orogen-parallel shear zones underwent ductile deformation mostly at *c*. 630–580 Ma. However, further shearing is recorded in both the Kaoko and Dom Feliciano Belts at *c*. 550 Ma, thus being coeval with shearing along the Colenso Fault of the Saldania Belt. Though the Brasiliano–Pan-African Orogeny led to a relative stabilization of the South American and African continental crust by the early Paleozoic, shear zones were subsequently reactivated under brittle conditions during the Phanerozoic. These fault zones were particularly active during the opening of the South Atlantic Ocean in the Cretaceous, controlling magmatism emplacement, basin development and crustal exhumation. Shear zones thus played a major role not only during the Neoproterozoic assembly but also during the subsequent break-up of Gondwana.

Keywords

Mylonites • Neoproterozoic • Basement • South Atlantic Opening • Reactivation • Cretaceous

22.1 Introduction

Shear zones are one of the most prominent features in the architecture of Brasiliano–Pan-African belts. They not only represent boundaries between different crustal domains and preferred channels for magma ascent and emplacement but also played a major role in the orogen construction and exhumation (e.g. Kisters et al. 2002; Konopásek et al. 2005; Goscombe and Gray 2008; Passarelli et al. 2011a; Ganade et al. 2016; Oriolo et al. 2017). As they constitute major crustal anisotropies, Brasiliano–Pan-African shear zones were subsequently reactivated as well, thus controlling the Phanerozoic exhumation and uplift of the South American and African crust (Raab et al. 2002; Salomon et al. 2014; Hueck et al. 2017).

The aim of this chapter is to provide an overview of shear zones present in Brasiliano–Pan-African belts of southwestern Gondwana. Shear zones separating major tectonostratigraphic domains are presented separately, whereas those that are subordinated are referred to as intrabelt shear zones. Structural, microstructural, kinematic and geochronological data are thus compiled in order to summarize the main characteristics of shear zones. The tectonic implications are also discussed, including all different models and interpretations regarding the role of shear zones during the assembly of Gondwana.

S. Oriolo (✉) · M. Hueck · K. Wemmer · S. Siegesmund
Geoscience Centre, Georg-August-Universität Göttingen, Goldschmidtstraße 3, 37077 Göttingen, Germany
e-mail: seba.oriolo@gmail.com; soriolo@gl.fcen.uba.ar

Present Address:
S. Oriolo
CONICET-Universidad de Buenos Aires. Instituto de Geociencias Básicas, Aplicadas y Ambientales de Buenos Aires (IGEBA), Intendente Güiraldes 2160, C1428EHA Buenos Aires, Argentina

P. Oyhantçabal
Departamento de Geología, Facultad de Ciencias, Universidad de la República, Iguá 4225, 11400 Montevideo, Uruguay

B. Goscombe
Integrated Terrane Analysis Research (ITAR), 18 Cambridge Rd, Aldgate, SA 5154, Australia

S. Siegesmund et al. (eds.), *Geology of Southwest Gondwana*, Regional Geology Reviews,
https://doi.org/10.1007/978-3-319-68920-3_22

22.2 Dom Feliciano Belt

The Dom Feliciano Belt (Fragoso César 1980, 1991) follows a north-northeast trend from the Brazilian state of Santa Catarina to southeastern Uruguay for more than 1000 km with a typical width of *c*. 150 km. Along its extension, it is divided into eastern, central and western domains (Basei et al. 2000), separated by major shear zones following a regional northeast orientation (Fig. 22.1). Phanerozoic sediments cover much of the belt extension, which is exposed in three basement domes in the Brazilian states of Santa Catarina and Rio Grande do Sul, and in Uruguay.

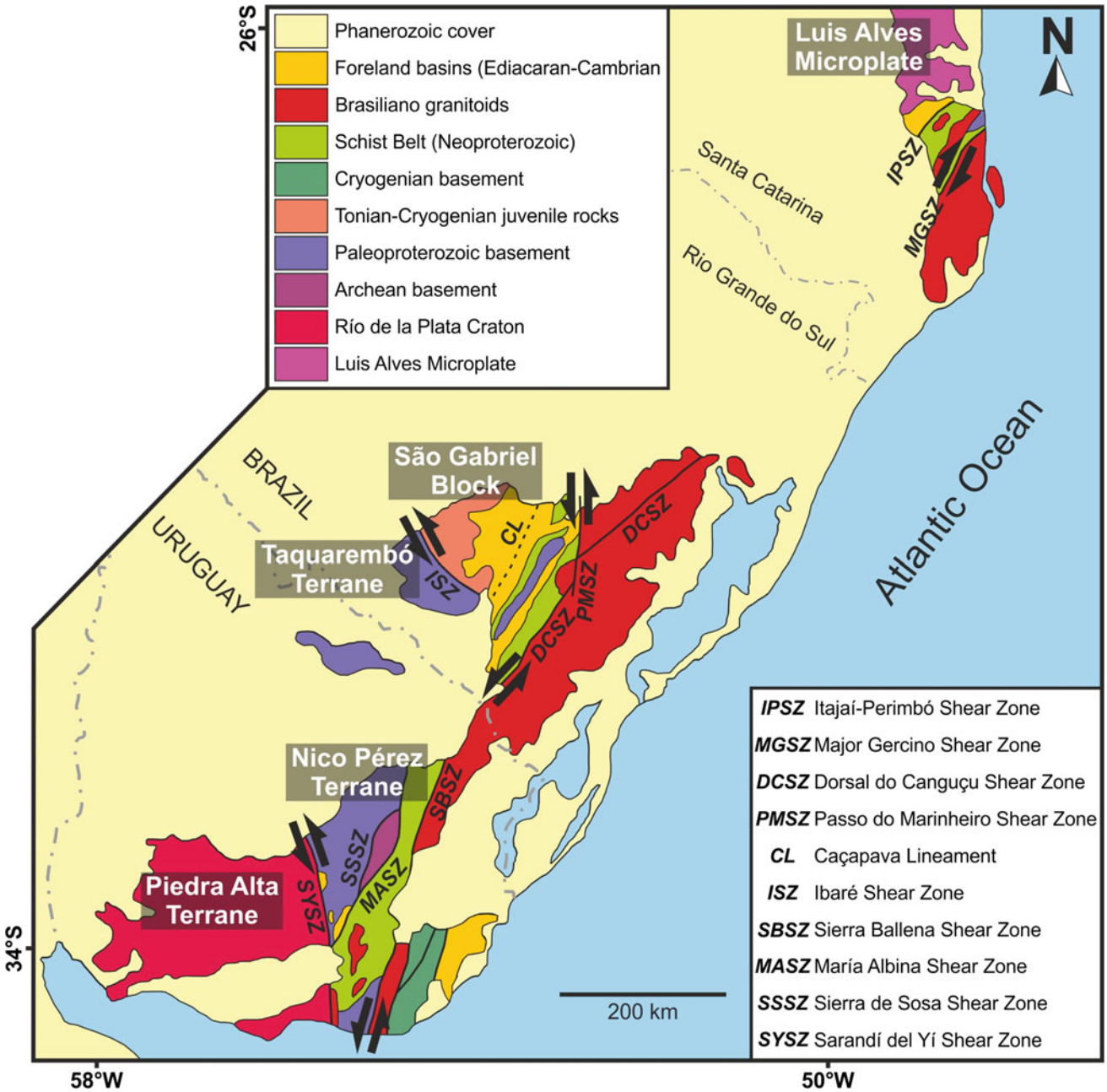

Fig. 22.1 Simplified geological map of the Dom Feliciano Belt (modified after Basei et al. 2000; Oyhantçabal et al. 2011a; Hueck et al. 2016)

22.2.1 Santa Catarina Sector

22.2.1.1 Introduction

The Precambrian basement in Santa Catarina constitutes a corridor approximately 70–100 km wide along the Atlantic coast north of the city of Tubarão. It comprises two main tectonostratigraphic domains: the Dom Feliciano Belt and the Luís Alves Microplate.

The Luís Alves Microplate is composed mostly of banded orthogneisses with TTG composition and subordinated quartzites, migmatites and banded iron formations, intruded in its eastern border by the Neoproterozoic Paranaguá Batholith. Archean crustal growth is indicated by U-Pb SHRIMP ages of zircon xenocrysts and whole-rock Sm–Nd model ages, but it was strongly reworked in the Paleoproterozoic by two high-grade metamorphic events (Basei 1985; Basei et al. 2000, 2009; Hartmann et al. 2000, 2001, 2003).

This microplate is limited to the southeast by the Dom Feliciano Belt, which is divided into three domains bounded by regional shear zones (Basei et al. 2000). These structures and those correlated with them further south are grouped into the South Brazilian Shear Belt (Bitencourt and Nardi 2000).

The northwestern domain consists of the Itajaí Basin, deposited on top of the Luís Alves Microplate and tectonically separated from the Schist Belt by the Itajaí-Perimbó Shear Zone. The sequence is deformed by northwest-verging thrust tectonics (Rostirolla et al. 1992, 1999; Schroeder 2006; Guadagnin et al. 2010; Basei et al. 2011a).

The central domain consists of a fold-and-thrust schist belt, an association of metavolcanosedimentary rocks metamorphosed in greenschist to amphibolite facies called the Brusque Group. Along with its crystalline basement, the Camboriú Complex, it is intruded by several generations of granitic plutons. Crustal growth is interpreted to be mostly Archean to Paleoproterozoic, but the unit was ultimately reworked in the Neoproterozoic (Basei 1985; da Silva 1991; Philipp et al. 2004; da Silva et al. 2005; Basei et al. 2011b, 2013; Florisbal et al. 2012a; Hueck et al. 2016).

The southeastern or external domain is the Florianópolis Batholith, part of a large granitic belt. It is divided into several suites and records a long-lasting magmatic history between *c*. 650 and 580 Ma. Many of the intrusions are spatially related to shear zones (Basei et al. 2000; Bitencourt and Nardi 2000; Bitencourt et al. 2008; Passarelli et al. 2010, 2011b; Florisbal et al. 2009, 2012b, c; Chemale et al. 2012).

22.2.1.2 Major Gercino Shear Zone

The transcurrent Major Gercino Shear Zone is the most evident structure in Santa Catarina and was recognized early on as the boundary between the granitic rocks of the Florianópolis Batholith and the metasedimentary succession of the Brusque Group (Caldasso et al. 1995a, b). As such, it constitutes one of the main shear zones of the Dom Feliciano Belt, separating its eastern and central domains (Basei et al. 2000). It stretches for more than 70 km with a general northeast strike, from the Porto Belo Peninsula at the Atlantic shore to the border of the Phanerozoic Paraná Basin, which covers it to the east of the town of Angelina.

The shear zone has a maximum width of 10 km, intercalating mylonites and transcurrence-related granitic intrusions. Two mylonitic belts containing proto- to ultramylonites are separated by an elongated granitic core (Passarelli et al. 1993, 2010, 2011a). Mylonitic foliation is subvertical and shows a systematic strike variation from 065° in the northeastern sector to 010° in the southwestern part. Stretching lineation, in turn, exhibits trends varying from 055° with shallow plunges in the northeast to intermediate to steep plunges towards 200° in the southwest, especially in its late stages.

In contrast to the central portion, mylonites of the northeastern tip of the Major Gercino Shear Zone do not define clear belts in the Porto Belo region, being rather restricted to local shearing within and along borders of the granitic intrusions (Bitencourt and Kruhl 2000; Florisbal et al. 2012b). Mylonitic foliations strike northeast.

Most shear sense indicators, such as mantled porphyroclasts, S-C shear bands and mica-fish, record a dextral strike-slip movement. There are, however, numerous occurrences of symmetrical and sinistral indicators, which, according to Passarelli et al. (2010, 2011a), indicate the influence of pure shear and general flattening, further supported by strain analysis.

The development of the shear zone is closely related to the emplacement of granitic intrusions, which acted as the protolith to the majority of the mylonites. The emplacement of granites was coeval with the shearing event, as continuous deformation is registered in these rocks from the magmatic stage to greenschist facies metamorphic conditions (Bitencourt and Kruhl 2000; Passarelli et al. 2010; Florisbal et al. 2012b). Therefore, most geochronological constraints of the shear zone come from these granitoids and reveal a long-term deformational history. The earliest shear-related intrusions are the Quatro Ilhas and Mariscal granitoids, dated between *c*. 625 and 610 Ma (Chemale et al. 2012; Florisbal et al. 2012c), which are very similar to the U-Pb TIMS zircon ages of the Fernandes (614 ± 2 Ma) and Rolador (609 ± 16 Ma) suites (Passarelli et al. 2010). Somewhat younger, the Estaleiro Granite is interpreted to constrain the main phase of shearing, and was dated at 602 ± 4.2 Ma (U-Pb TIMS zircon, Chemale et al. 2012). Finally, the late-transcurrent Zimbros Suite yields U-Pb zircon ages with different methods between *c*. 589 and 586 Ma (Chemale et al. 2012). According to Passarelli et al. (2010), K-Ar muscovite and biotite ages of *c*. 570 Ma of mylonites around

Major Gercino represent tectonic activity after the main phase of deformation and are approximately synchronic to cooling K-Ar biotite ages of the Fernandes and Rolador granites. A much younger K-Ar age in muscovite (539 ± 13 Ma) was also obtained for the southernmost mylonites (Passarelli et al. 2010).

22.2.1.3 Itajaí-Perimbó Shear Zone

The Itajaí-Perimbó Shear Zone constitutes one of the main shear zones of the Dom Feliciano Belt in the State of Santa Catarina, separating its Central and Western domains. Despite being recognized as an important geotectonic feature since early mappings (da Silva and Dias 1981), it is very badly exposed, and has mostly been studied in works concerning either the Brusque Group or the Itajaí Basin.

The shear zone is described as a 15 km-wide transcurrent corridor characterized by a braided network of mylonites, ultramylonites and phyllonites, affecting rocks from both the Luis Alves Microplate and the Brusque Group metavolcanosedimentary rocks (da Silva and Dias 1981; da Silva 1991; Hartmann et al. 2003, 2015; Schroeder 2006; Guadagnin et al. 2010). Mylonitic foliation is subvertical and shows a 045° strike. Although most authors indicate a dextral shear sense, sinistral indicators were also described by Schroeder (2006).

After deposition of the Itajaí Basin at *c*. 560–550 Ma, thrusting under brittle conditions deformed the sequence and reactivated the shear zone, placing the Brusque Group on top of the sedimentary package (Rostirolla et al. 1992, 1999; Schroeder 2006; Guadagnin et al. 2010). An alternative interpretation considers the juxtaposition of the central and western domains to be entirely due to thrusting, placing the Brusque Group on top of the sediments of the Itajaí Basin (Basei 1985; Basei et al. 2011a, b; Raposo et al. 2014).

22.2.1.4 Intrabelt Shear Zones

Smaller Neoproterozoic shear zones are a common feature of the central and eastern domain of the Dom Feliciano Belt in Santa Catarina. The late deformational stages of the Brusque Group during the Brasiliano include the development of transcurrent shear zones in high-strain areas (Basei et al. 2000, 2011b; Philipp et al. 2004). This is synchronic to the intrusion of the granitic intrusions, which record a continuous deformational evolution under magmatic to solid-state conditions (Peternell et al. 2010; Florisbal et al. 2012b; Hueck et al. 2016). This deformation extends to the crystalline basement in the Camboriú Complex, where the Corre-Mar granite is interpreted to have intruded within a transtensional northeast-striking shear zone, in a conjugate system with the domain boundaries during the main shear event (Peternell et al. 2010; Florisbal et al. 2012b; Martini and Bitencourt 2014; Martini et al. 2015). Microstructures indicate continuous deformation during magma cooling, reaching mylonitization under greenschist facies conditions.

As most of the Major Gercino Shear Zone developed in granitic rocks of the Florianópolis Batholith, this structure has received most of the interest among shear zones of the southeastern domain. Discreet unnamed dextral shear zones were described, however, parallel to the magmatic foliation of granitoids, especially along intrusion borders (Bitencourt et al. 2008; Florisbal et al. 2009). The latter authors attributed to these structures a decisive role during the magmatic evolution of the batholith, permitting the migration and assimilation of mantellic melts.

22.2.2 Rio Grande do Sul Sector

22.2.2.1 Introduction

The crystalline basement in Rio Grande do Sul is exposed in a dome-like window of the overlying Paraná Basin. It is traditionally divided into four terranes: Taquarembó, São Gabriel, Tijucas and Pelotas Batholith (Philipp et al. 2016 and references therein). The first three units are irregularly covered by sediments and subordinated volcanic rocks of the Camaquã Basin, which were deposited between *c*. 600 and 535 Ma (Almeida et al. 2010; Oliveira et al. 2014; Philipp et al. 2016 and references therein). In the traditional three-fold division of the Dom Feliciano Belt, the eastern and central domains correspond to the Tijucas Terrane and Pelotas Batholith, respectively, and the Western Domain consists of the Camaquã Basin.

The Taquarembó Terrane is separated to the north from the São Gabriel Terrane by the Ibaré Shear Zone and from the Tijucas Terrane to the east by the Caçapava Lineament, covered by sediments. It comprises Paleoproterozoic granulitic rocks (Hartmann et al. 1999, 2008) intruded by late to post-collisional granites associated with the Dom Feliciano Belt magmatism. The Taquarembó Terrane is an extension of the Nico Pérez Terrane in Uruguay (Rapela et al. 2011; Oriolo et al. 2016a; Philipp et al. 2016; Chap. 7).

In the westernmost portion of the Precambrian basement, the São Gabriel Terrane presents a distinct juvenile Neoproterozoic association. It is composed of the remains of two magmatic arcs, associated with ophiolitic complexes and marginal deposits, developed between *c*. 930–860 and 770–680 Ma (Leite et al. 1998; Saalmann et al. 2005, 2006a, 2011; Hartmann et al. 2011; Lena et al. 2014; Philipp et al. 2014, 2016; Lopes et al. 2015). Later, the whole sequence was intruded by Brasiliano granitoids (Philipp et al. 2016 and references therein).

The Tijucas Terrane (i.e., Encantadas Block; Saalmann et al. 2006b, 2007, 2011) constitutes a crustal block entrenched between the São Gabriel Terrane, west of the

Caçapava Lineament, and the Pelotas Batholith, separated by the Dorsal do Canguçu and Passo do Marinheiro Shear Zones. It consists of a mostly Paleoproterozoic crystalline core, the Encantadas Complex, covered by Neoproterozoic metasupracrustal rocks of the Porongos Complex, intensely reworked during the Brasiliano Orogeny (Hartmann et al. 2004; Saalmann et al. 2006b, 2007, 2011; Basei et al. 2008; Pertille et al. 2015a, b).

Finally, the Pelotas Batholith is separated to the west from the Tijucas Terrane by the Dorsal do Canguçu Shear Zone. It is a large association comprising syn- to post-collisional magmatism recorded by high-K calc-alkaline followed by alkaline and peralkaline intrusions (Philipp and Machado 2005; Nardi and Bitencourt 2009; Oliveira et al. 2015). Most intrusions are emplaced along shear zones (Philipp et al. 1993, 2013; Nardi and Frantz 1995; Koester et al. 2001a, b). The ages of the granite belt range between *c*. 650 and 550 Ma (Babinski et al. 1997; da Silva et al. 1997; Koester et al. 2001c; Frantz et al. 2003; Philipp and Machado 2005; Oliveira et al. 2015).

22.2.2.2 Dorsal Do Canguçu Shear Zone

The Dorsal do Canguçu Shear Zone is the main tectonic feature of the Dom Feliciano Belt in the Rio Grande do Sul State. It constitutes the boundary between the granitic intrusions of the Pelotas Batholith and the metavolcanosedimentary sequence of the Porongos Group. A number of concurring names have been suggested for this structure, such as 'Cordilheira Shear Zone' (Basei et al. 2000, 2005, 2008; Passarelli et al. 2011a) and 'Porto Alegre Suture' (Fernandes et al. 1995a, b; Fernandes and Koester 1999; Koester et al. 2001c, 2016, Masquelin et al. 2012). The latter is an interpretative term which was originally applied in the distinct context of the shear zone, but in later years it has occasionally been used in order to refer to the structure itself.

This shear zone crosscuts the entire crystalline shield in Rio Grande do Sul and extends for *c*. 200 km. It is usually limited to a band of synkinematic granites commonly around 8 km in width, but as wide as *c*. 20 km, in which mylonitic bands may be as thick as 2 km (Fernandes et al. 1993; Tommasi et al. 1994). The shear zone is transected in its central portion by the late Passo do Marinheiro Shear Zone, which is essentially brittle and has a northwards orientation.

Mylonitic foliation is subvertical or, subordinately, has steep dips to the northwest. Stretching lineations are mostly subhorizontal with northeast-southwest trends. Within high-strain zones, intrafolial folds are recognized with northeast-trending subhorizontal hinges, oriented parallel to the stretching lineation. Sinistral shear sense is recognized by the presence of macro- and microscale kinematic indicators, though there are some descriptions of dextral indicators in the northeastern segment of the structure. A later phase of deformation is also described as being responsible for folding the mylonites into open to tight folds with northeast hinges and axial planes parallel to the previous trend of the shear zone (Fernandes et al. 1992, 1993; Philipp et al. 1993; Tommasi et al. 1994; Fernandes and Koester 1999; Passarelli et al. 2011a).

The main transcurrent deformation in the Dorsal do Canguçu Shear Zone is synchronic with the intrusion of granitic bodies. According to Tommasi et al. (1994), most of the strain was accommodated during crystallization and subsequent cooling under high-temperature conditions, often resulting in microfractures filled with undeformed quartz crystals. The cooling from high- to low-temperature solid-state deformation is evidenced by the transition from ductile to brittle deformation of feldspar and variations in dynamic recrystallization mechanisms in quartz. This pattern is supported by crystallographic preferred orientation of quartz c-axes (Tommasi et al. 1994).

Geochronological constraints of the Dorsal do Canguçu Shear Zones are represented by synkinematic intrusions: the Quitéria and Cordilheira Suites. The first is a porphyritic granodiorite with mantle signature, while the second consists of peraluminous two-mica leucogranites (Nardi and Frantz 1995; Fernandes and Koester 1999; Koester et al. 2001a, b; Philipp and Machado 2005; Philipp et al. 2013). U-Pb zircon crystallization ages determine a wide age gap, with one age for the first suite of 658 ± 4 Ma and three ages between *c*. 635 and 605 Ma for the latter (Frantz et al. 2003). These are the oldest ages obtained for rocks of the Pelotas Batholith, including those related to tangential tectonics which is interpreted to be older than the strike-slip deformation. Late to post-kinematic intrusions are dated at *c*. 610–550 Ma (Philipp et al. 2016). Biotite of the Quitéria and Cordilheira suites yielded K-Ar ages beween 600 and 575 Ma, whereas muscovites of the latter were dated at 624 ± 41 and 586 ± 11 Ma (Koester et al. 1997). Although all ages are interpreted to represent cooling, mixture in the muscovite ages caused by neoformed crystals during sinistral shearing might be possible as well (Koester et al. 1997). In turn, biotite from mylonites yield Ar/Ar ages between *c*. 537 and 531 Ma (Philipp et al. 2003), indicating late tectonic activity.

22.2.2.3 Passo Do Marinheiro Shear Zone

The Passo do Marinheiro Shear Zone comprises a brittle fault system transecting the Dorsal do Canguçu Shear Zone. Nonetheless, it is a notable feature, not only for crosscutting one of the major shear zones in the system but also for establishing the boundary between the Florianópolis Batholith and the Tijucas Terrane.

The Passo do Marinheiro Shear Zone has an approximately north-northeast orientation, comprising subvertical cataclastic zones that strike between 005° and 020°

(Philipp 1998). Sinistral movements caused lateral displacements between 15 and 35 km, disrupting not only the Dorsal do Canguçu Shear Zone but also most intrusive suites from the Pelotas Batholith. The most notable case is the post-tectonic Encruzilhada do Sul Suite, of which the biggest intrusion is segmented by the fault zone. A U-Pb zircon crystallization age of *c*. 595 Ma of this suite (Babinski et al. 1997; Philipp et al. 2016) sets a maximum deformation age for the shear zone.

22.2.2.4 Caçapava Lineament

The presence of the juvenile São Gabriel Terrane implicates a Neoproterozoic accretion to the western border of the Tijucas Terrane, responsible for the juxtaposition of this exotic domain with the Paleoproterozoic Tijucas and Taquarembó Terranes. However, this structure, usually interpreted as a former suture zone, is completely covered by the deposition of the Ediacaran to Cambrian sedimentary rocks of the Camaquã Basin.

Though not exposed, the Caçapava Lineament is recognized based on aeromagnetic data (Fernandes et al. 1995a, b; Costa 1997; Saalmann et al. 2011), with an orientation between 020° and 035°. According to Saalmann et al. (2011), it is possible that, during collision of the São Gabriel Terrane, oblique collision along the suture represented by the Caçapava Lineament evolved to a strike-slip regime during escape tectonics caused by crustal thickening. In this case, sinistral displacements were responsible for the present configuration.

22.2.2.5 Ibaré Shear Zone

The Ibaré Shear Zone or Ibaré Lineament constitutes the boundary of the São Gabriel and Taquarembó Terranes. However, little attention has been paid to the structure itself, and most references only cite it as the given boundary (e.g., Hartmann et al. 2008, 2011; Saalmann et al. 2011; Lena et al. 2014; Philipp et al. 2016).

The structure presents a northwest orientation, which contrasts with the dominant northeast-north-northeast structural grain of the Dom Feliciano Belt. It stretches almost 100 km from its northwestern extension, where it is covered by Phanerozoic sediments of the Paraná Basin, south of the city of São Gabriel, until it is covered by the sediments of the Camaquã Basin northeast of Bagé, in its southeastern portion. Along its extension, the lineament has a maximum width of *c*. 3 km and it is recognizable in satellite images. Small grabens accommodated on it preserve sediments of the Paraná Basin, indicating Phanerozoic reactivation of the structure (Luzardo and Fernandes 1990; Fernandes et al. 1995a).

Mylonites of the shear zone are characterized by a southeast-northwest-trending subvertical foliation with a shallow-plunging stretching lineation to the northwest (Luzardo and Fernandes 1990). The foliation presents feldspar porphyroclasts and dynamic recrystallization of quartz ribbons, interpreted to result from greenschist metamorphic conditions. Sinistral shear was recognized based on few shear sense indicators.

22.2.2.6 Intrabelt Shear Zones

Most shear zones developed during the Dom Feliciano event other than the domain borders affect the Tijucas Terrane and the Pelotas Batholith. In the Tijucas terrane, both the Encantadas and the Porongos Complexes share a regional orientation aligned in a northeast-southwest direction, with subvertical shear zones that reach an extension of some tenths of kilometres, such as the Santana da Boa Vista Shear Zone (Philipp et al. 2016). According to Saalmann et al. (2006b, 2007, 2011), the main shearing event in the Porongos group accompanied tight isoclinal folding and had a dextral sense of shear localized on narrow bands. The metamorphic conditions in this event were limited to the greenschist facies. In the Pelotas Batholith, a late transcurrent deformation overprints all tangential deformation from early stages, forming numerous subvertical northeast-trending structures, such as the Erval, Vila Ayrosa, Arroio Grande and Canguçu Shear Zones.

22.2.3 Uruguayan Sector

22.2.3.1 Introduction

The main tectonostratigraphic units of the Precambrian shield of Uruguay are the Piedra Alta and Nico Pérez terranes together with the Dom Feliciano Belt (Oyhantçabal et al. 2011a). The Sarandí del Yí Shear Zone separates the Piedra Alta Terrane from the Nico Pérez Terrane and the western Dom Feliciano Belt, whereas the Sierra Ballena Shear Zone represents the boundary between the latter and the eastern Dom Feliciano Belt.

The Piedra Alta Terrane is located in western Uruguay and represents part of the Paleoproterozoic Río de la Plata Craton (Almeida et al. 1973; Dalla Salda et al. 1988), which also includes the Buenos Aires Complex of the Tandilia Belt in Argentina (Cingolani 2011 and references therein). It is made up of gneisses, granitoids and low- to medium-grade schist belts with ages of between 2.2 and 2.0 Ga, which are intruded by late Paleoproterozoic east-northeast-striking doleritic dykes (Oyhantçabal et al. 2011a; Chap. 7).

Further east, the Nico Pérez Terrane basement is made up of the Pavas Block, the Valentines-Rivera Granulitic Complex and the Campanero Unit (Oriolo et al. 2016a; Chap. 7). The Pavas Block comprises Archean orthogneisses, mafic and ultramafic rocks and metasediments (Preciozzi et al. 1979; Hartmann et al. 2001), whereas the Valentines-Rivera Granulitic Complex comprises 2.2–2.0 Ga granulites and

orthogneisses (Oyhantçabal et al. 2011a, 2012). The latter is intruded by the *c*. 1.7 Ga Illescas rapakivi granite (Campal and Schipilov 1995). The Campanero Unit, in turn, comprises migmatites, amphibolites, BIFs, micaschists and orthogneisses with zircon ages of 1.7 Ga and it is exposed further south as a basement inlier of the Dom Feliciano Belt (Sánchez Bettucci et al. 2003, 2004; Oyhantçabal 2005; Mallmann et al. 2007). Widespread Neoproterozoic magmatism, metamorphism and shear zones indicate crustal reworking of the Nico Pérez Terrane basement during the evolution of the Dom Feliciano Belt (Oyhantçabal et al. 2011a, 2012; Oriolo et al. 2016a, b).

Finally, the Dom Feliciano Belt represents a Neoproterozoic transpressional orogen, which is divided into three main geotectonic units: the Aiguá batolith, the schist belt and foreland deposits (Fig. 22.1; Basei et al. 2000). The western part of the Dom Feliciano Belt comprises the schist belt, whereas the Aiguá batholith is located to the east. Nevertheless, Neoproterozoic intrusions are present in the western part of the belt as well. Foreland deposits, in turn, are located on both sides.

22.2.3.2 Sarandí del Yí Shear Zone

The Sarandí del Yí Shear Zone is a *c*. 2 km-wide mylonitic belt that is exposed over at least 200 km in a north–south direction and represents the eastern boundary of the Río de la Plata Craton (Oyhantçabal et al. 2011a; Oriolo et al. 2015). Further north, it can be traced as a negative gravimetric anomaly, showing an orientation change from north–south to north-northwest-south-southeast (Oyhantçabal et al. 2011a). The Sarandí del Yí Shear Zone was first defined as a structural lineament by Preciozzi et al. (1979) and, subsequently, Bossi and Campal (1992) interpreted it as a dextral structure separating different tectonostratigraphic terranes. Oyhantçabal et al. (1993), in turn, recognized a Late Neoproterozoic sinistral reactivation, post-dating the pre-Brasiliano dextral shearing event.

In the eastern Piedra Alta Terrane, increasing clockwise rotations about a vertical axis towards the Sarandí del Yí Shear Zone were recognized based on the bending of the 1.79 Ga dyke swarm (Bossi and Campal 1992; Oriolo et al. 2015). Similar rotations were also observed in Paleoproterozoic east- to east-northeast-striking fabrics of the southeastern Piedra Alta Terrane (Spoturno et al. 2004; Sánchez Bettucci et al. 2016). Likewise, mylonites and protomylonites showing subvertical north-northwest-striking mylonitic foliations present S-C′ shear bands that indicate dextral shearing along the western Sarandí del Yí Shear Zone (Oriolo et al. 2015).

Further east, mylonites of the Sarandí del Yí Shear Zone present a subvertical north-northeast-south-southwest foliation with a mean orientation of 184°/81°W and a mean stretching lineation of 182°/06° (Oriolo et al. 2015). S-C′ shear bands and σ-type feldspar mantled porphyroclasts indicate a sinistral sense of shearing (Fig. 22.2a; Oriolo et al. 2015). Towards the east, tight to isoclinal symmetrical folds are recognizable and present fold axes with a mean orientation of 024°/01° and subvertical fold axial planes. The eastern margin of the shear zone is reworked by low-temperature deformation, as recorded by pseudotachylite veins, phyllonites and cataclasites (Oriolo et al. 2015).

Based on microstructures and quartz CPO data, deformation conditions for the dextral and sinistral shearing events were constrained at *c*. 650–600 and 550–450 °C, respectively (Oriolo et al. 2015). On the other hand, fold geometry, symmetrical quartz CPO textures and strain analysis indicate pure-shear-dominated deformation during sinistral shearing (Oriolo et al. 2015).

U-Pb zircon, Ar/Ar amphibole and U-Pb titanite data from mylonites of the Sarandí del Yi Shear Zone constrain the timing of dextral shearing at *c*. 630–600 Ma (Oriolo et al. 2016b, c). Subsequent sinistral shearing took place up to *c*. 584 Ma, as indicated by U-Pb zircon, Ar/Ar amphibole, Ar/Ar muscovite and U-Pb titanite data (Oriolo et al. 2016b, c). The age of the synkinematic Solís de Mataojo granitic complex further supports this timespan (584 ± 13 Ma, single-phase Pb–Pb stepwise leaching titanite; Oyhantçabal et al. 2007). The end of ductile deformation, in turn, is indicated by the post-kinematic Cerro Caperuza granite, which presents a U-Pb LA-ICP-MS zircon age of 570.9 ± 11.0 Ma (Oriolo et al. 2016c). However, deformation under brittle-ductile to brittle conditions took place up to the lower Paleozoic (Oriolo et al. 2015, 2016b, c; Hueck et al. 2017).

22.2.3.3 Sierra Ballena Shear Zone

The Sierra Ballena Shear Zone is a major structure that strikes north-northeast and presents a width of *c*. 4 km (Oyhantçabal 2005; Oyhantçabal et al. 2009). It separates the schist belt of the Dom Feliciano Belt to the west from the Aiguá batholith to the east. Further north, it was correlated with the Dorsal do Canguçú and Major Gercino shear zones from southern Brazil (Fernandes et al. 1992; Fernandes and Koester 1999; Oyhantçabal et al. 2009, 2011b; Passarelli et al. 2010, 2011a).

As in the case of the Sarandí del Yí Shear Zone, subvertical mylonitic foliations are dominant, showing a mean strike of 030°/85°W (Oyhantçabal et al. 2009). The stretching lineation, in turn, is normally subhorizontal with a mean orientation of 208°/12° (Oyhantçabal et al. 2009). A sinistral sense of shear is indicated by S-C shear bands, σ- and δ-type feldspar mantled porphyroclasts, and deflection of passive markers (Oyhantçabal et al. 2009). Tight to isoclinal folds are frequent and show axes that are parallel to stretching lineations, although the latter are sometimes

folded and exhibit a symmetric U-pattern (Oyhantçabal et al. 2009).

Microstructural and quartz CPO data indicate deformation conditions at *c*. 550–400 °C for the Sierra Ballena Shear Zone (Oyhantçabal 2005; Oyhantçabal et al. 2009, 2011b). In addition, fold geometry and quartz CPO data point to pure-shear-dominated deformation (Oyhantçabal 2005; Oyhantçabal et al. 2009).

Sinistral shearing along the Sierra Ballena Shear Zone is mostly constrained between 585.8 ± 1.6 (Ar/Ar muscovite plateau age; Oyhantçabal et al. 2009) and 551.0 ± 4.4 Ma (U-Pb SHRIMP zircon; Oyhantçabal et al. 2011b) (Fig. 22.2b). However, Phanerozoic brittle-ductile to brittle reactivation is indicated by K-Ar sericite fine-fraction and illite fault gouge ages (Hueck et al. 2017).

22.2.3.4 Sierra de Sosa Shear Zone

The Sierra de Sosa Shear Zone strikes northeast and separates the Paleoproterozoic Valentines-Rivera Granulitic Complex from the Archean La China Complex in the Nico Pérez Terrane (Fig. 22.1). The mylonitic foliation shows a mean orientation of 219°/70°W, whereas the mean stretching lineation is 225°/15° (Oriolo et al. 2016b).

S-C shear bands together with σ- and δ-type feldspar mantled porphyroclasts indicate a sinistral sense of shear (Oriolo et al. 2016b). Microstructures and quartz CPO data indicate that deformation started at *c*. 550 °C and continued below 300 °C (Oriolo et al. 2016b).

A U-Pb LA-ICP-MS zircon age of 598.1 ± 2.2 Ma constrains the protolith age of the Sierra de Sosa Shear Zone, thus indicating subsequent sinistral shearing (Oriolo et al. 2016b). Nevertheless, deformation might also take place prior to protolith emplacement, despite not being recorded by geochronological data.

22.2.3.5 María Albina Shear Zone

To the east of the Sierra de Sosa Shear Zone, the María Albina Shear Zone separates the La China Complex from metasedimentary rocks of the Las Tetas Complex. This northeast- to north-northeast-striking shear zone presents a mean mylonitic foliation of 192°/48°E and a mean stretching lineation of 017°/06° (Oriolo et al. 2016b). Folds of the mylonitic foliation, in turn, present a mean axis of 244°/56° and a mean axial plane of 223°/76°W (Oriolo et al. 2016b).

Shear bands and feldspar mantled porphyroclasts indicate sinistral shearing, whereas microstructures and quartz CPO data indicate maximum ductile deformation conditions of *c*. 550 °C (Oriolo et al. 2016b). The western part of the shear zone is cataclastically overprinted, indicating very low-grade deformation conditions after ductile deformation (Oriolo et al. 2016b).

The timing of sinistral shearing along the María Albina Shear Zone is constrained by two Ar/Ar muscovite plateau ages of 596.8 ± 1.1 and 597.2 ± 3.2 Ma (Oriolo et al. 2016b). Similar to the Sierra Ballena Shear Zone, brittle reactivation during the Cretaceous was indicated based on K-Ar illite fault gouge ages (Hueck et al. 2017).

22.2.3.6 Subordinated Shear Zones of the Dom Feliciano Belt of Uruguay

In the western Dom Feliciano Belt, subordinated northeast- to north-northeast-striking shear zones such as the Arroyo Corrales and Zapicán shear zones are present as well (Oriolo et al. 2016b). They form an anastomosing system of sinistral orogen-parallel shear zones that crosscut metasedimentary rocks of the schist belt.

Although orogen-parallel shear zones are widespread, oblique shear zones are also recognizable. The Rivera Shear Zone strikes west-northwest and crosscuts the Valentines-Rivera Granulitic Complex in the Isla Cristalina de Rivera. This shear zone underwent sinistral shearing recorded at 606 ± 10 Ma by Th-U-Pb CHIME-EPMA monazite and K-Ar muscovite data (Oyhantçabal et al. 2012). In turn, the Tupambaé Shear Zone, which also crosscuts the Valentines-Rivera Complex, strikes east-northeast and records dextral shearing. A U-Pb zircon age constrains the crystallization age of the protolith at 549.0 ± 2.9 Ma, indicating subsequent shearing (Oriolo et al. 2016b), though shearing prior to *c*. 549 Ma cannot be discarded.

On the other hand, several northeast- to north-northeast-striking shear zones are developed in the eastern Dom Feliciano Belt. Among them, the Cordillera, Punta de las Palmas, Paso de los Talas, Cañada del Sauce and Cerro Amaro are the most outstanding, and these underwent dominantly sinistral shearing (Oyhantçabal et al. 2009; Spoturno et al. 2012; Oriolo et al. 2016b). However, some segments of the Cordillera Shear Zone might also record dextral shearing (Oyhantçabal et al. 2009; Oriolo et al. 2016b). K-Ar data indicates shearing at 632.7 ± 6.1 and 615.2 ± 6.6 Ma for the Cordillera and Cerro Amaro shear zones, respectively (Oriolo et al. 2016b), though U-Pb zircon data from synkinematic intrusions points to shearing after *c*. 600 Ma (M. Basei, pers. comm.)

22.3 Kaoko Belt

22.3.1 Introduction

The Kaoko Belt, which is mostly exposed in Namibia, comprises three domains that are separated by major shear zones: the Western, Central and Eastern Kaoko zones (Miller 1983; Goscombe et al. 2003; Chap. 12). Alternatively, the terms ‘Escape Zone’ and ‘Foreland’ were considered for the Central and Eastern Kaoko zones,

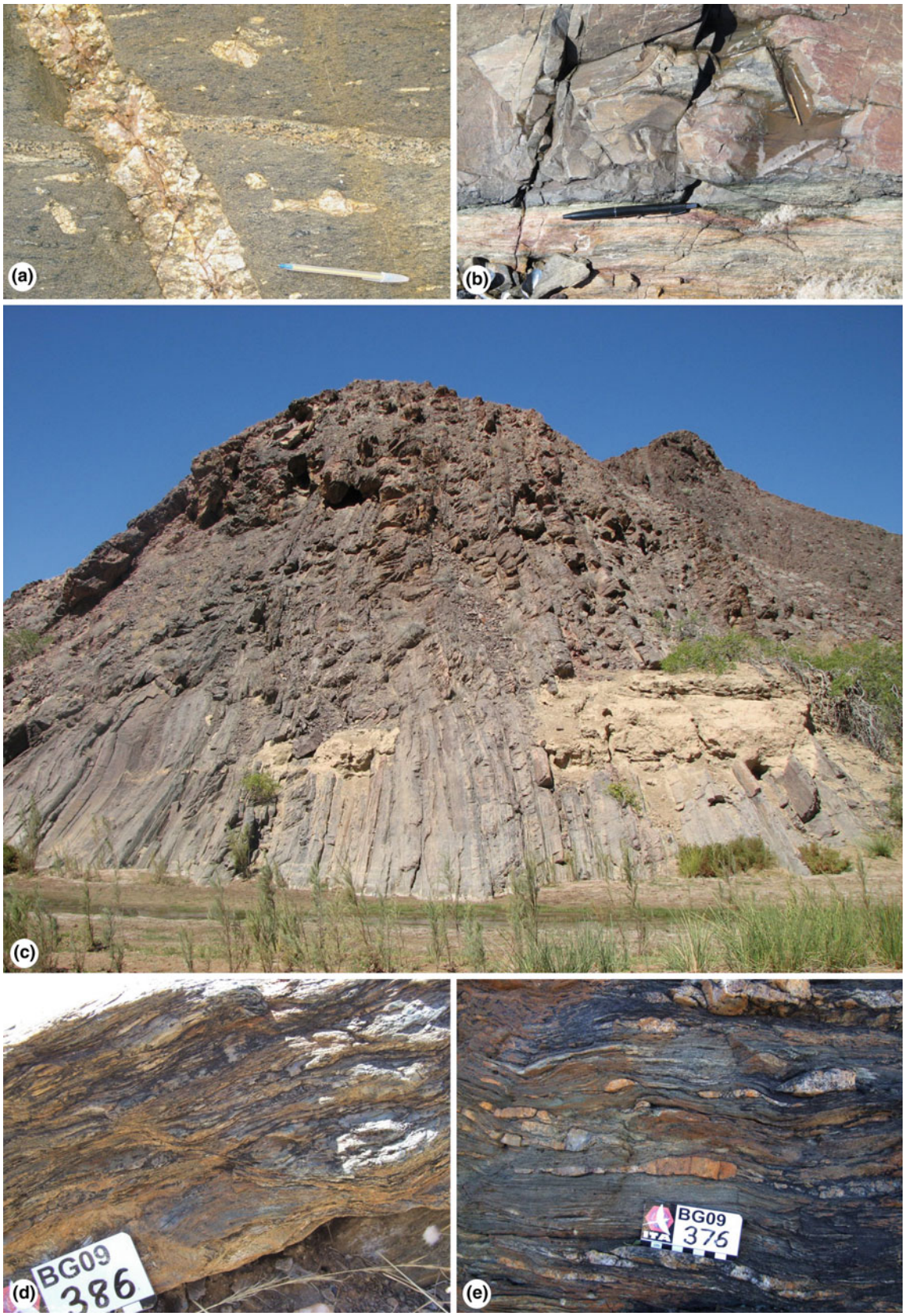
(a)
(b)
(c)
(d)
BG09
386
(e)
BG09
376

◀ **Fig. 22.2** Field photographs of shear zones in the Brasiliano–Pan-African belts. **a** Granitic mylonites of the Sarandí del Yí Shear Zone showing K-feldspar mantled porphyroclasts that indicate sinistral shearing. **b** Granitic mylonites (lower part) intruded by mylonitic porphyries (upper part) of the Sierra Ballena Shear Zone. Mylonitic porphyries were dated at 551.0 ± 4.4 Ma (Oyhantçabal et al. 2011b), constraining the timing of late synkinematic magmatism. **c** Steeply dipping granitic mylonites of the Purros Shear Zone close to the Purros locality. **d** Main phase north-over-south reverse shear fabric in Uis-Pass Suture zone, with S-C foliations and shear lenses of stretched early quartz veins. **e** Strong main phase shear foliation in Uis-Pass Suture zone, with shear lenses and extreme stretch of early bedding parallel quartz veins

respectively (Goscombe et al. 2005a). The Purros Mylonite Zone separates the Western from the Central Kaoko Zone, whereas the boundary between the latter and the Eastern Kaoko Zone is constituted by the Sesfontein Thrust (Fig. 22.3; Goscombe et al. 2003).

The Western Kaoko Zone can be subdivided into the Coastal Terrane and the Orogen Core, the Three Palms Mylonite Zone being the boundary between the two (Goscombe et al. 2005a, b; Goscombe and Gray 2007). Conversely, Konopásek et al. (2008) considered Ediacaran granitoids of the Boundary Igneous Complex as the limit between both domains (Seth et al. 1998; Kröner et al. 2004). The Coastal Terrane essentially comprises Cryogenian metasedimentary and metaigneous rocks and Ediacaran orthogneisses and granitoids (e.g., Seth et al. 1998; Goscombe et al. 2005a; Goscombe and Gray 2007; Konopásek et al. 2008, 2014, 2016). The Orogen Core, in turn, is made up of Mesoproterozoic basement slivers, Cryogenian metasedimentary rocks and metavolcanites, and Ediacaran granitoids (Goscombe et al. 2005a; Goscombe and Gray 2007; Konopásek et al. 2014).

On the other hand, the Central Kaoko Zone is mostly constituted of Archean-Paleoproterozoic basement inliers and Cryogenian metavolcanites and metasedimentary rocks (Miller 1983; Seth et al. 1998; Goscombe et al. 2003; Konopásek et al. 2008, 2014). Further east, the Eastern Kaoko Zone comprises Cryogenian-Ediacaran metasedimentary rocks, which overlie the Congo Craton margin (Goscombe et al. 2003; Hoffmann et al. 2004).

22.3.2 Three Palms Mylonite Zone

The Three Palms Mylonite Zone is the westernmost shear zone of the Kaoko Belt (Goscombe et al. 2003; Goscombe and Gray 2007). It occurs mostly as a 1–2 km wide mylonitic zone, despite being constituted by several discrete anastomosing shear zones in some areas. Though it was originally considered to be the eastern margin of the Coastal Terrane (Goscombe et al. 2003), Konopásek et al. (2008) recognized that the Three Palms Mylonite Zone partially crosscuts rocks of the Coastal Terrane.

North-northwest-striking mylonitic foliations exhibiting steep dips to the west dominate, although a north-northeast-striking trending domain in the central-northern area dips moderately to the east and a north-trending domain in the south has moderate to shallow dips to the west (Goscombe and Gray 2007, 2008). Dominant subhorizontal to gently south-southeast-plunging stretching lineations, together with kinematic indicators, point to dominant sinistral strike-slip with local normal or inverse components of dip displacement (Goscombe et al. 2005a; Goscombe and Gray 2007, 2008).

Two Ar/Ar muscovite plateau ages of 481 ± 3 and 492 ± 3 Ma were obtained for mylonitic orthogneisses of the Three Palms Mylonite Zone (Gray et al. 2006). However, the main phase of sinistral shearing was interpreted at *c*. 580–550 Ma, thus indicating that muscovite ages record isotopic resetting during further early Paleozoic deformation (Goscombe et al. 2003, 2005a; Gray et al. 2006, 2008; Goscombe and Gray 2007, 2008). In contrast, Ulrich et al. (2011) indicated sinistral shearing after *c*. 550 Ma. Transtensional reactivation was indicated for the Three Palms Mylonite Zone at *c*. 530–520 Ma after sinistral shearing (Foster et al. 2009).

22.3.3 Purros Mylonite Zone

The Purros Mylonite Zone is one of the most conspicuous structural features of the Kaoko Belt, extending for more than 600 km along strike and up to *c*. 5 km in thickness (Goscombe and Gray 2008). The mylonitic foliation dips steeply to the west-northwest-west-southwest in the northern part and exhibits moderate dips to the west-southwest further south, whereas the stretching lineation is typically subhorizontal (Fig. 22.2c; Goscombe et al. 2003; Goscombe and Gray 2008). Isoclinal folding of the mylonitic foliation is present as well, showing hinge lines parallel to stretching lineations (Goscombe and Gray 2008).

Feldspar mantled porphyroclasts indicate sinistral shearing, and dynamic recrystallization of quartz and feldspars point to maximum upper amphibolite facies deformation conditions (Goscombe and Gray 2008; Ulrich et al. 2011). Scarce pseudotachylyte zones and fault planes, in turn, indicate subsequent limited reactivation under brittle conditions (Goscombe and Gray 2008).

An Ar/Ar whole-rock apparent age of 467 ± 3 Ma was obtained for a mylonitized schist close to the Purros Shear Zone, which is interpreted as the result of K-Ar resetting

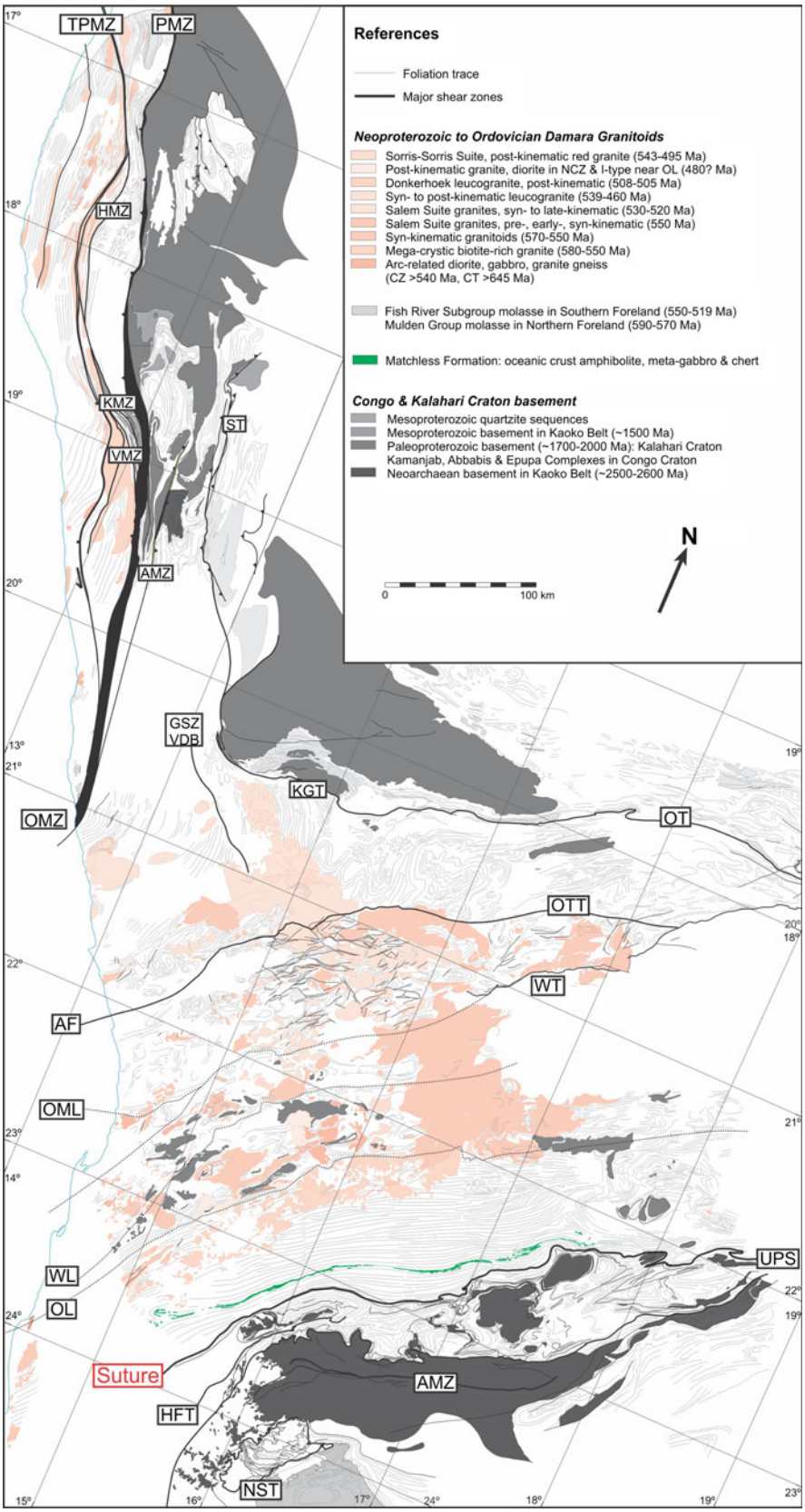

Fig. 22.3 Structural form map of the Damara Belt and Kaoko Belt, compiled primarily from the published 1:500000 geological map of Namibia for the Damara Belt component (Miller and Grote 1988), and published mapping of the Kaoko Belt (Guj 1970; Goscombe et al. 2003a, 2005a, b; Goscombe and Gray 2007, 2008). Modified after Goscombe et al. (2017a). Crustal-scale shear zones, thrusts or faults are indicated by abbreviations (ST, Sesfontain Thrust; PMZ, Purros Mylonite Zone; KMZ, Khumib Mylonite Zone; VMZ, Village Mylonite Zone; AMZ, Ahub Mylonite Zone; HMZ, Hartmann Mylonite Zone; TPMZ, Three Palms Mylonite Zone; OT, Outjo Thrust; AF, Autseib Fault; KGT, Khorixas-Gaseneirob Thrust; GSZ/VDB, Goantagab Shear Zone or Vrede-Doros-Brandberg line; OL, Okahandja Lineament; HFT, Hakos Frontal Thrust; ASZ, Areb Shear Zone; RTZ, Rehoboth Thrust Zone; WT, Waterberg Thrust; OTT, Otjorongo Thrust; OML, Omaruru Lineament; NST, Naukluft Sole Thrust; WL, Welwitchia Lineament; UPS, Uis-Pass Suture). The Uis-Pass Suture is a crustal thrust zone reactivated by extension, corresponding to the suture between stratigraphy deposited on either the Kalahari or Congo cratons, and containing dismembered serpentinites (Barnes 1983; Kasch 1983; Kukla and Stanistreet 1991)

during late stages of shearing (Gray et al. 2006). As in the case of the Three Palms Mylonite Zone, the main phase of deformation was alternatively placed at *c*. 580–550 Ma (Goscombe et al. 2003, 2005a; Gray et al. 2006, 2008; Goscombe and Gray 2007, 2008) and after *c*. 550 Ma (Ulrich et al. 2011).

22.3.4 Sesfontein Thrust

In contrast to ductile strike-slip shear zones that control the architecture of the Kaoko Belt, the Sesfontein Thrust comprises a series of discrete brittle thrusts at the western margin of the foreland (Goscombe and Gray 2007, 2008). It is interpreted as a system of reactivated faults of the passive margin (Prave 1996; Stanistreet and Charlesworth 2001). The timing of thrusting is constrained at *c*. 580–550 Ma (Goscombe et al. 2005a, Gray et al. 2006, 2008; Goscombe and Gray 2008), thus being contemporaneous with sinistral shearing further west.

22.3.5 Subordinated Shear Zones of the Kaoko Belt

The Orogen Core is crosscut by three main decimetre- to hectometre-wide shear zones—the Village, Khumib and Hartmann mylonite zones (Goscombe et al. 2003; Konopásek et al. 2005; Goscombe and Gray 2008)—which are located between the Three Palms and Purros mylonite zones and connect them. On the other hand, the Ahub Mylonite Zone is a 1 km-wide shear zone that is exposed in the southern part of the Central Kaoko Zone (Goscombe and Gray 2008).

The Village, Khumib and Hartmann mylonite zones comprise north-northwest-striking strike-slip-dominated sinistral shear zones that underwent protracted deformation from upper amphibolite to subgreenschist facies conditions (Goscombe et al. 2003; Konopásek et al. 2005; Goscombe and Gray 2008; Ulrich et al. 2011). In contrast, the Ahub Mylonite Zone is dominated by pure shear, although strike-slip displacements are also recorded (Goscombe and Gray 2008). In a similar way to major shear zones of the Kaoko Belt, the timing of shearing along intrabelt mylonite zones was placed at *c*. 580–550 Ma (Goscombe et al. 2003, 2005a; Gray et al. 2006, 2008; Goscombe and Gray 2007, 2008) and after *c*. 550 Ma (Konopásek et al. 2005; Ulrich et al. 2011). Likewise, transtensional reactivation was indicated for the Village and Khumib mylonite zones at *c*. 530–520 Ma (Foster et al. 2009).

22.4 Damara Belt

22.4.1 Introduction

The Damara Belt is mostly exposed in Namibia and comprises a central part, including the Northern, Central, Southern and Southern Marginal zones, and two external foreland domains that are located to the north and south along the Congo and Kalahari cratons margins, respectively (Miller 1983, 2008). The Northern and Central zones are separated by the Autseib Fault, which can be traced further east along the Otjohorongo Thrust. In turn, the Okahandja Lineament represents the boundary between the Central and Southern zones. All zones are made up of Cryogenian-Ediacaran metasedimentary rocks with subordinated volcanic intercalations of the Damara Sequence whereas, though Ediacaran-Cambrian granitoids are also exposed in the central part (Fig. 22.3; Foster et al. 2015 and references therein).

22.4.2 Shear Zones of the Damara Belt

The northern margin of the Northern Zone is marked by the steep crustal-scale Outjo Thrust that overrode the northern foreland (e.g., Coward 1983; Goscombe et al. 2004, 2017; Gray et al. 2008; Lehmann et al. 2015). Further west, the Ogden Mylonite Zone, which is correlated with the Purros Mylonite Zone of the Kaoko Belt, comprises the western margin of the Ugab Zone (Passchier et al. 2016; Goscombe et al. 2017a). This 5 km-wide shear zone comprises mylonites and protomylonites exhibiting subvertical foliations with shallow north-plunging stretching lineations (Foster et al. 2009). Sinistral shearing took place along the Ogden Mylonite Zone at *c*. 465–500 °C and 4.0–5.5 kbar (Foster et al. 2009). East of the Vrede-Doros-Brandberg line in the eastern Ugab Zone, passive margin carbonates are highly strained and preserve isoclinal folds and L-S fabrics in what may constitute an early crustal-scale shear zone, the Goantagab Shear Zone (Goscombe et al. 2004; Passchier et al. 2007, 2011, 2016).

Crustal-scale high-strain ductile shear zones are not present in the Central Zone, which is bound north and south by lineaments identified primarily by geophysics: the Okahandja Lineament and Autseib Fault (Corner 2000, 2008; Ritter et al. 2003). The Autseib Fault between the South Ugab Zone and Central Zone is largely unexposed and was possibly reactivated during exhumation under brittle conditions (Goscombe et al. 2017a). Structural grain and style, metamorphic grade and stratigraphy—all appear transitional across this fault zone. Shallow-dipping fault zones were recently identified at high stratigraphic levels in the Central

Zone and interpreted to root into the Autseib Fault (Goscombe et al. 2017a). These are interpreted to have formed at *c*. 505 Ma as a result of vertical flattening and north–south extension (Goscombe et al. 2017b). On the other hand, the Okahandja Zone is a broad zone of subvertical bedding and foliation centred on a steep, tight synclinorium (Miller and Grote 1988). Only small-scale inverse faults are present in the Okahandja Zone, whereas high-strain ductile shear zones of significant scale are absent.

Previous literature has hypothesized the basal unconformity between the Damara strata and basement as being a high-strain mylonitic detachment (e.g., Oliver 1994; Coward 1983; Kisters et al. 2004). However, units either side of the unconformity develop weakly aligned gneissose fabrics which are nowhere reworked; nor do they show signs of mylonitization (Chap. 12). Furthermore, a well-exposed basal unconformity in the upper Khan River region has a 10 m-thick Al–Fe-rich metapaleosoil horizon preserved intact in the basement.

Further south, the Uis-Pass Suture is the predominant high-strain crustal-scale structure between the Southern and Southern Marginal Zones (Kitt et al. 2016; Goscombe et al. 2017a). This suture represents the upper boundary of the Southern Marginal Zone between sequences deposited on the Kalahari Craton margin and accretionary prism sequences of the Khomas Complex with Congo provenance in the overlying Southern Zone (Hoffmann 1989; Foster et al. 2015; Kitt et al. 2016). This was the site of closure of the Khomas Ocean, contains dismembered Alpine-type serpentinites (Barnes 1983; Kasch 1983) and is the boundary between basinal sequences of different detrital zircon provenance (Foster et al. 2015). The Uis-Pass Suture is a 1–2 km-wide crustal-scale shear zone with a two-stage history: a main phase of top-to-the-south thrusting during prograde and peak metamorphism, and subsequent retrograde extensional reactivation producing chloritic-muscovitic schists and latter brittle structures (Figs. 22.2d, e; Goscombe et al. 2017b).

South of the suture, the Southern Margin Zone consists of very high-strain, intensely sheared passive margin sequences producing a fold-and-thrust belt with basement-cored nappes transported onto the Southern Foreland (Porada and Wittig 1983; Ritter et al. 2003; Kitt et al. 2016). The Southern Marginal Zone preserves a number of crustal-scale thrusts such as the Hakos Frontal Thrust, Areb Shear Zone, Naukluft Sole Thrust and Rehoboth Thrust Zone, large-sale nappes such as the Hakos Nappe and many minor thrusts.

22.5 Gariep Belt

The Gariep Belt crops out in southwestern Namibia and western South Africa, and it is made up of two main tectonostratigraphic units—the western Marmora Terrane and the eastern Porth Nolloth Group—which essentially comprise metamorphosed oceanic mafic and volcanosedimentary rocks (Fig. 22.4; Frimmel et al. 2011 and references therein). The Marmora Terrane overthrust the Porth Nolloth Group along the Schakalsberge Thrust (Frimmel et al. 2011). Thrusting along the Schakalsberge Thrust is constrained at *c*. 550–540 Ma by Ar/Ar hornblende and muscovite data of the Marmora Terrane (Frimmel and Frank 1998).

22.6 Saldania Belt

22.6.1 Introduction

The Saldania Belt is exposed along the southern coast of South Africa. From west to east, the Saldania Belt is made up of the Tygerberg, Swartland and Boland terranes (Rozendaal et al. 1999 and references therein), although the two former were considered as the Malmesbury Terrane (Frimmel et al. 2013). The Colenso Fault separates the Tygerberg from the Swartland Terrane, whereas the Piketberg-Wellington Fault represents the boundary between the latter and the Boland Terrane (Fig. 22.4).

The Tygerberg Terrane comprises essentially metagraywackes and phyllites of the homonymous formation (Rozendaal et al. 1999). On the other hand, the Swartland Terrane is constituted of metasandstones, metagraywackes, schists, phyllites and marbles of the Swartland Subgroup/Group, whereas the Boland Terrane is characterized by metaconglomerates, metasandstones and metapelites of the Malmesbury and/or Klipheuwel groups (Rozendaal et al. 1999; Belcher and Kisters 2003; Gresse et al. 2006; Frimmel et al. 2013). Volcanites and intrusions of the Cape Granite Suite, in turn, are also present within all three terranes (Rozendaal et al. 1999; Scheepers and Nortjé 2000; Scheepers and Armstrong 2002). Most metasedimentary and magmatic units of the Saldania Belt present Late Ediacaran-Early Cambrian ages (Scheepers and Armstrong 2002; Scheepers and Poujol 2002; Chemale et al. 2011; Frimmel et al. 2011).

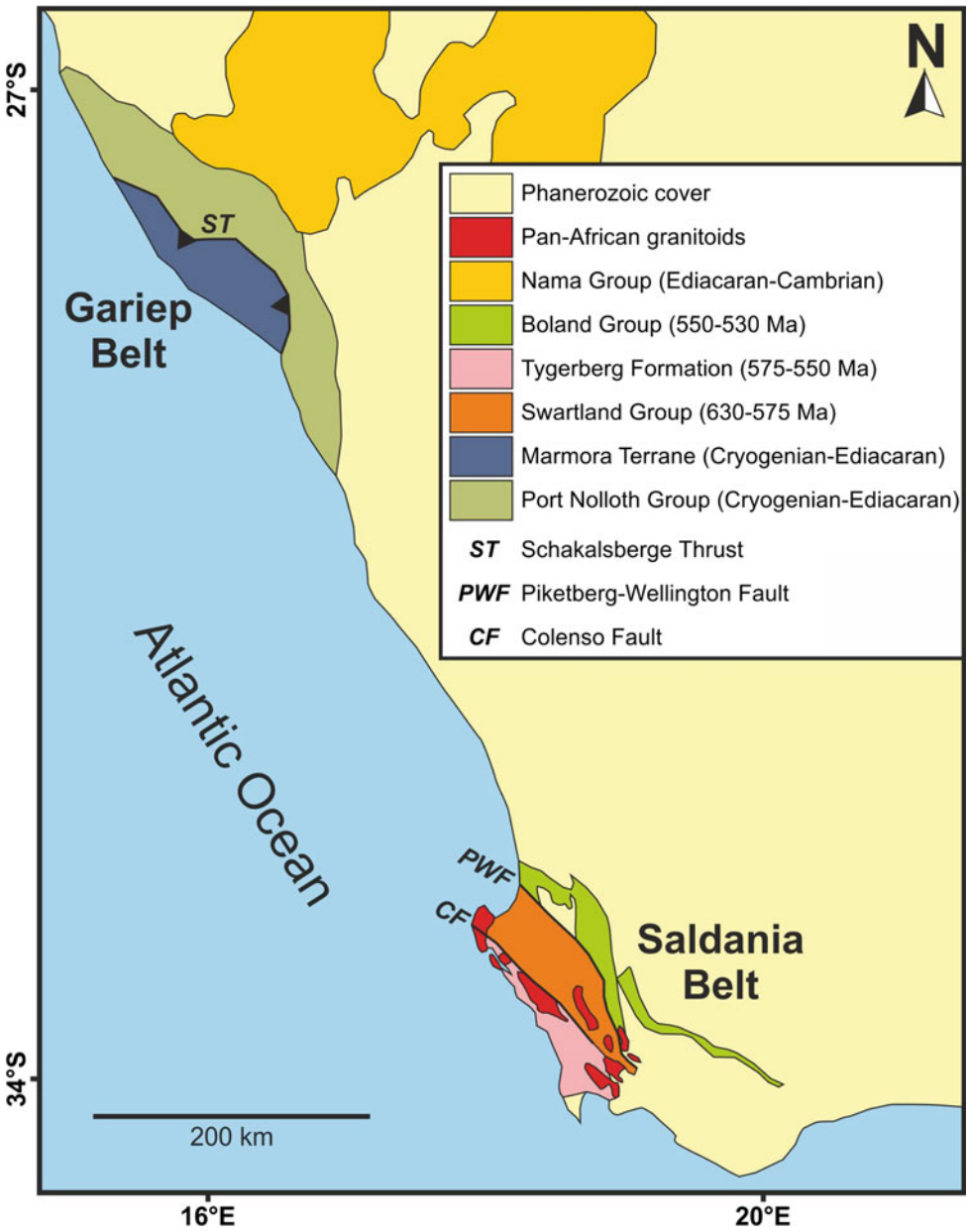

Fig. 22.4 Simplified geological map of the Saldania and Gariep Belts (modified after Frimmel et al. 2011, 2013 and references therein)

22.6.2 Colenso Fault

Though poorly exposed, the Colenso Fault extends for *c*. 150 km northwest, comprising an anastomosing system of mylonitic and cataclastic zones that can be correlated through magnetometric data (Schoch 1975; Theron et al. 1992; Kisters et al. 2002). Both mylonitic and cataclastic foliations are typically subvertical and strike northwest, whereas northwest-striking stretching lineations in mylonites are subhorizontal (Kisters et al. 2002).

Kinematic indicators such as S-C and S-C′ shear bands, feldspar mantled porphyroclasts, oblique foliation in quartz, passive markers and drag folds show a first phase of sinistral strike-slip shearing succeeded by dextral shearing (Kisters et al. 2002 and references therein). Microstructural data indicate dominant greenschist deformation conditions of *c*. 450–300 °C (Kisters et al. 2002).

The timing of deformation along the Colenso Fault is mostly constrained by associated intrusions (Kisters et al. 2002). U-Pb zircon ages of 547 ± 6 and 539 ± 4 Ma obtained in synkinematic intrusions (Darling batholith and Trekoskraal granite) constrain the timing of sinistral and subsequent dextral strike-slip shearing (da Silva et al. 2000; Kisters et al. 2002). Further dextral shearing is recorded until *c*. 520 Ma by the synkinematic Cape Columbine granite, whereas the end of deformation is constrained at

510 ± 4 Ma (Pb–Pb zircon; Chemale et al. 2011) by the post-kinematic Klipberg granite (Kisters et al. 2002).

22.6.3 Piketberg-Wellington Fault

Based on similarities with the Colenso Fault, a comparable evolution was inferred for the Piketberg-Wellington Fault in spite of the lack of detailed studies (Rozendaal et al. 1999). Likewise, it was correlated with the Schakalsberge Thrust of the Gariep Belt (Frimmel et al. 2013).

22.7 Discussion and Final Remarks

22.7.1 The Role of Shear Zones in the Brasiliano–Pan-African Orogeny

In the Dom Feliciano Belt, the Sierra Ballena-Dorsal do Canguçu-Major Gercino shear zone system has been classically interpreted as the main Brasiliano suture, juxtaposing the cratonic cores of South America and Africa (Basei et al. 2000, 2005, 2008; Bossi and Gaucher 2004; Gaucher et al. 2009; Passarelli et al. 2010, 2011a; Frimmel et al. 2011, 2013). However, different tectonic models were considered for the evolution of this shear zone system. Basei et al. (2000, 2005, 2008) considered east-directed subduction giving rise to the Aiguá-Pelotas-Florianópolis Batholith succeeded by collision at *c*. 600 Ma, especially based on the batholith significance as a terrane and contrasting isotopic signatures and zircon inheritance of both sides of the structure. In contrast, Bossi and Gaucher (2004), Gaucher et al. (2009) and Frimmel et al. (2011, 2013) considered ocean opening to the west of the shear zone since at least *c*. 580 Ma, west- or east-directed subduction and final collision at *c*. 530 Ma.

On the other hand, a number of authors consider both strike-slip shearing along the system and associated granitogenesis as the result of post-collisional processes during the Dom Feliciano Belt evolution. Similarities in the crystallization ages and geochemical signature of granites on both sides of the Sierra Ballena-Major Gercino system are commonly seen as evidence of a post-collisional setting after *c*. 650–630 Ma, age of the earliest shear-related intrusions (e.g., Fernandes et al. 1993, 1995; Fernandes and Koester 1999; Bitencourt and Kruhl 2000; Koester et al. 2001b; Philipp and Machado 2005; Oyhantçabal et al. 2007, 2009; Saalmann et al. 2011; Chemale et al. 2012; Florisbal et al. 2012a, b, c; Philipp et al. 2013, 2016; Lara et al. 2017). As a result, it is argued that, if the shear system once acted as a suture zone, this event pre-dated the shearing event responsible for its present configuration. In this sense, some authors (e.g., Fernandes et al. 1995a, b; Fernandes and Koester 1999; Koester et al. 2001c, 2016; Masquelin et al. 2012) propose the existence of the Porto Alegre Suture in the Rio Grande do Sul Shield, approximately parallel to the Dorsal do Canguçu Shear Zone, which would correspond to the suture zone of an older collision during the Tonian. More recently, other contributions have emphasized the role of the Sarandí del Yí Shear Zone as a terrane boundary that separate the Rio de la Plata Craton from Brasiliano-overprinted African domains (Oyhantçabal et al. 2011a; Rapela et al. 2011; Oriolo et al. 2015, 2016a, b, c, 2017). Within this framework, east-directed subduction prior to collision at *c*. 630 Ma was indicated, giving rise to dextral shearing along the Sarandí del Yí Shear Zone and regional deformation and metamorphism of the Dom Feliciano Belt between *c*. 630 and 600 Ma (Oriolo et al. 2016b, c, 2017).

On the other hand, major shear zones of the Kaoko Belt, namely the Purros and Three Palms shear zones, were interpreted as major boundaries between different crustal domains (e.g., Goscombe et al. Goscombe et al. 2003; Goscombe and Gray 2008). Alternatively, Ulrich et al. (2011) considered them to be the result of strain localization during sinistral shearing.

A similar scenario is observed in the Saldania Belt, where both the Colenso and Piketberg-Wellington faults were considered as terrane boundaries (Hartnady et al. 1974; Rozendaal et al. 1999). In contrast, Frimmel et al. (2013) indicated that the Colenso Fault does not represent a terrane boundary but an inherited basement structure of the Malmesbury Terrane. Nevertheless, the Piketberg-Wellington Fault and its continuation in the Gariep Belt, the the Schakalsberge Thrust, are still regarded as major terrane boundaries (Frimmel et al. 2011).

Despite the continuing controversy about whether some major shear zones represent major terrane boundaries or are just the result of strain localization, it is clear that most of them share a common history. In particular, shear zones of the Dom Feliciano and Kaoko belt have been correlated, considering that the latter might represent the foreland of the former (Goscombe et al. 2003, 2005a; Gray et al. 2006, 2008; Goscombe and Gray 2007, 2008; Oyhantçabal et al. 2011b; Oriolo et al. 2016b, c). Though diachronic, sinistral shearing after 600 Ma is ubiquitously recorded and clearly post-dates the main phase of crustal shortening in both areas. This was interpreted as the result of a major geodynamic change, resulting from the onset of the Kalahari Craton convergence with the Congo Craton (Lehmann et al. 2016; Oriolo et al. 2016c), already amalgamated with the Río de la Plata Craton (Oriolo et al. 2016b, c, 2017). Bedding-parallel mylonites with east-west-trending stretching lineations in the western and central Ugab Zone of the Damara Belt are interpreted as being the result of obduction of the Coastal Terrane at *c*. 590 Ma (Goscombe et al. 2004, 2017b).

Further sinistral shearing is recorded in both the Kaoko and Dom Feliciano Belts at *c*. 550 Ma (e.g., Oyhantçabal

et al. 2011b), thus being coeval with sinistral shearing along the Colenso Fault of the Saldania Belt (Kisters et al. 2002). The latter records a subsequent dextral shearing event (Kisters et al. 2002) which, in turn, might be related to oblique dextral shearing in the Dom Feliciano Belt (Oriolo et al. 2016c).

22.7.2 Structural Inheritance and Shear Zone Reactivation During the Phanerozoic

The amalgamation of major cratons during the Brasiliano–Pan-African Orogeny led to a relative stabilization of the South American and African continental crust by the early Paleozoic, though accretionary tectonics are recorded up to the late Paleozoic along the proto-Andean margin (e.g., Pankhurst and Rapela 1998). After Gondwana amalgamation, both areas underwent several episodes of intracontinental magmatism and basin development (Milani and Zalán 1999; Limarino and Spalletti 2006), culminating in the opening of the South Atlantic Ocean during the Cretaceous (e.g., Torsvik et al. 2009; Granot and Dyment 2015). The structural grain that resulted from late Neoproterozoic tectonics, however, also played a major role during Phanerozoic events, even controlling the lithospheric mantle anisotropy (James and Assumpção 1996; Vauchez et al. 1997; Tommasi and Vauchez 2001; Heintz et al. 2003).

In the southern Dom Feliciano Belt, K-Ar illite fault gouge data show reactivation of the Rivera Shear Zone during the late Paleozoic, contemporaneously with the development of regional angular unconformities in most southwestern Gondwana basins. K-Ar illite fault gouge data also reveal active faulting along the Sierra Ballena and María Albina shear zones during the opening of the South Atlantic Ocean at *c*. 140–130 and 100–80 Ma (Hueck et al. 2017). Likewise, thermochronological data indicates Cretaceous reactivation of the Sierra Ballena and Sarandí del Yí Shear Zones (Hueck et al. 2017). In southern Brazil, coeval faulting was reported for the Dorsal do Canguçu, Passo do Marinheiro and Porto Alegre shear zones (Oliveira et al. 2016), further supported by the presence of elongated Phanerozoic sedimentary deposits along lineaments such as the Dorsal do Canguçu and Ibaré shear zones. In addition, general exhumation is recorded in the Santa Catarina sector of the Dom Feliciano Belt (Karl et al. 2013).

In a similar way, Cretaceous reactivation was reported for the Three Palms and Purros shear zones of the Kaoko Belt (Salomon et al. 2014). Furthermore, Cretaceous dyke emplacement was controlled by the Pan-African structural grain in the Kaoko, Gariep and Saldania belts (Will and Frimmel 2013). Geophysical and thermochronological data of the Damara Belt, on the other hand, point to Triassic and Late Cretaceous reactivation of the Autseib Fault and Omaruru Lineament (Clemson et al. 1997; Corner 2000; Raab et al. 2002).

Though Paleozoic to Triassic shear zone reactivation is limited to some regions, fault activity seems to be ubiquitous along Brasiliano–Pan-African shear zones during the Cretaceous opening of the South Atlantic Ocean. Shear zones thus played a significant role not only during the Neoproterozoic assembly of Gondwana but also during the subsequent Gondwana break-up, controlling sedimentation, magmatism emplacement, exhumation and uplift.

References

Almeida FFM et al (1973) The precambrian evolution of the South American cratonic margin, South of Amazonas River. In: Nairn ACM et al (eds) The ocean basins and margins. Plenum, New York, pp 411–446

Almeida RP et al (2010) The ediacaran to Cambrian rift system of Southeastern South America: tectonic implications. J Geol 118:145–161

Babinski M et al (1997) U-Pb and Sm-Nd geochronology of the Neoproterozoic granitic-gneissic Dom Feliciano belt, southern Brazil. J S Am Earth Sci 10:263–274

Barnes SJ (1983) Pan-African serpentinites in central south West Africa/Namibia and the chemical classification of serpentinites. Spec Pub Geol Soc S Afr 11:147–155

Basei MAS (1985) O Cinturão Dom Feliciano em Santa Catarina. Dissertation, Universidade de São Paulo, São Paulo

Basei MAS et al (2000) The Dom Feliciano Belt of Brazil and Uruguay and its Foreland Domain the Rio de la Plata Craton: framework, tectonic evolution and correlation with similar provinces of Southwestern Africa. In: Cordani UG et al (eds) Tectonic evolution of South America. International Geological Congress, Rio de Janeiro, pp 311–334

Basei MAS et al (2005) The connection between the Neoproterozoic Dom Feliciano (Brazil/Uruguay) and Gariep (Namibia/South Africa) orogenic belts. Precambr Res 139:139–221

Basei MAS et al (2008) West Gondwana amalgamation based on detrital zircon ages from Neoproterozoic Ribeira and Dom Feliciano belts of South America and comparison with coeval sequences from SW Africa. In: Pankhurst RJ et al (eds) West Gondwana: pre-cenozoic correlations across the South Atlantic region. Geological Society of London Special Publications, London, vol 294, 239–256

Basei MAS et al (2009) The evolution and tectonic setting of the Luis Alves microplate of Southeastern Brazil: an exotic terrane during the assembly of Western Gondwana. In: Gaucher C et al (eds) Neoproterozoic-cambrian tectonics, global change and evolution: a focus on Southwestern Gondwana. Developments in Precambrian Geology, Amsterdam, Elsevier vol 16, pp 273–291

Basei MAS et al (2011a) The Itajaí foreland basin: a tectono-sedimentary record of the Ediacaran period, Southern Brazil. Int J Earth Sci 100:543–569

Basei MAS et al (2011b) Tectonic evolution of the Brusque group, Dom Feliciano belt, Santa Catarina, Southern Brazil. J S Am Earth Sci 32:324–350

Basei MAS et al (2013) Polycyclic evolution of Camboriú Complex migmatites, Santa Catarina, Southern Brazil: integrated Hf isotopic and U-Pb age zircon evidence of episodic reworking of a Mesoarchean juvenile crust. Braz J Geol 43:427–443

Belcher RW, Kisters AFM (2003) Lithostratigraphic correlations in the western branch of the Pan-African Saldania belt, South Africa: the Malmesbury Group revisited. S Arf J Geol 106:327–342
Bitencourt MF, Kruhl JH (2000) Crustal-scale shearing, magmatism and the development of deformation structures: an example from Santa Catarina (Southern Brazil). Z Angew Geol SH1, 229–236
Bitencourt MF, Nardi LVS (2000) Tectonic setting and sources of magmatism related to the Southern Brazilian shear Belt. Rev Bras Geociênc 30:186–189
Bitencourt MF et al (2008) Estratigrafia do Batólito Florianópolis, Cinturão Dom Feliciano, na Região de Garopaba-Paulo Lopes, SC. Pesqui Geociênc 35:109–136
Bossi J, Campal N (1992) Magmatismo y tectónica transcurrente durante el Paleozoico inferior del Uruguay. In: Gutiérrez J et al (eds) Paleozoico Inferior de Ibero-América. Universidad de Extremadura, Alicante, pp 343–356
Bossi J, Gaucher C (2004) The Cuchilla Dionisio Terrane, Uruguay: an allochthonous block accreted in the Cambrian to SW-Gondwana. Gondwana Res 7:661–674
Caldasso ALS et al (1995a) Programa de Levantamentos Geológicos Básicos 1: 100000; Folha Brusque (SG-22-Z-D-II-1), SC. Serviço Geológico do Brasil—CPRM, Brasília
Caldasso ALS et al (1995b) Programa de Levantamentos Geológicos Básicos 1: 100000; Folha Botuverá (SG-22-Z-D-I-2), SC. Serviço Geológico do Brasil—CPRM, Brasília
Campal N, Schipilov A (1995) The Illescas bluish quartz rapakivi granite (Uruguay-South America): some geological features. Symposium Rapakivi granites and related rocks, Abstracts, 18
Chemale F et al (2011) Geochronology and sources of late Neoproterozoic to Cambrian granites of the Saldania Belt. Int J Earth Sci 100:431–444
Chemale F et al (2012) Time constraints on magmatism along the Major Gercino Shear Zone, southern Brazil: implications for West Gondwana reconstruction. Gondwana Res 22:184–199
Cingolani CA (2011) The Tandilia system of Argentina as a southern extension of the Río de la Plata craton: an overview. Int J Earth Sci 100:221–242
Clemson J et al (1997) Structural segmentation and the influence of basement structure on the Namibian passive margin. J Geol Soc London 154:477–482
Corner B (2000) Crustal framework of Namibia derived from magnetic and gravity data. Communs Geol Surv Namibia 12:15–22
Corner B (2008) Crustal framework of Namibia derived from an integrated interpretation of geophysical and geological data. In: McG Miller R (ed) The geology of Namibia. Geological Survey of Namibia, Windhoek, pp 2-1–2-19
Costa AFU (1997) Teste de Modelagem geofisica da Estruturação das Associações Litotectônicas Pré-Cambrianas no Escudo Sul-riograndense. Dissertation, Universidade Federal de Rio Grande do Sul
Coward MP (1983) The tectonic history of the Damara belt. In: McG Miller R (ed) Evolution of the Damara Orogen of South West Africa/Namibia. Geological Society of South Africa, Johannesburg, vol 11, pp 409–421
Dalla Salda L et al (1988) The Río de la Plata cratonic region of southwestern Gondwanaland. Episodes 11:263–269
da Silva LC (1991) O cinturão metavulcanossedimentar Brusque e a evoluç ão policíclica das faixas dobradas proterozóicas no sul do Brasil: uma revisão. Rev Bras Geociênc 21:60–73
da Silva LC, Dias AA (1981) Projeto Timbó-Barra Velha. DNPM/CPRM Internal Report, Porto Alegre, Brazil
da Silva LC et al (1997) SHRIMP U/Pb zircon dating of Neoproterozoic granitic magmatism and collision in the Pelotas batholith, southernmost Brazil. Int Geol Rev 41:531–551
da Silva LC et al (2000) U-Pb SHRIMP and Sm-Nd age constraints on the timing and sources of the Pan-African Cape Granite Suite, South Africa. J Afr Earth Sci 30:795–815
da Silva LC et al (2005) The neoproterozoic Mantiqueira Province and its African connections: a zircon-based U-Pb geochronologic subdivision for the Brasiliano/Pan-African systems of orogens. Precambr Res 136:203–240
Fernandes LAD, Koester E (1999) The Neoproterozoic Dorsal de Canguqii strike-slip shear zone: Its nature and role in the tectonic evolution of southern Brazil. J Afr Earth Sci 29:3–24
Fernandes LAD et al (1992) Deformation patterns in the southern Brazilian branch of the Dom Feliciano Belt: a reappraisal. J S Am Earth Sci 5:77–96
Fernandes LAD et al (1993) Zona de cisalhamento transcorrente Dorsal de Canguçu: Caracterizacão e importancia na compartimentação tectônica do Cinturão Dom Feliciano. Rev Bras Geociênc 23:1–10
Fernandes LAD et al (1995a) Evolução Tectônica do Cinturão Dom Feliciano no Escudo Sul-riograndense: Parte I- Uma Contribuição a partir do registro geológico. Rev Bras Geociênc 25:351–374
Fernandes LAD et al (1995b) Evolução Tectônica do Cinturão Dom Feliciano no Escudo Sul-riograndense: Parte II- Uma Contribuição a partir do registro geofísico. Rev Bras Geociênc 25:375–384
Florisbal LM et al (2009) Early postcollisional granitic and coeval mafic magmatism of medium- to high-K tholeiitic affinity within the Neoproterozoic Southern Brazilian Shear Belt. Precambr Res 175:135–148
Florisbal LMF et al (2012a) Contrasted crustal sources as defined by whole-rock and Sr-Nd-Pb isotope geochemistry of Neoproterozoic early post-collisional granitic magmatism within the Southern Brazilian Shear Belt, Camboriú, Brazil. J S Am Earth Sci 39:24–43
Florisbal LMF et al (2012b) Petrogenesis of syntectonic granites emplaced at the transition from thrusting to transcurrent tectonics in post-collisional setting: whole-rock and Sr-Nd-Pb isotope geochemistry in the Neoproterozoic Quatro Ilhas and Mariscal granites, southern Brazil. Lithos 153:53–71
Florisbal LMF et al (2012c) Space-time relation of post-collisional granitic magmatism in Santa Catarina, southern Brazil: U-Pb LA-MC-ICP-MS zircon geochronology of coeval mafic-felsic magmatism related to the major Gercino Shear Zone. Precambr Res 216–219:132–151
Foster DA et al (2009) Rapid exhumation of deep crust in an obliquely convergent orogen: the Kaoko Belt of the Damara Orogen. Tectonics 28, TC4002. https://dx.doi.org/10.1029/2008TC002317
Foster DA et al (2015) U-Pb age and Lu-Hf isotopic data of detrital zircons from Neoproterozoic Damara Sequence: implications for pre-Gondwana proximity of Congo and Kalahari. Gondwana Res 28:179–190
Frantz JC et al (2003) SHRIMP U-Pb zircon ages of granitoids from southernmost Brazil: constrains on the temporal evolution of the Dorsal de Canguçu transcurrent Shear Zone and Eastern Dom Feliciano Belt. IV South American Symposium on Isotope Geology, Short Papers, pp 174–177
Frimmel HE, Frank W (1998) Neoproterozoic tectono-thermal evolution of the Gariep Belt and its basement, Namibia/South Africa. Precambr Res 90:1–28
Frimmel HE et al (2011) Neoproterozoic geodynamic evolution of SW-Gondwana: a southern African perspective. Int J Earth Sci 100:323–354
Frimmel HE et al (2013) A new lithostratigraphic subdivision and geodynamic model for the Pan-African western Saldania Belt, South Africa. Precambr Res 231:218–235
Ganade CE et al (2016) Tightening-up NE Brazil and NW Africa connections: new U–Pb/Lu–Hf zircon data of a complete plate tectonic cycle in the Dahomey belt of the West Gondwana Orogen in Togo and Benin. Precambrian Res 276:24–42

Gaucher C et al (2009) Tectonic events and palaeogeographic evolution of southwestern Gondwana in the Neoproterozoic and Cambrian. In: Gaucher C et al (eds) Neoproterozoic-cambrian tectonics, global change and evolution: a focus on Southwestern Gondwana. Developments in Precambrian Geology, Amsterdam, Elsevier, vol 16, pp 295–316

Goscombe BD, Gray DR (2007) The Coastal Terrane of the Kaoko Belt, Namibia: outboard arc-terrane and tectonic significance. Precambr Res 155:139–158

Goscombe BD, Gray DR (2008) Structure and strain variation at midcrustal levels in a transpressional orogen: a review of Kaoko Belt structure and the character of West Gondwana amalgamation and dispersal. Gondwana Res 13:45–85

Goscombe B et al (2003) Structure of the Kaoko Belt, Namibia: progressive evolution of a classic transpressional orogen. J Struct Geol 25:1049–1081

Goscombe BD et al (2004) Variation in metamorphic style along the northern margin of the Damara Orogen, Namibia. J Petrol 45:1261–1295

Goscombe B et al (2005a) Event geochronology of the Pan-African Kaoko Belt, Namibia. Precambrian Res vol 140, pp 103.e1–103.e41

Goscombe B et al (2005) Extrusional tectonics in the core of a transpressional orogen, the Kaoko Belt, Namibia. J Petrol 46:1203–1241

Goscombe B et al (2017a) Deformation correlations, stress field rotation and evolution of an orogenic intersection: the Pan-African Kaoko-Damara orogenic junction, Namibia. Geosci Front 8:1187–1232

Goscombe B et al (2017b) Metamorphic response and crustal architecture in a classic collisional orogen: the Damara Belt, Namibia. Gondwana Res 52:80–124

Granot R, Dyment J (2015) The Cretaceous opening of the South Atlantic Ocean. Earth Planet Sc Lett 414:156–163

Gray DR et al (2006) 40Ar/39Ar thermochronology of the PaneAfrican Damara Orogen, Namibia, with implications for tectonothermal and geodynamic evolution. Precambr Res 150:49–72

Gray DR et al (2008) A Damara orogeny perspective on the assembly of southwestern Gondwana. In: Pankhurst RJ et al (eds) West Gondwana: pre-cenozoic correlations across the South Atlantic Region. Geological Society of London Special Publications, London, vol 294, pp 257–278

Gresse PG et al (2006) Namibian (Neoproterozoic) to early Cambrian successions. In: Johnson MR et al (eds) The geology of South Africa. Geological Society of South Africa and Council for Geoscience, Johannesburg and Pretoria, pp 395–420

Guadagnin F et al (2010) Depositional age and provenance of the Itajaí Basin, Santa Catarina State, Brazil: implications for SW Gondwana correlation. Precambr Res 180:156–182

Guj P (1970) The Damara mobile belt in the South-Western Kaokoveld, South West Africa. PhD Thesis. University of Cape Town

Hartmann LA et al (1999) Deepest exposed crust of Brazil—SHRIMP establishes three events. Geology 27:947–950

Hartmann LA et al (2000) Advances in SHRIMP geochronology and their impact on understanding the tectonic and metallogenic evolution of southern Brazil. Aust J Earth Sci 47:829–844

Hartmann LA et al (2001) Archean crust in the Río de la Plata Craton, Uruguay—SHRIMP U-Pb zircon reconnaissance geochronology. J S Am Earth Sci 4:557–570

Hartmann LA et al (2003) Prolonged Paleoproterozoic magmatic participation in the Neoproterozoic Dom Feliciano belt, Santa Catarina, Brazil, based on zircon U-Pb SHRIMP geochronology. J S Am Earth Sci 16:477–492

Hartmann LA et al (2004) Paleoproterozoic provenance of detrital zircon, Porongos Complex quartzites, southern Brazilian Shield. Int Geol Rev 46:127–157

Hartmann LA et al (2008) Protolith age of Santa Maria Chico granulites dated on zircons from an associated amphibolite-facies granodiorite in southernmost Brazil. An Braz Acad Sci 80:543–551

Hartmann LA et al (2011) Time frame of 753–680 Ma juvenile accretion during the São Gabriel orogeny, southern Brazil. Gondwana Res 19:84–99

Hartmann LA et al (2015) Airborne geophysical characterization of geotectonic relationships in the southern Ribeira Belt, Luís Alves Craton, and northern Dom Feliciano Belt. Int Geol Rev, Brazilian Shield. https://doi.org/10.1080/00206814.2015.1089424

Hartnady CJH et al (1974) The stratigraphy and structure of the Malmesbury Group in the southwestern Cape. Bulletin of the Precambrian Research Unit, University of Cape Town 15:193–213

Heintz M et al (2003) Shear wave splitting in SE Brazil: an effect of active or fossile upper mantle flow, or both? Earth Planet Sc Lett 211:79–95

Hoffmann K-H (1989) New aspects of lithostratigraphic subdivision and correlation of late Proterozoic to early Cambrian rocks of the southern Damara Belt, and their correlation with central and northern Damara Belt and the Gariep Belt. Communs Geol Surv Namibia 5:59–67

Hoffmann K-H et al (2004) U-Pb zircon date from the Neoproterozoic Ghaub formation, Namibia: constraints on Marinoan glaciation. Geology 32:817–820

Hueck M et al (2016) Origin and evolution of the granitic intrusions in the Brusque group of the Dom Feliciano Belt, south Brazil: petrostructural analysis and whole-rock/isotope geochemistry. J S Am Earth Sci 69:131–151

Hueck M et al (2017) Phanerozoic low-temperature evolution of the Uruguayan Shield along the South American passive margin. J Geol Soc London. https://doi.org/10.1144/jgs2016-101

James DE, Assumpção M (1996) Tectonic implications of S-wave anisotropy beneath SE Brazil. Geophy J Int 126:1–10

Karl M et al (2013) Evolution of the South Atlantic passive continental margin in southern Brazil derived from zircon and apatite (U-Th-Sm)/He and fission-track data. Tectonophysics 604:224–244

Kasch KW (1983) Continental collision, suture propagation and thermal relaxation: a plate tectonic model for the Damara Orogen in central Namibia. Spec Pub Geol Soc S Afr 11:423–429

Kisters AFM et al (2002) Timing and kinematics of the Colenso Fault: the early paleozoic shift from collisional to extensional tectonics in the Pan-African Saldania Belt, South Africa. S Afr J Geol 56:257–270

Kisters AFM et al (2004) Thrust-related dome structures in the Karibib district and the origin of orthogonal fabric domains in the south Central Zone of the Pan-African Damara belt, Namibia. Precambr Res 133:283–303

Kitt S et al (2016) Shear-zone hosted copper mineralisation of the Omitiomire deposit—structural controls of fluid flow and mineralisation during subduction accretion in the Pan-African Damara Belt of Namibia. Ore Geol Rev 75:1–15

Koester E et al (1997) Geocronologia Rb/Sr e K/Ar dos granitóides sintectônicos à Zona de Cisalhamento Transcorrente Dorsal de Canguçu. Pesquis Geociênc 24:67–77

Koester E et al (2001a) Petrologia dos granitóides sintectônicos à Zona de Cisalhamento Transcorrente Dorsal de Canguçu, Encruzilhada do Sul, RS. Rev Bras Geociênc 31:131–140

Koester E et al (2001b) Geologia e geoquímica de granitóides sintectônicos à Zona de Cisalhamento Transcorrente Dorsal do Canguçu, Encruzilhada do Sul, RS. Rev Bras Geociênc 31:141–154

Koester E et al (2001c) SHRIMP U-Pb age for the emplacement of the Santana Granite and reactivation of the Porto Alegre Suture, southern Brazil. J S Am Earth Sci 14:91–99

Koester E et al (2016) Further evidence of 777 Ma subduction-related continental arc magmatism in Eastern Dom Feliciano Belt, southern

Brazil: the Chácara das Pedras Orthogneiss. J S Am Earth Sci 68:155–166
Konopásek J et al (2005) Oblique collision and evolution of large-scale transcurrent shear zones in the Kaoko belt, NW Namibia. Precambr Res 139:139–157
Konopásek J et al (2008) Neoproterozoic igneous complex emplaced along major tectonic boundary in the Kaoko Belt (NW Namibia): Ion probe and LAICP-MS dating of magmatic and metamorphic zircons. J Geol Soc London 165:153–165
Konopásek J et al (2014) Timing and sources of pre-collisional Neoproterozoic sedimentation along the SW margin of the Congo Craton (Kaoko Belt, NW Namibia). Gondwana Res 26:386–401
Konopásek J et al (2016) Linking the basement geology along the Africa-South America coasts in the South Atlantic. Precambr Res. https://doi.org/10.1016/j.precamres.2016.05.011
Kröner S et al (2004) U-Pb and Pb-Pb zircon ages for metamorphic rocks in the Kaoko Belt of Northwestern Namibia: a Palaeo- to Mesoproterozoic basement reworked during the Pan-African orogeny. S Afr J Geol 107:455–476
Kukla PA, Stanistreet IG (1991) The record of the Damaran Khomas Hochland accretionary prism in central Namibia: refutation of the "ensialic" origin of a Late Proterozoic orogenic belt. Geology 19: 473–476
Lara P et al (2017) Post-collisional, Late Neoproterozoic, high-Ba-Sr granitic magmatism from the Dom Feliciano Belt and its cratonic foreland, Uruguay: petrography, geochemistry, geochronology, and tectonic implications. Lithos 277:178–198
Lehmann J et al (2015) Structural and geochronological constraints of the Pan-African tectonic evolution of the northern Damara Belt. Tectonics 35:103–135. Namibia
Lehmann J et al (2016) Structural and geochronological constraints on the Pan-African tectonic evolution of the northern Damara Belt, Namibia. Tectonics 35:103–135
Leite JAD et al (1998) SHRIMP U/Pb zircon geochronology of Neoproterozoic juvenile and crustal-reworked terranes in southern-most Brazil. Int Geol Rev 40:688–705
Lena LOF et al (2014) The evolution of the Neoproterozoic São Gabriel juvenile terrane, southern Brazil based on high spatial resolution U-Pb ages and $\delta^{18}O$ data from detrital zircons. Precambr Res 247:126–138
Limarino CO, Spalletti LA (2006) Paleogeography of the upper Paleozoic basins of southern South America: an overview. J S Am Earth Sci 22:134–155
Lopes CG et al (2015) Provenance of the Passo Feio complex, São Gabriel Terrane, Dom Feliciano Belt, southern Brazil, implications for the tectonic setting of deposition, age of the São Gabriel Arc and origin of Paleoarchean detrital zircons (3.3–3.63 Ga). J S Am Earth Sci 58:9–17
Luzardo R, Fernandes LAD (1990) Análise estrutural do Lineamento do Ibaré parte I—Filitos de Ibaré—greenstone belt ou cobertura cratônica deformada? Acta Geol Leopoldensia 30:25–36
Mallmann G et al (2007) Isotope geochemistry and geochronology of the Nico Pérez Terrane, Rio de la Plata Craton, Uruguay. Gondwana Res 12:489–508
Martini A, Bitencourt MD (2014) Caacterização cinemática de uma zona de cisalhamento transcorrente de direção NNE marcada na evolução de seu magmatismo granítico sintectônico na região de Camboriú, SC. Geol USP Sér Cient 14:61–74
Martini A et al (2015) An integrated approach to the late stages of Neoproterozoic post-collisional magmatism from Southern Brazil: Structural geology, geochemistry and geochronology of the Corre-mar Granite. Precambr Res 261:25–39
Masquelin H et al (2012) The Cerro Olivo complex: a pre-collisional Neoproterozoic magmatic arc in eastern Uruguay. Int Geol Rev 54:1161–1183
Milani EJ, Zalán PV (1999) An outline of the geology and petroleum systems of the Paleozoic interior basins of South America. Episodes 22:199–205
Miller RMG (1983) Evolution of the Damara Orogen of South West Africa/Namibia. Geological Society of South Africa, Johannesburg
Miller RMG, Grote W (1988) Geological map of the Damara Orogen, Namibia (scale 1:500,000). Geological Survey of Namibia, Windhoek
Miller RMcG (2008) The geology of Namibia. Geological Survey of Namibia, Windhoek
Nardi LVS, Bitencourt MF (2009) A-type granitic rocks in post-collisional settings in southernmost Brazil: their classification and relationship with tectonics and magmatic series. Can Mineral 47:1493–1503
Nardi LVS, Frantz JC (1995) The Cordilheira Intrusive Suite: late-precambrian peralumious granitoids from southern Brazil. J S Am Earth Sci 8:55–64
Oliver GJH (1994) Mid-crustal detachment and domes in the central zone of the Damaran Orogen. J Afr Earth Sci 19:331–344. Namibia.
Oliveira CHE et al (2014) U-Pb and Lu-Hf Isotopes applied to the evolution of the late to post-orogenic transtensional basins of the Dom Feliciano Belt, Brazil. Precambr Res 246:240–255
Oliveira CHE et al (2016) Evidence of post-Gondwana breakup in Southern Brazilian Shield: insights from apatite and zircon fission track thermochronology. Tectonophysics 666:173–187
Oliveira DS et al (2015) Post-collisional subvolcanic rhyolites associated to the Neoproterozoic Batholith Pelotas, Southern Brazil. J S Am Earth Sci 63:84–100
Oriolo S et al (2015) Structural evolution of the Sarandí del Yí Shear Zone, Uruguay: Kinematics, deformation conditions and tectonic significance. Int J Earth Sci 104:1759–1777
Oriolo S et al (2016a) The Nico Pérez Terrane (Uruguay): from Archean crustal growth and connections with the Congo Craton to late Neoproterozoic accretion to the Río de la Plata Craton. Precambr Res 280:147–160
Oriolo S et al (2016b) Shear zone evolution and timing of deformation in the Neoproterozoic transpressional Dom Feliciano Belt, Uruguay. J Struct Geol 92:59–78
Oriolo S et al (2016c) Timing of deformation in the Sarandí del Yí Shear Zone, Uruguay: implications for the amalgamation of western Gondwana during the Neoproterozoic Brasiliano-Pan-African Orogeny. Tectonics 35:754–771
Oriolo S et al (2017) Contemporaneous assembly of Western Gondwana and final Rodinia break-up: implications for the supercontinent cycle. Geosci Frontiers. https://doi.org/10.1016/j.gsf.2017.01.009
Oyhantçabal P (2005) The Sierra Ballena shear zone: kinematics, timing and its significance for the geotectonic evolution of southeast Uruguay. Dissertation, Georg-August-Universität Göttingen
Oyhantçabal P et al (1993) Geología y aspectos estructurales del borde orogénico en el extremo sur del cinturón Dom Feliciano. Rev Bras Geociências 23:296–300
Oyhantçabal P et al (2007) Post-collisional transition from calc-alkaline to alkaline magmatism during transcurrent deformation in the southernmost Dom Feliciano Belt (Braziliano–Pan-African, Uruguay). Lithos 98:141–159
Oyhantçabal P et al (2009) The Sierra Ballena Shear Zone in the southernmost Dom Feliciano Belt (Uruguay): evolution, kinematics, and deformation conditions. Int J Earth Sci. https://doi.org/10.1007/s00531-009-0453-1
Oyhantçabal P et al (2011a) The Río de la Plata Craton: a review of units, boundaries, ages and isotopic signature. Int J Earth Sci 100:201–220
Oyhantçabal P et al (2011b) The transpressional connection between Dom Feliciano and Kaoko Belts at 580–550 Ma. Int J Earth Sci 100:379–390

Oyhantçabal P et al (2012) Paleo- and Neoproterozoic magmatic and tectonometamorphic evolution of the Isla Cristalina de Rivera (Nico Pérez Terrane, Uruguay). Int J Earth Sci 101:1745–1762

Pankhurst RJ, Rapela CW (1998) The Proto-Andean Margin of Gondwana. Geological Society of London Special Publications, London, p 142

Passarelli CR et al (1993) Caracterização geométrica e cinemática da Zona de Cisalhamento Major Gercino e sua importância na compartimentação dos terrenos Pré-Cambrianos de Santa Catarina. Rev Bras Geociênc 23:234–241

Passarelli CR et al (2010) Deformation and geochronology of syntectonic granitoids emplaced in the major Gercino Shear zone, southeastern South America. Gondwana Res 17:688–703

Passarelli CR et al (2011a) Major Shear Zones of southern Brazil and Uruguay: escape tectonics in the eastern border of Rio de La Plata and Paranapanema cratons during the Western Gondwana amalgamation. Int J Earth Sci 100:391–414

Passarelli CR et al (2011b) Heterogeneity in syntectonic granitoids emplaced in a major shear zone, southern Brazil. J S Am Earth Sci 32:369–378

Passchier CW et al (2007) Intrusion mechanisms in a turbidite sequence: the Voetspoor and Doros plutons in NW Namibia. J Struct Geol 29:481–496

Passchier CW et al (2011) Key-ring structure gradients and sheath folds in the Goantagab Domain of NW Namibia. J Struct Geol 33:280–291

Passchier CW et al (2016) How to make a transverse triple junction—New evidence for the assemblage of Gondwana along the Kaoko-Damara belts, Namibia. Geology 44:843–846

Peternell M et al (2010) Macro and microstructures as indicators of the development of syntectonic granitoids and host rocks in the Camboriú region, Santa Catarina, Brazil. J S Am Earth Sci 29:738–750

Pertille J et al (2015a) Zircon U-Pb age constraints on the Paleoproterozoic sedimentary basement of the Ediacaran Porongos Group, Sul-Riograndense Shield, southern Brazil. J S Am Earth Sci 63:334–345

Pertille J et al (2015b) Origin of the Ediacaran Porongos Group, Dom Feliciano Belt, southern Brazilian Shield, with emphasis on whole rock and detrital zircon geochemistry and U-Pb, Lu-Hf isotopes. J S Am Earth Sci 64:69–93

Philipp RP (1998) A Evolução Geológica e Tectônica do Batólito Pelotas no Rio Grande do Sul. Dissertation, Universidade de São Paulo, São Paulo

Philipp RP, Machado R (2005) The Neoproterozoic to Cambrian granitic magmatism of the Pelotas Batholith, southern Brazil. J S Am Earth Sci 19:461–478

Philipp RP et al (1993) Reconhecimento estrutural e geoquímico dos granitóides brasilianos da região de Pelotas-RS. Pesqui Geociênc 20:3–13

Philipp RP et al (2003) Reavaliação e novos dados geocronológicos (Ar/Ar, Rb/Sr e Sm/Nd) do Batólito Pelotas no Rio Grande do Sul: Implicações petrogenéticas e idade de reativação das zonas de cisalhamento. Geol USP Sér Cient 3:71–84

Philipp RP et al (2004) Caracterização litológica e evolução metamórfica da porção leste do Complexo Metamórfico Brusque, Santa Catarina. Rev Bras Geociênc 34:21–34

Philipp RP et al (2013) Peraluminous leucogranites of the Cordilheira Suite: a record of Neoproterozoic collision and the generation of the Pelotas Batholith, Dom Feliciano Belt, Southern Brazil. J S Am Earth Sci 43:8–24

Philipp RP et al (2014) Oldest age of magmatism in the Passinho Arc in the southwestern portion of Gondwana, Rio Grande do Sul, Brazil. In: IX South American Symposium on Isotope Geology, São Paulo, Abstracts, 186

Philipp RP et al (2016) Tectonic evolution of the Dom Feliciano Belt in Southern Brazil: geological relationships and U-Pb geochronology. Braz J Geol 46:83–104

Porada H, Wittig R (1983) Turbidites and their significance for the geosynclinal evolution of the Damara Orogen, South West Africa/Namibia. In: McG Miller R (ed) Evolution of the Damara Orogen of South West Africa/Namibia. Geological Society of South Africa, Johannesburg vol 11, pp 21–36

Prave AR (1996) Tale of three cratons: tectonostratigraphic anatomy of the Damara orogen in northwestern Namibia and the assembly of Gondwana. Geology 24:1115–1118

Preciozzi F et al (1979) Carta geo-estructural del Uruguay, escala 1:2.000.000. Instituto Geológico Ing. Terra Arocena, Montevideo

Raab MJ et al (2002) Late Cretaceous reactivation of major crustal shear zones in northern Namibia: constraints from apatite fission track analysis. Tectonophysics 349:75–92

Rapela CW et al (2011) The Río de la Plata craton and the adjoining Pan-African/brasiliano terranes: their origins and incorporation into south-west Gondwana. Gondwana Res 20:673–690

Raposo MI et al (2014) Deformation in rocks from Itajaí basin, Southern Brazil, revealed by magnetic fabrics. Tectonophysics 629:290–302

Ritter O et al (2003) A magnetotelluric study of the Damara Belt in Namibia 1. Regional scale conductivity anomalies. Phys Earth Planet In 138:71–90

Rostirolla SP et al (1992) O Grupo Itajaí, Estado de Santa Catarina, Brasil, exemplo de sedimentação em uma bacia flexural de antepaís. Bol Geociênc Petrobrás 6:109–122

Rostirolla SP et al (1999) Basin analysis and mineral endowment of the Proterozoic Itajaí Basin, south-east Brazil. Basin Res 11:127–142

Rozendaal A et al (1999) Neoproterozoic to early Cambrian crustal evolution of the Pan-African Saldania Belt, South Africa. Precambr Res 97:303–323

Saalmann K et al (2005) Tectonic evolution of two contrasting schist belts in southernmost Brazil: a plate tectonic model for the Brasiliano Orogeny. Int Geol Rev 47:1234–1259

Saalmann K et al (2006a) Tectonic evolution of the Neoproterozoic juvenile São Gabriel belt, southern Brazil—constraints on Brasiliano orogenic evolution of the La Plata Cratonic margin. J S Am Earth Sci 21:204–227

Saalmann K et al (2006b) Structural evolution and tectonic setting of the Porongos belt, southern Brazil. Geol Mag 143:59–88

Saalmann K et al (2007) The assembly of West Gondwana—the view from the Rio de la Plata craton. In: Linnemann U et al (eds) The evolution of the Rheic Ocean: from Avalonian-Cadomian active margin to Alleghenian-Variscan collision. Geological Society of America Special Paper, vol 423, pp 1–26

Saalmann K et al (2011) Multiple accretion at the eastern margin of the Rio de la Plata craton: the prolonged Brasiliano orogeny in southernmost Brazil. Int J Earth Sci 100:355–378

Salomon, E. et al. (2014) Brittle reactivation of ductile shear zones in NW Namibia in relation to South Atlantic rifting. *Tectonics* 34. https://dx.doi.org/10.1002/2014TC003728

Sánchez Bettucci L et al (2003) Petrography and geochemistry of the Carapé granitic complex (southeastern Uruguay). Gondwana Res 6:89–105

Sánchez Bettucci L et al (2004) Mineralizations of the Lavalleja group (Uruguay), a probable Neoproterozoic volcano-sedimentary sequence. Gondwana Res 7:745–751

Sánchez Bettucci L et al (2016) Análisis de la geofísica aérea en la zona sur de la Zona de Cizalla de Sarandí del Yí. In: VIII Geological Congress of Uruguay, Abstracts 22

Scheepers R, Armstrong R (2002) New U-Pb SHRIMP zircon ages of the Cape Granite Suite: implications for the magmatic evolution of the Saldania Belt. S Afr J Geol 105:241–256

Scheepers R, Nortjé AN (2000) Rhyolitic ignimbrites of the Cape Granite Suite, southwestern Cape Province, South Africa. J Afr Earth Sci 31:647–656

Scheepers R, Poujol M (2002) U-Pb zircon age of Cape Granite Suite ignimbrites: characteristics of the last phases of the Saldanian magmatism. S Afr J Geol 105:209–224

Schoch AE (1975) The darling granite batholith. Ann Univ Stellenbosch 1:1–104

Schroeder GS (2006) Análise tectônica da Bacia do Itajaí. M.Sc dissertation, Universidade Federal do Rio Grande do Sul, Porto Alegre

Seth B et al (1998) Archaean to Neoproterozoic magmatic events in the Kaoko belt of NW Namibia and their geodynamic significance. Precambr Res 92:341–363

Spoturno JJ et al (2004) Mapa geológico y de recursos minerales del Departamento de Canelones a escala 1:100.000. Proyecto CONICYT 6019, Montevideo

Spoturno JJ et al (2012) Mapa geológico del Departamento de Maldonado escala 1:100.000. Facultad de Ciencias (UdelaR)—Dirección Nacional de Minería y Geología (MIEM), Montevideo

Stanistreet IG, Charlesworth EG (2001) Damaran basement-cored fold nappes incorporating pre-collisional basins, Kaoko Belt, Namibia, and controls on Mesozoic supercontinent break-up. S Afr J Geol 104:1–12

Theron JN et al (1992) The geology of the cape town area. Geological Survey of South Africa, Explanation of Sheet, vol 3318, 140 pp

Tommasi A, Vauchez A (2001) Continental rifting parallel to ancient collisional belts: an effect of the mechanical anisotropy of the lithospheric mantle. Earth Planet Sc Lett 185:199–210

Tommasi A et al (1994) Orogen-parallel strike-slip faulting and synkinematic magmatism in the Dom Feliciano Belt, Southern Brazil. Tectonics 13:421–437

Torsvik TH et al (2009) A new scheme for the opening of the South Atlantic Ocean and the dissection of an Aptian salt basin. Geophys J Int 177:1315–1333

Ulrich S et al (2011) Transposition of structures in the Neoproterozoic Kaoko Belt (NW Namibia) and their absolute timing. Int J Earth Sci 100:415–429

Vauchez A et al (1997) Why do continents break-up parallel to ancient orogenic belts? Terra Nova 9:62–66

Will TM, Frimmel HE (2013) The influence of inherited structures on dike emplacement during Gondwana breakup in southwestern Africa. J Geol 121:455–474

The African Metallotects of Southwest Gondwana

23

Gregor Borg and Christoph Gauert

Abstract

The African portion of Southwest Gondwana is endowed with an enormous wealth of mineral resources. Certain types of ore deposits occur in metallotects that share common geological and metallogenetic features. These can include host rocks, the age and mode of origin of the mineralisation, the commodity elements or minerals, and the geodynamic significance of formation. This chapter describes metallotects that are significant for the regional and supraregional geological and plate tectonic evolution, and bear metallogenetically and economically important mineral resources. The size of metallotects or individual deposits described here is variable, from the world-class Cu-Co-resource of the Central African Copperbelt (CACB) to economically insignificant but metallogenetically relevant tin deposits in the Cape Peninsula of South Africa. The chapter includes settings such as Late Mesoproterozoic extensional, volcanosedimentary continental to shallow marine basins with the deposits contained therein. It also describes the Neoproterozoic, more continuous, deeper-water and locally seafloor-basalt-bearing Damara Belt with its metabasalt-hosted massive sulphide Cu–Zn deposits and sediment-hosted Pb–Zn deposits along the basin margins. However, for some of the metallotects, the age of the mineralisation is epigenetic and unrelated to the period of deposition of the host rocks. The comparatively poorly exposed, studied and explored West Congo Belt is also included, particularly since it bears a lithologically, structurally and metallogenetically strong resemblance to the Damara Belt further south. Orthomagmatic copper sulphide deposits, such as the ones of the Mesoproterozoic Okiep District, represent a comparatively small but historically and metallogenetically important metallotect in the Northern Cape Province of South Africa. In contrast, ore deposits related to highly fractionated felsic to exotic magmatic rocks have formed during the late to post-orogenic stages in collisional plate tectonic settings.

Keywords

Metallotects • Ore deposits • Geodynamic setting
VHMS • SHMS • Copper • Lead • Zinc
Gold • Tin • Tungsten • Uranium • REE

23.1 Introduction

Ore deposits, local mining districts, and regional metallotects make up the endowment of a region with mineral commodities used by human society for a large number of essential technical purposes. However, the general geological significance of ore deposits and the metallotects they occur in is far greater since districts that share common patterns of metallogenesis also characterise the geological setting and geological evolution of regions, and even of entire subcontinents or crustal plates. This chapter on the metallotects and ore deposits of SW Gondwana does not attempt to achieve any form of completeness because of the sheer number of ore deposits, mineral occurrences, and mineralised districts. National inventories with the aim of providing comprehensive catalogues have been published as substantial volumes for Namibia (Schneider and Seeger 1992), Southern Africa (Anhaeusser and Maske 1986), the whole of Africa as printed metallogenic maps (Milesi et al. 2004) and electronic GIS databases (Thiart and de Wit 2008).

G. Borg (✉)
Economic Geology and Petrology Research Unit,
Institute of Geosciences, Martin-Luther-University
Halle-Wittenberg, Halle, Germany
e-mail: gregor.borg@geo.uni-halle.de

C. Gauert
Landesamt für Geologie und Bergwesen (Geological Survey,
Sachsen-Anhalt), Halle, Germany
e-mail: Gauert@lagb.mw.sachsen-anhalt.de

C. Gauert
Department of Geology, University of the Free State,
250 Nelson-Mandela-Drive, Bloemfontein, 9300, South Africa

S. Siegesmund et al. (eds.), *Geology of Southwest Gondwana*, Regional Geology Reviews,
https://doi.org/10.1007/978-3-319-68920-3_23

In our contribution we have selected a number of technical mining districts, which represent geological metallotects in the African part of SW Gondwana (Fig. 23.1). These metallotects share common types of ore deposit, which offer an insight into the plate tectonic setting at a certain period from a metallogenetic perspective. The metallotects, mining districts, and ore deposits described in this chapter differ widely in size and economic significance from the world's largest Co resource, contained within the deposits of the Central African Copperbelt (CACB) in Zambia and the Democratic Republic of the Congo (DRC), to economically comparatively minute Sn-bearing pegmatite veins in the cupola of granites in the Southwestern Cape Province in South Africa. What these ore deposits have in common is that they represent significant and characteristic metallogenetic processes in the geodynamic evolution of their respective region within the African part of SW Gondwana. This summary does not include Archaean metallotects that have been inherited within the older crustal cores of Gondwana, such as the huge gold deposits of the Witwatersrand or the Platinum Group Element deposits of the Bushveld Complex. It cannot be ignored that our selection of metallotects and ore deposit types is influenced by our subjective familiarity, experience, and judgement of the particularities of the chosen examples. The depth of our descriptions and interpretations of the individual metallotects or classes of ore deposit varies also, depending on the available and published data and on the degree of general understanding and the specific complexity of the metallogenic processes involved. However, we hope that this selection and the general patterns and processes described here will add to the larger aim of furthering the understanding of the geological evolution of SW Gondwana.

The sheer number of metallotects and ore deposits contained therein with their enormous wealth of mineral resources can be subdivided and organised in different ways. One criterion that might come to mind first is the age of formation, but this is problematic since the age of the host sequence and the age of the mineralisation can differ widely from syngenetic to epigenetic and even to combined multistage metallogenetic histories [Kalahari Copper Belt (KCB) and CACB in Fig. 23.2]. Instead, here we have chosen to group the metallotects from extensional tectonic regimes to collisional orogenic and post-orogenic settings (Fig. 23.2), although we expect that this can also be debated in some cases. The period we consider covers the timespan from approximately 1600 Ma to approximately 520 Ma, thus comprising the Meso- and Neoproterozoic, and extending into the very early Cambrian with some of the post-orogenic deposits within the Damaran Mobile Belt.

23.2 Central African Copperbelt

The Central African Copperbelt (Figs. 23.1 and 23.3) is one of the world's largest copper metallotects and the largest cobalt district, situated within the Congo Craton both in Zambia and the Democratic Republic of the Congo (DRC), and it contains approximately 30% of the world's Cu reserves. The CACB, along with its possibly broad time equivalents in Botswana and Namibia (the KCB, Fig. 23.1), is the world's largest sediment-hosted, stratiform copper province (Sillitoe et al. 2010) with typical Cu grades of 2–3% and up to 1% Co, typically enriched in fold hinges. Considerable ore reserves exist in the Katangan Sequence of the 300 km-wide Zambian part of the basin but they extend far into the DRC, approximately 500 km to the northwest. Several world-class deposits, such as Nchanga (McGowan et al. 2003, 2006), Konkola (Sweeney et al. 1986), and Tenke Fungurume (Fay and Barton 2012), together with dozens of smaller mines make this region one of the largest Cu- and especially the most important Co-producing metallotects in the world. Although exploration and resource data for the entire CACB are unreliable, it has been estimated that the region still contains resources in excess of 150 million tons of Cu metal and 8 million tons of Co metal (Misra 2000).

Although it has been widely accepted by most authors that the disseminated mineralisation was introduced during sediment diagenesis in an extensional continental rift setting, alternative models with multiple events spanning several hundred million years or even an entirely late metallogenesis have been proposed by Sillitoe et al. (2010). The Katangan sediments were deposited in an intracratonic rift, formed on a Palaeoproterozoic, deformed but fertile magmatic arc that contained the ultimate source of Cu in porphyry-type intrusions (Unrug 1988; Rainaud et al. 1999, 2005; Master et al. 2005), and possibly Co from penecontemporaneous sills that intruded the Upper Roan Group (Annels 1974).

The initiation of rifting and siliciclastic deposition, playa lake and restricted marine incursions to form evaporites, shales, and carbonate rocks sediment followed relatively soon after the formation of the Nchanga granite basement rocks at 880 Ma. Ore genesis in the CACB was initially assumed to be syngenetic (Fleischer et al. 1976), but subsequently mineralisation was related to later, epigenetic fluids circulating through the sediments, either during diagenesis and compaction of the sequence (Sweeney et al. 1991) or significantly later during deformation and metamorphism (Unrug 1988). It seems likely that metals were sequentially precipitated by processes related to reduction–oxidation reactions between sedimentary host rocks and a

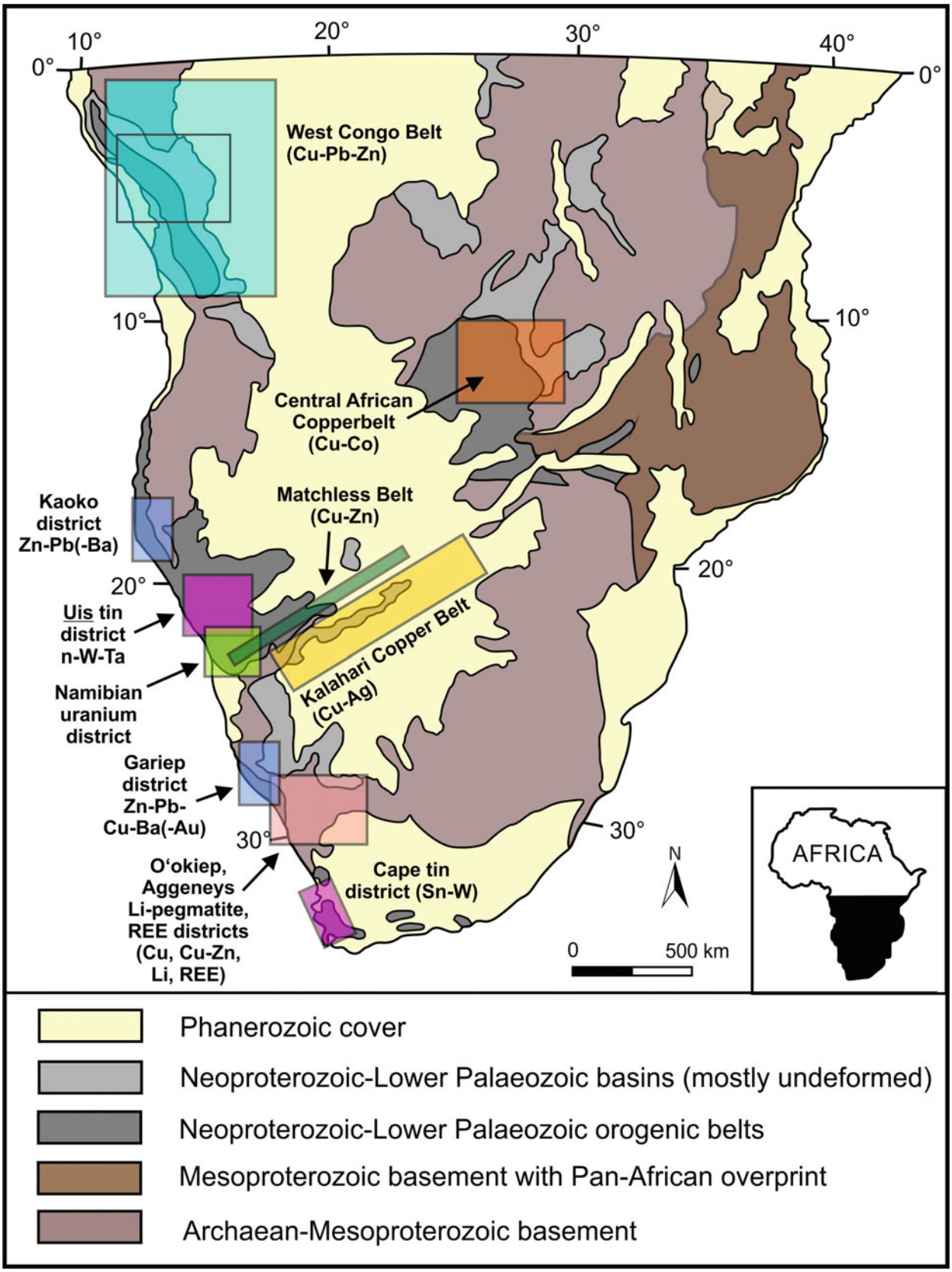

Fig. 23.1 Tectonic domains of subequatorial Africa with ore deposit districts that represent the most relevant metallotects of Southwest Gondwana described in this chapter. Tectonic domain map after Cailteux et al. (2015)

Period / Age	plate tectonic/ geodynamic stage	drifting stage/oceanic crust	continental rift/early ("failed") passive continental margin	epicontinental/failed rift	collisional intrusion-related		orogenic/syn-metamorphic/ syn-tectonic/late orogenic-intrusion-related
		mid-oceanic ridge	*hinge line/ marginal faults/ transfer faults*	*(arc-related?)*	*primitive mafic magmatic-related*	*highly evolved/ fractionated magmatic*	*strongly tectonically controlled*
541 Ma	*collisional*			Central African Copperbelt Cu-Co and Kalahari Copper Belt Cu-Ag (epigenetic emplacement)		Karibib-Usakos-Uis and Cape Granite Sn-W pegmatites and uranium-granites/pegmatites	Omitiomire Cu Navachab Au
Neoprotrozoic (Pan-African)	extensional/ stable	Matchless Belt Cu-Zn Gorob/Hope, Matchless, Otjihase		West Congo Belt Cu-Pb-Zn ?			
			Tsongoari, Rosh Pinah, Skorpion, Gergarup Pb-Zn(-Ba-Cu)				
1,000 Ma				West Congo Belt (host sequence), Central African Copperbelt Cu-Co and Kalahari Copper Belt Cu-Ag (diagenetic emplacement)			
Late Mesoproterozoic	*collisional*				O'okiep mafic sills Cu	Northern Cape Li-pegmatites	
						Steenkampskraal Th, REE, apatite-magnetite sills and veins	
1,600 Ma	*stable/ extensional*			Aggeneys District Cu-Zn (Gamsberg, Black Mountain, Broken Hill, Deeps)			

Fig. 23.2 Tabulated overview of the metallotects described in this chapter in relationship to their geodynamic setting and age of host sequence as well as age of ore formation

fertile, highly oxidised, saline, and sulphate-rich connate fluid (Muchez et al. 2010). This is regarded as the agent that scavenged Cu and Co from the sediments themselves and transported them as chloride complexes during diagenesis and oxidative alteration of the host rocks. Precipitation of these metals would occur as the fluid reacted, either with more reduced strata (containing organic carbon or diagenetic framboidal pyrite), or with a second, more reduced, fluid (El Desouky et al. 2009). Metal zonation, which is a feature of mineralisation throughout the Copperbelt (Annels and Simmonds 1984; Binda 1994; Porada and Druschel 2010), could, at least in part, be a product of the variable reduction potentials of metals such as Cu, Co, Pb, and Zn. An early or late diagenetic model for the origin of stratabound mineralisation in the CACB is consistent with the fact that it pre-dates the major period of compressive deformation that affected the entire region during the Lufilian Orogeny (590–510 Ma; Rainaud et al. 2002). Copper sulphide mineralisation at Konkola Mine has been Re–Os dated at 816 ± 62 Ma by Barra et al. (2004), which is regarded as synsedimentary to very early diagenetic. A Re–Os age of 800 Ma has also been presented by Muchez et al. (2015) for the syndiagenetic stage of the mineralisation during rifting and basin development, but the same authors also present evidence for epigenetic, synorogenic mineralisation at 682 ± 28 Ma. Molybdenite-monazite veins, which crosscut the mineralisation hosted by earlier chalcopyrite veins, have been dated by Re–Os ages of the molybdenite at 512 ± 1.2 Ma and 502.4 ± 1.2 Ma, respectively (Torrealday et al. 2000). Rainaud et al. (2005) also confirmed a major metamorphic pulse associated with regional mineralisation, dated at 512 ± 17 Ma on monazite from the Kalumbila deposit in northwestern Zambia.

Cu–Co mineralisation in the Zambian Copperbelt is concentrated in the 5–15 m thick 'ore shale' units of the Proterozoic Lower Roan Group, lying above variably thick metaconglomerate and arkosic meta-arenites. Sulphides occur in coarser-grained relict beds in weakly deformed rocks and along cleavage surfaces or metamorphic quartz(-carbonate) veins developed during deformation in more highly deformed rocks. Cu–Co sulphides are observed to replace euhedral to anhedral non-framboidal, probably diagenetic pyrite (McGowan et al. 2006). An inverse relationship between anhydrite (and scapolite as the metamorphic successor) and sulphide abundance in many layers suggests that sulphide sulphur was supplied in part by the reduction of anhydrite.

The 'ore shale' in these deformation zones is commonly much more highly recrystallised than underlying and overlying rocks and it displays well-developed shear textures both megascopically (Fig. 23.4) and microscopically. These zones generally contain coarse-grained Cu-Co sulphides and enhanced Cu–Co grades compared with the surrounding 'ore shale' (Sweeney et al. 1986). Such sulphide dissolution

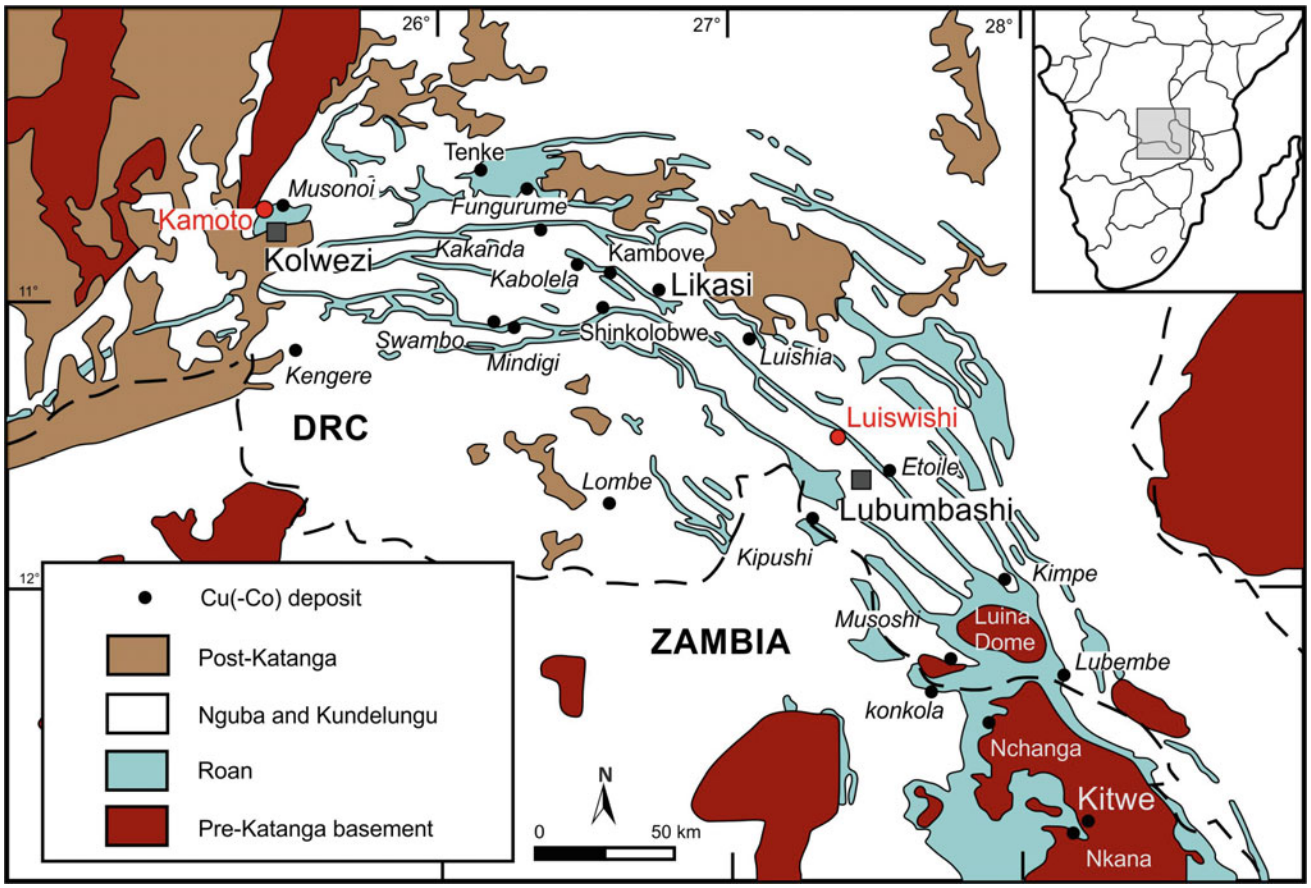

Fig. 23.3 Overview map of the Central African Copperbelt (after Cailteux et al. 2005)

during metamorphism, which has rarely been documented in other areas, may have occurred in the Copperbelt because of the unusually high salinity of the metamorphic fluids (Muchez et al. 2008; El Desouky et al. 2009; Eglinger et al. 2014). Such high salinity could have been produced by the dissolution of evaporites, which are much more common within the Proterozoic sequence than is commonly recognised.

The evaporite horizons may also have formed planes of weakness, along which low-angle faulting took place (Kampunzu and Cailteux 1999). New deposits may be found in stacked thrust repeats of 'ore shale' units along décollement zones and within other stratigraphic units of the Roan Group, which have undergone intensive shearing (Binda 1994; Kampunzu and Cailteux 1999; Jackson et al. 2003; Bernau et al. 2013). Some authors also hint that the Copperbelt may be allochthonous (Cailteux et al. 1995, 2005; Hitzman 2000; Hitzman et al. 2012; Wendorff 2001; Wendorff 2005a, b).

The formation of the vast, stratiform Cu–Co clastic sediment hosted ores of the CACB is also considered to have formed in an environment influenced by the Snowball Earth (El Desouky et al. 2010; Hitzman et al. 2010). The Katangan host sediments were deposited on a fertile Palaeoproterozoic basement representing a magmatic arc terrane (Rainaud et al. 2005). The Grand and Petit Conglomerats of the Katangan sequence (Wendorff 2005a, b), for example, represent glaciogenic sediments capped by carbonates (Wendorff and Key 2009), which are correlated, respectively, with the Sturtian and Marinoan events (Windley 1995). An influx of oxide-soluble Cu and Co, perhaps derived from the local basement, might have occurred as diagenetic fluids migrated along growth faults and through the basin during the post-glacial stages of deposition. The precipitation of ore sulphides would have occurred when the metal-charged oxidised fluids encountered reduced sediments or fluids either during diagenesis (Hitzman et al. 2010) or at epigenetic stages during orogenesis (Sillitoe et al. 2010).

Sillitoe et al. (2010) pointed out that the generally accepted timing of sediment-hosted, stratabound copper and associated cobalt mineralisation in the CACB, as well as in the geologically similar and broadly contemporaneous copper-silver prospects of Botswana and Namibia (the KCB; Borg 1988a, b; Borg and Maiden 1989), has changed radically over the past 50 years: from strictly syngenetic, during host-rock sedimentation (Garlick 1961), through early diagenetic, prior to final sediment cementation and compaction (e.g., Bartholomé

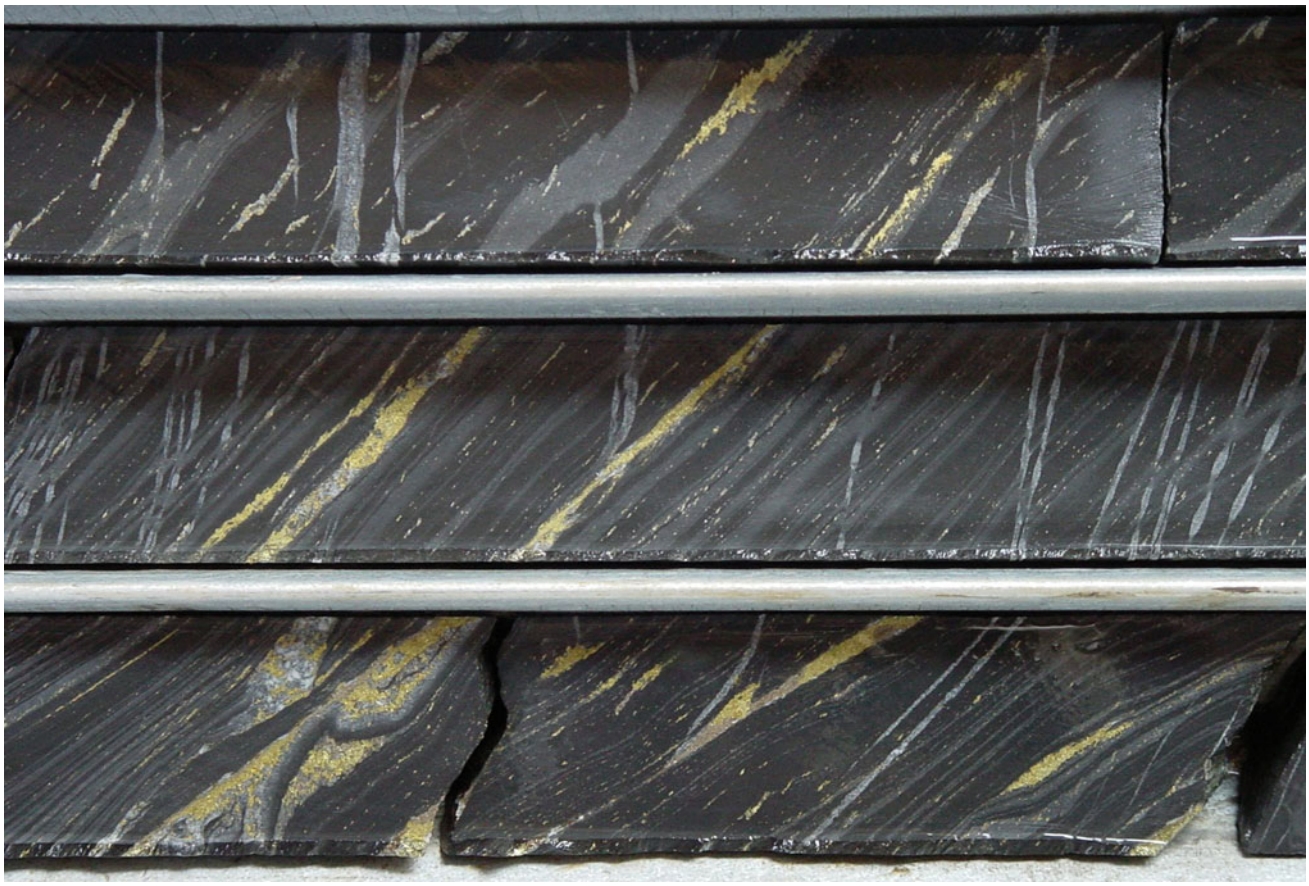

Fig. 23.4 Complex ore textures in drill core from Nchanga mine, Zambia, with chalcopyrite disseminated and in stringers and veinlets in metapelite crosscut by later calcite veins. Core diameter is NQ (47.6 mm). Photograph by Gregor Borg

et al. 1973; Annels 1974; van Eden 1974; Sweeney and Binda 1989; Sweeney et al. 1991; Cailteux et al. 2005), to the currently popular view of multiple, diagenetic to epigenetic stages spanning protracted basin evolution, including final tectonic inversion (e.g., Borg and Maiden 1989; Selley et al. 2005; El Desouky et al. 2009; Hitzman et al. 2010; Sillitoe et al. 2010).

Sillitoe et al. (2010) used field observations of sulphide-bearing veinlets that ubiquitously accompany the widespread stratabound, disseminated sulphide mineralisation as evidence to show that prelithifaction copper introduction is unlikely throughout the CACB of Zambia and the Democratic Republic of Congo as well as in the Kalahari Copperbelt of Botswana and Namibia. Sillitoe et al. (2010) argue that most of the veinlets are integral parts of the Cu–Co–Ag ore bodies, and formed essentially contemporaneously with the spatially associated, disseminated sulphide minerals, a view tacitly adopted by McGowan et al. (2006) in their study of the Nchanga deposit.

Both the disseminated and veinlet mineralisation styles lack ductile deformation features in many Congolese deposits but are variably metamorphosed and deformed in some deposits in Zambia, Botswana, and Namibia. In conjunction, these observations suggest that the stratiform copper ore bodies were the result of massive saline fluid expulsion by hydraulic fracturing after mafic magmatism (~765 to <715 Ma), most probably spanning peak Damara-Lufilian metamorphism and ductile deformation (~530 Ma) and continuing in places until at least ~500 Ma. Thus McGowan et al. (2006) claim that basin inversion, contractional tectonism, and associated uplift and exhumation, and not the earlier extension and rifting, seem more likely to have been the ultimate drivers for the fluid mobilisation and expulsion.

Sillitoe et al. (2017) characterised two intimately associated mineralisation styles of the sediment-hosted stratiform Cu–Co deposits and prospects of the CACB: disseminated sulphides and sulphide-bearing quartz-carbonate veins and veinlets (Fig. 23.5). The genetic model of disseminated sediment-hosted mineralisation that formed during diagenesis in a rift setting, possibly in multiple events, is in contrast to the idea that the veinlet-hosted mineralisation was either derived from remobilisation of the disseminated sulphides during the Lufilian collisional orogeny or introduced at broadly the same time(s) as the disseminated sulphides

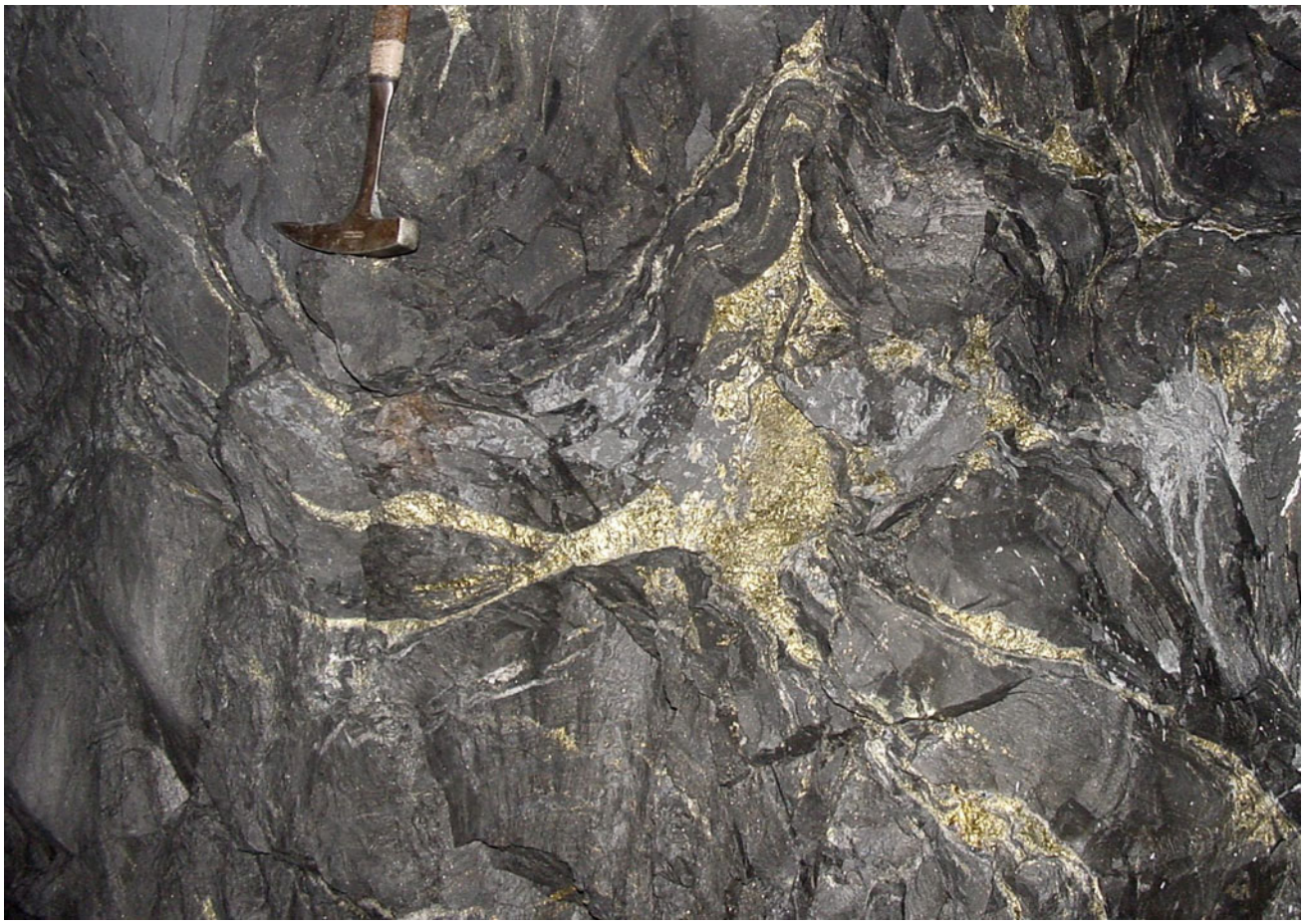

Fig. 23.5 Breccia- and vein-hosted chalcopyrite ore in dilatational fold structure, superimposed over disseminated laminated ore in metapelite underground at Nchanga Mine, Zambia. Photograph by Gregor Borg

during diagenesis and subsequent orogeny. Based on results of 15 Re–Os molybdenite age determinations from Cu–Co deposits and prospects across the Zambian part of the CACB, Sillitoe et al. (2017) provided strong evidence that both the disseminated and veinlet mineralisation styles were indeed generated together, but in a 50 myr or even shorter Cambrian time window (~540–490 Ma) during the later stages of the Lufilian Orogeny.

23.3 The Kalahari Copper Belt in Namibia and Botswana

The Late Mesoproterozoic Kalahari Copper Belt (KCB) has been recognised and named as such by Borg and Maiden (1989) and is laterally the most extensive copper-dominated metallotect of SW Gondwana. It represents the second-largest copper metallotect in Africa, second in size and metal endowment only to the CACB in Zambia and Zaire. Together, both of these metallotects represent the largest sediment-hosted stratabound copper province in the world (Sillitoe et al. 2010). The KCB extends from the Sinclair region in southern Namibia via Klein Aub, Dordabis, Witvlei, and Eiseb in Central and Central Eastern Namibia to Ghanzi, Lake N'Gami and the Goha, Gobatsa, and Shinamba Hills in the Chobe region in western, central, and northwestern Botswana (Fig. 23.6). A huge number of copper occurrences and copper showings are located along the entire outcropping part of the KCB, and even more copper mineralisation has been identified in exploration drilling, both in exposed parts and in parts under extensive cover by young Kalahari sediments. Copper has been mined in Namibia at the Sinclair Mine, at Klein Aub Mine from 1966 to 1987 (5.5 Mt at 2.0% Cu, 50 g/t Ag, with 7.5 Mt

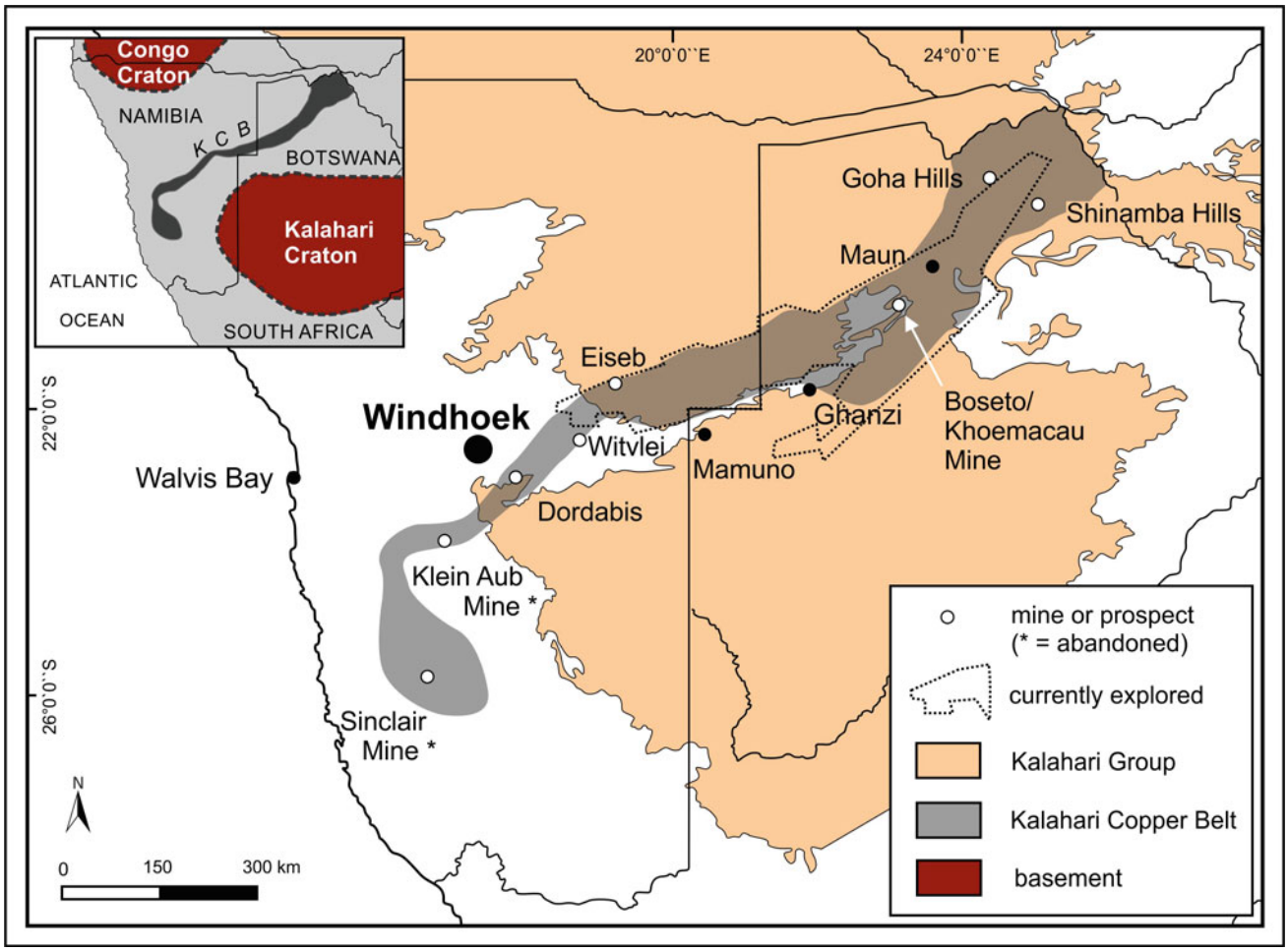

Fig. 23.6 Overview map of the Kalahari Copper Belt, which is orientated along the western and northeastern margin of the Kalahari Craton. Mineralised subprovinces, abandoned and producing mines are indicated. Geometry and extent of KCB adapted from Borg (1988a, b, 1995), Borg and Maiden (1989), and Lehmann et al. (2015)

pre-mining reserves), and, to a smaller extent, as erratic pieces of native copper at Dordabis (Schneider and Seeger 1992). Six small ore bodies, the largest up to 5 Mt, have been reported from the Witvlei area in central eastern Namibia, but mining has not exceeded initial trials (Ruxton and Clemmey 1986). In Botswana, copper-silver ore was mined at Boseto Mine between 2012 and 2015, when financial challenges led to the closure of the mining operation. A new mining operation is currently being developed in form of the succeeding Khoemacau Mine (www.cupriccanyon.com) in the Lake N'Gami region and the currently known reserves are shown in Fig. 23.7.

The general age of the rock sequence of the KCB has been variably attributed to the Late Mesoproterozoic (e.g., Borg and Maiden 1989; Kampunzu et al. 2000), to the Neoproterozoic (e.g., Schwartz et al. 1995; Sillitoe et al. 2010; and Piestrzynski et al. 2015), or comprising a lower, Late Mesoproterozoic and an upper Neoproterozoic part (Mapeo et al. 2000). The stratigraphic units and their probable correlations have been summarised by Rankin (2015) and are shown in Fig. 23.8. However, absolute age data on rocks from the units of the KCB range between 1200 and being just younger than 800 Ma (summarised in Schwartz et al. 1996; Kampunzu et al. 2000; Mapeo et al. 2000; Modie 2000; Rankin 2015), thus documenting a Late Mesoproterozoic to Early Neoproterozoic age for the rock units of the KCB (Fig. 23.8). Mineralisation, however, especially the post-tectonic replacement ores as well as the common

	tonnage (Mt)	Cu grade (%)	Ag grade (g/t)	Cu metal (Mt)	Ag metal (t)
Banana Zone	155	0.85	11	1.32	1,705
Chalcocite Zone	33	0.64	6	0.21	198
Mango NE2	21	1.69	18	0.35	378
Ophion	14	1.00	12	0.14	168
Plutus & Petra	82	1.31	13	1.07	1,066
Selene	17	1.00	16	0.17	272
Zeta UG	19	1.54	25	0.29	475
Zeta NE	25	2.19	44.6	0.55	1,115
Zone 5	100	1.95	19.9	1.95	1,990
Zone 5 North	17	2.27	43.4	0.39	737,8
Zone 6	17	0.86	4	0.15	68
Total	**500**			**6.59**	**8,172.8**

Fig. 23.7 Recent exploration results, including inferred tonnages, grades, and contained metal from the Botswana portion of the KCB (adapted from www.cupriccanyon.com, last access 10.04.2017). Note that the quoted and calculated reserves are not in accordance with any reporting standard

fracture- and vein-hosted ores (Figs. 23.9 and 23.10), is to a large extent epigenetic, and thus Neoproterozoic Pan-African to even Early Cambrian mineralisation ages apply. A relatively poorly constrained Pb-isotopic age of 600 Ma for the epigenetic mineralisation at the Klein Aub deposit in Namibia has been reported by Walraven and Borg (1992) as a first attempt to provide absolute age data on mineralisation. Relatively new Re–Os dating on a few mineralised samples has provided absolute age data but also delivered relatively ambiguous results (Hall 2013). Hall (2013) reports average Re–Os model age dates of 1012 ± 17 Ma and 914 ± 4 Ma for two samples of vein-hosted bornite and chalcopyrite, respectively, from the Zeta deposit, Lake N'Gami region, which is in general agreement with the age of early diagenesis, when the first diagenetic veinlets could have formed in this part of the KCB (Hall 2013). The third age from a vein-hosted chalcopyrite sample from the Plutus prospect, Botswana, yielded a Re–Os model age of 496 or even 442 Ma, depending on the applied $^{187}Os/^{188}Os$ ratio (Hall 2013). While the former would be roughly contemporaneous with a late stage of the Damaran Orogeny, the latter age date would even post-date any know deformation age of this orogenic event (Gray et al. 2006). However, such a late mineralisation age would be in agreement with the relative age date from textural evidence at the Klein Aub Mine, where the replacement of hard diagenetic pyrite cubes (Figs. 23.11 and 23.12) by soft but cube-shaped preserved chalcocite cubes (Figs. 23.13 and 23.14) document a metallogenetic emplacement of the chalcocite ore subsequent to peak deformation (Borg 1988a, b, 1995) adjacent to a major Damaran wrench fault system (Borg et al. 1987). Obviously one of the persisting challenges and open questions of this metallotect is the more precise and absolute dating of the timing of metallogenic events.

In a broad sense, the units of the KCB are located between the western and northwestern margin of the older Kalahari Craton and the younger Pan African Damara Belt in Namibia and Botswana. The detailed geometry and boundaries of these different units have recently been defined more precisely by comprehensive interpretations of new, high-quality airborne aeromagnetic data and stratigraphic comparisons and correlations (Lehmann et al. 2015; Rankin 2015; Gill 2016). However, the problems of stratigraphic correlations and precise age relationships, especially of the upper part of the stratigraphy of the KCB in Botswana, which are largely due to very limited surface exposure, is not really relevant to the metallogenic processes that have led to the formation of the mineralisation and ore deposits within the KCB.

The lithostratigraphic succession, structural, and geological setting of the exposed and drilled volcanosedimentary subsections of the KCB all display a striking similarity along the belt. The correlation of the volcanic units (Goha Hills, Kgwebe, Langberg Formations and Oorlogsende Porphyry Member, Nückopf Formation rhyolites) and the Ngwako Pan Formation with the Doornpoort Formation, and the D'Kar, Mamuno and Chinamba Formations with the Klein Aub Formation, and the use of directional, low-pass filtered

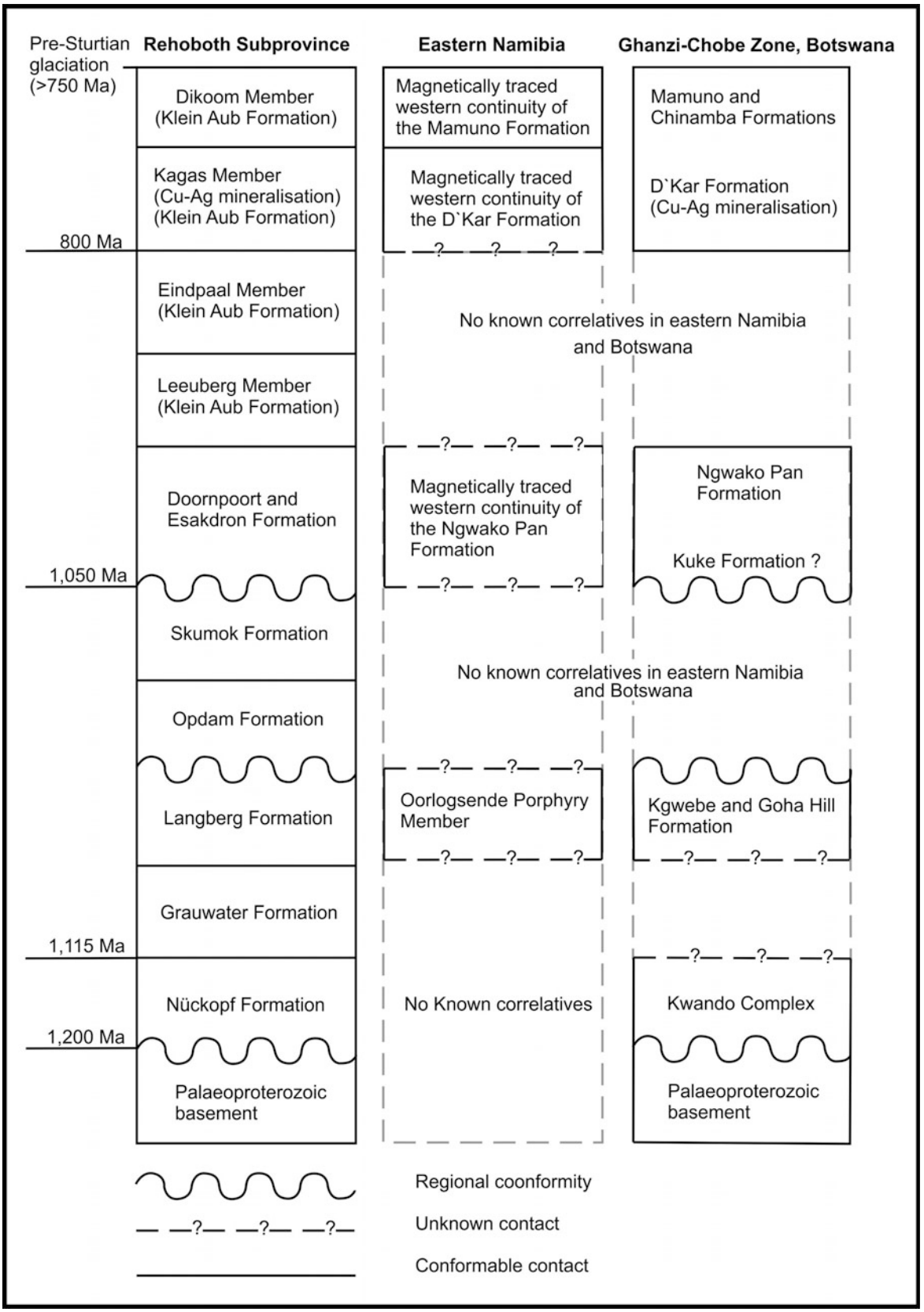

Fig. 23.8 Ages, stratigraphic subdivisions, and tentative correlation of litho- and chronostratigraphic units of the KCB and of relevant basement and cover units (from the compilation by Rankin 2015)

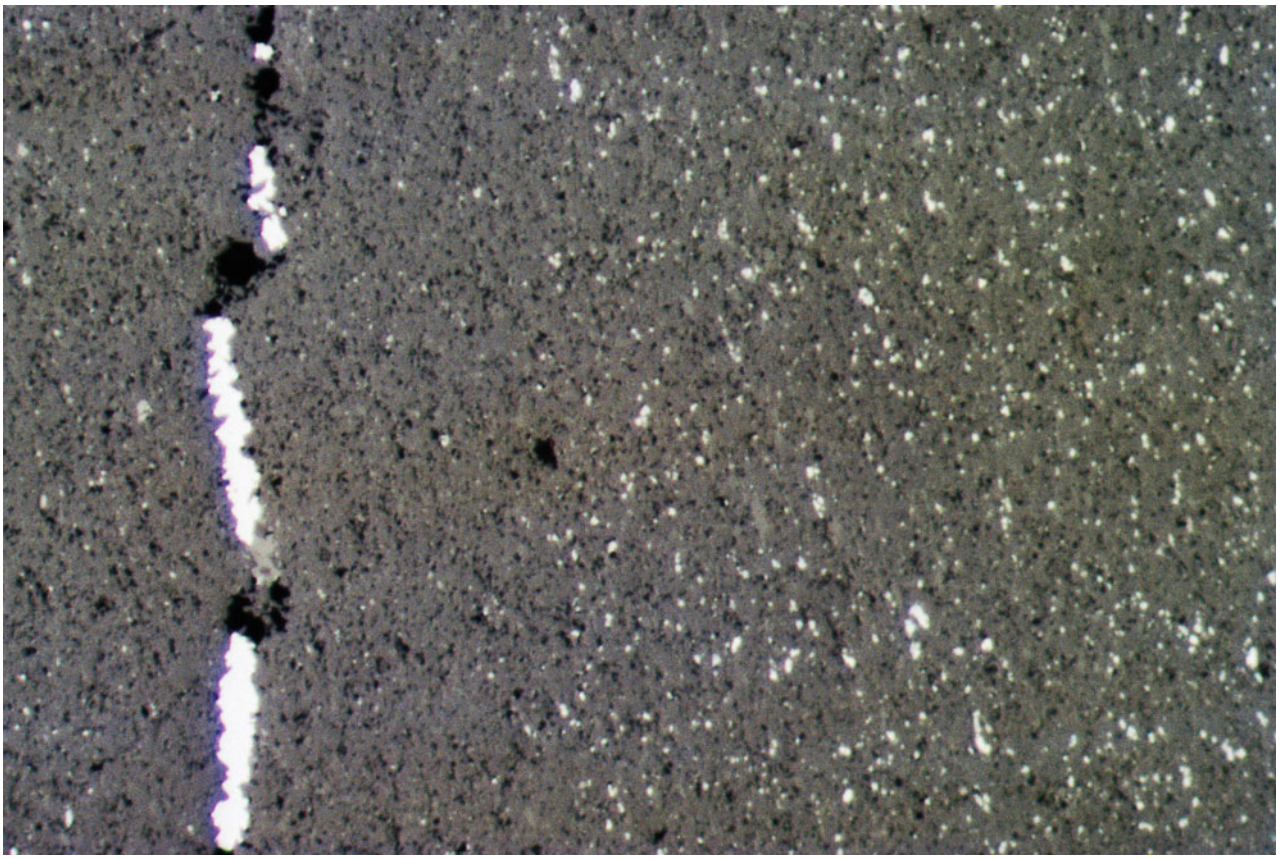

Fig. 23.9 Klein Aub Mine, Namibia. Photomicrograph, reflected light, polished section of disseminated chalcocite (white) in pores of metasiltstone with later remobilisation into veinlet with surrounding depletion halo (width of view 2.2 mm). Photograph by Gregor Borg

images from new aeromagnetic interpretations, suggest that the Ghanzi-Chobe Belt forms a continuous linear to curvilinear belt that can be traced from the Rehoboth subprovince through Botswana to the eastern Caprivi (Rankin 2015). The subprovinces, which represent at least partly discontinuous, fault-bounded sub-basins, all feature a common lithostratigraphic succession. The individual basins have been filled by basal portions of bimodal, basaltic and rhyolitic, subaerially extruded lava flows, as indicated by clastic sediment-filled and sediment-covered flow top breccias. These lower volcanic portions were deposited intercalated with and overlain by continental clastic red bed sequences, which comprise fault-scarp-related alluvial fan conglomerates, braided stream sediments, and aeolian sandstones, some of which directly cover flow top breccias, as in some Doornpoort metabasalts in the Klein Aub area in Central Namibia. During deposition these clastic continental red bed sediments were overlain by fine-clastic, chemically reducing, low-energy sediments such as tidalites, shallow submarine sandstones, and shallow water carbonates, including algal mat biostromes and locally laterally linked hemispheroidal stromatolites. Evaporites have occurred both in the continental red bed succession as documented by preserved hopper crystals in fine-grained meta-arenites (Namibia) and in laminated metamorphosed siltstone-mudstone units (Lake N'Gami, Botswana), where rhomb-shaped quartz-calcite pseudomorphs after gypsum crystals occur in their characteristic orientation, perpendicular to sedimentary layering in coarser laminae (Figs. 23.15 and 23.16, and summarised in Fig. 23.17). Diagenetic pyrite cubes of various sizes are common in the basal, chemically reducing grey-green units of the upper part of the stratigraphy.

Fig. 23.10 Klein Aub Mine. Chalcocite (white) in brittle fractures superimposed on disseminated chalcocite in meta-arenite and metapelite (underground 450 m level, stope 600 W). Photograph by Gregor Borg

The plate tectonic setting of the KCB has also been a matter of debate for some time. A diachronous, laterally progressing failed continental rift from Southern Namibia through Central and eastern Namibia and northeast-wards into and through Botswana has been proposed by Borg (1988a, b) and adopted by a number of other authors (Modie 1996, 2000; Hall 2013; Rankin 2015; Gill 2016) based on lithological and structural field geology and, at the time available, absolute age data. In contrast, Watters (1977), Becker and Schalk (2008), and Kampunzu et al. (2000) favoured a magmatic arc setting, based on geochemical signatures of the igneous rocks, although this is not in agreement with field geological evidence such as volcanosedimentary environments and the lack of intermediate magmatic rocks.

These 'fertile' metallogenic ingredients include sufficient volumes of suitable source rocks. These occur as extra-basinal rocks, in a faulted and shear-zone dissected older basement that includes mixed mafic, intermediate, and felsic magmatic rocks, and as intra-basinal rocks, with abundant mafic volcanic rocks that show signs of leaching and metal depletion (Borg and Maiden 1987). The lower part of the lithological basin fill has provided an oxidising fluid reservoir during active rifting stages and an oxidising rock volume during epigenetic stages for eventually chemically oxidising, chloride- and possibly sulphur-bearing, metalliferous fluids that were stored and channelled towards suitable trap sites. The chemically reducing, pyrite- and sulphate-bearing grey-green fine-clastic, low-energy sedimentary rocks were both chemical traps, causing pyrite-, anhydrite-, and carbonate cement-replacements, and also fluid-dynamically more impermeable rocks, which were more amenable to competent fracturing and veining during late diagenesis and especially later orogenic deformation. It is striking to see that the mineralised portions of the KCB all

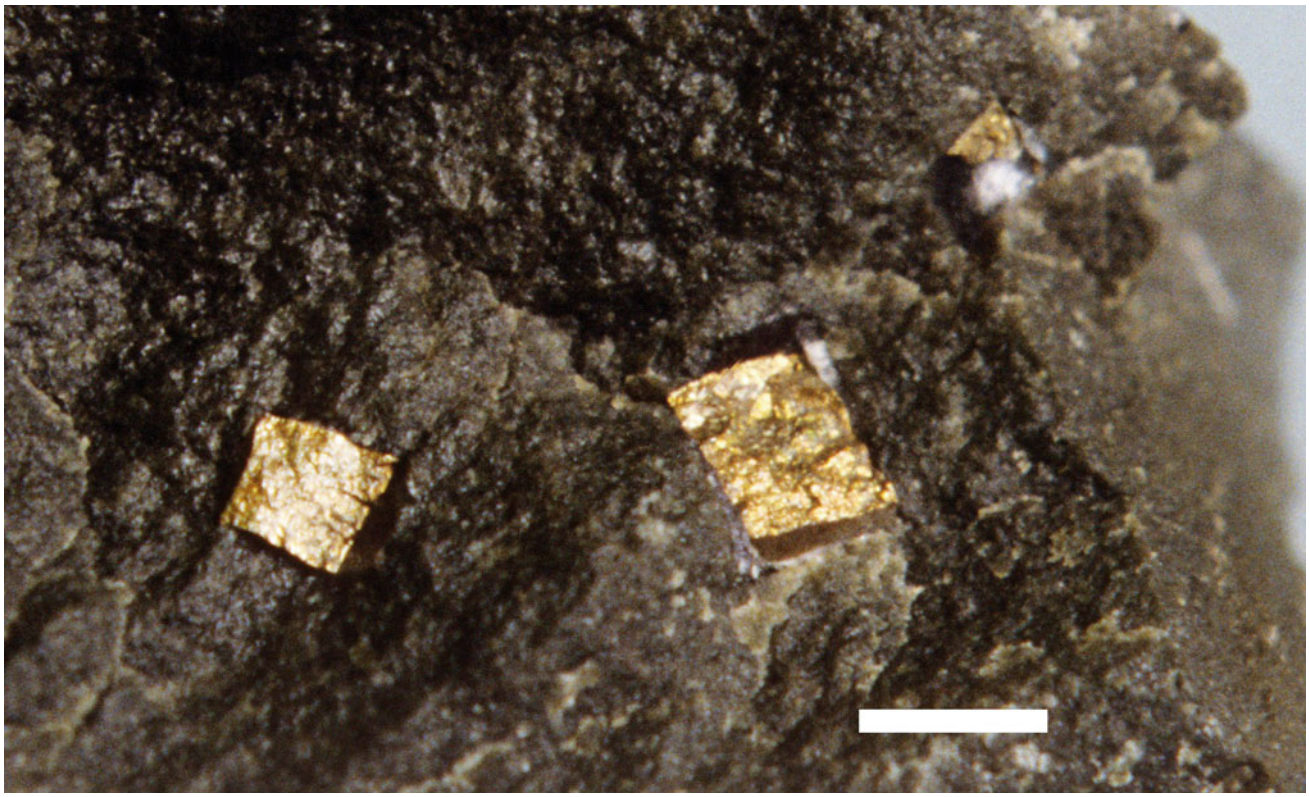

Fig. 23.11 Klein Aub Mine. Sharp angular pyrite cubes (golden-yellow) in barren meta-arenite layers adjacent to chalcocite ore body (underground 600 m level, stope 200 W). Compare with schematic diagram in Fig. 23.17. Scale: 5 mm. Photograph by Gregor Borg

contain disseminated mineralisation preferentially in the coarser layers and laminae of bedded siliciclastic rocks with superimposed fracture-hosted and vein-hosted mineralisation in the more competent layers. Sulphur sources have been provided by evaporitic sulphate minerals in the lower red bed portion, locally in the chemically reduced low-energy sediments and by abundant pyrite in the chemically reduced clastic sediments. This proposed model of sulphur sources has been supported by sulphur isotope data from Klein Aub Mine and Witvlei in Namibia (Ruxton 1986; Ruxton and Clemmey 1986) as well as from the Boseto Mine in Botswana (Hall 2013), documenting bacterial sulphur reduction from basin-internal sedimentary sources.

While initial, at least partly synsedimentary or groundwater-delivered, metallogenic explanations (Ruxton 1986; Ruxton and Clemmey 1986; Schwartz et al. 1995) have not been supported by evidence or other authors, there is understandable debate about whether the two observable styles of mineralisation stem from a first, diagenetic stage plus an epigenetic orogenic or late-orogenic stage (Borg 1988a, b; Borg and Maiden 1989; Schwartz et al. 1995) repeated later by Gorman et al. (2013), Morgan et al. (2013), or whether both styles may have formed simultaneously during a single late epigenetic stage (Sillitoe et al. 2010). However, both ore textural evidence and absolute age dating support a two-stage model of emplacement of mineralisation, as will be explained below.

The type of mineralisation is predominantly sediment-hosted stratabound copper with appreciable amounts of silver and traces of gold, and locally some rare anomalies of Platinum Group Elements in Namibia (Borg et al. 1987) and rare occurrences of Platinum Group Minerals in Botswana (Piestrzynski et al. 2015). Large but erratically occurring lumps of native copper have been found in the Klein Aub region and locally mined or rather collected at Dordabis on a very small scale from metabasalts, where they occur as fillings of amygdales and in breccias of metabasalts that show subaerial flow top breccias. Individual lumps

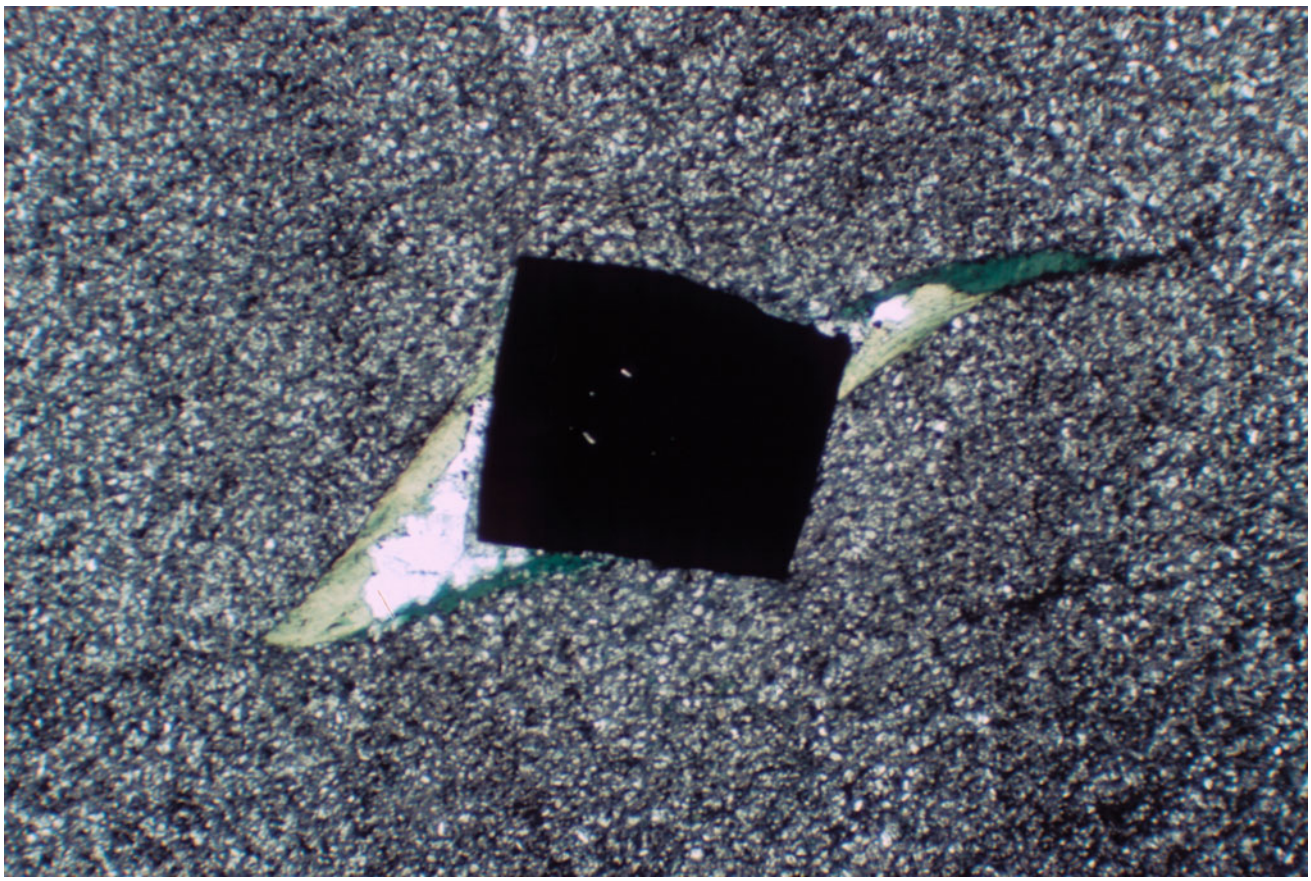

Fig. 23.12 Klein Aub Mine. Photomicrograph, plane polarised light, showing diagenetic, sharp angular pyrite cube (opaque, black) with pressure shadows in metasiltstone (underground 600 m level, stope 200 W), field of view is 10 × 4 mm. Photograph by Gregor Borg

Fig. 23.13 Klein Aub Mine. Angular chalcocite cubes (dark silver) with hematite halos (maroon-red) pseudomorph after pyrite cubes in mineralised meta-arenite (underground 450 m level, stope 600 W, scale is 5 mm). Note that the soft chalcocite has not been deformed and must thus post-date peak deformation. Photograph by Gregor Borg

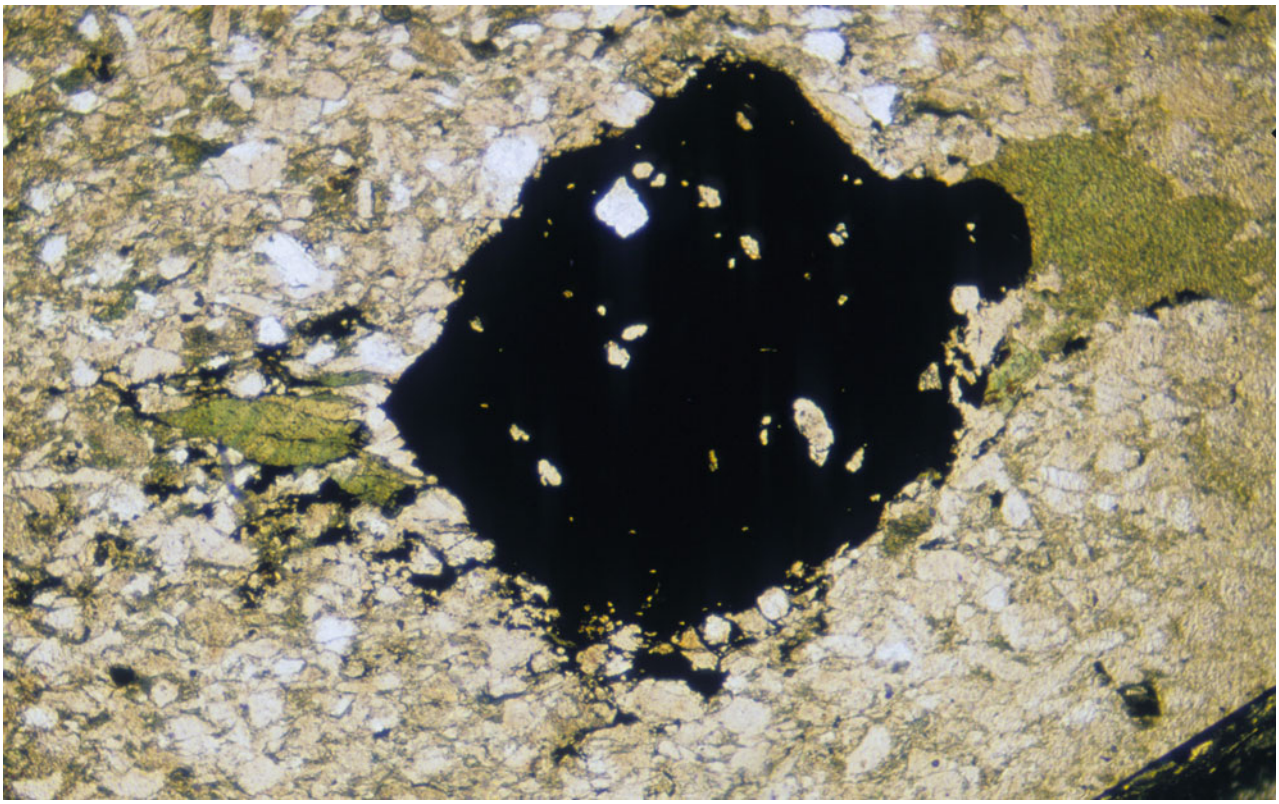

Fig. 23.14 Klein Aub Mine. Photomicrograph, plane polarised light, showing angular chalcocite cube (opaque, black) with pressure shadows in meta-arenite (underground 450 m level, stope 600 W). Field of view is 10 × 4 mm. Compare with schematic diagram in Fig. 23.17. Photograph by Gregor Borg

of copper that were recovered had a weight of up to 1.5 t (Borg and Maiden 1989). The sediment-hosted stratabound ores occur in chemically reduced low-energy metasedimentary rocks and the styles of mineralisation include ores that are finely disseminated, replacing former evaporite minerals and diagenetic pyrite cubes, and—as a substantial portion—as fillings of fractures, veinlets, and larger veins and breccias. The dominant ore minerals are bornite-chalcopyrite, but ores at the Klein Aub Mine were characterised by a strong predominance of chalcocite-digenite ore, which accounted for very high and thus economically advantageous copper grades of up to 58% Cu in the sulphide ore mineral concentrate (Borg and Maiden 1989; Maiden and Borg 2011). However, the ore bodies at Klein Aub Mine are possibly an exception in that they are structurally controlled by a local reverse fault within the northern part of a major wrench fault system, probably of late Damaran origin (Borg et al. 1987; Borg 1988a, b; Maiden and Borg 2011). The role of supergene modifications of the copper ores in Namibia and Botswana has not yet been studied but the presence of local portions of chalcocite-dominated (Cu–sulphide) and native silver-bearing ores in both Namibia and Botswana are strong

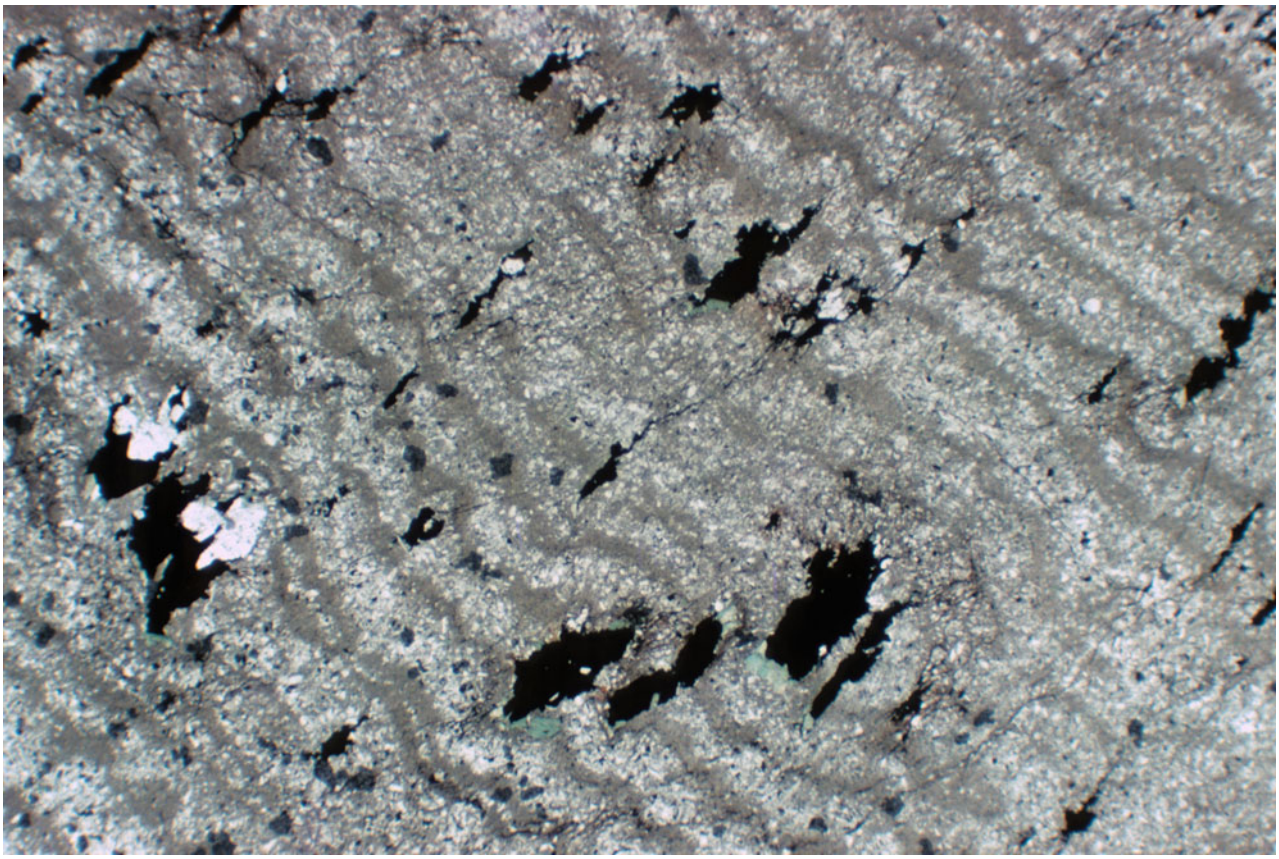

Fig. 23.15 Lake N'Gami area, Botswana. Photomicrograph, plane polarised light, of laminated meta-pelite and fine-grained meta-arenite with partly rhomb-shaped chalcocite (black) pseudomorph after evaporite minerals that had typically grown in the soft sediment, perpendicular to bedding (Borg 1988a, b, 1995; width of field of view is 8 mm). The sulphides also show signs of deformation and elongation into pressure shadows, indicating a pre-deformational origin of the mineralisation. Photograph by Gregor Borg

indications of subsequent, deep surface-related modifications and a possible upgrading of primary Cu–Fe–sulphide ores.

Metallogenetically critical ore textures from the Klein Aub Mine in Namibia have been presented by Borg (1995; Fig. 23.17), which give unequivocal evidence—although obviously no absolute ages—that post-deformational undeformed, hard, diagenetic pyrite cubes with marked pressure shadows in barren sandstone layers (Figs. 23.11 and 23.12), have been replaced by far softer, undeformed pseudomorphs of chalcocite cubes with hematite halos in mineralised layers (Figs. 23.13 and 23.14). Together with fracture- and vein-hosted mineralisation, this documents a partial or total late epigenetic origin of the mineralisation, even post-dating peak deformation during the Damaran Orogeny (Borg 1988a, b; Borg and Maiden 1989; Borg 1995; Maiden and Borg 2011). In the Lake N'Gami area of Botswana, however, rhomb-shaped evaporite minerals have been replaced by copper-iron sulphides prior to deformation and have been at least rotated into the direction of the schistosity, and locally deformed and smeared out during orogenic deformation (Borg 1995; Fig. 23.16).

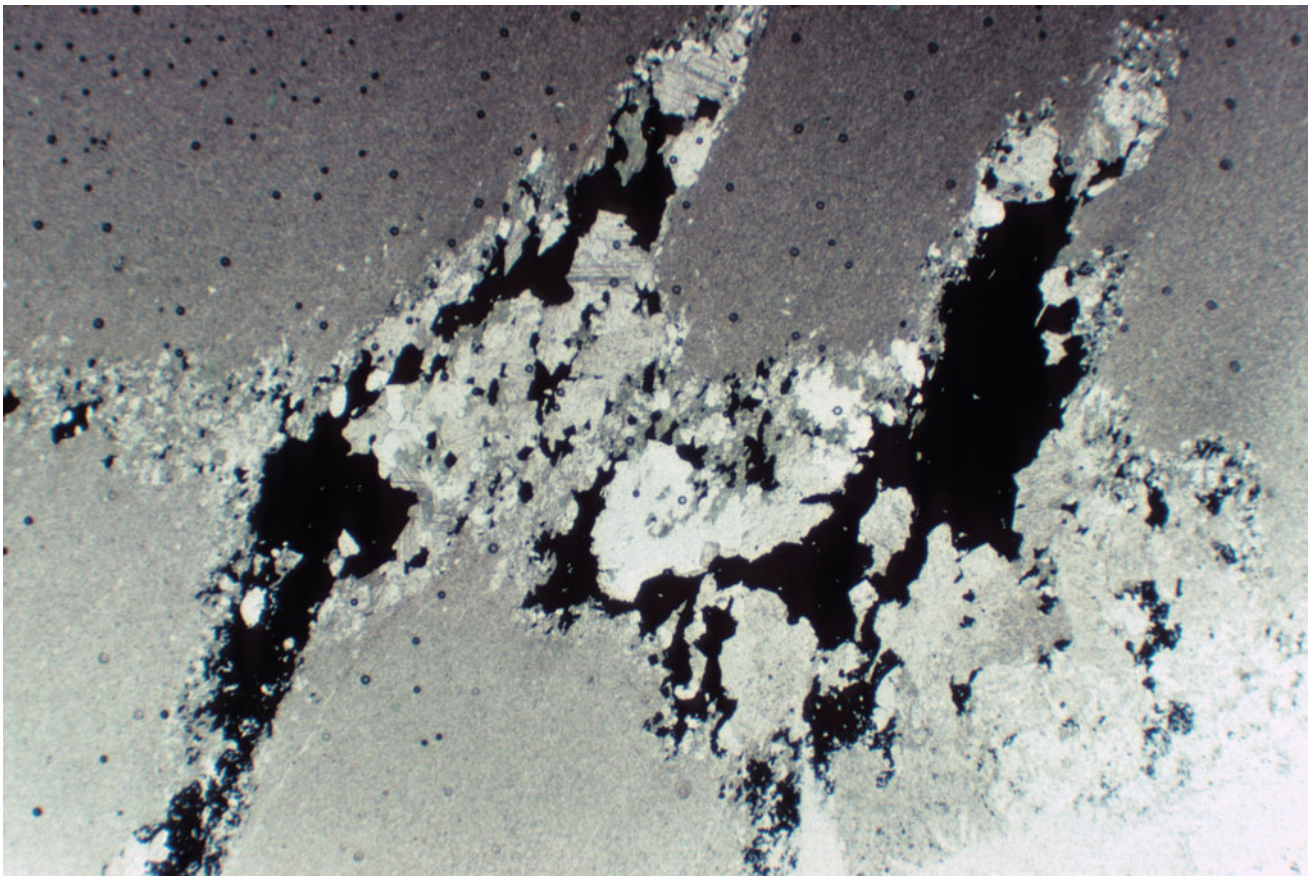

Fig. 23.16 Lake N'Gami area. Close-up photomicrograph, plane polarised light, of lamina of fine-grained meta-arenite in metapelite with two rhomb-shaped chalcocite-(black)calcite-quartz aggregates pseudomorph after gypsum with pressure shadows (Borg 1988a, b, 1995; width of field of view is 3 mm). Sulphides have been deformed and also mobilised into pressure shadows, indicating a pre-deformational origin of the mineralisation. Compare schematic diagram of Fig. 23.17. Photograph by Gregor Borg

Recent and current exploration activities are particularly targeting the Botswana portion of the KCB, but promising exploration results have also been reported from extensive exploration drilling in the Omaheke, Eiseb, Talismanis, and Gobabis regions in Central Eastern Namibia (Gill 2016; Simmonds, pers. comm). In Botswana, 11 target areas have been and are currently being prospected (www.cupriccanyon.com), and these contain substantial inferred resources of various tonnages and grades (Fig. 23.7). Although this does not yet allow any detailed or even J.O.R.C.-compliant estimation of the technical or economic viability of these projects, the overall tonnage of copper-silver ore is in the order of 500 Mt, with some 6.59 Mt of Cu metal and approximately 8170 t of Ag metal contained, which demonstrates the impressive size and metal endowment of this part of the KCB metallotect.

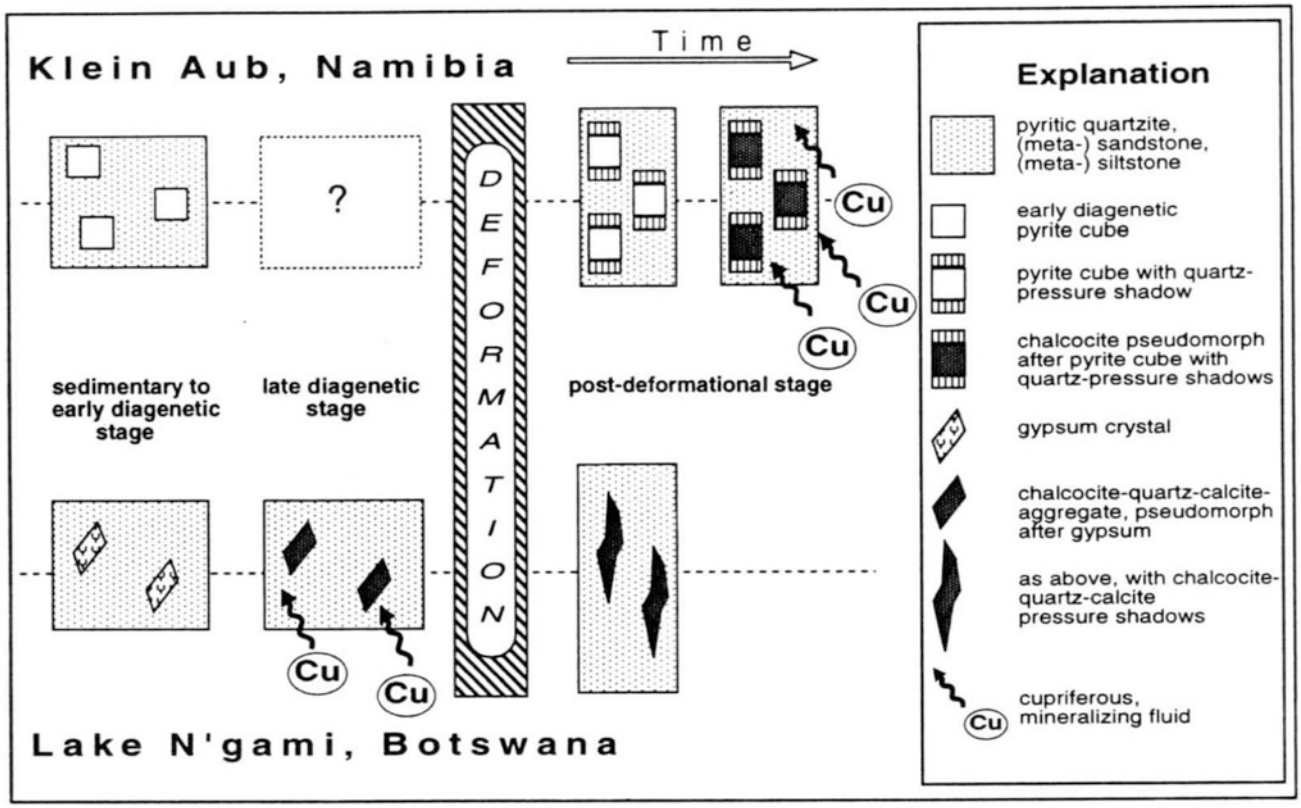

Fig. 23.17 Schematic illustration of unambiguous ore textures from the KCB at Klein Aub Mine, Namibia, and the Lake N'Gami area, Botswana explaining pre- and post-deformational emplacement of mineralisation (from Borg 1995)

23.4 The West Congo Belt

The West Congo Belt can be regarded as the northern continuation of the Kaokoveld part of the Damara Belt on the southwestern African Continent (Boudzoumou and Trompette 1988; Hanson 2003; de Wit et al. 2008; Frimmel 2009). The 'missing' link between the two belts is easily recognisable in South America, where the equivalent Dom Feliciano Belt is host to a number of sediment-hosted base metal deposits and occurrences (Frimmel and Miller 2009).

The Meso- to Neoproterozoic West Congo Belt extends over approximately 1000 km in Northern Angola (including the Cabinda exclave), the Democratic Republic of the Congo (DRC), Congo Brazzaville, and Gabon with its two coast-parallel and one inland branches representing a similar geometry and structure to the Damara-Kaokoveld-Gariep Belt in Namibia, Southern Angola and Northwestern South Africa (Fig. 23.1). During the last half-century, the Meso- and Neoproterozoic Belt, its litho- and chronostratigraphy, and its regional and supraregional correlatives have been described in a number of comprehensive publications by Cahen (1978, 1982), Tack et al. (2001), Frimmel et al. (2006), de Wit et al. (2008), de Wit and Linol (2015), and Cailteux et al. (2015). Basin and fault geometry, volcanosedimentary infill, litho- and chronostratigraphy, and marked clusters of base metal deposits and occurrences characterise this region as a fertile ground for yet undiscovered base metal sulphide deposits. However, deep weathering profiles and relatively dense vegetation cover limit geological exposure and obstruct modern exploration. Relatively few publications have described and summarised ore deposits, prospects and base metal occurrences (Nicolini 1958, 1959; Bigotte 1959; Michel and Scolari 1960; Stam 1960; Maurin et al. 1990, 1991; Maurin 1993), which have been complemented by more recent compilations of metallogenetic maps (Milesi et al. 2004) and geological and ore deposit GIS and databases (Thiart and de Wit 2008). The ore deposit map and GIS of Africa (Milesi et al. 2004; Thiart and de Wit 2008) illustrate the abundance of base metal occurrences in the Damara Belt sensu stricto, and the comparatively smaller clusters or lack of known occurrences, respectively, in the Gariep, Kaoko and West Congo Belts. Those parts of the WCB that are located within the DRC and Congo-Brazzaville include the Comba Basin, which hosts the biggest cluster of known mineral occurrences (Fig. 23.18). The apparent lack

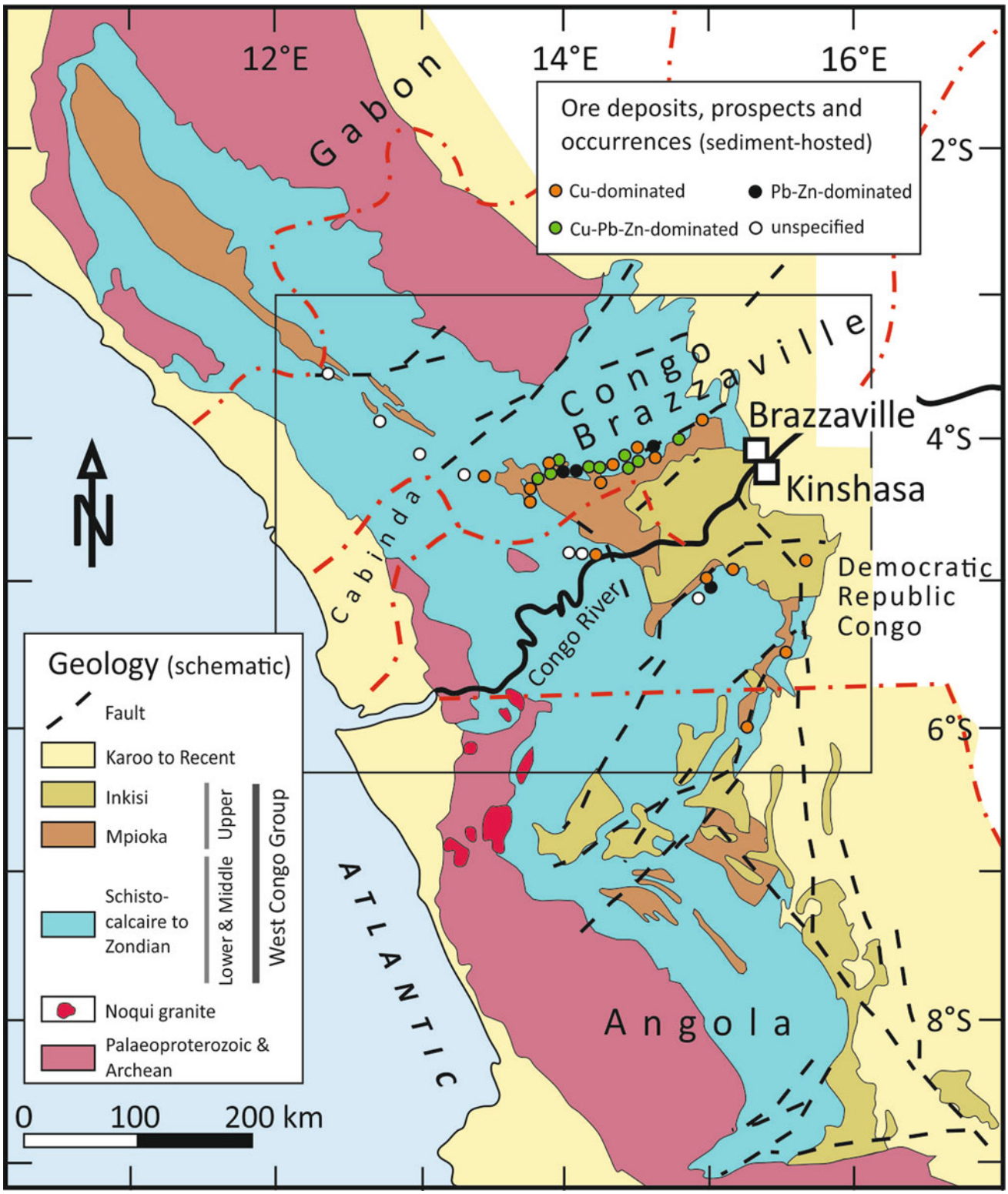

Fig. 23.18 Geological and metallogenic overview map of the West Congo Belt (compiled from Bigotte 1959; Cahen 1978; Maurin et al. 1990, 1991; Maurin 1993; Frimmel et al. 2006; Cailteux et al. 2015)

of known mineral occurrences in the northern, Gabonese part of the belt seems to be based more on a lack of information rather than on geological features. A lithologically and structurally highly fertile setting and major structural features extrapolated across from the originally adjacent S-American plate suggest strong exploration potential in the northern part of the WCB in its own right.

Potential magmatic source rocks for base metal sulphide deposits occur below and within the lower, initial, rift-related portion of the stratigraphy of the WCB (Fig. 23.19). These source rocks include mixed basement rocks of the Archaean and Palaeoproterozoic in the vicinity of deep-reaching basement faults and shear zones, mafic volcanic rocks of the Zandinian Group and Sansikwa Subgroup, as well as felsic volcanic rocks of the Mayumbian Group. The clastic basin fill provides a less fertile but nevertheless significant additional metal source, particularly for Pb and Zn.

This summary of the metallogenic endowment of the WCB does not attempt to list each individual deposit or occurrence but rather focuses on the overall pattern and possible controls on mineralisation. The regional overview map (Fig. 23.18) and the close-up map of the central portion of the WCB (Fig. 23.20), as well as the composite table of chrono- and lithostratigraphy, absolute age data and position of mineralisation (Fig. 23.19), highlight the stratigraphic and regional location of the base metal deposits. Generally, the maps and the stratigraphy follow the subdivisions proposed and established by Cahen (1978, 1982), Frimmel et al. (2006), and Cailteux et al. (2015), but here we group these units slightly differently. The abovementioned authors have given detailed lithological descriptions, which are not repeated here owing to limited space. However, both the maps and the stratigraphic table show that the base metal deposits and mineralisation occur in the upper part of the WCB stratigraphy (Fig. 23.19), where they straddle the boundary between the Schisto-Calcaire Subgroup and the overlying Mpoika Subgroup, but are locally also hosted by the uppermost unit of the WCB, the Inkisi Subgroup. The contact between the Schisto-Calcaire and the Mpoika subgroups is thus obviously of metallogenic relevance, possibly due to lithological, fluid dynamic, rheological and structural, or geochemical controls or to a combination of these. The base metal deposits and occurrences are generally sediment-hosted and occur both as impregnations in clastic meta-arenites and as replacement bodies in carbonate rocks of the upper parts of the stratigraphy, which represents the subsidence and widening part of the basins of the WCB. The ore deposit types can typically be classified as sandstone-hosted, Laisvall-type (Rickard et al. 1979; Saintilan et al. 2015, 2016) or Mississippi Valley Type (MVT) as described comprehensively by Leach et al. (2010). Gradual transitions between both types occur in the WCB and are also generally acknowledged as 'MVT sandstone-hosted' deposits by Saintilan et al. (2016).

The WCB lacks an extensive platformal carbonate unit similar to the carbonate platform of the northern Damara Belt in Namibia. However, a metallogenetically important basinal feature such as the hinge line between the deeper, subsiding basin and the marginal onlap of the sedimentary units onto the stable cratonic shoulders might be inferred from the curvilinear arrangements of ore deposits and occurrences within the WCB (Figs. 23.18 and 23.20). This hinge line is commonly a zone of synsedimentary basin margin faults and offers the potential for synsedimentary and early diagenetic mineralisation. However, such fault structures are typically reactivated during subsequent compressional tectonic stages and, during these stages, also offer possibilities for late epigenetic mineralising events. Besides a stratigraphic position in the upper part of the stratigraphy, there is a spatial and probably genetic relationship between the base metal deposits and faults (Stam 1960; de Boorder 1982) and shear zones (Maurin et al. 1990) as well as breccias (e.g., M'Passa deposit; Buffet et al. 1987). The densest cluster of base metal deposits and occurrences follows a quasilinear west-southwest-east-northeast trend, which appears to be a major sinistral wrench fault system (Maurin et al. 1990). Mineralisation between the deposits of Boko Songho and Mindouli is characterised by impregnations and replacement ores in the vicinity of fault structures and shear zones. In particular, the deposits of Mindouli, Mfouati, M'Passa, and Boko Songho occur in the DRC along the border with Congo-Brazzaville, and these are all hosted in a major transpressional strike-slip fault system (Maurin et al. 1990). The metallogenetic timing of the ore-forming processes has not been dated by absolute measures in any of the deposits within the WCB but rather interpreted from geological and ore textural evidence, also reflecting the metallogenetically favoured models of the respective times of publication. Thus the stratigraphic position of the ore deposits can initially give no more than a *terminus post quem* for the emplacement of the mineralisation. Various metallogenetic models from synsedimentary to early diagenetic—that is, prior to the loss of primary permeability—to late diagenetic replacements of cements in siliciclastic rocks or preferential replacement of intercalated carbonate units, to late epigenetic fault, thrust and shear

Era/ Characteristics	Supergroup	Group	Subgroup/Formation	Main Lithotypes	Carbonates/ Volcanics	Age Dating	Mineralisation
Recent - Mesozoic - Palaeozoic	Post-Cretaceous - Recent						
	Cretaceous			siliciclastic rocks	carbonates		yes
	Karoo			siliciclastic rocks			
Meso- and Neoproterozoic	West Congo Supergroup	West Congo Group	Inkisi Subgroup	siliciclastic rocks		pre-Karoo	yes
						566 Ma	
			Mpoika Subgroup	siliciclastic rocks	carbonates		yes, lower part
			Schisto-Calcaire Subgroup	siliciclastic and carbonate rocks	carbonates	> 635 Ma - 575 Ma	yes, upper part
			Upper Mixtite/Diamictite Formation	siliciclastic rocks	carbonates	635 ± 1.2 Ma	
			Haut Shiloango Subgroup	siliciclastic rocks			
			Lower Mixtite/Diamictite Formation	siliciclastic rocks		750 Ma - 713 Ma	
			Sansikwa Subgroup	siliciclastic rocks and mafic volcanics	basalt		
		Mayumbian Group		felsic volcanics, pyroclastics and siliciclastic rocks	rhyolite	920 ± 8 Ma - 912 ± 7 Ma	
		Zandinian Group		silciclastic rocks and mafic volcanics	basalt	1,000 Ma - 920 Ma	
		Noqui Granites		peralkaline granite		999 ± 7 Ma	
Palaeo-proterozoic	Kimezian Supergroup					≥ 2,100 Ma	
Archean							

Fig. 23.19 Composite stratigraphy of the West Congo Belt with stratigraphic subdivision, metallogenetically relevant host and source rocks and age data. Stratigraphic information and ore deposits after Bigotte (1959), Cahen (1978), Maurin et al. (1990, 1991), Maurin (1993), Frimmel et al. (2006). Age data from Tack et al. (2001), Hoffmann et al. (2004), Frimmel et al. (2006), Kampunzu et al. (2009), and Cailteux et al. (2015)

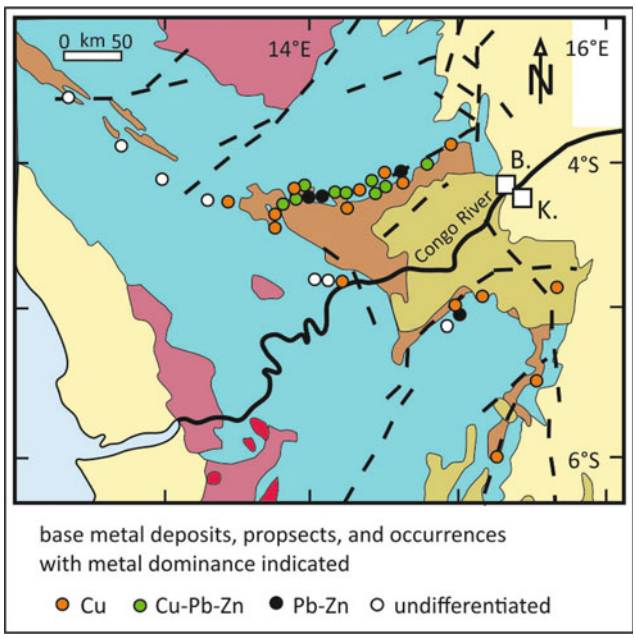

Fig. 23.20 Geological and metallogenic map of the central part of the West Congo Belt. (For stratigraphy and lithotypes, see overview map of Fig. 23.18.) K, Kinshasa; B, Brazzaville

zone-related emplacement from hydrothermal fluids have been proposed.

Absolute age data is comparatively sparse and is summarised in Fig. 23.19. However, the age of the upper part of the stratigraphic units gives a minimum age for the ore deposits, and this is given by the age of the Upper Mixtite/Diamictite Formation at 635 ± 1.2 Ma (Hoffmann et al. 2004; Kampunzu et al. 2009). However, epigenetic emplacement ages during the Pan-African orogenic or post-orogenic stages might apply to some of the mineralisation, but these events have not yet been dated for any of the WCB deposits.

The WCB is thus a major geological terrane, which features all components that make up a fertile sediment-hosted base metal metallotect. These features include a major volcanosedimentary basin, suitable bimodal mafic and felsic volcanic as well as siliciclastic and possibly crystalline basement source rocks, favourable carbonatic and coarse siliciclastic host rocks and fault, shear, and thrust systems that provided potential fluid conduits during various synsedimentary, diagenetic, and late epigenetic stages of the basin evolution. Owing to the thick soil and vegetation cover

of major parts of the WCB, the exploration potential for deeper, blind ore deposits must be considered as substantial.

23.5 The Matchless Belt in Namibia

The Southern Zone of the inland branch of the Damara Orogen in Namibia features the Matchless Amphibolite Belt, which is host to a number of volcanic-hosted massive sulphide occurrences and deposits, two of which are substantial mines: Otjihase Mine and Matchless Mine. The Matchless Belt extends for more than 250 km, trending west-southwest-east-northeast from close to the Atlantic coast, where trial mining has been carried out at the small but well-exposed Gorob Mine and Hope Mine, towards the northeast of Windhoek (Fig. 23.1), but it can be traced even further east magnetically. Volcanic-hosted massive sulphide (VHMS) ore bodies and base metal mineralisation occur in several separate clusters: the Gorob Cluster, Niedersachsen Cluster, Matchless Cluster, and Otjihase Cluster (Killick 2000). Although the deposits are spatially closely related to the Matchless amphibolite, the immediate host rocks are in several cases clastic metasedimentary rocks that enclose and intercalate the mafic volcanic rocks (Killick 2000). However, it is generally agreed that the basalts provided both the metal and heat source for hydrothermal cells and black smoker systems, from which not only Besshi-type massive and laminated sulphides but also local banded iron formations precipitated (Maiden et al. 1986; Breitkopf and Maiden 1988)

The Matchless Belt and its VHMS deposits were extensively studied in the 1970s and 1980s (Goldberg 1976; Killick 1983; Maiden et al. 1986; Klemd et al. 1987; Preussinger et al. 1987; Borg et al. 1987; Breitkopf and Maiden 1988; Klemd et al. 1989; Haeussinger et al. 1993). Reviews (Killick 2000) and modern follow-up investigations have been published on Re–Os dating (McCandless et al. 1998) and alteration mapping by remote sensing (Duke and Paterson 2007). The sulphide ore deposits are generally considered to be volcanogenic in origin and feature asymmetrical footwall and hangingwall alteration (Haeussinger et al. 1993). The effects of orogenic deformation of both wall rocks and ores have been very intense, with strong elongation of wall rocks such as pillow basalts at Gorob (Fig. 23.21) and brecciation, shearing, rotation and recrystallisation of massive sulphide ores at Otjihase

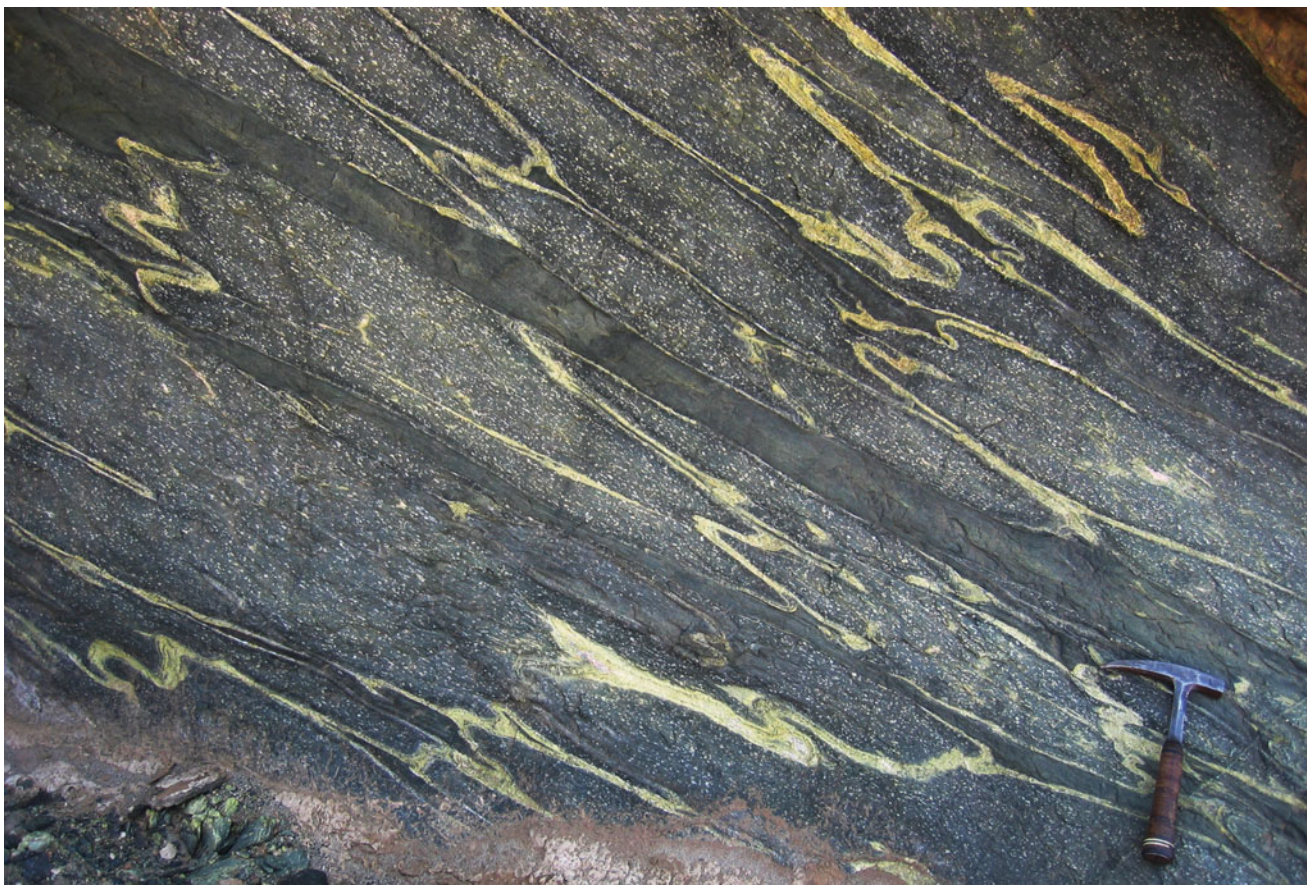

Fig. 23.21 Highly deformed and stretched pillow basalts and crosscutting basaltic sills of the Matchless Belt at Gorob, Namibia. The pillows feature Mg-chlorite-rich chilled rinds and epidotised inter-pillow margins. Photograph by Gregor Borg

Fig. 23.22 Massive sulphide ore (pyrite-chalcopyrite-sphalerite) hosted by the Matchless Belt at Otjihase Mine, Namibia. The brecciated and sheared amphibolite and metapelite show intensive brecciation, shearing, and rotation. Photograph by Gregor Borg

Mine (Fig. 23.22). However, a syntectonic emplacement of the ores, rather than an volcanogenic origin with subsequent deformation, has been offered as an alternative explanation (Maiden 1992).

The ore bodies are comparatively small (<1–30 Mt), are lens-shaped with average thicknesses of 1–10 m, and are typically copper-dominated (Killick 2000). Historical copper grades ranged between 1.3 and 3.9% with additional zinc grades at Otjihase (0.3%) and at the Ongombo prospect (0.01–0.1%). Historical grades of precious metals are reported from Otjihase Mine at 12 g/t Ag and 1.2 g/t Au, (Breitkopf and Maiden 1988) as well as from Matchless Mine with 10–20 g/t Ag and 0.5–1.5 g/t Au (Klemd et al. 1987). Both Matchless Western Extension Mine and Otjihase Mine are currently owned by Weatherly Mining Namibia (www.weatherlyplc.com) but they were put on care and maintenance in 2015. Current proved and probable reserves at Otjihase are 2.2 Mt at 1.48% Cu, 7 g/t Ag and 0.28 g/t Au, and at Matchless Western Extension are 0.3 Mt at 1.83% Cu, all at a cut-off grade of 1% (www.weatherlyplc.com). However, the company reports the measured, indicated, and inferred resources at Otjihase as 8.9 Mt at 1.78% Cu, 7 g/t Ag, and 0.32 g/t Au, and at Matchless Western Extension as 0.5 Mt at 2.77% Cu.

The Matchless Amphibolite Belt with its VHMS deposits in a narrow elongated metallotect, which documents the drifting stage of the Damara aulacogen with submarine, deep-water extrusion of basaltic magma (Killick 2000) and subsequent metallogenically fertile hydrothermal convection cells, which formed several typical high-grade, low-tonnage Cu–(Zn–Ag–Au) sulphide deposits that have been Re–Os-dated to 0.8 Ga (McCandless et al. 1998).

23.6 Ore Deposits of the Coastal Damaran Orogenic Belts

Significant Pb-Zn-Cu-Ba deposits developed in the marginal, fault-controlled portions of the Neoproterozoic Pan-African Damaran Belts, particularly in the northern coastal Kaokoveld Branch and in the southern coastal, Gariep Branch (Borg 2000; Borg and Gauert 2003). The metallogenetically most important deposits and exploration projects are briefly described below.

23.7 The Tsongoari–Omupokko Pb–Cu–Ba–Zn–Ag Prospects, Kaokoveld, NW-Namibia

The Neoproterozoic metasedimentary successions of the Kaoko Belt in the northern part of the Damara Orogen (Fig. 23.1) host several, mainly Pb-, Cu- and Ba-dominated sediment-hosted sulphide ore bodies with characteristics of exhalative deposits, formed during basin subsidence (Frimmel and Miller 2009). These ore bodies occur in metasedimentary rocks of the predominantly metapelitic basin facies rocks of the Swakop Group and were metamorphosed under amphibolite-facies conditions (Franz et al. 1999).

At Tsongoari–Omupokko (Fig. 23.23), several metamorphosed coticule, iron formation, and massive barite horizons with minor base metal sulphides are hosted by Neoproterozoic clastic to chemical metasedimentary rocks of the Ugab Subgroup within the Damara Sequence (Henry et al. 1992; Gauert 2005a). The depositional conditions of the host rocks included environments such as playa lacustrine, coastal or shallow marine, to submarine turbiditic and deep marine. Hydrothermal activity was confined to units that are now metapelitic and metapsammitic rocks, overlying carbonate layers, which represent unconformities expressed as paraconformities (Henry et al. 1992). The mineralised units of the Pb–Cu–Ba–Zn–Ag prospects vary considerably in their modal composition and to a lesser extent in their thickness and overall mineral content (Gauert 2005a). According to Henry and Bentley (1994) and Henry et al. (2002), the Tsongoari and Omupokko mineralised horizons show a vertical and lateral mineralogical variation in stratiform barite-sulphide horizons, containing base metal sulphides and oxides. Vertical changes in mineralogy and geochemistry indicate rhythmic exhalative cyclicity.

Reserves for Tsongoari East and Omupokko are 5.8 Mt of ore grading at 6.4% Pb, 0.8% Zn, 0.4% Cu, and 47 g/t Ag drilled to a depth of 350 m below the surface (Ministry of Mines and Energy of Namibia 1993). These comparatively small tonnages were regarded as not feasible for mining at the time.

Associated mica schist and feldspar-bearing quartzite host rocks contain Mn- and Cu-bearing biotite and muscovite, Zn-bearing amphibole, hyalophane, fluorite, and apatite (Gauert 2005a). At Tsongoari West, mineralisation consists of euhedral spessartine-rich garnet (coticule) and magnetite in a matrix of manganoan amphibole, quartz, mica, and carbonate. Considerable amounts of primary galena and secondary Cu-hydrocarbonate occur at the base of the mineralised horizon, at the transition to the metapelites (Gauert 2005a).

At Tsongoari East and Omupokko, aggregates of galena, chalcopyrite, digenite, and sphalerite occur in laterally and vertically consistent massive barite, magnetite, and coticule horizons, which have a maximum thickness of 10 m and a strike length of 4.5 km. Lateral thinning of the mineralised horizons occurs over tens of metres (Gauert 2005a). Sharp contacts of the mineralised horizons with the hangingwall and footwall suggest rapid transition from exhalative to detrital sedimentation. Barite and Mn-silicate mineralisation are regarded as the more distal exhalative facies types relative to a potential fluid discharge site (Fig. 23.24) and indicate variable oxidation and pH conditions during submarine hydrothermal activity. Field evidence points towards a laterally uniform hydrothermal-sedimentary depositional environment at Tsongoari/Omupokko where the size and geometry of the ore bodies was shaped by the relief of the sedimentary palaeosurface (Gauert 2005a).

Fluid inclusion data from barite and quartz mineralised zones yielded medium temperatures (150–280 °C) and medium salinity (3–7% NaCl-equivalent), characteristic of fluid compositions which are influenced by mixing with meteoric fluids during recrystallisation processes. Sulphur isotope ratios between 13 and 16‰ $\delta^{34}S$ for sulphide and 26‰ for sulphate at Tsongoari East, and −7‰ $\delta^{34}S$ for sulphide and 9.5‰ for sulphate at Tsongoari West, indicate overall strong seawater sulphur input (Gauert 2005a, b). During the Damaran Orogeny (~550 to ~490 Ma), the mineralised sections underwent strong compressional nappe- to thrust-dominated deformation and were metamorphosed to lower amphibolite-facies (~550 to ~610 °C at ~6.5 to ~9 kbar; Franz et al. 1999) as indicated by mineral assemblages in the coticules, without significantly affecting primary geochemical profiles.

Henry and Bentley (1994) and Gauert (2005a) confirmed a vertical cyclic exhalative activity for the Tsongoari West, East, and Omupokko mineralised horizons and similarities with Selwyn-type deposits (Cooke et al. 2000). Laterally, the relative uniform mineralogy of exhalative units over distances of kilometres at Tsongoari suggests a homogeneous depositional environment and quality and quantity of metal charge into the subaqueous metalliferous plume. Sedimentary dilution of the precipitates by detrital components during the main exhalative stage was weak. Cessation of emanative activity, as manifested at the transition of mineralised to barren units, occurred rapidly, possibly controlled by a substantial decrease in the discharge quantity of the hydrothermal feeder channels and the beginning of strong sedimentary input (Gauert 2005a).

Gauert (2005a) proposed the following chronology of events. After continental break-up at ~750 Ma, sedimentation took place during the closure of the Kaoko and Sesfontein rifts (Stanistreet and Charlesworth 2001). Through basin subsidence and dewatering of sediments of the central part of the Kaoko rift, basinal metalliferous brines moved along extension-related growth faults to the submarine sediment surface at the bottom of half-grabens.

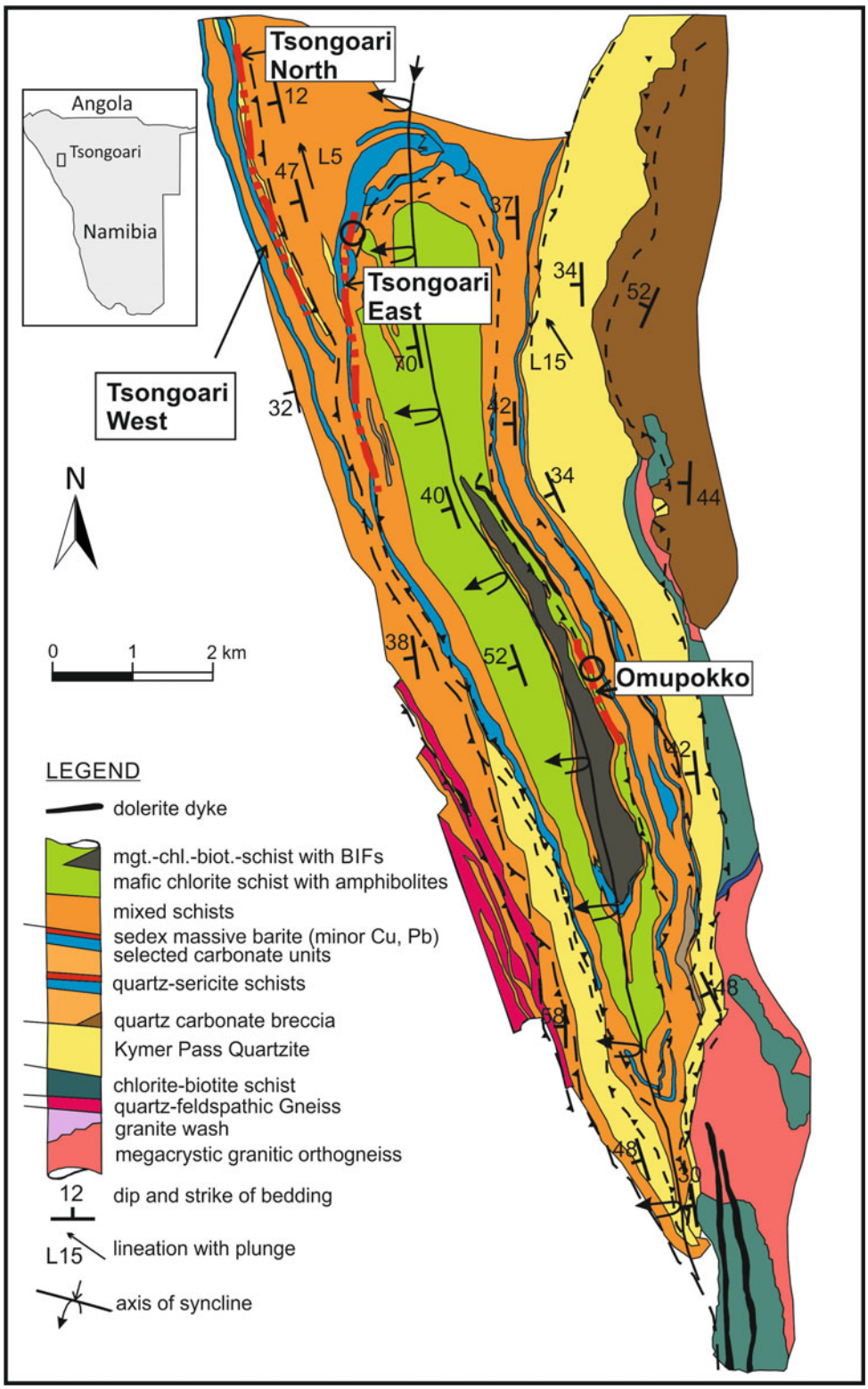

Fig. 23.23 Geological map of the Tsongoari deposit, Northern Namibia (compiled from Miller and Grote (1983), Schmerold (1992), open file map no. 1812 Opuwo, Geological Survey of Namibia, Bernd Teigler, pers. comm., and own mapping results

Extension-related growth faults, possibly at intersections with transfer/transform faults, facilitated the flow of basinal brines through the rift graben deposits and possibly locally also through fault and shear zones within the basement (Cooke et al. 2000). Evaporites within the sediments could have supplied the chloride necessary to leach sufficient metals from the lower volcanic rift graben filling (Chetty and Frimmel 2000). Ba, Pb, and Mn were dissolved from

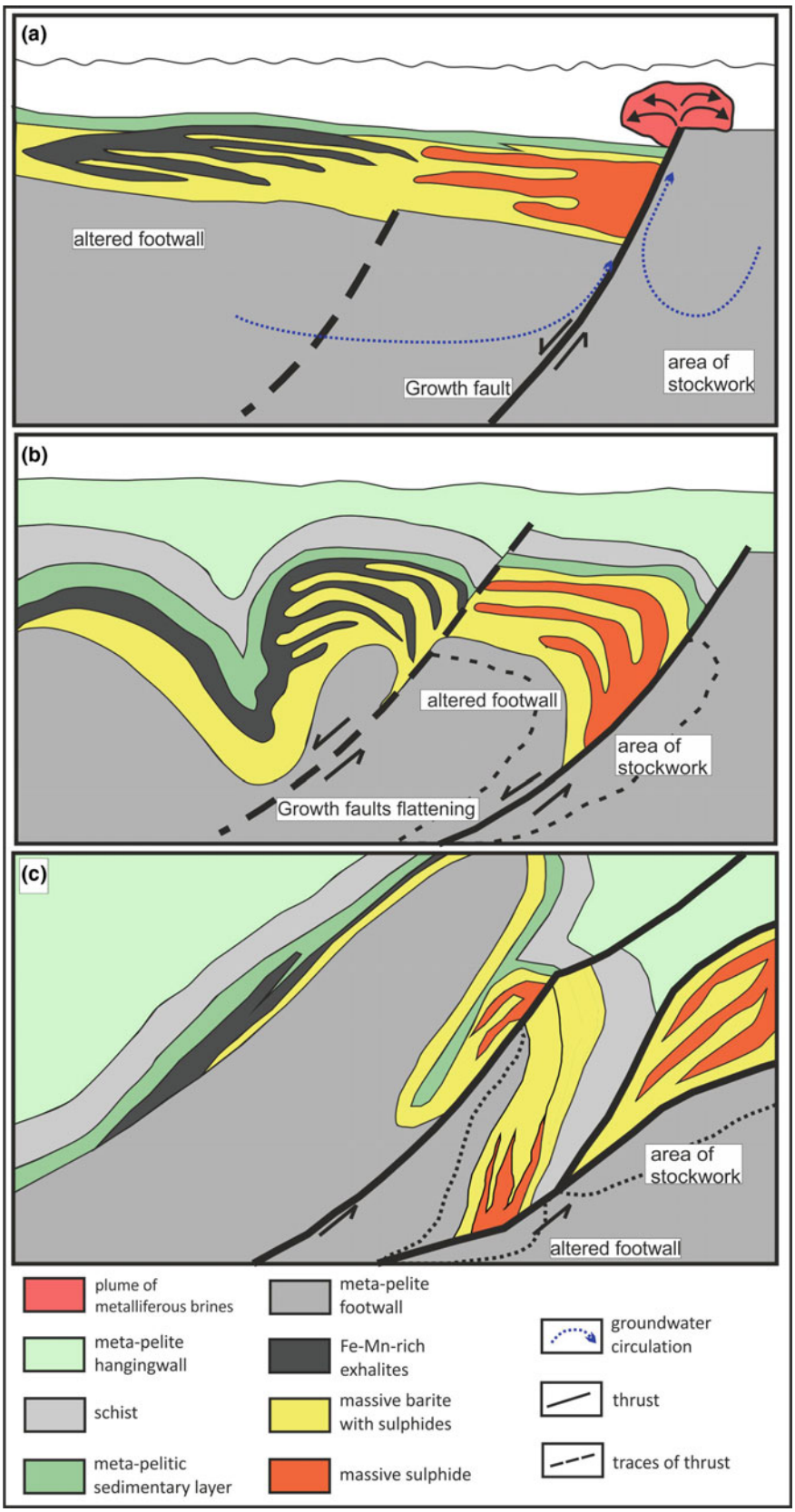

Fig. 23.24 Simplified cross-section and reconstruction of the metallogenesis and deformational evolution of the Tsongoari deposit

arkosic basin fills, whereas Cu was derived from mafic volcanic rocks of the basement. The fluids became buoyant and at the seafloor the depositional environment is postulated as isolated sub-basins within a larger north-northwest-trending depositional trough, with gentle currents and moderate bottom topography. The stratiform and stratabound mineralised beds formed by zoned sulphide, sulphate, oxide precipitation from a reduced brine. The Tsongoari prospects were never mined but represent the distal part of a vigorously emanating mineralising hydrothermal system that accumulated a large resource of sulphate and subeconomic base metal sulphides.

23.8 The Rosh Pinah, Skorpion, Gergarub Pb-Zn District

Regionally, the Rosh Pinah–Skorpion Zn–Pb(–Cu) district with its two operating mines and other promising exploration prospects is currently the only economically successful mining district within the Neoproterozoic Gariep Belt (Fig. 23.1). The metallogenetically fertile base metal district of Rosh Pinah, Skorpion, and Gergarub is shown in the schematic synthesis map in Fig. 23.25. The map has been compiled by Gregor Borg during extensive base metal exploration campaigns in the region. The geology of this

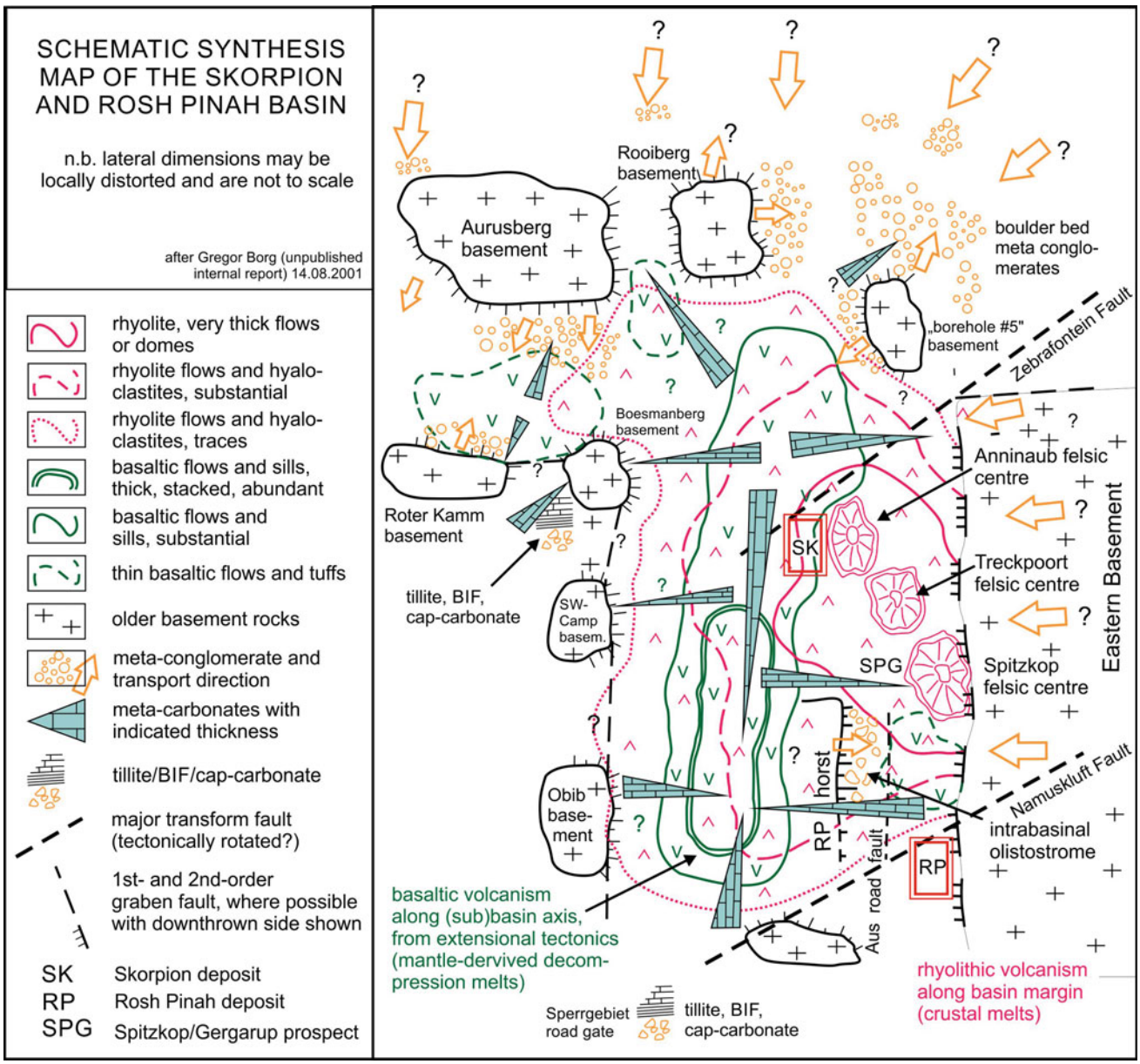

Fig. 23.25 Synthesis map of the Skorpion–Rosh Pinah volcanosedimentary basin showing critical features including bimodal volcanic rocks and metallogenetically relevant fault intersections

Neoproterozoic basin is very complex as a result of the lithologically, magmatically, and structurally highly variable inventory. The normal-fault-bounded graben and half-graben structures of both first- and second-order nature occur in a continental rift setting, bordered both to the north and west by older, Palaeoproterozoic to Early Mesoproterozoic basement, the Sperrgebiet Domain (Diener et al. 2017; Thomas et al. 2017). These older basement blocks, referred to as Aurus basement and Roter Kamm basement in Fig. 23.25, have recently been studied in great detail (Diener et al. 2017; Thomas et al. 2017). According to U–Pb zircon dating (Diener et al. 2017; Thomas et al. 2017), the basement consists of ~2020 Ma calcalkaline granodioritic orthogneiss, intruded by ~1885 Ma old alkali-granite and microgranodiorite and associated with the ~1700 Ma old Aurus Schist. The basement to the east is part of the wider Kalahari Craton margin sequence and Namaqua age rocks and is widely covered by younger Cambrian units.

The basin fill is a Neoproterozoic volcanosedimentary series in which the metavolcanic rocks comprise both basaltic, upper mantle derived, flows and sills as well as crustal melts of rhyolitic composition (Borg et al. 2003; Borg and Kottke-Levin 2007), extruded and deposited predominantly in a subaqueous environment. Characteristic metavolcanic rock types with basaltic composition include lava flows, sills, and very minor dykes of various thicknesses, with flows showing locally well-preserved pillow structures. Characteristic felsic metavolcanic rocks include massive rhyolitic domes and flows, hyaloclastic rhyolitic breccias, and, more rarely, accretionary lapilli tuffs. The rhyolitic magmas had unusually high melt temperatures between 1000 and 850 °C, as indicated by zircon saturation temperatures (Borg and Kottke-Levin 2007). The volcanic rocks were extruded and partly intruded into a mixed clastic-carbonate basin. The range of metasedimentary rocks includes both carbonate and clastic lithotypes. Clastic sedimentary rocks range from olistostromes with blocks up to 4.5 m in diameter and fault scarp-related alluvial fan conglomerates to black shale units deposited in restricted environments in local depot centres. Carbonate rocks include stromatolitic rocks, displaying laterally linked hemispheroidal stromatolites, reworked debris of broken stromatolites, and parallel, finely bedded carbonates of now recrystallised marble, interbedded with thin volcanic ash layers, as documented by the high-K content of former distal pyroclastic ash fall laminae (Lüttich et al. 2002).

The metasedimentary rock inventory documents a graben and half-graben environment with marked lateral facies changes from shallow marginal positions with strong clastic influx during more humid periods to strong carbonate deposition both with and without a strong organic component from the shallow, photic zone to deeper water zones in a tectonically active extensional environment. Magmatism has been markedly bimodal (Borg et al. 2003; Gauert 2005b) with basaltic volcanism focused predominantly along the southern half of the north–south graben axis (Fig. 23.25). Felsic proximal volcanism was focused primarily at and around three major rhyolitic domes (Fig. 23.25) with more distal volcanic facies such as thinner hyaloclastic brecciated flows, thin felsic sills and even more distal pyroclastic ash layers and accretionary lapilli. The tectonic inventory during the depositional period included (now) mainly north–south oriented extensional normal faults, which subdivided first- and second-order grabens and half-grabens as depot centres and basement highs of crystalline basement. These graben-bounding faults have been truncated by major transform-transfer faults (Fig. 23.25), which show up clearly in geophysical surveys and geomorphologically, where they are marked by wide, northeast-southwest-trending valleys. These transform faults have most likely been rotated counterclockwise during later deformation. It is important to note that the north–south orientation of the Rosh Pinah–Skorpion graben systems sensu stricto is deflected in its northern portion, where it has probably been deflected by major basement blocks of the Sperrgebiet Domain (Thomas et al. 2017). As a consequence, the graben system has split into a major west-northwest-east-southeast oriented arm and several very small graben systems between basement blocks trending north–south and eastward (Fig. 23.25).

The most important regional control for the localisation of this hybrid SHMS/VHMS district was the presence of high-temperature rhyolite melts as well as basaltic melts injected into the sedimentary basin fill. This bimodal suite not only provided an anomalously strong heat source to drive hydrothermal convection cells but was also a fertile source reservoir for Cu, Zn, Pb, Au, and Ba (Borg et al. 2003; Gauert 2005b). In more detail, the base metal sulphide deposits at Rosh Pinah and (the hypogene sulphides) at Skorpion, as well as numerous other, smaller base metal sulphide bodies, all cluster at and adjacent to intersections of first- and second-order graben bounding faults with major transform/transfer faults (Fig. 23.25). Here the necessary, deep-reaching, tectonically induced pathways allowed seawater to percolate through sufficiently large and fertile volumes of source rocks, become metal-charged, heated, buoyant and to ascend along fractures to form VHMS/SHMS deposits, both by impregnating and replacing the host sediments as well as partly exhaling onto the basin floor. No similar combination of metallogenetically necessary ingredients and controlling parameters has been identified anywhere else in the Gariep Belt to date.

23.8.1 Rosh Pinah Mine

The hybrid SHMS/VHMS Rosh Pinah Zn–Pb–Ag–(Cu–Au) deposit, situated in the Gariep Belt has been mined continuously since the mid-1960s following its discovery in 1963 (Figs. 23.25, 23.26 and 23.27).

After continental break-up around 750 Ma, sedimentation took place in the Gariep rift basin and the Rosh Pinah graben (Alchin et al. 2005). Early studies gave details on the range of host rocks and wall rocks, distinctly asymmetrical footwall and hangingwall alterations, and generally favoured a VHMS to SHMS metallogenesis for the base metal sulphide ores (Page and Watson 1976; van Vuuren 1986; De Kock 1987; Siegfried and Moore 1990; Clague and Alchin 2001). Feldspathic quartzites occur spatially related to major portions of the base metal sulphide ores and were initially interpreted as meta-arkose (Alchin et al. 2005). However, at least a substantial portion of the K-feldspar represents pervasive and intensive K-alteration that has replaced all detrital plagioclase, especially in the footwall of the mineralisation (Borg and Tornos 2009). Rozendaal et al. (2005) also studied the wall rock alteration haloes, inferring a Ba-rich reducing ore fluid which partly exhaled and partly impregnated the unconsolidated sediment in a subseafloor environment.

Frimmel and Board (2000) characterised two metallogenetically relevant fluid types and these include the pre-orogenic, VHMS/SHMS, rift-related Rosh Pinah ore-forming fluids and orogenic fluids that have been at least partly responsible for remobilisation of a portion of the sulphide ores at Rosh Pinah. Frimmel and Board (2000) found Pb isotopic evidence that the Pb and Zn of the mineralisation were derived from an Eburnian volcanic arc, most probably from the Sperrgebiet Domain of Thomas et al. (2017).

Four ore types can be distinguished at Rosh Pinah mine: (1) banded exhalative base metal sulphides (Fig. 23.28); (2) semi-massive carbonate replacement sulphides; (3) footwall stringer ore; and (4) vein- to shear zone-hosted sulphide ore, all being highly deformed and partly remobilised. Locally the footwall sequence displays silicified breccias (Fig. 23.29), which are generally interpreted to be part of the feeder zones for the SHMS/VHMS mineralisation.

Mineralogically, the banded ore (Fig. 23.28) consists of pyrite, pyrrhotite, sphalerite, and galena in an argillaceous carbon-bearing microquartzite, containing spessartine-rich garnet and chlorite, as well as quartzitic, feldspar-bearing lithic tuffs with abundant hyalophane, albite, Ba- and Mn-bearing biotite and muscovite, fluorite, and apatite, locally being almost completely replaced by pervasive K-Feldspar alteration (Borg and Tornos 2009). The carbonate-hosted replacement ore contains pyrite, interstitial Fe-poor manganiferous sphalerite, galena, chalcopyrite, and alabandite, as well as euhedral pyrite in a matrix of manganoan ankerite, and various Ba-rich carbonates. Quartz-carbonate veins and shear zones host pyrite-dominated ore, but also Zn and Pb sulphide ore, whereas the footwall stringer pyrite ore is richer in chalcopyrite.

The metallogenetic model that incorporates the widest range of observations and phenomena is as follows. Through basin subsidence and dewatering of sediments in the eastern part of the Gariep rift, basinal metalliferous

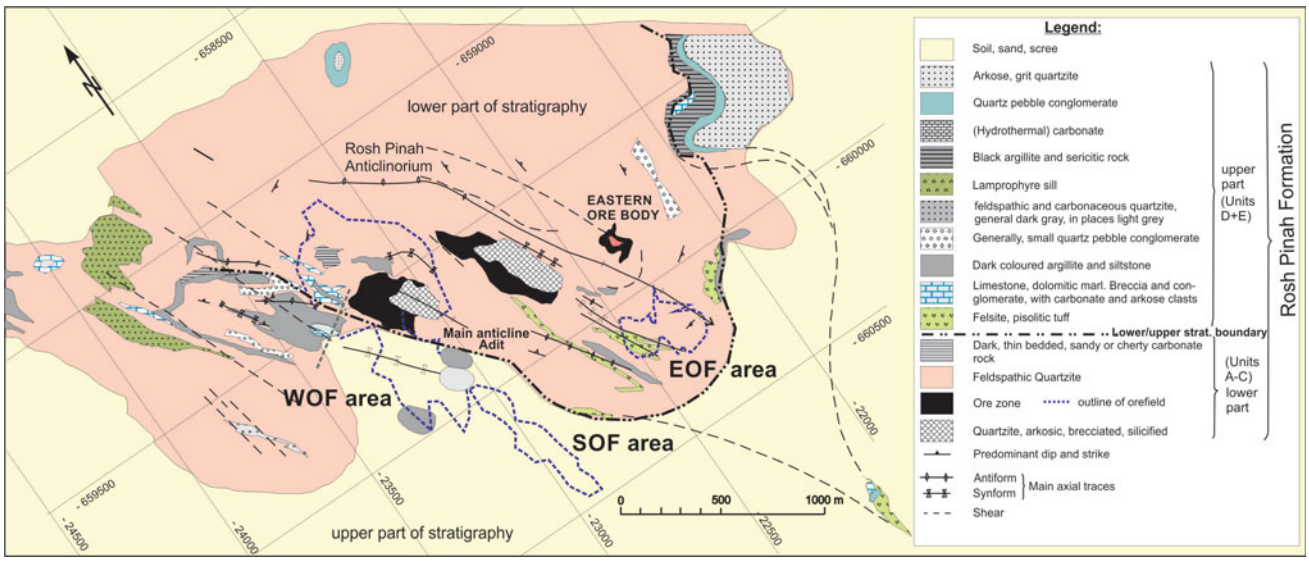

Fig. 23.26 Geological map of Rosh Pinah Mine, showing the various ore bodies and ore fields within the complexly folded and thrusted Neoproterozoic sequence. *WOF* western ore field; *SOF* southern ore field; *EOF* eastern ore field. Modified from van Vuuren (1986), data from Rosh Pinah Zinc Corporation and own data

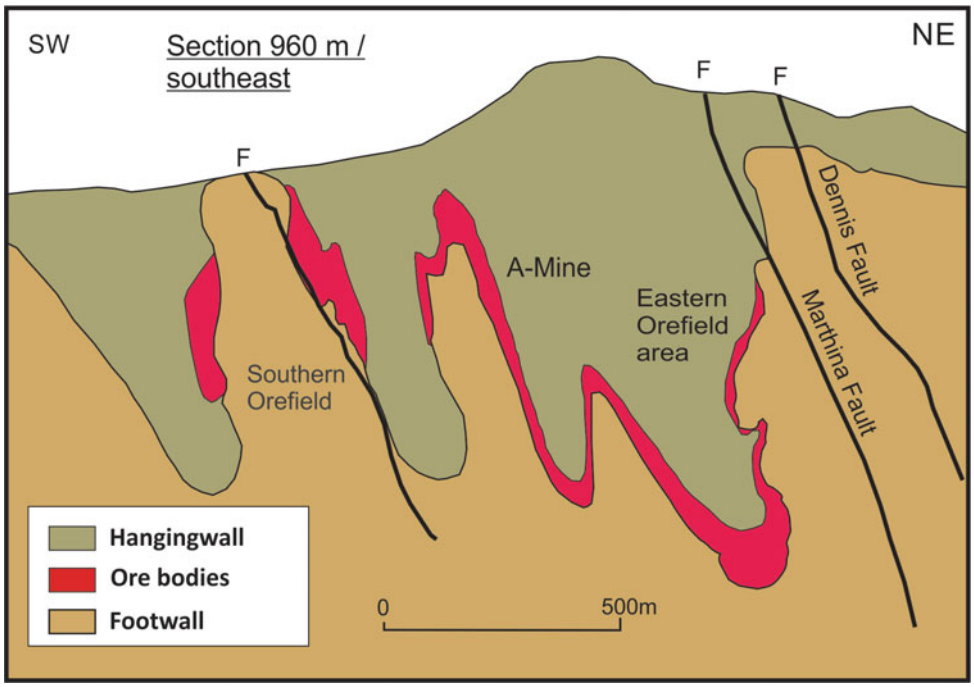

Fig. 23.27 East–west cross-section through Rosh Pinah Mine with typical ore bodies and immediate footwall and hangingwall rocks. Note the thickened fold noses and stretched and faulted limbs, especially in the massive sulphide ore bodies

Fig. 23.28 Banded pyrite-sphalerite-galena ore interlayered with K-feldspar-altered metapelite ('microquartzite'), underground at Rosh Pinah Mine. Photograph by Gregor Borg

brines moved along extensional growth faults, particularly where intersected by deep-reaching transfer-transform faults, to the sediment surface where the brines precipitated sulphides (Fig. 23.28). Growth faults that were active during this period might also have facilitated the locally restricted flow of basinal brines through basement rocks. Heat-driven convecting seawater within the sediments would have supplied the chloride, necessary to leach sufficient metals from the lower volcanic and volcanoclastic rift-fill. Judging from the Ba–Pb–Zn > Cu–Mn ratio of the hydrothermal metallogenetic system, the sedimentary fill and felsic volcanic rocks of the lower rift graben served as the Ba and Pb source, whereas mafic volcanic rocks in the basin and underlying basement contributed some Cu, Pb and Zn to the system.

The ore bodies at Rosh Pinah, originally discovered in 1963, were for a long time Namibia's main Zn producer, providing annually approximately 500,000 t of ore (Ministry of Mines and Energy of Namibia 1992). The remaining reserves are inferred to be in the order of 9 Mt of ore (Rosh Pinah Mine staff, pers. comm.). Total resources at the end of 2004 were 6.48 Mt at an average grade of 9.81% Zn, 2.77% Pb, 0.17% Cu, and 47 g/t Ag. Glencore International Plc's website (2011, 2012) stated a mine production of 89,000 t of zinc concentrate and 16,000 t of lead concentrate in 2011. Locally the ore contains appreciable amounts of Au, both as free gold and hosted in tetrahedrite-tennantite (Mukumbi 2011), although detailed studies as to the siting of the gold have not been carried out yet. The sulphide stringer ore in the footwall (feeder) zone carries approximately 0.35 g/t Au on average, and individual peak concentrations of Au in sulphide concentrate have been as high as 12 g/t (Danie van der Merwe, Rosh Pinah Zinc Corporation, pers. comm.). Our own analytical investigations of sphalerite and galena flotation concentrates from the Southern Orefield (Fig. 23.26) detected between 3.3 and 7.0 g/t of Au in the concentrates from microquartzite ore, massive ore, and arkose ore. Lower Au grades in sphalerite and galena concentrates between 0.5 and 3.8 g/t occur in breccia ore, whereas sulphide concentrates from carbonate ore are generally barren. Intensive on-mine exploration has added 8 Mt to the total mineral resource in 2012. The life of the mine in 2011 was stated as 8.5 years based on zinc concentrate production of 95,000 t per annum (Glencore International Plc 2011, 2012) but it has been steadily projected forward since then.

23.8.2 The Hypogene Skorpion Sulphide Zn (Cu–Pb) Deposit

The Skorpion deposit is a rare example of a siliciclastic-hosted supergene non-sulphide zinc deposit (Corrans et al. 1993; Borg et al. 2003) derived from a hypogene VHMS ore body, hosted in a volcanosedimentary succession of Neoproterozoic age (Fig. 23.29). Uplift and erosion of the host rocks and of the massive sulphides occurred long after the Damara Orogeny (<21 Ma; Kärner 2006) and allowed the supergene circulation of oxidising fluids, which then deposited zinc-silicates and minor zinc-carbonates in the secondary fracture porosity and by replacement of the same volcanosedimentary sequence. The mineralogy of the supergene zinc mineralisation at Skorpion is dominated by sauconite and hemimorphite with minor smithsonite. The supergene body has formed primarily in metavolcanic and meta-arenitic rocks next to a massive barren marble unit (Fig. 23.30). The non-sulphide ore minerals are non-deformed and were precipitated in open spaces, small veins, and replacing feldspar and mica (Borg et al. 2003). The total pre-mining resource of the supergene Skorpion Zn deposit is 29 Mt of ore containing 10.2% Zn, at a 3% cut-off grade (Markus Schaefer, Vedanta Resources plc, pers. comm.). Current ore reserves are in the order of 5 Mt at an annual production rate of 1.5 Mt and 150,000 t of refined Zn metal per year (www.vedanta-zincinternational.com).

However, more relevant to the mineral endowment of SW Gondwana are the relictic hypogene base metal sulphides in the felsic ore horizon adjacent to and below the supergene ore body (Fig. 23.30) down to a depth of at least 800 m. The hypogene ore occurs as stringers, disseminated sulphides, and thin but texturally massive sulphide layers with a systematic vertical zonation (Fig. 23.31). These base metal sulphides occur in metarhyolitic flows and felsic hyaloclastic rocks, structurally below the non-sulphide ore body (Fig. 23.29). The primary sulphide minerals comprise pyrite, pyrrhotite, sphalerite, minor chalcopyrite, and galena. Borg et al. (2004) revealed that the localisation and the metallogenesis of the hypogene sulphide mineralisation at the Skorpion deposit has been, at least partly, structurally controlled. The hypogene Neoproterozoic hybrid VHMS/SHMS Zn–(Cu–Pb–Ba) ores of this district have formed in an environment regionally controlled by the intersection of a first-order basin margin fault with a major transform/transfer fault (Fig. 23.25). Bimodal volcanism, anomalously high heat flow (Borg and Kottke-Levin 2007), and the resulting hydrothermal activity have been the other regionally significant controls for the hypogene ore formation. Age dating of zircon grains from a rhyolitic vesicular flow, extruded approximately contemporaneously with the hybrid VHMS/SHMS ores, yielded a U-Pb zircon age of 751.9 ± 5.5 Ma (Borg et al. 2003). The sulphide minerals are deformed and partly recrystallised, and thus of pre-metamorphic and pre-deformation origin. The rock sequence and the sulphide ores contained therein were affected by a major tectonometamorphic event, the Pan African-Brasiliano orogeny, at approximately 550–545 Ma.

Fig. 23.29 Footwall breccia in silicified meta-arkose stratigraphically below one of the Rosh Pinah ore bodies. Photograph by Gregor Borg

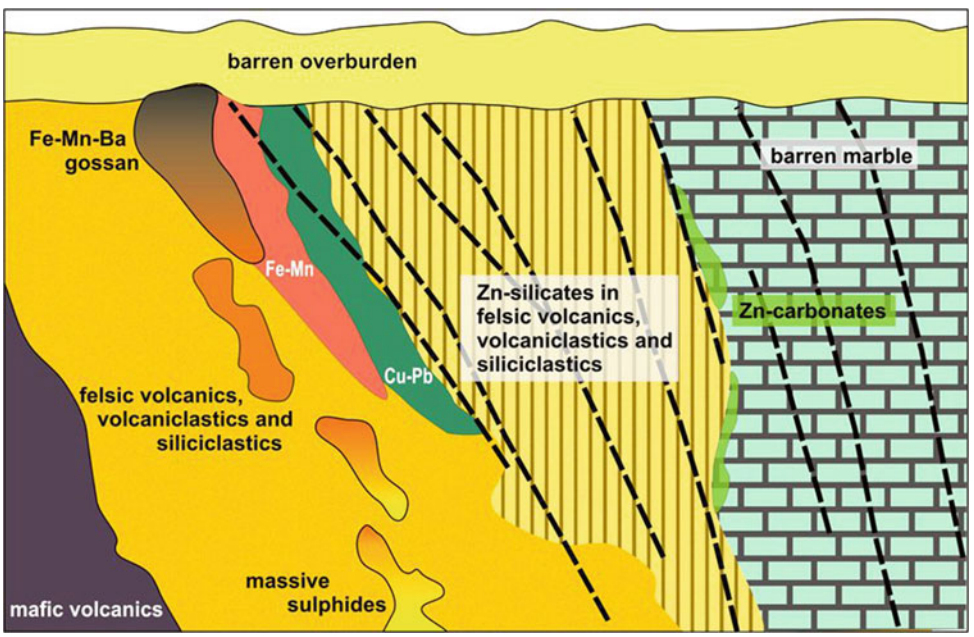

Fig. 23.30 Schematic west–east cross-section through the Skorpion deposit, showing hypogene sulphide mineralisation in the deep western portion below the supergene ore (after Borg 2015)

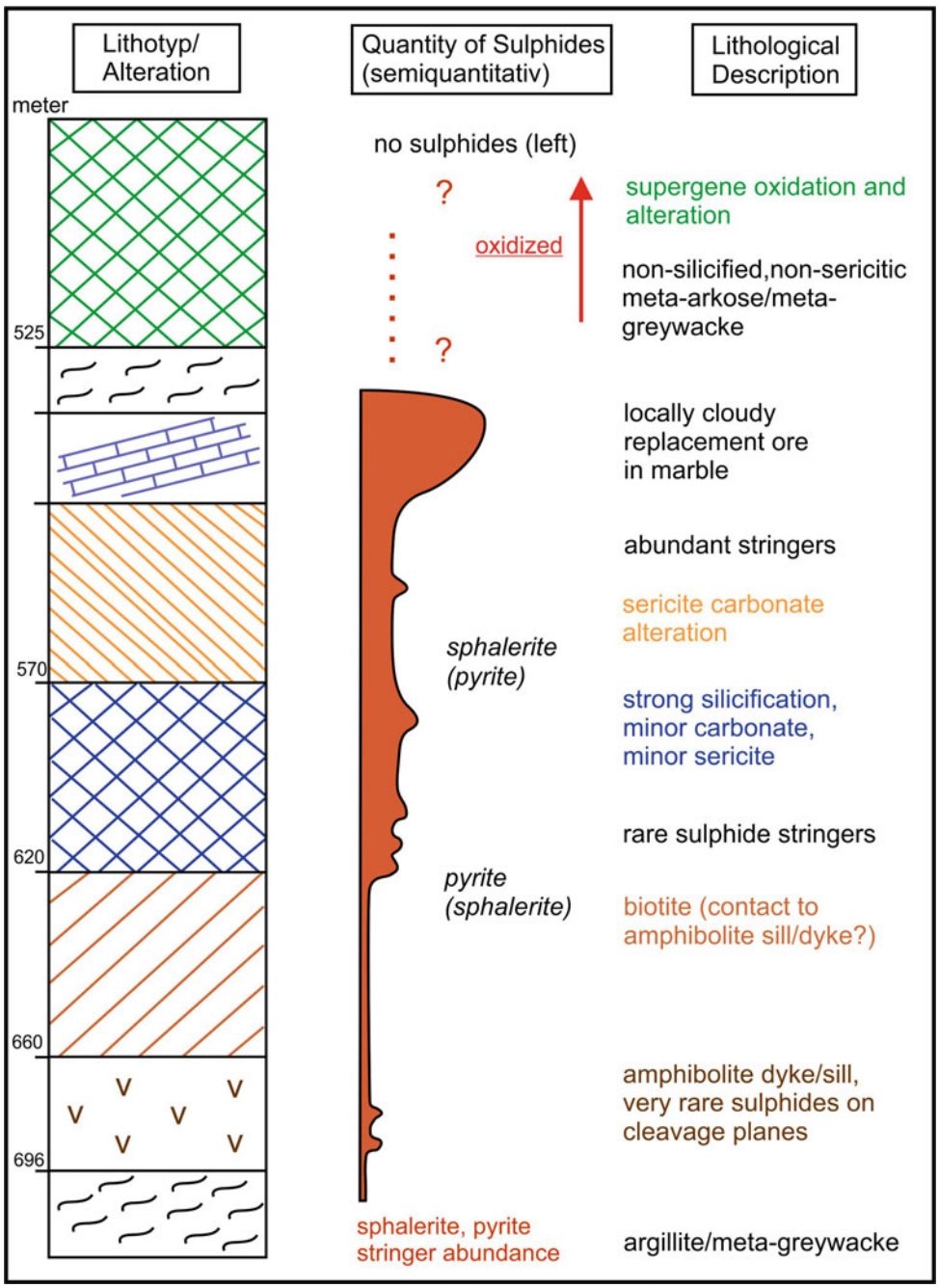

Fig. 23.31 Schematic borehole profile through the Skorpion sulphide ore body, showing systematic vertical VHMS zonation in the deeper part of borehole SD 107

Metamorphism reached uppermost greenschist to lowermost amphibolite-facies.

23.8.3 The Gergarub Pb–Zn Prospect

The Gergarub deposit, initially referred to as Spitzkop/Gergarub, is a newly discovered Pb-Zn deposit within the Gariep Belt, found in 2008, approximately between Skorpion Mine and Rosh Pinah Mine (Fig. 23.25) and it was undergoing a feasibility study until 2014. The deposit was discovered beneath 60–100 m of alluvial cover and extends to a depth of approximately 530 m (Enviro Dynamics 2014).

The Gergarub deposit is hosted by the Rosh Pinah Formation, similar to both the Skorpion and Rosh Pinah deposits (McMillan 2005). The host rocks of the Zn–Cu–Pb mineralisation are predominantly fine- to medium-grained meta-greywacke and subordinate felsic hyaloclastic rocks (Figs. 23.32 and 23.33). Locally the sphalerite occurs intergrown with blade-shaped barite (Fig. 23.34).

Fig. 23.32 Drill core from the sulphide ore at the Gergarub prospect, showing rich disseminated to semimassive pyrite-chalcopyrite-sphalerite ore in sheared and metamorphosed hyaloclastic rhyolite. Borehole SPDD 31 at approximately 462 m depth, core diameter NQ (47.6 mm). Photograph by Gregor Borg

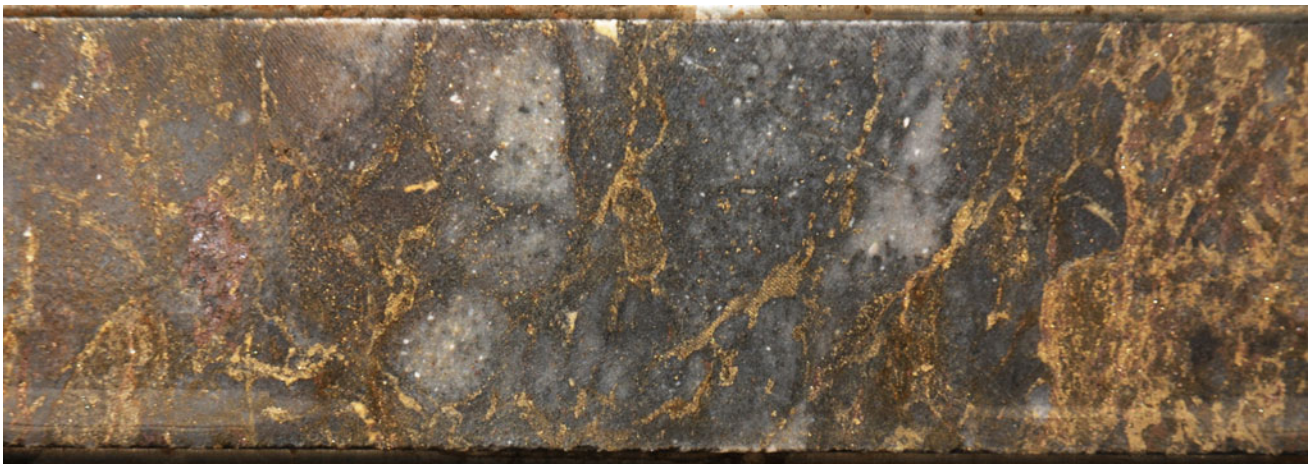

Fig. 23.33 Drill core with hypogene sulphides from the Gergarub prospect, showing pyrite-chalcopyrite-sphalerite in a brecciated coarse-clastic hyaloclastite with porphyritic rhyolite clasts. Borehole SPDD 29 at 217.50 m depth, core diameter NQ (47.6 mm). Photograph by Gregor Borg

Fig. 23.34 Gergarub drill core with hypogene sphalerite (brown) intergrown with blade-shaped barite (white). Borehole SPDD 48 at 259.70 m depth, core diameter NQ (47.6 mm). Photograph by Gregor Borg

The total pre-mining resource of the Gergarup prospect is 18 Mt of sulphide ore containing 8.68% Zn, 2.37% Pb, and 41 g/t Ag (Markus Schaefer, Vedanta Resources plc, pers. comm.).

23.9 The O'okiep Copper District

The O'okiep Copper District (Figs. 23.1, 23.35 and 23.36) contains numerous mafic intrusions of the so-called Koperberg noritoid Suite of Namaqualand in the northwestern Cape Province of South Africa (McIver et al. 1983; Gibson et al. 1996; Cornell et al. 2006). Copper mineralisation is associated with noritic and pyroxenitic rocks, which are interbanded on a scale of 1–10 m, in the granulite-facies metamorphic terrain of the O'okiep district (Cawthorn and Meyer 1993; Figs. 23.35 and 23.36). A typical feature of the entire Koperberg Suite is that the mafic intrusive rocks have no chilled margin against the country rocks. These Cu-mineralised mafic rocks of the Koperberg suite of Namaqualand constituted one of the three major copper producers in South Africa (O'okiep Copper Company) during their active mining period between 1980 and 2010 (first mined in 1685 by Governor Simon v. d. Stel and Company) with a pre-mining reserve of approximately 2 Mt of copper metal, most of which has now been mined out. Xtract Resources Ltd. Acquired the Carolusberg and O'okiep tailings dams in 2015 aiming to extract further Cu (Mining Atlas 2015).

Regionally, the mineralisation typically occurs in mafic intrusive bodies within the Nababeep granitic gneiss of the Klein Namaqualand Suite, just above the Springbok quartzite of the O'okiep Group (Fig. 23.36; Cawthorn and Meyer 1993). The mafic bodies of the Carolusberg mine, as one example, show a podiform shape, common lateral displacement, and are spatially related to so-called 'steep structures' (Fig. 23.37). The geometry of the O'okiep ore bodies has been documented by van Zyl (1967, 1978) and is shown as one example of the Carolusberg and East O'okiep mines in Fig. 23.36 (Cawthorn and Meyer 1993).

Many of these mafic bodies host Cu sulphide mineralisation, and some 30 deposits, ranging in size from 1 to >30 Mt, with grades between 1.75 and 14% Cu, have been mined (Lombaard et al. 1986). The origin of the mineralisation has been attributed to a combination of fractionation in mantle-derived magmas and contamination by crustal melts, followed by high-temperature oxidation during the Namaqua metamorphic peak and a subsequent lower-temperature overprint, probably associated with the Pan-African event (Boer et al. 1994; Brandriss and Cawthorn 1996; van Zwieten et al. 1996).

Numerous geochronological studies have been undertaken in the O'okiep Copper District of the western Namaqua Province, both on the Palaeoproterozoic regional basement and on the Mesoproterozoic sequence that hosts the O'okiep ore deposits (Clifford et al. 1975, 1981, 1995, 2004; Robb et al. 1999; Macey et al. 2017). Zircon grains from the Koperberg Suite have been dated at 1.160 ± 17 Ma (Clifford et al. 1981) as well as 1.168 ± 9 Ma and 1.063 ± 16 Ma (Robb et al. 1999).

The Namaqua orogenic event was associated with a subhorizontal deformation (D2) producing recumbent

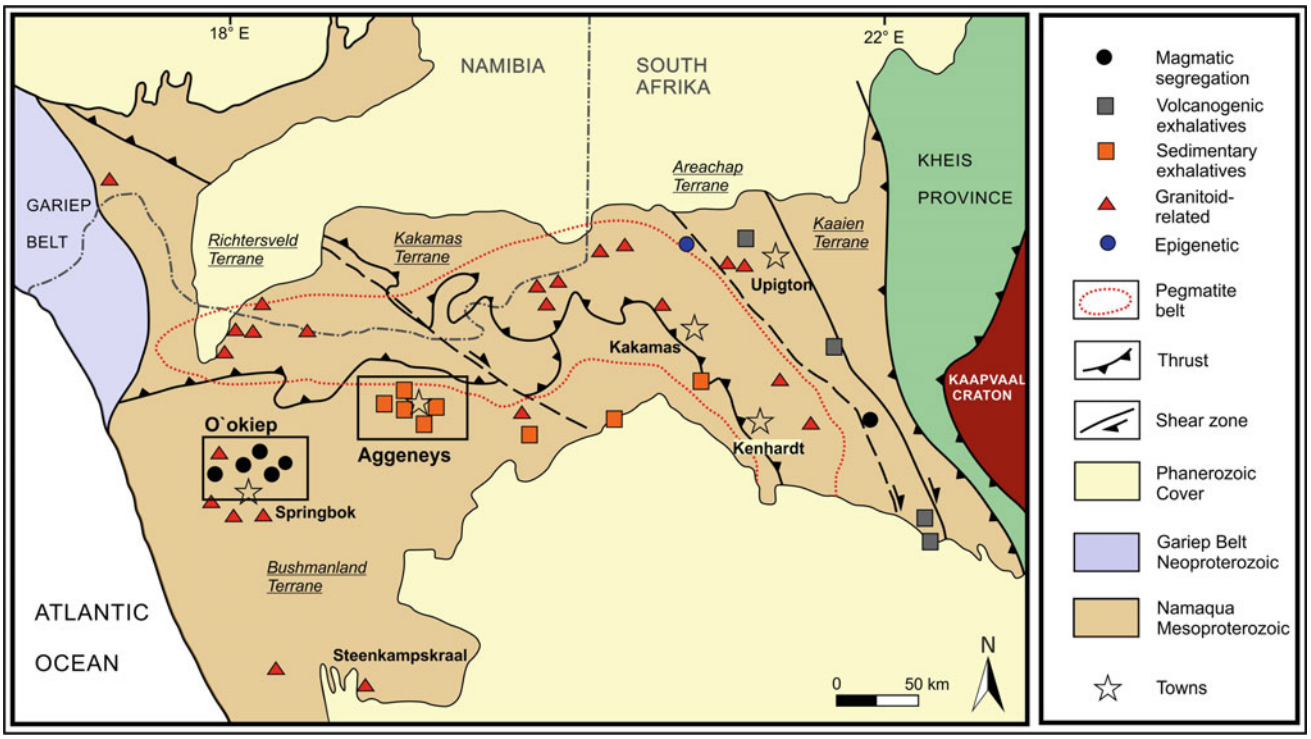

Fig. 23.35 Metallogenic map of Namaqualand showing the distribution of the most important mineral occurrences (after Thomas et al. 1994). Both the O'okiep and Aggeneys districts are marked by frames and shown in more detail in Figs. 23.35 and 23.37, respectively

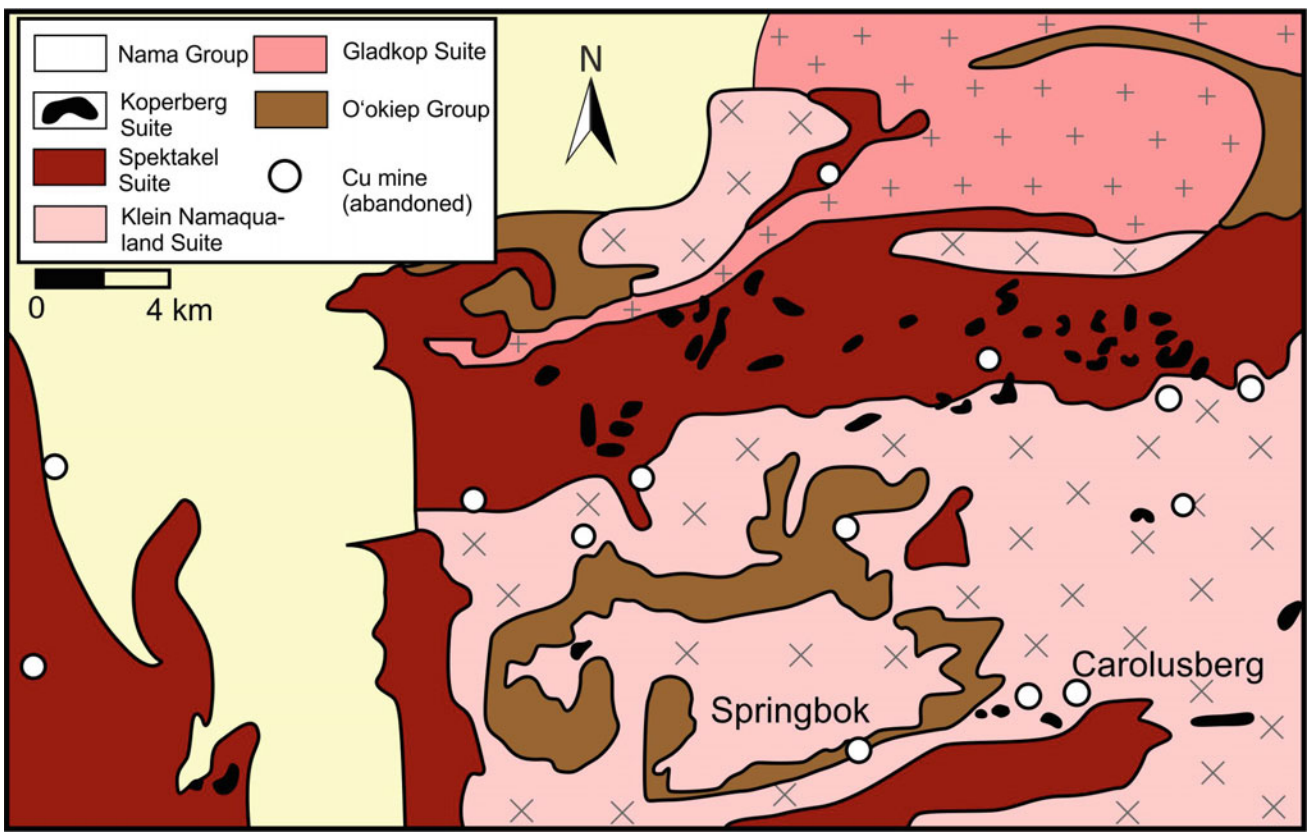

Fig. 23.36 Geological map of the O'okiep copper district (after Joubert 1986)

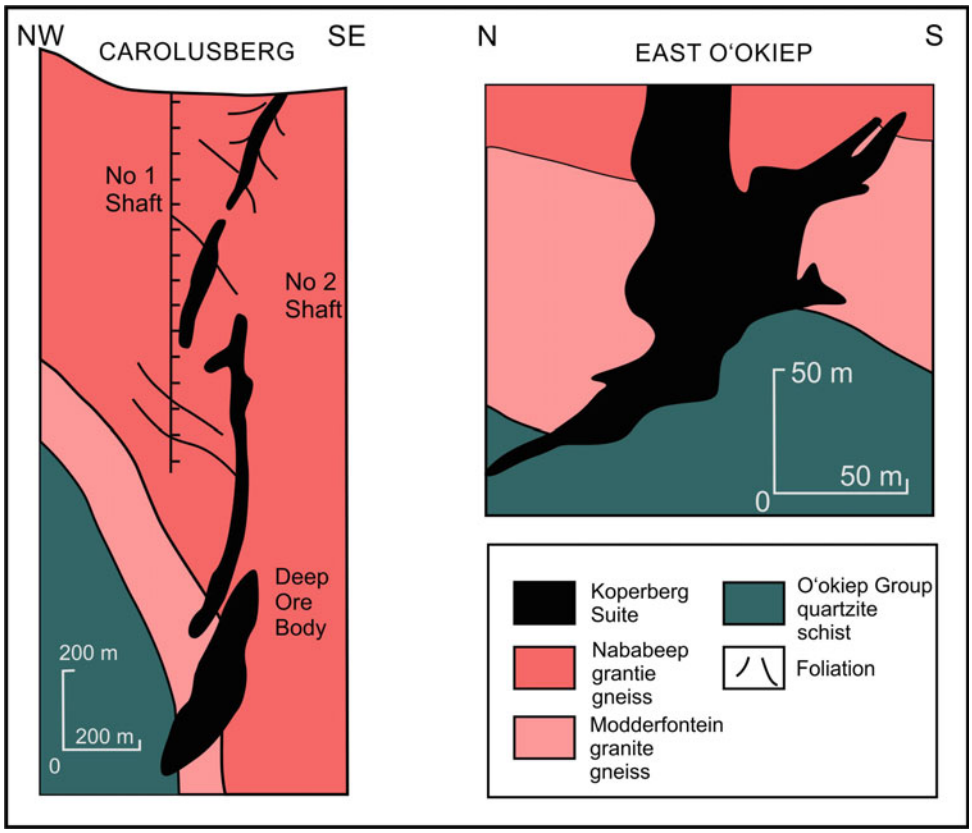

Fig. 23.37 Section through the Carolusberg and East O'okiep mines (after Cawthorn and Meyer 1993)

folding, and subsequent upright, gentle open folding (D3) (Joubert 1986). Related to the D3 event is the formation of the 'steep structures' (Joubert 1986), which possibly developed along periclinal axes or as piercement folds parallel to the Springbok antiform, in which an intense vertical fabric is locally developed (Clifford et al. 1981).

Kisters et al. (1996) explained the formation of steep structures in the O'okiep Copper District by bulk inhomogeneous shortening of the high-grade metamorphic granite-gneiss sequence. Subhorizontal gneissosities and lithotypes of the granite-gneiss terrane are cut by narrow, discontinuous, east-trending cusp-shaped and/or monoclinal structures, in which the regional gneissosity has been rotated to subvertical attitudes. Closely associated migmatisation and charnockitisation indicates that these 'steep structures' formed under high-grade metamorphic conditions. Subsequently, Kisters et al. (1998) emphasised the role of strain localisation in the segregation and ascent of anatectic melts, preserved in granulite-facies gneisses of the O'okiep Copper District and reflecting the initial stages of segregation and ascent of crustally derived magmas during high-grade metamorphism. While a metasomatic origin was briefly favoured for the noritoids, most researchers have emphasised the crosscutting nature of the noritoids relative to their host rocks and prefer an origin involving magmatic injection. Most authors have therefore concluded that these mafic bodies are post-metamorphic (Conradie and Schoch 1986; Schoch and Conradie 1990). However, McIver et al. (1983) argued that they were synmetamorphic and had been recrystallised under granulite-facies metamorphism, producing a mineralogy but not a texture similar to magmatic rocks.

Mclver et al. (1983) pointed out that high noritoid $^{87}Sr/^{86}Sr$ initial ratio values indicate that the mobilisation of suitable crustal materials was more probable than the intrusion of mantle-derived melts to account for the origin of the noritoid suite. The same authors suggested that the parent had been an alkaline mantle-derived magma, which suffered contamination by granitic anatects in the lower crust.

Latzky (1942) and van Zyl (1967) regarded the sulphides as having formed by the immiscibility of sulphide liquid from a basic magma. However, Stumpfl et al. (1976), in contrast, suggested that the sulphides formed from late-stage, magmatically derived hydrothermal fluids. In a refinement of this model, Clifford et al. (1990) recognised two end-member types of mineralisation, the Carolusberg type which was syngenetic and the Hoits type where Cu had undergone local remobilisation, redistribution, and recrystallisation (Cawthorn and Meyer 1993). They related the latter process to the 500–550 Ma Pan-African event, which

allows for two possible ages of mineralisation in the O'okiep Copper District: Mesoproterozoic or Late Neoproterozoic.

23.10 The Aggeneys Cu–Zn Deposits Within the Western Namaqua (-Natal) Metamorphic Belt

The southern African Kheis Orogeny (Windley 1995) was an event which focused tectonic activity and mineralisation within Southern Africa to the Namaqua-Natal Metamorphic Belt, situated to the south and west of the Kaapvaal Craton. A long period of cratonic stability ensued and Ur was subjected to rifting and intracontinental sedimentation between 1700 and 1600 Ma, forming large dominantly clastic sedimentary basins that host the world-class SHMS-/Broken Hill-type Pb–Zn ores of the Aggeneys district in the Northern Cape Province, South Africa (Figs. 23.1 and 23.35; Robb et al. 1999; Robb 2005). The ore deposits of the Aggeneys district represent an exception of a mineral camp, which formed in a period of orogenesis, affecting the continental margins of Ur in the 1060–1030 Ma Namaqua Orogen (Robb 2005).

The Namaqua-Natal Metamorphic Province forms an arcuate belt, up to 400 km wide, which is draped onto and around the western and southern margins of the Kaapvaal Craton. The rocks making up this province are believed to have formed adjacent to a foreland made up of the Kaapvaal Craton, Kheis Province and Kaaien Terrane (Thomas et al. 1994; Fig. 23.35). An orogenic event resulted in the welding together of the Areachap, Kakamas, Richtersveld, and Bushmanland accreted terranes, to form the Bushmanland Craton, by 1750 Ma (Macey et al. 2017). Rifting along northwest-trending axes, between 1600 and 1400 Ma, led to the formation of intracratonic basins in the thicker western part of the craton (Thomas et al. 1994).

In Namaqualand, 1300–1600 Ma-old supracrustal rocks, the high-grade Namaqua-Natal metamorphic belt, include arc-related sequences in the east and extensional foreland basin sequences in the west (Thomas et al. 1994). These sequences were deposited on a Palaeoproterozoic basement, with a western Domain, the Richtersveld Magmatic Arc, and an eastern part, the Pella Domain (Macey et al. 2017). The basement rocks consist of metavolcanic and equivalent plutonic rocks with a geochemical island arc signature, which formed between 1910 Ma and 1856 Ma and were variably affected by the ~1 Ga Namaqua Orogeny.

The metallogenic evolution of the dominantly convergent-collisional Namaqua-Natal Belt corresponds with its tectonomagmatic development, during which economically important stratiform exhalative VHMS and SHMS base-metal mineralisation was abundant throughout the belt (Thomas et al. 1994).

23.10.1 The Aggeneys District (Gamsberg, Black Mountain, Broken Hill)

The Pb–Zn–Cu–Ag deposits of the Aggeneys metallotect are world-class examples of the important Broken Hill-type mineralisation (Beeson 1990; Walters 1996) and are the biggest source of lead and zinc metal in South Africa (Ryan et al. 1986). The Aggeneys Zn–Pb–Cu–Ag district is situated some 110 km to the northeast of the town of Springbok and 80 km to the west of Pofadder within the Northern Cape Province (Fig. 23.35). The major deposits within the district are, from west to east, Black Mountain (Swartberg), Broken Hill, Deeps, Big Syncline, and Gamsberg (Fig. 23.38). The impressive tonnages and grades of the various ore deposits of the Aggeneys metallotect are as follows (Markus Schaefer, Vedanta Resources plc, pers. comm.):

Broken Hill including 'Deeps': 126 Mt @ 0.42% Cu, 3.99% Pb, 1.51% Zn, 59 g/t Ag
Black Mountain (Swartberg): 72 Mt @ 0.39% Cu, 3.14% Pb, 0.81% Zn, 48 g/t Ag
Gamsberg North: 183Mt @ 6.35% Zn, 0.52% Pb (at a 3% cut-off grade)
Gamsberg East: 32 Mt @ 9.83% Zn, 0.60% Pb (at a 7% cut-off grade) or
47 MT @ 8.6% Zn, 0.50% Pb (at a 4% cut-off grade)

The host rock sequence, the metavolcanic-metasedimentary Bushmanland Group, was deposited in the western part of the Namaqua Mobile Belt and subsequently tectonically emplaced as nappe structures (Cornell et al. 2006). The metallotect comprises several ore bodies, and numerous minor occurrences of Zn–Pb–Cu–Ag sulphides occur in association with manganese-rich iron formation and barite enclosed in wall rocks such as quartzite and mica-sillimanite schist of the Bushmanland Group (Rozendaal and Stumpfl 1984; Ryan et al. 1986). The deposits vary in size from 30 to >100 Mt and are interpreted as sedimentary-exhalative. Smaller (<20 Mt), laterally extensive but disrupted strata-bound deposits are present in the eastern portion of the terrane at Putsberg, south of Pofadder, and at Geelvloer. Cornell et al. (2006) found the Pb–Pb model ages of 1350–1300 Ma, obtained for the giant Aggeneys and Gamsberg deposits, to be reliable as it is difficult to see how such large quantities of lead could be reset.

The structural complexity of the region and the high grade of metamorphism have led to complications in correlating supracrustal rocks in complicated tectonic models for the area (Joubert 1986; Moore 1989). The importance of determining the tectonic evolution of the area lies not only in its economic potential as hosts of Broken Hill-type deposits but also in its role in the amalgamation of the southern African continental crust during the construction of the

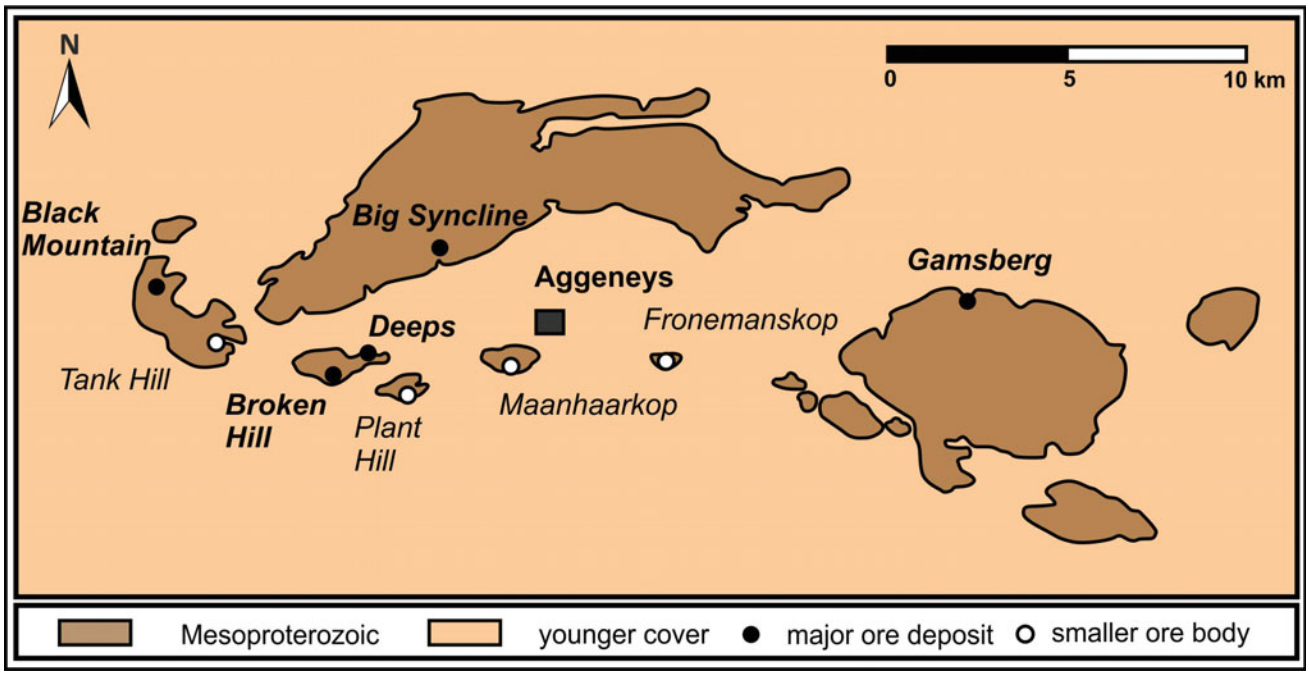

Fig. 23.38 Overview map of the Aggeneys mining district with the location of the major and smaller Broken Hill-type massive sulphide deposits

Rodinian supercontinent at ~1.2 to ~1.0 Ga (Thomas et al. 1994).

There has been protracted debate as to the provenance, basement and source of base metals of the supracrustal succession (Duncan et al. 1984, 1985; Watkeys 1986; Watkeys et al. 1988; Moore 1989; Lipson 1990; Moore et al. 1990; Reid et al. 1997a, b). These arguments have suggested that the present-day basement, a series of granitic gneisses termed the Achab and Hoogoor Gneisses, are older than the Bushmanland Group and acted as the basement and provenance to the metasedimentary rocks and source of the base metal mineralisation. The Bushmanland Group consists of metapelitic schists, metaquartzites, banded iron formations hosting massive sulphide mineralisation, and minor calcsilicate rocks, all deposited between approximately 1.64 and 1.2 Ga (Bailie and Reid 2005; Bailie et al. 2007a, b). The prominent inselbergs and ranges of hills, which characterise the arid landscape of the area, consist of metavolcanic-metasedimentary units of the Bushmanland Group that usually occur as major, commonly overturned, synformal infolds in the associated granitic gneisses (Joubert 1986). Apart from geochemical characteristics, the metasedimentary nature of the metapelites and metaquartzites is confirmed by the presence of heavy mineral layers and the presence of other sedimentary features, such as cross bedding within the metaquartzite units (Lipson et al. 1986). The deposits around Aggeneys have been subjected to upper amphibolite facies metamorphism (Ryan et al. 1986; Lipson 1990).

Lipson (1990) and Hoffmann (1993) conclude that mineralisation was deposited syndepositionally as a result of the presence of a large detrital component within the ore horizon, having similar geochemical characteristics to the hangingwall and footwall metasedimentary rocks and the presence of well-preserved banding within a mineralised iron formation (Fig. 23.40), considered to represent original sedimentary bedding (Hoffmann 1993). REE analyses of mineralised samples indicate transitions from detritally-dominated to hydrothermally-dominated signatures, characterised by the slopes of REE patterns and the nature of the Eu anomaly (Lottermoser 1989, 1992; Lottermoser and Ashley 1995). Lipson (1990) and Hoffmann (1993) report no physical evidence for a vent in the area of the mineralisation. However, the deposits grade from the Cu-rich Black Mountain and Broken Hill deposits in the west (Fig. 23.39) to progressively more zinc-rich and lead-poor (Ryan et al. 1986), to the large tonnage, low-grade Zn-rich Gamsberg deposit (Fig. 23.40) in the east (Rozendaal 1986). This zonation pattern supports models that see a general venting area towards the west with metal precipitation controlled by the specific solubility of the base metals. This district-wide zonation would argue more in favour of an exhalative nature of the mineralisation rather than a subseafloor impregnation and replacement within sediments.

The Aggeneys deposits are host to reserves of some 370 million tons of Pb, Zn, Cu and Ag-bearing ore. The biggest producer is the Broken Hill Mine, host to 38 Mt of ore with 7.8% Pb, 2.9% Zn, 0.5% Cu and 113 g/t Ag (Du Toit 1998).

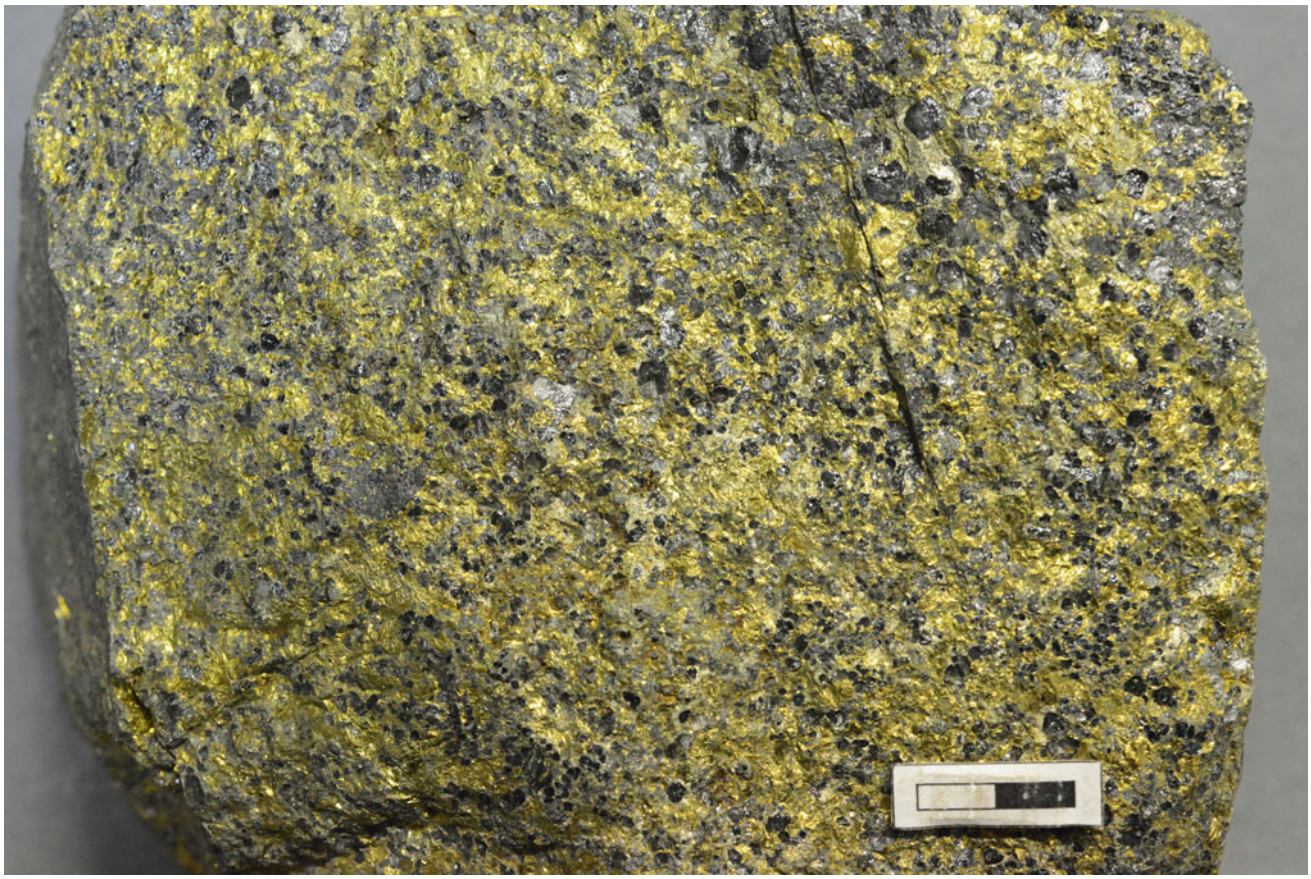

Fig. 23.39 Chalcopyrite-rich massive sulphide ore with euhedral garnet (blackish red) from Broken Hill Mine at Aggeneys. Note the Cu-rich ore in this western ore body of the Aggeneys district, showing a regional zonation from Cu-rich in the west to Zn-rich in the east. Photograph by Gregor Borg

The deposits conform with characteristics of typical Broken Hill-type deposits, which include host rock characteristics, specific tectonic settings with lithological variation in the sequence, metal ratios, a predominance of 'oxidised rock types' with facies variations, high Mn–Ca–Fe content, a vertical and lateral zonation in the base metal mineralisation, galena and sphalerite dominance, thin exhalite units, no obvious focused footwall feeder zones with intense alteration, and being affected by high-T/low-P metamorphic events and formed between 1900 and 1600 Ma (Beeson 1990; Walters 1996).

Previous workers have argued for hydrothermal venting onto the seafloor (Ryan et al. 1986; Lipson 1990), whereas others (e.g., Moore 1989) have argued for subseafloor replacement processes. Upgrading of the ore to economic levels occurred during peak metamorphism (Ryan et al. 1986). Ore mineralogy includes magnetite, sphalerite, galena, pyrrhotite, chalcopyrite and pyrite in varying proportions. The majority of the mineralisation occurs as massive ore, containing over 60% sulphides with coarse-grained, granoblastic textures featuring euhedral garnet (Fig. 23.39). The dominant alternating recrystallised magnetite- and quartz-rich bands, alternating with pyrite and sphalerite layers, especially at the Gamsberg Mine (Fig. 23.40) and extending over tens of metres in strike, are taken as evidence of the original banded sedimentary nature of the ore, prior to peak metamorphism (Lipson 1990; Hoffmann 1993).

The Gamsberg Zn-Pb deposit (150 Mt at 7% Zn and 0.5% Pb) is hosted by a multiply deformed and metamorphosed volcanosedimentary sequence composed of quartzite, metapelitic to metapsammitic schist, and amphibolite that overlie a suite of quartz-feldspar gneiss (Rozendaal 1986; Moore et al. 1990). Structurally, the deposit occurs within a large sheath-fold structure that has been exposed as a prominent inselberg. The ore-bearing horizon is referred to as the Gams Formation and consists of a sequence of metalliferous metasedimentary rocks and interbedded metapelite up to 100 m thick (Rozendaal and Stumpfl 1984; Rozendaal 1986). Base-metal and Fe sulphides are mostly confined to quartz-sillimanite-muscovite-graphite

Fig. 23.40 Laminated and interbedded sphalerite-pyrite-magnetite ore underground at Gamsberg Mine, Aggeneys. Note the Zn-rich ore in this eastern ore body of the Aggeneys district, showing a regional zonation from Cu rich in the west to zinc rich in the east. Photograph by Gregor Borg

and quartz-garnet-amphibole rocks of the middle unit of the Gams Formation (Stalder and Rozendaal 2005).

The Gamsberg ore body and associated metalliferous host rocks have been multiply deformed and metamorphosed along with the country rocks during the Kibaran and Namaquan orogenic events from 1220–1170 Ma and 1060–1030 Ma, respectively (Thomas et al. 1994; Robb et al. 1999). At least three phases of deformation are recognised, with the main fabric-forming event (D2) being represented by east–west-trending recumbent isoclinal folds (F2). These structures were reworked by east–west-trending open folds (F3) on a kilometre-scale wavelength, and later thrusts and shear zones that developed during subsequent compressional events (D3–D4). Conditions of metamorphism in the area are constrained by the presence of the assemblages cordierite + sillimanite + K-feldspar and quartz + muscovite in meta-pelite, with p–T estimates ranging from 630 to 670 °C and 3 to 4.5 kbar (Joubert 1986; Rozendaal 1986).

23.11 Felsic and Exotic Intrusion-Related Sn-/W-, U-, Li-, REE- and Au Deposits

A diverse group of metallogenetically relevant ore deposits is related to felsic and more highly fractionated orogenic intrusions such as granites, pegmatites and exotic melts. The group comprises technically and economically relevant commodity elements such as tin, uranium, lithium, gold, and rare earth elements. A narrow elongated cluster rather than a belt of such deposits with a range of Meso- to Neoproterozoic ages is located parallel to the present west coast of southern to equatorial Africa (Fig. 23.1). Geological and metallogenetic details of each type of deposit might yield persisting challenges and open questions, but generally the origin of many of these deposit types is not overly complex and comparatively straightforward. A brief summary will thus suffice in the present framework of this chapter and the

reader is referred to the most relevant papers for further references.

23.11.1 Tin-Tungsten Deposits

A well-documented and substantial tin-tungsten (Sn-W) district is located between Cape Cross and Uis in the central Damara Belt in western Namibia, but a small and typical tin deposit of similar geological setting has also been mined at the foot of the larger Table Mountain, precisely below Devils Peak in Cape Town.

The Central-Western Namibian tin-tungsten (niobium-tantalum) district extends for more than 230 km east–west and for more than 150 km north–south between Cape Cross, the Brandberg, and Karibib (Fig. 23.41; Diehl 1992a, b, 1993). The district consists of four west-southwest-east-northeast oriented belts with Sn–W-mineralised pegmatite and vein occurrences and two major deposits, the Uis tin Mine and the Brandberg West tin Mine (Gevers and Frommurze 1929; Richards 1986; Piranjo and Jacob 1987; Piranjo et al. 1987; Diehl 1992a, b, 1993; Kinnaird et al. 2016). The cassiterite-columbite-tantalite-bearing pegmatites hosted by biotite schist (Fig. 23.42) at Uis Mine and the cassiterite-bearing greisen at Brandberg West Mine (Fig. 23.43) were discovered in 1911 and were mined on a small scale until 1951 (Diehl 1992a, b).

Individual tin belts, such as the Uis tin belt, which runs from Cape Cross at the Atlantic coast to Uis, are more than 100 km long and over 10 km wide. The Central Western Namibian tin district has been comprehensively reviewed by Kinnaird et al. (2016 and references therein). Mineralisation is commonly dominated by cassiterite (Fig. 23.44), wolframite, and minor scheelite, locally with appreciable amounts of columbite-tantalite, lepidolite, and beryllium minerals in late- to post-tectonic pegmatites and subordinately in hydrothermal veins, skarns, and greisens (Piranjo and Jacob 1987; Diehl 1992a, b; Kinnaird et al. 2016). The age of the pegmatites and Sn-W-Ta mineralisation has been dated to 509 ± 11 Ma for mineralised veins in

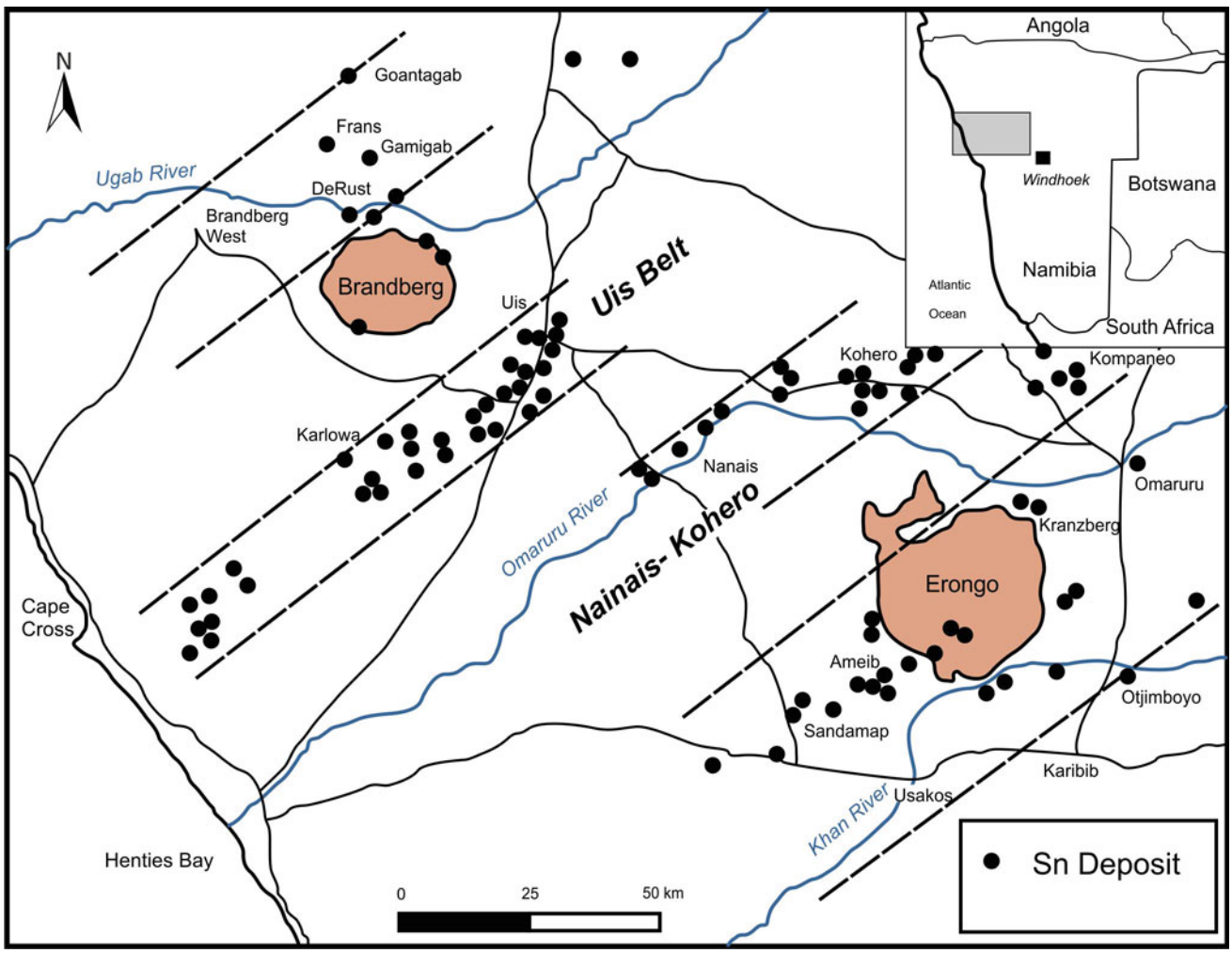

Fig. 23.41 Simplified overview map of the pegmatite-, vein-, and greisen-hosted tin-tungsten deposits and occurrences of the Uis tin district sensu lato (after Diehl 1992a)

Fig. 23.42 Cassiterite-bearing quartz-muscovite-feldspar pegmatite, intruded into metamorphosed turbidites at Uis Mine, Namibia. Photograph by Gregor Borg

metamorphosed turbidites at Brandberg West (Piranjo et al. 1987; Walraven 1989), to 503–486 Ma for cassiterite-bearing pegmatites at Uis (Haack and Gohn 1988), and to 505 Ma for columbite mineralisation near Karibib (Melcher et al. 2015). Production between 1924 and 1990 amounted to 35,000 t of tin concentrate, which was recovered from ore with grades of 0.125% Sn, which made Uis tin Mine the largest low-grade hard rock tin mine in the world between 1950 and 1970 (Richards 1986; Kinnaird et al. 2016). Economical operation at such extremely low grades was possible as a result of the International Tin Agreements between 1954 and 1986 (ITRI 2011, https://www.itri.co.uk/about-itri). A modern open-pit mine had been opened in 1951 and operated until 1990, when it had to close as a result of the collapse of the existing tin cartel (Fig. 23.45) and the resulting drastic drop in tin prices in 1986. The second largest producer of tin and tungsten in the district was Brandberg West Mine, where mineralisation occured in sheeted quartz veins and in greisen, hosted by greenschist-facies turbidites (Piranjo et al. 1987). Brandberg West produced a total of 14,374 t of concentrate grading at 32–56% Sn-oxide and 14.5–19% W-oxide (Piranjo et al. 1987; Diehl 1992a, b).

Situated relatively close to the southern margin of the Uis tin district *sensu lato* is another, although very different, type of ore deposit, formed in a felsic intrusion dominated regime, which is the Navachab gold deposit (see also elsewhere in this chapter). Navachab is the largest non-Witwatersrand-type gold deposit in Southern Africa (Steven et al. 2015) and it is worth mentioning, at least briefly, that several other authors consider Navachab to be a distant gold skarn (e.g., Piranjo and Jacob 1991; Nörtemann et al. 2000; Meinert et al. 2005), although formed in and around veins, which might alternatively be of late tectonometamorphic and/or hypozonal origin (e.g., Kisters 2005; Kolb et al. 2015; Wulff et al. 2010, 2017). Thompson et al. (1999) even pointed out the systematic and interrelated metallogenetic association of tin and gold mineralisation.

Fig. 23.43 Cassiterite-bearing greisen at Brandberg West Mine, Namibia. Photograph by Gregor Borg

At the far southern end of the trend of tin-tungsten-lithium-REE deposits along the southern west coast of Africa are the smaller tin-molybdenum Riviera deposit near Piketberg in the Western Cape Province and the economically incomparable tin deposits and mines of the Cape Peninsula in South Africa. The Riviera tungsten-molybdenum deposit is hosted by veins that have formed in the cupola of a granite pluton, which has intruded the Malmsbury Shales (Rozendaal et al. 1994; Walker 1994). Ore reserves have been estimated to be 46 Mt at 0.216% WO_3 and 0.02% Mo, with the main ore mineral being scheelite (Walker 1994).

Within the Cape Peninsula in total, there are six tin deposits associated with the granitic intrusive bodies of the Cape Granite Suite (Cole 2003; Miller 2006). Alluvial cassiterite was discovered and mined at Kuils River, some 25 km from Cape Town in the mid-nineteenth century and in streams on the slope of Table Mountain and Devils Peak in 1909/1910 (Spargo 1999). Alluvial tin mining, predominantly from the Kuils River area, produced a total of 700 t of tin concentrate and ceased only in 1956. The Vredehoek tin deposit was found in 1911, is located just above the so-called 'City Bowl' of Cape Town (Fig. 23.46), and was mined only very briefly and with interruptions between 1912 and 1916 (Spargo 1999). Mineralised veins (Fig. 23.47) were accessed by a 55 m-deep shaft, an additional blind shaft and several adits. In 1998 the area where the mine is located was incorporated into the Cape Peninsula National Park and only a few concrete foundations of the small mineral processing plant and part of an edit entrance, now closed, remain visible at the surface. The metallogenetic relevance of the Vredehoek tin Mine, however, is in the classical granitic-intrusion-related origin of the cassiterite-bearing quartz veins and granitic dykes in the Malmsbury Shales close to the intrusive contact of the Pan-African Cape Granite. The cassiterite occurs in quartz veins and fine-grained granite dykes intruded between 585 Ma (Visser 1998) and 510 Ma ago (Theron et al. 1992), and they also contain molybdenite, wolframite, arsenopyrite, tourmaline, and mica (Miller 2006).

Fig. 23.44 Coarse-crystalline anhedral cassiterite (brownish-black) in quartz-muscovite pegmatite from the Uis tin-pegmatite district, Namibia. Photograph by Gregor Borg

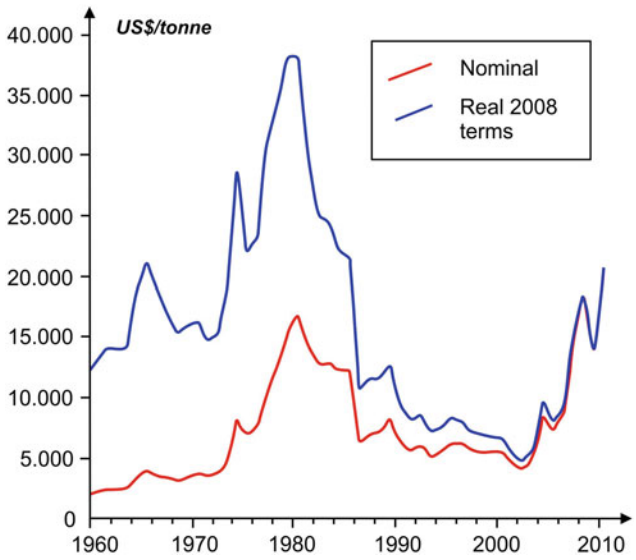

Fig. 23.45 Historical tin prices, nominal (red) and adjusted to 2008 real terms, showing the collapse of the tin market in 1986, which resulted in the closure of Uis Mine (ITRI 2011, https://www.itri.co.uk/about-itri)

Fig. 23.46 Location of Vredehoek Mine (arrow) at the foot of Devils Peak, Cape Town, with the northern part of Table Mountain at right. Photograph by Gregor Borg

Fig. 23.47 Subhorizontal cassiterite-bearing quartz veins underground at the Vredehoek Mine, Cape Town, South Africa. Width of field of view 1.6 m. Photograph by Gregor Borg

23.11.2 Uranium Deposits

Western Central Namibia is also host to one of the largest uranium districts in the world, and the Rössing Mine and deposit is briefly described here as one example of uraniferous granite intrusion mineralisation. Rössing Mine is located some 70 km inland from Swakopmund on the Atlantic coast and is one of the largest uranium mines and the longest in operation worldwide (Fig. 23.48). Although already discovered in 1928, operation only started in 1976 and the mine had produced 130,500 t of uranium oxide by the end of 2016 (www.rossing.com/history.html). A major discovery of a similar deposit has been made relatively recently very close by: the Rössing South deposit (Spivey et al. 2010). This deposit is also being developed into a mine now. A supergene uranium deposit, Langer Heinrich, has formed as secondary ore in a calcretised channel fill from the redistribution of primary mineralisation from another uraniferous granite source (Hartleb 1988; Becker and Kärner 2009). Several other deposits are currently being developed in the region and are at various advanced levels of development.

The uraniferous leucogranites intruded as sheet-like and crosscutting bodies (Fig. 23.49) into 780–746 Ma old Neoproterozoic metasedimentary rocks during the late-orogenic stage of the Damaran Orogeny at approximately 500 Ma (Kinnaird and Nex 2007). The district extends as a

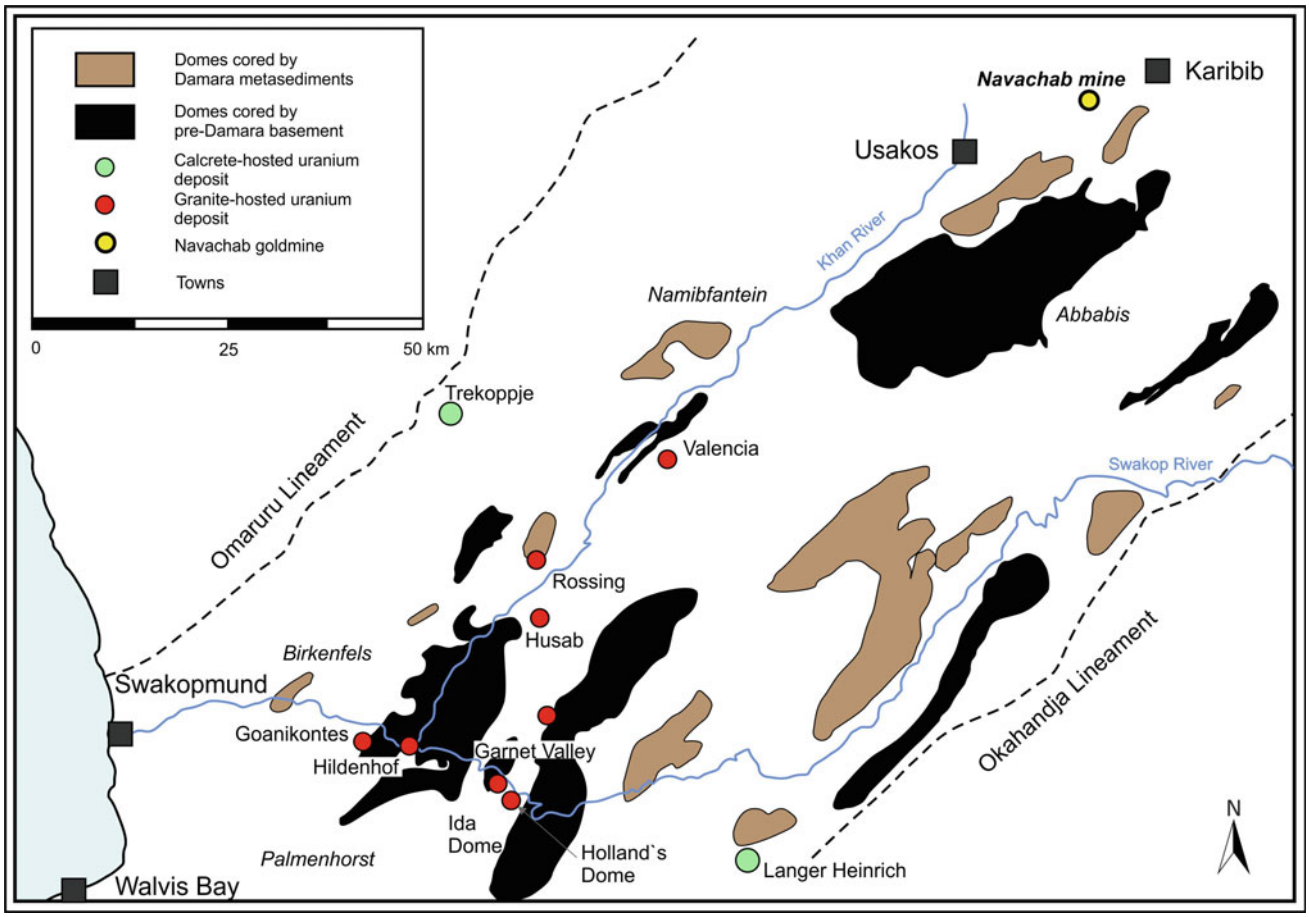

Fig. 23.48 Overview map of the Western Central Namibian uranium district, showing the primary, leucogranite-hosted deposits as well as the secondary supergene, calcrete-hosted deposits (modified after Kinnaird and Nex 2016). Navachab Mine is shown west-southwest of Karibib

70 × 30 km west-southwest-east-northeast-trending corridor (Fig. 23.48) and is located in the high-temperature, low-pressure metamorphic part of the Central Zone of the Damara Orogen (e.g., Bowden et al. 1995; Nex and Kinnaird 1995; Kinnaird and Nex 2007, 2016). The leucogranitic bodies were first described and classified as white alaskites (Marlow 1983), but Kinnaird and Nex (2007) documented a far greater variety of uranium-bearing granites, including granodiorite, monzogranite, syenogranite, and alkali feldspar granite. The emplacement of the uranium-mineralised leucogranite sheets was strongly structurally controlled and occurred late kinematically, preferentially in the apex of domal fold structures, which are locally either basement-controlled or had formed within the Damaran stratigraphy (Basson and Greenway 2004; Freemantle 2015). Absolute ages of emplacement range from 540 ± 33 to 508 ± 2 Ma and are thus indistinguishable from each other within error limits and have been summarised in the comprehensive studies by Basson and Greenway (2004), Freemantle (2015), and Kinnaird and Nex (2016). The uranium mineralisation consists of both primary magmatic and secondary ore minerals. The former comprise predominantly uraninite with subordinate amounts of betafite, brannerite and davidite (Kinnaird and Nex 2007, 2016). The latter, secondary ore minerals formed during alteration and partly during supergene processes, and they can account for a very substantial portion of the ore minerals, which can be as large as 50% (von Backström 1970). These secondary minerals include, in various proportions, betauranophane/uranophane, coffinite, metatorbernite, metahaiweeite, torbernite, uranothallite, carnotite, gummite, thorogummite, uranium-bearing monazite, and boltwoodite (von Backström 1970; Kinnaird and Nex 2007 and references therein). It is interesting to note that supergene carnotite is the predominant ore mineral at the surficial calcrete-hosted Langer Heinrich deposit (Becker and Kärner 2009).

In summary, the late-kinematically emplaced leucogranites that formed during the late orogenic stage of the Pan-African Damara Orogen have been enriched in uranium, together with other highly incompatible elements.

Fig. 23.49 Leucogranite, intrusive into Chuos Formation siliciclastic metasedimentary rocks, approximately 5 km southwest of Rössing Mine. Photograph by Gregor Borg

23.11.3 Rare Earth Element Deposits

A rare earth element (REE) deposit has been explored extensively at Lofdal, near Khorixas in the Kunene District of northwestern Namibia (Dodd et al. 2014). The mineralisation is associated with an alkali-carbonatite complex, intruded around 750 Ma, and, more precisely, with carbonatite dykes and carbonate 'dykes' and veins (Swindon and Siegfried 2011, Harmer and Nex 2016). The mineralisation has been dated from xenotime overgrowths that yielded an age of 765 ± 16 Ma (Wall et al. 2008). At least one generation of the carbonate veins is characterised by strong heavy rare earth element (HREE) enrichment over light rare earth element (LREE) enrichment, which is a peculiarity of this deposit (Swindon and Siegfried 2011; Harmer and Nex 2016). The HREE mineralisation is predominantly hosted by xenotime (Loye 2014) and probably represents the highly fractionated and incompatible element-enriched magmatic to hydrothermal stage of this highly evolved intrusion. Subordinate REE ore minerals comprise bastnaesite, parasite, synchisite, monazite and aeschynite (Loye 2014). An indicated resource of 2.88 Mt with a grade of 0.32% TREO and 9220 t of contained TREO, plus another inferred 8860 t of contained TREO, have been reported by the exploration company that currently holds the licence (http://www.namibiarareearths.com/).

Probably the most exotic ore deposit of SW Gondwana is the high-grade thorium, rare earth element (REE) deposit Steenkampskraal situated in the Bushmanland Subprovince of the Palaeo- to Mesoproterozoic Namaqua-Natal Metamorphic Belt (Eglington 2006; Basson et al. 2016), located some 350 km north of Cape Town (Fig. 23.35). Owing to its high REE grades, the deposit has attracted considerable attention, although in several different periods of the last century (Pike 1959; Andreoli et al. 1994) and more recently as described in the very comprehensive review and structural geology paper by Basson et al. (2016).

The Steenkampskraal deposit was mined from 1950 to 1963 and was the world-leading producer of thorium and REE during this period (Kremers 1958). The mine operated to a depth of 130 m and produced 50,000 t of monazite concentrate, containing remarkable 45% total REE oxides (TREO), 4% ThO_2, 10% P_2O_5, 1.075% Cu, 0.1–1.5% ZrO_2, 600 ppm U_3O_8 and traces of gold (Pike 1959; von Backström 1969). Renewed exploration efforts have recently resulted in extensive drilling and the reopening of old underground workings to investigate the remaining reserves both structurally (Basson et al. 2016) and economically. The current owner of the approved mining licence reports reserves of 605,000 t of ore at a grade of 14.4% TREO with a total of 86,900 t contained TREO and a measured and indicated thorium resource of 11,700 t ThO_2 (www.steenkampskraalrareearths.co.za/).

The ore occurs as monazite-rich, pinching and swelling, probably boudinaged, vein- and dyke-like bodies which dip at a moderate to steep angle (Andreoli et al. 1994; Basson et al. 2016). The rocks have a nelsonitic, silica-poor composition and consist of magnetite-ilmenite, apatite and monazite with minor pyrite and chalcopyrite plus a suite of accessory minerals (Pike 1959; Andreoli et al. 1994; Read et al. 2002; Basson et al. 2016). The ore bodies have a complex structural history, explained in great detail by Basson et al. (2016), and they most probably intruded along shallow dipping structures with subsequent boudination and rotation to a steeper structure, which led Andreoli et al. (1994) to propose an apparent similarity to the steep structures and mafic dykes of the Koperberg Suite at O'okiep. The melts were intruded at 1046 ± 75 Ma into granulite facies metamorphic rocks (Waters 1989). Initial explanations of the origin of the highly mineralised nelsonite bodies favoured a crustal hydrothermal origin of the veins (Pike 1959; Möller 1989). A subsequent, modified hydrothermal model proposed a deep mantle fluid source, based on near bulk earth values of the Nd isotope ratios (Andreoli et al. 1994). To date, a magmatic origin has been proposed, featuring a protracted fractionation of a REE-enriched magma, and this is now generally accepted (Kolker 1982; Andreoli et al. 1994; Read et al. 2002; Basson et al. 2016). Such a model involves a mantle derived LILE-enriched basaltic melt that fractionates and separates anorthosite-quartz-diorite cumulates, which is documented by the negative Eu anomaly (Andreoli et al. 1994). The resulting melt splits into two and segregates an immiscible nelsonitic melt that is rich in P, REE, Th, Fe, Cu, and S and forms the ore bodies (Andreoli et al. 1994).

Another deposit with lower grades of REE is located at Zandkops Drift in the southernmost part of the Northern Cape Province, South Africa. An indicated reserve of 22.92 Mt at 2.32% TREO is hosted in carbonate dykes that contain ore minerals such as churchite (Y/Dy/Nd-hydrophosphate), pyrochlore, apatite, betafite, uraninite and niobium rutile (Schürmann and Harmer 1998; Cole et al. 2014).

It is interesting to note that the absolute age of magmatic emplacement of these highly fractionated REE-rich melts in the Namaqua-Natal Metamorphic Belt is approximately contemporaneous with the formation of the volcanosedimentary basins and host rocks of the Kalahari Copper Belt, further north, although not with the (much later) mineralisation ages.

23.11.4 Lithium (Niobium-Tantalum-Feldspar) Deposits

Pegmatite-hosted lithium mineralisation, locally associated with or subordinate to niobium-tantalum-feldspar-REE ores, have formed during two major episodes and in two districts or belts (Fig. 23.35). The older of these districts is the Late Meso- to Early Neoproterozoic pegmatite province that straddles the border between South Africa and Namibia, stretching from Vioolsdrif and Steinkopf to Upington, and onwards to Kenhardt (Hugo 1970; Schutte 1972; Reid 1977; Minnaar and Theart 2006). The younger district comprises pegmatites intruded into deformed Damaran metasedimentary rocks in the Karibib-Usakos-Uis region of Western Central Namibia during Late Neoproterozoic to Early Cambrian times (Ashworth 2014 and references therein).

Economic interest has been highly variable over the last 60 years, with mining in the Namibian district being more active although at different times for various commodities such as beryl, lepidolite, tourmaline, and feldspar. Recent technically induced interests in strategic minerals such as lithium-bearing micas has seen renewed exploration activity (www.aurochminerals.com), although none of the deposits is currently mined. The largely undeformed pegmatites have been emplaced between 1.0 Ga and 950 Ma (Hugo 1970) during the closing stages of the Namaqua Orogeny into the 2.0–1.73 Ga Namaqualand Metamorphic Complex (Reid 1977) in southern Namibia and northwestern South Africa. These pegmatites have received comparatively less economic and scientific interest, except for the recent comprehensive review by Minnaar and Theart (2006), who point out that the only economic commodity mineral is feldspar, although with potentially commercial by-products such as lepidolite, spodumene, beryl, columbite-tantalite (e.g., at the Namibian Tantalite Valley pegmatite) and REE minerals. According to Minnaar and Theart (2006) the economically most promising pegmatite is located at Zebrakop, northeast of Steinkopf in the far Northern Cape Province.

The pegmatites in the Karibib-Usakos-Uis district in Namibia represent late orogenic intrusions, emplaced between 509 and 492 Ma into metamorphosed and deformed metasedimentary rocks of the Damara Orogen (Steven and Moore 1993;

Steven et al. 1994; Longridge 2012; Melcher et al. 2015; Ashworth 2014). The large number of mineralised pegmatites are comparatively well exposed in the Namib Desert and have been described in great detail by Diehl (1992c). Historically the most productive and currently the economically most promising pegmatite target area is located near Karibib with the former mines of Rubikon, with a major lepidolite zone, and Helikon, where the lithium-bearing ore minerals comprise lepidolite, petalite, and amblygonite (Roering and Gevers 1964; Diehl 1992c). The historical Namibian production of lithium minerals between 1939 and 1991 from this district amounted to 112,763 t of Petalite, 70,338 t of Lepidolite, 10,207 t of Amblygonite, and 6,667 t of beryl as a by-product. The Karibib Lithium Exploration Project, which includes the old Rubicon and Helikon mines, is targeting the area for new lithium resources (www.aurochminerals.com).

23.11.5 The Navachab Gold-Skarn and Vein-Type Gold Deposit, Namibia

The Navachab Au deposit is located in the southern Central Zone (sCZ) of the Pan-African northeast-trending Damara Belt relatively close to the triple junction of the three branches of this orogen (Figs. 23.1 and 23.48). There are several different types of ore deposits in the CZ including intrusion-hosted U- and Sn-deposits, pegmatitic REE occurrences, and a variety of base and precious metal ores hosted by Damaran metasedimentary rocks, many with skarn-type alteration, such as Navachab, (Pirajno and Jacob 1991; Pirajno et al. 1991; Meinert 1995, 1998; Nörtemann 1997), Otjimboyo (Nörtemann 1997), and Habis (Steven 1994).

The 750–550 Ma Damara metasedimentary sequence overlies the basement granitoid rocks of the Palaeoproterozoic Abbabis Inlier, which has a U–Pb zircon age of 2038 ± 5 Ma (Tack and Bowden 1999). The Navachab gold deposit is situated in amphibolite-facies metasedimentary rocks of the Damara Sequence, which represents a Neoproterozoic marble- and schist-dominated continental shelf succession (Miller 1983). The gold mineralisation was discovered in the early 1980s and production started in 1989 from an open pit operation. Some 900,000 oz of gold had been produced by 2002 with a current annual production of c. 2.4 t Au at average gold grades of approximately 2 g/t (Steven and Badenhorst 2002). The gold mineralisation is hosted by a composite system of quartz- and quartz-sulphide lodes (Fig. 23.50; Kisters 2005) and has partly replaced marble units in skarn-style mineralisation (Fig. 23.51). The auriferous quartz-vein system is located on the steep northwestern limb of a northeasterly-trending, kilometre-scale, shallow doubly-plunging anticline, the so-called Karibib dome.

Mining currently exploits two main, geometrically distinct ore bodies. Early mining concentrated on linear, massive sulphide shoots and an associated skarn-type alteration (Fig. 23.51) confined to the base of the marble-dominated Okawayo Formation, and most authors have emphasised the partly stratabound nature of the mineralisation (Moore and Jacob 1998; Nörtemann et al. 2000). The massive sulphide ore shoots and skarn alteration have tentatively been related to the intrusion of Pan-African granitoids into the metasedimentary Damara Sequence (Pirajno and Jacob 1991; Meinert 1995, 1998). Alternatively, skarn formation and mineralisation have been interpreted as a hybrid between a metamorphic and a plutonic gold skarn (Nörtemann et al. 2000). The bulk of the more recent mining, in contrast, focuses on a laterally extensive swarm of shallow northerly dipping gold-quartz veins (Fig. 23.50) that cut at high angles through the steeply dipping metasedimentary host rocks (Moore et al. 1999; Steven and Badenhorst 2002) and that are structurally controlled (Kisters 2005). This is in agreement with the observations of Moore and Jacob (1998), Moore et al. (1999), and Steven and Badenhorst (2002), who discovered numerous similarities in the style of mineralisation with orogenic lode-gold deposits. However, the setting of Navachab Mine in a marble-dominated, shelf-type host-rock sequence, which regionally has been intruded by large granitoid bodies and the high-grade, polyphase metamorphic evolution of the region together with the pervasive ductile deformation that has affected the wall rocks are certainly unique features and opposite to the majority of orogenic lode gold deposits. Furthermore, the detailed controls of the veining have remained controversial as a result of the highly variable orientations of the different quartz-vein sets (Moore and Jacob 1998; Moore et al. 1999; Steven and Badenhorst 2002). Kisters (2005) established the relationship between the auriferous veins, wall-rock fabrics, and the deposit-scale controlling structures in an attempt to constrain the formation of the Navachab gold mineralisation within the framework of regional deformation events in the Damara Belt.

In contrast, Nörtemann et al. (2000) regard the Navachab deposit as a reduced gold skarn and state similarities with deposits like Lucky Draw and Tillicum that are hybrids between a regional metamorphic environment and Phanerozoic plutonism at higher P-T conditions than typical gold skarns. Navachab's calcsilicate mineralogy is different from typical gold skarns with subcalcic garnets with up to 90 mol% pyralspite and pyroxene containing up to 16 mol% johannsenite similar to the Tillicum deposit. The metasomatic zonation from marble towards skarn involves an increase in Si, Fe and Mn, reflecting a banded marble protolith, as evidenced by the growth of garnet in thin pelitic layers, and laminae and clinopyroxene in marble layers (Fig. 23.50). An early base metal mineralisation paragenesis

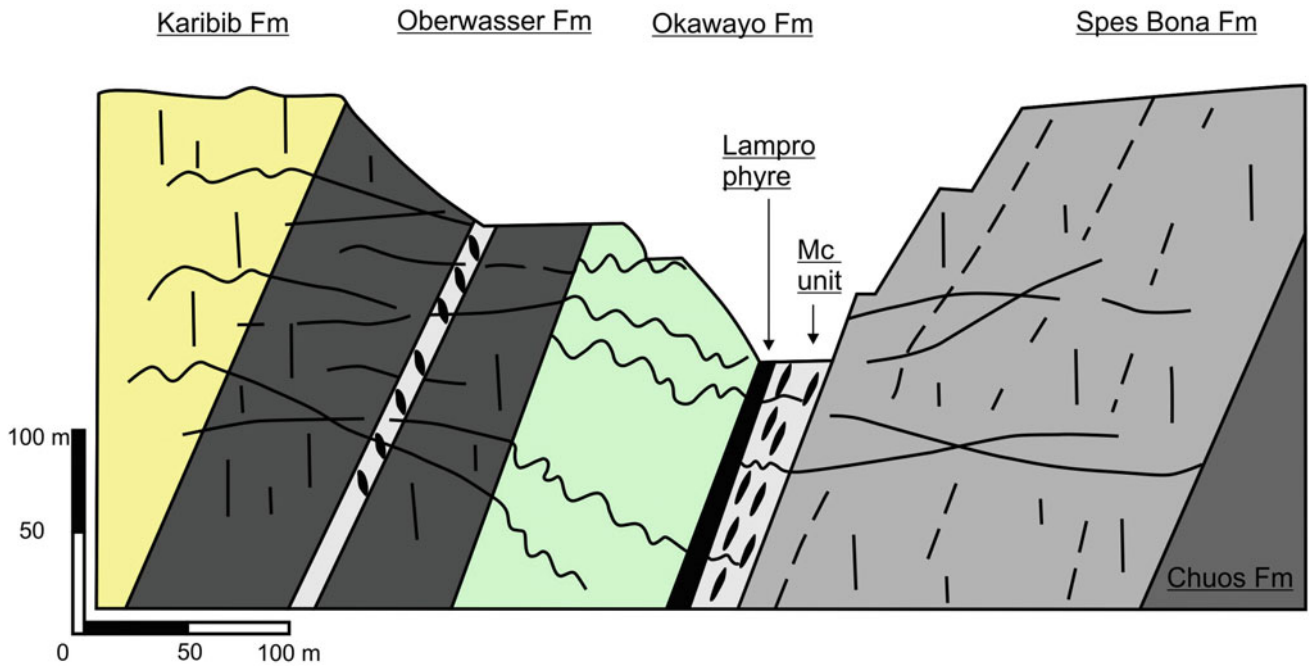

Fig. 23.50 Cross-section through the Navachab open pit and deposit (after Kisters 2005)

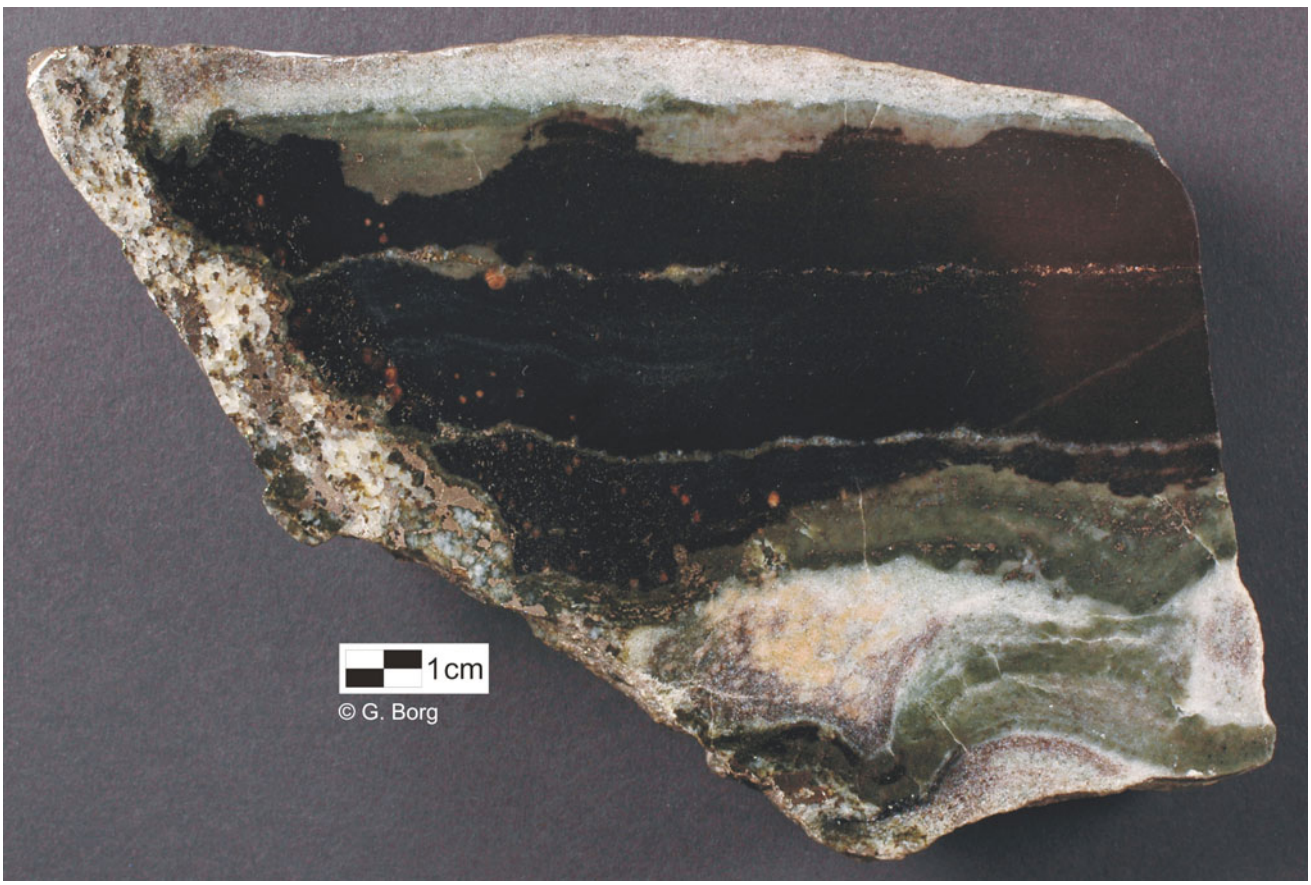

Fig. 23.51 Navachab Mine. Banded black and grey marble crosscut by a quartz-calcite-pyrrhotite vein at left. Euhedral garnet (brownish-red) and clinopyroxene (grey-green) have replaced the marble, partly along bedding planes, producing a typical distal exo-skarn texture. Photograph by Gregor Borg

containing pyrrhotite, chalcopyrite, arsenopyrite, and sphalerite was followed by a precious metal ore paragenesis of pyrite, maldonite, auriferous bismuth, and gold. Nörtemann et al. (2000) considered a barren, camptonitic metalamprophyre to represent a redox-trap for Au-bearing fluids and its unusual Mn- and Fe-rich composition, reflected in the skarn mineralogy. Gold occurs mainly as native gold, with minor maldonite (Au_2Bi) and as solid solution in bismuth (up to 4 mol% Au; Nörtemann 1997). The metalamprophyre MCH member is in general barren of gold.

Nörtemann et al. (2000) claim that Navachab has similar mineralogical, metamorphic, and structural features to several other skarns in the world, to a group that Meinert (1998) classified as 'mesothermal' regional metamorphic gold skarns. Like Navachab, the skarn mineralisation is situated at the contact to or within shoshonites. These authors concluded that the unusual mineralogy is the product of contact metamorphism and metasomatic alteration of metasedimentary rocks and interbedded mafic volcanic rocks. Deposits such as Navachab, Tillicum, and Lucky Draw are distinct from Phanerozoic gold skarns associated with relatively shallow plutons. In older, Precambrian orogenic belts, metamorphism reaches relatively high temperatures. In addition, the pressure conditions indicate deeper levels, more similar to W skarns rather than Au skarns. At Navachab, W occurs throughout the deposit as scheelite, confirming the similarities to W skarns.

According to Meinert (1998) these deposits are hybrids between a regional metamorphic environment and Phanerozoic plutonism. The occurrence of gold mineralisation in the vicinity of lamprophyres and the high content of volatiles in lamprophyres led Rock and Groves (1988) to the conclusion that lamprophyres represent the original transport media of significant volumes of gold-bearing fluids. Thus the lamprophyre of Navachab is considered to represent a redox trap for the circulating gold-bearing fluids. Dating of the early syntectonic Mon Repos diorite and leucogranites near Navachab by Moore and Jacob (1998) led them to the conclusion that these 540 Ma old intrusions represent the original source of the gold. These authors considered Navachab to be a sheeted vein mesothermal deposit developed distal to its related intrusion. However, these intrusions do not host any significant gold mineralisation or significant Fe–Cu sulphides. If the Damaran diorites and leucogranites are related to mineralisation and skarn formation at Navachab, and given the relatively large distance of fluid transport that this would require, it seems likely that the metal-bearing fluids of Navachab represent a mixture of fluid and metal sources, including those remobilised and derived from basement rocks. The key feature at Navachab is the presence of a lamprophyre that may have served as a redox trap for the circulating fluids.

Steven et al. (2015) provided the first Cambrian Re–Os molybdenite ages in two different types of aplite dyke from Navachab. Extensional auriferous quartz-bismuth-pyrite-pyrrhotite veins have slightly younger Re–Os ages around 520 Ma. The 525–520 Ma gold-mineralising event occurred slightly after the collisional metamorphic peak at 530 Ma, but subsequent gold redistribution and possibly melting of the Au–Bi minerals probably occurred at the late-stage thermal peak of the Damaran High-T/Low-P tectonothermal event.

Wulff et al. (2010) used stable isotope analyses to constrain the source of the mineralising fluid and the processes of fluid-rock interaction and ore deposition. Their data support earlier studies, which favour a metamorphic origin of the mineralising fluid (Dziggel et al. 2009a, b) and suggest that the most likely source of the mineralising fluid were deep-crustal equivalents of the Damaran metasedimentary rocks that underwent prograde metamorphism at amphibolite- to granulite-facies. Wulff et al. (2010) emphasise that the metasedimentary rock sequence at Navachab has been intruded by abundant syntectonic lamprophyre, aplite, and pegmatite dykes, documenting widespread igneous activity coeval with mineralisation. Gold is interpreted by these authors to have precipitated in equilibrium with a mid-crustal metamorphic fluid in equilibrium with the Damaran metapelites at peak metamorphic conditions, consistent with isotopic fractionations between coexisting calcite, garnet, and clinopyroxene in the alteration halos.

Although the deposit shares many characteristics with structurally controlled orogenic gold deposits (sensu Groves et al. 1998), the close spatial and temporal association of the deposit to igneous intrusions, the presence of skarn-type alteration assemblages, as well as an unusual metal association of Au–Bi–As–Cu–Ag (Dziggel et al. 2009a) have been used to suggest a possible genetic relationship with intrusion-related gold deposits (Thompson et al. 1999). As a result, most previously proposed genetic models have emphasised the role of igneous activity (1) as an agent for concentrating and redistributing gold and other metals into the ore bodies (Piranjo and Jacob 1991); (2) by acting as a redox trap for the gold-bearing fluid (Nörtemann et al. 2000); or 3) by contributing to elevated geothermal gradients and an overall hydraulic regime in the area of the deposit (Dziggel et al. 2009a).

The final, small group of deposits that have formed very late during the tectonometamorphic history of SW Gondwana orogens are described in an exemplary way for the following deposits.

23.12 Late Tectonic Deposits, Omitiomire and Similar Pan-African Cu Deposits

The Omitiomire deposit has been estimated to contain about 1 Mt of Cu metal, hosted by Mesoproterozoic (1115–1063 Ma) bimodal metavolcanic rocks, which were metamorphosed to amphibolite grade (7–8 kbar, 600 °C) during the Damaran orogenic event at ~535 Ma related to collision between the Congo and Kalahari Cratons. Maiden et al. (2013) describe the Omitiomire Cu deposit in the Pan-African Damara Belt of central Namibia as a late tectonic copper emplacement in a Neoproterozoic (Pan-African) imbricate shear system. The copper mineralisation occurs primarily as hypogene chalcocite in stacked ore lenses from 10 m to >100 m in thickness, hosted by mafic schists, dipping and plunging at moderate angles and extending for 4000 m 'open-ended' to the north-northeast. The chalcocite and associated epidote-sphene-magnetite paragenesis overprint the shear fabric, documenting the late tectonic emplacement of copper. Sphene ages (525–485 Ma) date the Cu-mineralising event(s) and Kitt et al. (2016) found Cu mineralisation confined to an anastomosing system of shallow-dipping, retrograde mylonitic shear zones within amphibolite gneiss domes. Mylonitisation and copper mineralisation are closely associated with the retrogression of particularly amphibolites and the partial or complete replacement of amphibolites by biotite-epidote and biotite-chlorite-epidote schists. The regional setting of the Omitiomire deposit, kinematics, and retrograde but high-temperature overprint of original mineral assemblages in the mineralised shear zones indicate deformation and fluid flow during the expulsion of the basement gneisses during northwards-directed subduction of the Kalahari Craton below the Congo Craton (Kitt et al. 2016). Lithological, geochronological, structural and P-T data suggest numerous similarities and, indeed, correlations between the Omitiomire-style copper mineralisation of the Damara Belt with the large copper deposits hosted by basement gneisses in the Domes Region of the Lufilian Arc in Zambia.

23.13 Conclusions

The African part of SW Gondwana is host to an enormous wealth of mineral deposits of commodities such as base metals (Cu, Pb, Zn, Co, Ni), precious metals (Au, Ag), and strategic metals (U, W, Sn, Li, Ta and REE). The ore deposits of SW Gondwana occur in several major regional to supraregional metallotects and formed during different geodynamic stages of crustal evolution and amalgamation of this supercontinent. The sheer number of metallotects and ore deposits does not allow any detailed summary or even condensed repetition at this point. It is important to note that ore formation in these metallotects has been systematically related to a number of distinct geodynamic settings and stages (Fig. 23.2). These include metallogenesis related to divergent crustal settings comprising VHMS deposit formation on the ocean floor, and VHMS/SHMS deposits formed in continental rifts at fault intersections in volcanosedimentary basins. The low-energy sedimentary, shallow marine, chemically reducing sediment package of more evolved, subsiding volcanosedimentary basins allowed the development of sediment-hosted stratabound Cu–Ag deposits during diagenetic stages. However, these metallotects show strong evidence of at least partial to substantial epigenetic introduction of metals at much later, collisional orogenic stages. Mantle derived mafic melts allowed the formation of orthomagmatic and related ore deposits of Cu, Co, and Ni, whereas the even more advanced collisional stages of orogens have been associated with varied increasing grades of metamorphism, regionally resulting in highly fractionated evolved and crustal granitic minimum melts. The ore deposits associated with these highly fractionated and locally exotic melts comprise a range of elements that share a highly incompatible geochemical behaviour during the evolution of the melts.

Overall, these geodynamic settings with multiple extensional and compressional regimes spanning large areas of Southern Africa have resulted in SW Gondwana's rich and diverse endowment with ore deposits. Many of these have been identified and mined in the past and present, mainly where the deposits occurred at or relatively close below the earth's surface. But there are, undoubtedly, more deposits to be discovered, particularly below surficial or deeper cover, where new metallogenetic and exploration concepts need to be developed for successful exploration.

Acknowledgements Staff of Skorpion Mine, Rosh Pinah Mine, the Aggeneys mines, Navachab Mine, and Eiseb Prospecting and Mining (Pty) Ltd. are acknowledged for allowing access to their operations and sharing valuable knowledge during informative discussions. Markus Schaefer, Vedanta Resources plc is acknowledged for providing up-to-date information about tonnages and grades for the Aggeneys and Skorpion deposits. Hartwig Frimmel is gratefully acknowledged for his thorough review of a first draft, which has helped to improve the quality of this chapter. We gratefully acknowledge Anna Friebel for her draft work on the maps and figures.

References

Alchin DJ, Rozendaal A, Cain AC, Hunt I, Lottering P (1999) Lithogeochemical haloes, metal zonation and geochemical vectors associated with the stratiform sediment-hosted Rosh Pinah Zn-Pb-Ag deposit, Namibia. J Afr Earth Sci 28(4):4

Alchin DJ, Moore JM (2005) A review of the Pan-African, Neoproterozoic Rosh Pinah Zn-Pb deposit, southwestern Namibia. S Afr J Geol 108(1):71–86

Alchin DJ, Frimmel HE, Jacobs LE (2005) Stratigraphic setting of the metalliferous Rosh Pinah Formation and the Spitzkop and Koivib suites in the Pan-African Gariep Belt, south-western Namibia. S Afr J Geol 108(1):19–34

Andreoli MAG, Smith CB, Watkeys MK, Moore JM, Ashwal LD, Hart RJ (1994) The geology of the Steenkampskraal monazite deposit, South Africa: implications for REE-Th-Cu mineralisation in charnockite-granulite terranes. Econ Geol 89:994–1016

Anhaeusser CR, Maske S (1998) Mineral deposits of southern Africa. Geol Soc S Afr 2:1020, Johannesburg

Annels AE, Simmonds JR (1984) Cobalt in the Zambian Copperbelt. Precambr Res 25:75–98

Annels AE (1974) Some aspects of the stratiform ore deposits of the Zambian Copperbelt and their genetic significance. In: Bartholomé P (ed) Gisements stratiformes et provinces cuprifères: Liège, Centenaire de la Société Géologique de Belgique: 235–254

Ashworth L (2014) Mineralised pegmatites of the Damara Belt, Namibia: Fluid inclusion and geochemical characteristics with implications for post-collisional mineralisation. Ph.D. thesis University of the Witwatersrand, Johannesburg, South Africa: 299p

Bailie RH, Reid DL (2005) Ore textures and possible sulphide partial melting at Broken Hill, Aggeneys, South Africa, I: Petrography. S Afr J Geol 108:51–70

Bailie R, Armstrong R, Reid D (2007a) The Bushmanland Group supracrustal succession, Aggeneys, Bushmanland, South Africa: provenance, age of deposition and metamorphism. S Afr J Geol 110:59–86

Bailie R, Armstrong R, Reid D (2007b) Composition and single zircon U-Pb emplacement and metamorphic ages of the Aggeneys Granite Suite, Bushmanland, South Africa. S Afr J Geol 110:87–110

Barra F, Broughton D, Ruiz J, Hitzman M (2004) Multi-stage mineralization in the Zambian Copperbett based on Re-Os isotope constraints. Geol Soc Am Abstr Progmms 36:516

Bartholomé P, Evrard P, Katekesha F, Lopez-Ruiz J, Ngongo M (1973) Diagenetic ore-forming processes at Kamoto, Katanga, Republic of the Congo, in Amstutz GC, Bernard AJ (eds) Ores in sediments. Springer, Berlin, pp 21–41

Basson IJ, Greenway G (2004) The Rössing uranium deposit: a product of late-kinematic localization of uraniferous granites in the Central Zone of the Damara Orogen, Namibia. J Afr Earth Sci 38:413–435

Basson IJ, Muntingh JA, Jellicoe BC, Anthonissen CJ (2016) Structural interpretation of the Steenkampskraal monazite deposit, Western Cape, South Africa. J Afr Earth Sci 121:301–315

Becker E, Kärner K (2009) Geological setting of the Langer Heinrich uranium mine, Namibia (No. IAEA-CN—175: p 15 (ADD.)). Addendum to the Book of Abstracts for the International Symposium on Uranium Raw Material for the Nuclear Fuel Cycle: Exploration, Mining, Production, Supply and Demand, Economics and Environmental Issues (URAM-2009) 22–26 June 2009, Vienna, Austria, 18p

Becker T, Schalk KEL (2008) The Sinclair Supergroup of the Rehoboth volcanic arc from the Sossusvlei-Gamsberg area to the Gobabis region. In: Miller RM (ed) The Geology of Namibia, in three volumes. Windhoek, Geological Survey of Namibia, vol 1, pp 8–68

Beeson R (1990) Broken Hill-type lead-zinc deposits – an overview of their occurrence and geological setting. Trans Inst Min Metall (Sect B) 99:163–175

Bernau R, Roberts S, Richards M, Nisbet B, Boyce A, Nowecki J (2013) The geology and geochemistry of the Lumwana Cu (± Co ± U) deposits, NW Zambia. Min Dep 48(2):137–153

Bigotte G (1959) Contribution a la geologie du bassin du Niari; etude sedimentologique et metallogenique de la region miniere. Bulletin de la Direction des Mines et de la Geologie 9, 188p

Binda PL (1994) Stratigraphy of Zambian Copperbelt orebodies. J Afr Earth Sci 19(4):251–264

Boer RH, Meyer FM, Cawthorn RG (1994) Stable isotopic evidence for crustal contamination and desulfidation of the cupriferous Koperberg Suite, Namaqualand, South Africa. Geochim Cosmochim Acta 58:2677–2687

Borg G (1988a) Controls on Stratabound Copper Mineralization at Klein Aub Mine and Similar Deposits within the Kalahari Copperbelt of South West Africa/ Namibia and Botswana. Unpubl. Ph.D. thesis, University of the Witwatersrand, Johannesburg, South Africa, 107p

Borg G (1988b) The Koras-Sinclair-Ghanzi Rift in Southern Africa. Volcanism, Sedimentation, Age Relationships and Geophysical Signature of a late Middle Proterozoic Rift System. Precambr Res 38:75–90

Borg G (1995) Metallogenesis of Neoproterozoic basins in Namibia and Botswana. Communs Geol Surv Namibia 10:109–119

Borg G (2000) Regional controls on sediment-hosted Pb-Zn (Ba-Cu) occurrences within the Pan-African orogenic belts of Namibia. Geol Surv Namibia Com 12:239–249

Borg G (2015) A Review of Supergene Nonsulphide Zinc (SNSZ) Deposits - the 2014 Update. In: Archibald SM, Piercey SJ (eds) Current Perspectives of Zinc Deposits. Irish Assoc Econ Geol, Dublin, pp 123–147

Borg G, Gauert C (2003) Sediment-hosted Pb-Zn (Cu-Ba) mineralisation within the coastal branches of the Damara Orogen, Namibia—a review. Geol Jahrb D 111:1–139

Borg G, Kärner K, Buxton M, Armstrong R, van der Merwe SW (2003) Geology of the Skorpion supergene zinc deposit, southern Namibia. Econ Geol 98(4):749–771

Borg G, Klein E, Kärner K, Botha R, Harney D (2004) Lithology, structure, and deep weathering characteristics of the supergene Skorpion zinc ore body. Abstract Geoscience Africa 2004–1:71–72

Borg G, Maiden KJ (1987) Basalt alteration and its relation to Middle Proterozoic stratabound copper—silver-gold deposits along the margin of the Kalahari Craton in SWA/Namibia and Botswana. In: Beckinsale RD, Rickards DT (eds) Pharaoh TC. Geochemistry and Mineralization of Proterozoic Volcanic Suites, Geol Soc Spec Publ, pp 347–354

Borg G, Maiden KJ (1989) The Middle Proterozoic Kalahari Copper Belt of Namibia and Botswana. In: Boyle RW, Brown AC, Jefferson CW, Jowett EC, Kirkham RV (eds) Sediment-hosted Stratiform Copper Deposits, Geol Ass Canada, Spec Pap, vol 36, pp 525–540

Borg G, Kottke-Levin J (2007) Recognition of high-T rhyolite melts in the Rosh Pinah – Skorpion Zn-Pb district, Southern Namibia. In: Andrew CJ et al (eds) Digging deeper—proceedings of the ninth biennial meeting, SGA, Dublin, Ireland, pp 1049–1052

Borg G, Tornos F (2009) Genetic Implications of a Pervasive K-alteration zone at the Rosh Pinah VHMS-SHMS deposit, Namibia. In: Williams PJ et al. (eds) Smart science for exploration and mining, proceedings of the 10th biennial SGA meeting, Townsville, Australia, pp 406–409

Borg G, Graf N, Maiden KJ (1987) The Klein Aub Fault Zone. A Wrench Fault System in Middle Proterozoic Metasediments in Central SWA/Namibia. Comm geol Surv SWA/Namibia 3:91–98

Borg G, Tredoux M, Maiden KJ, Sellschop JPF, Wayward, OFD (1987) PGE- and Au-Distribution in Rift-related Volcanics, Sediments and Stratabound Cu/Ag Ores of Middle Proterozoic Age in Central SWA/Namibia. In: Prichard HM, Potts PJ, Bowles JFW, Cribb SJ (eds) Geo-Platinum '87, Elsevier, pp 303–318

Boudzoumou F, Trompette R (1988) La chaine panafricaine ouest-congolienne au Congo (Afrique equatoriale): un socle polycyclique charrie sur un domaine subautochtone forme par l'aulacogene du Mayombe et le bassin de l'Ouest-Congo. Bull Soc Geol France 4(6):889–896

Bowden P, Herd D, Kinnaird JA (1995) The significance of Uranium and Thorium concentrations in pegmatitic leucogranites (alaskites), Rössing Mine, Swakopmund, Namibia. Comm Geol Surv Namibia 10:43–49

Brandriss ME, Cawthorn RG (1996) Formation of anorthosite and leucotonalite during magma hybridization in the Koperberg Suite of Namaqualand, South Africa. S Afr J Geol 99:135–152

Breitkopf JH, Maiden KJ (1988) Tectonic setting of the Matchless Belt pyritic copper deposits, Namibia. Econ Geol 83:710–723

Buffet G, Amosse J, Mouzita D, Giraud P (1987) Geochemistry of the M'Passa Pb-Zn deposit (Niari syncline, People's Republic of the Congo). Arguments in favour of a hydrothermal origin. Min Dep 22:64–77

Cahen L (1978) La stratigraphie et la tectonique du Supergroupe Ouest-Congolien dans les zones mediane et externe de l'Orogene Ouest-Congolien (Pan-Africain) au bas-Zaire et dans les regions Voisines. Koninklijk Museum voor Midden-Afrika – Annalen, Reeks in 80: Geologische Wetenschappen 83, 150p

Cahen L (1982) Geochronological correlations of the Late Precambrian sequence on and around the stable zones of equatorial Africa. Precambrian Res 18:73–86

Cailteux J, Binda PL, Kampunzu AB, Katekesha WM, Kaunda C, Wendorff M (1995) Results of lithostratigraphic correlation of the late Proterozoic Roan Supergroup between Zambia and Zaire, Central African Copperbelt, Royal Museum of Central Africa (Belgium) Ann Soc Geol, vol 101, pp 21–27

Cailteux JLH, Delpomdor FRA, Ngoie Ndobani J-P (2015) The Neoproterozoic West-Congo "Schisto-Calcaire" sedimentary succession from the Bas-Congo region (Democratic Republic of the Congo) in the frame of regional tentative correlations. Geological Belgica 18(2–4):126–146

Cailteux JLH, Kampunzu AB, Lerouge C, Kaputo AK, Milesi JP (2005) Genesis of sediment-hosted stratiform copper–cobalt deposits, Central African Copperbelt. J Afr Earth Sci 42:134–158

Cailteux JLH, Kampunzu AB, Lerouge C (2007) The Neoproterozoic Mwashya-Kansuki sedimentary succession in the Central African Copperbelt, its Cu–Co mineralisation, and regional correlations. Gondwana Res 11:414–431

Cawthorn RG, Meyer FM (1993) Petrochemistry of the Okiep Copper District Basic Intrusive Bodies, Northwestern Cape Province, South Africa. Econ Geol 88:590–605

Chetty D, Frimmel HE (2000) The role of evaporites in the genesis of base metal sulphide mineralisation in the northern Platform of the Pan-African Damara Belt, Namibia: geochemical and fluid inclusion evidence from carbonate wall rock alteration. Min Dep 35:364–376

Clague S, Alchin D (2001) The terrane setting and metallogenesis of the Rosh Pinah massive Zn-Pb sulfide deposit in the Gariep Terrane of southern Namibia. Abstract Geol Soc Am 33:271–272

Clifford TN, Barton ES, Retief EA, Rex DC (1990) The Koperberg Suite, Okiep copper district, Namaqualand, South Africa: new isotope data (abs): 15th Colloquium African Geology, Nancy, France

Clifford TN, Gronow L, Rex DC, Burger AJ (1975) Geochronological and petrological studies of high-grade metamorphic rocks and intrusives in Namaqualand, South Africa. J Petrol 16:154–188

Clifford TN, Stumpfl EF, Burger AJ, McCarthy TS, Rex DC (1981) Mineral-chemical and isotopic studies of Namaqualand granulites, South Africa: a Grenville analogue. Contr Mineral Petrol 77:225–250

Clifford TN, Barton ES, Retief EA, Rex DC, Fanning CM (1995) A Crustal Progenitor for the Intrusive Anorthosite—Charnockite Kindred of the Cupriferous Koperberg Suite, O'okiep District, Namaqualand, South Africa; New Isotope Data for the Country Rocks and the Intrusives. J Petrol 36:231–258

Clifford TN, Barton ES, Stern RA, Duschene J-C (2004) U-Pb zircon calendar for Namaquan (Grenville) crustal events in the granulite facies terrane of the O'okiep Copper District of South Africa. J Petrol 45:669–691

Cole DI (2003) The metallogeny of the Cape Town area. Explanation and metallogenic map of sheet 3318 (scale 1:250.000) Council for Geoscience, Pretoria, pp 1–80

Cole DI, Ngcofe L, Halenyane K (2014) Mineral Commodities in the Western Cape Province, South Africa. Council for Geoscience, Western Cape Regional Office, Report 2014-0012, 90 p

Conradie JA, Schoch AE (1986) Petrographical characteristics of the Koperberg Suite, South Africa: an anology to massif-type anorthosites? Precambrian Res 31:157–188

Cooke DR, Bull SW, Large RR, McGoldrick PJ (2000) The Importance of oxidised brines for the formation of Australian Proterozoic Stratiform Sediment-Hosted Pb-Zn (sedex) deposits. Econ Geol 95 (1):1–17

Cornell DH, Thomas RJ, Moen HFG, Reid DL, Moore JM, Gibson RL (2006) The Namaqua-Natal Province. In: The geology of South Africa, edited by Johnson MR, Anhaeusser CR, Thomas RJ (eds) Geological Society of South Africa and Council for Geoscience, Johannesburg, pp 325–379

Corrans RD, Gewald H, Whyte RM, Land BN (1993) The Skorpion SZ secondary zinc deposit–south western Namibia. In: Abstracts of conference on mining investment in Namibia, Windhoek, Namibia, pp 46–57

de Boorder H (1982) Deep-reaching fracture zones in the crystalline basement surrounding the West Congo System and their control of mineralization in Angola and Gabon. In: Hastings D (ed) Geophysics, tectonics and mineral deposits of Africa, pp 259–273

De Kock NJ, (1987) Die verandering van die wandgesteentes in die omgewing van die ertsliggame van Rosh Pinah. Unpublished M.Sc. thesis, University of Pretoria, South Africa, 155p

de Wit MJ, Linol B (2015) Precambrian basement of the Congo Basin and its flanking terrains. In: de Wit MJ, Guillocheau F, de Wit MCJ (eds) Geology and resource potential of the Congo Basin. Springer, Berlin, pp 19–37

de Wit MJ, Stankiewicz J, Reeves C (2008) Restoring Pan-African-Brasiliano connections: more Gondwana control, less Trans-Atlantic corruption. In: Pankurst RJ, Trouw RAJ, Brito Neves BB, de Wit MJ (eds) West Gondwana: Pre-Cenozoic correlations across the South Atlantic region. Geological Society of London, Special Publication, vol 294, pp 399–412

Diehl BJM (1992a) Tin. Mineral Resources of Namibia. Geological Survey of Namibia, Windhoek, pp 1–24

Diehl BJM (1992b) Tungsten. Mineral Resources of Namibia. Geological Survey of Namibia, Windhoek, pp 1–10

Diehl BJM (1992c) Lithium, beryllium, cesium. Mineral Resources of Namibia. Geological Survey of Namibia, Windhoek, pp 1–13

Diehl BJM (1993) Rare metal pegmatites of the Cape Cross-Uis pegmatites belt, Namibia: geology, mineralisation, rubidium-strontium characteristics and petrogenesis. J Afr Earth Sci 17:167–181

Diener JFA, Thomas RJ, Macey Paul H (2017) Pan-African accretionary metamorphism in the Sperrgebiet Domain, Gariep Belt, SW Namibia. Precambrian Res 292:152–162

Dodd DS, Hannon PJF, Roy WD, Siegfried PR, Hall MR (2014) Preliminary economic assessment of the Lofdal rare earths project, Namibia. NI 43-101, Technical Report. 363 p (available from www.sedar.com)

Duke EF, Paterson CJ (2007) Hyperspectral remote sensing and field spectral analysis of the stratigraphy, structure, and metamorphism of cupriferous volcanogenic massive sulfide occurrences near Gorob, Damara Orogen, west-central Namibia. Abstracts with Programs Geological Society of America, vol 39, p 628

Duncan AR, Watkeys MK, Moore JM (1984) Geochemistry of the "floor" rocks of Namaqualand. In: Abstracts of the Mid-late Proterozoic crustal evolution symposium, University of Cape Town, South Africa, pp 75–76

Duncan AR, Joubert P, Reid AM, Watkeys MK, Betton PJ, Reid DL, Erlank AJ, Cleverly RW (1985) Geochemical studies on the floor rocks of Namaqualand. Unpublished Final Report, National Geoscience Programme, Council for Scientific and Industrial Research, Pretoria, South Africa

Du Toit MC (1998) Lead. In: Wilson MGC, Anhaeusser CR (eds) The Mineral Resources of South Africa. Handbook of the Council for Geoscience, Pretoria, South Africa, pp 424–432

Dziggel A, Wulff K, Kolb J, Meyer FM (2009a) Processes of high-T fluid-rock interaction during gold mineralization in carbonate-bearing metasediments: the Navachab gold deposit. Min Dep, Namibia, pp 665–687

Dziggel A, Wulff K, Kolb J, Meyer FM, Lahaye Y (2009b) Significance of oscillatory and bell-shaped growth zoning in hydrothermal garnet: evidence from the Navachab gold deposit, Namibia. Chemical Geol 262:278–292

Eglinger A, Ferraina C, Tarantola A, Andre-Mayer AS, Vanderhaeghe O, Boiron MC, Dubessy J, Richard A, Brouand M (2014) Hypersaline fluids generated by high-grade metamorphism of evaporites: fluid inclusion study of uranium occurrences in the Western Zambian Copperbelt. Contrib Mineral Petrol 167:967

Eglington BM (2006) Evolution of the Namaqua-Natal Belt, southern Africa—a geochronological and isotope geochemical review. J Afr Earth Sci 46:93–111

El Desouky HA, Muchez P, Cailteux JLH (2009) Two Cu-Co sulphide phases and contrasting fluid systems in the Katanga Copperbelt, Democratic Republic of Congo. Ore Geol Rev 6(36):315–332

El Desouky HA, Muchez P, Boyce AJ, Schneider J, Cailteux JLH, Dewaele S, von Quadt A (2010) Genesis of sediment-hosted stratiform copper–cobalt mineralisation at Luiswishi and Kamoto, Katanga Copperbelt (Democratic Republic of Congo). Min Dep 45(8):735–763

Enviro Dynamics cc (2014) Environmental and social impact assessment (ESIA) for the proposed development of the Gergarub Mine, draft scoping report. Windhoek, Namibia

Fay I, Barton MD (2012) Alteration and ore distribution in the Proterozoic Mines Series, Tenke-Fungurume Cu–Co district, Democratic Republic of Congo. Min Dep 47(5):501–519

Fleischer VD, Garlick WG, Haldane R (1976) Geology of the Zambian Copperbelt. In: Wolf KH (ed) Handbook of strata-bound and stratiform ore deposits, vol 6, pp 223–352

Franz L, Romer RL, Dingeldey DP (1999) Diachronous Pan-African granulite-facies metamorphism (650 Ma and 550 Ma) in the Kaoko Belt, NW Namibia. Europ J Mineral 11(1):167–180

Freemantle GG (2015) Primary Uranium Mineralisation of the Central Damara Orogen, Namibia. Ph.D. thesis, University of the Witwatersrand, South Africa, 165p

Frimmel HE (2009) Configuration of Pan-African orogenic belts in southwestern Africa. eoproterozoic to Early Palaeozoic evolution of Southwestern Africa. In: Gaucher C, Sial AN, Halverson GP, Frimmel HE (eds) Neoproterozoic-Cambrian Tectonics, global change and evolution: a focus on Southwestern Gondwana, Developments in Precambrian Geology, Elsevier, Amsterdam, pp 145–151

Frimmel HE, Board WS (2000) Fluid evolution in and around the Rosh Pinah massive sulfide deposit in the external Pan-African Gariep belt, Namibia. S Afr J Geol 103:191–206

Frimmel HE, Miller RMcG (2009) Mineral deposits. Neoproterozoic to Early Palaeozoic evolution of Southwestern Africa. In Gaucher C, Sial AN, Halverson GP, Frimmel HE (eds) Neoproterozoic-Cambrian Tectonics, global change and evolution: a focus on Southwestern Gondwana, Developments in Precambrian Geology, Elsevier, Amsterdam, pp 227–229

Frimmel HE, Tack L, Basei MS, Nutman AP, Boven A (2006) Provenance and chemostratigraphy of the Neoproterozoic West Congolian Group in the Democratic Republic of Congo. J Afr Earth Sci 46:221–239

Garlick WG (1961) The syngenetic theory: In: Mendelsohn F (ed) The geology of the Northern Rhodesian Copperbelt: London, Macdonald & Co. (Publishers) Ltd., pp 146–165

Gauert CDK (2005a) Stratiform coticule-barite-sulphide horizons in the sediment-hosted Tsongoari-Omupokko Pb-Cu-Ba-Zn-Ag prospects, Kaokoland, Namibia. S Afr J Geol 108(1):87–118

Gauert CDK (2005b) Geochemistry and provenance of clastic metasedimentary host rocks of the Rosh Pinah Zn-Pb-Ag(-Cu-Au) deposit, Southern Namibia. In: Mao J, Bierlein FP (eds) Mineral Deposit Research: Meeting the Global Challenge. Springer, Berlin, Heidelberg, pp 123–126

Gevers TW, Frommurze HF (1929) The tin-bearing pegmatites of the Erongo area, South West Africa. Trans Geol Soc S Afr 32:111–149

Gibson RL, Robb LJ, Kisters AFM, Cawthorn RG (1996) Regional setting and geological evolution of the Okiep Copper District, Namaqualand, South Africa. S Afr Jl Geol 99(2):107–122

Gill SJ (2016) The Kalahari Copperbelt in central-eastern Namibia. Unpublished Ph.D. thesis, Birkbeck College, University of London, 407p

Glencore International Plc.'s website (2011) http://www.glencore.com/assets/media/doc/news/2011/201112150800-Glencore-enters-agreement-to-acquire-Rosh-Pinah.pdf. Accessed 2 May 2017

Glencore International Plc.'s website (2012) http://www.glencore.com/assets/media/doc/news/2012/201206110800-Glencore-completes-acquisition-of-controlling-interest-in-Rosh-Pinah.pdf. Accessed 2 May 2017

Goldberg I (1976) A preliminary account of the Otjihase copper deposit, South West Africa. Econ Geol 71:384–390

Gorman, AR, Jenkin GRT, Morgan KL, Catterall D (2013) Developing genetic models for copper-silver mineralisation in the Kalahari Copperbelt, Botswana: mineralogy, geochemistry and structure. In: 12th SGA biennial meeting, proceedings, vol 2, pp 624–627

Gray DR, Foster DA, Goscombe B, Passchier C, Trouw (2006) $^{40}Ar/^{30}Ar$ thermochronology of the Damara Orogen, Namibia, South West Africa, with implications for tectonothermal evolution. Precambrian Res 150:49–72

Groves DI, Phillips GN (1987) The genesis and tectonic control of archean gold deposits of the Western Australian Shield—a metamorphic replacement model. Ore Geol Rev 2:287–322

Groves DI, Goldfarb RJ, Gebre-Mariam M, Hagemann S, Robert F (1998) Orogenic gold deposits: a proposed classification in the context of their crustal distribution and relationship to other gold deposit types. Ore Geol Rev 13:7–28

Haack U, Gohn E (1988) Rb-Sr data on some pegmatites in the Damara Orogen, Namibia. Comm Geol Surv SW-Afr/Namibia 4:13–17

Haeussinger H, Okrusch M, Scheepers D (1993) Geochemistry of premetamorphic hydrothermal alteration of metasedimentary rocks associated with the Gorob massive sulfide prospect, Damara Orogen, Namibia. Econ Geo 88:72–90

Hall WS 2013 Geology and paragenesis of the Boseto Copper deposit, Kalahari Copperbelt, northwest Botswana. Unpublished M.Sc. thesis, Colorado School of Mines, Colorado, United States of America, 157 p

Hanson RE (2003) Proterozoic geochronology and tectonic evolution of southern Africa. In: Yoshida M, Windley B F, Dasgupta S (eds) Proterozoic East Gondwana: supercontinent assembly and breakup. Geological Society of London Special Publication, pp 427–463

Harmer RE, Nex PAM (2016) Rare earth deposits of Africa. Episodes 39(2):381–406
Hartleb JWO (1988) The Langer Heinrich uranium deposit; Southwest Africa/Namibia. Ore Geol Rev 3(1–3):277–287
Henry G, Bentley PN (1994) The Tsongoari Pb-Zn-Cu-Ba deposits, Namibia. In: Abstracts, conference on proterozoic crustal and metallogenic evolution, Geological Survey of Namibia, Abstract, vol 27
Henry G, Charlesworth EG, Master S, Stanistreet IG (2002) The Tsongoari sedimentary exhalative sulphide deposits, Kaokoland, Namibia. 11th quadrennial IAGOD symposium and geocongress 2002, abstract volume, pp 4–8
Henry G, Osborne MA, Schmerold RK (1992) Note: Proposed lithostratigraphic subdivision of the Ugab Subgroup (Damara Sequence) in Kaokoland, Namibia. Com Geol Surv Namibia 8:143–145
Hitzman MW (2000) Source basins for sediment-hosted stratiform Cu deposits: implications for the structure of the Zambian Copperbelt. J Afr Earth Sci 30(4):855–863
Hitzman MW, Selley D, Bull S (2010) Formation of sedimentary rock-hosted stratiform copper deposits through earth history. Econ Geol 105(3):627–639
Hitzman MW, Broughton D, Selley D (2012) The Central African Copperbelt: diverse stratigraphic, structural, and temporal settings in the world's largest sedimentary copper district. Econ Geol Spec Publ 16:487–514
Hoffmann D (1993) Aspects of the geology, geochemistry and metamorphism of the lower orebody, Broken Hill deposit, Aggeneys. Unpublished M.Sc. thesis, University of Cape Town, South Africa, 211p
Hoffmann KH, Condon DJ, Bowring SA, Crowley JL (2004) U-Pb zircon date for the Neoproterozoic Ghaub Formation, Namibia: constraints on Marinoan glaciation. Geology 32:817–820
Hugo PJ (1970) The pegmatites of the Kenhardt and Gordonia districts. Geological Survey. Department of Mines of South Africa, Pretoria, Memoir, pp 1–94
ITRI (2011) https://www.itri.co.uk/about-itri
Jackson MPA, Warin ON, Woad GM, Hudec MR (2003) Neoproterozoic allochthonous salt tectonics during the Lufilian orogeny in the Katangan Copperbelt, central Africa. Geol Soc America Bull 115 (3):314–330
Joubert P (1986) The Namaqualand metamorphic complex—a summary. In: Anhaeusser CR, Maske S (eds) Mineral deposits of southern Africa. Geological Society of South Africa, Johannesburg, pp 1395–1420
Kärner K (2006) The metallogenesis of the Skorpion non-sulphide zinc deposit, Namibia. Unpublished Ph.D. thesis, Martin-Luther-University Halle-Wittenberg, Germany, 133p
Kampunzu AB, Armstrong RA, Modis MP, Mapeo RBM (2000) Ion microprobe U-Pb ages on detrital zircon grains from the Ghanzi Group: implications for the identification of a Kibaran-age crust in northwest Botswana. J Afr Earth Sci 30:579–587
Kampunzu AB, Cailteux J (1999) Tectonic evolution of the Lufilian Arc (Central Africa Copperbelt) during Neoproterozoic Pan African orogenesis. Gondwana Res 3:401–421
Kampunzu AB, Cailteux JLH, Kamona AF, Intiomale MM, Melcher F (2009) Sediment-hosted Zn-Pb-Cu deposits in the Central African Copperbelt. Ore Geol Rev 35:263–297
Killick AM (1983) Sulphide mineralization at Gorob and its genetic relationship to the Matchless Member, Damara Sequence, SWA/Namibia. Geol Soc S Afr Spec Publ 11:381–384
Killick AM (2000) The Matchless Belt and associated sulphide mineral deposits, Damara Orogen, Namibia. Comm Geol Surv SW Afr/Namibia 12:73–80
Kinnaird JA, Nex PAM (2007) A review of geological controls on uranium mineralisation in sheeted leucogranites within the Damara Orogen, Namibia. Appl Earth Sci IMM Trans Sec B 116(2):68–85
Kinnaird JA, Nex PAM (2016) Uranium in Africa. Episodes 39 (2):335–359
Kinnaird JA, Nex PAM, Milani L (2016) Tin in Africa. Episodes 39 (2):362–380
Kisters AFM (2005) Controls of gold-quartz vein formation during regional folding in amphibolite-facies, marble-dominated metasediments of the Navachab Gold Mine in the Pan-African Damara Belt, Namibia. S Afr J Geol 108:365–380
Kisters AFM, Charlesworth EG, Gibson RL, Anhaeusser CR (1996) Steep structure formation in the Okiep Copper District, South Africa: bulk inhomogeneous shortening of a high-grade metamorphic granite-gneiss sequence. J Struct Geol 18(6):735–751
Kisters AFM, Charlesworth EG, Gibson RL, Anhaeusser CR (1998) The role of strain localization in the segregation and ascent of anatectic melts, Namaqualand, South Africa. J Struct Geol 20(2–3):229–242
Kitt S, Kisters A, Steven N, Maiden K, Hartmann K (2016) Shear-zone hosted copper mineralisation of the Omitiomire deposit—structural controls of fluid flow and mineralisation during subduction accretion in the Pan-African Damara Belt of Namibia. Ore Geol Rev 75:1–15
Klemd R, Maiden KJ, Okrusch M (1987) The Matchless copper deposit, South West Africa/Namibia; a deformed and metamorphosed massive sulfide deposit. Econ Geol 82:587–599
Klemd R, Maiden KJ, Okrusch M, Richter P (1989) Geochemistry of the Matchless metamorphosed massive sulfide deposit, South West Africa/Namibia; wall-rock alteration during submarine ore-forming processes. Econ Geol 84:603–617
Kolb J, Dziggel A, Bagas L (2015) Hypozonal lode gold deposits; a genetic concept based on a review of the New Consort, Renco, Hutti, Hira Buddini, Navachab, Nevoria and The Granites deposits. Precambrian Res 262:20–44
Kolker A (1982) Mineralogy and geochemistry of Fe-Ti oxide and apatite (nelsonite) deposits and evaluation of the liquid immiscibility hypothesis. Econ Geol 77:1146–1158
Kremers HE (1958) Rare Earths. Engineer Min J 159:145–146
Latzky R (1942) The magmatic copper ores of Namaqualand. Geol Soc S Afr Trans 45:109–150
Leach DL, Bradley DC, Huston D, Pisarevsky SA, Taylor RD, Gardoll SJ (2010) Sediment-hosted lead-zinc deposits in earth history. Econ Geol 105:593–625
Lehmann J, Master S, Rankin W, Milani L, Kinnaird JA, Naydenov KV, Saalmann K, Kumar M (2015) Regional aeromagnetic and stratigraphic correlations of the Kalahari Copperbelt in Namibia and Botswana. Ore Geol Rev 71:169–190
Lipson RD (1990) Lithogeochemistry and origin of metasediments hosting the Broken Hill Deposit, Aggeneys, South Africa, and implications for ore genesis. Unpublished Ph.D. thesis, University of Cape Town, South Africa, 250 p
Lipson RD, Martin GJ, Hobbs JBM (1986) Heavy mineral layers: evidence of a clastic origin for Bushmanland quartzite genesis at Aggeneys. Trans Geol Soc S Afr 89:367–372
Lombaard AF, the Exploration Department Staff of the O'okiep Copper Company Limited (1986) The copper deposits of the Okiep Copper District. In: Anhaeusser CR, Maske S (eds) Mineral deposits of Southern Africa, vol 2. Geological Society of South Africa, pp 1421–1445
Longridge L (2012) Tectonothermal Evolution of the southwestern Central Zone, Damara Belt, Namibia. Ph.D. thesis, University of the Witwatersrand, Johannesburg, South Africa, 524 p

Lottermoser BG (1989) Rare earth element study of exhalites within the Willyama Supergroup, Broken Hill Block, Australia. Min Dep 24:92–99
Lottermoser BG (1992) Rare earth elements and hydrothermal ore formation processes. Ore Geol Rev 7:25–41
Lottermoser BG, Ashley PM (1995) Exhalites within the Proterozoic Willyama Supergroup, Olary Block, South Australia. In: Pasăva J, Kríbek B, Zák K (eds) Mineral deposits: From their origin to their environmental impacts. Balkema, Rotterdam, The Netherlands, pp 237–240
Loye ER (2014) The Geological Controls on the heavy rare earth element enriched alteration zone of Area 4, Lofdal, Khorixas, Namibia. MSc thesis, Camborne School of Mines, University of Exeter, 114 p
Lüttich C, Borg G, Gauert C (2002) Contemporaneous carbonate deposition and rhyolitic volcanism as a setting for syngenetic Pb–Zn–Cu–Fe sulfides at the Spitskop III volcanic dome, Rosh Pinah [abs.]: 11th Quadrennial IAGOD Symposium and GEOCONGRESS 2002, Windhoek, Abstract Volume, 4 p
Macey PH, Thomas RJ, Minnaar HM, Gresse PG, Lambert CW, Groenewald CA, Miller JA, Indongo J, Angombe M, Shifotoka G, Frei D, Diener JFA, Kisters AFM, Dhansay T, Smith H, Doggart S, Le Roux P, Hartnady MI, Tinguely C (2017) Origin and evolution of the ~1.9 Ga Richtersveld Magmatic Arc, SW Africa. Precambr Res 292:417–451
Maiden K (1992) Massive sulphide Cu–Zn–Ag deposits of the Matchless amphibolite belt, Namibia; remobilised syngenetic deposits or syntectonic deposits? Int Geol Congr Abstr 3:792
Maiden KJ, Borg G (2011) The Kalahari Copperbelt in Central Namibia: controls on copper mineralization. Econ Geol Newsl 87:1 and 14–19
Maiden KJ, Breitkopf J, Klemd R, Okrusch M, Preussinger H (1986) Exhalative metasediments associated with the besshi-type massive sulphide deposits of the Matchless amphibolite belt, South West Africa/Namibia. Bur Miner Resour, Geol and Geophys Canberra, Australia, P 197
Maiden KJ, Hartmann K, Steven NM, Armstrong RA (2013) The Omitiomire deposit, Namibia: Late tectonic copper emplacement in a Neoproterozoic (Pan-African) imbricate shear system. Extended Abstract, SGA Meeting, Uppsala, Sweden, 12–15 Aug 2013
Mapeo RBM, Kampunzu AB, Armstrong RA (2000) Ages of detrital zircon grains from Neoproterozoic siliciclastic rocks in the Shakawe area: implications for the evolution of Proterozoic crust in northern Botswana. S Afr J Geol 103(2):156–161
Marlow AG (1983) Geology and geochronology of mineralised and anomalous granites and alaskites, Namibia. Geol Soc S Afr Spec Publ 11:289–298
Master S, Rainaud C, Armstrong RA, Phillips D, Robb LJ (2005) Provenance ages of the Neoproterozoic Katanga Supergroup (Central African Copperbelt), with implications for basin evolution. J Afr Earth Sci 42:41–60
Maurin JC (1993) The Pan-African West-Congo belt: links with eastern Brazil and geodynamical reconstruction. Internat Geol Rev 35 (5):436–452
Maurin JC, Alvarez P, Mouanda B (1990) Les Gisements de Cu-Pb-Zn du Congo: modele de structuration et hypotheses genetiques. In: Rocci G, Deschamps M (eds) Etudes recentes sur la geologie de l'Afrique, 15e colloque de geologie africaine, resumes detailles. Publication Occasionnelle - Centre International Pour la Formation et les Echanges Geologiques 22: 333–336
Maurin JC, Boudzoumou F, Djama LM, Gioan P, Michard A, Mpemba-Boni J, Peucat JJ, Pin C, Vicat J P (1991) La Chaine proterozoique ouest-congolienne et son avant-pays au Congo: nouvelles donnees geochronologiques et structurales, implications en Afrique centrale. Comptes Rendus de l'Academie des Sciences, Serie 2, 312, 11:1327–1334
McCandless TE, Mathur RD, Ruiz J (1998) The Re-Os isotopic composition of Precambrian massive sulphides in oceanic settings; a record of seawater-host rock interaction. Abstr Progr Geol Soc Am 30:185
McGowan RR, Roberts S, Foster RP, Boyce AJ, Coller D (2003) Origin of the copper-cobalt deposits of the Zambian Copperbelt: an epigenetic view from Nchanga. Geology 31(6):497–500
McGowan RR, Roberts S, Boyce AJ (2006) Origin of the Nchanga copper–cobalt deposits of the Zambian Copperbelt. Min Dep 40:617
McIver JP, McCarthy TS, Packham B de V (1983) The copper-bearing basic rocks of Namaqualand, South Africa. Mineralium Deposita 18:135–160
McMillan MD (2005) Exploration history of Rosh Pinah and Aggeneys. S Afr J Geol 108:3–4
Meinert LD (1995) Compositional variations of igneous rocks associated with skarn deposits. In: Thompson J (ed) Magmas, fluids and ore deposits. Mineralogical Association of Canada, pp 401–418
Meinert LD (1998) A review of skarns that contain gold. In: Lentz DR (ed) Mineralized Intrusion-related Skarn systems. Mineralogical Association of Canada, pp 359–414
Meinert LD, Dipple GM, Nicolescu S (2005) World Skarn Deposits. Econ Geo 100th Anniversary Volume, pp 299–336
Melcher F, Graupner T, Gäbler HE, Sitnikova M, Henjes-Kunst F, Oberthür T, Gerdes A, Dewaele S (2015) Tantalum-(niobium-tin) mineralisation in African pegmatites and rare metal granites: constraints from Ta-Nb oxide mineralogy, geochemistry and U-Pb geochronology. Ore Geol Rev 64:667–719
Michel H, Scolari G (1960) Le gisement de cuivre-plomb-zinc de M'Passa, vallee du Niari, Republique du Congo. International Geological Congress—Report of the Twenty-First Session, Part 16, pp 112–125
Milesi J-P, Feybesse J-L, Pinna P, Descamps Y, Kampunzu H A B, Muhongo S, Lescuyer J-L, Toteu S F (2004) Geologie et principaux gisements de l'Afrique. (Geological map 1:10.000.000), BGRM and Geol Soc Afr
Miller D (2006) The tin mines of Cape Town. S Afr Lapidary Mag 38 (3):12–20
Miller RMG (1983) Evolution of the Damara-Orogen of South West Africa/Namibia. In: Miller RMG (ed) Geodynamic evolution of the Damara Orogen. Special Publication of Geological Society of South Africa, pp 431–515
Miller RMG, Grote W (1983) Geological map of the Damara Orogen of South West Africa/Namibia, 1:500.000, 2 sheets. Geol Soc S Afr Spec Publ 11:431–515
Mining Atlas (2015) OKiep News. https://mining-atlas.com/operation/OKiep-Copper-Mine.php. Accessed 31 May 2017
Ministry of Mines and Energy of Namibia, Geological Survey of Namibia (1992) Lead and zinc: The Mineral Resources of Namibia, 1st edn. Republic of Namibia, Windhoek, pp 2.5–2.21
Ministry of Mines and Energy of Namibia (1993) Tsongoari Lead-Zinc Deposit. In: Mineral investment opportunities in Namibia—Project File, un-paginated
Minnaar H, Theart HFJ (2006) The exploitability of pegmatite deposits in the lower Orange River area (Vioolsdrif–Henkries–Steinkopf). S Afr J Geol 109(3):341–352
Misra KC (2000) Understanding mineral deposits. Kluwer Academic Publishers, Dordrecht, p 845
Modie BN (1996) Depositional environments of the Meso- to Neoproterozoic Ghanzi-Chobe belt, northwest Botswana. J Afr Earth Sci 22:255–268
Modie BN (2000) Geology and mineralisation in the Meso- and Neoproterozoic Ghanzi-Chobe Belt of northwest Botswana. J Afr Earth Sci 30(3):467–474

Möller P (1989) Rare Earth mineral deposits and their industrial importance. In: Möller P, Cerny P, Saupé F (eds) Lanthanides, tantalum and niobium. Springer, Berlin, pp 171–188

Moore JM (1989) A comparative study of metamorphosed supracrustal rocks from the western Namaqualand Metamorphic Complex. University of Cape Town, South Africa, Bull Precambrian Res Unit, p 37

Moore JM, Jacob RE (1998) The Navachab sheeted-vein/skarn Au deposit, Namibia. Abstr Conf Geol Assoc Canada/Mineral Assoc Canada, pp A125–A126

Moore JM, Jacob RE, Harris C, Armstrong RA (1999) The Navachab gold deposit, Namibia: a mesothermal sheeted-vein/skarn system related to the Pan-African Damara Orogen. Jl Afr Earth Sc 28:50–51

Moore JM, Watkeys MK, Reid DL (1990) The regional setting of the Aggeneys/ Gamsberg base metal deposits, Namaqualand, South Africa. In: Spry PG, Bryndzia LT (eds) Regional metamorphism of ore deposits. Science Press, Rotterdam, pp 77–95

Morgan KL, Jenkin GRT, Gorman, AR, Catterall D, Boyce AJ (2013) Formation of vein hosted copper-silver mineralisation in the Kalahari Copperbelt, Botswana: preliminary results. In: 12th SGA biennial meeting. Proceedings, vol 2, pp 655–658

Muchez P, André-Mayer AS, El Desouky HA, Reisberg L (2015) Diagenetic origin of the stratiform Cu–Co deposit at Kamoto in the Central African Copperbelt. Min Dep 50(4):437–447

Muchez P, Vanderhaeghen P, El Desouky H, Schneider J, Boyce AJ, Dewaele S, Cailteux J (2008) Anhydrite pseudomorphs and the origin of stratiform Cu–Co ores in the Katangan Copperbelt (Democratic Republic of Congo). Min Dep 43:575–590

Muchez P, Brems D, Clara E, De Cleyn A, Lammens L, Boyce A, De Muynck D, Mukumba W, Sikazwe O (2010) Evolution of Cu–Co mineralizing fluids at Nkana mine, central African copperbelt, Zambia. Jl Afr Earth Sci 58(3):457–474

Mukumbi A (2011) Occurrence of gold, copper and silver at the Rosh Pinah Mine. Unpublished B.Sc. thesis, University of Windhoek, Namibia, 43p

Nex PAM, Kinnaird JA (1995) Granites and their mineralisation in the Swakop River area around Goanikontes, Namibia. Comm Geol Surv Namibia 10:51–56

Nicolini P (1958) Etude bibliographique sur le cadre geologique et l'origine des mineralisations de l'Afrique centrale; discussion des hypotheses genetiques proposees. Chronique des Mines d'Outre--Mer et de la Recherche Minere 263:132–159

Nicolini P (1959) Le synclinal de la Nyanga (zone de la boucle du Niari): contribution a l'etude des mineralisations stratiformes du Moyen-Congo. Bulletin de la Direction des Mines et de la Geologie 10, 178p

Nörtemann MF-J (1997) Geological mapping of the Goldkuppe area on the farms Otjimbojo and Otjakatjongo in the central Damara-Orogen, Namibia, & Genesis, Petrography and Mineral Chemistry of the Goldskarn deposit Navachab in the central Damara-Orogen, Namibia. Unpubl. Diploma thesis, University of Göttingen, Germany, 265 p

Nörtemann MFJ, Mücke A, Weber K, Meinert LD (2000) Mineralogy of the Navachab deposit, Namibia: an unusual Au-bearing skarn in high grade metamorphic rocks. Comm Geol Surv Namibia 12:149–156

Page DC, Watson MD (1976) The Pb-Zn deposit of Rosh Pinah Mine, South West Africa. Econ Geol 71(1):306–327

Pike DR (1959) The monazite deposits of the Van Rynsdorp Division. Cape Province. M.Sc. Dissertation, University of Pretoria, 127p

Piranjo F, Jacob RE (1987) Sn-W metallogeny in the Damara Orogen, South West Africa/Namibia. S Afr J Geol 9(3):239–255

Piranjo F, Jacob RE (1991) Gold mineralisation in the intracontinental branch of the Damara-Orogen, Namibia: a preliminary survey. J Afr Earth Sci 13:305311

Piranjo F, Jacob RE, Petzel VFW (1991) Distal skarn-type mineralization in the Central Zone of the Damara Orogen, Namibia. In: Ladeira EA (ed) Proceedings of Brazil Gold '91: an International symposium on the Geology of Gold, Belo Horizonte. Balkema, Rotterdam, pp 95–100

Piranjo F, Petzel VFW, Jacob RE (1987) Geology and alteration-mineralisation of the Brandberg West Sn-W deposit, Damara Orogen, South West Africa/Namibia. S Afr J Geol 9(3):256–269

Piestrzynski A, Wendorf M, Letsholo M, Mackay W (2015) Platinum-group minerals in the Neoproterozoic stratabound copper-silver mineralisation, the Kalahari Copperbelt, northwestern Botswana. S Afr J Geol 118(3):275–284

Porada H, Druschel G (2010) Evidence for participation of microbial mats in the deposition of the siliciclastic 'ore formation' in the Copperbelt of Zambia. J Afr Earth Sci 58(3):427–444

Preussinger H, Maiden KJ, Okrusch M (1987) Contrasting styles of sedimentation in metasediments of the Kuiseb Formation near Gorob, SWA/Namibia. Comm Geol Surv SW-Africa/Namibia 3:105–109

Rainaud C, Armstrong RA, Master S, Robb LJ (1999) A fertile Palaeoproterozoic magmatic arc beneath the Central African Copperbelt. Mineral deposits: processes to processing 2:1427–1430

Rainaud CL, Armstrong RA, Master S, Robb LJ, Mumba PACC (2002) Contributions to the geology and mineralisation of the central African Copperbelt: I. Nature and geochronology of the pre-Katangan basement. In: 11th IAGOD quadrennial symposium and geocongress, Windhoek, Namibia. p 5

Rainaud C, Master S, Armstrong RA, Robb LJ (2005) Geochronology and nature of the Palaeoproterozoic basement in the Central African Copperbelt (Zambia and the Democratic Republic of Congo), with regional implications. J Afr Earth Sci 42:1–31

Rankin W (2015) Cross-border correlation of the Damara Belt in Namibia and equivalent lithologies in northwestern Botswana from potential field and magnetotelluric interpretations. Unpubl. Ph.D. thesis University of the Witwatersrand, Johannesburg, South Africa, 386 p

Read D, Andreoli MAG, Knoper M, Williams T, Jarvis N (2002) The degradation of monazite: implications for the mobility of rare-earth and actinide elements during low-temperature alteration. Euro J Min 14:487–498

Reid DL (1977) Geochemistry of Precambrian rocks in the lower Orange River Region. Bull Precambrian Res Unit Univ Cape Town S Afr 22:397

Reid DL, Smith CB, Watkeys MK, Welke HJ, Betton PJ (1997a) Whole-rock radiometric age patterns in the Aggeneys-Gamsberg ore district, central Bushmanland, South Africa. S Afr J Geol 100:11–22

Reid DL, Welke HJ, Smith CB, Moore JM (1997b) Lead isotope patterns in Proterozoic stratiform mineralisation in the Bushmanland Group, Namaqua Province, South Africa. Econ Geol 92:248–258

Richards TE (1986) Geological characteristics of rare metal bearing pegmatites of the Uis type in the Damara Orogen, South West Africa/Namibia. In: Anhaeusser CR, Maske S (eds) Mineral deposits of Southern Africa. Geological Society of South Africa, pp 1845–1862

Rickard DT, Willdén MY, Marinder NE, Donnelly TH (1979) Studies on the Genesis of the Laisvall sandstone lead-zinc deposit, Sweden. Econ Geol 74:1255–1285

Robb LJ (2005) Introduction to ore-forming processes. Blackwell Publishing, 373 p

Robb LJ, Armstrong RA, Waters DJ (1999) Nature and duration of mid-crustal granulite-facies metamorphism and crustal growth: evidence from single zircon U-Pb geochronology in Namaqualand, South Africa. J Petrol 40:1747–1770

Rock NM, Groves DI (1988) Can lamprophyres resolve the genetic controversy over mesothermal gold deposits? Geology 16(6):538–541

Roering C, Gevers TW (1964) Lithium- and beryllium-bearing pegmatites in the Karibib District, South West Africa. In: Haughton SH (ed) The geology of some ore deposits in Southern Africa. Geological Society of South Africa, pp 462–495

Rozendaal A (1986) The Gamsberg zinc deposit, Namaqualand District. In: Anhaeusser CR, Maske S (eds) Mineral deposits of Southern Africa. Geological Society of South Africa, pp 1477–1488

Rozendaal A, Gresse PG, Scheepers R, De Beer CH (1994) Structural setting of the Riviera W-Mo deposit, Western Cape, South Africa. S Afr J Geol 97:184–195

Rozendaal A, Stalder M, Alchin D (2005) Wall rock alteration and lithogeochemical haloes associated with the stratiform Rosh Pinah Zn-Pb-Ag deposit in the Pan African Gariep Belt, southwestern Namibia. S Afr J Geol 107:115–130

Rozendaal A, Stumpfl EF (1984) Mineral chemistry and genesis of Gamsberg zinc deposit, South Africa. Trans Inst Min Metall 93:131–175

Ruxton PA (1986) Sedimentology, isotopic signature and ore genesis of the Klein Aub copper mine, South West Africa/Namibia. In: Anhaeusser CR, Maske S (eds) Mineral deposits of Southern Africa II, Johannesburg. Geological Society of South Africa, pp 1725–1738

Ruxton PA, Clemmey H (1986) Late Proterozoic stratabound red-bed copper deposits of the Witvlei area, South West Africa. In: Anhaeusser CR, Maske S. (eds) Mineral deposits of Southern Africa II, Johannesburg. Geological Society of South Africa, pp 1739–1754

Ryan PJ, Lawrence AL, Lipson RD, Moore JM, Patterson A, Stedman DP, van Zyl D (1986) The Aggeneys base metal sulphide deposits, South Africa. In: Anhaeusser CR, Maske S (eds) Mineral deposits of Southern Africa, vol 2, Geological Society of South Africa, pp 1447–1474

Saintilan NJ, Schneider J, Stephens MB, Chiaradia M, Kouzmanov K, Wälle M, Fonboté L (2015) A Middle Ordovician age for the Laisvall sandstone-hosted Pb-Zn deposit, Sweden: a response to Early Caledonian orogenic activity. Econ Geol 110:1779–1801

Saintilan NJ, Spangenberg JE, Samankassou E, Kouzmanov K, Chiaradia M, Stephens MB, Fonboté L (2016) A refined genetic model for the Laisvall and Vassbo Mississippi Valley-type sandstone-hosted deposits, Sweden: constraints from paragenetic studies, organic geochemistry, and S, C, N, and Sr isotope data. Min Dep 51:639–664

Schmerold RK (1992) The Tsongoari project, Kaokoland, Namibia. Geological report on the field season 07.04.92–30.07.92. Unpublished report, Rand Mines Ltd., 32p

Schneider GI, Seeger K (1992) Copper. In: Mineral resources of Namibia. Geological Survey of Namibia, Windhoek, p 118

Schoch AE, Conradie JA (1990) Petrochemical and mineralogical relationships in the Koperberg Suite, Namaqualand, South Africa. Am Min 75:27–36

Schutte IC (1972) The main pegmatites of the area between Steinkopf, Vioolsdrif and Goodhouse. Mem Geol Surv S Afr 60:19

Schürmann LW, Harmer RE (1998) Rare-Earth Elements. In: Wilson MGC, Anhaeusser CR (eds) The mineral resources of South Africa. Handbook, pp 569–574

Schwartz MO, Akanyang P, Trippler K, Ngwisanyi TH (1995) The sediment-hosted Ngwako Pan copper deposit, Botswana. Econ Geol 90:1118–1147

Schwartz MO, Kwok YY, Davis D, Akanyang P (1996) Geology, geochronology and regional correlation of the Ghanzi Ridge, Botswana. S Afr J Geol 99:245–250

Selley D, Broughton D, Scott RJ, Hitzman M, Bull SW, Large RR, McGoldrick PJ, Croaker M, Pollington N (2005) A new look at the geology of the Zambian Copperbelt. Econ Geol 100th Anniversary, pp 965–1000

Siegfried PR, Moore JM (1990) The Rosh Pinah Zn-Pb-Cu-Ag massive sulphide deposit—a product of early rift-related volcanism? Abstracts Geocongress 1990, Geological Society of South Africa, Cape Town, South Africa, July 1990, pp 512–513

Sillitoe RH, Perelló J, García A (2010) Sulphide-bearing veinlets throughout the stratiform mineralisation of the Central African Copperbelt: temporal and genetic implications. Econ Geol 105 (8):1361–1368

Sillitoe RH, Perelló J, Creaser RA, Wilton J, Wilson AJ, Dawborn T (2017) Age of the Zambian Copperbelt. Min Dep, 24 p, https://doi.org/10.1007/s00126-017-0726-8

Spargo P (1999) The Vredehoek Tin Mine, Cape Town. Quart Bull Nat Lib S Afr 54(1):19–26

Spivey M, Penkethman A, Culpan N (2010) Geology and mineralization of the recently discovered Rössing South uranium deposit, Namibia. Econ Geol Spec Publ 15:729–746

Stalder M, Rozendaal A (2005) Calderite-rich garnet and Franklinite-rich spinel in Amphibolite-facies hydrothermal sediments, Gamsberg Zn–Pb Deposit Namaqua Province, South Africa. Can Mineral 43:585–599

Stam J (1960) Some ore occurrences of the Mississippi Valley type in equatorial Africa. Econ Geol 55(8):1708–1715

Stanistreet IG, Charlesworth EG (2001) Damaran basement-cored fold nappes incorporating pre-collisional basins, Kaoko Belt, Namibia, and controls on Mesozoic supercontinental break-up. S Afr J Geol 104(1):1–12

Steven NM (1993) A study of epigenetic mineralisation in the Central Zone of the Damara Orogen, Namibia, with special reference to gold, tungsten, tin and rare-earth elements. Mem Geol Surv Nam 16:166

Steven NM (1994) A review of gold occurrences in the northern and central zones of the Damara Orogen and the underlying mid-Proterozoic basement, central Namibia. Comm Geol Surv Namibia 9:63–77

Steven NM, Badenhorst F (2002) Mesothermal gold deposits of the Damara Orogen. Excursion guidebook, 11th Quadrennial IAGOD symposium and geocongress, Windhoek

Steven N, Creaser R, Wulff K, Kisters A, Eglington B, Miller J (2015) Implications of high-precision Re-Os molybdenite dating of the Navachab orogenic gold deposit, Namibia. Geochem Explor Environ Anal 15(2–3):125–130

Steven NM, Kuyper JL, Moore JM (1994) Late Proterozoic and early Palaeozoic metasediment hosted tungsten in central Namibia: recent advances in exploration and research. Explor Min Geol 3:337–348

Steven NM, Moore JM (1993) A Study of epigenetic mineralisation in the Central Zone of the Damara-Orogen, Namibia, with a special reference to gold, tungsten and rare earth elements. Mem Geol Surv Namibia 16

Swindon S, Siegfried P (2011) Amended 43–101, Technical Report on the Rare Earth Occurrences in the Lofdal Carbonatite Complex, Kunene Region, Khorixas District, Namibia. Namibia Rare Earths Inc., 210 p (available from www.sedar.com)

Stumpfl EF, Clifford TN, Burger AJ, van Zyl D (1976) The copper deposits of the Okiep district, South Africa: New data and concepts. Min Dep 11:46–70

Sweeney M, Turner P, Vaughan DJ (1986) Stable isotope and geochemical studies in the role of early diagenesis in ore formation, Konkola Basin, Zambian Copperbelt. Econ Geol 81:1838–1852

Sweeney MA, Binda PL (1989) The role of diagenesis in the formation of the Konkola Cu–Co orebody of the Zambian Copperbelt. Geol Ass Can Spec Pap 36:499–518

Sweeney MA, Binda PL, Vaughan DJ (1991) Genesis of the ores of the Zambian Copperbelt. Ore Geol Rev 6:51–76

Tack L, Bowden P (1999) Post-collisional granite magmatism in the central Damaran (Pan-African) Orogenic Belt, western Namibia. J Afr Earth Sci 28(3):653–674

Tack L, Wingate MTD, Lie´geois J-P, Fernandez-Alonso M, Deblond A (2001) Early Neoproterozoic magmatism (1000–910 Ma) of the Zadinian and Mayumbian Groups (Bas-Congo): onset of Rodinia rifting at the western edge of the Congo craton. Precambrian Res 110:277–306

Thiart C, de Wit MJ (2008) African Neoproterozoic mineral deposits and Pan African metallogenesis. In: Bonham-Carter G, Cheng W (eds) Progress in geomathematics. Springer, Berlin, pp 303–313. ISBN 978-3-540-69496-3

Theron JN, Gresse PG, Siegfried HP, Rogers J (1992) The geology of the Cape Town area. Geol Surv S Afr I-140

Thomas RJ, von Veh MW, McCourt S (1993) The tectonic evolution of southern Africa: an overview. J Afr Earth Sci 16:5–24

Thomas RJ, Agenbacht ALD, Cornell DH, Moore JM (1994) The Kibaran of southern Africa: tectonic evolution and metallogeny. Ore Geol Rev 9:131–160

Thomas RJ, Macey PH, Spencer C, Dhansey T, Diener JFA, Lambert CW, Frei D, Nguno A (2017) The Sperrgebiet Domain, Aurus Mountains, SW Namibia: a ~2020-850 Ma window within the Pan-African Gariep Orogen. Precambrian Res 286:35–58

Thompson JFH, Sillitoe RH, Baker T, Lang JR, Mortensen JK (1999) Intrusion-related gold deposits associated with tungsten-tin provinces. Min Dep 34:323–334

Torrealday HI, Hitzman MW, Stein HJ, Markley RJ, Armstrong R, Broughton D (2000) Re-Os and U-Pb dating of the vein-hosted mineralization at the Kansanshi copper deposit, Northern Zambia. Econ Geol 95(5):1165–1170

Unrug R (1988) Mineralization controls and source of metals in the Lufilian Fold Belt, Shaba (Zaire), Zambia, and Angola. Econ Geol 83:1247–1258

van Eden JG (1974) Depositional and diagenetic environment related to sulphide mineralisation, Mufulira, Zambia. Econ Geol 69:59–79

van Vuuren CCJ (1986) Regional setting and structure of the Rosh Pinah zinc-lead deposit, South West Africa/Namibia. In Anhaeusser CR, Maske S (eds) Mineral deposits of Southern Africa, vol 2, pp 1593–1607

van Zwieten AJM, McCarthy TS, Cawthorn RG (1996) A petrogenetic model for the Koperberg Suite: evidence from the Jubilee Mine, Namaqualand, South Africa. S Afr J Geol 99:121–134

van Zyl D (1967) The geology of the O'okiep copper mine, Namaqualand. Univ Stellenbosch Ann 42:68

van Zyl D (1978) A petrological approach towards the ore-bearing potentialities of the Okiep basic intrusives in Namaqualand. Geol Soc S Afr Spec Pub 4:323–329

Visser DJL (1998) The geotectonic evolution of South Africa and offshore islands. Geological Survey of South Africa, p I-319

von Backström JW (1969) Thorium. S Afr Geol Surv Handb 7:209–212

von Backström JW (1970) The Rössing uranium deposit near Swakopmund, South West Africa. A preliminary report, Uranium Exploration Geology. IAEA Report IAEA -PL-391/12 Vienna: 143–150

Wall F, Niku-Paavola VN, Storey C, Muller A, Jeffries T (2008) Xenotime-(Y) from carbonatite dykes at Lofdal, Namibia: unusually low LREE-HREE ratio in carbonatite, and the first dating of xenotime overgrowths on zircon. Can Min 46:861–877

Walraven FC (1989) Geology and alteration mineralization of the Gamigab tin prospect, Damaraland, Namibia. Unpubl. Ph.D. thesis, Rhodes University, 146 p

Walraven F, Borg G (1992) Lead isotopic signatures at the Klein Aub Mine, Namibia—implications for mineralisation models. Min Dep 27:115–121

Walker PWA (1994) Riviera tungsten—a discovery case history. Explor Min Geol 3:349–356

Walters SJ (1996) An overview of Broken Hill Type deposits. In: Pontgratz J, Davidson G (eds). New Developments in Broken Hill type deposits. Centre for Ore Deposit and Exploration Studies (CODES) Spec Publ 1. University of Tasmania, Hobart, Tasmania, Australia, pp 1–10

Waters DJ (1989) Metamorphic evidence for the heating and cooling of Namaqualand granulites. In: Daly JS, Cliff RA, Yardley BWD (eds) Evolution of metamorphic belts. Geological Society Special Publication, pp 357–363

Watkeys MK (1986) The Achab gneiss: A 'floor' in Bushmanland or a flaw in Namaqualand? Trans Geol Soc S Afr 89:103–116

Watkeys MK, Moore JM, Duncan AR (1988) Geochemical identification of Mid-Proterozoic felsic pyroclastic: a possible source for Aggeneys base metal mineralisation. Abstract of the International Symposium on Geochemistry and Mineralization in Proterozoic Mobile Belts. Tianjin, China

Watters BR (1977) The Sinclair Group: definition and regional correlation. Trans Geol Soc S Afr 80:9–16

Wendorff M (2001) Grey RAT orebodies with Cu-Co in the Katangan Copperbelt of the DRC: genetic implications of tectonostratigraphy. In: Piestrzynski A (ed) Mineral deposits at the beginning of the 21st century, Balkema Publishers, proceedings of the 6th joint SEG-SGA meeting, Krakow, Poland, Aug. 2001, pp 251–254

Wendorff M (2005a) Evolution of Neoproterozoic-Lower Palaeozoic Lufilian arc, Central Africa: a new model based on syntectonic conglomerates. J Geol Soc 162(1):5–8

Wendorff M (2005b) Sedimentary genesis and lithostratigraphy of Neoproterozoic megabreccia from Mufulira, Copperbelt of Zambia. J Afr Earth Sci 42(1–5):61–81

Wendorff M, Key RM (2009) The relevance of the sedimentary history of the Grand Conglomerat Formation (Central Africa) to the interpretation of the climate during a major Cryogenian glacial event. Precambrian Res 172(1–2):127–142

Windley BF (1995) The Evolving Continents, 3rd edn. Wiley, Chichester

Wulff K, Dziggel A, Kolb J, Vennemann T, Boettcher ME, Meyer FM (2010) Origin of mineralizing fluids of the sediment-hosted Navachab gold mine, Namibia; constraints from stable (O, H, C, S) isotopes. Econ Geol 105:285–302

Wulff K, Steven NM, Hein KAA, Kinnaird JA (2017) The Relationship between the structural orientation and the gold mineralisation of quartz-sulphide veins in the Navachab Gold Deposit, Namibia. Ore Geol Rev 80:504–521

The Impact Record of Southwest Gondwana

24

Wolf Uwe Reimold, Natalia Hauser, and Alvaro P. Crósta

Abstract

Impact cratering has been, and still is, a planetary process of utmost importance. Here, the limited impact record for Southwest Gondwana, amended by the record of Australia and the only two impact structures known from India in East Gondwana, is examined. Care is taken to distinguish between known impact events during the run-up to the completion of Gondwana—that is, prior to 1000 Ma—and in the interval 1000–500 Ma, the subsequent Pangea and Pangea-break-up phase till about 135 Ma, and in the post-135 Ma record. The overall record is simply too limited to allow a distinct evaluation of periods of possibly enhanced impact flux that, in turn, might have affected paleoenvironmental or even biological evolution. It stands to reason that at least a major part of the SW Gondwanan impact record was obliterated during the rifting stages related to the post-500 Ma break-up phase, but equally it cannot be excluded that large impact structures (or remnants of them) may still be discovered in future on the shields and in the orogenic belts/basins of Africa and South America. Finally, the SW Gondwanan impact record may be further expanded through careful observation aiming at identification of impact ejecta deposits, such as spherule layer beds, or through the discovery of shock metamorphosed zircon or monazite (derived from eroded impact structures) in the sedimentary records and the isotopic dating of these ancient impact-witness grains.

Keywords

Impact cratering • Terrestrial impact record
SW Gondwana record • Potential for future discoveries

24.1 Introduction

Some 60 years after the beginning of serious space exploration, it has become fundamental knowledge not only that impact cratering has been a major process since the very beginnings of the evolution of the solar system but also that it has been the most important process in the formation and modification of planetary surfaces (e.g., Melosh 2011; Reimold and Jourdan 2012b and references therein). The detailed photographic records of the surfaces of, for example, the Moon, Mercury, and Mars, as well as of many asteroids and some comet nuclei, have demonstrated the intensity with which the bodies of the inner solar system have been bombarded with projectiles ranging in size from microscopic to hundreds of kilometers wide. Zap pits (micrometeorite craters) on individual mineral grains in lunar rocks and, at the other extreme, the huge mare basins, with the >2000 km diameter South Pole-Aitken basin being the largest, illustrate this abundance and range of impact events on the Moon. While the bulk of this bombardment of the Moon can be related to the early stages of the evolution of the solar system, prior to what has been known as the Late Heavy Bombardment before ca. 3.8 Ga (e.g., Stöffler et al. 2006; Bottke et al. 2012; Marchi et al. 2012, 2013), there is ample evidence for later and still ongoing impact activity on this body, such as the observed impact on September 11, 2013 that produced a 40 m crater (Madiedo et al. 2014).

As part of the solar system, the Earth has obviously experienced a bombardment history of at least the same magnitude as the Moon (considering the much larger capture

W. U. Reimold (✉)
Museum für Naturkunde—Leibniz Institute for Evolution and Biodiversity Science, Invalidenstrasse 43, 10115 Berlin, Germany
e-mail: uwe.reimold@mfn-berlin.de

W. U. Reimold
Humboldt-Universität zu Berlin, Unter Den Linden 6, 10099 Berlin, Germany

W. U. Reimold · N. Hauser
Geochronology Laboratory, University of Brasília, Brasília, Brazil

A. P. Crósta
Geosciences Institute, State University of Campinas, 6152 13085-970 Campinas, SP, Brazil

S. Siegesmund et al. (eds.), *Geology of Southwest Gondwana*, Regional Geology Reviews,
https://doi.org/10.1007/978-3-319-68920-3_24

cross-section of the Earth and its much enhanced gravity compared to that of the Moon, the Earth's impact bombardment should actually have been much greater; see also Grieve et al. 2006; Bottke et al. 2012). However, the dynamic nature of our planet has obliterated much—in fact, most—of the effects of this activity. Only some 190 impact structures have been confirmed to date on Earth (Jourdan et al. 2012; Earth Impact Database, January 2017), in sharp contrast to the hundreds of thousands of impacts recognized on, for example, the lunar or mercurian surfaces. The age distribution of terrestrial impact structures covering the interval from *ca*. 3.5 Ga ((remnants of impact-generated ejecta layers in the form of Archean spherule layers, over 2.02 Ga (Vredefort, the oldest known terrestrial impact structure, South Africa) to recent (e.g., the Carancas impact of September 2007 in Peru)) demonstrates that impact has been an important force on the Earth for eons. Much has been written about impact having been, *inter alia*, the agent to destroy and modify the earliest terrestrial crust, to provide the primordial energy to jumpstart endogenic processes, to seed water on the planet, and having been a necessary agent for the development of earliest life on this planet (by providing locations with favorable physicochemical conditions for organic synthesis) or having been the process frustrating the development of earliest life, maybe for as much as 900 million years until the abatement of the Early Bombardment (e.g., Pierazzo and Artemieva 2012; review by Reimold and Koeberl 2014). It has also been speculated that impact could have influenced paleogeography, plate tectonics, and later evolution of life on Earth, throughout late Archean to Mesozoic times. At least one of the Big Five mass extinction events in Phanerozoic times was caused, or at least largely engineered, by a massive impact strike, at 66 Ma ago at Chicxulub on the Yucatán Peninsula (the K-Pg boundary mass extinction event; e.g., Schulte et al. 2010; Richards et al. 2015).

Some have mooted that large impact events could have played a role in the formation or break-up of supercontinents and been responsible for decisive changes in paleobiodiversity development, such as the Acraman impact event during Ediacaran times (e.g., Meert and Lieberman 2008) at *ca*. 590 Ma ago (Earth Impact Database 2016). It is therefore not trivial to examine the evidence of past impact flux against tectonic evolution, as is being done here.

We examine the impact record for the remnants of Southwest Gondwana, principally on the African and South American continents, but in comparison to the record of India and Australia, which were part of East Gondwana. We refrain here from reiterating the basics about impact cratering and impact structure recognition, which has been the subject of several recent publications that the interested reader may want to use as an entry into the related literature (e.g., French and Koeberl 2010; Reimold and Koeberl 2014; or the *Elements* issue entitled "IMPACT!" edited by Reimold and Jourdan 2012a).

24.2 The Terrestrial Impact Record

Before we examine the SW Gondwana impact database, it is necessary to speak briefly about the global terrestrial impact record. As stated, barely 190 impact structures are currently confirmed in the Earth Impact Database (http://www.unb.ca/passc/ImpactDatabase; compare with Fig. 24.1) at the time of finishing this manuscript (February 2017). We must emphasize that this database ought to be used with caution. For example, the authors do not accept at least one structure listed there for South America, Colônia (Brazil), because of the highly controversial and unconfirmed evidence alleged as shock metamorphism that has been cited as evidence pro impact in this case (Velázquez et al. 2013; discussion in Reimold et al. 2014; Velázquez et al. 2017). Other detail listed for a number of impact structures is also considered to be controversial and has required some modifications to the data from the Earth Science Database. (our view is presented in Table 24.1.)

What is more, there has been a lot of activity in the wider scientific community pushing alleged impact structures without proper adherence to the established and tested recognition criteria (exclusively, solid or chemical evidence for a projectile or projectile component, bona fide shock metamorphic evidence, shatter cones; see, e.g., French and Koeberl 2010; Reimold and Koeberl 2014). There are a number of non-reviewed listings of impact structures on the web that add up to many hundreds of alleged impact structures and that are not based on sound adherence to these recognized identification criteria. What is worse, as Reimold and Koeberl (2014, p. 87) wrote, a number of such doubtful records have entered even the peer-reviewed literature, which adds to the confusion of non-experts in the field. The rules and criteria for the recognition and confirmation of impact structures, as outlined above, are straightforward; so-called identifications (e.g., the alleged but unproven Chiemgau crater strewn field, southern Germany—Ernstson et al. 2010; the Bajada del Diablo, Argentina, strewn field—Acevedo et al. 2009—equally lacking bona fide impact evidence; the entirely unconfirmed Maniitsoq structure, Greenland—Garde et al. 2012, 2013) can easily be dismissed as not based on any established criteria (Reimold et al. 2014)."

Regarding the SW Gondwana region, this primarily concerns the alleged crater field at Bajada del Diablo in Patagonia, for which to date no accepted evidence for impact has been presented (Crósta and Reimold 2016).

The currently accepted impact structures are shown on a world map in Fig. 24.1. Several exemplary, confirmed

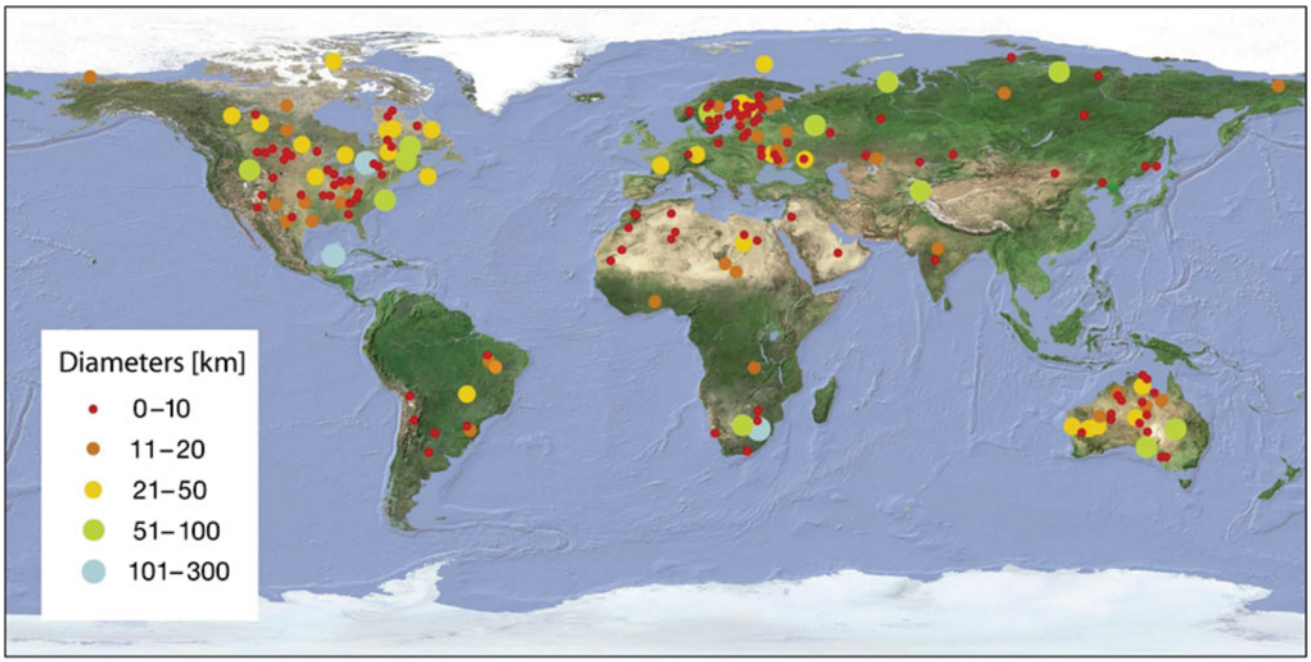

Fig. 24.1 The global terrestrial impact record of February 2017 (modified after Reimold and Koeberl 2014)

impact structures from Southwest Gondwana are introduced through their TanDEM-X satellite imagery in Fig. 24.2.

In the global distribution of impact structures, there are obvious regional variations in crater density, with most confirmed impact structures being located in North America and Eurasia. In addition, the record of Australia is comparatively strong. Obviously, in those countries where active space exploration has been pursued, and their allied nations, impact structures have been investigated, and searched for, since the 1950s. Other small, active groups with a strong interest in impact cratering have contributed extensively in Scandinavia, in southern Africa, and in Australia. A strong European research effort was supported by a European Science Network program in the 1990s, and the Nordic Countries' Impact Program of the last decade has also been highly successful in educating many geoscientists and, especially, students about this planetary process of fundamental importance. Many of the impact structures known in Australia must be credited to the efforts of the late Gene Shoemaker and his wife Carolyn, and their small number of dedicated collaborators. In South Africa, the Impact Cratering Research Group at the University of the Witwatersrand was instrumental in the analysis and confirmation of a number of impact sites. Recent enhanced efforts in South America should be noted as well, with centers of activity having been the universities of Campinas and São Paulo and, most recently, Brasilia and Salvador. There are, however, still many countries in Latin America where impact crater research is non-existent.

The preservation of impact structures is, generally, a first-order result of the regionally different geological histories of individual regions. For instance, young oceanic crust, recently exhumed continental crust, and vice versa, long exhumed, stable continental platforms must be expected to have had very different crater accumulation (and obliteration) rates. In particular, one can estimate that complete (i.e., global) oceanic resurfacing only requires some 150 Ma, thereby effectively erasing any impact structures formed on the seafloor and, partially, on shelf zones in a geologically relatively short interval.

Large parts of Asia, especially the eastern regions of Siberia and Mongolia, and then nearly all of China, are underrepresented on the global impact crater distribution map. Only a few relatively small impact structures have been identified in the Middle East and in Southeast Asia. The equatorial rain forest belt has not lent itself to detailed crater exploration because of the extensive vegetation cover hindering effective remote sensing observation, and difficult ground environments, largely covered by thick Quaternary deposits, that are adverse to extensive geological and geophysical coverage. Equally difficult are the hostile environments of Antarctica and Greenland, with large parts being covered by kilometer-thick ice.

Clearly, the terrestrial impact cratering record is incomplete, but the degree to which it is incomplete is a complex issue to tackle. A recent estimate by Stewart (2011) suggests that as many as 228 impact craters >2.5 km diameter have remained to be identified in the global Phanerozoic (younger than 540 Ma) sedimentary records.

Table 24.1 The impact record of SW Gondwana, modified after the Earth Impact Database (http://www.passc.net/EarthImpactDatabase/Africa.html, last accessed September 27, 2016

(a) The African record (see also Reimold and Koeberl 2014)

Crater name	Location	Latitude	Longitude	Diameter (km)	Age (Ma)	Exposed	Drilled	Target rock	Comment
Agoudal	Morocco	N 31°59′	W 5°30′	>1	*ca.* 120	(Y)	N	S	Chennaoui Aoudjehane et al. (2016)
Amguid	Algeria	N 26°5′	E 4°23′	0.45	<0.1	Y	N	S	–
Aorounga	Chad	N 19°6′	E 19°15′	12.6	<345	Y	N	S	–
Aouelloul	Mauritania	N 20°15′	W 12°41′	0.39	3.0 ± 0.3	Y	N	S	–
Bosumtwi	Ghana	N 6°30′	W 1°25′	10.5	1.07	Y	N	mS-C	–
B.P. Structure	Libya	N 25°19′	E 24°20′	2	<120	Y	N	S	–
Gweni-Fada	Chad	N 17°25′	E 21°45′	14	<345	Y	N	S	–
Kalkkop	South Africa	S 32°43′	E 24°26′	0.64	0.25 ± 0.05	Y	Y	S	–
Kamil	Egypt	N 22°01′	E 26°05′	0.045	*ca.* 0.004	Y	N	S	Sighinolfi et al. (2015)
Kgagodi	Botswana	S 22°29′	E 27°35′	3.5	<180	Y	Y	S	–
Luizi	DRCongo	S 10°10′	E 28°00′	17	<573	Y	N	S	–
Morokweng	South Africa	S 26°28′	E 23°32′	70	145 ± 2	N	Y	S-C	–
Oasis	Libya	N 24°35′	E 24°24′	18	<120	Y	N	S	–
Ouarkziz	Algeria	N 29°0′	W 7°33′	3.5	<70	Y	N	S	–
Roter Kamm	Namibia	S 27°46′	E 16°18′	2.5	<5	Y	N	S-C	–
Talemzane	Algeria	N 33°19′	E 4°2′	1.75	<3	N	Y	S	–
Tenoumer	Mauritania	N 22°55′	W 10°24′	1.9	1.57 ± 0.14	Y	N	mS-C	Schultze et al. (2016)
Tin Bider	Algeria	N 27°36′	E 5°7′	6	<70	Y	N	S	–
Tswaing (Pretoria Saltpan)	South Africa	S 25°24′	E 28°5′	1.13	0.220 ± 0.052	Y	Y	(S)-C	–
Vredefort	South Africa	S 27°0′	E 27°30′	250–300	2023 ± 4	Y	Y	mS-C	Gibson and Reimold (2008)
(b) The South American record (America: Earth Impact Database; for Brazil, see also Crósta and Vasconcelos 2013)									
Araguainha	Brazil	S 16°47′	W 52°59′	40	254.7 ± 2.5	Y	N	N	mS-C
Campo Del Cielo[a]	Argentina	S 27°38′	W 61°42′	Several in the range 0.02–0.115	<0.004	Y	Y	M	Finds of >100 t of an iron meteorite
Carancas	Peru	S 16°40′	W 69°03′	0.0135 km	0.000007	Y	N	S	Fall on September 15, 2007
Monturaqui	Chile	S 23°56′	S 23°56′	0.46	<1	Y	N	C	–
Riachão Ring	Brazil	S 7°43′	W 46°39′	4.5	<270	Y	N	S	Maziviero et al. (2013)
Rio Cuarto[b]	Argentina	S 32°52′	W 64°14′	Oblong structures of 4.5 × 1.1 km to a few m in length	<0.1	Y	N	M	Regionally occurring H chondrite
Santa Marta[c]	Brazil	S 10°10′	W45°15′	10	93–112	Y	N	M	Oliveira et al. (2014), Oliveira et al. (2018)
Serra da Cangalha	Brazil	S 8°5′	W 46°52′	12	<270	Y	Y	S	Vasconcelos et al. (2013)
Vargeão Dome	Brazil	S 26°50′	W 52°07′	12	123 ± 1.4	Y	N	M	Crósta et al. (2011), Nédélec et al .(2013)
Vista Alegre	Brazil	S 25°57′	W 52°41′	9.5	111–131	Y	N	–	Crósta et al. (2010, 2012)

[a]This strewn field comprises a number of craters, only the largest of which are possibly true impact ("explosion") craters, and the smaller ones simply formed as percussion funnels. [b]Controversial: these elongated, ovoid structures are variably discussed as the product of low-angle impact or as result of wind ablation (e.g., Glass and Simonson 2013). [c]Age range given by Oliveira et al. (2014) revised by Oliveira et al. (2018).

(continued)

Table 24.1 (continued)

(c) The Australian impact record (modified after Earth Impact Database, September 27, 2016)

Crater name	Location	Latitude	Longitude	Diameter (km)	Age (Ma)	Exposed	Drilled	Target Rock
Acraman	South Australia	S 32°1′	E 135°27′	90	~590	Y	N	C
Amelia Creek	Northern Territory	S 20°55′	E 134°50′	~20	1640–600	Y	N	mS
Boxhole	Northern Territory	S 22°37′	E 135°12′	0.17	0.0054 ± 0.0015	Y	N	C
Connolly Basin	Western Australia	S 23°32′	E 124°45′	9	<60	Y	N	S
Crawford	South Australia	S 34°43′	E 139°2′	8.5	>35	Y	N	C-mS
Dalgaranga	Western Australia	S 27°38′	E 117°17′	0.02	~0.27	Y	N	C
Flaxman	South Australia	S 34°37′	E 139°4′	10	>35	Y	N	C-mS
Foelsche	Northern Territory	S 16°40′	E 136°47′	6	>545	Y	N	C-S
Glikson	Western Australia	S 23°59′	E 121°34′	~19	<508	Y	N	C-S
Goat Paddock	Western Australia	S 18°20′	E 126°40′	5.1	<50	Y	N	S
Gosses Bluff	Northern Territory	S 23°49′	E 132°19′	22	142.5 ± 0.8	Y	Y	S
Goyder	Northern Territory	S 13°28′	E 135°2′	3	<1400	Y	N	S
Henbury	Northern Territory	S 24°34′	E 133°8′	0.15	0.0042 ± 0.0019	Y	N	S
Kelly West	Northern Territory	S 19°56′	E 133°57′	10	>550	N	N	C-mS
Lawn Hill	Queensland	S 18°40′	E 138°39′	18	>515	Y	N	C-S
Liverpool	Northern Territory	S 12°24′	E 134°3′	1.6	150 ± 70	Y	N	S
Matt Wilson	Northern Territory	S 15°30′	E 131°11′	~7.5	1402 ± 440	Y	N	S
Mount Toondina	South Australia	S 27°57′	E 135°22′	4	<110	Y	N	S
Piccaninny	Western Australia	S 17°32′	E 128°25′	7	<360	Y	N	S
Shoemaker (formerly Teague)	Western Australia	S 25°52′	E 120°53′	30	1630 ± 5	Y	N	C-S
Spider	Western Australia	S 16°44′	E 126°5′	13	> 570	Y	N	S
Strangways	Northern Territory	S 15°12′	E 133°35′	25	646 ± 42	Y	N	C-S
Tookoonooka	Queensland	S 27°7′	E 142°50′	55	128 ± 5	N	Y	C-S
Veevers	Western Australia	S 22°58′	E 125°22′	0.08	<1	Y	N	S
Wolfe Creek	Western Australia	S 19°10′	E 127°48′	0.87	<0.3	Y	N	S
Woodleigh	Western Australia	S 26°3′	E 114°39′	40	364 ± 8	N	Y	C-S
Yarrabubba	Western Australia	S 27°10′	E 118°50′	30	~2000	Y	N	C

(d) Impact glass occurrences in Argentina (modified, after Table 4.15 of Glass and Simonson 2013)

Location	Stratigraphic age	Radiometric age	References
Rio Cuarto	Holocene	6 ± 2 ka	Schultz et al. (2004)
	Pleistocene	114 ± 26 ka	Schultz et al. (2004)
		570 ± 100 ka	Bland et al. (2002)
Centinela del Mar	Pleistocene		
Lower Layer		230 ± 30 ka	Schultz et al. (2004)
Upper Layer (redeposited LL?)	445 ± 21 ka	Schultz et al. (2004)	
Mar del Plata	Pliocene	3.3 ± 0.2 Ma	Schultz et al. (1998)
Bahia Blanca	Late Miocene	5.28 ± 0.04 Ma	Schultz et al. (2006)
Chasicó	Late Miocene	9.24 ± 0.09 Ma	Schultz et al. (2006)

Also presented are the impact record of part of eastern Gondwana (Australia) and a list of distal impact ejecta occurrences in SW Gondwana. *S*, sedimentary rocks; *mS*, metasedimentary rocks; *C*, crystalline rocks; *Y*, yes; *N*, no

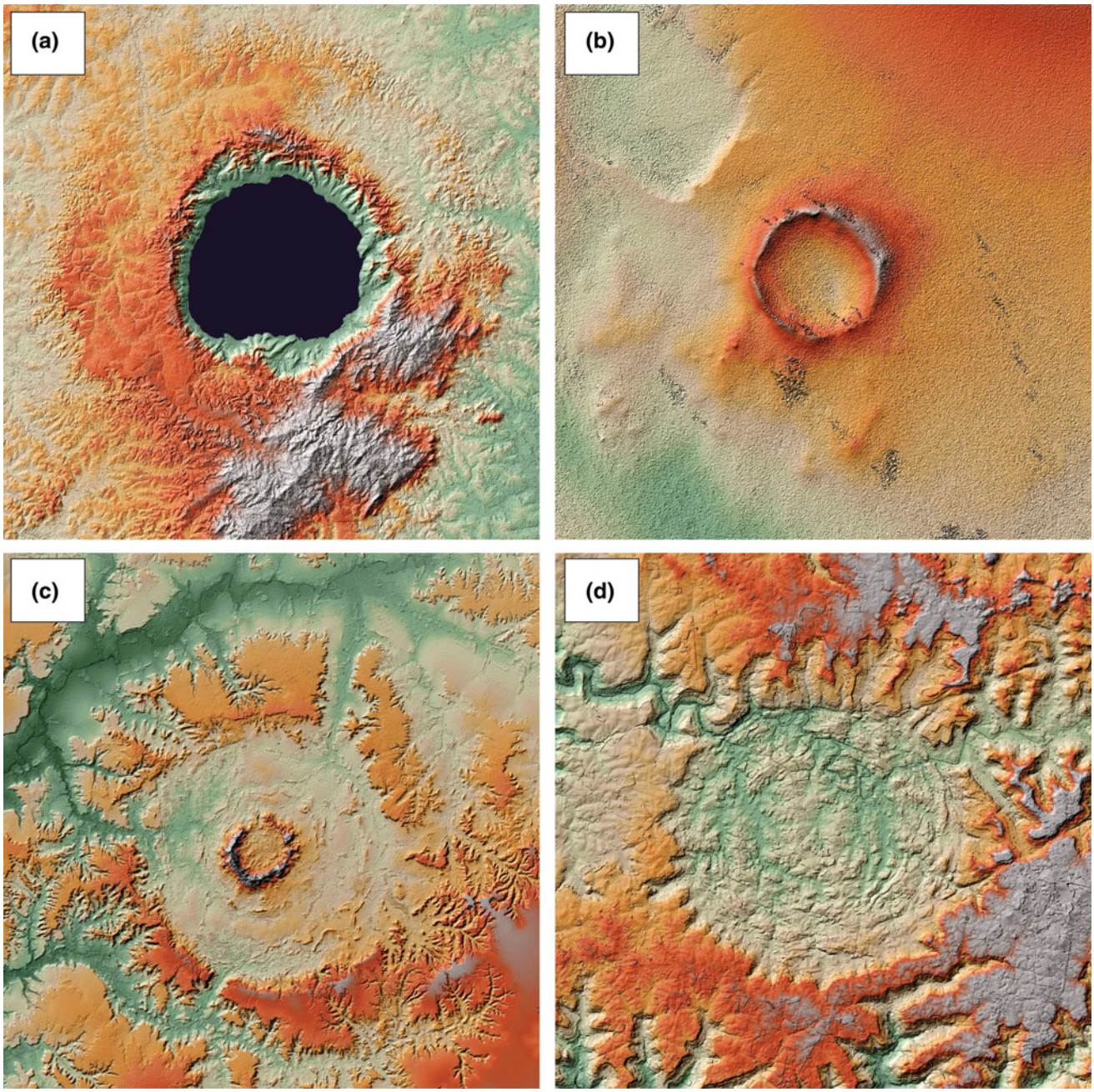

Stewart estimated for Africa that of the full <1 and >10 km diameter crater population, only some 15% had been discovered, and only <10% of the structures <210 km diameter had been accounted for. For African impact craters, >10 km diameter, *c*a. 45% (i.e., 5 out of 11), were known. A lot of variables (or, better, imponderables) have to go into such computations. Some pertinent questions would be: How much of the Phanerozoic sedimentary record has actually survived plate tectonics and surface degradation? Has the impact flux since the end of the Precambrian remained stable? Can the global rate of degradation be averaged? How would differential uplift rates be accounted for? And how can differential erosion rates be considered? Besides this work by Stewart concerning Phanerozoic sedimentary basins, how much evidence of impact remains to be discovered in the extensive regions of Precambrian crust in Africa (*ca*. 15–20 area% of the African continent)? Similar estimates could be attempted for South America, further emphasizing that it is safe to expect that additional discoveries of impact

◀ **Fig. 24.2** Four examples of confirmed impact structures from SW Gondwana (compare their locations in Fig. 24.3). All images are color-coded, hill-shaded digital elevation models generated by the German "TanDEM-X" spaceborne X-band radar mission (Gottwald et al. (2017); images courtesy Manfred Gottwald/DLR). In all four images (a–d), north is up. **a** Lake Bosumtwi impact crater (Φ = 10.5 km) in Ghana. The elevation ranges from 11 m (dark green) to 746 m (white). Scene size corresponds to about 25 × 25 km^2. A water mask, derived from the X-band amplitude, has been applied to the lake's surface. The structure encompasses Lake Bosumtwi and the surrounding prominent, up to a 300 m high (above lake level) crater rim. Note the asymmetry of the crater structure caused by the impact occurring against the flank of the Obuom mountain range trending northeast-soutwest along the structure's southern/southeastern side. There is also a ring structure indicated outside of the prominent crater rim, which was discussed in the past as possibly being the result of a fault scarp development or the erosional limit of the ejecta blanket (Wagner et al. 2002). For further detail about the geology and analysis of this impact structure, refer to Koeberl and Reimold (2005) and Reimold and Koeberl (2014). **b** Roter Kamm impact crater (Φ = 2.5 km) in Namibia. The elevation ranges from 306 m (dark green) to 1086 m (white). The scene size corresponds to about 11 × 11 km^2. The fine-grained black texture results from patches of sand where DEM generation is hampered. Some of these patches have a well-developed elongated shape. They coincide partially with prominent sand dunes, such as on, or against, the southern crater rim. A detailed review of the geology of Roter Kamm was provided by Miller (2008) and also Reimold and Koeberl (2014). **c** Serra da Cangalha impact crater (Φ = 12 km), formed on Paleozoic sedimentary strata of the Parnaíba Basin, Brazil. The elevation ranges from 157 m (dark green) to 669 m (white). The scene size corresponds to about 23 × 23 km^2. The eroded structure has nevertheless maintained a prominent crater rim along the outside, grading outward into the generally flat-lying sedimentary strata of the crater environs (brown), and a steep-walled central uplift feature. The ring basin in between displays several ring structures formed by more weathering-resistant chert layers. (For more detail, see Kenkmann et al. 2011.) **d** Vargeao Dome impact structure (Φ = 12 km) in Brazil, formed in volcanosedimentary sequences of the Paraná Basin; volcanic rocks are mostly continental flood basalts of the Paraná-Etendeka large igneous province (LIP). The elevation ranges from 519 m (dark green) to 1138 m (white). The scene size corresponds to about 28 × 28 km^2. A comprehensive study of this structure was reported by Crósta et al. (2012). The crater rim is well displayed in this image and the remnant of the deeply eroded central uplift can also still be discerned

structures of widely different sizes must be expected, worldwide, and certainly also for the continental regions of SW Gondwana.

24.3 The African and South American (SW Gondwana) Impact Record

The admittedly seriously limited impact record for Africa (Reimold and Koeberl 2014; Chennaoui Aoudjehane et al. 2016) and South America (Earth Impact Database; Crósta et al. 2011, 2012; Crósta and Vasconcelos 2013; Mazivieiro et al. 2013; Oliveira et al. 2014, 2018, for Brazil) is compiled in Tables 24.1a, b (compiled after modification of the information given by the Earth Impact Database (February 7, 2017)). Sites of the pre- and syn-Gondwana impact events have been transferred into the SW Gondwana map after Fig. 1 of Frimmel et al. (2011), shown as our Fig. 24.3.

The African impact record was recently discussed in great detail by Reimold and Koeberl (2014). Table 24.1a summarizes the known impact record for Africa, which comprises 19 impact structures plus the site at Agoudal (Morocco; Chennaoui Aoudjehane et al. 2016), where seemingly most of an original impact structure of >1 km size, as estimated by Chennaoui Aoudjehane et al., has been eroded, with the exception of a small fragment of shatter-cone-bearing marl and limestone.

The impact record for South America is even more restricted, to only 11 impact sites, of which two—Campo del Cielo and Rio Cuarto—are sites of meteorite falls or controversy about a fall, respectively. At Campo del Cielo, several "pits" of 20–115 m diameter have yielded meteorite samples. Only the largest of these holes could be termed impact craters, whereas the others are merely penetration funnels (Wright et al. 2007). At Rio Cuarto, hundreds of oblong, shallow structures ranging in size from a few meters length to 4.5 × 1.1 km have been variously discussed as the products of very low-angle (grazing) impact, as fragments of meteorites have been located in this area, or as wind-ablation features with only coincidental occurrence of a few meteorites (e.g., summary in Glass and Simonson 2013; see also Cione et al. 2002). Glass and meteorite fragments found in association with some of the Rio Cuarto structures were the basis for relating them to a low-angle impact event (Schultz and Lianza 1992). However, the glass fragments have been related by Bland et al. (2002) to a tektite-strewn field that covers a large area in southern Argentina, whereas the two meteorite fragments were shown to be of different nature (an ordinary chondrite and a basaltic achondrite) and terrestrial ages, likely accumulated in the blowout deflations of an eroded sand dune field (Bland et al. 2002).

As Table 24.1 demonstrates, the pre-1000 Ma impact record of SW Gondwana only comprises the oldest/largest known impact structure on Earth: Vredefort in South Africa (Gibson and Reimold 2008). The Rodinia-to-Gondwana phase, from 1000 to 500 Ma, is represented only by the Luizi structure in the Democratic Republic of Congo, with a poorly constrained age (<573 Ma; see Reimold and Koeberl 2014). The Gondwana-to-Pangea-to-supercontinent-break-up period from 500 to 135 Ma comprises seven known impact events. Related to these, only the largest impact structures of Morokweng (South Africa, 70 km, 145 ± 2 Ma) and Araguainha (Brazil, 40 km, 254.7 ± 2.5 Ma) have well-constrained ages. Of the remaining 19 events younger than 135 Ma, 11 must be considered recent with ages <5 Ma. This shift towards young structures clearly illustrates the effect of

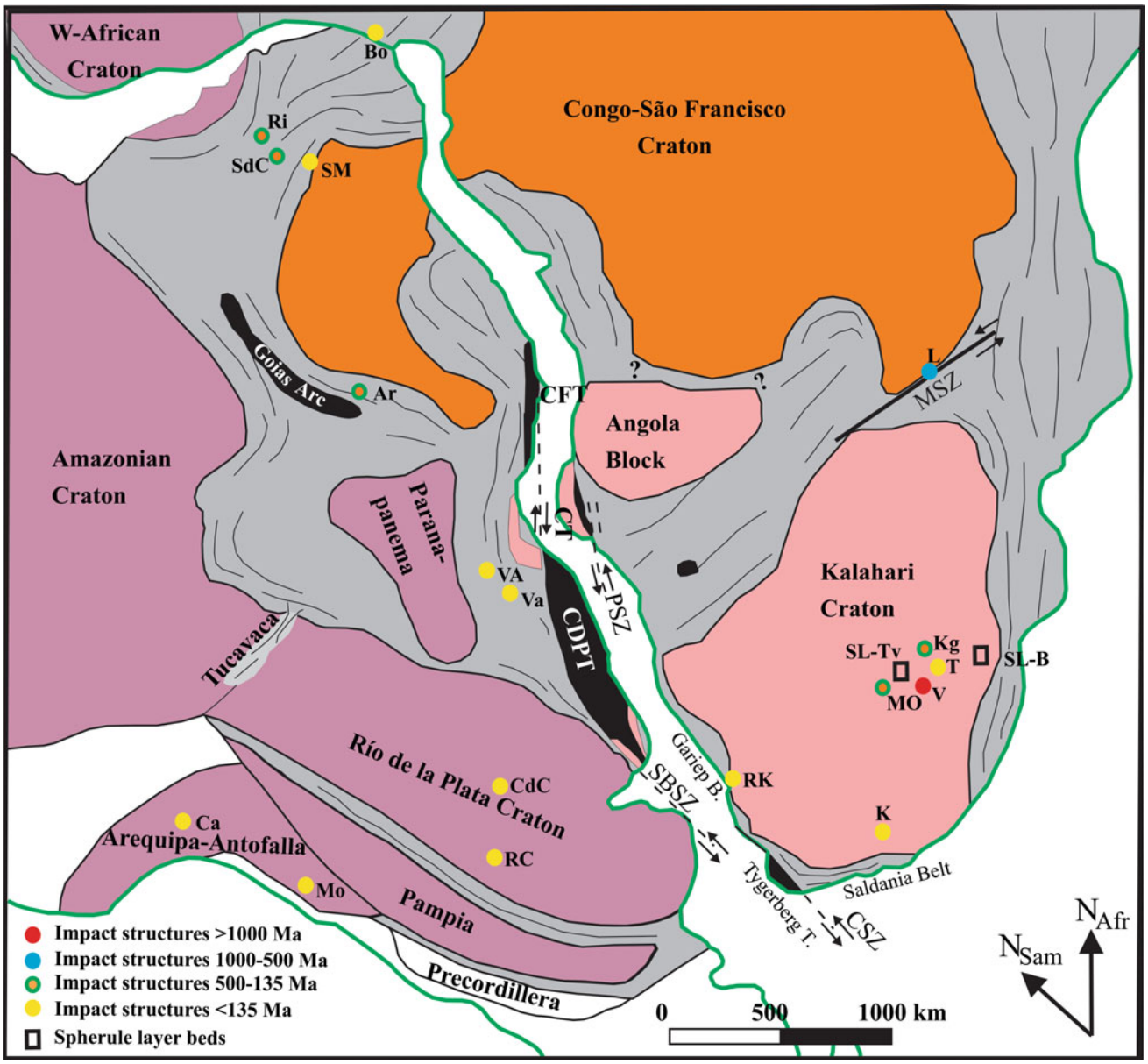

Fig. 24.3 The impact record of SW Gondwana superimposed onto a paleogeographic-tectonic map (modified after Fig. 1 of Frimmel et al. 2011, where abbreviations for rift basins/orogens can also be found). Further abbreviations: *1. South America:* Ri, Riachão; SdC, Serra da Cangalha; SM, Santa Marta; Ar, Araguainha; VA, Vista Alegre; Va, Vargeão; CdC, Campo del Cielo; RC, Rio Cuarto; Ca, Carancas; Mo, Monturaqui. *2. Africa:* Bo, Bosumtwi; L, Luizi; Kg, Kgagodi; T, Tswaing; V, Vredefort; MO, Morokweng; RK, Roter Kamm; K, Kalkkop; SL-B, Spherule layers of the Barberton Mountain Land (Swaziland Supergroup); SL-Tv, Spherule layers of the Transvaal Supergroup. For information about the impact structures, see Table 24.1

erosion of impact structures in geological time, whereby the very nature of such structures—relatively shallow sand in the uppermost crust—explains why impact structures are generally not long-lasting geological features.

Perhaps we should include the impact record of another part of Gondwana—the Australian continent—in our considerations. Australia, at first glance (Table 24.1c), has a quite extensive list of 27 recognized impact structures (compare with Table 24.1c). Indeed, there are four—Amelia Creek, Goyder, Shoemaker-Teague Ring, and Yarrabubba—that are listed with ages >1000 Ma. However, detailed perusal of the literature clarifies that none of these ages can be unequivocally interpreted to signify specific ages of impact events. Rather, these suggested ages are either related to dating of zircon from target rock or are subject to very large errors (hundreds of millions of years).

The interval relating to the build-up of Gondwana (1000–500 Ma) contains six impact structures, of which only one,

Strangways (see Earth Impact Database), is dated within a 40 Ma error limit (presumably at the 1 sigma confidence level though). The ages of the other five candidates are reported either with an "approximate" (~) symbol (the 90 km Acraman structure) or with a maximum age level (presumably based only on stratigraphic considerations). Five further events relate to the Pangea-to-break-up phase to *ca*. 130 Ma, with three well–dated craters (22 km Gosses Bluff at 142.5 ± 0.8 Ma; 55 km Tookoonooka at 128 ± 5 Ma; and 40 km Woodleigh at 364 ± 8 Ma) in evidence. The remaining 12 impact craters known in Australia were formed in more recent times.

Finally, a number of impact glass-bearing layers have been identified in Argentina, as summarized by Glass and Simonson (2013) and listed in Table 24.1d. At least six such glass occurrences have been identified based on radiometric dating, with one occurring in the Rio Cuarto area and, as some would like to have it, possibly related to a Rio Cuarto impact and/or meteorite fall, having yielded several ages in the range of 6000–570,000 years. Whether this finding might relate to several glass-forming events is still to be resolved. However, there seem to be fresh and dull looking varieties of glasses, possibly relating to Holocene and Pleistocene ages. The elongated depressions were apparently formed less than 10,000 years ago. The glass particles have been found associated with such depressions. Two small meteorite fragments were also recovered in the same area (Glass and Simonson 2013). However, it is obvious that these recent deposits are beyond the scope of this SW Gondwana contribution.

24.4 Discussion

In Fig. 24.3 the locations of the confirmed impact structures in SW Gondwana are shown against the background map of paleogeological information after Frimmel et al. (2011). The relatively few confirmed impact structures plot both into craton and into basin/orogen terranes, and there is no sorting by age for the bulk of the data of < 1000 – < 135 Ma ages. Considering the total extent of the continental regions shown, only limited clustering of impact sites is apparent, such as four structures formed over a 2 billion year interval in the inner Kalahari Craton, or three structures in the central South American Parnaíba Basin, spanning possibly as much as 200 Ma. Large areas of SW Gondwana have remained devoid of recorded impact sites, such as the entire Congo-São Francisco Craton, the Amazonian Craton, and the Rio de la Plata Craton and adjacent regions.

Furthermore, to date only a few Neoarchean (Barberton, Swaziland Supergroup) to Proterozoic (Transvaal Supergroup) impact spherule beds from South Africa are known (Glass and Simonson 2013) in SW Gondwana, whereas none such distal impact ejecta have been identified to date in similar successions on other parts of SW Gondwana. This is likely because little is known about such impact spherule occurrences in the wider geological community. Mapping and drilling activities could well unearth such occurrences in other parts as well and, thereby, decisively contribute to a better understanding of impact-related processes in the first half of the Earth's evolution.

With the exception of the 2.02 billion-year-old Vredefort structure in South Africa, which with an diameter of *ca*. 250–300 km had the potential of causing a major environmental catastrophe, with a mass extinction to be anticipated if there had been evolved life on the Earth at that time, none of the other structures in the study area seems to be large enough to have been responsible for a mass extinction event. However, it appears that the Gondwana-age Araguainha structure of 40 km diameter was formed in the Paraná Basin of Brazil at just about (within error limits) Permian-Triassic Boundary time (Tohver et al. 2012), with its associated major mass extinction. Tohver et al. (2013) suggested that seismic activity generated by this sizable impact over a major part of the basin could have released a vast amount of greenhouse gas from Paraná sediments that could have caused/contributed to a mega-environmental catastrophe.

In terms of major impact events in Gondwana, only the 90 km Acraman impact structure in southern Australia stands out, whose age is still only poorly constrained. Thus, an attempt at correlation with other geological events remains moot.

In Fig. 24.4 we compare the age distribution of impacts recorded in South America-Africa-Australia, plus two impact events in India (Dhala and Lonar—Earth Impact Database), whereby the age of Dhala at 1700–2500 Ma is too poorly constrained but was shown to be in excess of *ca*. 1000 Ma (Pati et al. 2010), and Lonar crater at 570 ka (Jourdan et al. 2011) is far too young for the topic discussed here. Figure 24.4 shows convincingly that there are several impact events that seemingly occurred between 500 and 650 Ma, and that since *ca*. 375 Ma a continuous but rather low flux of extraterrestrial projectiles is represented in the record. The last 20 Ma, and especially the last few million years, are recorded with a strong peak in this histogram but, obviously, there are a large number of relatively small and recent impact events among this subset of data. To attempt to compare this "scattergram" with other important geological events in Gondwana/Pangea history appears futile at this time, based on a too low statistical value of the impact database.

Much of the SW Gondwanan impact record was likely obliterated in the course of the rifting phases after 1000 Ma, and particularly during the post-500 Ma break-up phase. The known, rather limited impact record for this terrane contrasts sharply with the much stronger records of regions of, in particular, the northern hemisphere. Clearly there is ample scope

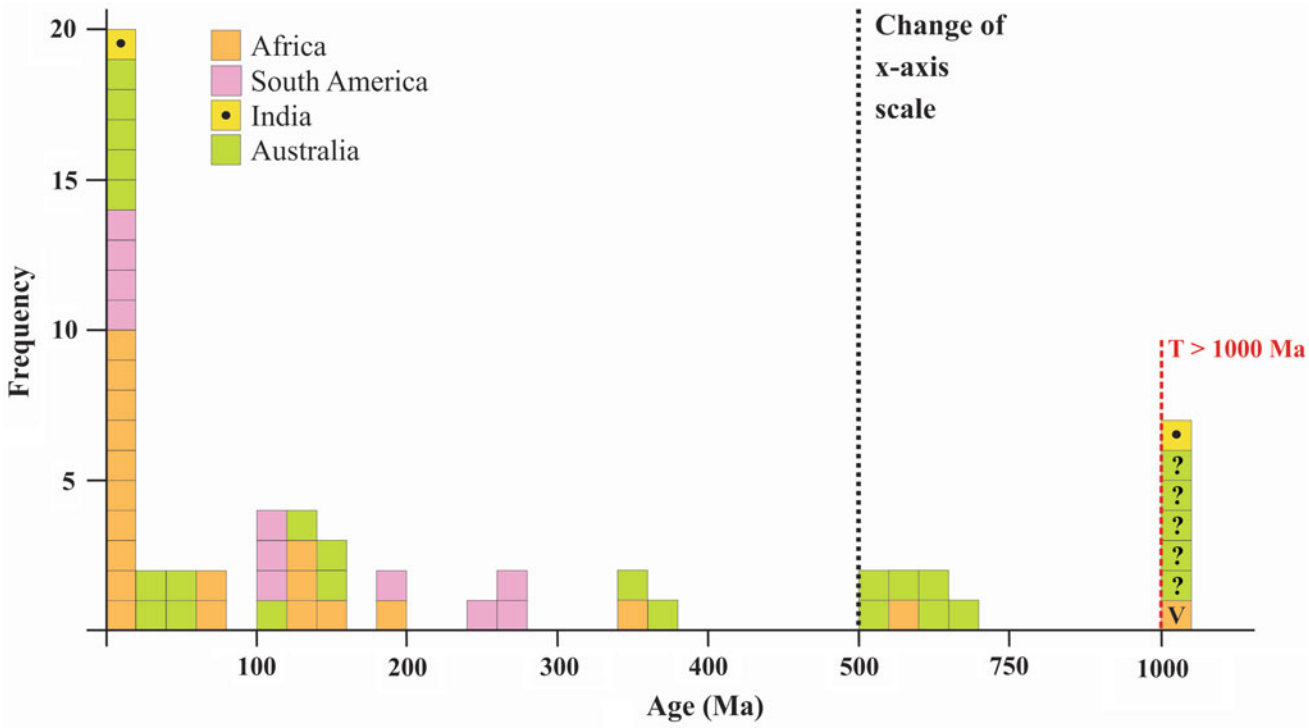

Fig. 24.4 Age histogram for the chronological data pertaining to the impact structures listed in Table 24.1, besides data for two Indian impact structures (compare with Earth Impact Database). Note the break in the x-axis scale at 500 Ma and structures with known (V: Vredefort in South Africa; filled black circle: Dhala in India) or possible yet unconfirmed ages (denoted by a ?, in Australia) >1000 Ma are plotted at the right edge of the figure

for further education about the fundamental importance of the impact process throughout geological time, in Africa as well as in South America. There is strong interest in this process among students. However, it has not yet become ingrained into the university curricula. Rarely does one find sessions with impact or meteorite, or general planetological themes in the programs of geoscientific conferences.

The dense vegetation covering major parts of these two continents does not favor remote sensing applications over much of Africa and South America, but outside the rainforest belt these techniques do have the potential to find first-order indications of possible impact structures. The applicants of widely applied geophysical methods should also be aware of impact structures and how to recognize them. And any geoscientist working on somewhat circular geological, geophysical, stratigraphic or hydrological anomalies ought to bear in mind the possibility that such anomalies could hint at the presence of impact structures. Finally, it has been shown conclusively (e.g., Erickson et al. 2013; Thomson et al. 2014) that shock (i.e., impact) deformed zircon and monazite grains from impact structures can survive erosion and weathering and can be traced from their source craters to distal depositories over 1000 km or more. Clearly any geoscientist working with such refractory minerals ought to know how to recognize shock-metamorphosed grains. Considering the wide application of zircon dating throughout Gondwana, we must expect to find new shock-zircon deposits and perhaps this will lead to discoveries of new impact structures. The products of impact (lithic, suevite, and melt breccias) and the telltale signs of impact deformation—shatter cones and shock microdeformation—ought to be known to every practicing geoscientist. French (1998), French and Koeberl (2010), and Reimold and Koeberl (2014) offer good introductory literature in this regard. Finally, the SW Gondwanan impact record —and, beyond that, the terrestrial impact record—may be further expanded through careful observation in the field and on drill cores, with the aim of identifying any possible impact ejecta deposits, such as spherule layer beds. Even if such beds cannot be dated radiometrically themselves, their stratigraphic position may be such that age bracketing could be attempted.

24.5 Conclusions

While the current impact record for Southwest Gondwana is limited and inadequate to identify any possible shift in the impact flux over the past 1000 Ma, or to attempt any correlation between impact activity and geological events in Gondwana/Pangea, we are making a case here for the need

to further improve this record. We consider this volume an opportunity to emphasize the importance of the impact process throughout solar system history, of past impact events on the Earth as on Gondwana, and the need to remain alert to the possibility that geological and petrographic studies of SW Gondwanan rock records may have the potential to still make significant contributions to the still fledgling impact record.

Acknowledgements This manuscript was prepared while WUR was on sabbatical at the University of Brasília. He wishes to thank the Institute of Geosciences there for their hospitality and support. His Brazilian research is also supported by an Innovationsfond grant from the Museum für Naturkunde Berlin to P. Zaag and WUR. APC acknowledges his CNPq research grant#305911/2013-9. Manfred Gottwald and the Deutsches Institut für Luft- und Raumfahrt (DLR) kindly provided permission to publish the TanDEM-X images in Fig. 24.2.

References

Acevedo RD, Ponce JF, Rocca M, Rabassa J, Corbella H (2009) Bajada del Diablo impact crater-strewn field: the largest crater field in the southern hemisphere. Geomorphologhy 110:58–67

Bland PA, de Souza Filho CR, Jull AJT, Kelley SP, Hough RM, Artemieva NA, Pierazzo E, Coniglio J, Pinotti L, Evers V, Kearsley AT (2002) A possible tektite strewn field in the Argentinian pampa. Science 296:1109–1111

Bottke WF, Vokrouhlický D, Minton D, Nesvorný D, Morbidelli A, Brasser A, Simonson B, Levison HF (2012) An Archaean heavy bombardment from a destabilized extension of the asteroid belt. Nature 485:78–81

Chennaoui Aoudjehane H, El Kerni H, Reimold WU, Baratoux D, Koeberl C, Bouley S (2016) The Agoudal (High Atlas Mountains, Morocco) shatter cone conundrum: a recent meteorite fall onto the remnant of an impact site. Meteorit Planet Sci 51:1497–1518

Cione AL, Tonni EP, San Cristóbal J, Hernández PJ, Benítez A, Bordignon F, Perí JA (2002) Putative meteoritic craters in Río Cuarto (Central Argentina) interpreted as eolian structures. Earth Moon Planet 91:9–24. https://doi.org/10.1023/A:1021209417252

Crósta AP, Koeberl C, Furuie RA, Kazzuo-Vieira C (2010) The first description and confirmation of the Vista Alegre impact structure in the Paraná flood basalts of southern Brazil. Meteorit Planet Sci 45:181–194

Crósta AP, Kazzuo-Vieira C, Pittarello L, Koeberl C, Kenkmann T (2011) Geology and impact features of Vargeão Dome, southern Brazil. Meteorit Planet Sci 47:51–71

Crósta AP, Jourdan F, Koeberl C (2012) $^{40}Ar/^{39}Ar$ dating of the Vista Alegre Crater, Brazil. In: 34th International Geological Congress. Brisbane, 1p. (abstract)

Crósta AP, Vasconcelos MAR (2013) Update on the current knowledge of the Brazilian impact craters. In: 44th lunar and planetary science conference (abstract#1318)

Crósta AP, Reimold WU (2016) Book review of: impact craters in South America by Acevedo, R.D., Rocca, M.C.L., Ponce, J. F., and Stinco, S.G., Heidelberg: Springer, 2015. 104 p., SpringerBriefs in Earth Sciences: South America and the Southern Hemisphere. ISBN 978-3-319-13092-7. Meteorit Planet Sci 51:996–999

Earth Impact Database (http://www.unb.ca/passc/ImpactDatabase) (last accessed February 2017)

Erickson T, Cavosie A, Moser D, Barker I, Radovan H, Wooden J (2013) Identification and provenance determination of distally transported, Vredefort-derived shocked minerals in the Vaal River, South Africa using SEM and SHRIMP-RG techniques. Geochim Cosmochim Acta 107:170–188

Ernstson K, Mayer W, Neumair A, Rappenglück B, Rappenglück MA, Sudhaus D, Zeller KW (2010) The Chiemgau crater strewn field: evidence for a holocene large impact event in Southeast Bavaria, Germany. J Sib Fed Univ Eng Technol 1(3):72–103

French BM, Koeberl C (2010) The convincing identification of terrestrial meteorite impact structures: what works, what doesn't, and why. Earth Sci Rev 98:123–170

Frimmel HE, Basei MS, Gaucher C (2011) Neoproterozoic geodynamic evolution of SW-Gondwana: A southern African perspective. Int J Earth Sci (Geologische Rundschau) 100:323–354

Garde AA, McDonald I, Dyck B, Keulen N (2012) Searching for giant, ancient impact structures on earth: the mesoarchaean Moniitsoq structure, West Greenland. Earth Planet Sci Lett 337–338:197–210

Garde AA, Keulen N, McDonald I, Dyck B (2013) Reply on "searching for giant, ancient impact structures on earth: the mesoarchaean Maniitsoq structure, West Greenland" by Garde et al. [Earth Planet. Sci. Lett. 337–338 (2012) 197-210]. Earth Planet Sci Lett 339–370: 336–343

Gibson RG, Reimold WU (2008) Geology of the Vredefort impact structure: a guide to sites of interest. Memoir 97, Council for Geoscience, Pretoria, 181 pp

Glass BP, Simonson BM (2013) Distal impact ejecta layers: a record of large impacts in sedimentary deposits. Impact Studies Series, Springer, Berlin, p 716

Gottwald M, Fritz T, Breit H, Schättler B, Harris A (2017) Remote sensing of terrestrial impact craters: the TanDEM-X digital elevation model. Meteorit Planet Sci 52:1412–1427

Grieve RAF, Cintala MJ, Therriault AM (2006) Large-scale impacts and the evolution of the Earth's crust. In Reimold WU, Gibson RL (eds) Processes on the early Earth. Geol Soc Am Spec Paper 405:23–31

Jourdan F, Moynier F, Koeberl C, Eroglu S (2011) 40Ar/39Ar age of the Lonar crater and consequence for the geochronology of planetary impacts. Geology 39:671–674. https://doi.org/10.1130/G31888.1

Jourdan F, Reimold WU, Deutsch A (2012) Dating terrestrial impact structures. Elements 8(1):49–54

Kenkmann T, Vasconcelos MAR, Crosta AP, Reimold WU (2011) The complex impact structure Serra da Cangalha, Tocantins State, Brazil. Meteorit Planet Sci 46:875–889

Koeberl C, Reimold WU (2005) Bosumtwi impact crater, Ghana (West Africa): an updated and revised geological map, with explanations. Jahrbuch der Geologischen Bundesanstalt, Wien, 145. Heft 1:31–70

Madiedo JM, Ortiz JL, Morales N, Cabrera-Caño J (2014) A large lunar impact blast on 2013 September 11. MNRAS (Monthly Notices of the Royal Astronomical Society), http://mnras.oxfordjournals.org/content/early/2014/02/19/mnras.stu083.full.pdf+html

Marchi S, Bottke WF, Kring DA, Morbidelli A (2012) The onset of the lunar cataclysm as recorded in its ancient crater populations. Earth Planet Sci Lett 325:27–38. https://doi.org/10.1016/j.epsl.2012.01.021

Marchi S, Bottke WF, Cohen BA, Wünnemann K, Kring DA, McSween HY, De Sanctis MC, O'Brien DP, Schenk P, Raymond CA, Russell CT (2013) High-velocity collisions from the lunar cataclysm recorded in asteroidal meteorites. Nat Geosci 6:303–307

Maziviero MV, Vasconcelos MAR, Crósta AP, Góes AM, Reimold WU, Carneiro CC (2013) Geology and impact features of Riachão structure, northern Brazil. Meteorit Planet Sci 48:2044–2058

Melosh HJ (2011) Planetary surface processes. Cambridge University Press, Cambridge, pp 500

Meert JG, Lieberman BS (2008) The neoproterozoic assembly of Gondwana and its relationship to the Ediacaran-Cambrian radiation. Gondwana Res 14:5–21

Miller RMcG (2008) Meteorite impact craters and meteorites. In Miller RMcG (ed) The geology of Namibia, vol 3. Ministry of mines and energy, Windhoek, Namibia, pp. 26–1 to 26-8 (Chapter 26)

Nédélec A, Paquette J-L, Yokoyama E, Trindade RIF, Aigouy T, Baratoux D (2013) In situ U/Pb dating of impact-produced zircons from the Vargeão Dome (Southern Brazil). Meteorit Planet Sci 48:420–431

Oliveira GJG, Vasconcelos MAR, Crósta AP, Reimold WU, Góes AM, Kowitz A (2014) Shatter cones and planar deformation features confirm Santa Marta in Piauí State, Brazil, as an impact structure. Meteorit Planet Sci 49:1915–1928

Oliveira GJG, Chamani MAC, Góes AM, Crósta AP, Vasconcelos MAR, Reimold WU (2018) Stratigraphic and structural characteristics of the central portion of the Santa Marta impact structure, Piauí State, Brazil. Braz J Geol 43:673–692

Pati JK, Jourdan F, Armstrong RA, Reimold WU, Prakash K, Renne PR (2010) First SHRIMP and $^{40}Ar/^{39}Ar$ chronological results from impact melt breccia from the Paleoproterozoic Dhala impact structure, India. In: Gibson RL, Reimold WU (eds) Geological society of Americe special paper 465, Large meteorite impacts and planetary evolution IV, pp 571–591

Pierazzo E, Artemieva N (2012) Local and global environmental effects of impacts on Earth. Elements 8(1):55–60. https://doi.org/10.2113/gselements.8.1.55

Reimold WU, Jourdan F (2012a) IMPACT! Special issue. Elements 8 (1):19–60

Reimold WU, Jourdan F (2012b) IMPACT!—Bolides, craters, and catastrophes. Elements 8(1):19–24

Reimold WU, Koeberl C (2014) Impact structures in Africa: a review. J Afr Earth Sci 93:57–175

Reimold WU, Ferrière L, Deutsch A, Koeberl C (2014) Impact controversies: impact recognition criteria and related issues. Meteorit Planet Sci 49:723–731

Richards MA, Alvarez WC, Self S, Karlstrom L, Renne PR, Manga M, Sprain CJ, Smit J, Vanderkluysen L, Gibson SA (2015) Triggering of the largest Deccan eruptions by the Chicxulub impact. Geol Soc Am Bull 127(11–12):1507–1520. https://doi.org/10.1130/B31167.1

Schulte P, Alegret L, Arenillas I, Arz JA, Barton P, Bown PR, Bralower TJ, Christeson GL, Claeys P, Cockell CS, Collins GS, Deutsch A, Goldin TJ, Goto K, Grajales-Nishimura JM, Grieve RAF, Gulick SPS, Johnson KR, Kiessling W, Koeberl C, Kring DA, MacLeod KG, Matsui T, Melosh J, Montanari A, Morgan JV, Neal CR, Nichols DJ, Norris RD, Pierazzo E, Ravizza G, Rebolledo-Vieyra M, Reimold WU, Robin E, Salge T, Speijer RP, Sweet AR, Urrutia-Fucugauchi J, Vajda V, Whalen MT, Willumsen PS (2010) The Chicxulub impact and mass extinction at the cretaceous-paleogene boundary. Science 327 (5970):1214–1218. https://doi.org/10.1126/science.1177265

Schultz PH, Lianza RE (1992) Recent grazing impacts on the Earth recorded in the Rio Cuarto crater field, Argentina. Nature 355: 234–237

Schultz PH, Zárate MA, Hames W, Camilión C, King J (1998) A 3.3-Ma impact in Argentina and possible consequences. Science 282(5396):2061–2063

Schultz P, Zárate MA, Hames W, Bunch T, Koeberl C (2004) Late cenozoic impact record in the Argentine pampas sediments. Meteorit Planet Sci 38(supplement):A95

Schultz PH, Zárate MA, Hames, Harris RS, Bunch TE, Koeberl C, Renne P, Wittke J (2006) The record of Miocene impacts in the Argentine pampas. Meteorit Planet Sci 41:749–771

Sighinolfi GP, Sibilia E, Contini G, Martini M (2015) Thermoluminescence dating of the Kamil impact crater (Egypt). Meteorit Planet Sci 50:204–215

Stewart SA (2011) Estimates of yet-to-find impact crater population on Earth. J Geol Soc Lond 168:1–14

Stöffler D, Ryder G, Artemieva NA, Cintala MJ, Grieve RAF, Ivanov BA (2006) Cratering history and lunar chronology. In: Joliff BL et al (eds) New views of the moon. Reviews in mineralogy and geochemistry 60. Mineralogical society of America, Chantilly, VA, USA, pp 519–596 (chapter 5)

Thomson O, Cavosie A, Moser D, Barker I, Radovan H, French BM (2014) Preservation of detrital shocked minerals derived from the 1.85 Ga Sudbury impact structure in modern alluvium and Holocene glacial deposits. Geol Soc Am Bull 126:720–737

Tohver E, Lana C, Cawood PA, Fletcher I, Sherlock S, Jourdan F, Rasmussen B,Trindade RIF, Yokoyama E, Souza Filho CR, Marangoni Y (2012) Geochronological constraints on a Permo-Triassic impact crater: U-Pb and $_{40}Ar/_{39}Ar$ results from the 40 km Araguainha crater of central Brazil. Geochim Cosmochim Acta 86:214–227

Tohver E, Cawood PA, Riccomini C, Lana C, Trindade RIF (2013) Shaking a methane fizz: seismicity from the Araguainha impact event and the permian–triassic global carbon isotope record. Palaeogeogr Palaeoclimatol Palaeoecol 387:66–75

Vasconcelos MAR, Crósta AP, Reimold WU, Góes AM, Kenkmann T, Poelchau MH (2013) The Serra da Cangalha impact structure, Brazil: geological, stratigraphic and petrographic aspects of a recently confirmed impact structure. J S Am Earth Sci 45:316–330

Velázquez VF, Riccomini C, Azevedo Sobrinho JM, Pletsch MAJS, Sallun AEM, Sallun Filho W, Hachiro J (2013) Evidence of shock metamorphism effects in allochthonous breccia deposits from the Colônia Crater, São Paulo, Brazil. Int J Geosci 4:274–282

Velázquez VF, Lucena RF, Sobrinho JMA, Sallun AEM, Sallun Filha W (2017) Petrographic investigation of target rock transformation under high shock pressures from the Colonia impact Crater, Brazil. Earth Sci Res 7(1):13–24

Wagner R, Reimold WU, Brandt D (2002) Bosumtwi impact crater, Ghana: a remote sensing investigation. In: Plado J, Pesonen L (eds) Impacts in precambrian shields. Impact Studies Series, Springer, Berlin, pp 189–210

Wright SP, Vesconi MA, Spagnuolo MG, Cerutti C, Jacob RW, Cassidy WA (2007) Explosion craters and penetration funnels in ther Campo del Cielo, Argentina, crater field. In: Lunar and planetary science conference XXVIII, abstract #2017 (CD-ROM), 2 p